Initial Reports of the Deep Sea Drilling Project

Volume XC, Part 2

Noumea, New Caledonia to Wellington, New Zealand
December 1982—January 1983

READEX FICHE best copy available

NATIONAL SCIENCE FOUNDATION
National Ocean Sediment Coring Program

NSFSP—90

January 1986

90/pt.2/car.

NEWARK PUBLIC LIBRARY
MAY 30 1986
U. S. GOVT. DEPOSITORY

Drilling locations

Leg	Location	Sites
Phase 1 1968-1970		
1	North Atlantic	1-7
2	North Atlantic	8-12
3	South Atlantic	13-22
4	Central Atlantic	23-31
5	North Pacific	32-43
6	North Pacific	44-60
7	Central Pacific	61-67
8	Central Pacific	68-75
9	Central Pacific	76-84
Phase 2 1970-1972		
10	Gulf of Mexico	85-97
11	North Atlantic	98-108
Re-entry trials		109-110
12	North Atlantic	111-119
13	Mediterranean	120-134
14	Central Atlantic	135-144
15	Caribbean	146-154
16	Central Pacific	155-163
17	Central Pacific	164-171
18	North Pacific	172-182
19	North Pacific	183-193
20	North Pacific	194-202
21	Coral Sea	203-210
22	Indian Ocean	211-218
23	Arabian Sea	219-230
24	Indian Ocean	231-238
25	Indian Ocean	239-249
Phase 3 1972-1975		
26	Indian Ocean	250-258
27	Indian Ocean	259-263
28	Antarctic	264-274
29	Tasman Sea	275-284
30	South Pacific	285-289
31	North Pacific	290-302
32	North Pacific	303-313
33	North Pacific	314-318
34	South Pacific	319-321
35	South Pacific	322-325
36	South Atlantic	326-331
37	North Atlantic	332-335
38	Arctic	336-352
39	Atlantic	353-359
40	South Atlantic	360-365
41	South Atlantic	366-370
42A	Mediterranean	371-378
42B	Black Sea	379-381
43	North Atlantic	382-387
44	North Atlantic	388-392
44A	North Atlantic	393-394
IPOD 1975-present		
45	North Atlantic	395-396
46	North Atlantic	396A-396B
47	North Atlantic	397-398
48	North Atlantic	399-406
49	North Atlantic	407-414
50	North Atlantic	415-416
51A	North Atlantic	417-417A
51B	North Atlantic	417B-417D
52	North Atlantic	417D-418A
53	North Atlantic	418A-418B
54	Central Pacific	419-429
55	North Pacific	430-433
56	North Pacific	434-437
57	North Pacific	438-441
58	North Pacific	442-446
59	North Pacific	447-451
60	North Pacific	452-461
61	Central Pacific	462
62	North Pacific	463-466
63	North Pacific	467-473
64	Gulf of California	474-481
65	Gulf of California	482-485
66	Central Pacific	486-493
67	Central Pacific	494-500
68	Central Pacific	502-503
69	Central Pacific	504-505, 501
70	Central Pacific	506-510, 504B
71	South Atlantic	511-514
72	South Atlantic	515-518
73	South Atlantic	519-524
74	South Atlantic	525-529
75	South Atlantic	530-532
76	North Atlantic	533-534
77	Caribbean	535-540
78	North Atlantic	541-543, 395A-B
79	North Atlantic	544-547
80	North Atlantic	548-551
81	North Atlantic	552-555
82	North Atlantic	556-564
83	Central Pacific	504B
84	Central Pacific	565-570
85	Central Pacific	571-575
86	North Pacific	576-581
87	North Pacific	582-584
88	North Pacific	581
89	Central Pacific	585-586, 462A
90	South Pacific	587-594

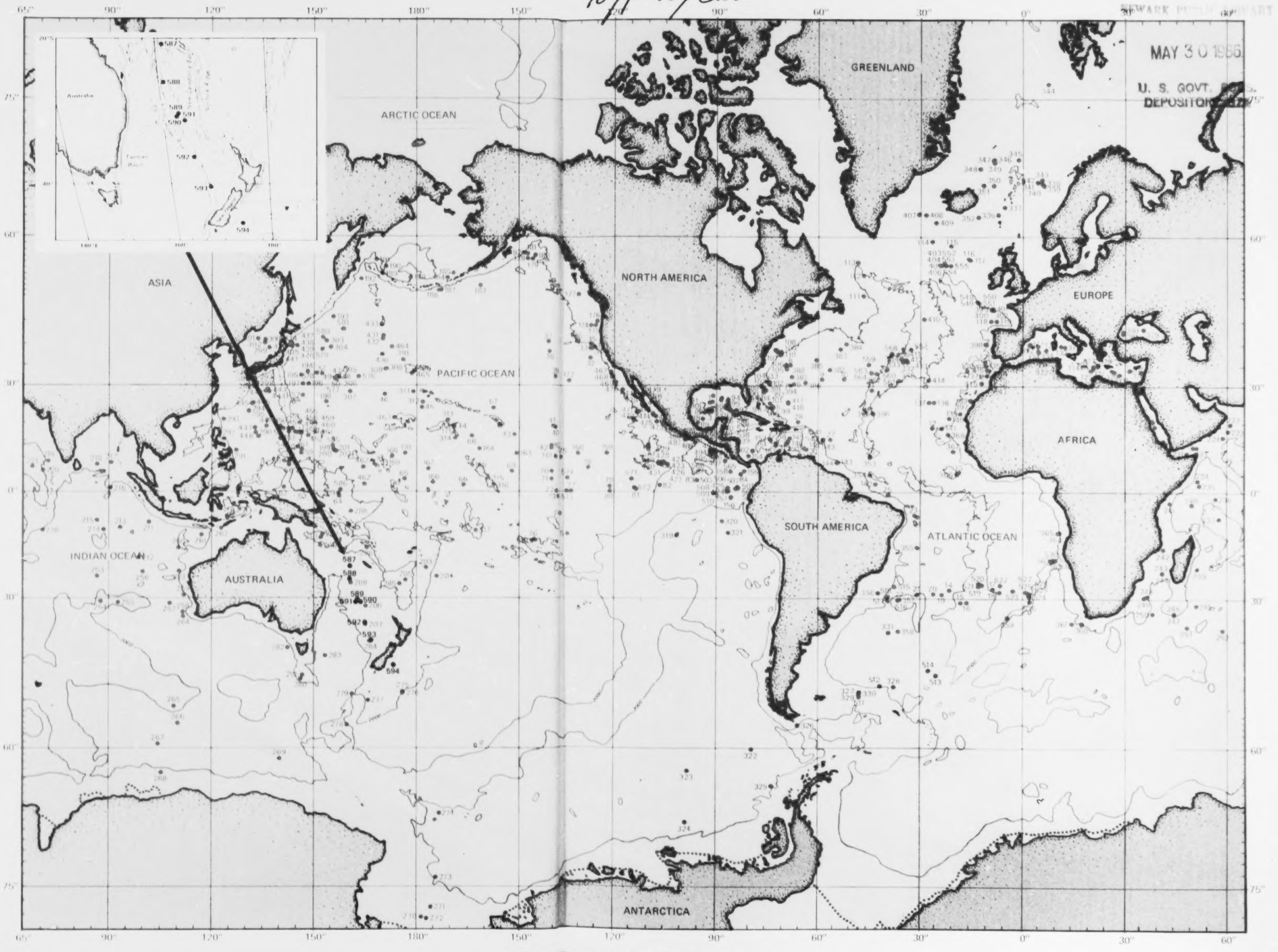

DEEP SEA DRILLING PROJECT

NS1.38:

P

F

Initial Reports of the Deep Sea Drilling Project

A Project Planned by and Carried Out With the Advice of the
JOINT OCEANOGRAPHIC INSTITUTIONS FOR DEEP EARTH SAMPLING (JOIDES)

VOLUME XC, Part 2

covering Leg 90 of the cruises of the Drilling Vessel *Glomar Challenger*
Noumea, New Caledonia, to Wellington, New Zealand
December 1982–January 1983

PARTICIPATING SCIENTISTS

James P. Kennett, Christopher C. von der Borch, Paul A. Baker,
Charles E. Barton, Anne Boersma, Jean Pierre Caulet,
Walter C. Dudley, Jr., James V. Gardner, D. Graham Jenkins,
William H. Lohman, Erlend Martini, Russell B. Merrill,
Roger Morin, Campbell S. Nelson, Christian Robert,
M. S. Srinivasan, Rüdiger Stein, and Akira Takeuchi

SHIPBOARD SCIENCE REPRESENTATIVE

Russell B. Merrill

EDITOR

Jan H. Blakeslee

Prepared for the
NATIONAL SCIENCE FOUNDATION
National Ocean Sediment Coring Program
Under Contract C-482
By the
UNIVERSITY OF CALIFORNIA
Scripps Institution of Oceanography
Prime Contractor for the Project

For sale by the Superintendent of Documents, U.S. Government Printing Office
Washington, D.C. 20402

Stock Number 038-000-00561-8 Second Printing

CONTENTS

Chapter Page

PART III: STRATIGRAPHIC AND PALEONTOLOGIC STUDIES

11. PALEOGENE CALCAREOUS NANNOPLANKTON FROM THE SOUTHWEST PACIFIC OCEAN, DEEP SEA DRILLING PROJECT LEG 90 747
E. Martini

12. CALCAREOUS NANNOPLANKTON BIOSTRATIGRAPHY OF THE SOUTHERN CORAL SEA, TASMAN SEA, AND SOUTHWESTERN PACIFIC OCEAN, DEEP SEA DRILLING PROJECT LEG 90: NEOGENE AND QUATERNARY 763
W. H. Lohman

13. CENOZOIC PLANKTONIC FORAMINIFERS FROM THE EQUATOR TO THE SUBANTARCTIC OF THE SOUTHWEST PACIFIC 795
D. G. Jenkins and M. S. Srinivasan

14. RADIOLARIANS FROM THE SOUTHWEST PACIFIC 835
J. P. Caulet

15. MIDDLE MIOCENE TO QUATERNARY DIATOM BIOSTRATIGRAPHY OF DEEP SEA DRILLING PROJECT SITE 594, CHATHAM RISE, SOUTHWEST PACIFIC... 863
P. F. Ciesielski

16. SILICOFLAGELLATES AND SOME SPONGE SPICULES FROM THE SOUTHWEST PACIFIC, DEEP SEA DRILLING PROJECT LEG 90 887
S. Locker and E. Martini

17. MIOCENE SILICOFLAGELLATES FROM CHATHAM RISE, DEEP SEA DRILLING PROJECT SITE 594........................ 925
D. Bukry

18. EBRIDIANS AND ACTINISCIDIANS FROM THE SOUTHWEST PACIFIC......... 939
S. Locker and E. Martini

19. QUATERNARY FISH OTOLITHS FROM SITES 587 AND 594, SOUTHWEST PACIFIC, DEEP SEA DRILLING PROJECT LEG 90 953
E. Martini and P. A. M. Gaemers

Chapter Page

20. BIOSTRATIGRAPHY AND BIOGEOGRAPHY OF TERTIARY BATHYAL BENTHIC FORAMINIFERS: TASMAN SEA, CORAL SEA, AND ON THE CHATHAM RISE (DEEP SEA DRILLING PROJECT, LEG 90)................................. 961
A. Boersma

21. NEOGENE BENTHIC FORAMINIFERS: DISTRIBUTION IN DEPTH TRAVERSE, SOUTHWEST PACIFIC 1037
K. Kurihara and J. P. Kennett

22. PHYTOLITHS FROM THE SOUTHWEST PACIFIC, SITE 591 1079
S. Locker and E. Martini

23. PALYNOLOGY OF SELECTED NEOGENE SAMPLES FROM HOLES 594 AND 594A, CHATHAM RISE..........................1085
L. E. Heusser

24. LATE PALEOGENE AND EARLY NEOGENE FORAMINIFERS OF DEEP SEA DRILLING PROJECT SITE 270, ROSS SEA, ANTARCTICA........................1093
R. M. Leckie and P.-N. Webb

PART IV: SEDIMENTOLOGIC STUDIES

25. DISTRIBUTION AND CHARACTER OF PALE GREEN LAMINAE IN SEDIMENT FROM LORD HOWE RISE: A PROBABLE LATE NEOGENE AND QUATERNARY TEPHROSTRATIGRAPHIC RECORD 1145
J. V. Gardner, C. S. Nelson, and P. A. Baker

26. NATURE, CHEMISTRY, AND ORIGIN OF LATE CENOZOIC MEGASCOPIC TEPHRAS IN LEG 90 CORES FROM THE SOUTHWEST PACIFIC 1161
C. S. Nelson, P. C. Froggatt, and G. J. Gosson

27. NATURE AND SIGNIFICANCE OF VOLCANOGENIC DEPOSITS AT THE EOCENE/OLIGOCENE BOUNDARY, HOLE 593, CHALLENGER PLATEAU, TASMAN SEA.............................1175
C. S. Nelson, R. M. Briggs, and P. J. J. Kamp

Chapter Page

28. BIOTURBATION IN MIDDLE BATHYAL, CENOZOIC NANNOFOSSIL OOZES AND CHALKS, SOUTHWEST PACIFIC 1189
C. S. Nelson

29. LATE NEOGENE AND QUATERNARY COARSE-FRACTION AND CARBONATE STRATIGRAPHIES FOR SITE 586 ON ONTONG-JAVA PLATEAU AND SITE 591 ON LORD HOWE RISE 1201
J. V. Gardner, W. E. Dean, L. Bisagno, and E. Hemphill

30. CENOZOIC EVOLUTION AND SIGNIFICANCE OF CLAY ASSOCIATIONS IN THE NEW ZEALAND REGION OF THE SOUTHWEST PACIFIC, DEEP SEA DRILLING PROJECT, LEG 90 1225
C. Robert, R. Stein, and M. Acquaviva

31. PHYSICAL PROPERTIES OF CALCAREOUS SEDIMENTS FROM THE SOUTHWEST PACIFIC 1239
R. H. Morin

PART V: GEOCHEMICAL STUDIES

32. PORE-WATER CHEMISTRY OF CARBONATE-RICH SEDIMENTS, LORD HOWE RISE, SOUTHWEST PACIFIC OCEAN 1249
P. A. Baker

33. ^{87}Sr/^{86}Sr RATIOS OF PLANKTONIC FORAMINIFERS AND INTERSTITIAL WATERS, DEEP SEA DRILLING PROJECT LEG 90, SITE 593 1257
J. Hess and J.-G. Schilling

34. ^{3}HE/^{4}HE RATIOS OF PORE GASES IN DEEP-SEA SEDIMENTS, LEGS 89 AND 90 .. 1261
H. Wakita, Y. Sano, N. Fujii, and A. Takeuchi

35. DIAGENESIS OF ORGANIC COMPOUNDS IN HOLE 593, LEG 90 (TASMAN SEA) 1265
B. Mycke, K.-C. Emeis, and E. T. Degens

PART VI. GEOPHYSICAL STUDIES

36. PALEOMAGNETISM OF SEDIMENTS COLLECTED DURING LEG 90, SOUTHWEST PACIFIC 1273
C. E. Barton and J. Bloemendal

Chapter Page

37. GEOTHERMAL MEASUREMENTS AT DEEP SEA DRILLING PROJECT SITE 587 .. 1317
R. H. Morin and R. P. Von Herzen

38. SEISMIC STRATIGRAPHY AND STRUCTURE ADJACENT TO AN EVOLVING PLATE BOUNDARY, WESTERN CHATHAM RISE, NEW ZEALAND 1325
K. B. Lewis, D. J. Bennett, R. H. Herzer, and C. C. von der Borch

39. SEISMIC STRATIGRAPHY OF THE NEOGENE SEQUENCE AT SITE 587 1339
A. Mignot and A. Mauffret

PART VII: PALEOCEANOGRAPHIC STUDIES

40. DEVELOPMENT OF LATITUDINAL THERMAL GRADIENTS DURING THE OLIGOCENE: OXYGEN-ISOTOPE EVIDENCE FROM THE SOUTHWEST PACIFIC 1347
M. G. Murphy and J. P. Kennett

41. LATE NEOGENE PALEOCEANOGRAPHIC EVOLUTION OF SITE 590: SOUTHWEST PACIFIC 1361
K. M. Elmstrom and J. P. Kennett

42. MIOCENE TO EARLY PLIOCENE OXYGEN AND CARBON ISOTOPE STRATIGRAPHY IN THE SOUTHWEST PACIFIC, DEEP SEA DRILLING PROJECT LEG 90 ... 1383
J. P. Kennett

43. QUATERNARY ISOTOPE STRATIGRAPHY OF HOLE 593, CHALLENGER PLATEAU, SOUTH TASMAN SEA: PRELIMINARY OBSERVATIONS BASED ON FORAMINIFERS AND CALCAREOUS NANNOFOSSILS 1413
C. S. Nelson, C. H. Hendy, and W. C. Dudley

44. LATE QUATERNARY CARBONATE AND ISOTOPE STRATIGRAPHY, SUBANTARCTIC SITE 594, SOUTHWEST PACIFIC 1425
C. S. Nelson, C. H. Hendy, A. M. Cuthbertson, and G. R. Jarrett

45. SILICICLASTIC SEDIMENTS AT SITES 588, 590, AND 591: NEOGENE AND PALEOGENE EVOLUTION IN THE SOUTHWEST PACIFIC AND AUSTRALIAN CLIMATE 1437
R. Stein and C. Robert

Chapter Page

PART VIII: SYNTHESES

46. BIOSTRATIGRAPHIC SYNTHESIS OF DEEP SEA DRILLING PROJECT LEG 90 IN THE SOUTHWEST PACIFIC OCEAN 1459
E. Martini and D. G. Jenkins

47. LITHOSTRATIGRAPHY OF DEEP SEA DRILLING PROJECT LEG 90 DRILL SITES IN THE SOUTHWEST PACIFIC: AN OVERVIEW 1471
C. S. Nelson

48. SOUTHWEST PACIFIC CENOZOIC PALEOCEANOGRAPHY....................1493
J. P. Kennett and C. C. von der Borch

BACK POCKET FIGURES

CHAPTER 15: FIGURE 3. POSITIONS OF SELECTED DIATOM, RADIOLARIAN, SILICOFLAGELLATE, AND FORAMINIFERAL DATUMS IN THE LATE MIOCENE AND PLIOCENE TO QUATERNARY OF HOLES 594 AND 594A AND THEIR CORRELATION TO PALEOMAGNETIC STRATIGRAPHY.

CHAPTER 15: FIGURE 4. POSITIONS OF SELECTED DIATOM, RADIOLARIAN, SILICOFLAGELLATE, AND CALCAREOUS NANNOFOSSIL DATUMS IN THE MIDDLE TO LATE MIOCENE OF HOLES 594 AND 594A AND THEIR CORRELATION TO PALEOMAGNETIC STRATIGRAPHY.

CHAPTER 38: FIGURE 5. TRACINGS OF *GLOMAR CHALLENGER* TRANSIT PROFILES BETWEEN COOK STRAIT AND SITE 594 EAST OF NEW ZEALAND, SHOWING MAIN SEISMIC SEQUENCES, FAULTS, AND UNCONFORMITIES.

PART III: STRATIGRAPHIC AND PALEONTOLOGIC STUDIES

11. PALEOGENE CALCAREOUS NANNOPLANKTON FROM THE SOUTHWEST PACIFIC OCEAN, DEEP SEA DRILLING PROJECT, LEG 90[1]

Erlend Martini, Geologisch-Paläontologisches Institut der Universität, Frankfurt am Main[2]

ABSTRACT

The positions of all cores recovered during Leg 90 in the southwest Pacific are shown within the standard calcareous nannoplankton zonation. The stratigraphic and regional occurrences and preservation of Paleogene calcareous nannoplankton found at Sites 588, 592, and 593 are discussed, and fossil lists are given for selected samples. Data on the Eocene/Oligocene boundary found in Holes 592 and 593 and on the Oligocene/Miocene boundary in Hole 588C are presented. Regional unconformities are noted in Hole 588C, where the upper Eocene to middle Oligocene interval (Zones NP17 to NP23) is missing, and in Hole 592, in which the middle Oligocene to lowest Miocene interval (Zones NP23 to NN1) is not represented.

INTRODUCTION

During Leg 90 of the Deep Sea Drilling Project, eight sites (587 to 594) were occupied and 18 holes drilled in the New Caledonia to New Zealand region (Fig. 1). All holes yielded common calcareous nannoplankton. Results for each hole are summarized and cores are located within the standard calcareous nannoplankton zonation in Table 1.

Holes 588C, 592, 593, and 593A yielded Paleogene calcareous nannoplankton. The Paleogene assemblages of these holes and their age assignments are discussed below. Fossil lists for selected samples from Holes 588C, 592, and 593 are presented in Tables 2 to 4, covering most of the middle Eocene to upper Oligocene interval. For the Neogene and Quaternary calcareous nannoplankton found during Leg 90 see Lohman, this volume.

CALCAREOUS NANNOPLANKTON ZONATION

For the Tertiary and Quaternary the standard calcareous nannoplankton zonation (Martini, 1971) is used. For the Paleogene nannoplankton zones some deviations are necessitated by the high latitudes of some of the Leg 90 sites (Fig. 2).

NP24/NP25$^{*}_{*}$ (combined *Sphenolithus distentus/ S. ciperoensis* Zone)[3]

Substitute definition. Interval from the last occurrence of *Blackites tenuis* (Bramlette and Sullivan) to the last occurrence of *Zygrhablithus bijugatus* (Deflandre).

Remarks. As sphenoliths commonly used to define the zonal boundaries in the middle and late Oligocene are too rare or missing in samples from Holes 593 and 593A because of its high latitude during the Paleogene, the two uppermost Paleogene nannoplankton zones had to be combined and the substitute species noted had to be used. The last occurrence of *B. tenuis* (Bramlette and Sullivan) is taken as the base of Zone NP24 in these holes, because in high latitudes it seems not to cross the NP23/NP24 boundary. The NP25/NN1 boundary is placed at the last occurrence of *Z. bijugatus* (Deflandre), as on the high latitude Legs 38 (Müller, 1976) and 49 (Martini, 1979).

NP 23* (*Sphenolithus predistentus* Zone)

Substitute definition. Interval from the last occurrence of *Reticulofenestra umbilica* (Levin) to the last occurrence of *Blackites tenuis* (Bramlette and Sullivan).

Remarks. Because of the high latitude of Hole 593 during the Paleogene, sphenoliths are commonly rare or missing, and the top of Zone NP23 in this case is defined by the last occurrence of *B. tenuis* (Bramlette and Sullivan) as discussed above.

NP19/NP20 (combined *Isthmolithus recurvus/Sphenolithus pseudoradians* Zone)

Definition. Interval from the first occurrence of *Isthmolithus recurvus* Deflandre to the last occurrence of *Discoaster saipanensis* Bramlette and Riedel.

Remarks. *Sphenolithus pseudoradians* Bramlette and Wilcoxon, the index species for the base of Zone NP20, first occurred in the equatorial Pacific much earlier than in high latitudes (Bukry, 1971), and differentiation is possible only in middle latitudes (Martini, 1981a). For the present area it seems more realistic to combine Zones NP19 and NP20.

NP15/NP16 (combined *Chiphragmalithus alatus/Discoaster tani nodifer* Zone)

Definition. Interval from the first occurrence of *Chiphragmalithus alatus* (Martini) to the last occurrence of *Chiasmolithus solitus* (Bramlette and Sullivan).

Remarks. In Hole 588C the index species of the boundary between Zones NP15 and NP16—*Blackites gladius* (Locker)—was not found (probably it is a nearshore spe-

---

[1] Kennett, J. P., von der Borch, C. C., et al., *Init. Repts. DSDP*, 90: Washington (U.S. Govt. Printing Office).

[2] Address: Geologisch-Paläontologisches Institut der Universität, Senckenberg-Anlage 32-34, D6000 Frankfurt am Main, Federal Republic of Germany.

[3] Superscript asterisk indicates that top marker species has been changed, subscript asterisk that base marker species has been changed.

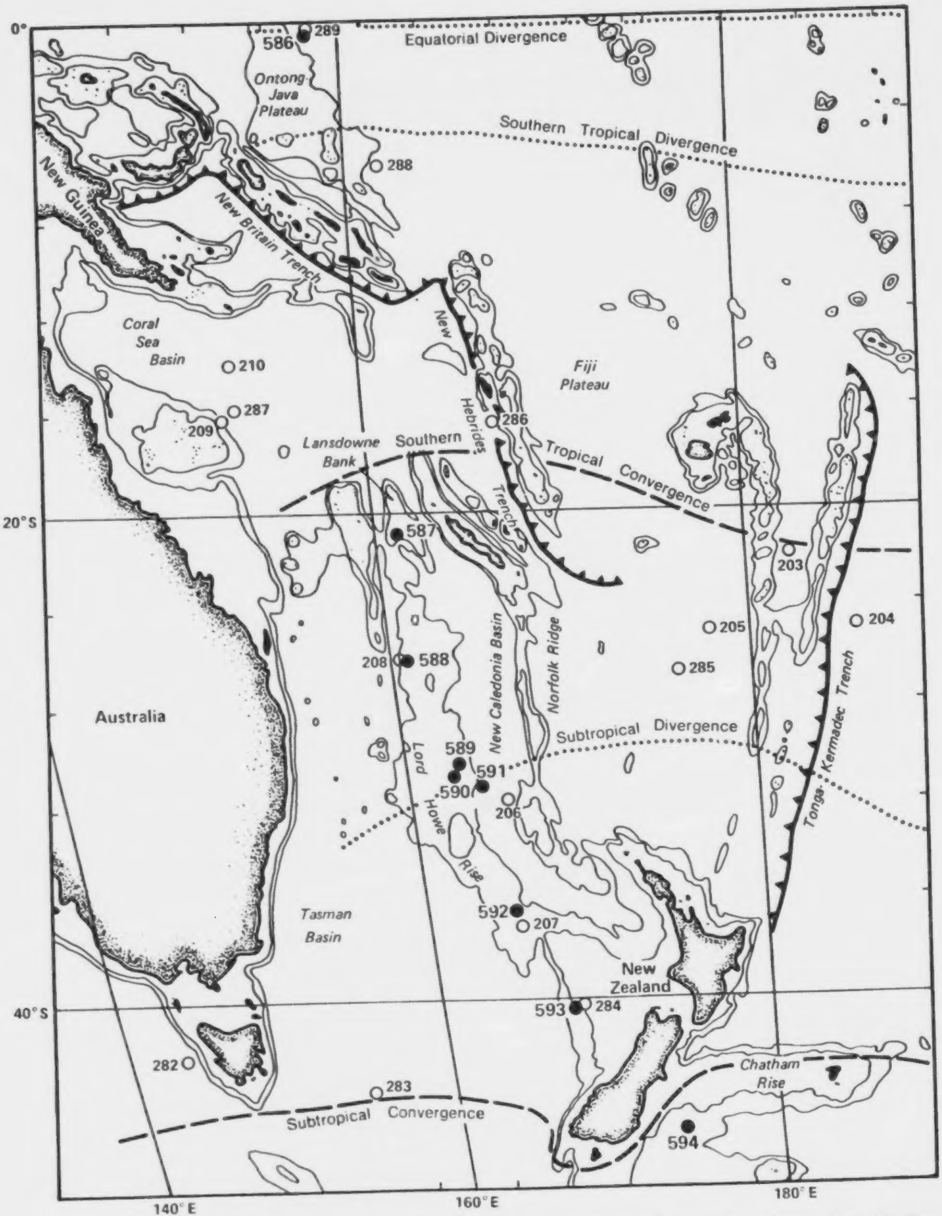
0°
20°S
40°S
140°E
160°E
180°E
586
289
Equatorial Divergence
Ontong Java Plateau
Southern Tropical Divergence
288
New Guinea
New Britain Trench
Coral Sea Basin
210
287
209
Lansdowne Bank
Southern Tropical Convergence
New Hebrides Trench
286
Fiji Plateau
587
203
205
204
208
588
285
Australia
Lord Howe Rise
New Caledonia Basin
Norfolk Ridge
Subtropical Divergence
Tonga-Kermadec Trench
589
591
590
206
592
207
Tasman Basin
New Zealand
593
284
282
283
Chatham Rise
Subtropical Convergence
594

Figure 1. Location of sites drilled during Leg 90 (solid circles) and other DSDP drill sites (open circles) in the southwest Pacific.

cies), and the only occurrence of *Chiphragmalithus alatus* is in Sample 588C-18-1, middle. Therefore a combination of the two zones for this hole seems necessary. However, a single specimen of *Chiasmolithus gigas* (Bramlette and Sullivan) was noted in Sample 588C-19-1, 10-12 cm, and the whole sequence between Samples 588C-18-1, middle, to 588C-19,CC may belong in Zone NP15 (*Chiphragmalithus alatus* Zone). The sequence could be in a position within this interval similar to the *Chiasmolithus gigas* Subzone of Bukry (1973).

SITE SUMMARIES

Site 588 (26°06.7′S, 161°13.6′E, water depth 1533 m)

In Hole 588C, on the northern part of Lord Howe Rise, Paleogene sediments were encountered form Core 6 (353.7 m sub-bottom) downward to the terminal depth of 488.1 m in Core 19. The interval between Samples 588C-6-2, 0-1 cm and 588C-17-1, 0-1 cm is placed in standard nannoplankton Zone NP25 (*Sphenolithus ciperoensis* Zone). Important species include *Helicosphae-*

Table 1. Calcareous nannoplankton stratigraphy of Holes 586–594.

	SNZ	586B	587	588	588A	588B	588C	589	590	590A	590B	591	591A	591B	592	593	593A	594	594A	594B
Quaternary	NN21	1	1–3	1		1		1	1		1	1	1		1	1	1	1–6	1	1–5
	NN20	1		1		1		1	1		1–2	1–2	1		1	1–2	1	6–7	2	
	NN19	1–5	3–4	1–3		1–2		1–4	2–3	1	2–4	2–6	2–5		2–3	2–5	2–4	7–11	(3)–5	
upper Pliocene (Piacenzian)	NN18	5–6	4	3–4		3		4		2	5–6	6–8	6–7		3–4	6	(5)	11–18	6–9	
	NN17	6	4	4		(4)				3	6	8	(8)		4	6	(5)			
	NN16	6–9	5	4–6		4–5				3–7	6–9	8–12	8–11		4–6	6–8	5–7			
lower Pliocene (Zanclian)	NN15	9–13	5–6	6–9		6–8				7–11	10–14	12–16	12–15		6–8	9	8–12	18–20	10	
	NN14	13–15	6–7	9–11		8–9				11–14	15–16	17–20	16–20		8–13	11–13	13–16	20–23	11	
	NN13	15	7	11		9				14–16	17–18	21	21–22		14	14–17				
	NN12	16–17	7	11–12		9–11				16–18	19–20	21–24	23							
upper Miocene (Tortonian–Messinian)	NN11b	18–21	7–10	12–18		12–17				18–27	21–30	24–28	24–27		15–17	17–22	17–20	23–26		
	NN11a	21–25	10–11	18–20		18–19					30–35	28–31	28–30	1–4	18–19	22–25	21–22			
	NN10			20–23		20–22					35–38			5–8	19–20	25–26		26–28		
	NN9			23–25		23–25					38–40			9–11	21–22	26–27		28–29		
middle Miocene (Langhian–Serravallian)	NN8			25	1	26					41			11	23	28–37		30–42		
	NN7			25	1–2	27–29					42–45			12	23–24					
	NN6				2–8	30–31					45–47			13–18	25–28	37–42		42–53	12–15	
	NN5				9–13						47–49			18–23	28–29	42–43			15–26	
lower Miocene (Aquitanian–Burdigalian)	NN4				13–15		1–2				50			24?	29–31	44				
	NN3				16–17		2–3				51–52				31–32	44–46				
	NN2				18		3–5				52–53				32–33	46				
	NN1						5								■	47–50	23–24			
upper Oligocene (Chattian)	NP25						6–17								■	50–55	24–27			
	NP24						17–18								■					
middle Oligocene (Rupelian)	NP23						■								■	55–56				
lower Oligocene (Latdorfian)	NP22						■								33–34	56–57				
	NP21						■								35–37	57–58				
upper Eocene (Bartonian–Priabonian)	NP20						■								37–41	59–60				
	NP19						■													
	NP18						■													
	NP17						■													
middle Eocene (Lutetian)	NP16						18–19													
	NP15																			
	NP14																			

Note: Numbers refer to cores. Hiatuses in black. SNZ = standard nannoplankton zone.

ra recta and *Zygrhablithus bijugatus*, which both last occur in Sample 588C-6-2, 0–1 cm, although the latter species occurs only sporadically. *Dictyococcites dictyodus* is present throughout this interval and is last noted in Sample 588C-4-5, 0–1 cm, of early Miocene age. *Dis- lithina enormis* and *S. ciperoensis* are rare or few and which last occur well below the Oligocene/Miocene boundary, which in this hole is defined by the last occurrences of *H. recta* (Table 2). *Triquetrorhabdulus carinatus* and *S. dissimilis*, both crossing the Oligocene/Miocene boundary, first occur in the lower part of Zone NP25. *Triquetrorhabdulus milowii*, which has a range from the base of Zone NP25 to the top of Zone NN1 in the Philippine Sea (Martini, 1980), seems to be restricted to the higher parts of Zone NP25 and lower part of Zone NN1 (last occurrence in Sample 588C-5-4, 0–1 cm) at Site 588. The interval between Sample 588C-17-3, 0–1 cm and 588C-18-1, top, belongs to nannoplankton Zone NP24 (*S. distentus* Zone), with the nominate species as well as *S. predistentus* and *Coccolithus abisectus* present. A hiatus was noted between Samples 588C-18-1, top, and 588C-18-1, middle part, dividing Zone NP24 and the combined Zones NP15/NP16, with the upper middle Eocene to middle Oligocene missing. Important species for the middle Eocene Zones NP15/NP16 include *Neococcolithes dubius*, *S. furcatolithoides*, *Chiasmolithus solitus*, and *Chiphragmalithus alatus*, which was noted in Sample 588C-18-1, middle. Above the hiatus reworked Eocene nannoplankton specimens were found in several samples (Table 2). Also reworked Paleogene species (*Fasciculithus* sp. and *Neochiastozygus concinnus*) were noted in Sample 588C-14-3, 0–1 cm, and Upper Cretaceous species (e.g., *Arkhangelskiella cymbiformis*) were found in Sample 588C-12-3, 0–1 cm.

Preservation of the Paleogene calcareous nannoplankton in Hole 588C varies from poor to moderate in white to light gray to light greenish gray foraminifer-bearing nannofossil chalk of late Oligocene age and in light greenish gray siliceous foraminifer-bearing nannofossil chalk of middle Eocene age. Discoasters, especially in the Oligocene, are overcalcified, which is also true for some of the Oligocene *Discolithina* occurrences.

Site 592 (36°28.40′S, 165°26.53′E, water depth 1098 m)

In Hole 592, situated on the southern part of the Lord Howe Rise, lower Oligocene (Zones NP21 and NP22) and upper Eocene (Zone NP19/NP20) sediments are present in the interval between Samples 592-33-3, 70 cm

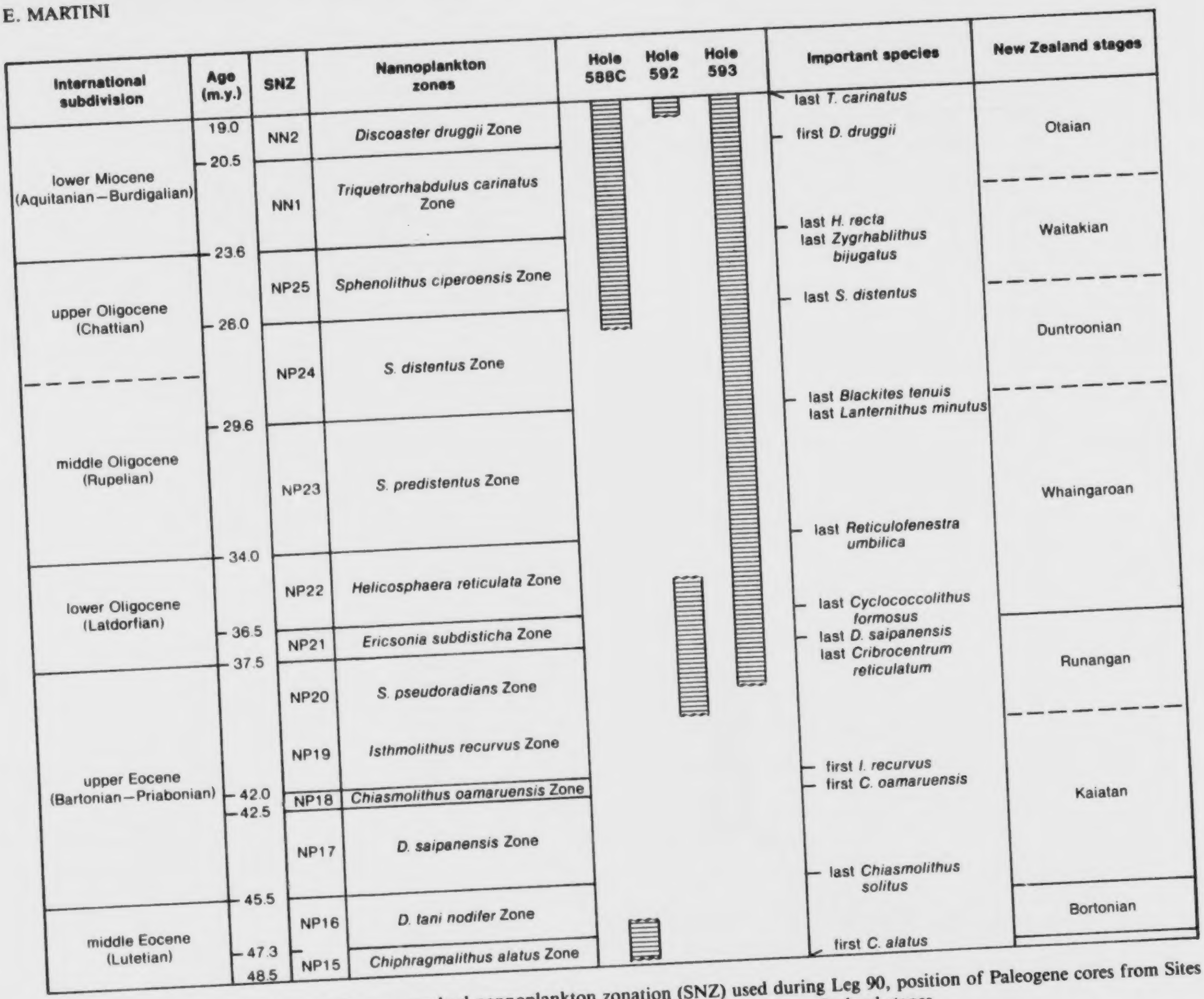

Figure 2. Middle Eocene to lowest Miocene standard nannoplankton zonation (SNZ) used during Leg 90, position of Paleogene cores from Sites 588, 592, and 593, first and last occurrences of important nannoplankton species, and New Zealand stages.

(305.8 m subbottom) and the terminal depth of 388.5 m in Sample 592-41,CC. Between Samples 592-33-3, 70 cm and 592-33-3, 5–6 cm a hiatus was identified, with the middle and upper Oligocene as well as the lowest Miocene missing.

The lower Oligocene Zones NP21 and NP22 were identified by the last occurrences of *Discoaster saipanensis* in Sample 592-37-2, 33–34 cm, *Cycloccolithus formosus* in Sample 592-35-1, 3–4 cm, and *Reticulofenestra umbilica* in Sample 592-33-3, 70 cm. For the late Eocene, nannoplankton Zones NP19 and NP20 were combined because the guide species *Sphenolithus pseudoradians* is not present in this area. It was also shown to have no time-equivalent first occurrence in the oceans (Bukry, 1971; Martini, 1976). For details on the ranges of calcareous nannoplankton species see Table 3.

Reworking of Eocene and Oligocene calcareous nannoplankton was noted in the lower Miocene above the hiatus. Reworked middle Eocene species, with *Neococcolithes dubius* most conspicuous, occurred also in the lowest part of Hole 592, attributed to the upper Eocene Zone NP19/NP20.

Preservation is moderate throughout the Paleogene interval, which consists of white to very light gray nannofossil ooze in the early Oligocene (Cores 33 to 37) and white to very light gray nannofossil chalk in the late Eocene (Cores 38 to 41), but is only poor to moderate just below and above the hiatus.

Site 593 (40°30.47′S, 167°40.47′E, water depth 1068 m)

Hole 593 on the Challenger Plateau to the west of New Zealand provided a continuous Paleogene sequence from Core 50 (~472 m sub-bottom) down to the terminal depth of 571.5 m in Core 60, including the upper Eocene and complete Oligocene. The Oligocene/Miocene boundary according to calcareous nannoplankton is placed between Samples 593-50-3, 3–4 cm and 593-50-5, 3–4 cm by the last occurrence of *Zygrhablithus bijuga-*

tus, because *Helicosphaera recta* and most *Sphenolithus* species are too rare or are missing, because of the high latitude of this site in the Paleogene.

Standard nannoplankton Zones NP24* (*Sphenolithus distentus* Zone) and NP25* (*S. ciperoensis* Zone) had to be combined because of the lack of sphenoliths. The top of Zone NP23* (*S. predistentus* Zone) is defined by the last occurrence of *Blackites tenuis* and *Lanternithus minutus* in Sample 593-55,CC. The tops of Zones NP22 (*Helicosphaera reticulata* Zone) and NP21 (*Ericsonia subdisticha* Zone) were identified by the last occurrence of *Reticulofenestra umbilica* and *Cyclococcolithus formosus*, respectively. The Eocene/Oligocene boundary based on calcareous nannoplankton is obscured in Hole 593 because of the volcanogenic material in the lower part of Core 58 and most of Core 59. Sample 593-59,CC clearly belongs in the late Eocene nannoplankton Zone NP19/NP20 based on the occurrence of *Cribrocentrum reticulatum*,which does not cross the Eocene/Oligocene boundary (Müller, 1978). The ranges of calcareous nannoplankton species found are listed in Table 4.

Reworked middle Eocene nannoplankton species (e.g., *Neococcolithes dubius*) occur throughout Core 60, but were not found in Sample 593-59,CC and above. A similar occurrence of reworked middle Eocene species at Site 592 also ceased before the end of the Eocene. A few reworked Eocene specimens were found at several levels in the middle and upper Oligocene.

Preservation in the Oligocene varies between poor to moderate and moderate, with the best preservation in the lower and middle Oligocene white nannofossil ooze. Unlike the Oligocene interval, there is little difference in preservation between the Eocene light greenish gray chalk and the white nannofossil chalk that is interbedded with lithified volcanogenic turbidites in the interval from 593-58-3 through Core 60.

In Hole 593A the late Oligocene calcareous nannoplankton Zone NP24/NP25* was encountered in Cores 24 (458.4 m sub-bottom) to the terminal depth of 496.8 m in Core 27; results duplicated those of part of Hole 593.

EOCENE/OLIGOCENE BOUNDARY

The Eocene/Oligocene boundary identified by means of the calcareous nannoplankton is commonly placed at the last occurrence of the rosette-shaped discoasters which dominate in the Eocene, especially the last occurrence of *Discoaster saipanensis* Bramlette and Riedel (top of Zone NP20) in deep sea sediments as well as in land-based sections (Martini, 1981b). The lower Oligocene (Latdorfian), including standard nannoplankton Zones NP21 and NP22, was clearly deposited prior to the Rupelian (= middle Oligocene), which includes the standard calcareous nannoplankton Zones NP23 and part of NP24, although a quite misleading version was recently published in Harland et al. (1982), which has some forerunners in papers by Berggren (e.g., Hardenbol and Berggren, 1978), and is also used in a few DSDP papers. There are several articles discussing the time-equivalence of the Eocene/Oligocene boundary using calcareous nannoplankton and foraminifers (e.g., Bombita and Rusu, 1981; Snyder et al., 1984); they may be summarized by saying that the boundary defined by the planktonic foraminifers (commonly the last occurrence of *Globorotalia cerroazulensis*) is slightly younger than that drawn using calcareous nannoplankton.

This is also true for Sites 592 and 593, in which the Eocene/Oligocene boundary was encountered. At Hole 592 the boundary based on calcareous nannoplankton is between Samples 592-37-2, 5–6 cm and 592-37-2, 33–34 cm, whereas based on planktonic foraminifers it is between Samples 592-36-3, 64 cm and 592-36-3, 90 cm, where the last *Globigerinatheka index* were noted. A similar offset was observed in Hole 593, where the boundary based on calcareous nannoplankton lies between Samples 593-59,CC and 593-58-2, 110–112 cm, (although it is somewhat obscured by volcanogenic material deposited at the site at this time) and just above Sample 593-57,CC, where *G. index* seems to have its last occurrence. At Site 593, discoasters are rare in the uppermost Eocene because of the position of Site 593 at that time, but are still noted in all samples just below the Eocene/Oligocene boundary (Table 4). However, the consistent presence of *Cribrocentrum reticulatum* (Gartner and Smith) up to Sample 593-59,CC is a reliable datum placing the boundary somewhere in the volcanogenic sequence. The last occurrence of *C. reticulatum* has always been placed prior to the Eocene/Oligocene boundary (top of Zone NP20, last occurrence of *D. saipanensis*) in low and middle latitudes, and the species can be used as a reliable substitute in high latitudes.

With an accumulation rate of 19.0 m/m.y. in the early Oligocene that may also be true for the latest Eocene at Site 592, the time difference between the two boundary "events" is about 0.4 m.y. No attempt is made to calculate the time difference at Site 593 because of the uncertainty of the nannoplankton-based Eocene/Oligocene boundary, which is somewhere within the volcanogenic interval.

OLIGOCENE/MIOCENE BOUNDARY

Continuous sequences across the Oligocene/Miocene boundary were recovered in Hole 588C and at Site 593. At Site 592 the boundary falls in a hiatus covering at least the interval between calcareous nannoplankton Zones NP23 (middle Oligocene) and NN1 (lower Miocene).

The Oligocene/Miocene boundary in terms of calcareous nannoplankton is generally placed at the top of standard nannoplankton Zone NP25 (Müller, 1981; Steininger, 1982), where several nannoplankton species have their last occurrences, for example *Sphenolithus ciperoensis* Bramlette and Wilcoxon, *Helicosphaera recta* (Haq), and *Zygrhablithus bijugatus* (Deflandre).

In Hole 588C the more delicate *S. ciperoensis* Bramlette and Wilcoxon and *S. distentus* (Martini) are rare, except in levels with moderate preservations, where they are better preserved. The last occurrence of *S. ciperoensis* in this hole is in Sample 588C-11,CC (Table 2), whereas *H. recta* and *Z. bijugatus* are found up to Sample 588C-6-2, 0–1 cm, although the latter are not continuously present and vary in frequency. *Discolithina enormis* Locker was noted in several samples up to Sample

Table 2. Distribution of calcareous nannoplankton in selected samples from Hole 588C and indication of standard nannoplankton zones.

Core Section (interval in cm)	*Blackites tenuis*	*Campylosphaera dela*	*Chiasmolithus altus*	*C. gigas*	*C. grandis*	*C. solitus*	*Chiphragmalithus alatus*	*Coccolithus abisectus*	*C. eopelagicus*	*C. miopelagicus*	*C. pelagicus*	*Coronocyclus nitescens*	*Cyclococcolithus floridanus*	*C. formosus*	*C. sp.*	*Dictyococcites dictyodus*	*D. aff. dictyodus*	*Discoaster barbadiensis*	*D. deflandrei group*	*D. wemmelensis*	*D. germanicus*	*D. lenticularis*	*D. desueta*	*D. distincta*	*D. enormis*	*Ericsonia fenestrata*	*H. carteri*
5-1, 21-22								R		R	C	R	C			R			C				R				R
5-4, 0-1								R		R	C	R	A			R			A				R				R
5,CC								R		R	C	R	C			R	R		C				R				R
6-2, 0-1								C		C	C	R	A			C			A				R				R
6,CC								C		C	C	R	C			R	R		C				R		R		R
7-2, 0-1*								C		R	C	R	A			C			A				R				
7-4, 0-1								C		C	C	R	A			R			A						R		R
8-1, 0-1*								C		C	R	R	C			R			C							R	R
8-3, 0-1								C		R	C	R	A			R			C				R		R		
8,CC								C		C	C	R	C				R		A				R				
9-3, 0-1								C		R	R	R	A			C			A				R				cf.
9,CC								C		C	C	R	A			C			A				R				
10-5, 0-1								C		C	C		A			R			C							R	
10,CC								C		C	C		A			R			A				cf.		cf.	R	
11-1, 0-1								R		C	C	R	A			R			A				cf.		cf.	R	
11-2, 0-1								C	cf.	R	C	R	A			C			A							R	
11,CC*								C	cf.	C	C		A			C	R		C							R	
12-3, 0-1			R					A		R	C	R	A			R			C				R		cf.	C	
12,CC			R					C		R	C	R	C			C	R		A				R			R	
13-3, 0-1			R					C	R	R	C		C			C	R		C				R		R	R	
13,CC								C	R	C	C		C			C	C		C						R	R	
14-3, 0-1			R					C	R	R	C	R	C			C	R		C				R			R	
14,CC			R					C	R	R	C	R	C			C	R		C							R	
15-3, 0-1			R					C	R	R	C		C			C			C							R	
15,CC			R					C	R	cf.	A		A			C			A								
16-3, 0-1			R					C	R		C	R	C			C			C				R				
16,CC			R					C	R		C		C			C			C								
17-1, 0-1			R					C	R		C		C			C			R								
17-3, 0-1			R					C	R		C		C			R			R							R	
17,CC			R					C	R		R	R	C			C			R								
18-1, top			R					A	R		C		C			C			C								
18-1, middle	R	R			R	C	R		R		C			R				C			R						
19-1, 10-12	R			R	R	C			R		R			R	R			R						R			
19-1, 55-57*	R				R	C			R		C			R	R			R		R	?						
19,CC*	R	R			R	C					C			R				C		cf.	cf.	R					

Note. R = rare to few, C = common, A = abundant. Preservation: P = poor, M = moderate, G = good. Reworking: C = Cretaceous, P = Paleocene, E = Eocene. * = samples studied with scanning electron microscope.

588C-6,CC. *Dictyococcites dictyodus* (Deflandre) [= *Reticulofenestra bisecta* (Hay, Mohler, and Wade) of some authors] and *Discolithina desueta* Müller range higher and have their last occurrences in Samples 588C-4-5, 0–1 cm and 588C-5-1, 0–1 cm, respectively. The Oligocene/Miocene boundary is taken to be just above Sample 588C-6-2, 0–1 cm with the last occurrences of *H. recta* and *Z. bijugatus*. The foraminifer-based boundary is indicated in this hole by the first appearance of *Globoquadrina dehiscens* (see Srinivasan and Kennett, 1983), which is first noted in Sample 588C-8,CC, and is considerably lower than at Site 593.

At Site 593 sphenoliths occur in a rather scattered fashion, except for *S. moriformis* (Brönnimann and Stradner), because of the position of this site at the time, and cannot be used as zonal markers. *Helicosphaera* species are rare and unreliable. The only species that occurs consistently and also commonly, indicating "shallow-water" conditions, is *Z. bijugatus*, which last occurs in Sample 593-50-5, 3–4 cm, and which is used in this hole to define the Oligocene/Miocene boundary in terms of calcareous nannoplankton. *Dictyococcites dictyodus* ranges higher up, as it does in Hole 588C. *Chiasmolithus altus* Bukry and Percival, which is widespread in cold water masses, is found up to Sample 593-50,CC (Table 4), whereas it ceased at Site 588 in Sample 588C-12-3, 0–1 cm, well below the supposed Oligocene/Miocene boundary.

The first occurrence of the planktonic foraminifer *G. dehiscens* was noted in Sample 593-50-4, 90 cm, and accordingly the Oligocene/Miocene boundary is placed between Samples 593-50-4, 90 cm and 593-50,CC, below the Oligocene/Miocene boundary based on calcareous nannoplankton. For further discussion see the biostratigraphic synthesis (Martini and Jenkins, this volume).

REGIONAL UNCONFORMITIES

In Leg 90 sites two major unconformities were noted in the Paleogene. One occurred in Hole 588C between Samples 588C-18-1, top and 588C-18-1, middle, dividing Zone NP24 and the combined Zone NP15/NP16, with the upper middle Eocene to middle Oligocene missing. In Hole 592 a hiatus was identified between Sam-

Table 2. (Continued).

H. compacta	*H. dinesenii*	*H. euphratis*	*H. intermedia*	*H. recta*	*H. seminulum*	*Markalius inversus*	*Neococcolithus dubius*	*Orthorhabdus serratus*	*Reticulofenestra insignita*	*R. umbilica*	*R.* sp. (small)	*Sphenolithus capricornutus*	*S. ciperoensis*	*S. delphix*	*S. dissimilis*	*S. distentus*	*S. furcatolithoides*	*S. moriformis*	*S. predistentus*	*S.* sp.	*Triquetrorhabdulus carinatus*	*T. inversus*	*T. milowii*	*Zygrhablithus bijugatus*	Reworking	Preservation	Standard nannoplankton zones
		R						R			C				R			C			R					PM	NN1
		R							R		C							C					R			PM	
		R									C				R			C								PM	
		R		R					R		A				C			C			R			R		PM	NP25
		R		R							C	R		R	R			C								PM	
		R		R					R		A			R	R			C			R		R			PM	
		R		C					R		A				R			C			R		R	R		PM	
		R		R							C				R			C					R	R		PM	
		R		R							C				R			C			C		R	C		PM	
		R	R	R							C							C			R		R			PM	
		R		R							C			R	R			A					R			PM	
R		R		R							A	R		R	C			C			R			R		PM	
		R		R							A			R	R			C			R			R		PM	
R		R		R							A				C			C			R			R		PM	
R		C	R	R					cf.		A				R			C			R			C		PM	
R		R		R					R		A				C			A			C			R		PM	
		R							R		A		R		C			C			R			C		PM	
		R		R					C		A		R		R			C			C			C	E C	M	
R		R							R		A		R		R			C			R			C	E	PM	
R		R	R	R					R		C		R		R			C			R			C	E	PM	
R		R		R					R		C		R		R			C			R			C	E	M	
R		C	R	R					R		A				R			C			R			C	P	PM	
R		R		R					R		A		R					C			R			C		PM	
R		R		R					R		A		C					C			R			C	E	M	
											A		cf.					C			cf.			R	E	P	
		R		R							C		R					C						C		M	
R		R	R						R		C		R					C						C		M	
		R	R						R		C		R					C						R	E	M	
											C		R			R		C	R					R		M	NP24
		R		R							C		R			R		C	R					C	E	M	
R		R							R		R							C						C	E	P	
	cf.					R	R			R	C						R	R		R		R		C		PM	NP15/NP16
							R			C	C							R		R				C		PM	
			R		R					C	C						R	R		R				C		M	
					R	R	R			C	R							R		R				C		M	

ples 592-33-3, 5–6 cm and 592-33-3, 70 cm, excluding at least the middle and upper Oligocene (Zones NP23 to NP25) as well as the lowest Miocene (Zone NN1).

Previous drilling in this area revealed a major hiatus at Site 207, which is close to Site 592 (Fig. 1), with part of the middle Eocene to part of the middle Miocene, representing ~30 m.y., missing (Edwards, 1973b). A hiatus was noted in Hole 206, also with the upper Eocene to lower middle Oligocene missing (~10 m.y.). Hole 206 is close to Sites 589 to 591, which unfortunately did not reach the corresponding depth to verify a widespread regional unconformity at this level. At Site 208 a hiatus described by Edwards (1973b) is more or less the same as that found at Site 588. In Hole 208 at least part of the middle Eocene (Zone NP16) to the middle Oligocene (Zone NP23) is missing. For a further discussion of the regional unconformities the biostratigraphic synthesis (Martini and Jenkins, this volume) should be consulted.

REMARKS ON SELECTED CALCAREOUS NANNOPLANKTON TAXA

Most of the Paleogene calcareous nannoplankton taxa found on Leg 90 are well documented elsewhere and need no discussion. Detailed information on calcareous nannoplankton from nearby DSDP legs and New Zealand can be found in Bukry, 1975; Edwards, 1971, 1973a; Edwards and Perch-Nielsen, 1975; Stradner and Edwards, 1968. However, a few taxa that cannot be differentiated by light microscope techniques because of their small size and one new species will be discussed.

***Cyclococcolithus* sp.** In Hole 588C some small circular forms with the general appearance of the genus *Cyclococcolithus* as seen with the light microscope were noted in the middle Eocene interval, and are listed as *Cyclococcolithus* sp. in Table 2.

***Discolithina* sp.** In Holes 592 and 593 a few small and poorly preserved specimens of the genus *Discolithina* found at various levels are grouped together as *Discolithina* sp. in Tables 3 and 4, although they actually may represent different species.

***Reticulofenestra* sp. (small).** Under this name all small *Reticulofenestra* species that cannot be differentiated with the light microscope are grouped together in Tables 2 to 4.

***Sphenolithus* sp.** In Hole 588C some sphenoliths were found in the middle Eocene interval; they may be related to *Sphenolithus radians* Deflandre, but were too small to be identified with certainty. They are listed in Table 2 as *Sphenolithus* sp.

Family SPHENOLITHACEAE Vekshina, 1959
Genus *SPHENOLITHUS* Deflandre, 1952

***Sphenolithus elongatus* n. sp.**
(Plate 2, Figs. 7, 8)

Holotype. SM.B 13507; Plate 2, Fig. 8.

Description. Basal part constructed of ~9 regularly placed calcite units (Plate 2, Fig. 7), followed by some irregularly placed smaller calcite particles, which form a collar from which a solid and prominent spine arises. The spine is clearly visible in normal light, showing maximum relief when parallel to polarizer. In polarized light it has its maximum birefringence with the long axis at 45° to crossed nicols. With the long axis parallel to crossed nicols only the base shows birefringence.

Size. 6 to 9 µm.

Remarks. *Sphenolithus elongatus* new species resembles *S. heteromorphus* Deflandre, but has a distinctly smaller base; the elongated spine is always slender and seems not to vary in size like that in *S. heteromorphus*. *Sphenolithus delphix* Bukry has longer crystals in the basal part, resulting in a different picture when viewed parallel to crossed nicols (see Martini, 1976, plate 13, figs. 22–24). Note: *S. elongatus* n. sp. is not listed in Table 2.

Type locality. Sample 588C-7-2, 0–1 cm, upper Oligocene, Zone NP25 (*S. ciperoensis* Zone).

Distribution. Few in Sample 588C-8-1, 0–1 cm and common in Sample 588C-7-2, 0–1 cm, Lord Howe Rise, upper Oligocene (Zone NP25).

ACKNOWLEDGMENTS

Thanks are due to the Deutsche Forschungsgemeinschaft (Bonn) for supporting the present study. SEM pictures were taken by J. Tochtenhagen with a Stereoscan Mark 2, which was provided to the Geologisch-Paläontologisches Institut der Universität Frankfurt am Main by the Volkswagenstiftung. My thanks also go to Dr. Stephen J. Percival (MEPSI, Dallas, Texas) and Dr. Sherwood W. Wise (Florida State University, Tallahassee) for reviewing this paper.

The type specimen of the new species and additional material is deposited in the Naturmuseum und Forschungsinstitut Senckenberg, Frankfurt am Main, Germany, Catalog No. SM.B 13507.

REFERENCES

Bombita, G., and Rusu, A., 1981. New data on the Eocene/Oligocene boundary in the Romanian Carpathians. *Palaeogeogr., Palaeoclimatol., Palaeoecol.*, 36:213–222.

Bukry, D., 1971. Coccolith stratigraphy Leg 6, Deep Sea Drilling Project. *In* Fisher, A. G., Heezen, B. C., et al., *Init. Repts. DSDP*, 6: Washington (U.S. Govt. Printing Office), 965–1004.

________, 1973a. Coccolith and silicoflagellate stratigraphy, Tasman Sea and southwestern Pacific Ocean. Deep Sea Drilling Project Leg 21. In Burns, R. E., Andrews, J. E., et al., *Init. Repts. DSDP*, 21: Washington (U.S. Govt. Printing Office), 885–891.

________, 1973b. Low-latitude coccolith biostratigraphic zonation. *In* Edgar, N. T., Saunders, J. B., et al., *Init. Repts. DSDP*, 15: Washington (U.S. Govt. Printing Office), 685–703.

________, 1975. Silicoflagellate and coccolith stratigraphy, Deep Sea Drilling Project, Leg 29. *In* Kennett, J. P., Houtz, R. E., et al., *Init. Repts. DSDP*, 29: Washington (U.S. Govt. Printing Office), 845–872.

Edwards, A. R., 1971. A calcareous nannoplankton zonation of the New Zealand Paleogene. *In* Farinacci, A. (Ed.), *Proc. II Planktonic Conf., Roma, 1970* (Vol. 1): Rome (Edizioni Tecnoscienza), 381–419.

________, 1973a. Calcareous nannofossils from the Southwest Pacific, Deep Sea Drilling Project, Leg 21. *In* Burns, R. E., Andrews, J. E., et al., *Init. Repts. DSDP*, 21: Washington (U.S. Govt. Printing Office), 641–691.

________, 1973b. Southwest Pacific regional unconformities encountered during Leg 21. *In* Burns, R. E., Andrews J. E., et al., *Init. Repts. DSDP*, 21: Washington (U.S. Govt. Printing Office), 701–720.

Edwards, A. R., and Perch-Nielsen, K., 1975. Calcareous nannofossils from the southern southwest Pacific, Deep Sea Drilling Project, Leg 29. *In* Kennett, J. P., Houtz, R. E., et al., *Init. Repts. DSDP*, 29: Washington (U.S. Govt. Printing Office), 469–539.

Hardenbol, J., and Berggren, W. A., 1978. A new Paleogene numeric timescale. *In* Cohee, G. V., Glaessner, M. F., and Hedberg, H. D. (Eds.), *Contributions to the Geologic Time Scale*. Am. Assoc. Pet. Geol. Stud. Geol., 6:213–234.

Harland, W. B., Cox, A. V., Llewellyn, P. G., Pickton, C. A. G., Smith, A. G., and Walters, R., 1982. *A Geologic Time Scale*. Cambridge Earth Science Series.

Martini, E., 1971. Standard Tertiary and Quaternary calcareous nannoplankton zonation. *Proc. II Planktonic Conf., Roma 1970* (Vol. 2): Rome (Edizioni Tecnoscienza), 739–785.

________, 1976. Cretaceous to Recent calcareous nannoplankton from the central Pacific Ocean (DSDP Leg 33). *In* Schlanger, S. O., Jackson, E. D., et al., *Init. Repts. DSDP*, 33: Washington (U.S. Govt. Printing Office), 383–423.

________, 1979. Calcareous nannoplankton and silicoflagellate biostratigraphy at Reykjanes Ridge, northeastern North Atlantic (DSDP Leg 49, Sites 407 and 409). *In* Luyendyk, B. P., Cann, J. R., et al., *Init. Repts. DSDP*, 49: Washington (U.S. Govt. Printing Office), 533–549.

________, 1980. Oligocene to Recent calcareous nannoplankton from the Philippine Sea, Deep Sea Drilling Project Leg 59. *In* Kroenke, L., Scott, R., et al., *Init. Repts. DSDP*, 59: Washington (U.S. Govt. Printing Office), 547–567.

________, 1981a. Nannoplankton in der Ober-Kreide, im Alttertiär und im tieferen Jungtertiär von Süddeutschland und dem angrenzenden Österreich. *Geol. Bavarica*, 82:345–356.

________, 1981b. Upper Eocene and Lower Oligocene calcareous nannoplankton from the Fore-Sudetic monocline. *Bull. Acad. Polon. Sci.*, 29:45–50.

Müller, C., 1976. Tertiary and Quaternary calcareous nannoplankton in the Norwegian-Greenland Sea, DSDP, Leg 38. *In* Talwani, M., Udintsev, G., et al., *Init. Repts. DSDP*, 38: Washington (U.S. Govt. Printing Office), 823–841.

________, 1978. Remarks on biostratigraphically useful nannofossils in the Paleogene of the northern hemisphere. *Strat. Newsl.*, 7:45–52.

________, 1981. Calcareous nannoplankton and silicoflagellates. *In* Cati, F. (Ed.), *In Search of the Paleogene/Neogene Boundary Stratotype. Part 1: Potential Boundary Stratotype Sections in Italy and Greece and a Comparison with Results from the Deep Sea. Giorn. Geol. Ser. 2a*, 44:33–38.

Snyder, S. W., Müller, C., and Mille, K. G., 1984. Eocene–Oligocene boundary: Biostratigraphic recognition and gradual paleoceanographic change at DSDP Site 549. *Geology*, 12:112–115.

Srinivasan, M. S., and Kennett, J. P., 1983. The Oligocene–Miocene boundary in the South Pacific. *Geol. Soc. Am. Bull.*, 94:798–812.

Steininger, F. F., 1982. The Palaeogene-Neogene (Oligocene-Miocene) boundary. *In* Odin, G. S. (Ed.), *Numerical Dating in Stratigraphy:* New York (John Wiley and Sons), pp. 652–658.

Stradner, H., and Edwards, A. R., 1968. Electron microscope studies on uper Eocene coccoliths from the Oamaru diatomite, New Zealand. *Jb. Geol. Bundesanst. Wien*, 13:1–66.

Date of Initial Receipt: 12 June 1984
Date of Acceptance: 26 October 1984

APPENDIX

Paleogene and Lowest Miocene Calcareous Nannoplankton from the Southwest Pacific

Blackites spinosus (Deflandre and Fert) Hay and Towe, 1962
B. tenuis (Bramlette and Sullivan) Hay and Mohler, 1967
Braarudosphaera bigelowi (Gran and Braarud) Deflandre, 1947
Campylosphaera dela (Bramlette and Sullivan) Hay and Mohler, 1967
Chiasmolithus altus Bukry and Percival, 1971
C. gigas (Bramlette and Sullivan) Gartner, 1970
C. grandis (Bramlette and Riedel) Radomski, 1968
C. oamaruensis (Deflandre) Hay, Mohler and Wade, 1966
C. solitus (Bramlette and Sullivan) Locker, 1968
Chiphragmalithus alatus (Martini) Martini, 1969
Coccolithus abisectus Müller, 1970
C. eopelagicus (Bramlette and Riedel) Bramlette and Sullivan, 1961
C. miopelagicus Bukry, 1971
C. pelagicus (Wallich) Schiller, 1930
Corannulus germanicus Stradner, 1962
Coronocyclus nitescens (Kamptner) Bramlette and Wilcoxon, 1967
Cribrocentrum reticulatum (Gartner and Smith) Perch-Nielsen, 1971
Cyclococcolithus floridanus (Roth and Hay) Müller, 1970
C. formosus Kamptner, 1963
Cyclococcolithus sp.
Dictyococcites dictyodus (Deflandre and Fert) Martini, 1969
D. aff. *dictyodus* (Deflandre and Fert) Martini, 1969
Discoaster barbadiensis Tan Sin Hok, 1927
D. binodosus Martini, 1958
D. deflandrei Bramlette and Riedel, 1954
D. druggii Bramlette and Wilcoxon, 1967
D. germanicus Martini, 1958

D. lenticularis Bramlette and Sullivan, 1961
D. saipanensis Bramlette and Riedel, 1954
D. tani Bramlette and Riedel, 1954
D. wemmelensis Achutan and Stradner, 1969
Discolithina desueta Müller, 1970
D. distincta (Bramlette and Sullivan) Levin and Joerger, 1967
D. enormis Locker, 1967
D. punctosa (Bramlette and Sullivan) Perch-Nielsen, 1971
Discolithina sp.
Ericsonia fenestrata (Deflandre and Fert) Stradner, 1968
E. subdisticha (Roth and Hay) Roth, 1969
Helicosphaera carteri (Wallich) Kamptner, 1964
H. compacta Bramlette and Wilcoxon, 1967
H. dinesenii (Perch-Nielsen) Jafar and Martini, 1975
H. euphratis Haq, 1966
H. granulata (Bukry and Percival) Jafar and Martini, 1975
H. intermedia Martini, 1965
H. recta (Haq) Jafar and Martini, 1975
H. seminulum (Bramlette and Sullivan) Jafar and Martini, 1975
Isthmolithus recurvus Deflandre, 1954
Lanternithus minutus Stradner, 1962
Markalius inversus (Deflandre) Bramlette and Martini, 1964
Neococcolithes dubius (Deflandre) Black, 1967
Orthorhabdus serratus Bramlette and Wilcoxon, 1967
Orthozygus aureus (Stradner) Bramlette and Wilcoxon, 1967
Reticulofenestra insignita Roth and Hay, 1967
R. oamaruensis (Deflandre) Stradner and Edwards, 1968
R. pseudoumbilica (Gartner) Gartner, 1969
R. umbilica (Levin) Martini and Ritzkowski, 1968
R. sp. (small)
Sphenolithus capricornutus Bukry and Percival, 1971
S. ciperoensis Bramlette and Wilcoxon, 1967
S. delphix Bukry, 1973
S. dissimilis Bukry and Percival, 1971
S. distentus (Martini) Bramlette and Wilcoxon, 1967
S. elongatus Martini, new species
S. furcatolithoides Locker, 1967
S. moriformis (Brönnimann and Stradner) Bramlette and Wilcoxon, 1967
S. predistentus Bramlette and Wilcoxon, 1967
S. sp.
Transversopontis pulcheroides (Sullivan) Perch-Nielsen, 1971
Triquetrorhabdulus carinatus Martini, 1965
T. inversus Bukry and Bramlette, 1969
T. milowii Bukry, 1971
Zygrhablithus bijugatus (Deflandre) Deflandre, 1959

Table 3. Distribution of calcareous nannoplankton in selected samples from Hole 592 and identification of standard nannoplankton zones.

Core-Section (interval in cm)	*Blackites spinosus*	*B. tenuis*	*Braarudosphaera bigelowi*	*Chiasmolithus altus*	*C. oamaruensis*	*Coccolithus abisectus*	*C. eopelagicus*	*C. miopelagicus*	*C. pelagicus*	*Corannulus germanicus*	*Coronocyclus nitescens*	*Cribrocentrum reticulatum*	*Cyclococcolithus floridanus*	*C. formosus*	*Dictyococcites dictyodus*	*D.* aff. *dictyodus*	*Discoaster barbadiensis*	*D. binodosus*	*D. deflandrei* group	*D. druggii*	*D. saipanensis*	*D. tani*	*Discolithina* sp.
32,CC						R		R	C		R		C						A	cf.			R
33-1, 5-6						R		C	C		R		A						A	cf.			
33-3, 5-6						C		C	C		R		A						C	cf.			
33-3, 70		R		C	R		R		C		R		C		A	R			R			R	
33-4, 5-6		R		C	R		R		C				C		A	R						R	
33,CC	R	C	R	C	R		C		C				C		A	R			R			R	R
34-3, 3-4		C		C	R		C		C		R		C		A	R						R	
34,CC		C	R	C	C		R		C				C		C			R	R			R	
35-1, 3-4		C		A	C		R		C				C	R	A	R						R	
35-5, 3-4		C		A	C		C		C				C	R	A	R						R	R
35,CC	R	C		C	C		R		C				C	R	A	R						R	
36-1, 3-4		R		C	R		R		C				C	R	A	R						R	
36-3, 3-4		R		C	C		C		C				C	R	A	R						R	
36,CC		R		R	C		R		C		R		C	C	A	R						R	
37-1, 4-5		C		R	C		R		C				C	C	A							R	
37-1, 5-6		C		C	C		R		A				C	R	A	R						R	
37-2, 33-34		C		C	C		R		C				C	R	A	R	R	R			R	R	
37-2, 93-94		C		C	C		R		C				R		A	R	R				R	R	
37-4, 4-5		R		R	C		R		C				C	R	A	R					R	R	
37,CC*		R	R	R	C		R		C			R	C	R	A	R					R	R	
38-2, 3-4		R			C		R		C				C	R	A	R					R		
38-4, 3-4		R			R		R		C		R		C	R	A	R					R	R	
38,CC		R					R		C	R		R	C	R	A	R					R	R	
39-1, 3-4		R			R		R		C				C	R	A	R					R		
39,CC		R			R		R		C	C		R	C	R	A	R					C	R	
40-3, 3-4		R			R		C		C			C	C	C	A	R					C	C	
40-4, 3-4		R			R		C		C	R		C	C	R	A	R					R	R	
40,CC		R	R		C		R		C		R	C	C	R	A	R					R	R	
41-1, 3-4		R			R		R		C			C	C	R	A	R					R	R	
41-4, 3-4		R			R		R		C			C	C	R	C						R	R	
41,CC*		R			C		R		C			C	C	R	C			R			R	R	

Note: R = rare to few, C = common, A = abundant, Preservation: P = poor, M = moderate, G = good. Reworking: E = Eocene, O = Oligocene. * = samples studied with scanning electron microscope.

Table 3. (Continued).

Ericsonia fenestrata	*E. subdisticha*	*Helicosphaera carteri*	*H. compacta*	*H. euphratis*	*H. intermedia*	*Isthmolithus recurvus*	*Lanternithus minutus*	*Markalius inversus*	*Reticulofenestra insignita*	*R. oamaruensis*	*R. pseudoumbilica*	*R. umbilica*	*R.* sp. (small)	*Sphenolithus dissimilis*	*S. moriformis*	*S. predistentus*	*Transversopontis pulcheroides*	*Triquetrorhabdulus carinatus*	*Zygrhablithus bijugatus*	Reworking	Preservation	Standard nannoplankton zones
		R		R							C		C	R	C			R		EO	PM	NN2
		cf.		R							R		A	R	C			R		EO	PM	
											R		A	R	C			R		EO	PM	
							R		R			C	C		R				R		PM	NP22
						R	R		C			R	C		R				R		M	
C	C					R	C	R	C			C	C		C				C		M	
R	C					R	C		R			C	C		C				A		M	
C	C				R	C	C		C			A	C		C	R	R		C		M	
R	C					C	R	R	C			A	C		R		R		C		M	NP21
	R					R	R		C			A	C		R				A		M	
R	R					C			A	R		A	C		R	R			A		M	
	R		R			C	R		C	R		C	C		R				C		M	
	R					C	R	R	C	R		C	C		R				A		M	
R	R		R			C		R	C	R		A	C		R		R		A		M	
	R		R		R	C			C	R		C	C		R		R		A		M	
			R			C		R	C	R		A	A		R		R		A		M	
	R		R			C	R	R	C	R		A	C		R		R		A		M	NP19/NP20
			R			C	R	R	C	R		A	C		R		R		C		M	
R						R			C	R		A	C		R		R		A		M	
					R	C			C			A	C		R		R		A		M	
						R	R		C			A	C		R				C		M	
	R		R			R	R	R	C			A	C		R				A		M	
			R			R		R	R			A	A		R				C		M	
	R					C	R	R	R			C	A		C				C		M	
						C	R	R				C	C		R				A		M	
						R	R		R			A	C		R				C		M	
						R		R	R			A	C		R				C		M	
							R	R				A	C		R				A	E	M	
							R	R	R			A	C		R				C	E	M	
						R	C	R				A	C		R				R	E	M	
						R	R	R				A	C		R				A	E	M	

Table 4. Distribution of calcareous nannoplankton in selected samples from Hole 593 and indication of standard nannoplankton zones.

Core-Section (interval in cm)	*Blackites spinosus*	*B. tenuis*	*Chiasmolithus altus*	*C. oamaruensis*	*Coccolithus abisectus*	*C. eopelagicus*	*C. miopelagicus*	*C. pelagicus*	*Coronocyclus nitescens*	*Cribrocentrum reticulatum*	*Cyclococcolithus floridanus*	*C. formosus*	*Dictyococcites dictyodus*	*D.* aff. *dictyodus*	*Discoaster barbadiensis*	*D. binodosus*	*D. deflandrei* group	*D. druggii* group	*D. saipanensis*	*D. tani*	*Discolithina desueta*	*D. enormis*	*D.* sp.	*Ericsonia fenestrata*
49,CC					C		C	C			A		R				A							
50-1, 3-4					A		R	A			C			R			A							
50-5, 3-4					R		R	C	R		A		R				C	cf.						
50,CC			R		C		R	A			C		A	R			C				R			R
52-1, 3-4			C		C	cf.	R	C			C		C				C				R	cf.		
52,CC			C		R		R	C	R		C		C	R			C				R			
53-1, 3-4			A		C	R		C	C		C		A	R										
53,CC			A		R	R		C			A		A	R									R	
54-1, 3-4			A		A	R		C			A		A	R										
54,CC			C	R	R	R		C	R		A		A	R										R
55-3, 3-4		R	A	R	C	R	cf.	C			C		A											
55,CC		C	C	R	cf.			C	C		C		A	R			R			cf.			R	
56-1, 3-4		C	C	R	cf.	R		C	R		C		A	R			R							
56-3, 3-4		R	C	R		R		C			C		A	R			R							
56,CC		C	A	R		R		C			R		A	R										
57-1, 3-4	R	C	A	C		R		C	R		R		A	R										
57-3, 3-4		C	A	A		R		C			R	R	A	R			R			R				
57,CC	R	C	A	C		C		C			C	R	A	R						R				R
58-1, 3-4		R	C	C		R		C			C	R	A	R						R				R
58-2, 5-6		R	A	A		C		C			C	R	C	R						R				R
58-2, 60-61		C	A	C		R		C			R	R	A	R		R				R				
58-2, 110-111		C	A	C		R		C	R		C	R	A	R		R				R				
58-3, 13			R	R				R			R	R	R											
58,CC		R	R	R				R			R		R							R				
59-4, 71-72			R					R			R		R											
59,CC	R	C		R		R		C		R	C		C	R										
60-1, 6-7	R	C		C		R		C	R	R	A		C						R	R				
60-3, 4-5		C		R		R		C		R	A	R	C	R					R					
60-5, 4-6		R	R	C		R		C		R	A		C	R	R				R	R				
60-6, 63-64		C	C	R		C		A		R	A		C	R					R	R				
60,CC*		C	C	C		C		A		R	A	R	C		R				R	R				

Note: R = rare to few, C = common, A = abundant. Preservation: P = poor, M = moderate, G = good. Reworking: E = Eocene. * = samples studied with scanning electron microscope.

Table 4. (Continued).

E. subdisticha	*Helicosphaera carteri*	*H. compacta*	*H. euphratis*	*H. intermedia*	*H. recta*	*Isthmolithus recurvus*	*Lanternithus minutus*	*Markalius inversus*	*Reticulofenestra insignita*	*R. oamaruensis*	*R. pseudoumbilica*	*R. umbilica*	*R.* sp. (small)	*Sphenolithus capricornutus*	*S. dissimilis*	*S. moriformis*	*S. predistentus*	*Transversopontis pulcheroides*	*Triquetrorhabdulus carinatus*	*Zygosphaera aurea*	*Zygrhablithus bijugatus*	Reworking	Preservation	Standard nannoplankton zones
	cf.										C		A		R	C			R				PM	NN1
													A	R	R	C			R				PM	
			R	R									A		R	C			C		R		PM	NP24/NP25*
			R						R		cf.		A			C			R		A	E	PM	
		R							R				C			R					C		PM	
									R				C			C					C		PM	
		R	R						C				A			R			R		A		M	
									C				C			R					A		M	
									R				A			R			cf.		A		PM	
									C				A			R	R				A	E	M	
					R				C				A			R	R				A	E	M	
							R	R	R				A			R					A		M	NP23*
							R		R				A			C	R				A	E	M	
						R	R		R			C	A			R					A		M	NP22
C						R	C		R			A	A			R					A		M	
A						C	A		R			C	A			C					A		M	
A						C	A		C			A	A			R					C		M	NP21
R						C			A			A	A			R					A		M	
R						C			A			A	A			R					C		M	
						C			A			A	A			R					C		M	
	R					C	R		A			A	A			R		cf.			A		M	
						C		R	R	R		A	A			R					A		M	
									R			R	R								R		PM	?
						R	R		R	R		R	R								R		M	
									R				R										M	
						R	R	R				R	C			R		R			C		M	NP19/NP20
						cf.	R	R	R			C	A			C		cf.			C	E	PM	
						R	R					A	A			R					C	E	M	
						cf.	R	R	R			A	C			R				R	C	E	PM	
						R	C					A	A			R					C	E	M	
						R	C					A	A			R					C	E	M	

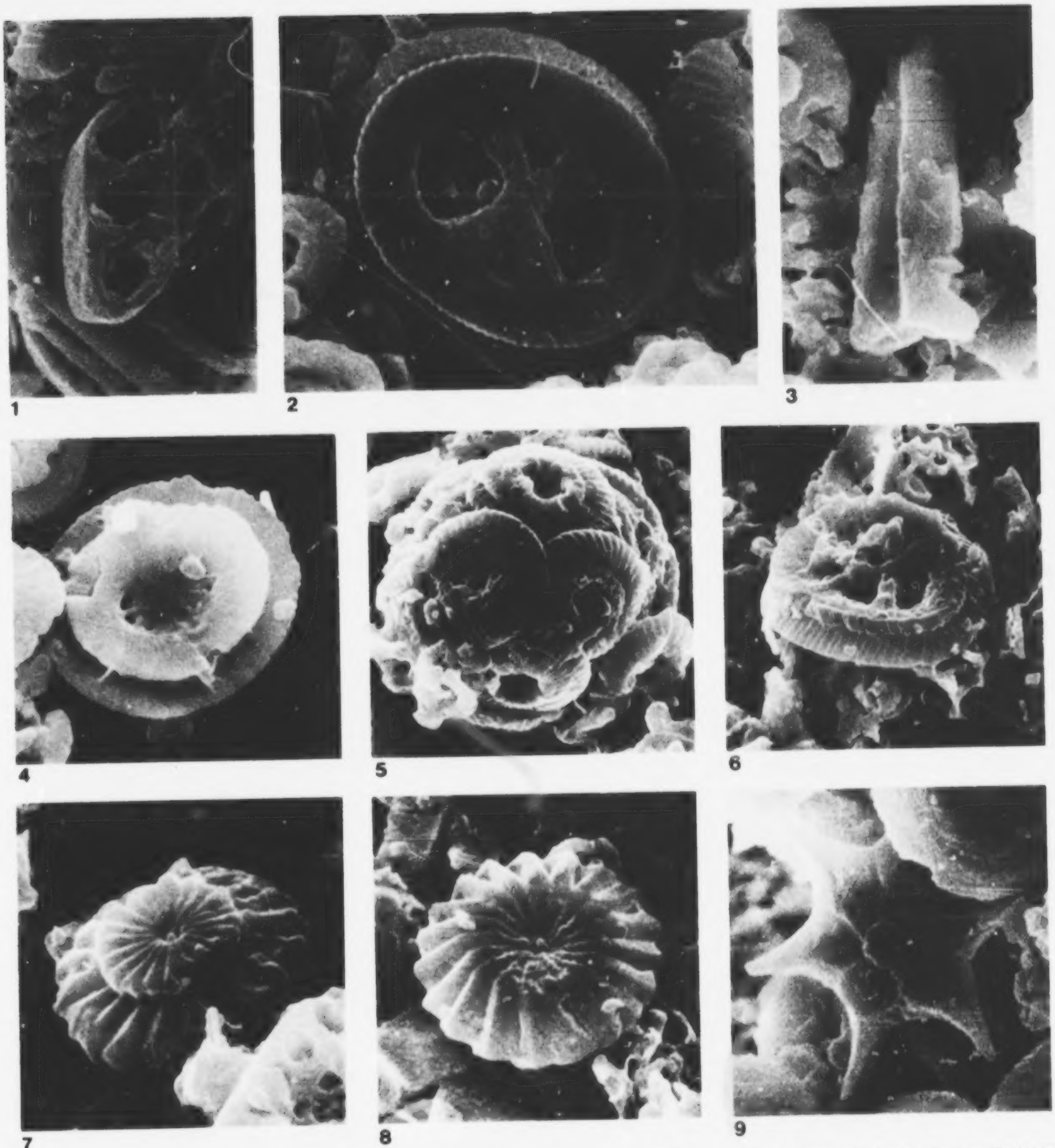

Plate 1. Eocene and Oligocene calcareous nannoplankton. **1.** *Isthmolithus recurvus* Deflandre, 1954, ×5000, distal side; Sample 592-37,CC, upper Eocene, Zones NP19/NP20. **2.** *Chiasmolithus oamaruensis* (Deflandre) Hay, Mohler, and Wade, 1966, ×5000, distal side; Sample 592-37,CC, upper Eocene, Zone NP19/NP20. **3.** *Zygrhablithus bijugatus* (Deflandre) Deflandre, 1959, ×5000, side view; Sample 588C-11,CC, upper Oligocene, Zone NP25. **4.** *Cribrocentrum reticulatum* (Gartner and Smith) Perch-Nielsen, 1971, ×5000, proximal side; Sample 592-37,CC, upper Eocene, Zone NP19/NP20. **5.** *Cycloccolithus floridanus* (Roth and Hay) Müller, 1970, ×4000, complete coccosphere; Sample 588C-11,CC, upper Oligocene, Zone NP25. **6.** *Chiasmolithus solitus* (Bramlette and Sullivan) Locker, 1968, ×4000, distal side; Sample 588C-19-1, 55–57 cm, middle Eocene, Zone NP15/NP16. **7.** *Discoaster wemmelensis* Achutan and Stradner, 1969, ×8000, distal? side; Sample 588C-19-1, 55–57 cm, middle Eocene, Zone NP15/NP16. **8.** *Discoaster* sp. ×8000, distal side; Sample 588C-19-1, 55–57 cm, middle Eocene, Zone NP15/NP16. **9.** *Discoaster saipanensis* Bramlette and Riedel, 1954, ×4500, proximal side; Sample 592-37,CC, upper Eocene, Zone NP19/NP20.

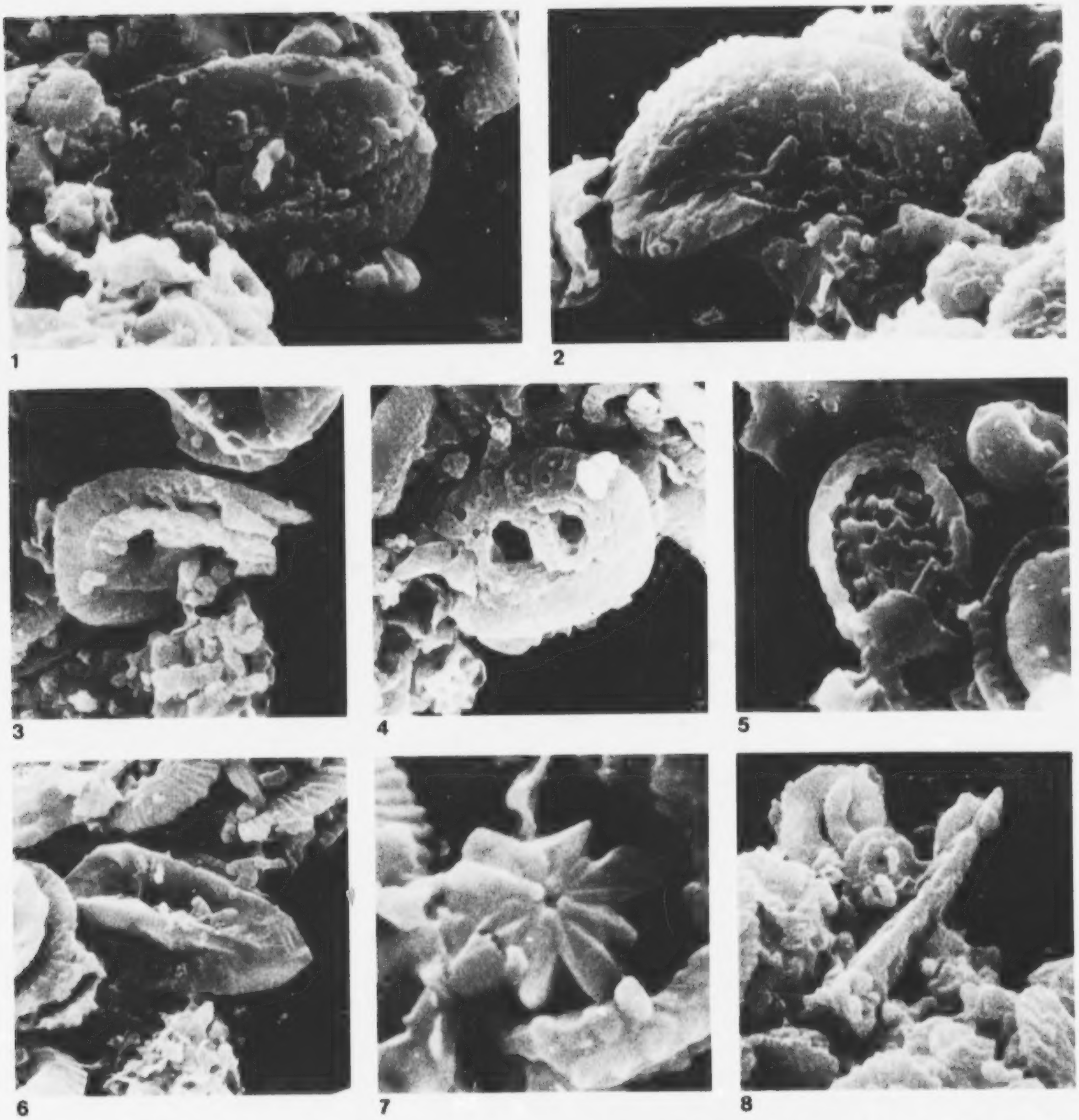

Plate 2. Eocene and Oligocene calcareous nannoplankton. **1, 2.** *Helicosphaera granulata* (Bukry and Percival) Jafar and Martini, 1975, × 5000, distal sides; Sample 588C-7-2, 0–1 cm, upper Oligocene, Zone NP25. **3, 4.** *Helicosphaera recta* (Haq) Jafar and Martini, 1975, Sample 588C-7-2, 0–1 cm, upper Oligocene, Zone NP25, (3) × 5000, proximal side; (4) × 4500, distal side. **5.** *Discolithina punctosa* (Bramlette and Sullivan) Perch-Nielsen, 1971, × 6000, distal side; Sample 588C-19-1, 55–57 cm, middle Eocene, Zone NP15/NP16. **6.** *Triquetrorhabdulus milowii* Bukry, 1971, × 4000, side view; Sample 588C-7-2, 0–1 cm, upper Oligocene, Zone NP25. **7.** *Sphenolithus elongatus* n. sp., × 10,000, basal part; Sample 588C-7-2, 0–1 cm, upper Oligocene, Zone NP25. **8.** *Sphenolithus elongatus* n. sp., holotype SM.B 13507, × 5000, side view; Sample 588C-7-2, 0–1 cm, upper Oligocene, Zone NP25.

12. CALCAREOUS NANNOPLANKTON BIOSTRATIGRAPHY OF THE SOUTHERN CORAL SEA, TASMAN SEA, AND SOUTHWESTERN PACIFIC OCEAN, DEEP SEA DRILLING PROJECT LEG 90: NEOGENE AND QUATERNARY[1]

William H. Lohman, Marathon Oil Company[2]

ABSTRACT

Leg 90 of the Deep Sea Drilling Project drilled 18 holes at eight sites (Sites 587–594) on several shallow-water platforms in the southern Coral Sea, Tasman Sea, and southwestern Pacific Ocean. The results from an additional hole (Hole 586B) drilled at Site 586 during Leg 89 are included in this report. Together, these sites form a latitudinal traverse which extends from the equator (Site 586) to 45°S (Site 594) and includes all the major water masses from tropical to subantarctic. Samples recovered at these sites range in age from middle Eocene to late Quaternary. The calcareous nannoplankton biostratigraphy for Leg 90 has divided into two parts: part 1, the Neogene and Quaternary of Sites 586-594. (this chapter); and part 2, the Paleogene of Sites 588, 592, and 593 (Martini, this volume). A slightly modified version of the Martini (1971) standard Tertiary and Quaternary zonation scheme was used to make age determinations on over 700 samples. All of the relevant Neogene and Quaternary zone-defining nannoplankton are present at Sites 586–591 (0°–30°S) but become increasingly rare or are absent at Sites 592–594 (35°–45°S). Species diversity increases southward from the equator (Site 586) and reaches a peak at 20°S (Site 587). A decrease at 25°S (Site 588) and 30°S (Sites 589–591) is followed by an increase in species diversity at 35°S (Site 592). South of 35°S, species diversity again decreases and reaches a low at 45°S (Site 594). Species diversity for all sites as a group generally increases through the early, middle, and late Miocene, reaches a peak in the early Pliocene, then gradually decreases through the late Pliocene and Quaternary.

INTRODUCTION

The southwest Pacific, unlike most other oceanic regions, contains numerous submarine topographic features. These bathymetric highs, or platforms, extend latitudinally over vast distances and are overlain by relatively uncomplicated middle to upper Cenozoic calcareous ooze and chalk, free of terrigenous content. One of the major platforms in the region, the Lord Howe Rise, is approximately 300 km wide and extends some 2000 km northward from central western New Zealand to about 20°S. The crest lies at water depths ranging from 750 to 1200 m.

Leg 90 of the Deep Sea Drilling Project (Noumea, New Caledonia, to Wellington, New Zealand) occupied eight sites (Fig. 1) in the southern Coral Sea, Tasman Sea, and southwestern Pacific east of New Zealand's South Island during December, 1982, and January, 1983. The sites are located on shallow-water platforms extending south from the southern slope of Lansdowne Bank (Site 587), northern to southern Lord Howe Rise (Sites 588–592), Challenger Plateau (Site 593), and the southern margin of the Chatham Rise (Site 594). Two methods of drilling, the hydraulic piston corer (HPC) and the extended core barrel (XCB), were used during Leg 90 to drill 18 holes in water depths ranging from 1068 m (from sea level) at Site 593 to 2131 m at Site 591. The XCB, first successfully used during Leg 90, is a core barrel that extends several centimeters ahead of the main rotary drill pipe bit and is used to core sediments after they have become too consolidated for coring with the HPC. The use of the HPC and XCB methods permitted greater core recovery with much less disturbance than with standard rotary coring and, as a result, a record 495 high-quality cores representing over 3700 m of sediment were recovered. An additional equatorial site (Site 586), located on the Ontong-Java Plateau at a water depth of 2207 m (from sea level), was drilled during Leg 89, and the 25 cores recovered from Hole 586B were set aside for study by Leg 90 scientists. The results from Hole 586B are included in the Leg 90 report. Samples recovered at these sites range in age from middle Eocene to late Quaternary. Only three sites (Sites 588, 592, and 593) penetrated pre-Miocene sediment.

The calcareous nannoplankton biostratigraphy for Leg 90 has been divided into two reports: part 1, the Neogene and Quaternary of Sites 586–594 (this chapter); and part 2, the Paleogene of Sites 588, 592, and 593 (Martini, this volume). Over 700 samples from the nine sites were examined for calcareous nannoplankton. All of the relevant Neogene and Quaternary zone-defining species used during Leg 90 are present at Sites 586–591 (0°–30°S) but become increasingly rare or are absent at Sites 592–594 (35°–45°S). The nannoplankton age determinations of Leg 90 samples made during this study agree very closely with those determined aboard the ship. Latitudinal effects on calcareous nannoplankton diversity are reflected in the changes in numbers of indigenous species observed from site to site along the traverse. Indigenous species range from a high of 48 in the early Pliocene at Site 587 (20°S) to a low of 13 in the late Pliocene at Site 594 (45°S).

---

[1] Kennett, J. P., von der Borch, C. C., et al., *Init. Repts. DSDP*, 90: Washington (U.S. Govt. Printing Office).

[2] Address: Marathon Oil Company, Denver Research Center, P.O. Box 269, Littleton, CO 80160

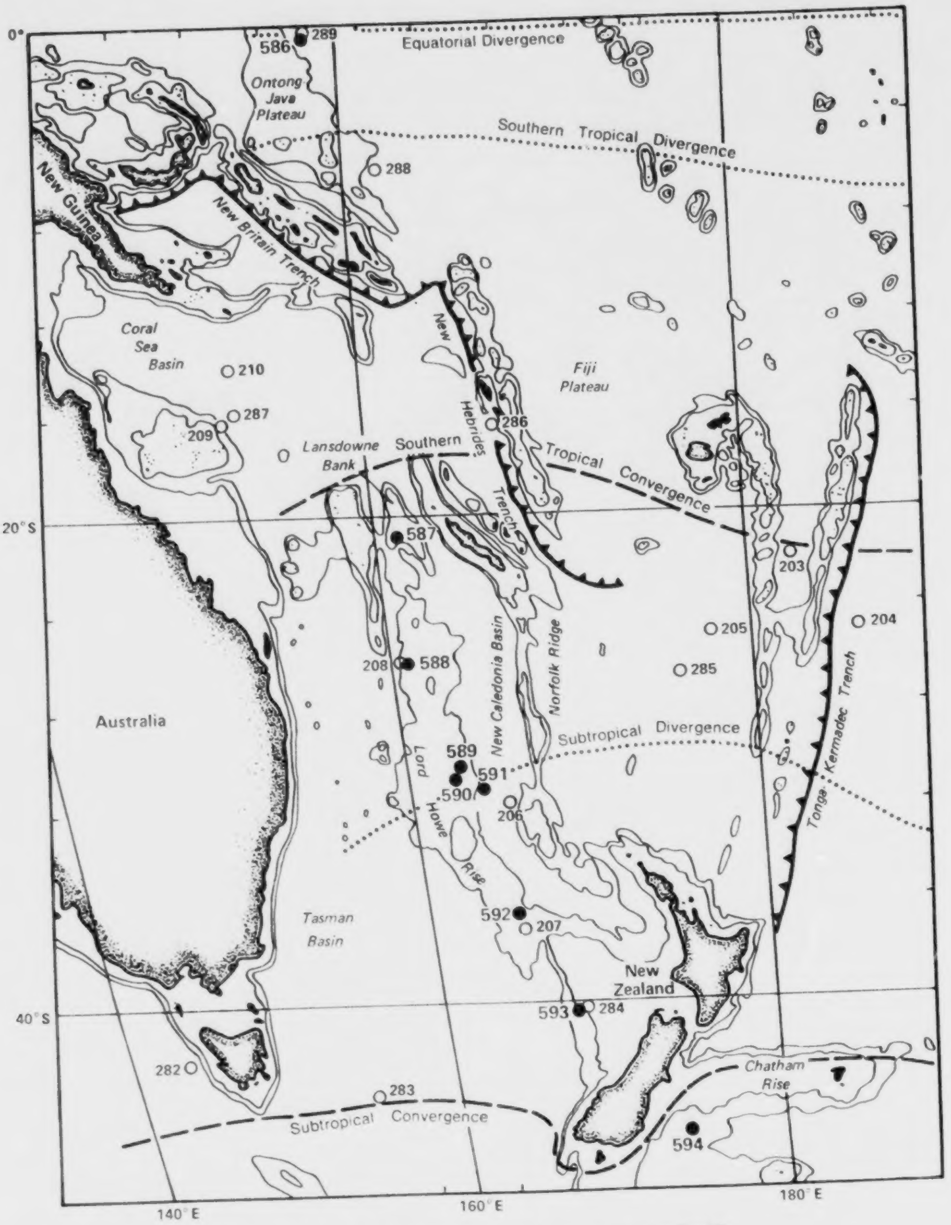
0°
586
289
Equatorial Divergence
Ontong Java Plateau
Southern Tropical Divergence
288
New Guinea
New Britain Trench
Coral Sea Basin
210
287
209
Lansdowne Bank
Southern
New Hebrides Trench
286
Fiji Plateau
Tropical Convergence
20°S
587
203
205
204
208
588
285
Australia
New Caledonia Basin
Norfolk Ridge
Subtropical Divergence
Tonga Kermadec Trench
589
591
590
206
Lord Howe Rise
Tasman Basin
592
207
New Zealand
40°S
593
284
282
283
Chatham Rise
Subtropical Convergence
594
140°E
160°E
180°E

Figure 1. DSDP drill sites from Leg 90 and other DSDP legs in the southwest Pacific.

NANNOPLANKTON ZONATION

A slightly modified version of the Martini (1971) standard Tertiary and Quaternary zonation scheme (Fig. 2) was used to make the initial calcareous nannoplankton age determinations during Leg 90. For consistency, the zonation scheme used aboard ship is also used in this chapter.

The zonal modifications include the subdivision of Zones NN19 and NN11 and the use of an alternate species to define the upper boundary of Zone NN4. The last occurrence of *Calcidiscus macintyrei* occurs within the early Quaternary *Emiliania ovata* (= *Pseudoemiliania lacunosa*) Zone (NN19) and is used to subdivide Zone NN19 into Subzones NN19a and NN19b. Subzone NN19a is equivalent to the *Calcidiscus macintyrei* (= *Cyclococcolithina macintyrei*) Zone of Gartner (1977) and Subzone WPN-30a of Ellis (1982). Subzone NN19b is equivalent to Subzones WPN-31a and WPN-30b of Ellis (1982). The late Miocene *Discoaster quinqueramus* Zone (NN11) is subdivided into Subzones NN11a and NN11b by the first occurrence of *Amaurolithus primus* within Zone NN11. Subzone NN11b is equivalent to the *Amaurolithus primus* (= *Ceratolithus primus*) Subzone of Bukry (1973b), Subzone CN9b of Okada and Bukry (1980), and Subzone WPN-26b of Ellis (1982). Subzone

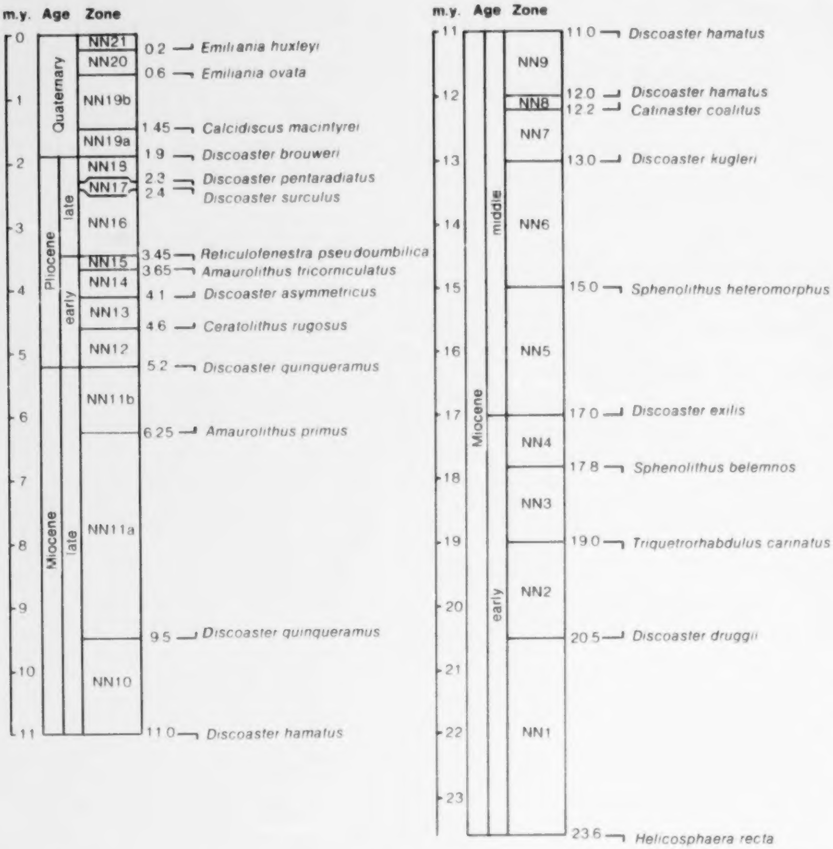
m.y.
Age
Zone
Quaternary
Pliocene
late
early
Miocene
NN21
NN20
NN19b
NN19a
NN18
NN17
NN16
NN15
NN14
NN13
NN12
NN11b
NN11a
NN10
0.2 Emiliania huxleyi
0.6 Emiliania ovata
1.45 Calcidiscus macintyrei
1.9 Discoaster brouweri
2.3 Discoaster pentaradiatus
2.4 Discoaster surculus
3.45 Reticulofenestra pseudoumbilica
3.65 Amaurolithus tricorniculatus
4.1 Discoaster asymmetricus
4.6 Ceratolithus rugosus
5.2 Discoaster quinqueramus
6.25 Amaurolithus primus
9.5 Discoaster quinqueramus
11.0 Discoaster hamatus
middle
NN9
NN8
NN7
NN6
NN5
NN4
NN3
NN2
NN1
11.0 Discoaster hamatus
12.0 Discoaster hamatus
12.2 Catinaster coalitus
13.0 Discoaster kugleri
15.0 Sphenolithus heteromorphus
17.0 Discoaster exilis
17.8 Sphenolithus belemnos
19.0 Triquetrorhabdulus carinatus
20.5 Discoaster druggii
23.6 Helicosphaera recta

Figure 2. Calcareous nannoplankton zonation scheme used for the Quaternary and Neogene of Leg 90; modified after Martini (1971). Ages for zonal boundaries are standardized for Leg 90 (Martini, this volume).

NN11a is equivalent to Subzone WPN-26a of Ellis (1982). Because *Helicosphaera ampliaperta* is apparently absent in the western Pacific, the upper boundary of the early Miocene *Helicosphaera ampliaperta* Zone (NN4), normally placed at the last occurrence of the nominal species, is instead marked by the first occurrence of *Discoaster exilis*, which closely approximates this level (Martini and Worsley, 1971).

NANNOPLANKTON ABUNDANCE AND DIVERSITY

The locations of Sites 587–594 (Leg 90), together with Site 586 (Leg 89), form a latitudinal traverse which extends from the equator to 45°S and includes all the major surface-water masses between the tropics and the sub-Antarctic. The effects of higher latitudes and cooler waters are reflected in the changes in abundance and diversity of calcareous nannoplankton observed at sites along this traverse.

The average abundance of each of the Neogene and Quaternary zonal and subzonal indicators at various southern latitudes is shown in Figure 3. The vertical axis indicates abundance in terms of A = abundant, C = common, R = rare, and B = barren (for quantitative estimates of A, C, R, see below). The abundance values for each taxon were obtained by assigning a value of A = 3, C = 2, R = 1, or B = O for each occurrence on the nannoplankton range charts and calculating the numerical average for each taxon at each site. The horizontal axis includes each of the nine sites plotted to the nearest increment of 5°S latitude. Abundance values for taxa at 30°S are the average of those obtained at Sites 589, 590, and 591. For some taxa there are no data in some sections, because drilling operations ended at those sites before the sections were penetrated. In general, the abundance of zone-defining discoasters declines steadily at higher latitudes; they are extremely rare at 45°S. However, three discoasters (*Discoaster pentaradiatus, D. asymmetricus*, and *D. quinqueramus*) reach an abundance peak at 25°S before declining sharply. The abundances of other zone-defining species, including *Amaurolithus primus, A. tricorniculatus, Calcidiscus macintyrei, Helicosphaera recta, Reticulofenestra pseudoumbilica*, and *Triquetrorhabdulus carinatus* appear to change very little with latitude. The abundance of one species, *Emiliania huxleyi*, increases with latitude, reaching a peak at 40°S.

Changes in nannoplankton diversity for indigenous species at various southern latitudes are shown in Figure 4. The highest diversity of nannoplankton (33 species) in Quaternary sediments occurs at 20°S (Site 587).

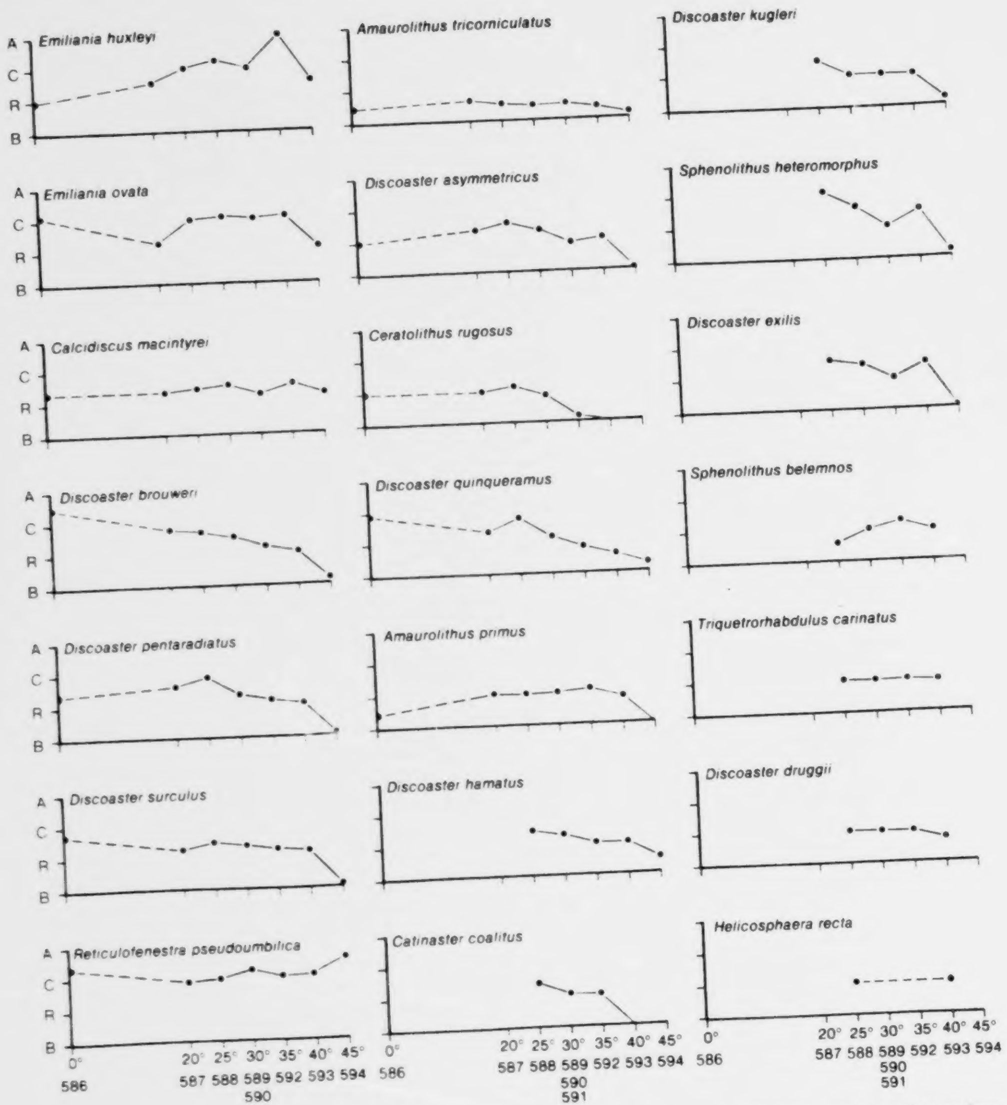

Figure 3. Relative abundances (●) of Quaternary and Neogene zonal and subzonal indicators encountered at various southern latitudes. Dashed lines indicate latitudes for which there are no data. Vertical axis: A = abundant, C = common, R = rare, and B = barren (fully defined in text). Horizontal axis: Approximate southern latitude of sites.

South of Site 587, there is a steady decline in diversity to a low of 20 species at 45°S (Site 594). In the late and early Pliocene and in the late Miocene, diversity peaks also occur at 20°S (Site 587), with a maximum of 48 species in the early Pliocene, South of Site 587, a decline in diversity at 25°S and 30°S (Sites 588–591) is followed by peaks of lesser diversity at 35°S (Site 592). The lowest diversity (13 species) occurs in the late Pliocene at 45°S (Site 594). The middle Miocene at Sites 588 and 590–594 and the early Miocene at Sites 588, 590, and 592–593 are marked by lower diversity.

The data presented in Figures 3 and 4 point out certain latitudinal abundance and diversity trends observed during Leg 90 and show the limitations of calcareous nannoplankton for zoning sediments south of 40°S.

SYSTEMATIC PALEONTOLOGY

Forty genera and 122 species of calcareous nannoplankton were recognized during the study of core samples from Sites 586–594 (Fig. 5). The genera are listed alphabetically for convenient reference and a brief synonymy of indigenous and reworked species is included.

Genus *AMAUROLITHUS* Gartner and Bukry, 1975

Amaurolithus amplificus (Bukry and Percival)

Ceratolithus amplificus Bukry and Percival, 1971, p. 125, pl. 1, figs. 9–11.

Amaurolithus amplificus (Bukry and Percival). Gartner and Bukry, 1975, pp. 455–456, figs. 6g–l.

Amaurolithus bizzarus (Bukry)

Ceratolithus bizzarus Bukry, 1973a, p. 676, pl. 1, figs. 6–10.

Amaurolithus bizzarus (Bukry). Gartner and Bukry, 1975, p. 456, figs. 8a–b.

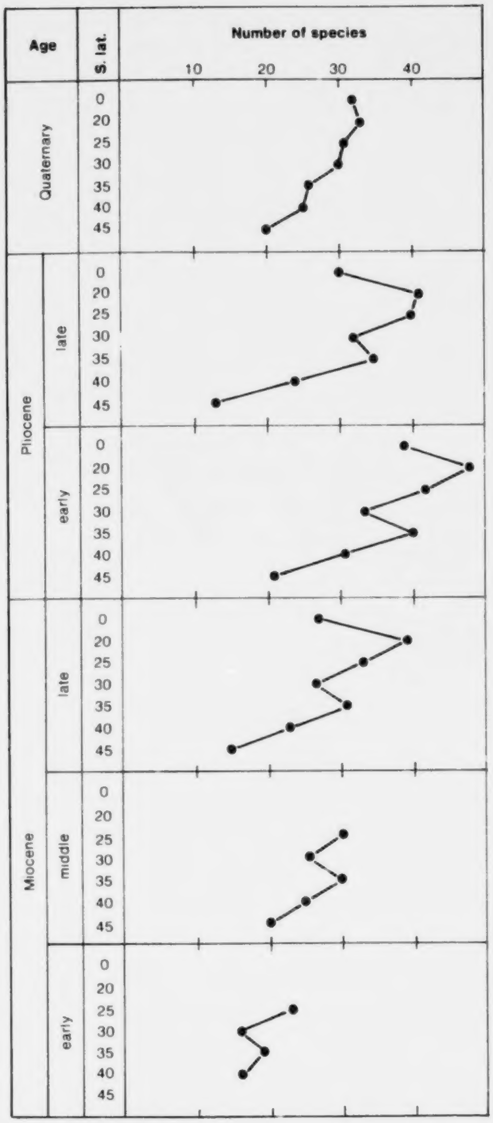

Figure 4. Total number of indigenous calcareous nannoplankton species observed in the Quaternary and Neogene at various southern latitudes.

Amaurolithus delicatus Gartner and Bukry

Amaurolithus delicatus Gartner and Bukry, 1975, p. 456, figs. 7a-f.

Amaurolithus primus (Bukry and Percival)

Ceratolithus primus Bukry and Percival, 1971, p. 126, pl. 1, figs. 12-14.

Amaurolithus primus (Bukry and Percival). Gartner and Bukry, 1975, p. 457, figs. 7g-1.

Amaurolithus tricorniculatus (Gartner)

Ceratolithus tricorniculatus Gartner, 1967, p. 5, pl. 10, figs. 4-6.

Amaurolithus tricorniculatus (Gartner). Gartner and Bukry, 1975, pp. 457-458, figs. 8c-h.

Genus *ANGULOLITHINA* Bukry, 1973

Angulolithina arca Bukry

Angulolithina arca Bukry, 1973a, p. 675, pl. 1, figs. 1-5.

Genus *BRAARUDOSPHAERA* Deflandre, 1947

Braarudosphaera bigelowii (Gran and Braarud)

Pontosphaera bigelowi Gran and Braarud, 1935, p. 389, fig. 67.

Braarudosphaera bigelowi (Gran and Braarud). Deflandre, 1947, p. 439, figs. 1-5.

Genus *CALCIDISCUS* Kamptner, 1950

Calcidiscus leptoporus (Murray and Blackman)

Coccosphaera leptopora Murray and Blackman, 1898, p. 430, pl. 15, figs. 1-7.

Calcidiscus leptoporus (Murray and Blackman). Loeblich and Tappan, 1978, p. 1391.

Calcidiscus macintyrei (Bukry and Bramlette)

Cyclococcolithus macintyrei Bukry and Bramlette, 1969, p. 132, pl. 1, figs. 1-3.

Calcidiscus macintyrei (Bukry and Bramlette). Loeblich and Tappan, 1978, p. 1392.

Genus *CATINASTER* Martini and Bramlette, 1963

Catinaster calyculus Martini and Bramlette

Catinaster calyculus Martini and Bramlette, 1963, p. 850, pl. 103, figs. 1-6.

Catinaster coalitus Martini and Bramlette

Catinaster coalitus Martini and Bramlette, 1963, p. 851, pl. 103, figs. 7-10.

Genus *CERATOLITHUS* Kamptner, 1950

Ceratolithus acutus Gartner and Bukry

Ceratolithus acutus Gartner and Bukry, 1974, pl. 115, pl. 1, figs. 1-4.

Ceratolithus armatus Müller

Ceratolithus armatus Müller, 1974, pl. 591, pl. 11, figs. 4-6; pl. 19, figs. 3-4.

Ceratolithus cristatus Kamptner

Ceratolithus cristatus Kamptner, 1954, p. 43, figs. 44-45.

Ceratolithus rugosus Bukry and Bramlette

Ceratolithus rugosus Bukry and Bramlette, 1968, p. 152, pl. 1, figs. 5-9.

Ceratolithus telesmus Norris

Ceratolithus telesmus Norris, 1965, p. 21, pl. 11, figs. 5-7; pl. 13, figs. 1-3.

Genus *CHIASMOLITHUS* Hay, Mohler, and Wade, 1966

Chiasmolithus altus Bukry and Percival

Chiasmolithus altus Bukry and Percival, 1971, p. 126, pl. 2, figs. 1-2.

Chiasmolithus bidens (Bramlette and Sullivan)

Coccolithus bidens Bramlette and Sullivan, 1961, p. 139, pl. 1, fig. 1.

Chiasmolithus bidens (Bramlette and Sullivan). Hay and Mohler, 1967, p. 1526, pl. 196, figs. 23-25.

Chiasmolithus californicus (Sullivan)

Coccolithus californicus Sullivan, 1964, p. 180, pl. 2, figs. 3a-b, 4a-b.

Chiasmolithus californicus (Sullivan). Hay and Mohler, 1967, p. 1527, pl. 196, figs. 18-20; pl. 198, fig. 5.

Genus	Species	Site 586	587	588	589	590	591	592	593	594
Amaurolithus	*amplificus*	●	●	●				●		
	bizzarus		●							
	delicatus		●	●		●	●	●	●	
	primus	●	●	●		●	●	●	●	
	tricorniculatus	●	●	●		●	●	●	●	●
Angulolithina	*arca*		●							
Braarudosphaera	*bigelowii*		●							
Calcidiscus	*leptoporus*	●	●	●	●	●	●	●	●	●
	macintyrei	●	●	●	●	●	●	●	●	●
Catinaster	*calyculus*			●		●				●
	coalitus			●		●	●	●		
Ceratolithus	*acutus*	●		●					●	
	armatus		●							
	cristatus	●	●	●	●	●	●	●		
	rugosus	●	●	●	●	●	●	●		
	telesmus	●	●	●	●	●	●	●		
Chiasmolithus	*altus*							x	●	x
	bidens									x
	californicus									x
	grandis									x
	oamaruensis									x
Coccolithus	*carteri*	●	●	●	●	●	●	●	●	●
	miopelagicus			●		●	●	●	●	●
	pelagicus	●	●	●	●	●	●	●	●	●
Coronocyclus	*nitiscens*			●		●	●	●	●	●
Crenalithus	*doronicoides*	●	●	●	●	●	●	●	●	●
Cricolithus	*jonesii*			●	●					●
Cyclicargolithus	*abisectus*			●		●	●	●	●	●
	floridanus			●		●	●	●	●	●
Dictyococcites	*bisectus*			●				●	●	x
	scrippsae			●					●	x
Discoaster	*asymmetricus*	●	●	●	x	●	●	●	●	
	barbadiensis									x
	bellus			●		●	●	●	●	
	berggrenii	●	●	●		●	●	●	●	
	blackstockae		●	●						
	bollii			●						
	brouweri	●	●	●	●	●	●	●	●	●
	calcaris			●						
	challengeri		●	●				●		
	decorus	●						●	●	
Discoaster	*deflandrei*			●		●	●	●	●	●
	druggii			●		●		●	●	
	exilis		x	●		●	●	●	●	●
	hamatus			●		●	●	●	●	●
	intercalaris									x
	kugleri			●		●	●	●	●	●
	lodoensis									x
	loeblichii		x							
	moorei	x		●			●		●	
	neohamatus		●	●		●	●	●	●	●
	pentaradiatus	●	●	●	x	●	●	●	●	●
	perclarus							●		
	quinqueramus	●	●	●		●	●	●	●	●
	stellulus						●			●
	surculus	●	●	●	x	●	●	●	●	●
	tamalis	●	●	●	x	●	●	●	●	
	tridenus	●	●	●		●	●	●	●	
	triradiatus	●	●	●	●	●	●	●	●	●
	variabilis	●	●	●	x	●	●	●	●	●
Discolithina	*japonica*	●	●	●	●	●	●	●	●	●
	multipora	●							●	●
Discosphaera	*tubifera*		●	●	●	●				
Emiliania	*annula*	●	●	●	●	●	●	●	●	
	huxleyi	●	●	●	●	●	●	●	●	●
	ovata	●	●	●	●	●	●	●	●	●
Fasciculithus	*tympaniformis*									x
Gephyrocapsa	*caribbeanica*	●	●	●	●	●	●	●	●	●
	oceanica	●	●	●	●	●	●	●	●	●
	protohuxleyi									●
Hayaster	*perplexus*	●	●	●	●	●	●	●		
Helicosphaera	*ampliaperta*					●				
	carteri	●	●	●	●	●	●	●	●	●
	euphratis		●	●		●	●	●	●	
	hyalina	●	●	●	●	●	●	●	●	●
	intermedia					●	●	●	●	●
	recta			●					●	
	sellii	●	●	●	●	●	●	●	●	●
	wallichii	●				●				
Heliolithus	*kleinpellii*									x
Isthmolithus	*recurvus*							●		x
Lithostromation	*perdurum*					●		●		
Lophodolithus	*nascens*									x
Oolithotus	*fragilis*	●	●	●	●	●	●	●	●	
Orthorhabdus	*serratus*			●						
Pontosphaera	*discopora*	●	●	●	●	●	●	●	●	●
Reticulofenestra	*hillae*									x
	pseudoumbilica	●	●	●	x	●	●	●	●	●
	umbilica			x				x		x
Rhabdosphaera	*clavigera*	●	●	●	●	●	●	●	●	
	procera	●	●	●	●	●	●	●	●	●
Scapholithus	*fossilis*	●	●	●	●	●	●	●	●	
Scyphosphaera	*amphora*	●					●			
	apsteinii	●	●			●				
	campanula		●							
	conica		●			●				
	cylindrica		●				●			
	globulata	●	●	●		●	●	●		
	intermedia	●	●	●		●	●	●	●	
	magna		●	●	●	●	●	●		
	pulcherrima	●	●	●	●	●	●	●	●	
	recurvata	●	●	●	●	●	●	●	●	●
Sphenolithus	*abies*	●	●	●		●	●	●	●	●
	belemnos			●		●		●	●	
	capricornutus			●						
	conicus			●						
	delphix			●						
	dissimilis			●					●	
	heteromorphus			●		●	●	●	●	●
	moriformis	x		●		●	●	●	●	●
	neoabies	●	●	●	x	●	●	●	●	●
Syracosphaera	*pulchra*	●	●	●	●	●	●	●	●	●
Thoracosphaera	*heimii*	●	●	●	●	●				
	saxea	●	●	●	●	●	●	●	●	●
Triquetro-rhabdulus	*carinatus*			●		●		●	●	●
	milowii			●						
	rugosus	●	●	●		●	●	●	●	●
Umbellosphaera	*irregularis*	●	●	●	●	●	●	●	●	●
Umbilicosphaera	*cricota*	●	●	●		●	●	●	●	●
	sibogae	●	●	●	●	●	●	●	●	
Watznaueria	*barnesae*	x								
Zygrhablithus	*bijugatus*			●				●	●	x

Figure 5. Occurrence plot of all species observed in Quaternary and Neogene sediments at Site 586 (Leg 89) and Sites 587-594 (Leg 90). Indigenous species (●) together with reworked species (×) are listed alphabetically for convenient reference.

Chiasmolithus grandis (Bramlette and Riedel)

Coccolithus grandis Bramlette and Riedel, 1954, p. 391, pl. 38, figs. 1a–b.

Chiasmolithus grandis (Bramlette and Riedel). Gartner, 1969b, p. 944, figs. 11-3, 14.

Chiasmolithus oamaruensis (Deflandre)

Tremalithus oamaruensis Deflandre *in* Deflandre and Fert, 1954, p. 154, pl. 11, fig. 22, text-figs. 72–74.

Chiasmolithus oamaruensis (Deflandre). Hay et al., 1966, p. 388, pl. 7, fig. 1.

Genus *COCCOLITHUS* Schwarz, 1894

Coccolithus carteri (Wallich)

Coccosphaera carteri Wallich, 1877, p. 348, pl. 17, figs. 3, 4, 6, 7, 17.

Coccolithus carteri (Wallich). Kamptner, 1941, p. 93.

Coccolithus miopelagicus Bukry

Coccolithus miopelagicus Bukry, 1971a, p. 310, pl. 2, figs. 6–9.

Coccolithus pelagicus (Wallich)

Coccosphaera pelagica Wallich, 1877, p. 348, pl. 17, figs. 1, 2, 5, 11, 12.

Coccolithus pelagicus (Wallich). Schiller, 1930, p. 246, figs. 123–124.

Genus *CORONOCYCLUS* Hay, Mohler, and Wade, 1966

Coronocyclus nitescens (Kamptner)

Umbilicosphaera nitescens Kamptner, 1963, pp. 187–188, pl. 1, fig. 5.

Coronocyclus nitescens (Kamptner). Bramlette and Wilcoxon, 1967, p. 103, pl. 1, fig. 4; pl. 5, figs. 7–8.

Genus *CRENALITHUS* Roth, 1973

Crenalithus doronicoides (Black and Barnes)

Coccolithus doronicoides Black and Barnes, 1961, p. 142, pl. 25, fig. 3.

Crenalithus doronicoides (Black and Barnes). Roth, 1973, p. 731, pl. 3, fig. 3.

Genus *CRICOLITHUS* Kamptner, 1958

Cricolithus jonesii Cohen

Cricolithus jonesi Cohen, 1965, p. 16, pl. 2, figs. j, k; pl. 16, figs. a–c.

Genus *CYCLICARGOLITHUS* Bukry, 1971

Cyclicargolithus abisectus (Müller)

Coccolithus? abisectus Müller, 1970, p. 92, pl. 9, figs. 9, 10; pl. 12, fig. 1.

Cyclicargolithus abisectus (Müller). Bukry, 1973b, p. 703.

Cyclicargolithus floridanus (Roth and Hay)

Coccolithus floridanus Roth and Hay *in* Hay et al., 1967, p. 445, pl. 6, figs. 1–4.

Cyclicargolithus floridanus (Roth and Hay). Bukry, 1971a, pp. 312–313.

Genus *DICTYOCOCCITES* Black, 1967

Dictyococcites bisectus (Hay, Mohler, and Wade)

Syracosphaera bisecta Hay, Mohler, and Wade, 1966, p. 393, pl. 10, figs. 1–6.

Dictyococcites bisectus (Hay, Mohler, and Wade). Bukry and Percival, 1971, p. 127, pl. 2, figs. 12, 13.

Dictyococcites scrippsae Bukry and Percival

Dictyococcites scrippsae Bukry and Percival, 1971, p. 128, pl. 2, figs. 7, 8.

Genus *DISCOASTER* Tan, 1927

Discoaster asymmetricus Gartner

Discoaster asymmetricus Gartner, 1969a, p. 598, pl. 1, figs. 1-3.

Discoaster barbadiensis Tan

Discoaster barbadiensis Tan, 1927, p. 119.

Discoaster bellus Bukry and Percival

Discoaster bellus Bukry and Percival, 1971, p. 128, pl. 3, figs. 1, 2.

Discoaster berggrenii Bukry

Discoaster berggrenii Bukry, 1971b, p. 45, pl. 2, figs. 4–6.

Discoaster blackstockae Bukry

Discoaster blackstockae Bukry, 1973c, p. 307, pl. 1, figs. 1–4.

Discoaster bollii Martini and Bramlette

Discoaster bollii Martini and Bramlette, 1963, p. 851, pl. 105, figs. 1–4, 7.

Discoaster brouweri Tan

Discoaster brouweri Tan, 1927, p. 120, figs. 8a–b.

Discoaster calcaris Gartner

Discoaster calcaris Gartner, 1967, p. 2, pl. 2, figs. 1–3.

Discoaster challengeri Bramlette and Riedel

Discoaster challengeri Bramlette and Riedel, 1954, p. 401, pl. 39, fig. 10.

Discoaster decorus (Bukry)

Discoaster variabilis decorus Bukry, 1971b, p. 48, pl. 3, figs. 5, 6.
Discoaster decorus (Bukry). Bukry, 1973a, p. 677, pl. 2, figs. 8, 9; pl. 4, fig. 11.

Discoaster deflandrei Bramlette and Riedel

Discoaster deflandrei Bramlette and Riedel, 1954, p. 399, pl. 39, fig. 6; text-figs. 1a–c.

Discoaster druggii Bramlette and Wilcoxon

Discoaster druggii Bramlette and Wilcoxon, 1967, p. 220 (nom. subst. pro *D. extensus* Bramlette and Wilcoxon, 1967, *non* Hay, 1967).

Discoaster exilis Martini and Bramlette

Discoaster exilis Martini and Bramlette, 1963, p. 852, pl. 104, figs. 1-3

Discoaster hamatus Martini and Bramlette

Discoaster hamatus Martini and Bramlette, 1963, p. 852, pl. 105, figs. 8, 10, 11.

Discoaster intercalaris Bukry

Discoaster intercalaris Bukry, 197[illegible], pl. 3, fig. 12; pl. 4, figs. 1, 2

Discoaster kugleri Martini and Bramlette

Discoaster kugleri Martini and Bramlette, 1963, p. 853, pl. 102, figs. 11-13.

Discoaster lodoensis Bramlette and Riedel

Discoaster lodoensis Bramlette and Riedel, 1954, p. 398, pl. 39, figs. 3a-b.

Discoaster loeblichii Bukry

Discoaster loeblichii Bukry, 1971a, pp. 315–316, pl. 4, figs. 3–5.

Discoaster moorei Bukry

Discoaster moorei Bukry, 1971b, p. 46, pl. 2, figs. 11, 12; pl. 3, figs. 1, 2.

Discoaster neohamatus Bukry and Bramlette

Discoaster neohamatus Bukry and Bramlette, 1969, p. 133, pl. 1, figs. 4–6.

Discoaster pentaradiatus Tan

Discoaster pentaradiatus Tan, 1927, p. 120, fig. 2.

Discoaster perclarus Hay

Discoaster perclarus Hay *in* Hay et al., 1967, p. 452, pl. 4, figs. 11, 12.

Discoaster quinqueramus Gartner

Discoaster quinqueramus Gartner, 1969a, p. 598, pl. 1, figs. 6, 7.

Discoaster stellulus Gartner

Discoaster stellulus Gartner, 1967, p. 3, pl. 4, figs. 1–3.

Discoaster surculus Martini and Bramlette

Discoaster surculus Martini and Bramlette, 1963, p. 854, pl. 104, figs. 10–12.

Discoaster tamalis Kamptner

Discoaster tamalis Kamptner, 1967, p. 166, pl. 24, fig. 131; text-fig. 28.

Discoaster tridenus Kamptner

Discoaster tridenus Kamptner, 1967, p. 166, text-fig. 30.

Discoaster triradiatus Tan

Discoaster triradiatus Tan, 1927, p. 417.

Discoaster variabilis Martini and Bramlette

Discoaster variabilis Martini and Bramlette, 1963, p. 854, pl. 104, figs. 4–8.

Genus *DISCOLITHINA* Loeblich and Tappan, 1963

Discolithina japonica Takayama

Discolithina japonica Takayama, 1967, p. 177, 181, 189, pl. 2, fig. 11; pl. 9; pl. 10, text-figs. 6, 7.

Discolithina multipora (Kamptner)

Discolithus multiporus Kamptner, 1948, p. 5, pl. 1, fig. 9.
Discolithina multipora (Kamptner). Martini, 1965, p. 400.

Genus *DISCOSPHAERA* Haeckel, 1894

Discosphaera tubifera (Murray and Blackman)

Rhabdosphaera tubifer Murray and Blackman, 1898, p. 438, pl. 15, figs. 8–11.
Discosphaera tubifera (Murray and Blackman). Ostenfeld, 1900, p. 200.

Genus *EMILIANIA* Hay and Mohler, 1967

Emiliania annula (Cohen)

Coccolithites annulus Cohen, 1964, p. 237, pl. 3, figs. 1a–c.
Emiliania annula (Cohen). Bukry, 1973a, p. 678.

Emiliania huxleyi (Lohmann)

Pontosphaera huxleyi Lohmann, 1902, p. 130, pl. 4, figs. 1–6; pl. 6, fig. 69.
Emiliania huxleyi (Lohmann). Hay and Mohler *in* Hay et al., 1967, p. 447, pl. 10, 11, figs. 1, 2.

Emiliania ovata Bukry

Emiliania ovata Bukry, 1973a, p. 678, pl. 2, figs. 10-12.

Genus *FASCICULITHUS* Bramlette and Sullivan, 1961

Fasciculithus tympaniformis Hay and Mohler

Fasciculithus tympaniformis Hay and Mohler *in* Hay et al., 1967, p. 447, pl. 8, figs. 1-5; pl. 9, figs. 1-5.

Genus *GEPHYROCAPSA* Kamptner, 1943

Gephyrocapsa caribbeanica Boudreaux and Hay

Gephyrocapsa caribbeanica Boudreaux and Hay *in* Hay et al., 1967, p. 447, pl. 12, 13, figs. 1-4.

Gephyrocapsa oceanica Kamptner

Gephyrocapsa oceanica Kamptner, 1943, pp. 43-49.

Gephyrocapsa protohuxleyi McIntyre

Gephyrocapsa protohuxley McIntyre, 1970, pp. 187-189, fig. 1a-g.

Genus *HAYASTER* Bukry, 1973

Hayaster perplexus (Bramlette and Riedel)

Discoaster perplexus Bramlette and Riedel, 1954, p. 400, pl. 39, fig. 9.
Hayaster perplexus (Bramlette and Riedel). Bukry, 1973c, p. 308.

Genus *HELICOSPHAERA* Kamptner, 1954

Helicosphaera ampliaperta (Bramlette and Wilcoxon)

Helicopontosphaera ampliaperta Bramlette and Wilcoxon, 1967, p. 105, pl. 6, figs. 1-4.
Helicosphaera ampliaperta (Bramlette and Wilcoxon). Jafar and Martini, 1975, p. 390.

Helicosphaera carteri (Wallich)

Helicosphaera carteri (Wallich). Kamptner, 1954, pp. 21-23, 73-74, text-figs. 17a-c, 18, 19. Jafar and Martini, 1975, pp. 381-397, pl. 1, figs. 1, 4, 5.
Helicopontosphaera kamptneri Hay and Mohler *in* Hay et al., 1967, p. 448, pl. 10, fig. 5; pl. 11, fig. 5.

Helicosphaera euphratis Haq

Helicosphaera euphratis Haq, 1966, p. 33, pl. 2, figs. 1, 3.
Helicopontosphaera euphratis (Haq). Martini, 1969, p. 136.

Helicosphaera hyalina Gaarder

Helicosphaera hyalina Gaarder, 1970, pp. 113-114, text-figs. 1-3.
Helicopontosphaera hyalina (Gaarder). Haq, 1973, p. 37.

Helicosphaera intermedia Martini

Helicosphaera intermedia Martini, 1965, p. 404, pl. 35, figs. 1, 2.
Helicopontosphaera intermedia (Martini). Hay and Mohler *in* Hay et al., 1967, p. 448.

Helicosphaera recta (Haq)

Helicosphaera seminulum recta Haq, 1966, p. 34, pl. 2, fig. 6; pl. 3, fig. 4.
Helicopontosphaera recta (Haq). Martini, 1969, p. 136.
Helicosphaera recta (Haq). Jafar and Martini, 1975, p. 391.

Helicosphaera sellii (Bukry and Bramlette)

Helicopontosphaera sellii Bukry and Bramlette, 1969, p. 134, pl. 2, figs. 3-7.
Helicosphaera sellii (Bukry and Bramlette). Jafar and Martini, 1975, p. 391; Ellis and Lohman, 1979, p. 76.
Helicosphaera inversa Gartner, 1977, p. 23, pl. 1, figs. 4a-b, 5a-c.

Helicosphaera wallichii (Lohmann)

Coccosphaera wallichi Lohmann, 1902, p. 138, pl. 5, figs. 58-60.
Helicopontosphaera wallichi (Lohmann). Boudreaux and Hay, 1969, pp. 272-273, pl. 6, fig. 9.
Helicosphaera wallichii (Lohmann). Okada and McIntyre, 1977, pp. 14-15, pl. 4, fig. 8.

Genus *HELIOLITHUS* Bramlette and Sullivan, 1961

Heliolithus kleinpellii Sullivan

Heliolithus kleinpellii Sullivan, 1964, p. 193, pl. 12, fig. 5.

Genus *ISTHMOLITHUS* Deflandre, 1954

Isthmolithus recurvus Deflandre

Isthmolithus recurvus Deflandre *in* Deflandre and Fert, 1954, p. 16, pl. 12, figs. 9-13, text-figs. 119-122.

Genus *LITHOSTROMATION* Deflandre, 1942

Lithostromation perdurum Deflandre

Lithostromation perdurum Deflandre, 1942b, p. 918, figs. 1-9.

Genus *LOPHODOLITHUS* Deflandre, 1954

Lophodolithus nascens Bramlette and Sullivan

Lophodolithus nascens Bramlette and Sullivan, 1961, p. 145, pl. 4, figs. 7a-c, 8a-c.

Genus *OOLITHOTUS* Reinhardt, *in* Cohen and Reinhardt, 1968

Oolithotus fragilis (Lohmann)

Coccolithophora fragilis Lohmann, 1912, pp. 49, 54, text-fig. 11.
Discolithus antillarum Cohen, 1964, p. 236, pl. 1, figs. 3a-e.
Oolithotus fragilis (Lohmann). Okada and McIntyre, 1977, p. 11, pl. 4, fig. 3.

Genus *ORTHORHABDUS* Bramlette and Wilcoxon, 1967

Orthorhabdus serratus Bramlette and Wilcoxon

Orthorhabdus serratus Bramlette and Wilcoxon, 1967, pp. 114-116, pl. 9, figs. 5-10.

Genus *PONTOSPHAERA* Lohmann, 1902

Pontosphaera discopora Schiller

Pontosphaera discopora Schiller, 1925, p. 11, pl. 1, fig. 4.

Genus *RETICULOFENESTRA* Hay, Mohler, and Wade, 1966

Reticulofenestra hillae Bukry and Percival

Reticulofenestra hillae Bukry and Percival, 1971, p. 136, pl. 6, figs. 1-3.

Reticulofenestra pseudoumbilica (Gartner)

Coccolithus pseudoumbilicus Gartner, 1967, p. 4, pl. 6, fig. 3.
Reticulofenestra pseudoumbilica (Gartner). Gartner, 1969a, pp. 587-589.

Reticulofenestra umbilica (Levin)

Coccolithus umbilicus Levin, 1965, p. 265, pl. 41, fig. 2.
Reticulofenestra umbilica (Levin). Martini and Ritzkowski, 196, p 245, pl. 1, figs. 11, 12.

Genus *RHABDOSPHAERA* Haeckel, 1894

Rhabdosphaera clavigera Murray and Blackman

Rhabdosphaera clavigera Murray and Blackman, 1898, p. 438, p. 15 figs. 13-15.

Rhabdosphaera procera Martini

Rhabdosphaera procera Martini, 1969, p. 289, pl. 26, figs. 10, 11.

Genus *SCAPHOLITHUS* Deflandre, 1954

Scapholithus fossilis Deflandre

Scapholithus fossilis Deflandre *in* Deflandre and Fert, 1954, p. 16 pl. 8, figs. 12, 16, 17.

Genus *SCYPHOSPHAERA* Lohmann, 1902

Scyphosphaera amphora Deflandre

Scyphosphaera amphora Deflandre, 1942a, p. 132, figs. 21, 22.

Scyphosphaera apsteinii Lohmann

Scyphosphaera apsteinii Lohmann, 1902, p. 132, pl. 4, figs. 26-30.

Scyphosphaera campanula Deflandre

Scyphosphaera campanula Deflandre, 1942a, pl. 134, figs. 23-27.

Scyphosphaera conica Kamptner

Scyphosphaera conica Kamptner, 1955, p. 26, figs. 130, 131.

Scyphosphaera cylindrica Kamptner

Scyphosphaera cylindrica Kamptner, 1955, p. 24, fig. 119.

Scyphosphaera globulata Bukry and Percival

Scyphosphaera globulata Bukry and Percival, 1971, pp. 138-140, pl. 7, figs. 1-6.

Scyphosphaera intermedia Deflandre

Scyphosphaera intermedia Deflandre, 1942a, p. 134, figs. 32-36.

Scyphosphaera magna Kamptner

Scyphosphaera magna Kamptner, 1967, p. 150, text-figs. 20.

Scyphosphaera pulcherrima Deflandre

Scyphosphaera pulcherrima Deflandre, 1942a, p. 133, figs. 28-31.

Scyphosphaera recurvata Deflandre

Scyphosphaera recurvata Deflandre, 1942a, p. 132, figs. 17-20.

Genus *SPHENOLITHUS* Deflandre, 1952

Sphenolithus abies Deflandre

Sphenolithus abies Deflandre *in* Deflandre and Fert, 1954, p. 164, pl. 10, figs. 1-4.

Sphenolithus belemnos Bramlette and Wilcoxon

Sphenolithus belemnos Bramlette and Wilcoxon, 1967, p. 118, pl. 2, figs. 1-3.

Sphenolithus capricornutus Bukry and Percival

Sphenolithus capricornutus Bukry and Percival, 1971, p. 140, pl. 6, figs. 4-6.

Sphenolithus conicus Bukry

Sphenolithus conicus Bukry, 1971a, p. 320, pl. 5, figs. 10-12.

Sphenolithus delphix Bukry

Sphenolithus delphix Bukry, 1973a, p. 679, pl. 3, figs. 19-22.

Sphenolithus dissimilis Bukry and Percival

Sphenolithus dissimilis Bukry and Percival, 1971, p. 140, pl. 6, figs. 7-9.

Sphenolithus heteromorphus Deflandre

Sphenolithus heteromorphus Deflandre, 1953, pp. 1785-1786, figs. 1, 2.

Sphenolithus moriformis (Brönnimann and Stradner)

Nannoturbella moriformis Brönnimann and Stradner, 1960, p. 368, figs. 11-16.
Sphenolithus moriformis (Brönniman and Stradner). Bramlette and Wilcoxon, 1967, pp. 124-126, pl. 3, figs. 1-6.

Sphenolithus neoabies Bukry and Bramlette

Sphenolithus neoabies Bukry and Bramlette, 1969, p. 140, pl. 3, figs. 9-11.

Genus *SYRACOSPHAERA* Lohmann, 1902

Syracosphaera pulchra Lohmann

Syracosphaera pulchra Lohmann, 1902, p. 134, pl. 4, figs. 33, 36, 37.

Genus *THORACOSPHAERA* Kamptner, 1927

Thoracosphaera heimii (Lohmann)

Syracosphaera heimii Lohmann, 1919, p. 117, fig. 29.
Thoracosphaera heimii (Lohmann). Kamptner, 1954, pp. 40-42, figs. 41, 42.

Thoracosphaera saxea Stradner

Thoracosphaera saxea Stradner, 1961, p. 84, fig. 71.

Genus *TRIQUETRORHABDULUS* Martini, 1965

Triquetrorhabdulus carinatus Martini

Triquetrorhabdulus carinatus Martini, 1965, p. 408, pl. 36, figs. 1-3.

Triquetrorhabdulus milowii Bukry

Triquetrorhabdulus milowii Bukry, 1971a, p. 325, pl. 7, figs. 9-12.

Triquetrorhabdulus rugosus Bramlette and Wilcoxon

Triquetrorhabdulus rugosus Bramlette and Wilcoxon, 1967, pp. 128-129, pl. 9, figs. 17, 18.

Genus *UMBELLOSPHAERA* Paasche, 1955

Umbellosphaera irregularis Paasche

Umbellosphaera irregularis Paasche *in* Markali and Paasche, 1955, p. 97, pl. 3-6.

Genus *UMBILICOSPHAERA* Lohmann, 1902

Umbilicosphaera cricota (Gartner)

Cyclococcolithus cricotus Gartner, 1967, p. 5, pl. 7, figs. 5-7.
Umbilicosphaera cricota (Gartner). Cohen and Reinhardt, 1968, p. 296, pl. 19, figs. 1, 5; pl. 21, fig. 3; text-fig. 6.

Umbilicosphaera sibogae (Weber-van Bosse)

Coccosphaera sibogae Weber-van Bosse, 1901, p. 137, 140, pl. 17, figs. 1, 2.
Umbilicosphaera mirabilis Lohmann, 1902, p. 139, pl. 5, figs. 66, 66a.
Umbilicosphaera sibogae (Weber-van Bosse). Gaarder, 1970, p. 126.

Genus *WATZNAUERIA* Reinhardt, 1964

Watznaueria barnesae (Black)

Tremalithus barnesae Black *in* Black and Barnes, 1959, p. 325, pl. 9, figs. 1, 2.
Watznaueria barnesae (Black). Perch-Nielsen, 1968, p. 69, pl. 22, figs. 1-7; pl. 23, figs. 1, 4, 5, 16; text-fig. 32.

Genus *ZYGRHABLITHUS* Deflandre, 1959

Zygrhablithus bijugatus (Deflandre)

Zygolithus bijugatus Deflandre *in* Deflandre and Fert, 1954, p. 148, pl. 11, figs. 20, 21.
Zygrhablithus bijugatus (Deflandre). Deflandre, 1959, p. 135.

SUMMARY OF NANNOPLANKTON BIOSTRATIGRAPHY

The nannoplankton biostratigraphy is summarized for each of the nine sites, together with brief site descriptions. The geologic age and nannoplankton zone or subzone assignment of the Quaternary and Neogene cores from Hole 586B (Leg 89) and the holes from Sites 587-594 (Leg 90) are shown in Table 1. In addition, a table of nannoplankton occurrences for each site has been prepared (Tables 2-10, later). For some sites where multiple holes were drilled, sets of samples from more than one

Table 1. Geologic age and nannoplankton zone assignment of Quaternary and Neogene cores from Site 586 (Leg 89) and Sites 587–594 (Leg 90).

Age		Zone or subzone	Leg 89	Leg 90 sites							
			Hole 586B	587	588	589	590	591	592	593	594
					Hole 588		**Hole 590**	**Hole 591**			**Hole 594**
Quaternary		NN21 NN20 NN19b	1-Top 1-3/1-4 1-5/4-2	1-1 3-3 3-4/4-4	1-1 1-2 1-3/1,CC	1-1/1-2 1-3 1-5/3-5	1-1/1-3 1-4/1-5 1,CC/3-2	1-1/1-3 1,CC/2-3 2-5/5-3	1-1/1-3 1,CC 2-1/3-1	1-1/1-3 1,CC/2-3 2-5/3-1	1-1/6-1 6-3/7-1 7,CC/11-3
							Hole 590A				
		NN19a	4-3/5-2	4-5	2-1/3-4	3-6/4-6	3-3/1,CC	5-5/6-5	3-2/3-5	3-3/5,CC	11-5
Pliocene	late	NN18 NN17 NN16	5-3/6-4 6-5/6-6 6-7/8,CC	4-6 4,CC 5-1/5-5	3-5/4-1 4-2 4-3/6-5	4,CC	2-1/2,CC 3-1 3-2/7-3	6,CC/8-1 8-3 8-5/12-3	3-6/4-1 4-2 4-3/6-3	6-1 6-2 6-3/8,CC	18-1
	early	NN15 NN14 NN13 NN12	9,CC/13-7 13,CC/15-1 15-2/15,CC 16-1/17,CC	5-6/6-4 6-5/7-1 7-2/7-3 7-4	6-6/9-2 9-3/11-1 11-2/11-3 11-4/12-1		7-4/11-7 11,CC/14-1 14-2/16-2 16-3/18-5	12-5/16,CC 17-1/20,CC 21-1/21-5 21,CC/24-1	6,CC/8-5 8,CC/13,CC 14-1 14,CC	9-1/9,CC 11-1/13,CC 14-1 17-3	18-3/20-5 20,CC 23-5
Miocene	late						**Hole 590B**				
		NN11b	18-1/21-4	7-5/10-1	12-2/18-3		18-6/30-3	24-3/28-3	15-1/17,CC	17-5/22-3	23,CC
								Hole 591B			
		NN11a NN10	21-5/25,CC	10-3/11,CC	18-4/20-7 20,CC/23-4		30-4/35-5 35,CC/38-5	28-5/4,CC 5-1/8,CC	18-1/19-1 19-3/20,CC	22,CC/25-1 25-3/26-5	26-5 26,CC/28-3
	middle	NN9 NN8			23-5/25-3 25-4/25-6		38,CC/40,CC 41-5/41,CC	9-2/11-1 11,CC	21-1/22,CC 23-1	26,CC/27,CC 28-1	28-5/29,CC 30-1
		NN7			**Hole 588A** 25,CC/2-4		42-1/45-1	12-1/12,CC	23-3/24,CC	37-1	42-3
		NN6			2,CC/8,CC		45-3/47-3	13-1/18-3	25-1/28-1	37-3/42-4	**Hole 594A** 42,CC/15-3
		NN5			**Hole 588C** 9-1/1,CC		47-5/49,CC	18-5/23,CC	28-3/29-3	42-4/43,CC	15,CC/26,CC
	early	NN4 NN3 NN2 NN1			2-1/2-5 2-6/3-6 3,CC/5-1 5-2/10-3		50-1/50,CC 51-1/52-5 52,CC/53-1 53-3/53,CC	24-1/24,CC	29-5/31-3 31-5/32-3 32-5/33-3	44-1/44-5 44,CC/46-5 46,CC 47-1/50-3	

Note: Slash separates first section of zonal interval from last section of interval.

hole were examined in order to provide complete stratigraphic coverage. For convenient reference, the index species are grouped together in the tables and the additional species are then listed alphabetically. The state of preservation is designated as G = good, little or no etching or overgrowth; F = fair, some etching or overgrowth which has damaged or obscured ornamentation; P = poor, considerable etching or overgrowth which has made many species difficult to recognize. Abundance values of each taxon were obtained by scanning an area measuring approximately 45 mm^2 and assigning the following values: A = abundant (>50 specimens), C = common (25–49 specimens), and R = rare (<25 specimens). Over 700 samples from the nine sites were examined with a light microscope to determine the Neogene and Quaternary nannoplankton biostratigraphy. In addition, 61 samples were further examined with a scanning electron microscope (SEM) to determine the range of *Emiliania huxleyi*. Time did not permit further SEM examination to determine the presence of other small Quaternary species.

All relevant zonal and subzonal indicators are present at Sites 586–591. However, at sites south of Site 591, some indicators become increasingly rare and consequently unusable, or they are absent. The paucity of *Ceratolithus rugosus* at Site 592 and its absence at Sites 593 and 594 prevents recognition of the NN13/NN12 boundary at these sites and the absence of *Catinaster coalitus* at Sites 593 and 594 prevents recognition of the NN8/NN7 boundary. At Site 594, 40% of the zonal and subzonal indicators are either missing or occur too sparsely to use. In addition to the absence of *Ceratolithus rugosus* and *Catinaster coalitus*, the absence of *Amaurolithus primus* and the sparse occurrences of *Discoaster brouweri, D. pentaradiatus, D. surculus*, and *D. asymmetricus* prevent recognition of the NN19/NN18, NN18/NN17, NN17/NN16, NN14/NN13, and NN11b/NN11a zonal and subzonal boundaries.

Site 586

Hole 586B

Site 586 is located on the northeastern upper slope of the Ontong-Java Plateau (00°29.84′S, 158°29.89′E) in tropical waters at a depth of 2207 m below sea level. Four holes were drilled at this site during DSDP Leg 89.

The 25 cores obtained from Hole 586B were set aside for study by DSDP Leg 90 scientists in order to complete the latitudinal traverse. Hole 586B was terminated at a depth of 240.3 m because equipment failed.

All of the zonal and subzonal indicators for Zones NN21 through NN11 are present and species diversity is good throughout Hole 586B (Table 2). Preservation changes from good to fair below Sample 586B-6-2, 30–31 cm, and only minor reworking was encountered.

Quaternary

The Quaternary includes Cores 1–4 and the upper part of Core 5 above the last occurrence of *Discoaster brouweri* in Sample 586B-5-3, 30–31 cm. Two rare occurrences of *D. brouweri* above this sample are reworked. The rare occurrence of *Emiliania huxleyi* in Sample 586B-1, top, places the uppermost part of Core 1 in Zone NN21. The two underlying samples (586B-1-3, 30–31 cm and 586B-1-4, 30–31 cm) belong in Zone NN20. The last occurrences of *E. ovata* in Sample 586B-1-5, 30–31 cm and *Calcidiscus macintyrei* in Sample 586B-4-3, 30–31 cm place Samples 586B-1-5, 30–31 cm through 586B-4-2, 30–31 cm in Subzone NN19b and Samples 586B-4-3, 30–31 cm through 586B-5-2, 30–31 cm in Subzone NN19a.

Pliocene

The Pliocene includes the lower part of Core 5 and Cores 6–17. The last occurrence of *Reticulofenestra pseudoumbilica* in Sample 586-9,CC marks the lower/upper Pliocene boundary. The last occurrences of *Discoaster pentaradiatus* in Sample 586B-6-5, 30–31 cm and *D. surculus* in Sample 586B-6-7, 30–31 cm place Samples 586B-5-3, 30–31 cm through 586B-6-4, 30–31 cm in Zone NN18, Samples 586B-6-5, 30–31 cm and 586B-6-6, 30–31 cm in Zone NN17, and Sample 586B-6-7, 30–31 cm through Core 8 in Zone NN16. The last occurrence of *Amaurolithus tricorniculatus* in Sample 586B-13,CC places Samples 586B-9,CC through 586B-13-7, 30–31 cm in Zone NN15. Zone NN14 includes Sample 586B-13,CC to the first consistent occurrence of *D. asymmetricus* in Sample 586B-15-1, 30–31 cm. The numerous occurrences of *D. asymmetricus* below this sample are probably due to contamination. The first occurrence of *Ceratolithus rugosus* in Sample 586B-15,CC places Samples 586B-15-2, 30–31 cm through 586B-15,CC in Zone NN13 and Samples 586B-16-1, 30–31 cm through 586B-17,CC in Zone NN12.

Miocene

The occurrence of *Discoaster quinqueramus* in Sample 586B-18-1, 30–31 cm through Core 25 determined that Hole 586B terminated within the late Miocene Zone NN11. This zone is subdivided into Subzones NN11b and NN11a by the first occurrence of *Amaurolithus primus* in Sample 586B-21-4, 30–31 cm.

Site 587

Hole 587

Site 587 is located on the southern slope of Lansdowne Bank (21°11.87′S, 161°19.99′E) in subtropical waters at a depth of 1101 m below sea level. One hole was cored to a depth of 147.0 m and 11 cores were obtained with good recovery. A sudden change in lithology at a depth of 99.1 m prevented further core recovery.

With the exception of the NN21/NN20 boundary, all of the nannoplankton zones and subzones through Subzone NN11a are recognized (Table 3). Species diversity is good throughout the hole. Preservation is good through Core 4, fair in Cores 5–10, and poor in Core 11. Rare reworked discoasters were observed in three of the Quaternary samples.

Quaternary

The Quaternary includes Cores 1–3 and most of Core 4. Rare to common occurrences of *Emiliania huxleyi* in all of the samples above the last occurrence of *E. ovata* in Sample 587-3-4, 20–21 cm prevent recognition of the boundary between Zones NN21 and NN20. Samples 587-1-1, 4–5 cm through 587-3-3, 20–21 cm are therefore placed in the combined Zone NN21/NN20. A thin Zone NN20 may, however, occur between Samples 587-3-3, 20–21 cm and 587-3-4, 20–21 cm. The last occurrence of *Discoaster brouweri* in Sample 587-4-6, 4–5 cm places Samples 587-3-4, 20–21 cm through 587-4-5, 4–5 cm in Zone NN19. The last occurrence of *Calcidiscus macintyrei* in Sample 587-4-5, 4–5 cm subdivides Zone NN19 into Subzones NN19b and NN19a.

Pliocene

The Pliocene includes the lower part of Core 4 through the upper part of Core 7. The last occurrence of *Reticulofenestra pseudoumbilica* in Sample 587-5-6, 4–5 cm marks the lower/upper Pliocene boundary. The presence of *Discoaster brouweri* and the absence of *D. pentaradiatus* in Sample 587-4-6, 4–5 cm places this sample in Zone NN18. The presence of *D. pentaradiatus* and the absence of *D. surculus* in Sample 587-4,CC places this sample in Zone NN17. The interval from the last occurrence of *D. surculus* down to Sample 587-5-5, 4–5 cm, above the last occurrence of *Reticulofenestra pseudoumbilica* in Sample 587-5-6, 4–5 cm, belongs in Zone NN16. Zone NN15 includes Samples 587-5-6, 4–5 cm through 587-6-4, 4–5 cm. The last occurrence of *Amaurolithus tricorniculatus* in Sample 587-6-5, 4–5 cm and the first occurrence of *D. asymmetricus* in Sample 587-7-1, 4–5 cm place this interval in Zone NN14. The first consistent occurrence of *Ceratolithus rugosus* in Sample 587-7-3, 4–5 cm places this sample and the overlying Sample 587-7-2, 4–5 cm in Zone NN13. Sample 587-7-4, 4–5 cm belongs in Zone NN12.

Miocene

The last occurrence of *Discoaster quinqueramus* in Sample 587-7-5, 4–5 cm and the first occurrence of *Amaurolithus primus* in Sample 587-10-1, 12–13 cm place this interval in Subzone NN11b. Sample 587-10-3, 12–13 cm through 587-11-1, 20–21 cm contain *D. quinqueramus* without *A. primus* and therefore belong in Subzone NN11a. Because preservation is poor and zonal indicators are missing below Sample 587-11-1, 20–21 cm, it can only be assumed that the remaining Core 11 samples also belong in Subzone NN11a.

Table 2. Nannoplankton occurrences, Hole 586B.

Age	Zone	Core	Section	Interval (cm)	Depth below seafloor (m)	Preservation	Index species												Additional species																																													
							Emiliania huxleyi	*Emiliania ovata*	*Ceratolithus rugosus*	*Calcidiscus macintyrei*	*Discoaster brouweri*	*Discoaster asymmetricus*	*Discoaster pentaradiatus*	*Discoaster surculus*	*Reticulofenestra pseudoumbilica*	*Amaurolithus tricorniculatus*	*Amaurolithus primus*	*Discoaster quinqueramus*	*Amaurolithus amplificus*	*Calcidiscus leptoporus*	*Ceratolithus acutus*	*Ceratolithus cristatus*	*Ceratolithus telesmus*	*Coccolithus carteri*	*Coccolithus pelagicus*	*Crenalithus doronicoides*	*Discoaster berggrenii*	*Discoaster decorus*	*Discoaster moorei*	*Discoaster tamalis*	*Discoaster tridenus*	*Discoaster triradiatus*	*Discoaster variabilis*	*Discolithina japonica*	*Emiliania annula*	*Gephyrocapsa caribbeanica*	*Gephyrocapsa oceanica*	*Hayaster perplexus*	*Helicosphaera carteri*	*Helicosphaera hyalina*	*Helicosphaera sellii*	*Helicosphaera wallichii*	*Oolithotus fragilis*	*Pontosphaera discopora*	*Rhabdosphaera clavigera*	*Rhabdosphaera procera*	*Scapholithus fossilis*	*Scyphosphaera amphora*	*Scyphosphaera apsteinii*	*Scyphosphaera globulata*	*Scyphosphaera intermedia*	*Scyphosphaera pulcherrima*	*Scyphosphaera recurvata*	*Sphenolithus abies*	*Sphenolithus moriformis*	*Sphenolithus neoabies*	*Syracosphaera pulchra*	*Thoracosphaera heimii*	*Thoracosphaera saxea*	*Triquetrorhabdulus rugosus*	*Umbellosphaera irregularis*	*Umbilicosphaera cricota*	*Umbilicosphaera sibogae*	*Watznaueria barnesae*
Quaternary	NN21	1		TOP	0.01	G	R													C		R	R			A								R		A	A		R	R	R	R		R	R	R	C									R		R	R				C	
	NN20		3	30-31	4.71	G															C		R	R			A								R		A	A		R	R	R	R	R	R			R						R		R	C	R	R				C	
			4	30-31	6.21	G					R										C			R		R	A										A	A		R	R	C	R	R				R						R			R	R	R				C	
	NN19b		5	30-31	7.71	G		R												C		R	R			A										A	A		R	R	C	R	R	R	R	R	R		R							R	C	R	R				C	
			6	30-31	9.21	G		A												C			R			A									C	A	A		R	R	R	R	R	R			R									R	R	R		R		R	
				CC	11.00	G		C	R											C			R			A									R	A	A		R	R	R	R	R	R			R							R		R	R	R		R	R	R	
		2		CC	20.60	G		A												C		R				A									R	C	C		R	R	R		R	R														R	R	R		R			
		3		CC	30.20	G		C	R											A		R	R			A									R	R	R		C		R			R			R						R			R	R	R	R					R
		4	2	30-31	32.01	G		A	R		R									C		R				A									R	R	R		C		R																R	R	R	R					
	NN19a		3	30-31	33.51	G		A	R	R										C		R	R			A									C	R	R		C		C			R									R	R					R	R					
			5	30-31	36.51	G		A	R	R					R						C		R	R	R	C	A									R	R	R		C		C		R			R										R	R	R					
				CC	39.80	G		A	R	C										C		R	R	R	C	A									C	R	R		C		C											R					R	R	R					
		5	1	30-31	40.11	G		A	R	R										C		R	R	R	R	A									C	R	R		C		C			R											R	R	R	R					
			2	30-31	41.61	G		A	R	C										C		R		R	C	A									C	R	R		R		C		R	R								R					R	R	R					
Pliocene late	NN18		3	30-31	43.11	G		A	R	R	R									C		R		R	C	A							R		R	R				C		C		R										R					R	R	R					
			5	30-31	46.11	G		C	R	R	R									C		R		R	C	A									R				C		R			R			R						R	R			R	R	R	R					
				CC	49.40	G		A	R	R	C									C				R	C	A									R				C		R					R	R											R	R	R					
		6	1	30-31	49.71	G		C	R	R	A	R		R							C				R	C	A					R			R				C		R		R	R								R					R	R	R					
			2	30-31	51.21	G		A	R	R	A	R									C				R	C	A					R			C				C		R		R	R								R					R	R	R					
			3	30-31	52.71	F		C	R	R	A	R									R					C	C									R				R		R																		R								
			4	30-31	54.21	F		C	R	R	A										R					C	C									R				R		R																		R								
	NN17		5	30-31	55.71	F		C	R	R	A	R	R								C					C	C						R			C				R		R			R								R					R								
			6	30-31	57.21	F		C	R	R	A	R	C								C					C	C									R			R	R		R			R														R	R					
	NN16		7	30-31	58.71	F		C	R	R	A	R	A	R							R					C	C									R				R		R			R								R	R					R	R					
				CC	59.00	F		C	R	C	A	R	C	R							C		R	R	R	C	A						R			R				C		R		R	R		R											R	R	R			R		
		7	3	30-31	62.31	F		C	R	C	A	R	C	R							C						C									R			R	C		R		R	R								R	R				R	R	R					
			5	30-31	65.31	F		C	R	C	A	R	C	R							C						C									R			R	C		R		R	R													R	R	R					
			6	30-31	66.81	F		R	R	C	A	R	R	R							C						A									R			R	C		R			R								R						R	R					
				CC	68.60	F		R	R	C	A	R	R	R							C					C	A				R		R			R				C		R			R								R					R	R	R			R		
		8		CC	78.20	F		R	R	C	C	R	C	R							C					R	A		R		R				R	R			R	C		R		R	R				R		R			R				R	R					
early	NN15	9		CC	87.80	F		R	R	C	C	R	C	R	R						C		R				A		C					R	R		R			R	R		R		R	R							R	R	R	R		R	R	R	R			R		
		10		CC	96.30	F		C	C	C	C	C	C	R	C						C						A		R		R		R	R	R	R				C		R		R	R							R	R	R	C		A		R	R			R		
		11		CC	105.90	F		R	R	C	A	R	C	R	A						C						A				R	R		R						C		R					R				R		R	R	C		A		R				C		
		12		CC	115.50	F			R	C	C	R	C	R	A						C						A				R	R		R						C		R			R							R		R	R	C		A		R	R			R		
		13	6	30-31	123.31	F			R	R	C	R	C	A	C						C						C					R	R							C		R			R							R		R	R	C		A							R		
			7	30-31	124.81	F			R	R	C	R	R	R	C						C						C					R	R							C		R													R	R	C		A		R	R					
	NN14			CC	125.10	F			R	R	A	R	A	C	C	R				C						C					R	R							C		R			R							R		R	R	R		A							C		
		14		CC	134.70	F			R	R	C	R	R	C	A	R				C	R					C					R	R					R	C		R										R			R	A		A							R		
		15	1	30-31	135.01	F			R	R	C	R	R	C	A						C	R					C					R	R	R						C		R										R		R	C	A		A								
	NN13		2	30-31	136.51	F			R	R	C		R	A	A						C	R			R	C					R			R					C		R							R		R		R	C	A		A								
			5	30-31	141.01	F			R	R	C		R	R	A		R				C	R			R	C			R		R		R	R					R		R										R		R	R	C		A								
				CC	144.30	F			R	R	A	R	R	A	C	R	R			C	C				C	C					R	R	R	R					C		R			R					R		R	C	A		A								
	NN12	16	1	30-31	144.60	F				R	A	R	R	C	C				R	C				R	A					R	R	R	R					C		R									R	R	R	C	C		A							R		
			3	30-31	147.60	F				R	A	R	R	A	A		R			C	R				R	C				R	R	R	R	R					R		R									R	R	R	C	C		A								
				CC	152.90	F				R	C		R	A	A				C	R				R	A					R	R	R							C		R			R					R	R	R	R	A		A								
		17		CC	162.50	F				R	C		R	C	C				R						C					R	R	R							R		R												R	R	C		A							R		
Miocene late	NN11b	18	1	30-31	163.81	F				R	C	R	R	C	C			R		R					C	C	R				R	R	R							R		R										R		R	R	C		A								
			2	30-31	165.31	F				R	C		R	C	C			C		R					R	C	R				R	R	R							R		R										R		R	R	A		A								
			4	30-31	168.31	F			R	R	A	R	R	A	C			R		R					R	C	R				R	R	R					R	R		R										R		R	R	A		A								
				CC	173.10	F				R	A	R	R	C	A			C		R					R	A	R				R	R	R	R				C		R											R	R	R	A		A							R		
		19		CC	182.70	F				R	A	R	R	R	C		R	A		R						A	C				R	R	R	R				R		R													C	C	A		A				R			
		20		CC	192.30	F				C	A	R	R	A	A		R	C	R	C				C	C	C				R	R							R												R		C	R	A		A							R		
		21	4	30-31	197.10	F				R	A	R	R	C	C		R	A	R	R				R	C	A					R						R		R												R	R	A		A				R		R		
	NN11a		5	30-31	198.60	F				R	A	R	R	C	C			A	R	R				R	C	C					R						R														R		A		A				R				
			6	30-31	200.10	F				R	A	R	R	R	C			C	R	R				R	C	R				R	R	R					R														R	R	A		A				R		R		
				CC	201.90	F				R	A	R	R	C	A			R		C				A	C	R				R	R	R					R		R										R		R	R	A		A								
		22		CC	211.50	F				R	C		R	R	C			R		R				C	C	R				R	R						R														R		C		A				R				
		23		CC	221.10	F				C	C	R	R	C	C			C		C				C	A	R				R	R	R					C		R												R		A		A							R		
		24		CC	230.70	F				C	C		R	R	C			A		R				C	A	R				R		R					C		R												R		A		A							R		
		25		CC	240.30	F				C	C	R	R	R				R		R				C	A	R				R		R					C		R												R		C		A								

Site 588

Holes 588, 588A, 588C

Site 588 is located on the northern Lord Howe Rise (26°06.70′S, 161°13.60′E) in subtropical waters at a depth of 1533 m below sea level. Four holes were drilled at this site. Hole 588 was cored to a depth of 236.0 m and 25 cores were obtained. Hole 588A was washed down to a depth of 236.0 m and then cored to a depth of 344.4 m. Eighteen cores were taken. Hole 588B, which duplicates Hole 588, was cored to a depth of 277.4 m and 31 cores were taken. Hole 588C was washed down to a depth of 305.7 m and then cored to a depth of 488.1 m. Nineteen cores were obtained. Core recovery was generally good throughout the four holes, but recovery was poor in the lowest sections of Holes 588A and 588C.

In order to obtain a complete stratigraphic section, cores from three holes (588, 588A, and 588C) were examined for calcareous nannoplankton (Table 4). Species diversity is good throughout the holes. Preservation changes from good to fair below Core 7 of Hole 588 and only minor reworking was encountered. The major regional unconformity of the southwest Pacific was encountered within Core 18 in the lower part of Hole 588C. It separates middle Eocene sediments (NP15/

Table 1. Nannoplankton occurrences, Site 587.

Age	Zone	Core	Section	Interval (cm)	Depth below seafloor (m)	Preservation	Index Species												Additional species																																																							
							Emiliania huxleyi	Ceratolithus rugosus	Emiliania ovata	Calcidiscus macintyrei	Discoaster brouweri	Discoaster asymmetricus	Discoaster pentaradiatus	Discoaster surculus	Reticulofenestra pseudoumbilica	Amaurolithus primus	Amaurolithus tricorniculatus	Discoaster quinqueramus	Amaurolithus amplificus	Amaurolithus bizzarus	Amaurolithus delicatus	Angulolithina arca	Braarudosphaera bigelowii	Calcidiscus leptoporus	Ceratolithus armatus	Ceratolithus cristatus	Ceratolithus telesmus	Coccolithus carteri	Coccolithus pelagicus	Crenalithus doronicoides	Discoaster berggrenii	Discoaster blackstockae	Discoaster challengeri	Discoaster exilis	Discoaster loeblichii	Discoaster neohamatus	Discoaster tamalis	Discoaster tridenus	Discoaster triradiatus	Discoaster variabilis	Discolithina japonica	Discolithina multipora	Discosphaera tubifera	Emiliania annula	Gephyrocapsa caribbeanica	Gephyrocapsa oceanica	Hayaster perplexus	Helicosphaera carteri	Helicosphaera euphratis	Helicosphaera hyalina	Helicosphaera sellii	Oolithotus fragilis	Pontosphaera discopora	Rhabdosphaera clavigera	Rhabdosphaera procera	Scapholithus fossilis	Scyphosphaera apsteinii	Scyphosphaera campanula	Scyphosphaera conica	Scyphosphaera cylindrica	Scyphosphaera globulata	Scyphosphaera intermedia	Scyphosphaera magna	Scyphosphaera pulcherrima	Scyphosphaera recurvata	Sphenolithus abies	Sphenolithus neoabies	Syracosphaera pulchra	Thoracosphaera heimii	Thoracosphaera saxea	Triquetrorhabdulus rugosus	Umbellosphaera irregularis	Umbilicosphaera cricota	Umbilicosphaera sibogae
Quaternary	NN21 — NN20	1	1	4-5	0.05	G	C																R	C		C	R			R											C		R		R	R	R	C		R	R	R	R	C	R	R									R			R	R	R				R
			2	5-6	1.55	G	C	R															R	R		R	R		R	R											R		R		R	R	R	R		R	R	C	R	R	R	R									R			R	R	R		R	R	R
				CC	3.10	G	C	R						R										R		R	R		R	R								R			R		R		R	R	R	R		R	R	C	R	R	R	R									R			R	R	R		R	R	R
		2	1	12-13	3.23	G	C	R															R	R		R	R			R											R		R		R	R	R	R		R	R	C	R	R	R	R									R			R	R	R		R	R	R
			2	12-13	4.73	G	R	R																R		R	R			R											R		R		R	R	R	R		R	R	R	R	R	R	R									R			R	R	R		R	R	R
			3	2-3	6.13	G	R	R																R		R	R		R	R											R		R		R	R	R	R		R	R	C	R	R	R	R									R			R	R	R		R	R	R
			4	2-3	7.63	G	R	R																R		R	R			R											R		R		R	R	R	R		R	R	A	R	R	R	R									R			R	R	R		R	R	R
			5	2-3	9.13	G	R	R			R												R	C		R	R			R											R		R		R	R	R	R		R	R	C	R	R	R	R									R			R	R	R		R	R	C
			6	2-3	10.63	G	C	R															R	C		R	R			C											R		R		R	C	R	C		R	R	C	R	R	R	R									R			R	R	R		R	R	R
				CC	12.70	G	C	R			R												R	C		R	R			A											R		R		C	C	R	R		R	R	C	R	R	R	R									R			R	R	R		R	R	R
		3	1	20-21	12.90	G	C	R																R		R				A											R		R		C	R	R	R		R	R	R	R	R	R	R									R			R	R	R		R	R	R
			2	20-21	14.40	G	C	R																C		R				A											R		R		C	R	R	R		R	R	R	R	R	R	R									R			R	R	R		R	R	R
			3	20-21	15.90	G	C	R																C		R			R	A											R		R		C	C	R	R		R	R	R	R	R	R	R									R			C	R	R		R	R	R
	NN19b		4	20-21	17.40	G		R	R															C		R				A											R		R		R	R	R	R		R	R	R	R	R	C	R									R			C	R	R		R	R	R
			5	50-51	19.20	G		R	R															C						A											R		R		C	R	R	R		R	R	R	R	R	R	R									R			C	R	R		R	R	R
			6	26-27	20.47	G		R	C															C						A											R		R	R	C	C	R	R		R	R	R	R	R	R	R									R			R	R	C		R	R	R
				CC	22.30	G		R	R															C						A											R		R	R	C	C	R	R		R	R	R	R	R	R	R									R			R	R	R		R	R	R
		4	2	4-5	23.85	G		R	R															C					R	A											R		R	R	C	R	R	C		R	R	R	R	R	R	R	R						R	R	R			C	R	R		R	R	R
			3	4-5	25.35	G		R	C															C						A											R		R	R	C	R	R	C		R	R	R	R	R	R	R	R						R	R	R			C	R	R			R	R
			4	4-5	26.85	G		R	R															C						A											R		R	R	R	R	R	R		R	R	R	R	R	R	R	R						R	R	R			R	R	R			R	
	NN19a		5	4-5	28.35	G		R	R	R													R	C						A											R		R	R	R	R	R	C		R	R	R	R	R	C	R	R						R	R	R			C	R	R			R	
	NN18		6	4-5	29.85	G		R	R	R	R													C					R	A											R			R	R	R	R	C		R	R	R	R	R	R	R	R						R	R	R			C	R	R			R	
	NN17			CC	31.90	G		R	C	C	C	R	R										R	C				R	R	A									R		R			R	R	R	R	C		R	R	R	R	R	R	R	R						R	R	R			C	R	R			R	
Pliocene, late	NN16	5	1	106-107	32.97	F		R	R	C	C	R	R	R										C				R	C	A							R		R		R			R			R	R			R	R	R	R	R	R	R	R						R	R	R			R	R	R			R	
			2	4-5	33.45	F		R	R	C	C	R	R	R										R					C	A							R		R		R			R			R	C			R	R	R	R	R	R	R	R		R				R	R	R		R	C	R	R			R	
			3	4-5	34.95	F		R	R	C	C	R	C	R										C					R	A		R	R				C	R	R	R	R			R			R	R			R	R	R	R	R	R	R	R		R			R	R	R	R			C	R	R			C	
			4	4-5	36.45	F		R	C	C	C	C	C	C										C					R	A		R					C	R	R	R	R			R			R	R			R	R	R	R	R	R	R	R		R			R	R	R	R			C	R	R			R	
			5	4-5	37.95	F		R	R	C	C	R	C	C										C					R	A		R					R	R	R	R	R			R			R	C			R	R	R	R	R	R	R	C		R			R	R	R	C			R	R	R			C	
	NN15		6	4-5	39.45	F		R	C	C	C	C	C	C	R									C						A							C	R	R	R	R			R			R	C			R	R	R		R	R	R		R	R		R	R	R	R	R	R	R	R	R			C	
				CC	41.50	F		R	R	R	C	R	R	R	R									C						A							R	R	R	R	R			R			R	R			R	R	R		R	R	R		R	R	R		R		R	R	C	C	R	R	R			R	
		6	1	2-3	41.53	F		R	R	C	C	C	R	C	R									C						A							R	R	R	R	R			R			R	C			R	R	R		R	R	R		R		R	R	C	C	R	R	R			R	
			2	4-5	43.05	F		R	R	C	C	C	C	C	C									C						A							R	R	R	R	R			R			R	C			R	R	R		R	R	R		R		R	R	C	C	R	R	R			R	
			3	4-5	44.55	F		R	C	C	C	C	C	C	C									C						A							R	R	R	R	R			R			R	C			R	R	R		R	R	R		R		R	R	C	C	R	R	R			C	
			4	4-5	46.05	F		R		C	C	C	C	C	C									C						C			R				R	R	R	C	R						R	C			R	R	R		R	R	R	R	R		R	R	C	C	R	R	R			R	
	NN14		5	4-5	47.55	F		R		C	C	R	C	C	C	R	R							C					C	C		R	R				R	R	R	R	R						R	C			R		R		R	R	R	R	R		R	R	C	C	R	R	R			C	
			6	4-5	49.05	F		R		C	C	R	C	C	C	R	R			R				C					R	C		R						R	R	R	R	R					R	C	R		R		R		R	R	R	R	R		R	R	C	C	R	R	R			R	
			7	4-5	50.55	F		R		C	C	R	C	C	C	R	R				R			C					C	R								R	R	R	R						R	C	R		R		R		R	R	R				R	R		R	R	C	C	R	R	R			R	
				CC	51.10	F		R		R	C	R	C	R	C	R	R		R		R			C	R				C	C			R					R	R	R	R						R	C	R		R		R		R	R	R				R	R		R	R	C	C	R	R	R			R	
		7	1	4-5	51.15	F		R		C	C	R	C	R	C	R	R		R		R			C					C	C			R						R	R	R						R	C	R		R		R		R	R	R	R			R	R		R	R	C	C	R	R	R			R	
	NN13		2	4-5	52.65	F		R		R	C		R	R	C	R			R		R			R					R	C								C	R	R	R						R	R	R		R		R		R	R	R				R	R		R		C	C		R	R			R	
			3	4-5	54.15	F		R		R	C		C	R	C	R			R		R			R					C	C								C	R	R	R						R	C	R		R		R		R	R	R				R	R		R		C	C		R	R			R	
	NN12		4	4-5	55.65	F				R	C		C	R	C	R			R		R			R					C	C								C	R	C	R						R	C	R		R		R		R	R	R				R	R		R		C	C		R	R			R	
Miocene, late	NN11b		5	4-5	57.15	F				R	C		C	R	C	R		R	R		R			R					R	C								C	R	R	R						R	C	R				R		R	R	R			R	R	R		R		C	C		R	R			R	
			6	4-5	58.65	F				R	R		R	R	C	R		R	R		R			R					C	C								C	R	C	R						R	R	R				R		R	R	R				R	R		R		C	C		R	R			R	
				CC	60.70	F				R	R		R	R	C	R	R	R	R		R			R					C	R								C	R	R	R						R	R	R				R		R	R	R				R	R		R		C	C		R				R	
		8	1	115-116	61.86	F				R	C		R	R	C	R		C	R		R			R					C	C								R	R	R	R						R	C	R				R		R	R	R					R		R		C	C		R				R	
			2	115-116	63.36	F		R		R	R		R	R	C	R		C	R		R			R					C	C				R				R	R	R	R						R	C					R		R	R	R					R		R		C	A		R				R	
			3	115-116	64.86	F				R	R		C	R	C	R		R	R		R	R		R					C	C				R				C	R	R	R						R	C							R	R	R					R		R		C	C						R	
			4	115-116	66.36	F				R	C	R	C	R	C	R		R	R		R			R					C	C				R				C	R	C	R						R	R	R						R		R							R		C	C			R			C	
			5	115-116	67.86	F				R	C		C	R	C	R		C	R		R			R					C	C				R	R	R		R	R	C	R							R							R		R							R		C	C						R	
			6	115-116	69.36	F				R	R		C	R	C	R		C	R		R			R					C	A	R			R		R		R	R	C								C	R								R							R		C	C						R	
				CC	70.30	F				R	R		C	R	C	R		C	R		R			R					C	C	R			R		R		R	R	C								C	R						R		R					R		R		C	A						R	
		9	1	70-71	71.01	F				R	C		C	R	C	R		C	R		R			R					C	C	R			R		R		R	R	C	R							C					R				R					R		R		C	C						R	
			2	30-31	72.10	F				R	C		C	R	C	R		R			R			R					C	C	R			R		R			R	C								C									R							R		C	C						R	
				CC	79.90	F				R	C		C	R	C	R		R			R			C					C	C	R			R		R		C	R	R	R														R		R					R		R		C	C		R		R		R	
		10	1	12-13	80.03	F				R	C		R	R	C	R		R			R			R					C	C	R					R		C	R	R							R	R	R								R									C	C		R				R	
	NN11a		3	12-13	83.03	F				R	C		R	R	C			R						C					C	C	R					R		R		R							R	R					R				R							R		C	C			R	R		C	
			5	12-13	86.03	F				R	C		R	R	C			R						R					R	R	R					R		R		R	R							R	R								R									R	R		R		R		R	
		11	1	20-21	89.71	P				R	R		R	R	R			R						R					R	R						R																					R									R	R							
			3	20-21	92.71	P									R				•											R																																							R								
			5	20-21	95.71	P									R																								R								R																					R								
				CC	99.10	P																		R					R	R																																															

Table 4. Nannoplankton occurrences, Holes 588, 588A, and 588C.

Age	Zone	Core	Section	Interval (cm)	Depth below seafloor (m)	Preservation	Index species																					Additional species																																																																
							Emiliania huxleyi	Emiliania ovata	Calcidiscus macintyrei	Discoaster brouweri	Ceratolithus rugosus	Discoaster asymmetricus	Discoaster pentaradiatus	Discoaster surculus	Reticulofenestra pseudoumbilica	Amaurolithus tricorniculatus	Amaurolithus primus	Discoaster quinqueramus	Discoaster hamatus	Catinaster coalitus	Discoaster exilis	Discoaster kugleri	Sphenolithus heteromorphus	Sphenolithus belemnos	Discoaster druggii	Triquetrorhabdulus carinatus	Helicosphaera recta	Amaurolithus amplificus	Amaurolithus delicatus	Calcidiscus leptoporus	Catinaster calyculus	Ceratolithus acutus	Ceratolithus cristatus	Ceratolithus telesmus	Coccolithus carteri	Coccolithus miopelagicus	Coccolithus pelagicus	Coronocyclus nitescens	Crenalithus doronicoides	Cricolithus jonesi	Cyclicargolithus abisectus	Cyclicargolithus floridanus	Dictyococcites bisectus	Dictyococcites scrippsae	Discoaster bellus	Discoaster berggrenii	Discoaster blackstockae	Discoaster bollii	Discoaster calcaris	Discoaster challengeri	Discoaster deflandrei	Discoaster moorei	Discoaster neohamatus	Discoaster tamalis	Discoaster tridenus	Discoaster triradiatus	Discoaster variabilis	Discolithina japonica	Discosphaera tubifera	Emiliania annula	Gephyrocapsa caribbeanica	Gephyrocapsa oceanica	Hayaster perplexus	Helicosphaera carteri	Helicosphaera euphratis	Helicosphaera hyalina	Helicosphaera sellii	Oolithotus fragilis	Orthorhabdus serratus	Pontosphaera discopora	Reticulofenestra umbilica	Rhabdosphaera clavigera	Rhabdosphaera procera	Scapholithus fossilis	Scyphosphaera globulata	Scyphosphaera intermedia	Scyphosphaera magna	Scyphosphaera pulcherrima	Scyphosphaera recurvata	Sphenolithus abies	Sphenolithus capricornutus	Sphenolithus conicus	Sphenolithus delphix	Sphenolithus dissimilis	Sphenolithus moriformis	Sphenolithus neoabies	Syracosphaera pulchra	Thoracosphaera heimii	Thoracosphaera saxea	Triquetrorhabdulus milowii	Triquetrorhabdulus rugosus	Umbellosphaera irregularis	Umbilicosphaera cricota	Umbilicosphaera sibogae	Zygrhablithus bijugatus
Quaternary	NN21	1	1	85-86	0.86	G	C																							A			R	R			R		A	R																		R	R		C	C	R	C		R	R	A		C		C	C	[illegible]													C	R	C			R		R	
	NN20		2	85-86	2.36	G																								A			R				R		A	R																		R			A	A	R	C		R	C	C		R		C	R	A					R								C	R	C			R	R	R	
	NN19b		3	85-86	3.86	G		R																						C			R				R		A	R																		R		R	A	C	R	C		R	R	R		R		R	C	C													C	R	R			R	R	R	
				CC	5.80	G		A																						A			R						A	R																		R		A	C	C	R	C		C	R	R		C		C	C	C					C								C	C	C			R	R	C	
	NN19a	2	1	85-86	6.46	G		C	R																					C			R	R					A	R																		R		C	C			C			R	R		R		[illegible]	C	R					R								C	R	R			R	R	R	
			3	85-86	9.45	G		C	R																					C			R						A	R																		R		R	C			C			R	C		R		R	R	R					R								C	R	[illegible]			R	R	R	
				CC	15.20	G		A	R																					C			R				R		A	R																		R		R	C			C			R	R		R		[illegible]	R	R					R								C	R	R			R	R	R	
		3	4	0-1	19.70	G		A	C																					C			R	R	R		R		A																			R		R				C			R	R		R		R	R	R					R								C	R	R			R	R	R	
Pliocene, late	NN18		5	0-1	21.20	G		A	C	C																				C			R				C		A																		R		R		R				C			R	R		R		C	C	R				R	R								C	R	R				R	R	
				CC	24.80	G		C	C	A																				C			R	R			C		A																		R		R		R			R	C			R	R		R		C	C	R	R	R	R	R	C								C		R						
		4	1	0-1	24.80	G		C	C	A	R																			C			R				R		A																		R		R		R				C			R	R		C		C	C	R	R			R	R								C		R						
	NN17		2	0-1	26.31	G		C	C	A	R	R	R																	C			R				R		A																		R		C		R			R	C			C	R		R		C	C	R	R	R		R	R								C		[illegible]						
	NN16		3	0-1	27.81	G		A	C	C	R	R	A	R																C				R	R		C		A																R		R		R		C			R	C			C	C		R		R	C	R	R	R		R	C								R		R				R		
		5		CC	44.00	G		C	C	C	R	C	A	C																C					R		R		A								R								C	R	R		R		R			R	C			C	C		R		R	C	[illegible]	R	[illegible]		R	R								R		R				C		
		6	5	0-1	50.01	G		R	C	C	R	C	C	C																A							R		A												R				C	R	R	R	R		R			R	C			C	C		R			R	R	R	R		R	R	R							R		R			R	R		
Pliocene, early	NN15		6	0-1	51.51	G		R	C	C	R	C	C	C	R															A					R		R		A												R				C	R	R	R	R		R			R	C			C	C					C	R	R	R	R	R	R	R						R	R		R			R	C		
		7	2	0-1	55.11	G		R	C	C	R	A	A	C	C														R	C							R		A												R				R	R	R	R	R		R			R	C			C	C					R	R	R	R	R	R	R	C						C	R						C		
			3	0-1	56.61	G		R	C	C	R	A	A	C	A		R												R	C							R		A												R				R	R	R	R	R		R			R	C			R	R					R	R	R	C	R	R	C	C						A	R						C		
				CC	63.20	G			C	C	C	C	C	C	A		R												R	C					R		R		A												R				R	R	R	C	C					R	C			R						R	R	R	R		R	C	A						A							C		
		8		CC	72.80	F			R	C	C	R	A	R	A		R												R	C							R		A												R					C	R	R	C					R	C			R						R		R	R		R	R	C						A							C		
		9	2	0-1	74.31	F			R	C	R	R	A	R	A		R												R	C							R		A												R					C	R	R	R					R	C			R						R		R	R		R	R	C						A							C		
	NN14		3	0-1	75.81	F			R	C	R	R	A	R	A	R	R												R	C							R		C												R					R	R	R	R					R	C			R						R		R	R		R	R	A						A							C		
				CC	82.40	F			R	C	R	R	A	C	A	R	R												R	C							R		C												R					R	R	R	R					R	C			R						R		R	R		R	R	A						A							C		
		10	5	0-1	88.41	F			R	C	R	R	C	C	A	R	R												R	C							C		C												R					R	R	R	R					R	C	R		R						R		R	R		R	R	A						A							R		
			6	0-1	89.91	F			R	C	R	R	C	C	A	R	R											R	R	C		R					C		C												R					R	R	R	R					R	C			R						R		R	R		R	R	A						A							R		
		11	1	0-1	92.01	F			C	C	R	R	C	C	A	R	R												R	C		R					A		C												R					C	R	R	R					R	C			R						R		R	R		R	R	A						A							C		
	NN13		2	0-1	93.51	F			C	C			C	C	A		R												R	C		R					C		C												R					R	R	R	R					R	C			R						R		R	R		R	R	A						A							R		
			3	0-1	95.01	F			C	C			C	C	A		R												R	C							C		C												R					R	R	R	R					R	C			R						R		R	R		R	R	A						A							R		
	NN12		4	0-1	96.51	F			C	C			C	C	A		R												R	C							C		C												R					R	R	R	R					R	C			R						R		R	R		R	R	A						A							R		
		12	1	0-1	101.60	F			C	C			C	C	A		R												R	C							C		C												R					R	R	C	R					R	C			R						R		R	R		R	R	A						A							R		
late	NN11b		2	0-1	103.10	F			C	C			C	C	A		R	R											R	C							C		C												R					R	R	C	R					R	C			R						R		R	R		R	R	A						A							R		
			3	0-1	104.60	F			C	C			A	C	A	R	C	C											R	C							A		A												R					R	R	C	R					R	C									R		R	R		R	R	A						A							C		
				CC	111.20	F			C	C			C	R	A		R	C											R	C							A		C												R					R	R	R	R					[illegible]	C										R	R	R		R	R	A						A							R		
		13		CC	120.80	F			R	R			C	R	A		C	C											R	C							C		C																	R	R	R	R						C												R		R	R	A						A							R		
		14		CC	130.40	F			R	R			C	R	A		C	C											R	C							C		A																	R	R	C	R						R												R		R	R	A						A							R		
		15		CC	140.00	F			R	C			C	R	A		R	C											R	C							C		C					R												R	R	R	R						R												R		R	R	A						A							R		
		16		CC	149.60	F			C	R			C	R	A		R	C											R	C							C		C					R												R	R	R	R						C												R		R	R	A						A							C		
		17		CC	159.20	F			R	R			C	R	C		R	C											R	R							C		C					R													R	R	R						C												R		R	R	A						A							R		
		18	3	0-1	162.21	F			R	R			C	R	C		R	C											R	R							C		C					R													R	C	R						C												R		R	R	A						A							R		
	NN11a		4	0-1	163.71	F			R	R			C	R	C			C												R							C		C					R													R	R	R						C												R		R	R	A						A							R		
				CC	168.80	F			R	R			R	R	C			C												R							C		R					R													R	R							C												R		R	R	C						C					R		R		
		19		CC	178.40	F			R	R			R	R	R			C												C							A		C					C								R				C							R														R	R	A						A					R		R		
		20	3	0-1	181.41	F			C	C			R	R	R			C												R							A		R					C								R				C							C														R		C						C					R		R		
			4	0-1	182.91	F			C	C			R	R	R			R												R							A		R					R								R				R							C														R		C						C					R		R		
			6	0-1	185.91	F			C	C			R	R	R			R												R							C		R					R								R				R							C														R		C						C					R		R		
			7	0-1	187.41	F			C	C			R	R	R			R												R						R	C		R					R	R							C				R							C														R		C						C					R		R		
				CC	188.00	F			C	C			R	R	R															C						R	C		R					R						R		C	R			R							C	R									R				R		C						C					R		R		

Miocene middle	NN10		21		CC	197.60	F	C	C	R	C										C			C						R					C	R	R					C						C		R	R	
			22		CC	207.20	F	C	C	R	A										R			C						R					C	C	R					C						C		R	R	
			23	4	0-1	211.71	F	C	R	R	A										R			C						R					C	C	R					C						C		R	R	
	NN9			5	0-1	213.21	F	C	R	R	A	R									C			C						R					C	C	R					R						R		R	R	
				6	0-1	214.71	F	C	C		A	R	R								C	C		C						R					C	C	R				R	R						R		R	R	
					CC	216.80	F	C	R		C	C	R								C	A		C						R	R	R			C	C	R					C						C		R	R	
			24		CC	226.40	F	C	C		C	C	C								R	R		C						R					C	C	R					R						C		R	R	
			25	2	0-1	227.91	F	R	C		A	R	R								R	C		C						R					R	C	R					R						R		R	R	
				3	0-1	229.41	F	R	C		A	R	R								R	R		C						R					R	C	R					R						R		R	R	
	NN8			4	0-1	230.91	F	R	C		C		C	R							R			C											R	C	R					R						R		R	R	
				5	0-1	232.41	F	R	C		C		C	R							R			C										R	R	C	R					R						R		R	R	
				6	0-1	233.91	F	R	C		C		R	R							R			C										R		C	R					R						R		R	R	
	NN7				CC	236.00	F	R	R		A			R							R			C										R		C	R					R						R		R	R	
		A	1	2	0-1	237.51	F	R	R		A			C							C		R	C												C	R					R						R		R	R	
				4	0-1	240.51	F	R	R		C			C							R		R	C												R	R					R						R		R	R	
				5	0-1	242.01	F	R	R		C			C	R						R		R	C												R	R					R						R		R	R	
					CC	245.60	F	C	R		A			C	C						C		R	A												C	R					C						C		R	R	
			2	2	0-1	247.10	F	C	R		C			C	C						C		R	C												C	R					R						R		R	R	
				4	0-1	250.10	F	C	R		C			C	R						C		R	C									R			C	R					R					R	R		R	R	
	NN6				CC	250.62	F	R	R		C			C							R		R	C									C			R	R					R					R	R		R	R	
			3		CC	255.60	F	R	R		C			C							R		R	C		C	R						C			R	C					R					R	R		R	R	
			4		CC	260.60	F	R	R		C			R							R		R	R		R	R						C			R	R					R					R	R		R	R	
			5		CC	265.60	F	R	R		R			R							R		R	R		R	R						R			R	R					R					R			R	R	
			6		CC	270.60	F	R	R		R			R							R		R	R		C	R						R			R	C					R					R			R	R	
			7		CC	275.60	F	R			C			C							R		R	C		C	R						R			R	C										R				R	
			8		CC	280.60	F	R	R		C			C							R		R	C		C	R						R			R	C	R									R				R	
	NN5		9	1	0-1	280.60	F	R			R			C		R					R		R	C		C	R						R			R	R										R				R	
				3	0-1	283.60	F	R			R			C		R					R		R	C		C	C						R			R	R										R				R	
					CC	285.60	F	R			R			C		C					R		R	C		C	C						R			R	R										R				R	
			10		CC	290.60	F	R			R			R		C					R		R	C		C	C						R			R	R										R				R	
			11		CC	295.60	F	R			R			R		C					R		R	R		C	C						R			R	R										R				R	
			12		CC	300.60	F	C			R			R		C					R		C	C		A	C						C			C	R										R				R	
		C	1		CC	315.30	F	C			R			R		C							C	A		A	C						C			C	R	R									C					
early	NN4		2	1	0-1	315.31	F	C			R					C							C	A		A	C						C			R	R										C					
				2	0-1	316.81	F	R			R					C							R	C		A	R						C				R										C					
				3	0-1	318.31	F	R			R					A							R	C		A	R						C				R										C					
				4	0-1	319.81	F	R			R					A							R	C		A	R						A				R										C					
				5	0-1	321.31	F	R			R					A							R	C		A	C						A				R										C					
	NN3			6	0-1	322.81	F	R			R					A	R						R	C		A	C						A				R	R									C					
					CC	324.90	F	R			R						C						C	C	R	A	C						A				R	R									A		R			
			3	1	0-1	324.91	F	R			R						A						R	C		A	C						A				R										C					
				2	0-1	326.41	F	R			R						A						R	C		A	C						A				R										C					
				3	0-1	327.91	F	R			R						C						R	C		A	C						A				R										C		R			
				4	0-1	329.41	F	R			R						C						R	C		A	C						A				R									R	C					
				5	0-1	330.91	F	R			R						C						R	C		A	C						A				R										C					
				6	0-1	332.41	F	R			R						A						R	C	R	A	C						A				R									R	C		R			
	NN2				CC	334.50	F	R			R						C	R	R				R	C		A	C						A				R									R	A					
			4		CC	344.10	F										R	R	R				R	C	R	C	R						C													R	C					
			5	1	21-22	344.32	F										R	R	R				R	C		C	R						C													R	C					
	NN1			2	0-1	345.61	F										R		R				C	C	R	C	C						C													R	C		R			
					CC	353.70	F										R		R				C	C	R	A	C	R	R				C													R	C					
			6	1	0-1	353.71	F												R				C	C	R	A	C	R	R				A					R								C	C					
Oligocene late	NP25			2	0-1	355.21	F												R	R			C	C	R	A	C	R	R				A					R								C	C					R
				3	0-1	356.23	F												R	R			C	C	R	C	C	R	R				C					R								R	C					
					CC	363.23	F												R	R			C	C	R	C	C	R	R				A					R								C	C		R			
			7		CC	372.90	F												R	R			R	C	R	C	C	R	R				C					R								R	C		R			
			8		CC	382.50	F												R	R			C	C	R	C	C	R	R				C					R								R	C		R			
			9		CC	392.10	F												R	R			R	C	R	A	C	R	R				C											R	R	R	R	C		R			R
			10	3	0-1	399.43	F												C	R			C	C		A	C	R	R				C					R		R			R	R		R	C		R			
					CC	401.70	F												R	R			C	A		C	C	R	R				A											R		C	C					C
			11	1	0-1	401.71	F												R	R			C	C		C	C	R	R				A					R	R					R			C		R			C

NP16) from immediately overlying upper Oligocene sediments (NP24). A complete Quaternary, Neogene, and upper Oligocene section overlies the unconformity.

Quaternary

The Quaternary includes Cores 1–2 and the upper part of Core 3. The presence of *Emiliania huxleyi* in Sample 588-1-1, 85–86 cm places this sample in Zone NN21. The last occurrence of *E. ovata* in Sample 588-1-3, 85–86 cm places the intervening Sample 588-1-2, 85–86 cm in Zone NN20. The last occurrence of *Discoaster brouweri* in Sample 588-3-5, 0–1 cm places Samples 588-1-3, 85–86 cm through 588-3-4, 0–1 cm in Zone NN19. The last occurrence of *Calcidiscus macintyrei* in Sample 588-2-1, 85–86 cm subdivides Zone NN19 into Subzones NN19b and NN19a.

Pliocene

The Pliocene section includes the lower part of Core 588-3 through the upper part of Core 588-12. The last occurrence of *Reticulofenestra pseudoumbilica* in Sample 588-6-6, 0–1 cm marks the lower/upper Pliocene boundary. The presence of *Discoaster brouweri* and the absence of *D. pentaradiatus* in Samples 588-3-5, 0–1 cm through 588-4-1, 0–1 cm place these samples in Zone NN18. Sample 588-4-2, 0–1 cm contains *D. pentaradiatus* without *D. surculus* and belongs in Zone NN17. The interval from the last occurrence of *D. surculus* in Sample 588-4-3, 0–1 cm through Sample 588-6-5, 0–1 cm is placed in Zone NN16. The last occurrences of *R. pseudoumbilica* in Sample 588-6-6, 0–1 cm and *Amaurolithus tricorniculatus* in Sample 588-9-3, 0–1 cm place Samples 588-6-6, 0–1 cm through 588-9-2, 0–1 cm in Zone NN15. The first occurrences of *D. asymmetricus* in Sample 588-11-1, 0–1 cm and *Ceratolithus rugosus* in Sample 588-11-3, 0–1 cm place Samples 588-9-3, 0–1 cm through 588-11-1, 0–1 cm in Zone NN14 and Samples 588-11-2, 0–1 cm and 588-11-3, 0–1 cm in Zone NN13. Samples 588-11-4, 0–1 cm and 588-12-1, 0–1 cm, between the first occurrence of *C. rugosus* and the last occurrence of *D. quinqueramus*, belong in Zone NN12.

Miocene

The Miocene includes the upper part of Core 12, Hole 588, through the upper part of Core 10, Hole 588C. The middle/upper Miocene boundary lies between Samples 588-23-4, 0–1 cm and 588-23-5, 0–1 cm and the lower/middle Miocene boundary lies between Core 588C-1 and Sample 588C-2-1, 0–1 cm. The range of *Discoaster quinqueramus*, Samples 588-12-2, 0–1 cm through 588-20-7, 0–1 cm, defines Zone NN11. The first occurrence of *Amaurolithus primus* in Sample 588-18-3, 0–1 cm subdivides Zone NN11 into Subzones NN11b and NN11a. The range of *D. hamatus*, from Samples 588-23-5, 0–1 cm through 588-25-3, 0–1 cm, places these samples in Zone NN9 and the overlying interval, Samples 588-20,CC through 588-23-4, 0–1 cm, in Zone NN10. The successive first occurrences of *Catinaster coalitus* in Sample 588-25-6, 0–1 cm and *D. kugleri* in Sample 588A-2-4, 0–1 cm place Samples 588-25-4, 0–1 cm through 588-25-6, 0–1 cm in Zone NN8 and Samples 588-25,CC through 588A-2-4, 0–1 cm in Zone NN7. The last occurrence of *Sphenolithus heteromorphus* in Sample 588A-9-1, 0–1 cm places Sample 588A-2,CC and Cores 3–8 of Hole 588A in Zone NN6. The first occurrence of *D. exilis* in Sample 588C-1,CC places Samples 588A-9-1, 0–1 cm through 588C-1,CC in Zone NN5. Zone NN4 includes Samples 588C-2-1, 0–1 cm through 588C-2-5, 0–1 cm. The last occurrences of *S. belemnos* in Sample 588C-2-6, 0–1 cm and *Triquetrorhabdulus carinatus* in Sample 588C-3,CC place Samples 588C-2-6, 0–1 cm through 588C-3-6, 0–1 cm in Zone NN3. Zone NN2 includes Sample 588C-3,CC down to the first occurrence of *D. druggii* in Sample 588C-5-1, 21–22 cm. The last occurrence of *Helicosphaera recta* in Sample 588C-6-2, 0–1 cm marks the Oligocene/Miocene boundary and places Samples 588C-5-2, 0–1 cm through 588C-6-1, 0–1 cm in Zone NN1.

Site 589

Hole 589

Site 589, at a water depth of 1391 m below sea level, is located east of the crest of Lord Howe Rise (30°42.72′S, 163°38.39′E) in waters transitional between subtropical and temperate water masses. One hole was drilled and four cores were obtained before the onboard positioning computer failed and drilling operations ended at a depth of 36.1 m. Hole 589 penetrated a complete Quaternary sequence and terminated in the latest Pliocene Zone NN18 (Table 5).

Species diversity and preservation are good throughout Hole 589. However, there was considerable reworking of some species, particularly several discoaster species in Cores 3 and 4.

Quaternary

Emiliania huxleyi occurs abundantly in Samples 589-1-1, 0–1 cm and 589-1-2, 0–1 cm. Therefore, these samples are placed in Zone NN21. The last common occurrence of *E. ovata* in Sample 589-1-5, 0–1 cm is taken as the top of Subzone NN19b, which places Sample 589-1-3, 0–1 cm in Zone NN20. Rare occurrences of *E. ovata* above Sample 589-1-5, 0–1 cm are interpreted as reworking. The last consistently common occurrence of *Calcidiscus macintyrei* in Sample 589-3-6, 0–1 cm marks the top of Subzone NN19a, placing Samples 589-1-5, 0–1 cm through 589-3-5, 0–1 cm in Subzone NN19b and Samples 589-3-6, 0–1 cm through 589-4-6, 0–1 cm in Subzone NN19a. Rare to common occurrences of *C. macintyrei* above Sample 589-3-6, 0–1 cm are interpreted as reworking.

Pliocene

The common occurrence of *Discoaster brouweri* in Sample 589-4,CC places this sample in the latest Pliocene Zone NN18. Rare occurrences of *D. brouweri* above this sample are interpreted as reworking.

Site 590

Holes 590, 590A, 590B

Site 590 is located on the crest of Lord Howe Rise (31°10.02′S, 163°21.51′E) immediately north of the sub-

Table 5. Nannoplankton occurrences, Hole 589.

							Index species				Additional species																																					
Age	Zone	Core	Section	Interval in cm	Depth below seafloor (m)	Preservation	*Emiliania huxleyi*	*Emiliania ovata*	*Calcidiscus macintyrei*	*Discoaster brouweri*	*Calcidiscus leptoporus*	*Ceratolithus cristatus*	*Ceratolithus rugosus*	*Ceratolithus telesmus*	*Coccolithus carteri*	*Coccolithus pelagicus*	*Crenalithus doronicoides*	*Cricolithus jonesi*	*Discoaster asymmetricus*	*Discoaster pentaradiatus*	*Discoaster surculus*	*Discoaster tamalis*	*Discoaster triradiatus*	*Discoaster variabilis*	*Discolithina japonica*	*Discosphaera tubifera*	*Emiliania annula*	*Gephyrocapsa caribbeanica*	*Gephyrocapsa oceanica*	*Hayaster perplexus*	*Helicosphaera carteri*	*Helicosphaera hyalina*	*Helicosphaera sellii*	*Oolithotus fragilis*	*Pontosphaera discopora*	*Reticulofenestra pseudoumbilica*	*Rhabdosphaera clavigera*	*Rhabdosphaera procera*	*Scapholithus fossilis*	*Scyphosphaera magna*	*Scyphosphaera pulcherrima*	*Scyphosphaera recurvata*	*Sphenolithus neoabies*	*Syracosphaera pulchra*	*Thoracosphaera heimii*	*Thoracosphaera saxea*	*Umbellosphaera irregularis*	*Umbilicosphaera sibogae*
Quaternary	NN21	1	1	0-1	0.01	G	A	R	C		A			R	R	R	C								R	R		C	C		R	C	R		R		C	C	C					C	R	R	R	C
			2	0-1	1.51	G	A	R	C		A	R		R	R	C	C	R							C	R		C	C		C	R	R		R	R	C	C	C	R		R		C	R	C	R	C
	NN20		3	0-1	3.01	G		R	C		C	R		R	R	R	C	R							R	R		C	C		C	R	R		R		R	C	R	R		R		R	R	C	R	R
	NN19b		5	0-1	6.01	G		C	C		R	R		R	R	R	A	R							R		R	A	C		C	R	R		R		R	R	R	R		R		R	R	R	R	R
			CC		7.30	G		C	R		R	R		R	R	R	A	R							R		R	C	C		C	R	R		R		R	R	R	R		R		R	R	R	R	R
		2	3	0-1	10.31	G		C	R		C	R	R	R	R	R	A	R							R		R	R	R		C	R	C	R	C		R	R	R	R		C		R	R	R	R	R
			4	0-1	11.81	G		C	R		R	R	R	R	R	R	A	R	R						R		R	R	R		C	R	C	R	R		R	R	R	R		R		R	R	R	R	R
			5	0-1	13.31	G		C	R		C	R	R	R		R	A	R			R				R		R	R	R		C	R	R	R	R		R	R	R	R		R		R	R	R	R	R
			6	0-1	14.81	G		C	R		C	R	R	R		R	A								R		R	R	R		C	R	R	R	R		R	R	R	R		R		R	R	R	R	R
			7	0-1	16.31	G		C	R		C	R	R		R	R	A								R		R	R	R		C	R	R	R	R		R	R	R	R	R	R		R	R	R	R	R
			CC		16.90	G		A	R		C	R	R	R		R	A			R				R	R		R	R	R		C	R	R	R	R		R	R	R		R	R		R	R	R	R	R
		3	1	0-1	16.91	G		A	R	R	C	R	R			R	A			R					R		R	R	R		C	R	R	R	R		R	R	R			R		R	R	R	R	R
			2	0-1	18.41	G		A	R	R	C	R	R		R	R	A		R						R		C	R	R		C	R	R	R	R		R	R	R			R		R	R	R	R	R
			3	0-1	19.91	G		A	R	R	C	R	R	R	R	R	A						R		R		C	R	R		C	R	R	R	R		R	R	R		R	R		R	R	R	R	R
			4	0-1	21.41	G		A	R	R	R	R	R	R		R	A			R					R		C	R	R		C		R	R	R		R	R	R			R		R	R	R	R	R
			5	0-1	22.91	G		C	R	R	R	R	R			R	A			R					R		C	R	R		C		R	R	R		R	R	R			R		R	R	R	R	R
	NN19a		6	0-1	24.41	G		A	C	R	R	R	R		R	R	A			R					R		C	R	R		C		R	R	R		R	R	R			R		R	R	R	R	R
			CC		26.17	G		A	C	R	R	R	R	R		R	A		R	R					R		C	R	R		C		R	R	R		R	R	R			R		R	R	R	R	R
		4	1	0-1	26.51	G		A	C	R	R	R	R		R	R	A			R	R				R		C	C	C		C		C	R	R		R	R	R			R	R	R	R	R	R	R
			2	0-1	28.01	G		A	C	R	R	R	R	R	R	R	A			R	R				R		R	C	R	R	C		C	R	R		R	R	C		R	R		C	R		R	
			3	0-1	29.51	G		A	C	R	R	R	R	R	R	R	A			R	R	R	R		R		R	R			C		R	R			R	R	R			R		R	R		R	
			4	0-1	31.01	G		A	C	R	R	R	R	R	R	C	A			R	R				R		C	R			C		C	R			R	R	R			R		R	R		R	
			5	0-1	32.51	G		C	C	R	R	R	R	R	R	C	A			R	R		R	R	R		R				C		C	R			R	R	R			R		R	R		R	
			6	0-1	34.01	G		A	C	R	R	R		R		C	A			R	R			R	R		C				C		C	R			R	R	R			R		C	R		R	
Plio. late	NN18			CC	36.10	G		A	C	C	R	R	R	R	R	C	A			R	R		C	R	R		C				C		C	R			R	R	R		R			C	R		R	

tropical divergence at a water depth of 1299 m below sea level. Site 590 consists of three holes: Hole 590 was cored to a depth of 26.2 m and three cores were taken; Hole 590A was washed down to the depth of Hole 590, then cored to a depth of 280.8 m, and 27 cores were obtained; and Hole 590B was cored to a depth of 499.1 m and 53 cores were taken. Core recovery was good throughout the three holes.

In order to obtain a complete stratigraphic section, the three cores from Hole 590 together with 18 cores from Hole 590A and 31 cores from Hole 590B were examined for calcareous nannoplankton. All of the Neogene and Quaternary nannoplankton zones are present at Site 590 (Table 6). Species diversity is good throughout Site 590 and little reworking was encountered. Preservation is good down through Sample 590A-14-1, 0–1 cm and fair below this level.

Quaternary

The Quaternary includes Cores 1–3 of Hole 590 and Core 1 of Hole 590A. The presence of *Emiliania huxleyi* in Samples 590-1-1, 5–6 cm through 590-1-3, 5–6 cm places these samples in Zone NN21. The last occurrence of *E. ovata* in Sample 590-1,CC places Samples 590-1-4, 5–6 cm and 590-1-5, 5–6 cm in Zone NN20. The last occurrence of *Discoaster brouweri* in Sample 590A-2-1, 5–6 cm places Samples 590-1,CC through 590A-1,CC in Zone NN19. The last occurrence of *Calcidiscus macintyrei* in Sample 590-3-3, 5–6 cm subdivides Zone NN19 into Subzones NN19b and NN19a. A rare occurrence of *C. macintyrei* is reworked in Sample 590-1-1, 5–6 cm. Rare occurrences of several discoaster species are reworked into Subzone NN19a and Zone NN18.

Pliocene

The interval from Core 2 of Hole 590A through Sample 590A-18-5, 5–6 cm belongs in the Pliocene. The lower/upper Pliocene boundary is placed between Samples 590A-7-3, 0–1 cm and 590A-7-4, 0–1 cm. The last consistent occurrences of *Discoaster brouweri* in Sample 590A-2-1, 5–6 cm, *D. pentaradiatus* in Sample 590A-3-1, 5–6 cm, *D. surculus* in Sample 590A-3-2, 5–6 cm, and *Reticulofenestra pseudoumbilica* in Sample 590A-7-4, 0–1 cm place Samples 590A-2-1, 5–6 cm through 590A-2,CC in Zone NN18, Sample 590A-3-1, 5–6 cm in Zone NN17, and Samples 590A-3-2, 5–6 cm through 590A-7-3, 0–1 cm in Zone NN16. The interval between the last occurrence of *R. pseudoumbilica* in Sample 590A-7-4, 0–1 cm and the last occurrence of *Amaurolithus tricorniculatus* in Sample 590A-11-7, 0–1 cm belongs in Zone NN15. Zone NN14 includes Samples 590A-11,CC through 590A-14-1, 0–1 cm, the first occurrence of *D. asymmetricus*. *Ceratolithus rugosus* has its first occurrence in Sample 590A-16-2, 5–6 cm, thus placing Samples 590A-14-2, 0–1 cm through 590A-16-2, 5–6 cm in Zone NN13. Zone NN12 includes samples from 590A-16-3, 5–6 cm down to Sample 590A-18-5, 5–6 cm.

Miocene

The Miocene includes the interval from Sample 590A-18-6, 5–6 cm through 590B-53,CC. The middle/upper Miocene boundary lies between Sample 590B-38-5, 5-

Table 6. Nannoplankton occurrences, Holes 589, 590A, and 590B.

Age		Zone	Core	Section	Interval (cm)	Depth below seafloor (m)	Preservation	Index species																			
								Emiliania huxleyi	Emiliania ovata	Calcidiscus macintyrei	Discoaster brouweri	Discoaster pentaradiatus	Discoaster asymmetricus	Discoaster surculus	Reticulofenestra pseudoumbilica	Amaurolithus tricorniculatus	Ceratolithus rugosus	Discoaster quinqueramus	Amaurolithus primus	Discoaster hamatus	Catinaster coalitus	Discoaster kugleri	Discoaster exilis	Sphenolithus heteromorphus	Sphenolithus belemnos	Discoaster druggii	Triquetrorhabdulus carinatus
Quaternary		NN21	1	1	5-6	0.06	G	A		R																	
				2	5-6	1.55	G	R																			
				3	5-6	3.05	G	R																			
		NN20		4	5-6	4.55	G																				
				5	5-6	6.06	G																				
		NN19b			CC	7.00	G		R																		
			2	3	5-6	10.06	G		C																		
					CC	16.60	G		C																		
			3	2	5-6	18.16	G		C																		
		NN19a		3	5-6	19.66	G		C	R																	
					CC	26.20	G		A	R							R										
			1		CC	35.80	G		A	C			R				R										
Pliocene	late	NN18	2	1	5-6	35.86	G		C	C	R	R		R													
				3	5-6	38.86	G		R	C	C																
				5	5-6	41.86	G		R	C	C				R												
					CC	45.40	G		R	C	C						R										
		NN17	3	1	5-6	45.46	G		R	R	C	R															
		NN16		2	5-6	46.96	G		R	R	C	C	R	R													
				3	5-6	48.46	G		R	C	C	C	R	R													
				4	5-6	49.96	G		R	C	C	C	R	R													
				5	5-6	51.46	G		C	C	C	C	R	R													
			4		CC	64.60	G		C	C	C	C	R	C			R										
			5		CC	74.20	G		C	C	R	C	R	R													
			6		CC	83.80	G		C	C	R	R	R	R													
			7	3	0-1	86.81	G		R	C	R	R	R	R			R										
	early	NN15		4	0-1	88.31	G			C	R	R	C	R	R		R										
				5	0-1	89.81	G			C	R	R	C	R	R		R										
				6	0-1	91.31	G			R	R	R	C	R	C		R										
					CC	93.40	G			R	C	R	C	R	C		R										
			8		CC	103.00	G			R	C	R	C	R	C		R										
			10		CC	122.20	G			R	R	R	R	C	C		R										
			11	7	0-1	131.21	G			R	R	R	R	R	C		R										
		NN14			CC	131.80	G			R	R	R	R	R	C	R	R		R								
			12		CC	141.40	G			R	C	R	R	C	C	R	R		R								
			13		CC	151.00	G			R	C	C	R	C	C	R	R		R								
			14	1	0-1	151.01	G			R	C	R	R	C	A	R	R		R								
		NN13		2	0-1	152.51	F			R	C	R		C	A	R	R		R								
					CC	160.60	F			R	C	R		R	A	R	R		R								
			15		CC	170.20	F			R	R	R		R	A		R		R								
			16	2	5-6	171.76	F			R	R	R		R	A		R		R								
		NN12		3	5-6	173.26	F			R	R	R		C	A				R								
					CC	179.80	F			R	R	C		C	A				R								
			17		CC	189.40	F			R	C	C		C	A				R								
			18	5	5-6	195.46	F			R	C	C		C	A				R								

Depth below seafloor (m)	Additional species																																
	Amaurolithus delicatus	Calcidiscus leptoporus	Catinaster calyculus	Ceratolithus cristatus	Ceratolithus telesmus	Coccolithus carteri	Coccolithus mopelagicus	Coccolithus pelagicus	Coronocyclus nitescens	Crenalithus doronicoides	Cyclicargolithus abisectus	Cyclicargolithus floridanus	Discoaster bellus	Discoaster berggrenii	Discoaster deflandrei	Discoaster neohamatus	Discoaster tamalis	Discoaster tridenus	Discoaster triradiatus	Discoaster variabilis	Discolithina japonica	Discosphaera tubifera	Emiliania annula	Gephyrocapsa caribbeanica	Gephyrocapsa oceanica	Hayaster perplexus	Helicosphaera ampliaperta	Helicosphaera carteri	Helicosphaera euphratis	Helicosphaera hyalina	Helicosphaera intermedia	Helicosphaera sellii	Helicosphaera wallichii
0.06		A			R			R		A											R	R		C	C			C		C		R	
1.55		C			R	R		R		C											R			C	C			R		R		R	
3.05		C				R		R		C											R			C	C			R		R		R	
4.55		C			R	R		R		A											R			C	C			R		R		R	
6.06		C				R		R		A											R			A	C			R		R		R	R
7.00		C			R			R		A											R			A	C			R		R		R	
10.06		C						R		A											C		R	C	C			C		C		R	
16.60		C						R		A											R		R	C	R			C		C		R	
18.16		C			R	R		R		A											C		R	C	C			C		C		R	
19.66		C			R			R		A											C		R	C	C			C		C		R	
26.20		C			R			R		A											R		R	C	R			C		R		R	
35.80		C				R		C		C											R	R	R	R				R		R		R	
35.86		C						C		A									R	R	R		R	R				C				R	
38.86		C						C		A									R		R		R					C				R	
41.86		C		R		R		A		A									R		R		R					C				R	
45.40		C						A		A									R		R		R					C				R	
45.46		C				R		A		A											R		R			R		C				C	
46.96		R						C		A											R		R					R				R	
48.46		C						C		A											R		R					C				R	
49.96		C						C		A							R				R		R					C				R	
51.46		C						A		A							R				R		R					C				R	
64.60		C						C		A							C				R		R					C				R	
74.20		C						R		A							R				R		R					C				R	
83.80		C				R		R		A							C			R	R		R					C				R	
86.81		R						R		C							R			R	R		R			R		R				R	
88.31		R						R		A							R			R	R							C				C	
89.81		R						R		C							R			R	R							C				R	
91.31		R						R		C							R			R	R							R				R	
93.40		R						R		C							R			R	R					R		R				R	
103.00		C						R		C							R			R	R							C				R	
122.20		C						R		C								R		R	R							R				R	
131.21	R	C						R		C								R		R								R				R	
131.80	R	C						R		C								R		R								R				R	
141.40	R	C						R		C								R		R								R					
151.00	R	C						C		C								R		R								C					
151.01	R	C						C		C								R		R								R					
152.51	R	C						R		R								R		R								R					
160.60	R	C						R		R								R		R								R					
170.20	R	C						C		R								R		R								R					
171.76	R	C						C		R								R		R								R					
173.26	R	C						A		R								R		R								R					
179.80	R	C						C		R								R		R								R					
189.40	R	C						C		R								C		R								R					
195.46	R	C						C		R								C		R								R					

Depth below seafloor (m)	Additional species																						
	Lithostromation perdurum	Oolithotus fragilis	Pontosphaera discopora	Rhabdosphaera clavigera	Rhabdosphaera procera	Scapholithus fossilis	Scyphosphaera apsteinii	Scyphosphaera conica	Scyphosphaera globulata	Scyphosphaera intermedia	Scyphosphaera magna	Scyphosphaera pulcherrima	Scyphosphaera recurvata	Sphenolithus abies	Sphenolithus moriformis	Sphenolithus neoabies	Syracosphaera pulchra	Thoracosphaera heimii	Thoracosphaera saxea	Triquetrorhabdulus rugosus	Umbellosphaera irregularis	Umbilicosphaera cricota	Umbilicosphaera sibogae
0.06			R	R	C	C							R				R	R	R		C	R	R
1.55			R	R	R	R							R				R	R	R		R	R	R
3.05			R	R	R	R							R				R	R	R		R	R	R
4.55		R	R	R	R	R							R				R	R	R		R	R	R
6.06		R	R	R	R	R							R				R	R	R		R	R	R
7.00		R	R	R	R	R							R				R	R	R		R	R	
10.06		R	C	R	R	R							R				R	R	R		R	R	
16.60		R	R	R	R	C	R						R				R	R	R		R	R	
18.16		R	R	R	R	R	R						R				R	R	R		R	R	
19.66		R	R	R	R	R	R				R		R				R	R	R		R	R	
26.20		R	R	R	R	R	R						R				R	R	R		R	R	R
35.80			R	R	R	R						R	R			R	R	R	R			R	
35.86			R	R	R	R						R	R				R	R	R			R	
38.86			R	R	R	R						R	R				R		R			R	
41.86			R	R	R	R						R	R				R		R			R	
45.40			R		R	R						R	R				R		R			R	
45.46			R		R	R						R	R				R		R			R	
46.96			R		R	R						R	R				R					R	
48.46			R		R	R						R	R				R					R	
49.96			R		R	R			R			R	R				R					R	
51.46			R		C	R						R	R				R					R	
64.60			R		C	R		R		R		R	R				R					R	
74.20			R		R	R		R		R		R	R				R					R	
83.80			R		R	R				R			R			R	R					R	
86.81			R		R	R				R			R	R		R	R					R	
88.31	R		R		R				R	R			R	R		R	R					R	
89.81			R		R					R				R		R	R					R	
91.31			R		R					R				R		C	R					R	
93.40			R		R					R		R		R		C	R					R	
103.00			R		R					R				R		C						R	
122.20			R		R					R				C		A						R	
131.21			R		R					R				C		A						R	
131.80			R		R	R			R	R		R		C		A						R	
141.40			R		R				R	R				C		A						R	
151.00			R		R				R	R		R		C		A						R	
151.01			R						R	R		R		C		A						R	
152.51			R						R	R		R		C		A						R	
160.60			R			R			R	R				C		A						R	
170.20			R						R	R				A		A						R	
171.76									R	R				A		A						R	
173.26					R				R	R		R		A		A						R	
179.80										R		R		A		A						R	
189.40										R		R		C		A						R	
195.46										R		R		C		A						R	

Miocene	late	NN11b		6	5-6	196.96	F	R	C	C	C	A	R	R									R	C			C		R							C	R		R			R	R	C		C			R
			B 22		CC	203.80	F	R	R	R	R	A	R	R									R	C			C		C							R	R	R	R					C		A			R
			24		CC	223.00	F	R	R	R	R	C	R	R									R	C			C		R				R			R	C		R					C		C			R
			26		CC	242.20	F	R	R	R	R	A	R	R									R	C			A		R							R	C		R				R	A		A			R
			28		CC	259.10	F	R	R	R	R	A	R	R									R	R			C		R								R		R					A		A			R
			30	3	5-6	271.76	F	R	R	R	R	A	R	R										R			C		R				R				R		R				R	A		A			R
		NN11a		4	5-6	273.26	F	R	R	R	R	A	R											R			A		R								C		R			R	R	A		A			R
				5	5-6	274.76	F	R	R	R	R	A	C											R			A		R								C		R			R		A		A	R		R
			32		CC	297.50	F	R	C	R		A	C											R			A		R				R				R		C				R	A		A	R		R
			34		CC	316.70	F	R	C	R		C	C											R			A		R			R	R	R	R		R		R	R				C		C			R
			35	5	5-6	322.76	F	R	C	R		R	R											R			C		R			R		R	R		R		C					C		C	R		R
		NN10			CC	326.30	F	C	C	R		R												R			C					R			R		R		R	R				R		R		R	R
			36		CC	335.90	F	R	C	R		C												R			R					R		R	R		R		R					R		R	R		R
			37		CC	345.50	F	R	C	R		A												R			R					R			R		R		R	R				R		R	R		R
			38	5	5-6	351.56	F	R	C			C												R			R					R			R		R		R					R		R	R		R
	middle	NN9			CC	355.10	F	R	C			A			R									R	R		C					R			R		R		R					R		R	R		R
			39		CC	364.70	F	C	R			A			C	R								C	R		C					R			R		R		R					R		R	R		R
			40		CC	374.30	F	C	R			A			R	R								R	R		C					R			R		R		R					R		R	R		R
		NN8	41	5	5-6	380.36	F	R	R			C				R								R			C					R			R		R		R					R		R	R		R
					CC	383.90	F	C	R			C				R		R						R			C										R		R					R		R	R		R
		NN7	42	1	5-6	383.96	F	R	R			A						R						R		R	C							R			R		R					R		R	R		R
					CC	393.50	F	C	R			A					R	C						C		C	A							R			R		R					R	R	C	R		R
			43		CC	403.10	F	R	R			A					R	C						C		C	C			R	C			R			R		R					R	R	R	R		R
			44		CC	412.70	F	R	R			C					R	R						R		C	C			R	C			R			R		R					R	R	R	R		R
			45	1	5-6	412.76	F	R				C					R	R						R		C	C			R	C			R			R		R					R	R	R	R		R
		NN6		3	5-6	415.76	F	R				C						C						R		C	C			R	R			R			R		R					R	R	R	R		R
					CC	422.30	F	C				A						C						R		C	C			R	R			R			R		R					R	R	R	R		R
			46		CC	431.90	F	R				C						C						R		R	A			C	C			R			C		R						C	R			R
			47	3	5-6	434.96	F	R				C						C						R		R	C			C	C			R			R		R						R	R			R
		NN5		5	5-6	437.96	F	R				C						C	R					R		R	C			R	C			R			R		R						C	R			R
			48		CC	451.10	F	R				R						C	R					R		R	C			R	C			C			R		R						C				
			49		CC	460.70	F	R				R						R	R					R		R	C			R	C			C			R		R						R				
	early	NN4	50	1	5-6	460.76	F	R				R							R							R	A			R	C			C					R		R				C				
				3	5-6	463.76	F	R				R							C							R	C			R	C			A					R						A				
					CC	470.30	F	R				R							C					R		R	C	R		R	C			A					R						C				
		NN3	51	1	5-6	470.36	F	R				R								R						R	C	R		R	C			A				R	R	R					A				
					CC	479.90	F	R				C								R	R					R	C	R		C	C			C					R						C				
			52	5	5-6	485.96	F	R				R								R	R					R	C	R		R	R			C					R	R	R				A				
		NN2			CC	489.50	F	R				R								R	R	R				R	C	R		R	C			C					R	R					C				
			53	1	5-6	489.56	F					R									R	R				R	C	R		R	C			C					R						C				
		NN1		3	5-6	492.56	F					R										R				R	C	R		R	C			C					R						C				
				5	5-6	495.56	F					R										R				C	A	R		R	C			A					R						C				
					CC	499.10	F					R										R				C	A	R		R	C			A					R						C				

6 cm and 590B-38,CC and the lower/middle Miocene boundary is placed between Samples 590B-49,CC and 590B-50-1, 5–6 cm. The range of *Discoaster quinqueramus* from Samples 590A-18-6, 5–6 cm through 590B-35-5, 5–6 cm defines Zone NN11. The first occurrence of *Amaurolithus primus* in Sample 590B-30-3, 5–6 cm subdivides this zone into Subzones NN11b and NN11a. The range of *D. hamatus* from Samples 590B-38,CC through 590B-40,CC places these samples in Zone NN9 and Samples 590B-35,CC through 590B-38-5, 5–6 cm in Zone NN10. The first occurrences of *Catinaster coalitus* in Sample 590B-41,CC and *D. kugleri* in Sample 590B-45-1, 5–6 cm place Samples 590B-41-5, 5–6 cm and 590B-41,CC in Zone NN8 and Samples 590B-42-1, 5–6 cm through 590B-45-1, 5–6 cm in Zone NN7. The interval from Sample 590B-45-3, 5–6 cm to Sample 590B-47-3, 5–6 cm, above the last occurrence of *Sphenolithus heteromorphus* in Sample 590B-47-5, 5–6 cm, belongs in Zone NN6. The interval from Sample 590B-47-5, 5–6 cm to 590B-49,CC, the first occurrence of *D. exilis,* is placed in Zone NN5. Although *Helicosphaera ampliaperta* is normally absent in samples from the western Pacific, a single specimen was observed in Sample 590B-51-1, 5–6 cm. The last occurrence of *S. belemnos* in Sample 590B-51-1, 5–6 cm places Core 50 in Zone NN4. The last occurrence of *Triquetrorhabdulus carinatus* in Sample 590B-52,CC and the first occurrence of *Discoaster druggii* in Sample 590B-53-1, 5–6 cm place Samples 590B-51-1, 5–6 cm through 590B-52-5, 5–6 cm in Zone NN3, Samples 590B-52,CC and 590B-53-1, 5–6 cm in Zone NN2, and Sample 590B-53-3, 5–6 cm through 590B-53,CC in Zone NN1.

Site 591

Holes 591, 591B

Site 591 is located on a spur of Lord Howe Rise (31°35.06′S, 164°26.92′E) and lies on the subtropical divergence at a water depth of 2131 m below sea level. Three holes were drilled at Site 591. Hole 591 was cored to a depth of 283.1 m and 31 cores were taken. Hole 591A, a duplication of Hole 591, was cored to a depth of 284.6 m and 30 cores were taken. Hole 591B was washed down to a depth of 270.6 m and then cored to a depth of 500.4 m. Twenty-four cores were taken. Core recovery was good throughout Hole 591 and most of Hole 591A and fair throughout Hole 591B.

In order to obtain a complete stratigraphic section, 31 cores from Hole 591 and 22 cores from Hole 591B were examined for calcareous nannoplankton. Species diversity is good throughout Site 591 and reworking is minimal. Preservation of calcareous nannoplankton is good throughout Cores 1–16 of Hole 591 and fair below this level. Hole 591B terminated in the early Miocene Zone NN4 and all of the overlying Neogene and Quaternary nannoplankton zones are recognized (Table 7).

Quaternary

The Quaternary includes Samples 591-1-1, 4–5 cm through 591-6-5, 3–4 cm. The occurrence of *Emiliania huxleyi* in Samples 591-1-1, 4–5 cm and 591-1-3, 4–5 cm places these samples in Zone NN21. The last common occurrence of *E. ovata* in Sample 591-2-5, 3–4 cm marks the top of Subzone NN19b. A rare occurrence of *E. ovata* above this level is interpreted as reworking. The intervening samples belong in Zone NN20. The last consistent occurrence of *Calcidiscus macintyrei* in Sample 591-5-5, 3–4 cm marks the top of Subzone NN19a. A single occurrence of *C. macintyrei* in Sample 591-1,CC is interpreted as reworking.

Pliocene

The Pliocene includes Samples 591-6,CC through 591-24-1, 3–4 cm. The lower/upper Pliocene boundary is located between Samples 591-12-3, 3–4 cm and 591-12-5, 3–4 cm. The top of Zone NN18 is marked by the last occurrence of *Discoaster brouweri* in Sample 591-6,CC. Zone NN18 extends down to the last occurrence of *D. pentaradiatus* in Sample 591-8-3, 3–4 cm. This sample is placed in Zone NN17. The last occurrence of *D. surculus* in Sample 591-8-5, 3–4 cm down to the last consistent occurrence of *Reticulofenestra pseudoumbilica* in Sample 591-12-5, 3–4 cm places Sample 591-8-5, 3–4 cm through 591-12-3, 3–4 cm in Zone NN16. Two occurrences of *R. pseudoumbilica* above this level are interpreted as reworking. The interval from the last occurrence of *Amaurolithus tricorniculatus* in Sample 591-17-1, 21–22 cm through Sample 591-20,CC, the first occurrence of *Discoaster asymmetricus*, is placed in Zone NN14. The next two samples, down to the first occurrence of *Ceratolithus rugosus* in Sample 591-21-5, 3–4 cm, belong in Zone NN13. The interval from Sample 591-21,CC to Sample 591-24-1, 3–4 cm, above the last occurrence of *D. quinqueramus* in Sample 591-24-3, 3–4 cm, is placed in Zone NN12.

Miocene

The Miocene ranges from Sample 591-24-3, 3–4 cm through Sample 591B-24,CC. Hole 591B penetrated just into the early Miocene Zone NN4. The middle/upper Miocene boundary lies between Samples 591B-8,CC and 591B-9-2, 4–5 cm and the lower/middle Miocene boundary lies between Samples 591B-23,CC and 591B-24-1, 3–4 cm. The range of *Discoaster quinqueramus*, down through Sample 591B-4,CC, defines Zone NN11. The first consistent occurrence of *Amaurolithus primus* in Sample 591-28-3, 3–4 cm marks the boundary between Subzones NN11b and NN11a. The interval from Sample 591B-5-1, 3–4 cm through Sample 591B-8,CC is placed in Zone NN10. The range of *D. hamatus*, from Sample 591B-9-2, 4–5 cm through Sample 591B-11-1, 4–5 cm, places these samples in Zone NN9. The occurrence of *Catinaster coalitus* in Sample 591B-11,CC places this sample in Zone NN8. The next two samples belong in Zone NN7, based on the first occurrence of *D. kugleri* in Sample 591B-12,CC. Zone NN6 includes Samples 591B-13-1, 3–4 cm through 591B-18-3, 3–4 cm. The interval from the last occurrence of *Sphenolithus heteromorphus* in Sample 591B-18-5, 3–4 cm down to the first occurrence of *D. exilis* in Sample 591B-23,CC is placed in Zone NN5. Core 24 belongs in Zone NN4.

Table 7. Nannoplankton occurrences, Holes 591 and 591B.

Age		Zone	Core	Section	Interval (cm)	Depth below seafloor (m)	Preservation	Index species																Additional species																																																			
								Emiliania huxleyi	Emiliania ovata	Calcidiscus macintyrei	Discoaster brouweri	Ceratolithus rugosus	Discoaster pentaradiatus	Discoaster asymmetricus	Discoaster surculus	Reticulofenestra pseudoumbilica	Amaurolithus primus	Amaurolithus tricorniculatus	Discoaster quinqueramus	Discoaster hamatus	Discoaster exilis	Catinaster coalitus	Discoaster kugleri	Sphenolithus heteromorphus	Amaurolithus delicatus	Calcidiscus leptoporus	Ceratolithus cristatus	Ceratolithus telesmus	Coccolithus carteri	Coccolithus miopelagicus	Coccolithus pelagicus	Coronocyclus nitescens	Crenalithus doronicoides	Cyclicargolithus abisectus	Cyclicargolithus floridanus	Discoaster bellus	Discoaster berggrenii	Discoaster deflandrei	Discoaster moorei	Discoaster neohamatus	Discoaster stellulus	Discoaster tamalis	Discoaster tridenus	Discoaster triradiatus	Discoaster variabilis	Discolithina japonica	Emiliania annula	Gephyrocapsa caribbeanica	Gephyrocapsa oceanica	Hayaster perplexus	Helicosphaera carteri	Helicosphaera euphratis	Helicosphaera hyalina	Helicosphaera intermedia	Helicosphaera sellii	Oolithotus fragilis	Pontosphaera discopora	Rhabdosphaera clavigera	Rhabdosphaera procera	Scapholithus fossilis	Scyphosphaera amphora	Scyphosphaera cyclindrica	Scyphosphaera globulata	Scyphosphaera intermedia	Scyphosphaera magna	Scyphosphaera pulcherrima	Scyphosphaera recurvata	Sphenolithus abies	Sphenolithus moriformis	Sphenolithus neoabies	Syracosphaera pulchra	Thoracosphaera saxea	Triquetrorhabdulus rugosus	Umbellosphaera irregularis	Umbilicosphaera cricola	Umbilicosphaera sibogae
Quaternary		NN21	1	1	4-5	0.05	G	C																		A		R	R		R		A												R		C	C		C		R		R	R	R	C	C	C											C	R		R	C	C
				3	4-5	3.05	G	R	R																C		R	R		R		C	R											R		C	C		C		R		R	R	R	C	R	C											C	R		R	C	R
		NN20			CC	3.40	G			R						R										C		R	R		R		C												R		R	R		C		R		R		R	R	R	R										R	C	R		R	R	R
			2	3	3-4	6.44	G																		C	R		R		R		A												R		R	R		C		R		R		R	R	R	R											C			R	R	R
		NN19b		5	3-4	9.44	G		C																R			R		R		A												R	R	R			R		R		R		R	R	R	R											C			R	R	
			3		CC	22.60	G		C							C										C	R		R		R		A												R		R			C		R		R		R	R	R	R											R				R	
			4		CC	32.20	G		C																C			R		R		C												R	C	C			C		R		R		C	R	R	R											R				R	
			5	3	3-4	35.24	G		C																C			R		R		C												R	C	C			C		R		R		C	R	R	R							R				R				R	
		NN19a		5	3-4	38.24	G		C	R															C			R		R		C												R	C				C		R		R		C	R	R	R							R				R	R			R	
			6	5	3-4	47.84	G		C	C															C			R		C		A												R	C				C		R		R		R	R	R	R											C				R	
Pliocene	late	NN18			CC	51.40	G		C	C	R														C			R		C		A										R	R	R	C				C		R		R		R	R	R	R											C				R	
			7		CC	61.00	G		C	R	C	R													C			C		C		A												R	C				C				R		R	R	R	R						R					C	R			R	
			8	1	3-4	61.04	G		C	C	C	R													C			R		C		A												R	R				C				R		R	R	R	R						R	R				R	R			R	
		NN17		3	3-4	64.04	G		C	C	C	R	R	R											C			R		C		C												R	R			R	C				R		R		R	R						R	R				R	R			R	
		NN16		5	3-4	67.04	G		C	C	C	R	C	R	R										C			R		C		C												R	R				C				R		R		R	R						R					R				R	
			9		CC	80.20	G		C	C	C	R	C	C	C										C			R		C		C								R			R	R	R				C				R		R		R													C				R	
			10		CC	89.80	G		R	C	C	R	C	C	C										C			R		C		C								R			R	R	R				C				R		R		R													C				R	
			11		CC	99.40	G			C	C	R	C	C	C										C			R		C		C								R			R	R					C				R		R		R													C				R	
			12	3	3-4	102.44	G			C	C	R	C	C	C										C			R		C		C								C			R	R					C				R		R		R					R		R	R				C	R			R	
	early	NN15		5	3-4	105.44	G			C	C	R	C	C	C	R									C			R		R		C								C			R	R					C				C		C		R					R		R					R				R	
			13		CC	118.30	G			C	C	R	C	C	R	A									R	C					C		C												R	R				R	C				C		C		R		R			R	R	R	R	C		C	R				R	
			14		CC	127.60	G			C	C	R	C	R	C	A									C					C		C												R						C				R		R		R		R	R		R			R	C		C					R	
			15		CC	136.90	G			C	C	R	C	R	C	A									C					C		C												R						C				R		R		R		R	R	R	R		R		C		C					R	
			16		CC	146.20	G			C	C	R	C	R	R	A	R								R	C					R		C												R						C				R		R		R				R	R				C		C					R	
		NN14	17	1	21-22	146.24	G			C	C	R	C	R	C	C	R	R							R	C					R		C												R						C				R		R		R	R				R			R	C		C					R	
					CC	155.50	G			R	C	R	C	R	C	A	R	R							R	C					R		C												R						C				R		R									R	C		C					R	
			18		CC	164.80	G			R	C	R	C	R	C	A	R	R							R	C					R		C												R					R	C				R		R									R	C		C					R	
			19		CC	174.30	F			R	C	R	C	R	C	C	R	R							R	C					C		A												R						R				R													R	C		C					R	
			20		CC	183.80	F			R	C	R	C	R	C	C	R	R							R	C					C		A												R						R				R													R	C		C			R		R	
		NN13	21	1	3-4	188.84	F			R	C	R	C		C	C	R								R	R					C		C									R		R						R				R					R				R				C		C			R		R	
				5	3-4	189.84	F			R	C	R	C		C	C	R									C					C		C									R		R						R				R													C		C			R		R	
		NN12			CC	193.30	F			R	R		R		R	C	R									C					C		C									R		R						R				R											R		C		C			R		R	
			22		CC	202.70	F			R	R		R		C	C	R									R					C		A									R		R						R				R									R			R	A		A			R		R	
			23		CC	212.10	F			R	C		R		C	C	R									R					C		C									R		R						R				R									R		R	R	A		A			R		R	
			24	1	3-4	212.14	F			C	R		R		R	C	R									C					C		C									C		R						R	R			R													C		C			R		R	
Miocene	late	NN11b		3	3-4	215.14	F			C	R		R		R	C	R		R						C					C		C									R		R						R				R													C		C			R		R	
			25		CC	231.10	F			R	C		R		R	C	R		R					R	C					C		A									R		R						R				R									R			R	C		C			R		R	
			26		CC	240.70	F			R	R		R		R	C	C		R						C					C		C									R		R						R																	R	C		A			R		R	
			27		CC	250.30	F			R	R		R		R	C	R		R						C					C		C									R		R						R												R			R	C		C			R		R	
			28	3	3-4	253.34	F			R	R		R		R	C	R		R						R					C		C									R		R						R																C		C			R		R	
		NN11a		5	3-4	256.34	F			R	R		R			C			R						R					C		C												R						R														R	C		C			R		R	
			29		CC	269.30	F			R	R		R		R	C	R		R						R					C		A												R						R			R													C		C			R		R	
			30		CC	274.30	F			R	R		R			C			R						R					C		C				R							R						R														R	C		C			R		R	
			31		CC	283.10	F			R	R		R			C			R						R					C		R				R							R						R															C		C			R		R	
			B 3		CC	299.40	F			R	R		R		R	C			R						R					C		R			R	R							R						R															C		C			R		R	
			4		CC	308.80	F			R	C		R			C			R						R					A		R			R	R		R					R						C	R													C		C			R		R	
		NN10	5	1	3-4	308.85	F			R	C		R			C									R					C		R		R		R		R					R						R															C		C			R		R	
					CC	318.20	F			R	C		R			C									R					C		R		R		R		R	R				R						R															C		C			R		R	
			6		CC	327.60	F			R	C		R			A									R					R		R		R		R		C	R				R						R															R		C			R		R	
			7		CC	337.20	F			R	C		R			A									R					R					R		R		C					R						R															R		R			R		R	
			8		CC	346.80	F			R	R					A									R					C					R		R	R	C					R						R															R		R			R		R	
	middle	NN9	9	2	4-5	348.35	F			R	R					A				R					R					C					R		R		C					R						R															R		R			R		R	
					CC	356.40	F			R	R					A				R					R					C					R		R	R	R	R				R						R															R		R			R		R	
			10		CC	366.00	F			C	R					A				R					R					C					R		R	R	R	R				R						R															R		R			C		R	
			11	1	4-5	366.05	F			C	R					A				C					R					C							R		R	R				R						R															C		C			R		R	
		NN8			CC	375.60	F			C	R					A					R	R			R					C							R							C						R															C		C			R		R	
		NN7	12	1	3-4	375.64	F			C	R					A					R		R		R					C							R	R						C						R															C		C			R		R	
					CC	385.20	F			C	R					A					R		R		R					C							R							C						R															R		R			R			
		NN6	13	1	3-4	385.24	F			C	R					A					R				R				R	C							R							R						C	R													R		R			R			
					CC	394.80	F			C	R					A					C				R				R	C							C							R						C															C		C			R			
			14		CC	404.40	F			R	R					A					C				R				R	C							C							R						R															R	R	R			R			
			15		CC	414.00	F			R						C					C					R				R	C			R	R			C							R						R															R	R	R			R			
			16		CC	423.60	F			R						C					C					R				R	C			C	C			R	R						R						R															R	R	R			R			
			17		CC	433.20	F			R						C					R					R				R	C	R		C	C			R							R						R	R													R	R	R			R			
			18	3	3-4	436.24	F			R						C					R					R				R	C	R		C	C			R							R						R															R	R	R						
		NN5		5	3-4	439.24	F			C						C					R			R		R				R	C	R		C	C			R							R						R																C	R						
					CC	442.80	F			C						C					R			C		R				R	C	R		C	C			R							R						R																C	R						
			19		CC	452.40	F			C						C					R			C		R				R	C	R		C	C			R							R						R																C	R						
			20		CC	462.00	F			C						C					R			C		R				R	C	R		C	C			R							R						R																C							
			21		CC	471.60	F			C						C					R			C		R				R	C	R		C	C			C							R						R	R														C							
			22		CC	481.20	F			C						C					R			C		R				R	C	R		C	C			C													R	R														C							
			23		CC	490.80	F			R						C					R			C						R	R	R		C	C			C													R																C							
	early	NN4	24	1	3-4	490.84	F									C								C						R	R	R		C	C			C													R																C							
					CC	500.50	F									C								C						R	R	R		C	C			C													R																C							

Site 592

Hole 592

Site 592 is located on the southern Lord Howe Rise (36°28.40′S, 165°26.53′E) at a water depth of 1098 m below sea level. Hole 592, which lies in the temperate water mass, was cored to a depth of 388.5 m (late Eocene Zone NP18). Forty-one cores were taken and recovery was good throughout the hole.

The major regional unconformity of the southwest Pacific was encountered within Core 33 at a depth of 306 m. It separates lower Oligocene sediment (Zone NP22) from immediately overlying lower Miocene sediment (Zone NN2). Except for the boundary between the early Pliocene Zones NN13 and NN12, the Neogene and Quaternary nannoplankton zonation is complete down to the unconformity (Table 8). The preservation of calcareous nannoplankton in Hole 592 is good in Cores 1–4

Table 8. Nannoplankton occurrences, Hole 592.

Age		Zone	Core	Section	Interval (cm)	Depth below seafloor (m)	Preservation	Index species																				Additional species																																																													
								Emiliania huxleyi	Emiliania ovata	Calcidiscus macintyrei	Discoaster brouweri	Discoaster pentaradiatus	Discoaster surculus	Discoaster asymmetricus	Reticulofenestra pseudoumbilica	Amaurolithus tricorniculatus	Amaurolithus primus	Discoaster quinqueramus	Discoaster hamatus	Discoaster exilis	Catinaster coalitus	Discoaster kugleri	Sphenolithus heteromorphus	Sphenolithus belemnos	Discoaster druggii	Triquetrorhabdulus carinatus	Reticulofenestra umbilica	Amaurolithus amplificus	Amaurolithus delicatus	Calcidiscus leptoporus	Ceratolithus cristatus	Ceratolithus rugosus	Ceratolithus telesmus	Chiasmolithus altus	Chiasmolithus sp.	Coccolithus carteri	Coccolithus miopelagicus	Coccolithus pelagicus	Coronocyclus nitescens	Crenalithus doronicoides	Cyclicargolithus abisectus	Cyclicargolithus floridanus	Dictyococcites bisectus	Discoaster bellus	Discoaster berggrenii	Discoaster challengeri	Discoaster decorus	Discoaster deflandrei	Discoaster neohamatus	Discoaster perclarus	Discoaster sp.	Discoaster tamalis	Discoaster tridenus	Discoaster triradiatus	Discoaster variabilis	Discolithina japonica	Discolithina sp.	Emiliania annula	Gephyrocapsa caribbeanica	Gephyrocapsa oceanica	Hayaster perplexus	Helicosphaera carteri	Helicosphaera euphratis	Helicosphaera hyalina	Helicosphaera intermedia	Helicosphaera sellii	Isthmolithus recurvus	Lithostromation perdurum	Oolithotus fragilis	Pontosphaera discopora	Rhabdosphaera clavigera	Rhabdosphaera procera	Scapholithus fossilis	Scyphosphaera globulata	Scyphosphaera intermedia	Scyphosphaera magna	Scyphosphaera pulcherrima	Scyphosphaera recurvata	Sphenolithus abies	Sphenolithus moriformis	Sphenolithus neoabies	Syracosphaera pulchra	Thoracosphaera saxea	Triquetrorhabdulus rugosus	Umbellosphaera irregularis	Umbilicosphaera cricota	Umbilicosphaera sibogae	Zygrhablithus bijugatus
Quaternary		NN21	1	1	3-4	0.04	G	A																						C	R		R			R		C		A																R			C	C		C		R		R			R		R	R	C									C	R		R	R	R	
				3	3-4	3.04	G	R																						C						R		C		A																R			C	C		C		R		R			R	R	R	R	C									C	R		R	R	R	
		NN20			CC	4.50	G																							C						R		C		A																R			A	C		C		R		R			R	R	R	R	C									R	R		R	R	R	
		NN19b	2	1	3-4	4.54	G		R																					C						R		C		A																R			A	C		C		R		R			R	R	R	R	C									C	R		R	R		
				3	3-4	7.54	G		A																					C						R		C		A																R		C	C	C		C		R		R			R	R	R	R	C									R	R		R	R		
				5	3-4	10.54	G		A																					C						R		R		A																R		R	R	R		C		R		R			R	R	R	R	R					R				R	R		R	R		
			3	1	3-4	14.14	G		A																					C	R					R		R		A																R		C	R	R		C				R			R	R	R	R	R			R		R				R			R	R		
		NN19a		2	3-4	15.64	G		C	R																				C						R		A		C																R		R	R	R		C				R			R	R	R	R	R					R				R			R	R		
				5	3-4	20.14	G		A	C																				C						R		C		C																R		C	R			C				C			R	R	R	R	R					R				R			R	R		
Pliocene	late	NN18		6	3-4	21.92	G		A	A	R																			C						R		A		C														R		R		C	R			C				R			R	R	R	R	R					R				R			R	R		
					CC	23.70	G		A	A	R																			C						R		A		C														R		R		C	R			C				R			R	R	R	R	R					R				C			R	R		
			4	1	3-4	23.74	G		A	A	C																			C						R		A		C														R		R		C				C				R			R	R	R	R	R					R				C			R	R		
		NN17		2	3-4	25.24	G		A	A	C	R																		C	R					R		A		A														R		R		R				C				R			R	R	R	R	R				R	R				C			R	R		
		NN16		3	3-4	26.74	G		C	C	C	R	R																	C						R		C		A																R		R				R				R				R		R	R				R	R				R			R	R		
				4	3-4	28.24	G		C	R	R	R	R	R																C						R		C		A																R		R				R				C				R		R	R				R	R				R			R	R		
				6	3-4	31.24	G		C	C	R	R	C	R																C						R		A		A														R	R	R		R				C				R				R		R	R					R				C				R		
				7	3-4	32.74	G		C	C	R	R	R	R	R															C						R		A		A															R	R		R				C				R				R		R	R					R				R				R		
					CC	33.30	G		C	C	C	C	C	R	R															C						R		A		A												R			R	R		R				C				R				R		R	R		R		R	R				C				R		
			5	3	3-4	36.34	F		R	C	C	R	C	R	R															C						R		A		A												R		R	R	R		R				R				R				R		R	R		R			R				R				R		
				6	3-4	40.84	F		R	C	R	R	C	R	R															C						R		A		A												R		R	R	R		R				R				R				R		R	R		R		R	R				R				R		
					CC	42.90	F		R	C	R	R	R	R	R															C		R		R		R		A		A												R			R	R		R				C				R				R		R	R	R	R	R	R	R				R				R		
			6	3	3-4	45.94	F		R	C	R	R	R	R	R															C						R		C		A												R			R	R						C				R				R		R	R		R			R				R				R		
	early	NN15			CC	52.50	F		R	C	R	R	R	R	C															C						R		C		A												C	R		R	R						C				R				R		R	R		R		R	R	R		R	R				R		
			7	1	3-4	52.54	F		R	R	R	R	R	R	C															C		R				R		C		A												R			R	R						R				R				R		R	R		R			R	R		R	R				R		
					CC	62.10	F			R	R	R	R	R	C															C						R		C		A														R	R						R				R						R			R			R	C		C	R				R		
			8	3	3-4	65.14	F			R	R	C	C	R	C															C						R		C		A														R	R						C				R						R			R		R	R	C		C	R				R		
				5	3-4	68.14	F			R	R	R	R	R	C															C								C		A														R	R						C				R						R			R			R	C		C	R				R		
		NN14			CC	71.70	F			R	C	C	C	R	C	R	R											R	R	C								C		A														R	R						R				R						R			R			R	C		C	R				R		
			9	3	3-4	74.74	F			R	C	C	C	R	C	R	R											R	R	C								C		A														R	R						R				R		R				R			R		R	R	C		C	R				R		
					CC	81.30	F			C	C	C	C	R	C	R	C												R	C		R						C		A													R	R	R	R				R	C				R						R		R	R		R	R	C		C	R				R		
			10	1	3-4	81.34	F			C	R	R	R	R	C	R	R												R	C		R						C		A						R							R		R	R	R						C				R		R				R			R		R	R	C		C	R				R		
				3	3-4	84.34	F			R	R	R	C	R	C	R	R												R	C		R						C		A														R	R						C				R						R			R		R	R	C		C	R				R		
					CC	90.90	F			C	C	R	C	R	R		R													R								C		A														R	R						C										R			R			R	C		C					R		
			11		CC	100.50	F			R	C	C	R	R	A															C								C		A						R	R								C	R						C										R			R		R	R	A		A					R		
			12	5	3-4	106.54	F			R	R	C	R	R	A															R								R		C							R								R	R						R										R					R	A		A					R		
					CC	110.10	F			R	R	R	R	R	C		R													R								R		C														R	R						R										R					R	R	C		A					R		
			13		CC	119.70	F			R	R	R	R	R	C		R													R								C		A												R		R							R															R	C		A					R		
		NN13	14	1	3-4	119.74	F				R	R	R		C	R	R													R								C		C												R		R							R															R	C		C					R		
				3	3-4	122.74	F				R	R	R		C		R													R								C		C												R		R							R													R		R	R	C		C					R		
		NN12		5	3-4	125.74	F			R	R	R	R		C	R	R		R	R										R								R		C												R		R	R						R													R		R	R	C		C					R		
					CC	129.30	F			R	R	R	R		C		R			R										R								R		C											R	R		R							R													R			R	C		C					R		

Miocene	late	NN11b	15	1	3-4	129 34	F		C	R	R	A	R	R	R											R			C		C														R			R					R		R	C		C		R
				3	3-4	132 34	F	R	R	R	R	A	R	R	R											R			C		C												R		R			R					R		R	C		C		R
				5	3-4	135 34	F	R	R	R	R	A	R	C											R	R			R		R												R		C			R					R	R	R	C		C		R
					CC	138 90	F	R	R	R	R	C	R	C	R									R	R	R			C		R													R	C			C					R	R	R	C		C		R
			16	1	3-4	138 94	F	R	R	R	R	C	R	C										R	R	R			C		R														R	R		C					R	R	R	C		A		R
				3	3-4	141 94	F	R	R	R	R	A	C	C	R									R	R	R			C		R														C			C	R				R	R	R	C		A		R
				5	3-4	144 94	F	R	R	R	R	C	R	R	R									R		R			C		C	R						R							R			C	R		R	R	R	R	R	C		A		R
					CC	148 50	F	R	R	R	R	C	R	R	R											R			C		C					R		R							R			R					R	R	R	C		C		R
			17		CC	158 10	F	R	R	R	R	A	R	C	R										R	R			A		R														R			R					R			C		C		R
		NN11a	16	1	3-4	158 14	F	R	R	R	R	A			R											R			A		R														R			R					R		R	C		C	R	R
					CC	167 70	F	R	R	R	R	A			R											R			A		R							R							R			R						R		C		C	R	R
			19	1	3-4	167 74	F	R	R	R	R	A			R											R			A		R									R					R			R					R	R		C		C	C	R
		NN10		3	3-4	170 74	F	R	R	R		A														R			A		R									R					R			R	R							C		C	R	R
			20		CC	186 90	F	R	C	R		C														R			C		R								R	R					R			R								C		C	R	R
	middle	NN9	21	1	3-4	186 94	F	C	R	R		R				R										C			C		R									R					C			C	R						R	C		C	R	R
				3	3-4	189 94	F	R	C	R		R				R										R			C								R			R					C			R								C		C	R	R
				5	3-4	192 94	F	R	R	R		R				R										R			C						R		R			C					C			R								R		C	R	R
					CC	196 50	F	R	R			A				R										C			C						R					R					R			R								R		C	R	R
			22		CC	206 10	F	C	R			A				R	R									C			A						R					R					C			C								C		C	R	R
		NN8	23	1	3-4	206 14	F	C	R			A					R	R								C			C						R					R					R			R								R		R	R	R
		NN7		3	3-4	209 14	F	R	R			A					R									C			C																R			R								R		R	R	R
			24	3	3-4	218 74	F	R	R			A					R									C		R	C										R						R			C								R		R	R	R
				5	3-4	221 74	F	R	R			A					R		R							C		R	C										R						R			R								R		R	R	R
					CC	225 30	F	R	R			A					R		R							C		R	C										C						R			R								R		R	R	R
		NN6	25	1	3-4	225 34	F	R	R			A					R									C		R	C										C						R			R								R		C	R	R
					CC	234 90	F	R	R			A					R									C		R	C			C	R						C			R			R			R								R		C	R	R
			26		CC	244 50	F	R	R			A					R									C		C	C			A	C						C			R			R			R								R		R	C	R
			28	1	3-4	254 14	F	C				C					R									R		R	A			A	C						C			R			R			R									R	R		R
		NN5		3	3-4	257 14	F	R				C					R			R						C		R	A			A	C						C			R			R		R	R									R			R
					CC	263 70	F	R				C					R			R						R		R	C			A	C						C		R	R			R			R									R			R
			29	3	3-4	266 74	F	R				R					R			C						R		R	C			A	C						C			R			R			R									R			R
	early	NN4		5	3-4	268 74	F	R				R								R						R		R	C			A	C						C			R						R									C			R
			30		CC	282 90	F	R				R								C						R		R	C			A	C						A									R									R			
			31	3	3-4	285 94	F					R								R						R		R	C	R		C	C						C									R									C			
		NN3		5	3-4	288 94	F	R				R									R					R		R	R	R		C	C	R					C									R									C			
					CC	292 50	F					R									C							R	C	R		C	C						A									R									C			
			32	3	3-4	295 54	F					R									R	R						R	R	R		C	R						A									R		R							C			
		NN2		5	3-4	298 54	F					R									R	R	R					C	R	R		C	R						A										R								C			
					CC	302 10	F					R										R	R					R	R			C	R						C																		C			
			33	3	5-6	305 14	F					R										R	R					C	C			C	R	R					C																		C			
Olig	e.	[illegible]22		4	5-6	308 64	F					R															C	R	C					A					R												R									

and fair in Cores 5–33. Species diversity is good throughout these cores.

Quaternary

The Quaternary includes Samples 592-1-1, 3–4 cm through 592-3-5, 3–4 cm. Zone NN21, based on the range of *Emiliania huxleyi*, includes Samples 592-1-1, 3–4 cm and 592-1-3, 3–4 cm. Sample 592-1,CC, above the last occurrence of *E. ovata* in Sample 592-2-1, 3–4 cm, belongs in Zone NN20. The last occurrence of *Calcidiscus macintyrei* in Sample 592-3-2, 3–4 cm places Samples 592-2-1, 3–4 cm to 592-3-1, 3–4 cm in Subzone NN19b. Subzone NN19a includes Samples 592-3-2, 3–4 cm and 592-3-5, 3–4 cm, above the last occurrence of *Discoaster brouweri* in Sample 592-3-6, 3–4 cm.

Pliocene

The Pliocene includes Sample 592-3-6, 3–4 cm through Core 14. The lower/upper Pliocene boundary is between Samples 592-6-3, 3–4 cm and 592-6,CC. The last occurrence of *Discoaster pentaradiatus* in Sample 592-4-2, 3–4 cm places Samples 592-3-6, 3–4 cm to 592-4-1, 3–4 cm in Zone NN18. One sample, Sample 592-4-2, 3–4 cm, belongs in Zone NN17. The interval between the last occurrence of *D. surculus* in Sample 592-4-3, 3–4 cm and the last common occurrence of *Reticulofenestra pseudoumbilica* in Sample 592-6,CC is placed in Zone NN16. Rare occurrences of *R. pseudoumbilica* above Sample 592-6,CC are interpreted as reworking. The last occurrence of *Amaurolithus tricorniculatus* in Sample 592-8,CC places Samples 592-6,CC to 592-8-5, 3–4 cm in Zone NN15. Samples 592-8,CC through 592-13,CC, the first occurrence of *D. asymmetricus*, are placed in Zone NN14. The paucity of *Ceratolithus rugosus* at Site 592 prevents determination of the NN13/NN12 boundary.

Miocene

Samples 592-15-1, 3–4 cm through 592-33-3, 5–6 cm are in the Miocene. The middle/upper Miocene boundary is between Samples 592-20,CC and 592-21-1, 3–4 cm and the lower/middle Miocene boundary is between Samples 592-29-3, 3–4 cm and 592-29-5, 3–4 cm. The range of *Discoaster quinqueramus* from Sample 592-15-1, 3–4 cm to Sample 592-19-1, 3–4 cm determines Zone NN11. The first occurrence of *Amaurolithus primus* in Sample 592-17,CC subdivides Zone NN11 into Subzones NN11b and NN11a. The range of *D. hamatus* from Sample 592-21-1, 3–4 cm to Sample 592-22,CC places this interval in Zone NN9. The overlying interval belongs in Zone NN10. The first occurrence of *Catinaster coalitus* in Sample 592-23-1, 3–4 cm places this sample in Zone NN8. Zone NN7 includes Sample 592-23-3, 3–4 cm to the first occurrence of *D. kugleri* in Sample 592-24,CC. *Sphenolithus heteromorphus* last occurs in Sample 592-28-3, 3–4 cm, placing Samples 592-25-1, 3–4 cm through 592-28-1, 3–4 cm in Zone NN6. The interval from Sample 592-28-3, 3–4 cm to the first occurrence of *D. exilis* in Sample 592-29-3, 3–4 cm is placed in Zone NN5. Samples 592-29-5, 3–4 cm to 592-31-3, 3–4 cm, above the last occurrence of *S. belemnos* in Sample 592-31-5, 3–4 cm, belong in Zone NN4. The last occurrence of *Triquetrorhabdulus carinatus* in Sample 592-32-5, 3–4 cm places Samples 592-31-5, 3–4 cm through 592-32-3, 3–4 cm in Zone NN3. Based upon the occurrence of *D. druggii* in Sample 592-33-3, 5–6 cm and the common occurrence of *Reticulofenestra umbilica* in Sample 592-33-4, 5–6 cm, the major regional unconformity of the southwest Pacific occurs between these samples, with early Miocene Zone NN2 lying immediately above early Oligocene Zone NP22. The missing NN1 and NP25/NP23 zones represent a hiatus of at least 15.5 m.y.

Site 593

Hole 593

Site 593 is located on the Challenger Plateau west of the northern tip of the South Island of New Zealand (40°30.47′S, 167°40.47′E) at a water depth of 1068 m below sea level. Site 593, which lies in the temperate water mass, is a reoccupation of Site 284 (DSDP Leg 29).

Two holes were drilled at Site 593. Hole 593 was cored to a depth of 571.5 m (late Eocene Zone NP18) and 60 cores were taken. Core recovery was good throughout most intervals. Hole 593A was cored to a depth of 209.3 m; then washed down to a depth of 448.8 m, where coring was resumed to a depth of 496.9 m. Twenty-seven cores were taken.

Only Cores 1–50 from Hole 593 were examined in order to determine the Neogene and Quaternary nannoplankton zonation, because the Oligocene/Miocene boundary occurs within Core 50 (Table 9). Preservation of calcareous nannoplankton in Hole 593 is good in Cores 1–11 and fair in Cores 12–50. Species diversity is good throughout the hole. With the exception of the NN13/NN12 and the NN8/NN7 boundaries, all of the Neogene and Quaternary nannoplankton zones are recognized. Hole 284 (DSDP Leg 29) was cored to a depth of 208.0 m (late Miocene). The placement of the lower/upper Pliocene and the upper Pliocene/Quaternary boundaries in Hole 593 and in Hole 284, as determined by Edwards and Perch-Nielsen (1973), agrees very closely. The Miocene/Pliocene boundary in Hole 284 was not recognized. Species diversity in upper Miocene/Quaternary sediments in Hole 593 is somewhat greater than in Hole 284.

Quaternary

The Quaternary includes Sample 593-1-1, 3–4 cm through Core 5. Samples 593-1-1, 3–4 cm and 593-1-3, 3–4 cm contain common to abundant *Emiliania huxleyi* and are placed in Zone NN21. The last occurrence of *E. ovata* in Sample 593-2-5, 3–4 cm places Samples 593-1,CC through 593-2-3, 3–4 cm in Zone NN20. Subzone NN19b includes Samples 593-2-5, 3–4 cm through 593-3-1, 3–4 cm, above the last occurrence of *Calcidiscus macintyrei* in Sample 593-3-3, 3–4 cm. Subzone NN19a extends down through Core 5.

Pliocene

The Pliocene includes Samples 593-6-1, 39–40 cm through 593-17-3, 3–4 cm. The lower/upper Pliocene boundary lies between Samples 593-8,CC and 593-9-1, 3–4 cm. The last occurrence of *Discoaster brouweri* in Sample 593-6-1, 39–40 cm marks the top of Zone NN18.

The two samples below contain the last occurrences of *D. pentaradiatus* and *D. surculus*, respectively, placing Sample 593-6-2, 3–4 cm in Zone NN17. The last occurrence of *Reticulofenestra pseudoumbilica* in Sample 593-9-1, 3–4 cm places Samples 593-6-3, 3–4 cm through 593-8,CC in Zone NN16. Zone NN15 includes all of Core 9. The last occurrence of *Amaurolithus tricorniculatus* in Sample 593-11-1, 3–4 cm and the first occurrence of *D. asymmetricus* in Sample 593-13,CC place Cores 11–13 in Zone NN14. The NN13/NN12 boundary cannot be recognized because *Ceratolithus rugosus* is absent at Site 593.

Miocene

The Miocene includes Samples 593-17-5, 3–4 cm through 593-50-3, 3–4 cm. The middle/upper Miocene boundary is between Samples 593-26-5, 3–4 cm and 593-26,CC and the lower/middle Miocene boundary lies between Samples 593-43,CC and 593-44-1, 3–4 cm. The last occurrence of *Discoaster quinqueramus* in Sample 593-17-5, 3–4 cm and the first occurrence of *Amaurolithus primus* in Sample 593-22-3, 3–4 cm places this interval in Subzone NN11b. Subzone NN11a extends from Sample 593-22,CC down to 593-25-1, 3–4 cm, the first occurrence of *D. quinqueramus.* Samples 593-26,CC and 593-27,CC contain *D. hamatus,* which places this interval in Zone NN9. The intervening Samples 593-25-3, 3–4 cm through 593-26-5, 3–4 cm belong in Zone NN10. The absence of *Catinaster coalitus* at Site 593 prevents the determination of the NN8/NN7 boundary. The first occurrence of *D. kugleri* in Sample 593-37-1, 3–4 cm and the last occurrence of *Sphenolithus heteromorphus* in Sample 593-42-4, 99–100 cm place Samples 593-37-3, 3–4 cm through 593-42-4, 3–4 cm in Zone NN6. The interval from Sample 593-42-4, 99–100 cm through Sample 593-43,CC, the first occurrence of *D. exilis,* belongs in Zone NN5. The last occurrence of *S. belemnos* in Sample 593-44,CC places Samples 593-44-1, 3–4 cm and 593-44-5, 3–4 cm in Zone NN4. Zone NN3 includes samples above the last occurrence of *Triquetrorhabdulus carinatus* and the first occurrence of *D. druggii* in Sample 593-46,CC, which here constitutes Zone NN2. Zone NN1 extends down to the Oligocene/Miocene boundary between Samples 593-50-3, 3–4 cm and 593-50-5, 3–4 cm. The top of Zone NP25 is based on the last occurrence of *Helicosphaera recta* in Sample 593-50-5, 3–4 cm.

Site 594

Holes 594, 594A

Site 594 is located on the southern margin of Chatham Rise east of the South Island of New Zealand (45°31.41′S, 174°56.88′E) at a water depth of 1204 m below sea level. The site lies in the subantarctic water mass south of the Subtropical Convergence and is the southernmost site of Leg 90.

Three holes were drilled at Site 594. Hole 594 reached the middle Miocene NN5/NN6 zones at a depth of 505.1 m. Fifty-three cores were taken and core recovery through Core 31 (293.9 m) was generally good; however, below Core 31, core recovery was poor. Twenty-six cores were obtained from Hole 594A which duplicates portions of Hole 594 and extends the total depth down to 639.5 m (Zone NN5). Core recovery below 495.5 m (top of Core 12) was generally poor. Hole 594B was drilled to a depth of 42.9 m and 5 cores were obtained.

Cores 1–53 from Hole 594 and Cores 13–26 from Hole 594A were examined in order to determine the nannoplankton biostratigraphy at Site 594. Because Site 594 is near the South Island of New Zealand, numerous Paleogene as well as some Neogene taxa are reworked into indigenous assemblages. Preservation is fair throughout the site but discoasters are poorly preserved and their numbers are markedly reduced. Most of the nannoplankton zones are recognized; however, because of the paucity of zonal indicators, the Miocene and Pliocene zonal boundaries are shown with dashed lines (Table 10). Zones NN18, NN17, NN13, and the boundary between NN8 and NN7 cannot be determined.

Quaternary

The Quaternary includes Samples 594-1-1, 3–4 cm through at least 594-11-5, 3–4 cm. The base of the Quaternary cannot be determined. Samples 594-1-1, 3–4 cm through 594-6-1, 25–26 cm contain *Emiliania huxleyi* and are assigned to Zone NN21. The last occurrence of *E. ovata* in Sample 594-7,CC places Samples 594-6-3, 3–4 cm through 594-7-1, 3–4 cm in Zone NN20. Subzone NN19b includes Samples 594-7,CC through 594-11-3, 3–4 cm, above the last occurrence of *Calcidiscus macintyrei* in Sample 594-11-5, 3–4 cm.

Pliocene

The top of the Pliocene cannot be determined. The lower/upper Pliocene boundary lies between Samples 594-18-1, 3–4 cm and 594-18-3, 3–4 cm and the base of the Pliocene is between Samples 594-23-5, 3–4 cm and 594-23,CC. The last common occurrence of *Reticulofenestra pseudoumbilica* in Sample 594-18-3, 3–4 cm marks the top of Zone NN15. The presence of *R. pseudoumbilica* above this sample is interpreted as reworking. The intervening zones and subzones (NN19a–NN16) cannot be determined. A single rare occurrence of *Amaurolithus tricorniculatus* in Sample 594-20,CC places Samples 594-18-3, 3–4 cm through 594-20-5, 3–4 cm in Zone NN15. The boundaries between Zones NN14 and Zones NN13 and between Zones NN13 and NN12 cannot be recognized.

Miocene

The Miocene includes Samples 594-23,CC through 594A-26,CC. The middle/upper Miocene boundary lies between Samples 594-28-3, 3–4 cm and 594-20-5, 3–4 cm. The rare occurrences of *Discoaster quinqueramus* in Samples 594-23,CC and 594-26-5, 3–4 cm place this interval in Zone NN11, but the absence of *Amaurolithus primus* at Site 594 prevents the subdivision of this zone. The rare occurrences of *D. hamatus* in Samples 594-28-5, 3–4 cm and 594-29,CC place this interval in Zone NN9. Samples 594-26,CC through 594-28-3, 3–4 cm therefore belong in Zone NN10. The boundary between Zones NN8 and NN7 cannot be determined. The rare occurrences of *D. kugleri* in Sample 594-42, 3–4 cm

Table 9. Nannoplankton occurrences, Hole 593.

Age	Zone	Core	Section	Interval (cm)	Depth below seafloor (m)	Preservation	Index species																			Additional species																																																							
							Emiliania huxleyi	*Emiliania ovata*	*Calcidiscus macintyrei*	*Discoaster brouweri*	*Discoaster pentaradiatus*	*Discoaster asymmetricus*	*Discoaster surculus*	*Reticulofenestra pseudoumbilica*	*Amaurolithus tricorniculatus*	*Amaurolithus primus*	*Discoaster quinqueramus*	*Discoaster hamatus*	*Discoaster exilis*	*Discoaster kugleri*	*Sphenolithus heteromorphus*	*Sphenolithus belemnos*	*Discoaster druggii*	*Triquetrorhabdulus carinatus*	*Helicosphaera recta*	*Amaurolithus delicatus*	*Calcidiscus leptoporus*	*Ceratolithus acutus*	*Chiasmolithus altus*	*Coccolithus carteri*	*Coccolithus miopelagicus*	*Coccolithus pelagicus*	*Coronocyclus nitescens*	*Crenalithus doronicoides*	*Cyclicargolithus abisectus*	*Cyclicargolithus floridanus*	*Dictyococcites bisectus*	*Dictyococcites scrippsae*	*Discoaster bellus*	*Discoaster berggrenii*	*Discoaster decorus*	*Discoaster deflandrei*	*Discoaster moorei*	*Discoaster neohamatus*	*Discoaster tamalis*	*Discoaster tridenus*	*Discoaster triradiatus*	*Discoaster variabilis*	*Discolithina japonica*	*Discosphaera tubifera*	*Emiliania annula*	*Gephyrocapsa caribbeanica*	*Gephyrocapsa oceanica*	*Helicosphaera carteri*	*Helicosphaera euphratis*	*Helicosphaera hyalina*	*Helicosphaera intermedia*	*Helicosphaera sellii*	*Oolithotus fragilis*	*Pontosphaera discopora*	*Rhabdosphaera clavigera*	*Rhabdosphaera procera*	*Scapholithus fossilis*	*Scyphosphaera intermedia*	*Scyphosphaera pulcherrima*	*Scyphosphaera recurvata*	*Sphenolithus abies*	*Sphenolithus dissimilis*	*Sphenolithus moriformis*	*Sphenolithus neoabies*	*Syracosphaera pulchra*	*Thoracosphaera saxea*	*Triquetrorhabdulus rugosus*	*Umbellosphaera irregularis*	*Umbilicosphaera sibogae*	*Umbilicosphaera cricota*	*Zygrhablithus bijugatus*
Quaternary	NN21	1	1	3-4	0.04	G	A		R																		A			R		A		C															R	R		C	C	R		R		R		R	R	R	R			R					C	R		R	R	R	
			3	3-4	3.04	G	C																				C			R		A		A															R			A	R	R		R		R		R	R	R	R								C			R	R	R	
	NN20			CC	5.10	G																					C			R		A		A															R			C	R	C		R		R	R	R	R	R	R								C			R	R	R	
		2	1	3-4	5.14	G																					C			R		C		A															R			C	R	R		R			R	R	R	R	R								C			R	R	R	
			3	3-4	8.14	G																					R			R		C		A															R			C	R	R		R		R	R	R	R	R	R								C			R	R	R	
	NN19b		5	3-4	11.14	G		R																			C			R		R		A															R			C	R	R		R			R	R	R	R	R								C				R	R	
				CC	14.70	G		A																			A			C		A		A															R		R	R		R		R			R	R	R	R	R			R					R	R			R	R	
		3	1	3-4	14.74	G		C																			C			C		A		A															R		R	R		R		R			R	R	R	R	R			R					R					R	
	NN19a		3	3-4	17.74	G		C	R																		C			R		R		C															R		R	R		C		R		R	R	R	R	R	R			R					R					R	
		4		CC	33.90	G		A	R																		C			R		C		A															R		R			R				R	R	R	R	R	R			R					R					R	
		5		CC	43.50	G		A	C																		C			R		C		A															R		R			R				R		R	R	R	R			R					R					R	
Pliocene, late	NN18	6	1	39-40	43.90	G		C	R	R																	C			R		C		A															R		R			R				C		R	R	R	R			R					R					R	
	NN17		2	3-4	45.04	G		C	R	R	R																C			R		C		A															R		R			R				C		R	R	R	R			R					R					R	
	NN16		3	3-4	46.54	G		C	C	R	R	R	R														C			R		C		C															R		R			R				R		R	R	R	R			R					R					R	
				CC	53.10	G		C	C	R	R	R	R														C			R		C		C											R		R		R		R			R				R		R	R	R	R			R					R					R	
		7		CC	62.70	G		R	C	R	R	R	R														C			R		C		A											R				R					R				R		R	R	R	R	R		R					R					R	
		8		CC	65.80	G			C	R	R	R	C														C			R		C		A											R				R					C				R		R	R	R		R	R	R					R					R	
Pliocene, early	NN15	9	1	3-4	70.54	G			C	R	R	R	R	R													C			R		C		A															R					C				R		R	R	R	R	R		R					R					R	
			3	3-4	73.54	G			C	R	R	R	C	C													C			R		C		A															R					C				R		R		C		R		C	R			R	R					R	
				CC	81.90	G			C	R	R	R	C	C													C					C		A															R					C				R		R		C		R	R	R	R			R	R					R	
	NN14	11	1	3-4	91.54	G			C	R	R	R	R	C	R	R										R	C					C		C														R	R					C				R		R		C	R	R	R		R			R	R					R	
			3	3-4	94.54	G			R	R	R	R	R	C	R	R										R	C					C		C														R	R					R				R		R		C				R	R			R	R					R	
			5	3-4	97.54	G			R	R	R	R	R	C	R	R										R	C					C		C														R	R					R				R		R		C		R			R			R	R					R	
				CC	101.10	G			R	R	R	R	R	C	R	R										R	C					C		C														R	R					R				R		R		C	R				R			R	R					R	
		12		CC	110.70	F			R	R	R	R	R	C		R										R	C					C		C														C	R					R				R		R		R		R	R		R			R						R	
		13		CC	120.30	F			C	R	C	R	R	C		R										R	C	R				C		A							R							R	R					R				R		R		R	R	R	R	R	C			R						R	
	NN13/NN12	14	1	3-4	120.34	F			C	R	R		R	C		R										R	C					C		C												R		R	R					R						R		R				R	R			R						R	
				CC	129.90	F			C	R	R		R	C		R										R	C					C		C												R		R	R					R						R		R		R		R	R			R						R	
		15		CC	139.50	F			R	R	R			C													C					C		C														R						R						R		R		R		R	R			R	R					R	
		16		CC	149.10	F			R	R	R			C		R											C					C		C														R						R													R			R						R	
		17	3	3-4	152.14	F			R	R	R			C		R										R	C					R		A														R						R	R												R			R						R	
late	NN11b		5	3-4	155.14	F			R	R	R			C			R										R					R		A						R								C						R										R		R	R			R						R	
				CC	158.70	F			R	R				C													R					C		A						R								C						R										R		R	R			R						R	
		18		CC	168.30	F			R	R				C		R	R										C					C		C														R						R											R	R	R			R						R	
		19		CC	177.90	F			R	R				C		R											C					C		C														R						R													R			R						R	
		20		CC	187.50	F			R	C				A		R											C					C		A														C						R									R				C			R						R	
		21		CC	197.10	F			R	R				C		R											C					C		C														R						R													C			R			R			R	
		22	3	3-4	200.14	F			R	R				C		R											C					C		C														R						R													C			C			R			R	

Miocene	late	NN11a			CC	206.70	F	R	R			C	R									R			C		C											C	R					C			C	C	R
			23		CC	216.30	F	R	R			C	R									R			C		C						R					R	R					C			C	C	R
			24		CC	225.90	F	R	R			C	R									C			C		C								R			C	R					C			C	C	R
			25	1	3-4	225.94	F	R	R			C	R									C			A		R											C	C	R		R	R	C			C	C	R
		NN10		3	3-4	228.94	F	R	R			C										C			C		R									R	R	C	R					C			C	C	R
					CC	235.50	F	R	C			C										C			C		R					R				R	R	C	R					C			C	C	R
			26	5	3-4	241.54	F	R	R			C										C			C		R					R			R	R	R	C	R					C			C	C	R
	middle	NN9			CC	245.10	F	C	C			C		R								C			C		R								R	R	R	C	C					C			C	C	R
			27		CC	254.70	F	C	R			A		R								C			C		R					R				R	R	A	C					C			C	R	R
		NN8 NN7	28	1	3-4	254.74	F	R	R			C			C							R			C		R									R		C	R					R			C	R	R
					CC	264.30	F	C	R			A			C							C			C		R									R		C	C					C			C	R	R
			29		CC	273.90	F	C	R			A			R							C			C		R					R						C	R					C			C	R	R
			30		CC	283.50	F	C	R			A			R							A			C		R											R	R					C			C	R	R
			31		CC	293.10	F	C	R			A			C							C			C		R					R						R	R					C			C	R	R
			32		CC	302.70	F	C	R			A			C							C			C		R											R	R					C			C	R	R
			33		CC	312.30	F	C				A			R							C			C		R											R	R	R				R			R	R	R
			34		CC	321.90	F	C				A			R							C			C		R											R	R					R			R	R	R
			35		CC	331.50	F	C				A			R							C		R	C		R											R	R					R			R	R	R
			36		CC	341.10	F	C				A			R	R						C		C	C		R								R			R	R					R			R	R	R
			37	1	3-4	341.14	F	C				A			R	R						C		C	C		R											R	R					R			R	R	R
		NN6		3	3-4	344.14	F	C				A			R							C		C	C		R											R	R					R			R	R	R
					CC	350.70	F	C	C	R	R	A			C							C		C	C		R		R					R	R			R	R					R			R	R	R
			38		CC	360.30	F	C	R		R	A			C							C		R	C		R	R	C						C			R	R					R			R	C	R
			39		CC	369.90	F	C				A			C							C		R	C		R	C	C						C	R		R	R					C			C	C	R
			40		CC	379.50	F	C				C			C							C		R	C			C	C						C			R	R					R			R	R	R
			41		CC	389.10	F	C				C			C							C		R	C			C	A						C			R	R	R				R		C	R		R
			42	1	2-3	389.13	F	C				R			C							C		R	C			A	A						C			R	R					R		C	R		R
				3	3-4	392.14	F	C				R			C							C		R	C	R		A	A						C			R	C							C	R		R
				4	28-29	393.89	F	C				R			R							C		C	C	R		C	C						C				R	R						C	R		
		NN5		4	99-100	394.60	F	C				R			R		R					C		C	C	R		C	C						C				R	R						C			
				5	3-4	395.14	F	C				R			R		C					C		R	C	R		A	A						C				R							C			
			43		CC	408.30	F	R				R			R		R					R		R	C	R		C	A						C				R							C			
	early	NN4	44	1	3-4	408.34	F	R				C					C					R		R	C	R		C	C						A				R							C			
				5	3-4	414.34	F	R				C					C					R		R	C	R		C	C						A				R							C			
		NN3			CC	417.90	F	R				C					R	R	R			R		R	C	R		C	C						C											C			
			45		CC	427.50	F					C						R						R	R	R		C	C						C										R	C			
			46	5	3-4	433.54	F					C						R	R					R	R	R		C	C						C										R	C			
		NN2			CC	437.10	F					C							R	R				R	R	R		C	C	R					C										R	C			
		NN1	47	1	3-4	437.14	F					R								R				R	C	R		C	C						A											C			
					CC	446.70	F					R								R				C	C	R		C	C	R					A											C			
			48		CC	456.30	F					C								R				C	C	R		C	C						C											C			
			49		CC	465.90	F					R								R				C	C	R		C	C						C											C			
			50	1	3-4	465.94	F					R								R				R	C	R		C	C						C											C			
				3	3-4	468.94	F					R								R				R	C	R		C	C						C											C			
Olig	late	NP25		5	3-4	471.94	F					R								R	P			C	C	R		C	C	R					C											C			R
					CC	475.50	F					R								R	R		R	R	C			C	C	C	R				C							R				C			C

Table 10. Nannoplankton occurrences, Holes 594 and 594A.

Age		Zone	Core	Section	Interval (cm)	Depth below seafloor (m)	Preservation	Index species									Additional species																																																									
								Emiliania huxleyi	Emiliania ovata	Calcidiscus macintyrei	Reticulofenestra pseudoumbilica	Amaurolithus tricorniculatus	Discoaster quinqueramus	Discoaster hamatus	Discoaster kugleri	Sphenolithus heteromorphus	Calcidiscus leptoporus	Catinaster calyculus	Chiasmolithus altus	Chiasmolithus bidens	Chiasmolithus californicus	Chiasmolithus grandis	Chiasmolithus oamaruensis	Chiasmolithus sp	Coccolithus carteri	Coccolithus miopelagicus	Coccolithus pelagicus	Coronocyclus nitescens	Crenalithus doronicoides	Cricolithus jonesi	Cyclicargolithus abisectus	Cyclicargolithus floridanus	Dictyococcites bisectus	Dictyococcites scrippsae	Discoaster barbadiensis	Discoaster brouweri	Discoaster deflandrei	Discoaster exilis	Discoaster intercalaris	Discoaster lodoensis	Discoaster neohamatus	Discoaster pentaradiatus	Discoaster stellulus	Discoaster surculus	Discoaster triradiatus	Discoaster variabilis	Discolithina japonica	Discolithina multipora	Fasciculithus tympaniformis	Gephyrocapsa caribbeanica	Gephyrocapsa oceanica	Gephyrocapsa protohuxleyi	Helicosphaera carteri	Helicosphaera hyalina	Helicosphaera intermedia	Helicosphaera sellii	Heliolithus kleinpellii	Isthmolithus recurvus	Lophodolithus nascens	Pontosphaera discopora	Reticulofenestra hillae	Reticulofenestra umbilica	Rhabdosphaera procera	Scyphosphaera recurvata	Sphenolithus abies	Sphenolithus moriformis	Sphenolithus neoabies	Syracosphaera pulchra	Thoracosphaera saxea	Triquetrorhabdulus carinatus	Triquetrorhabdulus rugosus	Umbellosphaera irregularis	Umbilicosphaera cricota	Zygrhablithus bijugatus
Quaternary		NN21	1	1	3-4	0.04	F	C			R						A								R		C		C																						R	R		C			R												R	R			R		
					CC	5.90	F	R			R						C						R		C		C		C	R		R					R													R	R		R			R														R				
			2	3	3-4	8.94	F	R			R						R								C		C		A			R					R													C	R		R			R																			
					CC	15.50	F	A									R								C		C		A																								A	R		R	R																					
			3	3	3-4	18.54	F	R			R						R			R					C	R	C		A	R						R		R								R		R	A	R		R			R	R		R			R												
					CC	25.10	F	A			R						A								C	R	A		C	R																				R	R	R		R			R			R				R										
			4	3	3-4	28.14	F	R			R						R								C	R	A		A	R		R		R																R	C	R		R					R		R	R											
					CC	34.70	F	R			R						C								C		A		A	R		R					R													A	R	C	R															R					
			5	3	3-4	37.74	F	C			R						R								C	R	A		A	R		R															R		R	C	C	C	R			R													R					
					CC	44.30	F	R			R						R								C		C		A	R																						C	R	R	R			R																		
			6	1	25-26	44.56	F	R			R						R								C		C		A	R																						C	R	R	R			R																		
		NN20		3	3-4	47.34	F				R						R								R		C		A		R	R	R	R			R													C	R		R					R			R						R					
					CC	53.90	F				R						R								R		C		C	R		R																				R	R		R			R																		
			7	1	3-4	53.94	F				R						R								R		C		A			R	R																			C	R		R														R					
		NN19b			CC	63.50	F		R		R													R		C		A		R		R																R	C	R		R															R						
			8	1	3-4	63.54	F		R		R						R				R				C		A		A	R	R		R																	C	R		R				R	R															
					CC	73.10	F		C		R						A				R				C		A		A				R																		C	R		C															R	R				
			9	3	3-4	76.14	F		R		R						R								C		A		A			R	R	R			R										R			A	C		R			R						R											
					CC	82.70	F		R		R						A								R		R		A			R		R																	A	C		R			R																		
			10		CC	92.30	F		R		R						R				R				R		C		C		R	R	R														R			C	R		R																R					
			11	3	3-4	95.34	F		R							C			R	R				R		A		C	R			R	R			R										R			C	R		R																			
		NN19a/NN16		5	3-4	98.34	F		C	R	R						C								R		A		C	R	R																R			R	R		A			R							R				R					
					CC	101.90	F		C	C	R						C				R				R		C		C					R														R			C	R		R			R						R						R					
			12	3	3-4	104.94	F		C	R	R						R			R			R		R		C		C			R															R			C	C		R			R											R	R		R			
					CC	111.50	F		C	R	R						R			R					R		A		C	R	R		R																		R			R			R											R	R					
			13	3	3-4	114.54	F		R	R	R						R								R		A		C	R			R	R																		R			R			R						R						R					
					CC	121.10	F				R														C		A		C	R		R													R																					R					
Pliocene	late		14	3	3-4	124.14	F		R	R	R									R					R		A		R	R																			R						R			R										R					
					CC	130.70	F			R	R						R								R		A		C								R													R			R		R																				
			15	3	3-4	133.74	F			R	R						R								R		C		C																													R			R											R	R					
					CC	140.30	F		R	R	R						R								R		A		A	R			R	R													R									R													R					
			16	3	3-4	143.34	F				R						R								R		A		A	R		R	R																																												
					CC	149.90	F				R						R										A		A	R																												R											R							
			18	1	3-4	159.54	F			R	R						R			R					R		A		A																													R						R												
	early	NN15		3	3-4	162.54	F				R						C				R				R		A		A	R																	R					R						R			R	R	R			R					
				5	3-4	165.54	F			R	C						R				R						A		A	R																	R					R			R							R					R					
					CC	169.10	F			R	C						R										A		A			R	R				R																	R			R				R		R											
			19	3	3-4	172.14	F			R	C						R			R								C		A	R	R	R	R	R																					R			R				R														
					CC	173.70	F			C	C						R								R	A		C		R	R	R				R																			R										R										
			20	3	3-4	181.74	F			C	A						R										C		R		R					R																			R																						
				5	3-4	184.74	F			R	A						R			R					R	C		R		R		R																																										
		NN14/NN12			CC	188.30	F			R	A	R					R			R								C		R		R		R																								R																						
			21	1	3-4	188.34	F			R	A						R				R				R	C		R		R		R				R						R		R							R									R												
				3	3-4	191.34	F			C	A						R								R	C		C		R	R	R				R																			R									R												
					CC	197.90	F			C	A															R	C		C		R		R				R																																												
			23	1	3-4	207.54	F			R	A						R										C		R							R	R									R																																
				3	3-4	210.54	F			R	A										R				R	C		R			R				R	R			R		R		R		R								R																		R			
				5	3-4	213.54	F			R	A						R						R		R	C		R																						R																												R			
	late	NN11			CC	217.10	F			R	A		R								R						C		R							R	R							R		R																											R			
			24	1	3-4	217.47	F			R	A						R			R			R				R		R								R									R						R					R									R				R			
				3	3-4	220.14	F			R	A						R						R			C		R		R			R			R									R		R				R			R						R				R				R			
					CC	226.70	F			R	A						R			R	R				R	C		R		R		R	R		R	R									R							R										R								
			25	3	3-4	229.74	F			R	A											R			R			C		R		R			R	R		R									R							R							R	R			R		R							
					CC	236.30	F			R	A													R	R		R	C		R		R			R			R																									R				R							
			26	3	3-4	239.34	F			C	A						R				R		R	R		R	C		R				R	R			R									R															R				R				R			
				5	3-4	242.34	F			R	A		R				R			R				R		R	C		R		R		R	R		R	R									R															R				R				R			

Miocene		NN10			CC	245.90	F	R	A				R				R		R	R	C		R	R		R		R		R	R		R	R	R							R		
			27	3	3 4	248.94	F	R	A				R						R	R	R		R	R				R			R													
					CC	255.50	F	R	A				R						R	R	C		R	R				R			R				R					R				
			28	3	3 4	258.54	F	R	A				R	R					R	R	C		R		R	R		R										R		R		R		
	middle	NN9		5	3 4	261.54	F	C	A	R			R						R	R	C		R	R		R		R			R				R		R	R		R				
					CC	265.10	F	R	A										R		C		R	R				R							R			R		R				
			29	3	3 4	268.14	F	R	A				R			R			R	R	C		R	R		R		R							R			R	R	R				
					CC	274.70	F	R	A	R										R	C			R				R			R							R		C				
		NN8/NN7	30	1	3 4	274.74	F	R	A										R		C		R	R				R						R				R		R				
				3	3 4	277.74	F	R	A												C							R										R		R				
					CC	284.30	F	R	A										R	R	C							R									R	R		R				
			31	3	3 4	287.34	F	R	A												R			R				R							R			R		C				
					CC	293.90	F	C	A				R								C		R	R				R										R		R				
			33		CC	313.10	F	C	A				R						R	R	R							R								R		R		C				
			34	3	3 4	315.14	F	R	A				R							R	R																	R		C		R		
					CC	322.70	F	R	C											R	C			R																R	R			
			35	3	3 4	324.74	F	C	A				R							R	R				R											R		R		R				
					CC	332.30	F	C	A				R			R				C	R																			R				
			36	3	3 4	334.34	F	R	A		R		R			R				C	R			R														R		R				
					CC	341.90	F	C	A				R							R	C							R												R				
			37		CC	351.50	F	R	A											C	C					R		R												R				
			38	3	3 4	353.56	F	C	A				R						R	C	C					R		R												R				
					CC	361.10	F	R	A											R	C					R	R											R						
			39		CC	370.10	F	R	A											R	C						R											R						
			40	3	3 4	372.76	F	R	A				R							R	C			R																R				
					CC	380.30	F	R	A				R							R	R						R											R	R	R				
			41	3	3 4	383.36	F	R	A										R		R						R	R											R	R				
					CC	389.90	F	R	A										R		R						R												R	R				
			42	3	3 4	392.96	F	C	A		R									R	R																R	R	R	R				
		NN6			CC	399.50	F	C	A											C	C			R	R										R									
			43		CC	409.10	F	R	A				R							R	C			R				R										R	R					
			44		CC	418.70	F	R	A				R						R	R	C																	R	R	R				
			45		CC	428.30	F	C	A				R							C	R																	R		R				
			46		CC	437.90	F	C	A				R							C	R																		R					
			47		CC	447.50	F	R	A				R							R	C			R				R										R		R				
			48	3	3 4	450.56	F	C	A				R						R	C	C	R		R		R		R									R	R	R	R				
					CC	457.10	F	C	A				R						R	R	C			R		R		R										R	R	R				
			49	3	3 4	460.16	F	C	A				R							R	A			R														R	R	C				
					CC	466.70	F	C	A				R							R	C			R														R	R	R				
			50		CC	476.30	F	R	A				R						R	R	C							R												R				
			51		CC	485.90	F	R	C											R	C			R				R											R	R				R
			52		CC	495.50	F	R	A				R							R	C			R																R			R	
			53		CC	505.10	F	C	A											C	C			R				R							R		R	R		C				
			A 13	3	3 4	508.14	F	R	A				R						R	C	A			R	R			R				R			R		R	R	R	R				
					CC	514.70	F	R	C				R						R		C			C	R	R		R											R					
			14	3	3 4	517.74	F	R	C				R					R		R	C			C				R							R		R	R	R	R				
					CC	524.30	F	C	C				R							R	C			C	R			R							R			R	R	R				
			15	3	3 4	527.33	F	R	C				R							R	C			C				R									R	R	R	R				
		NN5			CC	533.90	F	R	C			R	R						R	R	C			C	R			R	R									R	C	R				
			16	3	3 4	536.93	F	R	C				R							R	A			A	R			R							R		R	R	C	R				
					CC	543.50	F	R	R				R						R	C	A			A	R	R		R							R			R	C	R				
			17	3	3 4	546.53	F	R	R				R						R	C	A	R		A	R	R		R										R	C	R				R
					CC	553.10	F	R	R										R	A	A			A	C	R		R										R	C	R				
			18	3	3 4	556.14	F	C	R				R		R					A	A			A	C	R		C							R			C	R	C				
					CC	562.70	F	C	R				R		R				R	C	A			A	R	R		C							R		R	R	R	R				
			19		CC	572.30	F	R	R										R	R	A			A	R	R	R	R											C	R				
			20	3	3 4	575.30	F	C	R										R	R	A			A	R	R		R										R	C					
					CC	581.90	F	R	R											R	C			A	R			R									R		R	R				
			21		CC	591.50	F	R	R				R						R	R	A			C	R	R		C											R					
			22		CC	601.10	F	C	C				R		R				R	R	A			A	C		R	R									R		C					
			23		CC	610.70	F	R	C			R			R				R	R	A			A	C	R	R	C							R		R	R	A	R				
			24		CC	620.30	F	R	C				R						R	R	A			A	C	R	R	C							R		R	R	A	R				
			25		CC	629.80	F	R	C				R		R				R	R	C			A	C		R	C									R	R	A	R				R
			26		CC	639.50	F	R	C				R		R					R	C			A	C			R							R			R	C	R				

and *Sphenolithus heteromorphus* in Sample 594A-15,CC place Samples 594-42,CC through 594A-15-3, 3-4 cm in Zone NN6 and Samples 594A-15,CC through 594A-26,CC in Zone NN5.

ACKNOWLEDGMENTS

I thank D. Bukry and S. Gartner for their review of the manuscript and for their helpful suggestions. Marathon Oil Company supported my participation on Leg 90 and approved publication of the results.

REFERENCES

Black, M., 1967. New names for some coccolith taxa. *Proc. Geol. Soc. London*, 1640:139-145.

Black, M., Barnes, B., 1959. The structure of coccoliths from the English Chalk. *Geol. Mag.*, 96:321-328.

________, 1961. Coccoliths and discoasters from the floor of the South Atlantic Ocean. *J. R. Microsc. Soc.*, 80:137-147.

Boudreaux, J. E., and Hay, W. W., 1967. Zonation of the latest Pliocene-Recent interval. *In* Hay, W. W., Mohler, H. P., Roth, P. H., Schmidt, R. R., and Boudreaux, J. E., *Calcareous Nannoplankton Zonation of the Cenozoic of the Gulf Coast and Caribbean-Antillean area, and Transoceanic Correlation. Trans. Gulf Coast Assoc. Geol. Soc.*, 17:428-480.

________, 1969. Calcareous nannoplankton and biostratigraphy of the late Pliocene-Pleistocene-Recent sediments in the Submarex cores. *Rev. Espan. Micropaleontol.*, 1:249-292.

Bramlette, M. N., and Riedel, W. R., 1954. Stratigraphic value of discoasters and some other microfossils related to Recent coccolithophores. *J. Paleontol.*, 28:385-403.

Bramlette, M. N., and Sullivan, F. R., 1961. Coccolithophorids and related nannoplankton of the early Tertiary in California. *Micropaleontology*, 7:129-188.

Bramlette, M. N., and Wilcoxon, J. A., 1967. Middle Tertiary calcareous nannoplankton of the Cipero Section, Trinidad, W. I. *Tulane Stud. Geol. Paleontol.*, 5:93-131.

Brönnimann, P., and Stradner, H., 1960. Die Foraminiferen und Discoasteriden-zonen von Kuba and ihre interkontinentale Korrelation. *Erdoel-Z.*, 76:364-369.

Bukry, D., 1971a. Cenozoic calcareous nannofossils from the Pacific Ocean. *San Diego Soc. Nat. Hist. Trans.*, 16:303-328.

________, 1971b. Discoaster evolutionary trends. *Micropaleontology*, 17:43-52.

________, 1973a. Coccolith stratigraphy, eastern equatorial Pacific, Leg 16, Deep Sea Drilling Project. *In* van Andel, T. H., Heath, G. R., et al., *Init. Repts. DSDP*, 16:Washington (U.S. Govt. Printing Office), 653-711.

________, 1973b. Low-latitude coccolith biostratigraphic zonation. *In* Edgar, N. T., Saunders, J. B., et al., *Init. Repts. DSDP*, 15: Washington (U.S. Govt. Printing Office), 685-703.

________, 1973c. Phytoplankton stratigraphy, Deep Sea Drilling Project Leg 20, western Pacific Ocean. *In* Heezen, B. C., MacGregor, I. D., et al., *Init. Repts. DSDP*, 20: Washington (U.S. Govt. Printing Office), 307-317.

Bukry, D., and Bramlette, M. N., 1968. Stratigraphic significance of two genera of Tertiary calcareous nannofossils. *Tulane Stud. Geol. Paleontol.*, 6:149-155.

________, 1969. Some new and stratigraphically useful calcareous nannofossils of the Cenozoic. *Tulane Stud. Geol. Paleontol.*, 7:131-142.

Bukry, D., and Percival, S. F., 1971. New Tertiary calcareous nannofossils. *Tulane Stud. Geol. Paleontol.*, 8:123-146.

Cohen, C. L. D., 1964. Coccolithophorids from two Caribbean deep-sea cores. *Micropaleontology*, 10:231-250.

________, 1965. Coccoliths and discoasters from Adriatic bottom sediments. *Leidse Geol. Meded.*, 35:1-44.

Cohen, C. L. D., and Reinhardt, P., 1968. Coccolithophorids from the Pleistocene Caribbean deep-sea core CP-28. *N. Jb. Geol. Palaontol., Abhandl.*, 131:289-304.

Deflandre, G., 1942a. Coccolithophoridés fossiles d'Oranie. Genre *Scyphosphaera* Lohmann et *Thorosphaera* Ostenfeld. *Soc. Hist. Nat. Toulouse, Bull.*, 77:125-137.

________, 1942b. Possibilités morphogénétiques comparées du calcaire et de la silice, à propos d'un nouveau type de microfossile calcaire de structure complexe, *Lithostromation perdurum* n.g. n. sp. *C. R. Acad. Sci.*, 214:917-920.

________, 1947. *Braarudosphaera* nov. gen., type d'une famille nouvelle de Coccolithophoridés actuels à éléments composites. *C. R. Acad. Sci.*, 225:439-441.

________, 1952. Classe des Coccolithophoridés (Coccolithophoridae Lohmann, 1902). *In* Grassé, P. P. (Ed.), *Traité de Zoologie:* Paris (Masson), 1:439-470.

________, 1953. Hétérogénéité intrinsèque et pluralité des éléments dans les coccolithes actuels et fossiles. *C. R. Acad. Sci.*, 237: 1785-1787.

________, 1959. Sur les nannofossiles calcaires et leur systématique. *Rev. Micropaleontol.*, 2:127-152.

Deflandre, G., and Fert, C., 1954. Observations sur les Coccolithophoridés actuels et fossiles en microscopie ordinaire et électronique. *Ann. Paleontol.*, 40:115-176.

Edwards, A. R., and Perch-Nielsen, K., 1975. Calcareous nannofossils from the southern southwest Pacific, Deep Sea Drilling Project, Leg 29. *In* Kennett, J. P., Houtz, R. E., et al., *Init. Repts. DSDP*, 29: Washington (U.S. Govt. Printing Office), 469-539.

Ellis, C. H., 1982. Calcareous nannoplankton biostratigraphy—Deep Sea Drilling Project Leg 60. *In* Hussong, D. M., Uyeda, S., et al., *Init. Repts. DSDP*, 60: Washington (U.S. Govt. Printing Office), 507-535.

Ellis, C. H., and Lohman, W. H., 1979. Neogene calcareous nannoplankton biostratigraphy in eastern Mediterranean deep-sea sediments (DSDP Leg 42A, Sites 375 and 376). *Mar. Micropaleontol.*, 4:61-84.

Gaarder, K. R., 1970. Three new taxa of Coccolithineae. *Nytt. Mag. Bot.*, 17:113-126.

Gartner, S., Jr., 1967. Calcareous nannofossils from Neogene of Trinidad, Jamaica, and Gulf of Mexico. *Kans. Univ. Paleontol. Contr.*, Paper 29, 1-7.

________, 1969a. Correlation of Neogene planktonic foraminifer and calcareous nannofossil zones. *Trans. Gulf Coast Assoc. Geol. Soc.*, 19:585-599.

________, 1969b. Phylogenetic lineages in the lower Tertiary coccolith genus *Chiasmolithus*. *N. Am. Paleontol. Conv., Proc. G.*, 930-957.

________, 1977. Calcareous nannofossil biostratigraphy and revised zonation of the Pleistocene. *Mar. Microplaeontol.*, 2:1-25.

Gartner, S., Jr., and Bukry, D., 1974. *Ceratolithus acutus* Gartner and Bukry n.sp. and *Ceratolithus amplificus* Bukry and Percival—nomenclatural clarification. *Tulane Stud. Geol. Paleontol.*, 11: 115-118.

________, 1975. Morphology and phylogeny of the coccolithophycean family *Ceratolithaceae*. *J. Res. U.S. Geol. Surv.*, 3:451-465.

Gran, H. H., and Braarud, T., 1935. A qualitative study of the phytoplankton in the Bay of Fundy and the Gulf of Maine. *J. Biol. Board Canada*, 1:279-467.

Haeckel, E., 1894. *Systematische Phylogenie der Protisten und Pflanzen:* Berlin (Reimer).

Haq, B. U., 1966. Electron microscope studies on some upper Eocene calcareous nannoplankton from Syria. *Stockholm Contr. Geol.*, 15:23-37.

________, 1973. Evolutionary trends in the Cenozoic coccolithophore genus *Helicopontosphaera*. *Micropaleontology*, 19:32-52.

Hay, W. W., and Mohler, H. P., 1967. Calcareous nannoplankton from early Tertiary rocks at Point Labau, France, and Paleocene—early Eocene correlations. *J. Paleontol.*, 41:1505-1541.

Hay, W. W., Mohler, H. P., Roth, P. H., Schmidt, R. R., and Boudreaux, J. E., 1967. *Calcareous Nannoplankton Zonation of the Cenozoic of the Gulf Coast and Caribbean-Antillean area, and Transoceanic Correlation. Trans. Gulf Coast Assoc. Geol. Soc.*, 17.

Hay, W. W., Mohler, H. P., and Wade, M. E., 1966. Calcareous nannofossils from Nal'chik (northwest Caucasus). *Eclogae Geol. Helv.*, 59:379-400.

Jafar, S. A., and Martini, E., 1975. On the validity of the calcareou nannoplankton genus *Helicosphaera*. *Senckenberg. Lethaea*, 56 381-397.

Kamptner, E., 1927. Beitrag zur Kenntnis adriatischer Coccolithophoriden. *Arch. Protistenk.*, 58:173-184.

________, 1941. Die Coccolithineen der Südwestkuste von Istrien. *Ann Naturh. Mus. Wien*, 51:54-149.

_______, 1943. Zur revision der Coccolithineen-Spezies *Pontosphaera huxleyi*. *Anz. Akad. Wiss. Wien., Math-Naturw.*, 80:43–49.

_______, 1948. Coccolithen aus dem Torton des Inneralpinen Wiener Beckens. *Sitz-Ber. Osterr. Akad. Wiss., Math-Naturw. Kl., Abt. I*, 157:1–16.

_______, 1950. Über den submikroskopischen Aufbau der Coccolithen. *Anz. Osterr. Akad. Wiss., Math.-Naturw. Kl.*, 86:77–80.

_______, 1954. Untersuchungen über den Feinbau der Coccolithen. *Arch. Protistenk.*, 100:1–90.

_______, 1955. Fossile Coccolithineen-Skelettreste aus Insulinde. Eine mikropaläontologische Untersuchung. *Verh. K. Nederl. Akad. Wet., Afd. Natuurk., ser. 2*, 50:1–105.

_______, 1958. Betrachtungen zur Systematik der Kalkflagellaten, nebst Versuch einer neuen Gruppierung der Chrysomonadales. *Arch. Protistenk.*, 103:54–116.

_______, 1963. Coccolithineen-Skelettreste aus Tiefseeablagerungen des Pazifischen Ozeans. *Ann. Naturh. Mus. Wien*, 66:139–204.

_______, 1967. Kalkflagellaten-Skelettreste aus Tiefseeschlamm des Sudatlantik Ozeans. *Ann. Naturh. Mus. Wien*, 71:117–198.

Levin, H. L., 1965. Coccolithophoridae and related microfossils from the Yazoo Formation (Eocene) of Mississippi. *J. Paleontol.*, 39: 265–272.

Loeblich, A. R., and Tappan, H., 1963. Type fixation and validation of certain calcareous nannoplankton genera. *Proc. Biol. Soc. Wash.*, 76:191–196.

_______, 1978. The coccolithophorid genus *Calcidiscus* Kamptner and its synonyms. *J. Paleontol.*, 52:1390–1392.

Lohmann, H., 1902. Die Coccolithophoridae, eine monographie der coccolithen bildenden Flagellaten, zugleich ein Beitrag zür Kenntnis des Mittel-meerauftriebs. *Arch. Protistenk.*, 1:89–165.

_______, 1912. Untersuchungen über das Pflanzen und Tierleben der Hoschsee. Zugleich ein Bericht über die biologischen Arbeiten auf der Fahrt der "Deutschland" von Bremerhaven nach Buenos Aires in der Zeit vom 7 Mai bis 7 September 1911. *Univ. Berlin, Inst. Meeresk. Veroff., n. ser., Geogr. Naturw. Reihe*, 1:1–92.

_______, 1919. *Die Bevölkerung des Ozeans mit Plankton nach den Ergebnissen der Zentrifugenfänge während der Ausreise der "Deutschland" 1911. Arch. Biont. (Ges. Naturf. Freunde Berlin)*, 4.

McIntyre, A., 1970. *Gephyrocapsa protohuxleyi* sp. n., a possible phyletic link and index fossil for the Pleistocene. *Deep-Sea Res.*, 17:187–190.

Markali, J., and Paasche, E., 1955. On two species of *Umbellosphaera*, a new marine coccolithophorid genus. *Nytt. Mag. Bot.*, 4: 95–100.

Martini, E., 1965. Mid-Tertiary calcareous nannoplankton from Pacific deep-sea cores. *Symp. Colston Res. Soc. Proc. 17th. Symp.*, pp. 393–411.

_______, 1969. Nannoplankton aus dem Miozän von Gabon (Westafrika). *N. J. Geol. Palaont., Abhandl.*, 132:285–300.

_______, 1971. Standard Tertiary and Quaternary calcareous nannoplankton zonation. *In* Farinacci, A. (Ed.), *Proc II. Planktonic Conf., Roma, 1970*, 2:739–785.

Martini, E., and Bramlette, M. N., 1963. Calcareous nannoplankton from the experimental Mohole drilling. *J. Paleontol.*, 37:845–856.

Martini, E., and Ritzkowski, S., 1968. Was is das "Unter-Oligocän"? *Nachr. Akad. Wiss. Gottingen, II Math.-Phys., Kl., Jahrg. 1968*, pp. 231–249.

Martini, E., and Worsley, T., 1971. Tertiary calcareous nannoplankton from the western equatorial Pacific. *In* Winterer, E. L., Riedel, W. R., et al., *Init. Repts. DSDP*, 7, Pt. 2: Washington (U.S. Govt. Printing Office), 1471–1507.

Müller, C., 1970. Nannoplankton aus dem Mittel-Oligozän von Norddeutschland und Belgien. *N. Jb. Geol. Palaontol., Abhandl.*, 135: 82–101.

_______, 1974. Calcareous nannoplankton, Leg 25 (western Indian Ocean). *In* Simpson, E. S. W., Schlich, R., et al., *Init. Repts. DSDP*, 25: Washington (U.S. Govt. Printing Office), 579–633.

Murray, G., and Blackman, V. H., 1898. On the nature of the coccospheres and rhabdospheres. *Phil. Trans. R. Soc. Lond., Ser. B*, 190:427–441.

Norris, R. E., 1965. Living cells of *Ceratolithus cristatus* (Coccolithophorineae). *Archiv. Protestenk.*, 108:19–24.

Okada, H., and Bukry, D., 1980. Supplementary modification and introduction of code numbers to the low-latitude coccolith biostratigraphic zonation (Bukry, 1973; 1975). *Mar. Micropaleontol.*, 5: 321–325.

Okada, H., and McIntyre, A., 1977. Modern coccolithophores of the Pacific and North Atlantic Oceans. *Micropaleontology*, 23:1–55.

Ostenfeld, C. H., 1900. Über *Coccosphaera*. *Zool. Anz.*, 23:198–200.

Perch-Nielsen, K., 1968. Der Feinbau und die Klassifikation der Coccolithen aus dem Maastrichten von Danemark. *Biol. Skr. Dan. Vid. Selsk.*, 16:1–96.

Reinhardt, P., 1964. Einige Kalkflagellaten-Gattungen (Coccolithophoriden, Coccolithineen) aus dem Mesozoikum Deutschlands. *Monatsber., Deutsch. Akad. Wiss. Berlin.*, 6:749–759.

Roth, P. H., 1973. Calcareous nannofossils—Leg 17, Deep Sea Drilling Project. *In* Winterer, E. L., Ewing, J. I., et al., *Init. Repts. DSDP*, 17: Washington (U.S. Govt. Printing Office), 675–795.

Schiller, J., 1925. Die planktonischen Vegetationen des adriatischen Meeres. A. Die Coccolithophoriden-Vegetation in den Jahren 1911–1914. *Arch. Protistenk.*, 51:1–130.

_______, 1930. Coccolithineae. *In* Rabenhorst, L. (Ed.), *Kryptogamen-Flora von Deutschland, Österreich und der Schweiz:* Leipzig (Akad. Verlagsgesellschaft, 10:89–267.

Schwarz, E. H. L., 1894. Coccoliths. *Ann. Mag. Nat. Hist., Ser. 6*, 14:341–346.

Stradner, H., 1961. Vorkommen von Nannofossilien im Mesozoikum und Alttertiär. *Erdoel-Z.*, 77:77–88.

Sullivan, F. R., 1964. Lower Tertiary nannoplankton from the California Coast Ranges. I. Paleocene. *Calif. Univ. Publ. Geol. Sci.*, 44: 163–227.

Takayama, T., 1967. First report on nannoplankton of the Upper Tertiary and Quaternary of the Southern Kwanto Region, Japan. *Jb. Geol. Bundesanst. Wien*, 110:169–198.

Tan, S. H., 1927. Over de samenstelling en het onstaan van krijt en mergelgesteenten van de Molukken. *Jb. Mijnw. Nederl.-Indië*, 55: 111–122.

Wallich, G. G., 1877. Observations on the coccosphaere. *Ann. Mag. Nat. Hist.*, 19 (4th ser.):342–350.

Weber-van Bosse, A., 1901. Etudes sur les algues de l'Archipel Malaisien. III. Note préliminaire sur les résultats algologiques de l'expédition du *Siboga*. *Ann. Jard. Bott. Bitenzorg*, 17:126–141.

Date of Initial Receipt: 30 April 1984
Date of Acceptance: 22 August 1984

13. CENOZOIC PLANKTONIC FORAMINIFERS FROM THE EQUATOR TO THE SUB-ANTARCTIC OF THE SOUTHWEST PACIFIC[1]

D. Graham Jenkins, Department of Earth Sciences, Open University
and
M. S. Srinivasan, Banaras Hindu University[2]

ABSTRACT

Planktonic foraminifers from DSDP Site 586 on Leg 89 and Sites 587–594 on Leg 90, cored by the *Glomar Challenger* from the equator to subantarctic waters of the southwest Pacific, are recorded. Five zonal schemes were used because of latitudinal changes in faunal assemblages and these are discussed; intersite correlation was established by selected datum species. Major epoch boundaries were normally marked by the following species: Pliocene/Pleistocene, the appearance of *Globorotalia truncatulinoides;* Miocene/Pliocene, appearance of *G. tumida* in the north and the extinction of *G. conomiozea* in the south; Oligocene/Miocene, the appearance of *Globoquadrina dehiscens* at 586, 588, and 593; Eocene/Oligocene, at the extinction of *Globigerinatheka index*.

The appearances and extinctions of most datum species were regarded as isochronous but a few were demonstrably diachronous at their paleogeographic limits, such as the appearances of *G. truncatulinoides* at Site 594 and *G. inflata* at 587.

The presence of *Jenkinsina samwelli* in the late Oligocene at Site 593 is further support for the hypothesis that the Circum-Antarctic Current began about 30 Ma ago. At the same time, a major unconformity was formed and is widespread in the Tasman Sea area; sedimentation did not resume at Site 592 until the early Miocene.

Selected taxonomic problems are discussed and 39 species illustrated.

INTRODUCTION

During December 1982 and January 1983, Deep Sea Drilling Project Leg 90 recovered more than 3700 m of sediment cores from eight sites in a traverse by the *Glomar Challenger* from the tropics to the sub-Antarctic (Fig. 1, Table 1). Leg 90 sites were located in all the major surface-water masses between the tropics and the sub-Antarctic in order to compare and be able to correlate Cenozoic faunas across a wide range of latitudes from the equator to latitude 45°S. The cores were recovered from uncomplicated calcareous oozes and chalks of late Eocene–Pleistocene age, in relatively shallow water. Core recovery was 85% and the quality of the cored sequences was good; the cores were obtained by using the hydraulic piston corer (HPC) and extended core barrel (XCB).

Table 1. Locations and water depths of Leg 90 sites.

Site	Latitude (S)	Longitude (E)	Water depth (m)
587	21°11.87′	161°19.99′	1101
588	26°06.70′	161°13.60′	1533
589	30°42.72′	163°38.39′	1391
590	31°10.02′	163°21.51′	1299
591	31°35.06′	164°26.92′	2131
592	36°28.40′	165°26.53′	1098
593	40°30.47′	167°40.47′	1068
594	45°31.41′	174°56.88′	1204

PROCEDURES

On board ship core-catcher sediment samples were washed, dried, and sieved to fine, medium, and coarse fractions; the planktonic foraminifers were then examined. Subsequently, in order to determine the position of zonal boundaries, intermediate samples in the cores were examined. The species identified from Sites 586 to 594 were recorded in stratigraphic tables.

Previous relevant work on the southwest Pacific includes that of Jenkins (1971, 1975), Kennett (1973), Srinivasan and Kennett (1981a, b), and Kennett and Srinivasan (1983).

ZONAL SCHEMES

Zonal schemes are empirical and their identification is dependent on the paleogeographic limitations of zonal markers in the Cenozoic. Consequently, five main zonal schemes were employed. The tropical zonal scheme was used for Hole 586B (N22–N17a), drilled by leg 89; the warm subtropical zonal scheme was used at Sites 587, 588, 589, and 590; the cool subtropical scheme at Sites 591 and 592; the temperate scheme at Site 593 and the subantarctic scheme at Site 594. Figure 2 shows four zonal schemes and the intersite datums used for correlation from the warm subtropical to subantarctic sites; the zonal markers and zonal schemes for the tropical to subantarctic sites are shown in Tables 2–6. The latitudinal distribution of zonal markers and major boundary markers is shown later in Figure 3 and Table 7, the biostratigraphic details of *Jenkinsina samwelli* and *Chiloguembelina cubensis* at sites around Antarctica in Figure 4, and some unconformities in the Tasman Sea in Figure 5.

---

[1] Kennett, J. P., von der Borch, C. C., et al., *Init. Repts. DSDP*, 90: Washington (U.S. Govt. Printing Office).

[2] Addresses: (Jenkins) Department of Earth Sciences, Open University, Walton Hall, Milton Keynes, MK7 6AA, Buckinghamshire, United Kingdom; (Srinivasan) Banaras Hindu University, Varanasi, 221005, India.

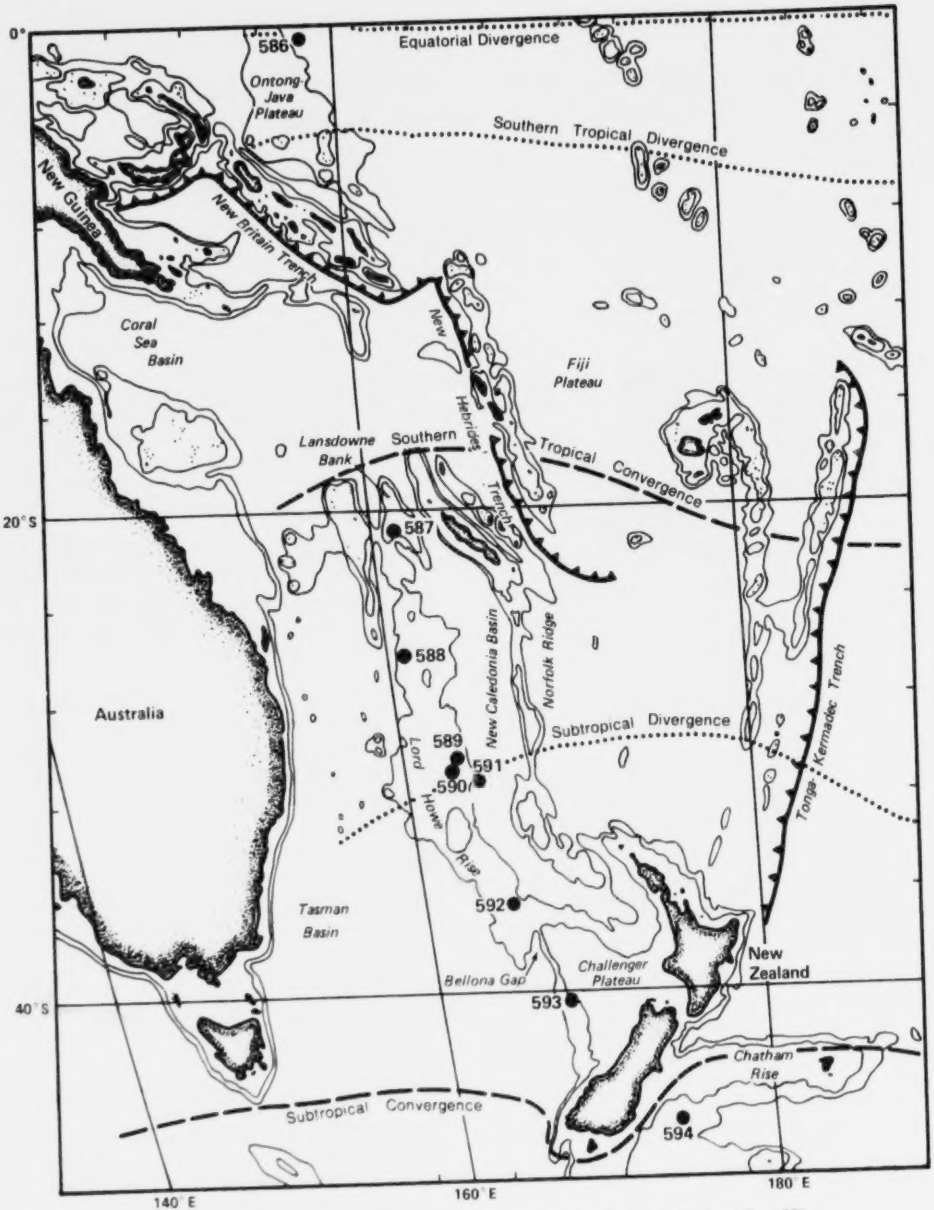
0°
586
Equatorial Divergence
Ontong Java Plateau
Southern Tropical Divergence
New Guinea
New Britain Trench
Coral Sea Basin
New Hebrides Trench
Fiji Plateau
Lansdowne Bank
Southern Tropical Convergence
20°S
587
588
New Caledonia Basin
Norfolk Ridge
Tonga-Kermadec Trench
Australia
Subtropical Divergence
589
591
590
Lord Howe Rise
Tasman Basin
592
Bellona Gap
Challenger Plateau
New Zealand
40°S
593
Chatham Rise
Subtropical Convergence
594
140°E
160°E
180°E

Figure 1. Location of Leg 90 sites (Site 586 is shown by solid circle but was drilled on Leg 89).

The zonal schemes are based on the stratigraphic distribution of species at Sites 586-594; the essential data are shown in Tables 8-16, later.

Tropical

The zonal scheme (Table 2) is similar to that of Srinivasan and Kennett (1981a, b) for Site 586 (N22-N17A). The top of Zone N19, however, could not be recognized in terms of Banner and Blow's zonal scheme. We have, therefore, included both Zones N19 and N20 within a zonal unit N19-N20 (Banner and Blow, 1965).

Warm Subtropical

The zonal scheme (Table 3) is similar to that of Kennett (1973) and Srinivasan and Kennett (1981a, b) for Site 208, but the following zones were not recognized: *Globorotalia conomiozea* Zone, *Globigerina nepenthes* Zone, and *Globorotalia peripheroacuta* Zone.

The *G. plesiotumida* Zone and the *G. margaritae* Zone have been used instead of both the *G. conomiozea* Zone and the *Globigerina nepenthes* Zone because of the late appearance of *Globorotalia conomiozea*. An added complication was that at Site 588, *G. conomiozea* had a squar-

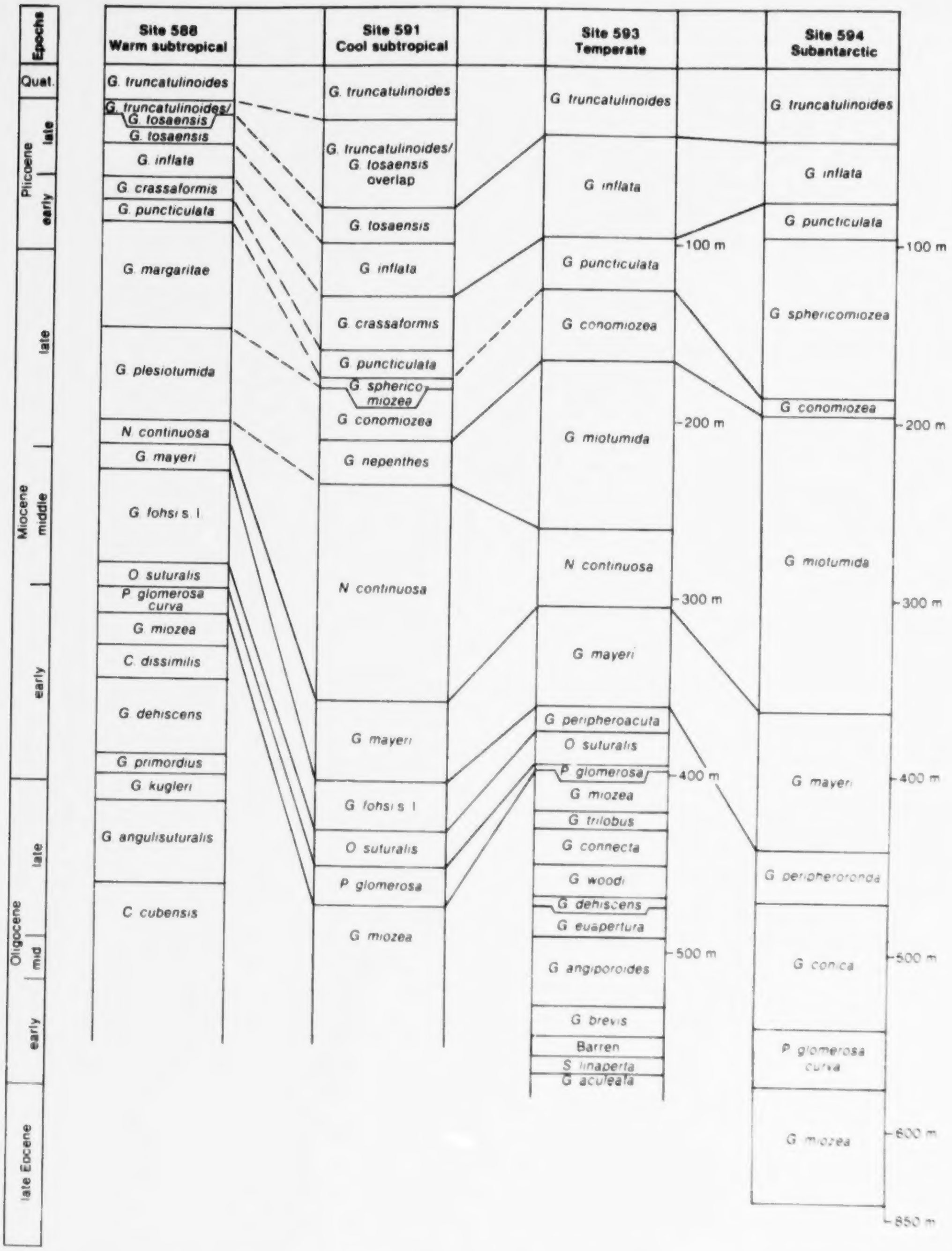
Epochs
Quat.
Pliocene
late
early
Miocene
late
middle
early
Oligocene
late
mid
early
late Eocene
Site 588
Warm subtropical
G. truncatulinoides
G. truncatulinoides/ G. tosaensis
G. tosaensis
G. inflata
G. crassaformis
G. puncticulata
G. margaritae
G. plesiotumida
N. continuosa
G. mayeri
G. fohsi s. l.
O. suturalis
P. glomerosa curva
G. miozea
C. dissimilis
G. dehiscens
G. primordius
G. kugleri
G. angulisuturalis
C. cubensis
Site 591
Cool subtropical
G. truncatulinoides
G. truncatulinoides/ G. tosaensis overlap
G. tosaensis
G. inflata
G. crassaformis
G. puncticulata
G. sphericomiozea
G. conomiozea
G. nepenthes
N. continuosa
G. mayeri
G. fohsi s. l.
O. suturalis
P. glomerosa
G. miozea
Site 593
Temperate
G. truncatulinoides
G. inflata
G. puncticulata
G. conomiozea
G. miotumida
N. continuosa
G. mayeri
G. peripheroacuta
O. suturalis
P. glomerosa
G. miozea
G. trilobus
G. connecta
G. woodi
G. dehiscens
G. euapertura
G. angiporoides
G. brevis
Barren
S. linaperta
G. aculeata
100 m
200 m
300 m
400 m
500 m
Site 594
Subantarctic
G. truncatulinoides
G. inflata
G. puncticulata
G. sphericomiozea
G. conomiozea
G. miotumida
G. mayeri
G. peripheroronda
G. conica
P. glomerosa curva
G. miozea
100 m
200 m
300 m
400 m
500 m
600 m
850 m

Figure 2. Four planktonic foraminiferal zonal schemes used for Leg 90 drilled sites with datums used for intersite correlation.

er outline in peripheral view when compared with typical forms (see taxonomic notes).

The *G. fohsi* s.l. Zone was used because it was difficult consistently to identify keeled *Globorotalia fohsi* in the upper part of the *G. fohsi* s.l. Zone at Site 588. The *G. fohsi* s.l. Zone is equivalent to the upper part of the *Orbulina suturalis* Zone of Kennett (1973) and to both the *G. fohsi* s.l. Zone and the *G. peripheroacuta* Zone of Srinivasan and Kennett (1981a, b).

Cool Subtropical

The main difference between the cool and warm subtropical zonal schemes is the recognition of the late Miocene zones that are noted in Table 4.

Table 2. Tropical zonal scheme with zonal markers.

Epochs	Tropical zonal scheme	Zonal markers
Pleistocene	N22	*Globorotalia truncatulinoides* I.A.
Pliocene	N21	*Globorotalia tosaensis* I.A.
	N19–N20	*Sphaeroidinella dehiscens* I.A.
	N18	*Globorotalia tumida* I.A.
Miocene l.	N17b	*Pulleniatina primalis* I.A.
	N17a	

Note: In Tables 2-6, I.A. = initial appearance, Ext. = Extinction.

Table 3. Warm subtropical zonal scheme with zonal markers.

Epochs		Warm subtropical zonal scheme	Zonal markers
Pleistocene		*Globorotalia truncatulinoides*	*Globorotalia tosaensis* Ext.
		G. truncatulinoides/G. tosaensis	*G. truncatulinoides* I.A.
Pliocene		*G. tosaensis*	*G. tosaensis* I.A.
		Globorotalia inflata	*G. inflata* I.A.
		Globorotalia crassaformis	*G. crassaformis* I.A.
		Globorotalia puncticulata	*G. puncticulata* I.A.
Miocene	l.	*Globorotalia margaritae*	*G. margaritae* I.A.
		Globorotalia plesiotumida	*G. plesiotumida* I.A.
		Neogloboquadrina continuosa	*G. mayeri* Ext.
	m.	*Globorotalia mayeri*	*Globorotalia peripheroacuta* Ext.
		Globorotalia fohsi (s.l.)	*G. peripheroacuta* I.A.
		Orbulina suturalis	*O. suturalis* I.A.
	e.	*Praeorbulina glomerosa curva*	*P. glomerosa curva* I.A.
		Globorotalia miozea	*C. dissimilis* Ext.
		Catapsydrax dissimilis	*Globorotalia kugleri* Ext.
		Globoquadrina dehiscens	*G. dehiscens* I.A.
Oligocene	l.	*Globigerinoides primordius*	*G. primordius* I.A.
		G. kugleri	*G. kugleri* I.A.
		Globigerina angulisuturalis	*C. cubensis* Ext.
		Chiloguembelina cubensis	

Table 4. Late Miocene cool subtropical zonal scheme with zonal markers.

Epoch		Zones	Zonal markers
Miocene	l.	*Globorotalia sphericomiozea*	*Globorotalia conomiozea* Ext.
		G. conomiozea	*G. conomiozea* I.A.
		Globigerina nepenthes	*Neogloboquadrina continuosa* Ext.

The cool subtropical zonal scheme is a modification of that used by Kennett (1973) and by Srinivasan and Kennett (1981a, b).

Temperate

Compared with the cool subtropical zonal scheme of Sites 591 and 592 the temperate scheme at 593 has been modified to account for the absence or paucity of some warmer-water zonal markers. Thus the *Globorotalia tosaensis* Zone and the *G. truncatulinoides/G. tosaensis* Zone are not recognized because of the low numbers of *Globorotalia tosaensis;* similarly because of the low numbers of *Neogloboquadrina continuosa*, the upper boundary of the *Neogloboquadrina continuosa* Zone was redefined on the extinction of *Globoquadrina dehiscens.* The zones and zonal markers are shown in Table 5. This zonal scheme is similar to that developed onshore in southeast Australia and New Zealand (Jenkins, 1960, 1966b, 1967) and on DSDP Leg 29 (Jenkins, 1975).

Table 5. Temperate zonal scheme with zonal markers.

Epochs		Temperate zonal scheme	Zonal markers
Pleistocene		*Globorotalia truncatulinoides*	*G. truncatulinoides* I.A.
Pliocene	l.	*Globorotalia inflata*	*G. inflata* I.A.
	e.	*Globorotalia puncticulata*	*G. puncticulata* I.A.
Miocene	l.	*Globorotalia conomiozea*	*G. conomiozea* I.A.
		Globorotalia miotumida	*Globoquadrina dehiscens* Ext.
		Neogloboquadrina continuosa	*Globorotalia mayeri* Ext.
	m.	*G. mayeri*	*Globorotalia peripheroacuta* Ext.
		G. peripheroacuta	*G. peripheroacuta* I.A.
		Orbulina suturalis	*O. suturalis* I.A.
	e.	*Praeorbulina glomerosa curva*	*P. glomerosa curva* I.A.
		Globorotalia miozea	*G. miozea* I.A.
		Globigerinoides trilobus	*G. trilobus* I.A.
		Globigerina connecta	*G. connecta* I.A.
		Globigerina woodi	*G. woodi* I.A.
		Globoquadrina dehiscens	*G. dehiscens* I.A.
Oligocene	l	*Globigerina euapertura*	*Globigerina angiporoides* Ext.
	e.	*G. angiporoides*	*Globigerina brevis* Ext.
		G. brevis	*G. brevis* I.A.
Eocene	l.	*Globigerina linaperta*	*Globorotalia aculeata* Ext.
		G. aculeata	

Table 6. Subantarctic zonal scheme with zonal markers.

Epochs		Subantarctic zonal scheme	Zonal markers
Pleistocene		*Globorotalia truncatulinoides*	*G. truncatulinoides* I.A.
Pliocene		*Globorotalia inflata*	*G. inflata* I.A.
		Globorotalia puncticulata	*Globorotalia sphericomiozea* Ext.
Miocene	l.	*G. sphericomiozea*	*Globorotalia conomiozea* Ext.
		G. conomiozea	*G. conomiozea* I.A.
		Globorotalia miotumida	*Globorotalia mayeri* Ext.
	m.	*G. mayeri*	*Globorotalia peripheroronda* Ext.
		G. peripheroronda	*Globorotalia conica* Ext.
		G. conica	*G. conica* I.A.
		Praeorbulina glomerosa curva?	*Globorotalia miozea:* change from random to sinistral coiling
	e.	*G. miozea*	

Subantarctic

Site 594 is located in subantarctic waters and the cooler waters in the Miocene to Pleistocene have affected the distribution of some of the taxa. Thus the initial appearance of *Globorotalia truncatulinoides* is within the late Pleistocene and the *Orbulina suturalis* Zone and the *Globigerinoides trilobus* Zone could not be identified because of the absence of zonal markers. The zonal scheme used for Site 594 (Table 6) is a modification of that used onshore in New Zealand (Jenkins, 1966a, 1967) and that developed on DSDP Leg 29 (Jenkins, 1975).

Zonal Markers

The intersite zonal markers used for correlation are shown in Figure 3. From a comparison with other mi-

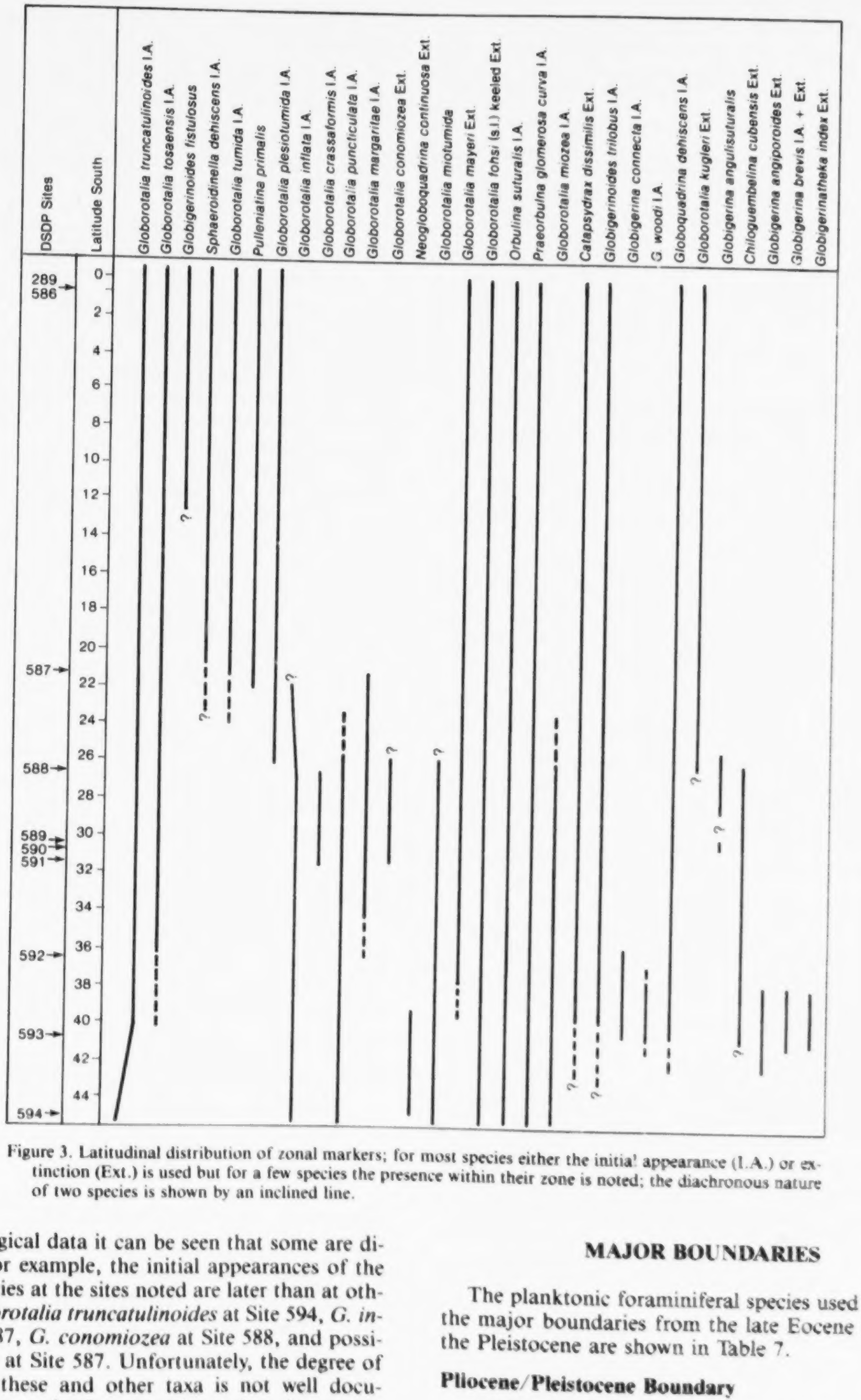

Figure 3. Latitudinal distribution of zonal markers; for most species either the initial appearance (I.A.) or extinction (Ext.) is used but for a few species the presence within their zone is noted; the diachronous nature of two species is shown by an inclined line.

cropaleontological data it can be seen that some are diachronous. For example, the initial appearances of the following species at the sites noted are later than at other sites: *Globorotalia truncatulinoides* at Site 594, *G. inflata* at Site 587, *G. conomiozea* at Site 588, and possibly *G. tumida* at Site 587. Unfortunately, the degree of diachrony of these and other taxa is not well documented because good paleomagnetic stratigraphy was not obtained.

MAJOR BOUNDARIES

The planktonic foraminiferal species used to identify the major boundaries from the late Eocene through to the Pleistocene are shown in Table 7.

Pliocene/Pleistocene Boundary

At Sites 586–592 the first evolutionary appearance of *Globorotalia truncatulinoides* was used with some con-

Table 7. Major boundary and zonal markers used on Leg 90.

Epoch		Boundary marker	Site
Pleistocene			
		← *Globorotalia truncatulinoides* I.A.	586–592
Pliocene	l.		
		← *Globorotalia inflata* I.A.	588–593
	e.		
		← *Globorotalia tumida* I.A. *Globorotalia conomiozea* Ext.	586, 587 588, 590–594
Miocene	l.		
		← *Neogloboquadrina acostaensis* I.A. *Globorotalia mayeri* Ext.	586 588–594
	m.		
		← *Orbulina suturalis* I.A.	586, 588–594
	e.		
		← *Globoquadrina dehiscens* I.A.	586, 588, 593
Oligocene	l.		
		← *Globigerina angiporoides* Ext.	592, 593
	e.		
		← *Globigerinatheka index* Ext.	592, 593
Eocene	l.		

fidence because its immediate ancestor *G. tosaensis* was present at these sites. Because of the low numbers of *G. tosaensis* at Site 593 and total absence of this species at 594, the first appearance of *G. truncatulinoides* could not be used to mark the Pliocene/Pleistocene boundary.

Miocene/Pliocene Boundary

At the tropical Sites 586 and 587 the first appearance of *Globorotalia tumida* was used, but further south, because this species became rare and then was not present, the extinction of *G. conomiozea* was used instead. This latter extinction is probably diachronous between sites.

Oligocene/Miocene Boundary

The first appearance of *Globoquadrina dehiscens* was used at Sites 586, 588, and 593. Srinivasan and Kennett (1983) have suggested that the first appearance of *G. dehiscens* can be used to mark the boundary in the southwest Pacific; this follows the work of Jenkins (1966b, 1971) in New Zealand. Srinivasan and Kennett (1983) have also suggested that the first appearance of *G. dehiscens* is isochronous in the North Atlantic and Pacific but Jenkins (1973, 1981) has argued that its first appearance is diachronous when plotted from the high-mid latitudes to low-latitude areas. It had been hoped that this problem could be resolved on the Leg 90 north-south traverse by comparing the taxonomic appearances at the various sites with the paleomagnetic record; unfortunately the intensities of magnetization were too low to produce a good paleomagnetic record.

Eocene/Oligocene Boundary

The extinction datum used for *Globigerinatheka index* follows the original work of Finlay (1939), Hornibrook (1958), and Jenkins (1963, 1966a) in New Zealand. It is probable that the extinction of this species is not too diachronous within the latitudinal belt 55°–35°S, but the extension of this event into the low latitudes will probably prove to be diachronous.

The species used to position the intraepoch boundaries are also shown in Table 7.

INITIATION OF THE CIRCUM-ANTARCTIC CURRENT

From the faunal evidence of planktonic foraminifers, the Circum-Antarctic Current began about 30 Ma ago (Jenkins, 1974, 1978a, b, c). An aid in dating this event was the documentation of *Jenkinsina samwelli*, and further evidence of its distribution has come from Site 593.

J. samwelli lived in the Austral Gulf between Antarctica and Australia from the earliest Oligocene to late Oligocene, according to the evidence from South Australia (Lindsay, 1969) (Fig. 4, [1]). At this time Antarctica was joined to Australia at the Tasman Rise and the only outlet of the Austral Gulf was toward the Indian Ocean. In the earlier part of the late Oligocene (*Globigerina euapertura* Zone), *J. samwelli* migrated eastward into the southwest Pacific with the parting of Australia and Antarctica; it migrated at least as far as the Campbell Plateau (Site 276), into marine incursions onto the South Island of New Zealand, and through Drake Passage to Site 360. As a result of Leg 90 the northern limit of *J. samwelli* can now be extended to latitude 40°30.47′S, because it was found at Site 593. In these areas *J. samwelli* lived for only a very brief interval (Fig. 4, [2]–[7]).

The ranges and extinctions of *Chiloguembelina cubensis* and *J. samwelli* are shown in Figure 4. The estimated age of 30 Ma for the beginning of the Circum-Antarctic Current and opening of Drake Passage is based on Berggren's (1972) date for the extinction of *C. cubensis*, 28.8–31.2 ± 1.5 Ma, because it approximates the extinction of *J. samwelli*, which happened soon after the current began.

UNCONFORMITIES

The oldest rocks below the unconformity at Site 592 are in the upper *Globigerina angiporoides* Zone of the Oligocene and the overlying rocks are in the lower Miocene *Globigerinoides trilobus* Zone. The probable cause of this and similarly aged unconformities in the Tasman Sea was the initiation of the Circum-Antarctic Current about 30 Ma ago. Some of the Tasman Sea unconformities are shown in Figure 5 and the ones formed by the bottom water of the Circum-Antarctic Current include those at Sites 209, 588, 207, and 592. The dating of the rocks above and below the unconformities at Sites 210 and 206 needs to be checked.

TAXONOMIC NOTES

In the recent publication by Kennett and Srinivasan (1983), most of the Neogene planktonic foraminiferal species of the southwestern Pacific have been illustrated by a Scanning Electron Microscope (SEM). Previously, mainly hand-drawn illustrations were available (Jenkins, 1966a, 1967, 1971). In this report most of the Paleogene species have been illustrated, plus a few from the Neogene which are of special interest (Plates 1–5), and the identified species from each of the Sites 586–594 are recorded in Tables 8–16. Specimens illustrated on Plates 1–5 have been deposited at the U.S. National Museum, Smithsonian Institute, Washington, D.C.

***Catapsydrax* cf. *echinatus* Bolli** (Plate 1, Fig. 1). Bolli, 1957a, p. 165, pl. 37, figs. 2a–5b. The illustrated specimen is not very spiny like *C. echinatus* but it is referred to this species because of its small size and the few spines which can be seen on the final chamber; the bulla is small and smooth.

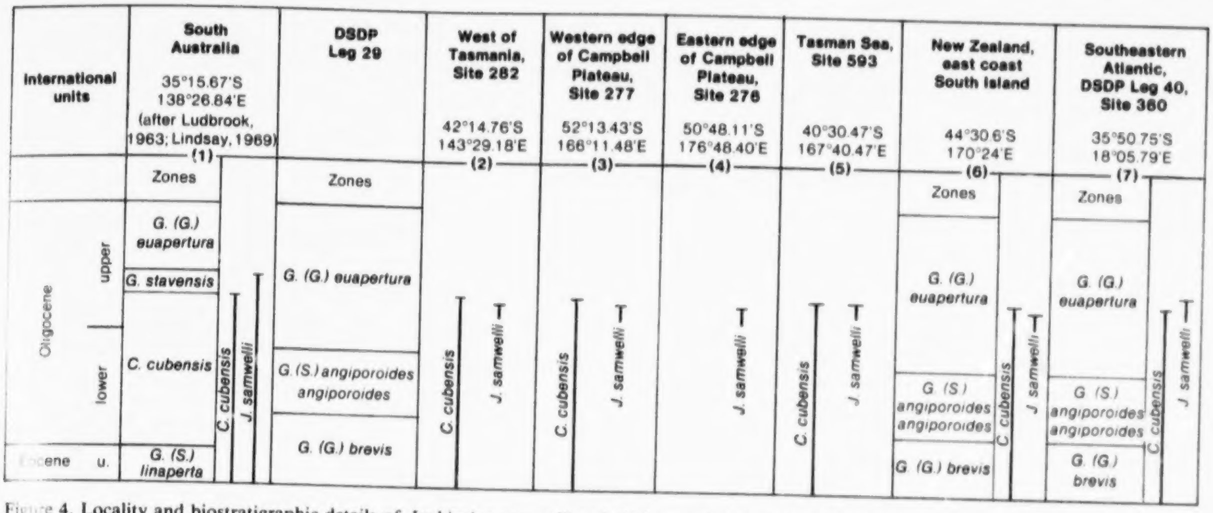

Figure 4. Locality and biostratigraphic details of *Jenkinsina samwelli* and *Chiloguembelina cubensis* in sites around Antarctica.

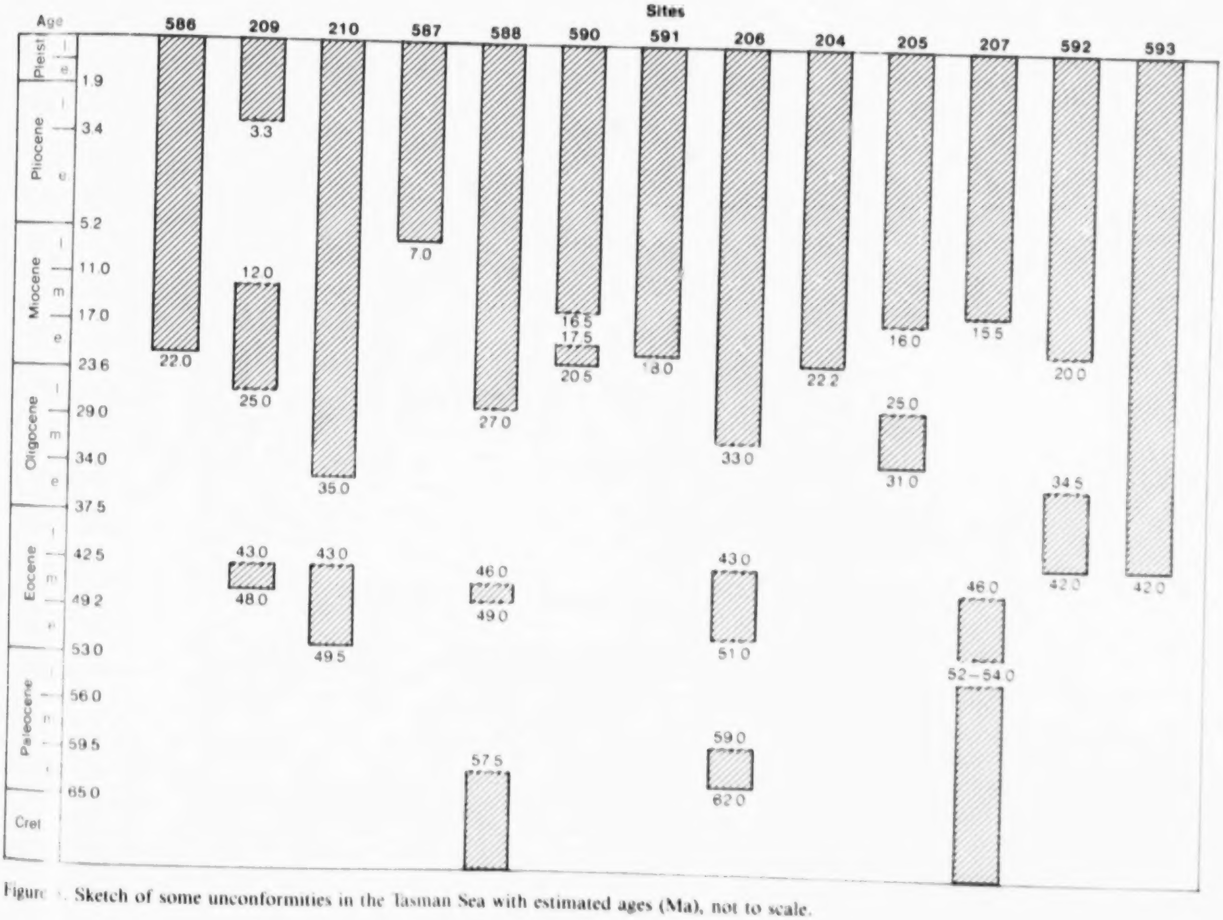

Figure 5. Sketch of some unconformities in the Tasman Sea with estimated ages (Ma), not to scale.

Table 8A. Occurrences of planktonic foraminifers in selected samples of Hole 586B, Sections 1-1 through 5-1.

Epoch	Zone	Core-Section (interval in cm)	Diversity (no. of species)	*Streptochilus globigerum*	*Globigerina quinqueloba*	*G. bulloides*	*G. falconensis*	*G. rubescens*	*G. pseudofoliata*	*Globigerinoides conglobatus*	*G. trilobus*	*G. quadrilobatus*	*G. sacculifer*	*G. fistulosus*	*G. ruber*	*G. ruber elongatus*	*G. tenellus*	*Orbulina universa*	*Globorotalia menardii*	*G. exilis*	*G. scitula*	*G. cibaoensis*	*G. theyeri*	*G. crassaformis*	*G. tosaensis*	*G. tosaensis/truncatulinoides*	*G. truncatulinoides*	*G. tumida tumida*	*Globoquadrina venezuelana*	*G. conglomerata*	*Neogloboquadrina pachyderma*	*N. humerosa*	*N. dutertrei*	*Pulleniatina primalis*	*P. obliquiloculata*	*Sphaeroidinella dehiscens*	*Globorotaloides hexagona*	*Globigerinita glutinata*	*Candeina nitida*	*Beela praedigitata*	*B. digitata*	*Globigerinella obesa*	*G. aequilateralis*	*G. calida*	*Hastigerina pelagica*
Pleistocene	N22	1-1, 51-53	19			x				x	x	x	x		x			x	x				x	x			x	x	x				x		x	x		x					x	x	
		1-2, 90-92	21					x		x	x	x	x		x			x	x		x		x	x			x	x	x	x			x		x	x		x					x	x	
		1-3, 90-93	22					x		x	x	x	x		x		x	x	x				x	x			x	x	x				x		x	x	x	x	x				x	x	
		1-4, 90-92	18						x	x	x	x	x		x			x	x					x				x	x				x		x	x	x	x	x				x		
		1-5, 90-92	22			x		x	x	x	x	x	x		x		x	x	x					x			x	x	x				x		x	x		x		x			x	x	
		1-6, 90-92	25		x	x		x	x	x	x	x	x		x		x		x		x		x	x			x	x	x			x	x		x		x	x	x				x	x	
		2-1, 50-52	22			x		x	x	x	x	x	x		x		x	x	x				x	x			x	x	x				x		x	x		x					x	x	
		2-1, 90-91	14	x									x		x				x					x			x	x		x			x		x	x		x					x	x	
		2-2, 50-52	26			x		x		x	x	x	x		x	x		x	x	x	x		x	x			x	x	x			x	x		x	x		x	x			x	x	x	
		2-2, 90-91	19			x				x			x		x			x	x		x		x	x			x	x		x			x		x	x	x	x					x	x	
		2-3, 50-52	24			x		x	x	x	x	x	x		x	x	x	x	x	x	x		x	x			x	x					x		x	x		x					x	x	
		2-3, 90-91	16			x				x			x		x			x	x	x	x						x	x					x		x	x	x		x				x		
		2-4, 90-91	13						x	x	x		x		x			x	x								x	x					x			x		x					x		
		2-5, 50-52	20					x		x	x	x	x		x	x		x	x	x				x			x	x					x		x	x	x	x	x				x		
		2-5, 90-91	17			x	x			x			x		x			x	x	x	x						x			x			x		x	x		x	x				x		
		2-6, 50-52	21				x	x		x	x	x	x		x		x	x	x		x		x	x			x	x					x		x	x		x	x				x		
		2-6, 90-91	12										x		x			x	x								x	x		x			x		x	x		x					x		
		3-1, 49-51	21					x		x	x	x	x		x	x		x	x	x			x	x			x	x					x		x	x		x	x				x	x	
		3-2, 50-52	18					x		x	x	x			x			x	x	x				x			x						x		x	x	x	x	x		x		x		
		3-3, 50-52	19			x			x	x	x	x	x		x				x	x	x		x	x			x	x					x		x	x		x					x		
		3-4, 50-52	22		x			x	x	x	x	x	x		x			x	x	x	x		x				x	x					x		x	x		x	x				x	x	
		3-5, 50-52	22		x	x	x	x		x	x	x	x		x		x	x	x		x		x				x	x					x		x	x		x	x				x	x	
		3-6, 50-52	23			x		x	x	x	x	x	x		x		x	x	x		x		x				x	x					x		x	x	x	x	x	x			x		
		4-1, 50-52	24		x			x	x	x	x	x	x		x	x	x	x	x		x		x				x	x					x		x	x		x	x		x		x		x
		4-2, 50-52	20			x			x	x	x	x	x		x	x		x	x					x	x		x	x			x		x		x	x						x	x		
		4-3, 50-52	19			x		x		x	x		x		x			x	x				x	x	x		x	x							x	x		x			x	x	x		
		4-4, 50-52	16				x					x	x		x			x					x		x	x	x	x					x		x	x		x					x		
		4-6, 50-52	22		x	x				x		x	x	x	x			x	x		x		x	x		x	cf.	x				x	x		x	x		x			x		x		
Pliocene	N21	5-1, 50-52	24			x	x	x		x	x	x	x	x	x	x	x	x	x		x			x	x	x						x			x	x		x				x	x		
		5-1, 90-91	14							x			x	x	x			x			x				x	x		x		x		x		x	x	x									

Table 8B. Occurrences of planktonic foraminifers in selected samples of Hole 586B, Sections 5-2 through 8-4.

Epoch	Zone	Core-Section (interval in cm)	Diversity (no. of species)	*Streptochilus tokelauae*	*Globigerina quinqueloba*	*G. bulloides*	*G. falconensis*	*G. woodi*	*G. apertura*	*G. decoraperta*	*G. rubescens*	*G. pseudofoliata*	*Globigerinoides obliquus*	*G. extremus*	*G. conglobatus*	*G. trilobus*	*G. quadrilobatus*	*G. sacculifer*	*G. fistulosus*	*G. ruber*	*G. ruber elongatus*	*Orbulina suturalis*	*O. universa*	*O. bilobata*	*Globorotalia menardii*	*G. multicamerata*	*G. exilis*	*G. scitula*	*G. theyeri*	*G. crassaformis*	*G. tosaensis*	*G. tosaensis/truncatulinoides*	*G. tumida tumida*	*G. ungulata*	*Globoquadrina venezuelana*	*G. altispira altispira*	*G. conglomerata*	*Neogloboquadrina pachyderma*	*N. humerosa*	*N. humerosa duterrei plexus*	*N. dutertrei*	*Pulleniatina primalis*	*P. obliquiloculata*	*Sphaeroidinella dehiscens*	*Globorotaloides hexagona*	*Globigerinita glutinata*	*Candeina nitida*	*Beela digitata*	*Globigerinella obesa*	*G. aequilateralis*
Pliocene l.	N21	5-2, 50-52	22							x	x				x	x	x	x	x	x	x	/	x		x					x	x	x	x						x				x	x		x		x		x
		5-2, 110-112	20				x	x		x				x	x				x	x			x		x	x		x			x	x	x				x			x		x	x	x						x
		5-3, 50-52	21								x	x			x		x	x	x	x	x		x		x					x	x	x	x		x				x		x		x	x		x			x	
		5-4, 50-52	22			x					x				x	x	x	x	x	x			x		x			x		x	x	x	x		x						x	x		x		x				x
		5-5, 50-52	24			x					x				x	x	x	x	x	x			x		x	x		x		x	x	x	x		x			x	x			x	x	x		x				x
		5-6, 50-52	24					x							x	x	x	x	x	x			x		x	x		/	x	x	x	x	x		x				x		x	x		x		x	x			x
		6-1, 50-51	21			x					x				x	x	x	x	x	x		x	x		x			x	/	x	x		x		x				x			x		x		x				x
		6-1, 60-61	23			x		x			x				x	x	x	x	x	x			x		x			x		x	x	x	x		x				x		x	x		x		x				x
		6-2, 50-51	25		x			x		x					x	x	x	x		x			x		x	x		x	x	x	x	x	x		x				x			x		x	x	x	x			x
		6-2, 60-61	19			x				x	x				x	x	x	x	x	x					x					x	x		x		x				x			x		x		x				x
		6-3, 50-51	20							x					x	x	x	x	x	x			x		x			x		x	x		x		x				x			x		x		x			x	x
		6-3, 60-61	20							x					x	x	x	x	x	x			x		x			x		x	x		x		x				x			x		x		x			x	x
		6-4, 50-51	19							x	x				x	x	x	x	x	x					x	x		x			x		x		x				x			x		x		x				x
		6-4, 60-61	20							x		x			x	x	x	x	x	x			x		x					x	x		x		x				x			x		x	x	x				x
		6-5, 50-51	22			x				x	x	x			x	x		x	x	x			x		x	x		x		x	x		x		x				x			x		x		x				x
		6-5, 60-61	17							/					x	x	x	x	x	x					x					x	x		x		x				x			x		x		x				x
		6-6, 50-51	25			x				x	x	x		x	x	x	x	x	x	x			x		x	x				x	x		x		x				x			x		x	x	x			x	x
		6-6, 60-61	22	x								x		x	x		x	/	x	x			x	x	x		x			x	x		x		x				x			x		x	x	x				x
		6-6, 108	22	x								x		x	x		x	x	x	x			x	x	x		x			x	x		x		x				x			x		x	x	x				x
		7-1, 50-52	22	x								x		x	x		x	x	x	x			x	x	x		x			x	x		x		x				x			x		x	x	x				x
		7-2, 50-52	22	x								x		x	x		x	x	x	x			x	x	x		x			x	x		x		x				x			x		x	x	x				x
		7-3, 50-52	22	x		x				x				x	x	x	x		x	x			x	x	x		x				R		x		x							x	cf.	x	x	x				x
		7-4, 50-52	22	x								x		x	x		x	x	x	x			x	x	x		x			x	x		x		x				x			x		x	x	x				x
		7-5, 50-52	22	x		x				x				x	x	x	x		x	x			x	x	x		x				R		x		x							x	cf.	x	x	x				x
		7-6, 50-52	22			x				x				x	x	x	x		x	x			x	x	x		x				R		x		x							x	cf.	x	x	x				x
		8-1, 50-52	20										x	x	x	x		x	x				x					x		x	x		x	x	x	x			x			x	cf.	x	x					x
		8-2, 20-21	18			x								x	x	x		x	x	x			x			x	x				x			x		x			x			x	cf.	x						x
		8-2, 50-52	18			x								x	x	x		x	x	x			x			x	x				x			x		x			x			x	cf.	x						x
		8-3, 50-52	18			x								x	x	x		x	x	x			x			x	x				x			x		x			x			x	cf.	x						x
		8-4, 50-52	21			x			x						x			x	x	x			x			x	x			x	x		x	x		x			x			x	cf.	x	x	x				x

Note: R = reworked.

Table 8C. Occurrences of planktonic foraminifers in selected samples of Hole 586B, Sections 8-5 through 15-3.

Epoch	Zone	Core-Section (interval in cm)	Diversity (no. of species)	*Streptochilus globigerum*	*Globigerina quinqueloba*	*G. bulloides*	*G. falconensis*	*G. nepenthes*	*G. decoraperta*	*Globigerinoides obliquus*	*G. extremus*	*G. conglobatus*	*G. trilobus*	*G. quadrilobatus*	*G. sacculifer*	*G. "praefistulosus"*	*G. fistulosus*	*G. bollii*	*G. ruber*	*Orbulina suturalis*	*O. universa*	*Globorotalia menardii*	*G. multicamerata*	*G. scitula*	*G. margaritae*	*G. crassaformis*	*G. tosaensis*	*G. plesiotumida*	*G. tumida tumida*	*Globoquadrina venezuelana*	*G. altispira altispira*	*G. conglomerata*	*Neogloboquadrina acostaensis*	*N. humerosa*	*Pulleniatina primalis*	*P. spectabilis*	*P. obliquiloculata*	*Sphaeroidinella seminulina*	*S. paenedehiscens*	*S. dehiscens*	*Globorotaloides variabilis*	*G. hexagona*	*Globigerinita glutinata*	*Beela praedigitata*	*Globigerinella obesa*	*G. aequilateralis*
Pliocene	N21	8-5, 20-21	26			x	x		x	x	x	x	x		x		x		x		x	x	x			x	x		x	x	x			x	x			x		x		x	x	x		x
	N19-N20	8-5, 50-52	25			x	x		x	x	x	x	x		x		x		x		x	x	x			x			x	x	x			x	x			x		x		x	x	x		x
		8-6, 20-21	17								x		x		x	x	cf.		x		x		x		x	x			x		x	x			x		x			x		x				x
		8-6, 50-52	18								x		x		x	x	cf.		x		x		x		x	x			x		x	x			x		x			x		x				x
		11-1, 50-52	21			x	x		x	x	x		x	x	x							x			x				x					x	x	x		x		x	x	x	x		x	x
		11-2, 50-52	21			x	x		x	x	x		x	x	x							x			x				x					x	x	x		x		x	x	x	x		x	x
		11-3, 50-52	21			x	x		x	x	x		x	x	x							x			x				x					x	x	/		x		x	x	x	x		x	x
		11-4, 50-52	21			x	x		x	x	x		x	x	x							x			x				x					x	x	x		x		x	x	x	x		x	x
		11-5, 50-52	21			x	x		x	x	x		x	x	x							x			x				x					x	x	x		x		x	x	x	x		x	x
		11-6, 50-52	21			x	x		x	x	x		x	x	x							x			x				x					x	x	x		x		x	x	x	x		x	x
		12-1, 50-52	26	x	x		x		x	x	x		x		x							x	x	x	x			x	x	x	x			x	x			x	x	x	x	x	x		x	x
		12-2, 50-52	27	x	x		x		x	x	x		x		x							x	x	x	x			x	x	x	x			x	x	x		x	x	x	x	x	x		x	x
		12-4, 50-52	27	x	x		x		x	x	x		x		x							x	x	x	x			x	x	x	x			x	x	x		x	x	x	x	x	x		x	x
		12-5, 50-52	27	x	x		x		x	x	x		x		x							x	x	x	x			x	x	x	x			x	x	x		x	x	x	x	x	x		x	x
		12-6, 50-52	27	x	x		x		x	x	x		x		x							x	x	x	x			x	x	x	x			x	x	x		x	x	x		x	x		x	x
		13-4, 50-52	23	x		x			x	x	x		x	x	x			x		x	x	x	x						x		x			x	x	x		x	x			x	x			x
		13-5, 18-19	23	x		x			x	x	x	x	x	x	x			x		x	x	x	x						x		x			x	x	x		x	x			x	x			x
		13-5, 50-52	20	x					x	x	x	x	x		x						x	x	x						x		x			x	x	x			x	x		x	x			x
		13-6, 50-52	20	x					x	x	x	x	x		x						x	x	x						x		x			x	x	x			x	x		x	x			x
		13-6, 50-52	20	x					x	x	x	x	x		x						x	x	x						x		x			x	x	x			x	x		x	x			x
		13-7, 18-19	20	x					x	x	x	x	x		x						x	x	x						x		x			x	x	x			x	x		x	x			x
	N18	14-1, 50-52	27	x			x	x	x	x	x	x	x	x	x					x	x	x	x	x	x				x	x	x		x	x	x	x			x				x		x	x
		14-2, 50-52	27	x			x	x	x	x	x	x	x	x	x					x	x	x	x	x	x				x	x	x		x	x	x	x			x				x		x	x
		14-3, 50-52	27	x			x	x	x	x	x	x	x	x	x					x	x	x	x	x	x				x	x	x		x	x	x	x			x				x		x	x
		14-4, 50-52	25	x				x	x	x	x	x	x		x			x				x	x		x			x	x	x	x		x	x	x	cf.		x	x				x		x	x
		14-5, 50-52	25	x				x	x	x	x	x	x		x			x				x	x		x			x	x	x	x		x	x	x	cf.		x	x				x		x	x
		14-6, 50-52	25	x				x	x	x	x	x	x		x			x				x	x		x			x	x	x	x		x	x	x	cf.		x	x				x		x	x
		15-1, 50-52	24	x				x	x	x	x	x	x	x	x					x	x	x			/			x	x	x	x	x			x	cf.		x	x				x		x	x
		15-2, 50-52	25	x				x	x	x	x	x	x	x	x					x	x	x			x			x	x	x	x	x			x	cf.		x	x				x		x	x
		15-3, 50-52	24	x				x	x	x	x	x	x	x	x					x	x	x						x	x	x	x	x			x	cf.		x	x				x		x	x

Table 8D. Occurrences of planktonic foraminifers in selected samples of Hole 586B, Sections 15-4 through 19-3.

Epoch	Zone	Core-Section (interval in cm)	Diversity (no. of species)	*Streptochilus globigerum*	*S. latum*	*Globigerina quinqueloba*	*G. bulloides*	*G. falconensis*	*G. woodi*	*G. nepenthes*	*G. decoraperta*	*Globigerinoides obliquus*	*G. extremus*	*G. conglobatus*	*G. bulloideus*	*G. trilobus*	*G. quadrilobatus*	*G. sacculifer*	*G. bolli*	*Orbulina suturalis*	*O. universa*	*O. bilobata*	*Globorotalia menardii*	*G. multicamerata*	*G. scitula*	*G. juanai*	*G. margaritae*	*G. cibaoensis*	*G. plesiotumida*	*G. plesiotumida/tumida plexus*	*G. tumida tumida*	*G. anfracta*	*Globoquadrina venezuelana*	*G. dehiscens*	*G. baroemoensis*	*G. altispira altispira*	*G. altispira globosa*	*G. conglomerata*	*Neogloboquadrina pachyderma*	*N. acostaensis*	*N. humerosa*	*Pulleniatina primalis*	*P. spectabilis*	*Sphaeroidinella seminulina*	*S. paenedehiscens*	*Globorotaloides hexagona*	*Globigerinella aequilateralis*
Pliocene e.	N18	15-4, 50–52	27	x						x	x	x	x	x		x	x	x	x		x	x	x	x	x				x		x		x			x		x				x	cf.	x	x		
		15-5, 50–52	27	x						x	x	x	x	x		x	x	x	x		x	x	x	x	x				x		x		x			x		x				x	cf.	x	x		
		15-6, 50–52	12							x		x						x			x										x		x			x				x		x		x	x		x
		16-1, 50–52	30	x		x				x	x	x	x	x		x	x	x	x	x	x		x						x		x		x			x		x		x	x	x	x	x	x	x	
		16-2, 50–52	30	x		x				x	x	x	x	x		x	x	x	x	x	x		x						x		x		x			x		x		x	x	x	x	x	x	x	
		16-3, 50–52	30	x		x				x	x	x	x	x		x	x	x	x	x	x		x						x		x		x			x		x		x	x	x	x	x	x	x	
		16-5, 50–52	24	x					x		x	x	x	x		x	x	x			x		x					cf.	x		x		x			x				x	x	x		x	x		
		16-6, 50–52	24	x					x		x	x	x	x		x	x	x			x		x					cf.	x		x		x			x				x	x	x		x	x		
		17-1, 50–52	21	x							x	x	x	x		x		x			x								x		x		x			x				x	x	x	cf.	x	x		
		17-1, 70–71	21	x							x	x	x	x		x		x			x								x		x		x			x				x	x	x	cf.	x	x		
		17-2, 50–52	21	x							x	x	x	x		x		x			x								x		x		x			x				x	x	x	cf.	x	x		
		17-2, 70–71	23	x							x	x	x	x		x		x			x		x			x			x		x		x			x				x	x	x	cf.	x	x		
		17-3, 50–52	20	x							x	x	x	x		x		x											x		x		x			x				x	x	x	cf.	x	x		
Miocene l.	N17b	17-4, 50–52	25	x				x	x		x	x	x	x		x	x	x			x	x	x						x	x			x	x	x					x	x	x		x	x	x	
		17-4, 70–71	25	x				x	x		x	x	x	x		x	x	x			x	x	x						x	x			x	x	x					x	x	x		x	x	x	
		17-5, 70–71	24	x							x	x	x	x		x		x	x	x	x		x						x	x			x	x		x				x	x	x		x	x		
		17-6, 50–52	24					x				x	x	x		x		x		x	x		x		x				x	x			x	x		x				x	x	x		x	x		
		17-6, 70–71	24					x				x	x	x		x		x		x	x		x		x				x				x	x		x				x	x	x		x	x		
		18-1, 50–52	30	x	x			x		x	x	x	x	x		x		x	x		x	x	x	x	x				x			x	x	x	x	x				x	x	x		x	x		
		18-1, 70–72	30	x	x			x		x	x	x	x	x		x		x	x		x	x	x	x	x				x			x	x	x	x	x				x	x	x		x	x		
		18-2, 50–52	30	x	x			x		x	x	x	x	x		x		x	x		x	x	x	x	x				x			x	x	x	x	x				x	x	x		x	x		
		18-2, 70–71	30	x	x			x		x	x	x	x	x		x		x	x		x	x	x	x	x				x			x	x	x	x	x				x	x	x		x	x		
		18-3, 50–52	30	x	x			x		x	x	x	x	x		x		x	x		x	x	x	x	x				x			x	x	x	x	x				x	x	x		x	x		
		18-4, 50–52	30	x	x			x		x	x	x	x	x		x		x	x		x	x	x	x	x				x			x	x	x	x	x				x	x	x		x	x		
		18-4, 70–71	30	x	x			x		x	x	x	x	x		x		x	x		x	x	x	x	x				x			x	x	x	x	x				x	x	x		x	x		
		18-5, 70–71	31	x		x	x	x		x	x	x	x	x		x		x	x	x	x	x	x	x	x				x	x				x	x	x				x	x	x		x	x		
		18-6, 50–52	31	x		x	x	x		x	x	x	x	x		x		x	x	x	x	x	x	x	x				x	x				x	x	x				x	x	x		x	x		
		19-1, 50–52	26	x						x	x	x	x	x		x	x	x					x	x			R			x	R			x	x	x		x	x	x	x	x		x	x		
		19-2, 50–52	32	x	x		x	x		x	x	x	x	x	x	x	x	x	x		x		x	x					x	x		x	x	x	x	x	x			x	x	x		x	x		
		19-3, 50–52	32	x	x		x	x		x	x	x	x	x	x	x	x	x	x		x	x	x	x					x	x		x	x	x	x	x	x			x	x	x		x	x		

Note: R = reworked.

Table 8E. Occurrences of planktonic foraminifers in selected samples of Hole 586B, Sections 19-4 through 25-5.

Epoch	Zone	Core-Section (interval in cm)	Diversity (no. of species)	*Streptochilus globigerum*	*S. latum*	*Globigerina bulloides*	*G. falconensis*	*G. apertura*	*G. nepenthes*	*G. decoraperta*	*Globigerinoides obliquus*	*G. extremus*	*G. conglobatus*	*G. bulloideus*	*G. trilobus*	*G. quadrilobatus*	*G. sacculifer*	*G. bolli*	*Orbulina suturalis*	*O. universa*	*O. bilobata*	*Globorotalia menardii*	*G. multicamerata*	*G. scitula*	*G. juanai*	*G. juanai/praemargaritae*	*G. praemargaritae*	*G. margaritae*	*G. plesiotumida*	*G. plesiotumida/tumida*	*G. tumida tumida*	*G. anfracta*	*G. cf. ichinosekiensis*	*Globoquadrina venezuelana*	*G. dehiscens*	*G. baroemoensis*	*G. altispira altispira*	*G. altispira globosa*	*G. conglomerata*	*Neogloboquadrina acostaensis*	*N. humerosa*	*Pulleniatina primalis*	*Sphaeroidinella seminulina*	*S. paenedehiscens*	*Globorotaloides variabilis*	*Globigerinita glutinata*	*Candeina nitida*	*Globigerinella aequilateralis*
Miocene l.	N17b	19-4, 50-52	31	x	x	x			x	x	x	x	x	x	x	x	x	x		x		x	x						x	x		x		x	x	x	x	x		x	x	x	x	x		x		x
		19-5, 50-52	31	x	x	x			x	x	x	x	x	x	x	x	x	x		x		x	x						x	x		x		x	x	x	x	x		x	x	x	x	x		x		x
		19-6, 50-52	31	x	x	x			x	x	x	x	x	x	x	x	x	x		x		x	x						x	x		x		x	x	x	x	x		x	x	x	x	x		x		x
		20-1, 50-52	26	x			x	x		x	x	x	x		x		x	x		x		x	x						x				x		x	x	x	x		x	x	x	x	x		x		x
		20-2, 50-52	26	x			x	x		x	x	x	x		x		x	x		x		x	x						x				x		x	x	x	x		x	x	x	x	x		x		x
		20-3, 50-52	27	x			x	x		x	x	x	x		x		x	x		x		x	x				x		x				x		x	x	x	x		x	x	x	x	x		x		x
		20-4, 50-52	26	x			x	x		x	x	x	x		x		x	x		x		x	x						x				x		x	x	x	x		x	x	x	x	x		x		x
		20-5, 50-52	27	x		x	x	x		x	x	x	x		x		x	x		x		x	x						x				x		x	x	x	x		x	x	x	x	x		x		x
	N17a	20-6, 50-52	25	x			x	x		x	x	x	x		x		x	x		x		x	x						x				x		x	x	x	x		x	x		x	x		x		x
		21-1, 50-52	25	x						x	x	x	x		x	x	x			x	x	x	x			x	cf.	R	x					x	x	x	x			x			x	x		x		x
		21-2, 50-52	24	x		x				x	x	x	x		x	x	x			x	x	x	x					R	x				x	x	x	x	x			x			x	x		x		x
		21-3, 50-52	25	x						x	x	x	x		x	x	x			x	x	x	x					R	x					x	x	x	x			x	x		x	x		x		x
		21-4, 50-52	23	x						x	x	x	x		x	x	x			x	x	x	x					R	x					x	x	x	x			x			x	x		x		x
		21-5, 50-52	23	x						x	x	x	x		x	x	x			x	x	x	x					R	x					x	x	x	x			x			x	x		x		x
		21-6, 50-52	23	x						x	x	x	x		x	x	x			x	x	x	x					R	x					x	x	x	x			x			x	x		x		x
		22-1, 50-52	25	x						x	x	x	x		x	x	x	x		x	x	x	x	x					x				x	x	x	x	x	x		x			x			x		x
		22-2, 50-52	29	x		x				x	x	x	x		x	x	x	x		x	x	x	x	x					x				x	x	x	x	x	x		x	cf.		x	x		x	x	x
		22-3, 50-52	29	x		x				x	x	x	x		x	x	x	x		x	x	x	x	x					x				x	x	x	x	x	x		x	cf.		x	x		x	x	x
		22-4, 50-52	25	xx						x	x	x	x		x	x	x	x		x	x	x	x	x					x				x	x	x	x	x	x		x			x			x		x
		22-5, 50-52	27	x		x				x	x	x	x	x	x		x	x		x	x	x	x	x	x				x					x	x	x	x		x	x			x	x		x		x
		22-6, 50-52	22	x						x	x	x	x		x		x			x		x	x	x	x				x					x	x	x	x		x	x			x			x		x
		23-1, 50-52	27	x		x	x		x	x	x	x	x		x		x			x		x	x	x					x					x	x	x	x			x	cf.		x	x		x	x	x
		23-2, 50-52	23	x					x	x	x	x	x		x		x	x		x		x	x	x					x					x	x	x	x			x			x	x	x			x
		23-3, 50-52	23	x					x	x	x	x	x		x		x	x		x		x	x	x					x				x	x	x	x	x			x			x		x			x
		23-4, 50-52	22	x					x	x	x	x	x		x		x	x		x		x	x	x					x					x	x	x	x			x			x		x			x
		23-5, 50-52	21	x					x	x	x	x	x		x		x	x		x		x	x	x					x					x	x	x	x			x			x		x			x
		23-6, 50-52	21	x					x	x	x	x	x		x	x	x	x		x		x	x						x						x	x	x			x			x			x		x
		24-1, 50-52	21	x					x	x	x	x	x		x	x	x	x		x		x	x						x						x	x	x			x			x			x		x
		24-2, 50-52	21	x					x	x	x	x	x		x	x	x	x		x		x	x						x						x	x	x			x			x			x		x
		24-3, 50-52	22	x					x	x	x	x	x		x	x	x	x		x		x	x						x		R				x	x	x			x			x			x		x
		24-5, 50-52	21	x					x	x	x	x	x		x	x	x	x		x		x	x						x						x	x	x			x			x			x		x
		24-6, 50-52	21	x					x	x	x	x	x		x	x	x	x		x		x	x						x						x	x	x			x			x			x		x
		25-1, 50-52	20	x						x	x	x	x		x		x	x	x	x		x	x		x				x						x	x	x			x			x					x
		25-2, 50-52	20	x						x	x	x	x		x		x	x	x	x		x	x		x				x						x	x	x			x			x					x
		25-3, 50-52	20	x						x	x	x	x		x		x	x	x	x		x	x		x				x						x	x	x			x			x					x
		25-4, 50-52	20	x						x	x	x	x		x		x	x	x	x		x	x		x				x						x	x	x			x			x					x
		25-5, 30-31	19	x							x	x	x		x		x			x		x	x	x	cf.				x						x	x	x			x			x			x		x
		25-5, 50-52	20	x						x	x	x	x		x		x	x	x	x		x	x		x				x						x	x	x			x			x					x

Note: R = reworked.

***Chiloguembelina cubensis* (Palmer)** (Plate 1, Fig. 2). *Guembelina cubensis* Palmer, 1934, p. 73, text-figs. 1–6. The extinction of *C. cubensis* appears to be a good marker in the southwest Pacific about 30 Ma ago and was first used by Jenkins and Orr (1972) to subdivide the *Globorotalia opima* Zone in the central Pacific.

***Globanomalina micra* (Cole)** (Plate 1, Fig. 3). *Nonion micrus* Cole, 1927, p. 22, pl. 5, fig. 12. At site 592, *G. micra* became extinct before *Globigerinatheka index;* this site differs from Site 593 and from New Zealand (Jenkins, 1971), where its extinction was slightly later than that of *G. index.*

***Globigerina ampliapertura* Bolli** (Plate 1, Fig. 4). Bolli, 1957b, p. 108, pl. 22, figs. 4a–7b.

***Globigerina angiporoides* Hornibrook** (Plate 1, Fig. 5). Hornibrook, 1965, p. 834, figs. 1, 2. The extinction of *G. angiporoides* in the early Oligocene is thought to be a good regional marker in the southwest Pacific; prior to its extinction there are large populations of the species.

***Globigerina angulisuturalis* Bolli** (Plate 1, Fig. 6). *Globigerina ciperoensis angulisuturalis* Bolli, 1957b, p. 109, pl. 22, fig. 11a–c. This distinctive species is common in the more northern Site 588 and was found at Site 593; it is rare in New Zealand at its southernmost limit.

***Globigerina brevis* Jenkins** (Plate 1, Fig. 7). Jenkins, 1966a, p. 1100, fig. 7, nos. 58–63. The distinctive feature of *G. brevis* is the deep-cut sutures on the umbilical side.

***Globigerina euapertura* Jenkins** (Plate 1, Fig. 8). Jenkins, 1960, p. 351, pl. 1, fig. 8a–c. *G. euapertura* is distinguished from *G. ampliapertura* in having a more umbilical and lower-arched aperture; *G. praesepsis* Blow is a junior synonym of *G. euapertura.*

***Globigerina labiacrassata* Jenkins** (Plate 1, Fig. 9). Jenkins, 1966a, p. 1102, fig. 8, nos. 64–71. The illustrated specimen has the distinctive thick lip but the general morphology of the test resembles that of *G. euapertura*, its probable ancestor.

***Globigerina linaperta* Finlay** (Plate 1, Fig. 10). Finlay, 1939, p. 125, pl. 23, figs. 54–57. Examination of the *G. patagonica* Todd and Knicker holotype at the Smithsonian Institution has shown that it is probably a junior synonym of *G. linaperta.*

***Globigerina ouachitaensis* Howe and Wallace** (Plate 1, Fig. 11). Howe and Wallace, 1932, p. 74, pl. 10, fig. 7a–b. This small, distinct species with an open umbilical aperture is relatively rare in the southwestern Pacific.

***Globigerinatheka index* (Finlay)** (Plate 1, Figs. 12, 13). *Globigerinoides index* Finlay, 1939, p. 125, pl. 14, figs. 85–88. *G. index* tends to be the dominant species in the late Eocene samples from Sites 592 and 593; its extinction is taken to mark the Eocene/Oligocene boundary. The test of *G. index* is normally thick, and thin-walled forms are hardly ever seen in deep-sea deposits; the broken specimen (Pl. 1, fig. 13) shows the thin-walled "*Globigerina*" stage.

***Globigerinatheka semiinvoluta* (Kiejzer)** (Plate 2, Fig. 1). *Globigerinoides semiinvolutus* Keijzer, 1945, p. 206, pl. 4, fig. 58a–e. This is a relatively short-ranging species which has also been described and figured from the late Eocene of New Zealand (Jenkins, 1971).

***Globigerinoides inusitatus* Jenkins** (Plate 2, Fig. 2). Jenkins, 1966a, p. 1108, fig. 9, nos. 72–80. *G. inusitatus* is exceedingly rare and has only been recorded from the *Globigerina euapertura-Globoquadrina dehiscens* zones of New Zealand (Jenkins, 1971). The illustrated specimen has a low arched umbilical aperture and another which is lipped and can be seen on the left side of the specimen. *G. inusitatus* is distinguished from *G. primordius* by its rather irregular shape and rimmed aperture on the spiral side.

***Globigerinoides tyrrhenicus* Borsetti and Cati** (Plate 2, Fig. 3). Borsetti and Cati, 1974, pp. 357, 358. The southwest Pacific specimens are fragile, and one distinctive feature, even in the broken specimens, is the spiny nature of the juvenile forms. Well-preserved specimens of *G. tyrrhenicus* were found at Sites 590 and 591.

***Globorotalia aculeata* Jenkins** (Plate 2, Fig. 4). *Globorotalia inconspicua aculeata* Jenkins, 1966a, p. 1118, fig. 13, nos. 119–125. This species has a widespread distribution in the southwest Pacific, southern United States, and Europe; work is in progress with D. Curry to establish its relationship to *Globorotalia danvillensis* (Howe), which is probably a senior synonym.

***Globorotalia conica* Jenkins** (Plate 2, Figs. 5–7). Jenkins, 1960, p. 358, pl. [illegible] fig. 4a–c. This species was originally described from the middle Miocene of southeast Australia and subsequently recorded from a similar level in New Zealand (Jenkins, 1971). On Leg 29 it was recorded at Sites 278, 279, and 281 and was used at subantarctic Site 278 as a zonal marker in the middle Miocene (Jenkins, 1975); it is also used at the Leg 90 Site 594 as a zonal marker in the lower middle Miocene.

G. conica appears to be better developed in the cooler subantarctic waters and its brief incursions into Australia and New Zealand may represent cooler-water episodes.

There is some evidence in Sample 594A-13,CC that *G. conica* may be related to and developed from *G. peripheroronda;* the latter species is also illustrated (Plate 4, Figs. 13, 14). There also seems to be some morphological affinity between *G. conica* and *G. zealandica*, with overlapping ranges at Site 281 and possibly at Site 594, although here the reworking masks the true stratigraphic relationship.

***Globorotalia* cf. *conomiozea* Kennett** (Plate 2, Fig. 8). Kennett, 1966, p. 235, text-fig. 10a–c. At the more northern Site 588 there is a slightly different form of *G. conomiozea;* it has 4 chambers in the final whorl, a lower conical umbilical side, and appears late stratigraphically compared with the range of *G. margaritae.*

Scott (1982) regards *G. conomiozea* as a variant of *G. conoidea* (= *G. miotumida*); at the more southern sites of Leg 90 it was possible to distinguish the two taxa and consequently use *G. conomiozea* as a zonal marker.

***Globorotalia explicationis* Jenkins** (Plate 2, Figs. 9–11). *Globorotalia miotumida explicationis* Jenkins, 1967, p. 1073, fig. 4, no. 14–19. *Globorotalia petaliformis* Boltovskoy, 1974, p. 707, pl. 14, figs. 1–16.

G. explicationis was recorded as well developed at Site 284 (Jenkins, 1975) and is similarly well developed at Site 593 in the *G. miotumida*–lower *G. conomiozea* zones. A similar uncoiling in the final whorl is present in the late Pleistocene–Recent *G. cavernula* Bé, which has also been recorded from Site 284 (Hornibrook, 1982); Hornibrook (1982) did not record *G. explicationis* from Site 284. Boltovskoy (1974) recorded *G. explicationis* as *G. petaliformis* from the Indian Ocean middle–late Miocene.

***Globorotalia gemma* Jenkins** (Plate 2, Figs. 12–14). Jenkins, 1966a, p. 1115, fig. 11, no. 971. This small species can be easily confused with *G. insolita:* the latter's aperture has a much higher arch (Pl. 3, Figs. 3–4) and much smoother wall than *G. gemma.*

***Globorotalia* cf. *ichinosekiensis* Takayanagi and Oda** (Plate 3, Figs. 1, 2). Takayanagi et al., 1976, pp. 344, 376. Specimens of *G.* cf. *ichinosekiensis* were found at Sites 586, 587, 588, 591, 592, 593, and 594; in order to confirm the identification of the species it will be necessary to obtain specimens from Japan; the southwestern Pacific specimens possibly belong to a new species.

***Globorotalia insolita* Jenkins** (Plate 3, Figs 3, 4). Jenkins, 1966a, p. 1120, fig. 13, nos. 113–118. The main diagnostic features of *G. insolita* are its small size, smooth test wall, square chambers on the spiral side, and very high arched aperture.

G. insolita was first described from the late Eocene of New Zealand and was next recorded at the same level at Site 77 in the equatorial Pacific (Jenkins and Orr, 1972). McDougall (1980) has recently recorded *G. insolita* from Rock Creek Section, Washington, United States, and it is present at Site 592, where there is an important stratigraphic overlap between it and *G. gemma* in the uppermost Eocene.

***Globorotalia mayeri* Cushman and Ellisor** (Plate 3, Figs 5, 6 and 9–11). Cushman and Ellisor, 1939, p. 11, pl. 2, figs. 4a–c. It has been long established that a species identified as *G. mayeri* evolved from *G. peripheroronda* in the middle Miocene of the southwest Pacific (Jenkins, 1960, 1966b, 1971, 1975). Specimens of *G. peripheroronda* and *G. mayeri* have been illustrated from Site 592. Also illustrated is *G. challengeri* Srinivasan and Kennett, which is a possible intermediate species linking *G. peripheroronda* to *G. mayeri.*

Forms showing a range of morphologies between *G. mayeri* and *G. challengeri* are shown (Plate 3, Figs. 9–11). It is possible that *G. challengeri* is a junior synonym of *G. rikuchuensis* Takayanagi and Oda; it is hoped that specimens of the latter species can be obtained from Japan to confirm this.

Hoskins (1984) has published evidence that *G. peripheroronda* is not related to the species identified as *G. mayeri* in the middle Miocene of New Zealand.

Table 9. Occurrences of planktonic foraminifers in selected samples of Hole 587.

Epoch	Zone	Core-Section (interval in cm)	Diversity (no. of species)	Streptochilus globigerum	S. latum	S. tokelauae	Globigerina quinqueloba	G. eamesi	G. bulloides	G. falconensis	G. woodi	G. nepenthes	G. decoraperta	G. foliata	Globigerinoides obliquus	G. extremus	G. conglobatus	G. trilobus	G. quadrilobatus	G. sacculifer	G. fistulosus	G. bollii	G. ruber	G. seiglei	G. tenellus	Orbulina suturalis	O. universa	O. bilobata	Globorotalia panda	G. puncticulata	G. inflata
Pleistocene	G. truncatulinoides	1-1, 5-6	25				x		x	x						R	x	x		x	R		x		x		x				x
		1-2, 6-7	20						x	x						R	x	x		x	R		x				x				x
		1,CC	18						x	x						R	x	x		x	R		x				x				x
		2-1, 15-16	10																	x							x			R	x
		2-2, 15-16	18							x						R	x	x	x	x			x				x			R	x
		2-3, 6-7	16							x							x	x	x	x			x				x			x	x
		2-4, 6-7	18						x	x							x	x	x	x			x				x			x	x
		2-5, 6-7	14														x	x		x			x				x			x	x
		2-6, 6-7	15														x	x		x			x				x			x	x
		2-7, 6-7	11				x										x	x		x			x								
		2,CC	7																											x	x
		3-1, 19-20	12															x					x								x
		3-2, 19-20	14															x	x	x			x				x				x
	G. truncatulinoides/ G. tosaensis	3-3, 19-20	18		x	x			x	x							x										x				x
		3-4, 19-20	19			x			x									x	x	x			x				x				x
		3-5, 80-81	22			x			x	x							x	x	x	x			x				x				x
		3-6, 25-26	14														x	x	x	x							x	x			x
		3,CC	20						x	x							x	x		x			x				x			x	
		4-1, 30-31	19							x							x	x		x			x				x				x
		4-2, 60-61	22						x	x							x	x		x			x				x	x			x
		4-3, 60-61	21						x	x								x		x			x				x	x			x
		4-4, 60-61	21						x	x								x		x			x				x	x			x
		4-5, 60-61	19						x	x								x		x			x				x	x			x
		4-6, 60-61	21				x		x	x							x			x	x		x				x			x	x
		4-7, 30-31	25				x		x	x							x	x		x	x		x				x	x		x	x
		4,CC	22							x						x	x	x		x	x		x				x			x	
Pliocene l	G. tosaensis	5-1, 114-115	20						x	x	x					x	x	x		x			x								x
		5-2, 80-81	20						x	x	x					x	x	x		x			x								x
		5-3, 94-95	24						x	x	x						x	x		x	x		x				x				x
		5-4, 90-91	24						x	x	x						x	x		x	x		x				x				x
	G. inflata	5-5, 80-81	24						x	x	x					x	x	x		x			x			x	x				x
		5-6, 80-81	27				x		x	x						x	x	x	x	x			x			x	x	x		x	x
		5-7, 80-81	27				x		x	x						x	x	x	x	x			x			x	x	x		x	x
		5,CC	21						x	x						x	x	x		x			x				x				x
	G. crassaformis	6-1, 85-86	21						x	x	x		x				x	x		x			x				x			x	
		6-2, 85-86	25						x	x			x		x	x	x	x		x			x							x	
		6-3, 89-90	24	x					x	x	x	x	x			x		x		x							x	x		x	
e	G. puncticulata	6-4, 85-86	22						x	x	x	x	x			x		x		x							x	x		x	
		6-5, 85-86	29	x					x	x	x	x	x			x	x			x							x	x		x	
	G. margaritae	6-6, 53-56	23						x	x	x	x	x			x	x	x		x		x					x	x			
		6-6, 124-125	21						x	x	x	x	x			x		x		x		x					x	x			
	G. tumida	6-7, 11-12	28	x					x	x		x	x		x	x		x	x	x		x					x	x			
		6,CC	27						x			x	x			x	x	x	x	x		x				x	x	x			
Miocene l	P. primalis	7-1, 59-60	27						x	x	x	x	x			x		x	x	x		x					x	x			
		7-2, 59-60	30						x	x		x	x			x		x	x	x		x		x		x	x	x			
		7-3, 59-60	31						x	x		x	x		x	x		x		x		x		x		x	x	x			
		7-4, 59-60	29	x			x		x	x	x	x	x			x		x		x		x					x	x			
		7-5, 59-60	31				x	x	x	x	x	x	x		x	x		x		x		x		x		x	x	x			
		7-6, 59-60	33	x			x		x	x	x	x	x			x		x		x		x		x		x	x	x			
		7,CC	37	x			x		x	x	x	x	x		x	x	x	x		x		x	x	x		x	x	x			
		8-1, 70-71	31	x			x		x	x	x	x	x		x	x		x		x		x		x		x	x	x			
		8-2, 70-71	31	x			x		x	x	x	x	x		x	x		x		x		x		x		x	x	x			
		8-3, 70-71	33	x			x		x	x	x	x	x		x	x		x		x		x		x		x	x	x			
		8-4, 70-71	28					x	x	x	x	x	x		x	x	x	x		x				x		x	x	x			
	G. plesiotumida	8-5, 70-71	27						x	x	x	x	x		x	x	x	x		x		x		x		x	x	x			
		8-6, 70-71	27						x	x	x	x	x		x	x		x		x		x		x		x	x	x			
		8-7, 46-47	29						x	x	x	x	x		x	x	x	x		x		x		x		x	x	x			
		8,CC	27						x	x	x	x	x		x	x	x	x		x		x		x			x	x			
		9-1, 56-57	30						x	x		x	x		x	x	x	x		x		x		x		x	x		x		
		9-2, 56-57	21						x	x		x	x		x	x		x		x		x		x					cf.		
		9,CC	25									x	x	x	x	x		x		x		x					x	x			
		10-1, 17-18	36		x		x		x	x	x	x	x	x	x		x	x		x		x					x	x			
		10-2, 17-18	31				x		x	x	x	x	x		x	x		x		x		x	x				x	x			
		10-3, 17-18	27				x		x	x	x	x	x										x				x	x			
		10-4, 17-18	28				x		x	x	x	x	x		x	x		x		x		x					x	x			
		10-5, 17-18	23						x	x		x	x		x	x		x		x							x	x			
		10-6, 17-18	20						x	x		x	x		x			x		x		x					x	x			
		10-7, 18-19	13									x						x		x							x	x			
		10,CC	17				x					x			x			x		x			x			x	x				
		11-1, 65-66	16							x		x					x	x		x							x				
		11-2, 65-66	19							x		x	x				x	x		x							x				
		11-3, 65-66	19				x		x	x	x	x	x					x				x					x				
		11-4, 65-66	20						x	x		x	x		x			x		x		x					x	x			
		11-5, 65-66	18							x		x	x		x			x		x							x	x			
		11,CC	19						x	x		x	x		x			x		x							x				
		13,CC	19							x		x			x			x		x						x		x			

Note: R = reworked.

Table 9. (Continued).

G. miotumida	*G. explicationis*	*G. menardii*	*G. multicamerata*	*G. scitula*	*G. cibaoensis*	*G. margaritae*	*G. hirsuta*	*G.* cf. *theyeri*	*G.* cf. *ichinosekiensis*	*G. crassaformis*	*G. crassaformis-tosaensis*	*G. tosaensis*	*G. tosaensis-truncatulinoides*	*G. truncatulinoides*	*G. merotumida*	*G. plesiotumida*	*G. plesiotumida-tumida*	*G. tumida tumida*	*G. tumida flexuosa*	*G. ungulata*	*Turborotalita cristata*	*Globoquadrina dehiscens*	*G. baroemoensis*	*G. altispira altispira*	*G. altispira globosa*	*Neogloboquadrina continuosa*	*N. pachyderma*	*N. acostaensis*	*N. humerosa*	*N. dutertrei*	*Pulleniatina primalis*	*P. obliquiloculata*	*Sphaeroidinella seminulina*	*S. paenedehiscens*	*S. dehiscens*	*Globigerinita glutinata*	*Candeina nitida*	*Beela digitata*	*Globigerinella obesa*	*G. pseudobesa*	*G. aequilateralis*	*C. calida*	*Hastigerina pelagica*
		x		x						x				x				x												x		x			x	x		x			x	x	x
		x								x				x				x												x		x				x		x			x	x	
		x								x				x				x												x		x									x	x	
		x												x				x												x		x			x								
		x	R							x				x				x												x		x									x		
		x	R							x				x																x						x					x		
		x								x				x																x		x				x					x	x	
		x								x				x				x														x			x						x		
		x								x				x				x												x		x			x						x		
										x			x	x																		x				x		x					
					x								x	x																		x									x		
		x								x			x	x				x												x		x					x				x		
		x											x	x																x		x			x			x			x		
				x			x	x		x		x		x							x											x				x		x					x
		x								x		x		x				x																	x	x		x	x		x		x
		x								x		x		x				x														x			x	x		x	x		x		x
										x		x		x																		x			x	x					x		
		x		x						x		x		x				x												x		x			x	x					x	x	
		x		x						x		x		x				x												x		x			x	x	x				x		
		x		x						x		x	x	x																x		x			x	x	x				x		x
		x		x						x		x	x	x																x		x			x	x	x				x		x
		x		x						x		x	x	x																x		x			x	x	x				x		x
		x								x		x	x	x				x												x		x						x			x		x
		x								x		x		x				x												x		x			x	x	x				x		
		x	x							x		x		x				x												x		x			x	x	x		x		x		
		x	x	x						x		x	x	x																x		x			x	x	x				x		
			x							x		x	x					x						x					x			x			x				x		x		
			x							x		x	x					x						x					x			x			x				x		x		
		x	x							x		x												x					x			x	x		x	x	x	x			x		x
		x	x							x		x												x					x			x	x		x	x	x	x			x		x
		x	x							x	x							x						x					x		x		x		x		x		x		x		
		x	x							x								x	x					x					x		x		x		x		x		x		x		
		x	x							x								x	x					x					x		x		x		x		x		x		x		
		x	x	x						x								x						x					x			x			x	x	x				x		
			x			x				x														x					x		x		x		x	x	x				x		
cf.		x	x			x				x							x							x				x	x		x		x	x			x		x		x		
cf.			x		x	x				x								x						x					x			x	x	x							x		
cf.		x	x			x													x					x							x		x				x		x		x		
cf.		x	x	x		x										cf.		x						x				x	x		x		x	x		x	x				x		x
cf.			x			x										x		x						x							x		x	x			x				x		
cf.			x			x												x						x							x		x			x	x				x		
x	x	x	x	x												x		x						x				x			x		x	x		x			x		x		
x		x	x	x												x		x						x				x			x		x	x		x	x		x		x		
		x	x	x	x											x	x							x				x			x		x	x		x	x		x		x		
x	x	x	x	x	x											x	x						x	x			cf.	x			x		x	x		x	x						
x	x	x	x		x			x								x							x	x			cf.	x			x		x	x		x	x		x		x		
x		x	x	x	x											x	x							x			cf.	x			x		x	x			x		x		x		
x			x	x	x											x							x	x			cf.	x			x		x	x			x		x		x		
x		x	x	x	x											x							x	x			cf.	x			x		x	x		x	x		x		x		x
x		x	x	x	x			x								x							x	x			cf.	x			x		x	x		x	x		x		x		x
x			x	x					cf.							x								x			cf.	x			x		x	x		x	x		x		x		
x			x	x					cf.							x								x			cf.	x			x		x	x		x	x		x		x		
x			x	x	x				cf.							x							x	x			cf.	x			x		x	x		x	x		x		x		
x				x	x											x								x			cf.	x			x		x	x			x		x		x		
x		x	x	x					x							x								x			cf.	x					x	x			x						
x			x	x	x				x							x								x				x					x	x			x		x		x		
x			x	x					x														x	x	x		cf.	x					x	x			x		x		x		
x			x	x												x							x	x	x		cf.	x					x				x		x		x		
x		x	x	x	cf.				x							x							x	x			cf.	x					x	x			x		x		x		
x					cf.											x								x			cf.	x					x	x		x	x						
x		x	x	x												x							x	x		x		x					x			x	x		x		x		x
x		x	x	x	x				x							x							x	x	x	x	cf.	x					x	x		x	x		x	x	x		x
x		x	x	x	x											x							x	x	x	x	cf.	x					x			x	x		x		x		
x		x	x	x	x											x							x	x	x	x	cf.	x					x			x	x		x	x	x		
x		x	x	x												x							x	x		x	cf.	x					x			x	x		x		x		
x		x														x						x	x	x	x			x					x			x	x		x		x		
x																x						x	x			x		x					x			x	x				x		
x															cf.	x						x						x					x			x					x		
x																x						x		x				x					x			x			x		x		
				x											cf.	x						x		x				x					x			x			x		x		
x				x											cf.	x						x		x			cf.	x					x			x			x		x		
															cf.	x						x				x	cf.	x					x			x			x		x		
x				x											cf.	x						x		x		x		x					x								x		
x			x													x						x	x	x		x	cf.	x													x		
x															x	x						x		x		x	cf.	x					x						x		x		
x		x		x	x										x	cf.						x		x		x		x					x								x		

Table 10A. Occurrences of planktonic foraminifers in selected samples of Hole 588.

Epoch		Zone	Core-Section (interval in cm)	Diversity (no. of species)	*Streptochilus globigerum*	*Catapsydrax parvulus*	*Globigerina quinqueloba*	*G. eamesi*	*G. bulloides*	*G. falconensis*	*G. woodi*	*G. apertura*	*G. nepenthes*	*G. decoraperta*	*G. foliata*	*Globigerinoides obliquus*	*G. extremus*	*G. conglobatus*	*G. bulloideus*	*G. trilobus*	*G. quadrilobatus*	*G. sacculifer*	*G. fistulosus*	*G. bollii*	*G. subquadratus*	*G. mitra*	*G. ruber*	*G. seiglei*	*G. tenellus*	*Orbulina suturalis*	*O. universa*	*O. bilobata*	*Globorotalia peripheroronda*	*G. peripheroacuta*	*G. fohsi fohsi*	*G. panda*	*G. conoidea*	*G. conomiozea*	*G. sphericomiozea*	*G. puncticulata*	*G. puncticulata-inflata plexus*	*G. inflata*	*G. miotumida*
Pleistocene	l	*G. truncatulinoides*	1,CC	19					x	x								x		x		x					x				x											x	
			2,CC	19					x	x								x		x		x					x				x											x	
		G. truncatulinoides *G. tosaensis*	3-1, 40-41	24			x		x					x				x		x		x					x				x											x	
			3-2, 40-41	30			x		x	x				x	x			x		x	x	x	x				x		x		x											x	
			3-3, 90-91	15					x	x										x	x	x					x				x											x	
			3,CC	15						x								x				x					x				x												
			4-2, 90-91	17		x				x				x				x				x					x				x											x	
			4-4, 90-91	12		x			x													x					x				x											x	
			4-5, 40-41	18					x	x								x		x		x					x				x	x										x	
Pliocene	l.	*G. tosaensis*	4-6, 40-41	30			x		x	x		x		x	x		x	x			x	x	x				x				x	x										x	
			4,CC	30			x		x	x		x		x	x		x	x			x	x	x				x				x	x										x	
			5-3, 90-91	15						x							x			x		x					x				x											x	
			5,CC	22					x	x				x			x			x	x		x				x				x											x	
			6-1, 40-41	32					x	x	x			x			x	x		x		x	x				x				x									x		x	
		G. inflata	6-2, 40-41	31					x	x	x			x			x	x		x		x					x				x									x		x	
			6-3, 40-41	30					x	x	x			x			x	x		x		x					x				x									x		x	
			6,CC	30					x	x	x			x			x	x		x		x					x				x									x		x	
			7-2, 94-95	29					x	x	x						x	x		x		x					x				x	x								x		x	
			7-3, 40-41	33					x	x	x			x			x	x		x	x	x					x				x	x										x	
			7-4, 40-41	25					x	x				x			x			x		x					x				x	x								x	x	x	
	e.	*G. crassaformis*	7-5, 94-95	16					x	x							x	x					x				x													x			
			7,CC	24					x	x		x		x	x		x	x		x	x	x									x									x			
			8,CC	32					x	x	x		x	x		x	x	x		x		x					x				x	x								x			
			9-1, 40-41	32					x	x	x		x	x		x	x	x		x		x					x				x	x								x			
			9-2, 40-41	25					x	x	x		x	x			x	x		x		x									x	x								x			
		G. puncticulata	9-3, 40-41	26					x	x	x		x	x		x	x	x		x		x									x	x								x			
			9-4, 90-91	19									x	x			x			x		x									x	x								x			x
			9-6, 40-41	29					x	x			x	x			x	x		x		x		x							x	x							x	x			x
		G. margaritae	9,CC	25	x				x	x		x	x	x	x		x	x		x		x									x												x
			10-2, 90-91	25	x				x	x		x	x	x	x		x	x		x		x									x												x
			10,CC	23	x				x	x			x	x	x		x	x		x		x																					x
			11,CC	21				x	x	x			x	x			x	x				x				x					x	x											x
			12,CC	30			x		x	x			x	x			x	x		x		x		x							x	x						x					
			13,CC	23					x	x			x	x			x			x		x															x	x					
			14,CC	16					x	x			x	x			x					x										x											x
			15-3, 90-91	15					x	x				x			x			x		x									x												x
			15,CC	16						x			x				x					x					x					x											x
			16-3, 90-91	12					x				x	x																		x											
Miocene	l.	*G. plesiotumida*	16-4, 40-41	21					x	x	x		x	x			x			x		x									x	x						x					x
			16,CC	15					x				x	x			x			x											x												x
			17,CC	17										x			x			x		x					x				x					x							x
			18,CC	22						x			x	x			x			x		x						x			x	x				x							x
			19,CC	22						x			x	x			x			x		x						x			x	x				x							x
			20-3, 90-92	22					x	x	x		x	x			x		x	x		x		x							x	x											x
			20-4, 40-42	22					x	x	x		x	x			x		x	x		x		x							x	x											x
			20-5, 40-42	22					x	x	x		x	x			x		x	x		x		x							x	x											x
			20-6, 40-42	22					x	x	x		x	x			x		x	x		x		x							x	x											x
		N. continuosa	20,CC	15									x				x			x											x												x
			21,CC	18							x		x			x				x		x									x												x
			22,CC	25			x				x		x	x		x				x	x									x		x											x
			23-1, 40-41	29		x			x	x	x		x	x		x	x			x		x					x			x	x	x											x
			23-2, 40-41	21					x	x	x		x	x			x			x		x									x					x							x
			23-3, 40-41	19	x	x	x			x	x		x	x																	x												x
			23-4, 40-41	21							x		x	x		x				x		x		x						x	x	x											x
			23-5, 40-41	25			x		x	x			x	x						x		x		x				x			x					x							x
	m.	*G. mayeri*	23,CC	18						x			x	x						x		x					x									x							x
			24-1, 40-41	23		x			x	x	x		x	x		x				x		x			x					x	x					x							x
			24-2, 40-41	21					x	x			x	x		x				x		x								x	x												x
			24-3, 40-41	21					x	x	x		x	x		x				x		x			x					x	x												x
	m.	*G. fohsi*	24-4, 40-41	23		x			x	x	x		x	x		x				x		x			x						x		x			x							x
			24-5, 40-41	22					x	x	x		x	x						x					x					x	x	x	x		x	x							x
			24-6, 40-41	22					x	x	x		x	x						x					x					x	x	x	x		x	x							x
			24,CC	26					x	x	x		x	x		x				x		x								x	x		x		x	x							x
			25-1, 40-41	31					x	x	x		x	x		x				x		x			x					x	x	x	x			x							x
			25-2, 40-41	31					x	x	x		x	x		x				x		x			x					x	x	x	x			x							x
			25-3, 40-41	31					x	x	x		x	x		x				x		x			x					x	x	x	x			x							x
			25-4, 40-41	31					x	x	x		x	x		x				x		x			x					x	x	x	x			x							x
			25-5, 40-41	31					x	x	x		x	x		x				x		x			x					x	x	x	x			x							x
			25-6, 40-41	31					x	x	x		x	x		x				x		x			x					x	x	x	x			x							x
			25,CC	27					x	x	x		x	x		x				x		x			x			x		x	x			x		x							x

Globorotalia challengeri **Srinivasan and Kennett** (Plate 3, Figs. 7, 8).
Srinivasan and Kennett, 1981b, p. 528, pl. 1, figs. 9–18

Specimens of *G. challengeri* have been illustrated from Site 592, the *G. mayeri* Zone; see discussion under *G. mayeri.*

Globorotalia miotumida **Jenkins** (Plate 3, Figs. 12–14). *Globorotalia menardii* (d'Orbigny) subsp. *miotumida* Jenkins, 1960, p. 362, pl. 4, figs. 9a–c. The holotype, described from the middle upper Miocene shallow-water deposits of southeast Australia, is relatively thin-walled and small (0.4 mm). The illustrations of the ontogeny of *G. miotumida* show its development into *G. conoidea* Walters, which is the adult thick-walled stage of development (Jenkins, 197). Note that in the juvenile form (Fig. 12) the pustules on the umbili-

Table 10A. (Continued).

	G. pliozea	G. praemenardii	G. menardii	G. multicamerata	G. exilis	G. miocenica	G. scitula	G. cibaoensis	G. margaritae	G. cf. ichinosekiensis	G. crassula	G. crassula-crassaformis	G. crassaformis	G. crassaformis-tosaensis	G. tosaensis	G. tosaensis-truncatulinoides	G. truncatulinoides	G. lenguaensis	G. merotumida	G. plesiotumida	G. tumida tumida	G. ungulata	G. anfracta	Turborotalia cristata	Globorotalia siakensis	G. mayeri	G. minutissima	Globoquadrina venezuelana	G. dehiscens	G. baroemoenensis	G. altispira altispira	G. altispira globosa	Neogloboquadrina continuosa	N. nympha	N. pachyderma	N. acostaensis	N. humerosa	N. dutertrei	Pulleniatina primalis	P. obliquiloculata	Sphaeroidinella seminulina seminulina	S. paenedehiscens	S. dehiscens	Globorotaloides hexagona	Globigerinita glutinata	G. uvula	Candeina nitida	Beela praedigitata	B. digitata	Globigerinella obesa	G. aequilateralis	G. calida	Hastigerina pelagica
			x				x						x				x				x														x			x		x			x		x						x	x	
			x	x			x						x		x	x	x				x	x													x			x		x			x		x				x	x	x	x	x
			x	x			x						x	x	x	x					x	x	x	x							x				x		x	x		x	x		x		x		x		x		x		x
			x	x	x	x	x		x	x			x	x							x	x		x							x				x		x		x	x	x		x		x		x		x		x		x
	x		x	x			x	x	x		x	x	x								x			x							x				x		x		x		x				x		x	x		x	x		
	x			x			x	x	x												x	x		x							x				x	x	x		x		x				x				x	x	x		
	x		x	x			x	x	x				x							x	x	x									x		x		x	x	x		x		x	x			x	x	x	x		x	x		x
x			x	x			x	x												x											x	x			x	x					x				x		x				x		
x			x			x	x	x		x								x	x	x					x				x		x	x	x	x	x	x					x				x	x	x			x	x		
			x															x								x		x	x	x	x		x	x	x	x					x				x					x	x		
		x	x				x											x							x	x	x	x	x	x	x		x								x			x	x	x				x	x		

cal [illegible]de are strongly developed but with the progressive thickening of the test (Figs. 13, 14) these are mainly lost from view, especially at the periphery (see further discussion under *G. pliozea*).

Globorotalia pliozea **Hornibrook** (Plate 4, Figs. 1-3). Hornibrook, 198[illegible] p. 95, fig. 7a-g. *G. pliozea* has four chambers in the final whorl whereas its ancestor *G. miotumida* has 4½-5. The *G. miotumida* precursor of *G. pliozea* seems to forecast some of the changes in its juvenile forms, including the pustules on the umbilical side and on the periphery which are a distinctive feature of *G. pliozea* (compare with Plate 3, Figs. 12, 13).

The chamber reduction in the final whorl in the *G. miotumida*-*G. pliozea* lineage also occurs in other *Globorotalia* lineages of the

Table 10B. Occurrences of planktonic foraminifers in selected samples of Hole 588A.

Epoch	Zone	Core-Section (interval in cm)	Diversity (no. of species)	*Cassigerinella chipolensis*	*Catapsydrax dissimilis*	*C. unicavus*	*C. parvulus*	*Globigerina ciperoensis*	*G. angustiumbilicata*	*G. quinqueloba*	*G. praebulloides*	*G. bulloides*	*G. falconensis*	*G. woodi*	*G. brazieri*	*G. connecta*	*G. druryi*	*G. nepenthes*	*G. decoraperta*	*Globigerinoides primordius*	*G. altiapertura*	*G. obliquus*	*G. trilobus*	*G. sacculifer*	*G. subquadratus*	*G. diminutus*	*G. ruber*	*G. bisphericus*	*Praeorbulina glomerosa curva*	*P. sicanus*	*P. transitoria*
Miocene m.	*G. fohsi* s.l.	1-1, 40-41	18															x	x				x	x	x						
		1-2, 40-41	18															x	x				x	x	x						
		1-3, 40-41	18									x	x	x					x			x	x	x	x						
		1-4, 40-41	20									x	x	x					x			x	x	x	x						
		1-6, 40-41	21											x				cf.	x				x	x	x						
		1,CC	15																x				x	x			x				
		2-3, 40-41	20									x	x	x					x				x		x						
		2,CC	15										x	x					x				x								
		3-3, 40-41	24									x	x	x					x				x	x	x						
		3,CC	11									x											x								
		4-3, 40-41	20									x	x	x					x				x		x						
		4,CC	9																				x		x						
		5-3, 40-41	24									x	x	x					x			x	x		x						
		5,CC	14															x									x				
		6-3, 40-41	19									x	x	x					x			x	x		x						
		6,CC	14																				x		x						
		7-3, 40-41	15									x	x	x					x			x	x		x						
		7,CC	13																					x							
		8-3, 40-41	21									x	x	x					x				x		x						
		8,CC	13																				x								
		9-3, 40-41	21									x	x	x					x				x		x						
	O. suturalis	9,CC	11																x				x								
		10-1, 40-41	18							x		x	x	x					x				x		x						
		10-2, 40-41	21							x			x	x					x				x	x	x						
		10-3, 40-41	20							x			x	x					x				x	x	x						
		10-3, 90-91	10																				x		x						
		10-4, 40-41	20							x			x	x					x				x	x	x						
		10,CC	10																x				x								
		11-3, 40-41	17													x							x		x	x			x		
		11-3, 90-91	12																					x		x			x		
e.	*P. glomerosa curva*	11,CC	16							x			x										x		x	x		cf.	x		
		12-3, 40-41	15				x																x		x	x		x	x		x
		13-3, 40-41	17				x								x	x							x		x			x	x	x	x
		13,CC	14												x										x			x	x		
		14-1, 40-41	16											x		x	x						x		x			x	x		
		14-2, 40-41	11											x									x		x			x	x		
		14-2, 90-91	11											x									x		x			x	x		
		14-3, 40-41	16									x	x			x	x						x		x			x	x		
	G. miozea	14,CC	10																				x		x			x			
		15-3, 40-41	16												x	x							x	x	x						
		15,CC	12											x		x							x		x						
		16,CC	15				x				x			x		x					x		x		x						
	C. dissimilis	17-1, 40-41	11		x	x					x																				
		17-1, 90-91	8		x	x					x																				
		17-2, 40-41	10		x	x					x																				
		17,CC	9		x	x					x									x											
		18-2, 40-41	9		x	x																									
		18-2, 90-91	9		x						x			x						x											
	G. dehiscens	18,CC	16	x	x			cf.	x					x	x	x															

mid and high latitudes; these include the *G. mayeri–Neogloboquadrina continuosa* and *G. sphericomiozea–G. puncticulata* lineages. Within these lineages the reduction in chamber numbers also involves fewer partitioning chamber walls and therefore there is less calcite in the test; this could have some advantage in buoyancy. In low latitudes the opposite trend takes place in many lineages: there is an increase of chamber numbers in the final whorl as in the *G. fohsi* and *G. menardii* lineages.

***Globorotalia munda* Jenkins** (Plate 4, Figs. 4–9). Jenkins, 1966a, p. 1121, fig. 14, nos. 126–133, pl. 13, nos. 152–166. Jenkins (1966a) illustrated the evolutionary transition of *G. munda* to *Globigerina juvenilis* Bolli; the main morphological changes are (1) the peripheral aperture in *Globorotalia munda* changes to the umbilical aperture of *Globigerina juvenilis;* (2) the spiral side of *Globorotalia munda* is flat and changes to the conical shape of *Globigerina juvenilis; G. juvenilis* acquires an umbilical bulla and thus evolves into *Globigerinita glutinata* (Egger). The migration of the aperture from the periphery in *Globorotalia munda* to the umbilicus as in *Globigerina juvenilis* is illustrated (Pl. 4, Figs. 4–9). Note that in the evolution of *Globorotalia munda* to *Globigerina juvenilis* the wall ornamentation is retained; this evolution takes place in the earlier part of the *Globigerina euapertura* Zone.

***Globorotalia nympha* Jenkins** (Plate 4, Figs. 10–11. *Globorotalia mayeri nympha* Jenkins, 1967, p. 1072, fig. 3, nos. 7–13. There are good transitional forms between *G. mayeri, Neogloboquadrina continuosa*, and *G. nympha* in 588-26,CC and in 592-24,CC. The bulla-like final chamber as illustrated is the feature that distinguishes *G. nympha* from *N. continuosa;* after the extinction of *G. nympha, N. continuosa* persists into the late Miocene, where a form similar to *G. nympha* evolves; this is *N. pachyderma* (Jenkins, 1967b).

***Globorotalia* cf. *opima* Bolli** (Plate 4, Fig. 12). *Globorotalia opima opima* Bolli, 1957b, p. 117, pl. 28, fig. 1a–2. This species is rare in New Zealand and in the southern sites of Leg 90. The holotype was recently examined at the Smithsonian Institution, Washington; it has 5 chambers in the final whorl and a lipped aperture. The illustrated specimen is closer to the 4-chambered paratype (Bolli, 1957b, plate 28, fig. 2).

***Globorotalia peripheroronda* Blow and Banner** (Plate 4, Figs. 13, 14). Blow and Banner, 1966, p. 294, pl. 1, figs. 1–3. In the mid latitudes of the Southern Hemisphere, *G. peripheroronda* is the middle Miocene ancestor of *G. mayeri* (Jenkins, 1960, 1966b). During its evolution, the recurved sutures became more radial on the spiral side and the aperture became enlarged (see Plate 3, Fig. 6). In New Zealand, *G. peripheroronda* appeared for the first time in the *Praeorbulina glomerosa curva* Zone (Jenkins, 1971), which is much later than in the lower latitudes; at Site 594 its initial appearance is in the *Globorotalia conica* Zone of the middle Miocene.

***Globorotalia nana* Bolli** (Plate 5, Fig. 1). *Globorotalia opima nana* Bolli, 1957b, p. 118, pl. 28, fig. 3a–c. *G. nana* originated in the

Table 10B. (Continued).

Orbulina suturalis	*O. universa*	*O. bilobata*	*Globorotalia kugleri*	*G. birnageae*	*G. kugleri/peripheroronda*	*G. peripheroronda*	*G. peripheroacuta*	*G. fohsi* s.l.	*G. fohsi lobata*	*G. nana*	*G. zealandica*	*G. praescitula*	*G. panda*	*G. miozea*	*G. praemenardii*	*G. menardii*	*G. scitula*	*G. miotumida*	*G. semivera*	*G. siakensis*	*G. bella*	*G. mayeri*	*G.* aff. *mayeri*	*G. acrostoma/mayeri*	*G. pseudocontinuosa*	*G. clemenciae*	*G. suteri*	*G. venezuelana*	*Globoquadrina dehiscens*	*G. baroemoenensis*	*G. altispira altispira*	*G. altispira globosa*	*G. tripartita*	*Neogloboquadrina continuosa*	*Sphaeroidinella disjuncta*	*Semiorbulina seminulina*	*Globigerinita glutinata*	*G. uvula*	*Globigerinatella insueta*	*Globigerinella obesa*	*G. aequilateralis*
x	x					x	x						x					x		x		x						x	x		x					x	x				
x	x					x	x						x					x		x		x						x	x		x					x	x				
						x	x	x					x			x		x				x							x		x										x
						x	x	x					x		x	x		x				x							x		x						x				x
x	x					x	x	x					x			x		x		x		x						x	x		x					x	x				
x							x	x										x		x		x						x	x		x				x		x				
x	x					x	x						x			x		x				x							x	x	x			x						x	x
x							x								x	x		x		x		x							x	/	x					x	x				
x	x					x	x	x	x				x		x	x		x		x		x						x	x	x	x					x					
						x	x								x			x				x							x		x				x		x				
x	x					x	x	x	x				x					x		x		x							x		x					x					x
	x					x							x					x				x							x		x										
x	x	x				x	x	x	x				x	cf.				x		x		x							x		x					x				x	x
x						x	x						x	x	x			x		x		x							x		x						x				
						x	x	x					x	cf.				x		x		x							x		x					x					x
x	x						x	x					x	x				x		x		x							x		x						x				
x	x					x	x															x							x		x										x
x							x						x	x	x			x		x		x							x		x				x		x				
x	x					x	x	x					x	cf.				x		x		x	x						x	x	x					x					
x	x					x	x	x					x		x					x		x							x		x						x				
x	x					x	x	x					x	cf.				x		x		x	x						x	x	x					x					
x						x	x							x			x					x							x		x						x				
x	x					x	x						x	x						x		x							x		x						x				
x	x					x	x							x	x					x		x						x	x	x	x				x		x				
x	x					x	x							x	x					x		x						x	x	x	x				x						
x						x						x								x		x							x		x						x				
x	x					x	x							x	x					x		x						x	x	x	x				x						
						x						x					x			x		x							x		x						x				
x				x		x						x		x						x		x							x		x				x		x		x		
x						x						x		x						x		x							x		x								x		
						x						x		x						x			x						x		x	x					x				
						x						x		x						x		x							x		x					x					
				x		x						x		x															x		x						x		x		
						x				x		x		x												x			x		x						x	x	x		
				x		x				x		x		x															x	x							x		x		
						x						x		x						x									x		x										
						x						x		x						x									x		x										
						x				x		x		x												x	x		x								x				
						x						x		x						x		x							x		x										
						x				x		x		x							x						x	x	x		x				x		x				
						x						x		x						x	x								x		x						x				
											x	x		x						x	x								x		x						x				
										x									x	x	x								x	x	x						x				
										x									x	x									x		x										
										x									x	x	x								x	x	x										
										x									x	x									x		x										
			cf.	x	x	x																						x	x								x				
										x									x	x			x						x												
			x																x	x					x			x	x		x		x				x				

middle Eocene and ranges through to the Miocene; it is the rootstock of species that have been referred to the subgenera *Paragloborotalia* and *Jenkinsella*. A number of species including *G. pseudocontinuosa* and *G. semivera* evolved from *G. nana* in the Oligocene of the southwest Pacific; in warmer waters of the Oligocene it gave rise to *G. opima* and *G. siakensis*.

Globorotalia pseudocontinuosa **Jenkins** (Plate 5, Figs. 2–4). Jenkins, 1967, p. 1074, fig. 4, nos. 20–25. In the *Globigerina angiporoides* Zone, *Globorotalia pseudocontinuosa* evolved from *G. nana* Bolli (Jenkins, 1967) and the change in the shape of the aperture can be seen by comparing illustrations (Pl. 5, Figs. 1 and 3). At about the same stratigraphic level, five-chambered forms appear in the populations, and these are *G. semivera* (Jenkins, 1971). Berggren et al. (1983) stated that in the southwest Atlantic *G. pseudocontinuosa* is a junior synonym of *G. incognita* Walters. The main morphological differences between the two are that (1) the aperture in *G. pseudocontinuosa* is well rounded, high-arched and extends from the umbilicus to about halfway to the periphery, whereas in *G. incognita* the aperture is isolated in a position halfway between the periphery and umbilicus; (2) the chambers of *G. pseudocontinuosa* are more inflated and globigerine; (3) there is a more rapid increase in size of chambers of the final whorl in *G. contin*[illegible] the spiral side in *G. incognita* is more flattened and the chambers are more globorotalid in shape.

Globorotaloides suteri **Bolli** (Plate 5, fig. 5). Bolli, 1957b, p. 117, pl. 27, figs. 9a–13b.

Globorotaloides testarugosa **Jenkins** (Plate 5, Fig. 6). Jenkins, 1960, p. 368, pl. 5, figs. 8a–c. This species is related to *G. suteri* but has a much coarser test wall and a much shorter stratigraphic range in the Oligocene of the southwest Pacific.

Globorotaloides turgida **(Finlay)** (Plate 5, Fig. 7). *Globigerina linaperta* Finlay var. *turgida* Finlay, 1939a, p. 125. *Globorotaloides turgida* Finlay, Jenkins, 1964, p. 117, pl. 7, figs. 1a–10b; Pl. 8, figs. 1a–13c (holotype figured). This species is restricted to the Paleocene-Eocene and is larger than *G. suteri*, which probably evolved from it in the Eocene.

Hantkenina alabamensis **Cushman** (Plate 5, Fig. 8). Cushman, 1925, p. 3, pl. 1, figs. 1–6, pl. 2, fig. 5. *H. alabamensis* was found in the late Eocene of Site 592; its presence probably represents a brief tropical incursion that also occurred in New Zealand at this level (Jenkins, 1971).

Jenkinsina samwelli **(Jenkins)** (Plate 5, Fig. 9). *Guembelitria samwelli* Jenkins, 1978b, p. 132, pl. 1, fig. 1–9.

J. samwelli appears to be a late Eocene–late Oligocene species of the Southern Hemisphere; outside South Australia it has only a very short stratigraphic range in the lower part of the *Globigerina euapertura* Zone. *J. samwelli* has a well-defined northern limit; it is found at Site 593 but not in the North Island of New Zealand (Jenkins, 1978b).

Streptochilus pristinum **Brönnimann and Resig** (Plate 5, Fig. 10). Brönnimann and Resig, 1971, p. 1289, pl. 51, fig. 4. *S. pristinum* was only found in the late Oligocene–early Miocene of Site 593; the

Table 10C. Occurrences of planktonic foraminifers in selected samples of Hole 588C.

Epoch	Zone	Core-Section (interval in cm)	Diversity (no. of species)	Cassigerinella chipolensis	Chiloguembelina cubensis	Catapsydrax dissimilis	C. unicavus	Globigerina ciperoensis	G. angustiumbilicata	G. angulisuturalis	G. praebulloides	G. bulloides	G. falconensis	G. woodi	G. brazieri	G. connecta	G. euapertura	G. druryi	G. cf. angiporoides	Globigerinoides primordius	G. altiapertura	G. trilobus	G. sacculifer	G. subquadratus	G. bisphericus	Praeorbulina sicanus	P. glomerosa	Globorotalia kugleri	G. birnageae	G. peripheroronda	G. nana	G. incognita	G. zealandica	G. zealandica-praescitula	G. praescitula	G. miozea	G. munda	G. semivera	G. cf. mayeri	G. pseudocontinuosa	G. opima	G. minutissima	G. siakensis	G. venezuelana	G. binaiensis	G. n. sp.	Globoquadrina dehiscens	G. altispira altispira	G. tripartita	Sphaeroidinella disjuncta	Globorotaloides suteri	G. testarugosa	Globigerinita glutinata	G. uvula	Globigerinatella insueta
Miocene e.	P. glomerosa curva	1,CC	11											x								x	x	x			x			x					x	x			x								x	x							
		2-2, 40-41	22	x									x	x		x		x			x	x		x	x	x	x		x	x	x				x	x											x	x		x			x	x	x
		2-4, 40-41	21	x									x	x		x		x			x	x		x	x	x	x			x	x				x	x											x	x		x			x	x	x
	G. miozea	2,CC	17											x	x	x					x	x		x						x		x	x		x	x			x				x				x	x			x		x		
		3-1, 40-41	12	x			x								x							x		x						x			x		x												x	x					x	x	
	C. dissimilis	3-3, 40-41	16	x		x	x		x			x		x	x							x											x		x				x				x				x	x					x	x	
		3-5, 40-41	7			x	x															x								x			x	x														x							
		3,CC	13	x		x	x		x													x											x		x				x				x				x	x	?				x	x	
		4,CC	9			x						x		x	x							x							x									x				x					x								
		5-1, 40-41	9			x						x		x	x							x							x									x				x					x								
		5-3, 40-41	8			x	x							x		x						x									x									x							x								
	G. dehiscens	5-5, 40-41	14	x		x	x							x	x													x			x												x	x	x		x		x				x	x	
		5,CC	15	x		x	x				x			x	x													x			x												x	x	x		x		x				x	x	
		6,CC	14	x		x	x		x		x			x	x					x	x							x															x				x						x	x	
		7,CC	14	x		x	x		x					x	x					x								x												x		x	x				x		x					x	
		8,CC	15	x		x	x	x	x											x	x							x				x								x			x				x				x		x	x	
		9-1, 40-41	13	x		x	x		x											x								x				x								x			x				x		x		x		x		
		9-3, 40-41	15	x		x	x	x	x											x	x							x				x								x			x				x				x		x	x	
Oligocene l.	G. primordius	9-5, 40-41	16	x		x	x		x		x			x	x					x	x							x										x		x			x			x							x	x	
		9,CC	14	x		x	x		x		x			x	x					x								x										x		x						x							x	x	
	G. kugleri	10-3, 40-41	15			x	x	x	x		x						x											x										x		x			x	x	x	x					x		x		
		10-5, 40-41	15			x	x	x	x		x						x											x										x		x			x	x	x	x					x		x		
		10,CC	12	x		x	x	x	x						x		x											x												x				x		x					x				
		11,CC	11			x			x	x				x			x											x										x		x									x		x		x		
	G. angulisuturalis	12-1, 40-41	13	x		x	x		x	x	x																	cf.			x										cf.			x					x		x		x		
		12-3, 40-41	11	x		x	x		x	x	x									cf.											x																				x	x	x		
		12-5, 40-41	7			x	x		x	x																					x																					x	x		
		12,CC	9			x			x					x			x														x							x		x									x		x				
		13,CC	8						x	x							x		x												x																					x	x	x	
		14,CC	6							x	x																	cf.																							x	x	x		
		15,CC	8	x		x		x		x																					x																								
		16,CC	8			x			x	x							x														x									x													x		
		17-1, 40-41	8			x	x		x	x							x														x										x			x											
	C. cubensis	17-3, 40-41	6		x	x	x										x														x										x														
		17,CC	8	x	x	x				x							x																				x				x							x	x			x			
		19,CC	2		x																																											x							
																																														x	x						

Table 11. Occurrences of planktonic foraminifers in selected samples of Hole 589.

Epoch	Zone	Core-Section (interval in cm)	Diversity (no. of species)	*Globigerina quinqueloba*	*G. bulloides*	*G. falconensis*	*Globigerinoides conglobatus*	*G. trilobus*	*G. sacculifer*	*G. ruber*	*Orbulina universa*	*Globorotalia inflata*	*G. menardii*	*G. scitula*	*G. crassaformis*	*G. tosaensis*	*G. truncatulinoides*	*G. tumida tumida*	*Neogloboquadrina pachyderma*	*N. dutertrei*	*Pulleniatina obliquiloculata*	*Sphaeroidinella dehiscens*	*Globigerinita glutinata*	*G. uvula*	*Beela digitata*	*Globigerinella aequilateralis*	*Globigerina calida*
Pleistocene	*G. truncatu-linoides*	1,CC	20	x	x	x	x	x	x	x	x	x	x	x	x		x	x	x	x	x		x			x	x
		2,CC	22	x	x	x	x	x	x	x	x	x	x	x	x	R	x	x	x	x	x		x		x	x	x
		3,CC	22	x	x	x	x	x	x	x	x	x		x	x	R	x	x	x	x	x		x	x	x	x	x
		4,CC	20	x		x	x	x	x	x	x	x		x	x	R	x	x	x	x	x	x	x			x	x

Note: R = reworked.

pecimens from this site are identical with the holotype deposited t the Smithsonian Institution, Washington

corotaloides collactea **(Finlay)** (Plate 5, Fig. 11) *Globorotalia collactea* Finlay, 1939, p. 327, pl. 29, figs. 164–165. *T. collactea* is laced in this genus because of the occasional small apertures on e spiral side.

NEW SPECIES

small number of possible new *Globorotalia* species have been discovered on Leg 90 and will be described elsewhere; these include *Globorotalia* sp.1. from the late Miocene of site 594; *G.* cf. *ichinosekiensis* of the middle–late Miocene of Sites 586 through 594; *G.* cf. *crassula* of the late Miocene–early Pliocene of Site 592; and a form of *G. miotumida*, recorded as *G.* sp.2, with a flattened spiral side, and found at Sites 592 and 593 (it has previously been recorded by Jenkins [1960] as *G. miocenica*). A possible ancestor of *Globoquadrina dehiscens* has been identified at Site 588 as *G.* sp.1.

ACKNOWLEDGMENTS

The SEM work was done at the Graduate School of Oceanography, University of Rhode Island, United States, with Julie Fisher; we are also grateful to J. Kennett for providing facilities and to DSDP for making funds available, to J. Jenkins who checked the manuscript and helped in the compilation of Tables 8–16, and to C. Whale, who typed the manuscript.

REFERENCES

Banner, F. T., and Blow, W. H., 1965. Progress in the planktonic foraminiferal biostratigraphy of the Neogene. *Nature*, 208:1164–1166.

Berggren, W. A., 1972. A Cenozoic time scale—some implications for general geology and paleobiogeography. *Lethaia*, 5:195–215.

Berggren, W. A., Aubry, M. P., and Hamilton, N., 1983. Neogene magnetobiostratigraphy of DSDP Site 516 (Rio Grande Rise, South Atlantic). *In* Barker, P. F., Carlson, R. L., Johnson, D. A., et al., *Init. Repts. DSDP*, 72: Washington (U.S. Govt. Printing Office), 675–706.

Blo . W. H., and Banner, F., 1966. The morphology, taxonomy and iostratigraphy of *Globorotalia barisanensis* LeRoy, *Globorotalia hsi* Cushman and Ellisor and related taxa. *Micropaleontology*, 2(3):294.

Bol , H. M., 1957a. Planktonic foraminifera from the Eocene Navet nd San Fernando Formations of Trinidad, B.W.I. *U.S. Nat. Mus. ull.*, 215:155–172.

———, 1957b. Planktonic foraminifera from the Oligocene–Mio ne Cipero and Lengua formations of Trinidad, B.W.I. *U.S. Nat. fus. Bull.*, 215:97–123.

Bo wskoy, E., 1974. Neogene planktonic foraminifera of the Indian cean (DSDP, Leg 26). *In* Davies, T. A., Luyendyk, B. P., et al., *nit. Repts. DSDP*, 26: Washington (U.S. Govt. Printing Office), 75–742.

Bo etti, A. M., and Cati, F., 1974. L'importanza di *Globigerinoides ber seigliei* nella stratigraphia del Miocene terminale e descrizione un nuova taxon. *Giorn. Geol. Bologna. Ser. 2*, 39:357–358.

Brönnimann, P., and Resig, J., 1971. A Neogene globigerinacean biochronologic time-scale of the south-western Pacific. *In* Winterer, E. L., Riedel, W. R., et al., *Init. Repts. DSDP*, 7, Pt. 2: Washington (U.S. Govt. Printing Office), 1235–1469.

Cole, W. S., 1927. A foraminiferal fauna from the Guayabal formation in Mexico. *Bull. Am. Paleont.*, 14(51):22.

Cushman, J. A., 1925. A new genus of Eocene foraminifera. *Proc. U.S. Nat. Mus.*, 66(2567):3.

Cushman, J. A., and Ellisor, A. C., 1939. New species of foraminifera from the Oligocene and Miocene. *Contr. Cushman Lab. Foram. Res.*, 15(pt.1):11.

Finlay, H. J., 1939. New Zealand Foraminifera: key species in stratigraphy—No. 3. *Trans. R. Soc. N. Z.*, 69(no.3):309–329.

Hornibrook, N. de B., 1958. New Zealand Upper Cretaceous and Tertiary foraminiferal zones and some overseas correlations. *Micropaleontology*, 4(1):25–38.

———, 1965. *Globigerina angiporoides* n.sp. from the upper Eocene and lower Oligocene of New Zealand and the status of *Globigerina angipora* Stache, 1865. *N. Z. J. Geol. Geophys.*, 8(5): 835–838.

———, 1982. Late Miocene to Pleistocene *Globorotalia* (Foraminiferida) from DSDP Leg 29, site 284, Southwest Pacific, *N.Z. J. Geol. Geophys.*, 25:83–99.

Hoskins, R. H., 1984. The taxonomy and stratigraphic record of *Globorotalia mayeri* Cushman and Ellisor in New Zealand. *Paleogeogr., Palaeoclimatol., Palaeoecol.*, 46:203–216.

Howe, H. V., and Wallace, W. E., 1932. Foraminifera of the Jackson Eocene at Danville Landing in the Ouachita, Catahoula Parish, Louisiana. *Bull. La. Conserv. Geol. Surv.*, 2:1–118.

Jenkins, D. G., 1960. Planktonic foraminifera from the Lakes Entrance oil shaft, Victoria, Australia. *Micropaleontology*, 6(no.4): 345–371.

———, 1963. The Eocene–Oligocene boundary in New Zealand. *N. Z. J. Geol. Geophys.*, 6:107.

———, 1964. A history of the holotype, ontogeny and dismorphism of *Globorotaloides turgida* (Finlay). *Contr. Cushman Found. Foram. Res.*, 15(pt.3):117–121.

———, 1966a. Planktonic foraminiferal zones and new taxa from the Danian to lower Miocene of New Zealand. *N. Z. J. Geol. Geophys.*, 8:1088–1125.

———, 1966b. Two lineages from the Neogene planktonic foraminifera of the Australian region. *Proc. Int. Un. Geol. Sci. Comm. Med. Neogene Strat., 3rd Sess.*, pp. 23–29.

———, 1967a. Planktonic foraminiferal zones and new taxa from the lower Miocene to Pleistocene of New Zealand. *N. Z. J. Geol. Geophys.*, 10:1064–1078.

———, 1967b. Recent distribution, origin, and coiling ratio changes in *Globorotalia pachyderma* (Ehrenberg). *Micropaleontology*, 13(2): 195–203.

———, 1971. *Cenozoic Planktonic Foraminifera of New Zealand.* N. Z. Geol. Surv. Paleont. Bull., 42.

———, 1973. The present status and future progress in the study of Cenozoic planktonic foraminifera. *Rev. Espan. Micropaleontol.*, 5:133–146.

Table 12A. Occurrences of planktonic foraminifers in selected samples of Holes 590 and 590A.

Epoch	Zone	Core-Section (interval in cm)	Diversity (no. of species)	Globigerina bulloides	G. falconensis	G. eamesi	G. woodi	G. decoraperta	G. nepenthes	G. apertura	G. quinqueloba	G. rubescens	G. foliata	Globigerinoides trilobus	G. quadrilobatus	G. sacculifer	G. fistulosus	G. ruber	G. conglobatus	G. obliquus	G. extremus	G. sieglini	G. tyrrhenicus	Globigerinella calida	G. aequilateralis	Hastigerina pelagica	Globigerinita glutinata	G. uvula
Pleistocene	G. truncatulinoides	Hole 590																										
		1,CC	23	x	x							x		x	x	x		x	x					x	x	x	x	x
		2,CC	25		x						x	x	x	x		x		x	x					x	x		x	
		3,CC	28	x	x						x	x		x	x	x		x	x					x	x		x	x
		Hole 590A																										
		1-3, 90-91	7											x				x										
		1,CC	26	x	x						x	x		x	x	x	x	x	x					x	x		x	
		2,CC	28	x	x						x	x		x	x	x		x	x						x		x	x
Pliocene l.	G. tosaensis	3,CC	19		x						x	x		x		x	x	x							x		x	x
		4,CC	19	x	x					x	x	x		x		x		x	x		x				x		x	
		5,CC	26	x	x			x			x	x		x	x	x		x			x				x		x	
		6-3, 90-91	8																						x			
	G. inflata	6,CC	27	x	x					x			x	x	x	x		x			x				x	x	x	
		7,CC	19	x	x		x	x				x		x		x		x	x		x				x		x	
		8-3, 90-91	13												x	x					x				x			
Pliocene e.	G. crassaformis	8,CC	19		x		x	x						x												x	x	
		10,CC	30	x	x	x		x	x	x	x		x	x	x	x					x				x		x	
		11,CC	24	x	x			x	x					x		x					x				x		x	
		12,CC	25	x	x			x	x					x		x		x			x				x		x	
		13,CC	21	x				x								x		x			x				x		x	
		14,CC	28	x	x			x						x		x					x				x		x	
		15-3, 90-91	15	x	x			x			x			x		x					x				x		x	
	G. puncticulata	15,CC	15	x				x				x		x		x		x			x		x					
		16,CC	22	x				x			x	x		x		x			x		x				x		x	x
		17,CC	18	x				x	x					x		x									x			
Miocene l.	G. conomiozea	18-3, 90-91	14		x										x						x							
		18-4, 90-91	17	x				x	x		x			x		x		x										
		18-5, 90-91	12		x			x								x					x				x		x	
		18,CC	18	x	x		x	x	x					x		x									x		x	
		19,CC	16	x					x		x			x							x	x	x					
		20,CC	14				x							x		x		x			x				x			x
		21,CC	14		x				x		x			x							x							x
		22,CC	18	x										x		x			x	x	x						x	
	G. nepenthes	23-3, 90-91	15				x		x					x		x		x			x						x	
		23,CC	15	x			x	x			x			x							x		x		x			
		24,CC	19	x	x		x	x	x					x		x		x		x	x						x	x
		25,CC	18	x	x		x		x					x		x			x	x	x				x		x	
		26,CC	19				x	x	x					x		x				x	x						x	x
		27,CC	14	x	x		x	x	x					x		x					x							

———, 1974. Initiation of the proto Circum-Antarctic Current. *Nature*, 252:371–373.

———, 1975. Cenozoic planktonic foraminiferal biostratigraphy of the southwestern Pacific and Tasman Sea—DSDP Leg 29. *In* Kennett, J. P., Houtz, R. E., et al., *Init. Repts. DSDP*, 29: Washington (U.S. Govt. Printing Office), 449–467.

———, 1978a. *Guembelitria* aff. *stavensis* Bandy, a paleoceanographic marker of the initiation of the circum-Antarctic current and the opening of the Drake Passage. *In* Bolli, H. M., Ryan, W. B. F., et al., *Init. Repts. DSDP*, Suppl. to Vols. 38, 39, 40, and 41: Washington (U.S. Govt. Printing Office), 687–693.

———, 1978b. *Guembelitria samwelli* Jenkins, a new species from the Oligocene of the southern Hemisphere. *J. Foraminiferal Res.*, 8(no.2):132–137.

———, 1978c. Neogene planktonic foraminifers from DSDP Leg 40 Sites 360 and 362 in the Southeastern Atlantic. *In* Bolli, H. M., Ryan, W. B. F., et al., *Init. Repts. DSDP*, 40: Washington (U.S. Govt. Printing Office), 723–739.

———, 1981. Planktonic foraminifera and the Palaeogene/Neogene boundary in the southwest Pacific. *In* Cati, F. (Ed.), *In Search of the Palaeogene/Neogene Boundary Stratotype. Giorni di Geologia, Ann. del Museo Geol. di Bologna, Ser. 2a*, 44:205–210.

Jenkins, D. G., and Orr, W. N., 1972. Planktonic foraminiferal biostratigraphy of the eastern equatorial Pacific—DSDP Leg 9. *In* Hays, J., et al., *Init. Repts. DSDP*, 9: Washington (U.S. Govt. Printing Office), 1060–1193.

Keijzer, F. G., 1945. Outline of the geology of the eastern province of Oriente, Cuba (E. cf. 76°WL) with notes on the geology of other parts of the Island. *Utrecht. Geogr. Geol. Meded. Phys-Geol. Reeks, Ser. 2*,6:206.

Kennett, J. P., 1966. The *Globorotalia crassaformis* bioseries in North Westland, and Marlborough, New Zealand. *Micropaleontology*, 12(2):235–245.

———, 1973. Middle and late Cenozoic planktonic foraminiferal biostratigraphy of the southwest Pacific—DSDP Leg 21. *In* Burns

Table 12A. (Continued).

Beella digitata	*B. praedigitata*	*Globoquadrina altispira*	*Globorotalia miotumida*	*G. conomiozea*	*G. sphericomiozea*	*G. pliozea*	*G. puncticulata*	*G. inflata*	*G. explicationis*	*G.* cf. *miocenica*	*G. menardii*	*G. multicamerata*	*G. scitula*	*G. cibaoensis*	*G. margaritae*	*G. crassaformis*	*G. tosaensis*	*G. truncatulinoides*	*G. merotumida*	*G. plesiotumida*	*G. tumida*	*G. ungulata*	*G. clemenciae*	*G. anfracta*	*G. humilis*	*G. siakensis*	*Orbulina universa*	*O. bilobata*	*Pulleniatina primalis*	*P. obliquiloculata*	*Neogloboquadrina acostaensis*	*N. pachyderma*	*N. humerosa*	*N. dutertrei*	*Sphaeroidinella seminulina*	*S. paenedehiscens*	*S. dehiscens*	*Candeina nitida*
x								x					x			x		x			x						x			x		x		x				
								x			x		x			x	x	x			x	x		x			x			x		x		x			x	
								x			x		x			x		x			x	x		x			x	x		x		x		x			x	x
																	x	x			x									x				x				
								x			x		x			x	x	x						x			x			x		x		x			x	
								x			x	x	x			x	x	x			x	x		x			x	x		x		x		x			x	
x								x				x	x			x	x										x	x				x		x				
								x					x			x	x										x					x		x				
		x						x			x	x	x			x	x				x						x					x	x	x	x		x	
		x						x			x					x	x				x																	
	x	x	x			x		x			x	x	x						x	x	x		x		x				x					x				
		x						x			x	x	x						x										x									
		x					x	x			x				x	x											x			x					x			
		x					x				x	x	x		x	x					x			x					x			x	x		x			
	x	x					x				x	x	x		x	x					x			x			x	x				x	x		x		x	
		x	x				x				x	x	x	x	x	x											x	x	x			x	x		x			
		x	x			x	x				x	x	x		x												x	x	x		x	x	x		x			
			x			x	x				x			x	x	x					x						x	x	x		x	x			x			
	x	x	x			x	x		x		x	x	x		x	x				x	x						x	x	x		x	x	x					
						x	x				x			x		x											x					x						
		x	x											x	x				x																			
		x	x			x	x				x			x	x				x				x													x		
				cf.	x		x				x			x	x				x	x			x			x							x					
				x	x						x			x	x					x							x	x	x			x			x			
			x	x							x			x						cf.							x	x			x	x			x			
			x	x							x																x				x	x			x			
	x		x	x							x		x	x					x				x										x					
		x	x	x					x		x			x					x	x																		
		x	x	x							x			x					x														x					
		x	x							x	x			x					x				x															
		x	x	x							x	x	x	x					x							x							x					
			x						x		x		x	x														x			x	x						
		x	x								x	x	x						x														x					
		x	x								x			x					x				x										x					
		x	x						x		x			x					x				x															
		x	x						x	x	x		x	x					x				x										x					
		x	x								x	x							x				x															

E., Andrews, J. E., *Init. Repts. DSDP*, 21: Washington (U.S. vt. Printing Office), 575–640.

ett, J. P., and Srinivasan, M. S., 1983. *Neogene Planktonic Fora- nifera:* Stroudsburg, Pa. (Hutchinson Ross).

ay, J. M., 1969. Cainozoic foraminifera and stratigraphy of the delaide plains sub-basin, South Australia. *Bull. Geol. Surv. South ust.*, 42:1–60.

ook, N. H., 1963. Correlation of the Tertiary rocks of South ustralia. *Trans. R. Soc. South Aust.*, 87:5–15.

ugall, K., 1980. Paleoecological evolution of late Eocene bio- atigraphy of the Pacific coast of North America. *J. Paleontol., leont. Monogr. No. 2*, 54:1–75.

r, D. K., 1934. The foraminiferal genus *Gubelina* in the Tertiary Cuba. *Mem. Soc. Cuba. Hist. "Filipe Poey"*, 8(no.2):74.

G. H., 1982. Review of Kapitean stratotype and boundary with poitian Stage (upper Neogene, New Zealand). *N. Z. J. Geol. eophys.*, 25:475–485.

Srinivasan, M. S., and Kennett, J. P., 1981a. Neogene planktonic foraminiferal biostratigraphy and evolution: Equatorial to subantarctic, South Pacific. *Mar. Micropal.*, 6(no. 5/6):499–533.

_______, 1981b. A review of Neogene planktonic foraminiferal biostratigraphy: Applications in the equatorial and South Pacific. *In* Warme, J. E., Douglas, R. G., and Winterer, E. L. (Eds.), *The Deep Sea Drilling Project: A Decade of Progress*. Soc. Econ. Paleont. Mineral. Spec. Publ., 32:395–432.

_______, 1983. The Oligocene-Miocene boundary in the South Pacific. *Geol. Soc. Am. Bull.*, 94:798–812.

Takayanagi, Y., Takayama, T., Sakai, T., Oda, M., and Kitazoto, H., 1976. Microbiostratigraphy of some middle Miocene sequences in Japan. *In* Takayanagi, Y., and Saito, T. (Eds.), *Progress in Micropaleontology:* New York (Am. Mus. Nat. Hist.), pp. 344–376.

Date of Initial Receipt: 18 June 1984
Date of Acceptance: 26 October 1984

Table 12B. Occurrences of planktonic foraminifers in selected samples of Hole 590B.

Epoch		Zone	Core-Section (interval in cm)	Diversity (no. of species)	*Cassigerinella chipolensis*	*Catapsydrax dissimilis*	*C. unicavus*	*C. parvulus*	*Globigerina angustiumbilicata*	*G. praebulloides*	*G. bulloides*	*G. falconensis*	*G. brazieri*	*G. woodi*	*G. connecta*	*G. decoraperta*	*G. nepenthes*	*G. quinqueloba*	*G. prenepenthes*	*G. druryi*	*Globigerinoides subquadratus*	*G. trilobus*	*G. quadrilobatus*	*G. sacculifer*	*G. ruber*	*G. obliquus*	*G. extremus*	*G. sieglei*	*Globigerinella obesa*	*G. aequilateralis*
Pliocene	e.	*G. crassformis*	11,CC	18							x	x				x						x		x			x			x
			12,CC	17							x	x										x		x						x
			13,CC	10							x	x										x								
Miocene	l.	*G. nepenthes*	30,CC	16												x	x	x				x		x		x		x		
		N. continuosa	31,CC	17								x		x			x					x				x				
			32,CC	19										x		x	x	x				x		x	x	x				
			33,CC	15										x		x	x	x				x				x				
			34,CC	19										x		x	x	x							x				x	
			35,CC	17							x	x		x		x	x	x				x				x				
			36,CC	17								x		x			x					x		x					x	
			37,CC	20							x	x		x		x	x					x		x		x			x	
			38,CC	18								x		x			x					x		x						
	m.	*G. mayeri*	39,CC	14							x	x		x		x	x					x							x	
			40,CC	23							x	x		x		x	x				x	x				x			x	
			41,CC	14							x			x		x						x								
			42,CC	29							x	x		x		x	x				x	x		x		x			x	
			43,CC	30							x	x		x		x		x			x	x	x	x		x			x	
			44,CC	22							x	x		x		x		x			x									
		G. fohsi s.l.	45,CC	28							x	x		x		x			x		x	x				x			x	
			46,CC	13							x										x					x				
			47,CC	17							x	x		x					x		x									
			48,CC	13										x		x													x	
	e.	*G. miozea*	49,CC	8				x							x					x	x	x								
			50,CC	8										x							x	x								
		C. dissimilis	51,CC	12		x	x		x	x			x	x																
			52,CC	14	x	x			x	x				x								x								
			53,CC	13		x	x		x					x				x			x	x								

Table 12B. (Continued).

Globigerinita glutinata	*G. uvula*	*Globoquadrina dehiscens*	*G. altispira*	*G. baroemoenensis*	*Globorotalia peripheroronda*	*G. peripheroacuta*	*G. fohsi*	*G. pseudocontinuosa*	*G. incognita*	*G. zealandica*	*F. miozea*	*G. miotumida*	*G. panda*	*G. puncticulata*	*G. explicationis*	*G.* cf. *miocenica*	*G. praemenardii*	*G. menardii*	*G. multicamerata*	*G. scitula*	*G. cibaoensis*	*G. margaritae*	*G. crassaformis*	*G. lenguaensis*	*G. tumida*	*G. siakensis*	*G. semivera*	*G. mayeri*	*G. nympha*	*Orbulina universa*	*O. bilobata*	*O. suturalis*	*Praeorbulina glomerosa curva*	*Neogloboquadrina continuosa*	*N. acostaensis*	*N. pachyderma*	*Sphaeroidinella disjuncta*	*S. seminulina*	*S. paenedehiscens*
x			x											x				x	x		x	x	x							x						x		x	
			x											x				x	x	x		x	x		x					x	x					x		x	
														x				x				x	x							x	x					x			
	x		x									x								x										x	x				x	x		x	
x			x									x			x	x		x		x										x				x	x	x		x	
x	x		x									x						x		x										x				x	x	x		x	
			x									x				x		x												x				x	x	x		x	
x	x		x									x				x		x		x										x		x		x	x	x		x	
			x									x				x		x												x				x	x	x		x	
x	x		x									x				x		x												x	x	x		x	x				
x	x	x	x									x				x		x												x				x	x	?			
x		x	x									x	x			x		x		x				x						x					x	x		x	
	x	x										x				x		x										x	x										
x	x	x	x	x								x				x		x		x				x				x		x								x	
x		x	x									x	x		x	x		x		x								x											
x	x	x	x	x								x	x			x	x	x		x				x		x		x		x		x		x				x	
x	x	x	x	x								x	x		x	x	x	x		x						x		x		x		x		x				x	
		x	x		?							x	x		x	x	x	x		x						x		x		x		x		x				x	
x	x	x	x	x	x	x	x					x	x				x	x		x						x		x		x		x		x				x	
		x	x		x	x						x					x									x		x		x								x	
x	x	x	x		x	x						x					x									x		x		x								x	
x		x	x		x	x					x															x				x							x		x
		x			x						x																												
					x					x	x															x							x						
		x						x	x	x																													
		x		x				x	x	?																x	x												
		x						x	x	x																	x												

Table 13. Occurrences of planktonic foraminifers in selected samples of Hole 591.

Epoch	Zone	Core-Section (interval in cm)	Diversity (no. of species)	*Globigerina umbilicata*	*G. foliata*	*G. bulloides*	*G. falconensis*	*G. woodi*	*G. decoraperta*	*G. nepenthes*	*G. quinqueloba*	*G. rubescens*	*Globigerinoides trilobus*	*G. quadrilobatus*	*G. sacculifer*	*G. ruber*	*G. conglobatus*	*G. extremus*	*G. seigliei*	*G. fragilis*	*Globigerina calida*	*Globigerinella obesa*	*G. aequilateralis*	*Hastigerina pelagica*	*Globigerinita glutinata*	*G. uvula*	*Beela digitata*
Pleistocene	*G. truncatulinoides*	1,CC	25			x	x				x	x		x	x	x	x				x		x	x	x		x
		2,CC	24			x	x				x	x		x	x	x					x		x	x	x		x
		3,CC	20			x	x				x	x	x		x	x							x		x		
		4-1, 66–68	18			x	x					x	x		x	x	x						x		x		
	G. truncatulinoides/ *G. tosaensis*	4-2, 66–68	18			x	x		x		x		x		x	x	x						x		x		
		4-3, 90–92	9												x								x				
		4,CC	21			x	x				x		x	x	x	x	x						x		x		x
		5,CC	21		x	x	x				x		x		x	x	x				x		x				
		6,CC	22			x	x				x		x	x	x	x	x				x		x		x		x
		7,CC	20			x	x						x		x	x					x		x		x	x	
		8,CC	26		x	x	x				x		x		x	x	x						x		x	x	x
		9-3, 90–92	4				x								x										x		
Pliocene l.	*G. tosaensis*	9-4, 66–68	18			x	x						x		x	x	x	x					x		x		x
		9-6, 66–68	24			x	x		x		x		x		x	x	x	x				x	x		x		
		9,CC	27		x	x	x	x	x		x		x	x	x	x	x					x	x		x		x
		10,CC	28		x	x	x		x				x	x	x	x	x	x				x	x		x		x
		11-3, 90–92	16				x	x					x			x		x					x				
		11-4, 66–68	22			x	x	x					x		x	x	x	x					x		x		
		11-5, 66–68	22			x	x	x					x		x	x	x	x					x		x		
	G. inflata	11-6, 66–68	19			x	x						x		x	x		x							x		
		11,CC	20			x	x		x				x		x	x		x					x		x		
		12,CC	20			x	x		x		x		x		x			x					x		x		
		13,CC	18				x		x				x		x			x					x		x		
		14-3, 90–91	18						x		x		x		x	x		x					x		x		
e.	*G. crassaformis*	14-4, 66–68	20			x	x	x									x						x		x		
		14-5, 66–68	19			x	x	x									x						x		x		
		14-6, 66–68	19			x	x	x									x						x		x		
		14,CC	22			x		x			x		x		x			x					x		x	x	
		15,CC	19	x		x	x						x		x			x					x		x		
		16,CC	23			x	x		x				x		x	x	x	x				x	x		x		
		17,CC	19			x							x		x	x	x	x									
		18-1, 66–68	25			x	x	x	x	x			x		x			x					x		x		
	G. puncticulata	18-2, 66–68	13			x		x	x		x		x					x									
		18-3, 90–92	15			x		x	x		x		x					x							x		
		18,CC	28			x	x		x		x		x	x	x	x		x				x	x		x		
		19,CC	21		x	x									x			x	x	x			x				
		20-1, 27–28	20			x	x			x	x		x		x								x		x		
Miocene l.	*G. sphericomiozea*	20-2, 27–28	15				x	x		x			x		x			x									
		20-3, 90–92	15				x	x		x			x												x		
		20-4, 27–28	16			x		x	x									x				x					
		20-5, 27–28	17			x					x		x									x					
		20-6, 27–28	18				x		x		x				x			x							x	x	
	G. conomiozea	20,CC	34		x	x	x		x	x			x	x	x	x	x	x	x			x	x		x		
		21,CC	22					x			x		x		x	x		x	x						x		
		22,CC	23				x		x	x			x		x			x		x			x		x		
		23-3, 90–91	14							x					x			x		x							
	G. nepenthes	23,CC	22			x	x		x	x			x	x				x		x			x		x	x	
		24,CC	23			x	x		x	x			x	x			x	x					x		x		
		25,CC	27			x	x	x	x	x			x		x			x					x		x		
	N. continuosa	26-1, 66–68	23			x	x	x	x	x			x		x		x	x							x		
		26-3, 90–92	7												x												
		26,CC	25			x	x		x	x			x		x		x	x							x		
		27,CC	23			x	x	x	x	x			x		x		x					x			x	x	
		28,CC	25			x	x	x		x	x		x		x			x		x		x			x	x	
		29,CC	26			x	x	x	x	x			x		x			x				x	x		x	x	
		30,CC	24				x	x	x	x	x		x		x			x				x	x		x	x	
		31,CC	16					x	x	x	x				x			x								x	

Note: R = reworked.

Table 13. (Continued).

B. praedigitata	*Globoquadrina dehiscens*	*G. altispira*	*Globorotalia miotumida*	*G.* sp.	*G. panda*	*G. explicationis*	*G. conomiozea*	*G. sphericomiozea*	*G. pliozea*	*G. puncticulata*	*G. inflata*	*G. menardii*	*G. multicamerata*	*G.* cf. *ichinosekiensis*	*G. scitula*	*G. cibaoensis*	*G. margaritae*	*G. crassula*	*G. crassaformis*	*G. tosaensis*	*G. truncatulinoides*	*G. lenguaensis*	*G. plesiotumida*	*G. tumida*	*Orbulina universa*	*O. bilobata*	*O. suturalis*	*Pulleniatina primalis*	*P. obliquiloculata*	*Neogloboquadrina continuosa*	*N. nympha*	*N. acostaensis*	*N. pachyderma*	*N. humerosa*	*N. dutertrei*	*Sphaeroidinella seminulina*	*S. dehiscens*	*Candeina nitida*
											x	x			x				x		x			R	x				x				x		x		x	x
											x	R			x				x		x			R	x		x		x				x		x		R	
											x	x			x				x		x			x	x				x				x		x		x	
											x				x				x		x			x	x				x				x		x			
											x				x					x	x			x					x				x		x			
											x								x	x	x			x	x				x									
											x	R			x				x	x	x			x	x				x				x					
											x				x					x	x			x	x				x				x		x		x	x
											x				x				R	R	x				x				x				x		x		x	
											x	x			x				x	x	x				x				x				x		x		x	
											x	x	x		x				x	x	x			x	x	x			R				x		R		x	
																					x																	
											x		x		x				x	x					x								x		x			
											x	x	x		x				x	x				x	x								x		x		x	x
											x	x	x		x				x	x				x	x	x							x				x	x
		x									x	x	x		x				x	x				x	x	x							x	x		x	x	
		x									x	x	x						x	x				x	x										x	x		
		x									x	x	x		x				x	x				x	x										x	x	x	
		x									x	x	x		x				x	x				x	x										x	x	x	
		x									x	x	x		x				x					x	x				x				x			x	x	
		x									x	x	x		x				x					x	x				x				x			x		
		x							cf.		x	x	x		x				x					x	x			x					x		?			
		x									x	x	x				x		x						x				x				x	x		x		
		x								x	x		x				x							x	x				x				x	x				
		x							x	x			x		x	cf.	x		x					x	x			x					x	x		x		
		x							x	x			x		x		x		x					x	x			x					x	x		x		
		x							x	x			x		x		x		x					x	x			x					x	x		x		
		x								x		x	x			x	x		x					x	x			x					x	x		x		
		x								x		x	x		x		x		x						x								x	x		x		
		x							x	x		x	x		x		x		x					?	x								x	x		x		
		x							x	x		x	x				x	cf.	R					x				x					x	x		x		
		x							x	x			x		x	cf.		x	x				x		x		x	x					x	x		x		
		x							x	x			x												x								x	x				
		x							x	x			x		x										x								x	x				
		x							x	x		x	x		x		?	cf.					x	x	x			x				x	x	x		x		x
		x							x	x		x	x			x	x	cf.					x		x			x					x	x		x		
			x			x		x	x	x		x											x		x			x				x	x			x		
			x			x		x	x			x					x											x				x	x					
			x					x	cf.			x				x	x	x							x								x			x		
		x	x			x		x								x	x								x			x				x	x			x		
		x	x			x		x	x							x	x								x	x		x				x	x			x		
			x			x		x	x			x					x								x			x				x	x			x		
x		x				x	x	x	?			x	x		x		x	cf.					x	x	x	x		x				x	x	x		x		
		x	x				x	x				x	x			x	cf.	cf.					x		x	x		x				x						
		x	x			x	x	x				x	x			x									x	x						x	x			x		x
		x	x				x					x				x		x							x	x						x				x		
		x											x			x	x	?					x		x	x		x				x	x			x		
		x	x									x	x		x	x							x		x	x	x					x	x			x		
		x	x	x	x							x	x	x	x	x						x	x		x	x	x					x	x			x		
		x	x	x								x	x		x	x							x		x					x	x	x				x		
		x	x			x								x		x														x								
		x	x	x								x		x	x	x		R					x		x	x	x			x		x	x			x		
		x	x	x								x	x		x								x		x					x		x	x			x		
	x	x	x	x								x		x									x		x	x				x		x	x			x		
	x	x	x	x								x		x	x								x		x	x				x		x	x			x		
		x	x									x		x	x								x		x	x				x		x	x			x		
		x	x											x	x								x		x					x			cf.			x		

Table 14A. Occurrences of planktonic foraminifers in Hole 592, Samples 592-1,CC through 592-29,CC.

Epoch		Zone	Core-Section (interval in cm)	Diversity (no. of species)	*Cassigerinella chipolensis*	*Globigerina foliata*	*G. angustiumbilicata*	*G. bulloides*	*G. falconensis*	*G. woodi*	*G. decoraperta*	*G. nepenthes*	*G. prenepenthes*	*G. quinqueloba*	*G. rubescens*	*Globigerinoides subquadratus*	*G. trilobus*	*G. sacculifer*	*G. bisphericus*	*G. ruber*	*G. conglobatus*	*G. extremus*	*G. tyrrhenicus*	*Globigerinella obesa*	*G. aequilateralis*	*Globigerinita glutinata*	*G. uvula*	*Beela praedigitata*	*Globoquadrina dehiscens*	*G. altispira*
Pleistocene		*G. truncatulinoides*	1,CC	12				x	x						x					x	x				x	x				
		G. truncatulinoides/ G. tosaensis	2-2, 90–91	2																										
			2,CC	15				x	x					x						x					x	x				
			3,CC	14				x	x					x						x					x	x				
			4-2, 90–91	3																										
			4-4, 90–91	8				x		x															x					
Pliocene	l.	*G. inflata*	4,CC	11				x						x			x			x					x	x				
			5,CC	12				x	x								x			x					x	x		x		
			6,CC	15		x				x	x			x											x	x				
			7,CC	17				x	x		x							x		x		x			x	x		x		
			8-3, 90–91	7				x														x			x					
	e.	*G. crassaformis*	8,CC	15		x		x						x			x					x				x				x
			9,CC	11				x		x				x				x				x								
			10-1, 90–91	5																						x				
			10-2, 90–91	8																		x			x					
		G. puncticulata	10-3, 90–91	5						x																				
			10,CC	23				x	x	x				x				x		x		x			x	x				x
			11-3, 90–91	5																										
			11,CC	12				x	x					x								x				x				
Miocene	l.	*G. sphericomiozea*	12-3, 90–91	6																										
			12,CC	15				x	x	x		x		x								x			x	x				
		G. conomiozea	13,CC	19				x	x	x		x		x			x	x				x			x	x				
			14,CC	11					x	x	x			x																
			15,CC	13				x	x	x	x			x										x	x	x				
			16,CC	17				x		x	x	x		x				x				x		x		x				x
			17-3, 90–91	7				x		x																				
		G. miotumida	17,CC	17				x	x	x	x			x			x						x	x		x				x
			18,CC	14				x		x	x	x		x									x			x				
			19,CC	17				x		x	x			x									x			x	x			
			20,CC	13				x		x				x			x	x							x		x			
			21,CC	11			x			x	x															x	x			
			22,CC	15				x		x		x					x									x			x	
			23-3, 90–91	6				x		x							x									x			x	
		N. continuosa	23,CC	14			x	x	x	x				x			x									x	x		x	
	m.	*G. mayeri*	24,CC	17				x	x	x	x			x			x									x	x		x	
			25,CC	14				x		x				x								x				x			x	
			26,CC	12						x			x	x			x									x			x	
		O. suturalis	28,CC	9					x	x				x															x	
	e.	*P. glomerosa curva*	29-3, 90–91	19	x		x	x	x	x				x		x	x		x							x				
		G. miozea	29,CC	11			x	x	x	x				x		x	x													

Table 14A. (Continued).

G. [illegible]	Globorotalia peripheroronda	G. praescitula	G. miozea	G. miotumida	G. panda	G. conomiozea	G. sphericomiozea	G. pliozea	G. puncticulata	G. inflata	G. explicationis	G. sp. 2	G. praemenardii	G. menardii	G. cf. ichinosekiensis	G. conica	G. scitula	G. cibaoensis	G. margaritae	G. hirsuta	G. crassaformis (conical)	G. crassaformis	G. crassula	G. tosaensis	G. truncatulinoides	G. cf. crassula	G. tumida	G. anfracta	G. mayeri	G. nympha	G. hexagona	Orbulina universa	O. bilobata	O. suturalis	Praeorbulina sicanus	P. curva	Pulleniatina primalis	Neogloboquadrina continuosa	N. pachyderma	N. humerosa	Sphaeroidinella disjuncta	S. seminulina
										x							x								x							x							x			
																								x	x																	
										x							x			x		x		x	x			x				x							x			
										x							x			x		x		x	x							x							x			
										x														x	x																	
										x												x		x	x							x										
										x							x					x										x							x			
										x							x					x										x							x			
										x				x			x		cf.			x					x					x							x			x
				x						x							x		x		x	x										x							x			
									x	x												x										x										
				x				x	x										x		x	x										x							x			
								x	x										x			x										x							x			
								x	x													x																	x			
						cf.		x	x										x			x																	x			
								x	x										x													x										
						cf.		x	x					x			x		x								x					x	x						x	x		x
								x	x										cf.													x					x					
							x	x	x										x							x						x							x			
				x		x	x	x											x				x																			
						x	x											x	cf.							x												cf.	x			
				x		x					x							x														x	x						x			x
				x		x												x								x						x		x					x	x		
				x		x											x															x							x			
				x		x												x														x							x	x		
				x		x					x							x														x		x								
				x								cf.					x	x														x		x					x			
				x											x			x														x		x				cf.	x			
				x	x						x	x			x																	x	x	x					x			x
				x							x	x			x																	x							x			
				x							x	x			x																	x							x			
x				x							x				x																x	x						cf.	x			x
				x																																						
				x							x				x																	x						x				
				x											x											x	x		x					x				x				x
				x	x								x		x														x			x						x				
	x			x									x			x													x					x								
	x			x									x			x																		x								
			x													cf.																			x	x					x	
			x		x								x																													

Table 14B. Occurrences of planktonic foraminifers in Hole 592, Samples 592-30,CC through 592-41,CC.

Epoch	Zone	Core-Section (interval in cm)	Diversity (no. of species)	*Chiloguembelina cubensis*	*Catapsydrax unicavus*	*C. echinatus*	*Globigerina angustiumbilicata*	*G. ampliapertura*	*G. angiporoides*	*G. bulloides*	*G. euapertura*	*G. brazieri*	*G. woodi*	*G. connecta*	*G. brevis*	*G. juvenilis*	*G. linaperta*	*G. quinqueloba*	*Globigerinoides trilobus*	*Globigerinatheka index*	*Globanomalina micra*	*Globorotalia aculeata*	*Globigerinella obesa*	*Globorotalia gemma*	*G. munda*	*G. insolita*	*Globigerinita glutinata*	*G. uvula*	*Hantkenina alabamensis*	*Globoquadrina dehiscens*	*G. venezuelana*	*Globorotalia peripheroronda*	*G. semivera*	*G. nana*	*G. pseudocontinuosa*	*G. incognita*	*G. zealandica*	*G. praescitula*	*G. miozea*	*G. praemenardii*	*G. minutissima*	*G. semivera*	*Globorotaloides suteri*	*G. turgida*	*Truncorotaloides collactea*
Miocene e.	*G. miozea*	30,CC	9							x			x					x	x													x						x	x	x					
	G. trilobus	31-3, 90-91	8							x			x						x				x				x			x							x	x							
		31,CC	11							x			x					x										x		x	x			x	x	x		x			x				
		32-3, 90-91	12		x		x			x			x	x		x											x	x		x	x		x		x										
		32,CC	12				x			x		x	x	x					x											x	x				x	x						x			
Oligocene e.	*G. angiporoides*	33-3, 90-91	6	x	x				x							cf.								cf.	x																				
		33-4, 90-91	7	x				x	x		x													x	x																		x		
		33,CC	9	x		x		x	x		x													x	x																	x	x		
	G. brevis	34-3, 90-91	5	x					x						x									x																			x		
		34,CC	5	x					x		x				x									x																					
		35-3, 90-91	6	x				x	x						x									x																			x		
		35,CC	5	x					x		x				x									x																					
		36-2, 90-91	7	x				x	x		x				x									x																			x		
Eocene l.		36-3, 90-91	7	x					x								x			x				x		x																	x		
		36,CC	3	x													x			x																									
		37-3, 90-91	8	x		x									x		x			x	x			x																			x		
	G. linaperta	37,CC	3														x			x	x																								
		38,CC	3														x			x									x																
		39,CC	5	x													x			x	x																						x		
		40-3, 90-91	6	x					x								x			x	x																							x	
		40,CC	7	x		x			x								x			x	x														x										
	G. aculeata	41,CC	6	x													x			x	x	x																							x

Table 15A. Occurrences of planktonic foraminifers in selected samples of Hole 593.

Epoch		Zone	Core-Section (interval in cm)	Diversity (no. of species)	*Globigerina angustiumbilicata*	*G. bulloides*	*G. falconensis*	*G. woodi*	*G. decoraperta*	*G. nepenthes*	*G. quinqueloba*	*Globigerinoides subquadratus*	*G. trilobus*	*G. sacculifer*	*G. ruber*	*G. extremus*	*G. tyrrhenicus*	*Globigerinella obesa*	*G. aequilateralis*	*G. pseudobesa*	*Globigerinita glutinata*	*G. uvula*	*Globoquadrina dehiscens*	*G. altispira*	*Globorotalia miotumida*	*G. conomiozea*	*G. sphericomiozea*	*G. pliozea*	*G. puncticulata*	*G. inflata*	*G. explicationis*	*G.* sp. 2	*G. ichinosekiensis*	*G. scitula*	*G. cibaoensis*	*G. margaritae*	*G. hirsuta*	*G. cibaoensis-crassula*	*G. crassaformis*	*G. crassula*	*G. truncatulinoides*	*G. crassaformis-tosaensis*	*Orbulina universa*	*O. bilobata*	*O. suturalis*	*Neogloboquadrina continuosa*	*N. nympha*	*N. pachyderma*
Pleistocene		*G. truncatulinoides*	1,CC	9		x	x														x									x				x							x		x					x
			2,CC	14		x	x								x				x			x								x				x			x		x		x		x	x				x
			3,CC	12		x	x												x		x									x				x					x		x		x		x			x
			4,CC	9		x													x											x				x			x		x		x		x					x
Pliocene	l.	*G. inflata*	5-3, 90-91	8		x	x		x						x				x											x									x				x					x
			5,CC	7															x											x				x			x		x				x					x
			6,CC	9		x			x							x			x											x				x					x				x					x
			7,CC	8		x													x										x	x				x					x				x					x
			8,CC	12		x	x								x				x		x				x				x	x				x								x	x					x
			9,CC	11		x	x		x		x				x				x										x	x												x	x					x
	e.	*G. puncticulata*	11-3, 90-91	12		x	x		x		x											x						x	x										x	cf.			x	x				x
			11,CC	12		x			x		x										x							x	x					x	x	x				x			x					x
			12,CC	11		x	x		x		x										x							x	x					x						x			x					x
			13,CC	10		x					x											x					x	x	x						x					x			x					x
Miocene		*G. conomiozea*	14,CC	8		x			x																	x	x								x					x			x					x
			15,CC	14		x	x		x		x										x				x	x	x							x	x			x		x			x					x
			16,CC	8		x																			x	x	x				x				x								x					x
			17,CC	15		x	x	x	x		x								x		x				x	x	cf.							x	x								x		x			x
			18-3, 90-91	11		x	x	x	x		x										x				x	x					x												x					x
	l.	*G. miotumida*	18,CC	14		x	x	x	x										x		x				x	cf.						x		x	x								x		x			x
			19,CC	10		x					x										x	x			x	cf.					x	x											x					x
			20,CC	17		x	x	x	x										x		x	x			x						x	x	x	x	x								x		x	cf.		x
			21,CC	18		x	x	x	x								x	x			x	x		x	x						x	x	x	x									x		x	cf.		x
			22,CC	18		x	x	x	x								x	x			x	x			x						x	x	x	x									x	x	x	cf.		x
			23,CC	17		x	x	x	x		x							x			x	x			x							x	x	x									x		x	x	x	cf.
			24,CC	17		x	x	x	x		x							x			x	x			x							x	x	x									x		x	x	x	cf.
			25,CC	16	x	x	x	x	x	cf.		x									x				x						x	x	x										x			x	x	x
			26,CC	13		x		x			x	x	x	x											x										x								x		x	x	x	x
			27,CC	18	x	x	x	x	x		x		x							x	x	x			x										x								x		x	x	x	x
		N. continuosa	28-3, 90-91	11		x	x	x	x												x		x		x																		x		x	x		cf.
			28,CC	18		x	x	x	x		x			x						x	x	x	x		x									x	cf.								x		x	x	x	cf.
			29,CC	18		x	x	x	x	x	x									x	x	x	x		x							x		x									x		x	x		cf.
			30,CC	15		x	x	x	x				x	x							x		x		x						x	x											x		x		x	x

Table 15B. Occurrences of planktonic foraminifers in Hole 593, Samples 593-31,CC through 593-60,CC.

Epoch		Zone	Core-Section (interval in cm)	Diversity (no. of species)	*Cassigerinella chipolensis*	*Streptochilus pristinum*	*Chiloguembelina cubensis*	*Catapsydrax dissimilis*	*C. unicavus*	*C. echinatus*	*Globigerina euapertura*	*G. angustiumbilicata*	*G. brevis*	*G. ampliapertura*	*G. linaperta*	*G. bulloides*	*G. falconensis*	*G. juvenilis*	*G. brazieri*	*G. woodi*	*G. connecta*	*G. decoraperta*	*G. nepenthes*	*G. ouachitaensis*	*G. quinqueloba*	*G. prenepenthes*	*G. angiporoides*	*G. labiacrassata*	*G. altiapertura*	*Globigerinoides subquadratus*	*G. trilobus*	*G. sacculifer*	*Globigerinatheka semiinvoluta*
Miocene	l.	*N. continuosa*	31,CC	15												x	x			x		x	x								x		
			32,CC	15												x	x			x		x	x		x						x		
			33-3, 90-91	11																x		x			x								
			33,CC	16												x	x			x		x									x		
	m	*G. mayeri*	34,CC	15												x	x			x		x									x		
			35,CC	14												x	x			x		x									x		
			36,CC	14												x	x			x		x									x		
			37,CC	18												x	x			x		x									x	cf.	
			38,CC	18												x	x			x		x				x				x	x		
			39-3, 90-91	12												x				x		x										x	
			39,CC	20												x	x			x		x				x					x	x	
			40-3, 90-91	14												x	x			x		x									x	x	
			40,CC	19																x		x				x					x	x	
		O. suturalis	41,CC	8												x	x			x											x		
	e	*P. glomerosa curva*	42-4, 6-8	12												x	x			x										x	x		
			42-4, 29-31	9													x			x										x	x		
		G. miozea	42,CC	12												x				x	x								x	x	x		
			43,CC	11												x				x											x		
			44,CC	13																x					x					x	x		
		G. trilobus	45,CC	8																x	x										x		
			45-3, 90-91	10																x	x										x		
		G. connecta	46,CC	11				x												x	x				x								
			47,CC	10				x												x	x				x								
			48,CC	10	x			x												x	x				x								
		G. woodi	49,CC	13				x				x						x	x	x					x								
		G. dehiscens	50-1, 90-91	7				x			x																						
Oligocene	l	*G. euapertura*	50,CC	10		x	x				x					x																	
	e	*G. angiporoides*	52,CC	11			x	x			x							x									x	x					
			53,CC	13			x	x	x		x	x												x			x						
			54,CC	13			x		x		x	x															x	x					
			55,CC	6			x	x																			x						
			56-3, 90-91	6			x		x																		x						
			56,CC	7			x																				x						
		G. brevis	57-1, 90-92	5			x			x			x														x						
			57-3, 90-92	6			x						x											cf.			x						
			57-6, 90-92	7						x			x	x										x			x						
Eocene	l		57,CC	11			x			x			x	x	x												x						
			58-1, 90-92	10			x			x			x	x	x												x						
			58-2, 90-92	10			x						x	x	x												x						
			58-2, 127-128	11			x						x	x	x												x						
		G. linaperta	58,CC	3				x							x												x						
			59,CC	7			x								x												x						
			60,CC	9			x							x	x												x						

Note: R = reworked.

Table 15B. (Continued).

G. [illegible]	[illegible]	Globigerinella obesa	G. pseudobesa	Globigerinita glutinata	G. uvula	Globoquadrina dehiscens	G. venezuelana	Globorotalia kugleri	G. peripheroronda	G. cf. peripheroacuta	G. opima	G. conica	G. nana	G. pseudocontinuosa	G. incognita	G. zealandica	G. praescitula	G. miozea	G. miotumida	G. panda	G. praemenardii	G. scitula	G. insolita	G. gemma	G. munda	G. minutissima	G. siakensis	G. seminvera	G. bella	G. mayeri	G. aculeata	Globorotaloides suteri	G. hexagona	G. testarugosa	G. turgida	Orbulina universa	O. suturalis	Praeorbulina glomerosa curva	Neogloboquadrina continuosa	N. nympha	N. pachyderma	Sphaeroidinella disjuncta	S. seminulina	Truncorotaloides collactea
				x		x													x	x																x	x		x	x	cf.			
				x		x													x	x																x	x		x		x			
				x		x													x	x		x														x			x		cf.			
			x	x		x													x	x	x												x			x	x		x		cf.			
				x		x													x	x	x									x						x	x		cf.	x				
				x		x													x								cf.			x						x	x		x	x				
				x		x											x		x											x						x	x		x	x				
				x		x											x		x	x	x	x								x						x	x		x					
				x		x											x		x	x	x									x						x	x		x	x				
		x								x									x											x						x	x						x	
		x		x		x			cf.	x		x					x		x	x	x									x						x	x		cf.					
				x		x			x	x		x							x											x						x	x		x					
		x		x		x			x			x					x	x	x		x									x							x						x	
						x			x			x						x	x		x								cf.								x							
				x		x			x					x			x	x																				x						
						x											x	x																				x						
						x							x	x				x			x																							
				x		x											x	x			x							x														x		
					x	x									x	x	x	x								x		x																
				x		x								x		x	x																											
				x	x	x								x			x											x	cf.															
					x	x							x	x	x	x												x																
				x	x	x								x												x		x																
				x		x		x						x												x																		
				x	x	x		x						x												x		x																
						x					cf.		x	x											x									x									
				x									x	x														x																
							x						x	x											x									x										
							x						x	x											x									x										
											cf.		x	x										cf.	x									x										
													x												x							x												
																								cf.	x									x										
																								cf.	x							x		x										
																								x								x												
																								x								x												
																								x																				
x																								x								x												
x																							x	x								x												
x																							x	x								x												
x																							x	x								x												
x													x											x																				
x																														R				x										R

Table 15C. Occurrences of planktonic foraminifers in Hole 593A.

Epoch		Zone	Core-Section (interval in cm)	Diversity (no. of species)	*Chiloguembelina cubensis*	*Streptochilus pristinum*	*Jenkinsina samwelli*	*Globoquadrina dehiscens*	*Catapsydrax unicava*	*C. dissimilis*	*Globorotalia opima*	*G. munda*	*G. nana*	*G. pseudocontinuosa*	*G. semivera*	*Globigerina juvenilis*	*G. angustiumbilicata*	*G. euapertura*	*G. angulisuturalis*	*G. bulloides*	*G. labiacrassata*	*G. brazieri*	*G. angiporoides*	*Globigerinoides inusitatus*	*Globigerinita glutinata*	*G. uvula*	*Globorotaloides testarugosa*
Miocene	e	*G. dehiscens*	23,CC	8				x									x	x		x	x				x	x	
			24-1, 90-91	12		x		x					x	x	x		x	x		x		x		x	x		cf.
Oligocene	l	*G. euapertura*	24-2, 90-91	13		x					x	x	x	x	x	x	x	x		x	x				x		x
			24,CC	15	x	x	x				cf.	x	x	x		cf.	x	x	x	x					x	x	x
			25,CC	15	x	x	x		x	x		x	x	x	x	x	x	x		x	cf.						x
	e	*G. angiporoides*	26,CC	10	x							x	x	x			x	x	x		cf.		x				x

Table 16A. Occurrences of planktonic foraminifers in Hole 594, Samples 594-1,CC through 594-30,CC.

Epoch		Zone	Core-Section (interval in cm)	Cold (C) Warmer (W)	Diversity	*Globigerina bulloides*	*G. woodi*	*G. connecta*	*G. quinqueloba*	*G. umbilicata*	*Globigerinella aequilateralis*	*Globigerinita glutinata*	*G. uvula*	*Globorotalia miotumida*	*G. panda*	*G. conomiozea*	*G. sphericomiozea*	*G. puncticulata*	*G. inflata*	*G. praemenardii*	*G. cf. ichinosekiensis*	*G. pseudomargaritae*	*G. scitula*	*G. crassaformis*	*G. crassula*	*G. tosaensis*	*G. truncatulinoides*	*G. cf. crassula*	*Orbulina universa*	*O. suturalis*	*Neogloboquadrina continuosa*	*N. pachyderma*
Pleistocene		*G. truncatulinoides*	1,CC	W	10	x			x	x		x	x						x				x			cf.	x					x
			2,CC	W	8	x			x	x			x						x							cf.	x					x
			3,CC	W	9	x			x	x			x						x				x				x		x			x
		G. inflata	4-3, 90-91	W	6	x			x				x						x				x									x
			4,CC	W	11	x			x	x	x	x	x						x				x	x					x			x
			5,CC	W	9	x			x	x		x	x						x				x	x								x
			6,CC	C	8	x			x	x			x						x				x	x								x
— ? — ? —			7,CC	W	6	x			x				x						x					x								x
	l		8,CC	W	8	x			x				x						x				x	x					x			x
Pliocene	e	*G. sphericomiozea*	9-3, 90-91	W	7	x			x			x	x					x						x								x
			9,CC	W	9	x			x		x							x					x	x	x				x			x
			10,CC	C	5	x			x									x						x								x
			11-3, 90-91	W	6	x							x				x	x														x
			11,CC		6	x			x			x	x				x	x														x
			12,CC		7	x	cf		x				x				x	x														x
			13,CC		6	x			x			x					x	x														x
			14,CC		4	x			x								x															x
			15,CC		8	x				x		x					x	x		x												x
			16,CC		8	x	x	x									x	x		x					cf							x
			18,CC		9	x	x	x	x			x	x				x	x											x			x
			19,CC		5	x							x																x			x
			20-3, 90-91		7	x			x				x	x			x											x	x			x
Miocene	l	*G. miotumida*	20,CC		9	x	x		x			x		x		x													x			x
			21-3, 90-91		7	x	x		x					x		x														x		x
			21,CC		8	x	x		x				x	x															x			x
			23,CC	C	10		x	x	x				x	x							x							x	x		x	x
			24,CC	C	8	x	x		x				x								x								x		x	x
			25,CC		7	x	x		x				x	x															x			x
			26,CC		11	x		x				x	x	x	cf.														x	x	x	x
			27,CC		8	x	x	x	x					x	x						x	x							x			
			28,CC		9	x	x		x				x								x	x							x	x		
			29,CC		9	x			x			x	x	x							x	x							x		x	
			30,CC		7	x	x		x				x	x															x		x	

Table 16B. Occurrences of planktonic foraminifers in Hole 594, Samples 594-31,CC through 594-53,CC and Hole 594A, Samples 594A-12,CC through 594A-26,CC.

Epoch	Zone	Core-Section (interval in cm)	Diversity	*Globigerina angustiumbilicata*	*G. bulloides*	*G. falconensis*	*G. eamesi*	*G. woodi*	*G. connecta*	*G. decoraperta*	*G. nepenthes*	*G. quinqueloba*	*Globigerinoides trilobus*	*Globigerinita glutinata*	*G. uvula*	*Globoquadrina dehiscens*	*Globorotalia peripheroronda*	*G. zealandica*	*G. praescitula*	*G. miozea*	*G. miotumida*	*G. panda*	*G. conica*	*G. explicationis*	*G. praemenardii*	*G. cf. archeomenardii*	*G. "pseudomiozea"*	*G. sp. 1*	*G. minutissima*	*G. semivera*	*G. mayeri*	*Orbulina universa*	*O. suturalis*	*Praeorbulina glomerosa*	*P. circularis*	*Neogloboquadrina continuosa*	*N. nympha*	*N. pachyderma*
		Hole 594																																				
l	*G. miotumida*	31,CC	8		x			x													x					x	x					x				x		x
		33,CC	8		x			x				x			x						x			x		x	x											
		34,CC	11		x			x				x		x	x						x					cf.	x									x	x	x
		35,CC	7		x			x				x			x						x					x	x											
		36,CC	4		x			x													cf.							x										
		37,CC	10					x		x				x	x						x	cf.						x					x			x		cf.
		38,CC	7		x			x				x									x						x	x								x		
Miocene m	*G. mayeri*	39-2, 90-91	8		x			x				x									x										x	x				x	x	
		39,CC	11		x			x				x			x						x					x	x				x	x				x	x	
		40,CC	10		x			x		x												cf.			cf.	x					x	x				x	x	
		41,CC	5	x	x			x																							x	x						
		42,CC	6		x			x				x			x						x										x							
		43,CC	5					x			cf.	x																			x					cf.		
		44,CC	9		x			x				x			x						x		x								x					x	x	
		45,CC	6		x			x											x	x														R	x			
		46-2, 90-91	10		x			x				x			x				x	x											x		x			x	x	
	G. peripheroronda	46,CC	9		x			x				x					x		x											x	x		x		x			
		47,CC	8	x	x	x		x								x	x		x											x			x					
		48,CC	11		x	x		x				x		x			x		x			cf.								x	x		x					
		49,CC	9		x							x		x			x		x	x											x		x					
	G. conica	50-1, 90-91	7		x			x				x					x			x			x										x					
		50,CC	8		x			x				x		x			x			x			x								x							
		51,CC	9					x	x			x					x	cf.	x	x			x						x									
		52-2, 90-91	6		x			x				x						x		x			x															
		52,CC	5														x	x	x				x		x													
		53,CC	8		x			x	x			x		x				x	x										x									
		Hole 594A																																				
m	*G. conica*	12,CC	11		x		cf.	x				x		x			cf.	R	x	cf.			x								cf.							
		13,CC	9		x			x	R	x							x	R		x			x								cf.							
		14,CC	7					x				x					x	R	x	x										R								
		15,CC	6	x	x			x												x			x										x					
		16,CC	9	x	x			x	R			x							x	x			x										x					
Miocene e	*P. glomerosa curva?*	17,CC	6					x	R			x	cf.					R		x																		
		18,CC	4		x			x	R											x																		
		19,CC	4		x			x											x	x																		
		20,CC	4					x	R										x	x																		
	G. miozea	21,CC	7		x			x	x			x						x	x	x																		
		22,CC	7		x			x	x							x		x	x	x																		
		23,CC	3					x										cf.		x																		
		24,CC	6		x			x	x			x							x	x																		
		25,CC	7					x	x					x	x			x	x	x																		
		26,CC	10		x	x		x	x			x		x	x			x	x	x																		

R = reworked.

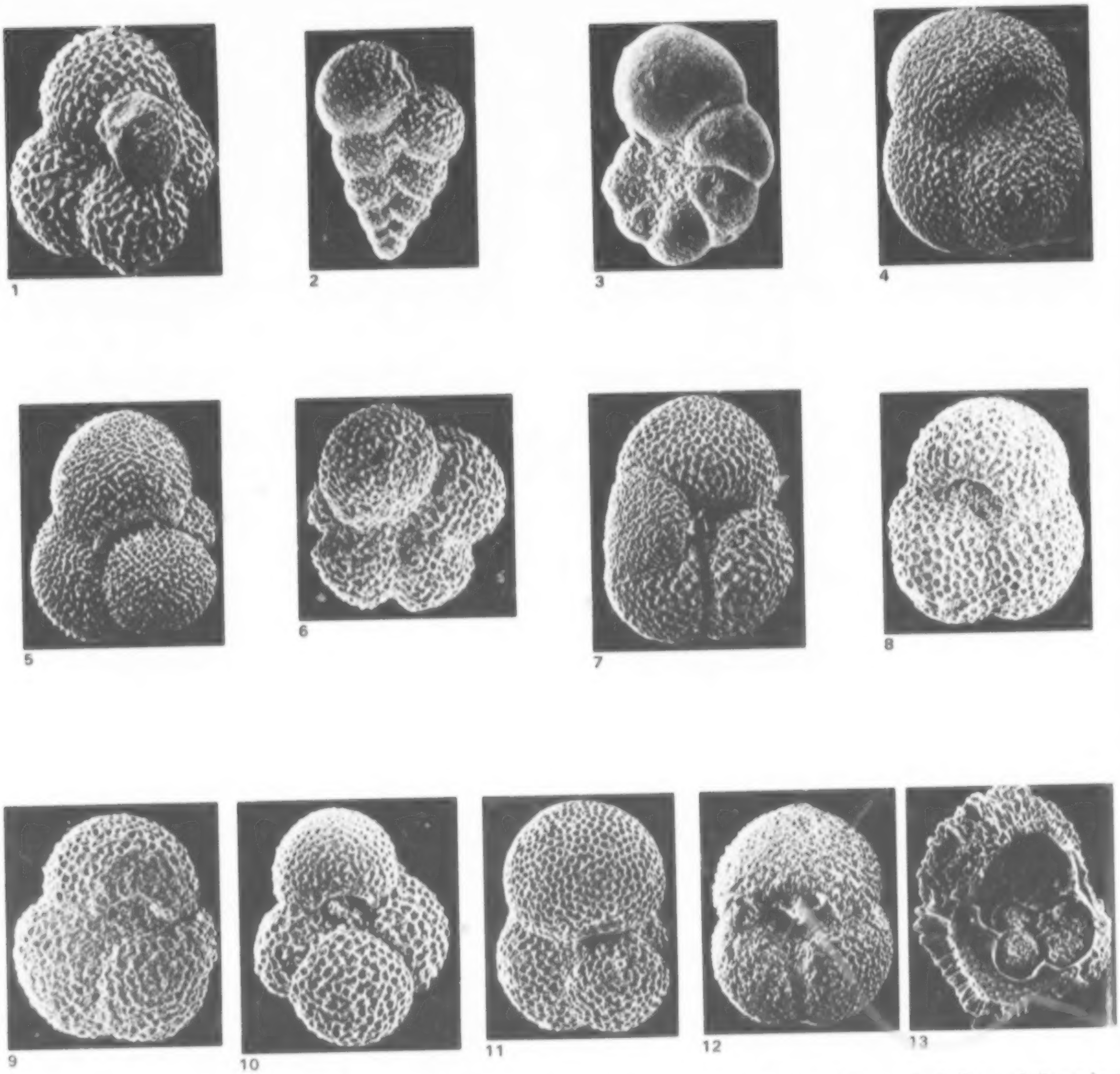

Plate 1. **1.** *Catapsydrax* cf. *echinatus*, umbilical view ×188; Sample 592-40,CC; *G. aculeata* Zone, late Eocene. **2.** *Chiloguembelina cubensis*, side view ×238; Sample 592-39,CC; *G. linaperta* Zone, late Eocene. **3.** *Globanomalina micra*, side view ×152; Sample 592-39,CC; *G. linaperta* Zone, late Eocene. **4.** *Globigerina ampliapertura*, umbilical view ×97; Sample 592-33,CC; *G. angiporoides* Zone, early Oligocene. **5.** *Globigerina angiporoides*, umbilical view ×94; Sample 592-36-2, 90-91 cm; *G. brevis* Zone, early Oligocene. **6.** *Globigerina angulisuturalis*, umbilical view ×155; Sample 588C-11,CC; *G. kugleri* Zone, late Oligocene. **7.** *Globigerina brevis*, umbilical view ×81; Sample 592-34,CC; *G. brevis* Zone, early Oligocene. **8.** *Globigerina euapertura*, umbilical view ×109; Sample 593-54,CC; *G. angiporoides* Zone, early Oligocene. **9.** *Globigerina labiacrassata*, umbilical view ×119; Sample 593-54,CC; *G. angiporoides* Zone, early Oligocene. **10.** *Globigerina linaperta*, umbilical view ×121; Sample 592-39,CC; *G. linaperta* Zone, late Eocene. **11.** *Globigerina ouachitaensis*, umbilical view ×76; Sample 592-34,CC; *G. brevis* Zone, early Oligocene. **12-13.** *Globigerinatheka index*, Sample 592-40,CC, *G. linaperta* Zone, late Eocene, (12) umbilical view ×84, (13) broken specimen showing juvenile stage ×107.

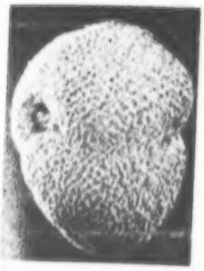

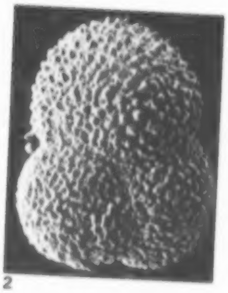
2

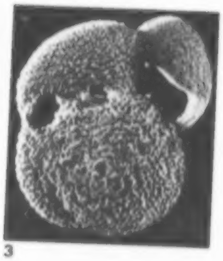
3

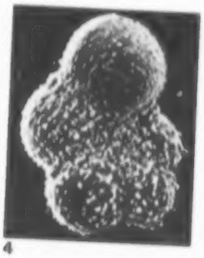
4

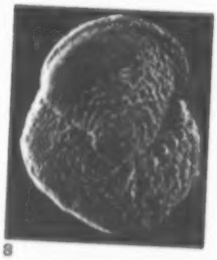
8

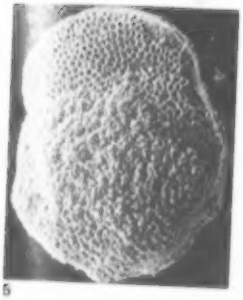
5

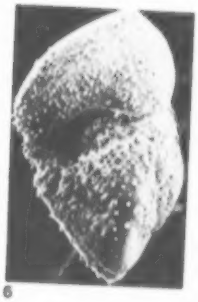
6

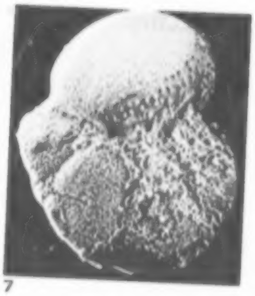
7

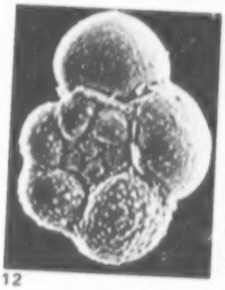
12

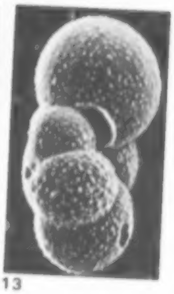
13

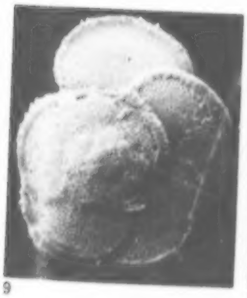
9

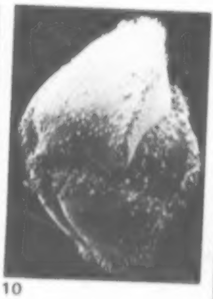
10

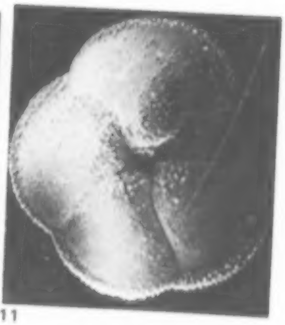
11

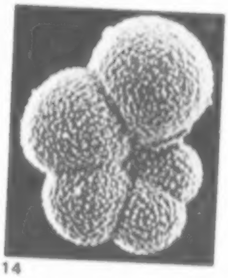
14

Plate 2. **1.** *Globigerinatheka semiinvoluta*, side view ×71; Sample 593-58-2, 90–91 cm; *G. linaperta* Zone, late Eocene. **2.** *Globigerinoides inusi-*
tat , umbilical view ×131; Sample 593A-24-1, 90–91 cm, *G. euapertura* Zone, late Oligocene. **3.** *Globigerinoides tyrrhenicus*, spiral view
×6 Sample 591-19,CC, *G. conomiozea* Zone, late Miocene. **4.** *Globorotalia aculeata*, umbilical view ×145; Sample 592-41,CC, *G. aculeata*
Zo , late Eocene. **5–7.** *Globorotalia conica*, three specimens; Sample 592-28,CC, *O. suturalis* Zone, middle Miocene, (5) spiral side ×93, (6)
sid view ×121, (7) umbilical view ×93. **8.** *Globorotalia* cf. *conomiozea*, umbilical view ×57; Sample 588B-11,CC, *G. margaritae* Zone, early
Pli ene. **9–11.** *Globorotalia explicationis*, three specimens; Sample 593-30,CC, *N. continuosa* Zone, late Miocene, (9) spiral side ×57, (10)
sid view ×57, (11) umbilical view ×57. **12–14.** *Globorotalia gemma*, three specimens; Sample 592-34,CC, *G. brevis* Zone, early Oligocene,
(12 piral side ×212, (13) side view ×215, (14) umbilical view ×215.

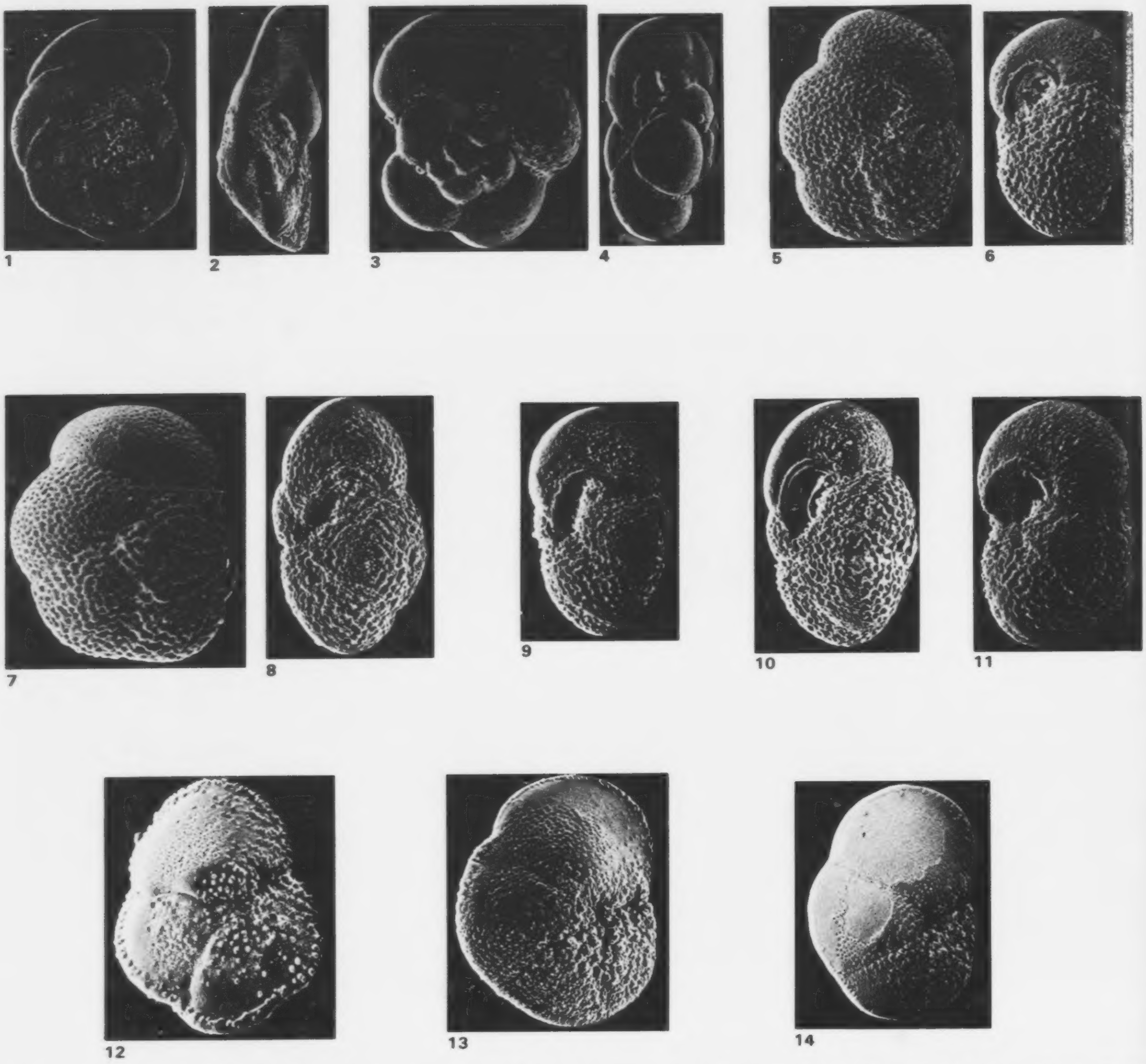

Plate 3. (Figs. 5–11 from Sample 592-26,CC, *G. mayeri* Zone, middle Miocene.) **1, 2.** *Globorotalia* cf. *ichinosekiensis*, two specimens; Sample 591-25,CC, *G. mayeri* Zone, middle Miocene, (1) spiral view ×94, (2) side view ×100. **3, 4.** *Globorotalia insolita*, two specimens; Sample 592-39,CC, *G. linaperta* Zone, late Eocene, (3) spiral view ×213, (4) side view ×213. **5, 6.** *Globorotalia mayeri*, two specimens, (5) spiral side ×114, (6) side view ×118. **7, 8.** *Globorotalia challengeri*, two specimens, (7) spiral side ×112, (8) side view ×131. **9–11.** *Globorotalia mayeri*, side views to show range of apertures, (9) ×113, (10) ×148, (11) ×112. **12–14.** *Globorotalia miotumida*, three specimens, umbilical views; Sample 593-30,CC, *N. continuosa* Zone, late Miocene, (12) ×109, (13) ×81, (14) ×58.

READEX FICHE best copy available

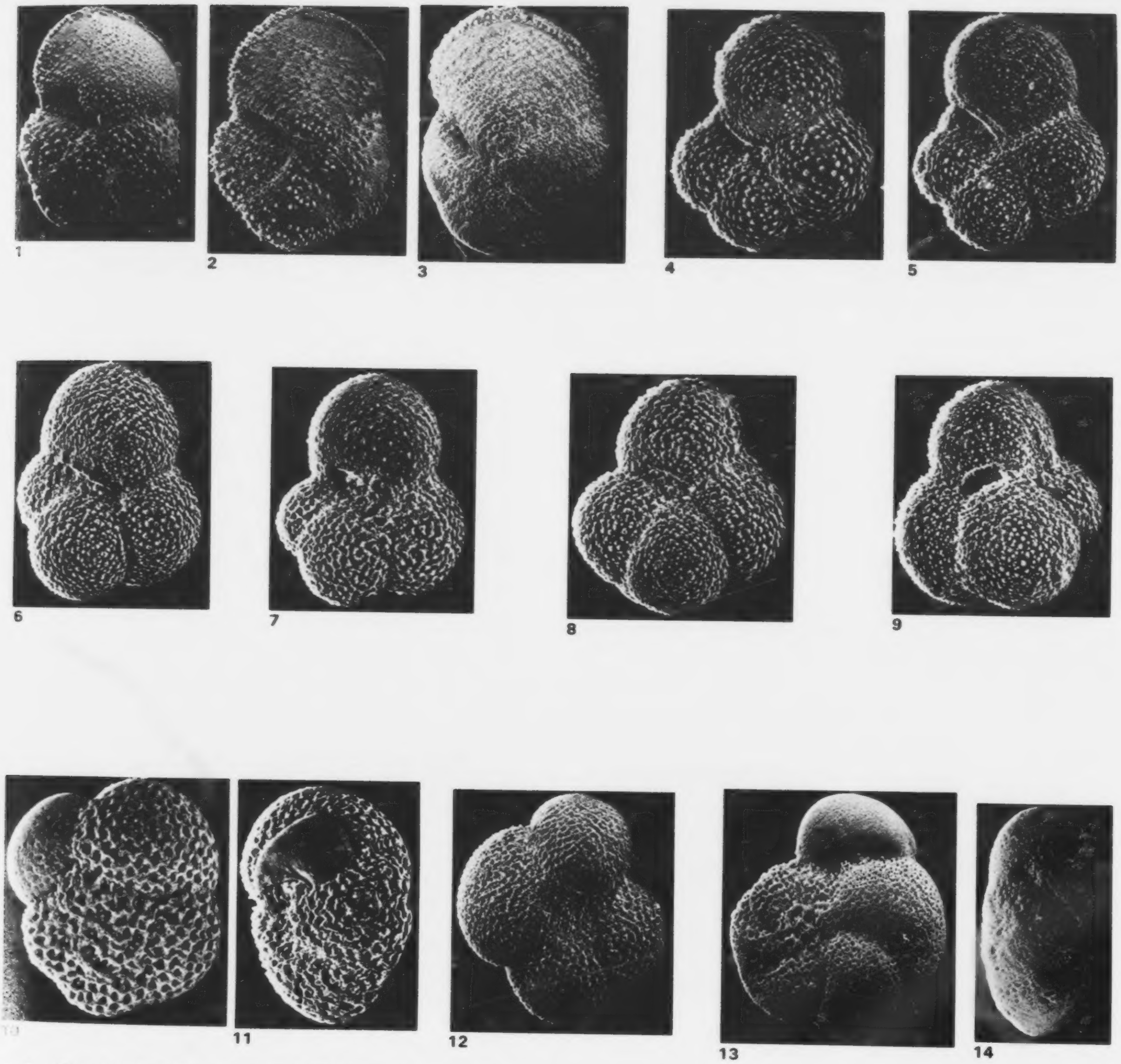

Plate 4. (Figs. 4–9 from Sample 591-30-3, 90–91 cm, *G. euapertura* Zone, late Oligocene.) **1–3.** ***Globorotalia pliozea***, three specimens, umbilical views, Sample 591-19,CC, *G. puncticulata* Zone, early Pliocene, (1) ×80, (2) ×72, (3) ×79. **4, 5.** ***Globorotalia munda***, two specimens, umbilical views, (4) ×223, (5) ×211. **6–9.** ***Globorotalia munda–Globigerina juvenilis*** intermediate morphologies, (6) ×183, (7) ×164, (8) ×184, (9) ×225. **10–11.** ***Globorotalia nympha***, two specimens, Sample 592-24,CC, *G. mayeri* Zone, middle Miocene, (10) spiral side ×200, (11) side view ×178. **12.** ***Globorotalia*** cf. ***opima***, umbilical view ×77; Sample 593A-24-2, 90–91 cm, *G. euapertura* Zone, late Oligocene. **13, 14.** ***Globorotalia peripheroronda***, two specimens; Sample 592-28,CC, *O. suturalis* Zone, middle Miocene, (13) spiral view ×100, (14) side view ×113.

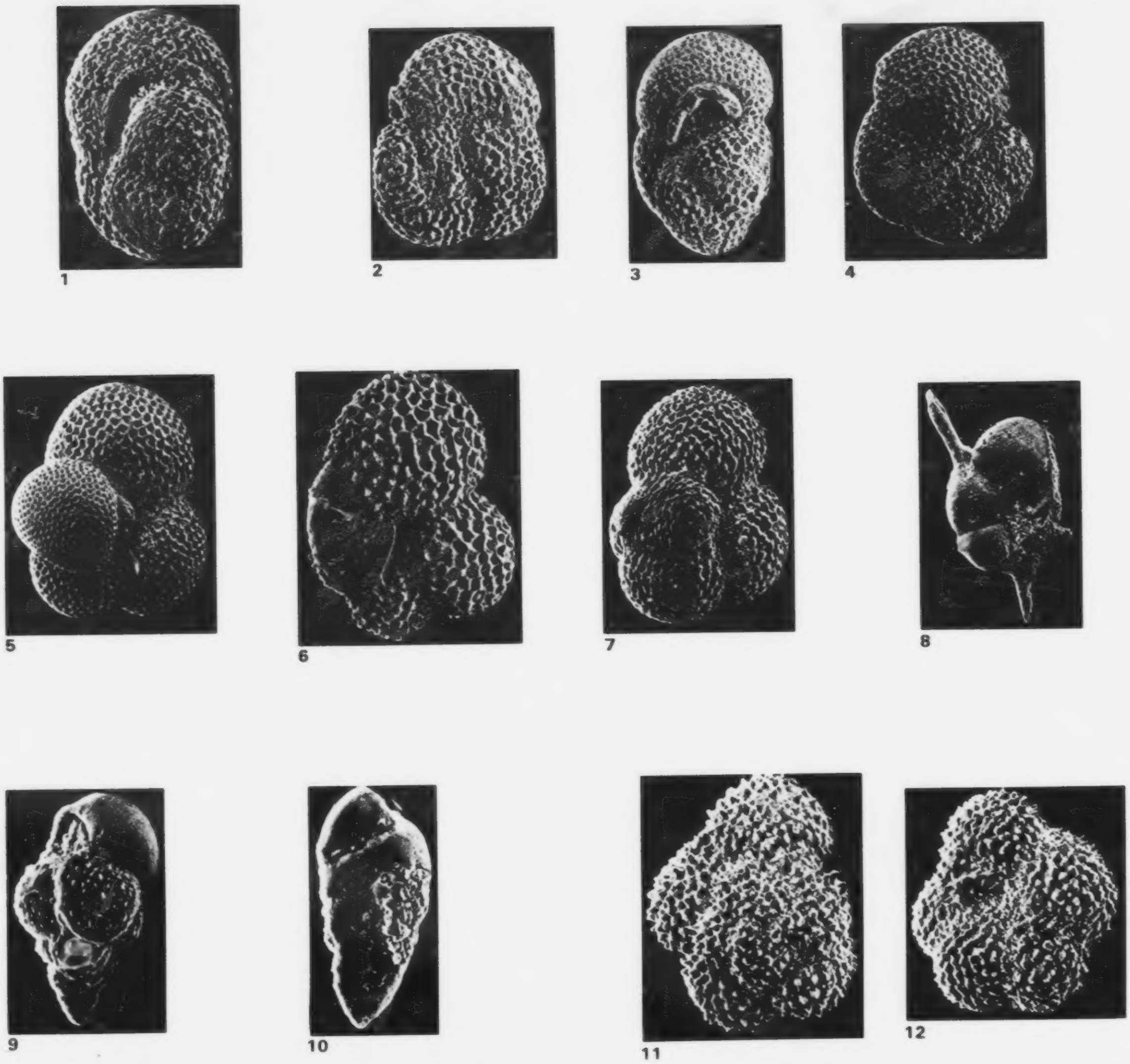

Plate 5. **1.** *Globorotalia nana*, side view ×83; Sample 592-40,CC, *G. aculeata* Zone, middle Eocene. **2–4.** *Globorotalia pseudocontinuosa*, three specimens; Sample 593-54,CC, *G. angiporoides* Zone, early Oligocene (2) spiral side ×106, (3) side view ×110, (4) umbilical view ×109. **5.** *Globorotaloides suteri*, umbilical view ×80; Sample 592-33,CC, *G. angiporoides* Zone, early Oligocene. **6.** *Globorotaloides testarugosa*, umbilical view ×161; Sample 592-33,CC, *G. angiporoides* Zone, early Oligocene. **7.** *Globorotaloides turgida*, umbilical view ×101; Sample 592-39,CC, *G. linaperta* Zone, late Eocene. **8.** *Hantkenina alabamensis*, umbilical view ×57; Sample 592-38,CC, *G. linaperta* Zone, late Eocene. **9.** *Jenkinsina samwelli*, side view ×319; Sample 593A-24-2, 90–91 cm, *G. euapertura* Zone, late Oligocene. **10.** *Streptochilus pristinum*, side view ×218; Sample 593A-24-2, 90–91 cm, *G. euapertura* Zone, late Oligocene. **11, 12.** *Truncorotaloides collactea*, two specimens; Sample 592-41,CC, *G. aculeata* Zone, late Eocene, (11) spiral view ×117, (12) umbilical view ×154.

14. RADIOLARIANS FROM THE SOUTHWEST PACIFIC[1]

J.-P. Caulet, Laboratoire de Géologie du Muséum National d'Histoire Naturelle[2]

ABSTRACT

Radiolarians are very rare in all Leg 90 sites. They are relatively more frequent only in Neogene sediments from Sites 586 and 594, and in Eocene sediments at Site 592. In this chapter radiolarian abundances are recorded as comparative percentages for 92 Neogene morphotypes at Site 586B. Relative abundances only are estimated at Sites 592 and 594, where preservation is poor to moderate. A tentative correlation of radiolarian events at Hole 586B and Site 594 shows that only a few species can be found in both tropical and subantarctic areas.

New evolutionary lineages are proposed. 1. Middle Miocene eucyrtids like *Eucyrtidium teuscheri* group evolved into a widespread species (*E. teuscheri teuscheri*) ranging from middle Miocene to Holocene and a temperate species (*E. teuscheri orthoporus*) ranging from middle Miocene to early Pleistocene. 2. *Phormostichoartus pitomorphus* appears to be a temperate descendant of the cosmopolitan *P. fistula* and disappears in early Pleistocene time. 3. The discovery of *Lamprocyrtis daniellae* n.sp. calls into question the lineage *L. heteroporos* → *L. nigriniae*. 4. The evolution of *Lamprocyclas maritalis* from an ancestor group (*L.* aff. *maritalis*) is located in the early part of the *Pterocanium prismatium* Zone.

INTRODUCTION

Because only carbonate-rich sediments deposited in relatively shallow environments were cored during Leg 90, radiolarians are generally absent or few in the material recovered. Moderately to well-preserved radiolarian assemblages occur throughout the sequences cored at equatorial Hole 586B (00°29.84′S, 158°29.89′E; water depth from rig floor, 2217 m) and at the subantarctic Site 594 (45°31.41′S, 174°56.88′E; water depth 1204 m). At Site 592 (36°28.40′S, 165°26.53′E; water depth 1098 m), radiolarians occur in small amounts, but only in upper Eocene sediments. Of particular interest at this site is a fine, complete boundary section between the Eocene and the Oligocene in Cores 592-36 and 592-37.

Hole 586B, with relatively well preserved specimens, provides a good sequence of late Neogene assemblages deposited in tropical shallow waters. Thus, it is important to verify if the radiolarian zonation is applicable to sediments accumulated below areas of high productivity and above the carbonate compensation depth (CCD).

Site 594 lies in the subantarctic water mass immediately south of the Subtropical Convergence. Thus the relative abundance of radiolarians allows studies of late Cenozoic paleoceanographic and paleoclimatic history. Moreover, Site 594 is important for establishing a radiolarian stratigraphy for upper Neogene sediments deposited during periods of temperate climate.

PROCEDURES

Except for Hole 592, where sampling for radiolarian studies was restricted to the Eocene/Oligocene boundary, one to five samples were taken from each core, acidified to remove carbonate, sieved at 50 µm, and the coarse fraction strewn on slides according to conventional methods.

Relative abundances are recorded in two ways. At Sites 592 and 594, where radiolarian occurrences are sporadic and preservation poor to moderate, four grades of abundance are used to indicate the abundance percentage of a taxon relative to the total assemblage of a strewn slide. These abundance grades and their symbols are explained in Table 2, later. At Hole 586B, where Cenozoic sediments contain well-preserved radiolarians, percentage estimates were used. The density of radiolarians on a slide having been estimated, the percentage of unbroken shells, which can be recognized at species level, was calculated by counting well-preserved individuals among 800 radiolarian whole specimens plus fragments. Next, 92 taxons were searched for and counted, if present, over the whole surface of the slide, and their abundance percentages were calculated relative to the number of unbroken shells. Radiolarian density is of the same order as in the study of Riedel and Westberg, 1982. The procedure developed by Westberg and Riedel (1982) for evaluating the stratigraphic reliability of upper and lower limits of taxa was applied at Hole 586B.

The radiolarian zones used in this paper for the Pliocene and Miocene at Site 586B are similar to the chronozones defined by Riedel and Sanfilippo (1978). The Quaternary zones are those defined by Caulet (1979).

At Site 594, the antarctic/subantarctic zonation proposed by Chen (1975) is not used because antarctic species occur so sporadically throughout the sequence and because some morphotypes are completely absent. Because equatorial and high-latitude assemblages are mixed, parts of both preexisting equatorial and antarctic event scales have been employed. Artostrobiidae are abundant, and the sequence of events proposed by Nigrini (1977) was successfully used and compared to occurrences of tropical and antarctic morphotypes. The Quaternary zones are those defined by Caulet (1982) for mid-latitude assemblages.

As part of the investigation of Leg 90 radiolarians, the data are supported by detailed radiolarian documentation from many *Marion Dufresne* (MD) piston cores from the South Indian Ocean region. These include the cores:

MD 73028: 49°25.9′S, 61°46.5′E, 2650 m water depth.
MD 75071: 38°24.9′S, 69°34.2′E, 4305 m water depth.
MD 75072: 37°55.7′S, 67°58.6′E, 4260 m water depth.
MD 75075: 34°23.4′S, 66°26.7′E, 4725 m water depth.
MD AET 75002: 34°34.5′S, 63°31.0′E, 4147 m water depth.
MD 77157: 4°48.2′S, 90°02.3′E, 4833 m water depth.

Detailed studies of these cores have been published (Caulet, 1977, 1982) or are in preparation.

RADIOLARIANS IN HOLES 586B, 592, AND 594

In Tables 1, 2, and 3 radiolarian occurrences are summarized for those stratigraphic intervals in which there are identifiable radiolarians.

---

[1] Kennett, J. P., von der Borch, C. C., et al., *Init. Repts. DSDP*, 90: Washington (U.S. Govt. Printing Office).

[2] Address: Laboratoire de Géologie du Muséum National d'Histoire Naturelle, 43, rue de Buffon, 75005 Paris, France.

Table 1. Relative abundance (%) of radiolarians from Hole 586B.

Age	Radiolarian zone	Core-Section (interval in cm)	Radiolaria density (thousands)	Preservation (% of entire shells)	Reworking (%)	*Buccinosphaera invaginata*	*Collosphaera* sp. A	*Pterocorys hertwigii*	*Collosphaera tuberosa*	*Pterocorys zancleus*	*Lamprocyrtis nigriniae*	*Eucecryphalus petrushevskaae*	*Androspyris anthropiscus*	*Anthocyrtidium angulare*	*Pterocorys c. variabilis*	? *(Axoprunum) monostylum*	*Lophosphaera hispida*	*Theocalyptra davisiana*	*Acanthodesmia circumflexa*	*Lamprocyclas maritalis*
Pleistocene	NR1	1-1, 60-62	7.9	24	0.2	0.16		0.32	0.05	0.42	0.05						1.05	0.79		0.84
		1-2, 60-62	5.0	25	0.1		0.48	0.32	0.08	0.64	0.24						0.72	0.96		1.2
	NR2	1-4, 60-62	3.6	30	0.1		0.09	0.74	0.19	0.37	0.09						0.28	0.74		0.93
	NR3	1-5, 60-62	7.0	30	0.1			0.19	0.14	0.57	0.14						0.71	0.76		0.86
		1-6, 60-62	4.6	8	0.2			0.27		0.54								1.36		0.54
		2-4, 60-62	0.8	9	0.2				5.71									2.86		
	NR4	2-5, 60-62	23.1	9	0					0.05	0.05							0.29		0.38
		3-1, 60-62	1.2	6	0						1.36								1.36	
		3-2, 60-62	15.1	9	0.1										0.22			0.37	0.15	0.66
	NR5	3-3, 60-62	8.4	4	0.1													1.78	0.30	0.30
		3-4, 60-62	0.7	4	0.1															
		4-1, 60-62	30.0	22	0.1							0.02		0.05	0.14		0.02	0.23	0.05	0.35
		4-2, 60-62	22.0	32	0.1							0.03	0.01	0.28	0.13		0.03	0.20	0.04	0.37
		4-4, 60-62	8.0	20	0.2										0.13		0.06	0.63	0.06	0.94
		4-5, 60-62	18.4	35	0.1								0.03	0.03	0.06		0.02	0.26	0.03	0.36
	Pterocanium prismatium	4-6, 60-62	15.0	17	0.1							0.04			0.20	0.12		0.31	0.08	0.98
		5-1, 60-62	35.0	17	0.2								0.02	0.02	0.10	0.02	0.02	0.20	0.02	0.76
		5-2, 60-62	7.6	13	0.1												0.20		0.20	1.42
Pliocene		5-3, 60-62	15.1	7	0.1											0.09	0.38	0.66	0.28	1.41
		5-4, 60-62	17.5	24	0.1									0.02	0.10	0.02				
		5-5, 60-62	7.7	15	0.1												0.26	1.13	0.09	0.52
		5-6, 60-62	3.5	7	0.1												0.41			2.04
		6-1, 60-62	9.4	29	0.1											0.04	0.11	0.55		0.36
		6-2, 60-62	4.5	12	0.1												0.37	0.37		1.11
		6-3, 60-62	7.6	10	0															
		6-4, 60-62	5.3	18	0.1													0.21		0.21
		6-5, 60-62	6.8	15	0														0.20	
		6-6, 60-62	6.6	18	0.1															0.08
		7-1, 60-62	8.0	22	0															
		7-2, 60-62	3.8	12	0															
	Spongaster pentas	7-3, 60-62	7.7	13	0															
		7-4, 60-62	3.5	13	0															
		7-5, 60-62	8.4	11	0															
		7-6, 60-62	10.5	8	0.1															
		8-1, 60-62	11.0	5	0															
		8-3, 60-62	10.2	10	0															
		8-5, 60-62	18.0	16	0															
		11-1, 60-62	12.0	2	0.1															
		11-3, 60-62	5.6	2	0															
		11-5, 60-62	12.0	4	0															
		12-1, 60-62	6.8	4	0.1															
		12-3, 60-62	11.4	2	0.1															
		12-5, 60-62	4.1	6	0															
		13-4, 60-62	3.7	5	0															
		14-1, 60-62	15.0	41	0															
		14-3, 60-62	11.5	15	0															
		14-5, 60-62	10.5	14	0															
		15-1, 60-62	6.6	12	0															
		15-3, 60-62	10.4	19	0															
	Stichocorys peregrina	15-5, 60-62	15.0	26	0															
		16-1, 60-62	13.2	16	0															
		16-3, 60-62	4.8	15	0															
		16-5, 60-62	11.5	27	0															
		17-2, 60-62	1.5	12	0															
		17-3, 60-62	11.0	13	0															
late Miocene		18-1, 60-62	13.7	14	0															
		18-5, 60-62	5.9	11	0															
		19-1, 60-62	0.9	27	0															
		19-3, 60-62	3.0	32	0															
		19-5, 60-62	6.5	17	0															
		20-1, 60-62	3.0	10	0															
		20-3, 60-62	6.7	15	0											0.10				
		20-5, 60-62	6.9	18	0															
		21-1, 60-62	2.5	15	0.1															
		21-3, 60-62	4.0	9	0.1															
		21-5, 60-62	1.0	18	0															
		22-1, 60-62	0.2	26	0															
		22-3, 60-62	1.0	9	0															
		22-5, 60-62	1.9	16	0															
		23-3, 60-62	4.2	8	0															
		23-5, 60-62	2.7	26	0															
		24-1, 60-62	6.9	30	0															
		24-3, 60-62	10.8	32	0															
		24-5, 60-62	7.3	27	0															
		25-1, 60-62	8.8	18	0															
		25-5, 60-62	4.2	32	0															

Note: Quantitative approach outlined in procedures. In the body of the table numbers indicate abundance in percent of total unbroken radiolarians on the slide. The following samples were barren of radiolarians: 586B-2-1, 60-62 cm, 586B-2-2, 60-62 cm, 586B-2-3, 60-62 cm, 586B-2-6, 60-62 cm, 586B-3-5, 60-62 cm, 582B-3-6, 60-62 cm.

Hole 586B

Radiolarians are rare and are poorly to moderately preserved in the samples from Core 586B-1 through 586B-25. A limited number of samples are barren (see Table 1), and there is some evidence of reworking.

The late and early Pleistocene faunas are well preserved but mid-Pleistocene Radiolaria are rare to absent and frequently dissolved. Zone NR1 (= *Buccinosphaera invaginata* Zone) yielded a rich fauna with the zone fossil, identified in Sample 586B-1-2, 60–62 cm. Zone NR2 extends from Samples 586B-1-2, 60–62 cm to 586B-1-4, 60–62 cm. Zone NR3 occurs between the first occurrence of *Collosphaera tuberosa* in Sample 586B-2-4, 60–62 cm and the last occurrence of *Stylatractus universus* in Sample 586B-1-5, 60–62 cm.

Table 1. (Continued).

Anthocyrtidium michelinae	*Theocorythium vetulum*	*Eucyrtidium indiensis*	*Lamprocyclas junonis*	*Lamprocyrtis neoheteroporos*	*Amphiropalum virchowi*	*Dictyophimus crisiae*	*Lophophaena cylindrica*	*Amphiropalum ypsilon*	*Anthocyrtidium nosicaae*	*Didymocyrtis tetrathalamus*	*Spirocyrtis scalaris*	*Spongaster tetras*	*Botryostrobus b. seriatus*	*Actinomma tetrapyla*	*Stylatractus aff. universus*	*Botryostrobus b. reedi*	*Eucyrtidium t. teuscheri*	*Spongaster pentas*	*Pterocorys longicollis*	*Phormostichoartus pitomorphus*	*Lamprocyrtis daniellae*	*Eucyrtidium t. orthoporus*
			0.37			0.79	0.21	0.32		1.58	0.05	1.84	0.21				0.53					
			0.48		0.48	0.64	0.4	0.48		2.08	0.08	2	0.24				0.4					
			0.46			0.83	0.74	1.39		2.31		2.13	0.37				0.56					
			0.43			0.57	0.67	0.86		1.29	0.05	0.71	0.10				0.24					
			0.54			0.54	2.72			1.36		1.09					0.54					
												12.9										
						0.10		0.24		0.29		0.43										
			0.37			0.44	0.22	0.66		1.54		1.10					0.44					
			0.60			1.49		1.79		1.79		2.38					0.89					
								17.9		17.9		21.4					7.14					
		0.02	0.33	0.18		0.38	0.15	0.24		0.47	0.02	0.35					0.09		0.02	0.03		0.03
			0.30	0.13		0.26	0.30	0.26	0.13	0.40		0.26	0.03				0.06		0.01	0.13		0.03
		0.06	0.63	0.06		0.75	0.63	1.00	0.25	1.25		0.44	0.13				0.19			0.13		0.06
0.17		0.02	0.34	0.06	0.05	0.36	0.19	0.39	0.15	0.59	0.02	0.09	0.02	0.02			0.03		0.02	0.08		0.02
0.35			0.35	0.24	0.08	0.31	0.39	0.59	0.16	0.47		0.71	0.12				0.08		0.08	0.24		
0.18		0.02	0.30	0.05	0.07	0.22	0.27	0.52	0.15	0.25	0.03	0.27	0.07	0.03			0.03	0.02	0.03	0.05		0.02
0.20			0.30	0.10		0.20	0.51	0.40	0.10	1.42		1.42					0.10					0.10
0.09			0.47	0.66		0.75	0.66	0.66	0.66	0.94	0.09	1.51			0.09		0.19		0.09			0.19
0.02				0.07			0.38	0.43	0.09	0.5	0.02	0.55	0.05							0.07		0.02
			0.78	0.09	0.26	0.95	1.04	0.43	0.26			1.04	0.17				0.17		0.09	0.26		0.09
			1.22		0.41	0.82	2.86	2.86		0.82			0.41				0.82			0.82		1.22
		0.07	0.11		0.18	0.36	0.18	0.69	0.04	0.08		0.15	0.11		0.22		0.26		0.07	0.11		0.04
			0.19		0.37	0.93	1.30	0.19		0.37		1.85	0.18				0.18		0.18	0.37		0.18
					0.53		0.53		0.39	0.39	0.13	0.26					0.13					0.13
			0.31	0.10	0.10	0.31	0.52			0.52	0.10	0.52			0.42		0.10			0.31		0.10
0.10						0.29	0.49		0.10	0.29	0.10	0.39	0.10				0.20	0.10	0.10	0.29		0.10
		0.08		0.17	0.08	0.42	0.50	0.34	0.08	0.50	0.08	0.59	0.08				0.08	0.17		0.08		
0.06	0.17		0.06		0.17		0.40	0.57	0.17	0.91		0.40					0.11		0.06	0.11		
							0.66	1.53		1.10		0.66	0.22									0.22
				0.10	0.20		0.50	2.09	0.20	0.30		0.10		0.10			0.20			0.10		0.10
		0.22			0.66			2.19	0.87	1.53		0.66		0.22			0.22					
			0.11	0.22	0.32	0.43	0.43	0.11	0.22	0.76		0.97	0.22		0.11		0.11	0.11	0.32			
					0.12			0.71	0.12	1.19		0.71					0.12	0.12				
					0.18	0.36	0.18	0.72	0.36	0.18	0.18	0.36							0.18	0.18		
							0.10	0.40	0.10	0.10		0.78					0.10			0.20		
									0.17	0.10	0.07							0.03		0.07		
												0.42	0.42							0.42		
															0.89							
													0.21		0.21							
																				0.44		
																	0.53					
															0.02			0.10	0.03	0.03		
														0.06								
														0.07	0.07		0.07	0.27		0.07		
																0.13				0.13		0.13
																0.05	0.05	0.05		0.10	0.15	
																			0.05	0.03	0.05	
																					0.05	0.05
																				0.39		

The first occurrence of *Lamprocyrtis nigriniae* in Sample 586B-1-5, 60–62 cm places this sample in Zone NR4 and the last occurrence of *Anthocyrtidium angulare* in Sample 586B-4-1, 60–62 cm places this sample in Zone NR5. But the limit between Zones NR4 and NR5 is difficult to position, because radiolarians are rare and dissolved in Sample 586B-3-2, 60–62 cm to 586B-3-6, 60–62 cm. The presence of *Pterocanium prismatium* in Sample 586B-4-6, 60–62 cm, places Samples 586B-4-1, 60–62 cm to 586B-4-5, 60–62 cm in the early Pleistocene Zone NR5. The first occurrence of *A. angulare* in Sample 586B-5-4, 60–62 cm is just below the Pliocene/Pleistocene boundary.

Radiolarians are rare and are moderately to well preserved in the upper Pliocene. Shells are often dissolved and poorly preserved in the middle to late *Spongaster pentas* Zone. The latest occurrence of *Stichocorys peregrina* marks the bottom of the *Pterocanium prismatium*

Table 1. (Continued).

Age	Radiolarian zone	Core-Section (interval in cm)	Radiolaria density (thousands)	Preservation (% of entire shells)	Reworking (%)	*Pterocorys c. campanula*	*Didymocyrtis avita*	*Spongaster berminghami*	*Botryostrobus b. tumidulus*	*Siphonosphaera hyalina*	*Phormostichoartus platycephala*	*Pterocanium prismatium*	*Spirocyrtis subscalaris*	*Lamprocyrtis heteroporos*	*Eucyrtidium anomalum*	*Eucyrtidium teuscheri* gr.	*Stylatractus universus*	*Botryostrobus praetumidulus*	*Botryostrobus aquilonaris* gr.	*Lamprocyclas* aff. *maritalis*
Pleistocene	NR1	1-1, 60–62	7.9	24	0.2				0.83		0.36				0.36				0.05	
		1-2, 60–62	3.0	25	0.1				0.96		0.32				0.24				0.08	
	NR2	1-4, 60–62	3.6	30	0.1				1.11		0.37				0.19				0.09	
	NR3	1-5, 60–62	7.0	30	0.1				0.33		0.24				0.24		0.57		0.10	
		1-6, 60–62	4.6	8	0.2				1.36		0.54						0.82		0.27	
		2-4, 60–62	0.8	9	0.2						2.86						1.43		2.86	
	NR4	2-5, 60–62	23.1	9	0				0.14		0.05						1.11		0.24	
		3-1, 60–62	1.2	6	0												5.42			
		3-2, 60–62	15.1	9	0.1				0.59		0.22				0.07		0.73		0.44	
	NR5	3-3, 60–62	8.4	4	0.1				1.79		0.60						0.89		1.49	
		3-4, 60–62	0.7	4	0.1				17.8		3.57						3.57		17.8	
		4-1, 60–62	30.0	22	0.1	0.06			0.18		0.08				0.05		0.20	0.06	0.12	
		4-2, 60–62	22.0	32	0.1	0.09			0.16		0.04				0.01		0.40	0.10	0.04	
		4-4, 60–62	8.0	20	0.2	0.19			0.56		0.06				0.13		1.25	0.50	0.38	
		4-5, 60–62	18.4	35	0.1	0.22			0.15	0.05	0.03			0.02	0.03		0.34	0.02	0.06	
	Pterocanium prismatium	4-6, 60–62	15.0	17	0.1	0.20			0.39	0.12		1.49	0.08	0.08	0.39		0.71	0.82	0.12	
		5-1, 60–62	35.0	17	0.2	0.30				0.08		0.24		0.03	0.15		0.29	0.37	0.05	
		5-2, 60–62	7.6	13	0.1	0.20						3.9	0.20		0.40		0.10	0.91	0.30	
Pliocene		5-3, 60–62	15.1	7	0.1	0.09			0.19	0.09		0.19	0.19				1.80	0.66	0.47	
		5-4, 60–62	17.5	24	0.1	0.19			0.14			0.57					0.52	0.36		
		5-5, 60–62	7.7	15	0.1	0.17			0.52			0.69	0.52		0.69		0.69	1.04	0.43	
		5-6, 60–62	3.5	7	0.1				0.92		0.41	0.41						3.67	1.22	
		6-1, 60–62	9.4	29	0.1	0.07			0.04		0.04	0.22	0.15	0.04	0.33		0.11	0.62	0.51	0.07
		6-2, 60–62	4.5	12	0.1	1.11			1.30			0.93	0.37		0.19		2.41	2.04	2.41	
		6-3, 60–62	7.6	10	0	0.79			1.45	0.13							1.05	2.37	2.11	
		6-4, 60–62	5.3	18	0.1	0.84			0.31	0.10		0.10	0.42		0.42		0.94	0.10	0.31	
		6-5, 60–62	6.8	15	0		0.20					0.10			0.10		0.59		0.20	0.49
		6-6, 60–62	6.6	18	0.1	0.50			0.25		0.08	0.17	0.08		0.25		0.17	0.34	0.42	0.25
		7-1, 60–62	8.0	22	0	0.11			0.17	0.06		0.45	0.06				0.34	0.06	0.68	
		7-2, 60–62	3.8	12	0	0.22	0.22					0.88		0.22			1.75	0.66	1.31	0.22
	Spongaster pentas	7-3, 60–62	7.7	13	0	0.20	0.80		0.10	0.20	0.10	0.30	0.10	0.10			0.70	0.30	0.80	
		7-4, 60–62	3.5	13	0	0.22			0.87	0.22		0.22		0.22			0.87		0.44	0.22
		7-5, 60–62	8.4	11	0	0.11	0.11		0.54		0.11		0.32	0.11	0.11		0.97	1.41	1.84	0.43
		7-6, 60–62	10.5	8	0.1		0.12		0.36			0.12	0.12				1.19	0.48	1.19	0.24
		8-1, 60–62	11.0	5	0		0.18		0.18				0.18	0.18			0.36	0.54	2.17	1.63
		8-3, 60–62	10.2	10	0				0.10		0.20	0.20					0.20	0.29	0.49	0.59
		8-5, 60–62	18.0	16	0	0.10			0.10		0.03	0.31	0.17				0.14	0.56	0.14	
		11-1, 60–62	12.0	2	0.1							0.42		0.42			0.84	0.42		1.25
		11-3, 60–62	5.6	2	0															4.46
		11-5, 60–62	12.0	4	0				0.21	0.21		2.29		0.21			1.04	0.42	0.21	2.29
		12-1, 60–62	6.8	4	0.1		0.37										1.10	0.74		0.74
		12-3, 60–62	11.4	2	0.1	0.44	0.88		0.44					0.44			0.44	1.32	3.07	1.75
		12-5, 60–62	4.1	6	0															
		13-4, 60–62	3.7	5	0		0.53		0.53	0.53			0.53				0.53	0.53	2.13	1.07
		14-1, 60–62	15.0	41	0	0.10	0.03			0.03		0.11	0.13		0.52		0.05	0.05	0.03	0.08
		14-3, 60–62	11.5	15	0		0.23			0.29		0.12	0.06		0.06		0.06	0.12		0.29
		14-5, 60–62	10.5	14	0	0.07	0.07			0.07		0.07					0.14	0.14	0.54	0.34
		15-1, 60–62	6.6	12	0		0.51		0.13	0.13		0.13					0.38	0.25	0.63	0.51
		15-3, 60–62	10.4	19	0		0.10		0.05			0.30					0.15	0.05	0.40	0.30
	Stichocorys peregrina	15-5, 60–62	15.0	26	0		0.05			0.03		0.10					0.03	0.03	0.18	
		16-1, 60–62	13.2	16	0	0.03	0.14			0.09	0.05		0.05				0.05	0.05		0.09
		16-3, 60–62	4.8	15	0	0.09	0.14	0.14		0.28							0.56		0.97	0.69
		16-5, 60–62	11.5	27	0				0.03	0.10			0.03	0.10	0.10	0.03	0.03		0.10	0.13
		17-2, 60–62	1.5	12	0					0.56								0.56	1.67	0.56
		17-3, 60–62	11.0	13	0						0.07		0.07		0.21		0.14	0.07	0.21	0.14
late Miocene		18-1, 60–62	13.7	14	0											0.05	0.16	0.05		
		18-5, 60–62	5.9	11	0									0.15					0.15	0.15
		19-1, 60–62	0.9	27	0															
		19-3, 60–62	3.0	32	0										0.20				0.20	0.81
		19-5, 60–62	6.5	17	0										0.27	0.18			0.36	0.36
		20-1, 60–62	3.0	10	0														0.67	
		20-3, 60–62	6.7	15	0										0.30					0.30
		20-5, 60–62	6.9	18	0										0.32		0.08	0.16	0.89	0.08
		21-1, 60–62	2.5	15	0.1												0.27	0.27		
		21-3, 60–62	4.0	9	0.1													0.28	1.40	
		21-5, 60–62	1.0	18	0														0.56	
		22-1, 60–62	0.2	26	0													3.85	5.77	
		22-3, 60–62	1.0	9	0														1.11	3.33
		22-5, 60–62	1.9	16	0														0.33	0.33
		23-3, 60–62	4.2	8	0															
		23-5, 60–62	2.7	26	0															
		24-1, 60–62	6.9	30	0															
		24-3, 60–62	10.8	32	0															
		24-5, 60–62	7.3	27	0															
		25-1, 60–62	8.8	18	0															
		25-5, 60–62	4.2	32	0															

Zone between Samples 586B-7-3, 60–62 cm and 586B-7-2, 60–62 cm. The event indicating the bottom of the *Spongaster pentas* Zone is the evolutionary transition between *Spongaster berminghami* and *S. pentas*. Because *S. berminghami* is rare, this event cannot be used in Hole 586B. Thus, the bottom of the *S. pentas* Zone occurs in the interval between Samples 586B-16-3, 60–62 cm (occurrence of *S. berminghami*) and 586B-15-3, 60–62 cm (first occurrence of *S. pentas*). This conclusion is supported by the first occurrence of *Didymocyrtis avita* in Sample 586B-16-3, 60–62 cm and the morphotypic bottom of *Pterocanium prismatium* in Sample 586B-15-5, 60–62 cm.

Although few individuals of *Stichocorys peregrina* and numerous ones of *S. delmontensis* occur in Samples 586B-24-3, 60–62 cm to 586B-25-5, 60–62 cm, the evolutionary transition between the two species cannot be reported, and the bottom of the *Stichocorys peregrina* Zone remains below the last sample cored. Thus, the interval

Table 1. (Continued).

Lamprocyclas margatensis	*Solenosphaera omnitubus* gr.	*Botryostrobus auri/aur.* gr.	*Dendrospyris bursa*	*Didymocyrtis penultima*	*Hexacontium hootsi*	*Hexacontium medusa*	*Lyriospyris ovalis*	*Platybursa clathrobursa*	*Spirocyrtis gyroscalaris*	*Stauroxiphos communis*	*Acrobotrys tritubus*	*Anthocyrtidium ehrenbergi*	*Botryostrobus b. bramlettei*	*Calocycletta caepa*	*Centrobotrys thermophila*	*Cyclampterium neatum*	*Desmospyris stabilis*	*Dictyophimus splendens*	*Didymocyrtis antepenultima*	*Spongodiscus klingi*	*Eucyrtidium anniae*	*Lamprocyclas hannai*
		1.30					0.10								0.05							
		1.84					0.08															
		2.13																				
		1.67																				
		1.36																				
		0.24																				
							0.07															
		1.79					0.60															
		7.14																				
		0.12					0.03															
		0.50					0.04															
		1.25																				
		0.54					0.02															
		1.49													0.08							
		0.76			0.02		0.02															
		0.81													0.10	0.10						
		0.94																				
		0.76													0.02							
		2.16			0.09																	0.09
		6.12													0.41							
		1.20			0.04																	0.04
		1.85			0.37																	0.56
		3.68																				
		1.15																				0.10
		0.69			0.10							0.10										0.39
		1.68			0.17										0.17							0.34
		1.70			0.06										0.11							
		1.54																				
		2.48										0.10										
		4.81													0.44							
		4.44			0.11		0.11								0.54	0.11						0.11
		1.43			0.12																	
		1.63														0.72						0.54
		1.47													0.29							
		1.11													0.17							
		1.67					0.42								2.51	0.84						0.42
		0.89													1.79	0.89						2.68
		1.46													308	38.5						135
		0.74													1.10					2.21		
		1.75													3.51	1.75				3.51		0.44
		1.07													1.07	1.07				1.07		1.07
0.02		0.15			0.07		0.05								0.59	0.02				0.11		0.03
0.06		0.23			0.06		0.12						0.06		0.17	0.17				0.46		
	0.07	0.20			0.27								0.07		0.20	0.14		0.07		0.14		0.07
	0.25												0.13		0.38	1.26						
	1.81	0.10		0.10	0.05										0.05	0.10		0.15		0.10		
	0.54	0.08		0.03											0.26	0.05				0.10		
0.05	2.08			0.09							0.05		0.05		0.38	0.24		0.09				
0.14	6.25			0.83											2.08	0.42		0.14		1.39		
	1.13	0.06		0.13									0.06		0.32	0.03		0.10		0.48		0.19
1.11	12.78			0.56									0.56		1.11	0.56				1.67		
	2.10	0.28		0.28	0.07		0.07						0.14		0.35	0.14		0.14		0.21		0.07
0.05	0.58	0.47		0.52									0.16		0.16			0.16		0.16		0.05
	5.89			0.46											0.31	0.15				0.15		
		0.39		0.39														0.39		0.39		0.39
	3.55	0.61		0.41							0.20		0.10		0.30	0.20	0.10			0.81		0.30
	3.63	0.45		0.18							0.45	0.09	0.27		0.63	0.09		0.36		0.36		0.09
	4.67			0.67			0.33											0.33		0.67		0.33
	2.28	0.10										0.10				0.10		0.20		0.30		0.40
0.08	2.42	0.08		0.56							0.16	0.16	0.56		0.08	0.16	0.08	0.40		0.48	0.32	0.08
0.13	0.27			0.53									0.53			0.8		0.53		0.8		
0.36	1.40	0.28														0.28		0.56		0.84		
	0.56															0.56				0.56		0.56
	15.38												1.92					3.85				1.92
[illegible]	1.11	1.11									1.11					1.11				2.22		
	32.57												0.33			0.33						
[illegible]	6.55		0.30	1.19			0.30				0.30	0.89	0.30		0.60	0.89		1.19		1.19	0.60	0.30
[illegible]	5.07	0.14		0.28			0.14				0.28		0.14		0.70	0.42		0.28		1.13		0.28
	2.32		0.05	0.19						0.05	0.10	0.14	0.05		0.10	0.05				0.14		
	1.74	0.03		0.20			0.03	0.03	0.06	0.09	0.12	0.12		0.14	0.12	0.06	0.20	0.03	0.03	0.20	0.12	0.06
	1.31					0.05	0.10			0.05	0.05	0.10	0.05		0.05	0.10		0.10	0.10	0.05	0.10	
		0.06	0.06	0.06	0.06	0.06	0.06	0.06	0.06	0.13	0.06	0.13	0.19	0.13	0.19	0.19	0.13	0.25	0.13	0.06	0.38	0.19
											0.07	0.15	0.15	0.15	0.07	0.07	0.07	0.07	0.22	0.07	0.37	0.07

between Samples 586B-15-3, 60–62 cm and 586B-25-5, 60–62 cm is placed in the late Miocene *S. peregrina* Zone.

Site 592

At Site 592, radiolarians are present in only part of the upper Eocene. Samples available for radiolarian studies range from Sections 592-37-1 to 592-40-5. Well-preserved radiolarian faunas are present in Sample 592-40-4, 40–42 cm, 592-40-3, 40–42 cm, 592-40-2, 40–42 cm, 592-40-1, 40–42 cm, 592-39-4, 40–42 cm, and 592-39-3, 40–42 cm. Very rare specimens are present in Samples 592-37-4, 15–16 cm and 592-37-3, 15–16 cm. Samples 592-37-1, 15–16 cm and 592-37-2, 15–16 cm contain only some fragments.

As radiolarian assemblages are different in tropical and polar areas, dating of temperate latitude sediments by the use of either the low-latitude or the high-latitude radiolarian biostratigraphy is often unsuccessful. Fortu-

Table 1. (Continued).

Age	Radiolarian zone	Core-Section (interval in cm)	Radiolaria density (thousands)	Preservation (% of entire shells)	Reworking (%)	*Lithomelissa ultima*	*Tessarastrum* sp.	*Phormostichoartus corbula*	*Phormostichoartus doliolum*	*Phormostichoartus fistula*	*Pterocanium trilobum* gr.	*Polysolenia s. hamospina*	*Polysolenia s. fasciculopora*	*Rhopalastrum oraculibrachium*	*Siphostichartus corona*	*Stichocorys delmontensis*	*Stichocorys peregrina*	*Stichocorys johnsoni*	*Stylosphaera angelina*	*Tricolospyris b. variabilis*	*Tricolospyris newtoniana*
Pleistocene	NR1	1-1, 60-62	7.9	24	0.2			0.89									0.05				
		1-2, 60-62	5.0	25	0.1			0.64													
	NR2	1-4, 60-62	3.6	30	0.1			0.37													
	NR3	1-5, 60-62	7.0	30	0.1			0.24													
		1-6, 60-62	4.6	8	0.2			0.82													
		2-4, 60-62	0.8	9	0.2																
	NR4	2-5, 60-62	23.1	9	0			0.29													
		3-1, 60-62	1.2	6	0																
		3-2, 60-62	15.1	9	0.1			0.51													
	NR5	3-3, 60-62	8.4	4	0.1																
		3-4, 60-62	0.7	4	0.1																
		4-1, 60-62	30.0	22	0.1	0.03		0.27													
		4-2, 60-62	22.0	32	0.1	0.01		0.21													
		4-4, 60-62	8.0	20	0.2	0.13		0.25													
		4-5, 60-62	18.4	35	0.1	0.05		0.09													
	Pterocanium prismatium	4-6, 60-62	15.0	17	0.1	0.04		0.24	0.04												
		5-1, 60-62	35.0	17	0.2	0.02		0.13	0.02												
		5-2, 60-62	7.6	13	0.1			0.20													
		5-3, 60-62	15.1	7	0.1			0.28											0.09		
Pliocene		5-4, 60-62	17.5	24	0.1	0.14		0.17	0.02												
		5-5, 60-62	7.7	15	0.1	0.78		0.35													
		5-6, 60-62	3.5	7	0.1	0.41		0.41													
		6-1, 60-62	9.4	29	0.1	0.22		0.29													
		6-2, 60-62	4.5	12	0.1	0.19		0.74											0.37		
		6-3, 60-62	7.6	10	0	0.26		0.26													
		6-4, 60-62	5.3	18	0.1	0.21		0.31													
		6-5, 60-62	6.8	15	0	0.10		0.59													
		6-6, 60-62	6.6	18	0.1	0.34		0.17													
		7-1, 60-62	8.0	22	0	0.23		0.23													
		7-2, 60-62	3.8	12	0			0.44											0.44		
	Spongaster pentas	7-3, 60-62	7.7	13	0	0.40		0.70									4.47				
		7-4, 60-62	3.5	13	0	0.66		0.44									9.40				
		7-5, 60-62	8.4	11	0	0.22		0.54									5.41		0.11		
		7-6, 60-62	10.5	8	0.1	0.12								0.24			6.55		0.36		
		8-1, 60-62	11.0	5	0	0.36											10.9				
		8-3, 60-62	10.2	10	0	0.10		0.20									5.30		0.10		
		8-5, 60-62	18.0	16	0	0.17		0.10	0.03							0.03	2.29				
		11-1, 60-62	12.0	2	0.1			0.42	0.42					1.25			8.78				
		11-3, 60-62	5.6	2	0												44.6		1.79		
		11-5, 60-62	12.0	4	0				57.7	19.2						19.2	865		76.9		
		12-1, 60-62	6.8	4	0.1				0.37	0.37							12.9				
		12-3, 60-62	11.4	2	0.1			0.44	0.44	0.44							17.9		2.19		
		12-5, 60-62	4.1	6	0																
		13-4, 60-62	3.7	5	0														1.07		
		14-1, 60-62	15.0	41	0	0.18		0.03	0.15	0.02		0.02					0.54		0.03	0.02	
		14-3, 60-62	11.5	15	0							0.29					2.96		0.23		
		14-5, 60-62	10.5	14	0	0.20			0.27			0.27					2.31		0.07		
		15-1, 60-62	6.6	12	0			0.51	0.13			1.16				0.38	5.68		0.13		
		15-3, 60-62	10.4	19	0			0.05	0.15	0.10		3.02					2.01		0.05		
	Stichocorys peregrina	15-5, 60-62	15.0	26	0			0.08	0.10			0.41					0.95				
		16-1, 60-62	13.2	16	0	0.09			0.09	0.05		2.60		0.05		0.05	1.99		0.09		
		16-3, 60-62	4.8	15	0	0.28			0.14	0.28		6.39	0.42	0.14					0.56		
		16-5, 60-62	11.5	27	0	0.03		0.03	0.19	0.03		0.19	2.51						0.29		
		17-2, 60-62	1.5	12	0					0.56		0.56	36.1				0.56		0.56		
late Miocene		17-3, 60-62	11.0	13	0	0.14			0.14		0.07	0.07	0.07			0.07	2.30			0.07	
		18-1, 60-62	13.7	14	0	0.10		0.10	0.05	0.05	0.05	0.26	0.16			0.10	2.23		0.21	0.05	
		18-5, 60-62	5.9	11	0							0.15					6.96				
		19-1, 60-62	0.9	27	0			0.39		0.39			0.39								
		19-3, 60-62	3.0	32	0			0.10			0.10		0.41				4.57				
		19-5, 60-62	6.5	17	0	0.09		0.18		0.18	0.45	1.09	0.36	0.09			3.45		0.09		
		20-1, 60-62	3.0	10	0					1.0		0.33	1.33			0.33	7.67				
		20-3, 60-62	6.7	15	0			0.10	0.10	0.20		0.20	0.60			0.30	2.08				
		20-5, 60-62	6.9	18	0			0.16	0.24		0.32	0.16	0.16			0.16	3.62	2.25	0.24	0.08	
		21-1, 60-62	2.5	15	0.1							0.27				0.27	6.4	1.07			
		21-3, 60-62	4.0	9	0.1						0.28	0.28	0.56	0.28			3.09	1.96	0.84		
		21-5, 60-62	1.0	18	0							0.56		0.56		0.56	0.56	0.56			
		22-1, 60-62	0.2	26	0					1.92	1.92			46.2		5.77	7.69				
		22-3, 60-62	1.0	9	0					1.11				68.9			5.56				
		22-5, 60-62	1.9	16	0							1.32		4.61			0.66	0.99	0.33		
		23-1, 60-62	4.2	8	0			0.30	0.89		1.19	10.4	0.60	1.19		9.23	3.27	3.27			
		23-5, 60-62	2.7	26	0	0.14		0.14			1.13	0.70	0.28	3.10		3.10	0.85	0.28	0.14	0.14	0.14
		24-1, 60-62	6.9	30	0						0.48	0.53	0.14	0.97	0.05	0.97	0.48	0.10	0.10		
		24-3, 60-62	10.8	32	0				0.41		0.49	0.38	0.06	0.43	0.26	1.01	0.46	0.55	0.23		0.0
		24-5, 60-62	7.3	27	0	0.05			0.15		0.20	0.71	0.10	1.01	0.10	2.02	0.30	0.30	0.40		
		25-1, 60-62	8.8	18	0		0.06	0.06	2.02	0.06	0.69	0.19	0.32	2.71	0.95	2.84	0.44	0.32	0.13		0.1
		25-5, 60-62	4.2	32	0		0.07	0.07	0.37		0.37	0.07	0.07	2.60	0.52	3.20	0.45	0.15	0.22	0.07	0.0

nately, late Eocene radiolarian assemblages from Site 592 are not very different from tropical faunas and thus the classic biostratigraphy of Riedel and Sanfilippo (1978) can be used.

Radiolarian abundances were roughly estimated from the density of radiolarians on strewn slides, from counts of 2000 to 5000 well-preserved tests for each sample. A large number of morphotypes were encountered, but only 39 well-known forms are tabulated in Table 2. A considerable amount of taxonomic work remains to be completed to describe the other morphotypes but because very little material is available, the descriptions and the ranges will be prepared for separate publication with other material cored on the Kerguelen Plateau.

Only one radiolarian zone was identified in Site 592: the *Cryptoprora ornata* Zone from Sections 592-39-3 to 592-40-4. The *C. ornata* Zone (= top of the former *Thyrsocyrtis bromia* Zone of Riedel and Sanfilippo,

Table 2. Abundance of some radiolarians from Hole 592.

Ag	Radiolarian zone	Core-Section (interval in cm)	Abundance	Preservation	Number of morphotypes	*Astatrobus elegans* gr.	*Astrophacus inca*	*Astrophacus linckiaeformis*	*Axoprunum euterpe* gr.	*Axoprunum polycentrum*	*Botryocella cribrosa* gr.	*Botryopera* gr.	*Calocycletta parva*	*Clathrocyclas spatiosa*	*Clathrocyclas universa*	*Cryptoprora ornata*	*Cyclampterium milowi*	*Desmospyris b. stabiloides*	*Dictyoprora urceolus*	*Tristylospyris triceros*	*Lithapium mitra*	*Lithomelissa haeckeli*	*Lithomitra* sp.	*Lithomitrella acephala*	*Lithomitrella elizabethae*	*Lithomitrella minuta*	*Lophocyrtis biaurita* gr.	*Lophocyrtis jacchia*	*Lychnocanium tripodium*	*Lychnocanoma bellum*	*Lychnocanoma amphitrite*	*Lychnocanoma babylonis*	*Periphaena decora*	*Periphaena heliasteriscus*	*Pseudodictyophimus callosus*	*Pseudodictyophimus gracilipes* gr.	*Pterocyrtidium barbadense* gr.	*Stylosphaera minor*	*Theocorys spongoconum*	*Theocorys cretica* gr.	*Thyrsocyrtis bromia*	*Tricolocapsa bergontiana* gr.	*Tripodiscinus clavipes*	*Velicucullus magnificum*
	?	37-3, 15-16	+	M	7				+								+		+	+				+		+														+				
		37-4, 15-16	+	P	4												+							+		+												+						
		39-3, 40-42	R	M	24			+			C	+	+	+	+	F	F	R	F	F	R			F	F	R		R		F	F	C					F	R		R	R	C		
la Eoc	C. ornata	39-4, 40-42	R	M	28	R	+			R	R		C		+	+	R	+	F	C	R	+		C	R	+		R		R	F	C	+	R			R		R	+	C	C		+
		40-1, 40-42	R	M	20	C		R		C	+		R		R	R			R	C	R			C		C		+			F	C		+			C		R		C	C		
		40-2, 40-42	R	G	28	F	+		C	R	R		R		R	R	C		C	R	C			R	R	C		R		R	F	C			+		C	R	R	R	R	C	+	+
		40-3, 40-42	R	G	31	F		R	R	R	R		C		R	F	F	R	F	R	F	R		+	R	R		+		R	F	C		+	+	+	F	R	R	+		F	R	R
		40-4, 40-42	R	G	33	F	+	R	+	C	R		F		C	F	F	+	F	R	F	+	+	C	R	F	+		R	C	F	F			R	+	R	+	R	R		C	C	C

Note: Morphotype abundances: + = one specimen; R = rare (less than 5 specimens); C = common (between 5 and 20 specimens); F = frequent (more than 20 specimens). Abundance of radiolarians in samples: very rare; R = rare. Preservation: P = poor; M = moderate; G = good.

emended by Maurrasse and Glass (1976) and Saunders et al. (in press), is the uppermost radiolarian zone of the Eocene. Since no radiolarian forms were found in sediments of early Oligocene age, the Eocene/Oligocene radiolarian boundary cannot be located at Site 592.

Late Eocene radiolarian assemblages from Site 592 are similar to tropical faunas but lack some typical morphotypes, like the *Lithocyclia* group. Other tropical species like *Thyrsocyrtis bromia* appear to be rare and are restricted to the upper part of the radiolarian zone. However, their skeletons are somewhat different from the tropical forms. The tests of *Cyclampterium(?) milowi* are frequent, but the test outline is narrower in the mid-latitude assemblages. Some forms like *Lychnocanoma amphitrite* and *Lithapium mitra* are more frequent than in the tropical assemblages. As shown by Chen (1975), high-latitude radiolarian assemblages "are similar to but less diverse than the late middle Eocene to late Eocene low-latitude assemblages previously described by Riedel and Sanfilippo (1971) and Foreman (1973)." Petrushevskaya (1975) reported that Eocene radiolarian faunas from the South Pacific sector of the Southern Ocean (DSDP Leg 29) are more similar to the Californian Eocene assemblages than those from the Caribbean. This is also the case for Eocene radiolarians from Site 592.

The preservation of the tests is good only in Samples 592-40-2, 40-42 cm, 592-40-3, 40-42 cm and 592-40-4, 40-42 cm. In these samples, the diversity of morphotypes is higher and diatoms are more abundant. In Sample 592-39-3, 40-42 cm the siliceous fraction is represented only by broken radiolarian tests. In Samples 592-37-3, 15-16 cm and 592-37-4, 15-16 cm, the number of the forms found is low and their state of preservation poor. It may be concluded that the deposition of radiolarians and other siliceous microfossils ceased at Site 592 before the very end of the late Eocene and that reworking processes are responsible for the rare latest Eocene siliceous accumulations near the Eocene/Oligocene boundary.

Site 594

Radiolarians are rare throughout the core recovered at Site 594; moderately to well-preserved faunas are encountered in all cores.

Stratigraphic correlation of Neogene Radiolaria from Site 594 is difficult because siliceous material is scarce and greatly diluted by terrigenous material, and paleoenvironments have changed. Because warm-water and polar assemblages are mixed, zonations proposed for both regions have been employed. Samples 594-1-1, 84-86 cm to 594-6-4, 84-86 cm contain a typical late Quaternary (less than 400,000 yr.) antarctic radiolarian assemblage that can be assigned to the *Antarctissa denticulata* Zone or NR1 Zone. Common species include *A. denticulata, A. strelkovi, Theocalyptra davisiana*, and *Rhizosphaera antarctica*.

Samples 594-7-2, 84-86 cm to 594-8-1, 84-86 cm, below the last appearance of *Stylatractus universus* in 594-7-2, 84-86 cm, are placed in Zone NR2 (Quaternary). The next marker observed was *Phormostichoartus pitomorphus* n. sp. (described in this chapter) whose last occurrence is in Sample 594-9-4, 84-86 cm. Therefore, Samples 594-9-4, 84-86 cm to 594-11-5, 84-86 cm are in the NR3/NR4 Zone (early to middle Pleistocene). It is not possible to distinguish between NR3 and NR4 because of the lack of warmer-water species.

Clathrocyclas bicornis occurs sporadically between Samples 594-11-6, 84-86 cm and 594-14-2, 84-86 cm. This occurrence is interpreted as reworking, because the first consistent occurrences of *A. denticulata* and *Theocalyptra bicornis* were found in Sample 594-12-3, 84-86 cm. Thus, Samples 594-11-6, 84-86 cm to 594-14-4, 84-86 cm are placed in the NR4 Zone.

The last consistent occurrence of *C. bicornis* in Sample 594-15-2, 84-86 cm is used to mark the top of the Pliocene. Rare radiolarians occur in Samples 594-15-2, 84-86 cm to 594-20-3, 84-86 cm. Typical Pliocene species like *Pseudocubus vema* occur sporadically. Because preservation was poor and markers were scarce the interval between Samples 594-15-2, 84-86 cm and 594-20-3, 84-86 cm remains unzoned.

Samples 594-20-4, 84-86 cm to 594-27-1, 84-86 cm, below the first occurrence of *Antarctissa ewingi* and above the first appearance of *Stichocorys peregrina*, are placed in the *Stichocorys peregrina* Zone (late Miocene). In the best preserved samples, forms like *Anthocyrtidium ehrenbergi* and *Hexacontium hootsi* indicate warmer condi-

Table 3. Abundance of some radiolarians from Hole 594.

Age	Radiolarian zone	Core-Section (interval in cm)	Abundance	Preservation	Reworking	*Theocalyptra bicornis*	*Antarctissa denticulata*	*Botryostrobus b. tumidulus*	*Antarctissa strelkovi*	*Phormostichoartus furcaspiculata*	*Triceraspyris antarctica*	*Theocalyptra davisiana*	*Actinomma popofskii*	*Pseudocubus vema*	*Antarctissa ewingi*	*Saccospyris antarctica*	*Stichopodium calvertense*	*Phormostichoartus multiseriatus*	*Rhizosphaera antarctica*	*Spongotrochus glacialis*	*Botryostrobus aquilonaris* gr.	*Botryostrobus b. seriatus*	*Druppatractus irregularis*	*Dictyophimus crisiae*	*Lonchosphaera spicata* gr.	*Clathocyclas bicornis*	*Botryostrobus b. pretumidulus*	*Eucyrtidium t. orthoporus*	*Stichopodium biconica*	*Stylatractus universus*	*Actinomma tetrapyla*	*Lamprocyrtis heteroporos*	*Stylatractus* aff. *universus*	*Botryostrobus aur./australis* gr.	*Saccospyris preantarctica*	*Spircyrtis subscalaris*
Quaternary	NR1	5-4, 84-86	R	G	O		F	R	R	R	F	F	F			F	R	R	F	C	F	R		+										C		
		6-4, 84-86	R	G	O		F	C	R	R	F	F	F			F	R	C	F	F	F	R		+										R		
	NR2	7-2, 84-86	R	M	)		F	C	R	C	C	F	F			F	R	C	F	C	C	R	+	+						+				C		
		8-1, 84-86	R	M	R		F	R	R	R	C	F	F			F	C	C	F	F	R	R		+						+				R		
	NR3 + 4	9-4, 84-86	R	M	R		F	R	R	R	C	F	F			F	C	R	F	F	C	R								+				C		
		10-2, 84-86	R	G	R		F	R	R	R	F	F	F			F	R	R	F	F	C	R	+				+			+				R		
		11-4, 84-86	R	G	O		F	R	R	+	C	F	F			C	R	R	F	F	F	C					+			+			+	R	+	
		11-5, 84-86	+	G	O		F	R	R	+	+	C	F			C	R	R	F	C	F	+					+			R				R		
	NR4	11-6, 84-86	R	G	O		F	R	R	+	C	C	F			R	+	R	C	C	F	+					+			+				R	+	
		12-2, 84-86	+	P	O	+	C	+	+		+	+	+			+	+		C		+					+	R			+				R		
		12-3, 84-86	+	M	O	+	C	R				R	R			+	R		+		F		+			+	+			+				C		
		12-4, 84-86	+	P	O														R		+									+						
		12-5, 84-86	+	P	O	+		+			+	+	+			+	+									+	+			+				+		
		13-3, 84-86	+	P	O	+				+	+		+			+	+				+		+	+		+			+	+		+		+	+	
		14-2, 84-86	+	P	O	+					+		+			+	C		+				+			+	+		+	+				+	+	
	Unzoned	15-2, 84-86	R	G	O	C	+	+	+	R	+	R	F	R		+	F		R	+		+	R	+	+	C	R	+	C	R			R	C	R	R
		16-2, 84-86	C	G	O			+					F	+		+	F		F	+			R		+	C	R	+	F	R		C		F	+	R
		16-4, 84-86	+	P	O			+				+	R	+		R	C		+	+			+	+		C			C	R		C		R	+	
		19-1, 84-86	+	P	O										+	+	+										+									
		19-4, 84-86	+	P	O										+	+	+	+				+		+			+	+	+							+
		20-1, 84-86	+	P	O										+	+	+									+	+							+		
late Miocene	*S. peregrina*	20-4, 84-86	R	M	O												+		+	R		R		R			R			+		+	+	R	C	
		21-2, 84-86	R	M	O																					C	+		R	+				R		
		23-1, 84-86	C	M	R													R	+	R	+					F	C		C		R			C	R	
		23-4, 84-86	C	M	R													R	+	+	+					F	C	+	C		R			C	R	
		24-1, 84-86	C	M	R																	R				C			C					C	+	
		24-4, 84-86	C	P	R																					F			R	+	R				+	
		25-1, 84-86	R	M	R																+		+			F	C		F	C	+			C		F
		25-4, 84-86	C	G	R																	+	+	+		F	C	+	C	C			R	C	+	C
		26-2, 84-86	C	G	R																			+	+	F	C	+	C	R	+		R	C	R	C
		26-4, 84-86	R	M	R					R																C	R	+	C	R	+	R	R	R	+	R
		27-1, 84-86	+	M	O																					C	R		C					R	+	R
	D. penultima + *D. ante-penultima*	27-4, 84-86	+	G	O																					C	C		C		+		R	R	+	
		28-1, 84-86	R	G	O					+																C	C		C		R		R	R	R	+
		28-3, 84-86	R	G	R					+																F	C		C				R	R	R	+
		29-2, 84-86	R	G	O					+																F	R		C		R		R	R	C	
		29-4, 84-86	R	G	O					+									+							C	R		C	+	+		C	R	C	
		30-1, 84-86	+	M	O																					R	+		C	+	+		R			
		31-1, 84-86	R	M	O																					+	+		C		+		C	R	+	
		31-2, 84-86	+	M	O																					+	+		R				+	R	R	
		31-3, 84-86	R	G	O					+																	+	R	C			+	C	R	R	+
		31-4, 84-86	R	G	R																						+	+	C				R	R	R	
		31-5, 84-86	R	G	O																							+	C	+			R	R	R	
	Unzoned	34-2, 84-86	+	P	O					+																					R					
		34-3, 84-86	+	P	R																															
		34-4, 84-86	+	P	O																															
		35-1, 84-86	+	P	O					+																						+			+	
		35-3, 84-85	+	P	R																															
		35-4, 84-86	R	M	O																															
		36-1, 84-86	+	M	O																												R	R		
		36-3, 84-86	+	M	O																													R		
		37-1, 84-86	R	M	O																															+
? middle Miocene	*D. pettersoni*	38-1, 84-86	+	P	O																												+		+	
		39-2, 84-85	+	P	O																															
		40-1, 84-86	R	M	O																															
		40-2, 84-85	+	P	O																						C									
		40-4, 84-86	+	P	O																															
		41-2, 84-86	R	G	O																						+	+						+		
		42-1, 84-86	+	P	O																										+			+		
		42-4, 84-86	+	P	+																								+							
		44-1, 84-86	+	P	O																								+							
		45-1, 84-86	R	G	R																														R	R
		46-1, 84-86	+	M	O																														+	+
		46-2, 84-86	+	P	O																														+	+
		47-1, 84-86	R	G	O																														R	R
		48-1, 84-86	R	M	O																														R	
		48-2, 84-86	R	M	O																															
		48-3, 84-86	R	M	O																														R	+
		49-1, 84-86	R	M	O																														R	+
		49-2, 84-86	+	M	O																														+	+
		49-3, 84-86	+	P	O																															+
		50-1, 84-86	+	P	O																															
		51-1, 84-86	+	P	O																														+	+
		52-1, 84-86	R	G	O																															+
		52-2, 84-86	R	G	O																															+

Note: Symbols as for Table 2. The following samples were barren of radiolarians: 594-18-1, 84-86 cm; 594-18-2, 84-86 cm; 594-18-4, 84-86 cm; 594-21-4, 84-86 cm; 594-34-1, 84-86 cm; 594-34-5, 84-86 cm; 594-38-2, 84-86 cm; 594-41-3, 84-86 cm; 594-41-4, 84-86 cm; 594-43-1, 84-86 cm.

Table 3. (Continued).

Anthocyrtidium ehrenbergi						R R C F C			
Lamprocyclas aff. *maritalis*						F F F F C C C			
Stichocorys peregrina					+ +	R C F F F F F C + +			
Stichopodium inflatum					+ +	C R R R + C C R R	+ + +		
Prunopyle titan						+ + + + R R R	R R R R R +		
Spongodiscus sp.						+ R +	R R R R +		
Didymocyrtis antepenultima						+ + +	+ + R R R + + +		
Diartus hughesi						+ R +	R R R C R R R + R		
Eucyrtidium punctatum					+		+ + +		
Phormostichoartus doliolum							+ + +		
Heliometta miocenica					F R	C C C C C C R C C	R C C R R R + + + +	+	
Lamprocyclas margatensis						C C C R	R R C C C R R R C C C	+ + C R R R R	
Eucyrtidium teuscheri gr.						+	+ + + + +	+	+
Lamprocyclas hannai							+ + + R R + + +	+	+
Stylosphaera angelina						R + + + +	+	R +	+
Phormostichoartus platycephala					+	F C + R +	R R + + R R R R F F	R + +	+ +
Dictyophimus splendens						+ C R	+ + + R + R +	R R + R	+
Lithopera neotera									+ + + + + +
Cyrtocapsella japonica						+ + +	+ + R R R	+ C C C C F F F	R R F F R C + F F F F F
Botryostrobus b. bramlettei						+ C R +	+ R R R R C R C C C	+ + + R R	+ C R R + +
Spirocyrtis subtilis									+ + +
Polysolenia aff. *murrayana*								+ + + + R	C + +
Cyrtocapsella elongata						+ +	+ + + +	+ R R C C C C	F C + + C C +
Botryostrobus miralestensis								+	+ + +
Lithomelissa ehrenbergi								+	+ + +
Siphostichartus corona									+ + + R + +
Prunopyle hayesi						+ +	R + R R C C R R R R	R R R R	R + R + + + F R +
Siphocampe modeloensis						R R + + R R R R R	R R R R C C + + R R R	R + + + R R R R	+ + + + F F R + R + + +
Botryostrobus sp.							+ +		+ + + +
Botryocella cribrosa gr.						+ R +			+ R R R + + + R R
Botryopyle dionisi									R R +
Circodiscus ellipticus						+		+ + R	R + R R R R R R + R R R
Clathrocyclas cabrilloensis						+ +		+ +	+ + + + + +
Clathrocyclas humerus						R R C	C R R C R R C C C C	C C C + + R	R + + C C R R R C R R + R F R
Cyrtocapsella cornuta									+ + R
Cyrtocapsella tetrapera						+ +	+ + +	+ +	+ + + + + + F C F R C C R R R F
Didymocyrtis laticonus						+ + + R +			R R R R R R C C
Eucyrtidium cienkowskii						+ + F F C F F F C C C	C C C C C C C C R C C	R R R R R C + R +	R + F R + R C R R C R R + R + + + R R
Lynchocanium grande						+ +	R R R R + + + +	+ R C C	+ + C C R + + R + +
Phormostichoartus corbula						+ + + R R R R +	+ R R R R R R R	+ + +	+ + + + R + + + + +
Phormostichoartus fistula					R +	+ + R R	+ + R R +		+ + +
Phormostichoartus marylandicus									+ R R R R R R
Collosphaera polygona gr.						C C R C C C C	+ + + + R		+ + + + R R
Stauroxiphos communis					+	C C R R + R R	C F F F + + C	R	+ F C + R R + C C R R R + C R R R R F F
Stichocorys delmontensis						+ R + R R + +	+ + R R R R R F F	R + R	+ + F + F F

tions. Reworked specimens of Eocene to middle Miocene age occur in Samples 594-23-1, 84–86 cm to 594-26-4, 84–86 cm.

The next markers observed were *Didymocyrtis antepenultima* and *Diartus hughesi*, whose first appearances are tabulated in Sample 594-31-5, 84–86 cm. Thus, Samples 594-27-4, 84–86 cm to 594-31-5, 84–86 cm are placed in the *Didymocyrtis antepenultima* Zone and the *D. penultima* Zone. The *D. penultima* and *D. antepenultima* zones are amalgamated because the species *D. penultima* was not found in the radiolarian assemblages. Moreover, the base of the *D. penultima* Zone, which is also recognized in tropical areas at the top of the range of *Diartus hughesi*, cannot be located in Site 594 because the last occurrence of *D. hughesi* is tabulated in the *S. peregrina* Zone. It is possible that *D. hughesi* as well as *Didymocyrtis laticonus* and *D. antepenultima* have different ranges in the mid-latitude sediments. Close examinations of numerous specimens show distinct morphological differences with tropical forms. Further studies, including size measurements, are needed to estimate the importance of these morphologic differences (Caulet, in preparation).

Samples 594-31-6, 84–86 cm to 594-37-1, 84–86 cm contain poorly preserved and rare radiolarian assemblages. Barren levels occur sporadically throughout this interval, which cannot be related to a well-defined zone.

Most radiolarian species recognized in the samples below 594-37-1, 84–86 cm are well known in the tropical assemblages of the *Diartus petterssoni* Zone (middle Miocene). The most significant transition in the radiolarian fauna is observed between Cores 594-23 and 594-21. In Core 21 and above, most temperate or warm-water radiolarians have disappeared. Radiolarian abundances are greatly reduced and antarctic or subantarctic species become more dominant. Their occurrence suggests a northward migration of the Antarctic Convergence.

DISCUSSION

Radiolarian Events and Potential Datum Levels

Figure 1 summarizes the sequence of events at Hole 586B and Site 594 for which adequate stratigraphic coverage is available. The list includes only those events which appear to be of potential stratigraphic significance.

Comparison between the sites shows that not all the available stratigraphically important species are reliable over the equatorial to subantarctic area. Only 14 events from a total of 38 (in the same stratigraphic interval) can be reported from both sites. Most of the correlation lines present no problem, but there are a few conflicts.

1. The discrepancy between the position of the upper limit of *Stichocorys delmontensis* in Holes 586B and 594 is resolved in favor of Hole 586B by the reliability indices (14 in Hole 586B and 7 in Hole 594). However, the last occurrence of this morphotype is very difficult to place because in temperate latitudes the shells of *S. peregrina* present many variations that are probably due to different local environments (W. R. Riedel, personal communication).

2. There is also a great discrepancy between the relative positions of the upper limit of *Phormostichoartus fistula*. The stratigraphic range assigned to this species by Nigrini (1977) is large: from the *Thyrsocyrtis bromia* Zone to the *Spongaster pentas* Zone. In Hole 586B, the upper limit of this species is located in the *S. pentas* Zone, but in Site 594, its last occurrence is tabulated in the *Stichocorys peregrina* Zone. However, the indices of reliability (20 at Hole 586B and 1 at Hole 594) show that the discrepancy is not due to different paleoenvironmental conditions.

3. The upper limit of *Lamprocyclas* aff. *maritalis* is also located in different radiolarian zones: the *Pterocanium prismatium* Zone at Hole 586B and the *S. peregrina* at Site 594. But the indices of reliability present the same value (25) and the discrepancy seems to be due to paleoecological fluctuations. However, the subantarctic morphotypes could be different from equatorial ones.

In addition to previously reported datum levels, several last occurrences that may be of stratigraphic significance (possibly only local) are worth noting here:

1. Top of *Phormostichoartus pitomorphus*. The last occurrence of this species is located in the early to middle Pleistocene in Hole 594 and near the Pliocene/Pleistocene boundary in Hole 586B. However, this species is consistently present in the sediments of the subantarctic area but is only scarce and sporadic in equatorial samples of the same age. The indices of reliability are difficult to calculate in the equatorial case and do not allow interpretation of the results. Data from current studies on Indian Ocean cores show this species gradually disappearing in cores located at different latitudes (Caulet, in preparation).

2. Top of *Lamprocyrtis heteroporos*. This species reaches an upper limit at the Pliocene/Pleistocene boundary in Hole 586B. However, it persists into the Pleistocene at Site 594.

3. As previously noted by Weaver (1983), the last occurrence of *Diartus hughesi* is higher in subantarctic material (in the *Didymocyrtis antepenultima/D. penultima* Zone in Hole 594, just below the first evolutionary transition to *S. peregrina*).

Evolutionary Lineages

Of importance for biostratigraphic application of the information included in this report are several suggested evolutionary transitions. Some of these are new, whereas others are modifications of trends previously reported in other areas.

1. *Eucyrtidium teuscheri* gr.–*E. teuscheri teuscheri* (Fig. 2) The *E. teuscheri* gr. evolves from large eucyrtids, which are rare in the middle Miocene, to slender forms in the late Miocene. These big specimens evolve into *E. teuscheri orthoporus* and *E. teuscheri teuscheri* In the temperate area (Site 594), the transition to *E. teuscheri orthoporus* occurs in the late Miocene. In the tropical area (Hole 586B), *E. teuscheri orthoporus* evolves from the *E. teuscheri* gr. in the beginning of the *Spongaster pentas* Zone. This species reaches extinction without apparent descendants in the early Pleistocene. Intermediate forms between the *E. teuscheri* gr. and its two descendants are reported in the late Miocene to early Pliocene. The modern *E. teuscheri teuscheri* morphotypes evolve in the early *S. pentas* Zone. As *E. teuscheri*

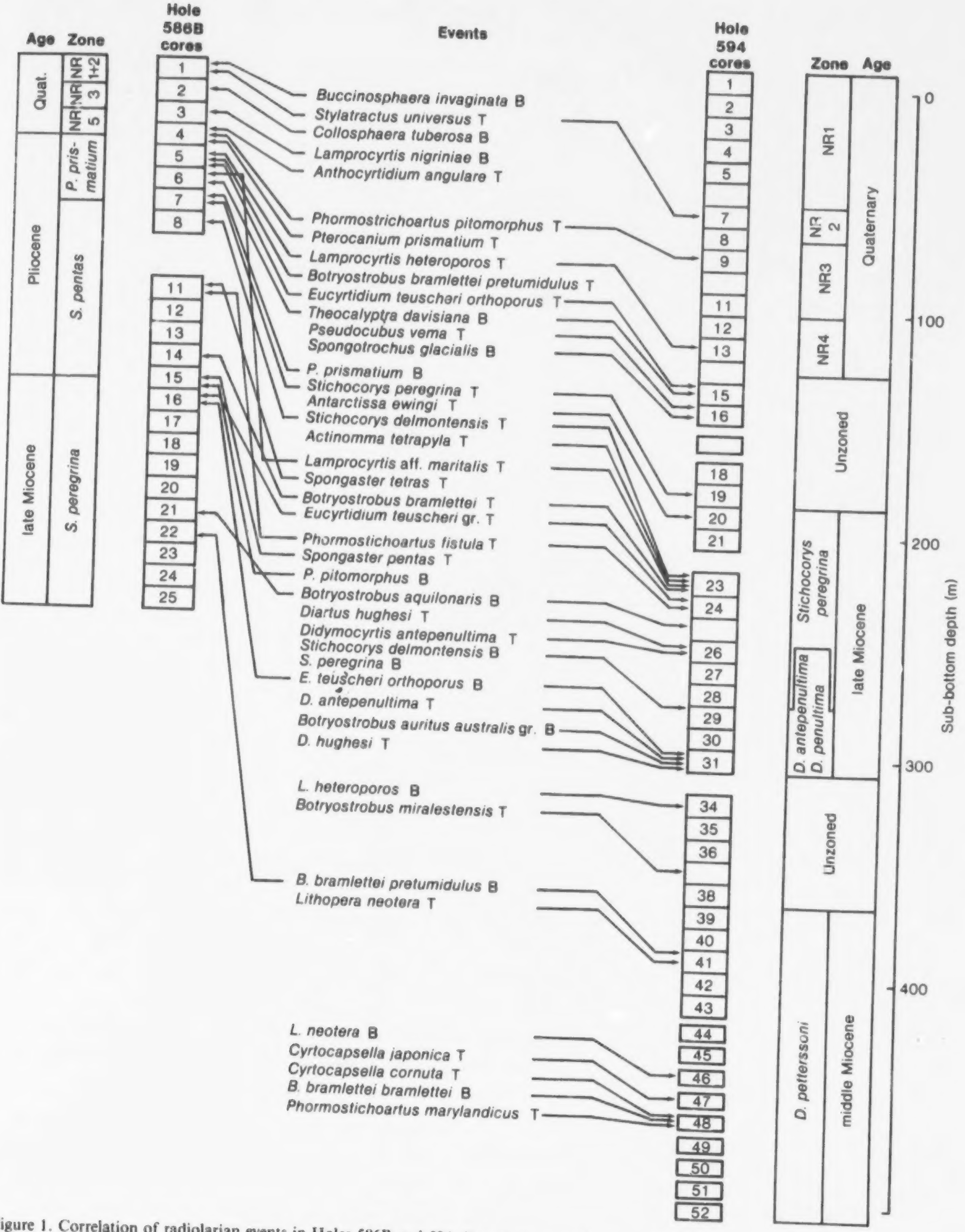
Age
Zone
Hole 586B cores
Events
Hole 594 cores
Zone
Age
Quat.
Pliocene
late Miocene
NR 1+2
NR 3
NR 5
P. pris-matium
S. pentas
S. peregrina
Buccinosphaera invaginata B
Stylatractus universus T
Collosphaera tuberosa B
Lamprocyrtis nigriniae B
Anthocyrtidium angulare T
Phormostrichoartus pitomorphus T
Pterocanium prismatium T
Lamprocyrtis heteroporos T
Botryostrobus bramlettei pretumidulus T
Eucyrtidium teuscheri orthoporus T
Theocalyptra davisiana B
Pseudocubus vema T
Spongotrochus glacialis B
P. prismatium B
Stichocorys peregrina T
Antarctissa ewingi T
Stichocorys delmontensis T
Actinomma tetrapyla T
Lamprocyrtis aff. maritalis T
Spongaster tetras T
Botryostrobus bramlettei T
Eucyrtidium teuscheri gr. T
Phormostichoartus fistula T
Spongaster pentas T
P. pitomorphus B
Botryostrobus aquilonaris B
Diartus hughesi T
Didymocyrtis antepenultima T
Stichocorys delmontensis B
S. peregrina B
E. teuscheri orthoporus B
D. antepenultima T
Botryostrobus auritus australis gr. B
D. hughesi T
L. heteroporos B
Botryostrobus miralestensis T
B. bramlettei pretumidulus B
Lithopera neotera T
L. neotera B
Cyrtocapsella japonica T
Cyrtocapsella cornuta T
B. bramlettei bramlettei B
Phormostichoartus marylandicus T
NR1
NR 2
NR3
NR4
Unzoned
Stichocorys peregrina
D. antepenultima
D. penultima
Unzoned
D. petterssoni
Quaternary
late Miocene
middle Miocene
0
100
200
300
400
Sub-bottom depth (m)

Figure 1. Correlation of radiolarian events in Holes 586B and 594. B = bottom marker, T = top marker.

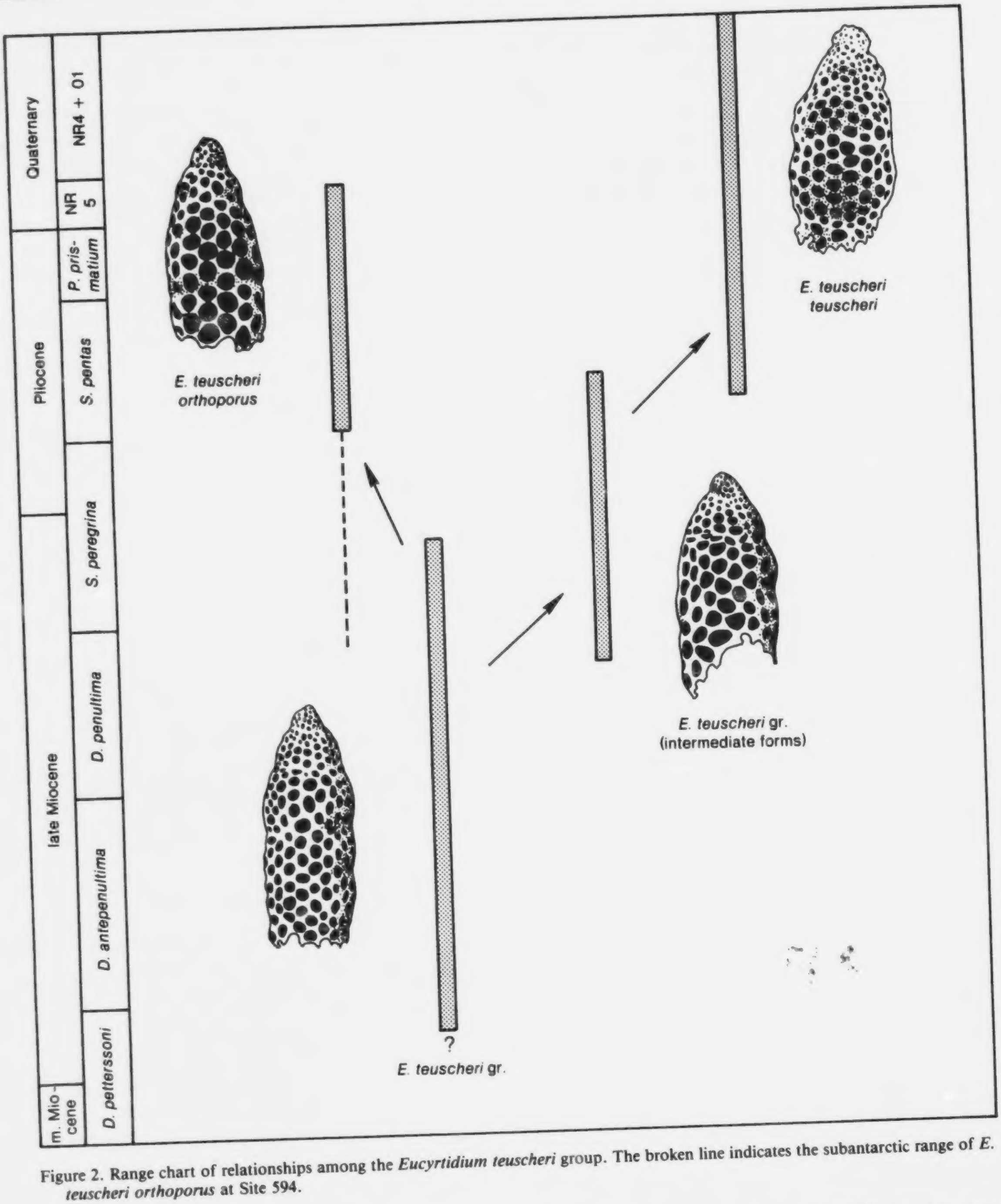

Figure 2. Range chart of relationships among the *Eucyrtidium teuscheri* group. The broken line indicates the subantarctic range of *E. teuscheri orthoporus* at Site 594.

orthoporus appears to be more frequent in the temperate sediments with a longer range, its evolution is probably controlled by paleoenvironmental conditions.

2. *Phormostichoartus fistula–P. pitomorphus* (Fig. 3) *Phormostichoartus fistula* is reported to appear in the late Eocene (Nigrini, 1977). It is rare in late Miocene sediments of both tropical and temperate areas. The transition to *P. pitomorphus* occurs in the early Pliocene. Transitional forms present gradually shorter tests and the width of the third segment increases. *P. pitomorphus* is more frequent in temperate to subtropical areas (Caulet, unpublished data), and becomes extinct in the early Pleistocene.

Intermediate forms with the *P. platycephala* gr. occur in the late Pliocene period: fourth segment smaller and enlarged cephalis. As *P. platycephala* gr. specimens are

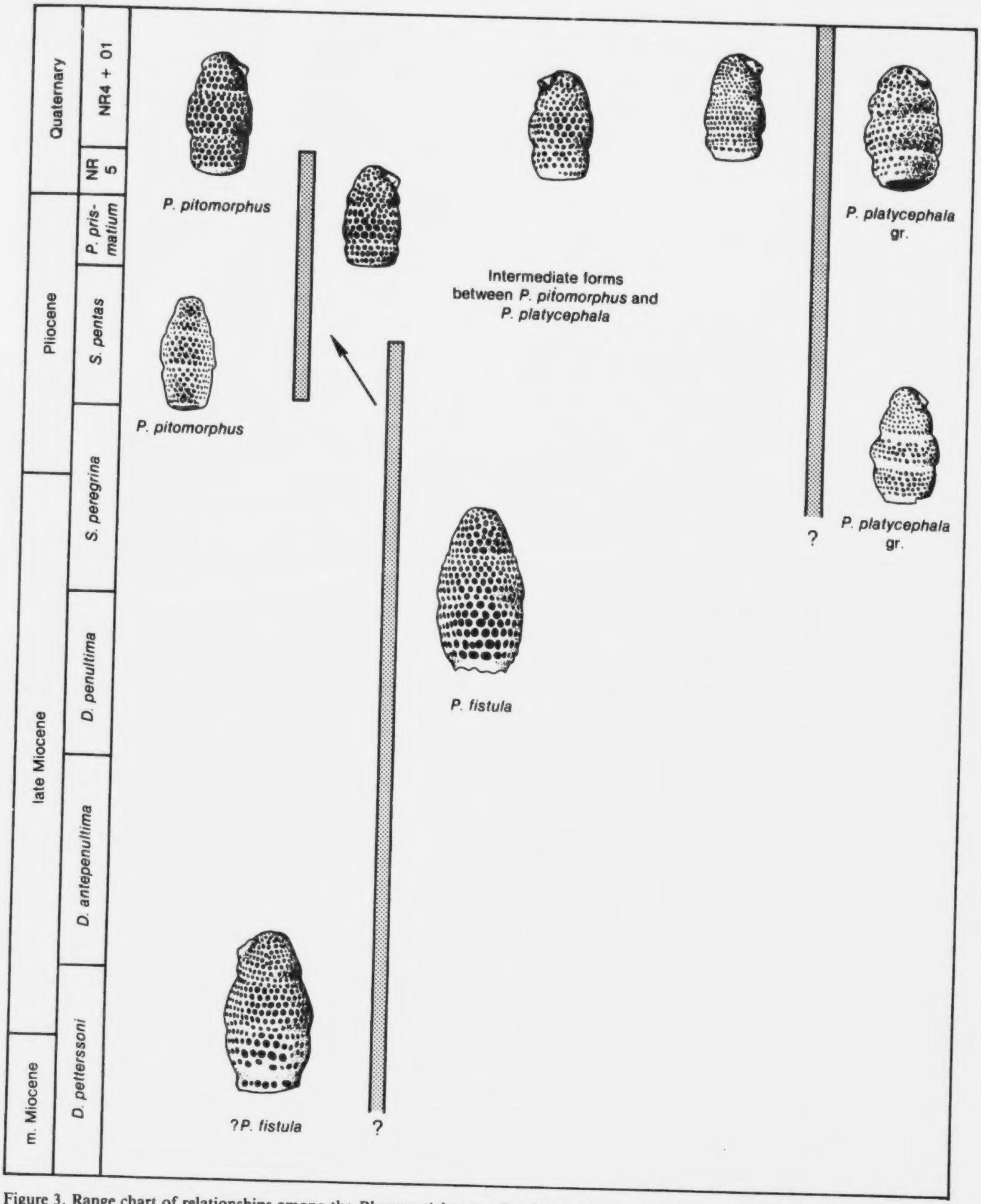

Figure 3. Range chart of relationships among the *Phormostichoartus fistula*–*P. pitomorphus* group. *P. fistula* has a widespread distribution in tropical and temperate areas. Its evolution into *P. pitomorphus* took place only in temperate areas. Intermediate forms between *P. pitomorphus* and *P. platycephala* group are commonly found in temperate sediments of Pliocene to early Pleistocene age. Relations between *P. platycephala* and *P. fistula* are not clear.

present in Messinian sediments (Caulet, unpublished data), it is possible that a hybridization takes place between the two groups of morphotypes. However, older ancestors of *P. platycephala* are unknown, and the phylogeny of the whole groups is not yet precise.

3. *Lamprocyclas* aff. *maritalis–L. maritalis. L. maritalis* appears approximately in the early *Pterocanium prismatium* Zone, where it probably evolves from the *L.* aff. *maritalis* gr. The relationships with the temperate forms of the same age are not clear.

4. *Lamprocyrtis heteroporos–L. nigriniae*. The discovery of *L. daniellae* calls into question the lineage proposed by Kling (1973) for the open-cephalis pterocoryds. But the distinction between *Lamprocyclas junonis* and *Lamprocyrtis neoheteroporos* and the range of *Lamprocyclas hannai* remain problematical. Before changing the phylogeny of this group, it is necessary to answer these questions, and to define precisely the stratigraphic range of *Lamprocyrtis daniellae*, which seems, unfortunately, to be very rare.

Preservation

Estimates of radiolarian preservation are generally imprecise. Preservation is considered "good" where a large number of species is present, and some skeletons of each species are reasonably complete. Samples in which incomplete specimens are frequent are considered to have "poor" preservation. Samples in which species diversity and specimen integrity are intermediate between the two are included in the "moderate" preservation category. The location of most Leg 90 sites under the mid-latitude water masses and in shallow depths is responsible for the absence or poor preservation of the radiolarian assemblages.

Some aspects of radiolarian preservation in Hole 586B are noteworthy (Fig. 4). Preservation appears to have been very poor during the middle Pleistocene and the middle Pliocene. Very good preservation occurred during the early Pleistocene and the early Pliocene. It is beyond the scope of this report to examine all the possible explanations for these events. However, some radiolarian and diatom contents measured in a few mid-latitude piston cores from the Indian Ocean have been shown to increase in the early Pleistocene and in the early Pliocene (Caulet, 1977). These greater amounts were interpreted as an increase of equatorial productivity. Thus, as biogenous silica dissolution is nearly constant in shallow-water sediments above the CCD (Johnson, 1975), the peaks of the preservation curve at Hole 586B can be interpreted as periods of increasing productivity.

SYSTEMATICS

The systematic study of radiolarians from Leg 90 is presented in two parts:

1. Taxonomic notes: descriptions of new species with or without revised concepts of the genus
2. Species list: bibliographic references for well-known taxa which are not discussed in the taxonomic notes.

The only literature references given are to the original description, and to my present concept of the species, if different from the original one. Type specimens are deposited in the Muséum National d'Histoire Naturelle, Paris. Measurements have been made on 20 specimens.

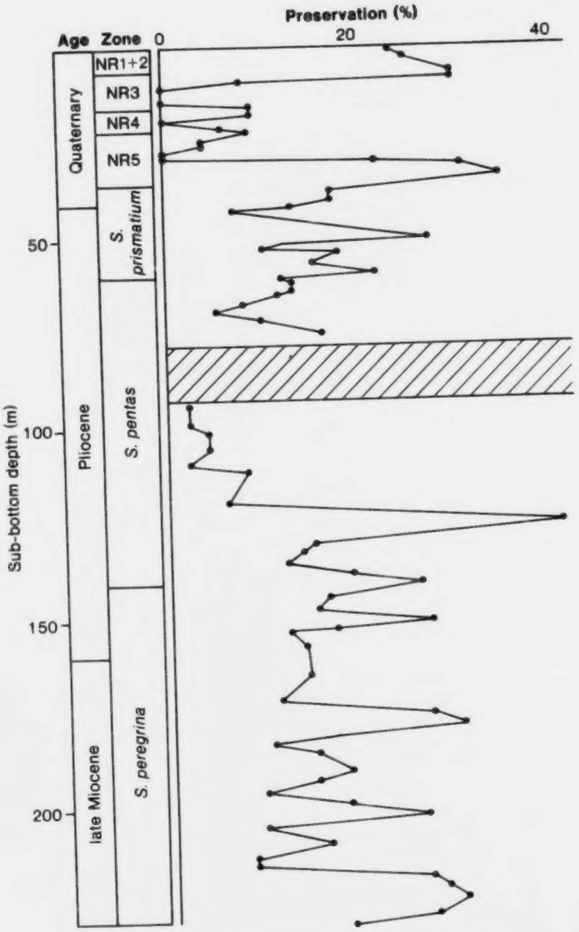

Figure 4. Fluctuations of radiolarian preservation in Hole 586B (in percentages of well-preserved individuals among 800 radiolarian shells). Hatched area shows barren samples.

Taxonomic Notes

Family COLLOSPHAERIDAE Müller, 1858
Genus *ACROSPHAERA* Haeckel, 1881

Type species. *Collosphaera spinosa* Haeckel, 1862, p. 536, pl. 34, figs. 12–13. Bjørklund and Goll (1979) gave a good discussion of thc genus. However, their choice of *A. echinoides* Haeckel, 1887 as the type species seems questionable (although technically correct), because they assign to *A. echinoides* the rank of a subspecies of *A. spinosa*, which was originally described by Haeckel in 1862.

Acrosphaera spinosa hamospina n.ssp.
(Plate 1, Figs. 2, 3)

Description. A subspecies of *Polysolenia spinosa* characterized b more than 10 strong spines ending in hooks.

Name. *Hamus* (Latin: hook) and *spina* (Latin: spine).

Holotype. Pl. 1, Fig. 2, Sample 586B-23-3, 60–62 cm, slide 2.

Dimensions. Shell diameter, 70–90 µm; spine length, 60–80 µm.

Distribution. The first occurrence is not recognized. But the firs consistent occurrence seems to be in the *Stichocorys peregrina* Zone a Sample 586B-24-5, 60–62 cm.

Remarks. This morphotype is closely related to the *Acrosphaer echinoides* gr. Haeckel and it could be included in that species. But it stratigraphic range is very short and its last appearance is an even with a good index of reliability. Very common in equatorial Indian Ocean material of the same age.

Acrosphaera spinosa fasciculopora n.ssp.
(Pl. 1, Fig. 1)

?*Acrosphaera spinosa echinoides* (Haeckel) Bjørklund and Goll, 1979, pl. 1, figs. 10, 11.

Description. *Acrosphaera spinosa* with 10–15 spines, strong, long, arising from a cluster of pores that are larger than the irregular small pores of the shell and that form small protuberances on the shell surface.

Name. *fasciculum* (Latin: cluster)

Holotype. Pl. 1, Fig. 1, Sample 586B-20-3, 60–62 cm, slide 1.

Dimensions. Shell diameter, 80–100 µm; Spine length, 30–100 µm.

Distribution. First occurrence not recognized. Very abundant in samples near the very end of the *Stichocorys peregrina* Zone (Sample 586B-16-5, 60–62 cm), a few meters below its last occurrence.

Remarks. This subspecies is closely related to the *A. echinoides* group but its external spines are less numerous, longer, and arise from a very typical cluster of larger pores. Its stratigraphic range is narrower, and the last occurrence seems to be a very good event.

Genus *SIPHONOSPHAERA* Müller, 1858

Type species. *Collosphaera tubulosa* Müller, 1855.

Siphonosphaera hyalina n.sp.
(Plate 2, Fig. 1)

Description. Subspherical shell with two distal tubes and numerous very small circular pores. Extremity of tubes not latticed, perforated by small pores.

Name. *hyalin* (Greek: glassy).

Holotype. Pl. 2, Fig. 1, Sample 586B-17-2, 60–62 cm, slide 1.

Dimensions: Total length, 100–130 µm.

Distribution. First occurrence in the early Pliocene (Sample 586B-17-2, 60–62 cm). Last occurrence in the early Pleistocene (Sample 586B-4-5, 60–62 cm).

Remarks. Bjørklund and Goll (1979) point out the problems that arise from collosphaerid taxonomy. They think that all morphotypes can be assigned to one or two genuses. Until a detailed study of tube-bearing collosphaerids is completed, it seems more reasonable to use the old genera.

Family ACTINOMMIDAE Haeckel, 1862, emend. Riedel 1967
Genus *AXOPRUNUM* Haeckel, 1887, emend. Koslova, 1972

Type species. *A. stauraxonium* Haeckel, 1887, pl. 48, fig. 4.

?*(Axoprunum) monostylum* n.sp.
(Plate 1, Figs. 9–11)

Description. *Axoprunum* with one single strong polar spine. Three shells subspherical to cuboid; 20–25 pores on the equatorial plane. The medullary and cortical shells are joined by rods (about 6) disposed in the equatorial plane, and by 2 rods going to the opposite poles of the shell. One rod penetrates the cortical shell and forms a strong spine, three-edged and thorny at its end. The other rod projects as a small thorn. Secondary spines, three-edged, often broken, arise from the bars of the third shell.

Name. *monostylus* (Latin: with one stylus).

Holotype. Pl. 1, Fig. 9, Sample 586B-5-4, 60–61 cm, slide 1.

Dimensions. Polar spine length: 100–120 µm. Shell diameter: 80–90 µm.

Distribution. Very rare in the sediments of the upper *Pterocanium prismatium* Zone. First common occurrence in Sample 586B-6-1, 60–61 cm. Last occurrence in Sample 586B-4-6, 60–61 cm.

Remarks. Very similar morphotypes can be found in some Langhian marls from Spain (Pl. 1, Fig. 11) (Caulet, unpublished results). But these older forms possess shells with 35–40 small pores. A nearly dissolved specimen was found in Sample 586B-20-3, 60–61 cm, but it is difficult to describe with precision.

Assignment of a generic name to this morphotype poses a difficult taxonomic problem. Vinassa (1900) describes two Prunoidea and two Sphaeroidea with a single polar spine (*Dorydruppa, Doryprunum* and *Dorysphaera, Dorylonchidium*). But the descriptions are very sketchy and the figures of his species cannot be compared to this species. As the inner structure of *A. monostylum* seems to be similar to the inner structure of *A. stauraxonium*, this new morphotype is provisionally ascribed to the genus *Axoprunum*.

Family SPONGODISCIDAE Haeckel, 1862, emend. Riedel, 1967
Genus *RHOPALASTRUM* Ehrenberg, 1847

Type species. *Haliomma lagena* Ehrenberg, 1840, p. 200. See discussion in Nigrini and Moore, 1979, p. 580.

Rhopalastrum oracutibrachium n.sp.
(Plate 2, Fig. 4)

Description. Spongodiscid with three simple, undivided, spongy arms. Triangular shells, equilateral. Patagium present. Central structure partly obscured by spongy network, consisting of 5 to 6 concentric chambered rings. Spongy arms with sharp edges and ragged ends.

Name. *ora* (Latin: edge), *acutus* (Latin: sharp), *brachium* (Latin: arm).

Holotype. Pl. 2, Fig. 4, Sample 586B-23-5, 60–62 cm, slide 2.

Dimensions. Arm length: 120–130 µm. Inner disk diameter: 70–80 µm.

Distribution. First occurrence not recognized. Abundant from Sample 586B-25-5, 60–62 cm to 586B-22-1, 60–62 cm. Last consistent occurrence in the *Stichocorys peregrina* Zone (Sample 586B-21-3, 60–62 cm). Sporadic occurrences in the *Spongaster pentas* Zone.

Remarks. Some Pleistocene forms present well-marked arm edges, but these forms are smaller and their arm edges less sharp and thick.

Genus *SPONGODISCUS* Ehrenberg, 1854

Type species. *S. resurgens* Ehrenberg, 1854c, p. 66.

Spongodiscus klingi n.sp.
(Plate 2, Figs. 2, 3)

Circular spongodiscid. Kling, 1971, p. 1086, pl. 1, fig. 8.

?Spongodiscid. Johnson, 1974, pl. 9, fig. 18.

?*Spongodiscus communis fragilis* Riedel, 1953, p. 809, pl. 84, fig. 6.

Description. Disc circular, spongy, subdivided into three concentric parts, with a regular margin. Inner disc with 4–5 chambered rows partly obscured by a spongy network. Median part of the disc a net of small irregular pores with 5–7 large meshes. External part of the disc strong and spongy with a delicate margin and fragile short spines, often broken.

Name. In honor of S. Kling, who first reported the species.

Holotype. Pl 2, Fig. 3, Sample 586B-18-1, 60–62 cm, slide 1.

Dimensions. Total diameter: 210–220 µm. Median thin area width: 40 µm. Maximum dimension of larger elliptical pores: 20 µm.

Distribution. First occurrence not recognized. Last occurrence at Sample 586B-12-1, 60–62 cm in the *S. pentas* Zone.

Remarks. This species differs from all other spongodiscid species in the broader pores located in the median part of the shell. Frequently, the fragile margin is not observed. The number of inner broad pores is variable. Riedel (1953) described a form with a thin region between a plain margin and a central chambered region, without larger pores. Relationships with other spongodiscids unknown.

Family PTEROCORYTHIDAE Haeckel, 1881, emend. Moore, 1972
Genus *LAMPROCYCLAS* Haeckel, 1881, emend. Nigrini, 1967

Type species. *Lamprocyclas nuptialis* Haeckel, 1887, p. 1390, pl. 74, fig. 15.

Lamprocyclas aff. *maritalis* gr.
(Plate 4, Figs. 1, 2)

Calocyclas margatensis Campbell and Clark *in* Riedel, 1953, p. 811, pl. 85, fig. 8.

?*Lamprocyclas aegles* gr. Petrushevskaya, 1975, pl. 16, figs. 2–4, *non* fig. 1. Weaver, 1983, pl. 4, figs. 4–5.

Description. Shell not entirely campanulate, thick-walled, and with a rough surface. Cephalis subspherical, with small subcircular pores, very thick-walled. Stout three-bladed apical horn, 2 or 3 times cephalis length. Lateral lobes not bulging. Primary and dorsal spines do not continue as ribs in the thoracic wall. Thorax cupola-shaped with subcircular pores, arranged in latitudinal rows and increasing slightly in size toward the third segment. Abdomen ovoid, 12–15 pores on a half equator. Peristome well differentiated, poreless, with two rows of teeth. Terminal teeth better developed than subterminal teeth.

Dimensions. Total length: 200–220 μm. Maximum width: 100 to 110 μm.

Distribution. In Hole 586B, the first occurrence is at Sample 586B-22-5, 60–62 cm in the *Stichocorys peregrina* Zone; the first common occurrence is in the same zone. In Hole 594, the first occurrence is in the same zone (Sample 594-26-2, 84–86 cm). But in the equatorial area the last occurrence of this species group is in the *Pterocanium prismatium* Zone (Sample 586B-6-5, 60–62 cm) and in the subantarctic area it is in the *S. peregrina* Zone (Sample 594-23-1, 84–86 cm).

Remarks. The individuals included in this species group are quite variable. They differ from *L. maritalis* by the shape of the cephalis and abdomen. Some specimens with intermediate morphology can be found in Hole 586B, where the first occurrence of *L. maritalis maritalis* Nigrini is reported 7 m below the last occurrence of *L.* aff. *maritalis*. Thus it can be assumed that *L.* aff. *maritalis* is the ancestor of *L. maritalis maritalis*. *L.* aff. *maritalis* gr. differs from *L. margatensis* Campbell and Clark by a longer shell, a more ovoid abdomen, and a strong terminal peristome (Pl. 4, Fig. 3). Moreover, the first occurrence of *L. margatensis* in Hole 586B is 10 m below the first occurrence of *L.* aff. *maritalis* gr., and the last occurrence of *L. margatensis*, in the early *Spongaster pentas* Zone, is reported 69 m below the last occurrence of *L.* aff. *maritalis* gr. A possible evolutionary lineage would be *L. margatensis* → *L.* aff. *maritalis* → *L. maritalis*. However, the mid- and high-latitude specimens of *L. maritalis* gr. have more ovoid shells than equatorial ones, with a spherical cephalis, and have a very different range. Relationships between these morphotypes are not well understood and more precise work, including size measurements, is necessary before a detailed description of this group can be presented (Caulet, in preparation).

Genus *LAMPROCYRTIS* Kling, 1973

Type species. *Lamprocyclas heteroporos* Hays, 1965, p. 179, pl. 3, fig. 1.

Lamprocyrtis daniellae n.sp.

(Plate 3, Figs. 13–16)

Description. Two-segmented form with very small cephalis, open, with irregularly circular pores and a small apical spine arising gradually from the periphery of the cephalis like a short beak. No accessory spines on the periphery of cephalic top. Collar stricture distinct. Thorax spindle-shaped, thick-walled, smooth with subcircular to irregular pores aligned in longitudinal rows. Thorax constricted distally, terminating in a peristome with an irregular row of strong irregular teeth.

Name. In memory of my wife Daniele.

Holotype. Pl. 3, Fig. 14, Sample 586B-16-1, 60–61 cm, slide 1.

Dimensions. Total length: 120–130 μm. Maximum width: 70 μm.

Distribution. Very rare in the sediments of the early *Spongaster pentas* Zone (Samples 586B-16-1, 60–62 cm to 586B-15-3, 60–62 cm).

Remarks. This morphotype is very similar to *L. nigriniae* (Caulet), with nearly the same shell. But the general shape and structure of the shell, the presence of a well-developed peristome, and the slightly developed apical spine are different. *L. daniellae* could be the ancestor of *L. nigriniae* and the *L. heteroporos–L. nigriniae* lineage may need to be revised. However, it is necessary to find evolutionary morphotypes between *L. daniellae* and *L. nigriniae*. As *L. heteroporos* is generally abundant in high-latitude sediments and *L. nigriniae* is restricted to the equatorial area, evolutionary morphotypes like *L. daniellae* must be found in mid-latitude sediments.

Genus *PTEROCORYS* Haeckel, 1881

Type species. *P. campanula* Haeckel, 1887, p. 1316, pl. 71, fig. 3.

Pterocorys longicollis n.sp.

(Plate 4, Figs. 4, 5)

Description. Shell rather thin-walled. Three-lobed cephalis subdivided into two parts: (1) upper portion, open, cylindrical, with circular pores, bearing a stout three-bladed apical horn, strong, with a great pore at its base; (2) lower "neck," formed by a very prominent dorsal lobe. Primary lateral and dorsal spines continue as ribs in the thoracic wall for about half its length. Sometimes, they are external, forming very small wings. Thorax is large, cupola-shaped with hexagonally framed, circular pores, quincuncially arranged and aligned longitudinally, 12–15 on a half-equator, 8–10 in a vertical series. Pronounced lumbar stricture. Abdomen campanulate. Distal end ragged; aperture never observed.

Name. *longus* (Latin: long), *collum* (Latin: neck).

Holotype. Pl. 4, fig. 4, Sample 586B-6-2, 60–61 cm, slide 2. (All specimens in Leg 90 samples are broken.)

Dimensions. Apical horn length: 50–60 μm. Total length of thorax: 40–50 μm. Maximum width: 80 μm.

Distribution. Very rare, with sporadic occurrences in Pliocene samples of Hole 586B. First occurrence in Sample 586B-15-5, 60–62 cm. Last occurrence in early Pleistocene, Sample 586B-4-1, 60–62 cm. More abundant in high-latitude sediments of Pliocene to early Pleistocene age from the Indian Ocean.

Remarks. Distinguished from the *P. campanula* group by pronounced bulging of the "D-lobe." Also more elongated, with abdomen walls not curved.

Family ARTOSTROBIIDAE Riedel, 1967, emend Foreman, 1973
Genus *PHORMOSTICHOARTUS* Campbell, 1951, emend. Nigrini, 1977

Type species. *Cyrtophormis cylindrica* Haeckel, 1887, p. 1461, pl. 77, fig. 17.

Phormostichoartus pitomorphus n.sp.

(Plate 3, Figs. 3, 4, 9, 10, 12)

Description. Shell smooth, spindle-shaped, consisting of four segments. Cephalis conical with well-developed, poreless, vertical tube lying along the thorax for about a third of its total length. Numerous circular pores, hexagonally framed, in regular horizontal rows. No apical horn.

Name. *pito* (Greek: barrel), *morphos* (Greek: shape).

Holotype. (Pl. 3, Fig. 12) Sample MD 75072-VI-100 cm.

Dimensions. Total length: 75–80 μm. Maximum width: 25–30 μm.

Distribution. Range is detailed in Figure 3. First common occurrence in early Pliocene at Sample 586B-16-1, 60–62 cm. Last occurrence in early Pleistocene (Sample 586B-4-1, 60–62 cm). The disappearance of this morphotype was previously documented in piston-core sediments from the southern Indian Ocean (Caulet, 1982).

Remarks. Relationships of this species with *P. fistula* and *P. platycephala* are described earlier in this chapter. In specimens of *P. pitomorphus*, the thorax is always longer then the abdomen.

Family THEOPERIDAE Heckel, 1881, emend. Riedel, 1967
Genus *EUCYRTIDIUM* Ehrenberg, 1847, emend. Nigrini, 1967

Type species. *Lithocampe acuminata* Ehrenberg, 1844b, p. 84.

Eucyrtidium anniae n.sp.

(Plate 5, Fig. 10)

Description. Five- to six-segmented shell, subcylindrical. Very small apical horn, often broken. Thorax longer than other segments. Longitudinal rows of circular pores on second and third segments. Horizontal rows on subsequent segments. Apertural margin rarely observed.

Name. After Annie Maurs who greatly helped in typing the tables.

Holotype. (Pl. 5, fig. 10) Sample 594-31-4, 84–86 cm.

Dimensions. Total length: 90–100 μm. Thoracic length: 40 μm. Thoracic width: 50 μm.

Distribution. First occurrence not recognized. Last common occurrence at Sample 586B-24-3, 60–62 cm (*Stichocorys peregrina* Zone). Last sporadic occurrence at Sample 586B-20-5, 60–62 cm, (*S. peregrina* Zone, late Miocene).

Remarks. This morphotype displays numerous resemblances to *E. punctatum* (broad second segment, shape of the shell). It differs by the longitudinal rows on the third segment and a less cylindrical shell. *E. anniae* could be the ancestor of *E. anomalum*, as the first occurrence of this species is recognized at Sample 586B-20-5, 60–62 cm. Close relationship seem to exist between *E. punctatum, E. anniae*, and *E. anomalum*, but the oldest species are very rare, occurring sporadically, and further examination is needed.

Eucyrtidium teuscheri gr. (Haeckel) sensu emend.

(Plate 5, Figs. 1–8)

Eucyrtidium teuscheri Haeckel, 1887, p. 1491, pl. 77, fig. 5.
Stichopilium variabilis Popofsky, 1908, p. 290, pl. 35, figs. 4–7.

Description. Four- to six-segmented shell; sinuous sutures between the segments. Cephalis hemispherical with a small, conical horn of the same length. Third segment longer and broader than the others. Fourth joint cylindrical. Apertural margin rarely observed. Cephalis and thorax with small subspherical pores and spiny walls. Vertical and dorsal spines prolonged as slight ribs along the thorax and the upper part of the abdomen. Pores large, subcircular, of variable sizes, and set in irregular, vertical rows.

Distribution. First occurrence not recognized. Rare in the *Diartus petterssoni* Zone in Hole 594 and in late Miocene to early Pliocene material. Common in late Pliocene to Pleistocene sediments from the subantarctic area, sparse in equatorial sediments of the same age.

Remarks. The individuals included in this group are quite variable. A provisional attempt is made to divide them into different subspecies when first and last occurrences of morphotypes are known. A subspecific name is not assigned to the oldest morphotypes because their first occurrence is unknown and individuals are too rare in the present material for an adequate description. An evolutionary lineage is proposed for late Miocene to living forms of this group (Fig. 2).

Eucyrtidium teuscheri s.sp.indet.

(Plate 5, Figs. 1–3)

Description. More than 10 vertical rows of pores on the third segment. Fifth segment very short but always recognized. Lateral and dorsal ribs not present on thorax.

Distribution. Rare and sporadic occurrences in the sediments of the *Diartus petterssoni* to *Stichocorys peregrina* Zone from Holes 586B and 594. Rare in Messinian samples from Spain and upper Miocene red clays from the South Indian Basin. Last occurrence in the *S. peregrina* Zone at Sample 586B-24-1, 60–62 cm and 594-24-4, 84–86 cm.

Remarks. The individuals included in this species group are quite variable. Further work is necessary to subdivide the group and understand its relationships with other eucyrtids of the same age.

Eucyrtidium teuscheri teuscheri n.ssp.

(Plate 5, Figs. 5–8)

Eucyrtidium teuscheri Haeckel, 1887, p. 1491, pl. 77, fig. 5.

Eucyrtidium (?) *teuscheri* Haeckel *in* Petrushevskaya, 1967, p. 121, pl. 68, fig. 1, 2.

Description. Four-segmented form with 8–10 vertical rows of pores on the third segment. External ribs very pronounced. Shell cylindrical after the third segment.

Holotype. Pl. 5, Fig. 6, Sample MD 75071-V-100 cm, slide 1.

Dimensions. Total length: 100–120 μm. Thoracic length: 20 μm. Maximum width: 40 μm.

Distribution. Very rare in the *Spongaster pentas* Zone. First common occurrence at Sample 586B-6-1, 60–61 cm in the *Pterocanium prismatium* Zone. Common in Pleistocene samples.

Remarks. Pleistocene forms are characterized by less cylindrical shells with more irregular pores.

Eucyrtidium teuscheri orthoporus n.ssp.

(Plate 5, Fig. 4)

Description. No internal ring between third and fourth segment, but slight stricture externally. Five to six vertical rows of subcircular pores. Shell cylindrical after the second segment.

Name. *orthos* (Greek: straight), *poros* (Greek: pore).

Holotype. Pl. 5, Fig. 4, Sample MD 73028-II-30 cm, slide 1 (Crozet Basin, Indian Ocean).

Dimensions. Nearly the same as for *E. teuscheri teuscheri*.

Distribution. Very rare in tropical sediments. Common in mid-latitude material from the subantarctic area. First occurrence at Sample 586B-16-1, 60–62 cm in the early *Spongaster pentas* Zone and at Sample 594-31-5, 84–86 cm (*Didymocyrtis antepenultima/penultima* Zone). Nonsporadic occurrences only in the *Pterocanium prismatium* Zone. Last occurrence at Sample 586B-4-1, 60–62 cm (early Pleistocene) and at Sample 594-15-1, 84–86 cm (late Pliocene to early Pleistocene). In both Hole 586B and Site 594, the last occurrence of this subspecies has no real significance because radiolarians are absent or very rare in all samples. Previous studies of Indian Ocean piston cores show that the last occurrence of *E. teuscheri orthoporus* occurs in the mid-Pleistocene period between 0.9 and 0.7 m.y. (Caulet, 1982).

Genus *STICHOCORYS* Haeckel, 1881

Type species. *S. wolffii* Haeckel, 1887, p. 1479, pl. 80, fig. 10.

Stichocorys johnsoni n.sp.

(Plate 6, Figs. 5, 6)

?Theoperid, gen. et sp. indet., Johnson, 1974, pl. 8, fig. 18.

Description. shell with four (or more ?) segments, distinctly separated by constrictions, the first three segments together forming a conical section. Cephalis subspherical, rough, poreless, and bearing a slightly curved apical horn generally longer than the first segment. Thorax subspherical, well developed, having 20–30 irregularly arranged subcircular pores. Third segment conical, longer and broader than any other, bearing two kinds of pores: ordinary small pores on the whole surface and a single row of pores twice as large as the others just below the lumbar stricture. Fourth segment generally ragged with smaller pores irregularly arranged. Entire apertural margin never observed.

Name. After D. A. Johnson, who first reported the morphotype.

Holotype. Pl. 6, Fig. 5, Sample 586B-20-5, 60–62 cm, slide 1.

Dimensions. Length of first, second, and third segments: 120–130 μm. Thoracic length: 40 μm. Abdominal length: 50–60 μm.

Distribution. First occurrence not recognized. Last occurrence in the *Stichocorys peregrina* Zone (Sample 586B-20-5, 60–62 cm) with a good reliability index.

Remarks. This morphotype seems to be related to the genus *Stichocorys* by the shape of the shell and the structure of the cephalis. It differs from other stichocorids in having a larger thorax and a big third segment (see figures of *S. peregrina* and *S. johnsoni* with same enlargement, Pl. 6, Figs. 4–6). Johnson and/or Nigrini (personal communication) show that Pacific Ocean forms (Pl. 6, Fig. 5) have no indentation on third segment like Indian Ocean forms (Pl. 6, Fig. 6). The species *Eucyrtidium diaphanes* (= *Calocyclas coronata* Carneval) is characterized by a single row of large pores just below the lumbar stricture but the shell has a different shape and the stratigraphic range is quite different. *E. diaphanes* could be a probable ancestor of *S. johnsoni* but the relationships between the two morphotypes must be studied more precisely.

Species List

Acanthodesmia circumflexa (Goll). *Giraffospyris circumflexa* Goll, 1969, p. 332, pl. 60, figs. 1–4, text-fig. 2. *Acanthodesmia circumflexa* (Goll) *in* Petrushevskaya, 1971, p. 274, pl. 142, figs. 4, 5.

Actinomma popofskii n. comb. *Echinomma popofskii* Petrushevskaya, 1967, p. 23, fig. 12 I–III.

Actinomma tetrapyla (Hays). *Prunopyle tetrapyla* Hays, 1965, p. 172, pl. 2, fig. 5. *Actinomma tetrapyla* (Hays) *in* Petrushevskaya, 1975, p. 569.

Acrobotrys tritubus Riedel, 1957, p. 80, pl. 1, fig. 5.

Amphirhopalum virchowii (Haeckel). *Euchitonia virchowii* Haeckel, 1862, p. 503, pl. 30, figs. 1–4. *Amphirhopalum virchowii* (Haeckel) *in* Dumitrică, 1973, p. 835, pl. 9, figs. 2–4; pl. 11, fig. 6; pl. 21, figs. 2–13.

Amphirhopalum ypsilon Haeckel, 1887, p. 522; Nigrini, 1971, p. 447, pl. 34.1, figs. 7a–c.

Androspyris anthropiscus Haeckel, 1887, p. 1093, pl. 83, fig. 8.

Antarctissa denticulata (Ehrenberg). *Lithobotrys ? denticulata* Ehrenberg, 1884a, p. 203. *Antarctissa denticulata* (Ehrenberg) *in* Petrushevskaya, 1967, p. 87, fig. 49, I–IV.

Antarctissa ewingi Chen, 1975, p. 457, pl. 16, figs. 5–9.

Antarctissa strelkovi Petrushevskaya, 1967, p. 89, fig. 51, III–VI.

Anthocyrtidium angulare Nigrini, 1971, p. 445, pl. 34.1, figs. 3a–b.

Anthocyrtidium ehrenbergi (Stöhr) gr. *Anthocyrtis ehrenbergi* Stöhr, 1880, p. 100, pl. 3, figs. 21a, b. *Anthocyrtidium ehrenbergi* (Stöhr) *in* Riedel et al., 1974, p. 712, pl. 60, fig. 10; pl. 61, fig. 1.

Anthocyrtidium michelinae Caulet, 1979, p. 132, pl. 2, figs. 8, 9.

Anthocyrtidium nosicaae Caulet, 1979, p. 132, pl. 2, fig. 6.

Artostrobus elegans (Ehrenberg) gr. n. comb. *Eucyrtidium elegans* Ehrenberg, 1854c, pl. 36, fig. 17; 1875, pl. 11, fig. 12.

Astrophacus inca (Clark and Campbell) n. comb. *Heliodiscus inca* Clark and Campbell, 1942, p. 38, pl. 3, fig. 17.

Astrophacus linckiaphormis (Clark and Campbell) n. comb. *Heliodiscus linckiaphormis* Clark and Campbell, 1942, p. 40, pl. 5, figs. 1, 2.

Axoprunum euterpe (Haeckel) gr. n. comb. *Stylosphaera euterpe* Haeckel, 1887, p. 135.

Axoprunum polycentrum (Campbell and Clark). *Druppatractus (Druppatractus) polycentrus* Campbell and Clark, 1942, p. 35, pl. 5, fig. 19. *Axoprunum polycentrum* (Campbell and Clark) *in* Petrushevskaya and Koslova, 1972, p. 521, pl. 10, figs. 11–12.

Botryocella cribrosa (Ehrenberg) gr. *? Lithobotrys cribrosa* Ehrenberg, 1873, p. 237; 1875, pl. 3, fig. 20. *Botryocella* aff. *B. cribrosa* (Ehrenberg) gr. *in* Petrushevskaya and Koslova, 1972, p. 554, pl. 39, figs. 4–6.

Botryopyle (?) dionisi Petrushevskaya, 1975, p. 589, pl. 13, fig. 18, pl. 26, fig. 10.

Botryostrobus aquilonaris (Bailey) gr. *Eucyrtidium aquilonaris* Bailey, 1856, p. 4, pl. 1, fig. 9. *Botryostrobus aquilonaris* (Bailey) *in* Nigrini, 1977, p. 246, pl. 1, fig. 1.

Botryostrobus auritus/australis (Ehrenberg) gr. *Lithocampe australe* Ehrenberg, 1844a, p. 187; 1854b, pl. 35A, 21, fig. 18. *Botryostrobus auritus/australis* (Ehrenberg) gr. *in* Nigrini, 1977, p. 246, pl. 1, figs. 2–5.

Botryostrobus bramlettei bramlettei (Campbell and Clark) *Lithomitra bramlettei* Campbell and Clark, 1944, p. 53, pl. 7, figs. 10–14. *Botryostrobus b. bramlettei* (Campbell and Clark) *in* Caulet, 1979, p. 129, pl. 1, fig. 8.

Botryostrobus bramlettei pretumidulus Caulet, 1979, p. 129, pl. 1, fig. 5.

Botryostrobus bramlettei reedi (Campbell and Clark) n. comb. *Siphocampe (Siphocampula) reedi* Campbell and Clark, 1944, p. 58, pl. 7, fig. 24.

Botryostrobus bramlettei seriatus (Jørgensen) *Eucyrtidium seriatum* Jørgensen, 1905, p. 150. *Botryostrobus bramlettei seriatus* (Jørgensen) *in* Caulet, 1979, p. 130, pl. 1, fig. 6, text-fig. 4.

Botryostrobus bramlettei tumidulus (Bailey) *Eucyrtidium tumidulus* Bailey, 1856, p. 5, pl. 1, fig. 11. *Botryostrobus bramlettei tumidulus* (Bailey) *in* Caulet, 1979, p. 131, pl. 1, fig. 9.

Botryostrobus miralestensis (Campbell and Clark) *Dictyocephalus miralestensis* Campbell and Clark, 1944, p. 45, pl. 6, figs. 12–14. *Botryostrobus miralestensis* (Campbell and Clark) *in* Petrushevskaya and Koslova, 1972, p. 539, pl. 24, fig. 31.

Buccinosphaera invaginata Haeckel. 1887, p. 99, pl. 5, fig. 11.

Calocycletta caepa Moore, 1972, p. 149, pl. 2, figs. 4–7.

Calocycletta parva Moore, 1972, p. 148, pl. 1, figs. 1–5.

Centrobotrys thermophila Petrushevskaya, 1965, p. 115.

Circodiscus ellipticus (Stöhr) *Trematodiscus ellipticus* Stöhr, 1880, p. 108, pl. 4, fig 16. *Circodiscus ellipticus* (Stöhr) gr. *in* Petrushevskaya, 1975, p. 575, pl. 6, figs. 1–6.

Clathrocyclas bicornis Hays, 1965, p. 179, pl. 3, fig. 3.

Clathrocyclas (Clathrocycloma) cabrilloensis Campbell and Clark, 1944, p. 48, figs. 1–3.

Clathrocyclas humerus Petrushevskaya, 1975, p. 586, pl. 15, figs. 7, 12, 22, 23, pl. 43, figs. 1, 2.

Clathrocyclas spatiosa (Ehrenberg) n. comb. *Cycladophora spatiosa* Ehrenberg, 1875, pl. 18, figs. 5, 6.

Clathrocyclas (Clathrocyclia) universa Clark and Campbell gr., 1942, p. 87–88, pl. 7, figs. 11–20.

Collosphaera polygona Haeckel gr., 1887, p. 96, pl. 13, fig. 15.

Collosphaera tuberosa Haeckel, 1887, p. 97; Nigrini, 1971, p. 445, pl. 34.1, fig. 1.

Collosphaera sp. A Knoll and Johnson, 1975, p. 63, pl. 1, figs. 1, 2, 7, pl. 2, figs. 4–6.

Cryptoprora ornata Ehrenberg, 1873, p. 222; 1875, pl. 5, fig. 8.

Cyclampterium (?) milowi Riedel and Sanfilippo, 1971, p. 1593, pl. 38, fig. 3; pl. 7, figs. 8, 9.

Cyclampterium ? neatum Sanfilippo and Riedel, 1970, p. 457, pl. 2, figs. 17, 18.

Cyrtocapsella cornuta Haeckel. *Cyrtocapsa (Cyrtocapsella) cornuta* Haeckel, 1887, p. 1513, pl. 78, fig. 9. *Cyrtocapsella cornuta* Haeckel *in* Sanfilippo and Riedel, 1970, p. 453, pl. 1, figs. 19–20.

Cyrtocapsella elongata (Nakaseko). *Theocapsa elongata* Nakaseko, 1963, p. 185, pl. 3, figs. 4–5. *Cyrtocapsella elongata* (Nakaseko) *in* Sanfilippo and Riedel, 1970, p. 452, pl. 1, figs. 11–12.

Cyrtocapsella japonica (Nakaseko). *Eusyringium japonicum* Nakaseko, 1963, p. 193, text-figs. 20–21, pl. 4, figs. 1–3. *Cyrtocapsella japonica* (Nakaseko) *in* Sanfilippo and Riedel, 1970, p. 452, pl. 1, figs. 13–15.

Cyrtocapsella tetrapera (Haeckel). *Cyrtocapsa (Cyrtocapsella) tetrapera* Haeckel, 1887, p. 1512, pl. 75, fig. 12. *Cyrtocapsella tetrapera* (Haeckel) *in* Sanfilippo and Riedel, 1970, p. 453, pl. 1, figs. 16–18.

Dendrospyris bursa Sanfilippo and Riedel, *in* Sanfilippo et al., 1973, p. 217, pl. 2, figs. 9–13.

Desmospyris biceps stabiloides (Petrushevskaya). *Desmospyris stabiloides* Petrushevskaya, 1972, fig. 1, no. 14. *Desmospyris biceps stabiloides* (Petrushevskaya) *in* Caulet, 1979, p. 136, pl. 4, fig. 8.

Desmospyris stabilis (Goll) n. comb. *Dendrospyris stabilis* Goll, 1968, p. 1422, pl. 173, figs. 16–18, 20, text-fig. 8.

Diartus hughesi (Campbell and Clark). *Ommatocampe hughesi* Campbell and Clark, 1944, p. 23, pl. 3, fig. 12. *Diartus hughesi* (Campbell and Clark) *in* Sanfilippo and Riedel, 1980, p. 1010, text-fig. 1, i.

Diartus petterssoni (Riedel and Sanfilippo). *Cannartus (?) petterssoni* Riedel and Sanfilippo, 1970, p. 520, pl. 14, fig. 3. *Diartus petterssoni* (Riedel and Sanfilippo) *in* Sanfilippo and Riedel, 1980, p. 1010, text-fig. 1, h.

Dictyophimus crisiae Ehrenberg, 1854a, p. 241.

Dictyophimus splendens (Campbell and Clark) n. comb. *Pterocorys (Pterocyrtidium) splendens* Campbell and Clark, 1944, p. 46, pl. 6, figs. 19, 20.

Dictyoprora mongolfieri (Ehrenberg). *Eucyrtidium mongolfieri* Ehrenberg, 1854c, pl. 36, fig. 18, B lower. *Dictyoprora mongolfieri* (Ehrenberg) *in* Nigrini, 1977, p. 250, pl. 4, figs. 1, 2.

Dictyoprora urceolus (Haeckel). *Dictyocephalus urceolus* Haeckel, 1887, p. 1305. *Dictyoprora urceolus* (Haeckel) *in* Nigrini, 1977, p. 251, pl. 4, figs. 9–10.

Didymocyrtis antepenultima (Riedel and Sanfilippo). *Ommatartus antepenultimus* Riedel and Sanfilippo, 1970, p. 521, pl. 14, fig. 4. *Didymocyrtis antepenultima* (Riedel and Sanfilippo) *in* Sanfilippo and Riedel, 1980, p. 1010, text-fig. 1.

Didymocyrtis avita (Riedel). *Panartus avitus* Riedel, 1953, p. 808, pl. 84, fig. 7. *Didymocyrtis avita* (Riedel) *in* Sanfilippo and Riedel, 1980, p. 1010, text-fig. 1.

Didymocyrtis laticonus (Riedel). *Cannartus laticonus* Riedel, 1959, p. 291, pl. 1, fig. 5. *Didymocyrtis laticonus* (Riedel) *in* Sanfilippo and Riedel, 1980, p. 1010, text-fig. 1, e.

Didymocyrtis penultima (Riedel). *Panarium penultimum* Riedel, 1957, p. 76, pl. 1, fig. 1. *Didymocyrtis penultima* (Riedel) *in* Sanfilippo and Riedel, 1980, p. 1010, text-fig. 1, f.

Didymocyrtis tetrathalamus (Haeckel). *Panartus tetrathalamus* Haeckel, 1887, p. 378, pl. 40, fig. 3. *Didymocyrtis tetrathalamus* (Haeckel) *in* Sanfilippo and Riedel, 1980, p. 1010, text-fig. 1, g.

Druppatractus irregularis Popofsky, 1912, p. 114, text-figs. 24–26.

Eucecryphalus petrushevskaae Caulet, 1979, p. 131, pl. 2, fig. 3.

Eucyrtidium anomalum (Haeckel). *Lithocampe anomala* Haeckel, 1860, p. 839. *Eucyrtidium anomalum* (Haeckel) *in* Haeckel, 1862, p. 323, pl. 7, figs. 11–13.

Eucyrtidium cienkowskii Haeckel gr. *Eucyrtidium cienkowskii* Haeckel, 1887, p. 1493, pl. 80, fig. 9.

Eucyrtidium indiensis Caulet, 1979, p. 134, pl. 4, fig. 5.

Eucyrtidium punctatum (Ehrenberg). *Lithocampe punctata* Ehrenberg, 1844b, p. 84. *Eucyrtidium punctatum* (Ehrenberg) Ehrenberg, 1847, p. 43; 1854c, pl. 22, fig. 24.

Haliometta miocenica (Campbell and Clark). *Heliosphaera miocenica* Campbell and Clark, 1944, p. 16, pl. 2, figs. 10–14. *Haliometta miocenica* (Campbell and Clark) *in* Petrushevskaya and Koslova, 1972, p. 517, pl. 9, figs. 8, 9.

Hexacontium hootsi Campbell and Clark, 1944, p. 14, pl. 2, fig. 5.

Hexacontium medusa (Ehrenberg) n. comb. *Haliomma medusa* Ehrenberg, 1854b, pl. 20, figs. 21, 22, 23, pl. 21, fig. 53, pl. 22, fig. 33.

Lamprocyclas hannai (Campbell and Clark) n. comb. *Calocyclas hannai* Campbell and Clark, 1944, p. 48, pl. 69, figs. 21, 22.

Lamprocyclas junonis (Haeckel) n. comb. *Theoconus junonis* Haeckel, 1887, p. 1401, pl. 69, fig. 7.

Lamprocyclas margatensis n. comb. *Calocyclas margatensis* Campbell and Clark, 1944, p. 47, pl. 6, figs. 17–18.

Lamprocyclas maritalis Haeckel, 1887, p. 1390, pl. 74, figs. 13, 14.

Lamprocyrtis heteroporos (Hays). *Lamprocyclas heteroporos* Hays, 1965, p. 179, pl. 3, fig. 1. *Lamprocyrtis heteroporos* (Hays) *in* Kling, 1973, p. 639, pl. 5, figs. 19–21, pl. 15, figs. 4, 5.

Lamprocyrtis neoheteroporos Kling. *Lamprocyrtis neoheteroporos* Kling, 1973, p. 639, pl. 5, figs. 17, 18, pl. 15, figs. 4, 5.

Lamprocyrtis nigriniae (Caulet). *Conarachnium nigriniae* Caulet, 1971, p. 3, pl. 3, figs. 1–4, pl. 4, figs. 1–4. *Lamprocyrtis nigriniae* (Caulet) *in* Kling, 1977, p. 217, pl. 1, fig. 17.

Liriospyris ovalis Goll, 1968, p. 1429, pl. 176, figs. 4, 6, 7; text-fig. 9.

Lithapium mitru (Ehrenberg) *Cornutella mitra* Ehrenberg, 1873, p. [illegible]; 1875, pl. 2, fig. 8. *Lithapium (?) mitra* (Ehrenberg) *in* Riedel and Sanfilippo, 1970, p. 520, pl. 4, figs. 6, 7.

Lithomelissa ehrenbergi Bütschli, 1882, p. 519, pl. 33, fig. 21.

?*Lithomelissa haeckeli* Bütschli, 1882, p. 519, pl. 33, fig. 23.

Lithomelissa ultima Caulet, 1979, p. 129, pl. 1, figs. 2, 3.

Lithomitrella acephala (Ehrenberg). *Eucyrtidium acephalum* Ehrenberg, 1875, p. 70, pl. 11, fig. 5. *Lithomitrella acephala* (Ehrenberg) *in* Petrushevskaya, 1979, p. 150, figs. 380, 409.

Lithomitrella elizabethae (Clark and Campbell) n. comb. *Lithomitra elizabethae* Clark and Campbell, 1942, p. 92, pl. 9, fig. 18.

Lithomitrella minuta (Clark and Campbell). *Lithocampe minuta* Clark and Campbell, 1942, p. 93, pl. 9, fig. 17. *Lithomitrella minuta* (Clark and Campbell) *in* Petrushevskaya, 1979, p. 154, figs. 412, 413, 478.

Lithopera neotera Sanfilippo and Riedel, 1970, p. 454, pl. 1, figs. 24–26, 28.

Lonchosphaera spicata Popofsky, 1908, p. 218, pl. 24, fig. 2, pl. 25, figs. 2, 7.

Lophocyrtis biaurita (Ehrenberg) gr. *Eucyrtidium biaurita* Ehrenberg, 1873, p. 226; 1875, pl. 70, pl. 10, fig. 7, 8. *Lophocyrtis biaurita* (Ehrenberg) *in* Foreman, 1973, p. 442, pl. 8, figs. 23–26.

Lophocyrtis (?) jacchia. Thyrsocyrtis jacchia Ehrenberg, 1873, p. 261; 1875, p. 84, pl. 12, fig. 7. *Lophocyrtis (?) jacchia* (Ehrenberg) *in* Riedel and Sanfilippo, 1970, p. 530; 1971, pl. 36, figs. 4, 5.

Lophophaena cylindrica (Cleve). *Dictyocephalus cylindricus* Cleve, 1900, p. 7, pl. 4, fig. 10. *Lophophaena cylindrica* (Cleve) *in* Petrushevskaya, 1971, p. 117, fig. 57, V; fig. 61, IV–VI.

Lophophaena hispida (Ehrenberg). *Dictyocephalus hispidus* Ehrenberg, 1872b, p. 289, pl. 5, fig. 18. *Lophophaena hispida* (Ehrenberg) *in* Petrushevskaya, 1971, p. 115, fig. 61, I–III.

Lychnocanium grande Campbell and Clark, 1944, p. 42, pl. 6, figs. 3–6.

Lychnocanium tripodium Ehrenberg, 1875, pl. 7, fig. 2.

Lychnocanoma amphitrite Foreman, 1973, p. 437, pl. 11, fig. 10.

Lychnocanoma babylonis (Clark and Campbell) gr. *Dictyophimus babylonis* Clark and Campbell, 1942, p. 67, pl. 9, figs. 32, 36. *Lychnocanoma babylonis* (Clark and Campbell) gr. *in* Foreman, 1973, p. 437, pl. 2, fig. 1.

Lychnocanoma bellum (Clark and Campbell). *Lychnocanium bellum* Clark and Campbell, 1942, p. 72, pl. 9, figs. 35, 39. *Lychnocanoma bellum* (Clark and Campbell) *in* Foreman, 1973, pl. 1, fig. 17, pl. 11, fig. 9.

Periphaena decora Ehrenberg, 1873, p. 246; 1875, pl. 28, fig. 6.

Periphaena heliasteriscus (Clark and Campbell). *Heliodiscus heliasteriscus* Clark and Campbell, 1942, p. 39, pl. 3, figs. 10, 11. *Periphaena heliasteriscus* (Clark and Campbell) *in* Sanfilippo and Riedel, 1973, p. 523, pl. 9, figs. 1–6, pl. 27, fig. 8.

Phormostichoartus corbula (Harting). *Lithocampe corbula* Harting, [illegible], p. 12, pl. 1, fig. 21. *Phormostichoartus corbula* (Harting) *in* Nigrini, 1977, p. 252, pl. 1, fig. 10.

Phormostichoartus doliolum (Riedel and Sanfilippo). *Artostrobium doliolum* Riedel and Sanfilippo, 1971, p. 1599, pl. 1H, figs. 1–3, pl. [illegible], figs. 14, 15. *Phormostichoartus doliolum* (Riedel and Sanfilippo) *in* Nigrini, 1977, p. 252, pl. 1, fig. 14.

Phormostichoartus fistula Nigrini, 1977, p. 153, pl. 1, figs. 11–13.

Phormostichoartus furcaspiculata (Popofsky) n. comb. *Lithamphora furcaspiculata* Popofsky, 1913, p. 408, text-figs. 138, 139.

Phormostichoartus marylandicus (Martin). *Lithocampe marylandica* Martin, 1904, p. 450, pl. 130, fig. 4. *Phormostichoartus marylandicus* (Martin) *in* Nigrini, 1977, p. 253, pl. 2, figs. 1–3.

Phormostichoartus multiseriatus (Ehrenberg) n. comb. *Eucyrticium multiseriatum* Ehrenberg, 1860, p. 768. *Lithocampe ? multiseriata* (Ehrenberg) *in* Petrushevskaya, 1967, p. 135, fig. 16, I–III.

Phormostichoartus platycephala (Ehrenberg) n. comb. *Eucyrtidium platycephalum* Ehrenberg, 1872b, pl. 3, fig. 16. *Lithocampe (?) platycephala* (Ehrenberg) *in* Petrushevskaya, 1967, p. 137, fig. 73, part; fig. 77, part.

Platybursa clathrobursa (Haeckel). *Tessarospyris clathrobursa* Haeckel, 1887, p. 1051, pl. 53, fig. 7. *Platybursa clathrobursa* (Haeckel) *in* Petrushevskaya, 1971, p. 259, fig. 130, II–V.

Prunopyle hayesi Chen, 1975, p. 454, pl. 9, figs. 3–5.

Prunopyle titan Campbell and Clark, 1944, p. 20, pl. 3, figs. 1–3.

Pseudocubus vema (Hays). *Helotholus vema* Hays, 1965, pl. 2, fig. 3, text-fig. A. *Pseudocubus vema* (Hays) *in* Petrushevskaya, 1971, p. 46, fig. 24, I–IV.

Pseudodictyophimus callosus (Petrushevskaya) n. comb. *Dictyophimus callosus* Petrushevskaya, 1979, p. 143, figs. 256, 257.

Pseudodictyophimus gracilipes (Bailey) gr. *Dictyophimus gracilipes* Bailey, 1856, p. 4, pl. 1, fig. 8. *Pseudodictyophimus gracilipes* (Bailey) *in* Petrushevskaya, 1971, p. 93, fig. 47–49.

Pterocanium prismatium Riedel, 1957, p. 87, pl. 3, figs. 4, 5.

Pterocanium trilobum (Haeckel). *Dictyopodium trilobum* Haeckel, 1860, p. 839; 1862, p. 340, pl. 8, figs. 6–10. *Pterocanium trilobum* (Haeckel) *in* Haeckel, 1887, p. 1333.

Pterocorys campanula campanula Haeckel. *Pterocorys campanula* Haeckel, 1887, p. 1316, pl. 71, fig. 3. *Pterocorys campanula campanula* Haeckel *in* Caulet, 1979, p. 133, pl. 3, figs. 3, 6.

Pterocorys campanula variabilis Caulet, 1979, p. 133, pl. 3, figs. 2, 5.

Pterocorys hertwigii (Haeckel). *Eucyrtidium hertwigii* Haeckel, 1887, p. 1491, pl. 80, fig. 12. *Pterocorys hertwigii* (Haeckel) *in* Nigrini, 1967, p. 73, pl. 7, figs. 4a, b.

Pterocorys zancleus (Müller). *Eucyrtidium zancleum* Müller, 1855, p. 492; 1858, p. 41, pl. 6, figs. 1–3. *Pterocorys zancleus* (Müller) *in* Petrushevskaya, 1971, p. 233, fig. 119, I–VII.

Pterocyrtidium barbadense (Ehrenberg) gr. *Pterocanium barbadense* Ehrenberg, 1873, p. 254; 1875, pl. 17, fig. 6. *Pterocyrtidium barbadense* (Ehrenberg) *in* Petrushevskaya, 1972, p. 352, pl. 27, figs. 18, 19.

Rhizosphaera antarcticum (Haeckel) n. comb. *Spongoplegma antarctica* Haeckel, 1887, p. 90.

Saccospyris antarctica Haecker, 1907, p. 124; 1908, p. 447, pl. 84, figs. 584, 589, 590.

Saccospyris preantarctica Petrushevskaya, 1975, p. 589, pl. 13, figs. 19, 20.

Siphocampe modeloensis (Campbell and Clark) n. comb. *Lithocampe modeloensis* Campbell and Clark, 1944, p. 59, pl. 7, figs. 28–30.

Siphostichartus corona (Haeckel). *Cyrtophormis (Acanthocyrtis) corona* Haeckel, 1887, p. 1462, pl. 77, fig. 15. *Siphostichartus corona* (Haeckel) *in* Nigrini, 1977, p. 257, pl. 2, figs. 5, 6, 7.

Solenosphaera omnitubus omnitubus Riedel and Sanfilippo, 1971, p. 1586, pl. 1A, fig. 24, pl. 4, figs. 1, 2.

Spirocyrtys gyroscalaris Nigrini, 1977, p. 258, pl. 2, figs. 10, 11.

Spirocyrtis scalaris Haeckel, 1887, p. 1509, pl. 76, fig. 14.

Spirocyrtis subscalaris Nigrini, 1977, p. 259, pl. 3, figs. 1, 2.

Spirocyrtis subtilis Petrushevskaya *in* Petrushevskaya and Koslova, 1972, p. 540, pl. 24, figs. 22–24.

Spongaster berminghami (Campbell and Clark). *Spongasteriscus berminghami* Campbell and Clark, 1944, p. 30, pl. 5, figs. 1, 2. *Spongaster berminghami* (Campbell and Clark) *in* Riedel and Sanfilippo, 1978, p. 73, pl. 2, figs. 14–16.

Spongaster pentas Riedel and Sanfilippo, 1970, p. 523, pl. 15, fig. 3.

Spongaster tetras Ehrenberg, 1860, p. 833.

Spongotrochus glacialis Popofsky, 1908, p. 228, pl. 26, fig. 8, pl. 27, fig. 1, pl. 28, fig. 2.

Stauroxiphos communis Carnevale, 1908, p. 15, pl. 2, fig. 9.

Stichocorys delmontensis (Campbell and Clark). *Eucyrtidium delmontense* Campbell and Clark, 1944, p. 56, pl. 7, figs. 19, 20. *Stichocorys delmontensis* (Campbell and Clark) *in* Sanfilippo and Riedel, 1970, p. 451, pl. 1, fig. 9.

Stichocorys peregrina (Riedel). *Eucyrtidium elongatum peregrinum* Riedel, 1953, p. 812, pl. 85, fig. 2. *Stichocorys peregrina* (Riedel) *in* Sanfilippo and Riedel, 1970, p. 451, pl. 1, fig. 10.

Stichopodium biconicum (Vinassa). *Lithocampe biconica* Vinassa, 1900, pl. 3, fig. 30. *Stichopodium biconicum* (Vinassa) *in* Petrushevskaya, 1975, p. 581, pl. 14, figs. 25–27, pl. 22, fig. 7.

Stichopodium calvertense (Martin). *Eucyrtidium calvertense* Martin, 1904, p. 450, pl. 130, fig. 5. *Stichopodium calvertense* (Martin) *in* Petrushevskaya and Kozlova, 1972, pl. 26, figs. 9, 10.

Stichopodium inflatum (Kling). *Eucyrtidium inflatum* Kling, 1973, p. 636, pl. 11, figs. 7, 8, pl. 15, fig. 7–10. *Stichopodium inflatum* (Kling) *in* Petrushevskaya, 1975, p. 581, pl. 26, figs. 7, 8.

Stylatractus universus Hays, 1970, p. 215, pl. 1, figs. 1, 2.

Stylosphaera angelina Campbell and Clark, 1944, p. 12, pl. 1, figs. 15, 20.

Stylosphaera minor Clark and Campbell, 1942, p. 27, pl. 5, figs. 1, 2.

Theocalyptra bicornis (Popofsky). *Pterocorys bicornis* Popofsky, 1908, p. 228, pl. 34, figs. 7, 8. *Theocalyptra bicornis* (Popofsky) *in* Riedel, 1958, p. 240, pl. 4, fig. 4.

Theocalyptra davisiana (Ehrenberg). *Cycladophora ? davisiana* Ehrenberg, 1861, p. 297. *Theocalyptra davisiana* (Ehrenberg) *in* Riedel, 1958, p. 239, pl. 4, figs. 2, 3, text-fig. 10.

Theocorys cretica (Ehrenberg) gr. *Eucyrtidium creticum* Ehrenberg, 1857, p. 559; 1872b, pl. 11, fig. 23. *Theocorys cretica* (Ehrenberg) *in* Haeckel, 1887, p. 1415.

Theocorys spongoconum (Kling). *Thecocorys spongoconus* Kling, 1971, pl. 5, fig. 6. *Theocorys spongoconum* Kling *in* Riedel and Sanfilippo, 1971, pl. 2F, fig. 4, pl. 3C, fig. 3.

Theocorythium vetulum Nigrini, 1971, p. 447, pl. 34.1, figs. 6a, 6b.

Thyrsocyrtis bromia Ehrenberg, 1873, p. 260; 1875, p. 84, pl. 12, fig. 2.

Triceraspyris antarctica (Haecker). *Phormospyris antarctica* Haecker, 1907, p. 124, fig. 9. *Triceraspyris antarctica* (Haecker) *in* Haecker, 1908, p. 445, pl. 84, fig. 586.

Tricolocapsa bergontiana (Carnevale) gr. n. comb. *Dictyocephalus bergontianum* Carnevale, 1908, p. 32, pl. 4, fig. 20.

Tricolospyris baconiana variabilis (Goll) n. comb. *Tholospyris baconiana variabilis* Goll, 1972, p. 452, pl. 8, figs. 1–8, pl. 9, figs. 1–12.

Tricolospyris newtoniana Haeckel, 1887, p. 1098, pl. 88, fig. 11.

Tripodiscinus clavipes (Clark and Campbell). *Tripilidium clavipes* Clark and Campbell, 1942, p. 64, pl. 9, fig. 29. *Tripodiscinus clavipes* (Clark and Campbell) *in* Petrushevskaya, 1979, p. 115, fig. 302.

Tristylospyris triceros (Ehrenberg). *Ceratospyris triceros* Ehrenberg, 1873, p. 220; 1875, pl. 21, fig. 5. *Tristylospyris triceros* (Ehrenberg) *in* Haeckel, 1887, p. 1033.

Velicucculus magnificum (Clark and Campbell). *Soreuma magnificum* Clark and Campbell, 1942, p. 51, pl. 4, fig. 15.

ACKNOWLEDGMENTS

Financial support for this study was provided by CNRS grant ATP no. 98.1012. The samples were kindly made available by the shipboard party. The author is much indebted to Catherine Nigrini who offered innumerable suggestions and kindly reviewed the structure of many sentences. Thanks are due to J. P. Kennett and F. M. Weaver for the critical review of the manuscript and to W. R. Riedel and A. Sanfilippo for informative discussions. The interest and support of Y. Lancelot and H. Chamley have also been of great value. A. Maurs, M. Destarac and A. Cambreleng assisted with photography and illustrations.

REFERENCES

Bailey, J. W., 1856. Notice of microscopic forms found in the soundings of the Sea of Kamtschatka—with a plate. *Am. J. Sci. Arts, Ser. 2*, 22:1–6.

Bjørklund, K. R., and Goll, R. M., 1979. Internal skeletal structures of *Collosphaera* and *Trisolenia*: a case of repetitive evolution in the Collosphaeridae (Radiolaria). *J. Paleontol.*, 53(no. 6):1293–1326.

Bütschli, O., 1882. Beiträge zur Kenntnis des Radiolarienskelette, insbesondere der Cyrtida. *Z. Wiss. Zool.*, 36:485–540.

Campbell, A. S., and Clark, B. L., 1944. *Miocene Radiolarian Faunas from Southern California*. Geol. Soc. Am., Spec. Pap. No. 51.

Carnevale, P., 1908. Radiolarie e Silicoflagellati di Bergonzano (Reggio Emilia). *Mem. R. Ist. Veneto Sci. Lett. Arti*, 28(no. 3):1–46.

Caulet, J. P., 1971. Contribution à l'étude de quelques radiolaires nassellaires des boues de la Méditerranée et du Pacifique. *Cah. Micropaléontol., Ser. 2*, 10:1–10.

________, 1977. La silice biogène dans les sédiments néogènes et quaternaires de l'océan indien austral. *Bull. Soc. Geol. France*, 19(no. 5):1021–1032.

________, 1979. Les dépôts à Radiolaires d'âge pliocène supérieur à pléistocène dans l'océan indien central: nouvelle zonation biostratigraphique. *Recherches Océanographiques dans l'Océan Indien. Paris 20-22 Juin 1977. Mem. Mus. Nat. Hist. Nat. Ser. C*, 43:119–141.

________, 1982. Faunes de radiolaires et fluctuations climatiques dans les sédiments de l'océan indien austral: une nouvelle biozonation. *Bull. Soc. Geol. France*, 24(no. 3):555–562.

Chen, P.-H., 1975. Antarctic radiolaria. *In* Hayes, D. E., Frakes, L. A., et al., *Init. Repts. DSDP*, 28: Washington (U.S. Govt. Printing Office), 437–513.

Clark, B. L., and Campbell, A. S., 1942. *Eocene Radiolarian Faunas from the Monte Diablo Area, California*. Geol. Soc. Am. Spec. Pap. No. 39.

Cleve, P. T., 1900. Notes on some Atlantic plankton-organisms. *Handl. Kgl. Svenska Vetensk.-Akad.*, 34(no. 1):1–22.

Dumitrica, P., 1973. Cretaceous and Quaternary Radiolaria in deep sea sediments from the northeast Atlantic Ocean and Mediterranean Sea. *In* Ryan, W. B. F., Hsü, K. J., et al., *Init. Repts. DSDP*, 13, Pt. 2: Washington (U.S. Govt. Printing Office), 829–901.

Ehrenberg, C. G., 1840. (Characteristik von 274 neuen Arten von Infusorien). Uber die auffalend rasche Entwicklung dieser Kenntnisse. *K. Preuss. Akad. Wiss. Berlin, Ber.*, 1840:197–219.

________, 1844a. Einige vorläufige Resultate seiner Untersuchungen der ihm von der Südpolreise des Capitain Ross, so wie von den Herren Schayer und Darwin zugekommen Materialen über das Verhalten des kleinsten Lebens in den Oceanen und den grössten bisher zugänglichen Tiefen des Weltmeeres. *K. Preuss. Akad. Wiss. Berlin, Monatsber.*, 1844:182–207.

________, 1844b. Uber 2 neue Lager von Gebirgsmassen aus Infusorien als Meeres-Absatz in Nord-Amerika und eine Vergleichung derselben mit den organischen Kreide-Gebilden in Europa und Afrika. *K. Preuss. Akad. Wiss. Berlin, Ber.*, 1844:57–97.

________, 1847. Uber die mikroskopischen kieselschaligen Polycystinen als mächtige Gebirgsmasse von Barbados und über das Verhältniss der aus mehr als 300 neuen Arten bestehenden ganz eigenthümlichen Formengruppe jener Felsmasse zu den jetzt legenden Thieren und zur Kriedebildung eine eue Anregung zur Erforschung des Erdlebens. *K. Preuss. Akad. Wiss. Berlin, Ber.*, 1847:40–60.

________, 1854a. Die systematische Charakteristik der neuen mikroskopischen Organismen des tiefen atlantischen Oceans. *K. Preuss. Akad. Wiss. Berlin*, 1854:236–250.

________, 1854b. *Mikrogeologie:* Leipzig (Leopold Voss).

________, 1854c. Uber das organische Leben des Meeresgrundes in bis 10800 und 12000 Fuss Tiefe. *K. Preuss. Akad. Wiss. Berlin, Monatsber.*, 1854:54–75.

________, 1857. Uber die organischen Lebensformen in unezwartet grossen Tiefen des Mittelmeeres. *K. Preuss. Akad. Wiss. Berlin, Monatsber.*, 1857:538–570.

________, 1860. Uber den Tiefgrund des stillen Oceans zwischen Californien und den Sandwich-Inseln aus bis 15600 Tief nach Lieut. Brooke. *K. Preuss. Akad. Wiss. Berlin, Monatsber.*, 1860:819–833.

________, 1861, Uber die Tiefgrund-Verhältnisse des Oceans am Einegange des Davisstrasse und bei Island. *K. Preuss. Akad. Wiss. Berlin, Monatsber.*, 1861:275–315.

________, 1872a. Mikrogeologischen Studien als Zusammenfassung der Beobachtungen des kleinsten Lebens des Meeres-Tiefgrunde aller Zonen und dessen geologischen Einfluss. *K. Preuss. Akad. Wiss. Berlin, Monatsber.*, 1872:265–322.

________, 1872b. Mikrogeologischen Studien über das kleinste Leben der Meeres-Tiefgrunde aller Zonen und dessen geologischen Einfluss. *K. Preuss. Akad. Wiss. Berlin, Abhandl.*, 1872:131–399.

________, 1873. Grössere Felsproben des Polycystinen-Mergels von Barbados mit weiteren Erläuterungen. *K. Preuss. Akad. Wiss. Berlin, Monatsber.*, 1873:213–263.

________, 1875. Fortsetzung der mikrogeologischen Studien als Gesammt-Uebersicht der mikroskopischen Paläeontologie gleichartig analysirter Gebirgsarten der Erde, mit specieller Rücksicht auf den Polycystinen-Mergel von Barbados. *K. Preuss. Akad. Wiss. Berlin, Abhandl.*, 1875:1–226.

Foreman, H. P., 1973. Radiolaria of Leg 10 with systematics and ranges for the families Amphypindacidae, Artostrobiidae, and Theoperidae. *In* Worzel, J. L., Bryant, W., et al., *Init. Repts. DSDP*, 10: Washington (U.S. Govt. Printing Office), 407–474.

Goll, R. M., 1968. Classification and phylogeny of Cenozoic Trissocyclidae (Radiolaria) in the Pacific and Caribbean basins. Part I. *J. Paleontol.*, 42(no. 6):1409–1432.

________, 1969. Classification and phylogeny of Cenozoic Trissocyclidae (Radiolaria) in the Pacific and Caribbean Basins. *J. Paleontol.*, 43(no. 2):322–339.

________, 1972. Systematics of eight *Tholospyris* taxa (Trissocyclidae, Radiolaria). *Micropaleontology*, 18(no. 4):443–475.

Haeckel, E., 1860. Abbildungen und Diagnosen neuer Gattungen und Arten von lebenden Radiolarien des Mittelmeeres. *K. Preuss. Akad. Wiss. Berlin, Monatsber.*, 1860:835–845.

_______, 1862. *Die Radiolarien (Rhizopoda Radiolaria):* Berlin (Reimer).

_______, 1887. *Report on the Radiolaria collected by H.M.S.* Challenger *during the Years 1873–1876. Report on the Scientific Results of the Voyage of H.M.S.* Challenger. *Zoology* (Vol. 18).

Haecker, V., 1907. Altertümlich Sphärellarien und Cyrtellarien aus grossen Meerestiefen. *Archiv. Protistenk.*, 10:114–126.

_______, 1908. Tiefsee-Radiolarien. Spezieller Teil, Lfg. 2. Die Tripyleen, Collodarien und Mikroradiolarien der Tiefsee. *Wiss. Ergebn. D. Tiefsee Exped. ("Valdivia")*, 14:337–476.

Harting, P., 1863. Bijdrage tot de kennis der mikroskopische faune en flora van de Banda-Zee. *Verh. K. Akad. Wetensh. Amsterdam*, 10: 1–34.

Hays, J. D., 1965. Radiolaria and late Tertiary and Quaternary history of Antarctic Seas. *Biology of Antarctic Seas II.* Am. Geophys. Un., Antarc. Res. Ser., 5:125–184.

_______, 1970. Stratigraphy and evolutionary trends of Radiolaria in North Pacific deep-sea sediments. *Geol. Soc. Am. Mem.*, 126: 185–218.

Johnson, D. A., 1974. Radiolaria from the eastern Indian Ocean, DSDP Leg 22. *In* von der Borch, C. C., Sclater, J. G., et al., *Init. Repts. DSDP*, 22: Washington (U.S. Govt. Printing Office), 521–575.

Johnson, T. C., 1975. The dissolution of siliceous microfossils in deep-sea sediments [Ph.D. dissert.]. University of California, San Diego.

Jørgensen, E., 1900. Protophyten und Protozoen im Plankton aus der norwegischen Westküste. *Bergens Museums Aarbog. (1899)*, no. 2, (no.6):1–112.

_______, 1905. The protist plankton and the diatoms in bottom samples. *Bergens Mus. Skr.*, pp. 49–151, 195–225.

Kling, S. A., 1971. Radiolaria. Leg 6 of the Deep Sea Drilling Project. *In* Fischer, A. G., Heezen, B. C., et al., *Init. Repts. DSDP*, 6: Washington (U.S. Govt. Printing Office), 1069–1117.

_______, 1973. Radiolaria from the eastern North Pacific, Deep Sea Drilling Project Leg 18: *In* Klum, L. D., von Huene, R., et al., *Init. Repts. DSDP*, 18: Washington (U.S. Govt. Printing Office), 617–671.

_______, 1977. Local and reigonal imprints on radiolarian assemblages from California coastal basin sediments. *Mar. Micropaleontol.*, 2(no. 2):207–221.

Knoll, A. H., and Johnson, D. A., 1975. late Pleistocene evolution of the collosphaerid radiolarian *Buccinosphaera invaginata* Haeckel. *Micropaleontology*, 21(no. 1):60–68.

Martin, G. C., 1904. *Radiolaria:* Baltimore (Maryland Geological Survey and John Hopkins Press).

Maurrasse, F., and Glass, B., 1976. Radiolarian stratigraphy and North American microtektites in Caribbean RC9-58: implications concerning late Eocene radiolarian chronology and the age of the Eocene-Oligocene boundary. *Publ. de la VII Conf. Géol. des Caraibes (30 Juin au 12 Juillet 1974), Cayenne*, pp. 205–212.

Moore, T. C., Jr., 1972. Mid-tertiary evolution of the radiolarian genus, *Calocycletta. Micropaleontology*, 18(no. 2):244–252.

Müller, J., 1855. Uber Sphaerozoum und Thallassicolla. *K. Preuss. Akad. Wiss. Berlin, Monatsber.*, 1855:229–253.

_______, 1858. Uber die Thalassicollen, Polycystinen und Acanthometren des Mittelmeeres. *K. Preuss. Akad. Wiss. Berlin, Abhandl.*, 1858:1–62.

Nakaseko, K., 1963. Neogene Cyrtoidea (Radiolaria) from the Isozaki Formation in Ibaraki Prefecture, Japan. *Sci. Rep. Coll. Gen. Ed., Osaka Univ.*, 12(no. 2):165–198.

Nigrini, C. A., 1967. *Radiolaria in Pelagic Sediments from the Indian and Atlantic Oceans.* Bull. Scripps Inst. Oceanogr., 11.

_______, 1971. Radiolarian zones in the Quaternary of the equatorial Pacific Ocean. *In* Funnell, B. M., and Riedel, W. R. (Eds.), *The Micropaleontology of Oceans:* Cambridge (Cambridge University Press), pp. 443–461.

_______, 1977. Tropical Cenozoic Artostrobiidae (Radiolaria). *Micropaleontology*, 23(no. 3):241–269.

Nigrini, C. A., and Moore, T. C., Jr., 1979. *A Guide to Modern Radiolaria.* Cushman Found. Foraminiferal Res. Spec. Publ., 16.

Petrushevskaya, M. G., 1965. Osobennosti i konstruktsii skeleta radiolaryii Botryoidae (otr. Nassellaria). *Trudy Zool. Inst.*, 35:79–118.

_______, 1967. Radiolarii otryadov spumellaria i nassellaria antarkticheskoi oblasti (po materialam sovetsko, antarkticheskoi ekspeditsii). *Issled. Fauny. morei*, 4(12). *Resultaty Biol. Issled. Sovetskoi Antarktic Eksped. (1950–1958), vyp. 3.*

_______, 1971. Radiolarians of the ocean. *Explorations of the Fauna of the Seas*, 9(17), Acad. Sci. USSR, Zool. Inst., Leningrad, 1971. (In Russian.)

_______, 1972. Biostratigraphy of deep-sea Quaternary sediments based on the radiolarian analysis data. *Okeanologia*, 12:71–86.

_______, 1975. Cenozoic radiolarians of the Antarctic, Leg 29, DSDP. *In* Kennett, J. P., Houtz, R. E., et al., *Init. Repts. DSDP*, 29: Washington (U.S. Govt. Printing Office), 541–675

_______, 1979. The history of the microplankton of the Norwegian Sea. *Explorations of the Fauna of the Seas*, 23(31), Acad. Sci USSR, Zool. Inst. Leningrad, 1979. (In Russian.)

Petrushevskaya, M. G., and Koslova, G. E., 1972. Radiolaria: Leg 14, Deep Sea Drilling Project. *In* Hayes, D. E., Pimm, A. C., et al., *Init. Repts. DSDP*, 14: Washington (U.S. Govt. Printing Office), 495–648.

Popofsky, A., 1908. Die Radiolarien der Antarktis (mit Ausnahme der Tripyleen). *D. Süd-Polar Exped. 1901–1903, Rept.* 10 (Zool., Vol. 2) (pt. 3):183–305.

_______, 1913. Die Nassellarien des Warmwassergebietes. *D. Südpolar-Exped. 1901–1903, Rept.*, 14(Zool., Vol. 6)(no.1):217–416.

Riedel, W. R., 1953. Mesozoic and late Tertiary Radiolaria of Rotti. *J. Paleontol.* 27(no. 6):805–813.

_______, 1957. Radiolaria. A preliminary stratigraphy. *Repts. Swed. Deep-Sea Exped. 1947–1948*, 6(no. 3):59–96.

_______, 1958. Radiolaria in antarctic sediments. *Repts. B.A.N.Z. Antarctic Res. Exped., Ser. B*, 6(10):217–255.

_______, 1959. Oligocene and lower Miocene Radiolaria in tropical Pacific sediments. *Micropaleontology*, 5(no. 3):285–302.

_______, 1967. Subclass Radiolaria. *In* Harland, W. B., et al. (Eds.), *The Fossil Record:* London (Geol. Soc. London), pp. 291–298.

Riedel, W. R., and Sanfilippo, A., 1970. Radiolaria, Leg 4, Deep Sea Drilling Project. *In* Bader, R. G., Gerard, R. D., et al., *Init. Repts. DSDP*, 4: Washington (U.S. Govt. Printing Office), 503–575.

_______, 1971. Cenozoic Radiolaria from the western tropical Pacific, Leg 7. *In* Winterer, E. L., Riedel, W. R., et al., *Init. Repts. DSDP*, 7, Pt. 2: Washington (U.S. Govt. Printing Office), 1529–1672.

_______, 1978. Stratigraphy and evolution of tropical Cenozoic radiolarians. *Micropaleontology*, 24(no. 1):61–96.

Riedel, W. R., Sanfilippo, A., and Cita, M. B., 1974. Radiolarians from the stratotype Zanclean (Lower Pliocene, Sicily). *Rev. Ital. Paleontol. Stratigr.*, 80(no. 4):699–734.

Riedel, W. R., and Westberg, J., 1982. Neogene radiolarians from the eastern tropical Pacific and Caribbean, DSDP Leg 68. *In* Prell, W. L., Gardner, J. V., et al., *Init. Repts. DSDP*, 68: Washington (U.S. Govt. Printing Office), 289–300.

Sanfilippo, A., and Riedel, W. R., 1970. Post-Eocene "closed" theoperid radiolarians. *Micropaleontology*, 16(no. 4):446–462.

_______, 1973. Cenozoic Radiolaria (exclusive of Theoperids, Artostrobiids and Amphipyndacids) from the Gulf of Mexico, DSDP Leg 10. *In* Worzel, J. L., Bryant, W., et al., *Init. Repts. DSDP*, 10: Washington (U.S. Govt. Printing Office), 475–612.

_______, 1980. A revised generic and suprageneric classification of the Artiscins (Radiolaria). *J. Paleontol.*, 54(no. 5):1008–1011.

Sanfilippo, A., Burckle, L. H., Martini, E., and Riedel, W. R., 1973. Radiolarians, diatoms, silicoflagellates and calcareous nannofossils in the Mediterranean Neogene. *Micropaleontology*, 19(no. 2): 209–234.

Saunders, J. B., Bernoulli, D., Müller-Merz, E., Oberhänsli, H., Perch-Nielsen, K., Riedel, W. R., Sanfilippo, A., and Torrini, R., Jr., in press. Stratigraphy of the late-middle Eocene to early Oligocene in the Bath Cliff section, Barbados, West Indies. *Micropaleontology.*

Stöhr, E., 1880. Die Radiolarienfauna der Tripoli von Grotte, Provinz Girgenti in Sicilien. *Palaeontographica*, 26(ser. 3, vol. 2):71–124.

Vinassa de Regny, P., 1900. Radiolari miocenici italiani. *Mem. R. Acad. Sci. Ist. Bologna Ser. 5*, 8:227–257.

Weaver, F. M., 1983. Cenozoic radiolarians from the southwest Atlantic, Falkland Plateau region, Deep Sea Drilling Project Leg 71. *In* Ludwig, W. J., Krasheninnikov, V. A., et al., *Init. Repts. DSDP*, 71, Pt. 2: Washington (U.S. Govt. Printing Office), 667–686.

Westberg, M. J., and Riedel, W. R., 1982. Radiolarians from the Middle America trench off Guatemala, Deep Sea Drilling Project Leg 67. *In* Aubouin, J., von Huene, R., et al., *Init. Repts. DSDP*, 67: Washington (U.S. Govt. Printing Office), 501–424.

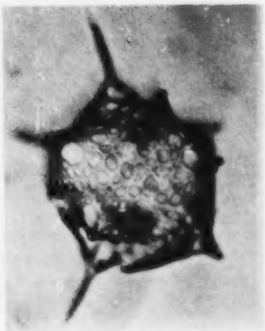
1

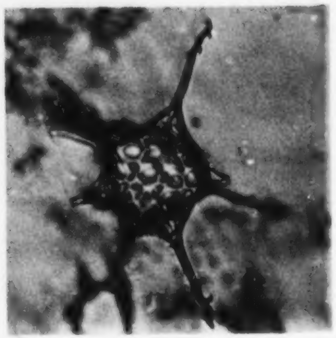
2

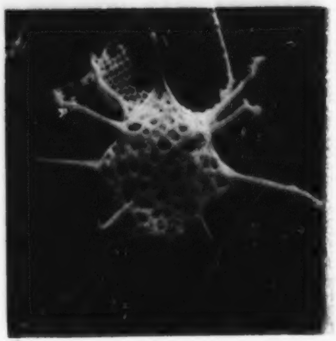
3

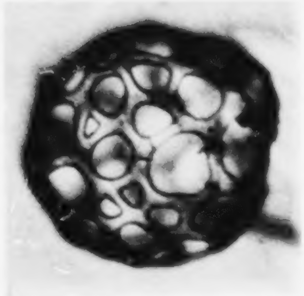
4

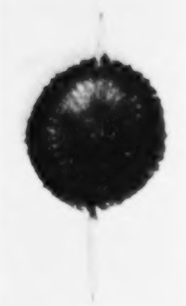
5

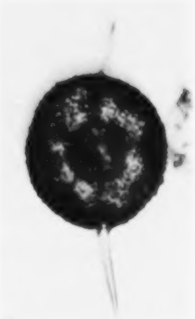
6

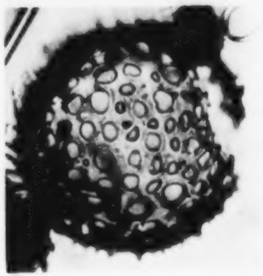
7

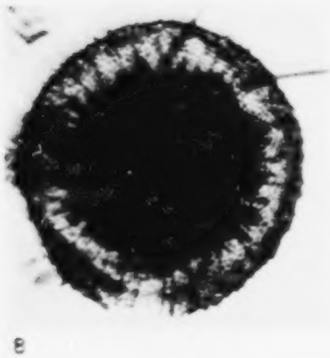
8

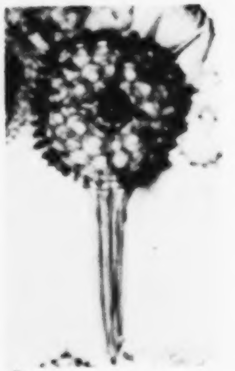
9

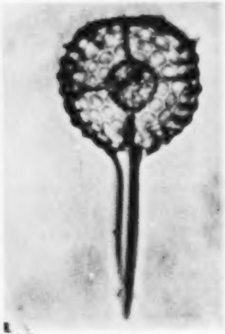
10

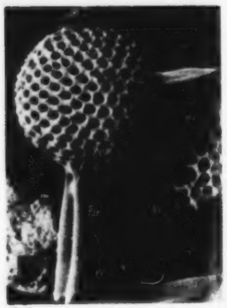
11

Plate 1. 1. *Acrosphaera spinosa fasciculopora*, holotype, Sample 586B-20-3, 60–62 cm; × 250. **2–3.** *Acrosphaera spinosa hamospina*, (2) holotype, Sample 586B-23-3, 60–62 cm; × 200; (3) Sample MD 77157-VII-0, 70 cm; × 200. **4.** *Collosphaera polygona* group, Sample 594-51-1, 84–86 cm; × 400. **5–6.** *Stylatractus* aff. *universus*, (5) Sample 594-29-4, 84–86 cm; × 270; (6) Sample 594-31-4, 84–86 cm; × 270. **7.** *Polysolenia murrayana* group, Sample 594-37-1, 84–86 cm; × 230. **8.** *Spongodiscus* sp., Sample 594-28-1, 84–86 cm; × 200. **9–11.** *Axoprunum(?) monostylum*, (9) holotype, Sample 586B-5-4, 60–62 cm; × 250; (10) Sample 586B-4-6, 60–62 cm; × 250; (11) Langhian, Spain, Sample 69-34; × 2[illegible].

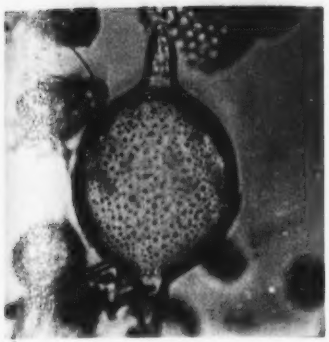
1

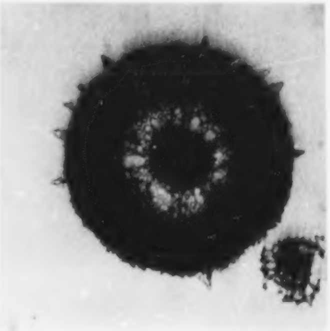
2

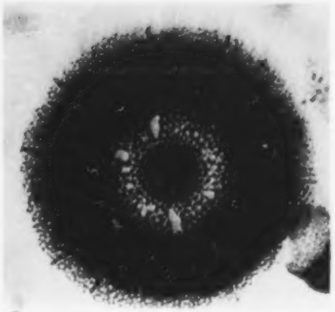
3

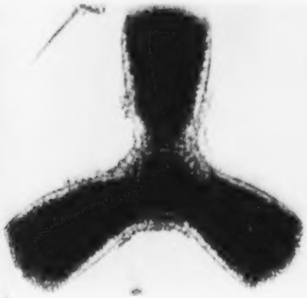
4

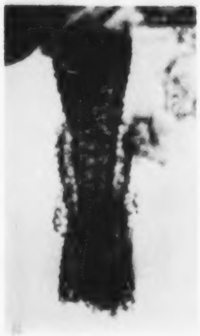
5

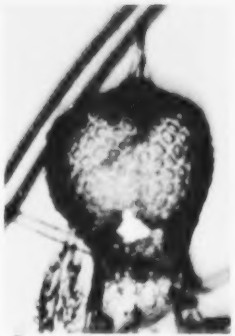
6

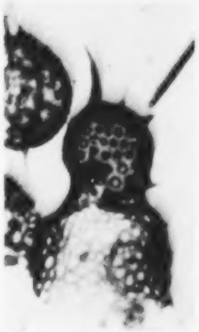
7

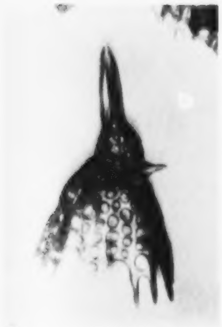
8

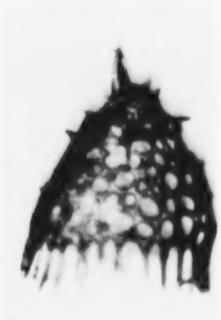
9

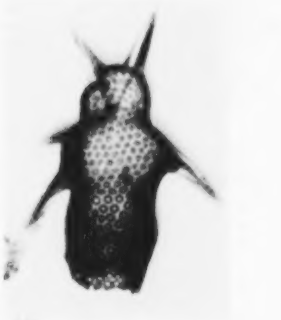
10

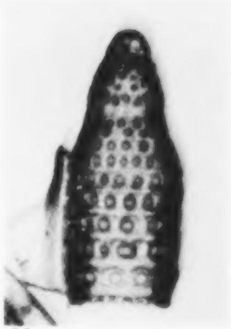
11

Pla[illegible] **1.** *Siphonosphaera hyalina*, holotype, Sample 586B-6-3, 60–62 cm; ×300. **2–3.** *Spongodiscus klingi*, (2) Sample 586B-18-1, 60–62 cm; [illegible]. (3) holotype, Sample 586B-19-3, 60–62 cm; ×200. **4.** *Rhopalastrum oracutibrachium*, holotype, Sample 586B-23-5, 60–62 cm; [illegible]. **5.** *Tessarastrum* sp., Sample MD 81481-III-24 cm; ×200. **6.** *Lithomelissa* sp., Sample 592-40-4, 40–42 cm; ×300. **7.** *Lithomelissa* [illegible]*bergi*, Sample 594-52-2, 84–86 cm; ×280. **8.** *Pseudodictyophimus* sp., Sample 594-41-2, 84–86 cm; ×250. **9.** *Ceratocyrtis* sp., Sample [illegible]2-2, 84–86 cm; ×320. **10.** *Nasselaria* gen. et sp. indet., Sample 594-49-1, 84–86 cm; ×300. **11.** *Siphocampe*(?), Sample 594-48-2, 84–86 [illegible] ×500.

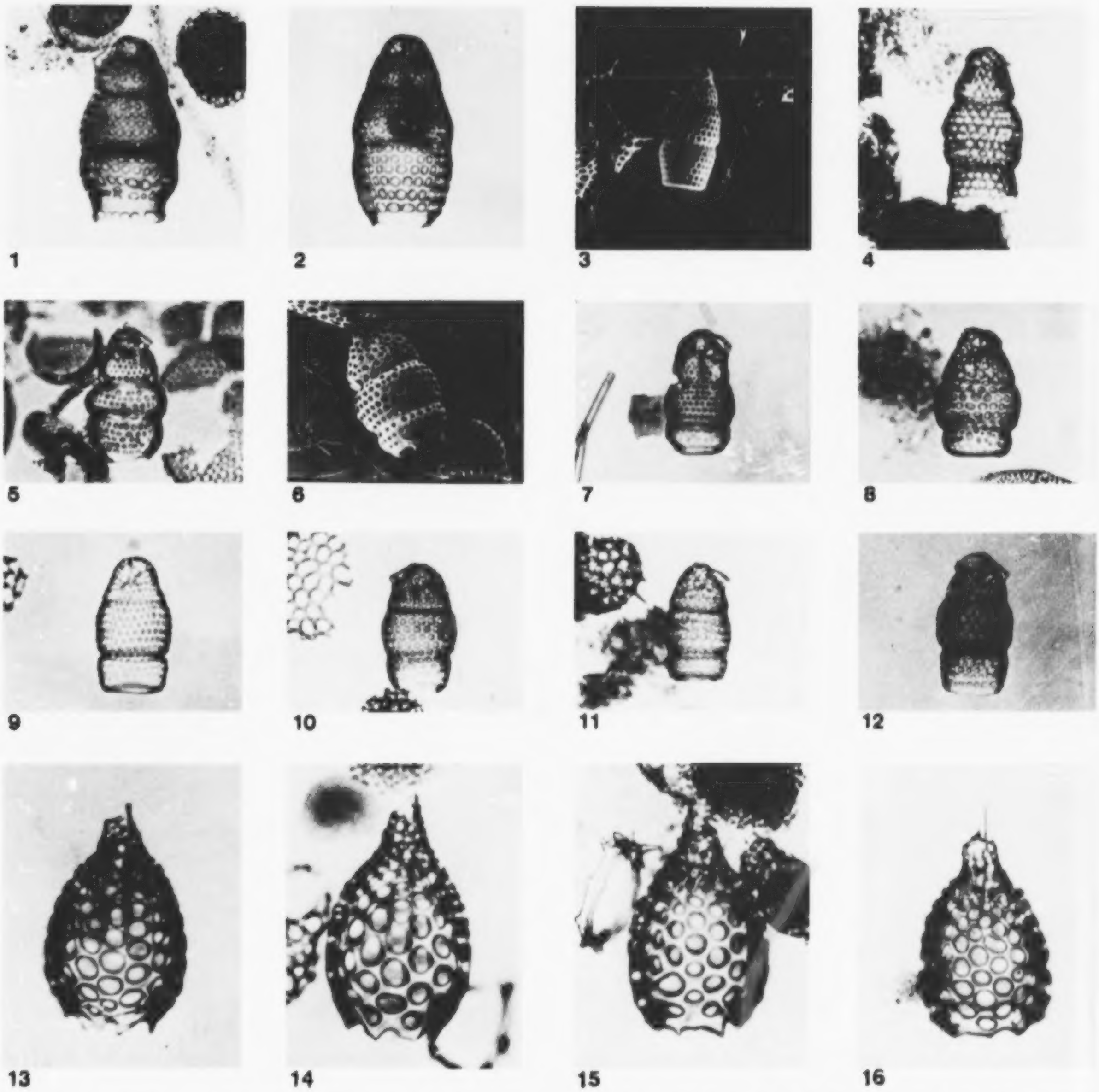

Plate 3. (Figs. 1-12 ×270; Figs. 13-16 ×310.) **1, 2.** ***Phormostichoartus(?) fistula***, (1) Sample 594-52-2, 84-86 cm; (2) Sample 594-30-4, 4-86 cm. **3, 4, 9, 10, 12.** ***Phormostichoartus pitomorphus***, (3) Sample "Valdivia" 62; (4) Sample 594-9-4, 84-86 cm; (9) Sample 586B-8-3, 0-62 cm, (10) Sample MD 75072-VIII-60 cm; (12) holotype, Sample MD 75072-VI-100 cm. **5, 6.** ***Phormostichoartus platycephala***, (5) Messini n, Spain, Sample 76285; (6) Sample MD 75072-IX-100 cm. **7, 8, 11.** ***Phormostichoartus pitomorphus–P. platycephala***, (7) Sample MD 8350 V-45 cm; (8) Sample MD 75075-X-48 cm; (11) Sample MD 75075-IX-140 cm. **13–16.** ***Lamprocyrtis daniellae***, (13) Sample 586B-15-3, 60–62 m; (14) holotype, Sample 586B-16-1, 60–62 cm, (15) Sample 586B-16-1, 60–62 cm; (16) Sample 586B-16-1, 60–62 cm.

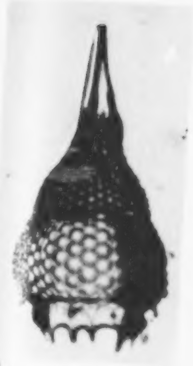
1

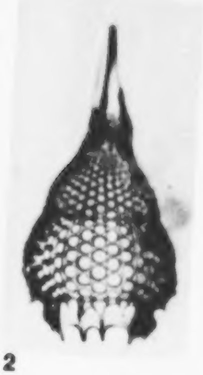
2

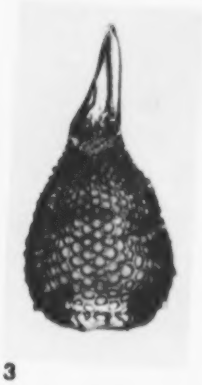
3

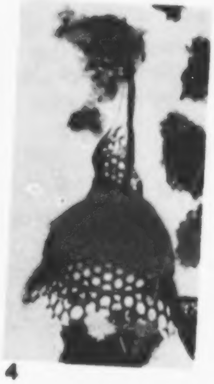
4

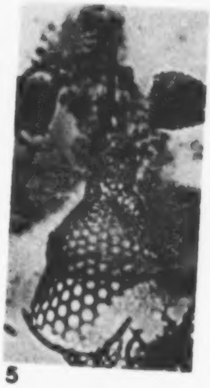
5

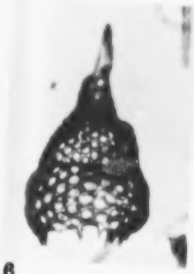
6

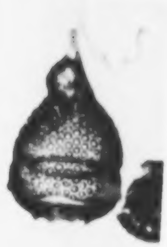
7

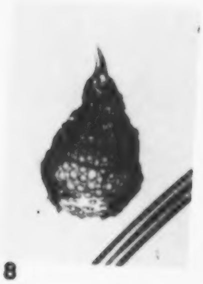
8

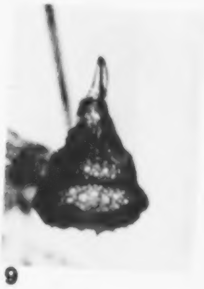
9

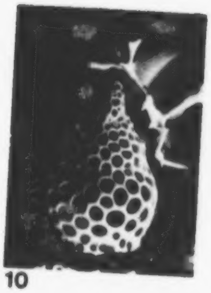
10

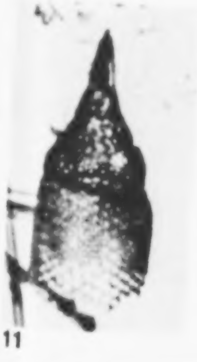
11

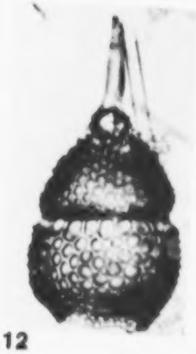
12

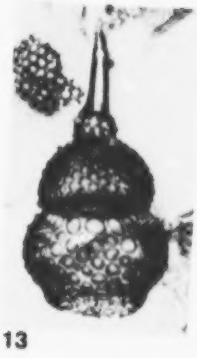
13

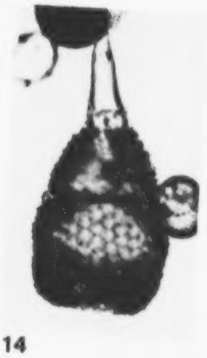
14

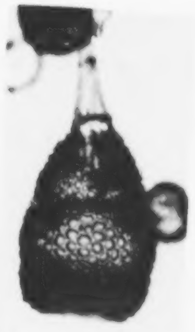
15

Plate 4. (Figs. 1–10 × 230.) **1, 2.** *Lamprocyclas* aff. *maritalis*, (1) Sample 594-29-4, 84–86 cm; (2) Sample 594-29-4, 84–86 cm. **3.** *Lamprocyclas margatensis*, Sample 586B-16-3, 60–62 cm. **4, 5.** *Pterocorys longicollis*, (4) holotype, Sample 586B-6-2, 60–62 cm; (5) Sample 586B-6-2, 60–6 cm. **6.** *Lamprocyclas* sp., Sample 594-41-2, 84–86 cm. **7.** *Lamprocyclas* sp., Sample 594-52-2, 84–86 cm. **8.** *Lamprocyclas* sp., Sample 5 4-29-4, 84–86 cm. **9.** *Lamprocyclas* sp., Sample 594-30-4, 84–86 cm. **10.** *Lamprocyclas junonis*, Sample "Valdivia" 62. **11.** *Pterocorys* s., Sample 592-40-2, 40–42 cm; × 300. **12, 13.** ?*Lophocyrtis* sp., Sample 592-40-1, 40–42 cm; × 200. **14, 15.** ?*Thyrsocyrtis* sp., Sample 592-3 -3, 40–42 cm; × 100.

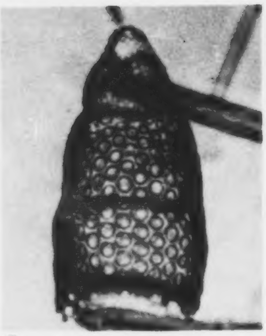
1

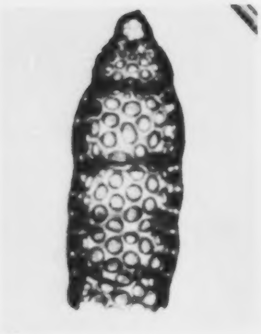
2

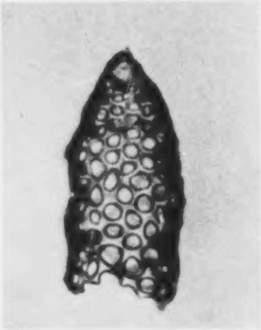
3

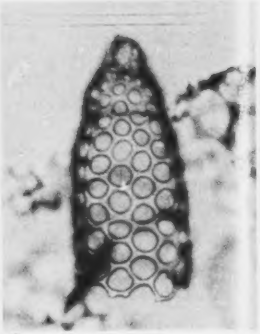
4

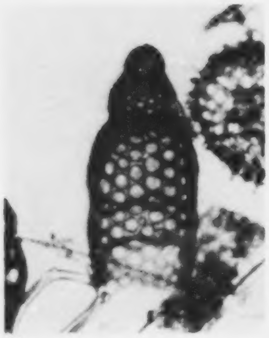
5

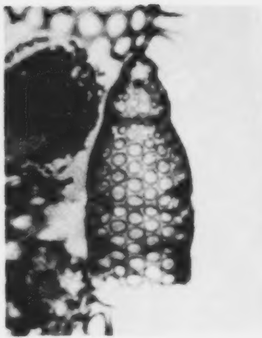
6

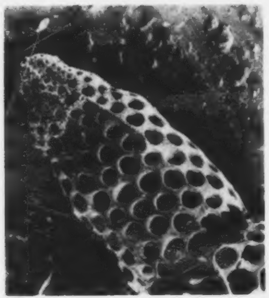
7

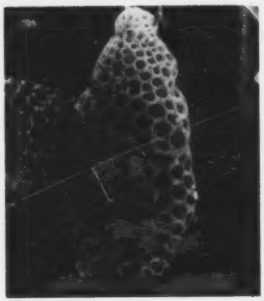
8

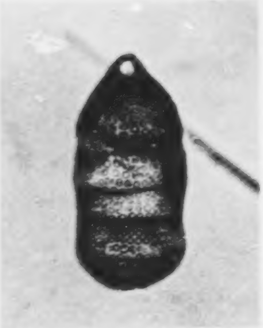
9

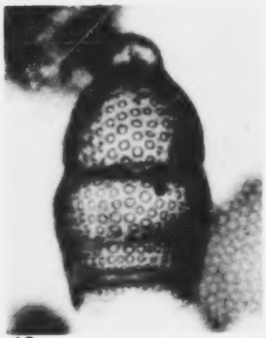
10

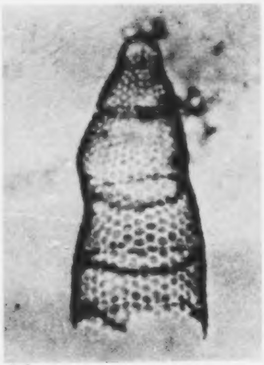
11

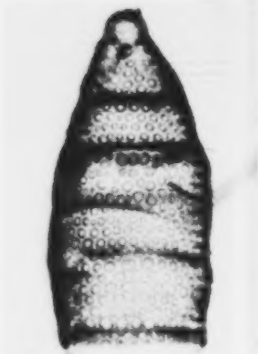
12

Plate 5. (All Figures × 380.) **1-3.** *Eucyrtidium* ? *teuscheri* gr., (1) Sample 594-52-1, 84-86 cm; (2) Sample 594-41-2, 84-86 cm; (3) Sample 52-6-3, 20-21 cm. **4.** *Eucyrtidium teuscheri orthoporus*, holotype, Sample MD 73028-II-30 cm. **5-8.** *Eucyrtidium teuscheri teuscheri*, (5) Sample MD 75072-VIII-111 cm; (6) holotype, Sample MD 75071-V-100 cm; (7) Sample MD 75072-IX-100 cm; (8) Sample MD 75072-II-60 cm. **9.** *Eucyrtidium punctatum*, Sample MD AET 75002-70 cm. **10.** *Eucyrtidium anniae*, holotype, Sample 594-31-4, 84-86 cm. **11.** *Eucyrtidium indiensis*, Sample 586B-15-1, 60-62 cm. **12.** *Eucyrtidium* sp., Sample 594-38-1, 84-86 cm.

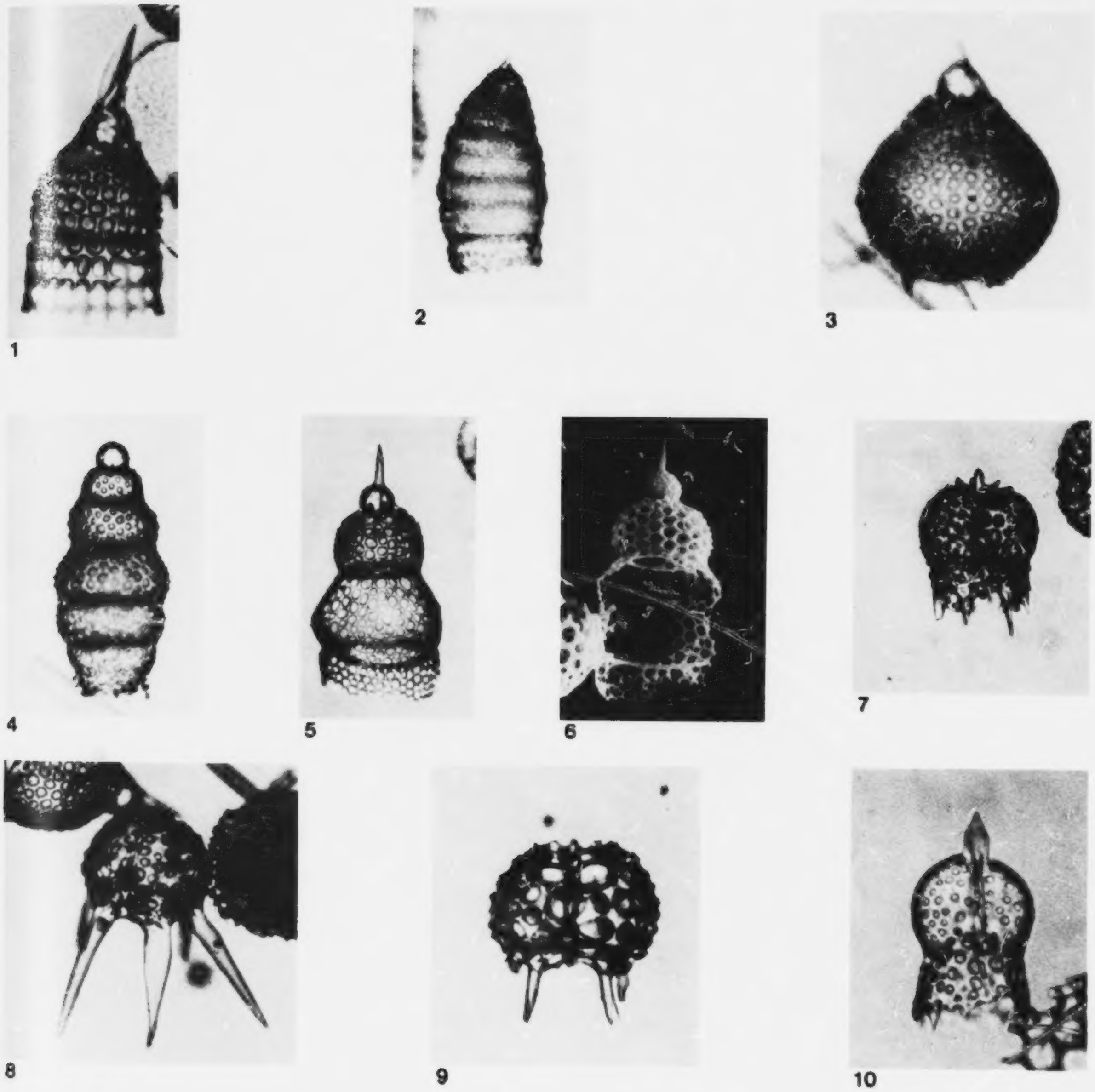

Plate [illegible] **1.** *Clathrocyclas* sp., Sample 592-39-3, 40–42 cm; ×450. 2. *Botryostrobus* sp., Sample 594-48-2, 84–86 cm; ×530. **3.** ?*Theocorys* sp., Sample 592-39-3, 40–42 cm; ×270. **4.** *Stichocorys peregrina*, Sample 594-24-4, 84–86 cm; ×400. **5, 6.** *Stichocorys johnsoni*, (5) holotype, Sample 586B-20-5, 60–62 cm; ×400; (6) Sample MD 77157-VI-20 cm; ×400. **7–10.** Acanthodesmiidae gen. et sp. indet., Sample 592-39-3, 40–42 cm; ×350.

15. MIDDLE MIOCENE TO QUATERNARY DIATOM BIOSTRATIGRAPHY OF DEEP SEA DRILLING PROJECT SITE 594, CHATHAM RISE, SOUTHWEST PACIFIC[1]

Paul F. Ciesielski, University of Florida[2]

ABSTRACT

A diatom biostratigraphy is presented for middle Miocene through Quaternary sediments recovered from the Chatham Rise east of New Zealand's South Island. The upper 590 m of the 639.5-m composite-section Site 594 represents approximately 16 m.y. and is characterized by moderately to very poorly preserved diatoms of antarctic to temperate affinity. Pliocene through Quaternary assemblages are poorly preserved and dominated by antarctic-subantarctic species which provide detailed biostratigraphic control. Recognized are 11 of 14 zones of the middle upper Miocene to Quaternary Neogene Southern Ocean diatom zonation (NSD 7–NSD 20) of Ciesielski (1983; this chapter).

Four Neogene Southern Ocean diatom zones (NSD 3–NSD 6) are recognized in the lower middle Miocene to middle upper Miocene of Site 594. Assemblages of this interval have a mixed high-latitude and temperate affinity; however, poor preservation limits correlation to high- and temperate-latitude zonal schemes.

Neogene North Pacific diatom zones and subzones of NNPD 3 through NNPD 5 (Barron, in press, b) are correlated to Neogene Southern Ocean diatom zones NSD 3 through NSD 7: the upper portions of the *Actinocyclus ingens* Zone (NNPD 3) is correlative to the upper *Nitzschia maleinterpretaria* Zone (NSD 3); the *Denticulopsis lauta* Zone (NNPD 4) and Subzones a and b are correlative to the lower *Coscinodiscus lewisianus* Zone (NSD 4); and the *D. hustedtii–D. lauta* Zone (NNPD 5) and its Subzones a through d encompass the upper *C. lewisianus* Zone (NSD 4), *N. grossepunctata* Zone (NSD 5), *N. denticuloides* Zone (NSD 6), and the lower *D. hustedtii–D. lauta* Zone (NSD 7).

A major disconformity spans the late Gilbert to early Gauss Chron (3.9–2.8 Ma). A second disconformity brackets the Miocene/Pliocene boundary; the section missing covers late Chron 5 and the early Gilbert chron (5.5–4.6 Ma). The remainder of the siliceous-fossil-bearing Miocene sediments at Site 594 appear to be correlative to lower paleomagnetic Chronozone 5 through upper Chronozone 16. Uppermost lower Miocene or lowermost middle Miocene sediments in the basal 50 m of Hole 594A are barren of diatoms.

INTRODUCTION

Site 594 is currently located in northern subantarctic waters immediately south of the Subtropical Convergence which separates the subantarctic from the cool-subtropical (temperate) water mass to the north. Upwelling associated with the Subtropical Convergence has produced high biogenic productivity, especially of the siliceous planktonic groups. As a result, diatoms are persistent and often abundant. This chapter describes the diatom biostratigraphy of Site 594, one of the best Neogene diatom sequences in the Southern Hemisphere.

Site 594 (45°31.41′S, 174°56.88′E, 1204 m water depth) is located at the southern margin of the Chatham Rise east of New Zealand's South Island (Fig. 1). The section studied consists of two holes cored to a maximum sub-bottom depth of 639.5 m (Fig. 2). Hole 594 consists of 53 cores obtained from 0 to 505.1 m sub-bottom depth, using the hydraulic piston corer (HPC) to 1[illegible]0.7 m. Hole 594A was discontinuously cored to a sub-bottom depth of 495.5 m; 11 cores were taken in the upper Miocene to Pleistocene intervals poorly recovered by Hole 594. Below 495.5 m, Hole 594A was continuously drilled to termination of the hole at 639.5 m. Depth relationships of cores from Hole 594 and 594A are shown in Figures 3–4, backpocket.

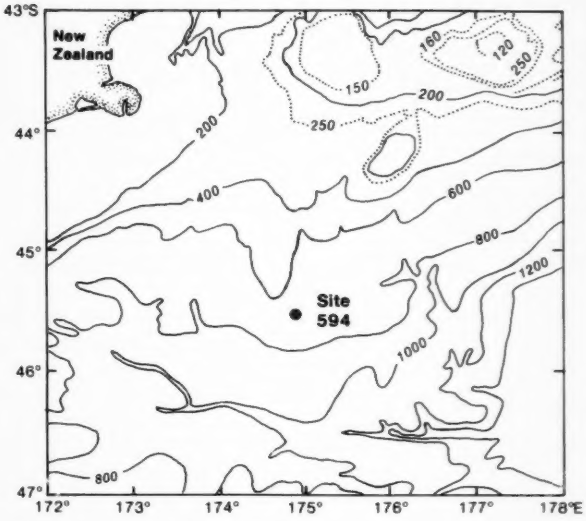

Figure 1. Location of DSDP Site 594.

PREPARATION OF SAMPLES AND METHOD OF STUDY

All samples used in this study were taken by scientists aboard the *Glomar Challenger*, Leg 90. A total of 85 samples were chemically processed to concentrate siliceous microfossils according to the procedure outlined by Ciesielski (1983).

Two strewn slides were prepared from the treated sample using Hyrax (n.d. = 1.71) mounting medium and 22 × 22 mm cover slips. In preparing slides an attempt was made to achieve uniform distribution of the sample material on the cover slips. Random-settling preparation

---

[1] Kennett, J. P., von der Borch, C. C., et al., *Init. Repts. DSDP*, 90: Washington (U.S. Govt. Printing Office).

[2] Address: Department of Geology, University of Florida, Gainesville, FL 32611.

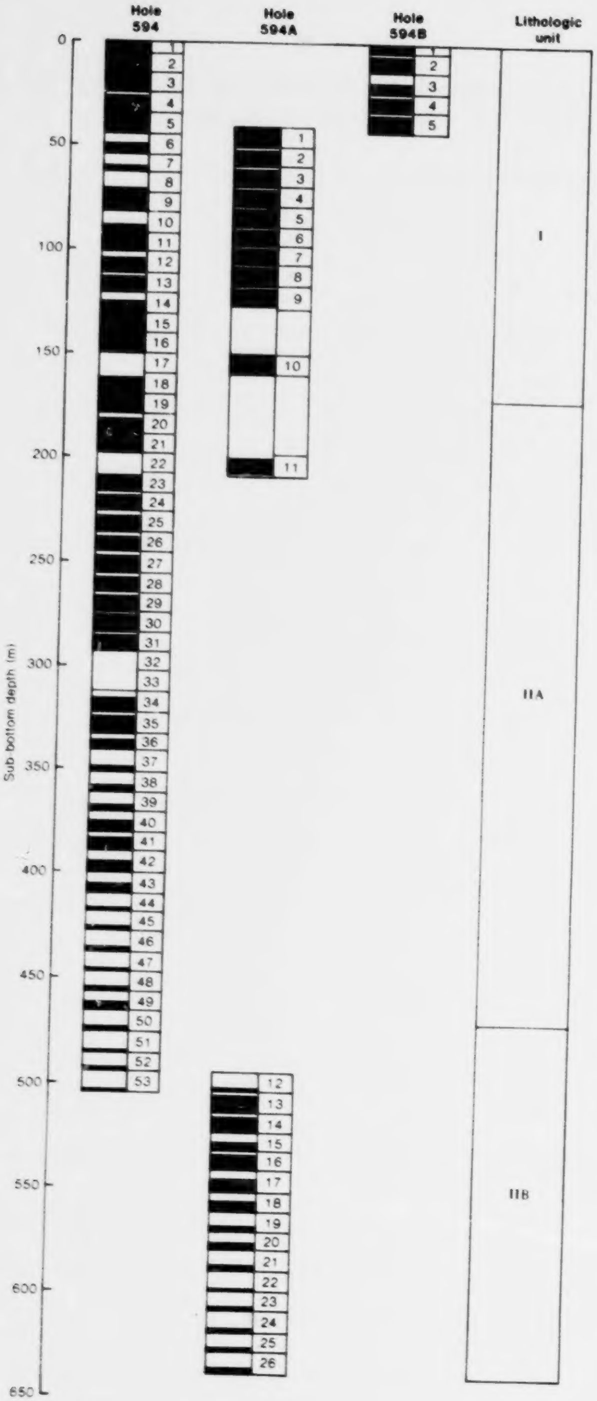

Figure 2. Lithologic columnar section of DSDP Site 594.

techniques were not used because of time restrictions on the preparation of this report.

All samples were sieved with a 45-μm sieve and a strewn slide was prepared from the coarse-fraction residue. Sieved residues were prepared in order to eliminate the extremely high clay content of most Miocene samples and to concentrate large diatoms and silicoflagellates of stratigraphic importance, such as *Mesocena circulus, M. diodon, Hemidiscus cuneiformis, Coscinodiscus lewisianus*, and others. For a more detailed discussion of the advantage of sieved-fraction examination the reader is referred to Gombos and Ciesielski (1983).

A Nikon Optiphot light microscope was used to determine the relative abundance of diatoms and silicoflagellates. Relative abundances are based on an examination of the entire whole-fraction slide (at 500×). Identifications were checked at 1250×. Relative abundances of species are designated as follows: D, dominant, more than one specimen in every field of view; A, abundant, at least one specimen in every field of view; C, common, at least one specimen in every two to five fields of view; F, frequent, at least one specimen in every six to ten fields of view; S, sparse, several specimens observed on the entire slide; R, rare, only one or two specimens observed on the entire slide.

Five traverses of sieved-fraction slides were made at 500× to check for rare species not present in whole-fraction slides. Species observed only in sieved-fraction slides are designated in Table 2 as Vr = very rare.

Estimates of the preservation of the diatom floras were made using the relative abundance of heavily silicified frustules versus less-silicified frustules. Five categories of preservation were noted: VP, very poor, sample with low diversity and abundance, generally dominated by sponge spicules and heavily silicified frustules, high fragmentation (e.g., *Coscinodiscus marginatus* and *Actinocyclus ingens*); P, poor, dominated by heavily silicified frustules but with less fragmentation and greater diversity; F, fair, dominated by heavily silicified frustules but with some moderately silicified frustules (e.g., *Asteromphalus* spp. and *Brunia mirabilis*) and rare, thinly silicified species, usually fragmented (e.g., *Nitzschia* spp.); M, moderate, greater diversity of heavily and moderately silicified diatoms (mostly unfragmented) and some well-preserved, thinly silicified species.

In general, only stratigraphically diagnostic diatoms are tabulated in Tables 1 and 2. The more important reference materials on the majority of the described taxa include McCollum (1975), Schrader (1973, 1976), Barron (1980a, b; 1981, 1983), and Ciesielski (1983). Silicoflagellate species listed in Tables 1 and 2 include only species of major stratigraphic importance.

PALEOMAGNETIC CORRELATIONS AND EPOCH BOUNDARIES

The paleomagnetic time scale utilized in this paper incorporates recent revisions of the middle Miocene portion of the time scale made by Kahn et al. (1984). These revisions are based on correlations of a long normal-polarity interval in DSDP Sites 563 and 558, which is associated with Zone NN9 (= Chron 11) and Zone N16, with marine Magnetic Anomaly 5. First-order magnetostratigraphic correlations of NN9 and N16 at these sites differ from previous second- and third-order correlations to Chron 9 by Berggren and van Couvering (1974), Ryan et al. (1974), and others. The reassignment of (Chron 11 = Anomaly 5 = Chron C5N) of Kahn et al. results in a 1.5–2.0 m.y. upward shift in the zonal boundaries of NN7/NN8 through NN10/NN11.

Correlation of Anomaly 5 with Chron 11 results in an absolute age assignment of 8.92–10.42 Ma for Chron 11 according to the Berggren et al. (in press) paleomagnetic time scale. Ages of Chrons 7 through 11 are also adjusted accordingly; however, traditional correlations of chrons and anomalies (Ryan et al. 1974; LaBrecque et al., 1977) younger than Chron 7 and older than Chron 14 appear correct and do not require adjustment (Berggren et al., in press).

Absolute ages of paleomagnetic boundaries shown in Figures 3–4 reflect the aforementioned revisions of Chrons 7 through 14 (Berggren et al., in press). Also indicated are the traditional chron boundaries with the revisions of Barron et al. (in press), the shortening of Chron 7 to include only Anomaly 4 (3 normal-polarity subchrons) and the lengthening of Chron 14 to include three additional normal-polarity subchrons below Anomaly 5A.

An alternate chron nomenclature system is now also in usage (Tauxe et al., 1983) and is also plotted in Figures 3–4 along with the more traditional nomenclature. This alternate nomenclature system labels successive chrons from the top of one numbered magnetic anomaly to the top of the next oldest anomaly; anomaly and chron numbers coincide.

Epoch Boundaries

The lower Miocene/middle Miocene boundary follows Ryan et al. (1974), with the upper part of the calcareous nannofossil NN4 (*Helicopontosphaera ampliaperta*) Zone of Martini (1971) within the upper part of paleomagnetic Chron 16 (= 16.0 Ma = Chron C5B = Anomaly 5B). As defined, this boundary is closely approximated by the initial occurrence of *Denticulopsis lauta* in the North Pacific (Barron, 1980a). The initial *D. lauta*, which marks the base of the *D. lauta* Zone (NNPD4), occurs in upper Chron 16 at approximately 16.1 Ma according to Barron et al.'s (in press) correlation to the Berggren et al. (in press) paleomagnetic time scale.

Kahn et al. (1984) have cited the base of the stratotype lower upper Miocene (Tortonian) as biostratigraphically within Zone NN8 and linked with the base of Anomaly 5. Their magnetochronology and revised magnetobiostratigraphy, therefore, places the middle/upper Miocene boundary (basal Tortonian) at approximately 10.4 Ma at the base of Chron 11.

The Miocene/Pliocene boundary lies within the lower reversed-polarity subchron of the Gilbert Chron at approximately 5.2 Ma (Cita, 1975; Burckle, 1978; and others). The Pliocene/Quaternary boundary is placed above the Olduvai Normal Subchron (1.6 Ma) according to recent paleomagnetic data from the proposed boundary stratotype at Vrica, Italy (Tauxe et al., 1983).

ZONATION

Holes 594 and 594A contain a nearly continuous 16-m.y. record of the uppermost lower Miocene through Quaternary. Middle upper Miocene to Quaternary diatom assemblages have a strong antarctic–subantarctic affinity which permits a biostratigraphic zonation of this interval utilizing well-established Neogene Southern Ocean diatom zones which have been correlated to magnetostratigraphy (McCollum, 1975; Weaver and Gombos, 1981; Ciesielski, 1983).

In the middle upper Miocene to Quaternary sediments of Samples 594-1-2, 4–5 cm through 594-50-2, 4–5 cm, 14 diatoms zones are recognized. These Neogene Southern Ocean diatom zones are those defined by Weaver and Gombos (1981) and amended by Ciesielski (1983). Definitions of these zones are provided in Figure 5.

Barron (in press, b) has presented a notation system for the Neogene Southern Ocean diatom (NSD) zonation of Weaver and Gombos (1981), designating Zones NSD 1 through NSD 16. This notation system is revised herein to include the additional Pliocene zones of Ciesielski (1983), resulting in 20 Neogene zones (NSD 1 through NSD 20, Fig. 5).

Samples 594-2-2, 4–5 cm through 594-43-1, 4–5 cm are representative of Zones NSD 7 through NSD 20. Below Sample 594-43-1, 4–5 cm, Neogene Southern Ocean diatom zones cannot be differentiated because of the absence of two species (*Nitzschia grossepunctata* and *N. maleinterpretaria*) used to define zonal boundaries of the base of the *Nitzschia maleinterpretaria* Zone (NSD 3). The only NSD zonal boundary identified in this lower portion of the section is the last occurrence of *Coscinodiscus lewisianus*, which defines the *Coscinodiscus lewisianus* Zone (NSD 4) boundary with the *N. grossepunctata* zone (NSD 5). Positions of the boundaries between the *N. maleinterpretaria* Zone (NSD 3) and *C. lewisianus* Zone (NSD 4) and the *Nitzschia grossepunctata* Zone (NSD 5) and *N. denticuloides* Zone (NSD 6), respectively, are inferred, using secondary datums present in Site 594 and the zonal type sections of Sites 266 and 278.

As previously noted by Barron (in press, b), the middle Miocene to lower upper Miocene diatom sequence of the Southern Ocean is very similar to that of the middle- to high-latitude North Pacific. Three North Pacific diatom zones are recognized between Sample 594-39-2, 4–5 cm and the base of Hole 594A; these include the *Denticulopsis hustedtii–D. lauta* Zone (NNPD 5), *D. lauta* Zone (NNPD 4), and *Actinocyclus ingens* Zone (NNPD 3). Table 2, later, reveals the relationship of NNPD and NSD zones in the upper lower Miocene to lower upper Miocene of Site 594. Further discussion of zonal occurrences and characteristics is presented in the following section.

BIOSTRATIGRAPHY OF SITE 594

Pliocene to Quaternary (Table 1, Figs. 3, 5)

Pliocene and Pleistocene diatoms of Hole 594 (Core 1 through Sample 594-20-2, 4–5 cm) and Hole 594A (Core 1 through Core 10) are generally characterized by fair to poor preservation and limited diversity. Throughout this entire sequence, antarctic–subantarctic diatoms predominate and are therefore zoned using the regional Southern Ocean diatom zonation of Ciesielski (1983). The occurrences of diatoms in each Pliocene–Pleistocene sample are recorded in Table 1, along with selected silicoflagellates and reworked diatoms and silicoflagellates. Figure 3 illustrates the depth in hole of major diatom, radiolarian, and foraminiferal datums and their correlation to paleomagnetic stratigraphy.

The upper ~124 m of Holes 594 and 594A, through 594A-10-2, 4–5 cm, contain an apparently continuous sequence of the upper Pliocene–Quaternary. Detailed chronostratigraphic control is provided throughout this sequence by numerous biostratigraphic datums and by a single paleomagnetic reversal boundary (the Brunhes/Matuyama boundary).

Paleomagnetic measurements were made at 50-cm intervals for samples from the HPC sections of Holes 594 and 594A. Unfortunately, below Core 594-13 intensities were too low for results to be reliable. One paleomagnetic boundary was identified within Sample 594-11-5,

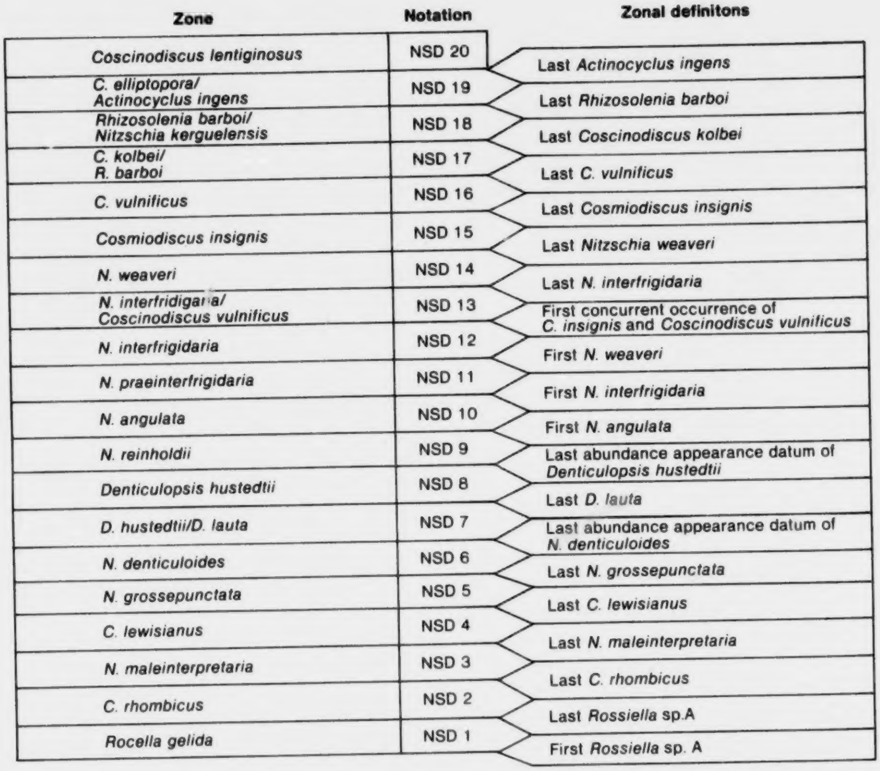

Zone	Notation	Zonal definitons
Coscinodiscus lentiginosus	NSD 20	Last *Actinocyclus ingens*
C. elliptopora/ Actinocyclus ingens	NSD 19	Last *Rhizosolenia barboi*
Rhizosolenia barboi/ Nitzschia kerguelensis	NSD 18	Last *Coscinodiscus kolbei*
C. kolbei/ R. barboi	NSD 17	Last *C. vulnificus*
C. vulnificus	NSD 16	Last *Cosmiodiscus insignis*
Cosmiodiscus insignis	NSD 15	Last *Nitzschia weaveri*
N. weaveri	NSD 14	Last *N. interfrigidaria*
N. interfridigaria/ Coscinodiscus vulnificus	NSD 13	First concurrent occurrence of *C. insignis* and *Coscinodiscus vulnificus*
N. interfrigidaria	NSD 12	First *N. weaveri*
N. praeinterfrigidaria	NSD 11	First *N. interfrigidaria*
N. angulata	NSD 10	First *N. angulata*
N. reinholdii	NSD 9	Last abundance appearance datum of *Denticulopsis hustedtii*
Denticulopsis hustedtii	NSD 8	Last *D. lauta*
D. hustedtii/D. lauta	NSD 7	Last abundance appearance datum of *N. denticuloides*
N. denticuloides	NSD 6	Last *N. grossepunctata*
N. grossepunctata	NSD 5	Last *C. lewisianus*
C. lewisianus	NSD 4	Last *N. maleinterpretaria*
N. maleinterpretaria	NSD 3	Last *C. rhombicus*
C. rhombicus	NSD 2	Last *Rossiella* sp.A
Rocella gelida	NSD 1	First *Rossiella* sp. A

Figure 5. The Neogene Southern Ocean diatom zonation of Weaver and Gombos (1981), as amended by Ciesielski (1983), with zonal definitions. The Neogene Southern Ocean diatom (NSD) notation is modified from Barron (in press, b) to include the Pliocene to Quaternary zonation of Ciesielski (1983).

75-77 cm; it was assumed to be the Brunhes/Matuyama Chronozone boundary (Barton and Bloemendal, this volume).

In spite of the great depth (99 m) of the Brunhes/Matuyama boundary (730 × 10^3 yr.), its identification is confirmed by the shallower occurrences of several well-defined Brunhes datums. Among these is the last appearance of *Actinocyclus ingens* (620 × 10^3 yr.) in Sample 594-9-5, 4-5 cm, marking the boundary between the overlying *Coscinodiscus lentiginosus* Zone (NSD 20, 0-620 × 10^3 yr.) and the *C. elliptopora/Actinocyclus ingens* Zone. Other important recognized datums of the Brunhes Chron include the last appearances of the radiolarian *Stylatractus universus* (425 × 10^3 yr.) in Section 594-7-2 and *Hemidiscus karstenii* (195 × 10^3 yr.) in Sample 594-3-5, 4-5 cm. Under the assumption of a constant Brunhes Chronozone sedimentation rate, the ages of the three aforementioned datums appear similar to previously published results.

The initial occurrence of the foraminifer *Globorotalia truncatulinoides* is in Sample 594-3,CC, immediately below the last occurrence of *Hemidiscus karstenii*, which is only slightly older than 200,000 yr. Even though the initial *G. truncatulinoides* approximates the Plio/Pleistocene boundary in lower latitudes, its first occurrence at this site is within the late Pleistocene, as in other subantarctic areas.

Rhizosolenia barboi and *C. kolbei* both last occur in Sample 594-15-2, 4-5 cm. The presence of these two species in the absence of *C. vulnificus* indicates the *Coscinodiscus kolbei/Rhizosolenia barboi* Zone (NSD 17, 2.22-1.89 Ma). Elsewhere in the subantarctic, the last appearance of *C. kolbei* (1.89 Ma) occurs earlier than the last appearance of *R. barboi* (1.5 Ma), thus defining the *R. barboi/Nitzschia kerguelensis* Zone (NSD 18, 1.89-1.58 Ma).

The joint last occurrences of *C. kolbei* and *R. barboi* and the absence of the *R. barboi/N. kerguelensis* Zone, however, is not thought to be conclusive evidence of a disconformity. This zone represents only 300,000 yr. and could be present in the 14.7-m unsampled interval between Samples 594-15-2, 4-5 cm and 594-13-5, 4-5 cm (Fig. 3).

Samples 594-15-2, 4-5 cm through 594A-10-2, 4-5 cm contain three of the four upper Gauss Chronozone to lower Matuyama Chronozone diatom zones of Ciesielski (1983). Diatom zones identified within this interval include: the *C. kolbei/R. barboi* Zone (NSD 17, 2.22-1.89 Ma) in Samples 594-15-2, 4-5 cm and 594-15-5, 4-5 cm; the *Cosmiodiscus insignis* Zone (NSD 15, 2.64-2.49 Ma) in Sample 594-16-2, 4-5 cm; and the *N. weaveri* Zone (NSD 14, 2.81-2.64 Ma) in Samples 594-16-5, 4-5 cm and 594A-10-2, 4-5 cm. The *Coscinodiscus vulnificus* Zone (NSD 16, 2.49-2.22 Ma) of the lower Matuyama-

Table 1. Stratigraphic distribution and relative abundances of selected diatom and silicoflagellate species in the Pliocene to Quaternary of Holes 594 and 594A.

Core-Section (interval in cm)	Diatoms																															Silicoflagellates					Reworked Diatoms and Silicoflagellates																									
	Actinocyclus ingens	*Actinoptychus undulatus*	*Asteromphalus parvulus*	*Charcotia actinochilus*	*Coscinodiscus elliptopora*	*C. endoi*	*C. kolbei*	*C. lentiginosus*	*C. lentiginosus* v. *obovatus*	*C. marginatus*	*C. vulnificus*	*Cosmiodiscus insignis*	***Denticulopsis hustedtii***	*Ethmodiscus rex*	*Eucampia antarctica*	*Hyalodiscus* spp.	*Hemidiscus cuneiformis*	*H. karstenii*	*Melosira* spp.	*Nitzschia angulata*	*N. fossilis*	*N. interfrigidaria*	*N. kerguelensis*	*N. reinholdii*	*N. weaveri*	*Rhizosolenia barboi*	*R. styliformis*	*Stephanopyxis turris*	*Stephanopyxis* sp. 1	*Thalassiothrix miocenica*	*Thalassiothrix* spp.	*Dictyocha* spp.	*Distephanus boliviensis*	*D. crux*	*D. polyactis*	*Mesocena diodon*	*Coscinodiscus praenitidus*	*Cosmiodiscus insignis* f. *triangula*	*Denticulopsis dimorpha*	*Hemiaulus polymorphus*	*H. polycistinorum*	*Mediaria splendida*	*Melosira architecturalis*	*Pterotheca aculeifera*	*Pyxilla* fragments	*Rocella vigilans*	*Sceptroneis* fragments	*Stephanopyxis hyalomarginata*	*Stictodiscus* spp. fragments	*Synedra jouseana*	*Triceratium* fragments	*Trinacria excavata*	*Xanthiopyxis acrolophra*	Benthic diatoms	Recrystallized diatoms	*Corbisema triacantha*	*Naviculopsis biapiculata*	*Mesocena apiculata*	*M. circulus*	Preservation	Reworking	Diatom zone
2-2, 4-5				R				F							R				F				F								F																							F						VP	•	*Coscinodiscus lentiginosus*
2-5, 4-5	r															R															F																				F									VP	•	
3-2, 4-5								R							R	F							R								F																													VP		
3-5, 4-5								F							R	F		F	R				F								c																							F						P	•	
4-2, 4-5	r									r				F				F					R			f		r			C		R		R										R			R							F					F	•	
4-5, 4-5	r				r			F	R						F			F					C								c																							R						F	•	
5-2, 4-5	r							R	R									R					C								C																							R						P	•	
1A-2, 4-5										T								R					F			r					F																													VP	•	
6-2, 4-5																R		R					R								F																				R									VP	•	
2A-2, 4-5	r							F							R	R			F				C								F																													VP		
7-2, 4-5	f	R	R					F		r									F				C					r			F														R															P	•	
3A-2, 4-5		R	R		R			F		f						R			R				C								C																													P		
8-1, 4-5	r				R														F				F								F																													VP		
9-2, 4-5	f	R			F					r						F			F				F					f			F		R																											P		
9-5, 4-5	C	R			F			S							S	S							C					r			C																													F		*C. elliptopora/ Actinocyclus ingens*
5A-2, 4-5	C				F			F						R	R				R				A								A																													M		
10-2, 4-5	C	F		R				R											F				C								F																													P		
5A-5, 4-5	C	F			F			F							R								C								C		R																											F		
6A-2, 4-5	C				F					r				R		C							C								C				F																									F		
11-2, 4-5	F				F		r	F		r				F		C							F								C		F																											P		
12-2, 4-5	C	R	F		F			C	R					F									C								C		R																										R	F	•	
12-5, 4-5	F							F															C								C											R			F															P	•	
13-2, 4-5										R													F								F																											R		VP	•	
13-5, 4-5	F									F						F							R					r			F																													VP		
15-2, 4-5	F						F	R		F				R		C		F	F		F	r				C					C	F								R					R							R		F		R				F	•	*C. kolbei/ Rhizosolenia barboi*
15-5, 4-5	F						R			F				F		F		R	F		F					C					A		F					R		R					F															P	•	
16-2, 4-5										R	R	C		F		F		F	F	F						R					A		F							R					R							R								P	•	*Cosmiodiscus insignis*
16-5, 4-5	F							R				C		F				C		R				C	C	R		F			A		F		R												C					F		C						F	•	*Nitzschia weaveri*
10A-2, 4-5																		F						F	F			F			F																							F						P	•	
10A-5, 4-5						R				F								R	R			F									C													R	F									F						P	•	*N. praeinterfrigidaria*
18-2, 4-5										R						R			R							R		R			F									R	R			R	R							R					R			VP	•	*N. angulata* and *N. reinholdii* undifferentiated
18-5, 4-5						R				F						R			F					R		R	R	R			C					r		R			R		R		F									F			R	R		VP	•	
19-2, 4-5	R											R	R					R						F	r	R	F		R		C		F	R					R	R	R		F	R	C				F		F		R	R						P	•	*Denticulopsis hustedii*
19-5, 4-5	F											R	R				R	R						F		R		F	F		F	F								F	R				F	R			R	R			R	F						VP	•	
20-2, 4-5	R												S				F	F						F		R	R	C	F	F	C	F	F			R	F		R		R				F												R			F	•	

Note: R, rare; S, sparse; F, frequent; C, common; A, abundant; lower-case abundance designators are interpreted as reworked occurrences; for explanation of abundances see Methods section. Reworked diatoms and silicoflagellates older than Pliocene listed separately. A after core number denotes cores from Hole 594A.

ma Chronozone is unrepresented; however, it may be present in the 4.5-m interval between Samples 594-15-2, 4-5 cm and 594-15-5, 4-5 cm (Fig. 3).

A major disconformity spanning the upper Gilbert to lower Gauss chronozones occurs within Core 12 of Hole 594A, between Samples 594A-10-2, 4-5 cm and 594A-10-5, 4-5 cm. This hiatus separates sediments of the upper Gauss *N. weaveri* Zone above from the upper Gilbert *N. praeinterfrigidaria* Zone (NSD 11, 4.02-3.88 Ma) found below. Encompassed by the hiatus are the entire *N. interfrigidaria* Zone (NSD 12, 3.88-3.1 Ma) and the *N. interfrigidaria/C. vulnificus* Zone (NSD 13, 3.10-2.81 Ma).

Sediment immediately beneath the hiatus (Sample 594A-10-5, 4-5 cm) contains the sole occurrence of *N. interfrigidaria* and is assigned to the *N. praeinterfrigidaria* Zone (NSD 11, 4.02-3.88 Ma). The apparent hiatus thus encompasses the interval from approximately 3.9 to 2.8 Ma, thus eliminating most of the stratigraphic range of index species such as *C. vulnificus, N. interfrigidaria, N. weaveri*, and the acme of *C. lentiginosus* var. *obovatus*. Alternatively, the 1.1 m.y. upper Gilbert-lower Gauss Chronozone interval may be present in the 4.5-m unsampled interval between Samples 594A-10-2, 4-5 cm and 594A-10-5, 4-5 cm. This explanation would appear unlikely, given the high sedimentation rates above and below this level (see Site 594 site chapter, this volume).

Approximately 24 m of middle Gilbert Chronozone sediment was identified in Samples 594A-10-5, 4-5 cm through 594-20-2, 4-5 cm. This sequence is bounded by the upper Gilbert-lower Gauss hiatus in Core 594A-10 and an upper Chron 5-lower Gilbert hiatus in Core 594-20. Samples 594A-10-5, 4-5 cm through 594-18-5, 4-5 cm are assigned to the *N. angulata* Zone (NSD 10, 4.2-4.02 Ma) and *N. reinholdii* Zone (NSD 9, 4.48-4.22 Ma) as this interval is above the last occurrence of *Denticulopsis hustedtii* and below the initial *N. interfrigidaria*. These two zones are not differentiated because of the absence of *N. angulata*, apparently as a result of the very poor to poor preservation of this interval.

Sediment from the last occurrence of *D. hustedtii* (4.5 Ma; Ciesielski, 1983) in Sample 594-19-2, 4-5 cm through 594-20-2, 4-5 cm is assigned to the lower Gilbert Chronozone portion of the *Denticulopsis hustedtii* Zone (NSD 8, 4.48-8.7 to 8.5 Ma). The last occurrence of the silicoflagellate *Mesocena diodon* (4.57 Ma; Ciesielski, 1983) occurs near the base of this interval (Sample 594-20-2, 4-5 cm), thus marking the top of the *Mesocena diodon* Zone. Based on previous paleomagnetic correlations of Ciesielski (1983), Core 594-19 and upper Core 594-20 represent only a portion of the reversed-polarity interval between the Sidufjall and Thvera subchronozones and a portion of the Thvera Subchronozone.

Miocene (Tables 2 and 3, Figs. 4, 6, 7)

Determining sediment ages of the Miocene sequence in Holes 594 and 594A is more difficult than in the Pliocene and Quaternary, where datums and diatom zones are correlated to magnetostratigraphy with high precision. In the southern mid to high latitudes, portions of the upper Miocene have been loosely correlated to paleomagnetic stratigraphy (Ciesielski, 1983), whereas the lower to middle Miocene zonal schemes have had no direct correlation to magnetostratigraphy. Unfortunately, paleomagnetic measurements of the Miocene section of Site 594 were too weak to provide a reliable magnetostratigraphy for direct correlation of Miocene Southern Ocean diatom zones.

Discussed in the following section are: (1) the occurrence of Miocene Southern Ocean diatom zones in Site 594, (2) a direct correlation of Miocene North Pacific diatom zones to Southern Ocean diatom zones, and (3) a correlation of the Miocene section at Site 594 to magnetostratigraphy.

Miocene Southern Ocean Diatom Zones

The *Denticulopsis hustedtii* Zone (NSD 8), as defined by McCollum (1975) and Weaver and Gombos (1981), brackets the Miocene/Pliocene boundary. This is true also in Hole 594, where the Miocene/Pliocene boundary appears to be a disconformity between Samples 594-20-2, 4-5 cm and 594-20-5, 4-5 cm (Fig. 4). Beneath this disconformity, the *D. hustedtii* Zone extends down to Sample 594-26-2, 4-5 cm.

The last occurrence of *Denticulopsis lauta* occurs in Sample 594-27-2, 4-5 cm, thus marking the boundary between the *D. hustedtii* Zone (NSD 8) and the underlying *D. hustedtii/D. lauta* Zone (NSD 7). The *D. hustedtii/D. lauta* Zone is a thick (~152 m) sequence extending down-section through Sample 594-43-1, 4-5 cm. Preservation is moderate to fair and diversity relatively high throughout the upper ~66 m of the zone; however, diversity declines significantly in the lower 86 m, where preservation is consistently poor to very poor (Table 2).

Sample 594-44-1, 4-5 cm contains the last appearance datum of *Nitzschia denticuloides*, defining the top of the *Nitzschia denticuloides* Zone (Weaver and Gombos, 1981; NSD 6) and coinciding closely with the middle/upper Miocene boundary (Ciesielski, 1983). The base of the *N. denticuloides* Zone is not recognized in Site 594 because of the absence of the high-latitude species *N. grossepunctata*. The next NSD zonal datum encountered downcore is the last occurrence of *Coscinodiscus lewisianus* in Sample 594-52-2, 4-5 cm, marking the upper boundary of the *Coscinodiscus lewisianus* Zone (Schrader, 1976; Weaver and Gombos, 1981; NSD 4). The aforementioned datums indicate that the *N. denticuloides* Zone (NSD 6) and *N. grossepunctata* Zone (NSD 5) occur between Samples 594-44-1, 4-5 cm and 594-51-1, 4-5 cm, although the datum defining the boundary between the zones (LAD *N. grossepunctata*) is unrecognized.

In the absence of *N. grossepunctata*, the boundary between the *N. denticuloides* Zone and *N. grossepunctata* Zone is inferred to be coincident with the first occurrence of *N. denticuloides*, as noted by Weaver and Gombos (1981). In Site 594, the first *N. denticuloides* occurs in Sample 594-50-2, 4-5 cm; therefore, the *N. denticuloides* Zone ranges from Sample 594-44-1, 4-5 cm through 594-50-2, 4-5 cm. The *N. grossepunctata* zonal equivalent is constrained to a single sample (594-51-1, 4-5 cm) by the last occurrence of *C. lewisianus* (594-52-2, 4-5 cm), which defines the top of the *C. lewisianus* Zone (Schrader, 1976).

The defined base of the *C. lewisianus* Zone (the last *N. maleinterpretaria*, Weaver and Gombos, 1981) is unrecognized in Site 594; however, its base is correlated to this site by the relationship of the *N. maleinterpretaria* datum in Sites 266 and 278 to the first occurrence of *D. lauta* at all three sites. In Site 278, the first *D. lauta* is coincident with the last *N. maleinterpretaria* in Sample 278-20-5, 80-81 cm (Schrader, 1976) and is used here as a substitute marker for the base of the *C. lewisianus* Zone. Thus, the base of the zone in Hole 594A is inferred to be at the first occurrence of *D. lauta* in Sample 594A-17-5, 4-5 cm (Table 2).

The interval from Sample 594A-18-2, 4-5 cm through Sample 594A-21-2, 4-5 cm, the lowermost diatom-bearing sample, appears to represent only a portion of the *N. maleinterpretaria* Zone (Weaver and Gombos, 1981; NSD 3). Several datums occur within the *N. maleinterpretaria* zonal equivalent at Site 278; these include the first occurrence of the genus *Denticulopsis*, *C. lewisianus*, and *Brunia mirabilis*. The absence of *C. rhombicus* in the lowermost diatom-bearing sample (594A-21-2, 4-5 cm) further supports a position within the *N. maleinterpretaria* Zone, because the last occurrence of this species defines its base. *Coscinodiscus rhombicus* occurs at a similar latitude in the Atlantic (Site 513, 47°35′S) and should be present at Site 594 if the stratigraphic horizon were reached.

Sample 594A-23-2, 4-5 cm through the base of Hole 594A (594A-26,CC) appears to be correlative to the *N. maleinterpretaria* Zone, even though the interval is barren of diatoms. This inference is based on Martini's (this volume) discovery of the calcareous nannofossil *Sphenolithus heteromorphus* in Sample 594A-26,CC. At Site 266, the first occurrence of *S. heteromorphus* occurs within the middle portion of the *N. maleinterpretaria* Zone (Sample 266-17-1, Weaver and Gombos, 1981). On this basis the interval between Sample 594-18A-2, 4-5 cm through 594A-26,CC is assigned to the *N. maleinterpretaria* Zone.

The base of Hole 549A is within calcareous nannofossil Zone NN5 (Martini, this volume); therefore, according to Ryan et al. (1974) and Berggren et al. (in press), the base of Hole 594A would be lowermost middle Miocene. Jenkins and Srinivasan (this volume) favor placement of the early/middle Miocene boundary between Samples 594A-20,CC and 594A-21,CC. Diatoms cannot be used to reconcile this discrepancy because of the effects of dissolution on age-diagnostic taxa in the lower portion of Hole 594A.

Correlation of Site 594 to Miocene North Pacific Diatom Zones

Uppermost lower Miocene through lower upper Miocene North Pacific diatom Zones NNPD 3 to NNPD 5 are recognized in Holes 594 and 594A and are correlated directly to Neogene Southern Ocean diatom Zones NSD 3 through NSD 7 (Table 2). The Neogene North Pacific diatom zones recognized herein and the respective authors of these zones are: *Actinocyclus ingens* Zone (NNPD 3, Barron, 1980a), *Denticulopsis lauta* zone (NNPD 4; Koizumi, 1973; Barron, 1980a; amended Barron and Keller, 1983), and the *D. hustedtii-D. lauta* Zone (NNPD 5; Koizumi, 1973; amended by Barron, 1980a, and Barron and Keller, 1983).

The Neogene North Pacific *D. hustedtii-D. lauta* Zone (NNPD 5) is defined as the interval from the evolutionary transition of *D. hyalina* to *D. hustedtii* (recognized by the first consistent dominance of *D. hustedtii* over *D. lauta;* Barron et al., in press) to the last occurrence of *D. dimorpha*. In Site 594 both of these datums are recognized in Samples 594A-14-2, 4-5 cm and 594-29-2, 4-5 cm, respectively. The *D. hustedtii-D. lauta* zone (NNPD 5) of the North Pacific, therefore, is inclusive of most of the *D. hustedtii/D. lauta* Zone (NSD 7), *N. denticuloides* Zone (NSD 6), *N. grossepunctata* Zone (NSD 5), and upper *Coscinodiscus lewisianus* Zone (NSD 4) (Table 2).

Barron (1980a) defined four subzones of the *D. hustedtii-D. lauta* zone which can also be correlated to Neogene Southern Ocean diatom zones. Subzone d, the youngest of these zones, is the interval from the last to the first occurrence of *D. dimorpha*. In Site 594, Subzone d extends from Sample 594-29-2, 4-5 cm to 594-47-1, 4-5 cm. The subzone contains the last occurrences of *Mediaria splendida* and *D. praedimorpha*, as was noted previously in the North Pacific by Barron (in press, b). Correlation of Subzone d to NSD zones in Site 594 reveals that it brackets the boundary between the *D. hustedtii/D. lauta* Zone (NSD 7) and the *N. denticuloides* Zone (NSD 6). This relationship of the NSD 7/NSD 6 boundary to Subzone d is the same at South Atlantic Site 512 (Ciesielski, 1983) and appears to be isochronous throughout the Southern Ocean.

The first occurrence of *D. praedimorpha* in Sample 594-49-2, 4-5 cm marks the base of Barron's (1980a) Subzone b. The base of Subzone c, the first occurrence of *Rhizosolenia barboi*, cannot be used to identify to Subzone b/c boundary because *R. barboi* has its first occurrence earlier in the southern high latitudes than in the North Pacific (McCollum, 1975; Schrader, 1976; Gombos and Ciesielski, 1983; and others). Even though *R. barboi* occurs sporadically in the basal portion of the Site 594 section, its first consistent occurrence is coincident with the first occurrence of *D. praedimorpha* and the base of Subzone b. Thus the first consistent occurrence of *R. barboi* at Site 594 (base of Subzone b) is slightly older than its North Pacific first occurrence (top of Subzone b).

Subzones c and b of the *D. hustedtii-D. lauta* Zone (NNPD 5) are confined to only two samples, Samples 594-48-2, 4-5 cm and 594-49-2, 4-5 cm. The poor stratigraphic representation of these subzones, as compared to many North Pacific sites, may be the consequence of low sedimentation rates, the presence of an undetected disconformity, or different ranges of species to define the top of Subzone c (FAD *D. dimorpha*) and the base of Subzone b (FAD *D. praedimorpha*). Both Subzones b

Table 2. Stratigraphic distribution and relative abundances of selected diatom and silicoflagellate species in the Miocene of Holes 594 and 594A.

Core-Section (interval in cm)	Preservation	Reworking	Neogene North Pacific diatom zones (NNPD) (1, 2, 3)		Neogene Southern Ocean diatom zones (NSD)	Silicoflagellate zones	Diatoms																	
							Actinocyclus ingens (flat)	*A. ingens* (undulated)	*A. ingens* var. *nodus*	*A. ellipticus*	*A. ellipticus* var. *spiralis*	*Actinoptychus undulatus*	*Asteromphalus* sp. 1	*A.* sp. 2	*A.* sp. 3	*Brunia mirabilis*	*Cestodiscus peplum*	*Coscinodiscus deformans*	*C. endoi*	*C. lewisianus*	*C. lewisianus* var. *robustus*	*C.* aff. *lineatus*	*C. marginatus*	*C. praenitidus*
20-5, 4-5	F	•			*Denticulopsis hustedtii* (NSD 8)	*Mesocena diodon*	F																F	
21-2, 4-5	M	•					R						R						R				R	R
21-5, 4-5	F	•					F						S			R							R	
23-2, 4-5	M	•				*M. diodon/ M. circulus*	C					R	S		R	R							F	
23-5, 4-5	M	•					C			R			R		S	S						S	R	
24-5, 4-5	M	•					A			R			S		S	R							S	
25-2, 4-5	M	•					S					R	S		F	R						S	S	
25-5, 4-5	M	•					S						C		R	S						R	C	
26-2, 4-5	M									R			F			S				r		S	C	
27-2, 4-5	M	•			*D. hustedtii/ D. lauta* (NSD 7)		S			S					F	F						F	F	
28-2, 4-5	M	•								F			C			R						S	F	
29-2, 4-5	M	•								S			F			S						R	S	
29-5, 4-5	F	•	*Denticulopsis hustedtii D. lauta* (NNPD5)	d									C			S						S	F	
30-5, 4-5	P	•								R			R		R	S			S			R	C	
31-5, 4-5	F	•				*M. circulus*	S			S			R		R			R	S				C	
34-2, 4-5	F	•					C	v		V			R			R							S	
35-2, 4-5	P	•					C									R							S	
36-2, 4-5	F	•					S																R	
37-1, 4-5	P	•					S													r			S	
38-2, 4-5	P	•					C					R			R	S							S	
39-2, 4-5	VP	•					S																C	
40-2, 4-5	P	•					C																S	
41-2, 4-5	VP						V																R	
41-5, 4-5	VP	•																						
42-2, 4-5	VP	•																					F	
43-1, 4-5	VP															R								
44-1, 4-5	F	•			*Nitzschia denticuloides* (NSD 6)		F									R							R	
45-2, 4-5	F	•					F									F							F	
46-2, 4-5	P	•					C									S			R				S	
47-1, 4-5	M	•					C									S							F	
48-2, 4-5	M	•		c			C	F								F		R					F	
49-2, 4-5	G	•		b			C	F								S							C	
50-2, 4-5	P	•		a	*N. grossepunctata*		F									R							C	
51-1, 4-5	VP	•					C									R							S	
52-2, 4-5		•			*Coscinodiscus lewisianus* (NSD 4)		F				R					R				F			C	
12A-2, 4-5	VP	•									R									R			R	
13A-2, 4-5	M	•					S									R				F			F	
14A-2, 4-5	M	•					S	S			R					S				F			F	
15A-2, 4-5	M	•	*D. lauta* (NNPD4)	b			S	S	S					R		S				F	R		F	
16A-2, 4-5	M	•		a			F	S	R		R			F						F			S	
17A-2, 4-5	M	•					C	F						R		R	R			F			F	
17A-5, 4-5	M	•					C	S	R							F				F			S	
18A-2, 4-5	P	•	? *Actinocyclus ingens* (NNPD3)		*N. male-interpretaria* Zonal equivalent (NSD 3)		S	S	R														S	
19A-2, 4-5	VP	•														S		R		R			R	
20A-2, 4-5	VP	•																					S	
21A-2, 4-5	VP	•																					R	
23A-2, 4-5							Barren																	
24A-2, 4-5																								
25A-2, 4-5																								
26A-1, 4-5																								

Note: V, very rare; R, rare; S, sparse; F, frequent; C, common; A, abundant; D, dominant; lower-case abundance designators are interpreted as reworked occurrences; for explanation of abundances see Methods section. Reworked diatoms and silicoflagellates older than middle Miocene listed separately. A after core number denotes cores from Hole 594A.

Table 2. (Continued).

Diatoms

C. [illegible]	*C. yabei*	*C.* aff. *marginatus*	*Cosmiodiscus insignis*	*C. insignis* var. *triangula*	*C. intersectus*	*Denticulopsis dimorpha*	*D. hustedtii*	*D. hyalina*	*D. lauta*	*D. nicobarica*	*D. punctata*	*D. praedimorpha*	*D. punctata* f. *hustedtii*	*Ethmodiscus rex*	*Eucampia antarctica*	*Hemidiscus cuneiformis*	*H. karstenii*	*H. karstenii* f. 1	*Lithodesmium* cf. *minusculum*	*L. reynoldsii*	*Macrora stella*	*Mediaria splendida*	*Nitzschia denticuloides*	*N.* aff. *donahuensis*	*N. fossilis*	*N. januaria*	*N. marina*	*N. miocenica*	*N. porteri*	*N. praereinholdii*	*N. reinholdii*	*N.* sp. 17	*Raphidiscus marylandicus*	*Rhaphoneis amphiceros*	*R. parilis*	*R.* sp. 1	*Rhizosolenia barboi*	*R. hebetata*	*R. hebetata* f. *hiemalis*	*R. praebarboi*	*R. styliformis*
			R	R	R		R							S	S	S															S						S				
			R	F			S							S		S	C	C									S	R			F						C	R	S		
			S	S			S								R	S	R	R	R												S						S				
				R			R							S		F	C	C													S						C	R			
							R								S	R	R									S				R	R						C				S
					R		F							S	R	F	S								S						R						C		R		S
						s	S					r			R	F	S		R						R			R									C	S	S		
						r	C							S	R	A	C		R										R								C		R		
		F					R							R	S	S	S		R									R	R	S							F				
						r	C		R						S	S	F		S						S	S		S	R	F						S	C				
							F								S	F	F													S						F	C				
		S					F		S			f				C	F								R				R							C	A		C		
		S				R	C		S						S	S	R		R	R																F	C	R			
		S				R	C		R						R		F		R																	F	C				
		C			R	S	F		S			s			S	S	S		R	R					R				R							S	C		S		
		S				R	F		R						S	R			R																		F				
							S		R																												S	S			
			R			S	S							S	R																						S				
						R	C		S																												S				S
	S					R	C																	R													F				
						C								R	S																										
					R	A	S		F			S			R																					S					
						F									R																						S				
					F	C	S		S			R			F							F														F					
						C	F		S																											F	F				
						C	R		R			S																									R				
			R		S	A	F		R			R	R	R	F								S														F				
					R	C	F		F													R	S										R				C				
						C	C		F			R										R	C														F				
	R					F	C		C	S		F	R									S	F														F			F	
							C		S			C	R									R	F														S			S	
					S		C		F			F											S														S				
					R		F		R				R										R																		
							S		R	S																										S					
R					R		S		S	C													R									R				S					
							R		R	F																														R	
R							F		F	C				S								S																		S	
							A	A	C	A																								S						S	
								A	S	A			R																					F		S	F			S	
							R		F	C	C		F																					F		S	R			S	
									S	A	C										R													F	S					R	
									F	C												S												S			R				
																																		S							
																						S																			
																																					R			R	
Barren																																									

and c of Barron (1980a) are shown to correlate to the lower *N. denticuloides* Zone (NSD 6) of the Southern Ocean.

The bottom of Subzone a, the basal subzone of NNPD 5, occurs in Sample 594A-14-2, 4–5 cm, where the evolutionary transition of *D. hyalina* to *D. hustedtii* is recognized by the first consistent dominance of *D. hustedtii* over *D. hyalina*. Subzone a occurs in Samples 594-50-2, 4–5 cm through 594A-14-2, 4–5 cm, encompassing the lowermost *N. denticuloides* Zone (NSD 6),

Table 2. (Continued).

Core-Section (interval in cm)	Diatoms										Silicoflagellates				Reworked diatoms													Reworked silicoflagellates										
	Rouxia naviculoides	*Stephanopyxis turris*	*Synedra jouseana*	*Thalassionema hirosakiensis*	*T. nitzschoides*	*Thalassiosira torokina*	*T.* sp. 10	*Thalassiothrix* spp.	*T. miocenica*	*Trinacria excavata*	*Corbisema triacantha*	*Mesocena circulus*	*M. diodon*	*Naviculopsis navicula* var. *naviculopsis*	*Goniothecium odontella*	*Hemiaulus incisus*	*H. polycystinorum* and *H. polymorphus*	*Lisitzinia ornata*	*Melosira architecturalis*	*Pyxilla* fragments	*Pterotheca aculeifera*	*Rocella gelida*	*R. gelida* var. *schraderi*	*R. vigilans*	*Stephanopyxis halomarginata*	*Triceratium groningensis*	*T. simulacrum*	*Corbisema apiculata*	*C. archangelskiana*	*C. disymmetrica communis*	*C. geometrica*	*Dictyocha frenguelii*	*Mesocena apiculata*	*N. oamaruensis*	*M. occidentalis*	*N. biapiculata*	*N. constricta*	*N. trispinosa*
20-5, 4-5		S			C			C					R				S			F													R			R		
21-2, 4-5	R	S			C	S		C					R				S	R		F		R								R				R		R		
21-5, 4-5	R	S		S	F			C					R							S																R		
23-2, 4-5	F	S		C	A	R		C	S			R	S		R	R	S			S	R	R									R							
23-5, 4-5	F			C	F			A			S	S	S							S				R			R	R										
24-5, 4-5	S			S				C	R			F	R				S						R										R					
25-2, 4-5	S	S	r	R	R		R	C	S	S	R	S	C				C	R		C	R	R			S		R									S		
25-5, 4-5	S	S			C			D	R			S	C				R																					
26-2, 4-5	S			S	C			A	S			S	F																									
27-2, 4-5	S	S			C			S	F			F	C							S	R		R															
28-2, 4-5	S			R	C			C	S			F	C							R									R								R	
29-2, 4-5	F			S	A		S	A	R	R	R	F	F											R												R		
29-5, 4-5	S	S		A	A		R	A	S			C	C							S	R																	
30-5, 4-5	S	S		C	A		R	A	R		R	F	C							S	R																	
31-5, 4-5	R	F			C		S	C			R	C					R			S	R	R	R			R							R					
34-2, 4-5		C	s	C	S			C			R						S			C				R													R	R
35-2, 4-5		R		F	R			C												S																		
36-2, 4-5		S		S				C												S																R		
37-1, 4-5				S	C			C			R						R			S																		
38-2, 4-5			r					C			R									R																		
39-2, 4-5		R						F									S			F			R															
40-2, 4-5					R		S	F					r								R																	
41-2, 4-5												R																										
41-5, 4-5		R	s					S			R						S			S			V													V		
42-2, 4-5		S						S									F	R		S																		
43-1, 4-5								F				R																										
44-1, 4-5		S			F			C												C			V	R														R
45-2, 4-5		S	S		R			C			R	R								F																		
46-2, 4-5			S					C			R	F								S																		
47-1, 4-5			r		C			C				S								S																	R	
48-2, 4-5								C													V						V					R					R	
49-2, 4-5		S						A									R			F																		
50-2, 4-5		R	S					F			R	R	r							S																		
51-1, 4-5			S		S			C												S																		
52-2, 4-5			R		F			C			R					R	S			S																		
12A-2, 4-5					S			C				R	r				R			S																		
13A-2, 4-5		S	F		F			C			R				R		F	S		F	S						R											R
14A-2, 4-5			F		R			A			S	F	r				S			F	R			R														
15A-2, 4-5			S		C			A			F						S			S																		
16A-2, 4-5			S		F			A		F							R			R																		V
17A-2, 4-5			S		F			C			R						S			S							V						V					
17A-5, 4-5		R	S		C			C			F			V			F			S	R		v													R		
18A-2, 4-5					S			F									S	R		S																		
19A-2, 4-5	R		S					F			S						S	R	S	F	R																	
20A-2, 4-5			R					S			S						F			F		R														S		
21A-2, 4-5			S					R			V						S			F	R												V		R	R		
23A-2, 4-5	Barren																																					
24A-2, 4-5																																						
25A-2, 4-5																																						
26A-1, 4-5																																						

N. grossepunctata Zone (NSD 5), and upper *C. lewisianus* Zone (NSD 4). At Site 594, *C. lewisianus* has its last occurrence in the upper part of Subzone a, similar to its position in the North Pacific (Barron, in press, b).

The North Pacific *D. lauta* Zone (NNPD 4, Koizumi, 1973; Barron, 1980a; Barron and Keller, 1983) is recognized in Sample 594A-15-2, 4–5 cm through the lowes occurrence of *D. lauta* in Sample 594A-17-5, 4–5 cm The first occurrence of *D. hyalina*, basal datum of Barron's (1980a) Subzone b, occurs in Sample 594A-15-2, 4–5 cm, the sole sample representing this subzone. Samples 594A-16-2, 4–5 cm through 594A-17-5, 4–5 cm rep-

Table 3. Ages of important stratigraphic diatom, radiolarian, silicoflagellate, and calcareous nannofossil datum levels in the Miocene of DSDP Holes 594 and 594A.

Core-Section (level in cm)			Datum	Age (Ma) (reference in parentheses)	Dating technique or direct paleomagnetic correlation
21-5, 4-5		LAD	*Brunia mirabilis*	5.6 (5)	Within Chron 5
23-2, 4-5	1.	FAD	*Cosmiodiscus insignis* var. *triangula*	6.4* (5)	Within (+) of Chron 6
	2.	LAD	*Mesocena circulus* (S)	6.4-5.9 (5)	upper Chron 6
	3.	LAD	*Thalassiothrix miocenica*	—	
	4.	FAD	*Thalassiosira torokina*	6.4-5.9 (5)	Upper (−) of Chron 6
23-5, 4-5		LAD	*Actinocyclus ellipticus*	—	
23,CC		LAD	*Discoaster quinqueramus* (N)	5.5* (1)	Top of (−), Chron 5
24-5, 4-5		FAD	*Nitzschia reinholdii*	5.6 (5)	Base of first (+), Chron 5
25-5, 4-5		LAD	*N. porteri*	6.7* (1)	upper Chron 7
26-2, 4-5	1. +	LAD	*Diartus hughesi* (R)	+ 8.5 (7), 7.0 (6)	mid to lower Chron 10 (7), lower Chron 7 (6)
	2.	LAD	*Coscinodiscus* aff. *marginatus*	—	—
26-5, 3-4		FAD	*Discoaster quinqueramus* (N)	7.3* (4)	2nd (−), Chron 7
27-2, 3-4		FAD	*Stichocorys peregrina* (R)	6.4 (12)	—
27-2, 4-5	1.	LAD	*Denticulopsis lauta*	8.5-8.7 (5)	lower Chron 10
				+ 9.5 (9)	K-Ar date
	2.	LAD	*Rhaphoneis* sp. 1	—	—
	3. +	FAD	*Nitzschia miocenica*	6.8* (1)	upper Chron 7
28-2, 4-5		FAD	*N. praereinholdii*	—	—
28-5, 4-5		LAD	*Discoaster hamatus* (N)	8.8* (3)	2nd (+), Chron 10
29-2, 4-5		LAD	*Thalassiosira* sp. 10	8.7 (7)	^{40}Ar/^{39}Ar date
29-5, 4-5	1.	FAD	*Thalassiothrix miocenica*	8.7 (7)	^{40}Ar/^{39}Ar date
	2.	LAD	*Denticulopsis dimorpha*		
			(temperate)	8.6 (8)	
			(subantarctic)	8.7 (7)	
29,CC	+	FAD	*Discoaster hamatus* (N)	10.0 (8)	
30-5, 4-5			First consistent *Mesocena diodon*(s)	—	
31-2, 3-4		LAD	*Cyrtocapsella japonica* (R)	8.7* (7, 6)	Uppermost Chron 11 and ^{40}Ar/^{39}Ar date
31-5, 3-4	1.	FAD	*Diartus hughesi* (R)	9.0* (1)	Uppermost Chron 11
	2.	FAD	*Stylatractus universus* (R)	8.7	^{40}Ar/^{39}Ar date
	3.	FAD	*Didymocyrtis antepenultima* (R)	9.0* (1)	Uppermost Chron 11
31-5, 4-5	4.	FAD	*Hemidiscus karstenii*	8.7 (7)	^{40}Ar/^{39}Ar date
	5.	FAD	*Nitzschia porteri*	—	
	6.	FAD	*N. fossilis*	—	
34-2, 4-5	1.	FAD	*Coscinodiscus* aff. *marginatus*	8.7 (7)	^{40}Ar/^{39}Ar date
	2.	FAD	*Actinocyclus ellipticus*	—	
	3.	FAD	*Lithodesmium* cf. *minusculum*	—	
	4.	FAD	*Asteromphalus* sp. 1	8.7 (7)	^{40}Ar/^{39}Ar date
	5.	FAD	*Hemidiscus cuneiformis*	8.7 (7)	^{40}Ar/^{39}Ar date
				+ 11.2 (4)	middle Chron 12
39-2, 4-5			Last common *Denticulopsis dimorpha*	—	
42-3, 3-4	+	FAD	*Discoaster kugleri* (N)	11.8 (8)	
44-1, 4-5	+	LAD	*Nitzschia denticuloides* (dissolutional)	—	
		LAD	*Denticulopsis punctata* f. *hustedtii*	10.7* (8)	Uppermost chron 12
47-1, 4-5	+	FAD	*D. dimorpha* (temperate)	8.9 (8)	
		LAD	*D. nicobaria* (isolated)	—	
49-2, 4-5	+	FAD	*D. praedimorpha* (temperate)	12.9 (8)	
51-1, 4-5			Last consistent *D. nicobaria*	12.6 (8)	
52-2, 4-5		LAD	*Conscinodiscus lewisianus*	12.9 (8)	
		FAD	*Nitzschia denticuloides*	—	
	+	LAD	*Actinocyclus ellipticus spiralis*	~ 11.0-10.8 (11)	
14A-2, 4-5	1. +	LAD	*Denticulopsis hyalina* (temperate)	15.0	
	2.	LAD	*Raphoneis amphiceros*	—	
	3.	LAD	*Actinocyclus ingens* (undulated)	—	
14A-5, 4-5			First common *Denticulopsis hustedtii* (main range, tropics)	13.9 (11)	
				14.0 (9)	K-Ar date
15A-2, 4-5	1.	LAD	*Actinocyclus ingens* var. *nodus*	—	
	2. +	FAD	*Denticulopsis hyalina*	15.0 (8)	
15A,CC		LAD	*Sphenolithus heteromorphus* (N)	14.0 (8)	
16A-2, 4-5	1.	FAD	*Denticulopsis punctata* f. *hustedtii*	13.7 (11)	
	2.	LAD	*D. punctata*	—	
	3.	FAD	*D. hustedtii* (isolated—tropics)	14.2 (11)	
	4.	FAD	*Actinocyclus ellipticus* var. *spiralis*	14.2 to 14.1 (11)	
17A-2, 4-5		FAD	*Denticulopsis punctata*	—	
17A-5, 4-5		FAD	*D.* spp. (dissolutional)	—	
18A-2, 4-5	1.	FAD	*Raphoneis amphiceros*	—	
	2.	FAD	*R. parilis*	—	
	3.	FAD	*Actinocyclus ingens* (dissolutional?)	15.5 (11)	

Note: Reference key is as follows: (1) Burckle, 1978; (2) Burckle, pers. comm. to Barron, in press, b; (3) Burckle et al., 1982; (4) Barron et al., in press; (5) Ciesielski, 1983; (6) Johnson and Wick, 1982; (7) based on position relative to ^{40}Ar/^{39}Ar date of 8.7 + 0.2 m.y. from DSDP Hole 513A (Ciesielski, 1983); (8) Barron et al., in press, b; (9) Koizumi, 1977; (10) Burckle, pers. comm. to Barron, 1978; (11) Barron, in press, a; age extrapolated from Barron, in press, b. Other symbols: * Direct paleomagnetic correlation. + Datum at left not considered reliable because of preservational problems or apparent diachrony relative to the lower latitudes. A after core number denotes cores from Hole 594A. N = calcareous nannoplankton; R = radiolarian; S = silicoflagellate. In right-hand column, (+) = normal polarity; (−) = reversed polarity.

resent Barron's (1980a) Subzone a of the *D. lauta* Zone (NNPD 4). The first occurrences of *D. hustedtii, D. hyalina, D. punctata*, and *D. punctata* var. *hustedtii* all fall within the *D. lauta* Zone. The portion of the *D. lauta* Zone (NNPD 4) represented here falls within the lower *C. lewisianus* Zone (NSD 4).

Samples 594A-18-2, 4–5 cm down to the basal barren zone of the hole beginning in Sample 594A-23-2, 4–5 cm are characterized by poor to very poor preservation and cannot be correlated with North Pacific diatom zones. Dissolution within this interval may have removed the lowermost occurrences of several diagnostic species, including the *A. ingens* group, *Brunia mirabilis, D. lauta*, and *D. nicobarica*. Dissolution is almost certainly responsible for the joint first occurrences of *D. lauta* and *D. nicobarica* in Sample 594A-17-5, 4–5 cm, because the first occurrence of *D. nicobarica* has been noted before the earliest *D. lauta* in the Southern Ocean (McCollum, 1975; Schrader, 1976) and throughout the low- to high-latitude Pacific (Barron, 1981, 1983; Schrader, 1976).

Samples 594A-18-5, 4–5 cm through the base of the hole (594A-26-1, 4–5 cm) probably fall within the lower *D. lauta* Zone (NNPD 4) and upper *A. ingens* Zone (NNPD 3). This conjecture is based on the placement of the early/middle Miocene boundary within this interval by Leg 90 paleontologists (Site 594 summary, this volume) and the paleomagnetic correlations (to follow herein) of microfossil datums in the lower part of Hole 594A. This interpretation would also agree with the correlation of the base of the *D. lauta* zone to approximately the early/middle Miocene boundary (Barron, 1980a; Barron and Keller, 1983).

CORRELATION OF THE MIOCENE OF SITE 594 TO PALEOMAGNETIC STRATIGRAPHY

Paleomagnetic studies of the HPC cores from the Miocene of Site 594 were unsuccessful in providing a magnetostratigraphy of the section because of low magnetic intensities (Barton and Bloemendal, this volume). The Miocene of Site 594 is here correlated to magnetostratigraphy generally, using microfossil datums which have been correlated directly or indirectly to magnetostratigraphy in middle- to lower-latitude sections. In the subantarctic and Antarctic, only a few diatom datums have been correlated to magnetostratigraphy (Ciesielski, 1983). These few correlations are not highly reliable because they are based on core sections bracketed by disconformities, making interpretations of the paleomagnetic record somewhat ambiguous.

A further complication of age interpretations at this site is the fact that the site lies just south of the Subtropical Convergence within the northern subantarctic zone. Temporal fluctuations of the Subtropical Convergence have resulted in a mixture of antarctic–subantarctic and temperate assemblages. Water mass migrations over the site have clearly resulted in microfossil datums which are diachronous with lower latitudes (Figs. 6 and 7, Table 3). In addition, dissolution may also have influenced the position of some datums.

Major foraminiferal, diatom, radiolarian, and silicoflagellate datums in the Miocene of Site 594 are illustrated in Figure 4. The absolute ages of many of these datums are given in Table 3 along with the source of the age information, the bulk of which are studies of low- to middle-latitude sequences.

An age versus depth diagram was constructed (Fig. 7) for datums listed in Table 3 to assist in determining those Miocene datums that are diachronous. Those datums considered unreliable because of apparent diachrony (greater than 0.5 m.y.) are identified by the symbol "+" preceding the datum designation in Table 3. Datums which appear to be significantly younger at Site 594 than their recorded occurrence elsewhere include the FAD and LAD of *Denticulopsis hyalina*, FAD of *D. praedimorpha*, LAD of *D. lauta*, FAD of *Hemidiscus cuneiformis*, FAD of *Discoaster kugleri*, LAD of *Diartus hughesi*, and FAD of *Discoaster hamatus*. Datums significantly older than their recorded occurrence elsewhere are the FAD of *Denticulopsis dimorpha* and the LAD of *Actinocyclus ellipticus spiralis*.

Reference to Figure 4 reveals that the Miocene of Site 594 represents upper Chronozone 16 through Chron 5. Cores 594-24 through 594-41 are difficult to correlate to magnetic stratigraphy because of problems of diachrony, dissolution, and a lack of reliable datums in much of this section. An exception to this generalization is found between Cores 594-28 and 594-34, where a number of datums occur in the same succession as at southwest Atlantic Site 513 (Fig. 6). At both sites these datums occur in close proximity to a radiometrically dated ash layer which is 8.7 ± 0.2 Ma. Cores 28–34 can be confidently considered to be approximately 9.0 to 8.5 Ma.

Cores 35 to 41 lack significant datums because of poor preservation and cannot be correlated accurately to magnetostratigraphy. Good biostratigraphic resolution within the lower part of the section suggests a correlation of Core 594-42 through Core 594A-18 to paleomagnetic Chronozones 13 through upper 16. The base of Hole 594 is barren of diatoms but is younger than the first occurrence of the calcareous nannofossil *Sphenolithus heteromorphus* (~17.5 Ma; Martini, this volume).

TAXONOMIC REFERENCES

Following is an alphabetical listing of diatom and silicoflagellate taxa cited in the range charts. It is not a complete list of all species in the assemblages. Since the emphasis in this study was on documenting the ranges of the predominant constituents of the assemblage, species represented by solitary occurrences were, in most cases, not included in the range charts. Because of time restrictions, emphasis was placed on species which characterize the assemblage or have potential use in biostratigraphy.

For each species, the first citation is the original description of the species. Subsequent citations are to more readily available references with descriptions, illustrations, and modern stratigraphic treatment. For species with more than one citation, only the more modern second citation is included in the reference list. The taxonomy follows that of Barron (1980a, b; 1983, in press) and Ciesielski (1983). References to the original species descriptions of the following taxa may be found in the publications already mentioned and in readily accessible papers dealing with Neogene subantarctic diatoms (McCollum, 1975; Schrader, 1976; Fenner et al., 1976; Gombos, 1976; Weaver and Gombos, 1981; and Ciesielski, 1983).

Diatoms

Actinocyclus ingens Rattray, 1890, p. 149, pl. 11, fig. 7; Schrader, 1973, pl. 18, figs. 2–4, 7; Kanaya, 1971, pl. 40.6, figs. 1–8. Re-

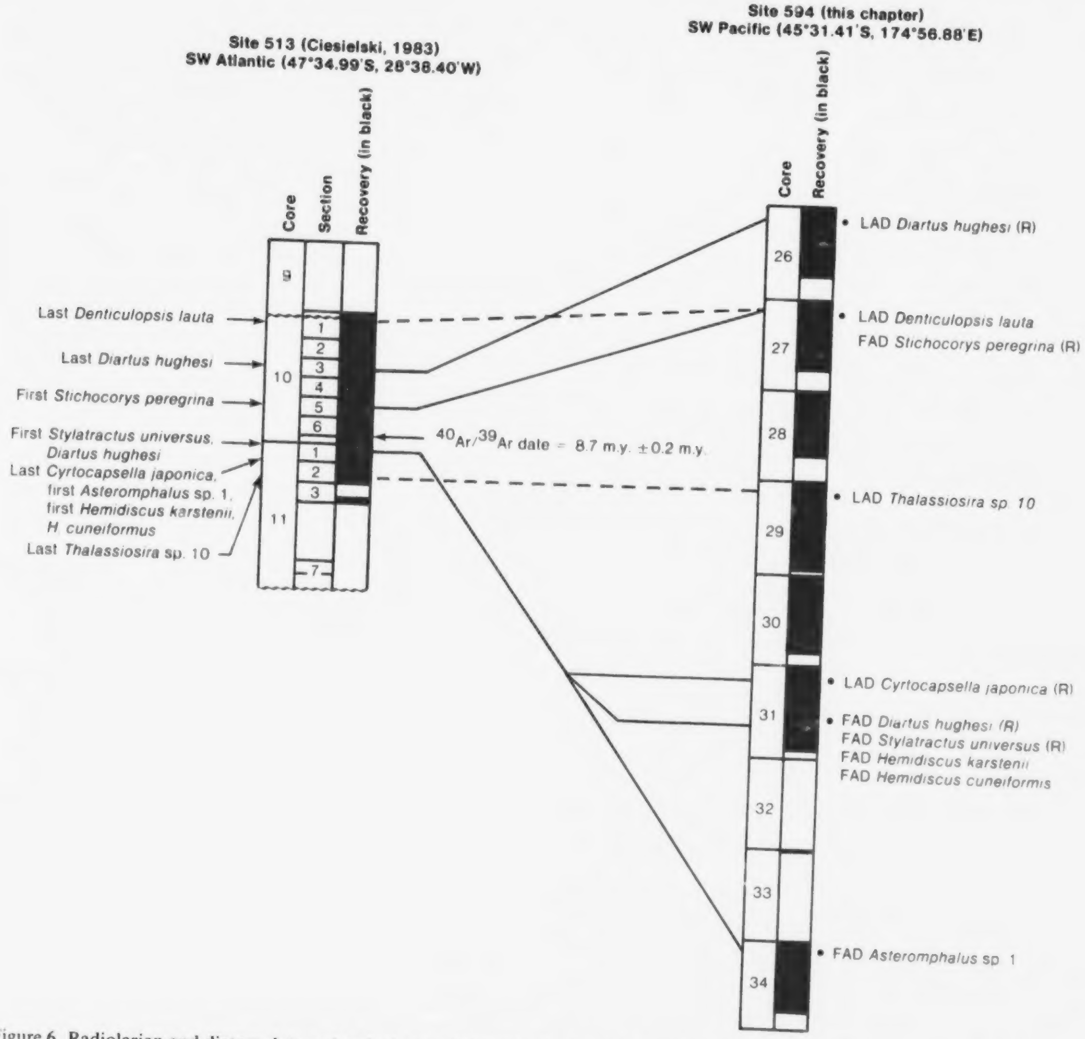
Site 513 (Ciesielski, 1983)
SW Atlantic (47°34.99'S, 28°38.40'W)
Core
Section
Recovery (in black)
Last Denticulopsis lauta
Last Diartus hughesi
First Stichocorys peregrina
First Stylatractus universus, Diartus hughesi
Last Cyrtocapsella japonica, first Asteromphalus sp. 1, first Hemidiscus karstenii, H. cuneiformus
Last Thalassiosira sp. 10
9
10
11
1
2
3
4
5
6
7
$^{40}Ar/^{39}Ar$ date = 8.7 m.y. ± 0.2 m.y.
Site 594 (this chapter)
SW Pacific (45°31.41'S, 174°56.88'E)
26
27
28
29
30
31
32
33
34
• LAD Diartus hughesi (R)
• LAD Denticulopsis lauta
FAD Stichocorys peregrina (R)
• LAD Thalassiosira sp. 10
• LAD Cyrtocapsella japonica (R)
• FAD Diartus hughesi (R)
FAD Stylatractus universus (R)
FAD Hemidiscus karstenii
FAD Hemidiscus cuneiformis
• FAD Asteromphalus sp. 1

Figure 6. Radiolarian and diatom datums bracketing a radiometrically dated volcanic ash (Dallmeyer *in* Ciesielski, 1983) in the upper Miocene to DSDP Site 513 and a correlation of these datums to DSDP Site 594. This comparison suggests a very high sediment accumulation rate in Cores 34–26 of Site 594. Based on this comparison, the 8.7 ± 0.2 Ma level in Site 594 falls between upper Core 29 and upper Core 27. Dashed lines represent slightly diachronous datums.

Remarks: Miocene representatives of this species are tabulated separately as "flat forms" or "undulated forms" according to the criteria of Baldauf and Barron (1980). (Plate 1, Fig. 10, "flat form".)

Actinocyclus ingens var. *nodus* Baldauf in Baldauf and Barron, 1980, p. 104, pl. 1, figs. 5–9. (Plate 1, Figs. 8–9.)

Actinocyclus ellipticus Grunow *in* Van Heurck, 1883, pl. 124, fig. 10; Schrader, 1973, pl. 8, figs. 7–9, 12–14, 16–17. (Plate 5, Fig. 8).

Actinocyclus ellipticus var. *spiralis* (Grunow) Barron, in press, a, pl. 7, figs. 9–10, pl. 9, fig. 5. (Plate 5, Figs. 6–7.)

Actinoptychus undulatus (Bailey) Ralfs in Pritchard, 1861; Hustedt, [illegible], pp. 475–478, fig. 264; Schrader, 1973, pl. 22, figs. 4, 12, 15.

Asteromphalus parvulus Karsten, 1905, p. 90, pl. 8, fig. 14; Hustedt, [illegible], p. 128, pl. 8, fig. 91; Schrader, 1976, pl. 8, figs. 3, 6.

Asteromphalus sp. 1 Ciesielski, 1983, p. 655, pl. 6, figs. 1–2, 6, 9.

Asteromphalus sp. 2 Schrader, 1976, pl. 8, fig. 1.

Asteromphalus sp. 3 Ciesielski, 1983, pl. 6, fig. 5.

Brunia mirabilis (Brun *in* Brun and Tempère) Tempère, 1890, plate 7, figs. 1–2. Barron, 1975, p. 127, pl. 4, fig. 16. Synonym: As *Bruniopsis mirabilis* (Brun) Karsten, referenced in Schrader, 1973, p. 702, pl. 13, fig. 16, and Gombos, 1977, p. 592, pl. 6, fig. 4.

Cestodiscus peplum Brun, 1891, p. 6, pl. 19, fig. 5; Lohman, 1974, pl. 3, fig. 2; Barron, 1983, pl. 1, figs. 1, 2. (Plate 5, Fig. 10.)

Charcotia actinochilus (Ehrenberg) Hustedt, 1958, pp. 122–126, figs. 57–80; Fenner et al., 1976, p. 771, pl. 5, fig. 5.

Coscinodiscus deformans Schrader, 1976, p. 630, pl. 11, figs. 1–2.

Coscinodiscus elliptopora Donahue, 1970, p. 201, pl. 4, figs. e, i–m; McCollum, 1975, pl. 16, fig. 10; Gombos, 1976, pl. 3, figs. 1–3, 6, pl. 9, fig. 3. (Plate 1, Fig. 6.)

Coscinodiscus endoi Kanaya, 1959, pp. 76–77, pl. 3, figs. 8–11; Schrader, 1976, p. 630, pl. 11, figs. 4, 8–10, 12.

Coscinodiscus kolbei Jousé, 1962, pl. 2, fig. 4; McCollum, 1975, pl. 4, figs. 7–9; Gombos, 1976, pl. 6, fig. 3. (Plate 4, Figs. 1–4.)

Coscinodiscus lentiginosus Janish *in* Schmidt et al., 1886, pl. 58, fig. 11; Gombos, 1976, pl. 3, figs. 4, 5.

Coscinodiscus lentiginosus var. *obovatus* (Castracane) Ciesielski, 1983, p. 653, pl. 4, figs. 6–8.

Coscinodiscus lewisianus Greville s.s.; Kolbe, 1954, pl. 2, fig. 21; Kanaya, 1971, pl. 40.5, figs. 4–6; Barron, 1983, pl. 1, fig. 5. Remarks: Included are specimens with length to width ratios of 5:3 or greater. (Plate 5, Figs. 1–4, 11.)

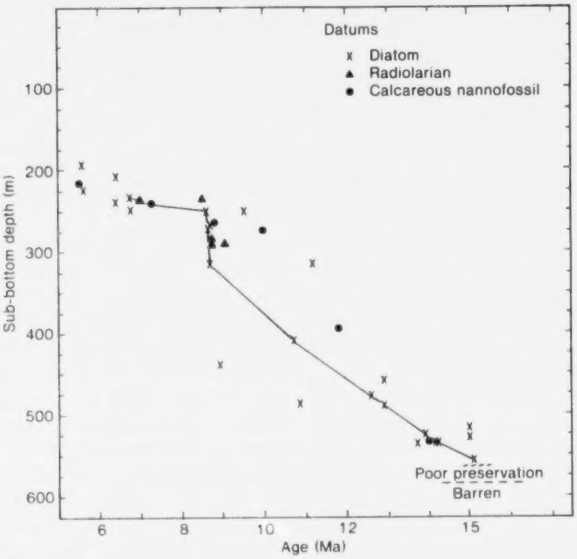

Figure 7. Age versus depth plot of the Miocene to Site 594 based on selected diatom, radiolarian, and calcareous nannofossil datums. Datum ages taken from Table 3.

Coscinodiscus lewisianus var. *robustus* Barron, 1983, p. 504, pl. 1, figs. 6-7. Remarks: Included are specimens with length to width ratios ranging from 4:3 to 8:7. (Plate 5, Fig. 5.)

Coscinodiscus aff. *lineatus* Ehrenberg, 1838; Schrader, 1976, p. 631, pl. 13, figs. 1, 2.

Coscinodiscus marginatus Ehrenberg, 1841, p. 142; Ehrenberg, 1854, pl. 18, fig. 44; Hustedt, 1930, p. 416, fig. 223.

Coscinodiscus praenitidus Fenner *in* Schrader and Fenner, 1976, p. 972, pl. 15, fig. 7, pl. 17, fig. 8.

Coscinodiscus ruboides Schrader, 1976, p. 631, pl. 6, figs. 4, 8.

Coscinodiscus vulnificus Gombos, 1977, p. 593, pl. 4, figs. 1-3, pl. 42, figs. 1-2.

Coscinodiscus yabei Kanaya, 1959, p. 86, pl. 5, figs. 6-9; Schrader, 1973, p. 704, pl. 6, figs. 1-6. (Plate 4, Figs. 7-10.)

Coscinodiscus aff. *C. marginatus* Ehrenberg, of Schrader, 1976, p. 631, pl. 10, fig. 3.

Cosmiodiscus insignis Jousé, 1961, p. 67, pl. 2, fig. 8; Koizumi, 1973, pl. 4, figs. 7-11; Gombos, 1976, pl. 4, figs. 4-5. Remarks: Whole valves of this species are rarely found intact in upper Gauss sediments of Southern Hemisphere mid-to high-latitude sediments. Plate 1, Figures 3-5 illustrate the most commonly recognized stages in the progressive dissolution of this species. (Plate 1, Figs. 1-5.)

Cosmiodiscus insignis f. *triangula* Jousé, 1977, pl. 79, fig. 2; Ciesielski, 1983, p. 656, pl. 5, figs. 1-10. (Plate 4, Figs. 5-6.)

Cosmiodiscus intersectus (Brun) Jousé, 1961, p. 68, pl. 2, figs. 9-10; Koizumi, 1973, p. 832, pl. 4, figs. 12-13.

Denticulopsis dimorpha (Schrader) Simonsen, 1979, p. 64. Synonym: *Denticula dimorpha* Schrader, 1973, p. 704, pl. 1, figs. 37-46; Barron, 1980a, pl. 1, fig. 21. (Plate 2, Figs. 5-8.)

Denticulopsis hustedtii (Simonsen and Kanaya) Simonsen, 1979, p. 64; Baldauf and Barron, 1982, pl. 7, figs. 7, 8. Synonym: *Denticula hustedtii* Simonsen and Kanaya, 1961, p. 501, pl. 1, figs. 19-25, pl. 2, figs. 36-47; Schrader, 1973, p. 704, pl. 2, figs. 28-34, 36-47. (Plate 2, Figs. 1-4.)

Denticulopsis hyalina (Schrader) Simonsen, 1979, p. 64; Baldauf and Barron, 1982, pl. 7, figs. 2, 4; Synonym: *Denticula hyalina* Schrader, 1973, p. 704, pl. 1, figs. 12-22. Remarks. In Site 594 this species is present in only two samples within the lower *Coscinodiscus lewisianus* Zone (NSD 4). In the North Pacific this species has a much longer range, having its last appearance in the upper Miocene *D. hustedtii* Zone, Subzone b. (Plate 2, Figs. 9-14.)

Denticulopsis lauta (Bailey) Simonsen, 1979, p. 64. Synonym: *Denticula lauta* Bailey, 1854, p. 9, figs. 1-2; Schrader, 1973, pl. 2, figs. 14-24, 35. Remarks: The lowermost range of this species may have been lost to dissolution.

Denticulopsis nicobarica (Grunow) Simonsen, 1979, p. 65; Baldauf and Barron, 1982, pl. 7, fig. 6; Synonym: *Denticula nicobarica* Grunow, 1868, p. 97, pl. 1a, fig. 5. Remarks: The lowermost range of this species may have been lost to dissolution. (Plate 2, Figs. 20-22.)

Denticulopsis praedimorpha (Akiba, 1979) Barron, 1981, p. 529, pl. 4, figs. 8-10; Synonym: *Denticula praedimorpha* (Akiba, 1979) Barron, 1980a, pl. 1, figs. 18-20.

Denticulopsis punctata (Schrader) Simonsen, 1979, p. 65; Baldauf and Barron, 1982, pl. 7, fig. 7. Synonym: *Denticula punctata* 1973 p. 705, pl. 1, figs. 25-30, pl. 3, figs. 16, 17. (Plate 2, Figs. 23-25.

Denticulopsis punctata f. *hustedtii* (Schrader) Simonsen, 1979; Barron, 1981, pl. 4, fig. 1; Synonym: *Denticula punctata* f. *hustedti* Schrader, 1973, p. 705, pl. 1, figs. 23, 24. (Plate 2, Figs. 15-19.)

Ethmodiscus rex (Wallich) Hendy *in* Wiseman and Hendy, 1953, p 51, pl. 1, fig. 1; Synonym: *Coscinodiscus rex* Wallich *in* Rattray 1980, p. 568, fig. 120.

Eucampia antarctica (Castracane) Mangin; Fenner et al., 1976, p. 774 pl. 5, figs. 7-9.

Goniothectum odontella Ehrenberg, 1844, p. 82; Gombos and Ciesielski, 1983, pl. 22, fig. 9. Reworked.

Hemiaulus incisus Hajós, 1976, p. 829, pl. 23, figs. 4-9. Reworked.

Hemiaulus polycystinorum Ehrenberg, 1854, pl. 36, figs. 43a, b; Fenner, 1978, p. 521, pl. 21, figs. 13, 14; pl. 22, figs. 4, 5, 7-10, pl. 23, figs. 1-4. Reworked.

Hemiaulus polymorphus Grunow, 1884, p. 66; Fenner, 1978, p. 522, pl. 21, fig. 11, pl. 23, figs. 10, 11, pl. 22, fig. 13. Reworked.

Hemidiscus cuneiformis Wallich, 1860, p. 42, pl. 2, figs. 3, 4; Barron 1980b, pl. 1, figs. 9, 10.

Hemidiscus karstenii Jousé *in* Jousé et al., 1962, p. 78, pl. 2, figs. 7-9; Abbott, 1974, pl. 1, figs. D-F; Gombos, 1976, pl. 4, fig. 8.

Hemidiscus karstenii f. 1 Ciesielski, 1983, p. 656, pl. 4, figs. 2-5.

Hyalodiscus spp. Remarks: No attempt to differentiate species of the genus was made in the present study.

Lithodesmium cf. *minusculum* Grunow *in* Van Heurck, 1883; Schrader, 1973, p. 706, pl. 12, figs. 15, 17; Barron, 1976, pl. 1, figs. 15, 16?; Ciesielski, 1983, p. 656. Remarks: Consistently present in the upper Miocene subantarctic DSDP Sites 594 and 513.

Lithodesmium aff. *reynoldsii* Barron, 1976, p. 53, pl. 1, figs. 17, 18?; Barron, 1981, pl. 5, fig. 7. Remarks: Specimens in Hole 594 are poorly preserved but appear to conform with the diagnosis by having punctae arranged in radial, linear rows, a small hyaline central area, one or two central nodules, straight or relatively straight valve margins, and a hyaline ring separating angles from the central body.

Lizitziana ornata Jousé, 1978, pp. 47-48, pl. 10, figs. 1-4; Gombos and Ciesielski, 1983, pl. 18, figs. 1-4. Synonym: *Triceratium cruciforme* Schmidt, 1887, pl. 77, fig. 41. Reworked.

Mediara splendida Scheschukova-Poretzkaja, 1962, p. 210, pl. 2, fig. 5; Baldauf and Barron, 1982, pl. 7, fig. 15.

Melosira architecturalis Brun, 1892, *in* Schmidt et al. (1874-____), pl. 177, figs. 45-50; Schrader and Fenner, 1976, p. 989, pl. 14, fig. 13, pl. 29, figs. 7-8, pl. 35, figs. 1-4. Reworked.

Nitzschia angulata (O'Meara) Hasle, 1972; Hasle, 1965, pp. 24-2 , pl. 1, fig. 6, pl. 4, fig. 19, pl. 9, figs. 1-6; Fenner et al., 197 , p. 775, pl. 1, figs. 17-39. (Plate 3, Fig. 13.)

Nitzschia denticuloides Schrader, 1976, p. 633, pl. 3, figs. 7-8, 10, 1 , 18-24; pl. 15, fig. 22. Remarks: Most specimens of this species are poorly preserved, particularly in the lower portion of its rang . (Plate 3, Fig. 18.)

Nitzschia aff. *donahuensis* Schrader, 1976, p. 633, pl. 2, fig. 30. Remarks: The specimen illustrated in Plate 3, Fig. 14 matches the description of Schrader (1976); however, the loss of one apex preven s a sure diagnosis because of the heteropolar nature of the speci .

Nitzschia fossilis (Frenguelli) Kanaya *in* Kanaya and Koizumi, 197 ; Schrader, 1974, p. 914, pl. 4, figs. 9-11, 24, 25; Barron, 198 , pl. 2, figs. 3, 4.

Nitzschia interfrigidaria (McCollum) Ciesielski, 1983, p. 655, pl. , figs. 11-13. (Plate 3, Figs. 6-7.)

Nitzschia januaria Schrader, 1976, p. 634, pl. 2, figs. 25-29. (Plate 3, Fig. 5.)

Nitzschia kerguelensis (O'Meara) Hasle, 1972; Hasle, 1965, pp. 14-18, pl. 4, figs. 11-18, pl. 7, fig. 9 (as *Fragilariopsis kerguelensis* O'Meara); Fenner et al., 1976, p. 776, pl. 2, figs. 19-30.

Nitzschia marina Grunow *in* Cleve and Grunow, 1880, p. 70; Grunow *in* Van Heurck, 1881, pl. 57, figs. 26–27; Schrader, 1973, pl. 4, figs. 17–19; Schrader, 1974, pl. 5, figs. 1–2, 5, 14?.

Nitzschia miocenica Burckle, 1972, pp. 240–241, pl. 2, figs. 10–15; Barron, 1980a, p. 672, pl. 2, fig. 8, pl. 3, figs. 3, 4.

Nitzschia porteri Frenguelli, 1949, p. 116, pl. 1, figs. 33–34; Schrader, 1973, p. 707, pl. 5, figs. 35, 36, 39–41, 43, 44.

Nitzschia praefossilis Schrader, 1973, p. 708, pl. 5, figs. 19, 21, 22.

Nitzschia praereinholdii Schrader, 1973, p. 708, pl. 5, figs. 20, 23, 26; Barron, 1981, pl. 4, fig. 16. (Plate 3, Fig. 15.)

Nitzschia reinholdii Kanaya and Koizumi, 1970; Schrader, 1973, p. 708, pl. 4, fig. 12–16, pl. 5, figs. 1–9; Barron, 1981, pl. 4, fig. 15. (Plate 3, Figs. 1–4.)

Nitzschia weaveri Ciesielski, 1983, p. 655, pl. 1, figs. 1–10. (Plate 3, Figs. 8–12.)

Nitzschia sp. 17 Schrader, 1976, p. 634, pl. 3, figs. 13–15, pl. 2, fig. 10.

Pterotheca aculeifera (Grunow) Van Heurck, 1896, p. 430, fig. 151; Fenner, 1978, p. 526, pl. 17, figs. 8–21; Synonym: *Pyxilla aculeifera* Grunow *in* Van Heurck, 1882, pl. 83, figs. 13, 14. Reworked.

Pyxilla fragments. Only reworked fragments of this genus were found in Neogene sediments.

Raphiodiscus marylandicus Christian, 1887; Schrader, 1973, p. 708, pl. 22, fig. 7; Andrews, 1974, p. 232, pls. 1–5, figs. 1–29.

Rhaphoneis amphiceros Ehrenberg, 1844; Hustedt, 1959, p. 174, figs. 680–681; Schrader, 1973, pp. 708–709, pl. 25, figs. 2–3. Remarks: The present study follows Schrader (1973) by including only specimens with finely punctate apices, with a single mucous pore situated at each apex and excentric to the axial area. (Plate 6, Figs. 1–3.)

Rhaphoneis parilis Hanna, 1932, pp. 214–215, pl. 16, figs. 2–4; Lohman, 1948, p. 182, pl. 11, fig. 10. (plate 6, Fig. 6.)

Rhaphoneis sp. 1. Remarks: A great deal of morphologic variability was found in *Rhaphoneis* specimens in the interval encompassed by the ranges of *R. amphiceros* and *R. parilis.* These specimens have one mucous pore located excentrically at each apex but do not have finely punctate apices. Valve surfaces on the opposite sides of the pseudoraphe are often asymmetric in outline. (Plate 3, Figs. 19–21.)

Rhizosolenia barboi (Brun) Tempère and Peragallo, 1908, p. 26, No. 47; Schrader, 1973, p. 709, pl. 24, figs. 4, 7; Synonym: *Pyxilla barboi* Brun, 1894, p. 87, pl. 5, figs. 16, 17, and 23. (Plate 3, Fig. 22.)

Rhizosolenia hebatata Bailey, 1856, p. 5, pl. 1, figs. 18, 19.

Rhizosolenia hebatata forma hiemalis Gran, 1904, p. 527, pl. 27, fig. 9; Schrader, 1973, pl. 9, figs. 11, 13–17, 19–21, 24, 25.

Rhizosolenia praebarboi Schrader, 1973, p. 709, pl. 24, figs. 1–3; Barron, 1980a, pl. 2, fig. 18.

Rhizosolenia styliformis Brightwell, 1858, p. 95, pl. 5, figs. 5a, b and d; Hustedt, 1930, pp. 584–588, figs. 333–335; Schrader, 1973, pl. 10, figs. 1, 18, 19, 20, 21; pl. 9, fig. 9?.

Rocella gelida (Mann) Bukry, 1978, p. 788, pl. 5, figs. 1–13; Gombos and Ciesielski, 1983, pl. 6, figs. 1–6, pl. 26, fig. 1. Reworked.

Rocella gelida var. *schraderi* (Bukry) Barron, in press b, fig. 4.15. Synonym: *Rocella schraderii* Bukry, 1978, p. 788, pl. 6, figs. 1–10, pl. 7, fig. 1; Gombos and Ciesielski, 1983, pl. 22, fig. 6. Reworked. (Plate 2, Fig. 26.)

Rocella vigilans (Schmidt) Fenner, 1982; Gombos and Ciesielski, 1983, p. 604, pl. 6, figs. 7–10; pl. 26, fig. 2. Synonym: *Coscinodiscus vigilans* Schmidt, Jousé, 1974, pl. 3, fig. 16; Kolbe, 1954, pl. 1, figs. 13, 14. Reworked.

Stephanopyxis hyalomarginata Hajós, 1976, p. 824, pl. 19, figs. 11–12; Gombos and Ciesielski, 1983, pl. 10, figs. 1–6. Reworked.

Stephanopyxis turris (Greville et Arnott) Ralfs *in* Pritchard, 1861, p. [illegible], pl. 5, fig. 74; Fenner, 1978, p. 532, pl. 12, figs. 8, 9. Synonym: *Cresswellia turris* Greville and Arnott, 1857, p. 538. (Plate 1, Fig. 7.)

Synedra jouseana Sheshukova-Poretzkaya, 1962, p. 208, fig. 4; Schrader, 1973, pl. 23, figs. 21–23, 25, 28.

Thalassionema hirosakiensis (Kanaya) Schrader, 1973, p. 711, pl. 23, figs. 31–33.

Thalassionema nitzschioides (Grunow) Van Heurck, 1896, p. 319, fig. 75; Schrader, 1973, pl. 23, figs. 2, 6, 8, 9, 10, 12–13, 26, 29, 34. (Plate 3, Fig. 17.)

Thalassiosira torokina Brady, 1977, pp. 122–123, figs. 1–5; Ciesielski, 1983, pl. 7, figs. 3–6.

Thalassiosira sp. 10 Schrader, 1976, p. 637, pl. 15, figs. 6–8.

Thalassiothrix spp. All species of *Thalassiothrix* are so tabulated in Table 2, except *T. miocenica*, which is tabulated separately.

Thalassiothrix miocenica Schrader, 1973, p. 713, pl. 23, figs. 2–5.

Triceratium groningensis Reinhold, 1937, p. 126, pl. 20, fig. 9; Fenner, 1979, p. 534, pl. 30, figs. 21–22. Reworked.

Trinacria excavata Heiberg, 1863; Hustedt, 1930, pp. 887–888, fig. 532; McCollum, 1975, pl. 13, fig. 6.

Trinacria simulacrum Grove and Sturt, 1887, p. 144, pl. 13, fig. 46; Fenner, 1978, p. 536, pl. 19, fig. 2; pl. 31, fig. 2.

Xanthiopyxis acrolophra Forti, 1913; Kanaya, 1959, p. 159, pl. 11, fig. 8.

Silicoflagellates

Corbisema apiculata (Lemmermann) Hanna, 1931; Shaw and Ciesielski, 1983, p. 706, pl. 1, figs. 1–3. Reworked.

Corbisema archangelskiana (Schulz) Frenguelli, 1940, fig. 12a; Shaw and Ciesielski, 1983, pl. 19, figs. 1–4, 6; pl. 20, fig. 1. Reworked.

Corbisema disymmetrica communis Bukry, 1976, p. 891, pl. 1, figs. 1–4; Synonym: *Corbisema navicula navicula* (Ehrenberg) Busen and Wise, 1977, p. 712, pl. 2, figs. 7–9. Reworked.

Corbisema geometrica Hanna, 1928, no. 4, p. 261, pl. 41, figs. 1, 2 (*fide* Loeblich et al., 1968, p. 75). Reworked.

Corbisema triacantha (Ehrenberg) Hanna, 1931; Ling, 1973, pl. 1, figs. 7, 8; Bukry and Foster, 1973, p. 826, pl. 2, fig. 3; Bukry, 1973, pl. 1, fig. 2.

Dictyocha frenguelli Deflandre, 1950, p. 194, figs. 188–193. Reworked.

Dictyocha spp. Remarks: *Dictyocha* species are not differentiated herein.

Distephanus boliviensis (Frenguelli) Bukry and Foster, 1973, p. 187, pl. 4, figs. 1–3; Shaw and Ciesielski, p. 713, pl. 10, figs. 5, 8.

Distephanus crux crux (Ehrenberg) Haeckel, 1887, p. 1563 (*fide* Glezer, 1966, pp. 279–280); Shaw and Ciesielski, 1983, p. 713, pl. 10, figs. 6–7; pl. 11, fig. 1.

Distephanus polyactis (Ehrenberg) Deflandre, 1932, p. 501, fig. 40.

Mesocena apiculata (Schulz) Hanna, 1931; Shaw and Ciesielski, 1983, p. 714, pl. 12, figs. 1–7. Reworked.

Mesocena circulus (Ehrenberg) Ehrenberg, 1844; Ling, 1972, p. 175, pl. 28, figs. 5, 6.

Mesocena diodon Ehrenberg, 1844, pp. 71, 84; Shaw and Ciesielski, 1983, p. 714; Ciesielski, 1975, p. 661, pl. 12, figs. 1–3.

Mesocena oamaruensis Schulz, 1928; Shaw and Ciesielski, 1983, p. 714, pl. 12, figs. 8–10, pl. 13, figs. 1–9, pl. 14, figs. 1–2. Reworked.

Mesocena occidentalis Hanna, 1931; Shaw and Ciesielski, 1983, p. 714, pl. 13, figs. 3–8. Reworked.

Naviculopsis biapiculata (Lemmermann) Frenguelli, 1940; Shaw and Ciesielski, 1983, p. 715, pl. 14, figs. 11–13, pl. 15, figs. 1–3. Reworked.

Naviculoposis constricta (Schulz) Frenguelli, 1940; Shaw and Ciesielski, 1983, p. 715, pl. 15, figs. 4–8. Reworked.

Naviculopsis navicula var. *naviculopsis* (Deflandre) Tsumura, 1963; Ciesielski, 1975, pl. 13, figs. 2, 3.

Naviculopsis trispinosa (Schulz) Glezer, 1966; Ciesielski, 1975, pl. 13, figs. 13, 14. Reworked.

Incertae Sedis

Macrora stella (Azpeitia) Hanna, 1932, p. 196, pl. 12, fig. 7; Schrader, 1973, pl. 12, figs. 21–24.

ACKNOWLEDGMENTS

Research supported by NSF grant DPP-81-13147 to M. T. Ledbetter and P. F. Ciesielski and NSF grant DPP-83-16679 to P. F. Ciesielski. Andrew M. Gombos, Jr., and John A. Barron are thanked for critical review of the manuscript.

REFERENCES

Baldauf, J. G., and Barron, J. A., 1980. *Actinocyclus ingens* var. *nodus:* A new, stratigraphically useful diatom of the circum-North Pacific. *Micropaleontology*, 26:103–110.

Barron, J. A., 1975. Late Miocene–early Pliocene marine diatoms from southern California. *Palaeontographica B*, 151:97–170.

———, 1976. Revised Miocene and Pliocene diatom biostratigraphy of Upper Newport Nay, Newport Beach, California. *Mar. Micropaleontol.*, 1:27–63.

________, 1980a. Lower Miocene to Quaternary diatom biostratigraphy of Leg 57, off northeastern Japan, Deep Sea Drilling Project *In* Scientific Party, *Init. Repts. DSDP*, 56, 57, Pt. 2: Washington (U.S. Govt. Printing Office), 641–685.

________, 1980b. Upper Pliocene and Quaternary diatom biostratigraphy of Deep Sea Drilling Project Leg 54, tropical Eastern Pacific. *In* Rosendahl, B. R., Hekinian, R., et al., *Init. Repts. DSDP*, 54: Washington (U.S. Govt. Printing Office), 455–462.

________, 1981. Late Cenozoic diatom biostratigraphy and paleoceanography of the middle-latitude eastern North pacific, Deep Sea Drilling Project Leg 63. *In* Yeats, R. S., Haq, B., et al., *Init. Repts. DSDP*, 63: Washington (U.S. Govt. Printing Office), 507–538.

________, 1983. Latest Oligocene through early middle Miocene diatom biostratigraphy of the eastern tropical Pacific. *Mar. Micropaleontol.*, 7:487–515.

________, in press, a. Late Eocene diatom biostratigraphy of the equatorial Pacific Ocean, DSDP Leg 85. *In* Mayer, L. Theyer, F., et al., *Init. Repts. DSDP*, 85: Washington (U.S. Govt. Printing Office).

________, in press, b. Neogene planktic diatom biostratigraphy. *In* Saunders, J. B., Bolli, H. M. (Eds.), *Biostratigraphy by Marine Plankton:* Cambridge (Cambridge Univ. Press).

Barron, J. A., and Keller, G., 1983. Paleotemperature oscillations in the middle and late Miocene of the northeastern Pacific. *Micropaleontology*, 29(2):150–181.

Barron, J. A., Keller, G., and Dunn, D. A., in press. A multiple microfossil biochronology for the Miocene. *Geol. Soc. Am. Mem.*

Berggren, W. A., 1981. Correlation of Atlantic, Mediterranean and Indo-Pacific Neogene stratigraphies: Geochronology and Chronostratigraphy. *Proc. IGCP-114 Int. Workshop Pacific Neogene Biostratigraphy*, Nov. 25–29, 1981, Osaka, Japan, pp. 29–60.

Berggren, W. A., Kent, D. V., and Flynn, J. J., in press. Paleogene geochronology and chronostratigraphy. *In* Snelling, N. J. (Ed.), *Geochronology and the Geological Record*. Geol. Soc. London, Spec. Paper.

Berggren, W. A., and Van Couvering, J. A., 1974. The Late Neogene: biostratigraphy, geochronology and paleoclimatology of the last 15 million years in marine and continental sequences. *Palaeogeogr., Palaeoclimatol., Palaeoecol.*, 16:1–216.

Brady, H. T., 1977. *Thalassiosira torokina* n.sp. (diatom) and its significance in Late Cenozoic biostratigraphy. *Antarctic J. U.S.*, 12: 122–123.

Bukry, D., 1976. Cenozoic silicoflagellate and coccolith stratigraphy, South Atlantic Ocean, Deep Sea Drilling Project Leg 36. *In* Hollister, C. D., Craddock, C., et al., *Init. Repts. DSDP*, 35: Washington (U.S. Govt. Printing Office), 845–872.

Burckle, L. H., 1972. Late Cenozoic planktonic diatom zones from the eastern equatorial Pacific: *Nova Hedw., Beihft.*, 39:217–250.

________, 1978. Early Miocene to Pliocene diatom datum levels for the equatorial Pacific. *Proc. Second Working Group Meeting, Biostratigraphic Datum-Planes of the Pacific Neogene, IGCP Project 114.* Republic of Indonesia Ministry of Mines and Energy, Directorate General of Mine, Geological Research and Development Center, Spec. Publ., 1:25–44.

Burckle, L. H., Keigwin, L. D., and Opdyke, N. D., 1982. Middle and late Miocene stable isotope stratigraphy: correlation to the paleomagnetic reversal record. *Micropaleontology*, 28:329–334.

Ciesielski, P. F., 1975. Biostratigraphy and paleoecology of Neogene and Oligocene silicoflagellates from cores recovered during Antarctic Leg 28, Deep Sea Drilling Project. *In* Hays, D. E., Frakes, L. A., et al., *Init. Repts. DSDP*, 28: Washington (U.S. Govt. Printing Office), 625–691.

________, 1983. The Neogene and Quaternary diatom biostratigraphy of subantarctic sediments, Deep Sea Drilling Project Leg 71. *In* Ludwig, W. J., Krasheninnikov, V. A., et al., *Init. Repts. DSDP*, 71: Washington (U.S. Govt. Printing Office), 635–665.

Cita, M. B., 1975. The Miocene/Pliocene boundary: history and definition. *In* Saito, T., and Burckle, L. H. (Eds.) *Late Neogene Epoch Boundaries:* New York (Micropaleontology Press), pp. 1–30.

Deflandre, G., 1932. Sur la systématique des silicoflagellés. *Soc. Bot. Fr. Bull.*, 79:494–506.

Donahue, J. G., 1970. *Pleistocene Diatoms as Climatic Indicators in North Pacific Sediments.* Geol. Soc. Am. Mem., 126.

Fenner, J., 1978. Cenozoic diatom biostratigraphy of the equatorial and southern Atlantic Ocean. *In* Supko, P. R., Perch-Nielsen, K., et al., *Init. Repts. DSDP*, Suppl. to Vols. 38, 39, 40, and 41: Washington (U.S. Govt. Printing Office), 491–623.

________, 1982. Diatoms in the Eocene and Oligocene sediments off N.W. Africa, their stratigraphic and paleogeographic occurrences [Ph.D. dissert.]: Kiel (University of Kiel).

Fenner, J., Schrader, H.-J., and Wienigk, H., 1976. Diatom phytoplankton studies in the southern Pacific Ocean, composition and correlation to the Antarctic Convergence and its paleoecological significance. *In* Hollister, C. D., and Craddock, C., et al., *Init. Repts. DSDP*, 35: Washington (U.S. Govt. Printing Office), 757–813.

Gombos, A. M., Jr., 1976. Paleogene and Neogene diatoms from the Falkland Plateau and Malvinas Outer Basin: Leg 36 Deep Sea Drilling Project. *In* Barker, P. F., Dalziel, I. W. D., et al., *Init. Repts. DSDP*, 36: Washington (U.S. Govt. Printing Office), 575–687.

Gombos, A. M., Jr., and Ciesielski, P. F., 1983. Late Eocene to Early Miocene diatoms from the southwest Atlantic. *In* Ludwig, W. F., Krasheninnikov, V. A., et al., *Init. Repts. DSDP*, 71: Washington (U.S. Govt. Printing Office), 583–634.

Hajós, M., 1976. Upper Eocene and lower Oligocene diatomaceae, Archaeomonadaceae, and Silicoflagellatae in Southwestern Pacific sediments, DSDP Leg 29. *In* Hollister, C. D., Craddock, C., et al., *Init. Repts. DSDP*, 35: Washington (U.S. Govt. Printing Office), 817–883.

Hanna, G. D., 1928. Silicoflagellatae from the Cretaceous of California. *J. Paleontol.*, 1(4):259–264.

________, 1931. Diatoms and silicoflagellates of the Kreyenhagen Shale. *Rept. State Mineral.*, pp. 187–201.

________, 1932. The diatoms of Sharktooth Hill, Kern County, California: *Calif. Acad. Sci. Proc.*, 20:161–263.

Hasle, G., 1965. *Nitzschia* and *Fragilariopsis*, species studied in the light and electron microscopes. III. The genus *Fragilariopsis: Skr. Nor. Videnskaps-Akad I. Mat.-Naturvidensk Kl.*, 21:1–49.

Hustedt, F., 1930. Die Kieselalgen Deutschlands, Osterreichs, und der Schweiz mit Berücksichtigung der übrigen Länder Europas sowie der angrenzenden Meeresgebiete. *In* Rabenhorst, L. (Ed.), *Kryptogamen-Flora von Deutschland, Osterreich und der Schweiz.* Vol. 7, Pt. 1: Leipzig (Akademische Verlagsgesellschaft).

________, 1958. *Diatomeen aus der Antarktik und dem Sudatlantik.* Deutsche Antarktische Exped. (Vol. 2).

Johnson, D. A., and Wick, B. J., 1982. Precision of correlation of radiolarian datum levels in the middle Miocene equatorial pacific. *Micropalentology*, 28:1–30.

Jousé, A. P., 1961. Miocene and Pliocene marine diatoms from the Far East. *Akad. Nauk SSSR, Bot. Inst. In. V. L. Komarova, Otd. Sporov. Rast., Bot. Mat.*, 14:59–70. (In Russian.)

________, 1962. *Stratigraphische und Palaogeographische Untersuchungen im Nordwestteil des Pazifik*, (vol. 5): Moscow (USSR Academy of Sciences).

________, 1978. New fossil genus of diatoms (*Lisitzinia* [Bacillariophyta]). *Marsk. Mikropaleontol.* (Moscow), pp. 47–48.

Kahn, M. J., Miller, K. G., Kent, D. V., Aubry, M.-P., and Berggren, W. A., 1984. Oligocene–Miocene magnetobiostratigraphy of the Western North Atlantic: Age of the middle/late Miocene boundary. *Trans. Am. Geophys. Union*, 65:199. (Abstract.)

Kanaya, T., 1959. Miocene diatom assemblages from the Onnagawa Formation and their distribution in the correlative formations in northeast Japan: *Sci. Rept. Tohoku Univ.*, Ser. 2 (Geol.), 30:1–1[illegible].

Koizumi, I., 1973. The Late Cenozoic diatoms of Sites 183–193, Leg 19, Deep Sea Drilling Project. *In* Creager, J. S., Scholl, D. W., et al., *Init. Repts. DSDP*, 19: Washington (U.S. Govt. Printing Office), 805–855.

________, 1977. Diatom biostratigraphy in the North Pacific region. *Proc. First Congr. Pacific Neogene Stratigraphy:* Tokyo (Kaiyo Shuppan), pp. 235–253.

Kolbe, R. W., 1954. Diatoms from equatorial Pacific cores. *In* Petterson, H. (ed.), *Rept. Swed. Deep-Sea Exped. 1947–1948*, 6:1–4[illegible]

LaBrecque, J. L., Kent, D. V., and Cande, S. C., 1977. Revised magnetic polarity time scale for Late Cretaceous and Cenozoic time. *Geology*, 5:330–335.

Ling, H. Y., 1972. Upper Cretaceous and Cenozoic silicoflagellates and ebridians. *Bull. Am. Paleontol.*, 62:125–229.

Lohman, K. E., 1974. Lower middle Miocene marine diatoms from Trinidad. *Verh. Nat. Ges. Basel*, pp. 1–47.

McCollum, D. W., 1975. Diatom stratigraphy of the Southern Ocean. *In* Hayes, D. and Frakes, L. A., et al., *Init. Repts. DSDP*, 28: Washington (U.S. Govt. Printing Office), 515–571.

Martini, E., 1971. Standard Tertiary and Quaternary calcareous nannoplankton zonation. *In* Farinacci, A. (Ed.), *Proc. II Planktonic Conf., Roma, 1970* (Vol. 2): Rome (Edizioni Tecnoscienza), 739–777.

Ryan, W. B. F., Cita, M. B., Rawson, M., Burckle, L. H., and Saito, T., 1974. A paleomagnetic assignment of Neogene stage boundaries and the development of isochronous datum planes between the Mediterranean, the Pacific, and Indian Oceans in order to investigate the response of the world ocean to the Mediterranean "salinity crisis." *Riv. Ital. Paleontol.*, 80:631–688.

Schrader, H.-J., 1973. Cenozoic diatoms from the northeast Pacific, Leg 18. *In* Kulm, L. D., von Huene, R., et al., *Init. Repts. DSDP*, 18: Washington (U.S. Govt. Printing Office), 673–797.

———, 1976. Cenozoic planktonic diatom biostratigraphy of the Southern Ocean. *In* Hollister, C. D., Craddock, C., et al., *Init. Repts. DSDP*, 35: Washington (U.S. Govt. Printing Office), 605–671.

Schrader, H.-J., and Fenner, J., 1976. Norwegian Sea Cenozoic diatom biostratigraphy and taxonomy. *In* Talwani, M., Udintsev, G., et al., *Init. Repts. DSDP*, 38: Washington (U.S. Govt. Printing Office), 921–1098.

Shaw, C. A., and Ciesielski, P. F., 1983. Silicoflagellate biostratigraphy of middle Eocene to Holocene subantarctic sediments recovered by Deep Sea Drilling Project Leg 71. *In* Ludwig, W. J., Krasheninnikov, V. A., et al., *Init. Repts. DSDP*, 71: Washington (U.S. Govt. Printing Office), 687–737.

Simonsen, R., 1979. The diatom system: Ideas on phylogeny. *Bacillaria*, 2:9–79.

Tauxe, L., Opdyke, N. D., Pasini, G., and Elmi, C., 1983. Age of the Plio–Pleistocene boundary in the Vrica section, southern Italy. *Nature*, 304:125–129.

Theyer, F., and Hammond, S. R., 1974. Paleomagnetic polarity sequence and radiolarian zones, Brunhes to polarity epoch 20. *Earth Planet. Sci. Lett.*, 22:307–319.

Theyer, F., Mato, C. Y., and Hammond, S. R., 1978. Paleomagnetic and geochronologic calibration of latest Oligocene to Pliocene radiolarian events, equatorial Pacific. *Mar. Micropaleontol.*, 3: 377–395.

Weaver, F. M., and Gombos, A. M., 1981. Southern high latitude diatom biostratigraphy. *In* Warme, T. E., Douglas, R. C., and Winterer, E. L. (Eds.), *The Deep Sea Drilling Project: A Decade of Progress*. Soc. Econ. Paleont. Mineral., Spec. Publ., 32:445–470.

Wiseman, D., and Hendy, N., 1953. The significance and diatom content of a deep-sea floor sample from the neighbourhood of the greatest oceanic depth. *Deep-Sea Res.*, 1:47–59.

Date of Initial Receipt: 24 September 1984
Date of Acceptance: 7 February 1985

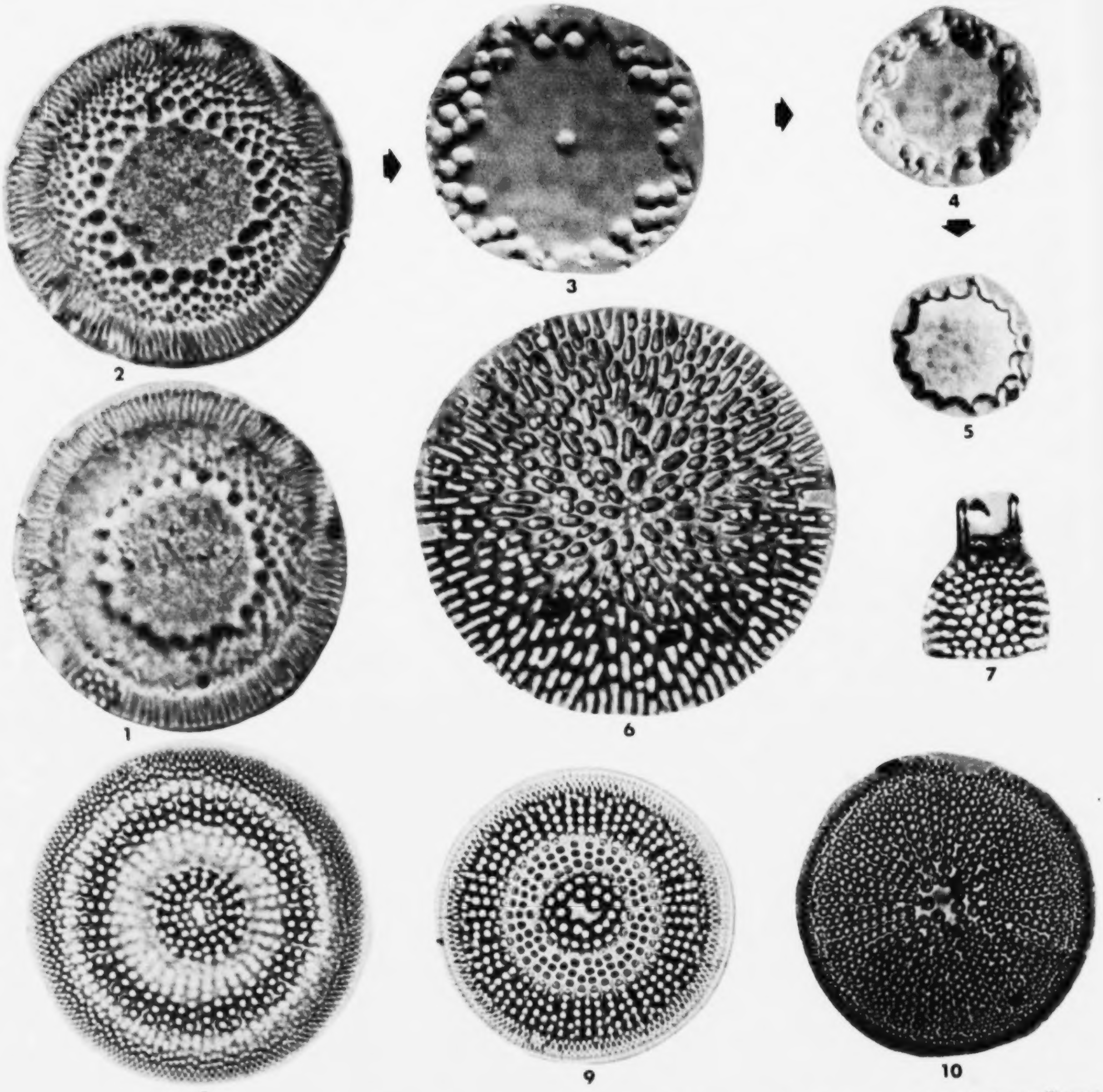

Plate 1. **1-5.** *Cosmiodiscus insignis* Jousé, × 1500, (1-2) Sample 594-16-5, 4-5 cm, (3-5) Sample 594-16-2, 4-5 cm. **6.** *Coscinodiscus elliptopo* Donahue, × 1000, Sample 594A-5-5, 4-5 cm. **7.** *Stephanopyxis turris* Ralfs, × 750, Sample 594-20-2, 4-5 cm. **8-9.** *Actinocyclus ingens* va *nodus* Baldauf, × 750, Sample 594A-18-2, 4-5 cm. **10.** *Actinocyclus ingens* Rattray (flat form), × 1000, Sample 594-9-5, 4-5 cm.

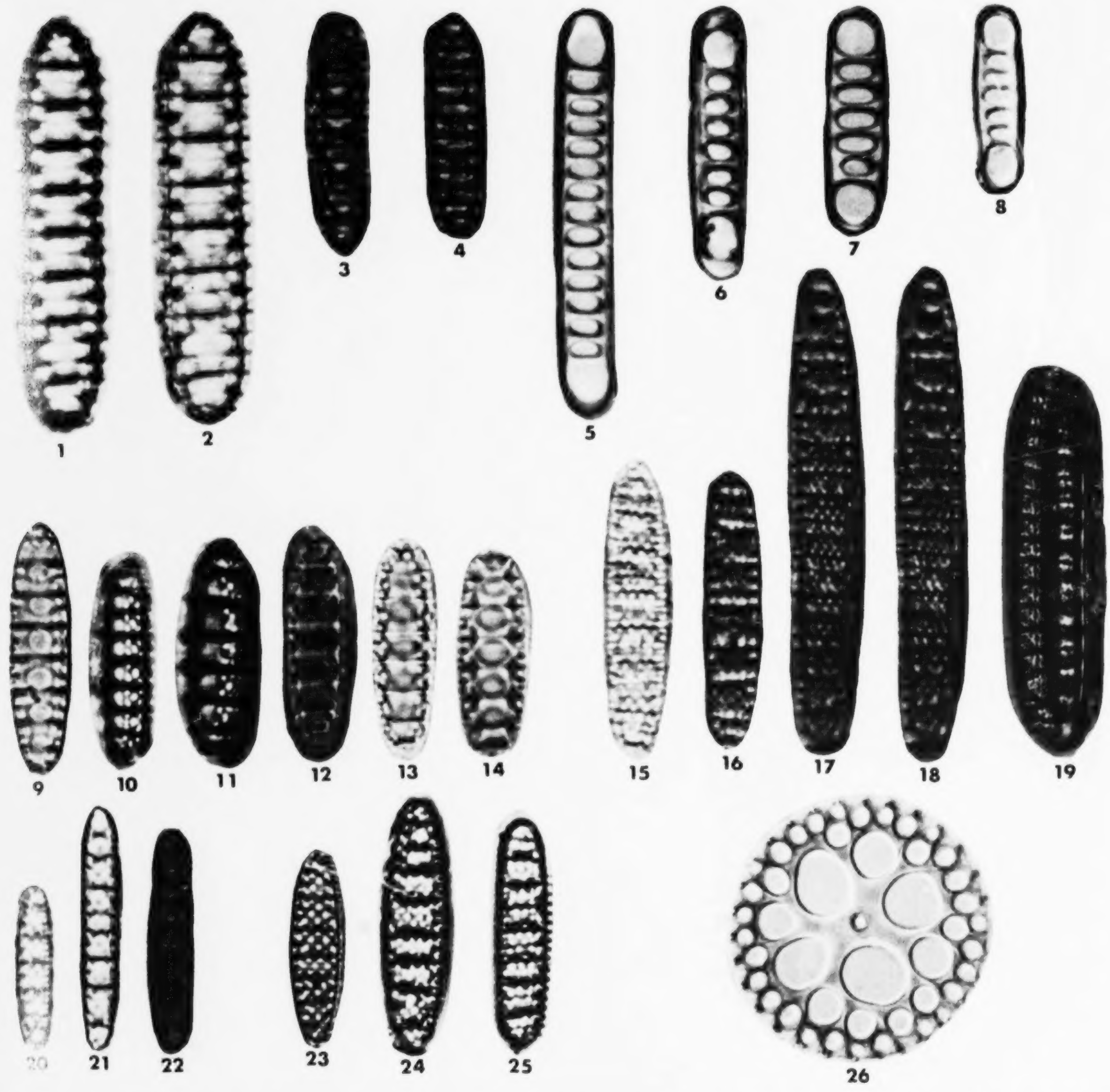

Plate 2. **1–4.** *Denticulopsis hustedtii* (Simonsen and Kanaya) Simonsen, × 1500, (1–2) Sample 594-49-2, 4–5 cm, (3–4) Sample 594-31-2, 4–5 cm. **5–8.** *Denticulopsis dimorpha* (Schrader) Simonsen, × 1500, (5, 7) Sample 594-44-1, 4–5 cm, (6) Sample 594-45-2, 4–5 cm, (8) Sample 594-47-1, 4–5 cm. **9–14.** *Denticulopsis hyalina* (Schrader) Simonsen, × 1500, (9–10, 12–14) Sample 594A-15-2, 4–5 cm, (11) Sample 594A-14-2, 4–5 cm. **15–19.** *Denticulopsis punctata* f. *hustedtii* (Schrader) Simonsen, × 1500, (15–18) Sample 594-47-1, 4–5 cm, (19) Sample 594A-15-2, 4–5 cm. **20–22.** *Denticulopsis nicobarica* (Grunow) Simonsen, × 1500, Sample 594A-16-5, 4–5 cm. **23–25.** *Denticulopsis punctata* (Schrader) Simonsen, × 1500, Sample 594A-16-2, 4–5 cm. **26.** *Rocella gelida* var. *schraderi* (Bukry) Barron, × 750, Sample 594-44-1, 4–5 cm.

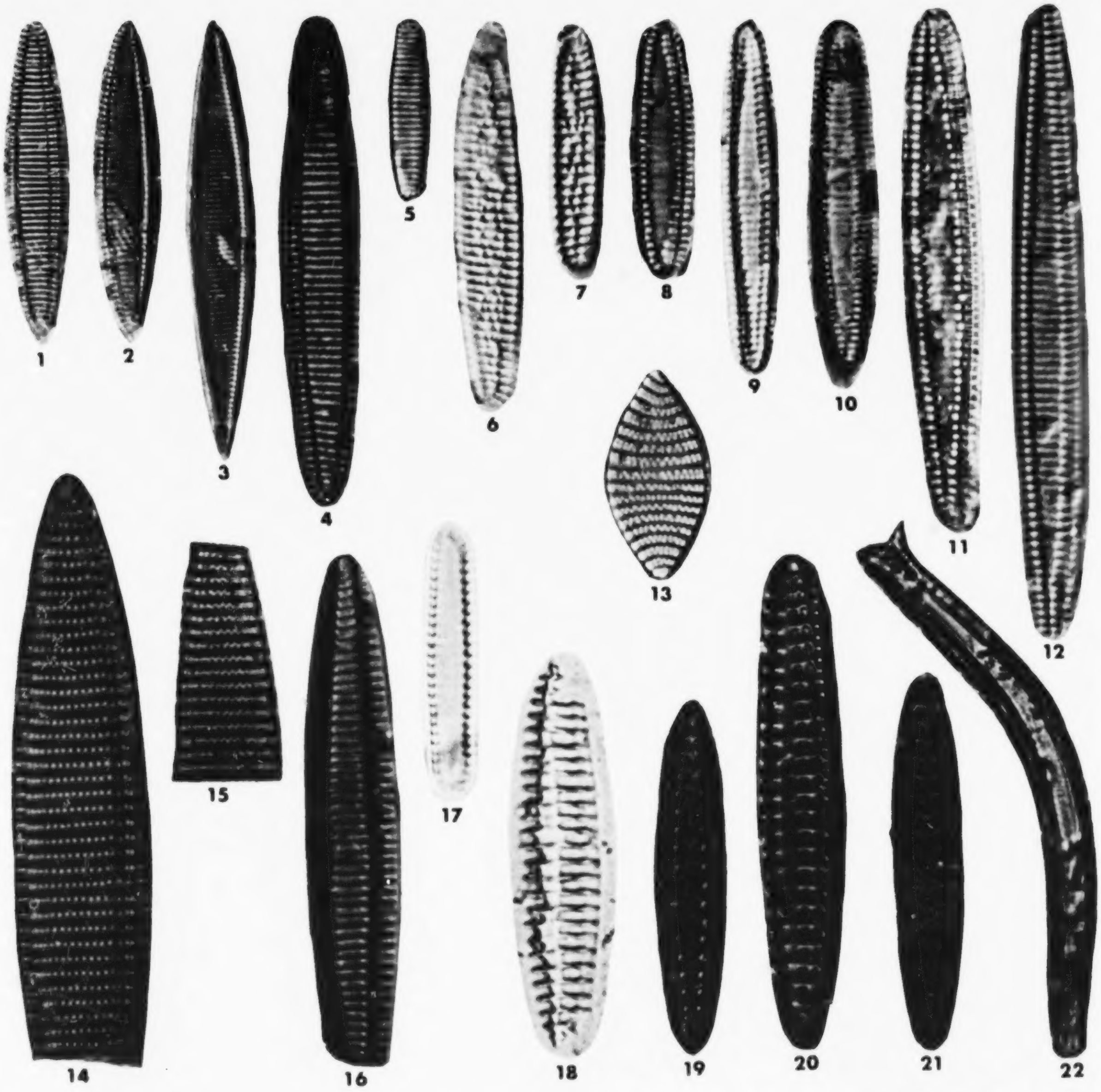

Plate 3. **1–4.** *Nitzschia reinholdii* Kanaya and Koizumi, × 1000, Sample 594-23-5, 4–5 cm. **5.** *Nitzschia januaria* Schrader, × 1500, Sampl 594-23-5, 4–5 cm. **6–7.** *Nitzschia interfrigidaria* (McCollum) Ciesielski, Sample 594A-10-5, 4–5 cm. **8–12.** *Nitzschia weaveri* Ciesielsk × 1500, Sample 594-16-5, 4–5 cm. **13.** *Nitzschia angulata* (O'Meara) Hasle, × 1500, Sample 594-15-2, 4–5 cm. **14.** *Nitzschia* aff. *donahuens* Schrader, × 1500, Sample 594-38-2, 4–5 cm. **15.** *Nitzschia praereinholdii* Schrader, × 1500, Sample 594-28-2, 4–5 cm. **16.** *Nitzschia miocen ca* (Burckle), × 1500, Sample 594-27-2, 4–5 cm. **17.** *Thalassionema nitzschioides* Grun, × 1500, Sample 594A-15-2, 4–5 cm. **18.** *Nitzsch denticuloides* Schrader, × 1500, Sample 594-47-1, 4–5 cm. **19–21.** *Rhaphoneis* sp. 1, × 1000, Sample 594-31-5, 4–5 cm. **22.** *Rhizosolenia ba boi* Brun, × 1000, Sample 594-21-5, 4–5 cm.

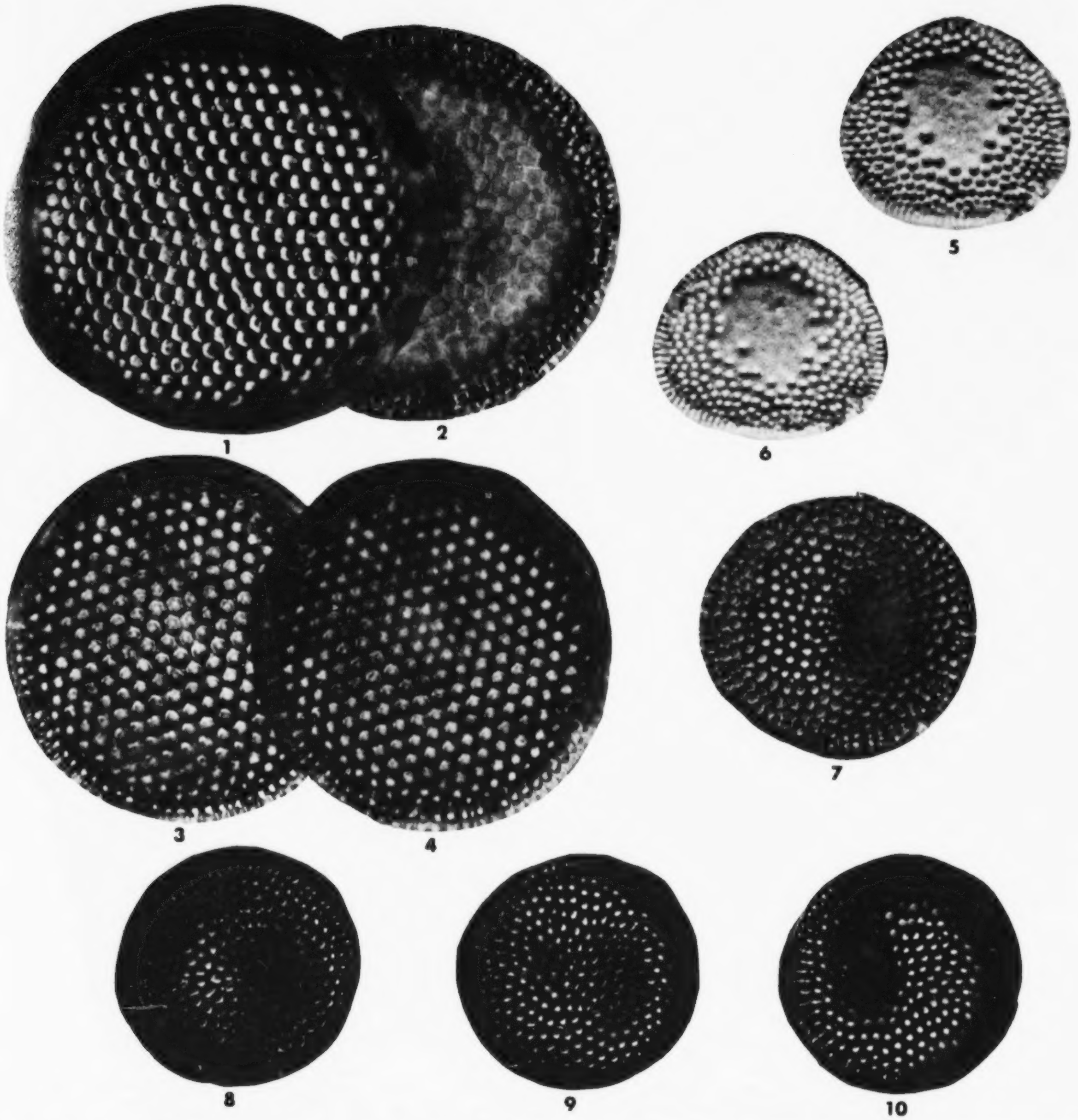

Plate 4. **1–4.** *Coscinodiscus kolbei* Jousé, × 1000, Sample 594-15-2, 4–5 cm. **5–6.** *Cosmiodiscus insignis* f. *triangula* Jousé, Sample 594-21-5, 4–5 cm. **7–10.** *Coscinodiscus yabei* Kanaya, × 1000, Sample 594-47-1, 4–5 cm.

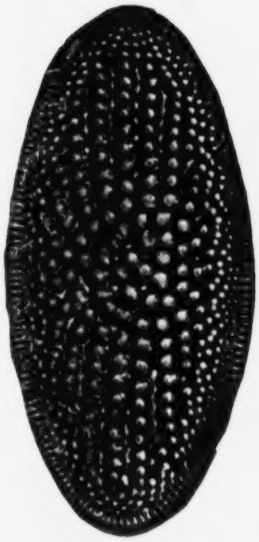
1

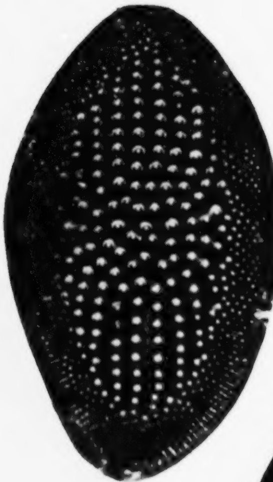
2

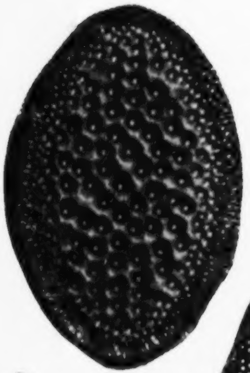
3

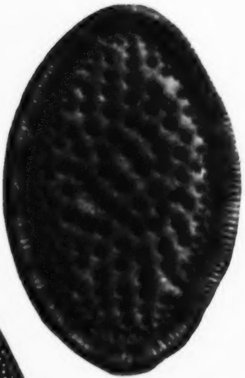
4

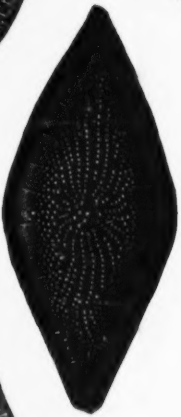
6

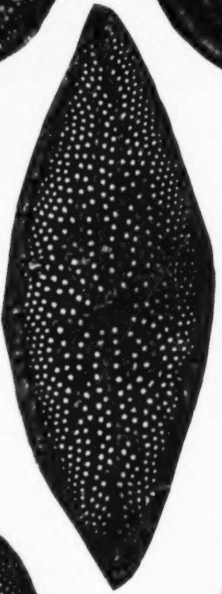
7

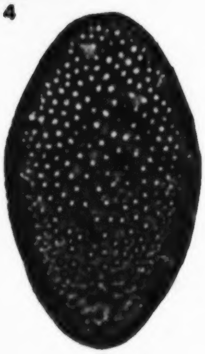
8

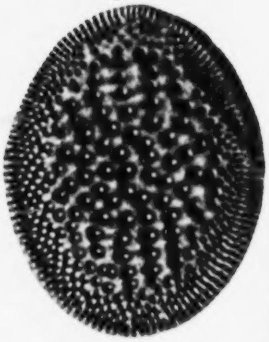
5

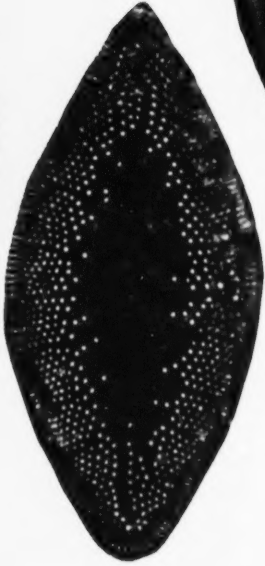
10

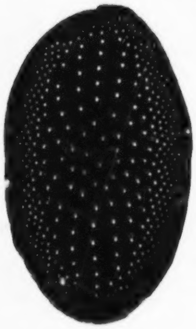
11

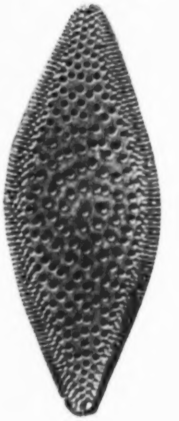
12

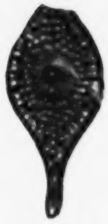
9

Plate 5. **1–4, 11.** *Coscinodiscus lewisianus* Greville, × 1000, (1–2) Sample 594A-15-2, 4–5 cm, (3–4, 11) Sample 594-52-2, 4–5 cm. **5.** *Coscinod cus lewisianus* var. *robustus* Barron, × 1000, Sample 594A-15-2, 4–5 cm. **6–7.** *Actinocyclus ellipticus* var. *spiralis* (Grunow) Barron, (6) × 100 (7) × 1500, Sample 594A-16-2, 4–5 cm. **8.** *Actinocyclus ellipticus* Grunow, × 1500, Sample 594-28-2, 4–5 cm. **9.** *Cymatosira* sp., × 150 Sample 594-31-5, 4–5 cm. **10.** *Cestodiscus peplum* Brun, × 1000, Sample 594A-17-2, 4–5 cm. **12.** *Coscinodiscus rhombicus* Castracan × 1000, Sample 594-47-1, 4–5 cm.

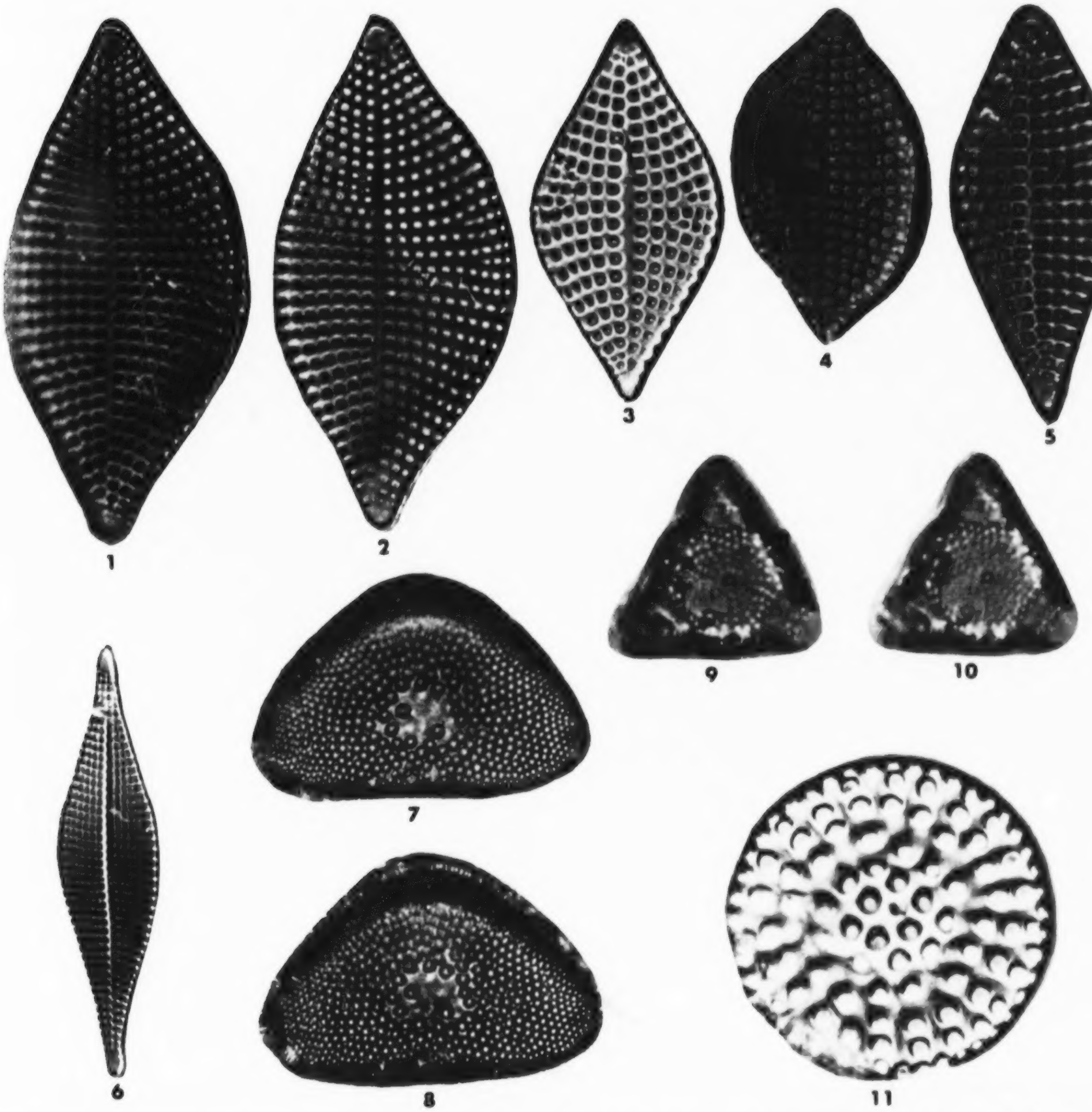

late 6. **1-3.** *Rhaphoneis amphiceros* Ehrenberg, × 1000, (1-2) Sample 594A-15-2, 4-5 cm, (3) Sample 594A-17-2, 4-5 cm. **4-5.** *Rhaphoneis* sp. 2, × 1000, (4) Sample 594A-15-2, 4-5 cm, (5) Sample 594A-16-2, 4-5 cm. **6.** *Rhaphoneis parilis* Hanna, × 1000, Sample 594A-17-2, 4-5 cm. **7-8.** *Cosmiodiscus insignis* f. *triangula* Jousé, × 1000, Sample 594-21-5, 4-5 cm. **9-10.** *Lithodesmium reynoldsii* Barron, × 1500, Sample 594-29-5, 4-5 cm. **11.** *Coscinodiscus praenitidus* Fenner, × 1500, Sample 594-21-2, 4-5 cm.

16. SILICOFLAGELLATES AND SOME SPONGE SPICULES FROM THE SOUTHWEST PACIFIC, DEEP SEA DRILLING PROJECT, LEG 90[1]

Sigurd Locker and Erlend Martini, Geologisch-Paläontologisches Institut der Universität, Frankfurt am Main[2]

ABSTRACT

Silicoflagellates are described from Sites 588 (middle Eocene), 591 (middle Miocene to lower Pliocene), and 594 (middle Miocene to Quaternary) in the southwest Pacific. At Sites 591 and 594 a detailed silicoflagellate zonation is possible, although there are some obvious differences arising from the latitudinal position of the sites in the silicoflagellate assemblages. Comparison between the sequences recovered at Sites 591 and 206 (Leg 21) revealed two hiatuses in the latter, but helped to establish a zonation for this area from the lower Miocene to the Pleistocene and a correlation to standard nannoplankton zones. The stratigraphic implications of the taxonomy used by various authors and the species concept presented here are discussed in detail. Special reference is made to types described by Ehrenberg and to later synonyma, because the Ehrenberg collection is the base for all subsequent descriptions and evaluations of silicoflagellate taxa.

Two new genera *(Neonaviculopsis, Paramesocena),* two new subspecies *(Dictyocha fibula* subsp. *asymmetrica, Neonaviculopsis neonautica* subsp. *praenautica),* and three new forms *(Dictyocha perlaevis* f. *pentaradiata, Distephanus speculum* subsp. *speculum* f. *nonarius,* and *Mesocena* ? *hexalitha* f. *heptalitha)* are described from the southwest Pacific Neogene and Pleistocene.

Associated sponge spicules were noted and will be described in detail in a later paper, but some are documented on Plate 13.

INTRODUCTION

During Leg 90 silicoflagellates and sponge spicules were found in three out of eight sites drilled in the New Caledonia to New Zealand region in the southwest Pacific Ocean (Fig. 1). They are commonly associated with diatoms, radiolarians, ebridians, and actiniscidians.

Hole 588C yielded Middle Eocene silicoflagellates in the lowest core (Core 19). At Site 591 silicoflagellates are rather common in the middle Miocene to lower Pliocene, with the exception of the upper middle Miocene, where they do not occur or are rare. At Site 594 silicoflagellates occur from the middle Miocene through the Pleistocene and are investigated in detail in Holes 594 and 594A. As at Site 591, the upper middle Miocene contains only rare silicoflagellates compared with the general distribution at this site. Reworked silicoflagellates from the Paleogene were noted at various levels and are marked by an asterisk in Table 3.

The assemblages of these sites and their age assignments are discussed below. Fossil lists for selected samples from Holes 588C, 591, 591A, 591B, 594, and 594A, and correlation to standard calcareous nannoplankton zones are presented in Tables 1 to 3, later. To obtain the abundances shown in these tables, a 120-mm traverse was made across the slides. Five categories are used: 1 1 specimen, 2 = 2 to 5 specimens, 3 = 6 to 15 specimens, 4 = 16 to 50 specimens, 5 = >50 specimens. Most silicoflagellate taxa described are documented by light microscopic photographs or by scanning electron microscope (SEM) pictures. Sponge spicules are not described in detail in this paper, but are documented by several photographs.

SILICOFLAGELLATE ZONATION

Investigations of various DSDP holes have shown that, with the exception of very few areas, the Paleogene silicoflagellate assemblages are relatively uniform in all oceans. But starting with the early to middle Miocene, distinct differentiation can be recognized between several regions of the oceans, especially between low and higher latitudes (Bukry, 1975; Ciesielski, 1975; Busen and Wise, 1977). This trend causes, in general, some difficulties in biostratigraphic correlations of Neogene sequences over long distances, for silicoflagellate assemblages that have different constituents and are adapted to warmer or cooler water conditions must be placed in somewhat different zonations. This is true for both the sections investigated from the southwest Pacific.

Sites 591, 206

The silicoflagellate zonation adopted here for the Neogene sequence at Site 591 is based on the stratigraphic occurrence of species which are found at Sites 591 and 206 (the latter investigated by Dumitricǎ, 1973b). The subdivision includes, from base to top, the *Naviculopsis iberica* Zone, *Corbisema triacantha* Zone, *Dictyocha varia* Zone, *Neonaviculopsis neonautica neonautica* Zone, *Paramesocena circulus* Zone, *D. perlaevis* Zone, and *D. messanensis aculeata* Zone (Fig. 2). Within the upper part of the *C. triacantha* Zone a *Distephanus stauracanthus* Horizon is distinguished and in the lower Quater-

---

[1] Kennett, J. P., von der Borch, C. C., et al., *Init. Repts. DSDP*, 90: Washington (U.S. Govt. Printing Office).

[2] Addresses: (Locker, present address) Geologisch-Paläontologisches Institut der Universität, Olshausenstr. 40-60, D-23 Kiel, Federal Republic of Germany; (Martini) Geologisch-Paläontologisches Institut der Universität, Senckenberg-Anlage 32-34, D-6000 Frankfurt am Main, Federal Republic of Germany.

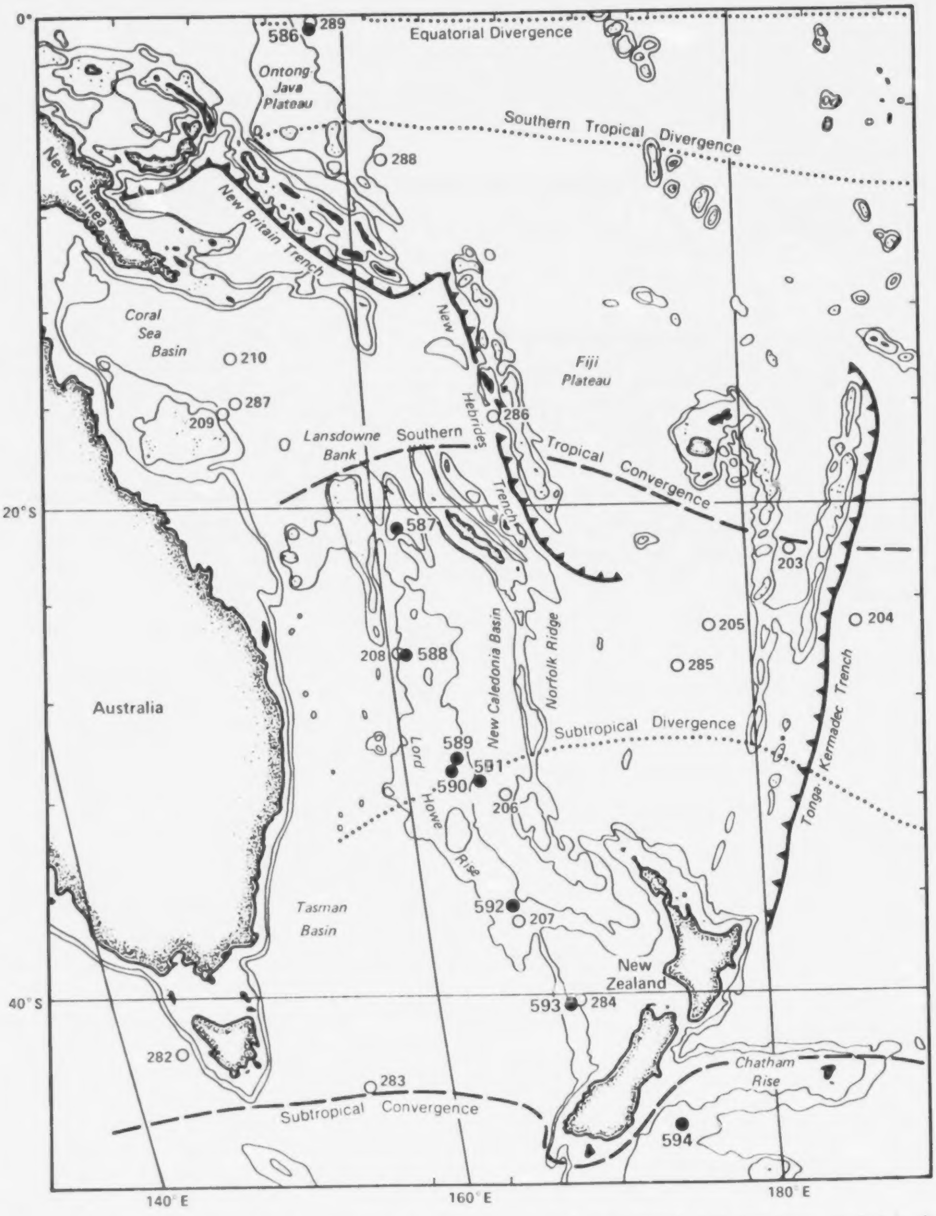
0°
586
289
Equatorial Divergence
Ontong Java Plateau
Southern Tropical Divergence
288
New Guinea
New Britain Trench
Coral Sea Basin
210
287
209
New Hebrides Trench
Fiji Plateau
286
Lansdowne Bank
Southern Tropical Convergence
20°S
587
203
205
204
208
588
285
New Caledonia Basin
Norfolk Ridge
Australia
Subtropical Divergence
Tonga-Kermadec Trench
589
591
590
206
Lord Howe Rise
Tasman Basin
592
207
New Zealand
40°S
593
284
282
283
Chatham Rise
Subtropical Convergence
594
140° E
160° E
180° E

Figure 1. Location of sites drilled during Leg 90 (solid circles) and other DSDP drill sites (open circles) in the southwest Pacific.

nary a *Mesocena quadrangula* Horizon. It should be noted that no material was available for a short interval between the *Naviculopsis iberica* and the *C. triacantha* Zone; therefore, no zonal assignment is given for this interval. Only the datum levels of some *Naviculopsis* species extrapolated from other regions are indicated. The zonation used is otherwise representative for the low and middle latitudes in many regions of the oceans, as is demonstrated in the remarks following the identification of zones.

Naviculopsis iberica Zone

Definition. Interval from the first occurrence of *N viculopsis iberica* to the last occurrence of *N. navicu a* (new zone). Upper Oligocene to lower Miocene.

Occurrence. Present at Site 206, but not cored at Sit s 591 and 594.

Remarks. The zone reflects a special development f late Oligocene to early Miocene silicoflagellate asse blages in the southern Pacific. In other regions the no

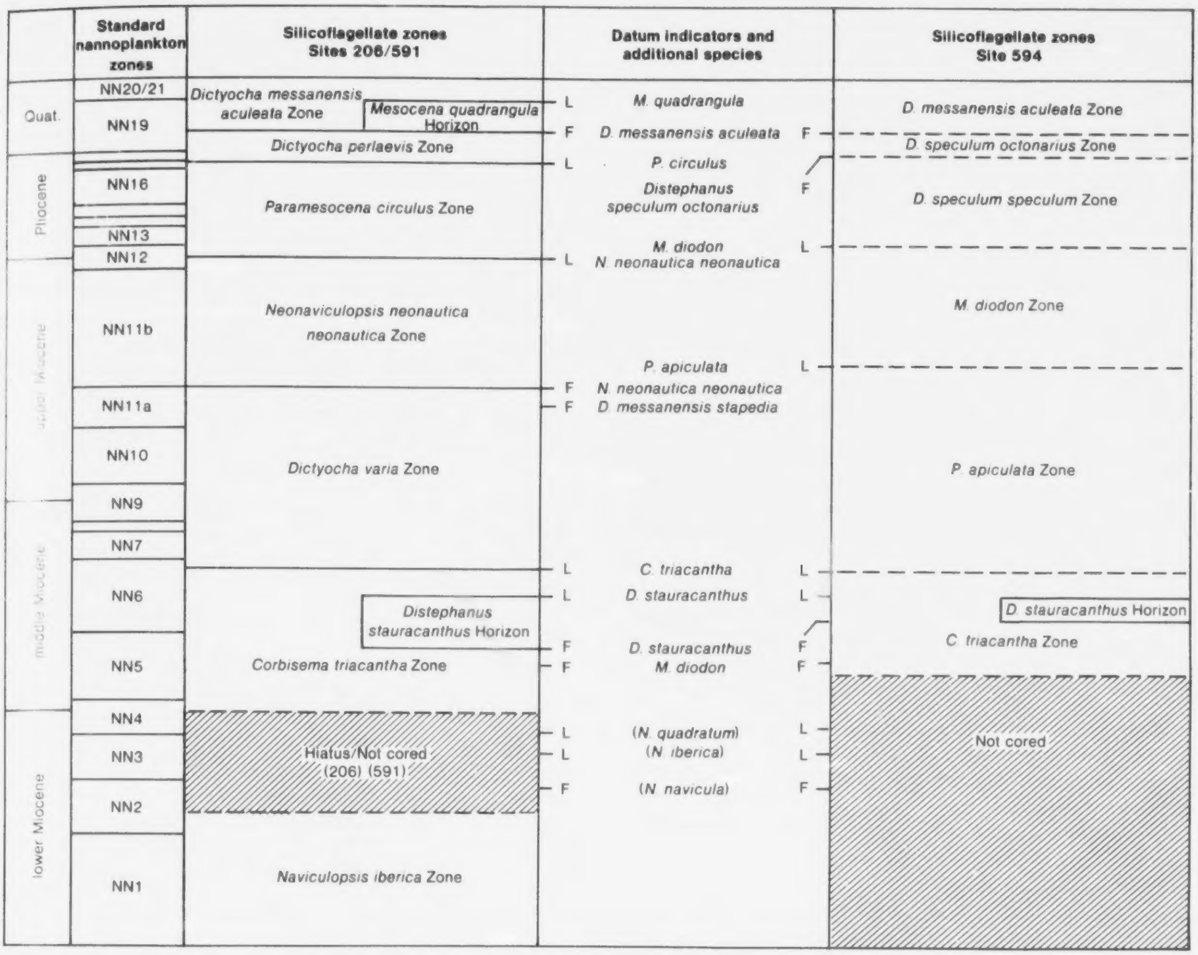
Standard nannoplankton zones
Silicoflagellate zones Sites 206/591
Datum indicators and additional species
Silicoflagellate zones Site 594
Quat.
Pliocene
upper Miocene
middle Miocene
lower Miocene
NN20/21
NN19
NN16
NN13
NN12
NN11b
NN11a
NN10
NN9
NN7
NN6
NN5
NN4
NN3
NN2
NN1
Dictyocha messanensis aculeata Zone
Mesocena quadrangula Horizon
Dictyocha perlaevis Zone
Paramesocena circulus Zone
Neonaviculopsis neonautica neonautica Zone
Dictyocha varia Zone
Distephanus stauracanthus Horizon
Corbisema triacantha Zone
Hiatus/Not cored (206) (591)
Naviculopsis iberica Zone
L M. quadrangula
F D. messanensis aculeata F
L P. circulus
Distephanus speculum octonarius F
M. diodon L
L N. neonautica neonautica
P. apiculata L
F N. neonautica neonautica
F D. messanensis stapedia
L C. triacantha L
L D. stauracanthus L
F D. stauracanthus F
F M. diodon F
L (N. quadratum) L
L (N. iberica) L
F (N. navicula) F
D. messanensis aculeata Zone
D. speculum octonarius Zone
D. speculum speculum Zone
M. diodon Zone
P. apiculata Zone
D. stauracanthus Horizon
C. triacantha Zone
Not cored

Figure 2. Silicoflagellate zones used at Sites 206/591 and Site 594, first (F) and last (L) occurrences of important silicoflagellate species, and correlation to standard nannoplankton zones. Parentheses indicate locations of datum levels within hiatus or uncored sections.

inate species may be associated with *N. lata* (Martini and Müller, 1976: Norwegian Sea, DSDP Site 338) indicating that the *N. iberica* Zone corresponds, more or less, to the *N. lata* Zone.

Corbisema triacantha Zone

Definition. Interval from the last occurrence of *Naviculopsis* species to the last occurrence of *Corbisema triacantha* (Martini, 1971a, 1972; base modified). Lower Miocene to middle Miocene.

Occurrence. Found at Site 591, Cores 591B-13 to 591B-21, and at Site 594, Cores 594A-12 to 594A-20 and Cores 594-46 to 594-53. Present also at Site 206.

Assemblage. At Site 591 *Corbisema triacantha, Dictyocha fibula,* and *D. varia* are common to abundant, and in the upper part, distinguished as *Distephanus stauracanthus* Horizon, some other species are also. *Dictyocha fibula asymmetrica, D. medusa, Distephanus crux crux*, and *D. speculum giganteus* are rare to few. The whole interval is characterized by the high number of *Cannopilus* species and the presence of *Macrora stella,* a synuracean species.

In contrast to Site 591, most of the species cited are sparse at Site 594. Only *Corbisema triacantha* and *Distephanus crux crux* are more or less consistently distributed throughout the zone. Most characteristic is the occurrence of *Cannopilus depressus. Macrora stella* is generally missing.

Remarks. The *Corbisema triacantha* Zone is rather uniformly developed in many regions. It was reported from low- and mid-latitude sites in the North Pacific (Experimental Mohole [EM] site, DSDP Sites 173, 469, 470, 472), central Pacific (DSDP Sites 65, 66, 71, 158, 495), South Pacific (DSDP Site 206), and North Atlantic (DSDP Sites 338, 369, 370, 391, 415, 416).

In higher latitudes identification of the zone may be difficult because *C. triacantha* specimens are fewer. But under these conditions, *Cannopilus depressus* may be used as a nearly time-equivalent indicator. High-latitude records with *Corbisema triacantha* scarcely present are known from the North Pacific (Sites 183, 433), the North Atlantic (Sites 407, 408), and the Antarctic (Sites 266, 323).

Distephanus stauracanthus Horizon

Definition. Interval in the upper *Corbisema triacantha* Zone characterized by the first and last appearance of *Distephanus stauracanthus* (Martini, 1972). Middle Miocene.

Occurrence. Found at Site 591, Cores 591B-15 to 591B-17, and at Site 594, Core 594A-12. Present also at Site 206.

Assemblage. At Site 591 *Corbisema triacantha, Dictyocha extensa, D. varia, Distephanus crux crux,* and *D. stauracanthus* are common to abundant.

Remarks. The horizon occupies an interval within the upper *Corbisema triacantha* Zone. It is distinguished by the rather short life-span of *Distephanus stauracanthus* (syn. *D. octacanthus*). Along with the *Corbisema triacantha* Zone, the horizon was reported from some low- and mid-latitude sections, mainly of the central and North Pacific. Clear indications exist, either as zone or by the nominate species, for the North Pacific (EM Site, DSDP Sites 173, 470, 472), central Pacific (Sites 66, 71), South Pacific (Site 206), and North Atlantic (Site 408).

Dictyocha varia Zone

Definition. Interval from the last occurrence of *Corbisema triacantha* to the first occurrence of *Neonaviculopsis neonautica neonautica* (new zone). Middle Miocene to upper Miocene.

Occurrence. Found at Site 591, Cores 591B-2 to 591B-12 and Cores 591-28 to 591-31, and partially present also at Site 206.

Assemblage. At Site 591 *Dictyocha fibula, D. varia,* and *Distephanus speculum speculum* are common to abundant; *Dictyocha extensa* and *D. medusa* are rare to few. *Dictyocha messanensis aspinosa* changes in the upper part of the interval to *D. messanensis stapedia. Distephanus crux hannai,* consistently distributed in the lower part, disappears toward the end of the zone. *Distephanus polyactis crassus* and *Paramesocena apiculata* are consistently present only in the lower part.

Remarks. The *Dictyocha varia* Zone describes an intermediate interval between the datum levels of two other species. It may be present in low- and mid-latitude subdivisions of some authors though other species names are cited (possibly as part of *D. rhombica, D. aspera, D. pulchella*). Setting aside the terminology, this zone probably occurs in sections of the North Pacific (DSDP Sites 469, 470, 472), central Pacific (Sites 65, 66, 158, 315, 495) and South Pacific (Site 206).

Neonaviculopsis neonautica neonautica Zone

Definition. Interval from the first to the last occurrence of *Neonaviculopsis neonautica neonautica* (in Bukry, 1981, as *Dictyocha neonautica* Subzone of his *D. fibula* Zone). Upper Miocene to lower Pliocene.

Occurrence. Found at Site 591, Cores 22 to 27.

Assemblage. *Dictyocha fibula, D. messanensis stapedia,* and *Distephanus speculum speculum* are common to abundant. Less common are *Dictyocha extensa, D. varia,* and also *N. neonautica neonautica.*

Remarks. The zone is distinguished by a species which is identical in its skeletal structure to *Naviculopsis* but generates first in the late Miocene, a long time after the extinction level of true *Naviculopsis* species in the early Miocene. *Neonaviculopsis neonautica* was cited or figured some years ago, but generally under other names (Bukry and Foster, 1973: *Naviculopsis navicula;* Martini, 1976: *Dictyocha* cf. *ausonia;* Ling, 1977: *Naviculopsis iberica*). These citations indicate the relatively wide distribution and usefulness of the zone.

The zone has been reported, or indicated by the species cited above, from sections in the North Pacific (DSDP Sites 469, 471), central Pacific (Sites 158, 315, 495, 503, 504), and now also from the South Pacific (Site 591).

Paramesocena circulus Zone

Definition. Interval from the last occurrence of *Neonaviculopsis neonautica neonautica* to the last occurrence of *Paramesocena circulus* (new zone). Lower Pliocene to upper Pliocene.

Occurrence. Found at Site 591, Cores 13 to 21, and also present at Site 206.

Assemblage. At Site 591 *Dictyocha fibula, D. messanensis stapedia,* and *Distephanus speculum speculum* are common to abundant, as are also, in different parts of this zone, *Dictyocha varia, Mesocena quadrangula,* and *Paramesocena circulus.* Few to common are *D. extensa, D. perlaevis,* and *Distephanus crux bispinosus,* the last being very characteristic.

Remarks. The zone is defined by the disappearance of *N. neonautica neonautica* at its base and the disappearance of *P. circulus,* or other evolved *Paramesocena* species, at the top. In this sense the zone does not correspond to the *Mesocena/Paradictyocha circulus* Zone of other authors, which circumscribes a late Miocene interval in higher latitudes. The late Miocene *M. circulus* Zone needs some further study because it may be related to *Paramesocena apiculata,* a quite similar species.

Although no *Paramesocena circulus* Zone has yet been used for the Pliocene, it may be recognized by its nominate species, mentioned in various publications. *Paramesocena circulus* has been reported from Pliocene sections in the North Pacific (DSDP Site 310), central Pacific (Sites 321, 425, 504), South Pacific (Sites 206, 278), North Atlantic (Site 410), and South Atlantic (Site 362).

Dictyocha perlaevis Zone

Definition. Interval from the last occurrence of *Paramesocena circulus* to the first occurrence of *Dictyocha messanensis aculeata* (Dumitrică, 1973b; base redefined). Upper Pliocene to lower Quaternary.

Occurrence. Present at Site 206, but not found at Sites 591 (barren interval) and 594 (not present).

Remarks. The *Dictyocha perlaevis* Zone describes an intermediate interval between the datum levels of two other species. Because of its short duration it may sometimes be difficult to distinguish, but usually it may be recognized by the presence of the nominate species below the occurrence of *D. messanensis aculeata* or the acme of *Mesocena quadrangula*.

The zone can be traced over large areas. It was reported, or indicated by its nominate species, from low- and mid-latitude sites in the North, central and South Pacific and the North and South Atlantic.

Mesocena quadrangula Horizon

Definition. Interval near or at the base of the *Dictyocha messanensis aculeata* Zone characterized by the acme of *Mesocena quadrangula*, which is limited by the disappearance of the nominate species (Martini, 1971a; base and top redefined by Bukry, 1979b). lower Pleistocene.

Occurrence. Present at Site 206, but not found at Sites 591 (barren interval) and 594 (not present).

Remarks. The horizon was originally defined from the first to the last occurrence of *Mesocena quadrangula*, but later it was restricted to the conspicuous acme interval of the species because of its indistinct first appearance. In some earlier publications the species is also related to *M. elliptica* (Ling, 1970; Dumitrică, 1973a; and others). The horizon was reported or indicated by its nominate species from many low- and mid-latitude sections in the North, central, and South Pacific and also from a few sites in the North and South Atlantic.

Dictyocha messanensis aculeata Zone

Definition. Interval above the first occurrence of *Dictyocha messanensis aculeata* (introduced by Ling, 1972, as *D. fibula* var. *aculeata* assemblage; defined as *D. aculeata* Zone by Dumitrică, 1973b; Bukry and Foster, 1973). Lower Pleistocene to Recent.

Occurrence. Not found at Site 591 (barren interval), but present at Site 206 and Site 594, Cores 594-6 to 594-11.

Assemblage. At Site 594 only *Distephanus speculum speculum* is consistently present, whereas *Dictyocha messanensis aculeata* occurs scattered and in low numbers.

Remarks. The zone is characterized by the multispined *D. messanensis aculeata*, which first appears in the early Pleistocene, corresponding to the beginning of the *Mesocena quadrangula* acme or shortly after that event. In some earlier publications this species was also referred to as *D. epiodon* (Bukry and Foster, 1973; and others) or noted as *D. mandrai* (Ling, 1977).

At Site 206 *D. messanensis aculeata* continues the warm to temperate species succession known from many sites at low and mid latitudes. But its presence at Site 594 does not reflect the general cooling trend from the middle/late Miocene to the early Pleistocene. The surprising appearance of *D. messanensis aculeata* at these latitudes may be normal or it might indicate a warming phase, as presumed for the same interval at Site 278 (Perch-Nielsen, 1975).

The *Dictyocha messanensis aculeata* Zone has been reported or is indicated by its nominate species from many low and mid-latitude sites in the North Pacific (TT sites in Ling, 1970; DSDP Sites 310, 466), central Pacific (Sites 84, 157, 315, 316, 321, 425, 427, 495, 504) South Pacific (Site 206), the North Atlantic (Sites 334, 397, 410, 412), Mediterranean Sea (Sites 127, 128), and South Atlantic (Site 358). However, it is documented also from some Pleistocene to Holocene higher-latitude sections in the North Pacific (TT sites of Ling; many sites described by Poelchau, 1976), South Pacific (Sites 278, 281), and South Atlantic (Site 328). The nominate species is sometimes associated with *Distephanus octangulatus* in the North Pacific.

Site 594

In the middle Miocene to early Pleistocene sequence at Site 594 a different subdivision is used because of the stronger affinities of the sequence with cool-water conditions. Above the *Corbisema triacantha* Zone, the zonation includes the *Paramesocena apiculata* Zone, *Mesocena diodon* Zone, *Distephanus speculum speculum* Zone, and the *D. speculum octonarius* Zone (Fig. 2). In the North Pacific this succession is terminated by the *D. octangulatus* Zone, but from other high-latitude regions no comparable subunit is known.

Paramesocena apiculata Zone

Definition. Interval from the last occurrence of *Corbisema triacantha* to the last occurrence of *Paramesocena apiculata* (introduced by Ling, 1973, as *Mesocena circulus* var. *apiculata* Zone; defined by Bukry, 1975, as *M. circulus* Subzone of his *Distephanus speculum speculum* Zone). Middle to upper Miocene.

Occurrence. Found at Site 594, Cores 24 to 45.

Assemblage. *Paramesocena apiculata* is the only species which occurs more or less consistently throughout this zone. In the upper part *Dictyocha varia, Distephanus crux crux*, and *D. speculum speculum* are also present.

Remarks. The zone is defined by an early *Paramesocena* species which still possesses two rows of spines. Its disappearance seems to be a wide-ranging event, although it is insufficiently documented at present. It may be presumed that the late Miocene *M./P. circulus* Zone distinguished in some high-latitude zonations is based on *Paramesocena apiculata*. But further investigations are needed.

Only a few indications exist for the *Paramesocena apiculata* Zone or the nominate species (North Pacific, DSDP Sites 173, 183, 192, EM site). Most reports register a *Paradictyocha circulus* or *Mesocena circulus* Zone in the middle to late Miocene interval: South Pacific (Site 278), Antarctic region (Sites 266, 274, 323), South Atlantic (Sites 328, 329, 358, 513), and North Atlantic (Sites 338, 348). But these reports may be taken as indications of the *Paramesocena apiculata* Zone, because the figured specimens often belong to *P. apiculata*.

Mesocena diodon Zone

Definition. Interval from the last occurrence of *Paramesocena apiculata* to the last occurrence of *Mesocena diodon* (introduced by Perch-Nielsen, 1975, as *M. diodon* Subzone of her *Paradictyocha dumitricae* Zone; base modified). Upper Miocene to lower Pliocene.

Occurrence. Found at Site 594, Cores 594-21 to 594-23.

Assemblage. Rare to few but consistently present are *Distephanus speculum speculum* and *Mesocena diodon*.

Remarks. The lower boundary of the zone may be difficult to place in some sections but the upper boundary seems to be a wide-ranging and distinct datum level. The zone was reported, or indicated by its nominate species, from the North Pacific (DSDP Sites 173, 183, 192), South Pacific (Site 278), Antarctic region (Site 266), North Atlantic (Sites 348, 407), and South Atlantic (Site 513).

Distephanus speculum speculum Zone

Definition. Interval from the last occurrence of *Mesocena diodon* to the first occurrence of *Distephanus speculum speculum* f. *octonarius* (Bukry, 1973; top redefined by Bukry, 1975; base modified). Lower to upper Pliocene.

Occurrence. Found at Site 594, Cores 594-14 to 594-20.

Assemblage. *Distephanus speculum speculum* with its hexagonal form is the only consistent species. *Dictyocha messanensis messanensis* appears sporadically.

Remarks. The *Distephanus speculum speculum* Zone describes an intermediate interval between the datum levels of two other species. The zone is characterized by the high number of specimens belonging to *D. speculum* and by the low species diversity. The zone was reported, or is indicated by the species assemblage, from many sites in the North Pacific (DSDP Sites 173, 183, 185, 186), South Pacific (Site 278), Antarctic region (Sites 266, 269, 274), North Atlantic (Sites 348, 407), and South Atlantic (Site 328).

Distephanus speculum octonarius Zone

Definition. Interval from the first occurrence of *Distephanus speculum speculum* f. *octonarius* to the first occurrence of *D. octangulatus* (Ling, 1973; base redefined by Bukry, 1975). Lower Pleistocene.

Occurrence. Found at Site 594, Cores 594-12 to 594-13.

Assemblage. Numerous forms of *Distephanus speculum speculum* including f. *octonarius* are present.

Remarks. The base of the zone is defined by the octogonal variants of *Distephanus speculum,* which are treated here as forms of the subspecies *D. speculum speculum,* because no precise and representative data on the true nature of the group are available. Statistical investigations might show that the *octonarius* forms represent a subspecies *Distephanus speculum octonarius,* which is characterized by a series of multispined morphes. But for practical stratigraphy such taxonomic problems are not considered here, and the zonal name is abbreviated to *D. speculum octonarius* Zone. Regarding taxonomy, it should be noted also that in some publications the species is called *D. polyactis* (Bukry, 1973; Busen and Wise, 1977; and others).

The top of the zone is defined by the first appearance of *Distephanus octangulatus,* which is known at present only from the North Pacific. Further investigations may show if this species can be used also for late Quaternary stratigraphy in other high-latitude regions. For Site 594 this question is irrelevant, because the succession is continued by *Dictyocha messanensis aculeata,* which is a good zonal indicator in low and mid latitudes (see also remarks for *D. messanensis aculeata* Zone). The *Distephanus speculum octonarius* Zone is reported, or indicated by its nominate species, from the North Pacific (DSDP Sites 173, 183, 185, 186, 190, 192), South Pacific (Site 278), Antarctic region (Sites 266, 269, 274), North Atlantic (Site 407), and South Atlantic (Sites 328, 513). To evaluate the distribution or presence of certain species the following papers, besides those already cited, were consulted: Bukry, 1976b, 1977, 1979a, 1980a, 1980b, 1981a, 1982a; Fuji and Bachmann, 1970; Hajós, 1976; Haq and Riley, 1976; Ling, 1975, 1980; Martini, 1979; Müller, 1981; Perch-Nielsen, 1977; Shaw and Ciesielski, 1983.

SITE SUMMARIES

Site 588 (26°06.70′S; 161°13.6′E; water depth 1533 m)

At Hole 588C, on the western part of Lord Howe Rise, Paleogene sediments containing silicoflagellates were encountered in Core 19, and are associated with diatoms, ebridians, radiolarians, rare sponge spicules, and calcareous nannoplankton. The silicoflagellate assemblage (Table 1) is dominated by *Naviculopsis foliacea* and *Corbisema apiculata,* and because *C. bimucronata* is also pres-

Table 1. Distribution of silicoflagellates in selected samples from Hole 588C, and indication of silicoflagellate and standard nannoplankton zones.

Series	Nannoplankton zone	Core-Section (interval in cm)	*Corbisema apiculata*	*C.* cf. *apiculata*	*C.* cf. *archangelskiana*	*C. bimucronata*	*C. convexa*	*C. hastata*	*C. spinosa*	*Dictyocha eocaenica*	*Distephanus speculum* s.l.	*D. speculum* s.l. f.1	*D. speculum* s.l. f.2	*Mesocena occidentalis*	*Naviculopsis biapiculata*	*N. foliacea*	Silicoflagellate specimens	Silicoflagellate zone
middle Eocene	NP15/ NP16	19-1, 10-12	1	2			1	1		1				1	1	2	10	*Naviculopsis foliacea* Zone
		19-1, 35-37	1	2	1		2			2	1	1	1	1	2	2	16	
		19-1, 55-57	1	2	1	1	1	1		1		1	1	1	1	3	18	
		19,CC		3		1	2		1	2			1	1	1	2	21	

Note: Numbers indicate frequency. 1 = 1 specimen, 2 = 2 to 5 specimens, 3 = 6 to 15 specimens, 4 = 16 to 50 specimens, 5 = > 50 specimens, counted on a 120-mm traverse across the slides.

ent the assemblage can be placed in the Middle Eocene *Naviculopsis foliacea* Zone (see Martini and Müller, 1976). A similar assemblage, although without *C. bimucronata* and slightly older, was found in Samples 208-27,CC and 208-28,CC, which were inspected for comparison from the nearby Site 208. For details on the silicoflagellates of this site see Dumitrică (1973b).

Associated calcareous nannoplankton indicate a middle Eocene age (Zone NP15/NP16), probably the middle part of Zone NP15 judging by a single specimen of *Chiasmolithus gigas* (Bramlette and Sullivan) in Sample 588C-19-1, 10–12 cm. This is in good agreement with the correlations indicated in Martini and Müller (1976, fig. 3).

Site 591 (31°35.0′S; 164°26.92′E; water depth 2131 m)

Site 591 is situated on the eastern part of Lord Howe Rise. Sediments recovered at this site consist mostly of foraminifer-bearing nannofossil ooze with low amounts of biosiliceous components, including diatoms, silicoflagellates, radiolarians, ebridians, actiniscidians, sponge spicules, and phytoliths. The investigated sequence, combined from Holes 591A, 591, and 591B, cover the middle Miocene to early Pleistocene interval. However, samples from above the lower Pliocene (591-11,CC and higher) are generally barren of silicoflagellates. The distribution of silicoflagellate taxa in the sequence and the correlations to calcareous nannoplankton zones (Martini, 1971b) are shown in Table 2.

The interval between Samples 591-13,CC and 591-21,CC is placed in the lower Pliocene *Paramesocena circulus* Zone, with the nominate species common in several samples. Abundant or common are *Dictyocha messanensis stapedia* f. *aspinosa, Distephanus speculum speculum* f. *speculum* and *D. crux bispinosus* f. *bispinosus*. Samples 591-22,CC to 591-27,CC belong to the *Neonaviculopsis neonautica neonautica* Zone, based on the occurrence of the nominate species. Other taxa present include *Dictyocha messanensis stapedia* f. *stapedia, D. varia,* and *Distephanus speculum speculum* f. *speculum*. This zone straddles the Miocene/Pliocene boundary, as is indicated by the associated calcareous nannoplankton. The interval between Samples 591-28,CC and 591B-12,CC is placed in the upper middle to upper Miocene *Dictyocha varia* Zone. The assemblages are dominated by *Dictyocha fibula fibula* and *D. varia,* and in the higher parts also by *Distephanus speculum speculum* f. *speculum*. Relatively common in this zone are *Dictyocha medusa, Distephanus crux hannai, D. polyactis crassus* and *Paramesocena apiculata*. In the lowest part of the *Dictyocha varia* Zone silicoflagellates are rare and rather insignificant. A barren interval follows, including Samples 591B-13,CC and 591B-14,CC. In Sample 591B-15,CC *Corbisema triacantha,* which is found down to Sample 591B-21,CC, last occurs. Accordingly, this interval belongs in the *Corbisema triacantha* Zone. Also *Macrora stella* was noted in all samples containing silicoflagellates in this interval. In Samples 591B-15,CC to 591B-17,CC, *Distephanus stauracanthus* occurs. This level is shown as the *Distephanus stauracanthus* Horizon in Table 2; it belongs to the middle Miocene and can be correlated to the uppermost part of standard nannoplankton Zone NN5 (*Sphenolithus heteromorphus* Zone) and the lower part of Zone NN6 (*Discoaster exilis* Zone). The lowest Samples 591B-22,CC to 591B-24,CC are again barren of silicoflagellates.

Site 591 is close to Site 206, from which silicoflagellates were described by Dumitrică (1973b) for the interval from the late Oligocene to the Pleistocene. Important species, correlation to standard nannoplankton zones, and placement in silicoflagellate zones for both sites are shown in Figure 3. In Hole 206 a hiatus between the upper Miocene and Pliocene (206-20,CC and 206-21,CC) has already been noted by Dumitrică (1973b, fig. 1). The hiatus includes the upper part of nannoplankton Zone NN10 (*Discoaster calcaris* Zone) to the lower part of Zone NN12 (*Ceratolithus tricorniculatus* Zone), or part of the *Dictyocha varia* Zone and probably the complete *Neonaviculopsis neonautica neonautica* Zone in the silicoflagellate zonation. Another hiatus can be noted between Samples 206-33, CC and 206-34,CC, with the upper lower Miocene and lower middle Miocene (Zones NN2, part to NN5, part) missing. This hiatus, if present at Site 591, is smaller, because the lowest Sample 591B-24,CC has already reached a level which is tentatively placed in the uppermost nannoplankton Zone NN4 (*Helicosphaera ampliaperta* Zone). The late Miocene hiatus of Site 206 was not observed at Site 591, where a complete sequence from the middle Miocene to the Recent was encountered.

Site 594 (45°31.41′S; 174°56.88′E; water depth 1204 m)

Holes 594 and 594A are located at the southern margin of the Chatham Rise, east of the South Island of New Zealand. The predominantly calcareous sediments contain as minor components diatoms, silicoflagellates, radiolarians, sponge spicules, and also some ebridians and actiniscidians throughout the Miocene to Quaternary sequence. A combination of core-catcher samples from Hole 594 (594-1,CC to 594-53,CC) for most of the sequence and from Hole 594A (594A-12,CC to 594A-25,CC) for the lowest part was used for detailed silicoflagellate investigation and correlation to calcareous nannoplankton zones (Table 3).

Severe reworking of silicoflagellates from older strata, especially from the Eocene and Oligocene, was noted throughout the sequence. Species obviously reworked are indicated by an asterisk beside the species name in Table 3. Some difficulties arise with species ranging into the Miocene, like *Corbisema triacantha,* which occurs, quite unusually, in the upper Miocene, lower Pliocene, and even in some Pleistocene samples. As they are in most cases associated with reworked *Naviculopsis* species, these occurrences are treated as erratics. Reworking was also noted in shipboard ebridian and diatom studies. Shore-based diatom studies (Ciesielski, this volume) even revealed several short hiatuses in the Pliocene and Pleistocene, which seem to occur just at calcareous nannoplankton zonal boundaries (between NN12/NN14 and NN15; NN15 and NN16/NN19A; NN16/NN19A and NN19B), but could not be detected in the silicoflagellate succession, probably because of low zonal resolution. In

Table 2. Distribution of silicoflagellates in selected samples from Site 591, indication of silicoflagellate zones, and correlation to standard nannoplankton zones.

Series	Nannoplankton zones	Core-catcher samples	*Cannopilus depressus*	*C. hemisphaericus*	*C. heptacanthus antarcticus*	*C. heptacanthus heptacanthus*	*C. schulzii*	*C. sidensis*	*C. latifenestratus*	*C. picassoi*	*Corbisema triacantha*	*Dictyocha aspera*	*D. epiodon*	*D. extensa*	*D. fibula asymmetrica*	*D. fibula fibula*	*D. fibula* s. l.	*D. mediata*	*D. messanensis messanensis* f. *aspinosa*	*D. messanensis messanensis* f. *speculum*	*D. messanensis aspinosa*	*D. messanensis stapedia* f. *aspinosa*	*D. messanensis stapedia* f. *stapedia*	*D. perlaevis* f. *pentaradiata*	*D. perlaevis* f. *perlaevis*	*D.* sp. 1	*D. pygmaea*	*D.* sp. 2	*D. subclinata*
Pleistocene-upper Pliocene	NN19 to NN16	A3,CC to A8,CC	Barren																										
		A9,CC																				1							
		11,CC	Barren																										
lower Pliocene	NN15	13,CC														1						1	2		1				
		14,CC												4		4	3					5	5		4				
		16,CC												4		4	3	1				5	3		3				
	NN14	17,CC												4		4	3					5	3						
		18,CC												3		2	1					5	3			1			
		19,CC												1		4	3					2	3		2	2			
		20,CC																1				1	3	1	4			4	
		21,CC												2		4		1				2	5		3			4	
	NN12	22,CC														3						2	4						
		23,CC														4						2	3						
upper Miocene	NN11b	24,CC												2		2							3					2	
		25,CC														2	2					2	4						
		26,CC												2		3	4		3			2	4					1	
		27,CC												2		5	3	1	5	3		3							
	NN11a	28,CC												2		4	1					4	2						
		29,CC												3		4	2	1			1								
		30,CC												1		4	2												
		31,CC												4		3		2			2				1				
		B2,CC												3		4	1	2							1				
		B3,CC												2		4		2			3								
		B4,CC		cf. 1										3		5	3	3			3				1				
	NN10	B5,CC										1		3	1	5	2	2											
		B6,CC												2	1	4	2	3			3								
		B7,CC												3		4		3			4								
		B8,CC												2		3		2			2						2		
	NN9	B9,CC													1	2	1	2			1								2
middle Miocene		B10,CC																1											
	NN8	B11,CC																									1		
	NN7	B12,CC																			2								
	NN6	B13,CC to B14,CC	Barren																										
		B15,CC									3			2		2		1			2								
		B16,CC			1						4			4	2	3	2	3			3						2		
		B17,CC		1						1	5			5	3	4	3	3			5								
	NN5	B18,CC	1	1			1				4			1	2	4	3	3			2								
		B19,CC				2			1		2				2	3	2	1											
		B20,CC				1		2			5			1		4	1	1			2								
		B21,CC		2		1					4		1		3	4	3	2			1								
	NN4-NN5	B22,CC to B24,CC	Barren																										

Note: Numbers indicate frequency (see Table 1). Species marked by an asterisk are reworked from the Paleogene.

view of these uncertainties, zonal boundaries for the silicoflagellates at Site 594 are tentative and are shown in dashed lines in Figure 2 and Table 3.

The uppermost samples from 594-1,CC to 594-5,CC, representing the late Quaternary, are barren of silicoflagellates. Samples 594-6,CC to 594-11,CC contain silicoflagellates in varying numbers, among these *Distephanus speculum speculum* and *Dictyocha messanensis,* each represented by several forms. *Dictyocha messanensis aculeata* has its first occurrence in Sample 594-11,CC, placing this interval in the middle Quaternary *Dictyocha messanensis aculeata* Zone. Samples 594-12,CC and 594-13,CC belong to the *Distephanus speculum octonarius* Zone of early Pleistocene age, with the nominate taxon present in Sample 594-13,CC.

The assemblages in most of the Pliocene, including Samples 594-14,CC to 594-20,CC, are dominated by *Distephanus speculum speculum* and are placed in the *D. speculum speculum* Zone. Also present in this interval are a few specimens of *Dictyocha fibula* and *D. messanensis.* A short interval (594-21,CC to 594-23,CC) around the Miocene/Pliocene boundary, where the last consistent occurrence of *Mesocena diodon* was noted, belongs to the *Mesocena diodon* Zone, which replaces the *Neonaviculopsis neonautica neonautica* Zone (Fig. 2) in these high southern latitudes. Below this interval *Paramesocena apiculata* is found consistently in most samples, together with *D. varia, Distephanus crux crux,* and *M. diodon* in the upper part. Accordingly Samples 594-24,CC down to 594-45,CC, just above what is considered the last autochthonous occurrence of *Corbisema triacantha,* are placed in the *Paramesocena apiculata* Zone of late middle to early late Miocene age. In the lower part of this interval silicoflagellates become rare. The *Corbisema triacantha* Zone below includes Samples 594-46,CC to 594A-20,CC. Other taxa present are *Cannopilus depressus, D. crux crux, Dictyocha varia, M. diodon,* and at level 594A-12,CC, *Distephanus stauracanthus,* which may be differentiated as the *Distephanus stauracanthus* Horizon, also found at Site 591 in the same position. The lowest part recovered in Hole 594A (Samples 594A-21,CC to 594A-25,CC), still belonging

Table 2. (Continued).

Distephanus aculeatus f. aculeatus	D. aculeatus f. binoculus	D. crux crux	D. crux bispinosus f. crux	D. crux bispinosus f. bispinosus	D. crux bispinosus f. mesophthalmus	D. crux hannai	D. polyactis crassus	D. polyactis polyactis	D. speculum giganteus f. giganteus	D. speculum giganteus f. pentagonus	D. speculum speculum f. cannopilea-hexacantha	D. speculum speculum f. pentagonus	D. speculum speculum f. septenarius	D. speculum speculum f. speculum	D. speculum speculum f. varians	D. sp.	D. stauracanthus f. octagonus	D. stauracanthus f. stauracanthus	Mesocena diodon	M. elliptica	M.? hexalitha	M. quadrangula	Naviculopsis cf. biapiculata*	Neonaviculopsis neonautica neonautica f. neonautica	N. neonautica neonautica f. praenautica	N. neonautica praenautica	Paramesocena apiculata	P. circulus	Septamesocena apiculata*	Silicoflagellate specimens	Macrora stella (chrysomonad)	Silicoflagellate zones
								Barren																						0		?
																														1		
								Barren																						0		
														1																6		*Paramesocena circulus* Zone
3														5									1					2		401		
2	1											2		5														4		226		
			3									4		5														4	1	342		
												3		5								4						5		581		
												2		4								3								462		
												1		5	1							5								339		
								1				3	1	5								1								533		
												2		4										3						124		*Neonaviculopsis neonautica neonautica* Zone
												2		5										4	1					139		
														5										1						170		
1								1			2	2		5																197		
2								1				1		5													1			298		
cf. 2					1			2			1	2		5										1	2					342		
												1		4		1										2				122		*Dictyocha varia* Zone
					1							1		4		1						1				4				89		
							1							5		2					2									113		
cf. 2						1						1		4		1						2								89		
1											1			4								3								67		
						2	1							4													3			102		
2		1				4		3	1		2		1	5																869		
						2	2	2						3													3			156		
						2	3				1			3													4			161		
						3	2					2		3					2								4			215		
						2	2		2			1		1													3			77		
cf. 1		3				cf. 1	1		2			1		1													2			56		
								1																						3		
								1																						5		
																														3		
								Barren																						0		?
								2						2				3	2											54	1	*Distephanus stauracanthus* Horizon
2	1	4							2		1			3			1	4	4								1			213	3	
		4							3					3				4	2											479	4	
		3							3										1											130	2	*Corbisema triacantha* Zone
		2							2											2										36	1	
		2				cf. 1			3	2										3										231	3	
		3							3											2										158	3	
								Barren																						0		

to calcareous nannoplankton Zone NN5 (*Sphenolithus heteromorphus* Zone), is barren of silicoflagellates.

All samples from Sites 591 and 594 can be correlated directly to standard nannoplankton zones (Martini, 1971b), which are indicated in Figures 2 and 3 as well as in Tables 1 to 3. The best correlations are possible between silicoflagellate and nannoplankton zones at Site 591 and also at Site 206, whereas correlations at Site 594 are somewhat hampered by ≈ steady reworking of Paleogene silicoflagellates into the Neogene to Quaternary sequence. A summary of correlations is given in Figure 2, with coverage best in the middle Miocene to Quaternary interval at Sites 591 and 206 and less reliable at Site 594, as indicated by dashed lines in Figure 2.

TAXONOMY

Stratigraphic Implications

Taxonomy is a special field of research in neontology and paleontology that aims to establish taxa both of plant and animal organisms that are clearly defined and stable in nomenclature, and that are generally in accordance with biological and phylogenetic data. Some of the problems still present in silicoflagellate stratigraphy are influenced by taxonomic ideas, especially by the species concepts used and synonymies hitherto not noted. The species concept upon which the following discussions are based is explained in the next section.

The species concept employed to determine silicoflagellate taxa of specific or intraspecific rank may have great importance in applied stratigraphy. If the population polymorphism of skeletons and the resulting interspecific and intergeneric homeomorphisms (present especially in the genera *Dictyocha, Distephanus,* and *Connopilus*) are not taken into account, subdividing and correlating geological sections will be difficult. Particular skeletal morphes produced by one species during different periods of its geological life-span may lead, for instance, to restricted or diachronous zones if datums are based on its range. (See the application of *Distephanus speculum* f. *pentagonus* as a time indicator for a late Miocene zone in Ling, 1973, and for an Oligocene–Miocene zone in Bukry, 1974.) Homologous skeletal morphes appearing in different species of the same genus or analogous morphes occurring in some species of different genera may lead to stratigraphic misinterpretations if they are

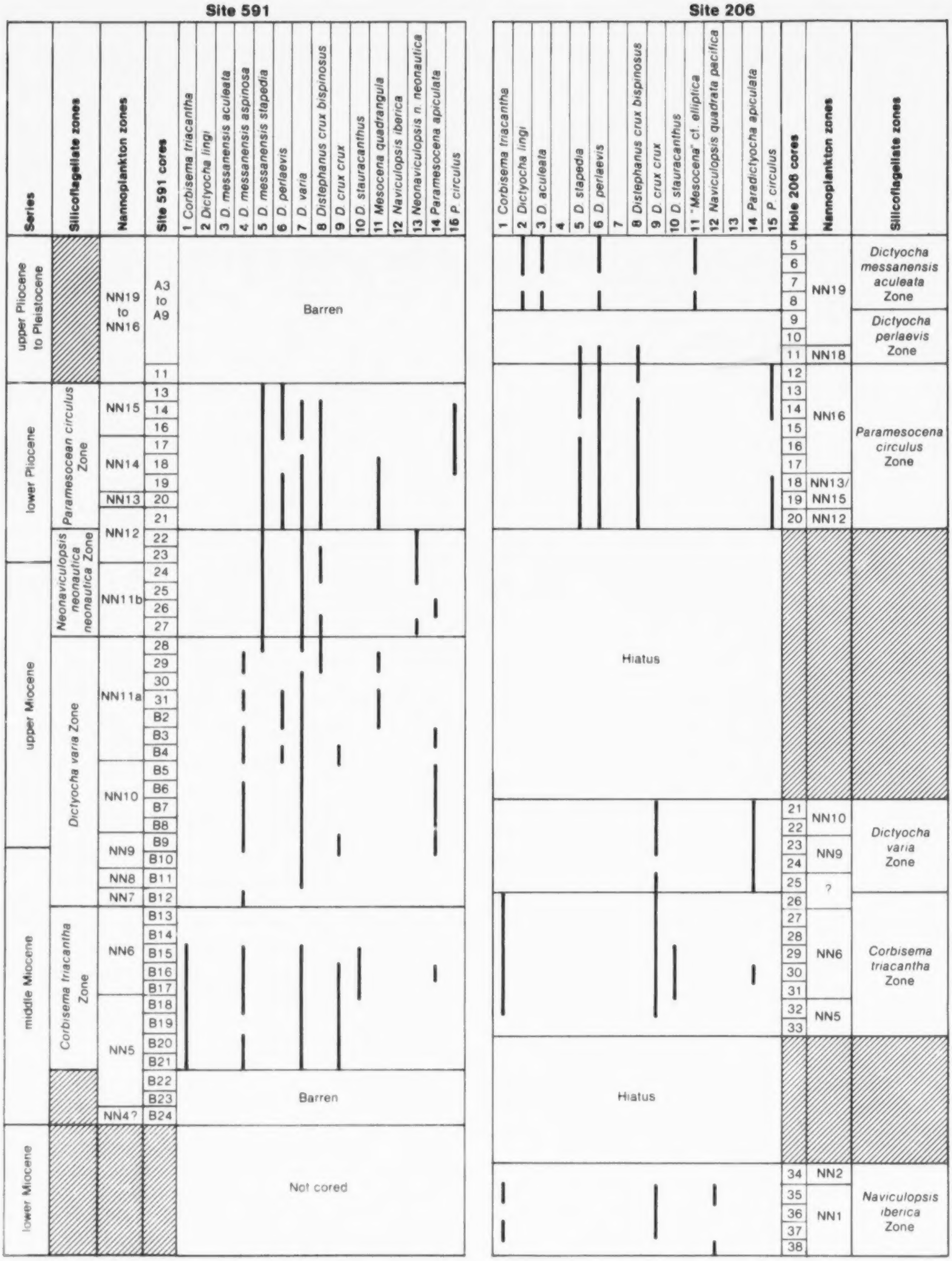

Figure 3. Distribution of important silicoflagellate taxa in core-catcher samples of Holes 591, 591B, and 206. Position of samples in the silicoflagellate and standard nannoplankton zonation and hiatuses are indicated. Standard nannoplankton zones in Hole 206 deduced from data shown in the Site 206 site chapter (Burns, Andrews, et al., 1973) and from Bukry (1973, fig. 2). Hole 591B cores indicated by B preceding core number. Corresponding species are marked by the same number. Site 591 species names, this chapter; Site 206 names, Dumitrică, 1973b.

given the same name (see the distinction of homologous forms of *Distephanus aculeatus* and *D. speculum* and analogous forms in *D. speculum* and *Cannopilus hemisphaericus,* this paper).

The intraspecific polytypism expressed in interpopulation differences of skeletal habitus comprises another field of stratigraphic implications. The differentiation of some species into subspecies realized in time and/or space may provide good possibilities for detailed age determinations, but often such variations are not known or documented (see the subdivision of *Distephanus crux* into the three subspecies *crux, bispinosus,* and *hannai,* and their stratigraphic distribution, this paper).

In general, the polymorphism and polytypism of species reflect a wide but not irregular range of skeletal variation in silicoflagellates. For some years it has been known that intraspecific variation may be very great under special conditions (Frenguelli, 1935, 1938; Van Valkenburg and Norris, 1970; Bachmann, 1971) but that normally it is limited. Investigations have shown that taxonomic distinction within a group of similar forms may be possible on the basis of statistical and biological considerations (see the distinction between *Mesocena elliptica,* tetragonal forms of *M. diodon,* and *M. quadrangula,* this paper).

In some cases synonyms and homonyms can mask conformities between stratigraphic successions of species in different areas. Fundamental in this respect are all species names introduced by C. G. Ehrenberg in the nineteenth century. Some of them that still influence the application of the Neogene silicoflagellate zonation scheme will be noted here. In general, the following names may be correlated on the species level (whereas intraspecific differentiation may be entirely possible): *Cannopilus sphaericus* Gemeinhardt to *C. depressus* (Ehrenberg), *Dictyocha ausonia* Deflandre and *D. aspera* (Lemmermann) to *D. fibula* Ehrenberg, *Distephanus boliviensis boliviensis* (Frenguelli) to *D. aculeatus* (Ehrenberg), *D. boliviensis major* (Frenguelli) to *C. heptacanthus* (Ehrenberg), *D. octacanthus* (Desikachary and Maheshwari) to *D. stauracanthus* (Ehrenberg), and *Naviculopsis rectangularis* (Schulz) to *N. quadratum* (Ehrenberg). Beside these synonyms, some equivalences have been published that cannot be confirmed: *Dictyocha epiodon* Ehrenberg does not correspond to the Quaternary *D. messanensis aculeata* (Lemmermann), and *Mesocena elliptica* Ehrenberg is distinctly separated from *M. quadrangula* Haeckel, both in time and habitus. It is to be hoped that confusion about the stratigraphic ranges of species caused by synonyms will be soon overcome by fixing the correct names, that is, the oldest legitimate names.

Additionally, there are some difficulties that may arise from the use of homonyms in species names. In Neogene stratigraphy especially, a clear decision must be made between *Dictyocha aculeata* Ehrenberg (now changed to *Distephanus aculeatus*) and *Dictyocha aculeata* (Lemmermann) (ex *D. fibula* var. *aculeata* Lemmermann, here given as *D. messanensis aculeata*); between *Mesocena apiculata* (Schulz) (ex *M. oamaruensis* var. *apiculata* Schulz, now changed to *Septamesocena apiculata*), and *M. apiculata* (Lemmermann) (ex. *M. circulus* var. *apiculata* Lemmermann, here transferred to *Paramesocena apiculata*); between *Naviculopsis ponticulus* (Ehrenberg) (ex *Dictyocha ponticulus* Ehrenberg, really a taxon belonging to *Naviculopsis*) and *N. ponticula* Perch-Nielsen.

Last but not least must be mentioned the provincialism of various silicoflagellate species, a biological–taxonomic phenomenon which bears strong stratigraphic implications. As now known (Gemeinhardt, 1934; Mandra, 1969; Martini, 1971a; Ciesielski, 1975; Busen and Wise, 1977; Bukry, 1983), some silicoflagellate species are adapted predominantly to tropical–subtropical or warm-water conditions (many *Dictyocha* species) and other species mainly to nontropical or cool-water conditions (some *Distephanus* and *Mesocena* species). This large-scale mode of geographic distribution may produce considerable difficulties if low-latitude and high-latitude sections are compared. The picture may be modified, furthermore, by some intraspecific taxa which are adapted to special conditions of limited water masses (in *Distephanus speculum* and *Mesocena diodon,* for example). The patchwork geographic distribution occurring in some subspecies or varieties may also cause difficulties in stratigraphic investigations because these taxa may have different time-ranges in separate areas.

Species Concept

Silicoflagellates are unicellular marine algae which produce a siliceous endoskeleton consisting of hollow rods. Because they are plants, the *ICBN* rules must be applied to discriminate and define taxa. According to the rules, in addition to the species some intraspecific taxa may be included in a species concept.

The species concept used here is based on statistical investigations made to clarify the taxonomic position of the species introduced by C. G. Ehrenberg (Locker, unpublished data), and on published empirical data (selected citations below). The statistical investigations have shown that the difficulties still present in silicoflagellate taxonomy can be solved only if species are treated exclusively as biological entities (groups of individuals sometimes differing in habitus but generally linked by genetic processes) rather than typological entities (groups of individuals exhibiting only a similar habitus).

The concept introduced some years ago (Locker, 1974) and explained now in more detail is based on the axiom that silicoflagellates possess temporary phases of sexual reproduction. Such phases have not yet been demonstrated but may be deduced from the relatively high stability of fossil and recent species. The persistent homogeneity of silicoflagellate species, a homogeneity often threatened by strong and divergent variation, can only be understood if sexual processes are presumed.

If sexual processes do indeed exist in silicoflagellates, some of Mayr's (1967) criteria for determining taxa in bisexually reproducing animals can also be used in silicoflagellates, although they are unicellular plants. Thus in Table 4, in addition to the categories *species* and *subspecies,* which are covered by the zoological criteria of Mayr, the two intraspecific but solely botanical catego-

Table 3. Distribution of silicoflagellates in selected samples from Site 594, indication of silicoflagellate zones, and correlation to standard nannoplankton zones.

	Nannoplankton zones	Core-catcher samples	*Cannopilus depressus*	*C. hemisphaericus*	*Corbisema apiculata**	*C.* cf. *apiculata**	*C. inermis* f. *disymmetrica**	*C. triacantha*	*Dictyocha fibula asymmetrica*	*D. fibula fibula*	*D. fibula* s. l.	*D. medusa*	*D. messanensis aculeata*	*D. messanensis aspinosa*	*D. messanensis messanensis* f. *aspinosa*	*D. messanensis messanensis* f. *messanensis*	*D. pygmaea*	*D.* sp. 3	*D. varia*	*Distephanus aculeatus* f. *aculeatus*	
Quaternary	NN20	1,CC to 5,CC										Barren									
		6,CC																			
	NN19b	7,CC											2								
		8,CC																			
		9,CC											2		1	3					
		10,CC						1													
		11,CC						1					1		1						
		12,CC														1					
		13,CC																			
"upper Pliocene"	NN16/NN19a	14,CC																			
		15,CC																		1	
		16,CC													2	3					
lower Pliocene	NN15	18,CC									1										
		19,CC							1							1					
	NN12/NN14	20,CC						1											1		
		21,CC						1											2	1	
upper Miocene		23,CC																			
	NN11	24,CC						1											1	2	
		25,CC			1			1		2		1							1		
	NN10	26,CC						2						2			1		2		
		27,CC						1			2			4					2	2	1
	NN9	28,CC		2															2		
middle Miocene		29,CC																			
	NN7/NN8	30,CC				1															
		31,CC																			
		33,CC																			
		34,CC																			
		35,CC						cf. 1													
		36,CC						2													
		37,CC						cf. 1													
		38,CC																			
		39,CC																	1		
		40,CC																			
	NN6	41,CC																			
		42,CC																			
		43,CC																			
		44,CC	3							3	2			2					2		
		45,CC															1				
		46,CC						1		1				1				2	3		
		47,CC						1		1											
		48,CC								1											
		49,CC																			
		50,CC																			
		51,CC																			
		52,CC										1									
		53,CC						2											1		
		A12,CC	2	1				2	2										2		
		A13,CC															cf. 1				
		A14,CC	1					1				1		1							
	NN5	A15,CC	2				1	3			2	2							3		
		A16,CC	2																		
		A17,CC		1		2		3			2								3		
		A18,CC			1			1				1							1		
		A19,CC						1													
		A20,CC						2									cf. 1				
		A21,CC to 25,CC										Barren									

Note: Numbers indicate frequency (see Table 1). Species marked by an asterisk are reworked from the Paleogene.

Table 3. (Continued).

D. crux crux	*D. crux hannai*	*D. speculum giganteus* f. *giganteus*	*D. speculum giganteus* f. *pentagonus*	*D. speculum speculum* f. *cannopilea-hexacantha*	*D. speculum speculum* f. *nonarius*	*D. speculum speculum* f. *octonarius*	*D. speculum speculum* f. *pentagonus*	*D. speculum speculum* f. *pseudofibula*	*D. speculum speculum* f. *septenarius*	*D. speculum speculum* f. *speculum*	*D. stauracanthus* f. *octagonus*	*D. stauracanthus* f. *stauracanthus*	*Mesocena diodon*	*M. quadrangula*	*Naviculopsis biapiculata**	*N.* cf. *biapiculata**	*N.* cf. *constricta**	*Paramesocena apiculata*	*P. circulus*	*P. dumitricae*	*Septamesocena apiculata**	Silicoflagellate specimens	Silicoflagellate zone
										Barren												0	*Dictyocha messanensis aculeata* Zone
																						1	
										4												24	
									1	2												6	
										2												23	
				1					2	4												50	
																						3	
											1											2	*Distephanus speculum octonarius* Zone
					1	2		cf. 1	1	4												31	
										2												2	*D. speculum speculum* Zone
										5					2							78	
										3												23	
										1			1		1							4	
										2					1							5	
										1								1				4	
								1		3			1	2					2			20	*Mesocena diodon* Zone
										1			3									8	
										3			2			1		2	3	1		40	*Paramesocena apiculata* Zone
1										3			2					3	2			33	
1		1								1			4		1		1	2		2		42	
2		2								4			5			1		2			1	145	
													4					4				51	
1		1											4		2			3				41	
1																		3		1	1	13	
2															1			2				8	
															cf. 1							1	
																1					1	2	
																	1					2	
2															1			2			1	11	
																		1				2	
1															1							2	
															1							2	
1																						1	
																		1				1	
																1					1	3	
										1								1				2	
1															1			2				32	
										1					1							3	
1	2																	1				26	*Corbisema triacantha* Zone
															1			1				4	
1																					1	3	
1																						1	
																						1	
																						1	
															1							2	
2										1			2									11	
3										1		2	2		1	2	1				1	34	*D. stauracanthus* Horizon
1															2							4	
2		1											2									10	
4		1	1												2		1					56	
1															1							4	
3													1		2							34	
1															1	1	1					8	
2															2		1				1	12	
1															2						2	8	
										Barren												0	

Table 4. Principles of a species concept: biological and typological characters for distinguishing silicoflagellate taxa.

Biological characters	Typological characters
Species (*species*)	**Species**
Based on a unique population or various populations. Strongly separated genetically and commonly also in skeletal morphology from other species. Geographically and/or stratigraphically co-occurring with closely related species (allopatric or sympatric distribution).	Comprises skeletons with special habitus. May be taxonomically fixed by features which vary continuously but sometimes also discontinuously. Examples: •*Dictyocha fibula—Dictyocha varia* (distinguishing features continuously varying = dimensions and proportions of the basal ring and apical bar). •*Cannopilus hemisphaericus—Cannopilus schulzii* (features discontinuously varying = number of radial spines)
Subspecies (*subspecies*)	**Subspecies**
Based on a single population or several populations. Slightly distinct genetically from other subspecies of the same species, but distinctly differentiated in skeletal morphology. Geographically and/or stratigraphically separated from other subspecies of the species (allopatric distribution).	Comprises skeletons which are distinctly different in habitus compared to other subspecies of the same species (habitual polytypism). May be taxonomically fixed by features which vary continuously but sometimes also discontinuously. Examples: •*Distephanus crux crux—Distephanus crux hannai* (discriminating features varying continuously - dimensions and proportions of the basal and apical ring). •*Dictyocha messanensis stapedia—Dictyocha messanensis aspinosa* (features varying discontinuously = presence or absence of variants with an apical pike).
Variety (*varietas*)	**Variety**
Based on a single population or several populations, often including clones. Presumably not genetically distinct or only slightly distinct from other varieties of the same species or subspecies, but differentiated in skeletal morphology (characters predominantly forced by ecology). Sometimes geographically and/or stratigraphically separated from other varieties of the species (allopatric or sympatric distribution).	Comprises skeletons which are slightly different in habitus compared to other varieties of the same species or subspecies. May be taxonomically fixed by features which vary continuously.
Form (*forma*)	**Form**
Based on a special group of individuals in a population, often including clones. Strongly separated genetically and in skeletal morphology from other forms of the same population. Generally cooccurring with other forms of the population (sympatric distribution).	Comprises skeletons which are strongly different in habitus compared to other forms of the same population (habitual polymorphism). May be taxonomically fixed by features which vary discontinuously. Examples: •*Distephanus speculum speculum* f. *speculum—Distephanus speculum speculum* f. *septenarius* (number of radial spines).

ries *variety* and *form* are used. All these categories are characterized by biological and typological features which assist in taxonomic discrimination within both fossil and recent species.

Practical considerations suggest using only the categories listed in Table 4. Taxa of species rank can be established mainly by features that vary continuously (dimensions of skeletal elements and proportions of skeleton) but generally within the limits of generic characters that are phylogenetically founded. Habitual polytypism may distinguish subspecies that can also be established mainly by features which vary continuously.

Generally speaking, it should be possible to enumerate silicoflagellate varieties, but investigations have shown that most intraspecific variations in habitus are linked to larger areas or to different time-levels. This spatial and temporal distribution suggests that the subspecies may be the more appropriate category. But, if necessary, varieties can also be described by features which vary continuously.

One of the most important categories of the species concept used here is the *form*. Forms are regarded as intrapopulation variants which can be fixed by features that vary discontinuously (number of radial spines, number and kind of apical elements, presence of pikes, etc.). In terms of genetics, these forms must be quoted as *morphes*. The concept of intrapopulation polymorphism agrees well with the empirical data received from recent populations of silicoflagellates and also with statistical evaluations of fossil populations (recent populations: Hovasse, 1932; Frenguelli, 1935, 1938; Van Valkenburg and Norris, 1970; fossil populations: Deflandre, 1950, 1952; Bachmann, 1970, 1971; Locker, unpublished data). Nevertheless, in some cases it may be difficult to apply the concept because similar morphes may be developed in different species of the same genus (homologous morphes). Making distinctions will be further complicated by populations containing, in addition to the normal variants, morphes which correspond in habitus to forms of other genera (analogous morphes). Morphes of the last type are known especially from the genera *Corbisema* (dictyochid forms), *Dictyocha* (mainly distephanoid and cannopiloid forms), and *Distephanus* (dictyochid and cannopiloid forms). Therefore, a taxonomy satisfactory on the specific and intraspecific level can only be established if all data—genetic, habitual, geographic, stratigraphic, and statistical—are considered.

Finally, variation patterns can be modified by polymorphisms in size which are caused, presumably, by ecological conditions. Populations with relatively small skeletons occur as well as populations with larger skeletons. This mode of variation can be roughly registered empirically, but more exact statistical methods are desirable. In this chapter, variations expressed only in size are regarded as taxonomically insignificant; that is, no special names should be introduced.

The large number of variations possible in any given homogeneous group of silicoflagellate skeletons explains the difficulty in making completely satisfactory taxonomic evaluations. The species concept proposed here is intended to establish precise criteria for distinguishing intraspecific taxa, criteria that are biologically based and that may be reproduced in fossil populations.

Remarks on Ehrenberg's Species

As indicated earlier, the species names introduced by C. G. Ehrenberg (1795–1876) from 1838 to 1873 are fundamental in silicoflagellate taxonomy because they are the oldest citations. Most of the names were validated by Ehrenberg with a description but for many he provided no figure, and some were published only as nomina nuda. Therefore, Locker (1974) undertook a revision of types.

The revision of Ehrenberg's species was accomplished using the following general scheme: (1) selection of the type locality by means of the first description; (2) examination of the type series; and (3) fixing of a lectotype or corroboration of a holotype. Because this procedure was in accordance with the rules of nomenclature, the typifications must be accepted (*ICBN*, article 8.1; *ICZN*, article 24a). The only exception concerns the type of *Dictyocha crux*. Because of special circumstances in the Ehrenberg collection, the two species *D. crux* and *D. mesophthalma* were confused by use of the same type specimen. But in all other cases the types fixed in 1974 can be taken as a base for further taxonomic procedures, such as fusion of names used by Ehrenberg or establishing equivalences with names of later authors.

In this context we should mention a typical source of error. As indicated by Ehrenberg's original publications, many of the species names must be treated as substantives in apposition; that is, if such species are transferred to other genera, the Latin endings should not be altered (*ICBN*, articles 23.5, 24.2; *ICZN*, article 11g). Among others, the names *circulus, heptacanthus, ornamentum, ponticulus, quadratum, speculum,* and *stauracanthus* are affected by this rule.

Systematic Descriptions

In this chapter all autochthonous species are discussed (allochthonous species are marked with an asterisk in Tables 2 and 3). Without exception, genera and species are described in alphabetical order, according to the rules of the *ICBN*. Following the species concept explained above, intraspecific taxa, like subspecies and forms, are distinguished within some species. These taxa are generally indicated by a rank-denoting term (*ICBN*, article 24.1). But in other sections we have done so only in the case of forms, because for subspecies the third position in a name is indicative enough.

Referring to the species concept, homologous forms occurring in different subspecies of the same species are given the same name, because it may be assumed that equivalent forms within one species are produced by the same alleles or combinations of alleles. Only in nominate taxa were different homonymic combinations used, according to the rules of nomenclature (*ICBN*, article 26.1). For example, *Distephanus speculum speculum* f. *speculum* corresponds, in skeletal structure, exactly with *D. speculum giganteus* f. *giganteus*.

Below the species name only the most important synonyms are cited. In descriptive terminology we followed mainly Bukry (1976b), but some other terms were also used. The term "apical structure" was replaced by the more unwieldy "apical apparatus," because "structure" is treated here in its systemological sense as indicating relations between the elements of any given system.

Class CHRYSOPHYCEAE
Order SILICOFLAGELLATA Borgert, 1891
Genus *CANNOPILUS* Haeckel, 1887

Type species. *Cannopilus hemisphaericus* (Ehrenberg, 1845) Haeckel, 1887 ex *Dictyocha hemisphaerica* Ehrenberg, 1845.

Typification. In Loeblich et al. (1968) it is suggested that the genus *Cannopilus* Haeckel, 1887, might belong in the synonymy of *Halicalyptra* Ehrenberg, 1854. But according to Locker (1974) the genus *Halicalyptra* must be placed with the Radiolaria, and the two silicoflagellate species included by Ehrenberg himself must be transferred to *Cannopilus*.

In 1974, Locker noted that the selection of *H. virginica* Ehrenberg, 1854, as type of the genus *Halicalyptra* (Campbell, 1954) was mistaken because the species name had been introduced with a genus in question (cited as *Halicalyptra*? *virginica*)—a designation prohibited by Article 67h of the *ICZN* (exclusion of species inquirenda or species incertae sedis), and recommendation 7B or article 8.1 of the *ICBN* (nomination in accordance with the protologue). Locker, therefore, corrected the determination and appointed *H. fimbriata* Ehrenberg, 1854, as the type genus of *Halicalyptra*.

Description. Skeleton consisting of a basal ring and an apical apparatus. Basal ring polygonal or circular, with 5 to 12 radial spines or spines absent; usually with basal pikes, but sometimes pikes absent. Apical apparatus semiglobular or nearly globular, furnished with 2 or more apical windows, often bearing accessory pikes.

Remarks. All species of *Cannopilus* are provided with 2 or more apical windows. The fenestrate apical apparatus of *Cannopilus* generally represents a relatively high and late evolutionary stage in silicoflagellates which obviously arises from some late Oligocene *Distephanus* species. The normal variants of these *Distephanus* species are furnished with a simple apical ring but generalist forms with a fenestrate apparatus—so-called cannopiloid morphes—are produced. During a relatively short geological time-span these early cannopiloid variants were transformed by phylogenetic selection and stabilization processes into obligatory fenestrate species.

Usually the cannopiloid specimens of *Distephanus* and normal individuals of *Cannopilus* found in the same material may be distinguished by additional skeletal features, but in some cases only statistical or genetic methods may lead to sufficient taxonomic discrimination.

Cannopilus depressus (Ehrenberg) Locker
(Plate 1, Fig. 1)

1854 *Halicalyptra depressa* Ehrenberg, *Mikrogeologie*, plate 18, fig. 111.

1931 *Cannopilus sphaericus* Gemeinhardt, *Ber. D. Bot. Ges.*, 49:105, plate 10, figs. 3–4.

1974 *Cannopilus depressus* (Ehrenberg) *in* Locker, *Eclog. Geol. Helv.*, 67:639, plate 4, fig. 3 (= lectotype).

Remarks. The specimens have a globular apical apparatus which is perforated by many large apical windows.

Cannopilus hemisphaericus (Ehrenberg) Haeckel
(Plate 1, Fig. 7)

1845 *Dictyocha hemisphaerica* Ehrenberg, *Ber. Akad. Wiss. Berlin*, 1844:266–267.

1887 *Cannopilus hemisphaericus* (Ehrenberg) *in* Haeckel, *Rep. Sci. Res. Voy.* Challenger, 18:1569.

1974 *Cannopilus hemisphaericus* (Ehrenberg) *in* Locker, *Eclog. Geol. Helv.*, 67:639, plate 4, fig. 1 (= lectotype), figs. 4, 5, 7, 8 (= other types).

Remarks. This species shows a basal ring with spines arranged in the plane of the ring. The semiglobular apical apparatus usually bears only a few apical windows.

Cannopilus heptacanthus (Ehrenberg) Locker

Remarks. *Cannopilus heptacanthus* is characterized by a large basal ring armed with 7 or more radial spines. Basal pikes are usually not developed. The apical apparatus generally exhibits several windows. The subspecies may be distinguished by the width of the apical apparatus in relation to the basal ring and by the number of apical windows.

Cannopilus heptacanthus ssp. *antarcticus* (Ciesielski) n. comb.
(Plate 1, Fig. 10)

1975 *Cannopilus antarcticus* Ciesielski, *Init. Repts. DSDP*, 28:654, plate 1, figs. 1–9.

Remarks. This large subspecies displays an apical apparatus which is divided into many small windows. The lateral windows are remarkably large.

Cannopilus heptacanthus (Ehrenberg) ssp. *heptacanthus*
(Plate 1, Fig. 9)

1841 *Dictyocha heptacanthus* Ehrenberg, *Ber. Akad. Wiss. Berlin*, 1840:208.

1854 *Dictyocha heptacanthus* Ehrenberg *in* Ehrenberg, *Mikrogeologie*, plate 19, fig. 39.

1951 *Dictyocha boliviensis* var. *major* Frenguelli, *Physis*, 20:277, fig. 3a–c.

1974 *Cannopilus heptacanthus* (Ehrenberg) *in* Locker, *Eclog. Geol. Helv.*, 67:639, plate 4, fig. 9 (= holotype).

Remarks. This large subspecies generally possesses 7 radial spines in the material investigated. The apical apparatus is furnished with a few large windows.

Cannopilus ichikawai Bachmann
(Plate 1, Figs. 2, 3)

1964 *Cannopilus ichikawai* Bachmann, *Sci. Rep. Kanazawa Univ.*, 9: 110, plate 6, figs. 59–61.

Remarks. This large globular species shows no radial spines but has long basal pikes which are oriented toward the center.

Cannopilus iidaensis Bachmann
(Plate 1, Figs. 5, 6)

1967 *Cannopilus iidaensis* Bachmann, *Sci. Rep. Kanazawa Univ.*, 12: 162, plate 3, figs. 1–7.

Remarks. The specimens are furnished with 9 radial spines and an apical apparatus perforated by many small windows.

Cannopilus latifenestratus Bachmann
(Plate 1, Fig. 8)

1964 *Cannopilus latifenestratus* Bachmann, *Sci. Rep. Kanazawa Univ.*, 9:111, plate 6, figs. 62–64.

Remarks. The large, broken specimen possesses no radial spines. The apical windows are nearly as wide as the lateral ones.

Cannopilus picassoi Stradner
(Plate 1, Fig. 4)

1961 *Cannopilus picassoi* Stradner, *Erdöl Kohle*, 14:92, plate 3, figs. 101–104.

Remarks. The single specimen found shows a globular apical apparatus pierced by many small windows.

Genus *CORBISEMA* Hanna, 1928

Type species. *Corbisema geometrica* Hanna, 1928.

Description. Skeleton consisting of a basal ring and an apical apparatus. Basal ring trigonal, with radial spines or spines absent, often bearing septate corners; basal pikes below the struts or pikes absent. Apical apparatus triradiate, sometimes with apical plate. Skeleton seldom tetragonal and with cross-shaped apical apparatus (dictyochid morphes) or digonal and then with apical bridge (naviculopsoid morphes).

Remarks. Usually the species of *Corbisema* are constructed trigonally but sometimes the main morphes are accompanied by tetragonal forms or, more seldom, also by diagonal ones. At present, there is no sufficient argument to include pentagonal forms in this genus.

Corbisema apiculata (Lemmermann) Hanna
(not figured)

1901 *Dictyocha triacantha* var. *apiculata* Lemmermann, *Ber. D. Bot. Ges.*, 19:259, plate 10, figs. 19, 20.

1975 *Corbisema apiculata* (Lemmermann) *in* Perch-Nielsen, *Init. Repts. DSDP*, 29:685, plate 2, figs. 15, 16, 19, plate 3, figs. 19, 20, 24, plate 5, figs. 1, 2.

Remarks. Specimens included here have a triangular basal ring, short radial spines, and also basal pikes. Present in the middle Eocene of Hole 588C, and rare reworked specimens in the middle and upper Miocene at Site 594.

Corbisema cf. *apiculata* (Lemmermann) Hanna
(not figured)

Remarks. Specimens found in Hole 588C are somewhat smaller than the nominate species and have less prominent basal pikes. Present (few to common) in the middle Eocene samples of Hole 588C, and also found reworked in a few Miocene samples of Site 594.

Corbisema cf. *archangelskiana* (Schulz) Frenguelli
(not figured)

1928 *Dictyocha triacantha* var. *archangelskiana* Schulz, *Bot. Archiv*, 21:250, figs. 33a–c, 77, 78.

1975 *Corbisema archangelskiana* (Schulz) *in* Perch-Nielsen, *Init. Repts. DSDP*, 29:685, plate 3, figs. 17, 22.

Remarks. Some rare specimens found in the middle Eocene of Hole 588C may be attributed to this species; they are identical to fig. 5 of plate 7 in Martini and Müller (1976).

Corbisema bimucronata Deflandre
(not figured)

1950 *Corbisema bimucronata* Deflandre, *Microscopie*, 2:191, figs. 174–177.

Remarks. Rare specimens found in the lower part of Hole 588C, Core 19, in the middle Eocene (Table 1).

Corbisema convexa (Bukry) n. comb.
(not figured)

1978 *Corbisema triacantha* ssp. *convexa* Bukry, *Init. Repts. DSDP*, 44: 815, plate 1, figs. 13–17.

Remarks. Specimens found in the middle Eocene of Hole 588C, Core 19, seem to represent this species, which was also found in the *Naviculopsis foliacea* Zone sensu Bukry of DSDP Hole 390A (Core 7), western North Atlantic (Bukry, 1978b).

Corbisema hastata (Lemmermann) Frenguelli
(not figured)

1901 *Dictyocha triacantha* var. *hastata* Lemmermann, *Ber. D. Bot. Ges.*, 19:259, plate 10, figs. 16, 17.

1975 *Corbisema hastata* (Lemmermann), *in* Perch-Nielsen, *Init. Repts. DSDP*, 29:685, plate 3, figs. 2–4, 8.

Remarks. Rare specimens were found in samples from Core 19 of Hole 588C, which can be placed in the middle Eocene *Naviculopsis foliacea* Zone.

Corbisema spinosa Deflandre
(not figured)

1950 *Corbisema spinosa* Deflandre, *Microscopie*, 2:193, figs. 178–182.

1976 *Corbisema spinosa* Deflandre, *in* Martini and Müller, *Init. Repts. DSDP*, 38:869, plate 7, fig. 9.

Remarks. Rare specimens were encountered in Sample 588C-19,CC (middle Eocene, *Naviculopsis foliacea* Zone).

Corbisema triacantha (Ehrenberg) Hanna
(Plate 2, figs. 1, 2; Plate 11, Fig. 1)

1845 *Dictyocha triancantha* Ehrenberg, *Ber. Akad. Wiss. Berlin*, 1844: 80.

1931 *Corbisema triacantha* (Ehrenberg) *in* Hanna, *Mining Calif.*, p. 198, plate D, fig. 1.

1974 *Corbisema triacantha* (Ehrenberg) *in* Locker, *Eclog. Geol. Helv.*, 67:634, plate 1, fig. 10 (=holotype).

Remarks. The specimens included range from smaller to larger ones. Smaller skeletons are provided with basal bars which are more convex than in larger specimens. Radial spines are usually long.

Genus *DICTYOCHA* Ehrenberg, 1840

1838 *Dictyocha* Ehrenberg, *Abh. Akad. Wiss. Berlin*, 1836:132 (nomen nudum).

1840 *Dictyocha* Ehrenberg, *Abh. Akad. Wiss. Berlin*, 1838:128–129.

Type species. *Dictyocha fibula* Ehrenberg, 1840.

Typification. Frenguelli (1940) selected *Dictyocha fibula* Ehrenberg, 1840, as type of the genus. This selection was generally acknowledged but several questions remained about the nature of the type. As shown in the species description, Ehrenberg's intentions about the species and also the protologue belonging to the diagnosis (Ehrenberg, 1840) were neglected for more than a century.

Description. Skeleton consisting of a basal ring and an apical apparatus. Basal ring tetragonal, pentagonal, or hexagonal?, usually with radial spines; basal pikes below or close to the struts, or pikes absent. Apical apparatus composed of struts and an apical bar, the bar simple or complex?, sometimes with an apical pike. Skeleton seldom trigonal (corbisemoid variants) or digonal (naviculopsoid variants) and then often supporting a reduced apical apparatus. The regular basal ring sometimes surmounted by an apical ring (distephanoid morphes) or a fenestrate apical apparatus (cannopiloid morphes). For details see Table 5.

Remarks. Most of the *Dictyocha* species are provided with a tetragonal basal ring and a simple apical bar, but relatively often pentagonal forms with an additional strut are developed in addition to the main morphes. Trigonal or digonal specimens with a reduced apical apparatus are rarely present in the populations, and they are probably more abnormal variants. Most of the hexagonal skeletons possessing a complex apical bar certainly belong to populations of *Distephanus* (dictyochid morphes), but some of them may in fact exhibit independent species of *Dictyocha*.

The bulk of the *Dictyocha* species are distinguished by the orientation of the apical bar and the general outline of the basal ring. Differences among species where the apical bar is aligned with the long axis are usually slight, but in many cases they are significant. This is also true for species with the bar along the short axis.

Dictyocha aegea Stradner and Bachmann
(Plate 2, Fig. 13)

1978 *Dictyocha aegea* Stradner and Bachmann, *Init. Repts. DSDP*, 42:805–806, text-fig. 1, plate 1, figs. 12(?), 13–16.

Remarks. The relatively robust specimen found in Sample 591B-5,CC (upper Miocene) corresponds in shape and dimensions to those from the type material.

Dictyocha eocaenica (Krotow)
(not figured)

1960 *Dictyocha fibula* f. *eocaenica* Krotov *in* Gleser, *Geol. Inst. Inf. Sborn.*, 35:131, plate 2, fig. 9.

Remarks. The fibuloid silicoflagellates in the Paleocene and Eocene in general need detailed study. Currently, specimens found in the middle Eocene of Hole 588C (Core 19) are best placed with *Dictyocha eocaenica*.

Dictyocha epiodon Ehrenberg
(Plate 2, Fig. 16)

1845 *Dictyocha epiodon* Ehrenberg, *Ber. Akad. Wiss. Berlin*, 1844: 79.

1854 *Dictyocha epiodon* Ehrenberg *in* Ehrenberg, *Mikrogeologie*, plate 18, fig. 55; *non* plate 35A and 35B (=other taxa).

1974 *Dictyocha epiodon* Ehrenberg *in* Locker, *Eclog. Geol. Helv.*, 67: 634–635, plate 1, figs. 4, 5 (=lectotype, syntype), *non* figs. 1, 7, 8 (= other taxa).

Remarks. The single but typical specimen possesses a large basal ring surmounted by a short apical bar. Basal pikes are present. Found in Sample 591B-21,CC (middle Miocene).

Dictyocha extensa (Locker) n. comb.
(Plate 2, Figs. 10–12; Plate 11, Fig. 3)

1975 *Dictyocha varia* f. *extensa* Locker, *Z. Geol. Wiss. Berlin*, 3:99–101, figs. 1/2, 3/3.

Remarks. This taxon is separated here from *Dictyocha varia* and includes specimens with an elongated basal ring and basal bars which

Table 5. Structure of some *Dictyocha* and *Distephanus* species: subspecies and common forms.

Dictyocha messanensis H *D. messanensis* ssp. *aculeata* (L) *D. messanensis* ssp. *aspinosa* (B) *D. messanensis* H ssp. *messanensis* *D. messanensis* ssp. *stapedia* (H)	4 rs/ab/1 ap f. *aculeata* f. *messanensis* f. *stapedia*	4 rs/ab/0 ap f. *aspinosa* (nm) f. *aspinosa* f. *aspinosa* (nm) f. *aspinosa* (nm)	4 rs/ar/0–1 ap f. *speculum* (F)	5 rs/ab/0–1 ap f. *abnormis* (E)
Dictyocha perlaevis F	4 rs/ab f. *perlaevis*			5 rs/ab f. *pentaradiata* n. f.
Distephanus crux (E) *Distephanus crux* ssp. *bispinosus* D *D. crux* (E) ssp. *crux* *D. crux* ssp. *hannai* B	4 rs/ar/0 ap f. *crux* (nm) f. *crux* f. *hannai*	4 rs/ar/1–2 ap f. *bispinosus*	4 rs/ar/3–4 ap f. *mesophthalmus* (E)	4 rs/>1 aw Known, not named Known, not named
Distephanus aculeatus (E)	5 rs/ar Known, not named	6 rs/ar f. *aculeatus*	7 rs/ar f. *ornamentum* (E)	8 rs/ar
	5 rs/>1 aw Known, not named	6 rs/>1 aw f. *binoculus* (E)	7 rs/>1 aw Known, not named	
Distephanus speculum (E)	5 rs/ar f. *pentagonus* (L)	6 rs/ar f. *speculum*	7 rs/ar f. *septenarius* (E)	8 rs/ar f. *octonarius* (E)
	5 rs/>1 aw f. *cannopilus-pentagona* (F)	6 rs/>1 aw f. *cannopilus-hexacantha* (F)	7 rs/>1 aw Known, not named	
	5 rs/ab f. *pentagonalis* (A)	6 rs/ab f. *varians* G + B f. *pseudofibula* S	7 rs/ab	

Note: Nominate forms or antonyms are given without author; non-nominate but structurally identical forms within different subspecies are marked (nm); described forms and transferred taxa are cited with author (A = Aurivillius, B = Bukry, D = Dumitrică, E = Ehrenberg, F = Frenguelli, G + B = Gran and Braarud, H = Haeckel, L = Lemmermann, S = Schulz). Abbreviations refer to combinations of skeletal elements (ab = apical bar, ap = apical pike, ar = apical ring, aw = apical window, rs = radial spine).

are distinctly convex. The short apical bar is aligned with the long axis. Few to common in the middle Miocene to lower Pliocene of Site 591.

Dictyocha fibula Ehrenberg

Remarks. *Dictyocha fibula* is treated here as a group of subspecies. The species is generally characterized by a large basal ring, usually tetragonal in outline, and an apical bar arranged along the short axis. The subspecies indicated may be distinguished by the shape of the skeleton and the proportions of the skeletal elements.

D. fibula ssp. *asymmetrica* n. ssp.
(Plate 4, Figs. 1–6)

Holotype. SM.B 13508; Plate 4, Fig. 1.

Type locality. Lord Howe Rise, DSDP Sample 591B-21,CC (middle Miocene).

Description. Basal ring tetragonal, usually asymmetrical, furnished with four radial spines. Basal pikes generally small and directly beneath the struts. Apical apparatus composed of an apical bar and four struts, the bar along the short axis, reaching one-third of the short diameter. Length, 62–93 μm.

Remarks. This new subspecies may be distinguished from similar taxa by the rather conspicuous shape of the skeleton. The basal ring usually exhibits an asymmetrical outline, causing slight divergence of the radial spines aligned with the long axis. Commonly all apical elements, bar and struts, are more delicate than the basal ones.

D. fibula Ehrenberg ssp. *fibula*
(Plate 5, Figs. 1, 2; Plate 11, Figs. 8, 9)

1838 *Dictyocha fibula* Ehrenberg, *Abh. Akad. Wiss. Berlin*, 1836:132 (nomen nudum)

1840 *Dictyocha fibula* Ehrenberg, *Abh. Akad. Wiss. Berlin*, 1838:129.

1854 *Dictyocha fibula* Ehrenberg *in* Ehrenberg, *Mikrogeologie*, plate 21, figs. 42a–b, plate 22, figs. 42a–b, *non* figure 42c, plate 36, fig. C 37, *non* plates 18–20, 33B (= other taxa).

1974 *Dictyocha fibula* Ehrenberg *in* Locker, *Eclog. Geol. Helv.*, 67: 636, plate 1, fig. 6 (= lectotype), figures 3, 9, 11 (= other types).

Typification. The species was first indicated without a description or figure from Oran in Algeria (Ehrenberg, 1838). Therefore the type selection by Locker (1974) was in accordance to *ICBN* rules (recommendation 7B and article 8.1), and the species must now be restricted to the large Miocene specimens bearing the apical bar along the short axis.

Remarks. The specimens referred to this subspecies correspond in shape and dimensions to the type specimens. The basal ring generally shows a rhomboidal outline with bars usually slightly convex. The apical bar may vary in length.

Dictyocha fibula Ehrenberg s.l.
(Plate 5, Fig. 3)

Remarks. The specimens placed into this group are heterogeneous in their habitus. Angulate rhomboidal skeletons, elongate rounded, and angulate specimens are included. This group needs special investigation so that specimens may be better discriminated.

Dictyocha medusa Haeckel
(Plate 2, Figs. 14, 15; Plate 11, Fig. 6)

1887 *Dictyocha medusa* Haeckel, *Rep. Sci. Res. Voy.* Challenger, 18: 1560, plate 101, figs. 13, 14.

Remarks. This species is characterized by a cross-shaped apical apparatus. It may be polyphyletic because one group of individuals shows affinities to *Dictyocha varia* and another to *D. extensa*. The first group exhibits an apical cross slightly broadened along the short axis, the latter group a cross slightly broadened along the long axis.

Another possible explanation of the relationship would be to assume a variational continuum across the three taxa indicated, forming a line *Dictyocha varia*—*D. medusa*—*D. extensa*. This would at least enable us to erect three forms within one species.

Dictyocha messanensis Haeckel

Remarks. *Dictyocha messanensis* demonstrates a very complicated intraspecific structure. As illustrated in Table 5, some subspecies containing forms may be distinguished. The species is generally characterized by a basal ring, usually tetragonal in outline, and by an apical bar strongly aligned with the long axis. The subspecies may be distinguished by the outline of the skeleton and the presence of an apical pike. The forms may be discriminated by the number of radial spines and the structure of the apical apparatus.

The early Miocene *D. messanensis* ssp. *aspinosa* has no apical pike (only f. *aspinosa*). This feature is first developed in the late Miocene *D. messanensis* ssp. *stapedia*, which also contains spineless specimens in its population (f. *stapedia* and f. *aspinosa*). Besides the last mentioned subspecies, *D. messanensis* ssp. *messanensis* occurs in some areas, and also comprises variants with and without an apical pike (f. *messanensis* and f. *aspinosa*). The same mode of variation appears in the Quaternary *D. messanensis* ssp. *aculeata* (f. *aculeata* and f. *aspinosa*).

Typification. The species as a whole is here called *D. messanensis*. The name *D. trifenestra* given by Ehrenberg (1843) would have priority in at least one subgroup, but because the name of Haeckel is widely accepted in oceanographic literature and the name of Ehrenberg has been neglected for over a hundred years, *D. messanensis* is preferred even though this is not fully in accordance with the *ICBN*.

Dictyocha messanensis ssp. *aculeata* (Lemmermann) n. comb.

1901 *Dictyocha fibula* var. *aculeata* Lemmermann, *Ber. D. Bot. Ges.*, 19:261, Plate 11, Figs. 1, 2.

1973 *Dictyocha aculeata* (Lemmermann) *in* Dumitrică, *Init. Repts. DSDP*, 13:907, plate 9, figs. 5–10.

1977 *Dictyocha mandrai* Ling, *Proc. First Int. Cong. Pacific Neogene Strat.*, pp. 209–210, plate 1, figs. 13, 14.

Remarks. This subspecies possesses a basal ring which is more or less rhomboidal in outline. The basal bars are distinctly bent outward and have additional pikes between the radial spines. Specimens found can be placed into f. *aculeata* and f. *aspinosa* (for characters see Table 5).

Dictyocha messanensis ssp. *aculeata* (Lemmermann) f. *aculeata*
(Plate 3, Figs. 11, 12)

Dictyocha messanensis ssp. *aculeata* (Lemmermann) f. *aspinosa* (nm)
(not figured)

Dictyocha messanensis ssp. *aspinosa* (Bukry) n. comb.
(Plate 3, Figs. 3–5; Plate 12, Fig. 2)

1976 *Dictyocha stapedia* ssp. *aspinosa* Bukry, *Init. Repts. DSDP*, 34: 724, plate 2, figs. 6–9.

Remarks. This subspecies shows a basal ring slightly elongated. The radial spines are relatively short but also elongated parallel to the long axis. The apical bar does not have a pike.

D. messanensis Haeckel ssp. *messanensis*

1843 *Dictyocha fibula* var. β Ehrenberg, *Abh. Akad. Wiss. Berlin*, 1841:312, plate 2, fig. IV 11.

1861 *Dictyocha messanensis* Haeckel *in* Peters, *Ber. Akad. Wiss. Berlin*, 1860:799–800.

1861 *Dictyocha tenella* Ehrenberg, *Ber. Akad. Wiss. Berlin*, 1860:767.

Remarks. This subspecies exhibits a distinctly rhomboidal basal ring; the radial spines are relatively long. The apical bar varies in length but often may be short. Most of the specimens found belong to f. *aspinosa*, but some specimens can be placed with f. *messanensis* and f. *speculum* (for characters see Table 5).

D. messanensis Haeckel ssp. *messanensis* f. *aspinosa* (nm)
(Plate 3, Figs. 1, 9)

Dictyocha messanensis Haeckel ssp. *messanensis* f. *messanensis*
(Plate 3, Fig. 10)

Dictyocha messanensis ssp. *messanensis* f. *speculum* (Frenguelli) n. comb.
(Plate 3, Fig. 8)

1935 *Dictyocha fibula* f. *speculum* Frenguelli, *An. Mus. Argent. Cienc. Nat.*, 38 (Protistol. 4):277, plate 5, figs. 1–9, plate 6, figs. 1–8.

Dictyocha messanensis ssp. *stapedia* (Haeckel) n. comb.

1887 *Dictyocha stapedia* Haeckel, *Rep. Sci. Res. Voy.* Challenger, 18: 1561, plate 101, figs. 10–12.

Remarks. This subspecies shows a basal ring usually elongated; the radial spines are also elongated parallel to the long axis. Basal bars are generally more bent than in *D. messanensis* ssp. *messanensis*. The apical bar varies in length from one-third to one-half of the basal ring. Specimens found belong to f. *aspinosa* and f. *stapedia* (for characters see Table 5).

Dictyocha messanensis ssp. *stapedia* (Haeckel) f. *aspinosa* (nm)
(Plate 3, Fig. 2; Plate 11, Fig. 2)

D. messanensis ssp. *stapedia* (Haeckel) f. *stapedia*
(Plate 3, Figs. 6, 7)

Dictyocha perlaevis Frenguelli

1951 *Dictyocha perlaevis* Frenguelli, *Physis*, 20:279, figs. 4b–c.

Remarks. This species resembles *D. messanensis* ssp. *aspinosa* and ssp. *stapedia* in shape but is generally larger. Commonly, basal pikes are not developed. The apical bar ranges in length from one-fifth to one-third of the basal ring. Most of the specimens found belong to f. *perlaevis;* only a few specimens could be placed into f. *pentaradiata*.

Dictyocha perlaevis f. *pentaradiata* n. f.
(Plate 5, Fig. 6)

Holotype. SM.B 13509; Plate 5, Fig. 6.

Type locality. Lord Howe Rise, DSDP Sample 591-20,CC (lower Pliocene).

Description. Basal ring pentagonal, with 5 radial spines, but usually without pikes. Basal bars slightly constricted at junctions of struts. Apical apparatus composed of a crooked apical bar supported by 5 struts. Size: 55 μm.

Remarks. This new form may be differentiated from similar taxa of other species by the dimensions of the skeleton and the shape of basal bars, which are bent like the nominal form.

Dictyocha perlaevis Frenguelli f. *perlaevis*
(Plate 5, Fig. 5; Plate 12, Fig. 1)

Dictyocha sp. 1
(Plate 5, Fig. 4)

Remarks. The specimens found in the lower Pliocene of Site 591 consist of a tetragonal basal ring which is surmounted by some remnants of an apical apparatus. The apical bar, aligned with the long axis, appears reduced or aberrantly joined with the basal ring. They may be related to *D. perlaevis*.

Dictyocha pygmaea (Ciesielski) n. comb.
(Plate 2, Fig. 6)

1975 *Dictyocha aspera* var. *pygmaea* Ciesielski, *Init. Repts. DSDP*, 28:655, plate 4, figs. 1, 3, 4, 6.

Remarks. The small specimens exhibit a basal ring more or less rhomboidal in outline and an apical bar aligned with the short axis. Radial spines are relatively long. Rare in the Miocene of Sites 591 and 594.

Dictyocha sp. 2
(Plate 2, Fig. 7; Plate 11, Fig. 7)

Remarks. Specimens are small and consist of a tetragonal basal ring which has distinctly curved bars. The apical bar is arranged along the short axis. Radial spines are short. The species may be related to *D. pygmaea* or *D. varia*. Present in the uppermost Miocene and lower Pliocene of Site 591.

Dictyocha sp. 3
(Plate 2, Fig. 8)

Remarks. The small specimens show a basal ring which is more or less rhomboidal in outline. The apical bar is aligned with the short axis. Radial spines are short. Relationships to *D. pygmaea* and also to *Dictyocha* sp. 2 may be possible. Rare in the middle Miocene of Site 594.

Dictyocha subclinata Bukry
(Plate 2, Fig. 9)

1981 *Dictyocha subclinata* Bukry, *Init. Repts. DSDP*, 63:546–547, plate 1, figs. 4–8, plate 2, figs. 1–5, *non* figs. 6–10 (= other taxon).

Remarks. Specimens found are similar in shape to *Dictyocha varia* except that the bar is arranged more obliquely. The radial spines parallel to the long axis are rather long. Present in the basal upper Miocene of Site 591.

Dictyocha varia Locker
(Plate 2, Figs. 3–5; Plate 11, Figs. 4, 5)

1975 *Dictyocha varia* Locker, *Z. Geol. Wiss. Berlin*, 3:99–100, text-figs. 1/1, 3/1, *non* 1/2, 1/3, 3/2, 3/3 (= other taxon).

1975 *Dictyocha pulchella* Bukry, *Init. Repts. DSDP*, 32:687, plate 4, figs. 1–3.

Remarks. In typical cases specimens exhibit a basal ring with bars which are distinctly convex. But variation may also include more rhomboidal skeletons. The apical bar is generally aligned with the short axis. Radial spines vary in length. The species is rather abundant throughout the middle Miocene to lower Pliocene at Site 591; it is less common and occurs sporadically at Site 594.

Genus DISTEPHANUS Stöhr, 1880

Type species. *Distephanus rotundus* Stöhr, 1880, probably = *Dictyocha speculum* Ehrenberg, 1840.

Description. Skeleton consisting of a basal ring and an apical apparatus. Basal ring tetragonal to polygonal, usually with radial spines; basal pikes below or close to the struts, or pikes absent. Apical apparatus composed of struts and an apical ring which may be large or narrow, sometimes with apical pikes. The regular basal ring in some cases surmounted by a complex apical bar (dictyochid morphes) or a fenestrate apical apparatus (cannopiloid morphes).

Remarks. Species of *Distephanus* normally have an apical ring but in some populations morphes with a complex apical bar or, more often, with an apical apparatus showing several windows, are present in greater numbers. Distinguishing cannopiloid forms belonging to *Distephanus* from normal variants of *Cannopilus* may be difficult, especially if they are found in the same material. But in many cases differentiation is possible by the size range of the basal ring, its general shape, and the number of apical windows.

Distephanus aculeatus (Ehrenberg) Haeckel

1841 *Dictyocha aculeata* Ehrenberg, *Abh. Akad. Wiss. Berlin*, 1839: 148–149.

1854 *Dictyocha aculeata* Ehrenberg *in* Ehrenberg, *Mikrogeologie*, plate 19, fig. 40, *non* plates 21, 22 (= other taxa).

1887 *Distephanus aculeatus* (Ehrenberg) *in* Haeckel, *Rep. Sci. Res. Voy.* Challenger, 18:1565.

1940 *Dictyocha boliviensis* Frenguelli, *Rev. Mus. La Plata*, 2(Pal. 7): 44, fig. 4a, *non* figs. 4b–d (= other taxon).

1974 *Distephanus aculeatus* (Ehrenberg) *in* Locker, *Eclog. Geol. Helv.*, 67:637, plate 3, fig. 5 (= lectotype), figs. 6, 9 (= intraspecific taxa of *Distephanus aculeatus*).

Remarks. This large species shows a basal ring with radial spines which are usually about equal in length. The apical ring normally has no pikes. Most of the specimens found scattered throughout the middle Miocene to Pliocene at Sites 591 and 594 belong to f. *aculeatus* but some can be placed into f. *binoculus* (for characters see Table 5).

Distephanus aculeatus (Ehrenberg) f. *aculeatus*
(Plate 6, Fig. 5)

Distephanus aculeatus f. *binoculus* (Ehrenberg) n. comb.
(Plate 6, Figs. 11, 12)

1843 *Dictyocha binoculus* Ehrenberg, *Ber. Akad. Wiss. Berlin*, 1842: 265 (nomen nudum).

1845 *Dictyocha binoculus* Ehrenberg, *Ber. Akad. Wiss. Berlin*, 1844: 79.

1854 *Dictyocha binoculus* Ehrenberg *in* Ehrenberg, *Mikrogeologie*, plate 19, fig. 42.

1974 pars *Distephanus aculeatus* (Ehrenberg) *in* Locker, *Eclog. Geol. Helv.*, 67:637, plate 3, fig. 6 (= holotype), *non* figs. 5, 9 (= other intraspecific taxa of *D. aculeatus*).

Distephanus crux (Ehrenberg) Haeckel

Remarks. *Distephanus crux* is regarded here as a group of subspecific taxa. The species is generally characterized by a tetragonal basal ring surmounted by an apical ring. The subspecies indicated may be distinguished by the outline of the skeleton and the presence of apical pikes.

Distephanus crux ssp. *bispinosus* Dumitrică

1973 *Distephanus crux* ssp. *bispinosus* Dumitrică, *Init. Repts. DSDP*, 21:850, plate 6, figs. 3, 6, 7.

Remarks. This subspecies has a basal ring very similar in shape to *Distephanus crux* ssp. *crux*, but the apical ring generally supports apical pikes. According to the number of pikes, 3 forms can be distinguished: f. *crux*, f. *bispinosus*, and f. *mesophthalmus* (for characters see Table 5).

Distephanus crux ssp. *bispinosus* Dumitrică f. *bispinosus*

(Plate 6, Figs. 1-3)

Distephanus crux ssp. *bispinosus* Dumitrică f. *crux* (nm)

(not figured)

Distephanus crux ssp. *bispinosus* f. *mesophthalmus* (Ehrenberg) n. comb.

(Plate 6, Fig. 4)

1845 *Dictyocha mesophthalma* Ehrenberg, *Ber. Akad. Wiss. Berlin*, 1844:80.
1854 *Dictyocha mesophthalma* Ehrenberg *in* Ehrenberg, *Mikrogeologie*, plate 22, fig. 43.
1887 *Distephanus mesophthalmus* (Ehrenberg) *in* Haeckel, *Rep. Sci. Res. Voy.* Challenger, 18:1563-1564.
1974 pars *Distephanus crux* (Ehrenberg) *in* Locker, *Eclog. Geol. Helv.*, 67:637, plate 3, fig. 8 (= holotype, revised), *non* fig. 10 (= other intraspecific taxon of *Distephanus crux*).

Distephanus crux (Ehrenberg) ssp. *crux*

(Plate 6, Figs. 6, 7)

1841 *Dictyocha crux* Ehrenberg, *Ber. Akad. Wiss. Berlin*, 1840: 207-208.
1845 *Dictyocha staurodon* Ehrenberg, *Ber, Akad. Wiss. Berlin*, 1844: 80.
1854 *Dictyocha crux* Ehrenberg *in* Ehrenberg, *Mikrogeologie*, plate 18, figs. 56a-c, plate 20, fig. I 46, plate 33, figs. B XV 9, B XVI 9, B XVII 5.
1854 *Dictyocha staurodon* Ehrenberg *in* Ehrenberg, *Mikrogeologie*, plate 18, fig. 58.
1887 *Distephanus crux* (Ehrenberg) *in* Haeckel, *Rep. Sci. Res. Voy.* Challenger, 18:1563.
1974 *Distephanus crux* (Ehrenberg) *in* Locker, *Eclog. Geol. Helv.*, 67: 637, plate 3, fig. 10 (= lectotype of *Dictyocha staurodon*), *non* fig. 8 (= holotype of *Dictyocha mesophthalma*, revised).

Remarks. This subspecies exhibits a basal ring that is commonly rhomboidal in outline. The apical ring varies in width. The radial spines are arranged parallel to the long axis, normally reaching one-half the length of the basal ring.

Typification. Under the name *"Dictyocha Crux"* Ehrenberg figured on plates 411 and 2319 in his "Microgeological Collection" at Berlin the specimens previously indicated as lectotype (Locker, 1974). Because no other syntypes could be detected in the collection, this selection seemed to solve the problem, but it must be revised. It seems possible that Ehrenberg used on two other occasions the specimen figured in the collection and in his *Mikrogeologie* (1854): first in 1841 as part of the *Dictyocha crux* type series, and secondly in 1845 as type for the new taxon *Dictyocha mesophthalma*. To distinguish between both taxa, the "lectotype" of *Dictyocha crux* (Locker, 1974) is revised here to represent the holotype of *D. mesophthalma*. Consequently, no type specimen is at present available for *D. crux*.

Distephanus crux ssp. *hannai* Bukry

(Plate 6, Fig. 13)

1975 *Distephanus crux* ssp. *hannai* Bukry, *Init. Repts. DSDP*, 29:855, plate 4, figs. 4-6.

1977 *Distephanus pussiltus* Ling, *Proc. 1st Int. Cong. Pacific Neog. Strat., Tokyo*, pp. 211-212, plate 2, figs. 18-21.

Remarks. This large subspecies possesses a basal ring distinctly constricted at the struts. The basal bars are therefore commonly strongly curved. The apical ring is rather narrow.

Distephanus polyactis (Ehrenberg) Deflandre

Remarks. *Distephanus polyactis* is characterized by a wide basal ring possessing many radial spines but never pikes, and a rather large apical ring. The two subspecies may be distinguished by their dimensions, by the compactness of the skeleton, and by the proportions of main skeletal elements.

Distephanus polyactis ssp. *crassus* Bukry

(Plate 5, Fig. 7)

1977 *Distephanus polyactis* ssp. *crassus* Bukry, *Init. Repts. DSDP*, 37:922, plate 1, figs. 7-14.

Remarks. This subspecies has a basal ring armed with 6 to 9 short radial spines, more or less equal in length. The basal ring, missing any pikes, is surmounted by a very high and wide apical ring. The subspecies may be distinguished from the similar *Distephanus speculum* ssp. *giganteus* by the length of radial spines and the absence of basal pikes.

Distephanus polyactis (Ehrenberg) ssp. *polyactis*

(Plate 5, Figs. 8, 9)

1840 *Dictyocha polyactis* Ehrenberg, *Abh. Akad. Wiss. Berlin*, 1838: 129.
1854 *Dictyocha polyactis* Ehrenberg *in* Ehrenberg, *Mikrogeologie*, plate 22, fig. 50.
1932 *Distephanus polyactis* (Ehrenberg) *in* Deflandre, *Bull. Soc. Bot. France*, 79:497, 501.
1940 *Paradictyocha polyactis* (Ehrenberg) *in* Frenguelli, *Rev. Mus. La Plata*, 2(Pal. 7):51, text-figs. 7f-g, 8a; *non* 8b-e (= other taxon).
1974 *Distephanus polyactis* (Ehrenberg) *in* Locker, *Eclog. Geol. Helv.*, 67:637, plate 4, fig. 2 (= holotype).

Remarks. This subspecies shows a very large basal ring with 7 to 16 radial spines, rather short and nearly equal in length. The basal ring has no pikes and supports a very large diameter apical ring. The subspecies may be distinguished from *D. polyactis* ssp. *crassus* by the greater dimensions and the higher number of radial spines.

Distephanus speculum (Ehrenberg) Haeckel

Remarks. *Distephanus speculum* has a very complex intraspecific structure. As illustrated in Table 5, two subspecies and many forms may be distinguished. The species is generally characterized by a basal ring, commonly hexagonal in outline, and by an apical ring decorated with pikes. The subspecies indicated may be discriminated by their dimensions, by the compactness of the skeleton, and by the presence of apical pikes. The forms may be determined by the number of radial spines and the structure of the apical apparatus. Note that for undifferentiated middle Eocene taxa *D. speculum* s.l. is used.

Distephanus speculum ssp. *giganteus* Bukry

1976 *Distephanus speculum* ssp. *giganteus* Bukry, *Init. Repts. DSDP*, 38:848-849, plate 1, fig. 19, plate 2, figs. 1, 2.

Remarks. This subspecies possesses a very robust basal ring and commonly has 6 radial spines, but basal pikes are often minute. The apical ring does not support any pikes. Most specimens encountered belong to f. *giganteus*, but some specimens with 5 radial spines can be placed into f. *pentagonus*.

Distephanus speculum ssp. *giganteus* Bukry f. *giganteus*

(Plate 7, Figs. 14, 15)

D. speculum ssp. *giganteus* Bukry f. *pentagonus* (nm)

(not figured)

D. speculum (Ehrenberg) ssp. *speculum*

1838 *Dictyocha speculum* Ehrenberg, *Abh. Akad. Wiss. Berlin*, 1836: 132 (nomen nudum).

1840 *Dictyocha speculum* Ehrenberg, *Abh. Akad. Wiss. Berlin*, 1838: 129, plate 4, figure X n.

1854 *Dictyocha speculum* Ehrenberg *in* Ehrenberg, *Mikrogeologie*, plate 18, fig. 57, plate 19, fig. 41b, plate 21, fig. 44a, plate 33, fig. B XIII 6, *non* plate 19, fig. 41a, *non* plate 21, fig. 44b, *non* plate 22 (= other taxon).

1887 *Distephanus speculum* (Ehrenberg) *in* Haeckel, *Rep. Sci. Res. Voy.* Challenger, 18:1565.

1974 *Distephanus speculum* (Ehrenberg) *in* Locker, *Eclog. Geol. Helv.*, 67:638, plate 3, fig. 2 (= lectotype), figs. 1, 3, 4, 7, 11 (= other types of *D. speculum*).

Remarks. This subspecies sometimes has a rather small basal ring which commonly bears 6 radial spines. Basal pikes are usually distinct. The apical ring often shows pikes, in the most typical case 2, but any number from 0 to 6 may occur. Besides the most common f. *speculum*, other forms found in the material were f. *pentagonus*, f. *septenarius*, f. *octonarius*, f. *nonarius*, f. *cannopilea-hexagona*, f. *pseudofibula*, and f. *varians* (for characters see Table 5).

Distephanus speculum ssp. *speculum* f. *cannopilea-hexacantha* (Frenguelli) n. comb.

(Plate 7, Fig. 1)

1935 *Dictyocha fibula* f. *cannopilea-hexacantha* Frenguelli, *An. Mus. Argent. Cienc. Nat.*, 38 (Protist. 4): plate 12, figs. 1, 2.

Distephanus speculum ssp. *speculum* f. *nonarius* n. f.

(Plate 7, Fig. 7)

Holotype. SM.B 13510; Plate 7, Fig. 7.

Type locality. Chatham Rise, DSDP Sample 594-13,CC (lower Pleistocene).

Description. Basal ring polygonal with 9 radial spines, and basal pikes. Basal bars are slightly concave. Apical apparatus composed of a large apical ring supported by 9 struts. Pikes may be present at the apical ring. Diameter 45 μm.

Remarks. This new form is distinguished from similar taxa of other species by the dimensions and proportions of the skeleton, by the curvature of basal bars, and the presence of apical pikes.

Distephanus speculum ssp. *speculum* f. *octonarius* (Ehrenberg) n. comb.

(Plate 7, Fig. 6)

1845 *Dictyocha octonaria* Ehrenberg, *Ber. Akad. Wiss, Berlin*, 1844: 201.

1887 *Distephanus octonarius* (Ehrenberg) *in* Haeckel, *Rep. Sci. Res. Voy.* Challenger, 18:1566.

1959 *Dictyocha speculum* f. *octonarius* (Ehrenberg) *in* Proshkina-Lavrenko, *Trudy Bot. Inst. Akad. Nauk SSSR, Ser. 2*, 12:153.

Remarks. The octogonal form of *D. speculum speculum* may represent one of the more frequent morphes in its own subspecific unit of the Quaternary *D. speculum*. Size relations indicate that the subspecies may comprise a line from six- to nine-spined forms, but this must yet be demonstrated.

Distephanus speculum ssp. *speculum* f. *pentagonus*

(Plate 7, Fig. 8)

1901 *Distephanus speculum* var. *pentagonus* Lemmermann, *Ber. D. Bot. Ges.*, 19:264, plate 11, fig. 19.

Distephanus speculum ssp. *speculum* f. *pseudofibula* Schulz

(Plate 7, Fig. 11)

1928 *Distephanus speculum* f. *pseudofibula* Schulz, *Bot. Archiv*, 21: 262, figs. 51a-b.

Distephanus speculum ssp. *speculum* f. *septenarius* (Ehrenberg) n. comb.

(Plate 7, Fig. 5)

1845 *Dictyocha septenaria* Ehrenberg, *Ber. Akad. Wiss. Berlin*, 1844: 80.

1854 *Dictyocha septenaria* Ehrenberg *in* Ehrenberg, *Mikrogeologie*, plate 21, fig. 45, plate 35A, fig. B XXI 8.

1974 pars *Distephanus speculum* (Ehrenberg) *in* Locker, *Eclog. Geol. Helv.*, 67:638, plate 3, fig. 1 (= holotype), *non* figs. 2-4, 7, 11 (= other intraspecific taxa of *D. speculum*).

Distephanus speculum (Ehrenberg) ssp. *speculum* f. *speculum*

(Plate 7, Figs. 2-4)

Distephanus speculum ssp. *speculum* f. *varians* Gran and Braarud

(Plate 7, Figs. 9, 10)

1935 *Distephanus speculum* f. *varians* Gran and Braarud, *J. Biol. Board Can.*, 1:390, text-figs. 68A-B.

Distephanus sp.

(Plate 7, Fig. 12)

Remarks. The specimens included here have a hexagonal basal ring without any apical elements. Only short basal pikes are present and are oriented toward the center. The skeletons usually are very delicate; they were treated as a new taxon by Bukry (1982b), *Distephanus speculum* ssp. *tenuis*, which indicates the relationship to *D. speculum*.

Distephanus speculum (Ehrenberg) Haeckel s.l.

(not figured)

Remarks. In the middle Eocene of Hole 588C several 6-sided specimens having the general appearance of *D. speculum* were found in Core 19. For a detailed study more material is needed, but at present 3 groups are differentiated for practical use (see Table 1). *D. speculum* s.l. is hexagonal, with a 6-sided single apical window, *D. speculum* s.l. f.1 includes specimens which also have 6 struts supporting an apical apparatus of 3 windows, but *D. speculum* s.l. f.2 includes specimens in which the apical structure is reduced to a trifurcated bar supported by 6 struts. Specimens of the latter variant are frequently found in the middle Eocene of Hole 588C.

Distephanus stauracanthus (Ehrenberg) Haeckel

1846 *Dictyocha stauracanthus* Ehrenberg, *Ber. Akad. Wiss. Berlin*, 1845:76.

1854 *Dictyocha stauracanthus* Ehrenberg *in* Ehrenberg, *Mikrogeologie*, plate 33, fig. B XV 10, *non* plate 33 (= other taxon).

1887 *Distephanus stauracanthus* (Ehrenberg) *in* Haeckel, *Rep. Sci. Res. Voy.* Challenger, 18:1564.

1956 *Distephanus crux* var. *octacanthus* Desikachary and Maheshwari, *J. Ind. Bot. Soc.*, 35:260, text-figs. 10, 12, 13, plate 13, figs. 8, 9.

1971 *Dictyocha octacantha* (Desikachary and Maheshwari) *in* Martini, *Init. Repts. DSDP*, 7:1697, plate 1, fig. 16.

1974 *Distephanus stauracanthus* (Ehrenberg) *in* Locker, *Eclog. Geol. Helv.*, 67:638, plate 3, fig. 12 (= lectotype).

Remarks. This species is characterized by an octogonal basal ring armed with 4 radial spines. The rather narrow apical ring shows 4 corners, indicating some relationship to *Distephanus crux*. Besides f. *stauracanthus*, one specimen of f. *octagonus* showing only a single apical bar was found in the present material.

D. stauracanthus f. *octagonus* (Tsumura) n. comb.

(Plate 6, Fig. 8)

1963 *Dictyocha fibula* var. *octagona* Tsumura, *J. Yokohama Univ.*, C45, no. 146:55-56, plate 2, fig. 4, plate 10, figs. 11-13, plate 23, figs. 8-10.

1971 *Dictyocha octagona* (Tsumura) *in* Martini, *Init. Repts. DSDP*, 7:1697, plate 1, fig. 15.

D. stauracanthus (Ehrenberg) f. *stauracanthus*

(Plate 6, Figs. 9, 10)

Remarks. According to available data this form seems to be restricted to the middle Miocene. It is listed as *Distephanus stauracanthus* Horizon in Tables 2 and 3 (Sites 591 and 594), but is less conspicuous in the high-latitude Site 594.

Genus MESOCENA Ehrenberg, 1841

1841 *Dictyocha (Mesocena)* Ehrenberg, *Ber. Akad. Wiss. Berlin*, 1840: 208.

1843 *Mesocena* Ehrenberg *in* Ehrenberg, *Abh. Akad. Wiss. Berlin*, 1841:401.

1974 *Bachmannocena* Locker, *Eclog. Geol. Helvet.*, 67:635.

Type species. *Mesocena elliptica* Ehrenberg, 1841, ex *Dictyocha (Mesocena) elliptica* Ehrenberg, 1841.

Typification. Ehrenberg (1841) introduced the taxon *Mesocena* as subgenus of the genus *Dictyocha* without a description. In the same paper he described the species *D. (M.) circulus*, *D. (M.) elliptica* and *D. (M.) triangula* as being new. Therefore, according to articles 12 and 16a–v of the *ICZN* (validity by indication) and article 45.4 of the *ICBN* (validity of algal taxa published under the *ICZN*) the genus *Mesocena* dates from 1841 and not from 1843, as Loeblich et al. (1968) wrote. It also follows that *M. elliptica* Ehrenberg, 1841, has to be taken as type species; this is in accordance with the first selection of Frenguelli (1940).

Description. Skeleton consisting only of a basal ring, which is digonal to hexagonal, mainly tetragonal, usually with radial spines, but also without spines; basal pikes generally absent.

Remarks. All species with a single skeletal ring can be assigned to three or four genera, depending on their phylogenetic origin. According to the concept of Bachmann (1970), the genus *Mesocena* is regarded here as derived from *Dictyocha*, and tetragonal forms are most frequently represented in many populations.

Some species of *Mesocena* always show 4 radial spines, but most populations are composed of more than one form. In general, the main morphe has an even number (2, 4, 6) of radial spines, because of the greater morphological stability of symmetrical constructions. Six-rayed mesocenoid species are known, but they are rare. In some cases they may be derived, not from tetragonal *Mesocena* species along a variation line of 4, 5, or 6 radial spines, but from hexagonal species of *Distephanus*. If this can be demonstrated, the hexagonal species generated from *Distephanus* must be removed from *Mesocena* and placed in a separate genus.

Mesocena diodon Ehrenberg
(Plate 8, Figs. 3, 4)

1845 *Mesocena diodon* Ehrenberg, *Ber. Akad. Wiss. Berlin*, 1844:84.

1854 *Mesocena diodon* Ehrenberg, *in* Ehrenberg, *Mikrogeologie*, plate 33, fig. XV 18.

1974 *Bachmannocena diodon* (Ehrenberg) *in* Locker, *Eclog. Geol. Helv.*, 67:636, plate 2, fig. 9 (= lectotype).

Remarks. The species has a large basal ring which is distinctly oval in shape. Usually 2 short radial spines are developed, but in some cases 3 spines or only 1 spine may be present. Size and shape are important in differentiating this species from others.

Mesocena elliptica Ehrenberg
(Plate 9, Fig. 6)

1841 *Dictyocha (Mesocena) elliptica* Ehrenberg, *Ber. Akad. Wiss. Berlin*, 1840:208.

1845 *Mesocena elliptica* Ehrenberg *in* Ehrenberg, *Ber. Akad. Wiss. Berlin*, 1844:71, 84.

1854 *Mesocena elliptica* Ehrenberg *in* Ehrenberg, *Mikrogeologie*, plate 20, figs. I 44a–b.

1974 *Mesocena elliptica* Ehrenberg *in* Locker, *Eclog. Geol. Helv.*, 67: 634, plate 2, fig. 4 (= lectotype).

Remarks. Specimens so far known have a tetragonal basal ring. Basal bars are usually slightly wavy. Radial spines are short.

Mesocena? hexalitha Bukry

1981 *Mesocena hexalitha* Bukry, *Init. Repts. DSDP*, 63:547–548, plate 5, Figs. 5–10.

Remarks. This species usually has a hexagonal basal ring; the bars are distinctly convex. Hexagonal variants are common (f. *hexalitha*), but one heptagonal skeleton (f. *heptalitha*) was also found in the present material. The question mark after the genus name should indicate some questions about the phylogenetic origin of this species, which may have developed from *Distephanus*, in contrast to all other *Mesocena* species, which are regarded as derivates of *Dictyocha*.

Mesocena? hexalitha f. *heptalitha* n. f.
(Plate 8, Fig. 6)

Holotype. SM.B 13511; Plate 8, Fig. 6.

Type locality. Lord Howe Rise, DSDP 591-30,CC (upper Miocene).

Description. Basal ring heptagonal, the bars distinctly convex, with 7 short radial spines. Diameter 62 μm.

Remarks. The new form might be confused with specimens described by Schulz (1928) as *Mesocena polymorpha* f. *septenaria*, but the latter has distinctly straight basal bars.

Mesocena? hexalitha Bukry f. *hexalitha*
(Plate 8, Fig. 5)

Mesocena occidentalis Hanna ex Mandra
(not figured)

1931 *Mesocena occidentalis* Hanna, *Calif. Div. Mines Dept., State Mineral.*, 27(2):200, plate E, fig. 1 (invalid).

1968 *Mesocena occidentalis* Hanna ex Mandra, *Proc. Calif. Acad. Sci.* 36(9):260, figs. 29, 32, 33.

Remarks. Robust quadrate ring, with distinct spine at each corner Present in low numbers in all middle Eocene samples at Site 588 (*Naviculopsis foliacea* Zone).

Mesocena quadrangula Ehrenberg ex Haeckel
(Plate 8, Figs. 1, 2; Plate 12, Figs. 6, 7)

1873 *Mesocena quadrangula* Ehrenberg, *Abh. Akad. Wiss. Berlin* 1872:145, 273 (nomen nudum).

1887 *Mesocena quadrangula* Ehrenberg ex Haeckel, *Rep. Sci. Res Voy.* Challenger, 18:1556.

Remarks. This species usually has a tetragonal basal ring. Basal bars may vary from straight to rounded or slightly waved. The radial spines are rather long.

Genus *NAVICULOPSIS* Frenguelli, 1940

Type species. *Naviculopsis biapiculata* (Lemmermann, 1901) Frenguelli, 1940, ex *Dictyocha navicula* var. *biapiculata* Lemmermann, 1901.

Description. Skeleton consisting of a basal ring and an apical apparatus. Basal ring digonal or elliptical, with 2 radial spines, or spines absent; generally without basal pikes. Apical apparatus usually barlike or bandlike, but sometimes also composed of short struts and an apical bar, seldom bearing an apical pike.

Remarks. No generic differentiation is made here between species supporting radial spines and those without them, because the latter are clearly derived from the spiny forms.

Naviculopsis biapiculata (Lemmermann) Frenguelli
(not figured)

1901 *Dictyocha navicula* var. *biapiculata* Lemmermann, *Ber. D. Bot. Ges.*, 19:258, plate 10, figs. 14, 15.

1940 *Naviculopsis biapiculata* (Lemmermann) *in* Frenguelli, *Rev. Mus. La Plata*, 2 (Pal. 7):60, text-figs. 11 c–d.

1975 *Naviculopsis biapiculata* (Lemmermann) *in* Perch-Nielsen, *Init. Repts. DSDP*, 29:689, plate 12, figs. 18–22.

Remarks. Navicular skeleton with two long spines along the main axis and a small apical bridge. The basal ring is slightly concave at the connecting points of the apical bridge. Rare or few specimens are present in all middle Eocene samples at Site 588, but the species is also found reworked throughout the middle Miocene to upper Pliocene sequence at Site 594.

Naviculopsis foliacea Deflandre
(not figured)

1950 *Naviculopsis foliacea* Deflandre, *Microscopie*, 2:204, text-figs. 235–240.

1960 *Naviculopsis foliacea* Deflandre *in* Martini and Müller, *Init. Repts. DSDP*, 38:837, plate 12, fig. 4.

Remarks. This slender navicular species is present in all middle Eocene samples at Hole 588C (*Naviculopsis foliacea* Zone).

Genus *NEONAVICULOPSIS* n. gen.

Type species. *Neonaviculopsis neonautica* (Bukry, 1981) n. comb ex *Dictyocha neonautica* Bukry, 1981.

Description. Skeleton consisting of a basal ring and an apical apparatus. Basal ring digonal with two radial spines, but basal pikes are absent. Apical apparatus usually constructed of a simple bar (naviculopsoid morphes), but sometimes also composed of struts and an apical bar (dictyochid morphes). Differentiation from *Naviculopsis* is based mainly on the stratigraphic ranges of the two genera rather than on morphological features.

Remarks. The new genus includes a special group of naviculopsoid taxa which developed in the late Miocene from the *Dictyocha fibula* group. These naviculopsoid taxa, all placed in *Neonaviculopsis neo-*

nautica, reflect the typical habitus of *Naviculopsis*, a genus known from the early Paleocene to the early Micocene. Because the development of the *neonautica* group marks a second radiation of naviculopsoid taxa, a new genus was introduced.

The taxa united in *Neonaviculopsis* most probably indicate a unique evolutionary line. Therefore, the different members are treated only as subspecies and forms of one species. It seems especially remarkable that in younger populations 2 different morphes are present, one reflecting its derivation from *Dictyocha* and the other one an evolved stage of *Neonaviculopsis.*

Neonaviculopsis neonautica (Bukry) n. comb.

Remarks. *Neonaviculopsis neonautica* is characterized by an elongated basal ring bearing 2 short radial spines and an apical apparatus, usually bar-shaped. The subspecies may be distinguished by the proportions of the skeleton, the forms by the structure of the apical apparatus.

Neonaviculopsis neonautica (Bukry) ssp. *neonautica*

1981 *Dictyocha neonautica* Bukry, *Spec. Publ. Soc. Econ. Paleontol. Mineral.*, 32:442.

Remarks. This subspecies has a strikingly slender basal ring, more than twice as long as it is wide. Besides f. *neonautica*, specimens of f. *praenautica* supporting a dictyochid apical apparatus were found.

Neonaviculopsis neonautica (Bukry) ssp. *neonautica* f. *neonautica*
(Plate 10, Figs. 6–11)

Neonaviculopsis neonautica (Bukry) ssp. *neonautica* f. *praenautica* (nm)
(Plate 10, Fig. 12)

Neonaviculopsis neonautica ssp. *praenautica* n. ssp.
(Plate 10, Figs. 1–5)

Holotype. SM.B 13512; Plate 10, Fig. 5.

Type locality. Lord Howe Rise, DSDP 591-29,CC (upper Miocene).

Description. Basal ring oval with 2 radial spines aligned with the long axis. Apical apparatus composed of a long apical bar and 4 struts. Length 44 to 55 μm.

Remarks. This new subspecies resembles in outline some specimens of *Dictyocha fibula*, indicating close evolutionary relations, but the radial spines along the short axis are generally missing. The apical apparatus consists of a large bar which nearly reaches the basal ring. In the material investigated only the typical f. *praenautica* could be found.

Genus *PARAMESOCENA* n. gen.

Type species. *Paramesocena apiculata* (Lemmermann, 1901) n. comb, ex *Mesocena circulus* var. *apiculata* Lemmermann, 1901.

Typification. The new genus is erected here to solve the many questions related to discrimination of the mesocenoid *apiculata–circulus* group from the genus *Distephanus.* As several authors have indicated, this species group represents a special evolutionary line which certainly originates from the *D. polyactis* group (Frenguelli, 1940; Ling, 1972; Dumitrică, 1973b; Perch-Nielsen, 1975). If the ancestor is included in a separate genus covering this line, *Paradictyocha* Frenguelli, 1940, can be employed. But if one maintains the opinion that *D. polyactis* still belongs to *Distephanus*, another genus must be used, because *D. polyactis* has clearly been indicated as type of the genus *Paradictyocha* (Frenguelli, 1940). According to article 48.1 of the *ICBN*, it is not permitted to designate a new type species for *Paradictyocha* as Dumitrică (1973b) did solely to preserve the genus name. Because no genus was available to comprise this group, the new genus was introduced.

Description. Skeleton consisting only of a basal ring, which is wide, polygonal, or circular, with numerous radial spines or nodes; basal pikes are generally absent. Distinguished from *Mesocena* and *Septamesocena* by the high number of radial spines displayed in all species.

Paramesocena apiculata (Lemmermann) n. comb.
(Plate 9, Figs. 1, 5; Plate 12, Fig. 3)

1901 *Mesocena circulus* var. *apiculata* Lemmermann, *Ber. D. Bot. Ges.*, 19:257, plate 10, figs. 9, 10.

1940 *Paradictyocha apiculata* (Lemmermann) *in* Frenguelli, *Rev. Mus. La Plata*, 2(Pal. 7):52 plate 4, fig. 4.

Remarks. This species shows a basal ring with many short spines, arranged in 2 slightly diverging rows.

Paramesocena circulus (Ehrenberg) n. comb.
(Plate 9, Figs. 2–4; Plate 12, Figs. 4, 5)

1841 *Dictyocha (Mesocena) circulus* Ehrenberg, *Ber. Akad. Wiss. Berlin*, 1840:208.

1845 *Mesocena circulus* Ehrenberg *in* Ehrenberg, *Ber. Akad. Wiss. Berlin*, 1844:65.

1854 *Mesocena circulus* Ehrenberg *in* Ehrenberg, *Mikrogeologie*, plate 19, fig. 44.

1974 *Bachmannocena circulus* (Ehrenberg) *in* Locker, *Eclog. Geol. Helv.*, 67:636, plate 2, fig. 11 (= lectotype).

Remarks. This species possesses a basal ring with many small, sometimes nodular spines, arranged at varying distances from another, but generally in one plane.

Paramesocena dumitricae (Perch-Nielsen) n. comb.
(Plate 9, Fig. 7)

1975 *Paradictyocha dumitricae* Perch-Nielsen, *Init. Repts. DSDP*, 29: 689, plate 11, figs. 1, 5–8.

Remarks. The species has a basal ring with many spines that are usually larger than in other species of the genus and that are arranged farther from each other.

Genus *SEPTAMESOCENA* Bachmann, 1970

Type species. Septamesocena apiculata (Schulz, 1928) Bachmann, 1970, ex *Mesocena oamaruensis* var, *apiculata* Schulz, 1928.

Description. Skeleton consisting only of a basal ring that is trigonal or tetragonal, usually with radial spines but also without spines, and often bearing septate corners; basal pikes generally absent.

Remarks. According to Bachmann (1970) the genus *Septamesocena* is regarded as derived from *Corbisema.* Therefore, the species are most frequently furnished with 3 radial spines; but besides the trigonal main morphes tetragonal forms may also be developed in the populations. The septate corners present in some species clearly indicate phylogenetic relations to *Corbisema.*

Septamesocena apiculata (Schulz) Bachmann
(not figured)

1928 *Mesocena oamaruensis* var. *apiculata* Schulz, *Bot. Arch.*, 21: 240, text-fig. 11.

1931 *Mesocena apiculata* (Schulz) *in* Hanna, *State Mineral.*, 27:198, plate D, fig. 3.

1970 *Septamesocena apiculata* (Schulz) *in* Bachmann, *Cat. Foss. Austria*, 1b:13–14.

Remarks. The triangular specimens vary in shape from distinctly angular to rounded. Radial spines are usually short. In several cases septa are visible. The species occurs reworked in several Miocene samples at Site 594.

Class CHRYSOPHYCEAE
Order CHRYSOMONADALES
Family SYNURACEAE
Genus *MACRORA* Hanna, 1932

1932 *Macrora* Hanna, *Proc. Calif. Acad. Sci., ser. 4*, 20:196.

1938 *Pseudorocella* Deflandre, *Bull. Soc. Fr. Microsc.*, 7:91.

Type species. *Macrora stella* (Azpeitia, 1911) Hanna, 1932, ex *Pyxidicula? stella* Azpeitia, 1911 (syn. *Pseudorocella corona* Deflandre, 1947).

Macrora stella (Azpeitia) Hanna
(Plate 7, Fig. 13; Plate 12, Figs. 8, 9)

1911 *Pyxidicula? stella* Azpeitia, *Ass. Esp. Progr. Cien. Congr. Zaragoza*, 4:150, plate 1, fig. 1.

1932 *Macrora stella* (Azpeitia) *in* Hanna, *Proc. Calif. Acad. Sci., ser. 4*, 20:196, plate 12, fig. 7.

1947 *Pseudorocella corona* Deflandre, *Bull. Soc. Bot. Fr.*, 93:337, text-fig. 4.

Remarks. The platelike elements, appearing slightly serrate in outline, are penetrated by several openings varying in number and size. The center of each plate is occupied by a domeshaped elevation. Present in the middle Miocene (*Corbisema triacantha* Zone) of Site 591.

SPONGE SPICULES

Sponge spicules are present throughout the Neogene of Sites 591 and 594, probably indicating that the water depth in both areas was relatively shallow during Neogene time. From base to top of the sections the sponge spicules change slightly in number and type, and a detailed investigation is intended. Some sponge spicules are figured on Plate 13. For terminology and some general remarks the reader is referred to papers by Rauff (1893/94), Bukry (1978b) and Martini (1981).

The most common types found in both sequences are amphioxes (Plate 13, figs. 1, 12, 13). But besides these simple forms there are present some very complicated types which may be significant for defining time intervals. For example, a special tetractin with branched terminations (Plate 13, Fig. 7) seems to be characteristic of the early Pliocene.

ACKNOWLEDGMENTS

Thanks are due to the Deutsche Forschungsgemeinschaft (Bonn) for supporting the present study. The Geologisch-Paläontologisches Institut der Universität Kiel provided space for laboratory work (S.L.). SEM pictures were taken by J. Tochtenhagen with a Stereoscan Mark 2, which was made available to the Geologisch-Paläontologisches Institut der Universität Frankfurt am Main by the Volkswagenstiftung. Our thanks go also to Dr. Amanda Palmer (Texas A&M University) and Dr. Cynthia Shaw (Exxon, U.S.A., Houston) for reviewing this paper.

The type specimens of the new taxa are deposited in the Naturmuseum und Forschungsinstitut Senckenberg, Frankfurt am Main, Federal Republic of Germany, Catalog Nos. SM.B 13508 to 13512.

REFERENCES

Bachmann, A., 1970. Flagellata (Silicoflagellata). *In* Zapfe, H. (Ed.), *Catalogus Fossilium Austriae*.

________, 1971. Silicoflagellaten aus dem oberen Badenien von Walbersdorf, Burgenland. *Sitz.-Ber. Österr. Akad. Wiss., Math.-Nat. Kl.*, 179:55-72.

Bukry, D., 1973. Coccolith and silicoflagellate stratigraphy, Deep Sea Drilling Project, Leg 18, eastern North Pacific. *In* Klum, L. D., von Huene, R., et al., *Init. Repts. DSDP*, 18: Washington (U.S. Govt. Printing Office), 817-831.

________, 1974. Stratigraphic value of silicoflagellates in nontropical regions. *Geol. Soc. Am. Bull.*, 85:1905-1906.

________, 1975. Silicoflagellate and coccolith stratigraphy, Deep Sea Drilling Project, Leg 29. *In* Kennett, J. P., Houtz, R. E., et al., *Init. Repts. DSDP*, 29: Washington (U.S. Govt. Printing Office), 845-872.

________, 1976a. Cenozoic silicoflagellate and coccolith stratigraphy, South Atlantic Ocean, Deep Sea Drilling Project, Leg 36. *In* Hollister, C. D., Craddock, C., et al., *Init. Repts. DSDP*, 35: Washington (U.S. Govt. Printing Office), 885-917.

________, 1976b. Silicoflagellate and coccolith stratigraphy, southeastern Pacific Ocean, Deep Sea Drilling Project Leg 34. *In* Yeats, R. S., Hart, S. R., et al., *Init. Repts. DSDP*, 34: Washington (U.S. Govt. Printing Office), 715-735.

________, 1977. Coccolith and silicoflagellate stratigraphy, central North Atlantic Ocean, Deep Sea Drilling Project Leg 37. *In* Aumento, F., Melson, W. G., et al., *Init. Repts. DSDP*, 37: Washington (U.S. Govt. Printing Office), 917-927.

________, 1978a. Cenozoic coccolith and silicoflagellate stratigraphy, offshore Northwest Africa, Deep Sea Drilling Project, Leg 41. *In* Lancelot, Y., Seibold, E., et al., *Init. Repts. DSDP*, 41: Washington (U.S. Govt. Printing Office), 689-707.

________, 1978b. Cenozoic coccolith, silicoflagellate, and diatom stratigraphy, Deep Sea Drilling Project, Leg 44. *In* Benson, W. E., Sheridan, R. E., et al., *Init. Repts. DSDP*, 44: Washington (U.S. Govt. Printing Office), 807-863.

________, 1978c. Cenozoic silicoflagellate and coccolith stratigraphy, southeastern Atlantic Ocean, Deep Sea Drilling Project, Leg 40. *In* Bolli, H. M., Ryan, W. B. F., et al., *Init. Repts. DSDP*, 40: Washington (U.S. Govt. Printing Office), 635-649.

________, 1979a. Coccolith and silicoflagellate stratigraphy, northern Mid-Atlantic Ridge and Reykjanes Ridge, Deep Sea Drilling Project Leg 49. *In* Luyendyk, B. P., Cann, J. R., et al., *Init. Repts. DSDP*, 49: Washington (U.S. Govt. Printing Office), 551-581.

________, 1979b. Comments on opal phytoliths and stratigraphy of Neogene silicoflagellates and coccoliths at Deep Sea Drilling Project Site 397 off Northwest Africa. *In* Luyendyk, B. P., Cann, J. R., et al., *Init. Repts. DSDP*, 49: Washington (U.S. Govt. Printing Office), 977-1009.

________, 1980a. Miocene *Corbisema triacantha* Zone phytoplankton from Deep Sea Drilling Project Sites 415 and 416, off northwest Africa. *In* Lancelot, Y., Winterer, E. L., et al., *Init. Repts. DSDP*, 50: Washington (U.S. Govt. Printing Office), 507-523.

________, 1980b. Silicoflagellate biostratigraphy and paleoecology in the eastern equatorial Pacific, Deep Sea Drilling Project Leg 54. *In* Rosendahl, B. R., Hekinian, R., et al., *Init. Repts. DSDP*, 54: Washington (U.S. Govt. Printing Office), 545-573.

________, 1981a. Silicoflagellate stratigraphy of offshore California and Baja California, Deep Sea Drilling Project Leg 63. *In* Yeats, R. S., Haq, B. U., et al., *Init. Repts. DSDP*, 63: Washington (U.S. Govt. Printing Office), 539-557.

________, 1981b. Synthesis of silicoflagellate stratigraphy for Maestrichtian to Quaternary marine sediment. *In* Warme, I. E., Douglas, R. G., and Winterer, E. L. (Eds.), *The Deep Sea Drilling Project: A Decade of Progress*. Soc. Econ. Paleont. Mineral., Spec. Publ., 32:433-444.

________, 1982a. Cenozoic silicoflagellates from offshore Guatemala, Deep Sea Drilling Project Site 495. *In* Aubouin, J., von Huene, R., et al., *Init. Repts. DSDP*, 67: Washington (U.S. Govt. Printing Office), 425-445.

________, 1982b. Neogene silicoflagellates of the eastern equatorial Pacific, Deep Sea Drilling Project Hole 503A. *In* Prell, W. L., Gardner, J. V., et al., *Init. Repts. DSDP*, 68: Washington (U.S. Govt. Printing Office), 311-323.

________, 1983. Upper Cenozoic silicoflagellates from offshore Ecuador, Deep Sea Drilling Project Site 504. *In* Cann, J. R., Langseth, M. G., Honnorez, J., Von Herzen, R. P., White, S. M., et al., *Init. Repts. DSDP*, 69: Washington (U.S. Govt. Printing Office), 321-342.

Bukry, D., and Foster, J. H., 1973. Silicoflagellate and diatom stratigraphy, Leg 16, Deep Sea Drilling Project. *In* van Andel, T. H., Heath, G. R., et al., *Init. Repts. DSDP*, 16: Washington (U.S. Govt. Printing Office), 815-871.

Burns, R. E., Andrews, J. E., et al., 1973. Site 206. *In* Burns, R. E., Andrews, J. E., et al., *Init. Repts. DSDP*, 21: Washington (U.S. Govt. Printing Office), 103-195.

Busen, K. E., and Wise, S. W., Jr., 1977. Silicoflagellate stratigraphy, Deep Sea Drilling Project, Leg 36. *In* Barker, P. F., Dalziel, I. W. D., et al., *Init. Repts. DSDP*, 36: Washington (U.S. Govt. Printing Office), 697-743.

Campbell, A. S., 1954. Radiolaria. *In* Moore, R. C. (Ed.) *Treatise on Invertebrate Paleontology*, D, 11-163.

Ciesielski, P. F., 1975. Biostratigraphy and paleoecology of Neogene and Oligocene silicoflagellates from cores recovered during Arctic Leg 28, Deep Sea Drilling Project. *In* Hayes, D. E., Frakes, L. A., et al., *Init. Repts. DSDP*, 28: Washington (U.S. Govt. Printing Office), 625-691.

Deflandre, G., 1950. Contribution à l'étude des Silicoflagellidés actuels et fossiles. *Microscopie*, 2:72-108, 117-142, 191-210.

________, 1952. Classe des Silicoflagellidés. *In* Grassé, P. P. (Ed.), *Traité de Zoologie*, 1:425-438.

Dumitrica, P., 1973a. Miocene and Quaternary silicoflagellates in sediments from the Mediterranean Sea. *In* Ryan, W. B. F., Hsü, K. J., et al., *Init. Repts. DSDP*, 13, Pt. 2: Washington (U.S. Govt. Printing Office), 902-933.

________, 1973b. Paleocene, late Oligocene, and post-Oligocene silicoflagellates in southwestern Pacific sediments cored on DSDP Leg 21. *In* Burns, R. E., Andrews, J. E., et al., *Init. Repts. DSDP*, 21: Washington (U.S. Govt. Printing Office), 837-883.

Ehrenberg, C. G., 1838. Über das Massenverhältniss der jetzt lebenden Kiesel-Infusorien und über ein neues Infusorien-Conglomerat als Polirschiefer von Jastraba in Ungarn. *Abh. Akad. Wiss. Berlin, 1836, Phys. Abh.*, pp. 109-135.

________, 1843. Verbreitung und Einfluss des mikroskopischen Lebens in Süd- und Nordamerika. *Abh. Akad. Wiss. Berlin, 1841, Phys. Abh.*, pp. 291-446.

———, 1854. *Mikrogeologie: Das Erden und Felsen schaffende Wirken des unsichtbar kleinen selbstständigen Lebens auf der Erde:* Leipzig (Leopold Voss).

Frenguelli, J., 1935. Variaciones de *Dictyocha fibula* en el Golfo de San Matías (Patagonia Septentrional). *An. Mus. Argent. Cienc. Nat., 38, Protist.*, 4:265–281.

———, 1938. Variaciones de *"Dictyocha speculum"* Ehr. en el Golfo de San Jorge (Patagonia). *Notas Mus. La Plata, 3, Zool.*, 11: 117–123.

———, 1940. Consideraciones sobre los silicoflagelados fósiles. *Rev. Mus. La Plata, 2, Paleont.*, 7:37–112.

Fuji, N., and Bachmann, A., 1970. Fossile Pollen, Sporen und Silicoflagellaten aus den Hijirikawa-Schichten (Obermiozän) der Halbinsel Noto, Zentral-Japan (III). Silicoflagellaten in den Hijirikawa-Schichten. *Bull. Fac. Educ. Kanazawa Univ.*, 19:77–91.

Gemeinhardt, K., 1934. Die Silicoflagellaten des Südatlantischen Ozeans. *Wiss. Erg. D. Atlant. Exp. "Meteor," 1925–1927*, 12:274–312.

Hajós, M., 1976. Upper Eocene and lower Oligocene diatomaceae, archaemonadaceae, and silicoflagellatae in southwestern Pacific sediments, DSDP Leg 29. *In* Hollister, C. D., Craddock, C., et al., *Init. Repts. DSDP*, 35: Washington (U.S. Govt. Printing Office), 817–883.

Haq, B. U., and Riley, A., 1976. Antarctic silicoflagellates from the Southeast Pacific, Deep Sea Drilling Project Leg 35. *In* Hollister, C. D., Craddock, C., et al., *Init. Repts. DSDP*, 35: Washington (U.S. Govt. Printing Office), 673–691.

Hovasse, R., 1932. Contribution à l'étude des silicoflagellés. Multiplication, variabilité, hérédité, affinités. *Bull. Biol. Fr. Belg.*, 66:448–501.

ICBN. See Stafleu (Ed.).

Kraus, O. (Ed.), 1962. *Internationale Regeln für die Zoologische Nomenklatur, beschlossen vom XV. Internationalen Kongress für Zoologie:* Frankfurt am Main (Senck. Naturf. Ges.).

Ling, H. Y., 1970. Silicoflagellates from central North Pacific core sediments. *Bull. Am. Paleont.*, 58:85–129.

———, 1972. Upper Cretaceous and Cenozoic silicoflagellates and ebridians. *Bull. Am. Paleont.*, 62:135–229.

———, 1973. Silicoflagellates and ebridians from Leg 19. *In* Creager, J. S., Scholl, D. W., et al., *Init. Repts. DSDP*, 19: Washington (U.S. Govt. Printing Office), 751–775.

———, 1975. Silicoflagellates and ebridians from Leg 31. *In* Karig, D. E., Ingle, J. C. Jr., et al., *Init. Repts. DSDP*, 31: Washington (U.S. Govt. Printing Office), 763–777.

———, 1977. Late Cenozoic silicoflagellates and ebridians from the eastern North Pacific Region. *Proc. 1st Int. Cong. Pacific Neog. Strat., Tokyo 1976*, pp. 205–233.

———, 1980. Silicoflagellates and ebridians from Leg 55. *In* Jackson, E. D., Koizumi, I., et al., *Init. Repts. DSDP*, 55: Washington (U.S. Govt. Printing Office), 375–385.

Locker, S., 1974. Revision der Silicoflagellaten aus der Mikrogeologischen Sammlung von C. G. Ehrenberg. *Eclog. Geol. Helv.*, 67:631–646.

Loeblich, A. R. III, Loeblich, L. A., Tappan, H., and Loeblich, A. R., Jr., 1968. *Annotated Index of Fossil and Recent Silicoflagellates and Ebridians.* Geol. Soc. Am. Mem., 106.

Mandra, Y. T., 1969. Silicoflagellates: a new tool for the study of Antarctic tertiary climates. *Ant. J. U.S.*, 4:172–174.

Martini, E., 1971a. Neogene silicoflagellates from the equatorial Pacific. *In* Winterer, E. L., Riedel, W. R., et al., *Init. Repts. DSDP*, 7, Pt. 2: Washington (U.S. Govt. Printing Office), 1695–1708.

———, 1971b. Standard Tertiary and Quaternary calcareous nannoplankton zonation. *Proc. II Planktonic Conf., Roma 1970*, (Vol. 2): Rome (Edizioni: Tecnoscienza), 739–785.

———, 1972. Der stratigraphische Wert von Silicoflagellaten im Jungtertiär von Kalifornien und des östlichen Pazifischen Ozeans. *Nachr. D. Geol. Ges.*, 5:47–49.

———, 1976. Neogene and Quaternary silicoflagellates from the central Pacific Ocean (DSDP Leg 33). *In* Schlanger, S. O., Jackson, E. D., et al., *Init. Repts. DSDP*, 33: Washington (U.S. Govt. Printing Office), 439–449.

———, 1979. Calcareous nannoplankton and silicoflagellate biostratigraphy at Reykjanes Ridge, northeastern North Atlantic (DSDP Leg 49, Sites 407 and 409). *In* Luyendyk, B. P., Cann, J. R., et al., *Init. Repts. DSDP*, 49: Washington (U.S. Govt. Printing Office), 533–549.

———, 1982. Pliocene and Quaternary diatoms, silicoflagellates, sponge spicules, and endoskeletal dinoflagellates from the Philippine Sea, Deep Sea Drilling Project Legs 59 and 60. *In* Hussong, D. M., Uyeda, S., et al., *Init. Repts. DSDP*, 60: Washington (U.S. Govt. Printing Office), 565–574.

Martini, E., and Müller, C., 1976. Eocene to Pleistocene silicoflagellates from the Norwegian–Greenland Sea (DSDP Leg 38). *In* Talwani, M., Udintsev, G., et al., *Init. Repts. DSDP*, 38: Washington (U.S. Govt. Printing Office), 857–895.

Mayr, E., 1967. *Artbegriff und Evolution.* Hamburg and Berlin (Paul Parey).

Müller, C., 1981. Miocene to Pleistocene silicoflagellates from the central North Pacific, Deep Sea Drilling Project Leg 62. *In* Thiede, J., Vallier, T. L., et al., *Init. Repts. DSDP*, 62: Washington (U.S. Govt. Printing Office), 361–364.

Perch-Nielsen, K., 1975. Late Cretaceous to Pleistocene silicoflagellates from the southern Southwest Pacific, DSDP, Leg 29. *In* Kennett, J. P., Houtz, R. E., et al., *Init. Repts. DSDP*, 29: Washington (U.S. Govt. Printing Office), 677–721.

———, 1977. Tertiary silicoflagellates and other siliceous microfossils from the western South Atlantic, Deep Sea Drilling Project Leg 39. *In* Supko, P. R., Perch-Nielsen, K., et al., *Init. Repts. DSDP*, 39: Washington (U.S. Govt. Printing Office), 863–867.

Poelchau, H. S., 1976. Distribution of Holocene silicoflagellates in North Pacific sediments. *Micropaleontology*, 22:164–193.

Rauff, H., 1893/94. Palaeospongiologie: allgemeiner Teil. *Palaeontographica*, 40:1–232.

Schulz, P., 1928. Beiträge zur Kenntnis fossiler und rezenter Silicoflagellaten. *Botan. Archiv.*, 21:225–292.

Shaw, C. A., and Ciesielski, P. F., 1983. Silicoflagellate biostratigraphy of Middle Eocene to Holocene subantarctic sediments recovered by Deep Sea Drilling Project Leg 71. *In* Ludwig, W. J., Krasheninnikov, V. A., et al., *Init. Repts. DSDP*, 71: Washington (U.S. Govt. Printing Office), 687–737.

Stafleu, F. A. (Ed.), 1978. *International Code of Botanical Nomenclature, Adopted by the Twelfth International Botanical Congress, Leningrad, July 1975.* Utrecht (Bohn, Scheltema and Holkema).

Van Valkenburg, S. D., and Norris, R. E., 1970. The growth and morphology of the silicoflagellate *Dictyocha fibula* Ehrenberg in culture. *J. Phycol.*, 6:48–54.

Date of Initial Receipt: 19 July 1984
Date of Acceptance: 30 October 1984

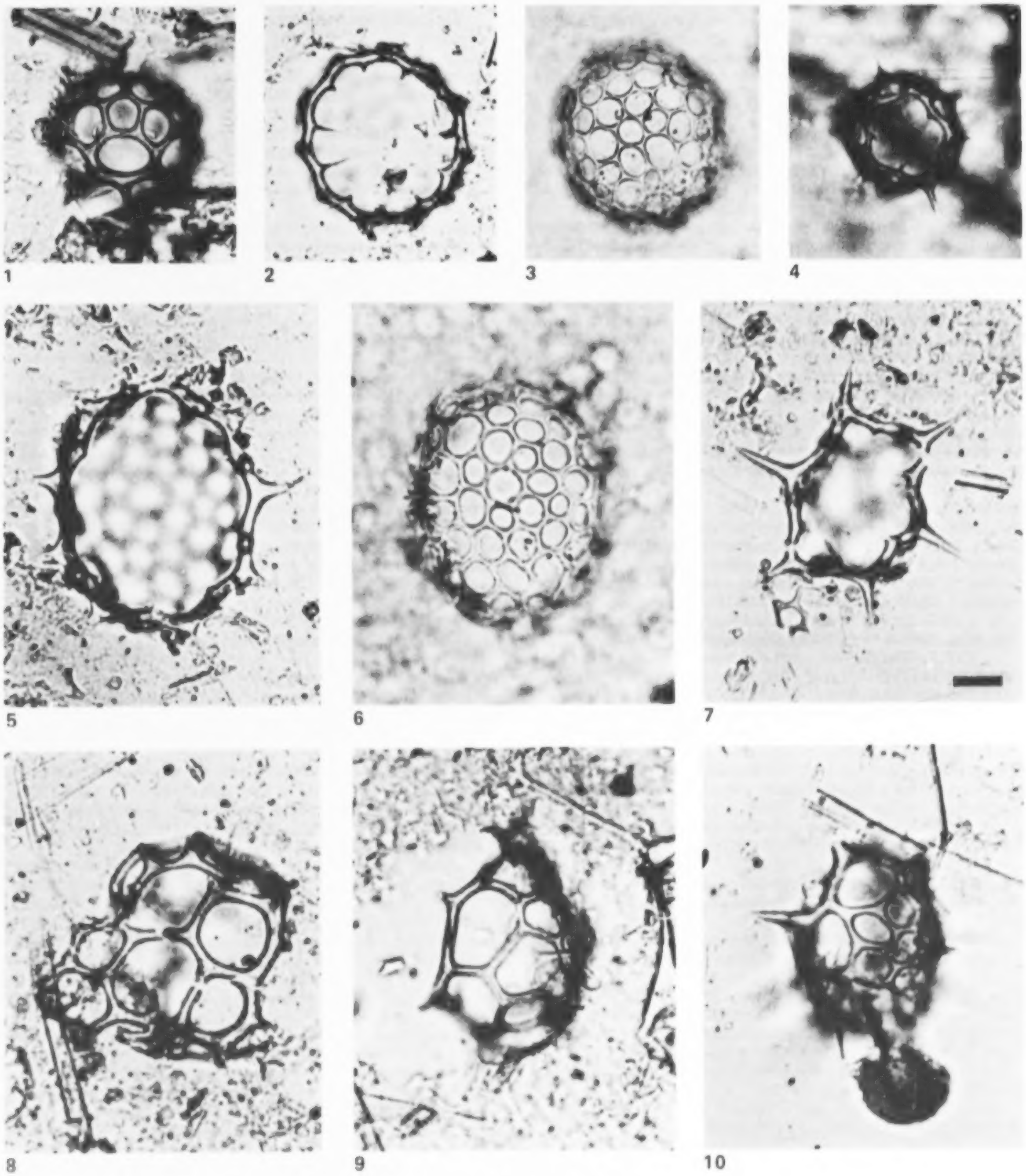

Plate 1. Middle Miocene silicoflagellates. (All specimens magnified ×800, bar = 10 μm.) **1.** *Cannopilus depressus* (Ehrenberg), Sample 594-44,CC. **2, 3.** *Cannopilus ichikawai* Bachmann, high and low focus; Sample 591B-18,CC. **4.** *Cannopilus picassoi* Stradner, Sample 591B-17,CC. **5, 6.** *Cannopilus iidaensis* Bachmann, high and low focus; Sample 591B-20,CC. **7.** *Cannopilus hemisphaericus* (Ehrenberg), Sample 591B-18,CC. **8.** *Cannopilus latifenestratus* Bachmann, Sample 591B-19,CC. **9.** *Cannopilus heptacanthus* (Ehrenberg) ssp. *heptacanthus*, Sample 591B-21,CC. **10.** *Cannopilus heptacanthus* ssp. *antarcticus* (Ciesielski), Sample 591B-16,CC.

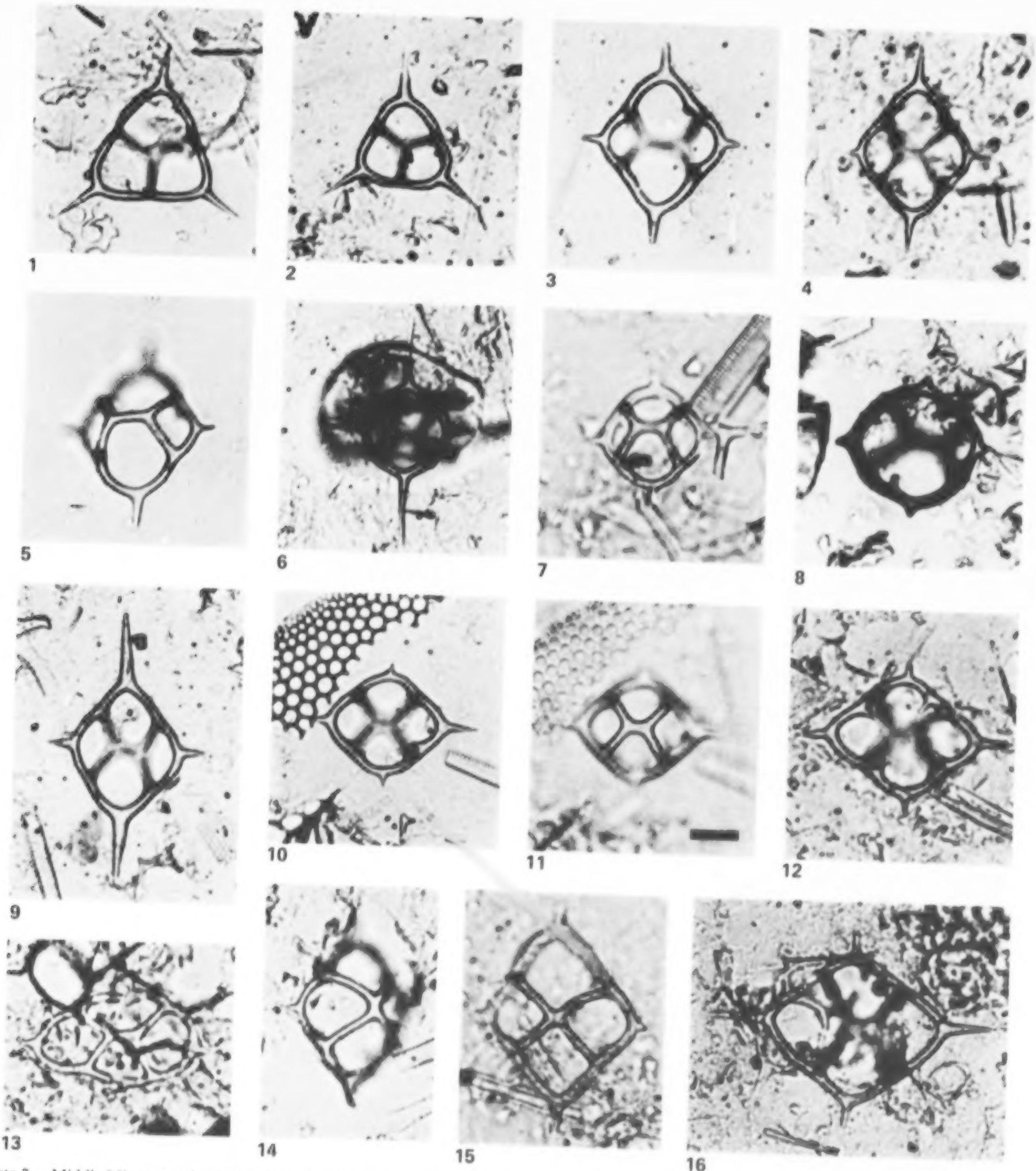

Plate 2. Middle Miocene to lower Pliocene silicoflagellates. (All specimens magnified × 800, bar = 10 μm.) **1, 2.** *Corbisema triacantha* (Ehrenberg), (1) Sample 591B-16,CC, middle Miocene; (2) Sample 591B-20,CC, middle Miocene. **3–5.** *Dictyocha varia* Locker, (3) Sample 591-22,CC, lower Pliocene; (4) Sample 591B-6,CC, upper Miocene; (5) Sample 591-19,CC, lower Pliocene. **6.** *Dictyocha pygmaea* (Ciesielski), Sample 591B-16,CC, middle Miocene. **7.** *Dictyocha* sp. 2, Sample 591-20,CC, lower Pliocene. **8.** *Dictyocha* sp. 3, Sample 594-46,CC, middle Miocene. **9.** *Dictyocha subclinata* Bukry, Sample 591B-9,CC, upper Miocene. **10–12.** *Dictyocha extensa* (Locker), (10, 11) high and low focus, Sample 591B-2,CC, upper Miocene; (12) Sample 591B-16,CC, middle Miocene. **13.** *Dictyocha aegea* Stradner and Bachmann, Sample 591B-5,CC, upper Miocene. **14, 15.** *Dictyocha medusa* Haeckel, (14) Sample 591B-17,CC, middle Miocene; (15) Sample 591B-19,CC, middle Miocene. **16.** *Dictyocha epiodon* Ehrenberg, Sample 591B-21,CC, middle Miocene.

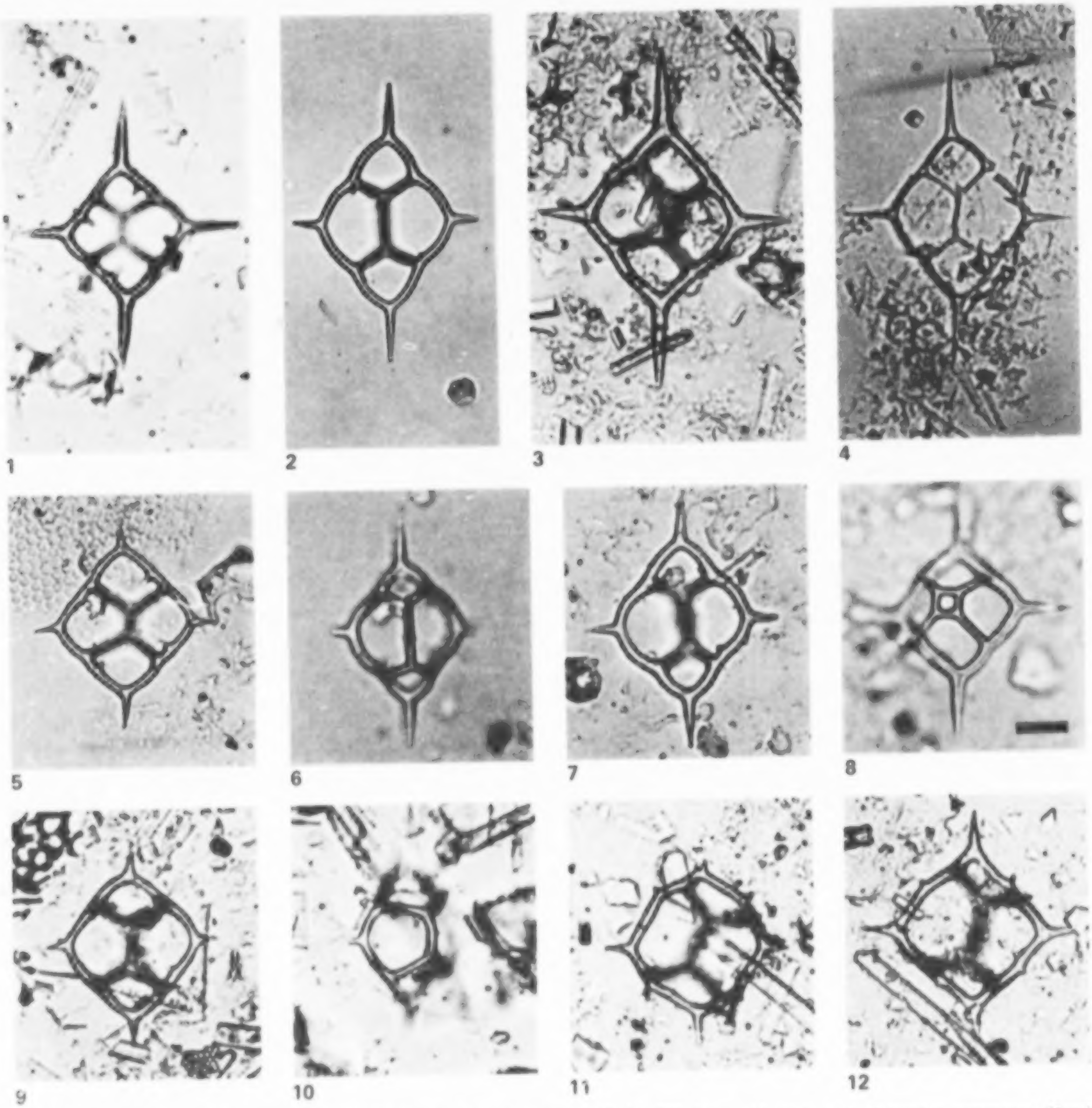

Plate 3. Middle Miocene to Quaternary silicoflagellates. (All specimens magnified × 800, bar = 10 μm.) **1, 9.** *Dictyocha messanensis* Haeckel ssp. *messanensis* f. *aspinosa*, (1) Sample 591-26,CC, upper Miocene; (9) Sample 594-16,CC, upper Pliocene. **2.** *Dictyocha messanensis* ssp. *stapedia* (Haeckel) f. *aspinosa*, Sample 591-14,CC, lower Pliocene. **3–5.** *Dictyocha messanensis* ssp. *aspinosa* (Bukry), (3) Sample 594-44,CC, middle Miocene; (4) Sample 591B-7,CC, upper Miocene; (5) Sample 591B-16,CC, middle Miocene. **6, 7.** *Dictyocha messanensis* ssp. *stapedia* (Haeckel) f. *stapedia*, (6) Sample 591-14,CC, lower Pliocene, (7) Sample 591-21,CC, lower Pliocene. **8.** *Dictyocha messanensis* ssp. *messanensis* f. *speculum* (Frenguelli), Sample 591-27,CC, upper Miocene. **10.** *Dictyocha messanensis* Haeckel ssp. *messanensis* f. *messanensis*, Sample 594-16,CC, upper Pliocene. **11, 12.** *Dictyocha messanensis* ssp. *aculeata* (Lemmermann) f. *aculeata*, (11) Sample 594-7,CC, Quaternary; (12) Sample 594-9,CC, Quaternary.

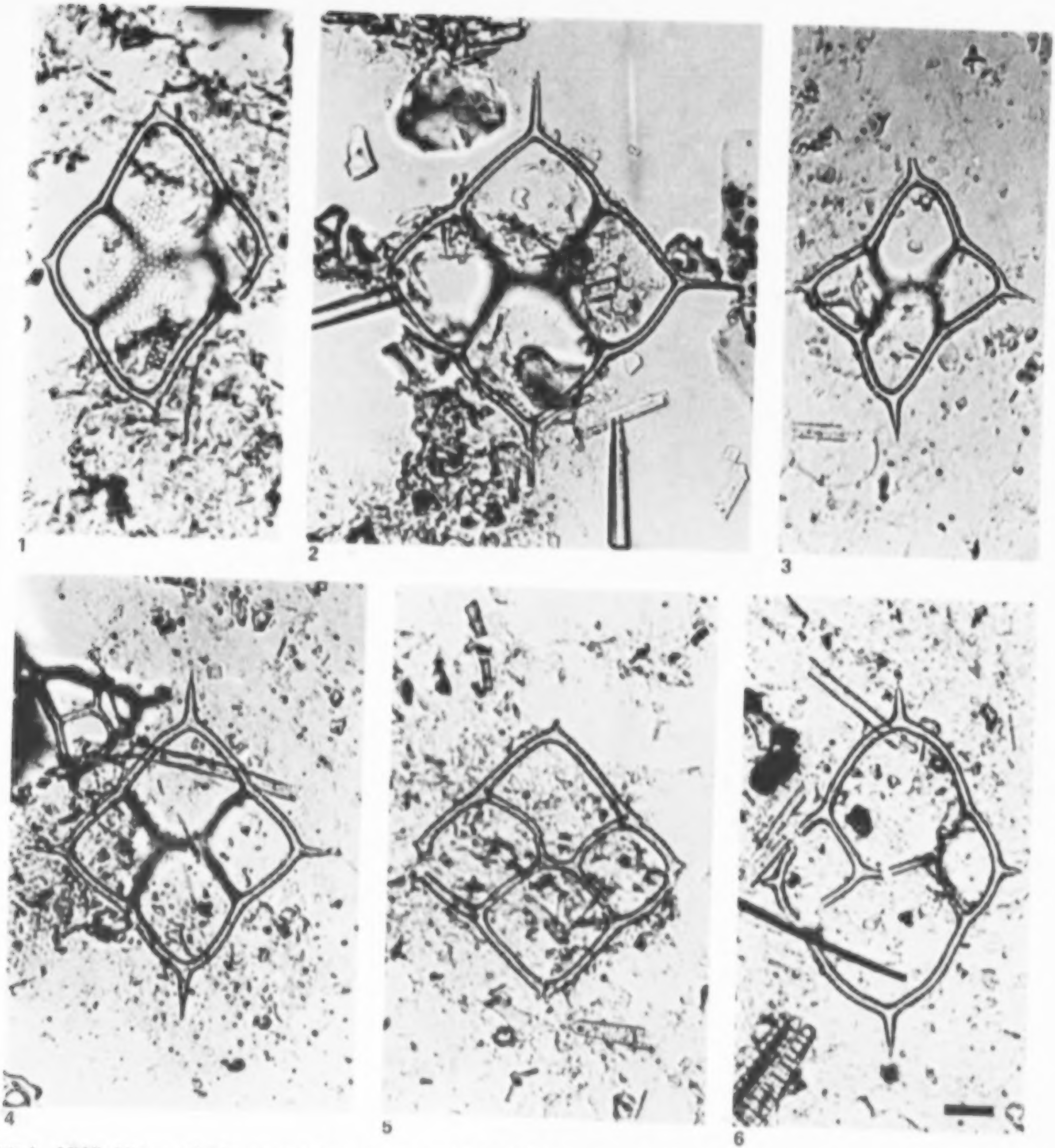

late 4. Middle Miocene silicoflagellates. (All specimens magnified ×800, bar = 10 μm.) **1-6.** *Dictyocha fibula* ssp. *asymmetrica* n. ssp., (1) holotype SM.B 13508, Sample 591B-21,CC; (2) Sample 594A-12,CC; (3, 4) Sample 591B-19,CC; (5) Sample 591B-21,CC; (6) Sample 591B-17,CC.

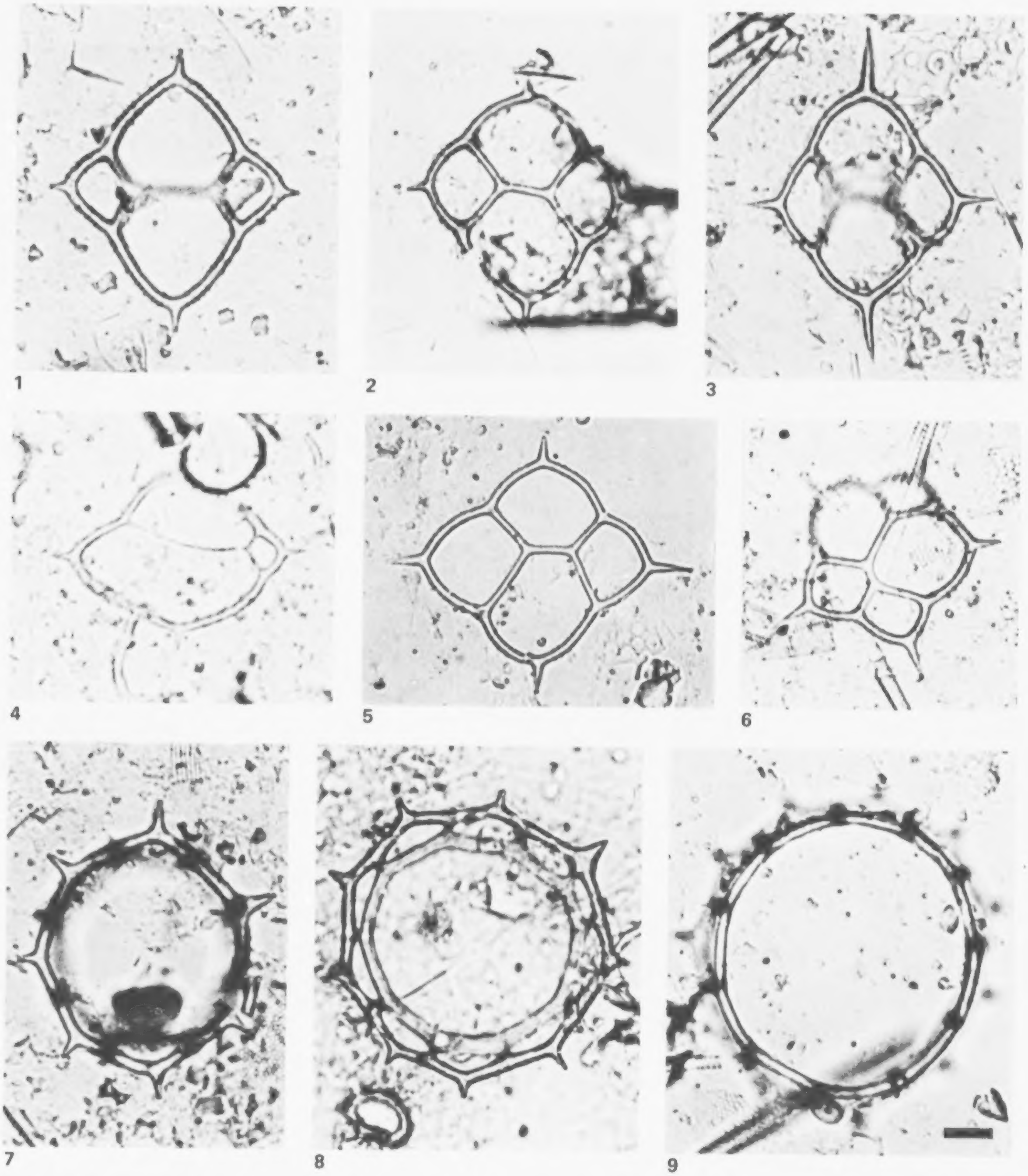

Plate 5. Middle Miocene to lower Pliocene silicoflagellates. (All specimens magnified ×800, bar = 10 μm.) **1, 2.** *Dictyocha fibula* Ehrenber ssp. *fibula*. (1) Sample 591-21,CC, lower Pliocene; (2) Sample 591B-16,CC, middle Miocene. **3.** *Dictyocha fibula* Ehrenberg s. l., Sampl 591B-18,CC, middle Miocene. **4.** *Dictyocha* sp. 1, Sample 591-19,CC, lower Pliocene. **5.** *Dictyocha perlaevis* Frenguelli f. *perlaevis*, Sampl 591-14,CC, lower Pliocene. **6.** *Dictyocha perlaevis* f. *pentaradiata* n. f., holotype SM.B 13509, Sample 591-20,CC, lower Pliocene. **7.** *Distephanus polyactis* ssp. *crassus* Bukry, Sample 591B-8,CC, upper Miocene. **8, 9.** *Distephanus polyactis* (Ehrenberg) ssp. *polyactis*, (8) Sampl 591B-4,CC, upper Miocene; (9) Sample 591-21,CC, lower Pliocene.

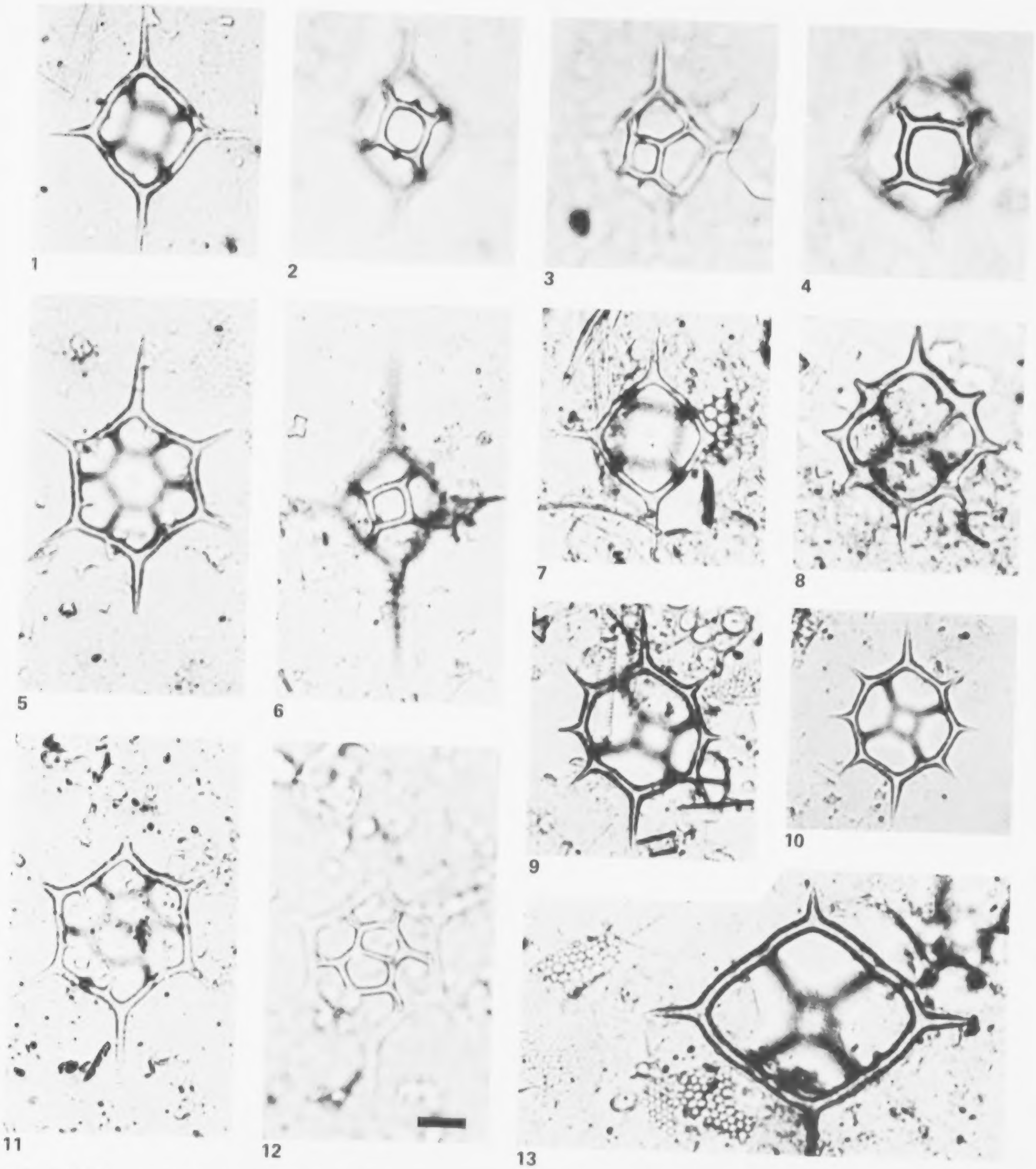

Plate 6. Middle Miocene to Quaternary silicoflagellates. (All specimens magnified × 800, bar = 10 μm.) **1–3.** *Distephanus crux* ssp. *bispinosus* Dumitrică f. *bispinosus*, (1, 2) high and low focus, Sample 591-21,CC, lower Pliocene; (3) Sample 591-24,CC, upper Miocene. **4.** *Distephanus crux* ssp. *bispinosus* f. *mesophthalmus* (Ehrenberg), Sample 591-29,CC, upper Miocene. **5.** *Distephanus aculeatus* (Ehrenberg) f. *aculeatus*, Sample 591-25,CC, upper Miocene. **6, 7.** *Distephanus crux* (Ehrenberg) ssp. *crux*. (6) Sample 591B-18,CC, middle Miocene; (7) Sample 594A-12,CC, middle Miocene. **8.** *Distephanus stauracanthus* f. *octagonus* (Tsumura), Sample 594-12,CC, Quaternary, allochthonous. **9, 10.** *Distephanus stauracanthus* (Ehrenberg) f. *stauracanthus*; (9) Sample 591B-16,CC, middle Miocene; (10) Sample 591B-17,CC, middle Miocene. **11, 12.** *Distephanus aculeatus* f. *binoculus* (Ehrenberg), high and low focus, Sample 591-16,CC, lower Pliocene. **13.** *Distephanus crux* ssp. *hannai* Bukry, Sample 591B-4,CC, upper Miocene.

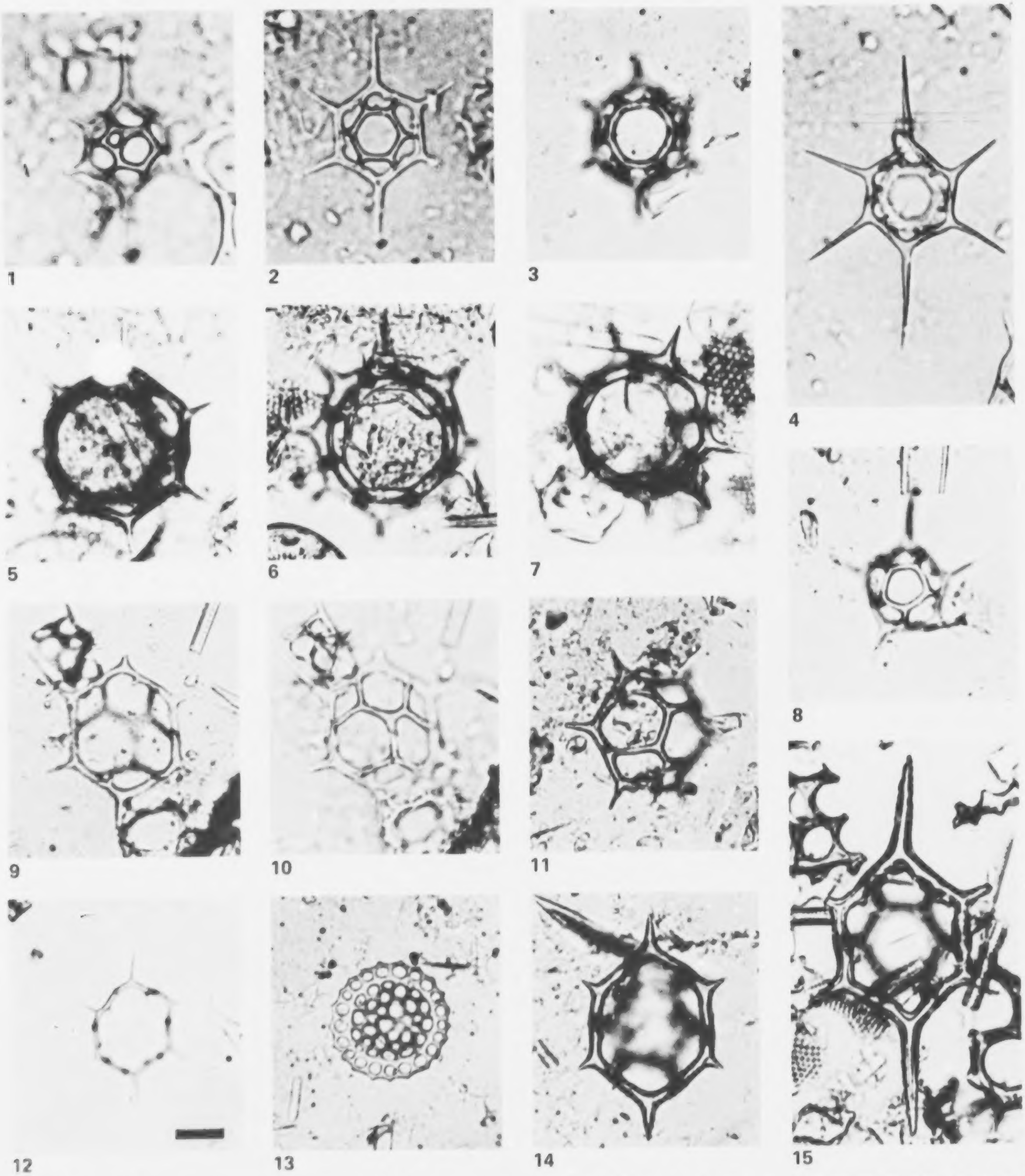

Plate 7. Middle Miocene to Quaternary silicoflagellates. (All specimens magnified ×800, bar = 10 μm.) **1.** *Distephanus speculum* ssp. *speculu* f. *cannopilea-hexacantha* (Frenguelli), Sample 591B-1,CC upper Miocene. **2-4.** *Distephanus speculum* (Ehrenberg) ssp. *speculum* f. *speculum* (2) Sample 591-17,CC, lower Pliocene; (3) Sample 594-19,CC, lower Pliocene; (4) Sample 591-21,CC, lower Pliocene. **5.** *Distephanus speculu* ssp. *speculum* f. *septenarius* (Ehrenberg), Sample 594-13,CC, Quaternary. **6.** *Distephanus speculum* ssp. *speculum* f. *octonarius* (Ehrenberg) Sample 594-13, Quaternary. **7.** *Distephanus speculum* ssp. *speculum* f. *nonarius* n.f., holotype SM.B 13510; Sample 594-13,CC, Quaternar **8.** *Distephanus speculum* ssp. *speculum* f. *pentagonus* (Lemmermann), Sample 591-21,CC, lower Pliocene. **9, 10.** *Distephanus speculum* ssp *speculum* f. *varians* Gran and Braarud, high and low focus, Sample 591-20,CC, lower Pliocene. **11.** *Distephanus speculum* ssp. *speculum* *pseudofibula* Schulz, Sample 594-21,CC, lower Pliocene. **12.** *Distephanus* sp., Sample 591-29,CC, upper Miocene. **13.** *Macrora stella* (A peitia), a synuracean sklerite, Sample 591B-17,CC, middle Miocene. **14, 15.** *Distephanus speculum* ssp. *giganteus* Bukry f. *giganteus*, (14) Sample 591B-21,CC, middle Miocene; (15) Sample 594-27,CC, upper Miocene.

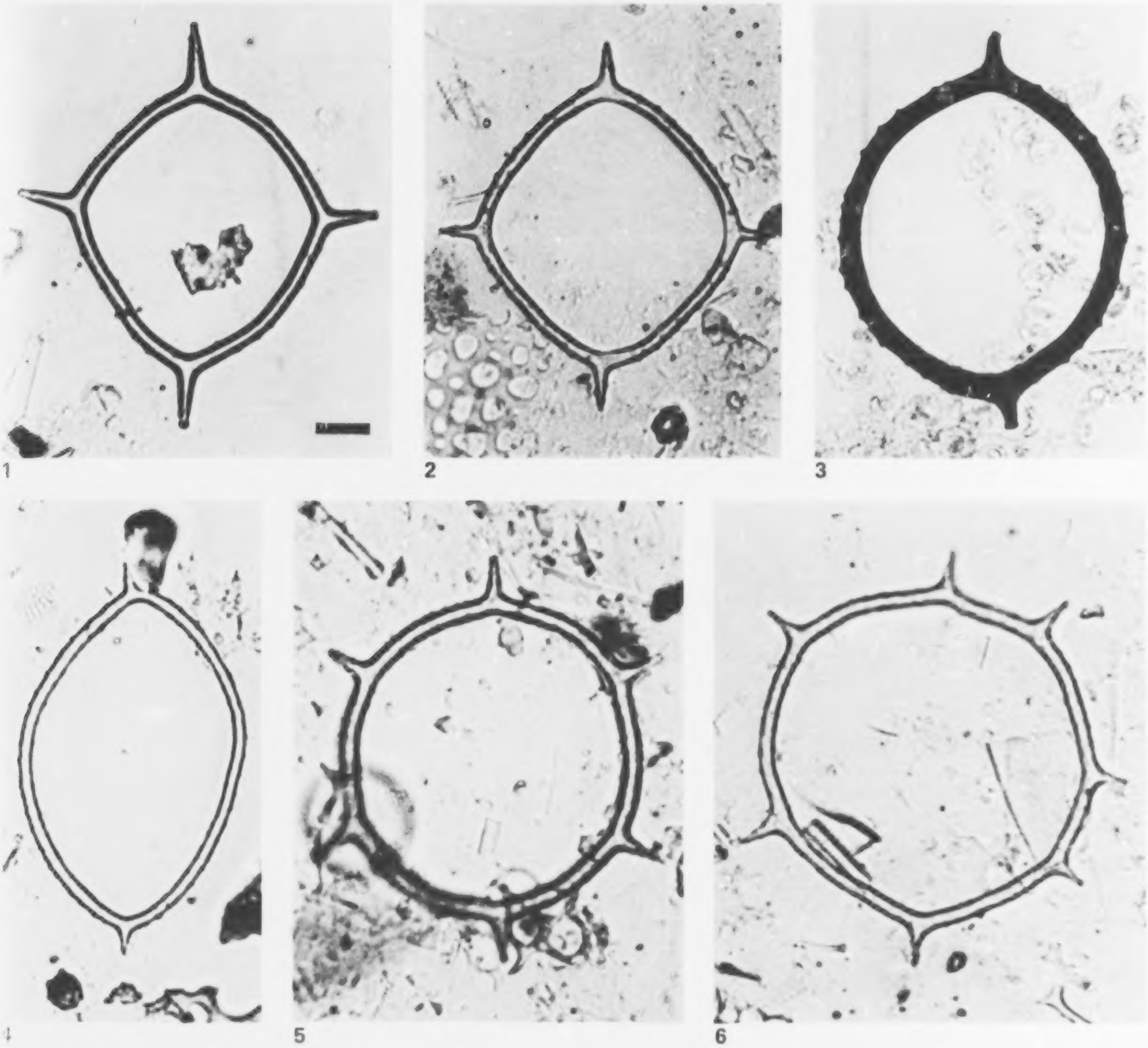

Plate 8. Middle Miocene to lower Pliocene silicoflagellates. (All specimens magnified × 800, bar = 10 µm.) **1, 2.** *Mesocena quadrangula* Ehrenberg ex Haeckel, (1) Sample 591-18,CC, lower Pliocene; (2) Sample 591-20,CC, lower Pliocene. **3, 4.** *Mesocena diodon* Ehrenberg, (3) Sample 594-29,CC, middle Miocene; (4) Sample 591B-15,CC, middle Miocene. **5.** *Mesocena? hexalitha* Bukry f. *hexalitha*, Sample 591-30,CC, upper Miocene. **6.** *Mesocena? hexalitha* f. *heptalitha* n. f., holotype SM.B 13511, Sample 591-30,CC, upper Miocene.

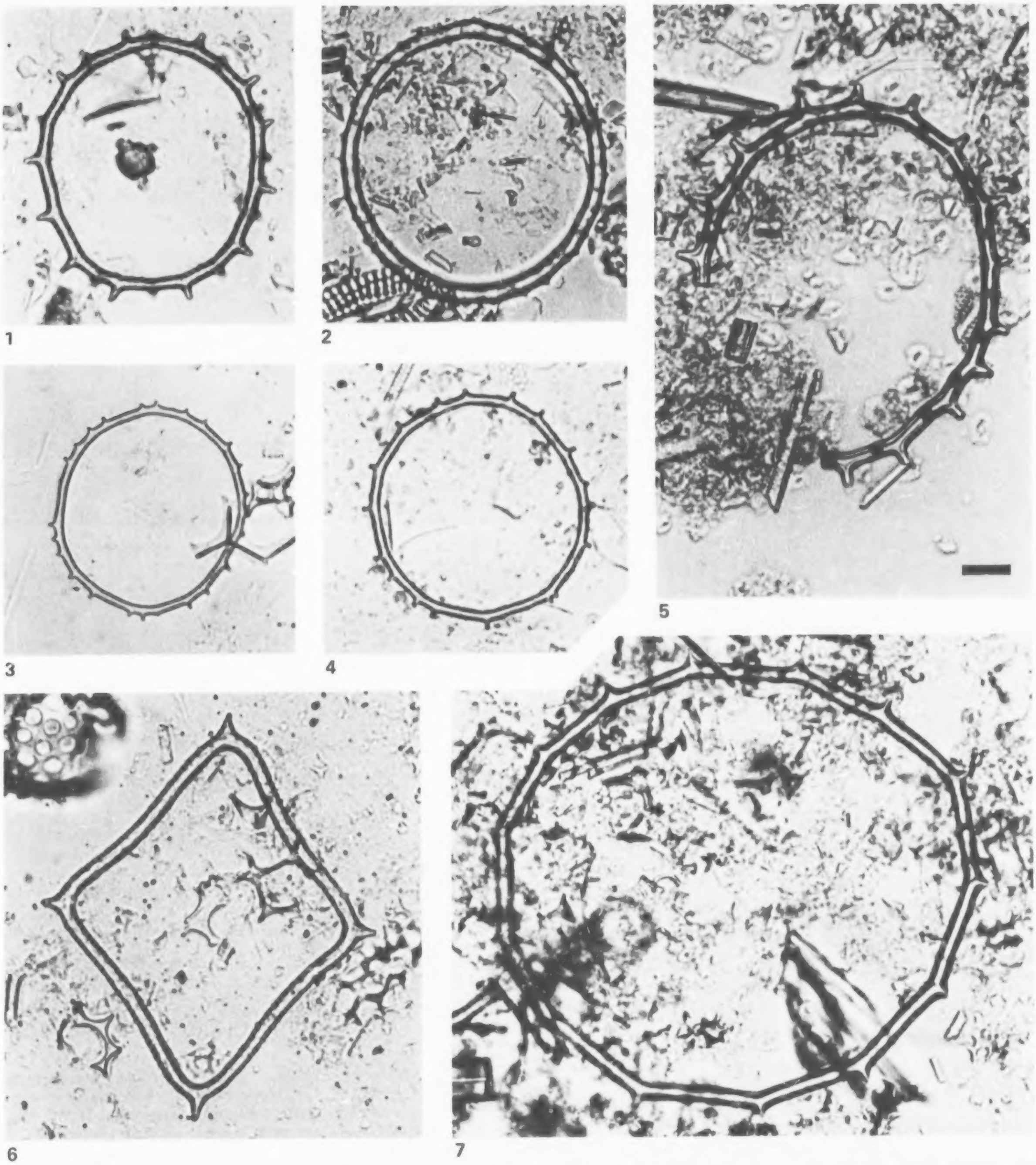

Plate 9. Middle Miocene to lower Pliocene silicoflagellates. (All specimens magnified × 800, bar = 10 μm.) **1, 5.** *Paramesocena apiculata* (Lemmermann), (1) Sample 591B-9,CC, upper Miocene; (5) Sample 594-28,CC, upper Miocene. **2–4.** *Paramesocena circulus* (Ehrenberg), (2) Sample 594-25,CC, upper Miocene; (3) Sample 591-18,CC, lower Pliocene; (4) Sample 591-18,CC, lower Pliocene. **6.** *Mesocena elliptica* Ehrenberg, Sample 591B-20,CC, middle Miocene. **7.** *Paramesocena dumitricae* (Perch-Nielsen), Sample 594-26,CC, upper Miocene.

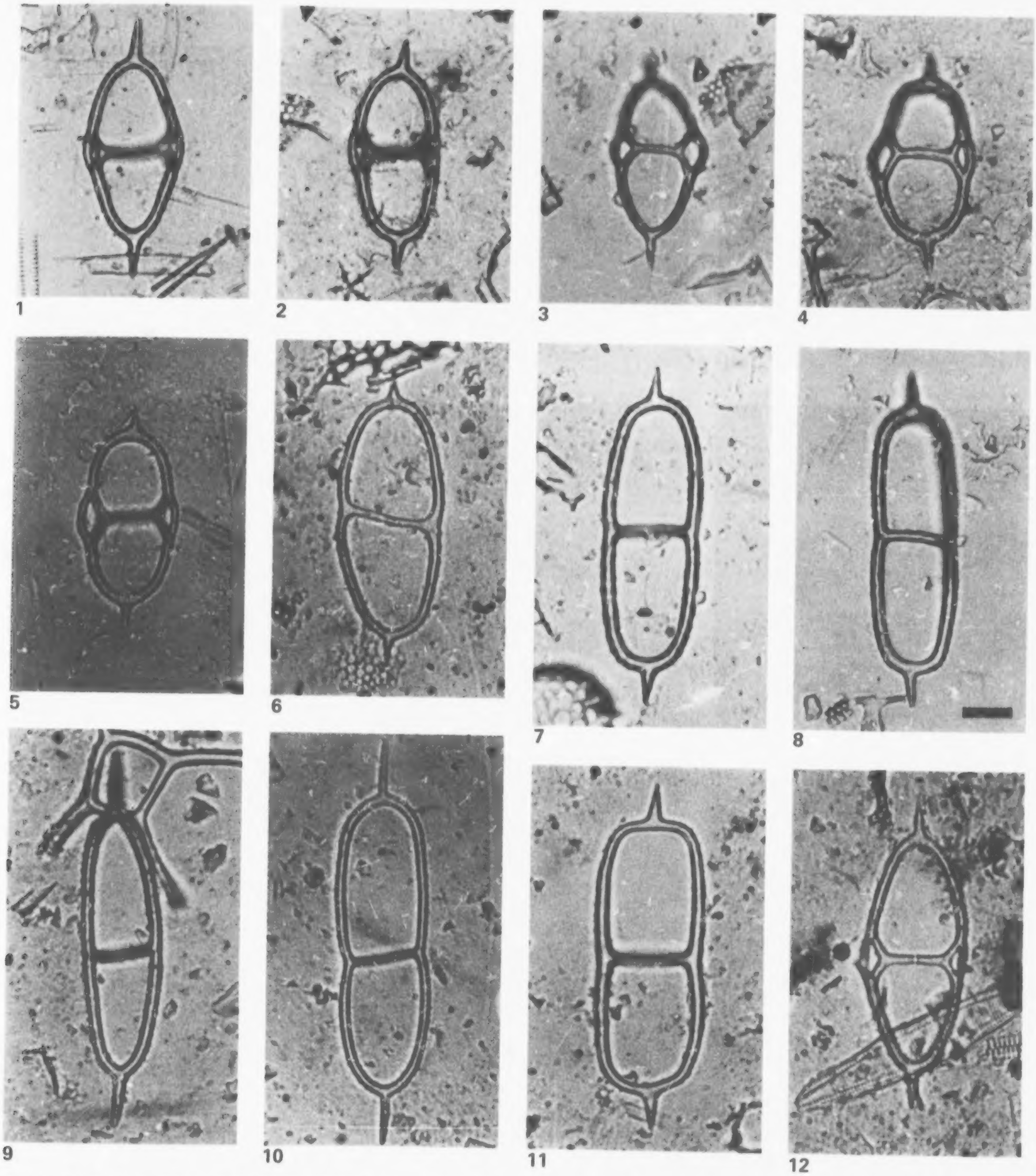

late 10. Upper Miocene to lower Pliocene silicoflagellates. (All specimens magnified ×800, bar = 10 µm.) **1–5.** *Neonaviculopsis neonautica* ssp. *praenautica* n. ssp., (1, 2, 4) Sample 591-29,CC, upper Miocene; (3) Sample 591-28,CC, upper Miocene; (5) holotype SM.B 13512, Sample 591-29,CC, upper Miocene. **6–11.** *Neonaviculopsis neonautica* (Bukry) ssp. *neonautica* f. *neonautica*, (6–8) Sample 591-23,CC, lower Pliocene; (9–11) Sample 591-22,CC, lower Pliocene. **12.** *Neonaviculopsis neonautica* (Bukry) ssp. *neonautica* f. *praenautica*, Sample 591-23,CC, lower Pliocene.

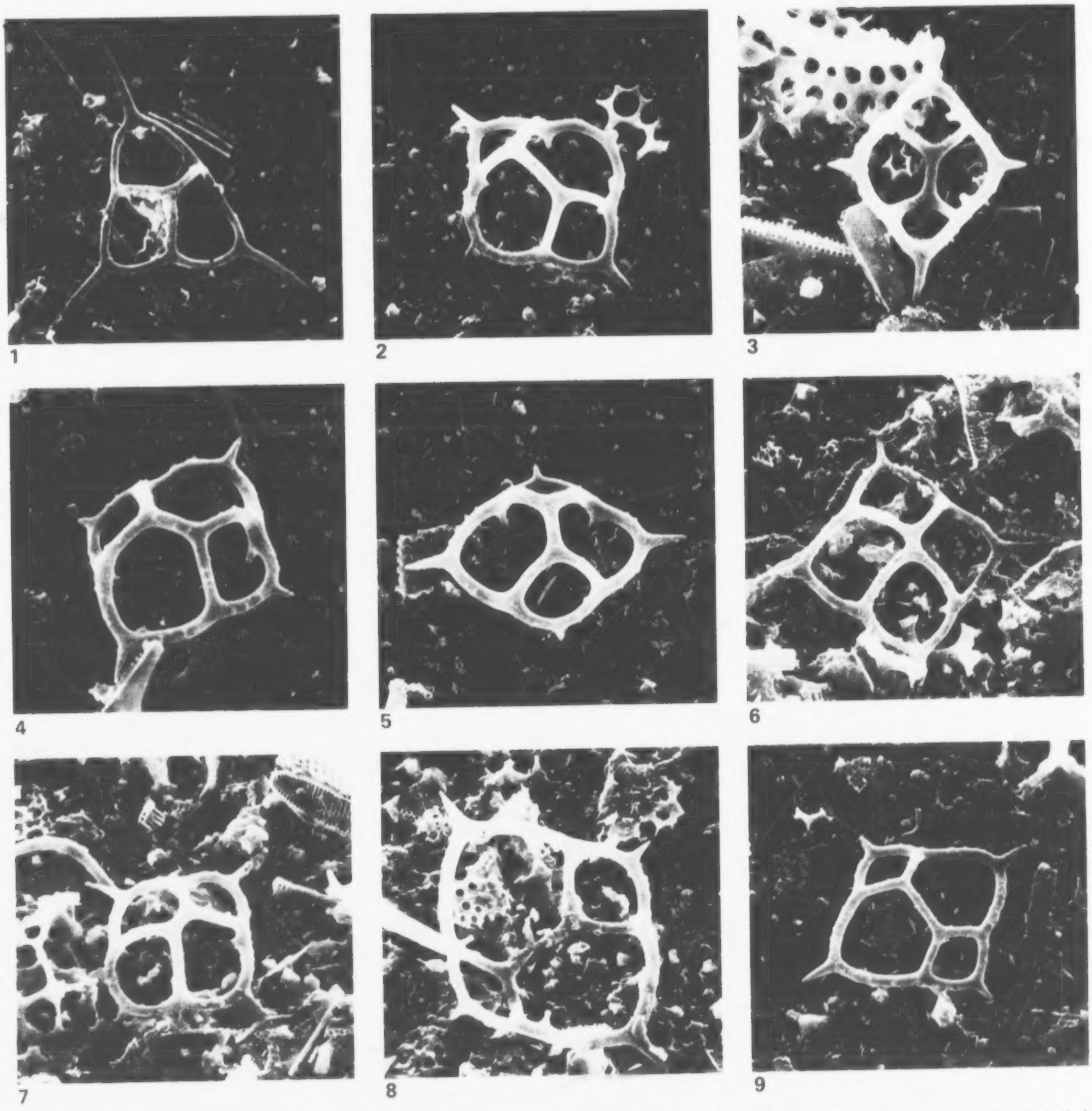

Plate 11. Middle Miocene to Lower Pliocene silicoflagellates (Scanning electron micrographs.) **1.** *Corbisema triacantha* (Ehrenberg), apical view, 1200 ×; Sample 591B-18,CC, middle Miocene. **2.** *Dictyocha messanensis* ssp. *stapedia* (Haeckel) f. *aspinosa*, apical view, 1300 ×; Sample 591-18,CC, lower Pliocene. **3.** *Dictyocha extensa* (Locker), antapical view, 1200 ×; Sample 591-29,CC, upper Miocene. **4, 5.** *Dictyocha varia* Locker, (4) apical view, 1800 ×, Sample 591-20,CC, lower Pliocene; (5) apical view, 1500 ×, Sample 591-20,CC, lower Pliocene. **6.** *Dictyocha medusa* Haeckel, apical view, 1200 ×; Sample 591B-4,CC, upper Miocene. **7.** *Dictyocha* sp. 2, apical view, 1200 ×; Sample 591B-4,CC, upper Miocene. **8, 9.** *Dictyocha fibula* Ehrenberg ssp. *fibula*, (8) antapical view, 1100 ×, Sample 591B-4,CC, upper Miocene; (9) apical view, 1050 ×, Sample 591-29,CC, upper Miocene.

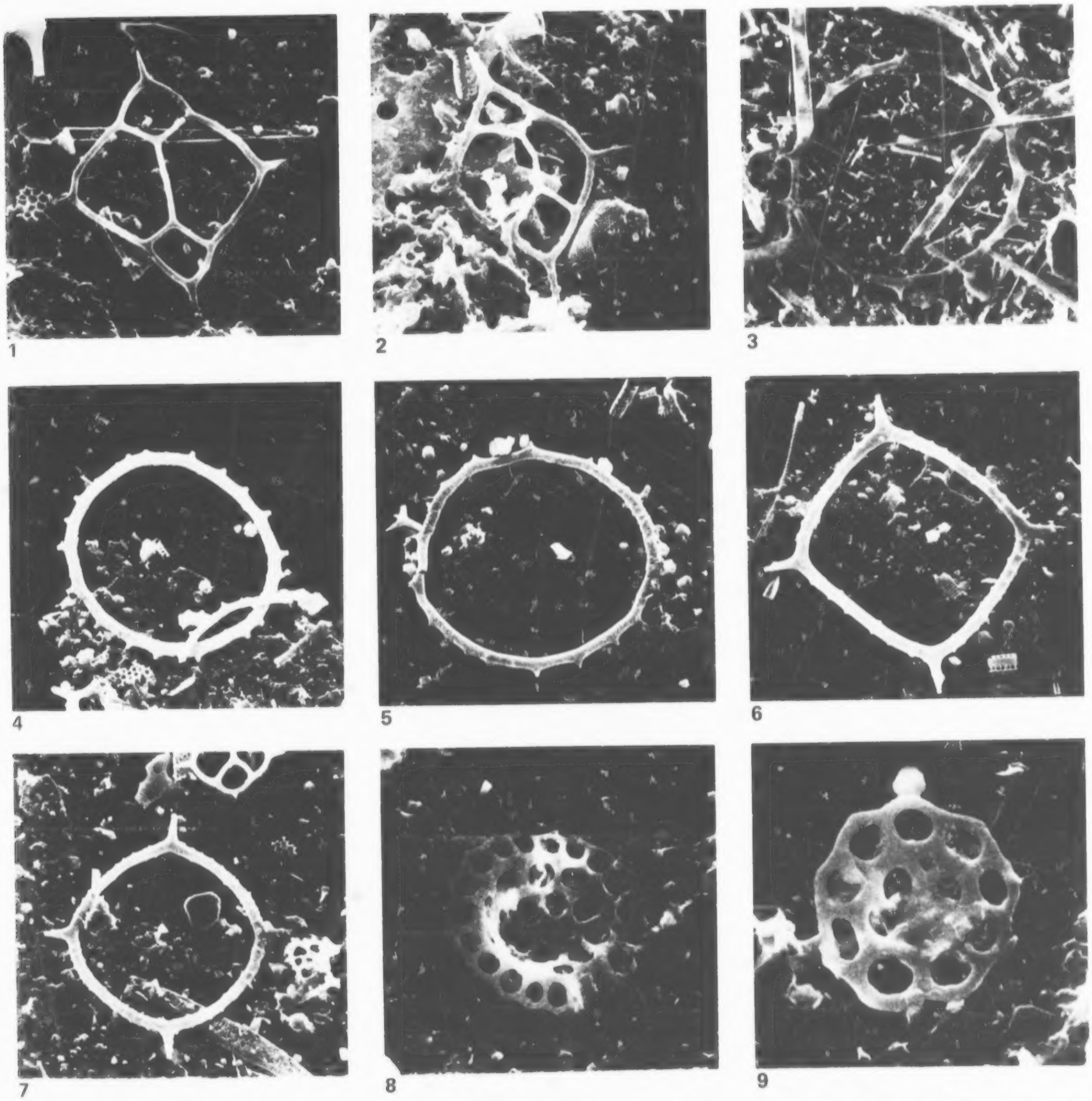

Plate 12. Middle Miocene to Lower Pliocene silicoflagellates. (Scanning electron micrographs.) **1.** *Dictyocha perlaevis* Frenguelli f. *perlaevis*, 900×; Sample 591-20,CC, lower Pliocene. **2.** *Dictyocha messanensis* ssp. *aspinosa* (Bukry), 1200×; Sample 591B-7,CC, upper Miocene. **3.** *Paramesocena apiculata* (Lemmermann), 650×; Sample 594-28,CC, upper Miocene. **4, 5.** *Paramesocena circulus* (Ehrenberg), 1050× and 1100×; Sample 591-18,CC, lower Pliocene. **6, 7.** *Mesocena quadrangula* Ehrenberg ex Haeckel, 1000× and 550×; Sample 591-20,CC, lower Pliocene. **8, 9.** *Macrora stella* (Azpeitia), 1400× and 3500×; Sample 591B-20,CC, middle Miocene.

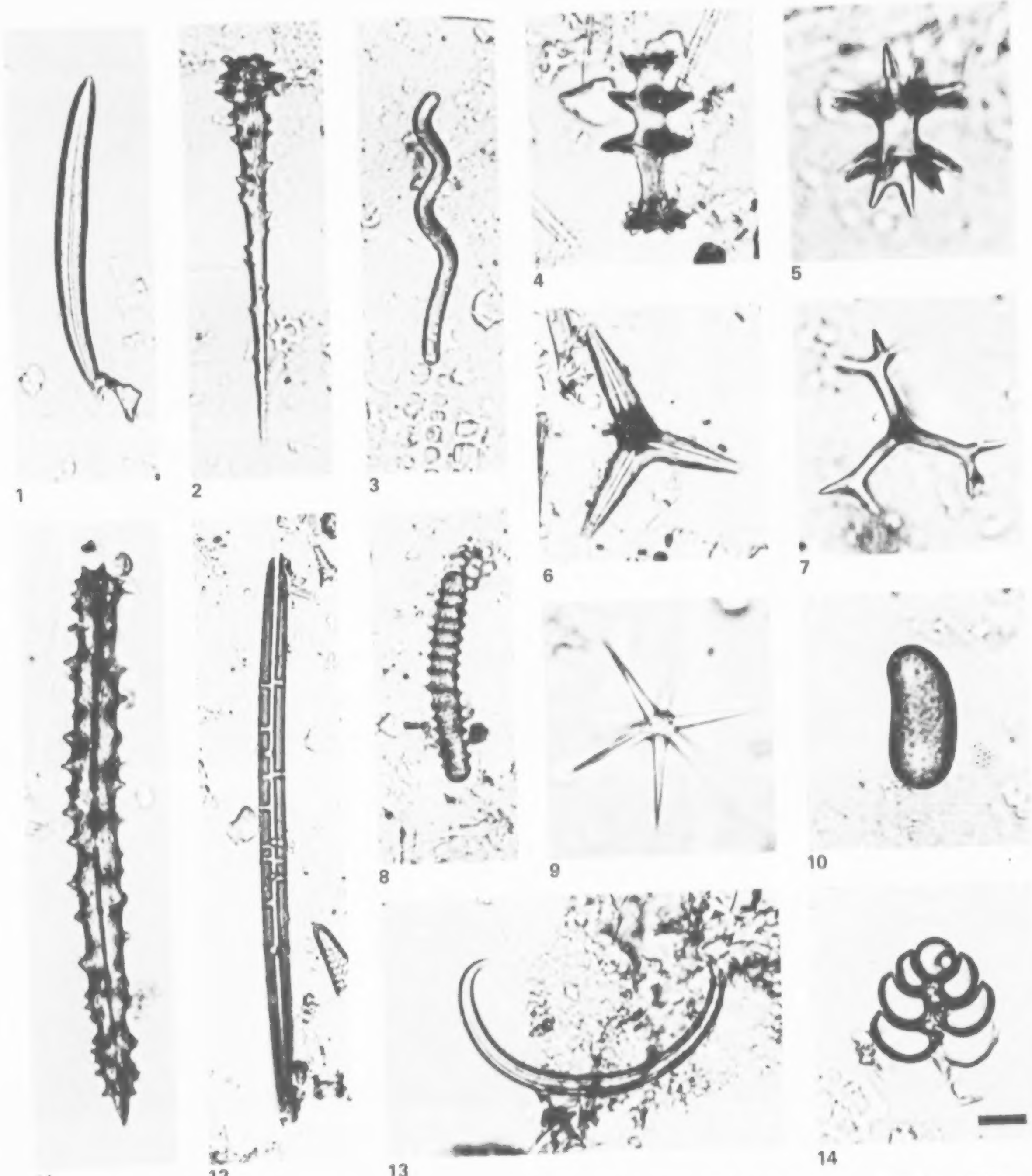

Plate 13. Middle Miocene to lower Pliocene sponge spicules; terminology according to Rauff, 1893/94. (All specimens magnified ×800, bar = 10 μm.) **1.** Amphiox, Sample 591-29,CC, upper Miocene. **2.** Acanthostyl, Sample 591-31,CC, upper Miocene. **3.** Spirul, Sample 591-31,CC, upper Miocene. **4.** Discorabd, Sample 594-47,CC, middle Miocene. **5.** Amphiaster, Sample 591-31,CC, upper Miocene. **6.** Oxycalthrop, Sample 594A-17,CC, middle Miocene. **7.** Calthrop with branched terminations, Sample 591-18,CC, lower Pliocene. **8.** Criccostrongyl, Sample 591B-2,CC, upper Miocene. **9.** Oxyaster, Sample 591-17,CC, lower Pliocene. **10.** Nephroid rhax, Sample 591-20,CC, lower Pliocene **11.** Acanthostyl, Sample 594-18,CC, lower Pliocene. **12.** Amphiox with short accessary channels, Sample 594A-18,CC, middle Miocene. **13.** Hooked amphiox, Sample 594A-12,CC, middle Miocene. **14.** Silicified biserial foraminifer, Sample 591-26,CC, upper Miocene.

17. MIOCENE SILICOFLAGELLATES FROM CHATHAM RISE, DEEP SEA DRILLING PROJECT SITE 594[1]

David Bukry, United States Geological Survey, Scripps Institution of Oceanography[2]

ABSTRACT

Miocene silicoflagellates, dominated by *Mesocena*, are identified and correlated from Site 594 to other Deep Sea Drilling Project sites. Relative paleotemperature values from silicoflagellates at Site 594 are very low, supporting the evidence of the associated cold-water, low-diversity coccolith assemblages. The greatest abundances of *Mesocena diodon nodosa* yet recorded occur at Site 594, which is near the present Subtropical Convergence. Similarities in the ecostratigraphic records between Chatham Rise (Site 594) and the Falkland Plateau (Site 329) in the late Miocene indicate widespread events within the circum-Antarctic water mass.

INTRODUCTION

Neogene silicoflagellate assemblages occur in Hole 594 of Deep Sea Drilling Project (DSDP) Leg 90 on Chatham Rise, east of New Zealand. This is the southernmost of a series of holes drilled during Leg 90 between New Zealand and the equator, to provide a latitudinal transect for paleoceanographic analysis. Although sparse Eocene silicoflagellates occur in Hole 588C (Core 19) and Hole 592 (Core 40), the only Neogene silicoflagellate sequence is from Hole 594 (Cores 20 to 48). Most of the Leg 90 sections that were examined lack silicoflagellates. Site 594 (45°31.41′S, 174°56.88′E, water depth 1204 m) is presently under the Subantarctic Water Mass, just south of the Subtropical Convergence. Cold-water silicoflagellates and coccoliths that are identified from Hole 594 support a similar water-mass pattern in the late Miocene.

A quantitative investigation of the Neogene silicoflagellate assemblages from Hole 594 was done to permit comparison of the species array to those in similar and contrasting regions, such as Site 329 (Falkland Plateau, 50°39.31′S, 46°05.73′W, water depth 1519 m) and Site 285 (South Fiji Basin, 26°49.16′S, 175°48.24′E, water depth 4658 m) and to determine relative paleotemperature values. In addition to the autochthonous late Miocene silicoflagellates, the samples from Hole 594 contain persistent reworked Paleogene specimens. Eocene and Oligocene biosiliceous deposits of similar age are now well exposed on New Zealand, as in the Oamaru section (Mandra et al., 1973), and form a potential local source for reworked Paleogene silicoflagellates.

The systematic paleontology covers the species of genus *Mesocena* which predominate in most samples of the upper Miocene at Hole 594. The distribution of abundant occurrences of these species at other DSDP localities is analyzed to help explain the high abundances in Hole 594.

METHODS

The samples taken aboard ship for shore-based silicoflagellate studies from the biosiliceous upper Miocene section of DSDP Site 594 were processed using HCl and H_2O_2 to help concentrate the silicoflagellates. Permanent strewn slides were prepared and a light microscope at 250× and 500× magnification, with mechanical stage translation, was used to systematically track the slide areas of 40 × 22 mm. Species were enumerated using a mechanical counter. All specimens encountered were recorded. Fragmented specimens were included in the counts by mental accumulation into whole specimens. Relative paleotemperature values (Ts) were calculated according to the scheme described by Bukry (1981, 1983).

Coccolith slides were prepared as standard whole-sediment smear slides as described in Bukry and Kennedy (1969). A light microscope with 250× and 500× magnification, rotating mechanical stage, and cross-polarized light was used to study the coccolith assemblages for identification of zones.

ZONATION

Several *Distephanus speculum speculum* zones representing partly different time intervals have been proposed for correlation of cool-water assemblages (Bukry, 1973b, 1976a; Ciesielski, 1975; Martini and Müller, 1976; Busen and Wise, 1977). In the late Miocene to early Pleistocene cool-water assemblages of the Northern Hemisphere, the *D. speculum speculum* zones are dominated by *D. speculum speculum* (Bukry, 1973b; Martini and Müller, 1976). At mid latitudes in the Northern Hemisphere, the *Distephanus longispinus* Zone and *Distephanus pseudofibula* Zone may also be recognized in the upper Miocene sediment below the *D. speculum speculum* Zone (Bukry, 1981). But the guide species for these zones are sparse in high-latitude assemblages from the Southern Hemisphere and limit recognition of these zones (Bukry, 1975c; Haq and Riley, 1976; specimens attributed to *D. pseudofibula* by Ciesielski, 1975, all show the morphology of *D. speculum varians*, a possibly cooler water phenotype). In the Southern Hemisphere a longer *D. speculum speculum* Zone has been identified by the first abundant occurrence of *Mesocena circulus* at the base (Bukry, 1975c, 1976a) and the first common occurrence of *Distephanus octonarius* at the top (Bukry, 1975c). The longer *D. speculum speculum* Zone in the Southern Hemisphere zone is used here, with the Miocene *Mesocena circulus* Subzone (Bukry,

---

[1] Kennett, J. P., von der Borch, C. C., et al., *Init. Repts. DSDP*, 90: Washington (U.S. Govt. Printing Office).

[2] Address: U.S. Geological Survey, Scripps Institution of Oceanography, La Jolla, CA 92093.

1975c) identified by the common occurrences of *Mesocena circulus* and *M. diodon nodosa* (Fig. 1).

RELATIVE PALEOTEMPERATURES (Ts)

The percentages of cool- and warm-indicator taxa in a silicoflagellate assemblage have been used to indicate latitudinal paleotemperature trends (Bukry, 1981) and have permitted interregional paleotemperature comparisons between the Pacific and Atlantic oceans for coeval intervals (Bukry, 1984; in press). Late Miocene assemblages at Site 594 have low relative paleotemperature values (Ts = 0 to 39) which are similar to the low values (Ts = 0 to 57) that occur at Site 329 (see Bukry, 1976b), at similar latitude and in the same Subantarctic Water Mass, east of the Falkland Islands. By contrast, late Miocene values (Ts = 85 to 97) are distinctly warmer at Site 285 (Bukry, 1975b), in the Fiji Basin, to the north of Site 594.

Large abundances of *Mesocena* and *Distephanus* at Site 594 indicate very cool conditions for most of the examined sample levels. Warm-water *Dictyocha* and temperate *Distephanus* (quadrate) are common in only a few samples. The contrasting assemblages of Site 285 (Bukry, 1975b), nearer the equator, contain practically no *Mesocena* and only moderate numbers of *Distephanus*. Warm-water *Dictyocha* predominates (>50%) throughout.

A comparison of relative paleotemperature values between the late Miocene samples from Site 594 and from North Pacific Site 581 (lat 43°55.62′N, long 159°47.76′E, depth 5476 m) shows much higher values (warmer) for the North Pacific because of the predominance of the genus *Dictyocha*. Late Miocene values at Site 581 range from Ts = 52 to 94 (Bukry and Monechi, in press), instead of the lower values of Ts = 0 to 39 at Site 594, even though they are located at similar north (44°) and south (45°) latitudes. The great contrast between the assemblages is the predominance of *Mesocena* at Site 594, which reflects cool and nutrient-rich waters. At the eastern end of the North Pacific Current the relative paleotemperature values off the coast of California for late Miocene samples are also lower than at Site 581 and the assemblages contain more *Mesocena* (Bukry, 1981). Therefore, it is possible that the warm Kuroshio Current was intensified and advanced farther north during the late Miocene, enhancing the productivity of *Dictyocha* over *Mesocena* at Site 581. Late Quaternary assemblages in the area of Site 581 contain cool-water *Distephanus octangulatus* (Ling, 1980; Bukry and Monechi, in press).

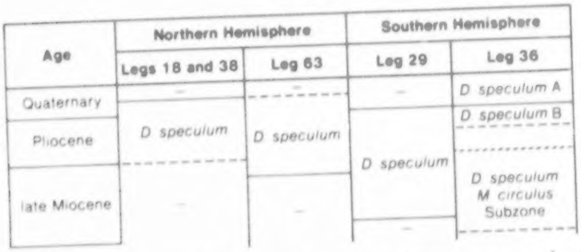

Age	Northern Hemisphere		Southern Hemisphere	
	Legs 18 and 38	Leg 63	Leg 29	Leg 36
Quaternary	—	—	—	D speculum A
Pliocene	D speculum	D speculum	D speculum	D speculum B
late Miocene	—	—	—	D speculum M circulus Subzone

Figure 1. Comparison of age ranges for various *Distephanus speculum* zones from Deep Sea Drilling Project Legs.

This poleward heat transfer (Csanady, 1984) by the warm-water mass in the Kuroshio Current might be linked to overall cooling in the late Miocene. There are advected cool-water pulses recorded in the late Miocene of the central equatorial Pacific Hole 572D (Bukry, in press) and a general North Pacific cooling has been described (Keller, 1981). But there is a notable lack of *Mesocena* in the samples with cool-water pulses at the equatorial Pacific hole (Ts = 18, 30, 32, and 36). Thus the *Mesocena* abundances for Site 594, which yield low Ts values, result from both cool temperature and rich nutrient levels. Although better time scales will be needed to make coeval comparisons, the distinctive silicoflagellate assemblage of Site 594 represents an important new reference for analysis of silicoflagellate ecostratigraphy in the Pacific.

Diatom chronostratigraphic correlations (*Denticula hustedtii* Zone) of DSDP Sites 158, 329, 470, 472, 572, 581, and 594 (J. A. Barron, written communication, 1984) were used to make a preliminary check of silicoflagellate Ts trends for the early late Miocene. The sampling array in the *Initial Reports* is inadequate for detailed silicoflagellate comparisons, but similar, consistent low Ts values occur at Sites 173, 329, and 594, where cool or transitional waters probably occurred in the late Miocene. The only changing trend observed for the interval was one of the declining Ts values at the Pacific equatorial Site 158 (Ts = 92 to 63) and Site 572 (Ts = 96 to 36).

The four silicoflagellate samples from Cores 594-23 to 594-25 (214 to 228 m) occur in the interval assigned to the late Miocene cool-water *Thalassiosira antiqua* Zone by Ciesielski (J. A. Barron, written communication, 1984). The Ts values are very low (Ts = 2 or 3) except at the bottom of this interval (Ts = 30) in Sample 594-25-2, 8–9 cm. A comparison of the same diatom zone at offshore California Sites 469 and 470 shows that the coolest value is Ts = 27 and the warmest Ts = 61. Farther south, off Baja California at Site 472, warmer values occur, Ts = 58 to 94. This zone was not used for Site 581 and was not cored at Site 329. The coeval interval according to diatoms at northwest Pacific Site 581 is in Cores 581-5 to 581-6; at equatorial Pacific Hole 572D it is in Cores 572D-6 to 572D-11 (J. A. Barron, verbal communication, 1984). At both locations there is a general warming upward through the interval. Maximum Ts values at Site 581 (Ts = 96) are higher than at Hole 572D (Ts = 82), but minimum values are more disparate, with a minimum of Ts = 32 for Hole 572D and Ts = 79 for Site 581. The exceptionally cold conditions at Site 594 appear to have persisted through the late Miocene, according to the relative paleotemperature values of silicoflagellates, correlated by diatom zonation.

COMPARISON OF *MESOCENA* OCCURRENCES

Mesocena circulus s. ampl. is most numerous at oceanic locations where cool-water currents or upwelling are most intense. Comparison of peak abundances at DSDP sites shows generally higher numbers at higher latitudes but equatorial abundances up to 34% at Site 157 show that the local cool, nutrient-rich waters of the Peru Current determine the productivity of *M. circulus* s. ampl.

Actual latitude is too general a guide. Other fairly high abundances at low latitudes (Table 1) are noted for Holes 321 and 572A, which are also influenced by the Peru Current. In the South Atlantic, the cool nutrient-rich upwelled waters at the Walvis Ridge account for the relatively high 19% abundance of *M. circulus* s. ampl. at Site 362. At high-latitude Site 594 the highest value of 95% follows moderate values of 28%.

A comparison of the maximum abundance for *M. diodon nodosa* s. ampl. in the Atlantic and Pacific oceans shows similar maximum values near Ts = 40 (Table 2), except for Site 594. As with *M. circulus* s. ampl., data are more numerous for the Pacific Ocean. Comparison of the relative timing of the maximum abundances between these two taxa shows that *M. diodon nodosa* s. ampl. typically precedes *M. circulus* s. ampl. At 17 localities compared, *M. diodon nodosa* s. ampl. has an earlier maximum abundance peak at 11 sites (DSDP 157, 158, 285, 303, 304, 472, 503A, 504, 579A, and 581, and EM site). The order is reversed at five sites (DSDP 173, 310, 278, 469, and 470). The general stratigraphic range of *M. diodon nodosa* s. ampl. is briefer and earlier than for *M. circulus* s. ampl. Site 594 does show the reverse relation in maximum abundances but the base of the section is not established. More significantly, the highest abundances of *M. diodon nodosa* ever recorded (86%, 77%, 75%, etc.) are in Cores 594-23 through 594-30. This pre-eminence of *M. diodon nodosa* indicates a specialized condition for this area.

Table 1. Maximum abundance (percent) of *Mesocena circulus* s. ampl. recorded from Deep Sea Drilling Project (DSDP) and Experimental Mohole (EM) coring locations in the Pacific and Atlantic oceans, arranged from north to south.

Site or Hole	Latitude	Abundance	Age	Total range
Pacific Ocean				
433A	44°46.60′N	X	—	l. Miocene to Pliocene or Pleistocene
581	43°55.62′N	7	l. Miocene	l. Miocene
580	41°37.47′N	34	l. Miocene	l. Miocene
303	40°48.50′N	7	l. Miocene or e. Pliocene	m. or l. Miocene to l. Miocene or e. Pliocene
173	39°57.71′N	3	m. Miocene and Pleistocene	m. Miocene to Pleistocene
464	39°51.64′N	24	e. Pliocene	l. Miocene to e. Pleistocene
304	39°20.27′N	17	l. Miocene or e. Pliocene	l. Miocene to l. Miocene or e. Pliocene
579A	38°37.61′N	26	e. Pliocene	e. and l. Pliocene
310	36°52.11′N	20	l. Pliocene	l. Miocene to Pleistocene
466	34°11.46′N	13	Pleistocene	Pleistocene
469	32°37.00′N	74	l. Miocene	m. and l. Miocene to l. Miocene or Pliocene
577	32°26.51′N	22	e. Pliocene	e. and l. Pliocene
470	28°54.46′N	45	m. Miocene	m. and l. Miocene
EM	28°00.58′N	20	m. and l. Miocene	m. and l. Miocene
472	23°00.35′N	4	l. Miocene	l. Miocene
495	12°29.78′N	1	l. Miocene and Pliocene	l. Miocene and Pliocene
158	6°37.36′N	5	m. and l. Miocene	m. and l. Miocene
65.0	4°21.21′N	X	—	l. Miocene or Pleistocene
503A	4°04.04′N	2	l. Pliocene	e. and l. Pliocene
166	3°45.70′N	X	—	Miocene or Pliocene
572A	1°26.09′N	12	e. Pliocene	e. Pliocene
572D	1°26.09′N	2	m. Miocene	m. and l. Miocene
425	1°23.68′N	2	Pleistocene	Pleistocene
504	1°13.58′N	6	e. Pliocene	Pliocene and Pleistocene
157	1°45.70′S	34	e. Pliocene	l. Miocene to Pleistocene
157A	1°45.70′S	1	Pleistocene	Pleistocene
321	12°01.29′S	13	l. Pliocene	l. Pliocene
205	25°30.99′S	6	l. Miocene	l. Miocene
285	26°49.16′S	1	l. Miocene	l. Miocene
278	56°33.42′S	48	Pliocene	l. Miocene or Pliocene
322	60°01.45′S	4	Pliocene	Pliocene
Atlantic Ocean				
348	68°30.18′N	X	—	m. or l. Miocene
338	67°47.11′N	X	—	m. or l. Miocene
407	63°56.32′N	18	Pliocene	Pliocene
408	63°22.63′N	41	m. Miocene	m. Miocene to Pliocene
555	56°33.70′N	16	m. Miocene	m. and l. Miocene
554A	56°17.40′N	5	l. Miocene	l. Miocene
552A	56°02.56′N	4	e. Pliocene	e. Pliocene
410	45°30.53′N	4	l. Pliocene	l. Pliocene
335	37°17.74′N	4	Pleistocene	Pleistocene
334	37°02.13′N	4	l. Miocene	l. Miocene
332B	36°52.72′N	<1	l. Pliocene	l. Pliocene
333	36°50.45′N	6	l. Pliocene	l. Pliocene
397	26°50.70′N	3	l. Pliocene	l. Pliocene
362	19°45.45′S	19	l. Pliocene	Pliocene and Miocene or Pliocene
328	49°48.67′S	6	l. Miocene	l. Miocene
329	50°39.31′S	92	Miocene	Miocene
327	50°52.28′S	1	Pleistocene	Miocene to Pleistocene

Note: Ages for the maximum abundance event and the range of *M. circulus* s. ampl. are also shown. X = present, but too sparse for accurate percentage.

Table 2. Maximum abundance (percent) of *Mesocena diodon* s. ampl. recorded from Deep Sea Drilling Project (DSDP) and Experimental Mohole (EM) coring locations in the Pacific and Atlantic oceans, arranged from north to south.

Site or Hole	Latitude	Abundance	Age	Total range
Pacific Ocean				
192	53°00.57′N	6	l. Miocene	l. Miocene
433A	44°46.60′N	X	—	m. Miocene to Pleistocene
581	43°55.62′N	10	l. Miocene	l. Miocene
303	40°48.50′N	4	m. or l. Miocene	m. Miocene to e. Pliocene
173	39°57.71′N	4	l. Miocene	m. and l. Miocene
464	39°51.64′N	6	e. Pliocene	e. Pliocene
33	39°28.48′N	8	l. Miocene	m. and l. Miocene
304	39°20.27′N	1	l. Miocene and e. Pliocene	l. Miocene to e. Pliocene
579A	38°37.61′N	6	e. Pliocene	e. Pliocene
310	36°52.11′N	2	Pliocene	Pliocene
466	34°11.46′N	33	e. Pliocene	e. Pliocene
469	32°37.00′N	5	l. Miocene	m. and l. Miocene
470	28°54.46′N	20	l. Miocene	m. and l. Miocene
EM	28°00.58′N	10	m. Miocene	m. Miocene
472	23°00.35′N	5	m. Miocene	m. and l. Miocene
495	12°29.78′N	1	m. Miocene	m. Miocene
158	6°37.36′N	8	m. Miocene	m. and l. Miocene
503A	4°04.04′N	40	l. Miocene	l. Miocene to l. Pliocene
572A	1°26.09′N	0	—	e. Pliocene
572D	1°26.09′N	0	—	m. and l. Miocene
504	1°13.58′N	1	l. Miocene	l. Miocene
157	1°45.70′S	1	l. Miocene	l. Miocene to Pleistocene
285	26°49.16′S	<1	m. Miocene	m. Miocene
206	32°00.75′S	X	—	m. and l. Miocene
281	47°54.84′S	20	l. Miocene	l. Miocene
278	56°33.42′S	16	l. Miocene	l. Miocene or Pliocene
322	60°01.45′S	6	Pliocene	Pliocene
323	63°40.84′S	X	m. Pliocene	m. Pliocene
Atlantic Ocean				
348	68°30.18′N	X	m. Miocene to e. Pliocene	m. Miocene to e. Pliocene
338	67°47.11′N	34	m. Miocene	m. Miocene
407	63°56.32′N	X	e. Pliocene	e. Pliocene
408	63°22.63′N	14	l. Miocene	m. Miocene to Pliocene
555	56°33.70′N	1	m. Miocene	m. Miocene
554A	56°17.40′N	37	l. Miocene	l. Miocene
552	56°02.56′N	22	l. Miocene	l. Miocene
552A	56°02.56′N	1	l. Miocene	l. Miocene to e. Pliocene
334	37°02.13′N	<1	l. Miocene	l. Miocene
391A	28°13.61′N	3	m. Miocene	m. Miocene
394A	28°11.70′N	2	m. Miocene	m. Miocene
358	37°39.31′S	X	l. Miocene	l. Miocene
328B	49°48.67′S	X	l. Pliocene	l. Pliocene
329	50°39.31′S	33	l. Miocene	l. Miocene
327	50°52.28′S	<1	Pleistocene	Miocene to Pleistocene

Note: Ages for the maximum abundance event and the range of *M. diodon* s. ampl. are also shown. X = present, but too sparse for accurate percentage.

Previous studies from the Southern Ocean, off Antarctica (Ciesielski, 1975; Perch-Nielsen, 1975; Bukry, 1975c; Haq and Riley, 1976; Busen and Wise, 1977), have shown low and sporadic abundances except at one site (Site 329) where 2 to 33% *M. diodon nodosa* occur. The location of Site 329 at 50°39′S latitude, at 1519 m water depth on the Falkland Plateau, is also analogous to Site 594, at 45°31.41′S and 1204 m, east of New Zealand. Higher-latitude sites to the south (nearer Antarctica) lack *M. diodon nodosa* or have only sparse (1–3%) occurrences. The highest abundances of *M. diodon nodosa* at Sites 594 and 329 identify intensified activity at the Subtropical Convergence in the late Miocene. High abundance of *M. diodon nodosa* elsewhere may also signify convergence zone conditions.

DSDP HOLE 594 COMPARED TO DSDP HOLE 329

The presence of *Mesocena triangula* and reworked Paleogene silicoflagellates in samples from Cores 20 to 31 at Site 594 suggested a potential similarity and ecostratigraphic correlation to Site 329, which was cored earlier on the Falkland Plateau. A comparison of quantitative silicoflagellate occurrences for Site 594 (Table 3) and Site 329 (Bukry, 1976b) demonstrates a sequence of similar events (Table 4). Three lower correlation events in the upper Miocene are the boundary between moderate (Ts = 26 to 57) and very low (Ts = 0 to 9) relative paleotemperature values (Ts) and the bracketing by major and minor concentrations of *Distephanus crux crux* above and below. The middle three events are an increase of Paleogene reworked silicoflagellates, bracketed by concentrations of *Mesocena circulus* below and *Dictyocha aspera clinata* above. The final trio of correlation events includes a dominance reversal of *M. diodon* s. ampl. and *M. circulus* s. ampl. followed by the highest Ts values (Ts = 30 and 10) above the lower part of the section, and finally the conjunction of *M. triangula* with *M. quadrangula*. These events are believed to represent interregional changes that are probably related to circum-Antarctic ocean circulation. Both drill sites lie within the present area of Subantarctic Water, south of the Subtropical Convergence (see Kennett, 1980, fig. 2) and just south of the Subantarctic Convergence (Burkov, 1966). Periods of major current scour may be recorded by the reworked Paleogene taxa at both areas. Similarities in temperature and nutrient changes account for the species correlations.

Some of the species events compared between the two sites did not prove to be sequentially correlative between the two regions. These included the local acmes of *Dictyocha brevispina, D. fibula augusta, D. pentagona, Distephanus speculum minutus*, and *D. speculum speculum*.

The similarity in the sequence of silicoflagellate events between Site 594, Cores 23 to 31, and Site 329, Cores 2 to 17, suggests that the late Miocene age of Site 329 may be applied to Site 594.

Shipboard identification of a fairly complete middle Miocene to early Pliocene sequence of coccolith Zones NN7/8, NN9, NN10, NN11, and NN12/14 for Cores 20 to 31 at Site 594 is not supported by shore-based examination of the section. The samples contain limited coolwater assemblages that lack all of the zonal guide species which define these numbered zones (Martini, 1971), including *Discoaster kugleri, D. hamatus, D. quinqueramus*, and *Amaurolithus tricorniculatus*. Among the low-diversity, placolith-dominated assemblages, only a few contained coccolith species with ranges useful for stratigraphic correlation. Cores 26 and 29 contain sparse *D. brouweri* s. ampl. and *D. bellus*, and Cores 23 and 26 contain *Triquetrorhabdulus rugosus* which, together, indicate a probable late Miocene correlation of these cores, if the specimens are stratigraphically in place. Actually, there is a significant number of reworked Paleogene species such as *Chiasmolithus oamaruensis* and *Isthmolithus recurvus* in these samples. Therefore, identification of coccolith zonal boundaries should be considered as tenuous and only a general late Miocene age is indicated.

SUMMARY

The main results of this initial study of silicoflagellates from Site 594 are summarized below.

1. Very high abundances of *Mesocena diodon nodosa* occur in the upper Miocene from Site 594, and may be a guide to convergence zone conditions.
2. A sequence of similar silicoflagellate events between Site 594 and Site 329 in the Atlantic suggest possible ecostratigraphic correlation throughout the circum-Antarctic water mass. The increase in Paleogene reworking at both sites shows timing for widespread scour and current activity.
3. Comparison of low relative paleotemperatures from Site 594 (lat. 45°S) with high values at North Pacific Site 581 (lat. 44°N) supports an intensified and more northerly warm Kuroshio Current in the North Pacific for the late Miocene. The late Quaternary flora just south of Site 581 yields low Ts values typical of cool water conditions.
4. Taxonomic distinction of *M. circulus* var. *apiculata* from *M. dumitricae* may be useful for paleoecological reconstructions, as the latter appears to be favored by cooler conditions.

SYSTEMATIC PALEONTOLOGY OF GENUS *MESOCENA* EHRENBERG, 1843, FROM DSDP HOLE 594

Mesocena circulus (Ehrenberg) Ehrenberg

(Plate 3, Figs. 3–6)

Dictyocha (*Mesocena*) *circulus* Ehrenberg, 1840, p. 208. Figured by Ehrenberg, 1854, pl. 19, fig. 44.

Mesocena circulus (Ehrenberg) Ehrenberg, 1844, p. 65.

Mesocena circulus (Ehrenberg), Mandra and Mandra, 1972, pl. 31, fig. 36.

Mesocena circula (Ehrenberg), Bukry and Foster, 1973 (in part), p. 828, pl. 5, fig. 9.

Paradictyocha circulus (Ehrenberg) Dumitricá, 1973, p. 853, pl. 9, figs. 7–10.

Bachmannocena circulus (Ehrenberg) Locker, 1974, p. 636, pl. 2, fig. 11.

Mesocena circulus (Ehrenberg), Bukry, 1975a (in part), p. 718, pl. 2, fig. 4.

Paradictyocha circulus (Ehrenberg), Perch-Nielsen, 1975, p. 689, pl. 11, fig. 12.

Paradictyocha circulus (Ehrenberg) Dumitricá, Stradner and Bachmann, 1978, p. 808, pl. 2, figs. 13–15.

Remarks. For Site 594, *Mesocena circulus* is identified in a restricted sense which is limited to the morphology with numerous, small, irregular spines that was originally illustrated by Ehrenberg (1854) and repeated in lectotype material by Locker (1974). Previously, *M. circulus* s. ampl. of some authors has also included long-spined specimens of *M. dumitricae* (see Bukry, 1975a; Busen and Wise, 1977) and speci-

pages tightly bound

Table 3. Late Miocene silicoflagellates recorded as percentages from Cores 20 to 48 of Hole DSDP 594.

Age	late Miocene																	—	
Zone	*Distephanus speculum speculum* Zone																	—	
Subzone	*Mesocena circulus* Subzone																		
Depth (m)	180	190	214	219	223	228	233	241	247	252	257	262	267	276	281	286	290	438	449
Sample (interval in cm) / Taxa	20-2, 8-9	21-2, 8-9	23-5, 8-9	24-2, 8-9	24-5, 8-9	25-2, 8-9	25-5, 8-9	26-4, 8-9	27-2, 8-9	27-5, 8-9	28-2, 8-9	28-5, 8-9	29-2, 8-9	30-2, 8-9	30-5, 8-9	31-2, 8-9	31-5, 8-9	47-1, 8-9	48-2, 8-9
Caryocha sp.	1																	3	P
Dictyocha aspera aspera								1											
D. aspera clinata s. ampl.								4	4									1	P
D. brevispina		11																	
D. fibula augusta		1						1	*	11									
D. fibula fibula						3			9		1	4	1						P
D. pentagona					2														
D. pulchella		3		2		16		1	2	6		1	4			1	2		P
D. sp. aff. *pulchella* var. *inflata*																		25	
D. sp. (asperoid)	1				1	7										1	2	3	
D. sp. (fibuloid)	1				1			5	1				1			1	2	5	
Distephanus crux crux		5	2		1	7		*	1		2	1	5	2	12	4	66	32	P
D. frugalis				1															
D. polyactis crassus																			P
D. pseudofibula						1													
D. quinquangellus	2	2					1	1						1					P
D. speculum diommata									1										
D. speculum minutus	67	8	1	1	1														
D. speculum speculum	24	43	13	18	76	16	23	4	6	30	11	9	27	1	1	1			P
D. speculum triommata								1											
D. xenus		23																	
Mesocena circulus		1		1		22	1												
M. circulus var. *apiculata*	1				14	19		18	2	16	8	30	14	61	1	94	24	31	
M. circulus var. *apiculata* (knobby)								4						4		1	4		
M. dumitricae									24							1			
M. sp. cf. *diodon borderlandensis*									1										
M. diodon nodosa	3	3	70	77	4	9	75	59	51	29	78	44	38	29	86				
N. diodon nodosa (circular)			1						1	9	1	14	8	2		1			
M. diodon nodosa (oblate)			2										3						
M. quadrangula		1	2																P
M. triangula			9								1								
M. triodon								1			1			1					
Reworked																			
Corbisema apiculata		X			X	■				X					X	X	X	X	
C. sp. cf. *C. glezerae*								X								X			
C. hastata globulata								X											
C. hastata hastata		X				X						X				X			X
C. inermis							X									X			
C. triacantha s. ampl.		X			X				X				X		X			X	
C. spp.						X										X			
Dictyocha deflandrei completa		X		X				X	X	X					X			X	
D. sp. (asperoid)					X		X												
D. sp. (fibuloid)					X														
Mesocena apiculata apiculata		X			X	X		X			X			X	X	X	X		
M. apiculata curvata																			X
M. apiculata glabra								X											
Naviculopsis aspera									X										
N. biapiculata		■				X	X	X	X	X			X	X				X	
N. sp. aff. *N. biapiculata*									X										
N. constricta	X	X	X	X	X	X		X	■		X	■	X			X		■	X
N. eobiapiculata		X	X												X	X			
N. sp. cf. *N. trispinosa*		X											X						
Naviculopsis spp.																X			
Reworked diatoms																			
Rocella gelida		X			X	X					X	X	X	X		X	X		X
R. schraderi						X			X							X			X
Total specimens (plus reworked)	100 (1)	103 (25)	100 (2)	100 (2)	100 (7)	100 (10)	100 (3)	100 (7)	201 (11)	200 (3)	200 (4)	200 (2)	100 (4)	200 (3)	100 (5)	200 (31)	50 (4)	100 (11)	19 (7)
Paleotemperature value	2	17	2	2	3	30	0	12	17	17	2	6	9	1	6	5	39	50	—

Note: X = presence of reworked specimens; ■ = numerically predominant. * = recorded after counts. P = too sparse for percent.

Table 4. Matching silicoflagellate events between Site 594, east of New Zealand, and Site 329, east of the Falkland Islands, both within the present Subantarctic Water Mass.

Silicoflagellate event	Core or Section at Site 594	Core at Site 329
Mesocena triangula and *M. quadrangula* conjunction	23	2
Highest relative paleotemperature (Ts) above the basal interval	25-2	4
Coincident decline of *M. diodon* s. ampl. and concentration of *M. circulus* s. ampl.	25-2 and 25-5	8 and 9
Dictyocha aspera clinata s. ampl. concentration	26-4 and 27-2	11 and 12
Increase in Paleogene reworking	27-2	15
Mesocena circulus s. ampl. concentration	30-2	14
Distephanus crux crux minor concentration	30-5	15
Major reduction in relative paleotemperature values (Ts)	31-5 to 31-2	17 to 16
Distephanus crux crux major concentration	31-5	17

mens of *M. circulus* var. *apiculata* (see Bukry and Foster, 1973). Although the small spines of *M. circulus* may lie in the plane of the ring, they may also have variable positions along the outer periphery of the ring. The inner circumference lacks spines.

According to a subsequent designation by Loeblich et al. (1968), *Mesocena*? *octogona* is the type species for genus *Mesocena*. Previous designations of *M. circulus* or *M. elliptica* as type species could not be accepted by Loeblich et al. (1968) because they were not taken from the paper in which the genus name was defined. The simplistic illustration of *M.*? *octogona* could ambiguously represent several silica bodies. And its Holocene age separates it in time from all other taxa classified in *Mesocena* (Paleocene to mid Pleistocene). Locker's (1974) reexamination of Ehrenberg materials purports to reillustrate the holotype of *M.*? *octogona* and shows that it is the basal ring of *Octactis*. This is reasonable on the basis of the morphology and age of the specimen. Therefore, the status of the name *Mesocena* is in doubt; parenthetically, so is the status of *Octactis*. The other available species for *Mesocena* in the Ehrenberg publication, *M.*? *heptagona*, is simply a polymorph of *M.*? *octogona*. *Mesocena circulus* (Ehrenberg) Ehrenberg (1844, p. 65) appears to be the next best choice if the name *Mesocena*, with 140 years of continuous usage, is to be retained. If *Mesocena* were not conserved, then *Bachmannocena* of Locker (1974) could be substituted.

For this publication, the name *Mesocena* is retained for silicoflagellate skeletons composed of a single ring, with or without spines of various sizes and orientations. This includes the widely reported forms *M. circulus* and *M. circulus* var. *apiculata* among others. Resolution of the *Mesocena* problem will have to treat *Bachmannocena*, *Paradictyocha*, and *Septamesocena*, also.

***Mesocena circulus* var. *apiculata* Lemmermann**
(Plate 2, Figs. 3–7; Plate 3, Figs. 1, 2)

Mesocena circulus var. *apiculata* Lemmermann, 1901, p. 257, pl. 10, figs. 9, 10.

Mesocena circulus Ehrenberg, Martini and Müller, 1976, p. 872, pl. 4, figs. 7, 8.

Mesocena circulus var. *apiculata* Lemmermann, Ling, 1972, p. 176, pl. 28, figs. 7, 8.

Mesocena circula (Ehrenberg), Bukry and Foster, 1973 (in part), p. 828, pl. 6, fig. 1.

Paradictyocha apiculata (Lemmermann), Perch-Nielsen, 1975, p. 689, pl. 11, figs. 14, 15.

Mesocena circulus apiculata (Lemmermann) Ling, 1977, p. 214, pl. 2, fig. 24.

Remarks. The moderate-length spines of *Mesocena circulus* var. *apiculata* are equal to or longer than those on *M. circulus* and are more regularly spaced into two rows, or peripheral cycles, with offset between the spines of the two cycles. The regularity of the spine spacing and the limitation to two parallel cycles distinguishes *M. circulus* var. *apiculata* from *M. circulus* and *M. dumitricae*. Some variants with knobby spines or small nodes are illustrated.

***Mesocena diodon borderlandensis* Bukry**
(Plate 4, Fig. 1)

Mesocena diodon borderlandensis Bukry, 1981, p. 547, pl. 4, figs. 5–9; pl. 5, figs. 1, 2.

Remarks. Only two compared specimens of *Mesocena diodon borderlandensis* were found among the abundant *Mesocena* at Site 594. The elongate morphology of *M. diodon borderlandensis* is most prominent at Site 469, off California, in the lower upper Miocene.

***Mesocena diodon nodosa* Bukry**
(Plate 4, Figs. 2–6)

Mesocena diodon nodosa Bukry, 1978 (in part), p. 818, pl. 5, figs. 14, 15; pl. 6, figs. 1–3 (not figs. 4, 5 which are now classified as *Mesocena diodon borderlandensis* Bukry).

Mesocena diodon nodosa Bukry, Bukry and Monechi, in press, pl. 9, figs. 1–3; pl. 16, fig. 4.

Remarks. The most abundant populations of *Mesocena diodon nodosa* occur in the middle and upper Miocene. Aside from the normal specimens with prolate elliptic rings, two minor varieties that are circular or oblate were also found and recorded at Site 594. The circular variety is most common (14%) in Sample 594-28-5, 8–9 cm, whereas the oblate is most common (3%) just below in Sample 594-29-2, 8–9 cm.

***Mesocena dumitricae* (Perch-Nielsen) emend. Bukry, n. comb.**
(Plate 5, Figs. 1, 2)

Mesocena circulus Ehrenberg, Ling, 1972 (in part), p. 175, pl. 28, figs. 5, 6.

Mesocena circulus Ehrenberg, Stadum and Burckle, 1973, p. 108, pl. 1, figs. 1–5.

Mesocena circulus Ehrenberg, Ciesielski, 1975, p. 661, pl. 11, figs. 6, 8, 9.

Mesocena circulus (Ehrenberg), Bukry, 1975a (in part), p. 718, pl. 2, fig. 5.

Paradictyocha dumitricae Perch-Nielsen, 1975, p. 689, pl. 11, figs. 1, 5–8.

Mesocena circulus Ehrenberg, Busen and Wise, 1977, p. 715, pl. 7, figs. 2, 3, 4? 6?; pl. 11, figs. 1, 2.

Remarks. *Mesocena dumitricae* was described as having a polygonal rather than round outline (Perch-Nielsen, 1975); however, four of the five type specimens show nearly continuous curvature around the ring. Also, the spines were characterized as short, but moderate to moderately long spines are also known in populations from different areas (see Stadum and Burckle, 1973; and Bukry, 1975a, c). The most diagnostic features of *M. dumitricae*, as emended herein, are the single cycle of regularly spaced equant spines which lie in the plane of the ring. Specimens of *M. dumitricae* with polygonal and essentially circular rings may occur together (Perch-Nielsen, 1975, pl. 11).

Occurrence. *Mesocena dumitricae* emend. has previously been tabulated as *M. circulus*, so the full stratigraphic and geographic range are not known, but the illustrations of high-latitude *Mesocena* by Busen and Wise (1977) and Stadum and Burckle (1973) suggest that *M. dumitricae* may favor cooler areas where upwelling is strong.

***Mesocena quadrangula* Ehrenberg ex Haeckel**
(Plate 5, Fig. 3)

Mesocena quadrangula Ehrenberg ex Haeckel, 1887, p. 1556.

Mesocena quadrangula Ehrenberg ex Haeckel, Bukry, 1979, p. 574, pl. 5, figs. 5, 6.

Remarks. *Mesocena quadrangula* is largely missing from the assemblages at Site 594. Sparse specimens occur only in two sample from Cores 21 and 23 near the top of the silicoflagellate-bearing section. The conjunction of *M. quadrangula* and *M. triangula* in Core 2 suggests a correlation to the upper part of Site 329, which is considered upper Miocene.

***Mesocena triangula* (Ehrenberg)**
(Plate 5, Figs. 3–6)

Dictyocha triangula Ehrenberg, 1839, p. 129. Figured by Ehrenberg 1854, pl. 22, fig. 41.

READEX FICHE best copy available

Mesocena triangula (Ehrenberg) Ehrenberg, 1844, p. 65, 71.
Mesocena triangula (Ehrenberg), Bukry and Foster, 1973 (in part), p. 829, pl. 6, figs. 9, 10.
Mesocena triangula (Ehrenberg), Ling, 1977, p. 214, pl. 3, fig. 6.

Remarks. *Mesocena triangula* has surface texture and stratigraphic distribution which suggest derivation from *Mesocena quadrangula* or possibly *M. circulus*. A triangular variant of *M. diodon nodosa* from Site 594 (Plate 4, Figs. 5, 6) shows distinctive crenulate surface texture suggesting different affinities than *M. triangula* at Site 594.

Occurrence. The highest abundances reported for *Mesocena triangula* are 8% at Site 555 in the North Atlantic and 9% at Site 594 in the South Pacific. Both are in late Miocene samples. Infrequent occurrences in other areas are typically 1 or 2% in assemblages from Oligocene (Busen and Wise, 1977) to Quaternary (Bukry, 1975c). This long range supports polyphyletic or secondary origins for many of the occurrences of the species. But the late Miocene occurrences at Site 594, 555, and 329 show a potential correlation between the *Dictyocha brevispina* Zone and *Distephanus speculum* Zone. Because *M. triangula* occurs in cool (Ts = 2) to relatively warm (Ts = 42) assemblages no single temperature regime seems responsible for its occurrence.

Mesocena triodon Bukry

Mesocena triodon Bukry, 1973a, p. 860, pl. 2, fig. 11.
Mesocena triodon Bukry, Bukry, 1978, p. 819, pl. 7, figs. 9, 10.

Remarks. The occurrence of rare specimens of *Mesocena triodon* at Site 594, in assemblages lacking *M. quadrangula*, indicates that *M. triodon* is more closely related to *M. diodon nodosa* than to *M. quadrangula*.

OTHER TAXA CITED

Silicoflagellates

Bachmannocena Locker
Caryocha Bukry and Monechi
Corbisema apiculata (Lemmermann) Hanna
C. disymmetrica angulata Bukry
C. glezerae Bukry
C. hastata globulata Bukry
C. hastata hastata (Lemmermann) Frenguelli
C. inermis (Lemmermann) Dumitrică
C. triacantha (Ehrenberg) Hanna
Dictyocha aspera aspera (Lemmermann) Frenguelli
D. aspera clinata Bukry
D. brevispina (Lemmermann) Bukry
D. deflandrei completa (Glezer) Bukry
D. fibula augusta Bukry
D. fibula fibula Ehrenberg
D. pentagona (Schulz) Bukry and Foster
D. pulchella Bukry
D. pulchella var. *inflata* Bukry
Distephanus crux crux (Ehrenberg) Haeckel
D. frugalis (Bukry) Bukry
D. octangulatus Wailes
D. octonarius (Ehrenberg) Haeckel
D. polyactis crassus Bukry
D. pseudofibula (Schulz) Bukry
D. quinquangellus Bukry and Foster
D. speculum diommata (Ehrenberg) Bukry
D. speculum minutus (Bachmann) emend. Bukry
D. speculum speculum (Ehrenberg) Haeckel
D. speculum triommata (Ehrenberg) Bukry
D. varians (Gran and Braarud) Bukry
D. xenus Bukry
Mesocena apiculata apiculata (Schulz) Hanna
M. apiculata curvata Bukry
M. apiculata glabra (Schulz) Bukry
Naviculopsis aspera (Schulz) Perch-Nielsen
N. biapiculata (Lemmermann) Frenguelli
N. constricta (Schulz) emend. Bukry
N. eobiapiculata Bukry
N. trispinosa (Schulz) Glezer
Octactis Schiller
Paradictyocha Frenguelli
Septamesocena Bachmann

Diatoms

Rocella gelida (Mann) Bukry
R. schraderi Bukry

Coccoliths

Amaurolithus tricorniculatus (Gartner) Gartner and Bukry
Chiasmolithus oamaruensis (Deflandre) Hay et al.
Discoaster bellus Bukry and Percival
D. brouweri Tan, emend. Bramlette and Riedel
D. hamatus Martini and Bramlette
D. kugleri Martini and Bramlette
D. quinqueramus Gartner
Isthmolithus recurvus Deflandre
Triquetrorhabdulus rugosus Bramlette and Wilcoxon

ACKNOWLEDGMENTS

I thank Jack G. Baldauf and John A. Barron, U.S. Geological Survey, Menlo Park, for their helpful reviews and comments. John A. Barron provided valuable diatom correlations to assist in time-slice comparisons of relative paleotemperature values. The manuscript was typed and proofed with usual thoroughness and aplomb by Dorothy L. Blackstock, U.S. Geological Survey, La Jolla.

REFERENCES

Bukry, D., 1973a. Coccoliths and silicoflagellates from Deep Sea Drilling Project Leg 19, North Pacific Ocean and Bering Sea. *In* Creager, J. S., Scholl, D. W., et al., *Init. Repts. DSDP*, 19: Washington (U.S. Govt. Printing Office), 857–867.

________, 1973b. Coccolith and silicoflagellate stratigraphy, Deep Sea Drilling Project Leg 18, eastern North Pacific. *In* Kulm, L. D., von Huene, R., et al., *Init. Repts. DSDP*, 18: Washington (U.S. Govt. Printing Office), 817–831.

________, 1975a. Coccolith and silicoflagellate stratigraphy near Antarctica, Deep Sea Drilling Project Leg 28. *In* Hayes, D. E., Frakes, L. A., et al., *Init. Repts. DSDP*, 28: Washington (U.S. Govt. Printing Office), 709–723.

________, 1975b. Phytoplankton stratigraphy, southwest Pacific, Deep Sea Drilling Project Leg 30. *In* Andrews, J. E., Packham, G., et al., *Init. Repts. DSDP*, 30: Washington (U.S. Govt. Printing Office), 539–547.

________, 1975c. Silicoflagellate and coccolith stratigraphy, Deep Sea Drilling Project Leg 29. *In* Kennett, J. P., Houtz, R. E., et al., *Init. Repts. DSDP*, 29: Washington (U.S. Govt. Printing Office), 845–872.

________, 1976a. Cenozoic silicoflagellate and coccolith stratigraphy, South Atlantic Ocean, Deep Sea Drilling Project Leg 36. *In* Hollister, C. D., Craddock, C., et al., *Init. Repts. DSDP*, 35: Washington (U.S. Govt. Printing Office), 885–917.

________, 1976b. Comments on some coccoliths and silicoflagellates from Deep Sea Drilling Project Leg 35. *In* Hollister, C. D., Craddock, C., et al., *Init. Repts. DSDP*, 35: Washington (U.S. Govt. Printing Office), 693–699.

________, 1978. Cenozoic coccolith, silicoflagellate, and diatom stratigraphy, Deep Sea Drilling Project Leg 44. *In* Benson, W. E., Sheridan, R. E., et al., *Init. Repts. DSDP*, 44: Washington (U.S. Govt. Printing Office), 807–863.

________, 1979. Coccolith and silicoflagellate stratigraphy, northern Mid-Atlantic Ridge and Reykjanes Ridge, Deep Sea Drilling Project Leg 49. *In* Luyendyk, B. P., Cann, J. R., et al., *Init. Repts. DSDP*, 49: Washington (U.S. Govt. Printing Office), 551–581.

________, 1981. Silicoflagellate stratigraphy of offshore California and Baja California, Deep Sea Drilling Project Leg 63. *In* Yeats, R. S., Haq, B. U., et al., *Init. Repts. DSDP*, 63: Washington (U.S. Govt. Printing Office), 539–557.

________, 1983. Upper Cenozoic silicoflagellates from offshore Ecuador, Deep Sea Drilling Project Site 504. *In* Cann, J. R., Langseth, M. G., et al., *Init. Repts. DSDP*, 69: Washington (U.S. Govt. Printing Office), 321–342.

________, 1984. Cenozoic silicoflagellates from Rockall Plateau, Deep Sea Drilling Project Leg 81. *In* Roberts, D. G., Schnitker, D., et al., *Init. Repts. DSDP*, 81: Washington (U.S. Govt. Printing Office) 547–563.

________, in press. Tropical Pacific Pacific silicoflagellate zonation and paleotemperature trends of the Late Cenozoic. *In* Mayer, L., They-

pages tightly bound

er, F., et al., *Init. Repts. DSDP*, 85: Washington (U.S. Govt. Printing Office).

Bukry, D., and Foster, J. H., 1973. Silicoflagellate and diatom stratigraphy, Leg 16, Deep Sea Drilling Project. *In* van Andel, T. H., Heath, G. R., et al., *Init. Repts. DSDP*, 16: Washington (U.S. Govt. Printing Office), 815-871.

Bukry, D., and Kennedy, M. P., 1969. Cretaceous and Eocene coccoliths at San Diego, California. *Calif. Div. Min. Geol. Spec. Rept.*, 100:33-43.

Bukry, D., and Monechi, S., in press. Late Cenozoic silicoflagellates from the Northwest Pacific, Deep Sea Drilling Project Leg 86: Paleotemperature trends and texture Classification. *In* Heath, G. R., Burckle, L. H., et al., *Init. Repts. DSDP*, 86: Washington (U.S. Govt. Printing Office).

Burkov, V. A., 1966. Structure and nomenclature of Pacific Ocean currents. *Oceanology*, 6:1-10.

Busen, K. E., and Wise, S. W., Jr., 1977. Silicoflagellate stratigraphy, Deep Sea Drilling Project, Leg 36. *In* Barker, P., Dalziel, I. W. D., et al., *Init. Repts. DSDP*, 36: Washington (U.S. Govt. Printing Office), 697-743.

Ciesielski, P. F., 1975. Biostratigraphy and paleoecology of Neogene and Oligocene silicoflagellates from cores recovered during Antarctic Leg 28, Deep Sea Drilling Project. *In* Hayes, D. E., Frakes, L. A., et al., *Init. Repts. DSDP*, 28: Washington (U.S. Govt. Printing Office), 625-691.

Csanady, G. T., 1984. Warm water mass formation. *J. Phys. Oceanogr.*, 14:264-275.

Dumitrică, P., 1973. Paleocene, late Oligocene and post-Oligocene silicoflagellates in southwestern Pacific sediments cored on DSDP Leg 21. *In* Burns, R. E., Andrews, J. E., et al., *Init. Repts. DSDP*, 21: Washington (U.S. Govt. Printing Office), 837-883.

Ehrenberg, C. G., 1839. Über die Bildung der Kreidefelsen und des Kreidemergels durch unsichtbare Organismen. *K. Akad. Wiss. Berlin, Abh., Jahr.* 1838 (1840, separate 1839):59-148.

________, 1840. Blätter von ihm selbst ausgeführter Zeichnungen von ebenso vielen Arten. *K. Preuss. Akad. Wiss. Berlin Ber., Jahr.* 1840:197-219 (Nov.)

________, 1844. Untersuchungen über die kleinsten Lebensformen im Quellenlande des Euphrats und Araxes, so wie über eine an neuen Formen sehr reiche marine Tripelbildung von den Bermuda-Inseln vor. *K. Preuss. Akad. Wiss. Berlin Ber., Jahr.* 1844:253-275.

________, 1854. *Mikrogeologie:* Leipzig (Leopold Voss), 1-374.

Haeckel, E. H. P. A., 1887. Cannorrhaphida. *Challenger Rept.* 18: 1546-1569.

Haq, B. U., and Riley, A., 1976. Antarctic silicoflagellates from the southeast Pacific, Deep Sea Drilling Project Leg 35. *In* Hollister, C. D., Craddock, C., et al., *Init. Repts. DSDP*, 35: Washington (U.S. Govt. Printing Office), 673-691.

Keller, G., 1981. Miocene biochronology and paleoceanography of the North Pacific. *Mar. Micropaleontol.*, 6:535-551.

Kennett, J. P., 1980. Paleoceanographic and biogeographic evolution of the Southern Ocean during the Cenozoic, and Cenozoic microfossil datums. *Palaeogeogr., Palaeoclimatol., Palaeoecol.*, 31: 123-152.

Lemmermann, E., 1901. Silicoflagellatae. *Ber. Dtsch. Bot. Ges.*, 19: 247-271.

Ling, H. Y., 1972. Upper Cretaceous and Cenozoic silicoflagellates and ebridians. *Bull. Am. Paleontology*, 62:135-229.

________, 1977. Late Cenozoic silicoflagellates and ebridians from the eastern North Pacific region. *Proc. 1st Int. Congr. Pacific Neogene Stratigraphy*, Tokyo, 205-233.

________, 1980. Silicoflagellates and ebridians from Leg 55. *In* Jackson, E. D., Koizumi, I., et al., *Init. Repts. DSDP*, 55: Washington (U.S. Govt. Printing Office), 375-385.

Locker, S., 1974. Revision der Silicoflagellaten aus der Mikrogeologischen Sammlung von C. G. Ehrenberg. *Eclog. Geol. Helv.*, 67: 631-646.

Loeblich, A. R., III, Loeblich, L. A., Tappan, H., and Loeblich, A. R. Jr., 1968. Annotated index of fossil and recent silicoflagellates and ebridians with descriptions and illustrations of validly proposed taxa. *Mem. Geol. Soc. Am.*, 106:1-319.

Mandra, Y. T., Brigger, A. L., and Mandra, H., 1973. Preliminary report on a study of fossil silicoflagellates from Oamaru, New Zealand. *Occas. Pap. Calif. Acad. Sci.*, 107:1-11.

Mandra, Y. T., and Mandra, H., 1972. Paleoecology and taxonomy of silicoflagellates from an upper Miocene diatomite near San Felipe, Baja California, Mexico. *Occas. Pap., Calif. Acad. Sci.*, 99:1-35.

Martini, E., 1971. Standard Tertiary and Quaternary calcareous nannoplankton zonation. *In* Farinacci, A. (Ed.), *Proc. 2nd Planktonic Conf., Roma:* Rome (Edizioni Tecnoscienza), 739-785.

Martini, E., and Müller, C., 1976. Eocene to Pleistocene silicoflagellates from the Norwegian-Greenland Sea (DSDP Leg 38). *In* Talwani, M., Edintsev, G., et al., *Init. Repts. DSDP*, 38: Washington (U.S. Govt. Printing Office), 857-895.

Perch-Nielsen, K., 1975. Late Cretaceous to Pleistocene archaemonads, ebridians, endoskeletal dinoflagellates, and other siliceous microfossils from the subantarctic southwest Pacific, DSDP Leg 29. *In* Kennett, J. P., Houtz, R. E., et al., *Init. Repts. DSDP*, 29: Washington (U.S. Govt. Printing Office), 873-907.

Stadum, C. J., and Burckle, L. H., 1973. A silicoflagellate ooze from the east Falkland Plateau. *Micropaleontology*, 19:104-109.

Stradner, H., and Bachmann, A., 1978. Late Pliocene and early Pleistocene silicoflagellates and ebridians from DSDP Site 378 in the Aegean Basin, north of Crete. *In* Hsü, K. J., Montadert, L., et al., *Init. Repts. DSDP*, 42, Pt. 1: Washington (U.S. Govt. Printing Office), 805-815.

Date of Initial Receipt: 24 August 1984
Date of Acceptance: 8 September 1984

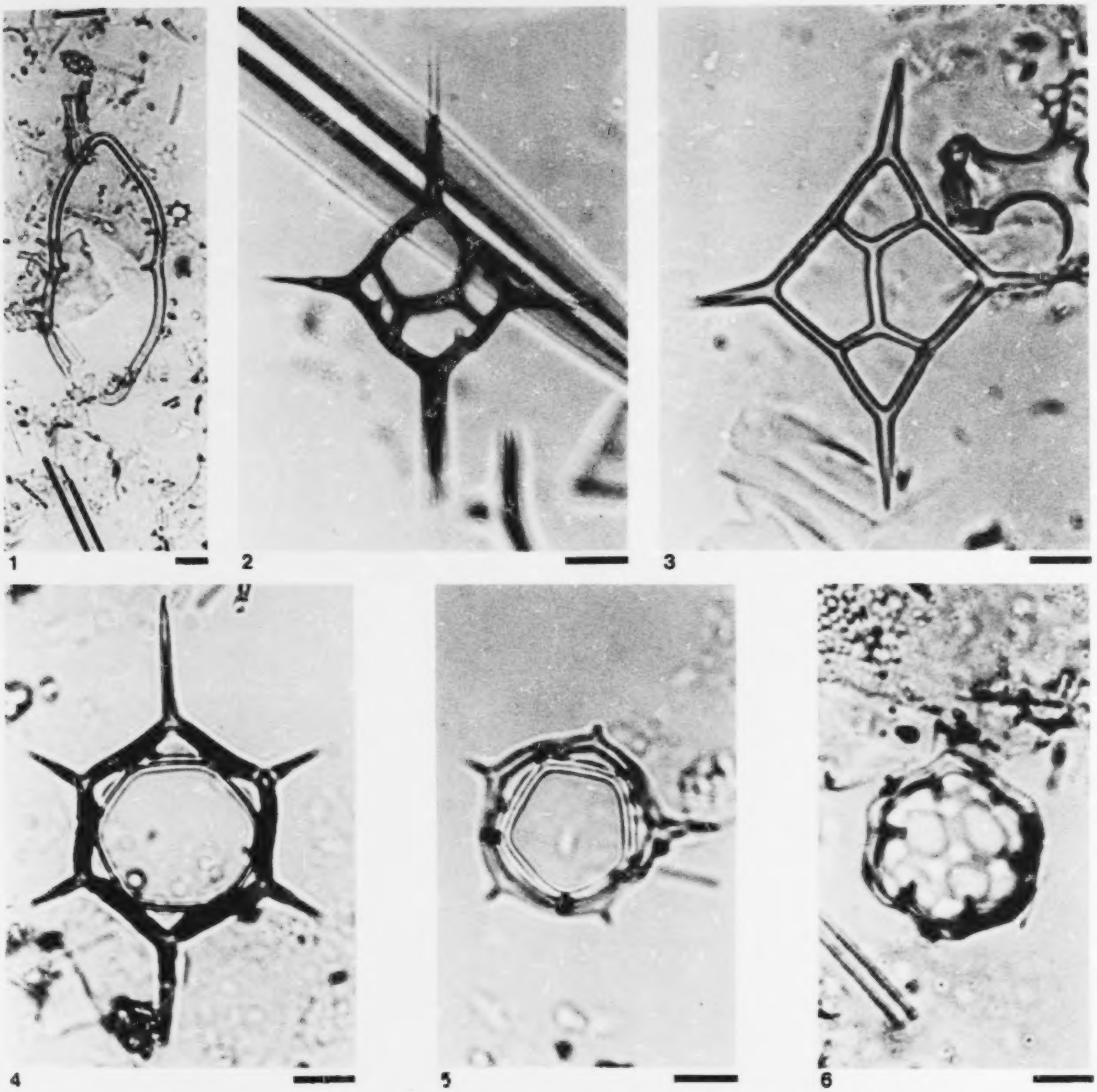

Plate 1. Silicoflagellates from DSDP Leg 90. (Scale bar equals 10 μm.) **1.** *Corbisema* sp; compare *Corbisema disymmetrica angulata* Bukry, Sample 594-31-2, 8–9 cm. **2.** *Dictyocha aspera clinata* Bukry s. ampl., Sample 594-27-2, 8–9 cm. **3.** *Dictyocha fibula augusta* Bukry, Sample 594-27-2, 8–9 cm. **4, 5.** *Distephanus speculum minutus* (Bachmann), Sample 594-20-2, 8–9 cm, (4) normal specimen, (5) pentagonal variant. **6.** *Distephanus xenus* Bukry, Sample 594-21-2, 8–9 cm; basal focus.

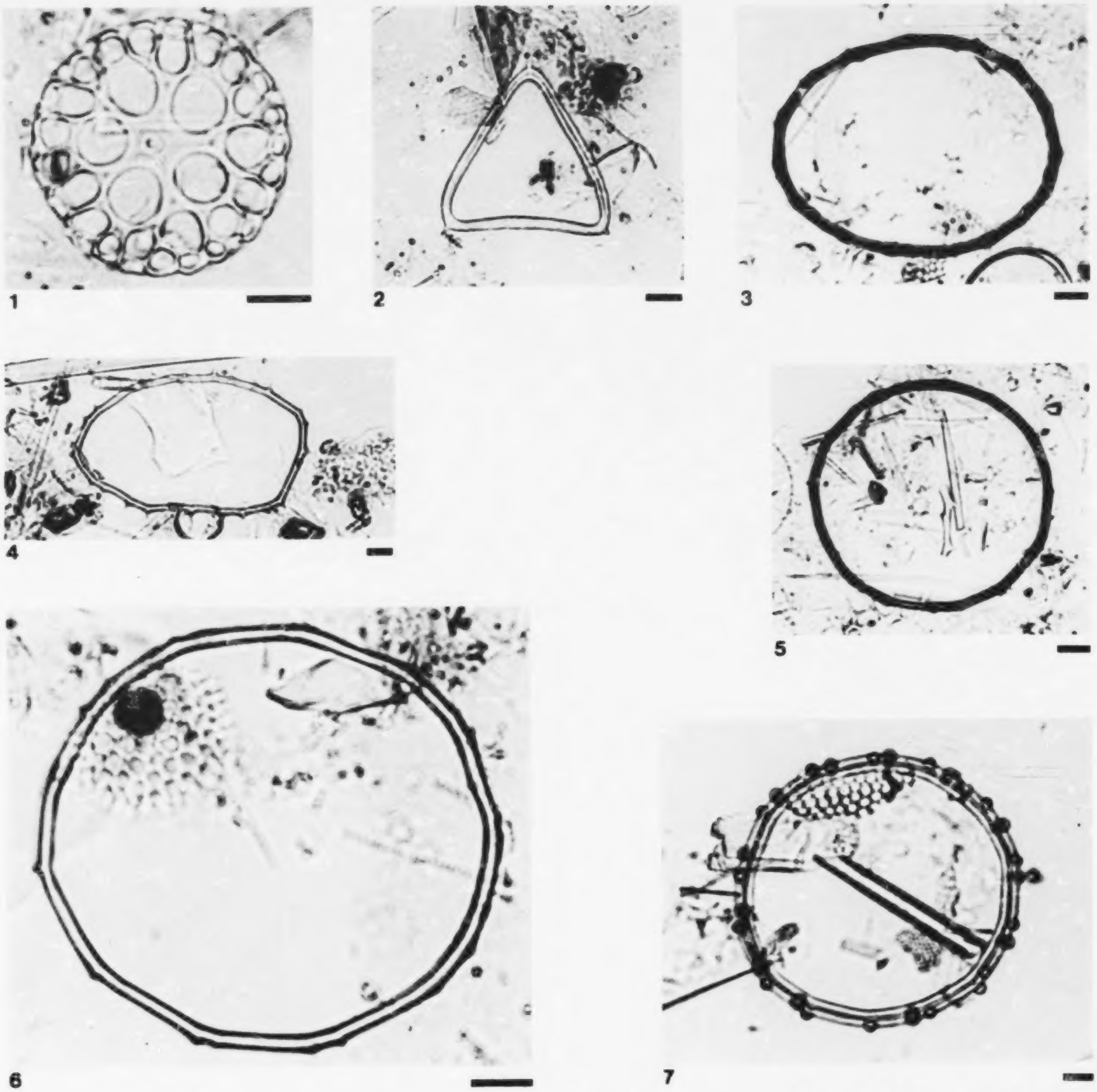

Plate 2. Diatom and silicoflagellates from DSDP Leg 90. (Scale bar equals 10 μm.) **1.** *Rocella schraderi* Bukry, Sample 594-31-2, 8–9 cm (diatom). **2.** *Mesocena apiculata curvata* Bukry, Sample 594-48-2, 8–9 cm. **3–7.** *Mesocena circulus* var. *apiculata* Lemmermann, (3) elliptic, Sample 594-31-2, 8–9 cm, (4) oblong, Sample 594-47-1, 8–9 cm, (5, 6) circular and nearly spineless, Sample 594-31-2, 8–9 cm, (7) knobby variant, Sample 594-30-2, 8–9 cm.

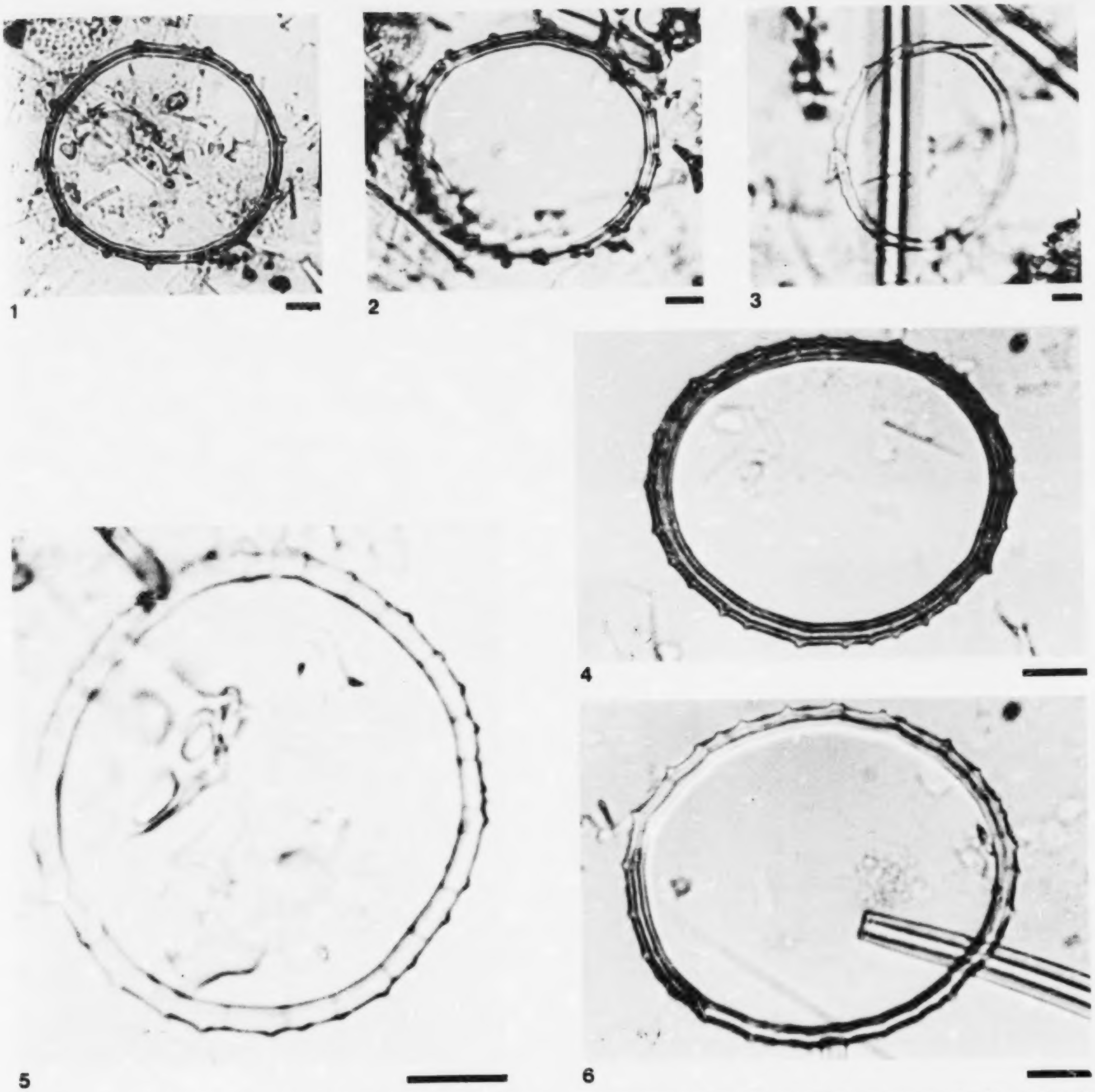

Plate 3. Silicoflagellates from DSDP Leg 90. (Scale bar equals 10 μm.) **1, 2.** *Mesocena circulus* var. *apiculata* Lemmermann, knobby variant, (1) Sample 594-31-2, 8–9 cm, (2) Sample 594-30-2, 8–9 cm. **3–6.** *Mesocena circulus* (Ehrenberg), (3) Sample 594-27-2, 8–9 cm, (4, 5) verticillate nodes suggest affinities with *Mesocena diodon nodosa;* Sample 594-25-2, 8–9 cm, (6) Sample 594-25-2, 8–9 cm.

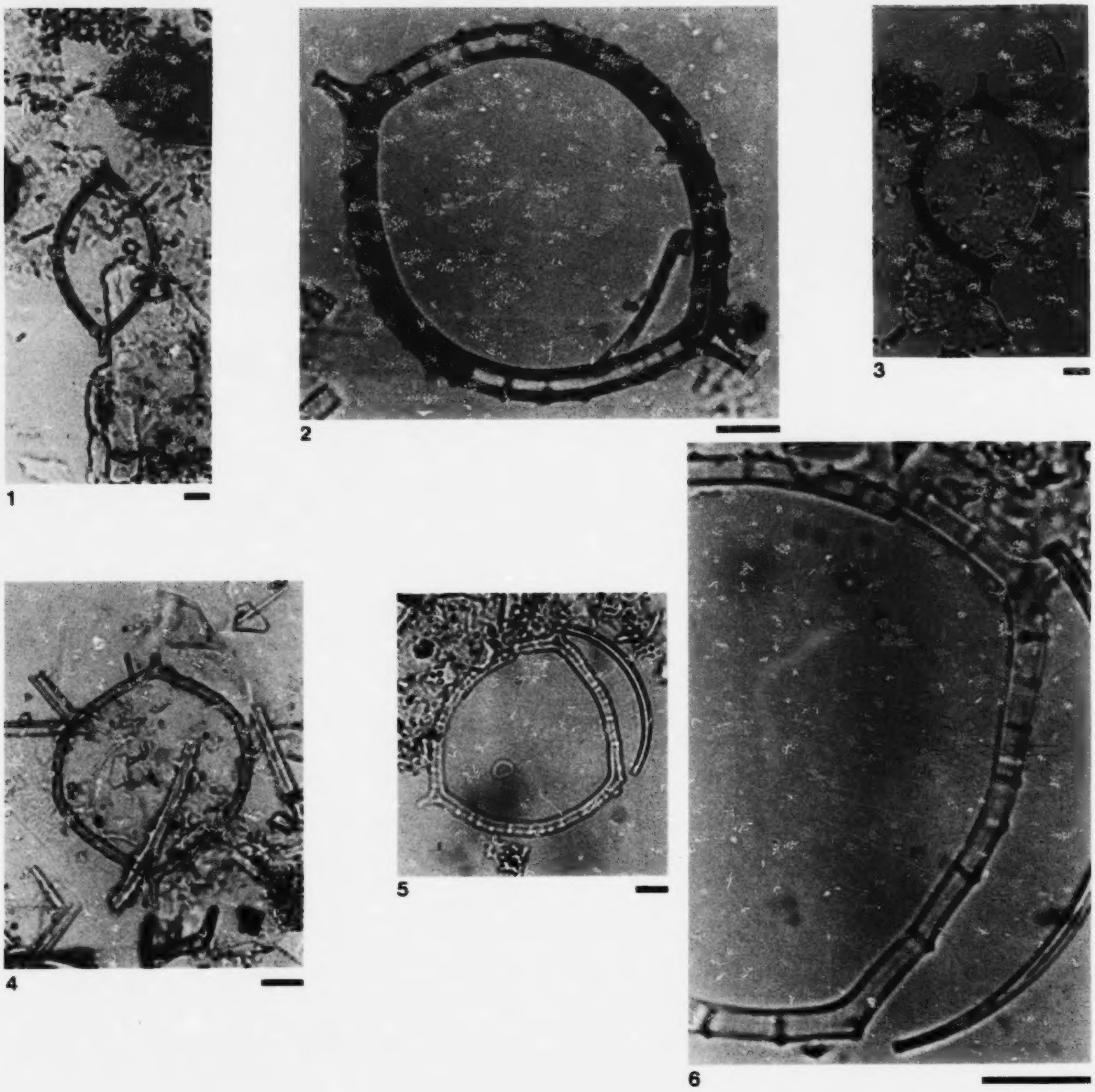

Plate 4. Silicoflagellates from DSDP Leg 90. (Scale bar equals 10 μm.) **1.** *Mesocena* sp. cf. *M. diodon borderlandensis* Bukry, Sample 594-27-2, 8–9 cm. **2–6.** *Mesocena diodon nodosa* Bukry, (2) Sample 594-30-2, 8–9 cm, (3) Sample 594-27-2, 8–9 cm, (4) oblate, Sample 594-23-5, 8–9 cm, (5, 6) triangular variant, Sample 594-23-5, 8–9 cm.

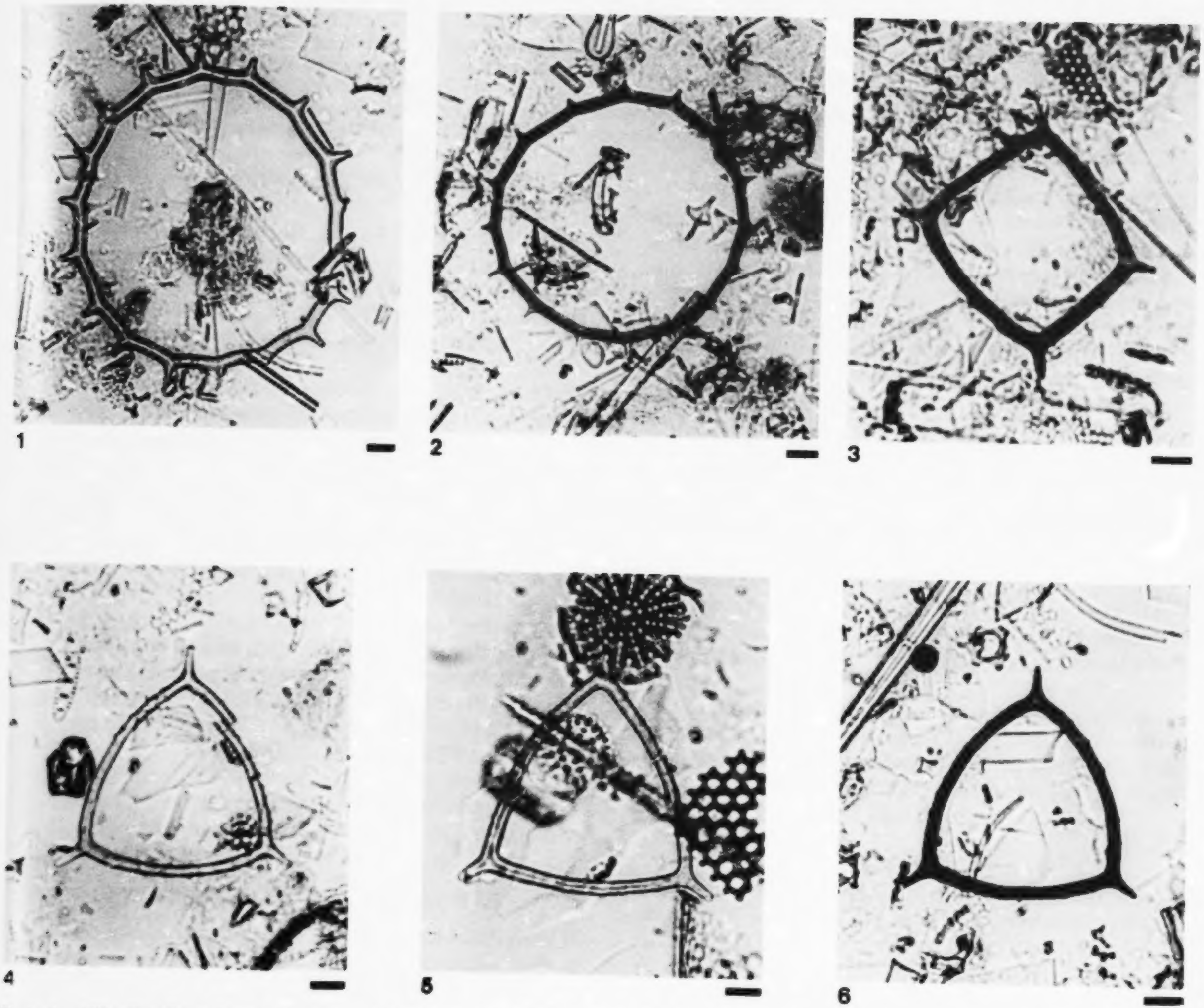

Plate 5. Silicoflagellates from DSDP Leg 90. (Scale bar equals 10 μm.) 1, 2. *Mesocena dumitricae* (Perch-Nielsen), Sample 594-27-2, 8-9 cm. 3. *Mesocena quadrangula* Ehrenberg ex Haeckel, Sample 594-23-5, 8-9 cm. 4-6. *Mesocena triangula* (Ehrenberg), Sample 594-23-5, 8-9 cm.

18. EBRIDIANS AND ACTINISCIDIANS FROM THE SOUTHWEST PACIFIC[1]

Sigurd Locker and Erlend Martini, Geologisch-Paläontologisches Institut der Universität, Frankfurt am Main[2]

ABSTRACT

Ebridians and actiniscidians are described from Sites 588, 591, and 594 in the southwest Pacific. The middle Miocene to early Pliocene interval at Site 591 can be subdivided into five ebridian–actiniscidian zones. These are correlated to standard nannoplankton zones.

Five new species are described from the Neogene of the southwest Pacific: *Ammodochium serotinum, Hermesinum obliquum, Actiniscus flosculus, A. laciniatus,* and *A. squamosus.*

INTRODUCTION

During Leg 90 ebridians and actiniscidians—so-called endoskeletal dinoflagellates—were found in three out of eight sites in the New Caledonia to New Zealand region in the southwest Pacific Ocean (Fig. 1). They are commonly associated with diatoms, silicoflagellates, and radiolarians.

Hole 588C yielded middle Eocene ebridians. In Holes 591 and 591B ebridians and actiniscidians are rather common in the middle Miocene to early Pliocene interval, and are investigated in detail. In Holes 594 and 594A both groups were noted sporadically in the middle Miocene to Pleistocene, including reworked forms from the Paleogene. The assemblages of these sites and their age assignments are discussed below. Fossil lists for selected samples from Holes 588C, 591, and 591B and corelation to standard nannoplankton zones are presented in Tables 1 and 2. The abundances shown in these tables refer to the specimens counted in three traverses on the slides, comprising a total length of 120 mm. Five counting classes are used: 1 = 1 specimen, 2 = 2 to 5 specimens, 3 = 6 to 15 specimens, 4 = 16 to 50 specimens, 5 = more than 50 specimens. All species described are documented by light microscopic photographs (Plates 1 to 3), and some actiniscidians are also shown in scanning electron microscope pictures (Plate 4).

EBRIDIAN–ACTINISCIDIAN ZONES

Although many species of ebridians and actiniscidians have been described from various locations, only a few continuous sequences containing these fossils are known. Therefore, the continuously cored sequence at Site 591 covering the middle Miocene to early Pliocene interval is of some importance. The core-catcher samples investigated can be grouped into five ebridian–actiniscidian zones, which may be regarded partly as concurrent range zones and partly as local range zones.

At present the zonation used reflects more or less local conditions, but some of these zones may have more than local value. This is true especially for the *Actiniscus elongatus* Zone, the *Thranium crassipes* Zone, the *Ebriopsis cornuta* Zone, and the *Ammodochium serotinum* Zone, which lies above the sequence at Site 591 containing ebridians and actiniscidians. The zones used in this report and correlations to standard nannoplankton zones (Martini, 1971) are shown in Table 2.

Actiniscus elongatus Zone

Definition. Interval from the first occurrence of *Actiniscus? elongatus* to the first occurrence of *Hermesinella conata*. Lower Miocene to lowermost middle Miocene

Assemblage. *Actiniscus flosculus* and *A. pentasterias* are few to common, *Hermesinum adriaticum, H. obliquum,* and *Parathranium clathratum* are rare to few. The nominate actiniscidian species occurs rarely to commonly.

Remarks. *Actiniscus? elongatus* seems to have its first occurrence in the lowest middle Miocene, according to different authors (Dumitrică, 1973a, southwest Pacific Site 206; Perch-Nielsen, 1975, southwest Pacific Site 278; this paper, Southwest Pacific Site 591).

Hermesinella conata Zone

Definition. Interval from the first occurrence of *Hermesinella conata* to the first occurrence of *Thranium crassipes*. Middle Miocene to lower upper Miocene.

Assemblage. Actiniscus? elongatus, A. flosculus, and *A. pentasterias* are common or abundant in some samples. *Hermesinum adriaticum* and *H. obliquum* are few to common, and in the lower part of this zone *Ammodochium serotinum* is also present.

Remarks. *Hermesinella conata* has a distinct first occurrence at Site 591, but at present no further data are available from other areas.

Thranium crassipes Zone

Definition. Interval from the first to the last occurrence of *Thranium crassipes*. Upper Miocene.

Assemblage. *Actiniscus? elongatus, A. flosculus* and *A. pentasterias* are common to abundant. *Hermesinum*

---

[1] Kennett, J. P., von der Borch, C. C., et al., *Init. Repts. DSDP*, 90: Washington (U.S. Govt. Printing Office).

[2] (Locker, present address) Geologisch-Paläontologisches Institut der Universität, Olshausenstr. 40-60, D-23 Kiel, Federal Republic of Germany; (Martini) Geologisch-Paläontologisches Institut der Universität, Frankfurt am Main, Federal Republic of Germany.

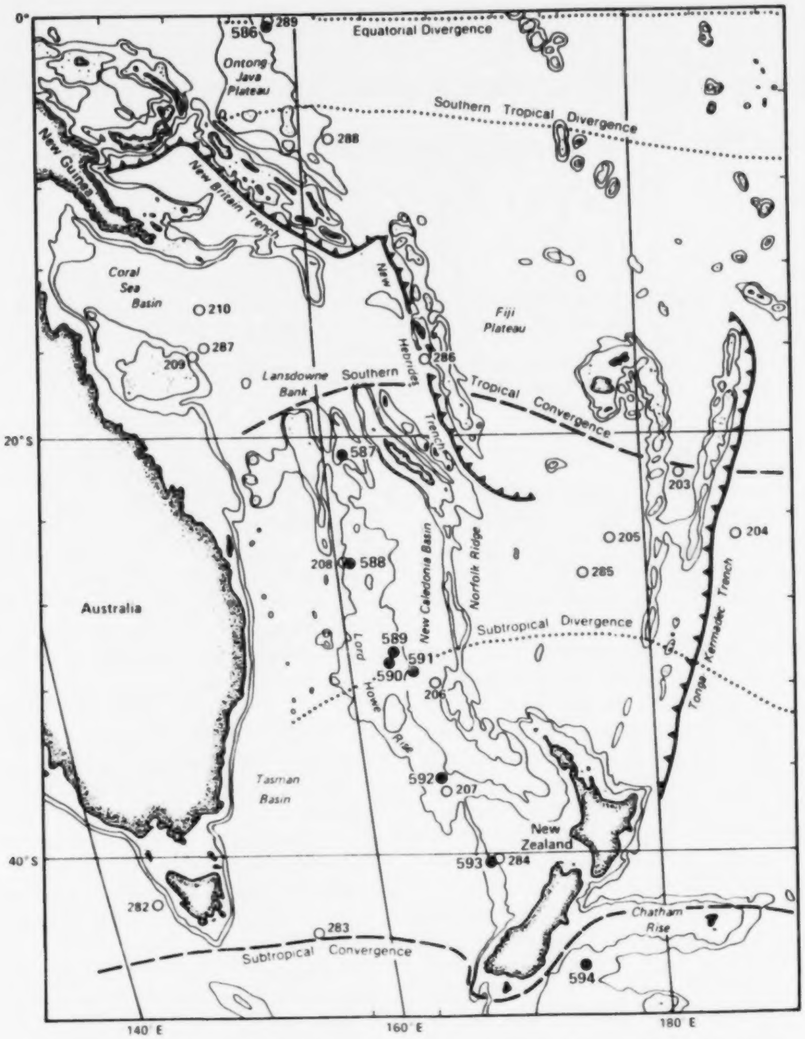
0°
20°S
40°S
140°E
160°E
180°E
586
289
Equatorial Divergence
Ontong Java Plateau
Southern Tropical Divergence
288
New Guinea
New Britain Trench
Coral Sea Basin
210
287
209
Lansdowne Bank
Southern Tropical Convergence
New Hebrides Trench
286
Fiji Plateau
587
203
204
205
285
208
588
Australia
New Caledonia Basin
Norfolk Ridge
Subtropical Divergence
Tonga Kermadec Trench
589
591
590
206
Lord Howe Rise
Tasman Basin
592
207
New Zealand
593
284
282
283
Subtropical Convergence
Chatham Rise
594

Figure 1. Location of sites drilled during Leg 90 (solid circles) and other DSDP drill sites (open circles) in the southwest Pacific.

adriaticum and *H. obliquum* are few to common, and *Hermesinella conata* and *H. fenestrata* rare to few.

Remarks. The short total range of the nominate species at Site 591 and other known occurrences (Hovasse, 1932) may indicate a more than regional value for this zone.

Hermesinum obliquum Zone

Definition. Interval from the last occurrence of Thranium crassipes to the first occurrence of *Ebriopsis cornuta*. Upper Miocene to lower Pliocene.

Assemblage. *Hermesinum adriaticum, H. obliquum,* and *Foliactiniscus mirabilis* are rare to few. Generally, the number of ebridian and actiniscidian specimens distinctly decreases in this zone.

Remarks. Although the assemblage of this zone is not very distinctive, at least the base seems to be well defined. In the only comparable section at Site 206 (Dumitrică, 1973a) this zone falls in a local hiatus.

Ebriopsis cornuta Zone

Definition. Interval from the first to the last occurrence of *Ebriopsis cornuta* (introduced by Ling, 1973, as *Ebriopsis antiqua* Zone; base modified). Lower Pliocene.

Assemblage. *Actiniscus? elongatus* and *Cinctactiniscus?* sp. are common to abundant, *A. flosculus* and *Foliactiniscus mirabilis* are few to common. All other species occur only sporadically and in low numbers. This is also true for the nominate ebridian species.

Remarks. *Ebriopsis cornuta* (here including spiny and spineless forms; see taxonomy) has already been reported from the upper Miocene of other sections, but its last occurrence seems to be consistently at or near the top of the lower Pliocene (Ling, 1973, North Pacific Sites 184, 185, 188, 190, 192; Ling, 1975, northwest Pacific Site 301; Ling, 1977, northeast Pacific Site 173).

Ammodochium serotinum Zone

Definition. Interval from the last occurrence of *Ebriopsis cornuta* to the last occurrence of *Ammodochium serotinum* (introduced by Ling, 1973, as *Ammodochium rectangulare* Zone). Upper Pliocene.

Assemblage. *Ammodochium serotinum* and *Actiniscus pentasterias* are among the few species found in this zone.

Remarks. This distinctive zone is not represented at Site 591, because the upper Pliocene is barren of ebridians and actiniscidians. However, it seems to have wide distribution, because the last occurrence of *Ammodochium serotinum* (= *A. rectangulare* of some authors) has been reported from several sites in the Pacific (Ling, 1973, North Pacific Sites 184, 185, 190, 192; Ling, 1975, northeast Pacific Site 301; Ling, 1977, northeast Pacific Site 177).

Further papers consulted to evaluate the distribution or presence of certain species include Bukry, 1976; Dumitricǎ, 1973b; Ling, 1971, 1972, 1980; Orr and Conyley, 1976; Perch-Nielsen, 1977, 1978; Stradner and Bachmann, 1978.

SITE SUMMARIES

Site 588 (26°06.7′S; 161°13.6′E; water depth 1533 m)

In Hole 588C, on the northern part of Lord Howe Rise, Paleogene sediments containing ebridians were encountered in Core 19, and are associated with common diatoms, silicoflagellates, and calcareous nannoplankton. The assemblage (Table 1) is dominated by *Ebriopsis crenulata*, and contains also *Ammodochium rectangulare*, *Craniopsis* sp., and *Micromarsupium anceps*. A number of *E. crenulata* show a well-developed lorica (Plate 1, Figs. 10–11), and most *M. anceps* are in an advanced lorica stage (Fig. 2). Associated calcareous nannoplankton indicate a middle Eocene age (Zone NP15/16) for this interval.

Table 1. Distribution of ebridians in selected samples from Hole 588C, and correlation to standard nannoplankton zones.

Epoch and nannoplankton zone	Core-Section (interval in cm)	*Ammodochium rectangulare*	*Craniopsis* sp.	*Ebriopsis crenulata*	*Micromarsupium anceps*	Ebridian specimens
middle Eocene NP15/16	19-1, 10–12	1	1	3		11
	19-1, 35–37	1	1	4	2	27
	19-1, 55–57	1	1	3	1	15
	19,CC	1		4	1	17

Note: Numbers indicate frequency: 1 = 1 specimen, 2 = 2 to 5 specimens, 3 = 6 to 15 specimens, 4 = 16 to 50 specimens, 5 = more than 50 specimens.

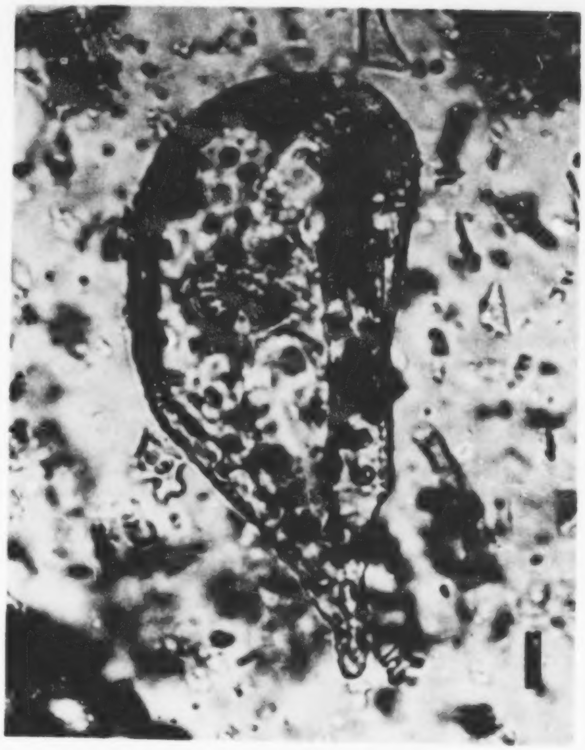

Figure 2. *Micromarsupium anceps* Deflandre, highly developed lorica stage; Sample 588C-19,CC, middle Eocene. LM, ×800 (bar = 10 μm).

Similar ebridian assemblages were found in the upper Eocene and lower Oligocene recovered during Legs 29 and 38 (Perch-Nielsen, 1975, 1978).

Site 591 (31°35.06′S; 164°26.92′E; depth 2131 m)

Site 591 is situated on the eastern part of the Lord Howe Rise. Sediments recovered at this site consists mostly of foraminifer-bearing or foraminifer-rich nannofossil ooze. Biosiliceous components are present in low numbers compared with the calcareous material and include diatoms, silicoflagellates, radiolarians, phytoliths, ebridians, and actiniscidians. The investigated section, combined from Holes 591A, 591, and 591B, cover the middle Miocene to Pleistocene interval.

The Pleistocene and upper Pliocene, represented by Samples 591A-3,CC to 591A-10,CC and 591-11,CC, is barren of ebridians and actiniscidians. In the lower Pliocene actiniscidians are especially common in Samples 591-14,CC to 591-20,CC (Table 2), which are placed in the *Ebriopsis cornuta* Zone with the nominate species present in several samples and rather common *Actiniscus? elongatus* and *Cinctactiniscus?* sp. The interval between Samples 591-21,CC and 591-30,CC belongs in the *Hermesium obliquum* Zone, with rather meager assemblages in the middle part covering the Miocene/Pliocene boundary, but with abundant *A. flosculus* and *A. pentasterias* in the lowest part. The early late Miocene Samples 591-31,CC and 591B-2,CC to 591B-8,CC contain

Table 2. Distribution of ebridians and actiniscidians in selected samples from Holes 591 and 591B, indication of ebridian–actiniscidian zones, and correlation to standard nannoplankton zones. Numbers indicate frequency (see Table 1).

Epoch	Nannoplankton zones	Sample	*Ammodochium serotinum*	*Ditripodium latum*	*Ebriopsis cornuta*	*Haplohermesinum?* sp.	*Hermesinella conata*	*H. fenestrata*	*H.* aff. *fenestrata*	*Hermesinum adriaticum*	*H. obliquum*	*Parathranium clathratum*	*Thranium crassipes*	Ebridian specimens	*Actiniscus? elongatus*	*A. flosculus*	*A. lancearius*	*A. pentasterias*	*A. squamosus*	*A.* indet.	*A.?* sp.	*Cinctactiniscus?* sp.	*Foliactiniscus* cf. *folia*	*F. mirabilis*	Actiniscidian specimens	Ebridian-actiniscidian horizons
upper Pliocene	NN16	591-11,CC						Barren																		?
lower Pliocene	NN15	13,CC												0	1										2	*Ebriopsis cornuta* Zone
		14,CC								3	3			14	4	3		2	2	4		4		3	108	
		16,CC			2									3	4					4		3		1	87	
	NN14	17,CC			1						2	2 cf.		8	5	3		2		4		4		2	190	
		18,CC										1		1	5	2		2		2		5		2	230	
		19,CC	2											3	5	3				3		4		2	111	
		20,CC			2							1		4	4	2		1		3		4		2	109	
	NN12	21,CC										2		2	3	2		3		3		2		2	39	*Hermesinum obliquum* Zone
		22,CC								2	2			5				1						2	6	
		23,CC								1	2			3											0	
upper Miocene	NN11B	24,CC								2	2	1		5		1				1				2	4	
		25,CC									2			2						1				1	2	
		26,CC								1				1						3					9	
		27,CC	2										1	5			1			2				2	6	
	NN11A	28,CC	2				1			2	2			13	3	3		3		3					38	
		29,CC				1								1	4	5	2	4	1	5					434	
		30,CC								1				1		5	2	5	3	5				1	658	
		31,CC										2	2	5	5	5	2	5	1	5		1			639	*Thranium crassipes* Zone
		591B-2,CC					2	1			2	3	2	16	5	5	2	5		5					534	
		3,CC					2	2		1	2	4	2	34	4	5	2	5	1	5	1			1	336	
		4,CC					2	2		2	2		1	16	5	5	1	5		5			1		550	
	NN10	5,CC					2	2		2	2		3	21	4	5	1	4		4					184	
		6,CC	3							3	3		2	35	5	5	2	5		4					209	
		7,CC				1	1	2		3	4	4	2	56	4	5	2	5	1	5					296	
		8,CC	2					1		2	2	2	1	16	4	5	1	4		4					191	
	NN9	9,CC								3	3			21	4	5	1	5		5					257	*Hermesinella conata* Zone
middle Miocene		10,CC												3	4	4		3		4					87	
	NN8	11,CC					2	2		1				9	3	2		3		3					36	
	NN7	12,CC								1	1			2	3	1		1		2					14	
	NN6	13,CC												0						2					2	
		14,CC						Barren																		
		15,CC	2							2	2	1		12	4	3		4		3	2			1	87	
		16,CC	3				2			3	4			49	5	5	2	5		4	2		2	2	367	
	NN5	17,CC	3			2	3	2	2	4	5			115	4	5	2	4		4	1		3	1	280	
		18,CC	3	2			1			3	3	4		64	4	4	2	4		4	1				116	
		19,CC								3	1	2		10	2	3		3		2				1	23	*Actiniscus elongatus* Zone
		20,CC								2	3	2		20	4	4	2 cf.	4		4			1	1	125	
		21,CC	1							3	3	3		32	2	3	3 cf.	3		3				1	47	
		22,CC												0				1							1	?
	NN4/5	23,CC to 24,CC						Barren																		

Thranium crassipes in varying numbers and also abundant *Actiniscus* species, and are placed in the *Thranium crassipes* Zone. The late middle Miocene *Hermesinella conata* Zone is represented by Samples 591B-9,CC to 591B-18,CC, in which *Hermesinella conata* was found in several samples together with *Hermesinum obliquum, Foliactiniscus* cf. *folia,* and several common *Actiniscus* species. In the middle part of this zone assemblages are again rather meager, and Sample 591B-14,CC is barren of ebridians and actiniscidians. The early middle Miocene Samples 591B-19,CC to 591B-24,CC include the *Actiniscus elongatus* Zone in Samples 591B-19,CC to 591B-21,CC, with the nominate species first occurring in this sample. The lowest available Samples 591B-22,CC to 591B-24,CC are barren or nearly barren and cannot be placed in any zone.

Similar Neogene assemblages were described from the nearby DSDP Site 206 by Dumitricá (1973a), although most of the late Miocene is not represented because of a hiatus.

Site 594 (45°31.41'S; 174°56.88'E; depth 1204 m)

In Holes 594 and 594A, located at the southern margin of the Chatham Rise east of New Zealand, the predominantly calcareous sediments contain as minor components diatoms, silicoflagellates, radiolarians, and also a few ebridians and actiniscidians throughout the Miocene to Quaternary sequence. Actiniscidians are present rather continuously in the section, whereas ebridians seem to occur less continuously but were noted in Samples 594-19,CC to 594-31,CC and 594A-12,CC to 594A-20,CC in some abundance. However, both groups were not investigated in detail at this site because of severe mixing with reworked species from the Paleogene, including *Ammodochium rectangulare* in Samples 594-24,CC and 594-27,CC (late Miocene) and 594-47,CC (middle Miocene), *Ebriopsis antiqua* in Samples 594-39,CC and 594A-20,CC (both of middle Miocene age), and *E. crenulata* in Samples 594-13,CC (late Miocene) and 594-43,CC (middle Miocene). *Micromarsupium anceps* was found in Sample 594A-12,CC, which is of middle Miocene age.

SYSTEMATIC PALEONTOLOGY

Ebridians and actiniscidians are treated here as unicellular marine algae which may be grouped together as "endoskeletal" or siliceous dinoflagellates. The actiniscidians are true dinoflagellates, possessing a dinocaryon and many chromatophores. The ebridians, in contrast, are heterotrophic protistans, but they may be also placed with the dinoflagellates because they show similar nuclear relations (Tappan, 1980).

The skeleton of ebridians consists of massive siliceous rods composing a three-dimensional structure. In describing the elements of the skeleton the terminology of Deflandre (1951, 1952) is followed, with some exceptions. The term "upper window" has been changed to "procladian window" to indicate the position and relations of the feature, and the combination of three opisthoclades with the rhabde is called "opisthocladian basket."

The skeleton of actiniscidians comprises a single siliceous element which is usually star-shaped. In describing features of the skeleton the terminology of Dumitricǎ (1973b) has been adopted. The terms used are formalized for more precise comparisons between the species (Fig. 3).

Within both groups, the genera and species are described in alphabetical order, and in accordance with the rules of the International Code of Biological Nomenclature. Although in some actiniscidian species morphes can be distinguished by the number of skeletal arms, no special forms have been erected. Below the species name are generally cited the most important synonyms, that is, other specific combinations and generic emendations.

Class DINOPHYCEAE Fritsch, 1929
Order EBRIALES Fott, 1959
Genus *AMMODOCHIUM* Hovasse, 1932

Type species. *Ammodochium prismaticum* Hovasse, 1932 = *A. rectangulare* (Schulz, 1928) Deflandre, 1933 ex *Ebria antiqua* var. *rectangularis* Schulz, 1928.

Ammodochium rectangulare (Schulz)
(Plate 1, Fig. 7)

1928 *Ebria antiqua* var. *rectangularis* Schulz, *Bot. Arch.*, 21:274, text-fig. 72a–d.

1932 *Ebria rectangularis* (Schulz) *in* Deflandre, *Bull. Soc. France Microsc.*, 1:19, figs. 59, 60.

1932 *Ammodochium prismaticum* Hovasse, *Bull. Soc. Zool. France,* 57:462.

1932 *Ammodochium rectangulare* (Schulz) *in* Deflandre, *Bull. Soc. Zool. France,* 57:517–518.

Remarks. The specimens usually show massive pro- and ophisthoclades and slightly curved synclades. Both the openings visible between the triode and the surrounding clades are more or less oval in outline.

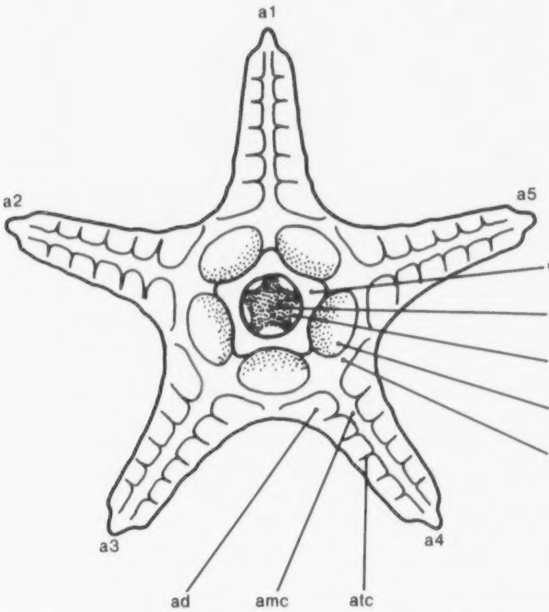

Figure 3. Morphological elements of the *Actiniscus* skeleton.
c = central field
cd = central depression; ck = central knob; cr = central ring; pc = peripheral crest; pd = peripheral depression.
a = arm
amc = median crest of the arm; atc = transversal crest of the arm; ad = depression of the arm.

Occurrence. Moler Formation of Denmark (upper Paleocene to lower Eocene); DSDP Hole 588C, Core 19 (middle Eocene). Other occurrences have to be re-evaluated, but probably are restricted to the Paleogene.

Ammodochium serotinum n. sp.
(Plate 2, Figs. 1, 2)

Holotype. SM.B 13502, Plate 2, Fig. 1.

Type locality. Lord Howe Rise, Sample 591B-18,CC (middle Miocene).

Description. Proclades and opisthoclades slightly but evenly bent from the triode to the synclades, the synclades highly arched, the proclades or opisthoclades without a window.

Size. 17 to 19 μm.

Remarks. This new species is closely related to *Ammodochium rectangulare,* the ancestor, but it may be distinguished by its more gracile skeleton, the highly arched synclades, and the shape of the openings visible between the triode and the surrounding clades. These openings are more or less semicircular in outline, since the triode appears bandlike in lateral view.

In earlier publications of different authors the new species is generally labeled as *Ammodochium rectangulare.* Here the latter is restricted to the specimens figured by Schulz (1928) from the lower Eocene of Mors, Denmark.

Occurrence. Sporadically distributed throughout the section investigated from the middle Miocene to lower Pliocene.

Genus *CRANIOPSIS* Hovasse ex Frenguelli, 1940

Type species. *Craniopsis octo* Hovasse ex Frenguelli, 1940.

Craniopsis sp.
(Not figured)

Remarks. A few specimens which seem to belong to the genus *Craniopsis* were noted in samples from Hole 588C, Core 19 (see Table 1).

Genus *DITRIPODIUM* Hovasse, 1932

Type species. *Ditripodium elephantinum* Hovasse, 1932.

Ditripodium latum Hovasse
(Plate 2, Figs. 5, 6)

1932 *Ditripodium latum* Hovasse, *Bull. Soc. Zool. France,* 57:282, text-fig. 6.

Remarks. The specimens are furnished with a large apical ring, short proclades, and short opisthoclades. The mesoclades are sometimes corroded or broken off. The terminations of the opisthoclades are usually trifurcated.

Occurrence. Only four specimens found in Sample 591B-18,CC middle Miocene.

Genus *EBRIOPSIS* Hovasse, 1932

Type species. *Ebriopsis antiqua* (Schulz, 1928) Hovasse, 1932, ex *Ebria antiqua* Schulz, 1928.

Ebriopsis crenulata Hovasse
(Plate 1, Figs. 10, 11)

1932 *Ebriopsis crenulata* Hovasse, *Bull. Soc. Zool. France,* 57:281, text-fig. 4.

Remarks. Only 8 out of 200 specimens showed a well-developed lorica in samples from Hole 588C.

Occurrence. This species is rather common in the middle Eocene of Hole 588C, Core 19, and was present reworked in several Miocene samples from Hole 594 (see Hole 594 site report). It was also recently figured from the "Lower Eocene 4" in northern Germany (Martini, 1981).

Ebriopsis cornuta (Ling) nov. comb.
(Plate 2, Figs. 14, 15)

1973 *Ebriopsis antiqua cornuta* Ling, *Pro. 1st Int. Cong. Pacific Neogene Stratigraphy,* pp. 215–216, plate 3, figs. 19–22.

1975 non *Ebriopsis cornuta* Dumitricǎ and Perch-Nielsen *in* Perch-Nielsen, *Init. Repts. DSDP,* 29:880, text-fig. 2, plate 7, figs. 8, 9 (= *Hermesinella*)

Remarks. The skeletons are more gracile than in other species of this genus. The two tripods are generally connected by strongly arched clades, leaving distinct indentations at the junctions with the arms. In some specimens a small spine may be developed at the apex, and rarely also at the antapex. The species probably comprises spiny and spineless forms comparable to *Parathranium clathratum,* which shows specimens with or without nodes at the upper synclades. In earlier publications of various authors the species is cited as *Ebriopsis antiqua,* but the latter name is here restricted to the specimen figured by Schulz (1928) from the lower Eocene of Mors, Denmark. Confusion with the homonymic *E. cornuta* Dumitrică and Perch-Nielsen (in Perch-Nielsen, 1975) may be avoided if the latter is placed in the genus *Hermesinella.*

Occurrence. Found only in the lower Pliocene part of the section investigated.

Genus *HAPLOHERMESINUM* Hovasse, 1943

Type species. *Haplohermesinum simplex* (Schulz, 1928) Hovasse, 1943 ex *Ebria tripartita* var. *simplex* Schulz, 1928.

Haplohermesinum? sp.

(Plate 2, Fig. 16)

Remarks. The specimens consist of a tripode united by three strongly curved clades. They may represent broken pieces of a known ebridian species, but the relations are uncertain.

Occurrence. Only four specimens found in three samples, ranging from the middle to late Miocene in age.

Genus *HERMESINELLA* Deflandre, 1934

Type species. *Hermesinella transversa* Deflandre, 1934.

Hermesinella conata (Deflandre) nov. comb.

(Plate 2, Figs. 9, 10)

1951 *Hermesinum conatum* Deflandre, *Bull. Biol. France Belg.,* 85: 44, text-fig. 141.

Remarks. This species shows one of the upper synclades highly arched. The opisthoclades are generally different in length, making the opisthocladian basket irregular in shape.

Occurrence. More or less consistently distributed from the middle to upper Miocene at Site 591.

Hermesinella fenestrata Frenguelli

(Plate 2, Fig. 13)

1951 *Hermesinella fenestrata* Frenguelli, *Physis,* 20:279, text-fig. 5a.

Remarks. This species exhibits a very regularly developed apical ring. The opisthocladian basket is asymmetrical in shape, comparable to that of *Hermesinella conata.*

Occurrence. Sporadically distributed in the middle Miocene and consistently present in the lower part of the upper Miocene of Site 591.

Hermesinella aff. *fenestrata* Frenguelli

(Plate 2, Figs. 11, 12)

Remarks. The specimens superficially resemble *Hermesinella fenestrata,* but they have larger procladian windows. At the junction point between the opisthoclades and the central rhabde an indention exists. Specimens found may be compared with skeletons described by Hovasse (1943) as *Hermesinum schulzii,* but the relationship to these forms, recovered at Saint-Laurent-La-Vernède, France, needs further study.

Occurrence. Only two specimens found in Sample 591B-17,CC, middle Miocene.

Genus *HERMESINUM* Zacharias, 1906

Type species. *Hermesinum adriaticum* Zacharias, 1906 (syn. *Bosporella triaenoides* Hovasse, 1931).

Hermesinum adriaticum Zacharias

(Plate 1, Figs. 5, 6)

1906 *Hermesinum adriaticum* Zacharias, *Arch. Hydrobiol. Planktonk.,* 1:394, figs. a–d.

1931 *Bosporella triaenoides* Hovasse, *C.R. Acad. Sci. Paris,* 193:781, figs. A–E.

1932 *Hermesinum adriaticum* var. *longispinosum* Hovasse, *Bull. Soc. Zool. France,* 57:466, fig. 20.

Remarks. This species shows one of the upper synclades highly arched and decorated by a long spine. Two of the opisthoclades are generally reduced, leaving only short remnants of the clades.

Occurrence. Consistently present from the middle Miocene to the lowermost Pliocene in Hole 591. Above this level found only in one sample (Table 2).

Hermesinum obliquum n. sp.

(Plate 1, Figs. 1–4)

Holotype. SM.B 13503, Plate 1, Figs. 1, 2.

Type locality. Lord Howe Rise, Sample 591B-15,CC (middle Miocene).

Description. Proclades connected by a flat syncladian ring, which supports a spine. The spine asymmetrically adjoins one of the large procladian windows. The opisthocladian basket is reduced to only one completely developed clade.

Size. 32–38 μm.

Remarks. This new species may be distinguished from *Hermesinum adriaticum* by the flat upper syncladian ring and the asymmetrical spine. In contrary to *H. adriaticum,* the complete opisthoclade generally lies to the right if viewed from the procladian window in front of the observer. In earlier publications of different authors, this species is commonly placed with *H. adriaticum.*

Occurrence. Consistently distributed from the middle Miocene to the lower Pliocene in Hole 591, but common only at the base of the *Hermesinella conata* Zone (middle Miocene) and near the base of the *Thranium crassipes* Zone (upper Miocene).

Genus *MICROMARSUPIUM* Deflandre, 1934

Type species. *Micromarsupium anceps* Deflandre, 1934.

Micromarsupium anceps Deflandre

(Plate 1, Figs. 8, 9; Text-fig. 2)

1934 *Micromarsupium anceps* Deflandre, *Ann. Protistol.,* 4:86, text-figs. 20–32.

Remarks. This species was observed in Leg 29 material (Perch-Nielsen, 1975) and corresponds to the original description of specimens from the upper Eocene of Oamaru, New Zealand, by Deflandre. Specimens found in the middle Eocene of Hole 588C are in most cases in the lorica stage (Text-fig. 3). There seems to exist a phylogenetic relationship between *M. anceps* Deflandre, *M. curticannum* Deflandre, and *M. rostovense* Martini (Martini, 1976).

Occurrence. Middle Eocene to early Oligocene (Deflandre, 1934, Oamaru; Perch-Nielsen, 1975, DSDP Sites 280, 281, and 283; this paper, DSDP Hole 588C).

Genus *PARATHRANIUM* Hovasse, 1932

Type species. *Parathranium tenuipes* Hovasse, 1932, = *Parathranium clathratum* (Ehrenberg, 1845) Deflandre, 1944, ex *Dicladia? clathrata* Ehrenberg, 1845.

Parathranium clathratum (Ehrenberg)

(Plate 2, Figs. 3, 4)

1845 *Dicladia? clathrata* Ehrenberg, *Ber. Akad. Wiss. Berlin, Jahrg. 1844,* p. 79.

1854 *Dicladia? clathrata* Ehrenberg *in* Ehrenberg, *Microgeologie,* plate 18, fig. 100.

1932 *Thranium tenuipes* Hovasse, *Bull. Soc. Zool. France,* 57:123, fig. 5 (invalid).

1932 *Parathranium tenuipes* Hovasse, *Bull. Soc. Zool. France,* 57: 464–465.

1944 *Parathranium clathratum* (Ehrenberg) *in* Deflandre, *Bull. Biol. France Belg.,* 78:67.

1968 *Parathranium biclathratum* Hajós, *Geol. Hung., Palaeontol.,* 37:72, plate 6, figs. 18–20.

Remarks. The specimens found have an apical ring, short proclades, and long opisthoclades. In some specimens the opisthoclades are relatively short and diverge from the triode. All apical clades may be decorated with a node. Investigation of the Ehrenberg type material has shown that the opisthoclades may vary arbitrarily in length, so no differentiation has been made between specimens bearing larger opisthoclades and shorter ones.

In contrast to Ling and McPherson (1974), but in accordance with Deflandre (1936, 1971), it must be stated that the type specimen of *Dicladia? clathrata* really belongs to *Parathranium*. The drawing of the type (Locker *in* Ling and McPherson, plate 1, fig. 9) was taken from the slide indicated by Ehrenberg himself on the original drawing sheet in his collection. The specimen was drawn with a high magnification objective from the lower side of the slide because it could not be focused from the upper side, owing to a thick layer of canada balsam. The new drawing, therefore, represents a mirror image of Ehrenberg's figure. Note also, that the drawing, although made with Abbéan drawing equipment, was primarily intended as a sketch and not for publication. The missing middle opisthoclade was indicated for better comparison only (S.L.).

Occurrence. Sporadically distributed throughout the sequence investigated at site 591 (middle Miocene to lower Pliocene).

Genus *THRANIUM* Hovasse, 1932

Type species. *Thranium crassipes* Hovasse, 1932.

Thranium crassipes Hovasse
(Plate 2, Figs. 7, 8)

1932 *Thranium crassipes* Hovasse, *Bull. Soc. Zool. France*, 57:122, figs. 4a–c (invalid).

1932 *Thranium crassipes* Hovasse, *Bull. Soc. Zool. France*, 57:464.

Remarks. The specimens are composed of an apical ring, short proclades, and short opisthoclades. The terminations of the opisthoclades are usually trifurcated.

Occurrence. Restricted to a horizon in the upper Miocene in the present material.

Class DINOPHYCEAE Fritsch, 1929
Order PERIDINIALES Ehrenberg, 1830
Family ACTINISCACEAE Kützing, 1849
Genus *ACTINISCUS* Ehrenberg, 1841

1841 *Dictyocha (Actiniscus)* Ehrenberg, *Abh. Akad. Wiss. Berlin, Jahrg. 1839*, p. 149.

1844 *Actiniscus* Ehrenberg *in* Ehrenberg, *Ber. Akad. Wiss. Berlin*, Jahrg. 1843, p. 103.

1891 *Gymnaster* Schütt, *Neptunia*, 1:407.

Type species. *Actiniscus pentasterias* Ehrenberg, 1841, ex *Dictyocha (Actiniscus) pentasterias* Ehrenberg, 1841.

Remarks. The genus *Actiniscus* is subdivided here into four species, which all show the typical alveolar structure of the external surface *(Actiniscus flosculus, A. laciniarius, A. pentasterias, A. squamosus)*, and two species which have a central knob but no peripheral depressions enclosed by a crest (*A.? elongatus, Actiniscus?* sp.).

Actiniscus? elongatus Dumitricǎ
(Plate 3, Figs. 1, 2; Plate 4, Figs. 1, 2)

1968 *Actiniscus elongatus* Dumitricǎ, *Stud. Cerc. Geol. Geofiz. Geogr., Geol.*, 13:240, plate 4, figs. 22, 26.

1974 *Actiniscus talmadgei* Parke, *Rev. Micropal.*, 17:81–82, plate 1, figs. 1–9.

Remarks. The starlike specimens, usually bilaterally symmetrical, consist of a thickened central part and a thin margin. The central part seems to correspond to the central knob of larger *Actiniscus* species. Besides the most common five-rayed variants, some six-rayed were also found. The question mark after the genus name indicates the unclear relationship to other *Actiniscus* species. All other species of the genus (*Actiniscus?* sp. excluded) show in larger specimens the typical alveolar structure on the external side.

Occurrence. Consistently present from the middle Miocene to the lower Pliocene at Site 591.

Actiniscus flosculus n. sp.
(Plate 3, Fig. 15; Plate 4, Figs. 4–7)

Holotype. SM.B 13504, Plate 3, Fig. 15.

Type locality. Lord Howe Rise, Sample 591B-1,CC (upper Miocene).

Description. Central field relatively large, with peripheral depressions distinctly developed, surrounded by a strong peripheral crest. Arms usually long, covered with depressions. Besides the most common five-rayed specimens, six- and seven-rayed ones were also found.

Size. 23 to 55 μm.

Remarks. This new species may be distinguished from other *Actiniscus* species by its regular shape and the appearance of the central field, which resembles, more or less, a flower composed of five leaves. The outer margin of the peripheral crest commonly appears smooth.

Occurrence. Consistently present from the middle Miocene to the lower Pliocene at Site 591.

Actiniscus laciniatus n. sp.
(Plate 3, Fig. 9)

Holotype. SM.B 13505, Plate 3, Fig. 9.

Type locality. Lord Howe Rise, Sample 591B-6,CC (upper Miocene).

Description. Central field relatively large, with peripheral depressions usually shallow, surrounded by an angular peripheral crest. Arms often asymmetrical, covered by depressions.

Size. 28 to 42 μm.

Remarks. *A. laciniatus* may be distinguished from other taxa by its shape, which is often irregular, and its general appearance. The central field commonly shows a distinctly angular peripheral crest, and the median crest of the arms may also be slightly creased. In connection with the transversal crests of the arms, an impression of patches or irregular grooves is created.

Occurrence. Consistently found in the middle and upper Miocene of Site 591, but not encountered in the lower Pliocene.

Actiniscus pentasterias Ehrenberg
(Plate 3, Figs. 11–14; Plate 4, Figs. 8, 9)

1841 *Dictyocha (Actiniscus) pentasterias* Ehrenberg, *Abh. Akad. Wiss. Berlin, Jahrg. 1839*, pp. 149–150.

1854 *Actiniscus pentasterias* Ehrenberg *in* Ehrenberg, *Mikrogeologie*, plate 18, fig. 61, plate 19, fig. 45, non plate 20, fig. 48 (=?), plate 33, fig. B XVII 1, plate 35A, fig. B XXIII 1, plate 36, fig. C36.

1895 *Gymnaster pentasterias* (Ehrenberg) *in* Schütt, *Wiss. Ergeb. Plankton-Exped. Humboldt-St.*, 1889 (4):31–35, plate 27, fig. 100/1–4.

Description. Central field large, with peripheral depressions usually shallow, surrounded by a strong peripheral crest. Arms relatively long, covered with depressions. Most common are five-rayed specimens, but six- and seven-rayed specimens were also found.

Remarks. This species may be distiguished from other taxa by its regular shape and by the appearance of the central field, which resembles a wheel. The outer margin of the peripheral crest commonly shows two small crestlike projections central to each interradial incision. The specimens found at Site 591 have been compared only with the figures given from the type locality, Aegina, Greece (subsequent designation in Locker, 1974). No additional investigations could be made.

Occurrence. Consistently present from the middle Miocene to the lower Pliocene, but most common in the *Thranium crassipes* Zone, upper Miocene.

Actiniscus squamosus n. sp.
(Plate 3, Fig. 10)

Holotype. SM.B 13506, Plate 3, Fig. 10.

Type locality. Lord Howe Rise, Sample 591B-3,CC (upper Miocene).

Description. Central field relatively large, with peripheral depressions usually shallow, surrounded by a wavy peripheral crest. Arms commonly short, covered with many drepressions.

Size. 21 to 27 μm.

Remarks. This new species can be distinguished from other taxa by its regular shape and the appearance of the central field, which is bordered by a wavy peripheral crest. The waves of the peripheral crest continue into the transversal crests of the arms, thus producing the impression of sheds.

Occurrence. Sporadically present in the upper Miocene and lower Pliocene of Site 591.

Actiniscus? sp.
(Plate 3, Fig. 3)

Remarks. The starlike specimens show four arms radiating from a central knob. The arms are constructed of a median crest framed by a thin margin. Specimens placed in *Actiniscus?* sp. here are often described as *A. tetrasterias* Ehrenberg, but the relations are unclear. *A. tetrasterias* was originally figured by Ehrenberg (1854) from Richmond, Virginia, but the Richmond specimens resemble some variants of *A. pentasterias* more than do the specimens found at Site 591.

Occurrence. Sporadically found in the middle and upper Miocene at Site 591.

Genus *CINCTACTINISCUS* Dumitrică, 1973

Type species. *Cinctactiniscus cinctus* (Hovasse, 1943) Dumitrică, 1973, ex *Gymnaster cinctus* Hovasse, 1943.

Cinctactiniscus? sp.

(Plate 3, Figs. 7, 8)

Remarks. Specimens are crescent-shaped in lateral view. The three or four arms developed are covered with shallow drepressions. The outer margin of the arms often has strong transversal crests. Specimens found generally resemble *Cinctactiniscus cinctus* as described and figured by Dumitrică (1973a). Because relations between *C. cinctus* and *Actiniscus? elongatus,* which are very similar in lateral view, and the present specimens are somewhat uncertain, we prefer an open species nomenclature for our specimens.

Occurrence. Consistently present in the lower Pliocene of Site 591.

Genus *FOLIACTINISCUS* Dumitrică, 1973

Type species. *Foliactiniscus folia* (Hovasse, 1943) Dumitrică, 1973, ex *Actiniscus folia* Hovasse, 1943.

Foliactiniscus cf. *folia* (Hovasse)

(Plate 3, Fig. 4)

Remarks. The starlike specimens show a central part occupied by a system of crests. The margin is rather thin. Specimens found are only tentatively placed with *Foliactiniscus folia* because questions remain about variations in proportions and shape in the material investigated.

Occurrence. Only sporadically present in the middle and upper Miocene of Site 591.

Foliactiniscus mirabilis Dumitrică, 1973

(Plate 3, Figs. 5, 6)

1973 *Foliactiniscus mirabilis* Dumitrică, *Init. Repts. DSDP*, 21:823, plate 1, figs. 12, 13, 20, plate 2, figs. 4, 12, 13.

Remarks. *F. mirabilis* displays large depressions around the central crest, and, very characteristically, the starlike specimens may be elongated along the central crest.

Occurrence. More or less consistently distributed from the middle Miocene to the lower Pliocene of Site 591, but generally in low numbers. Rare in the lower Pleistocene of Site 451, Philippine Sea (Martini, 1982).

ACKNOWLEDGMENTS

Thanks are due to the Deutsche Forschungsgemeinschaft (Bonn) for supporting the present study. The Geologisch-Paläontologisches Institut der Universität Kiel provided space for laboratory work (S.L.). SEM pictures were taken by J. Tochtenhagen with a Stereoscan Mark 2, which was made available to the Geologisch-Paläontologisches Institut der Universität Frankfurt am Main by the Volkswagenstiftung. Our thanks go also to Dr. Hsin Yi Ling (DeKalb, Illinois) and Dr. Katharina Perch-Nielsen (Zürich) for reviewing this paper.

The type specimens of the five new species are deposited in the Naturmuseum und Forschungsinstitut Senckenberg, Frankfurt am Main, Germany, Catalogue Nos. SM.B 13502 to 13506.

REFERENCES

Bukry, D., 1976. Comments on some coccoliths and silicoflagellates from Deep Sea Drilling Project Leg 35. *In* Hollister, C. D., Craddock, C., et al., *Init. Repts. DSDP*, 35: Washington (U.S. Govt. Printing Office), 693–699.

Deflandre G., 1934. Nomenclature du squelette des Ebriacées et description de quelques formes nouvelles. *Ann. Protist.*, 4:75–96.

________, 1936. *Les Flagellés Fossiles Aperçu Biologique et Paléontologique. Rôle Géologique.* Actual. Sci. indust., No. 335.

________, 1951. Recherches sur les Ebriédiens: paléobiologie, évolution, systématique. *Bull. Biol. France Belg.*, 85:1–84.

________, 1952. Classe des Ebriédiens. *In* Piveteau, J. (Ed.), *Traité de Paléontologie* (Vol. 1): Paris (Masson), 125–128.

________, 1971. Rejet du genre *Dicladia* Ehrenberg (diatomée) introduit fallacieusement dans les Ebriédiens. *Proc. II Plankt. Conf., Roma 1970* (Vol. 1): Rome (Edisioni Tecnoscienza), 349–353.

Dumitrică, P., 1973a. Cenozoic endoskeletal dinoflagellates in southwestern pacific sediments cored in Leg 21 of the Deep Sea Drilling Project. *In* Burns, P. E., Andrews, J. E., et al., *Init. Repts. DSDP*, 21: Washington (U.S. Govt. Printing Office), 819–835.

________, 1973b. Miocene and Quaternary ebridians in sediments from the Mediterranean Sea, Deep Sea Drilling Project Leg 13. *In* Ryan, W. B. F., Hsü, K. J., et al., *Init. Repts. DSDP*, 13, Pt 2: Washington (U.S. Govt. Printing Office), 934–939.

Ehrenberg, C. G., 1854. *Mikrogeologie. Das Erden und Felsen schaffende Wirken des unsichtbar kleinen selbständigen Legens auf der Erde:* Leipzig (Leopold Voss).

Hajós, M., 1968. Die Diatomeen der miozänen Ablagerungen des Mátravorlandes. *Geol. Hung., Palaeont.*, 37:1–262.

Hovasse, R., 1932. Troisième note sur les Ebriacées. *Bull. Soc. Zool. France*, 57:457–476.

________, 1943. Nouvelles recherches sur les flagellés à squelettes siliceux: Ebriidés et silicoflagellés fossiles de la diatomite de Saint-Laurent-La-Vernède (Gard). *Bull. Biol. France Belg.*, 77:271–284, 285–294.

Ling, H. Y., 1971. Silicoflagellates and ebridians from the Shinzan diatomaceous mudstone member of the Onnagowa formation (Miocene), Northeast Japan. *Proc. II Plankt. Conf. Roma 1970* (Vol. 2): Rome (Edizioni Tecnoscienza), 689–703.

________, 1972. Upper Cretaceous and Cenozoic silicoflagellates and ebridians. *Bull. Amer. Paleont.*, 62:135–229.

________, 1973. Silicoflagellates and ebridians from Leg 19. *In* Creager, J. S., Scholl, D. W., et al., *Init. Repts. DSDP*, 19: Washington (U.S. Govt. Printing Office), 751–775.

________, 1975. Silicoflagellates and ebridians from Leg 31. *In* Karig, D. E., Ingle, J. C., Jr., et al., *Init. Repts. DSDP*, 31: Washington (U.S. Govt. Printing Office), 763–777.

________, 1977. Late Cenozoic silicoflagellates and ebridians from the eastern North Pacific region. *Proc. 1st Int. Cong. Pacific Neogene Stratigraphy,* pp. 205–233.

________, 1980. Silicoflagellates and ebridians from Leg 55. *In* Jackson, E. D., Koizumi, I., et al., *Init. Repts. DSDP*, 55: Washington (U.S. Govt. Printing Office), 375–385.

Ling, H. Y., and McPherson, L. M., 1974. Study on the ebridian genus *Parathranium* Hovasse. *Rev. Espan. Micropal.*, 6:191–200.

Locker, S., 1974. Revision der Silicoflagellaten aus der Sammlang von C. G. Ehrenberg. *Eclog. Geol. Helv.*, 67:631–646.

Loeblich, A. R. III, Loeblich, L. A., Tappan, H., and Loeblich, A. R., Jr., 1968. *Annotated Index of Fossil and Recent Silicoflagellates and Ebridians with Descriptions and Illustrations of Validly Proposed Taxa.* Geol. Soc. Am., Mem. 106.

Martini, E., 1976. *Micromarsupium rostovense,* eine neue Ebriiden-Art aus dem Paläogen der Umgebung von Rostow, UdSSR. *Senckenb. Leth.*, 56(6):453–461.

________, 1981. Silicoflagellaten aus dem Paläogen von Norddeutschland. *Senckenb. Leth.*, 62(2/6):277–283.

________, 1982. Pliocene and Quaternary diatoms, silicoflagellates, sponge spicules, and endoskeletal dinoflagellates from the Philippine Sea, Deep Sea Drilling Project Legs 59 and 60. *In* Hussong, D. M., Uyeda, S., et al., *Init. Repts. DSDP*, 60: Washington (U.S. Govt. Printing Office), 565–574.

Orr, W. N., and Conyley, S., 1976. Siliceous dinoflagellates in the northeast Pacific rim. *Micropaleontology,* 22:92–99.

Perch-Nielsen, K., 1975. Late Cretaceous to Pleistocene archaeomonads, ebridians, endoskeletal dinoflagellates, and other siliceous microfossils from the subantarctic southwest Pacific, DSDP, Leg 29. *In* Kennett, J. P., Houtz, R. E., et al., *Init. Repts. DSDP*, 29: Washington (U.S. Govt. Printing Office), 873–907.

________, 1977. Tertiary silicoflagellates and other siliceous microfossils from the western South Atlantic, Deep Sea Drilling Project Leg 39. *In* Supko, P. R., Perch-Nielsen, K., et al., *Init. Repts. DSDP*, 39: Washington (U.S. Govt. Printing Office), 863–867.

———, 1978. Eocene to Pliocene archaeomonads, ebridians, and endoskeletal dinoflagellates from the Norwegian Sea, DSDP Leg 38. *In* Talwani, M., Udintsev, G., et al., *Init. Repts. DSDP*, Suppl. to Vols. 38, 39, 40, and 41: Washington (U.S. Govt. Printing Office), 147–175.

Schulz, P., 1928. Beiträge zur Kenntnis fossiler und rezenter Silicoflagellaten. *Bot. Arch.*, 21:225–292.

Stradner, H., and Bachmann, A., 1978. Late Pliocene and early Pleistocene silicoflagellates and ebridians from DSDP Site 378 in the Aegean Basin, north of Crete. *In* Hsü, K., Montadert, L., et al., *Init. Repts. DSDP*, 42, Pt. 1: Washington (U.S. Govt. Printing Office), 805–815.

Tappan, H., 1980. *The Paleobiology of Plant Protists:* San Francisco (Freeman and Co.).

Date of Initial Receipt: 12 June 1984
Date of Acceptance: 29 October 1984

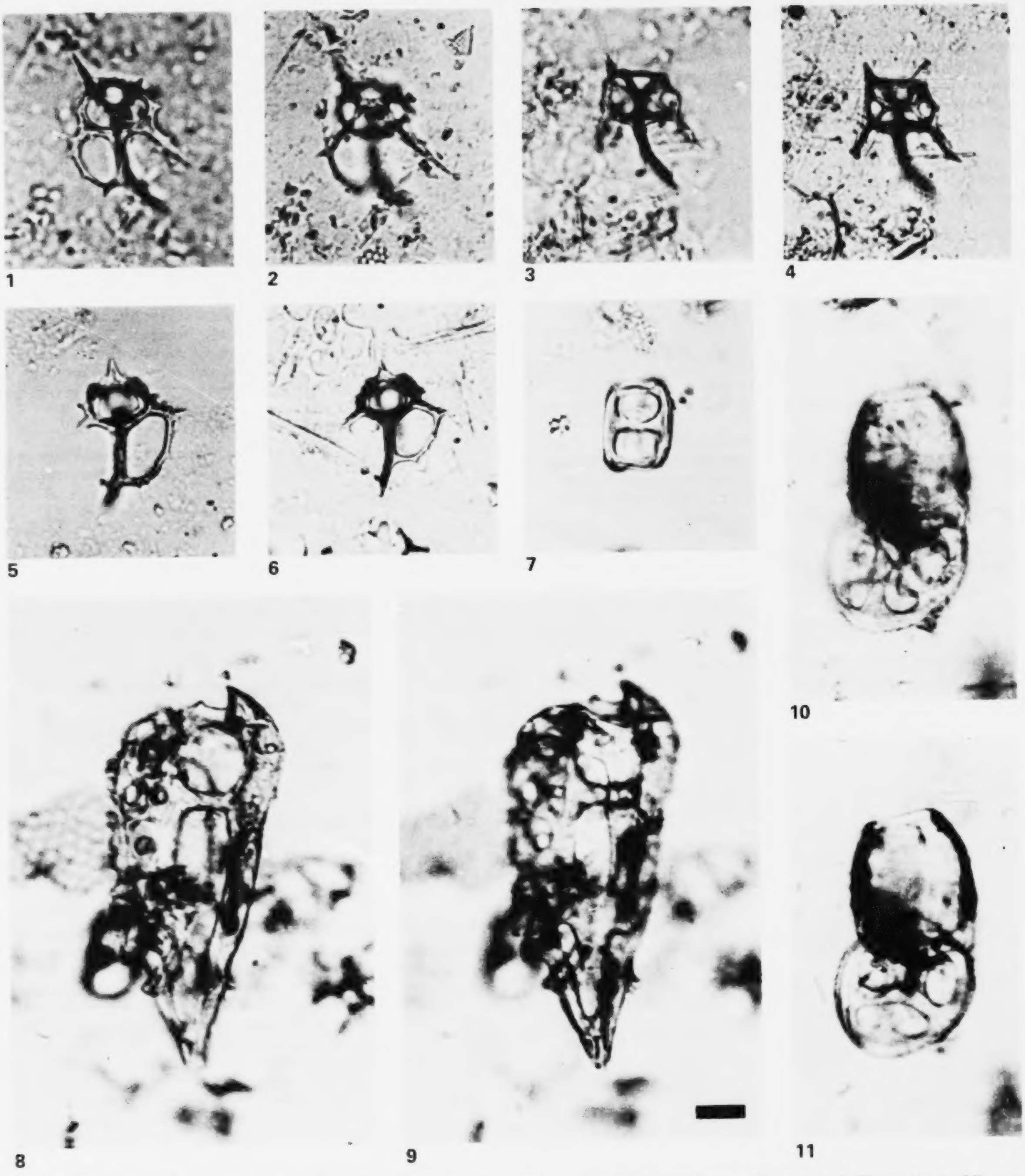

Plate 1. Middle Eocene and middle to upper Miocene ebridians. (All specimens magnified ×800, bar = 10 μm.) **1–4.** ***Hermesinum obliquum*** n. sp., (1, 2) holotype, low and high focus, SM.B 13503; Sample 591B-15,CC, middle Miocene; (3, 4) low and high focus, Sample 591B-7,CC, upper Miocene. **5, 6.** ***Hermesinum adriaticum*** Zacharias, (5) Sample 591-24,CC upper Miocene; (6) Sample 591B-7,CC, upper Miocene. **7.** ***Ammodochium rectangulare*** (Schulz), Sample 588C-19-1, 35–37 cm, middle Eocene. **8, 9.** ***Micromarsupium anceps*** Deflandre, different focus; Sample 588C-19-1, 35–37 cm, middle Eocene. **10, 11.** ***Ebriopsis crenulata*** Hovasse with lorica, different focus; Sample 588C-19,CC, middle Eocene.

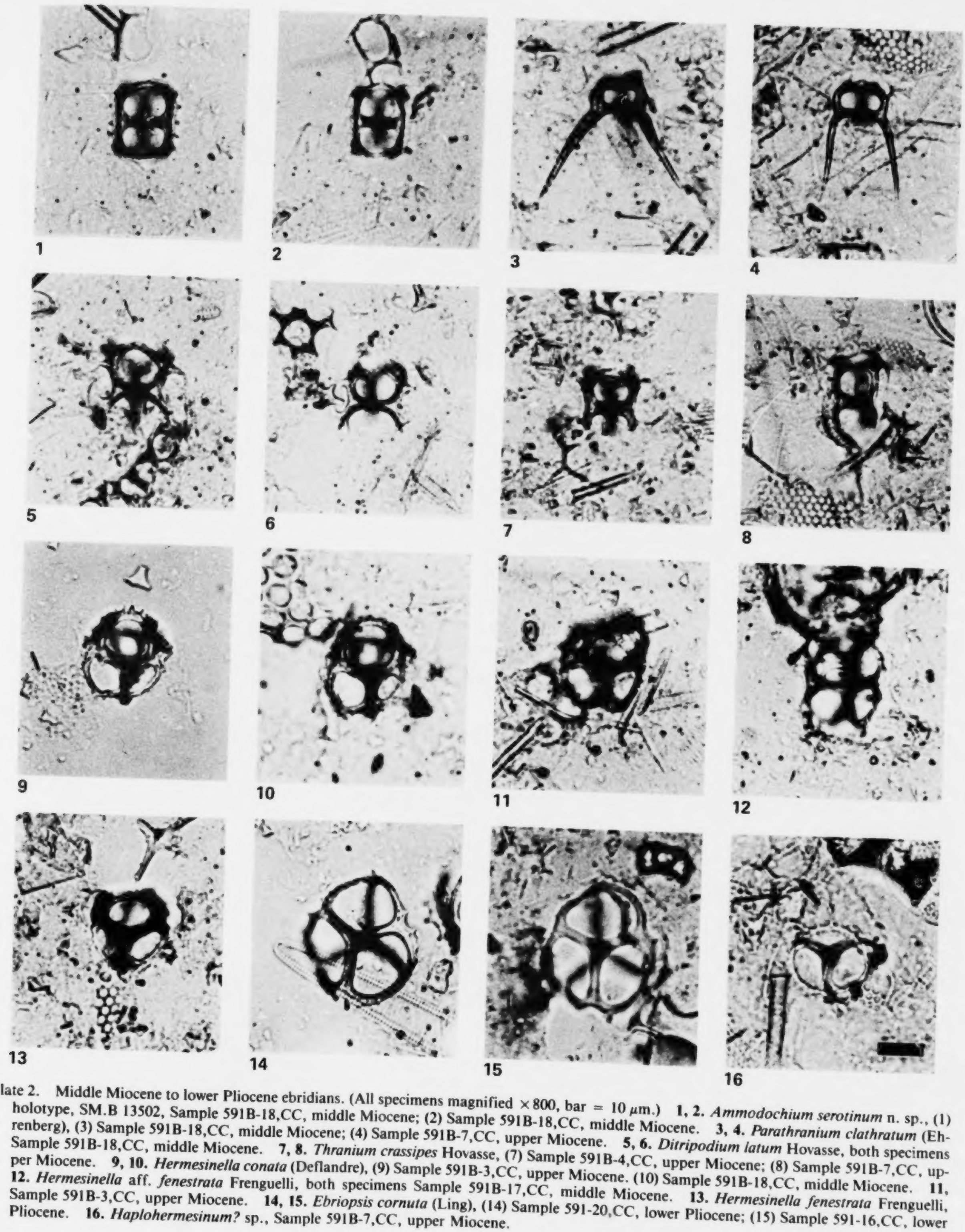

Plate 2. Middle Miocene to lower Pliocene ebridians. (All specimens magnified ×800, bar = 10 µm.) **1, 2.** *Ammodochium serotinum* n. sp., (1) holotype, SM.B 13502, Sample 591B-18,CC, middle Miocene; (2) Sample 591B-18,CC, middle Miocene. **3, 4.** *Parathranium clathratum* (Ehrenberg), (3) Sample 591B-18,CC, middle Miocene; (4) Sample 591B-7,CC, upper Miocene. **5, 6.** *Ditripodium latum* Hovasse, both specimens Sample 591B-18,CC, middle Miocene. **7, 8.** *Thranium crassipes* Hovasse, (7) Sample 591B-4,CC, upper Miocene; (8) Sample 591B-7,CC, upper Miocene. **9, 10.** *Hermesinella conata* (Deflandre), (9) Sample 591B-3,CC, upper Miocene. (10) Sample 591B-18,CC, middle Miocene. **11, 12.** *Hermesinella* aff. *fenestrata* Frenguelli, both specimens Sample 591B-17,CC, middle Miocene. **13.** *Hermesinella fenestrata* Frenguelli, Sample 591B-3,CC, upper Miocene. **14, 15.** *Ebriopsis cornuta* (Ling), (14) Sample 591-20,CC, lower Pliocene; (15) Sample 591-16,CC, lower Pliocene. **16.** *Haplohermesinum?* sp., Sample 591B-7,CC, upper Miocene.

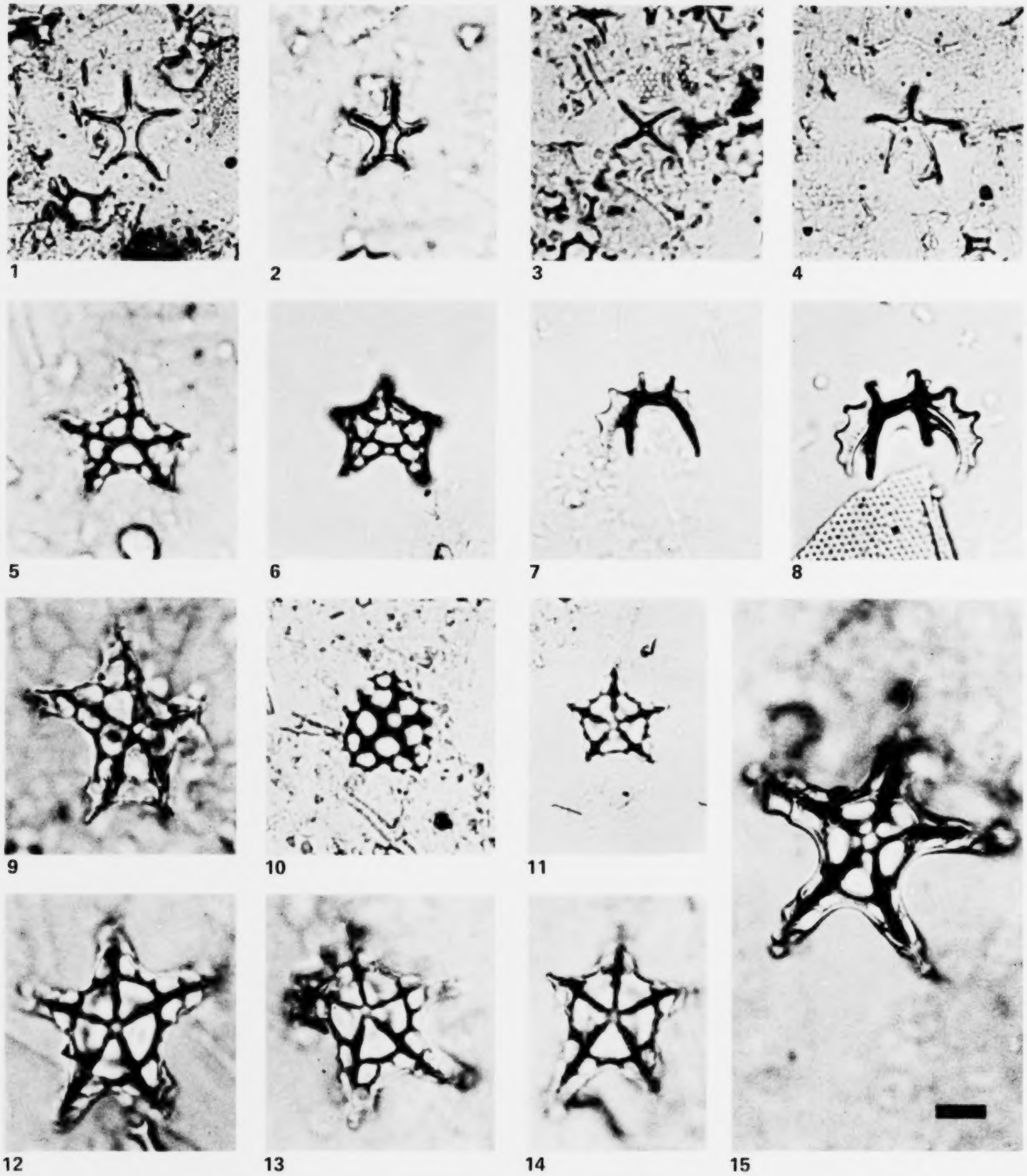

Plate 3. Middle Miocene to lower Pliocene actiniscidians. (All specimens magnified ×800, bar = 10 μm.) **1, 2.** *Actiniscus? elongatus* Dumitrică, (1) Sample 591B-2,CC, upper Miocene; (2) Sample 591-17,CC, lower Pliocene. **3.** *Actiniscus?* sp., Sample 591B-3,CC, upper Miocene. **4.** *Foliactiniscus* cf. *folia* Hovasse, Sample 591B-4,CC, upper Miocene. **5, 6.** *Foliactiniscus mirabilis* Dumitrică, (5) Sample 591-24,CC, upper Miocene; (6) Sample 591-19,CC, lower Pliocene. **7, 8.** *Cinctactiniscus?* sp., (7) Sample 591-18,CC, lower Pliocene; (8) Sample 591-20,CC, lower Pliocene. **9.** *Actiniscus laciniatus* n. sp., holotype, SM.B 13505; Sample 591B-6,CC, upper Miocene. **10.** *Actiniscus squamosus* n. sp., holotype, SM.B 13506; Sample 591B-3,CC, upper Miocene. **11–14.** *Actiniscus pentasterias* Ehrenberg, (11) Sample 591B-21,CC, middle Miocene; (12–14) Sample 591B-1,CC, upper Miocene. **15.** *Actiniscus flosculus* n. sp., holotype, SM.B 13504; Sample 591B-1,CC, upper Miocene.

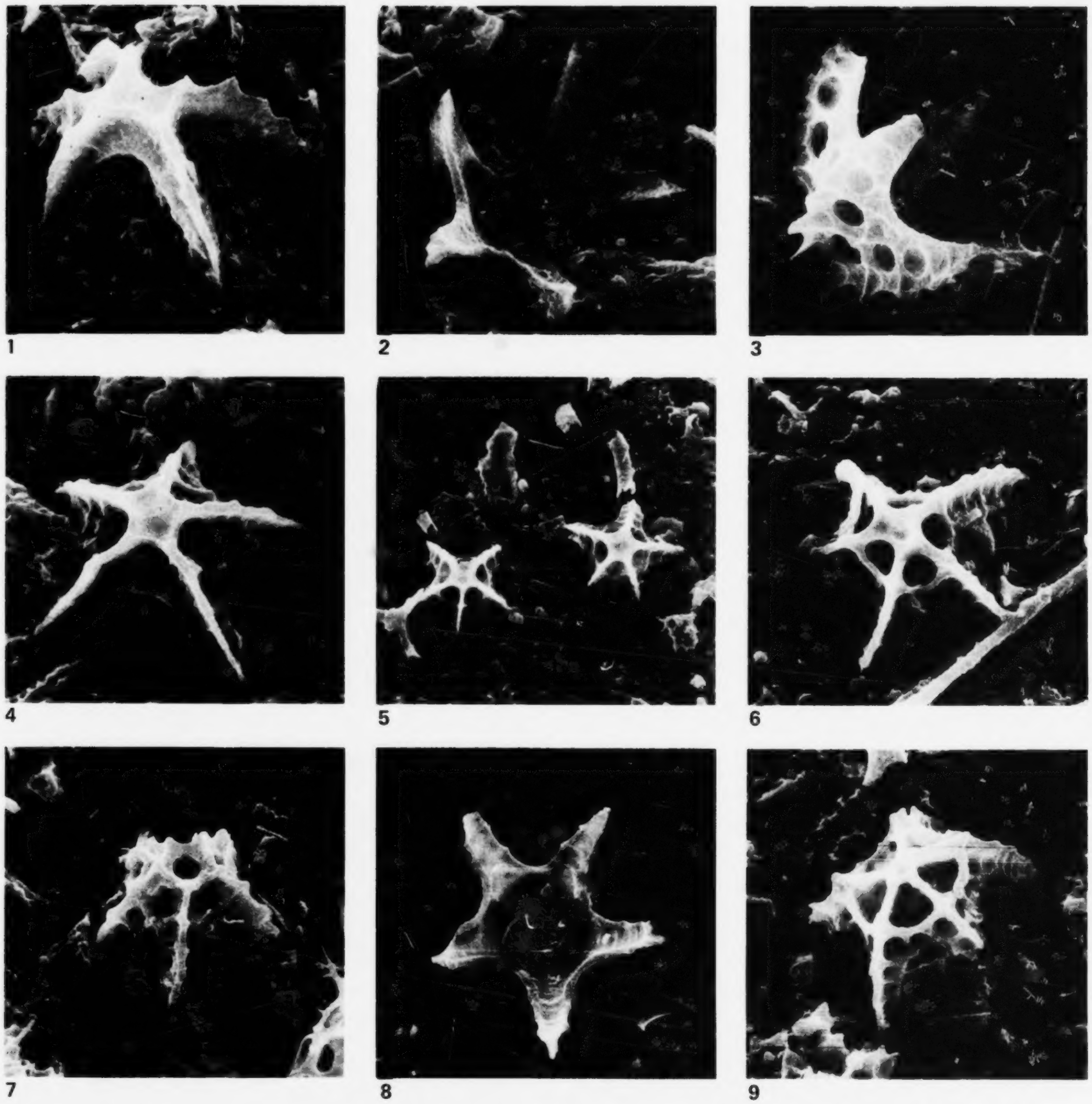

Plate 4. Middle Miocene to upper Miocene actiniscidians. (Scanning electron micrographs.) **1, 2.** *Actiniscus? elongatus* Dumitricǎ, (1) external view, 2800 ×, Sample 591B-16,CC, middle Miocene; (2) internal view, 2750 ×, Sample 591B-16,CC, middle Miocene. **3.** *Actiniscus* sp., oblique view, 1900 ×, Sample 591-30,CC, upper Miocene. **4–7.** *Actiniscus flosculus* n. sp., (4) juvenile specimen, external view, 2800 ×, Sample 591B-17,CC, middle Miocene; (5) juvenile specimens, external view, 1200 ×, Sample 591-30,CC, upper Miocene; (6) adult specimen, external view, 1200 ×, Sample 591-30,CC, upper Miocene; (7) adult specimen, oblique view, 1100 ×, Sample 591B-16,CC, middle Miocene. **8, 9.** *Actiniscus pentasterias* Ehrenberg, (8) internal view, 2100 ×, Sample 591-30,CC, upper Miocene; (9) external view, 2000 ×, Sample 591B-4,CC, upper Miocene.

19. QUATERNARY FISH OTOLITHS FROM SITES 587 AND 594, SOUTHWEST PACIFIC, DEEP SEA DRILLING PROJECT, LEG 90[1]

Erlend Martini, Geologisch-Paläontologisches Institut der Universität, Frankfurt am Main
and
Pieter A. M. Gaemers, Rijksmuseum van Geologie en Mineralogie, Leiden[2]

ABSTRACT

Otoliths, predominantly from Lanternfishes (Myctophidae), from two species belonging to the Deepsea Bristlemouths (Gonostomidae), and from one stromatoid species are described from the Quaternary of Sites 587 and 594 in the southwest Pacific. Their occurrences and preservation as well as their present distribution are discussed. Growth layers of some otoliths are described in detail and figured using SEM techniques.

INTRODUCTION

During Leg 90, fish otoliths were found at two out of eight sites (Fig. 1). At Site 587 (21°11.87′S, 161°19.99′E, Lord Howe Rise west of New Caledonia, water depth 1101 m) approximately 60 otoliths were recovered in the core-catcher samples of Cores 1 to 3, and at Site 594 (45°31.41′S, 174°56.88′E, Chatham Rise southeast of New Zealand, water depth 1204 m) a single otolith was found in Sample 594-3,CC. Most of the otoliths are badly worn, especially in Sample 587-3,CC, but some are fairly well preserved and the genus can be identified.

STRATIGRAPHIC POSITION AND LITHOLOGY

Samples 587-1,CC, 587-2,CC, and 594-3,CC can be placed in the late Pleistocene to Recent calcareous nannoplankton Zone NN21 (*Emiliana huxleyi* Zone) and in the planktonic foraminiferal *Globorotalia truncatulinoides* Zone. Sample 587-3,CC belongs in the Pleistocene calcareous nannoplankton Zone NN19B (upper part of the *Pseudoemiliania lacunosa* Zone) and in the planktonic foraminiferal *Globorotalia truncatulinoides/G. tosaensis* overlap Zone used on Leg 90.

Core-catcher Samples 587-1,CC to 587-3,CC consist of very light grey to white foraminifer-bearing nannofossil ooze to foraminifer nannofossil ooze with disrupted pyritized laminae, blebs, and rare burrows. Sample 587-4,CC is a white to bluish white foraminifer-bearing nannofossil ooze. Besides planktonic and benthic foraminifers, the sieved material contains pteropods, echinoid spines, ostracodes, and rare bryozoans. Sample 594-3,CC is a firm, light bluish grey foraminifer- and clay-bearing nannofossil ooze with H_2S odor, containing mica and some small mollusk shells.

PRESERVATION AND ABUNDANCE

In Hole 587 only Cores 1 to 3 (only core-catcher samples investigated) contained fish otoliths in numbers rising with depth (Table 1); no specimens were found in Sample 587-4,CC and below, although the same amount of sediment was checked for each level. The preservation declines rapidly with depth, and otoliths from Sample 587-3,CC are badly corroded, especially on the inner face; this is probably due to the coarser crystal arrangement along the sulcus (Martini, 1974). Accordingly the genus of most cannot be identified with certainty. The single otolith from Sample 594-3,CC from the clay-bearing nannofossil ooze is much better preserved (Plate 1, Figs. 1, 2) than those from Hole 587. It seems possible that in samples from Cores 587-1 to -3, which show generally coarser material and winnowing of the fine fraction, otoliths became concentrated.

DEEP SEA OCCURRENCES OF FISH OTOLITHS

Fish otoliths are built of aragonite, which is less solution-resistant than calcite (Berger, 1978); accordingly, their occurrence in deep sea sediments is restricted by depth. Only a few papers have mentioned otoliths from deep sea sediments, although under certain conditions they may be found in sufficient numbers. The only detailed account of fish otoliths within the *Initial Reports* of the Deep Sea Drilling Project is for Leg 25 (Martini, 1974), where Recent to late Pleistocene assemblages were described from present water depths of 2275 m (Site 242, Mozambique Channel) and 1030 m (Site 246, Madagascar Ridge) in the Indian Ocean.

Two otoliths were figured by Beckmann (1976) from Site 318; they were recovered during Leg 33 on the Tuamotu Ridge (Sample 318-2-2, 15–17 cm), from Pleistocene sediments placed in calcareous nannoplankton Zone NN19 (*Pseudoemiliania lacunosa* Zone) at a present water depth of 2641 m. As they were associated with a shallow-water fauna they may represent displaced specimens.

For the Mediterranean Leg 42A, Bizon et al. (1978) noted fish otoliths in several holes but did not describe them in detail. Occurrences were more or less restricted to the Quaternary and included Holes 371 (present water depth 2792 m), 372 (present water depth 2699 m), 376 (present water depth 2101 m), and 378 (present water depth 1835 m). Some Pliocene occurrences were noted

---

[1] Kennett, J. P., von der Borch, C. C., et al., *Init. Repts. DSDP*, 90: Washington (U.S. Govt. Printing Office).

[2] Addresses: (Martini) Geologisch-Paläontologisches Institut der Universität, Frankfurt am Main, Federal Republic of Germany; (Gaemers) Rijksmuseum van Geologie en Mineralogie, Leiden, Netherlands.

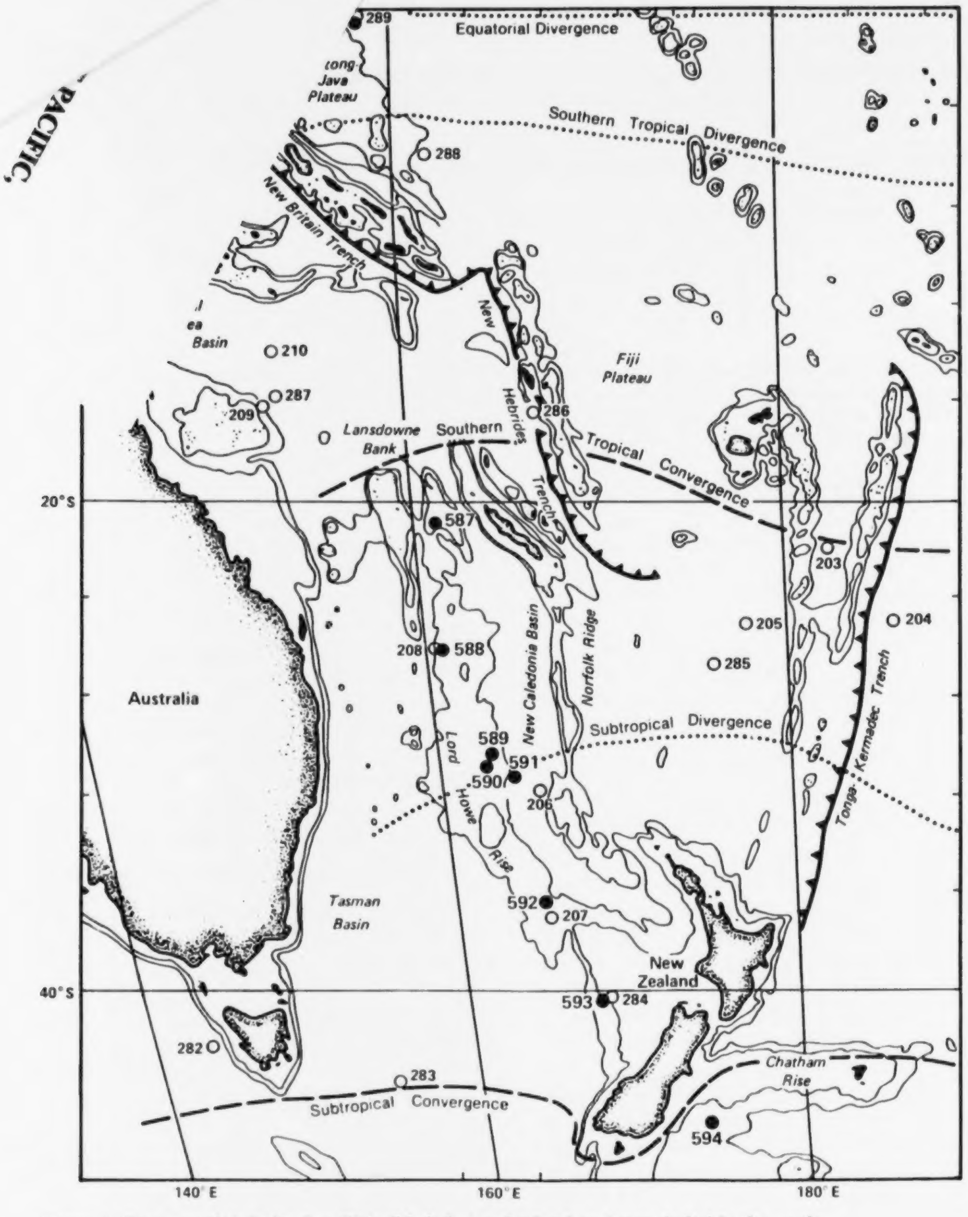
289
Equatorial Divergence
Ontong Java Plateau
Southern Tropical Divergence
288
New Britain Trench
New Hebrides Trench
Fiji Plateau
Coral Sea Basin
210
287
209
Lansdowne Bank
286
Southern Tropical Convergence
20°S
587
203
204
205
285
208
588
New Caledonia Basin
Norfolk Ridge
Australia
Subtropical Divergence
Tonga - Kermadec Trench
589
591
590
206
Lord Howe Rise
Tasman Basin
592
207
New Zealand
40°S
593
284
282
283
Chatham Rise
Subtropical Convergence
594
140°E
160°E
180°E

Figure 1. Sites occupied during Leg 90 (solid circles) and other legs (open circles) in the southwest Pacific. Fish otoliths were encountered only at Sites 587 and 594.

in Hole 373A in the Tyrrhenian Basin at the exceptional present water depth of 3517 m—later subsidence is a possible explanation—and in Holes 376 (present water depth 1900 m) and 378 (present water depth 1835 m).

SYSTEMATIC DESCRIPTION

Family GONOSTOMIDAE Gill, 1892
(Lightfish or Deepsea Bristlemouths)
Genus *BONAPARTIA* Goode and Bean, 1896

Bonapartia sp.
(Plate 1, Figs. 15, 16)

One eroded specimen from Sample 587-2,CC belongs to this genus. The shape of the sulcus is characteristic for the family. The middle part of the cauda is the widest and deepest part. The ostium is only vaguely visible because of erosion. The shape of the outline is very similar to that of *B. pedalotia*, apart from a clearly concave part directly behind the antirostrum. It is not clear whether this is an erosional phenomenon or a primary structure. The otolith length/height ratio agrees well with that of *B. pedalotia* (Kotthaus, 1972a, fig. 27).

Genus *VALENCIENNELUS* Jordan and Evermann in Goode and Bean, 1896

Valenciennellus tripunctulatus **(Esmark, 1871)**
(Plate 1, Figs. 9, 10, 23, 24)

Two sagittae found in Samples 587-1,CC and 587-2,CC are assigned to this species. Both specimens are rounded and the height is greater than the length. Rostrum and antirostrum are nearly of equal

Table 1. Distribution and preservation of fish otoliths in samples from Holes 587 and 594.

Sample	*Bonapartia* sp.	*Valenciennellus tripunctulatus*	? *Nomeidarum* sp.	*Hygophum macrochir*	*H. benoiti*	? *Centrobranchus* sp.	*Diaphus subtilis*	*Diaphus* spp.	*Lampanyctodes* aff. *hectoris*	*Ceratoscopelus* spp.	*Lampanyctus* spp.	Unidentifiable	Total number of specimens	Preservation
587-1,CC		1			1		1			1	1	1	6	M
587-2,CC	1	1	1	1			1			4		2	11	M
587-3,CC						2		5		7	1	29	44	P
594-3,CC									1				1	G

Note: For preservation, G = good, M = moderate, P = poor.

size. A small excisura is present in both specimens. The ventral rim of the sulcus is prominent and bent downward along the ostium. The ostium is relatively small compared with the elongated cauda. The outer face is smooth, but may be affected by corrosion. Both sagittae are very similar to the specimen of *Valenciennellus tripunctulatus* (Esmark, 1871) figured in Kotthaus (1972a, fig. 30). Other illustrations of this species can be found in Kotthaus (1967, text-fig. 31) and Weitzman (1974, text-fig. 42D). The species is widespread and is caught in all oceans (Kotthaus, 1972a, p. 8).

Family MYCTOPHIDAE Gill, 1892
(Lanternfishes)
Genus *HYGOPHUM* Tåning, 1932

Hygophum macrochir (Günther, 1864)
(Plate 1, Figs. 5, 6)

One specimen in Sample 587-2,CC can be assigned to this species. Length and height are more or less equal, the antirostrum is a little less prominent than the rostrum and is separated from the latter by a distinct excisura. The postventral part is steep and straight. The ostium is larger than the cauda, the base of which does not reach the same level as the base of the ostium. The dorsal margin is characteristic for the species. It shows some undulation and has a rounded predorsal angle and a more prominent postdorsal angle; the parts between the angles and between postdorsal angle and caudal end are nearly straight (see Schwarzhans, 1980, text-fig. 104; Hecht and Hecht, 1981, text-fig. 49).

Hygophum atratum (Garman, 1891) shows many similarities with *H. macrochir.* It differs from the latter species by having more prominent dorsal angles lying farther apart, less ornamentation along its margins, and more oblique otoliths which are rather pointed in the middle of the ventral rim (otolith in Gaemers collection, donated by the late J. E. Fitch; see also Weiler, 1971, plate 1, fig. 23, although this specimen seems to be more strongly ornamented). The specimen illustrated as *H. atratum* by Schwarzhans, 1980, however, differs in many respects; it is therefore doubtful if it belongs to the same species, unless the otoliths show a strong allometrical growth.

Hygophum benoiti (Cocco, 1838)
(Plate 1, Figs. 3, 4)

A left sagitta assigned to this species was found in Sample 587-1,CC. The height is slightly greater than the length. It has a distinct rostrum and a smaller antirostrum, separated by an excisura. The antirostrum is somewhat blunt (probably caused by erosion), leading to an angle on the dorsal margin of the sagitta, which shows some undulation related to two grooves on the outer face. The inner face is worn, but ostium and cauda seem to be of about equal length with the bases in line. The regularly rounded dorsal rim is characteristic for *H. benoiti* (see Schwarzhans, 1980, text-fig. 105; Hecht and Hecht, 1981, text-fig. 48; Nolf and Steurbaut, 1983, plate 2, figs. 28–33).

Genus *CENTROBRANCHUS* Fowler, 1904

?*Centrobranchus* sp.
(not figured)

Two small otoliths from Sample 587-3,CC may belong to the genus *Centrobranchus*. Their length is greater than their height. The rostrum is small and an antirostrum is not developed. Both specimens have a distinct postdorsal angle. The ostium is larger than the cauda in the better-preserved specimen. At present they can be best compared with *Centrobranchus nigroocellatus* in Kotthaus (1972a, text-fig. 64).

Genus *DIAPHUS* Eigenmann, 1891

Diaphus subtilis Nafpaktitis, 1968
(Plate 1, Figs. 21, 22, 25, 26)

Two otoliths belonging to the genus *Diaphus* were recovered at Site 587. In Sample 587-1,CC (Plate 1, Figs. 25, 26) a small left sagitta with a distinct rostrum can be assigned to *Diaphus subtilis* (see Kotthaus, 1972a, text-fig. 73), but differs in having no antirostrum and an excisura that is reduced to a groove on the outer face. As the dentation on the ventral rim and the outer face is rather smooth this may represent a corroded specimen with details lost. The ostium is slightly larger than the cauda and a faint area is present on the dorsal part. The left sagitta found in Sample 587-2,CC (Plate 1, Figs. 21, 22) is slightly larger, having a somewhat blunt rostrum and a small excisura and antirostrum. Two incisions followed by grooves on both faces are developed on the dorsal rim. On the ventral rim a small projection can be noted. Otherwise the sagitta looks corroded, with an obscured sulcus. The asymmetrical, triangular outline is typical for *D. subtilis* (several otoliths available for comparison in Gaemers collection, donation J. Craddock, Woods Hole).

?*Diaphus* sp.
(not figured)

Five badly worn otoliths from Sample 587-3,CC seem to belong to the genus *Diaphus*. One worn otolith from Sample 587-3,CC still shows some faint radial grooves on the outer face.

Genus *LAMPANYCTODES* Fraser-Brunner, 1949

Lampanyctodes aff. *hectoris* (Günther, 1876)
(Plate 1, Figs. 1, 2)

The single right sagitta from Sample 594-3,CC is somewhat eroded. The ventral rim is undulated, the incisions resulting in grooves on the outer face. It has a prominent antirostrum, whereas the rostrum is less distinct because of erosion. Originally antirostrum and rostrum were probably equally prominent. The ostium is large and about one and a half times the length of the cauda. A crista superior is well developed and separates the sulcus from the area. The otolith very much resembles that figured in Karrer, 1973 as *L. hectoris* in the gradually rising dorsal rim from antirostrum to the rounded postdorsal angle. Other characteristics which are very similar are antirostrum, excisura, ventral furrow, and sulcus (see the specimens of *L. mimiensis* in Schwarzhans, 1980). The ostial colliculum in the specimen figured by Karrer must erroneously have been confined to the posterior part of the ostium as she also incorrectly did in the otoliths of *Diaphus dumerili* and *D. taaningi.* The dentation, which is clearly visible in Karrer's drawing, was probably smoothed in the fossil specimen by erosion. This otolith differs from Karrer's illustration in having a stronger ornamentation on the outer face and a more rounded posterior rim. The latter may be the result of a somewhat stronger erosion along the ventral part of this rim.

Genus *CERATOSCOPELUS* Günther, 1864

Ceratoscopelus sp.
(Plate 1, Figs. 11–14, 17–20, and 29–30)

Several otoliths from Hole 587 belong to the genus *Ceratoscopelus*. One right sagitta from Sample 587-1,CC (Plate 1, Figs. 29, 30) is tentatively assigned to the genus *Ceratoscopelus*, as it is elongated and rounded, has a small excisura, a distinctive rostrum, and a very indistinct antirostrum. Several specimens from Sample 587-2,CC (Plate 1, Figs. 13, 14, and 17–20) are more or less corroded, but still show a distinct rostrum, a less distinct antirostrum, and the general outline of otoliths of the genus *Ceratoscopelus*. If the inner face is less corroded the ostium is definitely larger than the cauda. One specimen (Plate 1, Figs. 19, 20) shows some similarities with *Ceratoscopelus madarensis* (Kotthaus, 1972a, text-fig. 92) in having a rather angular outline, which is obvious in the postdorsal angle and the posterior end. Three specimens (Plate 1, Figs. 13–14, 17–18, and 29–30) seem to represent *Ceratoscopelus warmingi* (Kotthaus, 1972a, text-fig. 91) as they have a more rounded outline. Seven badly worn otoliths from Sample 587-3,CC are also placed into this genus, as the outline seems to fit the general description of the genus. A large, badly worn otolith from Sample 587-2,CC probably also belongs to this genus.

Genus *LAMPANYCTUS* Bonaparte, 1840

Lampanyctus sp.

(Plate 1, Figs. 7, 8)

One left sagitta from Sample 587-1,CC is assigned to the genus *Lampanyctus* because the rostrum is short, the excisura is small, and the antirostrum not very prominent. The ventral rim and the outer face are smooth. The specimen has a distinct postdorsal angle, and the ostium is about twice the size of the cauda. The sagitta is similar to some *Lampanyctus* species figured in Nolf and Steurbaut (1983, plate 2, figs. 34–41 and 46–51), one of which comes from the Tortonian stratotype in Italy. Another otolith found in Sample 587-3,CC is badly worn and is only tentatively assigned to this genus.

Family NOMEIDAE Günther, 1880

?*Nomeidarum* sp.

(Plate 1, Figs. 27, 28)

A single, right, probably juvenile sagitta from Sample 587-2,CC having clear perciform characters belongs to the suborder Stromateoidei. It is somewhat elongated, with a prominent rostrum and a small antirostrum which is separated from the rostrum by a distinct excisura. The sulcus is wide and long, and slightly bent downward at the posterior end. The ventral part of the outer face shows distinct radiating grooves.

Otoliths of many species of this suborder are still unknown and no Recent material is available from the Tetragonuridae and Pampidae. The outline of the otolith shows some resemblances to otoliths of the Stromateidae family (see Schmidt, 1968, plate 10, figs. 142–144, and plate 22). The present otolith does not belong to the Centrolophidae family, which possesses otoliths with a narrow sulcus. Butler (1979) illustrates otoliths of four *Cubiceps* species belonging to the Nomeidae family. The fossil otolith resembles *C. baxteri* the most in general outline, rostrum, antirostrum, and excisura. It resembles *C. pauciradiatus* the most in the shape of the sulcus and ornamentation. It may belong to a genus of the Nomeidae of which the otoliths are still unknown. Judging by the otoliths of the four *Cubiceps* species illustrated by Butler (1979), it seems indeed inevitable that these species belong to three different genera: the differences in the shapes of the outline and sulcus are too large for inclusion in only one genus.

Unidentifiable otoliths

(Plate 2, Figs. 1–5)

In Samples 587-1,CC and 587-2,CC three broken pieces of otoliths were recovered but could not be identified. In Sample 587-3,CC, 29 otoliths could not be identified because they are heavily worn, with the inner face more or less dissolved. Most probably they belong to the lanternfish family (Myctophidae). Some of these are split along the median axis, showing excellent growth patterns discussed below.

Heavy corrosion and solution signs are always noted on the inner face, where deep depressions, including the central core, are visible. The marked differences in the fine structure within and outside the sulcus probably caused the selective corrosion of the inner face of deep sea fish otoliths, as discussed by Martini (1974)[3]. The present material supports this assumption, as only the inner faces are dissolved and the outer faces are commonly better preserved.

FINE STRUCTURE AND GROWTH LAYERS

Growth layers in fish otoliths are commonly considered as seasonal accretions of calcium carbonate in the form of aragonite prisms and an organic matrix consisting of protein (Degens et al., 1969). The larger and transparent layers are built during spring and summer. The smaller and darker layers represent slower accretion during late summer and autumn (Weiler, 1958). They are termed "summer" and "winter" layers, although pluvial and dry periods or changes in temperature may also result in different growth layers. Pannella (1971) demonstrated that growth takes place by daily increments, and recurrent patterns show a fortnightly and monthly periodicity. Also spawning rings were microscopically distinguishable from "winter"-rings.

Several otoliths from Sample 587-3,CC are split along their median axis and are somewhat etched, revealing detailed growth layers. A typical specimen, which unfortunately cannot be assigned to any family, is figured on Plate 2 using scanning electron microscope (SEM) techniques. The embryonal core is clearly visible (Plate 2, Fig. 1) and the aragonite fibers show only faint layering (Plate 2, Fig. 2). The more prominent rings succeeding each other in declining thickness may indicate an age of 4.5 yr. for the present specimen. Within the supposed seasonal sections a series of additional layers is visible in the first two cycles; they consist of about 15 layers in the second cycle. In the third and fourth cycle the total thickness is smaller than in the first and second cycles; this may be related to sexual maturity (Pannella, 1971). With this age the accretion of aragonite slows down, resulting in slower growth of the otoliths. Within the third and fourth cycle several distinct accretion layers of somewhat spongy aragonite fibers can be observed (Plate 2, Figs. 3–5). At present these cannot be related to any seasonal fluctuation in the life cycles of deep sea fishes, although one possibility, besides those discussed by Pannella (1979), may also be dependence on the life cycle of copepods. Additional investigations of better-preserved material are necessary to evaluate the nature of growth layers in deep sea fish otoliths.

DISCUSSION

The Quaternary otolith association of Hole 587 on Lord Howe Rise is clearly dominated (86.5%) by otoliths of the Lanternfish family (Myctophidae); 10% are from Deepsea Bristlemouths (Gonostomidae), and only 3.5% can be attributed to the ?Stromatoidei, if one leaves aside the unidentifiable otoliths.

The Myctophidae are mesopelagic fishes forming gigantic swarms at between 200 and 1000 m. On dark nights they rise close to the surface following copepods, their favorite food (Schwarzhans, 1980). Myctophidae otoliths also dominate Recent otolith assemblages in oceanic sediments below approximately 150 m (Wigley and Stinton, 1973). The Deepsea Bristlemouths commonly inhabit the seas offshore New Zealand below 1000 m

---

[3] Magnification for figs. 1b and 1c in Martini, 1974, should read × 450 rather than × 900.

(Ayling and Cox, 1982), whereas most Stromateoids are epi- and mesopelagic fishes in all oceans.

The otolith association of Hole 587 is very similar to the assemblages of Holes 242 and 246 in the Indian Ocean (Martini, 1974), where the Myctophidae also clearly dominate. The present water depths of these localities are all below 1000 m. In depths not exceeding 407 m around southern Norway, Gaemers (1978) reported the importance of Gadidae together with Myctophidae in the deeper assemblages, quite different in this aspect from true deep sea occurrences.

In Hole 587 pteropod shells are found in all core-catcher samples (587-1,CC–587-4,CC) investigated for the present study. As pteropod shells, like the otoliths, are built of aragonite, their dissolution patterns in the world oceans are closely related. Berger (1978) reported the critical depth for pteropod shell preservation in the area of Site 587 as between 1100 and 1300 m, in accordance with the present water depth at Site 587, in which fish otoliths are rather common. At Site 594 only one well-preserved otolith was found in Sample 594-3,CC. Core-catcher samples from Hole 594B were checked in detail from 594B-1,CC to 594B-5,CC, but no further otoliths were found. Pteropod shells are missing, in accordance with data given in Berger (1978, fig. 1). The sieved fraction (greater than 63 μm) contains abundant planktonic foraminifers and, in varying frequency, benthic foraminifers, chinoid spines, sponge spicules, ostracodes, and very rare *Chlamys* in Sample 594B-3,CC. Some of this material may be redeposited from higher levels, as discussed in the Site 594 site chapter; the single otolith of the genus *Lampanyctodes* may also be erratic.

Fish otoliths from the New Zealand Tertiary are described in several papers by Frost (1924, 1928, 1933), Stinton (1957), Schwarzhans (1980), and Grenfell (1984). Schwarzhans revised the earlier literature and he also figured otoliths from Recent species for comparison. The Myctophidae played an important role in the Tertiary fish assemblages of New Zealand, as they do today. From the myctophid otoliths from Holes 587 and 594 only the genera *Centrobranchus* and *Ceratoscopelus* seem not to be represented in the Tertiary of New Zealand. Furthermore, representatives of the genus *Valenciennellus* (Family Gonostomidae) may be restricted to the Quaternary. For occurrences of Recent species compared with the otoliths found in Holes 587 and 594, the detailed papers by Kawaguchi et al. (1972), Kawaguchi and Shimizu (1978), and Kotthaus (1972a, b) should be consulted.

ACKNOWLEDGMENTS

Thanks are due to the Deutsche Forschungsgemeinschaft (Bonn-Bad Godesberg) for supporting the present study. B. Kahl (Geologisch-Paläontologisches Institut der Universität, Frankfurt am Main) made the excellent photographs of the otoliths (Plate 1). SEM pictures (Plate 2) were taken by J. Tochtenhagen with a Stereoscan Mark 2, which was provided to the Geologisch-Paläontologisches Institut der Universität, Frankfurt am Main, by the VW-Stiftung. Our thanks also go to Dr. W. Schwarzhans (Berlin) for valuable discussions and for reviewing this paper.

REFERENCES

Ayling, T., and Cox, G. J., 1982. *Collins Guide to the Sea Fishes of New Zealand:* Auckland (Collins Publ. Ltd.).

Beckmann, J. P., 1976. Shallow-water foraminifers and associated microfossils from Sites 315, 316, and 318, DSDP Leg 33. *In* Schlanger, S. O., Jackson, E. D., et al., *Init. Repts. DSDP*, 33: Washington (U.S. Govt. Printing Office), 467–489.

Berger, W. H., 1978. Deep-sea carbonate: pteropod distribution and the aragonite compensation depth. *Deep-Sea Res.*, 25:447–452.

Bizon, G., Cita, M. B., Müller, C. and Wright, R., 1978. DSDP Leg 42A biostratigraphic range charts. *In* Hsü. K. J., Montadert, L., et al., *Init. Repts. DSDP*, 42, Pt. 1: Washington (U.S. Govt. Printing Office), 1095–1138.

Butler, J. L., 1979. The nomeid genus *Cubiceps* (Pisces) with a description of a new species. *Bull. Mar. Sci.*, 29(2):226–241.

Degens, E. T., Deuser, W. G., and Haedrich, R. L., 1969. Molecular structure and composition of fish otoliths. *Mar. Biol.*, 2(2):105–113.

Frost, E. A., 1924. Otoliths of fishes from the Tertiary formations of New Zealand. *Trans. Proc. N. Z. Inst.*, 55:605–614.

———, 1928. Otoliths of fishes from the Tertiary formations of New Zealand and Balcombe Bay, Victoria. *Trans. Proc. N. Z. Inst.*, 59:91–97.

———, 1933. Otoliths of fishes from the Tertiary formations of New Zealand. *Trans. Proc. N. Z. Inst.*, 63:133–142.

Gaemers, P. A. M., 1978. Late Quaternary and Recent otoliths from the seas around southern Norway. *Meded. Werkgr. Tert. Kwart. Geol.*, 15:101–117.

Grenfell, H. R., 1984. Early Miocene teleost otoliths from Parengarenga Harbour, New Zealand. *N. Z. J. Geol. Geophys.*, 27:51–96.

Hecht, T., and Hecht, A., 1981. A descriptive systematic study of the otoliths of the neopterygean marine fishes of South Africa. Part IV: Siluriformes and Myctophiformes. *Trans. R. Soc. S. Afr.*, 44(3): 401–440.

Karrer, C., 1973. Ueber Fische aus dem Südostatlantik. *Mitt. Zool. Mus. Berlin*, 49(1):191–257.

Kawaguchi, K., Ikeda, H., Tamura, M., and Ueyanagi, S., 1972. Geographical distribution of surface-migrating myctophid fishes (genus Myctophum) in the tropical and subtropical Pacific and Indian Oceans. *Bull. Far Seas Fish Res. Lab.*, 6:23–37.

Kawaguchi, K., and Shimizu, H., 1978. Taxonomy and distribution of the lanternfishes, genus *Diaphus* (pisces, Myctophidae) in the western Pacific, eastern Indian Oceans and the southeast Asian Seas. *Bull. Ocean Res. Inst. Univ. Tokyo*, 10:1–145.

Kotthaus, A., 1967. Fische des Indischen Ozeans. Ergebnisse der ichthyologischen Untersuchungen während der Expedition des Forschungsschiffes "Meteor" in den Indischen Ozean, Oktober 1964 bis Mai 1965. *"Meteor" Forsch., D1*, pp. 1–84.

———, 1972a. Die meso- und bathypelagischen Fische der "Meteor"-Rossbreiten-Expedition 1970 (2. und 3. Fahrtabschnitt). *"Meteor" Forsch., D11*, pp. 1–28.

———, 1972b. Fische des Indischen Ozeans. Ergebnisse der ichthyologischen Untersuchungen während der Expedition des Forschungsschiffes "Meteor" in den Indischen Ozean. Oktober 1964 bis Mai 1965. A. Systematischer Teil, IX. Iniomi (Nachtrag: Fam. Myctophidae). *"Meteor"-Forsch., D12*, pp. 12–35.

Martini, E., 1974. Quaternary fish otoliths from Sites 242 and 246—Leg 25, Deep Sea Drilling Project. *In* Simpson, E. S. W., Schlich, R., et al., *Init. Repts. DSDP*, 25: Washington (U.S. Govt. Printing Office), 647–655.

Nolf, D., and Steurbaut, E., 1983. Révision des otolithes de téléostéens du Tortonien stratotypique et de Montegibbo (Miocène Supérieur d'Italie septentrionale). *Meded. Werkgr. Tert. Kwart. Geol.*, 20(4):143–197.

Pannella, G., 1971. Fish otoliths: daily growth layer and periodical patterns. *Science*, 173:1124–1127.

Schmidt, W., 1968. Vergleichend morphologische Studie über die Otolithen mariner Knochenfische. *Arch. Fischereiwiss.*, 19,1:1–96.

Schwarzhans, W., 1980. Die tertiäre Teleosteer-Fauna Neuseelands, rekonstruiert anhand von Otolithen. *Berl. Geowissensch. Abh.*, A 26:1–211.

Steurbaut, E., 1982. Les otolithes de téléostéens du gisement de Peyrère à Peyrehorade (couches de passage de l'Oligocène au Miocène d'Aquitaine méridionale, France). *Meded. Werkgr. Tert. Kwart. Geol.*, 19(2):35–57.

Stinton, F., 1957. Teleostean otoliths from the Tertiary of New Zealand. *Trans. R. Soc. N.Z.*, 84:513–517.

Weiler, W., 1958. Fischreste, insbesondere Otolithen. *In* Freund, H. (Ed.), *Handbuch der Mikroskopie in der Technik* (Vol. 2) (3): Frankfurt am Main (Umschau Verlag), pp. 265–280.

________, 1971. Fisch-Otolithen aus dem Jungtertiär Süd-Siziliens. *Senckenb. Leth.* 52(1):5–37.

Weitzman, S. H., 1974. Osteology and evolutionary relationships of the Sternoptychidae, with a new classification of Stomatoid otoliths. *Bull. Am. Mus. Nat. Hist.*, 153(3):331–478.

Wigley, R. L., and Stinton, F. C., 1973. Distribution of macroscopic remains of Recent animals from marine sediments off Massachusetts. *Fish. Bull. (U.S.)*, 71(1):1–40.

Date of Initial Receipt: 4 June 1984
Date of Acceptance: 26 October 1984

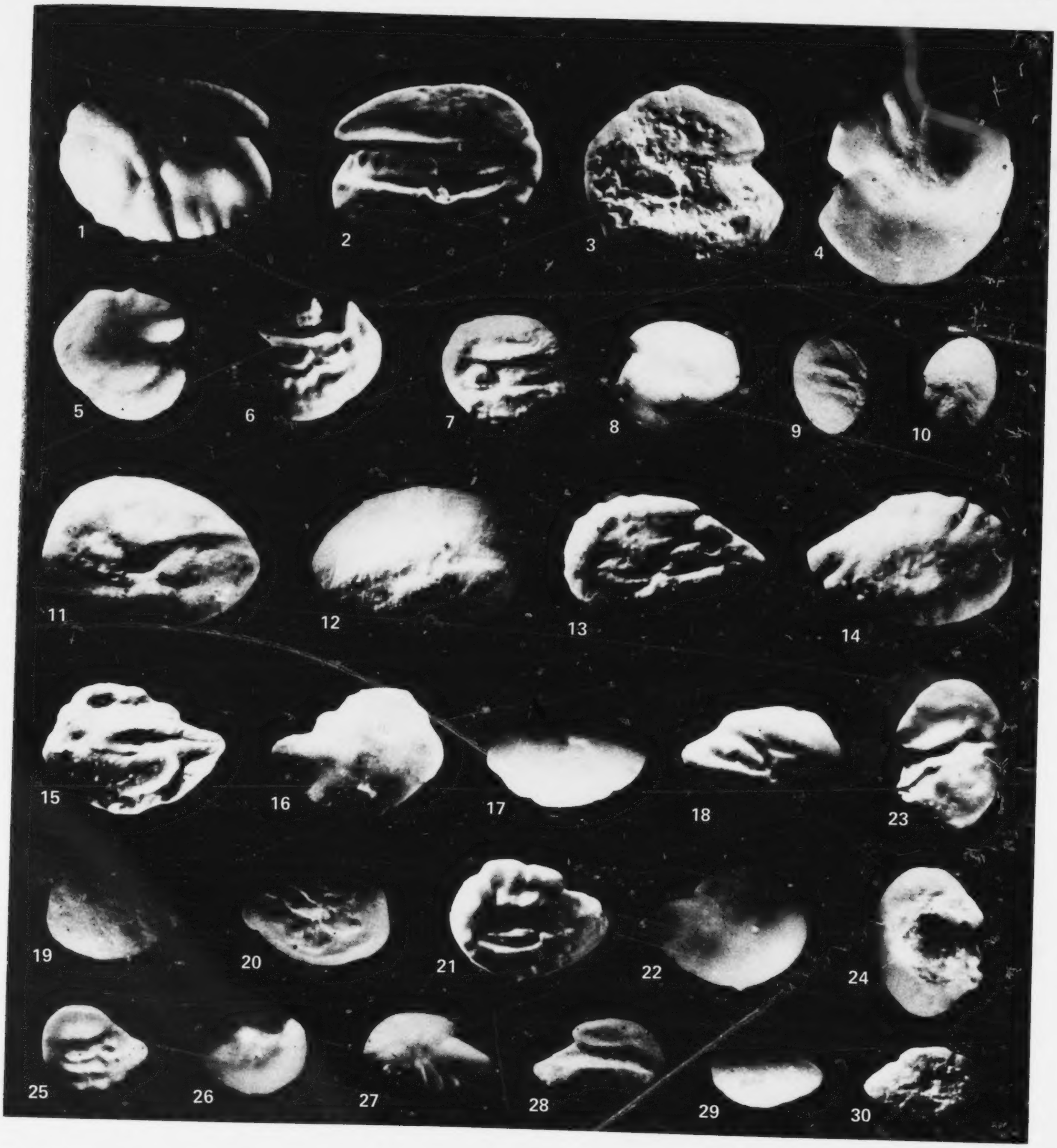

Plate 1. (All specimens approximately ×20) **1, 2.** *Lampanyctodes* aff. *hectoris*, right sagitta, Sample 594-3,CC, (1) outer face; (2) inner face. **3, 4.** *Hygophum benoiti*, left sagitta, Sample 587-1,CC, (3) inner face; (4) outer face. **5, 6.** *Hygophum macrochir*, right sagitta, Sample 587-2,CC, (5) inner face; (6) outer face. **7, 8.** *Lampanyctus* sp., left sagitta, Sample 587-1,CC, (7) inner face; (8) outer face. **9, 10.** *Valenciennellus tripunctulatus*, left sagitta, Sample 587-2,CC, (9) inner face; (10) outer face. **11, 12.** *Ceratoscopelus* sp., left sagitta, Sample 587-2,CC, (11) inner face; (12) outer face. **13, 14.** *Ceratoscopelus* sp. cf. *C. warmingi*, left sagitta, Sample 587-2,CC, (13) inner face; (14) outer face. **15, 16.** *Bonapartia* sp., left sagitta, Sample 587-2,CC, (15) inner face; (16) outer face. **17, 18.** *Ceratoscopelus* sp. cf. *C. warmingi*, right sagitta, Sample 587-2,CC, (17) outer face; (18) inner face. **19, 20.** *Ceratoscopelus* sp. cf. *C. maderensis*, right sagitta, Sample 587-2,CC, (19) outer face; (20) inner face. **21, 22.** *Diaphus subtilis*, left sagitta, Sample 587-2,CC, (21) inner face; (22) outer face. **23, 24.** *Valenciennellus tripunctulatus*, right sagitta, Sample 587-1,CC, (23) inner face; (24) outer face. **25, 26.** *Diaphus subtilis*, left sagitta, Sample 587-1,CC, (25) inner face; (26) outer face. **27, 28.** ?*Nomeidarum* sp., right sagitta, Sample 587-2,CC, (27) outer face; (28) inner face. **29, 30.** *Ceratoscopelus* sp. cf. *C. warmingi*, left sagitta, Sample 587-1,CC, (29) inner face; (30) outer face.

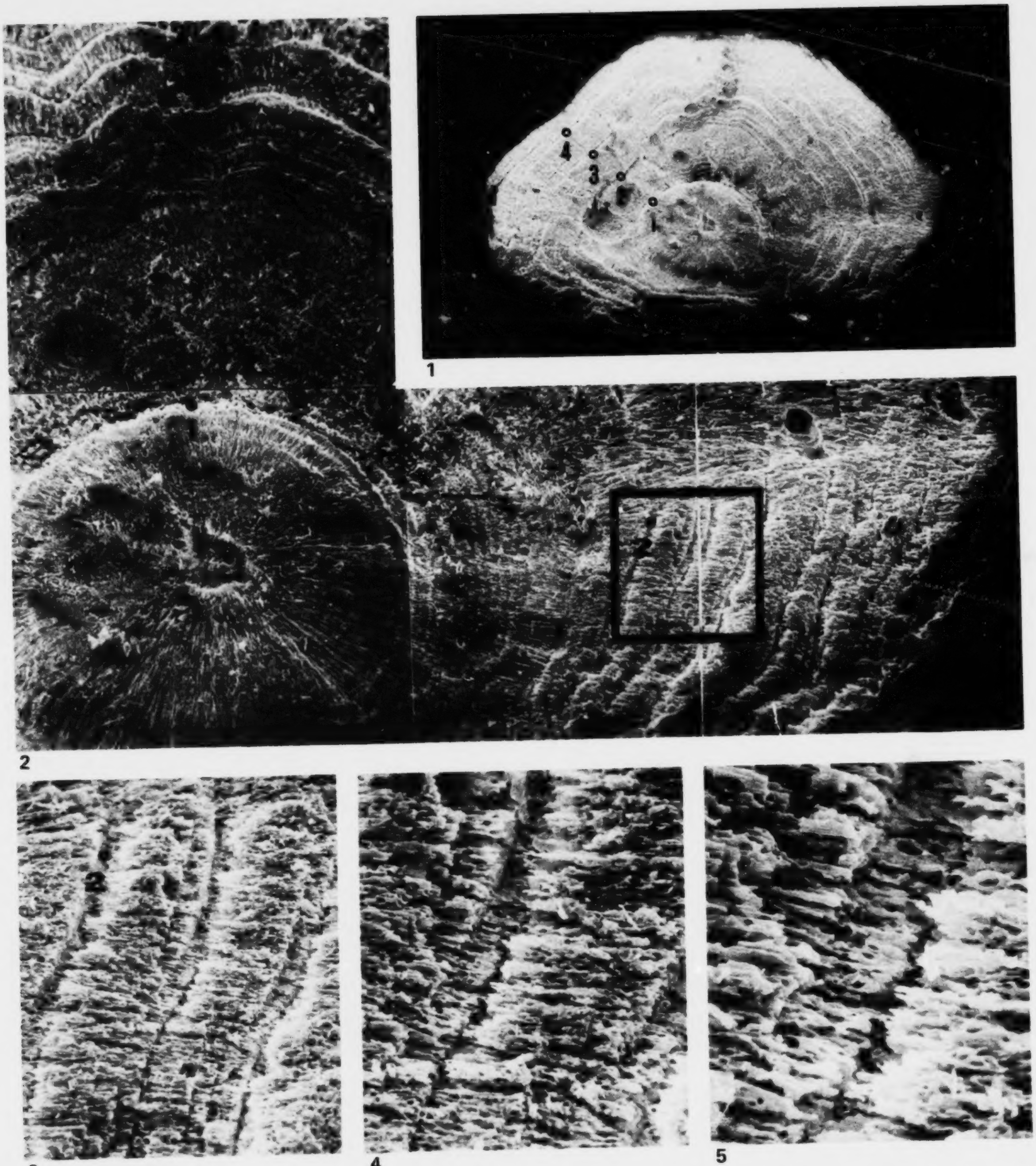

Plate 2. SEM pictures of unidentified otolith, corroded inner face showing growth layers, from Sample 587-3,CC. **1.** Overall view, × 42. **2.** Enlarged section of Figure 1, × 145. **3–5.** Details of growth layers in the right part of Fig. 2 (square), (3) × 365; (4) × 730, (5) × 1460.

20. BIOSTRATIGRAPHY AND BIOGEOGRAPHY OF TERTIARY BATHYAL BENTHIC FORAMINIFERS: TASMAN SEA, CORAL SEA, AND ON THE CHATHAM RISE (DEEP SEA DRILLING PROJECT, LEG 90)[1]

Anne Boersma[2]

ABSTRACT

Eocene through Pliocene benthic foraminifers were examined from seven sites located at middle and lower bathyal depths on the Lord Howe Rise in the Tasman Sea, from another site at lower bathyal depths in the Coral Sea, and from a site in the intermediate-depth, hemipelagic province of the Chatham Rise, east of southern New Zealand. Age-related, depth-related, and bioprovincial faunal variations are documented in this chapter. One new species, *Rectuvigerina tasmana*, is named. The paleoecologic indications of several key groups, including the miliolids, uvigerinids, nuttallitids, and cibicidids, are combined with sedimentologic and stable isotopic tracers to interpret paleoceanographic changes in the Tasman Sea.

Because the total stratigraphic ranges of many bathyal benthic foraminifers are not yet known, most endpoints in the Tasman Sea are considered ecologically controlled events. The disappearances of *Uvigerina rippensis* and *Cibicidoides parki* and the first appearances of *U. pigmaea, Sphaeroidina bulloides*, and *Rotaliatina sulcigera* at the Eocene/Oligocene boundary can be considered evolutionary events, as also can the first appearance of *Cibicides wuellerstorfi* in Zone NN5.

Species which are restricted to the lower bathyal zone except during discrete pulses, most of which are related to the development of glacial conditions, include *Melonis pompilioides, M. sphaeroides, Pullenia quinqueloba, Nuttallides umbonifera*, and *U. hispido-costata*. Middle bathyal indigenes include *U. spinulosa, U. gemmaeformis, Ehrenbergina marwicki, R. sulcigera*, and all rectuvigerinids except *Rectuvigerina spinea*. Although the miliolids first occurred at lower bathyal depths, they were more common in the middle bathyal zone. Although the Neogene hispido-costate uvigerinids first developed at lower bathyal depths and at higher middle latitude sites, in the later Neogene this group migrated to shallower depths and became predominant also in the middle bathyal zone.

Despite the relatively similar sedimentologic settings at the six middle bathyal Tasman sites, there was extensive intrageneric and intraspecific geographic variation. Mililiolids, strongly ornamented brizalinids, bolivinitids, *Bulimina aculeata, Osangularia culter*, and strongly porous morphotypes were more common at higher latitudes. *Osangularia bengalensis*, striate brizalinids such as *Brizalina subaenariensis, Gaudryina solida*, osangularids in general, and finely porous morphotypes were more common in the subtropics. There was strong covariance between faunas at lower middle latitude, lower bathyal Site 591, and higher middle latitude, middle bathyal Site 593.

The following oceanographic history of the Tasman Sea is proposed; using the stable isotopic record as evidence for glacials and examining the ecologic correlations between (1) miliolids and carbonate saturation, (2) nuttallitids and undersaturated, cooled, or "new" water masses, (3) uvigerinids with high organic carbon in the sediment and high rates of sediment accumulation, and (4) cibicidids and terrestrial organic carbon. The glacial located near the Eocene/Oligocene boundary is characterized by the penetration of cooler, more corrosive waters at intermediate depths in high southern latitudes. This may have caused overturn, upwelling pulses, in other Tasman areas. The development of Neogene-like conditions began in the late Oligocene (Zone NP24/NP25) with the evolution of several common Neogene species. A large number of Paleogene benthics disappeared gradually through the course of the early Miocene, which was not well preserved at any Tasman site. Corrosive conditions shallowed into the middle bathyal zone in several pulses during the early Miocene.

The development of glacial conditions in the middle Miocene was accompanied by major changes throughout the Tasman Sea. Sediment accumulation rates increased and high-productivity faunas and corrosive conditions developed at all but the lowest-latitude Site 588. This increase in productivity and accumulation rate is attributed to the eutrophication of Antarctic water masses feeding Tasman current systems, as well as to invigorated circulation in general. It overlaps with the beginning of the Pacific High-productivity Episode (10–5 Ma). During the latest Miocene glacial episode, corrosive conditions developed at lower bathyal depths, while cooler water and lower nutrient levels shallowed to middle bathyal depths. Lower input of terrestrial organic carbon may be related to the lower nutrient levels of this time and to the termination of the Pacific High-productivity Episode.

The moderate glacial episode during the mid-Pliocene (Zone NN15/NN16, ~3.2 Ma) corresponds to a decline in sediment accumulation rates and a reorganization of faunas unlike that of all other times. New genera proliferate and indices for cool, noncorrosive conditions and high organic carbon expand throughout the middle bathyal zone coeval with the sedimentation rate decreases. By the latest Pliocene (about 2.5 Ma), however, during another glacial episode, faunal patterns typical of this and later glacials develop throughout the Tasman Sea. Benthic foraminiferal patterns suggest increased input of terrestrial organic matter to Tasman Sea sediments during this episode and during later glacials.

INTRODUCTION

During DSDP Leg 90, seven sites were drilled along the Lord Howe Rise, the medial ridge of the Tasman Sea. These sites occupied a latitudinal range of from near 21°S to over 40°S, and all but one were drilled at depths of between 1000 and 2000 m (Table 1). An additional high-latitude site, Site 594, was drilled on the Chatham Rise, in the hemipelagic province to the southeast of New Zealand. In order to construct a latitudinal traverse extending to the equator, Site 586, drilled on Leg 89 in 2,207 m water depth on the Ontong-Java Plateau (Fig. 1), was made available for this study.

---

[1] Kennett, J. P., von der Borch, C. C., et al., *Init. Repts. DSDP*, 90: Washington (U.S. Govt. Printing Office).

[2] Address: Microclimates, P.O. Box 404, RR1, Stony Point, NY 10980.

Table 1. Location and drilling data for Leg 90 sites.

Site	Water depth (m)	Latitude (S)	Longitude (E)
586	2207	0°29	158°29
587	1101	21°11	161°19
588	1533	26°06	161°13
589	1391	30°42	163°38
590	1299	31°10	163°21
591	2131	31°35	164°26
592	1098	36°28	165°26
593	1068	40°30	167°40
594	1204	45°31	174°56

Cenozoic sediments were recovered from all sites; the only Paleogene samples were cored at Sites 588, 592, and 593. Faunas of the late Eocene through the late Pliocene only are described here.

This chapter documents, with extensive faunal lists, scanning electron microscopy, and detailed species descriptions the large and unique intermediate-depth benthic foraminiferal faunas of the Tasman Sea. In addition, faunal and specific variability through depth and latitude have been analyzed during the following climatic and sedimentologic events: (1) the Eocene/Oligocene boundary; (2) the mid-Miocene glacial; (3) the late Miocene carbon isotope excursion; and (4) the late Miocene through early Pliocene sedimentation increase.

METHODS

Between 15 and 35 samples from each series (lower, middle, or upper) were processed on >149 μm sieve. An aliquot of 0.5 mg was split out of the washed fraction, and all benthic foraminifers were picked from that 0.5 mg. All species in faunas consisting of several hundred individuals are listed for each series recovered at each site.

Biostratigraphic subdivision of each site and intersite correlations follow the schemes of Jenkins and Srinivasan (this volume). Sedimentation rates were calculated on the basis of the nannofossil biostratigraphy (see site chapters, this volume).

TAXONOMY

For this report I have made an extensive search of the older literature and of topotypic faunas described in that literature in order to update some of the benthic foraminiferal taxonomy. For the most part benthic foraminifers described in Deep Sea Drilling volumes are still reported according to the taxonomy developed largely in the western hemisphere by Cushman, Bermudez, Beckmann, Renz, and others. Tertiary-age middle to lower bathyal benthic foraminifers were, however, cosmopolitan and ranged into areas as far removed as the Vienna Basin, the Cape Basin, and the type Bortonian of New Zealand. Benthic foraminiferal faunas of the eastern hemisphere were, for the most part, described much earlier (for example, d'Orbigny, 1846; Reuss, 1851; Schwager, 1866) and many of those names should take precedence.

Many of the synonyms found in the literature on bathyal benthics reflect the process of geographic variation which has, throughout the Tertiary, produced specific morphotypes in each biogeographic province of the world ocean. Thus, the lower bathyal hispido-costate uvigerinid of the Caribbean province in the early Oligocene is called *Uvigerina spinicostata* Cushman and Bermudez; the austral variant is named *U. bortotara* Finlay. The two taxa reflect the fact that more costae are consistently developed on this form in the southwest Pacific than in the Caribbean.

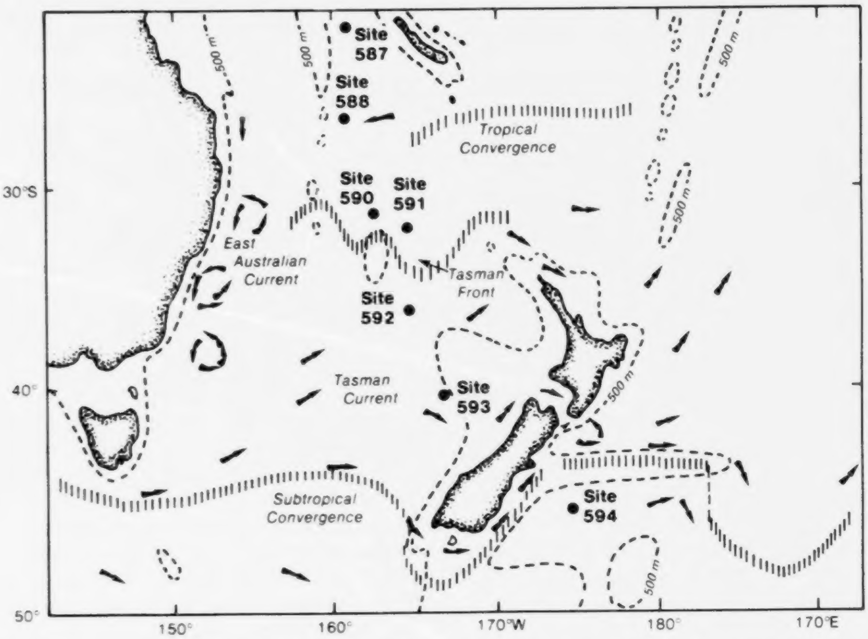

Figure 1. Location map of Leg 90 sites in the Tasman Sea, Coral Sea, and on the Chatham Rise.

The correct procedure for distinguishing this type of ecophenotypic variation is to erect *forma* for the younger, distinguishable variants. Because this taxonomy is so ponderous and because many variants do have determinable features which differentiate them, I have, for the most part, retained the geographically defined names in this report.

SITE DESCRIPTIONS

For each site the following aspects of the faunas will be briefly described: (1) general faunal aspects; (2) most consistently appearing species; (3) species unique to the site; (4) dominant species; (5) other fossils; and (6) the total number of species.

Hole 586B

Sediments of latest Miocene (Zone N17a) through latest Pliocene (Zone N21) age were recovered in this hole, which was drilled at 2,207 m water depth on the Ontong-Java Plateau near DSDP Site 289. Preservation of benthic foraminifers is only fair to moderate through most of this interval; it improves during the latest Pliocene Zone N21, when it is generally good.

The 63 species of benthic foraminifers identified in the late Miocene at this site are listed in Appendix Table 1. Highly dominant species are *Uvigerina proboscidea* Schwager, *Uvigerina hispido-costata* Cushman and Todd, and *Uvigerina auberiana* d'Orbigny—this species last primarily at the very end of the Miocene, in sediments which also contain moderate amounts of radiolarians in the coarse fractions. The most consistently occurring species include *Oridorsalis umbonatus* (Reuss), *Cibicides wuellerstorfi* (Schwager), *Globocassidulina subglobosa* (Brady), and diverse miliolids. Unique elements in these faunas include *Melonis sphaeroides* (Voloshnaya), the genus *Bulava*, named by Boltovskoy (1978) from the Ninetyeast Ridge in the Indian Ocean, a new uvigerinid named *Uvigerina tasmana* (Boersma, 1984a), and specimens of *Brizalina aenariensis* (Costa). Species which occur consistently at this site, as well as at the other 2,000-m-deep Site 591, include *Melonis pompilioides* (Fichtel and Moll), *Pullenia quinqueloba* (Reuss), and the spiroplectaminid-form of *Vulvulina pennatula* Batsch. Other similarities between these two deeper-water sites include: (1) consistent appearance of *U. hispido-costata;* (2) absence of most species of rectuvigerinids, *Hopkinsina mioindex* Finlay, or *Osangularia culter* (Parker and Jones); and (3) the occasional presence of *Favocassidulina favus* (Brady).

From Pliocene sediments a total of 63 benthic foraminiferal species were identified (Appendix Table 2). Above the Miocene/Pliocene boundary, *U. auberiana*, the only highly dominant species in this section, occurs during Zones N19–N20, equivalent to nannofossil Zone NN15. Other consistent elements of these faunas include *C. wuellerstorfi* and diverse miliolids. *Nuttallides umbonifera* (Cushman) occurs more consistently here than at any other site; it is absent, however, during the uvigerinid maxima in Zones N19–N20. Species occurring frequently, but not consistently, include *Pyrgo murrhina* Schwager, *U. hispido-costata, Pullenia bulloides* (d'Orbigny), *G. subglobosa*, and *Oridorsalis umbonatus*. Species of *Osangularia, Ehrenbergina*, and *Heterolepa* are much less common here than at other sites.

Site 587

The 13 cores of late Miocene to Quaternary age recovered at Site 587 contained mixed benthic foraminiferal faunas: mixed into an apparently typical intermediate-depth benthic fauna composed of such species as *Textularia lythostrota* (Schwager), *Brizalina aenariensis*, and *Globocassidulina subglobosa*, there were calcareous algae, pteropods, mollusk shells, and shallow-water benthic foraminifers of the genera *Tretomphalus, Amphistegina, Spiropthalmidium, Miliolinella*, and *Elphidium*. From Core 10 to Core 13 (late Miocene), sediments consisted of recrystallizing carbonate sands with rare, larger, benthic foraminifers.

Core 7, of latest Miocene age, contained floods of bolivinids, uvigerinids, and rectuvigerinids, among which there is a new species characterized by very abundant, fine, and wavey striations, most of which are continuous from one chamber to the next; this species, *Rectuvigerina tasmana*, is described in the Annotated List of Species at the end of this chapter.

Site 588

The section recovered at Site 588 extends from upper Oligocene Zone P21a, called the *Chiloguembelina cubensis* Zone in this area, through the upper Pliocene. The lower part of the section, from the Oligocene through the lower Miocene into the *Globorotalia fohsi* Zone, is poorly preserved, benthics are very rare to infrequent, the sediment is recrystallized, and much of the coarse fraction is missing. Poor preservation continues from Cores 588C-19 through 588C-1, and into Core 588B-31; preservation improves, however, and faunas become very diverse in Cores 588B-27 through 588B-25.

Oligocene

Late Oligocene faunas are found in Cores 588C-19 through 588C-9 in recrystallized sediments containing radiolarians, glauconite, and frequently, iron oxides. Most faunas include the solution-resistant forms *Cibicidoides tuxpamensis* (Cole), *Pullenia bulloides, Globocassidulina subglobosa, Oridorsalis umbonatus, Heterolepa kullenbergi* (Parker), *Bulimina semicostata* Nuttall, *Vulvulina spinosa* Cushman, and *Gyroidinoides* spp. (Appendix Table 3).

Despite dissolution, many modern forms appear in the faunas beginning in the latest Oligocene *Globigerina angulisuturalis* Zone (Sample 588-16,CC). These species include *Osangularia bengalensis* (Schwager), *H. kullenbergi, Textularia lythostrata, P. quinqueloba, Uvigerina pigmaea* d'Orbigny, *Bulimina striata* d'Orbigny, *Stilostomella lepidula* (Schwager) and *Melonis barleeanum* (Williamson).

Early to middle Miocene

Sediments of early to middle Miocene age are found in Cores 588C-8 to 588C-1 and 588B-31 to 588B-25. Sediments are more chalky than those underlying. Faunas are slightly larger; a total of 75 species was recognized. The only highly dominant species is *Eggerella bradyi* (Cushman). The most consistently occurring species are *Globocassidulina subglobosa, O. umbonatus, Anomalinoides semicribrata*, the rectuvigerinids, and *Heterolepa kullenbergi. Nuttallides umbonifera* first appears at the base of the section and occurs through the lower Miocene in small numbers (Appendix Table 3).

Uvigerinids found at this site include very spinose forms such as *Uvigerina proboscidea* Schwager and the two species related to *Uvigerina spinulosa* Hadley, *Rectuvigerina ongleyi* Finlay and *Rectuvigerina spinea* (Bermudez).

Within the *Globorotalia fohsi* Zone, preservation improves and the number of benthic foraminifers increases dramatically. *Heterolepa rugosa* (Phleger and Parker) and *Cibicides wuellerstorfi* (Schwager) first occur in this zone.

Middle through late Miocene

Sixty-nine species were identified in middle to upper Miocene sediments in which microfossil preservation was good to moderate (588-25,CC to 588-13-2, 19 cm; Appendix Table 4). Preservation was consistently good through the *Neogloboquadrina continuosa* Zone (Cores 22 through 20).

Highly dominant species occurred only during the late Miocene: *Textularia lythostrota* during the *Globorotalia plesiotumida* Zone and the miliolids in several samples from Cores 13 and 14 at the top of the *G. margaritae* Zone (equivalent to nannofossil Zone NN11b). Species consistently present include *Oridorsalis umbonatus, Sphaeroidina bulloides, T. lythostrata, Stilostomella consobrina* d'Orbigny, *Eggerella bradyi, Heterolepa kullenbergi*, and *Gaudryina solida* Schwager. Whereas *Melonis* cf. *barleeanum* occurred consistently only before the *Globorotalia plesiotumida* Zone, *Osangularia bengalensis* and *Uvigerina hispida* Schwager were consistently present only during the *Globorotalia plesiotumida* Zone and later.

During a latest Miocene episode of miliolid abundance, faunas were characterized by a decrease in *Globocassidulina subglobosa* and *Oridorsalis umbonatus*, and the consistent occurrence of *U. hispida, Bulimina truncana, H. kullenbergi*, and *Gaudryina solida*.

Pliocene

Pliocene sediments at this site are moderately well preserved and contained 77 species of benthic foraminifers, 37 of which were rectilinear (Appendix Table 5). The dominant species were, in the early Pliocene, *Gaudryina solida; Cibicides wuellerstorfi* and *Bolivinopsis praelonga* Schwager in the mid-Pliocene *Globorotalia puncticulata* Zone; and at the very end of the Pliocene *B. praelonga* (Sample 588-4,CC). Species appearing consistently through this section include *Globocassidulina subglobosa, C. wuellerstorfi, Osangularia bengalensis, Bulimina truncana*, and *Eggerella bradyi. Uvigerina proboscidea, Stilostomella lepidula* Schwager, and *H. kullenbergi* are also common. The miliolids and *G. solida* are common only during the early part of the Pliocene, whereas *C. wuellerstorfi, S. lepidula*, and *U. proboscidea* are more common in the *Globorotalia crassaformis* Zone and later.

A large variety of uvigerinids is present in these samples. The hispid types and the small hispido-costate *U. pigmaea* occur with the large costate form *U. gemmaeformis* and the new striate species, *U. tasmana* (Boersma, 1984a). Although *U. spinulosa* and *Rectuvigerina spinea* range into the *Globorotalia tosaensis* Zone, only the hispido-costate species *U. hispido-costata* and *U. dirupta* occur in the latest Pliocene. Both are strongly spinose in this area.

Site 589

Only four cores of Quaternary age were recovered before this site was abandoned. Sediment preservation is good and benthic foraminifers are abundant. In two cores volcanic glass constitutes almost 50% of the sediment. Typical species through this section are *Cassidulina laevigata carinata* Cushman, *Uvigerina dirupta, Heterolepa kullenbergi, Cibicides wuellerstorfi, Oridorsalis umbonatus, U. auberiana, Globocassidulina subglobosa*, and *Stilostomella lepidula*.

Site 590

A uniform sequence of carbonate oozes was recovered at Site 590, in both Holes 590A and 590B. The lower to middle Miocene section is poorly preserved except for Cores 44 to 46, in which preservation is moderate. Middle to upper Miocene sediments (590B-28 to 590B-40,CC and 590A-18 to 590A-27,CC) are fairly to moderately well preserved; good preservation was found only in Sample 590A-26,CC. Preservation improves in the Pliocene, where it is moderate to good from 590A-17,CC to 590A-7,CC, and good in Cores 6 through 14. Radiolarians occur in sediments of the coarse fractions only during the *Neogloboquadrina continuosa* and basal *Globigerina nepenthes* zones of the upper Miocene and in core 590B-47 during the middle Miocene *Globorotalia fohsi* Zone.

Early to middle Miocene

Sediments of early Miocene age were recovered in Cores 590B-53 through 590B-49. The preservation of these levels is extremely poor because of dissolution and recrystallization. Only the dissolution-resistant species, *Globocassidulina subglobosa, Heterolepa kullenbergi, H. rugosa, Oridorsalis umbonatus, Brizalina pusilla* (Schwager), and *Gyroidinoides* spp. were preserved in most levels (Appendix Table 6).

Beginning in the middle Miocene *Globorotalia fohsi* Zone (equivalent to Zone NN6) in Core 590B-46, faunas become slightly more diverse and usually contain *Hopkinsina mioindex* along with the solution-resistant forms. Faunas of the *G. mayeri* Zone are moderately well preserved and more diverse. Consistent elements during this interval include *Eggerella bradyi* along with the solution-resistant group of the early Miocene. Occasionally present are *Melonis barleeanum, Pullenia bulloides*, and *Uvigerina spinulosa* (Appendix Table 6).

Middle to late Miocene

Sediments of middle to late Miocene age are fairly well to moderately well preserved; preservation improves in general toward the end of this interval. Eighty-four benthic species were recognized and are listed in Appendix Table 7.

The *Neogloboquadrina continuosa* and earliest *Globigerina nepenthes* zones are present in Cores 590B-28 through 590B-40. Radiolarians occur throughout these cores. Highly dominant species include *Heterolepa kullenbergi, Eggerella bradyi*, and *Rectuvigerina spinea*, which was consistent and highly dominant in the later part of the *N. continuosa* Zone and earlier *G. nepenthes* Zone. Other consistently occurring species include *Oridorsalis umbonatus* throughout this time; *Uvigerina proboscidea, Hopkinsina mioindex*, and *Brizalina pusilla* occur consistently only from the *G. nepenthes* Zone to the end of the Miocene.

A large faunal shift takes place midway in the *N. continuosa* Zone (Cores 590B-34 to 590B-33). Accompanying an improvement in the preservation and a change in dominance from *H. kullenbergi* to *R. spinea* are large numbers of brizalinids and *Melonis pompilioides*. Radiolarians become much less common above this level.

The late Miocene *G. nepenthes* and *Globorotalia conomiozea* zones are represented from Section 590A-28-5 through 590A-18,CC (Appendix Table 7). Faunas in this interval are generally better preserved and more diverse than those below. Benthic foraminifers become very abundant in one well-preserved fauna (590A-26,CC) which lacks coarse-fraction radiolarians and is dominated by *R. spinea*. Uvigerinids, brizalinids, and cibicidids are the most common forms and *Nuttallides umbonifera, Osangularia bengalensis*, and *U. auberiana* all first occur during this time. The miliolids occur only during the latest Miocene *G. conomiozea* Zone, which is also characterized by the consistent presence of *Bulimina truncana, Stilostomella lepidula, Oridorsalis umbonatus, H. kullenbergi*, and *Globocassidulina subglobosa*, which is not common before this time.

Throughout the late Miocene, *Osangularia bengalensis* is more common than *O. culter*. The spinose uvigerinids and the spinose rectuvigerinids predominate, although *U. gemmaeformis*, a large, striate species, does occur in some samples. *Uvigerina hispido-costata* first occurs near the end of the Miocene. Species of *Laticarinina, Alabamina*, and *Anomalinoides* are not common, and both *C. wuellerstorfi* and *G. subglobosa* are noteworthy by their absence from many samples.

Pliocene

Eighty-three benthic foraminiferal species were identified from Pliocene sediments in Core 590A-17 through Sample 590A-4-4, 19 cm (Appendix Table 8). Preservation varies from moderate to good; the good preservation is typical of the beginning and the end of this interval. Highly dominant species include *Uvigerina proboscidea, U. hispida*, and *Uvigerina striata* d'Orbigny in the *Globorotalia crassaformis* Zone and *U. proboscidea, U. auberiana, U. striata, U. hispido-costata*, and *Uvigerina asperula* Czjeck during the *Globorotalia inflata* Zone. The uvigerinids occurred less consistently than *Heterolepa kullenbergi, T. lythostrota, S. lepidula*, or *G. subglobosa*.

In the late Pliocene, before Zone NN19–NN20, rectilinear genera such as *Stilostomella, Ehrenbergina*, and *Uvigerina* are most common, whereas cibicidids are rare; the pattern reverses in Zone NN19–NN20.

Site 591

A section ranging in age from early Miocene through late Pliocene was recovered from Holes 591 and 591B. As at several other sites, the preservation in the early Miocene is poor, improves to fair to moderate in the late Miocene, and is generally moderate throughout the Pliocene. Radiolarians occur in the coarse fractions only during the *Globorotalia mayeri* Zone (Core 591B-11) and in the later Miocene *G. conomiozea* Zone (Cores 591-22 and 591-21).

Early to middle Miocene

Early to middle Miocene faunas were found in Cores 591B-24 to 591B-8 (Appendix Table 9). From Cores 24 through 20, sediments are recrystallized and most of the foraminifers are broken. Solution-resistant species in this type of sediment are *Oridorsalis umbonatus* and *Eggerella bradyi*. Faunas become more diverse beginning in Core 18, but even in the late Miocene faunas are smaller than those at other sites and sediments are generally less well preserved.

In this section where species abundances may be largely the result of the dissolution process, dominant species include *Globocassidulina subglobosa* and *Nuttalides umbonifera*. The most consistently occurring species are *O. umbonatus, E. bradyi, Cibicides wuellerstorfi, G. subglobosa*, and *Heterolepa kullenbergi*.

Twelve species first occur in the Tasman Sea at Site 591 during the early middle Miocene (see section on biostratigraphy). *Nuttallides umbonifera* first appears at this site during the *Orbulina suturalis* Zone (equivalent to nannofossil Zone NN5). It recurs, along with frequent *C. wuellerstorfi*, during the mid *Globorotalia fohsi* Zone (591B-15,CC). During the *G. mayeri* Zone in Cores 591B-12 and 591B-11 (equivalent to nannofossil Zone NN7 and NN8), *Pullenia bulloides* and *N. umbonifera* both become dominant faunal elements, and *N. umbonifera* is very large. Faunas containing large-sized, abundant *N. umbonifera* occur at Site 594 at this same time.

Late Miocene

In the fairly to moderately well preserved late Miocene faunas (591-31,CC to 591-20-4, 19 cm) 65 species of benthic foraminifers were recognized (Appendix Table 10). Beginning in the *Globigerina nepenthes* Zone, the dominant species are *Uvigerina hispido-costata, Pyrgo comata* (Schwager), and other diverse miliolids. The most consistently occurring species besides *U. hispido-costata* are *Bulimina truncana, Heterolepa kullenbergi, Oridorsalis umbonatus* and, to a lesser degree, *Sigmoilopsis schlumbergeri* (Silvestri) and *Pyrgo* spp. *Globocassidulina subglobosa* is usually rare.

Faunas in Cores 591-21 to 591-27 (*Neogloboquadrina continuosa* into *Globorotalia conomiozea* zones) contain very abundant miliolid fragments. Typically there are few species, but many specimens of each. The residue fauna found in very dissolved sediments in Core 21 is different from those of the earlier Miocene at this site; it includes *P. murrhina, O. umbonatus, Nuttalides umbonifera, Quinqueloculina seminulina* Linne, *Cibicidoides cicatricosus* (Schwager), *Ehrenbergina* spp., and *Gyroidinoides* spp.

Near the end of the sequence faunas are more diverse, contain few agglutinated species, rare *Globocassidulina subglobosa*, and very few anomalinids. *Uvigerina hispido-costata* has been replaced by *U. hispida* and several different species such as *Laticarinina halophora* (Stache) and *Brizalina finlayi* (Hornibrook) reappear.

Pliocene

The 66 species of benthic foraminifers that are identified through this section are listed in Appendix Table 11. Twenty-six of these species are rectilinear and approximately six are agglutinated. Species which become strongly dominant include *Pyrgo* spp. and *Bulimina truncana*, and the most consistently occurring forms along with *B. truncana* are *Stilostomella consobrina, Globocassidulina subglobosa, Oridorsalis umbonatus*, and *Cibicidoides bradyi* (Trauth). Cibicidids become frequent at the end of the Pliocene.

Osangularia bengalensis, but not *O. culter*, occurs at this site. Uvigerinids are primarily hispido-costate with the addition of the spinose *U. proboscidea*. *Hopkinsina mioindex* recurs during the middle *Globorotalia crassaformis* Zone and occurs consistently into the mid *G. tosaensis* Zone.

Site 592

The section at this site extends from the upper Eocene *Globigerina aculeata* Zone through the upper Pliocene. However, the entire upper Oligocene and the first zone of the Miocene are missing. Sediments of the upper Eocene and lower Miocene are fairly well preserved, those of the upper Miocene moderately well preserved, and preservation throughout the Pliocene is good. Few radiolarians were found in the coarse fractions.

Paleogene

Seventy-five species were identified from sediments of late Eocene through early Oligocene age at this site. Preservation in the upper Eocene sediments was fair to moderate; it improved in the lower Oligocene (Appendix Table 12). Highly dominant species in this section include *Cibicidoides parki* (Finlay), *Uvigerina bortotara* Finlay, *Anomalinoides aragonensis* (Nuttall), and *Oridorsalis umbonatus*. There are many species which occur very consistently throughout this sequence; they include *Globocassidulina subglobosa, U. bortotara, Hanzawaia cushmani, C. parki, O. umbonatus, Cibicidoides grimsdalei* Cole, *Anomalinoides alazanensis* (Nuttall), *Anomalinoides semiteres* Finlay, *Cibicidoides* cf. *ungerianus* d'Orbigny, and *Heterolepa* trans. *kullenbergi*.

The Eocene/Oligocene boundary is located between Sample 592-36-2, 19 cm and 592-35,CC. Radiolarians appear just within this interval, but disappear immediately afterwards. Species which disappear at this time include *C. parki, Uvigerina rippensis* Cole, *Rotaliatina sulcigera* Finlay, and *Cibicidoides tuxpamensis* Nuttall. Just above the boundary *Pullenia bulloides, U. bortotara*, and *U.* cf. *pigmaea* also disappear. In the earliest Oligocene two species of *Laticarinina, L. halophora* and *L. altocamerata* Chapman and Parr, first appear. *Oridorsalis umbonatus* becomes the dominant species for the first time.

Several modern species which appear for the first time in the *Globigerina angiporoides* Zone (592-34-2, 19 cm) include *Pullenia quinqueloba, Hopkinsina mioindex*, and *Eggerella bradyi*.

Early to middle Miocene

In the early to middle Miocene sequence (592-32,CC to 529-24-6, 19 cm) 67 species were recognized (Appendix Table 13). In sediments where preservation is only fair, the only highly dominant species is *Cassidulina laevigata carinata*. The consistently appearing species are *Heterolepa kullenbergi, Globocassidulina subglobosa, Brizalina reticulata* (Hantken), and *Oridorsalis umbonatus*. Frequently present are *Laticarinina bullbrooki* and *Cibicides* trans. *wuellerstorfi*.

A major origination episode takes place during the *Globorotalia mayeri* Zone (equivalent to nannofossil Zone NN6) in Core 26, producing 12 new species. Among these are *Pleurostomella alternans* Schwager, *Cibicides lobatulus* (Walker and Jacob), *Anomalinoides globulosa* Chapman and Parr, *Cibicidoides* trans. *cicatricosus, Stilostomella subspinosa*, and *Siphotextularia solita* Schwager. *Hopkinsina mioindex* reappears at this time and *Marginulinopsis mammilligera* (Karrer) becomes extinct. *Nuttallides umbonifera* becomes more abundant during this same interval.

Late Miocene

Sediments of late Miocene age (592-23-2, 19 cm to 592-12,CC) are fairly to moderately well preserved. Radiolarians occur only in the coarse fraction of Sample 592-21-3, 19 cm. Although benthic foraminifers are not common, 79 species were identified and are listed in Appendix Table 14.

In this section the highly dominant and consistent species are very different in the early part (that part of the *G. miotumida* Zone prior to nannofossil Zone NN11a in Core 18) and the late *G. miotumida* Zone through the *G. conomiozea* Zone (Cores 18 to 12). Dominant species of the early part are *Hopkinsina mioindex* and *Rectuvigerina spinea;* in the later part, *Uvigerina hispida* predominates. Although *H. mioindex, Oridorsalis umbonatus, Heterolepa kullenbergi*, and *Brizalina pusilla* are consistent throughout the section, only during the early part are *R. spinea, Laticarinina halophora*, and *Globocassidulina subglobosa* consistently present. In the later part, consistent species are *Cibicides lobatulus, Heterolepa rugosa, Textularia lythostrota, Cibicidoides* cf. *un-*

gerianus, and *Pullenia bulloides*. Several new species of miliolids and uvigerinids first occur during this interval and agglutinated forms are more common. *Cibicides wuellerstorfi* becomes rare, however. At the very end of the section both *U. hispido-costata* and the miliolids increase in import.

Pliocene

Seventy-eight species were recognized (Appendix Table 15) in this sequence, which is well preserved throughout. No one species becomes highly dominant, but there are many species which occur consistently: *Brizalina pusilla, Sphaeroidina bulloides, Sigmoilopsis schlumbergeri, Globocassidulina subglobosa, Oridorsalis umbonatus, Stilostomella lepidula*, and *Melonis barleeanum*.

There is one marked faunal change during the mid-Pliocene at the *Globorotalia crassaformis/G. inflata* zonal boundary (equivalent to the NN15/NN16 boundary). Several uvigerinids, miliolids, and anomalinids, *Bulimina truncana*, and *Melonis affinis* (Reuss) all disappear at this time. *Osangularia culter* enters the area for the first time and species of *Pyrgo* increase in import. Overlying faunas contain similar genera, but different species of those genera. For example, *B. striata* replaces *B. truncana, Uvigerina proboscidea* replaces *U. hispida*, and *Cibicidoides cicatricosus* replaces *C.* cf. *ungerianus.*

Site 593

A section ranging from latest Eocene (*Globigerina linaperta* Zone) through the Pliocene was recovered at this site. The Eocene and Oligocene sediments are moderately well preserved. Only moderately preserved at its beginning, the Miocene is well preserved in the middle part, but only moderately well preserved at its end. The Pliocene is well preserved throughout.

Paleogene

Paleogene sediments were found in Cores 593-60 to 593-49; the Eocene/Oligocene boundary is placed between Sections 2 and 3 of Core 58. The 79 species identified in this sequence are listed in Appendix Table 16.

The only highly dominant species at this site was large-sized *Globocassidulina subglobosa*, which predominated in the late Eocene but dropped off markedly in the earliest Oligocene. Species which occurred consistently throughout the section include *G. subglobosa, Oridorsalus umbonatus, Heterolepa grimsdalei, Bolivinopsis cubensis*, and *Laticarinina altocamerata. Rotaliatina sulcigera, Anomalinoides alazanensis, Rectuvigerina prisca* Finlay, *Vulvulina pennatula* Batsch, *Laticarinina halophora, Brizalina reticulata* Hantken, and *Stilostomella basicarinata* Hornibrook all occurred consistently during parts of the Oligocene.

Substantial faunal overturn characterized the Eocene/Oligocene boundary interval. Termination of the high dominance of *G. subglobosa* accompanied the extinctions of *Cibicidoides parki, Uvigerina rippensis*, and several rare lagenids. Occurring just above the boundary were *R. prisca, Rotaliatina sulcigera, Uvigerina wanzea* Finlay, *Nuttallides umbonifera, Vulvulina pennatula, Cassidulina cuneata* Finlay, and *Pleurostomella tenuis* Hantken.

In the late Oligocene *Globigerina angiporoides* Zone (equivalent to nannofossil zones NP24–NP25), *R. sulcigera* disappeared, although it reappeared briefly in the Miocene. At this same time (Core 53) several modern species occurred for the first time at this site; these include *H. kullenbergi, U. spinulosa, U. pigmaea, P. quinqueloba*, and the variant of *B. pusilla* with several costae which extend almost the length of the test.

Early to middle Miocene

Despite the relatively good preservation of these sediments, only 69 species were identified (Appendix Table 17). No species becomes dominant, but several occur consistently; these are *Globocassidulina subglobosa, Heterolepa kullenbergi, Oridorsalis umbonatus, Hopkinsina mioindex, Pullenia bulloides, Melonis barleeanum, Karreriella bradyi* (Cushman), and *Brizalina anastomosa* (Finlay).

Numerous species first named from sections on New Zealand are found at Site 593, in larger numbers than at any other site. Among these are *H. mioindex, Anomalinoides orbiculus* Stache, *Trifarina costornata* (Hornibrook), *Rectuvigerina striatissima* (Stache), *Rectuvigerina rerensis* Finlay, *R. vesca, Siphonina australis* Finlay and *B. anastomosa.*

A yellow interval, termed the "oxidized zone," was recovered in Cores 593-43 and 593-42, belonging to the *Globorotalia miozea* Zone, which at this latitude is considered equivalent to nannofossil Zones NN4–NN5. In these sediments *U. auberiana* occurs in large numbers, cibicidids occur in larger numbers than in other samples at this site, and *Lenticulina calcar* d'Orbigny makes its one and only appearance in the Leg 90 Tasman Sea sites. The spirally limbate *Cibicidoides trincherasensis* (Bermudez) first occurs in this interval, as do *Planulina harangensis* Cushman and Ellisor and the more fully striate morphotype of *B. pusilla. Brizalina anastomosa* for the first time is consistently present and common through this interval.

First appearances of several important species occur in Core 40 (*G. peripheroacuta* Zone). These include *Uvigerina rugosa, Nuttallides umbonifera, Alabamina haitiensis, Cibicides wuellerstorfi, Martinottiella communis* d'Orbigny, and *Bolivinopsis praelonga* Schwager.

Middle to late Miocene

Despite only moderate sediment preservation, faunas from the mid to late Miocene at Site 593 contained the largest assortment of benthic foraminifers of any site at any time. One hundred and two species were identified and are listed in Appendix Table 18. At least 13 of these species were agglutinated and 45 were rectilinear.

Species dominance was pronounced in many samples, but different species were dominant during four discrete times intervals: the early *Neogloboquadrina continuosa* Zone equivalent to NN6–NN9, the later *N. continuosa* Zone equivalent to NN9–NN11a, the *Globorotalia miotumida* into the early *G. conomiozea* Zones, equivalent to Zones NN11a *partim* and NN11b to NN12; and the late *G. conomiozea* Zone. During the earliest interval highly dominant species were *Cibicides wuellerstorfi* and *Rectuvigerina spinea*. These were superseded in the late *N. continuosa* Zone by the more ornamented brizalinids *Brizalina pusilla* and *B. finlayi*, and during the *G. miotumida* Zone by the striate brizalinids of the *B. pusilla* group. In the late *G. conomiozea* Zone, however, a very different group of species dominates, including highly dominant miliolids, *Heterolepa rugosa*, and *Uvigerina asperula*.

Species which occur throughout the section consistently and in relatively large numbers are *H. kullenbergi*, *Oridorsalis umbonatus*, *Hopkinsina mioindex*, *Heterolepa rugosa*, and *Bulimina striata* d'Orbigny. Spinose uvigerinids are relatively diverse at this site and *U. hispida* is present in most samples of the *G. miotumida* Zone and later. Striate rectuvigerinids are less frequent; only *R. ongleyi* and *R. postprandia* occur at this site. *Osangularia culter* and *O. bengalensis* both occur at this site and with the same frequency. The one species unique to this site is the horned cassidulinid, *Globocassidulina bicornis* Cushman, which occurs only at the very end of the Miocene.

Rather unusual radiolarian-bearing samples are intercalated into the calcareous sequence of the early *Neogloboquadrina continuosa* Zone in Cores 593-39 to 593-34 and 593-27 to 593-28. These unusual samples contain large amounts of large-sized *N. umbonifera* and floods of small virgulinids. Throughout this interval they alternate with a *R. spinea-Cibicides wuellerstorfi* fauna. At the very end of this episode *Pullenia quinqueloba* joins the *N. umbonifera* fauna. Both of these species are more frequent at deeper-water Sites 591 and 586, except at this time.

Pliocene

The 85 species identified in the Pliocene at Site 593 are listed in Appendix Table 19. These faunas occurred in sediments which were generally well preserved throughout. Approximately 33 species were rectilinear and 10 were agglutinated.

The dominant species of the early Pliocene was *Uvigerina hispida*. The miliolids, particularly *Pyrgo murrhina*, and *Pullenia bulloides* dominated samples during the later Pliocene. The most consistently occurring species, however, were *Heterolepa kullenbergi*, *H. rugosa*, *Textularia lythostrota*, *Cibicidoides* cf. *ungerianus*, and *Oridorsalis umbonatus*. Various miliolids also were present throughout and were much more common here than in Site 592 some 5° farther to the north.

Faunal overturn is concentrated at a level equivalent to the nannofossil NN15/NN16 boundary in the *G. inflata* Zone. *Hopkinsina mioindex*, *C. cicatricosus*, *Brizalina reticulata*, and *Siphonina australis* all disappear permanently from the faunas at this time. Coincidentally, *Cibicides wuellerstorfi* and *Osangularia bengalensis* return to the faunas, both having been absent since the latest Miocene. Diversity (species richness) and the percentages of rectilinear species also increase at this same level (593-8,CC).

Site 594

An entirely different sedimentary sequence was recovered at Site 594, including radiolarian oozes with greater or lesser amounts of hemipelagic input. These hemipelagic sediments include large amounts of mica, volcanic glass, and quartz. In the majority of samples prior to the Pliocene the calcareous fossils are poorly preserved; at some levels few if any calcareous particles could be identified. The fact that each sediment type contained a unique foraminiferal fauna explains the disjunct distributions seen in Appendix Tables 20 to 22.

Early to middle Miocene

Throughout this interval benthic foraminiferal faunas are poorly preserved. They occur in radiolarian oozes which contain large amounts of diatoms and sponge spicules. In a few samples there is enough carbonate material to qualify the sediments as a radiolarian-foraminifer ooze. Frequently these siliceous oozes contain large amounts of mica, quartz, and glass. Carbonate material is relatively common.

Along with the variable lithologies, the benthic faunas are varied and species distributions are disjunct (see Appendix Table 20). In the radiolarian oozes containing the least amount of carbonate material, resistant benthic species are *Cassidulina crassa*, *Stilostomella lepidula*, and *Stilostomella pomuligera* Stache. This fauna is entirely different from the solution-resistant fauna in dissolved carbonate oozes; in generic composition it closely resembles faunas from radiolarian-rich levels in the Oceanic Formation of Barbados.

When sediments contain large amounts of hemipelagic materials, benthic faunas consist of many specimens of *Heterolepa kullenbergi*, *Anomalinoides globulosa*, several species of *Stilostomella*, *Bolivinopsis praelonga*, and *Uvigerina spinulosa*. *Bolivinopsis praelonga* is the dominant species in such samples.

In samples containing larger amounts of carbonate, benthic foraminifers are more diverse. Common species include *Brizalina finlayi*, *Globocassidulina subglobosa*, *Hopkinsina mioindex*, relatively frequent cibicidids, species of *Laticarinina*, and *Trifarina*. Samples of this sort in Cores 40–45 and 47–50 contain huge specimens of *N. umbonifera* which are very commonly accompanied by spherical, ornamented radiolarians.

Middle to late Miocene

Sixty-two species of benthic foraminifers were identified from the fairly well to poorly preserved sediments (Appendix Table 21). Most samples contain large amounts of radiolarians, mica, and siliceous spicules, and the carbonate is largely dissolved, leaving only fine-fraction residues in many cases.

In such lithologies, benthic faunas have large numbers of a few highly dominant species, including *Heterolepa kullenbergi*, *Uvigerina auberiana*, and *Nuttalides umbonifera*. Species very frequent, but not dominant, include *Bolivinopsis praelonga*, *Brizalina reticulata*, and *Oridorsalis umbonatus*. The only species consistently present throughout this time interval is *Bolivinopsis praelonga.*

The species of *Bulimina* differ in these levels from those at other sites and/or at other times. *Bulimina truncana* is relatively rare and *B. striata* is common. *Bulimina aculeata*, present only at Site 593 and here, first occurs during the early part of the *Globorotalia miotumida* Zone equivalent to nannofossil zones NN7–NN8, in radiolarian ooze.

As at other sites, the uvigerinids become particularly abundant and more diverse at the end of the Miocene (Appendix Table 21). The hispid species *U. auberiana*, very frequent at the beginning of this interval, is gradually replaced by spinose types such as *U. proboscidea* and *U. aculeata* toward the end of the Miocene. At the very end, the hispido-costate form *U. hispido-costata* predominates, along with the coarsely spinose *U. hispida.*

Miliolids appear at the end of the Miocene along with the hispido-costate uvigerinids. They occur in samples composed largely of radiolarians and spicules along with another, typically deeper water species, *Pullenia quinqueloba.* Unique to this site is *Hoeglundina elegans* (d'Orbigny), which becomes more frequent later in the Pliocene.

Unusual benthic faunas (Cores 594-36 to 594-38) are composed almost totally of giant-sized specimens of *N. umbonifera* accompanied by an occasional specimen of *P. quinqueloba*, in a matrix of spherical radiolarians. Although similar to the *N. umbonifera*–radiolarian samples of the early Miocene, the size and numbers of *N. umbonifera* in these samples are much greater.

Pliocene

In the Pliocene the benthic foraminiferal faunas are more diverse (See Appendix Table 22) because there are more carbonate-rich samples and less dissolution. Preservation varies from fair to moderate throughout the Pliocene. In the latest Pliocene (and in the Pleistocene, not discussed in this report) there are two distinct carbonate lithologies: in the first, foraminifers are opaque, and large amounts of hemipelagic sediments may be present; in the second, the foraminifers are clear and glassy, and the sediment is largely carbonate. Both lithologies contain distinctive foraminiferal faunas.

Carbonate and siliceous sediments alternate from core to core and contain different benthic faunas. In the earliest Pliocene, sediments composed entirely of radiolarians and some benthic foraminifers contain frequent specimens of *Sigmoilopsis schlumbergeri*, along with solution-resistant, cosmopolitan forms such as *Globocassidulina subglobosa, Oridorsalis umbonatus*, and *Heterolepa kullenbergi.* Carbonate samples of this age are rich in uvigerinids (only a few of which are rectuvigerinids), have high benthic diversity, and a fauna typical of the 1000-m depth sites in the Tasman Sea.

Higher in the Pliocene, in sediments which contain not only radiolarians but diatoms and detrital micas, quartz, and glauconite, an entirely new, unique benthic fauna occurs. In Core 594-6 *Bulimina aculeata* becomes common, accompanying a new species of *Bolivinita* in Core 594-10; it occurs with large amounts of *Trifarina angulosa* and/or *T. eximia*, which are opaque.

In Core 594-12 in samples composed primarily of hemipelagic sediments, *Hoeglundina elegans* is accompanied by relatively large numbers of cassidulinids belonging to either of the species *Cassidulina crassa* or *C. laevigata carinata, Brizalina alata* (Sequenza), *S. lepidula*, and several lagenids.

Unlike other sites, the Pliocene at Site 594 is dominated by the hispido-costate uvigerinids, has at least one sample (594-14-3, 19 cm) dominated by *Melonis pompilioides*, and contains faunas similar to those at DSDP Site 532, located under the west African upwelling and receiving large amounts of detrital sediments from the African continent (Boersma, 1984c).

BIOSTRATIGRAPHY

The stratigraphic ranges of the most common benthic foraminifers have been extracted from Appendix Tables 1–22 and are shown in Figure 2; Figure 3 depicts only the ranges of all uvigerinids. Because of the large latitudinal range of the sites, correlation was difficult. This difficulty was compounded by the fact that the foraminiferal zones became longer and fewer at the two highest latitude Sites 594 and 593. Although use of the nannofossil zones, particularly at Site 594, was also problematic, their greater number and their reputation for better synchrony through latitude seemed to provide the better means for intersite correlation. Therefore, the ranges of the benthics are interpreted using the nannofossil biostratigraphy.

Because the total stratigraphic ranges of many bathyal benthic foraminifers are not yet known, it has not been possible to establish first or last appearances in the evolutionary sense. The majority of species occurrences in these sites are probably ecologically controlled events. Exceptions, that is, appearances likely to be evolutionary originations, are discussed later.

The majority of changes across the Eocene/Oligocene boundary involve faunal reorganization, changes in dominant species, or the reappearance of species already present in the late Eocene of either Sites 592 or 593. At both sites, however, *Cibicidoides parki* and *Uvigerina rippensis* disappear at the boundary, and *U. pigmaea* appears just above it. Based on my extensive knowledge of uvigerinids, it is possible to state that these are first and last occurrence datums of the uvigerinids, and probably the LAD of *C. parki* as well.

The Oligocene, and particularly the late Oligocene, is characterized by disappearances of typically Eocene species such as *Bolivinopsis cubensis, Heterolepa grimsdalei, Marginulinopsis hochstetteri, Rectuvigerina prisca*, and a cibicidid transitional to *H. kullenbergi. Rotaliatina sulcigera*, which in New Zealand sections is a good index for the early Oligocene, ranges in the Tasman Sea to the mid-Oligocene at Site 592, but into early Miocene Zone NN2 at Site 593.

The one notable species to originate in the Oligocene is *H. kullenbergi*, which first appeared during the Interval Zone NP24/NP25 at Sites 593 and 588. The fact

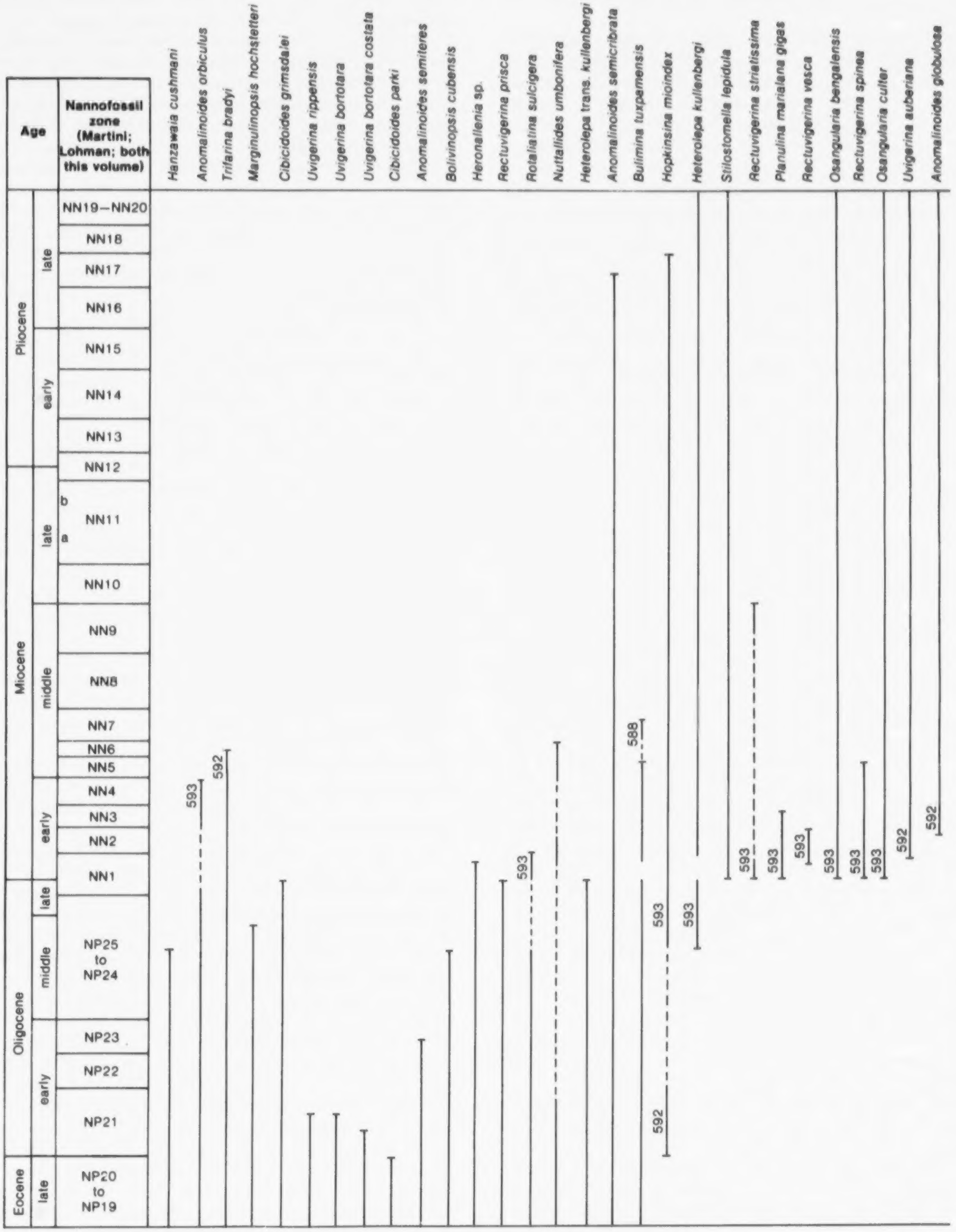

Figure 2. Stratigraphic ranges of benthic foraminifers through the Tertiary at Leg 90 sites in the Tasman Sea, Coral Sea, and on the Chatham Rise. Ranges are combined from all the range data in Appendix Tables 1-22. Biostratigraphic zonation follows Martini; Lohman; both this volume.

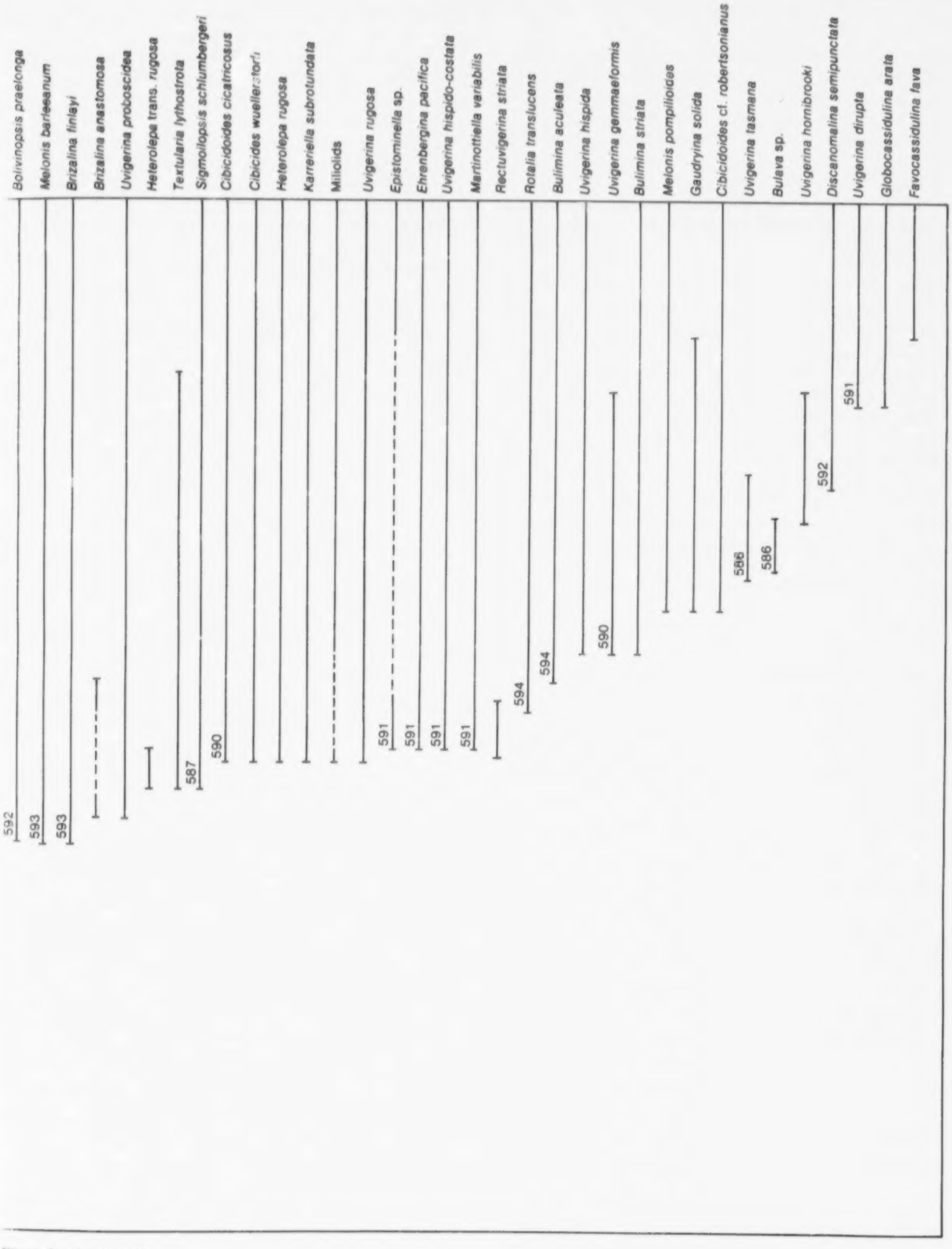

Figure 2. (Continued).

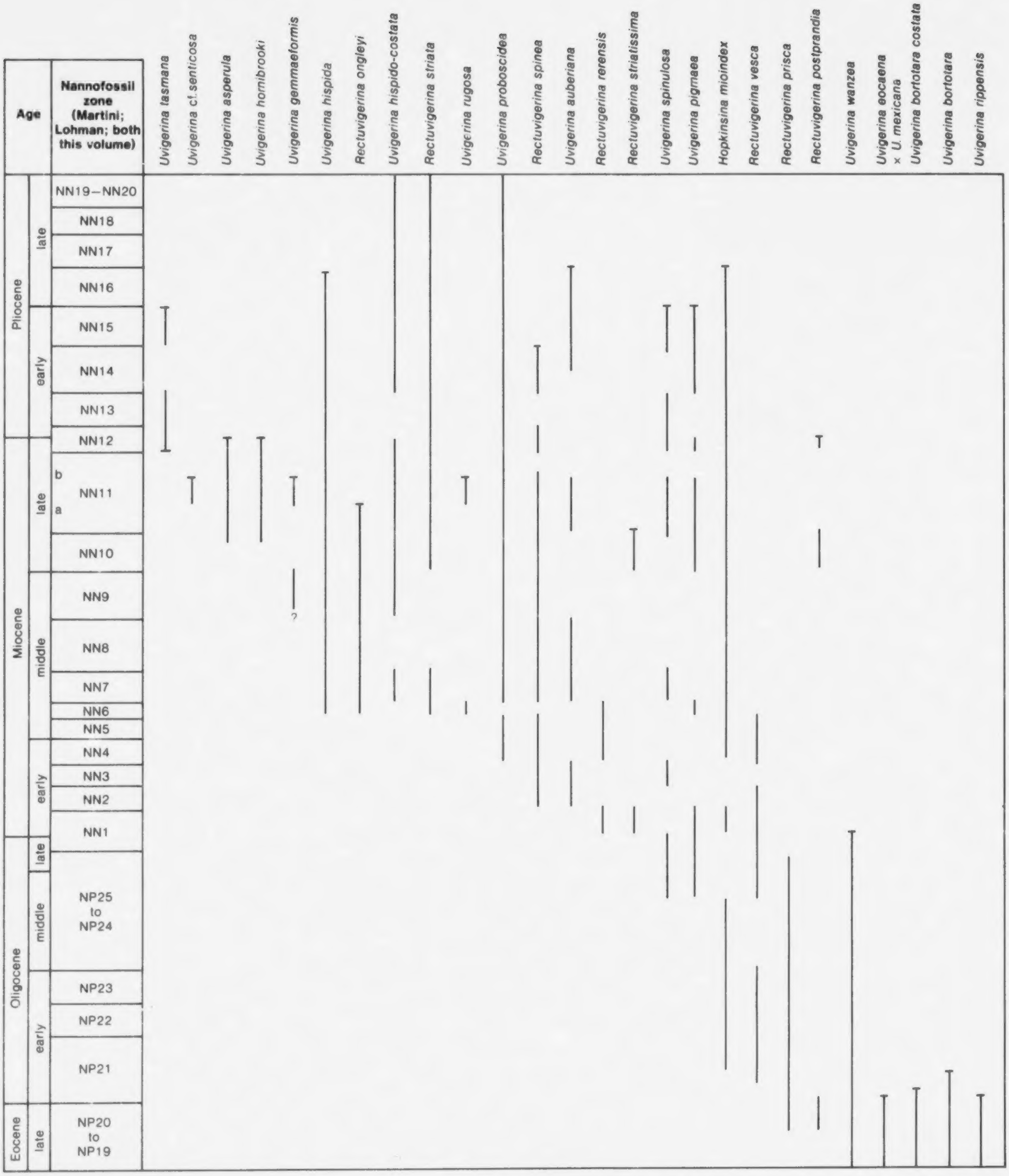

Figure 3. Stratigraphic ranges of species of the genera *Uvigerina* and *Rectuvigerina* through the Tertiary in the Tasman Sea, the Coral Sea, and on the Chatham Rise. Biostratigraphic zonation follows Martini; Lohman; both this volume.

that this species first occurs during the late Oligocene in other areas, for example at Sites 516 and 526 in the South Atlantic (Tjalsma, 1983; Boersma, 1984b), suggests that its appearance here may be an evolutionary event.

Approximately 20 species first appear during the course of the early Miocene. Seven of these, occurring synchronously during Zone NN1 at Sites 588 and 593, include species of the genera *Osangularia, Uvigerina, Rectuvigerina*, and *Brizalina*. These newly evolved species tend to predominate in the few well-preserved samples of early Miocene age. A relatively thin species of *Melonis*, tentatively referred to *M. barleeanum*, also first occurs at this time at both sites.

Several typically Paleogene buliminids disappear during the course of the early to middle Miocene. Of these, *Bulimina tuxpamensis* disappears diachronously through the Tasman Sea, persisting longest at Site 588, where it lasts until the middle Miocene (Zone NN8). *Heronallenia* sp. and *Rotaliatina sulcigera* disappear in Zones NN1 and NN2, respectively.

The largest number of first appearances of the entire Tertiary was found during Zones NN5/NN6, and to a lesser degree, Zone NN7. Of the 13 new taxa, 5 belong to the cibicidids and 3 to the uvigerinids. The appearance of *Cibicides wuellerstorfi, Heterolepa rugosa*,and *C. cicatricosus* in Zones NN5/NN6 and of *Rectuvigerina striata* and *Rotalia translucens* in Zone NN7 are considered first appearance datums. It is interesting that all of the originations during Zone NN7 took place at the deeper-water Site 591.

Primarily buliminids and uvigerinids appear during the course of the middle Miocene. *Bulimina aculeata*, later typical of both higher-latitude Sites 593 and 594, first occurs at Site 594 and reaches 593 only by the later Miocene.

Melonis pompilioides, a species more common at the two deeper-water Sites 586 and 591, first appears at Site 591 in Zone NN10; its occurrence at shallower sites is delayed until Zone NN11. Few other species first occur during the late Miocene, with the notable exception of a bizarre genus, *Bulava*, first named from Ninetyeast Ridge in the Indian Ocean, where it ranges through middle and late Miocene (Boltovskoy, 1978). At Site 586 *Bulava* occurs only in Zone NN11a. Also at Site 586 a new species, *U. tasmana*, first evolves. It ranges through late Miocene Zones NN11–NN12.

At the very end of the Miocene, in levels dominated by miliolids and uvigerinids at all sites, a spined anomalinid, *Discanomalina semipunctata*, first appears and ranges into the Pliocene.

Only two new species appear in the Pliocene, both at the deeper-water Site 591. A reticulate form, *Globocassidulina arata*, first appears in Zone NN14 at the two deeper Sites 591 and 586 and remains confined to these deeper areas. *Uvigerina dirupta*, a very common Pleistocene to Recent species worldwide, first appears at Site 591 in Zone NN14, but spreads to several other sites diachronously through the course of the Pliocene. This is probably the first appearance datum of this species.

BIOGEOGRAPHY

The preceding faunal descriptions indicate several species or genera whose presence, absence, and frequency suggest depth and latitudinal provincialization. Lacking other quantitative data, frequency, normalized for sample number, was computed for several species, genera, or cohesive groups of species. In this discussion, all of the sites whose depth was approximately 1,000 m will be termed mid-bathyal, and the two deeper Sites 591 and 586, located near 2,000 m paleodepth, will be called lower bathyal.

Osangularids

The distributions of the genus *Osangularia* and its two species show the most pronounced latitudinal trends of any of the benthic foraminifers. The genus (Fig. 4) is less frequent with increasing latitude; it is absent altogether in the early Miocene at Sites 593 and outside the Tasman Sea, at Site 594. The gradient toward higher frequency at lower latitudes increases through the later Miocene. In the Pliocene the genus appears more commonly at lower bathyal Site 591 and most commonly at adjacent middle bathyal Site 590. The two species, *O. bengalensis* and *O. culter*, behave inversely through latitude (Fig. 5). *Osangularia culter* is more frequent at mid to higher middle latitudes, whereas *O. bengalensis* is more frequent both at lower latitudes and at greater depths.

Miliolids

Like the osangularids, the porcellaneous miliolids demonstrate latitudinal frequency gradients; they appear more commonly at higher latitudes. The miliolids first occur in the lower bathyal zone and are more common there than in the mid-bathyal sites. Like the osangularids, this group increases in import and frequency after the early Miocene.

Brizalinids

Among the brizalinid species there is a trend toward greater, thicker reticulation at higher latitudes. Peripheral flanges such as those on *Brizalina aenariensis* and dense striations are more typical of equatorial latitudes. A frequency gradient increasing toward Site 593 is maintained throughout the Miocene and Pliocene (shown in Fig. 7, later), despite the marked decrease in brizalinid abundance after the early Miocene. In the Pliocene, the number of species at Site 593 is greater and their frequency still increases at Sites 593 and 592 at this time.

Lower Bathyal Species—the "Deep Group"

Because of their greater frequency at the two lower bathyal Sites 591 and 586, a suite of six species has been termed the lower bathyal group. Figure 6 indicates their concentration at the two deeper-water sites. When these species do occur at the mid-bathyal sites, it is in pulses, at least some of which appear to be related to the several steps in the buildup of polar glaciation. These species are *Melonis pompilioides, Stilostomella subspinosa, Pul-*

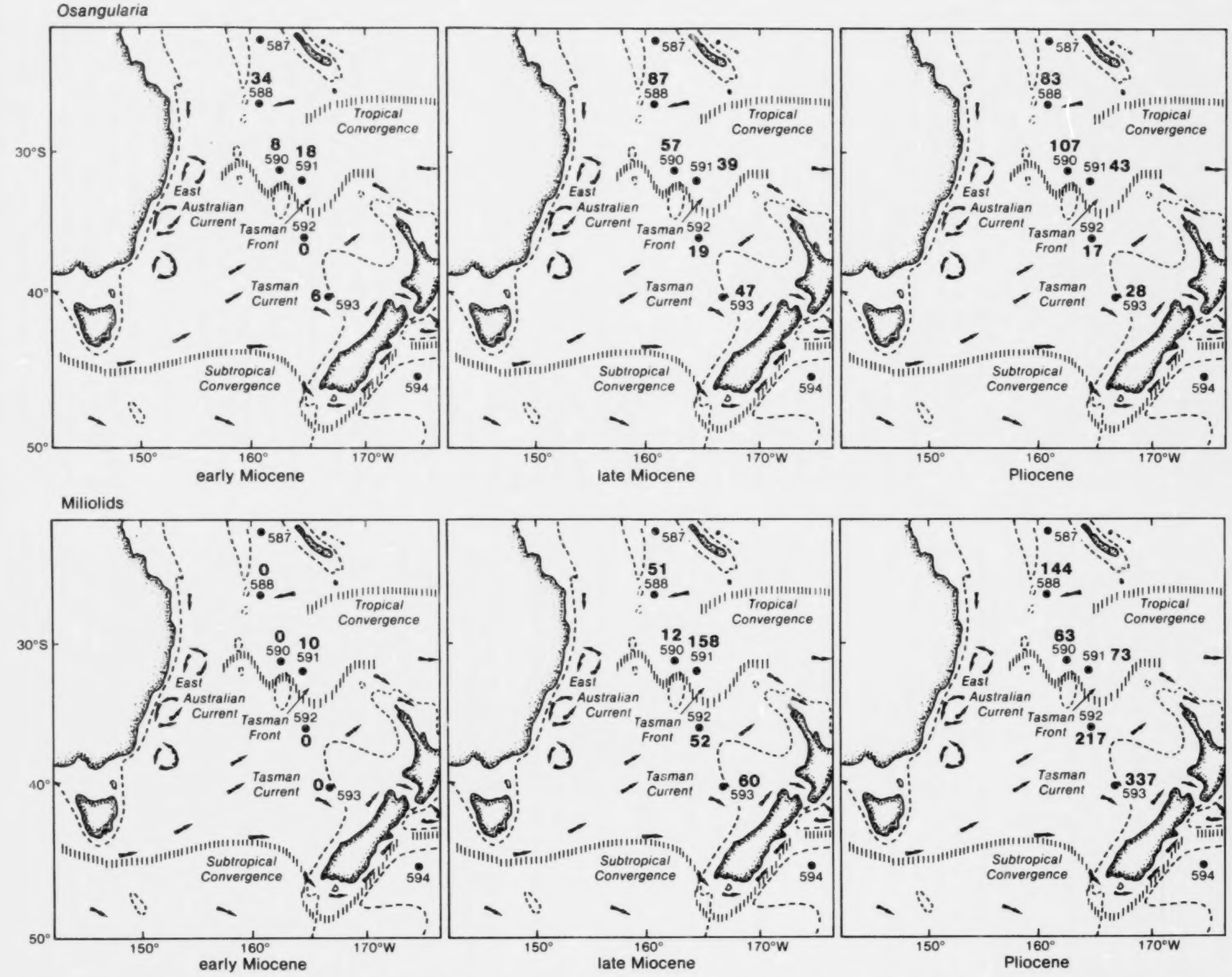
Osangularia
587
34
588
8
590
18
591
592
0
6
593
594
East
Australian
Current
Tasman
Front
Tasman
Current
Tropical
Convergence
Subtropical
Convergence
30°S
40°
50°
150°
160°
170°W
early Miocene
587
87
588
57
590
591
39
592
19
47
593
594
late Miocene
587
83
588
107
590
591
43
592
17
28
593
594
Pliocene
Miliolids
587
0
588
0
590
10
591
592
0
0
593
594
early Miocene
587
51
588
12
590
158
591
592
52
60
593
594
late Miocene
587
144
588
63
590
591
73
592
217
337
593
594
Pliocene

Figure 4. Frequency of osangularids and miliolids in the early and late Miocene and the Pliocene in the Tasman Sea. The number of total occurrences is normalized to the number of samples examined, and expressed as a percentage.

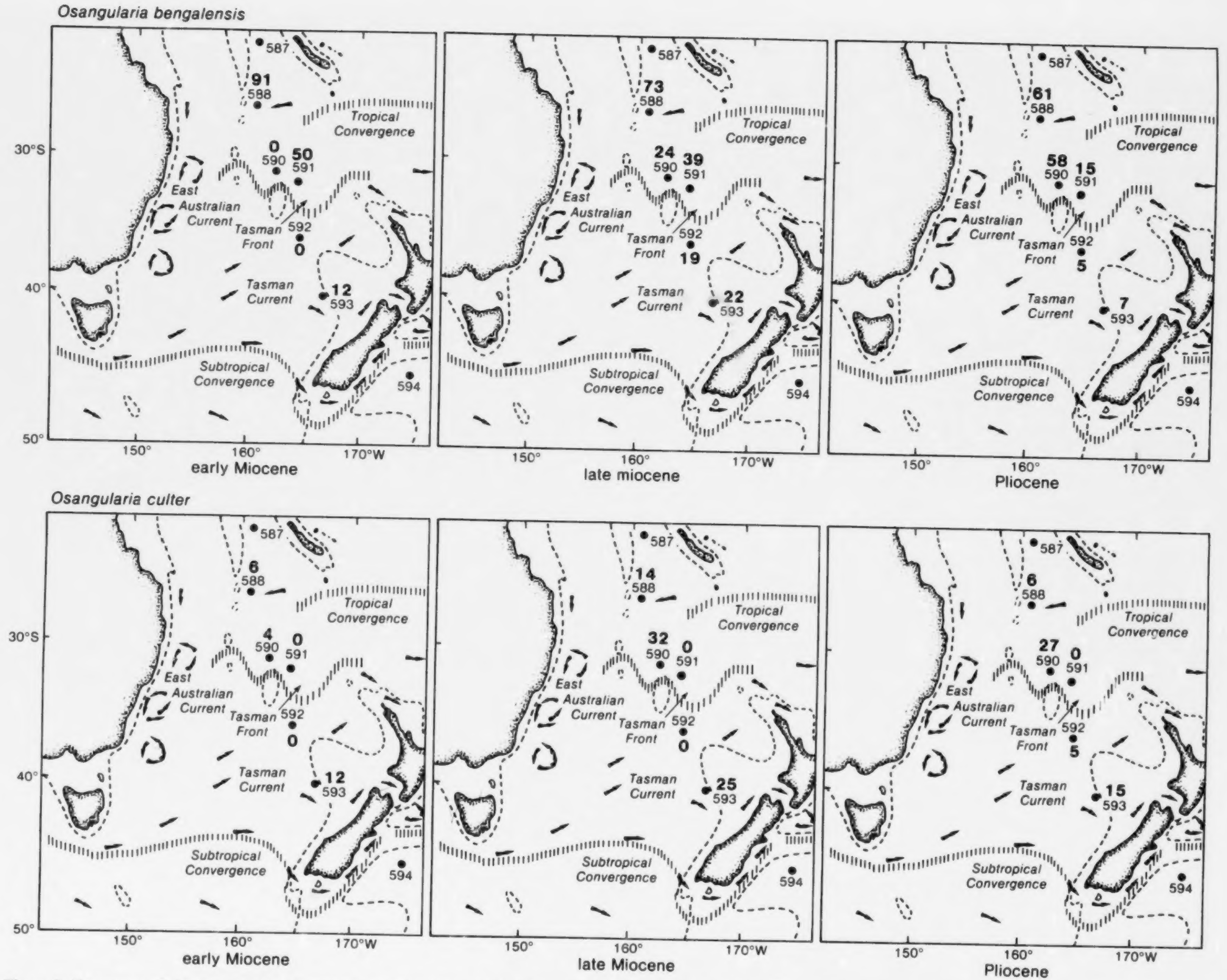

Osangularia bengalensis

Osangularia culter

587
91
588
0
590
50
591
592
0
12
593
594
73
24
39
19
22
61
58
15
5
7
6
4
14
32
25
27
Tropical Convergence
East Australian Current
Tasman Front
Tasman Current
Subtropical Convergence
30°S
40°
50°
150°
160°
170°W
early Miocene
late miocene
Pliocene
late Miocene

Figure 5. Frequency of the two species *Osangularia* in the early and late Miocene and the Pliocene in the Tasman Sea. Percentages determined as in Figure 4.

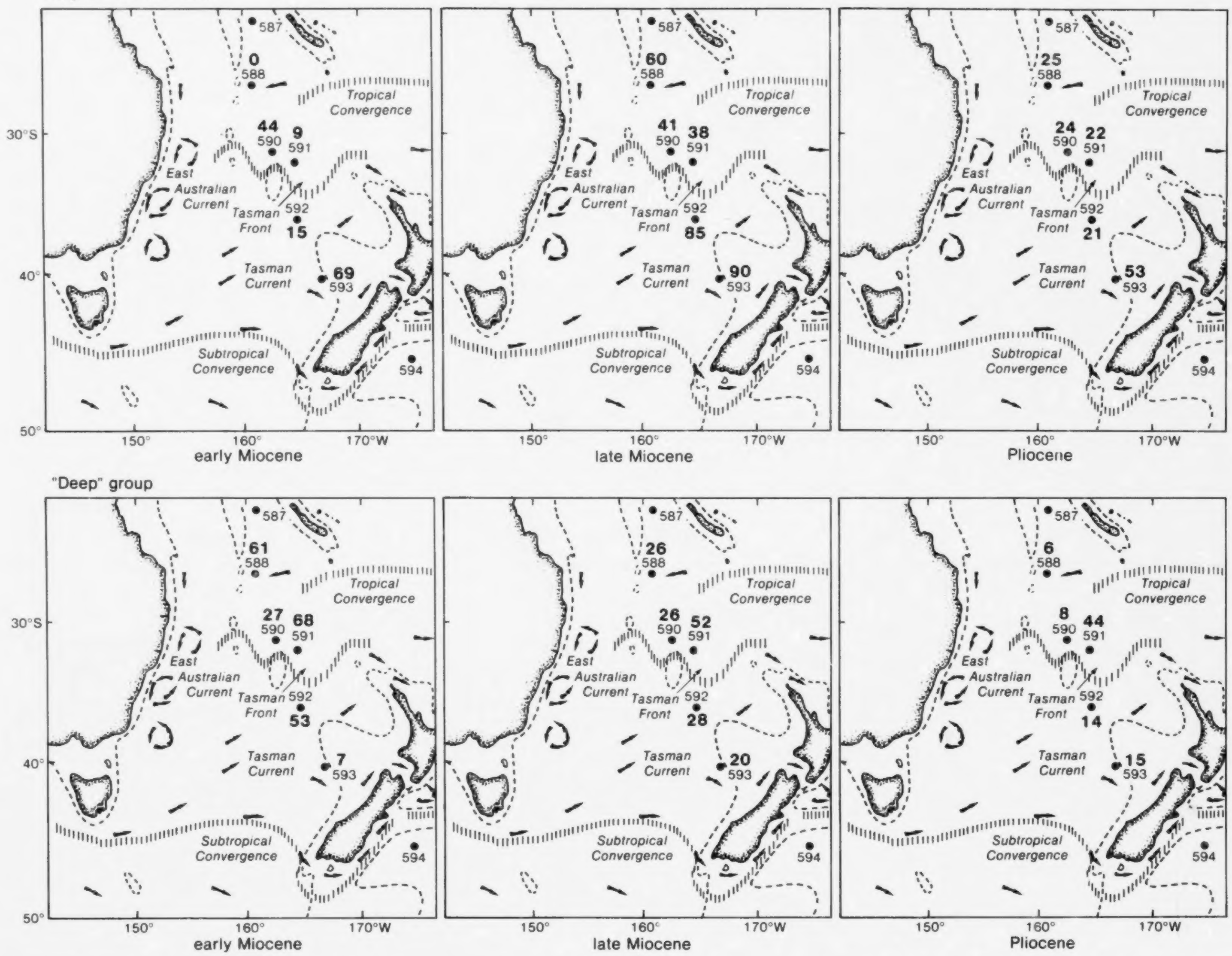
Hopkinsina mioindex
"Deep" group
30°S
40°
50°
150°
160°
170°W
early Miocene
late Miocene
Pliocene
587
588
590
591
592
593
594
0
44
9
15
69
60
41
38
85
90
25
24
22
21
53
61
27
68
53
7
26
26
52
28
20
6
8
44
14
15
East
Australian
Current
Tasman
Front
Tasman
Current
Tropical
Convergence
Subtropical
Convergence

Figure 6. Frequency of *Hopkinsina mioindex* and the "deeper" group of benthics in the early and late Miocene and the Pliocene in the Tasman Sea. The deeper group of species includes *Melonis pompilioides, Pullenia quinqueloba, Uvigerina hispido-costata, Nuttallides umbonifera, Stilostomella subspinosa*, and *Melonis sphaeroides*. Percentages determined as in Figure 4.

lenia quinqueloba, M. sphaeroides, Uvigerina hispidocostata, and *Nuttallides umbonifera.*

Cibicidids

This group provided the largest taxonomic problems, with the result that only about one-half of the species could be positively identified. The group is much more diversified in the Pacific than in the Atlantic during the Neogene. At mid-bathyal sites, the overall diversity of cibicidids decreases from the early Miocene into the Pliocene; for example, early Miocene samples at Site 593 contain 10 species, contrasted to an average of 3 in the Pliocene (Fig. 7). The opposite pattern emerges at Site 591, where cibicidid diversity increases from the early Miocene into the Pliocene. The few Pliocene species, however, become much more abundant, particularly at the very end of the Pliocene.

Species of *Planulina* and *Cibicides* are equally distributed at each site. *Heterolepa* is the most frequently occurring genus, and *H. kullenbergi* the most common species. The only species limited to the mid-bathyal zone was *Cibicidoides tuxpamensis.* Other patterns in the numbers of species or types at different sites are difficult to recognize. A decrease in the number of species with depth is illustrated in Figure 7.

Hopkinsina mioindex

In general, *H. mioindex* is both more abundant and more frequent at Site 593 (Fig. 6). It decreases in frequency in lower latitudes and in the lower bathyal zone, where it occurs only in pulses, the most intense of which was in the late Pliocene.

The inferred depth or latitudinal preferences of several other species or species groups are depicted qualitatively in Figure 8. Species apparently preferring lower-latitude, mid-bathyal regions include the very finely striate rectuvigerinids, *Globocassidulina arata, Uvigerina tasmana*, and *Brizalina aenariensis*. Those which flourish toward higher middle latitudes in the mid-bathyal zone are *Discanomalina semipunctata, Bulimina aculeata, Bolivinita pliozea, Hoeglundina elegans*, and the coarsely striate rectuvigerinids such as *Rectuvigerina prisca* and *R. postprandia.*

Depth preferences are depicted qualitatively in Figure 9. *Melonis sphaeroides* and *Bulimina consanguinea* are restricted to the lower bathyal zone. Only the costate uvigerinids such as *U. hornibrooki* and *U. tasmana* are confined to the mid-bathyal zone. Other species which have strong depth correlation nevertheless transcend depth in discrete pulses relatable to oceanographic changes in the area.

Species restricted to the hemipelagic environment of Site 594 include *Brizalina alata, Trifarina eximia*, and *Sigmavirgulina tortuosa.* Only in this environment do *Bulimina aculeata, M. pompilioides*, and *T. angulosa* occur in floods. Of the cibicidids, *Cibicides wuellerstorfi* is the most common species. This species is concentrated in other hemipelagic areas, for example, DSDP Site 532 off Angola; and in the nutrient-rich peripheral areas of the North Pacific Ocean (Woodruff and Douglas, 1981).

COMPARATIVE FAUNAL HISTORIES AND SUMMARY

In general, Tasman Sea benthic foraminiferal faunas contain large percentages of cosmopolitan species including *Oridorsalis umbonatus, Globocassidulina subglobosa, Stilostomella lepidula, Hopkinsina mioindex, Pullenia bulloides, Sphaeroidina bulloides, Eggerella bradyi*, and *Heterolepa kullenbergi.* The numbers of stilostomellids, uvigerinids, brizalinids, cibicidids, and anomalinids are usually high, the numbers of buliminids, lagenids, and lenticulinids are low. Very similar Neogene faunas have been reported from Car Nicobar (Srinivasan and Sharma, 1980), from the Ninetyeast Ridge in the Indian Ocean (Boltovskoy, 1978), and from Site 289 on the Ontong-Java Plateau (Woodruff, 1979). Faunas of the later Neogene on the Chatham Rise are similar to those from the carbonate sediments at DSDP Site 532 located under an eastern boundary upwelling off the coast of Angola (Boersma, 1984c).

Unique to Tasman Sea faunas, particularly in the Paleogene, are the large numbers of austral species originally named from New Zealand (Finlay, 1939), the large ornamented nodosarids such as *Nodosaria costornata* and *N. scalaris* (see Plate 13) first named from Car Nicobar (Schwager, 1866), and the very high numbers of uvigerinids and miliolids. Austral species include, *inter alia, Bolivinita pliozea, Rectuvigerina rerensis, R. vesca, R. striatissima, Cibicidoides notocenicus, Uvigerina bortotara, Rotaliatina sulcigera, Siphonina australis, Trifarina costornata, Anomalinoides orbiculus, Brizalina anastomosa, B. finlayi, R. prisca, U. wanzea, Stilostomella basispinata*, and *Margulinopsis hochstetteri.* Although spinose uvigerinids occurred in large numbers worldwide during the late Miocene *Globorotalia plesiotumida* Zone (Lutze, 1978; Woodruff and Savin, 1981; Vincent et al., 1980), their abundance and persistence, along with marked decreases in *Cibicides wuellerstorfi* and *Globocassidulina subglobosa* but relatively diverse rectuvigerinid and miliolid faunas, is unique to the Tasman Sea.

Diversity (species richness) of Tasman Sea faunas varies from a low near 63 to a high near 102 species per series. Diversities, particularly in the early Miocene at lower-latitude Site 588, are somewhat higher than in Atlantic Ocean middle bathyal oceanic regions such as Site 526 on the Walvis Ridge, but similar to those on the Ninetyeast Ridge (Boltovskoy, 1978; Boersma, 1984b). However, from the late Oligocene through late Pliocene, the number of individuals per gram of sediment (the Benthic Number) is especially high in the Tasman Sea compared with these other intermediate-depth, open ocean areas.

Paleogene

The Paleogene was drilled in Hole 588C and Sites 592 and 593, but the record at 588 is obscured by diagenesis. In the latest Eocene, there is marked faunal and sedimentary differentiation between the closely situated Sites 592 and 593. Faunas at Site 592 contained large numbers of cibicidid species and were dominated by species

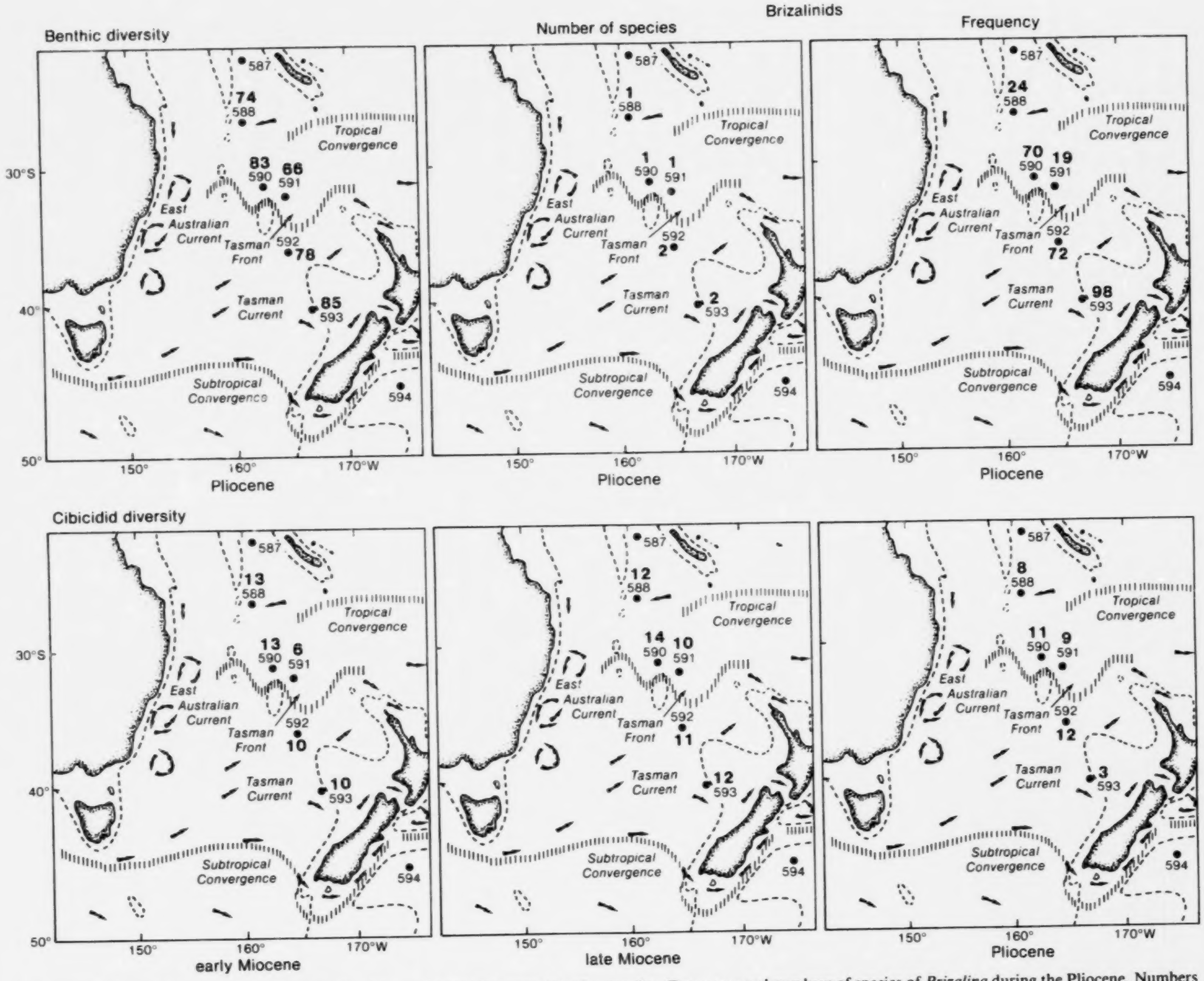
Benthic diversity
Brizalinids
Number of species
Frequency
Cibicidid diversity
30°S
40°
50°
150°
160°
170°W
Pliocene
early Miocene
late Miocene
587
588
590
591
592
593
594
74
83
66
78
85
1
2
24
70
19
72
98
13
6
10
12
14
11
8
9
3
East Australian Current
Tasman Front
Tasman Current
Tropical Convergence
Subtropical Convergence

Figure 7. Benthic diversity, expressed as species richness, in the Pliocene of the Tasman Sea. Frequency and numbers of species of *Brizalina* during the Pliocene. Numbers of cibicidid species in the early, late Miocene, and Pliocene throughout the Tasman Sea. Genera included in this estimate are *Cibicides, Planulina, Cibicidoides*, and *Heterolepa*. Percentages determined as in Figure 4.

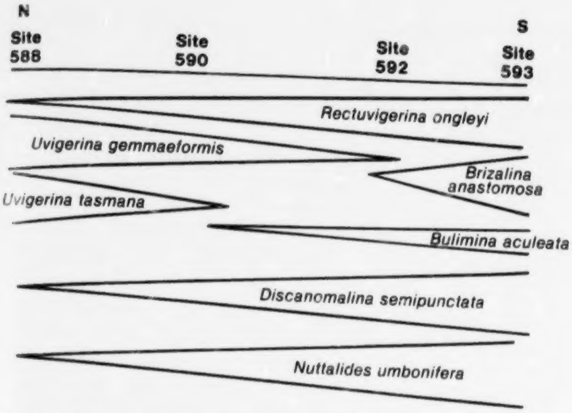

igure 8. Schematic depiction of the abundance, with latitude, of seven benthic foraminiferal species through the mid-bathyal sites in the Tasman Sea. This geographic provincialization occurs between 21° and 35°S. Increasing species abundance is indicated by widening, diminishing abundance by narrowing of the V.

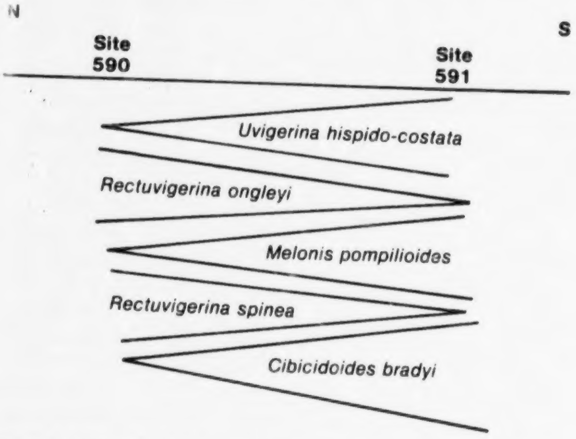

Figure 9. Schematic depiction of the abundance with depth of five benthic foraminiferal species through the mid- to lower bathyal zone in the Tasman Sea. Increasing species abundance is indicated by widening, diminishing abundance by narrowing of the V.

of *Anomalinoides*, such as *A. aragonensis*, and by the spinocostate uvigerinid, *U. bortotara*. By contrast, at Site 593, more species typical of New Zealand land sections, larger specimens of *Marginulinopsis hochstetteri*, and very large and abundant specimens of *Globocassidulina subglobosa* characterize most faunas.

Faunal overturn is similar at the two sites at the Eocene/Oligocene boundary when *Cibicidoides parki* and *Uvigerina rippensis* both become extinct, whereas *Sphaeroidina bulloides, U. pigmaea, Rectuvigerina prisca, Laticarinina altocamerata, L. halophora*, and *Rotaliatina sulcigera* first appear. However, faunal compositional and sedimentary changes are different at the two sites. At Site 593 large *G. subglobosa* disappears, whereas *Nuttalides umbonifera* occurs in a short pulse at the boundary. Most uvigerinids, except for an unusual smooth species, disappear at the boundary, but return immediately above. Faunas above the boundary are characterized by large numbers of cibicidids, anomalinids, and *O. umbonatus*. At Site 592 the boundary is punctuated by a pulse of radiolarians and spino-costate uvigerinids, followed by the disappearance of the uvigerinids and *Pullenia bulloides*. For the first time, *O. umbonatus* becomes the dominant species in a fauna characterized by anomalinids such as *A. orbiculus*, stilostomellids such as *Stilostomella basispinata*, and the rectuvigerinids.

Early Oligocene faunas are more homogeneous than those of the late Eocene. At both sites generalists, cibicidids, anomalinids, and *O. umbonatus* are common faunal elements. In Zone NP21, the remaining uvigerinids are replaced in import by rectuvigerinids, many of which, like *Rectuvigerina postprandia*, were originally named in New Zealand (Hornibrook, 1971).

Late Oligocene faunas of Zones NP24/NP25 were found at Site 593 and in very recrystallized sediments in Hole 588C. A marked change in faunas at Site 593 is characterized by a decrease in anomalinids and cibicidids, the extinctions of such Eocene holdovers as *M. hochstetteri* and *Cibicidoides notocenicus*, the temporary disappearance of *R. sulcigera*, and the appearance of a number of typically Neogene species such as *Heterolepa kullenbergi, Hopkinsina mioindex, Pullenia quinqueloba, Brizalina pusilla*, and *Eggerella bradyi*. Here, as in New Zealand, *R. sulcigera* disappears from faunas in the middle Oligocene; however, this taxon returns for a short time in early Miocene faunas (Zones NN1–NN2) at Site 593 before its final disappearance from the Tasman Sea. Despite very poor preservation, the first specimens of *H. kullenbergi, H. mioindex, P. quinqueloba, Textularia lythostrota*, and *C.* cf. *wuellerstorfi* are found in Hole 588C in the late Oligocene.

Preservation at all but Site 593 is poor to barely moderate through the early Miocene. Solution-residue faunas at all sites are strongly dominated by a few resistant species such as *H. kullenbergi, S. lepidula, O. umbonatus, E. bradyi*, and *G. subglobosa*. *Nuttallides umbonifera* first occurs, at the base of the section only, at Site 588 and appears in small numbers in several samples through the early Miocene. In the South Atlantic also, *N. umbonifera* migrates into mid-bathyal sites in the earliest Miocene (Tjalsma, 1983; Boersma, 1984b). By contrast, this species does not occur at the deeper-water Site 591 until Zone NN5. Several Oligocene holdovers such as *Bulimina semicostata, B. jarvisi*, and *R. sulcigera* become extinct through this time interval, but poor preservation make it impossible to specify their endpoints.

By contrast, the moderately well preserved faunas at Site 593 contain new species of cibicidids and a relatively large number of species typical of New Zealand, including *Rectuvigerina vesca, R. rerensis, Brizalina anastomosa, B. finlayi*, and *Siphonina australis*. At this time the brizalinids become established as consistent and highly dominant faunal elements at Site 593. The elongate rectuvigerinids of the *R. striatissima–R. rerensis* type were located at Site 593, whereas the forms related to *R. ongleyi* and *R. spinea* were confined to lower latitudes at Site 588. Despite the superior preservation, species richness at Site 593 was lower (67 species) than in the very poorly preserved sediments at Site 588, which contained 93 species.

Major evolutionary overturn, species migration, faunal reorganization, and depth or latitudinal compartmentalization characterized the beginning of the middle Miocene (NN5–NN6) at all sites, including Site 594 on the Chatham Rise. This corresponds to a global episode of climatic and benthic faunal change attributed to the development of permanent Antarctic glaciation (Shackleton and Kennett, 1975; Woodruff and Douglas, 1981; Boltovskoy, 1978; Boersma, 1984b). Evolutionary overturn involved originations rather than extinctions. Twelve new species appeared at Sites 591 and 592, but only six at the middle bathyal Site 593 (Fig. 2). These include *Pleurostomella alternans, Anomalinoides globulosa, Cassidulina laevigata carinata, Cibicides wuellerstorfi*, and *Heterolepa rugosa*. *Heterolepa rugosa* occurred only at lower-latitude sites, but *C. wuellerstorfi* first occurred synchronously at all sites in the Tasman Sea. *Uvigerina hispido-costata*, which first evolved slightly later at Site 591 only, became common along with several newly evolved miliolids. *Nuttallides umbonifera* reappeared at all but Site 588, and became very abundant in conjunction with floods of spherical radiolarians at Sites 591, 593, and 594. The waxing and waning of these radiolarian–*N. umbonifera* faunas were diachronous through latitude and depth; they endured longest at deeper Site 591, and at higher latitudes; disappearing in Zone NN9 at Site 593 and in the late Miocene at Site 594. More diverse radiolarian faunas appeared also at Site 590 during Zone NN6.

The result of this earliest middle Miocene event was the first real compartmentalization of benthics into depth- and latitudinally related faunas with different consistent or very abundant species. Only deeper-water faunas at Site 591 contained miliolids and hispido-costate uvigerinids (beginning in Zone NN7). No rectuvigerinids except *R. spinea* penetrated this depth. Faunas dominated by *R. spinea* or *C. wuellerstorfi* alternated with the radiolarian–*N. umbonifera* faunas through most of the early Miocene (to Zone NN9) at Site 593. Brizalinids, particularly those with reticulate or anastomosing striae, predominated at Site 593 and extended in abundance also to Site 592. The higher-diversity, lower-latitude faunas at Sites 590 and 588 contained large numbers of generalists and cosmopolitan species typical of areas like Car Nicobar (Srinivasan and Sharma, 1980) such as *P. bulloides, S. lepidula, Melonis barleeanum, Hopkinsina mioindex, Heterolepa kullenbergi, E. bradyi*, and the first spinose and hispid uvigerinids such as *U. proboscidea*.

The persistence of these faunas through the early part of the late Miocene was terminated near the Zone 11a/11b boundary by a second basinwide event involving migration and faunal reorganization rather than evolutionary overturn. Key forms which spread to all sites were the miliolids, such as *Pyrgo murrhina*, previously found only at the deeper Site 591, and the spinose uvigerinids such as *U. hispida*, which migrated into all sites including Site 594 but were particularly numerous at Site 590. Site 593 demonstrated the highest specific diversity (102 species) and the least faunal disturbance at this time; reticulate brizalinids such as *Brizalina finlayi* continued to be highly dominant, although the spinose uvigerinids and miliolids did appear in small numbers.

Similar taxa persisted into the latest Miocene (Zone NN12) when radiolarians disappeared from Site 590 and benthic faunal transformations at all sites involved (1) replacement of spinose by spino-costate uvigerinids and the appearance of new species such as *U. asperula* and *U. hornibrooki;* (2) decreased abundance of *G. subglobosa* and *C. wuellerstorfi;* (3) originations of several new rotaloid species such as *Discanomalina semipunctata* (see Fig. 2); and (3) continuing abundance of the miliolids, including new species such as *Triloculina lucernula* and *P. comata*. At Site 593, where faunas were still typified by high abundances of brizalinids, *B. pusilla* became the dominant species of the latest Miocene and the early Pliocene and reticulate brizalinids did not again become abundant at this or any site after this time. The deep-water, more robust variant, *M. sphaeroides* occurred for the first time accompanying *M. pompilioides* at lower bathyal Site 586. Increased dissolution at lower bathyal Site 591 removed a large amount of the fauna just below the Miocene/Pliocene boundary. Dissolution at the middle bathyal depths was less evident, but did produce some diminished faunas at Site 593.

Faunal compositions established in the late Miocene continued through the early Pliocene up to Zone NN14. Diversities ranged from a low of 66 species at the lower bathyal Site 591 to highs of near 85 species at Sites 590 and 593. Although faunas were relatively homogeneous through latitude, higher numbers of agglutinants and heterolepids occurred at Site 590, greater percentages of *Hopkinsina mioindex* at Site 593, and osangularids were generally more common at lower latitudes (see Figs. 4–7). The genus *Ehrenbergina* became a more prominent faunal component at all sites. Depth-restricted species increased in numbers at this same time; these included *Pullenia quinqueloba, M. pompilioides, Favocassidulina fava*, and *Globocassidulina arata*. *Nuttallides umbonifera* occurred most consistently at Site 586, but was present in small numbers in each zone of the early Pliocene at the middle bathyal sites as well.

Faunas at Site 588 contain more genera but the same approximate number of species as the equivalent-depth Site 590, farther to the south. Miliolids are more common, and rectilinear species more frequent than at Site 590. Cibicidids, particularly the turbinate forms which could not be assigned to any species, osangularids in general and *O. culter* in particular, and ornamented brizalinids such as *B. pusilla* are more frequent at Site 590.

By comparison with Site 590, located slightly to the north but at equivalent depths, Site 592 has a greater percentage of miliolids, but fewer osangularids. This site contains the lowest numbers of uvigerinids of any site; the hispido-costate and costate types such as *U. hornibrooki* found commonly at Site 593 do not occur at Site 592.

Faunas are temporarily modified in Zone NN14 by a short-lived influx of large numbers of spinose uvigerinids such as *U. proboscidea* and *U. hispida* at Site 590 and an apparently coeval acme of *N. umbonifera* at Site

592. Faunas following this event are similar to those preceding it.

At all sites, faunas above the Zone NN15/NN16 boundary are significantly different from those below. Hispido-costate uvigerinids such as *U. hispido-costata* and *U. dirupta* reach peak frequencies just below the boundary, then spread into all sites regardless of depth or latitude; *U. dirupta* is more common in the lower bathyal sites. Previously uncommon species such as *Rotalia translucens, Cassidulina laevigata carinata, Ehrenbergina pacifica, Bulimina truncana*, and *B. aculeata* increase in import along with the osangularids, the stilostomellids, and several agglutinated forms such as *B. praelonga*. Agglutinated species are still more frequent at Site 588 and the buliminids, such as *B. truncana*, at the lower bathyal sites. *Bulimina aculeata*, however, occurs only at middle bathyal Sites 593 and 594, where improved preservation in the early Pliocene resulted in the first consistent carbonate sedimentary sequences. In the late Pliocene, these *in situ* carbonate sediments alternate with mixed carbonate and redeposited clays containing outer-shelf benthics such as *Trifarina angulosa* and *T. eximia.*

Latest Pliocene faunas (Zone NN19–NN20) are transformed by the increased frequencies of the cibicidids at all sites; heterolepids such as *Heterolepa kullenbergi* and *H. rugosa* are more common at lower latitudes, whereas *Cibicides wuellerstorfi* and the planulinids predominate at higher middle latitudes and at the lower bathyal sites. After this time, at all Tasman sites except 593, cibicidid-rich samples containing high proportions of other rotaloid species alternate with faunas rich in uvigerinids and other rectilinear forms. Several unique species occurring only at the higher middle latitude sites include *Bolivinita pliozea* and *Bolivinita* sp. at Sites 592 and 594, and *B. aculeata* at Sites 593 and 594. In general at this time faunas at Site 593 become more similar to those in the carbonate levels at Site 594.

BENTHIC FORAMINIFERAL RESPONSE TO OCEANOGRAPHIC CHANGES IN THE TASMAN SEA

The fact that Tasman Sea benthic foraminiferal faunas differ from north to south at sites located at the same approximate paleodepths indicates the complexity of the interactive processes of biogeographic provincialization, geographic variation, and diachronous alteration of environments which result from the discontinuous distributions of oceanic fronts. Like oceanic fronts, faunas may be in different "states" when subjected to major environmental changes, and faunal response then will not necessarily be uniform oceanwide or even regionally. This notion forms the philosophic basis of the planktonic foraminiferal biostratigraphy in this volume. Its complexity is an accurate reflection of the temporal and spatial heterogeneity of foraminiferal distributions. Only biologic evolution and the oceanic dynamic equivalent should produce coeval and identical faunal developments worldwide.

The extensive descriptions of faunas in this report (Appendices 1–21, Figures 2–7) document the differing "states" of mid- to lower bathyal faunas of the Tasman Sea through latitude and depth. Development of these faunas through the Neogene at Sites 588, 590, 591, 592, and 593 is summarized in Figure 10, using key taxa which demonstrate changes in very high dominance, consistency, rarity, or first and last occurrences.

Monitors of Oceanographic Change

Three standard monitors of oceanographic conditions have been measured in Tasman Sea sediments. The oxygen isotope record of paleotemperatures and glacial alteration of ocean isotopic composition has been analyzed through the Paleogene at Sites 592 and 593, and the Miocene and Pliocene at Sites 588, 590, and 591 (Murphy and Kennett; Elmstrom and Kennett; Kennett, this volume). The major features at least of the Neogene oxygen isotope record are by now well established (Savin et al., 1981). In the Tasman Sea $\delta^{18}O$ becomes heavier at the Eocene/Oligocene boundary, in the mid-Oligocene (Zone NP24/NP25), in middle Miocene Zone NN5/NN6, in an excursion near the end of the Miocene (NN11b), at the early/late Pliocene boundary (NN15/NN16), and in the latest Pliocene (NN18) (Fig. 11).

The carbon isotope records, monitors of the oceanic carbon budget, were measured at the same sites. The Tertiary carbon isotope record is less well analyzed and more problematic to interpret (Keigwin and Shackleton, 1980). Tasman Sea records are difficult to interpret because of the species used in the Paleogene and the lack of a planktonic record for the Miocene, so that the surface-to-bottom gradient cannot be estimated. Records at the Eocene/Oligocene boundary differ at Sites 592 and 593. A lightening both at the surface and at depth is found at Site 592, but both values become heavier at Site 593. In the Oligocene there is a slight decrease in the surface-to-bottom gradient caused by heavier values at the bottom, coeval with the positive excursion in oxygen isotope values during the NP24–NP25 zonal interval. The Miocene benthic record includes positive values of $\delta^{13}C$ coeval with the lightest oxygen isotope values at the beginning of the middle Miocene (Zone NN5). Through the remainder of the Miocene, carbon isotope values become gradually lighter until, near the Zone NN11a/NN11b boundary, there is a negative excursion at the bottom. The Pliocene record at Site 590 is punctuated in Zone NN14 (about 4.3–4.4 Ma) and in Zone NN19 (about 2.3 Ma) by increases in the surface-to-bottom gradient caused by lightening both at the surface and at depth, coeval with more positive oxygen isotope values both at the bottom and through the water column.

Sediment accumulation rate records depict the ultimate balance between sediment input and removal at a site. The Tasman Sea records are likely to be representative of original sediment delivery because most sites are located on the upper areas of the Lord Howe Rise, out of the influence of corrosive bottom water and land-derived sediment fluxes. Shipboard seismic records gave no evidence of extensive bottom current activity. If anything, rates may be too low because of the winnowing of fine-fraction nannofossils common at sites on mid-oceanic topographic highs (Shackleton et al., 1984).

Age		Nannofossil zones (Martini; Lohman; both this volume)	Planktonic foraminifer zones (Jenkins and Srinivasan, this volume)	Site 588	Site 590	Site 591	Site 592	Site 593
Pliocene	late	NN19–NN20	*G. tosaensis/ G. truncatulinoides*	*H. kullenbergi* (C) *B. praelonga* (H)	*H. rugosa* (C) *C. wuellerstorfi* (C)	*Cibicides* (C) *Planulina* (C)	*Cibicides* (C) *Bolivinita* (U)	*B. aculeata* (U) Cibicidids (C)
		NN18				*Pyrgo* (C) *U. hispido-costata* (C) *H. mioindex* (C)	*Cibicides–Heterolepa* (C) *B. pusilla* (C)	*U. hispido-costata* (C) Miliolids (C) *O. bengalensis* ⊥̲ *A. haitiensis* (C)
		NN17		*O. bengalensis* (C) *U. proboscidea* (C) *U. hispido-costata* (C) *S. lepidula* (C)	Spinose uvigerinids (C) *S. lepidula* (C) *E. pacifica* (C)			
		NN16	*G. tosaensis*		Cibicidids ↓	*N. umbonifera* ↑	Uvigerinids ↓ Miliolids ↓ *G. subglobosa* ↓	Faunal overturn
	early	NN15	*G. inflata* *G. crassa.*	*C. wuellerstorfi* (H) *B. praelonga* (H)	*S. lepidula* (C)	*B. truncana* (C) *C. bradyi* (C) *O. bengalensis* (U) Miliolids (C)	*Ehrenbergina* (C) Agglutinants (C) Miliolids (C)	*Ehrenbergina* (C) Cibicidids (C)
		NN14	*G. margaritae*	*G. solida* (H) *B. truncana* (C) Miliolids (C) *H. kullenbergi* (C)	*Uvigerina* interval (H)		*N. umbonifera* ↑	Generalists and *H. rugosa* (H) Miliolids (H)
		NN13			*G. subglobosa* (C)	*U. hispida* ⊥ *B. finlayi* ⊥̲ *L. halophora* ⊥̲		
Miocene	late	NN12		Cibicidids ↓ *G. subglobosa* ↓ Miliolids (H)	*U. hispido-costata* (H)	Dissolution	*C. wuellerstorfi* ↓ *U. hispido-costata*, *Miliolids* (C)	*U. asperula* (H)
		NN11 b			Miliolids (C) *U. proboscidea* (C)	*G. subglobosa* ↓ *O. seminulina* (C)	*U. hispida* (H) *G. subglobosa* ↓	*B. pusilla* (H) *U. hispida* (H)
		NN11 a	*G. plesiotumida*	*T. lythostrota* (H) *U. hispida* (C)	Radiolarians T *R. spinea* (H) *Brizalina* (C) *H. kullenbergi* (C)	Miliolids (C) *U. hispido-costata* (C) *B. truncana* (C)	*R. spinea* (H)	
		NN10	*N. continuosa*				*L. halophora* (C) *B. reticulata* (C)	*B. finlayi* (H) *B. pusilla* (H)
	middle	NN9	*G. mayeri*	*O. bengalensis* (C) *E. bradyi* (C)		*P. bulloides* (C) Generalists (C)		
		NN8	*G. fohsi* s.l.	*M.* cf. *barleeanum* (C) *E. bradyi* (C)			*R. striata* (C)	*P. quinqueloba* ⊥ *N. umbonifera*–radiolarians ↑ *R. spinea/C. wuellerstorfi*
		NN7		*C. wuellerstorfi–H. rugosa* ⊥	Rads (H) *H. mioindex* ⊥	Radiolarian–*N. umbonifera* ↑ *C. wuellerstorfi* ⊥ 12 appearances	*H. mioindex* ⊥̲ *N. umbonifera* ↑ 12 appearances	6 appearances
		NN6						
		NN5	*O. suturalis*			*N. umbonifera* ⊥		*B. anastomosa* (U)
	early	NN4	*P. glom. curva*	Generalists and *U. spinulosa* *R. ongleyi* *R. spinea*	Dissolution faunas		Oxidized interval *U. auberiana* (C)	New Zealand rectuvigerinids (U)
		NN3	*G. miozea*			Generalists		*H. mioindex* (C)
		NN2	*G. dissimilis*				Generalists and *B. reticulata*	
		NN1	*G. dehiscens*	*N. umbonifera* ⊥				

↑ = Increases ⊥ = Appears C = Consistently present ↓ = Decreases
H = Highly dominant ⊥̲ = Reappears U = Unique T = Disappears

Figure 10. Subdivision of Tasman Sea mid- to lower bathyal sections of the Miocene through Pliocene into intervals with distinctive faunas and/or short, marked faunal-change episodes. Index species for each interval were chosen on the basis of high abundance, endemism to the site at that time, high frequency, or sudden rarity at that site.

The sediment accumulation rate diagram for Site 590 computed aboard ship has been converted to a curve and is plotted in Figure 12. Rates at Site 590 are the highest in the Tasman Sea; nevertheless, the shape of the histogram is typical of the Tasman Sea in general and contains evidence of several basinwide sedimentation events, most of which are attenuated at Site 588, which typically has the lowest accumulation rates (~2000 g/cm²/per m.y.) than the other sites. Episodes of increased rate of sediment accumulation occur during Zones NN6–NN9, increase at the NN11a/NN11b boundary, drop off during Zone NN12, but return to late Miocene highs in the early Pliocene at most sites, and increase to a final high in Zone NN18–NN19.

Benthic Faunas and Sediment Accumulation

Comparison of foraminiferal fluctuations summarized in Figure 10 and the stable isotope and accumulation rate records indicates a consistent parallelism between sediment accumulation at all sites and their faunal histories. Species evolution, large-scale faunal overturn, and depth migrations all occur synchronously with basin-

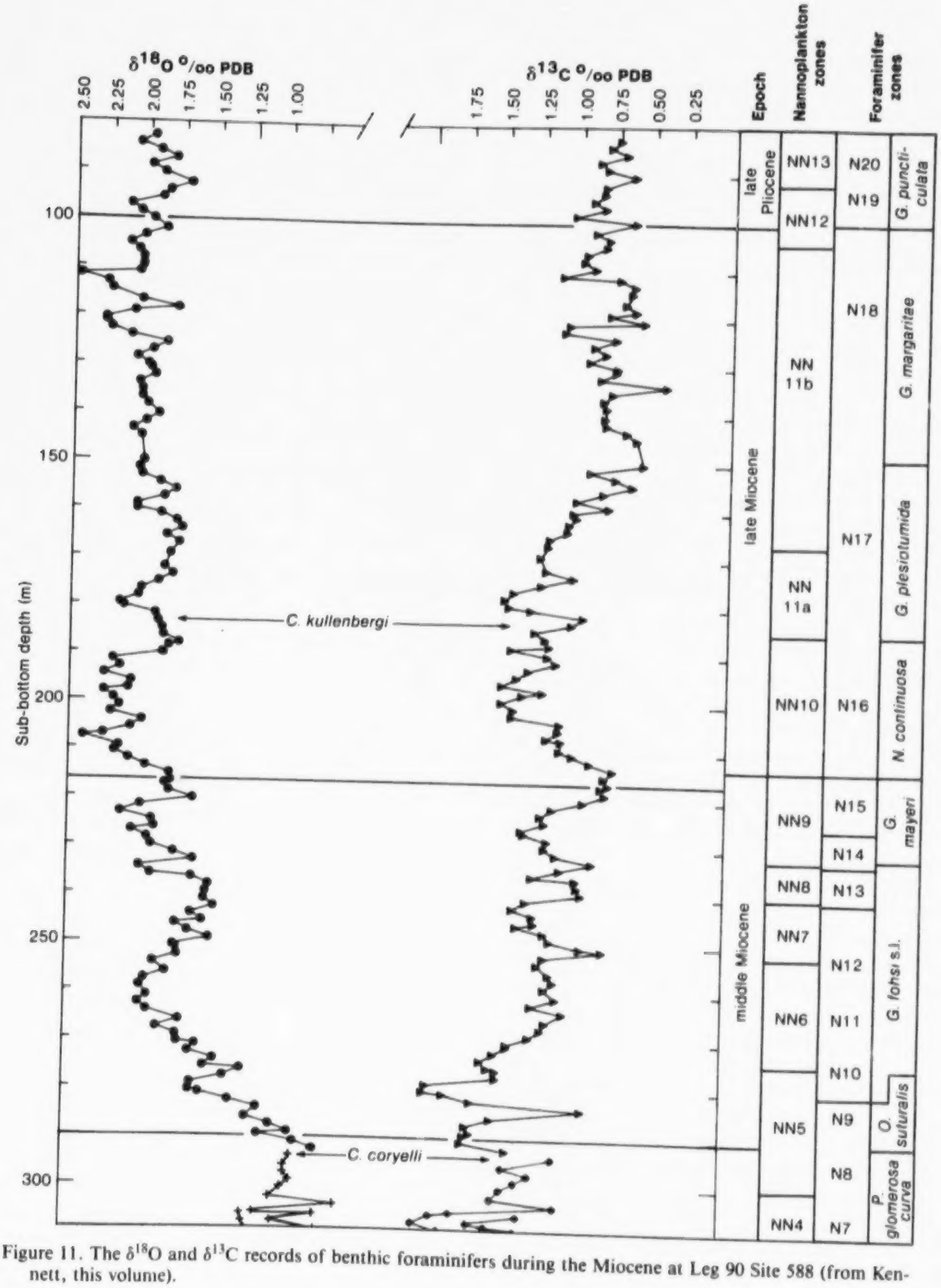

Figure 11. The $\delta^{18}O$ and $\delta^{13}C$ records of benthic foraminifers during the Miocene at Leg 90 Site 588 (from Kennett, this volume).

wide fluctuations in the sediment accumulation rate records, interpreted here to represent fluctuations in surface-water productivity.

Whether by production or preservation, sediment accumulation rates in the Tasman Sea are high (Worsley and Davies, 1979); Tertiary maxima are two to two and one half times greater than at equivalent depths in the southeastern Atlantic Ocean (Shackleton et al., 1984). Benthic faunas are more diverse and have higher numbers of specimens per sample at these sites with high sedimentation rates than in other oceanic areas (Boersma, 1984b).

The idea that increased rates of sediment accumulation indicate increased sediment supply generated by surface-water productivity is supported by the carbon isotopic record of the early Pliocene (Elmstrom and Kennett, this volume). Increased biotic production at the surface is usually represented in the carbon isotopic record in one of two ways. Oceanwide productivity events associated with reorganization of oceanic carbon cycling

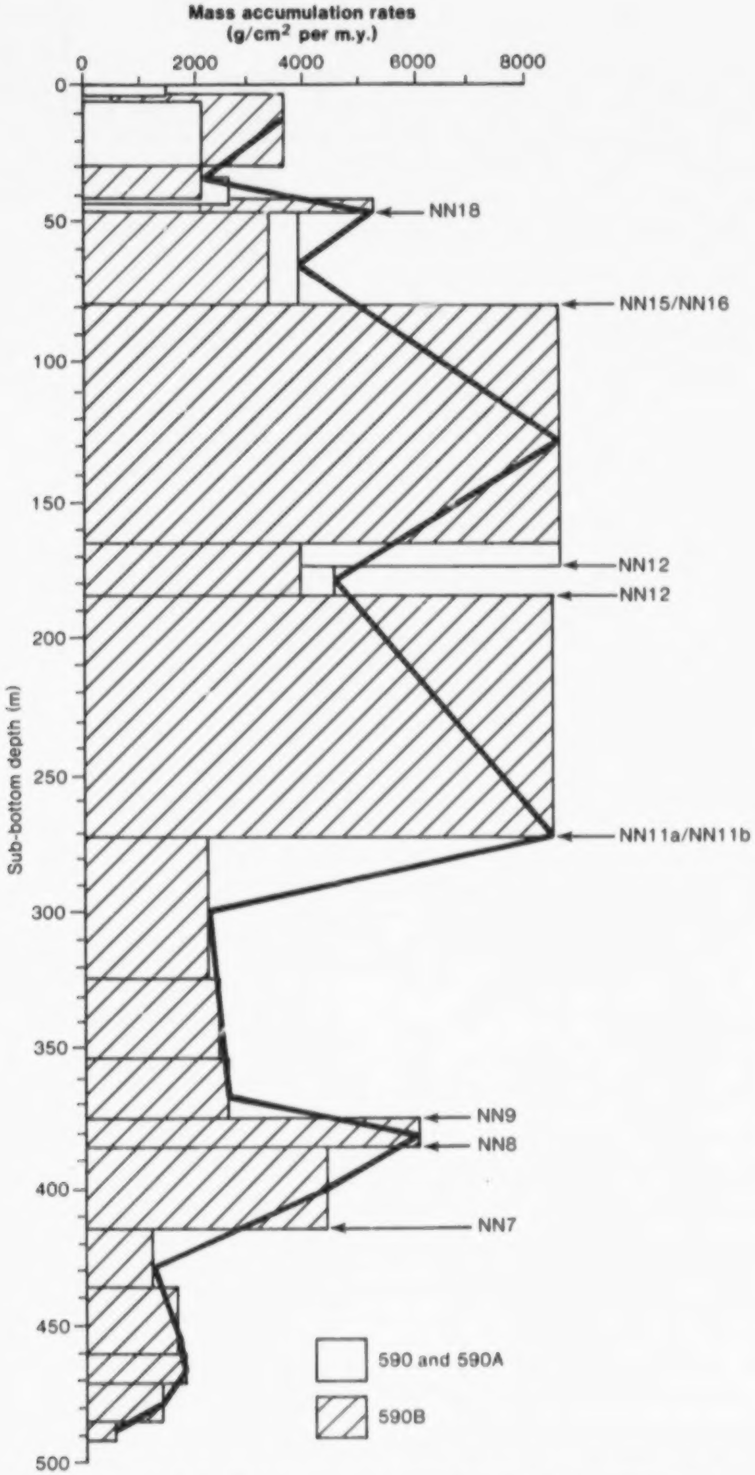

Figure 12. The record of sediment accumulation rates plotted with the combined frequencies of all *Uvigerina* species in each zone through the Miocene and Pliocene at Site 590. Frequencies are normalized to the number of samples examined in each zone. Rates were calculated using the nannofossil biostratigraphy of Martini; Lohman; both this volume. Nannofossil zonal age of each major shift in the record is indicated to the right of the diagram.

are reflected by an increase in the surface-to-bottom gradient involving more positive values both at the surface and at depth. Light carbon is being stored in biologic systems, and not recycled. Heavy values at the bottom are the ocean-atmosphere response to this situation. By contrast, heightened productivity resulting from local upwelling is evidenced by light carbon values at the surface and at depth, which indicate that light carbon is being recycled; more positive oxygen isotope values among the planktonics demonstrate that cooler temperatures are being distributed higher in the water column (Prell and Curry, 1981). The early Pliocene stable isotope records at Site 590 exemplify this scenario in Zone NN14 and suggest heightened surface-water productivity in a local upwelling correlative with high rates of sediment accumulation (see Fig. 12). Figure 10 shows the *Uvigerina* maximum which is coeval with this upwelling event.

A further indication of episodes of high surface-water productivity over the Lord Howe Rise is provided by the radiolarians (see Appendices 1–21 for presence–absence data). Large numbers of nearly monospecific spherical radiolarian assemblages first appear in coarse-fraction residues at the beginning of the middle Miocene at Sites 591 and 593 and persist through Zone NN9. They appear slightly later at Site 590, where they are common throughout the middle Miocene, and disappear in the late Miocene near the NN11a/NN11b boundary. Radiolarians occur sporadically at the Miocene/Pliocene boundary and throughout the Pliocene, most commonly at Site 590, but never in great abundance. These radiolarian occurrences suggest the migration of high-productivity surface currents into the areas of Sites 591 and 593, both of which lie near the Tasman eastern boundary current system, and at Site 590, which lies within the path of a subtropical divergence, called the Tasman Front. Their absence at Site 592 indicates a pronounced frontal zone between Sites 592 and 593; the foraminiferal faunas shown in Figure 10 corroborate this.

Radiolarians disappear from Site 590 near the Zone NN11a/NN11b boundary (about 10 Ma), coeval with the major increase in sediment accumulation rates there and throughout the Tasman Sea (Fig. 11). This Tasman event corresponds in time with the heightened productivity episode in the Pacific during the late Miocene from 10–5 Ma, when silica production increased in high northern latitudes (Woodruff and Savin, in press) and in the western equatorial Pacific (Leinen, 1979), but decreased dramatically in the southwestern sector. If productivity is not reflected in abundance of siliceous organisms, then another source must be postulated. In the early Pliocene, high rates of sediment accumulation in the Tasman area have been attributed to increased productivity of nannofossils (Elmstrom and Kennett, this volume). This may have been the case also in the late Miocene, with or without enhanced conditions for carbonate preservation. However, increasing productivity is also likely, in Pacific intermediate waters, to cause an expansion of the oxygen minimum zone (Woodruff and Douglas, 1981), which then acts to preserve carbonate and residual organic matter by decreasing oxidation and CO_2 release to sediment. Furthermore, this residual organic matter should support a greater biomass at the bottom.

The very high rates of sediment accumulation despite the absence of radiolarians, the benthic carbon isotope lightening in the late Miocene records at Sites 588, 590, and 591, the high late Miocene diversities of benthic foraminifers, and the high Benthic Numbers in general in the Tasman Sea all suggest that there was a productivity increase in the Tasman Sea coeval with the high-productivity episode in the Pacific from 10–5 Ma, and that enhanced preservation of organic matter supported the large foraminiferal faunas.

Further support for a direct relation among increased surface-water productivity, sediment accumulation, and benthic faunal composition can be drawn from the foraminiferal species themselves. One of the most unique features of these benthic faunas is the large numbers and high frequencies of uvigerinids, including the diverse and occasionally endemic species of *Rectuvigerina*. Several lines of evidence demonstrate a relationship between uvigerinids and high surface-water productivity and/or high rates of sediment accumulation. Lutze (1979) included uvigerinids among his "cool" group which predominated in *Meteor* cores off West Africa during higher-productivity glacial episodes. In Recent sediments taken in *Meteor* cores in the same area, the uvigerinids and rectuvigerinids correlated with areas of highest organic carbon resulting from high surface-water productivity (Lutze and Coubourn, 1983). This relationship is previewed by the first consistent appearance of uvigerinids in the open ocean during the high-productivity episode of the late Paleocene (Boersma, 1984a) that involved oceanwide increases in sedimentation rates (Worsley and Davies, 1979). It is reiterated by the first diversification of the rectuvigerinids during the episode of high sedimentation rates in the late Oligocene to early Miocene (Worsley and Davies, 1979). And at Quaternary glacial/interglacial boundaries it is most visible in the disappearance of uvigerinids from most open ocean sites, particularly in high-productivity areas such as the Panama Basin—a disappearance correlated with the decrease or disappearance of siliceous fossils.

The relationship of uvigerinids to high rates of sediment accumulation and heightened surface-water productivity in the Tasman Sea is corroborated by their involvement in almost every major faunal reorganization coeval with sedimentation rate changes (Figs. 10, 12), their evolutionary diversification during the first episode of high sedimentation rates in the middle Miocene (Fig. 3), their great abundance and frequency at Site 590, where sediment accumulation rates are highest, and their abundance peak at Site 590 during the upwelling episode in Zone NN14.

To test this relationship, uvigerinid frequencies through the Neogene are plotted against the curve of sediment accumulation for Site 590 (Fig. 12). These curves have several drawbacks: (1) frequency per zone is not the best monitor of the uvigerinids; an abundance peak such as that in Zone NN14 is lost; (2) uvigerinid frequencies are averaged over a whole zone; and (3) spacing of sample points on the two curves is not the same. Nevertheless, there is good correspondence between the curves of uvigerinid frequency and rates of sediment accumulation at Site 590. Slight offsets between the two curves are attributable to sample point offset.

Faunas and Glacial Events

Several glacial events of differing magnitude and duration are represented in the stable isotope records from the Tasman Sea (Kennett, this volume). These include the short-lived event coeval in this area with the Eocene/Oligocene boundary, ~36.5 Ma; (Mathews and Poore, 1983, have demonstrated that this glacial actually occured in the earliest Oligocene elsewhere); the development of Antarctic glaciation in the early middle Miocene, ~14 Ma (Shackleton and Kennett, 1975); the further glacial buildups just below the Miocene/Pliocene boundary, ~5 Ma (Savin et al., 1981) and in the mid-Pliocene, ~3.2 Ma (Shackleton and others, 1984a; Prell, 1982); and the development of Northern Hemisphere glaciation, ~2.5 Ma (Backman, 1979). Glacials correspond with periods of high sediment accumulation in the Tasman Sea in the middle Miocene and the latest Pliocene, but not at the Eocene/Oligocene, Miocene/Pliocene, or early/late Pliocene boundaries. Rates of sediment accumulation actually plummet in the latter two instances, and are generally low in the early Oligocene.

Three glacially correlated faunal patterns which first develop during the Eocene/Oligocene boundary event and recur with each later glacial are (1) the covariance of uvigerinids with signals of heightened productivity, in this case a pulse of radiolarians and carbon isotopic evidence of upwelling at mid-bathyal Site 592; (2) migration toward shallower depths of lower bathyal species, which at this time involved the first appearance of *Nuttallides umbonifera* at mid-bathyal Site 593; and (3) disappearance of large specimens of *Globocassidulina subglobosa* above the boundary and their replacement by low-diversity faunas containing cosmopolitan and austral species.

The appearance of *N. umbonifera* at middle bathyal sites is anomalous and suggests unusual oceanographic conditions. Evidence on the ecology of *N. umbonifera* comes from several sources. In the Quaternary abundances of this species frequently parallel the path of Antarctic Bottom Water (AABW), but correlate with a strongly corrosive bottom environment and carbonate undersaturation in areas not overlain by AABW (Lohman, 1978; Bremer and Lohman, 1982). In the Neogene, *N. umbonifera* reaches high percentages in abyssal sites located at over 3000 m water depth in both the Atlantic and Pacific oceans. It occurs in middle bathyal areas in very low numbers, if at all, and in discrete pulses (Woodruff, 1979; Tjalsma, 1983). In the Paleogene, *N. umbonifera* first appears in lower bathyal and abyssal areas where sedimentologic and isotopic evidence demonstrate the first development of cooled, corrosive and/or low oxygen conditions at the bottom (Tjalsma and Lohman, 1983; Boersma, 1985). It occurs at middle bathyal depths only during short episodes of dissolution just above the Eocene/Oligocene boundary (Boersma, in press) and in the mid Oligocene (Boersma, 1985). In most cases it varies inversely with the miliolids and uvigerinids. Together these studies suggest that in the Tertiary, as well as the Quaternary, it is justifiable to use the presence of *N. umbonifera* to trace corrosive conditions and, where dissolution is not prominent, cooled and well-oxygenated conditions. Therefore the presence of *N. umbonifera* at Site 593 is interpreted to represent the glacially forced, short-lived penetration into shallower depths of cooled, "new" waters and related conditions at the bottom at the Eocene/Oligocene boundary.

Eutrophication of Tasman Sea current systems, indicated by a large influx of radiolarians at Sites 590, 591, and 593 (Fig. 10) as well as in New Zealand land sections (Hornibrook, 1971) occurred during the middle Miocene glaciation that is recognized worldwide in stable isotope records (Shackleton and Kennett, 1975; Savin et al., 1981). This glacial can be traced in the Tasman Sea by (1) increased rates of sediment accumulation (Fig. 12) beginning in Zone NN6 and persisting through most of the middle Miocene at Sites 591 and 593 and (2) the characteristic heavy benthic isotope values (Kennett, this volume). Several faunal patterns reiterate those of the Eocene/Oligocene glacial, with important differences and additions: (1) the faunal changes are long-lived, not episodic; (2) during the sediment accumulation increase miliolids first appear, followed later by an influx of spinocostate uvigerinids at lower bathyal depths; (3) updepth migration of *N. umbonifera* into middle bathyal Sites 593 and 594 accompanies very large, monospecific, radiolarian faunas and intense dissolution at Site 594; (4) at Sites 591 and 593 cibicidid-rich faunas alternate with uvigerinid-bearing samples, previewing a pattern which will occur in all later glacials and will eventually occur throughout depth; and (5) radiolarians first commonly appear at Site 590, located at lower middle latitudes under the Tasman Front, coevally with the first appearance of striate hopkinsinids and rectuvigerinids.

Based on the acknowledged relationship between uvigerinids and high organic carbon in sediments, the high sediment accumulation rates, and the expansion of radiolarians through the Tasman Sea, I conclude that the middle Miocene glacial period brought invigorated oceanic circulation, increased rates of upwelling, and heightened productivity in divergence zones, under the Tasman Current system both within the Tasman Sea in the area of Site 593 and on the Chatham Rise, as well as at higher middle latitudes in the eastern boundary current system. Because the Antarctic was transformed from an oligotrophic to a eutrophic region at this same time (Schnitker, 1980), it is probable that Antarctic-derived waters feeding this circulation were themselves more nutrient-rich. Schnitker (1980) has suggested that eutrophication of the Antarctic and invigorated circulation resulted from the increased production of North Atlantic Deep Water (NADW), which disrupted stratification of Antarctic water masses, allowing upwelling of more nutrient-rich underwaters. Along similar lines Blanc and Duplessy (1982) determined a single, southern source of deep water to the Pacific (probably a type of NADW) beginning in the middle Miocene. It appears that eutrophication of the Antarctic, high fertility of the southern Pacific, and compartmentalization of nutrients in the Pacific all occurred during this same glacial episode and are reflected in the benthic faunas.

The glacial episode at the termination of the Miocene is signalled by heavy oxygen isotope values at Sites 588 and 590 (Kennett, this volume) but decreased sediment accumulation rates at most sites. Dissolution, which may have contributed to the low accumulation rates, was intense at lower bathyal sites, but only moderate at middle bathyal depths. At this time (Fig. 10), miliolids and uvigerinids became highly dominant at middle bathyal sites, miliolids disappeared from lower bathyal Site 591, spino-costate replaced spinose uvigerinids, uvigerinids developed at the expense of *Cibicides wuellerstorfi* and *G. subglobosa*, and the lower bathyal species, *Melonis pompilioides* and *Pullenia quinqueloba*, migrated updepth into the middle bathyal zone, whereas *N. umbonifera* remained important only at lower bathyal sites. These were temporary changes, and faunas typical of the later Miocene returned in the early Pliocene.

Interpretation of the faunal patterns of this glacial is based on the relation between uvigerinids and high organic carbon content; the usual restriction of spino-costate uvigerinids to deeper, cooler sites; and the inverse correlation between miliolid abundance and *N. umbonifera* and carbonate undersaturation (Bremer and Lohman, 1982). These patterns suggest that whereas lower bathyal depths became more corrosive to carbonate, sediment at middle bathyal depth was relatively well preserved and waters were well saturated with respect to calcium carbonate. This may reflect penetration of the lysocline into shallower depths. However, cooler water conditions typical of the lower bathyal zone moved updepth into the middle bathyal zone at this time. The spino-costate uvigerinids which now dominated at middle bathyal depths originally inhabited the cooler, slightly less organic carbon rich lower bathyal zone. In other words, these was slightly lower nutrient availability at cooler temperatures at shallower depths.

This glacial event is coeval with the termination of the High-productivity Episode (10–5 Ma) in the Pacific, and the lower sediment accumulation rates in Tasman Sea sites conform to this pattern. The decreased abundance of *C. wuellerstorfi* and other cibicidids may lend evidence which explains this decrease in sediment accumulation. In the Holocene, cibicidids, particularly *C. wuellerstorfi*, are associated with high-productivity regions receiving large amounts of hemipelagic material. Under the West African upwelling during the Holocene, the abundance of *C. wuellerstorfi* is correlated with high accumulation rates of terrestrial organic carbon, not marine organic carbon, which is correlated with higher numbers of uvigerinids (Lutze and Coubourn, 1983). It is suggested, therefore, that both the lower productivity and the major decrease in cibicidids in the latest Miocene reflect the decreased input of carbon to the ocean from terrestrial sources.

The glacial buildup near the NN15/NN16 boundary is accompanied by plummeting rates of sediment accumulation at all sites. Uvigerinids increase to a mid-Pliocene high coeval with the peak in sediment accumulation (Fig. 12), but decrease dramatically and become more geographically compartmentalized in Zone NN16; spinose forms are concentrated in the lower latitudes, spino-costate taxa in the higher middle latitudes and at lower bathyal depths. The miliolids also decrease generally across the boundary into Zone NN16. By contrast with the previous glacial buildup, however, cibicidids expand and new genera such as *Osangularia, Rotalia*, and *Cassidulina* are more commonly found in the faunas. Expansion of the cibicids may indicate the persistent presence of terrestrial organic matter. These faunal events represent the transition into a fully glacial pattern. Lack of miliolids and uvigerinids suggests the lowered productivity which the sediment accumulation rates corroborate. The less intense benthic oxygen isotope signal (Kennett and Elmstrom, this volume), lack of upwelling signals, and the restriction of *N. umbonifera* to middle bathyal depths at Site 591 and (in greater abundance) Site 586, suggest mild restratification and the development of different intermediate and deep-water types and related conditions at the bottom in the Tasman Sea after this time.

The final Pliocene glaciation, about 2.5 Ma, is reflected in (1) a peak in sediment accumulation rates; (2) a positive excursion in the oxygen isotopes; (3) proliferation of the cibicidids, which alternate with uvigerinid-bearing samples, indicating the initiation of permanent glacial–interglacial faunal patterns and oceanographic conditions at this time.

SUMMARY

The unique compositions of Tertiary-age middle to lower bathyal benthic foraminiferal faunas are largely modulated by (1) fluctuations in oceanic surface productivity developed in several oceanographic fronts which migrate through the Tasman Sea and (2) glacially forced vertical displacements in hydrochemical boundaries. Heightened productivity during the numerous steps in glacial buildup, from the latest Eocene to the latest Pliocene or during the late Miocene high-productivity episode in the Pacific, is reflected in the very high rates of sediment accumulation in the Tasman Sea. Evolutionary overturn, all major faunal reorganization, and depth migrations are coeval with the large-scale features of the sediment accumulation rate curves for the Tasman Sea sites.

Faunal overturn reflecting high productivity and expansion of the oxygen-minimum zone involves the uvigerinids and miliolids. Uvigerinid frequencies vary directly with the the large-scale features in the sediment accumulation rate records, and uvigerinids reach peak abundance during local upwelling events. Glacial fluctuations involving heightened productivity are expressed by alternating cibicid-rich and uvigerinid-bearing samples.

Lower bathyal faunal elements migrated to shallower, mid-bathyal sites during glacial episodes; overturn which causes shallowing of oxygen-rich, corrosive, and cool bottom waters is indicated by high abundances of *Nuttallides umbonifera* at middle bathyal sites. Shallowing

of deep-water, less corrosive conditions in the latest Miocene glacial resulted in migration into shallower depths of *Melonis pompilioides, Pullenia quinqueloba*, and spino-costate uvigerinids, high dominance of miliolids, and minimal dissolution at middle bathyal depths.

ANNOTATED LIST OF SELECTED SPECIES

The following list is not inclusive, but contains species for which information exists on taxonomy and morphotypic variation. A new species is described and is figured in Plate 17.

***Anomalinoides globulosa* (Chapman and Parr).** Plate 2, Figs. 1-3. This species varies markedly in thickness and in the eccentricity of the final chamber. Specimens closely resemble *Anomalinoides badensis* (d'Orbigny), first described from the Vienna Basin (d'Orbigny, 1846). Specimens from higher latitudes tend to have squarer, less inflated chambers and a more lobulate periphery. Ranges from early Miocene through the Pliocene.

***Anomalinoides orbiculus* (Stache).** First named from New Zealand, this species is relatively common in the Paleogene levels of Site 592 and 593. Specimens from the higher-latitude Site 593 are rounder and resemble *Anomalinoides ammonoides* (Reuss). At Site 592, this species is squarer, thinner, the periphery is more angled and the umbilical flaps are more articulated.

***Anomalinoides semicribrata* (Beckman).** Plate 1, Figs. 1-6. This species possesses a peripheral aperture which extends slightly onto the spiral side. The umbilical side is not umbilicate and both sides lack umbonal knobs; nevertheless it is closer to the genus *Anomalinoides* than *Gavelinella*, to which it was later assigned. This species usually has 4 to 5 chambers in the final whorl; more tightly coiled forms with the larger chamber number are typical at Site 593 during the Paleogene. At Site 592 all degrees of coiling tightness are present. In the early Miocene, specimens at Site 593 are much larger and more evolute, and the chambers are less inflated than in lower latitudes (Hole 588C). Comparison of late Miocene forms at Site 590 with the deeper-water Site 591 demonstrates that the deeper-dwelling specimens are smaller and dextrally coiled, whereas the coiling of those at Site 590 is sinistral. Toward lower latitudes the numbers of pores decrease, but they become larger in size (Plate 1, Figs. 4-6).

***Bolivinopsis praelonga* (Schwager).** Plate 3, Figs. 3-4. As figured by Srinivasan and Sharma (1980), this species is both large and especially long. Comparison of specimens which would be called *Bolivinopsis cubensis* in the Paleogene (Plate 3, Figs. 1, 2) demonstrates that the two species are identical except for the larger size and longer biserial portion on *B. praelonga*. Elongation is a common feature of the evolution of long-lived rectilinear benthic species; most of them receive different names when they have added more chambers. In the case of *Bolivinopsis*, the addition of more chambers does not involve a change in coiling, which would be sufficient reason to use a different species name. Therefore the species *cubensis* should probably be referred to the level of *forma* of the species *praelonga*.

***Brizalina finlayi* (Hornibrook).** Plate 4, Figs. 3-4. This species has ornament which is intermediate between that on *Brizalina pusilla* and *B. reticulata*. It is generally smaller and more delicate than those two species. In the early Miocene individuals at higher latitudes are generally larger, have more pointed initial ends, and are longer. Their costae are more wavy and finer than those at low-latitude Site 588.

***Brizalina pusilla* (Schwager).** Plate 4, Figs. 1-2. As is the case with many other long-lived bathyal benthics, there appear to be two names, one applied in the Paleogene and the other in the Neogene. In this case one Paleogene name is *B. tectiformis* (Beckman). Comparison of populations from the Atlantic province and from Barbados, where it was named (Beckman, 1953), indicate that *B. tectiformis* is almost identical with *B. pusilla* from the Tasman Sea and from Car Nicobar. Boltovskoy (1978) pictures Indian Ocean populations of this species which are identical to those from the Tasman Sea.

***Brizalina reticulata* (Hantken).** Plate 4, Fig. 5. This species occurs worldwide during the Oligocene and Miocene. Although some authors believe that it is conspecific with *Brizalina anastomosa* (Finlay), there is a clear distinction between the two in the Tasman Sea. *Brizalina anastomosa* is the more common form at Site 593, where it is shorter, broader, and has more strongly developed ornament.

***Bulimina aculeata* d'Orbigny.** Plate 5, Fig. 1. This species is not common in the Tasman Sea, but is very frequent at Site 594 on the Chatham Rise in hemipelagic sediments containing large amounts of siliceous fossils. At higher latitudes the spines of this species are blunter and much shorter.

***Bulimina striata* d'Orbigny.** Specimens from the Tasman Sea are identical with forms from the Miocene of the Vienna Basin and from the Atlantic province. There seems no good reason to use Cushman's taxon, *B. striata mexicana*.

***Bulimina truncana* Guembel.** Plate 5, Figs. 2-5. This species varies greatly both through latitude and depth. This variability is expressed in the number of costae, their height, their orientation relative to the test axis, and the number of smooth chambers at the apertural end. Such variability has resulted in a large number of names in the literature: small, inflated forms with few costae which begin almost at the aperture have been called *B. rostrata* Brady forms with numerous, slightly wavy costae which begin on the third chamber are usually called *B. alazanensis* Nuttall (Plate 2 Fig. 7); when the costae anastomose, the name is *Bulimina consanguinea* Sequenza. *Bulimina truncana* is very similar to *B. alazanensis*, except the costae are slightly fewer in number, more bladelike and straight, and begin on the first or second chamber (rather than the third, as on *B. alazanensis* or *B. consanguinea*). Because both types occur in populations from the Tasman Sea, the older taxon, *B. truncana*, has been used.

There are two main latitudinal trends: lower-latitude forms are much larger and have fewer costae which usually begin on the first or second chamber, but more frequently on the first chamber. With increasing depth, costae become more numerous and more narrow, and individuals are generally smaller. Forms with a few anastomosing costae occur only at Site 593 in the early Miocene and have been called *B. consanguinea*.

***Cibicides wuellerstorfi* (Schwager).** This is a common and well-known species which is cosmopolitan at bathyal to abyssal depths. Following Srinivasan and Sharma (1980), *inter alia*, it is placed in the genus *Cibicides* because of its sharp apertural face and the peripheral aperture which continues onto the spiral side. In the Tasman Sea this species is most common during the middle Miocene. During the middle Miocene, intergrodes between *C. wuellerstorfi, H. kullenbergi*, and *H. rugosa* occur in several samples. This is especially true of samples in the *Globorotalia fohsi* Zone, where morphotypes of *H. rugosa* are very flat and less porous. It is larger at lower latitudes in both the shallower and deeper Sites 588 and 586. There is marked variation in the porosity of this species; lower-latitude forms seem to have fewer pores in the middle Miocene. At the very end of the Miocene, during the miliolid-uvigerinid acme intervals, it becomes much less porous, along with the other rotaloid species. This demonstrates that there is more than a latitudinal pattern to its porosity.

***Cibicidoides parki* (Finlay).** Plate 7, Figs. 1-5; Plate 8, Figs. 1-5. This is a well-known index species in New Zealand sections. It has been identified in the Possagno section of Italy and in the American Gulf Coast where it has been called *Cibicidoides cancelata* (Cushman), which name is actually older. However, it appears that this species was first named *Cibicides truncanus* (Guembel) in the Monte Brione section of Italy. Because this synonomy could not be confirmed by the samples I have from this section, the local taxon, *C parki*, has temporarily been retained for the lower-spired, less strongly ornamented forms from the Tasman Sea.

Suggestions that this species should be referred to the genus *Osangularia*, seem unwarranted because of the distinctive cibicidid aperture seen on Plates 7-8, as compared with that on *O. culter* in Plate 12, Figs. 4-6.

***Cibicidoides* cf. *ungerianus* (d'Orbigny).** Several intermediate-depth sites of the Pacific and the Atlantic contain a cibicidid which closely resembles *C. ungerianus* from the Vienna Basin. Comparison of specimens from the Tasman Sea and Viennese material has shown that the Tasman forms are very similar, but larger, similarly flat have a similarly pinched periphery and keel, possess the same number of slightly depressed, curved sutures, but lack the ornamented or limbate spiral and the slight umbilical fosse on the ventral side. This is probably a deep-water ecophenotype of *C. ungerianus*. Because of its widespread distribution in oceanic sites, the species should be in some of the older literature, but I have yet to find it.

Discanomalina semipunctata **(Bailey).** Plate 2, Figs. 4–6. Originally this species was classed as an *Anomalina*, but the character of the umbilical side, the peripheral aperture, and the partially evolute dorsal side all locate it in the newer genus, *Discanomalina*. It has been suggested that this species is one generation of the attached, shallow-water genus *Carpentaria*, but the interpretation is difficult to accept in view of the distribution and frequency of this species at middle and lower bathyal depths in the Tasman Sea.

Ehrenbergina pacifica **Cushman.** Of the several species of *Ehrenbergina* present in the Tasman Sea, only *E. pacifica* is present at all sites by the Pliocene. There are definite latitudinal gradients both in the degree of spinosity and in the number of chambers in the adult. At higher latitudes specimens are more spinose and are usually shorter and broader, adding fewer chambers which enlarge more rapidly. In general, the ehrenberginids of the Tasman Sea are less angular and more rounded, almost bulbous, like *E. marwicki* Finlay in Plate 11, Figs. 1–2.

Globocassidulina subglobosa **(Brady)** This well-known, cosmopolitan species occurs consistently but not in abundance at most of the Tasman Sea Sites. The one exception is in the late Eocene at Site 593, when *G. subglobosa* is both very common and very large. Such large specimens do not again occur in the Tasman Sea.

Hanzawaia cushmani. This species becomes much higher-spired at Site 592 than at Site 593. It has been placed in synonymy with *H. ammophila* (Guembel), as repictured by Hagn (1956). However, comparison of material from Monte Brione indicates that *H. ammophila* is a much smaller, flatter species with many more chambers in the final whorl, thicker sutures, and a much less domed shape than Tasman forms.

Heterolepa kullenbergi **(Phleger and Parker).** The species is placed in the genus *Heterolepa* because it is plano-convex to slightly biconvex, but not biumbonate, and possesses an aperture which is not only peripheral with a lip, but extends onto the umbilical side as well as onto the spiral side. The apertural features are those of a *Heterolepa*, not a *Cibicidoides*.

There is marked variation in the roundness of the test and the spire height, but no latitudinal or depth-related pattern could be inferred. Populations are, however, much larger at the deeper Site 591 than in the shallower sites. The species appears to be a solution-resistant form in both carbonate and siliceous facies.

It first appears during the *G. angulisuturalis* Zone at Site 588, apparently evolving from an ancestral form which was smaller, chunkier, and possessed a distinct keel.

Heterolepa rugosa **(Phleger and Parker).** This species varies geographically in the development of its porosity, the degree of reticulation and spiral limbation, and in the spiral height. Oldest populations demonstrate pores on only one-half of the chambers in the final whorl. Reticulation is barely developed and the walls appear coarse on only about half of the chambers. After its expansion in the *Globorotalia fohsi* Zone, the species shows definite gradients; lower-latitude forms are flatter and more ornamented. Such forms appear to grade into *C. wuellerstorfi* and *H. kullenbergi*. Reticulations, well developed at Site 590, are reduced to a coarsening of the wall texture at Sites 592 and 593. None of the specimens from the Tasman Sea, however, show the same degree of reticulation as typical forms from the Atlantic. Whereas those at the deeper Site 591 are larger than their counterparts at the shallower Site 590, they also lack well-developed reticulation or pronounced spiral limbation.

Hopkinsina mioindex **Finlay.** The species is more or less angular from site to site, but demonstrates marked variation in the development of the striae. Striae are always fewer and finer at Site 594. At Site 591 striae are higher and somewhat less numerous than on individuals from shallower-water Site 590. There is a consistent trend for this species to become longer, thinner, and to possess many fine costae toward higher latitudes in the shallow Tasman Sea sites. Lower-latitude forms are consistently shorter, wider, and have fewer uniserial chambers.

Laticarinina halophora **(Stache).** This species is commonly called *Laticarinina pauperata* (Parker et al., 1865), although Brady indicated that Stache's species, named in 1864, was identical (Barker, 1960). The older taxon, *L. halophora*, is therefore retained here. It is easily differentiated from *L. bullbrooki* and *L. altocamerata*, both of which occur frequently in Tasman Sea sections, by its much larger number of chambers, which are barely convex above the plane of the wide-flanging keel.

Marginulinopsis hochstetteri **(Finlay).** This very large and distinctive species is an index for the Bortonian of New Zealand (Hornibrook, 1971); it occurs into the Oligocene in the Tasman Sea at both Sites 592 and 593. At the latter site individuals are much larger, spines are much more numerous and acute, and even the periphery is serrate to spiny.

Melonis **cf.** ***barleeanum*** **(Williamson).** This form is distinguished from typical specimens by being much flatter and slightly less porous. It is more common in the Tasman Sea than typical *M. barleeanum*, particularly earlier in the species' ranges.

Melonis pompilioides **(d'Orbigny).** Typical specimens of this species occur in the Tasman Sea primarily at the two deeper Sites 591 and 586, where *M. sphaeroides* is also found briefly. The species occurs in pulses in the shallower sites, where it is distinctly smaller and very slightly thinner than the deeper-water indigenes. A second difference is found in the degree of chamber inflation; at Sites 588 and 590 the earlier chambers are less inflated than the final ones. At Site 591, chamber inflation is relatively constant throughout the final whorl. At middle bathyal depths there is a tendency for size to decrease at progressively lower latitudes.

Nuttallides umbonifera **(Cushman).** This species is not common in the Tasman Sea except in discrete pulses in the early to middle Miocene, when it occurs in very large numbers in coarse fractions consisting largely of spherical radiolarians. These pulses seem to be coeval between Sites 591, 593 in the Tasman Sea, and Site 594 on Chatham Rise, where *N. umbonifera* may be the only species in the entire sample. The radiolarian–*N. umbonifera* pulses continue at Site 594 through the middle and into the later Miocene. *Nuttallides umbonifera* is consistently larger at the higher-latitude sites, and always larger at Site 594 than elsewhere.

Osangularia bengalensis **(Schwager).** This demonstrates definite latitudinal and depth-related gradients which persist through the Miocene and Pliocene. It is more frequent in the deeper Site 591 than in the equatorial, deep Site 586. In the shallower-water sites there is a marked gradient in its abundance; it is more common toward lower latitudes.

Osangularia culter **(Parker and Jones).** Plate 12, Figs. 4–6. Like *O. bengalensis*, this species demonstrates latitudinal and depth-related frequency gradients; they are the inverse of those of *O. bengalensis*. *Osangularia culter* is more common at deeper-water Site 586 than at Site 591; it is more frequent at the sites toward higher than toward lower latitudes. However, the genus *Osangularia* is consistently less common at higher latitudes and is absent altogether at Site 594 in the Pliocene.

Pullenia quinqueloba **d'Orbigny.** Like *M. pompilioides*, this species shows a preference for the deeper sites. It occurs in discrete pulses in shallower sites.

Rectuvigerina ongleyi **(Finlay).** Plate 17, Fig. 2. This species is an index for the late Oligocene into early Miocene in New Zealand. In the Tasman Sea it ranges through the middle and late Miocene; in the early Miocene, only its predecessor, *Uvigerina spinulosa*, is present. That is to say, specimens of this group do not begin to add uniserial chambers in Tasman Sea sites until middle Miocene Zone NN6. It occurs at all of the shallower Tasman sites, but is not found at the deeper Site 591. More spinose morphotypes are found at Site 593 in the later Miocene.

Rectuvigerina postprandia **(Finlay).** Plate 17, Fig. 6. In New Zealand sections this species is an index for the late Eocene into early Oligocene (Hornibrook, 1971), and is restricted to this same interval in the Tasman Sea. In the Atlantic, however, it occurs later in the Oligocene (Boersma, 1984b).

Rectuvigerina prisca **(Finlay).** Plate 17, Figs. 1, 7. Although in New Zealand this species is an index for the late Eocene (Hornibrook, 1971), it occurs from the late Eocene through the Oligocene in the Tasman Sea. In older populations, individuals add only one or two uniserial chambers. In the late Oligocene, however, many specimens possess 2–4 uniserially added chambers. Striae are attenuated on these uniserial chambers (Plate 17, Fig. 1).

Rectuvigerina spinea **(Bermudez).** Plate 18, Fig. 5. These very spinose rectuvigerinids are the only ones to appear in the deeper-water sites; other groups are restricted to the shallower parts of the Tasman Sea and New Zealand land sections. Individuals from the deeper Site 591 are more strongly striate and very much more spinose than those at the shallower Site 590. Upper bathyal morphotypes with very few spines have been called *Siphogenerina opima* Cushman, which species should probably be referred to the genus, *Rectuvigerina*.

***Rectuvigerina striata* (Schwager).** Plate 17, Fig. 5. This unique species is characterized by its very lobulate periphery resulting from the almost spherical shape of the uniserially added chambers. Irregular, occasionally anastomosing costae are usually present on several chambers. It is differentiated from the similar *Rectuvigerina striatissima* (Stache), which also occurs in the Tasman Sea, by the fact that the striations on the latter species are continuous across the chamber margins. Figure 5 is taken from topotype material from Car Nicobar; forms in the Tasman Sea are identical. Another New Zealand species, *Rectuvigerina vesca* (Finlay), is conspecific with *R. striata*, differing only in the smaller number of uniserially added chambers.

***Rectuvigerina tasmana* n. sp.** Plate 17, Fig. 4.

Description. Test very elongate, thin, medium-sized, about 0.6 mm in length; about 3 times as long as broad; coiling triserial in initial whorl, rapidly becoming uniserial in following 3 or 4 whorls; chambers inflated, increasing in size very slowly and regularly, so that sides are subparallel; periphery lobulate; sutures indistinct behind the ornament; porous wall ornamented with longitudinal, very fine, spinose striations, about 40 in total circumference; most of the spinose striations or lines of joined spines are restricted to individual chambers; a few anastomose, and a few may cross the sutures and join those above or below; neck terminal, short, and tubelike; rarely found with a reverted lip.

Holotype. Plate 17, Fig. 4, will be deposited in the Cushman Collection at the United States National Museum.

This species is differentiated from other rectuvigerinids by its very large number of totally spinose striations. It is found only at Site 587 in samples with mixed middle bathyal and shelf benthic foraminiferal faunas, so the ecology of this species is uncertain. It is very likely to be a shallower-water species that was moved downslope with the amphisteginids, bryozoans, and elphidiums in these samples.

***Siphonodosaria insecta* (Schwager).** Plate 16, Figs. 6–7. This is a common species in the Tasman Sea. It occurs along with *Stilostomella lepidula*, transitional forms to which are also shown in Plate 16. The species is identical with Paleogene, smooth siphonodosarids, one of which is called *S. nuttalli* (Cushman and Jarvis). Although *S. nuttalli* is more curvilinear than typical *S. insecta*, the species are essentially identical, and Schwager's name takes precedence.

***Stilostomella lepidula* (Schwager).** Plate 16, Figs. 1–4. As already discussed by Boltovskoy (1978) and Srinivasan and Sharma (1980), this is a very variable group which, through time, has produced a large number of morphotypes, most of which have been given a separate name in both the Paleogene and the Neogene. These multiple taxa have been based largely on the number and location of spines. Although Srinivasan and Sharma (1980) mention that the older taxon, *S. adolphina* of d'Orbigny, exemplifies some of the variation in the group, they do not adopt the older name. In Vienna Basin material, *S. adolphina* contains relatively few, very regularly placed large spines, which form a ring skirting the base of each chamber. It is thus most similar to the Paleogene species, *Stilostomella basicarinata* Hornibrook, which contains many more spines aligned into a basal, skirting, rim. Accepting these as valid species leaves *S. lepidula* to include those species more or less curvilinear, which possess few or many randomly distributed spines on the chambers, some of which may line up on the chamber margins. *Stilostomella lepidula* is also conspecific with *Stilostomella antillea* (Cushman) and the plexus of *Stilostomella curvatura* (Cushman).

In the Tasman Sea the species is relatively common at all sites. At Site 594 it is frequently found associated with radiolarian oozes and appears to be a solution-resistant species in this facies.

***Textularia lythostrota* (Schwager).** Plate 3, Figs. 8–9. This species appears to be conspecific with *Textularia bermudezi* (Cushman and Todd); it is closely related to *Textularia leuzingeri* (Cushman and Renz), but in most cases lack the pinched periphery of that species. This is probably an intergrading plexus, because in some instances populations of *T. lythostrota* include the features of both these other species, while ranging to the wider, flatter *Textularia yasicaensis* Bermudez as well. In this case, they could all be lumped under the older taxon, *T. lythostrota*.

There is marked variation in the development of ridges paralleling the chamber widths; the ridges are higher at higher-latitude sites. The species is smaller at the deeper-water Site 591, and in the hemipelagic sediments at Site 594 where it is also composed of much finer grains.

***Uvigerina asperula* Czjeck.** This uncommon species is ornamented with very numerous, discrete, and sharp spines which are all aligned longitudinally on the chambers. By this alignment it differs from the other spinose species, *U. hispida* (Plate 20, Figs. 5–6). Like *U. hispido-costata* it is more common at the deeper than at the shallower sites.

***Uvigerina bortotara* Finlay.** Plate 19, Figs. 6. This species is very close morphologically to *Uvigerina spinicostata* Cushman and Jarvis, first named from Trinidad. However, the New Zealand species consistently has more low costae per chamber, and they are usually more spinose than those on the Caribbean taxon.

***Uvigerina eocaena* Guembel × *Uvigerina mexicana* Nuttall.** Plate 18, Fig. 2. This little-known species is actually very frequent in upper middle bathyal basinal facies of the late Eocene, and in the open ocean on topographic highs such as the Lord Howe Rise, the Walvis Ridge, and Rockall Bank, and in Oligocene faunas from Mediterranean slope basins (Boersma, 1984a). It occurs onshore in New Zealand in the late Eocene, and in the late Eocene and early Oligocene in the Tasman Sea where, however, it is not very common. Tasman forms demonstrate more rapid chamber enlargement resulting in a broader, more squat test than typical Mediterranean types. Tasman *U. eocaena* × *U. mexicana* also possesses more costae which, however, are less continuous than in the Mediterranean and adjacent areas.

***Uvigerina interruptata-costata* Le Roy.** Plate 20, Fig. 7. This species is common in the Tasman Sea. Although it closely resembles *U. dirupta* (Plate 19, Figs. 3–4), it is distinguishable by the fact that the costae are barely more than striae and the aligned, broken segments of the costae are also very fine. Like the other hispido-costate uvigerinids, this species is more common at the deeper than at the shallower sites.

***Uvigerina hornibrooki* Boersma.** Plate 18, Fig. 1. This species, described in 1984 from the Tasman Sea (Boersma, 1984a) is somewhat similar to *U. macrocarinata* Papp and Turnovsky from the Vienna Basin. That species, however, has several costae which are continuous over one or more chambers. Its costae are much less bladelike, more numerous, and the wall is distinctly less porous.

Uvigerina hornibrooki occurs only in the latest Miocene and early Pliocene in the Tasman Sea and only at the middle bathyal sites. It was not found on the Tasman Rise.

***Uvigerina tasmana* Boersma.** Plate 18, Fig. 4. This is a very unusual uvigerinid because of its loosely appressed chambers and relatively platy costae which wind around the neck, forming spinelike projections out from the neck. It is consistently wider and more bulbous in the lower half of the test. It is also restricted in its distribution to subtropical and lower latitudes, but it occurs in both the shallower and the deeper lower-latitude sites. It is not frequent in either the latest Miocene or early Pliocene.

***Vulvulina pennatula* (Batsch).** This species occurs through the entire section from the late Eocene through the Pliocene. It is generally found without final spiroplectaminid chambers, except at Site 586 where a long uniserial portion is developed. The character of the ridges varies markedly from one location to the next.

ACKNOWLEDGMENTS

The author wishes to express her special thanks to Dr. Bill Ventress and Mr. Dennis Greig of Chevron, U.S.A., in New Orleans, for providing the excellent scanning micrographs of Tasman Sea benthics. Dr. C. Srinivasan very kindly aided in the identification and picking of some of the benthic foraminifers. Drs. J. Kennett, B. Corliss, and D. Schnitker reviewed and improved the manuscript. This research was sponsored under the Bathyal Benthic Project administrated by Dr. W. A. Berggren at Woods Hole. I am profoundly grateful to Dr. Berggren for his continuing support.

REFERENCES

Backman, J., 1979. Pliocene biostratigraphy of DSDP sites 111 and 116 from the North Atlantic Ocean and the age of Northern Hemisphere glaciation. *Stockholm Contrib. Geol.*, 32:115–137.

Barker, R. W., 1960. *Taxonomic Notes on the Species Figured by H. B. Brady in his Report on the Foraminifera Dredged by H.M.S.*

Challenger *during the Years 1873-1876*. Soc. Econ. Paleontol. Mineral. Spec. Publ., 9.

Beckman, J. P., 1953. Die Foraminiferen der Oceanic Formation (Eocaen–Oligocaen) von Barbados Kl. Antillen. *Eclogae Geol. Helv.*, 46:301–412.

Blanc, P., and Duplessy, J., 1982. The deep-water circulation during the Neogene and the impact of the Messinian salinity crisis. *Deep-Sea Res.*, 29:1391–1414.

Boersma, A., 1984a. *Handbook of Common Tertiary* Uvigerina: Stony Point, N.Y. (Microclimates Press).

________, 1984b. Oligocene and other Tertiary benthic foraminifers from a depth traverse down Walvis Ridge, Deep Sea Drilling Project Leg 74, Southeast Atlantic. *In* Hay, W. W., Sibuet, J. C., et al., *Init. Repts. DSDP*, 75: Washington (U.S. Govt. Printing Office), 1273–1299.

________, 1984c. Pliocene planktonic and benthic foraminifers from the southeastern Atlantic Angola Margin: Leg 75, Site 532, Deep Sea Drilling Project. *In* Hay, W. W., Sibuet, J. C., et al., *Init. Repts. DSDP*, 75: Washington (U.S. Govt. Printing Office), 657–670.

________, 1985. Oligocene benthic Foraminifers from North Atlantic sites: Benthic foraminifers as water-mass indexes in the North and South Atlantic. *In* Bougault, H., Cande, S. C., et al., *Init. Repts. DSDP*, 82: Washington (U.S. Govt. Printing Office), 611–628.

________, in press. Eocene/Oligocene Atlantic paleoceanography using benthic foraminifera. *Palaeogeogr. Palaeoclimatol. Palaeoecol.*

Boersma, A., Shackleton, N., Hall, M., and Given, Q., 1979. Carbon and oxygen isotope records at DSDP Site 384 (North Atlantic) and some Paleocene paleotemperatures and carbon isotope variations in the Atlantic Ocean. *In* Tucholke, B. E., Vogt, P. R., et al., *Init. Repts. DSDP*, 43: Washington (U.S. Govt. Printing Office), 695–717.

Boltovskoy, E., 1978. Late Cenozoic benthonic foraminifera of the Ninetyeast Ridge (Indian Ocean). *Mar. Geol.*, 26:139–175.

Bremer, M., and Lohman, G., 1982. Evidence for primary control of the distribution of certain Atlantic Ocean benthonic foraminifera by degree of carbonate saturation. *Deep Sea Res.*, 29:987–998.

Corliss, B. H., 1981. Deep sea benthonic foraminiferal faunal turnover near the Eocene/Oligocene boundary. *Mar. Micropaleontol.*, 6:367–384.

Finlay, H. J., 1939. New Zealand Foraminifera: key species in stratigraphy. *Trans. R. Soc. N.Z.*, 69:89–128.

Hagn, H., 1956. Geologische und paläontologische Untersuchungen im Tertiär des Monte Brione und seiner Umgebung. *Palaeontographia, A*, 107(3–6):67–210

Heath, G. R., Moore, T. C., and Dauphin, J. P., 1977. Organic carbon in deep-sea sediments. *In* Andersen, N. R., and Malahoff, A. (Eds.), *The Fate of Fossil Fuel CO_2 in the Oceans:* New York (Plenum Press), pp. 605–625.

Hornibrook, N. de B., 1971. A revision of the Oligocene and Miocene Foraminifera from New Zealand described by Karrer and Stache in the Reports of the "Novara" Expedition (1864). *Bull. N.Z. Geol. Surv. Paleont.*, 43:5–85.

Keigwin, L. D., Jr., and Shackleton, N. J., 1980. Uppermost Miocene carbon isotope stratigraphy of a piston core in the equatorial Pacific. *Nature*, 284:613–314.

Leinen, M., 1979. Biogenic silica accumulation in the central equatorial Pacific and its implications for Cenozoic paleoceanography: summary. *Geol. Soc. Am. Bull.*, 90:803–810.

Lohman, G. D., 1978. Abyssal benthonic foraminifera as hydrographic indicators in the Western South Atlantic. *J. Foraminiferal Res.*, 8: 6–34.

Lutze, G. F., 1978. Neogene Benthonic foraminifera from Site 369, Leg 41, Deep Sea Drilling Project, *In* Lancelot, Y., Seibold, E., et al., *Init. Repts. DSDP*, 41: Washington (U.S. Govt. Printing Office), 41:659–666.

Lutze, G., and Coubourn, J., 1983. Recent benthic foraminifera from the continental margin of northwest Africa—community structure and distribution. *Mar. Micropaleontol.*, 8:361–401.

Matthews, R. K., and Poore, R. Z., 1980. Tertiary $\delta^{18}O$ record and glacioeustatic sea-level fluctuations. *Geology*, 8:501–504.

Orbigny, Alcide d', 1846. *Foraminifères fossiles du bassin tertiaire de Vienne (Autriche) [Die fossilen Foraminiferen des tertiaren Beckens von Wien]:* Paris (Gide).

Parker, W. K., Jones, T. R., and Brady, H. B., 1865. On the nomenclature of the foraminifera. Pt. 12. The Species enumerated by d'Orbigny in the "Annales des Sciences Naturelles", Vol. 7, 1826. *Ann and Mac. Nat. Hist.*, Ser 3. 16:15–41.

Prell, W. L., 1982. Temporal and spatial patterns of monsoonal upswelling along Arabia: a modern analogue for the interpretation of Quaternary SST anomalies. *J. Mar. Res.*, 40:143–155.

Prell, W. L., and Curry, W. B., 1981. Faunal and isotopic indices of monsoonal upwelling: western Arabian Sea. *Oceanol. Acta*, 4: 91–98.

Reuss, A. E., 1851. Über die fossilen Foraminiferen und Entomostracen der Septarienthone der Umgegend von Berlin. *Z. Geol. Ges.*, 3:49–91.

Savin, S. M., Douglas, R. G., Keller, G., Killingley, J. S., Shaughnessy, L., Sommer, M. A., Vincent, E., and Woodruff, F., 1981. Miocene benthic foraminiferal isotope records: a synthesis. *Mar. Micropaleontol.*, 6:423–450.

Schwager, C., 1866. Fossile Foraminiferen von Kar Nicobar. *Novara Exped., Geol.*, Pt. 2:187–268.

Shackleton, N. J., Backman, J., Zimmerman, H., Kent, D. V., Hall, M. A., Roberts, D. G., Schnitker, D., Bauldauf, J. G., Desprairies, A., Homrighausen, R., Huddlestun, P., Keene, J. B., Kaltenback, A. J., Krumsiek, K. A. O., Morton, A. C., Murray, J. W., and Westberg-Smith, J., 1984. Oxygen isotopic calibration of the onset of ice rafting and history of glaciation in the North Atlantic region. *Nature*, 307:620–623.

Shackleton, N. J., Hall, M. A., and Boersma, A., 1984. Oxygen and carbon isotope data from leg 74 foraminifers. *In* Moore, T. C., Jr., Rabinowitz, P. D., et al., *Init. Repts. DSDP*, 74: Washington (U.S. Govt. Printing Office), 599–612.

Shackleton, N. J., and Kennett, J. P., 1975. Paleotemperature history of the Cenozoic and the initiation of Antarctic glaciation: oxygen and carbon isotope analyses in DSDP Sites 277, 279 and 281. *In* Kennett, J. P., Houtz, R. E., et al., *Init. Repts. DSDP*, 29: Washington (U.S. Govt. Printing Office), 743–755.

Schnitker, D., 1980. North Atlantic oceanography as possible cause of Antarctic glaciation and eutrophication. *Nature*, 284:615–616.

Srinivasan, M. S., and Sharma, V., 1980. *Schwager's Car Nicobar Foraminifera in the Reports of the Novara Expedition: a Revision.* New Delhi (Today and Tomorrow Press).

Tjalsma, L. C., 1983. Eocene to Miocene benthic foraminifers from DSDP Site 516, Rio Grande Rise, South Atlantic *In* Barker, P. F., Carlson, R. L., Johnson, D. A., et al., *Init. Repts. DSDP*, 72: Washington (U.S. Govt. Printing Office), 731–755.

Tjalsma, L. C., and Lohman, G., 1983. Paleocene–Eocene bathyal and abyssal benthic foraminifera from the Atlantic Ocean. *Micropaleontology Spec. Publ.*, 4.

Vincent, E., Killingley, J., and Berger, W., 1980. The Magnetic Epoch-6 carbon shift: a change in the ocean's $^{13}C/^{12}C$ ratio 6.2 million years ago. *Mar. Micropaleontol.*, 5:185–203.

Woodruff, F., 1979. Deep sea benthic foraminiferal changes associated with the middle Miocene oxygen isotopic event, DSDP Site 289, equatorial Pacific [Ph.D. dissert.]. Univ. of Southern California.

Woodruff, F., and Douglas, R. G., 1981. Response of deep sea benthic foraminifera to Miocene paleoclimatic events, DSDP Site 289. *Mar. Micropaleontol.*, 6:617–632.

Woodruff, F., and Savin, S., 1981. Miocene stable isotope record: a detailed deep Pacific Ocean study and its paleoclimatic implications. *Science*, 122:665–668.

________, in press. $\delta^{13}C$ values of Miocene Pacific benthic foraminifera: correlations with sea level and biological productivity. *Geology*.

Date of Initial Receipt: 1 November 1984
Date of Acceptance: 8 April 1985

APPENDIX

Appendix Tables 1–22 include the presence–absence data for all common benthic foraminiferal species identified at each site. Presence is indicated by x; if a species is very abundant in any particular sample, that is signalled by A. Preservation of the carbonate in each sample is ranked on the scale P, poor; F, fair, M, moderate; G, good; E, excellent. For most time periods the total number of species identified is indicated also on the diagram. In all Pliocene sections, the number of species per sample and the number of rectilinear species per sample is indicated. Also counted were the total number of species identified at the site in that time period, and the total number of rectilinear and agglutinated species. All data are plotted against the zonation of Jenkins and Srinivasan, this volume.

Table 1. Benthic foraminifers, Hole 586B, late Miocene.

Age	Planktonic foraminifer zone	Core-Section (interval in cm)	Preservation	Radiolarians	*Uvigerina proboscidea*	*Bulimina truncana*	*Oridorsalis umbonatus*	*Cibicides wuellerstorfi*	*Heterolepa kullenbergi*	*Brizalina aenariensis*	*Pullenia bulloides*	*Anomalinoides semicribrata*	*Stilostomella pomuligera*	*Buliminella* sp.	*Dentalina neugeboreni*	*Vulvulina pennatula*	*Globocassidulina subglobosa*	*Melonis pacificum*	*Uvigerina hispido-costata*	*Pullenia quinqueloba*	*Melonis affinis*	*Pleurostomella alternans*	*Laticarinina halophora*	*Cibicidoides cicatricosus*	*Sphaeroidina bulloides*	*Textularia* sp. 1	*Melonis pompilioides*	*Melonis* cf. *barleeanum*
late Miocene	N17a	18-1, 19	M	x	A	x		x	x					x			x	x		x					x		x	x
		18-7, 19	M		x	x	x	x	x		x						x		x		x			x	x	x	x	
		19-6, 20	M				x	x	x						x				A		x							
		20-2, 20	M				x	x	x					x			x		x					x	x			x
		20-7, 20	F			x		x	x		x						x				x							
		22-11, 19	F			x	x	x	x	x				x				x			x		x		x			x
		22-4, 19	M	x	x	x	x	x				x			x		x		x	x	x		x	x		x		
		23-1, 19	P				x	x		x	x						x			x	x						x	x
		23-4, 19	M	x	x		x			x	x	x		x			x			x			x				x	x
		24-5, 19	M	x	x		x	x	x	x				x	x		x				x			x				
		25-5, 19	G	x	A	x	x	x	x	x	x	x	x	x	x	x	x	x	x	x	x	x	x	x	x	x	x	x

Table 2. Benthic foraminifers, Hole 586B, Pliocene.

Age	Planktonic foraminifer zone	Core-Section (interval in cm)	Preservation	Radiolarians	*Uvigerina auberiana*	*Cibicides wuellerstorfi*	*Globocassidulina subglobosa*	*Oridorsalis umbonatus*	*Pullenia quinqueloba*	*Anomalinoides globulosa*	*Brizalina aenariensis*	*Cibicidoides cicatricosus*	*Martinottiella variabilis*	*Melonis pompilioides*	*Heterolepa kullenbergi*	*Nuttallides umbonifera*	*Gyroidinoides altiformis*	*Dentalina neugeboreni*	*Melonis* cf. *barleeanum*	*Pullenia bulloides*	*Cassidulina* sp. 1	*Anomalinoides semicribrata*	*Melonis affinis*	*Sphaeroidina bulloides*	*Cibicidoides bradyi*	*Pyrgo murrhina*	*Siphotextularia catenata*	*Gaudryina solida*	*Textularis lythostrota*	*Nodosaria stiliformis*
Pliocene	N21	5-1, 90	P	x	x	x			x					x		x				x			x			x				
		5-2, 110	M	x	x	x	x		x							x				x										x
		5-3, 108	G	x	x			x																		x				
		5-4, 106	G		x	x									x		x			x			x							x
		5-6, 56	G	x	x	x	x	x						x	x	x						x	x	x	x					
		6-1, 108	G		x	x					x									x						x				
		6-3, 108	M		x	x		x																		x				
		6-6, 108	M	x				x			x			x		x				x		x			x					
		8-7,20	F	x	x	x	x															x				x				
	N19-20	11-4, 66	F	x	A	x	x	x					x						x				x					x		
		12-1, 66	F	x	A		x	x			x			x				x	x			x				x				
		13-4, 18	F		x	x										x				x		x		x		x			x	
	N18	14-1, 66	M	x	x	x	x	x			x	x			x	x			x					x						
		15-4, 66	M	x	A	x	x			x					x	x			x							x	x	x	x	x
		17-2, 70	F			x								x								x	x	x	x					
	N17b	17-6, 19	M		x	x	x	x	x	x	x	x	x	x	x	x	x	x	x	x	x									

Table 1. (Continued).

Chrysalogonium equisetiformis	*Uvigerina asperula*	*Melonis sphaeroides*	*Heterolepa* cf. *rugosa*	Miliolids	*Nuttallides umbonifera*	*Siphonodosaria insecta*	*Uvigerina tasmana*	*Laticarinina altocamerata*	*Sigmoilopsis schlumbergeri*	*Textularia lythostrota*	*Quinqueloculina* cf. *seminulina*	*Cassidulina bradyi*	*Bulava* sp.	*Ehrenbergina pacifica*	*Bolivinopsis praelonga*	*Pullenia quadriloba*	*Brizalina silvestrina*	*Cibicidoides trincherasensis*	*Alabamina haitiensis*	*Pleurostomella brevis*	*Martinotiella variabilis*	*Favocassidulina fava*	*Pleurostomella tenuis*	*Uvigerina auberiana*	*Eggerella bradyi*	*Pyrgo comata*	*Karreriella baccata*	*Nodosaria skobina*	*Pyrgo serrata*	*Rotalia translucens*	*Alabamina haitiensis*	*Ehrenbergina spinosissima*	*Pyrgo lucernula*	*Osangularia bengalensis*	*Stilostomella lepidula*	*Cbicidoides* cf. *robertsonianus*
				x	x	x																		A	x											x
x				x				x																x		x		x					x	x	x	
				x				x														x		x			x	x	x	x	x	x				
x				x																				x	x											
				x																			x	x	x	x										
	x			x												x	x					x														
				x																x	x															
x					x											x	x	x	x																	
					x						x	x	x	x	x																					
				x	x	x	x	x	x	x	x																									
x	x	x	x	x																																

Table 2. (Continued).

Chrysalogonium equisetiformis	*Pyrgo lucernula*	*Rotalia translucens*	*Cibicidoides bradyi*	*Pyrgo comata*	*Heterolepa* cf. *rugosa*	*Gyroidina soldanii*	*Uvigerina proboscidea*	*Pullenia quinqueloba*	*Nodosaria skobina*	*Nodosaria consobrina*	*Cibicidoides subhaidingeri*	*Bulimina truncana*	*Eggerella bradyi*	*Sigmoilopsis schlumbergeri*	*Stilostomella insecta*	*Uvigerina hispido-costata*	*Laticarinina halophora*	*Stilostomella lepidula*	*Globocassidulina arata*	*Osangularia bengalensis*	*Melonis barleeanum*	*Laticarinina bullbrooki*	*Pleurostomella alternans*	*Brizalina pusilla*	Miliolids	*Nodosaria stilifomis*	*Uvigerina pigmaea*	*Planulina* cf. *ariminensis*	*Epistominella exigua*	*Melonis nicobarense*	*Osangularia culter*	*Trifarina bradyi*	*Uvigerina senticosa*	*Pyrgo serrata*	*Karreriella bradyi*	*Ehrenbergina pacifica*	No. of rectilinear (total, 20)	No. of species (total, 63)
													x																	x					x		2	11
		x																		x			x	x	x				x							x	3	14
																x		x											x						x		3	7
																	x								x							x	x	x			4	12
								x		x								x				x			x						x						3	18
																					x				x				x								2	8
						x		x					x			x									x				x	x							2	12
								x				x	x			x					x					x	x										5	14
													x		x	x	x				x		x	x	x												3	13
x						x	x								x							x															4	13
x													x	x	x	x	x	x	x	x	x																7	19
			x							x	x	x	x																								5	13
x	x	x	x	x	x	x	x	x	x																												7	20
																																					5	11
																																					1	6
																																					4	17

Table 3. Benthic foraminifers, Site 588, early–middle Miocene.

Age		Planktonic foraminifer zone	Core-Section (level in cm)	Preservation	*Globocassidulina subglobosa*	*Bolivinopsis praelonga*	*Laticarinina bullbrooki*	*Osangularia bengalensis*	Eponid-form biumbonate–cibicidid	*Uvigerina wanzea*	*Melonis barleeanum*	*Pleurostomella tenuis*	*Uvigerina auberiana*	*Heterolepa kullenbergi*	*Brizalina finlayi*	Eponid-form cibicidid	*Cibicidoides* trans. *cicatricosus*	*Vulvulina pennatula*	*Oridorsalis umbonatus*	*Karreriella subrotundata*	*Anomalinoides globulosa*	*Anomalinoides semicribrata*	Coarsely punctate cibicidid	*Nodosaria stiliformis*	*Nuttallides umbonifera*	*Planulina* sp.	*Bulimina tuxpamensis*	*Eggerella bradyi*	*Bulimina truncana*	*Stilostomella lepidula*	*Alabamina haitiensis*	*Cibicidoides trincherasensis*	*Karreriella* sp.	*Pullenia bulloides*
Miocene	middle	*G. mayeri*	B25,CC	M										x							x							A	x					
			26,CC	G	x						x			x		x			x	x	x							x					x	
		G. fohsi	27,CC	M	x	x										x		x	x	x								x		x	x	x		x
			28,CC	M	x			x						x			x		x									x	x		x			
			29,CC	M	x		x				x	x		x				x	x	x									x			x		
			30,CC	M			x							x					x															x
			31,CC	M	x						x			x					x												x			x
		P. glomerosa curva	C1-4, 32	P	x												x		x			x		x								x		
			1,CC	F	x						x			x				x						x	x					x				x
	early	*G. miozea*	2-5, 19	F	x	x						x		x	x			x	x			x				x				x				x
			2,CC	F				x										x							x	x								
		G. dissimilis	3-5, 19	F	x						x		x	x				x	x									x				x		x
			3,CC	P	x									x					x								x	x						
			4-4, 19	F	x									x				x	x								x	x						x
			4,CC	F	x		x	x										x	x			x		x										
			5-1, 22	P										x					x														x	x
			5,CC	P	x														x			x									x			
			6-1, 19	P										x			x							x									x	x
			6,CC	F	x	x								x								x			x					x	x	x		
		G. dehiscens	7-4, 19	P	x												x		x				x	x	x	x	x	x	x					
			7,CC	P	x		x											x	x	x	x	x												
			8-7, 19	P	x						x	x	x	x	x	x	x																	
			8,CC	P	x	x																												
Oligocene	late	*T. kugleri*	10,CC	P	x	x	x	x	x	x																								

Note: B and C indicate cores from Holes 588B and 588C, respectively.

Table 3. (Continued).

Pullenia quadriloba	*Cibicidoides bradyi*	*Anomalinoides aragonensis*	*Rectuvigerina spinea*	*Pullenia* cf. *quinqueloba*	*Stilostomella* trans. *lepidula*	*Bulimina semicostata*	*Stilostomella subspinosa*	*Sphaeroidina bulloides*	*Osangularia culter*	*Pleurostomella alternans*	*Cassidulina laevigata*	*Uvigerina spinulosa*	*Trifarina bradyi*	*Cibicidoides io*	*Uvigerina* cf. *gemmaeformis*	*Pullenia quinqueloba*	*Siphonodosaria insecta*	*Dentalina neugeboreni*	*Stilostomella consobrina*	*Sigmoilopsis schlumbergeri*	*Ehrenbergina* cf. *spinosissima*	*Orthomorphina perversa*	*Karreriella sub-baccata*	*Melonis affinis*	*Cibicides* cf. *wuellerstorfi*	*Cassidulina crassa*	*Laticarinina halophora*	*Textularia lythostrota*	*Chrysalogonium equisetiformis*	*Siphonodosaria modesta*	*Brizalina reticulata*	*Uvigerina gemmaeformis*	*Martinottiella variabilis*	*Bulimina striata*	Umbilically reticulate cibicidid	Planispiral cibicidids	*Textularia agglutinans*	*Rectuvigerina ongleyi*	*Uvigerina pigmaea*	*Heterolepa* trans. *rugosa*	*Heterolepa rugosa*	*Cibicides wuellerstorfi*
			x					x													x								x	x			x				x				x	x
			x		x		x			x								x			x				x															x		
			x				x			x	x								x					x	x		x	x			x				x	x	x	x	x			
			x								x	x				x		x		x				x	x		x		x	x	x	x	x	x								
				x						x								x		x				x			x	x	x													
		x	x					x								x		x		x			x	x	x	x																
						x	x	x				x									x	x																				
												x								x																						
						x											x			x																						
	x					x							x				x	x	x																							
x																x																										
					x		x	x			x	x	x	x	x																											
									x	x																																
					x	x	x	x																																		
x			x			x	x																																			
				x	x																																					
x	x	x	x																																							

Table 4. Benthic foraminifers, Site 588, middle to late Miocene.

Age	Planktonic foraminifer zone	Core-Section (level in cm)	Preservation	*Globocassidulina subglobosa*	*Oridorsalis umbonatus*	*Heterolepa kullenbergi*	*Eggerella bradyi*	*Bulimina truncana*	*Pullenia bulloides*	*Uvigerina proboscidea*	*Heterolepa* cf. *rugosa*	*Osangularia bengalensis*	*Rectuvigerina tasmana*	*Nodosaria consobrina*	*Stilostomella subspinosa*	*Ehrenbergina trigona*	*Bulimina spicata*	*Bulimina tuxpamensis*	*Vulvulina spinosa*	*Nuttallides umbonifera*	*Martinottiella variabilis*	*Pullenia quadriloba*	*Uvigerina auberiana*	*Melonis* cf. *barleeanum*	*Brizalina pusilla* (long striae)	*Pleurostomella alternans*	*Alabamina haitiensis*	*Cibicides lobatulus*	*Stilostomella insecta*	*Anomalinoides globulosa*
Miocene	*G. margaritae*	13-2, 19	M	x		x	x	x			x	x	x									x					x			
		13,CC	M			x	x	x	x	x		x											x			x				
		14-4, 19	M		x	x		x			x				x												x	x		
		14,CC	M	x	x	x	x	x		x			x	x															x	
		15-6, 19	F	x	x		x					x																		
		15,CC	G	x				x				x				x	x								x					
		16-1, 19	F		x			x			x	x	x	x														x		
	G. plesiotumida	16,CC	M	x	x	x	x	x	x			x											x							
		17,CC	G	x		x	x	x	x	x		x	x										x		x			x		
		18,CC	M		x	x										x	x				x				x					x
		19,CC	M		x		x																	x						
	T. continuosa	20,CC	G		x		x	x	x															x						
		21-6, 19	G	x		x	x	x	x	x	x											x		x	x	x	x			
		21,CC	G	x	x	x	x														x			x		x	x			
		22,CC	G	x	x	x	x	x				x		x										x						
	G. mayeri	23,CC	M	x	x		x					x							x				x			x				
	G. fohsi	24-4, 19	M	x	x	x																x								
		24,CC	M	x	x	x	x		x				x			x						x	x	x	x	x	x	x	x	x
		25,CC	M	x	x	x	x	x	x	x	x	x	x	x	x	x	x	x	x	x	x									

Note: Total no. of species, 60.

Table 5. Benthic foraminifers, Site 588, Pliocene.

Age	Planktonic foraminifer zone	Core-Section (level in cm)	Preservation	Miliolids	*Anomalinoides globulosa*	*Nodosaria consobrina*	*Globocassidulina subglobosa*	*Osangularia bengalensis*	*Pyrgo comata*	*Oridorsalis umbonatus*	*Cibicides wuellerstorfi*	*Brizalina pusilla*	*Sphaeroidina bulloides*	*Alabamina haitiensis*	*Textularia lythostrota*	*Heterolepa kullenbergi*	*Sigmoilopsis schlumbergeri*	*Bulimina truncana*	*Ehrenbergina spinosissima*	*Pleurostomella tenuis*	*Laticarinina altocamerata*	*Uvigerina striata*	*Stilostomella lepidula*	*Gaudryina solida*	*Cibicidoides trincherasensis*	*Uvigerina spinulosa*	*Heterolepa rugosa*	*Cibicidoides cicatricosus*	*Hopkinsina mioindex*	*Textularia* sp. 1	*Orthomorphina koina*	*Uvigerina hispida*	*Melonis barleeanum*	*Triloculina lucernula*	*Cibicidoides bradyi*	*Pyrgo murrhina*
Pliocene	*G. tosaensis*	4,CC	M		x					x	x		x	x		x	x	x					x					x								
		5-1, 19	M			x				x	x					x		x					x	x	x						x			x		
		5,CC	M	x	x	x	x			x	x	x	x		x								x					x				x				
	G. inflata	6-2, 19	M				x	x			x	x		x			x	x					x		x											
		6,CC	M				x	x		x			x		x	x	x	x					x		x	x			x			x		x		x
	G. crassaformis	7-4, 19	M				x			x				x	x	x									x	x							x			
		7,CC	M	x	x		x	x			x		x			x		x					x			x						x	x	x		x
	G. puncticulata	8,CC	G				x	x		x	x	x		x			x	x	x	x		x		x	x			x					x		x	
		9-1, 19	G			x	x	x			A		x	x			x	x					x							x						
		9,CC	M				x	x		x	x		x			x																				
	G. margaritae	10-5, 19	M				x	x								x	x	x					x		x				x							
		10,CC	M	x			x	x		x			x					x	x						x	x		x	x			x	x			
		1-6, 19	G							x						x	x								x											
		11,CC	M	x		x	x	x		x	x		x	x	x	x	x	x	x							x		x	x	x	x	x	x	x	x	x
		12-2, 19	M	x							x		x	x	x		x		x	x	x	x	x	A	x	x	x									
		12,CC	M	x	x	x	x	x	x	x	x	x	x	x	x	x	x	x																		

Table 4. (Continued)

Brizalina pusilla	*Bolivinopsis praelonga*	*Stilostomella lepidula*	*Discorbis* sp. 1	*Bulimina striata*	*Sphaeroidina bulloides*	*Heterolepa rugosa*	*Uvigerina hispida*	*Cibicidoides bradyi*	*Cibicides wuellerstorfi*	*Pullenia quinqueloba*	*Cassidulina crassa*	Miliolids	*Nodosaria crassitesta*	*Trifarina bradyi*	*Karreriella bradyi*	*Melonis pompilioides*	*Laticarinina bullbrooki*	*Melonis nicobarense*	*Brizalina pacifica*	*Chrysalogonium equisetiformis*	*Cibicidoides kullenbergi* × *C. wuellerstorfi*	*Gaudryina solida*	*Uvigerina striata*	*Cibicidoides cicatricosus*	*Rectuvigeria spinea*	*Karreriella subrotundata*	Small virgulinids	*Textularia lythostrota*	*Uvigerina hispido-costata*	*Nodosaria consobrina*	*Sigmoilopsis schlumbergeri*	*Textularia* sp. 1	*Osangularia culter*	Domed cibicids	*Uvigerina gemmaeformis*	*Spiroplectamina haeringensis*	*Anomalinoides semicribrata*	*Textularia agglutinans*	*Melonis affinis*	*Cibicidoides* cf. *ungerianus*
				x			x					A			x		x	x		x		x						x		x	x				x		x	x	x	x
	x	x				x	x	x	x			A					x					x		x									x							
				x	x		x					A										x			x					x	x									
		x				x	x		x			x										x						x		x	x									
							x		x									x				x		x					x								x			
	x				x												x					x						x	x	x			x	x	x	x				
					x			x									x					x			x			x				x								
							x											x							x			x	x	x	x									
	x				x			x				x																x	x	x	x									
		x			x			x										x									A													
					x																																			
	x	x			x		x	x	x					x		x									x	x														
	x			x	x							x					x	x	x	x	x	x	x	x																
	x			x	x			x							x	x	x	x																						
										x			x	x	x	x																								
		x			x	x	x	x	x	x	x	x																												
x	x	x	x	x	x																																			

Table 5 (Continued).

Chrysalogonium equisetiformis	*Dentalina neugeboreni*	*Rotalina translucens*	*Rectuvigerina spinea*	*Gaudryina solida*	*Uvigerina tasmana*	*Pullenia bulloides*	*Uvigerina pigmaea*	*Laticarinina halophora*	*Heterolepa* cf. *rugosa*	*Uvigerina proboscidea*	*Uvigerina gemmaeformis*	*Bulimina striata*	*Melonis affinis*	*Cibicides lobatulus*	*Bolivinopsis praelonga*	*Pleurostomella alternans*	*Osangularia culter*	*Ehrenbergina amina*	*Stilostomella insecta*	*Trifarina bradyi*	*Fissurina capillosa*	*Orthomorphina perversa*	*Eggerella bradyi*	*Bulimina* sp. 1	*Cibicidoides* cf. *ungerianus*	*Alabamina haitiensis*	*Karreriella bradyi*	*Textularia* sp. 1	*Martinotiella variabilis*	*Melonis pompilioides*	*Uvigerina hispido-costata* (spinose)	*Siphotextularia solita*	*Buliminella basicostata*	*Discanomalina semipunctata*	*Textularia agglutinans*	*Anomalinoides semicribrata*	*Pullenia quadriloba*	*Cassidulina crassa*	*Lenticulina nicobarensis*	*Uvigerina dirupta*	*Cassidulina laevigata*	*Pleurostomella brevis*	No. of Species (total, 77)	No. of Rectilinear (total, 37)	Total agglutinants 8
	x									x					A						x		x									x				x				x			18	9	
	x								x	x					x							x	x								x						x			x	x	x	21	12	
										x	x				x								x		x				x									x	x				19	10	
							x					x	x										x												x	x	x						16	7	
				x	x		x			x			x						x				x				x		x				x	x									25	15	
		x	x					x	x						x									x						x	x	x											17	7	
		x		x	x	x			x	x	x		x		x	x			x		x		x		x				x														29	13	
						x	x			x	x	x		x	x	x										x	x	x															27	13	
															A							x	x	x	x	x	x																18	11	
															x	x							x																				9	3	
	x			x	x										x				x	x	x	x																					16	10	
			x	x		x			x	x	x	x	x	x	x	x	x	x																									26	11	
	x	x	x	x	x	x	x	x																																			25	5	
																																											24	10	
																																											15	7	
																																											15	5	

Table 6. Benthic foraminifers, Hole 590B, early–middle Miocene.

Age		Planktonic foraminifer zone	Core-Section (level in cm)	Preservation	*Oridorsalis umbonatus*	*Heterolepa kullenbergi*	*Brizalina pusilla*	*Orthomorphina rohri*	*Uvigerina spinulosa*	*Lenticulina* sp.	*Bulimina tuxpamensis*	Eponid-form *Cibicidoides*	*Uvigerina pigmaea*	*Karreriella bradyi*	*Cibicidoides haitiensis*	*Cassidulina laevigata*	*Melonis* cf. *barleeanum*	*Gyroidinoides planulata*	*Cibicidoides dicatricosus*	*Marginulinopsis* sp.	*Stilostomella subspinosa*	*Globocassidulina subglobosa*	*Heterolepa rugosa*	*Brizalina subaenariensis*	*Eggerella bradyi*	*Pullenia bulloides*	*Hopkinsina mioindex*	*Cibicidoides tuxpamensis*	*Sphaeroidina bulloides*	*Nuttallides umbonifera*	*Cibicides wuellerstorfi*
Miocene	middle	*G. mayeri*	41,CC		x	x									x												x				
			42-4, 19	M		x	x		x			x				x	x					x	x		x		x		x	x	x
			42,CC	P	x	x	x		x						x							x	x		x		x				
			43,CC	P	x	x															x	x	x		x		x	x			
			44-6, 19	M	x	x	x		x						x		x		x				x			x	x	x			x
			44,CC	P	x	x															x	x				x	x				
		G. fohsi	45-3, 19	M	x	x				x				x									x		x					x	x
			45,CC	P	x	x																		x	x	x	x				
			46-1, 19	P		x	x									x	x					x	x			x			x	x	x
			46,CC	P	x												x				x				x	x	x	x			
			47,CC	P	x	x	x								x	x	x	x	x	x	x	x	x	x							
			48,CC	P	x	x																									
		G. miozea	49,CC	P	x	x																									
			50,CC	P	x	x																									
	early	*G. dissimilis*	51-3, 19	P		x	x	x	x	x	x	x	x	x																	
			51,CC	P	x	x																									
			52,CC	P	x	x																									
			53,CC	P	x	x																									

Table 7. Benthic foraminifers, Site 590, middle–late Miocene.

Age		Planktonic foraminifer zone	Core-Section (level in cm)	Preservation	Radiolarians	*Globocassidulina subglobosa*	*Bulimina striata*	*Uvigerina proboscidea*	*Alabamina haitiensis*	*Planulina* sp. 1	*Melonis* cf. *barleeanum*	*Laticarinina altocamerata*	*Holmanella* sp.	*Epistominella* sp.	*Heterolepa kullenbergi*	*Pullenia quadriloba*	*Brizalina finlayi*	*Oridorsalis umbonatus*	*Cibicides wuellerstorfi*	*Pullenia bulloides*	Domed cibicidids	*Sphaeroidina bulloides*	*Pullenia quinqueloba*	*Stilostomella subspinosa*	*Martinottiella variabilis*	*Uvigerina gemmaeformis*	*Eggerella bradyi*	*Stilostomella lepidula*	*Bolivinopsis praelonga*	*Karreriella bradyi*	*Hopkinsina mioindex*	*Cibicidoides bradyi*	*Matanzia* sp.	*Heterolepa rugosa*	*Cibicidoides* cf. *subhaidingeri*	*Anomalinoides globulosa*	*Bulimina truncana*	*Brizalina pusilla*	*Cassidulina crassa*
Miocene	late	*G. conomiozea*	A18,CC	M		x		x							x			x				x						x						x			x		
			19-3, 19	F		x						x			x			x										x			x							x	
			19,CC	M		x		x			x				x			x		x		x					x	x				x		x			x		x
			20-5, 19	M		x		x			x				x	x	x	x				x						x					x		x		x		x
			20,CC	M		x		x				x			x		x	x				x					x	x				x		x		x	x		
		G. nepenthes	21-1, 19	F				x							x		x			x									x					x				x	
			21,CC	M			x	x			x				x							x			x		x	x				x		x				x	
			22,CC	M		x	x	x			x				x			x				x		x			x	x			x	x		x				x	
			23-2, 19	M		x					x		x				x	x							x		x	x			x	x		x	x		x		
			23,CC	M			x	x			x				x			x		x		x					x			x	x			x			x	x	
			24,CC	M			x				x				x		x	x					x								x						x	x	
			25,CC	F		x		x							x							x						x			x	x						x	
			26,CC	G			x	x							x		x	x		x								x			x								
			27,CC	P				x			x				x													x	x								x		
			B28-5, 19	F	x										x			x	x	x		x									x						x	x	x
			29-5	M	x		x	x							x							x		x			x		x		x			x	x			x	
			30-5, 19	M		x		x				x			x	x				x							x		x		x	x		x	x				
			30,CC	M			x	x			x									x		x		x			x		x			x		x		x		x	
		N. continuosa	31-5, 19	M		x		x									x	x									x					x		x	x			x	
			31,CC	M											x										x		x	x	x			x		x				x	
			32,CC	P											x			x									x							x					
			33-6, 19	M	x		x	x			x				x									x	x									x	x				
			33,CC	M		x									x			x											x			x					x		
			34-4, 19	F	x										A	x		x		x					x		x		x					x			x		
			34,CC	F	x				x		x				x			x	x			x					x												
			35,CC	F	x						x				x			x									x												
			36-5, 19	M	x		x				x				x													x			x			x	x				
			36,CC	F	x							x			x		x	x													x			x	x	x			
			37-2, 19	M	A					x					x	x	x	x		x				x			A		x			x	x	x			x	x	
			37,CC	M	x	x		x	x						x		x	x						x															x
			38,CC	F							x				x			x		x				x			x	x		x	x								
	mid.	*G. mayeri*	39-1, 19	F	x	x					x				x		x	x		x							x	x									x	x	x
			39,CC	F	x						x				x			x	x			x		x			x		x	x	x	x	x	x	x	x			
			40-6, 19	F			x	x	x	x	x	x	x	x	x	x	x	x	x	x	x	x	x	x	x	x	x	x	x										

Note: A and B indicate cores from Holes 590A and 590B.

Table 6. (Continued).

Planulina renzi	Pullenia quinqueloba	Nodosaria stiliformis	Globocassidulina subglobosa	Anomalinoides semicribrata	Bulimina striata	Pullenia quadriloba	Rectuvigerina striatissima	Laticarinina altocamerata	Punctuate cibicidids	Bulimina alazanensis	Pleurostomella trans. alternans	Brizalina anastomosa	Rectuvigerina spinea	Melonis nicobarensis	Stilostomella consobrina	Osangularia culter	Textularia sp. 1	Laticarinina halophora	Pleurostomella brevis	Uvigerina auberiana	Bolivinopsis praelonga	Cibicides cf. laurisae	Uvigerina striata	Karreriella subrotundata	Ehrenbergina pacifica	Dentalina neugeboreni	Cibicidoides trincherasensis	Textularia lythostrota	Sigmoilopsis schlumbergeri	Karreriella sub-baccata	Siphonodosaria insecta	Melonis affinis	Stilostomella lepidula	Martinottiella variabilis	Orthomorphina sp.	Siphotextularia catenata	Osangularia bengalensis	Alabamina haitiensis	Anomalinoides globulosa	Laticarinina bullbrooki
															x						x				x			x	x		x				x	x	x	x	x	x
	x									x			x						x		x		x			x	x	x	x	x	x	x	x	x						
													x												x															
																								x																
			x		x				x		x				x		x	x	x	x	x	x	x																	
														x	x	x																								
						x			x	x	x	x	x	x																										
				x	x	x	x	x																																
x	x	x	x	x																																				

Table 7. (Continued).

Cibicidoides trincherasensis	Sphaeroidina bulloides	Nodosaria consobrina	Anomalinoides semicribrata	Chrysalogonium equisetiformis	Brizalina pusilla (long striae)	Stilostomella insecta	Pleurostomella alternans	Pleurostomella brevis	Uvigerina pygmaea	Trifarina bradyi	Uvigerina hispida	Rectuvigerina spinea	Sigmoilopsis schlumbergeri	Textularia lythostrota	Osangularia culter	Melonis pompilioides	Laticarinina halophora	Melonis affinis	Pleurostomella tenuis	Rectuvigerina ongleyi	Siphonodosaria modesta	Planulina cf. foveolata	Lenticulina nicobarensis	Laticarinina bullbrooki	Melonis nicobarense	Cibicidoides cf. subhaidingeri	Uvigerina spinulosa	Cibicides lobatulus	Eggerella bradyi	Nodosaria stiliformis	Ehrenbergina pacifica	Osangularia bengalensis	Nuttalides umbonifera	Cibicidoides cf. robertsonianus	Planulina renzi	Cibicidoides cicatricosus	Uvigerina auberiana	Siphotextularia solita	Cibicidoides cf. ungerianus	Uvigerina hispido-costata	Rotalia translucens	Orthomorphina perversa	Pyrgo ovata	Cassidulina laevigata	Textularia lassata	Miliolids	Siphotextularia catenata	Gaudryina solida
		x			x	x				x															x			x			x		x														x	x
		x									x																			x	x					x						x				x	x	
		x	x		x	x	x					x		x										x		x					x	x						x	x	x				x				
											x		x	x																	x					x						x						
		x	x		x									x														x			x			x					x	x	x				x	x		
				x							x		x						x							x										x			x	x				x				
						x				x			x	x							x				x			x			x					x					x		x					
		x	x			x																			x						x		x						x									
x									x	x		x		x														x	x	x					x						x						
					x	x				x	x		x																		x	x					x		x	x	x							
		x				x	x					x			x											x	x				x							x		x									
					x						x	x			x					x													x															
			x			x	x			x		A	x	x	x												x				x	x					x	x	x									
										x		x		x																																		
												x															x											x										
x						x					x		x														x						x	x	x		x	x											
				x								A	x		x				x																													
					x						x	x		x												x									x													
x												x		x																		x	x	x														
					x				x			x											x		x			x			x	x																
						x						x			x									x		x				x																		
												A	x													x			x																			
												x																																				
			x																	x							x	x																				
					x											x							x	x	x	x																						
		x			x		x					x											x																									
													x	x	x	x	x	x	x	x	x																											
			x	x	x			x				x																																				
	x					x					x	x																																				
								x	x	x	x	x	x																																			
					x	x	x																																									
x	x	x	x	x																																												

Table 8. Benthic foraminifers, Hole 590A, Pliocene.

Age	Magnetic polarity	Planktonic foraminifer zone (Jenkins and Srinivasan, this volume)	Core-Section (level in cm)	Preservation	Radiolarians	*Gyroidina solida*	*Heterolepa kullenbergi*	*Textularia lythostrota*	*Laticarinina halophora*	*Oridorsalis umbonatus*	*Brizalina anastomosa*	*Alabamina haitiensis*	*Martinottiella variabilis*	*Sphaeroidina bulloides*	*Cibicidoides* cf. *ungerianus*	*Melonis affinis*	*Pullenia quadriloba*	*Anomalinoides semicribrata*	*Uvigerina hispida*	*Ehrenbergina spinosissima*	*Orthomorphina koina*	*Pullenia bulloides*	*Textularia agglutinans*	*Uvigerina proboscidea*	*Cibicides lobatulus*	*Heterolepa* cf. *rugosa*	*Stilostomella lepidula*	*Eggerella bradyi*	*Gaudryina solida*	*Sigmoilopsis schlumbergeri*	*Cibicidoides cicatricosus*	*Bulimina truncana*	*Globocassidulina subglobosa*	Miliolids	*Laticarinina bullbrooki*	*Brizalina pusilla* (long striae)	*Brizalina reticulata*	*Pleurostomella alternans*	*Orthomorphina skobina*	*Brizalina pusilla*
Pliocene	■	*G. tosaensis*	4-4, 19	M		x	x	x		x				x	x	x		x		x		x		x	x		x				x		x							
			4,CC	G		x	x	x	x	x				x	x	x	x	x		x		x		x	x		x	x					x				x	x		
	■		5,CC	G			x	x		x				x				x		x					x		x	x			x	x	x			x		x		
	■		6-2, 19	M				x		x				x	x		x			x							x	x			x		x		x					
		G. inflata	6,CC	G		x	x	x		x					x					x		x		x	x	x	x	x			x		x			x				
			7-2, 19	G			x			x					x	x		x						A	x	x		x		x	x		x		x					
	■		7,CC	M		x		x						x		x		x			x				x		x	x			x	x				x	x			
			8-3, 19	M		x	x	x						x		x					x	x			x		x	x			x	x	x							x
		G. crassaformis	8,CC	M		x	x	x	x					x	x									x	x								x			x		x		
			10-3, 19	M		x	x			x				x	x	x			x			x			x		x	x			x		x							
			10,CC	G			x			x		x				x	x		x		x			x	x						x	x	x			x	x	x		
			11-5, 19	G		x	x	x	x	x		x		x		x	x			x							x	x		x	x		x							x
			11,CC	M						x				x	x	x		x		x	x	x	x		x		x				x	x	x	x		x			x	x
			12,CC	M		x	x	x	x	x				x								x		x	x		x	x		x									x	
			13-4, 19	M									x		x	x								A			x				x		x						x	x
			13,CC	M		x	x	x						x													x	x	x	x	x	x	x			x		x		
			14-4, 19	F		x	x	x	x	x		x		x		x						x					x					x	x							
			14,CC	M				x	x	x					x			x	x					x			x						x	x				x		
		G. punctiulata	15-7, 19	M			x	x							x	x						x		x	x	x	x	x	x	x		x	x							x
			15,CC	G		x	x			x						x			x			x			x	x		x					x							x
			16-5, 19	F						x	x															x		x				x	x							x
			16,CC	G			x	x		x					x		x		x	x		x		x	x		x	x				x								x
			17-3, 19	G			x		x	x			x		x		x					x			x	x					x									
			17,CC	G		x	x	x	x	x	x	x	x	x	x	x	x	x	x	x	x	x	x	x	x	x	x	x	x	x	x	x	x	x	x	x	x	x	x	

Note: Total no. of species, 83.

Table 9. Benthic foraminifers, Hole 591B, early–middle Miocene.

Age		Planktonic foraminifer zone	Core-Section (level in cm)	Preservation	*Oridorsalis umbonatus*	*Eggerella bradyi*	*Pullenia bulloides*	*Cibicides wuellerstorfi*	*Globocassidulina subglobosa*	*Heterolepa kullenbergi*	*Brizalina pusilla* (long striae)	*Melonis barleeanum*	*Rectuvigerina spinea*	*Laticarinina bullbrooki*	*Stilostomella subspinosa*	*Pullenia quinqueloba*	*Cassidulina laevigata*	*Bulimina semicostata*	*Laticarinina altocamerata*	Eponid-form cibicidids	*Nuttallides umbonifera*	*Karreriella bradyi*	*Stilostomella consobrina*	*Stilostomella lepidula*	*Melonis nicobarense*	*Cibicides wuellerstorfi*
Miocene	late	*N. continuosa*	8,CC	F	x	x	x			x			x	x						x	x			x		
	middle		9,CC	F	x	x		x			x			x	x						x		x	x		
		G. mayeri	10,CC	P	x	x			x					x							x	x				
			11-1, 19	P		x		x	x	x						x			x		A					
			11,CC	P	x			x	x																x	
			12-1, 19	P	x	x	A			x											A					
			12,CC	F	x	x		x	x	x	x		x		x		x				x	x				
			13-1, 19	P		x	x					x														
			13,CC	P	x	x		x	x	x	x	x														
		G. fohsi	14,CC	P	x				x	x	x												x	x	x	
			15-3, 19	F		x		x		x										x						
			15,CC	F	x	x		x		A											x		x	x	x	
			16,CC	P	x	x		x	x										x						x	
			17-4, 19	P	x		x		x	x															x	x
			17,CC	P				x		x		x							x							
		O. suturalis	18-4, 19	M	x	x	x	x	x			x				x		x			x					x
			18,CC	P	x		x		x	x						x		x	x	x	x	x	x	x	x	
			19,CC	P	x					x		x			x	x	x	x	x							
		O. glomerosa curva	20,CC	P	x	x	x	x	x	x	x	x	x	x												
			21,CC	P	x	x																				
	early	*G. miozea*	22,CC	P	x	x																				
			23,CC	P	x	x																				
			24,CC	P	x	x																				

Table 8. (Continued).

[illegible]	*Chrysalogonium equisetiformis*	*Karreriella bradyi*	*Karreriella subrotundata*	*Discanomalina semipunctata*	*Stilostomella consobrina*	*Globocassidulina arata*	*Heterolepa rugosa*	*Cibicidoides bradyi*	*Fissurina capillosa*	*Trifarina bradyi*	*Anomalinoides semicribrata*	*Rectuvigerina spinea*	*Bolivinopsis praelonga*	*Rotalia translucens*	*Melonis nicobarense*	*Hopkinsina mioindex*	*Lenticulina nicobarensis*	*Martinottiella communis*	Scalloped, turbinate cibicidid	*Osangularia bengalensis*	*Cassidulina crassa*	*Stilostomella insecta*	*Siphotextularia solita*	*Melonis barleeanum*	*Osangularia culter*	*Uvigerina auberiana*	*Nodosaria stiliformis*	*Textularia* sp. 1	*Uvigerina striata*	*Uvigerina hispido-costata*	*Pyrgo murrhina*	*Bulimina striata*	*Karreriella baccata*	*Nodosaria tholigera*	*Uvigerina asperula*	*Nodosaria pseudoinconstans*	*Cibicides wuellerstorfi*	Large porous cibicidids	*Uvigerina* cf. *macrocarinata*	*Anomalinoides* sp.	*Pleurostomella brevis*	*Melonis affinis*	*Planulina* cf. *ariminensis*	*Planulina* cf. *renzi*	*Stilostomella pomuligera*	*Cibicidoides subhaidingeri*	*Nuttallides umbonifera*	Total no. species	No. rectilinear
		x		x			x										x			x					x		x				x						x	x			x							26	7
	x				x		x		x		x		x	x								x		x			x	x									x	x										32	11
							x	x			x											x				x				x	x						x									x		23	9
				x	x									x											x					x		x				x												18	7
				x	x			x	x			x	x	x						x		x		x						x	x				x		x	x								x	x	32	9
	x				x			x												x					x	A			A						A		x				x				x			24	5
		x		x	x			x						x	x					x		x		x				x	x	x		x		x									x	x				29	15
x				x						x			x	x										x											x		x			x		x						24	18
				x				x			x			x						x		x	x		x	x									x		x				x							23	5
							x													x		x									x	x			x		x			x								22	8
					x		x	x			x		x							x		x		x	x				x						x				x	x								28	6
				x									x				x	x		x										x					x		x											23	6
								x		x			x		x					x				x									x	x	x	x												28	12
																				x		x																										15	5
					x		x	x			x		x			x				x				x	x				A	A	x	x																22	7
								x			x		x			x				x		x		x		x	x	x																				23	12
							x	x								x					x																											16	4
				x	x			x	x						x	x	x	x	x	x	x	x	x	x	x																							26	9
x	x	x	x		x	x	x	x	x			x	x			x	x				x	x	x	x	x																							33	12
																x	x	x	x	x																												16	6
					x																																											8	4
x	x	x	x	x																																												19	11
																																																10	2
																																																30	14

Table 9. (Continued).

Siphonodosaria insecta	*Palmula* sp.	*Melonis* cf. *affinis*	*Karreriella subrotundata*	*Melonis affinis*	*Cibicidoides bradyi*	*Anomalinoides semicribrata*	*Bulimina alazanensis*	*Cassidulina bradyi*	*Stilostomella* cf. *lepidula*	*Hopkinsina mioindex*	*Bolivinopsis praelonga*	Miliolids	*Melonis pacificum*	*Dentalina soluta*	*Trifarina angulosa*	*Sphaeroidina bulloides*	*Osangularia bengalensis*	*Cibicidoides* cf. *tuxpamensis*	*Cibicidoides* trans. *cicatricosus*	*Eggerella* sp.	*Uvigerina striata*	*Uvigerina pigmaea*	*Pleurostomella brevis*	*Pleurostomella tenuis*	*Brizalina reticulata*	*Ehrenbergina pacifica*	*Epistominella* sp.	*Uvigerina hispido-costata*	*Anomalinoides globulosa*	*Pullenia quadriloba*	*Lenticulina* sp.	*Alabamina haitiensis*	*Textularia* sp. 1	*Ehrenbergina* cf. *amina*	*Pyrgo murrhina*	*Pleurostomella alternens*	*Melonis pompilioides*
							x	x					x	x			x									x		x									x
							x								x										x	x		x						x	x	x	
						x																				x			x		x	x	x				
			x						x													x									x						
							x				x			x														x	x	x							
																	x							x				x									
																	x								x	x	x										
									x													x	x	x													
							x															x															
												x			x																						
						x				x									x	x	x																
							x								x	x	x	x																			
x						x		x					x	x																							
		x							x	x	x	x																									
x					x																																
x	x	x	x	x	x	x	x	x	x																												

Table 10. Benthic foraminifers, Hole 591, late Miocene.

Age	Planktonic foraminifer zone	Core-Section (level in cm)	Preservation	Radiolarians	*Bulimina truncana*	*Chrysalogonium equisetiformis*	*Eggerella bradyi*	*Heterolepa kullenbergi*	*Hopkinsina mioindex*	*Cibicidoides bradyi*	*Stilostomella lepidula*	*Pleurostomella tenuis*	*Uvigerina hispido-costata*	*Osangularia bengalensis*	*Oridorsalis umbonatus*	*Brizalina pusilla*	*Ehrenbergina* cf. *amina*	*Uvigerina striata*	*Quinqueloculina* cf. *seminulina*	*Laticarinina halophora*	*Brizalina finlayi*	*Stilostomella subspinosa*	*Melonis* cf. *barleeanum*	*Globocassidulina subglobosa*	*Brizalina pusilla* (long striae)	*Melonis* cf. *affinis*	*Cibicidoides trincherasensis*	*Rectuvigerina spinea*	*Siphonodosaria insecta*
late Miocene	*G. sphericomiozea*	20-4, 19	M			x	x	x	x	x	x				x				x	x	x				x				x
	G. conomiozea	20,CC	M		x			x	x				x		x	x						x							
		21-5, 19	F		x	x			x			x	x	x		x		x											
		21,CC	VP						x						x				x										
		22-2, 19	F	x	x			x					x	x	x			x						x					
		22,CC	P			x		x		x			x	x	x				x					x					
		23-1, 19	M	x	x			x				x	A		x	x						x		x					
	G. nepenthes	23,CC	M		x		x	x		x	x		x		x							x		x					
		24-4, 19	F		x		x	x				x	x		x									x					
		24,CC	F		x			x		x			x		x			x	x										x
		25-5, 19	M		x			x					A	x	x	x		x	A										
		25,CC	M		x			x					A						A										
	N. continuosa	26,CC	M		x			x							x			x	x					x					
		27,CC	M		x		x		x		x		x					x	x				x	x					
		28-4, 19	M				x	x		x	x				x	x					x			x					
		28,CC	M		x			x					x		x	x			x				x					x	x
		29-3, 19	F				x	x		x		x		x	x	x					x			x		x	x		x
		29,CC	F		x			x											x										x
		30,CC	M		x	x		x	x	x	x				x			x		x				x				x	x
		31-2, 19	M		x	x	x	x	x	x	x	x								x	x	x	x	x	x	x	x		
		31,CC	M		x	x	x	x	x	x	x	x	x	x	x	x	x	x	x										

Note: Total no. of species, 65.

Table 11. Benthic foraminifers, Hole 591, Pliocene.

Age	Planktonic foraminifer zone	Core-Section (level in cm)	Preservation	*Osangularia bengalensis*	*Cibicides wuellerstorfi*	*Globocassidulina subglobosa*	*Oridorsalis umbonatus*	*Laticarinina altocamerata*	*Bulimina truncana*	*Melonis pompilioides*	*Pyrgo murrhina*	*Melonis affinis*	*Nodosaria consobrina*	*Heterolepa kullenbergi*	*Gyroidina* sp. 1	*Pullenia bulloides*	*Eggerella bradyi*	*Favocassidulina fava*	*Uvigerina interrupta-costata*	*Karreriella subrotundata*	*Stilostomella subspinosa*	*Stilostomella lepidulina*	*Brizalina pusilla*	*Uvigerina dirupta*	*Pyrgo lucernula*	*Uvigerina hispida*	*Sphaeroidina bulloides*	*Nodosaria skobina*	*Cibicidoides bradyi*	*Alabamina haitiensis*	*Ehrenbergina pacifica*
Pliocene	*G. tosaensis*	9-9, 19	G	x		x	x	x				x		x															x		
		9,CC	M	x		x	x		x	x	x		x	x		x	x		x			x	x		x				x		
		10-3, 19	M				x	x	x		x	x			x		x		x					x		x	x		x		
		10,CC	M	x		x	x	x	x	x	x		x				x	x						x		x				x	x
	G. inflata	11,CC	M	x	x	x	x	x	x		x		x	x		x						x							x		x
		12-3, 19	G				x		x	x	x	x		x		x						x				x					
		12,CC	M			x	x	x	x		A		x					x			x	x	x		x				x		
		13-3, 19	G		x	x			x			x		x			x			x											
		13,CC	M		x	x	x		A				x									x	x				x		x		
	G. crassaformis	14-4, 40	M		x		x		x		x	x		x	x		x	x		x	x										
		14,CC	M	x	x		x				x		x			x	x												x		x
		15,CC	M	x	x	x			x	x	x	x	x	x			x					x			x				x		
		16,CC	M	x	x	x	x		x		x	x										x		x			x		x		
		17,CC	M	x			x		x		x			x								x	x	x	x	x	x	x	x	x	
	G. puncticulata	19,CC	M	x	x	x	x	x	x	x	x	x	x	x	x	x	x	x	x	x	x	x									

Table 10. (Continued).

Bolivinopsis praelonga	*Pullenia bulloides*	*Gaudryina solida*	*Pyrgo murrhina*	*Stilostomella consobrina*	*Cibicides wuellerstorfi*	*Melonis pompilioides*	*Anomalinoides semicribrata*	*Alabamina haitiensis*	*Sigmoilopsis schlumbergeri*	*Dentalina neugeboreni*	Domed cibicidids	*Heterolepa rugosa*	*Martinottiella variabilis*	*Uvigerina auberiana*	*Pullenia quinqueloba*	*Laticarinina altocamerata*	*Textularia agglutinans*	*Textularia* sp. 1	*Uvigerina spinulosa*	*Uvigerina proboscidea*	*Pyrgo comata*	*Uvigerina hispida*	*Triloculina lucernula*	*Bulimina striata*	*Ehrenbergina pacifica*	*Cibicidoides cicatricosus*	*Pleurostomella alternans*	*Nodosaria longiscata*	*Uvigerina pigmaea*	*Nuttallides umbonifera*	*Nodosaria spirostriolata*	Eponid-form cibicidids	*Ehrenbergina* cf. *amina*	*Stilostomella pomuligera*	*Martinottiella* cf. *antarctica*	*Sphaeroidina bulloides*	*Trifarina bradyi*	*Cassidulina laevigata*
x				x			x		x			x	x			x				x																x	x	x
			x	x	x													x												x		x						
			x													x										x				x					x			
			x																						x	x				x								
			x		x			x				x				x					x																	
			x		x				x				x				x				x																	
		x							x	x	x					x	x				x											x	x	x				
		x	x		x				x				x			A	x	x			A										x							
		x			x											x													x	x								
		x				x			x				x							x		x	x	x	x	x	x	x										
								x	x			x				A					x																	
			x	x													x			x																		
	x		x		x				x						x			x	x																			
x		x	x	x				x	x							x	x	x																				
									x	x		x			x	x																						
	x		x	x		x		x				x	x	x																								
		x					x	x	x	x	x																											
		x	x	x	x	x																																
x	x	x	x																																			

Table 11. (Continued).

Globocassidulina arata	*Textularia lythostrota*	*Cibicidoides* cf. *ungerianus*	*Cibicidoides* spp.	*Textularia* sp. 1	*Laticarinina halophophora*	*Quinqueloculina seminulina*	*Martinottiella variabilis*	*Bolivinopsis praelonga*	*Sigmoilopsis schlumbergeri*	*Cassidulina laevigata*	*Hopkinsina mioindex*	*Nuttallides umbonifera*	*Uvigerina hispido-costata*	*Nodosaria holoserica*	*Textularia agglutinans*	*Melonis nicobarense*	*Uvigerina proboscidea*	*Cibicidoides bradyi*	*Rotalia translucens*	*Melonis barleeanum*	*Pullenia quadriloba*	*Ehrenbergina spinosissima*	*Pullenia quinqueloba*	*Stilostomella insecta*	*Brizalina reticulata*	*Uvigerina striata*	*Anomalinoides globulosa*	*Pyrgo comata*	*Laticarinina bullbrooki*	*Heterolepa rugosa*	*Pyrgo ovata*	*Siphotextularia catenata*	*Fissurina capillosa*	*Pleurostomella alternans*	*Cibicides lobatulus*	*Planulina* cf. *ariminensis*	Stilostomella pomuligera	No. of species (total species, 66)	No. of rectilinear (total, 26)
												x																							x	x	x	11	1
			x				x				x	x	x			x		x					x			x							x	x				26	11
							x				x				x			x				x		x						x	x	x						30	10
						x					x				x		x										x	x	x									21	8
				x							x	x					x	x					x	x	x	x												24	9
									x		x				x			x																				13	4
	x	x							x						x						x																	17	8
							x						x					x																				10	5
				x							x				x			x	x	x		x																16	7
			x										x																									13	5
						x			x							x	x																					13	4
	x					x			x	x	x	x	x	x	x																							13	7
		x	x	x	x	x	x	x																														22	6
																																						14	6
																																						19	7

Table 12. Benthic foraminifers, Hole 592, Eocene–Oligocene.

Age		Planktonic foraminifer zone	Core-Section (level in cm)	Preservation	Radiolarians	*Bulimina alazanensis*	*Hanzawaia cushmani*	*Globocassidulina subglobosa*	*Anomalinoides orbiculus*	*Trifarina bradyi*	*Pullenia eocaena*	*Stilostomella antillea*	*Oridorsalis umbonatus*	*Gyroidinoides* sp.	*Karreriella subglabra*	*Heterolepa grimsdalei*	*Uvigerina rippensis*	*Anomalinoides alazanensis*	*Heterolepa subspirata*	*Anomalinoides semicribrata*	*Vulvulina carinata*	*Lenticulina* sp.	*Cibicidoides havanensis*	*Cibicidoides parki*	*Anomalinoides semiteres*	*Bolivinopsis cubensis*	*Alabamina haitiensis*	*Rectuvigerina prisca*	*Rotaliatina sulcigera*	Porous cibicidids	*Gyroidinoides planulatus*	*Anomalinoides aragonensis*	*Cibicidoides* cf. *havanensis*	*Marginulinopsis hochstetteri*
Oligocene	early	*G. angiporoides*	33,CC				x	x					x		x	x				x		x				x	x						x	x
		G. brevis	34-2, 19	M			x	x					x		x	x				x		x				x	x			x			x	x
			34,CC	G			x	x		x	x	x	x	x	x	x		x	x			x			x			x		x		x	x	x
			35,CC	G				x			x	x	A	x		x		x				x			x	x				x			x	
		G. linaperta	36-2, 119	G	x		x	x	x	x	x		x	x	x	x	x	x	x			x		A	x	x		x	x				x	x
			36-3, 92	F			x	x					x			x		x			x				x	x		x						x
Eocene	late		37-3, 88	P			x	x			x	x				x				x	x			x	x				x			x		x
			37-4, 30	M		x	x	x	x		x		A	x		x				x		x		x		x							x	x
			38-3, 19	F		x		x			x	x	x	x		x		x	x		x			x	x	x	x		x				x	x
			38,CC	M			x	x		x		x	x	x		x		x	x		x			x	x				x				x	
			39-3	M		x	x	x	x	x			x			x		x	x	x	x	x		x					x	x			x	x
			39,CC	F	x	x	x	x	x		x	x	x		x		x	x			x	x		x		x		x	x	x			x	
			40-5, 19	F		x	x	x		x	x		x	x		x	x	x	x	x				x	x	x	x							x
			40,CC	F		x	x	x	x	x	x		x	x		x		x	x					x	x	x	x		x				x	
		G. aculeata	41-4, 19	M		x		x			x		x	x		x	x	x	x	x	x		x						x	x		A	x	x
			41,CC	F	x	x	x	x	x	x	x	x	x	x	x	x	x	x	x	x	x	x	x	x	x	x	x	x	x	x	x	x		

Note: Total no. of species, 75.

Table 13. Benthic foraminifers, Hole 592, early–mid Miocene.

Age		Planktonic foraminifer zone	Core-Section (level in cm)	Preservation	*Rectuvigerina spinea*	*Pullenia quadriloba*	*Stilostomella pomuligera*	*Anomalinoides alazanensis*	*Heterolepa rugosa*	*Anomalinoides pompilioides*	*Nuttallides umbonifera*	*Oridorsalis umbonatus*	*Cibicidoides tuxpamensis*	*Uvigerina auberiana*	*Stilostomella* trans. *lepidula*	*Brizalina reticulata*	*Heterolepa kullenbergi*	*Globocassidulina subglobosa*	*Cibicidoides* sp. 1	*Sphaeroidina bulloides*	*Pullenia bulloides*	*Siphonina australis*	*Melonis* cf. *barleeanum*	*Ehrenbergina* sp. 1	*Stilostomella consobrina*	*Rectuvigerina vesca*	*Lenticulina gyroscalpra*	*Bolivinopsis praelonga*	*Discorbis* sp.
Miocene	middle	*G. mayeri*	24-6, 19						x			x				x	x	x	x				x						
			24,CC	F					x			x				x	x	x					x						
			25-7, 19	F									x	x	x		x	x	x						x				
			25,CC	F			x		x			x				x	x	x											
			26-3, 19	M						x	x	x					x	x					x				x		
			26,CC	F			x				x	x				x	x	x											
		O. suturalis	28-5, 19	F								x				x	x		x	x			x					x	x
			28,CC	F						x	x	x				x	x	x	x		x								
		O. glomerosa	29,CC	F	x			x				x			x			x											
	early	*G. miozea*	30-2, 19	M								x	x				x												
			30,CC	F	x											x	x	x											
			31,CC	F	x								x	x	x	x	x	x	x	x	x	x	x	x	x	x	x	x	x
		G. trilobus	32,CC	F	x	x	x	x	x	x	x	x	x	x	x	x	x												

Note: Total no. of species, 67.

Table 12. (Continued).

Stilostomella curvatura	*Fissurina capillosa*	*Uvigerina bortotara costata*	*Lenticulina* cf. *vortex*	*Cibicides vortex*	*Pleurostomella tenuis*	*Nuttallides umbonifera*	*Cibicidoides* cf. *ungerianus*	*Textularia* sp. 2	*Uvigerina wanzea*	*Pullenia bulloides*	*Textularia* sp. 2	Planispiral cibicidid	*Uvigerina bortotara*	*Osangularia mexicana*	*Uvigerina* cf. *pigmaea*	*Orthomorphina perversa*	*Vulvulina pennatula*	*Brizalina reticulata*	*Marginulinopsis* sp.	*Rectuvigerina postprandia*	*Orthomorphina rohri*	*Heterolepa* trans. *kullenbergi*	*Stilostomella basicarinata*	*Planulina* sp.	*Karreriella bradyi*	*Cibicidoides notocenicus*	*Cibicides lobatulus*	*Siphonodosaria nuttalli*	*Cibicidoides tuxpamensis*	*Stilostomella subspinosa*	*Cibicides laurisae*	*Pullenia multiloba*	*Pullenia quadriloba*	*Laticarinina altocamerata*	*Laticarinina halophora*	*Martinottiella* cf. *antarctica*	*Rectuvigerina vesca*	*Cassidulina crassa*	*Cibicidoides tholus*	*Eggerella bradyi*	*Hopkinsina mioindex*	*Cibicidoides* cf. *havanensis*	*Pullenia quinqueloba*
				x	x		x										x					x											x			x		x	x		x	x	x
x				x	x		x	x				x					x					x											x			x					x	x	x
				x	x		x	x									x					x			x		x	x								x	x	x	x	x			
		x		x	x		x			x			x		x							x			x								x	x	x								
					x		x			x			x		x	x	x					x				x		x		x	x	x											
							x						x									x			x	x	x	x	x														
							x						x													x																	
		x	x				x			x		x	x				x					x	x	x	x																		
	x	x	x				x			x			x					x	x	x	x																						
x						x				x			x	x				x	x																								
							x			x			A		x	x	x																										
												x	x	x																													
x	x	x					x	x	x	x	x																																
x	x	x		x			x		x	x																																	
x	x	x	x	x	x	x	x																																				

Table 13. (Continued).

Nodosaria skobina	*Hopkinsina mioindex*	*Laticarina bullbrooki*	*Pullenia quadriloba*	*Bulimina alazanensis*	*Karreriella bradyi*	*Cibicidoides trincherasensis*	*Gyroidinoides* sp.	*Cibicidoides subhaidingeri*	*Marginulinopsis mammilligera*	*Planulina* sp.	*Cassidulina crassa*	*Textularia lythostrota*	*Cibicidoides* cf. *wuellerstorfi*	Domed cibicidids	*Cibicidoides* cf. *io*	*Pleurostomella alternans*	*Cassidulina laevigata carinata*	*Brizalina reticulata*	*Trifarina bradyi*	*Melonis barleeanum*	*Heterolepa* trans. *rugosa*	*Eggerela bradyi*	*Pleurostomella alternans*	*Cibicides lobatulus*	*Siphotextularia solita*	*Anomalinoides globulosa*	*Hopkinsina mioindex*	*Alabamina haitiensis*	*Uvigerina* cf. *pigmaea*	*Stilostomella subspinosa*	*Cibicidoides* trans. *cicatricosus*	*Orthomorphina rohri*	*Karreriella subrotundata*	*Melonis affinis*	*Laticarinina altocamerata*	*Stilostomella lepidula*	*Cibicidoides cicatricosus*	*Karreriella sub-baccata*	*Brizalina finlayi*	*Martinottiella variabilis*
	x									x							A					x						x		x				x			x	x	x	x
		x	x									x					A										x								x	x				
	x					x	x						x	x		x					x		x	x									x	x						
				x				x					x										x																	
	x	x				x						x		x								x																		
		x	x		x							x	x									x	x	x	x	x	x	x	x	x	x	x								
		x					x		x	x		x	x							x	x																			
	x		x	x						x		x	x	x	x	x	x	x	x																					
		x							x	x	x																													
							x	x																																
				x	x	x																																		
		x	x																																					

Table 14. Benthic foraminifers, Hole 592, late Miocene.

Age	Planktonic foraminifer zone	Core-Section (level in cm)	Preservation	Radiolarians	*Globocassidulina subglobosa*	*Textularia lythostrota*	*Melonis barleeanum*	*Ehrenbergina pacifica*	*Cibicides wuellerstorfi*	*Uvigerina striatissima*	*Stilostomella subspinosa*	*Holmanella* sp.	*Brizalina reticulata*	*Heterolepa kullenbergi*	*Nodosaria consobrina*	*Hopkinsina mioindex*	Domed cibicidids	*Siphotextularia catenata*	*Stilostomella lepidula*	*Heterolepa rugosa*	*Pullenia coryelli*	*Cibicidoides* cf. *ungerianus*	*Eggerella bradyi*	*Oridorsalis umbonatus*	*Karreriella bradyi*	*Laticarinina bullbrooki*	*Cibicides lobatulus*	*Pullenia bulloides*	*Sigmoilopsis schlumbergeri*	*Brizalina pusilla* (long striae)	*Brizalina reticulata*	*Brizalina pusilla*	*Melonis affinis*	*Pullenia quadriloba*	*Alabamina haitiensis*	*Uvigerina proboscidea*	*Sphaeroidina bulloides*
late Miocene	*G. conomiozea*	12,CC	M		x			x						x	x	x							x				x		x		x					x	
		13-2, 19	M					x							x	x				x			x									x	x				x
		13,CC	M		x			x						x		x			x	x		x			x		x		x	x				x			
		14-2, 1	M			x		x							x	x			x	x		x	x	x				x	x			x				x	
		14,CC	M		x	x		x						x	x	x						x	x	x			x			x					x		
		15-2, 19	M		x	x	x	x						x	x	x				x			x				x	x					x			x	
		15,CC	M		x		x							x		x				x		x		x				x	x								
		16,CC	M			x		x	x					x		x				x		x		x			x		x	x						x	
		17-2, 19	M				x	x							x	x				x		x		x			x	x	x			x				x	
		17,CC	M			x		x						x		x			x	x		x	x	x						x					x		x
	G. miotumida	18-1, 19	F			x	x					x			x		x					x	x	x	x		x	x				x	x				x
		18,CC	M			x		x						x									x	x			x	x		x				x		x	x
		19-5, 19	F										x	x		x								x								x	x	x			
		19,CC	F		x									x		x			x	x			x	x			x			x							
		20-6, 19	M		x					x		x	x	x	x	A							x									x					
		20,CC	M		x			x						x		x			x					x						x	x	x					
		21-3, 19	F	x	x	x						x	x	x	x	x							x			x						x					
		21,CC	M		x	x										x								x			x			x	x				x	x	x
	N. continuosa	22-4, 19	M		x						x		x						x				x	x	x							x	x	x	x		
		22,CC	M		x		x				x			x		x			x								x	x	x	x	x						
		23-2, 19	M		x	x	x	x	x	x	x	x	x	x	x	x	x	x	x	x	x	x	x	x	x												

Table 15. Benthic foraminifers, Hole 592, Pliocene.

Age	Planktonic foraminifer zone	Core-Section (level in cm)	Preservation	*Brizalina pusilla*	*Textularia lythostrota*	*Uvigerina hispido-costata*	*Heterolepa kullenbergi*	*Sphaeroidina bulloides*	*Bulimina truncana*	*Uvigerina auberiana*	*Cibicidoides mundulus*	*Eggerella bradyi*	*Spiroloculina* sp.	*Pullenia bulloides*	*Sigmoilopsis schlumbergeri*	*Hopkinsina mioindex*	*Gyroidinoides* sp. 1	*Oridorsalis umbonatus*	*Pleurostomella alternans*	*Martinottiella communis*	*Melonis barleeanum*	*Pyrgo murrhina*	*Laticarinina bullbrooki*	*Cassidulina crassa*	*Laticarinina halophora*	*Pullenia quadriloba*	*Uvigerina hispida*	*Discanomalina semipunctata*	*Stilostomella lepidula*	Domed cibicidids	*Chrysalogonium equisetiformis*	Miliolids	*Siphotextularia solita*	*Heterolepa rugosa*	*Gaudryina solida*	*Laticarinina altocamerata*
Pliocene	*G. truncatulinoides*-*G. tosaensis*	3,CC	G		x	x	x	x										x			x								x					x		
	G. inflata	4-6, 35	G	x		x		x			x			x	x		x	x	x					x				x						x		
		4,CC	G	x			x	x		x	x		x		x			x			x		x		x	x		x	x					x		x
		5,CC	G	x		x		x			x		x		x			x	x		x							x	x							x
		6-2, 19	G	x	x		x	x			x	x		x	x			x	x	x	x				x				x					x		x
		6,CC	G	x		x		x		x				x				x			x	x						x	x							x
		7,CC	G	x	x		x	x			x				x			x	x		x	x	x					x						x		x
	G. crassaformis	8-6, 19	G	x		x		x			x	x		x	x		x	x					x		x	x	x	x	x					x	x	
		8,CC	G			x				x		x		x	x			x	x		x	x			x				x				x	x		x
		9-3, 19	G	x	x	x	x	x	x			x		x	x	x					x							x	x			x		x		
		9,CC	G		x		x	x		x					x	x		x	x		x			x				x	x						x	
	G. puncticulata	10,CC	G	x			x	x										x		x		x	x				x	x	x			x				x
	G. sphericomiozea	11-4, 19	G	x	x		x			x	x	x			x		x			x	x		x	x				x	x					x		x
		11,CC	G	x	x	x	x	x	x	x	x	x	x	x	x	x	x	x	x	x	x	x	x	x	x	x	x	x	x	x	x	x	x	x	x	x

Table 14. (Continued).

Cibicidoides subhaidingeri	Uvigerina striata	Cibicidoides bradyi	Laticarinina altocamerata	Rectuvigerina ongleyi	Cibicidoides cicatricosus	Laticarinina halophora	Bulimina striata	Rectuvigerina spinea	Siphonina australis	Cibicidoides cf. cicatricosus	Pleurostomella alternans	Stilostomella pomuligera	Uvigerina hispida	Martinottiella variabilis	Uvigerina proboscidea	Anomalinoides cf. alazanensis	Melonis nicobarense	Pullenia quinqueloba	Fissurina capillosa	Miliolids	Orthomorphina perversa	Karreriella subrotundata	Osangularia bengalensis	Bolivinopsis praelonga	Planulina sp. 1	Karreriella cf. baccata	Anomalina semicribrata	Anomalina globulosa	Textularia agglutinans	Ehrenbergina pacifica	Martinottiella communis	Uvigerina hornibrooki	Bulimina truncana	Stilostomella insecta	Chrysalogonium equisetiformis	Discanomalina semipunctata	Cassidulina crassa	Siphonina australis	Textularia sp. 2	Dentalina neugeboreni	Martinottiella antarctica	Uvigerina hispido-costata	Uvigerina gemmaeformis	Pyrgo murrhina	Nodosaria stiliformis
	x	x			x					x		x	x				x	x		x																x									x
		x																		x							x						x												
												x			x							x					x						x			x	x				x	x		x	
										x			^		x																														
	x									x		x	x					x		x		x					x	x			x	x	x									x	x		
										x			x		x																										x	x			
		x	x			x					x		x				x	x		x					x			x										x	x	x					
						x	x				x	x						x		x								x	x					x	x	x	x								
				x	x	x	x						x		x					x			x	x			x			x	x	x	x	x											
	x	x					x			x			x										x	x					x																
			x		x	x	x					x			x			x				x	x	x	x	x	x	x																	
x		x				x	x	x		x	x	x				x		x	x	x	x																								
				x	x			x																																					
x												x	x		x	x	x																												
						x	x	^						x																															
x		x				x	x	x		x	x	x	x																																
		x	x	x	x	x	x	x	x																																				

Table 15. (Continued).

Stilostomella consobrina	Cibicides lobatulus	Brizalina pusilla (long striae)	Karreriella bradyi	Cibicidoides cicatricosus	Globocassidulina subglobosa	Melonis affinis	Nodosaria stiliformis	Karreriella baccata	Osangularia bengalensis	Martinottiella cf. antarctica	Stilostomella pomuligera	Martinottiella variabilis	Alabamina haitiensis	Uvigerina striata	Lenticulina nicobarensis	Nuttallides umbonifera	Triloculina lucernula	Karreriella subcylindrica	Textularia agglutinans	Ehrenbergina pacifica	Cibicidoides cf. io	Anomalinoides globulosa	Cibicides laurisae	Uvigerina hornibrooki	Anomalinoides semicribrata	Osangularia culter	Siphonina sp.	Rotalia translucens	Quinqueloculina seminulina	Pyrgo ovata	Gyroidinoides nitidula	Bulimina striata	Uvigerina auberiana	Uvigerina proboscidea	Melonis pacificum	Cibicidoides trincherasensis	Cibicides trans. wuellerstorfi	Pullenia quinqueloba	Bolivinita pliozea	Cibicidoides cf. havanensis	Cibicidoides cf. robertsonianus	Eponides sp.	Siphonodosaria insecta	# Species (total, 78)	# Rectilinear (total, 30)	Total agglutinated, 9
	x				x									x				x	x													x							x	x	x	x	x	20	8	
			x	x	x										x							x						x			x		x	x	x	x	x	x						25	6	
x	x		x	x	x			x										x														x			x									25	8	
x	x			x	x			x												x								x						x										20	8	
					x														x	x													x											20	10	
	x		x		x															x		x								x		x												20	6	
x	x		x		x						x							x	x								x	x	x	x	x													26	6	
x	x			x		x		x												x				x		x	x																	26	9	
x	x	x			x			x														x		x	x																			22	9	
x	x			x	x			x												x	x	x	x																					24	10	
x				x	x									x		x	x	x	x	x																								22	11	
x		x			x			x	x	x	x	x	x	x	x																													24	10	
x			x	x	x	x	x																																					23	9	
x		x	x																																									38	16	

Table 16. Benthic foraminifers, Hole 593, Eocene-Oligocene.

Age	Planktonic foraminifer zone	Core-Section (level in cm)	Preservation	*Bulimina alazanensis*	*Hanzawaia cushmani*	*Globocassidulina subglobosa*	*Anomalinoides orbiculus*	*Trifarina bradyi*	*Pullenia eocaena*	*Heterolepa* trans. *kullenbergi*	*Stilostomella antillea*	*Marginulinopsis hochstetteri*	*Eponides* sp.	*Oridorsalis umbonatus*	*Gyroidinoides* sp.	Planispiral cibicidids	*Karreriella subglabra*	*Heterolepa grimsdalei*	*Stilostomella curvatura*	*Uvigerina rippensis*	*Anomalinoides alazanensis*	*Fissurina capillosa*	*Uvigerina bortotara costata*	*Uvigerina bortotara*	*Heterolepa subspirata*	*Anomalinoides semicribrata*	*Eponides* sp.	*Vulvulina pennatula*	*Pullenia quadriloba*	*Lenticulina* sp.	*Cibicidoides parki*	*Globulina* sp.	*Anomalinoides* cf. *alazanensis*	*Bolivinopsis cubensis*	*Cibicidoides notocenicus*	*Anomalinoides aragonensis*
Oligocene	*G. woodi*	49,CC	M	x		x			x		x			x				x											x	x						
	G. euaperta	50-1, 19	M	x		x			x		x			x				x			x								x	x						
		50-3, 19	F			x			x		x			x				x											x	x						
		50-5, 19	F																																	
		50,CC	M	x		x	x				x			x		x		x											x	x						
	G. angiporoides	52-3, 96	F	x		x					x				x																					
		52,CC	M			x				x		x	x	x											x				x					x		
		53-3, 19	F	x		x				x				x				x	x															x		
		53,CC	G	x	x	x			x		x			x	x			x			x					x		x								
		54,CC	M	x		x	x			x	x			x	x			x																x	x	
		55-2, 19	G	x	x	x	x	x	x		x	x		x				x	x		x								x	x				x		
		55,CC	M		x		x	x		x	x	x	x					x	x		x								x					x	x	
	G. brevis	56-3, 19	M		x	x	x	x						x				x			x							x						x	x	
		56,CC	M		x	x	x			x	x	x		x	x		x	x			x	x				x							x			
		57-2, 96	M		x	x	x		x	x	x	x			x	x	x	x			x				x					x				x	x	x
		57,CC	M			x	x			x	x			x			x	x	x					x	x				x					x		
	G. linaperta	58-1, 19	F	x		x	x		x	x	x			x		x	x	x		x	x		x						x	x				x		
		58-2, 19	M		x	x	x	x			x			x	x	x	x	x	x		x		x	x	x				x					x		
Eocene		60-1, 7	F	x	x	A	x	x		x	x	x		x	x				x		x		x	x	x		x		x	x	x		x			
		60,CC	G	x	x	A	x	x	x	x	x	x	x	x	x	x	x	x	x	x	x	x	x	x	x	x	x	x	x	x	x	x	x	x	x	x

Note: Total no. of species, 79.

Table 17. Benthic foraminifers, Hole 593, early Miocene.

Age	Planktonic foraminifer zone	Core-Section (level in cm)	Preservation	*Oridorsalis umbonatus*	*Laticarinina halophora*	*Heterolepa kullenbergi*	*Stilostomella lepidula*	*Globocassidulina subglobosa*	*Bulimina truncana*	*Hopkinsina mioindex*	*Osangularia culter*	*Osangularia bengalensis*	*Eggerella bradyi*	*Pleurostomella alternans*	*Cibicidoides bradyi*	*Stilostomella pomuligera*	*Cassidulina crassa*	*Laticarinina bullbrooki*	*Melonis nicobarense*	*Gyroidinoides nitidula*	*Nodosaria consobrina*	*Trifarina costornata*	*Rectuvigerina striatissima*	*Uvigerina pigmaea*	*Planulina* sp. 2	*Cibicides lobatulus*	*Vulvulina haeringensis*
early Miocene	*G. peripheroacuta*	40-3, 19	G		x	x	x	x		x				x					x			x					
	O. suturalis	40,CC	G		x	x	x	x																			
		41,CC	G			x	x	x		x								x	x			x					
	G. miozea	42-5, 19	F	x		x				x																	
		42,CC	G	x	x	x	x	x		x			x					x									
		43-5, 19	M	x		x			x										x								
		43,CC	M	x	x	x	x			x			x						x			x					
	G. trilobus	45-4, 19	M		x	x		x								x		x		x					x		
		45,CC	M	x		x	x								x			x						x			x
	G. woodi connecta	47-5, 19	M	x	x	x		x										x		x	x	x	x	x			
		47,CC	M	x		x	x		x	x	x	x	x			x		x					x			x	x
		48-6, 19	M	x		x		x	x	x								x	x	x	x	x	x	x	x		
		48,CC	M	x	x	x	x	x	x	x	x	x	x	x	x	x	x										

Note: Total no. of species, 64.

Table 16. (Continued).

[illegible]																				x
Siphonodosaria puttalli																				x
Pullenia bulloides		x						x		x	x		x							x
Osangularia mexicana										x										x
Domed cibicidids																				x
Cibicides lobatulus															x					x
Cibicidoides tholus										x										x
Lenticulina cf. *vortex*											x				x				x	
Alabamina haitiensis							x					x	x						x	
Laticarinina altocamerata	x	x	x		x	x	x	x	x	x	x	x		x	x			x	x	
Martinottiella cf. *antarctica*										x	x	x							x	
Heronallenia sp.	x	x	x	x	x														x	
Cibicides vortex														x			x		x	
Cassidulina cuneata					x												x	x		
Pullenia multiloba		x			x													x		
Rectuvigerina prisca					x	x	x				x	x	x		x		x	x		
Rotaliatina sulcigera								x	x	x	x	x	x	x	x		x	x		
Uvigerina wanzea					x			x										x		
Porous cibicidids						x		x		x	x		x	x	x	x		x		
Pleurostomella tenuis						x					x					x	x	x		
Vulvulina pennatula	x	x	x		x	x			x		x	x	x	x		x		x		
Nuttallides umbonifera					x			x				x				x		x		
Laticarinina halophora							x	x		x	x	x		x		x	x			
Brizalina reticulata	x	x	x		x	x		x	x	x	x				x		x			
Siphonodosaria modesta	x						x			x					x		x			
Stilostomella basicarinata									x		x	x		x	x	x				
Gyroidinoides planulata											x				x					
Marginulinopsis sp.															x					
Vulvulina spinosa														x						
Stilostomella consobrina		x									x		x							
Cibicidoides haitiensis												x								
Planulina sp.							x				x									
Rectuvigerina vesca	x	x	x			x	x	x	x	x	x									
Hopkinsina mioindex	x	x	x								x									
Eggerella bradyi											x									
Orthomorphina perversa	x						x			x										
Stilostomella cf. *lepidula*										x										
Karreriella bradyi		x						x		x										
Cibicidoides havanensis								x		x										
Orthomorphina rohri	x	x			x				x											
Uvigerina spinulosa						x	x	x	x											
Heterolepa kullenbergi	x	x	x	x	x	x	x		x											
Uvigerina pigmaea	x	x	x		x		x		x											
Brizalina pusilla					x			x	x											
Pullenia quinqueloba						x	x	x												

Table 17. (Continued).

Planulina mariaiana gigas	x		x						x	x	x
Pullenia quadriloba			x				x	x			x
Pullenia bulloides	x		x		x	x	x			x	x
Rectuvigerina rerensis	x				x		x				x
Laticarinina altocamerata											x
Cibicidoides haitiensis	x		x								x
Finely punctate cibicidids											x
Stilostomella lepidula (smooth)								x		x	
Melonis barleeanum			x		x		x	x	x	x	
Cibicidoides cf. *ungerianus*										x	
Anomalinoides pompilioides										x	
Rectuvigerina vesca				x						x	
Bulimina tuxpamensis					x					x	
Cibicides lobatulus	x		x						x		
Karreriella bradyi	x		x		x		x	x	x		
Siphonina australis									x		
Martinottiella variabilis									x		
Anomalinoides orbiculus					x	x		x			
Vulvulina pennatula								x			
High-spired cibicidids								x			
Brizalina finlayi								x			
Brizalina anastomosa	x		x	x	x	x	x				
Cibicides cf. *laurisae*							x				
Uvigerina proboscidea					x		x				
Karreriella subglabra	x	x	x			x					
Cibicidoides trincherasensis			x			x					
Lenticulina calcar						x					
Planulina harangensis			x		x						
Brizalina pusilla (long striae)					x						
Domed cibicidids	x	x	x	x							
Anomalinoides globulosa			x								
Sigmoilopsis schlumbergeri	x		x								
Uvigerina rugosa	x										
Cibicides wuellerstorfi	x										
Martinottiella communis	x										
Alabamina haitiensis	x										
Bolivinopsis praelonga	x										
Nuttallides umbonifera	x										

Table 18. Benthic foraminifers, Hole 593, late Miocene.

Age	Planktonic foraminifer zone	Core-Section (level in cm)	Preservation	Radiolarians	*Planulina renzi*	*Pleurostomella alternans*	*Pullenia quadriloba*	*Cibicidoides cicatricosus*	*Laticarinina altocamerata*	*Stilostomella subspinosa*	*Uvigerina striata*	*Textularia lythostrota*	*Heterolepa kullenbergi*	*Hopkinsina mioindex*	*Cibicides wuellerstorfi*	*Globocassidulina subglobosa*	*Oridorsalis umbonatus*	*Karreriella bradyi*	*Cibicidoides bradyi*	*Nuttallides umbonifera*	*Brizalina silvestrina*	Dotted cibicids	Eponid form cibicids	*Laticarinina bullbrooki*	*Nodosaria consobrina*	*Anomalinoides semicribrata*	*Pleurostomella tenuis*	*Brizalina finlayi*	*Pullenia bulloides*	*Bulimina truncana*	*Heterolepa rugosa*	*Brizalina reticulata*	*Melonis affinis*	*Cibicidoides* cf. *ungerianus*	*Gyroidinoides soldanii*	*Karreriella subrotundata*	*Planulina ariminensis*	*Stilostomella lepidula*	*Brizalina anastomosa*	*Sigmoilopsis schlumbergeri*	*Melonis barleeanum*	*Sphaeroidina bulloides*	*Laticarinina halophora*	*Cibicidoides trincherasensis*	*Chrysalogonium equisetiformis*	*Rectuvigerina ongleyi*	*Cassidulina laevigata*	*Martinottiella* sp.
late Miocene	*G. conomiozea*	14-1, 19	F					x	x			x	x	x	x	x			x										x		x													x				x
		14,CC	G			x	x	x			x	x	x	x			x	x	x		x								x	x	x							x				x	x					
		15-3, 19	G					x				x	x	x	x		x								x						A					x				x		x	x					x
		15,CC	G					x	x		x	x	x	x	x		x	x			x			x						x	x							x		x	x	x						
		16-1, 19	G					x					x	x			x							x	x						x							x		x								
		16,CC	G								x	x	x	x					x										x	x	x	x						x										
		17-3, 19	M						x			x	x	x	x	x	x	x			x	x		x							x		x		x					x	x	x		x				
		17,CC	M					x	x			x	x	x		x	x											x	x	x	x											x						
	G. miotumida	18-3, 19	G					x				x	x	x			x	x				x		x							x		x			x	x			x				x				
		18,CC	G			x	x					x	x	x		x	x	x	x		x							x			x							x				x	x					
		19-2, 19	M					x	x					x			x														x									x		x		x				
		19,CC	G		x	x		x					x	x	x		x		x										x		x									x	x		x					
		20,CC	G			x		x				x		x			x		x												x					x				x	x	x	x					
		21-4, 19	G										x	x			x					x	x		x			x			x				x			x		x		x						
		21,CC	G					x	x			x	x	x			x		x							x			x		x							x		x	x	x	x					
		22-3, 19	G					x				x	x	x			x					x							x		x													x				
		22,CC	G					x			x		x				x												x		x									x	x		x					
	N. continuosa	23-1, 19	F		x		x	x				x	x	x							x	x		x	x	x		x			x																	
		23,CC	G				x							x			x		x		x								x		x	x									x		x					x
		24-2, 19	M										x	x			x						x	x				x				x								x						x		
		24,CC	G								x		x	x			x											x	x	x	x											x			x		x	
		25-1, 19	M				x							x	x	x									x						x										x					x		
		25,CC	M								x		x			x															x				x						x		x					
		26-4, 19	M				x	x					x	x	x	x	x								x										x							x				x		
		26,CC	M						x					x	x	x	x		x										x		x							x				x						
		27,CC	M	x		x								x	x	x	x		x									x			x	x			x				x									
late Miocene	*N. continuosa*	28-3, 19	F				x	x	x				x	x	x		x											x			x		x								x					x		
		28,CC	G				x	x	x				x				x	x	x	x											x	x			x				x									
		29-6, 19	M				x					x		x	x	x	x			x								A	x		x												x	x				
		29,CC	M		x		x					x	x	x	x	x	x							x							x	x						x	x				x					
		30-4, 19	M							x	x		x	x	x													x			x	x			x						x							
		30,CC	M	x	x		x		x			x	x	x	x		x		x											x	x								x									
		31,CC	M		x					x	x	x		x	x		x							x						x								x					x					
		32-1, 19	M							x		x	x			x	x										x	x	x	x		x						x					x				x	
		32,CC	M		x		x		x				x	x		x		x		x									x	x		x						x	x		x	x	x					
		33,CC	F					x		x			x	x	A		x											x		x								x	x	x								
		34-1, 19	M	x									x	x	A	x	x						x					x	x	x			x								x		x			x		
		34,CC	M										x	x		x	x													x									x		x	x					x	
		36,CC	M		x		x		x		x		x	x		x	x									x				x								x			x		x			x	x	x
		37,CC	M				x	x		x	x		x	x	x	x	x	x						x						x	x							x	x				x	x	x			
		38-5, 19	M										x	x	x	x	x	x		x	x	x	x						x	x	x					x					x	x						
		38,CC	M							x			x		x	x	x		x									x		x		x					x	x	x	x								
		39-6, 19	M								x	x	x	x	x	x	x	x	x	x	x	x	x	x	x	x	x	x	x	x	x	x	x	x	x	x												
		39,CC	M	x	x	x	x	x	x	x	x	x	x	x	x	x	x																															

Table 19. Benthic foraminifers, Hole 593, Pliocene.

Age	Planktonic foraminifer zone	Core-Section (level in cm)	Preservation	*Gyroidina* sp. 1	*Uvigerina hispida*	*Eggerella bradyi*	*Oridorsalis umbonatus*	*Textularia lythostrota*	*Heterolepa kullenbergi*	*Hopkinsina mioindex*	*Sphaeroidina bulloides*	*Heterolepa rugosa*	*Martinottiella communis*	*Sigmoilopsis schlumbergeri*	*Cibicidoides cicatricosus*	*Laticarinina halophora*	*Pleurostomella alternans*	*Brizalina pusilla*	*Cassidulina crassa*	*Cibicides lobatulus*	*Globocassidulina subglobosa*	*Martinottiella variabilis*	*Brizalina silvestrina*	*Pyrgo murrhina*	Miliolids	*Stilostomella pomuligera*	*Uvigerina striata*	*Stilostomella insecta*	*Uvigerina proboscidea*	*Cibicidoides bradyi*	*Stilostomella lepidula* (smooth)	*Discanomalina semipunctata*	*Gaudryina solida*	*Laticarinina altocamerata*	*Bulimina consanguinea*	*Pullenia bulloides*
Pliocene	*G. inflata*	5-5, 19	G				x	x	x			x	x											A												
		5,CC	G				x	x	x		x	x		x						x				x	x			x			x		x	x		x
		6-3, 19	G	x			x				x	x		x																	x					A
	G. puncticulata	6,CC	G			x	x	x	x					x			x	x		x	x		x	x	A	x	x	x	x		x					x
		7,CC	G			x	x	x	x		x		x	x				x		x	x	x		x	x				x		x	x				
		8,CC	G			x	x	x	x		x				x						x				x					x	x	x				
		9-6, 19	G				x		x	x		x			x	x		x							x											x
		9,CC	G		x				x	x	x	x	x		x			x		x	x			x	x							x				x
		11-4, 19	M	x			x		x	x	x	x	x	x		x		x	x													x				
		11,CC	G			x	x	x	x	x		x			x	x		x	x		x			x	x		x			x	x	x	x			
		12-6, 19	G	x	A	x	x	x	x	x	x	x	x	x	x	x	x	x	x						x			x		x		x				
		12,CC	G		x		x	x	x	x	x	x	x	x	x	x		x	x	x	x			x	x	x	x	x	x	x	x	x	x	x	x	x
		13,CC	G	x	x	x	x	x	x	x	x	x	x	x	x	x	x	x	x	x	x	x	x	x	x	x	x	x								

Table 18. (Continued).

Rectuvigerina spinea	Stilostomella insecta	Alabamina haitiensis	Cibicidoides cf. mundulus	Cibicidoides cf. subhaidingeri	Eggerella bradyi	Uvigerina proboscidea	Uvigerina hispida	Cibicides cf. lobatulus	Pullenia quinqueloba	Nodosaria crassitesta	Bolivinopsis praelonga	Coarsely punctate cibicidids	Bolivinopsis praelonga	Textularia agglutinans	Bulimina striata	Ehrenbergina amina	Brizalina pusilla (long striae)	Rotalia translucens	Karreriella cf. baccata	Brizalina pusilla	Quinqueloculina seminulina	Textularia sp. 1	Discorbis sp.	Gaudryina solida	Orthomorphina perversa	Stilostomella pomuligera	Melonis nicobarense	Pyrgo murrhina	Rectuvigerina postprandia	Anomalinoides pompilioides	Siphotextularia catenata	Osangularia culter	Martinottiella variabilis	Cibicidoides cf. robertsonianus	Anomalina globulosa	Osangularia bengalensis	Uvigerina hispido-costata	Uvigerina hornibrooki	Cassidulina crassa	Miliolids	Dentalina neugeboreni	Uvigerina senticosa	Martinottiella communis	Uvigerina rugosa	Ehrenbergina pacifica	Pyrgo lucernula	Cibicides laurisae	Siphotextularia solita	Bulimina consanguinea	Fissurina capillosa	Anomalinoides semicribrata	Uvigeria asperula	Discanomalina semipunctata	Globocassidulina bicornis	Pyrgo comata
			x			x		x							x					x						x			x					x			x		x	x			x			x						x			x
			x			x	x								x											x	x						x		x					x							x				x		x	x	
		x	x		x		x							x						x				x									x		x					x													x	x	
			x				x																			x		x							x							x										x		
									x					x										x								x			x					x	x		x		x							A			
							x	x						x	x					x	x			x		x		x			x							x		x					x			x	x	x	x				
			x		x		x	x							x					x																	x								x										
		x					x											x		x				x			x				x								x						x		x								
						x								x		A	x		A					x														x	x																
			x	x		x	x	x					x		x			x								x																		x	x	x									
			x			x						x								x												x				x				x															
	x		x	x	x		x						x	x	x						x					x					x	x		x	x	x																			
	x			x		x	x	x						x	x						x			x			x					x		x									x												
x					x	x		x						x	x					x						x							x					x				x													
x			x	x	x	x		x							x		x				x					x						x				x																			
x			x			x	x	x	x						x			x		x												x	x								x														
		x	x		x		x						x	x	x						x					x	x				x				x	x	x	x	x	x															
x						x		x									x							x														x																	
x	x				x	x		x									x										x							x	x	x	x																		
x							x													x																																			
x					x			x					x	x	x						x					x										x																			
			x		x										x		x															x				x																			
x					x	x	x						x	x									x			x					x	x	x	x	x																				
		x			A	x										x												x	x																									
x					x										x											x	x	x																										
		x						x	x						x										x																														
		x	x		x			x	x										x	x		x	x	x	x																														
x		x			x										x						x																																		
		x			x				x			x					x	x		A																																			
		x			x										x																																									
		x			x																																																			
		x			x						x					x	x	x	x																																				
	x				x	x							x	x	x																																								
x		x			x			x	x	x	x	x																																											
		x			x		x																																																	
A				x	x	x																																																		
		x	x																																																				
x	x	x																																																					
x																																																							

Table 19. (Continued).

Laticarinina bullbrooki	Siphotextularia catenata	Osangularia culter	Melonis affinis	Dentalina neugeboreni	Cibicidoides cf. ungerianus	Anomalinoides globulosa	Orthomorphina koina	Cassidulina crassa	Bulimina spicata	Nodosaria stiliformis	High-spiral Gyroidinoides	Pyrgo comata	Gyroidinoides altiformis	Textularia agglutinans	Uvigerina hispido-costata	Nuttalides umbonifera	Pullenia quadriloba	Alabamina haitiensis	Pyrgo lucernula	Melonis barleeanum	Ehrenbergina pacifica	Brizalina reticulata	Rotalia translucens	Uvigerina hornibrooki	Siphonina australis	Melonis nicobarense	Bulimina truncana	Chrysalogonium equisetiformis	Karreriella subrotundata	Osangularia bengalensis	Cibicides wuellerstorfi	Anomalinoides semicribrata	Brizalina pusilla (long striae)	Karreriella bradyi	Cassidulina laevigata carinata	Pullenia quinqueloba	Anomalina cf. aotea	Bulimina striata	Pyrgo ovata	Karreriella cf. siphonella	Bulimina aculeata	# Species (total, 85)	# Rectilinear (total, 33)	Total agglutinants, 10
					x		x					x	x																													10	3	
	x				x										x			x		x			x	x			x									x					x	24	7	
							x		x	x			x	x	x		x	x									x								x			x	x	x		20	10	
										x							x	x	x				x			x					x	x		x			x					28	12	
	x				x					x					x			x	x		x										x			x	x	x						27	10	
x					x							x			x		x	x		x	x					x				x	x	x	x									23	5	
			x		x					x									x		x		x		x			x	x													18	5	
					x														x	x		x		x		x	x															21	4	
					x	x							x					x	x	x	x																					19	2	
x					x	x									x	x	x	x																								25	6	
x		x	x	x	x	x	x	x	x	x	x	x	x																													34	12	
x	x																																									30	12	
																																										25	12	

Table 20. Benthic foraminifers, Hole 594, early Miocene.

Age	Planktonic foraminifer zone	Core-Section (level in cm)	Preservation	Radiolarians	*Laticarinata altocamerata*	*Heterolepa kullenbergi*	*Globocassidulina subglobosa*	*Cibicides wuellerstorfi*	Milliolids	*Melonis* cf. *barleeanum*	*Sphaeroidina bulloides*	*Valvulina haeringensis*	*Alabamina haitensis*	*Epistominella* sp.	*Gyroidinoides* spp.	*Oridorsalis umbonatus*	*Bolivinopsis praelonga*	*Laticarinina halophora*	*Stilostomella lepidula*	*Trifarina angulosa*	*Bulimina striata*	Umbilically reticulate cibicidid
early Miocene	*Globorotalia mayeri*	39-1, 11	F	x	x	x							x		x	x	A	A				
		40-4, 19	F	x		x		x				x	x			x						x
		41,CC	F	x				x					x						x			
		42,CC	P	x	x														x			
		43,CC	F	x		x	x	x			x				x	x			x			
		44,CC	M	x		x				x			x			x	x		x			
		45-1, 19	F	x		x		x		x								x				
	G. peripheroronda	46,CC	F	x		x													x			
		47,CC	F	x			x	x								x				x	x	
		48,CC	P	x													x					
		49,CC	M	x	x	x		x		x			x		x		x			x	x	
	G. miozea	50,CC	M	x		x				x			x			x	x					
		51,CC	M	x	x	x	x	x		x		x	x			x	x		x	x	x	x
	G. zealandica	52,CC	M	x		x				x			x			x	x			x	x	x
		53,CC	F	x	x	x	x	x	x	x	x	x	x	x	x	x	x	x	x	x	x	

Table 21. Benthic foraminifers, Hole 594, middle Miocene.

Age	Planktonic foraminifer zone	Core-Section (level in cm)	Preservation	Radiolarians	*Heterolepa kullenbergi*	*Nodosaria consobrina*	*Oridorsalis umbonatus*	*Hopkinsina mioindex*	*Cibicidoides* cf. *ungerianus*	*Chrysalogonium equisetiformis*	*Pullenia quinqueloba*	*Martinottiella variabilis*	*Uvigerina auberiana*	*Gyroidinoides altiformis*	*Stilostomella lepidula*	Umbilically reticulate cibicidids	*Textularia lythostrota*	*Pullenia bulloides*	*Alabamina haitiensis*	*Epistominella* sp.	*Bulimina striata*	*Bolivinopsis praelonga*	*Melonis pacificum*	*Cibicidoides trincherasensis*	*Nuttallides umbonifera*	*Cibicidoides* cf. *subhaidingeri*	*Globocassidulina subglobosa*	*Laticarinina bullbrooki*
middle Miocene	*G. conomiozea*	20,CC	P	x	x		x												x			x						
	G. miotumida	21,CC	F	x	x		x														x					x	x	
		23-2	P	x	x		x															x						
		23,CC	M	x	x				x		x	x	x					x	x		x	x					x	
		24,CC	P	x	x		x															x						
		25-1, 19	M	x	x		x	x	x			x							x		x	x					x	x
		25,CC	P	A																								
		26,CC	P	A											x													
		27,CC	P	A																								
		28-5	P	A	x			x				x									x	x						
		28,CC	P	A																								
		29,CC	P	A	x																							
		30-4, 19	P		x			x											x				x					
		30,CC	P										x		x													
		31,CC	P		x																	x						
		33,CC	P		x		x	x					x						x									x
		34-2, 19	P	x	x		x	x		x		x												x				x
		34,CC	P	x	x								A									x						
		35,CC	P	x	x								x						x			x						
		36-3, 19	F	x		x	x	x	x			x						x						x	x			
		36,CC	F	A	x		x	x					x						x			x			A	x	x	x
		37-1, 19	F		A		x	x	x	x		x	x			x			x	x	x	x			A		x	x
		37,CC	F	A	x			x					x		x			x	x		x			x	x	x	x	x
		38-3, 19	P		A	x	x	x	x	x	x	x	x	x	x	x	x	x	x	x	x	x	x	x				

Table 20. (Continued).

Eggerella bradyi	Brizalina silvestrina	Martinottiella communis	Pleurostomella alternans	Laticarinina bullbrooki	Cibicidoides cicatricosus	Hopkinsina mioindex	Cibicidoides cf. pseudoungerianus	Karreriella bradyi	Stilostomella insecta	Lenticulina spp.	Sigmoilopsis schlumbergeri	Favocassidulina fava	Nuttallides umbonifera	Cassidulina crassa	Pullenia bulloides	Cyclammina sp.	Stilostomella subspinosa	Cibicidoides cf. cicatricosus	Scalloped cibicidid	Cibicidoides tuxpamensis	Uvigerina proboscidea	Cibicidoides trincherasensis	Pullenia quinqueloba	Uvigerina spinulosa	Bulimina truncana	Anomalinoides globulosa	Pullenia coryelli	Anomalinoides semicribrata	Karreriella baccata	Uvigerina	Brizalina
									x				x		x																x
					x						x		A										x			x	x				
		x											A																		
														x																	
											x	x						x													x
x									x				x		x															x	
						x																x	x				x	x	x		
																										x					
x						x			x				x											x	x						
																								x							
		x		x			x	x			x		x		x	x	x	x	x	x	x	x	x								
				x								x	x	x	x																
x		x		x	x	x	x	x	x	x	x																				
x	x	x	x	x																											

Table 21. (Continued).

Cibicidoides bradyi	Martinottiella communis	Stilostomella pomuligera	Heterolepa rugosa	Rectuvigerina ongleyi	Cibicides wuellerstorfi	Bulimina aculeata	Eggerella bradyi	Laticarinina altocamerata	Sigmoilopsis schlumbergeri	Bulimina truncana	Textularia agglutinans	Chrysalogonium equisetiformis	Cassidulina crassa	Trifarina angulosa	Brizalina reticulata	Holmanella sp.	Laticarinina halophora	Sphaeroidina bulloides	Rotalia translucens	Anomalinoides globulosa	Cibicidoides cicatricosa	Pleurostomella alternans	Textularia cf. baccata	Uvigerina striata	Uvigerina proboscidea	Uvigerina asperula	Miliolids	Uvigerina pigmaea	Chrysalogonium equisetiformis	Brizalina silvestrina	Uvigerina hispida	Uvigerina hispido-costata	Trifarina bradyi	Cibicides cf. lobatulus	Hoeglundina elegans	Melonis barleeanum	Siphonodosaria insecta
		x						x	x								x	x									x	x			x					x	x
x								x	x						x		x								x				x	x		x	x	x	x		
					x									x														x	x								
		x	x	x					x						x					x					x		x	x		x	x						
					x									x														x	x								
x										x							x				x	x	x	x	x	x	x	x									
															x					x																	
														x																							
							x								x																						
														x																							
															x		x																				
								x										x	x																		
									x						x																						
		x							x						x																						
								x								x	x																				
	x														x																						
									x							x																					
x							x				x		x	x	x																						
							x	x	x	x	x	x																									
x	x	x	x	x	x	x																															

Table 22. Benthic foraminifers, Hole 594, Pliocene.

Age	Planktonic foraminifer zone	Core-Section (level in cm)	Preservation	Radiolarians	*Heterolepa rugosa*	*Stilostomella pomuligera*	*Textularia lythostrota*	*Stilostomella lepidula*	*Uvigerina interrupta-costata*	*Pullenia bulloides*	*Oridorsalis umbonatus*	*Cibicides wuellerstorfi*	*Cibicidoides* cf. *ungerianus*	*Laticarinina bullbrooki*	*Gyroidina* sp. 1	*Martinottiella communis*	*Uvigerina hispido-costata*	*Planulina* sp. 2	*Bulimina striata*	*Alabamina haitiensis*	*Sphaeroidina bulloides*	*Uvigerina proboscidea*	*Sigmoilopsis schlumbergeri*	*Nodosaria consobrina*	*Karreriella bradyi*	*Gyroidina soldanii*	*Hopkinsina mioindex*	*Nodosaria stiliformis*	*Heterolepa kullenbergi*	*Pyrgo* spp.	*Pullenia quinqueloba*	*Trifarina angulosa*	*Brizalina silvestrina*	*Uvigerina auberiana*	*Cibicidoides bradyi*	*Pullenia quadriloba*
late Pliocene	*G. inflata*	4-3, 19	M				x			x	x												x									x				
		4,CC	M				x			x	x												x		x				x	x		x			x	
		5-7, 19	M						A		x									x						x			x							
		5,CC	F							x	x	x					x			x									x	x	x	x	x			
		6-1, 19	M								x	x								x			x							x	x					x
		6,CC	F	x						x																						x				x
		7,CC	M	x						x	x	x					x						x						x							
		8-1, 19	M	x							x	x																								
		8,CC	M	x								x																		x	x	x			x	
	G. puncticulata	9-3, 19	M				x					x																	x							
		9,CC	M				x				x	x					x												x						x	x
		10-1, 19	P	x						x																			x							
		10,CC	F	x						x	x																		x				x			
	G. sphericomiozea	11-3, 19	F								A	x											x			x						x				
		11,CC	M	x				x			x			x			x						x						x	x		x				
		12-2, 19	F	x						x	x	x											x	x		x			x	x		x				
		12,CC	F	x						x							x												x							
		13-4, 19	M	x				x				A												x				x		x						x
		13,CC	P	x				x		x	x						x												x							
		14-3, 19	P	x							x																									
		14,CC	P	x				x			x																									x
		15-7, 19	P	x							x						x		x				A						x							
		15,CC	P	x				x									x																			
		16-1, 19	P	x													x						A													
early		16,CC	P	x				x		x	x						x						x						x					x		
		18-1, 19	F				x				x	x	x	x			A						x								x					
		18,CC	G	x		x		x		x	x		x						x	x	x						x		x	x	x	x	x	x	x	x
		19-1, 19	F							x	x	x	x	x	x	x	x	x	x	x	x	x	x	x	x	x	x	x								
		19,CC	P		x	x	x	x	x	x	x	x																								

Table 22. (Continued).

Miliolids	*Stilostomella insecta*	*Melonis barleeanum*	*Pyrgo serrata*	*Karreriella baccata*	*Lenticulina peregrina*	*Siphotextularia solita*	*Rotalia translucens*	*Pyrgo murrhina*	*Globocassidulina subglobosa*	*Cibicidoides cicatricosus*	*Hoeglundina elegans*	*Brizalina alata*	*Cassidulina crassa*	*Bulimina aculeata*	*Melonis pompilioides*	*Melonis nicobarense*	*Trifarina carinata*	*Brizalina pusilla* (many striae)	*Laticarinina altocamerata*	*Melonis affinis*	*Nodosaria skobina*	*Cassidulina laevigata carinata*	*Trifarina exima*	*Cibicides lobatulus*	*Trifarina bradyi*	*Melonis nicobarense*	*Pleurostomella alternans*	*Anomalinoides globulosa*	*Bulimina truncata*	*Uvigerina dirupta*	*Uvigerina striata*	*Cibicidoides* cf. *io*	*Bolivinita quadrilatera*	*Siphotextularia catenata*	*Sigmavirgulina tortuosa*	*Ehrenbergina pacifica*	*Eggerella bradyi*	*Textularia* sp. 1	*Planulina* cf. *ariminensis*	*Cibicidoides trincherasensis*	*Epistominella exigua*	No. of species (total, 75)	No. of rectilinear (total, 33)	Total agglutinants, 6
		x					x			x	x								x				x			x																12	2	
x			x				x	x	x					x		x	x									x		x	x					x							x	21	5	
							x		x	x																				x									x	x		11	2	
						x	x	x						x								x					x						x				x					18	8	
			x				x		x													x								x								x				13	2	
x			x					x	x			x	x	A								x	x			x	x						x									15	6	
								x		x				x		x						x					x	x	x	x							x					14	6	
										x	x																			x	x					x						7	3	
x									x																		x			x				x	x							11	4	
							x			x												x								x	x											8	3	
			x					x	x		x		x	x		x	x						x							x		x										18	5	
		x	x											A																			x									6	2	
A									A					x		x						x	x				x															11	4	
	x	x	x				x			x	x			x																x		x										14	5	
x						x	x	x	x		x					x	x					x					x			x	x											18	7	
	x										x		x					x				A							x													16	6	
x																x						x	x	x	x	x	x	x														12	5	
	x		x	x						x	x	x							x	x	x																					15	7	
																x		x																								6	2	
											x	x		A	A																											5	2	
											x	x	x																													6	2	
		x										x	x																													8	3	
								x		x																																6	3	
		x							x																																	4	2	
	x						x	x																																		4	2	
x	x	x	x	x	x	x																																				10	5	
																																										16	5	
																																										17	7	
																																										16	8	

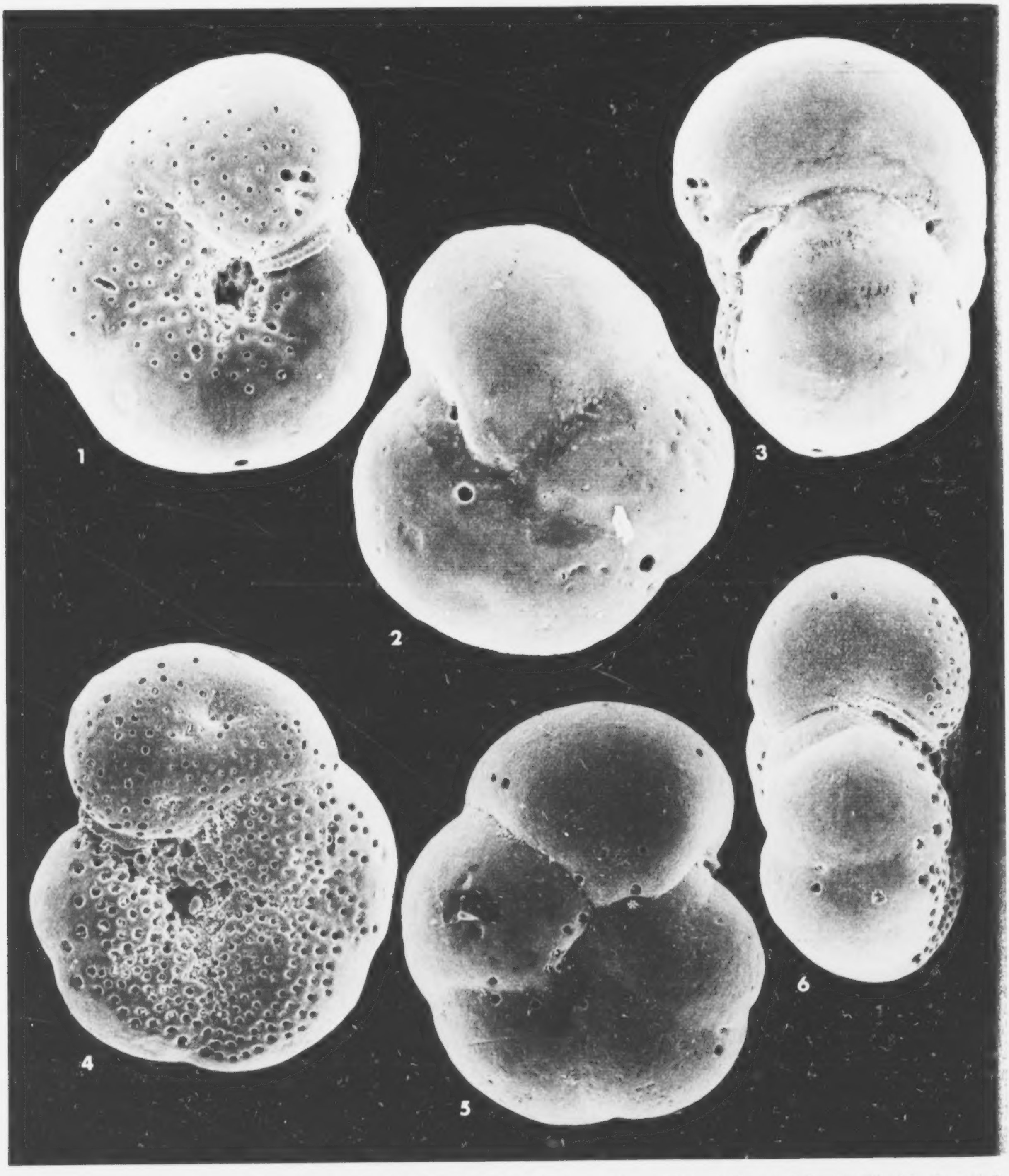

Plate 1. **1–6.** *Anomalinoides semicribrata* (Beckman), (1–3) Sample 590A-5,CC (1, × 330; 2, × 290; 3, × 330); (4–6) Sample 588-16-3, 40 cm (4, 5
× 160; 6, × 150).

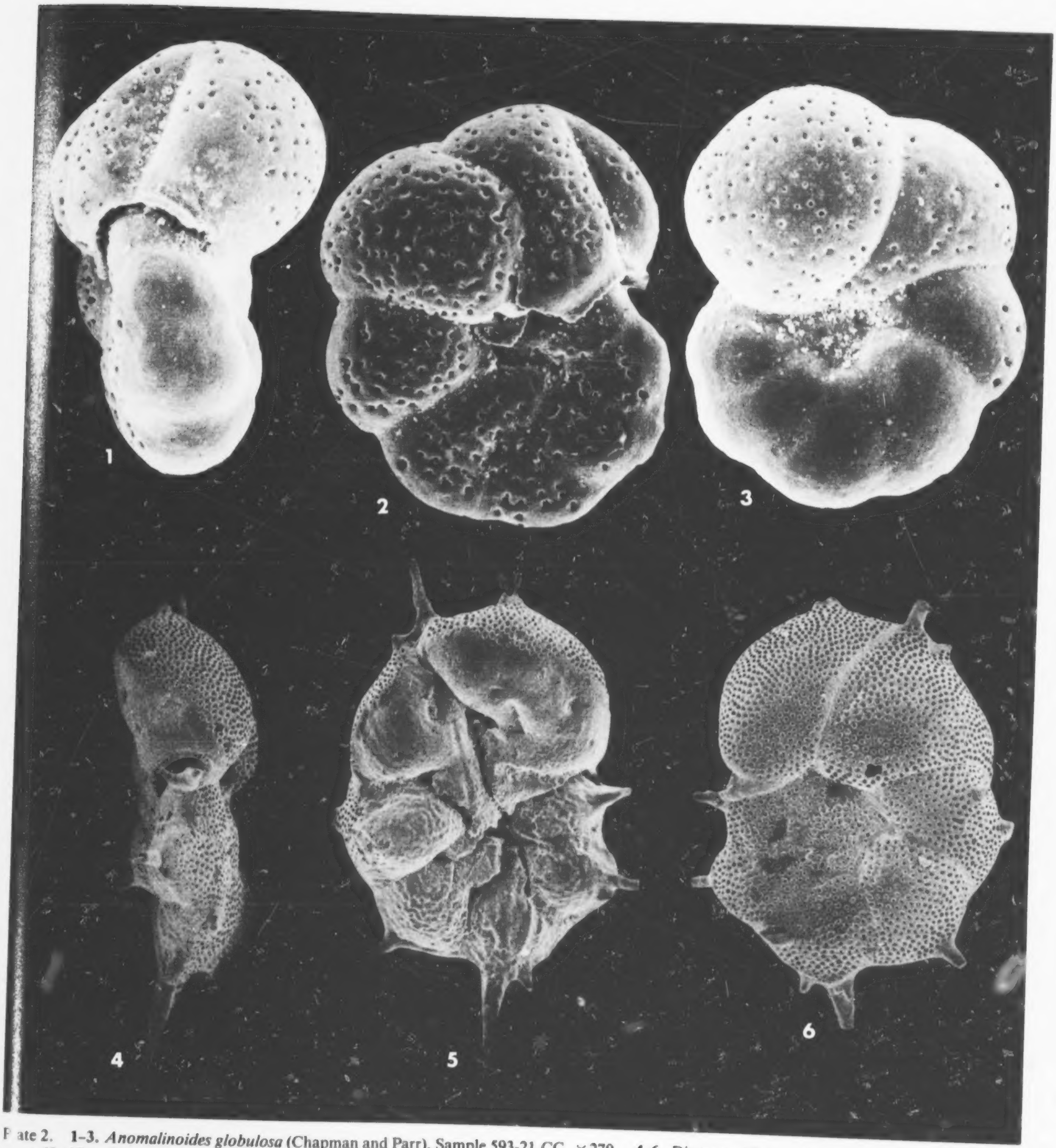

Plate 2. **1–3.** ***Anomalinoides globulosa*** (Chapman and Parr), Sample 593-21,CC, × 270. **4–6.** ***Discanomalina semipunctata*** (Bailey), (4) × 60, (5) × 63, (6) × 58.

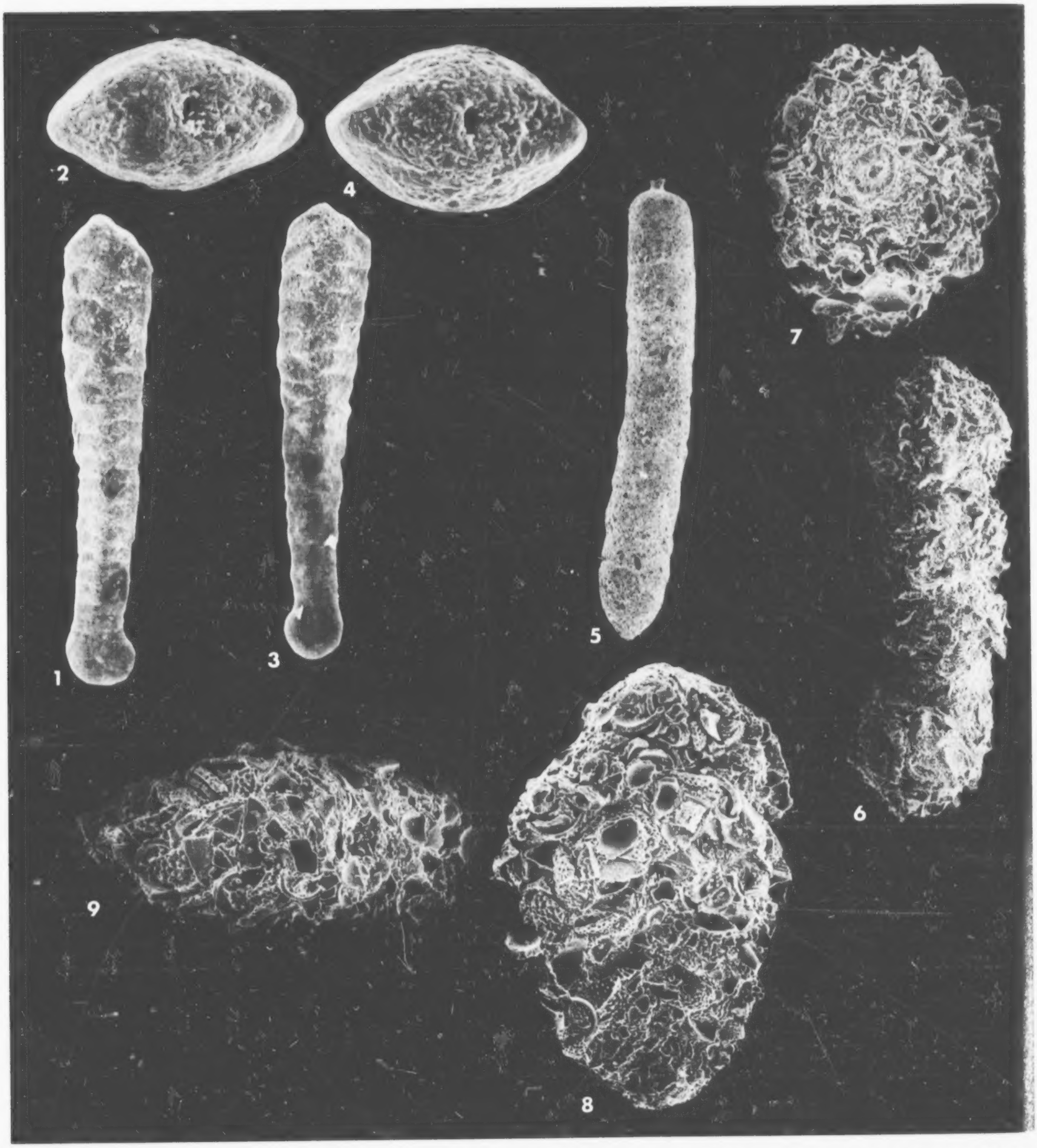

Plate 3. **1–2.** *Bolivinopsis cubensis*, Sample 592-23-2, 19 cm, (1) × 146, (2) × 400. **3–4.** *Bolivinopsis praelonga* (Schwager), Sample 594-30,CC (3) × 101, (4) × 250. **5.** *Martinottiella communis* (d'Orbigny), Sample 590A-6,CC, × 39. **6–7.** *Martinottiella variabilis* (Schwager), Samp 591-16,CC, (6) × 69, (7) × 115. **8–9.** *Textularia lythostrota*, Sample 593-1,C, (8) × 100, (9) × 120.

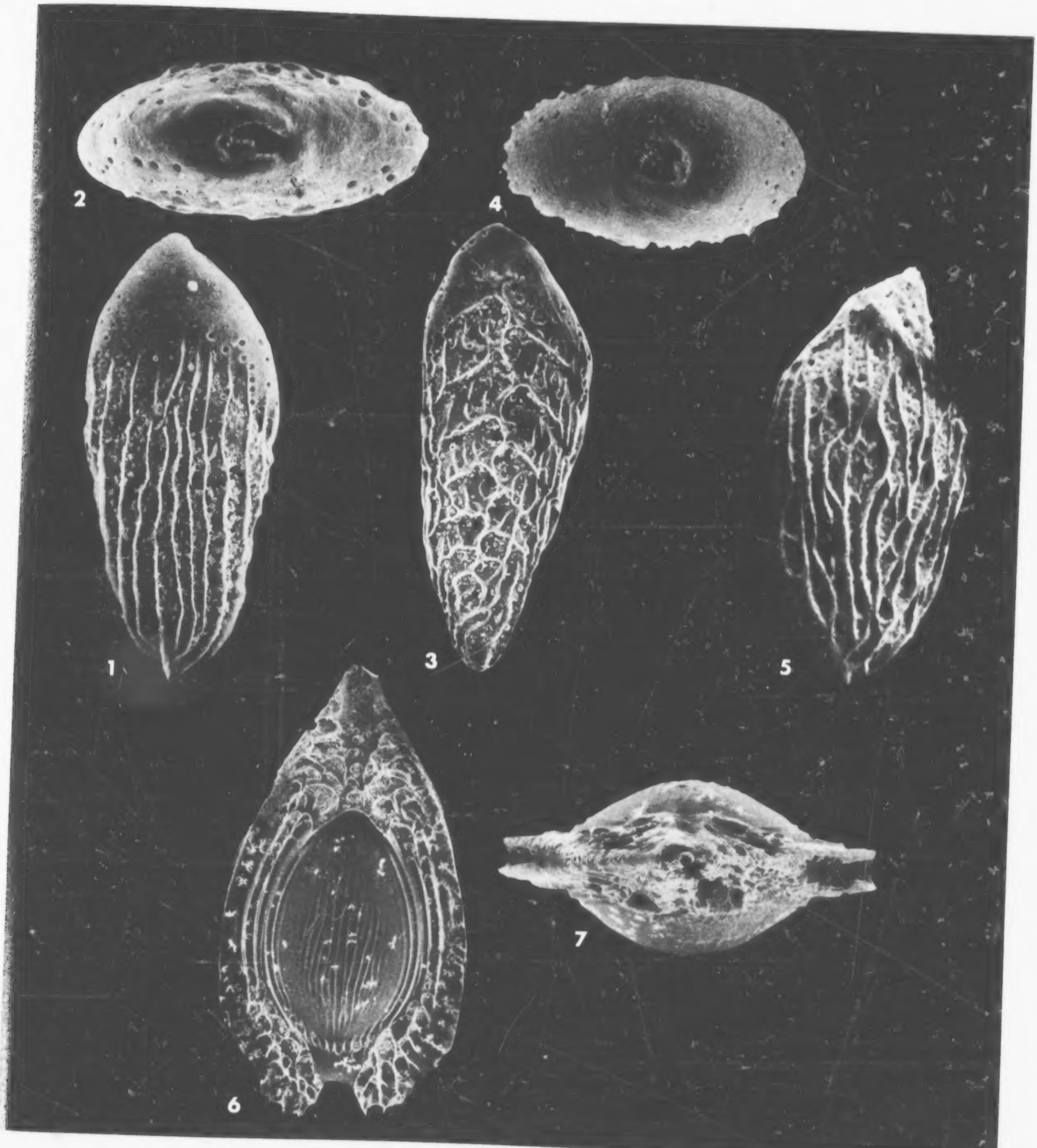

Pla 4. **1–2.** *Brizalina pusilla* (Schwager), Sample 591-12,CC, (1) ×280, (2) ×470. **3–4.** *Brizalina finlayi* (Hornibrook), Sample 593-27,CC, (3) ×220, (4) ×470. **5.** *Brizalina reticulata* (Hantken), Sample 525B-19,CC, ×220. **6–7.** *Fissurina capillosa* Schwager, Sample 591-4,CC, (6) ×101, (7) ×160.

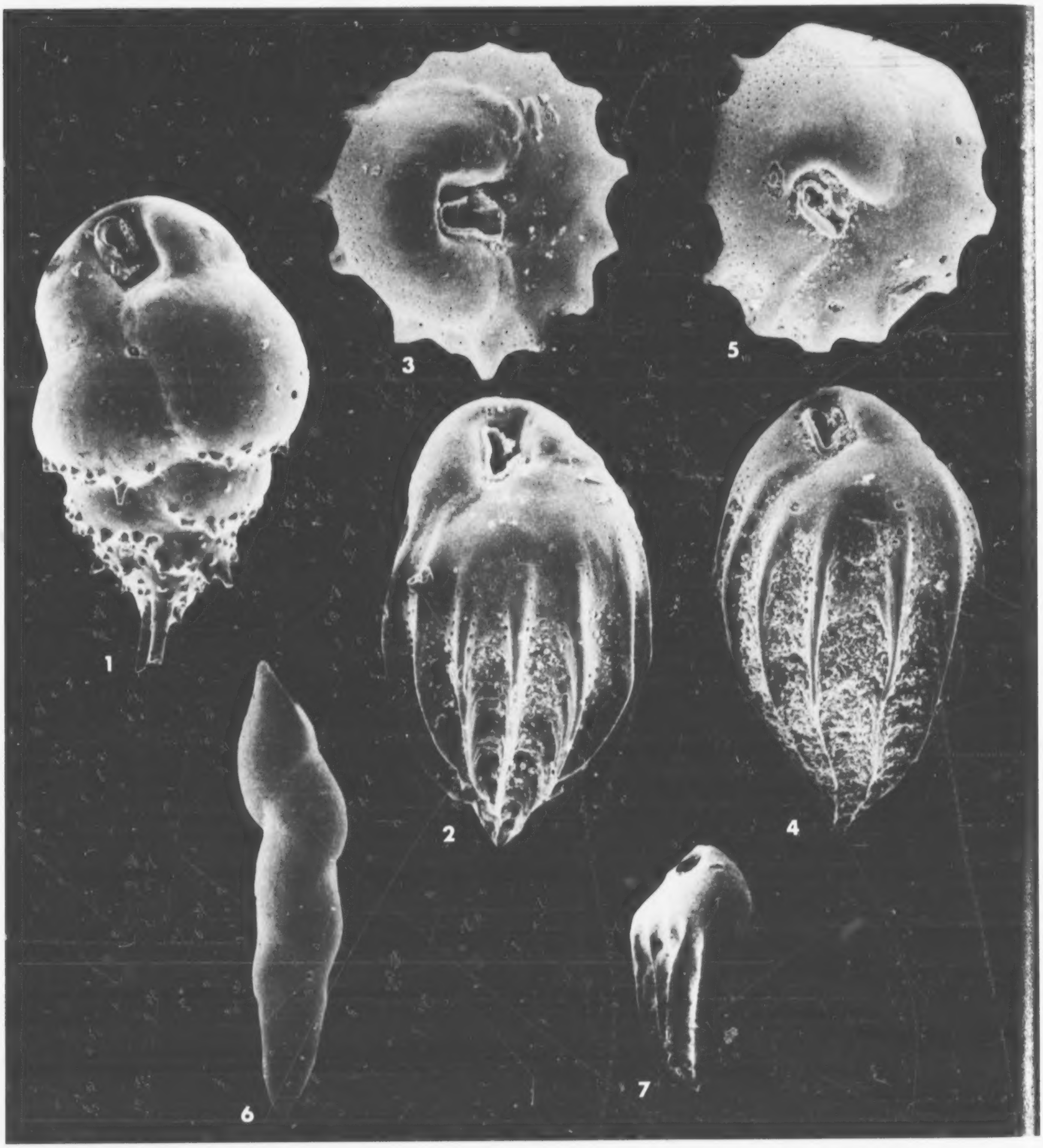

Plate 5. **1.** *Bulimina aculeata* d'Orbigny, Sample 590A-16,CC, × 120. **2-5.** *Bulimina truncana* Guembel, (2-3) Sample 591-16,CC (2, × 230; × 196); (4-5) Sample 591-12,CC (4, × 200; 5, × 230). **6.** *Pleurostomella alternans* Schwager, Sample 590-3,CC, × 66. **7.** *Bulimina alazanen* Nuttall, Sample 526A-41-2, 44 cm, × 110.

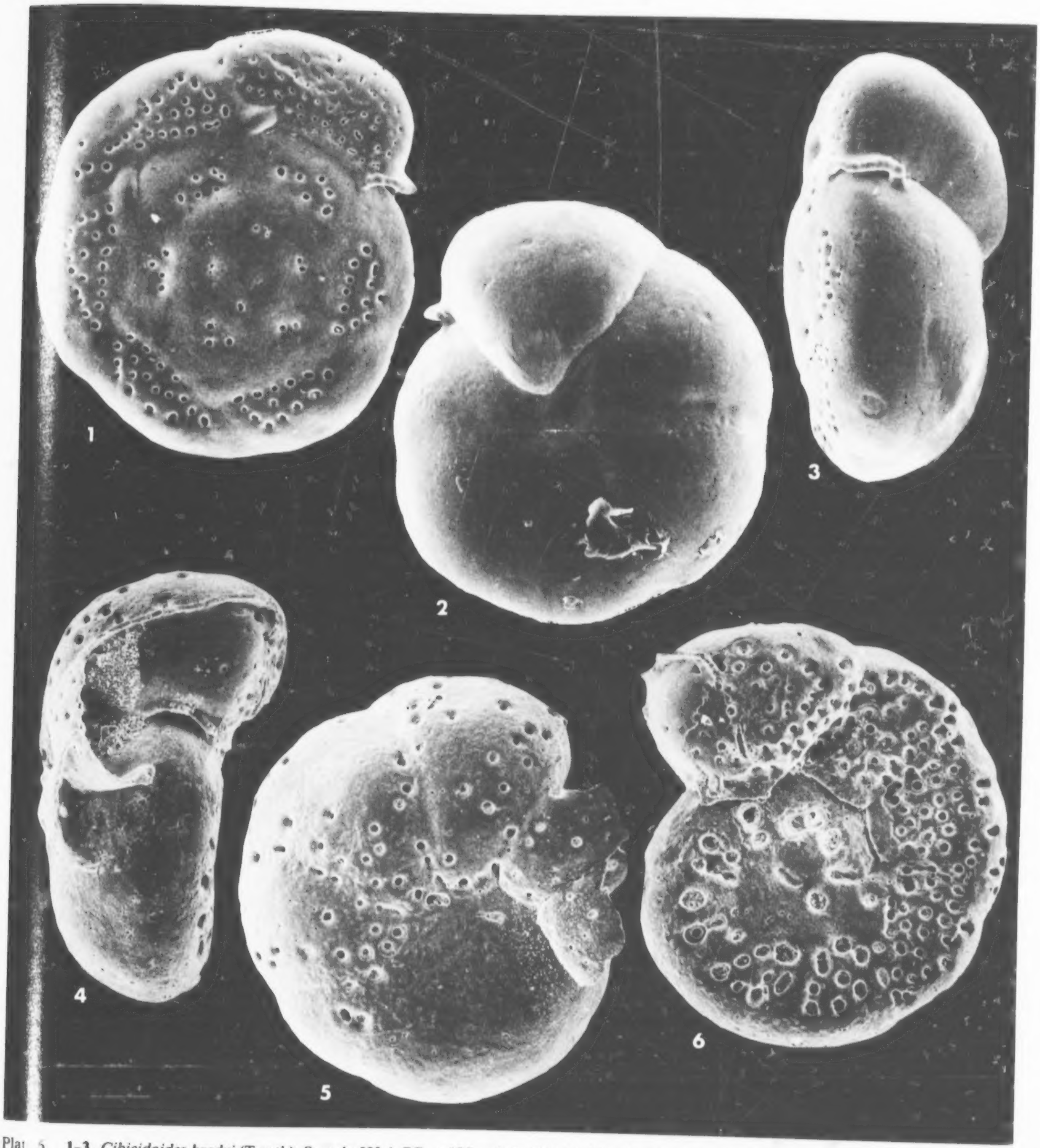

Plate 6. **1–3.** *Cibicidoides bradyi* (Trauth), Sample 593-1,CC, × 195. **4–6.** *Cibicidoides cicatricosus* (Schwager), Sample 589-1,CC, (4, × 142; 5, 6, × 145).

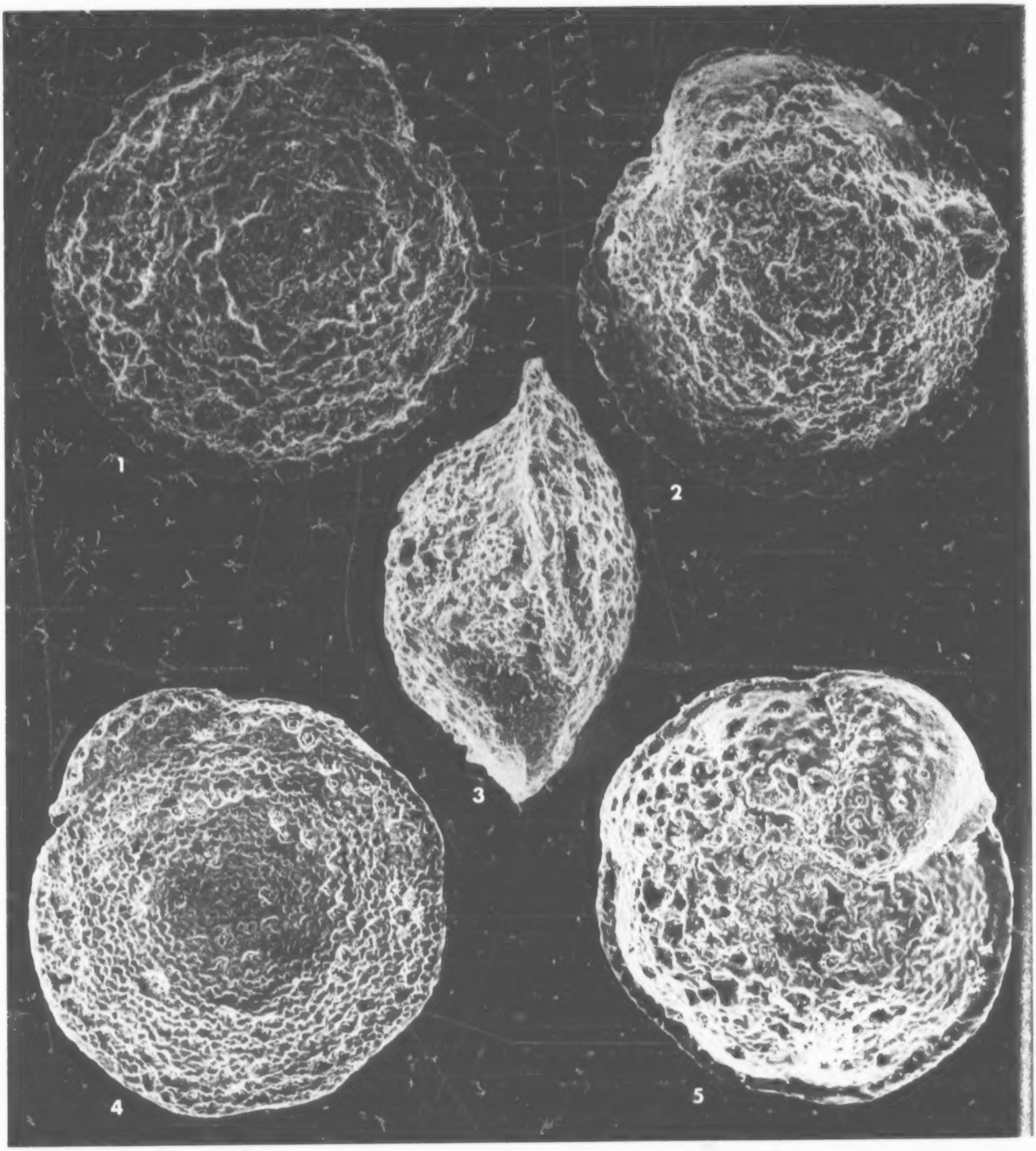

Plate 7. **1–5.** *Cibicidoides parki* (Finlay), (1–3) Sample 548A-18-1, 65 cm, × 180; (4–5) Sample 592-36-3, 92 cm (4, × 140; 5, × 147).

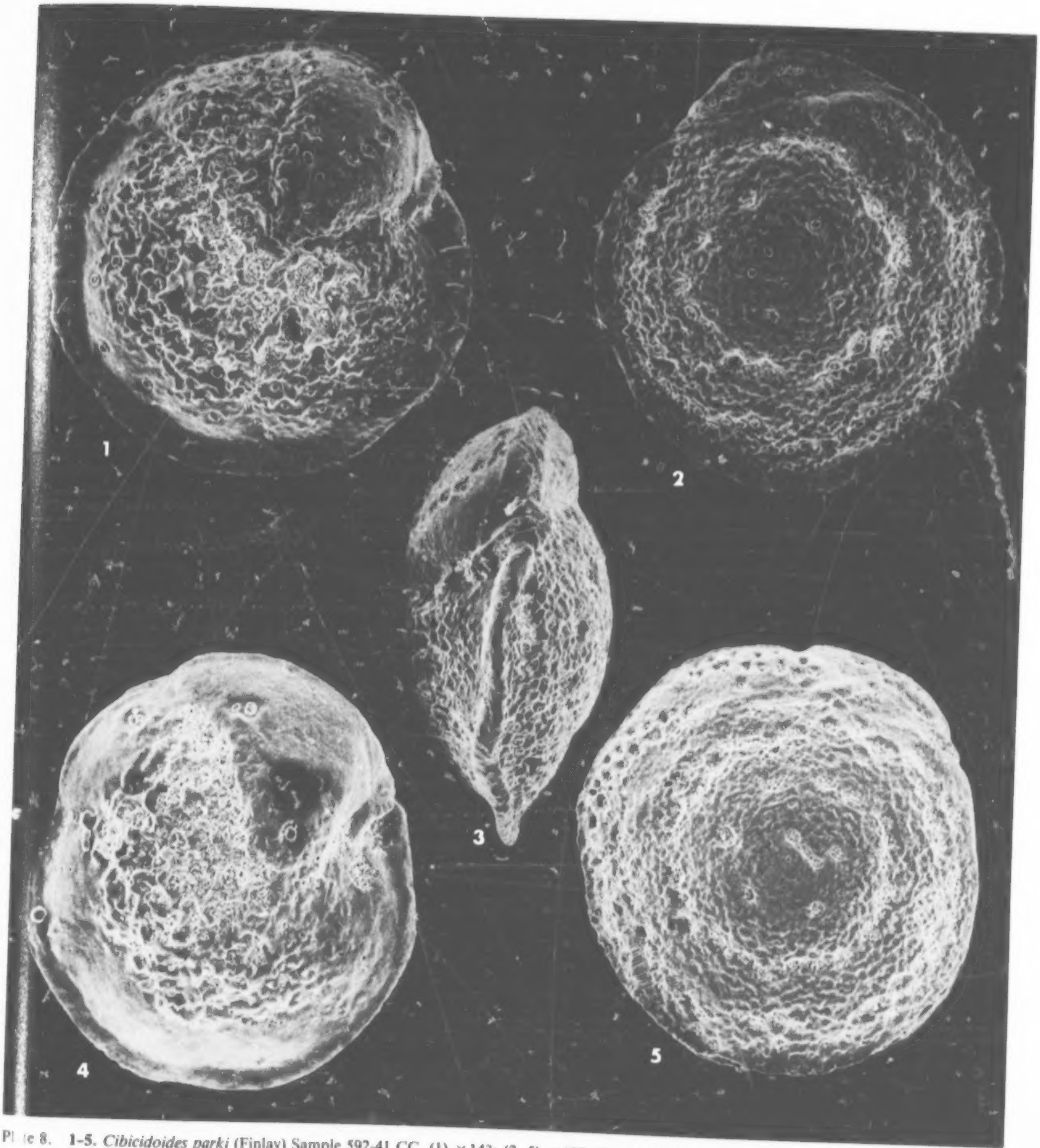

Plate 8. **1-5.** *Cibicidoides parki* (Finlay) Sample 592-41,CC, (1) × 143; (2, 5) × 137; (3) × 140; (4) × 180.

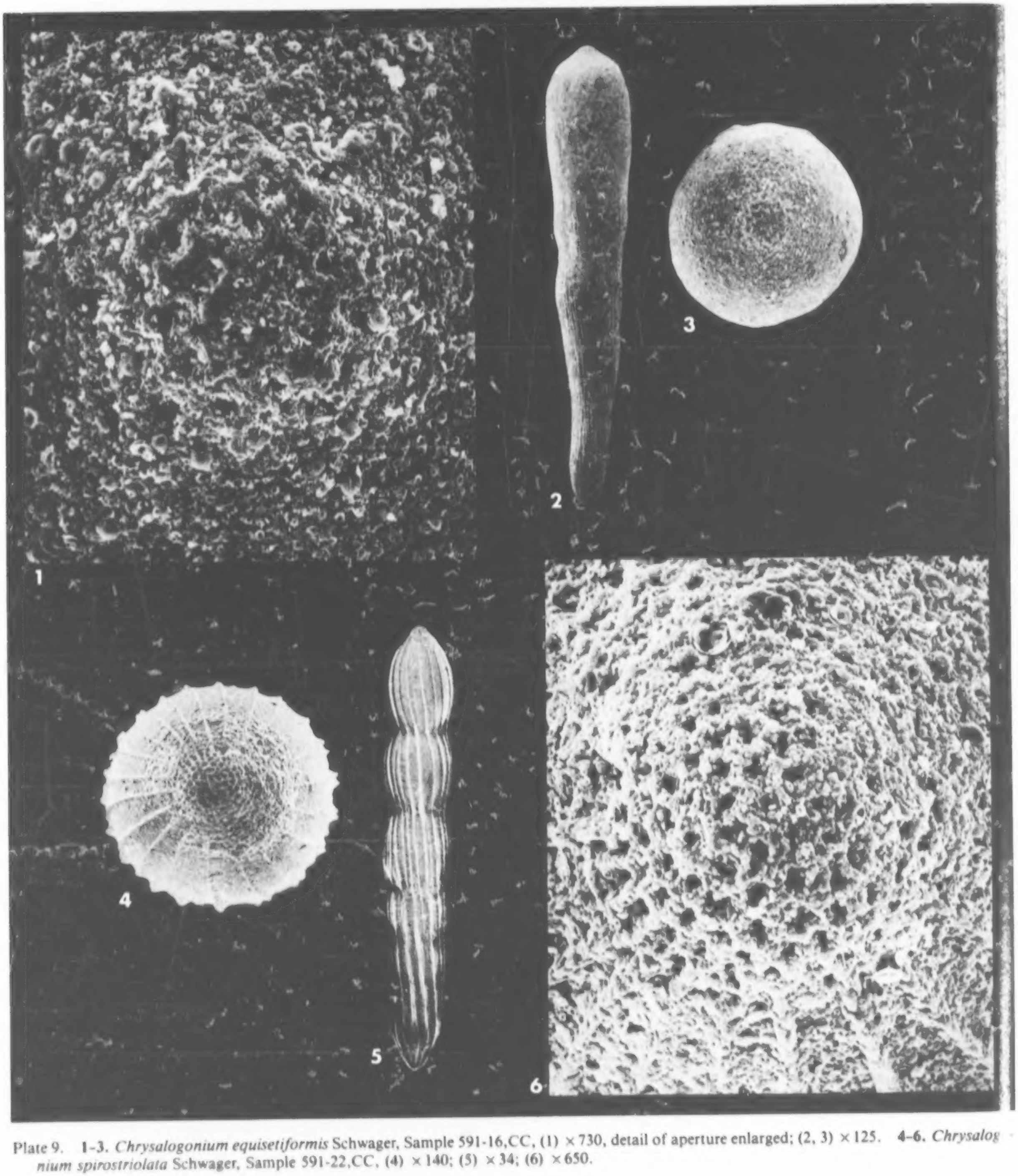

Plate 9. **1-3.** *Chrysalogonium equisetiformis* Schwager, Sample 591-16,CC, (1) × 730, detail of aperture enlarged; (2, 3) × 125. **4-6.** *Chrysalog nium spirostriolata* Schwager, Sample 591-22,CC, (4) × 140; (5) × 34; (6) × 650.

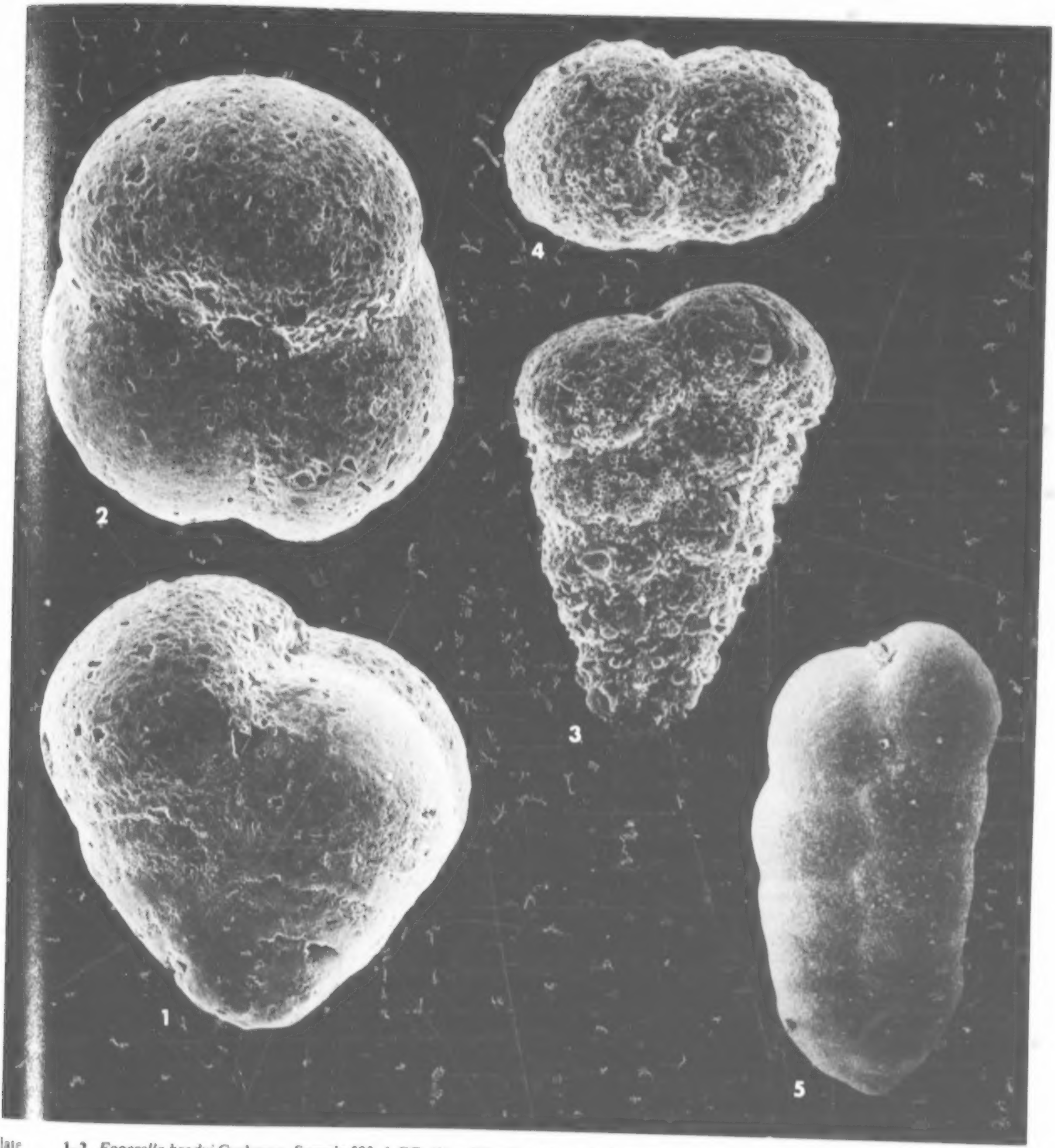

Plate 1–2. *Eggerella bradyi* Cushman, Sample 593, 1,CC, (1) × 220; (2) × 190. 3–4. *Textularia agglutinans* d'Orbigny, Sample 591-12,CC, (3) × 5; (4) × 300. 5. *Karreriella bradyi* Cushman, Sample 591-7,CC, × 90.

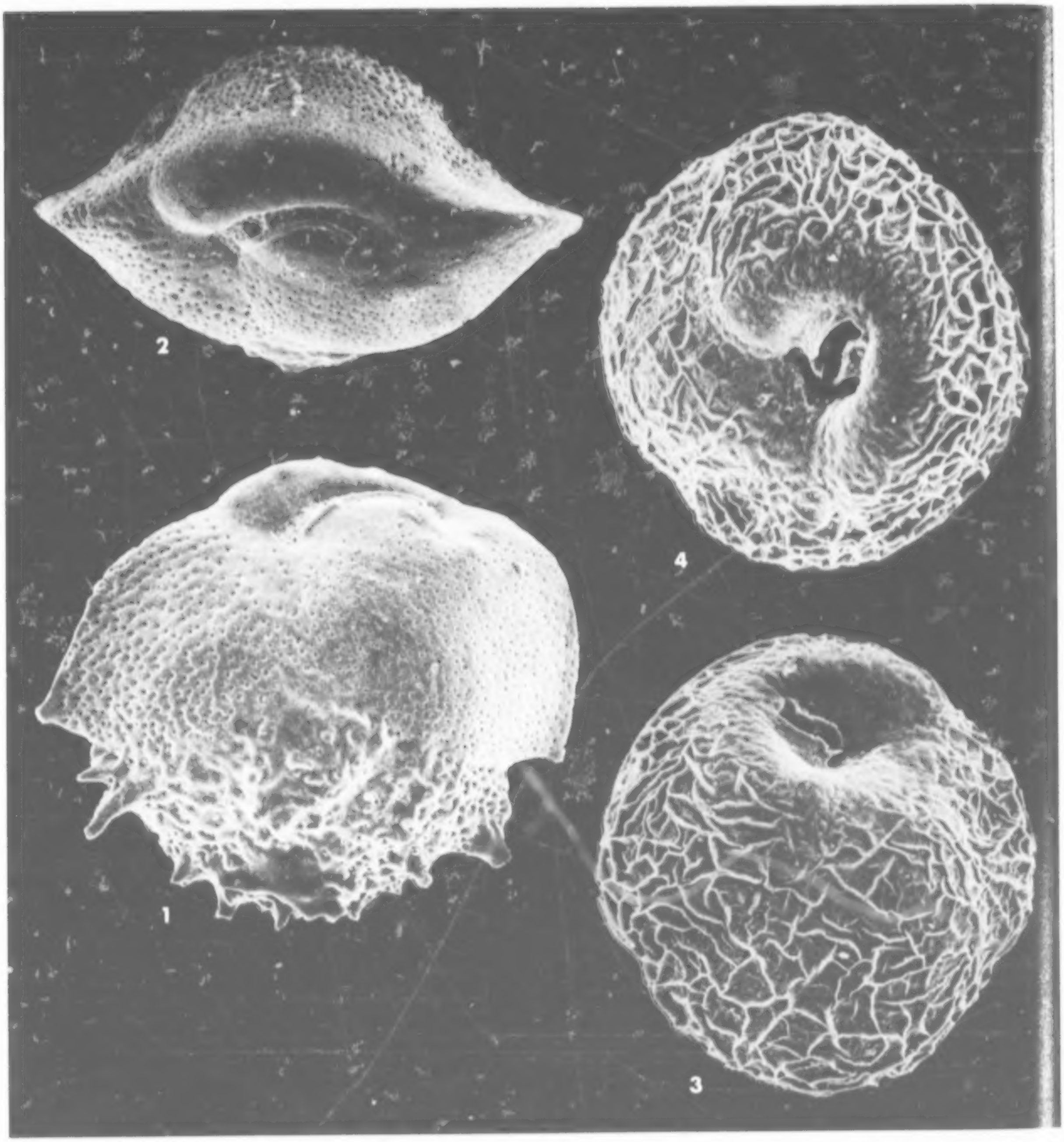

Plate 11. 1–2. *Ehrenbergina marwicki* Finlay, Sample 590-16,CC, (1) × 290; (2) × 280. 3–4. *Globocassidulina arata* (Finlay), Sample 590-3,C (3) × 250; (4) × 200.

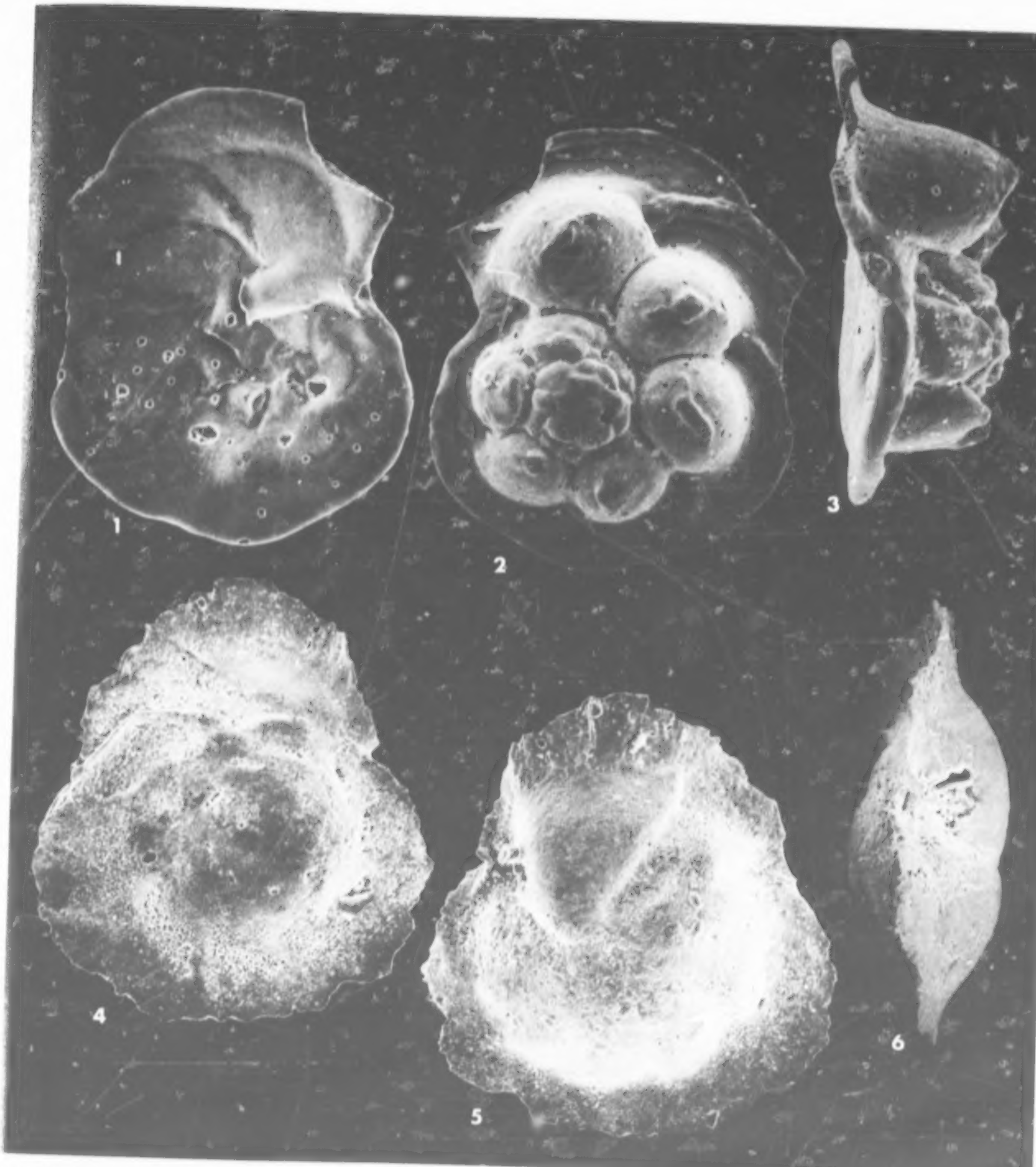

Plate 12. **1–3.** *Laticarinina altocamerata* Chapman and Parr, Sample 590A-1,CC, (1) × 155; (2) × 155; (3) × 163. **4–6.** *Osangularia culter* (Parker and Jones), Sample 593-21,CC, (1) × 110; (2, 3) × 125.

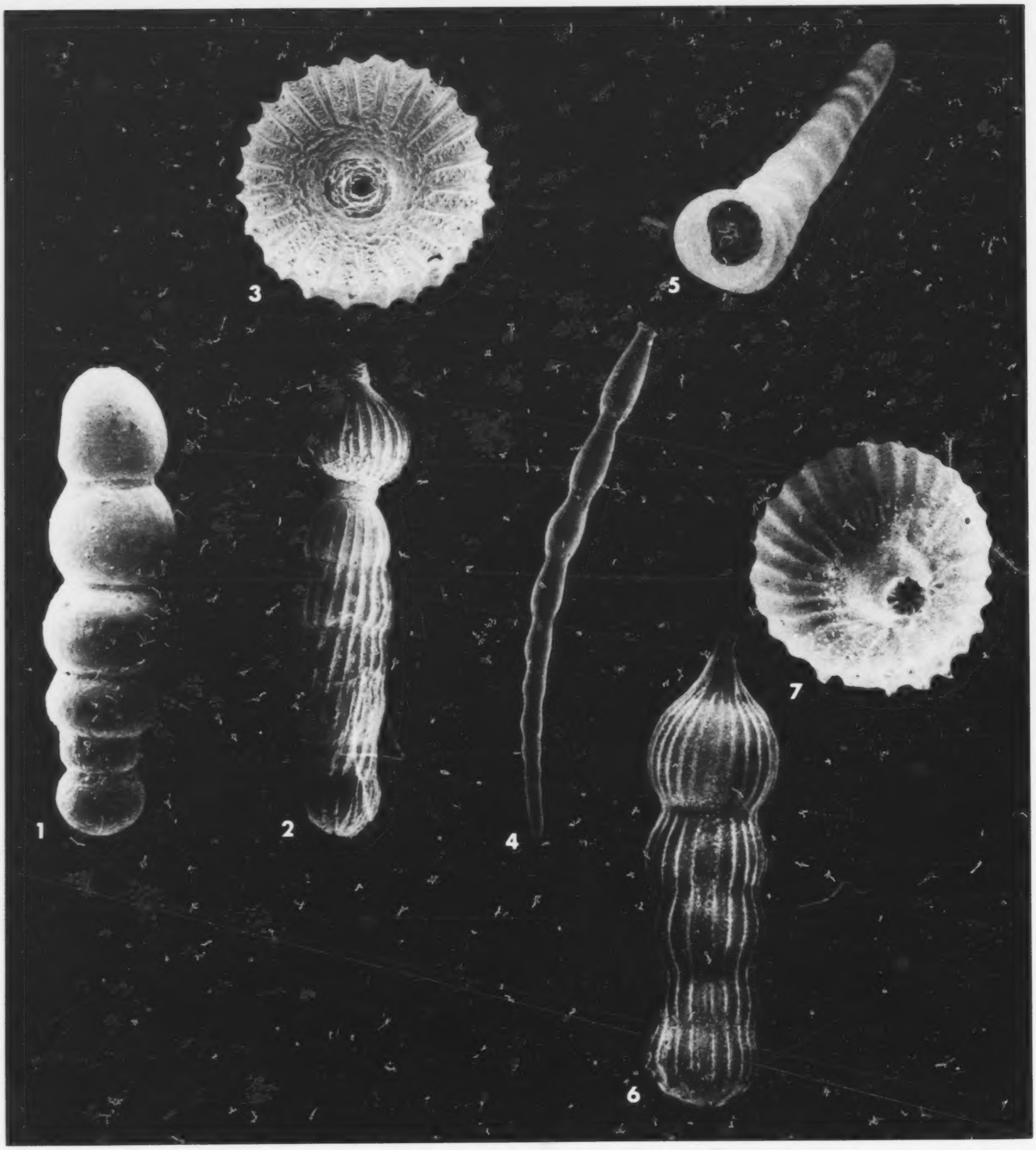

Plate 13. **1.** *Orthomorphina koina* Schwager, Sample 591-7,CC, ×95. **2–3.** *Nodosaria scalaris* Schwager, Sample 591-16,CC, (2) ×29; (3) ×85 **4–5.** *Stilostomella consobrina* (d'Orbigny), Sample 591-17,CC, (4) ×40; (5) ×152. **6–7.** *Nodosaria costornata* Schwager, sample 591-22,CC (6, ×45; 7, ×120).

READEX FICHE best copy available

pages tightly bound

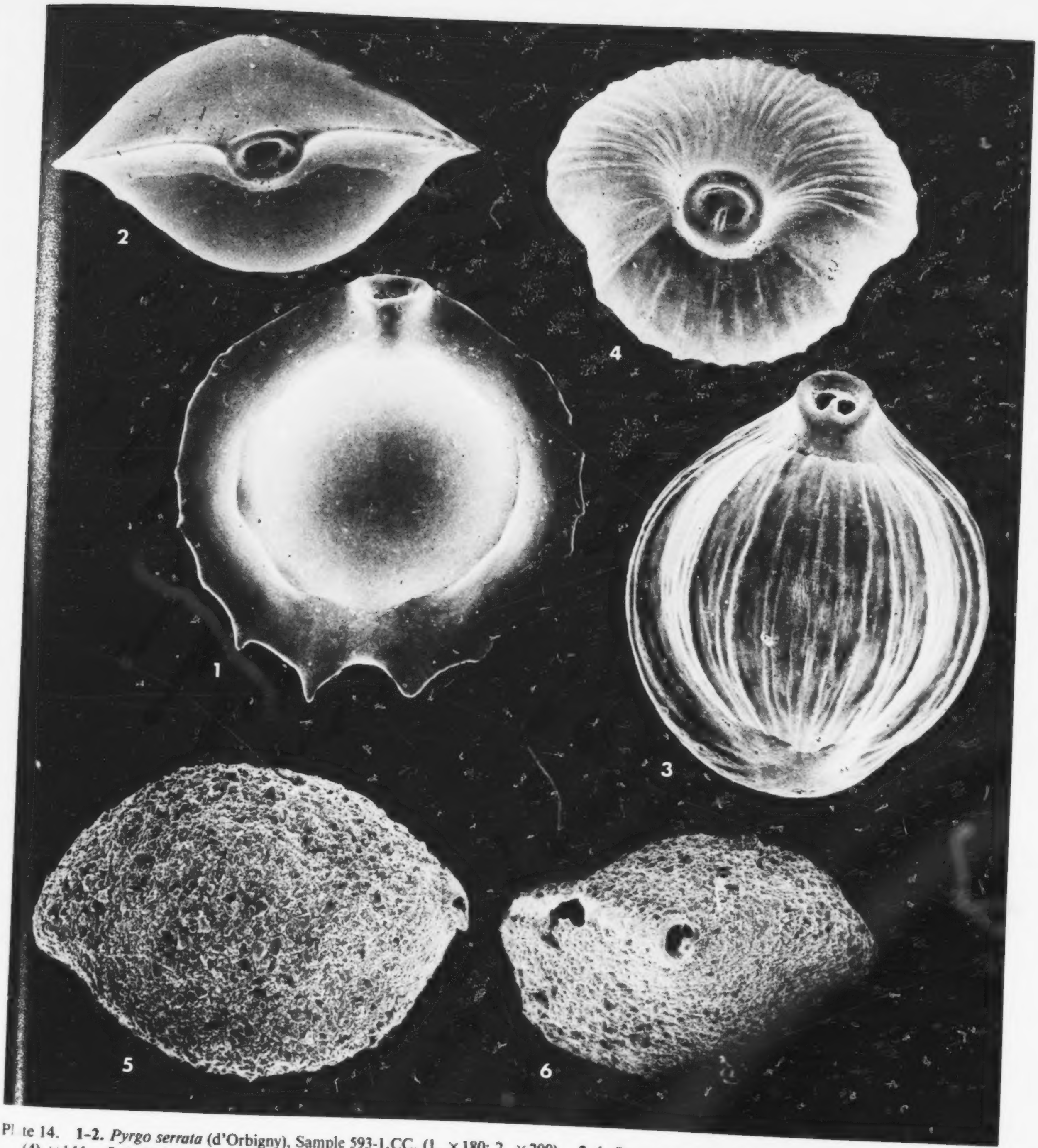

Plate 14. **1–2.** *Pyrgo serrata* (d'Orbigny), Sample 593-1,CC, (1, × 180; 2, × 200). **3–4.** *Pyrgo comata* (Schwager), Sample 593-1,CC, (3) × 143; (4) × 144. **5–6.** *Sigmoilopsis schlumbergeri* (Silvestri), Sample 590-1,CC, × 120.

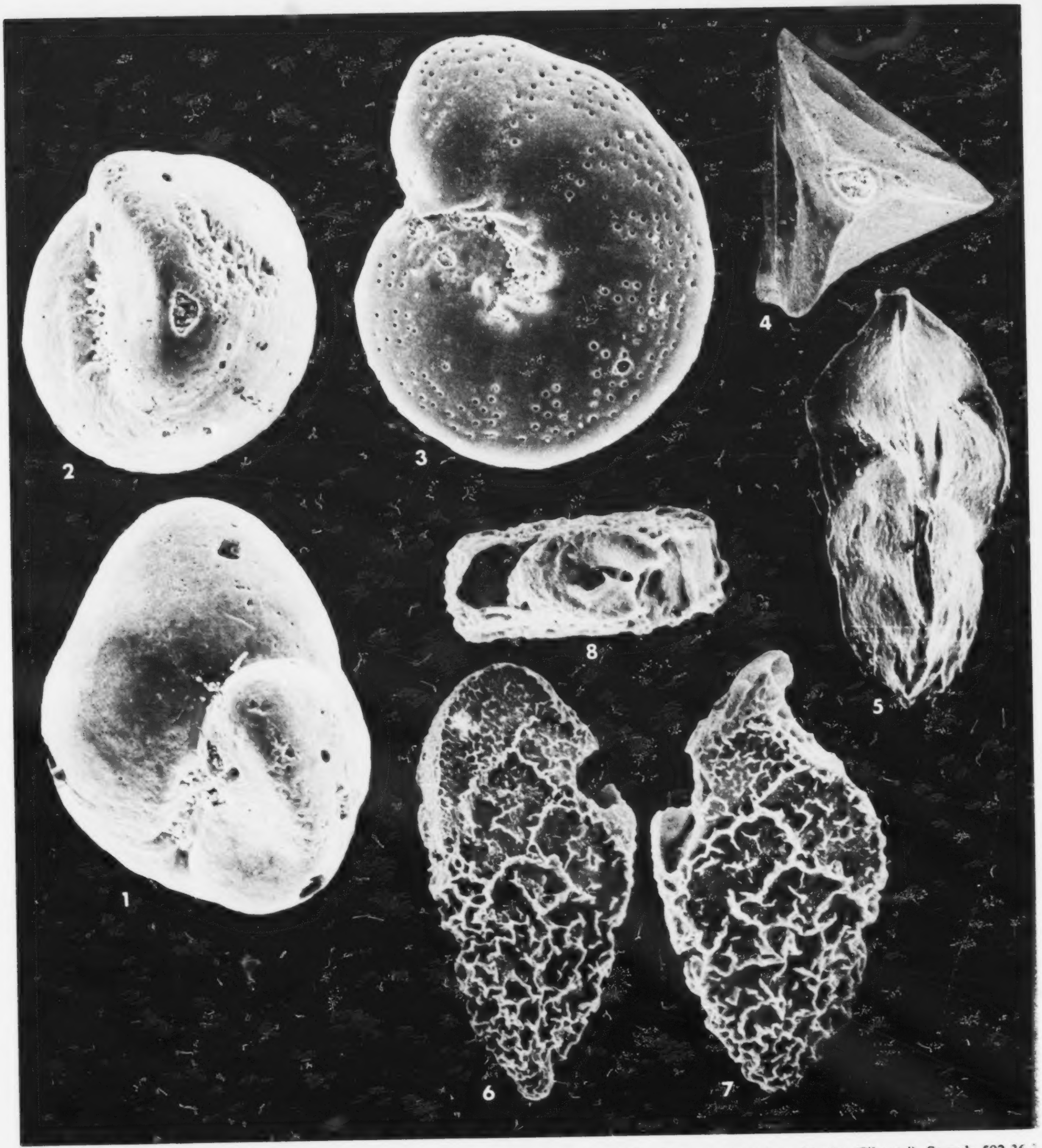

Plate 15. **1–2.** *Rotaliatina sulcigera* Finlay, Sample 592-36-3, 92 cm, (1) × 260; (2) × 290. **3.** *Anomalinoides orbiculus* (Silvestri), Sample 592-36- 92 cm, × 200. **4–5.** *Trifarina costornata* (Hornibrook), Sample 590A-16,CC, (4) × 270; (5) × 400. **6–8.** *Bolivinita* sp., Sample 594-9-3, 90 cm (6–7) × 350; (8) × 410.

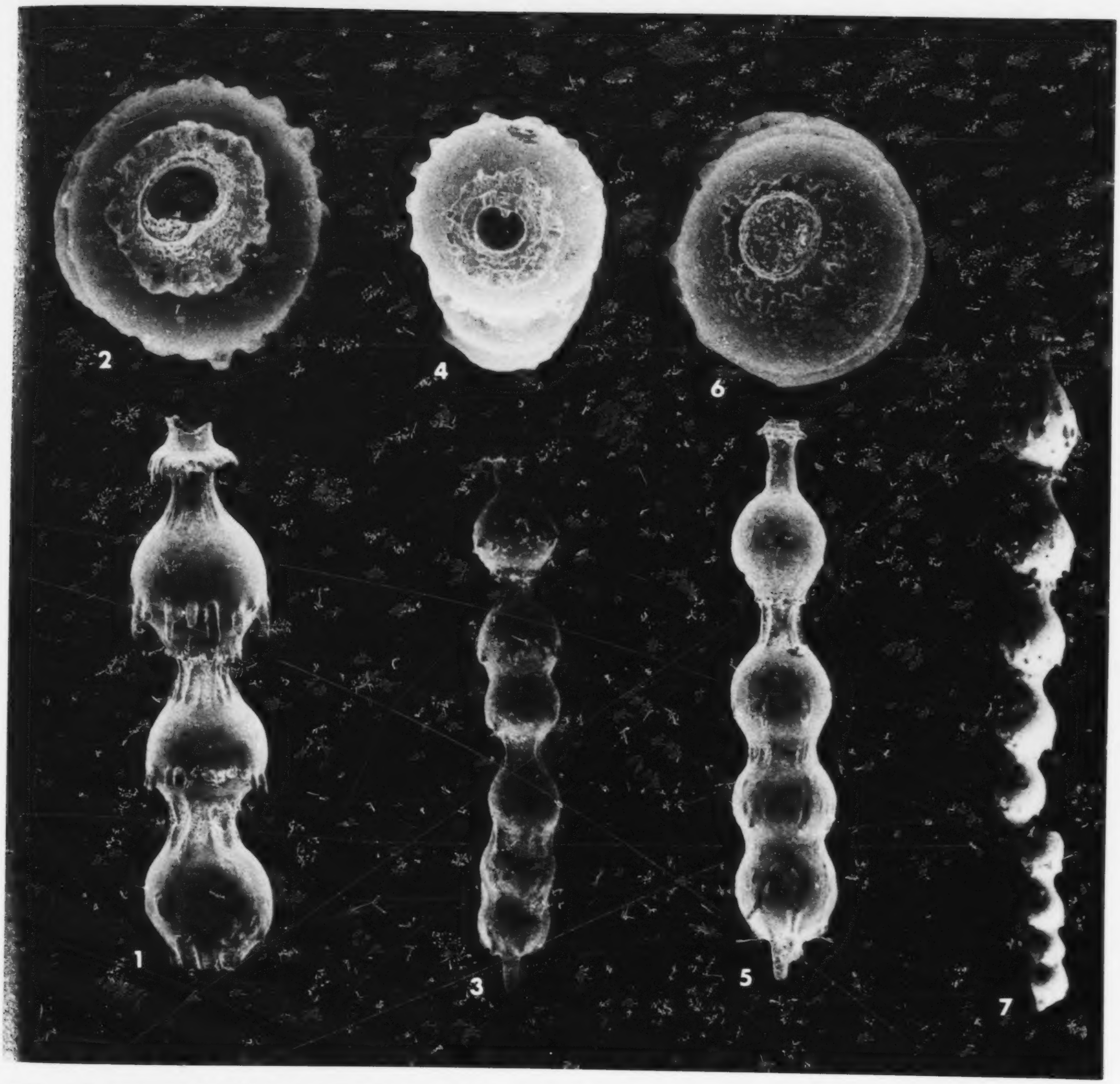

Pl 16. **1–2.** *Stilostomella lepidula* Schwager, Sample 591-24,CC, (1) × 54; (2) × 115. **3–4.** *Stilostomella lepidula* trans. *Siphonodosaria insecta* Schwager), Sample 591-29,CC, (3) × 49; (4) × 115. **5–6.** *Siphonodosaria insecta* (Schwager), Sample 591-24,CC, (5) × 69; (6) × 175. **7.** *Sti- stomella basicarinata* Hornibrook, Sample 529-19,CC, × 100.

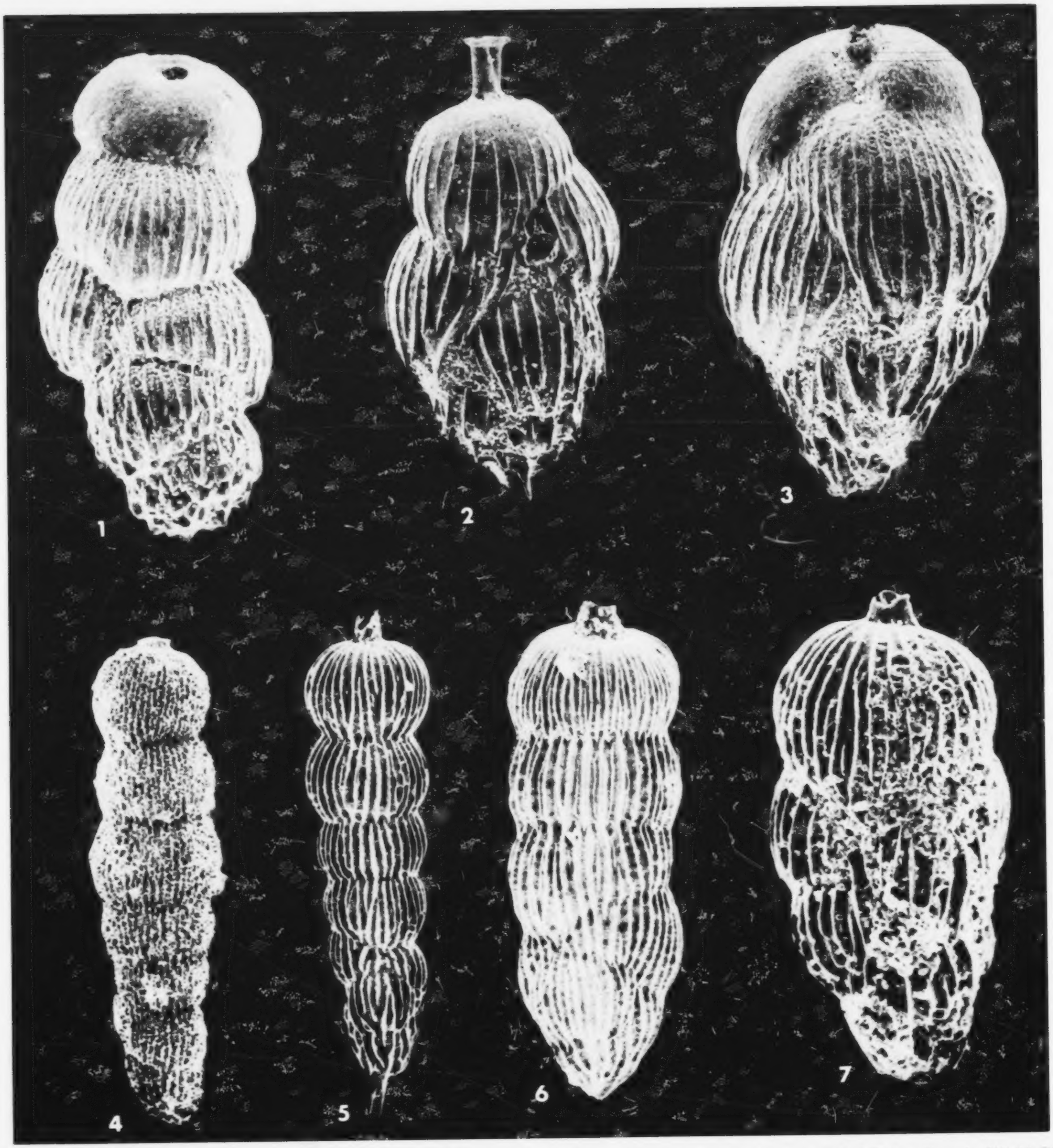

Plate 17. **1, 7.** *Rectuvigerina prisca* Finlay, Sample 592-36-3, 92 cm, (1) ×136; (7) ×270. **2.** *Rectuvigerina ongleyi* Finlay, Sample 592-24,CC ×127. **3.** *Uvigerina spinulosa* Hadley, Sample 590B-21,CC, ×150. **4.** *Rectuvigerina tasmana* n. sp., Sample 587-11,CC, ×108. **5.** *Rectuvigerina striata* Schwager, Car Nicobar, CM 1, ×132. **6.** *Rectuvigerina postprandia* Finlay, Site 593-24,CC, ×163.

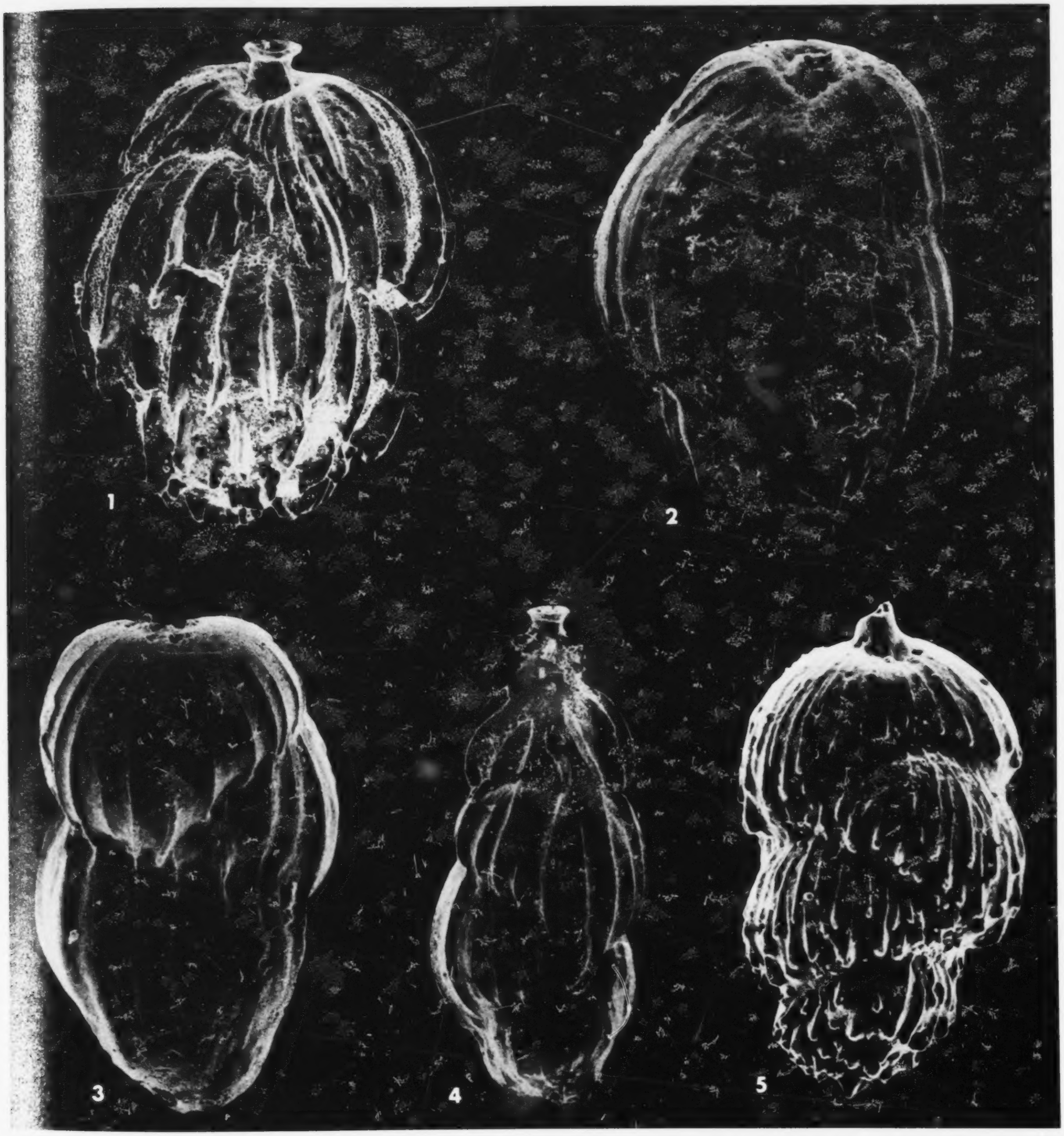

e 18. **1.** *Uvigerina hornibrooki* Boersma, Sample 590A-12,CC, ×167. **2.** *Uvigerina eocaena* Guembel × *Uvigerina mexicana* Nuttall, Sample 93-58-2, 19 cm, ×175. **3.** *Uvigerina picki* Finlay, Sample 590A-12,CC, ×140. **4.** *Uvigerina tasmana* Boersma, Sample 588-6,CC, ×144. 5. *Rectuvigerina spinea* (Bermudez), Sample 590B-37,CC, ×180.

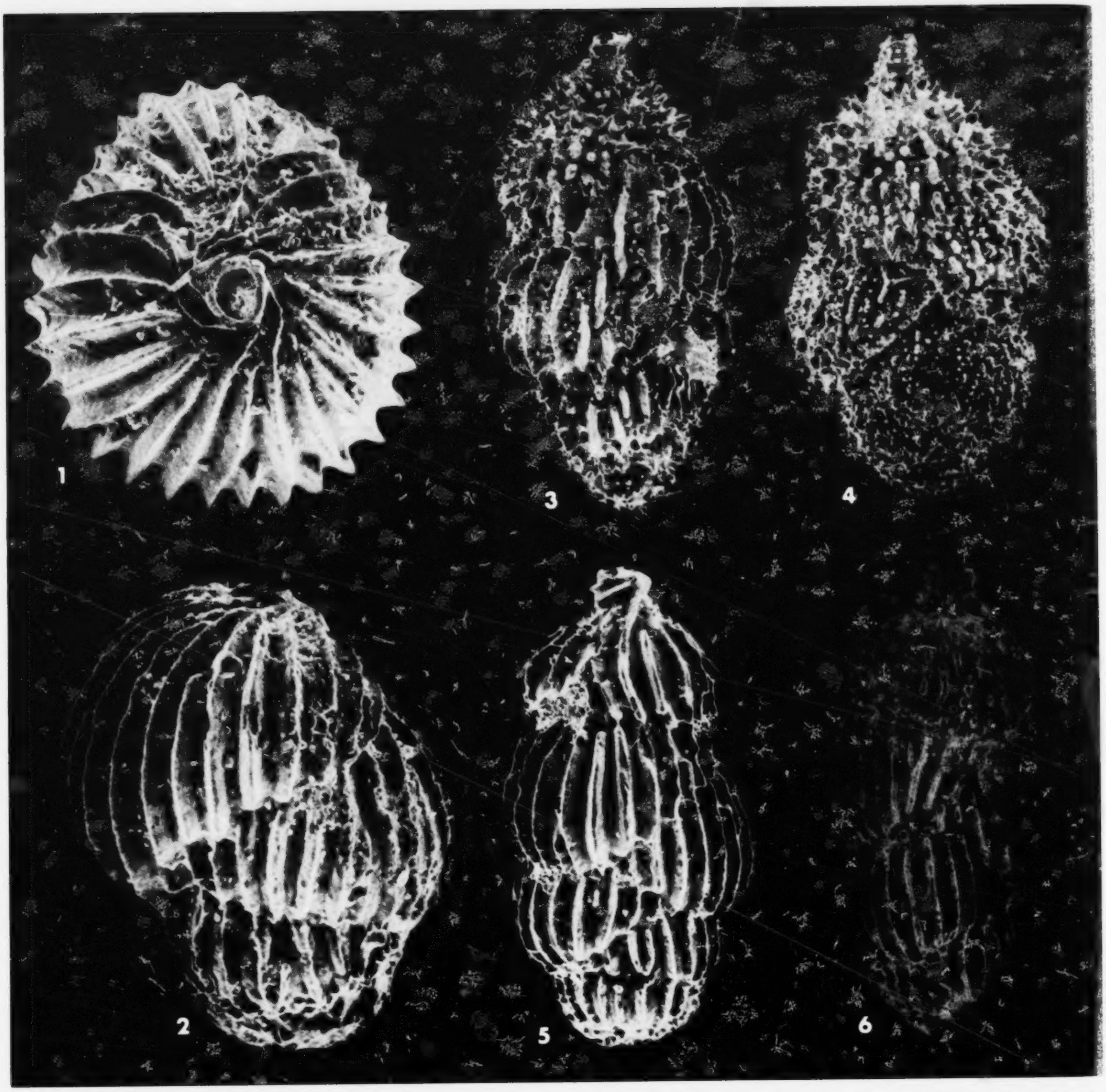

Plate 19. **1–2.** *Uvigerina rippensis* Cole, Sample 592-41,CC, (1) ×240; (2) ×260. **3–4.** *Uvigerina dirupta* Cushman and Todd, (3) Sample 593 1,CC, ×116; (4) Sample 593-6,CC, ×142. **5.** *Uvigerina costata* Finlay, Sample 592-41,CC, ×140. **6.** *Uvigerina bortotara* Finlay, Sampl 592-41,CC, ×150.

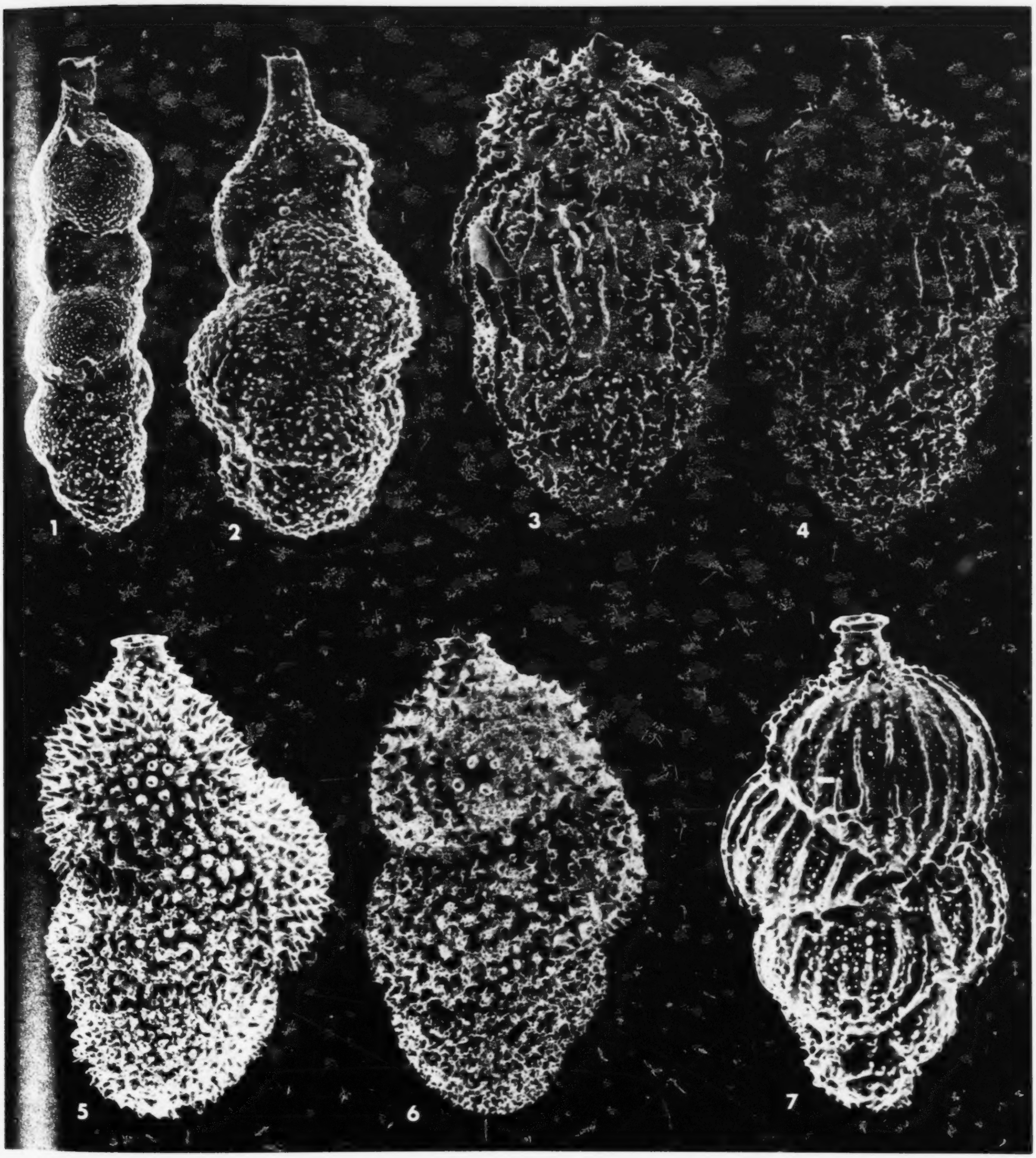

Plate 10. **1.** *Uvigerina auberiana* d'Orbigny, Sample 586B-6,CC, × 155. **2.** *Uvigerina proboscidea* Schwager, Sample 588C-24,CC, × 270. **3–4.** *Uvigerina hispido-costata* Cushman and Todd, (3) Sample 592-6,CC, × 172; (4) Sample 590A-5,CC, × 131. **5–6.** *Uvigerina hispida* Schwager, (5) Sample 590A-16,CC, × 116; (6) Sample 591-27,CC, × 87. **7.** *Uvigerina interrupta-costata* Le Roy, Sample 586B-6,CC, × 150.

21. NEOGENE BENTHIC FORAMINIFERS: DISTRIBUTION IN DEPTH TRAVERSE, SOUTHWEST PACIFIC[1]

Kenji Kurihara and James P. Kennett, Graduate School of Oceanography, University of Rhode Island[2]

ABSTRACT

Early Miocene to Quaternary benthic foraminifers have been quantitatively studied (>63 μm size fraction) in a southwest Pacific traverse of DSDP sites at depths from about 1300 to 3200 m down the Lord Howe Rise (Site 590, 1299 m; Site 591, 2131 m; Site 206, 3196 m). Benthic foraminiferal species smaller than 150 μm are by far dominant in the samples, averaging from 78 to 89% of the total benthic foraminiferal assemblages in the three sites examined. Although about 150 benthic foraminiferal species or taxonomic groups have been identified, only a few species dominate the assemblages. These dominant species include *Epistominella exigua*, *E. rotunda*, and *Globocassidulina subglobosa*, which prevail in the three sites, and *Oridorsalis umbonatus*, *E. umbonifera*, and *Cassidulina carinata*, which occur usually in frequencies of between 10 and 30%.

Faunal changes in Neogene benthic foraminiferal assemblages are not similar in each of the three sites, but faunal successions are most similar between the two shallowest sites. The deepest site differs in composition and distribution of dominant species. There are three intervals during which the most important changes occur in benthic foraminiferal assemblages: the early middle Miocene (14 Ma; the *Orbulina suturalis* Zone and the *Globorotalia fohsi* s.l. Zone); the late Miocene (6 Ma; the *Globigerina nepenthes* Zone) and near the Pliocene/Pleistocene boundary at about 2 Ma.

A Q-mode factor analysis of the faunal data has assisted in recognizing assemblage changes during the Neogene at each of the sites. Early Miocene assemblages were dominated by *Globocassidulina subglobosa* at Site 590 (1299 m), by *G. subglobosa* and *Oridorsalis umbonatus* at Site 591 (2131 m), and by *G. subglobosa*, *E. exigua*, and *Bolivina pusilla* at Site 206 (3196 m). In the early middle Miocene at Sites 590 and 591, a marked increase occurred in the frequencies of *E. exigua*. *Epistominella exigua* reached maximum abundance in the early Miocene in the deeper Site 206, and in the middle and early late Miocene in the shallower Sites 590 and 591. In the late Miocene, a spike occurred in the frequencies of *E. umbonifera* in Site 206, whereas the dominant species changed from *E. exigua* to *E. rotunda* at Site 590. Latest Miocene to late Pliocene assemblages were dominated by *E. rotunda* at Site 590, by *E. exigua* at Site 591, and by *G. subglobosa–E. exigua* (early Pliocene) and *E. rotunda–E. exigua* (late Pliocene) at Site 206. At the Pliocene/Pleistocene boundary, *E. exigua* temporarily diminished in importance at Sites 591 and 206. Quaternary assemblages were dominated by *E. rotunda* and *Cassidulina carinata* at Site 590, by *E. rotunda* at Site 591, and by *E. exigua* at Site 206.

These major faunal changes are all associated with known major paleoceanographic events—the middle Miocene development of the Antarctic ice sheet; the latest Miocene global cooling and increased polar glaciation; and the onset of quasiperiodic glaciation of the Northern Hemisphere. These major paleoceanographic events undoubtedly had a profound effect on the intermediate and deep water mass structure of the Tasman Sea as recorded by changes in benthic foraminiferal assemblages.

INTRODUCTION

Early Miocene to Quaternary benthic foraminifers have been studied from three sites in the Tasman Sea, southwest Pacific: Site 590 (31°10.02′S, 163°21.51′E), Site 591 (31°35.06′S, 164°26.92′E), both DSDP Leg 90, and Site 206 (32°00.75′S, 165°27.15′E), DSDP Leg 21. Sites 590 and 591 were cored on the Lord Howe Rise in water depths of 1299 m and 2131 m respectively. Site 206 is located in the New Caledonia Basin to the east of the Lord Howe Rise at greater water depth (3196 m).

We selected these three sites because they form a suite of cores ranging from intermediate to deep water between about 1000 m and 3000 m. The purpose of this study was to examine changes in benthic foraminiferal assemblages at different water depths during the Neogene. This, in turn, should provide information about paleoceanographic changes in the vertical water mass structure of the Tasman Sea. Changes in benthic foraminifers are known to be associated with certain deep and intermediate water masses (Douglas and Woodruff, 1981). Changes in assemblages through geologic time have also been shown to be sensitive monitors of changes in the distribution of deep and bottom water masses (Schnitker, 1974; Streeter, 1973; and others).

The three sequences are also appropriate for this investigation for several other reasons: (1) they all consist of continuous or nearly continuous early Miocene to Quaternary sequences; (2) the three sections are all well correlated using the same planktonic foraminiferal zonation (Kennett and Srinivasan, 1983); (3) the three sites are located above the foraminiferal lysocline and yield rich assemblages of benthic foraminifers throughout; and (4) no displaced benthic faunas were recognized in any of the sites.

METHOD OF STUDY

Benthic foraminifers were studied from ~9 m intervals from 149 core-catcher samples: 51 from Site 590, 55 from Site 591, and 43 from Site 206 (Fig. 2). The core-catcher samples were washed over a 63 μm Tyler screen. Benthic foraminiferal assemblages were quantitatively examined from the >63 μm fraction, chosen because relatively small individuals between 63 and 150 μm completely dominate the assemblages.

Kennett, J. P., von der Borch, C. C., et al., *Init. Repts. DSDP*, 90: Washington (U.S. Gov Printing Office).

Addresses: (Kurihara, permanent address) Rikkyo (St. Paul's) University, Nishi-ikebukur Tokyo, Japan; (Kennett) Graduate School of Oceanography, University of Rhode Island Kingston, RI 02881.

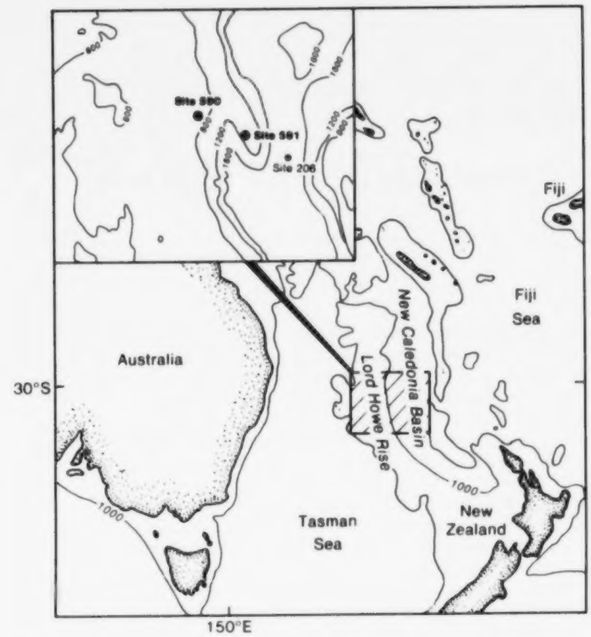

Figure 1. Location of DSDP Sites 590, 591, and 206 on the Lord Howe Rise and in the New Caledonia Basin. Depth is shown in fathoms.

Different workers have studied rather different size fractions of benthic foraminiferal assemblages. For example, fractions greater than 300 μm were studied by Lutze (1979); >250 μm by Lohmann (1978); >150 μm by Woodruff and Douglas (1981); >125 μm by Schnitker (1979); >100 μm by Douglas (1973); >73 μm by Boltovskoy (1983); and >62 μm by Resig (1976). Unfortunately, the size distribution of benthic foraminiferal tests has not previously been examined in deep-sea sediments. We examined the relative abundances of benthic foraminiferal tests larger and smaller than 150 μm. A number of important studies of Recent deep-sea benthic foraminiferal distribution patterns have been analyzed from the >150 μm size fractions (Parker, 1958; Phleger et al., 1953). Foraminiferal tests smaller than 150 μm range from 50 to 99% of the assemblages (Fig. 3), and average 78 to 89% of the assemblages in the three sites examined:

Site	>150 μm (avg.) (%)	<150 μm (avg.) (%)
590	1-35 (11)	65-99 (89)
591	8-50 (22)	50-92 (78)
206	5-37 (15)	63-95 (85)

The number of individuals >150 μm were not always sufficiently abundant to allow a quantitative study of this size fraction alone.

Washed samples were split to a size containing about 150 to 300 individuals using a microsplitter. The split samples were spread on a counting tray, and all benthic foraminifers were removed and mounted in taxonomic groups on slides. The procedure of spreading samples and removing benthic foraminifers was repeated three times or more for each sample to insure that no specimens were missed. The average number of benthic foraminifers counted was 164 individuals per sample at Site 590, 212 at Site 591, and 224 at Site 206.

Planktonic to benthic foraminiferal ratios (P/B ratios) were also determined in the fractions larger than 63 μm. In order to estimate the number of planktonic foraminifers contained in the samples, the samples used for benthic forms were microsplit, and 300 to 1000 planktonic individuals were counted.

The data for each site were also separately analyzed using Q-mode factor analysis (Klovan and Imbrie, 1971) to assist in evaluating the major changes in faunal components within each site.

RESULTS

Site 590

Site 590 lies near the crest of the Lord Howe Rise at a water depth of 1299 m and is the shallowest of the three sites studied. The section is a 499 m-thick sequence of mostly foraminifer-bearing nannofossil ooze from early Miocene (*Catapsydrax dissimilis* Zone) to Quaternary (*Globorotalia truncatulinoides* Zone). An unconformity exists at the early/middle Miocene boundary where the *Praeorbulina glomerosa curva* and *Orbulina suturalis* Zones are missing.

Benthic foraminifers were studied from 51 samples of Hole 590 (590-1,CC to 3,CC), Hole 590A (590A-1,CC to 27,CC), and Hole 590B (590B-30,CC to 53,CC) (Fig 2). Benthic foraminifers are well preserved in the Quaternary to late Miocene, but are recrystallized during most of the middle and early Miocene. There is a large range of planktonic to benthic foraminiferal ratios, from 45:1 to 4469:1 (Fig. 4). The largest ratios occur in the early Miocene and decrease over the early/middle Miocene boundary. For the remainder of the Miocene to the Quaternary, the ratios are rather constant and relatively low, mostly within the range of 50:1 to 300:1.

The stratigraphic distribution of benthic foraminifers in Site 590 is shown in Table 1. Benthic foraminiferal faunas are dominated by *Epistominella, Globocassidulina, Cassidulina, Bolivina, Oridorsalis*, and *Gyroidina*. Most of the abundant species range throughout the section from the early Miocene to the Quaternary. There are many species with rare or sporadic occurrences (Table 1) and hence their stratigraphic ranges are difficult to determine with accuracy.

Early Miocene assemblages at Site 590 were dominated by *Globocassidulina subglobosa* (Brady). Other important species include *Oridorsalis umbonatus* (Reuss), *Cibicidoides mundulus* (Brady, Parker, and Jones) and *Bolivina pusilla* Schwager. In one sample within the *Catapsydrax dissimilis* Zone, *Bolivina* sp. A was found with exceptionally high frequencies (48%).

In the middle Miocene, the benthic foraminiferal assemblages were dominated by *Epistominella exigua* (Brady) usually in frequencies between 10 and 25%. Other important species include *Epistominella rotunda* (Husezima and Maruhasi), *Cassidulina* sp. A, *B. pusilla, O. umbonatus, G. subglobosa*, and *Cibicidoides wuellerstorfi* (Schwager). *Globocassidulina subglobosa*, which was the dominant species of the early Miocene assemblages, tended to decrease in abundance during the middle Miocene.

Late Miocene assemblages were also dominated by *E exigua*. The frequencies of this dominant species decrease in the *Globigerina nepenthes* Zone and *E. rotunda* was dominant in the late late Miocene. Other important species include *Cassidulina* sp. A, *B. pusilla*, and *O. umbonatus*. At the same time as the dominant species changed from *E. exigua* to *E. rotunda*, several species showed interesting occurrences in the late Miocene. *Rectuvigerina* sp. appears only in the *Neogloboquadrina continuosa* and *Globigerina nepenthes* zones. *Pyrgo* and *Quinqueloculina* first occur in the *G. nepenthes* Zone and *Globorotalia conomiozea* Zone, respectively. *Bulimina stri*

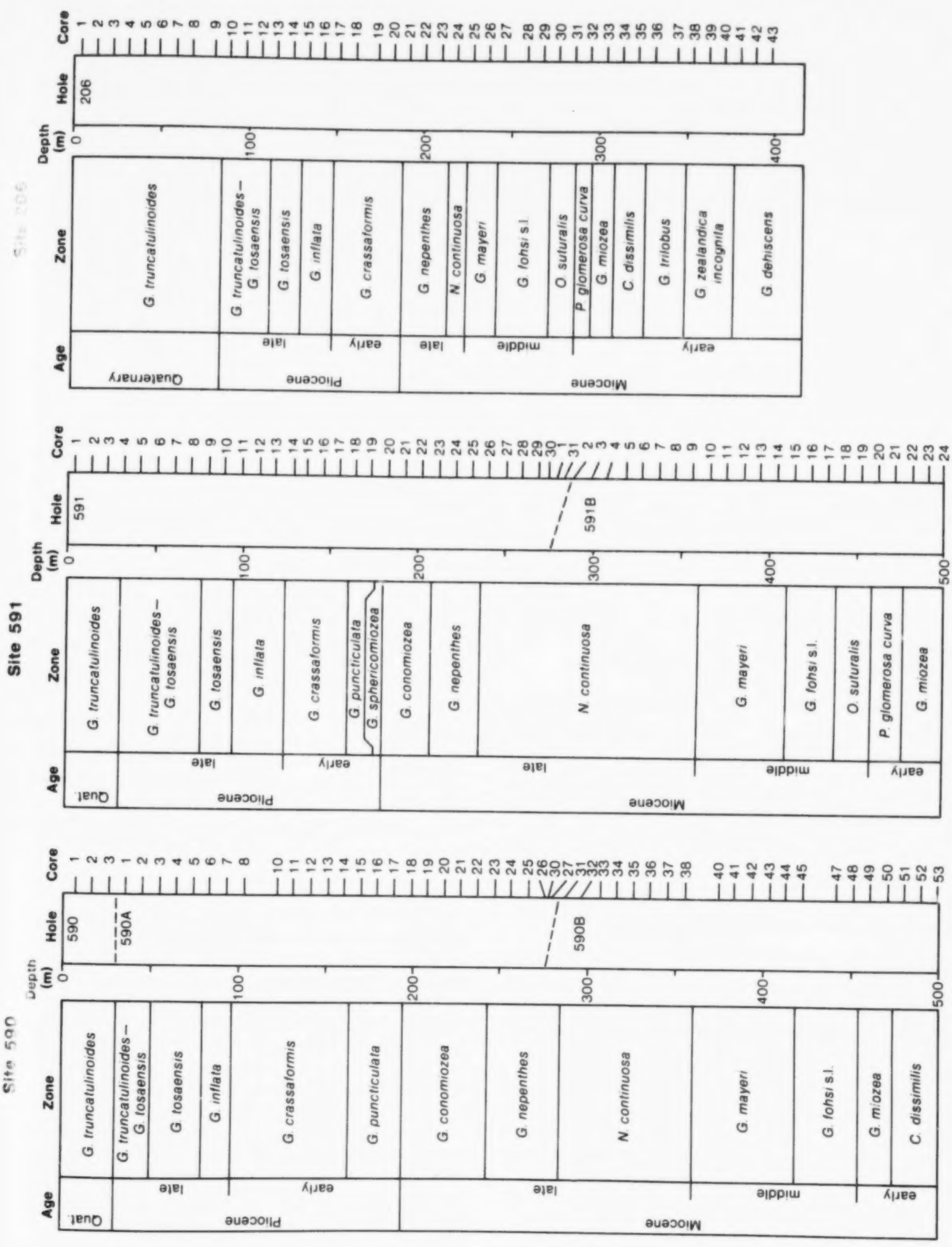
Site 590
Age
Zone
Depth (m)
Hole
Core
Quat.
Pliocene
late
early
Miocene
late
middle
early
G. truncatulinoides
G. truncatulinoides – G. tosaensis
G. tosaensis
G. inflata
G. crassaformis
G. puncticulata
G. conomiozea
G. nepenthes
N. continuosa
G. mayeri
G. fohsi s.l.
G. miozea
C. dissimilis
0
100
200
300
400
500
590
590A
590B
1 2 3 1 2 3 4 5 6 7 8 10 11 12 13 14 15 16 17 18 19 20 21 22 23 24 25 26 30 27 31 32 33 34 35 36 37 38 40 41 42 43 44 45 47 48 49 50 51 52 53
Site 591
Age
Zone
Depth (m)
Hole
Core
Qual.
Pliocene
late
early
Miocene
late
middle
early
G. truncatulinoides
G. truncatulinoides – G. tosaensis
G. tosaensis
G. inflata
G. crassaformis
G. puncticulata
G. sphericomiozea
G. conomiozea
G. nepenthes
N. continuosa
G. mayeri
G. fohsi s.l.
O. suturalis
P. glomerosa curva
G. miozea
0
100
200
300
400
500
591
591B
1 2 3 4 5 6 7 8 9 10 11 12 13 14 15 16 17 18 19 20 21 22 23 24 25 26 27 28 29 30 1 31 2 3 4 5 6 7 8 9 10 11 12 13 14 15 16 17 18 19 20 21 22 23 24
Site 206
Age
Zone
Depth (m)
Hole
Core
Quaternary
Pliocene
late
early
Miocene
late
middle
early
G. truncatulinoides
G. truncatulinoides – G. tosaensis
G. tosaensis
G. inflata
G. crassaformis
G. nepenthes
N. continuosa
G. mayeri
G. fohsi s.l.
O. suturalis
P. glomerosa curva
G. miozea
C. dissimilis
G. trilobus
G. zealandica incognita
G. dehiscens
0
100
200
300
400
206
1 2 3 4 5 6 7 8 9 10 11 12 13 14 15 16 17 18 19 20 21 22 23 24 25 26 27 28 29 30 31 32 33 34 35 36 37 38 39 40 41 42 43

Figure 2. Planktonic foraminiferal zones and stratigraphic position of core-catcher samples of Sites 590, 591, and 206.

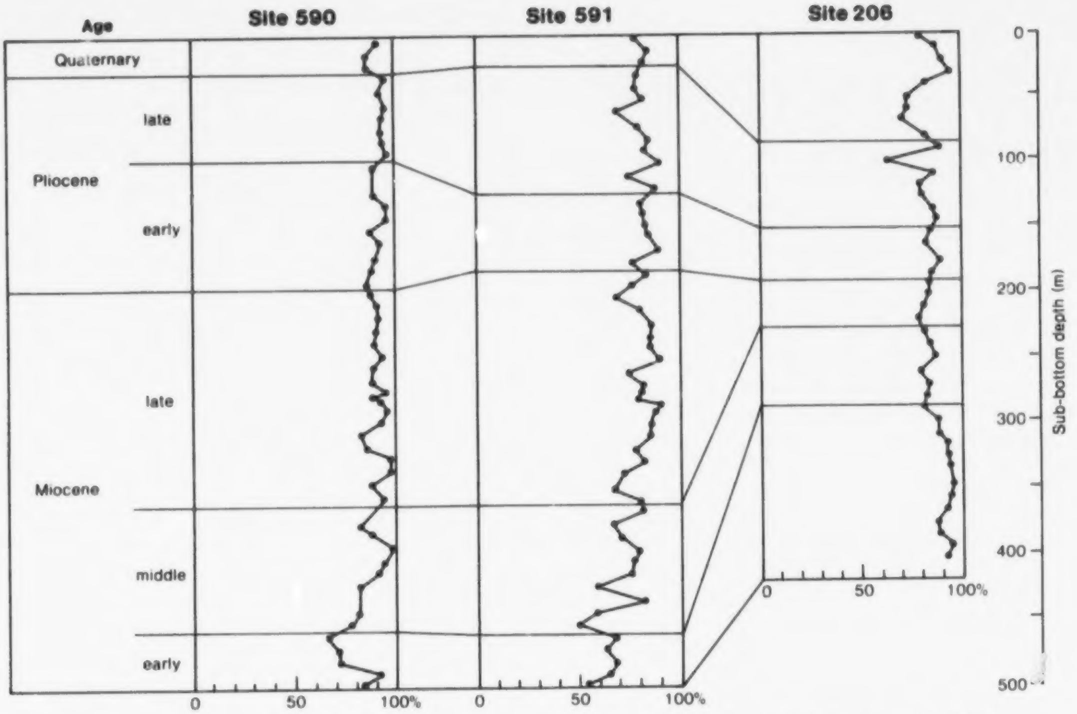

Figure 3. Percentages of benthic foraminifers < 150 μm within the total benthic assemblages at Sites 590, 591, and 206.

ata d'Orbigny and *Epistominella rugosa* (Phleger and Parker) temporarily disappear in the upper part of the *Globigerina nepenthes* Zone, while *Uvigerina peregrina* Cushman first appears within this zone.

Pliocene and Quaternary assemblages were dominated by *E. rotunda*, usually with frequencies between 10 and 25%, and the late Quaternary assemblage was dominated by *Cassidulina carinata* Silvestri. Other important species include *E. exigua, Cassidulina* sp. A, *Globocassidulina subglobosa, Bolivina decussata* Brady, *Virgulopsis* sp., *Gyroidina* cf. *quinqueloba* Uchio and *Anomalinoides* sp. B. *Globocassidulina subglobosa* increased again in the latest Pliocene and Quaternary. The changing species dominance of benthic foraminiferal assemblages for Site 590 is summarized in Figure 5.

Site 591

Site 591 lies near the crest of a southern spur on the eastern part of the Lord Howe Rise at a water depth of 2130 m. The crest of the spur, separated from the main part of the Lord Howe Rise by a valley, is largely isolated from sediment transportation from the main part of the Lord Howe Rise. The sedimentary sequence recovered at Site 591 is a calcareous biogenic facies consisting mainly of calcareous nannofossil and foraminiferal ooze. It is a 500-m-thick continuous sequence from the late early Miocene (*Globorotalia miozea* Zone) to the Quaternary (*Globorotalia truncatulinoides* Zone).

Fifty-five samples were studied from Hole 591 (591-1,CC to 591-31,CC) and Hole 591B (591B-1,CC to 591B-24,CC), as shown in Figure 2. Benthic foraminifers are well preserved in the upper part of the sequence, from Quaternary to late Miocene in age. In the early and middle Miocene, benthic foraminifers are rarer than in sediments of younger age. Recrystallization of benthic foraminiferal tests at Site 591 becomes conspicuous, especially during the early Miocene. P/B ratios are higher than at the other two sites (Fig. 4) ranging from 179:1 to 10674:1. Maximal P/B values occur in the early Miocene and average about 6400:1 in this interval. As in Site 590, P/B ratios decrease near the early/middle Miocene boundary. Beginning in the early middle Miocene, the ratios become less than 100:1, with several peaks of up to about 2000:1 to 3000:1.

Table 2 shows the stratigraphic distribution of benthic foraminifers at Site 591. The following species are the most abundant at this site: *Epistominella exigua, E. rotunda, Globocassidulina subglobosa, Cassidulina* sp. A, *Oridorsalis umbonatus, Bolivina decussata, B. pusilla, Gyroidina* sp. A, *Virgulopsis* sp., *Cibicidoides wuellerstorfi, Pullenia osloensis* Feyling-Hanssen, and *Siphonaperta* sp.

Early Miocene assemblages were dominated by *Globocassidulina subglobosa* and *Oridorsalis umbonatus* with frequencies up to 31 and 20%, respectively.

In the middle Miocene, the assemblages were dominated by *E. exigua*. This species increased in frequencies in the early middle Miocene as in Site 590. Other important species include *G. subglobosa, O. umbonatus, Cassidulina* sp. A, *Cibicidoides wuellerstorfi, C.* cf. *opacus* (Carter), and *Virgulopsis* sp.

Late Miocene and Pliocene assemblages were also dominated by *Epistominella exigua*. This dominant species

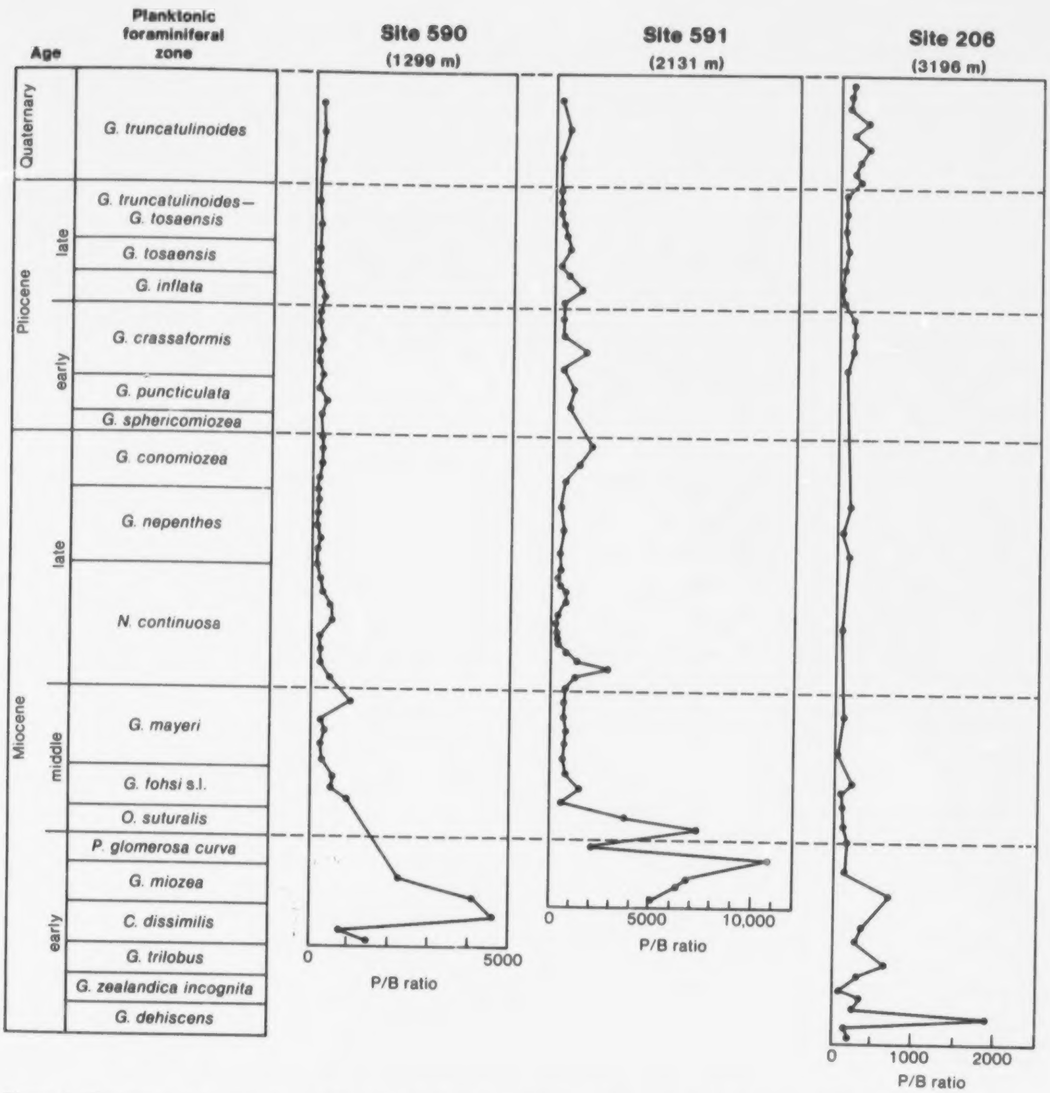

Figure 4. Planktonic to benthic foraminiferal ratios (P/B ratios) at Sites 590, 591, and 206 (water depth in parentheses).

showed highest frequencies in the early late Miocene (15 to 30%). Other important species include *G. subglobosa, O. umbonatus, E. rotunda, Cassidulina* sp. A, *Siphonaperta* sp., and *B. decussata. Quinqueloculina* and *Pyrgo* were found to occur beginning in the *Neogloboquadrina continuosa* Zone, as in Site 590, but there are some sporadic occurrences in the early and middle Miocene.

Quaternary assemblages were dominated by *E. rotunda.* Near the Pliocene/Quaternary boundary, *E. exigua* temporarily decreased in frequency and was even absent just below the boundary (591-4,CC). *Epistominella rotunda* and *O. umbonatus* also increased in frequency near the boundary and remained important throughout the Quaternary. Other important species are similar to those of late Miocene and Pliocene age. The changing species dominance of benthic foraminiferal assemblages for Site 591 is summarized in Figure 5.

Site 206

Site 206 is located about 220 km to the southeast of Site 590. It lies at the bottom of the New Caledonia Basin, and is the deepest of the three sites studied (3196 m). The Neogene of Site 206 is represented by 440 m of foraminifer-rich nannofossii ooze. Planktonic foraminifers at this site were studied by Kennett (1973) and Srinivasan and Kennett (1981), and 16 planktonic foraminiferal zones were well recognized, from the *Globoquadrina dehiscens* Zone of the early early Miocene to the *Globorotalia truncatulinoides* Zone of the Quaternary. There is an unconformity between the late Miocene and the early Pliocene, where the *G. conomiozea* Zone to the *G. puncticulata* Zone are missing.

Benthic foraminifers were studied from 43 samples of Hole 206 (206-1,CC to 43,CC). They are not as well preserved as they are at the other two sites, but rich calcare-

Table 1. Distribution of benthic foraminifers at Site 590.

	Quat.			Pliocene																Miocene		
				late							early									late		
	G. truncatulinoides			G. truncatulinoides-G. tosaensis		G. tosaensis			G. inflata		G. crassaformis							G. puncticulata			G. conomiozea		
Benthic foraminifers	590-1,CC	590-2,CC	590-3,CC	590A-1,CC	590A-2,CC	590A-3,CC	590A-4,CC	590A-5,CC	590A-6,CC	590A-7,CC	590A-8,CC	590A-10,CC	590A-11,CC	590A-12,CC	590A-13,CC	590A-14,CC	590A-15,CC	590A-16,CC	590A-17,CC	590A-18,CC	590A-19,CC	590A-20,CC
Bolivinopsis sp. A															1							
Spiroplectammina sp.																						
Textularia lythostrota		1								1						1			2			
T. spp.				1				1							1				3	2		1
Siphotextularia rolshauseni			2				2					1	1			1						
S. sp.										1												
Gaudryina sp.									1													
Eggerella sp. A					1			1	1	5		1		2		4		3	2			3
E. sp. B		2	3			1					2	2		1	1				1		1	
Karreriella bradyi																			1			
Martinottiella spp.											1											
Ophthalmidium pusillum			1																			
Spiroloculina sp.								1														
Quinqueloculina sp.		1																				
Pyrgo murrhina			2																			
P. spp.		1	2	1					1		1		1						1			1
Sigmoilina edwardsi	1																			1		
S. tenuis																						
Sigmoilopsis schlumbergeri										1					1	3		1		1		1
Siphonaperta sp.	2		5	4				2	1	6	1	6	1	3	8							
Triloculina tricarinata		1	1	1																		
Nodosaria spp.		1		3	2		2	2	1	1	2	5	2		1	2	5		1	2	2	
Dentalina spp.					1			1		1	1				1	1	1				1	3
Lagena spp.	2	2	1	4					3			3	1	2	3		2	3	3		3	1
Lenticulina spp.					1		1						1		1		1	2		3	1	1
Vaginulina sp. A																						
V. spp.	1									2			1							1		
Pyrulina spp.																						1
Seabrookia earlandi												1									1	
Oolina spp.	1	1	1	1	2	2	2		3	2	5	1							1	1	1	
Fissurina spp.	1	6	1	4	4	2	2	5	4	3	3			2		1	1	1		1	3	2
Parafissurina spp.		1						1								1		1		1		
Sphaeroidina bulloides		1	1	2	1	2	2	4	1	2	1	1			1	1	2	1			1	2
Bolivina cf. *anastomosa*																						
B. decussata	9	1	1	3	2	1	3			3	7	15	11	13	2	13	3	7		8	22	1
B. minuta	2	2	2	2				12	4							1	1					
B. pusilla	4			2	1	1	1	3	4	10	1	1	3	2	1	7		7	5		9	7
B. robusta	1				1	2				1												
B. seminuda	1	1	2	1	2	1		6	2				1									2
B. sp. A	2															2	4	10	2	1		
B. sp. B																						
B. sp. C										2										3	1	1
B. spp.										2												1
Stilostomella spp.		9	7	12	13	5	3	10	7	7	5	5	6	3		6	6	7	4	7	7	6
Bulimina aculeata	11	1		6																		
B. rostrata	8	5	6	2			1		2			5	1		1		2	2	2	3	8	3
B. striata		2																				
B. spp.	1							1												2		
Stainforthia complanata		1		4	3	1		3	1					1	2	1		3	4	1	1	4
Virgulopsis sp.								1	1			20	1	7	6	3	6	16	15	6	6	3
Uvigerina hispida																			1			
U. peregrina	3	2	1	1		1	2	1													1	
U. proboscidea				2	1	1		2	6		1	5	1	1			1	1	1			1
U. vadescens																						
U. sp. A			1			1	2				1		1		2	4	9		5	3	3	4
U. sp. D								1														
U. spp.																						
Rectuvigerina sp.																						
Trifarina sp.	2		3		4	2	1	1	2		1						3	1		4		
Discorbis sp.																			1			
Discorbinella bertheloti	1			1	1			2				2	2									
Epistominella exigua	36	17	14	30	12	29	15	35	33	12	12	18	19	17	14	25	5	3	18	13	4	15
E. rotunda	25	20	9	34	24	45	23	22	44	15	25	20	32	26	40	31	24	19	10	22	21	29
E. rugosa			1	1		1	5	1	1			1	2				2					
E. umbonifera								1								1	2			2		

Note: Number represents no. specimens counted in >63 µm. Planktonic foraminifer zones and DSDP sample nos. in column heads.

Table 1. (Continued).

Miocene																												
late																middle								early				
G. conomiozea		*G. nepenthes*						*N. continuosa*								*G. mayeri*					*G. fohsi* s.l.			*G. miozea*		*C. dissimilis*		
590A-21,CC	590A-22,CC	590A-23,CC	590A-24,CC	590A-25,CC	590A-26,CC	590A-27,CC	590B-30,CC	590B-31,CC	590B-32,CC	590B-33,CC	590B-34,CC	590B-35,CC	590B-36,CC	590B-37,CC	590B-38,CC	590B-40,CC	590B-41,CC	590B-42,CC	590B-43,CC	590B-44,CC	590B-45,CC	590B-47,CC	590B-48,CC	590B-49,CC	590B-50,CC	590B-51,CC	590B-52,CC	590B-53,CC
1			2			1	1		1	1					1	1								1		1		3
																			1									
	1						1																					
		1	1																2									
1			1		1	1				2	1					1		1	1									
	4							1	2	2	1	1		2		1			1	2	3							
	2		2							1																		
				3											2	1												
		1																							1			
2																												
		1																										
																			1									
		2	1												1									1				
								12	1	4			1	1				30		4	1	1	3	1		4	1	
	1	1	3	1	1			2	4	8	1	1	3	1	4	1	1		2	1	4	2	8	3	3	3	1	2
1	1			1			1		2						1	2	2				2			1	2	4	1	1
	1		1				1		6	1		2		2			1	3	1	2	1				2			
1	2			2	1	2							1	2	1					1					3	1		4
																						1	3	1	1	1		
																							1			1		
														1														
1		1																										
					4	1				1	1		2											1				
3		2	3	2	1		4		2				2		2			1		1			2	1	1		2	1
										1	1	1				1		1									2	1
1				2	2		2	1			1																	
																		1		1	2		4	1			1	
					1	4	7		3		9	1	3		6		1	3	3	10	5	1		2		3	9	8
8	8	3	8	1		4	5	2	2	3	7	12	2	10	10	10	5	3			16	10	14		1	8	12	2
		3												1														
				1				3	2			1	2			4	1		1					9			79	
								3		6			6					6		1		10	2		3	1	1	1
	1		1												1													
								2									1						1			1		1
3	8		1	4	2	3	3		1	8	3		1	5	8	5	3	3		1	3	4		5	10	9	3	5
1																												
	2	1	3		1	2		3		2			1		3	2	1		1		2			1				
			4	3	1	3	2	2			3		1	1	1	1	1	1		1								
														1														
			2									1		1	2						1					1		
5	6	2	2	3	1	7	1	1		1	11	4	4	3		3		1	4	1	5	5	6	2	3	1		8
1			1				2		1																			
					1	1	3																					
	1			1		2	1	1						1		2			4			1				2		
1		1										1		2	7					1						1	3	
2	7		3	3	2			3	5		1		2	1	5	3	4	4	1	12	2		5	2	1	4		4
			1	1		2								1					1		1	1		2				1
					3		1			1																		
		2	2	1	4	4		1	1	3	2	4	2	1					2		1		1	2				
					1		1	3					3															
																				2								
13	17	8	35	53	59	31	9	14	45	5	19	9	48	26	12	24	35	36	22	21	16	21	4	12			3	2
26	37	24	41	19	35	20	32	26	18	5	13	36	33	19	20	13	17	22	21	22	1	3	1	3	1	2	2	2
			16	14	5	10	8	4	5	3	4	9	15	2	3	1	3				1	1	1					
										1		1	2						4				7	8				

Table 1. (Continued).

	Quat.			Pliocene																Miocene		
				late							early									late		
	G. truncatulinoides			*G. truncatulinoides*- *G. tosaensis*		*G. tosaensis*			*G. inflata*		*G. crassaformis*							*G. puncticulata*			*G. conomiozea*	
Benthic foraminifers	590-1,CC	590-2,CC	590-3,CC	590A-1,CC	590A-2,CC	590A-3,CC	590A-4,CC	590A-5,CC	590A-6,CC	590A-7,CC	590A-8,CC	590A-10,CC	590A-11,CC	590A-12,CC	590A-13,CC	590A-14,CC	590A-15,CC	590A-16,CC	590A-17,CC	590A-18,CC	590A-19,CC	590A-20,CC
E. sp.																						
Gavelinopsis lobatulus	6	7	8	4	3		2	2	9	10	8	8					3	2	2		1	15
Laticarinina alto-camerata				1												1						
L. pauperata																1				1		
Valvulineria sp.						1					1											
Heronallenia sp.A			2	1				1					1	1	2							
Siphonina australis																						
Pleurostomella spp.		2	4	2	1	1	2	3	6	4	2	6	1	1	1	2	1	5		4	1	
Cassidella bradyi			1																			
Cassidulina carinata	43	2	1	11	1																	8
C. sp.A	7	17	19	22	22	15	22	20	18	14	11	7	10	16	10	16	12	17	5	23	23	23
C. sp.B	8	4	2	7	4	4			2	3	1	1	3	3	2		1	2	2	6	1	3
C. sp.C											1		3									
C. sp.D																	2					
C. spp.	3	1	2	2		2						1	1	1	1	1	1		1	2	1	1
Globocassidulina subglobosa	8	20	20	33	10	8	3	2	4	4	12	9	6	9	8	6	6	5	4	4		3
G. ornata																	2	1				
Cassidulinoides spp.																						
Ehrenbergina hystrix																1						
E. trigona																				1	2	
Chilostomella oolina										1												1
Allomorphina pacifica		3				1																
Astrononion spp.	3	2	1	16	1	1	4	5	6	3	10	2	6	2	2	4	4	4	4	5	1	4
Nonionella spp.	2	2		2	1			3	1			1				1			1		1	
Pullenia bulloides	1	4	1						3						2	1		2				2
P. osoloensis		2	1	7	4	1	1	1			3	2			3		1	2	1	1		3
P. quinqueloba			2					1									1			1	1	1
P. sp.A																						
P. sp.B												1					1					
P. spp.		1											1									
Gyroidina acuta				1	2			1						1	3			6	1			1
G. broeckhiana		1	1							1					1	1	1		1	1		
G. lamarckiana		1					1		1				1					2				
G. neosoldanii																						
G. cf. *quinqueloba*	5	3	10	13	10	4	2	4	7	6	1	4	3	3	6	7	3		5	2	7	2
G. sp.A	3	2	3	2	2	3	2	1	4	1		2		1	3		2	4	3	2	1	6
G. sp.B			1				1	1								1	3				3	
G. sp.C												2										
G. sp.D																1	2		1			
G. spp.	3		2		2		1	3						2					1	2	2	2
Oridorsalis umbonatus	7	8	4	4	3	1	2		8		8	5	3	2	1	9	7	7	7	1	11	2
O. sp.																						
Osangularia culter			1	2	1	1		1		1		3	1		2	5	4		1		1	
O. bengalensis																						
Anomalina sp.																						
Anomalinoides globulosus					2			1	1		1								1			7
A. sp.A	2	3	2					1														1
A. sp.B	1	9	8	11	8		3	8	14	5	6	8	3	6	5	5	5	5	6	3	5	
A. sp.C						3	2	1				3	3	1	2							
A. spp.	1			4	9		1	2	1	4	3			1		1		1	1	1	1	1
Cibicidoides bradyi	1	1	3	1	2		2			2								1		2		
C. kullenbergi		1	4		1							1			3	1	5	4	1	1	4	
C. labatulus						1	1				2						1	1				
C. mundulus									2									1		1	1	3
C. cf. *opacus*									1					1								
C. pseudoungerianus							1	1	1		1	1						3	2		4	1
C. wuellerstorfi	1		3	1	1		1	1		1			1		1							
C. sp.A				1		1		3	3		2				2	1	1		1	4		
C. spp.		2	1	1			1				1		1		2	1	1		1	1	2	2
Gavelinella sp.																						
Hanzawaia cf. *cushmani*													1						1	2	1	1
Melonis barleeanum	1	1	2	2	2	1	2	1	2			1	1							1		1
M. cf. *nicobarensis*			1		1												1	1	3	1		
M. sp.A																						
M. spp.						1	1							1			1					
Miscellaneous benthic foraminifers	9	7	7	6	7	13	5	5	7	14	9	5	3	2	3	4	6	3	2	5	2	3
Total number of specimens	229	185	184	279	177	160	130	193	224	151	153	186	141	134	152	180	158	167	142	166	174	190

Table 1. (Continued).

Miocene																												
late																middle								early				
G. conomiozea		G. nepenthes						N. continuosa								G. mayeri					G. fohsi s.l.			G. miozea		C. dissimilis		
590A-21,CC	590A-22,CC	590A-23,CC	590A-24,CC	590A-25,CC	590A-26,CC	590A-27,CC	590B-30,CC	590B-31,CC	590B-32,CC	590B-33,CC	590B-34,CC	590B-35,CC	590B-36,CC	590B-37,CC	590B-38,CC	590B-40,CC	590B-41,CC	590B-42,CC	590B-43,CC	590B-44,CC	590B-45,CC	590B-47,CC	590B-48,CC	590B-49,CC	590B-50,CC	590B-51,CC	590B-52,CC	590B-53,CC
																4												
8	8	11	13	8	1	3	1	1					2					1							1			1
																								1				
										1																		
			1	1			1	1					1					1					1				2	2
																									1	1		
		1	4			2	1		1	3	1		1	3		1	3		1	2	8	1	2	1	5	8	3	6
	2	2																										
																											2	
23	18	21	13	4	5	5	9	13	7	7	11	12	12	8	4	6	1	15	19	12	6	4	9	4			3	3
	2	1	2	2	2	4	2	1	1	2	1	1		1	3			3	1				1	2	1		1	
				1	1						1			1	4			7	3									
																1	1						2					
				2				1		1			2	3	13		3	2	4	2	2	1	4		7	2	3	1
4	1	5	1	1	6		7	5	5	1	4	6	7	11	10	8	4	2	13	9	6	4	13	19	18	1	2	15
						1					1		2			1		2										
																	3											
3	4	3	2	8	4	5	6	3																				
														1														
	2					1																						
5	8	2	7	6	1	4	1	1	12	8	4	2	8	10	7	6	1	2	3	2	7	10	5	4	2			1
1	2	1	2		4	3							1	2						1	1				1			
			1			1					1			1	1						1						1	
1	1	1	2	2		1		1	3	2	1	1		2	1	2	2	3	1	3	5	5	2	3	5		2	3
	1						1				2					1					1	1		1		1		1
					1				1				1	1	1		1											
					1									2														
																				2				1				1
1	1	2	2	1		1	2			2	1					4	1	1	2	3	2	1		2	2	2	1	2
1			2																				1	1				
	1					1	1			1	1												2					
1		1												1														
8	6		1		3		2	4	3	3			2	2	2	2	2	3	1	5			2	2				
4	1	1	3	1				4	8	5	3	2	2	3	6	1	2			1		3	1					
4		4	9	4	2	1	1	1		2	1	1	3														1	
				1						2		1		2	1		2				4			2		2		
	1			1	1				2						1						1		1		1			
		1	4	3	1		1	1			4	3	1	1	3	1	2		2	1		5	4	3	3		1	1
5	2		12	5	7	5	2	3	8	6	6	3	4	12	12	11	2	1	13	15	7	5	4	13	15	6	5	7
														1									1					
1	2			4	2						1			1	1	1	1	1										
							1				1													1				
																						1						1
		1	1				2											1		1		3	2					
																				1					1			
2	11	6	8	1	7	1	6	3	3	1	3	3	3	1	1	3	2	8	2	3	3	4					1	3
3							1											2									1	3
	2	2			1		2		1	1		2		2			2	2	1	2		1	1					
	1					2	1							2		1	1						1				1	2
	1	3	2	4			1		1	5	4	3		1	3													
						1		1			1										1		1					
														3							2		3	7	4	4	3	6
																			1	1	1	1		2				
	2		2	1			2			1														3	3			
			1				1				1			2		4	1		3	7	4	6	4	2	1			
4	2		1	1							2		1	1		1	2				2	1						
4	2	1	2	2	1			1	1	1	2			1		1	3	2			1	3	3	3	2	2	5	
									1							1												
	3	5				2	2			2			1			2		2	2	2								
							1			1	4				2	2					1	1	2	1	1		1	
						1																				1		
																							1	3		3		2
		1																	2					1	2			1
2	2	3	3	3	1	3	2	4	5	2	6	3	6	1	7	3	1	6	7	5	5	2	4	5	6	3	4	4
156	188	132	235	182	178	146	145	133	164	119	146	127	194	167	173	144	119	183	154	164	138	124	140	146	114	84	163	112

Table 2. Distribution of benthic foraminifers at Site 591.

	Quat.			Pliocene																Miocene				
				late										early						late				
	G. truncatulinoides			*G. truncatulinoides*–*G. tosaensis*					*G. tosaensis*		*G. inflata*			*G. crassaformis*				*G. puncticulata*		*G. conomiozea*			*G. nepenthes*	
Benthic foraminifers	591-1,CC	591-2,CC	591-3,CC	591-4,CC	591-5,CC	591-6,CC	591-7,CC	591-8,CC	591-9,CC	591-10,CC	591-11,CC	591-12,CC	591-13,CC	591-14,CC	591-15,CC	591-16,CC	591-17,CC	591-18,CC	591-19,CC	591-20,CC	591-21,CC	591-22,CC	591-23,CC	591-24,CC
Bolivinopsis cubensis									1					1										
B. sp. A																		2						
B. sp. B																								
Textularia lythostrota												3						2	2					
T. spp.				1								3				2	1		3	2		1		
Siphotextularia rolshauseni	2	2		1	3		1	2						1	1	1			2	2	1	5	1	1
Gaudryina sp.																						4		
Dorothia brevis																1								
Eggerella sp. A		2	1	2	8	2	3	2		5	2		5	2			3		6	3	2	1	2	
E. sp. B							1	1	1			1							2				2	
Karreriella bradyi																								
Martinottiella spp.																								
Ophthalmidium pusillum		1																						1
Quinqueloculina venusta		1		1			1				4		1			1	1		2		3	6	2	1
Q. spp.			1								1													
Pyrgo murrhina	2	3	1	1		1		1	1	2	2		1	1	2		1	2		2			2	
P. spp.	1		2	2	5	1	3	6	2	3		1	1		2	1	2	1		2	6	4	2	1
Sigmoilina edwardsi	2		4							2	3	3			1	1	1		3	1	5	1	1	
S. tenuis																								
Sigmoilopsis schlumbergeri		2	2												1	1					1		1	
Siphonaperta sp.		1					1	6	1	2	17	1	27		1	5	3	16	5	11	2	5	20	8
Triloculina spp.						3	1						2					1						
Nodosaria spp.					1		5	1	2	1	1	1			1	1		1	3	1	1	1		
Amphicoryna sp.																								
Dentalina spp.	1	1	1	3		1		1		2	3	3	2	2				1			1	5	4	1
Lagena spp.		1	1	2		1	4	1	3	1	4		5	1	4	4	1	3	5		3	1	1	2
Lenticulina spp.		4			2				2			1	1				1		1					
Vaginulina sp. A																								
Pyrulina spp.		1	3	3	1				1		1	1	2		2		1	2	2	2	1	1		
Seabrookia earlandi																				1	7			
Oolina spp.	3		1	2	2	3	2	1	2	4	3	2	3			1	7	2	2	3	3		3	
Fissurina spp.	5	4	10	6	11	7	8	3	7	2	3	9	3	2	3	9	5	6	8	5	11	5	7	2
Parafissurina spp.		2	1					2	1		1					1		2	3				1	3
Buliminella sp.																								
Sphaeroidina bulloides			2	2	1	1	3	3	1		1				1				1		1		2	
Bolivina anastomosa																								
B. decussata	2	1		8		8	1	6	5	7	4		3	2	6	8	4		7	3	8	3	28	7
B. minuta	2																							
B. pusilla	1	7	2		4	2	3		2	2	3	8		4	3	3	6	5	1	1	2	5	10	3
B. seminuda	5	7		4	1	6	7	1		1	3	5	1						1				1	2
B. sp. A							1						3	15		1	8	5	5	2	1	6	2	2
B. sp. B											2		22											
B. spp.										1						3		5						
Stilostomella spp.			7	5	7	8	5	8	5	5	2	10	10	3	4	5	11	2	5	8	8	8	6	8
Bulimina miolaevis																								
B. rostrata	6	6	4	1	2	1			4	8	6	9	7	6	5	1	3	5	4		6	4	3	5
B. striata	1											1												
B. spp.				1			2	2	2					1		1								1
Stainforthia complanata	2	3	2	4	3	1			1	1	6	4	12	2	1		1	1		1	1	1		1
Virgulopsis sp.				9	7	7	7	3	7	1	7	10	3	1	1	1	2	5	5	1	7	1	5	5
Uvigerina hispida																	1							
U. peregrina				2	2	5	10	1	5	2			1	2			2		1		2	5		
U. proboscidea												1				1						2		
U. vadescens																								1
U. sp. A									1	1	5	7	2	1	1			2	3	3	3	1	2	1
U. sp. B																								
U. sp. C																								
U. sp. D																								
U. spp.																								
Rectuvigerina sp.																								
Trifarina sp.													1	4	1	3				1	1	1	7	7
Discorbis sp.																			7					
Discorbinella bertheloti			1																					
Epistominella exigua	26	32	8		50	19	35	17	11	42	36	26	27	20	20	21	41	8	18	39	25	17	16	23
E. rotunda	50	22	19	18	11	12	24	13	16	25	10	8	14	9	12	11	9	9	7	12	1	3	6	8
E. rugosa	4	4	8		1		1	1	2	4	6	2	5	1	2	11	6	5	4	13	2	1		1
E. umbonifera			1	1				2									1	1			2	2		2
E. sp.																								
Gavelinopsis lobatulus												1	1											1
Laticarinina alto-camerata					1																			

Note: Number represents no. specimens counted in >63 μm. Planktonic foraminifer zones and DSDP sample nos. in column heads.

Table 2. (Continued).

Miocene																														
late																middle										early				
G. nepenthes	*N. continuosa*															*G. mayeri*					*G. fohsi* s.l.			*O. suturalis*		*P. glomerosa curva*		*G. miozea*		
591-25,CC	591-26,CC	591-27,CC	591-28,CC	591-29,CC	591-30,CC	591-31,CC	591B-1,CC	591B-2,CC	591B-3,CC	591B-4,CC	591B-5,CC	591B-6,CC	591B-7,CC	591B-8,CC	591B-9,CC	591B-10,CC	591B-11,CC	591B-12,CC	591B-13,CC	591B-14,CC	591B-15,CC	591B-16,CC	591B-17,CC	591B-18,CC	591B-19,CC	591B-20,CC	591B-21,CC	591B-22,CC	591B-23,CC	591B-24,CC
		2		1			3			2			3		2	2	1	4	2	2	2	3	2	1	1		2		1	
																						1								
	4		1												2		2						1			1				
					4	1		2	1	1	2		1		3		1		3		2									
	1	1					2																							
											1				1															
	3		7	4		1		1	1		6		2	9	2	4	8	7	4		3	6				1			1	
							1	1			1	1		3		1	2							1						
												1		2		2						3		1						
						1	1								1														1	
	1																					1								
2	6	2			1	1	1			1		1			1															
		1																												
1	5				1	1				1				1				1	1		1									
1		1	2	1	1						3				1												1			
																								1						
30	17	11		14	2				2	2	3		1	1	1							1	1		1	3	1			
		3	1	2	2		1	1	2	2	3		5	5	3		4	1	2	6	5	4	5	7	5	2		1		3
																								1						
	2	1	2	1	4	1					2		3	4	4	4	2	2	4	4	4	2	4	11	6	4				4
1	2		3	2		1	1	3	3	2	1	2	4	3	1	5	2			2		1		2	1					1
		1					1	2	1				2		2	2	1			1			1		2			1		
																	3	1	1	1	1		2	3	6	1		1		6
	1	3		1	2			1	3	1	3	4	5					2	1		4	5	1	2	4	1				2
1																														
2	3	1	2		2	3	3	4		1	1	1	7	1	5				3	1	2		1	4			2	1		1
4	10	8	2	3	2		5	1	3	2	1	4	1	1	3	2	8	2	2	8	6	3	2	4	4	4				2
1	1	1	1	1	2	1				1	1		2			2		2		3		1			2		1			
																								1						
	2		1			1				1														2		1	1			
	1					1																								
	5	4	3	1	2	26	5	8	3	2	2	5	4	5	6	2	14	8	4	12	7	1	1	8		3				1
1			3	1	3	7		7			3	11	3	1	1	20			9	6	4	1	12		3	3	2			2
1	1	4	4	9	5	1	1		10		1				1			2		1										
4	5	4		2				1				3		1	1	2	1	3							8					
											2				1	1									1					
																				1	1			1						1
3		11	11	10	6	2	10	5	5	11	7	4	6	15	10	2	7	15	8	11	11	8	7	19	10	6	1	2	2	11
														1					1								1			
2	7	5	5	1	1	2	5	2	1	3	3	1	2		4	6	7	3	5	5		7	7		1	1				
									1		2									1		1								
					1													2			1							1		
	3		7	2	4	5	5	7			1		2				2		15	21	9		18	1	4	6	1	2		
	1	1	11		1	1			2		1					1														
																							1							
																4														
1	1	3	2		6	18		2			4	1	1	2	6	1	3	5	1		2				1					
														2				1							1	1				
																		5		4	1									
2															2				3	11		3		2		2				
							1																	1						
																								1	1	1			2	
3	3	4	1	4	5	8	4	5			1						1									1				
				1	2						1	1																		
		1																												
10	15	56	44	24	17	28	69	34	40	31	40	52	30	26	28	48	24	33	32	39	30	11	26		6	23	1	1	2	12
6	5	5	3	14	4	11	9	7	20	9	4	12	1	5	15	22	7	8	3			1	3	3	1					1
10	17	12	6	4	5	6	10	9	4	2	4	1	2	1	5	6	10	3	1	1	1									
4	1			1	1		2	1		2	2	2	2	5	2	4	1	20	10	5	8	2	2	14	4		1		1	
2																														
			2	2	1			1																						
						1																								

Table 2. (Continued).

	Quat.			Pliocene																Miocene				
				late										early						late				
	G. truncatulinoides			*G. truncatulinoides*-*G. tosaensis*					*G. tosaensis*		*G. inflata*			*G. crassaformis*				*G. puncticulata*		*G. conomiozea*			*G. nepenthes*	
Benthic foraminifers	591-1,CC	591-2,CC	591-3,CC	591-4,CC	591-5,CC	591-6,CC	591-7,CC	591-8,CC	591-9,CC	591-10,CC	591-11,CC	591-12,CC	591-13,CC	591-14,CC	591-15,CC	591-16,CC	591-17,CC	591-18,CC	591-19,CC	591-20,CC	591-21,CC	591-22,CC	591-23,CC	591-24,CC
L. pauperata																2		1			1			
Stetsonia sp. A																			2					
Valvulineria spp.			1						1				5											
Heronallenia sp. A															2	1					1			
Siphonina australis																								
Eponides tumidulus	5	4																						
Pleurostomella spp.				2	2	1	1	3	3	4	4	5	1	2	1	4	2	7	12	1	8	6	3	2
Cassidella bradyi		1	1		1		1	1				1	2	1	1					3			1	
Francesita advena			1								1				1	1				1		1		
Cassidulina carinata	6		2		6	3																		
C. sp. A	16	15	9	17	12	9	12	6	14	10	20	6	4	4	3	10	19	5	4	5	2	8	6	5
C. sp. B			2	1					2		1	3	2	4	2	1	4	1	3			2		
C. sp. C								1	1	7	6	1	2	1	6	1		2	3					
C. sp. D		1		1		1					1		1					1			2			
C. spp.	2	2		1			4	1	2		3	1	2	1	1		3	5	1	1		1	2	
Globocassidulina subglobosa	6	15	6	7	10	5	14	8	10	16	13	8	6	23	10	12	23	3	14	13	4	6	9	
G. ornata										1		2				1								
Cassidulinoides spp.								1		2					1				1					
Favocassidulina favus														1										
Ehrenbergina hystrix																					1			
E. trigona		1	4	1							2	1												
E. sp.										10	6	2				1	2				1	2	3	
Chilostomella oolina																								
Allomorphina pacifica												1									1			1
Astrononion spp.	5	15	2	4	22	6	7		2		8	5	2	3	4	5	6	1	5	9	2	4	3	4
Nonionella spp.	1		4			2		1			1	4	2	2	2		2			2				
Pullenia bulloides				2			5			1		2	1			1			2	1				1
P. osloensis	6	4	1	3	5	1	6	6	2	4	2	2		5	2	4	7	1	13	3	5		1	
P. quinqueloba	5	4					4	2		1			1				1			3			1	2
P. sp. A		5	2	1	3		1		1	2	2	4	2				1	2	3			3	1	2
P. sp. B			4	2		2		2	2	1	2	1	2		2	2	1	1			1		1	1
P. spp.																		1						
Gyroidina acuta	1		1	2	3	1	2	1			1	1	1		1					2	2	1		1
G. broeckhiana				1																				
G. lamarckiana	2										2	2		1	1		1	1						
G. neosoldanii		1													1				1		1			
G. cf. *quinqueloba*	7	14	2	3	3	4	2	2	3	3	2	1	6		4	2		4					4	7
G. sp. A	4	6	1	3	7	1	3	6	3	3	9	3		1	3	1	4	11	1	1	5	2	2	
G. sp. B			1			9			1	1	3					1								
G. sp. C		1		2	2		4						3							1			3	
G. sp. D															1				1					1
G. spp.		2	6	3	8	8	4	5	3	9	2	2	3	4	2		1		4	4	1	1	1	2
Oridorsalis umbonatus	12	28	18	25	28	16	20	12	5	16	6	10	7	5	2	14	8	2	12	12	15	4	5	12
O. sp.				1				1												1				
Osangularia culter				1		2	3	1	1			1	1	2	1	1		1	4	4	4		1	2
Anomalina sp.																								
Anomalinoides globulosus		1			1					1						2			1					
A. sp. A	5	9		9		4		4	1		7	7	2	2	5	3			2	1	1			6
A. sp. B		7	3	1	3	2	3	2	3	3		1	4	3	5	14				1	2		4	1
A. spp.	6		1	6	2	3	2		4	2	1			1	1	1	2		3			1		1
Cibicidoides bradyi						1	2	1	1	2	2		1	1			1						1	
C. kullenbergi				2		7	1		1	1	3	4	1	3	2	5	3	1	7		2	1	7	
C. mundulus	2	3		2			1		1	1	1	1			3		1			1		2		
C. cf. *opacus*												3	2	3	2	2	4		4	1		1		3
C. pseudoungerianus																								
C. wuellerstorfi	6	1	1	4	3	4	2	6	1	4	1	6	3		1	4	1	1			6	1	6	
C. sp. A	1				3	1	6	1		3	1						2		1					2
C. spp.					1					5	3							1						
Gavelinella sp.															1	1								
Hanzawaia cf. *cushmani*			2		1	1	2							1										
Melonis barleeanum	5		4	4	2		1	2	1	1		2		1			2		2	1				
M. cf. *nicobarensis*	2							1		1		2	1	1	1				2	2				
M. pompilioides	5	5	1	4	14	2	17		1			5	3		1	1	1							
M. cf. *pompilioides*				1			2	2	1			1				2								
M. sp. A																	1		1					
M. spp.									1	1			1											
Hoeglundina elegans	1																							
Miscellaneous benthic foraminifers	10	17	1	4	5	7	1	6	5	3	6	8	2	2	1	3	1	1		5			2	2
Total number of specimens	236	269	163	199	270	192	262	169	163	243	258	230	241	159	152	202	226	148	227	198	185	147	204	156

Table 2. (Continued).

Miocene																														
late																middle										early				
G. nepenthes	*N. continuosa*															*G. mayeri*					*G. fohsi* s.l.			*O. suturalis*		*P. glomerosa curva*		*G. miozea*		
591-25,CC	591-26,CC	591-27,CC	591-28,CC	591-29,CC	591-30,CC	591-31,CC	591B-1,CC	591B-2,CC	591B-3,CC	591B-4,CC	591B-5,CC	591B-6,CC	591B-7,CC	591B-8,CC	591B-9,CC	591B-10,CC	591B-11,CC	591B-12,CC	591B-13,CC	591B-14,CC	591B-15,CC	591B-16,CC	591B-17,CC	591B-18,CC	591B-19,CC	591B-20,CC	591B-21,CC	591B-22,CC	591B-23,CC	591B-24,CC
	1													2	1	1								3	1	3		2		1
																	3	2				1				1			1	
1														1																4
3	4	3		4	3	2	2	6	5	5	11	2	5	22	9	3	12	17	4	7	13	22	5	11	11	5	5	8	3	3
	1	1						4				1	1	1	1	1				1	1		1							
						1	2		1	3					1				1		1				1					
5	10	5	7	3	6	10	10	12	5	10	9	1	14	28	7	14	4	5	10	23	13	9	30	15	17	3		1		4
1									1		1				1	1		3	1		1		1	6	1					
		1	3									1	1				1				1									1
															1			1							2					
1		1		1			1	2		1		1	2			2			1		3	4	4		1	2	2	2		10
6	12	8	8	20	30	19	19	23	14	26	19	12	9	31	15	19	50	41	21	42	8	11	8	56	24	17	1	8	14	10
			1	1								1			2			2		3		3				1				
						1	2		2		3	1		13	7	4	4	1	2											
								2			1				1															
2	1			2																										
									1																					
								1											1											
	4	6	10	2	2	4	6	10	9	15	7			8	3	6	10	6	2	8	10		13	21	14	6	1	2	2	5
	1		1	1	1	1	2		1				3	1	2				2	1			1	1		4				
			1						1	2			2	5	1		3	3	1					1				1		
4	2	1	2	3	1	1		8		8	1	1	3	16	3	5	8	6	1	8	1	7	3	5	10	5	1	3		1
						2	1	1		1	1			3		2		2	6				2		2	3	2			
1				4		2			2	5	6				6	2	3	3	1	4	4	2		5	3	1	2			2
1		1			1					2	2		3	1	1	2	2	1			2	2		2	2					
	1		1		1								1																	
2	2	2		1				1	1		1	1	2	6	2	2	1	3		2	1	4		3	6	9	1		2	4
							1											1		1	1	2			4	1				
		1						2						2					1	1										
				2						2	2		2	1				1		2	1	1			1	1	1			
6	3		3	1	1			1	2	1	5	1		3					6	2	1	1		1			1			
	6	3	6	2	5	6	3	1	4	9	8	7	15	9	9	7	6	4	5	5		1	6			4	3	1	1	4
		1		10	1			1		7	3	1	1	1	6	2	1	3	1	1	3		1	1						
		1							3		4	1	5	4	2	4	4	5	3	2	5	3	1	1		1		2		
		1					9				1					3	2	1				1	1							
1	3	3	4	4	6	2			5	9	4		5	6	5	3	4	4	3	3	2	2	10	5	3	3	3			6
7	7	5	9	17	8	5	16	16	9	14	10	5	20	26	16	21	26	20	17	12	21	26	26	27	30	19	7	11	5	18
		1									1			1			1		2	3	1	1								3
		3	1	1	3			3		1	2	3	2	4	4		3	1	2		4				1		2		2	
														1					2									1		
				2	1		1	2					1				1	2		2	1	2	2				1			1
4				2	1	4	2		1	1	9	6				3	6	1	6	7	6	4			1	5	1	1		
4	4		1	2		5	1	2	1	1		2		1							2		1							
1	1	1	2	3	1		1	1					5	9	5	14	3	2	1	1	3	5	6		1	1	1		1	
					3						4			7	2	1		1		3					3					3
	9		2	9	2	3	13	3	5	5	13	6		13	6	7	30	3												
		1					2	2	6			4		7	2	1		3	6	2	2	2	2	6	2	9	5			3
6							3		2	1	3					7	10	4	8	13	9	9	3	17		3		1	1	1
																									1					1
		1		2				2		1	1	2	11	1	1			8	10	18	11	14	11	12	29	13				1
		1	2					1		2	3	2																		1
											1		1		1			2		1	1	3		2	2				1	1
											1									1	1			1	1					
				1					2		1	5	1	1																
									3	2		1	3		1	1		1	5	6	4	6	5		7	4				
													2		1		1	2		3		1								
					2						1	2	9		4															
										1																				
													1		1								2			4	1	1		1
	1																								1				1	
2	2	3	2	4			3	6	4	1	3	1	1	3		3	4	4	2	6	1	1		3		1	1		1	9
150	198	201	190	210	166	197	240	218	192	213	248	178	220	332	244	284	314	299	249	340	244	216	242	296	255	194	57	55	45	145

ous faunas are contained throughout the Neogene section. P/B ratios are lower than at the two shallower sites, probably because some planktonic foraminiferal tests were dissolved or broken at this greater water depth. The ratios range from 8:1 to 1864:1 (Fig. 4). In the early Miocene, the ratios are high and average value is 454:1. P/B ratios are rather constant after the early Miocene and mostly average less than 100:1.

The stratigraphic distribution of benthic foraminifers is shown in Table 3. The most important species in this site include *Epistominella exigua, Globocassidulina subglobosa, E. rotunda, Epistominella umbonifera* (Cushman), *Bolivina pusilla, B. decussata, Oridorsalis umbonatus*, and *Cassidulina* sp. A. Almost all species at this site are also commonly found at the other two sites. Species occurring more frequently than at the other two sites are *Buliminella* sp., *E. umbonifera, Favocassidulina favus* (Brady), and *Stetsonia* sp. A. The following species, which occur at the other two sites and are absent from this site include *Seabrookia earlandi* Wright, *Cibicidoides kullenbergi* (Parker), and *Gyroidina broeckhiana* (Karrer).

Early Miocene assemblages were dominated by *G. subglobosa* and *E. exigua*. Other important species include *Bolivina pusilla, B. decussata, Oridorsalis umbonatus, Cassidulina* sp. A, and *Stetsonia* sp. A.

In the middle Miocene and early late Miocene (*Neogloboquadrina continuosa* Zone), the assemblages were also dominated by *G. subglobosa* and *E. exigua*. No significant change of dominant species was recognized between the early and middle Miocene assemblages at this deepest site. Other important species include *O. umbonatus, Bulimina rostrata* Brady, *Cassidulina* sp. A, and *Bolivina decussata*.

In the late late Miocene (*Globigerina nepenthes* Zone), the assemblages were dominated by *E. umbonifera*. Other important species include *E. exigua, Globocassidulina subglobosa*, and *Cassidulina* sp. C. *Cassidulina* sp. A almost disappeared during this interval.

Early Pliocene assemblages were again dominated by *G. subglobosa* and *E. exigua* as in the early to early late Miocene. Other important species include *E. rotunda, Oridorsalis umbonatus*, and *Virgulopsis* sp.

In the late Pliocene, the assemblages were dominated by *E. rotunda* and *E. exigua*. *Epistominella rotunda* markedly increased in abundance during this interval. Other important species include *O. umbonatus, G. subglobosa, E. umbonifera*, and *Melonis pompilioides* (Fichtel and Moll).

Quaternary assemblages were dominated by *E. exigua*. This species slightly decreased in frequencies near the Pliocene/Pleistocene boundary. Other important species include *E. rotunda, Cassidulina* sp. A, *O. umbonatus, G. subglobosa*, and *Virgulospsis* sp. The changing species dominance of benthic foraminiferal assemblages for Site 206 is summarized in Figure 5.

COMPARISON OF BENTHIC FORAMINIFERS AMONG THE THREE SITES

The distribution of important benthic foraminiferal species among the three sites is shown in Figure 6. Among the genera occurring in the three sections, *Epistominella* shows highest frequencies in most part of the sections. *Globocassidulina, Cassidulina, Oridorsalis, Gyroidina*, and *Bolivina* occur frequently in the three sites. Other genera, including *Cibicidoides, Uvigerina, Pullenia*, and *Stilostomella*, rarely exceed 10% of the fauna. *Bolivina* was found to occur in high frequencies in the early Miocene.

Dominant species prevailing in the three sections are *E. exigua, E. rotunda*, and *Globocassidulina subglobosa*, which usually occur in frequencies between 10 and 30%. The average size of specimens of these three species is small (< 150 μm). Other dominant species, such as *Oridorsalis umbonatus, E. umbonifera*, and *Cassidulina carinata*, show a more restricted stratigraphic distribution.

In the early Miocene, *G. subglobosa* was the dominant element of benthic foraminiferal assemblages in all three sites. *Globocassidulina subglobosa* was associated with other dominant species such as *E. exigua* in the deepest site and *O. umbonatus* at the intermediate site. In the early middle Miocene, *E. exigua* migrated upslope and became dominant at the intermediate and shallowest sites (Sites 590 and 591), whereas *G. subglobosa* decreased in importance at these two sites. However, *G. subglobosa* remained dominant with *E. exigua* at the deepest site for much of the remainder of the Neogene. The stratigraphic range over which *E. exigua* dominated varies from site to site, but *E. exigua* maintained near constant abundance in the deepest site. This species remained the dominant form until the beginning of the Quaternary at intermediate Site 591, but was replaced as the dominant species by *E. rotunda* in the shallowest Site 590 during the late Miocene. *Epistominella umbonifera* was dominant during the late Miocene only at deepest Site 206. *Epistominella rotunda* appeared earlier as an important form at shallower Site 590 in the late Miocene and remained dominant in the Pliocene and Quaternary. This species appeared as a dominant species at the deepest Site 206 in the late Pliocene and at intermediate Site 591 in the Quaternary. Assemblages dominated by *Cassidulina carinata* appeared in the late Quaternary only at the shallower site.

Among the three sites, faunal successions are most similar between the two shallowest sites (Sites 590 and 591). The deepest site (Site 206) differs in composition and distribution of dominant species. Major faunal changes of benthic foraminiferal assemblages often occurred during the same time intervals among the three sites (Fig. 5). Major changes in benthic foraminiferal assemblages occurred during the middle Miocene at Sites 590 and 591; the late Miocene at Sites 590 and 206; and near the Pliocene/Pleistocene boundary at Sites 591 and 206.

RESULTS OF FACTOR ANALYSIS

Site 590

The factor analysis of the benthic foraminifers of Site 590, which employs 5 factors, incorporates 88% of the faunal variance. Four distinct faunal assemblages are recognizable as follows (Fig. 7):

Factor 1: This assemblage (factor) is dominated by *Epistominella rotunda* and *Cassidulina* sp. A (39% of the faunal variance).

Factor 2: This assemblage is dominated by *Globocassidulina subglobosa* and *Oridorsalis umbonatus* (10% of the faunal variance).

Factor 3: This assemblage is dominated by *E. exigua* (28% of the faunal variance).

Factor 4: This assemblage is dominated by *Bolivina pusilla*. Other important species include *Cassidulina* sp. A, *Virgulopsis* sp., *E. rotunda*, and *Siphonaperta* sp. (7% of the faunal variance).

Distribution of these four assemblages in Site 590 is summarized as follows. The early and early middle Miocene was characterized by oscillating dominance of the *G. subglobosa-O. umbonatus* assemblage (factor 2) and the *B. pusilla* assemblage (factor 4). During the middle middle Miocene to middle late Miocene, the *E. exigua* assemblage (factor 3) became dominant and the *E. rotunda-Cassidulina* sp. A assemblage (factor 1) increased in importance. During the middle late Miocene to Quaternary, the fauna was dominated by the *E. rotunda-C.* sp. A assemblage. In the Quaternary the *G. subglobosa-O. umbonatus* assemblage increased once again in importance.

Site 591

Factor analysis of the benthic foraminifers at this site (5 factors; 87% of the faunal variance) shows that five distinct faunal assemblages are recognizable, as follows (Fig. 8):

Factor 1: This assemblage is dominated by *Epistominella exigua* (35% of the faunal variance).

Factor 2: This assemblage is dominated by *Globocassidulina subglobosa* (16% of the faunal variance).

Factor 3: This assemblage is dominated by *E. rotunda*. Other important species are *Cassidulina* sp. A and *Oridorsalis umbonatus* (12% of the faunal variance).

Factor 4: This assemblage is dominated by *Siphonaperta* sp. Another important species is *E. rugosa* (11% of the faunal variance).

Factor 5: This assemblage is dominated by *O. umbonatus* and *Cibicidoides wuellerstorfi*. Other important species include *E. rotunda, Virgulopsis* sp., and *Cassidulina* sp. A (14% of the faunal variance).

Distribution of the five assemblages in Site 591 is summarized as follows. The early Miocene to early middle Miocene was dominated by the *O. umbonatus-C. wuellerstorfi* assemblage (factor 5) and at times by the *G. subglobosa* assemblage (factor 2). During the early middle Miocene to middle late Miocene the fauna was dominated by the *E. exigua* assemblage (factor 1). During the middle late Miocene to earliest Pliocene the *Siphonaperta* sp. assemblage (factor 4) increased in importance, while the *E. exigua* assemblage still remained important. During the early late Pliocene to Quaternary the *E. rotunda* assemblage (factor 3) became dominant.

Site 206

Factor analysis of the benthic foraminifers of Site 206 (5 factors; 88% of the faunal variance) shows that five distinct faunal assemblages are recognizable, as follows (Fig. 9):

Factor 1: This assemblage is dominated by *Globocassidulina subglobosa*. Another important species is *Oridorsalis umbonatus* (24% of the faunal variance).

Factor 2: This assemblage is dominated by *Epistominella rotunda*. Other important species include *O. umbonatus, Cassidulina* sp. A, and *Uvigerina peregrina* (23% of the faunal variance).

Factor 3: This assemblage is dominated by *E. umbonifera*. Another important species is *Cassidulina* sp. C (12% of the faunal variance).

Factor 4: This assemblage is dominated by *E. exigua*. Another important species is *E. rotunda* (20% of the faunal variance).

Factor 5: This assemblage is dominated by *Bolivina pusilla*. Other important species include *B. decussata* and *E. exigua* (9% of the faunal variance).

Distribution of the five assemblages in Site 206 is summarized as follows. The early early Miocene was dominated by the *G. subglobosa* assemblage (factor 1) and the *E. exigua* assemblage (factor 4), which, in turn, were replaced during the late early Miocene by the *B. pusilla* assemblage (factor 5). This, in turn, was replaced during the latest early Miocene by the *E. exigua* assemblage (factor 4). During the early middle Miocene to early Pliocene faunas were mostly dominated again by the *G. subglobosa* assemblage as well as at times by the *E. umbonifera* assemblage (factor 3), which particularly dominated during the late Miocene. During the late Pliocene, faunas were dominated by the *E. rotunda* assemblage (factor 2). The late Quaternary was again dominated by the *E. exigua* assemblage.

The distribution of the benthic foraminiferal assemblages revealed by the factor analysis is shown in Figure 10 for the three sites. The analysis shows that the most of the assemblages tend to be dominated by single, rather than multiple, species. Only about eight species can be considered to represent dominant Neogene forms at these locations and depths on the Lord Howe Rise. Other species may be persistent, but are never dominant elements in the assemblages.

Changes in the assemblages revealed by the factor analysis (Fig. 10) are generally similar to observations based on the changes in species frequencies as summarized in Figure 5. The factor analysis allows greater assemblage subdivision in the early Miocene, when there tended to be more rapid oscillations in faunal dominance.

DISCUSSION

Paleoceanography

Benthic foraminifers tend to be relatively unchanging for long intervals of time because of the relative conservatism of the deep-sea environment. Although large numbers of benthic foraminiferal species are present in deep-sea assemblages, only a few species tend to dominate the assemblages, and it is their fluctuations that mark the important changes in the assemblages through time. The frequency changes of dominant forms usually vary from 10 to 30%, which is quite large compared with most other species. The changing relative dominance

Table 3. Distribution of benthic foraminifers at Site 206.

	Quaternary									Pliocene								
										late							early	
	G. truncatulinoides									*G. truncatulinoides*-*G. tosaensis*			*G. tosaensis*		*G. inflata*		*G. crassaformis*	
Benthic foraminifers	206-1,CC	206-2,CC	206-3,CC	206-4,CC	206-5,CC	206-6,CC	206-7,CC	206-8,CC	206-9,CC	206-10,CC	206-11,CC	206-12,CC	206-13,CC	206-14,CC	206-15,CC	206-16,CC	206-17,CC	206-18,CC
Bolivinopsis cubensis																		
B. sp. A																		
B. sp. B																		
Vulvulina pennatula																		
Textularia spp.	3	1		1	1		1		1		1		1	1				2
Siphotextularia rolshauseni	2				3	1			1	1	1		4		2	1		1
Dorothia brevis	1																1	
Eggerella sp. A	4	1	2	2	1	2	6	3	5	2	7		2	5		4	10	6
E. sp. B				1										1	1		2	
Karreriella bradyi																		
Martinottiella spp.										2						1		
Ophthalmidium pusillum		1			1		1					1					1	
Quinqueloculina venusta	3	1	2		6	4	1	1	2		1	2	1	1			2	
Q. spp.																		
Pyrgo murrhina							5	1	1		3			1		1	2	1
P. serrata											1							
P. spp.					3					1				1				
Sigmoilina edwardsi			1	1		3	1					2			2	1	2	1
S. tenuis																		
Siphonaperta sp.				1	2			1				3		1	1			
Triloculina tricarinata	1																	
Nodosaria spp.									1	1	2	1	3			1		1
Astacolus sp.																		
Dentalina spp.			1	1	1	2		1	1			2	1	1		1	1	
Lagena spp.	4	1	3	1	1	1		1			2			1		3		
Lenticulina spp.								1						1	1	1		1
Marginulina sp.																		
Vaginulina sp. A																		
Pyrulina spp.	1	1				1		1					1		1	1	2	2
Oolina spp.	1	2		1	1		1	1	3		2		2	2	2	1		1
Fissurina spp.	1	1	2		3	4	6	5	4		3	1	2	3	2	4	8	2
Parafissurina spp.	1	1	2		1							1				3		
Buliminella sp.													4			1		
Sphaeroidina bulloides	1		2		1		1		1		3		1	6	1			1
Bolivina decussata				3					1				4	2	2	1	6	
B. minuta				2									1					
B. pusilla				1							1							
B. cf. *robusta*																		
B. seminuda	1	4	6	1	1	2	5		5	2	3	5	4	2	10	4	8	
B. sp. A	1	1					1											
B. sp. B																		
B. sp. D				4														
B. spp.				2	1					1								
Stilostomella spp.				8		1	1	1	7			5			3	3	8	4
Bulimina miolaevis																		
B. rostrata						1	2									1		
B. striata							1											
B. translucens																		
B. spp.	2		2							1	1		1	1				3
Stainforthia complanata	3	4	2	1	2		2	3	2	2				1				
Virgulopsis sp.	6	6	1	1	14	13	9	5	11	3	3	6	6	3	1	9	9	5
Uvigerina peregrina	7	6	2	1	22	8	17	16	3	1		2	2	6	4	2	4	5
U. vadescens				1														
U. sp. A													5	4	3	2	5	
U. sp. B													1	1				
U. sp. C																		
U. spp.																		
Trifarina spp.			1	7													1	1
Epistominella exigua	48	30	36	19	42	24	23	11	9	15	17	33	12	46	22	42	23	20
E. rotunda	18	11	11	7	32	8	14	26	28	47	12	36	11	22	38	28	12	19
E. rugosa	1			5	1		2	3	1		1	1		1		7		
E. umbonifera									2	1	3		24	28	14	2	13	5
E. sp.			1															

Note: Number represents no. specimens counted in >63 μm. Planktonic foraminifer zones and DSDP sample nos. in column heads.

Table 3. (Continued).

Pliocene		Miocene																						
early		late				middle						early												
G. crassaformis		*G. nepenthes*			*N. continuosa*	*G. mayeri*		*G. fohsi* s.l.			*O. suturalis*	*P. glomerosa curva*	*G. miozea*		*C. dissimilis*		*G. trilobus*		*G. zealandica incognita*			*G. dehiscens*		
206-19,CC	206-20,CC	206-21,CC	206-22,CC	206-23,CC	206-24,CC	206-25,CC	206-26,CC	206-27,CC	206-28,CC	206-29,CC	206-30,CC	206-31,CC	206-32,CC	206-33,CC	206-34,CC	206-35,CC	206-36,CC	206-37,CC	206-38,CC	206-39,CC	206-40,CC	206-41,CC	206-42,CC	206-43,CC
							1	2	1	1														2
														1	2	1		1		2	2	2	3	3
														1										
											1													
								1		1			1											
						1		1			2					1	1			1				
					1			1																
5		9	2	3	1	1	2	2	4	6	1	3	2		3		2		1		1	3		2
			2		1	2					1	1							1			2		
										1							2							
		1																						1
															1									
		1		1					1	4	1													
													1										1	
		1																						
1	2	4										1												
1	2	2			1					1			2											
					1						1													
				1			2	3					7			1		1						
		5	5	2	1		1	2	2	1	3			1			1	2	1		5	1	3	
														1			2		1					
		3		2	4	5	6	5	4		2	3	4	3		1	4	3	2	3	5	1	1	
2		1	2	1			2				1	2	2	3	1	1	1		2	1	1	1	1	
1			1		2							1					2	2	2	1		2		
										1														
								1						1		1						1		
1	2			1				1					2			1						1		
2		3	3		1		1	2		1	3	1	2		2		1	1		1		2	5	
5	7	5		2	1	5	1			1	2	5		1	2	3	4	3	2	1		5	4	
	1		1		2		1				1		1				1		1	3	1	3	1	
		1			2			1								1	1	3	1	5	2			
2	1				1																			
6	23	1	7	4	2	2	5	9	3	1	6	6	8	7	9	17	9	55	6	2	27	4	7	6
				3																				
										18		6	5	8	29	21	64	7	26	2	21			
1								1			1			4	1	2	3	1	1				8	7
3	4		1	1			1																	
																						3	8	
													1			1			1			1	3	
								1						1		3	3	4	2	1	3	3	17	5
														2			1	1					1	
4	4		6	9	6	9	9	10	7	12	9	7	31	13	8	14	19	18	18	17	29	8	7	6
														1										
1	3	3	3	1	7	7		7	2	11	6	6	3											
																								1
												3	2	4	2	3	5	2	15	4	8	1	3	
						1						2	4		4	4	4	5	3		5	3	4	2
	1																							
10	11								2						2	1	2	1	2	1	1			14
	2					1													1		1			
8	15		1	3	5	5	15			4					2			3		1		1	8	3
	1	4		2		1	2																	
									4	7	4				1									
			1							1											1		1	
							5							1			1							
37	29	29	14	22	22	5	21	38	37	30	14	27	47	70	25	39	38	25	45	28	9	36	16	48
6	9	6		1	5	3	3	1		1	6	2			5	18	6	3	5	3			1	1
23	18	1			2	2	3	1	1	2	4	7	8			5	3	4	2	1	2		1	1
		37	50	29	2	1	2	5	4	6	6	3	7	1	3	2	1	2	13	4	8	2	2	

Table 3. (Continued).

	Quaternary									Pliocene								
										late							early	
	G. truncatulinoides									G. truncatulinoides–G. tosaensis			G. tosaensis		G. inflata		G. crassaformis	
Benthic foraminifers	206-1,CC	206-2,CC	206-3,CC	206-4,CC	206-5,CC	206-6,CC	206-7,CC	206-8,CC	206-9,CC	206-10,CC	206-11,CC	206-12,CC	206-13,CC	206-14,CC	206-15,CC	206-16,CC	206-17,CC	206-18,CC
Laticarinina alto-camerata																		
L. pauperata						1					3			2			1	1
Stetsonia sp. A																		1
S. sp. B						1			1	4								
S. sp. C								1					2					1
Heronallenia sp. A																		
H. sp. B																		
Eponides tumidulus	8	2			1				2		2		1					
Pleurostomella spp.				3	3	1			1		1	1	6	5	2	5	7	2
Cassidella bradyi	12	3	2		2	1			1	4					3			1
Francesita advena					1			1	2		1	3	1		2	6	2	
Cassidulina carinata		1	12	2		1			1								1	
C. sp. A	15	11	17	26	14	4	11	12	13	20	2	3	2	10		5	6	12
C. sp. B		1		3									1	5	12	4	5	2
C. sp. C									1	5		4	8	7	6	11	4	
C. spp.	2	4			4	3	4	3	3	13		1	3	2		3	3	2
Globocassidulina subglobosa	15	12	13	21	11	9	10	9	16	9	7	22	13	8	5	9	19	28
G. ornata																		
Cassidulinoides spp.				1										2				
Favocassidulina favus	3						1	1	3			1	1	1		3		
Ehrenbergina hystrix																		1
E. trigona	2																1	1
Chilostomella oolina		2			1	1							1					
Allomorphina pacifica													1					
Astrononion spp.		1	1	3	6	3	2		5	1	10	1	2				4	1
Nonionella spp.									1			1	4		1	1		
Pullenia bulloides			1				1	2			1		3	1	1			
P. osloensis	14	7	4		5	3	10	5	6	3	5	5	2	3		4	4	2
P. quinqueloba						2	3		1		2		3			2	1	
P. sp. A	7	2	6		29	9	9	11	3	6	5	8		4	1	3	5	1
P. sp. B	3	3			1			2	1		3	4	4	3		2	1	1
P. spp.				1	1			1			1					2		
Gyroidina acuta				1				1			2	1	2			2		
G. lamarckiana			1					1					2			1		1
G. neosoldanii																	3	
G. cf. *quinqueloba*				2					1		3	2	7	11	5	2	7	5
G. sp. A	1	1		1	1	5	5	1	4		5	1	2	1	1	1	9	1
G. sp. B				1						3	1	4	1	10			4	
G. sp. C							1		1			4						
G. spp.	3	5	9	2	9	4	1	8	4	6	8	9	3	16	4	10	1	5
Oridorsalis umbonatus	8	11	12	5	20	12	18	17	18	11	16	15	6	9	16	13	16	8
O. sp.													3					
Osangularia culter				1														
Anomalina sp.												5						
Anomalinoides globulosus		1				2											1	
A. sp. A	2	3	4	1	6	8	3			1	4		1	1			5	
A. sp. B		1	1				1											
A. sp. C		1				1										2		2
A. spp.	1	5	10	3	1	1	5		1	4	1	3		4	1	2	1	1
Cibicidoides bradyi	2					1	2	2		2	4				1		2	
C. lobatulus							1		1									
C. mundulus					1		1	2		1	3		2			1	2	3
C. cf. *opacus*																		3
C. wuellerstorfi	4		2		5	3	3	3	5	1	11	1	3	6	3		7	1
C. sp. A	1				2		2			2		1	1		2			
C. spp.	1		1							3	1	2	2	1		1		
Gavelinella sp.																		
Melonis barleeanum	3					4		2	4		2	2	1	1	1	6	2	2
M. cf. *nicobarensis*	2	3		1									1	1	1		2	1
M. pompilioides	7	3	1	1	2	1	1	2	6	2	14	6	9	4		1	2	1
M. sp. A																		
M. spp.				1			1											
Miscellaneous benthic foraminifers		8	6	7	6		1		5	1	1	4	7	2	6	3	2	1
Total number of specimens	226	163	180	159	272	156	197	168	200	182	186	215	204	262	184	230	250	173

Table 3. (Continued).

Pliocene		Miocene																						
early		late				middle						early												
G. crassaformis		G. nepenthes			N. continuosa	G. mayeri		G. fohsi s.l.			O. suturalis	P. glomerosa curva	G. miozea		C. dissimilis		G. trilobus		G. zealandica incognita			G. dehiscens		
206-19,CC	206-20,CC	206-21,CC	206-22,CC	206-23,CC	206-24,CC	206-25,CC	206-26,CC	206-27,CC	206-28,CC	206-29,CC	206-30,CC	206-31,CC	206-32,CC	206-33,CC	206-34,CC	206-35,CC	206-36,CC	206-37,CC	206-38,CC	206-39,CC	206-40,CC	206-41,CC	206-42,CC	206-43,CC
																					1			
1		2		2		1					1				1							1		
		2	1	2	2	2		6	1	1	4		2	4		15	11	4	14		9	6	4	1
													1											
				2	1	1							2		2	1	1	1	1	1		1	2	
					1																1		3	6
	1																							
8	5	5	3	7	8	9	6	13	5	4	4	7		11	5	5	5	8	9	5	8	15	6	6
		2	2																8	1				
	3	1		1		1		1			1	1	2			1								
2		1				2	3	10	1	7	10	5	6	9	6	17	4	15	7	21	5	1	5	3
1	1											1		1										
	7	14	12		4	2	1	1	1		1	14				9	5	4	1		4			
1	3	2	1	2		1	4	2	3	3		1	6		2	7	11	12	2	7	5	14	15	4
38	34	14	21	11	31	17	20	43	40	21	36	5	15	42	23	13	32	47	20	50	51	25	65	27
	2																							
				1		4					4		1											
2	2																							
		1		1			8																	
									1		1													
1	2		2	2	3	6				1		6	3	7	8	6	4	3	1	5	2	3	7	14
			1							2			1				3	1			1	2	1	
	1		1	1		1	2		1	2		4	2	2				3				3	1	3
1	1	3	1	3	8	1	1	2	3	4	2	11	4	3	4		2	3	1	5		11	2	6
	6	7	1					3	1		1	3				4			5			2	1	4
3	9	1	14	2	12	3	2	4	2	4		1	2			1	1			1	1	10		
	4		2	9	2	4	10			1			4			3	1		1			2		
4	1			1	2		2				2			1	1		1	1			1	1		1
	2	1		1			2	1	2	6	2	5	1	6	4	2	3		10	1	1	6	5	
1										2			1											1
																		1						
3	4	3	6	6	5	4	4	1	3	4	8	2		3		4	2	1	5	5	2	3	1	4
		8	5	3	15	11	3		1	5			1	5	1	1			9	2	2	2	4	3
7	2	5	1	2	2	4	8	1	3	6	5	2	10	6	2	4	1	4	6	4		1	1	2
		3						1	2		4	1		1	1	3	4		3	3	3	1	1	2
1	1	5	3	4	8	3	7	10	2	2		4	3	4	2	2	4	4	1	3	4	1	3	1
7	16	16	5	7	13	15	16	17	14	7	10	3	13	7	9	16	33	8	11	15	17	17	25	4
	1			1	1				1	1		2												
						2																		
		2			3		2	1		3		2	2		1	2	2	1	2					1
1		5	1	3	1		2	10	11	5	4			2	1	1			4	3	2			6
													4	2										
2	2	4	5	1	1	1	2	3	1	6	3	4	4	2	2	1	1	1	3	5		7	13	3
	1			1			1				1			1	1		3				2	1		
1	5	2	1	5	3	6		1	3		3	8	3	3	1	4	4	1	4	4	6	3	5	2
									1															
3		1		2	3	2	1	1	2	1		1												
3						1																		
	2				1						1			3	1		2	5		1		5	2	2
1																	1							
1	2	1	1	1	2	2	5	5	5		2	4	5							1		7	8	
	1																							
1	1	1											1			1								
										1														
	3				3		2								1			1		1	1	1		
4	10	8	2	6	10	4	7	3	8	3	5	6	4	25	4	6	4	4	4	4	5	5	9	1
217	270	237	191	178	215	161	204	235	190	213	190	189	243	274	185	270	326	280	286	230	266	243	295	210

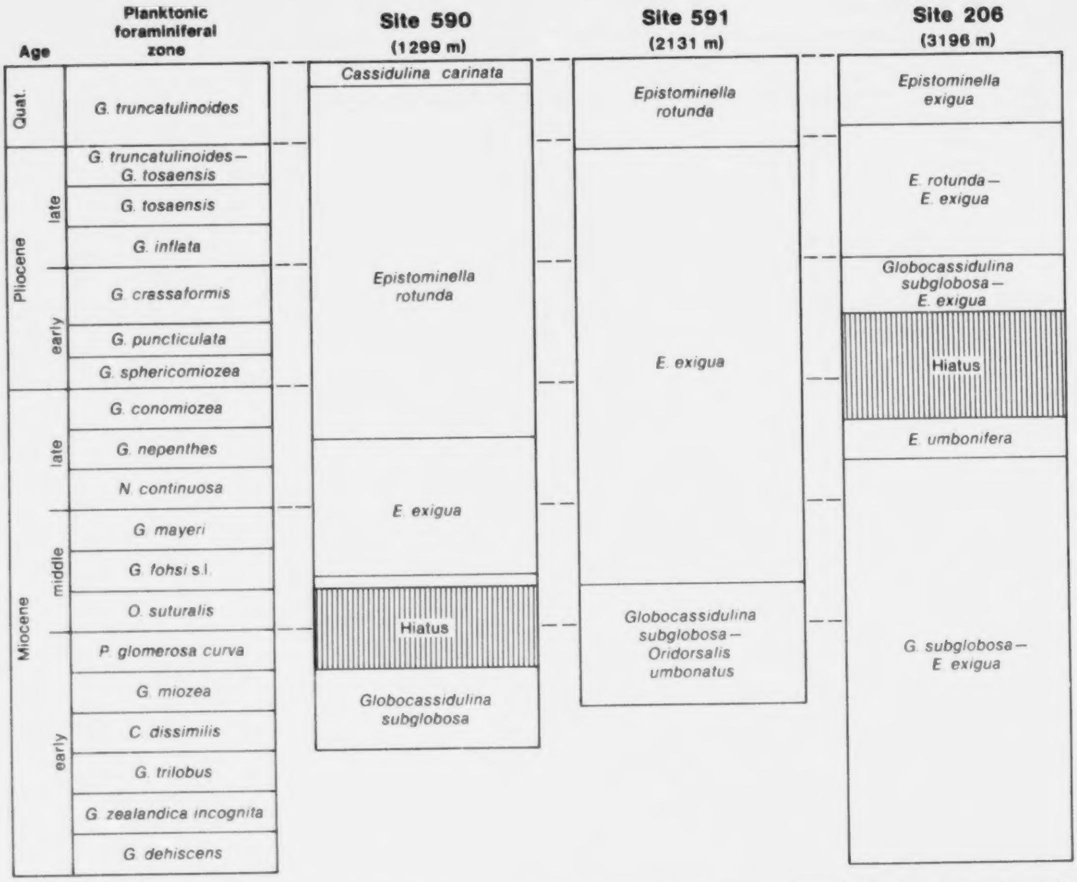
Age
Planktonic foraminiferal zone
Site 590
(1299 m)
Site 591
(2131 m)
Site 206
(3196 m)
Quat.
Pliocene
late
early
Miocene
late
middle
early
G. truncatulinoides
G. truncatulinoides– G. tosaensis
G. tosaensis
G. inflata
G. crassaformis
G. puncticulata
G. sphericomiozea
G. conomiozea
G. nepenthes
N. continuosa
G. mayeri
G. fohsi s.l.
O. suturalis
P. glomerosa curva
G. miozea
C. dissimilis
G. trilobus
G. zealandica incognita
G. dehiscens
Cassidulina carinata
Epistominella rotunda
E. exigua
Hiatus
Globocassidulina subglobosa
Epistominella rotunda
E. exigua
Globocassidulina subglobosa– Oridorsalis umbonatus
Epistominella exigua
E. rotunda– E. exigua
Globocassidulina subglobosa– E. exigua
Hiatus
E. umbonifera
G. subglobosa– E. exigua

Figure 5. Dominant benthic foraminiferal species in assemblages at Sites 590, 591, and 206, as determined using changes in species frequencies (water depths in parentheses).

of a few species, particularly *Epistominella exigua, E. rotunda, and Globocassidulina subglobosa*, as well as *E. umbonifera, Cassidulina carinata*, and *Oridorsalis umbonatus*, define the major faunal changes that have occurred in these three sites.

Major faunal changes of benthic foraminiferal assemblages occurred in the early middle Miocene, late Miocene, and near the Pliocene/Pleistocene boundary. These faunal changes reflect global paleoceanographic events. A marked faunal change occurred in the early middle Miocene at about 14 Ma. *Globocassidulina subglobosa*, which prevailed as the dominant element in the early Miocene assemblages, was replaced by *E. exigua*, which had been the dominant element at the deepest Site 206 during the early Miocene. *Epistominella exigua* was probably associated with the water mass at the bottom of the New Caledonia Basin and migrated upslope to shallower depths during the early middle Miocene. Accordingly, dominant species of the early Miocene assemblage at the shallower two sites, namely, *G. subglobosa* at Site 590 and *G. subglobosa* and *O. umbonatus* at Site 591, were replaced by *E. exigua* in the early middle Miocene. This may suggest a shallowing of the deeper water masses within the New Caledonia Basin to water depths of at least 1300 m during the early middle Miocene. This circulation change was probably related to the development of the Antarctic ice sheet, which caused a change in the intermediate water mass structure of the southern oceans. In the three Leg 90 sites studied, high P/B ratios were recognized in the early Miocene; they decrease dramatically during the middle Miocene event (Fig. 4). In contrast, P/B ratios at Site 289 in the equatorial Pacific were shown to increase during the early middle Miocene, synchronously with the characteristic middle Miocene enrichment in $\delta^{18}O$ (Woodruff and Douglas, 1981). The differences in the P/B ratio changes probably resulted from the different size fractions studied. However, the reasons for these differences remain unresolved.

Another faunal change is found in the *Globigerina nepenthes* Zone of the late Miocene. By then, *E. exigua* prevailed as the dominant species in all three sites. However, *E. exigua* shows a decrease in frequencies during the *G. nepenthes* Zone at Site 590, and was replaced by *E. rotunda* at this time. Synchronously with this faunal change, assemblages at Site 206 became temporarily dominated by *E. umbonifera*. This species is abundant in Cenozoic sections of deeper DSDP sites of the Pacific

(Resig, 1976), and is associated with Antarctic Bottom Water in the Atlantic Ocean (Streeter, 1973; Schnitker, 1974) and in the Indian Ocean (Corliss, 1978). The temporary dominance of *E. umbonifera* at Site 206 may indicate the influence of deep water masses, probably Antarctic Bottom Water, during the late Miocene. Bottom-water temperatures may have cooled at the three sites during this time. This faunal change coincided with the latest Miocene carbon isotope shift (6.2 Ma) in marine sequences (Keigwin, 1979; Loutit and Kennett, 1979; and others), and with other numerous paleoceanographic changes which occurred during the latest Miocene (Kennett, 1983).

Remarkably high sedimentation rates were also found in the early Pliocene of Site 591 and were calculated to be as high as 131 m/m.y. High sedimentation rates were also recognized in the Pliocene of Site 590 (57 m/m.y.). Such high rates of calcareous biogenic materials are considered to be due to high biogenic productivity. The sediments consist mostly of planktonic foraminifers and calcareous nannofossils. An increase in the P/B ratio at this time may be expected because of the increased productivity of planktonic foraminifers. The average P/B ratio of Site 591 in the early Pliocene, during which the highest sedimentation rates were recognized, is only slightly higher than ratios in the Quaternary and the late Pliocene, and is comparable to late Miocene ratios (Table 4). The early Pliocene P/B ratios are an order of magnitude smaller than the early Miocene ratios. P/B ratios are not significantly higher during the high sedimentation rate interval in Sites 591 and 590. However, it is noteworthy that Site 591, at which highest sedimentation rates were calculated, shows higher P/B ratios than Sites 590 and 206 throughout the section. Site 591 has been marked by higher productivity of planktonic foraminifers than the other two sites since the early Miocene.

A number of interesting changes in the composition of benthic foraminiferal assemblages can be found in the latest Pliocene and early Quaternary within the *Globorotalia truncatulinoides–G. tosaensis* Zone and the *G. truncatulinoides* Zone. Major changes occurred in the distribution of *E. exigua*, which became more dominant at the deeper Site 206 and less dominant at the shallower Site 591 (Fig. 5). The data suggest that *E. rotunda* migrated to deeper water in the latest Pliocene, probably in association with an expansion of intermediate water masses. *E. exigua* became more restricted as an abundant form to deeper waters. Distinct surface-water cooling of the southern oceans was associated with the development of Northern Hemisphere glaciation during the late Pliocene. This cooling of high-latitude surface waters may have played an important role in the final development of intermediate water structure in the southwest Pacific.

Table 4. Planktonic/benthic ratios at Sites 590 and 591.

Age	Site 591 P/B ratios	Site 591 Avg.	Site 590 avg.
Quaternary	210:1–593:1	343:1	153:1
late Pliocene	179:1–753:1	490:1	79:1
early Pliocene	420:1–1662:1	756:1	141:1
late Miocene	151:1–2775:1	713:1	181:1
early Miocene	2121:1–10,674:1	6147:1	2522:1

CONCLUSIONS

1. All samples examined from Sites 590, 591, and 206 are dominated by relatively small individuals of benthic foraminifers in the size fractions between 63 and 150 μm. Foraminiferal tests smaller than 150 μm make up from 50 to 99% of the assemblages and average 78 to 89% at the three sites. This demonstrates the importance of studying the small size fraction of Neogene deep-sea benthic foraminifers.

2. Planktonic to benthic foraminiferal ratios (P/B ratios) were examined in the fractions larger than 63 μm. The ratios range approximately from 50:1 to 10,000:1. Benthic foraminifers comprise between 0.01 and 2% of the total planktonic and benthic populations. P/B ratios indicate similar trends at the three sites. High P/B ratios occur in the early Miocene, and decrease over the early/middle Miocene boundary. The ratio remains low and almost constant with several minor peaks from the middle Miocene to the Quaternary. The decrease of the P/B ratios at the early/middle Miocene boundary is the most remarkable change during the Neogene, and was recognized at all three sites. This faunal change is almost certainly associated with middle Miocene oceanographic changes related to increased Antarctic glaciation. Increased numbers of benthic specimens relative to planktonic forms at this time may have resulted from increased supply of organic material to the deep sea as a result of increased surface-water productivity.

3. Benthic foraminifers were studied in the fractions larger than 63 μm at the three sites. The most dominant species, which prevailed in the three Neogene sections, are *Epistominella exigua, E. rotunda*, and *Globocassidulina subglobosa*. Most specimens of these three species are small (<150 μm), and each usually occurs in frequencies of between 10 and 30%. The assemblages are dominated by only a few forms. Single species usually dominated the assemblages at any interval of time.

4. Faunal changes of benthic foraminiferal assemblages, as shown by species frequency changes and factor analysis, occurred in the three sites through the Neogene. Faunal successions are most similar between the two shallowest sites (Sites 590 and 591). The deepest site (Site 206) has a different faunal sequence. The most important faunal changes of benthic foraminiferal assemblages occurred in the early middle Miocene (14 Ma; the *Orbulina suturalis* Zone and the *Globorotalia fohsi* s.l. Zone), in the late Miocene (6 Ma; the *Globigerina nepenthes* Zone), and closely associated with the Pliocene/Pleistocene boundary (2 Ma; the *Globorotalia truncatulinoides–G. tosaensis* Zone and the *G. truncatulinoides* Zone).

5. These major faunal changes of benthic foraminiferal assemblages at the three sites are associated with known major paleoceanographic events: the middle Miocene development of the Antarctic ice sheet, the latest Miocene global cooling and increased polar glaciation, and quasiperiodic glacial oscillations of the Quaternary.

ACKNOWLEDGMENTS

We thank D. Hodell for his assistance with the factor analysis. J. Resig and J. Ingle kindly reviewed the paper and offered useful suggestions. Financial support for K. Kurihara was provided by Rikkyo University, Tokyo. Partial support was also provided by U.S. National Science Foundation Grant OCE82-14937 (Marine Geology and Geophysics).

REFERENCES

Boltovskoy, E., 1983. Late Cenozoic deep-sea benthic foraminifera off the coast of northwest Africa (DSDP Site 369). *J. African Earth Sci.*, 1(2):83–102.

Corliss, B. H., 1978. Studies of deep-sea benthonic foraminifera in the southeast Indian Ocean. *Antarctic J. U. S.*, 13:116–118.

Douglas, R. G., 1973. Benthonic foraminiferal biostratigraphy in the central North Pacific, Leg 17, Deep Sea Drilling Project. *In* Winterer, E. L., Ewing, J. I., et al., *Init. Repts. DSDP*, 17: Washington (U.S. Govt. Printing Office), 607–671.

Douglas, R. G., and Woodruff, F., 1981. Deep-sea benthic foraminifera. *In* Emiliani, C. (Ed.), *The Oceanic Lithosphere* (Vol. 7): New York (John Wiley), 1233–1327.

Keigwin, L. D., Jr., 1979. Late Cenozoic stable isotope stratigraphy and paleoceanography of Deep Sea Drilling Project Sites from the East Equatorial and central North Pacific Oceans. *Earth Planet. Sci. Lett.*, 45:361–382.

Kennett, J. P., 1973. Middle and Late Cenozoic planktonic foraminiferal biostratigraphy of the southwest Pacific—DSDP, Leg 21. *In* Burns, R. E., Andrews, J. E., et al., *Init. Repts. DSDP*, 21: Washington (U.S. Govt. Printing Office), 575–639.

________, 1983. Paleo-oceanography: global ocean evolution. *Rev. Geophys. Space Phys.* 5:1258–1274.

Kennett, J. P., and Srinivasan, M. S., 1983. *Neogene Planktonic Foraminifera: A Phylogenetic Atlas:* Stroudsburg, PA (Hutchinson Ross).

Klovan, J. E., and Imbrie, J., 1971. An algorithm and Fortran IV for large scale Q-mode factor analysis. *Int. Assoc. Math. Geol. J.*, 3: 61–78.

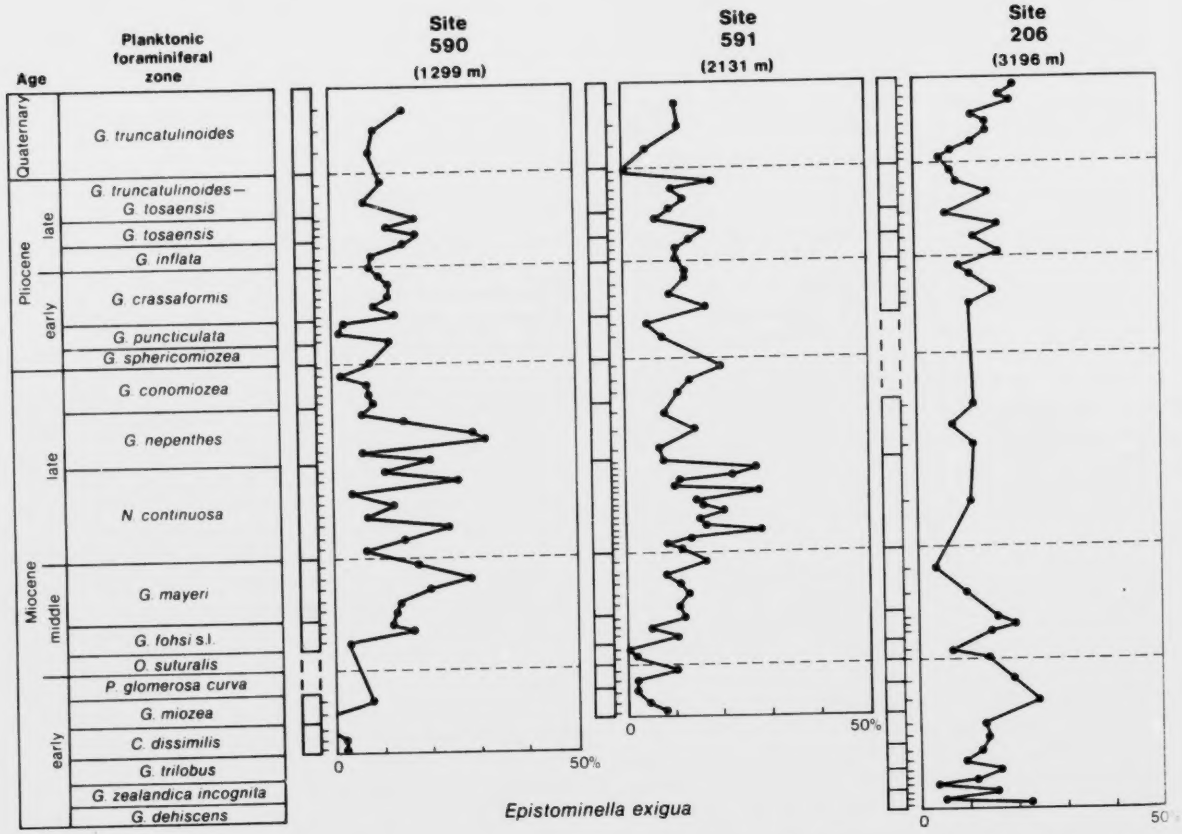

Figure 6. Distribution (species frequencies) of benthic foraminiferal species (>63 μm) at Sites 590, 591, and 206 (water depths in parentheses

Lohmann, G. P., 1978. Abyssal benthonic foraminifera as hydrographic indicators in the Western South Atlantic Ocean. *J. Foram. Res.*, 8: 6–34.

Loutit, T., and Kennett, J. P., 1979. Application of carbon isotope stratigraphy and correlation of Late Miocene shallow marine sediments, New Zealand. *Science*, 204:1196–1199.

Lutze, G. F., 1979. Benthic foraminifers at Site 397: Faunal fluctuation and ranges in the Quaternary. *In* von Rad, U., Ryan, W. B. F., et al., *Init. Repts. DSDP*, 47, Pt. 1: Washington (U.S. Govt. Printing Office), 419–431.

Parker, F. L., 1958. Eastern Mediterranean foraminifera. *Rept. Swedish Deep-Sea Expedition*, 8(4):219–283.

Phleger, F. B., Parker, F. L., and Peirson, J. F., 1953. North Atlantic foraminifera. *Rept. Swedish Deep-Sea Expedition*, 7(1):3–121.

Resig, J. M., 1976. Benthic foraminiferal stratigraphy, eastern margin, Nazca Plate. *In* Yeats, R. S., Hart, S. R., et al., *Init. Repts. DSDP*, 34: Washington (U.S. Govt. Printing Office), 743–759.

Schnitker, D., 1974. West Atlantic abyssal circulation during the past 120,000 years. *Nature*, 248:385–387.

________, 1979. Cenozoic deep water benthic foraminifers, Bay of Biscay. *In* Montadert, L., Roberts, D. G., et al., *Init. Repts. DSDP*, 48: Washington (U.S. Govt. Printing Office), 377–413.

Srinivasan, M. S., and Kennett, J. P., 1981. Neogene planktonic foraminiferal biostratigraphy and evolution: equatorial to Subantarctic, South Pacific. *Mar. Micropaleontol.*, 6:499–533.

Streeter, S. S., 1973. Bottom water and benthonic foraminifera in the North Atlantic—glacial-interglacial contrasts. *Quat. Res.*, 3: 131–141.

Woodruff, F., and Douglas, R. G., 1981. Response of deep-sea benthic foraminifera to Miocene paleoclimatic events, DSDP Site 289. *Mar. Micropaleontol.*, 6:617–632.

Date of Initial Receipt: 17 August 1984
Date of Acceptance: 7 December 1984

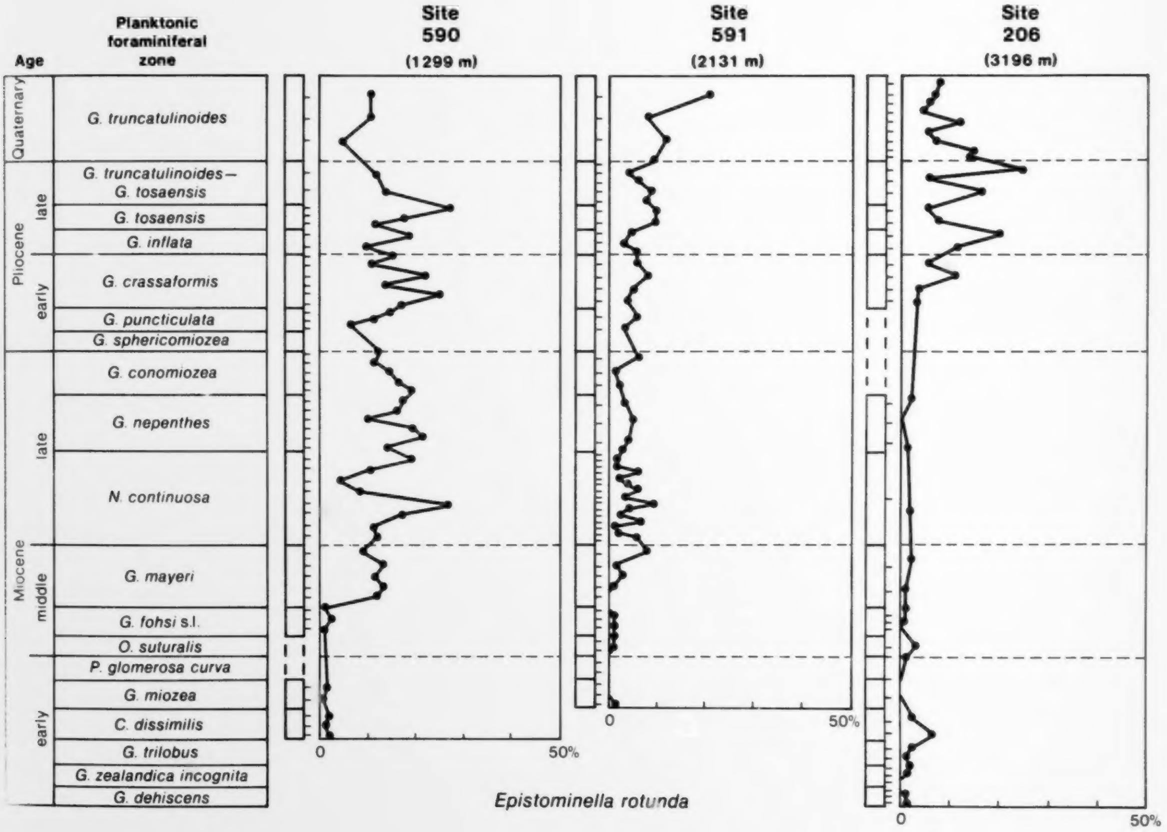

Figure 6. (Continued).

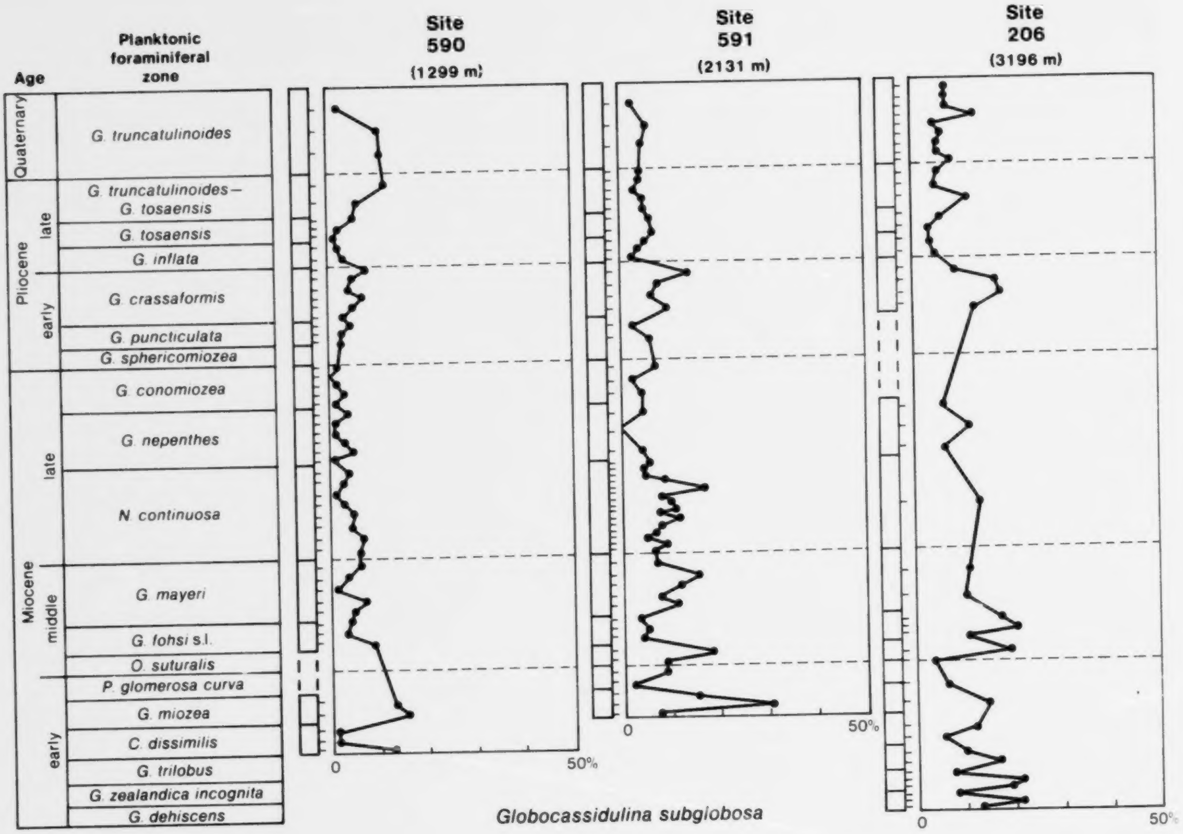

Figure 6. (Continued).

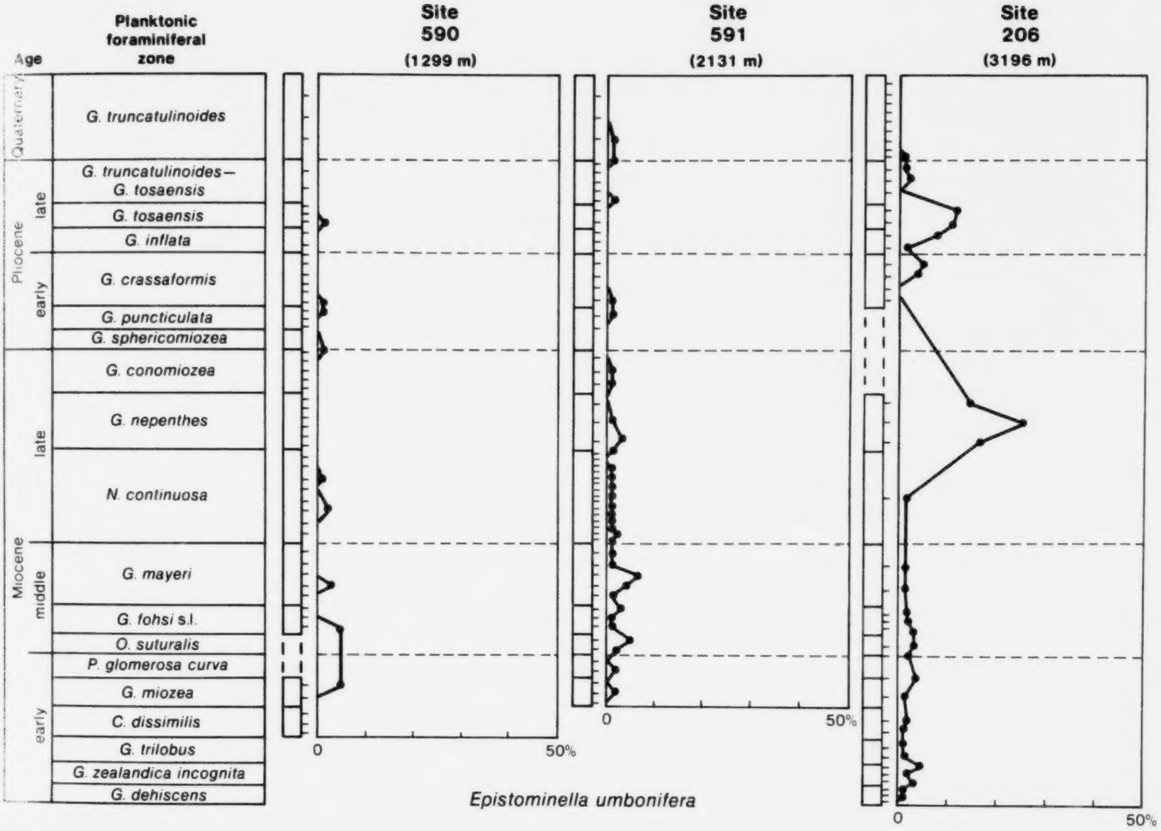

Figure 6. (Continued).

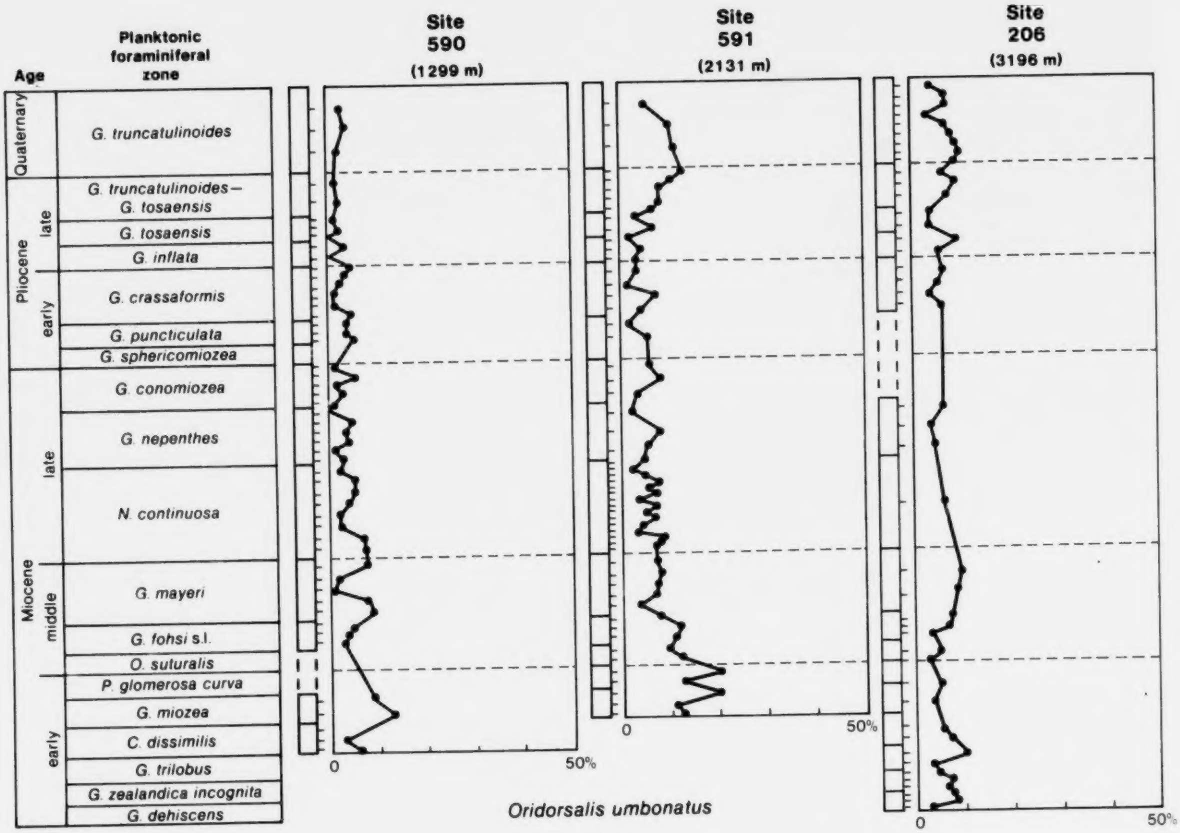

Figure 6. (Continued).

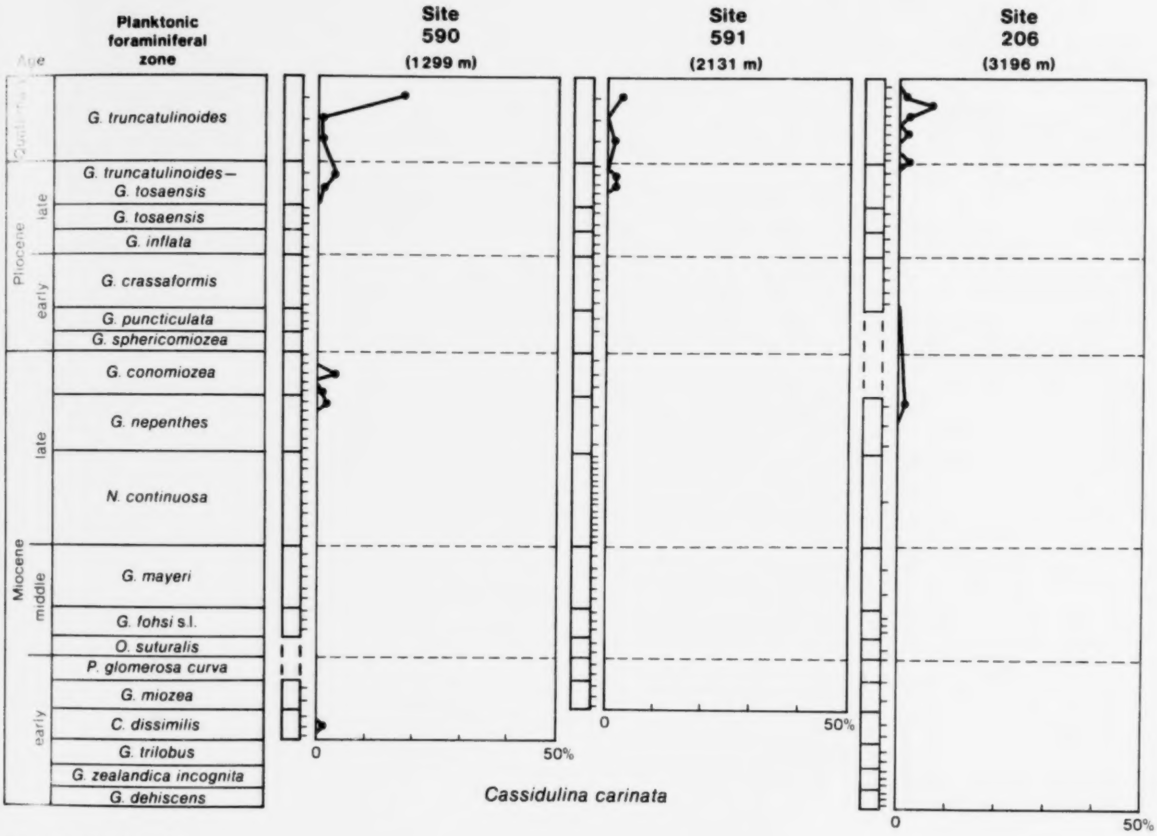

Figure 6. (Continued).

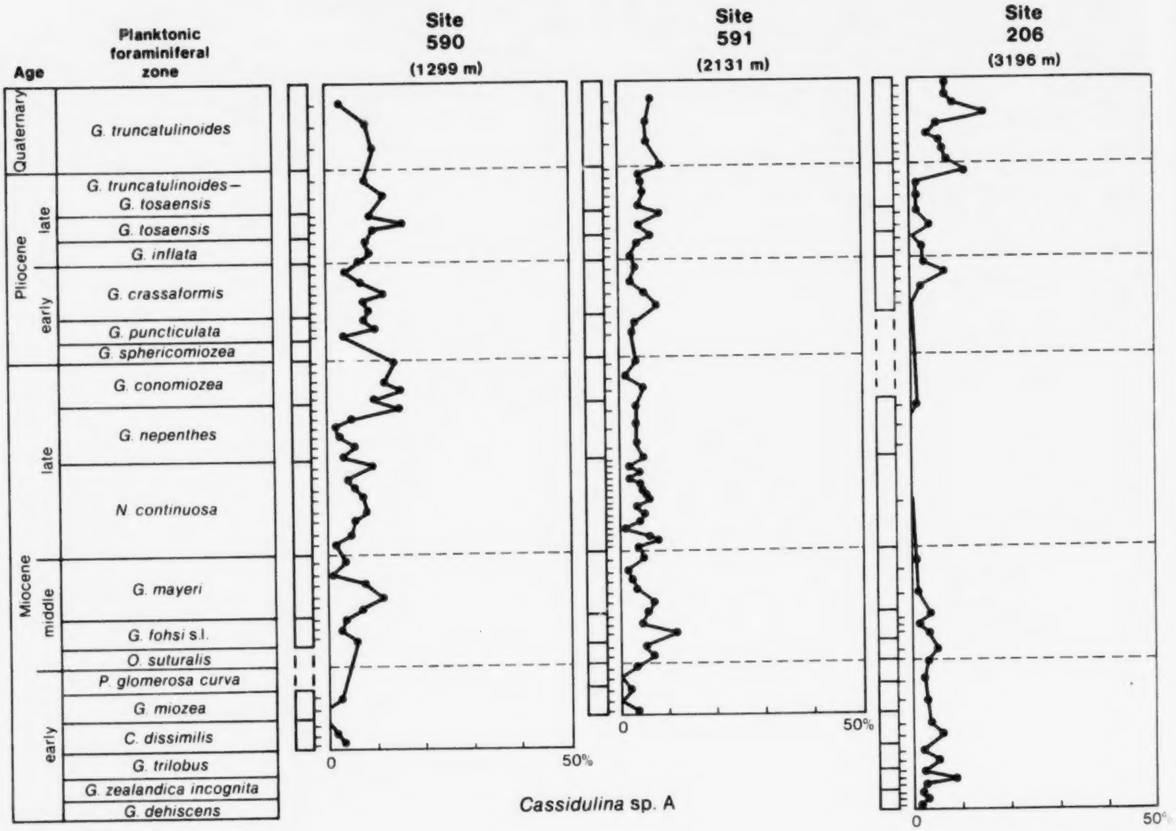

Figure 6. (Continued).

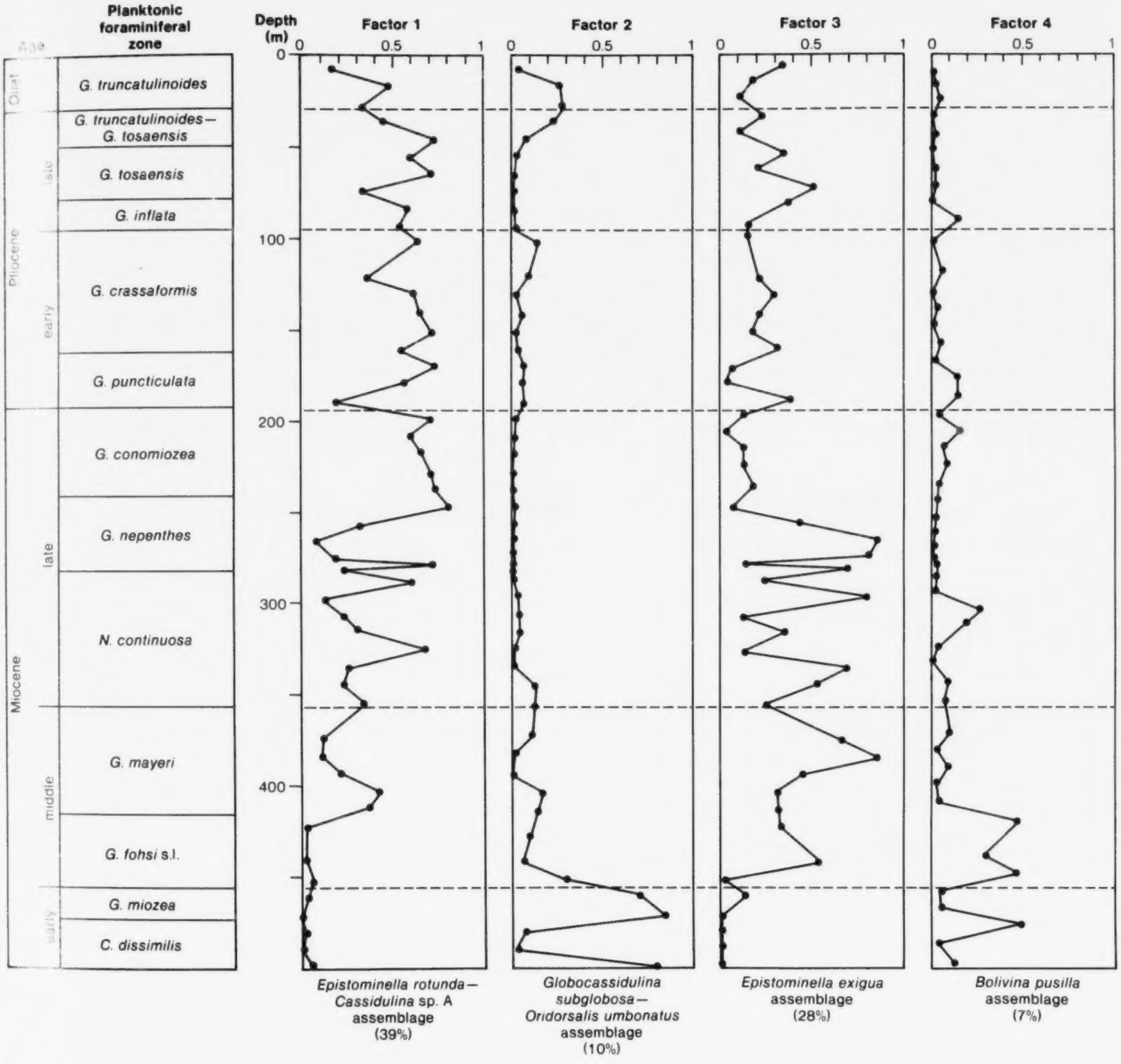

Figure 7. Factor analysis scores (5 factors analyzed) for Site 590, showing changes in the relative importance of four benthic foraminiferal assemblages (factors) in >63 μm fraction. Factor 5 was relatively unimportant quantitatively. Percentages indicate the amount of faunal variance within the data set contained within each of the factors.

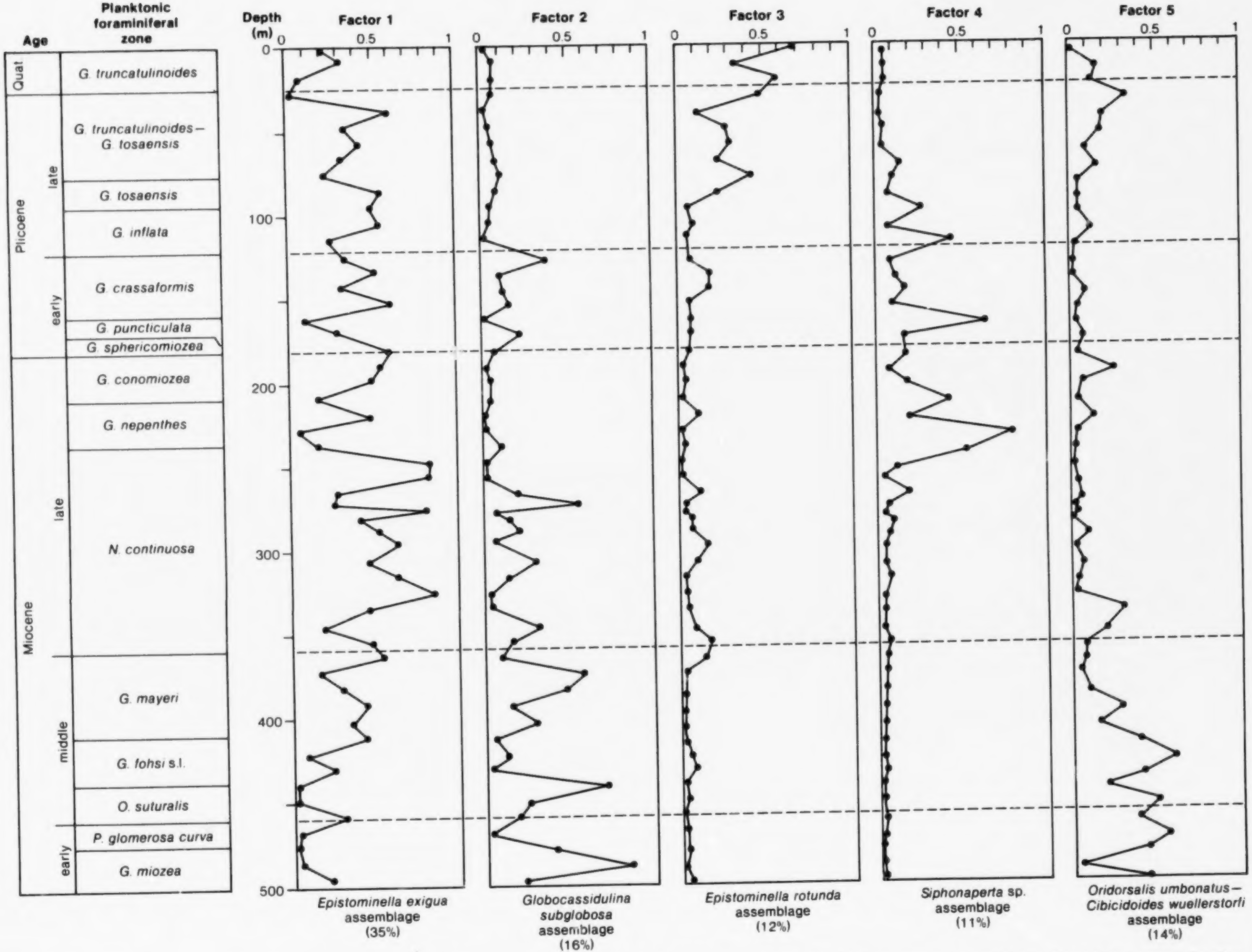

Figure 8. Factor analysis scores (5 factors analyzed) for Site 591, showing changes in the relative importance of five benthic foraminiferal assemblages (factors) in >63 µm fraction. Percentages indicate the amount of faunal variance within the data set contained within each of the factors.

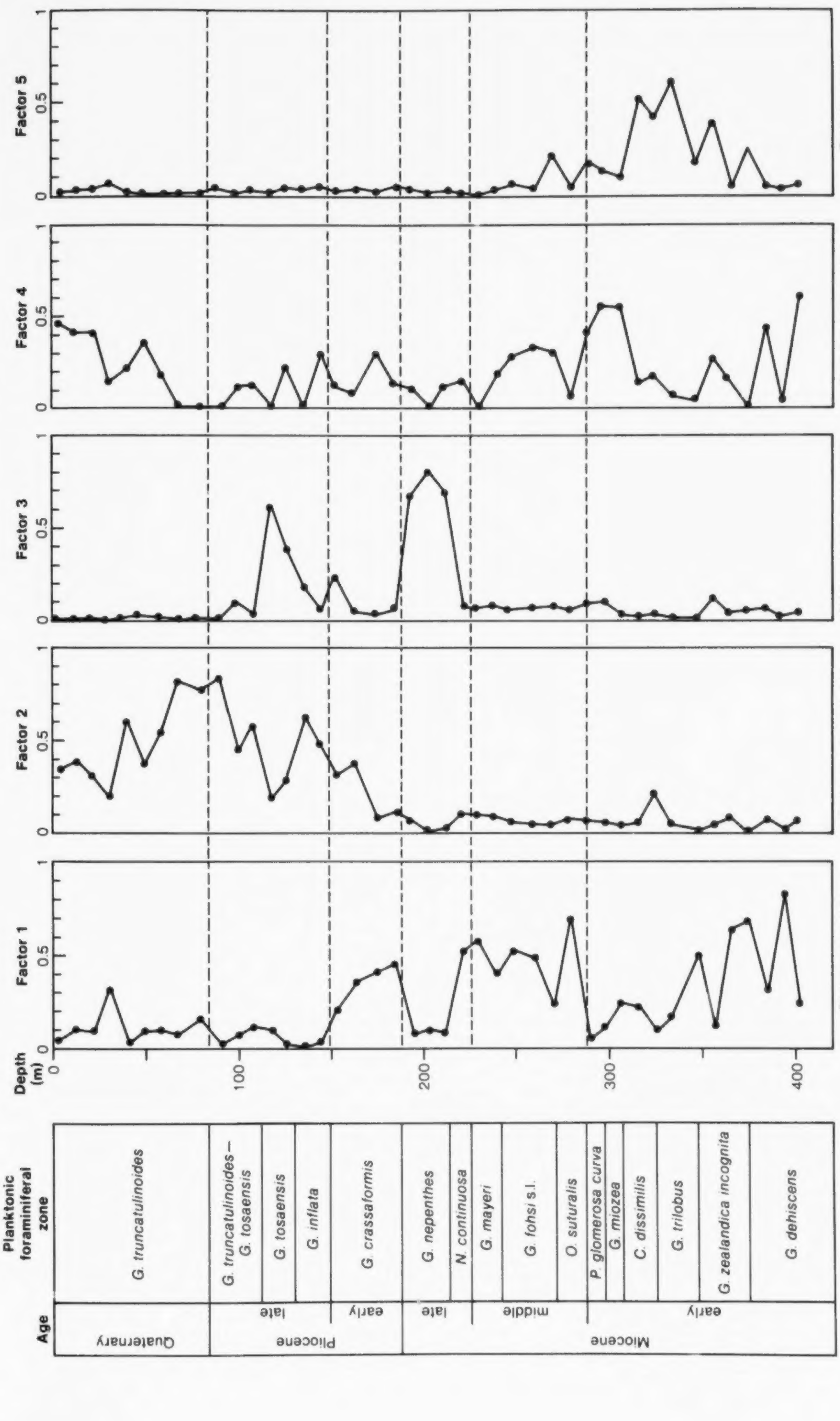

Figure 9. Factor analysis scores (5 factors analyzed) for Site 206, showing changes in the relative importance of five benthic foraminiferal assemblages (factors) in >63 μm fraction. Percentages indicate the amount of faunal variance within the data set contained within each of the factors.

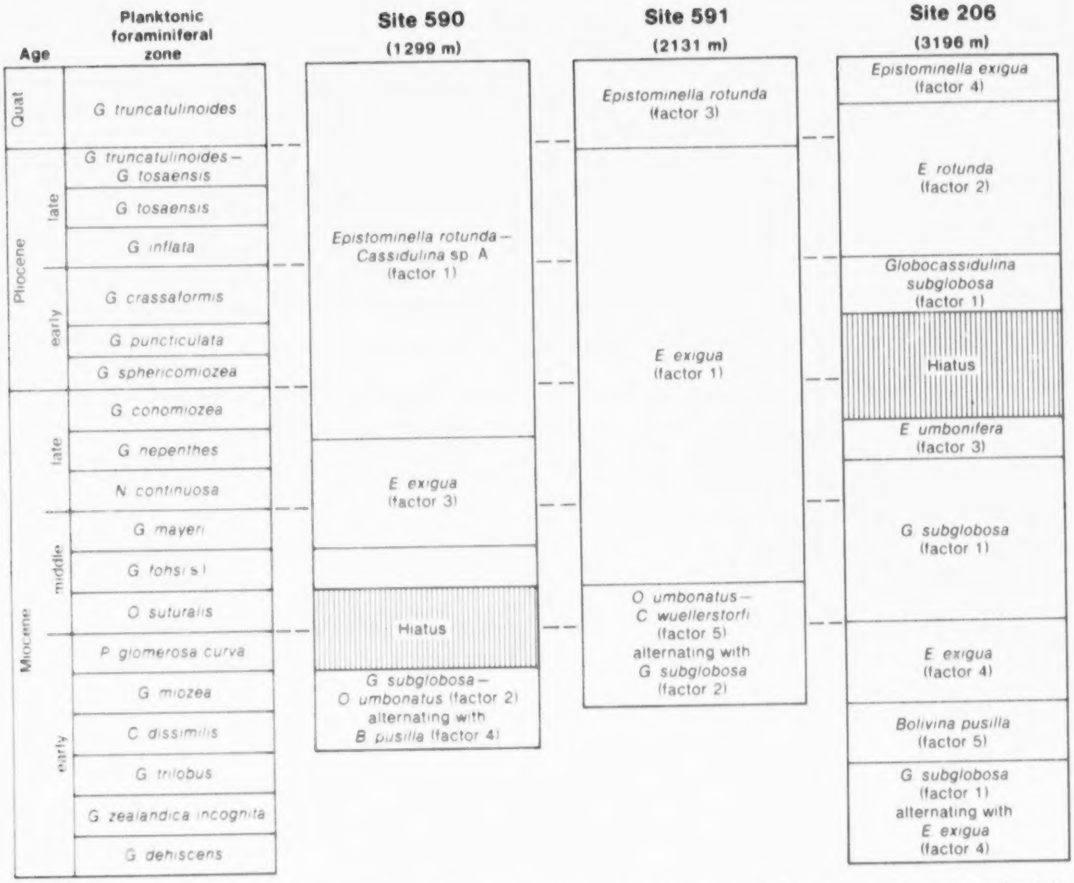
Age
Planktonic foraminiferal zone
Site 590
(1299 m)
Site 591
(2131 m)
Site 206
(3196 m)
Quat
Pliocene
late
early
Miocene
late
middle
early
G truncatulinoides
G truncatulinoides – G tosaensis
G tosaensis
G inflata
G crassaformis
G puncticulata
G sphericomiozea
G conomiozea
G nepenthes
N continuosa
G mayeri
G fohsi s l
O suturalis
P glomerosa curva
G miozea
C dissimilis
G trilobus
G zealandica incognita
G dehiscens
Epistominella rotunda – Cassidulina sp A (factor 1)
E exigua (factor 3)
Hiatus
G subglobosa – O umbonatus (factor 2) alternating with B pusilla (factor 4)
Epistominella rotunda (factor 3)
E exigua (factor 1)
O umbonatus – C wuellerstorfi (factor 5) alternating with G subglobosa (factor 2)
Epistominella exigua (factor 4)
E rotunda (factor 2)
Globocassidulina subglobosa (factor 1)
Hiatus
E umbonifera (factor 3)
G subglobosa (factor 1)
E exigua (factor 4)
Bolivina pusilla (factor 5)
G subglobosa (factor 1) alternating with E exigua (factor 4)

Figure 10. Dominant benthic foraminiferal assemblages at Sites 590, 591, and 206 as revealed by factor analysis (water depth in parentheses).

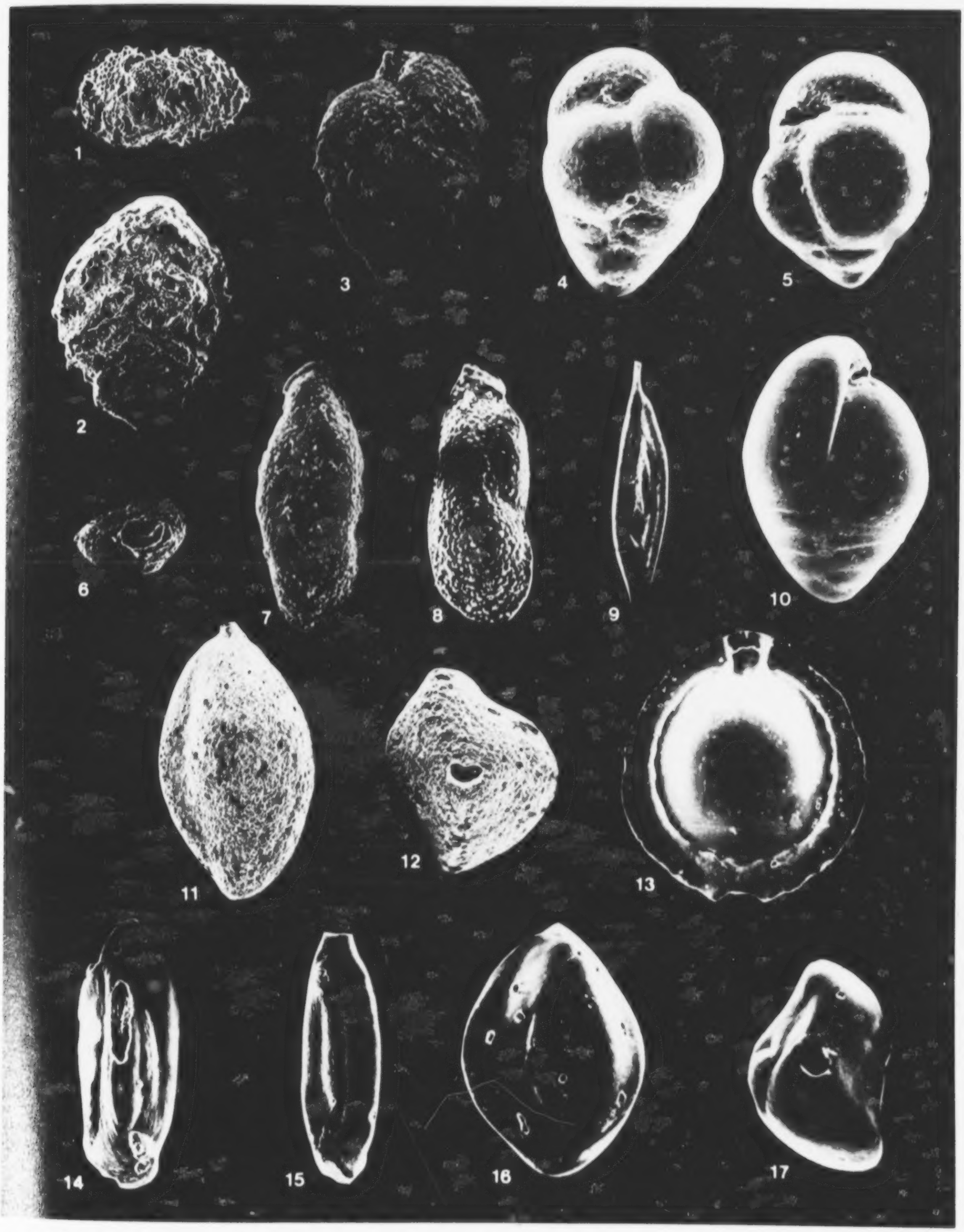

Pla **1, 2.** *Textularia lythostrota* (Schwager), ×75, Sample 591-12,CC. **3.** *Siphotextularia rolshauseni* Phleger and Parker, ×220, Sample ,CC. **4.** *Eggerella* sp. B, ×80, Sample 591-5,CC. **5.** *Eggerella* sp. A, ×133, Sample 591-5,CC. **6–8.** *Siphonaperta* sp., (6) ×513, le 591B-16,CC; (7) ×367, Sample 591-18,CC; (8) ×343, Sample 591-25,CC. **9.** *Ophthalmidium pusillum* (Earland), ×96, Sample CC. **10.** *Dorothia brevis* Cushman and Stainforth, ×49, Sample 591-5,CC. **11, 12.** *Sigmoilopsis schlumbergeri* (Silvestri), (11) ×70; ×125, Sample 591-3,CC. **13.** *Pyrgo murrhina* (Schwager), ×160, Sample 591-5,CC. **14, 15.** *Quinqueloculina venusta* Karrer, (14) Sample 591-21,CC; (15) ×133, Sample 591-25,CC. **16, 17.** *Sigmoilina edwardsi* (Schlumberger), (16) ×133; (17) ×213, Sample ,CC.

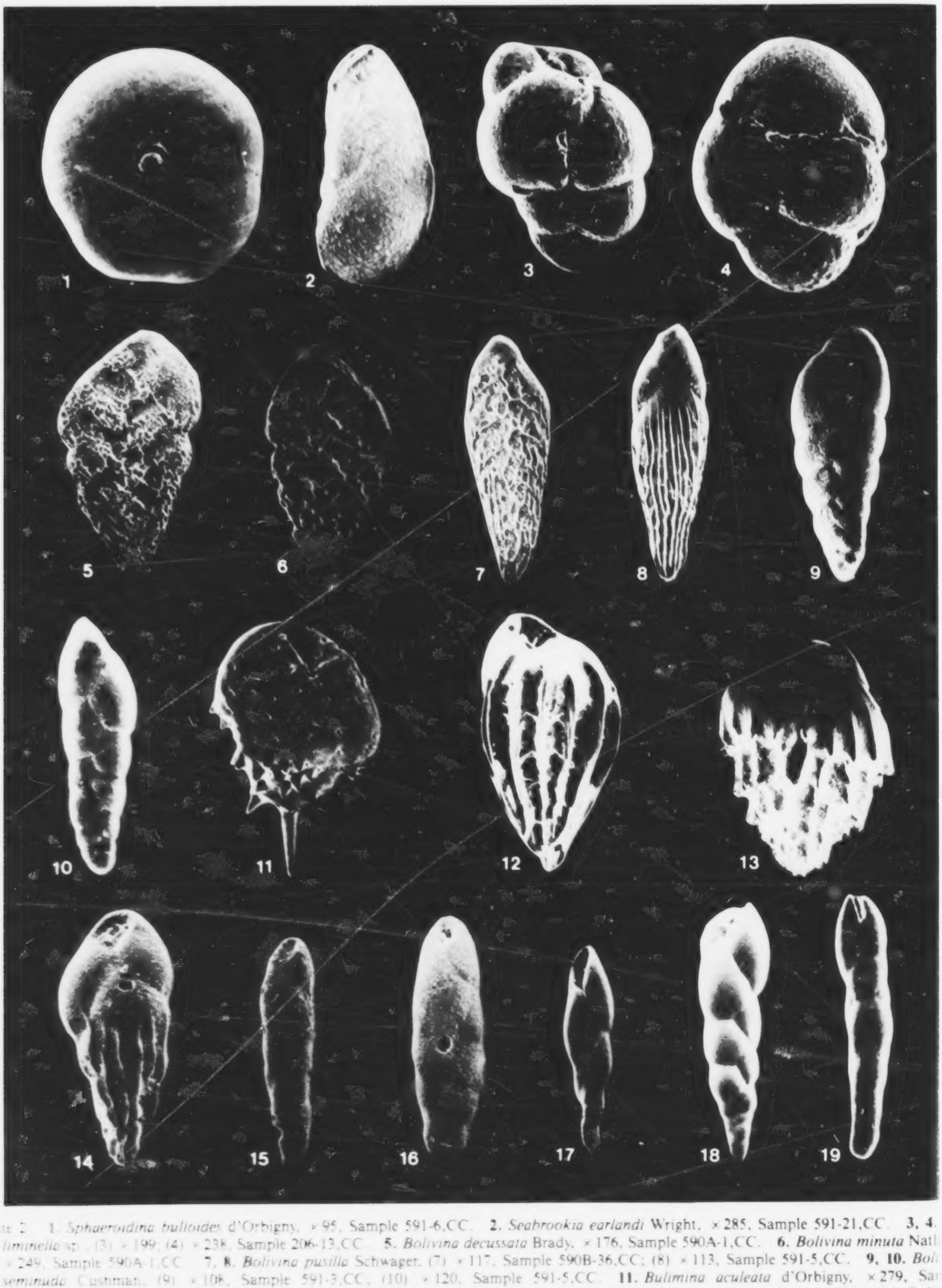

Plate 2. 1. *Sphaeroidina bulloides* d'Orbigny, × 95, Sample 591-6,CC. **2.** *Seabrookia earlandi* Wright, × 285, Sample 591-21,CC. **3, 4.** *Buliminella* sp., (3) × 199; (4) × 238, Sample 206-13,CC. **5.** *Bolivina decussata* Brady, × 176, Sample 590A-1,CC. **6.** *Bolivina minuta* Natland, × 249, Sample 590A-1,CC. **7, 8.** *Bolivina pusilla* Schwager, (7) × 117, Sample 590B-36,CC; (8) × 113, Sample 591-5,CC. **9, 10.** *Bolivina seminuda* Cushman, (9) × 108, Sample 591-3,CC; (10) × 120, Sample 591-5,CC. **11.** *Bulimina aculeata* d'Orbigny, × 279, Sample 590A-1,CC. **12.** *Bulimina rostrata* Brady, × 176, Sample 591-5,CC. **13.** *Bulimina striata* d'Orbigny, × 83, Sample 591-3,CC. **14.** *Bulimina translucens* Parker, × 274, Sample 206-38,CC. **15, 16.** *Virgulopsis* sp., (15) × 132, Sample 590B-52,CC; (16) × 220, Sample 590A-11,CC. **17.** *Stainforthia complanata* (Egger), × 135, Sample 591-5,CC. **18, 19.** *Cassidella bradyi* (Cushman), (18) × 50; (19) × 44, Sample 591-5,CC

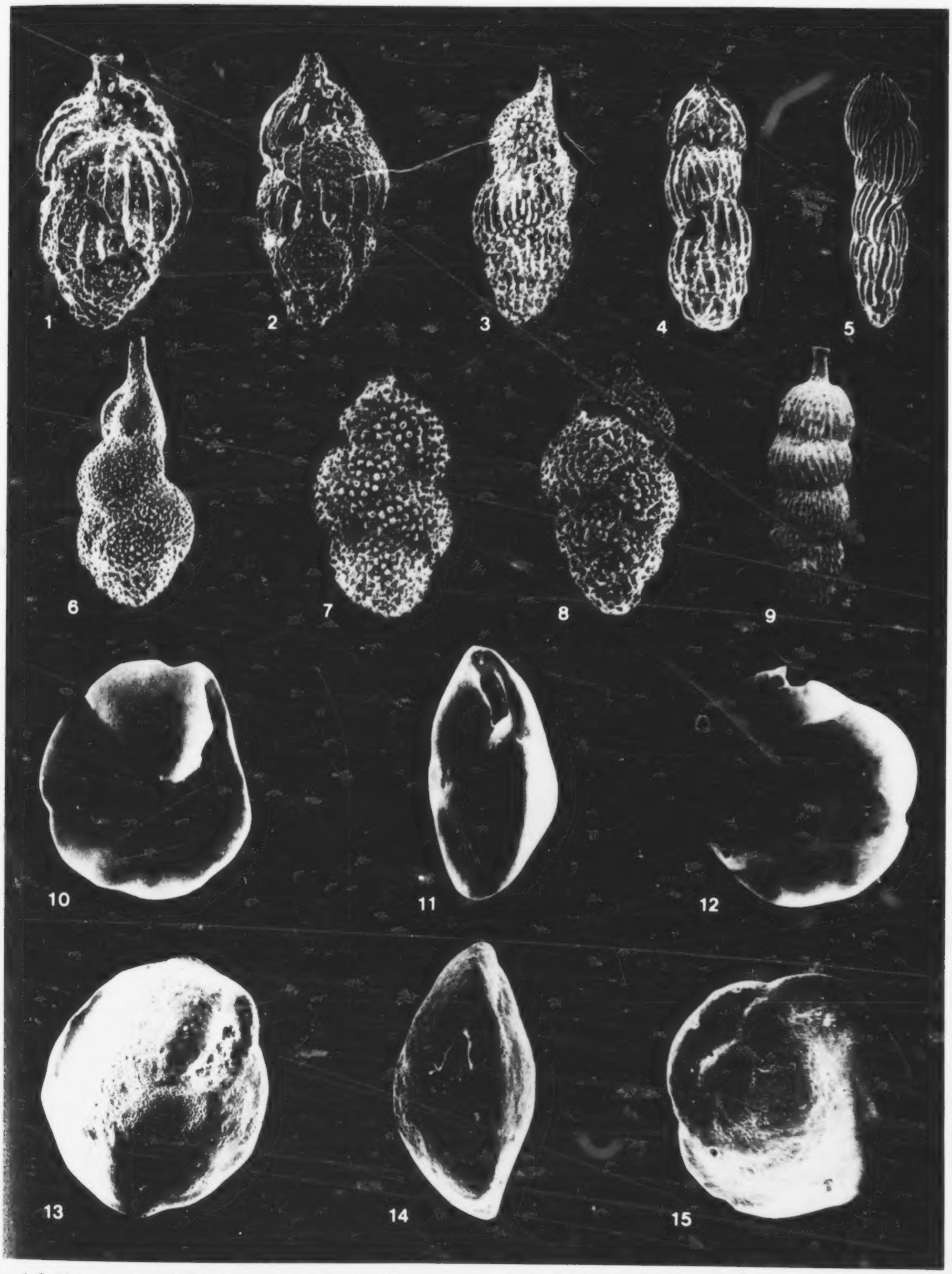

1-3. *Uvigerina peregrina* Cushman, (1) × 107; (2) × 93; (3) × 67, Sample 591-5,CC. **4, 5.** *Uvigerina* sp. A, (4) × 133, Sample 591-27,CC; (5) 69, Sample 591-9,CC. **6.** *Uvigerina proboscidea* Schwager, × 103, Sample 591-5,CC. **7, 8.** *Uvigerina hispida* Schwager, (7) × 63; (8) × 64, mple 591-24,CC. **9.** *Rectuvigerina* sp, × 73, Sample 590A-27,CC. **10-12.** *Epistominella exigua* (Brady), (10) × 227; (11) × 213; (12) × 175, mple 591-1,CC. **13-15.** *Epistominella rugosa* (Phleger and Parker), (13) × 128; (14) × 266; (15) × 208, Sample 206-13,CC.

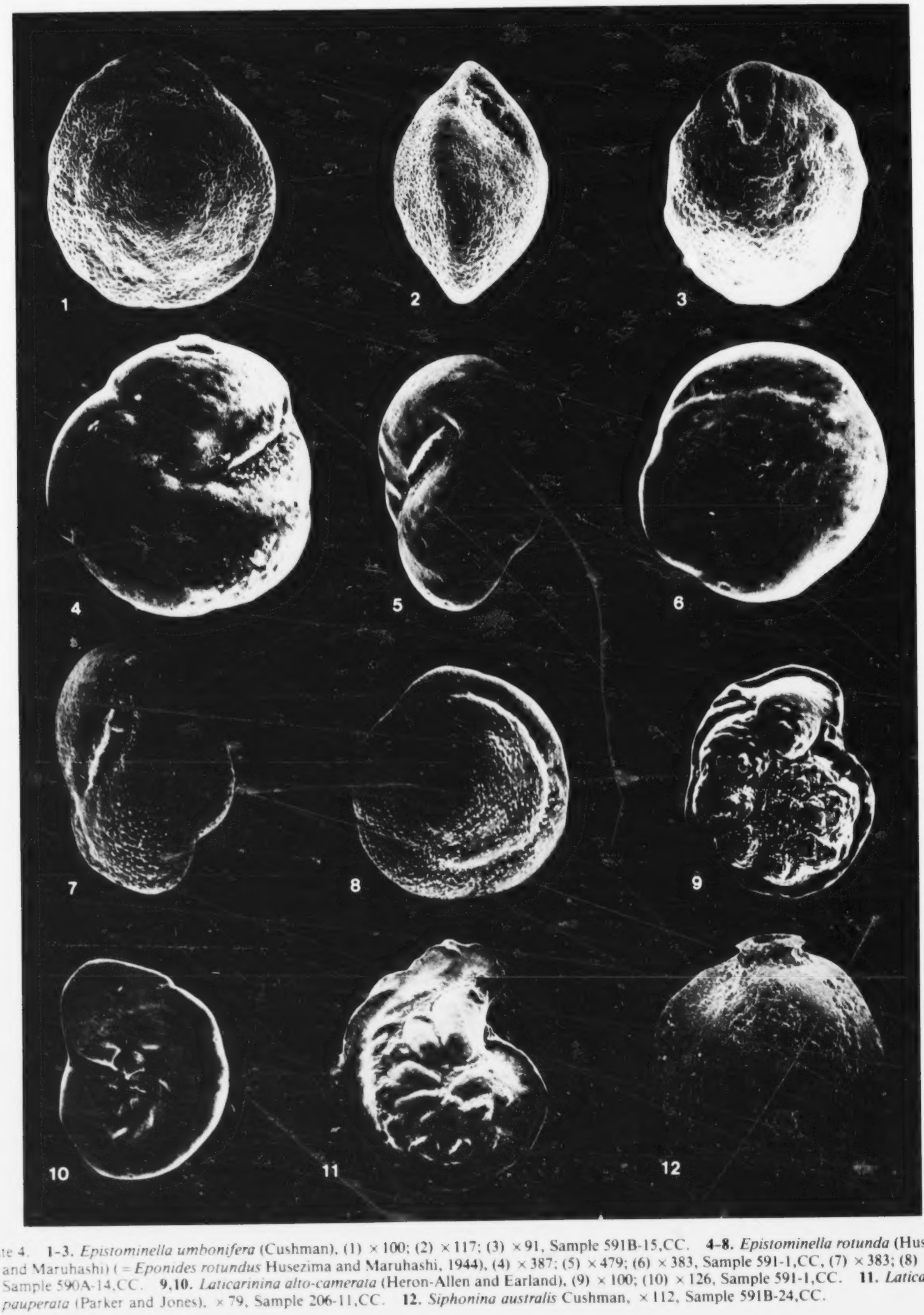

Plate 4. **1-3.** *Epistominella umbonifera* (Cushman), (1) × 100; (2) × 117; (3) × 91, Sample 591B-15,CC. **4-8.** *Epistominella rotunda* (Husezin and Maruhashi) (= *Eponides rotundus* Husezima and Maruhashi, 1944), (4) × 387; (5) × 479; (6) × 383, Sample 591-1,CC, (7) × 383; (8) × 36 Sample 590A-14,CC. **9,10.** *Laticarinina alto-camerata* (Heron-Allen and Earland), (9) × 100; (10) × 126, Sample 591-1,CC. **11.** *Laticarinin pauperata* (Parker and Jones), × 79, Sample 206-11,CC. **12.** *Siphonina australis* Cushman, × 112, Sample 591B-24,CC.

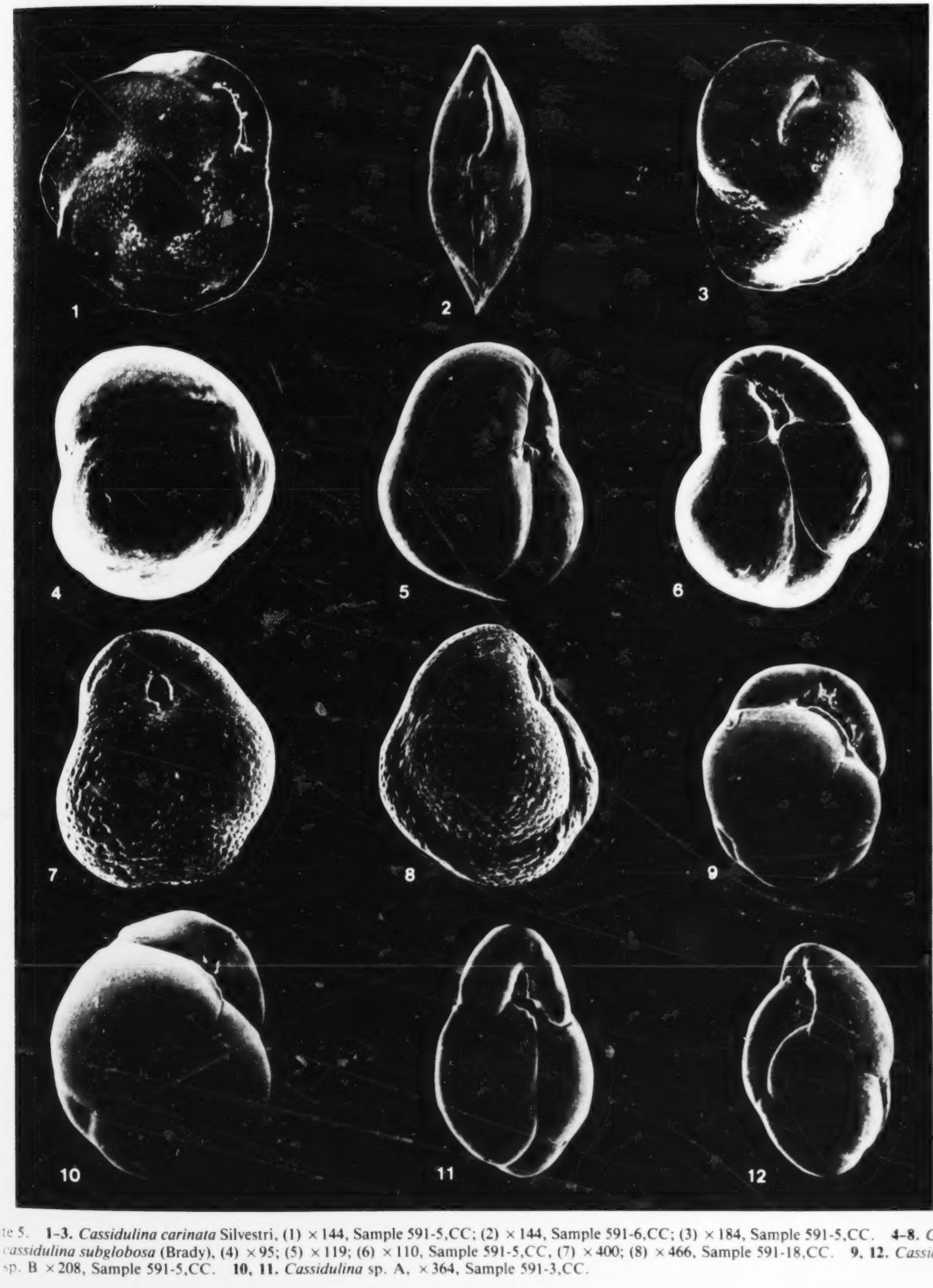

Plate 5. **1–3.** *Cassidulina carinata* Silvestri, (1) × 144, Sample 591-5,CC; (2) × 144, Sample 591-6,CC; (3) × 184, Sample 591-5,CC. **4–8.** *Globocassidulina subglobosa* (Brady), (4) × 95; (5) × 119; (6) × 110, Sample 591-5,CC, (7) × 400; (8) × 466, Sample 591-18,CC. **9, 12.** *Cassidulina* sp. B × 208, Sample 591-5,CC. **10, 11.** *Cassidulina* sp. A, × 364, Sample 591-3,CC.

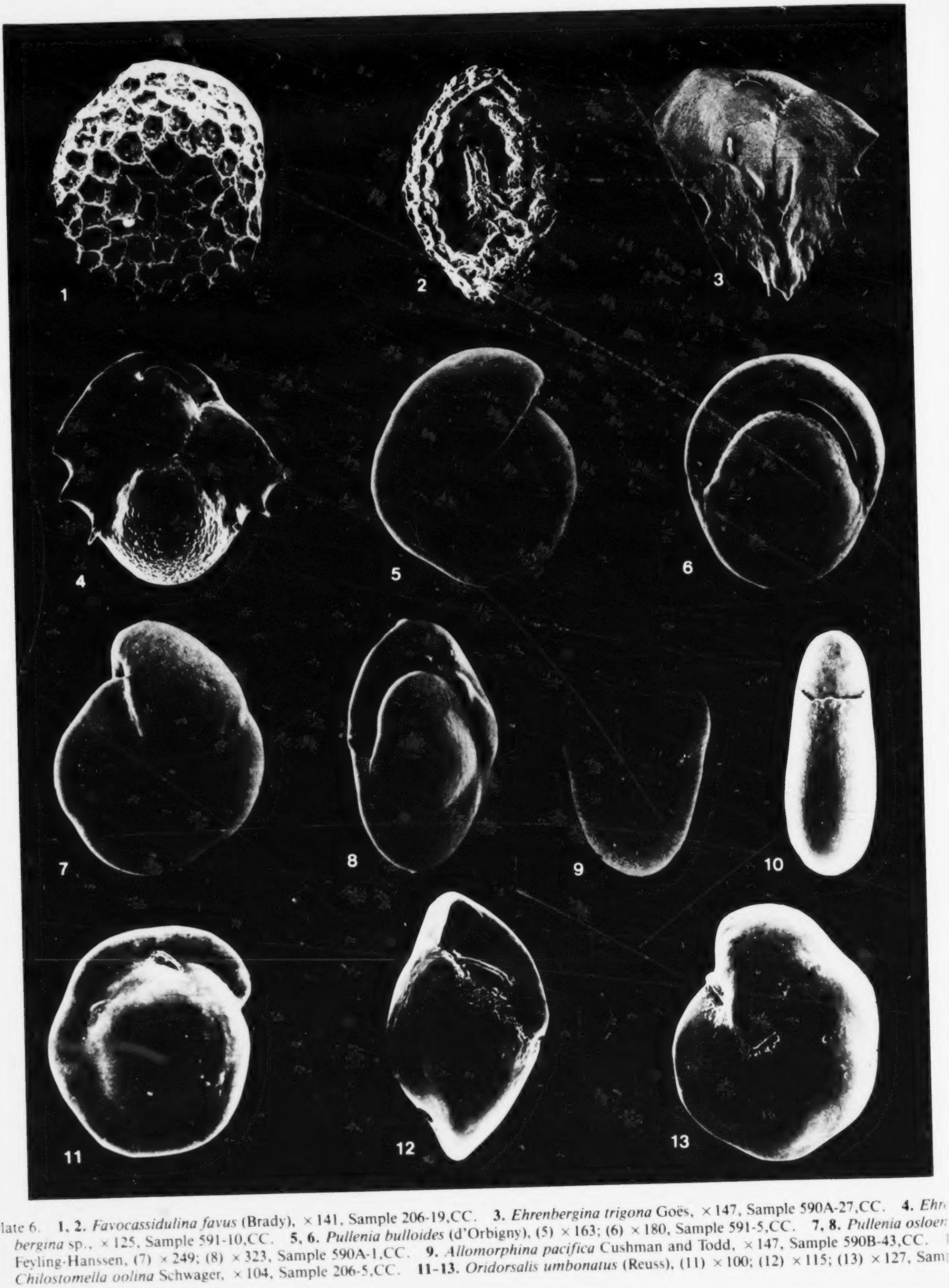

Plate 6. **1, 2.** *Favocassidulina favus* (Brady), × 141, Sample 206-19,CC. **3.** *Ehrenbergina trigona* Goës, × 147, Sample 590A-27,CC. **4.** *Ehrenbergina* sp., × 125, Sample 591-10,CC. **5, 6.** *Pullenia bulloides* (d'Orbigny), (5) × 163; (6) × 180, Sample 591-5,CC. **7, 8.** *Pullenia osloensis* Feyling-Hanssen, (7) × 249; (8) × 323, Sample 590A-1,CC. **9.** *Allomorphina pacifica* Cushman and Todd, × 147, Sample 590B-43,CC. **10.** *Chilostomella oolina* Schwager, × 104, Sample 206-5,CC. **11-13.** *Oridorsalis umbonatus* (Reuss), (11) × 100; (12) × 115; (13) × 127, Sample 591-5,CC.

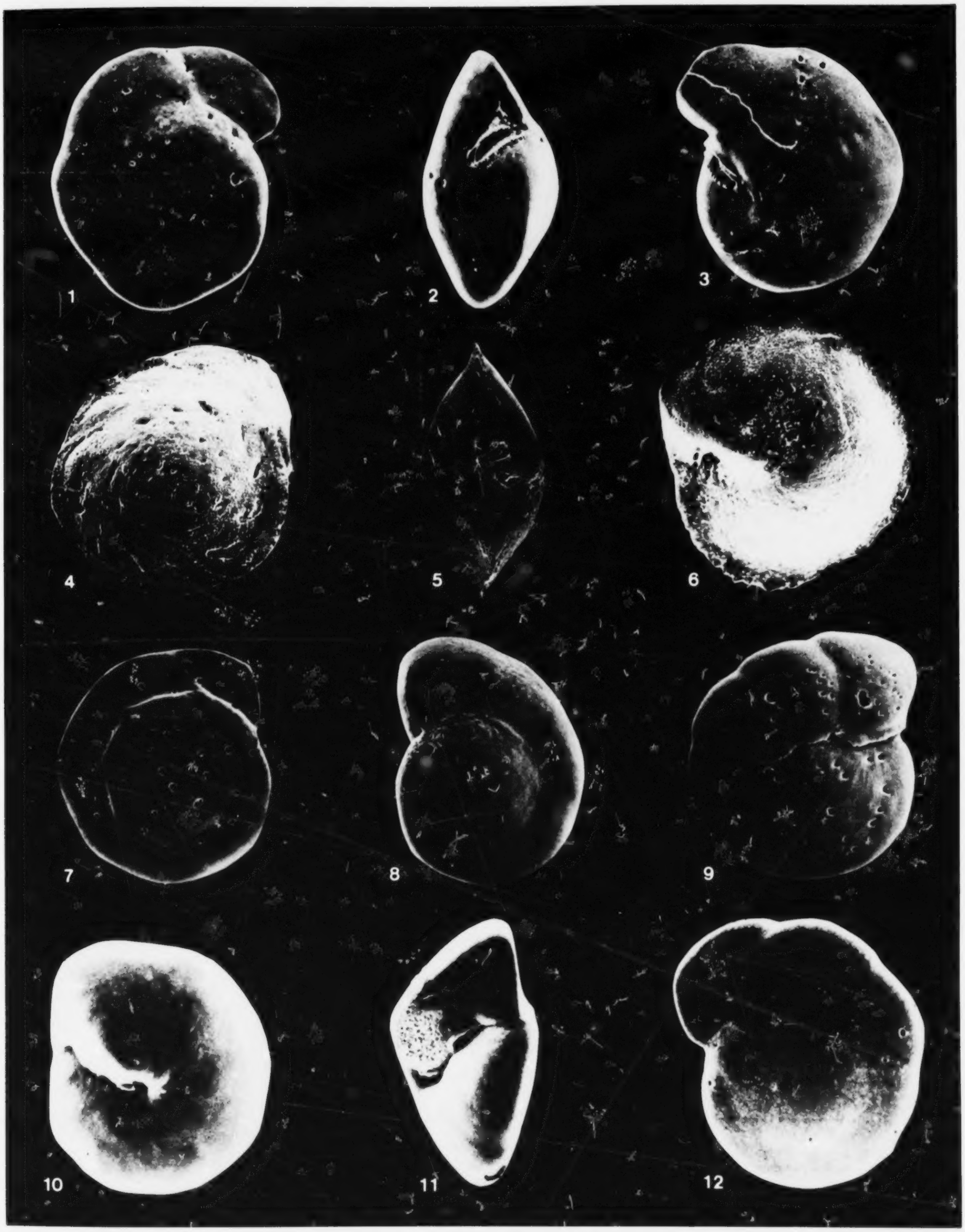

Plate 7. **1-3.** *Oridorsalis* sp. (1, 2) ×93; (3) ×96, Sample 591-5,CC. **4-6.** *Osangularia culter* (Parker and Jones), (4) ×105; (5) ×125; (6) ×123, Sample 591-14,CC. **7.** *Gyroidina acuta* Boomgaart, ×73, Sample 591-7,CC. **8.** *Gyroidina neosoldanii* Brotzen, ×61, Sample 591-7,CC. **9.** *Anomalinoides* sp. A, ×213, Sample 591-6,CC. **10-12.** *Gyroidina* sp. A, (10) ×207; (11) ×230; (12) ×240, Sample 591-5,CC.

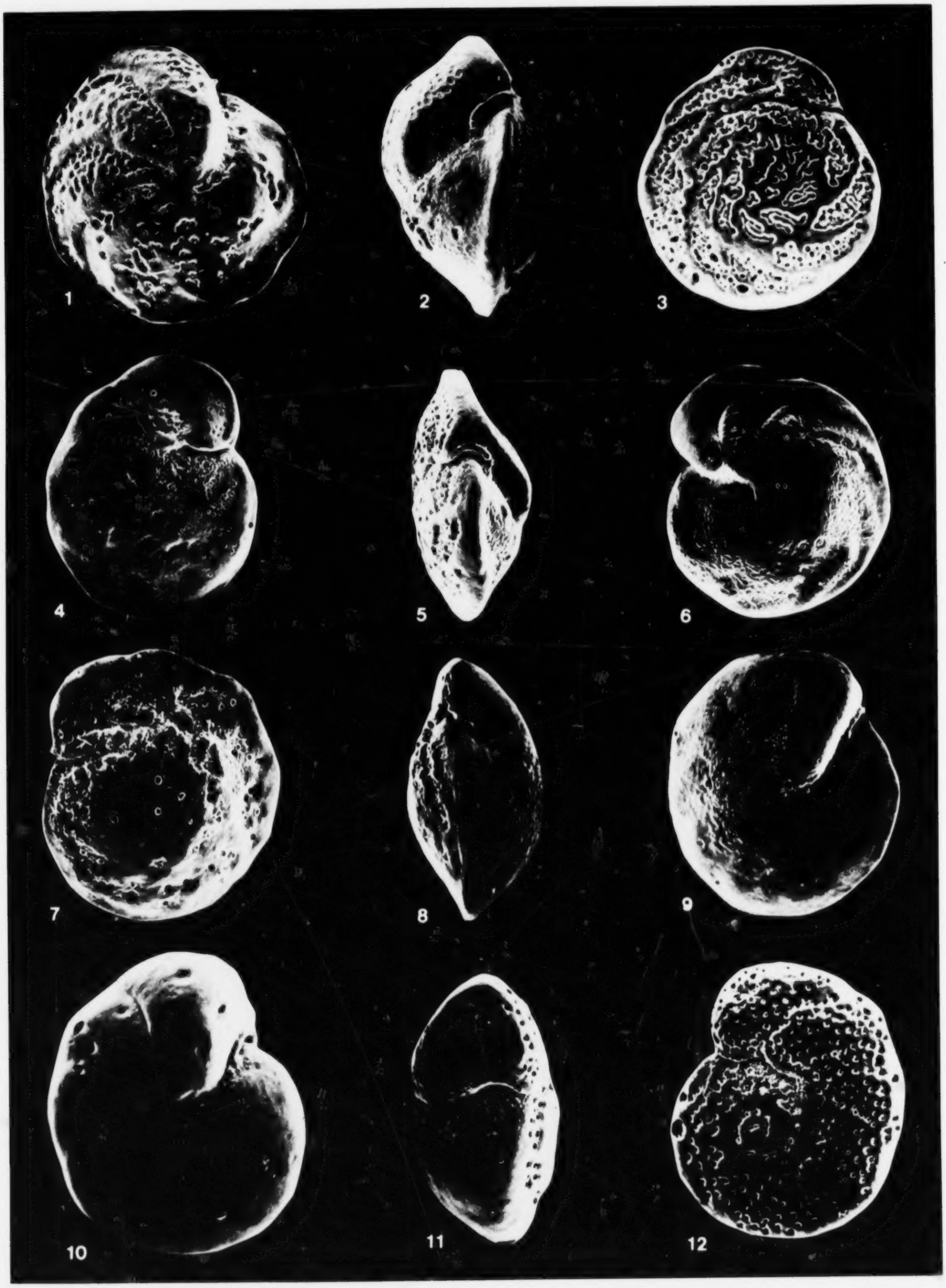

Plate 8. **1–3.** *Cibicidoides kullenbergi* (Parker), (1) × 80; (2) × 74; (3) × 69, Sample 591-14,CC. **4–6.** *Cibicidoides wuellerstorfi* (Schwager), (4, × 74; (6) × 68, Sample 591-8,CC. **7–9.** *Cibicidoides mundulus* (Brady, Parker, and Jones), × 107, (7, 9) Sample 591-11,CC; (8) Sampl 591-10,CC. **10–12.** *Cibicidoides* sp. A, (10) × 110; (11) × 122; (12) × 100, Sample 591-6,CC.

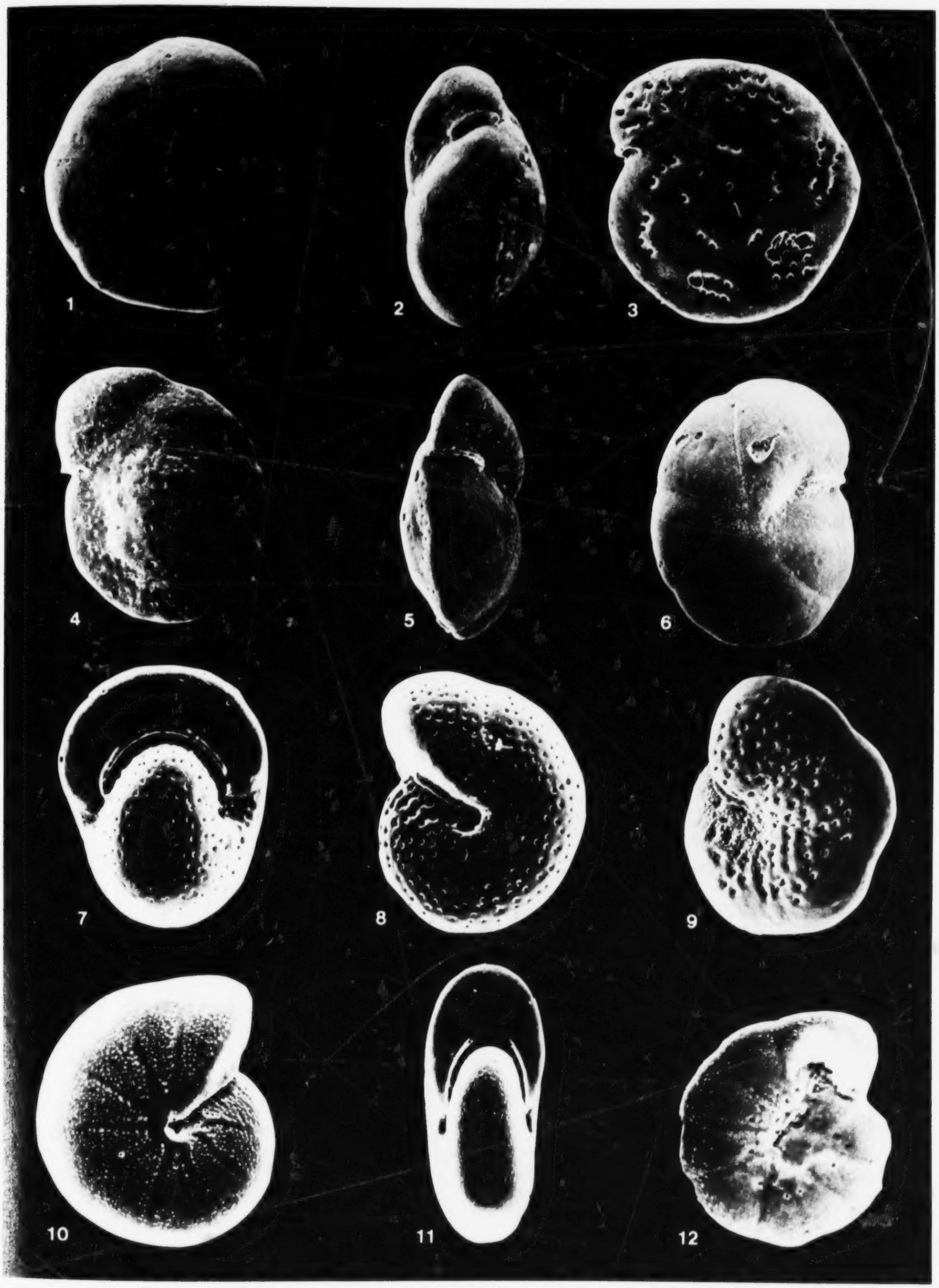

Plate [illegible]. **1–3.** *Cibicidoides bradyi* (Trauth), (1) ×81; (2) ×152; (3) ×129, Sample 591-6,CC. **4–6.** *Cibicidoides* cf. *opacus* (Carter), (4) ×137; (5) ×[illegible]90; (6) ×161, Sample 591B-15,CC. **7, 8.** *Melonis pompilioides* (Fichtel and Moll), (7) ×161; (8) ×173, Sample 591-5,CC. **9.** *Anomalinoides globulosus* (Chapman and Parr), ×148, Sample 591-8,CC. **10, 11.** *Melonis barleeanum* (Williamson), (10) ×132; (11) ×147, Sample 591-5,CC. **12.** *Anomalinoides* sp. B, ×375, Sample 590-1,CC.

22. PHYTOLITHS FROM THE SOUTHWEST PACIFIC, SITE 591[1]

Sigurd Locker and Erlend Martini, Geologisch-Paläontologisches Institut der Universität, Frankfurt am Main[2]

ABSTRACT

Phytoliths are described from deep sea sediments at Site 591 in the southwestern Pacific. Their regional distribution is related to the arid and semiarid regions of Australia, from where they were blown by westerly winds into the Tasman Sea area. The stratigraphic record ranges from the middle Miocene, at about 14.4 m.y., until the early Pleistocene. A distinct increase in frequencies observed during the Pliocene and a maximum at about 2.5 m.y. coincide with important trends in paleogeography and paleoclimatology: the development of the Antarctic ice cap, the northward drift of the Australian Plate, and the generation of arid conditions on the Australian continent.

INTRODUCTION

During Leg 90 phytoliths were found in fair numbers in Holes 591, 591A, and 591B, and very sporadically also in Hole 594A. They were investigated in detail only in the first three holes. Site 591 is situated on the eastern flank of the Lord Howe Rise (31°35.06′S; 164°26.92′E) in a present water depth of 2131 m (Fig. 1). Sediments recovered at this site consist mainly of foraminifer-bearing or foraminifer-rich nannofossil ooze. Biosiliceous components are present in low numbers compared with calcareous components, and include diatoms, silicoflagellates, radiolarians, and phytoliths. The investigated sections cover the middle Miocene to early Pleistocene interval.

PHYTOLITHS IN MARINE SEDIMENTS

Phytoliths are siliceous casts of various shapes that occur mainly in epidermal cells of grasses. They generally indicate that a certain fraction of a sediment sample is derived from a terrestial source.

Phytoliths have been described from terrestial localities (Ehrenberg, 1854; Baker, 1960a; Deflandre, 1963; Hajós, 1968) as well as from marine sections (see Table 1). In marine sediments they commonly occur in areas which are close to continents and where permanent eolian transport of dust in particular directions is possible (Folger et al., 1967; Folger, 1970). The main areas of phytolith distribution are in the Atlantic Ocean off the coast of northwest Africa and in the eastern equatorial Pacific. In both areas easterly winds, that is, winds blowing in a westerly direction, cause phytoliths to occur in Recent and ancient sediments. To these occurrences we can now add the southwest Pacific, where phytoliths were found in fair numbers during Leg 90 of the Deep Sea Drilling Project, distributed from Australia by westerly winds.

The stratigraphic occurrence of phytoliths in marine sediments is presently known to cover the middle Eocene to the Quaternary, with a distinct increase in frequencies in several sections of the Pliocene and Pleistocene (Table 1).

PHYTOLITH CLASSIFICATION

Phytoliths are composed of opaline silica. Their appearance under the microscope is colorless in normal light but may also tend to grey or brown. Size is commonly below 30 μm but can reach 60 μm and more. Their shape varies from simple, rounded, or angular bodies to dumbbell-shaped or rodlike bodies.

Two systematic concepts are in use to describe the variety found in phytoliths, but neither is very satisfactory. One concept uses only a descriptive nomenclature (Twiss et al., 1969; Bukry, 1980), and the other one a fixed nomenclature with parataxa (Deflandre, 1963; Dumitricá 1973), because phytoliths of identical shape may occur in grasses of quite different taxonomic positions.

In the present study we prefer the concept of Deflandre (1963), which is based on Ehrenberg (1854), and includes the three genera *Lithodontium*, *Lithomesites*, and *Lithostylidium*. However, we treat these genera in the following sense: (1) lithodontioid group = phytoliths commonly conical or tetragonal, but also polygonal in outline; (2) lithomesitoid group = dumbbell-shaped phytoliths composed of two globules connected by a neck; (3) lithostyloid group = rodlike phytoliths showing a smooth, undulate, serrate, or spiny margin.

SITE 591 SUMMARY

The section for the present phytolith study is combined from the following intervals: Hole 591A-3,CC to 591A-10,CC for the upper part (upper Pliocene and Pleistocene); Hole 591-11,CC to 591-31,CC for the middle part (upper Miocene to lower upper Pliocene); and Hole 591B-2,CC to 591B-24,CC for the lower part (middle Miocene to lower upper Miocene). Only core-catcher samples were investigated, and as a result no phytolith data are available for calcareous nannoplankton Zones NN13 and NN17 in Table 2.

As shown in Table 2 and Figure 2, phytoliths commonly occur in low numbers in the middle and upper

---

[1] Kennett, J. P., von der Borch, C. C., et al., *Init. Repts. DSDP*, 90: Washington (U.S. Govt. Printing Office).

[2] Addresses: (Locker, present address) Geologisch-Paläontologisches Institut der Universität, Olshausenstrasse 40/60, D-2300 Kiel, Federal Republic of Germany; (Martini) Geologisch-Paläontologisches Institut der Universität, Senckenberg-Anlage 32–34, D-6000 Frankfurt am Main, Federal Republic of Germany.

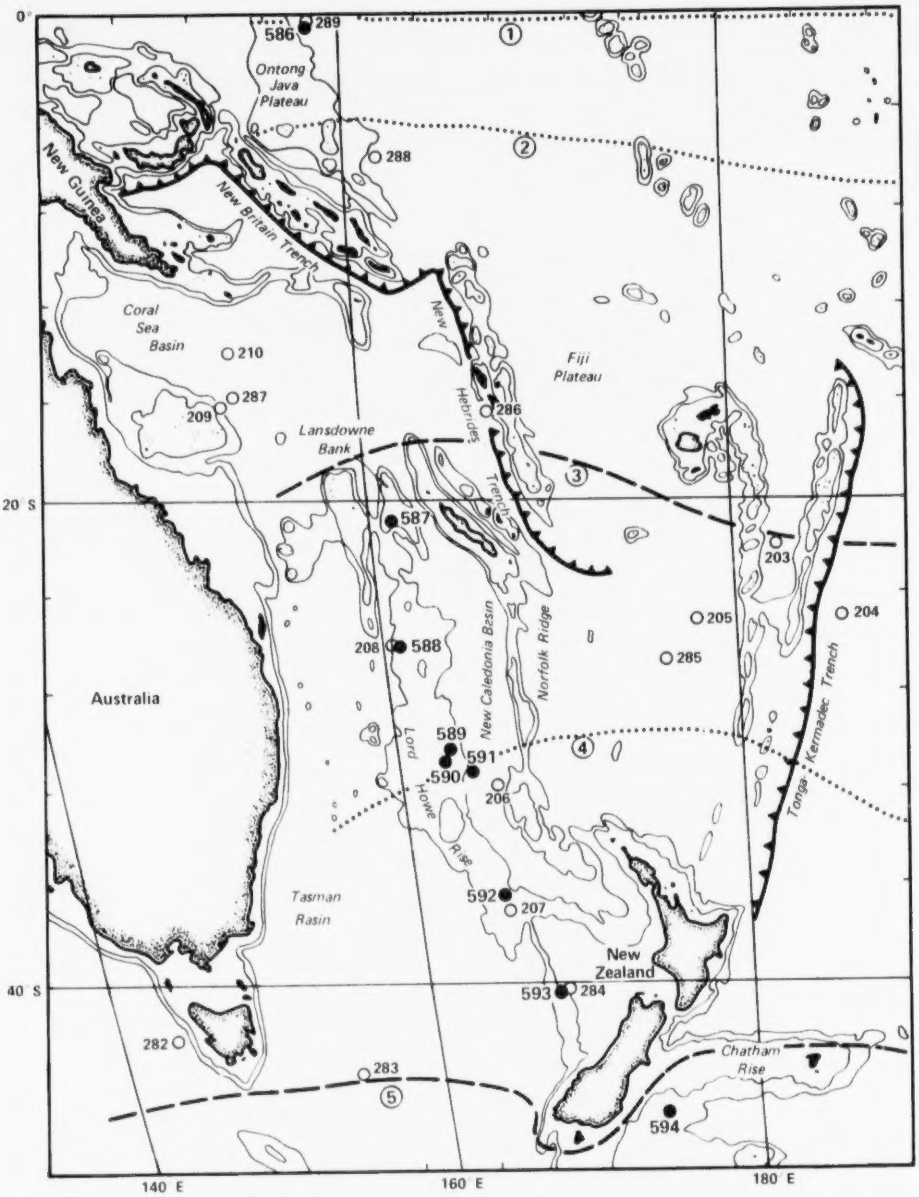
0°
20°S
40°S
140°E
160°E
180°E
①
②
③
④
⑤
586
289
288
210
287
209
286
587
203
205
204
208
588
285
589
591
590
206
592
207
593
284
282
283
594
Ontong Java Plateau
New Guinea
New Britain Trench
Coral Sea Basin
Lansdowne Bank
New Hebrides Trench
Fiji Plateau
Australia
New Caledonia Basin
Norfolk Ridge
Tonga-Kermadec Trench
Lord Howe Rise
Tasman Basin
New Zealand
Chatham Rise

Figure 1. Locations of sites drilled during Leg 90 (solid circles) and other DSDP drill sites (open circles) in the southwest Pacific. Phytoliths are described only from Site 591.

Miocene part of the section, and some levels are barren, especially in the lowest part, comparable with nannoplankton zones NN4 and NN5 (Samples 591B-17,CC to 591B-24,CC). A rather sudden increase in frequencies can be noted with the early Pliocene: lithodontioid, lithomesitoid, and lithostyloid phytoliths are rather common in the upper lower Pliocene and upper Pliocene. Around the Pliocene/Pleistocene boundary two samples (591A-5,CC and 591A-6,CC) are barren of phytoliths, but they reappear in Pleistocene Samples 591A-3,CC and 591A-4,CC.

PALEOCLIMATOLOGICAL INTERPRETATION

Judging by frequencies of occurrence and assumed transport mechanisms, the phytoliths are considered to be derived mainly from the Australian continent. As proved by palynological studies, large, open grasslands developed during the late Neogene in the northern and central regions of Australia (Kemp, 1978), supplying the phytoliths found at Site 591. By analogy with recent conditions (Baker, 1960b; Healy, 1970; Ramage, 1970; Thiede, 1979), strong westerly winds must have blown phyto-

Table 1. Known distribution of phytoliths in marine sediments.

Author	Locality	Time interval	Geographic source
	Atlantic Ocean and Mediterranean Sea		
Kolbe, 1955, 1957	N Atlantic, off NW Africa	Quaternary	Africa
Dumitrică, 1973	Mediterranean Sea (DSDP Sites 124, 130, 131)	Miocene (Site 124), Quaternary (Sites 130, 131)	Mediterranean Region
Hajós, 1973	Mediterranean Sea (DSDP Sites 124, 130)	Miocene (Site 124), Quaternary (Site 130)	Mediterranean Region
Schrader, 1978b	SE Atlantic, Walvis Ridge (DSDP Site 362)	Miocene, Pliocene, Quaternary	Africa
Schrader, 1978a	N Atlantic, off NW Africa (DSDP Site 369)	Eocene, Oligocene, Miocene	Africa
	Equatorial E Atlantic, Sierra Leone Rise (DSDP Site 366)	Oligocene, Miocene, Quaternary	
Bukry, 1979b	N Atlantic, off NW Africa (DSDP Site 397)	Pliocene, Quaternary	Africa
Bukry, 1979a	N Atlantic, Mid-Atlantic Ridge (DSDP Sites 410, 412)	Pliocene/Quaternary	Africa?
	Off SW Iceland (DSDP Site 408)	Pliocene	Iceland?
	Pacific Ocean		
Bukry, 1980	Equatorial E Pacific (DSDP Site 425)	Quaternary	Mexico and Central America
	East Pacific Rise (DSDP Sites 419, 420, 422, 427, 428)	Pliocene, Quaternary	
Locker and Martini, this paper	SW Pacific (DSDP Sites 591, 594)	Miocene, Pliocene, Quaternary	Australia

lith-bearing dusts from the arid and semiarid regions of Australia into the investigated area, which is situated more than 1000 km off the coast. We can deduce from recent conditions that the phytoliths were probably swept from the ground by gusts during cyclonal activity, and lifted up into higher layers of the troposphere. There, in the zone of upper westerly winds, they may have been transported over long distances, especially if enclosed in the subtropical jetstream (recent data in Healy, 1970, and Lamb, 1972).

As shown in Figure 2, phytoliths were first found at about 14.4 m.y., comparable to nannoplankton Zone NN6, middle Miocene. This record provides a more precise date for the initial phase of open grassland formation in Australia than hitherto determined from palynological studies (Kemp, 1978). Generally, the middle Miocene appearance of phytoliths seems to reflect the complex co-operation of various geographical and climatological factors such as:

1. The permanent northward drift of the Indo-Australian Plate after its separation from Antarctica, and its successive penetration into the mid-latitudes (Edwards, 1975; Kemp, 1978), that is, to zones of increased solar radiation (recent data in Lamb, 1972).

2. The development of a large Antarctic ice mass associated with steeper temperature gradients between high and low southern latitudes (Hayes and Frakes, 1975; Kennett, Houtz, et al., 1975; Shackleton and Kennett, 1975; Kennett, 1977; Keigwin, 1979) and the intensification of the wind system (Hayes and Frakes, 1975; Kemp, 1978). Accompanying these processes, came:

3. The initiation of arid conditions in the northern and northwestern parts of Australia, followed by the development of open grasslands (Kemp, 1978). From their first appearance up to the uppermost Miocene, phytoliths are distributed in relatively low frequency. But starting with nannoplankton Zone NN12, at about 5.1 m.y. (early Pliocene), they suddenly occur in higher numbers. After that, phytolith quantities are drastically increased towards the late Pliocene, showing a maximum in nannoplankton Zone NN16, at about 2.5 m.y.

This evolution may be related to developments in the trends described above. It has been demonstrated that:

1. The Antarctic ice sheet attained its maximum dimensions in the latest Miocene to earliest Pliocene (Hayes and Frakes, 1975; Kennett, Houtz, et al., 1975; Kennett, 1977; Mercer and Sutter, 1982; Ciesielski and Weaver, 1983). This was surely accompanied by stronger winds in mid and low latitudes (Hayes and Frakes, 1975; Stein, 1984).

2. The Australian Plate shifted to nearly its recent position in the late Miocene (Edwards, 1975; Kemp, 1978). This must have effected the aridification of vast areas.

The coincidence of both processes obviously led to an expansion of open grasslands in Australia, to the production of large quantities of phytoliths, and to an intensified transport of dust into the eastern seas. It is noteworthy that phytolith frequency does not increase in

Table 2. Distribution of phytoliths in selected samples from Holes 591, 591A, and 591B, and correlation to standard nannoplankton zones.

Age	Nannoplankton zones	Samples	Lithodontioid	Lithomesioid	Lithostyloid	Indet.	Specimens
Quaternary	NN19	591A 3,CC	4	3	2		31
		4,CC	4	4	4	1	102
		5,CC			Barren		
upper Pliocene	NN18	6,CC			Barren		
	NN16	7,CC	4	3	3		51
		8,CC	5	4	4	1	113
		9,CC	4	4	3		65
		10,CC	5	4	4		96
		591 11,CC	4	4	3	1	75
lower Pliocene	NN15	13,CC	4	4	4	2	87
		14,CC	4	4	4	3	84
		16,CC	4	4	3	2	59
	NN14	17,CC	4	4	2	1	52
		18,CC	3	3	2	2	22
		19,CC	4	4	2	1	51
		20,CC	3	3	3	1	29
	NN12	21,CC	3	3	2		24
		22,CC	3	3	2		18
		23,CC	3	3	2		18
upper Miocene	NN11B	24,CC	2	2	2		10
		25,CC	2	2	2		10
		26,CC	2	2	1		9
		27,CC	3	2	2		12
	NN11A	28,CC		2	1		3
		29,CC	2	2	2	1	10
		30,CC	1	3	1		8
		591B 2,CC	2	3	1		13
		3,CC	1	1	2	1	6
		4,CC	1	2	2		8
	NN10	5,CC	2	2	2		11
		6,CC	2	2	2		6
		7,CC			Barren		
		8,CC		2	2		5
	NN9	9,CC	2	1	1		6
middle Miocene		10,CC	2	2			8
	NN8	11,CC	2	2			6
	NN7	12,CC		2	1		3
	NN6	13,CC	1	2			5
		14,CC	1	2	1		6
		15,CC			Barren		
		16,CC	1	1	1		3
	NN4/NN6	17,CC to 24,CC			Barren		

Note: Numbers indicate frequency of particular forms: 1 = 1 specimen, 2 = 2 to 5 specimens, 3 = 6 to 15 specimens, 4 = 16 to 50 specimens, 5 = more than 50 specimens, counted in 4 rows (= 120 mm) across the slides.

the late Miocene, with the assumed beginning of Antarctic ice expansion, but in the early Pliocene. Thus the rise apparently follows, after a slight delay, the prominent cooling event across the Miocene/Pliocene boundary that is evidenced by studies of oxygen isotopes (Shackleton and Kennett, 1975) and planktonic foraminifers in the Tasman Sea area (Kennett and Vella, 1975) and by investigations of ice rafting and the distribution of siliceous and calcareous sediments around Antarctica (Hayes and Frakes, 1975).

The distinct peak of phytolith frequency at about 2.5 m.y., late Pliocene, seems to be in response to the global decrease of temperature and the intensification of westerly winds which had been caused by the formation of the Northern Hemisphere ice sheet at about 3 m.y. (Berggren, 1972; Shackleton and Opdyke, 1977; Keigwin, 1979; Stein, 1984). But the processes causing the absence of phytoliths at the Pliocene/Pleistocene boundary remain unclear. On the one hand, the disappearance might be related to the glacial maximum around 2 m.y. (Shackleton and Opdyke, 1977; Keigwin, 1979; Stein, 1984), which might have changed common meteorological conditions, especially the winds. But on the other hand, selective dissolution of phytolith opal could also be responsible.

ACKNOWLEDGMENTS

Thanks are due to the Deutsche Forschungsgemeinschaft (Bonn Bad Godesberg) for supporting the present study. The Geologisch-P läontologisches Institut der Universität Kiel provided space for labor tory work. Our thanks go also to J. Fenner, M. Sarnthein, and Stein (Kiel) for valuable discussions and to J. P. Kennett (University Rhode Island) for comments and suggestions.

REFERENCES

Baker, G., 1960a. Fossil opal-phytoliths. *Micropaleontology*, 6:79-8

________, 1960b. Phytoliths in some Australian dusts. *Proc. R. So Victoria*, 72:21-40.

Berggren, W. A., 1972. Late Pliocene-Pleistocene glaciation. *In* Laugh ton, A. S., Berggren, W. A., et al., *Init. Repts. DSDP*, 12: Wash ington (U.S. Govt. Printing Office), 953-963.

________, 1979a. Coccolith and silicoflagellate stratigraphy, northern Mid-Atlantic Ridge and Reykjanes Ridge, Deep Sea Drilling Proj ect Leg 49. *In* Luyendyk, B. P., Cann, J. R., et al., *Init. Repts DSDP*,49: Washington (U.S. Govt. Printing Office), 551-581

Bukry, D., 1979b. Comments on opal phytoliths and stratigraphy of Neogene silicoflagellates and coccoliths at Deep Sea Drilling Proj ect Site 397 off northwest Africa. *In* Luyendyk, B. P., Cann, J. R., et al., *Init. Repts. DSDP*, 49: Washington (U.S. Govt. Printing Office), 977-1009.

________, 1980. Opal phytoliths from the tropical Pacific Ocean, Deep Sea Drilling Project Leg 54. In Rosendahl, B. R., Hekinian, R., et al., *Init. Repts. DSDP*, 54: Washington (U.S. Govt. Printing Office), 575-589.

Ciesielski, P. F., and Weaver, F. M., 1983. Neogene and Quaternary paleoenvironmental history of Deep Sea Drilling Project Leg 71 sediments, southwest Atlantic Ocean. *In* Ludwig, W. J., Krasheninnikov, V. A., et al., *Init. Repts. DSDP*, 71, Pt 1: Washington (U.S. Govt. Printing Office), 461-477.

Deflandre, G., 1963. Les Phytolithaires (Ehrenberg). *Protoplasma*, 57 234-259.

Dumitricà, P., 1973. Phytolitharia. *In* Ryan, W. B. F., Hsü, K. J., et al., *Init. Repts. DSDP*, 13, Pt. 2: Washington (U.S. Govt. Printing Office), 940-943.

Edwards, A. R., 1975. Southwest Pacific Cenozoic paleogeography and an integrated Neogene paleocirculation model. *In* Andrews, E., Packham, G., et al., *Init. Repts. DSDP*, 30: Washington (U Govt. Printing Office), 667-684.

Ehrenberg, C. G., 1854. *Mikrogeologie. Das Erden und Felsen scha fende Wirken des unsichtbar kleinen selbststädigen Lebens auf Erde:* Leipzig (Leopold Voss).

Folger, D. W., 1970. Wind transport of land-derived mineral, biog ic, and industrial matter over the North Atlantic. *Deep-Sea Re* 17:337-352.

Folger, D. W., Burckle, L. H., and Heezen, B. C., 1967. Opal phy liths in North Atlantic dust fall. *Science*, 155:1243-1244.

Hajós, M., 1968. Magyarországi neogén Phytolithariák. *Magyar Földt. Int., 1966*, pp. 225-240.

________, 1973. The Mediterranean diatoms. *In* Ryan, W. B. F., H K. J., et al., *Init. Repts. DSDP*, 13: Pt. 2: Washington (U.S. Go Printing Office), 944-969.

Hayes D. E., and Frakes, L. A., 1975. General synthesis, Deep Drilling Project Leg 28. *In* Hayes, D. E., Frakes, L. A., et al., *it. Repts. DSDP*, 28: Washington (U.S. Govt. Printing Offic 919-942.

Healy, T. R., 1970. Dust from Australia. *Earth Sci. J.*, 4:106-116.

Keigwin, L. D., 1979. Late Cenozoic stable isotope stratigraphy and paleoceanography of DSDP sites from the east equatorial and central north Pacific Ocean. *Earth Planet Sci. Lett.*, 45:361-382.

Kemp, E. M., 1978. Tertiary climatic evolution and vegetation history in the Southeast Indian Ocean region. *Palaeogeogr., Palaeoclimatol., Palaeoecol.*, 24:169-208.

Kennett, J. P., 1977. Cenozoic evolution of Antarctic glaciation, the Circum-Antarctic Ocean, and their impact on global paleoceanography. *J. Geophys. Res.*, 82:3843-3860.

Kennett, J. P., Houtz, R. E., et al., 1975. Cenozoic paleoceanography in the southwest Pacific Ocean, Antarctic glaciation, and the development of the Circum-Antarctic Current. *In* Kennett, J. P., Houtz, R. E., et al., *Init. Repts. DSDP*, 29: Washington (U.S. Govt. Printing Office), 1155-1169.

Kennett, J. P., and Vella, P., 1975. Late Cenozoic planktonic foraminifera and paleoceanography at DSDP Site 284 in the cool subtropical South Pacific. *In* Kennett, J. P., Houtz, R. E., et al., *Init. Repts. DSDP*, 29: Washington (U.S. Govt. Printing Office), [illegible]9-799.

K[illegible], R. W., 1955. Diatoms from equatorial Atlantic cores. *Rep. Swedish Deep-Sea Exp.*, 7:150-184.

———, 1957. Fresh-water diatoms from Atlantic deep-sea sediments. *Science*, 126:1053-1056.

L[illegible], H. H., 1972. *Climate: Present, Past and Future* (Vol. 1): *Fundamentals and Climate Now:* London (Methuen and Co.).

M[illegible]er, J. H., and Sutter, J. F., 1982. Late Miocene—earliest Pliocene glaciation in southern Argentina: implications for global ice-sheet history. *Palaeogeogr., Palaeoclimatol., Palaeoecol.*, 38:185-206.

Ramage, C. S., 1970. Meterology of the South Pacific tropical and middle latitudes. *In* Wooster, W. S. (Ed.), *Scientific Exploration of the South Pacific:* Washington (National Academy of Sciences), pp. 16-29.

———, 1978a. Diatoms in DSDP Leg 41 Sites. *In* Lancelot, Y., Seibold, E., et al., *Init. Repts. DSDP*, 41: Washington (U.S. Govt. Printing Office), 791-812.

Schrader, H.-J., 1978b. Opal phytoplankton remains at DSDP Leg 40 Sites. *In* Bolli, H. M. Ryan, W. B. F., et al., *Init. Repts. DSDP*, Suppl. to Vols. 38, 39, 40, and 41: Washington (U.S. Govt. Printing Office), 735-741.

Shackleton, N. J., and Kennett, J. P., 1975. Paleotemperature history of the Cenozoic and the initiation of Antarctic glaciation: oxygen and carbon isotope analysis in DSDP Sites 277, 279, and 281. *In* Kennett, J. P., Houtz, R. E., et al., *Init. Repts. DSDP*, 29: Washington (U.S. Govt. Printing Office), 743-755.

Shackleton, N. J., and Opdyke, N. D., 1977. Oxygen isotope and paleomagnetic evidence for early Northern Hemisphere glaciation. *Nature*, 270:216-219.

Stein, R., 1984. *Zur neogenen Klimaentwicklung in Nordwest-Afrika und Paläo-Ozeanographie im Nordost-Atlantik: Ergebnisse von DSDP-Sites 141, 366, 397 und 544B.* Ber. Geol. Paläont. Inst. Univ. Kiel, 4.

Thiede, J., 1979. Wind regimes over the late Quaternary southwest Pacific Ocean. *Geology*, 7:259-262.

Twiss, P. C., Suess, E., and Smith, R. M., 1969. Morphological classification of grass phytoliths. *Proc. Soil Sci. Soc. Am.*, 33:109-115.

Date of Initial Receipt: 12 June 1984
Date of Acceptance: 26 October 1984

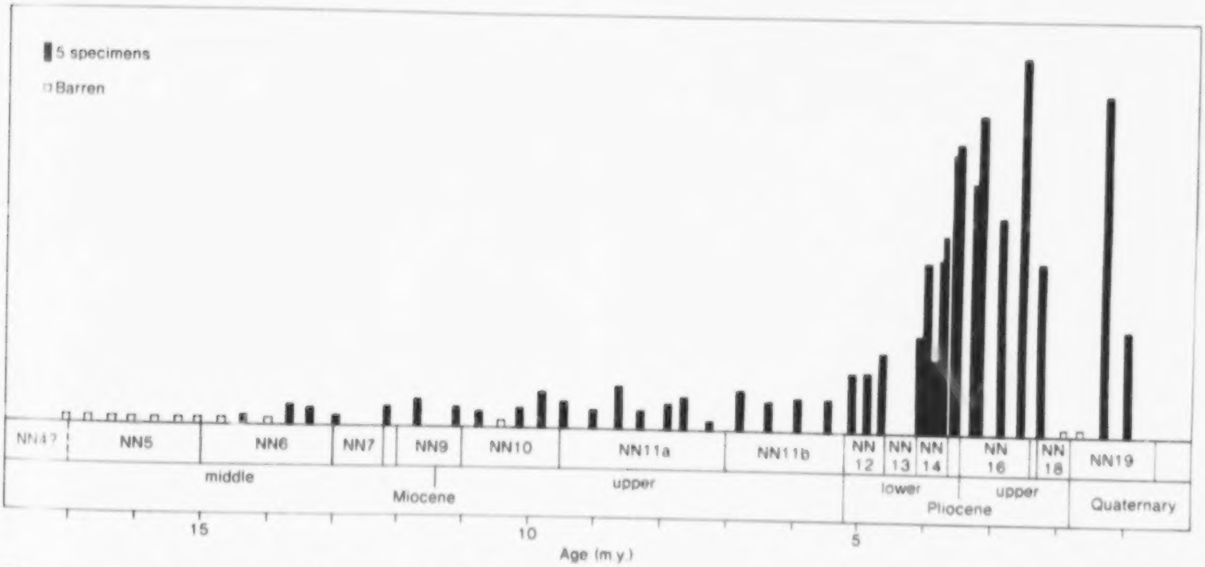

Figure 2. Frequency distribution of phytoliths found at Site 591, and correlation to standard nannoplankton zones.

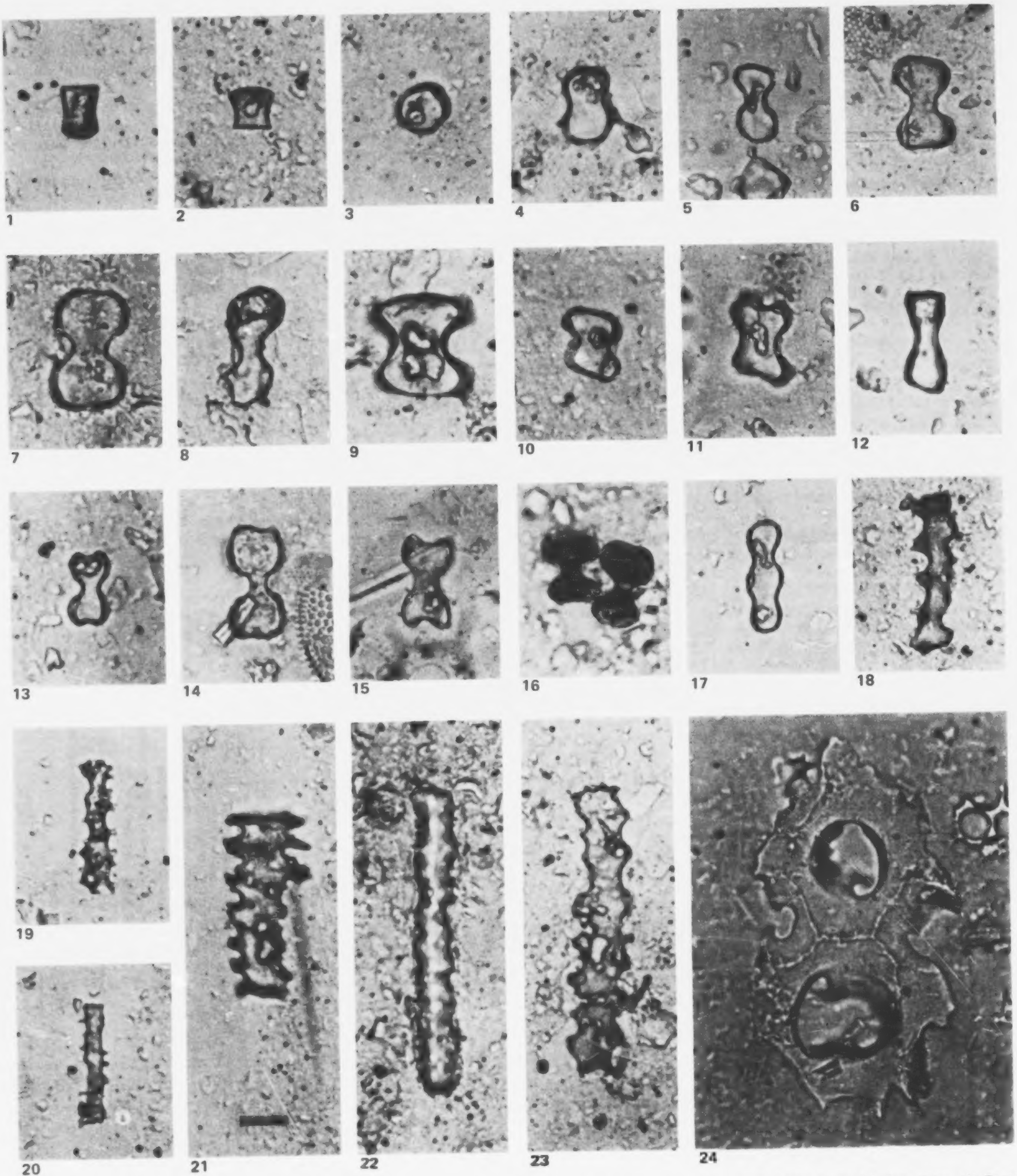

Plate 1. Middle Miocene to Pleistocene phytoliths. (All specimens magnified ×800, bar = 10 μm). **1–3.** Lithodontioid phytoliths, (1) Samp 591A-4,CC, Quaternary; (2) Sample 591A-7,CC, upper Pliocene; (3) Sample 591-11,CC, upper Pliocene. **4–17.** Lithomesitoid phytoliths, (Sample 591-14,CC, lower Pliocene; (5) Sample 591A-4,CC, Quaternary; (6) Sample 591-31,CC, upper Miocene; (7) Sample 591-17,CC, low Pliocene; (8) Sample 591B-16,CC, middle Miocene; (9) Sample 591A-4,CC, Quaternary; (10) Sample 591-21,CC, lower Pliocene; (11) Samp 591-17,CC, lower Pliocene; (12) Sample 591A-4,CC, Quaternary; (13) Sample 591-11,CC, upper Pliocene; (14) Sample 591-20,CC, lower Pli cene; (15) Sample 591-22,CC, lower Pliocene; (16) Sample 591-13,CC, lower Pliocene; (17) Sample 591A-7,CC, upper Pliocene. **18–23.** Lith styloid phytoliths, (18) Sample 591A-8,CC, upper Pliocene; (19) Sample 591A-4,CC, Quaternary; (20) Sample 591-13,CC, lower Pliocene; (2 Sample 591A-9,CC, upper Pliocene; (22) Sample 591A-4,CC, Quaternary; (23) Sample 591A-3,CC, Quaternary. **24.** Silicified epidermis, Sa ple 591-28,CC, upper Miocene.

23. PALYNOLOGY OF SELECTED NEOGENE SAMPLES FROM HOLES 594 AND 594A, CHATHAM RISE[1]

Linda E. Heusser, Lamont-Doherty Geological Observatory[2]

ABSTRACT

This chapter presents the results of preliminary palynologic analyses of 132 samples from Holes 594 and 594A from Deep Sea Drilling Project Leg 90. Palynomorph abundance, diversity, and preservation vary, with minimum concentration in the late early to middle Miocene nannofossil chalk. In the upper part of the late Miocene foraminifer-bearing nannofossil ooze, pollen concentration rises close to the maximum amounts (~400 grains/cm ^{3}) found in the Pliocene, Pleistocene, and Quaternary hemipelagic silts and clays.

Pollen spectra in all samples are mainly arboreal pollen. Early Miocene pollen assemblages are dominated by *Nothofagus brassi*, with subsidiary podocarpaceous pollen. In mid-Miocene samples, *N. fusca* is the major type of beech pollen present. Late Miocene, Pliocene, and Quaternary pollen assemblages show decreasing representation of extinct Tertiary pollen types and evidence of climatic fluctuations.

INTRODUCTION

The purpose of this preliminary survey of palynomorphs in cores recovered from DSDP Holes 594 and 594A on the Chatham Rise in the southwest Pacific east of South Island, New Zealand, is to evaluate the stratigraphic, paleogeographic, and paleoclimatic potential of the marine pollen record from Site 594. Although few papers discuss pollen in marine sediments near New Zealand (Koroneva, 1968), pollen analyses of marine sediments in fjords of western South Island (Harris, 1964; Mildenhall, 1978d) demonstrate the stratigraphic and ecologic usefulness of marine pollen. Elsewhere in the Antipodes, Kemp (1975, 1981; Kemp and Harris, 1975) used pollen from deep-sea cores to reconstruct Antarctic and Australian Tertiary vegetation and climates. Pollen analyses of samples from DSDP sites near western North American (Fournier, 1981; Heusser, 1982) and in the Black Sea (Koroneva and Kartashova, 1978; Traverse, 1978) provide age determinations, palynostratigraphic zonations, and floral and climatic information about nearby land masses.

New Zealand Tertiary and Quaternary pollen stratigraphy and vegetation/climatic history are well known from pollen analyses of late Cenozoic shallow-water marine and nonmarine deposits, work begun by New Zealand palynologists such as Cranwell (Cranwell and von Post, 1936), Couper (1951a, b), and Moar (1958). Tertiary pollen zonations are usually related to the exceptionally complete and well-correlated New Zealand Tertiary marine sequence. Paleoclimatic interpretations of [illegible] Cenozoic pollen assemblages are based on detailed studies of present relationships between pollen and vegetation distributions in New Zealand (e.g., McGlone, 1982; Moar, 1970; Pocknall, 1980).

SETTING

The plants of New Zealand (South Island and, to a lesser extent, North Island) are the primary source of pollen in sediments of Site 594. Vegetation of these mountainous islands can be simplistically divided into two plant formations, forest and tussock grassland, the first widely distributed in both islands, and the second well-developed in South Island east of the forest-covered Southern Alps (Cockayne and Phillips-Turner, 1967). Two broad categories of temperate, board-leaved evergreen forests are recognized: lowland, conifer–broadleaf forest (including podocarps such as *Podocarpus, Dacrydium*, and *Phyllocladus*, hardwoods such as *Weinmannia*, and tree ferns like *Cyathea*), and subalpine *Nothofagus* (southern beech) stands (including *N. fusca* and *N. solandri;* Wardle et al., 1983).

Present distribution of plant associations in New Zealand is related to climatic patterns, controlled by latitude, oceanic environment, and relief, as well as to historical factors (Wardle et al., 1983). Located between ~34° and 47°S, the long, narrow (<300 km) land mass lies in the convergence of atmospheric pressure systems (subtropical high and Southern Ocean low) and oceanic water masses (subantarctic, temperate, and warm subtropical) (Griggs, et al., 1983). Precipitation is high, with strong, circumpolar westerly winds and high relief causing marked differences in average annual rainfall (from 6250 mm on the west coast of South Island to <600 mm in the east). Moderate mean annual temperatures range from 8°C on South Island to 13°C on North Island (Allan, 1961; Moar and Suggate, 1979).

METHODS

For this preliminary survey, two to three samples were taken from each core from Holes 594 and 594A (Table 1). Sampling intervals ranged from 3 to 10 m. In all, 132 samples were processed, 94 from Hole 594 and 38 from Hole 594A. Sample size ranged from 10 cm^3 to 20 cm^3 wet sediment. Preparations involved mechanical and chemical extraction techniques described in Heusser and Stock (1984). Palynomorphs were identified using a reference collection made from plants

---

[1] Kennett, J. P., von der Borch, C. C., et al., *Init. Repts. DSDP*, 90: Washington (U.S. Govt. Printing Office).

[2] Address: Lamont-Doherty Geological Observatory, Colombia University, Palisades, N.Y. 10964.

Table 1. Samples analyzed for pollen from Holes 594 and 594A.

Sample (interval in cm)	Depth below Seafloor (m)	Lithology	Age
Hole 594			
1-2, 43-47	1.95	Unit I Alternating bluish gray foraminifer-bearing nannofossil ooze and greenish gray nannofossil-bearing clayey silt	Quaternary
1-4, 43-47	4.95		
2-2, 43-47	7.85		
2-4, 43-47	10.85		
2-6, 43-47	13.85		
3-1, 43-47	16.95		
3-2, 43-47	17.45		
3-4, 43-47	20.45		
3-5, 43-47	21.45		
3-6, 43-47	23.45		
4-2, 43-47	27.05		
4-4, 43-47	30.05		
4-6, 43-47	33.05		
5-2, 43-47	36.65		
5-4, 43-47	39.65		
5-6, 43-47	42.65		
6-2, 43-47	46.25		
6-4, 43-47	49.25		
7-2, 43-47	55.85		
9-2, 43-47	75.05		
9-4, 43-47	78.05		
9-6, 43-47	81.05		
10-2, 43-47	84.65		
11-2, 43-47	94.25		
11-4, 43-47	97.25		
11-6, 43-47	100.25		
12-2, 43-47	103.85		
12-4, 43-47	106.85		
13-2, 43-47	113.45		
13-4, 43-47	116.45		
14-2, 43-47	123.05		
14-4, 43-47	126.05		late Pliocene
15-2, 43-47	132.65		
15-4, 43-47	135.65		
15-6, 43-47	138.65		
16-2, 43-47	142.25		
16-4, 43-47	145.25		
18-2, 43-47	161.45		early Pliocene
18-4, 43-47	164.45		
18-6, 43-47	167.45		
19-2, 43-47	171.05	Subunit IIA Light to very light gray foraminifer-bearing nannofossil ooze to nannofossil ooze	
19-4, 43-47	174.05		
19-6, 43-47	177.05		
20-2, 43-47	180.65		
20-4, 43-47	183.65		
21-2, 43-47	190.25		late Miocene
21-4, 43-47	193.25		
21-6, 43-47	196.25		
23-2, 43-47	209.45		
23-4, 43-47	212.45		
23-6, 43-47	215.45		
24-2, 43-47	219.05		
24-4, 43-47	222.05		
24-6, 43-47	225.05		
25-2, 43-47	228.65		
25-4, 43-47	231.65		
26-2, 43-47	238.25		
26-4, 43-47	241.25		
27-2, 43-47	247.05		
27-4, 43-47	250.85		
28-2, 43-47	257.45		
28-4, 43-47	260.45		
29-2, 43-47	267.05		
29-4, 43-47	270.05		
29-6, 43-47	273.05		
30-2, 43-47	276.65		
30-4, 43-47	279.65		
30-6, 43-47	282.65		
31-2, 43-47	286.25		
31-4, 43-47	289.25		
31-6, 43-47	292.25		
Hole 594 (Cont.)			
34-2, 43-47	314.05		
34-4, 43-47	317.05		
35-2, 43-47	323.65		
35-4, 43-47	326.65		
36-2, 43-47	333.25		
36-4, 43-47	336.25		
38-2, 43-47	352.45		
39-2, 43-47	362.05		mid Mioce
40-2, 43-47	371.65		
40-4, 43-47	374.65		
41-2, 43-47	382.25		
41-4, 43-47	385.25		
42-2, 43-47	391.85		
42-4, 43-47	394.85		
45-2, 43-47	420.65		
46-2, 43-47	430.25		
47-1, 43-47	438.35		
48-2, 43-47	449.45		
49-2, 43-47	459.05		
49-4, 43-47	462.05		
50-2, 43-47	468.65		
51-1, 43-47	476.75	Subunit IIB Very light gray nannofossil chalk with occasional interbeds of olive gray silt-bearing clayey nannofossil chalk	
52-2, 43-47	487.85		
Hole 594A			
1-2, 43-47	43.25	Unit I Alternating bluish gray foraminifer-bearing nannofossil ooze and greenish gray nannofossil bearing clayey silt	Quaternary
1-4, 43-47	46.25		
1-6, 43-47	49.25		
2-2, 43-47	52.85		
2-4, 43-47	55.85		
2-6, 43-47	58.85		
3-2, 43-47	62.45		
3-4, 43-47	65.45		
3-6, 43-47	68.45		
4-2, 43-47	72.05		
5-2, 43-47	81.65		
5-4, 43-47	84.65		
5-6, 43-47	87.65		
6-2, 43-47	91.25		
10-2, 43-47	129.65		late Pliocene
10-4, 43-47	132.65		early Pliocene
10-6, 43-47	135.65		
11-2, 43-47	199.85	Subunit IIA Light to very light gray foraminifer-bearing nannofossil ooze to nannofossil ooze	late Miocene
11-4, 43-47	202.85		
13-2, 43-47	507.05	Subunit IIB Very light gray nannofossil chalk with occasional interbeds of olive gray silt-bearing clayey nannofossil chalk	mid-Miocene
13-4, 43-47	510.05		
13-6, 43-47	513.05		
14-2, 43-47	516.65		
14-4, 43-47	519.65		
15-2, 43-47	526.25		
16-2, 43-47	535.85		
16-4, 43-47	538.85		
16-6, 43-47	540.85		
17-2, 43-47	545.45		
17-4, 43-47	548.45		
20-1, 10-14	572.42		
20-2, 43-47	574.25		
21,CC	584.34		early Miocene
22,CC	592.45		
23-1, 127-130	602.39		
24-1, 110-112	611.81		
25-1, 100-102	621.31		
26-1, 32-34	630.23		

collected in New Zealand by the author, C. J. Heusser, and L. B. Moore; from reference slides and photographs graciously lent by L. M. Cranwell; and from illustrations and descriptions published by Cookson, 1959; Couper, 1953c; Cranwell, 1938–1963. Hanks and Fairbrothers, 1976; Harris, 1955; and Truswell 1982b, 1983. Poor preservation and the presence of numerous opaque (pyrite ?) particles often made identification difficult; therefore, many groups were not differentiated and classifications should be regarded as tentative, pending further detailed study. For example, *Dacrydium kirkii-biforme-bidwilli* types were not differentiated and may be included in the *Podocarpus* group or mistakenly assigned to *Dacrydium cupressinum* (Mildenhall, 1978c). Tertiary bisaccate grains with small sacci placed in the *Phyllocladus* group may include *Phyllocladites mawsoni* (Couper, 1953c; Tulip, et al., 1982), and some small, trisaccate grains may represent *Microcachrys*, *Microstrobus (Pherosphaera)* species, *Microcachryidites*, or possibly *Acmopyle pancheri* and *A. alba* from New Caledonia (Cranwell, 1961; personal communication, 1983).

SITE 594 (45°31.41′S; 174°56.88′E)

Site 594 is located in the South Pacific Ocean at a depth of 1204 m on the southern margin of the Chatham Rise about 250 km east of South Island, New Zealand (Fig. 1). The site, downslope from Waitaki Canyon, is situated in a transitional area between ocean (subantarctic waters immediately south of the Subtropical Convergence) and terrigenous influences, particularly the Waitaki River drainage.

Holocene through lower Miocene sediments were recovered from three holes cored to a maximum sub-bottom depth of 639 m, with four unconformities detected (about 8.3–6.5 Ma, about 5.4–4.5 Ma, about 3.85–2.7 Ma, and about 1.6–0.74 Ma). Both the Miocene/Pliocene boundary and the early/late Pliocene boundary fall within disconformities. Two lithostratigraphic units were defined (Table 1). Unit I (earliest Pliocene to Quaternary age) consists of an alternating sequence of greenish gray hemipelagic and bluish gray pelagic lithofacies separated from the lower units by a gradational contact. Unit II (late early Miocene to earliest Pliocene age) is a pelagic facies consisting mainly of light gray foraminifer-bearing nannofossil ooze (Subunit IIA, middle Miocene to earliest Pliocene age), and light gray nannofossil chalk with occasional interbeds of olive gray silt-bearing nannofossil chalk (Subunit IIB, late early to middle Miocene).

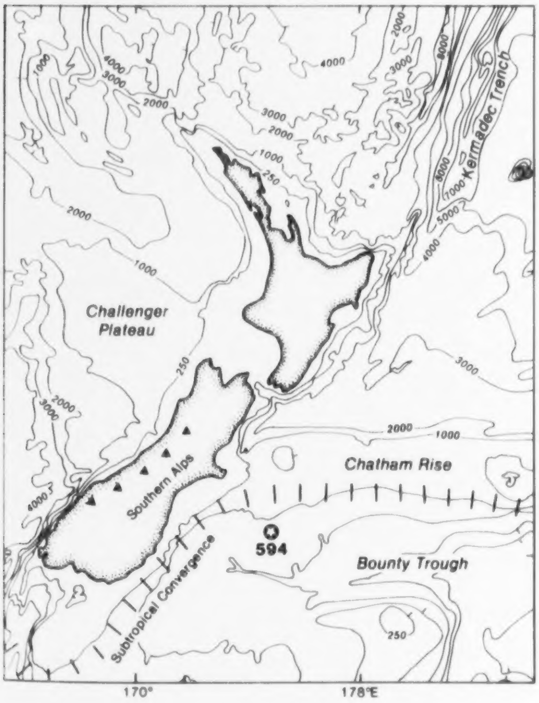

Figure 1. Location of Site 594 off South Island, New Zealand.

Two major tectonic episodes are recorded in sediments of Site 594. The clay turbidites of Subunit IIB provide evidence of an early tectonic pulse about 17 Ma, which coincides with strike-slip motion along the Alpine Fault sector of the Indian/Pacific plate boundary (site chapter, this volume). At 6 Ma, the first late Neogene influx of hemipelagic sediments dates the beginning of the Kaikoura Orogeny and the emergence of a fairly substantial, continuous, northeast-to-southwest-trending landmass (site chapter, this volume; Nelson, this volume; Suggate, 1978). In the upper 200 m below the seafloor, 25 major hemipelagic depositional episodes are recorded. Shipboard investigations indicate that this sequence of alternating dark hemipelagic and light pelagic biogenic sediments of latest Miocene to Pleistocene age is related to climatic change: warm climates (interglacials) and high sea levels are associated with pelagic sediment containing warm planktonic foraminifer faunas, and cold climates (glacials) and low sea levels are associated with pelagic sediments containing much biosiliceous material and cold planktonic foraminifer faunas (site chapter, this volume). High-resolution carbonate and isotope stratigraphies provide detailed confirmation of the correlation between sedimentary parameters and late Quaternary climatic changes, and provide a correlation between New Zealand Quaternary records and fluctuations of northern hemisphere ice sheets (Nelson, Hendy, et al., this volume).

RESULTS

The results presented in this preliminary report cannot do justice to the paleoecological potential of the pollen record in the sediments of Site 594. Palynomorphs in samples from Holes 594 and 594A (Table 1) are *Nothofagus fusca* type, *Nothofagus menziesii* type, *Nothofagus brassi* type, *Podocarpus* types, *Dacrydium* types, *Phyllocladus* type, *Michrocachrys* type, inaperturate cupressaceous types, Myrtaceae, *Coprosma* types, Ericaceae, Gramineae, Cyperaceae, Compositae, Chenopodiaceae, Polypodiaceae, and Lycopodiaceae. Dinoflagellates, microforaminifers, and recycled pollen and spores are frequently present. Pollen types identified, but not tabulated, include *Haloragacidites* (al. *Triorites*) *harrisii* and *H. trioratus*, extinct species probably belonging to the Haloragaceae or Betulaceae (Couper, 1953a–c; Mildenhall and Harris, 1970), *Proteacidites*, and members of the Umbelliferae, Rosaceae, Loranthaceae, Cupressaceae, Proteaceae, and Cunoniaceae (Allan, 1961; Moore and Edgar, 1970).

Pollen spectra from samples from Sites 594 and 594A are not correlated with New Zealand stratigraphic units because rare diagnostic forms (Couper, 1951–1960; Couper and McQueen, 1954; Couper and Harris, 1960; Mildenhall, 1972–1980. Moar and Suggate, 1979) were not often identified. Future preparation of larger samples from cores taken at Site 594 to isolate diagnostic pollen types may prove useful for late Cenozoic correlations; however, Mildenhall and Suggate (1981) suggest that palynological subdivision using extinct species may be of only local value in the upper Pliocene and basal Quaternary. In deep-sea sediments, rare extinct or extant pollen types must be interpreted with caution because of the increased possibilities for contamination by long-distance transport or the addition of recycled pollen.

Palynomorphs were recovered from both lithostratigraphic units (Unit I, and Subunits IIA and IIB). Early Pliocene–Quaternary samples from the interbedded hemipelagic and pelagic facies of Unit I and late Miocene–early Pliocene Samples 594A-11-2, 43–47 cm and 594-21-6, 43–47 cm through 594-19-2, 43–47 cm from Subunit IIA were generally more productive than the nannofossil ooze of Subunit IIB, with the exception of turbidite samples 594A-17-2, 43–47 cm, 594A-17-4, 43–47 cm, and 594A-20-1, 10–14 cm. Pollen concentration is low (<400 pollen grains/cm^3), and shows no apparent correlation with the detailed changes in sedimentary properties of the Quaternary pelagic and hemipelagic oozes at Site 594 described by Nelson (Nelson et al., this volume). Preservation and pollen diversity vary: more pollen groups are identified in well-preserved assemblages with relatively high pollen counts (50 to 100 grains), samples which often, but not always, have high pollen density.

Pteridophyte spores (Filicopsida and Lycopsida) and redeposited pollen and spores occur in all three sedimentary units. A few grains identified as *Sphagnum* appear at the base of Subunit IIA. Dinoflagellates are commonly present and frequently abundant in samples from Unit I and Subunit IIA, and are rare in Subunit IIB. Units I and II contain microforaminifers, ranging from abundant in Unit I to absent in Subunit IIB. Other components of the organic residue include fungal spores, blackened and degraded plant fragments, amorphous organic material (<5 μm), and algal fragments.

Early Miocene

In the six early Miocene samples, pollen assemblages are dominated by *Nothofagus*, primarily *N. brassi* with lesser *N. menziesii. Nothofagus fusca* is present in small amounts. Podocarp and *Microcachryidites*-type pollen occurs throughout. *Haloragacidites harrisii* and *Proteacidites* are present, along with recycled pollen and spores. Herb and shrub pollen is essentially absent (one Gramineae grain was identified), and no dinoflagellates or microforaminifers were found.

Mid-Miocene

Pollen concentration is very low in most mid-Miocene samples. Eight samples are barren and four other samples have <10 pollen grains. Samples 594A-20-1, 43–47 cm, 594A-13-6, 43–47 cm, 594-49-2, 43–47 cm, 594-46-2, 43–47 cm, and 594-45-2, 43–47 cm, are very productive, with >50 pollen grains identified from each sample. *Nothofagus fusca* is the most important arboreal pollen type, and replaces *N. brassi* in prominence. *N. menziesii*, podocarpaceous pollen, and *Microchachryidites*-types are present, along with representatives of the Gramineae, Compositae, Chenopodiaceae, and Cyperaceae. Pteridophyte spores, including *Cyathea*-types, increase in abundance upwards, Dinoflagellates are present in each sample, and recycled palynomorphs, microforaminifer cysts, and a few *Sphagnum*-like grains occasionally appear.

Late Miocene

Basal late Miocene Samples 594-38-2, 43–47 cm through 594-31-4, 43–47 cm are relatively unproductive. Pollen becomes more numerous in Samples 594-31-[illegible], 43–47 cm, through 594-28-2, 43–47 cm, with 65 grains identified in Samples 594-28-4, 43–47 cm. Podocarpaceous pollen types (including *Dacrydium cupressinum*) are more numerous than *Nothofagus* types. Fern spores and dinoflagellate are frequent, microforaminifers appear occasionally, and lycopod spores occur in a few samples. Between 250 and 212 m (Samples 594-27-4, 43–47 cm through 594-23-6, 43–47 cm), podocarps (*Dacrydium cupressinum, Podocarpus dacrydiodes*, and trisaccate types) outnumber *Nothofagus* types (*N. fusca, N. menziesii, and N. brassi*, in order of prominence). Fern (polypod) spores and dinoflagellates are consistently abundant. Nonarboreal pollen, lycopod spores, and microforaminifers appear occasionally.

The podocarp/*Nothofagus* ratio reverses in pollen-rich (>100 pollen grains/sample), younger late Miocene samples (594-23-4, 43–47 cm, through 594-21-2, 43–47 cm, 594A-11-4, 43–47 cm, and 594A-11-2, 43–47 cm), with *Nothofagus fusca* the leading arboreal pollen group. Compositae pollen is present in each sample, and *Coprosma*, Chenopodiaceae, Gramineae, and Cyperaceae pollen are occasional components of these pollen assemblages. Pteridophyte spores (polypod and lycopod) are more prominent than dinoflagellates and microforaminifers. *Microcachryidites* is present. A few grains of *Haloragacidites harrisii* and *Protaecidites* were identified, apparently marking the last appearance of these grains.

Pliocene–Quaternary

Plio-Pleistocene samples are characterized by large fluctuations in pollen density, changing from 400 to 5 grains/cm^3 in one sample interval. *Nothofagus fusca* is the leading pollen type, and *Nothofagus* types usually occur more frequently than podocarps, although some levels do have larger numbers of conifer pollen. Nonarboreal pollen is always less numerous than arboreal pollen; only 2 samples (594-5-6, 43–47 cm and 594A-2-6, 43–47 cm) have $>25\%$ herb pollen. As in older samples, fern spores are more abundant than lycopod spores. Dinoflagellates and microforaminifers vary in relative frequency of total palynomorphs, the latter increasing in the upper 36 m below the seafloor. Characteristic older Tertiary types, *N. brassi* and trisaccate conifers, gradually decrease in younger sediment. Sample 594-18-2, 43–47 cm (161 m sub-bottom depth) marks the last fairly continuous appearance of *N. brassi*, although (?recycled) pollen grains which appear to be *N. brassi* occur occasionally in younger sediments up to 43 m sub-bottom depth (Sample 594-1-2, 43–47 cm).

DISCUSSION

Pollen concentration ($< 400/cm^3$) in all samples analyzed from Site 594 is unexpectedly low, although larger than concentration values of marine pollen in piston cores taken off North Island, New Zealand (Koroneva, 1968). In similar marine sedimentary environments adjacent to North America and Japan (continental slope at ~40° latitude near large river systems draining temperate vegetation), pollen concentrations are 2 to 20 times greater than in sediments east of New Zealand (Heusser, 1983; Heusser and Balsam, 1977; Heusser, L. E., unpublished data). Perhaps the relatively small area from which pollen is derived (both the present surface area of North and South Island and the even smaller area capable of supporting vegetation in the Tertiary; Walcott, 1984) accounts for the low amount of pollen in cores from Holes 594 and 594A. Sedimentation and preservation are also important determinants in pollen concentration in sediments from Chatham Rise. Dilution by terrigenous and pelagic sedimentary components may account for the scarcity of pollen at Site 594. Oxidation and winnowing related to vigorous current action may have differentially destroyed or removed pollen (Heusser and Balsam, 1977), and oxidizing depositional environments are noted for poor pollen preservation (Tschudy and Scott, 1969). Pollen concentration is broadly correlated with intervals of terrigenous influx, with greatest pollen influx in the Plio-Pleistocene hemipelagic sequence (Samples 594-1-2, 43–47 cm through 594-11-2, 43–47 cm, and 594A-1-2, 43–47 cm through 594A-6-2, 43–47 cm), and in basal Miocene turbidites (Samples 594A-20-1, 10–14 cm and 594A-25-1, 100–102 cm). Lowest pollen influx, in middle Miocene nannofossil oozes (Sample 594-49-4, 43–47 cm through 594-28-2, 43–47 cm) is associated with pelagic carbonates and virtual lack of terrigenous input (site chapter, this volume). The sparseness of pollen in these mid-Miocene samples may also be related to the increased corrosiveness of Pacific Ocean bottom waters associated with Antarctic glaciation and the formation of Antarctic Bottom Water (Shackleton and Kennett, 1975).

Broad changes in marine plankton in the pollen concentrate of samples analyzed from Sites 594 and 594A, an absence of dinoflagellate and microforaminifer cysts in the lower Miocene, and abundance variations in younger sediments probably relate to the paleoceanographic changes (i.e., changes in sea surface temperature and salinity, sediment supply, current velocity, and glacioeustatic sea level). Increased numbers of dinoflagellates in the upper Miocene may be associated with development of the Subtropical Convergence at this time (site chapter, this volume). In the northeast Pacific Ocean, late Miocene dinoflagellate abundance and diversity indicate changes in surface waters of the California Current (Ballog and Malloy, 1981). Further south off Mexico, Fournier (1981) related dinoflagellate abundance to water depth and turbulence: high dinoflagellate density is associated with low sea level in shallow depositional sites.

Pollen spectra from marine sediments of Site 594 can be interpreted only in relation to late Cenozoic pollen assemblages found on land (New Zealand) because there are no comprehensive studies relating New Zealand vegetation and pollen deposition in marine environments offshore. In comparing marine pollen assemblages from DSDP cores taken on Chatham Rise with pollen assemblages from South and North Island, differences in pollen source and sedimentation should be noted. Pollen from most peats, lignites, or nonmarine sediment is largely wind-transported short distances from small plant communities and rapidly deposited in lakes and bogs, environments with excellent pollen preservation. Pollen from shallow-water marine sediments (the fjords of South Island, or the mudstones and siltstones of the Wanganui Series) is derived from large vegetation formations, and shows effects of differential sorting and preservation during aerial and fluviomarine transport before final deposition in high-energy environments. Pollen and spores in deep-water marine sediments reflect vegetation of broad regions, as well as eolian and fluviomarine transport and deposition (Heusser, 1983; Heusser and Balsam, 1977).

Late Cenozoic pollen assemblages from Site 594 are dominated by arboreal pollen: *Nothofagus* (southern beech), the most common Cretaceous and Tertiary pollen type of New Zealand (Couper, 1951a), and representatives of the Podocarpaceae (conifers), including *Dacrydium, Podocarpus*, and *Phyllocladus* species (Allan, 1961). Pollen and macrofossils from these wind-pollinated trees are prominent in Tertiary marine and nonmarine sediments in the southern hemisphere, and relative differences in representation of beech and conifer pollen are criteria for stratigraphic assignments and climatologic interpretations of Tertiary and Quaternary polliniferous sediments from New Zealand, Australia, and Antarctica (Couper, 1951–60; Cranwell, 1969; Kemp, 1975; Mildenhall, 1978a, b).

Despite differences in source and sedimentation, late Cenozoic pollen spectra in samples analyzed from Site 594 are broadly correlative with pollen obtained from marine and nonmarine sediments on New Zealand. Early Miocene floras are characterized by the presence of numerous extinct pollen and spore types. The mid-Miocene marks a transition, with some older pollen types (*N. brassi, Haloragacidites harrisii*) continuing in a minor role and others (*N. fusca*) playing a major role. As on North and South islands, new groups (Compositae and Chenopodiaceae) appear in greater numbers. Upper Miocene and Pliocene marine samples show a gradual decline in extinct species, and no abrupt changes in floral assemblage appear between ~2.47 and ~5.5 Ma. On New Zealand, no evidence exists of exceptional climatic changes (Suggate et al., 1978), or of abrupt floral extinctions at the Miocene/Pliocene boundary or in latest Miocene (Kapitean) pollen sequences. Pliocene–Quaternary pollen assemblages also record an apparent gradual loss of extinct taxa, although a substantial number of extinct species make their last appearance in the Pliocene Taranaki Series (Suggate et al., 1978; Mildenhall and Suggate, 1981). The progressive extinction of Tertiary groups includes forms with interrupted ranges, such as the *Nothofagus brassi* group which appears in interglacial deposits after absence in earlier glacial periods (Suggate et al., 1978).

In New Zealand, Quaternary pollen stratigraphic units are defined by climatic criteria supported by physiography, lithostratigraphy, and radioisotope and tephrochronology (Fleming, 1970; 1975; Moar, 1982). Generally, nonarboreal pollen assemblages are present in glacial intervals, and arboreal-dominated pollen assemblages are more prominent in interstadial or interglacial intervals. All Quaternary spectra in samples analyzed from Site 594 are dominated by arboreal pollen. Arboreal pollen dominates interglacial as well as glacial intervals, as defined by oxygen isotope stratigraphy of samples from the last ~400,000 yr. (Nelson, Hendy, et al., this volume). Samples 594-1-2, 43–47 cm and 594-1-4, 43–47 cm deposited during isotope Stage 2, the last glacial maximum, have a prominence of cool-temperate forest pollen.[3] Interstadial intervals are characterized by podocarp pollen in sediments from Site 594 and on North Island (Otamangakau interstadial; McGlone and Topping, 1983).

Climatic interpretations of pollen in samples analyzed from Site 594 are restricted to broad observations by the preliminary nature of the data. Early Miocene pollen assemblages from Chatham Rise probably represent subtropical (frost-intolerant) vegetation (trees similar to those now growing in New Guinea and New Caledonia—*N. brassi* group), as well as temperate and cool-temperate vegetation (trees now growing in lowland and montane parts of New Zealand). Rainfall estimates, based on requirements of modern species, range from 1800 mm/yr. (inferred from *N. brassi*) to as low as 400 mm/yr. (inferred from *N. fusca*) (Truswell, 1982a). Miocene pollen assemblages from Site 594 appear transitional between warm-temperate to subtropical early Cenozoic vegetation (Wardle et al., 1983) and temperate vegetation of the late Cenozoic glacial mode. Variations in key pollen types suggest that climate was not static during the Miocene. Using the prominence of conifers (podocarps) and southern beech (*Nothofagus* groups) as a general guide[4] to climate suggests that in the late Miocene, a warm, moist interval preceeded cooler, drier conditions in which herbs and shrubs (vegetation of more open forests or shrublands and grasslands) developed. Miocene New Zealand apparently was ecologically and topographically diverse, with local montane and arid habitats (Wardle, 1978).

Pollen and spores deposited on Chatham Rise during the last 5 m.y. document the gradual disappearance of subtropical environments supporting *N. brassi*, and the expansion of temperate forests on both South and North Island. Changing climatic modes are suggested by variations in arboreal pollen in the upper 200 m taken from Site 594. Climatic interpretations of the broadly spaced pollen data appear to correlate with similar levels in the high-resolution sedimentary and geochemical data from the upper 80 meters of Site 594 (Nelson, Hendy, et al., this volume). Cool-temperature (glacial) pollen assemblages occur in hemipelagic ooze enriched in silt, with low carbonate content, high $\delta^{18}O$ values and low $\delta^{13}C$ values. Warm-temperate (interstadial and interglacial) pollen assemblages occur in pelagic oozes high in sand and clay, with high carbonate content, low $\delta^{18}O$ values, and high $\delta^{13}C$ values (Nelson et al., this volume).

CONCLUSIONS

Preparation and preliminary analyses of 132 samples from Holes 594 and 594A produce the following results:

1. Pollen is present in low concentration (<400 pollen grains/cm^3 wet sediment) in both pelagic and hemipelagic facies. Preparation of large samples (on the order of 20 cm^3 is recommended for future pollen analyses.
2. Early Miocene samples are dominated by *Nothofagus brassi* type pollen, along with other extinct Tertiary pollen types.
3. In mid-Miocene samples, pollen is scarce and *N. fusca* becomes more important than *N. brassi*.
4. Pollen concentration increases in late Miocene samples, which show fluctuations in the importance of conifers (podocarps) and beech (*Nothofagus*), suggesting vegetational and climatic changes on New Zealand.
5. Extinct Tertiary pollen types appear gradually to drop out of the record. Evidence for abrupt, major climatic change from late Miocene pollen assemblages in the samples analyzed from Site 594 is not apparent.
6. Pliocene/Quaternary samples show fluctuations in pollen concentration and in arboreal-dominated pollen assemblages. Climatic interpretations of changes in these arboreal pollen types appear to correlate with climatic changes indicated by oxygen isotope analyses of samples from Site 594.
7. Detailed analyses of pollen from Holes 594 and 594A will produce high-frequency stratigraphic and climatic information.

ACKNOWLEDGMENTS

Thanks are extended to L. Burckle, L., Cranwell, J. Morley, E, Stern, and to the shipboard and editorial staffs of the Deep Sea Drilling Project. This research was partially supported by NSF Grant ATM82-13609.

REFERENCES

Allan, H. H., 1961. *Flora of New Zealand* (Vol. 1): Wellington, N.Z. (R. E. Owen).

Ballog, R. A., and Malloy, R. E., 1981. Neogene palynology from the Southern California Continental Borderland, Site 467, Deep Sea Drilling Project Leg 63. *In* Yeats, R. S., Haq, B. U., et al. *Init. Repts. DSDP*, 63: Washington (U.S. Govt. Printing Office), 565–576.

Cockayne, L., and Turner, E. P., 1967. *The Trees of New Zealand*: Wellington, N. Z., (R. E. Owen).

Cookson, I. C., 1959. Fossil pollen grains of *Nothofagus* from Australia. *Proc. R. Soc. Victoria*, 71: 25–30.

Couper, R. A., 1951a. Evidence from earlier times. *N.Z. Sci. Rev.*, 5–14.

———, 1951b. Microflora of a submarine lignite from Toetoes Bay, near Bluff, New Zealand. *N.Z. J. Sci. Tech. B*, 33:179–186.

---

[3] The absence of herb-dominated pollen spectra from glacial sediments in Site 594 suggests that *Nothofagus* persisted in favorable sites on South Island during Plio-Pleistocene glaciations. This agrees with previous observations that scattered clumps of trees now present in South Island forests grew on the east coast of South Island during the last glaciation (Wardle, 1963, 1978; Wardle et al., 1983).

[4] High values in the Podocarpus/*Nothofagus* ratio are interpreted as warm intervals and low values as cold intervals (Mildenhall, 1976). Although the ratio of conifers (Podocarpaceae) and southern beech (*Nothofagus*) pollen and macrofossils is used extensively in New Zealand Tertiary and Quaternary paleoclimatic reconstructions to indicate warmer and cooler conditions, recent ecological work in New Zealand stressing the variability of modern New Zealand forests questions the validity of such interpretations (Moar, 1973).

———, 1953a. Distribution of Proteaceae, Fagaceae, and Podocarpaceae in some southern hemisphere Cretaceous and Tertiary beds. *N.Z. J. Sci. Tech. B*, 35:247–250.

———, 1953b. Plant microfossil dating of some New Zealand Upper Tertiary volcanic rocks. *N.Z. J. Sci. Tech. B*, 34:373–377.

———, 1953c. *Upper Mesozoic and Cainozoic Spores and Pollen Grains from New Zealand*. N.Z. Geol. Surv. Paleo. Bull. 22.

———, 1954. Lower Pleistocene plant microfossils from the Glenhope Beds and Moutere gravels, Nelson, New Zealand. *N.Z. J. Sci Tech. B*, 36:136–139.

———, 1960. Southern Hemisphere Mesozoic and Tertiary Podocarpaceae and Fagaceae and their palaeogeographic significance. *Proc. R. Soc. London B*, 152:491–500.

Couper, R. A., and Harris, W. F., 1960. Pliocene and Pleistocene plant microfossils from drillholes near Frankton, New Zealand, *N.Z J. Geol. Geophys.*, 3:15–22.

Couper, R. A., and McQueen, D. R., 1954. Pliocene and Pleistocene plant fossils of New Zealand and their climatic interpretation. *N.Z. J. Sci. Tech. B*, 35:398–420.

Cranwell, L. M., 1938. Fossil pollens. *N.Z. J. Sci. Tech.*, 19:628–645.

———, 1939. Southern beech pollens. *Records Auckland Inst. Museum*, 2:175–196.

———, 1940. Pollen grains of New Zealand conifers. *N.Z. J. Sci. Tech.*, 22(18):1–17.

———, 1942. New Zealand pollen studies. 1. Key to the pollen grains of families and genera in the native flora. *Records Auckland Inst. Mus.*, 2:280–308.

———, 1953. New Zealand pollen studies: the monocotyledons. *Bull. Auckland Inst. Mus.*, 3:1–91.

———, 1959. Fossil pollen from Seymour Island, Antarctica. *Nature*, 184:1782–1785.

———, 1961. Coniferous pollen types of the southern hemisphere, I. Aberration in *Acmopyle* and *Podocarps dacridiodes, J. Arnold Arboretum*, 42:416–425.

———, 1962. Endemism and isolation in the Three Kings Islands, New Zealand—with notes on pollen and spore types of the endemics. *Records Auckland Inst. Mus.*, 5:215–237.

———, 1963. The Hectorellaceae: pollen type and taxonomic speculation. *Grana Palynol.*, 4:195–202.

———, 1969. Antarctic and circum-Anarctic palynological contributions. *Antarct. J. U.S.*, 4:197–198.

Cranwell, L. M., Harrington, H. J., and Speden, I. G., 1960. Lower Tertiary microfossils from McMurdo Sound, Antarctica. *Nature*, 186:700–702.

Cranwell, L. M., and von Post, L., 1936. Post-Pleistocene pollen diagrams from the Southern Hemisphere. I: New Zealand. *Geogr. Ann.*, 18:308–347.

Fleming, C. A., 1970. Radiocarbon dating and pollen analyses of the Otiran Periglacial fans in western Wellington. *Trans. R. Soc. N.Z.*, 7:197–208.

———, 1975. The Quaternary record of New Zealand and Australia. *In* Suggate, R. P., Cresswell, M. M., (Eds.), *Quaternary Studies:* Wellington (R. Soc. N.Z.), pp. 1–20.

Fournier, G. R., 1981. Palynostratigraphic analysis of cores from Site 493, Deep Sea Drilling Project Leg 66. *In* Watkins, J. S., Moore, J. C., et al., *Init. Repts. DSDP*, 66: Washington (U.S. Govt. Printing Office), 661–670.

Griggs, G. B., Carter, L., Kennett, J. P., and Carter, R. V., 1983. Late Quaternary marine stratigraphy southeast of New Zealand. *Geol. Soc. Am. Bull.*, 94:791–797.

Hanks, S. L., and Fairbrothers, D. E., 1976. Palynotaxonomic investigation of *Fagus* L. and *Nothofagus* BL.: microscopy, scanning electron microscopy, and computer analyses. *Bot. System.* 1:1–141.

Harris, W. F., 1955. *A Manual of the Spores of New Zealand Pteridophyta*. N.Z. D.S.I.R. Bull. 116.

———, 1964. A note on pollen distribution in a core from Milford Sound. *In* Skerman, T. M. (Ed.), *Mem. N.Z. Oceanogr. Inst.* 17 (N.Z. D.S.I.R. Bull. 157).

Heusser, L. E., 1982. Pollen analysis of laminated and homogeneous sediment from the Guaymas Basin, Gulf of California. *In* Curray, J. R., Moore, D. G., et al., *Init. Repts. DSDP*, 64, Pt 2: Washington (U.S. Govt. Printing Office), 1217–1223.

———, 1983. Pollen distribution in the bottom sediments of the western North Atlantic Ocean. *Mar. Micropaleontol.*, 8:77–88.

Heusser, L. E., and Balsam, W. L., 1977. Pollen distribution in the northeast Pacific Ocean. *Quat. Res.* 7:45–62.

Heusser, L. E., and Stock, C., 1984. Preparation techniques for concentrating pollen from marine sediments and other sediments with low pollen density *Palynology*, 8:225–227.

Kemp, E. M., 1975. Palynology of Leg 28 Drill Sites, Deep Sea Drilling Project. *In* Hayes, D. E., Frakes, L. A., et al., *Init. Repts. DSDP*, 28: Washington (U.S. Govt. Printing Office), 599–623.

———, 1981. Tertiary palaeogeography and the evolution of Australian climate. *In* Keast, A. (Ed.), *Ecological Biogeography of Australian:* Boston (Junk), 33–49.

Kemp, E. M., and Harris, W. K., 1975. The vegetation of Tertiary islands on the Ninetyeast Ridge. *Nature*, 258:303–307.

Koroneva, E. V., 1968. *Distribution and Preservation of Pollen in Sediments in the Western Part of the Pacific Ocean.* Queens College, New York, Dept. Geol., Geol. Bull. 2.

Koroneva, E. V., and Kartashova, G. G., 1978. Palynological study of samples from Holes 379A, 380A, Leg 42B. *In* Ross, D. A., Neprochnov, Y. P., et al., *Init. Repts. DSDP*, 62: Washington (U.S. Govt. Printing Office), 951–992.

McGlone, M. S., 1982. Modern pollen rain, Egmont National Park, New Zealand. *N.Z. J. Bot.*, 20:253–262.

McGlone, M. S., and Topping, W. W., 1983. Late Quaternary vegetation, Tongariro region, central North Island, New Zealand, *N.Z. J. Bot.*, 21:53–76.

Mildenhall, D. C., 1972. Fossil pollen of Acacia Type from New Zealand *N.Z. J. Bot.*, 10:485–494.

———, 1975a. Lower Pleistocene palynomorphs from the Ohuka Carbonaceous Sandstone, south-west Auckland, New Zealand. *N.Z. J. Geol. Geophys.*, 18:675–681.

———, 1975b. New fossil spores from the Pakihikura Pumice (Okehuan, Quaternary), Rangitikei Valley, New Zealand. *N.Z. J. Geol. Geophys.*, 18:667–673.

———, 1975c. Palynology of the *Acacia*-bearing beds in the Konako District, Pohangiani Valley, North Island, New Zealand. *N.Z. J. Geol. Geophys.*, 18:209–228.

———, 1976. Exotic pollen rain on the Chatham Islands during the Late Pleistocene. *N.Z. J. Geol. Geophys.*, 19:327–333.

———, 1978a. Palynology of the Waipipian and Hautawan States, (Pliocene and Pleistocene) Wanganui, New Zealand. *N.Z. J. Geol. Geophys.*, 21:775–777.

———, 1978b. *Palynomorphs from Miocene-Pliocene sediments Grey Valley (K31-metric), South Island, New Zealand.* N.Z. Geol. Surv. Report PAL 24.

———, 1978c. *Pollen Counts from Quaternary Sediments in the Wellington Area (N160, N164).* N.Z. Geol. Surv. Rep. Paleontol., 25.

———, 1978d. Pollen distribution in sediments from Caswell, Nancy, and Milford Sounds. *In* Glasby, G. P. (Ed.), *Fiord Studies Caswell and Nancy Sounds, New Zealand.* N.Z. Oceanogr. Inst. Mem., 79:45–61.

———, 1980. New Zealand Late Cretaceous and Cenozoic plant biogeography: a contribution. *Palaeogeogr., Palaeoclimatol., Palaeoecol.*, 31:197–233.

Mildenhall, D. C., and Harris, W. F., 1970. A cool climate pollen assemblage from the type Waipipian (Middle Pliocene). *N.Z. J. Geol. Geophys.*, 13:586–91.

Mildenhall, D. C., and Suggate, R. P., 1981. Palynology and age of the Tadmor Group (late Miocene–Pliocene) and Porika Formation (early Pleistocene), South Island, New Zealand. *N.Z. J. Geol. Geophys.*, 24:515–528.

Moar, N. T., 1958. Contribution to the Quaternary history of the New Zealand Flora I. Auckland Island Peat Studies. *N.Z. J. Sci.*, 1: 449–465.

———, 1970. Recent pollen spectra from three localities in the South Island, New Zealand. *N.Z. J. Bot.*, 8:210–221.

———, 1973. Late Pleistocene vegetation and environment in southern South Island. *In* Bakker, E. M. van Zinderen (Ed.), *Palaeoecology of Africa and of the Surrounding Islands and Antarctica* (Vol. 8): Cape Town (Balkema), 179–198.

———, 1982. Chronostratigraphy and the New Zealand post-glacial. Striae, 16:10–16.

Moar, N. T., and Suggate, R. P., 1979. Contributions to the Quaternary history of the New Zealand Flora 8. Interglacial and glacial vegetation in the Westport District, South Island. *N.Z. J. Bot.*, 17: 361–389.

Moore, L. B., and Edgar, E., 1970. *Flora of New Zealand, Volume II:* Wellington, N.Z. (A. R. Shearer).

Pocknall, D. T., 1980. Modern pollen rain and Aranuian vegetation from Lady Lake, north Westland, New Zealand. *N.Z. J. Bot.*, 18: 275–284.

Shackleton, N. J., and Kennett, J. P., 1975. Paleotemperature history of the Cenozoic and the initiation of Antarctic glaciation: oxygen and caroon isotope analyses in DSDP Sites 277, 279, and 281. *In* Kennett, J. P., Houtz, R. E., et al., *Init. Repts. DSDP*, 29: Washington (U.S. Govt. Printing Office), 743–755.

Suggate, R. P., et al., 1978. *The Geology of New Zealand:* Wellington (Keating).

Traverse, A., 1978. Palynological analysis of DSDP Leg 42B (1975) cores from the Black Sea. *In* Ross, D. A., Neprochnov, Y. P., et al., *Init. Repts. DSDP*, 42, Pt. 2: Washington (U.S. Govt. Printing Office), 993–1015.

Tschudy, R. H., and Scott, R. A., 1969. *Aspects of Palynology:* New York (Wiley-Interscience).

Truswell, E. M., 1982a. Antarctica: the vegetation of the past and its climatic implications. *Aust. Met. Mag.*, 30:169–173.

________, 1982b. Palynology of seafloor samples collected by the 1911–14 Australasian Antarctic Expedition: implications for the geology of coastal East Antarctica. *J. Geol. Soc. Aust.*, 29:343–356.

________, 1983. Recycled Cretaceous and Tertiary pollen and spores in Antarctic marine sediments: a catalogue. *Palaeontographica B*, 186:121–174.

Tulip, J. R., Taylor, G., and Truswell, E. M., 1982. Palynology of Tertiary Lake Bunyan, Cooma, New South Wales. *BMR J. Aust. Geol. Geophys.*, 7:255–268.

Walcott, R. I., 1984. Reconstructions of the New Zealand Regio for the Neogene. *Palaeogeogr., Palaeoclimatol., Palaeoecol.*, 4 217–231.

Wardle, P., 1963. Evolution and distribution of the New Zealand fl ras, as affected by Quaternary climates. *N.Z. J. Bot.*, 1:3–17.

________, 1978. Origin of the New Zealand mountain flora, with sp cial reference to trans-Tasman relationships. *N.Z. J. Bot.*, 1 535–560.

________, Bulfin, M.J.A., and Dugdale, J., 1983. Temperate broa leaved evergreen forests of New Zealand. *In* Ovington, J. D. (Ed *Temperate Broad-leaved Evergreen Forests*. Amstérdam (Elsevie pp. 33–71.

Date of Initial Receipt: 2 July 1984
Date of Acceptance: 30 October 1984

24. LATE PALEOGENE AND EARLY NEOGENE FORAMINIFERS OF DEEP SEA DRILLING PROJECT SITE 270, ROSS SEA, ANTARCTICA[1]

R. Mark Leckie, University of Massachusetts
and
Peter-Noel Webb, Ohio State University[2]

ABSTRACT

Foraminifers from the upper Oligocene, lower Miocene, and Pleistocene at Site 270 in the southern Ross Sea, Antarctica, are discussed and illustrated. The total fauna comprises 74 genera and 163 species. A small number of taxa are recycled from Cretaceous and older Paleogene sediments. Four assemblage zones are proposed, the age of informal lithologic units discussed, and potentially important hiatuses identified. Microfaunas reflect a mixing of biogeographic affinities with one element exhibiting similarities to temperate late Paleogene assemblages in New Zealand, and another representing the early cold-water assemblages of the antarctic Neogene.

INTRODUCTION

Rich foraminiferal faunas have long been known from the Quaternary of the Ross Sea and other parts of Antarctica (Chapman, 1916; Heron-Allen and Earland, 1922; McKnight, 1962; Pflum, 1966; Kennett, 1968; Fillon, 1974; Anderson, 1975; Osterman and Kellogg, 1979; and Ward, 1979). Studies of Tertiary microfaunas have been hampered by lack of exposures on land and paucity of stratigraphic drill holes in the Ross Sea and coastal areas near the Transantarctic Mountains. However, in the last decade, drill cores provided by such projects as the Deep Sea Drilling Project (Leg 28), Dry Valley Drilling Project, Ross Ice Shelf Project, and the McMurdo Sound Sediment and Tectonic Studies have facilitated the study of late Neogene (D'Agostino, 1980; Webb and Wrenn, 1982) and Paleogene foraminifers (Webb, 1982a, b; Webb et al., 1982, in press). Microfaunas from very limited land outcrops of upper Neogene sediments have also been investigated (Webb, 1972, 1974; Webb et al., 1984). Only at Site 270 has the upper Paleogene and lower Neogene transition been recovered. This time interval is particularly significant in that it marks the intensification of cooling in the Ross Sea (Leckie and Webb, 1983). The present study documents the faunas of this transition, from cosmopolitan and temperate Paleogene faunas to more restricted polar assemblages of the Neogene. Another important objective of this paper is to establish the foraminiferal biostratigraphy at Site 270 with an emphasis on the problems of southern high-latitude biostratigraphic control during the mid-Tertiary and lack of reliable correlation beyond Antarctica. A companion paper (Leckie and Webb, 1983) addresses our paleoenvironmental interpretations of the upper Oligocene–lower Miocene sedimentary sequence at Site 270.

LITHOSTRATIGRAPHIC FRAMEWORK

DSDP Site 270 is located in the south-central Ross Sea on the western flank of a broad sedimentary basin on the eastern Ross Sea continental shelf (Figs. 1, 2). The *Glomar Challenger* penetrated a total section of 422.5 m at Site 270. Details of the drilling operations and a coring summary are published in Volume 28 of the *Initial Reports* (Hayes, Frakes, et al., 1975).

A sedimentary succession of 412 m overlies a metasedimentary basement complex (marble and calc-silicate gneiss) that is tentatively correlated with the early Paleozoic Koettlitz Marble of the Transantarctic Mountains (Ford, 1975) (Fig. 2). The lowermost sedimentary unit, Unit 5, rests unconformably on the basement and is a subaerial breccia of supposed Tertiary age. Two thin, upper Oligocene shallow marine sandstones, a carbonaceous quartz sand (Unit 4), and a glauconitic greensand

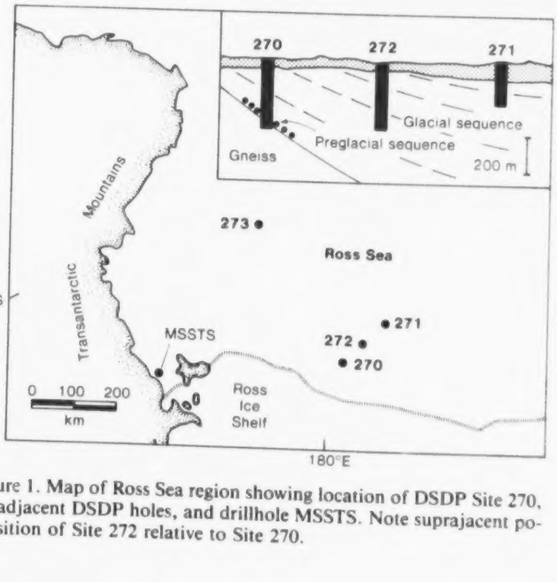

Figure 1. Map of Ross Sea region showing location of DSDP Site 270, adjacent DSDP holes, and drillhole MSSTS. Note suprajacent position of Site 272 relative to Site 270.

---

[1] Kennett, J. P., von der Borch, C. C., et al., *Init. Repts. DSDP*, 90: Washington (U.S. Govt. Printing Office).

[2] Addresses: (Leckie) Dept. of Geology and Geography, University of Massachusetts, Amherst, MA 01003; (Webb) Dept. of Geology and Mineralogy and Institute of Polar Studies, Ohio State University, Columbus, OH 43210.

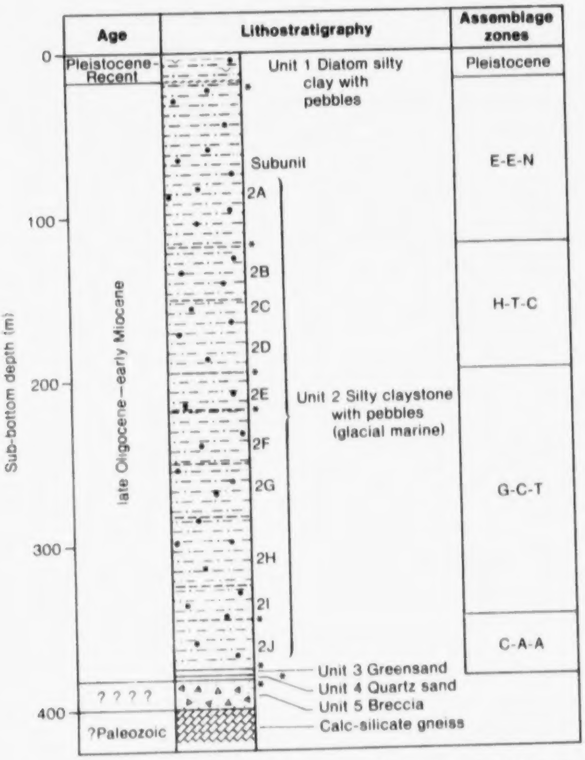

Figure 2. Stratigraphic column at Site 270, showing foraminiferal assemblage zones. Asterisks mark position of suspected diastems or minor hiatuses as discussed in text. See Figure 3 for assemblage zones.

(Unit 3) overlie this breccia. These sands may represent the thin marginal facies of an extensive late Mesozoic—early Cenozoic preglacial basin (Fig. 1). Above the sandstone units lie the thick (365 m) upper Oligocene–lower Miocene glaciomarine sediments of Unit 2, composed of silty claystones with granules and pebbles distributed throughout. Unit 2 is divided into 10 subunits, each delineated by subtle bedding features and clast abundance (Barrett, 1975). Unit 1, also of glaciomarine origin, caps the sequence at Site 270. A lower Miocene to Pliocene-Pleistocene angular unconformity separates Unit 2 from Unit 1 above.

Paleontologic, magnetostratigraphic, and radiometric dating has suggested that the late Oligocene–early Miocene marine phase of sedimentation at Site 270 spans a 9-m.y. interval, from 26 to 17 Ma (Allis and others, 1975; McDougall, 1977). According to Savage and Ciesielski's (1983) reinvestigation of diatom biostratigraphy at nearby suprajacent Site 272, the age of the uppermost Miocene sediments at Site 270 could be no younger than 19 Ma.

AGE OF UNITS FOUR THROUGH TWO AT SITE 270

Preliminary comments on the paleontology and biostratigraphy of Site 270 yielded a broad late Oligocene-early Miocene age for Units 4 through 2 (Hayes, Frakes et al., 1975). Burns (1975) noted small calcareous nannoplankton floras in Subunits 2C–2D and suggested an Oligocene or Miocene age. Ten samples from Unit 2 were recently examined for calcareous nannofossils by Marie-Pierre Aubry (WHOI). Samples from Subunits 2A, 2B, 2D, and 2F yielded low-diversity assemblages that concur with an early Miocene age for the upper part of Unit 2. A fairly diverse and well-preserved flora is recorded in Sample 270-18-2, 66–68 cm (Subunit 2B); it includes *Cyclococcolithus macintyrei, C. floridanus, Helicosphaera* cf. *H. carterii, Coccolithus pelagicus, Reticulofenestra* cf. *R. pseudoumbilica, Sphenolithus moriformis/neoabies, Umbilicosphaera* sp., *R. bisecta*, and *R. hesslandi*. The last two taxa are probably reworked from Paleogene deposits.

Webb (in Hayes, Frakes, et al., 1975, p. 227) assigned an Oligocene–early Miocene age to the diverse benthic foraminiferal taxa of Units 2, 3, and 4, citing their affinities with the New Zealand mid-Tertiary in the lower part of the succession but noting the development of a strong polar endemism in the middle and upper parts of Unit 2. Chen (1975) reported fragmented radiolarians in Unit 1 and Subunit 2B but these did not provide useful ages. McCollum (1975) noted Brunhes-age diatoms in Unit 1 and no diatoms in Units 2, 3, or 4. However, Subunits 2A, 2B, and 2C originally contained abundant diatoms, as is suggested by the persistent occurrence of cristobalite (Hayes, Frakes, et al., 1975, p. 216; Cook et al., 1975).

Kemp (1975) and Kemp and Barrett (1975) reported abundant wood fragments in the carbonaceous sandstone (Unit 4) and a sparse dinoflagellate cyst assemblage in the glauconitic sandstone (Unit 3). Unit 3 was assigned a "mid" to late Oligocene age based on the presence of *Selenopemphix nephroides*. This taxon also occurs in the lowermost sample of the overlying glaciomarine sequence (Subunit 2J). However, there may be a synonymous form, *Protoperidinium subinera*, which ranges into the Pleistocene and would render the biostratigraphic utility of "*S. nephroides*" tenuous (J. H. Wrenn, pers. comm., 1984).

Preglacial Units 4 and 3 contain no pollen or spores, but all samples from the glaciomarine strata contain these palynomorphs (Kemp, 1975; Kemp and Barrett, 1975). The basal Subunit 2J contains the richest assemblages. These assemblages are interpreted as *in situ* because there are no forms which are obviously recycled. The sparse assemblages of Subunits 2E and 2F (Cores 270-24, 270-25, and 270-29) contain Eocene–early Oligocene dinoflagellate cysts, suggesting that reworking is more common in the upper parts of the glaciomarine sequence of Unit 2 (Kemp, 1975; Kemp and Barrett, 1975). Most of the spore and pollen species are known to have relatively long stratigraphic ranges and therefore have limited biostratigraphic value. A mid-Tertiary age is, however, consistent with other dating techniques.

A potassium/argon date of 26.0 ± 0.5 Ma was determined from glauconite in the calcareous greensand of Unit 3, immediately beneath the basal glaciomarine sediments of Unit 2 (McDougall, 1977; Fig. 2). McDougall noted that glauconite commonly yields K-Ar ages that are too young, but he concluded that the 26 Ma age is probably a reliable minimum. Revised decay constants would put this age at about 26.7 Ma.

Allis et al. (1975) conducted a paleomagnetic study of the thick glaciomarine sequence of Unit 2. The reversal stratigraphy for 30 to 240 m sub-bottom compares closely with the early Miocene part of the Heirtzler et al. (1968) seafloor anomaly scale. This interval includes magnetic anomaly numbers 5C through the upper part of 6A of LaBrecque et al. (1977), which, according to a revised Neogene geochronology by Berggren et al. (in press), represents an absolute age of about 16 to 21 Ma (Fig. 5, later). This translates into an average sediment accumulation rate of about 42 m/m.y. for the upper 210 m of Unit 2. The linear relationship between the Site 270 reversal stratigraphy and the seafloor anomaly record implies that the sedimentation rate was constant (fig. 6 of Allis et al., 1975). Although Unit 2 is nearly homogeneous and composed mainly of poorly sorted silty claystone with granules and pebbles throughout, there are several distinct stratigraphic intervals with very different average clast densities: Subunit 2A = 13.7 pebbles/m; Subunits 2B–2E = 2.2 pebbles/m; Subunits 2F–2I = 14 pebbles/m; Subunit 2J = 3.2 pebbles/m (from fig. 9 of Barrett, 1975). These variations in clast abundance perhaps could be interpreted to indicate changes in intensity of ice-rafting and therefore presumably changes in sedimentation rate. Foraminiferal trends through Unit 2 also suggest changing rather than static paleoenvironmental conditions (Leckie and Webb, 1983). Barrett (1975) attributes the changes in pebble density to differences in size distribution caused by erosional processes. This remains an unresolved problem and therefore biases our confidence in the paleomagnetic record.

The interval from 240–370 m sub-bottom is entirely normally magnetized (Allis et al., 1975). Three reversals are present from 370–384 m but cannot be uniquely correlated to the Heirtzler et al. seafloor anomaly scale. Allis et al. (1975) attribute the long interval of normal magnetization to growth of authigenic minerals with unstable magnetization. If, however, a constant sedimentation rate of 42 m/m.y. is assumed for the lower 144 m of Unit 2, the extrapolated age of the base of the glacial sequence is about 24 to 25 Ma, which is in good agreement with the glauconite age of Unit 3. Are these results fortuitous or are they substantiating evidence of a reliable paleomagnetic record?

In lieu of high-resolution biostratigraphy at DSDP Site 270, we must assume that the age control provided by the paleomagnetic stratigraphy of Unit 2 and the 26 Ma K-Ar date of Unit 3 represents the best first approximation to the age of the glaciomarine sequence at Site 270. This latest Oligocene–early Miocene age is corroborated by benthic and planktonic foraminifers (discussed in a later section). Diatoms, foraminifers, palynomorphs, and microplankton appear to hold the greatest promise for future biostratigraphic refinement in the antarctic Cenozoic, although a reevaluation of calcareous nannofossil biostratigraphy at Site 270 may also prove valuable.

AGE OF THE LOWER GLACIOMARINE SECTION AT SITE 272

Savage and Ciesielski (1983) used diatoms and silicoflagellates in determining a date of 19.2 Ma (early Miocene) for the lower glaciomarine section of Site 272, located close to Site 270 and at a slightly higher stratigraphic level than Subunit 2A of Site 270 (Figs. 1, 2). The lower 296 m of Site 272 (Subunits 2B and 2C) contain rare diatoms indicative of the *Coscinodiscus rhombicus* Zone (18.34–19.23 Ma) and perhaps the lower *Nitzschia maleinterpretaria* Zone (18.19–18.34 Ma) according to Savage and Ciesielski (1983). At Site 272, the top of the *C. rhombicus* Zone is tentatively placed at the last occurrence of *Coscinodiscus* sp. 1 (of McCollum, 1975), a datum recognized by Weaver and Gombos (1981) in the original definition of this zone. Although *C. rhombicus* and *N. maleinterpretaria* were not recorded in the Site 272 sequence, the presence of the silicoflagellate *Mesocena apiculata* concurs with the *C. rhombicus* Zone assignment. Where originally defined at DSDP Site 266, the top of the *C. rhombicus* Zone (Section 266-18-1; Weaver and Gombos, 1981) is coincident with an overlap between the last occurrence of *Catapsydrax* spp. and the first appearance of *Globorotalia zealandica* (Kaneps, 1975). This suggests foraminiferal zones N6 or N7 (about 19.0 to 16.6 Ma, according to Berggren et al., in press). Nannofossil data from the same interval at Site 266 are in close agreement with the foraminifer age assignment (i.e., NN4 or 17.5 to 16.0 Ma) based on the last occurrence of *Sphenolithus belemnos* in Section 266-19-2 (top of NN3) and the first occurrence of *S. heteromorphus* in Core 266-17-1 (NN4–NN5; Burns, 1975). The last occurrence of the silicoflagellate *M. apiculata* is just above the top of the *C. rhombicus* Zone at Site 266 (Section 266-17-4; Ciesielski, 1975) and therefore may lend support to the reliability of the *Coscinodiscus* sp. 1 datum at Site 272. From this information we can infer that Subunits 2B and 2C of Site 272 are probably at least 16–17 Ma in age if *Coscinodiscus* sp. 1 and *M. apiculata* are indeed *in situ* and if our reassessment of the age of the upper *C. rhombicus* Zone applies to the antarctic region.

Savage and Ciesielski (1983) assume that the basal sediments of Site 272 (Subunit 2C) correspond with the *C. rhombicus* Zone although no age-diagnostic species were recorded. They note that the diatom assemblage of Subunit 2C is very similar to that of Subunit 2B and therefore assume an early Miocene age. However, the age-diagnostic species of Subunit 2B, *Coscinodiscus* sp. 1 and *M. apiculata*, may be useful in defining the top of the *C. rhombicus* Zone but not necessarily its base: *Coscinodiscus* sp. 1 has an unspecified first occurrence and *M. apiculata* first appears in the middle Eocene (Bukry, 1981). All we can say with reasonable confidence is that Subunits 2B and 2C of Site 272 (145 to 441 m sub-bottom) are probably older than about 16 Ma. Acoustic reflection profiles across Sites 270 and 272 indicate that there probably is only a slight stratigraphic overlap, if any, between the two sites (Hayes, Frakes, et al., 1975).

Indeed, Subunit 2C of Site 272 (365 to 441 m sub-bottom) bears strong resemblance to Subunits 2A through 2C of Site 270 (20 to 177 m sub-bottom), based on sedimentology, bulk x-ray mineralogy, and persistence of cristobalite (Hayes, Frakes, et al., 1975; Cook et al., 1975).

Conflicting age assignments apparently exist between the lower two-thirds of Site 272 and the top of Unit 2 at Site 270. Subunits 2B and 2C of Site 272 are probably older than about 16 Ma and represent a sedimentary section of nearly 300 m. If the top of Subunit 2B is 16 Ma, estimates of the basal age of Site 272 could range from about 23 Ma (based on a sedimentation rate of 42 m/m.y.) to 17 Ma (based on a rate of 275 m/m.y., proposed by Savage and Ciesielski, 1983). These figures do not agree with the paleomagnetic stratigraphy of Site 270, which puts the age of the top of Unit 2 at about 16 Ma (Allis et al., 1975). What do we believe? If we assume that the paleomagnetic record of Site 270 is indeed correct, what might account for the "old" age for Subunits 2B and 2C of Site 272? Perhaps there is more stratigraphic overlap between Sites 270 and 272 than interpreted from the reflection profiles. This is doubtful because there is no lithologic equivalent of Subunit 2B (of Site 272) at Site 270. Perhaps *Coscinodiscus* sp. 1 and *M. apiculata*, the siliceous species used by Savage and Ciesielski (1983) to define the early Miocene *C. rhombicus* Zone at Site 272, have different stratigraphic ranges in antarctic compared with subantarctic or temperate areas. This is a potential problem with other southern high-latitude siliceous microfossils and calcareous groups as well. Future drilling in the Antarctic is necessary in order to refine polar late Paleogene and Neogene microfossil zonations. At present, too few antarctic drill sites have penetrated strata below the upper Miocene, and as is often the case in Antarctica, incomplete sedimentary sequences, reworking and poor microfossil abundance or preservation have hindered our ability to establish high-resolution biostratigraphy. Recycling of microfaunas and floras could also be responsible for an older apparent age, particularly if the background species are all long-ranging. A case may be made for this interpretation at Site 272. The absence of age-diagnostic diatoms in Subunit 2C and strong lithologic similarity to the upper part of Unit 2 at Site 270 contrasts with Subunit 2B at Site 272, which contains only two "age-diagnostic" species in a lithology much different from any at Site 270. Perhaps there is an unconformity between diatom-rich Subunit 2B and diatom-poor, cristobalite-rich Subunit 2C at Site 272.

FORAMINIFERAL TRENDS AND ZONATION AT SITE 270

Foraminifers were found to be moderately abundant in the thin preglacial strata (Unit 4), the thick glaciomarine succession of Unit 2, and the overlying and much younger Unit 1 (Fig. 2; Leckie and Webb, 1980, 1983). One hundred and ten samples from Units 2 and 4 were examined for foraminifers (Table 1). Twenty-six samples containing the greatest number of specimens were used to delineate four late Oligocene–early Miocene assemblage zones (Leckie and Webb, 1980; 1983) (Fig. 3). Throughout Unit 2 there are numerous intervals that contain deformed soft-sediment clasts suggesting bottom-current scour or slump of semilithified claystone. Twenty-five of the 26 representative samples, however, are not from such intervals and therefore may contain truly autochthonous faunas. Assemblage zones are based on generic abundance, species diversity, and the composition of individual assemblages (Fig. 3; Leckie and Webb, 1983, fig. 4).

Cyclammina–Ammoscalaria–Anomalinoides Assemblage Zone

Definition. The C-A-A Assemblage Zone is 36 m thick. The base of the zone is placed at the lithologic contact between Unit 4 and the sedimentary breccia of Unit 3, 388 m sub-bottom (1022 m below present sea level). The top of the zone is coincident with the sharp lithologic contact between Subunits 2J and 2I, at 352 m sub-bottom (986 m below sea level) (Fig. 2).

Faunal content. The C-A-A Assemblage Zone contains 44 genera and 77 species (Table 1). Distribution of genera is 18 agglutinated, 24 calcareous benthic, and 2 planktonic; of species is 32 agglutinated, 43 calcareous benthic, and 2 planktonic. Sixty percent of C-A-A taxa range into the suprajacent G-C-T Assemblage Zone. The proportion of calcareous benthic to agglutinated species increases from the lower to higher levels of the zone. Planktonic taxa occur in the uppermost part of the C-A-A Assemblage Zone (Samples 270-39-6, 24–36 cm and 270-40-3, 123–131 cm).

Species of *Cyclammina*, *Anomalinoides*, and *Ammoscalaria pseudospiralis* are prominent taxa throughout the C-A-A Assemblage Zone (Figs. 3, 4). Unit 4 contains only 11 species. Most are large specimens. The four agglutinated species dominate the assemblage in Section 270-44-1 (Table 1). Large specimens of *Globobulimina* sp. are also common in this fauna. Although all 11 species in Unit 4 are also present in the more diverse faunas of Subunit 2J, the presence of hiatuses between Units 4, 3, and 2J (Leckie and Webb, 1983, fig. 2) might require further subdivision of the C-A-A Assemblage Zone. The upper part is characterized by much more diverse assemblages of calcareous benthic taxa, including species of *Astacolus*, *Lenticulina*, *Dentalina*, *Nodosaria*, and the small and delicate *Fissurina*, *Oolina*, and *Parafissurina* (Table 1). Planktonic foraminifers appear in the uppermost strata of the C-A-A Assemblage Zone (Subunit 2J), *Candeina antarctica* in Sample 270-40-3, 123–131 cm, and *Globorotalia* cf. *G. siakensis* in Sample 270-39-6, 24–26 cm.

Globocassidulina–Cassidulinoides–Trochoelphidiella Assemblage Zone

Definition. The G-C-T Assemblage Zone encompasses Subunits 2I through 2E, a stratigraphic thickness of 156 m. The base is marked by the sharp paraconformable contact between Subunits 2J and 2I at 352 m sub-bottom (986 m below sea level). The top of the G-C-T Assemblage Zone is arbitrarily placed between Subunits 2E and 2D by foraminiferal and sedimentary characteristics. The contact between these two subunits was not recovered. The top of the zone corresponds to 196 m sub-bottom or 830 m below present sea level (Fig. 2).

Faunal Content. The G-C-T Assemblage Zone contains 50 genera and 77 species (Table 1). Distribution of genera is 11 agglutinated, 34 calcareous benthic, and 6 planktonic; of species is 11 agglutinated, 70 calcareous benthic, and 6 planktonic. About 53% of these species also occur in the underlying *Cyclammina-Ammoscalaria-Anomalinoides* Assemblage Zone and 52% continue into the succeeding *Haplophragmoides-Trifarina-Cibicides* Assemblage Zone.

Globocassidulina subglobosa is the most common and persistent calcareous benthic in the G-C-T Assemblage Zone (Figs. 3, 4). *Cassidulinoides* is also a characteristic genus, being represented by *C. bradyi, C. braziliensis*, and *C. parkerianus*. These taxa disappear just below the G-C-T/H-T-C Assemblage Zone boundary. Another key taxon of the G-C-T Assemblage Zone is *Trochoelphidiella*, the genotype of which occurs in the Pliocene Pecten gravels of Wright Valley (Webb, 1974). The earliest known species of this genus, *T. pustulosa* n. sp. appears near the base of the G-C-T Assemblage Zone (Subunit 21) in Sample 270-38-3, 86–93 cm. A second species, *T. uniforamina* D'Agostino n. sp. appears slightly higher in the succession, in Sample 270-35-3, 112–121 cm (Subunit 2H). Several variants of these species are also present in the G-C-T Assemblage Zone. Both *T. pustulosa* and *T. uniforamina* continue up into the H-T-C Assemblage Zone and the latter species is also found in the E-E-N Assemblage Zone and the Miocene of Site 273 (D'Agostino, 1980). *Trochoelphidiella* appears to be endemic to Antarctica and provides a potentially useful lineage. Other members of the Elphididae are also persistent throughout the G-C-T Assemblage Zone. The first appearance of *Elphidium magellanicum* s.l. in Sample 270-38,CC (Subunit 21) just above the C-A-A/G-C-T Assemblage Zone boundary may also provide a useful regional biostratigraphic datum.

The planktonic *Candeina antarctica* has a first appearance near the top of the C-A-A Assemblage Zone and occurs persistently throughout the G-C-T Assemblage Zone. Other occurrences of planktonic species are confined to single or a few specimens. These include *Chiloguembelina cubensis, Globorotalia* cf. *G. gemma, Globigerina* cf. *G. ouachitaensis, Globigerinita* cf. *G. glutinata*, and *Globigerinoides trilobus*. These will be discussed below.

A wide diversity exists among the small and fragile taxa such as *Fissurina, Oolina*, and *Parafissurina*. Although the G-C-T Assemblage Zone exhibits the highest diversity among the five assemblage zones, the occurrence of individual species is sporadic (Table 1). In Figure 3 it is apparent that species diversity declines steadily towards the top of the G-C-T Assemblage Zone. Low-diversity agglutinated fauna occur in the basal and uppermost G-C-T Assemblage Zone sediments (Subunits 21 and 2E, respectively).

Haplophragmoides–Trifarina–Cibicides Assemblage Zone

Definition. The H-T-C Assemblage Zone embraces Subunits 2D through 2B, a stratigraphic thickness of 75 m (Fig. 2). The base of the zone is placed between Subunits 2E and 2D, 196 m sub-bottom (830 m below present sea level). The top of the H-T-C Assemblage Zone is placed at the lithologic boundary between Subunit 2B and the thick, unstratified glaciomarine sediments of Subunit 2A (121 m sub-bottom, 755 m below sea level; Fig. 2).

Faunal content. The H-T-C Assemblage Zone contains 47 genera and 84 species (Table 1). Distribution of genera is 16 agglutinated, 28 calcareous benthic, and 3 planktonic; of species is 24 agglutinated, 57 calcareous benthic, and 3 planktonic. Of the H-T-C Assemblage Zone taxa, 55% are common to the underlying G-C-T Assemblage Zone whereas only 25% continue up into Zone E-E-N.

The agglutinated fauna of the H-T-C Assemblage Zone differs markedly from the faunas rich in agglutinated species in the lower part of the C-A-A Assemblage Zone (Figs. 3, 4). The conspicuous occurrence of *Haplophragmoides* sp. in the H-T-C Assemblage Zone may be used to distinguish the two assemblages. *Ammoscalaria pseudospiralis* is present in the C-A-A Assemblage Zone but absent in the H-T-C Assemblage Zone. *Cyclammina incisa* remains a common member of the H-T-C assemblages. Calcareous benthics are also an important element in this zone. Although *Trifarina fueguina* ranges through all zones it is particularly common here. Species of *Cibicides*, long-ranging in most cases, are also represented in high numbers. Of the H-T-C calcareous benthics, 64% are also common to the G-C-T Assemblage Zone. As noted above, species of *Globocassidulina* and *Cassidulinoides* disappear below the G-T-C/H-T-C Assemblage Zone boundary. The influx of new agglutinated taxa in the H-T-C Assemblage Zone and loss of certain calcareous taxa in the uppermost G-C-T Assemblage Zone may signify the presence of an hiatus. The most diverse assemblage encountered in this study is present in Sample 270-19-5, 113–122 cm (Subunit 2C), near the middle of the zone.

Epistominella–Elphidium–Nonionella Assemblage Zone

Definition. The E-E-N Assemblage Zone is represented by the 101-m-thick succession of unstratified glaciomarine sediments of Subunit 2A (Fig. 2). This is the youngest Neogene assemblage zone documented at Site 270. It is bounded at its base by what has been described as a gradational contact with Subunit 2B at 121 m sub-bottom (755 m below present sea level) and at its top by a major disconformity which separates lower Miocene Subunit 2A from Pleistocene Subunit 1B at 20 m sub-bottom, or 654 m below present sea level.

Faunal content. The E-E-N Assemblage Zone contains 19 genera and 29 species (Table 1), a sharp drop from the much more diverse assemblages of the underlying zone (Fig. 2; Leckie and Webb, 1983, fig. 4). Distribution of genera is 0 agglutinated, 18 calcareous benthic, and 1 planktonic; of species is 0 agglutinated, 28 calcareous benthic, 1 planktonic. Of these species, 72% are found in the H-T-C Assemblage Zone while 86% are present in the three underlying zones.

The most obvious aspect of the E-E-N Assemblage Zone is the very low diversity and absence of agglutinated taxa (Figs. 3, 4). The few taxa present in significant

Table 1. Distribution of foraminifers at Site 270.

Lithologic unit	Core-Section (interval in cm)	*Ammodiscus* cf. *A. glabratus*	*Ammobaculites* cf. *A. caprolithiformis*	*Ammoscalaria pseudospiralis*	*Cyclammina incisa*	*Parafissurina groenlandica*	*Parafissurina lateralis*	*Elphidium* sp.	*Gyroidina zelandica*	*Anomalinoides globulosa*	*Melonis barleeanus*	*Globobulimina* sp.	*Cyclammina* cf. *C. complanata*	*Hyperammina cylindrica*	*Rhizammina algaeformis*	*Trifarina* aff. *T. fueguina*	*Cibicides lobatulus*	*Cibicides temperata* s.l.	*Pullenia subcarinata*	*Astacolus crepidulus*	*Cassidulinoides bradyi*	*Epistominella vitrea*	*Nonionella magnalingua*	*Melonis affinis*	*Oolina apiculata*	*Elphidium* cf. *E. nitidum*	*Cyclammina rotundata*	*Pullenia bulloides*	?*Bathysiphon* sp. 1	*Haplophragmoides* sp.	?*Gaudryina* spp.	*Fissurina laevigata*	*Globocassidulina subglobosa*	*Anomalinoides* cf. *A. macraglabra*	*Cibicides pseudoungerianus*	
1	1-2, 52-54																																			
	1,CC																															x				
	2,CC																					x														
	3-1, 123-125																																			
	3,CC																x					x											x			
2A	4,CC																																			
	5-2, 122-132																																			
	6-1, 113-123																																			
	6-2, 123-126																																			
	7-3, 135-150																																			
	8-3, 113-128								x		x						?					x														
	9-3, 134-142																																			
	9,CC																		x		x	x		x											x	
	10-2, 110-120																																			
	10,CC																?		x			x											?			
	11-2, 112-122																	x																	x	
	12-1 (top of section)																					x		x											?	
	12-4, 123-134																																			
	13-3, 114-125										x						x	x				x		x											x	
	13,CC																	x	x			x		x												
	14-3										x						x		x			x														
	14,CC																x	x				x		x												
	15-1 (top of section)																																			
2B	15-3, 50-57				x													x	x			x							x	x						
	15-3, 97-110		x		x							x		x		x		x				x						x	x						x	x
	15,CC										x					x		x										x							x	
	16-4, 123-133																													x						
	17-5, 130-140				x							x				x	x	x	x											x						
	17,CC		?		?						x	x		x		x		x										x	x	x						
2C	18-5, 129-139	x			x																															
	19-5, 113-122		x			x	x		x	x	x	x				x		x	x					x				x				?			x	
	20-6, 85-95	x			x					x	x			x		x		x											x	x						x
2D	21-5, 102-112	x			x											x		x				x		x												
	22-6, 135-145	x																x	x			x			x											
2E	23-4, 72-82				x												x				x	x											x			
	24-3, 110-120																					x		x	?								x			
	24,CC																					x											x			
2F	25-2, 50-60	x			x						x							x				x		x	x								x		x	
	26-4, 100-114								x												x												x			
	26,CC																	x			x												x			
	27-4, 108-118															x				x	x	x											x		x	
	28-3, 54-56																																			
	28-6 (bottom of section)										x					x		x	x		x	x		x									x			
	28,CC				?																x	x											x			
	29-1, 3-5																																			
	29-1, 21-23																																			
	29-2, 52-54																																			
	29-3, 50-52																																			
	29-4, 48-50																																			
2G	29-6, 8-18								x		x							x			x	x		x								x	x		x	
	29-6, 50-52																																			
	30-2, 50-52																																			
	30-4, 24-35										x											x											x			
	31-3, 59-67																				x	x		x	x								x		x	
	31-5, 58-60																																			

Note: Most samples are too poor in foraminifers to yield realistic abundance data. Relative abundance data for 27 of the richest samples are presented in Figure 4. Note that he samples representing 2-3 cm intervals are very poor in foraminifers. Species from *Ceratobulimina* to *Uvigerina* sp. not present in Samples 270-31,CC to 270-44-2, 5-7 c

Table 1. (Continued).

	Rosalina globularis	Fissurina marginata	Cassidulinoides braziliensis	Lagena striata	Nodosaria calomorpha	Anomalinoides pinguiglabra	Bathysiphon discreta	Textularia cf. T. plummerae	Karreriella obscura	Nodosaria sp. 3	Fissurina bisulcata	Sphaeroidina bulloides	Fissurina agassizi	Astrorhiza cf. A. granulosa	Protobotellina cylindrica	Hormosina globulifera	Reophax scorpiurus	Ammobaculites cf. A. expansus	Textularia sp. 2	Psammosphaera fusca	Bathysiphon cf. B. alba	Rhabdammina cf. R. abyssorum	Oolina apiopleura	Oolina globosa	?Bathysiphon sp. 2	Marsipella sp.	Reophax sp. 1	Ammodiscus cf. A. incertus	Dentalina cf. D. advena	Lenticulina lenticula	Gyroidina cf. G. obicularis	Reophax cf. R. nodulosus	Eponides cf. E. weddellensis	Fursenkoina schriebersiana	Nonionella iridea	Fissurina lucida	Lagena laevis	Candeina antarctica	Globorotalia cf. G. siakensis	Textularia sp. 1	Fissurina annectens	Fissurina sp. 4	Oridorsalis tenera	Elphidium magellanicum s.l.
																																												x
																																			?									
																																			x									
																																			x									
	x																																		x									x
																																			x									x
																								x																				
	x																																											x
																																			x									x
																																			x									x
	x										x																								x			x						x
																								x											x									x
	x											x																										x						x
																																			x									x
																																												x
x																		x		x															x									x
x																	x	x		x			x	x			x				x	x					x							x
																																			x	x		x						x
																													x															x
																																						x						x
	x						x										x	x								x											x							x
				x																				x																				x
	x	x									x	x	x	x			x	x					x	x							x													x
x																	x																		?			x						
				x							x	x			x								x										x					x			x			
	x																						x												x			x						x
	x		x																																			?						
	x		x									x																										x				x		x
			x																					x														x						
																																												x
	x		x																																x			x			x			x
	x			?																			x												x		x					x		x
			x																																									x
																																												x
			x																																			x			?			x
	x																																					x			x			x
						x																																						x

Table 1. (Continued).

Lithologic unit	Core-Section (interval in cm)	*Articulina* sp.	*Pyrgo* cf. *P. vespertilio*	*Quinqueloculina seminula*	*Trochoelphidiella pustulosa* n.sp.	*Quinqueloculina triangularis*	*Trochoelphidiella* sp.	*Jaculella* cf. *J. acuta*	*Vaginulina* cf. *V. rheophagica*	*Cassidulinoides* cf. *C. parkerianus*	*Globigerinita* cf. *G. glutinata*	*Gyroidina parva*	*Cibicides* cf. *C. mediocris*	*Nonionella bradii*	*Trochoelphidiella uniforamina*	*Saracenaria kellumi*	*Saracenaria* sp.	*Fissurina* sp. 3	*Triloculina rotundata*	*Chiloguembelina cubensis*	*Globigerina* cf. *G. ouachitaensis*	*Cassidulinoides* cf. *C. chapmani*	*Lagena* cf. *L. laevigata*	*Nodosaria* sp. 2	?*Astacolus* sp.	*Flintina* cf. *F. droogeri*	*Parafissurina subcarinata*	*Eponides bradyi*	*Uvigerina* cf. *U. miozea*	*Globigerinoides trilobus*	*Globocassidulina crassa*	*Parafissurina curta*	*Globorotalia* cf. *G. gemma*	*Globorotaloides* cf. *G. suteri*	*Lenticulina* cf. *L. punctata*	
1	1-2, 52-54																														x					
	1,CC																																			
	2,CC																																			
	3-1, 123-125																																			
	3,CC										x																									
2A	4,CC																																			
	5-2, 122-132														x																					
	6-1, 113-123						x																													
	6-2, 123-126																																			
	7-3, 135-150																																			
	8-3, 113-128						x			x				x													x									
	9-3, 134-142																																			
	9,CC																																			
	10-2, 110-120																																			
	10,CC											?																								
	11-2, 112-122																																			
	12-1 (top of section)																																			
	12-4, 123-134																																			
	13-3, 114-125											?																								
	13,CC													x																						
	14-3																																			
	14,CC			x																																
	15-1 (top of section)																																			
2B	15-3, 50-57																																			
	15-3, 97-110		x					x					x										x													
	15,CC														x																					
	16-4, 123-135																																			
	17-5, 130-140				x																															
	17,CC							x																				x								
2C	18-5, 129-139																																			
	19-5, 113-122													x													?	x				x				
	20-6, 85-95												?					x																		
2D	21-5, 102-112																																			
	22-6, 135-145			x																																
2E	23-4, 72-82			x		x				x																										x
	24-3, 110-120														x	x																			x	
	24,CC																																x	x		
2F	25-2, 50-60					x												x	x																	
	26-4, 100-114																								x											
	26,CC									?																										
	27-4, 108-118				x	x						x							x																	
	28-3, 54-56																																			
	28-6 (bottom of section)				x										x																x	x				
	28,CC				x										?														x	x						
	29-1, 3-5																																			
	29-1, 21-23																																			
	29-2, 52-54																																			
	29-3, 50-52																																			
	29-4, 48-50																																			
2G	29-6, 8-18				x		x					x											x				x									
	29-6, 50-52																																			
	30-2, 50-52																											x								
	30-4, 24-35		x		x																		x				x									
	31-3, 59-67				x																					x										
	31-5, 58-60																								x											

Table 1. (Continued).

Ceratobulimina spp.	*Lagena gracilis*	*Cancris laevinflatus*	*Rhabdammina linearis*	*Reophax* cf. *R. cushmani*	*Arenodosaria antipoda*	*Cibicides* cf. *C. thiara*	*Gaudryina reussi*	*Marginulina tumida*	*Lagena sequenziana*	*Lenticulina callifera*	*Nodosaria* sp. 1	*Vaginulina awamoana*	*Fissurina danica*	*Cibicides refulgens*	*Cibicides vortex*	?*Rhizammina* sp.	*Siphonia* spp.	*Marginulina* cf. *M. cocoaensis*	*Lagena elongata*	*Lenticulina* sp.	*Fissurina fimbricata*	*Globigerina* cf. *G. angiporoides*	*Parafissurina* cf. *P. tasmanica*	*Lagena nebulosa*	*Marginulinopsis* cf. *M. pedum*	*Lagena sulcata*	*Fissurina kerguelenensis*	*Islandiella norcrossi*	*Islandiella teretis*	*Eponides tumidulus*	*Ehrenbergina glabra*	*Globocassidulina biora*	*Astrononion echolsi*	*Globorotalia* sp.	*Globigerina* sp.	*Globigerina megastoma*	*Neogloboquadrina pachyderma*	*Trifarina earlandi*	*Miliammina lata*	*Trochammina* sp.	*Trifarina pauperata*	*Uvigerina* sp.
																																							x	x	x	x
																																		x								
																																	x									
														x											x	x	x	x	x	x	x	x	x	x	x	x	x	x				
																							x																			
																								x																		
																							x																			
x																					x																					
														x																												
																						x																				
					x								x				x	x	x	x	x																					
						x											x																									
																x																										
	x			x		x	x	x	x	x	x	x	x	x	x																											
			x	x	x	x																																				
		x																																								
	x																																									
x																																										

Table 1. (Continued).

Lithologic unit	Core-Section (interval in cm)	*Ammodiscus* cf. *A. glabratus*	*Ammobaculites* cf. *A. coprolithiformis*	*Ammoscalaria pseudospiralis*	*Cyclammina incisa*	*Parafissurina groenlandica*	*Parafissurina lateralis*	*Elphidium* sp.	*Gyroidina zelandica*	*Anomalinoides globulosa*	*Melonis barleeanus*	*Globobulimina* sp.	*Cyclammina* cf. *C. complanata*	*Hyperammina cylindrica*	*Rhizammina algaeformis*	*Trifarina* aff. *T. fueguina*	*Cibicides lobatulus*	*Cibicides temperata* s.l.	*Pullenia subcarinata*	*Astacolus crepidulus*	*Cassidulinoides bradyi*	*Epistominella vitrea*	*Nonionella magnalingua*	*Melonis affinis*	*Oolina apiculata*	*Elphidium* cf. *E. nitidum*	*Cyclammina rotundata*	*Pullenia bulloides*	?*Bathysiphon* sp. 1	*Haplophragmoides* sp.	?*Gaudryina* spp.	*Fissurina laevigata*	*Globocassidulina subglobosa*	*Anomalinoides* cf. *A. macraglabra*	*Cibicides pseudoungerianus*
2G	31,CC								?								x		x		x	x	x	x									x		
	32-2, 53-55			x																															
	32-3, 114-123										x					x	x				x	x											x		x
	32,CC										x							x			x	x											x		
2H	33-1, 50-52																																		
	33-3, 102-110															x	x		x			x		x									x		x
	33-5, 52-54																																		
	34-2, 70-72																																		
	34-3, 28-38								?	x	x					x	?		x				?	x								x	x		
	34-5, 59-61																																		
	34,CC																x					x		x								x	x		
	35-1, 49-51																																		
	35-3, 112-121				?				x	x	x					x	x	x			x	x		x				x					x		x
	35-5, 53-55																																		
	35,CC										x					x	x	x			x			x								x	x		x
	36-2, 53-55																																		
	36-3, 97-104						x										x	x						x											x
	36-5, 100-102				x																														
	36-6, 115-123		?	?	x		x				x			x	x				x		x			x					x				x		
	37-2, 58-60																x																		
	37-2, 123-132																																		
2I	37-4, 133-142									x	x					x	?	x			x			x	x			x					x		x
	38-3, 87-96								x	x	x					x	x	x	x		x		x	x											
	38-6, 114-124				?				x	x							x	x			x							x							x
	38,CC		x		x						x	x				x	x	x	x		x	x	x	x				x		?			x		x
	39-3, 133-144				x						x							x				x								x					
2J	39-5 (top of section)	x			x												x	x												?					?
	39-6, 24-36				x					x	x							x				x		x			x			?				x	x
	40-3, 123-131		?		x					x	x	x				x	x		x									x		?		x		x	x
	40-5 (top of section)	x		x	x	x											?					x						x		x				x	
	40-5, 70-79	x			x						?	?		x				x																	
	41-2, 0-10			x	x						x			x		?		?	x		x			x			x			x				x	x
	41-3, 36-40			x	x									x										?						x					
	41-3, 134-142			x	x								x					x									x			x	x				
	41,CC	x		x	x									x				x			x									x			x		
	42-2, 21-31			x	x						x			x		?		x											x	x				x	x
	42-2, 131-141			x	x					x	x	?			x	x		x	x								x	x		?		x	?	x	x
	42-3, 19-29	x		x	x						x	x		x		x		x												x	x		x	?	x
	42-3, 94-107			x	x			x						x		x		x									x		x						
	42-4, 13-23				x			x								?		x																	?
	42-4, 93-103			x	x			?								x		x												x				x	
	43-1, 130-140	x		x	x				x	x						x	x	x	?						x					x					x
	43-2, 46-56	x		x	x					x				x		x	x	?				x												x	
	43-2, 120-133				x						x	x				x		x	?		x												x	x	?
	43-3, 29-39			x	x					x	x	?	x			x		x						x				x	x	x	x	x			
	43-3, 90-100																																		
	43-4, 20-30				x																						x	?							
	43-4, 90-100																																		
	43-5, 18-31																									x									
	43-5, 50-52																																		
	43-5, 70-72			x																															
	43-5, 121-132				x						x	x				x			x		x	x	x	x	?										
	43-6, 65-79		x	x	x			x	x	x		x	x	x	x	x	x	x	x	?															
3	43-6, 129-132	Barren																																	
	43,CC																																		
4	44-1	x	x	x	x	x	x	x	x	x	x	x																							
	44-1, 130-140																																		
	44-1, 142-150																																		
	44-2, 5-7																																		

Table 1. (Continued).

Rosalina globularis	*Fissurina marginata*	*Cassidulinoides braziliensis*	*Lagena striata*	*Nodosaria calomorpha*	*Anomalinoides pinguiglabra*	*Bathysiphon discreta*	*Textularia* cf. *T. plummerae*	*Karreriella obscura*	*Nodosaria* sp. 3	*Fissurina bisulcata*	*Sphaeroidina bulloides*	*Fissurina agassizi*	*Astrorhiza* cf. *A. granulosa*	*Protobotellina cylindrica*	*Hormosina globulifera*	*Reophax scorpiurus*	*Ammobaculites* cf. *A. expansus*	*Textularia* sp. 2	*Psammosphaera fusca*	*Bathysiphon* cf. *B. alba*	*Rhabdammina* cf. *R. abyssorum*	*Oolina apiopleura*	*Oolina globosa*	?*Bathysiphon* sp. 2	*Marsipella* sp.	*Reophax* sp. 1	*Ammodiscus* cf. *A. incertus*	*Dentalina* cf. *D. advena*	*Lenticulina lenticula*	*Gyroidina* cf. *G. obicularis*	*Reophax* cf. *R. nodulosus*	*Eponides* cf. *E. weddellensis*	*Fursenkoina schreibersiana*	*Nonionella iridea*	*Fissurina lucida*	*Lagena laevis*	*Candeina antarctica*	*Globorotalia* cf. *G. siakensis*	*Textularia* sp. 1	*Fissurina annectens*	*Fissurina* sp. 4	*Oridorsalis tenera*	*Elphidium magellanicum* s.l.
x										x												x												x			x				x		x
		x			?					x													x														x			x			x
x		x																																								x	x
x																																					x						x
x		x		x	x					x																								x			x			x			x
x											x																																x
x		x									x																							x			x				x	x	x
										x																																	
x	x				x						x																									x	x						x
					x																																						
		x		x													?					x			x									?		x				x			
																																		x									
x		x		x	x				x	x	x																		x								x					x	x
x		x							x	x	x											x																		x		x	x
	x	x			x		x				x																										x			x			x
x	x	x									x	x										x												x			x			x	x	x	x
																x																		x			x	x	x				
	x	x		x	x						x	x		x								x													x	x	x						
		x			x												x															x	x	x	x								
																x									x						x												
		x															?					x			x					x													
		x			?												x												x														
						x											x		x						x																		
x		x				x							x	x		x	x																										
				x								x					x							x			x	x															
						x					x		x				x							x	x	x																	
		x	x		?	x					x	x	x						x	x	x	x	x																				
						x							x	x	x	x	x	x	x																								
	x				?	x	x	x	x	x	x	?																															
			x	x	x																																						
	x	x																																									
x																																					?						
								?																																			
Barren																																											

Table 1. (Continued).

Lithologic unit	Core-Section (interval in cm)	*Articulina* sp.	*Pyrgo* cf. *P. vespertilio*	*Quinqueloculina seminula*	*Trochoelphidiella pustulosa* n.sp.	*Quinqueloculina triangularis*	*Trochoelphidiella* sp.	*Jaculella* cf. *J. acuta*	*Vaginulina* cf. *V. rheophagica*	*Cassidulinoides* cf. *C. parkerianus*	*Globigerinita* cf. *G. glutinata*	*Gyroidina parva*	*Cibicides* cf. *C. mediocris*	*Nonionella bradii*	*Trochoelphidiella uniforamina*	*Saracenaria kellumi*	*Saracenaria* sp.	*Fissurina* sp. 3	*Triloculina rotundata*	*Chiloguembelina cubensis*	*Globigerina* cf. *G. ouachitaensis*	*Cassidulinoides* cf. *C. chapmani*	*Lagena* cf. *L. laevigata*	*Nodosaria* sp. 2	?*Astacolus* sp.	*Flintina* cf. *F. droogeri*	*Parafissurina subcarinata*	*Eponides bradyi*	*Uvigerina* cf. *U. miozea*	*Globigerinoides trilobus*	*Globocassidulina crassa*	*Parafissurina curta*	*Globorotalia* cf. *G. gemma*	*Globorotaloides* cf. *G. suteri*	*Lenticulina* cf. *L. punctata*	*Robertina tasmanica*
2G	31,CC				x										?								x	x												
	32-2, 53-55																																			
	32-3, 114-123				x		x								?																					
	32,CC				x																															
2H	33-1, 50-52																																			
	33-3, 102-110			x	x												x		x			x														
	33-5, 52-54																																			
	34-2, 70-72																																			
	34-3, 28-38			x	x									x																						
	34-5, 59-61																				x															
	34,CC			x	x										x				x	x																
	35-1, 49-51																																			
	35-3, 112-121			x	x										x	x	x	x																		
	35-5, 53-55																																			
	35,CC			x	x					x		x	x	?	?																					
	36-2, 53-55																																			
	36-3, 97-104																																			
	36-5, 100-102																																			
	36-6, 115-123			x		x		x	x	x	x																									
	37-2, 58-60																																			
	37-2, 123-132																																			
2I	37-4, 133-142			x		x	x																													
	38-3, 87-96		x	x	x																															
	38-6, 114-124	x																																		
	38,CC																																			
	39-3, 133-144																																			
2J	39-5 (top of section)																																			
	39-6, 24-36																																			
	40-3, 123-131																																			
	40-5 (top of section)																																			
	40-5, 70-79																																			
	41-2, 0-10																																			
	41-3, 36-40																																			
	41-3, 134-142																																			
	41,CC																																			
	42-2, 21-31																																			
	42-2, 131-141																																			
	42-3, 19-29																																			
	42-3, 94-107																																			
	42-4, 13-23																																			
	42-4, 93-103																																			
	43-1, 130-140																																			
	43-2, 46-56																																			
	43-2, 120-133																																			
	43-3, 29-39																																			
	43-3, 90-100																																			
	43-4, 20-30																																			
	43-4, 90-100																																			
	43-5, 18-31																																			
	43-5, 50-52																																			
	43-5, 70-72																																			
	43-5, 121-132																																			
	43-6, 65-79																																			
3	43-6, 129-132	Barren																																		
	43,CC																																			
4	44-1																																			
	44-1, 130-140																																			
	44-1, 142-150																																			
	44-2, 5-7																																			

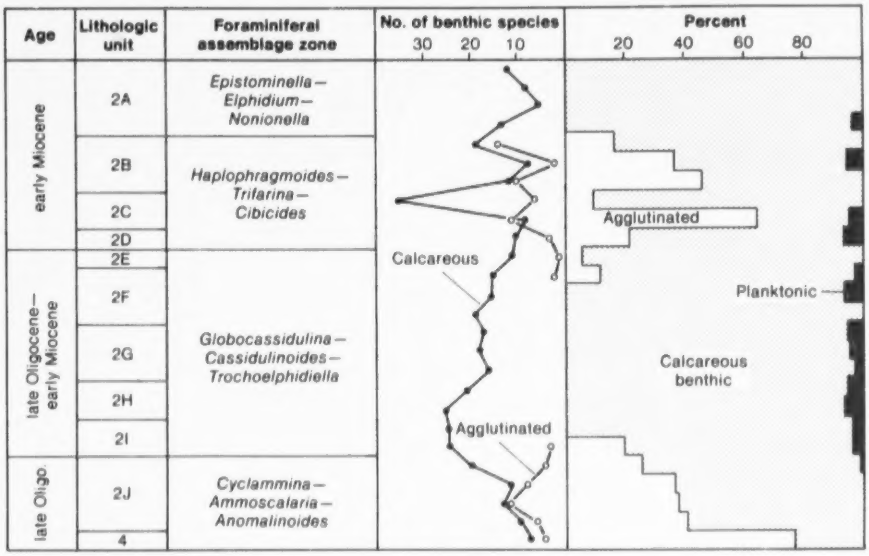

Figure 3. Diversity trends of agglutinated and calcareous benthic species and proportions of agglutinated, calcareous benthic, and planktonic taxa expressed as percentages. Based on 26 of 110 samples investigated in Units 2–4 at Site 270. Selection determined by size of population and stratigraphic distribution. Thin (1 m) glauconitic sand of Unit 3 (between 2J and 4) is apparently devoid of foraminifers.

numbers include *Epistominella vitrea, Elphidium magellanicum* s.l., and *Nonionella iridea* as well as *Melonis* spp. and *Cibicides* spp. Although the Subunit 2B/2A contact is regarded as gradational, the sudden loss of agglutinated taxa and drop in diversity and test numbers at the H-T-C/E-E-N Assemblage Zone boundary is striking and points to a possible hiatus.

Pleistocene Foraminifers (Unit 1)

The floor of the Ross Sea is capped by a widespread cover of Pliocene-Pleistocene diamictons. These sediments have been labeled Subunits 1A and 1B and vary in thickness across the Ross Sea. Unit 1A, at Site 270 only 20 cm thick, has not been studied here. Unit 1B is approximately 20 cm thick.

Unit 1 has been studied extensively both sedimentologically and paleontologically. Paleontological studies have revealed that the composition of the population is very sensitive to depth, salinity, temperature, and oxygen and carbon dioxide concentration (e.g., Kennett, 1968; Osterman and Kellogg, 1979). Unit 1 clearly does not have a consistent lateral microfossil composition and also contains an appreciable component of recycled taxa. (Many of the factors affecting the microfaunas of Unit 1 also apply, of course, to those of Unit 2.)

Faunal content. At Site 270 Unit 1B contains 21 genera and 26 species (Table 1). Distribution of genera is 2 agglutinated, 14 calcareous benthic, 5 planktonic; of species is 2 agglutinated, 19 calcareous benthic, 5 planktonic. Only 29% of these species are common to Unit 2 assemblages. Some of these may be recycled. Assemblages are marked by a near absence of agglutinated forms. Taxa common in Unit 1 but not represented in the late Oligocene–early Miocene assemblage zones include *Islandiella norcrossi, I. teretis, Trifarina earlandi, T. pauperata, Eponides tumidulus, Ehrenbergina glabra, Globocassidulina biora, Astrononion echolsi, Globigerina megastoma*, and *Neogloboquadrina pachyderma*. Specimens of the late Oligocene-Miocene-Pliocene *Trochoelphidiella* species complex and late Oligocene-Miocene *Candeina antarctica* do not occur in Pleistocene assemblages.

FORAMINIFER AGE DETERMINATIONS AND FAUNAL AFFINITIES

Although foraminifers have proven useful in delineating paleoecological and basin history trends, their usefulness in providing high-resolution biostratigraphy in the Ross Sea, with a potential for correlation northward to calibrated temperate zonations, is limited (Leckie and Webb, 1983). The predominantly neritic nature of the benthic assemblages and the paucity of planktonic taxa greatly restricts correlation to periantarctic deep-sea zonations. The nearest neritic benthic zonations are located in New Zealand, which by late Oligocene–early Miocene times lay beneath temperate water masses, whereas the Ross Sea lay within much cooler water masses. The Site 270 assemblages exhibit, within a span of about 7 to 10 m.y., an important high-latitude late Paleogene–early Neogene transition. The C-A-A Assemblage Zone is cool-temperate in character, whereas the G-C-T, H-T-C, and E-E-N Assemblage Zones demonstrate a distinctive polar aspect (Leckie and Webb, 1983). Many of the Site 270 benthic taxa with known extra-antarctic records have ranges of Eocene–Oligocene, Eocene–Miocene, and Oligocene–Miocene. Benthic taxa known to be confined to the high southern latitudes have long ranges which span the late Oligocene–Miocene or Miocene. Pliocene and Pleistocene benthic taxa are significantly different from those of the Miocene. Planktonic taxa found in Site 270

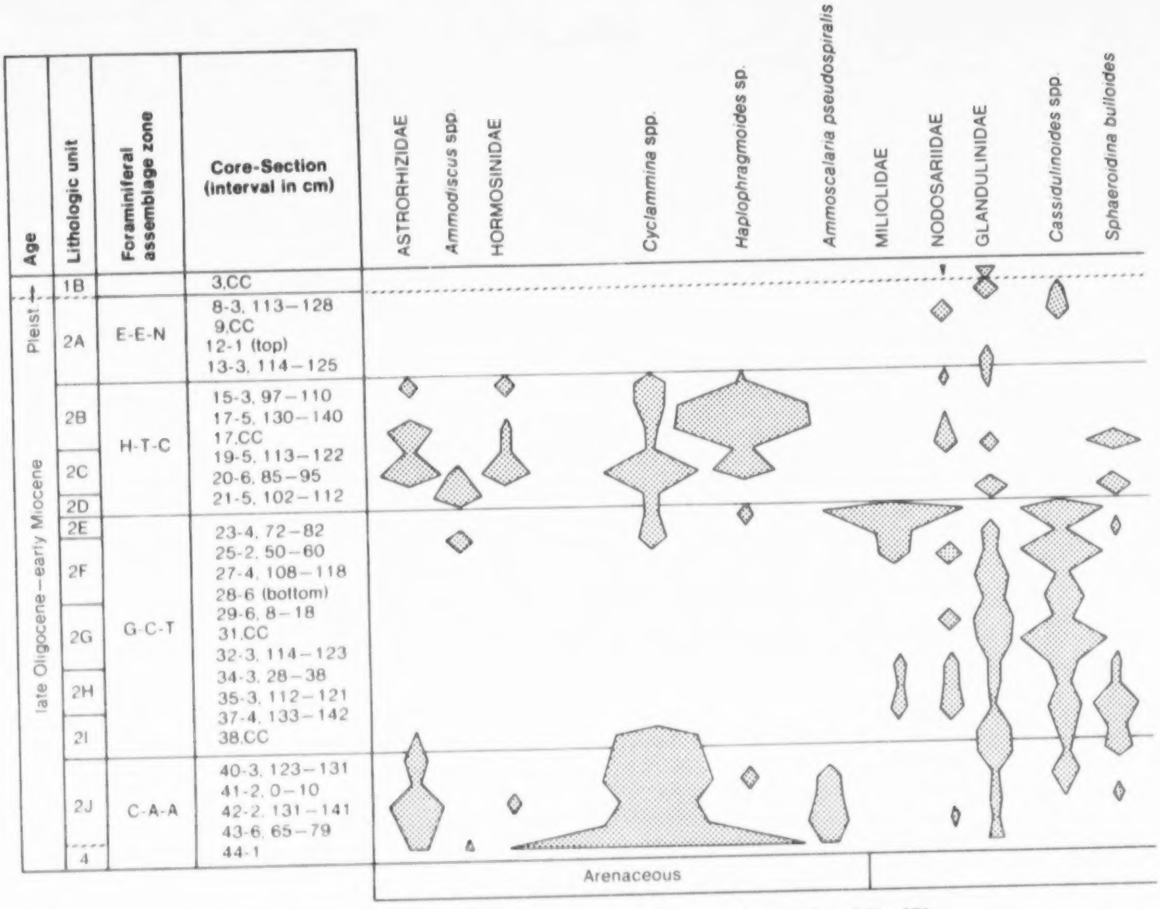

Figure 4. Percentage occurrences of the key taxa or faunal groups in the 27 representative samples of Site 270.

appear to be of very limited use. Late Paleogene-Neogene planktonic assemblages never achieved a diversity greater than one to three species, and apparently temperate planktonics only made sporadic appearances in the southern high latitudes. Their extreme rarity in these glaciomarine sediments reduces their importance owing to the possibility of recycling into younger sediments.

C-A-A Assemblage Zone (Unit 4, Subunit 2J)

Globorotalia cf. *G. siakensis* is present in the upper part of Subunit 2J (270-39-6, 24–26 cm). In lower-latitude zonations this taxon ranges from the base of Zone P22 (late Oligocene) to the top of Zone N14 (middle Miocene, about 11 Ma; Kennett and Srinivasan, 1983; Fig. 5). The only other planktonic, *Candeina antarctica*, is apparently endemic to antarctic areas in the Pacific Ocean and is the only persistent planktonic taxon in upper Oligocene-mid Miocene strata of the Ross Sea (Leckie and Webb, 1985). *Cyclammina incisa* has a New Zealand range of Eocene through Oligocene (Arnold and Landon Series; Hornibrook, 1961, 1971) and is reported to range into the early Miocene in Australia (Ludbrook, 1977). *Gyroidinoides zelandica*, common in the C-A-A Assemblage Zone, appears in the New Zealand late Oligocene (Waitakian) but ranges to the Pleistocene (Hornibrook, 1961). *Anomalinoides pinguiglabra* ranges from the early Oligocene to mid-Miocene (Whaingaroan-upper Southland Series), while *A. macraglabra* spans the New Zealand late Eocene to mid-Miocene (Runangan-Waiauan). The general compositional aspects of the C-A-A Assemblage Zone suggest an affinity with the relatively shallow water late Oligocene assemblages of the Oamaru district of New Zealand (Hornibrook, 1961), a relationship not so obvious in the overlying G-C-T Assemblage Zone.

G-C-T Assemblage Zone (Subunits 2I to 2E)

Six planktonic species are recorded within this interval (Fig. 5). With the exception of *Candeina antarctica*, all are well known in the lower latitudes. Because of their extreme paucity, recycling must be considered a possibility. *Chiloguembelina cubensis* (270-34,CC, Subunit 2H) ranges from the middle Eocene to late Oligocene (*Globigerina euapertura* Zone) in New Zealand (Jenkins, 1971), but according to Blow (1969, p. 222), *Chiloguembelina* spp. ex-group *cubensis* ranges "throughout most, if not all, of N3 (= P22)" and also "has been noted to occur with *Globigerinoides primordius* and,

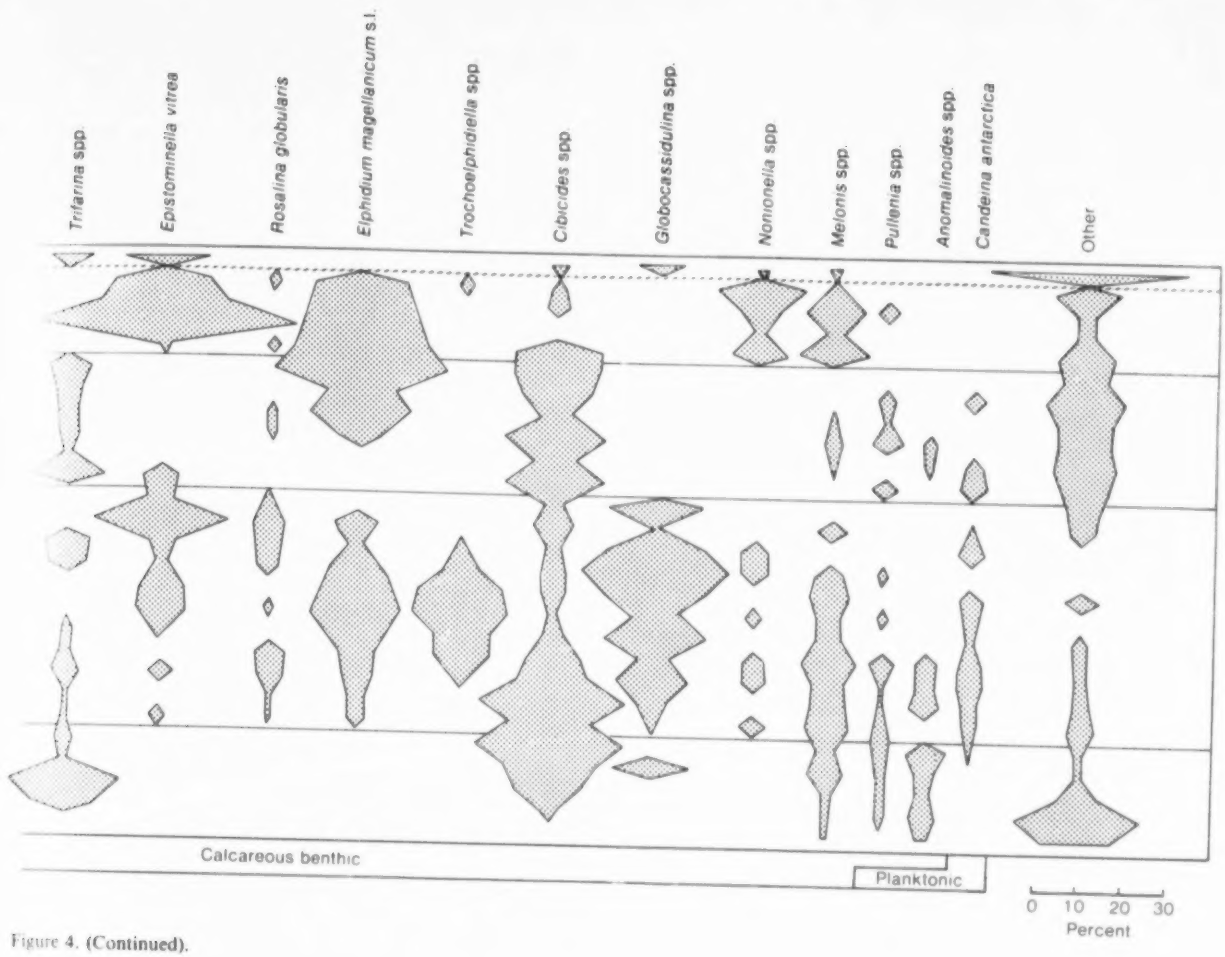

Figure 4. (Continued).

thus, to range into the early part of Zone N4" (latest Oligocene–earliest Miocene). *Globigerina ouachitaensis* (270-34-5, 59–61 cm, Subunit 2H) ranges from the middle Eocene (*Globigerapsis index index* Zone) to early Miocene (*Globigerinoides trilobus trilobus* Zone) in New Zealand (Jenkins, 1971). *Globigerinita* cf. *G. glutinata* is also present in Subunit 2H (270-36-6, 115–123 cm) and ranges in New Zealand (as *G. juvenilis*) from early Oligocene (*Globigerina angiporoides angiporoides* Zone) to Pleistocene (Jenkins, 1974). Kennett and Srinivasan (1983) state a range for *Globigerinita glutinata* as late Oligocene (Zone P22) to Recent. A single specimen of *Globigerinoides trilobus* occurs in 270-28,CC (Subunit 2F). This species first appears in early Miocene Zone N4 (about 23 Ma; Kennett and Srinivasan, 1983). *Globigerina* cf. *G. angiporoides* (270-15-3, 50–57 cm; Subunit 2B) and *Globorotalia* cf. *G. gemma* (270-24,CC, Subunit 2E) have New Zealand ranges of late Eocene–early Oligocene (Jenkins, 1971). These occurrences in Site 270 are clearly recycled. If we assume that *Chiloguembelina cubensis* and *Globigerinoides trilobus* are not recycled, the Oligocene–Miocene boundary would lie between 270-34,CC (Subunit 2H) and 270-28,CC (Subunit 2F).

Calcareous benthic taxa characterize the G-C-T Assemblage Zone and a number of these species also occur in the lower member of the Carmen Silva Formation of Tierra Del Fuego (lower to middle Miocene, local Gaviotian Stage; Codignotto and Malumian, 1981; Malumian, 1982). These taxa include *Trifarina fueguina*, *Globobulimina* sp., "*Buccella*" sp., and *Pullenia* spp. (see Malumian, 1982).

H-T-C Assemblage Zone (Subunits 2D to 2B)

Although some of the taxa are also documented in New Zealand, most are long-ranging late Paleogene–Neogene forms. *Cyclammina incisa* probably ranges no younger than the early Miocene (Ludbrook, 1977), as does *Gaudryina reussi* (Hornibrook, 1961, 1971).

E-E-N Assemblage Zone (Subunit 2A)

No age-definitive taxa are present. The zone contains what is regarded here as typical Miocene polar assemblages.

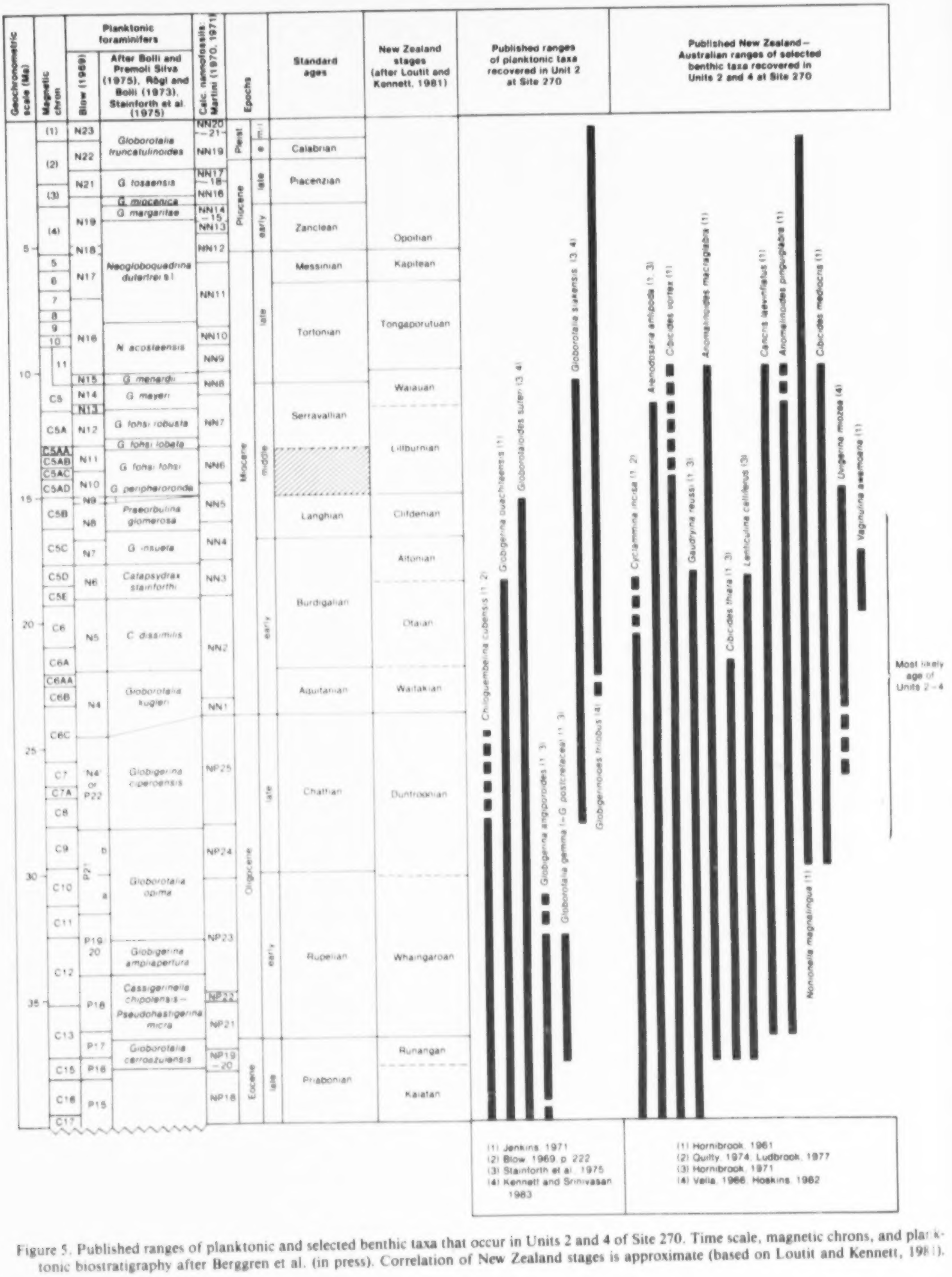

Figure 5. Published ranges of planktonic and selected benthic taxa that occur in Units 2 and 4 of Site 270. Time scale, magnetic chrons, and planktonic biostratigraphy after Berggren et al. (in press). Correlation of New Zealand stages is approximate (based on Loutit and Kennett, 1981).

Pleistocene (Subunit 1B)

Contains typical polar Quaternary assemblages (e.g., McKnight, 1962; Pflum, 1966; Kennett, 1968; Fillon, 1974; Anderson, 1975; Osterman and Kellogg, 1979). These assemblages differ significantly from Pliocene assemblages (Webb, 1974; Webb and Wrenn, 1982) and are markedly different from the late Oligocene–early Miocene assemblages discussed earlier.

SYSTEMATIC NOTES

This investigation of upper Oligocene–lower Miocene and Quaternary sediments from Site 270 results in the identification and description of 74 genera and 163 species of foraminifers. This includes 22 genera and 40 species of agglutinated taxa, 43 genera and 109 species of calcareous benthic taxa and 9 genera and 14 species of planktonic taxa. Of the 163 species, 144 are present in the upper Oligocene–lower Miocene sediments (Units 4 and 2) whereas 27 species are present in the Quaternary sediments (Unit 1). Eight of the taxa in Unit 1 are also found in Unit 2. Some of these may be recycled from Unit 2.

Among the agglutinated taxa, members of the Astrorhizidae, Hormosinidae, and Lituolidae were found to be dominant. Astrorhizidae are the most diverse, with 8 genera and 14 species. Species diversity is highest in *Bathysiphon*. Hormosinidae are also prominent with 6 species (5 species of *Reophax*). The Lituolidae (7 species) are dominated by *Cyclammina* (3 species). *Textularidae* are poorly represented by 3 species of *Textularia*.

Prominent calcareous benthic families include the Nodosariidae, Glandulinidae, Islandiellidae, Uvigerinidae, Elphidiidae, Cibicididae, and Nonionidae. Nodosariidae are the most diverse, with 8 genera and 26 species (8 species of *Lagena*). Glandulinidae are also prominent with 3 genera and 21 species—*Fissurina* (13 species), *Parafissurina* (5 species), and *Oolina* (3 species). The Islandiellidae are represented by 2 genera (*Cassidulinoides* and *Islandiella*) and 6 species. The Uvigerinidae are represented by 2 genera (*Trifarina* and *Uvigerina*) and 4 species. The family Elphidiidae is represented by 2 genera (*Elphidium* and *Trochoelphidiella*) and 6 species. The Cibicididae include 1 genus (*Cibicides*) and 7 species. Three genera (*Astrononion*, *Nonionella*, and *Pullenia*) and 6 species from the Nonionidae are documented.

The planktonic fauna contains 9 genera and 14 species and includes members of the Globorotalidae, Globigerinidae, Heterohelicidae, Candeinidae, and Planomalinidae. The Globigerinidae are the most diverse, with 5 genera and 8 species, and include species of *Globigerina*, *Globigerinita*, *Globigerinoides*, *Globorotaloides*, and *Neogloboquadrina*. The Family Globorotalidae is represented by 3 species of *Globorotalia*. Four species are possibly recycled into Unit 2 from other Cenozoic sediments. One is recycled from Cretaceous sediments.

Classification and Identification

The family and generic classification of Loeblich and Tappan (1964) is followed here. For taxa with Paleogene benthic affinities we have relied on the New Zealand works of Hornibrook (1961, 1971). Jenkins's (1971) treatment of New Zealand Cenozoic planktonic foraminifers was also an important source of comparative information. Many of the taxa identified here were compared with primary type and other materials held in the collections of the New Zealand Geological Survey, Lower Hutt, New Zealand. For identification of many of the cool-water polar Neogene taxa, we have relied on studies of Recent assemblages published by Brady, Parr, Heron-Allen and Earland, and others.

***Astrorhiza* cf. *A. granulosa* Brady**
(P. 1, Fig. 8)

Astrorhiza granulosa Brady, 1884, pl. 20, figs. 14–23.

***Bathysiphon* cf. *B. alba* (Heron-Allen and Earland)**
(Pl. 1, Fig. 3)

Hippocrepinella alba Heron-Allen and Earland, 1932, p. 259, pl. 1, figs. 16–18.

***Bathysiphon* aff. *B. cylindrica* (Glaessner)**
(Pl. 1, Figs. 1–2)

Rhabdammina cylindrica Glaessner, 1937, pl. 1, fig. 1
Bathysiphon cylindrica (Glaessner). Webb, 1975, p. 834, pl. 1, fig. 4.

***Bathysiphon discreta* (Brady)**
(Pl. 1, Fig. 4)

Rhabdammina discreta Brady. Brady, 1884, pl. 22, figs. 7–10.

***Bathysiphon* sp. 1**
(Pl. 1, Fig. 5)

Description. Test an elongate narrow tube, coarsely arenaceous with carbonate cement, open at both ends in most instances.

Discussion. This form is narrower and more coarsely agglutinated than *B. discreta* of this study. These specimens resemble *Rhabdammina linearis* Brady except that they possess a central, subglobular chamber. Because these forms are obviously fragments, generic classification is uncertain. This species occurs in Subunits 2J, 2H, 2C, and 2B.

***Bathysiphon* sp. 2**

Description. Test an elongate tube with a thick wall constructed of well-sorted, silt-sized quartz grains in a milky white clay matrix; exterior smoothly finished, both ends of tube open.

***Hyperammina cylindrica* Parr**
(Pl. 1, Fig. 7)

Hyperammina elongata Brady, 1878, p. 433, pl. 20, fig. 2.
Hyperammina cylindrica Parr, 1950, p. 254, pl. 3, fig. 5. Anderson, 1975, p. 88, pl. 1, fig. 6.

***Jacuella* cf. *J. acuta* Brady**
(Pl. 1, Fig. 11)

Jacuella acuta Brady, 1884, pl. 22, figs. 14–18.

***Marsipella* sp.**
(Pl. 1, Fig. 13)

Description. Test a single undivided chamber, elongate-fusiform, slightly compressed and twisted, wall smooth and consisting of very fine agglutinated quartz grains in a micritic cement. Most specimens are white but a few are iron-stained.

***Protobotellina cylindrica* Heron-Allen and Earland**
(Pl. 1, Fig. 14)

Protobotellina cylindrica Heron-Allen and Earland, 1929, p. 326, pl. 2, figs. 9–13.

***Rhabdammina* cf. *R. abyssorum* M. Sars**

Rhabdammina abyssorum M. Sars, 1868, p. 248 (nomen nudum) *in* Carpenter, 1869, p. 288.

***Rhabdammina linearis* Brady**
(Pl. 1, Fig. 9)

Rhabdammina linearis Brady, 1879, p. 37, pl. 3, figs. 10–11.

***Rhizammina algaeformis* Brady**
(Pl. 1, Fig. 12)

Rhizammina algaeformis Brady, 1879.

***Psammosphaera fusca* Schulze**
(Pl. 1, Fig. 10)

Psammosphaera fusca Schulze, 1875, p. 113. McKnight, 1962, p. 99, pl. 9, fig. 3.

***Ammodiscus* cf. *A. glabratus* Cushman and Jarvis**
(Pl. 2, Fig. 13)

Ammodiscus glabratus Cushman and Jarvis, 1928, p. 86, pl. 12, fig. 6.

Ammodiscus cf. *A. incertus* (d'Orbigny)

Ammodiscus cf. *incertus* (d'Orbigny). Cushman and Stainforth, 1945, p. 14, pl. 1, figs. 10–11.

Hormosina cf. *H. globulifera* Brady

Hormosina globulifera Brady, 1879, p. 60, pl. 4, figs. 4–5.

Reophax cf. *R. cushmani* Heron-Allen and Earland
(Pl. 2, Fig. 5)

Reophax cushmani Heron-Allen and Earland, 1932, p. 339, pl. 7, figs. 22–24.

Reophax cf. *R. nodulosus* Brady
(Pl. 2, Fig. 6)

Reophax nodulosus Brady, 1884, p. 295, pl. 31, figs. 1–9. McKnight, 1962, p. 100, pl. 9, fig. 11. Anderson, 1975, p. 92, pl. 1, fig. 19.

Reophax scorpiurus Montfort
(Pl. 2, Fig. 7)

Reophax scorpiurus Montfort, 1808, p. 331. Anderson, 1975, p. 92, pl. 2, fig. 2.

Miliammina lata Heron-Allen and Earland

Miliammina lata Heron-Allen and Earland, 1930, p. 43, pl. 1, figs. 13–17.

Ammobaculites cf. *A. coprolithiformis* (Schwager)
(Pl. 2, Fig. 8)

Ammobaculites coprolithiformis (Schwager). Cushman, 1946, p. 22, pl. 3, figs. 7–9.

Ammobaculites cf. *A. expansus* Plummer
(Pl. 2, Figs. 9–10)

Ammobaculites expansus Plummer. Cushman, 1951, p. 4, pl. 1, figs. 5–7.

Ammoscalaria pseudospiralis (Williamson)
(Pl. 2, Figs. 11–12)

Proteonina pseudospiralis Williamson, 1858, p. 2, pl. 1, figs. 2–3.

Ammoscalaria pseudospiralis (Williamson). Parker et al., 1953, p. 6, pl. 1, figs. 29, 35. Murray, 1971, p. 29, pl. 7, fig. 105.

Cyclammina cf. *C. complanata* Chapman

Cyclammina complanata Chapman, 1904, p. 228, pl. 22, fig. 7.

Haplophragmoides complanata (Chapman). Taylor, 1965, p. 148, fig. 3.

Cyclammina complanata Chapman. Ludbrook, 1977, p. 187, pl. 2, figs. 28–30; pl. 4, figs. 41–44.

Discussion. These specimens resemble *Cyclammina incisa* (Stache) but are larger in diameter and have sinuous sutures which join at the umbilicus at a greater angle. *C.* cf. *complanata* also has 13–14 chambers in its final whorl instead of the 10–11 characteristic of *C. incisa*. Taylor (1965) believes that *C. incisa* developed from *C. complanata*.

Cyclammina incisa (Stache)
(Pl. 3, Figs. 1–5)

Haplophragmium incisum Stache, 1864, p. 165, pl. 21, fig. 1.

Cyclammina incisa (Stache). Chapman, 1926, p. 29, pl. 2, fig. 1. Crespin, 1950, p. 72, pl. 10, fig. 3. Asano, 1950, p. 77, pl. 12, figs. 8–9. Hornibrook, 1961, p. 30.

Haplophragmoides cf. *incisa* (Stache). Taylor, 1965, p. 150, figs. 2A–3.

Cyclammina incisa (Stache). Hornibrook, 1971, p. 34, pl. 6, figs. 1–3.

Cyclammina cf. *incisa* (Stache). Quilty, 1974, p. 33, pl. 1, figs. 1–3.

Cyclammina incisa (Stache). Ludbrook, 1977, p. 188, pl. 1, figs. 5–8; pl. 3, figs. 31–35; pl. 5, figs. 45–46; pl. 6, figs. 47–49; pl. 7, figs. 50–51; pl. 8, figs. 52–53.

Discussion. Crespin (1950) recognized that this species is widespread in the Oligocene and Miocene. Asano (1950) also assigned the occurrence of *C. incisa* to the Oligocene and Miocene in Japan. Hornibrook (1961) doubted Asano's identification of *C. incisa* and restricted the range of this species to the Eocene–Oligocene (Arnold to Landon Series; Hornibrook, 1971). Quilty (1974) extended the range into the Tasmanian Early Miocene. Likewise, Ludbrook (1977) notes the widespread occurrence of *C. incisa* in southern Australia and New Zealand from Late Paleocene to Early Miocene. Common in Unit 4 and Subunits 2J, and occurs sporadically in Subunits 2I, 2H, 2E, 2D, 2C, and 2B.

Cyclammina rotundata Chapman and Crespin
(Pl. 3, Figs. 6–7)

Cyclammina rotundata Chapman and Crespin, 1930, p. 96, pl. [illegible], figs. 1–2. Crespin, 1950, p. 72, pl. 10, fig. 5.

Haplophragmoides rotundata (Chapman and Crespin). Taylor, 1965, p. 153, fig. 4.

Cyclammina rotundata Chapman and Crespin. Ludbrook, 1977, p. 193, pl. 1, figs. 9–12, 14–17; pl. 3, fig. 36.

Discussion. This species is smaller in size and broader in cross section than *Cyclammina incisa* (Stache). *C. rotundata* is also differentiated by possessing fewer chambers, straight sutures, and a shallow umbilicus. Ludbrook (1977) reports an association with *C. incisa* in Australia and New Zealand from the late Paleocene to the Oligocene and possibly in lower Miocene sediments. Occurs sporadically in Subunit 2J.

Haplophragmoides sp.
(Pl. 3, Fig. 8–13)

Description. Test planispirally coiled, wall coarsely agglutinated, 5-6 chambers in final whorl, subcircular in outline but compressed in axial view.

Discussion. A persistent member of Subunit 2J assemblages (middle and upper part) and common in assemblages of Subunits 2B and 2C.

Textularia cf. *T. plummerae* Lalicker

Textularia cf. *plummerae* (Lalicker). Webb, 1975, p. 835, pl. 3, fig. 4.

Discussion. Numerous specimens occur in the intervals 270-42-4, 13–23 cm (Subunit 2J), and 270-36-6, 115–123 cm (Subunit 2H).

Arenodosaria antipoda (Stache)
(Pl. 2, Fig. 2)

Clavulina antipodum Stache, 1864, p. 167, pl. 21, figs. 3–8.

Clavulina robusta Stache, 1864, p. 169, pl. 21, figs. 9–10.

Arenodosaria antipodum (Stache). Hornibrook, 1961, p. 29, pl. 3, fig. 36.

Arenodosaria robusta (Stache). Hornibrook, 1961, p. 29, pl. 3, fig. 37.

Arenodosaria antipoda (Stache). Hornibrook, 1971, p. 32, pl. 5, figs. 7–8, text-fig. 8, p. 33.

Discussion. Hornibrook (1971) reports a stratigraphic range for *A. antipoda* in New Zealand of middle Eocene to middle Miocene (Bortonian to Waiauan stages) and states that this was a rare form above the lower Miocene (lower Southland Series) (Hornibrook, 1968, p. 54).

Gaudyrina reussi Stache

Gaudyrina reussi Stache, 1864, p. 171, pl. 21, fig. 11. Hornibrook, 1971, p. 32, pl. 6, figs. 83-87.

Discussion. Hornibrook (1971) notes that *G. reussi* ranges in New Zealand from late Eocene to early Miocene (Kaiatan to Otaian stages).

Karreriella obscura Srinivasan

Karreriella obscura Srinivasan, 1966, p. 233, pl. 1, figs. 1–2.

Flintina cf. *F. droogeri* Marks
(Pl. 17, Figs. 18–20)

Flintina droogeri Marks, 1951, p. 41, pl. 5, figs. 2–3.

Pyrgo cf. *P. vespertilio* (Schlumberger)
(Pl. 17, Figs. 16–17)

Biloculina vespertilio Sclumberger, 1891, p. 174, pl. 10, figs. 7[illegible]–76; text-figs. 20–22.

Pyrgo vespertilio (Schlumberger). Quilty, 1974, p. 48, pl. 2, fig. 38.

Discussion. Quilty (1974) reports *P. vespertilio* from the early Miocene of Tasmania.

Quinqueloculina seminula (Linné)
(Pl. 4, Figs. 1–2; Pl. 17, Figs. 2–5)

Serpula seminulum Linnaeus, 1758, p. 786, pl. 2, fig. 1.

Quinqueloculina seminulum (Linne). Hayward and Buzas, 1979, p. 36, pl. 3, fig. 34.

Discussion. Reported by Hayward and Buzas (1979) from the early Miocene of New Zealand and by Quilty (1974) from the early Miocene of Tasmania.

Quinqueloculina triangularis d'Orbigny
(Pl. 4, Fig. 3; Pl. 17, Figs. 6–10)

Quinqueloculina triangularis d'Orbigny, 1846, p. 288, pl. 18, figs. 7–9. Vella, 1957, p. 23, pl. 6, figs. 100, 101, 108.

Triloculina rotunda d'Orbigny
(Pl. 17, Figs. 11–13)

Triloculina rotunda d'Orbigny, 1826, p. 299. McKnight, 1962, p. 107, pl. 12, fig. 38. Quilty, 1974, p. 59, pl. 2, figs. 78–79.

Discussion. Quilty (1974) reports this species from the early Miocene of Tasmania.

Astacolus crepidulus (Fichtel and Moll)
(Pl. 19, Figs. 6–7)

Nautilus crepidula Fichtel and Moll, 1798, p. 107, pl. 19, figs. g–i.

Dentalina cf. *D. advena* (Cushman)
(Pl. 19, Figs. 13–15)

Nodosaria advena Cushman, 1923, p. 79, pl. 14, fig. 12.

Marginulina cf. *M. cocoaensis* Cushman
(Pl. 19, Fig. 10)

Marginulina cocoaensis Cushman, 1925, p. 67, pl. 10, figs. 9–10.

Marginulina tumida Reuss
(Pl. 19, Figs. 8–9)

Marginulina tumida Reuss, 1851, p. 64, pl. 3, fig. 14.

Marginulinopsis cf. *M. pedum* (d'Orbigny)
(Pl. 20, Figs. 3–4)

Marginulina pedum d'Orbigny, 1846, p. 68, pl. 3, figs. 13–14.

Lagena elongata (Ehrenberg)

Miliola elongata Ehrenberg, 1844, p. 274.

Lagena elongata (Ehrenberg). Anderson, 1975, pl. 5, fig. 5. Hayward and Buzas, 1979, p. 61, pl. 19, fig. 239.

Lagena gracilis Williamson

Lagena gracilis Williamson, 1848, p. 13, pl. 1, figs. 3–4. Pflum, 1966, p. 180, pl. 16, fig. 27. Hayward and Buzas, 1979, p. 61, pl. 19, fig. 237.

Lagena cf. *L. laevigata* (d'Orbigny)
(Pl. 19, Fig. 3)

Oolina laevigata d'Orbigny, 1839, p. 19, pl. 5, fig. 3.

Lagena laevigata (d'Orbigny). Heron-Allen and Earland, 1932, p. 361, pl. 10, fig. 4.

Lagena laevis Montagu
(Pl. 4, Fig. 6)

Lagena laevis Montagu, 1803, p. 524. Quilty, 1974, p. 68, pl. 3, figs. 101–102.

Lagena nebulosa Cushman
(Pl. 19, Fig. 2)

Lagena laevis (Montagu) var. *nebulosa* Cushman, 1923, p. 29, pl. 5, figs. 4–5.

Lagena nebulosa Cushman. McKnight, 1962, p. 115, pl. 16, fig. 85.

Lagena sequenziana Fornasini
(Pl. 19, Figs. 4–5)

Lagena sequenziana Fornasini, 1886, p. 352, pl. 8, figs. 1–6.

Lagena striata (d'Orbigny)
(Pl. 4, Fig. 5)

Oolina striata d'Orbigny, 1839, p. 21, pl. 5, fig. 12.

Lagena striata (d'Orbigny). Quilty, 1974, p. 69, pl. 3, fig. 105.

Lagena sulcata (Walker and Jacob)
(Pl. 4, Fig. 7)

Serpula (Lagena) sulcata Walker and Jacob, 1798, p. 634, pl. 14, fig. 5.

Lagena sulcata (Walker and Jacob). Murray, 1971, p. 87, pl. 34, figs. 5–8.

Lenticulina callifera (Stache)
(Pl. 20, figs. 11–12)

Cristellaria callifera Stache, 1864, p. 236, pl. 23, fig. 15.

Robulus calliferus (Stache). Hornibrook, 1971, p. 42, pl. 9, figs. 148–149.

Lenticulina callifera (Stache). Hayward and Buzas, 1979, p. 62, pl. 19, figs. 244–246.

Discussion. Hornibrook (1971) records a New Zealand stratigraphic range of late Eocene to early Miocene (Runangan to Otaian stages).

Lenticulina lenticula (Stache)
(Pl. 20, Fig. 15)

Robulina lenticula Stache, 1864, p. 246, pl. 23, fig. 25.

Robulus lenticulus (Stache). Hornibrook, 1971, p. 43, pl. 9, figs. 158–159.

Discussion. Recorded from the Oligocene (Whaingaroan Stage) in New Zealand (Hornibrook, 1971).

Nodosaria calomorpha Reuss
(Pl. 19, Fig. 1)

Nodosaria calomorpha Reuss, 1866, p. 129, pl. 1, figs. 15–19. Hornibrook, 1961, p. 47, pl. 5, fig. 95.

Saracenaria kellumi Dorreen
(Pl. 20, Figs. 5–8)

Saracenaria kellumi Dorreen, 1948, p. 289, pl. 37, fig. 4.

Vaginulina awamoana Hornibrook
(Pl. 19, Figs. 11–12)

Vaginulina awamoana Hornibrook, 1961, p. 44, pl. 5, figs. 77, 81, 82.

Discussion. *V. awamoana* occurs in the early Miocene of New Zealand (Hutchinsonian and Awamoan stages).

Vaginulina cf. *V. rheophagica* Sidebottom

Vaginulina rheophagica Sidebottom, 1918, p. 139, pl. 5, figs. 5, 7.

Fissurina agassizi Todd and Brönnimann
(Pl. 18, Figs. 15–16)

Fissurina agassizi Todd and Brönnimann, 1957, p. 36, pl. 9, fig. 14.

Fissurina annectens (Burrows and Holland)
(Pl. 4, Fig. 15)

Lagena annectens Burrows and Holland, 1866, p. 203, pl. 7, fig. 11.

Fissurina annectens (Burrows and Holland). Quilty, 1974, p. 89, pl. 4, fig. 150.

***Fissurina bisulcata* (Heron-Allen and Earland)**
(Pl. 4, Figs. 13–14)

Lagena bisulcata Heron-Allen and Earland, 1932, p. 380, pl. 11, figs. 29–32.

***Fissurina danica* (Madsen)**
(Pl. 4, Fig. 12; Pl. 18, Figs. 5–6)

Lagena danica Madsen, 1895, p. 196, pl. O, fig. 4.

***Fissurina fimbriata* (Brady)**
(Pl. 4, Figs. 18–19)

Lagena fimbriata Brady, 1884, p. 486, pl. 60, figs. 26–28. McKnight, 1962, p. 114, pl. 16, fig. 78.

***Fissurina kerguelenensis* Parr**
(Pl. 4, Fig. 16)

Fissurina kerguelenensis Parr, 1950, p. 305, pl. 8, fig. 7. Hayward and Buzas, 1979, p. 57, pl. 16, fig. 206.

***Fissurina laevigata* Reuss**
(Pl. 18, Figs. 11–12)

Fissurina laevigata Reuss, 1850, p. 366, pl. 46, fig. 1.

***Fissurina lucida* (Williamson)**
(Pl. 18, Figs. 7–8)

Entosolenia marginata (Montagu) var. *lucida* Williamson, 1848, p. 17, pl. 2, fig. 7.

***Fissurina marginata* (Montagu)**
(Pl. 18, Figs. 9–10)

Vermiculum marginatum Montagu, 1803, p. 524.
Fissurina marginata (Montagu). Quilty, 1974, p. 90, pl. 4, fig. 153. Hayward and Buzas, 1979, p. 57, pl. 16, fig. 207.

***Oolina apiculata* Reuss**
(Pl. 4, Fig. 11)

Oolina apiculata Reuss, 1851, p. 22, pl. 2, fig. 1.
Lagena apiculata (Reuss). McKnight, 1962, p. 113, pl. 15, fig. 71.
Oolina apiculata Reuss. Quilty, 1974, p. 92, pl. 4, fig. 157.

***Oolina apiopleura* (Loeblich and Tappan)**
(Pl. 4, Figs. 8–9)

Lagena apiopleura Loeblich and Tappan, 1953, p. 59, pl. 10, figs. 14–15.

***Oolina globosa* (Montagu)**
(Pl. 4, Fig. 10; Pl. 18, Fig. 17)

Vermiculum globosa Montagu, 1803, p. 523.
Oolina globosa (Montagu). Quilty, 1974, p. 92, pl. 4, fig. 158. Hayward and Buzas, 1979, p. 68, pl. 23, figs. 284–285.

***Parafissurina curta* Parr**
(Pl. 18, Figs. 24–25)

Parafissurina curta Parr, 1950, p. 318, pl. 10, figs. 6–7.

***Parafissurina groenlandica* (Stschedrina)**

Entosolenia groenlandica Stschedrina, 1946, p. 144, 147, pl. 4, fig. 19.

***Parafissurina lateralis* (Cushman)**
(Pl. 18, Figs. 22–23)

Lagena lateralis Cushman, 1913, pl. 1, fig. 1.
Entosolenia lateralis (Cushman). McKnight, 1962, p. 121, pl. 19, fig. 117.
Parafissurina lateralis (Cushman). Hayward and Buzas, 1979, p. 69, pl. 23, fig. 294.

***Parafissurina subcarinata* Parr**
(Pl. 18, Figs. 20–21)

Parafissurina subcarinata Parr, 1950, p. 318, pl. 10, fig. 9.

***Parafissurina* cf. *P. tasmanica* Parr**
(Pl. 18, Figs. 18–19)

Parafissurina tasmanica Parr, 1950, p. 319, pl. 10, fig. 15.

***Sphaeroidina bulloides* d'Orbigny**
(Pl. 5, Figs. 1–4)

Sphaeroidina bulloides d'Orbigny, 1826, p. 267, modèles no. 65. Boltovskoy, 1978, p. 169, pl. 7, fig. 11. Hayward and Buzas, 19[illegible], p. 74, pl. 27, fig. 335.

***Cassidulinoides bradyi* (Norman)**
(Pl. 5, Figs. 9–10)

Cassidulina bradyi Norman *in* Brady, 1881, p. 59. Brady, 1884, pl. [illegible], figs. 6–10.
Evolvocassidulina bradyi (Norman). Hayward and Buzas, 1979, p. [illegible], pl. 14, fig. 179.

Discussion. A common taxon in Subunits 2J, 2I, 2H, 2G, 2F, [illegible], and rare in 2A. The main difference between *C. bradyi* and *C. parkerianus* appears to be inflation of chambers; *C. parkerianus* being the more inflated form.

***Cassidulinoides braziliensis* (Cushman)**
(Pl. 5, Figs. 13–14)

Cassidulina braziliensis Cushman, 1922, p. 130, pl. 25, figs. 4–5. Uchio, 1960, pl. 9, figs. 13–14.

Discussion. This species does not have wide distribution in the literature, probably because it is morphologically similar to other species of *Cassidulinoides*. Hayward and Buzas (1979, p. 56, pl. 14, fig. 181) figure a specimen of *Evolvocassidulina orientalis* (Cushman) which looks similar to *C. braziliensis* of this study. Further investigation reveals that *C. orientalis* is a "more compressed, broader form" (Cushman, 1922, p. 129). Figures by Barker (1960, pl. 54, fig. 10) and Hornibrook (1961, pl. 10, fig. 201) indicate that the aperture is elongate in the direction of test compression, normal to what is found in specimens of *C. braziliensis*. These specimens also resemble the smaller, less inflated tests of *C. porrectus* (Heron-Allen and Earland) from antarctic Recent sediments. Recent *C. porrectus* is a larger form, with its longest dimension generally ranging between 0.7 and 0.9 mm, as compared with *C. braziliensis*, which is less than 0.5 mm long. A common taxon in Subunits 2J, 2I, 2H, 2G, 2F, and 2E.

***Cassidulinoides* cf. *C. chapmani* Parr**
(Pl. 5, Fig. 12)

Cassidulinoides chapmani Parr, 1931, p. 100, figs. a–c.
Evolvocassidulina cf. *chapmani* (Parr). Hayward and Buzas, 1979, p. 55, pl. 15, fig. 180.

***Cassidulinoides* cf. *C. parkerianus* (Brady)**
(Pl. 5, Fig. 11)

Cassidulina parkeriana Brady, 1884, p. 432, pl. 54, figs. 11–16.
Cassidulinoides parkerianus (Brady). McKnight, 1962, p. 127, pl. 22, fig. 141.

Discussion. Specimens referred here to *C. parkerianus* are distinguished from *C. bradyi* (Norman) by possessing slightly more inflated chambers.

***Islandiella norcrossi* (Cushman)**
(Pl. 5, Figs. 7–8)

Cassidulina norcrossi Cushman, 1933, p. 7, pl. 2, fig. 7.

***Islandiella teretis* (Tappan)**
(Pl. 5, Fig. 5–6)

Cassidulina teretis Tappan, 1951, pl. 1, fig. 30.

***Globobulimina* sp.**
(Pl. 5, Figs. 15–16)

Globobulimina sp. Malumian, 1982, p. 58, pl. 4, figs. 15–16.

Discussion. This taxon closely resembles *Globobulimina* sp. from lower Miocene strata of Tierra del Fuego Island (local Gaviotian Stage; Malumian, 1982). At Site 270, *Globobulimina* sp. is closely associated with the characteristically agglutinated faunas.

Trifarina earlandi (Parr)
(Pl. 6, Figs. 15–16)

Uvigerina angulosa Heron-Allen and Earland (non Williamson), 1932, p. 397, pl. 12, figs. 32–39.

Angulogerina earlandi Parr. McKnight, 1962, p. 123, pl. 20, fig. 125. Echols, 1971, pl. 12, fig. 8. *Trifarina earlandi* (Parr). Anderson, 1975, p. 92, pl. 8, fig. 6.

Trifarina aff. *T. fueguina* Malumian
(Pl. 6, Figs. 10–12)

Trifarina angulosa fueguina Malumian, 1982, pp. 63–64, pl. 6, figs. 1–6.

Discussion. Specimens of Site 270 closely resemble *T. fueguina* from the lower and middle Miocene of Tierra del Fuego Island (local Gaviotian Stage) but they differ in possessing weaker ribs than the type material. Also, there appears to be some significant variability in the type material as exemplified by figs. 4, 5, and 6. Our specimens closely resemble fig. 4, one of the paratypes. *T.* aff. *fueguina* also resembles *T. fluens* (Todd) but is less angular and lacks the well-defined apertural lip of *T. fluens*. *T.* aff. *fueguina* is common at Site 270.

Trifarina pauperata (Heron-Allen and Earland)
(Pl. 6, Figs. 13–14)

Uvigerina angulosa Williamson, var. *pauperata* Heron-Allen and Earland, 1932, p. 398, pl. 12, figs. 40–43.

Angulogerina pauperta (Heron-Allen and Earland). Fillon, 1974, pl. 4, fig. 8.

Uvigerina cf. *U. miozea* Finlay

Uvigerina miozea Finlay, 1939, p. 102, pl. 12, figs. 12–14.

Hofkeruva (Trigonouva) miozea (Finlay). Vella, 1961, p. 477, pl. 1, figs. 5, 8, 9; pl. 2, fig. 6.

Uvigerina miozea Finlay. Hornibrook, 1961, p. 65, pl. 8, fig. 144.

Trigonouva miozea (Finlay). Vella, 1966, p. 97, pl. 27, fig. 23.

Euuvigerina miozea (Finlay). Hayward and Buzas, 1979, p. 55, pl. 14, fig. 178.

Discussion. The *Uvigerina miozea* species group first appears in the Waitakian Stage of New Zealand (early Miocene) or possibly in the Duntroonian Stage (late Oligocene) (Hornibrook, 1961; Hoskins, 1982). Although the name *U. miozea* has been applied to forms ranging as young as Pleistocene, Vella (1961, 1966) emphasizes that *U. miozea* s.s. ranges no younger than the Clifdenian Stage (early middle Miocene).

Buccella sp.
(Pl. 8, Fig. 13)

Description. Six-chambered, planoconvex form with subacute periphery. Umbilical region partially obscured by prominent pustules. Aperture interiomarginal, halfway between umbilicus and periphery. Supplementary sutural apertures clearly visible beyond umbilical region. Surficial resemblance to *Trochoelphidiella*. *Bucella* sp. has also been recorded in Oligocene–lower Miocene strata at the MSSTS drill site (Webb et al., in press).

Cancris laevinflatus Hornibrook
(Pl. 6, Figs. 8–9)

Cancris laevinflatus Hornibrook, 1961, p. 120, pl. 15, figs. 328, 331, 33

Discussion. Hornibrook (1961) notes a stratigraphic range of late Oligocene to middle Miocene (Whaingaroan to Waiauan stages) for this taxon in New Zealand.

Epistominella vitrea Parker
(Pl. 6, Figs. 1–5)

Epistominella vitrea Parker, 1953, *in* Parker et al., 1953, p. 9, pl. 4, figs. 34–36, 40, 41. Murray, 1971, p. 130, pl. 54, figs. 1–6.

Discussion. This tiny species is a dominant taxon through most of the succession at Site 270; absent in Unit 4 and Subunit 2C, present and common in Subunits 2J, 2I, 2H, 2G, 2F, 2E, 2D, 2B, 2A, and Unit 1

Rosalina globularis d'Orbigny
(Pl. 6, Figs. 6–7)

Rosalina globularis d'Orbigny, 1826, p. 271, pl. 13, figs. 1–2.

Discorbis globularis (d'Orbigny). McKnight, 1962, p. 125, pl. 20, fig. 133.

Rosalina globularis d'Orbigny. Fillon, 1974, pl. 4, figs. 11–12.

Discussion. Absent in Unit 4, present in only two intervals from Subunit 2J, but a persistent member of assemblages from Subunits 2I through 2A.

Elphidium magellanicum s.l. Heron-Allen and Earland
(Pl. 7, Figs. 1–9)

Elphidium (Polystomella) magellanicum Heron-Allen and Earland, 1932, p. 440, pl. 16, figs. 26–28. Murray, 1971, p. 163, pl. 68, figs. 1–7.

Description. Test planispiral, involute. Periphery rounded, slightly lobate in outline. Chambers inflated, 5 to 8½ in final whorl; 5½ to 6½ most common. Sutures depressed, slightly curved. Dense pustulation fills umbilical areas and sutures, obscuring sutural foramina and apertural face (Pl. 7, Figs. 8–9). Aperture a series of interiomarginal foramina, usually three (Pl. 7, Fig. 6).

Discussion. A variable species group with 5 to 8½ chambers in the final whorl. *E. magellanicum* previously described as having 5–7 (Hansen and Lykke-Andersen, 1976). Specimens from Site 270 with 7 to 8½ chambers in the final whorl are somewhat similar to *Protelphidium obiculare* (Brady) or *Elphidium barletti* Cushman (Pl. 7, Figs. 5, 7). *P. obiculare* characteristically has 7–10 chambers in the final whorl and is a much broader form than *E. magellanicum*. *E. barletti* has more numerous chambers, 10–12 in the final whorl, and better defined sutural foramina. This is a dominant taxon throughout most of the succession of Site 270, first appearing in Subunit 2I and ranging through Subunit 2A.

Elphidium cf. *E. nitidum* Dorreen
(Pl. 7, Fig. 11)

Elphidium nitidum Dorreen, 1948, p. 290, pl. 37, fig. 11.

Elphidium sp.
(Pl. 7, Fig. 10)

Description. Seven inflated chambers, periphery broadly rounded. Tests of several specimens are longer than broad. Appears to have 5–7 poorly preserved retral processes per lumen. Aperture not discernible. All specimens poorly preserved.

Discussion. Differs from *E. magellanicum* in possessing recognizable retral processes. In gross morphology it resembles *E. poeyanum* (d'Orbigny). Rare specimens occur in Unit 4 and the lower part of Subunit 2J.

Trochoelphidiella pustulosa n. sp.
(Pl. 8, Figs. 1–12, 14–15; Pl. 21, Figs. 14–19)

Holotype. Pl. 21, Figs. 14–16, Sample 270-32,CC (Subunit 2G), length 0.26 mm, width 0.21 mm, breadth 0.15 mm (megalospheric).

Paratypes. Pl. 8, Figs. 1,2, 15, Sample 270-31-3, 59–67 cm (Subunit 2G), length 0.30 mm, width 0.25 mm, breadth 0.15 mm (megalospheric); Pl. 8, Figs. 9–11, Sample 270-29-6, 8–18 cm (Subunit 2G), length 0.25 mm, width 0.20 mm, breadth 0.14 mm (megalospheric); Pl. 21, Figs. 17–18, Sample 270-31-3, 59–67 cm (Subunit 2G), length 0.33 mm, width 0.25 mm, breadth 0.18 mm (microspheric); Pl. 8, Fig. 3, Sample 270-29-6, 8–18 cm, length 0.26 mm, width 0.20 mm, breadth 0.15 mm (megalospheric); Pl. 8, Figs. 4, 12, Sample 270-32-3, 114–123 cm (Subunit 2G), length 0.24 mm, width, 0.20 mm, breadth 0.13 mm (megalospheric); Pl. 8, Figs. 5–6 and Pl. 21, Fig. 19, Sample 270-29-6, 8–18 cm (Subunit 2G), length 0.38 mm, width 0.30 mm (megalospheric); Pl. 8, Figs. 7, 8, 14, Sample 270-33-3, 102–110 cm (Subunit 2G), length 0.20 mm, width 0.17 mm, breadth 0.13 mm (megalospheric).

Description. Test calcareous, trochospirally coiled, never planispiral. Spiral side nearly flat, umbilical side slightly convex with depressed umbilicus. Periphery rounded. Dimorphic; the megalospheric form is the most common, possessing a total of about 13 chambers arranged in 2 whorls. the microspheric generation commonly has about 22 chambers in 3 whorls. Chambers increase rapidly in size as added, inflated on umbilical side, especially so in the last-formed chambers. The final chamber is rarely found intact. Sutures moderately curved on the spiral side, nearly radial on the umbilical side. The aperture consists of one to three small foramina at the base of the final chamber and extending from the periphery to the umbilicus (Pl. 8, Figs. 12, 14, 15). Apertures usually obscured by pustulation where complete final chambers are preserved; readily observable at the base of the penultimate chamber where pustulation is poorly developed. The umbilicus is depressed and contains dense pustulation. The umbilical extensions of each chamber cover a primitive canal system. Coarse pustules emerge through the chambers in the umbilical area from the underlying canals. In some specimens, primitive sutural canals are apparent as fissures between the umbilical extensions of the chambers. These extensions fuse together toward the periphery (Pl. 8, Figs. 1, 4, 11). No septal foramina or retral processes are apparent. However, an irregular pattern of foramina is developed in the umbilical area. The spiral side is generally smooth and devoid of pustulation. The simple sutural canal system may extend around the periphery to the spiral side, there expressed externally as small foramina at the base of the spiral chambers. The surface texture of the test is smooth to finely granular. Finely perforate. The microspheric and megalospheric forms are similar in size. Both range in diameter from 0.24 to 0.38 mm, width from 0.19 to 0.30 mm, and breadth from 0.10 to 0.15 mm. The proloculus of the microspheric generation is about 0.008 mm compared with 0.040 to 0.050 mm in the dominant megalospheric generation.

Discussion. *Trochoelphidiella pustulosa* n. sp. shares several characteristics with the Pliocene genotype, *T. onyxi* (Webb, 1974). The attitude of the septal walls, both dorsally and ventrally, is similar in both species. The presence of a canal system, though crudely developed in *T. pustulosa*, establishes an affinity with *T. onyxi*. Both possess interiomarginal multiple apertures and exhibit a prominent pustulation on the umbilical side. Dimorphism, with a dominance of the megalospheric generation, is another shared feature. *Trochoelphidiella pustulosa* differs from Pliocene *T. onyxi* in several respects. The chambers of *T. onyxi* increase gradually as added, producing a test that is circular in outline in contrast to the more oblong shape of *T. pustulosa*, which is produced by chambers that increase rapidly in size. *T. pustulosa* lacks the distinctive, paired, septal canal foramina of *T. onyxi*. The canal system of *T. pustulosa* is rather simple and is developed primarily in the umbilical area. The pustulation of *T. pustulosa* is coarser than that of the Pliocene *T. onyxi*. The spiral side of *T. onyxi* is convex, and low to highly elevated, whereas the spiral side of *T. pustulosa* is nearly flat. The apertures of *T. pustulosa* also differ somewhat from *T. onyxi* in that they are confined to a single row of small foramina at the base of the final chamber and extend only from the periphery to the umbilicus. Those of *T. onyxi* consist to one to two rows of small foramina that may extend across the entire base of the apertural lumen (interiomarginal). A further distinction between the two species is in the size of their two generations; the megalospheric and microspheric forms of *T. pustulosa* are similar in size, whereas the two generations of *T. onyxi* demonstrate a marked difference in size, the microspheric form being the larger. *Trochoelphidella pustulosa* is biostratigraphically significant at Site 270. It first appears in 270-38-3, 87–96 cm (Subunit 2I) and ranges up through Subunits 2H, 2G, 2F, with a single occurrence in Subunit 2B. It is probably ancestral to *T. uniforamina* D'Agostino (early to middle and ?late Miocene) and *T. onyxi* Webb (Pliocene). Type specimens to be placed in the U.S. National Museum, Washington, D.C.

Trochoelphidiella uniforamina D'Agostino

(Pl. 9, Figs. 1–12; Pl. 10, Figs. 11–13; Pl. 21, Figs. 8–13)

Trochoelphidiella uniforamina D'Agostino, 1980, p. 76, pl. 5, figs. 1–12.

Hypotypes. Pl. 9, Figs. 1–3, 9–12, and Pl. 21, Figs. 11–13, Sample 270-5-2, 122–132 cm (Subunit 2A), length 0.56 mm, width 0.46 mm, breadth 0.30 mm (microspheric); Pl. 9, Fig. 4, Section 270-28-6, bottom (Subunit 2F), length 0.25 mm, width 0.23 mm, breadth 0.13 mm (megalospheric); Pl. 9, Figs. 5–6 and Pl. 21, Figs. 8–10, Sample 270-15,CC (Subunit 2B), length 0.18 mm, width 0.15 mm, breadth 0.07 mm (megalospheric); Pl. 9, Figs. 7–8, Section 270-28-6, bottom (Subunit 2F), length 0.23 mm, width 0.20 mm, breadth 0.13 mm (megalospheric).

Description. Test calcareous, trochospirally coiled, never planispiral. Circular in outline, biconvex in edge view. Dimorphism pronounced, with the megalospheric form the most common. Chambers increase gradually in size as added, slightly inflated on the spiral side, more so on the umbilical side. Sutures moderately curved on the spiral side, nearly radial on the umbilical side. Aperture consists of one to three small interiomarginal foramina. Apertures usually obscured by pustulation (Pl. 9, Fig. 9). The umbilicus is slightly depressed and covered by pustulose ornament, which also covers sutures on the umbilical side. A sutural canal system is developed by septal doubling and chamber overlap. The canal system does not appear to extend to the spiral side. Communication with the exterior is via a series of single, elongate sutural foramina (Pl. 9, Figs. 9–12). The spiral side is generally smooth and devoid of pustulation. The surface texture of the test is finely granular.

Discussion. *Trochoelphidiella uniforamina* D'Agostino is morphologically similar to the Pliocene genotype *T. onyxi* (Webb, 1974). There are several significant differences. *T. uniforamina* lacks an umbilical lumen, a feature present in *T. onyxi*. The series of sutural canal foramina of *T. uniforamina* occur in a single row and are elongate parallel to the septa. This differs from the characteristic paired septal canal foramina of *T. onyxi* which are elongate normal to the septa. This canal system extends around the periphery to the spiral side in *T. onyxi* whereas in *T. uniforamina* it is restricted to the umbilical side. A further difference is in the multiple apertures, which in *T. onyxi* may be in one or two rows, compared with a single row in *T. uniforamina*.

Although *Trochoelphidiella uniforamina* is closely related to *T. onyxi*, it also shares similarities with *T. pustulosa* n. sp. The nature of the multiple apertures, lack of an umbilical lumen, and presence of a canal system restricted to the umbilical side are all characteristics common to both *T. uniforamina* and *T. pustulosa*. In all other respects, *T. pustulosa* differs from *T. uniforamina* as it does from *T. onyxi*.

Trochoelphidiella uniforamina appears to be intermediate between *T. pustulosa* and *T. onyxi*. Its first appearance in the early Miocene (270-35-3, 112–121 cm, Subunit 2H) is preceded stratigraphically by *T. pustulosa* (270-38-3, 87–96 cm, Subunit 2I) with several transitional specimens (270-35,CC) which do not exhibit the true characteristics of *T. uniforamina* (Pl. 10, Figs. 11–13). *T. uniforamina* is most prolific by the middle Miocene, as documented by D'Agostino (1980). It is not known at present whether a late Miocene precursor to Pliocene *T. onyxi* exists (Webb, 1974). *T. uniforamina* occurs sporadically through Subunits 2H, 2G, 2F, 2E, 2B, and 2A.

Trochoelphidiella sp.

(Pl. 10, Figs. 1–10; Pl. 21 Figs. 1–7)

Hypotypes. Pl. 10, Figs. 1–2, and Pl. 21, Figs. 1–2, Sample 270-37-4, 133–142 cm (Subunit 2I), length 0.62 mm, width 0.55 mm, breadth, 0.25 mm; Pl. 10, Figs. 3–4 and Pl. 21, Figs. 3–4, Sample 270-29-6, 8–18 cm (Subunit 2G), length 0.27 mm, width 0.22 mm, breadth 0.11 mm; Pl. 10, Figs. 5–7, 10, Sample 270-8-3, 113–128 cm, breadth 0.15 mm; Pl. 10, Figs. 8–9, Sample 270-6-1, 113–123 cm (Subunit 2A), width 0.23 mm, breadth 0.14 mm; Pl. 21, Figs. 5–7, Sample 270-32-3, 114–123 cm (Subunit 2G), length 0.34 mm, width 0.30 mm, breadth 0.16 mm.

Description. Test calcareous, low trochospiral coil. Periphery rounded to subangular (Pl. 10, Figs. 6, 9; Pl. 21, Figs. 1, 3, 6). Circular to oblong in outline, biconvex in side view with tendency to be flat on the umbilical side. Dimorphism not observed. Chambers increasing gradually as added, slightly inflated on the umbilical side. Aperture consists of one or two small interiomarginal foramina. Umbilicus slightly depressed, pustulose to coarsely granular as are the umbilical sutures. A septal canal system is present but it is uncertain if the sutural foramina are paired or singular. The canal system is best developed on the umbilical side and may or may not extend to the spiral side. About 8 chambers in the final whorl. Surface texture of the test is finely to coarsely granular.

Discussion. These rare specimens of *Trochoelphidiella* possess morphologic characteristics different from *T. pustulosa* n.sp., *T. uniforamina* D'Agostino, or *T. onyxi* Webb. The low trochospiral coil and tendency for the umbilical side to be flat distinguish this group. They may represent a new species. All tests appear megalospheric. *Trochoelphidiella* sp. is rare in Subunits 2G and 2A.

***Eponides bradyi* Earland**
(Pl. 23, Figs. 11-13)

Truncatulina pygmaea Hantken. Brady, 1884, pl. 95, figs. 9-10.
Eponides bradyi Earland, 1934, p. 187, pl. 8, figs. 36-38. Boltovskoy, 1978, p. 15, pl. 4, figs. 1-3.

***Eponides tumidulus* (Brady)**
(Pl. 12, Fig. 2)

Truncatulina tumidulus Brady, 1884, pl. 95, fig. 8.

***Eponides* cf. *E. weddellensis* Earland**
(Pl. 12, Fig. 1)

Eponides weddellensis Earland, 1936, p. 57, pl. 1, figs. 65-67.

***Cibicides lobatulus* (Walker and Jacob)**
(Pl. 11, Figs. 10-12)

Nautilus lobatus Walker and Jacob, 1798, p. 642, pl. 14, fig. 36.
Cibicides lobatulus (Walker and Jacob). Murray, 1971, p. 175, pl. 73, figs. 1-7.

***Cibicides* cf. *C. mediocris* Finlay**
(Pl. 22, Figs. 13-16)

Cibicides mediocris Finlay, 1940, p. 464, pl. 67, figs. 198, 199. Hornibrook, 1961, p. 160, pl. 25, figs. 499, 500, 502. Hayward and Buzas, 1979, p. 48, pl. 10, figs. 127-129.

Discussion. Hornibrook (1961) gives the range of this species in New Zealand as early Oligocene to late Miocene (Duntroonian to Tongaporutuan).

***Cibicides pseudoungerianus* (Cushman)**
(Pl. 22, Figs. 4-6)

Truncatulina pseudoungeriana Cushman, 1922, p. 97, pl. 20, fig. 9
Cibicides pseudoungerianus (Cushman). Murray, 1971, p. 176, pl. 74, figs. 1-6.

***Cibicides refulgens* Montfort**
(Pl. 11, Figs. 13-15)

Cibicides refulgens Montfort, 1808-1810, p. 122. McKnight, 1962, p. 129, pl. 23, fig. 150. Anderson, 1975, p. 84, pl. 10, fig. 3.

***Cibicides temperata* s.l. Vella**
(Pl. 11, Figs. 1-9; Pl. 22, Figs. 1-3)

Cibicides temperata Vella, 1957, p. 40, pl. 9, figs. 201-203. Hornibrook, 1961, p. 162, pl. 24, figs. 476, 477, 482.
Cibicidoides temperatus (Vella). Hayward and Buzas, 1979, p. 49, pl. 11, figs. 135-137.

Discussion. *Cibicides temperata* displays considerable morphologic variation. The height of the ventral surfaces is illustrated in Pl. 11, Figs. 2, 6. The height of the dorsal surface also varies, from nearly flat (Pl. 11, Fig. 4) to biconvex (Pl. 11, Fig. 2). The attitude of the sutures on the umbilical side ranges from slightly curved to nearly radial. The characteristics that distinguish this species group are the 6-8 chambers in the final whorl (6½ to 7 most common) and the low but wide aperture. *C. temperata* is common and persistent throughout Unit 2 (late Oligocene-early Miocene) at Site 270. Hornibrook (1961) gives the range of this species in New Zealand as late Eocene (Runangan Stage to Recent.

***Cibicides* cf. *C. thiara* (Stache)**
(Pl. 22, Figs. 7-9)

Rosalina thiara Stache, 1864, p. 279, pl. 24, figs. 29-30.
Cibicides thiara (Stache). Hornibrook, 1961, p. 159, pl. 25, figs. 495, 497. Hornibrook, 1971, p. 52, pl. 11, figs. 188-190.

Discussion. Hornibrook (1961) records the range of this species in New Zealand as late Eocene to late Oligocene (upper Arnold Series to Waitakian Stage).

***Cibicides vortex* Dorreen**
(Pl. 22, Figs. 10-12)

Cibicides vortex Dorreen, 1948, p. 299, pl. 41, fig. 5. Hornibrook, 1961, p. 160, pl. 24, figs. 490-492. Hayward and Buzas, 1979, p. 49, pl. 11, figs. 138-139.

Discussion. In New Zealand this species ranges from middle Eocene to middle Miocene (Bortonian to Lillburnian stages; Hornibrook, 1961).

***Fursenkoina schreibersiana* (Czjzek)**
(Pl. 12, Fig. 3)

Virgulina schreibersiana Czjzek, 1848, p. 11, pl. 13, figs. 18-21. Hornibrook, 1961 p. 64, pl. 8, fig. 138.

***Ehrenbergina glabra* Heron-Allen and Earland**
(Pl. 12, Figs. 11-12)

Ehrenbergina hystrix Brady var. *glabra* Heron-Allen and Earland, 1922 p. 140, pl. 5, figs. 1-6.
Ehrenbergina glabra Heron-Allen and Earland. McKnight, 1962, p. 127, pl. 22, fig. 142. Fillon, 1974, pl. 5, figs. 9-10.

***Globocassidulina biora* (Crespin)**
(Pl. 12, Fig. 10)

Cassidulina biora Crespin, 1960, p. 28, pl. 3, figs. 1-10.
Globocassidulina biora (Crespin). Fillon, 1974, p. 133, pl. 1, figs. 8-15.

***Globocassidulina crassa* (d'Orbigny)**
(Pl. 12, Figs. 7-9)

Cassidulina crassa d'Orbigny, 1839, p. 56, pl. 7, figs. 18-20.
Globocassidulina crassa (d'Orbigny) var. *rossensis* Kennett, 1967, p. 134, pl. 11, figs. 4-6.
Globocassidulina crassa rossensis Kennett. Fillon, 1974, p. 132, pl. 1, figs. 1-7.

***Globocassidulina subglobosa* (Brady)**
(Pl. 12, Figs. 4-6)

Cassidulina subglobosa Brady, 1884, p. 60, pl. 54, fig. 17.
Cassidulina subglobosa subglobosa Brady. Boltovskoy, 1978, p. 155, pl. 2, fig. 34.
Globocassidulina subglobosa (Brady). Hayward and Buzas, 1979, p. 59, pl. 17, figs. 219-220.

***Astrononion echolsi* Kennett**
(Pl. 13, Figs. 1-2)

Astrononion echolsi Kennett, 1967, p. 134, pl. 11, figs. 7-8. Fillon, 1974, p. 139, pl. 6, figs. 1-3.

***Nonionella bradii* (Chapman)**
(Pl. 13, Fig. 6; Pl. 23, Figs. 1-2)

Nonionina scapha (Fichtel and Moll) var. *bradii* Chapman, 1916, p. 71, pl. 5, fig. 42.
Nonionella bradii (Chapman). McKnight, 1962, p. 118, pl. 17, fig. 99. Fillon, 1974, pl. 5, figs. 12-13. Anderson, 1975, p. 90, pl. 11, fig. 6.

***Nonionella iridea* Heron-Allen and Earland**
(Pl. 13, Figs. 3-4; Pl. 23, Figs. 5-7)

Nonionella iridea Heron-Allen and Earland, 1932, p. 438, pl. 16, figs. 14-16. Fillon, 1974, p. 140, pl. 5, figs. 11, 14.

***Nonionella magnalingua* Finlay**
(Pl. 13, Fig. 5; Pl. 23, Figs. 3-4)

Nonionella magnalingua Finlay, 1940, p. 456, pl. 65, figs. 144, 146. Hornibrook, 1961, p. 94, pl. 12, figs. 226, 232, 233.

***Pullenia bulloides* (d'Orbigny)**
(Pl. 13, Fig. 10)

Nonionina bulloides d'Orbigny, 1846, p. 107, pl. 5, figs. 9-10.
Pullenia bulloides (d'Orbigny). Hornibrook, 1961, p. 90, pl. 11, figs. 205-206.

Pullenia subcarinata (d'Orbigny)

(Pl. 13, Figs. 7-9)

Nonionina subcarinata d'Orbigny, 1839, p. 28, pl. 5, figs. 23-24.
Pullenia subcarinata (d'Orbigny). McKnight, 1962, p. 128, pl. 22, fig. 44.

Gyroidina cf. *G. obicularis* d'Orbigny

(Pl. 13, Figs. 15-16)

Gyroidina obicularis d'Orbigny, 1826, p. 278, no. 1, modèles no. 13. Boltovskoy, 1978, p. 160, pl. 4, figs. 16-17.
Gyroidinoides obicularis (d'Orbigny). Corliss, 1979, p. 9, pl. 5, figs. 1-3.

Gyroidina parva Cushman and Renz

(Pl. 13, Figs. 11-12)

Gyroidina parva Cushman and Renz, 1941, p. 23, pl. 4, fig. 2.
Gyroidina parva Cushman and Renz. Becker and Dusenbury, 1958, p. 39, pl. 7, fig. 8.

Gyroidina zelandica Finlay

(Pl. 13, Figs. 13-14; Pl. 23, Figs. 8-10)

Gyroidina zelandica Finlay, 1939, p. 323, pl. 28, figs. 138-140.
Gyroidinoides zelandica (Finlay). Hornibrook, 1961, p. 113, pl. 16, figs. 339, 334.
Gyroidina zelandica Finlay. Douglas, 1973, pl. 12, figs. 4-9; pl. 24, figs. 5-6. Hayward and Buzas, 1979, p. 60, pl. 18, figs. 221-223.

Oridorsalis tenera (Brady)

(Pl. 13, fig. 17)

Truncatulina tenera Brady, 1884, pl. 95, fig. 11.
Eponides tenera (Brady). McKnight, 1962, p. 126, pl. 21, fig. 136.
Oridorsalis tenera (Brady). Fillon, 1974, pl. 6, figs. 10-11.

Anomalinoides globulosa (Chapman and Parr)

(Pl. 14, Figs. 13-16)

Anomalina grosserugosa (Guembel). Brady, 1884, pl. 94, figs. 4-5.
Anomalina globulosa Chapman and Parr, 1937, p. 117, pl. 9, fig. 27. Boltovskoy, 1978, p. 152, pl. 1, figs. 5, 8.
Anomalinoides globulosa (Chapman and Parr). Hayward and Buzas, 1979, p. 39, pl. 4, figs. 50-51.

Discussion. Reported from the Oligocene of Ninetyeast Ridge (Indian Ocean) by Boltovskoy (1978) and from the early Miocene of New Zealand by Hayward and Buzas (1979).

Anomalinoides cf. *A. macraglabra* (Finlay)

(Pl. 14, Figs. 8-9)

Anomalina macraglabra Finlay, 1940, p. 460, pl. 65, figs. 141-143.
Anomalinoides macraglabra (Finlay). Hornibrook, 1961, p. 155, pl. 24, figs. 473-475. Hayward and Buzas, 1979, p. 40, pl. 5, figs. 52-53.

Discussion. In New Zealand, *A. macraglabra* ranges from the late Eocene to middle Miocene (Runangan to Waiauan stages) (Hornibrook, 1961).

Anomalinoides pinguiglabra (Finlay)

(Pl. 14, Figs. 10-12)

Anomalina pinguiglabra Finlay, 1940, p. 460, pl. 66, figs. 160-165.
Anomalina pineuiglabra (Finlay). Hornibrook, 1961, p. 156, pl. 23, figs. 464-466.

Discussion. *A. pinguiglabra* ranges from the early Oligocene to middle Miocene in New Zealand (Whaingaroan Stage to upper Southland Series) (Hornibrook, 1961).

Melonis affinis (Reuss)

(Pl. 14, Figs. 5-7)

Nonionina affinis Reuss, 1851, p. 72, pl. 5, fig. 32.
Nonion affine (Reuss). Boltovskoy, 1978, p. 162, pl. 5, figs. 1-2.
Melonis affinis (Reuss). Hayward and Buzas, 1979, p. 65, pl. 20, fig. 256.

Melonis barleeanus (Williamson)

(Pl. 14, Figs. 1-4)

Nonionina barleeana Williamson, 1858, p. 32, pl. 3, figs. 68-69.
Melonis barleeanum (Williamson). Corliss, 1979, p. 10, pl. 5, figs. 7-8.

Robertina tasmanica Parr

(Pl. 23, Figs. 14-15)

Robertina tasmanica Parr, 1950, p. 369, pl. 15, figs. 10-11.

Chiloguembelina cubensis (Palmer)

(Pl. 15, Fig. 11)

Guembelina cubensis Palmer, 1934, p. 74, text-figs. 1-6.
Chiloguembelina spp. ex group *cubensis* (Palmer). Blow, 1969, p. 2, 378, pl. 54, figs. 4-6.
Chiloguembelina cubensis (Palmer). Jenkins, 1971, p. 66, pl. 1, figs. 3-5.

Globigerinelloides cf. *G. volutus* (White)

(Pl. 16, Fig. 16)

Globigerina volutus White, 1928, p. 197, pl. 28, fig. 5.
Globigerinelloides volutus (White). Webb, 1973, p. 552, pl. 2, figs. -7.

Discussion. Recycled from Cretaceous sediments.

Globorotalia sp.

(Pl. 16, Figs. 10-15)

Discussion. The very small size, umbilical-extraumbilical arched aperture, five inflated chambers in the final whorl, and chambers that rapidly increase in size as added are characteristic features of this species and not known in named antarctic Quaternary taxa. The specimens have a weakly to moderately pustulose surface. An extensive literature search failed to find an adequate reference to this species. Engelhardt (1980) notes a similar form from the late Miocene of the southeast Indian Ocean.

Globorotalia cf. *G. gemma* Jenkins

(Pl. 15, Figs. 12-13)

Globorotalia (Turborotalia) postcretacea (Myatliuk). Blow and Banner, 1962, p. 120, pl. 12, figs. g-j.
Globorolatia gemma Jenkins, 1966, p. 1115, fig. 11, no. 97-103.
Turborotalia gemma (Jenkins). Srinivasan, 1968, p. 146, pl. 14, figs. 3-4.
Globorotalia gemma Jenkins. Blow, 1969, p. 348, pl. 34, fig. 9.
Globorotalia (Turborotalia) gemma Jenkins. Jenkins, 1971, p. 115, pl. 10, figs. 263-269.

Globorotalia cf. *G. siakensis* LeRoy

(Pl. 15, Figs. 14-16)

Globorotalia siakensis Leroy, 1939, pl. 3, figs. 30-31.
Globorotalia (Turborotalia) siakensis Leroy. Blow, 1969, p. 356, pl. 10, figs. 7-9; pl. 34, figs. 4-5.
Globorotalia (Jenkinsella) siakensis Leroy. Kennett and Srinivasan, 1983, p. 172, pl. 42, figs. 1, 6-8.

Globigerina cf. *G. angiporoides* Hornibrook

(Pl. 15, Figs. 5-7)

Globigerina angipora Stache. Hornibrook, 1961, p. 145, text-figs. 3a-d.
Globigerina (Subbotina) angiporoides angiporoides Hornibrook. Jenkins, 1971, p. 160, Pl. 20, figs. 588-594.

Globigerina megastoma Earland

(Pl. 16, Figs. 6-8)

Globigerina megastoma Earland, 1934, p. 177, pl. 8, figs. 9-12. Banner and Blow, 1960, p. 14, pl. 1, fig. 3. Kennett, 1968, p. 42

Discussion. This species closely resembles *Globorotalia anfracta* Parker. The nature of the aperture appears to be the only criterion to distinguish the two species. The aperture of *Globorotalia anfracta* is extraumbilical-umbilical, whereas that of *Globigerina megastoma* is umbilical, with a strong tendency toward an extraumbilical position. Is is this extraumbilical tendency that makes some specimens of *G.*

megastoma look more like *Globorotalia*. In Earland's (1934, p. 177) original description of *G. megastoma*, he states that the test is large; "maximum breadth of the final convolution about 0.60 mm." Banner and Blow (1960, p. 15) examined Heron-Allen and Earland's collections in the British Museum and noted that there were "very many small specimens of this species". Antarctic collections of *Globigerina megastoma* discussed by Ward (1979) and D'Agostino (1980) have been examined by the authors and found to contain specimens ranging in maximum diameter from 0.11 to 0.35 mm. These populations also demonstrate the full range of aperture position from extraumbilical-umbilical to umbilical.

Globigerina cf. *G. ouachitaensis* Howe and Wallace

(Pl. 15, Figs. 8–10)

Globigerina ouachitaensis Howe and Wallace, 1932, p. 74, pl. 10, figs. 7a, b. Jenkins, 1971, p. 153, pl. 16, figs. 489–490.

Globorotaloides cf. *G. suteri* Bolli

(Pl. 15, Figs. 3–4)

Globorotaloides suteri Bolli, 1957, p. 117, pl. 27, figs. 9–13. Jenkins, 1971, p. 189, pl. 22, figs. 646–648. Kennett and Srinivasan, 1983, p. 214, pl. 53, figs. 1, 3–5.

Globigerinita cf. *G. glutinata* (Egger)

(Pl. 16, Figs. 3–5)

Globigerina glutinata Egger, 1893, p. 371, pl. 13, figs. 19–21.

Globigerinita glutinata (Egger). Kennett and Srinivasan, 1983, p. 224, pl. 56, figs. 1, 3–5.

Globigerinoides trilobus (Reuss)

(Pl. 15, Figs. 1–2)

Globigerina triloba Reuss, 1850, p. 374, pl. 47, fig. 11.

Globigerinoides quadrilobatus trilobus (Reuss). Blow, 1969, p. 326.

Globigerinoides trilobus trilobus (Reuss). Jenkins, 1971, p. 180, pl. 19, figs. 571–581.

Globigerinoides triloba (Reuss). Kennett and Srinivasan, 1983, p. 62, pl. 13, figs. 1–3.

Neogloboquadrina pachyderma (Ehrenberg)

(Pl. 16, Figs. 1–2)

Aristerospira pachyderma Ehrenberg, 1861, p. 303.

Neogloboquadrina pachyderma (Ehrenberg), Kennett and Srinivasan, 1983, p. 192, pl. 47, figs. 3–5.

Candeina antarctica Leckie and Webb

Candeina antarctica Leckie and Webb, 1985, pl. 1, figs. 1–15; pl. 2, figs. 1–9; pl. 3, figs. 3, 6, 8.

Discussion. *Candeina antarctica* was the dominant, virtually monospecific planktonic foraminiferal species throughout the Ross Sector of Antarctica during the latest Oligocene to middle Miocene (Leckie and Webb, 1985).

ACKNOWLEDGMENTS

We would like to thank N. de B. Hornibrook (N. Z. Geological Survey), who kindly provided access to New Zealand foraminiferal assemblages and types. Dr. Marie-Pierre Aubry (Woods Hole Oceanographic Institution) examined Site 270 material for calcareous nannoplankton; her efforts are greatly appreciated. Dr. John Wrenn (Amoco Research) discussed the problems of palynological biostratigraphy in the Ross Sea and Dave Harwood (Ohio State University) discussed diatom biostratigraphy. The assistance of Sue Shipley, Pamela Bar[illegible], Brian Huber, and Robert Tope is acknowledged. A special thanks to Pamela Leckie and Helen Jones for enduring the many format changes. This paper greatly benefitted from reviews by Dr. Ken Miller (Lamont-Doherty Geological Observatory) and an anonymous referee. DSDP and ODP kindly provided samples for this study. This work was supported by National Science Foundation grants DPP 76-20[illegible], DPP 79-07043 and DPP 80-018749. Illustration of the microfauna was undertaken with scanning electron microscope facilities at Northern Illinois University, DeKalb. Postdoctoral research support to R.M.L. at Woods Hole Oceanographic Institution is gratefully acknowledged.

REFERENCES

References not cited here can be found in the foraminifer treatise by Loeblich and Tappan (1964).

Allis, R. G., Barrett, P. J., and Christoffel, D. A., 1975. A paleomagnetic stratigraphy for Oligocene and early Miocene marine glacial sediments at Site 270, Ross Sea, Antarctica. *In* Hayes, D. E., Frakes, L. A., et al., *Init. Repts. DSDP*, 28: Washington (U.S. Govt. Printing Office), 879–884.

Anderson, J. B., 1975. Ecology and distribution of foraminifera in the Weddell Sea of Antarctica. *Micropaleontology*, 21:69–96.

Asano, K., 1950. Some Lituolidae from the Tertiary of Japan. *Contr. Cushman Found. Foram. Res.*, 1:75–79.

Banner, F. T., and Blow, W. H., 1960. Some primary types of species belonging to the superfamily Globigerinaceae. *Contr. Cushman Found. Foram. Res.*, 11:1–41.

Barker, R. W., 1960. *Taxonomic Notes on the Species Figured by H. B. Brady in His Report on the Foraminifera dredged by H.M.S.* Challenger *during the Years 1873–1876.* Soc. Econ. Paleont. Mineral. Spec. Publ. 9.

Barrett, P. J., 1975. Textural characteristics of Cenozoic preglacial and glacial sediments at Site 270, Ross Sea, Antarctica. *In* Hayes, D. E., Frakes, L. A., et al., *Init. Repts. DSDP*, 28: Washington (U.S. Govt. Printing Office), 757–767.

Becker, L. E., and Dusenbury, A. N., Jr., 1958. *Mio-Oligocene (Aquitanian) Foraminifera from the Goajira Peninsula, Colombia.* Cushman Found. Foram. Res., Spec. Publ., 4.

Berggren, W. A., Kent, D. V., Flynn, J. J., and Van Couvering, J. A., in press. Cenozoic geochronology. *In* Snelling, N. J. (Ed.), *Geochronology and the Geologic Time Scale.* Geol. Soc., London, Spec. Pap.

Blow, W. H., 1969. Late Middle Eocene to Recent planktonic foraminiferal biostratigraphy. *In* Brönnimann, P., and Renz, H. H. (Eds.), *Proc. 1st Int. Conf. Planktonic Microfossils, Geneva, 1967*: Leiden (E. J. Brill), 199–421.

Blow, W. H., and Banner, F. T., 1962. The Mid-Tertiary (Upper Eocene to Aquitanian) Globigerinaceae. *In* Eames, F. E., Banner, F. T., Blow, W. H., and Clarke, W. J. (Eds.), *Fundamentals of Mid-Tertiary Stratigraphical Correlation*: Cambridge (Cambridge Univ. Press), pp. 61–152.

Boltovskoy, E., 1978. Late Cenozoic benthonic foraminifera of the Ninetyeast Ridge (Indian Ocean). *Mar. Geol.*, 26:139–175.

Bukry, D., 1981. Cenozoic coccoliths from the Deep Sea Drilling Project. *In* Warme, J. E., Douglas, R. G., and Winterer, E. L. (Eds.), *The Deep Sea Drilling Project: A Decade of Progress*, Soc. Econ. Paleontol. Mineral., Spec. Publ., 32:335–353.

Burns, D. A., 1975. Nannofossil biostratigraphy for Antarctic sediments, Leg 28, DSDP. *In* Hayes, D. E., Frakes, L. A. et al., *Init. Repts. DSDP*, 28: Washington (U.S. Govt. Printing Office), 589–598.

Chapman, F., 1904. On some Cainozoic foraminifera from Brown's Creek, Otway Coast. *Rec. Geol. Surv. Vict.*, 1:227–230.

Chapman, F., 1916. Report on the Foraminifera and Ostracoda out of marine muds from soundings in the Ross Sea. *British Antarct. Exped. 1907-1909, Repts. Sci. Investig., Geol.*, 2(3):53–80.

Chapman, F., and Parr, W. J., 1937. *Foraminifera, Australian Antarctic Expedition, 1911-1914: Scientific Reports, Series C—Zoology and Botany*, 1(pt. 2):1–190.

Chen, P.-H., 1975. Antarctic radiolaria. *In* Hayes, D. E., Frakes, L. A., et al., *Init. Repts. DSDP*, 28: Washington (U.S. Govt. Printing Office), 437–513.

Ciesielski, P. F., 1975. Biostratigraphy and paleoecology of Neogene and Oligocene silicoflagellates from cores recovered during Antarctic Leg 28, Deep Sea Drilling Project. *In* Hayes, D. E., Frakes, L. A., et al., *Init. Repts. DSDP*, 28: Washington (U.S. Govt. Printing Office), 625–691.

Codignotto, J. O., and Malumian, N., 1981. Geología de la region al norte del paralelo 54°S de la Isla Grande de la Tierra del Fuego. *Rev. Assoc. Geol. Argentina*, 36:44–88.

Cook, H. E., Zemmels, I., and Matti, J. C., 1975. X-ray mineralogy data, Austral-Antarctic region, Deep Sea Drilling Project Leg 28.

In Hayes, D. E., Frakes, L. A., et al., *Init. Repts. DSDP*, 28: Washington (U.S. Govt. Printing Office), 981–998.

Corliss, B. H., 1979. Taxonomy of Recent deep-sea benthonic foraminifera from the southeast Indian Ocean. *Micropaleontology*, 25: 1–19.

Crespin, I., 1950. Some Tertiary Foraminifera from Victoria, Australia. *Contr. Cushman Found. Foram. Res.*, 1:70–74.

_______, 1960. Some Recent foraminifera from Vestfold Hills, Antarctica. *Sci. Rep. Tohoku Univ.* Ser. 2 (Geol.), Spec. Vol. 4:19–31.

Cushman, J. A., 1925. New foraminifera from the upper Eocene of Mexico. *Contr. Cushman Lab. Foram. Res.*, 1(1):4–8.

_______, 1933. New Arctic foraminifera collected by Capt. R. A. Bartlett from Fox Basin and off the northeast coast of Greenland. *Smithsonian Misc. Coll.*, 89(9):1–8.

_______, 1951. *Paleocene Foraminifera of the Gulf Coast Region of the United States and Adjacent Areas.* U.S. Geol. Surv. Prof. Paper, 232.

Cushman, J. A., and Jarvis, P. W., 1928. Cretaceous foraminifera from Trinidad. *Contr. Cushman Lab. Foram. Res.*, 4:85–103.

D'Agostino, A. E., 1980. Foraminiferal biostratigraphy, paleoecology, and systematics of DSDP Site 273, Ross Sea, Antarctica [M.S. thesis]. Northern Illinois University, DeKalb.

Dorreen, J. M., 1948. A foraminiferal fauna from the Kaiatan Stage (Upper Eocene) of New Zealand. *J. Paleontol.*, 22:281–300.

Douglas, R. G., 1973. Benthonic foraminiferal biostratigraphy in the central North Pacific, Leg 17, Deep Sea Drilling Project. *In* Winterer, E. L.,Ewing, J. I. et al., *Init. Repts. DSDP*, 17: Washington (U.S. Govt. Printing Office), 607–671.

Earland, A., 1934. Foraminifera, part III. The Falklands sector of the Antarctic (excluding South Georgia). *Discovery Repts*, 10:1–208.

_______, 1936. Foraminifera, Part IV. Additional records from the Weddell Sea Sector from material obtained by S. Y. *Scotia. Discovery Repts.*, 13:1–76.

Echols, R. J., 1971. Distribution of foraminifera in sediments of the Scotia Sea area, Antarctic waters. *In* Reid, J. L. (Ed.), *Antarctic Oceanology I.* Antarct. Res. Ser., 15:93–168.

Engelhardt, N. L., 1980. Paleoecologic and biostratigraphic interpretations of late Miocene foraminifera at DSDP Site 265 (Leg 28), southeast Indian Ocean [M.S. thesis]. Northern Illinois University, DeKalb.

Fillon, R. H., 1974. Late Cenozoic foraminiferal paleoecology of the Ross Sea, Antarctica. *Micropaleontology*, 20:129–151.

Ford, A. B., and Barrett, P. J., 1975. Basement rocks of the south-central Ross Sea, Site 270, DSDP Leg 28. *In* Hayes, D. E., Frakes, L. A., et al., *Init. Repts. DSDP*, 28: Washington (U.S. Govt. Printing Office), 861–868.

Hansen, H. J., and Lykke-Anderson, A-L., 1976. Wall structure and classification of fossil and recent elphidiid and nonionid foraminifera. *Fossils and Strata*, 10:1–37.

Hayes, D. E., Frakes, L. A., et al., 1975. *Init. Repts. DSDP*, 28: Washington (U.S. Govt. Printing Office).

Hayward, B. W., and Buzas, M. A., 1979. *Taxonomy and Paleoecology of Early Miocene Benthic Foraminifera of Northern New Zealand and the North Tasman Sea.* Smithsonian Contr. Paleobiol., 36.

Heirtzler, J. R., Dickinson, G. O., Herron, E. M., Pitman, W. C. III, and Le Pichon, X., 1968. Marine magnetic anomalies, geomagnetic field reversals and motions of the ocean floor and continents. *J. Geophys. Res.*, 73:2119–2136.

Heron-Allen, E., and Earland, A., 1922. Protozoa, Part II. Foraminifera. *British Antarct. Exped. 1910, Zool.*, 6(2):25–268.

Hornibrook, N. de B., 1961. *Tertiary Foraminifera from Oamaru District (N.Z.) Part I—Systematics and Distribution.* N. Z. Geol. Surv. Paleontol. Bull., 34(1).

_______, 1968. *A Handbook of New Zealand Microfossils (Foraminifera and Ostracoda).* N. Z. Geol. Surv., Info. Ser. 62.

_______, 1971. *A Revision of the Oligocene and Miocene Foraminifera from New Zealand Described by Karrer and Stache in the Reports of the "Novara" Expedition (1864).* N. Z. Geol. Surv. Paleontol. Bull., 43.

Hoskins, R. H., 1982. *Stages of the New Zealand Marine Cenozoic: A Synopsis.* N. Z. Geol. Surv. Rept., 107.

Jenkins, D. G., 1966. Planktonic foraminiferal zones and new taxa from the Danian to Lower Miocene of New Zealand. *N. Z. J. Geol. Geophys.*, 8:1088–1126.

_______, 1971. *New Zealand Cenozoic Planktonic Foraminifera.* N. Z. Geol. Surv. Paleontol. Bull., 42.

Kaneps, A., 1975. Cenozoic planktonic foraminifera from Antarctic deep-sea sediments, Leg 28, DSDP. *In* Hayes, D. E., Frakes, L. A., et al., *Init. Repts. DSDP*, 28: Washington (U.S. Govt. Printing Office), 573–583.

Kemp, E. M., 1975. Palynology of Leg 28 drillsites, Deep Sea Drilling Project. *In* Hayes, D. E., Frakes, L. A., et al., *Init. Repts. DSDP*, 28: Washington (U.S. Govt. Printing Office), 599–608.

Kemp, E. M., and Barrett, P. J., 1975. Antarctic glaciation and early Tertiary vegetation. *Nature*, 258(5535):507–508.

Kennett, J. P., 1967. New foraminifera from the Ross Sea, Antarctica. *Contr. Cushman Found. Foram. Res.*, 18:133–135.

_______, 1968. The fauna of the Ross Sea: Part 6, Ecology and distribution of foraminifera. *N. Z. Dept. Sci. Industr. Res. Mem.* 46: 1–48.

Kennett, J. P., and Srinivasan, M. S., 1983. *Neogene Planktonic Foraminifera, A Phylogenetic Atlas*: Stroudsburg, PA (Hutchinson Ross).

LaBrecque, J. L., Kent, D. V., and Cande, S. C., 1977. Revised magnetic polarity time scale for Late Cretaceous and Cenozoic time. *Geology*, 5:330–335.

Leckie, R. M., and Webb, P. N., 1980. A provisional late Oligocene–early Miocene foraminiferal zonation, Ross Sea Continental Shelf, Antarctica. *Geol. Soc. Am. Abstr. Progr.*, 12:469.

_______, 1983. Late Oligocene–early Miocene glacial record of the Ross Sea, Antarctica: Evidence from DSDP Site 270. *Geology*, 11: 578–582.

_______, 1985. *Candeina antarctica* n.sp. and the phylogenetic history and distribution of *Candeina* spp. in the Paleogene–early Neogene of the Southern Ocean. *J. Foram. Res.*, 15(2):65–78.

LeRoy, D. O., 1939. Some small foraminifera, ostracods and otoliths from the Neogene ("Miocene") of the Rokan-Tapanoeli area, central Sumatra. *Natuurk. Tijdschr. Nederl.-Indie*, 99(6):215–296.

Loeblich, A. R., Jr., and Tappan, H., 1964. Sarcodina, chiefly "Thecamoebians" and Foraminiferida. *In* Moore, R. C. (Ed.), *Treatise in Invertebrate Paleontology*, Protista 2, Pt. C: Lawrence (Univ. Kansas Press.).

Loutit, T. S., and Kennett, J. P., 1981. New Zealand and Australian Cenozoic sedimentary cycles and global sea-level changes. *Am. Assoc. Pet. Geol. Bull.*, 65:1586–1601.

Ludbrook, N. H., 1977. Early Tertiary *Cyclammina* and *Haplophragmoides* (Foraminifera: Lituolidae) in southern Australia. *Trans. R. Soc. S. Aust.*, 101(7):165–198.

McCollum, D. W., 1975. Diatom stratigraphy of the Southern Ocean. *In* Hayes, D. E., Frakes, L. A., et al., *Init. Repts. DSDP*, 28: Washington (U.S. Govt. Printing Office), 515–571.

McDougall, I., 1977. Potassium-argon dating of glauconite from a greensand drilled at Site 270 in the Ross Sea, DSDP Leg 28. *In* Barker, P. F., Dalziel, I. W. D., et al., *Init. Repts. DSDP*, 36: Washington (U.S. Govt. Printing Office), 1071–1072.

McKnight, W. M., Jr., 1962. The distribution of foraminifera off parts of the Antarctic coast. *Bull. Am. Paleontol.*, 44(201):61–158.

Malumian, N., 1982. Foraminiferos benthicos de la Formacion Carmen Silva, Mioceno, Isla Grande de la Tierra del Fuego. *Rev. Asoc. Paleont. Argentina*, 19:37–66.

Marks, P., Jr., 1951. A revision of the smaller foraminifera from the Miocene of the Vienna Basin. *Contr. Cushman Found. Foram. Res.*, 2:33–73.

Murray, J. W., 1971. *An Atlas of British Recent Foraminiferids.* New York (Elsevier Publ. Co.).

Osterman, L. E., and Kellogg, T. B., 1979. Recent benthic foraminifera distributions from the Ross Sea, Antarctica: relation to ecologic and oceanographic conditions. *J. Foram. Res.*, 9:250–269.

Palmer, D. K., 1934. The foraminiferal genus *Guembelina* in the Tertiary of Cuba. *Mem. Soc. Cubana Hist. Nat.*, 8:73–76.

Parker, F. L., Phleger, F. B., and Peirson, J. F., 1953. *Ecology of Foraminifera from San Antonio Bay and Environs, Southwest Texas.* Cushman Found. Foram. Res., Spec. Publ. 2.

Parr, W. J., 1931. A new species of the foraminifera: *Cassidulinoides chapmani. Victorian Naturalist*, 48:99-100.

________, 1950. Foraminifera: *Repts. B.A.N.Z. Antarct. Res. Exped., 1929-1931, Ser. B*, 5:235-392.

Pflum, C. E., 1966. The distribution of Foraminifera in the eastern Ross Sea, Amundsen Sea and Bellingshausen Sea, Antarctica. *Bull. Am. Paleontol.*, 50(226):151-209.

Quilty, P. G., 1974. Tasmanian Tertiary Foraminifera. Part 1. Textulariina, Miliolina, Nodosariacea. *R. Soc. Tasmania, Pap. Proc.*, 108:31-106.

Savage, M. L., and Ciesielski, P. F., 1983. A revised history of glacial sedimentation in the Ross Sea region. *In* Oliver, R. L., James, P. R., and Jago, J. B. (Eds.), *Proc. Int. Symp. Antarct. Earth Sci., 4th, Adelaide, Australia, 1982*: (Australian National Academy of Sciences), pp. 555-559.

Srinivasan, M. S., 1966. Descriptions of new species and notes on taxonomy of foraminifera from the Upper Eocene and Lower Oligocene of New Zealand. *Trans. R. Soc. N. Z., Geol.*, 3:231-256.

________, 1968. Late Eocene and early Oligocene planktonic foraminifera from Port Elizabeth and Cape Foulwind, New Zealand. *Contr. Cushman Found. Foram. Res.*, 19:142-159.

Stainforth, R. M., Lamb, J. L., Luterbacher, H., Beard, J. H., and Jeffords, R. M., 1975. *Cenozoic Planktonic Foraminiferal Zonation and Characteristics of Index Forms*. Univ. Kansas Paleontol. Contrib., Art. 62.

Stschedrina, Z. G., 1946. *New Species of Foraminifera from the Arctic Ocean*. Trans. Arctic Sci. Res. Inst. Northern Sea Route Board Drifting Expedition on the Icebreaker *G. Sedov* in 1937-1940, Moscow-Leningrad (Vol. 3, Biology).

Tappan, H., 1951. Northern Alaska index foraminifera. *Contr. Cushman Found. Foram. Res.*, 2:1-8.

Taylor, D. J., 1965. Preservation, composition, and significance of Victorian Lower Tertiary *Cyclammina* faunas. *R. Soc. Victoria*, 78:143-160.

Vella, P., 1957. *Studies in New Zealand Foraminifera*. N. Z. Geol. Surv. Paleontol. Bull., 28.

________, 1961. Upper Oligocene and Miocene uvigerinid foraminifera from Raukumara Peninsula, New Zealand. *Micropaleontology*, 7:467-483.

________, 1966. Some foraminiferal lineages in New Zealand. *In* Drooger, C. W., Reiss, Z., Rutsch, R. F., and Marks, P. (Eds.), *Proc. 3rd Session in Berne, Int. Union Geol. Sci. Medit. Neogene Strat., 1964*: Leiden (E. J. Brill), 87-102.

Ward, B. L., 1979. Late Quaternary foraminifera from elevated deposits of the Cape Royds-Barne areas, Ross Island, Antarctica [M.S. Thesis]. Northern Illinois University, DeKalb.

Weaver, F. M., and Gombos, A. M., Jr., 1981. Southern high-latitude diatom biostratigraphy. *In* Warme, J. E., Douglas, R. G., and Winterer, E. L. (Eds.), *The Deep Sea Drilling Project: A Decade of Progress*. Soc. Econ. Paleontol. Mineral., Spec. Publ., 32:445-470.

Webb, P. N., 1972. Wright Fjord, Pliocene marine transgression of an Antarctic dry valley. *Antarct. J. U. S.*, 7:225-232.

________, 1973. Upper Cretaceous-Paleocene Foraminifera from Site 208 (Lord Howe Rise, Tasman Sea), DSDP Leg 21. *In* Burns, R. E., Andrews, J. E., et al., *Init. Repts. DSDP*, 21: Washington (U.S. Govt. Printing Office), 541-573.

________, 1974. Micropaleontology, paleoecology and correlation of the Pecten Gravels, Wright Valley, Antarctica, and description of *Trochoelphidiella onyxi* n. gen. n. sp. *J. Foram. Res.*, 4:184-199.

________, 1975. Paleocene Foraminifera from DSDP Site 283, south Tasman Basin. *In* Kennett, J. P., Houtz, R. E., et al., *Init. Repts. DSDP*, 29: Washington (U.S. Govt. Printing Office), 833-843.

________, 1982a. Climatic, paleoceanographic and tectonic interpretation of Paleogene-Neogene biostratigraphy from MSSTS-1 drillhole, McMurdo Sound, Antarctica (abstract). *In* Oliver, R. L., James, P. R., Jago, J. B. (Eds.), *Proc. Int. Symp. Antarct. Earth Sci., 4th, Adelaide, Australia, 1982*: (Australian National Academy of Sciences), p. 175.

________, 1982b. Review of Late Cretaceous-Cenozoic stratigraphy, tectonics, paleontology and climate in the Ross Sector (abstract). *In* Oliver, R. L., James, P. R., Jago, J. B. (Eds.), *Proc. Int. Symp. Antarct. Earth Sci., 4th, Adelaide, Australia, 1982*: (Australian National Academy of Sciences), p. 174.

Webb, P. N., Harwood, D. M., McKelvey, B. C., Mercer, J. H., and Stott, L. D., 1984. Cenozoic marine sedimentation and ice-volume variation on the east Antarctic craton. *Geology*, 12:287-291.

Webb, P. N., Leckie, R. M., and Ward, B. L., 1982. Cenozoic foraminiferal biostratigraphy of MSSTS-1 drillhole, McMurdo Sound, Antarctica. *Geol. Soc. Am. Abstr. Progr.*, 14:643.

________, in press. Late Oligocene foraminifera from MSSTS-1 drillhole, McMurdo Sound, Antarctica. *Bull. N.Z. Dept. Indust. Sci. Res., Misc. Ser.*

Webb, P. N., and Wrenn, J. H., 1982. Late Cenozoic micropaleontology and biostratigraphy of eastern Taylor Valley, Antarctica. *In* Craddock, C., (Ed.), *SCAR Symposium on Geology and Solid-Earth Geophysics, 1977*: Madison (University of Wisconsin Press), pp. 1117-1122.

White, M. P., 1928. Some index Foraminifera of the Tempico Embayment area of Mexico. *J. Paleontol.*, 2:197-198.

Date of Initial Receipt: 18 July 1984
Date of Acceptance: 7 December 1984

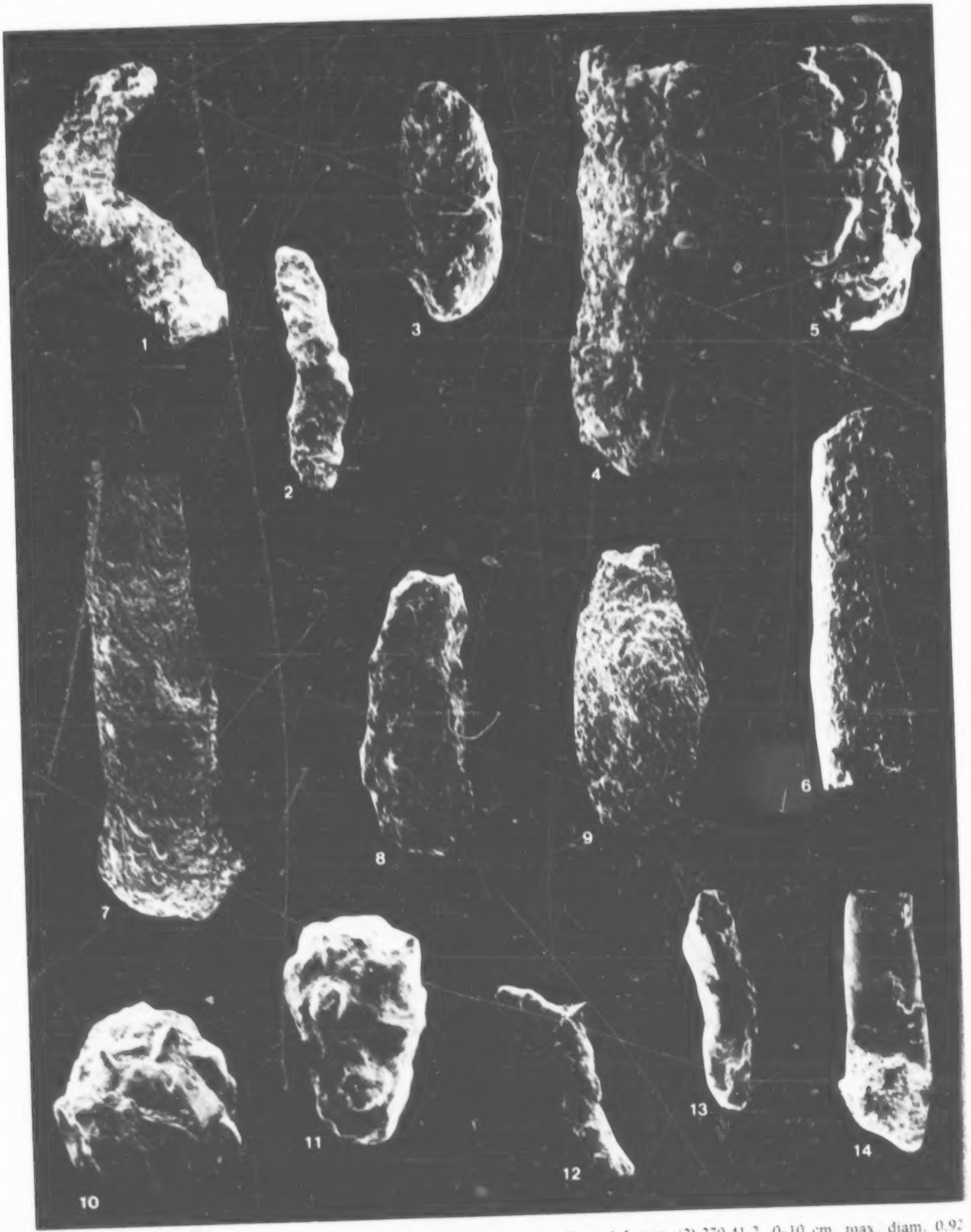

Plate 1. **1-2.** *Bathysiphon* aff. *B. cylindrica*, (1) 270-15-3, 97-110 cm, max. diam. 1.5 mm; (2) 270-41-2, 0-10 cm, max. diam. 0.92 mm
3. *Bathysiphon* cf. *B. alba*, 270-42-3, 19-29 cm, max. diam. 0.79 mm. **4.** *Bathysiphon discreta*, 270-42-3, 94-107 cm, max. diam. 2.9 mm
5. *Bathysiphon* sp. 1, 270-42-3, 94-107 cm, max. diam. 2.1 mm. **6.** *Bathysiphon* sp. 2, 270-42-2, 131-141 cm, max. diam. 2.8 mm. **7.** *I. pe*
ammina cylindrica, 270-15-3, 97-110 cm, max. diam. 3.2 mm. **8.** *Astrorhiza* cf. *A. granulosa*, 270-42-3, 19-29 cm, max. diam. 1.07 mm
Rhabdammina linearis, 270-20-6, 85-95 cm, max. diam. 1.78 mm. **10.** *Psammosphaera fusca*, 270-42-3, 94-107 cm, max. diam. 1.05 mm
11. *Jaculella* cf. *J. acuta*, 270-36-6, 115-123 cm, max. diam. 1.0 mm. **12.** *Rhizammina algaeformis*, 270-42-2, 131-141 cm, max.
1.22 mm. 13. *Marsipella* sp., 270-36-6, 115-123 cm, max. diam. 0.85 mm. **14.** *Protobotellina cylindrica*, 270-42-3, 94-107 cm, max.
1.8 mm.

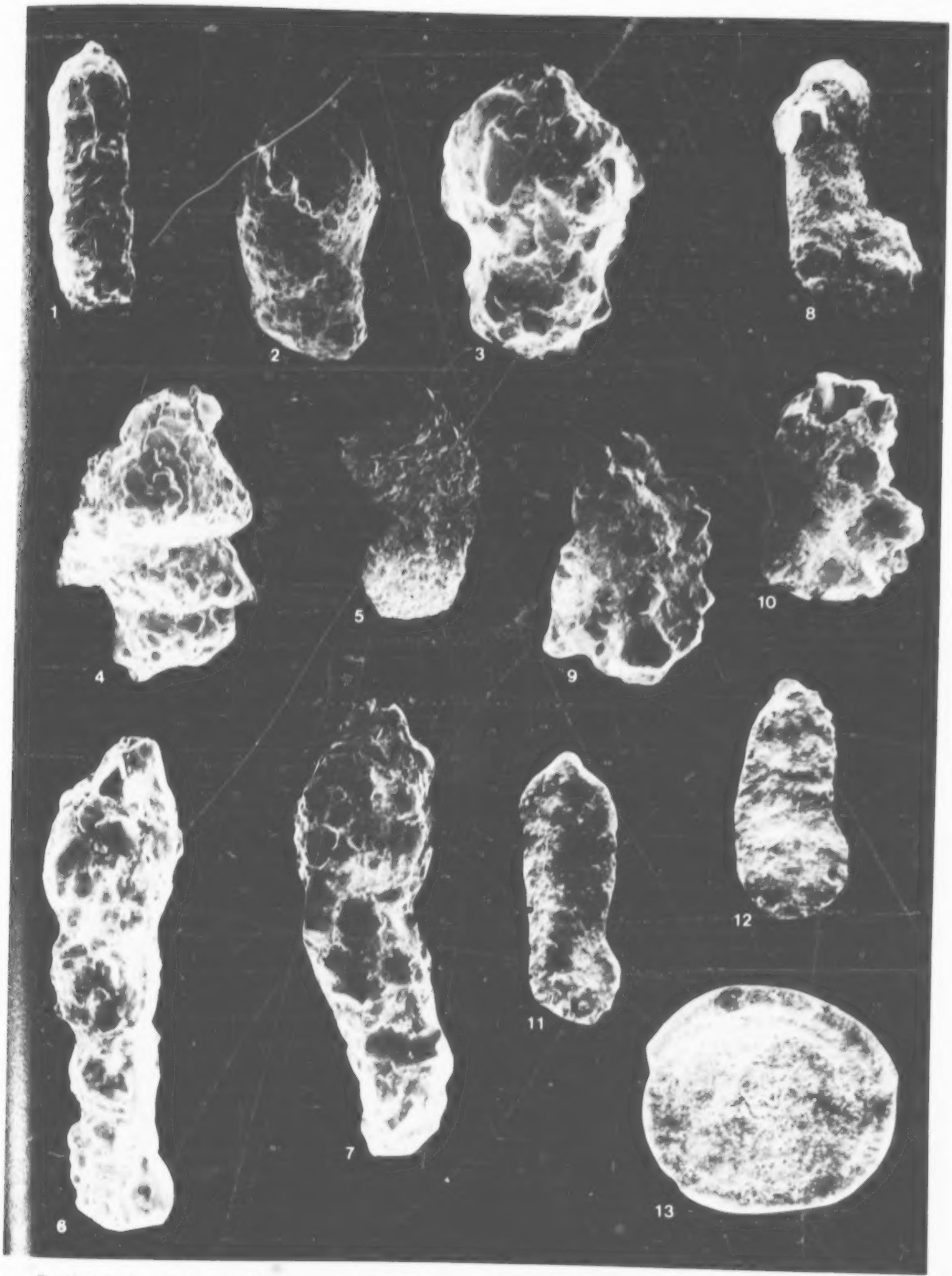

Plate 2. [illegible] *Reophax* sp. 1, 270-42-2, 131-141 cm, max. diam. 1.05 mm. **2.** ***Arenodosaria antipoda***, 270-20-6, 85-95 cm, max. diam. 1.36 mm. **3.** ***Re[illegible]ax*** sp. 2, 270-15-3, 50-57 cm, max. diam. 1.0 mm. **4.** ***Reophax*** sp. 2, 270-15-3, 97-110 cm, max. diam. 1.9 mm. **5.** ***Reophax*** cf. ***R. cushn[illegible]i***, 270-20-6, 85-95 cm, max. diam. 1.8 mm. **6.** ***Reophax*** cf. ***R. nodulosus***, 270-40-5, 70-79 cm, max. diam. 1.8 mm. **7.** ***Reophax scorpiuru[illegible]*** [illegible]70-42-3, 94-107 cm, max. diam. 1.62 mm. **8.** ***Ammobaculites*** cf. ***A. coprolithiformis***, 270-19-5, 113-122 cm, max. diam. 2.3 mm. **9-10.** ***[illegible]nmobaculites*** cf. ***A. expansus***, (9) 270-15-3, 50-57 cm, max. diam. 0.80 mm; (10) 270-15-3, 97-110 cm, max. diam. 0.70 mm. **11-12.** ***A[illegible]noscalaria pseudospiralis***, 270-43-6, 65-79 cm, (11) max. diam. 1.18 mm; (12) max. diam. 1.43 mm. **13.** ***Ammodiscus*** cf. ***A. glabratus***, 270-18[illegible], 129-139 cm, max. diam. 0.30 mm.

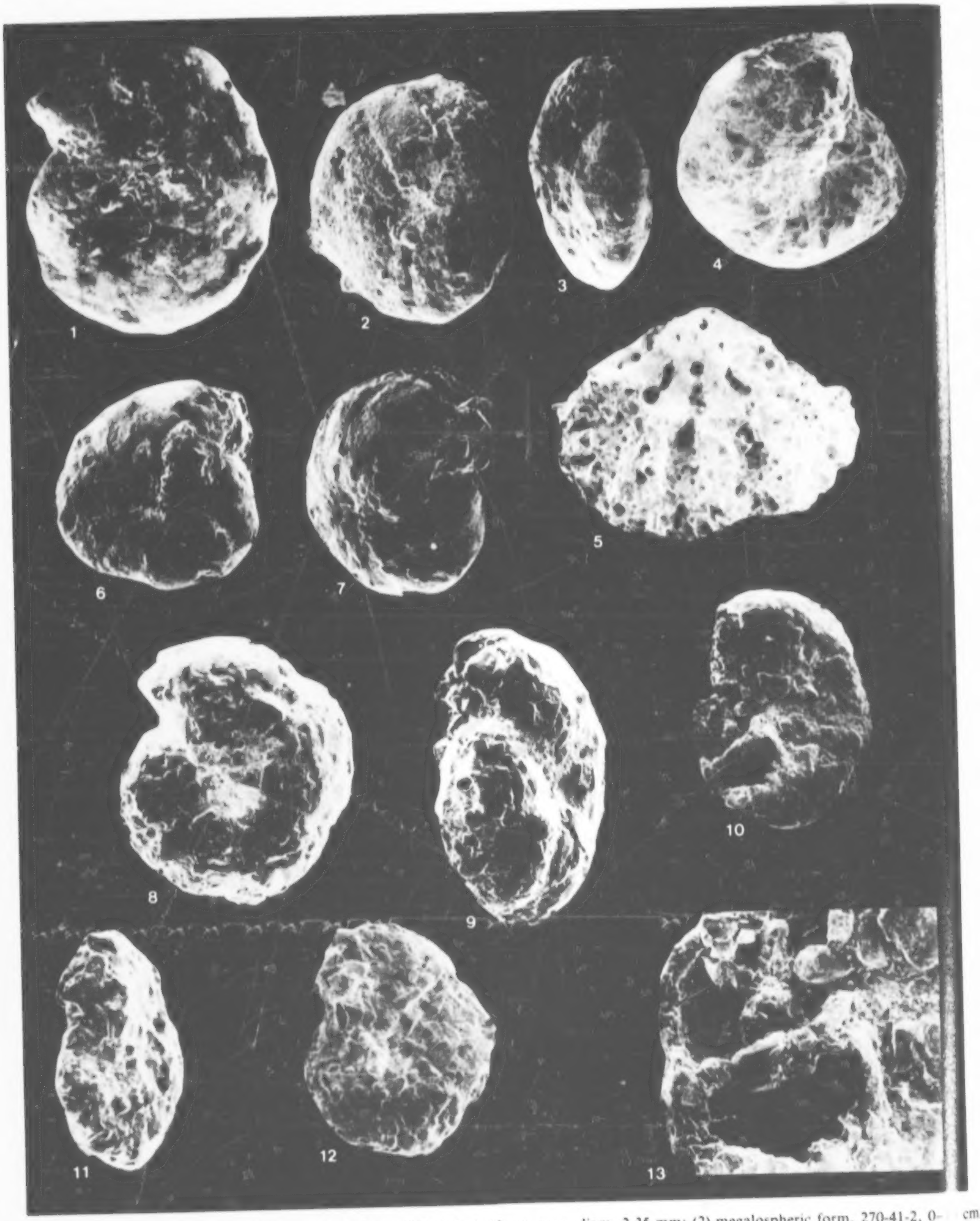

Plate 3. **1-5.** *Cyclammina incisa*, (1) microspheric form, 270-41-2, 0-10 cm, max. diam. 2.35 mm; (2) megalospheric form, 270-41-2, 0- cm
max. diam. 0.75 mm; (3) same specimen, oblique apertural view; (4) microspheric form, 270-15-3, 97-110 cm, max. diam. 1.60 mm; (5) i rna
view of broken specimen, 270-18-5, 129-139 cm. **6-7.** *Cyclammina rotundata*, (6) 270-41-3, 134-142 cm, max. diam. 1.15 mm; (7) same peci
men, oblique apertural view. **8-13.** *Haplophragmoides* sp., (8) 270-15-3, 50-57 cm, max. diam. 1.0 mm; (9) same specimen, oblique ap tura
view; (10) 270-17-5, 130-140 cm, max. diam. 0.80 mm; (11) oblique apertural view, 270-17-5, 130-140 cm, max. diam. 0.60 mm; (12) same peci
men, side view; (13) closeup of broken chambers.

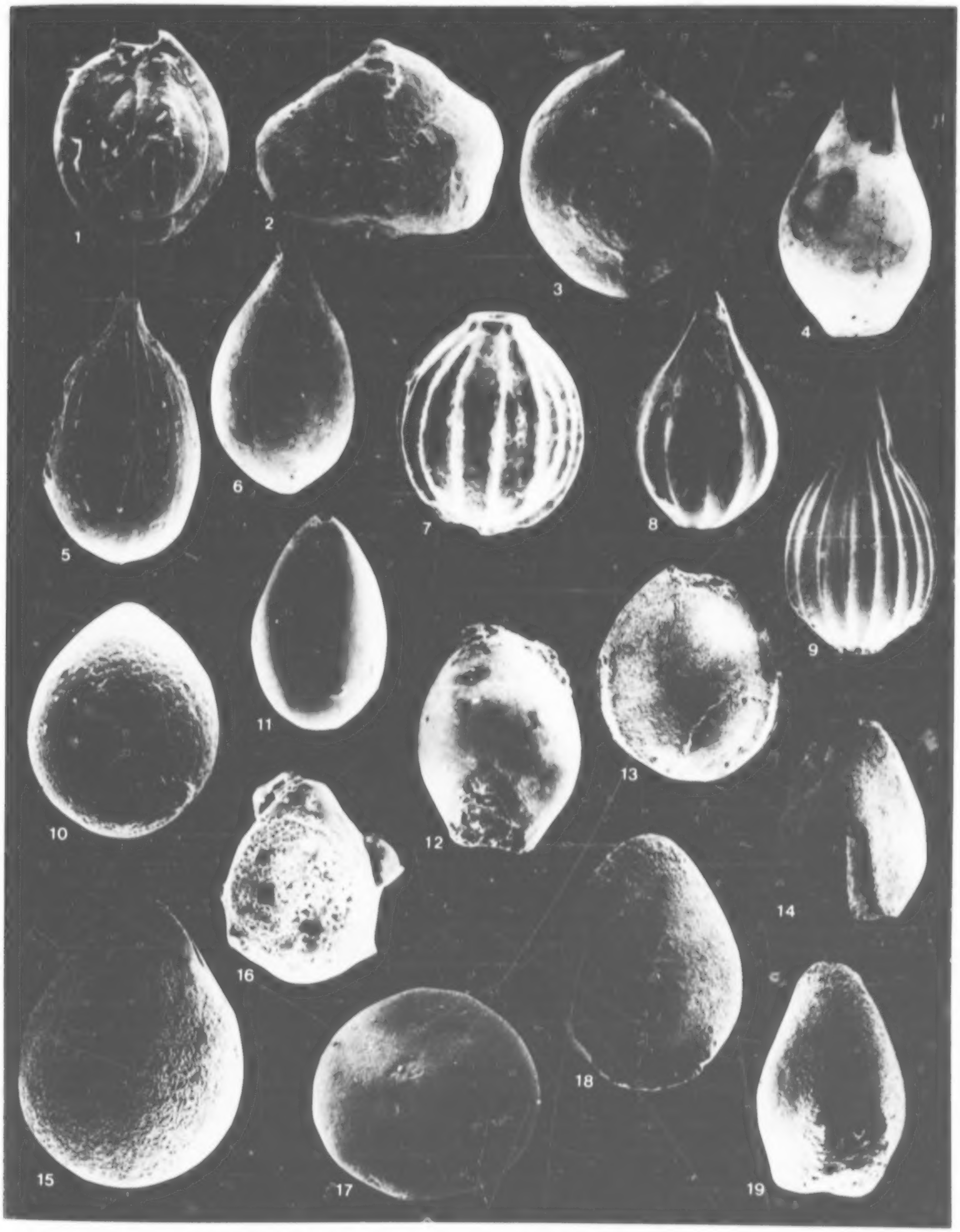

4 **1-2.** *Quinqueloculina seminula*, (1) 270-22-6, 135-145 cm, max. diam. 0.23 mm; (2) same specimen, apertural view. **3.** *Quinqueloculina nqularis*, 270-23-4, 72-82 cm, max. diam. 0.40 mm. **4.** *Nodosaria* sp. 1, 270-19-5, 113-122 cm, max. diam. 0.83 mm. **5.** *Lagena striata*, 0-22-6, 135-145 cm, max. diam. 0.32 mm. **6.** *Lagena laevis*, 270-17,CC, max. diam. 0.50 mm. **7.** *Lagena sulcata*, 270-3,CC, max, diam. 11 mm. **8-9.** *Oolina apiopleura*, (8) 270-22-6, 135-145 cm, max. diam. 0.24 mm; (9) 270-19-5, 113-122 cm, max. diam. 0.38 mm. **10.** *olina globosa*, 270-13,CC, max. diam. 0.15 mm. **11.** *Oolina apiculata*, 270-22-6, 135-145 cm, max. diam. 0.24 mm. **12.** *Fissurina danica*, ge view, 270-19-5, 113-122 cm, max. diam. 0.32 mm. **13-14.** *Fissurina bisulcata*, (13) 270-37-4, 133-142 cm, max. diam. 0.35 mm; (14) edge w, same specimen. **15.** *Fissurina annectens*, 270-32-3, 114-123 cm, max. diam. 0.30 mm. **16.** *Fissurina kerguelenensis*, 270-3,CC, max. am. 0.12 mm. **17.** *Fissurina* sp. 1, 270-29-6, 8-18 cm, max. diam. 0.23 mm. **18-19.** *Fissurina fimbriata*, (18) 270-13-3, 114-125 cm, max. am. 0.23 mm; (19) edge view, same specimen.

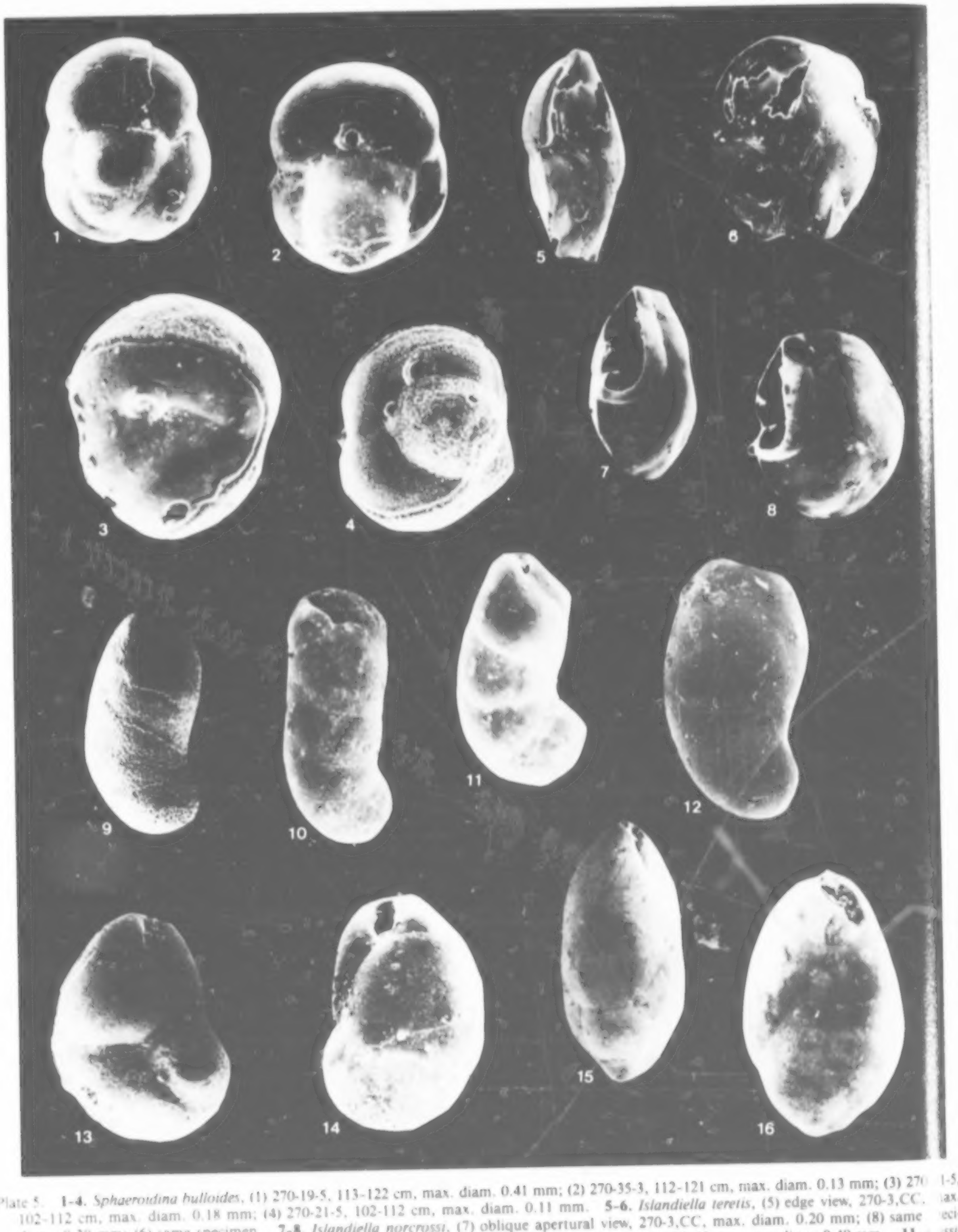

Plate 5. **1-4.** *Sphaeroidina bulloides*, (1) 270-19-5, 113-122 cm, max. diam. 0.41 mm; (2) 270-35-3, 112-121 cm, max. diam. 0.13 mm; (3) 270 1-5, 102-112 cm, max. diam. 0.18 mm; (4) 270-21-5, 102-112 cm, max. diam. 0.11 mm. **5-6.** *Islandiella teretis*, (5) edge view, 270-3,CC, ax. diam. 0.30 mm; (6) same specimen. **7-8.** *Islandiella norcrossi*, (7) oblique apertural view, 270-3,CC, max. diam. 0.20 mm; (8) same eci- men. **9-10.** *Cassidulinoides bradyi*, (9) 270-31-3, 59-67 cm, max. diam. 0.50 mm; (10) 270-23-4, 72-82 cm, max. diam. 0.49 mm. **11.** ssi- *dulinoides* cf. *C. parkerianus*, 270-23-4, 72-82 cm, max. diam. 0.70 mm. **12.** *Cassidulinoides* cf. *C. chapmanni*, 270-33-3, 102-112 cm. ax diam. 0.57 mm. **13-14.** *Cassidulinoides braziliensis*, (13) 270-34-3, 28-38 cm, max. diam. 0.37 mm; (14) 270-32,CC, max. diam. 0.5 im **15-16.** *Globobulimina* sp., (15) 270-19-5, 113-122 cm, max. diam. 1.05 mm; (16) 270-19-6, 113-122 cm, max. diam. 0.92 mm.

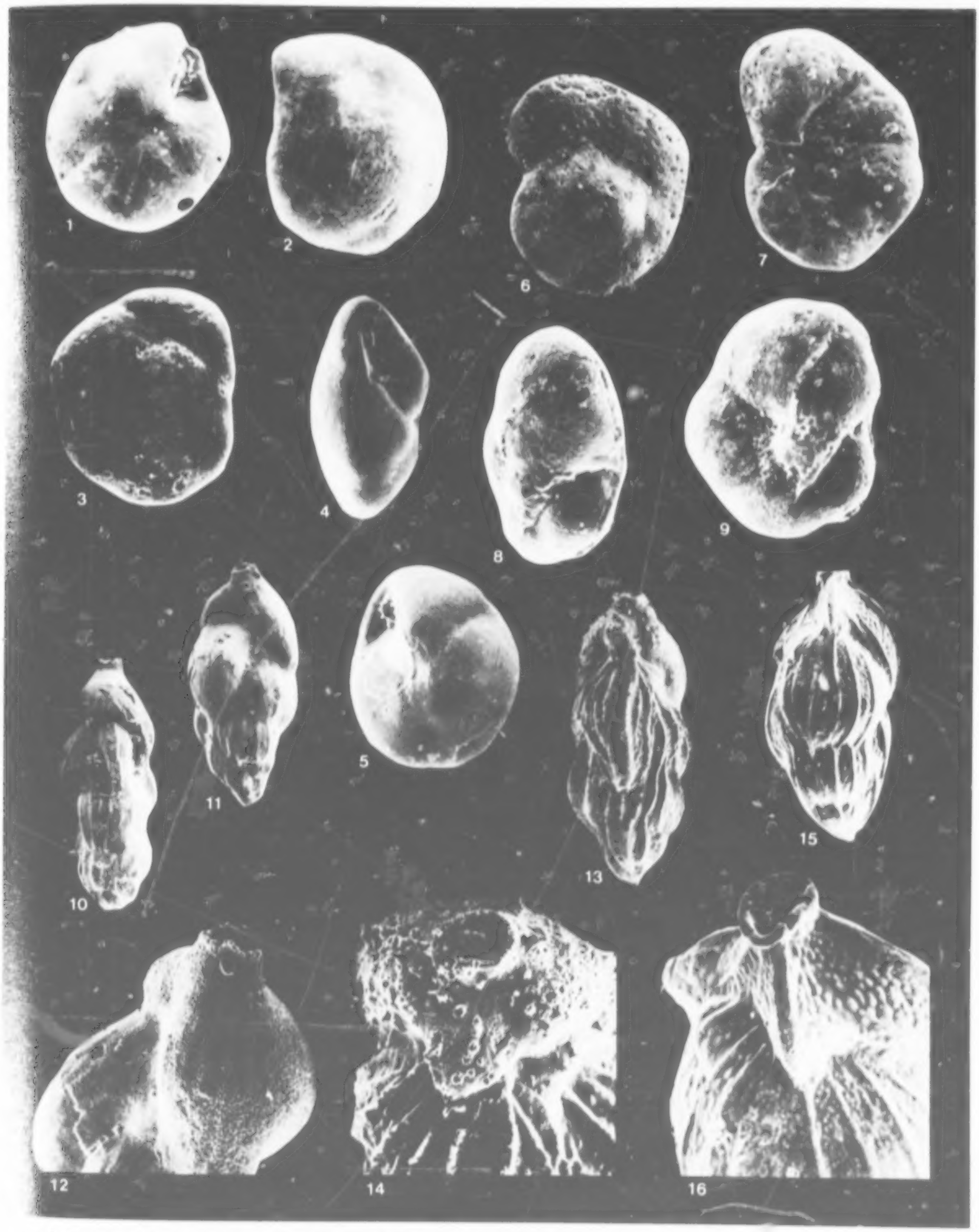

P 1-5. *Epistominella vitrea*, (1) umbilical side, 270-3,CC, max. diam. 0.13 mm; (2) spiral side, 270-3,CC, max. diam. 0.13 mm; (3) spiral 70-12-3, (top of section), max. diam. 0.16 mm; (4) apertural view, same specimen; (5) umbilical side, 270-12-1 (top of section), max. diam. m. **6-7.** *Rosalina globularis*, (6) spiral side, 270-34-3, 28-38 cm, max. diam. 0.37 mm; (7) umbilical side, 270-34,CC, max. diam. m. **8-9.** *Cancris laevinflatus*, (8) oblique apertural view, 270-21-5, 102-112 cm, max. diam. 0.18 mm; (9) umbilical side, same speci- **10-12.** *Trifarina* aff. *T. fueguina*, (10) 270-15-3, 97-110 cm, max. diam. 0.42 mm; (11) 270-15-3, 97-110 cm, max. diam. 0.41 mm; (12) te, same specimen. **13-14.** *Trifarina pauperata*, (13) 270-1-2, 52-54 cm, max. diam. 0.54 mm; (14) aperture, same specimen. **15-16.** *na earlandi*, (15) 270-3,CC, max. diam. 0.58 mm; (16) aperture, same specimen.

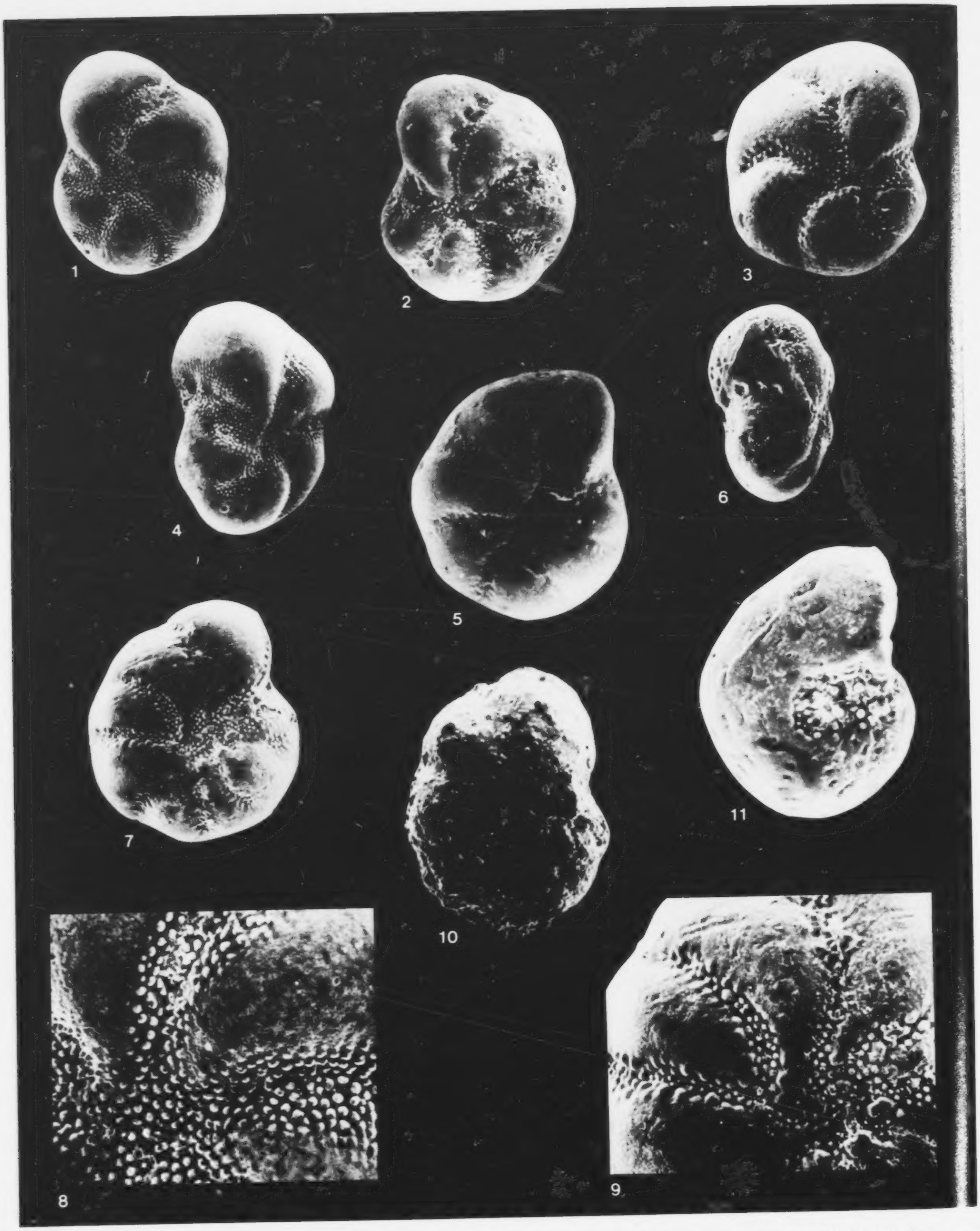

Plate 7. **1–4, 6, 8.** *Elphidium magellanicum*, (1) 270-15-3, 50–57 cm, max. diam. 0.33 mm; (4, 8) same specimen; (2) 270-8-3, 113–128 cm, ax. diam. 0.42 mm; (3) 270-8-3, 113–128 cm, max. diam. 0.25 mm; (6) edge view, 270-12-1 (top of section), max. diam. 0.30 mm. **5, 7, 9.** *Elp idium* cf. *E. magellanicum*, (5) 270-33-3, 102–110 cm, max. diam. 0.41 mm; (7) 270-8-3, 113–128 cm, max. diam. 0.37 mm; (9) same speci en. **10.** *Elphidium* sp., 270-43-6, 65–79 cm, max. diam. 0.40 mm. **11.** *Elphidium* cf. *E. nitidum*, 270-43-5, 18–31 cm, max. diam. 0.20 mm

READEX FICHE best copy available pages tightly bound

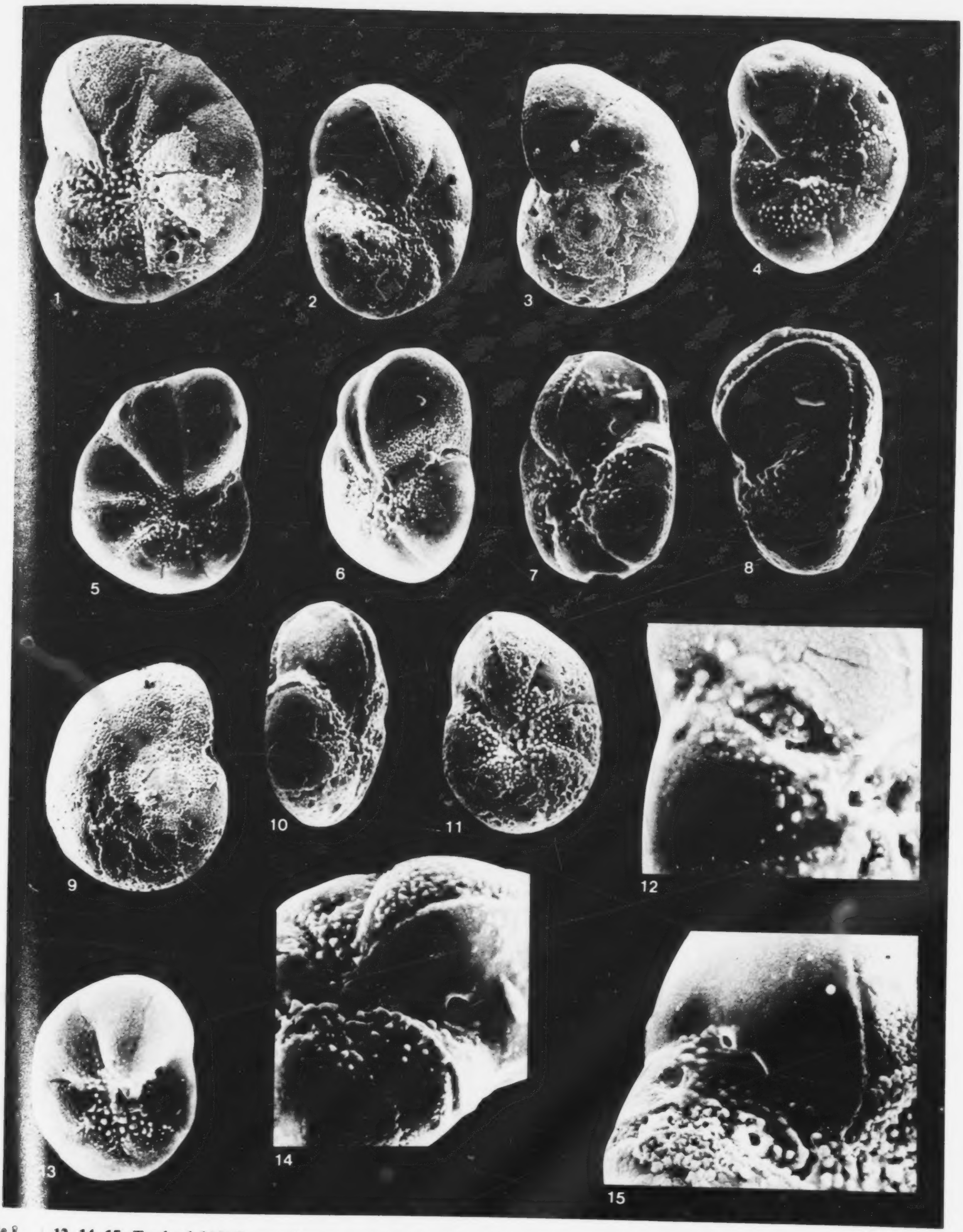

Plate 8 –**12, 14, 15.** ***Trochoelphidiella pustulosa*** n. sp., all megalospheric forms, (1) umbilical view, 270-31-3, 59–67 cm, max. diam. 0.30 mm; (2) s e specimen; (15) aperture, same specimen; (3) spiral view, 270-29-6, 8–18 cm, max. diam. 0.26 mm; (4) umbilical view, 270-32-3, 114–123 , max. diam. 0.24 mm; (12) aperture, same specimen; (5) umbilical view, 270-29-6, 8–18 cm, max. diam. 0.38 mm; (6) oblique apertural view, me specimen; (7) oblique edge view, 270-33-3, 102–110 cm, max. diam. 0.20 mm; (8) edge view, same specimen; (14) aperture, same specimen) spiral view, 270-29-6, 8–18 cm, max. diam. 0.25 mm; (10) edge view, same specimen; (11) umbilical view, same specimen. **13.** ***Buccella*** sp., bilical view, 270-29-6, 8–18 cm, max. diam. 0.18 mm.

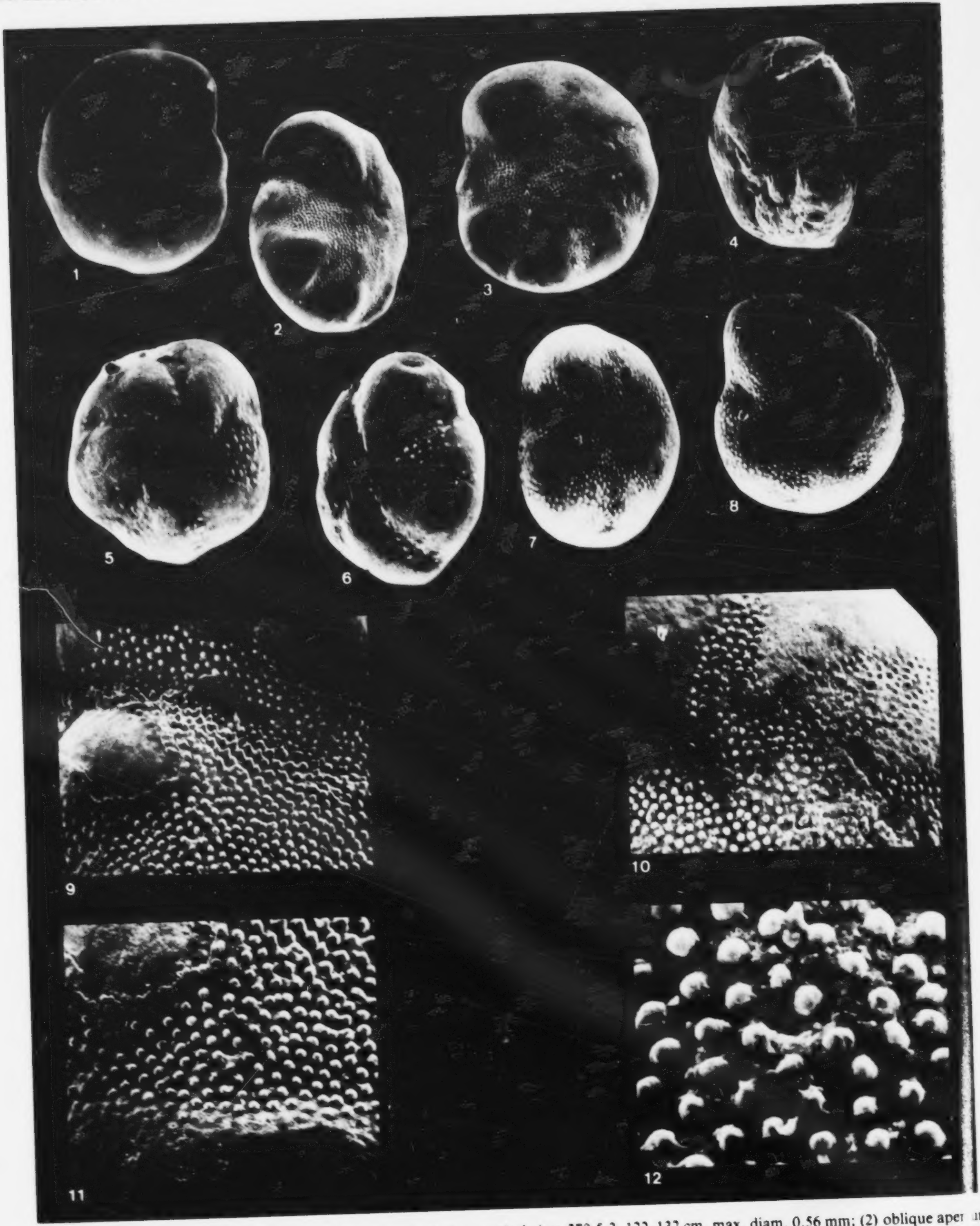

Plate 9. 1-12. *Trochoelphidiella uniforamina*, (1) microspheric form, spiral view, 270-5-2, 122–132 cm, max. diam. 0.56 mm; (2) oblique apertural view, same specimen; (3) umbilical view, same specimen; (9) aperture, same specimen; (10) sutural foramina, same specimen; (11) sutural foramina, same specimen; (12) sutural foramina, same specimen; (4) oblique edge view, 270-28-6 (bottom of section), max. diam. 0.25 mm; (5) megalospheric form, umbilical view, 270-15,CC, max. diam. 0.18 mm; (6) oblique apertural view, same specimen; (7) megalospheric form, oblique apertural view, 270-28-6 (bottom of section), max. diam. 0.23 mm; (8) umbilical view, same specimen.

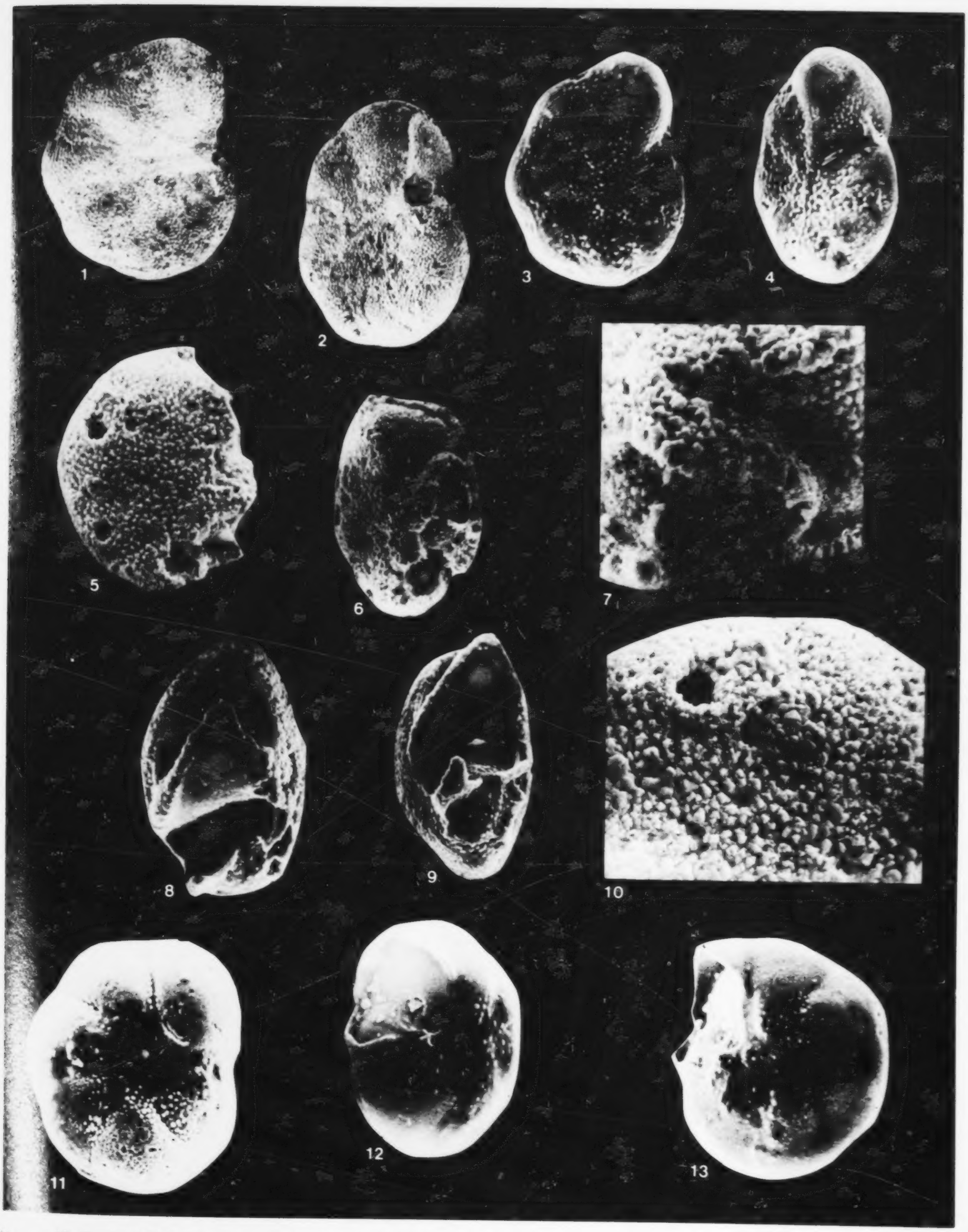

Plate [illegible]–10. *Trochoelphidiella* sp., (1) umbilical view, 270-37-4, 133–142 cm, max. diam. 0.62 mm; (2) oblique edge view, same specimen; (3) umbilical view 270-29-6, 8–18 cm, max. diam. 0.27 mm; (4) oblique apertural view, same specimen; (5) umbilical view, 270-8-3, 113–128 cm, max. diam. 0.15 mm; (6) edge view, same specimen; (7) remnant apertures, same specimen; (10) same specimen; (8) edge view, 270-6-1, 113–123 cm, width 0.14 mm; (9) edge view, same specimen. **11–13.** *Trochoelphidiella* aff. *T. uniforamina*, (11) umbilical view, 270-35,CC, max. diam. 0.22 mm; (12) oblique apertural view, 270-35-3, 112–121 cm, max. diam. 0.21 mm; (13) umbilical view, same specimen.

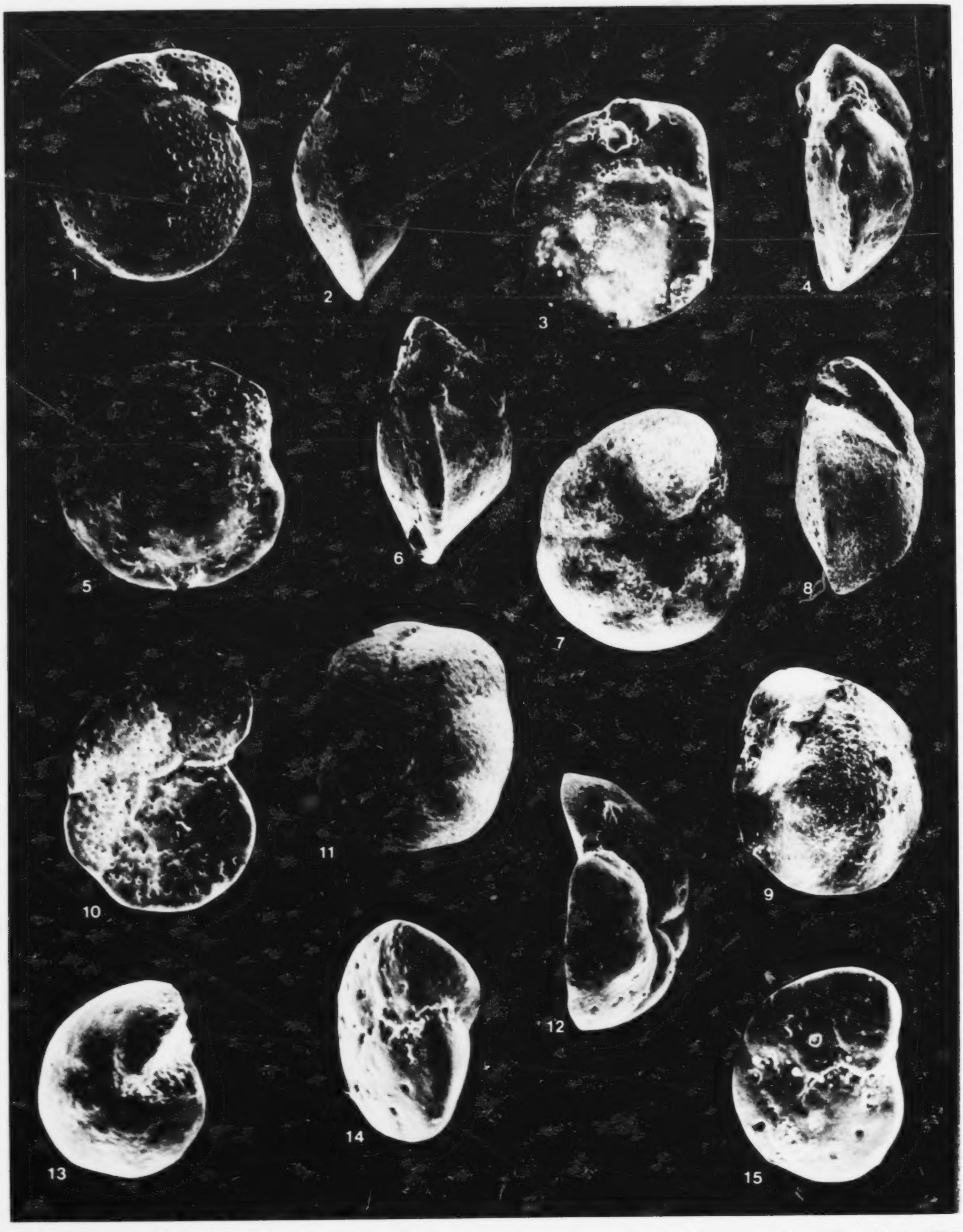

Plate 11. **1–9.** *Cibicides temperata*, (1) spiral side, 270-25-2, 50–60 cm, max. diam. 0.51 mm; (2) edge view, same specimen; (3) spiral side, 270-1[illegible]-5, 113–122 cm, max. diam. 0.56 mm; (4) edge view, same specimen; (5) spiral side, 270-19-5, 113–122 cm, max. diam. 0.46 mm; (6) edge view, same specimen; (7) umbilical view, 270-19-5, 113–122 cm, max. diam. 0.62 mm; (8) edge view, 270-14,CC, max. diam. 0.35 mm; (9) umbilical view, 270-19-5, 113–122 cm, max. diam. 0.40 mm. **10–12.** *Cibicides lobatulus*, (10) spiral side, 270-33-3, 102–110 cm, max. diam. 0.35 mm; (12) edge view, same specimen; (11) umbilical side, 270-13-3, 114–125 cm, max. diam. 0.38 mm. **13–15.** *Cibicides refulgens*, (13) umbilical side, 270-3,CC, max. diam. 0.15 mm; (14) oblique apertural view, 270-3,CC, max. diam. 0.14 mm; (15) spiral side, same specimen.

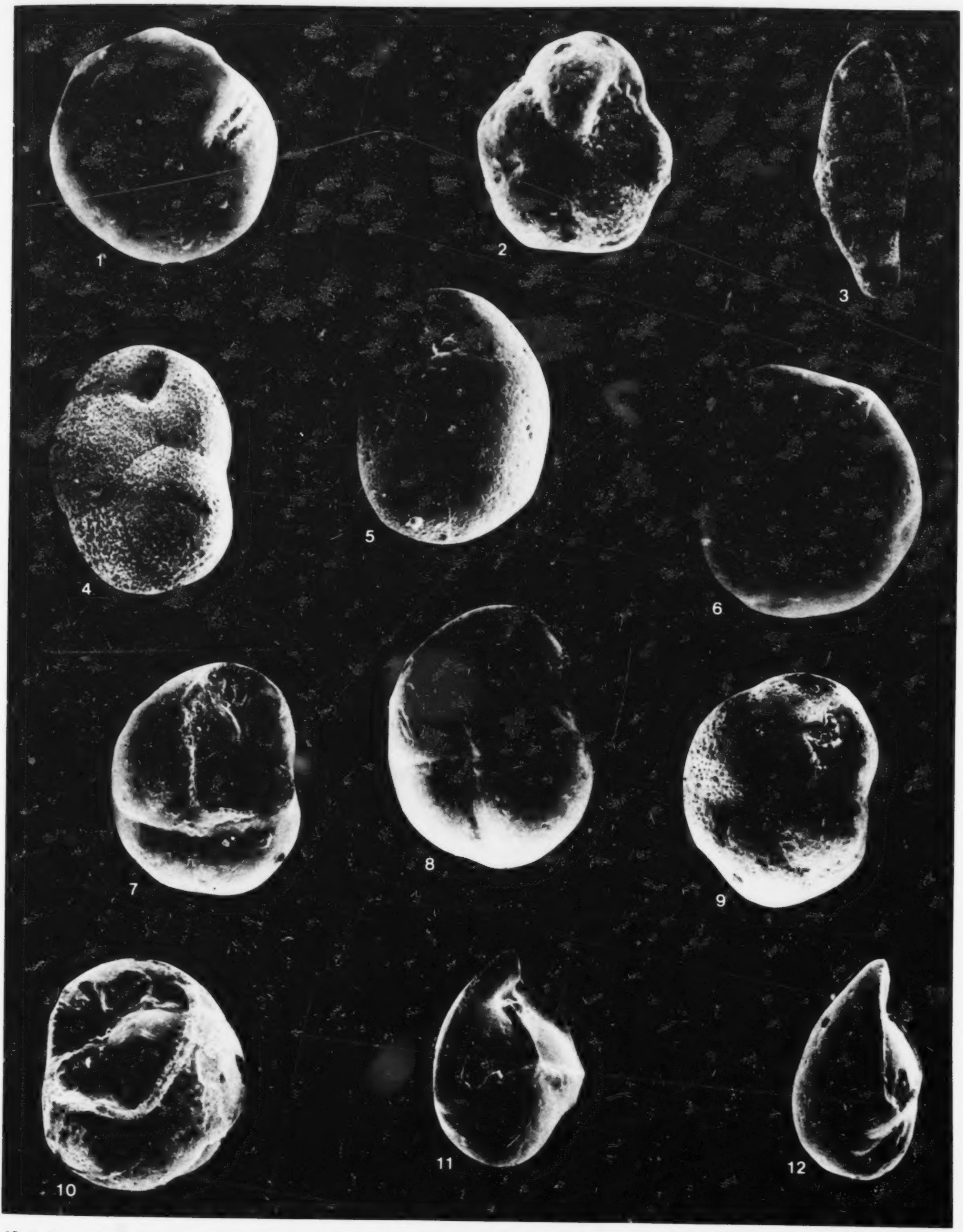

Plate 12. **1.** *Eponides* cf. *E. weddellensis*, umbilical side, 270-21-5, 102–112 cm, max. diam. 0.15 mm. **2.** *Eponides tumidulus*, umbilical side, 270-3,CC, max. diam. 0.11 mm. **3.** *Fursenkoina schreibersiana*, 270-40-5, (top of section), max. diam. 0.27 mm. **4–6.** *Globocassidulina subglobosa*, (4) 270-23-4, 72–82 cm, max. diam. 0.32 mm; (5) 270-23-4, 72–82 cm, max. diam. 0.20 mm; (6) 270-19-5, 113–122 cm, max. diam. 0.51 mm. **7–9.** *Globocassidulina crassa*, (7) 270-1-2, 52–54 cm, max. diam. 0.37 mm; (8) 270-28-6 (bottom of section), max. diam. 0.27 mm; (9) 270-1-2, 52–54 cm, max. diam. 0.40 mm. **10.** *Globocassidulina biora*, 270-3,CC, max. diam. 0.58 mm. **11–12.** *Ehrenbergina glabra*, (11) 270-3,CC, max. diam. 0.27 mm; (12) edge view, same specimen.

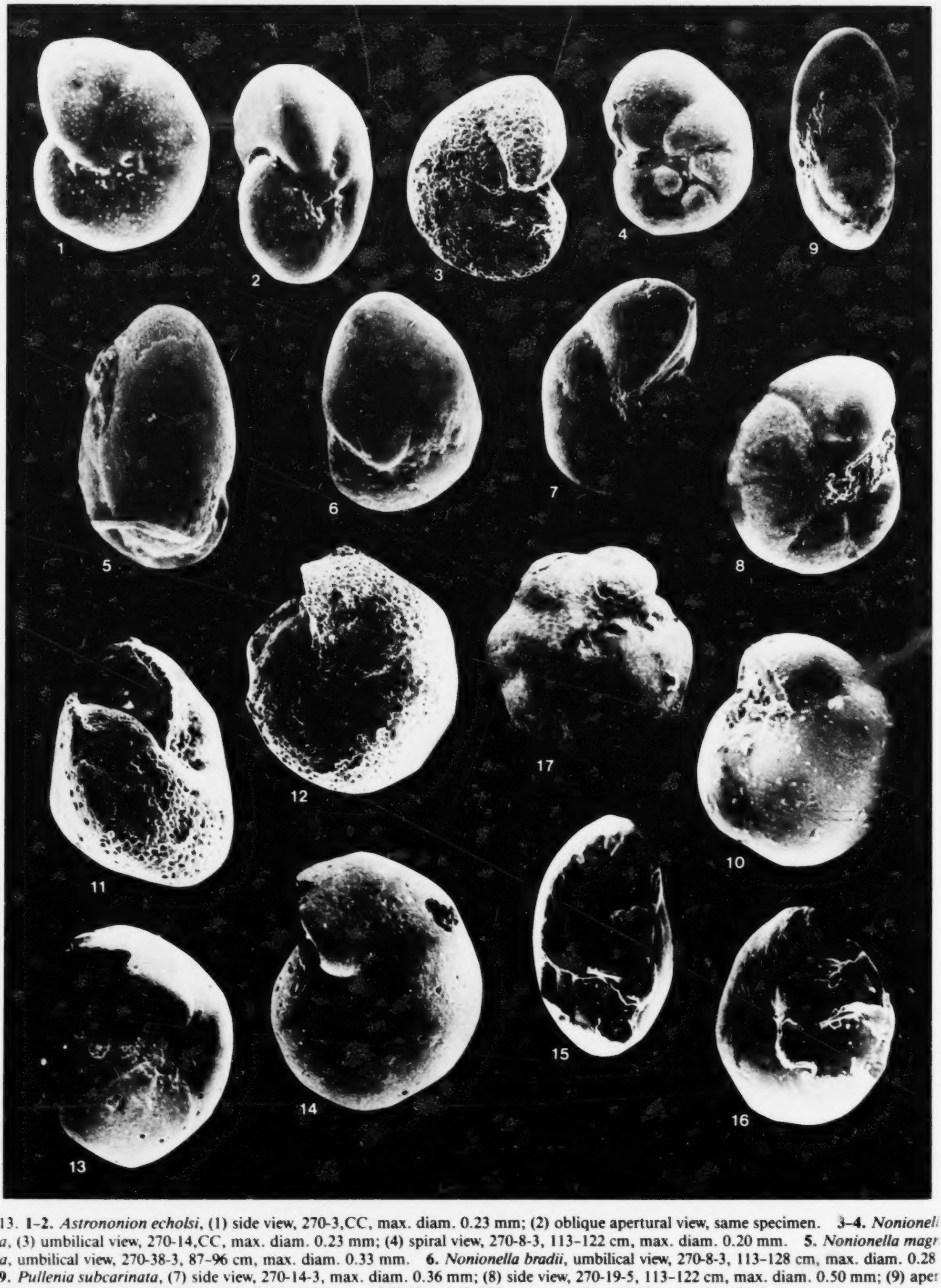

Plate 13. **1–2.** *Astrononion echolsi*, (1) side view, 270-3,CC, max. diam. 0.23 mm; (2) oblique apertural view, same specimen. **3–4.** *Nonionel* *iridea*, (3) umbilical view, 270-14,CC, max. diam. 0.23 mm; (4) spiral view, 270-8-3, 113–122 cm, max. diam. 0.20 mm. **5.** *Nonionella mag* *lingua*, umbilical view, 270-38-3, 87–96 cm, max. diam. 0.33 mm. **6.** *Nonionella bradii*, umbilical view, 270-8-3, 113–128 cm, max. diam. 0.28 m. **7–9.** *Pullenia subcarinata*, (7) side view, 270-14-3, max. diam. 0.36 mm; (8) side view, 270-19-5, 113–122 cm, max. diam. 0.50 mm; (9) ape ural view, same specimen. **10.** *Pullenia bulloides*, side view, 270-19-5, 113–122 cm, max. diam. 0.33 mm. **11–12.** *Gyroidina parva*, (11) ape ural view, 270-27-4, 108–118 cm, max. diam. 0.29 mm; (12) umbilical view, same specimen. **13–14.** *Gyroidina zelandica*, (13) oblique ape ural view, 270-19-5, 113–122 cm, max. diam. 0.42 mm; (14) umbilical view, same specimen. **15–16.** *Gyroidina* cf. *G. obicularis*, (15) apertural iew, 270-15-3, 97–110 cm, max. diam. 0.36 mm; (16) oblique umbilical view, same specimen. **17.** *Oridorsalis tenera*, umbilical view, 270-32 CC max. diam. 0.57 mm.

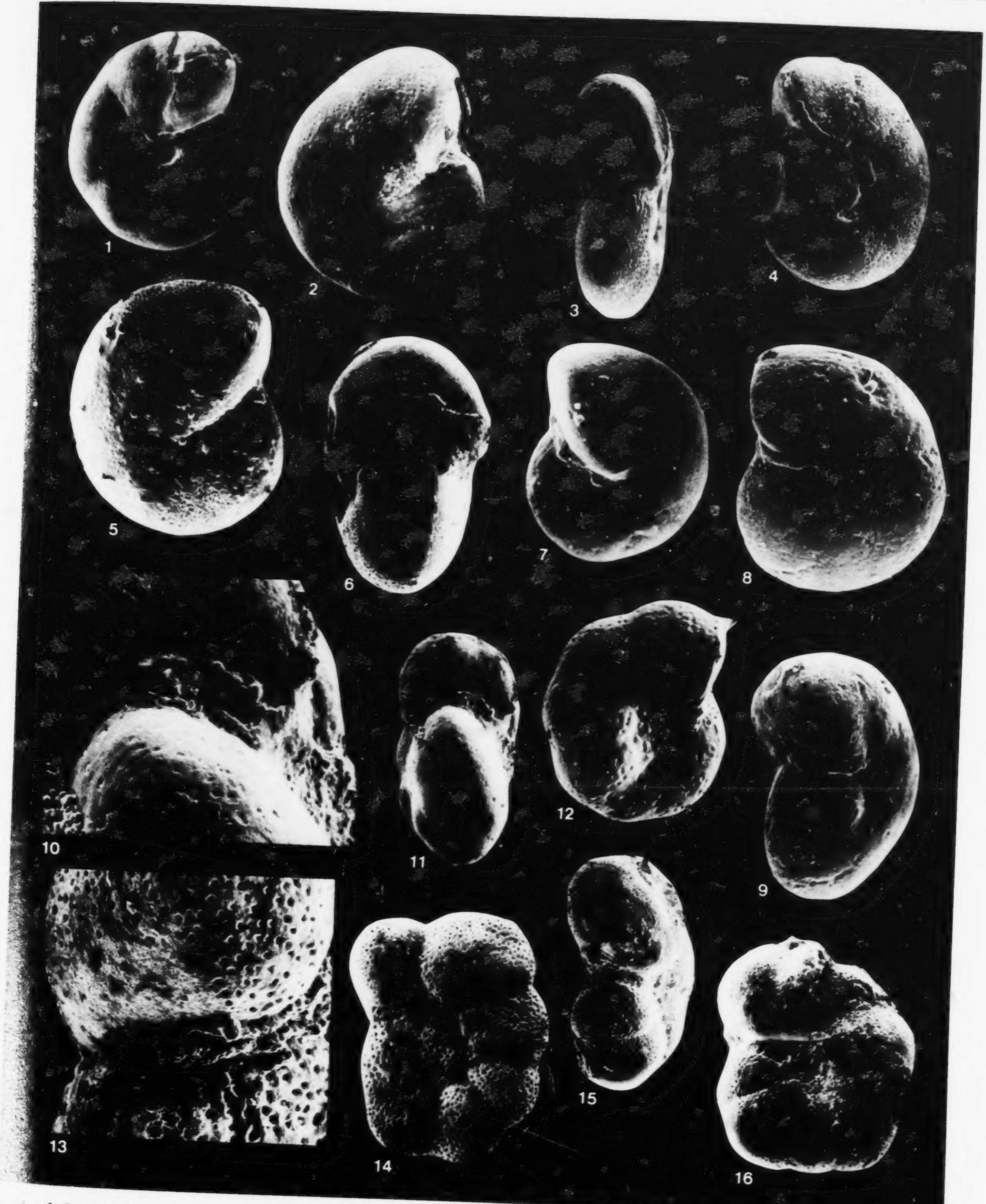

Plate 4. **1-4.** *Melonis barleeanus*, (1) 270-14-3, max. diam. 0.45 mm; (2) 270-12-1 (top of section), max. diam. 0.27 mm; (3) apertural view, 270- C, max. diam. 0.48 mm; (4) same specimen. **5-7.** *Melonis affinis*, (5) side view, 270-37-4, 133-142 cm, max. diam. 0.27 mm; (6) edge view, 270-37-4, 133-142 cm, max. diam. 0.43 mm; (7) 270-38,CC, max. diam. 0.27 mm. **8-9.** *Anomalinoides* cf. *A. macraglabra*, (8) spiral view, 270-40-3, 123-131 cm, max. diam. 0.37 mm; (9) oblique edge view, same specimen. **10-12.** *Anomalinoides pinguiglabra*, (10) aperture, 270-34-3, 28-38 cm, max. diam. 0.52 mm; (11) edge view, same specimen; (12) umbilical view, 270-34-3, 28-38 cm, max. diam. 0.52 mm. **13-16.** *Anomalinoides globulosa*, (13) aperture, 270-19-5, 113-122 cm, max. diam. 1.05 mm; (14) spiral view, same specimen; (15) edge view, 270-19-5, 113-122 cm, max. diam. 1.05 mm; (16) umbilical view, same specimen.

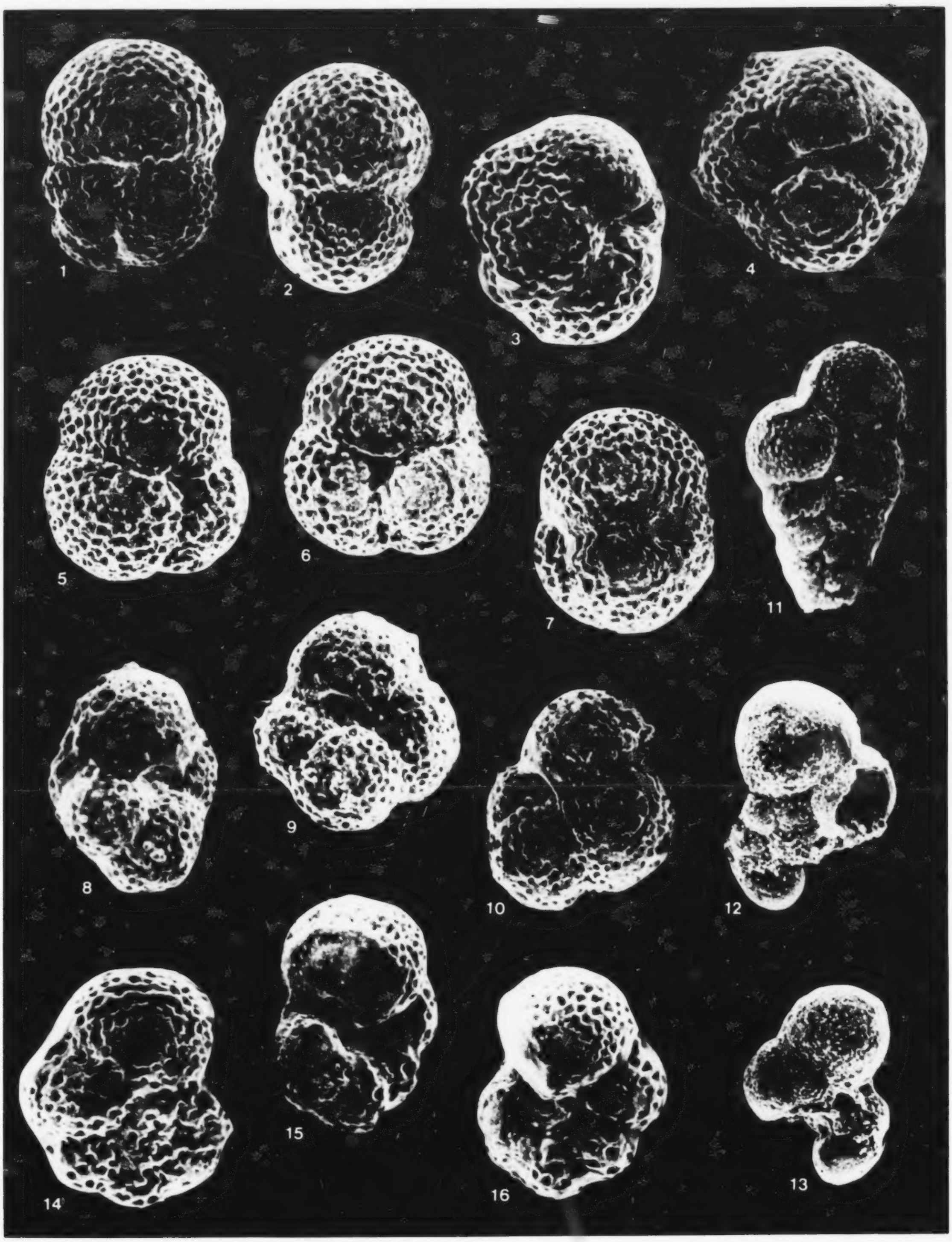

Plate 15. **1-2.** *Globigerinoides trilobus*, (1) 270-28,CC, max. diam. 0.40 mm; (2) side view, same specimen. **3-4.** *Globorotaloides* cf. *G. suteri*, (3) side view, 270-24,CC, max. diam. 0.18 mm; (4) umbilical view, same specimen. **5-7.** *Globigerina* cf. *G. angiporoides*, (5) side view, 270-15-3, 50-57 cm, max. diam. 0.23 mm; (6) umbilical view, same specimen; (7) side view, same specimen. **8-10.** *Globigerina* cf. *G. ouachitaensis*, (8) side view, 270-34-5, 59-61 cm, max. diam. 0.14 mm; (9) umbilical view, same specimen; (10) side view, same specimen. **11.** *Chiloguembelina cubensis*, 270-34,CC, max. diam. 0.15 mm. **12-13.** *Globorotalia* cf. *G. gemma*, (12) spiral view, 270-24,CC, max. diam. 0.12 mm; (13) umbilical view, same specimen. **14-16.** *Globorotalia* cf. *G. siakensis*, (14) spiral view, 270-39-6, 24-36 cm, max. diam. 0.17 mm; (15) edge view, same specimen; (16) umbilical view, same specimen.

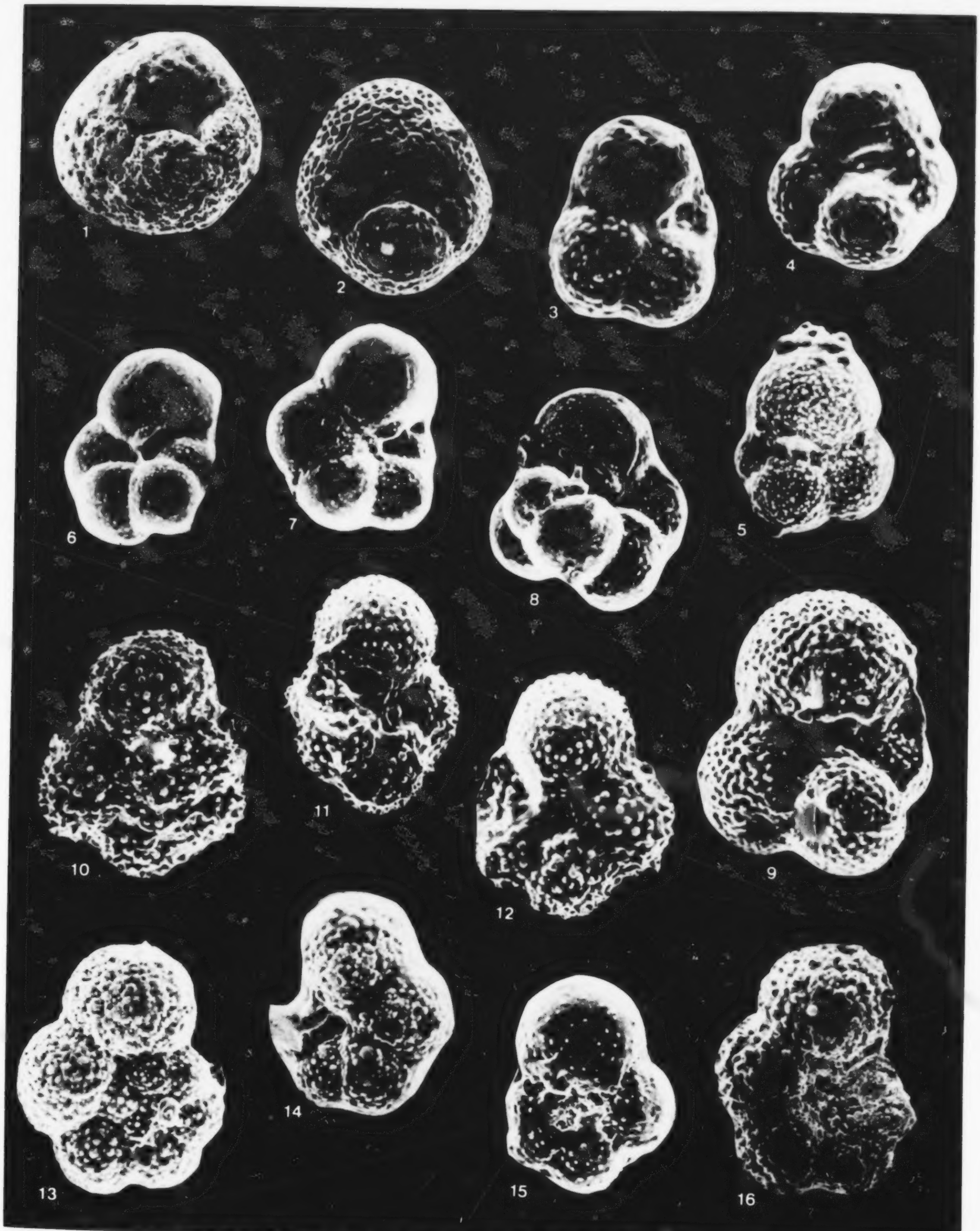

Plate 16. **1–2.** *Neogloboquadrina pachyderma*, (1) 270-1-2, 52–54 cm, max. diam. 0.20 mm; (2) 270-3,CC, max. diam. 0.31 m. **3–5.** *Globigerinita* cf. *G. glutinata*, (3) side view, 270-3,CC, max. diam. 0.13 mm; (4) umbilical view, same specimen; (5) umbilical view, 270-36-6, 115–123 cm, max. diam. 0.10 mm. **6–8.** *Globigerina megastoma*, (6) oblique apertural view, 270-3,CC, max. diam. 0.13 mm; (7) umbilical view, same specimen; (8) apertural view, 270-3,CC, max. diam. 0.13 mm. **9.** *Globigerina* sp., umbilical view, 270-3,CC, max. diam. 0.17 mm. **10–15.** *Globorotalia* sp., (10) spiral view, 270-3,CC, max. diam. 0.18 mm; (11) apertural view, same specimen; (12) umbilical view, same specimen; (13) spiral view, 270-1,CC, max. diam. 0.12 mm); (14) umbilical view, same specimen; (15) umbilical view, 270-3,CC, max. diam. 0.16 mm. **16.** *Globigerinelloides* cf. *G. volutus*, 270-19-5, 113–122 cm, max. diam. 0.15 mm.

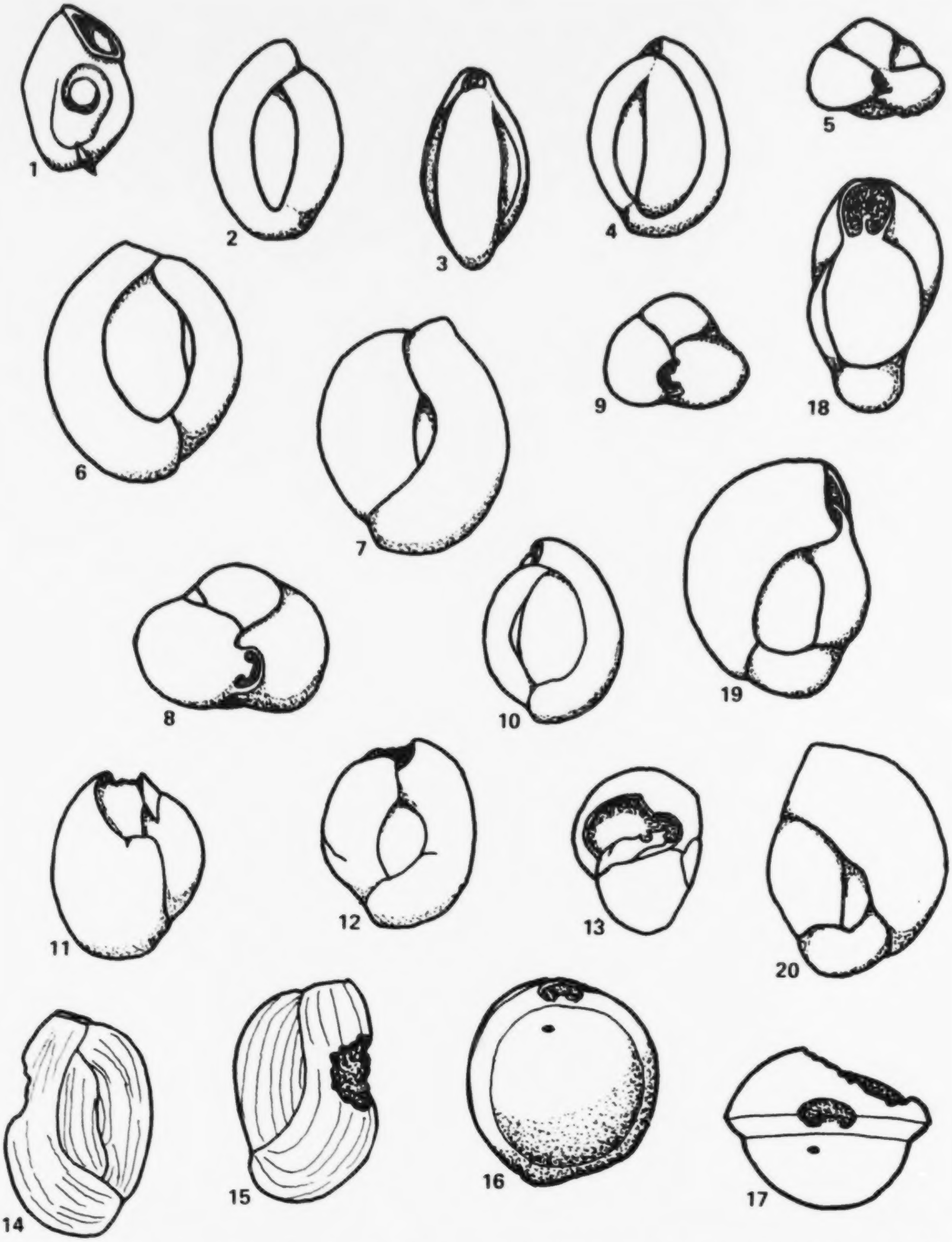

Plate 17. **1.** *Articulina* sp., 270-38-6, 114–124 cm, max. diam. 0.15 mm. **2–5.** ***Quinqueloculina seminula***, (2) 270-14,CC, max. diam. 0.43 mm; (3) edge view, same specimen; (4) same specimen; (5) apertural view, same specimen. **6–10.** ***Quinqueloculina triangularis***, (6) 270-23-4, 72–82 cm, max. diam. 0.54 mm; (7) same specimen; (8) apertural view, same specimen; (9) apertural view, 270-23-4, 72–82 cm, max. diam. 0.42 mm; (10) same specimen. **11–13.** *Triloculina rotundata*, (11) 270-33-3, 102–110 cm, max. diam. 0.68 mm; (12) same specimen; (13) apertural view, same specimen. **14–15.** *Triloculina* cf. *T. brongniartiana*, (14) 270-29-1, 3–5 cm, max. diam. 0.21 mm; (15) same specimen. **16–17.** *Pyrgo* cf. *P. vespertilio*, (16) 270-15-3, 97–110 cm, max. diam. 1.90 mm; (17) apertural view, same specimen. **18–20.** ***Flintina*** cf. *F. droogeri*, (18) 270-31-3, 59–67 cm, max. diam. 0.52 mm; (19) apertural view, same specimen; (20) same specimen.

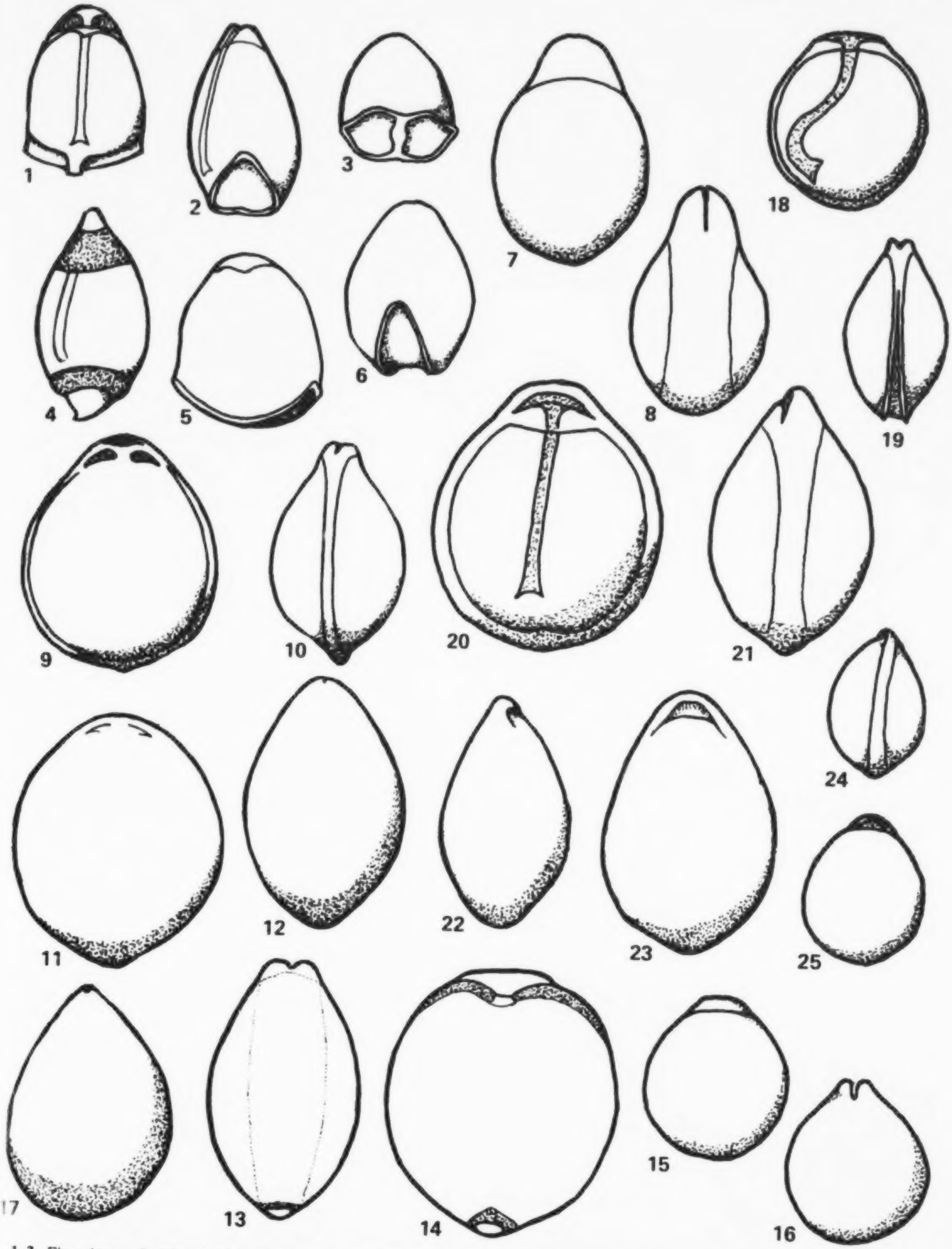

Pla **1-3.** *Fissurina* sp. 3, (1) 270-25-2, 50-60 cm, max. diam. 0.19 mm; (2) edge view, same specimen; (3) basal view, same specimen. **4.** *Fis-* sp. 4, 270-25-2, 50-60 cm, max. diam. 0.22 mm. **5-6.** *Fissurina danica*, (5) 270-15-3, 97-110 cm, max. diam. 0.17 mm; (6) edge view, specimen. **7-8.** *Fissurina lucida*, (7) 270-40-3, 123-131 cm, max. diam. 0.21 mm; (8) edge view, same specimen. **9-10.** *Fissurina marginata*, (9) 270-19-5, 113-122 cm, max. diam. 0.25 mm; (10) edge view, same specimen. **11-12**. *Fissurina laevigata*, (11) 270-19-5, 113-122 cm, max. diam. 0.27 mm; (12) edge view, same specimen. **13-14.** *Fissurina* sp. 2, (13) edge view, 270-27-4, 108-118 cm, max. diam. 0.25 mm; (14) same specimen. **15-16.** *Fissurina agassizi*, (15) 270-38,CC, max. diam. 0.36 mm; (16) side view, same specimen. **17.** *Oolina globosa*, 270-19-5, 113-122 cm, max. diam. 0.24 mm. **18-19.** *Parafissurina* cf. *P. tasmanica*, (18) 270-8-3, 113-128 cm, max. diam. 0.16 mm; (19) edge view, same specimen. **20-21.** *Parafissurina subcarinata*, (20) 270-8-3, 113-128 cm, max. diam. 0.24 mm; (21) edge view, same specimen. **22-23.** *Parafissurina lateralis*, (22) edge view, 270-19-5, 113-122 cm, max. diam. 0.24 mm; (23) same specimen. **24-25.** *Parafissurina curta*, (24) edge view, 270-28-6 (bottom of section), max. diam. 0.34 mm; (25) same specimen.

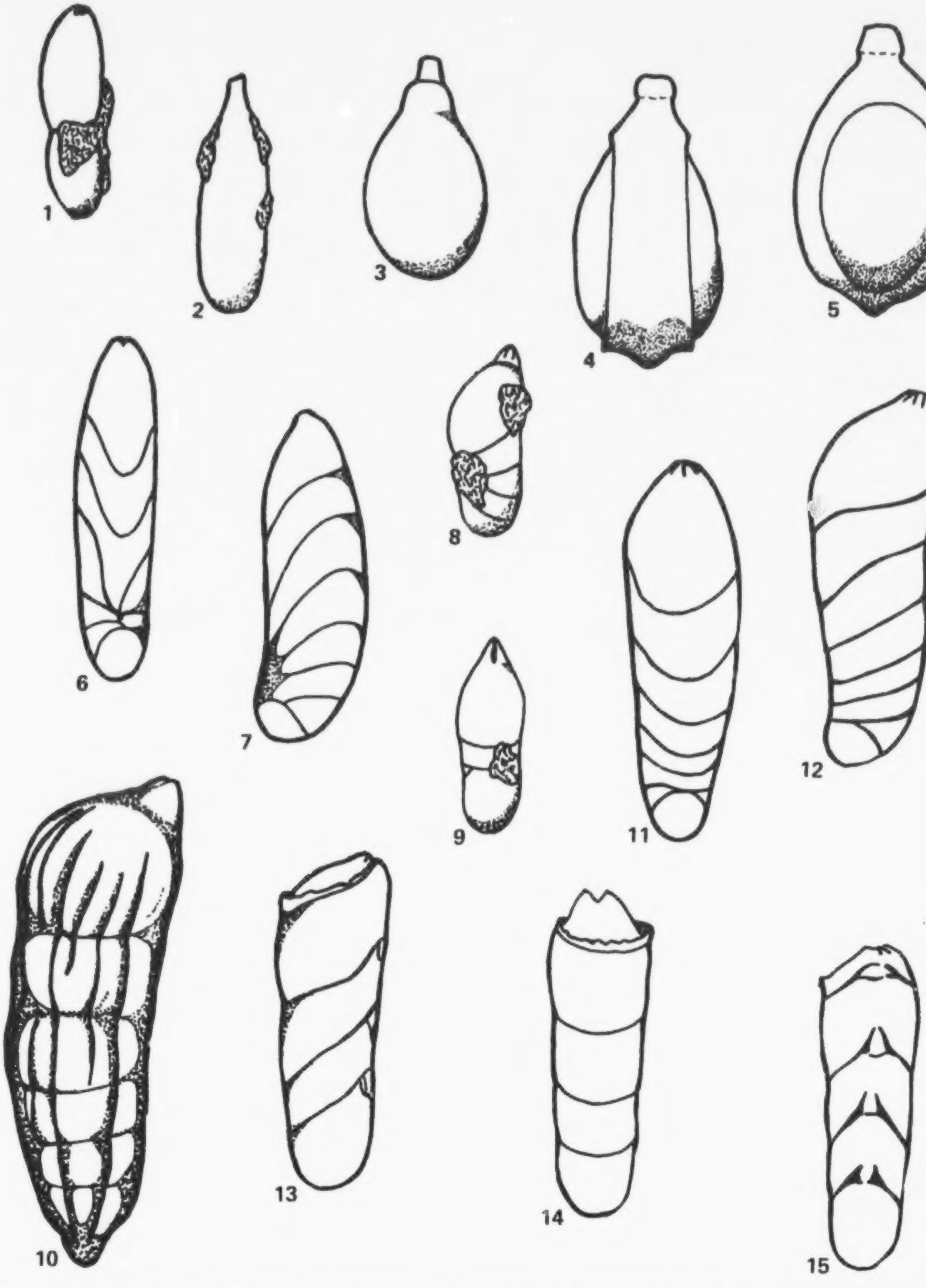

Plate 19. **1.** *Nodosaria calomorpha*, 270-34-3, 28–38 cm (max. diam. 0.45 mm). **2.** *Lagena nebulosa*, 270-9,CC, max. diam. 0.50 mm. **3.** *Lagena* cf. *L. laevigata*, 270-15-3, 97–110 cm, max. diam. 0.23 mm. **4–5.** *Lagena sequenziana*, (4) edge view, 270-19-5, 113–122 cm, max. diam. 0.32 mm; (5) same specimen. **6–7.** *Astacolus crepidulus*, (6) edge view, 270-27-4, 108–118 cm, max. diam. 0.85 mm; (7) same specimen **8–9.** *Marginulina tumida*, (8) 270-19-5, 113–122 cm, max. diam. 0.42 mm; (9) edge view, same specimen. **10.** *Marginulina* cf. *M. cocoaensis*, 270-15-3, 97–110 cm, max. diam. 1.07 mm. **11–12.** *Vaginulina awamoana*, (11) edge view, 270-19-5, 113–122 cm, max. diam. 1.27 mm; (12) same specimen. **13–15.** *Dentalina* cf. *D. advena*, (13) 270-16-4, 123–135 cm, max. diam. 0.67 mm; (14) same specimen; (15) same specimen.

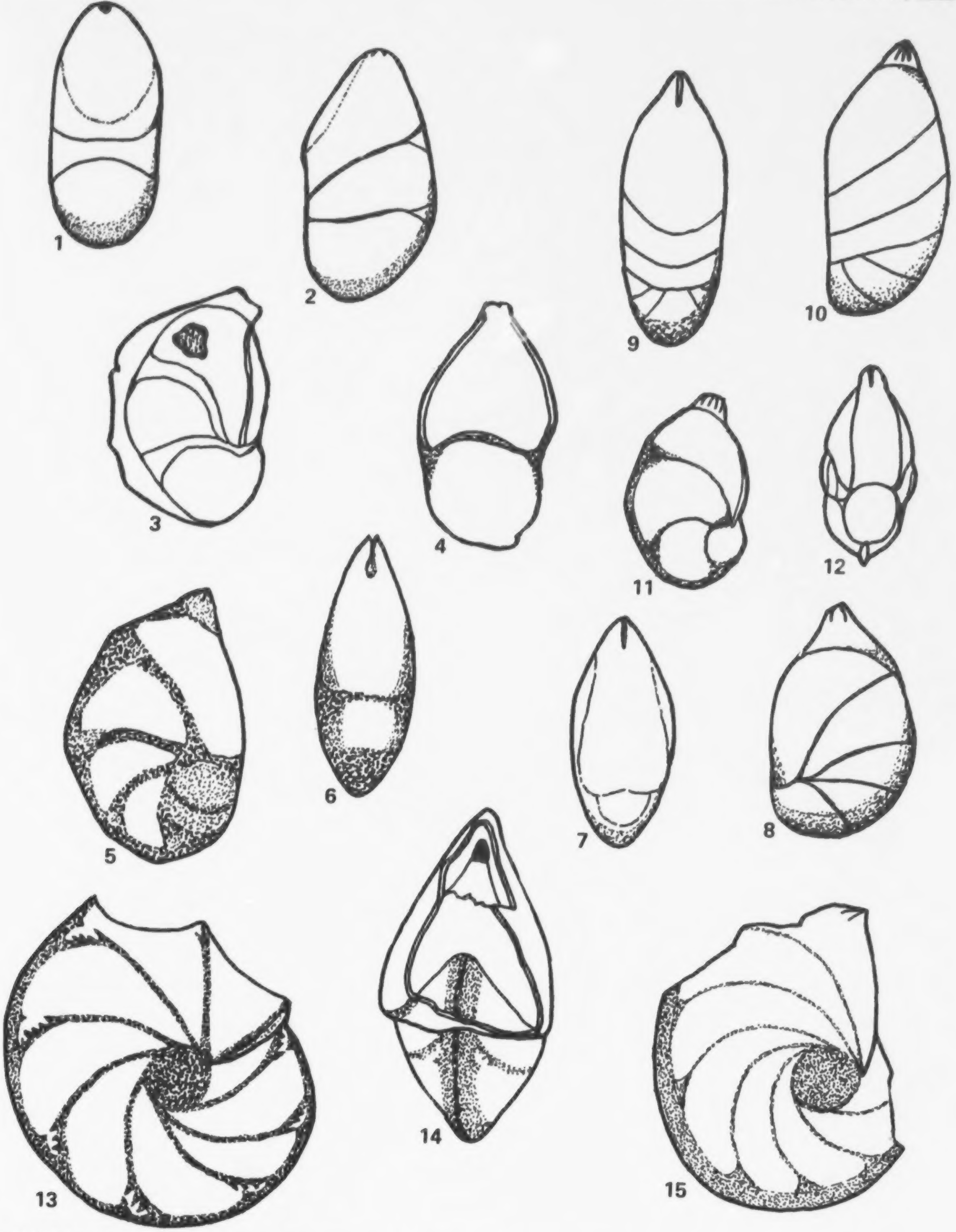

Plate 20. **1–2.** ?*Astacolus* sp., (1) edge view, 270-26-4, 100–114 cm, max. diam. 0.52 mm; (2) side view, same specimen. **3–4.** *Marginulinopsis* cf. *M. pedum*, (3) 270-3,CC, max. diam. 0.21 mm; (4) edge view, same specimen. **5–8.** *Saracenaria kellumi*, (5) 270-24-3, 110–120 cm, max. diam. 0.59 mm; (6) edge view, same specimen; (7) edge view, 270-35-3, 112–121 cm, max. diam. 0.53 mm; (8) same specimen. **9–10.** *Saracenaria* sp., (9) edge view, 270-35-3, 112–121 cm, max. diam. 0.66 mm; (10) same specimen. **11–12.** *Lenticulina callifera*, (11) 270-19-5, 113–122 cm, max. diam. 0.45 mm; (12) edge view, same specimen. **13–14.** *Lenticulina* sp., (13) 270-15-3, 97–110 cm, max. diam. 2.95 mm; (14) edge view, same specimen. **15.** *Lenticulina lenticula*, 270-37-4, 133–142 cm, max. diam. 1.15 mm.

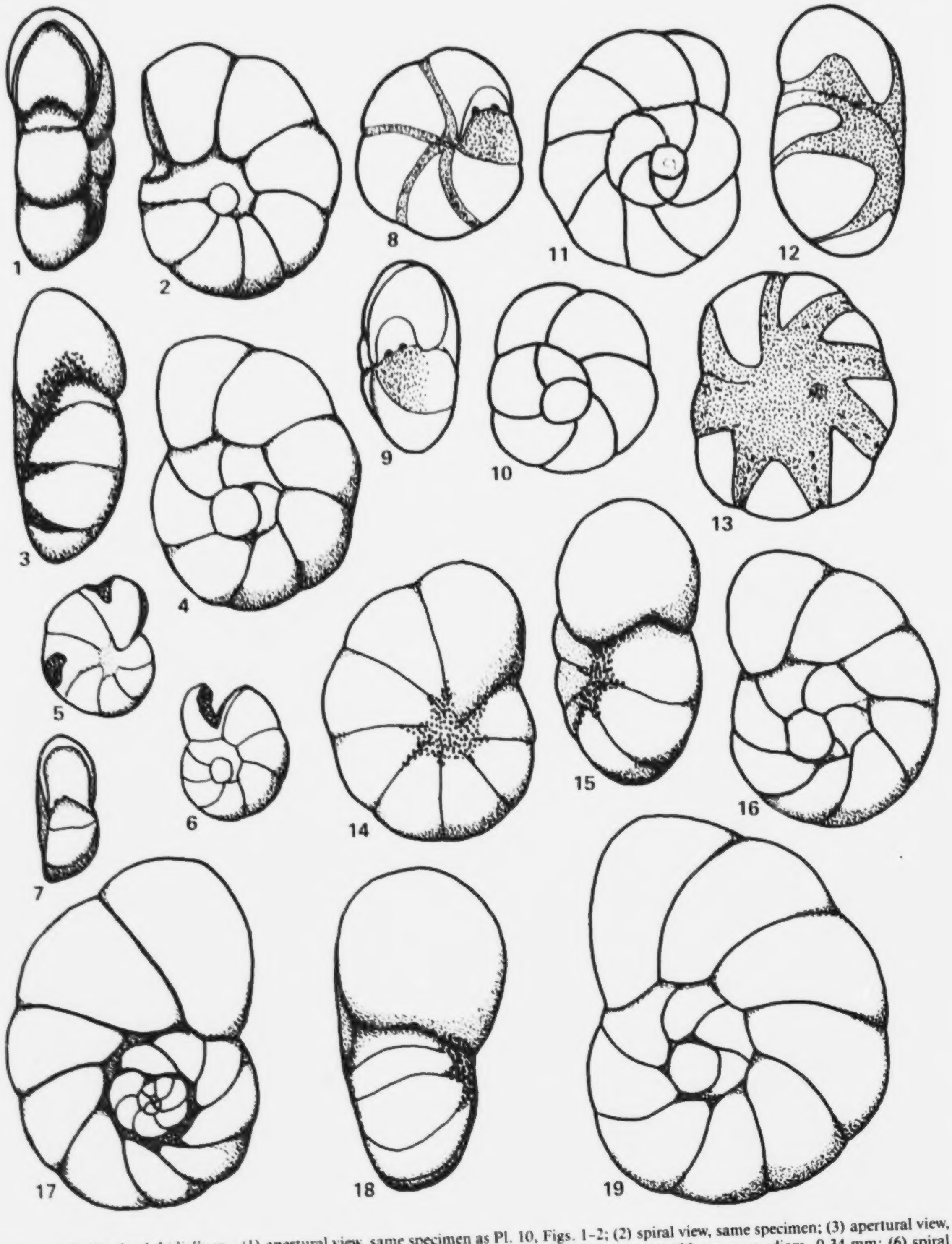

Plate 21. **1–7.** *Trochoelphidiella* sp., (1) apertural view, same specimen as Pl. 10, Figs. 1–2; (2) spiral view, same specimen; (3) apertural view, same specimen as Pl. 10, Figs. 3–4; (4) spiral view, same specimen; (5) umbilical view, 270-32-3, 114–123 cm, max. diam. 0.34 mm; (6) spiral view, same specimen; (7) apertural view, same specimen. **8–13.** *Trochoelphidiella uniforamina*, (8) megalospheric form, umbilical view, same specimen as Pl. 9, Figs. 5–6; (9) apertural view, same specimen; (10) spiral view, same specimen; (11) microspheric form, spiral view, same specimen as Pl. 9, Figs. 1–3, 9–12; (12) apertural view, same specimen; (13) umbilical view, same specimen. **14–19.** *Trochoeiphidiella pustulosa* n. sp., (14) holotype, umbilical view, 270-32,CC, max. diam. 0.26 mm; (15) edge view, same specimen; (16) spiral view, same specimen; (17) microspheric form, spiral view, 270-31-3, 59–67 cm, max. diam. 0.33 mm; (18) edge view, same specimen; (19) spiral view, same specimen as Pl. 8, Figs. 5–6.

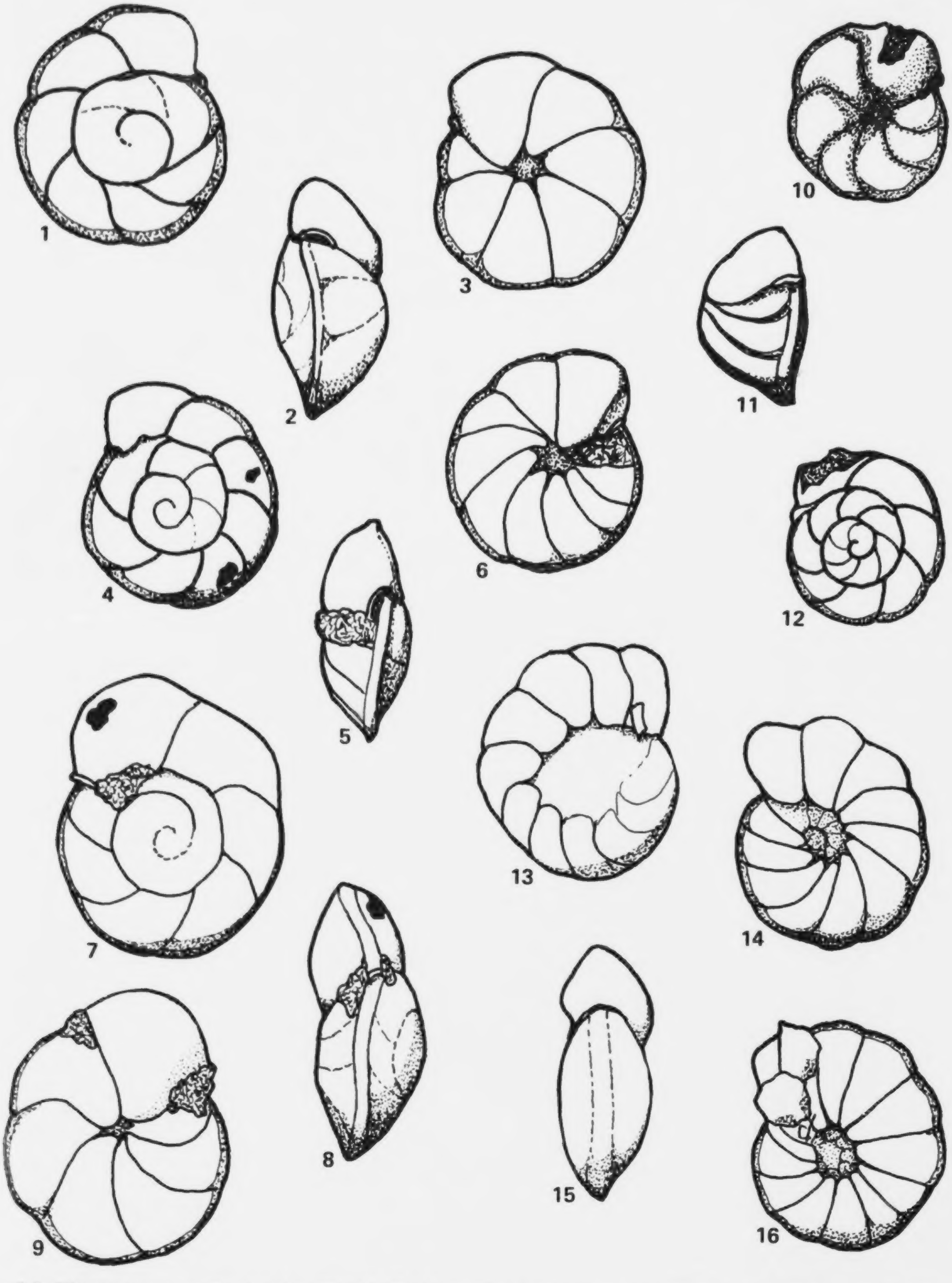

Plate [illegible] **1-3.** *Cibicides temperata*, (1) spiral view, 270-15-3, 97-110 cm, max. diam. 0.53 mm; (2) edge view, same specimen; (3) umbilical view, same specimen. **4-6.** *Cibicides pseudoungerianus*, (4) spiral view, 270-15-3, 97-110 cm, max. diam. 0.72 mm; (5) edge view, same specimen; (6) umbilical view, same specimen. **7-9.** *Cibicides* cf. *C. thiara*, (7) spiral side, 270-19-5, 113-122 cm, max. diam. 0.63 mm; (8) edge view, same specimen; (9) umbilical side, same specimen. **10-12.** *Cibicides vortex*, (10) umbilical view, 270-19-5, 113-122 cm, max. diam. 0.41 mm; (11) edge view, same specimen; (12) spiral view, same specimen. **13-16.** *Cibicides* cf. *C. mediocris*, (13) spiral side, 270-15-3, 97-110 cm, max. diam. 0.52 mm; (16) umbilical view, same specimen; (14) umbilical side, 270-15-3, 97-110 cm, max. diam. 0.55 mm; (15) edge view, same specimen.

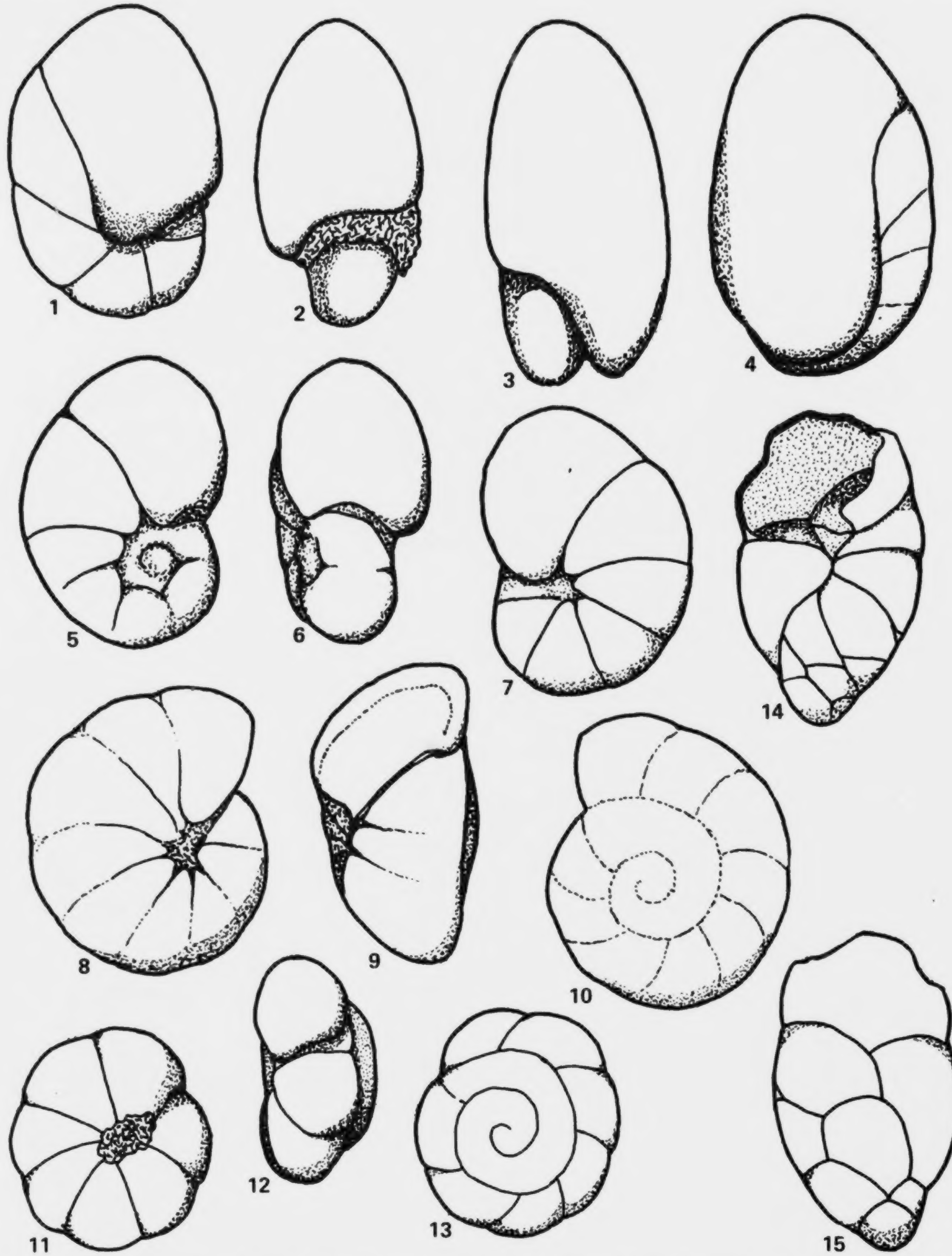

Plate 23. **1–2.** *Nonionella bradii*, (1) umbilical view, 270-19-5, 113–122 cm, max. diam. 0.26 mm; (2) apertural view, same specimen. **3–4.** *Nonionella magnalingua*, (3) apertural view, 270-38,CC, max. diam. 0.32 mm; (4) umbilical side, same specimen. **5–7.** *Nonionella iridea*, (5) spiral side, 270-38,CC, max. diam. 0.25 mm; (6) apertural view, same specimen; (7) umbilical side, same specimen. **8–10.** *Gyroidina zelandica*, (8) umbilical view, 270-19-5, 113–122 cm, max. diam. 0.42 mm; (9) apertural view, same specimen; (10) spiral view, same specimen. **11–13.** *Eponides bradyi*, (11) umbilical view, 270-19-5, 113–122 cm, max. diam. 0.21 mm; (12) edge view, same specimen; (13) spiral view, same specimen. **14–15.** *Robertina tasmanica*, (14) 270-23-4, 72–82 cm, max. diam. 0.27 mm; (15) same specimen.

PART IV: SEDIMENTOLOGIC STUDIES

25. DISTRIBUTION AND CHARACTER OF PALE GREEN LAMINAE IN SEDIMENT FROM LORD HOWE RISE: A PROBABLE LATE NEOGENE AND QUATERNARY TEPHROSTRATIGRAPHIC RECORD [1]

James V. Gardner, U.S. Geological Survey
Campbell S. Nelson, University of Waikato
and
Paul A. Baker, Duke University[2]

ABSTRACT

Pale green laminae <2 mm thick are common features of the Neogene and Quaternary sediment of Lord Howe Rise. We believe these laminae represent diagenetically altered volcanic ash layers from regional volcanic events. Although no consistent high abundances of volcanic glass are found within the laminae, the volcanic origin of the laminae is suggested by (1) similar temporal distribution of the laminae and the distribution of volcanic ash layers elsewhere in the southwest Pacific; (2) the high abundances of authigenic smectite in the laminae; and (3) the common occurrence of iron sulfides in proximity to most of the laminae. The resulting tephrostratigraphy is considerably more complex and detailed than was previously known.

INTRODUCTION

During the shipboard descriptions of the sediment recovered from Lord Howe Rise on Deep Sea Drilling Project (DSDP) Leg 90, we observed numerous, thin, pale green laminations (PGLs) that persist through long intervals of the cores. We tabulated the frequency of occurrence of these PGLs and have attempted to identify their origin. Our purpose in this paper is to (1) describe the PGLs, (2) report on a series of analyses of these laminae, (3) discuss the possibilities for their origin, and (4) argue that the PGLs are bentonites, a term used here in a general way for altered tephra layers. We present data from five sites (Sites 588, 590, 591, 592, and 593) (Fig. 1) where we recovered virtually complete sequences of the upper Neogene and Quaternary.

DESCRIPTION AND OCCURRENCE OF THE PALE GREEN LAMINAE

The general lithofacies of sediment from all the sites is foraminifer-bearing nannofossil ooze or nannofossil ooze to chalk. Fragments of siliceous microfossils, when they occur, are only in trace (<1%) amounts. Rare, clear volcanic glass, pyrite, quartz, and feldspars were observed in smear slides of some samples. The PGLs are typically 0.5 to about 2 mm thick; a few are about 5 mm thick. The laminae occur as an isolated or as a composite sets of laminae. They range in color from hues of pale green (5G) and yellow green (5GY) to greenish yellow (10Y), appearing as more or less distinct layers within the otherwise white (N9) to light gray (N7) or light greenish gray (5G8/1) bioturbated and mottled pelagic facies. The PGLs are not burrows, and all are horizontal or nearly so. There were no observations of a PGL cross-cutting a trace fossil or other sedimentary structures that might suggest a secondary origin for the laminae. The PGLs commonly occur a few centimeters above a lens or pocket of iron sulfides.

Attempts to photograph the PGLs were not very successful because of the subtle differences between the green hues of the dominant carbonate facies and the PGLs. However, a few of the more obvious PGLs did photograph well enough to demonstrate their general appearance (Fig. 2).

Figure 3 is a plot of the occurrence of volcanic glass identified in routine shipboard smear slides and the number of PGLs per core for each site. The counts were made on each section of each core as it was described and are not necessarily represented on the core summaries at the end of each site chapter (this volume). The smear-slide data are compilations of analyses by the six shipboard sedimentologists. The smear-slide data are semiquantitative, with abundance ranges of trace (T) = <1%, rare (R) = 1-5%, common (C) = 5-25%, abundant (A) = 25-75%, and dominant (D) = >75%. Figure 4 is a plot of the number of PGLs observed versus age. To construct this plot, we used the detailed nannofossil stratigraphy and nannofossil zonal ages (site chapters, this volume) and interpolated the ages for the top and bottom of each recovered core assuming a constant sedimentation rate between each of the consecutive nannofossil datums (Table 1). The age of the top and bottom of each core was calculated using Equations 1 and 2, respectively.

$$A_T = \frac{(C_T - NNZ)}{NNR} + NNA \qquad (1)$$

---

[1] Kennett, J. P., von der Borch, C. C., et al., *Init. Repts. DSDP*, 90: Washington (U.S. Govt. Printing Office).

[2] Address: (Gardner) U.S. Geological Survey, Menlo Park, CA 94025; (Nelson) University of Waikato, Hamilton, New Zealand; (Baker) Duke University, Durham, NC 27708.

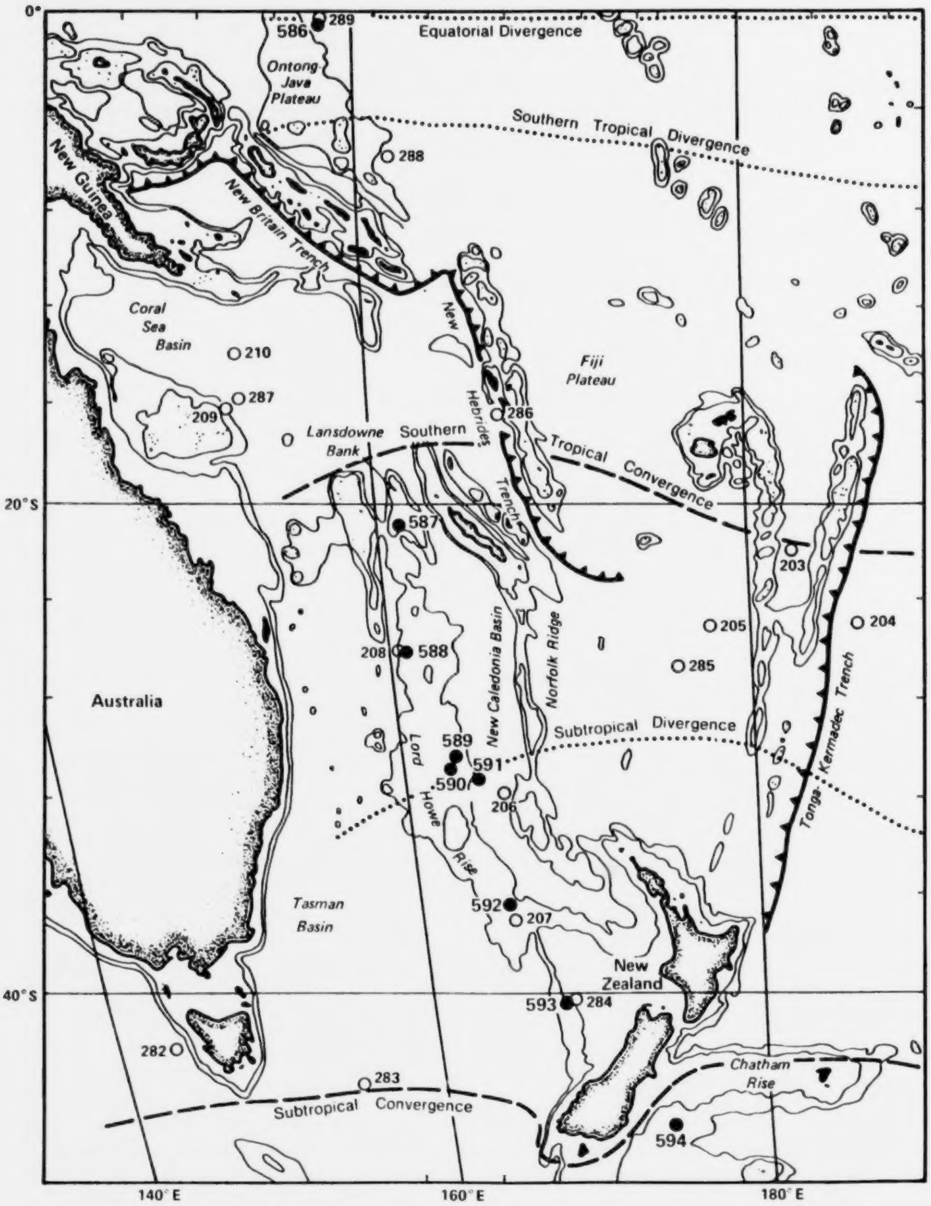
0°
20°S
40°S
140° E
160° E
180° E
Equatorial Divergence
Southern Tropical Divergence
Ontong Java Plateau
New Guinea
New Britain Trench
Coral Sea Basin
Fiji Plateau
New Hebrides Trench
Lansdowne Bank
Southern Tropical Convergence
New Caledonia Basin
Norfolk Ridge
Subtropical Divergence
Tonga-Kermadec Trench
Australia
Lord Howe Rise
Tasman Basin
New Zealand
Chatham Rise
Subtropical Convergence
586
289
288
210
287
209
286
587
203
205
204
208
588
285
589
590
591
206
592
207
593
284
282
283
594

Figure 1. Location map of Lord Howe Rise, locations of Leg 90 sites, and the generalized bathymetric and surface oceanographic features of the region.

$$A_B = \frac{(C_B - NNZ)}{NNR} + NNA \qquad (2)$$

where

A_T = age at the top of a core,
A_B = age at the bottom of a core,
NNZ = sub-bottom depth of top of an NN zone,
NNA = age of top of an NN zone,
NNR = accumulation rate of the NN zone,
C_T = sub-bottom depth of core top, and
C_B = sub-bottom depth of core bottom.

Sites in the central part of Lord Howe Rise (Sites 5 8, 590, and 591) have a higher abundance of PGLs in he middle and lower upper Miocene sections relative to he sites farther to the south (Sites 592 and 593). Convers ly, southern sites (Sites 592 and 593) have a higher ab ndance of PGLs in the Quaternary section than the c ntral sites (Sites 588 and 590).

POSSIBLE ORIGINS OF THE PALE GREEN LAMINAE

We believe the PGLs are the products of discrete sh falls. However, as will be seen, our evidence is equivo-

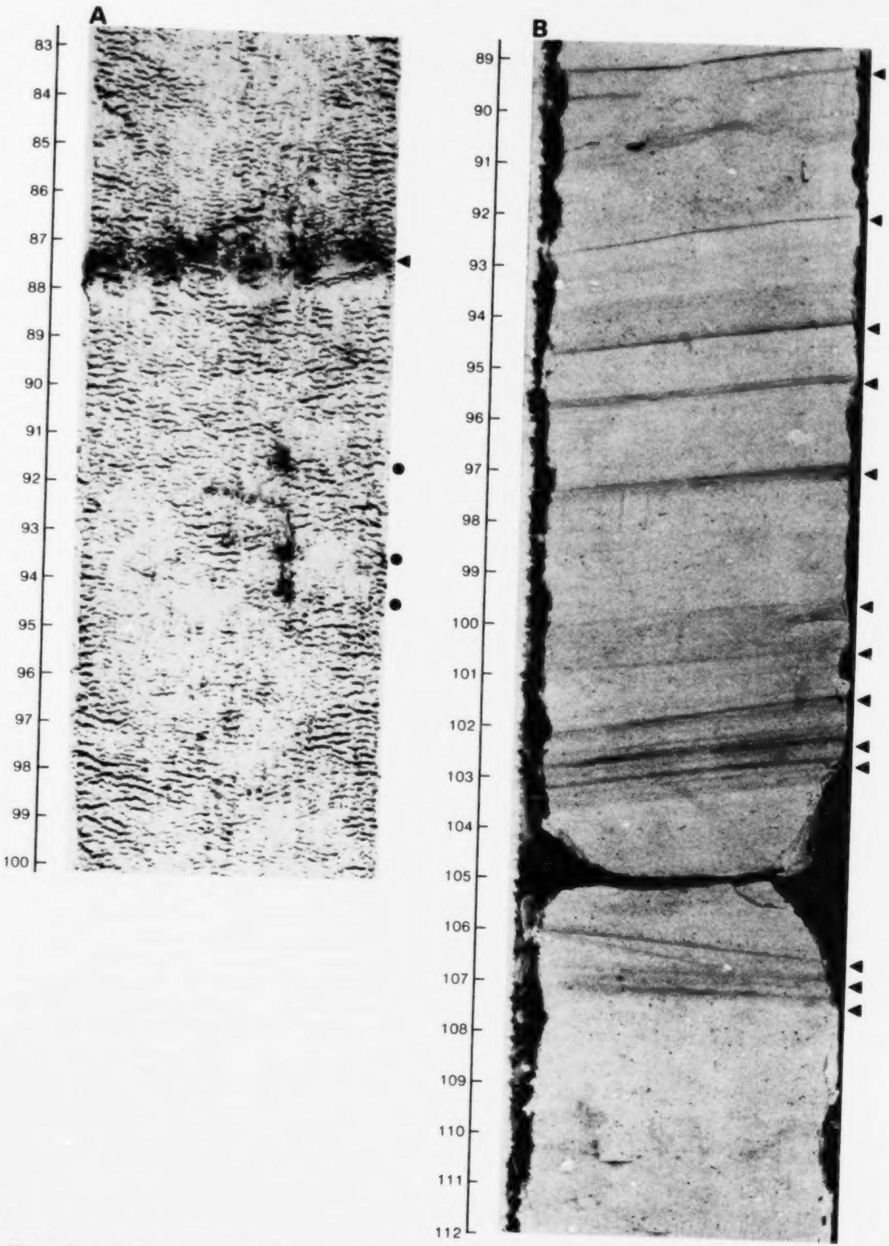

Figure 2. A. Sample 588B-22-4, 83–100 cm (205 m sub-bottom) showing a pale green lamina (solid triangles) and pockets of iron sulfides (solid circles). Sample 599C-16-3, 89–112 cm (453 m sub-bottom) showing several PGLs (solid triangles). Notice several of the zones of PGLs are composite laminae. The circular feature at 89 to 92 cm is a Planolites-type burrow that has itself been burrowed.

cal, so first we will discuss briefly some other possibilities for their origin.

Dean et al. (1977; 1981) and Arthur et al. (in press) discussed Jurassic to Holocene cycles of oxidation, reduction, and dissolution in deep-sea sediment. The cycles discussed by them have roughly equal hemicycles; that is, the reduced section is about the same length (in time or stratigraphic thickness) as the oxidized hemicycle. The same relationship follows for dissolution cycles (Gardner, 1975). In contrast to these sedimentary cycles, the PGLs do not represent a roughly equal segment of stratigraphic thickness with the surrounding facies; the PGLs are generally <2 mm thick but the surrounding facies is often >50 cm thick. There does not appear to be any difference in preservation of calcareous microfossils between the two facies, nor does there appear to be any difference in grain size. These two observations preclude dissolution cycles and winnowing events.

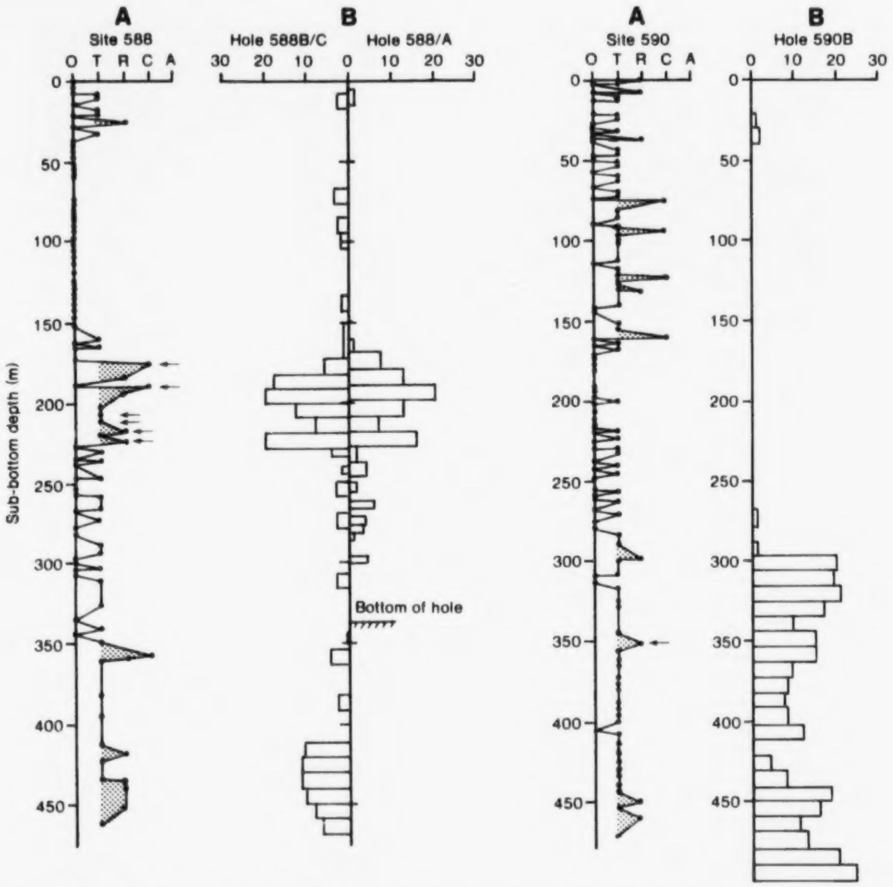

Figure 3. The distribution of pale green laminae (PGLs) and volcanic glass shards in smear slides from DSDP Sites 590, 591, 592, and 593. For each site, column A indicates amounts of volcanic glass in smear slides, column B the number of PGLs per core. Smear-slide estimates are T (trace) = <1%, R (rare) = 1-5%, C (common) = 5-25%, A (abundant) = 25-75%, and D (dominant) = >75%. The distribution of PGLs is number of PGLs per core, scaled to the sub-bottom depth interval of each core (see specific site chapters for intervals of recovery). Arrows indicate the occurrence of observed discrete ash layers.

Conceivably, the PGLs could have been produced by local differences in the oxidation state of the sediment. This is discounted by the observation that the entire sediment section, from approximately 1 to 2 m sub-bottom to the bottom of the holes, is anoxic and mildly sulfate-reducing, as is demonstrated by the common presence of pyrite and iron sulfide staining throughout the sections as well as by lower-than-seawater concentrations of sulfate in pore water at every site (Baker, this volume). Another possibility is that the pale green laminae represent brief episodes of dilution by some exotic (other than tephra) material. Again, smear-slide and scanning electron microscopy (SEM) observations and X-ray diffraction (XRD) analyses did not reveal any notable differences between PGLs and surrounding sediment, other than in clay mineralogy.

In light of the preceding discussion of the general characteristics of the lithofacies, we have discounted cyclic sedimentation and cyclic diagenesis as the origin of the pale green laminae.

EVIDENCE SUPPORTING A TEPHRA ORIGIN

Circumstantial evidence led us to propose tephra as the origin of the PGLs. The temporal distribution of PGLs and the previously published record of discrete volcanic ash layers in the southwest Pacific (Fig. 5) show striking similarities. The occurrence of volcanism in the southwest Pacific shows a pronounced middle to early late Miocene high followed by relative quiescence through the Pliocene and renewed volcanism in the Quaternary. This distribution is found throughout the margin of the Pacific (Kennett et al., 1977), but is especially strong in the southwest Pacific (Kennett and Thunell, 1975). However, several problems arise when attempting to compile data on ash layers in deep-sea sediment. The occurrence of ash initially depends on the intensity of the eruption and the climatic conditions, especially the direction and strength of the winds. An ash bed, once deposited, may be significantly modified or destroyed by reworking by currents, slumping, bioturbation, diagenesis, and, with

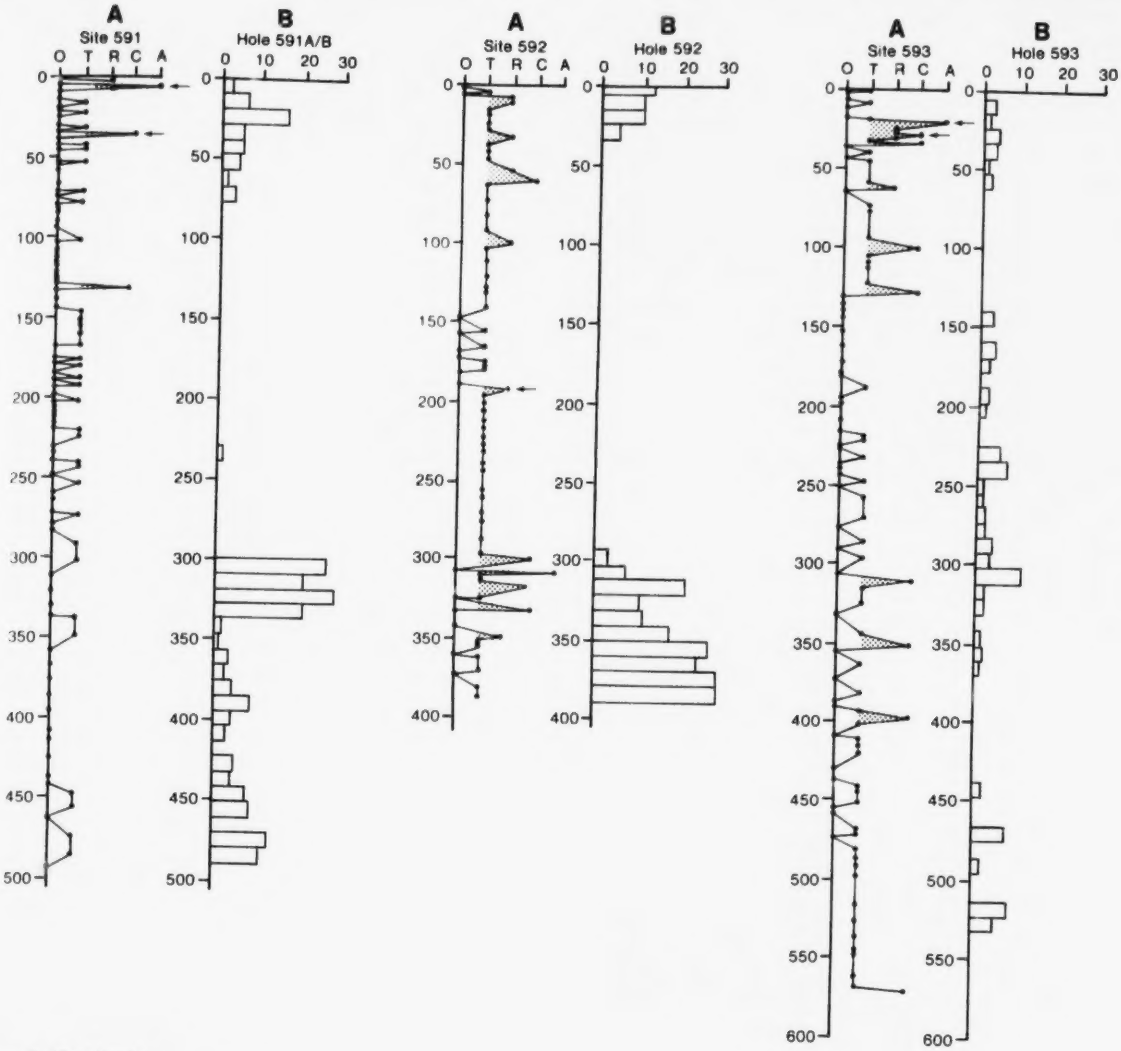

Figure 3. (Continued).

rotary drilling, by the coring process itself. An ash can be preserved as a discrete bed, a pod, or dispersed shards. Shards generally cannot be detected megascopically and require detailed analyses of channel samples to produce frequency data on volcanic activity (Ledbetter, 1982).

Hein et al. (1978) discussed the inconsistent counting techniques used by different workers and the effects this inconsistency has on the interpretation of ash layers in DSDP cores. They also emphasized how diagenesis can obscure the tephrostratigraphy by alteration of volcanic ash beds to bentonite. Many bentonite beds in North Pacific DSDP sites are developed in the older (pre-Pliocene) deposits of diatomaceous muds and are largely indistinguishable from them except by mineralogical analysis (Hein et al., 1978).

All the Lord Howe Rise holes discussed here show a pattern of PGLs that is similar to the distribution of tephra in other Pacific Ocean sites; the highest abundances of PGLs occur in the middle and lower upper Miocene intervals, generally followed by few PGLs in the Pliocene intervals, then by numerous PGLs in the Quaternary sections. The correspondence between abundances of volcanic glass in smear slides greater than trace amounts (< 1%) and the abundances of PGLs (Fig. 3) is good only at Site 588 and fair at Site 592. However, at all sites where the abundance estimates of volcanic glass indicates the presence of greater than trace amounts, there are numerous PGLs.

Volcanic glass and biogenic silica are scarce to absent from intervals with high counts of PGLs. Subtropical- to temperate-latitude deep-sea sediment deposited well above the lysocline should have an appreciable component of diatoms and radiolarians. The relatively fast accumulation rates of the sediment at Leg 90 sites (10 to >50 m/m.y.) suggest high productivity, which in turn implies that biosiliceous components must have been supplied to the sediment (Diester-Haass and Schrader, 1979; Schuette and Schrader, 1981; de Vries and Schrader, 1981).

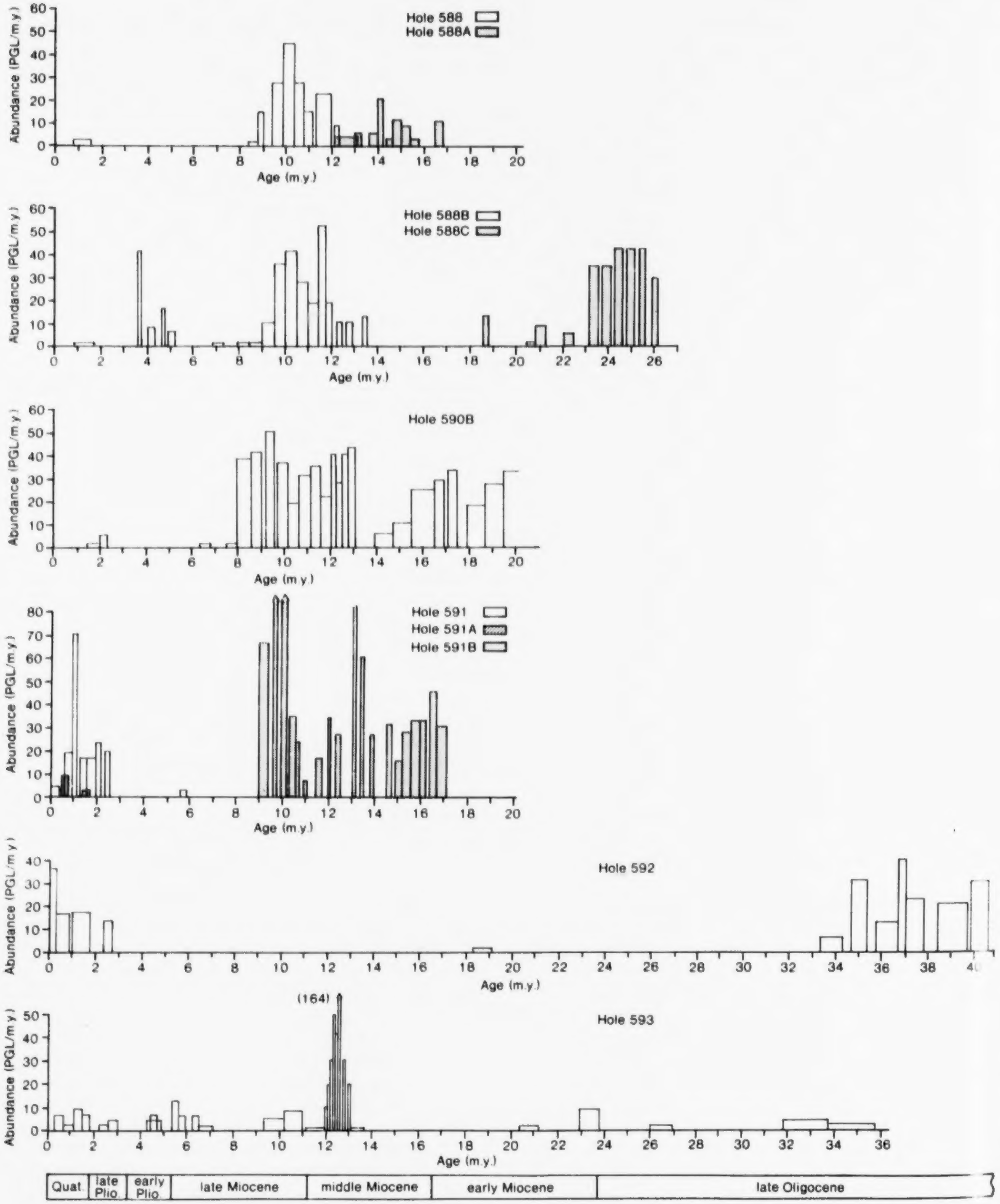

Figure 4. The number of pale green laminae (PGLs) per million years for DSDP Sites 588, 590, 591, 592, and 593. The ages of each recovered nannofossil zone (Table 1) was used to extrapolate the ages of the top and bottom ages of each core. The duration represented by each core was used to normalize the number of PGLs per m.y.

Table 1. Ages (m.y.) of tops of nannofossil zones used to interpolate age in Figure 2 (from Introduction, this volume).

Nannofossil zone	Age	Nannofossil zone	Age
NN21	0.00	NN7	12.20
20	0.20	6	13.00
19	0.55	5	15.00
18	1.90	4	17.00
17	2.30	3	17.80
16	2.40	2	19.00
15	3.45	1	20.50
14	3.65	NP25	23.6
13	4.10	24	26.0
12	4.60	23	32.0
11b	5.20	22	34.0
11a	6.25	21	36.5
10	9.50	20	37.5
9	11.00	19	41.0
8	12.00		

Insoluble residues of 25–50 cm^3 of sediment have, if any, only traces of biosiliceous material in them (see site chapters, this volume). Site 591 is an exception; it contains biogenic silica in trace amounts throughout the section. Site 591 is located in the deepest waters of all the Leg 90 sites, and, as will be discussed later, this may explain the presence of biosiliceous components. Consequently, we believe there must have been severe postdepositional dissolution of the biogenic silica. Analyses of pore waters indicate consistently very low concentrations of dissolved silica at all sites (except Site 591) in sediment younger than late Miocene, which reflects the low content of solid biogenic silica. The low concentrations of dissolved silica promote the congruent dissolution of volcanic glass. Alternately, volcanic glass can devitrify to palagonite (Peterson and Griffin, 1964) or incongruently dissolve to yield palygorskite (Hathaway and Sachs, 1965; Siever and Kastner, 1967), smectite (Peterson and Griffin, 1964; Nayudu, 1964; von Rad and Rösch, 1972), and zeolites (Arrhenius, 1963; Bonatti, 1972; Stonecipher, 1974).

To investigate further the possibility that the PGLs are bentonites, several PGLs were sampled for clay mineralogy by XRD analyses. In addition, samples were taken in sections where no PGLs occur. Approximately 10 cm^3 was collected for each sample. Standard techniques were used to prepare the samples (Hein et al., 1976), and the weighted peak area techniques of Biscaye (1965) were used to analyze the diffractograms. The results (Table 2) clearly show that the dominant clay mineral in almost all PGL samples is smectite (Fig. 6). Several of the PGL samples analyzed have no clays present,

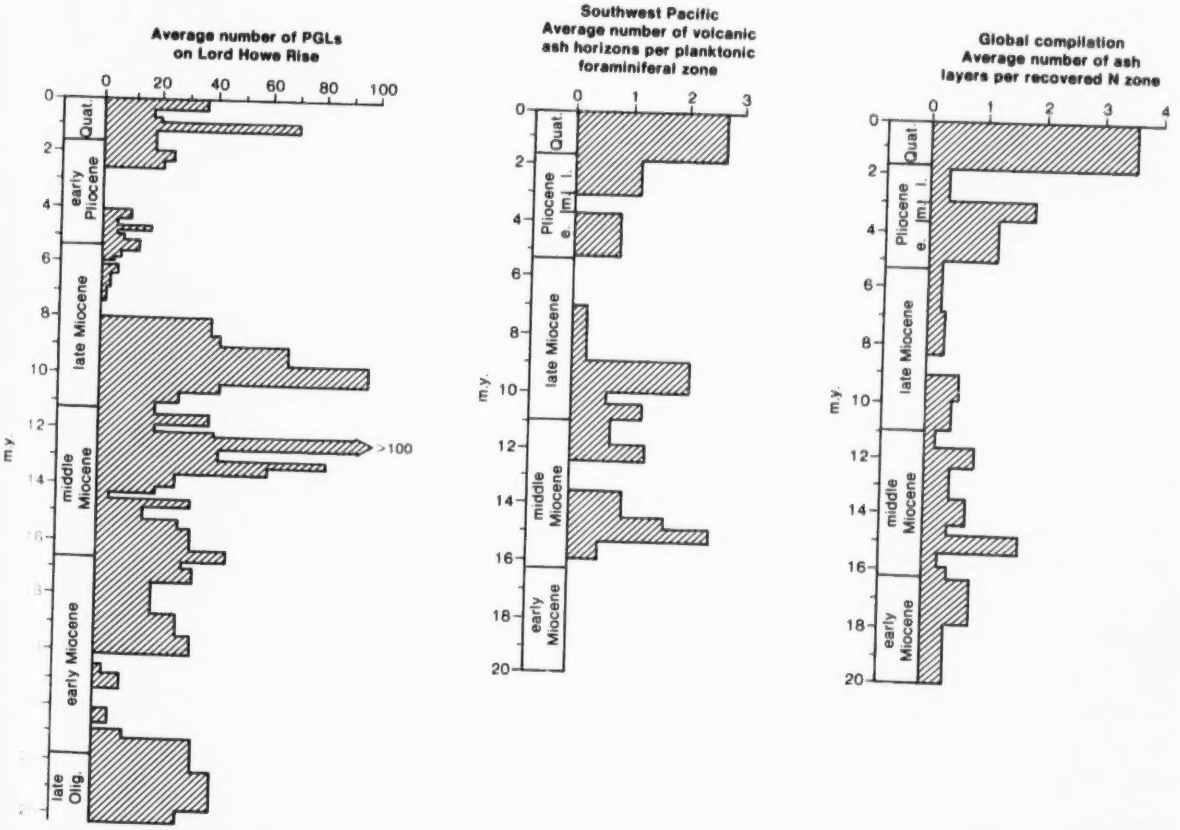

Figure 5. The distribution of PGLs on Lord Howe Rise and the distribution of discrete volcanic ash layers from the southwest Pacific and the global distribution of volcanic ash (after Kennett et al., 1977).

Table 2. Results of XRD analyses. Clay mineralogy is the relative percentages of the <2-μm fraction where sm = smectite, ill = illite, and ch + k = chlorite plus kaolinite.

Sample (interval in cm)	Sub-bottom depth (m)	Age	Clay mineralogy		
			sm	ill	ch + k
		Pale green laminae			
591A-3-3, 26	22.06	Quat. (NN19)	50	16	33
591A-3-3, 68	22.48	Quat. (NN19)	76	6	17
591A-3-3, 86	22.66	Quat. (NN19)	50	19	32
591A-3-3, 92	22.72	Quat. (NN19)	48	18	34
591A-3-3, 104	22.84	Quat. (NN19)	46	20	34
591A-3-4, 5	23.35	Quat. (NN19)	25	23	52
591A-3-4, 15	23.45	Quat. (NN19)	62	12	26
591A-3-5, 20	25.00	Quat. (NN19)	63	8	20
591A-3-5, 27	25.07	Quat. (NN19)	54	22	24
591A-3-6, 50	26.80	Quat. (NN19)	51	18	30
591-19-2, 110	167.40	Plio. (NN14)	57	20	23
591-19-4, 40	169.70	Plio. (NN14)	55	20	25
591-19-5, 110	171.90	Plio. (NN14)	69	12	19
		Nonpale green laminae			
591-15-1, 40	128.00	Plio. (NN15)		—	
591-15-2, 70	129.80	Plio. (NN15)		—	
591-15-3, 110	131.70	Plio. (NN15)		—	
591-15-5, 40	134.00	Plio. (NN15)		—	
591-15-6, 40	135.50	Plio. (NN15)		—	
591-16-1, 110	138.00	Plio. (NN15)		—	
591-16-3, 40	140.30	Plio. (NN15)		—	
591-16-6, 40	144.80	Plio. (NN15)	67	11	23
591-17-3, 40	149.60	Plio. (NN15)	64	15	21
591-17-4, 110	151.80	Plio. (NN15)		—	
591-17-6, 40	154.10	Plio. (NN15)		—	
591-18-4, 40	160.40	Plio. (NN15)		—	
591-18-5, 110[a]	162.60	Plio. (NN15)	60	14	24
591-20-1, 40	174.70	Plio. (NN14)		—	
591-20-2, 110	176.90	Plio. (NN14)		—	
591-20-4, 40[a]	179.20	Plio. (NN14)	60	17	23
591-20-5, 110	181.40	Plio. (NN14)		—	
591-20-6, 110	182.90	Plio. (NN14)		—	

Note: — = no clays present.
[a] Samples within 15 cm of a zone of pale green laminae.

but those samples are either older than 5 m.y. and occur deeper than 300 m sub-bottom, or contain so little clay-sized material that the analyses are questionable. Scanning electron micrographs of PGLs (Fig. 7) clearly show the presence of authigenic smectite as highly wrinkled or honeycomb-like flakes and sheets (Wilson and Pittman, 1977). The abundances of smectite in PGL samples (avg. = 55.2%; S.D. = 11.6%) are well within the range that Hein and Scholl (1978) used to identify bentonites. The lack of smectite in the pre-Pliocene PGL samples suggests that diagenetic processes have broken down the clays and remobilized the elements. However, the PGLs remain visible in the pre-Pliocene sediment. Interestingly, Hein and Scholl (1978) did not observe smectites in volcanogenic sediment any younger than Miocene in sediment from the Bering Sea.

These results encouraged additional, more detailed research into the clay mineralogy. Eight samples of sediment containing PGLs from Sites 588 and 591 were dissolved in 4M acetic acid, known not to alter clay minerals (Carroll and Starkey, 1971). The residue was washed several times with distilled water and then wet-sieved through a 63-μm screen. The <63-μm fraction was centrifuged and a slurry was drawn off, dropped onto a

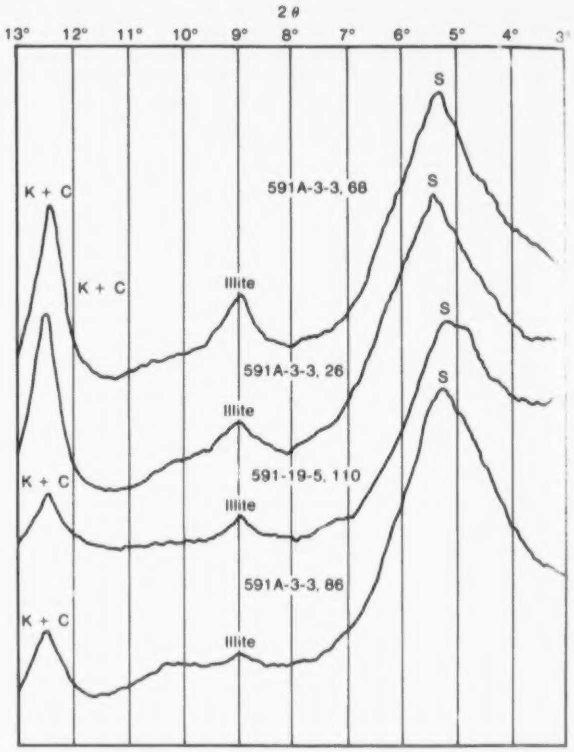

Figure 6. X-ray diffractograms of the glycolated <2-μm fraction of sediment comprising a pale green laminae. S = smectite, Ill = illite, and K + C = kaolinite plus chlorite.

glass slide, and rapidly dried with a low-intensity infrared lamp for about 20 min. Three X-ray runs were performed on aliquots of each sample: (1) an untreated sample; (2) following ethylene glycolation for 12 hr. to test for smectite; and (3) after heating to 500°C for 1 hr. to test for dehydration of smectite and the nature of any chlorite components (Hume and Nelson, 1982). In addition, suspensions were boiled in 10% HCl for 5 min. to distinguish between kaolinite and chlorite (Brindley, 1972), then saturated in 1N KOH for 15 hr. and heated in 1N KOH at 90°C for 1 hr. to note the degree of contraction of smectite through K^+ uptake, which can indicate the general nature of the parent material (Weaver, 1958).

The results of these treatments show that the clay mineralogy of the PGLs is similar for all samples analyzed (Fig. 8). A broad, major (001) reflection between 14.3 and 16.0Å expanded to 15.5–17.7 Å upon glycolation and collapsed to 9.8Å after heating. These are characteristics of dominant smectite clays in the samples. The (001) smectite peak showed only partial contraction to 12–13Å after the KOH treatments, which supports the derivation of the smectite from materials with a low inherited charge, such as volcanic ash, rather than from the argillization of sheet silicates such as muscovite or biotite (Weaver, 1958; Hume and Nelson, 1982). The (060) spacing of the smectites is from 1.49 to 1.52Å, which suggests that their octahedral layer is of a dioctahedral

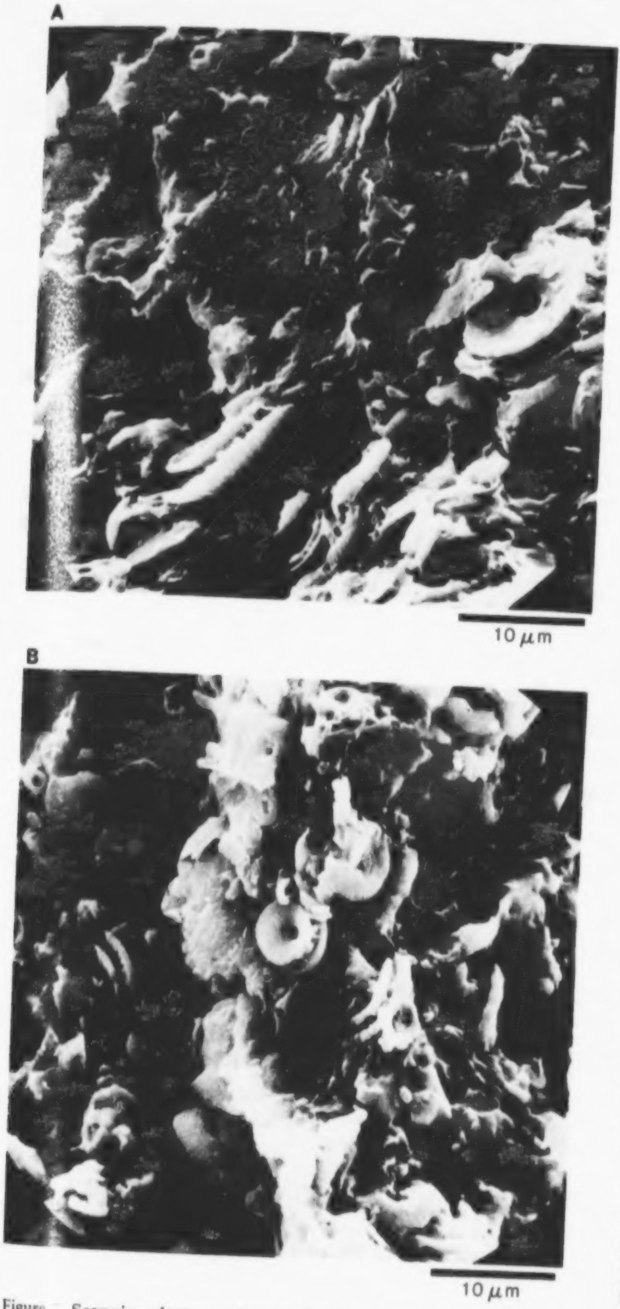

Figure 7. Scanning electron micrographs of two samples of PGLs. A. From Sample 588C-13-4, 38–40 cm. B. from 588C-16-2, 74–75 cm. Magnification ×2000.

type (MacEwan, 1972). The asymmetry of the smectite peak on its high-angle side, with superimposed minor peaks between 14 and 10Å, is mainly due to random interstratification of smectite with some illite, and possibly small amounts of other clay species. A consistent set of subdominant peaks at 7.2 and 3.57Å, unaffected by glycolation and acid treatment but destroyed by heating, is caused by kaolinite and not chlorite.

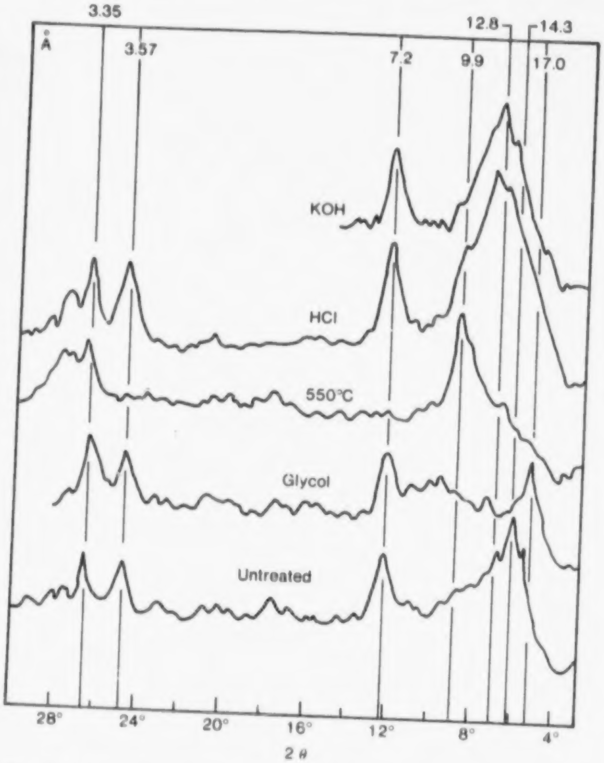

Figure 8. X-ray diffractograms of specially treated PGL samples (see text for a discussion of each of the treatments).

Thus, the detailed clay mineralogy of the <63-μm fraction of the PGLs mainly consists of smectite, with small to moderate amounts of mixed-layer illite-smectite (illite < smectite) and kaolinite. The evidence strongly suggests that the smectites resulted from the argillization of ash material that has settled onto Lord Howe Rise and that the PGLs represent bentonite layers. The presence of some interlayered illite in authigenic volcanogenic smectites is expected (Hein and Scholl, 1978) and is a characteristic feature of K-bentonites (Weaver, 1958; Mossler and Hayes, 1966).

The next piece of evidence suggesting a tephra origin for the PGLs is the common occurrence of concentrations of iron sulfides immediately below a PGL within the surrounding facies (Fig. 2). The iron sulfide layer probably formed as a result of microbial sulfate reduction, a process presently taking place at each of the sites (Baker, this volume). Volcanic ash provides a good reactive source of dissolved iron for combination with the dissolved sulfide. We postulate that the distance of the sulfide layer beneath the PGL, typically 5–10 cm, was approximately the thickness of the oxic zone of bioturbation.

Lastly, Lord Howe Rise is surrounded by regions of active Neogene and Quaternary volcanism, especially explosive rhyolitic and andesitic centers in New Zealand, along the Tonga–Kermadec Arc, the New Hebrides Arc, and the New Britain Arc (Figs. 9 and 10). Ample sources exist for tephra to have been transported to the Tasman

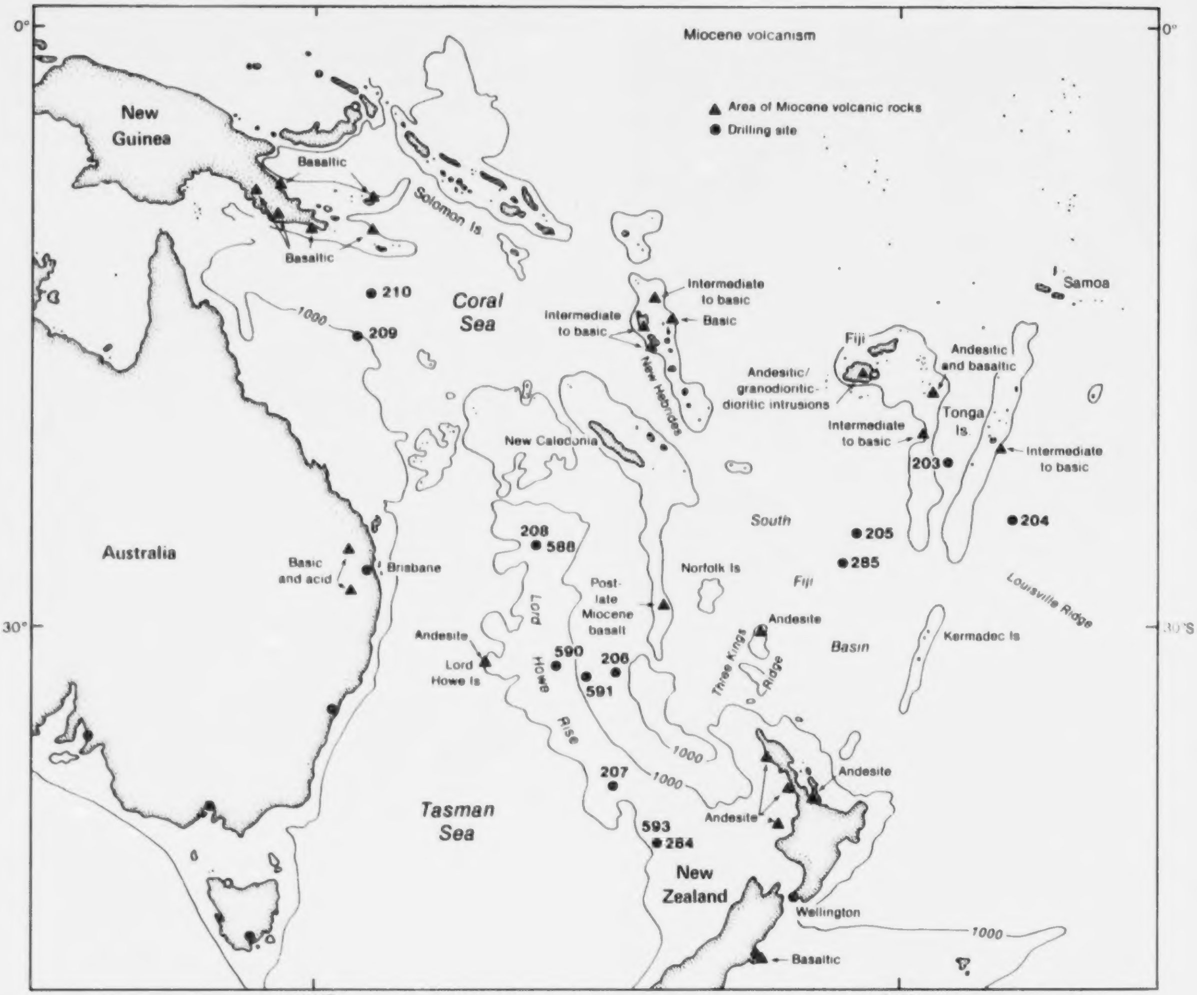
Miocene volcanism
▲ Area of Miocene volcanic rocks
● Drilling site
0°
0°
30°
30°S
150°E
180°
New Guinea
Basaltic
Basaltic
Solomon Is
210
209
1000
Coral Sea
Intermediate to basic
Intermediate to basic
Basic
New Hebrides
Fiji
Andesitic/ granodioritic-dioritic intrusions
Andesitic and basaltic
Samoa
Tonga Is
Intermediate to basic
Intermediate to basic
203
204
New Caledonia
South
205
285
Fiji
Basin
Louisville Ridge
Kermadec Is
Australia
Basic and acid
Brisbane
208
588
Lord Howe Rise
Post-late Miocene basalt
Norfolk Is
Andesite
Three Kings Ridge
Andesite
Lord Howe Is
590
206
591
1000
1000
207
Andesite
Andesite
Tasman Sea
593
284
New Zealand
Wellington
1000
Basaltic

Figure 9. Distribution of known Miocene volcanic rocks in the region of Lord Howe Rise (modified after Churkin and Packham, 1973).

Sea. Explosive volcanoes can produce discrete ash layers in deep-sea sediment several thousand kilometers from the source eruption (Nayudu, 1964; Huang et al., 1973, 1975; Shaw et al., 1974).

DISCUSSION

One of the most convincing lines of evidence that the PGLs are tephra layers is the correlation of their temporal distribution with the temporal distribution of discrete ash layers in the southwest Pacific and with the global pattern (Fig. 5). Ninkovich and Donn (1976) and Stewart (1975) have cautioned against conclusions about tephrostratigraphy in regions of convergent plate boundaries. Very little relative convergence has occurred between Lord Howe Rise and potential volcanic sources in Australia, New Zealand, and the seamounts within the Tasman Sea. If these regions are the sources for the tephra, then the tephrostratigraphy is a direct record of volcanism. However, convergence of about 6 cm/yr. has occurred during the Neogene and Quaternary along the northern boundary between the Pacific and Australian plates at the New Britain and New Hebrides arcs (McDougall et al., 1981). Although northern sources for the volcanic ash are a distinct possibility, the pattern of high abundances of tephra in the middle and early late Miocene and relatively low abundances in the Quaternary is opposite to that expected by convergence alone. However, the Pacific/Australian plate boundary in the vicinity of New Zealand is a potential source for the tephra.

The Pacific/Australian plate boundary in the vicinity of New Zealand formed about 24 m.y. ago, at about the end of the Oligocene (Carter and Norris, 1976; Nelson and Hume, 1977; Sporli, 1980). Island arc volcanism has characterized the boundary during the Neogene and Quaternary (Ballance, 1976; Coleman and Packham, 1976). The tephrostratigraphic record from Lord Howe Rise can be compared with the tectonic nature of the Pacific/Australian plate boundary in the southwest Pacific

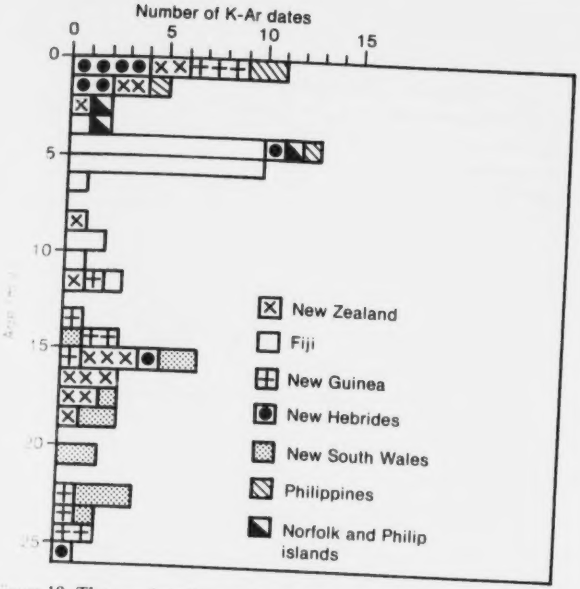

Figure 10. The age, location, and number of K-Ar dates of volcanism in the southwest Pacific for the past 26 m.y. (after Kennett et al., 1977).

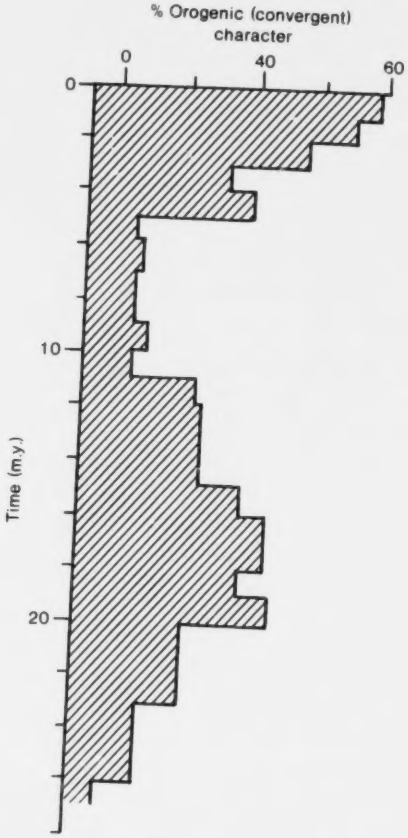

Figure 11. The orogenic convergence of the Pacific/Australian plate boundary in the New Zealand region through the Neogene and Quaternary as it relates to convergent velocity at the boundary (after Hodder, in press). The small negative percentage from 26 to 27 m.y. implies that the boundary was slightly extensional at this time.

over the same period to determine any correlation between volcanism and changes in the rates of seafloor spreading and subduction.

Hodder (in press) used a vectorial approach to analyze tectonism at the Pacific/Australian plate boundary, primarily based on the velocities of plate motions determined from the distribution and age of successive intraplate volcanoes on the two plates. The results of his analysis of boundary convergence velocities at 1-m.y. intervals are shown in Figure 11. Two main periods of relatively accelerated plate convergence are evident in Figure 11, a moderately fast convergence from late early through middle Miocene (20–11 m.y. ago) and a rapidly increased tempo of movement in post-Miocene times (5–0 m.y. ago) that culminated in maximum convergence during the Quaternary. A broad correlation is apparent between these periods of increased intensity of convergent boundary tectonics and the history of Neogene and Quaternary explosive volcanism as interpreted from the PGL record. Two apparent anomalies inciude the marked period of early late Miocene volcanism (11–8 m.y.) during a time of very slow convergence, and a record of generally sparse volcanism during a period of relatively increased plate movement in the Pliocene (5–2 m.y. ago). Both situations may be partly related to the lag time of volcanism associated with periods of increased tectonic convergence that Hodder (in press) determined can be about 3 m.y. for the northern New Zealand region. Thus, the relatively fast rates of plate motion recorded during late middle Miocene (14–11 m.y. ago) and Pliocene (5–2 m.y. ago) may not have been manifested in the PGL record until the early late Miocene (11–8 m.y. ago) and Quaternary (2–0 m.y. ago), respectively.

Figure 4 shows that tephra from Quaternary volcanism is limited to the sites relatively close to New Zealand. It is curious that Site 591, the site mentioned earlier that has siliceous biogenic fragments in rare to trace amounts throughout the recovered section, also has numerous bentonites throughout the Quaternary section, whereas nearby Site 590 shows only a few PGLs in the lower Quaternary section. However, Site 590 is a 1299 m water depth, whereas Site 591 is at 2131 m. It may well be that the Quaternary tephra from the shallower Site 590 has been winnowed out of the sediment or that the bentonites are so subtle as to be indistinguishable to the unaided eye from the surrounding sediment. Nevertheless, Quaternary volcanism in the New Zealand region appears not to have produced as many tephra layers as have episodes of middle and early late Miocene volcanism.

The compilations of Kennett and Thunell (1975) and Kennett et al. (1977) indicate that, on a worldwide basis, Quaternary explosive volcanism was more extensive than middle and early late Miocene volcanism (Fig. 5). However, the numbers of bentonites on Lord Howe Rise suggest that middle and early late Miocene volcanism was much more active in this sector of the southwest Pacific than it was during the Quaternary. Middle and early late Miocene explosive volcanism is well documented throughout the southwest Pacific (Mitchell and Warden, 1971; Churkin and Packham, 1973; Kennett and Thunell, 1975; Kennett et al., 1977; Kennett, 1981). The Leg 90 sites on Lord Howe Rise north of New Zealand clearly show a maximum of middle and early late Miocene volcanism, whereas those sites closer to New Zealand do not. This suggests that the tephras from the middle and early late Miocene volcanism came from the island arcs to the north or northeast rather than from New Zealand. An episode of explosive volcanism from island arcs suggests an increase in the rates of subduction or a change in plate motion (Hays et al., 1972) or possibly an increase in global magmatic activity related to deep convective properties (Vogt, 1972). Whatever the cause, the resultant tephra covered northern Lord Howe Rise more frequently than it did the southern area.

There is a curious abundance of PGLs (bentonites) in the lower Miocene section at Site 590 (Fig. 4). Neither the global averages nor the southwest Pacific averages of explosive volcanism show much activity during this time (Fig. 5), although other areas around the Pacific rim do; for example, the Aleutian Arc (Hein and Scholl, 1978). However, the entire Miocene section at both DSDP Site 205 (Burns, Andrews, et al., 1973) and Site 285 (Andrews, Packham, et al., 1975) have facies of predominantly glass shard tuffs. Bentonites in the lower Miocene at Site 590 may have been ashes that originated along the Tonga-Kermadec area, as is suggested by early Miocene fast rates of convergence (Fig. 11). The timing coincides with the first record of voluminous andesitic volcanism in northern New Zealand (Ballance, 1976) that is associated with the propagation of the Pacific/Australian plate boundary through the New Zealand region. Other possible sources include Norfolk Island and Three Kings Ridge (Davey, 1982).

Many upper Oligocene to lower lower Miocene bentonites occur at Site 588 but not at Sites 592 and 593. The distribution of these bentonites at the central region of Lord Howe Rise suggests a northern source of the tephras that displayed relatively minor explosivity. The South Fiji Basin is thought to have been forming during Oligocene time (Watts et al., 1977; Malahoff et al., 1982; Davey, 1982); consequently, this region is a potential source for the tephras. The lower upper Oligocene bentonites appear to have a New Zealand source, but there is only one stratigraphic record (Site 592) that goes that far back in time.

Another curious aspect of the sediment from Lord Howe Rise is the generally low abundances of discrete volcanic glass even in the Quaternary section. Hein and Scholl (1978) and Hein et al. (1978) discussed the diagenesis of tephra and concluded that it generally takes 4 or 5 m.y. to alter ash to bentonites. But, as pointed out earlier, the biosiliceous fossils from Lord Howe Rise have been dissolved even from Quaternary sediment. The cause of the very rapid devitrification of the volcanic ash, as well as the dissolution of biosiliceous material, may well be tied directly to biological processes and water masses (Calvert, 1974). Antarctic Intermediate Water (AAIW) is greatly undersaturated in silica at the Antarctic Divergence (Fig. 12) because of the intense upwelling (Heath, 1974; Calvert, 1974). AAIW is formed at about 60-65°S but submerges to about 1000 m depth by 55°S. This highly silica-undersaturated water then spreads north, and the first sediment it comes in contact with in the Tasman Sea is on Lord Howe Rise. Any silica within the upper few meters of sediment that was biogenically mixed (Thompson and Wilson, 1980; Weaver and Schultheiss, 1983) should have been subjected to silica dissolution. Although a postdepositional dissolution process such as this appears to have been discounted by Berger (19[illegible]) and Bogoyavlenskiy (1967), this mechanism alone could account for the lack of biosiliceous fossils and volcanic glass. Dissolution of silica by AAIW may also explain the presence of biogenic and volcanic silica at Site 591, which is located in 2131 m water depth, below the direct influence of AAIW. Consequently, severe silica dissolution may not be as prevalent at Site 591 as at the other Leg 90 sites on Lord Howe Rise.

If the PGLs in Leg 90 sediment do indeed correspond to diagenetically altered volcanic ash layers, then whether or not they are identified will significantly affect the interpretation of the frequency of volcanic activity in the region. For example, our data are derived from five sites drilled on Lord Howe Rise with the hydraulic piston corer (HPC) and extended core barrel (XCB). Kennett and Thunell (1975) considered four sites that were rotary drilled on Lord Howe Rise in their global compilation of volcanic ash layers in deep-sea sediment. They recorded no volcanic ash layers in two sites and only multiple ash layers in the Quaternary sections of the other two sites. Compare their observations of an apparently very simple volcanic history with the complexity of our Neogene and Quaternary tephrostratigraphies in Figure 4. The difference partly reflects the far better quality of the Leg 90 cores, as well as the recognition that PGLs represent altered ash layers. If, in fact, we had counted only the number of truly megascopic, glass-rich ash layers and pods in the Leg 90 sediments, then we would have recorded a total of only 11 volcanic episodes, seven of Quaternary age and two each from lower and upper Miocene sequences (Nelson et al., this volume).

CONCLUSIONS

Pale green laminae that occur conspicuously in sediment from Lord Howe Rise reflect episodes of volcanism from sources in the southwest Pacific. The evidence that leads to this interpretation includes the following: (1) The timing of the occurrences of the laminae matches the periods of known volcanism from the circum-Pacific and the southwest Pacific. (2) There is a general correspondence between the occurrence of laminae and the presence of volcanic glass in smear slides. (3) The flow of corrosive Antarctic Intermediate Water in contact with the surface of Lord Howe Rise, depleted in silica at its source region at the Antarctic Divergence, accounts for the lack of both biogenic and volcanic silica in the sediments of Lord Howe Rise. (4) The pale green laminae generally occur in association with iron sulfide. The iron necessary for the formation of the iron sulfides proba-

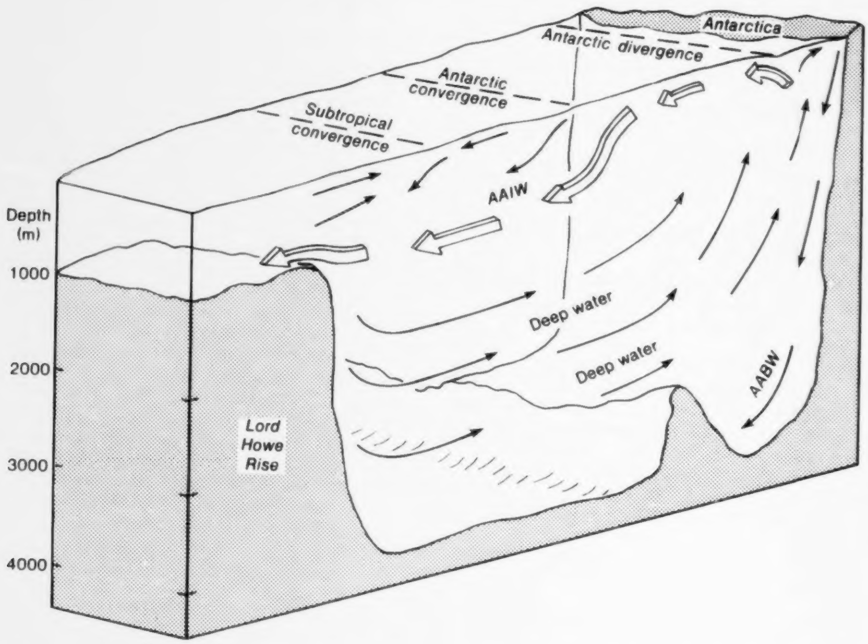

Figure 12. The generalized circulation of subsurface water masses in the southwest Pacific, showing the relationship between Antarctic Intermediate Water (AAIW) and the topographic expression of Lord Howe Rise (modified after Knox, 1970).

bly was supplied by the alteration of the overlying volcanic ash, and the sulfur was supplied by sulfate reduction occurring within pore water. (5) Clay mineralogy of the PGLs indicates that authigenic smectite is dominant over other clay minerals. High contents of smectite where the smectite contains only few crystallographically intermixed illite layers is considered to be derived from the alteration of volcanic ash. (6) Lord Howe Rise is surrounded by regions of active Neogene and Quaternary volcanism; consequently, volcanic ash is an expected component of the sediment.

Despite the reasonably good correlation between our composite PGL stratigraphy and the changes in intensity of plate motions at the Pacific/Australian plate boundary, lending support to Kennett et al.'s (1977) interpretation of synchronous episodes of especially intense volcanism in the circum-Pacific region in the middle and early late Miocene and in the Quaternary, it is clear that the record at individual Leg 90 sites does not necessarily follow the general trend. More refined interpretations concerning the significance of the PGL stratigraphy is presently hampered by the lack of information on the specific source areas of the ashes. Potential sources include not only the major New Zealand, Tonga–Kermadec, and Melanesian calc-alkaline volcanic arcs at the Pacific/Australian plate boundary (Ballance, 1976; Coleman and Packham, 1976), but also the central volcanoes of eastern Australia (Wellman and McDougall, 1974), the chains of volcanic seamounts in western Tasman Sea (McDougall et al., 1981), and the back-arc basins of eastern Tasman Sea and Coral Sea (Karig, 1971; Malahoff et al., 1982). The pervasive diagenesis of the PGLs poses a challenging geochemical and mineralogical analytical problem if they are to be ultimately fingerprinted as to source.

ACKNOWLEDGMENTS

We thank A. P. W. Hodder, University of Waikato, for access to unpublished information on the convergence of the Pacific and Australian plates and C. K. Beltz, University of Waikato, for SEM assistance. Eileen Hemphill, U.S. Geological Survey, analyzed many of the samples for clay mineralogy, and our thanks go to J. R. Hein for allowing her the use of his XRD. We thank the staff of the West Coast DSDP Repository for their help in resampling some cores. We appreciate the constructive reviews by W. E. Dean, J. R. Hein, and T. L. Vallier. This work was supported, in part, by the U.S.G.S. Climate Program.

REFERENCES

Andrews, J. E., Packham, G., et al., 1975. *Init. Repts. DSDP*, 30: Washington (U.S. Govt. Printing Office).

Arrhenius, G., 1963. Pelagic sediments. *In* Hill, M. N. (Ed.), *The Sea* (Vol. 3): New York (Interscience Publ.), pp. 655–727.

Arthur, M. A., Dean, W. E., Bottjer, D., and Scholle, P. A., in press. Rhythmic bedding in Mesozoic–Cenozoic pelagic carbonate sequences: the primary and diagenetic origin of Milankovitch-like cycles. *In* Berger, A., Imbrie, J., and Hays. J. D. (Eds.), *Milankovitch and Climate:* NATO Advanced Workshop Series. (Riedel Publ. Co.).

Ballance, P. F., 1976. Evolution of the upper Cenozoic magmatic arc and plate boundary in northern New Zealand. *Earth Planet Sci. Lett.*, 28:356–370.

Berger, W. H., 1968. Radiolarian skeletons: solution at depths. *Science*, 159:1237–1238.

Biscaye, P. E., 1965. Mineralogy and sedimentation of Recent deep-sea clay in the Atlantic Ocean and adjacent seas and oceans. *Geol. Soc. Am. Bull.*, 76:803–832.

Bogoyavlenskiy, A. N., 1967. Distribution and migration of dissolved silica in oceans. *Intl. Geol. Rev.*, 9:133–153.

Bonatti, E., 1972. Authigenesis of minerals—marine. *In* Fairbridge, R. W. (Ed.), *Encyclopedia of Geochemistry and Environmental Sciences:* New York (Van Nostrand Reinhold Co.), pp. 48–56.

Brindley, G. W., 1972. Chlorite minerals. *In* Brown, G. (Ed.), *X-ray Identification and Crystal Structures of Clay Minerals.* London (Mineralogical Soc.) pp. 242–296.

Burns, R. E., Andrews, J. E., et al., 1973. *Init. Repts. DSDP*, 21: Washington (U.S. Govt. Printing Office).

Calvert, S. E., 1974. Deposition and diagenesis of silica in marine sediments. *In* Hsü, K. J., and Jenkyns, H. C. (Eds.), *Pelagic Sediments: On Land and Under the Sea.* Intl. Assoc. Sedimentol. Spec. Publ. 1, pp. 273–299.

Carroll, D. and Starkey, H. C., 1971. Reactivity of clay minerals with acids and alkalies. *Clays Clay Min.* 19:321–335.

Carter, R. M., and Norris, R. J., 1976. Cainozoic history of southern New Zealand: an accord between geological observations and plate tectonic predictions. *Earth Planet. Sci. Lett.*, 31:85–94.

Churkin, M., Jr., and Packham, G. H., 1973. Volcanic rocks and volcanic constituents in sediments, Leg 21, Deep Sea Drilling Project. *In* Burns, R. E., Andrews, J. E., et al., *Init. Repts. DSDP*, 21: Washington (U.S. Govt. Printing Office), 481–493.

Coleman, P. J., and Packham, G. H., 1976. The Melanesian borderlands and India-Pacific plates' boundary. *Earth Sci. Rev.*, 12: 197–233.

Davey, F. J., 1982. The structure of the South Fiji Basin. *Tectonophysics*, 87:185–241.

Dean W. E., Gardner, J. V., and Čepek, P., 1981. Tertiary carbonate-dissolution cycles on the Sierra Leone Rise, eastern equatorial Atlantic Ocean. *Mar. Geol.*, 39:81–101.

Dean, W. E., Gardner, J. V., Jansa, L. F., Čepek, P., and Seibold, E., 1977. Cyclic sedimentation along the continental margin of northwest Africa. *In* Lancelot, Y., Seibold, E., et al., *Init. Repts. DSDP*, 41: Washington (U.S. Govt. Printing Office), 965–986.

de Vries, T. J., and Schrader, H. J., 1981. Variation of upwelling/oceanic conditions during the latest Pleistocene through Holocene off the central Peruvian coast: A diatom record. *Mar. Micropaleontol.*, 6:57:–167.

Diester-Haass, L., and Schrader, H. J., 1979. Neogene coastal upwelling history off northwest and southwest Africa. *Mar. Geol.*, 29: 39–53.

Gardner, J. V., 1975. Late Pleistocene carbonate dissolution cycles in the eastern equatorial Atlantic. *In* Sliter, W. V., Bé, A. W. H., and Berger, W. H., (Eds.), *Dissolution of Deep-Sea Carbonates*. Cushman Foundation Foram. Res., Spec. Publ. 13, pp. 129–141.

Hathaway, J. C., and Sachs, P. L., 1965. Sepiolite and clinoptilolite from the Mid-Atlantic Ridge. *Am. Mineralogist.*, 50:852–867.

Hays, J. D. Cook, H. E., Jenkins, G., Orr, W., Goll, R., Cook, F., Milow, D., and Fuller, J., 1972. An interpretation of the geologic history of the eastern equatorial Pacific from the drilling results of *Glomar Challenger*, Leg 9. *In* Hays, J. D., et al., *Init. Repts. DSDP*, 9: Washington (U.S. Govt. Printing Office), 909–931.

Heath, G. R., 1974. Dissolved silica and deep-sea sediments. *In* Hay, W. W. (Ed.), *Studies in Paleo-oceanography*. Soc. Econ. Paleontol. Mineral. Spec. Publ. 20, pp. 77–93.

Hein, J. R., and Scholl, D. W., 1978. Diagenesis and distribution of late Cenozoic volcanic sediment in the southern Bering Sea. *Geol. Soc. Am. Bull.*, 89:197–210.

Hein, J. R., Scholl, D. W., and Gutmacher, C. E., 1976. Neogene clay minerals of the far NW Pacific and southern Bering Sea: Sedimentation and diagenesis. *In* Bailey, S. W. (Ed.), *AIPEA* Proceedings, International Clay Conf. Mexico City, 1975: Wilmette, Ill. (Aied Publishing Ltd.), pp. 71–80.

Hein, J. R., Scholl, D. W., and Miller, J., 1978. Episodes of Aleutian Ridge explosive volcanism. *Science*, 199:137–141.

Hodder, A. P. W., in press. Neogene tectonic intensity at the Australian-Pacific plate boundary at New Guinea and New Zealand; A vectorial approach. *J. Geol. Soc. Australia.*

Huang, T. C., Watkins, N. D., and Shaw, D. M., 1975. Atmospherically transported volcanic glass in deep-sea sediment: volcanism in sub-Antarctic latitudes of the South Pacific during late Pliocene and Pleistocene time. *Geol. Soc. Am. Bull.*, 86:1305–1315.

Huang, T. C., Watkins, N. D., Shaw, D. M., and Kennett, J. P., 1973. Atmospherically transported volcanic dust in South Pacific deep sea sediment cores at distances over 3000 km from the eruptive source. *Earth Planet. Sci. Lett.*, 20:119–124.

Hume, T. M., and Nelson, C. S., 1982. X-ray diffraction analytical procedure and some mineralogical characteristics for South Auckland region sediments and sedimentary rocks, with special reference to their clay fraction. *Occasional Rept. 10*, Univ. Waikato

Karig, D. E., 1971. Origin and development of marginal basins in the Western Pacific. *J. Geophys. Res.*, 76:2542–2561.

Kennett, J. P., 1981. Marine tephrochronology. *In* Emiliani, C. (Ed.), *The Sea* (Vol. 7): New York (John Wiley), pp. 1373–1436.

Kennett, J. P., McBirney, A. R., and Thunell, R. C., 1977. Episodes of Cenozoic volcanism in the circum-Pacific region. *J. Volc. Geotherm. Res.*, 2:145–163.

Kennett, J. P., and Thunell, R. C., 1975. Global increase in Quaternary explosive volcanism. *Science*, 187:497–503.

Knox, G. A., 1970. Biological oceanography of the South Pacific. *In* Wooster, W. S. (Ed.), *Scientific Exploration of the South Pacific:* Washington (National Academy of Sciences), pp. 155–182.

Ledbetter, M. T., 1982. Tephrochronology at Sites 502 and 503. *In* Prell, W. L., Gardner, J. V., et al., *Init. Repts. DSDP*, 68: Washington (U.S. Govt. Printing Office), 403–408.

McDougall, E., Embleton, B. J. J., and Stone, D. B., 1981. Origin and evolution of Lord Howe Island, southwest Pacific Ocean. *J. Geol. Soc. Australia*, 28:155–176.

MacEwan, D. M. C., 1972. Montmorillonite minerals. *In* Brown, G. (Ed.), *X-ray Identification and Crystal Structures of Clay Minerals*. London (Mineralogical Soc.), pp. 143–207.

Malahoff, A., Feden, R. H., and Fleming, H. S., 1982. Magnetic anomalies and tectonic fabric of marginal basins north of New Zealand. *J. Geophys. Res.*, 87:4109–4125.

Mitchell, A. H. G., and Warden, A. J., 1971. Geological evolution of the New Hebrides island arc. *J. Geol. Soc. London*, 127:501–529.

Mossler, J. M., Hayes, J. B., 1966. Ordovician K-bentonites of Iowa. *J. Sed. Petrol.*, 36:414–424.

Nayudu, Y. R., 1964. Palgonite tuffs (hyaloclastites) and the products of posteruptive processes. *Bull. Volcanolog.*, 27:332–341.

Nelson, C. S., and Hume, T. M., 1977. Relative intensity of tectonic events revealed by the Tertiary sedimentary record in the North Wanganui basin and adjacent areas, New Zealand. *N.Z. J. Geol. Geophys.*, 20:369–392.

Ninkovich, D., and Donn, W. L., 1976. Explosive Cenozoic volcanism and climatic implications. *Science*, 194:899–906.

Peterson, M. N. A., and Griffin, J. J., 1964. Volcanism and clay minerals in the southeastern Pacific. *J. Mar. Res.*, 22:287–312.

Schuette, G., and Schrader, J. J., 1981. Diatom taphocoenoses in the coastal upwelling area off southwest Africa. *Mar. Micropaleontol.*, 6:131–155.

Shaw, D. M., Watkins, N. D., and Huang, T. C., 1974. Atmospherically transported volcanic glass in deep-sea sediment: theroretical calculations. *J. Geophys. Res.*, 79:3087–3094.

Siever, R., and Kastner, M., 1967. Mineralogy and petrology of some Mid-Atlantic Ridge sediments. *Mar. Res.*, 25:263–278.

Sporli, K. B., 1980. New Zealand and oblique-slip margins: tectonic development up to and during the Cainozoic. *Spec. Publ. Internat. Assoc. Sedimentol.*, 4:147–170.

Stewart, R. J., 1975. Late Cainozoic explosive eruptions in the Aleutian and Kuril island arcs. *Nature*, 258:505–507.

Stonecipher, S. A., 1974. Distribution of zeolites in marine sediments, *Geol. Soc. Am. Abstr. with Progr.* 6:262–263. (Abstract)

Thompson, J., and Wilson, T. R. S., 1980. Burrow-like structures at depth in a Cape Basin red clay core. *Deep-Sea Res.*, 27A:97–102.

Vogt, P. R., 1972. Evidence for global synchronism in mantle plume convection, and possible significance for geology. *Nature*, 240: 87–118.

von Rad, U., and Rösch, H., 1972. Mineralogy and origin of clay minerals, silica and authigenic silicates in Leg 14 sediments. *In* Hayes,

D. E., Pimm, A. C., et al., *Init. Repts. DSDP*, 14: Washington (U.S. Govt. Printing Office), 727–751.

Watts, A. B., Weissel, J. K., and Davey, F. J., 1977. Tectonic evolution of South Fiji marginal basins. *In* Talwani, M., and Pittman, W. C. (Eds.), *Island Arcs Deep-Sea Trenches, and Back-arc Basins*. Am. Geophys. Un. Maurice Ewing Ser. 1:419–427.

Weaver, C. E., 1958. The effects and geological significance of potassium "fixation" by expandable clay minerals derived from muscovite, biotite, chlorite and volcanic material. *Am. Mineralogist*, 43: 839–861.

Weaver, P. P. E., and Schultheiss, P. J., 1983. Vertical open burrows in deep-sea sediments 2 m in length. *Nature*, 301:329–331.

Wellman, P., McDougall, I., 1974. Cainozoic igneous activity in eastern Australia. *Tectonophysics*, 23:49–65.

Wilson, M. D., and Pittman, E. D., 1977. Authigenic clays in sandstones: Recognition and influence on reservoir properties and paleoenvironmental analysis. *J. Sed. Petrol.*, 47:3–31.

Date of Initial Receipt: 11 May 1984
Date of Acceptance: 3 August 1984

26. NATURE, CHEMISTRY, AND ORIGIN OF LATE CENOZOIC MEGASCOPIC TEPHRAS IN LEG 90 CORES FROM THE SOUTHWEST PACIFIC[1]

Campbell S. Nelson, University of Waikato
and
Paul C. Froggatt and Gregory J. Gosson, Victoria University[2]

ABSTRACT

Several thin (1-10 cm) megascopic vitric tephras occur in the late Cenozoic calcareous oozes on Lord Howe Rise in the Tasman Sea and off eastern South Island, New Zealand. Of the 18 tephras analyzed 15 are silicic (75-78% SiO_2) with abundant clear glass shards and a biotite ± hypersthene ± green hornblende ferromagnesian mineralogy. The Neogene silicic tephras were derived from the now-extinct Coromandel volcanic area in New Zealand, and the Quaternary ones from the presently active Central Volcanic Region of New Zealand. On the basis of glass chemistry and age, several of the Quaternary tephras are probably correlatives, and at least two can be matched to the major on-land Mt. Curl tephra (~0.25 m.y.). The occurrence of correlative silicic tephras both northwest and southeast of New Zealand may result from particularly violent eruptions, the ash below and above an altitude of ~20 km being dispersed in opposite directions toward the Pacific Ocean and Tasman Sea, respectively. Ash drifting eastward into the southeasterly trade wind belt off northeastern New Zealand could also be carried into the central and northern Tasman Sea.

Three megascopic tephras consist of altered basic shards and common labradorite crystals. They record Neogene explosive basaltic to andesitic activity from nearby ocean island or ridge sources in the Ontong-Java Plateau and Vanuatu regions.

The megascopic tephras are a very incomplete and biased record of late Cenozoic explosive volcanism in the southwest Pacific because the innumerable, thin, green argillaceous layers in the cores (Gardner et al., this volume) probably represent devitrified intermediate to basic tephras derived mainly from oceanic arc volcanism along the Pacific/Australia plate boundary. In contrast to the New Zealand-derived silicic glass shards, the preservation potential of these more basic shards in Leg 90 calcareous sediments was low.

INTRODUCTION

The southwest Pacific region has been characterized by extensive volcanism throughout the late Cenozoic (Fig. 1). Volcanic ash deposited in deep-sea sediments accumulating in the vicinity and downwind of eruptive centers can provide an accurate record of explosive volcanic activity (Kennett, 1981). In turn, the tephras form invaluable stratigraphic marker horizons with the potential for dating the associated sediments and correlating them over considerable distances.

Leg 90 drilling obtained high-quality cores through middle to late Cenozoic sediments at nine sites (586-594) in the southwest Pacific (Fig. 1). All sites were located in water depths of between 1000 and 2200 m, principally on the Lord Howe Rise in Tasman Sea, but also on the Ontong-Java Plateau in the western Pacific and off eastern South Island, New Zealand. The cores consist predominantly of foraminifer-bearing nannofossil oozes and chalks, with few and minor unconformities in their Neogene-Quaternary part. Hemipelagic oozes occur at the southernmost site (Site 594) close to New Zealand. The sediments were drilled using the hydraulic piston corer and extended core barrel systems (see Introductory chapter, this volume). These provided not only high core recovery (average 90%), but also excellent sections that are much less disturbed than the rotary cores previously obtained from the region on DSDP Legs 21 and 29 (Burns, Andrews, et al., 1973; Kennett, Houtz, et al., 1975). Conditions were optimal for detecting discrete tephra layers and other minor lithologies within the soft oozes. In anticipation of this, one of the precruise objectives of Leg 90 was the development of a deep-sea tephrostratigraphy for the region (see Introductory chapter, this volume).

Only a relative small number of visible vitric tephra layers were detected during core description (Appendix). However, trace amounts (<1%) of colorless and occasional brown glass shards were ubiquitous sediment components; their occurrence as revealed in routine shipboard smear slides has been summarized for five sites by Gardner, Nelson, et al. (this volume). Conceivably, careful processing of channel samples from cores may ultimately provide a useful tephrostratigraphy based on this finely dispersed volcanic glass fraction (e.g., Watkins and Huang, 1977). On the other hand, Gardner, Nelson, et al. (this volume) have suggested that diagenetic processes played a major role in determining and possibly masking the distribution of volcanic material in the Tasman Sea sites. They inferred that a proportion of the glassy component may have been dissolved from those sediments in contact with silica-undersaturated Antarctic Intermediate Water on Lord Howe Rise and, moreover, that common pale green laminae in the nannofossil oozes and chalks may represent the smectitized alteration products of former thin ash layers.

---

[1] Kennett, J. P., von der Borch, C. C., et al., *Init. Repts. DSDP*, 90: Washington (U.S. Govt. Printing Office).

[2] Addresses:(Nelson) Department of Earth Sciences, University of Waikato, Hamilton, New Zealand; (Froggatt) Centre for Continuing Education and Department of Geology, Victoria University, Wellington, New Zealand; (Gosson) Department of Geology, Victoria University, Wellington, New Zealand.

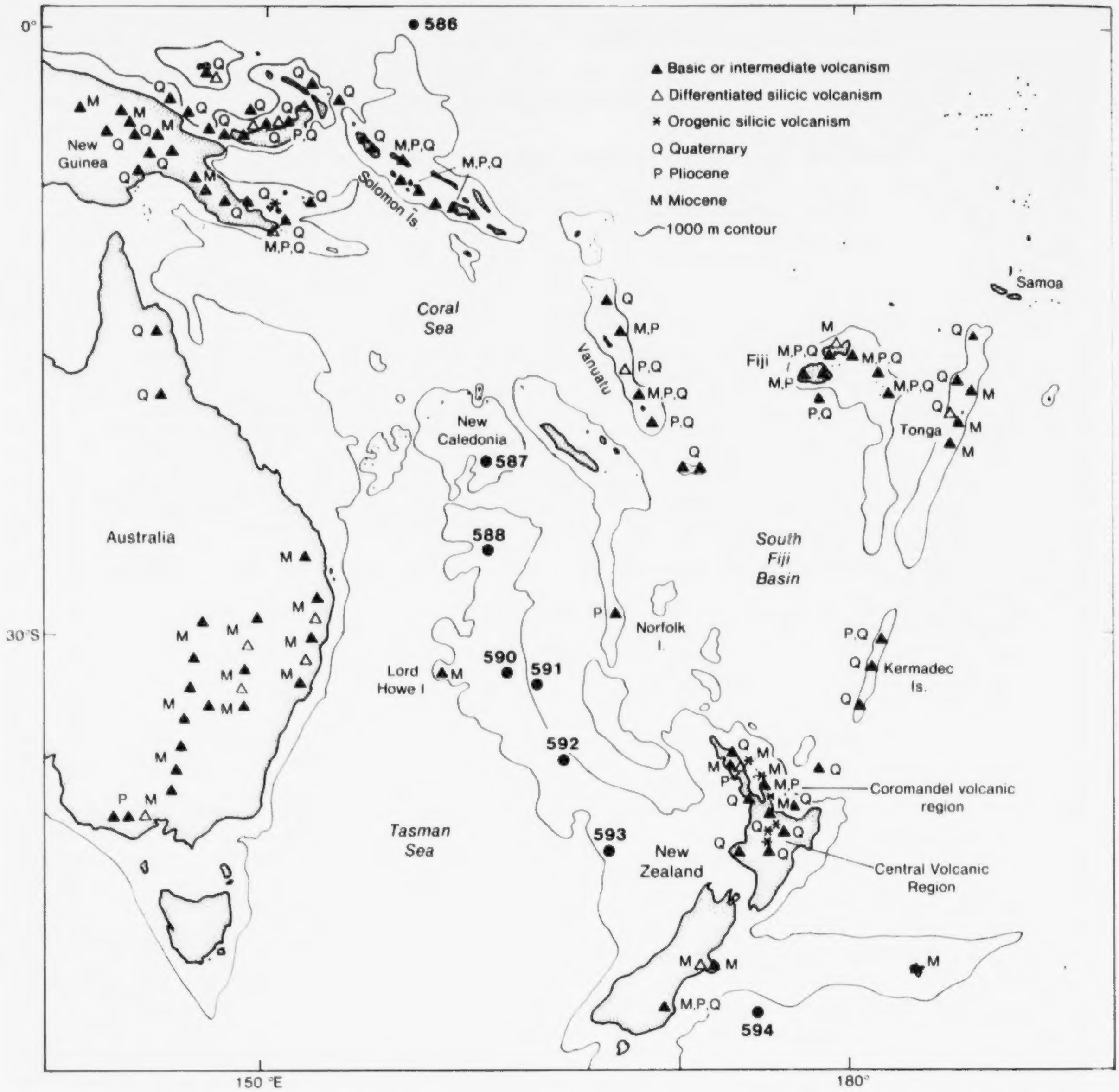
0°
30°S
150 °E
180°
▲ Basic or intermediate volcanism
△ Differentiated silicic volcanism
* Orogenic silicic volcanism
Q Quaternary
P Pliocene
M Miocene
1000 m contour
586
587
588
590
591
592
593
594
New Guinea
Solomon Is
Coral Sea
Vanuatu
Fiji
Samoa
Tonga
New Caledonia
Australia
South Fiji Basin
Norfolk I.
Lord Howe I
Kermadec Is.
Tasman Sea
New Zealand
Coromandel volcanic region
Central Volcanic Region
M,P,Q

Figure 1. Distribution and character of Neogene and Quaternary subaerial volcanism in the southwest Pacific region (modified from Churkin and Packham, 1973; after Gosson, in prep.) in relation to DSDP Leg 90 Sites 586 to 594.

This chapter describes only those glass-dominated ash layers forming discrete, megascopic layers (= tephras) in Leg 90 cores. The principal objectives are to note the mineralogy of the tephras; determine the chemical composition of their glass shards, and hence the nature of the magmas; investigate the possibility of intercore tephra correlations; and suggest possible eruptive sources for the tephras.

RECOGNITION AND COLLECTION OF MEGASCOPIC TEPHRAS

During routine shipboard description of Leg 90 cores, special attention was paid to the occasional minor lithologies encountered within the lithologically monotonous sequences of calcareous oozes and chalks. The majority of these minor lithologies were pale green (bentonitic) laminae (Gardner, Nelson, et al., this volume); sediment layers enriched in pyrite, biosiliceous material, or glauconite; and diagenetic color-enhanced bioturbation structures (Nelson, this volume). The minor lithologies occasionally contained conspicuous glass shards, suggesting they represented primary air-fall tephra that had settled through the water column to the sea bed. In these cases, 5–10 cm^3 samples of the ash material plus contaminating host ooze were collected by the sedimentologists on duty. On shore, the summary core and smear slide descriptions were perused again and additional, supposedly glass-rich, samples were requested to fill in some of the gaps in the collection of megascopic ash samples. A total of 54 samples was examined finally, but only 18 (T1 to T18) contained sufficiently abundant glass undisputedly to represent discrete tephra layers (see Appendix).

ANALYTIC METHODS

To determine the tephra sand mineralogy, samples were wet-sieved through a 63-μm mesh sieve, cleaned in an ultrasonic bath, wet-sieved again to remove impurities, and dried at 70°C. At this stage samples consisted of glass shards, varying amounts of foraminiferal tests, and small quantities of felsic, mafic, and opaque minerals. After first being checked for magnetite with a hand magnet, these components were separated by repeated passage of the sample through a Frantz Isodynamic electromagnetic separator (20° forward and 15° side slope). The majority of mafic and felsic minerals (other than pyrite) was contained in the magnetic fraction at 0.5–0.8 A, whereas glass and foraminifer grains were concentrated in the magnetic and nonmagnetic fractions, respectively, at 1.8 A. Any foraminifers remaining in the glass shard extract at this stage were removed. Minerals were identified in detrital slide mounts using a petrographic microscope, and the glass shards were examined both in thin section and with a scanning electron microscope.

The chemical composition of glass shards from 16 of the 18 megascopic tephras has been determined using an electron microprobe. A beam of 8 nA and 20 μm diameter was used to minimize alkali loss. Instrumental conditions and standard analyses are in Froggatt (1983). All of the analyzed shards were visually isotropic and free of microlites and inclusions. Homogeneity of each sample was checked by analyzing freshly polished internal surfaces of 12 to 15 shards. All glass analyses are recalculated to 100%, the deficiency being recorded as H_2O. This water is presumed to be gained by postdepositional hydration and values are typical of silicic tephras (see Froggatt, 1983). Tephras T2 and T3 contained too few unaltered shards for analysis, but the chemical composition of the plagioclase crystals in T3 (and also T1) has been determined.

DISTRIBUTION, APPEARANCE, AND AGE OF TEPHRAS

The stratigraphic locations of the 18 megascopic tephras studied are shown in Figure 2 and their appearance in cores in Figure 3. Samples, stratigraphy, and descriptive information for the individual tephras are summarized in Table 1.

Compared to the white (N9) to very light gray (N8) color of the host calcareous oozes (chalks), the tephras have distinctly greenish hues, ranging from light to dark greenish gray. They are typically only a centimeter or two thick, occasionally reaching 10 cm and exceptionally (T5) 25 cm. Several have sharp lower contacts, some exhibit normal size grading, and most have diffuse upper contacts with evidence of upward dissemination of ash by bioturbation into the overlying ooze (Fig. 3). Bioturbate structures are discernible within the thicker tephras, and biogenic reworking has totally disrupted some of the thinner ash layers and concentrated ash material as diffuse wisps, blebs, and pods within the host ooze.

Ten of the tephras are of Quaternary age, three are Pliocene, and five are Miocene (Fig. 2). Biostratigraphic age estimates are shown in Table 1. Absolute ages have been estimated by assuming a constant rate of sedimentation between an ash layer and the nearest paleomagnetic chron or subchron boundary in the case of each of the Quaternary tephras, and the nearest calcareous nannoplankton zone boundary for each of the Tertiary tephras (see Site chapters, this volume). In several cases two separate ages have been estimated, one using paleomagnetic and the other biostratigraphic information, or by employing datums both above and below an ash layer. In those cases the preferred age estimate of the tephra is italicized in Table 1.

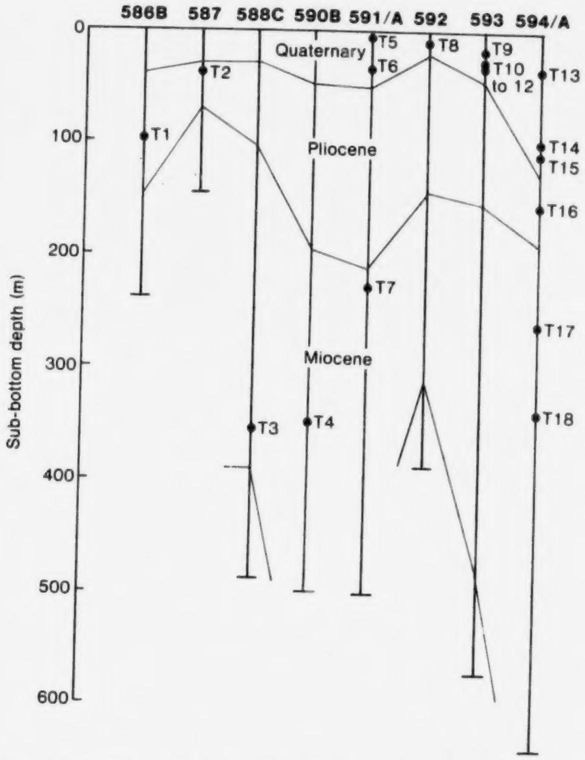

Figure 2. Stratigraphic distribution of the analyzed 18 megascopic tephras (T1 to T18) from Leg 90 sediments.

PETROGRAPHY OF TEPHRAS

Because many of the sampled tephras included host calcareous ooze material, it was not possible to determine detailed textural properties for the discrete tephra layers. However, all were noticeably coarser than the associated oozes, and most had very fine to fine sandy textures (Table 2). The coarsest ash material occurred in samples (T1 to T3) from the three northernmost sites.

The sand fraction mineralogy of the 18 megascopic tephras is summarized in Table 2. Except for tephra T3, they are dominated by clear and/or milky glass shards (Plate 1). The minor crystalline components consist mainly of plagioclase, biotite, hypersthene, and green hornblende. White to pale green smectite-dominated aggregates occur in several samples and have formed possibly from the alteration of former glass or glassy rock fragments (cf. Gardner, Nelson, et al., this volume). Other alteration products include limonitized and leucoxene-coated (?) grains. In tephra T2 the glass is mostly devitrified but retains its shard morphology; in tephra T3 no free glass shards remain and the ash consists principally of feldspars, some with remnant glass jackets, and clay aggregates. Diagenetic pyrite (Table 3) occurs in some

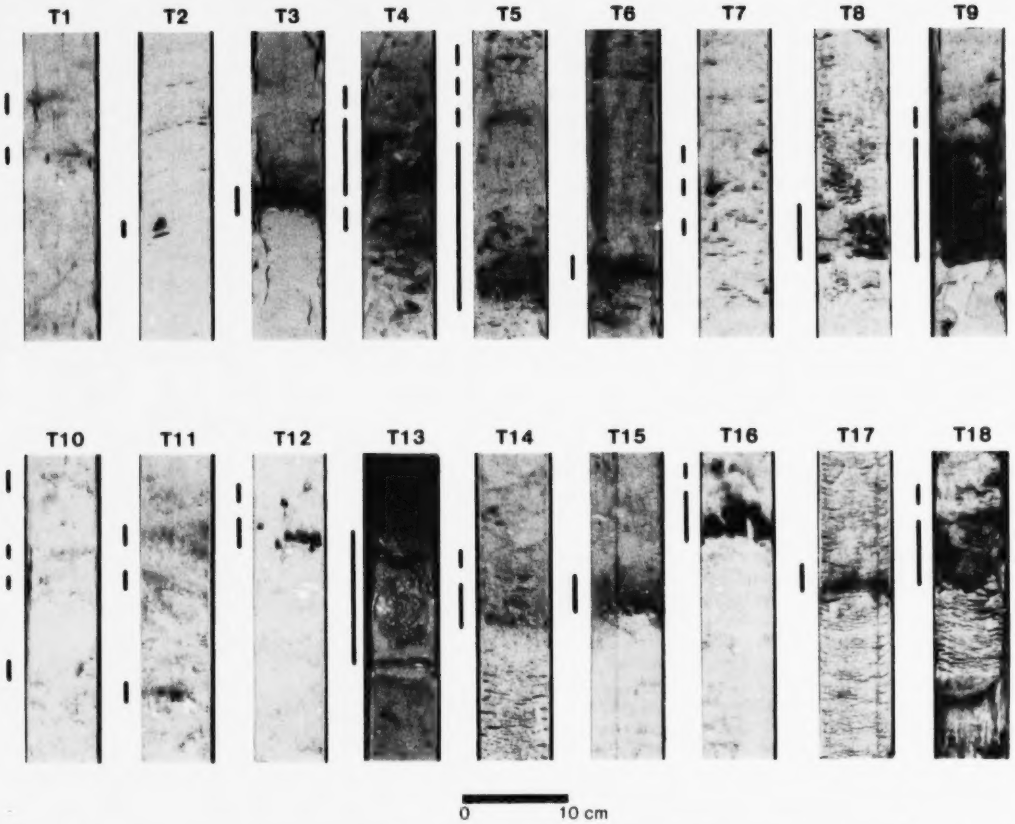

Figure 3. Appearance of the 18 megascopic tephras (T1 to T18) in Leg 90 cores (see Table 1 for descriptions of individual tephras). The bar to the left of each 30-cm-long core section indicates the position of the tephras. Core sections are located as follows: T1, 586B-11-3, 100–130 cm; T2, 587-5-5, 30–60 cm; T3, 588C-6-3, 35–65 cm; T4, 590B-38-4, 100–130 cm; T5, 591-2-2, 30–60 cm; T6, 591-5-3, 120–150 cm; T7, 591A-25-3, 10–40 cm; T8, 592-2-6, 65–95 cm; T9, 593-3-5, 65–95 cm; T10, 593-4-4, 20–50 cm; T11, 593-4-4, 60–90 cm; T12, 593-4-4, 90–120 cm; T13, 594-5-2, 20–50 cm; T14, 594-12-2, 25–55 cm; T15, 594A-8-3, 35–65 cm; T16, 594A-10-6, 0–30 cm; T17, 594-28-5, 45–75 cm; T18, 594-36,CC (0–30 cm).

samples. It forms a coating on glass shards in tephra T1 (Plate 1, Fig. 1; Fig. 4A) and is a microcrystalline replacement of the glass in tephra T4 (Fig. 4B), forming completely pyritized shards in some.

A scheme (Fig. 5) developed by G. J. Gosson (in prep.) is used here to classify the dominant glass shard morphologies in the 60–250 μm size range of the megascopic tephras (Table 4). The bulk of the Leg 90 shards are only slightly stretched with relatively few vesicles, and bubbles are moderately large with moderately thick walls (Tables 4). As a consequence, many of the shards form subequant- to rectangular-shaped, flat to gently curved plates, with up to two or three low-amplitude parallel ridges in some. Tephras T1 and T2 are distinctive because they are highly vesicular with relatively small bubble sizes and thin walls. A small percentage of shards in tephras T7, T8, T14, T15, and T17 are very stretched and highly vesicular. A feature of Miocene samples T17 and T18 is the polygonal shape of some bubble walls.

TEPHRA CHEMISTRY AND MAGMA TYPES

The glass analyses (Table 5) indicate that tephras T4 to T18 are all silicic (SiO_2 from 73.7 to 78.3 wt. % on an anhydrous basis) with broadly similar chemistry but varying amounts of most elements, especially the alkalis and iron and calcium. The variation in glass chemistry is evident on a plot of CaO versus FeO (Fig. 6) where, apart from tephra T15 (= 0 on Fig. 6), the glass analyses from individual tephras are relatively tightly clustered and many are unique. The occurrence of biotite, hypersthene, and/or green hornblende in the majority of these tephras (Table 2) is also consistent with a silicic volcanic source (Ewart, 1966; Kohn, 1973; Ewart et al., 1975; Seward, 1976; Cole, 1979). In contrast, tephra T1 is basaltic and has K_2O, TiO_2, SiO_2, and MgO values typical of ocean island or a more evolved mid-ocean ridge basalt (Table 6). Normative mineralogy of tephra T1 glass composition indicates it is quartz tholeiite, and the feldspar is calcic-labradorite (Table 7). Despite the lack of suitable glass for analysis in samples T2 and T3, both probably are basic also because (1) the abundant plagioclase crystals in T3 are sodic-labradorite (Table 7); (2) the devitrified glass shard morphologies in T2 are very similar to those in T1 (Table 4), and, in particular, both have very thin bubble walls suggestive of a low-viscosity magma; and (3) all three tephras (T1 to T3) lack the ferromagnesian

Table 1. Stratigraphy of megascopic vitric tephras in Leg 90 cores.

Tephra	Site	Core-Section (interval in cm)	Sub-bottom depth (m)	Thickness (cm)	Age		Lithologic description
					Period	m.y.^{a}	
T1	586	11B-3, 114	100.44	<1	early Plio.	3.87^{1}	Diffuse light greenish gray (5G 8/1) ash pods formed by bioturbation
T2	587	5-5, 48	38.28	<1	early Plio.	2.91^{2} *3.70*^{1}	Distinct dark gray (N3) ash pod formed by bioturbation
T3	588	6C-3, 52	357.25	2	early Mio.	22.0^{1}	Distinct dark bluish gray (5BG 4/1) ash layer, sharp base, burrowed diffuse top
T4	590	38B-4, 113	351.15	10	late Mio.	11.0^{1}	Prominently bioturbated, disrupted dark greenish gray (5GY 4/1) ash bed, pyritiferous, associated PGLs^{b}
T5	591	2-2, 54	5.45	25	late Pleist.	0.24^{2}	Diffuse light gray to light greenish gray (N7 to 5G 8/1) ash bed, sharp base, subtle normal grading into overlying ooze
T6	591	5-3, 144	36.64	1.5	early Pleist.	*1.37*^{2} 1.33^{2}	Distinct greenish gray (5GY 6/2) ash layer, sharp base, diffuse bioturbated top
T7	591	25A-3, 25	230.75	1	late Mio.	7.0^{1}	Scattered grayish olive (10Y 4/2) ash pods formed by bioturbation
T8	592	2-6, 83	12.83	5	middle Pleist.	*0.85*^{2} 0.95^{2}	Distinct light gray (N6) ash bed, sharp base, irregular top and disrupted by bioturbation
T9	593	3-5, 78	21.50	10	middle Pleist.	0.93^{2}	Distinct medium gray (N5) ash bed, sharp base, burrowed irregular top
T10	593	4-4, 30	29.10	<1	early Pleist.	*1.26*^{2} 1.38^{2}	Diffuse grayish yellow green (5GY 7/2) ash layer and wisps possibly due to bioturbation
T11	593	4-4, 80	29.60	1	early Pleist.	*1.26*^{2} 1.38^{2}	Diffuse grayish yellow green (5GY 7/2) ash pods and wisps formed by bioturbation
T12	593	4-4, 100	29.80	2	early Pleist.	*1.26*^{2} 1.38^{2}	Distinct grayish yellow green (5GY 7/2) ash layer, sharp base, disrupted by bioturbation
T13	594	5-2, 30	36.50	10	late Pleist.	0.28^{1} *0.27*^{2}	Diffuse, soupy-textured, massive bluish gray (5B 6/1) ash with moderately sharp contacts
T14	594	12-2, 40	103.80	2	middle Pleist.	*0.77*^{2} 0.73 to 1.66^{2}	Diffuse dark greenish gray (5GY 6/1) ash bed with abruptly gradational contacts with ooze
T15	594	8A-3, 50	112.00	1	middle Pleist.	*0.85*^{2} 0.73 to 1.66^{2}	Diffuse light olive gray (5Y 6/1) ash layer disrupted by bioturbation
T16	594	10A-6, 6	157.46	3	early Plio.	*3.9*^{1} 2.2 to >2.47^{2}	Distinct but partly disrupted dark gray (N3) ash bed with upward dissemination of ash
T17	594	28-5, 56	262.06	2	late Mio.	8.6^{1}	Diffuse light olive gray (5Y 6/1) ash layer with sharp lower and gradational upper contact with ooze
T18	594	36, CC	341.75	7	mid Mio.	9.4^{1}	Diffuse olive gray (5Y 4/1) ash bed, sharp base, gradational top

[a] Estimated age assuming constant rates of sedimentation between dated boundaries of associated nannofossil (1) or paleomagnetic (2) zones. Where two ages are given, the italicized age is preferred.

[b] PGL = pale green laminae (Gardner, Nelson, et al., this volume).

Table 2. General grain size classification and mineralogic composition[a] of megascopic tephras in Leg 90 sediments.

	T1	T2	T3	T4	T5	T6	T7	T8	T9	T10	T11	T12	T13	T14	T15	T16	T17	T18
Grain size (mm)																		
Dominant[b]	fsu	vfsu	msl	vfsl	fsl	vfsu	vfsu	fsu	fsl	vfsu	fsl	vfsu	fsl	vfsu	vfsu	fsu	fsu	vfsl
Maximum	0.4	0.4	0.8	0.2	0.3	0.3	0.3	0.3	0.3	0.2	0.3	0.2	0.3	0.2	0.2	0.3	0.3	0.2
Mineralogy																		
Magnetite			R															
Pyrite	R			C	R		T					R			R	R	R	
Altered fragments[c]		A	C	C	C		R	C	C	R	R	C	C	C	C	C	R	C
Hypersthene								R	R	T	T	T	R	T	R	R	T	
Green hornblende					T				T	T			T		R	T	T	
Brown hornblende																T		T
Biotite				C	R			R	T		T		T	R			C	R
Muscovite																		C
Plagioclase	R	R	A	T	T			T	T	T	T	T	T	T		T		
Quartz								T	T	T			T					T
Glass shards																		
Clear	A	R		C	A	A	A	A	A	A	A	A	A	A	A	A	A	C
Brown					R				R				R	R	T	T		

A = abundant; C = common; R = rare; T = trace.

vfsl and vfsu = very fine sand lower (0.06–0.10 mm) and upper (0.10–0.13 mm), respectively; fsl and fsu = fine sand lower (0.13–0.19 mm) and upper (0.19–0.25 mm), respectively; msl = medium sand lower (0.25–0.35 mm).

Includes argillized shards, limonitized fragments, and grains with ?leucoxene coatings.

Table 3. Microprobe analysis of pyrite replacing glass shard in tephra T1, Site 586.

	T1 pyrite	
	Wt.%	Atom
Fe	47.00	1.01
S	53.28	1.99
Cu	0.03	—
Mn	—	—
Ni	0.02	—
	100.33	3.00

mineralogy typical of silicic tephras (Table 2). Thus, whereas most of the megascopic tephras (T4 to T18) in Leg 90 sediments were derived from silicic magmas, tephras T1 to T3 had a basic or intermediate magma source.

INTERCORE CORRELATION

Several of the megascopic tephra samples have a glass chemistry (Table 5) distinctive enough to be positively differentiated (Fig. 6). Some of the tephras overlap in their glass chemistry, and those of a similar age probably are correlative. None of the analyzed Miocene or Pliocene tephras (T1 to T4, T7, and T16 to T18) are sufficiently similar in composition and age (Tables 1 and 5; Fig. 6) to be regarded as correlatives so that eight separate explosive events are indicated by the Neogene megascopic tephras—three basaltic and five silicic. Of the 10 Quaternary tephras (T5, T6, and T8 to T15), samples T5 and T13 are chemically identical and of similar late Pleistocene age, samples T6 and T10 to T12 are likewise chemically similar and of comparable early Pleistocene age, and samples T8 and T9 form a third chemical cluster and are of middle Pleistocene age. Of the two remaining Quaternary tephras, both are middle Pleistocene, but T14 is chemically unique, and T15 clearly plots as two distinct clusters on Figure 6, one falling within the T6/T10/T11/T12 field and the other being unique. The cause of this bimodality is not clear and, although biologic mixing of tephras may be represented, interpretation is hampered by the uncertain paleomagnetic zones at Site 594 (see Site chapter, this volume). Thus the between-core correlation implied on the basis of age and glass chemistry indicates that the 10 Quaternary tephras analyzed record at most five eruptive events, all silicic (Fig. 7).

TEPHRA SOURCES

Since New Zealand is the only area in the southwest Pacific with voluminous silicic volcanism during the late Cenozoic (Fig. 1), it is the most likely source of the silicic ash layers in all Leg 90 cores. The Coromandel region and the Central Volcanic Region of North Island have produced large-volume silicic eruptions from middle Miocene to Pliocene and throughout the Quaternary, respectively (Fig. 1; Ballance, 1976; Suggate et al., 1978; Cole, 1979). The glass chemistry of the Leg 90 silicic tephras is compatible with the known chemistry of the volcanic products from North Island sources (Ewart, 1963, 1966; Froggatt, 1983; Gosson, in prep.).

The Leg 90 silicic tephras are still not correlated with specific source eruptions. Of several silicic tephras in

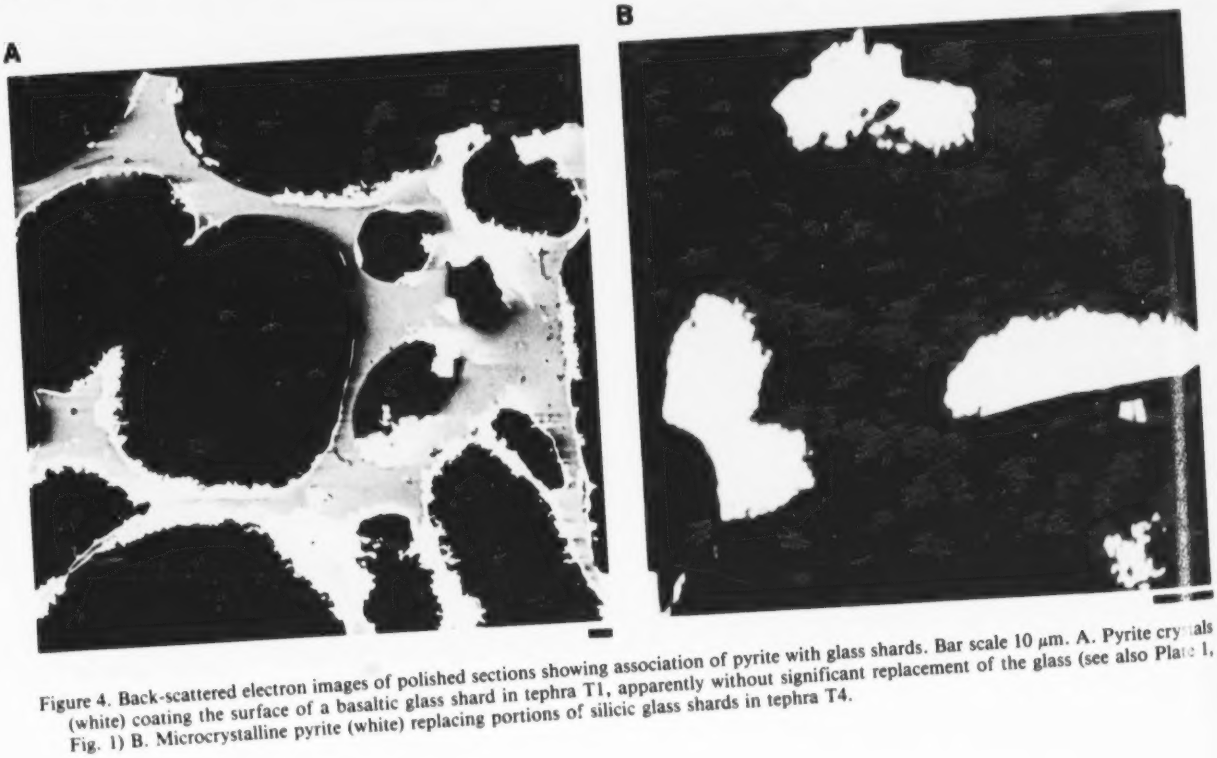

Figure 4. Back-scattered electron images of polished sections showing association of pyrite with glass shards. Bar scale 10 μm. A. Pyrite crystals (white) coating the surface of a basaltic glass shard in tephra T1, apparently without significant replacement of the glass (see also Plate 1, Fig. 1) B. Microcrystalline pyrite (white) replacing portions of silicic glass shards in tephra T4.

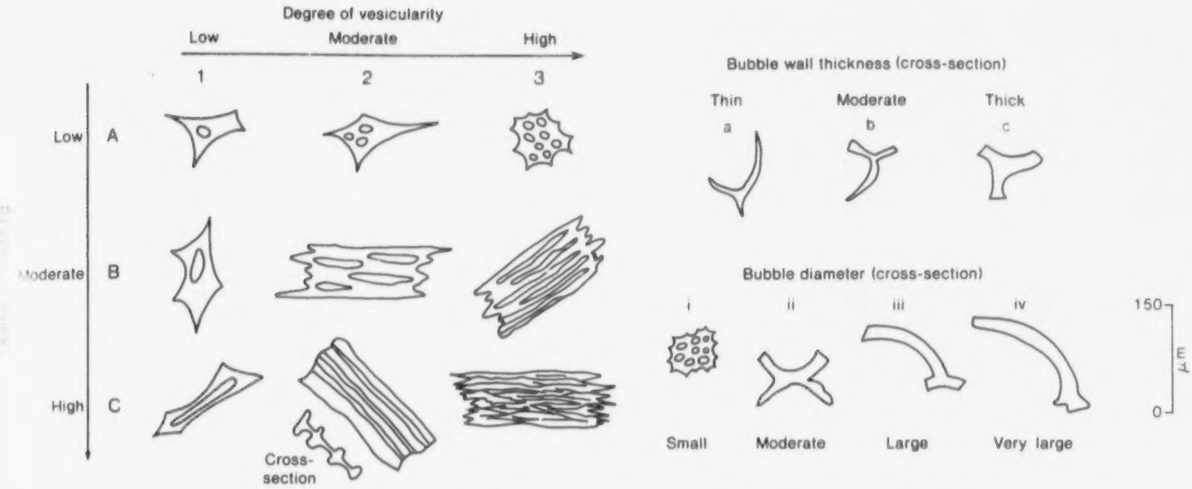

Figure 5. Descriptive terminology for morphologic classification of glass shards in the 60–250 μm size fraction (from Gosson, in prep.).

Table 4. General morphologic features of dominant glass shard types in megascopic tephras from Leg 90 cores. Categories defined in Figure 5.

	Vesicularity			Stretching			Bubble diameter				Bubble wall thickness		
Tephra	1	2	3	A	B	C	i	ii	iii	iv	a	b	c
T1		X	X	X				X			X		
T2			X	X			X	X			X		
T4	X			X				X	X			X	X
T5	X	X			X				X		X	X	
T6	X			X				X				X	X
T7	X	X		X	X			X	X			X	
T8		X			X				X			X	
T9	X	X		X	X			X	X				X
T10	X			X				X	X		X	X	
T11	X	X		X				X	X		X	X	X
T12	X	X		X				X			X		X
T13	X			X					X			X	
T14		X	X	X			X					X	X
T15	X			X						X		X	
T16		X	X	X	X		X	X			X		
T17	X			X				X	X				X
T18	X			X	X			X	X			X	X

piston cores of abyssal sediments from east of New Zealand, five, labeled A to E by Ninkovich (1968), were tentatively correlated using paleomagnetic dating (Watkins and Huang, 1977) with tephras in Pleistocene marine sediments on land (Seward, 1974, 1976). Using glass analyses, Froggatt (1983) has suggested that land equivalents of three of Ninkovich's deep-sea tephras are widespread in North Island and has related two of them to specific ignimbrites. The glasses in deep-sea tephras A and D are compositionally similar to and likely correlatives of two separate sets of equivalently aged tephras in Leg 90 cores (Fig. 7). Froggatt (1983) has correlated tephra D with the widespread Mt. Curl tephra of New Zealand, and the Whakamaru ignimbrite of the Central Volcanic Region, the source vent for which was probably Lake Taupo (Briggs, 1976). The evidence is a combination of similar stratigraphic position and a common distinctive glass chemistry, with high K_2O values (>4.00%) and a Na_2O/K_2O ratio much less than 1.0 (typically 0.8). The Leg 90 tephras T5 and T13 are chemically indistinguishable (Table 5), have similar stratigraphic position, and thus are possibly distal air-fall correlatives of Whakamaru ignimbrite. Moreover, tephras T5 and T13 are among the thickest recorded in Leg 90 cores (Table 1). Tephra T5 is located over 500 km northwest of New Zealand (Site 591), whereas tephra T13 was cored at Site 594, 250 km off eastern South Island (Fig. 1). An extremely large eruptive event is implied.

The Coromandel region of northern North Island (Ballance, 1976; Suggate et al., 1978) is probably the eruptive source of the pre-Quaternary silicic tephras in Leg 90 cores, but specific centers cannot be determined. The volcanic history of Coromandel is poorly understood, and the Neogene tephrostratigraphy there virtually is unknown. A partial record of Coromandel volcanic activity is preserved as primary and reworked tephras in thick (>7 km) marine sequences now uplifted in eastern North Island (Gosson, in prep.). Tentative correlations of Leg 90 tephras with these tephras can be made as follows. Figure 8 is a graphical means (after Sarna-Wojcicki et al., 1984) of displaying the similarities and differences between the shard chemistry of two samples. Ratios are calculated by dividing the mean weight percent of an element in a Neogene tephra sample from land by the mean weight percent of the same element in a Leg 90 tephra sample. Chemically similar samples will have ratios close to 1.00 for each element, whereas differences will be shown by ratios greater or less than 1.00. Seven eastern North Island late Miocene tephras that are closest in chemistry to tephra T17 (Table 5) are compared with tephra T17 in Figure 8A. Samples G019, G255, and G256 are most similar to tephra T17 and, being comparable in age, could be correlatives. The abundance of biotite in both tephras T17 (Table 2) and G019 (Gosson, in prep.) strengthens the suggested correlation between these two tephras. A similar approach for late Miocene tephra T7

Table 5. Chemical composition of glass shards from megascopic tephras in Leg 90 cores.

	T1	T4	T5	T6	T7	T8	T9	T10
Si_2O	51.48 (0.25)	77.40 (0.24)	77.14 (0.21)	75.26 (0.30)	77.62 (0.27)	77.82 (0.24)	77.62 (0.22)	75.63 (0.56)
Al_2O_3	14.02 (0.10)	12.55 (0.10)	12.42 (0.10)	13.26 (0.13)	12.16 (0.11)	12.24 (0.08)	12.40 (0.12)	12.99 (0.20)
TiO_2	2.35 (0.07)	0.07 (0.05)	0.16 (0.03)	0.14 (0.05)	0.18 (0.04)	0.12 (0.04)	0.12 (0.04)	0.16 (0.05)
FeO*	10.94 (0.21)	0.94 (0.19)	1.07 (0.08)	1.95 (0.12)	1.18 (0.09)	1.06 (0.12)	1.08 (0.13)	2.00 (0.19)
MgO	6.74 (0.13)	0.06 (0.04)	0.12 (0.03)	0.08 (0.01)	0.14 (0.02)	0.10 (0.03)	0.09 (0.04)	0.09 (0.02)
CaO	11.27 (0.10)	0.57 (0.21)	0.82 (0.03)	0.98 (0.05)	1.10 (0.08)	0.89 (0.12)	0.86 (0.13)	1.04 (0.12)
Na_2O	2.75 (0.06)	3.66 (0.24)	3.60 (0.13)	4.59 (0.21)	3.38 (0.11)	3.74 (0.15)	3.89 (0.11)	4.36 (0.19)
K_2O	0.32 (0.05)	4.63 (0.76)	4.46 (0.17)	3.57 (0.13)	4.05 (0.15)	3.80 (0.33)	3.73 (0.25)	3.55 (0.18)
Cl	0.13 (0.05)	0.12 (0.02)	0.23 (0.03)	0.16 (0.04)	0.19 (0.03)	0.22 (0.03)	0.22 (0.03)	0.17 (0.03)
Water[a]	2.33 (0.53)	6.14 (0.78)	5.21 (0.45)	5.79 (1.04)	6.89 (1.62)	4.96 (1.04)	5.53 (0.56)	5.38 (1.04)
N	15	14	14	13	14	15	15	15
Na/K	8.59	0.79	0.81	1.29	0.83	0.98	1.04	1.23
	T11	T12	T13	T14	T15	T16	T17	T18
SiO_2	75.41 (0.39)	75.53 (0.74)	77.06 (0.37)	74.88 (0.97)	76.25 (0.72)	76.25 (0.32)	77.41 (0.36)	77.11 (0.23)
Al_2O_3	13.20 (0.21)	12.87 (0.36)	12.47 (0.19)	13.46 (0.34)	12.58 (0.33)	13.05 (0.22)	12.79 (0.16)	12.75 (0.10)
TiO_2	0.16 (0.04)	0.15 (0.04)	0.15 (0.03)	0.22 (0.05)	0.13 (0.07)	0.17 (0.04)	0.05 (0.03)	0.07 (0.03)
FeO*	1.97 (0.10)	1.95 (0.23)	1.03 (0.09)	2.33 (0.20)	1.80 (0.28)	1.58 (0.17)	0.76 (0.11)	0.95 (0.06)
MgO	0.09 (0.03)	0.10 (0.02)	0.11 (0.03)	0.18 (0.07)	0.07 (0.02)	0.16 (0.07)	0.04 (0.03)	0.05 (0.03)
CaO	1.01 (0.09)	1.01 (0.15)	0.81 (0.04)	1.36 (0.18)	0.92 (0.15)	1.26 (0.16)	0.49 (0.14)	0.72 (0.03)
Na_2O	4.51 (0.17)	4.55 (0.21)	3.67 (0.13)	4.26 (0.33)	4.33 (0.25)	3.99 (0.28)	3.67 (0.19)	3.52 (0.19)
K_2O	3.44 (0.10)	3.65 (0.17)	4.46 (0.12)	3.12 (0.17)	3.72 (0.24)	3.39 (0.41)	4.67 (0.39)	4 67 (0.17)
Cl	0.21 (0.04)	0.20 (0.04)	0.24 (0.03)	0.19 (0.01)	0.20 (0.05)	0.16 (0.03)	0.12 (0.02)	0.16 (0.03)
Water[a]	5.60 (0.81)	5.86 (1.99)	6.14 (1.77)	6.10 (0.81)	6.31 (1.27)	6.33 (1.45)	6.86 (1.54)	6.07 (0.89)
N	15	15	12	15	15	15	14	15
Na/K	1.31	1.25	0.82	1.37	1.16	1.18	0.79	0.75

Note: * All Fe calculated as FeO. *N* = number of analyses in mean. Numbers in parentheses are 1 standard deviation.
[a] Water by difference.

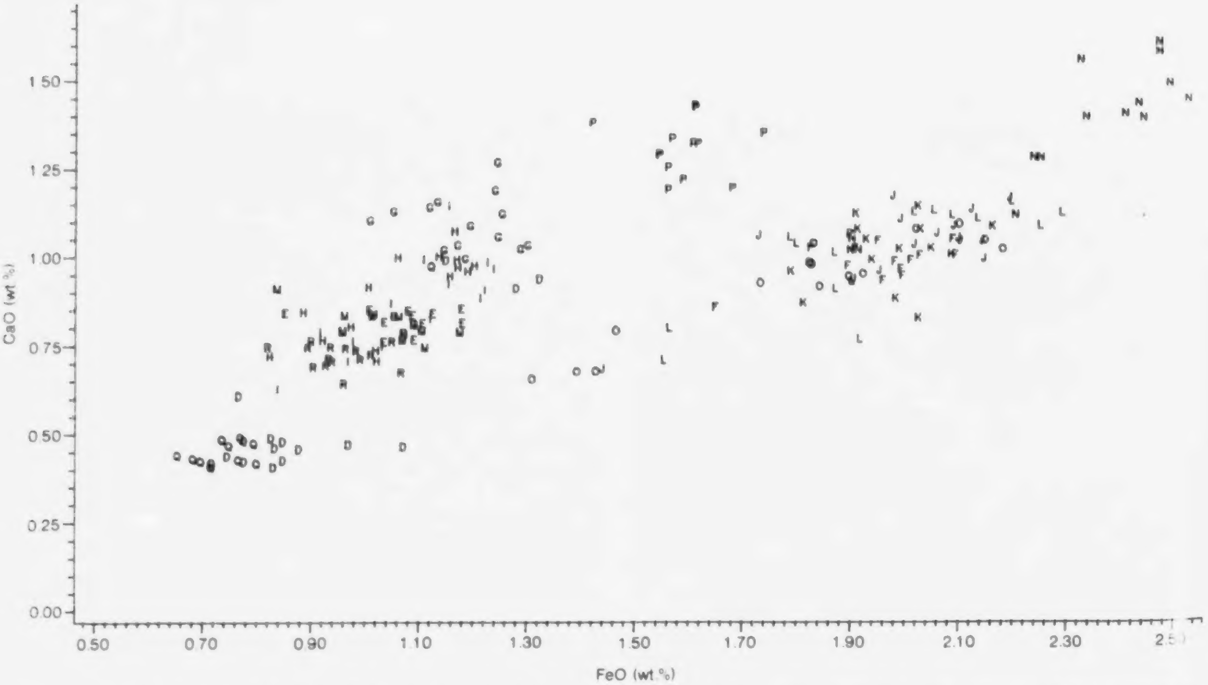

Figure 6. Plot of CaO versus FeO (Table 5) for the glass shards from 15 megascopic tephras (T4 to T18) in Leg 90 sediments. Letter symbols D through R correspond to tephras T4 through T18, respectively.

Table 6. Comparison of chemical composition of basaltic glasses from mid-ocean ridge (1,2), ocean island (3,4,5), and island arc (6) settings (from Basaltic Volcanism Study Project, 1981) with glass from tephra T1 (Site 586).

	1	2	3	4	5	6	T1
SiO_2	50.19	50.93	49.60	48.70	50.40	50.90	51.48
Al_2O_3	14.86	15.15	13.60	12.20	13.30	17.80	14.02
TiO_2	1.77	1.19	2.88	2.50	3.80	0.95	2.35
FeO^*	11.33	10.32	11.00	11.40	12.20	9.50	10.94
MnO	—	—	0.10	0.10	0.10	0.19	—
MgO	7.10	7.69	6.24	9.69	5.20	6.00	6.74
CaO	11.44	11.84	11.00	10.80	9.59	10.40	11.27
Na_2O	2.66	2.32	2.37	2.05	2.74	2.73	2.75
K_2O	0.16	0.14	0.57	0.47	0.75	0.82	0.32
Cr_2O_3	—	—	0.01	0.01	—	—	—
P_2O_5	0.14	0.10	—	—	—	0.23	—
	99.65	99.68	97.37	98.01	98.08	99.52	99.87

Note: 1,2 = Average basaltic glass from East Pacific Rise and Indian Ocean spreading centers. 3,4,5 = Average composition of Hawaiian glasses HAW-21, HAW-23, HAW-25, respectively. 6 = Average composition of island arc basalts. * All Fe calculated as FeO. — = not detected.

Table 7. Representative chemical composition of plagioclase crystals from Sites 586 and 587.

	T1	T3
SiO_2	51.93	54.83
Al_2O_3	29.41	28.54
TiO_2	0.08	0.02
FeO^*	0.94	0.21
MnO	0.01	0.02
MgO	0.29	0.01
CaO	14.02	11.46
Na_2O	3.65	4.93
K_2O	0.07	0.34
NiO	0.01	0.01
Cr_2O_3	0.03	
	100.44	100.37
Number of ions based on 8(0)		
Si	2.362	2.469
Al	1.577	1.515
Ti	0.003	0.001
Fe^*	0.035	0.008
Mn	—	0.001
Mg	0.020	0.001
Ca	0.683	0.553
Na	0.322	0.431
K	0.004	0.020
	5.006	4.999
Ab	31.9	42.9
An	67.7	55.1
Or	0.4	2.0
N	4	4

Note: * All Fe calculated as ferrous. *N* = number of analyses in mean. — = not considered.

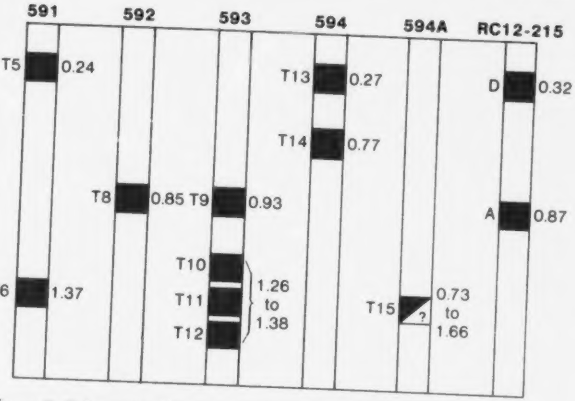

Figure 7. Schematic diagram illustrating possible correlation of Quaternary megascopic tephras in Leg 90 cores with each other and with the deep-sea tephras A and D described from core RC12-215 off eastern New Zealand by Ninkovich (1968) and Watkins and Huang (1977). Estimated ages (m.y.) of tephras (Table 1) shown to right of each column.

(Fig. 8B) indicates chemical similarity and possible correlation with tephra G052, an eastern North Island tephra with an estimated age between 7 and 7.5 m.y.

Surface winds from between the northwest and southwest prevail over New Zealand (Fig. 9) so that volcanic ash from North Island should be transported to the east of New Zealand. Dispersal in this anticipated direction was confirmed by Ninkovich (1968) and Watkins and Huang (1977). Here we have documented the occurrence of North Island–derived Neogene and Quaternary megascopic silicic tephras west and northwest of New Zealand at Sites 590 through 593 in the Tasman Sea. Moreover, disseminated silicic shards of a probable New Zealand origin occur in the Lord Howe Rise oozes at least as far north as Site 588 (Site chapter, this volume). Possible explanations for the transport of ash from New Zealand into the central and northern Tasman Sea include: (a) eruption at a time when upper-level winds were blowing from the east which, at the present day, occurs up to 5 to 20% of the time over northern New Zealand, the frequency varying with altitude (Table 8); (b) dispersal of ash first east and northeast of North Island by the prevailing westerlies (Fig. 9; Reid, 1982) and then west and northwest into the Tasman Sea, either because of the natural anticyclonic curvature of surface winds in the region (Ramage, 1970; Steiner, 1980) or because the ash enters into the belt of southeasterly through easterly trade winds off northern New Zealand (Fig. 9); and (c) direct northwestward transport by stratospheric (south)easterly winds which, at the present day, prevail above 20 km altitude between September and March over New Zealand (J. W. D. Hessell, New Zealand Meteorological Service, pers. comm., 1984). This last option can account for the opposing directions of ash dispersal implied, for example, by correlating tephra T5 with tephra T13 and D, and tephras T8 and T9 with tephra A (cf. Figs. 1 and 7), the ash below and above about 20 km altitude being "simultaneously" dispersed in opposite directions toward the Pacific Ocean and Tasman Sea, respectively.

The source regions of the nonsilicic tephras T1 to T3 are less readily identified. Tephra T1 (Site 586) has a glass chemistry typical of an ocean island source (Table 6), which abound in the vicinity of the Ontong-Java Plateau. Tephras T2 (Site 587) and T3 (Site 588) also are basic or intermediate (see earlier) and are derived from

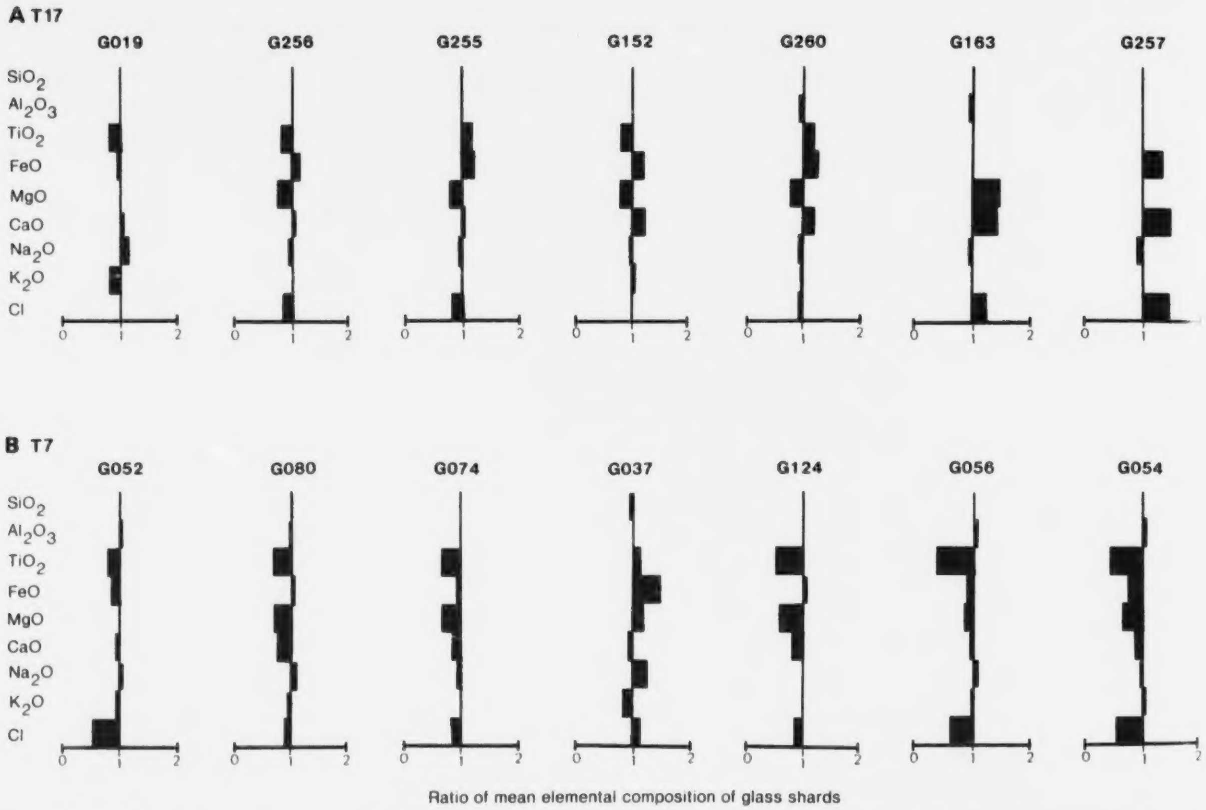

Figure 8. Comparison of elemental composition (as ratio of means) of glass shards from late Miocene deep-sea tephras T17 (A) and T7 (B) with several equivalently aged tephras from New Zealand as a possible way of determining correlative eruptive events. Tephra chemistry for land samples (labeled G) from Gosson (in prep.). Chemical affinity is indicated where the ratios are very close to 1.00 for each element. See text for discussion.

ocean ridge or ocean island volcanoes. Churkin and Packham (1973) suggested that prevailing wind and ocean current directions in the northern South Fiji Basin are both toward the southwest so that a source from Vanuatu (New Hebrides) arc is favored (Fig. 1). Tephras T1 to T3 are each generally coarser than the silicic ashes (Table 2), suggesting closer volcanic sources.

CONCLUSIONS

Eighteen late Cenozoic megascopic vitric tephras are described from Leg 90 sediments in the Tasman Sea and off eastern South Island, New Zealand. Fifteen of these are silicic, derived from eruptions in North Island, New Zealand. Several of the Quaternary silicic tephras are correlatives, and at least two are matched to the on-land Mt. Curl tephra (~0.25 m.y.), possibly associated with eruption of Whakamaru ignimbrite from Lake Taupo, North Island. The occurrence of North Island-derived tephras in Tasman Sea sediments suggests that ash transported eastward by the prevailing westerly airstream across New Zealand may be diverted northwest and west on entering the southeasterly trade wind belt off northeastern New Zealand. In the case of large eruptions, ash ascending above 20 km altitude may be carried directly toward the Tasman Sea by easterly stratospheric winds, while coeval lower-level ash drifts east of New Zealand into the southern Pacific Ocean.

The three analyzed nonsilicic megascopic tephras comprise altered basic shards and common labradorite crystals derived from ocean island or ridge explosive volcanism in the Ontong-Java Plateau and Vanuatu regions.

The megascopic tephras are a fragmentary record of late Cenozoic volcanism in the southwest Pacific since New Zealand-derived silicic shards are a ubiquitous but disseminated minor component in many of the sediments. More importantly, innumerable thin bentonite layers occur in Leg 90 cores, probably representing devitrified intermediate to basic tephras derived mainly from oceanic arc volcanism at the Pacific/Australian plate boundary (Gardner, Nelson, et al., this volume). In contrast to the silicic shards, the preservation potential of more basic shards was low in the calcareous sediments.

ACKNOWLEDGMENTS

We thank Professor Paul Vella (Department of Geology, Victoria University, Wellington) and Dr. William G. Melson (Smithsonian Institution) for their reviews of this paper.

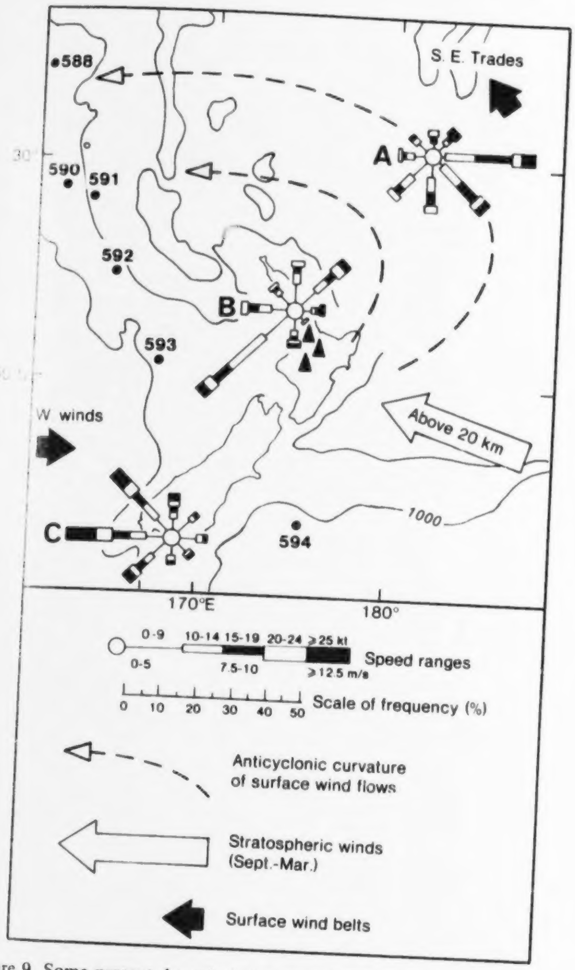

Figure 9. Some present-day wind characteristics in the New Zealand sector of the southwest Pacific. Open-ocean surface wind frequency diagrams for upper wind stations A, B, and C for Raoul Island, Auckland, and Invercargill, respectively, are from Reid (1982). See text for discussion.

Table 8. Some upper-level wind frequencies and mean speeds measured above Auckland over the period 1966–1979 (data from Reid and Penney, 1982).

mb	Altitude (km)	Mean wind speed (mps)	% time wind occurs from SE	E	NE
100	16	15	1.2	0.6	0.5
200	12	28	1.7	0.6	0.6
300	9	24	3.4	1.8	2.0
500	6	15	4.7	2.9	3.3
700	3	11	6.3	5.3	5.6
900	1	9	5.8	8.0	10.2

REFERENCES

Ballance, P. F., 1976. Evolution of the Upper Cenozoic magmatic arc and plate boundary in northern New Zealand. *Earth Planet. Sci. Lett.*, 28:356–370.

Basaltic Volcanism Study Project, 1981. *Basaltic Volcanism on the Terrestrial Planets:* New York (Pergamon Press, Inc.).

Briggs, N. D., 1976. Welding and crystallization zonation in Whakamaru Ignimbrite, central North Island, New Zealand. *N.Z. J. Geol. Geophys.*, 19:189–212.

Burns, R. E., Andrews, J. E., et al., 1973. *Init. Repts. DSDP*, 21: Washington (U.S. Govt. Printing Office).

Churkin, M., and Packham, G. H., 1973. Volcanic rocks and volcanic constituents in sediments, Leg 21, Deep Sea Drilling Project. *In* Burns, R. E., Andrews, J. E., et al., *Init. Repts. DSDP*, 21: Washington (U.S. Govt. Printing Office), 481–493.

Cole, J. W., 1979. Structure, petrology, and genesis of Cenozoic volcanism, Taupo Volcanic Zone, New Zealand—a review. *N.Z. J. Geol. Geophys.*, 22:631–657.

Ewart, A., 1963. Petrology and petrogenesis of the Quaternary pumice ash in the Taupo area, New Zealand. *J. Petrol.*, 4:392–431.

————, 1966. Review of mineralogy and chemistry of the acidic rocks of Taupo Volcanic Zone, New Zealand. *Bull. Volcanol.*, 29: 147–172.

Ewart, A., Hildreth, W., and Carmichael, I. S. E., 1975. Quaternary acid magma in New Zealand. *Contrib. Mineral. Petrol.*, 51:1–27.

Froggatt, P. C., 1983. Toward a comprehensive Upper Quaternary tephra and ignimbrite stratigraphy in New Zealand using electron microprobe analysis of glass shards. *Quat. Res.*, 19:188–200.

Kennett, J. P., 1981. Marine tephrochronology. *In* Emiliani, C. (Ed.), *The Sea* (Vol. 7): New York (John Wiley), 1373–1436.

Kennett, J. P., Houtz, R. E., et al., 1975. *Init. Repts. DSDP*, 29: Washington (U.S. Govt. Printing Office).

Kohn, B. P., 1973. Some studies of New Zealand Quaternary pyroclastic rocks [Ph.D. dissert.]. Victoria University, Wellington.

Ninkovich, D., 1968. Pleistocene volcanic eruptions in New Zealand recorded in deep sea sediments. *Earth Planet. Sci. Lett.*, 4:89–102.

Ramage, C. S., 1970. Meteorology of the South Pacific tropical and middle latitudes. *In* Wooster, W. S., (Ed.), *Scientific Exploration of the South Pacific:* Washington (National Academy of Sciences), pp. 16–29.

Reid, S. J., 1982. Surface wind frequencies in the southwest Pacific estimated from radar-wind data. *N.Z. J. Sci.*, 25:303–311.

Reid, S. J., and Penney, A. C., 1982. Upper-level wind frequencies and mean speeds for New Zealand and Pacific Island stations. *N.Z. Met. Serv. Misc. Publ.*, 174.

Sarna-Wojcicki, A. M., Bowman, H. R., Meyer, C. E., Russell, P. C., Woodward, M. J., McCoy, G., Rowe, J. J., Jr., Baedecker, P. A., Asaro, F., and Michael, H., 1984. Chemical analyses, correlations, and ages of upper Pliocene and Pleistocene ash layers of east-central and southern California. *U.S. Geol. Surv. Prof. Paper*, 1293.

Seward, D., 1974. Age of New Zealand Pleistocene substages by fission track dating of glass shards from tephra horizons. *Earth Planet. Sci. Lett.*, 24:242–248.

————, 1976. Tephrostratigraphy of the marine sediments of the Wanganui Basin, New Zealand. *N.Z. J. Geol, Geophys.*, 19:9–20.

Steiner, J. T., 1980. The climate of the South-West Pacific region. *N.Z. Met. Serv. Misc. Publ.*, 166.

Suggate, R. P., Stevens, G. R., and Te Punga, M. T. (Eds.), 1978. *The Geology of New Zealand* (Vol. 2): Wellington (Govt. Printer).

Watkins, N. D., and Huang, T. C., 1977. Tephras in abyssal sediments east of the North Island, New Zealand: chronology, paleowind velocity, and paleoexplosivity. *N.Z. J. Geol. Geophys.*, 20:179–198.

Date of Initial Receipt: 25 June 1984
Date of Acceptance: 31 October 1984

APPENDIX

Listed here are the 54 samples originally obtained from supposedly megascopic vitric tephra layers in the course of shipboard sampling. Subsequent laboratory analyses indicated that only 18 of these samples had sufficiently abundant glass undisputedly to represent primary airfall tephras, and only these are the subject of this study. Many of the remaining samples may represent argillized ash layers (Gardner, Nelson, et al., this volume). The relative abundance of mainly fresh glass shards in the samples is shown by the letter (A, abundant; C, common; T, trace; O, absent) in parentheses next to each sample.

Site 586

11B-11, 114 cm	(A)

Site 587

5-5, 49 cm	(C)

Site 588

19-5, 63 cm	(O)
21-2, 10 cm	(O)
23-2, 145 cm	(O)
3B-5, 77 cm	(O)
3B-5, 83 cm	(O)
3B-6, 56 cm	(O)
3C-3, 74 cm	(O)
6C-3, 52 cm	(T)
6C-3, 149 cm	(T)
12C-5, 100 cm	(O)

Site 590

1-4, 71 cm	(O)
4B-3, 112 cm	(O)
5B-2, 82 cm	(O)
5B-5, 66 cm	(T)
38B-4, 113 cm	(C)

Site 591

2-2, 54 cm	(A)
3-2, 80 cm	(O)
3-4, 48 cm	(O)
3-4, 80 cm	(O)
5-3, 144 cm	(C)
13-6, 49 cm	(T)
1A-3, 62 cm	(O)
25A-3, 25 cm	(C)

Site 592

2-6, 83 cm	(A)
21-6, 12 cm	(O)
33-5, 77 cm	(T)
34-4, 143 cm	(T)

Site 593

3-2, 96 cm	(O)
3-5, 80 cm	(A)
4-1, 80 cm	(T)
4-2, 80 cm	(T)
4-4, 30 cm	(C)
4-4, 80 cm	(C)
4-4, 100 cm	(C)
25-6, 122 cm	(O)
25,CC	(O)
26-6, 30 cm	(T)
29-5, 105 cm	(O)
32-4, 118 cm	(O)
33-4, 2 cm	(T)
47-5, 39 cm	(O)

Site 594

5-2, 33 cm	(A)
12-2, 40 cm	(A)
13,CC	(O)
15-5, 15 cm	(O)
15-5, 20 cm	(O)
20-4, 19 cm	(O)
28-5, 57 cm	(A)
36,CC	(A)
51-1, 105 cm	(O)
8A-3, 50 cm	(A)
10A-6, 6 cm	(A)

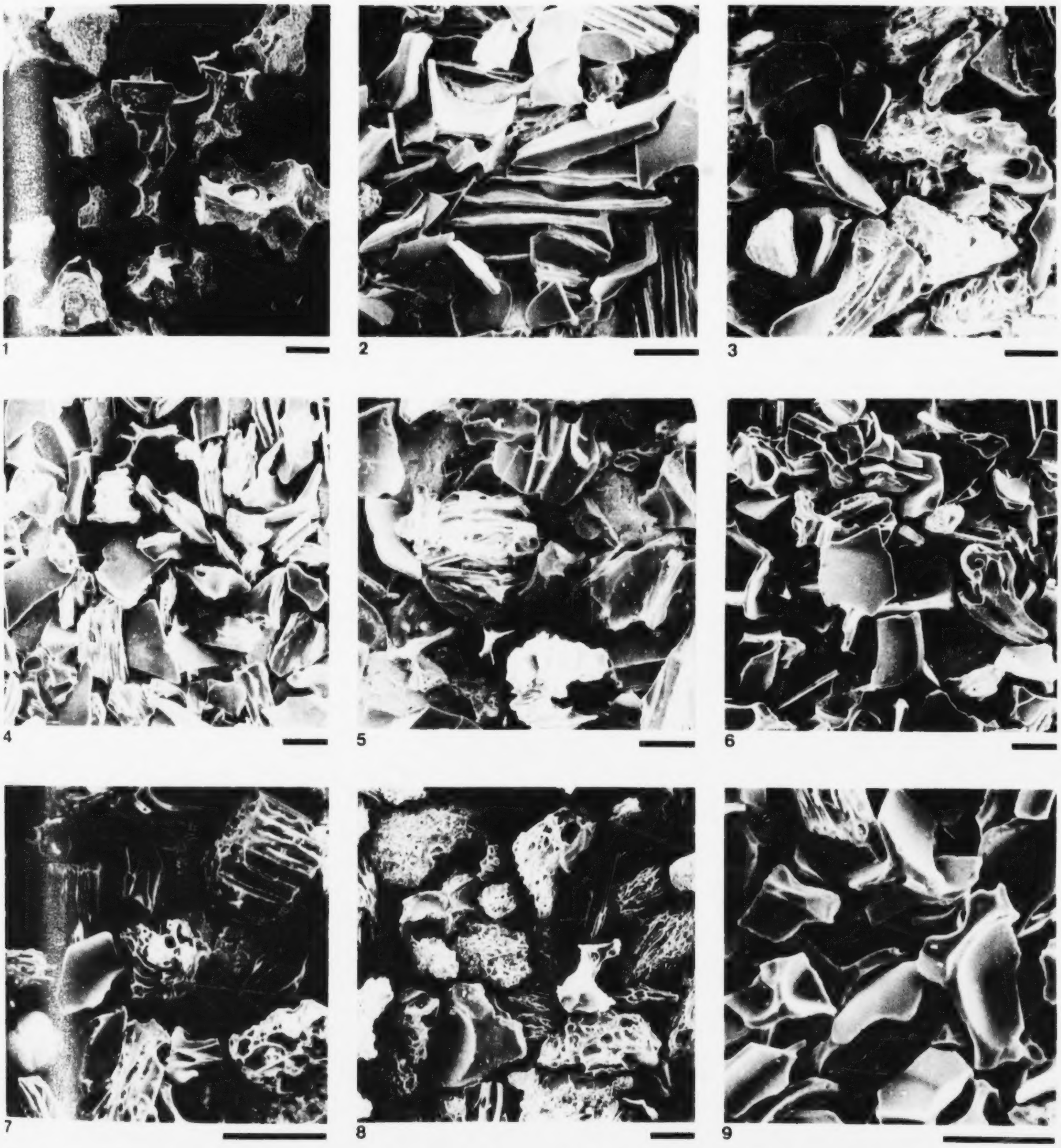

Plate 1. Scanning electron micrographs of glass shards from several megascopic tephras in Leg 90 cores. Dominant morphologic features are summarized in Table 4. Bar scale is 100 μm. Tephras are as follows: **1.** T1, 586B-11-3, 114 cm. **2.** T5, 591-2-2, 54 cm. **3.** T8, 592-2-6, 83 cm. **4.** T[illegible] [illegible]93-3-5, 80 cm. **5.** T11, 593-4-4, 80 cm. **6.** T13, 594-5-2, 33 cm. **7.** T14, 594-12-2, 40 cm. **8.** T16, 594A-10-6, 6 cm. **9.** T18, 594-[illegible]C.

27. NATURE AND SIGNIFICANCE OF VOLCANOGENIC DEPOSITS AT THE EOCENE/OLIGOCENE BOUNDARY, HOLE 593, CHALLENGER PLATEAU, TASMAN SEA[1]

Campbell S. Nelson, Roger M. Briggs, and Peter J. J. Kamp, University of Waikato[2]

ABSTRACT

Hole 593 includes a spectacular 16.4-m-sequence of thinly bedded, grayish black, lithified volcanogenic sandstones, mudstones, and occasional breccias near its base within chalks. Sandstone-mudstone couplets (up to 50 cm thick) have sharp basal contacts, are normally graded, and include Bouma A, B, occasional C, and E divisions, whereas breccia-dominated units are thicker (up to 140 cm), massive or inversely graded, and unsorted. The beds were deposited rapidly at bathyal depths, close to the Eocene/Oligocene boundary, from turbidity currents and/or subaqueous pyroclastic flows originating on the slopes of "Lalitha pinnacle," a now-buried ~500-m-high volcanic shield (average 6–8° slopes) located only ~3 km from Site 593.

The occurrence in the deposits of rare primary augite and olivine crystals, the abundance of the low Si/Al zeolite phillipsite, and certain chemical considerations support a basaltic parentage. However, as a result of low-temperature oxidative alteration by pore fluids following emplacement, the original basaltic glass fragments that formed the bulk of the deposits have been palagonitized extensively and replaced by phillipsite, smectite, and calcite.

"Lalitha pinnacle" is similar to several other (buried) "pinnacles" evident on seismic records from southern Lord Howe Rise, both in its seismic character and structural and age relations to surrounding sediments. This suggests that submarine basaltic volcanism and associated sedimentary redeposition was widespread in the southeast Tasman Sea during the late Eocene to early Oligocene. The activity is viewed as off-rift (western) volcanism that is related to regional extension and the formation of a major western New Zealand rift system associated with eastward propagation of the mid-ocean Southeast Indian Ridge into the south Tasman Sea and through the New Zealand subcontinent at this time. Analogous occurrences of submarine Eocene-Oligocene basalts east of the rift system now crop out on land in eastern South Island, New Zealand.

INTRODUCTION

Nearly all of the record total of about 3700 m of sediment cored on DSDP Leg 90 at eight sites (587–594) in the southwest Pacific consisted of middle to late Cenozoic calcareous oozes and chalks. On two counts the sequence encountered at the bottom of Hole 593 generated considerable shipboard interest. First, it was one of only three holes to penetrate Eocene strata. Second, the Eocene chalks included a conspicuous 16.4-m-thick sequence of dark-colored volcanogenic deposits, the only relatively thick nonbiogenic lithology cored on Leg 90. In this chapter, we describe briefly the stratigraphy and nature of the volcanogenic materials, present chemical analyses of bulk samples and mineral separates, and speculate on the tectonic and environmental significance of the volcanics in the southwest Pacific region.

Site 593 (40°30.47′S, 167°47.48′E) was drilled in 1068 m water depth near the western edge of Challenger Plateau, southern Lord Howe Rise, Tasman Sea (Fig. 1). Hole 593 was continuously cored with the hydraulic piston corer from 0 to 245.1 m sub-bottom and continued to a total depth of 571.5 m with the extended core barrel. The volcanic sequence is contained within the bottom three cores (Cores 58–60) from 542.7 to 571.5 m sub-bottom, for which recovery rate averaged about 70%.

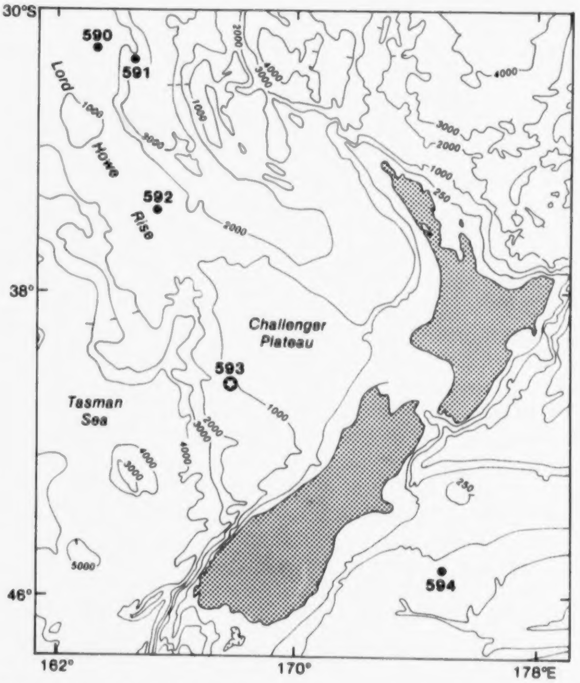

Figure 1. Location of Site 593 on western Challenger Plateau, west of New Zealand.

---

[1] Kennett, J. P., von der Borch, C., et al., *Init. Repts. DSDP*, 90: Washington (U.S. Govt. Printing Office).

[2] Addresses: Department of Earth Sciences, University of Waikato, Private Bag, Hamilton, New Zealand.

THE VOLCANOGENIC SECTION

Lithostratigraphy

The volcanogenic sequence is illustrated in Figure 2 and a summary lithologic log, showing "cyclic" units and sample locations, in Figure 3.

The lowermost Core 60 (561.9–571.5 m) is white (N9) to light greenish gray (5GY 8/1) foraminifer-bearing nannofossil chalk with many pale green (10G 8/1) thin (<2 mm) laminae, possibly altered basic tephra layers (Gardner, Nelson, et al., this volume). The chalk includes three prominent, thin (5–20 cm) interbeds of grayish black (N2 to N5), massive to horizontally laminated, volcanogenic fine sandstone and mudstone, the lower two of which are normally graded and burrowed.

Core 59 (552.3–561.9 m) and the basal 1.5 m of Core 58 (542.7–552.3 m) comprise a thinly bedded sequence of lithified volcanogenic breccias, sandstones, and mudstones, which, despite some disturbance by drilling (cf. Leggett, 1982), retain their stratigraphic entity (Fig. 2). Overall, grayish black (N2) colors dominate, although many of the sandstones have distinctive dark greenish hues (5G 2/1, greenish black; 5G 6/1, greenish gray; 5G 3/2, dusky green) and some are rather paler green (5GY 3/2 and 10G 4/2, grayish green; 10Y 6/2, pale olive). Locally, the darker-colored beds include subtranslucent white or very pale green blotches (Fig. 4) of secondary calcite, smectite, and/or zeolite. Gross variations of grain size are used to subdivide the sequence into a repetitive series of fining-upward sandstone–mudstone units, each ranging from only a few to as much as 50 cm thick (Figs. 3, 4). The lower boundary of each cyclic unit is usually sharp and sometimes wavy, with relief up to 1 cm, suggestive of predepositional erosion and/or postdepositional loading. The immediately overlying sandstone is mainly massive and medium to fine grained, rarely coarse grained. The sandstone fines upward, develops horizontal laminae, and passes gradationally or abruptly into massive or horizontally laminated, and sometimes convolute-laminated, vitric siltstones or mudstones, superficially resembling black obsidian (Fig. 4). Unit boundaries are not always clear, and several of those numbered in Figure 3 (e.g., Units 24, 26, and 31) are composite. The sharp basal contacts, normal grading, and presence of Bouma A, B, occasional C, and E divisions indicate that the majority of the sandstone–mudstone couplets are turbidity current deposits that originated as either cold sedimentary (e.g., Walker, 1979) or pyroclastic flows (e.g., Lajoie, 1979).

In contrast, at least five of the coarser-grained units (i.e., Units 18, 20, 21, 27 and 29), including three thick (40–139 cm) breccia beds, generally coarsen upward and support a thin capping mudstone. The breccias comprise an unsorted assemblage of clast-supported, angular, black glassy fragments, up to 8 mm in size, in a dark glassy interstitial matrix of sand and mud. They are mainly massive, although the more sandy portions at the base may include poorly developed horizontal laminations. The lithology and structure of these thicker, inversely (-to-normally) graded coarse units are consistent with them being either sedimentary mass flow deposits (e.g., Carter, 1975) or primary subaqueous pyroclastic flows (e.g., Lajoie, 1979) of more proximal aspect than the associated sandstone–mudstone couplets.

Veins of white sparry calcite are locally conspicuous, especially in the fine-grained tops of cyclic units (Figs. 2 to 4). They are 0.1 to 4 mm wide, most form subhorizontal anastomosing stringers parallel to bedding, and some heal high-angle tension cracks. The subhorizontal veins possibly originated by recrystallization of thin layers of interbedded calcareous ooze, an interpretation supported by the close association of veining with partly recrystallized ooze layers near the top of Section 593-58-3 (Fig. 2).

The uppermost contact of the volcanogenic deposits at 545.5 m sub-bottom depth is sharp and irregular (Fig. 2). It is overlain by homogeneous, white (N9) to very light gray (N8) nannofossil ooze, alternating in consistency from firm to stiff, with no megascopic volcanic components.

Age

The preliminary fossil evidence (Site 593 report, this volume) indicates that the volcanogenic deposits straddle the Eocene/Oligocene boundary (Fig. 5). The planktonic foraminiferal data place the Eocene/Oligocene boundary a few centimeters above the volcanic material, at about Sample 593-58-2, 120 cm. On the other hand, the boundary as defined by the extinction of two calcareous nannoplankton species occurs within the volcanic sequence, between Units 19 and 34. At Site 592 to the north, which contains an excellent extended ooze sequence over the boundary, the critical nannofossil species also disappear about 7 m below the zonal planktonic foraminiferal species. Thus, the microfossil succession appears uninterrupted, a view supported by continuity of a uniformly low sedimentation rate of 4.6 m/m.y. (Site 593 report, this volume) across the boundary. The best age estimate for emplacement of the volcanogenic deposits is very latest Eocene to possibly earliest Oligocene. This is consistent with the reversed geomagnetic polarity values throughout the volcanogenic sequence (Site 593 report, this volume), suggesting deposition during magnetic Subchron C13R, 37–36 m.y. ago (LaBrecque et al., 1983; Poore et al., 1983). The volcanic material is too altered to provide a reliable radiometric age (I. McDougall, pers. comm., 1983).

Petrography

Eleven small samples (S1–S11) representative of a range of textures and structures in the volcanogenic sequence were slabbed from coherent core sections aboard ship (Fig. 3).

In thin section the rock fabrics are varied and complex, their most obvious feature being the abundance of brown palagonite (cf., Hay and Iijima, 1968). Alteration is such that original clastic textures are often difficult to distinguish (Plate 1, Fig. 1). In one sample (S9) relict outlines of glass shards are discernible (Plate 1, Fig. 2), where cuspate curved vitric fragments are concentrated in thin layers (Plate 1, Fig. 3), possibly representing primary volcanic ash. All other samples show

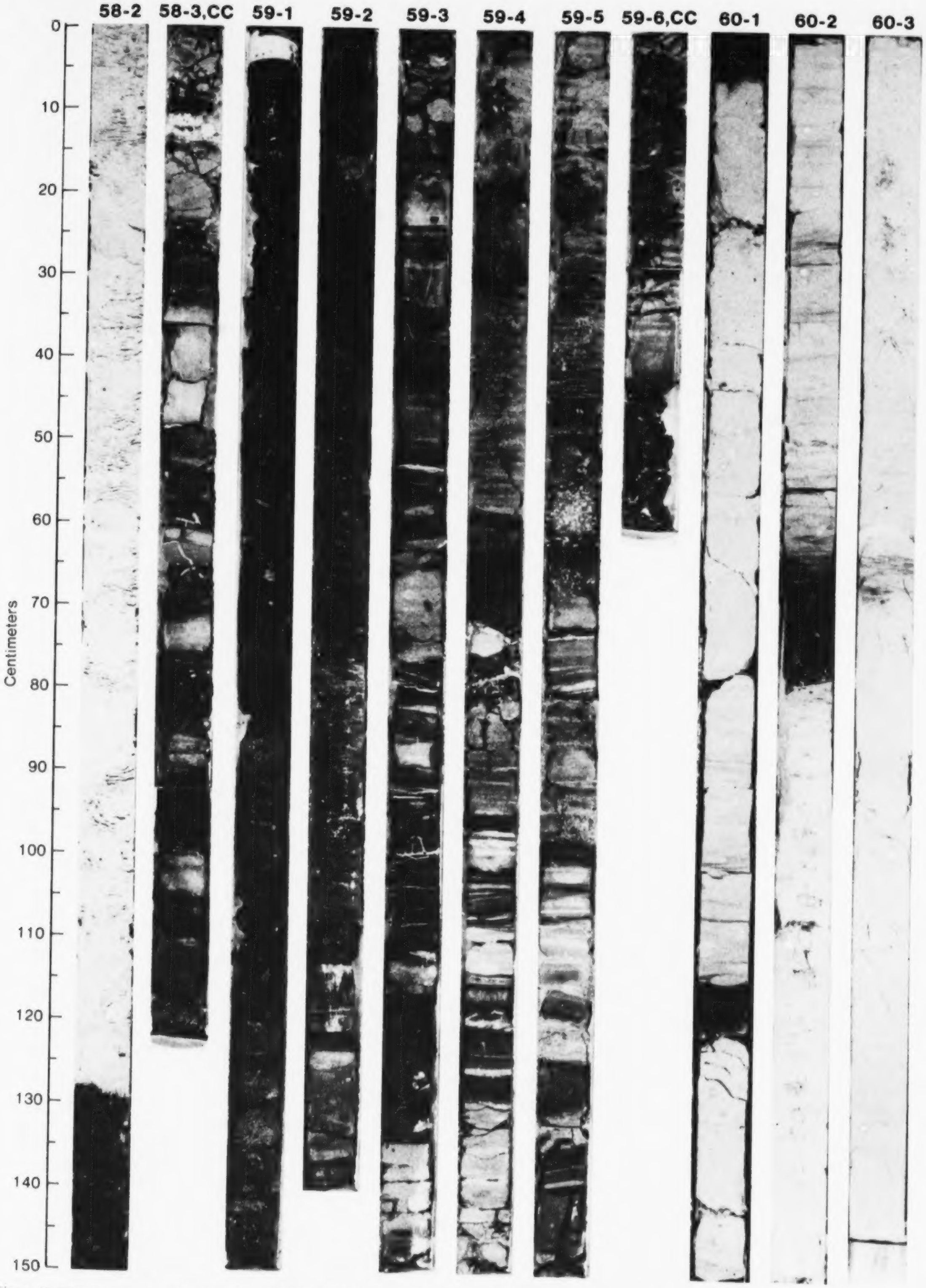
58-2
58-3,CC
59-1
59-2
59-3
59-4
59-5
59-6,CC
60-1
60-2
60-3
0
10
20
30
40
50
60
70
80
90
100
110
120
130
140
150
Centimeters

Figure 2. The recovered volcanogenic sequence within Paleogene chalk from the basal three cores (544.2–566.4 m sub-bottom) in Hole 593. Based on key foraminifers, the Eocene/Oligocene boundary occurs at about Sample 593-58-2, 120 cm, whereas critical nannofossil species suggest the same boundary is in Core 59.

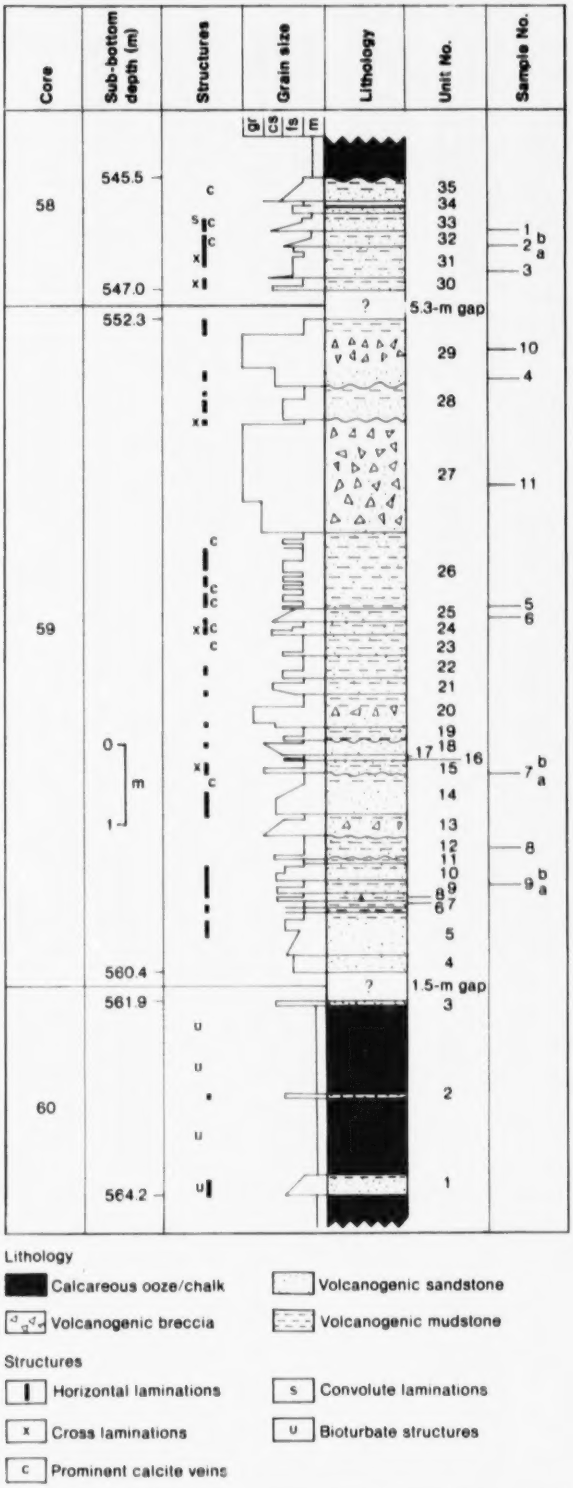
Core
Sub-bottom depth (m)
Structures
Grain size
Lithology
Unit No.
Sample No.
gr
cs
fs
m
58
59
60
545.5
547.0
552.3
560.4
561.9
564.2
0
m
1
5.3-m gap
1.5-m gap
35
34
33
32
31
30
29
28
27
26
25
24
23
22
21
20
19
18
17
16
15
14
13
12
11
10
9
8
7
6
5
4
3
2
1
1
2
3
b
a
10
4
11
5
6
7
8
9
Lithology
Calcareous ooze/chalk
Volcanogenic breccia
Volcanogenic sandstone
Volcanogenic mudstone
Structures
Horizontal laminations
Cross laminations
Prominent calcite veins
Convolute laminations
Bioturbate structures

Figure 3. Lithologic log of the volcanogenic sequence at the base of Hole 593 showing sample positions and sedimentation units defined on the basis of size grading and contact types. Modal sizes are: gr = gravel (>2.0 mm), cs = coarse sand (0.5–2.0 mm), fs = fine sand (0.06–0.5 mm), m = mud (<0.06 mm).

blotchy, globular, or spherulitic masses of dark brown palagonitic material, with irregular patches of the secondary minerals calcite, phillipsite, and smectite (Plate 1, Figs. 4, 5). The lithologic layering evident from color and grain-size variations in the core (Fig. 2) corresponds to variations in the abundance of palagonite and secondary minerals in the deposits. In particular, the lighter gray coarser sediment intervals are relatively enriched in coarsely crystalline sparry calcite (Plate 1, Fig. 6), and sometimes phillipsite, probably because of the originally coarser grain size and higher porosity of the primary volcanogenic sediment at these levels. Compared to the coarser-grained sediments, the associated mudstones (e.g., S2a, 5, 7a, and 9a) are relatively enriched in smectite and phillipsite, but depleted in calcite (confirmed by semiquantitative x-ray diffraction data).

The only primary minerals observed in thin section are occasional pale green prismatic or anhedral augite up to 0.1 mm in length, and a single tiny grain of olivine. Magnetite is a minor constituent and occurs as small (0.02 mm) irregular anhedral grains. Feldspar is absent. Occasionally foraminifers occur in the palagonitic mudstone beds (Plate 1, Fig. 7).

Palagonite varies in color from buff, brown, dark brown to black and occurs either as irregular blotchy masses or in globular, spherulitic, or colloform habit (Plate 1). Some globules or spherulites show a zonal concentric arrangement from phillipsite or calcite cores to outer layers containing smectite or calcite, and an outermost selvage of palagonite (Plate 1, Fig. 8); however, this secondary mineralogic sequence is highly variable. Also, some cores of aggregated globular palagonite may consist of a single secondary mineral, so that globules containing calcite or smectite or phillipsite may be adjacent to each other in the aggregate (Plate 1, Fig. 4), suggesting that extensive metasomatism between palagonite globules has taken place. Radial cracks in globular or spherulitic masses are common features, and many massive palagonite patches contain curved perlitic cracks. Such microfractures probably allowed seawater extensively to pervade the deposits; this has enhanced secondary alteration.

Smectite is a common secondary mineral, has a light to dark green color, and forms irregular patches within palagonite, cross-cutting veins, or globules, the latter probably representing pseudomorphs after globular palagonite.

Phillipsite is colorless to yellow, and its presence has been confirmed by x-ray diffraction (XRD) and microprobe data. The composition of phillipsite in S5 is given in Table 1; it has a Si/Al ratio of 2.49, consistent with Si/Al ratios in the range 2.44–2.87 for deep-sea phillipsites generally (Boles, 1977). The Na_2O content is probably low because of volatilization under the probe beam. Phillipsite forms radiating splays in patches and pools (Plate 1, Fig. 9) and in globules after palagonite.

Calcite is ubiquitous and often abundant and occurs as irregular aggregates, rounded masses after palagonite, coarsely crystalline pseudospar, or as stringers and veins that both parallel and cross cut bedding. The calcite is a low magnesian variety; microprobe analyses of two calcites gave MgO contents of 0.84–0.94 wt.%, total Fe as

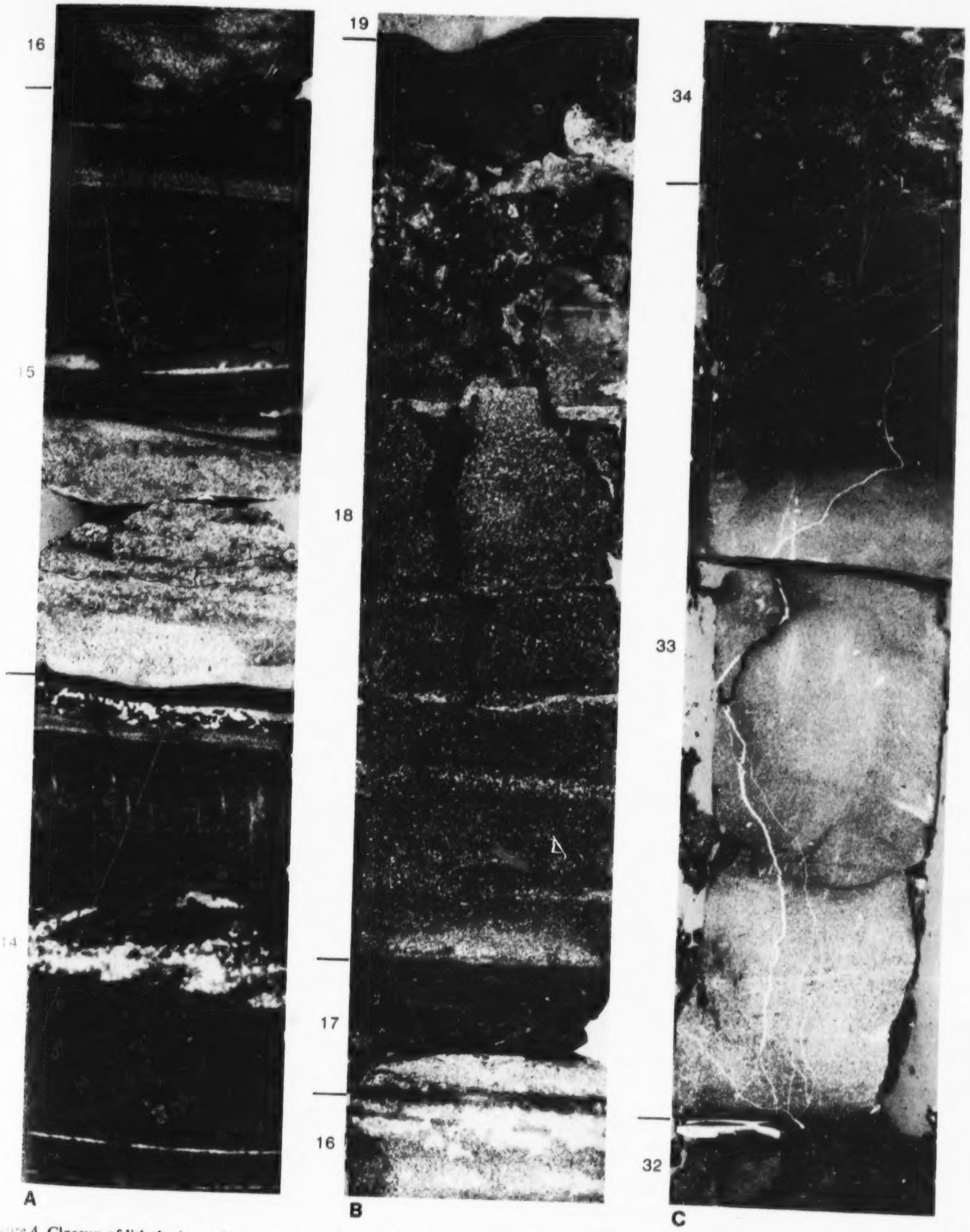

Figure 4. Closeup of lithologies and structures typical of Hole 593 volcanogenic deposits. Core sections are 25 cm long each, and unit numbers (see Fig. 3) are indicated. (A) From Sample 593-59-4, 100–125 cm showing light-colored, vaguely laminated sandstones forming the lower part of Units 15 and 16 in sharp lower contact with massive, laminated or cross-laminated, dark vitric siltstones and mudstones, those in Unit 14 including light blotchy areas due to concentrations of secondary calcite and zeolite. (B) From Sample 593-59-4, 75–100 cm showing massive laminated sandstones with thin, massive, dark mudstones. Note the sharp, irregular contact between Units 18 and 19. (C) From Sample 593-58-3, 25–50 cm showing sharp lower and upper contacts, normal grading, some horizontal and convolute laminae, and both horizontal and vertical calcite veining in Unit 33.

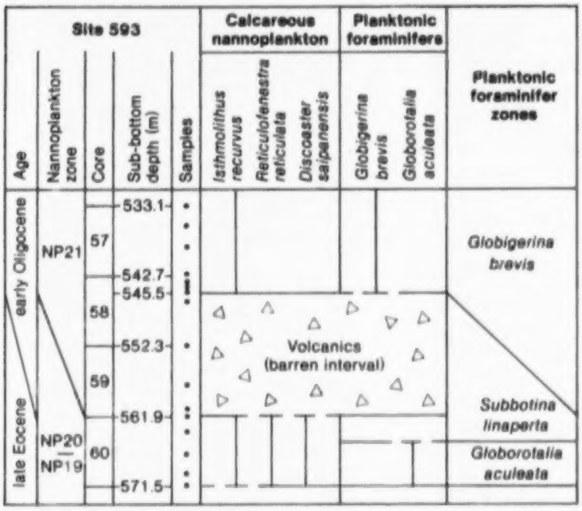

Figure 5. Distribution of key planktonic foraminiferal and nannofossil species used to define the Eocene/Oligocene boundary in relation to the volcanogenic deposits near the base of Hole 593. The occurrence of *Isthmolithus recurvus* shows the core terminated in sediments no older than the late Eocene NN19 Zone. The absence of *Sphenolithus pseudoradians* prevents recognition of the NN20/NN19 boundary. The last occurrence of *Reticulofenestra reticulata* (= *Cribrocentrum reticulatum*) and *Discoaster saipanensis* marks the Eocene/Oligocene boundary.

Table 1. Microprobe analysis of phillipsite in Sample 593-59-3, 60 cm (Sample 5, Fig. 3).

		Cations on basis of 31(0)
SiO_2	51.40	11.16
Al_2O_3	17.54	4.49
FeO*	1.29	0.24
MgO	0.10	0.03
CaO	0.14	0.03
Na_2O	3.71	1.56
K_2O	6.26	1.74
H_2O	n.d.	-
Total	80.44	
	Si/Al	2.49

Note: * = total Fe. n.d. = not determined.

FeO of 0.57–0.69 wt.%, and MnO abundances of 0.33–0.44 wt.%.

Iron oxy-hydroxides occur as alteration products of magnetite and in veins associated with calcite.

Major Element Chemistry

Several samples were analyzed in an attempt to determine the original composition of the volcanogenic material. Five samples of palagonite separates and five whole-rock samples were analyzed by routine x-ray fluorescence (XRF) methods, and palagonite material was analyzed by microprobe in eight samples. The microprobe analyses were determined first, and when these showed widely variable compositions, it was considered that although large-scale metasomatism had obviously occurred, analyses of whole-rock samples might be closer to the original composition. However, this was proved not to be the case, and because of the extreme variability in composition of all oxides, only averaged analyses are shown together with ranges in composition in Table 2.

The microprobe analyses of palagonite indicated that intrasample variation was as much as the variation between samples, and no sensible trends in composition with respect to stratigraphic position of the samples could be detected. The very large loss on ignition (LOI) values of samples analyzed by XRF indicate that extensive hydration has occurred. Samples with the largest CaO contents are also those with the largest LOI values, suggesting that calcite was probably a significant constituent, especially in bulk samples.

Nature of Primary Volcanic Materials

The major element compositions of the volcanogenic material show that it is severely altered and hydrated, and none of the analytical data are considered to represent the primary composition of the volcanogenic material. However, the glass is thought to have been most likely basaltic rather than andesitic or rhyolitic in composition for the following reasons:

1. Unaltered pale green augite, minor magnetite, and rare olivine are the only primary minerals present. If the original composition of the material was silicic or intermediate, then feldspars would be expected. We have not detected any textural evidence to indicate that feldspar was formerly present but now completely altered. Orthopyroxene is also absent. Hence, a mineralogy dominated by augite favors an original basaltic composition.

2. Most studies on low-temperature oxidative alteration and weathering of basaltic glass by seawater (e.g., Hart, 1970; Scheidegger and Corliss, 1981) indicate there is depletion in MgO, SiO_2, and CaO, and enrichment in K_2O, total iron, TiO_2, P_2O_5, MnO, and Na_2O, whereas Al_2O_3 is little affected. These changes in major element abundances, caused by oxidative seawater alteration, are

Table 2. Chemical composition of bulk samples (XRF), palagonite-enriched samples (XRF), and palagonitic material (microprobe) from the volcanogenic deposits at Site 593.

	Composition (XRF) of bulk samples (*N* = 5)		Composition (XRF) of palagonite-enriched samples (*N* = 5)		Composition (microprobe) of palagonite (*N* = 8)	
	Average	Range	Average	Range	Average	Range
SiO_2	32.28	24.26-41.57	39.38	31.97-43.80	41.37	31.4[illegible]-49.92
TiO_2	2.44	2.07-2.70	2.64	2.38-2.93	3.30	0.3[illegible]-6.54
Al_2O_3	9.47	7.53-11.93	10.81	9.67-11.96	13.32	8.3[illegible]-18.38
FeO*	9.28	7.05-12.38	12.44	7.90-15.22	10.43	4.1[illegible]-17.08
MnO	0.17	0.09-0.25	0.09	0.03-0.21	0.08	0.0[illegible]-0.30
MgO	7.96	4.85-12.12	9.75	5.54-13.96	6.87	3.3[illegible]-11.33
CaO	16.02	5.34-24.61	7.68	2.32-18.26	2.71	0.[illegible]-11.25
Na_2O	2.48	1.43-2.99	2.53	2.11-2.86	1.82	1.[illegible]-2.93
K_2O	0.96	0.49-1.41	1.09	0.30-3.28	1.26	0.[illegible]-2.33
P_2O_5	1.13	0.83-1.58	1.32	0.86-2.06	n.d.	
LOI	17.73	10.21-22.79	12.06	6.54-18.25	n.d.	
Total	99.92		99.79		81.13	
ppm						
Sc	22	18-25	20	14-22		
V	207	196-228	213	128-251		
Cr	103	33-250	111	22-274		
Ba	744	259-1209	323	101-889		

Note: * = total Fe. LOI = loss on ignition. n.d. = not determined. XRF analyses by K. Palmer, Analytical Facility, Victoria University, Wellington.

very significant and are suggested by the extreme variation in composition in our samples. Conversely, higher temperature nonoxidative hydrothermal alteration of basalts can produce slight enrichments in the alkali metals, TiO_2, and MgO, and depletion in total iron (Campsie et al., 1983).

Because our samples were recovered from within 600 m of the seafloor, we assume that palagonitization resulted from oxidative low-temperature, low-pressure alteration by pore fluids, and so depletion of MgO is more likely. The smallest averaged MgO content is 6.87 wt.% in palagonite determined by microprobe (Table 2), and the total range in MgO abundance is 3.3–11.3 wt.%. If MgO depletion has occurred, then the original composition is more likely to be basaltic rather than andesitic because the average MORB contains 7.6 wt.% MgO, whereas the average andesite contains only 3.6 wt.% MgO (Gill, 1981).

Furthermore, although Sc and V abundances (average 21 and 210 ppm, respectively) are not considered diagnostic because these values by themselves could represent either abundances in a basaltic or andesitic composition, the average Cr content (107 ppm) is regarded as more typical of a basaltic composition. Le Roex and Dick (1981) noted that Cr (and V) in basalts are relatively unaffected by alteration processes, and so these Cr contents are unlikely to represent enriched values. Also, most andesites, apart from some continental medium- and high-K calcalkaline varieties, have Cr abundances less than about 40 ppm (Gill, 1981), whereas Cr abundances in excess of 100 ppm are typical of basalts.

3. Phillipsite is the only zeolite identified, and clinoptilolite has notably not been detected. In a review of zeolites in deep-sea sediments, Kastner (1979) concluded that phillipsite almost always coexists with basaltic glass. Petzing and Chester (1979) also found that the Si/Al ratio of the parent glass in marine environments generally controlled the type of zeolitic alteration product; phillipsite, with a low Si/Al ratio (2.4–2.8), characteristically forms from basic, alkaline glasses (low Si/Al), whereas deep-sea clinoptilolites, with Si/Al ratios ranging from 4.1 to 4.9 (Boles, 1977), form from alteration of silicic glass (high Si/Al). The abundance of low Si/Al ratio phillipsite (2.49; Table 1) in the volcanogenic deposits in Hole 593 favors a primary basaltic composition.

Although we consider it most likely that the primary composition of the volcanic material was basaltic, it may be possible to speculate further that the high Ti content and Ti/V ratios, and absence of feldspars, could indicate an alkalic, within-plate composition rather than an arc or spreading center environment (Shervais, 1982).

SOURCE AND EMPLACEMENT OF VOLCANOGENIC DEPOSITS

An *Eltanin* seismic profile over western Challenger Plateau (Hayes et al., 1975) had indicated the presence of a prominent sub-bottom knoll in the vicinity of proposed Site 593. While approaching Site 593 from the north, a careful watch was kept on the shipboard seismic record to ensure the chosen drill site did not sit over any such buried feature. None was located, and Hole 593 was successfully spudded and cored. However, within half an hour of departing Site 593, the seismic profiling system was again deployed to reveal the ship's eastward track passing across the eastern slope of a buried cone. This cone, named by lottery after a shipboard scientist's wife as "Lalitha pinnacle" (a Sanskrit name meaning beautiful), lay only ~3 km from Site 593. A seismic profile over Lalitha pinnacle (Fig. 6), recorded by Geophysics Division of New Zealand Department of Scientific and Industrial Research, Wellington, shows an edifice rising about 500 m from a 6–7-km-wide base. With an average profile slope of 6–8°, the form is compatible with that of a central basaltic shield. The downbowing of reflectors adjacent to the cone may result partly from progressive sediment infilling of a seafloor moat formed around the volcano by increased bottom current activity.

Lalitha pinnacle is logically the source of the volcanogenic deposits at Site 593, and possibly also some of the numerous thin ash layers occurring in the late Eocene–early Oligocene carbonate sediments at the site, as well as at Site 592 to the north (Gardner, Nelson, et al., this volume). It remains uncertain whether the graded volcanogenic units (Fig. 3) are cold sedimentary turbidites, each triggered by some disturbance of the volcanic materials on the slopes of Lalitha, or whether they represent discrete subaqueous pyroclastic flow deposits. Existing facies models for the latter (e.g., Tassé et al., 1978; Lajoie, 1979) closely mimic those for turbidites and associated coarse clastic sedimentary deposits (e.g., Walker, 1979), with more proximal deposits exhibiting a higher proportion of massive or reversely graded beds than distal deposits, which are mainly normally graded and include common traction structures such as horizontal and cross laminations. In either case, the majority of the normally graded volcanogenic units represent deposition at bathyal depths from relatively low-density, decelerating turbulent suspensions of basic glass-dominated material, whereas the less abundant and thicker breccia units accumulated from laminar suspensions resembling debris flows, or possibly hyaloclastites.

Based on the seismic evidence, the sequence of flows (possibly Acoustic Unit C, see Site 593 report, this volume) appears to be traceable for at least several tens of kilometers north of Site 593. Moreover, the character of the seismic profile suggests the volcanogenic deposits are probably confined to the relatively short time interval in the vicinity of the Eocene/Oligocene boundary. One slightly deeper (650–700 m sub-bottom) interval of strong reflectors (Acoustic Unit E), resembling Acoustic Unit C, does occur above acoustic basement (see Site 593 report, this volume) and may either represent earlier activity or could actually correlate with the cored volcanogenic turbidite sequence. The numerous laminae of altered volcanic ash of late Eocene through early Oligocene age at Sites 592 and 593 (Gardner, Nelson, et al., this volume) suggest when Lalitha was active.

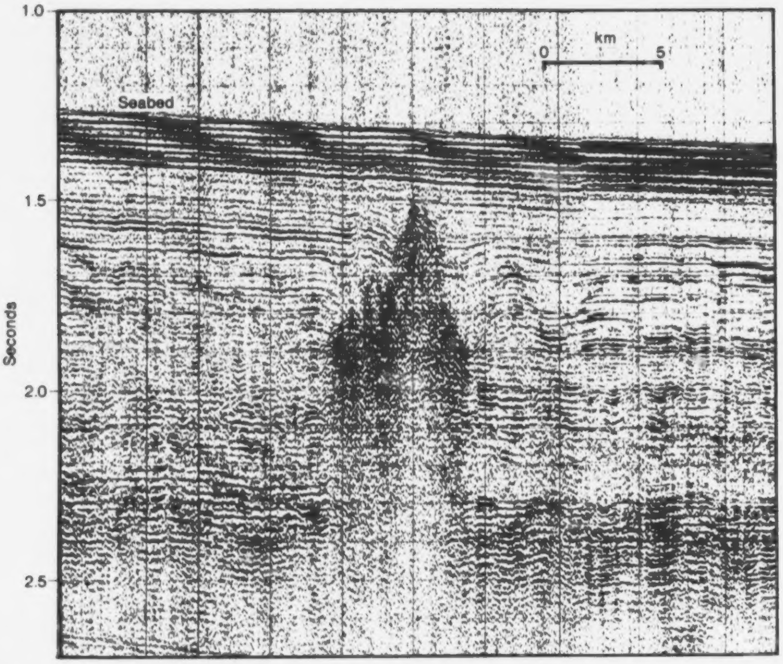

Figure 6. Single-channel seismic profile over a portion of the buried Lalitha pinnacle on western Challenger Plateau in the vicinity of Site 593. The record was kindly provided by the Geophysics Division of the New Zealand Department of Scientific and Industrial Research, Wellington. Horizontal and vertical scales are marked at 15-min. (approximately 3.1 km) and 0.1-s two-way traveltime (approximately 100 m) intervals, respectively.

EXTENT OF EOCENE–OLIGOCENE SUBMARINE VOLCANISM ON SOUTHERN LORD HOWE RISE

A conspicuous feature of several of the published seismic reflection profiles from the southern Lord Howe Rise–Challenger Plateau region is the occurrence of isolated seafloor and buried pinnacles, resembling "piercement" structures (e.g., Brodie, 1952; Houtz et al., 1967; Andrews and Eade, 1973; Bentz, 1974; Davey, 1977). Although an igneous origin has generally been accepted for these features, considerable difference of opinion exists as to their age(s) and composition and whether they represent predominantly intrusive or extrusive masses. For example, Andrews and Eade (1973) favored an early and middle Miocene age and an intrusive origin with associated volcanism; Bentz (1974) suggested explosive rhyolitic eruptions throughout the Neogene into the present, and possibly also in the Paleogene; whereas Davey (1977) commented on some evidence for a post-Miocene age and intrusive formation.

The pinnacles typically rise a few to several hundred meters from 4–10-km-wide bases, and have calculated slopes in the range 5–12°. Thus, like Lalitha, they are technically not pinnacles, but, rather, have a form typical of volcanic shields. This and their association with large-amplitude, isolated, subcircular positive magnetic anomalies (van der Linden, 1967; Heirtzler et al., 1969; Bentz, 1974; Davey and Robinson, 1978) lend support to the contention that they are basaltic. In at least some cases the apparent steepness and downward continuity of pinnacles may result simply from a masking of deeper-seated structures within the shadow zone cast by a cone of volcanic materials. For example, several of the subcone reflectors below the triangular top of Lalitha pinnacle appear to pass without interruption from one side of the structure to the other, suggesting that the cone was constructed from rather small, localized feeder pipes (Fig. 6).

Available seismic evidence suggests a possible correlation between several of the southern Lord Howe Rise "pinnacles" and the inferred Eocene–Oligocene basaltic volcanism represented by the buried Lalitha shield. The products of coeval volcanism on Challenger Plateau up to 500 km from Site 593 are evident on *Eltanin* seismic Profiles 26 and 34 (e.g., Fig. 7). Here the volcanics are closely associated with a prominent reflector (labeled X by Davey, 1977) which, in the vicinity of Site 593, corresponds to an unconformity of late Eocene and/or early Oligocene age (see Site 593 seismic stratigraphy, this volume). Away from Site 593 this unconformity becomes more profound (e.g., top middle Eocene to base middle Miocene at DSDP Site 207; Kennett et al., 1975) and corresponds to a well-documented regional Paleogene-Neogene unconformity in the Tasman Sea (Bentz, 1974; Kennett et al., 1975). Seismic profiles from the southern Lord Howe Rise (e.g., Houtz et al., 1967; Andrews and Eade, 1973; Bentz, 1974), 500 km and more north of Site 593 (Fig. 8), also show that isolated (volcanic) pinnacles are sometimes associated with this unconformity. For example, Houtz et al. (1967, p. 4726) noted that the

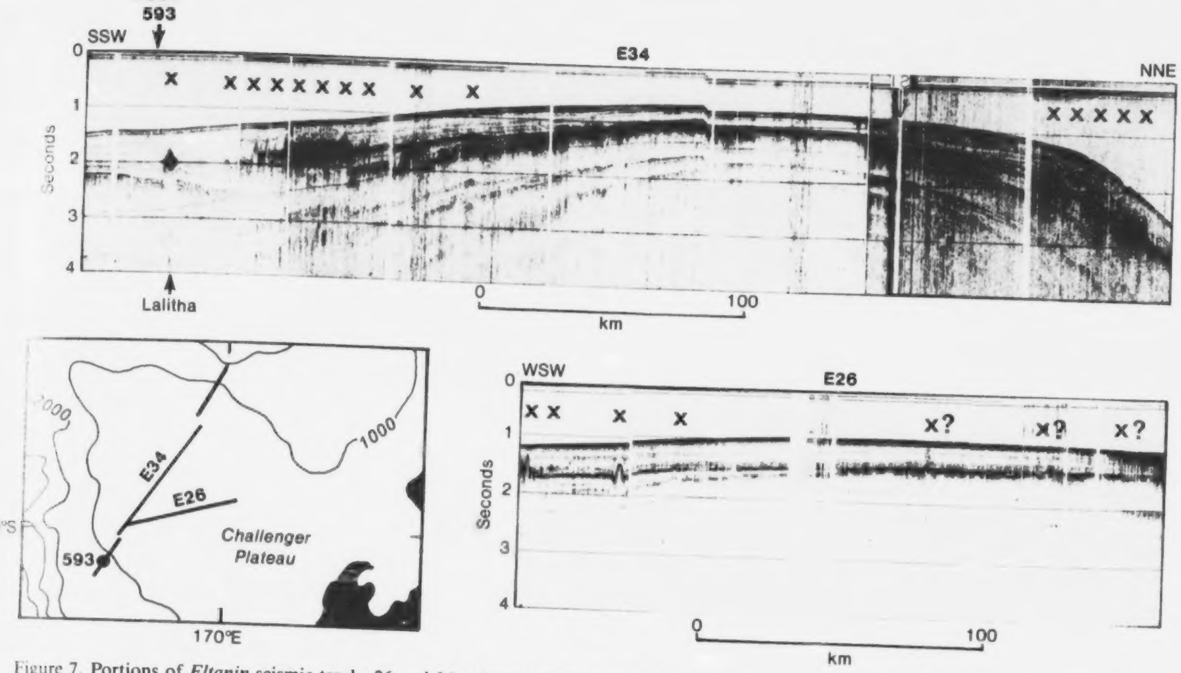

Figure 7. Portions of *Eltanin* seismic tracks 26 and 34 (adapted from Houtz and Aitkin, 1973; and Hayes et al., 1975) in the vicinity and northeast of Site 593 showing Lalitha pinnacle and other probably correlative buried basaltic volcanoes (marked by overlying crosses) on Challenger Plateau. Other seismic examples of volcanic features from as far as 500 km and more north of these profiles are illustrated by Houtz et al. (1967), Andrews and Eade (1973), and Bentz (1974). Bathymetry on locality map in meters.

"volcanics have poured out on a surface...which appears to correlate with the unconformity," whereas Andrews and Eade (1973, p. 3095) indicated that the volcanics "have been buried by sediments above the reflector," which corresponds to the mid-Eocene to mid-Miocene unconformity.

Obviously considerably more specific seismic and drill core data are needed to resolve the origin(s) of these (buried) pinnacles. However, their seismic character and structural and age relations to surrounding sediments, which are similar to those of Lalitha pinnacle, suggest that submarine basaltic volcanism was scattered but widespread over at least 250,000 km^2 in the southeast Tasman Sea region during late Eocene to early Oligocene times.

TECTONIC IMPLICATIONS OF LATE EOCENE-EARLY OLIGOCENE SUBMARINE VOLCANISM

The similar character and age of the widely distributed submarine volcanics over the southern Lord Howe Rise and Challenger Plateau are suggestive of a regional tectonic control on their eruption. A subduction origin of these basalts, either as island arc or back-arc volcanics, is precluded by the location and orientation of the nearest trench at that time, the Tonga-Kermadec Trench (Kamp, 1984). The widespread eruption of these volcanics near the Eocene/Oligocene boundary also precludes any suggestion of migratory control, as established for Cenozoic volcanics in eastern Australia by Wellman and McDougall (1974) and Sutherland (1981). The location of the submarine volcanics above the Lord Howe Rise rift system and adjacent to the New Caledonia Basin (Fig. 8) may, however, be indicative of a rift-related origin.

That there is not a simple and direct relationship between the basaltic eruptions and either the Lord Howe Rise or New Caledonia Basin rifting is evident from the great disparity in ages between rifting and volcanism. In both cases active rifting preceded Tasman Sea spreading, dated from 76–57 m.y. ago (Jongsma and Mutter, 1978; Wilcox et al., 1980), whereas the basaltic volcanism occurred near the Eocene/Oligocene boundary. The occurrence of the volcanics upon Paleogene bathyal nannofossil chalk also indicates that the eruptions followed passive foundering of the Lord Howe Rise, which in turn postdated the active rifting.

We consider that the submarine volcanism originated from the reactivation of underlying Late Cretaceous rift structures. That these faults were reactivated in the late Eocene–Oligocene can be inferred from the seismic sections presented by Bentz (1974). He showed that many of the basement faults within what later came to be identified as the Lord Howe Rise rift system (Jongsma and Mutter, 1978), and on the eastern flank of the New Caledonia Basin, extended through the Paleogene sequence up to the widespread Paleogene–Neogene unconformity in the Tasman Sea (Kennett et al., 1975), of which the underlying beds are variously aged from middle Eocene to early Oligocene. Bentz (1974) considered that these faults originated by differential displacements as the Lord Howe Rise foundered through the Paleogene. This is chal-

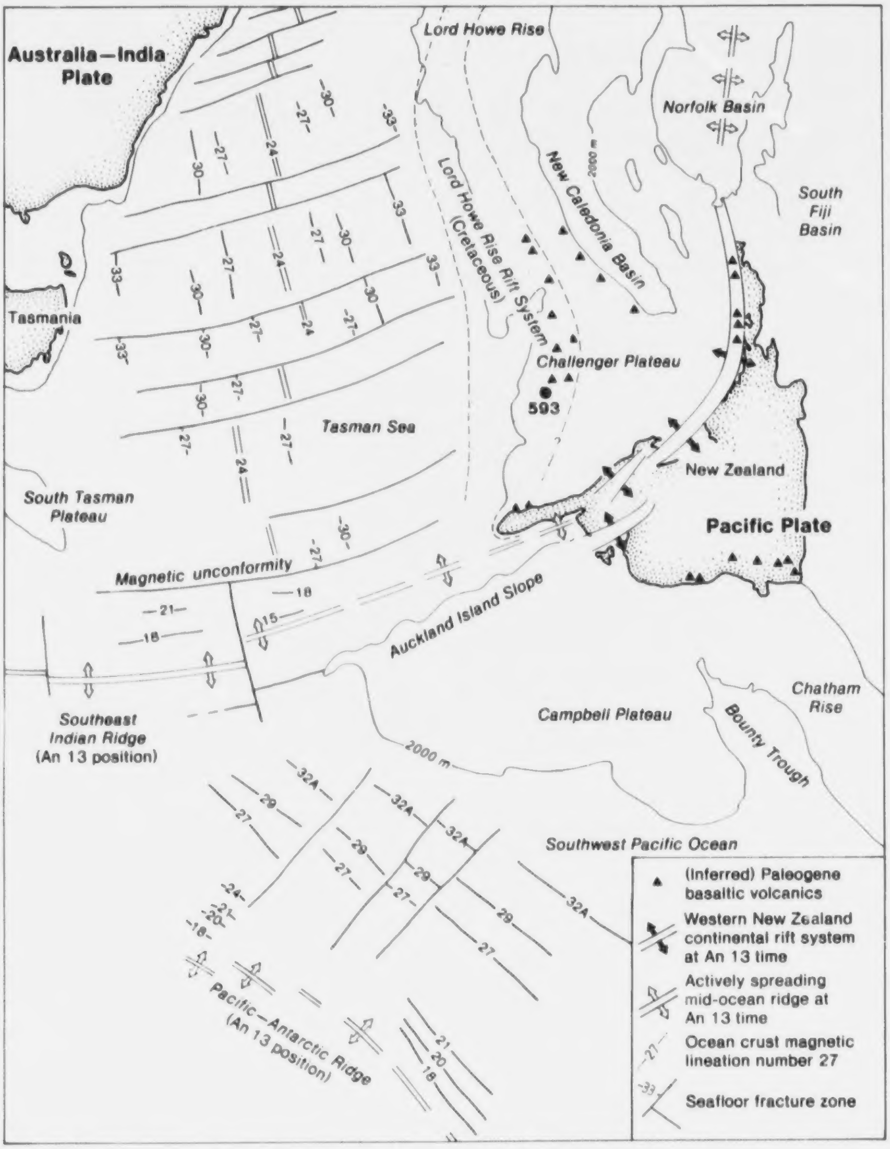
Australia—India Plate
Lord Howe Rise
Norfolk Basin
South Fiji Basin
Lord Howe Rise Rift System (Cretaceous)
New Caledonia Basin
2000 m
Tasmania
Challenger Plateau
593
Tasman Sea
New Zealand
Pacific Plate
South Tasman Plateau
Magnetic unconformity
Auckland Island Slope
Southeast Indian Ridge (An 13 position)
Campbell Plateau
Bounty Trough
Chatham Rise
2000 m
Southwest Pacific Ocean
Pacific—Antarctic Ridge (An 13 position)
33
30
27
24
21
18
15
32A
29
20
(Inferred) Paleogene basaltic volcanics
Western New Zealand continental rift system at An 13 time
Actively spreading mid-ocean ridge at An 13 time
Ocean crust magnetic lineation number 27
Seafloor fracture zone

Figure 8. Plate tectonic reconstruction of the Tasman Sea-southwest Pacific region at Anomaly (An) 13 time (37 m.y. ago), during eruption of the DSDP Site 593 Eocene/Oligocene boundary volcanics, showing the distribution of these and other possible (offshore geophysical evidence) and definite (on land in New Zealand) early Tertiary basaltic volcanoes in the region in relation to spreading on the Southeast Indian Ridge and the postulated New Zealand continental rift system of the time.

lenged on the basis that there is no perceptible evidence of sequences below the unconformity thickening toward growth faults, as one would expect. Also, closely spaced faulting would not be consistent with the evidence from other passive margins (e.g., Montadert et al., 1979) that subsidence of a continental margin following rifting is not characterized by differential faulting, nor with geophysical modeling that suggests that the flexural rigidity of continental crust increases after rifting (Karner and Watts, 1982). We prefer to interpret the faults cutting the Paleogene sequence in Bentz's (1974) sections as mainly postdepositional faults that displaced the lower Paleogene sequence vertically, thereby facilitating the rapid upward passage of basaltic magmas and subsequently their extrusion.

We propose that the reactivation of the rift structures was a local response to the regional extension accompanying a middle to late Eocene change in the seafloor spreading pattern southwest of New Zealand. Kamp (unpubl. data) has suggested that following the cessation of Tasman Sea spreading, the Southeast Indian Ridge propagated eastward into the New Zealand subcontinent during the middle to late Eocene (Anomaly 18–Anomaly 13) and caused the development of a continental rift system through western New Zealand (Fig. 8). Coincidentally, the Eocene/Oligocene boundary age of the transition from slow infrarift subsidence to active axial trough subsidence in the western rift system is the same age as the submarine volcanism, as determined previously. The vigorous eastward propagation of the mid-ocean ridge into New Zealand and the associated continental rifting offer a compelling geodynamic reason for the reactivation of the Late Cretaceous structures of the Lord Howe Rise–Challenger Plateau. This mechanism may also explain the occurrence of Eocene–Oligocene submarine basaltic lavas and tuffs of tholeiitic to alkaline composition in eastern South Island (Schofield, 1951; Coombs and Dickey, 1965; Challis, 1978); these are disposed off the rift to the east the same distance (~300 km) as the Lord Howe Rise and Challenger Plateau volcanics are to the west (Fig. 8).

CONCLUSIONS

1. A 16.4-m-thick sequence of volcanogenic deposits is enclosed within bathyal chalks about 550 m below the seafloor at DSDP Site 593, western Challenger Plateau, Tasman Sea.

2. The sequence of deposits was emplaced rapidly at bathyal depths close to the time of the Eocene/Oligocene boundary, about 37–36 m.y. ago.

3. It consists of a stacked series of normally graded volcanogenic sandstone–mudstone couplets with Bouma sequences of sedimentary structures, indicating deposition from decelerating turbidity currents, and occasional thicker interbeds of massive or inversely graded, unsorted volcanogenic breccia, suggestive more of deposition from high-concentration laminar suspensions resembling debris flows. It is not possible, based on present evidence, to distinguish positively between cold sedimentary redeposition or subaqueous pyroclastic flow origins for the beds, since generally similar structures can result from both emplacement mechanisms.

4. Petrographic, chemical, and geophysical data supports a basaltic heritage for the sequence. However, the original glassy components that formed the bulk of the deposits have been pervasively palagonitized and replaced by a complex association of the secondary minerals phillipsite, smectite, and calcite as a result of low-temperature oxidative alteration by pore fluids. It is inferred that alteration commenced soon after emplacement of the deposits and has continued throughout burial diagenesis.

5. The probable source of the deposits is Lalitha pinnacle, a now-buried 500-m-high volcanic shield situated near Site 593.

6. Seismic evidence indicates that volcanic centers of similar character and age to Lalitha pinnacle are dotted over at least 250,000 km² of southern Lord Howe Rise and Challenger Plateau. This implies that submarine basaltic volcanism and associated sedimentary redeposition were widespread in the southeast Tasman Sea region during the late Eocene to early Oligocene. Previously, this period has been regarded as one of little volcanism in the area.

7. Volcanism is genetically related to the eastward propagation in the late Eocene–early Oligocene of the mid-ocean Southeast Indian Ridge into the south Tasman Sea and through the New Zealand subcontinent, forming a major western New Zealand rift system. The southern Lord Howe Rise basalts are viewed as off-rift (western) volcanics erupted along reactivated major Late Cretaceous faults on the Rise in response to regional extension across the New Zealand platform accompanying development of the western rift system. Analogous occurrences of submarine Eocene–Oligocene basalts east of the rift system now crop out on land in eastern South Island, New Zealand.

ACKNOWLEDGMENTS

We thank Drs. P. F. Ballance, Geology Department, University of Auckland; F. J. Davey, Geophysics Division, Department of Scientific and Industrial Research, Wellington; J. B. Gill, University of California, Santa Cruz; and J. H. Natland, Scripps Institution of Oceanography, for constructive reviews of this manuscript. The age data forming Figure 5 were kindly provided by Dr. W. H. Lohman (Marathon Oil Company, Denver) and the core photographs of Figures 2 and 4 were prepared aboard ship by Mr. V. Sotelo.

REFERENCES

Andrews, J. E., and Eade, J. V., 1973. Structure of the western continental margin, New Zealand, and the Challenger Plateau, eastern Tasman Sea. *Geol. Soc. Am. Bull.*, 84:3093–3100.

Bentz, F. P., 1974. Marine geology of the southern Lord Howe Rise, Southwest Pacific. *In* Burk, C. A., and Drake, C. L. (Eds.), *The Geology of Continental Margins:* New York (Springer-Verlag), pp. 537–547.

Boles, J. R., 1977. Zeolites in deep-sea sediments. *In* Mumpton, F. A. (Ed.), *Reviews in Mineralogy (Vol. 4) Mineralogy and Geology of Natural Zeolites:* Mineral. Soc. Am., pp. 137–163.

Brodie, J. W., 1952. Features of the sea-floor west of New Zealand. *N.Z. J. Sci. Technol.*, B33:373–384.

Campsie, J., Neumann, E. R., and Johnson, L., 1983. Dredged volcanic rocks from the southern oceans: the Eltanin collection. *N. Z. J. Geol. Geophys.*, 26:31–45.

Carter, R. M., 1975. A discussion and classification of subaqueous mass-transport with particular application to grain-flow, slurry-flow, and fluxoturbidites. *Earth Sci. Rev.*, 11:145–177.

Challis, G. A., 1978. (Tertiary) Volcanism. *In* Suggate, R. P., Stevens, G. R., and Te Punga, M. T. (Eds.), *The Geology of New Zealand:* Wellington (Govt. Printer), pp. 632–637.

Coombs, D. S., and Dickey, J. S., 1965. The early Tertiary petrographic province of north-east Otago: Waiareka and Deborah Volcanic formations. *N. Z. Volcanol. South Island. N. Z. Dept. Sci. Industr. Res. Info. Ser.*, 51:38–50.

Davey, F. J., 1977. Marine seismic measurements in the New Zealand region. *N. Z. J. Geol. Geophys.*, 20:719–777.

Davey, F. J., and Robinson, A. G., 1978. Cook (1st Ed.). *Magnetic total force anomaly map, Oceanic Series, 1:1000 000.* Wellington, N. Z., Dept. Sci. Indust. Res.

Gill, J. B., 1981. *Orogenic Andesites and Plate Tectonics:* Berlin (Springer-Verlag).

Hart, R., 1970. Chemical exchange between sea water and deep ocean basalts. *Earth Planet. Sci. Lett.*, 9:269–279.

Hay, R. L., and Iijima, A., 1968. Nature and origin of palagonite tuffs of the Honolulu Group on Oahu, Hawaii. *Geol. Soc. Am. Mem.*, 116:331–376.

Hayes, D. E., Houtz, R., Talwani, M., Watts, A. B., Weissel, J., and Aitken, T., 1975. Preliminary Report of Volume 23, USNS *Eltanin*, Cruises 33–38, March 1968–May 1969. Parts A, B and C. *Tech. Rept. Lamont-Doherty Geol. Obs. Columbia Univ., Palisades, N. Y.*, Cu-1-75.

Heirtzler, R. J., Hayes, D. E., Herron, E. M., and Pitman, W. C., III, 1969. Preliminary Report of Volume 20, USNS *Eltanin*, Cruises 16–21, January 1965–January 1966. Parts A and B. *Tech. Rept. Lamont-Doherty Geol. Obs., Columbia Univ., Palisades, N. Y.*, 3-CU-3-69.

Houtz, R., and Aitkin, T. D., 1973. Preliminary Report of Volumes 20 and 21, USNS *Eltanin* Cruises 16–21 and 22–27, January 1965–

February 1967. Part C. *Tech. Rept. Lamont-Doherty Geol. Obs., Columbia Univ., Palisades, N. Y.*, CU-1-73.

Houtz, R. E., Ewing, J., Ewing, M., and Leonard, A. G., 1967. Seismic reflection profiles of the New Zealand Plateau. *J. Geophys. Res.*, 72:4713–4739.

Jongsma, D., and Mutter, J. C., 1978. Non-axial breaching of a rift valley: evidence from the Lord Howe Rise and the southeastern Australian margin. *Earth Planet. Sci. Lett.*, 39:226–234.

Kamp, P. J. J., 1984. Neogene and Quaternary extent and geometry of the subducted Pacific Plate beneath North Island, New Zealand: implications for Kaikoura tectonics. *Tectonophysics*, 108:241–266.

Karner, G. D., and Watts, A. B., 1982. On isostasy at Atlantic-type continental margins. *J. Geophys. Res.*, 87:2923–2948.

Kastner, M., 1979. Zeolites. *In* Burns, R. G. (Ed.), *Reviews in Mineralogy (Vol. 6) Marine Minerals:* Mineral. Soc. Am., pp. 111–122.

Kennett, J. P., Houtz, R. E., Andrews, P. B., Edwards, A. R., Gostin, V. A., Hajòs, M., Hampton, M., Jenkins, D. G., Margolis, S. V., Ovenshine, A. T., and Perch-Nielsen, K., 1975. Cenozoic paleoceanography in the southwest Pacific Ocean, Antarctic glaciation, and the development of the Circum-Antarctic Current. *In* Kennett, J. P., Houtz, R. E., et al., *Init. Repts. DSDP*, 29: Washington (U.S. Govt. Printing Office), 1155–1169.

LaBrecque, J. L., Hsü, K. J., Carman, M. F., Jr., Karpoff, A-M., McKenzie, J. A., Percival, S. F., Jr., Petersen, N. P., Pisciotto, K. A., Schreiber, E., Tauxe, L., Tucker, P., Weissert, H. J., and Wright, R., 1983. DSDP Leg 73: contributions to Palaeogene stratigraphy in nomenclature, chronology and sedimentation rates. *Palaeogeogr., Palaeoclimatol., Palaeoecol.*, 42:91–125.

Lajoie, J., 1979. Facies models 17. Volcaniclastic rocks. *In* Walker, R. G. (Ed.), *Facies Models:* Canada (Geoscience Canada), Repr. Ser. 1, pp. 191–200.

Leggett, J. K., 1982. Drilling-induced structures in Leg 66 cores. *In* Watkins, J. S., Moore, J. C., et al., *Init. Repts. DSDP*, 66: Washington (U.S. Govt. Printing Office), 531–532.

Le Roex, A. P., and Dick, H. J. B., 1981. Petrography and geochemistry of basaltic rocks from the Conrad fracture zone on the America-Antarctic Rise. *Earth Planet. Sci. Lett.*, 54:117–138.

Montadert, L., de Charpal, O., Roberts, D. G., Guennoc, P., and Sibuet, J.-C., 1979. Northeast Atlantic passive margins: rifting and subsidence process. *In* Talwani, M., Hay, W. W., and Ryan, W. B. F. (Eds.), *Deep Drilling Results in the Atlantic Ocean: Continental Margins and Paleo-environment.* Am. Geophys. Un., Maurice Ewing Ser., 3:154–186.

Petzing, J., and Chester, R., 1979. Authigenic marine zeolites and their relationship to global volcanism. *Marine Geol.*, 29:253–271.

Poore, R. Z., Tauxe, L., Percival, S. F., Jr., LaBrecque, J. L., Wright, R., Petersen, N. P., Smith, C. C., Tucker, P., and Hsü, K. J., 1983. Late Cretaceous-Cenozoic magnetostratigraphic and biostratigraphic correlations of the South Atlantic Ocean: DSDP Leg 73. *Palaeogeogr., Palaeoclimatol., Palaeoecol.*, 42:127–149.

Scheidegger, K. F., and Corliss, J. B., 1981. Petrogenesis and secondary alteration of upper layer 2 basalts of the Nazca plate. *Geol. Soc. Am. Mem.*, 154:77–107.

Schofield, J. C., 1951. Distribution of lower Oligocene volcanics in New Zealand. *N. Z. J. Sci. Technol.*, B33:201–217.

Shervais, J. W., 1982. Ti–V plots and the petrogenesis of modern and ophiolitic lavas. *Earth Planet. Sci. Lett.*, 59:101–118.

Sutherland, F. L., 1981. Migration in relation to possible tectonic and regional controls in eastern Australian volcanism. *J. Volcanol. Geotherm. Res.*, 9:181–213.

Tassé, N., Lajoie, J., and Dimroth, E., 1978. The anatomy and interpretation of an Archean volcaniclastic sequence, Noranda region, Quebec. *Can. J. Earth Sci.*, 15:874–888.

van der Linden, W. J. M., 1967. Structural relationships in the Tasman Sea and south-west Pacific Ocean. *N. Z. J. Geol. Geophys.*, 10: 1280–1301.

Walker, R. G., 1979. Facies Models 8. Turbidites and associated coarse clastic deposits. *In* Walker, R. G. (Ed.), *Facies Models:* Canada (Geoscience Canada), Repr. Ser. 1, pp. 91–103.

Wellman, P., and McDougall, I., 1974. Cenozoic igneous activity in eastern Australia. *Tectonophysics*, 23:49–65.

Wilcox, J. B., Symonds, P. A., Hinz, K., and Bennett, D., 1980. Lord Howe Rise, Tasman Sea—preliminary geophysical results and petroleum prospects. *BMR J. Austral. Geol. Geophys.*, 5:225–236.

Date of Initial Receipt: 14 May 1984
Date of Acceptance: 31 October 1984

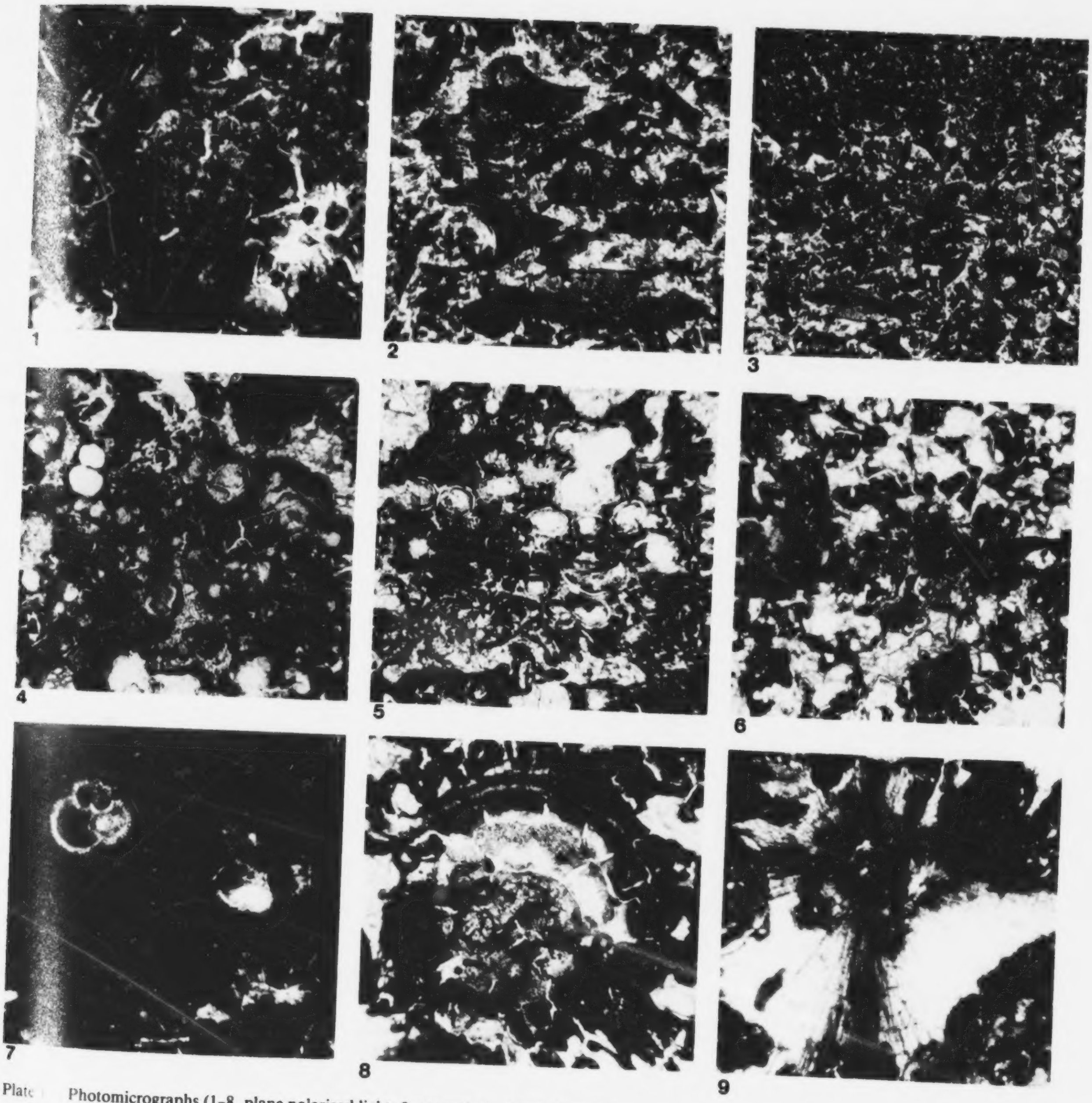

Plate Photomicrographs (1–8, plane polarized light; 9, crossed-nicols) of altered volcanogenic material at Site 593. For Figs. 1, 2, 4, 7, 8, and 9 the bottom edge of the photomicrograph measures 0.7 mm; for Figs. 3, 5, and 6 about 1.7 mm. **1.** Palagonite masses (black or dark gray) with irregular patches and veinlets of calcite and phillipsite (white or light gray). **2.** Relict, cuspate, curved glass shards set in a calcite-phillipsite cement. **3.** Lithologic layering defined by palagonitized, fine (top), and coarse shard-rich bands; light-colored cement is mainly calcite, phillipsite, and smectite. **4.** Globular masses of palagonitic material with smectite, calcite, and phillipsite in concentric layers within globules, and surrounded by coarse-grained sparry calcite. **5.** Globular palagonite in sparry calcite cement. **6.** Palagonite masses in a cement of calcite, phillipsite, and smectite. **7.** Black palagonite-rich layer containing planktonic foraminifers. **8.** Radial and concentric perlitic cracks in globular palagonite containing secondary minerals in concentric layers. **9.** Radiating splay of phillipsite.

28. BIOTURBATION IN MIDDLE BATHYAL, CENOZOIC NANNOFOSSIL OOZES AND CHALKS, SOUTHWEST PACIFIC[1]

Campbell S. Nelson, University of Waikato, Hamilton, New Zealand[2]

ABSTRACT

The high-quality cores obtained on Leg 90 have enabled preliminary qualitative study of the trace fossils in middle to late Cenozoic oozes and chalks at sites from equatorial to subantarctic latitudes in the southwest Pacific. Cores are dominated by a range of biogenic hieroglyphs that are in the main taxonomically nondiagnostic and are identified principally by subtle color contrasts with the host sediment, or by pyritization. Structures include abundant mottles, blebs and spots, common streaks and wisps, and rarer threads, tubes, rinds, halos, rings, and pockets. Planolites-like and possibly Trichichnus burrows occur, and below some critical sub-bottom depth in most holes a Planolites–Chondrites-Zoophycos ichnofaunal assemblage is developed. The megascopically apparent intensity of bioturbation in cores is summarized on stratigraphic logs for each site, and ranges widely both within and between sites. Controlling factors were unlikely to have been variations in either substrate character or water depth as primary sediments were almost wholly pure (foraminifer-bearing) nannofossil oozes deposited at middle bathyal (1–2 km) depths. Instead, fluctuations in sedimentation rates and in the rate of supply of organic nutrients at the seafloor were probably the influential controls on the degree of sediment bioturbation. Overall increases in both these parameters in the Neogene can explain the upward disappearance of the Planolites–Chondrites–Zoophycos assemblage in cores. Fundamental causes probably relate to the Cenozoic evolution and fluctuations in position and level of productivity of surface and intermediate-depth water masses in the southwest Pacific.

INTRODUCTION

Trace fossils provide useful information about ecology, sedimentation processes, water depth, and depositional environments of sediments (e.g., Frey, 1975; Basan, 1978). In deep-sea cores they are often the only or dominant structures in the sediments and may be the only preserved record of benthic faunal activity. The understanding of the nature and paleoecology of deep-sea fossil communities has resulted from several detailed studies of trace fossils in DSDP cores from a range of oceanic environments (e.g., Tracey et al., 1971; Fullman et al., 1973; Piper and Schrader, 1973; van der Lingen, 1973; Warme et al., 1973; Ekdale, 1978, 1980; Okado, 1980; McMillen and Lundberg, 1982). Useful overviews of trace fossils and their significance in DSDP sediments generally have been made by Chamberlain (1975) for the Pacific Ocean, and Ekdale (1977) for all oceans.

DSDP Leg 90 obtained a traverse of nine middle to late Cenozoic cores (Sites 586 to 594) between equatorial and northern subantarctic water masses in the southwest Pacific (Fig. 1). All the sites are located at relatively shallow water depths of between 1000 and 2200 m, principally on Lord Howe Rise in the Tasman Sea. Drilled sequences are dominantly pure calcareous oozes and chalks, mainly continuously deposited and uncomplicated by unconformities in their Neogene–Quaternary parts. Lord Howe Rise had subsided everywhere to present-day upper to middle bathyal depths by the middle Eocene (introductory chapter, this volume), so that the cored sediments were deposited at depths comparable to those of the present drill sites. Most cores were obtained with the hydraulic piston corer and extended core barrel systems (introductory chapter, this volume), which provided both high (average ~90%) core recovery and good quality sections with minimal core disturbance, even in soft oozes.

These high-quality cores provided an excellent opportunity to record the biogenic structures in Cenozoic foraminifer-bearing nannofossil oozes deposited on open ocean platforms at middle bathyal (1000–2000 m) depths (classification scheme of Edwards, 1979) across a wide range of latitudes. Previously, the rotary drilling method used on Legs 21 and 29 in this region had mainly smeared or destroyed trace fossils in the thick ooze sequences, restricting observations to the more indurated sediments (van der Lingen, 1973). Moreover, in Chamberlain's (1975) general review of trace fossils in Pacific DSDP cores only 4 of his 38 sites yielding bioturbation data came from water depths as shallow as middle bathyal, and none were as shallow as most Leg 90 sites, from 1000 to 1500 m depth. Since a major aim of DSDP Leg 90 is to gain detailed information on Neogene paleoceanography in the southwest Pacific from high-resolution biostratigraphic and isotopic studies of the sediments, the intention is to provide future researchers with some information on bioturbation in the cores.

METHODS

A specialized study of bioturbation has not been attempted. In describing core lithologies, the shipboard sedimentologists arbitrarily classified the extent of bioturbation as minor (<30%), moderate (30–60%), or intense (>60%) and noted certain other properties such as color, geometry, and location of trace fossils. After the cruise, a complete set of black-and-white core photographs was obtained and, in conjunction with the shipboard core descriptions, was used to determine the nature of visible trace fossil markings in the sediments and to

---

[1] Kennett, J. P., von der Borch, C. C., et al., *Init. Repts. DSDP*, 90: Washington (U.S. Govt. Printing Office).

[2] Address: Department of Earth Sciences, University of Waikato, Hamilton, New Zealand.

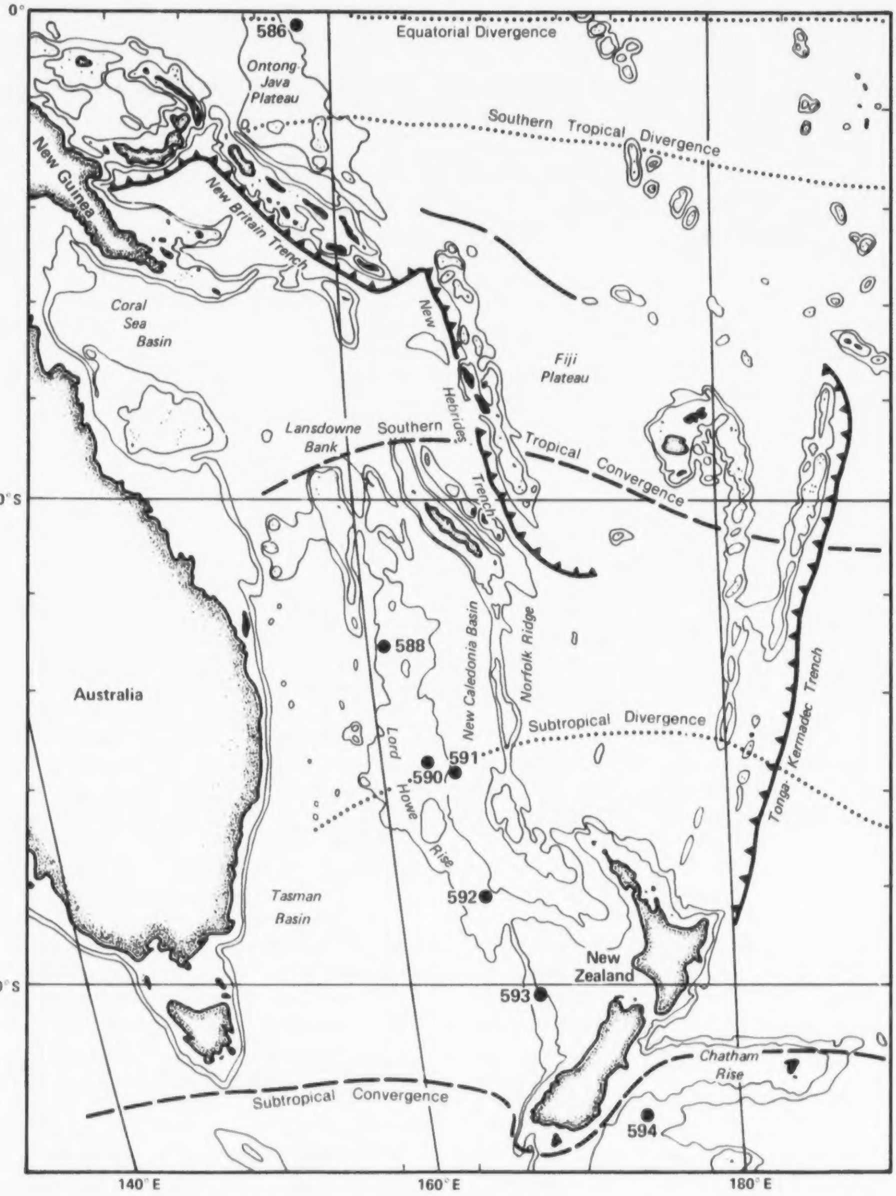
0°
586
Ontong Java Plateau
Equatorial Divergence
Southern Tropical Divergence
New Guinea
New Britain Trench
Coral Sea Basin
New Hebrides Trench
Fiji Plateau
Lansdowne Bank
Southern Tropical Convergence
20° S
588
Australia
New Caledonia Basin
Norfolk Ridge
Subtropical Divergence
Tonga-Kermadec Trench
Lord Howe Rise
591
590
Tasman Basin
592
New Zealand
40° S
593
Chatham Rise
Subtropical Convergence
594
140° E
160° E
180° E

Figure 1. Location of DSDP Leg 90 sites in the southwest Pacific for which bioturbation data are presented. The approximate positions of major water mass boundaries are taken from Knox (1970). Depth contours are for 1000 and 2000 m.

construct logs showing the apparent degree of bioturbation in Leg 90 cores from seven principal sites (586, 588, 590–594). This megascopic approach to describing the degree of bioturbation is potentially subject to several errors, but is nevertheless that normally used when logging DSDP core materials generally. For example, a totally featureless ooze can indicate complete homogenization of the sediment by meiofaunal burrowers, but outward proof of this is visibly lacking and the ooze would probably be logged as showing little evidence of bioturbation. Burrow preservation is a complex function of the rates of burrow production and destruction, the rate of sediment burial, the type and strength of sediment, and its early diagenetic history (Berger et al., 1979). Diagenesis, in particular, commonly imparts visual color contrasts between the organic traces and the surrounding burrowed or nonburrowed sediment. This is the principal basis for differentiating bioturbation in Leg 90 cores. The visual extent of bioturbation in Leg 90 cores has been placed within an arbitrary 10-point scale in which 3, 6, and 9 correspond approximately to the shipboard categories of minor, moderate, and intense bioturbation, respectively (Fig. 2). It is stressed, however, that only with more specialized core study, such as by X-ray radiography (e.g., Werner and Wetzel, 1981), can a more truly quantitative assessment of bioturbation be attempted.

DESCRIPTION AND GENERAL DISTRIBUTION OF SPECIFIC BIOGENIC TRACES

Burrow traces are ubiquitous in Leg 90 cores, but only rarely are they assignable to a specific ichnogenus. They

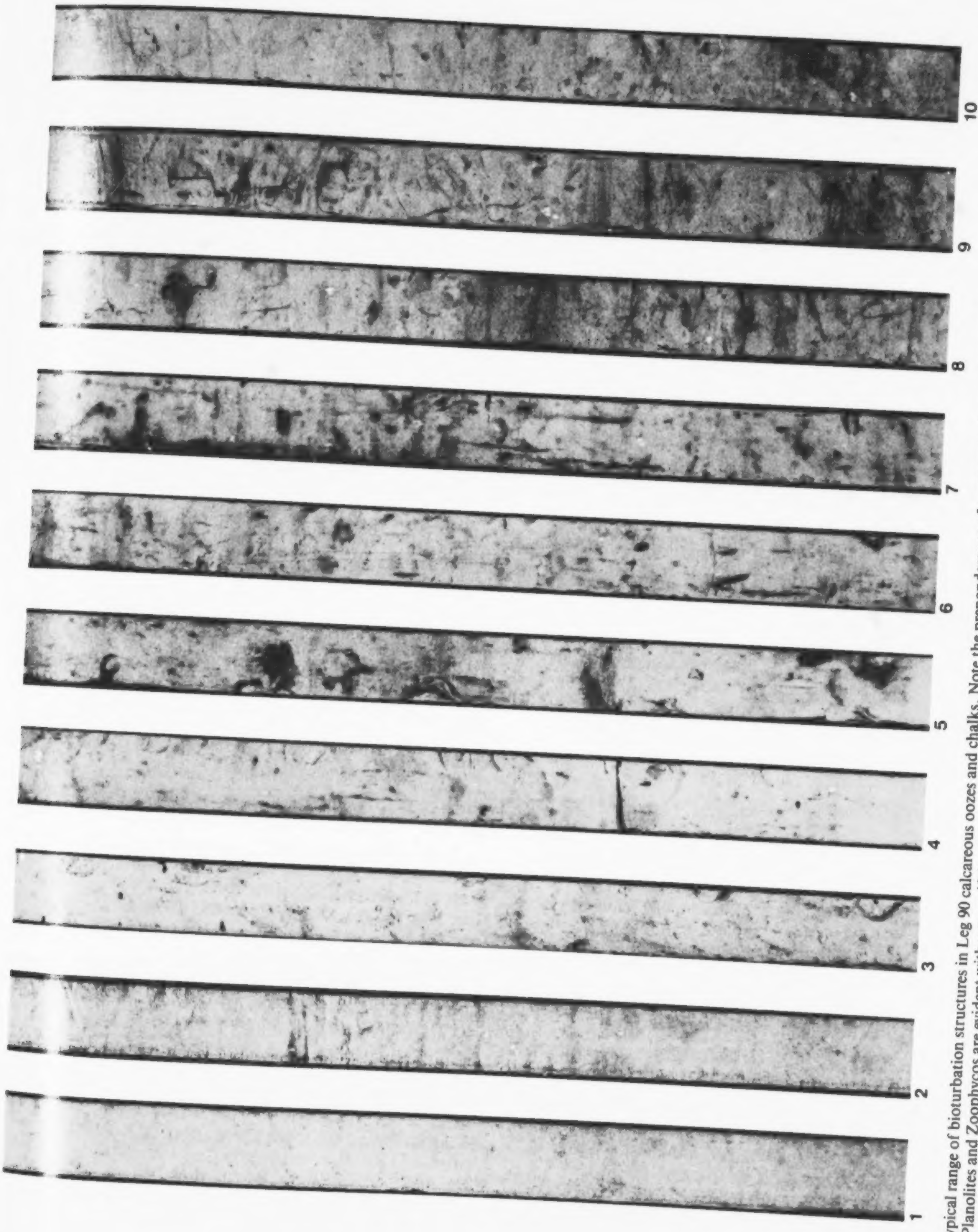

Figure 2. Typical range of bioturbation structures in Leg 90 calcareous oozes and chalks. Note the preponderance of taxonomically nondiagnostic biogenic hieroglyphs and mottles, although examples of Planolites and Zoophycos are evident with a magnifying lens in Samples H to J. Based principally on the intensity of color contrast patterns, the sequence from A to J is arranged in order of megascopically apparent increasing intensity of sediment bioturbation (see discussion under Methods). Core locations are 1. 588A-1-6, 65–145 cm; 2. 588-22-4, 60–140 cm; 3. 588-11-1, 60–140 cm; 4. 588-17-1, 10–90 cm; 5. 588-5-5, 0–80 cm; 6. 586B-12-2, 20–100 cm; 7. 586B-15-1, 10–90 cm; 8. 590B-33-6, 30–110 cm; 9. 590B-45-4, 45–125 cm; 10. 590B-37-5, 70–150 cm.

are recognized primarily by color and/or subtle textural contrasts with the surrounding sediment. The host calcareous oozes and chalks are mainly white (N9), very light gray (N8), or light gray (N7), whereas burrows are mainly yellowish gray (5Y 8/1, 5Y 7/2), greenish gray (5GY 6/1, 5GY 7/1, 5GY 7/2, 5GY 8/1), pale olive (10Y 6/2), or light to dark gray (N7 to N3). Smear slides from the burrowed sediment and the host sediment seldom reveal major differences in composition or texture. Some mottles with yellowish hues include more foraminiferal material than the host nannofossil-dominated oozes; those with greenish hues may contain concentrations of altered volcanic ash components (Gardner, Nelson, et al., this volume); and dark gray mottles may be relatively enriched in authigenic iron sulfides, commonly pyrite framboids.

The geometry of burrows in split cores is highly variable with a preponderance of mainly nondiagnostic biogenic hieroglyphs, informally described as spots, blebs, pockets, threads, tubes, streaks, wisps, eddies, rinds, halos, rings, and circular, ovoid, or irregular mottles. Their boundaries with the host sediment are mainly diffuse and often abruptly color gradational. Some characteristics of specific traces are mentioned in the following and illustrated in Figures 2 and 3, and in Plate 1.

1. Spots and Blebs:

Spots and blebs, often formed of pyritized sediment, range up to a few millimeters across and may be isolated "pods" or sections through short threads or tubes. They are ubiquitous and common in Leg 90 cores, especially throughout the upper Miocene–Quaternary oozes at Sites 586 and 588, and the Pliocene–Quaternary oozes at Sites 590 and 591. The strong tendency to pyritization suggests that at least some of these structures may be cross-sections of Trichichnus burrows (Werner and Wetzel, 1981). Others may represent fecal pellets or disrupted fecal strings.

2. Pockets:

Pockets are typically a few to several millimeters in size, with irregular or vertically elliptical shapes, infilled by mud-depleted sediment, commonly foraminiferal material and pyrite, sometimes preferentially cemented by ?celestite (e.g., Cores 593-11, 593-12, and 593-13). They are generally rare but are conspicuous in the Pliocene–Quaternary oozes at the southern sites (591–594). Highly selective sediment sorting within capsular structures is indicated, but the organism responsible is unknown.

3. Threads and Tubes:

Threads and tubes have small diameters (0.2–2.0 mm), range up to several centimeters long, rarely to 30 cm, and consist dominantly of pyritized sediment. They are ubiquitous but rare in Leg 90 cores, are most obvious in the upper Neogene oozes at northern sites (586–590), and some may be Trichichnus burrows. Bundles of fine tubes sometimes form the nucleus of pyritized nodules in the sediments (Fig. 4).

4. Streaks, Wisps, and Eddies:

Nebulous streaks and wisps are mainly horizontally to obliquely oriented and, along with occasional eddies, may be mainly biodeformational structures associated with the indiscriminant tracking, burrowing, and churning of surficial sediment layers (e.g., Werner and Wetzel, 1981). They are detected by generally subtle diagenetic color contrasts in the sediment and are one of the most common bioturbate structures in Leg 90 cores, particularly at Sites 586 through 591. They are of unknown taxonomic affinity.

5. Rinds, Halos, and Rings:

Rinds and halos are (sub)circular sections of cylindrical burrows, typically 5 to 40 mm across, defined by diagenetic color contrasts at the margins of burrows. Diffusion color rings, resembling Liesegang rings, are sometimes also developed about the burrows, rarely as far as 10–15 cm from the (inferred) burrow shaft. Gray, green, or purple hues dominate, suggesting they have formed by mobilization and precipitation of iron compounds under more or less reducing Eh conditions around the preferred sites of sulfate reduction provided by the organic-rich burrows. Rinds, halos, and rings occur infrequently in all cores, and are most common at Sites 586, 590, and 591. They are taxonomically nondiagnostic, but are widely reported from deep-sea cores (e.g., Chamberlain, 1975, 1978).

6. Mottles:

Circular and ovoid mottles are typically 5–30 mm or more across, internally structureless, and are the cross or oblique sections of mainly horizontal to inclined burrows of similar width. They are nearly always associated with similarly sized or larger irregular blebs, patches and mottles, and rarely with more vertically oriented shafts up to 10–15 cm long (e.g., Fig. 3). Blebs and mottles are the dominant bioturbation structure in Leg 90 sediments and occur to a greater or lesser extent in practically every core studied. They can be difficult to discern because of diffuse contacts with, and only subtle color differences from, the host sediment. In some firmer oozes they appear to be sites of preferential cementation (e.g., Fig. 3H), Plate 1, Fig. 7; Cores 593-29 and 594-36). Those mottles representing subhorizontal burrows with subcircular cross-sections are a form of Planolites (e.g., Plate 1, Figs. 2, 7, 9–12) referred to as Planolites-like in the core barrel descriptions (Site chapters, this volume). They occur sporadically at all sites in oozes of Miocene to Quaternary age and are most obvious in several of the Pliocene cores from Sites 590 and 591.

7. Planolites–Chondrites–Zoophycos Association:

Only three trace fossil genera have been positively identified in Leg 90 cores: Planolites, Chondrites, and Zoophycos. The morphologic characteristics of these traces are similar to those previously detailed by several workers (e.g., Hantzschel, 1975; Chamberlain, 1975, 1978;

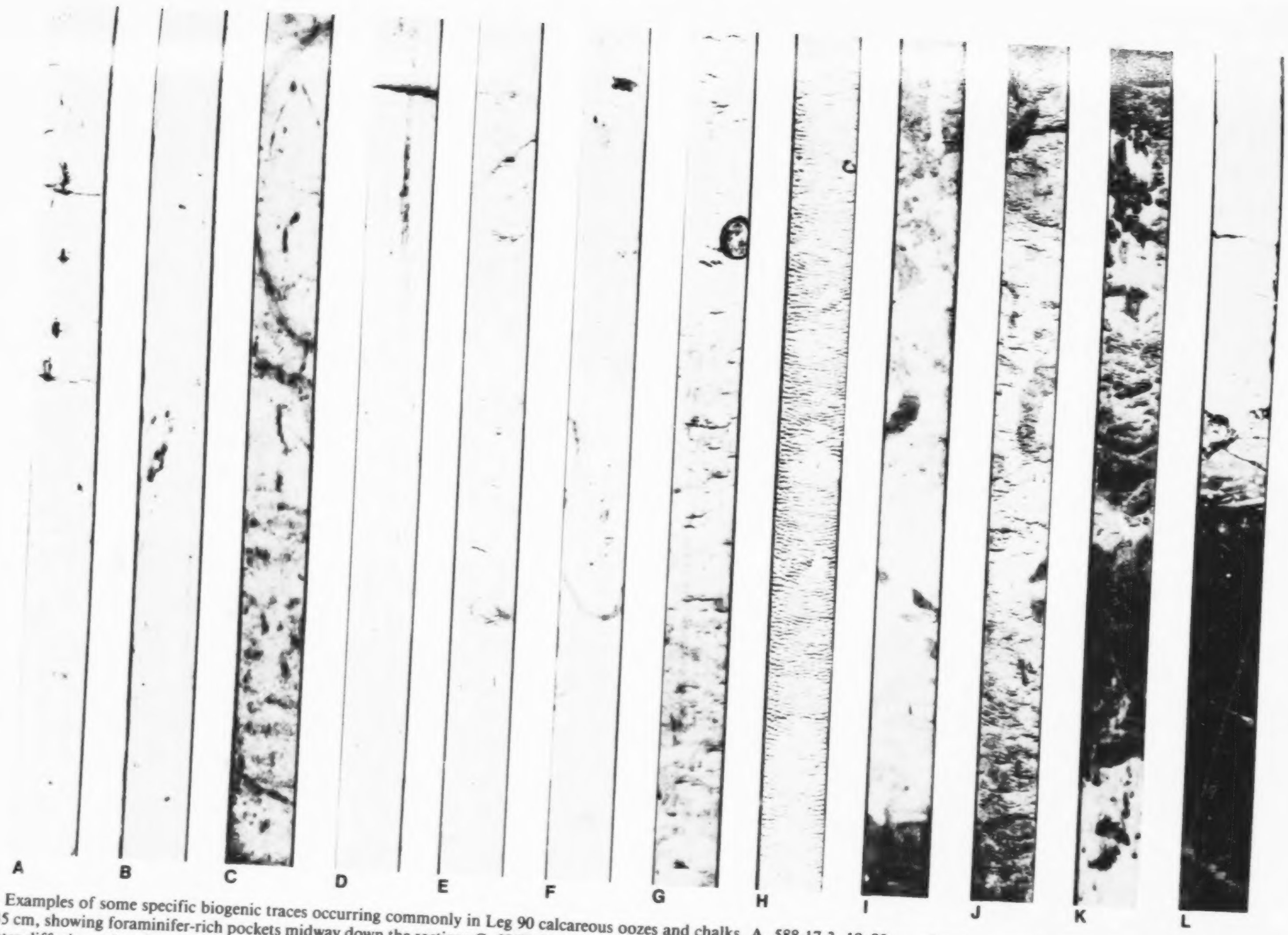

Figure 3. Examples of some specific biogenic traces occurring commonly in Leg 90 calcareous oozes and chalks. A. 588-17-3, 10–90 cm, showing scattered pyritized spots and blebs; B. 592-13-3, 55–135 cm, showing foraminifer-rich pockets midway down the section; C. 586B-21-3, 65–145 cm, showing common pyritized spots, threads and streaks, irregular blebs and mottles, and a large diameter diffusion color ring; D. 588-11-6, 5–85 cm, showing scattered pyritized spots and a long tube; E. 591-29-5, 5–85 cm, showing solitary Planolites-like halo burrow; F. 590B-7-3, 45–125 cm, showing biogenic streaks, wisps and mottles, a color diffusion ring structure, and pyritized spots and blebs; G. 591-24-4, 70–150 cm, showing diffuse mottles and a solitary Planolites-like rind burrow with reburrowed fill; H. 594-36-2, 5–85 cm, showing preferentially cemented Planolites-like burrows in stiff ooze, one including a color diffusion ring; I. 594-15-6, 10–90 cm, showing irregular and Planolites-like mottles across the contacts between pelagic (light) and hemipelagic (dark) sediment and within the pelagic interval; J. 594-16-1, 50–130 cm, as for I; K. 594-20-1, 45–125 cm, as for I showing severe biogenic disruption and displacement of sediment across the lithologic boundaries; L. 594A-23-1, 55–135 cm, showing well developed Planolites, Chondrites, and Zoophycos burrows at the top of a silty turbidite (dark) in chalk (light), the later preserving mainly scattered Planolites burrows and diffuse mottles.

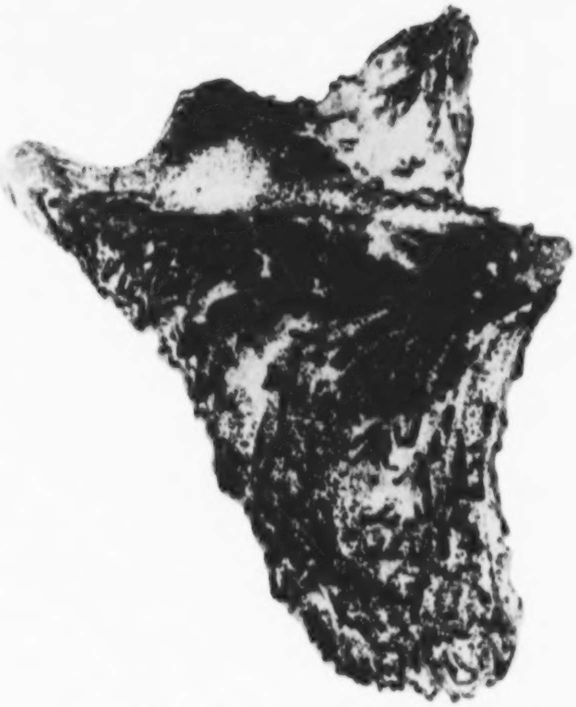

Figure 4. A spectacular 5-cm-long pyritized nodule from Sample 588-17-2, 143-148 cm, consisting of tapering bundles of overlapping fine tubes of unknown taxonomy.

Ekdale, 1977). Planolites is a simple, subhorizontal to inclined burrow seen mainly as subcircular, elliptical, or lenticular shapes in cross-section (e.g., Plate 1, Figs. 2, 7, 9-12). Chondrites comprises a three-dimensional dendritic network of obliquely to horizontally orientated burrows, typically only 1-2 mm in diameter, spreading down and out from a central shaft. On split core faces it usually appears as tiny ovoid blebs, a millimeter or so across, with associated small Y-shaped branching tubes (Plate 1, Figs. 6, 9-12). Zoophycos consists of a horizontal or inclined web or spreiten (up to 8 mm thick) of burrowed and back-filled sediment producing characteristic crescentic arcs in split core faces (Plate 1, Figs. 1, 5, 6, 10, 12).

Two striking features concerning Planolites, Chondrites, and Zoophycos are noted for Leg 90 cores. First, although the Planolites-like traces discussed previously can and do occur by themselves, the Planolites, Zoophycos, and Chondrites traces typically occur in association. In no core has only Zoophycos or only Chondrites been identified without the nearby presence of the other trace or of Planolites (Plate 1). Thus a definite Planolites-Chondrites-Zoophycos assemblage exists in Leg 90 sediments. Second, this assemblage is not uniformly distributed through the cores, but appears to be absent at each site down to some critical sub-bottom depth below which it persists to a greater or lesser extent to the bottom of the drilled sequence (Table 1; Fig. 5). This critical depth level differs from site to site, generally becomes progressively deeper from north to south, and varies widely in age in a nonsystematic way from as young as latest Miocene (Site 590) to as old as latest Eocene (Site 593). Possible reasons for this distribution pattern are discussed later.

BIOTURBATION HISTORY AND SOME ENVIRONMENTAL RELATIONSHIPS

Given the reservations outlined earlier, the apparent degree of bioturbation in Leg 90 cores from each site is summarized on stratigraphic logs in Figure 5. Also plotted are the general lithology, age, and sedimentation rates, as well as the sub-bottom depth below which the Planolites-Chondrites-Zoophycos assemblages occurs in cores.

Site 586 (2207 m): Tropical

Bioturbation here is moderate to moderately intense throughout the upper Miocene to Quaternary sequence of foraminifer-bearing nannofossil oozes. Overall, the apparent degree of bioturbation is consistently greater than in comparably aged lithologies at all other sites, despite the persistently moderate rates of sedimentation. This may relate to uniformly high productivity in the water column at Site 586, located beneath the Equatorial Divergence (Fig. 1). The most intensely bioturbated interval, from the late late Miocene to early early Pliocene, coincides with the lowest rates of sedimentation in the section. Nondescript biogenic hieroglyphs, often pyritized, completely dominate the sequence. The Planolites-Chondrites-Zoophycos assemblage was not encountered at Site 586.

Site 588 (1533 m): Warm Subtropical

The sequence is a foraminifer-bearing nannofossil ooze or chalk of middle Eocene to Quaternary age. Bioturbation appears moderately intense in the middle Eocene to early Miocene, drops to very low in the middle Miocene, and fluctuates from low to moderate in the late Miocene to Quaternary. Nondiagnostic biogenic markings, commonly pyritized in the late Miocene to Quaternary interval, dominate. The Planolites-Chondrites-Zoophycos assemblage is restricted to the moderately bioturbated pre-middle Miocene chalks, appearing about 60 m below the ooze/chalk transition level. No clear relation exists between apparent degree of bioturbation and rates of sedimentation, although the middle Miocene to Quaternary interval of reduced bioturbation coincides with a general increase in the mass accumulation rate of sediments compared to pre-middle Miocene values. The bioturbation curve may reflect productivity variations associated with changes in intermediate water masses during the Neogene. This is exemplified by several significant changes in the benthic foraminiferal assemblages at Site 588 (Site 588 chapter, this volume), especially across the early/middle Miocene boundary and within the Pliocene, periods of notable changes in degree of sediment bioturbation.

Site 590 (1299 m): Transitional Warm Subtropical to Temperate

This late early Miocene to Quaternary sequence consists of foraminifer, foraminifer-bearing, and pure nannofossil oozes and chalks. The apparent degree of bioturbation is moderate in the early Miocene, generally in-

Table 1. Sub-bottom depth and age of first downhole appearance of the Planolites–Chrondrites–Zoophycos trace fossil assemblage and of the ooze/chalk transition level at drill sites on Leg 90.

Site	Water depth (m)	Total core penetration (m)	First appearance downhole of Planolites–Chrondrites–Zoophycos			Level of ooze/chalk transition		
			Core	Depth (m)	~ Age (m.y.)	Core	Depth (m)	~ Age (m.y.)
586	2207	305.3	—	—	—	25A	?260	?8
588	1533	488.1	1C	306	17	2A	245	13
590	1299	499.1	28B	251	7.5	30B	269	8
591	2131	500.4	4B	299	9.5	3B	290	9
592	1098	388.5	34	312	35	30	273	17
593	1068	571.5	60	562	40	60	562	40
594	1204	639.5	13A	505	14	50	476	13

Note: — = not present.

tense in the middle and early late Miocene, and low to moderate thereafter. The rather abrupt upward change from moderately high to generally low amounts of bioturbation within the late Miocene interval coincides with a significant increase in sediment accumulation rate since the middle late Miocene. It also corresponds to the ooze/chalk transition at 269 m sub-bottom depth and, in the latest Miocene, to a distinctive cooling as temperate waters migrated northward across the area (Site 590 chapter, this volume). Nondiagnostic biogenic markings dominate the record and are joined by many examples of Planolites, Zoophycos, and rarer Chondrites traces below 251 m. The increased amount of bioturbation of the entire Neogene sequence compared to both more northern (Site 588) and southern (Site 592) sites may relate to an overall higher delivery rate of organic material to the ocean floor at the site, which lies below the Subtropical Divergence in the Tasman Sea (Fig. 1).

Site 591 (2131 m): Transitional Warm Subtropical to Temperate

This late early Miocene to Quaternary sequence is comparable in age and lithology to adjacent Site 590, but was deposited in deeper (~2000 m) water. The apparent intensity of bioturbation is consistently low to moderate throughout and bears little relation to either variations in rates of sedimentation at the site or to the bioturbation log at the nearby shallower Site 590. Perhaps the supply of organic nutrients at the seafloor was influenced independently by the development and history of an intermediate water mass at the site, as suggested by important shifts in benthic foraminiferal assemblages in the late middle Miocene, early late Miocene, latest Miocene, and late Pliocene (Site 591 chapter, this volume). Biogenic hieroglyphs continue to dominate the trace fossil record and are joined by scattered Planolites, Zoophycos, and occasional Chondrites below 299 m sub-bottom, 9 m below the ooze/chalk transition.

Site 592 (1098 m): Cool Temperate

The late Eocene to Quaternary foraminifer-bearing and pure nannofossil oozes (and chalks) show major differences in their apparent degree of bioturbation. They are moderately intensely bioturbated in the Paleogene, show a decrease through the early Miocene to very low levels of bioturbation in the middle Miocene, moderate values in the late Miocene, a drop to mainly low values in the early Pliocene, and a return to moderately intense values in the late Pliocene and Quaternary. The overall reduction in sediment accumulation rates at Site 592 compared to the more northerly sites is not matched by an apparent increase in sediment bioturbation, although a rough inverse relationship occurs between bioturbation and sedimentation rates for the late Neogene–Quaternary interval of core. The Planolites–Chondrites–Zoophycos assemblage is evident only in the Eocene–Oligocene oozes and chalks below the well-defined Paleogene-Neogene unconformity at ~306 m sub-bottom. Persistence of mild bottom current activity at this site throughout the entire Neogene–Quaternary is suggested both by relatively thin sequences and by stratigraphic wedging on the seismic profile (Site 592 chapter, this volume) and may account for the reduced rates of both sediment accumulation and bioturbation at Site 592.

Site 593 (1068 m): Cool Temperate

This late Eocene to Quaternary sequence comprises foraminifer-bearing nannofossil ooze that grades to nannofossil ooze (and chalk) with depth. Despite some significant changes in sedimentation rates, the apparent degree of bioturbation is mainly uniformly low throughout the core. Only in the late Pliocene–Quaternary and late Eocene–Oligocene intervals, when sedimentation rates were relatively reduced, does the intensity of bioturbation increase. Nondiagnostic traces are ubiquitous and the Planolites–Chondrites–Zoophycos assemblage appears only in the upper Eocene chalk at the bottom of the hole, beneath a conspicuous volcanogenic deposit marking the Eocene/Oligocene boundary (Nelson, Briggs, et al., this volume).

Site 594 (1204 m): Northern Subantarctic

The core comprises a foraminifer-bearing to pure nannofossil ooze (chalk) of latest early Miocene to late Miocene age, below a thick (~180 m) Pliocene–Quaternary sequence of alternating pelagic and hemipelagic oozes. The apparent degree of bioturbation ranges widely and is moderate in the late early Miocene to early middle Miocene, very low in the late middle Miocene, increases to moderate values by the close of the Miocene, is moderately intense in the Pliocene, and fluctuates from low to moderately intense throughout the Quaternary. The generally low values through the late middle Miocene and late Miocene occur during relatively high rates

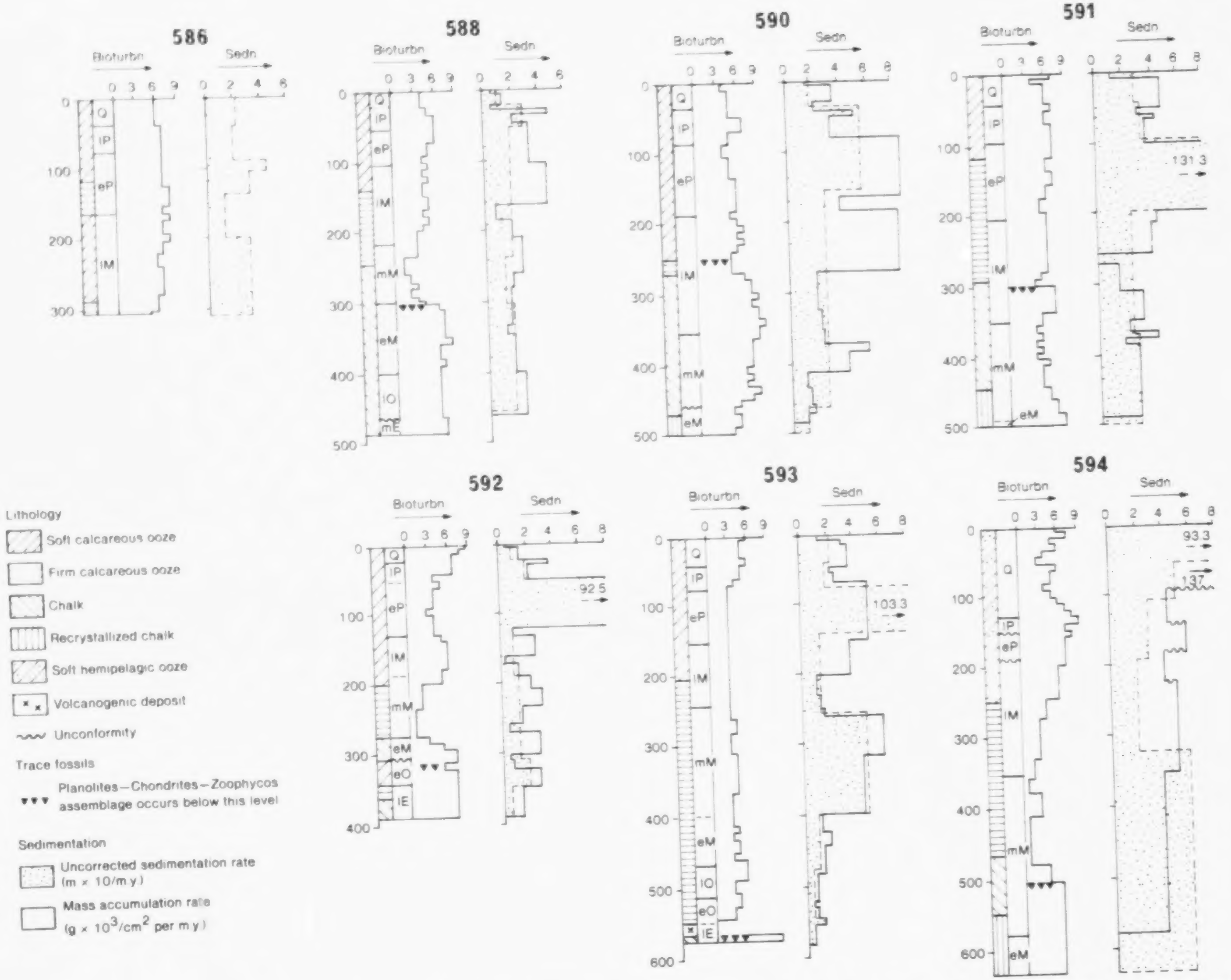

Figure 5. Stratigraphic logs showing the changing relative intensity (increases from 0 to 9) of megascopically visible bioturbation (see Fig. 2) in Leg 90 cores, and the level below which the Planolites-Chondrites-Zoophycos assemblage occurs at each site. Sediment age (E, Eocene; O, Oligocene; M, Miocene; Pl, Pliocene; Q, Quaternary; e, early; m, middle; l, late), degree of induration, and rate of sedimentation, both uncorrected for sediment porosity (m × 10/m.y. and g × 10^3/cm^2 per m.y.), are also shown (data from site chapters, this volume).

of ooze accumulation, especially compared with similarly aged oozes at other sites. The fluctuating but moderately high degree of bioturbation in the Pliocene-Quaternary, despite the rapid rates of sediment accumulation, may be related to nutrient enrichment at the seafloor associated with hemipelagic sedimentation and/or the proximity of the Subtropical Convergence (Fig. 1). The record is dominated by biogenic hieroglyphs, especially diffuse color blebs and mottles, which are conspicuous across the boundaries of the rapidly alternating pelagic-hemipelagic oozes in the upper part of the core. The Planolites-Chondrites-Zoophycos assemblage occurs only below 505 m sub-bottom depth, about 30 m below the ooze/chalk transition level, and is especially evident in silt-bearing clayey chalk turbidite interbeds. These show a pronounced habitat stratification of infaunal burrow types in their upper levels, with Planolites between 0 and about 5 cm, Chondrites to depths of 10 cm, and Zoophycos to depths of 15-20 cm in the beds (Fig. 3L) and Plate 1, Figs. 11, 12). The ecologic stratification is similar to that described by Seilacher (1978) for the burrowed tops of turbidites and by Werner and Wetzel (1981) in their story sequence model of bioturbation in oceanic sediments generally.

DISCUSSION

The character of bioturbation in Leg 90 cores is similar at all sites and is dominated by mainly nondiagnostic biogenic traces and Planolites-like burrow mottles, with variable development of a Planolites-Chondrites-Zoophycos ichnofaunal assemblage at depth in the cores. However, the megascopically apparent intensity of bioturbation in sediments ranges widely, both within and between sites. These variations are unlikely to have been controlled primarily by significant differences in substrate (i.e., grain size, composition, consistency, or induration), water depth, or redox conditions since the primary sediments were nearly all (foraminifer-bearing) nannofossil oozes deposited in aerobic bottom waters at middle bathyal depths (~1000-2000 m; see site chapters, this volume).

The two most important factors influencing the bioturbation record are considered to have been the rate of sediment accumulation and the availability of organic nutrients at the seafloor. As specifically mentioned earlier, a rough inverse relationship is evident between sedimentation rate and sediment bioturbation over several stratigraphic intervals at the various sites (Fig. 5). For example, at Site 590 the overall apparent decrease in intensity of bioturbation since the late late Miocene is associated with a significant increase in sediment accumulation rates, and the sharp increase in bioturbation in the late Pliocene-Quaternary oozes at Site 592 corresponds with a sudden drop in sedimentation rates. However, in Leg 90 sediments generally, the apparent bioturbation response does vary within and between cores for otherwise similar changes in the rate of sediment accumulation. Moreover, sometimes no obvious correlation occurs between rates of sedimentation and intensity of bioturbation. In these instances the rate of supply of organic matter to the ocean floor may have been an influential factor. With due regard for sedimentation rates, it is noticeable that the apparent degree of bioturbation in the late Neogene-Quaternary oozes is proportionately greater at those sites (Sites 586, 590, 591, and 594) located near the boundary of contrasting water masses in the southwest Pacific than at intervening sites (Fig. 1). Oceanic fronts are commonly regions of enhanced primary productivity in the water column (Knox, 1970; Lisitzin, 1972; Bradford and Roberts, 1978; Bradford, 1983), and it can be inferred that there will be a corresponding increase in the availability of organic nutrients at the seafloor in their vicinity (Suess, 1980). Under these conditions the potential exists for an increase both in the number and diversity of benthic fauna and in their extent and depth of sediment reworking.

It is possible, therefore, that the more significant spatial and temporal variations recorded by the bioturbation logs for Leg 90 sediments are related to the Cenozoic history of development, migration, and level of fertility of the various surface and intermediate-depth water masses in the southwest Pacific (e.g., Rochford, 1960a, b; Knox, 1970). The relationship is supported by a degree of parallelism between the bioturbation record and major shifts in the nature and diversity of microfossil assemblages at several sites (e.g., see earlier discussion of Sites 588 and 591). However, only with high resolution micropaleontologic and isotope studies of the core sediments, perhaps in conjunction with organic carbon measurements (e.g., Müller and Suess, 1979), can the interrelationships between water masses, organic nutrient availability, sedimentation rates, and intensity of sediment bioturbation be investigated more closely.

An outstanding problem in Leg 90 sediments concerns the interpretation of the distribution of the Planolites-Chondrites-Zoophycos trace fossil assemblage and, specifically, why it appears to be restricted to the lower part of holes (Fig. 5). The fact that it occurs mainly below the ooze/chalk transition depth (Table 1) originally suggested that diagenetic enhancement controlled the distribution, but several factors argue against a purely diagenetic control:

1. Many chalk cores lack the assemblage, sometimes over long intervals (e.g., Cores 588A-2 to 588A-13).
2. The assemblage is well developed in both soft and firm oozes below the first ooze/chalk transition level at Site 592 and also occurs in firm oozes immediately above the transition level at Site 590.
3. Scattered occurrences of Planolites and Planolites-like burrows are evident by themselves in both oozes and chalks at most sites (e.g., Plate 1).
4. Although several examples of the Planolites-Chondrites-Zoophycos assemblage in Leg 90 chalks occur in association with rare turbidite or volcanic ash interbeds, where their burrow fills are emphasized by strong color contrasts (e.g., see Plate 1, Figs. 9-12), the majority are differentiated by the same yellowish or greenish gray tones that distinguish the biogenic traces generally in Leg 90 oozes and chalks (compare Figs. 1 and 2 with Plate 1, Figs. 1, 5, 6, 8). Consequently, it is unlikely that the distinctive chevron traces of Zoophycos, for example, if genuinely common in the oozes, could have totally escaped being identified during the detailed examination and description of 2-3 km of core sediments.

An age control based on extinction of the animals responsible for the trace fossils cannot explain the upward disappearance of the association because (a) there is considerable variation in age (late Eocene to late Miocene) of the last occurrence of the trace fossil association in the different holes (Table 1), and (b) the stratigraphic range of each of the three trace fossils concerned extends to the Recent (Chamberlain, 1978).

One is forced to seek some environmental reason(s) for the apparent upward disappearance of the Planolites-Chondrites-Zoophycos assemblage in cores. It is notable that at each site, irrespective of age, the assemblage occurs in mainly moderately to moderately intensely bioturbated sequences deposited under conditions of relatively low rates of sediment accumulation for that site. Disappearance of the assemblage coincides generally with a significant decrease in the apparent intensity of bioturbation and an overall increase in the long-term rate of sediment accumulation. On this basis, and using the environmental preferences established by Werner and Wetzel (1981) for the same trace fossils on the modern North Atlantic slope, a possible explanation is given in Figure 6 for the upward loss of the Planolites-Chondrites-Zoophycos assemblage and its replacement by Planolites(-like) burrows and nondiagnostic biogenic hieroglyphs in Leg 90 cores. Note especially that depositional depths and substrate characteristics remain similar throughout, and that the major controls are variations in rate of sediment accumulation and/or supply of organic nutrients at the seafloor. It has been mentioned earlier that these factors are probably linked to the evolution and history of contrasting surface and intermediate water masses in the southwest Pacific. If this is so, then detailed studies of the character, distribution, and intensity of bioturbation in oceanic cores can make a useful contribution to the developing science of paleoceanography.

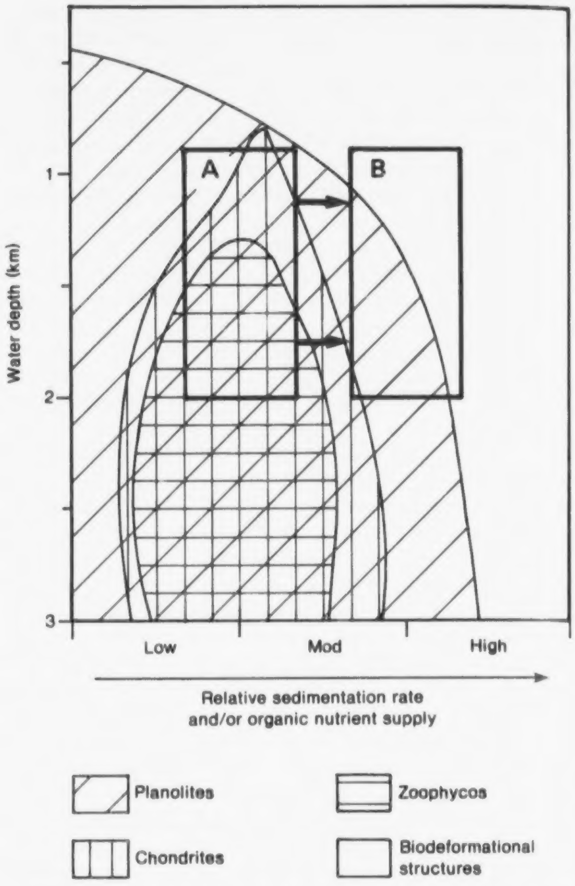
1
2
3
Water depth (km)
A
B
Low
Mod
High
Relative sedimentation rate
and/or organic nutrient supply
Planolites
Zoophycos
Chondrites
Biodeformational structures

Figure 6. Schematic illustration of how changes in the relative rates of sedimentation and availability of organic nutrients at the seafloor could alone or together be responsible for the upward disappearance of the Planolites-Chondrites-Zoophycos assemblage in Leg 90 cores by passage from within area A to area B. The preferred environmental distribution fields for the various trace fossil types are adapted from those summarized by Werner and Wetzel (1981).

ACKNOWLEDGMENTS

I thank Janet Bradford and Keith Probert (N. Z. Oceanographic Institute, Wellington) for helpful discussion on the topics of bioturbation and primary productivity, and Gerrit van der Lingen (N. Z. Geological Survey, Christchurch), Wolfgang Berger (Scripps Institution of Oceanography), and Allan Ekdale (Department of Geology and Geophysics, University of Utah, Salt Lake City) for their useful comments on a draft of the paper.

REFERENCES

Basan, P. (Ed.), 1978. *Trace Fossil Concepts*: Tulsa (Society of Economic Paleontologists and Mineralogists Short Course 5).

Berger, W. H., Ekdale, A. A., and Bryant, P. P., 1979. Selective preservation of burrows in deep-sea carbonates. *Mar. Geol.*, 32:205-230.

Bradford, J. M., 1983. Plankton and primary productivity in the vicinity of Chatham Rise. *N.Z.O.I. Oceanog. Summary*, 21:1-14.

Bradford, J. M., and Roberts, P. E., 1978. Distribution of reactive phosphorus and plankton in relation to upwelling and surface circulation around New Zealand. *N.Z. J. Mar. Freshw. Res.*, 12:1-15.

Chamberlain, C. K., 1975. Trace fossils in DSDP cores of the Pacific. *J. Paleontol.*, 49:1074-1096.

________, 1978. Recognition of trace fossils in cores. *In* Basan, P. (Ed.), *Trace Fossil Concepts*: Tulsa (Society of Economic Paleontologists and Mineralogists Short Course 5), pp. 133-184.

Edwards, A. R., 1979. Classification of marine paleoenvironments. *Geol. Soc. N.Z. Newsl.*, 47:17-19.

Ekdale, A. A., 1977. Abyssal trace fossils in worldwide Deep Sea Drilling Project cores. *In* Crimes, T. P., and Harper, J. C. (Eds.), *Trace Fossils II*: Liverpool (Seel House), pp. 163-182.

________, 1978. Trace fossils in Leg 42A cores. *In* Hsü, K., Montadert, L., et al., *Init. Repts. DSDP*, 42, Pt. 1: Washington (U.S. Govt. Printing Office), 821-827.

________, 1980. Trace fossils in Deep Sea Drilling Project Leg 58 cores. *In* Klein, G. deV., Kobayashi, K., et al., *Init. Repts. DSDP*, 58: Washington (U.S. Govt. Printing Office), 601-606.

Frey, R. W. (Ed.), 1975. *The Study of Trace Fossils*. New York (Springer Verlag).

Fullam, T. J., Supko, P. R., Boyce, R. E., and Stewart, R. J., 1973. Some aspects of late Cenozoic sedimentation in the Bering Sea and North Pacific Ocean. *In* Creager, J. S., Scholl, D. W., et al., *Init. Repts. DSDP*, 19: Washington (U.S. Govt. Printing Office), 887-896.

Hantzschel, W., 1975. Trace fossils and problematica, *In* Teichert, C. (Ed.), *Treatise on Invertebrate Paleontology, Part W, Supplement 1, Miscellanea*: Lawrence (University of Kansas and Geological Society of America).

Knox, G. A., 1970. Biological oceanography of the South Pacific. *In* Wooster, W. S., (Ed.), *Scientific Exploration of the South Pacific*: Washington (National Academy of Sciences), pp. 155-182.

Lisitzin, A. P., 1972. Sedimentation in the world ocean. *Soc. Econ. Paleontol. Mineral. Publ.*, 17.

McMillen, K. J., and Lundberg, N. F., 1982. Trace fossil assemblages in Leg 66 sediments. *In* Watkins, J. S., Moore, J. C., et al., *Init. Repts. DSDP*, 66: Washington (U.S. Govt. Printing Office), 653–657.

Muller, P. J., and Suess, E., 1979. Productivity, sedimentation rate, and sedimentary organic matter in the oceans—I. Organic carbon preservation. *Deep-Sea Res.*, 26A:1347–1362.

Okado, H., 1980. Trace fossils in cores from Deep Sea Drilling Project Sites 434, 435, and 436 (Japan Trench Transect). *In* Scientific Party (Co-Chiefs: von Huene, R., Nasu, N.,), *Init. Repts. DSDP*, 56, 57, Pt. 2: Washington (U.S. Govt. Printing Office), 911–913.

Piper, D. J., and Schrader, J. H., 1973. Bioturbation of sediments. *In* Kulm, L. D., von Huene, R., et al., *Init. Repts. DSDP*, 18: Washington (U.S. Govt. Printing Office), 869–875.

Rochford, D. J., 1960a. The intermediate depth water of the Tasman and Coral Seas. I. The $27.20\sigma t$ surface. *Aust. J. Mar. Freshw. Res.*, 11:127–147.

———, 1960b. The intermediate depth water of the Tasman and Coral Seas, II. The $26.80\sigma t$ surface. *Aust. J. Mar. Freshw. Res.*, 11: 148–165.

Seilacher, A., 1978. Use of trace fossil assemblages for recognizing depositional environments. *In* Basan, P. (Ed.), *Trace Fossil Concepts*: Tulsa (Society of Economic Paleontologists and Mineralogists Short Course 5), pp. 167–181.

Suess, E., 1980. Particulate organic carbon flux in the oceans—surface productivity and oxygen utilization. *Nature*, 288:260–263.

Tracey, J. I., Jr., Sutton, G. H., et al., 1971. Site 71. *In* Tracey, J. I., Jr., et al., *Init. Repts. DSDP*, 8: Washington (U.S. Govt. Printing Office), 285–458.

van der Lingen, G. J., 1973. Ichnofossils in deep-sea cores from the Southwest Pacific. *In* Burns, R. E., Andrews, J. E., et al., *Init. Repts. DSDP*, 21: Washington (U.S. Govt. Printing Office), 693–700.

Warme, J. E., Kennedy, W. J., and Schneidermann, N., 1973. Biogenic sedimentary structures (trace fossils) in Leg 15 cores. *In* Edgar, N. T., Saunders, J. B., et al., *Init. Repts. DSDP*, 15: Washington (U.S. Govt. Printing Office), 813–831.

Werner, F., and Wetzel, A., 1981. Interpretation of biogenic structures in oceanic sediments. *Bull. Inst. Geol. Bassin d'Aquitaine, Bordeaux*, 31:275–288.

Date of Initial Receipt: 25 June 1984
Date of Acceptance: 31 October 1984

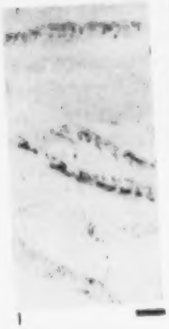
1

2

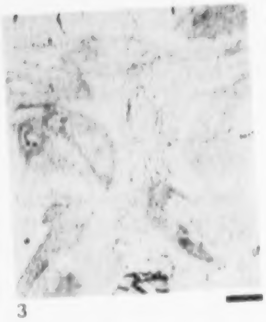
3

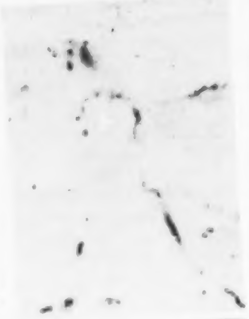
4

5

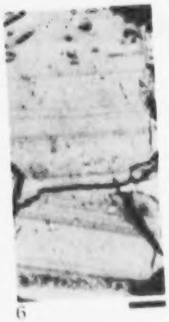
6

7

8

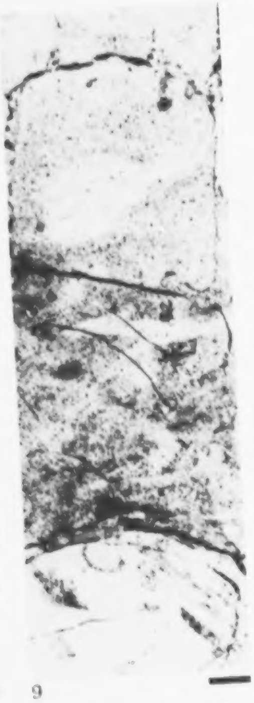
9

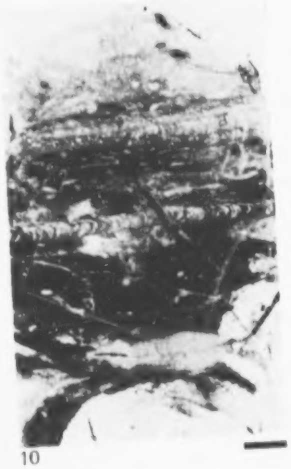
10

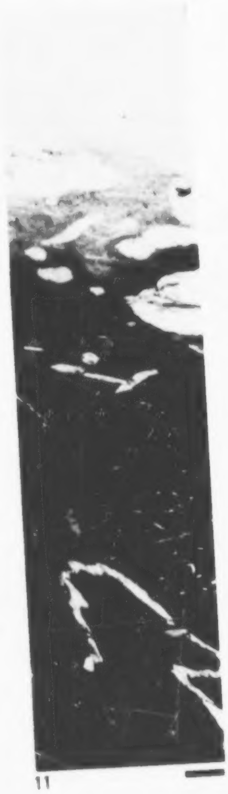
11

12

Plate 1. Examples of biogenic traces in Leg 90 calcareous oozes and chalks. Bar scale equals 1 cm. **1.** 594A-13-1, 131-142 cm, showing Zoophycos spreiten and diffuse blebs and mottles of Planolites-like burrows in chalk. **2.** 588-12-5, 31-41 cm, showing diffuse Planolites-like yellowish gray burrow mottles in soft white ooze. **3.** 591B-9-2, 52-60 cm, showing Planolites and halo burrows smeared by coring in soft chalk. **4.** 591B-6-5, 94-100 cm, showing pyritized spots, threads and halo burrows, and diffuse burrows in chalk with vaguely discernible small normal fault at top right. **5.** 591B-7-3, 19-27 cm showing diffuse Zoophycos, Planolites-like, and ?Chondrites traces in chalk offset by small normal fault at top left. Pyritized lamina near base. **6.** 588C-13-6, 71-80 cm, showing Chondrites burrows and a Zoophycos trace in chalk with pale greenish gray laminae formed from altered volcanic ash materials. **7.** 591B-18-3, 83-92 cm, showing common Planolites burrows in chalk with prominent flaser-like structures formed by selective dissolution and cementation processes, possibly controlled partly by burrow morphology and distribution. **8.** 590B-44-1, 128-148 cm, showing diffuse color blebs and mottles, and streaks and wisps in moderately intensely burrowed chalk. **9.** 588C-4-6, 20-37 cm, showing complex color mottling and common pyritized spots associated with Planolites, Chondrites, and [illegible]ind burrows in intensely bioturbated altered ?ash bed overlying chalk. **10.** 594A-13-2, 128-139 cm, showing Planolites-Chondrites-Zoophycos assemblage of trace fossils in silty sponge spicule-bearing interbed in chalk. **11.** 594A-24-1, 37-58 cm, showing coarse ecologic stratification of Planolites, Chondrites, and Zoophycos (or ?Teichichnus) in top of redeposited interbed (dark) of silt and clay-bearing chalk in pure chalk (white). **12.** 594A-25-1, 76-100 cm, as for Fig. 11, although depth of reworking by Chondrites and Planolites-like burrows is more variable.

29. LATE NEOGENE AND QUATERNARY COARSE-FRACTION AND CARBONATE STRATIGRAPHIES FOR SITE 586 ON ONTONG-JAVA PLATEAU AND SITE 591 ON LORD HOWE RISE[1]

James V. Gardner, Walter E. Dean, Lynne Bisagno, and Eileen Hemphill, U.S. Geological Survey[2]

ABSTRACT

Carbonate oozes recovered by hydraulic piston coring at DSDP Site 586 on Ontong-Java Plateau and Site 591 on Lord Howe Rise have carbonate contents that are consistently higher than 90% with only minor variations. Consequently, paleoceanographic signals were not recorded in detail in the carbonate contents. However, mass accumulation rates of carbonate increased in the late Miocene to mid-Pliocene, reflecting an increase in productivity, then abruptly decreased from mid-Pliocene to the present. Variations in relative abundances of coarse material (foraminifers) and fine material (mostly calcareous nannofossils) do reflect histories of current winnowing and biogenic productivity at the two sites. The late Miocene from 10.5 to 6.5 m.y. ago was a time of relatively constant, quiet, pelagic sedimentation with typical southwest Pacific sedimentation rates of 20–25 m/m.y. The average coarse-fraction abundances are always higher at Site 586 than at Site 591, which reflects winnowing at Site 586. These conditions were interrupted between 6.5 to 4.0 m.y. ago when increased upwelling at the Subtropical Divergence and the Equatorial Divergence produced greater productivity of calcareous planktonic organisms. The increased productivity is suggested by large increases in both fine- and coarse-fraction material and constant ratios of foraminifers to nannofossils. The maximum of productivity was about 4.0 m.y. ago. This period of increased upwelling is coincident with the inferred development of the West Antarctic ice sheet. The high productivity was followed by an abrupt increase in winnowing about 2.5 m.y. ago at Site 591, but not until about 2.0 m.y. ago at Site 586. By 2.0 m.y. ago in the late Pliocene, quiet, pelagic sedimentation conditions prevailed, similar to those of the late Miocene. The last 0.7 m.y. has been a period of relatively intense winnowing on Lord Howe Rise but not on Ontong-Java Plateau.

The coarse-fraction data have both long- and short-period fluctuations. Long-period fluctuations at Site 591 average about 850 × 10^3 yr./cycle and those at Site 586 average 430 × 10^3 yr./cycle. The highest amplitudes are found in the Pliocene and Quaternary sections. The short-period fluctuations range from 100 to 48 × 10^3 yr./cycle at Site 586 and from 250 to 33 × 10^3 yr./cycle at Site 591. The effects of local fluctuations of productivity and winnowing have modified the primary orbital forcing signals at these two sites to yield complex paleoceanographic records.

INTRODUCTION

Shackleton and Opdyke (1976) published their classic study of the oxygen-isotope composition of late Pliocene and Quaternary planktonic foraminifers from piston Core V28-239 from Ontong-Java Plateau, and also presented a high-resolution (1 sample/5 10^3 yr.) stratigraphy of the percent coarse fraction (>180 μm). The coarse-fraction record in Core V28-239 is strongly correlated with the oxygen-isotope record; the oxygen-isotope stages with higher values of $\delta^{18}O$ (i.e., colder periods; Stages 2, 4, 6, etc.) have more coarse material than do those with lighter $\delta^{18}O$ values. Because Core V28-239 was collected in a water depth of 3490 m, below the foraminiferal lysocline, Shackleton and Opdyke (1976) assumed that the increases in coarse fraction were due to carbonate dissolution. Studies of carbonate dissolution on Ontong-Java Plateau place the top of the calcite lysocline at about 3400 m (Johnson et al., 1977; Berger et al., 1982); consequently, dissolution is likely to have occurred in Core V28-239. Shackleton and Opdyke (1976) did not discuss the details of the coarse-fraction data from Core V28-239, but focused on the significance of the oxygen-isotope data.

On Leg 90, during the splitting of the cores, the shipboard sedimentologists noticed that there appeared to be fluctuations of observable foraminiferal tests with depth, especially in sediment from Site 586 on Ontong-Java Plateau. This observation prompted us to sample Site 586 for coarse-fraction analyses and, for a comparison, we also chose to sample sediment from Site 591, adjacent to the Subtropical Divergence on Lord Howe Rise. We reasoned that fluctuations in the coarse fraction must be a response to (1) dissolution of carbonate, (2) winnowing of fine-grained material, or (3) deposition of fine-grained material. All three of these processes are responses to oceanographic conditions; therefore, the coarse-fraction stratigraphies should provide insights into late Neogene paleoceanographic changes that occurred in the southwest Pacific.

Site 586 is located within 2 km of DSDP Site 289 (Andrews, Packham, et al., 1975) in 2208 m of water on the eastern flank of Ontong-Java Plateau (Fig. 1). The hydraulic piston corer (HPC) was used to obtain 98% recovery of a virtually undisturbed 300-m composite section. The sediment is foraminifer–nannofossil ooze to foraminifer-bearing nannofossil ooze, and the oldest sediment recovered is earliest late Miocene in age. The Quaternary section on Ontong-Java Plateau has been extensively studied, principally by Thompson and Saito (1974), Shackleton and Opdyke (1973; 1976), Berger and Johnson (1976), Berger et al. (1977; 1979), Thompson and Sciarrillo (1978), Krishnamurthy et al. (1979), Bonneau

---

[1] Kennett, J. P., von der Borch, C. C., et al., *Init. Repts. DSDP*, 90: Washington (U.S. Govt. Printing Office).

[2] Addresses: (Gardner, Bisagno, Hemphill) U.S. Geological Survey, Menlo Park, CA 94025; (Dean) U.S. Geological Survey, Denver, CO 80303.

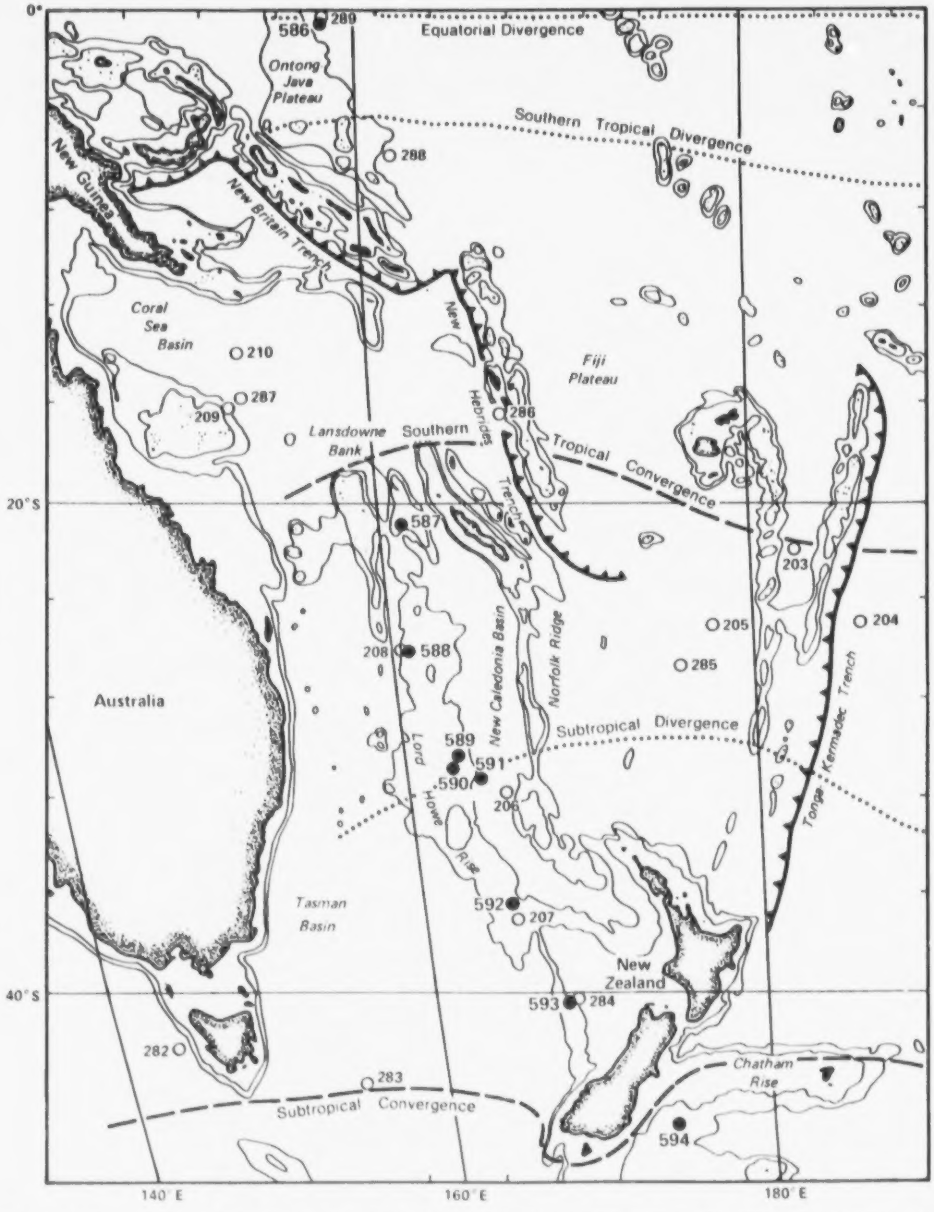
0°
586
289
Equatorial Divergence
Ontong Java Plateau
Southern Tropical Divergence
288
New Guinea
New Britain Trench
Coral Sea Basin
210
287
209
New Hebrides Trench
Fiji Plateau
286
Lansdowne Bank
Southern Tropical Convergence
20°S
587
203
205
204
285
208
588
Australia
New Caledonia Basin
Norfolk Ridge
Subtropical Divergence
Tonga-Kermadec Trench
589
591
590
206
Lord Howe Rise
Tasman Basin
592
207
New Zealand
40°S
593
284
282
283
Chatham Rise
Subtropical Convergence
594
140°E
160°E
180°E

Figure 1. Map of the southwest Pacific Ocean showing the locations of DSDP Sites 206, 289, 586, and 591, and major water-mass boundaries.

et al. (1980), and Vincent et al. (1981). The rotary-drilled late Neogene section at Site 289 on Ontong-Java Plateau was investigated (Klein, 1975; van der Lingen and Packham, 1975; Holdsworth, 1975; Woodruff, et al., 1981), but those studies are based on widely separated samples of sediment that were severely disturbed by drilling.

Site 591 is located on the eastern flank of Lord Howe Rise in 2142 m of water (Fig. 1). The upper 284 m of the site was drilled with the HPC and recovered 98% section; below 284 m the section was drilled with the extended core barrel and averaged only 44% recovery. The undisturbed sediment is foraminifer-bearing nannofossil ooze that grades to chalk at about 300 m sub-bottom. The oldest sediment recovered is latest early Miocene in age.

METHODS

Samples for coarse-fraction analyses were collected approximately every 40 cm at Site 586 and every 50 cm at Site 591. Average sedimentation rates, based on nannofossil biostratigraphy (Introduction, this volume), average about 27 m/m.y. for Site 586 and about 32 m/m.y. for Site 591. The sample spacing yields an approximate time series with an average of one sample every 15 × 10^3 yr. for Site 586 and one sample every 16 × 10^3 yr. for Site 591. The highest frequency of cycles that may be defined from a periodic series is twice the sampling interval (Davis, 1973; also see Ledbetter and Ellwood, 1976). This highest frequency, called the Nyquist frequency, is therefore about 30×10^3 yr./cycle for our time series from Sites 586 and 591.

Samples were first split into three subsamples: one for calculation of a water-content correction factor so that it was not necessary to dry the coarse-fraction samples before they were disaggregated; a second split for coarse-fraction analysis; and a third, very small split for smear-slide examination. Each correction-factor split was weighed, dried in an oven at 60°C for 24 hr., cooled in a desiccator, and weighed again. The correction factor was calculated using Equation 1:

$$\mathrm{CORR} = \frac{\mathrm{DWa}}{\mathrm{WWa}} \tag{1}$$

where DWa is the dried weight of the sample and WWa is the initial wet weight of the sample. The correction factor was used to calculate the weight of dry sediment in the split used for coarse-fraction analysis using Equation 2:

$$P_{147} = \frac{W_{147}}{\mathrm{WWb} \times \mathrm{CORR}} \times 100 \tag{2}$$

where P_{147} is the percentage of the sample >147 μm, W_{147} is the weight of the >147 μm fraction, and WWb is the wet weight of the original coarse-fraction split. The same calculations were carried out on the fraction between 63 and 147 μm. The percentages of coarse fraction (>63 μm) and fine fraction (<63 μm) were calculated by difference from the analytical results.

Nearly all the carbonate data presented here were analyzed aboard ship using the carbonate bomb (Müller and Gastner, 1971). The shipboard data from both sites show step increases in carbonate with depth (Fig. 2A, B) that we suspect are calibration errors. Consequently, we reanalyzed some of the original bomb samples from the intervals that bridge the step increases using a coulometric carbon analyzer with a precision and accuracy that are both better than ± 1% (Huffman, 1977). To correct these errors, the upper sections were adjusted by adding the difference between the mean values of the reruns and the mean of the carbonate bomb analyses to each data point above the step change. The resulting adjusted curves (Fig. 2C, D) are considered to be more representative of the carbonate stratigraphy than are the original curves.

In order to investigate the timing of events in the coarse-fraction record and to calculate periodicities of the cycles, we had to apply an age model to each site. We used the nannofossil zonation and age boundaries established for Leg 90 (Introduction, this volume; Table 1) but with some apparent difficulties. A plot of age versus sedimentation rate for Site 591 (Fig. 3) shows that nannofossil Zones NN12 to NN15 have anomalously high sedimentation rates. When similar plots were constructed for all of the Leg 90 sites and for Site 586 (Fig. 3), the same nannofossil zones between 3.5 and 5.0 m.y. have very high sedimentation rates, often an order of magnitude greater than those for the other zones. It is possible that either the ages of the nannofossil zone boundaries, or the criteria for their recognition, or both, may be in error but we assumed that the biostratigraphy and ages are correct. We used the Leg 90 biostratigraphy (Introduction, this volume) for Site 591, but we had difficulties with the data from Site 586. We plotted several different age models for Site 586 using different biostratigraphic zonations and compared different sections of the record (Fig. 4). When the western North Pacific nannofossil zonation of Ellis ([illegible]) is used, a severe compression of the data occurs in the interval from 1.8 to 2.1 m.y., and an expansion of the data occurs in the interval from 0.9 to 1.8 m.y. Similar compressions and expansions occur when the nannofossil zonation of Okada and Bukry (1980) or the planktonic foraminiferal zonation (Moberly, Schlanger, et al., in press) are used. We used the nannoplankton zonation of Leg 90 for Site 586 because it gives the least severe compressions and expansions of the record and it allows us to compare the records from Sites 586 and 591 without major distortions caused by different age models. However, accepting this biostratigraphic and age model results in the acceptance of the high sedimentation rates for the early to middle Pliocene (Fig. 3). The data for coarse fraction versus depth (Appendix A) were converted to coarse fraction versus age by calculating a sedimentation rate between each of the nannofossil zone boundaries and linearly interpolating the age of each data point. Bulk-sediment mass accumulation rates (MAR) in g/cm² per m.y. were calculated for 0.5-m.y. intervals in order to eliminate the effects of compaction on linear sedimentation rates and so that calculations of fluxes of components could be made (Fig. 5). Bulk-sediment MAR was calculated using Equations 4 and 5:

$$\mathrm{DBD} = (1\text{-}P/100) \times 2.7 \tag{4}$$

$$\mathrm{MAR} = \mathrm{DBD} \times \mathrm{SR} \times 100 \tag{5}$$

where P is the average porosity, DBD is the average dry bulk density, both calculated from the physical properties data (Site 586 and 591 chapters, this volume). SR is the average sedimentation rate, and 2.7 is the average density of calcite.

RESULTS

Carbonate Data

The carbonate concentrations for Sites 586 and 591 are plotted versus depth in Figure 2, and the data are tabulated in Appendix B. The carbonate values are so high that even large fluctuations in the flux of carbonate will cause only subtle changes in the carbonate percentages (Gardner, 1975; Dean et al., 1981). There are only 34 data points on the carbonate curve for Site 586 (Fig. 2C), but there appears to be a trend of decreasing carbonate from about 100 m sub-bottom to the top of the section. The decrease in carbonate began about 4.2 m.y. ago in the early Pliocene. There also appear to be fluctuations of carbonate about the mean throughout the sequence, although, again, it is difficult to detect any character in a curve with so few data points.

The carbonate curve for Site 591 (Fig. 2D) is based on 232 data points, representing an average sample interval of about one sample per meter from the surface to 300 m sub-bottom. High- and low-frequency cycles of carbonate occur throughout the record. The most noticeable change in the character of the carbonate curve occurs at about 75 m sub-bottom where the amplitude of carbonate fluctuations changes from about 2 to 3% below 75 m, to amplitudes of 8 to 10% above 75 m. This change in the variation occurs at about 2.5 m.y. in the late Pliocene.

The changes in flux of $CaCO_3$ at the two sites are shown by plots of the MAR of $CaCO_3$ for 0.5-m.y. intervals (Fig. 6). Both sites have very pronounced increases in $CaCO_3$ flux in the late Miocene through mid-Pliocene, then dramatic decreases in $CaCO_3$ flux to the present. Fluxes of $CaCO_3$ were consistently higher at Site 591 than at Site 586 except for the period between 10.5 and 6.5 m.y., when Site 586 received about 50% more carbonate than did Site 591 and the period of the last 0.5 m.y. when Site 586 received about twice the flux of $CaCO_3$ as did Site 591.

Coarse-Fraction Data

The coarse-fraction data are presented in Figures 7 and 8 in four size fractions; the fraction >147 μm, the fraction 63–147 μm, the fraction >63 μm, and the fraction <63 μm. Observations from smear slides indicate that the size fractions of >147 μm and 63–147 μm are

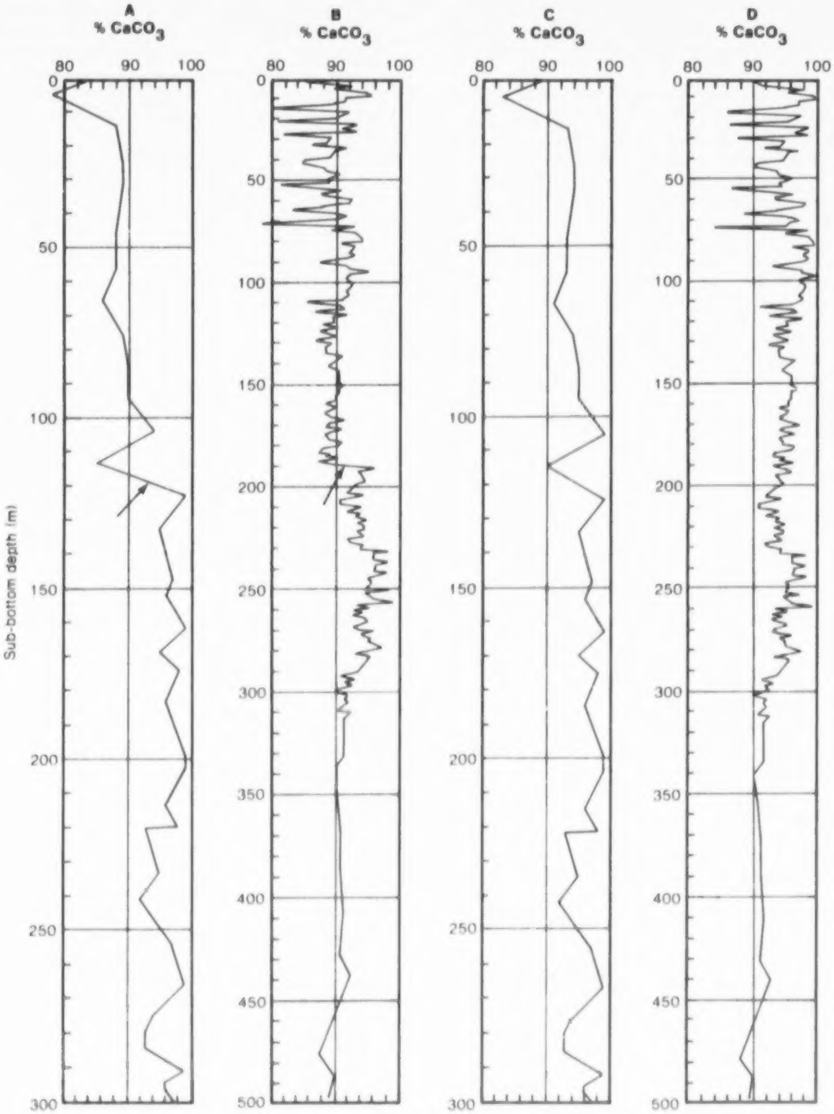

Figure 2. Plots of percent CaCO$_3$ determined by shipboard carbonate bomb for Site 586 (A) and Site 591 (B), and adjusted for shipboard calibration errors for Site 586 (C) and Site 591 (D). See text for method of adjustment. The arrows on Figure 2A,B indicate the location of the step changes in carbonate caused by the shipboard calibration error.

composed entirely of planktonic foraminifers. The <63 μm fraction is composed almost entirely of nannofossils and juvenile planktonic foraminifers.

The coarse-fraction data from all four size fractions from Site 586 (Fig. 7) show persistent long-term and short-term trends. In general, the concentrations of the >147-μm fraction are lower than the mean value below 100 m sub-bottom and higher than the mean value above 100 m. However, there is a persistent trend of increasing >147-μm fraction from 120 m to the surface. The percentage of the <63-μm fraction is consistently above the mean from 300 to 140 m sub-bottom, then generally decreases to the top of the core. The concentrations of the 63–147-μm fraction vary around the mean value with no consistent trends.

The coarse-fraction data for Site 591 are complete only for the >63-μm and <63-μm fractions (Fig. 8). The >147-μm percentages are consistently less than about 4% below 120 m sub-bottom, and the amounts of material >147-μm were so small that significant errors in weighing could occur. We therefore stopped sieving for the >147-μm fraction at the 120-m level but continued to measure the >63-μm fraction. The <63-μm fraction shows trends that are similar to those from Site 586 with both high- and low-frequency cycles of grain size, but the details of the distributions of grain size with depth are somewhat different. The <63-μm fraction is generally above the mean value from 480 to about 120 m sub-bottom but with zones of below mean values, especially between 440 and 420 m and between 302 and 295 m.

Table 1. Ages (m.y.) of tops of nannofossil zones used to interpolate age for each sample (from Introduction, this volume).

Nannofossil zone	Age (m.y.)
NN21	0.00
NN20	0.20
NN19	0.55
NN18	1.90
NN17	2.30
NN16	2.40
NN15	3.45
NN14	3.65
NN13	4.10
NN12	4.60
NN11b	5.20
NN11a	6.25
NN10	9.50
NN9	11.00
NN8	12.00

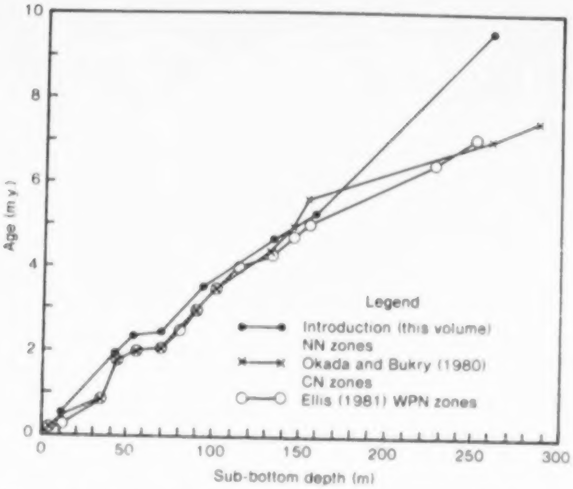

Figure 4. Age versus depth curves for Site 586 using nannofossil zonations and ages from Introduction (this volume), Okada and Bukry (1980), and Ellis (1981).

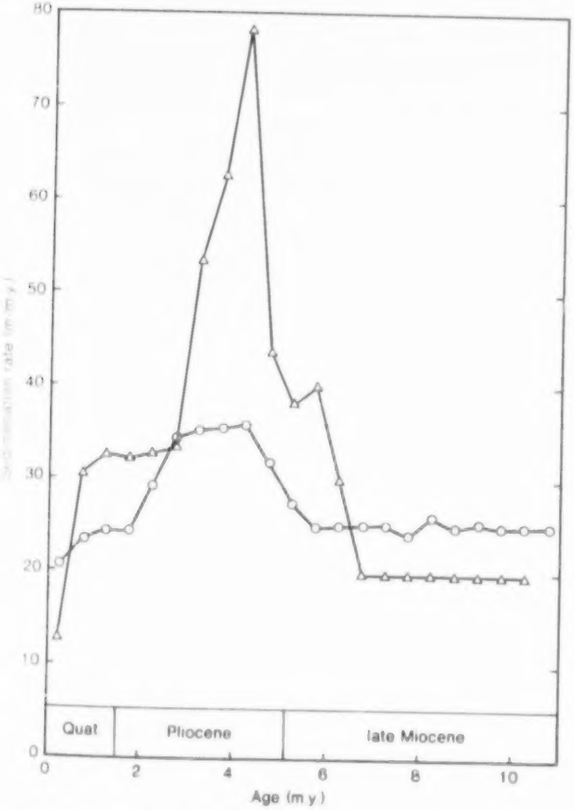

ure 3. Plots of sedimentation rates in m/m.y. averaged for 0.5-m.y. intervals versus age for Site 586 (circles) and Site 591 (triangles).

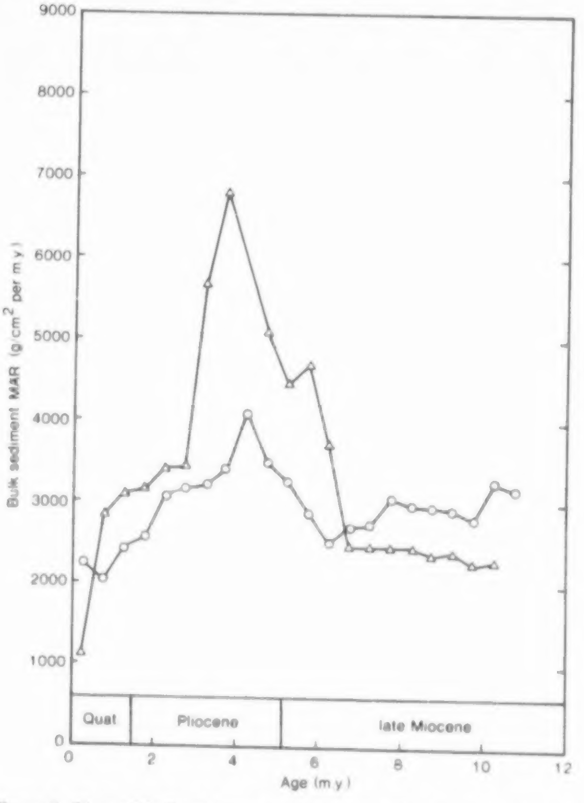

Figure 5. Plots of bulk-sediment mass accumulation rates (MAR; in g/cm^2 per m.y.) averaged for 0.5-m.y. intervals versus age for Site 586 (circles) and Site 591 (triangles).

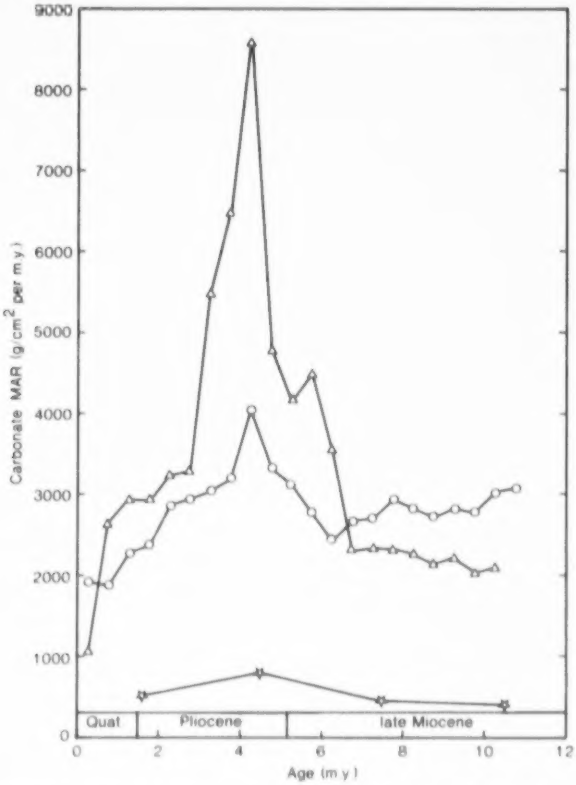

Figure 6. Plots of $CaCO_3$ mass accumulation rates (MAR; g/cm^2 per m.y.) averaged for 0.5-m.y. intervals versus age for Site 586 (circles) and Site 591 (triangles). The lowest plot (stars) represents the average carbonate MARs for the entire Pacific Ocean (from Davies and Worsley, 1981).

The <63-μm fraction has a persistent trend of decreasing percentages from about 230 m to the top of the section, similar to the trend above 100 m at Site 586.

In order to investigate the nature of the variations in coarse fraction and to compare the coarse-fraction stratigraphies from Sites 586 and 591, it was necessary to replot the coarse-fraction abundance data versus age (Figs. 9, 10). These data were subdivided into 0.5-m.y. intervals and various parameters were calculated for each interval (Tables 2, 3).

Plots of the mean percentage of coarse fraction >63-μm in each 0.5-m.y. interval (Fig. 11) show that the two sites have similar trends in coarse fraction with time, but that Site 586 consistently has more than twice the percentage (and as much as five times) of the >63-μm fraction than does Site 591. The overall trend in coarse fraction is a pronounced low abundance at both sites that lasted from the late Miocene into the early Pliocene (about 9 to 4.5 m.y. ago). Coarse fraction generally increased from about 4.5 m.y. to the late Quaternary at both sites, but there are significant fluctuations, particularly at Site 586.

The variation in coarse-fraction values is shown in Figure 11 as the coefficient of variation (c.v.), which is the standard deviation expressed as a percentage of the mean [(X/SD) · 100]. The variations in the coarse-fraction data from the two sites are different in magnitude, although they are similar in trend. Clearly, there is greater variability in coarse fraction at Site 591 than at Site 586. The >63-μm fraction from Site 586 has c.v. values that range between 15 and 30%, whereas the same size fraction from Site 591 has c.v. values that range from less than 10 to greater than 30%.

CAUSES OF COARSE-FRACTION VARIATION

The entire coarse-fraction component >63 μm from Sites 586 and 591 is composed of planktonic foraminifers. The material <63 μm is principally composed of nannofossils and juvenile foraminifers. The shipboard smear-slide summaries (see site chapters, this volume) and shore-based observations reveal that very little material other than foraminifers and nannofossils is present in the sediment. Consequently, the significance of fluctuations in coarse fraction can be interpreted as the result of one or a combination of the following conditions: (1) fluctuations in size-selective dissolution of biogenic carbonate; (2) fluctuations in the rates of production and accumulation of nannofossils relative of those of foraminifers; and (3) fluctuations in amount of winnowing of the fine biogenic components.

Dissolution would tend to break down the foraminiferal tests into fragments and produce a decrease in coarse fraction (>63 μm) and an increase in fine fraction (<63 μm) (Berger et al., 1982). However, we have discounted dissolution as a cause of fluctuations in coarse fraction because both sites are well above the depth of the present lysocline of 3400 to 3600 m (Berger et al., 1977, 1982). The depths of the Pacific lysocline and calcite compensation depth (CCD) have been below their present depths since the early Oligocene (van Andel et al., 1977), and there are no indications that either Ontong-Java Plateau or Lord Howe Rise were ever significantly deeper than their present depths (Burns, Andrews, et al., 1973; Andrews, Packham, et al., 1975). Shipboard paleontologists noted good to excellent preservation of calcareous microfossils in Quaternary through lower Pliocene sediment at both sites but, in general, the preservation of nannofossils decreases with depth. Noticeable overgrowths were observed on nannofossils in the lowermost Pliocene and older sediment at Site 586 and in upper Miocene and older sediment at Site 591. The fluctuations in coarse fraction do not follow the pattern of observed overgrowths, but occur throughout the record from the late Miocene through the Holocene. This is another reason why we believe that dissolution can be discounted here.

The second process that can cause fluctuations in coarse fraction is variation in accumulation of fine (<63 μm) material. If a locality was a depocenter of material that had been winnowed from upstream, or if productivity in the surface waters significantly increased, thus producing a higher flux of nannofossils than normal, then the fine-fraction (<63 μm) component would dilute the coarser foraminiferal component. There is no evidence from the bathymetry of either area to suggest that they may have periodically been preferred sites of

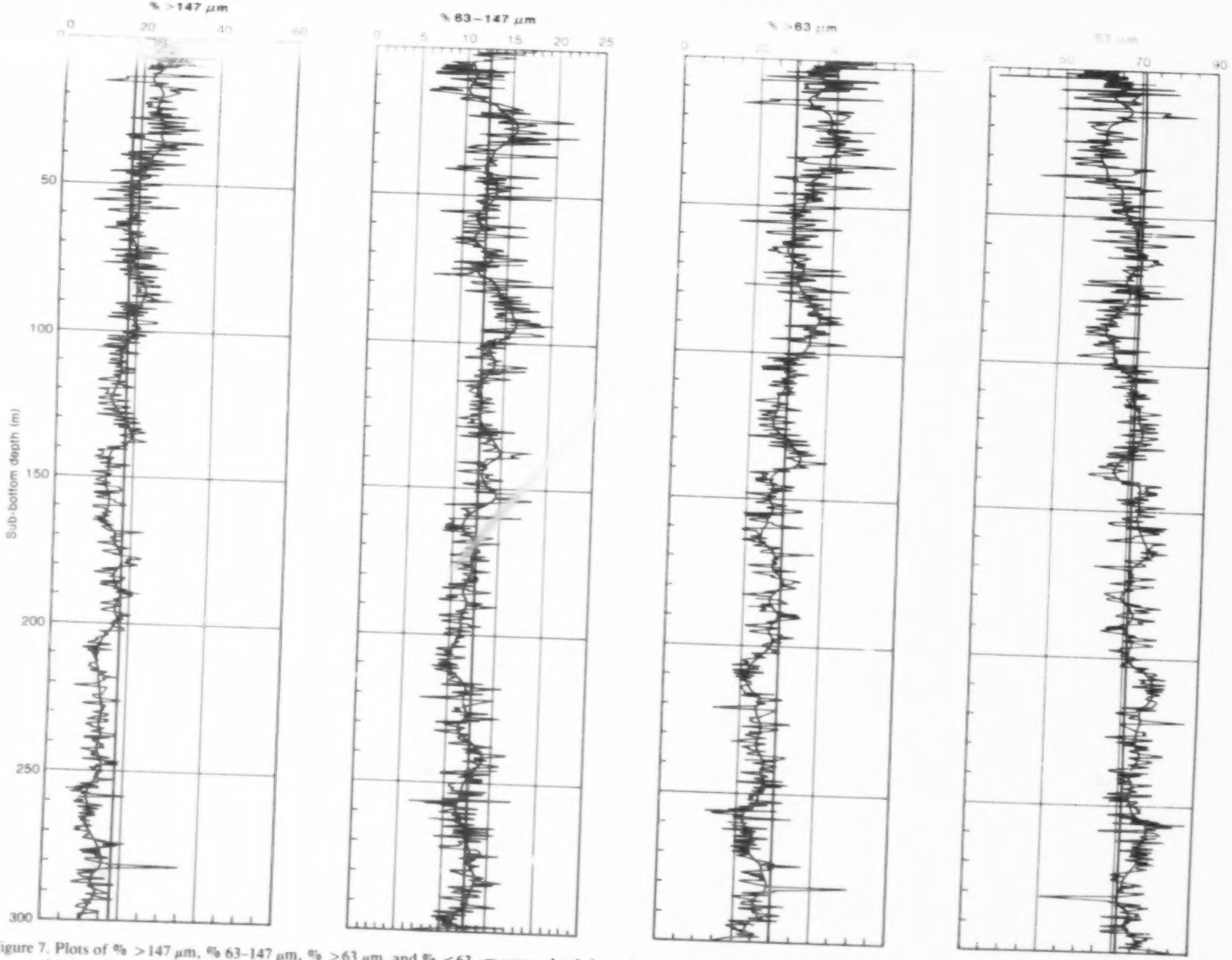

Figure 7. Plots of % >147 μm, % 63–147 μm, % >63 μm, and % <63 μm versus depth for sediments from Site 586. Heavy lines through the data plots are smoothed curves computed using a 21-point moving average. The heavy vertical line through each plot is located at the mean value for each parameter.

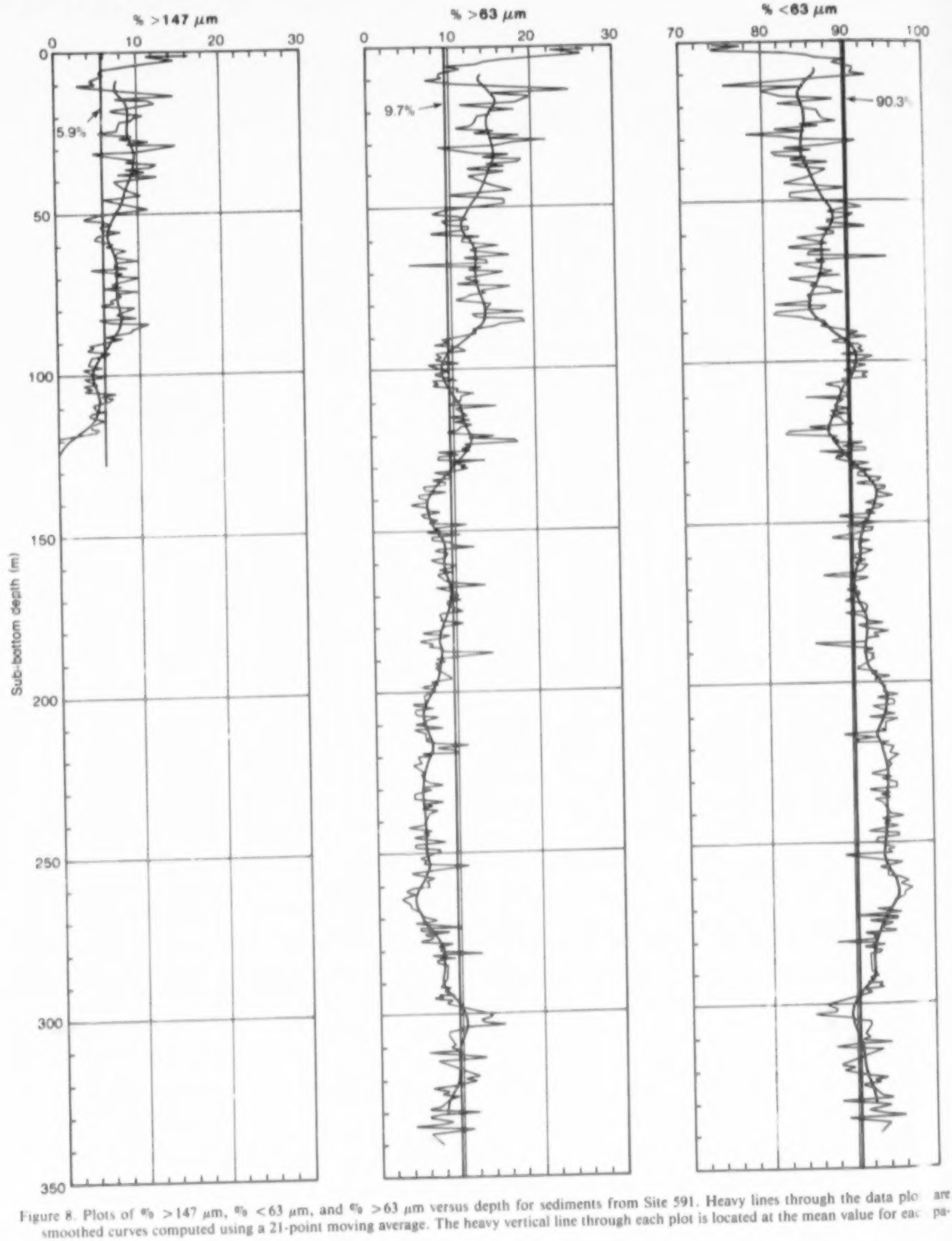

Figure 8. Plots of % >147 µm, % <63 µm, and % >63 µm versus depth for sediments from Site 591. Heavy lines through the data plo are smoothed curves computed using a 21-point moving average. The heavy vertical line through each plot is located at the mean value for eac parameter.

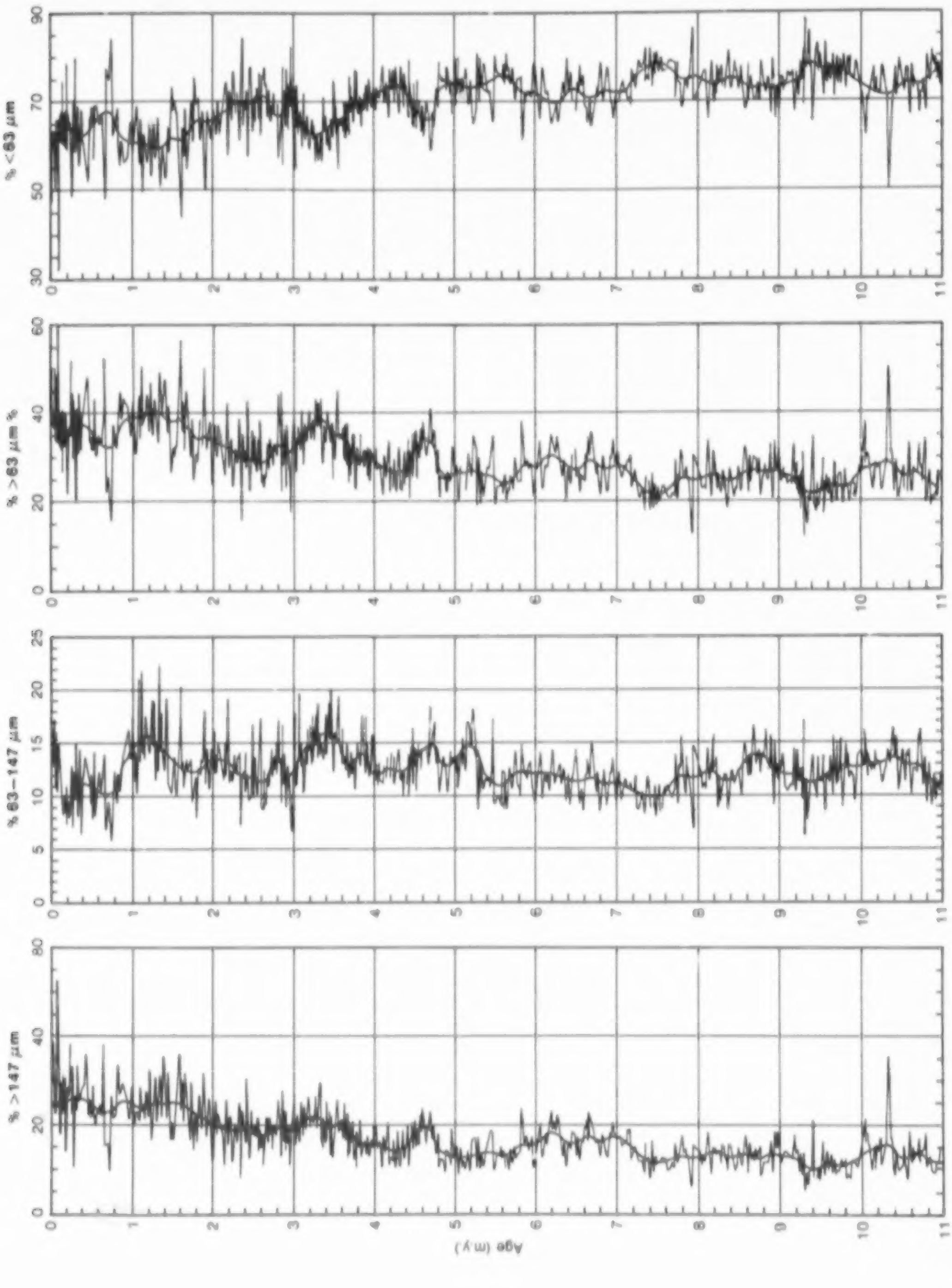

Figure 9. Plots of % >147 μm, % 63–147 μm, % >63 μm, and % <63 μm versus age for sediments from Site 586. Heavy lines through the data plots are smoothed curves computed using a 21-point moving average.

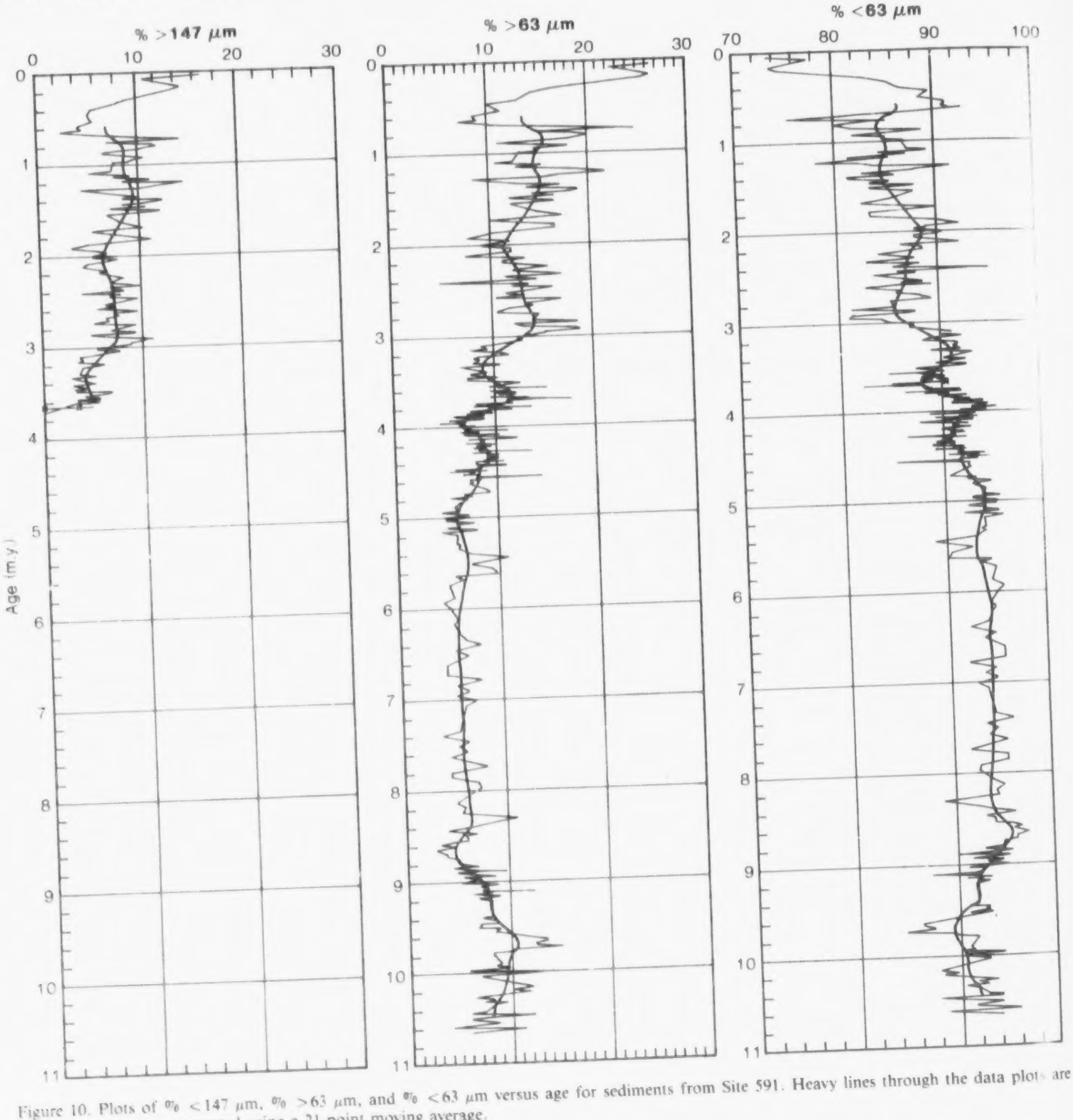

Figure 10. Plots of % <147 μm, % >63 μm, and % <63 μm versus age for sediments from Site 591. Heavy lines through the data plots are smoothed curves computed using a 21-point moving average.

accumulation of current-transported fine materials. Variations in nannofossil productivity, however, may have occurred. Both sites are presently located close to oceanographic diverences (Fig. 1); Site 586 is near the Equatorial Divergence and Site 591 is beneath the Subtropical Divergence. Any overall change in the strength of regional surface circulation should have had exaggerated effects at both sites and in the same way; that is, if circulation strengthened, then the divergence should have become stronger and productivity should have increased. An area of high primary production, such as an upwelling region or a divergence, preferentially should produce a larger flux of phytoplankton (nannofossils and iatoms) than zooplankton (foraminifers and radiolaria s). Consequently, an area of high productivity might ell produce sediment with higher percentages of finer m terial relative to an area with low productivity. This rocess would allow the coarse-fraction record to be i erpreted as a record of paleoproductivity.

The third process that can produce changes in the coarse-fraction content is variation in winnowing eff cts. Currents competent to erode and transport fine (63 μm) material would increase the coarse fraction (63 μm) at the expense of the fine fraction (see, e.g., Thi de,

Table 2. Summary of the mass accumulation rates (MAR) of the grain-size fractions for DSDP Site 586.

Depth range (m)	Age range (m.y.)	Sed. rate (m/m.y.)	Avg. >147 μm	Avg. 63-147 μm	Avg. <63 μm	Avg. >63 μm	Avg. carb.	MAR bulk	MAR >147 μm	MAR 63-147 μm	MAR <63 μm	MAR >63 μm	MAR carb.
0.0-10.3	0.0-0.5	20.6	26.6	11.4	62.0	38.0	86	2241.4	596.2	255.5	1389.7	851.7	1927.6
10.4-22.0	0.5-1.0	23.4	23.5	11.2	65.3	34.7	93	2021.7	475.1	226.4	1320.2	701.5	1880.2
22.1-34.3	1.0-1.5	24.4	24.7	14.9	60.4	39.6	94	2424.3	598.8	361.2	1464.3	960.0	2278.9
34.4-46.4	1.5-2.0	24.2	23.5	12.6	63.9	36.1	93	2548.2	598.8	321.0	1628.3	919.9	2369.8
46.5-61.0	2.0-2.5	29.2	18.6	12.6	68.8	31.2	93	3074.7	571.9	387.4	2115.4	959.3	2859.5
61.1-78.2	2.5-3.0	34.4	18.6	12.0	69.4	30.6	93	3157.9	587.3	378.9	2191.6	966.3	2936.8
78.3-95.8	3.0-3.5	35.2	20.6	15.1	64.3	35.7	95	3193.3	657.8	482.1	2053.3	1140.0	3033.6
95.9-113.5	3.5-4.0	35.4	17.6	13.7	68.7	31.3	94	3393.0	597.1	464.8	2331.0	1062.0	3189.5
113.6-131.4	4.0-4.5	35.8	15.3	12.5	72.2	27.8	99	4079.0	624.0	509.8	2945.0	1133.9	4038.2
131.5-147.3	4.5-5.0	31.8	16.7	13.8	69.5	30.5	95	3485.9	582.1	481.0	2422.7	1063.2	3311.6
147.4-160.3	5.0-5.5	27.4	13.2	13.2	73.6	26.4	96	3255.1	429.6	429.6	2395.7	859.3	3124.9
160.4-173.4	5.5-6.0	24.8	14.4	11.6	74.0	26.0	97	2859.1	411.7	331.6	2115.8	743.3	2773.4
173.5-185.9	6.0-6.5	25.0	17.0	12.0	71.0	29.0	97	2497.5	424.5	299.7	1773.2	724.2	2422.5
186.0-198.4	6.5-7.0	25.0	17.0	11.3	71.7	28.3	99	2700.0	459.0	305.1	1935.9	764.1	2673.0
198.5-211.0	7.0-7.5	25.2	14.0	10.3	75.7	24.3	99	2721.6	381.0	280.3	2060.2	661.3	2694.3
211.1-223.0	7.5-8.0	24.0	12.4	11.2	76.4	23.6	96	3058.5	379.2	342.5	2336.7	721.8	2936.2
223.1-236.0	8.0-8.5	26.0	13.4	11.6	75.0	25.0	95	2962.4	396.9	343.6	2221.8	740.6	2814.3
236.1-248.4	8.5-9.0	24.8	13.6	13.4	73.0	27.0	92	2946.2	400.6	394.7	2150.7	795.4	2710.5
248.5-261.0	9.0-9.5	25.2	11.8	11.6	76.6	23.4	97	2912.1	343.6	337.8	2230.6	681.4	2824.7
261.1-273.4	9.5-10.0	24.8	11.4	12.6	76.0	24.0	99	2798.9	319.0	352.6	2127.1	671.7	2770.9
273.5-285.9	10.0-10.5	25.0	14.8	13.3	71.9	28.1	93	3253.5	481.5	432.7	2339.2	914.2	3025.7
286.0-298.4	10.5-11.0	25.0	12.8	12.3	74.9	25.1	97	3159.0	404.3	388.5	2366.0	792.9	3064.2

Table 3. Summary of the mass accumulation rate (MAR) of the grain-size fractions for DSDP Site 591.

Depth range (m)	Age range (m.y.)	Sed. rate (m/m.y.)	Avg. >147 μm	Avg. 63-147 μm	Avg. <63 μm	Avg. >63 μm	Avg. carb.	MAR bulk	MAR >147 μm	MAR 63-147 μm	MAR <63 μm	MAR >63 μm	MAR carb.
0.00-6.35	0.0-0.5	12.7	10.7	19.4	69.9	30.1	94.0	1114.4	119.2	216.2	779.0	335.4	1047.6
6.35-21.67	0.5-1.0	30.6	8.3	14.3	77.6	22.4	94.6	2817.3	233.8	402.9	2186.3	631.1	2665.2
21.67-37.97	1.0-1.5	32.6	9.3	15.0	75.8	24.2	95.2	3098.3	288.1	464.7	2348.5	749.8	2949.6
37.97-54.00	1.5-2.0	32.1	7.7	13.0	78.8	21.2	92.7	3146.1	242.3	409.0	2479.1	667.0	2916.5
54.00-70.33	2.0-2.5	32.7	7.0	12.4	80.8	19.2	95.1	3408.0	238.6	422.6	2753.7	654.3	3241.0
70.33-86.98	2.5-3.0	33.3	7.8	14.2	78.0	22.0	96.8	3398.6	265.1	482.6	2650.9	747.7	3289.8
86.98-113.74	3.0-3.5	53.5	4.7	9.4	85.8	14.2	97.3	5648.0	265.5	530.9	4846.0	802.0	5495.5
113.74-145.06	3.5-4.0	62.6			88.6	11.4	95.0	6794.6			6020.0	774.6	6454.9
145.06-184.22	4.0-4.5	78.3			91.2	8.8	95.3	9006.1			8213.5	792.5	8482.8
184.22-206.00	4.5-5.0	43.6			92.7	7.3	94.0	5085.5			4714.3	371.2	4780.4
206.00-225.00	5.0-5.5	38.0			93.5	6.5	93.4	4442.6			4153.8	288.8	4149.4
225.00-245.00	5.5-6.0	40.0			94.1	5.9	95.7	4687.2			4410.7	276.5	4485.7
245.00-259.95	6.0-6.5	29.9			93.7	6.2	95.5	3713.6			3479.6	230.2	3546.5
259.95-269.85	6.5-7.0	19.8			95.3	4.7	94.0	2459.2			2343.6	115.6	2311.6
269.85-279.75	7.0-7.5	19.8			94.1	5.9	95.4	2459.2			2314.1	145.1	2346.0
279.75-289.65	7.5-8.0	19.8			92.2	7.8	94.8	2459.2			2267.3	191.8	2331.3
289.65-299.55	8.0-8.5	19.8			92.1	7.9	92.2	2459.2			2264.9	194.3	2267.3
299.55-309.45	8.5-9.0	19.8			88.6	11.4	91.4	2352.2			2084.1	268.2	2149.9
309.45-319.35	9.0-9.5	19.8			90.9	9.1	92.1	2405.7			2186.8	218.9	2215.6
319.35-329.25	9.5-10.0	19.8			91.0	9.0	90.8	2245.3			2043.2	202.1	2038.8
329.25-339.15	10.0-10.5	19.8			92.4	7.6	91.6	2298.8			2124.1	174.7	2105.7

1977). We use winnowing to mean a process that either erodes and transports some, but not necessarily all, of the fine components or causes selective nondeposition of that fine fraction leaving the coarse components relatively intact. We do not mean an erosive process that eliminates entire deposits. Erosion of an entire deposit will cause a hiatus and should be recognized by absent or highly compressed biostratigraphic zones and very slow sedimentation rates. The recovery of all biostratigraphic zones of both planktonic foraminifers and nannofossils at Sites 586 and 591 indicates that there were no erosional events strong enough to remove an entire biostratigraphic zone, although minor erosional events of up to several tens of thousands of years may have occurred.

Long-Term Trends

From our discussion on causes of coarse-fraction variations in the previous section, we concluded that dissolution could not be an important process at either Sites 586 or 591, but that productivity of calcareous plankton and current winnowing both may have been important processes. In this section we discuss how these two processes may have been responsible for the observed variations in the coarse-fraction records on Lord Howe Rise and Ontong-Java Plateau. The basis for this discussion will be the plots for 0.5-m.y. intervals of average values of the >63-μm fraction (Fig. 11), average sedmentation rates (Fig. 3), average bulk-sediment MAR (Fig. 5), and average MAR for each size fraction (Fig. 12).

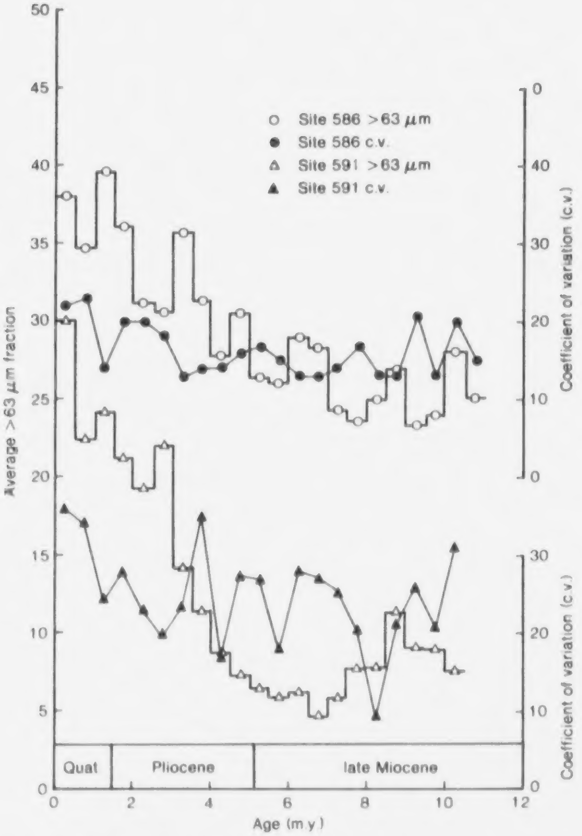

Figure 11. Histograms of percent coarse fraction (>63 μm) averaged for 0.5-m.y. intervals versus age for Sites 586 and 591. Plots of the coefficient of variation (c.v.; standard deviation as the percent of mean) for each 0.5-m.y. interval are shown for each site below the appropriate histogram.

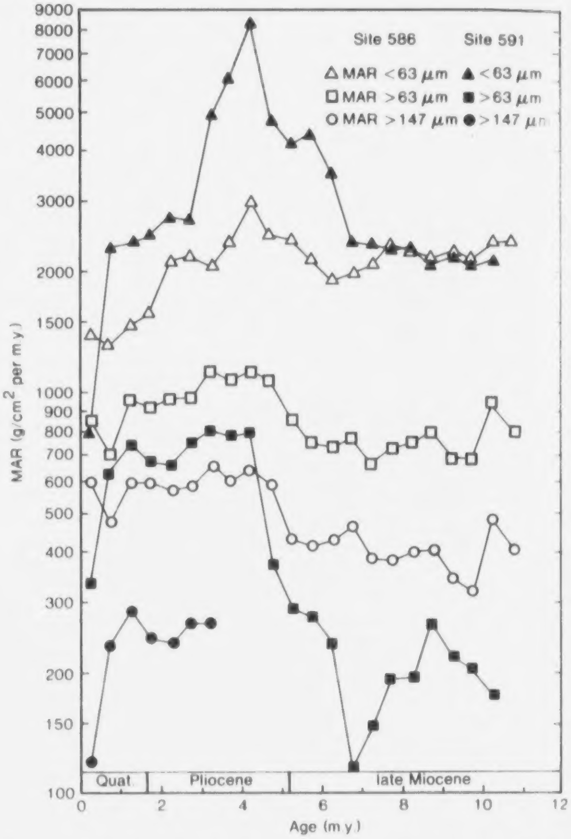

Figure 12. Semilogarithmic plots of mass accumulation rates (MAR; in g/cm² per m.y.) averaged for 0.5-m.y. intervals versus age for the >147 μm, >63 μm, and <63 μm size fractions in sediments from Sites 586 and 591.

Based on the plots in Figures 3, 5, 11, and 12, we have subdivided the records at Sites 586 and 591 into five time intervals for purposes of discussion: 10.5 to 6.5 m.y.; 6.5 to 4.0 m.y.; 4.0 to 2.5 m.y.; 2.5 to 0.7 m.y.; 0.7 to the present. Each interval represents different conditions of sediment accumulation at Lord Howe Rise and Ontong-Java Plateau. During the early late Miocene (10.5 to 6.5 m.y.) sedimentation rates at Sites 586 and 591 were relatively typical for sedimentation rates on carbonate platforms outside of high-productivity regions. The sedimentation rate on Lord Howe Rise during this interval was about 20 m/m.y. and that on Ontong-Java Plateau was about 25 m/m.y. (Fig. 3). The bulk-sediment MARs of the two areas during this interval were about 2500 g/cm² per m.y. for Lord Howe Rise and about 3000 g/cm² per m.y. for Ontong-Java Plateau (Fig. 5). These MARs are typical for the southwestern Pacific at that time (Worsley and Davies, 1979). The average coarse-fraction (>63 μm percentages (Fig. 11) and MARs (Fig. 12) were always higher at Site 586 than at Site 591. We interpret this difference to be the result of winnowing of rather nominal sediment fluxes on Ontong-Java Plateau during the early late Miocene. Site 586 has about 30% coarse fraction and about 70% fine fraction (Fig. 11). If we assume all coarse fraction is foraminifers and 10% of the fine fraction is juvenile foraminifers, then the ratio of foraminifers to nannofossils is 40:60. The same assumptions applied to Site 591 yield a ratio of foraminifers to nannofossils of 15:85. Consequently, it is apparent that Site 586 witnessed stronger winnowing efficiently than did Site 591 during the early late Miocene. We use this period from 10.5 to 6.5 m.y. ago as a baseline for "normal" conditions of productivity and sediment accumulation at both Lord Howe Rise and Ontong-Java Plateau from which to measure changes that occurred later in the records from these two areas. It is important to note that during this period the main Antarctic ice sheet was already formed (Kennett, 1977), but the West Antarctic ice sheet was not yet developed (Ciesielski et al., 1982; Kennett, 1982).

The period of relatively normal sedimentation was followed by a period of very high productivity in the latest Miocene to early Pliocene from 6.5 to 4.0 m.y. ago. The effects apparently were much greater and began about 1 m.y. earlier on Lord Howe Rise than on Ontong-Java Plateau. Increased productivity is suggested by the large increases in sedimentation rates (Fig. 3) and bulk-sediment MARs (Fig. 5), but, more importantly, by the relationships between the size-fraction MARs (Fig. 12). At Site 591, there is a very large increase in the <63-μm MAR from about 2100 to greater than 8000 g/cm² per m.y. (Fig. 12). During this same interval, the >63-μm MAR rose from less than 200 to about 800 g/cm² per m.y. Less dramatic but significant increases in size-fraction MARs also occurred on Ontong-Java Plateau where the <63-μm MAR went from 2000 to 3000 g/cm² per m.y. and the >63-μm MAR went from 700 to 1100 g/cm² per m.y. The ratio of the coarse- to fine-fraction components changed very little from 6.5 to 4.0 m.y. ago (Fig. 12), further supporting increased productivity during this time. Maximum productivity at Sites 586 and 591 from 6.5 to 4.0 m.y. ago supports the suggestion by Ciesielski et al. (1982) that one effect of the expansion of the Antarctic ice sheet and the growth of the West Antarctic ice sheet beginning about 6.2 m.y. ago was to increase the surface circulation at least of the Southern Ocean. The grain-size stratigraphies suggest that there was increased productivity probably caused by increased upwelling that resulted from the intensification of the Subtropical and Equatorial divergences during this time. This early Pliocene period of maximum productivity on both Lord Howe Rise and Ontong-Java Plateau corresponds to a period of maximum sedimentation rates on the Falkland Plateau (Ciesielski et al., 1982) and maximum carbonate MAR averaged for the entire Pacific Ocean (Davies and Worsley, 1981; Fig. 6).

Productivity appears to have been at a maximum at both Lord Howe Rise and Ontong-Java Plateau in the early Pliocene, about 4 m.y ago. Sedimentation rates at Site 591 abruptly decreased from the maximum of almost 80 m/m.y. 4.0 m.y. ago to about 32 m./m.y. by 2.5 m.y. ago. However, sedimentation rates at Site 586 remained high at about 35 m/m.y. from 4.0 m.y. to about 2.5 m.y. ago and then decreased to a minimum of about 22 m/m.y. about 2.0 m.y. ago. There appears to have been a lag of about 0.5 m.y. in the response of sedimentation rates and mass accumulation rates at Ontong-Java Plateau relative to Lord Howe Rise.

The cause of the decreased sedimentation rates can be determined from the grain size MARs (Fig. 12). At both Ontong-Java Plateau and Lord Howe Rise the coarse-fraction component MAR (>63 μm) persisted at high values of about 700 to 1000 g/cm² per m.y. between 4.0 and 2.5 m.y. ago, whereas the fine-fraction component MAR (<63 μm) significantly decreased. At Site 591 the decrease was from a high of greater than 8000 to a low of about 2500 g/cm² per m.y.; at Site 586 the decrease was from a high of 2900 to a low of about 1500 g/cm² per m.y. These decreases in fine fraction together with persistently high values of coarse fraction suggest a significant period of winnowing between 4.0 and 2.5 m.y. ago.

By 2.0 m.y. ago sedimentation rates at Ontong-Java Plateau had returned to values similar to those of the late Miocene (~25 m/m.y.), but sedimentation rates on Lord Howe Rise remained about 50% higher than late Miocene rates. Both fine fraction and coarse fraction significantly decreased, yet the sedimentation rates do not suggest a hiatus. Consequently, dissolution probably is not the cause of the decreases. It is not possible to determine how much of the sharp decrease in sedimentation rates and sediment MARs between 4.0 and 2.0 m.y. ago was due to winnowing and how much was due to decreased productivity. However, the middle Pliocene (4 to 3 m.y. ago) was a period of erosion on the Falkland Plateau (Ciesielski et al., 1982); increase Antarctic Bottom Water circulation in Vema Channel in the South Atlantic (Ledbetter et al., 1978); and high abundance of cold-water Antarctic radiolarians (Keany, 1978). Further, it is represented by a disconformity in the Ross Sea (Hayes, Frakes, et al., 1975). All of these suggest that winnowing was important. A decrease of about 50% in the carbonate MAR for the entire Pacific Ocean beginning about 4.0 m.y. ago (Davies and Worsley, 1981), however, suggests that productivity also may have decreased.

Significant winnowing and possibly decreased productivity continued between 3.0 and 0.7 m.y. ago, as indicated by the shoulders on the sedimentation rate and MAR curves for this time interval (Figs. 3, 5, 12). Erosion on Lord Howe Rise and Ontong-Java Plateau during this time interval coincides with a period of maximum post-Miocene erosion on the Falkland Plateau (2 to 1 m.y. ago; Ciesielski et al., 1982); several Patagonia glaciations (Fleck et al., 1972; Mercer, 1976); severe glaciation in the Weddell Sea (2.5 to 1.9 m.y. ago; Anderson, 1972); and initiation of Northern Hemisphere glaciation about 2.5 m.y. ago (Kent et al., 1971; Berggren, 1972; Shackleton and Kennett, 1975; Shackleton and Opdyke, 1977; Backman, 1979; Poore, 1981; Kennett, 1983).

The intensity of winnowing increased on Lord Howe Rise during the late Quaternary from 0.7 m.y. ago to the present, but this event did not affect the Ontong-Java Plateau. The evidence for winnowing on Lord Howe Rise can be seen by the marked decreases in MARs of both the fine and coarse fractions (Fig. 12). The <63-μm MAR decreased from 2300 to less than 800 g/cm² per m.y., the >63-μm MAR decreased from 650 to 340 g/cm² per m.y., the >147-μm MAR decreased from 250 to 120 g/cm² per m.y., the bulk-sediment MAR decreased from 3000 to 1200 g/cm² per m.y. (Fig. 5), and the sedimentation rates decreased from 32 to 12 m/m.y. (Fig. 3). The average percentage of the coarse fraction also increased considerably during the Pliocene and Quaternary (Fig. 11), lending further support for winnowing during the last 1.0 m.y. This interval of increased winnowing on Lord Howe Rise may have been a local event because it is not found on Ontong-Java Plateau and the last 0.7 m.y. was a period of increased sedimentation on the Falkland Plateau (Ciesielski et al., 1982).

10^5 and 10^4 Year Cycles

The plots of coarse fraction versus time (Figs. 9, 10) show that there are distinct fluctuations in grain size on scales of 10^5 and 10^4 yr. cycle. The 10^4 yr. cycles are best seen in the raw data, but the 10^5 yr. cycles are better seen in the 21-point running averages that are drawn through the data. The average periodicity of eleven 10^5 yr. cycles over the past 10 m.y. at Site 591 is 850 × 10^3 yr. The average periodicity of 25 × 10^5 yr. cycles over the past 11 m.y. at Site 586 is 430 × 10^3 yr. The 10^5 yr. cycles at both sites are best developed (have the highest amplitudes) in the last 5 m.y.; prior to 5 m.y. ago, the amplitudes of the cycles are greatly reduced.

In order to determine the periodicities of the 10^4 yr. cycles, we plotted the grain-size data versus age but at a much larger scale than in Figures 9 and 10. We subdivide the age axis into 0.5-m.y. intervals and counted the number of cycles for each 0.5-m.y. interval. The periodicities for each 0.5-m.y. interval at each site are plotted on Figure 13.

The periodicities of the 10^4 yr. cycles range from 100 to 48 × 10^3 yr./cycle at Site 586 and from 250 to 33 × 10^3 yr./cycle at Site 591 (Fig. 13). The most noticeable characteristic of the grain-size cycles is the change in periodicities that occurred about 5 m.y. ago at both sites. Prior to 5 m.y. ago, in the late Miocene, periodicities of grain-size cycles at Site 586 varied between about 55 and 80 × 10^3 yr./cycle with an average periodicity of about 65 × 10^3 yr./cycle. Then, at about the Miocene/Pliocene boundary, the periodicities of the cycles decreased to an average of about 40 × 10^3 yr./cycle between 5 and 2.5 m.y. ago, and increased back to an average periodicity of about 65 × 10^3 yr./cycle between 2.5 and 0.7 m.y. ago. Because the sedimentation rates and MARs are relatively constant at Site 586 between 11 and 6 m.y. ago and between 2.5 and 0.7 m.y. ago (Figs. 3, 5, 12), the range in periodicities (55 to 80 × 10^3 yr./cycle) for these parts of the section probably represents an average range of periodicities for cycles in sediment from this area deposited under relatively stable conditions. The amplitudes of the 10^4 yr. cycles, like the amplitudes of the 10^5 yr. cycles, are much less in the Miocene part of the section. In the post-Miocene part of the section the amplitudes of variation in grain size at all scales are considerably greater.

At Site 591, periodicities of grain-size cycles were generally greater than 100 × 10^3 yr./cycle during the late Miocene, with considerable variation. Periodicities decreased markedly in the latest Miocene to about 40 × 10^3 yr./cycle by the early Pliocene, and then increased to between 70 and 130 × 10^3 yr./cycle in the upper Pliocene section and greater than 100 × 10^3 yr./cycle in the Quaternary section. The shortest periodicities at both sites occur in the Pliocene.

The observed variations in grain-size parameters are the result of fluctuations in winnowing strength and productivity that are directly linked to climatic forcing through fluctuations in surface and subsurface circulation. The periodicities of all of the grain-size cycles are within the range of orbital cycles that have been used to interpret the mechanism of global climate change (Hays et al., 1976; Pisias and Moore, 1981). However, because the periodicities of 10^4 and 10^5 yr. grain-size cycles at Sites 586 and 591 are not similar for any given period and because the periodicities are highly variable over the past 10 m.y., particularly on Lord Howe Rise, we believe that local effects of fluctuations in productivity and winnowing have modified the primary record of climatic forcing. Consequently, the resultant records are complex products of primary climate signals with superimposed local effects.

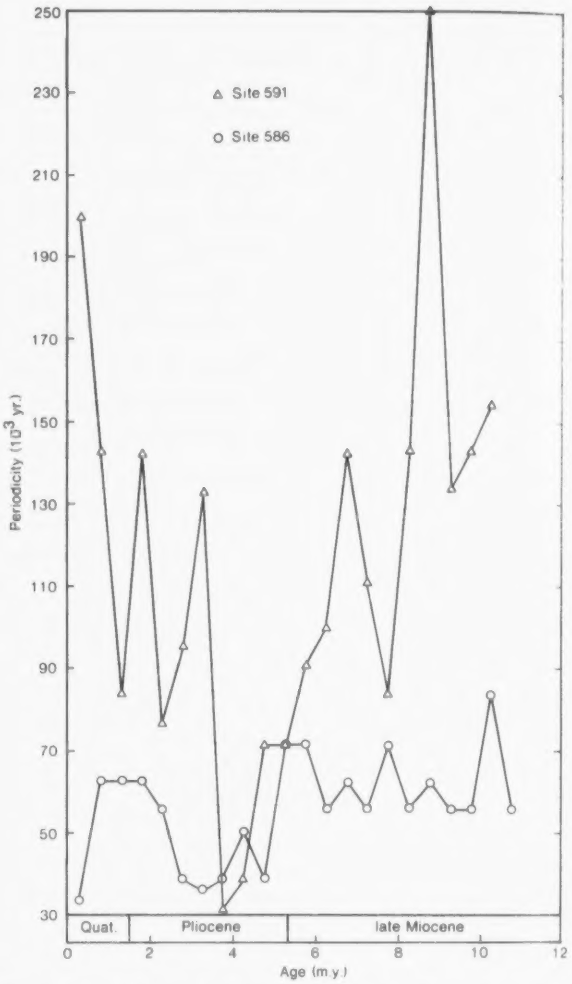

Figure 13. Periodicities of shorter-period cycles in the >63 μm size-fraction records for Site 586 (circles) and Site 591 (triangles) averaged for 0.5-m.y. intervals.

CONCLUSIONS

Ontong-Java Plateau and Lord Howe Rise have both been well above the foraminiferal lysocline and the CCD for at least the last 10 m.y. Therefore, carbonate concentrations are too high to preserve any variations that might be correlated with established carbonate stratigraphies that reflect climate change. However, the grain-size stratigraphies of Sites 586 and 591 do show histories of the influences of current winnowing and phytoplankton productivity on the sediment of Ontong-Java Plateau and Lord Howe Rise that are related to climatic changes.

Conditions of sediment accumulation at both sites were relatively stable during the late Miocene from 10 to 6.5 m.y. ago. The latest Miocene and early Pliocene was a period of greatly increased nannoplankton productivity, influencing the sediment of Lord Howe Rise much more than the sediment of Ontong-Java Plateau. The increased productivity at Lord Howe Rise probably was caused by increased upwelling at the Subtropical Divergence and at Ontong-Java Plateau by increased upwelling at the Equatorial Divergence. The increased upwelling is inferred to have been caused by increased circulation related to the development and expansion of the West Antarctic ice sheet. The period of increased productivity was followed by a period of current winnowing during the late Pliocene (4.0 to 2.0 m.y.). The conditions returned to quieter pelagic sedimentation until about 0.7 m.y. ago when another episode of current winnowing commenced on Lord Howe Rise but not on Ontong-Java Plateau.

The periodicities of the cycles of grain-size fluctuations are within the range of cycles of the Earth's orbital parameters that are thought to be the main forcing mechanism of global climate change. However, local influences of current winnowing and productivity have altered any primary climatic signal of orbital forcing at both Lord Howe Rise and Ontong-Java Plateau.

ACKNOWLEDGMENTS

We thank the shipboard scientific parties of Legs 89 and 90 for their help in sampling the cores and for providing physical property, carbonate, and biostratigraphic data. We appreciate the helpful reviews of this manuscript by M. T. Ledbetter and J. P. Kennett. This work was supported by the U.S. Geological Survey Climate Program.

REFERENCES

Anderson, J. B., 1972. The marine geology of the Weddell Sea. *Florida State Univ. Sediment. Res. Lab., Contrib.*, 35.

Andrews, J. E., Packham, G. H., et al., 1975. *Init. Repts. DSDP*, 30: Washington (U.S. Govt. Printing Office).

Backman, J., 1979. Pliocene biostratigraphy of DSDP Sites 111 and 116 from the North Atlantic Ocean and the age of Northern Hemisphere glaciation. *Stockholm Contrib. Geol.*, 32(3):115–137.

Berger, W. H., Bonneau, M.-C., and Parker, F. L., 1982. Foraminifera on the deep-sea floor: Lysocline and dissolution rate. *Oceanol. Acta*, 5:249–258.

Berger, W. H., Ekdale, A. A., and Bryant, P. P., 1979. Selective preservation of burrows in deep-sea carbonates. *Mar. Geol.*, 32:205–230.

Berger, W. H., and Johnson, T. C., 1976. Deep-sea carbonates: Dissolution and mass wasting on Ontong-Java Plateau. *Science*, 192: 785–787.

Berger, W. H., Johnson, T. C., and Hamilton, E. L., 1977. Sedimentation on Ontong-Java Plateau: Observations on a classic "carbonate monitor." *In* Anderson, N. R., and Malahoff, A. (Eds.), *The Fate of Fossil Fuel CO_2 in the Oceans*: New York (Plenum Publ. Corp.), pp. 543–567.

Berggren, W. A., 1972. Late Pliocene-Pleistocene glaciation. *In* Laughton, A. S., Berggren, W. A., et al., *Init. Repts. DSDP*, 12: Washington (U.S. Govt. Printing Office), 953–963.

Bonneau, M.-C., Vergnaud Grazzini, C., and Berger, W. H., 1980. Stable isotope fractionation and differential dissolution in recent planktonic foraminifera from Pacific box-cores. *Oceanol. Acta*, 3: 377–[illegible]2.

Burns, [illegible] E., Andrews, J. E., 1973. *Init. Repts. DSDP*, 21: Washington (U.S. Govt. Printing Office).

Ciesielski, P. F., Ledbetter, M. T., and Ellwood, B. B., 1982. The development of Antarctic glaciation and the Neogene paleoenvironment of the Maurice Ewing Bank. *Mar. Geol.*, 46:1–51.

Davies, [illegible] C., 1973. *Statistics and Data Analysis in Geology*: New York (John Wiley and Sons, Inc.).

Davies, [illegible] A., and Worsley, T. R., 1981. Paleoenvironmental implications of oceanic carbonate sedimentation rates. *In* Warme, J. E., Douglas, R. G., and Winterer, E. L. (Eds.), *The Deep Sea Drilling Project: A Decade of Progress*. Soc. Econ. Paleont. Mineral. Spec. Publ., 32:169–179.

Dean, W. E., Gardner, J. V., and Čepek, P., 1981. Tertiary carbonate-dissolution cycles on the Sierra Leone Rise, Eastern Equatorial Atlantic Ocean. *Mar. Geol.*, 39:81–101.

Ellis, H., 1981. Calcareous nannoplankton biostratigraphy—(Deep Sea Drilling Project) Leg 60. *In* Hussong, D. M., Uyeda, S., et al., *Init. Repts. DSDP*, 60: Washington (U.S. Govt. Printing Office), 507–535.

Fleck, R. J., Mercer, J. H., Nairn, A. E. M., and Peterson, D. N., 1972. Chronology of late Pliocene and early Pleistocene glacial and magnetic events in Southern Argentina. *Earth Planet. Sci. Lett.*, 16:15–22.

Gardner, J. V., 1975. Late Pleistocene carbonate dissolution cycles in the eastern equatorial Atlantic. *In* Sliter, W. V., Bé, A. W. H., and Berger, W. H. (Eds.), *Dissolution of Deep-Sea Carbonates*. Cushman Found. Foram. Res., Spec. Publ., 13:129–141.

Hayes, D. E., Frakes, L. A., et al., 1975. *Init. Repts. DSDP*, 28: Washington (U.S. Govt. Printing Office).

Hays, J. D., Imbrie, J., and Shackleton, N. J., 1976. Variations in the Earth's orbit: Pacemaker of the Ice Ages. *Science*, 194:1121–1132.

Holdsworth, B. K., 1975. Cenozoic Radiolaria biostratigraphy; Leg 30: Tropical and equatorial Pacific. *In* Andrews, J. E., Packham, G. H., et al., *Init. Repts. DSDP*, 30: Washington (U.S. Govt. Printing Office), 499–537.

Huffman, E. W. D., 1977. Performance o a new automatic carbon dioxide coulometer. *Microchem. J.*, 22:567–573.

Johnson, T. C., Hamilton, E. L., and Berger, W. H., 1977. Physical properties of calcareous ooze: Control by dissolution at depth. *Mar. Geol.*, 24:259–277.

Keany, J., 1978. Paleoclimatic trends in early and middle Pliocene deep-sea sediments of the Antarctic. *Mar. Micropaleontol.*, 3:35–49.

Kennett, J. P., 1977. Cenozoic evolution of Antarctic glaciation, the Circum-Antarctic Ocean, and their impact on global paleoceanography. *J. Geophys. Res.*, 82:3843–3860.

———, 1982. *Marine Geology*: Englewood Cliffs, N. J., (Prentice-Hall, Inc).

———, 1983. Paleo-oceanography: Global ocean evolution. *In* James, D. E. (Ed.), *Reviews of Geophysics and Space Physics*, 21: 1258–1274.

Kent, D., Opdyke, N. D., and Ewing, M., 1971. Climatic change in the North Pacific using ice-rafted detritus as a climatic indicator. *Geol. Soc. Am. Bull.*, 82:2741–2754.

Klein, G. deV., 1975. Depositional facies of Leg 30 Deep Sea Drilling Project sediment cores. *In* Andrews, J. E., Packham, G. H., et al., *Init. Repts. DSDP*, 30: Washington (U.S. Govt. Printing Office), 423–442.

Krishnamurthy, R. V., Lal, D., Somayajulu, B. L. K., and Berger, W. H., 1979. Radiometric studies of box cores from the Ontong-Java Plateau. *Proc. Indian Acad. Sci.*, 88A:273–283.

Ledbetter, M. T., and Ellwood, B. B., 1976. Selection of sample intervals in deep-sea sedimentary cores. *Geology*, 4:303–304.

Ledbetter, M. T., Williams, D. F., and Ellwood, B. B., 1978. Late Pliocene climate and southwest Atlantic abyssal circulation. *Nature*, 272:237–239.

Mercer, J. H., 1976. Glacial history of southernmost South America. *Quat. Res.*, 6:125–166.

Moberly, R., Schlanger, S. O., et al., in press. *Init. Repts. DSDP*, 89: Washington (U.S. Govt. Printing Office).

Müller, G., and Gastner, M., 1971. The "Karbonate bomb," a simple device for the determination of carbonate content in sediment, soils, and other materials. *N. Jahrb. Mineral. Mh.*, 10:466–469.

Okada, H., and Bukry, D., 1980. Supplementary modifications and introduction of code numbers to the low-latitude coccolith biostratigraphic zonation (Bukry, 1973; 1975). *Mar. Micropaleontol.*, 5:321–325.

Pisias, N. G., and Moore, T. C., 1981. The evolution of Pleistocene climate: A time series approach. *Earth Planet. Sci. Lett.*, 52: 450–458.

Poore, R, Z., 1981. Temporal and spartial distribution of ice-rafted mineral grains in Pliocene sediments of the North Atlantic: Implications for Late Cenozoic climatic history. *Soc. Econ. Paleont. Mineral. Spec. Publ.*, 32:505–515.

Shackleton, N. J., and Kennett, J. P., 1975. Late Cenozoic oxygen and carbon isotope changes at Deep Sea Drilling Project Site 284: Implications for glacial history of the Northern Hemisphere and Antarctica. *In* Kennett, J. P., Houtz, R. E., et al., *Init. Repts. DSDP*, 29: Washington (U.S. Govt. Printing Office), 801-807.

Shackleton, N. J., and Opdyke, N. D., 1973. Oxygen isotope and paleomagnetic stratigraphy of equatorial Pacific core V28-238: Oxygen isotope temperatures on a 10^5 and 10^6 year time scale. *Quat. Res.*, 3:39-55.

________, 1976. Oxygen-isotope and paleomagnetic stratigraphy of Pacific core V28-239 late Pliocene to latest Pleistocene. *Geol. Soc. Am. Mem.*, 145:449-464.

________, 1977. Oxygen isotope and paleomagnetic evidence for early Northern Hemisphere glaciation. *Nature*, 270:216-219.

Thiede, J., 1977. Textural variations of calcareous coarse fractions in the Panama Basin (Eastern Equatorial Pacific Ocean). *In* Anderson, N. R., and Malahoff, A. (Eds.), *The Fate of Fossil Fuel CO_2 in the Oceans*: New York (Plenum Publ. Corp.), pp. 673-692.

Thompson, P. R., and Saito, T., 1974. Pacific Pleistocene sediments: Planktonic Foraminifera dissolution cycles and geochronology. *Geology*, 2:333-335.

Thompson, P. R., and Sciarrillo, J. R., 1978. Planktonic foraminiferal biostratigraphy in the Equatorial Pacific. *Nature*, 275:29-33.

van Andel, Tj. H., Heath, G. R., and Moore, T. C., 1977. Cenozoic history and paleoceanography of the central equatorial Pacific Ocean. *Geol. Soc. Am. Mem.*, 143.

van der Lingen, G. J., and Packham, G. H., 1975. Relationships between diagenesis and physical properties of biogenic sediments of the Ontong-Java Plateau (Sites 288 and 289; Deep Sea Drilling Project). *In* Andrews, J. E., Packham, G. H., et al., *Init. Repts. DSDP*, 30: Washington (U.S. Govt. Printing Office), 443-481.

Vincent E., Killingley, J. S., and Berger, W. H., 1981. Stable isotope composition of benthic foraminifera from the equatorial Pacific. *Nature*, 289:639-643.

Woodruff, F., Savin, S. M., and Douglas, R. G., 1981. Miocene stable isotope record: A detailed deep Pacific Ocean study and its paleoclimatic implications. *Science*, 212:665-668.

Worsley, T. R., and Davies, T. A., 1979. Cenozoic sedimentation in the Pacific Ocean: Steps toward a quantitative evaluation. *J. Sediment. Petrol.*, 49:1131-1146.

Date of Initial Receipt: 5 October 1984
Date of Acceptance: 5 April 1985

APPENDIX A
Coarse- and Fine-Fraction Percentages, Sites 586 and 591

Site	Core	Section	Interval (cm)	Sub-bottom depth (m)	>147 μm	>63 μm	63-147 μm	<63 μm
586	1	1	0	0.0	36.5	53.4	16.9	46.6
586	1	1	39	0.4	25.9	39.0	13.1	61.0
586	1	1	80	0.8	19.8	36.7	16.9	63.3
586	1	1	0	1.4	38.5	49.5	11.0	50.5
586	1	1	40	1.8	22.6	33.7	11.1	66.3
586	1	1	120	2.6	52.9	68.0	15.1	32.0
586	1	2	0	2.9	28.7	41.8	13.1	58.2
586	1	2	40	3.3	18.6	33.4	14.8	66.6
586	1	2	80	3.7	13.0	25.5	12.5	74.5
586	1	2	120	4.1	27.0	38.8	11.8	61.2
586	1	3	0	4.4	17.7	26.7	9.0	73.3
586	1	3	40	4.8	22.5	32.5	10.0	67.5
586	1	3	80	5.2	24.4	33.2	8.8	66.8
586	1	3	120	5.6	25.6	35.6	10.0	64.4
586	1	4	0	5.9	29.5	40.3	10.8	59.7
586	1	4	40	6.3	18.5	28.3	9.8	71.7
586	2	1	1	6.4	24.9	37.5	12.6	62.5
586	1	4	80	6.7	28.2	36.2	8.0	63.8
586	2	1	40	6.8	32.6	48.4	15.8	51.6
586	1	4	120	7.1	38.2	51.1	12.9	48.9
586	2	1	80	7.2	25.0	35.4	10.4	64.6
586	1	5	0	7.4	32.1	44.6	12.5	55.4
586	2	1	120	7.6	22.5	34.0	11.5	66.0
586	1	5	40	7.8	26.2	41.2	15.0	58.8
586	2	2	10	8.0	25.4	37.4	12.0	62.6
586	1	5	80	8.2	31.7	44.6	12.9	55.4
586	2	2	50	8.4	32.8	46.3	13.5	53.7
586	1	5	120	8.6	25.3	31.8	6.5	68.2
586	2	2	90	8.8	27.6	38.9	11.3	61.1
586	1	6	0	8.9	23.5	31.5	8.0	68.5
586	2	2	139	9.3	27.3	38.3	11.0	61.7
586	1	6	40	9.3	26.4	37.8	11.4	62.2
586	2	3	20	9.6	26.8	35.2	8.4	64.8
586	1	6	80	9.7	39.4	50.2	10.8	49.8
586	2	3	60	10.0	31.3	40.1	8.8	59.9
586	1	6	120	10.1	22.5	31.8	9.3	68.2
586	2	3	100	10.4	27.6	36.9	9.3	63.1
586	1	7	0	10.4	25.0	32.9	7.9	67.1
586	2	3	140	10.8	22.8	32.2	9.4	67.8
586	1	7	40	10.8	22.3	30.7	8.4	69.3
586	2	4	30	11.2	14.1	21.5	7.4	78.5
586	2	4	70	11.6	25.3	34.1	8.8	65.9
586	2	4	110	12.0	26.6	35.0	8.4	65.0
586	2	4	149	12.4	22.7	29.9	7.2	70.1
586	2	5	40	12.8	10.5	20.1	9.6	79.9
586	2	5	80	13.2	23.3	31.3	8.0	68.7
586	2	5	120	13.6	25.5	39.9	14.4	60.1
586	2	6	10	14.0	31.5	46.9	15.4	53.1
586	2	6	50	14.4	31.8	47.5	15.7	52.5
586	2	6	90	14.8	32.3	46.1	13.8	53.9
586	3	1	0	15.1	22.2	33.6	11.4	66.4
586	2	6	130	15.2	27.4	38.4	11.0	61.6
586	3	1	40	15.4	21.7	33.5	11.8	66.5
586	2	7	21	15.6	22.1	32.1	10.0	67.9
586	3	1	80	15.8	28.8	43.0	14.2	57.0
586	3	1	120	16.2	20.1	30.5	10.4	69.5
586	3	2	10	16.7	23.7	34.4	10.7	65.6
586	3	2	50	17.1	22.8	35.0	12.2	65.0
586	3	2	90	17.5	24.2	34.5	10.3	65.5
586	3	2	130	17.9	22.1	33.3	11.2	66.7
586	3	3	20	18.3	25.7	37.5	11.8	62.5
586	3	3	60	18.7	38.1	52.0	13.9	48.0
586	3	3	100	19.1	13.1	18.4	5.3	81.6
586	3	3	141	19.5	17.7	26.3	8.6	73.7
586	3	4	30	19.9	15.7	25.0	9.3	75.0
586	3	4	70	20.3	14.4	21.6	7.2	78.4
586	3	4	110	20.7	9.9	15.7	5.8	84.3
586	3	4	149	21.1	26.6	37.1	10.5	62.9
586	3	5	42	21.5	23.0	34.4	11.4	65.6
586	3	5	79	21.9	21.7	34.0	12.3	66.0
586	3	5	120	22.3	22.3	31.8	9.5	68.2
586	3	6	10	22.7	28.8	40.3	11.5	59.7
586	3	6	52	23.1	33.8	44.3	10.5	55.7
586	3	6	92	23.5	26.8	39.0	12.2	61.0
586	3	6	131	23.9	28.1	40.9	12.8	59.1
586	3	7	20	24.3	29.5	43.4	13.9	56.6
586	4	1	40	25.6	26.2	41.7	15.5	58.3
586	4	1	80	26.0	22.9	39.0	16.1	61.0
586	4	1	120	26.4	21.4	35.0	13.6	65.0
586	4	2	10	27.0	25.5	42.4	16.9	57.6
586	4	2	50	27.4	27.6	39.1	11.5	60.9
586	4	2	90	27.8	21.9	35.9	14.0	64.1
586	4	2	130	28.2	20.7	31.0	10.3	69.0
586	4	3	20	28.6	22.9	37.0	14.1	63.0
586	4	3	60	29.0	23.1	44.2	21.1	55.8
586	4	3	100	29.4	21.2	34.6	13.4	65.4
586	4	3	140	29.8	28.8	50.5	21.7	49.5
586	4	4	30	30.2	23.3	37.5	14.2	62.5
586	4	4	70	30.6	24.5	38.0	13.5	62.0
586	4	4	110	31.0	21.7	39.4	17.7	60.6
586	4	4	149	31.4	27.5	43.7	16.2	56.3
586	4	5	40	31.8	26.1	41.2	15.1	58.8
586	4	5	80	32.2	21.9	35.9	14.0	64.1
586	4	5	110	32.5	32.0	46.8	14.8	53.2
586	4	6	10	33.1	16.8	35.7	18.9	64.3
586	4	6	50	33.4	20.2	35.0	14.8	65.0
586	4	6	90	33.8	24.3	42.8	18.5	57.2
586	4	6	130	34.2	30.9	42.4	11.5	57.6
586	4	7	10	34.5	25.1	39.9	14.8	60.1
586	4	7	43	34.8	21.4	33.7	12.3	66.3
586	5	1	0	34.9	24.4	38.1	13.7	61.9
586	5	1	40	35.3	26.7	48.9	22.2	51.1
586	5	1	80	35.7	31.0	45.4	14.4	54.6
586	5	1	120	36.1	22.0	39.9	17.9	60.1
586	5	2	10	36.5	29.0	42.2	13.2	57.8
586	5	2	50	36.9	35.1	47.5	12.4	52.5

Appendix A. (Continued).

Site	Core	Section	Interval (cm)	Sub-bottom depth (m)	>147 μm	>63 μm	63-147 μm	<63 μm
586	5	2	90	37.3	27.9	46.9	19.0	53.1
586	5	2	130	37.7	21.7	35.8	14.1	64.2
586	5	3	20	38.1	30.2	41.4	11.2	58.6
586	5	3	60	38.5	59.8	72.9	13.1	27.1
586	5	3	100	38.9	16.6	26.8	10.2	73.2
586	5	3	140	39.3	20.4	32.0	11.6	68.0
586	5	4	30	39.7	16.8	30.2	13.4	69.8
586	5	4	70	40.1	21.3	32.0	10.7	68.0
586	5	4	110	40.5	22.7	32.7	10.0	67.3
586	5	4	149	40.9	28.1	41.2	13.1	58.8
586	5	5	40	41.3	33.7	48.8	15.1	51.2
586	5	5	80	41.7	36.1	56.2	20.1	43.8
586	5	5	120	42.1	23.5	35.8	12.3	64.2
586	5	6	10	42.5	29.2	42.2	13.0	57.8
586	5	6	50	42.9	20.8	31.8	11.0	68.2
586	5	6	90	43.3	31.6	45.0	13.4	55.0
586	5	6	130	43.7	27.0	39.5	12.5	60.5
586	1	1	40	44.8	16.9	30.3	13.4	69.7
586	1	1	78	45.2	30.6	40.4	9.8	59.6
586	1	1	80	45.2	28.1	37.6	9.5	62.4
586	1	1	120	45.6	14.3	24.5	10.2	75.5
586	1	2	10	46.0	17.2	28.7	11.5	71.3
586	1	2	50	46.4	22.6	30.5	7.9	69.5
586	1	2	90	46.8	16.3	29.1	12.8	70.9
586	1	2	130	47.2	21.7	34.8	13.1	65.2
586	1	3	20	47.6	26.2	38.4	12.2	61.6
586	1	3	60	48.0	19.8	33.2	13.4	66.8
586	1	3	100	48.4	19.3	32.6	13.3	67.4
586	1	3	140	48.8	31.8	49.8	18.0	50.2
586	1	4	30	49.2	23.9	35.3	11.4	64.7
586	1	4	70	49.6	17.6	32.1	14.5	67.9
586	1	4	110	50.0	21.7	34.3	12.6	65.7
586	1	4	149	50.4	26.0	36.9	10.9	63.1
586	1	5	40	50.8	23.7	38.0	14.3	62.0
586	1	5	80	51.2	11.9	23.9	12.0	76.1
586	1	5	120	51.6	21.0	35.0	14.0	65.0
586	1	6	10	52.0	16.1	32.2	16.1	67.8
586	1	6	50	52.4	24.7	36.9	12.2	63.1
586	1	6	90	52.8	17.9	30.2	12.3	69.8
586	1	6	130	53.2	22.4	37.3	14.9	62.7
586	1	7	20	53.6	21.4	35.5	14.1	64.5
586	2	1	80	54.8	17.5	29.0	11.5	71.0
586	2	1	120	55.2	10.9	25.8	14.9	74.2
586	2	2	10	55.6	25.6	37.5	11.9	62.5
586	2	2	50	56.0	22.9	42.2	19.3	57.8
586	2	2	90	56.4	15.5	27.9	12.4	72.1
586	2	2	130	56.8	21.9	33.2	11.3	66.8
586	2	3	20	57.2	21.7	34.0	12.3	66.0
586	2	3	60	57.6	11.7	23.5	11.8	76.5
586	2	3	100	58.0	13.7	27.5	13.8	72.5
586	2	3	140	58.4	19.6	32.2	12.6	67.8
586	2	4	30	58.8	16.7	28.8	12.1	71.2
586	2	4	70	59.2	16.1	29.5	13.4	70.5
586	2	4	110	59.6	22.5	34.7	12.2	65.3
586	2	4	149	60.0	24.7	38.7	14.0	61.3
586	2	5	40	60.4	10.9	20.6	9.7	79.4
586	2	5	80	60.8	8.3	15.7	7.4	84.3
586	2	5	120	61.2	23.1	35.1	12.0	64.9
586	2	6	10	61.6	21.9	33.4	11.5	66.6
586	2	6	50	62.0	19.9	30.3	10.4	69.7
586	2	6	90	62.4	17.9	31.8	13.9	68.2
586	2	6	130	62.8	16.1	27.7	11.6	72.3
586	2	7	20	63.2	30.3	42.5	12.2	57.5
586	3	1	40	64.0	14.0	23.7	9.7	76.3
586	3	1	80	64.4	12.6	22.5	9.9	77.5
586	3	1	120	64.8	14.2	24.1	9.9	75.9
586	3	2	10	65.2	22.4	36.3	13.9	63.7
586	3	2	50	65.6	18.1	34.9	16.8	65.1
586	3	2	90	66.0	19.1	29.1	10.0	70.9
586	3	2	130	66.4	20.2	33.9	13.7	66.1
586	3	3	20	66.8	17.6	28.8	11.2	71.2
586	3	3	60	67.2	19.7	30.0	10.3	70.0
586	3	3	100	67.6	17.1	27.2	10.1	72.8
586	3	3	140	68.0	21.6	33.1	11.5	66.9
586	3	4	30	68.4	14.1	27.2	13.1	72.8
586	3	4	70	68.8	20.4	37.6	17.2	62.4
586	3	4	110	69.2	14.7	24.2	9.5	75.8
586	3	4	149	69.6	17.0	25.9	8.9	74.1
586	3	5	40	70.0	15.7	24.4	8.7	75.6
586	3	5	80	70.4	11.0	23.3	12.3	76.7
586	3	5	120	70.8	16.5	26.5	10.0	73.5
586	3	6	10	71.2	16.4	25.7	9.3	74.3
586	3	6	50	71.6	21.1	32.6	11.5	67.4
586	3	6	90	72.0	21.2	33.1	11.9	66.9
586	3	6	130	72.4	16.3	27.3	11.0	72.7
586	3	7	20	72.8	21.7	34.1	12.4	65.9
586	4	1	40	73.6	18.4	32.8	14.4	67.2
586	4	1	80	74.0	18.7	30.8	12.1	69.2
586	4	1	120	74.4	14.9	28.1	13.2	71.9
586	4	2	10	74.8	19.1	32.8	13.7	67.2
586	4	2	50	75.2	18.5	31.2	12.7	68.8
586	4	2	90	75.6	17.7	32.6	14.9	67.4
586	4	2	130	76.0	18.2	30.4	12.2	69.6
586	4	3	20	76.4	19.8	34.0	14.2	66.0
586	4	3	60	76.8	25.5	42.7	17.2	57.3
586	4	3	100	77.2	23.2	36.7	13.5	63.3
586	4	3	140	77.6	21.0	34.1	13.1	65.9
586	4	4	30	78.0	12.9	22.2	9.3	77.8
586	4	4	70	78.4	27.6	44.3	16.7	55.7
586	4	4	110	78.8	17.0	28.1	11.1	71.9
586	4	4	149	79.2	16.4	30.4	14.0	69.6
586	4	5	40	79.6	23.5	35.5	12.0	64.5
586	4	5	80	80.0	14.3	23.4	9.1	76.6
586	4	5	120	80.4	23.4	36.2	12.8	63.8
586	4	6	10	80.8	16.8	28.3	11.5	71.7
586	4	6	50	81.2	15.9	26.7	10.8	73.3

Appendix A. (Continued).

Site	Core	Section	Interval (cm)	Sub-bottom depth (m)	>147 µm	>63 µm	63-147 µm	<63 µm
586	4	6	90	81.6	18.9	30.2	11.3	69.8
586	4	6	130	82.0	10.9	17.7	6.8	82.3
586	4	7	20	82.4	20.6	31.9	11.3	68.1
586	5	1	40	83.2	25.2	38.7	13.5	61.3
586	5	1	80	83.6	18.1	33.2	15.1	66.8
586	5	1	120	84.0	27.4	45.1	17.7	54.9
586	5	2	10	84.4	15.5	26.5	11.0	73.5
586	5	2	50	84.8	17.2	28.6	11.4	71.4
586	5	2	90	85.2	21.6	34.4	12.8	65.6
586	5	2	130	85.6	17.0	36.8	19.8	63.2
586	5	3	20	86.0	16.6	31.9	15.3	68.1
586	5	3	60	86.4	19.9	32.7	12.8	67.3
586	5	3	100	86.8	25.1	40.2	15.1	59.8
586	5	3	140	87.2	17.6	30.7	13.1	69.3
586	5	4	30	87.6	17.9	28.2	10.3	71.8
586	5	4	70	88.0	24.2	36.8	12.6	63.2
586	5	4	110	88.4	23.5	38.2	14.7	61.8
586	5	4	149	88.8	19.1	33.5	14.4	66.5
586	5	5	40	89.2	20.7	33.8	13.1	66.2
586	5	5	80	89.6	23.0	39.3	16.3	60.7
586	5	5	120	90.0	26.1	40.3	14.2	59.7
586	5	6	10	90.4	19.5	36.2	16.7	63.8
586	5	6	50	90.8	20.6	35.4	14.8	64.6
586	5	6	90	91.2	21.4	34.4	13.0	65.6
586	5	6	130	91.6	20.7	38.4	17.7	61.6
586	5	7	20	92.0	20.5	34.2	13.7	65.8
586	6	1	40	92.8	26.3	43.1	16.8	56.9
586	6	1	80	93.2	19.2	36.8	17.6	63.2
586	6	1	120	93.6	23.8	37.5	13.7	62.5
586	6	2	10	94.0	23.9	42.6	18.7	57.4
586	6	2	50	94.4	24.9	41.3	16.4	58.7
586	6	2	90	94.8	22.3	37.2	14.9	62.8
586	6	2	130	95.2	29.3	43.4	14.1	56.6
586	6	3	20	95.6	17.2	32.1	14.9	67.9
586	6	3	60	96.0	14.9	28.6	13.7	71.4
586	6	3	100	96.4	21.7	35.7	14.0	64.3
586	6	4	30	97.2	15.8	33.4	17.6	66.6
586	6	4	70	97.6	25.3	39.4	14.1	60.6
586	6	4	110	98.0	16.7	35.1	18.4	64.9
586	6	4	149	98.4	21.9	40.6	18.7	59.4
586	6	5	40	98.8	23.0	38.4	15.4	61.6
586	6	5	80	99.2	13.5	33.7	20.2	66.3
586	6	5	120	99.6	19.3	36.8	17.5	63.2
586	6	6	10	100.0	21.7	37.0	15.3	63.0
586	6	6	50	100.4	12.9	25.3	12.4	74.7
586	6	6	90	100.8	17.9	34.0	16.1	66.0
586	6	6	130	101.2	17.0	29.5	12.5	70.5
586	6	7	20	101.6	21.8	39.3	17.5	60.7
586	7	1	40	102.4	25.6	44.9	19.3	55.1
586	7	1	80	102.8	19.5	34.5	15.0	65.5
586	7	1	120	103.2	18.9	34.3	15.4	65.7
586	7	2	10	103.6	20.7	34.7	14.0	65.3
586	7	2	48	104.0	20.3	34.4	14.1	65.6
586	7	2	90	104.4	21.3	34.3	13.0	65.7
586	7	2	130	104.8	20.2	36.5	16.3	63.5
586	7	3	20	105.2	17.1	29.8	12.7	70.2
586	7	3	60	105.6	24.5	37.7	13.2	62.3
586	7	3	100	106.0	16.7	29.0	12.3	71.0
586	7	3	140	106.4	21.9	36.4	14.5	63.6
586	7	4	30	106.8	22.8	37.8	15.0	62.2
586	7	4	70	107.2	12.9	24.6	11.7	75.4
586	7	4	110	107.6	20.5	32.9	12.4	67.1
586	7	4	149	108.0	13.4	26.3	12.9	73.7
586	7	5	40	108.4	17.7	31.9	14.2	68.1
586	7	5	80	108.8	16.3	28.5	12.2	71.5
586	7	5	120	109.2	20.9	34.3	13.4	65.7
586	7	6	10	109.6	13.9	27.3	13.4	72.7
586	7	6	50	110.0	12.1	22.8	10.7	77.2
586	7	6	90	110.4	17.8	31.2	13.4	68.8
586	7	6	130	110.8	10.4	23.1	12.7	76.9
586	7	7	20	111.2	17.5	32.3	14.8	67.7
586	8	1	40	112.0	15.1	28.5	13.4	71.5
586	8	1	80	112.4	18.9	32.0	13.1	68.0
586	8	1	120	112.8	20.7	35.2	14.5	64.8
586	8	2	10	113.2	12.9	30.4	17.5	69.6
586	8	2	50	113.6	15.9	31.6	15.7	68.4
586	8	2	90	114.0	15.4	28.2	12.8	71.8
586	8	2	130	114.4	16.4	28.6	12.2	71.4
586	8	3	20	114.8	13.9	31.3	17.4	68.7
586	8	3	60	115.2	13.5	26.1	12.6	73.9
586	8	3	100	115.6	17.4	32.2	14.8	67.8
586	8	3	140	116.0	17.5	29.5	12.0	70.5
586	8	4	30	116.4	13.1	24.9	11.8	75.1
586	8	4	70	116.8	15.2	27.8	12.6	72.2
586	8	4	110	117.2	16.5	31.2	14.7	68.8
586	8	4	149	117.6	14.7	30.5	15.8	69.5
586	8	5	40	118.0	18.6	30.0	11.4	70.0
586	8	5	80	118.4	20.2	30.1	9.9	69.9
586	8	5	120	118.8	18.4	31.9	13.5	68.1
586	8	6	50	119.6	19.6	31.5	11.9	68.5
586	8	6	90	120.0	16.5	27.4	10.9	72.6
586	8	6	130	120.4	15.0	27.8	12.8	72.2
586	8	7	20	120.8	16.1	27.7	11.6	72.3
586	9	1	40	121.6	13.4	24.7	11.3	75.3
586	9	1	80	122.0	10.5	21.8	11.3	78.2
586	9	1	120	122.4	15.6	27.2	11.6	72.8
586	9	2	10	122.8	17.6	30.3	12.7	69.7
586	9	2	50	123.2	15.9	28.6	12.7	71.4
586	9	2	90	123.6	13.8	25.6	11.8	74.4
586	9	2	130	124.0	16.8	29.0	12.2	71.0
586	9	3	20	124.4	17.4	31.0	13.6	69.0
586	9	3	60	124.8	19.9	33.6	13.7	66.4
586	9	3	100	125.2	10.9	22.5	11.6	77.5
586	9	3	140	125.6	13.1	26.1	13.0	73.9
586	9	4	30	126.0	13.0	27.1	14.1	72.9
586	9	4	70	126.4	13.3	25.1	11.8	74.9
586	9	4	110	126.8	12.1	23.4	11.3	76.6
586	9	4	149	127.2	16.1	29.6	13.5	70.4
586	9	5	40	127.6	16.7	29.5	12.8	[illegible]
586	9	5	80	128.0	11.2	22.4	11.2	[illegible]
586	9	5	120	128.4	10.6	22.7	12.1	[illegible]
586	9	6	10	128.8	12.9	27.1	14.2	[illegible]
586	9	6	50	129.2	18.8	32.5	13.7	[illegible]
586	9	6	90	129.6	14.3	26.7	12.4	[illegible]
586	9	6	130	130.0	11.1	22.6	11.5	[illegible]
586	9	7	20	130.4	10.7	22.8	12.1	[illegible]
586	10	1	40	131.2	16.3	26.6	10.3	[illegible]
586	10	1	80	131.6	18.9	31.1	12.2	[illegible]
586	10	1	120	132.0	12.4	24.0	11.6	[illegible]
586	10	2	10	132.4	14.8	26.6	11.8	[illegible]
586	10	2	50	132.8	14.5	25.6	11.1	[illegible]
586	10	2	90	133.2	19.8	33.7	13.9	[illegible]
586	10	2	130	133.6	19.4	33.2	13.8	[illegible]
586	10	3	20	134.0	10.6	20.7	10.1	[illegible]
586	10	3	60	134.4	16.0	30.6	14.6	[illegible]
586	10	3	100	134.8	15.3	27.8	12.5	[illegible]
586	10	3	140	135.2	20.5	34.1	13.6	[illegible]
586	10	4	30	135.6	19.2	35.5	16.3	[illegible]
586	10	4	70	136.0	14.6	25.8	11.2	[illegible]
586	10	4	110	136.4	19.6	34.1	14.5	[illegible]
586	10	4	149	136.8	21.5	35.8	14.3	[illegible]
586	10	5	40	137.2	15.0	25.4	10.4	[illegible]
586	10	5	80	137.6	18.3	31.7	13.4	[illegible]
586	10	5	120	138.0	16.3	31.3	15.0	[illegible]
586	10	6	10	138.4	16.1	29.8	13.7	[illegible]
586	10	6	50	138.8	21.5	35.0	13.5	[illegible]
586	10	6	130	139.6	18.5	31.0	12.5	[illegible]
586	10	7	20	140.0	23.4	37.9	14.5	[illegible]
586	11	1	40	140.8	19.4	33.9	14.5	[illegible]
586	11	1	80	141.2	15.9	30.3	14.4	[illegible]
586	11	1	120	141.6	18.4	32.3	13.9	[illegible]
586	11	2	10	142.0	19.6	32.5	12.9	[illegible]
586	11	2	50	142.4	19.9	35.3	15.4	64.7
586	11	2	90	142.8	22.5	40.8	18.3	59.2
586	11	2	130	143.2	23.3	39.6	16.3	60.4
586	11	3	20	143.6	17.4	33.4	16.0	66.6
586	11	3	60	144.0	20.2	36.1	15.9	63.9
586	11	3	100	144.4	18.9	35.9	17.0	64.1
586	11	3	140	144.8	16.8	31.0	14.2	69.0
586	11	4	30	145.2	13.4	26.7	13.3	73.3
586	11	4	70	145.6	15.6	28.9	13.3	71.1
586	11	4	110	146.0	17.9	31.5	13.6	68.5
586	11	4	149	146.4	10.6	20.9	10.3	79.1
586	11	5	40	146.8	12.2	25.4	13.2	74.6
586	11	5	80	147.2	29.4	61.9	32.5	38.1
586	11	5	120	147.6	12.0	24.4	12.4	75.6
586	11	6	10	148.0	11.9	25.6	13.7	74.4
586	11	6	130	148.2	10.8	22.6	11.8	77.4
586	11	6	50	148.4	14.2	24.5	10.3	75.5
586	11	7	20	148.6	9.6	22.4	12.8	77.6
586	11	6	90	148.8	14.4	27.3	12.9	72.7
586	12	1	40	150.4	14.0	28.2	14.2	71.8
586	12	1	80	150.8	11.3	24.9	13.6	75.1
586	12	1	120	151.2	19.2	32.6	13.4	67.4
586	12	2	10	151.6	16.6	30.2	13.6	69.8
586	12	2	50	152.0	12.7	25.8	13.1	74.2
586	12	2	90	152.4	16.7	32.0	15.3	68.0
586	12	2	130	152.8	15.3	27.6	12.3	72.4
586	12	3	20	153.2	14.4	28.2	13.8	71.8
586	12	3	60	153.6	9.2	20.0	10.8	80.0
586	12	3	100	154.0	13.2	25.1	11.9	74.9
586	12	3	140	154.4	14.4	27.7	13.3	72.3
586	12	4	30	154.8	12.4	25.0	12.6	75.0
586	12	4	70	155.2	10.5	24.6	14.1	75.4
586	12	4	110	155.6	11.7	27.1	15.4	72.9
586	12	4	149	156.0	11.2	25.4	14.2	74.6
586	12	5	40	156.4	10.0	22.5	12.5	77.5
586	12	5	80	156.8	11.2	28.2	17.0	71.8
586	12	6	10	157.6	14.0	30.9	16.9	69.1
586	12	6	50	158.0	9.7	26.5	16.8	73.5
586	12	6	90	158.4	10.8	25.4	14.6	74.6
586	12	6	130	158.8	15.9	33.4	17.5	66.6
586	12	7	20	159.2	17.0	35.2	18.2	64.8
586	13	1	40	160.0	17.0	31.8	14.8	68.2
586	13	1	80	160.4	10.3	19.2	8.9	80.8
586	13	1	120	160.8	16.6	30.0	13.4	70.0
586	13	2	10	161.2	10.1	20.4	10.3	79.6
586	13	2	50	161.6	13.6	26.8	13.2	73.2
586	13	2	90	162.0	10.8	22.3	11.5	77.7
586	13	2	130	162.4	10.5	21.2	10.7	78.8
586	13	3	20	162.8	11.3	22.9	11.6	77.1
586	13	3	60	163.2	14.8	26.2	11.4	73.8
586	13	3	100	163.6	15.6	27.7	12.1	72.3
586	13	3	140	164.0	16.2	27.6	11.4	72.4
586	13	4	30	164.4	17.4	28.4	11.0	71.6
586	13	4	70	164.8	18.5	31.3	12.8	68.7
586	13	4	110	165.2	17.7	35.0	17.3	65.0
586	13	4	149	165.6	10.1	20.5	10.4	79.5
586	13	5	40	166.0	10.0	19.3	9.3	80.7
586	13	5	80	166.4	12.8	22.9	10.1	77.1
586	14	1	40	167.3	13.6	23.4	9.8	76.6
586	14	1	80	167.7	14.7	23.8	9.1	76.2
586	14	1	120	168.1	12.3	24.7	12.4	75.3
586	14	2	10	168.5	12.7	21.6	8.9	78.4
586	14	2	50	168.9	14.2	26.0	11.8	74.0
586	14	2	90	169.3	10.4	19.2	8.8	80.8
586	14	2	130	169.7	12.7	22.7	10.0	77.3
586	14	3	20	170.1	10.1	22.5	12.4	77.5
586	14	3	60	170.5	12.9	25.6	12.7	74.4
586	14	3	100	170.9	14.3	25.1	10.8	74.9
586	14	3	140	171.3	11.9	22.8	10.9	77.2
586	15	1	40	172.2	15.1	29.4	14.3	70.6

Appendix A. (Continued).

Site	Core	Section	Interval (cm)	Sub-bottom depth (m)	> 147 μm	> 63 μm	63-147 μm	< 63 μm
586	15	1	80	172.6	12.5	26.3	13.8	73.7
586	15	1	120	173.0	13.6	24.8	11.2	75.2
586	15	2	10	173.4	13.8	24.7	10.9	75.3
586	15	2	50	173.8	14.6	24.6	10.0	75.4
586	15	2	90	174.2	23.3	38.2	14.9	61.8
586	15	2	130	174.6	20.0	33.2	13.2	66.8
586	15	3	20	175.0	16.5	28.7	12.2	71.3
586	15	3	60	175.4	17.2	29.4	12.2	70.6
586	15	3	100	175.8	17.5	29.1	11.6	70.9
586	15	3	140	176.2	14.5	27.5	13.0	72.5
586	15	4	30	176.6	14.9	27.6	12.7	72.4
586	15	4	70	177.0	15.7	28.9	13.2	71.1
586	15	4	110	177.4	17.4	28.6	11.2	71.4
586	15	4	149	177.8	11.0	21.8	10.8	78.2
586	15	5	40	178.2	12.5	22.1	9.6	77.9
586	15	5	80	178.6	15.9	29.6	13.7	70.4
586	15	5	120	179.0	15.2	27.1	11.9	72.9
586	15	6	10	179.4	17.1	29.5	12.4	70.5
586	15	6	50	179.8	19.6	33.7	14.1	66.3
586	15	6	90	180.2	15.6	28.3	12.7	71.7
586	15	6	130	180.6	12.7	22.5	9.8	77.5
586	16	1	40	181.2	15.0	27.0	12.0	73.0
586	16	1	80	181.6	17.0	28.3	11.3	71.7
586	16	1	120	182.0	15.6	27.7	12.1	72.3
586	16	2	10	182.4	53.0	86.0	33.0	14.0
586	16	2	50	182.8	20.7	31.4	10.7	68.6
586	16	2	90	183.2	22.9	35.1	12.2	64.9
586	16	2	130	183.6	19.1	33.4	14.3	66.6
586	16	3	20	184.0	19.5	33.1	13.6	66.9
586	16	3	60	184.4	20.3	31.6	11.3	68.4
586	16	3	100	184.8	18.9	30.7	11.8	69.3
586	16	3	140	185.2	22.2	34.3	12.1	65.7
586	16	4	30	185.6	20.1	32.9	12.8	67.1
586	16	4	70	186.0	17.7	30.6	12.9	69.4
586	16	4	110	186.4	17.6	28.7	11.1	71.3
586	16	4	149	186.8	13.1	25.7	12.6	74.3
586	16	5	40	187.2	16.8	29.1	12.3	70.9
586	16	5	80	187.6	13.1	24.8	11.7	75.2
586	16	5	120	188.0	10.7	20.3	9.6	79.7
586	16	6	10	188.4	15.4	27.5	12.1	72.5
586	16	6	50	188.8	15.8	25.9	10.1	74.1
586	16	6	90	189.2	14.6	23.7	9.1	76.3
586	16	6	130	189.6	18.0	29.7	11.7	70.3
586	16	7	20	190.0	18.5	30.5	12.0	69.5
586	17	1	40	190.8	17.7	32.1	14.4	67.9
586	17	1	80	191.2	12.9	25.1	12.2	74.9
586	17	1	120	191.6	17.1	27.9	10.8	72.1
586	17	2	10	192.0	12.4	21.8	9.4	78.2
586	17	2	50	192.4	14.8	25.5	10.7	74.5
586	17	2	90	192.8	16.0	26.4	10.4	73.6
586	17	2	130	193.2	16.0	24.6	8.6	75.4
586	17	3	20	193.6	19.0	30.8	11.8	69.2
586	17	3	60	194.0	18.8	30.8	12.0	69.2
586	17	3	100	194.4	20.8	34.2	13.4	65.8
586	17	3	140	194.8	16.5	29.6	13.1	70.4
586	17	4	110	195.0	22.7	34.6	11.9	65.4
586	17	4	30	195.2	18.4	30.6	12.2	69.4
586	17	4	70	195.6	20.7	35.7	15.0	64.3
586	17	4	149	196.4	18.9	30.6	11.7	69.4
586	17	5	80	197.2	16.1	26.5	10.4	73.5
586	17	5	120	197.6	17.1	29.2	12.1	70.8
586	17	6	10	198.0	14.0	25.1	11.1	74.9
586	17	5	60	198.4	12.4	21.0	8.6	79.0
586	17	6	90	198.8	15.4	25.1	9.7	74.9
586	17	6	130	199.2	18.1	30.0	11.9	70.0
586	17	7	20	199.6	15.4	27.9	12.5	72.1
586	18	1	40	200.4	13.0	22.0	9.0	78.0
586	18	1	80	200.8	12.9	23.1	10.2	76.9
586	18	1	120	201.2	15.4	26.5	11.1	73.5
586	18	2	10	201.6	18.2	30.5	12.3	69.5
586	18	2	50	202.0	17.6	30.0	12.4	70.0
586	18	2	90	202.4	20.4	33.8	13.4	66.2
586	18	2	130	202.8	17.6	28.9	11.3	71.1
586	18	3	20	203.2	18.5	28.0	9.5	72.0
586	18	3	60	203.6	18.8	30.1	11.3	69.9
586	18	3	100	204.0	18.2	30.4	12.2	69.6
586	18	3	140	204.4	16.5	27.1	10.6	72.9
586	18	4	30	204.8	16.9	26.4	9.5	73.6
586	18	4	70	205.2	15.1	25.3	10.2	74.7
586	18	4	110	205.6	16.5	27.3	10.8	72.7
586	18	4	149	206.0	16.5	28.0	11.5	72.0
586	18	5	40	206.4	16.3	27.6	11.3	72.4
586	18	5	80	206.8	18.9	29.5	10.6	70.5
586	18	5	120	207.2	17.9	28.7	10.8	71.3
586	18	6	10	207.6	19.2	30.3	11.1	69.7
586	18	6	50	208.0	12.3	23.0	10.7	77.0
586	18	6	90	208.4	14.2	24.8	10.6	75.2
586	18	6	130	208.8	14.2	24.3	10.1	75.7
586	18	7	20	209.2	15.0	26.8	11.8	73.2
586		1	40	210.0	13.1	22.0	8.9	78.0
586		1	80	210.4	11.7	20.6	8.9	79.4
586		1	120	210.8	11.9	22.2	10.3	77.8
586		2	10	211.2	12.0	21.7	9.7	78.3
586		2	50	211.6	11.5	22.0	10.5	78.0
586		2	90	212.0	9.6	18.1	8.5	81.9
586		2	130	212.4	15.7	25.5	9.8	74.5
586		3	20	212.8	12.1	23.9	11.8	76.1
586		3	60	213.2	13.0	24.9	11.9	75.1
586		3	100	213.6	8.2	18.2	10.0	81.8
586		3	140	214.0	13.3	22.2	8.9	77.8
586		4	30	214.4	16.3	26.4	10.1	73.6
586		4	70	214.8	9.8	18.8	9.0	81.2
586		4	110	215.2	12.7	23.7	11.0	76.3
586		4	149	215.6	10.9	19.1	8.2	80.9
586		5	40	216.0	11.7	21.0	9.3	79.0
586		5	80	216.4	12.0	23.1	11.1	76.9

Appendix A. (Continued).

Site	Core	Section	Interval (cm)	Sub-bottom depth (m)	> 147 μm	> 63 μm	63-147 μm	< 63 μm
586	19	5	120	216.8	11.7	20.2	8.5	79.8
586	19	6	10	217.2	11.5	20.2	8.7	79.8
586	19	6	50	217.6	12.7	23.0	10.3	77.0
586	20	1	40	218.5	12.3	23.3	11.0	76.7
586	20	1	80	218.9	11.5	22.3	10.8	77.7
586	20	1	120	219.3	9.8	20.9	11.1	79.1
586	20	2	10	219.7	10.4	20.6	10.2	79.4
586	20	2	50	220.1	10.2	20.5	10.3	79.5
586	20	2	90	220.5	11.2	21.0	9.8	79.0
586	20	2	130	220.9	11.5	21.6	10.1	78.4
586	20	3	20	221.3	10.5	21.5	11.0	78.5
586	20	3	60	221.7	15.3	29.2	13.9	70.8
586	20	3	100	222.1	11.6	20.9	9.3	79.1
586	20	3	140	222.5	12.8	25.7	12.9	74.3
586	20	4	30	222.9	13.3	25.9	12.6	74.1
586	20	4	70	223.3	15.7	31.4	15.7	68.6
586	20	4	110	223.7	17.6	31.1	13.5	68.9
586	20	4	149	224.2	13.6	24.9	11.3	75.1
586	20	5	40	224.6	14.7	25.1	10.4	74.9
586	20	5	80	225.0	13.4	27.2	13.8	72.8
586	20	5	120	225.4	13.2	24.6	11.4	75.4
586	20	6	10	225.8	12.6	24.3	11.7	75.7
586	20	6	50	226.2	10.5	21.0	10.5	79.0
586	20	6	90	226.6	6.2	13.2	7.0	86.8
586	20	6	130	227.0	15.3	30.1	14.8	69.9
586	21	2	10	229.3	13.8	25.7	11.9	74.3
586	21	2	50	229.7	11.2	23.2	12.0	76.8
586	21	2	90	230.1	12.9	23.7	10.8	76.3
586	21	2	130	230.5	11.9	23.3	11.4	76.7
586	21	3	20	230.9	12.6	23.2	10.6	76.8
586	21	3	60	231.3	15.8	30.2	14.4	69.8
586	21	3	100	231.7	18.9	33.6	14.7	66.4
586	21	3	140	232.1	13.7	25.2	11.5	74.8
586	21	4	30	232.5	8.9	21.2	12.3	78.8
586	21	4	70	232.9	13.2	25.6	12.4	74.4
586	21	4	110	233.3	15.1	30.8	15.7	69.2
586	21	4	149	233.7	13.8	26.3	12.5	73.7
586	21	5	40	234.1	15.0	28.6	13.6	71.4
586	21	5	80	234.5	14.1	23.0	8.9	77.0
586	21	5	120	234.9	14.2	26.2	12.0	73.8
586	21	6	10	235.3	14.1	23.8	9.7	76.2
586	21	6	50	235.7	11.7	22.1	10.4	77.9
586	21	6	90	236.1	15.8	26.7	10.9	73.3
586	21	6	130	236.5	15.2	27.3	12.1	72.7
586	21	7	20	236.9	12.2	23.8	11.6	76.2
586	21	7	20	236.9	12.2	23.8	11.6	76.2
586	21	7	60	237.3	13.5	25.0	11.5	75.0
586	21	7	100	237.7	11.8	22.5	10.7	77.5
586	22	1	40	237.7	8.3	14.9	6.6	85.1
586	21	7	140	238.1	15.6	25.1	9.5	74.9
586	22	1	80	238.1	15.6	26.6	11.0	73.4
586	21	8	30	238.5	17.9	29.4	11.5	70.6
586	22	1	120	238.5	13.3	25.6	12.3	74.4
586	22	2	10	238.9	12.6	25.1	12.5	74.9
586	22	2	50	239.3	12.8	25.0	12.2	75.0
586	22	2	90	239.7	10.0	21.2	11.2	78.8
586	22	2	130	240.1	11.6	23.1	11.5	76.9
586	22	3	20	240.5	11.3	23.3	12.0	76.7
586	22	3	60	240.9	15.0	27.5	12.5	72.5
586	22	3	100	241.3	12.9	24.9	12.0	75.1
586	22	3	140	241.7	12.0	22.3	10.3	77.7
586	22	4	30	242.1	11.1	24.4	13.3	75.6
586	22	4	70	242.5	14.5	28.8	14.3	71.2
586	22	4	110	242.9	17.4	32.5	15.1	67.5
586	22	4	149	243.4	17.9	30.7	12.8	69.3
586	22	5	40	243.8	9.8	21.8	12.0	78.2
586	22	5	80	244.2	15.8	29.7	13.9	70.3
586	22	5	120	244.6	12.2	24.4	12.2	75.6
586	22	6	10	245.0	12.8	27.3	14.5	72.7
586	22	6	50	245.4	12.1	28.6	16.5	71.4
586	22	6	90	245.8	13.9	30.2	16.3	69.8
586	22	6	130	246.2	14.9	29.9	15.0	70.1
586	22	7	20	246.6	13.2	26.3	13.1	73.7
586	23	1	40	247.3	15.2	29.5	14.3	70.5
586	23	1	80	247.7	8.8	21.0	12.2	79.0
586	23	1	120	248.1	9.5	23.4	13.9	76.6
586	23	2	10	248.5	12.5	25.9	13.4	74.1
586	23	2	50	248.9	11.6	26.2	14.6	73.8
586	23	2	90	249.3	12.3	28.3	16.0	71.7
586	23	2	130	249.7	12.1	25.6	13.5	74.4
586	23	3	20	250.1	11.7	24.7	13.0	75.3
586	23	3	60	250.5	15.3	27.8	12.5	72.2
586	23	3	100	250.9	16.8	32.6	15.8	67.4
586	23	3	140	251.3	9.5	20.7	11.2	79.3
586	23	4	30	251.7	13.8	23.2	9.4	76.8
586	23	4	70	252.1	18.8	33.7	14.9	66.3
586	23	4	110	252.5	15.6	27.5	11.9	72.5
586	23	4	149	252.9	18.8	31.8	13.0	68.2
586	23	5	40	253.3	13.2	24.7	11.5	75.3
586	23	5	80	253.7	13.8	27.8	14.0	72.2
586	23	5	120	254.1	11.7	24.4	12.7	75.6
586	23	6	10	254.5	13.5	27.3	13.8	72.7
586	23	6	50	254.9	13.5	25.5	12.0	74.5
586	23	6	90	255.3	14.4	25.3	10.9	74.7
586	23	6	130	255.7	14.5	25.2	10.7	74.8
586	23	7	20	256.1	13.1	23.6	10.5	76.4
586	24	1	40	256.9	13.6	24.7	11.1	75.3
586	24	1	80	257.3	12.6	23.5	10.9	76.5
586	24	1	120	257.7	14.4	28.0	13.6	72.0
586	24	2	10	258.1	17.9	32.4	14.5	67.6
586	24	2	50	258.5	13.9	24.4	10.5	75.6
586	24	2	90	258.9	14.4	28.7	14.3	71.3
586	24	2	130	259.3	13.3	25.7	12.4	74.3
586	24	3	20	259.7	9.7	21.3	11.6	78.7
586	24	3	60	260.1	13.2	25.7	12.5	74.3
586	24	3	100	260.5	8.7	18.6	9.9	81.4

Appendix A. (Continued).

Site	Core	Section	Interval (cm)	Sub-bottom depth (m)	> 147 µm	> 63 µm	63-147 µm	< 63 µm
586	24	3	140	260.9	13.9	30.9	17.0	69.1
586	24	4	30	261.3	5.5	11.8	6.3	88.2
586	24	4	70	261.7	9.4	21.0	11.6	79.0
586	24	4	110	262.1	6.8	14.7	7.9	85.3
586	24	4	149	262.5	9.8	21.2	11.4	78.8
586	24	5	40	262.9	9.6	19.7	10.1	80.3
586	24	5	80	263.3	10.2	22.5	12.3	77.5
586	24	5	120	263.7	20.9	34.6	13.7	65.4
586	24	6	10	264.1	8.7	19.9	11.2	80.1
586	24	6	50	264.5	8.4	18.8	10.4	81.2
586	24	6	90	264.9	8.3	17.9	9.6	82.1
586	24	6	130	265.3	10.1	23.6	13.5	76.4
586	24	7	20	265.7	7.8	19.4	11.6	80.6
586	25	1	40	266.5	11.1	22.5	11.4	77.5
586	25	1	80	266.9	15.4	29.0	13.6	71.0
586	25	1	120	267.3	8.8	17.2	8.4	82.8
586	25	2	10	267.7	13.6	25.5	11.9	74.5
586	25	2	50	268.1	14.0	25.8	11.8	74.2
586	25	2	90	268.5	10.5	21.9	11.4	78.1
586	25	2	130	268.9	11.4	25.0	13.6	75.0
586	25	3	20	269.3	12.9	25.0	12.1	75.0
586	25	3	60	269.7	9.4	19.8	10.4	80.2
586	25	3	100	270.1	13.2	28.8	15.6	71.2
586	25	3	140	270.5	11.8	24.7	12.9	75.3
586	25	4	30	270.9	9.1	20.5	11.4	79.5
586	25	4	70	271.3	10.7	25.7	15.0	74.3
586	25	4	110	271.7	9.8	21.2	11.4	78.8
586	25	4	149	272.1	12.1	25.8	13.7	74.2
586	25	5	40	272.5	10.5	26.0	15.5	74.0
586	25	5	80	272.9	10.6	19.6	9.0	80.4
586	25	5	120	273.3	10.5	24.2	13.7	75.8
586	25	6	10	273.7	12.4	27.2	14.8	72.8
586	25	6	50	274.1	8.2	20.9	12.7	79.1
586	25	6	90	274.5	9.6	23.6	14.0	76.4
586	25	6	130	274.9	8.0	19.8	11.8	80.2
586	25	7	20	275.3	10.8	23.1	12.3	76.9
586	26	1	40	276.1	12.3	24.0	11.7	76.0
586	26	1	80	276.5	11.5	21.2	9.7	78.8
586	26	1	120	276.9	12.1	23.6	11.5	76.4
586	26	2	10	277.3	10.7	24.4	13.7	75.6
586	26	2	50	278.7	16.4	30.7	14.3	69.3
586	26	2	90	279.1	13.9	26.7	12.8	73.3
586	26	2	130	279.5	21.3	37.4	16.1	62.6
586	26	3	20	279.9	16.2	29.1	12.9	70.9
586	26	3	60	280.3	18.4	30.4	12.0	69.6
586	26	3	87	280.6	16.0	29.8	13.8	70.2
586	27	1	40	281.6	13.1	25.6	12.5	74.4
586	27	1	80	282.0	9.6	22.5	12.9	77.5
586	27	1	120	282.4	15.1	27.6	12.5	72.4
586	27	2	10	282.8	10.3	24.6	14.3	75.4
586	27	2	50	283.2	14.2	27.5	13.3	72.5
586	27	2	90	283.6	14.5	27.8	13.3	72.2
586	27	2	130	284.0	14.1	27.3	13.2	72.7
586	27	3	20	284.4	17.1	28.4	11.3	71.6
586	27	3	60	284.8	11.0	22.1	11.1	77.9
586	28	2	10	286.0	15.1	27.6	12.5	72.4
586	28	2	50	286.4	16.8	30.7	13.9	69.3
586	28	2	90	286.8	35.2	49.7	14.5	50.3
586	28	3	20	287.6	17.6	30.8	13.2	69.2
586	28	3	60	288.0	16.5	31.3	14.8	68.7
586	28	3	100	288.4	10.8	27.3	16.5	72.7
586	28	3	140	288.8	8.9	22.8	13.9	77.2
586	28	4	30	289.2	13.5	29.2	15.7	70.8
586	28	4	70	289.6	11.2	24.4	13.2	75.6
586	28	5	105	290.0	9.7	20.5	10.8	79.5
586	29	1	40	290.7	11.1	24.2	13.1	75.8
586	29	1	80	291.1	10.8	25.2	14.4	74.8
586	29	1	120	291.5	15.7	27.8	12.1	72.2
586	29	2	10	291.9	11.3	22.7	11.4	77.3
586	29	2	50	292.3	9.7	23.5	13.8	76.5
586	29	2	90	292.7	8.0	22.3	14.3	77.7
586	29	2	130	293.1	18.8	33.1	14.3	66.9
586	29	3	20	293.5	15.1	27.7	12.6	72.3
586	29	3	60	293.9	11.7	22.0	10.3	78.0
586	29	3	100	294.3	14.8	27.4	12.6	72.6
586	29	3	140	294.7	12.5	25.0	12.5	75.0
586	29	4	30	295.1	13.9	26.4	12.5	73.6
586	30	1	40	295.7	14.1	26.4	12.3	73.6
586	30	1	80	296.1	17.2	32.7	15.5	67.3
586	30	1	120	296.5	11.7	27.8	16.1	72.2
586	30	2	10	296.9	14.1	28.3	14.2	71.7
586	30	2	50	297.3	14.6	25.7	11.1	74.3
586	30	2	90	297.7	15.2	27.5	12.3	72.5
586	30	2	130	298.1	18.3	32.0	13.7	68.0
586	30	3	20	298.5	10.6	19.9	9.3	80.1
586	30	3	60	298.9	12.2	22.0	9.8	78.0
586	30	3	100	299.3	13.1	26.1	13.0	73.9
586	30	4	30	300.1	9.7	18.8	9.1	81.2
586	31	1	40	300.7	9.4	21.3	11.9	78.7
586	31	1	80	301.1	10.8	20.5	9.7	79.5
586	31	1	120	301.5	12.2	23.6	11.4	76.4
586	31	2	10	301.9	11.0	21.4	10.4	78.6
586	31	2	50	302.3	15.2	26.2	11.0	73.8
586	31	2	90	302.7	14.2	26.0	11.8	74.0
586	31	2	130	303.1	11.5	21.7	10.2	78.3
586	31	3	20	303.5	10.5	27.6	17.1	72.4
586	31	3	60	303.9	10.6	23.4	12.8	76.6
586	31	3	100	304.3	10.5	19.3	8.8	80.7
586	31	3	140	304.7	9.4	17.0	7.6	83.0
586	31	4	30	305.1	10.5	19.1	8.6	80.9
SITE 591								
591	1	1	66	.7	16.6	26.5	9.9	73.5
591	1	1	105	1.0	11.1	22.5	11.4	77.5
591	1	2	66	2.2	14.7	26.3	11.6	73.7
591	1	2	105	2.5	14.5	25.6	11.1	74.4

Appendix A. (Continued).

Site	Core	Section	Interval (cm)	Sub-bottom depth (m)	> 147 µm	> 63 µm	63-147 µm	< 63 µm
591	2	1	40	3.8	9.3	16.5	7.2	83.5
591	2	1	105	4.4	8.3	14.4	6.1	85.6
591	2	2	40	5.3	5.7	13.3	7.6	86.7
591	2	2	105	5.9	5.5	10.0	4.5	90.0
591	2	3	40	6.8	5.9	11.4	5.5	88.6
591	2	4	40	8.3	4.6	8.7	4.1	[illegible]
591	2	4	105	8.9	4.4	8.7	4.3	[illegible]
591	2	5	40	9.8	4.9	9.1	4.2	[illegible]
591	2	5	105	10.4	2.7	7.2	4.5	[illegible]
591	2	6	40	11.3	5.8	10.7	4.9	[illegible]
591	2	6	105	11.9	8.5	15.4	6.9	[illegible]
591	3	1	40	13.4	14.6	24.7	10.1	[illegible]
591	3	1	105	14.1	7.2	14.8	7.6	[illegible]
591	3	2	40	14.9	11.5	18.5	7.0	[illegible]
591	3	2	105	15.6	12.1	20.0	7.9	[illegible]
591	3	3	40	16.4	10.6	18.8	8.2	[illegible]
591	3	3	105	17.0	8.7	18.2	9.5	[illegible]
591	3	4	40	17.9	6.7	11.1	4.4	[illegible]
591	3	4	105	18.5	7.2	14.0	6.8	[illegible]
591	3	5	40	19.4	10.7	18.1	7.4	[illegible]
591	3	5	105	20.0	9.7	14.8	5.1	[illegible]
591	3	6	40	20.9	9.2	14.9	5.7	[illegible]
591	3	6	105	21.5	7.8	13.4	5.6	[illegible]
591	4	1	105	23.6	7.6	12.9	5.3	[illegible]
591	4	2	40	24.5	7.5	12.5	5.0	[illegible]
591	4	2	105	25.1	5.3	10.8	5.5	[illegible]
591	4	3	40	26.0	9.4	15.4	6.0	[illegible]
591	4	3	105	26.6	7.8	12.9	5.1	[illegible]
591	4	4	40	27.5	11.4	18.5	7.1	[illegible]
591	4	4	105	28.1	8.7	14.7	6.0	[illegible]
591	4	5	40	29.0	14.8	21.7	6.9	[illegible]
591	4	5	105	29.6	12.7	17.3	4.6	[illegible]
591	4	6	40	30.5	9.8	15.6	5.8	[illegible]
591	4	6	105	31.1	4.5	8.5	4.0	[illegible]
591	5	1	40	32.6	7.6	12.7	5.1	[illegible]
591	5	1	105	33.3	9.9	17.2	7.3	82.8
591	5	2	40	34.1	8.6	13.9	5.3	86.1
591	5	2	105	34.8	12.4	18.8	6.4	81.2
591	5	3	40	35.6	11.5	18.3	6.8	81.7
591	5	3	105	36.3	8.4	14.5	6.1	85.5
591	5	4	40	37.1	10.8	16.6	5.8	83.4
591	5	4	105	37.8	7.4	12.0	4.6	88.0
591	5	5	40	38.6	12.4	16.6	4.2	83.4
591	5	5	105	39.3	9.5	15.3	5.8	84.7
591	5	6	40	40.1	7.0	12.2	5.2	87.8
591	6	1	110	42.8	8.6	14.9	6.3	85.1
591	6	2	110	44.3	10.4	17.4	7.0	82.6
591	6	3	110	45.8	5.5	10.1	4.6	89.9
591	6	4	110	47.3	8.8	16.6	7.8	83.4
591	6	5	110	48.8	11.4	16.6	5.2	83.4
591	6	6	110	50.3	5.4	9.9	4.5	90.1
591	7	1	40	51.8	3.4	7.8	4.4	92.2
591	7	1	105	52.5	5.8	10.6	4.8	89.4
591	7	2	40	53.3	6.8	12.1	5.3	87.9
591	7	2	105	54.0	5.5	8.9	3.4	91.1
591	7	3	40	54.8	5.6	9.7	4.1	90.3
591	7	3	105	55.5	7.9	12.2	4.3	87.8
591	7	4	40	56.3	6.7	12.1	5.4	87.9
591	7	4	105	57.0	5.0	9.9	4.9	90.1
591	7	5	40	57.8	4.6	7.6	3.0	92.4
591	7	5	105	58.5	5.7	13.6	7.9	86.4
591	7	6	40	59.3	6.9	11.4	4.5	88.6
591	7	6	105	60.0	6.2	11.3	5.1	88.7
591	8	1	40	61.4	8.5	15.9	7.4	84.1
591	8	1	105	62.0	7.6	13.6	6.0	86.4
591	8	2	40	62.9	7.1	12.2	5.1	87.8
591	8	2	105	63.5	7.4	14.9	7.5	85.1
591	8	3	40	64.4	9.9	17.1	7.2	82.9
591	8	3	105	65.1	7.1	11.6	4.5	88.4
591	8	4	40	65.9	7.1	14.3	7.2	85.7
591	8	4	105	66.6	8.6	14.5	5.9	85.5
591	8	5	40	67.4	4.1	4.9	.8	95.1
591	8	5	105	68.1	8.1	13.8	5.7	86.2
591	8	6	40	68.9	7.1	12.1	5.0	87.9
591	8	6	105	69.6	9.8	16.3	6.5	83.7
591	9	1	110	71.7	6.6	11.5	4.9	88.5
591	9	2	40	72.5	7.8	13.5	5.7	86.5
591	9	2	110	73.2	5.7	10.6	4.9	89.4
591	9	3	40	74.0	9.8	17.1	7.3	82.9
591	9	3	110	74.7	7.3	15.3	8.0	84.7
591	9	4	40	75.5	7.9	13.4	5.5	86.6
591	9	4	110	76.2	7.4	14.2	6.8	85.8
591	9	5	40	77.0	6.5	11.9	5.4	88.1
591	9	5	110	77.7	6.9	11.6	4.7	88.4
591	9	6	40	78.5	5.3	10.5	5.2	89.5
591	9	6	110	79.2	9.5	14.8	5.3	85.2
591	10	1	110	81.3	7.0	14.2	7.2	85.8
591	10	2	40	82.1	9.6	18.7	9.1	81.3
591	10	2	110	82.8	5.1	12.3	7.2	87.7
591	10	3	40	83.6	6.5	13.2	6.7	86.8
591	10	3	110	84.3	11.3	18.5	7.2	81.5
591	10	4	40	85.1	10.0	18.9	8.9	81.1
591	10	4	110	85.8	8.9	15.7	6.8	84.3
591	10	5	40	86.6	8.8	15.0	6.2	85.0
591	10	5	110	87.3	7.6	12.7	5.1	87.3
591	10	6	40	88.1	5.6	12.5	6.9	87.5
591	10	6	110	88.8	7.9	13.0	5.1	87.0
591	11	1	110	90.9	3.8	8.7	4.9	91.3
591	11	2	40	91.7	4.3	9.7	5.4	90.3
591	11	2	110	92.4	3.6	7.7	4.1	92.3
591	11	3	40	93.2	6.3	10.9	4.6	89.1
591	11	3	110	93.9	5.9	11.7	5.8	88.3
591	11	4	40	94.7	4.1	8.5	4.4	91.5
591	11	4	110	95.4	4.0	8.1	4.1	91.9
591	11	5	40	96.2	3.8	8.7	4.9	91.3
591	11	5	110	96.9	3.8	7.9	4.1	92.1
591	11	6	40	97.7	5.4	10.8	5.4	89.2
591	11	6	110	98.4	3.0	6.8	3.8	93.2

Appendix A. (Continued).

Site	Core	Section	Interval (cm)	Sub-bottom depth (m)	>147 μm	>63 μm	63-147 μm	<63 μm
591	12	1	110	100.5	5.5	9.6	4.1	90.4
591	12	2	40	101.3	3.1	7.6	4.5	92.4
591	12	2	110	102.0	4.1	8.7	4.6	91.3
591	12	3	40	102.8	4.8	10.5	5.7	89.5
591	12	3	110	103.5	3.2	7.4	4.2	92.6
591	12	4	40	104.3	4.2	8.2	4.0	91.8
591	12	4	110	105.0	3.4	7.5	4.1	92.5
591	12	5	40	105.8	7.0	10.7	3.7	89.3
591	12	5	110	106.5	5.3	10.4	5.1	89.6
591	12	6	40	107.3	6.7	12.5	5.8	87.5
591	12	6	110	108.0	6.4	11.0	4.6	89.0
591	13	1	40	109.4	4.2	11.0	6.8	89.0
591	13	1	110	110.1	4.5	9.9	5.4	90.1
591	13	2	40	110.9	4.6	9.6	5.0	90.4
591	13	2	70	111.2	5.8	15.3	9.5	84.7
591	13	2	110	111.6	3.9	10.4	6.5	89.6
591	13	3	40	112.4	3.6	10.9	7.3	89.1
591	13	3	110	113.1	4.7	11.4	6.7	88.6
591	13	4	40	113.9	5.6	11.7	6.1	88.3
591	13	5	110	114.6	4.8	9.7	4.9	90.3
591	13	5	40	115.4	4.0	12.1	8.1	87.9
591	13	5	110	116.1	4.0	10.1	6.1	89.9
591	13	6	40	116.9	5.0	12.2	7.2	87.8
591	13	6	110	117.6	4.5	10.8	6.3	89.2
591	13	7	70	118.7	3.6	9.6	6.0	90.4
591	14	1	40	118.7	0	11.5	11.5	88.5
591	14	1	110	119.4	0	9.2	9.2	90.8
591	14	2	40	120.2	0	12.9	12.9	87.1
591	14	2	70	120.5	0	14.9	14.9	85.1
591	14	2	110	120.9	0	11.9	11.9	88.1
591	14	3	40	121.7	0	17.3	17.3	82.7
591	14	3	110	122.4	0	17.8	17.8	82.2
591	14	4	40	123.2	0	11.3	11.3	88.7
591	14	4	110	123.9	0	11.9	11.9	88.1
591	14	5	40	124.7	0	11.0	11.0	89.0
591	14	5	70	125.0	0	11.8	11.8	88.2
591	14	5	110	125.4	0	8.2	8.2	91.8
591	14	6	40	126.2	0	10.6	10.6	89.4
591	14	6	110	126.9	0	8.0	8.0	92.0
591	14	7	40	127.7	0	8.0	8.0	92.0
591	15	1	40	128.0	0	13.6	13.6	86.4
591	15	1	110	128.7	0	9.6	9.6	90.4
591	15	2	40	129.5	0	11.4	11.4	88.6
591	15	2	70	129.8	0	10.8	10.8	89.2
591	15	2	110	130.2	0	11.6	11.6	88.4
591	15	3	40	131.0	0	10.3	10.3	89.7
591	15	3	110	131.7	0	7.5	7.5	92.5
591	15	4	40	132.5	0	9.4	9.4	90.6
591	15	4	110	133.2	0	9.7	9.7	90.3
591	15	5	40	134.0	0	7.2	7.2	92.8
591	15	5	70	134.3	0	7.9	7.9	92.1
591	15	5	110	134.7	0	8.9	8.9	91.1
591	15	6	40	135.5	0	8.8	8.8	91.2
591	15	6	110	136.2	0	6.0	6.0	94.0
591	16	1	40	137.1	0	6.6	6.6	93.4
591	16	1	110	138.0	0	9.0	9.0	91.0
591	16	2	40	138.8	0	5.5	5.5	94.5
591	16	2	110	139.5	0	5.5	5.5	94.5
591	16	3	40	140.3	0	6.8	6.8	93.2
591	16	3	110	141.0	0	6.5	6.5	93.5
591	16	4	40	141.8	0	4.6	4.6	95.4
591	16	4	110	142.5	0	6.7	6.7	93.3
591	16	5	40	143.3	0	6.7	6.7	93.3
591	16	5	110	144.0	0	8.2	8.2	91.8
591	16	6	40	144.8	0	5.7	5.7	94.3
591	16	6	110	145.5	0	6.2	6.2	93.8
591	17	1	40	146.6	0	7.9	7.9	92.1
591	17	1	110	147.3	0	6.8	6.8	93.2
591	17	2	40	148.1	0	11.3	11.3	88.7
591	17	2	110	148.8	0	7.3	7.3	92.7
591	17	3	40	149.6	0	8.1	8.1	91.9
591	17	3	110	150.3	0	6.6	6.6	93.4
591	17	4	40	151.1	0	10.5	10.5	89.5
591	17	4	110	151.8	0	7.0	7.0	93.0
591	17	5	40	152.6	0	7.2	7.2	92.8
591	17	5	110	153.3	0	9.1	9.1	90.9
591	17	6	40	154.1	0	9.9	9.9	90.1
591	17	6	110	154.8	0	12.3	12.3	87.7
591	17	7	40	155.6	0	7.8	7.8	92.2
591	18	1	40	155.9	0	7.4	7.4	92.6
591	18	1	110	156.6	0	9.0	9.0	91.0
591	18	2	40	157.4	0	8.8	8.8	91.2
591	18	2	110	158.1	0	8.9	8.9	91.1
591	18	3	40	158.9	0	7.1	7.1	92.9
591	18	3	110	159.6	0	8.1	8.1	91.9
591	18	4	40	160.4	0	9.9	9.9	90.1
591	18	4	110	161.1	0	9.3	9.3	90.7
591	18	5	40	161.9	0	8.0	8.0	92.0
591	18	5	110	162.6	0	9.5	9.5	90.5
591	18	6	40	163.4	0	7.7	7.7	92.3
591	18	6	110	164.1	0	8.3	8.3	91.7
591	19	1	40	165.2	0	8.6	8.6	91.4
591	19	1	110	165.9	0	9.8	9.8	90.2
591	19	2	40	166.7	0	13.5	13.5	86.5
591	19	2	110	167.4	0	7.7	7.7	92.3
591	19	3	40	168.2	0	9.3	9.3	90.7
591	19	3	110	168.9	0	10.1	10.1	89.9
591	19	4	40	169.7	0	10.2	10.2	89.8
591	19	4	110	170.4	0	9.2	9.2	90.8
591	19	5	40	171.2	0	10.6	10.6	89.4
591	19	5	110	171.9	0	8.9	8.9	91.1
591	19	6	40	172.7	0	8.9	8.9	91.1
591	19	6	110	173.4	0	9.3	9.3	90.7
591	20	1	40	174.7	0	10.8	10.8	89.2
591	20	1	110	175.4	0	8.2	8.2	91.8
591	20	2	40	176.2	0	7.9	7.9	92.1

Appendix A. (Continued).

Site	Core	Section	Interval (cm)	Sub-bottom depth (m)	>147 μm	>63 μm	63-147 μm	<63 μm
591	20	2	110	176.9	0	8.2	8.2	91.8
591	20	3	40	177.7	0	8.1	8.1	91.9
591	20	3	110	178.4	0	10.8	10.8	89.2
591	20	4	40	179.2	0	8.8	8.8	91.2
591	20	4	110	179.9	0	8.3	8.3	91.7
591	20	5	40	180.7	0	8.1	8.1	91.9
591	20	5	110	181.4	0	5.9	5.9	94.1
591	20	6	40	182.2	0	9.2	9.2	90.8
591	20	6	110	182.9	0	8.1	8.1	91.9
591	21	1	40	184.2	0	5.1	5.1	94.9
591	21	1	40	184.2	0	5.1	5.1	94.9
591	21	1	110	184.9	0	7.4	7.4	92.6
591	21	1	110	184.9	0	7.4	7.4	92.6
591	21	2	40	185.7	0	6.7	6.7	93.3
591	21	2	110	186.4	0	8.3	8.3	91.7
591	21	3	40	187.2	0	8.3	8.3	91.7
591	21	3	110	187.9	0	14.6	14.6	85.4
591	21	4	40	188.9	0	9.1	9.1	90.9
591	21	4	110	189.4	0	7.3	7.3	92.7
591	21	5	40	190.2	0	8.6	8.6	91.4
591	21	5	110	190.9	0	7.3	7.3	92.7
591	21	6	40	191.7	0	7.7	7.7	92.3
591	21	6	110	192.4	0	7.3	7.3	92.7
591	22	2	40	195.2	0	9.1	9.1	90.9
591	22	2	110	195.9	0	9.3	9.3	90.7
591	22	3	40	196.7	0	6.8	6.8	93.2
591	22	3	110	197.4	0	7.6	7.6	92.4
591	22	4	40	198.2	0	5.4	5.4	94.6
591	22	4	110	198.9	0	7.2	7.2	92.8
591	22	5	40	199.7	0	7.0	7.0	93.0
591	22	5	110	200.4	0	6.2	6.2	93.8
591	22	6	40	201.2	0	5.8	5.8	94.2
591	23	1	40	203.1	0	6.2	6.2	93.8
591	23	1	110	203.8	0	4.5	4.5	95.5
591	23	2	40	204.6	0	7.0	7.0	93.0
591	23	2	110	205.3	0	4.9	4.9	95.1
591	23	3	40	206.1	0	4.8	4.8	95.2
591	23	3	110	206.8	0	5.1	5.1	94.9
591	23	4	40	207.6	0	7.6	7.6	92.4
591	23	4	110	208.3	0	6.2	6.2	93.8
591	23	5	40	209.1	0	6.2	6.2	93.8
591	23	5	110	209.8	0	4.9	4.9	95.1
591	23	6	40	210.6	0	8.1	8.1	91.9
591	23	6	110	211.3	0	4.5	4.5	95.5
591	24	1	40	212.5	0	6.1	6.1	93.9
591	24	1	110	213.2	0	6.0	6.0	94.0
591	24	2	40	214.0	0	5.9	5.9	94.1
591	24	2	70	214.3	0	6.3	6.3	93.7
591	24	2	110	214.7	0	6.0	6.0	94.0
591	24	3	40	215.5	0	7.2	7.2	92.8
591	24	3	110	216.2	0	11.1	11.1	88.9
591	24	4	40	217.0	0	7.3	7.3	92.7
591	24	4	110	217.7	0	9.4	9.4	90.6
591	24	5	40	218.5	0	9.9	9.9	90.1
591	24	5	70	218.8	0	5.4	5.4	94.6
591	24	5	110	219.2	0	6.6	6.6	93.4
591	24	6	40	220.0	0	5.0	5.0	95.0
591	25	1	40	221.9	0	5.5	5.5	94.5
591	25	1	110	222.6	0	4.4	4.4	95.6
591	25	2	40	223.4	0	5.1	5.1	94.9
591	25	2	110	224.1	0	5.3	5.3	94.7
591	25	3	40	224.9	0	5.8	5.8	94.2
591	25	3	110	225.6	0	5.3	5.3	94.7
591	25	4	40	226.4	0	5.7	5.7	94.3
591	25	4	110	227.1	0	5.8	5.8	94.2
591	25	5	40	227.9	0	6.4	6.4	93.6
591	25	5	110	228.6	0	7.9	7.9	92.1
591	25	6	40	229.4	0	5.4	5.4	94.6
591	25	6	110	230.1	0	6.6	6.6	93.4
591	26	1	40	231.5	0	4.5	4.5	95.5
591	26	1	110	232.2	0	4.5	4.5	95.5
591	26	2	40	233.0	0	4.5	4.5	95.5
591	26	2	110	233.7	0	8.1	8.1	91.9
591	26	3	40	234.5	0	5.5	5.5	94.5
591	26	3	110	235.3	0	6.7	6.7	93.3
591	26	4	40	236.0	0	5.4	5.4	94.6
591	26	4	110	236.7	0	7.3	7.3	92.7
591	26	5	40	237.5	0	6.3	6.3	93.7
591	27	1	40	241.1	0	5.6	5.6	94.4
591	27	1	110	241.8	0	3.8	3.8	96.2
591	27	2	40	242.6	0	6.6	6.6	93.4
591	27	2	110	243.3	0	5.5	5.5	94.5
591	27	3	40	244.1	0	6.3	6.3	93.7
591	27	3	110	244.8	0	4.6	4.6	95.4
591	27	4	40	245.6	0	6.3	6.3	93.7
591	27	4	110	246.3	0	8.3	8.3	91.7
591	27	5	40	247.1	0	4.6	4.6	95.4
591	27	5	110	247.8	0	4.6	4.6	95.4
591	27	6	40	248.6	0	7.3	7.3	92.7
591	27	6	110	249.3	0	7.5	7.5	92.5
591	28	1	40	250.7	0	6.0	6.0	94.0
591	28	1	110	251.4	0	5.1	5.1	94.9
591	28	2	40	252.2	0	5.9	5.9	94.1
591	28	2	110	252.9	0	5.5	5.5	94.5
591	28	3	40	253.7	0	11.2	11.2	88.8
591	28	3	110	254.4	0	7.9	7.9	92.1
591	28	4	40	255.2	0	6.0	6.0	94.0
591	28	4	110	255.9	0	3.9	3.9	96.1
591	28	5	40	256.7	0	5.3	5.3	94.7
591	28	5	110	257.4	0	7.0	7.0	93.0
591	28	6	40	258.2	0	5.8	5.8	94.2
591	28	6	110	258.9	0	6.1	6.1	93.9
591	29	1	40	260.2	0	6.1	6.1	93.9
591	29	1	110	260.7	0	4.3	4.3	95.7
591	29	2	40	261.7	0	3.4	3.4	96.6
591	29	2	110	262.4	0	4.5	4.5	95.5

Appendix A. (Continued).

Site	Core	Section	Interval (cm)	Sub-bottom depth (m)	>147 μm	>63 μm	63-147 μm	<63 μm
591	29	3	40	263.2	0	3.5	3.5	96.5
591	29	3	110	263.9	0	2.9	2.9	97.1
591	29	4	40	264.7	0	3.6	3.6	96.4
591	29	4	110	265.4	0	3.9	3.9	96.1
591	29	5	40	266.2	0	3.9	3.9	96.1
591	29	5	110	266.9	0	4.4	4.4	95.6
591	29	6	40	267.7	0	5.2	5.2	94.8
591	29	6	110	268.4	0	5.2	5.2	94.8
591	30	1	40	269.7	0	5.5	5.5	94.5
591	30	1	110	270.4	0	7.1	7.1	92.9
591	1	1	36	271.0	0	5.7	5.7	94.3
591	30	2	40	271.2	0	4.4	4.4	95.6
591	1	1	110	271.7	0	6.4	6.4	93.6
591	30	2	110	271.9	0	6.0	6.0	94.0
591	1	2	36	272.5	0	9.8	9.8	90.2
591	30	3	40	272.7	0	4.9	4.9	95.1
591	1	2	110	273.2	0	4.9	4.9	95.1
591	30	3	110	273.4	0	6.3	6.3	93.7
591	1	3	36	274.0	0	8.5	8.5	91.5
591	31	1	40	274.7	0	5.5	5.5	94.5
591	31	1	110	275.4	0	6.8	6.8	93.2
591	31	2	40	276.2	0	6.5	6.5	93.5
591	31	2	110	276.9	0	5.2	5.2	94.8
591	31	3	40	277.7	0	8.9	8.9	91.1
591	31	3	110	278.4	0	7.2	7.2	92.8
591	31	4	40	279.2	0	8.0	8.0	92.0
591	31	4	110	279.9	0	7.4	7.4	92.6
591	2	1	36	280.6	0	12.6	12.6	87.4
591	31	5	40	280.7	0	7.6	7.6	92.4
591	2	1	110	281.3	0	8.1	8.1	91.9
591	31	5	110	281.4	0	6.6	6.6	93.4
591	2	2	36	282.1	0	9.1	9.1	90.9
591	31	6	40	282.2	0	7.5	7.5	92.5
591	2	2	110	282.8	0	7.7	7.7	92.3
591	31	6	100	282.9	0	6.9	6.9	93.1
591	2	3	36	283.6	0	7.1	7.1	92.9
591	2	3	110	284.3	0	8.3	8.3	91.7
591	3	1	37	290.2	0	7.7	7.7	92.3
591	3	1	43	290.2	0	8.5	8.5	91.5
591	3	1	101	290.8	0	7.3	7.3	92.7
591	3	2	37	291.7	0	8.2	8.2	91.8
591	3	2	43	291.7	0	8.0	8.0	92.0
591	3	2	101	292.3	0	8.5	8.5	91.5
591	3	3	37	293.2	0	8.8	8.8	91.2
591	3	3	47	293.3	0	7.0	7.0	93.0
591	3	3	101	293.8	0	7.3	7.3	92.7
591	3	4	37	294.7	0	7.1	7.1	92.9
591	3	4	43	294.7	0	6.9	6.9	93.1
591	3	4	99	295.3	0	8.9	8.9	91.1
591	3	5	37	296.2	0	8.9	8.9	91.1
591	3	5	43	296.2	0	7.6	7.6	92.4
591	3	5	105	296.9	0	9.4	9.4	90.6
591	4	1	38	299.8	0	13.7	13.7	86.3
591	4	1	110	300.5	0	13.5	13.5	86.5
591	4	2	38	301.3	0	12.4	12.4	87.6
591	4	2	110	302.0	0	12.7	12.7	87.3
591	4	3	38	302.8	0	15.2	15.2	84.8
591	4	3	110	303.5	0	10.6	10.6	89.4
591	4	4	38	304.3	0	10.0	10.0	90.0
591	4	4	110	305.0	0	8.3	8.3	91.7
591	4	5	38	305.8	0	8.3	8.3	91.7
591	5	1	36	309.2	0	9.1	9.1	90.9
591	5	1	110	309.9	0	8.5	8.5	91.5
591	5	2	36	310.7	0	9.9	9.9	90.1
591	5	2	110	311.4	0	5.7	5.7	94.3
591	5	3	36	312.2	0	10.6	10.6	89.4
591	5	3	110	312.9	0	12.9	12.9	87.1
591	5	4	36	313.7	0	7.0	7.0	93.0
591	6	1	36	318.6	0	12.1	12.1	87.9
591	6	1	110	319.3	0	10.2	10.2	89.8
591	6	2	36	320.1	0	11.7	11.7	88.3
591	6	2	110	320.8	0	10.2	10.2	89.8
591	6	3	36	321.6	0	8.5	8.5	91.5

Appendix A. (Continued).

Site	Core	Section	Interval (cm)	Sub-bottom depth (m)	>147 μm	>63 μm	63-147 μm	< m
591	6	3	110	322.3	0	6.3	6.3	[illegible]
591	6	4	36	323.1	0	8.2	8.2	[illegible]
591	6	4	110	323.8	0	7.3	7.3	[illegible]
591	6	5	36	324.6	0	9.5	9.5	[illegible]
591	6	5	110	325.3	0	8.3	8.3	[illegible]
591	7	1	36	328.0	0	7.1	7.1	[illegible]
591	7	1	110	328.7	0	5.9	5.9	[illegible]
591	7	2	36	329.5	0	12.1	12.1	[illegible]
591	7	2	110	330.2	0	7.2	7.2	[illegible]
591	7	3	36	331.0	0	5.9	5.9	[illegible]
591	7	3	110	331.7	0	7.1	7.1	[illegible]
591	7	4	36	332.5	0	8.7	8.7	[illegible]
591	7	4	110	333.2	0	7.3	7.3	[illegible]
591	7	5	36	334.0	0	4.1	4.1	[illegible]
591	7	5	110	334.7	0	11.3	11.3	[illegible]
591	7	6	36	335.5	0	8.2	8.2	[illegible]
591	7	6	110	336.2	0	5.9	5.9	[illegible]
591	8	2	40	339.1	0	7.3	7.3	[illegible]
591	10	1	40	356.8	0	6.6	6.6	[illegible]
591	10	1	110	357.5	0	9.7	9.7	90.3
591	10	2	40	358.3	0	9.3	9.3	90.7
591	10	2	110	359.0	0	10.6	10.6	89.4
591	11	1	40	366.4	0	9.9	9.9	90.1
591	11	1	110	367.1	0	9.8	9.8	90.2
591	12	1	40	376.0	0	7.9	7.9	92.1
591	12	2	40	377.5	0	5.9	5.9	94.1
591	13	1	40	385.6	0	6.4	6.4	93.6
591	13	1	110	386.3	0	6.5	6.5	93.5
591	13	2	40	387.1	0	9.6	9.6	90.4
591	13	2	110	387.8	0	7.7	7.7	92.3
591	14	1	40	395.2	0	6.4	6.4	93.6
591	15	1	40	404.8	0	9.5	9.5	90.5
591	15	1	110	405.5	0	11.7	11.7	88.1
591	15	2	40	406.3	0	21.6	21.6	78.4
591	15	2	110	407.0	0	9.5	9.5	90.5
591	15	3	40	407.8	0	7.9	7.9	92.1
591	17	1	40	424.0	0	10.5	10.5	89.5
591	17	1	110	424.7	0	11.0	11.0	89.0
591	17	2	40	425.5	0	7.9	7.9	92.1
591	17	2	110	426.2	0	12.4	12.4	87.6
591	17	3	40	427.0	0	7.6	7.6	92.4
591	17	3	110	427.7	0	14.0	14.0	86.0
591	17	4	40	428.5	0	13.4	13.4	86.6
591	18	1	40	433.6	0	10.8	10.8	89.2
591	18	1	110	434.3	0	13.1	13.1	86.9
591	18	2	40	435.1	0	9.0	9.0	91.0
591	18	2	110	435.8	0	10.4	10.4	89.6
591	18	3	40	436.6	0	12.8	12.8	87.2
591	18	3	110	437.3	0	12.3	12.3	87.7
591	18	4	40	438.1	0	9.8	9.8	90.2
591	18	4	110	438.8	0	17.2	17.2	82.8
591	18	5	40	439.6	0	14.9	14.9	85.1
591	18	5	110	440.3	0	16.2	16.2	83.8
591	18	6	40	441.1	0	12.4	12.4	87.6
591	18	6	110	441.8	0	11.9	11.9	88.1
591	19	1	40	443.2	0	16.5	16.5	83.5
591	19	1	110	443.9	0	31.7	31.7	68.3
591	19	2	40	444.7	0	15.0	15.0	85.0
591	19	2	110	445.4	0	12.9	12.9	87.1
591	19	3	40	446.2	0	8.9	8.9	91.1
591	19	4	40	447.7	0	7.7	7.7	92.3
591	19	4	110	448.4	0	17.3	17.3	82.7
591	19	5	40	449.2	0	7.1	7.1	92.9
591	20	1	40	452.8	0	6.0	6.0	94.0
591	20	1	110	453.5	0	13.3	13.3	86.7
591	20	2	40	454.3	0	5.3	5.3	94.7
591	20	3	40	455.8	0	11.9	11.9	88.1
591	20	4	40	457.3	0	4.0	4.0	96.0
591	20	5	40	458.8	0	5.9	5.9	94.1
591	21	1	40	462.4	0	8.6	8.6	91.4
591	21	2	40	463.9	0	7.4	7.4	92.6
591	21	3	40	465.4	0	9.9	9.9	90.1
591	22	1	40	472.0	0	10.5	10.5	89.5

APPENDIX B
Carbonate Percentages, Sites 586 and 591

Hole	Core	Section	Interval (cm)	Sub-bottom depth (m)	%CaCO$_3$
586	1	1	31	0.79	84.0
586	2	3	110	5.40	78.0
586	3	3	76	14.56	88.0
586	4	4	92	25.72	89.0
586	5	2	105	32.35	89.0
586A	1	2	79	45.69	88.0
586A	2	1	75	54.75	88.0
586A	2	1	70	56.70	88.0
586A	3	2	69	65.79	86.0
586A	4	2	48	75.18	89.0
586A	5	2	75	85.05	90.0
586A	6	2	29	94.19	90.0
586A	7	2	35	103.85	94.0
586A	8	2	31	113.41	85.0
586A	9	2	27	122.97	99.0
586A	10	2	30	132.60	95.0
586A	11	5	100	147.40	97.0
586A	12	2	64	152.14	96.0
586A	13	2	60	161.70	99.0
586A	14	2	24	168.64	95.0
586A	15	2	60	173.90	98.0
586A	16	2	70	183.00	96.0
586A	17	6	70	198.60	99.0
586A	18	2	60	202.10	99.0
586A	19	3	49	213.09	96.0
586A	20	2	20	219.80	98.0
586A	20	2	82	220.42	93.0
586A	21	4	108	233.28	95.0
586A	22	3	60	240.90	92.0
586A	23	5	82	253.72	97.0
586A	24	6	145	265.45	99.0
586A	25	6	137	274.97	94.0
586A	26	3	75	279.45	97.0
586A	27	2	105	284.25	93.0
586A	28	4	45	290.85	99.0
586A	29	3	99	294.29	96.0
586A	30	1	54	295.84	96.0
586A	31	1	121	301.51	98.0

SITE 591

Hole	Core	Section	Interval (cm)	Sub-bottom depth (m)	%CaCO$_3$
591	1	1	5	0.05	88.8
591	1	1	75	0.75	84.6
591	1	2	75	2.25	85.6
591	2	1	5	3.45	88.8
591	2	1	75	4.15	92.5
591	2	2	75	5.65	89.9
591	2	3	75	7.15	93.6
591	2	4	75	8.65	95.6
591	2	5	75	10.15	91.4
591	2	6	75	11.65	91.4
591	3	1	5	13.05	88.8
591	3	1	75	13.75	85.6
591	3	2	75	15.25	80.4
591	3	3	75	16.75	92.0
591	3	4	75	18.25	90.9
591	3	5	75	19.75	89.9
591	3	6	75	21.25	80.9
591	4	1	5	22.65	92.5
591	4	1	75	23.35	93.0
591	4	2	75	24.85	90.9
591	4	3	75	26.35	93.0
591	4	4	75	27.85	81.9
591	4	5	75	29.35	89.3
591	4	6	75	30.85	88.8
591	5	1	5	32.25	88.3
591	5	1	75	32.95	86.2
591	5	2	75	34.45	91.4
591	5	3	75	35.95	90.0
591	5	4	75	37.45	90.1
591	5	5	75	38.95	89.0
591	5	6	75	40.45	84.9
591	6	1	5	41.85	84.4
591	6	1	75	42.55	86.0
591	6	2	75	44.05	88.0
591	6	3	75	45.55	88.5
591	6	4	75	47.05	90.6
591	6	5	75	48.55	89.5
591	6	6	75	50.05	88.0
591	7	1	5	51.45	89.0
591	7	1	75	52.15	81.3
591	7	2	75	53.65	86.0
591	7	3	75	55.15	90.6
591	7	4	75	56.65	87.5
591	7	5	75	58.15	88.5
591	7	6	75	59.65	92.6
591	8	1	5	61.05	92.1
591	8	1	75	61.75	90.6
591	8	2	75	63.25	88.0
591	8	3	75	64.75	82.9
591	8	4	75	66.25	89.5
591	8	5	75	67.75	91.6
591	8	6	75	69.25	90.1
591	9	1	5	70.65	89.5
591	9	1	75	71.35	78.3
591	9	2	75	72.82	93.0
591	9	3	75	74.35	89.4
591	9	4	75	75.85	93.0
591	9	5	75	77.35	93.5
591	9	6	75	78.85	94.0
591	10	1	5	80.25	94.0
591	10	1	75	80.95	90.5
591	10	2	75	82.45	93.0
591	10	3	75	83.95	92.5
591	10	4	75	85.45	92.0

Appendix B. (Continued).

Hole	Core	Section	Interval (cm)	Sub-bottom depth (m)	%CaCO$_3$
591	10	5	75	86.95	93.0
591	10	6	75	88.45	91.5
591	11	1	75	90.55	87.4
591	11	2	75	92.05	91.5
591	11	3	75	93.55	92.0
591	11	4	75	95.05	95.1
591	11	5	75	96.55	92.0
591	11	6	75	98.05	91.5
591	12	1	75	100.15	92.5
591	12	2	75	101.65	92.5
591	12	3	75	103.15	92.0
591	12	4	75	104.65	91.5
591	12	5	75	106.15	92.0
591	12	6	75	107.65	91.5
591	13	1	0	109.00	90.5
591	13	1	75	109.75	85.4
591	13	2	75	111.25	90.5
591	13	3	75	112.75	91.5
591	13	4	75	114.25	86.9
591	13	5	75	115.75	92.0
591	13	6	75	117.25	89.4
591	14	1	75	119.05	90.0
591	14	2	75	120.55	87.9
591	14	3	75	122.05	90.5
591	14	4	75	123.55	87.4
591	14	5	75	125.05	88.4
591	14	6	75	126.55	90.0
591	15	1	75	128.35	86.9
591	15	2	75	129.85	89.4
591	15	3	75	131.35	88.4
591	15	4	75	132.85	88.4
591	15	5	75	134.35	88.4
591	15	6	75	135.85	91.0
591	16	1	75	140.65	88.9
591	16	4	75	142.15	90.0
591	16	5	75	143.65	90.5
591	16	6	75	145.15	90.5
591	17	2	75	148.45	90.5
591	17	3	75	149.95	91.5
591	17	4	75	151.45	90.5
591	17	5	75	152.95	90.5
591	17	6	75	154.45	90.5
591	18	1	75	156.25	90.0
591	18	2	75	157.75	90.0
591	18	3	75	159.25	88.4
591	18	4	75	160.75	90.0
591	18	5	75	162.25	89.4
591	18	6	75	163.75	88.4
591	19	1	75	165.55	89.4
591	19	2	75	167.05	91.5
591	19	3	75	168.55	89.4
591	19	4	75	170.05	88.4
591	19	5	75	171.55	91.0
591	19	6	75	173.05	89.4
591	20	1	5	174.35	88.4
591	20	1	75	175.05	88.9
591	20	2	75	176.55	88.9
591	20	3	75	178.05	91.0
591	20	4	75	179.55	90.5
591	20	5	75	181.05	87.9
591	20	6	75	182.55	87.4
591	21	1	5	183.85	89.4
591	21	1	75	184.55	88.4
591	21	2	75	186.05	90.5
591	21	3	75	187.55	87.4
591	21	4	75	189.05	89.4
591	21	5	75	190.55	96.1
591	21	6	75	192.05	93.4
591	22	1	5	193.35	94.0
591	22	1	75	194.05	94.0
591	22	2	75	195.55	94.5
591	22	3	75	197.05	94.5
591	22	4	75	198.55	93.4
591	22	5	75	200.05	92.9
591	23	1	5	202.75	91.9
591	23	1	75	203.45	94.5
591	23	2	75	204.95	92.9
591	23	3	75	206.45	90.8
591	23	4	75	207.95	90.8
591	23	5	75	209.45	94.0
591	23	6	75	212.05	93.4
591	34	1	5	212.15	91.9
591	24	1	75	212.85	94.0
591	24	2	75	214.35	93.4
591	24	3	75	215.85	95.0
591	24	4	75	217.35	93.4
591	24	5	75	218.85	94.5
591	24	6	75	220.35	94.5
591	25	1	5	221.55	93.4
591	25	1	75	222.25	94.0
591	25	2	75	223.75	94.5
591	25	3	75	225.25	91.9
591	25	4	75	226.75	92.4
591	25	5	75	228.25	94.5
591	25	6	75	229.75	94.0
591	26	1	5	231.15	98.2
591	26	1	75	231.85	96.1
591	26	2	75	233.35	96.1
591	26	3	75	234.85	96.1
591	26	4	75	236.35	98.2
591	26	5	75	237.85	96.6
591	27	1	5	240.75	96.1
591	27	1	75	241.45	98.2
591	27	2	75	242.95	96.6
591	27	3	75	244.45	95.0
591	27	4	75	245.95	95.5

Appendix B. (Continued).

Hole	Core	Section	Interval (cm)	Sub-bottom depth (m)	%$CaCO_3$
591	27	5	75	247.45	95.5
591	27	6	75	248.95	95.0
591	28	1	5	250.35	97.1
591	28	1	75	251.05	94.5
591	28	2	75	252.55	95.5
591	28	3	75	254.05	96.1
591	28	4	75	255.55	99.2
591	28	5	75	257.05	93.4
591	28	6	75	258.55	95.5
591	29	1	5	259.85	92.9
591	29	1	75	260.55	94.5
591	29	2	75	262.05	92.9
591	29	3	75	263.55	94.5
591	29	4	75	265.05	95.5
591	29	5	75	266.55	94.0
591	29	6	75	268.05	92.9
591	30	1	5	269.35	94.0
591	30	1	75	270.05	96.1
591	30	2	75	271.55	94.0
591	30	3	75	273.05	95.0
591	31	1	75	275.05	95.0
591	31	2	75	276.55	96.6
591	31	3	75	278.05	97.6
591	31	4	75	279.55	94.5
591	31	5	75	281.05	95.0
591	31	6	75	282.55	95.5
591B	2	3	75	283.95	95.2
591B	3	1	5	289.85	93.7
591B	3	1	75	290.55	92.7
591B	3	2	75	292.05	91.1
591B	3	3	75	293.55	93.2
591B	3	4	75	295.05	91.6
591B	3	5	75	296.55	92.7
591B	4	1	5	299.45	90.1
591B	4	1	75	300.15	90.6
591B	4	2	75	301.65	92.1
591B	4	3	75	303.15	91.6
591B	4	4	75	304.65	92.1
591B	4	5	75	306.15	91.6
591B	5	1	5	308.85	90.6
591B	5	1	75	309.55	92.7
591B	5	2	75	311.05	92.1
591B	5	3	75	312.55	91.6
591B	7	3	75	331.35	91.6
591B	8	1	75	337.95	90.1
591B	9	2	75	349.05	90.6
591B	11	1	75	366.75	91.1
591B	13	1	75	385.95	91.1
591B	15	3	75	408.15	91.6
591B	17	3	75	427.35	91.1
591B	18	3	70	436.90	92.7
591B	19	3	75	446.55	91.6
591B	20	1	80	453.20	90.6
591B	22	3	75	475.35	88.0
591B	23	3	85	485.05	90.1
591B	24	3	85	494.65	89.6

READEX FICHE best copy available

pages tightly bound

30. CENOZOIC EVOLUTION AND SIGNIFICANCE OF CLAY ASSOCIATIONS IN THE NEW ZEALAND REGION OF THE SOUTH PACIFIC, DEEP SEA DRILLING PROJECT, LEG 90[1]

Christian Robert, Faculté des Sciences de Luminy,
Rüdiger Stein, Geologisch-Paläontologisches Institut und Museum der Universität Kiel
and
Monique Acquaviva, Faculté des Sciences de Luminy[2]

ABSTRACT

Clay minerals, flux rates, and the size distribution of terrigenous matter in DSDP Sites 592, 593, and 594 have been used to reconstruct continental and marine paleoenvironments in the New Zealand sector of the southwest Pacific. Five stages are recognized from late Eocene to Pleistocene times.

1. At the Eocene–Oligocene boundary, illite and mixed-layer clays marked a period of tectonic extension related to graben formation and volcanic activity.
2. During the Oligocene, smectites formed abundantly in plains and perimarine lagoons which developed during subsidence-induced peneplanation of the relief.
3. During the early Miocene, greater abundances of chlorite, illite, and irregular mixed-layer clays, and the appearance of kaolinite were due to an increase in the relief of New Zealand that followed the inception of a compressive regime; in the Tasman Sea, part of the detrital supply (smectites) was derived from the north and was deposited by southward-flowing currents.
4. From middle Miocene to early late Miocene time, abundant chlorite, illite, mixed-layer clays, and kaolinite, and the appearance of stilpnomelane marked an important tectonic event in New Zealand which increased the detrital supply to the whole South Tasman Sea; on the Chatham Rise, abundant smectites from the north diluted the detrital supply influenced by the tectonic activity in New Zealand.
5. From early late Miocene to Pleistocene time, abundant chlorite, illite, mixed-layer clays, kaolinite, and stilpnomelane were eroded from New Zealand, where the Kaikoura orogeny increased the relief, and deposited in the South Tasman Sea; during the late Pliocene, both grain size and amounts of clay particles eroded from New Zealand increased, related to reinforced bottom-current activity on the Lord Howe Rise; on the Chatham Rise, increased detrital components from the Southern Alps (chlorite, illite, mixed-layer clays, stilpnomelane) were supplied by northward-flowing currents.

INTRODUCTION

During Leg 90 of the Deep Sea Drilling Project in the southwest Pacific, holes were drilled at three sites at depths coinciding with upper water masses, close to New Zealand, in an area marked by the convergence of the Indo-Australian and Pacific plates. As shown in Figure 1, DSDP holes were drilled on the southern part of the Lord Howe Rise (Site 592), on the Challenger Plateau (Site 593), and on the Chatham Rise (Site 594). Basic data about the sites is given in Table 1.

The purpose of this study is to determine the effect of structural evolution, climatic changes, and current interactions on sedimentation, using variations in clay minerals, flux rates, and size distribution of terrigenous matter. Similar approaches have previously been used to determine the paleoenvironmental evolution of the Atlantic Ocean (Chamley, 1979; Robert, 1982; Stein, 1984).

METHODS

Clay Mineralogy

In each sample, the $<63\ \mu m$ size fraction was leached in $0.2N$ hydrochloric acid. The excess acid was removed by repeated centrifugations followed by homogenization. The $<2\ \mu m$ size fraction was separated by decantation (settling time based on Stokes' Law), and oriented aggregates were made on glass slides. Three X-ray diffractograms were made: (!) untreated sample; (2) glycolated sample; (3) sample heated for 2 hr. at 490°C. A C.G.R. Thêta 60 diffractometer (copper $K\alpha$ radiation focused by a quartz curved monochromator) was used at scan speeds of $1°2\Theta$/min. A receiving slit of 1.25 mm allowed a more precise resolution of poorly crystallized minerals.

Semiquantitative evaluations were based on the peak heights and areas. Data are given in percentages, the relative error being ±5%. The relative abundances of smectites versus illite (S/I index) and of kaolinite versus illite (K/I index) were obtained from the ratios of the 001 smectite (18Å), illite (10Å), and kaolinite (7Å) peaks on the glycolated sample.

Some samples were selected for transmission electron microscopy analysis. The $<8\ \mu m$ size fraction was separated by decantation, and the particles were scattered into a solution of tert-butylamin. A drop of the suspension was then deposited on a copper grid, which had been previously covered by a membrane of collodion. The samples were analyzed using a Philips EM 300 microscope.

Grain Size and Flux Rates of Terrigenous Matter

The carbonate content was determined by infrared absorption of CO_2 released by phosphoric acid treatment. The $<63\ \mu m$ size fraction was treated successively with hydrogen peroxide and acetic acid in or-

---

[1] Kennett, J. P., von der Borch, C. C., et al., *Init. Repts. DSDP*, 90: Washington (U.S. Govt. Printing Office).

[2] Addresses: (Robert, Acquaviva) Géologie Marine, UA CNRS 41, Faculté des Sciences de Luminy, Case 901, 13288 Marseille Cedex 9, France; (Stein, present address) Institute of Petroleum and Organic Geochemistry (ICH-5), KFA Jülich, P.O. Box 1913, 5170 Jülich, Federal Republic of Germany.

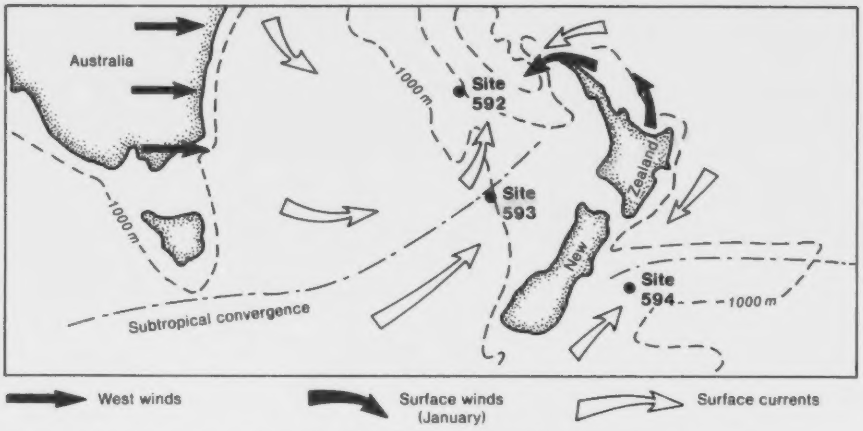

Figure 1. Location of Leg 90 Sites 592, 593, and 594. 1000 m isobath shown.

Table 1. Site data for Sites 592, 593, and 594.

Site	Latitude (S)	Longitude (E)	Water depth (m)	Penetration (m)	Oldest sediment recovered
592	36°28.40′	165°26.53′	1098	388.5	late Eocene
593	40°30.47′	167°40.47′	1068	571.5	late Eocene
594	45°31.41′	174°56.88′	1204	639.5	middle Miocene

der to remove both organic matter and calcium carbonate, respectively. The carbonate-free fraction was separated into >6 μm and <6 μm size fractions according to the method of Atterberg. The composition of the >6 μm size fraction was analyzed using a microscope, and its grain size was measured with a Coulter counter. The mass accumulation rates were calculated according to the method of Thiede et al. (1982), using the shipboard porosity and wet-bulk density data of Morin (site chapters, this volume). Details of the methodology are given by Stein and Robert (this volume).

ORIGIN AND SIGNIFICANCE OF THE PARTICLES

The sediments consist mainly of nannofossil to foraminifer-bearing nannofossil oozes and chalks. At Site 594 (Chatham Rise), foraminifer and clay-bearing nannofossil oozes, clayey silty nannofossil oozes, nannofossil silty clays and silty clays, sometimes associated with diatomaceous sponge spicule silts, are present in late Miocene to Pleistocene sediments. At Site 593 on the Challenger Plateau, volcanogenic turbidites are surrounded by upper Eocene and lower Oligocene sediments (site chapters, this volume).

General Results

Clay minerals include smectites, illite, chlorite, irregular mixed-layer clays (illite-smectite and chlorite-smectite), kaolinite, and stilpnomelane (Figs. 2–5). Abundant illite and irregular mixed-layer clays (up to 40%) were deposited on the southern Lord Howe Rise (Site 592) during the late Eocene and the early Oligocene, when dominant smectites (up to 95%) were deposited on the Challenger Plateau (Site 593). During the Neogene, chlorite, illite, irregular mixed-layer clays, and sometimes kaolinite increased at all sites, but in a different way. On the southern Lord Howe Rise (Site 592), smectites remained dominant (up to 100%) during the early Miocene, decreasing, however, in the middle Miocene. Minimum values of smectites (<25%), also indicated by extremely low S/I ratios, occurred during the last 4 m.y. This change in the sediment record of Site 592 coincided with a distinct coarsening of both bulk sediment and terrigenous sediment fractions, and a distinct decrease in accumulation rates of terrigenous matter. On the Challenger Plateau (Site 593), chlorite, illite, irregular mixed-layer clays, and kaolinite increased as early as the early Miocene. On the Chatham Rise (Site 594), smectites were abundant until the late Pliocene and then decreased, being replaced by dominant chlorite, illite, and irregular mixed-layer clays (Figs. 2, 4, 5).

Electron micrographs show very rare palygorskite-like fibers at Sites 592 and 593 (Plate 1). During the late Eocene, while volcanogenic turbidites were deposited at Site 593, the clay fraction temporarily consisted of up to 90% smectites on the southern Lord Howe Rise (Site 592). At this level, the clay particles consist mainly of thick laths and associated globular packs of fine laths (Plate 1). The latter are also present in the sedimentary record at levels where volcanic glass is present, as well as in the vicinity of greenish gray laminae attributed to the presence of devitrified volcanic ash. This observation can be extended to the other sites of the Lord Howe Rise (Stein and Robert, this volume). In the Leg 90 sediments marked by abundant smectites (up to 95% of the clay fraction), there is a general occurrence of very fine, transparent, and apparently fragile laths (Plate 2). These laths are more abundant in Eocene to Miocene sediments, and become sparse in Pliocene and Quaternary sediments. The fine laths scattered in the background of the micrographs are often associated in geometrical figures with 60° angles (Plate 2). These laths are also present at the periphery of fleecy packs and large particles (Plate 2). They are sometimes arranged in urchinlike groups (Plate 2). Lastly, biosiliceous fragments occasionally show traces of dissolution, and small tufts of fibers are present at the periphery and within the frustules (Plate 2).

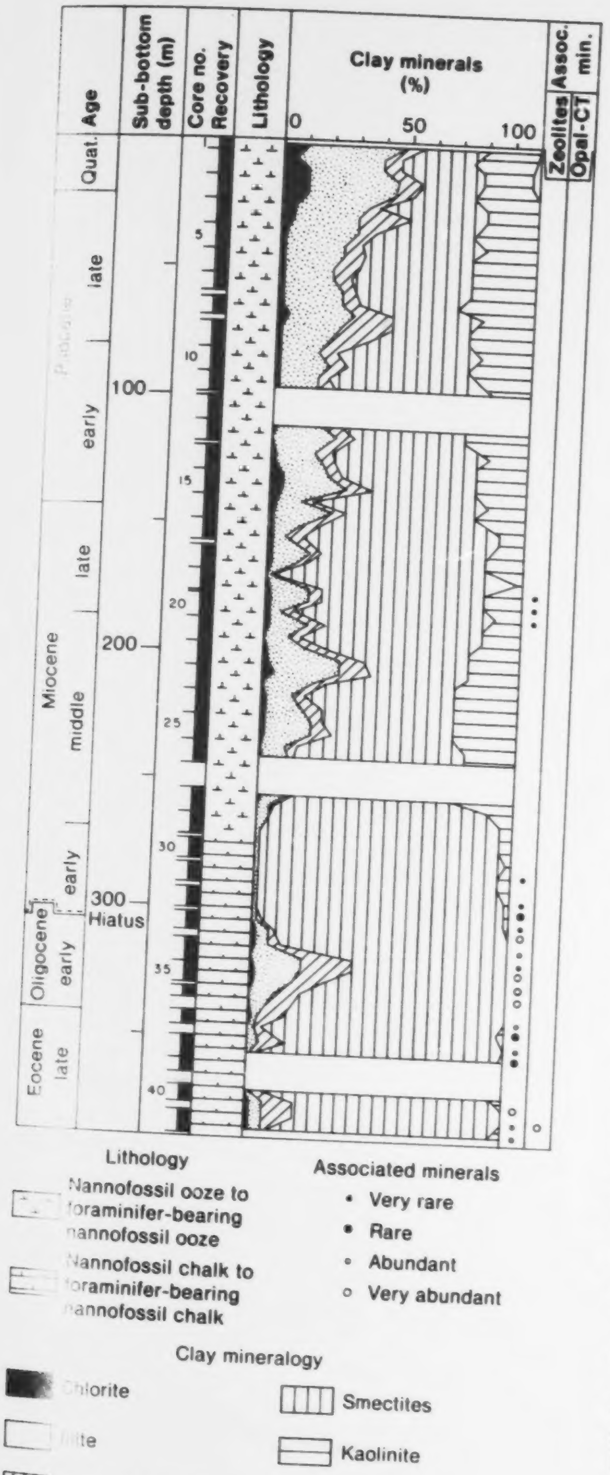

Figure 2. Site 592 results.

Early Diagenesis

Generally, smectites appear in the soil on land, in the form of fleecy particles (Chamley and Bonnot-Courtois, 1981; Robert, 1982). In the Leg 90 sediments characterized by abundant smectites, electron micrographs often show that this morphological type is scarce. Instead, fine laths are present; their fineness and apparent fragility, as well as their ubiquity, suggest that they were formed *in situ*. Similar morphological types of smectites were described in the North Atlantic during Aptian–Albian and early Cenozoic times (Holtzapffel et al., in press). These studies show that fine laths of smectites originated during *in situ* recrystallization of smectites, within the interstitial sedimentary environment, without significant chemical or mineralogical change. In the dominantly terrigenous environments of the Atlantic, the formation of fine-lathed smectites was favored by low sedimentation rates. In the southwest Pacific, sedimentation rates are high, but the terrigenous component of the sediment is highly diluted by the biogenic elements. Possibly recrystallization of smectites is favored when terrigenous supply is weak.

In biosiliceous fragments, tufts of fibers are probably small particles of smectites, formed in these microenvironments from the silica of the skeletons. Similar processes of smectite formation were described by Hoffert (1980) in the central Pacific. In the southwest Pacific, the scarcity of siliceous microfossils excludes this mechanism as a major contributor to smectite genesis.

Volcanic Influence

The thick laths and globular packs of fine laths in the sediments of the south Tasman Sea are generally associated with volcanic elements. Similar thick laths, sometimes associated with packs of laths, were observed near the Daito Ridge in the Philippine Sea (Chamley, 1980), and on the Walvis Ridge in the South Atlantic (Chamley et al., 1984). In both of these regions, smectites were chiefly formed during subaerial alteration processes in volcanic products. At Site 592, thick laths of smectites appear contemporaneously with the volcanogenic turbidites which were emplaced at Site 593. During the late Eocene, volcanic events were common in the southwest Pacific (Site 593 site chapter, this volume). Volcanogenic smectites observed on the southern Lord Howe Rise (Site 592) and on the Challenger Plateau (Site 593) were probably derived from erosion of altered volcanic material, transported by winds and currents.

Detrital Supply

Chlorite, illite, and irregular mixed-layer clays, which are associated with stilpnomelane, are abundant at all sites, especially from the late Miocene to the Pleistocene. Chlorite and illite are partly derived from the erosion of crystalline and metamorphic rocks. During alteration, chlorite, illite, and irregular mixed-layer clays are formed preferentially under humid, temperate climatic conditions, and their formation is also favored by continental mountain relief with active tectonism and erosion (Millot, 1964; Chamley, 1979). These conditions

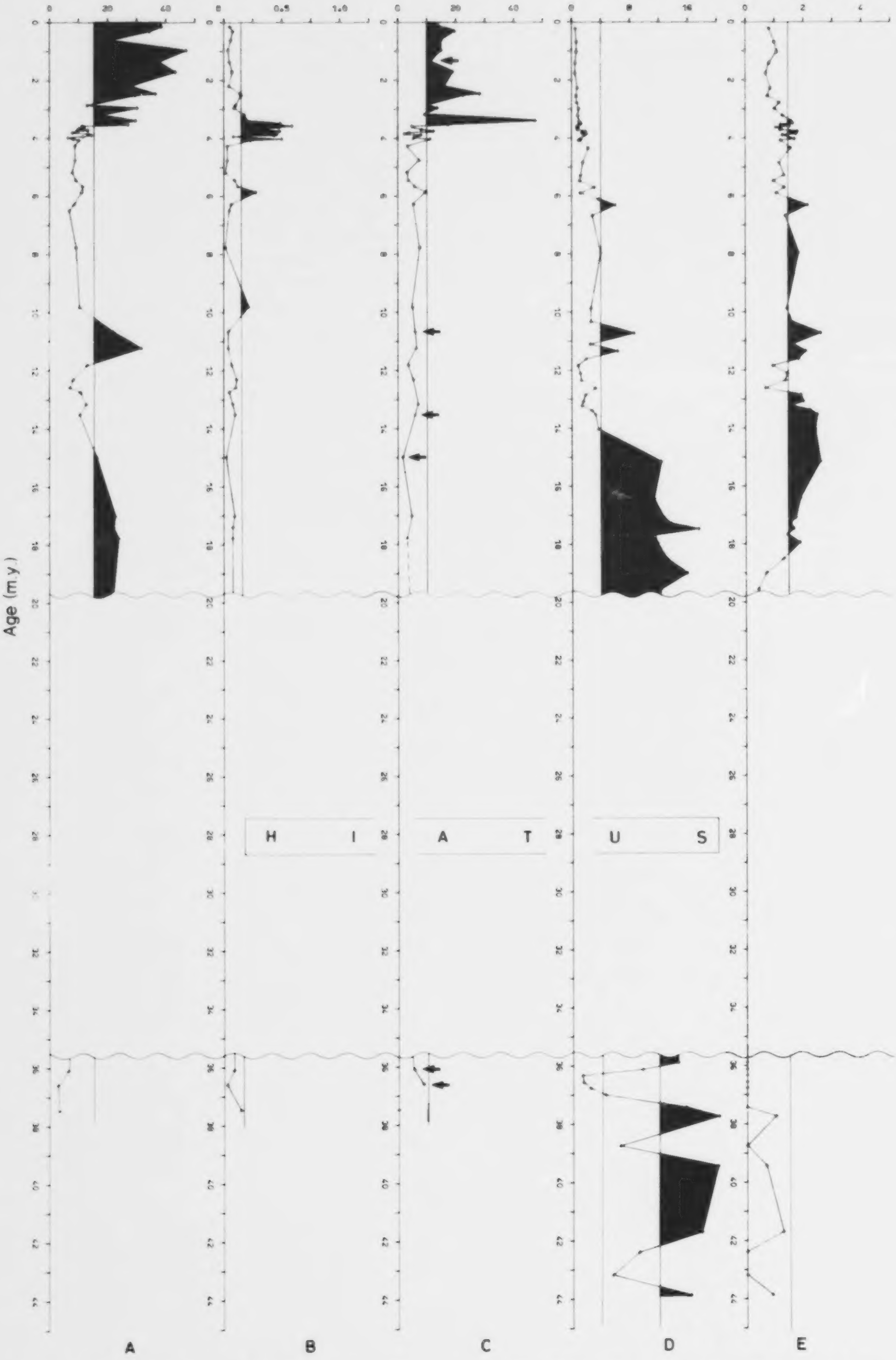

Figure 3. Site 592 results. A. Percentages of the <63 μm size fraction of the sediment. B. Accumulation rate of the carbonate-free fraction in g/(cm^2 × 10^3 yr.). C. Percentages of the terrigenous sediment fraction >6 μm of the carbonate-free sediment fraction. Arrows indicate samples with significant amounts of volcanic glass. D. Smectite/illite ratio. E. Kaolinite/illite ratio. Age determination according to the nannofossil biostratigraphy (Lohman; Martini; both this volume). Auxiliary lines emphasizing the major changes in the sediment record are arbitrary.

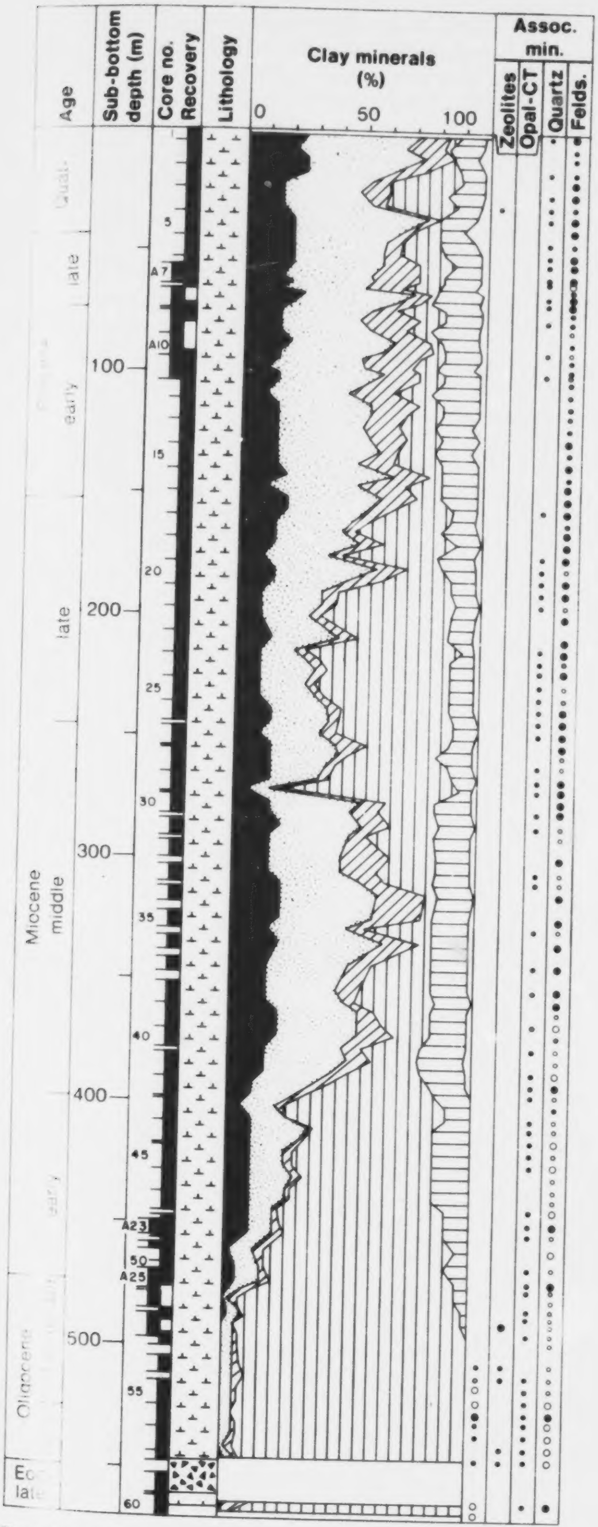

Figure 4. Site 593. Results. See Figure 2 for explanation of symbols.

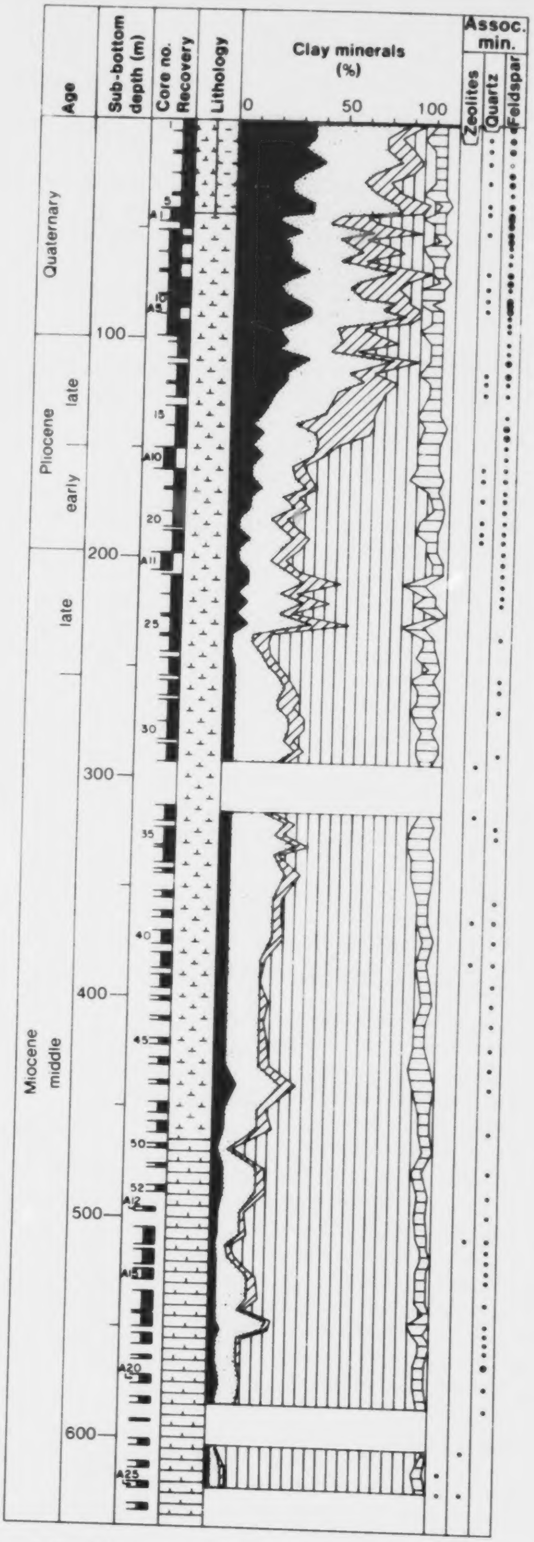

Figure 5. Site 594. Results. See Figure 2 for explanation of symbols.

are present today over a large portion of New Zealand. Moreover, stilpnomelane, mineral characteristic of low-grade, regionally metamorphosed terranes, is present in the sediment. Stilpnomelane is known as a widespread, abundant constituent of the schists of western Otago, in the South Island of New Zealand (Hutton, 1956; Deer et al., 1969). This mineral is present from the middle Miocene to the Pleistocene in the vicinity of New Zealand, at Site 593 on the Challenger Plateau and at Site 594 on the Chatham Rise. It also appears during the Quaternary at Site 592, on the southern Lord Howe Rise. These data suggest that the detrital supply from New Zealand had strong influence in this sector of the southwest Pacific.

The particles may have been transported by the currents which flow southward along the western coasts of New Zealand (Stanton, 1976; Ridgway, 1980) and then northward out at sea (Wyrtki, 1962). Taking into account meteorological data (Ramage, 1970), a portion of the particles could also have been transported by surface winds from northern New Zealand and by mid to high tropospheric westerly winds from Australia, toward the southern Lord Howe Rise. Rare palygorskite-like fibers are present in the Tasman Sea. Similar fibers, often associated in clusters, have been described previously in eolian dusts transported from Africa by trade winds and sampled in the Mediterranean (Robert et al., in press). During the last 15 m.y. (middle Miocene), the modes of the grain-size distribution of the terrigenous silt fraction from Site 592 are very similar to those from Sites 588 and 590 on the northern and middle Lord Howe Rise. This may indicate that the terrigenous silt at all three sites has the same source area (Dauphin, 1980; Sarnthein et al., 1982), that is, probably the Australian continent (Stein and Robert, this volume). East of New Zealand, the particles are transported by currents directed toward the northeast (Heath, 1981).

Main Significance of the Clay Minerals

Sites 592, 593, and 594 (Figs. 2–5) are subject principally to the detrital influence of New Zealand. Strong variations in the clay mineral associations are sometimes inconsistent with the climatic evolution of the Cenozoic (Kennett, 1977; Robert, 1982). Indeed, Eocene climates favored the formation of abundant smectites. Then, from the Eocene/Oligocene boundary to the Pleistocene, chlorite, illite, and irregular mixed-layer clays increased progressively (Chamley, 1979; Robert, 1982). On the southern Lord Howe Rise (Site 592), abundant illite and irregular mixed-layer clays were deposited during the late Eocene and the early Oligocene. On the Challenger Plateau and Chatham Rise, Sites 593 and 594, drilled at similar latitudes in the temperate zone, show very different abundances of illite and irregular mixed-layer clays during the middle and late Miocene. Climatic conditions strongly influenced clay mineral genesis on the Lord Howe Rise, but in the New Zealand area the data suggest that the morphology of the continental areas, driven by structural evolution, had the most important influence on the clay mineral assemblages at the DSDP sites, as in the Cape Basin of the South Atlantic (Robert, 1982).

Regions of rugged relief favor the removal of soluble ions and allow the development of soils in which chlorite and illite, then kaolinite, form. In contrast, regions with low relief, where soluble ions accumulate in the soils of poorly drained plains and sometimes in perimarine lagoons, are characterized by abundant smectites. Rifting stages or other tectonic activity, permit removal of the clay particles formed during previous periods, and the detrital supply is enriched in chlorite, illite, irregular mixed-layer clays, and kaolinite issued from the rejuvenated relief. Alternatively, the subsidence of the continental margins and the peneplanation of pre-existing relief favor the development of the poorly drained soils and perimarine lagoons where smectites accumulate (Chamley, 1979; Robert, 1982).

The abundances of clay minerals show large temporal changes which suggest that important shifts have occurred in the continental morphology, as well as in the climatic conditions and oceanic circulation in the southwest Pacific.

CENOZOIC CHANGES IN DETRITAL PARTICLES OFF NEW ZEALAND

Around New Zealand, five mineralogical units can be distinguished during the Cenozoic (Figs. 2–5).

Late Eocene–Early Oligocene

On the Challenger Plateau (Hole 593, Cores 56 to 60), volcanogenic turbidites were deposited, surrounded by calcareous biogenic sediments containing 85–100% smectites. When these turbidites were deposited, the calcareous biogenic sediments on the southern Lord Howe Rise (Hole 592, Cores 33 to 41) contained relatively abundant illite (5 to 20%) and irregular mixed-layer clays (5 to 20%), accompanied by chlorite and kaolinite (trace amounts to 5%). Smectites, however, remained the most abundant minerals (60 to 95%). In Cores 34 and 35, the carbonate-free silt fraction shows significant amounts of relatively coarse yellowish volcanic glass.

Middle Oligocene–Late Oligocene

During this period, a hiatus occurred on the Lord Howe Rise (Site 592), while on the Challenger Plateau (Cores 593-50 to 593-56; Cores 593A-25 to 593A-27), smectites were the dominant minerals (95%), and were accompanied by 5% illite and trace amounts of irregular mixed-layer clays.

Early Miocene

Above the hiatus, on the southern Lord Howe Rise (Cores 592-29 to 592-33), smectites were dominant (95%), accompanied by kaolinite (5%) and illite (trace amounts). On the Challenger Plateau (Cores 593-43 to 593-50; Cores 593A-23 to 593A-25), smectites prevailed (50 to 70%). Kaolinite (10 to 15%), illite (10 to 15%), chlorite (trace amounts to 10%), and irregular mixed-layer clays (trace amounts to 5%) were also present.

Middle Miocene–Late Miocene

During this period on the south Lord Howe Rise (Cores 592-19 to 592-29), smectites dominated the clay fraction (35 to 100%). They were accompanied by illite (trace amounts to 30%), kaolinite (trace amounts to 25%), irregular mixed-layer clays (trace amounts to 10%), and chlorite (0 to 5%). Significant amounts of yellowish volcanic glass, relatively coarse, were distinguished in the carbonate-free silt fraction, in Cores 20 (10.5 m.y.), 25, and 26 (13 to 14 m.y.).

On the Challenger Plateau (Cores 593-23 to 593-42), illite dominated (10 to 45%), associated with chlorite (5 to 20%), kaolinite (5 to 20%), and irregular mixed-layer clays (trace amounts to 20%). Smectites remained intermittently important (5 to 80%). Stilpnomelane appeared in trace amounts.

On the Chatham Rise, east of New Zealand (Cores 594-26 to 594-52; Cores 594A-12 to 594A-26), smectites were very abundant (45 to 95%). They were accompanied by illite (trace amounts to 30%), kaolinite (trace amounts to 10%), chlorite (trace amounts to 10%), and irregular mixed-layer clays (trace amounts to 5%). Stilpnomelane (0 to 5%) was also present.

Late Miocene–Pleistocene

On the southern Lord Howe Rise (Cores 592-1 to 592-18), illite increased (5 to 40%) and smectites decreased (75 to 25%). These minerals were accompanied by kaolinite (10 to 30%), irregular mixed-layer clays (trace amounts to 20%), and chlorite (0 to 10%). Trace amounts of stilpnomelane were present during Pleistocene time. The accumulation rates of the carbonate-free silt fraction show its first maxima near 10 and 6 m.y. (late Miocene), followed by a distinct maximum near 4 m.y. (early Pliocene). The last 3.5 m.y. (late Pliocene–Pleistocene) were characterized by a distinct coarsening of the grain size of the >63 µm fraction and the terrigenous silt fraction, and accumulation rates decreased. This change occurred at the same time also at Sites 588, 590, and 591 (Stein and Robert, this volume).

On the Challenger Plateau at this time as earlier (Cores 593-1 to 593-23; Cores 593A-7 to 593A-11), illite increased (15 to 55%) and smectites decreased (60% to 0). They were associated with chlorite (10 to 25%), irregular mixed-layer clays (5 to 25%), kaolinite (10 to 20%), and stilpnomelane (0 to 10%).

During the same period to the east of New Zealand (Cores 594-1 to 594-25; Cores 594A-1 to 594A-11), illite also increased (15 to 45%), as did chlorite (5 to 40%), irregular mixed-layer clays (5 to 35%), and stilpnomelane (trace amounts to 10%); smectites (60% to 0) and kaolinite (10 to 5%), however, decreased. During the late Pliocene, in particular, smectites decreased abruptly, from [illegible] to 10%, and chlorite, illite and mixed-layer clays increased in the same proportions. This change in the mineralogy immediately followed increased terrigenous supply in the bulk sediment, marked by alternations of detritus-rich and detritus-poor deposits. The presence of this event at Site 594 suggests that a drastic change in the detrital supply on the Chatham Rise occurred during the late Pliocene (Site 594 site chapter, this volume).

EVOLUTION OF TECTONICS AND CURRENTS IN THE NEW ZEALAND SECTOR

The important differences in the temporal and geographical distribution of the clay minerals suggest that the New Zealand area underwent a complex evolutionary history during the Cenozoic (Fig. 6, Table 2).

Late Eocene–Early Oligocene

After the Rangitata orogenesis during the Cretaceous, New Zealand became a passive margin until Oligocene time, while active spreading separated Antarctica and Australia (Crook and Feary, 1982). However, at the end of the late Eocene, an increase in illite and irregular mixed-layer clays appeared at Site 592 on the southern Lord Howe Rise. The composition of the clay fraction points to the local formation of continuously rejuvenated relief, because kaolinite does not form abundantly in soils. The presence of a youthful relief was possibly due to a distensive stage in New Zealand. Following a change in the rotation of the plates at 40 m.y. (Malahoff et al., 1982), a suite of faults and grabens formed in the South Island of New Zealand, especially in the region now corresponding to the Moonlight Tectonic Zone (Norris et al., 1978). At the end of the Eocene, volcanogenic turbidites were emplaced at Site 593 and volcanic glasses were deposited at Site 592. During this interval, lathed particles, sometimes associated with volcanic glass, suggest that volcanic activity also played a role in the formation of the smectites. Volcanic activity was present in New Zealand and as far north as New Caledonia (Lillie and Brothers, 1969). In other parts of New Zealand, the topography consisted of plains where smectites formed.

Middle Oligocene–Late Oligocene

During this period, smectites became dominant, indicating peneplanation of the relief, corresponding to subsidence of the continental margin. Volcanism was absent, and smectites developed in poorly drained soils or in perimarine lagoons. Smectite abundance may also indicate hot climatic conditions, with alternating periods of humidity and aridity, as in the Chad basin (Africa) today (Gac, 1979) or in the Mediterranean basin during the Messinian (Chamley et al., 1977). The observations made on the Challenger Plateau (Site 593) agree with the onshore data of Hume (1978) in northern New Zealand. During the Oligocene, the effects of subsidence were also recorded in the South Island of New Zealand (Norris et al., 1978), while tectonic quiescence induced a decrease in the volume of terrigenous particles eroded from New Zealand, and calcareous formations developed along the shore (Nelson, 1977). By this time, the presence of strong currents flowing southward across the Tasman Sea prevented deposition and eroded sediments in different regions of the southwest Pacific (Kennett, 1982), as evidenced by a hiatus on the southern Lord Howe Rise (Site 592).

Early Miocene

During the earliest Miocene, the detrital supply on the Challenger Plateau (Site 593) was marked by an increase in chlorite, illite, irregular mixed-layer clays, and

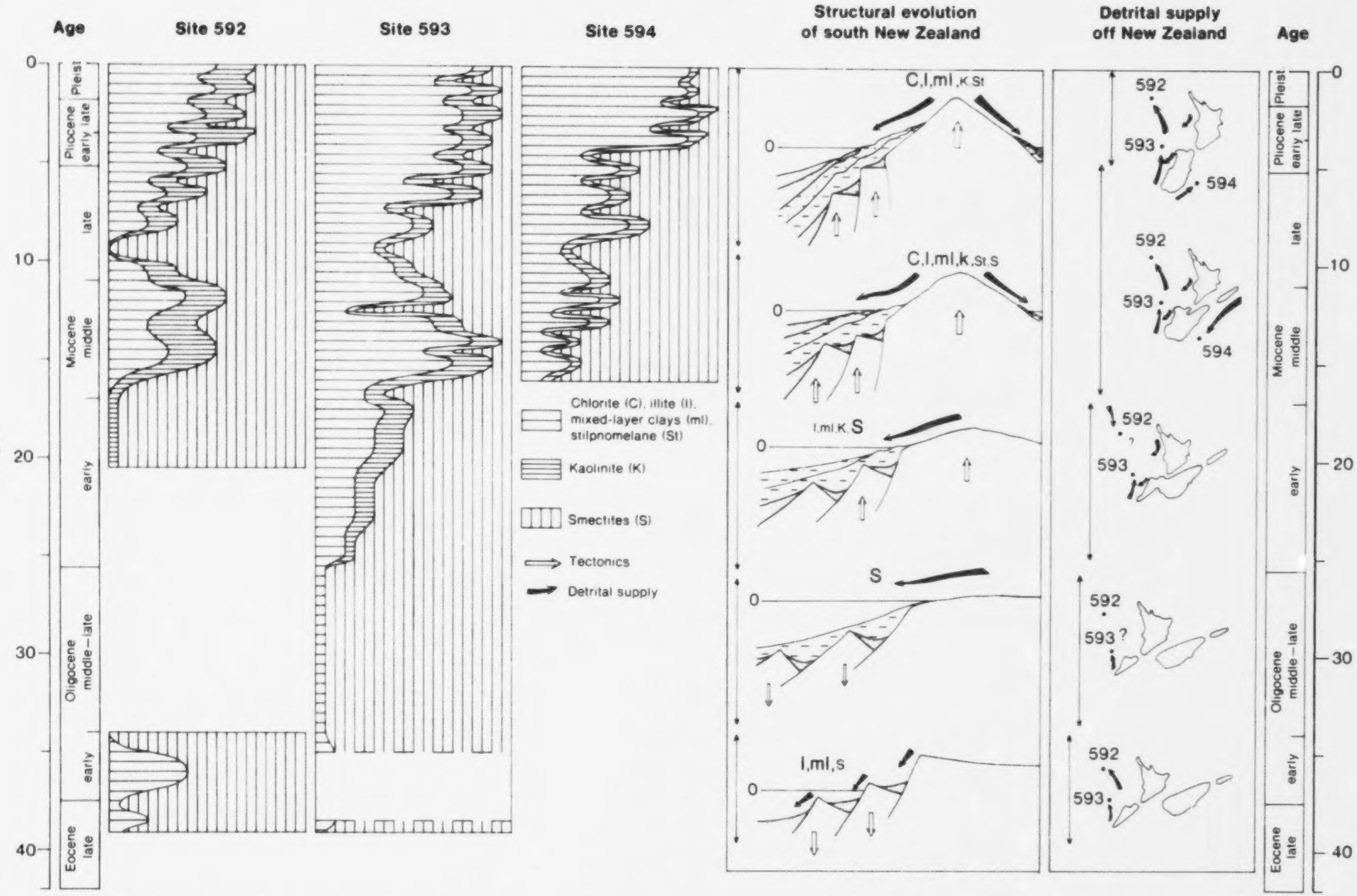

Figure 6. Evolution and significance of Cenozoic clay associations around New Zealand. Larger letters indicate more abundant minerals.

Table 2. Chronology and interpretation of the main mineralogic events, correlated with the geologic and oceanographic history of the southwest Pacific.

Age (m.y.)	Signals in the sediment	Interpretation	Major events
0			
	Stilpnomelane at 592	Increased detrital supply from New Zealand on the southern Lord Howe Rise. Increased circulation in the Tasman Sea	
	Coarsening of grain size at 592		Development of major Arctic ice sheets
5	Drastic increase in chlorite, illite, and mixed-layer clays at 594 and maximum accumulation rate of detritus at 592	Increased detrital supply from New Zealand on the Chatham and Lord Howe rises by northward currents	
	Strong increase in chlorite, illite, and mixed-layer clays at 592-593	Major rejuvenation of continental relief, related to a tectonic event	Kaikoura orogeny in New Zealand Change in the rotation of the plates
10	Short increase in smectites	Short tectonic relaxation	
	Abundant smectites at 594 until 4 m.y.	Detrital supply by southward currents on the Chatham Rise	
15	Drastic increase in chlorite, illite, mixed-layer clays, kaolinite at 592 and 593 Stilpnomelane appeared	Major rejuvenation of continental relief, related to a tectonic event Otago schists outcropped in New Zealand	Tectonic activity in New Zealand
20	Dominant smectites at 592	Detrital supply from plains, probably located in Australia, by southward currents and westerly winds	
25	Illite, mixed-layer clays, kaolinite appeared at 593	Weak rejuvenation of continental relief	Compression started in New Zealand Change in the rotation of the plates Strong southward currents in the Tasman Sea
30 Hiatus, Site 592			
35	Dominant smectites at 593	Strong influence of plains and perimarine basins	Subsidence and peneplanation in New Zealand
	Thick laths, globular packs of fine-lathed smectites at 592 Volcanogenic turbidites at 593	Strong influence of volcanism	Active volcanism in western New Zealand
40	Illite and mixed-layer clays at 592 until 34 m.y.	Rejuvenation of continental relief	Fracturing and graben formation in South Island, New Zealand Change in the rotation of the plates

Note: major events from Crook and Feary (1982), Hume (1978), Kennett (1977, 1982), Malahoff et al. (1982), Nelson (1977), Nelson and Hume (1977), Norris et al. (1978), Stock and Molnar (1982).

olinite eroded from areas of high relief, probably re- venated by tectonism. At this time, terrigenous clays ch as chlorite and illite also increased in abundance in nshore sediments (Hume, 1978). Sedimentological studies based on grain size, sedimentation rates, and mineralogy point to tectonic activity in the North Island during the early Miocene (Nelson and Hume, 1977). The Oligocene/Miocene boundary is marked by a change in the poles of rotation of the Pacific and Indo-Australian plates (Stock and Molnar, 1982). As a consequence, a compressive regime began in New Zealand (Crook and Feary, 1982), resulting in regional uplift of the South Island (Norris et al., 1978).

Above the hiatus on the southern Lord Howe Rise (Site 592), the clay mineral analysis shows 95% smectites and 5% kaolinite. This association of minerals, derived from continental regions where poorly drained plains dominate, is inconsistent with the geological history of New Zealand and with the clay mineral record on the Challenger Plateau (Site 593). Detrital supply on the southern Lord Howe Rise during the early Miocene came from a more stable and tectonically more quiescent area, probably Australia, where uplift in the eastern highlands did not begin before the end of the early Miocene (Plumb, 1979). Strong southward currents, active during the Oligocene and earliest Miocene, decreased in intensity toward 20 m.y., when northward currents developed in the south Tasman Sea (Kennett, 1982). This change in circulation permitted the deposition of clay particles eroded from Australia and transported southward by currents (pre-East Australian Current). Additionally, eolian input from Australia by the westerlies also provided detrital particles to sediments, as on the northern and middle Lord Howe Rise (Stein and Robert, this volume).

Middle Miocene-Late Miocene

During the middle and the early late Miocene, a strong increase in the abundances of chlorite, illite, irregular mixed-layer clays, and kaolinite on the Challenger Plateau (Site 593) and the southern Lord Howe Rise (Site 592) suggests the presence of continental relief, where soils formed on slopes rejuvenated by tectonic activity in New Zealand. The detrital supply of clays from New Zealand settled on the southern Lord Howe Rise, probably because of the increased influence of northward-flowing currents in the Tasman Sea. During the middle Miocene, reverse faulting began in the South Island contemporaneously with increased continental relief and erosion, marked by coarse conglomerates on land (Norris et al., 1978). This uplift favored the outcropping and erosion of old, metamorphosed terranes containing stilpnomelane. From this time onward, stilpnomelane was present in the detrital sediments around New Zealand. On the North Island, the influence of tectonism progressively increased (Nelson and Hume, 1977). More extensive volcanic activity (Crook and Feary, 1982) led to increased abundances of smectites in the sedimentary basins located on land (Hume, 1978). This increase in abundance of smectites was not observed in Tasman Sea sediments. There, detrital supply related to tectonic activity was largely dominant, though silty volcanic glasses were present in the sediment. Similar volcanic glasses were recovered on the northern and middle Lord Howe Rise (Sites 588 and 590), where they were more frequent during the same period (Stein and Robert, this volume). They may have originated from New Zealand, transported by surface winds. They may also have been supplied from tropical regions (Melanesia, New Hebrides) by hurricanes which flow southward in the Coral and Tasman seas (Ramage, 1970). However, at the end of the period under consideration, an increased supply of smectites in the sediments points to an increased influence of plain areas or volcanic activity on the southern Lord Howe Rise.

East of New Zealand, on the Chatham Rise (Site 594), chlorite, illite, irregular mixed-layer clays, and kaolinite are present in weak abundances at this site, located close to the South Island. Fluctuations in the mineral abundances are related to tectonic pulses, as at other sites. During the middle and the late Miocene, radiolarian associations include species of tropical origin (Caulet, this volume). As a consequence, it seems probable that the clay minerals supplied by erosion of proximal areas under tectonic influence were diluted by distal supplies of smectites, brought by currents flowing southward from the central Pacific (Caulet and Robert, in press).

Late Miocene-Pleistocene

This last period began with increased abundance of chlorite, illite, irregular mixed-layer clays, and stilpnomelane. On the southern Lord Howe Rise (Site 592), this increase seems too important to be related to climatic cooling at this latitude (Robert, 1982), where present-day climatic conditions favor smectite formation (Pedro, 1968). Furthermore, the relatively high kaolinite abundances present during that time are inconsistent with a climatic interpretation of the clay mineral association at Site 592. The data suggest rather, a resurgence of tectonic activity. During the late Miocene, at about 10 m.y., a new shift in the poles of rotation of the plates induced a more important compression, at the origin of the Kaikoura Orogeny (Crook and Feary, 1982). The effects of this tectonic stage on clay minerals appear clearly on the Challenger Plateau (Site 593) between the middle late Miocene (late NN11a, Core 23) and the middle early Pliocene (NN12-NN13, Core 16). Tectonic influences reached a climax close to the Miocene/Pliocene boundary and during the early Pliocene. Mass accumulation rates also record this evolution, characterized by maxima at 10 and 6 m.y. (late Miocene), then at 4 m.y. (early Pliocene) on the southern Lord Howe Rise. These maxima were interpreted as increased inputs of terrigenous matter, with negligible content of biogenic opal (Fig. 3). These important tectonic influences correspond to the Kaikoura Orogeny. The earlier maximum is also in agreement with sedimentological data from the North Island, based on sedimentation rates and mineralogy, which point to a maximum influence of tectonism at 5 m.y. (Nelson and Hume, 1977). Since that time, clay minerals have not shown any important change, suggesting that New Zealand had by then acquired its present morphology.

On the southern Lord Howe Rise, increased percentages of the sediment fraction >63 μm and terrigenous matter >6 μm suggest that currents exercised increased influence during the late Pliocene and the Quaternary (Fig. 3). During the Quaternary, stilpnomelane from South New Zealand appeared at Site 592, suggesting that the detrital supply from New Zealand had an increased influence on the southern Lord Howe Rise, induced by reinforced northward currents in the Tasman Sea.

On the Chatham Rise (Site 594), tectonic influence increased during the middle late Miocene, but the maximum abundance of chlorite, illite, and irregular mixed-layer clays occurred during the late Pliocene, following the onset of the cyclic terrigenous supply (Site 594 site chapter, this volume). During the same period, radiolarian associations show replacement of tropical by antarctic species, suggesting an inversion of the surface current system east of New Zealand. As northward currents replaced southward currents, increased abundances of clay minerals from the Southern Alps were supplied to Site 594 (Caulet and Robert, in press) and climatic cycles, marked by alternating detritus-rich and detritus-poor levels (Site 594 site chapter, this volume) appeared in the sedimentary record. On the North Island, mainly during the Pleistocene, an increase in abundance of smectites occurred in the sedimentary basins close to the volcanics which developed with the initiation of the Havre Trough-Taupo Graben (Hume, 1978). This increase in smectite abundance does not appear in the marine sediments recovered on the southern Lord Howe Rise, the Challenger Plateau, and the Chatham Rise, though light volcanic glass was observed in the carbonate-free silty fraction near 1.4 m.y. on the southern Lord Howe Rise. This is probably caused by preferential sedimentation toward the graben itself, and by dilution of the particles transported out of the graben into the detrital supply eroded from the New Zealand Alps.

CONCLUSION

In the New Zealand sector of the southwest Pacific, temporal variations in the clay mineral associations and grain-size distribution are mainly controlled by continental morphology, which is intimately tied to the structural evolution of the region. From the late Eocene onward, a continental margin evolves. A distensive stage occurred near the Eocene/Oligocene boundary, followed by subsidence during the Oligocene. A compressional regime began at the Oligocene/Miocene boundary and increased during the late Miocene, leading to several tectonic stages. Moreover, a comparison of the data obtained at these three sites suggests changes in oceanic circulation: the slowing of southward currents during the early Miocene, and transition from southward to northward currents in the Tasman Sea at the beginning of the middle Miocene, and east of New Zealand during the late Pliocene.

ACKNOWLEDGMENTS

Financial support for this study was provided by the Centre National de la Recherche Scientifique (A.T.P. Géologie et Géophysique des Océans) and the Deutsche Forschungsgemeinschaft. We should like to express our thanks to T. Allert, J. P. Ripert, F. Sirocko, R. Spielhagen, and M. Stransky for technical assistance. We are grateful to H. Chamley, J. P. Kennett, C. S. Nelson, M. Sarnthein, H. Zimmerman, and an anonymous colleague who offered aid and constructive comments during the genesis of this paper or during its review.

REFERENCES

Caulet, J. P., and Robert, C., in press. Reconstruction of Neogene paleoenvironments at Site 594 (Chatham Rise, Leg 90) from radiolarian and clay mineral study. *Paleogeogr., Paleoclimatol., Paleocol.*

Chamley, H., 1979. North Atlantic clay sedimentation and paleoenvironment since the late Jurassic. *In* Talwani, M., Hay, W., and Ryan, W. B. F. (Eds.), *Deep Drilling Results in the Atlantic Ocean: Continental Margins and Paleoenvironments*: Washington (Am. Geophys. Union), pp. 342-360.

________, 1980. Clay sedimentation and paleoenvironment in the area of the Daito Ridge (Northwest Philippine Sea) since the early Eocene. *In* Klein, G. de V., Kobayashi, K., et al., *Init. Repts. DSDP*, 58: Washington (U.S. Govt. Printing Office), 683-693.

Chamley, H., and Bonnot-Courtois, C., 1981. Argiles authigènes et terrigènes de l'Atlantique et du Pacifique N.W. (legs 11 et 58 DSDP): apport des terres rares. *Oceanol. Acta*, 4(2):229-238.

Chamley, H., Giroud d'Argoud, G., and Robert, C., 1977. Genèse des smectites messiniennes de Sicile. Implications paléoclimatiques. *Geol. Medit.*, 4(4):371-378.

Chamley, H., Maillot, H., Duée, G., and Robert, C., 1984. Paleoenvironmental history of the Walvis Ridge at the Cretaceous-Tertiary transition, from mineralogical and geochemical investigations. *In* Moore, T. C., Rabinowitz, P. D., et al., *Init. Repts. DSDP*, 74: Washington (U.S. Govt. Printing Office), 685-695.

Crook, K. A. W., and Feary, D. A., 1982. Development of New Zealand according to the fore-arc model of crustal evolution. *Tectonophysics*, 87:65-107.

Dauphin, J. P., 1980. Size distribution of chemically extracted quartz used to characterize fine-grained sediments. *J. Sed. Petrol.*, 50: 205-214.

Deer, W. A., Howie, R. A., and Züssmann, J., 1969. *An Introduction to the Rock-forming Minerals:* London (Longmans).

Gac, J. Y., 1979. Géochimie du bassin du lac Tchad. Bilan de l'altération, de l'érosion et de la sédimentation [D. Sci. dissert.]. University of Strasbourg.

Heath, R. A., 1981. Oceanic fronts around southern New Zealand. *Deep-Sea Res.*, 28A(6):547-560.

Hoffert, M., 1980. Les argiles rouges des grands fonds dans le Pacifique Centre-Est. Authigenèse, transport, diagenèse [D. Sci. dissert.]. University of Strasbourg.

Holtzapffel, T., Bonnot-Courtois, C., Chamley, H., and Clauer, N., in press. Héritage et diagenèse dans la constitution des smectites nord-atlantiques (Crétacé-Paléogène). *Bull. Soc. Géol. France.*

Hume, T. M., 1978. Clay petrology of Mesozoic to recent sediments of central western North Island, New Zealand [Ph. D. dissert.]. Waikato University, Hamilton, N.Z.

Hutton, C. O., 1956. Further data on the stilpnomelane mineral group. *Am. Mineral.*, 41:608-615.

Kennett, J. P., 1977. Cenozoic evolution of Antarctic glaciation, the circum-Antarctic Ocean, and their impact on global paleoceanography. *J. Geophys. Res.*, 82(27):3843-3860.

________, 1982. *Marine Geology:* Englewood Cliffs (Prentice-Hall).

Lillie, A. R., and Brothers, R. N., 1970. The geology of New Caledonia. *N.Z.J. Geol. Geophys.*, 13(1):145-183.

Malahoff, A., Feden, R. H., and Fleming, H. S., 1982. Magnetic anomalies and tectonic fabric of marginal basins north of New Zealand. *J. Geophys. Res.*, 87(B5):4109-4125.

Millot, G., 1964. *Géologie des argiles:* Paris (Masson).

Nelson, C. S., 1977. *Geological History of New Zealand.* Auckland Geogr. Teachers Group, 4.

Nelson, C. S., and Hume, T. M., 1977. Relative intensity of tectonic events revealed by the Tertiary sedimentary record in the North Wanganui basin and adjacent areas, New Zealand. *N.Z.J. Geol. Geophys.*, 20(2):369-392.

Norris, R. J., Carter, R. M., and Turnbull, I. M., 1978.Cainozoic sedimentation in basins adjacent to a major continental transform boundary in southern New Zealand. *J. Geol. Soc. London*, 135: 191-205.

Pedro, G., 1968. Distribution des principaux types d'altération chimique à la surface du globe. *Rev. Géogr. Phys. Géol. Dyn.*, 10(5): 457-470.

Plumb, K. A., 1979. The tectonic evolution of Australia. *Earth Sci. Rev.*, 14:205-249.

Ramage, C. S., 1970. Meteorology of the South Pacific, tropical and middle latitudes. *In* Wooster, W. S., (Ed.), *Scientific Exploration of the Southwest Pacific:* Washington (National Academy of Sciences), pp. 32-60.

Ridgway, N. M., 1980. Hydrological conditions and circulation off the West coast of the North Island, New Zealand. *N.Z.J. Marine Freshwater Res.*, 14(2):155-167.

Robert, C., 1982. Modalité de la sédimentation argileuse en relation avec l'histoire géologique de l'Atlantique Sud [D. Sci. dissert.]. University of Aix-Marseille 2.

Robert, C., Gauthier, A., and Chamley, H., in press. Origine autochtone et allochtone des argiles récentes de haute altitude en Corse. *Rev. Géol. Médit.*

Sarnthein, M., Thiede, J., Pflaumann, U., Erlenkeuser, H., Fuetterer, D., Koopmann, B., Lange, H., and Seibold, E., 1982. Atmospheric and oceanic circulation patterns off Northwest Africa during the past 25 million years. In von Rad, U., Hinz, K., Sarnthein, M., and Seibold, E. (Eds.), *Geology of the Northwest African Continental Margin:* Berlin (Springer-Verlag), pp. 545–604.

Stanton, B. R., 1976. Circulation and hydrology off the west coast of the South Island, New Zealand. *N.Z.J. Marine Freshwater Res.*, 10(3):445–467.

Stein, R., 1984. *Zur neogenen Klimaentwicklung in Nordwest Afrika und Paläo-Ozeanographie im Nordost-Atlantik: Ergebnisse von DSDP Sites 141, 366, 397 und 544B.* Ber. Rep., Geol. Paläontol. Inst. Univ. Kiel, 4. [Ph. D. dissert.]

Stock, J., and Molnar, P., 1982. Uncertainties in the relative positions of the Australia, Antarctica, Lord Howe and Pacific plates since the Late Cretaceous. *J. Geophys. Res.*, 87(B6):4697–4714.

Thiede, J., Suess, E., and Mueller, P. J., 1982. Late Quaternary fluxes of major sedimentary components to the seafloor at the Northwest African continental slope. In von Rad, U., Hinz, K., Sarnthein, M., and Seibold, E. (Eds.), *Geology of the Northwest African Continental Margin:* Berlin (Springer-Verlag), pp. 605–631.

Wyrtki, K., 1962. Geopotential topographies and associated circulation in the western South Pacific Ocean. *Aust. J. Marine Freshwater Res.*, 13(2):89–105.

Date of Initial Receipt: 28 June 1984
Date of Acceptance: 10 May 1985

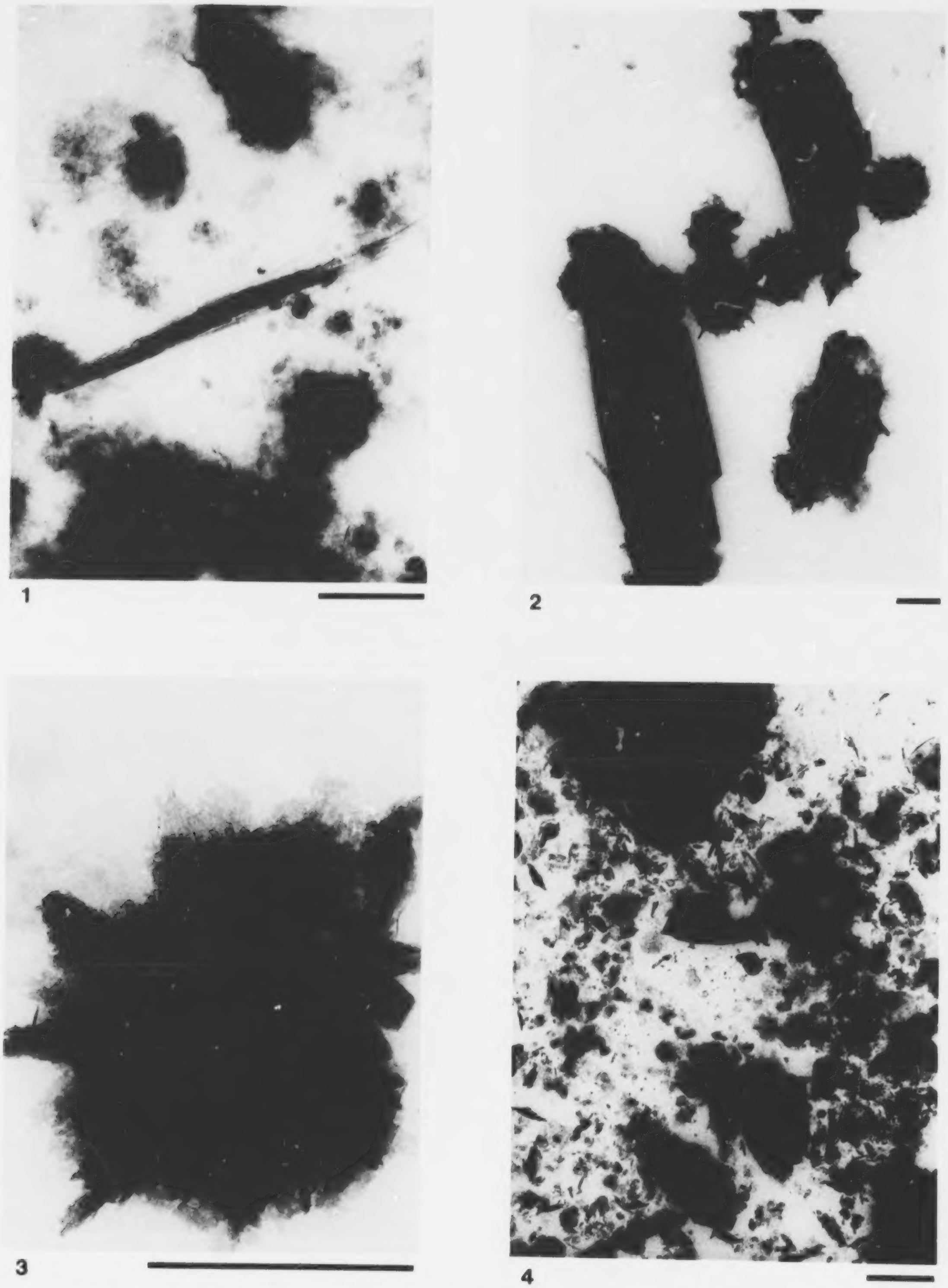

Plate 1. Electromicrographs. (Scale bar = 1 μm.) **1.** Sample 592-19-2, 50 cm, late Miocene; association of palygorskite-like fibers, abundant fleecy particles, and very fine laths in clay fraction containing up to 100% smectites. **2–3.** Sample 592-41-2, 50 cm, late Eocene, (2) thick-lathed particles and globular packs of fine laths, dominant in sample containing 85% smectites; (3) globular pack of fine laths. **4.** Sample 593-3-2, 50 cm, Quaternary; Fleecy particles, particles with sharp outlines, and rare hexagons in clay fraction containing 15% smectites, 10% irregular mixed-layer clays, 25% chlorite, 40% illite, and 10% kaolinite.

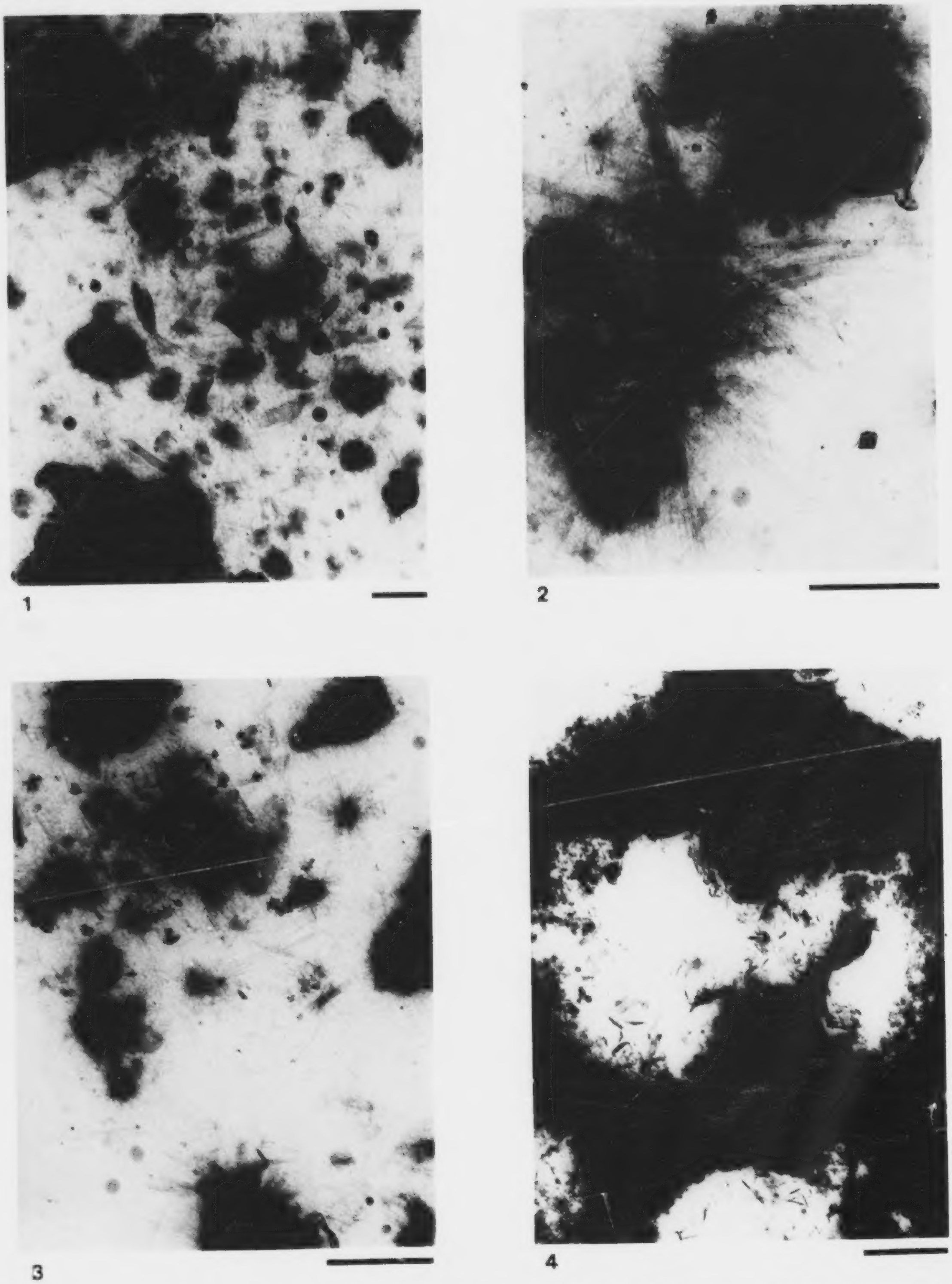

Plate 2. Electromicrographs. (Scale bar = 1 μm.) **1.** Sample 593-55-2, 50 cm, middle to late Oligocene; very fine laths, dispersed in the background or in the vicinity of fleecy particles, in clay fraction containing 95% smectites associated with 5% illite. **2.** Sample 593-58-2, 50 cm, early Oligocene; very fine laths associated in geometrical figures with 60° angles, in a clay fraction containing 95% smectites associated with 5% illite. **3–4.** Sample 594-26-2, 60 cm, middle to late Miocene, (3) very fine laths growing at the periphery of big particles (probably illite) or grouped in urchins, in clay fraction containing 75% smectites associated with 10% illite, 5% irregular mixed-layer clays, and 5% kaolinite; (4) small tufts of fibers, present at the periphery and in badly preserved diatom frustules.

31. PHYSICAL PROPERTIES OF CALCAREOUS SEDIMENTS FROM THE SOUTHWEST PACIFIC[1]

Roger H. Morin, Massachusetts Institute of Technology, Cambridge[2]

ABSTRACT

The extensive hydraulic piston coring activity on Leg 90 provided hundreds of meters of good quality sediment from which to conduct a comprehensive physical properties examination of nannofossil ooze and chalk. Most sites exhibit a well-defined transitional zone between the soft ooze and the indurated chalk, and a clear correlation is established between the onset of this region and sharp increases in sediment shear strength. Distinct increases in the values of compressional velocity and thermal conductivity across the ooze-to-chalk transformation are less evident. In a few instances, the porosity-versus-depth profiles depict zones where sediment porosity remains relatively constant across substantial depth intervals. Porosity is seemingly unaffected by large increases in overburden pressure, and no significant compaction occurs across several hundred meters of the sediment column. This behavior is attributed to a combination of several environmental factors. It is postulated that remarkably high sedimentation rates, a high diagenetic potential, and, perhaps, an appropriate grain size distribution all have had some relative influence in promoting sediment rigidity and retarding compaction.

INTRODUCTION

Leg 90 was principally organized as a paleoenvironmental expedition, with an ambitious and extensive program of hydraulic piston coring scheduled at eight sites traversing tropical to subantarctic areas of the southwest Pacific. Over the last few years, the hydraulic piston corer (HPC) has demonstrated the ability to recover high-quality geologic samples to depths of several hundred meters into the seafloor; this tool was utilized once again for the high-resolution paleoceanographic studies proposed for the region. Several thousand meters of relatively undisturbed core were retrieved by the HPC, and these provided a valuable opportunity to examine sediment physical properties in light of the depositional and lithification processes that occur in the ocean basins.

A comprehensive physical properties program was initiated during the course of the cruise, and a vast quantity of scientific data was generated. The shipboard experiments included the Gamma Ray Attenuation Porosity Evaluator (GRAPE) (Boyce, 1976b); gravimetric determination of wet-bulk density, grain density, and porosity (Boyce, 1976b); estimation of thermal conductivity (Chaney et al., 1983); measurement of compressional wave acoustic velocity (Boyce, 1976a); and evaluation of sediment shear strength (Boyce, 1976a).

Most of these experimental results have been presented in the individual site chapters of this volume, and deailed descriptions of the laboratory equipment and methodology are contained in the introductory chapter. This hapter attempts to correlate and compare data from arious sites, and focuses upon the physical characteriscs of calcareous sediments only. For all of the sites except Site 594, $CaCO_3$ content remained high, consistently above 90%, and physical properties profiles versus depth share the same trends (Sites 587, 588, 590, 591, 592, 593). These sites consisted almost exclusively of nannofossil ooze (grading into chalk) and/or foraminifer-bearing nannofossil ooze (grading into chalk) with occasional trace amounts of siliceous material, such as radiolarians, sponge spicules, and volcanic glass. Sediments at Site 594 contained numerous intervals of terrigenous material, such as clayey silt, and data from this final hole are not included in this review.

GRAPE ANALYSES

The Gamma Ray Attenuation Porosity Evaluator was used in a continuous scanning mode in order to estimate sediment wet-bulk density. Boyce (1976b) describes the instrument and operational procedure in detail and considers the sources of error associated with the measurement. These include liner variation, integrity of the geologic material, and change in gamma-ray path length. The greatest problem in reliability of the data has arisen where hard rocks or indurated sediments have not completely filled the core liners. In these cases, geometric concerns caused by a shorter gamma-ray path length through the geologic sample have made the values of wet-bulk density suspect.

During HPC deployment in soft sediments, the liner was completely filled with relatively undisturbed material, and no geometric adjustments to the GRAPE data were required. Mayer (1982) has addressed the issue of sediment disturbance and has found specimen quality to be very high when the HPC has functioned properly. HPC refusal began to occur during this cruise at coring depths near 250 m, coincident with the appearance of the stiffer chalks, and a newly developed extended core barrel (XCB) was utilized for subsequent core retrieval. Site 590 represented the first successful deployment of the XCB. Cores obtained with this apparatus were slightly to moderately disturbed, often consisting of biscuits of indurated sediments surrounded by an annular slurry of soft ooze injected during the coring process. This soft material is expected to cause GRAPE wet-bulk density estimates to be slightly less than the actual values; a 3 mm-thick slurry wall adjacent to the 6.61-cm inside diameter of the core liner should decrease the average density by 1 to 2%. Gravimetric analyses of chunk samples (Boyce, 1976b) taken from these deep cores, however, yielded wet-bulk density results that were in very good agreement with the uncorrected GRAPE-generated data. Thus, the GRAPE results presented in this chapter, measured on both the HPC and the XCB cores, have not been adjusted for possible geometric errors.

---

[1] Kennett, J. P., von der Borch, C. C., et al., *Init. Repts. DSDP*, 90: Washington (U.S. t. Printing Office).

[2] (Present address): U.S. Geological Survey, Denver, CO 80225.

The porosity-versus-depth profiles displayed in Figure 1 were derived from the GRAPE saturated wet-bulk density data. Carbonate content is one parameter that directly controls porosity and density; it was uniformly high throughout the sediment columns at all pertinent sites. The grain density of biogenic calcite is 2.72 g/cm^3, whereas that of silica is 2.1 to 2.3 g/cm^3 (Baas Becking and Moore, 1959). An average grain density was assumed to be 2.69 g/cm^3, and the saturated wet-bulk density results were accordingly converted to values of sediment porosity.

In this situation of constant grain density, porosity essentially mirrors the bulk density profile. The dashed lines in Figure 1 identify the individual depths where an ooze-to-chalk transition was observed. The corresponding transitional porosities range from approximately 50 to 53%. Hole 592 contains two separate transitional appearances. An initial onset of chalk is observed at 260 m, followed by a reintroduction of calcareous ooze. This sequence quickly undergoes a transition to chalk again at a depth of approximately 330 m. The gap in porosity data for Site 593 (360–500 m) was caused by a GRAPE instrument malfunction that was not detected immediately.

The effective overburden pressure at each site was computed from the GRAPE wet-bulk density data averaged across the incremental depth intervals, assuming no excess pore pressures. Plots of cumulative effective stress versus depth are presented in Figure 2, again with the dashed horizontal lines representing the ooze-to-chalk transitional levels. By comparing Figures 1 and 2, it is interesting to note the instances where little or no obvious consolidation has occurred across substantial depth intervals, even with significant, systematic increases in lithostatic load. At Site 590, for example, average porosity remains effectively constant, apart from high frequency fluctuations, across a 250-m span of the sediment column (200–450 m). Similar behavior is observed, but to a lesser extent, at Sites 591 and 592. At Site 593, porosity is shown to decrease through the upper 50 m, but to remain relatively constant over the next 300 m as sediment overburden pressure is gradually increased from approximately 4 to 26 kg/cm^2.

THERMAL CONDUCTIVITY

Sediment thermal conductivity was measured through the core liner at Sites 587 and 588 utilizing the needle probe method (Chaney et al., 1983); the results are plotted versus depth in Figure 3. These data were obtained aboard ship and have not been corrected for *in situ* pressure and temperature conditions. Morin and Von Herzen (this volume) have performed this exercise at selected depths in order to compute oceanic heat flow and report a total correction of only 2.6%. The experimental error in this particular case is approximately ±4%.

The thermal conductivity values were cross correlated with the porosity profiles of Sites 587 and 588 in order to arrive at a relationship between conductivity and porosity for calcareous sediments (Fig. 4). Numerous models designed to provide a suitable estimate for the thermal conductivity of two-phase media with static liquid component have been proposed (Wyllie and Southwick, 1954; Jeffrey, 1973; Crane and Vachon, 1977). A detailed solution of this conduction problem, however, requires that the shape, size, location, and conductivity of each particle be known. Analytical models have attempted to overcome this difficulty in describing the microstructure by proposing a number of simplifying assumptions.

Ohm's Law models, for instance, are designed to represent randomly packed granular systems by equivalent electrical analogs. Broad constraints are placed on the bulk thermal conductivity of the system by considering two different phase networks. The series and the parallel arrangements correspond to the minimum and maximum possible values for conductivity, respectively. Curves A and B in Figure 4 illustrate these bounds, assuming the fluid and solid conductivities to be 0.61 and 2.85 W/m-K, respectively (Clark, 1966).

If the values of the separate phase conductivities differ significantly, the established bounds are so broad as to fail to provide useful limits. Hashin and Shtrikman (1962) have shown that their exact, rigorous solution produces the narrowest possible constraints on thermal conductivity for macroscopically heterogeneous, isotropic media. Their model consists of a well-separated suspension of spheres of varying size; one phase is continuous and the other discrete. Curves C and D in Figure 4 are the conductivity bounds determined by the Hashin and Shtrikman (1962) analysis. Curve C defines the case of a dominant fluid component, with sediment grains suspended in seawater. Curve D assumes a continuous solid matrix containing individual pores. Theoretically, as a calcareous sediment gradually undergoes consolidation, the thermal conductivity data are expected to deviate from Curve C (liquid dominated—ooze) and approach curve D (solid dominated—chalk). This behavior is not clearly substantiated by the results plotted in Figure 4. However, the narrow limits imposed by the Hashin and Shtrikman (1962) model do successfully constrain all of the individual data points.

SHEAR STRENGTH

Shear strength was measured on split cores in the original horizontal direction with a modified Wykeham Farrance laboratory vane apparatus (Boyce, 1976a). The test procedure was repeated until the sediment became so lithified that its strength exceeded the capability of the

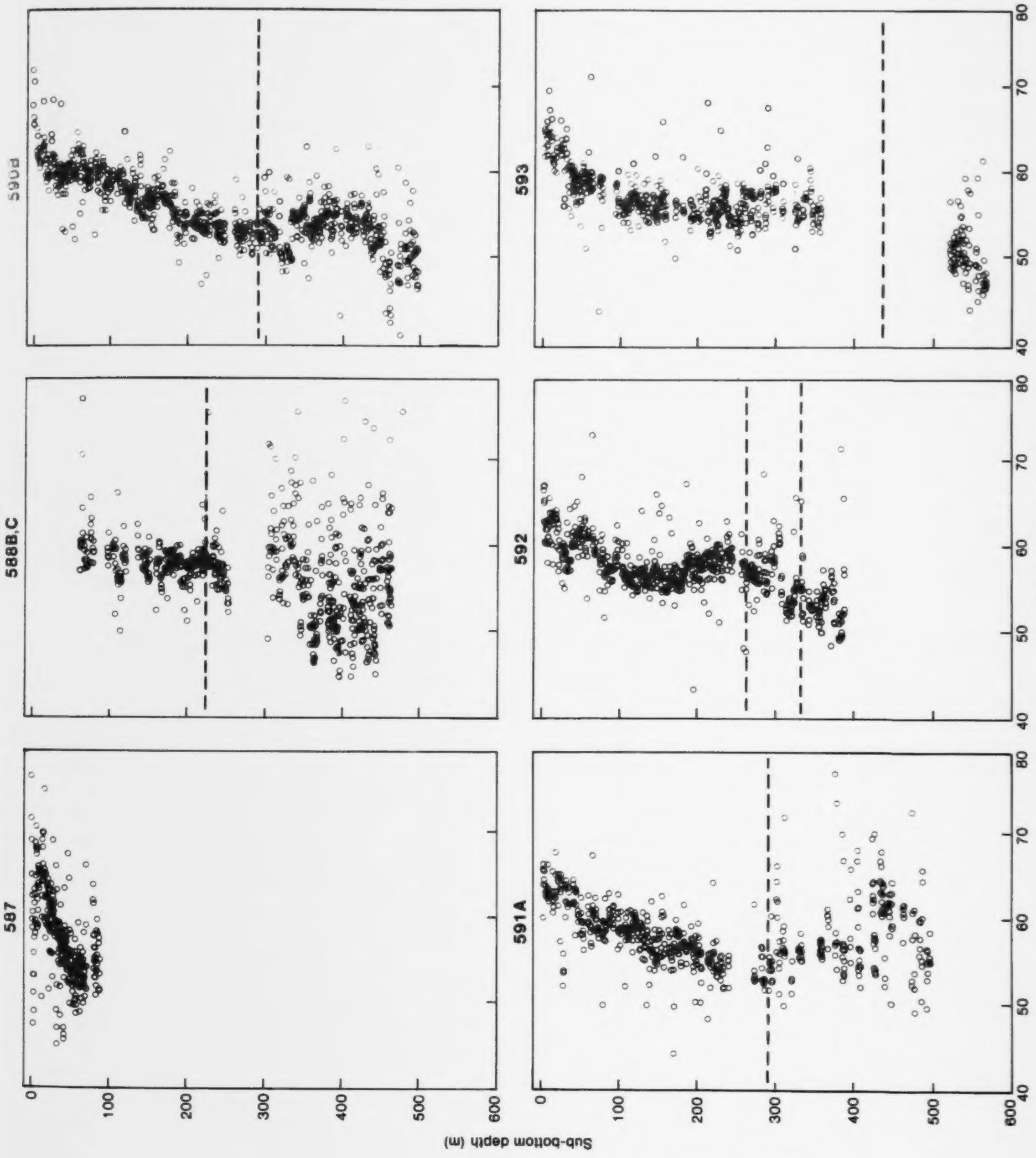

Figure 1. Multiple plot of porosity (GRAPE) versus depth for six sites. Dashed line indicates ooze-to-chalk transitional depth.

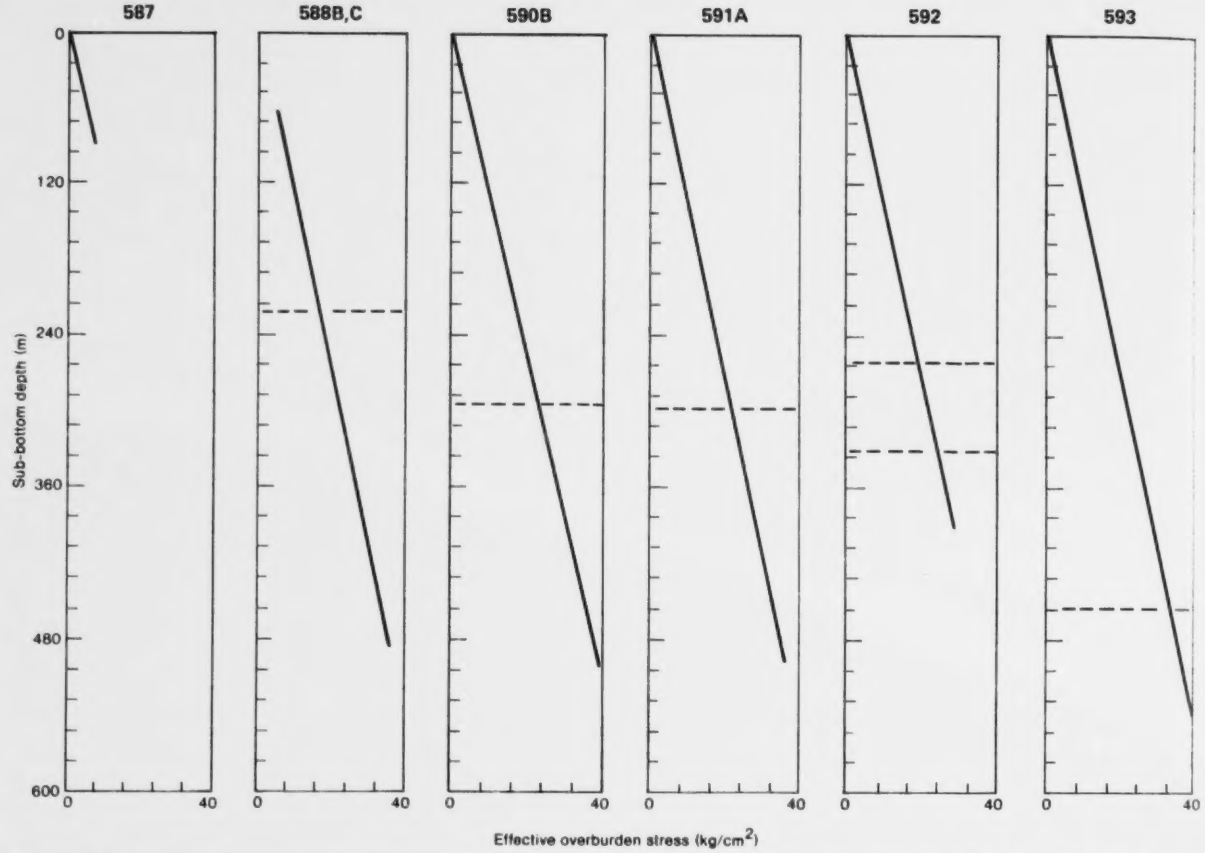

Figure 2. Multiple plot of effective overburden pressure versus depth for six sites. Dashed line indicates ooze-to-chalk transitional depth.

instrument. This condition coincided with the appearance of chalk and closely followed the retooling of coring operations from the HPC to the XCB. Results are recorded versus depth in Figure 5 for Sites 590, 591, and 592. At Site 592, where there were two transitional depths, a sizable increase in shear strength at the initial onset of chalk was followed by a gradual decline and, finally, by another sharp increase in this property at the second ooze-to-chalk transition. When these results are cross correlated with the individual site porosity profiles, a clear dependence of shear strength upon porosity is observed. This relationship is illustrated in Figure 6; the dashed line represents a least-squares polynomial fit of the data. This best-fit approximation is described by the following equation.

$$S = 40461.3 - 1956.7\phi + 31.60\phi^2 - 0.170\phi^3$$

where S = shear strength (g/cm^2) and ϕ = porosity (%). A sudden increase in shear strength is observed as the porosity approaches the transitional region, estimated as being in the range of 50 to 53% for all sites considered. At porosities below the ooze-to-chalk transformation, lithification is so pronounced that the miniature vane device can no longer penetrate the sediments to produce an accurate estimate of shear strength.

ACOUSTIC VELOCITY

Sediment acoustic velocity was measured on board ship on split cores, parallel to bedding (Boyce, 1976b), and the results from four sites are plotted versus depth in Figure 7. Unlike the shear strength determination, which was limited by the range of the laboratory instrument, seismic velocity results continued to be collected below the ooze-to-chalk transformation. The data obtained from Sites 588, 590, and 592 show little change in compressional wave velocity over the top 300 m of the sediment column. In their physical properties study, Wilkens and Langseth (1983) report that seismic velocity exhibited the least variation with depth of any of the parameters measured; Mayer (1979, 1982) arrived at a similar conclusion. Fluctuations in this elastic property remained small across large depth intervals, even as other physical properties changed significantly. Small velocity increases became evident as porosities declined into the chalk region, though this shift to higher values was not nearly so pronounced as that observed with the shear strength data. The Site 591 profile shows greater variations in acoustic velocity at the lower depths because of early diagenetic alteration produced by a spectacular sedimentation rate of 131 m/m.y. during the early Pliocene. Calcareous nannofossils begin to exhibit signs of overgrowths

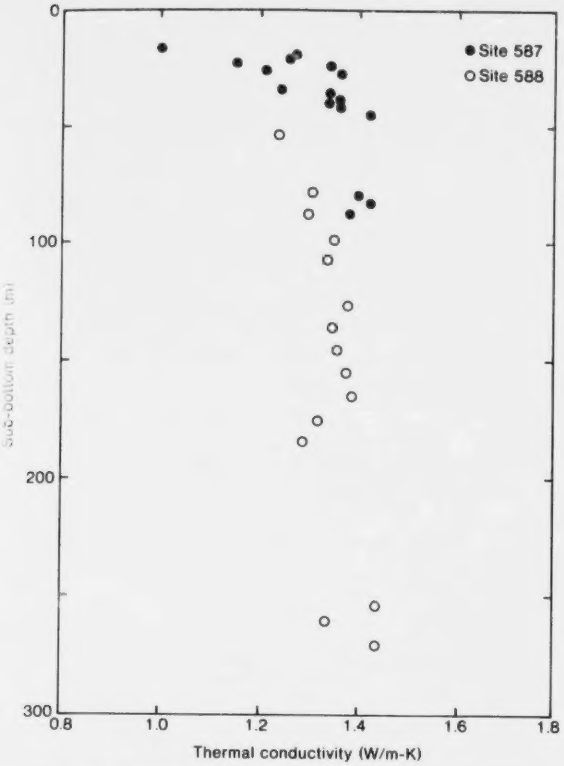

Figure 3. Plot of sediment thermal conductivity (Sites 587 and 588) versus depth.

at a depth of 260 m. These cementing agents develop sediment framework, increase matrix rigidity, and allow elastic energy to be more readily transmitted.

DISCUSSION

The set of physical properties data presented in this chapter provides a good base from which to investigate the consolidation characteristics of calcareous ooze and chalk. Coogan and Manus (1975) have presented a comprehensive review of this complex subject, with its numerous interrelated facets. They categorize the sets of conditions that directly affect the compaction of carbonates as the following: (1) inherited factors such as grain size, packing arrangement, and sorting; (2) inhibitory factors that discourage compaction, principally cementation; and (3) dynamic factors such as rate of loading, pore pressure, overburden pressure, and nature of formation fluid. It is significant to this discussion to note that if compactive stresses are high enough, deformation will occur regardless of the relative influences of any other factors. Instances are found from the profiles depicted in Figure 1 where the sediment column displayed little or no evidence of systematic lithostatic compaction, and where porosity remained essentially constant across hundreds of meters of depth. This behavior is now considered in terms of the primary factors classified previously.

Apart from Site 588, all locations experienced remarkably high sedimentation rates during the late to early Pliocene. These ranged from 57 to 131 m/m.y. and correspond to depths of approximately 40 to 200 m. It is

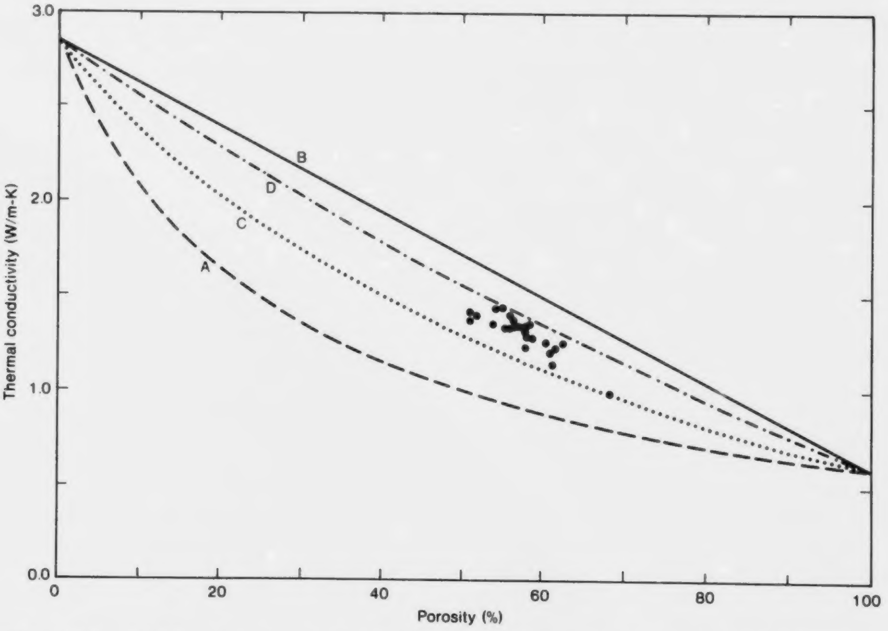

Figure 4. Plot of sediment thermal conductivity (Sites 587 and 588) versus porosity. Curves A and B are series and parallel bounds, respectively. Curves C and D are constraints defined by Hashin and Shtrikman (1962).

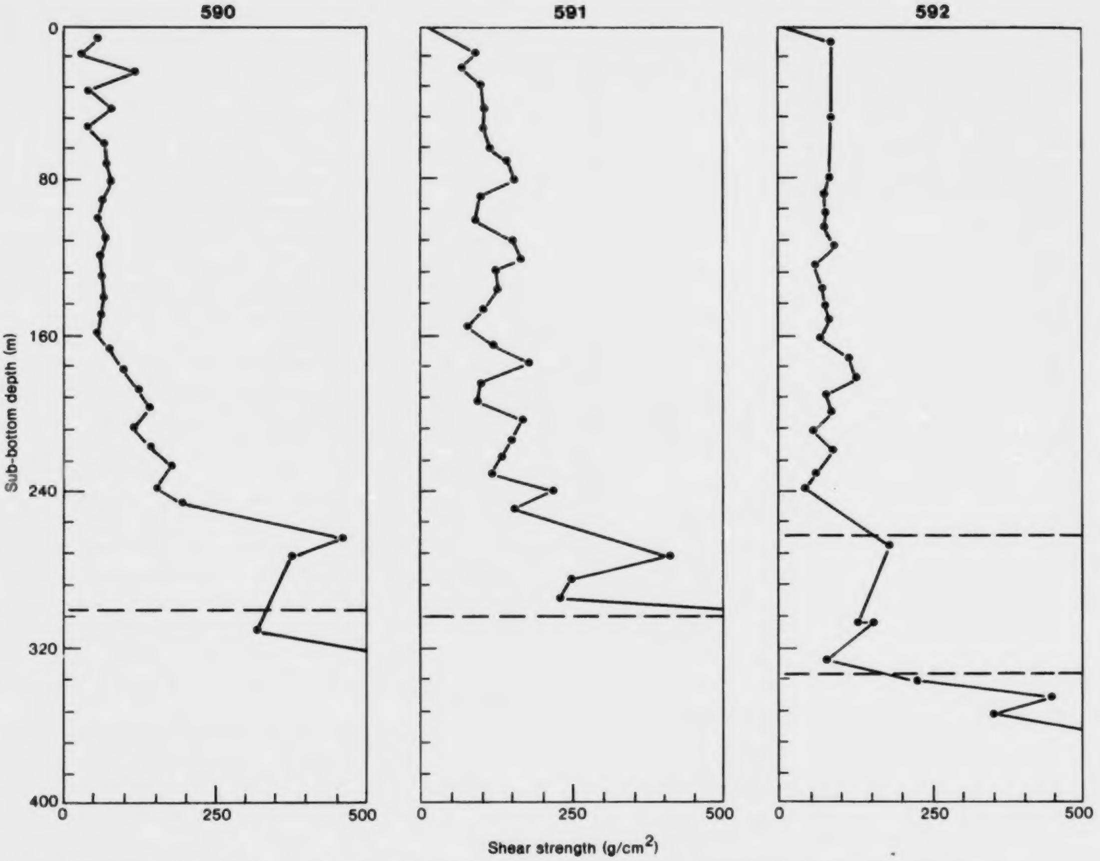

Figure 5. Multiple plot of shear strength versus depth for three sites. Dashed line indicates ooze-to-chalk transitional depth.

possible that excess pore pressures induced by these large depositional rates delayed initial consolidation, enabling the sediment particles to establish a competent, solid matrix before complete dissipation of pore pressures occurred.

The phenomenon of early lithification of carbonate sediments has been addressed by Bathurst (1971) and Schlanger (1963), among others. Weller (1959) attributes the relatively high porosities and lack of compaction in carbonate sands to early and widespread cementation. At Site 591, a premature introduction of chalk is caused by a diagenetic change in the state of fossil preservation. Schlanger and Douglas (1974) have defined the concept of diagenetic potential, whereby the variations in the degree of cementation and textural changes across ooze-chalk-limestone sequences are ascribed to paleoceanographic conditions or events. The ease with which diagenesis may occur becomes a function of, among other parameters, plankton productivity and, correspondingly, sedimentation rate. Milholland et al. (1980) have applied this concept to pure carbonate sediments in order to develop a geoacoustic model that accounts for observed physical property variations with depth. Thus, it is possible that the high sedimentation rates not only produced the initial excess pore pressures, but also contributed to a condition of high diagenetic potential, thereby promoting a dissolution and recrystallization process among grains which, in turn, enhanced the rigidity of the open framework.

An additional mechanism that could account for the absence of compaction across various depth intervals at these pertinent sites relates to proper grain size and sorting. Both cementation and mechanical compaction are influenced by these two particle properties. Heald and Renton (1966) have demonstrated that fine sands, with their considerable surface area, are much more susceptible to dissolution effects than are coarser ones. Robertson (1967) has reported laboratory results that illustrate the effects of grain size and rate of loading upon the consolidation of a carbonate sediment. Coogan and Manus (1975) describe a condition known as bridging, whereby large grains form an interlocking network during the initial steps of consolidation and receive the majority of the overburden load. The smaller grains are located between these prominent particles and contribute little to the overall sediment compressibility. This phenomenon produces a stiff matrix early during the consolidation process and is a direct function of grain size distribution. Well-sorted grains make compaction more likely, whereas poorly sorted, fine grains encourage bridging and cementation. Grain size and sorting characteristics should have a primary effect upon the consolidation be-

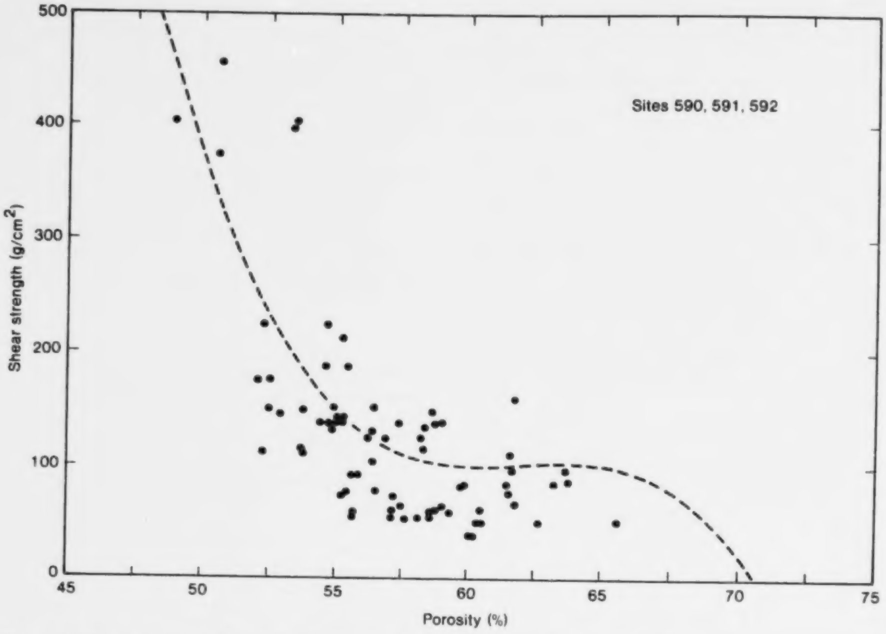

Figure 6. Plot of sediment shear strength versus porosity for three sites. Dashed line represents least-squares polynomial fit.

havior of calcareous ooze and chalk. Grain size distribution analyses on specific Leg 90 samples are currently being conducted at shore-based geotechnical laboratories.

It is hypothesized, therefore, that some combination of the three following factors may have contributed to the unusually constant porosity-versus-depth profiles evidenced at these sites.

1. Excess pore pressures caused by spectacular sedimentation rates retarded initial compaction and promoted the formation of an open sediment microstructure.

2. Excessive sedimentation rates increased the diagenetic potential of the calcareous sediments, thereby accelerating cementation processes among grains and increasing sediment rigidity.

3. Appropriate grain size distributions provided a good mechanical fit among particles and prevented further consolidation from occurring until a threshhold overburden stress finally initiated additional compaction. A small median grain size also encouraged dissolution and reprecipitation.

The ooze-to-chalk transition, whether it was simply the product of mechanical compaction and particle reorientation or brought about through diagenetic alteration, coincides clearly with sharp, substantial increases in shear strength. Variations in compressional velocity at this stage are also present, though the relationship is much less distinct. The thermal conductivity results all fall within the limits established by the Hashin and Shtrikman (1962) model, but a uniform shift in the data from Curve C to Curve D with declining porosity is not obvious (Fig. 4). It does not appear, therefore, that the ooze-to-chalk transformation affects this property to the extent that it does the shear strength; a transitional porosity range cannot be identified from the plots presented in Figure 4. It is interesting to consider, as a final note, that the porosity range over which the sediment undergoes this major lithological change is very narrow, perhaps only 1 or 2%.

ACKNOWLEDGMENTS

J. Gardner assisted in collecting the physical properties data throughout the cruise; J. Pine performed all of the carbonate bomb tests. Their help is gratefully appreciated.

REFERENCES

Baas Becking, L. G. M., and Moore, D., 1959. Density distribution in sediments. *J. Sediment. Petrol.*, 29:45–55.

Bathurst, R. G. C., 1971. *Carbonate Sediments and Their Diagenesis:* Amsterdam (Elsevier).

Boyce, R. E., 1976a. Deep Sea Drilling Project procedures for shear strength measurements of clayey sediments using modified Wykeham-Farrance Laboratory vane apparatus. *In* Barker, P. F., Dalziel, I. W. D., et al., *Init. Repts. DSDP*, 36: Washington (U.S. Govt. Printing Office), 1059–1068.

Boyce, R. E., 1976b. Definitions and laboratory techniques of compression sound velocity parameters and wet-water content, wet-bulk density, and porosity parameters by gravimetric and gamma ray attenuation techniques. *In* Schlanger, S. O., Jackson, E. D., et al., *Init. Repts. DSDP*, 33: Washington (U.S. Govt. Printing Office), 931–958.

Chaney, R. C., Ramanjaneya, G., Hencey, G., Kanchanastit, P., and Fang, H. Y., 1983. Suggested test method for determination of thermal conductivity of soil by thermal-needle procedure. *Geotech. Testing J.*, 6:220–225.

Clark, S. P. (Ed.), 1966. *Handbook of Physical Constants:* Boulder (Geological Society of America).

Coogan, A. H., and Manus, R. W., 1975. Compaction and diagenesis of carbonate sands. *In* Chilingarian, G. V., and Wolf, K. H., (Ed.), *Developments in Sedimentology: Compaction of Coarse-Grained Sediments:* Amsterdam (Elsevier), pp. 79–166.

Crane, R. A., and Vachon, R. I., 1977. A prediction of the bounds on the effective thermal conductivity of granular materials. *Int. J. Heat Mass Transfer*, 20:711–723.

Hashin, Z., and Shtrikman, S., 1962. A variational approach to the theory of the effective magnetic permeability of multiphase materials. *J. Appl. Phys.*, 33:3125–3131.

Heald, M. T., and Renton, J. J., 1966. Experimental study of sandstone cementation. *J. Sediment. Petrol.*, 36:977–991.

Jeffrey, D. J., 1973. Conduction through a random suspension of spheres. *Proc. Roy. Soc. London*, 335:355–367.

Mayer, L. A., 1979. Deep sea carbonate: acoustic, physical, and stratigraphic properties. *J. Sediment. Petrol.*, 49:819–836.

________, 1982. Physical properties of sediment recovered on DSDP Leg 68 with the hydraulic piston corer. *In* Prell, W. L., Gardner, J. V., et al., *Init. Repts. DSDP*, 68: Washington (U.S. Govt. Printing Office), 365–382.

Milholland, P., Manghnani, M. H., Schlanger, S. O., and Sutton, G. H., 1980. Geoacoustic modeling of deep-sea carbonate sediments. *J. Acoust. Soc. Am.*, 68:1351–1360.

Robertson, E. C., 1967. Laboratory consolidation of carbonate sediment. *In* Richards, A. F. (Ed.), *Marine Geotechnique:* Urbana (Univ. of Ill. Press), pp. 118–127.

Schlanger, S. O., 1963. Subsurface geology of Eniwetok Atoll. *U.S. Geol. Survey Prof. Paper*, 260BB:991–1066.

Schlanger, S. O., and Douglas, R. G., 1974. The pelagic ooze-chalk-limestone transition and its implications for marine stratigraphy. *Int. Assoc. Sedimentol.*, Spec. Publ., 1:117–148.

Weller, J. M., 1959. Compaction of sediments. *Am. Assoc. Petrol. Geol. Bull.*, 43:273–310.

Wilkens, R. H., and Langseth, M. G., 1983. Physical properties of sediments of the Costa Rica Rift, Deep Sea Drilling Project Sites 504 and 505. *In* Cann, J. R., Langseth, M. G., et al., *Init. Repts. DSDP*, 69: Washington (U.S. Govt. Printing Office), 659–674

Wyllie, M. R. J., and Southwick, P. F., 1954. An experimental investigation of the s.p. and resistivity phenomena in dirty sands. *J. Petrol. Tech.*, 44–57.

Date of Initial Receipt: 18 June 1984
Date of Acceptance: 26 October 1984

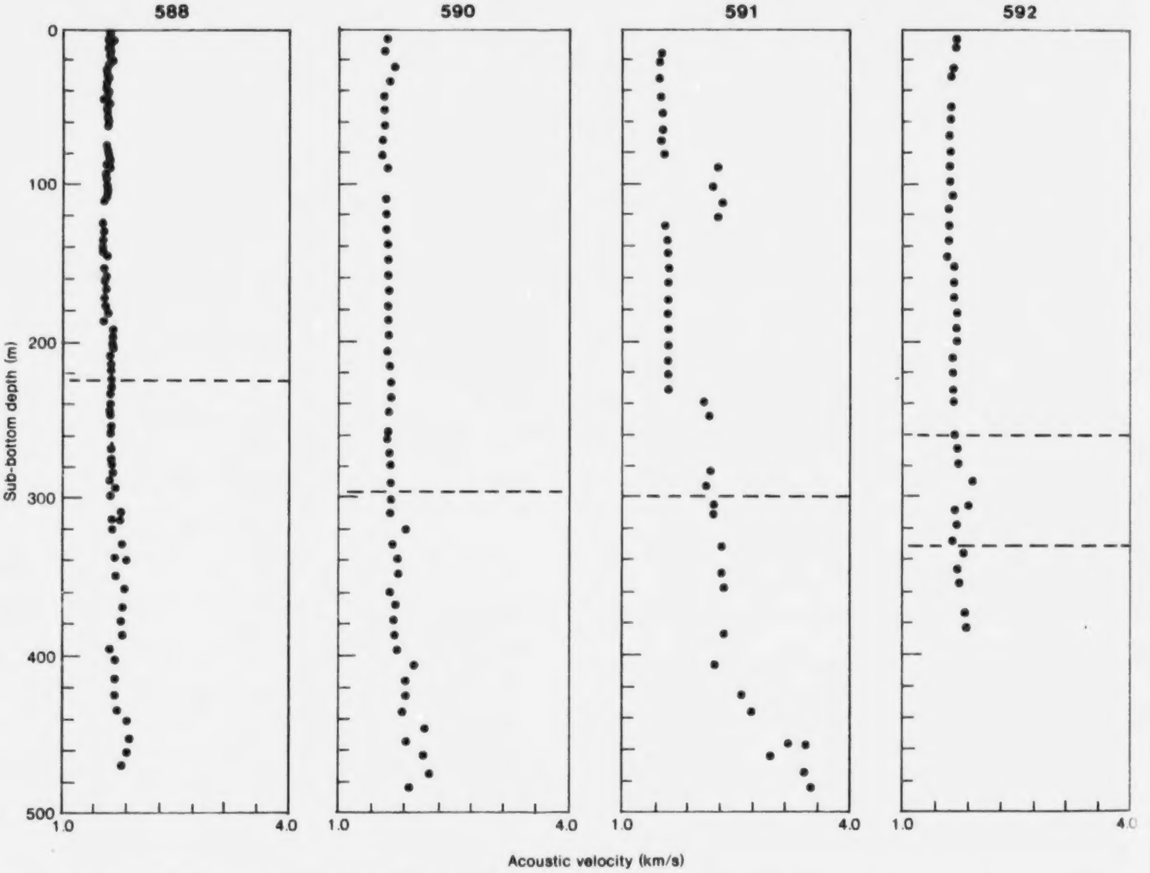

Figure 7. Multiple plot of acoustic compressional velocity versus depth for four sites. Dashed line indicates ooze-to-chalk transitional depth

PART V: GEOCHEMICAL STUDIES

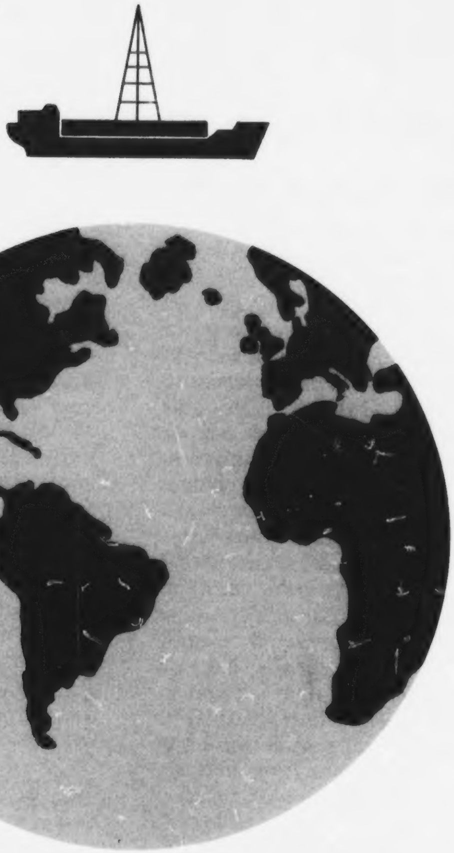

32. PORE-WATER CHEMISTRY OF CARBONATE-RICH SEDIMENTS, LORD HOWE RISE, SOUTHWEST PACIFIC OCEAN[1]

Paul A. Baker, Department of Geology, Duke University[2]

ABSTRACT

About 200 pore-water samples were recovered and analyzed from eight sites of DSDP Leg 90. At all sites on the carbonate-rich Lord Howe Rise, Ca^{2+} concentrations increase and Mg^{2+} concentrations decrease with increasing sub-bottom depth. The value of $\Delta Ca^{2+}/\Delta Mg^{2+}$ averages -0.45 mol/mol at these sites, an unusually small negative value in comparison with sites on basaltic crust. This supports the argument that the crust of the Lord Howe Rise is siliceous. Li^{+} concentrations increase and K^{+} concentrations decrease with depth. Both of these constituents are affected by reactions within the sediment column. Microbial sulfate reduction occurs to a small extent at all sites. In the upper 200 m of Site 594 on the south side of the Chatham Rise, sulfate reduction and alkalinity production are more pronounced.

Carbonate recrystallization is indicated by large increases in Sr^{2+} concentrations with depth at all sites. The exact value of the Sr^{2+} maximum at each site is determined by equilibrium with respect to celestite ($SrSO_4$). The greater the degree of microbial sulfate reduction, the higher is the pore water Sr^{2+} concentration. The diffusive flux of Sr^{2} out of the pore waters is consistent with an initial rate of carbonate recrystallization of 10%/m.y. This recrystallization must alter the isotopic and trace elemental compositions of some carbonate components.

INTRODUCTION

Leg 90 of the Deep Sea Drilling Project consisted of a north–south transect from 26°S to 41°S along the shallow (about 1000 m deep), carbonate-rich, Lord Howe Rise between New Caledonia, New Zealand, and Australia. An additional site, Site 594, was cored on the south side of the Chatham Rise at 46°S in a region presently characterized by more hemipelagic sedimentation. The major objective of this expedition was the recovery of complete Neogene sections for high-resolution paleoceanographic studies. We also obtained an atypically large number of interstitial water samples. Combined with detailed studies of sediment isotopic, chemical, and textural composition, the chemistry of Leg 90 pore waters provides important insights into the processes and rates of carbonate diagenesis.

ANALYTICAL METHODS

All interstitial waters analyzed in this study were obtained by shipboard extraction using the procedure and equipment described by Manheim and Sayles (1974). Extraction was effected as soon as possible after sediment recovery and was conducted at laboratory ambient temperature and pressure. Comparison of this extraction method with *in situ* sampling has established previously that temperature- and pressure-of-squeezing effects on the analyzed constituents are quite small (see Gieskes, 1973, 1974).

All analyses reported in this paper were carried out ashore. Prior to analysis, samples were stored unrefrigerated in either linear polyethylene bottles or sealed polyethylene or glass ampules. On the basis of previous experience, this storage procedure is acceptable for the reported constituents. Measurements that are in progress, but not published here, include the strontium and oxygen isotopic ratios of dissolved strontium and water, respectively.

Analytical methods for determination of chloride, calcium, magnesium, silica, alkalinity, and strontium are similar to those of Gieskes (1974) and Gieskes and Lawrence (1976). Lithium, potassium, and sulfate methodologies are similar to those of Presley (1971).

RESULTS AND DISCUSSION

All the pore-water data are shown in Table 1 and Figures 1–6. The Lord Howe Rise sites (588, 590, 591, 592, and 593) and the lower 400 m of Site 594 display increasing Ca^{2+} and decreasing Mg^{2+} concentrations with increasing sub-bottom depth. The changes in Ca^{2+} and Mg^{2+} concentrations with depth at these sites are approximately linearly correlated (Fig. 7) with an average slope $\Delta Ca^{2+}/\Delta Mg^{2+}$ of about -0.45 mol/mol. This slope is similar to those observed previously at drill sites overlying presumed siliceous basement rocks. Examples include (1) DSDP Sites 346 and 349 on the Jan-Mayen Ridge, north of Iceland, where $\Delta Ca^{2+}/\Delta Mg^{2+}$ is about -0.4 and -0.2, respectively (Gieskes et al., 1978); (2) DSDP Site 116 on the Rockall Bank in the North Atlantic Ocean where $\Delta Ca^{2+}/\Delta Mg^{2+}$ is about -0.4 (Manheim et al., 1972); and (3) DSDP Site 237 on the Mascarene Ridge in the western Indian Ocean where $\Delta Ca^{2+}/\Delta Mg^{2+}$ is -0.57 (Sandstrom and Gieskes, 1974). By contrast, of those sites listed by McDuff (1981) in a compilation of DSDP sites displaying nonzero Ca^{2+}/Mg^{2+} gradients and linear correlations of Ca^{2+} versus Mg^{2+}, not a single one overlying basaltic basement had a value of $-\Delta Ca^{2+}/\Delta Mg^{2+}$ as low as any of these on siliceous crust. A typical value of $\Delta Ca^{2+}/\Delta Mg^{2+}$ for sites on basaltic crust is -1.5 (McDuff, 1981). It has previously been shown (McDuff and Gieskes, 1976, McDuff, 1981) that linear correlation of Ca^{2+} and Mg^{2+} is usually indicative of conservative chemical behavior in the sediment column. As basement rocks alter, they take up magnesium from the pore waters and release calcium to the pore waters. Apparently, as basement rocks of the Lord Howe Rise alter, they take up more magnesium and release less calcium than do basaltic basement rocks. The implication of these observations for Leg 90 sites is sup-

---

[1] Kennett, J. P., von der Borch, C. C., et al., *Init. Repts. DSDP*, 90: Washington (U.S. Govt. Printing Office).

[2] Address: Department of Geology, Duke University, Box 6729, College Station, Durham, NC 27708.

Table 1. Interstitial water concentration data.

Core-Section (interval in cm)	Depth (m)	Ca^{2+} (mM)	Mg^{2+} (mM)	Sr^{2+} (mM)	K^+ (mM)	Li^+ (μM)	Sio_2 (μM)	Alkalinity (meq/l)	SO_4^{2-} (mM)
Site 587									
2-3, 144–150	7.57	9.03	54.66	0.147	10.49	—	186	3.64	26.7
3-6, 0–6	20.23	8.79	55.40	0.287	11.54	—	214	3.51	28.0
5-3, 144–150	36.37	9.30	53.98	0.293	11.54	—	147	3.36	27.4
7-3, 144–150	55.57	9.74	53.54	0.306	10.68	—	—	3.28	25.7
9-1, 144–150	71.77	9.83	53.74	0.363	11.75	—	—	3.09	—
Hole 588									
1-3, 144–150	4.47	10.63	51.03	—	10.49	31.0	220	2.84	25.0
2-5, 144–150	13.07	10.47	51.23	0.249	11.76	32.8	190	2.74	26.1
3-4, 144–150	21.17	10.51	51.03	0.300	11.50	34.2	169	2.83	25.7
4-4, 144–150	30.77	10.72	51.07	0.395	11.54	36.3	149	2.77	25.8
5-4, 144–150	40.37	11.01	50.56	0.446	10.91	37.0	158	2.84	25.4
6-4, 144–150	49.97	11.20	49.95	0.523	10.75	39.0	156	3.04	24.7
7-4, 144–150	59.57	11.15	49.97	0.561	10.75	39.6	141	—	
9-4, 144–150	78.77	11.76	49.25	0.644	10.18	41.4	152	3.06	23.3
10-4, 144–150	88.37	11.93	47.79	0.638	10.31	42.8	164	2.78	24.7
11-4, 144–150	97.97	12.10	48.04	0.701	10.23	43.6	160	2.97	23.7
12-4, 144–150	107.57	12.11	48.15	0.714	10.16	44.3	165	2.95	23.6
13-4, 144–150	117.47	12.47	47.19	0.746	10.44	46.6	201	2.90	23.6
14-3, 144–150	125.27	12.71	46.45	0.708	—	48.1	211	2.91	23.4
15-3, 144–150	134.87	12.77	46.33	0.714	10.01	47.8	182	2.86	23.3
16-3, 144–150	144.47	12.97	46.25	0.708	10.01	49.1	210	2.79	22.9
17-3, 144–150	154.07	13.17	45.80	0.708	10.12	51.1	226	2.74	23.3
18-5, 144–150	166.67	13.38	46.75	0.714	10.01	55.7	233	2.72	23.3
19-5, 144–150	176.27	13.23	45.59	0.733	9.79	54.2	226	2.71	22.6
20-3, 144–150	182.87	13.32	44.58	0.663	9.62	55.0	222	2.75	22.9
21-4, 144–150	193.97	13.36	44.91	0.689	9.63	58.7	228	2.50	22.3
22-4, 144–150	203.57	13.58	44.43	0.682	10.16	59.6	324	2.22	22.9
23-3, 144–150	211.67	13.42	43.57	0.676	10.16	61.7	258	1.98	23.4
24-3, 144–150	221.27	11.79	45.57	0.689	9.96	63.0	246	—	23.6
25-3, 144–150	230.87	11.81	45.57	0.669	10.12	66.2	284	1.90	22.9
Hole 588A									
1-4, 144–150	241.97	13.62	37.42	0.701	10.49	69.7	150	1.67	22.7
3-2, 144–150	253.57	14.28	42.30	0.714	10.15	73.9	158	1.99	22.6
5-2, 144–150	263.57	14.13	42.33	0.695	10.03	77.1	158	1.71	21.7
7-2, 144–150	273.57	14.31	42.71	0.720	9.24	80.0	169	1.78	21.6
9-2, 144–150	283.57	14.20	42.00	0.708	—	84.8	—	—	22.9
12-2, 140–150	298.55	14.31	39.95	0.701	10.35	84.5	166	0.46	22.1
14-1, 140–150	307.05	14.62	41.37	0.708	10.18	84.3	169	0.97	22.0
17-1, 140–150	326.65	—	—	0.701	—	94.0	—	0.80	23.0
Hole 588C									
1-5, 140–150	313.15	14.22	41.64	0.720	—	88.2	81	—	22.7
3-3, 140–150	329.35	14.94	40.90	0.752	9.64	92.0	105	0.80	22.4
5-4, 140–150	350.05	—	—	0.720	10.23	99.1	—	0.21	22.6
7-2, 140–150	366.25	—	—	0.740	9.84	102.2	—	0.44	22.6
9-5, 140–150	398.95	—	—	0.759	9.74	105.2	—	0.54	22.0
11-1, 140–150	403.15	—	—	0.765	8.67	107.0	—	0.59	21.7
13-3, 140–150	425.35	—	—	0.759	9.41	118.5	—	0.43	21.4
15-4, 140–150	446.05	—	—	0.822	9.79	124.3	—	0.58	22.6
17-3, 140–150	463.75	—	—	0.746	9.05	115.5	—	—	22.4
Site 589									
1-4, 140–150	5.95	10.68	52.41	0.191	12.38	34.9	252	3.70	26.3
2-5, 144–150	14.77	10.96	49.99	0.300	11.25	36.0	277	4.01	25.1
3-5, 144–150	24.37	10.70	48.84	0.402	12.62	39.2	261	3.86	24.1
4-4, 144–150	32.47	11.22	47.74	0.491	12.38	41.0	233	4.46	23.4
Hole 590									
1-3, 144–150	4.47	10.66	50.89	0.172	11.39	33.2	263	3.42	26.1
2-3, 144–150	11.47	10.85	49.59	0.300	11.23	38.1	278	4.31	25.1
3-3, 144–150	21.07	10.78	50.90	0.274	11.04	37.2	260	3.97	25.6
Hole 590A									
1-3, 144–150	30.65	11.23	47.73	0.504	11.17	38.6	241	4.84	21.7
2-3, 144–150	40.27	11.39	46.49	0.587	11.02	40.8	188	4.52	22.6
3-3, 144–150	49.87	11.48	45.13	0.657	11.02	41.4	182	4.02	21.1
4-5, 144–150	62.47	11.84	44.49	0.797	11.20	42.8	177	4.30	20.7
5-3, 144–150	69.07	12.29	44.07	0.759	10.69	42.8	175	3.77	19.7

Table 1. (Continued).

Core-Section (interval in cm)	Depth (m)	Ca^{2+} (mM)	Mg^{2+} (mM)	Sr^{2+} (mM)	K^{+} (mM)	Li^{+} (μM)	Sio_2 (μM)	Alkalinity (meq/l)	SO_4^{2-} (mM)
Hole 590A (cont.)									
6-3, 144–150	78.67	12.93	43.31	0.848	—	—	186	3.90	—
7-3, 144–150	88.27	12.78	43.12	0.880	10.71	42.6	177	4.56	18.4
8-3, 144–150	97.87	12.66	41.25	0.854	11.09	43.6	181	3.63	19.1
10-3, 144–150	117.07	13.64	40.17	0.842	10.71	41.6	192	2.96	18.3
11-3, 144–150	126.67	13.81	40.21	0.880	—	40.7	194	2.53	—
12-3, 144–150	136.27	13.76	38.84	0.874	10.61	40.8	201	2.95	17.4
13-3, 144–150	145.87	14.54	38.58	0.880	10.73	40.5	214	3.36	17.3
14-3, 144–150	155.47	13.99	38.63	0.854	9.88	39.7	216	2.46	17.3
15-3, 144–150	165.07	14.71	36.73	0.893	10.31	40.2	235	—	16.1
16-3, 144–150	174.67	14.89	37.72	0.880	10.27	39.7	246	3.65	16.4
17-3, 144–150	184.27	14.75	36.11	0.880	10.42	39.5	260	2.89	15.7
18-3, 144–150	193.87	15.50	37.10	0.893	—	39.8	284	3.09	16.6
19-3, 144–150	203.47	15.37	34.96	0.905	—	45.6	310	2.19	16.6
20-3, 144–150	213.07	15.72	37.00	0.899	10.06	47.2	337	2.38	15.1
21-3, 144–150	222.67	15.70	34.95	0.905	10.66	42.1	395	2.17	14.4
23-3, 144–150	241.87	16.17	33.88	0.842	10.49	46.0	504	2.04	15.4
24-3, 144–150	251.47	16.64	33.92	0.848	10.71	47.7	609	—	15.6
25-3, 144–150	261.07	16.37	34.06	0.842	10.39	48.9	781	2.17	15.9
26-3, 144–150	270.67	17.27	33.56	0.822	10.07	51.0	899	—	16.0
27-2, 144–150	278.77	16.68	33.63	0.829	9.92	53.7	976	1.99	14.9
Hole 590B									
33-5, 140–150	304.95	17.52	33.36	0.842	10.30	65.8	1035	—	16.0
35-4, 140–150	322.65	18.23	32.59	0.829	10.23	79.6	1060	—	15.7
37-4, 140–150	341.85	18.72	31.89	0.867	10.37	92.4	1135	2.12	15.9
39-5, 140–150	362.55	19.73	32.57	0.854	10.30	104.4	840	—	16.4
41-5, 140–150	381.75	19.98	32.38	0.867	9.92	115.5	622	2.22	17.0
43-3, 140–150	397.95	19.45	31.69	0.848	10.01	125.2	574	—	16.3
45-4, 140–150	418.65	20.44	31.65	0.886	9.77	137.5	672	—	16.6
47-6, 140–150	440.85	20.24	31.53	0.867	9.73	148.7	647	1.80	16.6
49-4, 1401–50	457.05	19.28	33.06	0.791	9.59	143.2	357	—	17.6
51-3, 140–150	474.75	19.52	33.37	0.835	9.88	135.2	361	1.91	17.7
53-4, 1401–50	495.45	19.42	34.06	0.822	9.76	131.7	378	—	18.1
Hole 591									
2-3, 144–150	7.87	10.53	50.88	0.198	11.95	34.5	354	4.44	24.3
4-3, 144–150	27.07	11.35	49.94	0.389	11.81	33.4	492	3.21	22.7
6-3, 144–150	46.27	11.28	44.81	0.548	12.76	35.2	497	3.87	21.4
8-3, 144–150	65.47	12.24	45.15	0.759	11.90	34.6	583	4.68	20.7
10-3, 144–150	84.67	13.20	41.89	0.829	12.00	33.4	672	5.05	19.6
12-3, 144–150	103.87	12.98	40.59	0.880	11.40	30.5	700	4.32	18.7
14-2, 144–150	121.27	13.27	39.70	0.925	12.14	29.6	831	3.30	18.9
16-4, 144–150	142.87	14.04	37.63	0.931	12.31	27.0	935	2.52	17.3
18-4, 144–150	161.47	15.29	36.52	0.925	12.07	27.1	950	2.64	18.0
20-2, 144–150	177.27	14.60	36.16	0.944	12.18	25.3	988	—	17.9
22-4, 144–150	199.27	15.27	36.15	0.918	12.09	24.9	1001	2.58	17.0
24-3, 144–150	216.57	15.99	34.39	0.931	12.18	25.5	1026	2.34	16.9
26-3, 144–150	235.57	15.31	34.01	0.969	12.03	28.9	1236	—	15.7
28-3, 144–150	254.77	16.53	32.14	0.969	12.04	27.3	1048	—	16.9
30-2, 144–150	272.27	17.74	31.59	0.950	11.97	26.6	1073	2.21	16.7
Hole 591B									
2-3, 140–150	284.67	18.64	31.74	0.925	12.06	29.6	1056	1.84	17.0
4-3, 140–150	303.85	18.36	31.56	0.931	11.54	28.7	1037	—	—
6-3, 140–150	322.65	18.61	31.33	0.912	11.87	31.7	1071	1.85	—
10-2, 140–150	359.35	19.13	31.59	0.905	11.23	42.1	1005	—	—
12-1, 140–150	377.05	19.44	29.79	0.912	11.87	46.2	1039	2.15	—
14-1, 140–150	396.25	19.96	31.02	0.899	11.45	52.2	1082	1.86	—
18-3, 140–150	437.65	20.32	30.07	0.918	11.72	66.1	980	—	—
20-3, 140–150	456.85	20.02	29.09	0.889	—	70.9	1012	2.26	—
22-4, 140–150	477.55	19.63	28.91	0.880	12.10	76.1	990	2.43	—
24-4, 140–150	496.75	19.58	29.42	0.867	11.85	76.4	—	2.23	—
Hole 592									
2-3, 144–150	8.97	11.14	50.72	0.185	11.16	33.9	—	2.85	27.3
4-4, 144–150	29.67	11.39	—	0.370	11.26	—	207	3.39	26.0
6-3, 144–150	47.37	11.89	47.56	0.497	10.67	40.1	—	3.32	24.9
8-3, 144–150	66.57	12.26	46.91	0.580	10.49	41.4	184	3.90	24.3
10-3, 144–150	85.77	13.15	45.38	0.676	10.69	44.3	186	3.84	22.9
12-3, 144–150	104.97	13.23	45.58	0.752	10.12	46.1	190	4.00	22.4
14-3, 144–150	124.17	13.65	44.25	0.769	9.21	48.3	199	4.12	22.7
16-3, 144–150	143.37	14.15	43.99	0.784	9.81	49.2	213	4.04	21.6

Table 1. (Continued).

Core-Section (interval in cm)	Depth (m)	Ca^{2+} (mM)	Mg^{2+} (mM)	Sr^{2+} (mM)	K^{+} (mM)	Li^{+} (μM)	Sio$_2$ (μM)	Alkalinity (meq/l)	SO$_4^{2-}$ (mM)
Hole 592 (cont.)									
18-3, 144–150	162.57	14.50	43.07	0.784	8.61	50.9	222	3.92	20.9
20-3, 144–150	181.77	15.00	42.65	0.740	9.36	51.9	224	3.99	21.1
22-3, 144–150	200.97	15.38	41.36	0.778	9.58	54.7	199	3.98	20.9
24-3, 144–150	220.17	15.70	40.90	0.784	9.81	57.5	190	3.63	20.3
26-3, 144–150	239.37	15.86	40.67	0.797	9.05	58.6	196	3.65	20.9
28-3, 144–150	258.57	15.66	40.75	0.784	9.47	60.7	211	3.28	20.7
31-3, 140–150	287.35	16.10	39.60	0.791	8.61	62.7	286	2.71	19.7
33-3, 140–150	306.55	16.71	38.54	0.771	8.93	65.2	465	3.02	20.1
35-3, 140–150	325.75	17.16	38.08	0.791	8.35	66.4	—	—	19.7
37-3, 140–150	344.95	17.20	38.04	0.797	8.49	77.4	925	3.29	19.1
39-3, 140–150	364.15	17.34	37.44	0.797	8.37	80.0	1033	3.27	18.7
41-3, 140–150	383.35	17.54	36.86	0.797	8.30	83.0	946	3.18	18.9
Site 593									
1-4, 144–150	5.97	10.56	51.96	0.166	11.07	31.6	—	3.42	27.0
4-3, 144–150	28.77	10.54	51.42	0.236	11.74	29.2	405	3.34	27.1
6-3, 144–150	47.97	10.68	49.99	0.338	11.30	32.6	—	3.34	26.4
8-1, 144–150	62.37	10.74	49.90	0.389	10.92	35.8	182	3.36	25.0
12-3, 144–150	105.57	11.24	48.99	0.529	10.81	38.3	—	4.12	24.9
14-3, 144–150	124.77	11.66	48.69	0.671	10.08	39.4	—	3.35	25.0
16-3, 144–150	143.17	11.62	48.23	0.631	9.95	39.6	177	3.94	25.0
18-3, 144–150	163.17	11.74	47.97	0.657	9.91	41.0	—	3.54	24.1
20-3, 144–150	182.37	12.18	46.37	—	10.12	42.5	—	—	24.6
22-3, 144–150	201.57	12.15	46.82	0.701	9.33	45.5	254	3.55	23.9
24-3, 144–150	220.77	12.64	46.06	0.733	9.44	45.1	241	3.78	24.3
26-3, 144–150	239.97	12.79	45.91	0.720	9.65	47.3	203	3.14	23.1
28-3, 144–150	259.17	13.17	44.02	0.733	9.37	49.8	190	2.73	22.6
30-3, 144–150	278.37	13.44	43.04	0.752	9.35	51.5	—	—	23.1
32-2, 144–150	296.07	13.84	42.68	0.695	9.16	53.1	—	2.99	23.4
34-2, 144–150	315.27	13.94	42.67	0.759	9.16	54.3	171	2.81	22.4
36-2, 144–150	334.47	14.16	42.93	0.714	9.09	57.3	—	2.28	22.4
38-3, 144–150	355.17	14.31	41.73	0.752	9.02	58.2	162	2.93	21.4
40-3, 144–150	374.37	14.77	40.57	0.733	8.51	61.0	—	2.91	21.6
42-3, 144–150	393.57	14.81	39.48	0.759	—	62.8	—	2.64	21.0
44-3, 144–150	412.77	15.46	38.69	0.765	8.30	68.4	—	2.52	21.9
46-3, 144–150	431.97	15.86	37.65	0.771	8.49	71.6	—	2.44	21.4
47-3, 144–150	441.57	15.49	—	0.746	9.28	71.9	—	1.99	21.9
48-3, 144–150	451.17	15.71	37.24	0.733	8.45	69.7	186	—	22.1
50-3, 144–150	470.37	15.69	36.60	0.759	9.21	95.5	—	2.08	21.3
54-2, 144–150	507.27	16.71	34.13	0.708	8.72	83.8	459	—	20.9
56-3, 144–150	527.97	17.12	33.50	0.746	—	—	—	—	20.6
58-1, 140–150	544.15	16.02	34.81	0.714	8.84	88.3	425	2.14	21.4
60-3, 144–150	566.37	15.14	30.16	0.689	7.79	179.5	—	—	—
Hole 594									
2-3, 144–150	10.37	6.45	51.80	0.070	11.52	32.3	689	9.57	19.6
4-3, 144–150	29.57	6.46	47.66	0.064	12.16	34.2	761	9.83	15.3
6-3, 144–150	48.77	5.83	45.45	0.070	11.54	36.1	859	14.94	10.1
8-3, 144–150	64.97	3.96	44.53	0.102	12.18	—	—	—	9.0
10-1, 144–150	84.17	5.03	41.96	0.134	10.85	43.7	808	13.06	—
12-3, 144–150	106.37	5.14	41.84	0.140	11.63	47.7	819	9.38	10.6
15-3, 144–150	135.17	5.90	43.82	0.191	11.04	40.4	931	9.28	13.3
18-3, 144–150	163.97	8.01	44.03	0.306	10.88	—	—	7.80	16.3
20-3, 144–150	183.17	9.24	43.17	0.338	10.67	31.5	954	5.62	18.0
24-3, 144–150	221.57	12.44	41.07	0.555	9.01	27.6	1039	4.84	18.9
26-3, 144–150	240.77	14.17	39.63	0.620	9.51	—	—	—	20.1
28-3, 144–150	259.97	15.02	38.88	0.657	9.70	24.8	1137	2.48	19.4
30-3, 144–150	279.17	16.34	38.62	0.720	9.23	—	1043	2.97	20.3
34-3, 144–150	316.57	17.83	36.33	0.759	9.46	—	—	—	19.1
36-3, 144–150	335.77	18.31	35.25	0.797	7.79	24.8	—	2.44	19.0
38-2, 144–150	353.47	19.31	33.98	0.810	8.23	26.1	—	2.23	19.3
40-3, 144–150	374.17	20.05	32.34	0.816	8.54	27.9	1205	—	19.6
42-3, 144–150	394.37	20.49	32.66	0.835	8.65	30.8	—	3.16	19.0
44-3, 144–150	414.57	21.44	29.63	0.861	8.16	35.5	1139	3.22	18.3
46-1, 144–150	429.77	22.00	29.07	0.861	6.58	39.8	1173	3.18	19.1
48-2, 144–150	450.47	22.58	28.94	0.867	7.24	43.7	1196	3.06	18.9
Hole 594A									
11-3, 144–150	202.37	12.08	40.89	0.478	—	30.2	908	3.11	17.6
12-1, 138–144	496.91	24.82	24.59	0.931	7.10	52.1	1364	2.99	17.1
14-3, 140–150	519.15	24.76	25.49	0.931	6.82	56.5	1340	2.68	17.0
16-3, 140–150	538.35	24.56	25.43	0.937	—	59.7	1132	2.82	17.6
19-1, 140–150	564.15	25.23	23.83	0.976	6.44	63.1	795	1.99	16.6

Table 1. (Continued).

Core-Section (interval in cm)	Depth (m)	Ca^{2+} (mM)	Mg^{2+} (mM)	Sr^{2+} (mM)	K^+ (mM)	Li^+ (μM)	SiO_2 (μM)	Alkalinity (meq/l)	SO_4^{2-} (mM)
Hole 594A (cont.)									
21-1, 140–150	583.35	24.94	23.10	0.956	6.34	68.1	—	—	15.9
23-2, 140–150	604.05	—	—	—	—	—	—	—	—
25-2, 140–150	623.25	25.11	23.05	0.963	5.48	69.0	692	1.81	16.1

Note: Dashes indicate that no analysis was performed.

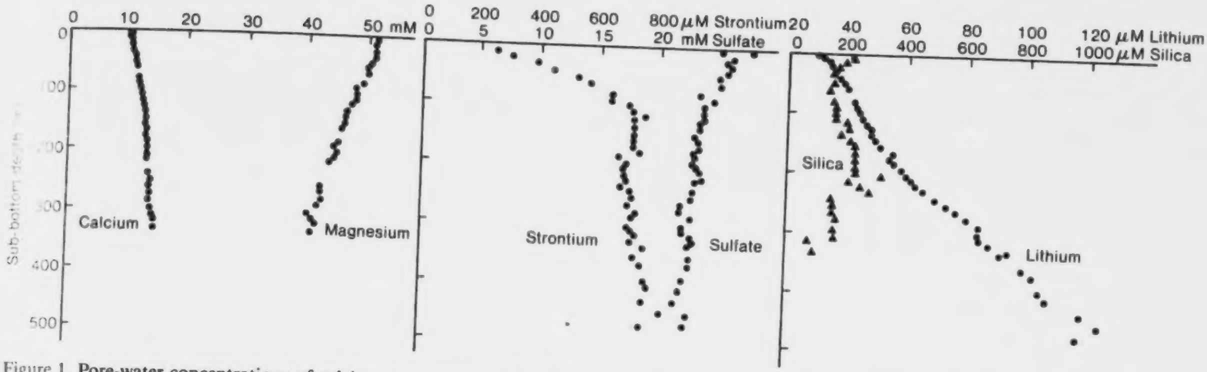

Figure 1. Pore-water concentrations of calcium, magnesium, strontium, sulfate, lithium, and silica as a function of sub-bottom depth of Site 588.

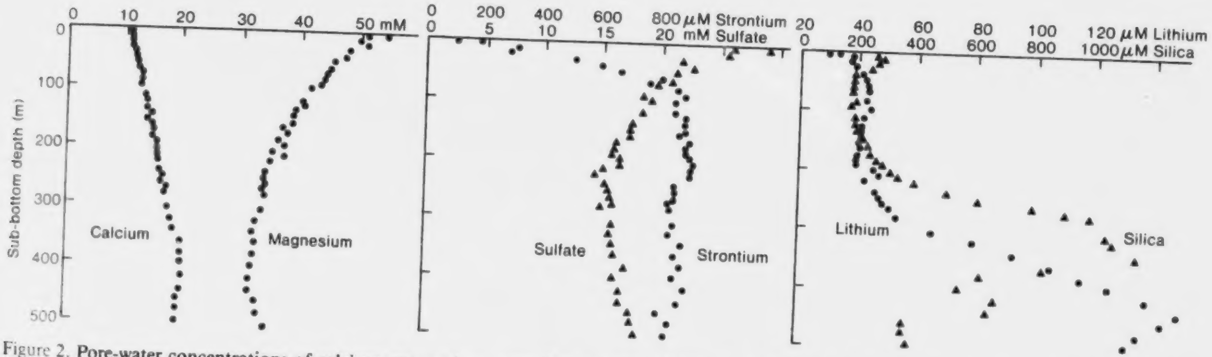

Figure 2. Pore-water concentrations of calcium, magnesium, strontium, sulfate, lithium, and silica as a function of sub-bottom depth at Site 590.

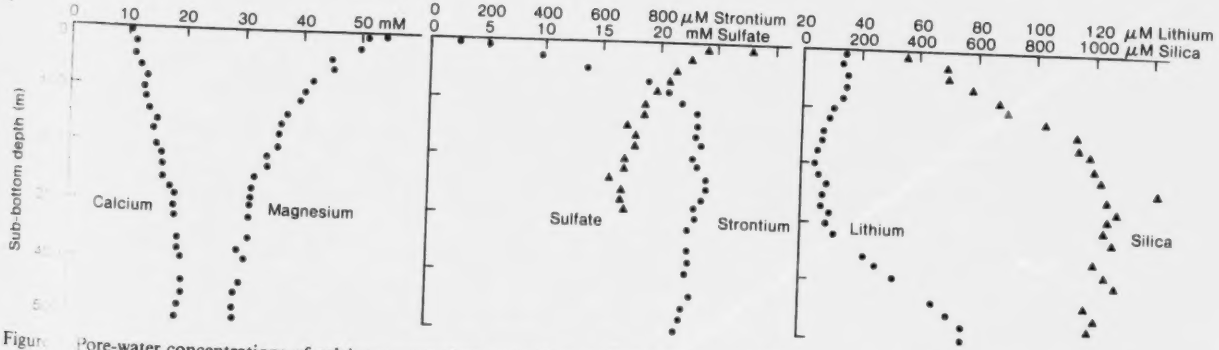

Figur[illegible] Pore-water concentrations of calcium, magnesium, strontium, sulfate, lithium, and silica as a function of sub-bottom depth at Site 591.

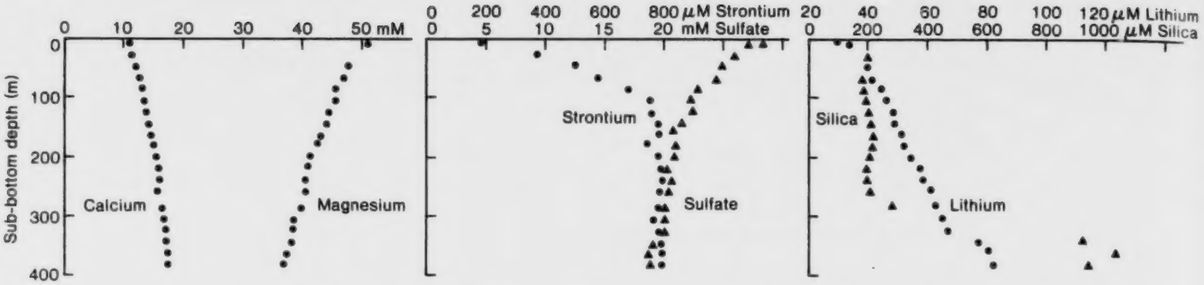

Figure 4. Pore-water concentrations of calcium, magnesium, strontium, sulfate, lithium, and silica as a function of sub-bottom depth at Site 592.

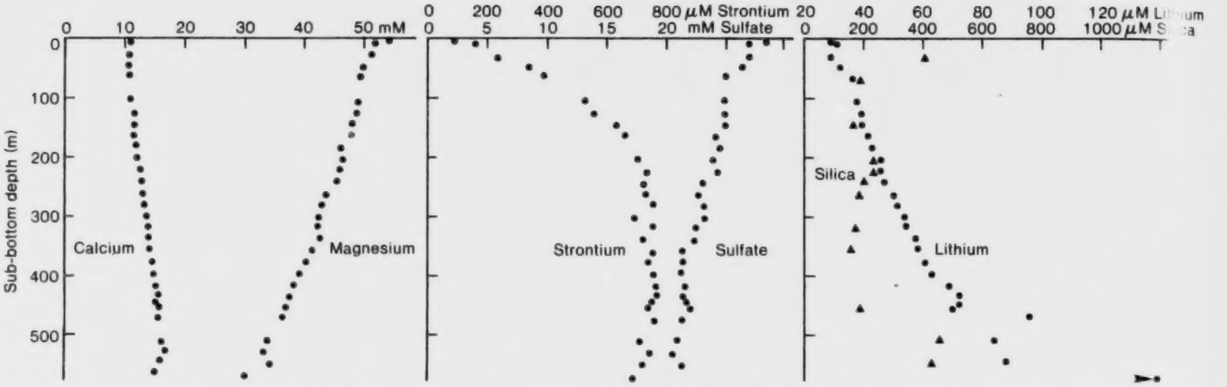

Figure 5. Pore-water concentrations of calcium, magnesium, strontium, sulfate, lithium, and silica as a function of sub-bottom depth at Site 593.

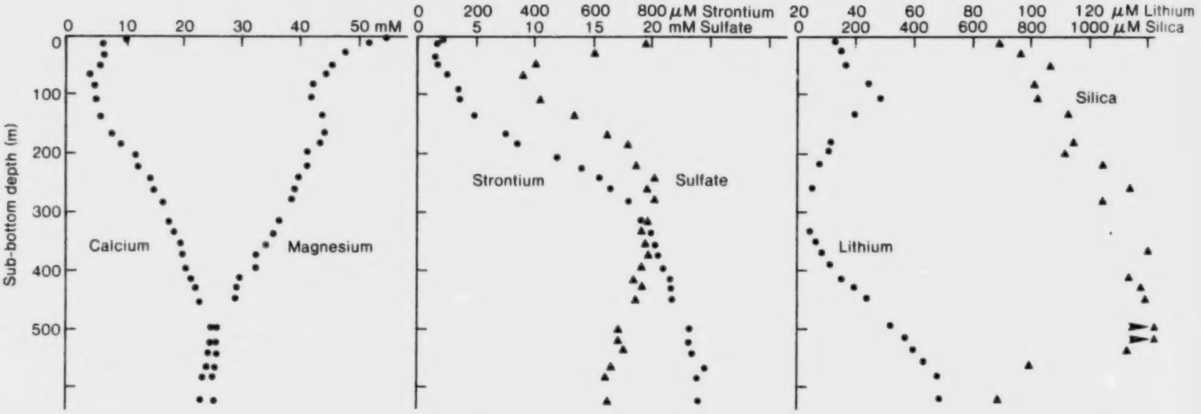

Figure 6. Pore-water concentrations of calcium, magnesium, strontium, sulfate, lithium, and silica as a function of sub-bottom depth at Site 594.

port for the hypothesis that the entire Lord Howe Rise has an affinity with continental crust (van der Lingen, 1973; Willcox et al., 1980). The minor amount of curvature (toward lower magnesium values) displayed in Figure 7 is consistent with some volcanic ash alteration within the sediment column (Gieskes and Lawrence, 1981), particularly at Sites 590 and 591.

The alkali metals, lithium and potassium, exhibit trends similar to those observed at many other DSDP sites (e.g., Gieskes, 1983). At all sites except Site 591 there is a slight tendency for potassium concentrations to decrease and lithium concentrations to increase with increasing burial depth. It is clear from the shapes of the lithium concentration-depth curves, that sources and sinks for lithium must occur within the sediment column. At the present time, the nature of these sources and sinks is unknown (Gieskes, 1983).

Dissolved silica concentrations reflect the amount of biogenic silica present in the surrounding sediments (e.g., Gieskes, 1981). Thus, high values of dissolved silica are

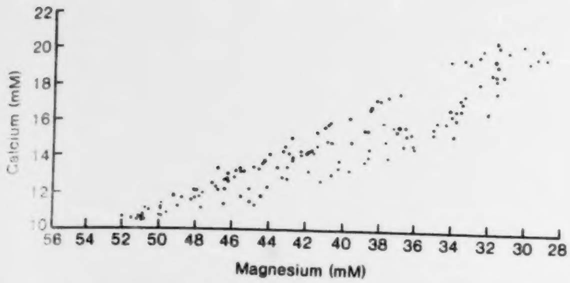

Figure 7. Pore-water concentrations of calcium and magnesium for every sample from the Lord Howe Rise Sites 588, 590, 591, 592, and 593. The data from Sites 590 and 591 lie beneath the general trend.

found at Sites 591 and 594, the two sites that contain the most abundant solid silica. Elsewhere, silica concentrations increase at depth at Sites 590 and 592. The transformation of biogenic silica to opal-CT is associated with a decrease in dissolved silica as observed at Sites 590, 592, and 594. This "silica front" occurs at depths of about 350, 375, and 550 m at the respective sites. Chert was recovered at 335 and 380 m sub-bottom at Site 592, but was not identified at Sites 590 or 594.

Because of the relatively high rates of carbonate sedimentation, microbial sulfate reduction occurs to some degree at all sites of Leg 90. There is some correlation between the degree of sulfate reduction and the rate of sedimentation, with Sites 590 and 591 having slightly lower sulfate concentrations and higher sedimentation rates than at other sites. Site 594, with its thick hemipelagic Pleistocene section, has a much greater degree of sulfate reduction than any of the Lord Howe Rise sites. At Site 594 an increase in alkalinity accompanies the decrease in sulfate. In turn, the alkalinity increase causes the precipitation of calcium carbonate and a decrease in the Ca^{2+} concentration.

The strontium concentration profiles are a product of two reactions: carbonate recrystallization and celestite ($SrSO_4$) precipitation. As previously shown by Baker et al. (1982), the calcium carbonate tests of foraminifers and coccoliths are enriched in strontium relative to recrystallized calcium carbonate precipitated during burial diagenesis. As a result, there is a net input of strontium to the pore waters of carbonate-rich sediments during the calcite dissolution–reprecipitation reaction. The amount of strontium incorporated into diagenetic carbonate is predicted by the product of the distribution coefficient of strontium in calcite, k_{sr}, and the ratio of dissolved strontium to dissolved calcium Sr^{2+}/Ca^{2+}:

$$\left(\frac{Sr}{Ca}\right)_{calcite} = k_{sr}\left(\frac{Sr^{2+}}{Ca^{2+}}\right).$$

As the amount of recrystallization increases in older and deeper carbonate sediments, the Sr^{2+} concentration increases, more strontium is incorporated into the reprecipitated calcite, and eventually a steady-state plateau concentration of Sr^{2+} is achieved.

The Sr^{2+} concentration at the plateau is typically 0.4 to 0.7 mM in deep-sea carbonate porewaters (Baker et al., 1982). The relatively high sedimentation rates at the Leg 90 sites has led to higher plateau concentrations, ranging from 0.7 mM at Site 588 to 0.9 mM at Sites 591 and 594. As a consequence of these higher concentrations, celestite precipitation occurs. Small nodules of celestite were recovered at Sites 590, 591, and 592. The observed concentration product of strontium sulfate at depth in all the Leg 90 sites averages about 15.2×10^{-6} mol^2/l^2. The exact value of the Sr^{2+} concentrations are controlled by celestite precipitation and thus, by the degree of sulfate reduction at each site.

The concentration gradients of Sr^{2+} versus depth over the upper 100 m of core at Sites 588, 590, 591, and 592, average 7×10^{-11} mol Sr^{2+}/cm^4. The average diffusive flux of Sr^{2+} out of the pore waters at these sites can be calculated simply from Fick's law:

$$\text{Flux} = -D\frac{dc}{dx}$$

where D is the diffusion coefficient of Sr^{2+} in pore waters and dc/dx is the average concentration–depth gradient of Sr^{2+}. Substituting a value of 4×10^{-6} cm^2/s for D, we calculate an average flux of Sr^{2+} out of the sediments of 2.8×10^{-16} mol/cm^2 per s or 8.8×10^{-3} mol/cm^2 per m.y. In a column of sediment that is 100 m thick, with a porosity of 67%, an average carbonate content of 90% and an average Sr/Ca ratio in the carbonate of 2.0×10^{-3} (Baker et al., 1982), there are about

$$(0.9 \times 5 \times 10^3\text{cm}^3\ \text{CaCO}_3\left(\frac{2.7\text{ g CaCO}_3}{\text{cm}^3\ \text{CaCO}_3}\right)$$

$$\left(\frac{1\text{ mol Ca}}{100\text{ g CaCO}_3}\right)\left(\frac{2.0 \times 10^{-3}\text{ mol Sr}}{\text{mol Ca}}\right)$$

$= 0.24$ mol Sr in the solid phase per cm^2 of pore water.

The average age of the sediments at 100 m sub-bottom is about 3 m.y. The diffusive flux of Sr^{2+} over a 3-m.y. time span amounts to a loss to seawater of 0.026 mol or 11% of the total amount of strontium contained in the original sediment. Thus, the *minimum* rate of recrystallization of the surface sediments is 11% in 3 m.y. However, much of the strontium released during the dissolution of biogenic calcite is immediately sequestered during the reprecipitation of authigenic calcite. In fact, the "efficiency" of strontium release is probably only about one-third in the upper 100 m of sediment (and almost zero below 100 m). This implies that as much as 30–35% of the carbonate in the upper 100 m of sediment is recrystallized!

Values for the distribution coefficient, k_{sr}, have previously been derived mostly from experimental studies. A limiting value also can be derived in the following manner. The amount of strontium incorporated into authigenic calcite cannot exceed the average amount of strontium in the biogenic calcite. The latter value, as used, is about 2×10^{-3} mol Sr/mol Ca. At the Sr^{2+} concentration plateau:

$$2 \times 10^{-3} \geq k_{sr} \left(\frac{Sr^{2+}}{Ca^{2+}}\right)_{plateau}$$

Using an average value of 5×10^{-2} mol/mol for the $(Sr^{2+}/Ca^{2+})_{plateau}$, yields a value of $k_{sr} \leq 0.04$. This number agrees very well with the results of Katz et al. (1972) and Baker et al. (1982). In the latter paper, we predicted a value of $k_{sr} \approx 0.04$ at 5°C and 0.08 mM Sr^{2+}.

CONCLUSIONS

In summary, we can make the following statements on the basis of the observed pore-water chemistry of Leg 90 drill sites. (1) The calcium and magnesium concentration–depth gradients are dominated by silicate alteration reactions occurring mostly at depth beneath the sampled sediments. The unusual value of $\Delta Ca^{2+}/\Delta Mg^{2+} \approx -0.45$ mol/mol is consistent with the observation that the entire Lord Howe Rise is underlain by siliceous rocks. Some volcanic ash alteration can be detected within the sediments at Sites 590 and 591. (2) Minor amounts of microbial sulfate reduction occur at all sites on the Lord Howe Rise. A much higher amount of sulfate reduction occurs in the hemipelagic sediments at Site 594. (3) Strontium pore-water concentrations are determined by carbonate recrystallization reactions. Dissolved strontium concentrations increase downcore until celestite precipitation occurs. At greater depths, strontium concentrations are controlled by thermodynamic equilibrium with respect to celestite, thus Lord Howe Rise sites with lower rates of sulfate reduction have lower concentrations of dissolved strontium. (4) The diffusive flux of strontium in the upper 100 m of the pore waters can only reasonably be explained by recrystallization of the bulk carbonate sediment at an initial rate of about 10%/m.y. To verify paleoceanographic conclusions based on isotopic and/or chemical compositions of the carbonate constituents therefore will require detailed study of the relative reaction rates of different sediment components.

ACKNOWLEDGMENTS

This work has benefited from detailed reviews by Joris M. Gieskes and Douglas B. Kent. In addition, I thank Paul M. Stout and James V. Gardner for their helpful discussions. Jim Pine extracted all the pore waters aboard the *Glomar Challenger*. Support was provided for this work by NSF-OCE-8219917.

REFERENCES

Baker, P. A., Gieskes, J. M., and Elderfield, H., 1982. Diagenesis of carbonates in deep-sea sediments—evidence from Sr/Ca ratios and interstitial dissolved Sr^{2+} data. *J. Sediment. Petrol.*, 52:71–82.

Gieskes, J. M., 1973. Interstitial water studies, Leg 15—alkalinity, pH, Mg, Ca, Si, PO_4, and NH_4. *In* Heezen, B. C., MacGregor, I. D., et al., *Init. Repts. DSDP*, 15: Washington (U.S. Govt. Printing Office), 813–829.

________, 1974. Interstitial water studies, Leg 25. *In* Simpson, E. S. W., Schlich, R., et al., *Init. Repts. DSDP*, 25: Washington (U.S. Govt. Printing Office), 361–394.

________, 1981. Deep-sea drilling interstitial water studies: implications for chemical alteration of the oceanic crust, layers I and II. *SEPM Spec. Pub.*, 32:149–167.

________, 1983. The chemistry of interstitial waters of deep sea sediments: interpretation of deep sea drilling data. *In* Riley, J. P., and Chester, R. (Eds.), *Chemical Oceanography* (Vol. 8): London (Academic Press), pp. 221–269.

Gieskes, J. M., and Lawrence, J. R., 1976. Interstitial water studies, Leg 35. *In* Hollister, C. D., Craddock, C., et al., *Init. Repts. DSDP*, 35: Washington (U.S. Govt. Printing Office), 407–423.

________, 1981. Alteration of volcanic matter in deep sea sediments: evidence from the chemical composition of interstitial waters from deep sea drilling cores. *Geochim. Cosmochim. Acta*, 45:1687–1703.

Gieskes, J. M., Lawrence, J. R., and Galleisky, G., 1978. Interstitial water studies, Leg 38. *In* Talwani, M., Udintsev, G., et al., *Init. Repts. DSDP*, Suppl. to Vols. 38, 39, 40, and 41: Washington (U.S. Govt. Printing Office), 121–133.

Katz, A., Sass, E., Starinsky, A., and Holland, H. D., 1972. Strontium behavior in the aragonite-calcite transformation: an experimental study at 40–98°C. *Geochim. Cosmochim. Acta*, 36:481–496.

Manheim, F. T., and Sayles, F. L., 1974. Composition and origin of interstitial waters of marine sediments based on deep sea drill cores. *In* Goldberg, E. D. (Ed.), *The Sea* (Vol. 5): New York (Wiley-Interscience), 527–568.

Manheim, F. T., Sayles, F. L., and Waterman, L. S., 1972. Interstitial water studies on small core samples, Deep Sea Drilling Project, Leg 12. *In* Laughton, A. S., Berggren, W. A., et al., *Init. Repts. DSDP*, 12: Washington (U.S. Govt. Printing Office), 1193–1200.

McDuff, R. E., 1981. Major cation gradients in DSDP interstitial waters: The role of diffusive exchange between seawater and upper oceanic crust. *Geochim. Cosmochim. Acta*, 45:1705–1713.

McDuff, R. E., and Gieskes, J. M., 1976. Calcium and magnesium in DSDP interstitial waters: diffusion or reaction? *Earth Planet. Sci. Lett.*, 33:1–10.

Presley, B. J., 1971. Techniques for analyzing interstitial water samples. I. Determination of selected minor and major inorganic constituents. *In* Winterer, E. L., Riedel, W. R., et al., *Init. Repts. DSDP*, 7, Pt. 2: Washington (U.S. Govt. Printing Office), 1749–1755.

Sandstrom, M., and Gieskes, J. M., 1974. Interstitial water studies, Leg 24. *In* Fisher, R. L., Bunce, E. T., et al., *Init. Repts. DSDP*, 24: Washington (U.S. Govt. Printing Office), 799–810.

van der Lingen, G. J., 1973. The Lord Howe Rise rhyolites. *In* Burns, R. E., Andrews, J. E., et al., *Init. Repts. DSDP*, 21: Washington (U.S. Govt. Printing Office), 523–540.

Willcox, J. B., Symonds, P. A., Hinz, K., and Bennett, D., 1980. Lord Howe Rise, Tasman Sea—preliminary geophysical results and petroleum prospects. *B.M.R. J. Aust. Geol. Geophys.*, 5:225–236.

Date of Initial Receipt: 18 June 1984
Date of Acceptance: 31 October 1984

33. ^{87}Sr/^{86}Sr RATIOS OF PLANKTONIC FORAMINIFERS AND INTERSTITIAL WATERS, DEEP SEA DRILLING PROJECT LEG 90, SITE 593[1]

Jennifer Hess and Jean-Guy Schilling, Graduate School of Oceanography, University of Rhode Island[2]

ABSTRACT

Detailed profiles of the Sr isotopic compositions of fossil planktonic foraminifers and interstitial waters have been measured from DSDP Site 593 to determine the Sr isotopic composition of seawater during the last 40 m.y. Foraminiferal recrystallization was assessed through scanning electron microscopy (SEM) and Sr/Ca ratios. Foraminifers were shown to be well preserved. Results document that the seawater ^{87}Sr/^{86}Sr has increased continuously but not uniformly, since the latest Eocene.

INTRODUCTION

The chemical and isotopic composition of seawater has varied significantly over the course of geologic time (see, e.g., Broecker, 1971; Shackleton and Kennett, 1975; Bender and Keigwin, 1979; Claypool et al., 1980; Burke et al., 1982; Graham et al., 1982; Delaney, 1983). Efforts to constrain the geological forcing functions responsible for these changes rely on paleochemical tracers. One such tracer, important in deciphering the long-term record of oceanic chemical changes, is the Sr isotopic composition of ancient seawater.

Because the chemistry of Sr is similar to that of Ca, high concentrations of Sr are substituted for Ca during biogenic carbonate precipitation. The isotopic composition of Sr incorporated into calcite records the contemporaneous seawater ^{87}Sr/^{86}Sr ratio, which in turn integrates the weighted fluxes and isotope compositions of the oceanic Sr sources. The long-term variations in the marine ^{87}Sr/^{86}Sr ratio arise from changes in the fluxes of Sr from the various isotopically different oceanic sources. These include deep-sea hydrothermal activity, continental erosion, and submarine sedimentary recycling (Peterman et al., 1970; Brass, 1976; Spooner, 1976; Albarède et al., 1981; Armstrong, 1971). Estimates of the mass fluxes for each of the source terms can be used to assess the relative contribution of each process in fixing the seawater ^{87}Sr/^{86}Sr and hence in regulating seawater chemistry.

We are determining the Cenozoic record of the marine ^{87}Sr/^{86}Sr variations by measuring the ^{87}Sr/^{86}Sr ratio of well-preserved and well-dated fossil foraminifers from several DSDP cores of overlapping ages. Site 593 on the shallow Lord Howe Rise provides a complete, high-quality, carbonate-rich sequence from the latest Eocene to the present for use in our work. We report here the measurements of foraminiferal and interstitial water ^{87}Sr/^{86}Sr ratios for Site 593. Because carbonate recrystallization can obscure the true ancient seawater ^{87}Sr/^{86}Sr, all samples were carefully checked for evidence of diagenetic alteration through the use of scanning electron microscopy (SEM) and Sr/Ca ratios.

ANALYTICAL METHODS

Sediment samples for Site 593 were collected by J. P. Kennett and the shipboard scientific party of DSDP Leg 90. Interstitial water samples were provided by P. A. Baker of Duke University from splits of his shipboard sampling. All Sr isotope analyses were done in the thermal ionization mass spectrometry laboratory at the University of Rhode Island.

Sample preparation is similar to procedures reported by other workers (Dasch and Biscaye, 1971; Brass, 1976; Elderfield, personal communication). Sediment samples were disaggregated in a hot Calgon solution, wet-sieved though a 63 μm screen, and dried at 50°C. Whole foraminifer tests (mixed planktonic species, >150-μm size fraction) were hand-picked from the sample, repeatedly cleaned ultrasonically to remove clay minerals trapped within the tests, and dried at 50°C. The cleaned tests were dissolved in 0.25 ml of 2× quartz-distilled 2.5*N* HCl and loaded onto a Dowex 50W-8×, 200–400 mesh cation exchange column. The Sr fraction was eluted with ultrapure 2.5*N* HCl, evaporated to dryness, and redissolved in 1μl of dilute phosphoric acid. This Sr-phosphoric acid solution was then loaded in a drop of tantalum oxide slurry on a single Re filament for isotopic analysis. Pore water samples were evaporated to dryness before going through the same procedure.

For Sr and Ca determinations, foraminifers were hand-picked, cleaned ultrasonically, dried at 50°C, weighed, and then dissolved in dilute HCl for analysis. Sr and Ca concentrations were measured on these solutions by atomic absorption spectrometry. Ca was analyzed by flame techniques; Sr was analyzed by graphite furnace techniques.

RESULTS

Foraminiferal and interstitial water ^{87}Sr/^{86}Sr are shown in Figure 1 and Tables 1 and 2, respectively. All Sr isotope values have been normalized to an ^{86}Sr/^{88}Sr value of 0.1194 to correct for mass discrimination and an Eimer and Amend $SrCO_3$ standard ^{87}Sr/^{86}Sr value of 0.70800. Our laboratory value for this standard, covering the period of analysis, is $0.708075 \pm 22 \times 10^{-6}$, at the 95% confidence level (19 replicate analyses). Results of foraminiferal Sr/Ca ratio measurements and scanning electron microscopy examinations are given in Table 1.

At Site 593, the foraminiferal ^{87}Sr/^{86}Sr is relatively constant to a depth of approximately 400 m (early middle Miocene), after which the ratio decreases rather linearly for the remainder of the section (early Miocene to

---

[1] Kennett, J. P., von der Borch, C. C., et al., *Init. Repts. DSDP*, 90: Washington (U.S. Govt. Printing Office).

[2] Address: Graduate School of Oceanography, University of Rhode Island, Kingston, RI 02881.

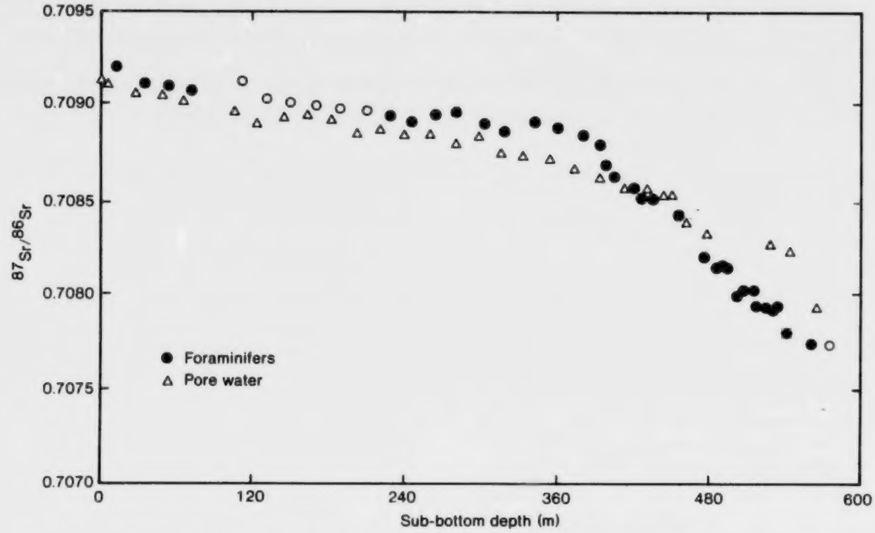

Figure 1. Foraminiferal and interstitial water $^{87}Sr/^{86}Sr$ as a function of depth for Hole 593. Closed circles represent well-preserved foraminifer samples. Open circles indicate foraminifer samples that showed trace amounts of euhedral calcite crystals indicative of recrystallization when viewed under the SEM.

Table 1. Foraminiferal $^{87}Sr/^{86}Sr$, Sr/Ca, and SEM examinations for Hole 593.

Sample Core-Section (interval in cm)	Sub-bottom depth (m)	Ratio ± 2σ × 10^{-6}	Sr/Ca Atom ratio (× 1000)	SEM observations
2-6, 2-4	12.6	0.709205 ± 41	1.41	No recrystallization
4,CC	33.9	0.709117 ± 32	1.39	No recrystallization
6,CC	53.1	0.709105 ± 26	1.40	No recrystallization
8,CC	72.3	0.709080 ± 26	1.34	No recrystallization
12,CC	110.7	0.709064 ± 32	1.36	Minor recrystallization
14,CC	129.9	0.709035 ± 34	1.36	Minor recrystallization
16,CC	149.1	0.709020 ± 34	1.32	Minor recrystallization
18,CC	168.3	0.709003 ± 30	1.28	Minor recrystallization
20,CC	187.5	0.708988 ± 24	1.30	Minor recrystallization
22,CC	206.7	0.708974 ± 30	1.28	Minor recrystallization
24,CC	225.9	0.708949 ± 28	1.40	No recrystallization
26,CC	245.1	0.708917 ± 22	1.30	No recrystallization
28,CC	264.3	0.708961 ± 26	1.38	No recrystallization
30-5, 1-2	279.9	0.708969 ± 26	1.39	No recrystallization
32,CC	302.7	0.708910 ± 36	1.41	No recrystallization
34-5, 1-2	318.3	0.708868 ± 28	1.41	No recrystallization
36,CC	341.1	0.708911 ± 36	1.36	No recrystallization
38,CC	360.3	0.708876 ± 30	1.39	No recrystallization
40,CC	379.5	0.708848 ± 24	1.26	No recrystallization
42-3, 70-72	392.8	0.708802 ± 14	1.35	No recrystallization
42,CC	398.7	0.708698 ± 24	1.35	No recrystallization
44-1, 35-37	408.7	0.708637 ± 16	1.28	No recrystallization
44,CC	417.9	0.708557 ± 20	1.35	No recrystallization
46-1, 35-37	427.9	0.708515 ± 32	1.37	No recrystallization
46,CC	437.1	0.708515 ± 24	1.35	No recrystallization
48,CC	456.3	0.708446 ± 20	1.36	No recrystallization
50,CC	475.5	0.708211 ± 28	1.39	No recrystallization
52-2, 35-37	487.0	0.708161 ± 12	1.32	No recrystallization
52-4, 35-37	490.0	0.708159 ± 28	1.35	No recrystallization
52,CC	494.7	0.708145 ± 32	1.39	No recrystallization
53-3, 35-37	498.1	0.708003 ± 16	1.35	No recrystallization
54-1, 35-37	504.7	0.708027 ± 28	1.35	No recrystallization
54-2, 35-37	506.2	0.708038 ± 16	1.39	No recrystallization
54,CC	513.9	0.708030 ± 20	1.41	No recrystallization
55-2, 35-37	516.8	0.707959 ± 18	1.41	No recrystallization
56-2, 35-37	525.4	0.707932 ± 36	1.43	No recrystallization
56-5, 35-36	529.9	0.707911 ± 24	1.39	No recrystallization
56,CC	533.1	0.707945 ± 32	1.40	No recrystallization
57-6, 35-37	540.1	0.707809 ± 24	1.36	No recrystallization
58-2, 35-37	544.6	0.707816 ± 14	1.41	No recrystallization
60-2, 35-37	563.8	0.707752 ± 20	1.45	No recrystallization
60,CC	571.5	0.707747 ± 34	1.45	Minor recrystallization

Note: Errors are 2 standard errors of the mean $^{87}Sr/^{86}Sr$ in 10^{-6} abd represent in-run precision.

Table 2. Pore-water $^{87}Sr/^{86}Sr$ for Hole 593.

Core-Section	Depth (m)	Ratio ± 2σ × 10^{-6}
Surface seawater		0.709131 ± 20
1-4	4.8	0.709115 ± 36
4-3	28.0	0.709063 ± 22
6-3	47.3	0.709050 ± 28
8-1	63.5	0.709032 ± 24
12-3	104.9	0.708967 ± 18
14-3	124.1	0.708907 ± 30
16-3	143.3	0.708939 ± 28
18-3	163.5	0.708952 ± 22
20-3	181.7	0.708927 ± 28
22-3	200.9	0.708858 ± 30
24-3	220.1	0.708883 ± 32
26-3	239.3	0.708849 ± 18
28-3	258.5	0.708864 ± 18
30-3	277.7	0.708806 ± 20
32-2	296.9	0.708842 ± 24
34-2	314.6	0.708762 ± 20
36-2	333.8	0.708745 ± 18
38-3	354.5	0.708721 ± 26
40-3	373.7	0.708665 ± 24
42-3	392.9	0.708629 ± 14
44-3	412.1	0.708564 ± 24
46-3	431.3	0.708557 ± 14
47-3	440.9	0.708532 ± 14
48-3	450.5	0.708533 ± 22
50-3	469.7	0.708392 ± 26
54-2	506.6	0.708345 ± 14
56-3	527.3	0.708275 ± 22
58-1	543.5	0.708244 ± 18
60-3	565.7	0.707945 ± 18

Note: Errors are 2 standard errors of the mean $^{87}Sr/^{86}Sr$ in 10^{-6} and represent in-run precision.

latest Eocene). This observation is consistent with $^{87}Sr/^{86}Sr$ ratios measured at other DSDP sites and from other marine samples (Burke et al., 1982; Hess et al., 1984, and unpubl. data; DePaolo and Ingram, 1985; Palmer and Elderfield, in press). Pore-water $^{87}Sr/^{86}Sr$ displays roughly the same pattern as do the foraminifers. The pore-water Sr isotope ratios are fairly constant but c nsistently lower than the foraminiferal $^{87}Sr/^{86}Sr$ to ab ut 400 m, at which point the pore-water $^{87}Sr/^{86}Sr$ decrea es along with the foraminiferal $^{87}Sr/^{86}Sr$, but with con istently higher $^{87}Sr/^{86}Sr$ ratios than the foraminiferal atios. The crossover point between the two curves is between 400 and 440 m, close to the ooze/chalk transition at 462 m.

DISCUSSION

The measured foraminiferal ^{87}Sr/^{86}Sr accurately records the ^{87}Sr/^{86}Sr of contemporaneous seawater only if the foraminifers are pristine or the effects of diagenetic alteration are minimal. Two criteria were used to screen for diagenetic alteration: scanning electron microscopy and Sr/Ca ratios. Physical evidence for recrystallization was evident in scanning electron micrographs by the presence of large, blocky, euhedral calcite crystals, cementation, or overgrowth. Seven foraminiferal samples from Site 593, indicated by the open circles in Figure 1, showed trace amounts of euhedral calcite crystals indicative of recrystallization. All other samples were free of any physical evidence of recrystallization (Table 1).

Diagenesis also affects the foraminiferal Sr/Ca ratio. Lorens (1981) showed that the magnitude of the calcite distribution coefficient for Sr is dependent on the rate of carbonate precipitation. At slower growth rates, the Sr distribution coefficient is lower. Because inorganic recrystallization rates are much slower than biogenic calcite precipitation rates, the foraminiferal Sr/Ca is lowered during diagenetic alteration. Sr/Ca ratios for the foraminifer samples are given in Table 1. Comparison of the measured Sr/Ca ratio to the Sr/Ca age curve determined from well-preserved fossil foraminifers (Graham et al., 1982; Delaney, 1983) provide a second check on sample alteration. Samples with Sr/Ca ratios that were low relative to contemporaneous samples were suspected of being recrystallized. For Site 593, all Sr/Ca ratios were comparable to values on the Sr/Ca age curve.

As a final check on the integrity of our ancient seawater ^{87}Sr/^{86}Sr determinations, we measured the ^{87}Sr/^{86}Sr of contemporaneous pore-water samples. If the foraminifers had recrystallized in some way that was not detected by our screening criteria, their ^{87}Sr/^{86}Sr ratio would be influenced by the interstitial water ^{87}Sr/^{86}Sr with which they equilibrated. As pore-water ^{87}Sr/^{86}Sr ratios are affected by diffusion and advection as well as alteration of sedimentary volcanic matter and continental debris (Elderfield et al., 1982; Elderfield and Gieskes, 1982), the ^{87}Sr/^{86}Sr of pore waters may differ from that of sedimentary biogenic calcite. Pore-water ^{87}Sr/^{86}Sr are shown in Figure 1 and Table 2. Pore-water Sr isotope ratios are nearly identical to foraminiferal ^{87}Sr/^{86}Sr. Thus, even if the samples were partially recrystallized, the influence on the foraminiferal Sr isotope composition would be minimal.

With the exception of seven slightly altered foraminifer samples (open circles, Fig. 1), our analyses found no evidence for foraminiferal recrystallization. Therefore, we interpret our measured foraminiferal ^{87}Sr/^{86}Sr ratios as representative of ancient seawater ^{87}Sr/^{86}Sr. The fact that our measurements for Site 593 agree well with ^{87}Sr/^{86}Sr ratios from other DSDP sites supports this conclusion. On the other hand, on the basis of pore-water Sr^{+2} concentration increases with depth, Baker (this volume) calculated an initial bulk carbonate recrystallization rate of 10%/m.y. for Site 593. Since most of the carbonate at Site 593 is composed of calcareous nannofossils, which may be more susceptible to alteration than most foraminifers, it is probable that this fine fraction provides most of Sr^{+2} excess to the pore water. A detailed study of the Sr isotopic composition of fine-fraction carbonates is planned to test this hypothesis.

CONCLUSIONS

The ^{87}Sr/^{86}Sr ratio of seawater, as reflected by the ^{87}Sr/^{86}Sr ratio of fossil foraminifers, has increased from the latest Eocene to the present. The rise was extremely rapid from the late Eocene to the early Miocene and very gradual from the middle Miocene to the present. This trend is consistent with Sr isotopic measurements from other DSDP cores. SEM examinations and Sr/Ca ratios showed that planktonic foraminifers (<150-μm size fraction) were well preserved.

ACKNOWLEDGMENTS

We thank the shipboard scientific team of DSDP Leg 90, in particular J. P. Kennett and P. A. Baker, for providing the samples used in this study and Michael Bender, Paul Baker, and Martin Palmer for reviewing this manuscript. Support for this project was provided by NSF-OCE-8207787.

REFERENCES

Albarède, F., Michard, A., Minster, J. F., and Michard, G., 1981. ^{87}Sr/^{86}Sr ratios in hydrothermal waters and deposits from the East Pacific Rise at 21°N. *Earth Planet Sci. Lett.*, 55:229-236.

Armstrong, R. L., 1971. Glacial erosion and the variable isotopic composition of strontium in sea water. *Nature Phys. Sci.*, 230:132-133.

Bender, M. L., and Keiwig, L. D., Jr., 1979. Speculations about the Upper Miocene change in abyssal Pacific dissolved bicarbonate ^{13}C. *Earth Planet. Sci. Lett.*, 45:383-393.

Brass, G. W., 1976. The variation of marine ^{87}Sr/^{86}Sr ratio during Phanerozoic time: interpretation using a flux model. Geochim. Cosmochim. Acta, 40:721-730.

Broecker, W. S., 1971. A kinetic model for the chemical composition of seawater. *Quat. Res.*, 1:188-207.

Burke, W. H., Dennison, R. E., Hetherington, E. A., Koepnick, R. B., Nelson, H. F., and Otto, J. B., 1982. Variation of seawater ^{87}Sr/^{86}Sr throughout Phanerozoic time. *Geology*, 10:516-519.

Claypool, G. E., Holser, W. T., Kaplan, I. R., Sakai, H., and Zak, I., 1980. The age curves of sulfur and oxygen isotopes in marine sulfate and their mutual interpretation. *Chem. Geol.*, 28:199-260.

Dasch, E. J., and Biscaye, P. E., 1971. Isotopic composition of strontium in Cretaceous-to-Recent pelagic foraminifera. *Earth Planet. Sci. Lett.*, 11:201-204.

Delaney, M. L., 1983. Foraminiferal trace elements: uptake, diagenesis, and 100 m.y. paleochemical history [Ph.D. Dissert.] Massachusetts Institute of Technology.

DePaolo, D., and Ingram, B., 1985. High resolution stratigraphy with Sr isotopes. *Science*, 277:187-191.

Elderfield, H., and Gieskes, J. M., 1982. Sr isotopes in interstitial waters of marine sediments from Deep Sea Drilling Project cores. *Nature*, 300:(5982):493-497.

Elderfield, H., Gieskes, J. M., Baker, P. A., Oldfield, R. K., Hawkesworth, C. J., and Miller, R., 1982. ^{87}Sr/^{86}Sr and ^{18}O/^{16}O ratios, interstitial water chemistry and diagenesis in deep-sea carbonate sediments of the Ontong-Java Plateau. *Geochim. Cosmochim. Acta*, 46:2259-2267.

Graham, D. W., Bender, M. L., Williams, D. F., and Keigwin, L. D., Jr., 1982. Strontium-calcium ratios in Cenozoic planktonic foraminifera. *Geochim. Cosmochim. Acta*, 46:1281-1292.

Hess, J., Bender, M. L., and Schilling, J. -G., 1984. The marine ^{87}Sr/^{86}Sr record during the last 100 million years. *EOS*, 65(45):976. (Abstract)

Lorens, R. B., 1981. Sr, Cd, Mn and Co distribution coefficients in calcite as a function of calcite precipitation rate. *Geochim. Cosmochim. Acta*, 45,553-562.

Palmer, M., and Elderfield, H., in press. The strontium isotopic composition of seawater over the past 75 million years. *Nature*.

Peterman, Z. E., Hedge, C. E., and Tourtelot, H. A., 1970. Isotopic composition of strontium in seawater throughout Phanerozoic time. *Geochim. Cosmochim. Acta*, 34:105–120.

Shackleton, N. J., and Kennett, J. P., 1975. Paleotemperature history of the Cenozoic and initiation of Antarctic glaciation: oxygen and carbon isotope analyses in DSDP Sites 277, 279, and 281. *In* Kennett, J. P., Houtz, R. E., et al., *Init. Repts. DSDP*, 29: Washington (U.S. Govt. Printing Office), 743–775.

Spooner, E.T.C., 1976. The strontium isotopic composition of seawater and seawater-oceanic crust interaction: *Earth Planet. Sci. Lett.*, 31:167–174.

Date of Initial Receipt: 10 December 1984
Date of Acceptance: 1 April 1985

34. ^{3}He/^{4}He RATIOS OF PORE GASES IN DEEP-SEA SEDIMENTS, LEGS 89 AND 90[1]

Hiroshi Wakita and Yuji Sano, University of Tokyo
Naoyuki Fujii, Kobe University
and
Akira Takeuchi, Toyama University[2]

INTRODUCTION

Studies on He isotope ratios of gas and rock samples in various parts of the world have shown a close relation between the ^{3}He/^{4}He ratio and geotectonic features of the sampling area (Tolstikhin 1978; Craig and Lupton, 1982; Lupton, 1983; Sano and Wakita, in press, a). Emission of primordial He is commonly found in gases and fluid in Cenozoic volcanic areas (mid-ocean ridges, hot spots, and subduction zones), whereas that of radiogenic He is predominant in continental areas. Thus, the ^{3}He/^{4}He ratio is considered a useful tool for evaluating a variety of geotectonic environments.

Investigations on He isotope ratios in oceanic areas have been carried out mainly for fresh basalt glasses obtained from mid-ocean ridges (Lupton and Craig, 1975; Craig and Lupton, 1976; Rison, 1980; Kyser and Rison, 1982; Allegre et al., 1983; Ozima and Zashu, 1983). Because of the genetic configuration of sampling sites, the investigated area is rather limited. Alternatively, using deep-seawater samples, previous workers have reported enrichment of ^{3}He in the Atlantic Ocean (Jenkins and Clarke, 1976), Pacific Ocean (Jenkins et al., 1978), and Red Sea (Lupton et al., 1977). Lupton and Craig (1981) found an extensive plume of water enriched with ^{3}He in the Pacific Ocean. These data, however, provide indirect information on outgassing of the oceanic crust. Deep-sea sediment is considered to be an ideal material for investigating the ocean floor because of its preservation of gases emitted from the interior of the Earth. Furthermore, sampling sites can be selected all over the oceanic area. In the existing data base, however, helium studies on gases dissolved in pore water of oceanic sediment are quite sparse (Clarke et al., 1973; Barnes and Clarke, 1980; Sayles and Jenkins, 1982; Sano and Wakita, in press, b). The purpose of this study is to reveal the isotopic signature of He in an ocean floor of continental crust character in relation to its tectonic features. We report the ^{3}He/^{4}He and ^{4}He/^{20}Ne ratios of gases dissolved in pore water of sediments in the Ontong-Java Plateau (Site 586) and Chatham Rise (Site 594).

EXPERIMENTAL

Sampling Method

A sample container with a vacuum valve at one end was used for gas samples. Prior to gas collection, the lead glass container, with inside volume of about 50 cm^3, was evacuated in the laboratory by a rotary pump and a sorption pump. On the deck, both ends of 1.5-m sections of the core sample recovered in the plastic liner were capped with plastic caps. On reaching room temperature, some of the liner began to swell slightly because of gas released from the sediments. The core section was held vertically, and a plastic vessel was attached to the top of the liner and filled with deionized water. An inverted funnel was connected with the glass container by a thick rubber tube in the water (Fig. 1). Then the middle part of the plastic cap was cut to release gas into the funnel, and the gas was transferred to the container by opening the stop valve. The samples were stored about one month before analysis. Considering the low permeation velocity of He in lead glass, penetration of atmospheric He is negligible for the storage time.

Helium Isotope Measurements

After the sample container was brought back to the laboratory, about 1 cm^3 STP of gaseous sample was introduced into a metallic ultra-high vacuum line. Purification was carried out using a CuO furnace and a three-stage charcoal trap kept at 196°C. The ^{3}He/^{4}He and ^{4}He/^{20}Ne ratios were measured with a static mass spectrometer (6-60-SGA, Nuclide Co.). Ion beams of ^{3}He and ^{4}He were detected by a double collector system. Resolving power of about 600 at 1% peak height was attained for complete separation of ^{3}He beam from those of H_3 and HD. An in-house standard for ^{3}He/^{4}He measurements was prepared by mixing known amount of pure ^{3}He and ^{4}He gases. The mass discrimination factor of the measuring system was calculated using this standard. The atmospheric He was used as a running standard. Isotopic ratios were determined as an average of six sets of measurements of the peak heights. The mean value of the ^{3}He/^{4}He ratios in Tokyo air is $(1.42 \pm 0.04) \times 10^{-6}$ from 31 individual runs. ^{4}He/^{20}Ne ratio measurements were conducted by adjusting the magnet current. A detailed description of the measurement was given in a previous paper (Sano et al., 1982).

RESULTS AND DISCUSSIONS

Three samples were obtained at Site 586 in the Ontong-Java Plateau and six sample in Holes 594 and 594B in the Chatham Rise (Fig. 2). The observed ^{3}He/^{4}He and ^{4}He/^{20}Ne ratios are shown in Table 1, together with depths of the sampling sites. The ^{3}He/^{4}He and ^{4}He/^{20}Ne ratios vary significantly, from 4.39×10^{-7} to 1.26×10^{-6} and from 0.39 to 4.35, respectively. No correlation between the ^{3}He/^{4}He ratios and locations of sampling sites is found.

Clarke et al. (1973) measured the ^{3}He/^{4}He ratios of pore water from sections of core at three locations (Sites 148, 149, and 150) in the Caribbean Sea. Their ratios were principally radiogenic, varying from 6.6×10^{-7} to 1.4×10^{-6}. Barnes and Clarke (1980) reported that the

---

[1] Kennett, J. P., von der Borch, C. C., et al., *Init. Repts. DSDP*, 90: Washington (U.S. Govt. Printing Office).

[2] Addresses (Wakita, Sano) Laboratory for Earthquake Chemistry, Faculty of Science, The University of Tokyo, Bunkyo-ku, Tokyo, Japan; (Fujii) Department of Earth Science, Faculty of Science, Kobe University, Nada-ku, Kobe, Japan; (Takeuchi) Department of Earth Science, Faculty of Science, Toyama University, Gohuku, Toyama, Japan.

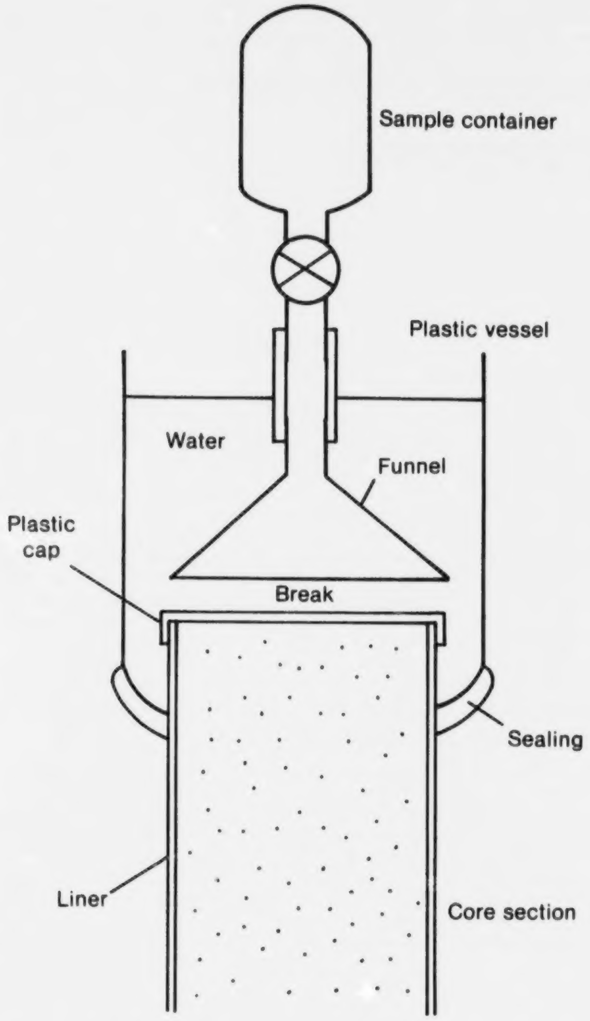

Figure 1. Sampling method of pore gases in sediment.

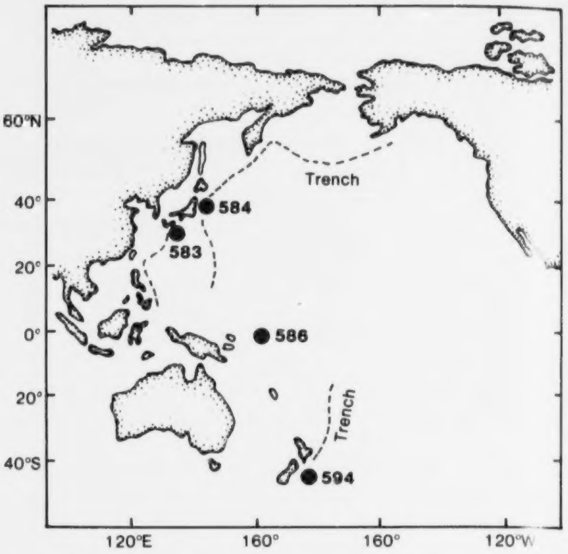

Figure 2. Sampling sites of pore gases in sediment. Three samples were collected in the Ontong-Java Plateau (Site 586) and six samples in the Chatham Rise (Holes 594 and 594B).

Table 1. $^3He/^4He$ and $^4He/^{20}Ne$ ratios of pore gases in sediment from the Ontong-Java Plateau and the Chatham Rise.

No.	Depth (m)	Location	$^3He/^4He$ ($\times 10^{-6}$)	$^4He/^{20}Ne$
Ontong-Java Plateau (Site 568)				
SG-1	191.9	0°30′S, 158°30′E	0.639 ± 0.013	4.4
SG-2	240.3		0.990 ± 0.020	0.57
SG-3	261		0.974 ± 0.009	0.52
Chatham Rise (Site 594)				
SG-4	399.5	45°31′S, 174°57′E	0.439 ± 0.007	3.2
SG-5	447.5		0.568 ± 0.021	2.6
SG-6	449.0		0.536 ± 0.009	1.4
SG-7	466.7		0.549 ± 0.030	2.2
SG-8	466.7		0.503 ± 0.011	2.9
SG-9	18.6		1.26 ± 0.03	0.39

$^3He/^4He$ ratios of pore fluids at Sites 398, 410, 419, 424, 436, and 438 were generally higher than the atmospheric ratio, with values varying from 5.0×10^{-7} to 1.05×10^{-5}. The discrepancy in the ratio between the Caribbean Sea and the Pacific Ocean was interpreted as a possible difference in the He isotope signature of the upper mantle and the crust in the two ocean basins (Barnes and Clarke, 1980).

We already reported the $^3He/^4He$ ratios of gases dissolved in pore water in sediments from the Nankai Trough (Site 583) and the Japan Trench (Site 584) (Sano and Wakita, in press, b). The $^3He/^4He$ ratios, ranging from 2.15×10^{-7} to 1.23×10^{-6}, agree well with the present value (4.39×10^{-7} to 1.26×10^{-6}). As a whole, the He isotope signature of our study is practically radiogenic and is significantly different from that of Barnes and Clarke (1980).

Helium in pore gases of deep-sea sediments is considered to be a mixture of the following components: (1) atmospheric He dissolved in seawater and air contamination during sampling and/or analysis with the $^3He/^4He$ ratio of 1.4×10^{-6}. This component is easily distinguished from the other components by its low $^4He/^{20}Ne$ ratio. (2) *In situ* radiogenic He in the sediments with the ratio of $(1–2) \times 10^{-8}$. The $^3He/^4He$ ratio of this component depends on the chemical composition of the sediment. (3) Trapped He from the degassing of the basement rock beneath the sediment. Large variation in the $^3He/^4He$ ratio (1.0×10^{-7}–1.0×10[illegible]) is explained by the differences in components, varying ages of the crust and initial contents of He, U, and Th in material generating He. (4) Extraterrestrial He caused by fallout of meteoritic materials with the extraordinarily high ratio of (1×10^{-4} to 1.0). The possible existence of the component was reported by Krylov et al. (1973) and Ozima et al. (1984).

The $^3He/^4He$ ratios of the present samples are plotted against the $^4He/^{20}Ne$ ratios in Figure 3. There is a negative correlation between $^3He/^4He$ and $^4He/^{20}Ne$ ra-

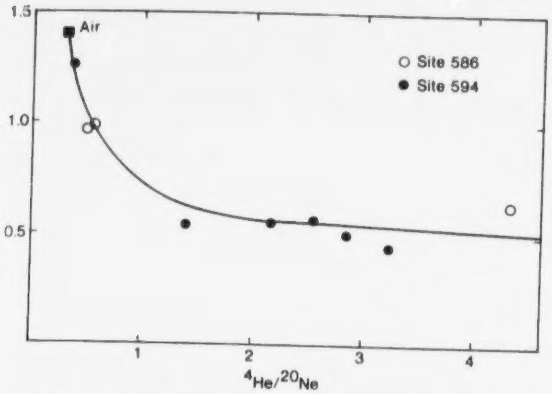

igure 3. The ^{3}He/^{4}He ratios for samples are plotted against the ^{4}He/^{20}Ne ratios. Solid line shows the mixing line between atmospheric He and He with ^{3}He/^{4}He ratio of 4×10^{-7}.

tios. All data lie on a mixing line between the atmospheric He and gas with a ^{3}He/^{4}He ratio of about 5×10^{-7}. This suggests that He in the present sediments can be explained by the mixing of two end-members: atmospheric He and radiogenic He.

For the ^{3}He/^{4}He ratios from the Nankai Trough (Site 583) and Japan Trench (Site 584), we found two-component mixing between the atmospheric He and radiogenic He with the ^{3}He/^{4}He ratio of $(2\text{–}3) \times 10^{-7}$ (Sano and Wakita, 1983). The *in situ* radiogenic ^{3}He/^{4}He ratio was calculated to be 2.0×10^{-8} based on the nuclear reactions of ^{6}Li$(n,\alpha)^3$H$\rightarrow{}^3$He. The value was lower by a factor of 10 than the ratio of the estimated end-member, that is, $(2\text{–}3) \times 10^{-7}$. We attributed the discrepancy to the radiogenic end-member with a much higher ^{3}He/^{4}He ratio. Such a component might be the trapped He in the sediment associated with degassing of the basement rocks beneath the sediment. The assigned end-member may be an admixture of He from basement rocks and sediments.

In the present samples, the ^{3}He/^{4}He ratio of the radiogenic end-member in the mixing is calculated to be 4×10^{-7}. The value is two times higher than that of the Nankai Trough (Site 583) or the Japan Trench (Site 584). If we consider that the ^{3}He/^{4}He ratios of *in situ* radiogenic He of estimated pelagic clay of the area investigated in this study (1.5×10^{-8}) are almost the same as hat of trench sediment (2.0×10^{-8}), the discrepancy nay be explained by some enhancement of trapped He rom the basement rocks or extraterrestrial He.

If the trapped He from the basement rocks is a major ause of the discrepancy, there should be some relation etween the tectonic features of the sites where samples ere taken and observed ^{3}He/^{4}He ratios. The degassing ate of He from basement rocks may reflect changes in ectonic conditions such as distance from a mid-ocean idge, rock type, age of the crust, thickness of the sediment, alteration stage, and others. Sites 583 and 584 re located in the outer slope of the Nankai Trough and he Japan Trench, respectively, and both are on oceanic rust. Site 586 on the Ontong-Java Plateau is known to e composed of continental crust. If the observed ^{3}He/^{4}He ratios reflect outgassing from basement plus sediment, Site 594 on the Chatham Rise may be in a tectonic feature similar to the Ontong-Java Plateau.

ACKNOWLEDGMENTS

We thank I. Kaneoka, University of Tokyo, and K. Nagao, Okayama University of Science, for providing valuable comments on the original manuscript. We also thank D. Fisher and an anonymous reviewer for critical comments.

REFERENCES

Allegre, C. J., Staudacher, T., Sarda, P., and Kurz, M., 1983. Constraint on evolution of Earth's mantle from rare gas systematics. *Nature*, 303:762–766.

Barnes, R. O., and Clarke, W. B., 1980. ^{3}He/^{4}He, He, Ne and Ar concentrations in pore fluids of DSDP Sites 398 to 438. *EOS, Trans. Am. Geophys. Un.*, 61:996.

Clarke, W. B., Horowitz, R. M., and Broecker, W. S., 1973. Interstitial water studies, Leg 15—inert gases. *In* Edgar, N. T., Saunders, J. B., et al., *Init. Repts. DSDP*, 15: Washington (U.S. Govt. Printing Office), 777–781.

Craig, H., and Lupton, J. E., 1976. Primordial neon, helium and hydrogen in oceanic basalts. *Earth Planet. Sci. Lett.*, 31:369–385.

————, 1982. Helius-3 and mantle volatiles in the ocean and the oceanic crust. *In* Emiliani, C. (Ed.), *The Sea* (Vol. 7): New York (Wiley), 391–428.

Jenkins, W. J., and Clarke, W. B., 1976. The distribution of ^{3}He in the western Atlantic Ocean. *Deep-Sea Res.*, 23:481–494.

Jenkins, W. J., Edmond, J. M., and Corliss, J. B., 1978. Excess ^{3}He and ^{4}He in Galapagos submarine hydrothermal waters. *Nature*, 272:156–158.

Krylov, A. Ya, Mamyrin, B. A., Silin, Yu. I., and Khabarin, L. U., 1973. Helium isotopes in ocean sediments. *Geochem. Int.*, 1973: 202–205.

Kyser, M. D., and Rison, W., 1982. Systematics of rare gas isotopes in basic lavas and ultramafic xenoliths. *J. Geophys. Res.*, 87: 5611–5630.

Lupton, J. E., 1981. A major helium-3 source at 15°S on the East Pacific Rise. *Science*, 214:13–18.

————, 1983. Terrestrial inert gases: isotope tracer studies and clues to primordial components in the mantle. *Ann. Rev. Earth Planet. Sci.*, 11:371–414.

Lupton, J. E., and Craig, H., 1975. Excess ^{3}He in oceanic basalts: evidence for terrestrial primordial helium. *Earth Planet. Sci. Lett.*, 26:133–139.

Lupton, J. E., Weiss, R. F., and Craig, H., 1977. Mantle helium in the Red Sea brines. *Nature*, 266:244–246.

Ozima, M., Takayanagi, M., Zashu, S., and Amari, S., 1984. High ^{3}He/^{4}He ratio in ocean sediments. *Nature*, 311:448–450.

Ozima, M., and Zashu, S., 1983. Noble gases in submarine pillow volcanic glasses. *Earth Planet. Sci. Lett.*, 62:24–40.

Rison, W., 1980. Isotopic studies of the rare gases in igneous rocks: implications for the mantle and atmosphere [Ph. D. Thesis]. Univ. Calif., Berkeley.

Sano, Y., Tominaga, T., Nakamura, Y., and Wakita, H., 1982. ^{3}He/^{4}He ratios of methane-rich natural gases in Japan. *Geochem. J.*, 16:337–345.

Sano, Y., and Wakita, H., in press, a. Geographical distribution of ^{3}He/^{4}He ratios and its implications for geotectonic structure of the Japanese Islands. *J. Geophys. Res.*

————, in press, b. ^{3}He/^{4}He ratios of pore gases in pore water, Leg 87, Sites 583 and 584. *In* Kagami, H., Karig, D. E., Coulbourn, W. T., et al., *Init. Repts. DSDP*, 87: Washington (U.S. Govt. Printing Office).

Sayles, F. L., and Jenkins, W. J., 1982. Advection of pore fluids through sediments in the equatorial East Pacific. *Science*, 217:245–248.

Tolstikhin, I. N., 1978. Some recent advances in isotope geochemistry light rare gases. *In* Alexander, E. C., and Ozima, M. (Eds.), *Terrestrial Rare Gases*. Japan Sci. Soc. Press. Adv. Earth Planet. Sci., 3: 33–62.

Date of Initial Receipt: 28 June 1984
Date of Acceptance: 26 October 1984

35. DIAGENESIS OF ORGANIC COMPOUNDS IN HOLE 593, LEG 90 (TASMAN SEA)[1]

B. Mycke, K.-C. Emeis, and E. T. Degens, Geologisch-Paläontologisches Institut und Museum,
Universität Hamburg[2]

ABSTRACT

C_{org} and N_{org} contents in the acid insoluble mineral fraction were studied in sediments of Site 593. Both decrease systematically from Recent to early Miocene over 425 m of carbonate facies. C/N ratios (7–11) are typically marine and indicate that residual organic matter, bound to clay minerals, was originally scavenged from the marine habitat rather than being of terrigenous origin. Variations of C_{org} and N_{org} are almost entirely controlled by rates of sedimentation, which gradually increase from Recent to early Miocene. Preliminary results of carbohydrate distribution indicate that epigenetic and diagenetic processes alter both the concentrations and the ratios of individual monomers with depth. Total carbohydrate concentrations in the samples diminish from 91 μg/g sediment at 18 m sub-bottom depth to 49 μg/g at 335 m. In contrast, sugars in the acid insoluble residue increase with depth, suggesting release of structural polysaccharides and their subsequent association with clay minerals. Ratios of arabinose to fucose, which are about 6:1 in Recent carbonaceous sediments intercepted by sediment traps, vary from 1:1 in the youngest sample to 1:2.5 in the oldest.

INTRODUCTION

Amount and type of organic matter in deep-sea sediments is controlled by a series of factors, most notably: (1) primary production in the euphotic zone, (2) vertical and horizontal advection of particles, (3) rate of sedimentation, (4) burrowing activities, and (5) microbial degradation. Changes in any one of these variables will have an effect on C_{org} compounds.

Hole 593 from the Tasman Sea (southwest Pacific) exhibits a typical carbonate facies starved of clastic sediment input. This hole was analyzed for C_{org}, N_{org}, and carbohydrates (CH) to discover the diagenetic fate of the organic matter. Emphasis was placed on organic matter associated with the acid insoluble fraction. Most of this organic matter is thought to be bound to clay minerals. Its point of origin could be terrestrial soils or the marine dissolved organic-carbon pool. In both instances organic matter was scavenged from an aqueous phase. It is of note that labile organic matter derived, for example, from calcified tissue was lost during the analytical operation.

Previous work has focused attention on the biogeochemistry of labile organic templates in foraminiferal tests and their rate of decay (Bada et al., 1978). Furthermore, variability in C/N ratios as a measure of this decay has been discussed at length (e.g., Müller, 1977; Waples and Sloan, 1980; Müller and Suess, 1979). Because organic matter scavenged by clay minerals is rendered structurally more resistant, microbial degradation during early diagenesis should be minor. Because of its inertia, this type of organic matter is expected to survive diagenesis for an extended period of time.

METHODS

Preparatory and analytical methods employed during this study are as follows. For the carbonate, ground and homogenized bulk samples were subjected to an acid treatment in a closed system (0.1 *N* H_3PO_4). The amount of CO_2 released was measured conductometrically by means of a Charmograph Model 6 CO_2 analyzer against reagent grade $CaCO_3$ standards. For C_{org} and N_{org}, ground and homogenized samples were acidified with 2 *N* HCl and washed to neutrality with distilled water. Liquid was removed by centrifugation and was subsequently decanted. An aliquot of the vacuum-dried (40°C) residue was combusted in an elemental analyzer (Carlo Erba Model 1104). For carbohydrates, following acid hydrolysis of ground bulk samples by 2 *N* HCl, individual monosaccharides were quantitatively analyzed by ion-exchange chromatography. Further details on analytical techniques are given elsewhere (Mopper, 1977).

RESULTS

Carbonate, C_{org}, and N_{org} values are given in Table 1 and Figures 1 and 2. Except for two anomalous data points between 180 and 200 m sub-bottom depth, there is a general decrease (with wide scatter) in C_{org} to a depth of 475 m in Hole 593. The increase in organic carbon below 475 m coincides with an unconformity (lower Miocene/lower Pliocene). C_{org} values of the carbonate-free residue generally range from 0.2 to 1.2%, whereas the corresponding N_{org} values are an order of magnitude lower at ~0.02 to 0.1%. The resulting C/N ratios fall mostly in the range from 7 to 11 and thus correspond to ratios commonly found in marine sediments (e.g., Emery and Rittenberg, 1952; Degens, 1970; Müller and Suess, 1979) and in the dissolved marine organic-carbon pool (Holm-Hansen et al., 1966; Degens and Ittekkot, 1983).

In contrast, C/N ratios in terrestrial humic compounds of soil and riverine provenance are considerably higher (15–40). Some of the scattering of C/N ratios in our samples can be attributed to the low N_{org} contents in a number of samples just barely above the detection limit. The reported increase in C/N ratios with depth for pelagic sediments (e.g., Trask and Patnode, 1942; Waples and Sloan, 1980) could not be corroborated by our data set.

---

[1] Kennett, J. P., von der Borch, C. C., et al., *Init. Repts. DSDP*, 90: Washington (U.S. Govt. Printing Office).

[2] Address: Geologisch-Paläontologisches Institut und Museum, Universität Hamburg, Bundesstrasse 55, D-2000 Hamburg 13, Federal Republic of Germany.

Table 1. Organic matter data for Hole 593.

Depth (m)	$CaCO_3$ (%)	C_{min} (%)	C_{org} (%)[a]	N_{org} (%)[a]	C/N[a]	Total C_{org} (%)[b]
3.6	85.1	10.1	0.50	0.06	8.3	0.07
8.7	89.7	10.6	0.99	0.13	7.6	0.10
18.3	83.8	9.9	0.85	0.06	14.2	0.14
27.5	89.0	10.5	0.71	0.07	10.1	0.08
47.1	91.2	10.8	0.63	0.06	10.5	0.06
56.7	92.4	10.9	0.40	0.06	6.7	0.05
75.9	92.1	10.9	0.50	0.05	10.2	0.04
95.1	94.0	11.1	0.86	0.06	14.3	0.05
114.3	95.9	11.4	0.67	0.05	13.4	0.03
123.9	nd	nd	1.03	0.09	11.4	nd
133.5	95.7	11.3	0.92	0.06	15.3	0.04
143.1	96.8	11.5	0.93	0.03	31.0	0.03
152.7	94.9	11.2	0.57	0.05	11.4	0.03
162.3	95.2	11.3	0.63	0.04	15.7	0.03
171.9	94.8	11.3	0.59	0.05	11.8	0.03
181.5	96.0	11.4	1.66	0.09	18.4	0.07
191.1	nd	nd	1.42	0.10	14.2	nd
210.3	95.9	11.5	0.62	0.03	20.7	0.03
219.9	95.1	11.3	0.45	0.06	7.5	0.02
229.5	93.6	11.1	0.64	0.08	8.0	0.04
239.1	95.2	11.3	0.35	0.06	5.8	0.02
258.3	91.9	10.9	0.67	0.07	9.6	0.05
267.9	94.0	11.2	0.67	0.05	13.4	0.04
277.5	97.0	11.5	0.41	0.04	10.3	0.01
287.1	95.2	11.3	0.68	0.04	17.0	0.03
296.7	93.3	11.1	0.41	0.03	13.7	0.03
306.3	96.1	11.4	0.73	0.02	36.5	0.03
315.9	91.0	10.8	0.73	0.09	8.1	0.07
325.5	94.3	11.2	0.34	0.01	48.6	0.02
335.1	93.1	11.1	0.53	0.03	17.7	0.04
344.7	92.6	11.0	0.35	0.03	11.7	0.03
354.3	90.5	10.8	0.51	0.06	8.5	0.05
363.9	93.4	11.1	0.31	0.04	7.8	0.02
373.5	92.8	11.0	0.40	0.05	8.0	0.03
383.1	93.7	11.2	0.40	0.05	8.0	0.03
392.7	92.0	10.9	0.45	0.07	6.4	0.04
402.3	95.3	11.3	0.30	0.04	7.5	0.03
421.5	92.8	11.0	0.36	0.04	9.0	0.03
431.1	94.4	11.2	0.27	0.04	6.8	0.02
450.3	95.3	11.3	0.23	0.03	7.7	0.01
469.5	95.0	11.3	0.29	0.04	7.3	0.01
488.7	95.5	11.4	0.93	0.08	11.6	0.04
498.3	95.0	11.3	0.88	0.07	12.6	0.04
507.9	96.4	11.5	0.56	0.06	9.3	0.02
517.5	95.6	11.3	0.76	0.06	12.7	0.03
565.5	90.6	10.8	1.09	0.18	6.1	0.06

Note: nd = no data.

[a] In acid insoluble residue.

[b] Percentage of acid insoluble C_{org} computed for bulk sample.

DISCUSSION

Organic Carbon and Nitrogen

The decrease of C_{org} in the residue fraction of Hole 593 is substantiated by the calculation of a regression analysis. Including or excluding the two data points at 181.5 and 191.1 m does not significantly change the slope of regression (-1.0×10^{-3} versus -1.1×10^{-3}). The higher C_{org} values in lower Oligocene sediments were excluded in this calculation, because they belong to a different sedimentation regime.

Eq. (1) describes C_{org} loss with depth:

$$x_C = (-1.0 \times 10^{-3})y_d + 0.8 \qquad (1)$$

where x_C is C_{org} loss (%) with depth and y_d is sub-bottom depth (m).

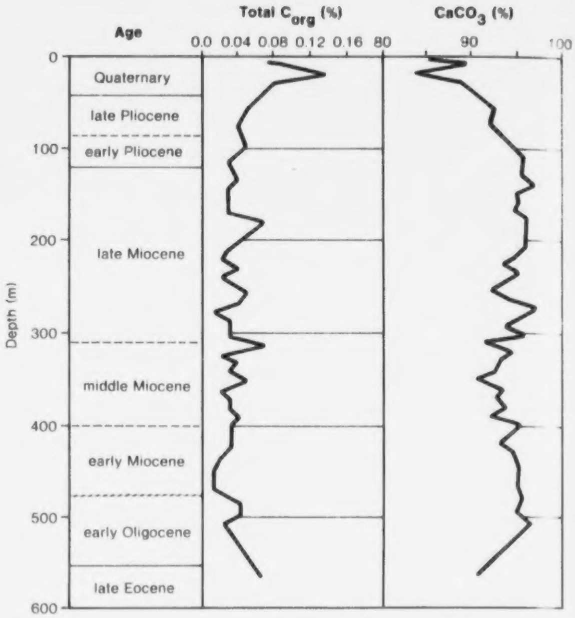

Figure 1. Plot of carbonate ($CaCO_3$) content and computed total C_{org} through time for Hole 593.

A plot of C_{org} decrease versus time allows the estimation of diagenetic C_{org} loss in the noncarbonate residue of calcareous sediments. For this purpose, five geological time markers in Hole 593 were selected. C_{org} concentrations at their respective depths were calculated according to Eq. (1) leading to Eq. (2), which describes C_{org} loss with time:

$$x_C = (-3.0 \times 10^{-2})y_t + 0.82 \qquad (2)$$

where y_t is time duration (m.y.). The rate constant for the C_{org} loss of the residual fraction can thus be inferred by the slope of Eq. (2).

The following conclusions can be reached. A total of 0.03% C_{org} contained in the acid insoluble residue is consumed every 1 m.y. C_{org} gradually decreases from 0.82% at the top of the hole to 0.4% at a depth of 475 m, i.e., from Recent to early Miocene (Fig. 3). Comparable calculations by Waples and Sloan (1980) indicate total diagenetic loss of C_{org} at a depth of about 100 m, which coincides with the Pliocene/Pleistocene boundary. Below this interface they observed constant C_{org} values.

The same calculations were performed for N_{org}. Loss of N_{org} with depth follows the C_{org} pattern, but with a different slope:

$$x_N = (-7.07 \times 10^{-5})y_d + 0.07 \qquad (3)$$

The depletion of residual nitrogen is also a simple time-dependent process, as can be deduced from the highly significant correlation ($r = 0.9998$) between the calculated decrease with depth and time. Calculation of the regression for N_{org} content versus time yields Eq. (4).

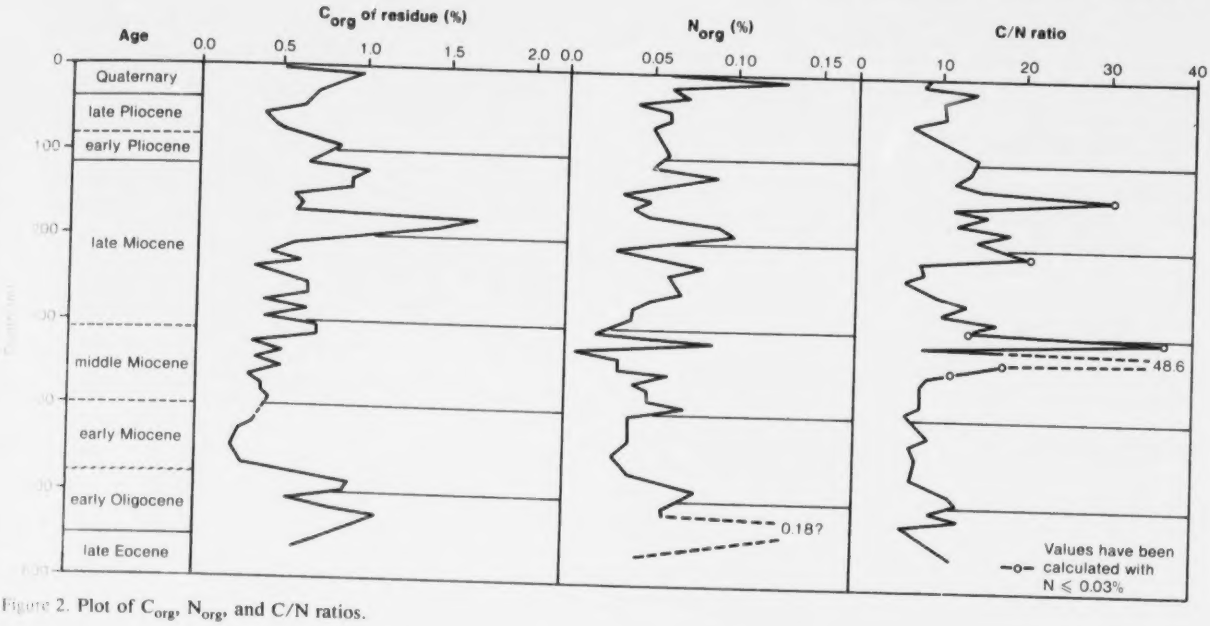

Figure 2. Plot of C_{org}, N_{org}, and C/N ratios.

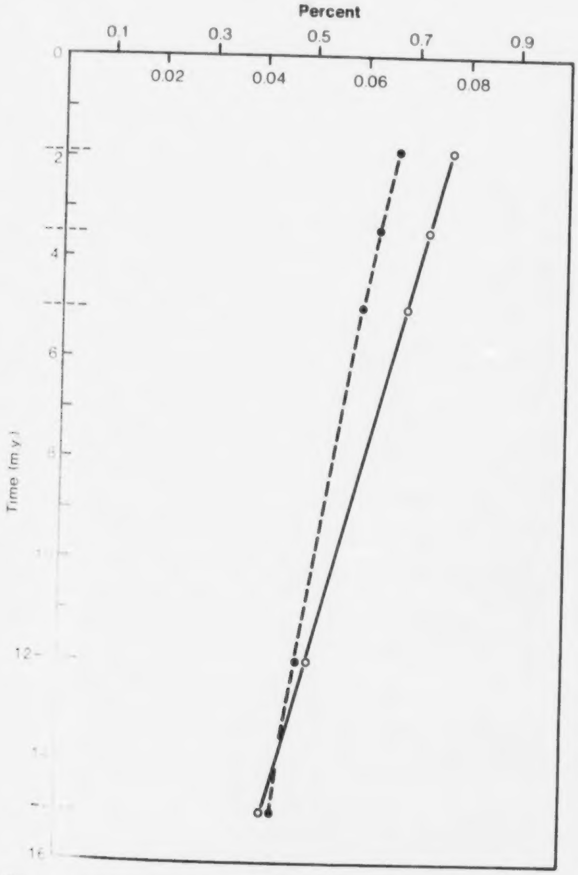

Figure . Regression analysis plot of C_{org} (solid line) and N_{org} (dashed line) in residue through time.

$$x_N = (-1.9 \times 10^{-3})y_t + 0.07 \quad (4)$$

These findings are consistent with those of Waples and Sloan (1980) who described the loss of N_{org} as a continuous process, although their decrease follows first-order kinetics. An explanation for this can be found in the source of nitrogenous matter in deep-sea sediments. A major part of N_{org} delivered to the ocean floor stems from proteinaceous matter in tests of planktonic organisms (Ittekkot, Degens et al., 1984; Ittekkot, Deuser et al., 1984).

The diagenetic fate of such proteinaceous templates in foraminiferal tests has been studied by Bada et al. (1978). They reached the conclusion that amino acid decomposition follows first-order kinetics and comes to completion within 1 m.y. Because we removed the labile or acid hydrolyzable N_{org} fraction, the depth distribution of residual N_{org} can be used to reinterpret the data set of Waples and Sloan (1980) and Bada et al. (1978). Namely, their observed exponential decrease of N_{org} is simply a reflection of the decomposition rate of labile N_{org} compounds, but not of total N_{org}:

$$N_{org(total)} = N_{org(labile)} + N_{org(residual)} \quad (5)$$

The different slopes for C_{org} and N_{org} loss mirror decreasing C/N ratios with depth (Table 1 and Figs. 2 and 3). Müller (1977) explains this relationship by sorption of nitrogeneous compounds to clay minerals. Although his inferences were drawn only from a study of a 5-m core section, they appear to be applicable also for the 475-m core section of Hole 593. It should be noted that the residual fraction of that core, measuring about 5 to 15%, is predominantly clay.

The simultaneous (but not parallel) decrease of C_{org} and N_{org} with depth could be explained by changes in the rate of sedimentation. This would correspond to the interpretation offered by Müller and Suess (1979) for a similar situation. In the present case this would indicate a decrease in the rate of deposition since middle Miocene. Because the ratio of carbonate to residue is about the same for the whole length of the core below 100 m, contributions from primary production and terrigenous matter have apparently decreased proportionally.

This observation is in agreement with recent findings on the biological control of the removal of clay-sized detritus from the water column (Deuser et al., 1983; Honjo, 1980; Ittekkot, Degens et al., 1984; Ittekkot, Deuser et al., 1984; Degens et al., 1984). The decreasing trend in the rate of sedimentation becomes even more obvious by considering compaction effects. Einsele (1977) has shown that the porosity of a chalk ooze decreases exponentially to a depth of 200 m. Because the facies of sediments recovered from Hole 593 is identical to that of sediments studied by Einsele (1977), sedimentation rates given in Table 2 for the Pliocene–Quaternary section could be in error by as much as 20%. The validity of our calculation and its inherent error can be appreciated when it is compared to calculations of sedimentation rates based on mass accumulation rate data presented in Kennett (this vol.). These revised sedimentation rates based on his data, which are also given in Table 2, do not significantly alter the trend observed in our model.

In summary, the C_{org} and N_{org} relationships in the residual fraction of Hole 593 suggest the following conclusions. (1) C_{org} and N_{org} originated in the marine habitat and were extracted from the dissolved organic-matter pool or from aqueous solutions in the "benthic layer" or topmost sediment; (2) the low C/N ratios argue against terrestrial sources; (3) the geothermal gradient is too low to significantly alter C/N ratios or to introduce catagenesis of organic matter; (4) changes in C_{org} and N_{org} content are principally related to changes in the rate of deposition; and (5) the systematic decrease in C_{org} and N_{org} with depth implies that rates of deposition have decreased from middle Miocene to Recent.

Carbohydrates

Preliminary data on the carbohydrate (CH) content of bulk carbonates (Hole 593) and of the carbonate-free residue are summarized in Table 3. Total CH content is low because of low C_{org} values. A decrease with depth is indicated, and some sugars are more affected than others (Fig. 4). The relative abundances of mannose, galactose, and xylose decrease, resulting in a predominance of fructose and glucose in deeper samples. The ratio or arabinose to fucose has been used to distinguish periods of dominantly calcareous input from periods of opaline biogenic input in sediment trap experiments (Ittekkot, Degens et al., 1984; Ittekkot, Deuser et al., 1984). They report a ratio of about 6:1 in purely carbonaceous trap material.

Table 2. Estimated sedimentation rates in Hole 593.

Thickness (m)	Deposition time span (m.y.)[a]	Age	Sedimentation rate (m/m.y.)	
			Uncorrected[b]	MAR[c]
38	1.9	Quaternary	20.0	23.3
44	1.6	late Pliocene	27.7	16.7
38	1.5	early Pliocene	25.3	33.3
190	7.0	late Miocene	27.1	26.7
90	3.0	middle Miocene	30.0	33.3

[a] After Van Eysinga (1975).
[b] Calculated without correction for compaction of the sediment.
[c] Calculated from mass accumulation rates (MAR); site chapter (this vol.).

Table 3A. Carbohydrates in Hole 593: Total sugars (μg/g sediment).

Sugar	Sub-bottom depth (m)			
	18.3	133.5	229.5	335.1
Mannose	3.64	1.96	1.58	nd
Fructose	31.97	27.35	22.01	21.21
Arabinose	7.87	6.69	2.99	3.46
Fucose	9.36	8.49	8.54	9.88
Galactose	7.74	2.63	1.14	0.68
Xylose	6.39	3.10	0.55	0.43
Glucose	24.4	25.86	20.81	13.37
Total sugars	91.37	76.09	57.90	49.03

Table 3B. Carbohydrates in Hole 593: Sugars in residue (μg/g residue).

Sugar	Sub-bottom depth (m)		
	37.5	56.7	191.1
Rhamnose	12.42	12.56	43.53
Mannose	15.19	58.93	138.16
Fructose	11.44	37.29	133.5
Arabinose	23.91	37.63	101.87
Fucose	11.45	16.99	86.32
Galactose	30.82	48.36	90.90
Xylose	18.91	116.51	282.62
Glucose	32.29	168.88	575.76
Total sugars	156.43	497.15	1452.67

Although sediments in Hole 593 are very pure biogenic chalks, the arabinose to fucose ratio decreases from 1:1 in surface samples to 1:2.5 in the deepest sample, suggesting mechanisms at the water/sediment interface that invert this ratio (Table 3A). In addition, the relative enrichment of fucose with depth is indicative of selective removal of other CH during diagenesis. The CH fraction in residual material, after removal of biogenic carbonates and associated CH, consists predominantly of glucose and xylose. The increase of these sugars with depth (Table 3B) is notable and is tentatively explained by diagenetic release of structural polysaccharides during recrystallization. The polysaccharides then associate with clay minerals.

ACKNOWLEDGMENT

Financial support was given by the Deutsche Forschungsgemeinschaft, Bonn–Bad Godesberg. Laboratory assistance of M. St[illegible]nhagen is gratefully acknowledged.

REFERENCES

Bada, J. L., Shou, M.-J., Manx, E. H., and Schroeder, R. A., 1978. Decomposition of hydroxy amino acids in foraminiferal tests: Kinetics mechanism and geochronological implications. *Earth Planet. Sci. Lett.*, 41:67–76.

Degens, E. T., 1970. Molecular nature of nitrogenous compounds in sea water and recent marine sediments. *In* Wood, D. W. (Ed.), *Or-*

ganic Matter in Natural Waters. Institute of Marine Sciences, Alaska, 1:77–106.

Degens, E. T., and Ittekkot, V., 1983. A new look at clay–organic interactions. *In* Degens, E. T., Krumbein, W. E., and Prashnowsky, A. A. (Eds.), *Ein Norg–Süd Profil: Zentraleuropa-Mittelmeerraum-Afrika.* Mitt. Geol.-Paläont. Inst. Univ. Hamburg, Festband Georg Knetsch, 56:229–248.

Degens, E. T., Kempe, S., and Spitzy, A., 1984. CO_2: A biogeochemical portrayal. *In* Hutzinger, O. (Ed.), *Handbook of Environmental Chemistry*, (Vol. 1/C): Berlin (Springer-Verlag), pp. 127–215.

Deuser, W. G., Brewer, P. G., Jickells, T. D., and Commeau, R. D., 1983. Biological control of the removal of abiogenic particles from the surface ocean. *Science* (Washington, D.C.), 219:388–391.

Einsele, G., 1977. Range, velocity, and material flux of compaction flow in growing sedimentary sequences. *Sedimentology*. 24:639–655.

Emery, K. O., and Rittenberg, S. C., 1952. Early diagenesis of California Basin sediments in relation to origin of oil. *Am. Assoc. Pet. Geol. Bull.*, 36:735–806.

Hecky, E., Mopper, K., Kilham, P., and Degens, E. T., 1973. The amino acid and sugar composition of diatom cell walls. *Mar. Biol.*, 19:323–331.

Holm-Hansen, O., Strickland, J. D. H., and Williams, P. M., 1966. A detailed analysis of biologically important substances in a profile off Southern California. *Limnol. Oceanogr.*, 11:548–561.

Honjo, S., 1980. Material fluxes and modes of sedimentation in the mesopelagic and bathypelagic zones. *J. Mar. Res.*, 38:53–97.

Ittekkot, V., Degens, E. T., and Honjo, S., 1984. Seasonality in the fluxes of sugars, amino acids, and amino sugars to the deep ocean: Panama Basin. *Deep-Sea Res.*, 31/9A:1071–1083.

Ittekkot, V., Deuser, W. G., and Degens, E. T., 1984. Seasonality in the fluxes of sugars, amino acids, and amino sugars to the deep ocean: Sargasso Sea. *Deep-Sea Res.*, 31/9A:1057–1069.

Mopper, K., 1977. Sugars and uronic acids in sediments and water from Black Sea and North Sea with emphasis on analytical techniques. *Mar. Chem.*, 5:585–603.

Müller, P. J., 1977. C/N ratios in Pacific deep sea sediments: Effect of inorganic ammonium and organic nitrogen compounds sorbed by clays. *Geochim. Cosmochim. Acta*, 41:765–776.

Müller, P. J., and Suess, E., 1979. Productivity, sedimentation rate, and sedimentary organic matter in the oceans, I: Organic carbon preservation. *Deep-Sea Res.*, 26A:1347–1362.

Trask, P. D., and Patnode, H. W., 1942. *Source Beds of Petroleum*: Tulsa (Am. Assoc. Pet. Geol. Memoir).

Van Eysinga, F. W. B., 1975. *Geological Time Table.* Amsterdam (Elsevier).

Waples, D. W., and Sloan, J. R., 1980. Carbon and nitrogen diagenesis in deep sea sediments. *Geochim. Cosmochim. Acta*, 44:1463–1470.

Date of Initial Receipt: 2 January 1985
Date of Acceptance: 15 April 1985

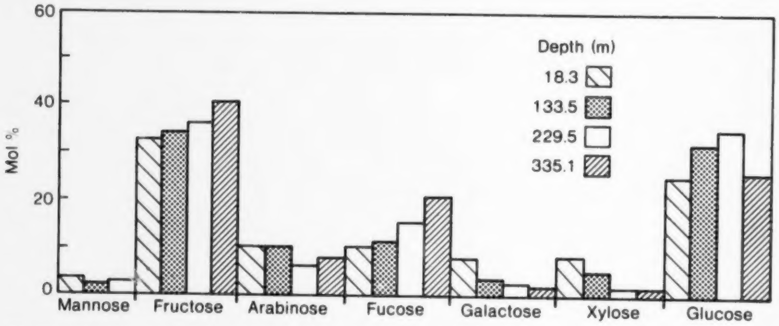

Figure 4. Amount of acid hydrolyzable sugars with depth in bulk samples from Hole 593.

PART VI. GEOPHYSICAL STUDIES

36. PALEOMAGNETISM OF SEDIMENTS COLLECTED DURING LEG 90, SOUTHWEST PACIFIC[1]

C. E. Barton, University of Rhode Island and Bureau of Mineral Resources, Canberra, Australia
and
J. Bloemendal, University of Rhode Island[2]

ABSTRACT

Sediments recovered during Leg 90 (Sites 587–594, plus Site 586 cored during Leg 89) are, in general, extremely weakly magnetized carbonate oozes and chalks with NRM intensities seldom greater than 0.05 μG. The quality of the paleomagnetic records deteriorates with increasing depth caused by the combined effects of removal of primary magnetic oxides by sulfate reduction processes and the dispersal of magnetic grains during compaction.

Magnetic reversal sequences are generally recognizable back to the Gilbert, 3.4 to 5.35 m.y., except at equatorial Site 586 where only the Brunhes/Matuyama boundary could be identified. Longer reversal records were obtained at Site 588 (to Chron 13, about 13 m.y.) and Site 594 (base of Chron 5, about 5.9 m.y.).

Sediments are characterized by extremely high calcium carbonate contents (90–100%) with almost no biosiliceous components. Blebs and streaks of pyrite are common, and the presence of iron sulfides with poor magnetic stabilities is suspected, although not yet positively identified. Viscous components of magnetization are common, sometimes to the extent of dominating the primary remanence, and there is evidence to suggest that a magnetic remanence is imparted during core recovery. Siliceous carbonate oozes provide better paleomagnetic records than pure carbonate oozes.

INTRODUCTION

During Leg 90, long sequences of Neogene and late Paleogene shallow-water (1000–2000 m) carbonate sediments were recovered from Sites 587 to 593 along a north-northwest to south-southeast traverse of the Lord Howe Rise, and from Site 594 on the southern margin of the Chatham Rise, southeast of New Zealand. Site 586 on the northeastern edge of the Ontong-Java Plateau, cored during Leg 89, was included in the study. The principal objective of the paleomagnetic work was to provide a stratigraphic and chronological framework for biostratigraphic and paleoceanographic studies. Because of the relatively unconsolidated nature of the sediments, much of the coring was accomplished with the variable-length hydraulic piston corer (HPC) and the extended core barrel (XCB) rotary drilling technique. Most of the paleomagnetic results discussed here pertain to the HPC cores. Collection of duplicate HPC cores proved to be valuable.

The magnetic polarity time scale used is that of Berggren et al. (1983). Depths are given in meters below the top of the hole, which is nominally coincident with the seafloor. Intensities of magnetization are in microgauss: 1 μG = 10^{-6}emu·cm^{-3} = 10^{-3}Am^{-1}. Low-field magnetic susceptibilities are quoted per unit volume in units of microgauss per oersted: 1 μG Oe^{-1} = 10^{-6}emu·cm^{-3} 4 $\pi \times 10^{-6}$ SI units.

Note on Magnetic Chron Nomenclature[3]

The old system for naming magnetic chrons, as it appears in Berggren et al. (1983), is used throughout this chapter—namely, a succession of numbered chrons: C1 to C4 assigned to the Brunhes, Matuyama, Gauss, and Gilbert intervals, and C5 to C30 thereafter. It provides a convenient and widely adopted method of labelling the magnetic polarity timescale, but is somewhat arbitrary (Kent, personal communication, 1985).

The new nomenclature (LaBrecque et al., 1983; Berggren et al., in press) directly links magnetic chrons to the numbered and lettered marine magnetic anomaly sequence, using a "C" prefix. Each chron spans an upper, predominantly normal interval which corresponds to the magnetic anomaly, together with the preceding, lower, predominantly reversed interval, e.g., C5AN and C5AR for anomaly 5A. Comparisons between the two systems are illustrated in Figures 23 and 27.

GENERAL PROPERTIES OF THE SEDIMENTS

Sequences are largely composed of one lithological unit: a foraminifer-nannofossil ooze generally grading to chalk at depths of less than 300 meters. Carbonate contents are very high, typically 95 to 100%, and biosiliceous components are very low or absent, with only trace amounts of terrigenous material.

With the exception of the alternating pelagic and hemipelagic sediments of the upper 170 m at Site 594 (Unit I), all sequences display similar magnetic properties. This is true even for Site 586 on the Ontong-Java Plateau, de-

---

[1] Kennett, J. P., von der Borch, C. C., et al., *Init. Repts. DSDP*, Washington (U.S. Govt. Printing Office).

[2] Addresses: (Barton) Bureau of Mineral Resources, P.O. Box 378, Canberra, Australia; (Bloemendal) Graduate School of Oceanography, University of Rhode Island, Narragansett, RI 02882.

[3] Added after preparation of the manuscript.

spite its remoteness from the Lord Howe Rise. There is a surficial layer of a few tens of centimeters of oxidized sediment, pale brown-orange-yellow in color, which retains a strong magnetic remanence (1-10 μG). Reducing conditions prevail below this and iron sulfides (pyrite) are dispersed throughout as blebs, gray streaks, and gray coloration. Sediments are generally very pale gray to pale olive green to white in color. Green laminae and bands of altered volcanic ash are common. Neither these nor the iron sulfide concentrations carry a magnetic remanence noticeably higher than the surrounding sediments. Thus, it is unlikely that pyrrhotite and the less stable magnetic iron monosulfides play a significant role. Localized intensity and susceptibility spikes occur (see site chapters, this volume), but are uncorrelated with any obvious visible characteristics of the sediments.

Maximum intensities of magnetization occur in the surface oxidized layer and thereafter taper off with depth to extremely low values at typically 100 m, which are often below the noise threshold of the cryogenic magnetometer used (~0.005 μG). Reduced porosity at greater depths leads to slightly higher intensities, and in a few sequences there is a region of enhanced intensity within the Miocene.

Geometric mean intensities (Table 1) are in the range 0.03 to 0.08 μG, except for Site 588 (0.115 μG), which gave the best paleomagnetic record. These very low levels of magnetization result from dilution of the ferromagnetic content by very high carbonate contents and from diagenetic removal of primary magnetic oxides by sulfate-reducing reactions, with the accompanying production of iron sulfides (Berner, 1964; Karlin and Levi, 1983).

Deterioration, that is, increased scatter, of the paleomagnetic record with depth generally precludes polarity interpretation prior to the Gilbert (Chron 4), except at Sites 588 and 594. Median destructive field (MDF) values show considerable variation, but tend to follow the overall pattern of intensity and susceptibility variation—higher at the tops of sequences and in the deeper, more indurated sediments (a few 100 Oe), with lesser values (~50–150 Oe) in the most weakly magnetized sediments. The latter is consistent with preferential removal of the finer-grained, more stable magnetic oxides during diagenesis (Karlin and Levi, 1983).

Table 1. Some paleomagnetic statistics for Leg 90 sites.

Hole	Treatment	Axial dipole inclination (°)	Arithmetic mean inclination (°)	Geometric mean intensity (μG)	Depth range (m)
586	NRM	−1.0	5.0 ± 19.0	0.084 ± 0.72	0.00-044.4
586A	NRM		1.5 ± 32.7	0.031 ± 0.94	44.4-305.3
586B	NRM		−3.2 ± 35.2	0.044 ± 1.34	1.4-240.3
587	NRM	−37.8	−10.3 ± 42.2[a]	0.054 ± 1.51	14.4-096.2
588	NRM	−44.4	−5.0 ± 39.7[a]	0.115 ± 1.79	0.2-235.1
588A	NRM		−6.7 ± 51.6[a]	1.54 ± 1.08	236.2-336.5
588B	NRM		−10.5 ± 41.6	0.168 ± 1.76	1.0-271.8
589	NRM	−49.9	5.7 ± 48.6[a]	0.159 ± 1.14	0.2-035.0
590	NRM	−50.4	−26.5 ± 39.0[a]	0.335 ± 1.66	0.2-025.9
590A	NRM		−12.9 ± 37.6[a]	0.043 ± 1.05	27.2-280.5
590B	NRM		−5.2 ± 39.0	0.044 ± 1.14	0.1-334.3
591	NRM	−50.9	−9.1 ± 43.7[a]	0.066 ± 1.22	0.2-282.5
	AF				0.8-282.5
591A	NRM		−7.2 ± 44.0[a]	0.059 ± 1.33	0.4-253.3
592	NRM	−55.9	−5.8 ± 41.9	0.056 ± 1.14	0.2-387.1
	AF		−2.9 ± 39.8	0.021 ± 1.04	0.7-184.0
593	NRM	−59.7	−3.9 ± 41.7[a]	0.110 ± 1.63	0.1-569.6
	AF		9.8 ± 43.9	0.038 ± 1.72	0.1-569.6
593A	NRM		−2.3 ± 43.0	0.054 ± 1.10	0.2-256.4
	AF		−1.2 ± 42.1	0.025 ± 1.12	0.2-256.4
594	NRM	−20.7	−20.7 ± 38.4[a]	0.086 ± 1.21	0.2-488.1
	AF		−15.9 ± 42.3	0.050 ± 1.18	0.2-488.1
594A	NRM		−30.4 ± 33.7	0.133 ± 0.80	47.0-252.6

[a] After filtering.

The surface high-intensity zone extends up to a few tens of meters below the oxidized surficial layer, indicating that the bulk of the primary iron oxides survive the early stage of diagenesis. By far the best polarity record comes from this zone.

Bioturbation is common and intense in some sequences (e.g., Hole 586B). Because of high sedimentation rates, the length of the bioturbated zone (up to a few tens of centimeters) is very short compared with a typical polarity interval. The paleomagnetic record does not appear to be adversely affected by bioturbation.

INFLUENCE OF BIOGENIC SILICA

Previous studies of Cenozoic marine calcareous sequences have usually provided good paleomagnetic records (e.g., eastern equatorial Pacific—Kent and Spariosu, 1982b; northwest Pacific—Weinreich and Theyer, in press; Bleil, in press; South Atlantic—Tauxe et al., 1983, 1984), although seldom have NRM intensities been as low as encountered in this study. A characteristic of carbonate sequences that provide good paleomagnetic data is the presence of biogenic siliceous material (Kent and Spariosu's, 1982a, work on Caribbean cores is an exception, but these contained relatively large terrigenous components). Siliceous material is noticeably absent from or only present in trace amounts in most Leg 90 sediments. This is despite normal abundances in the present-day water column. Bleil (in press) comments "biosiliceous sediments carry a predominantly strong remanent magnetism, whereas increasing amounts of calcareous components result in drastic reduction of the NRM intensities." A contributing factor to this contrast may be differences in the sediment matrix created by calcareous fossils, which tend to be rounded, and siliceous fossils, which are generally "skeletal." This must affect the physical stability of very fine-grained interstitial magnetic particles during compaction.

CARBONATE DILUTION

On the Lord Howe Rise, which is well above the calcium carbonate compensation depth and has high carbonate productivity, dilution of the ferromagnetic input results in very low levels of magnetization. The scale of the effect is illustrated in Figure 1, which is based on a starting composition of 99% nonmagnetic matrix ($CaCO_3$ in this case), and 1% magnetic component. At these dilutions the NRM intensity is very sensitive to small fluctuations in carbonate content. The sensitivity drops off fairly rapidly for lower initial carbonate contents. Since carbonate contents close to 100% are not uncommon, a substantial part of the observed intensity variation could thus be caused by small fluctuations in carbonate content. However, this explanation is not sufficient to explain the intensity variations completely since a positive correlation exists between NRM intensity and modified Koenigsberger-ratio variations. Based on a sim-

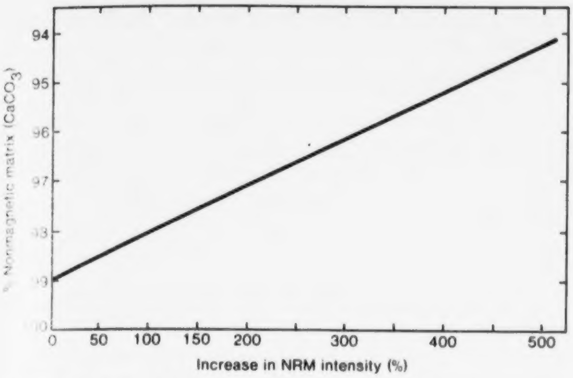

Figure 1. Variation of NRM intensity with calcium carbonate content, assuming a constant rate of input of magnetic material. The curve is based on an initial composition of 99% nonmagnetic matrix and 1% magnetic component.

ple dilution model, these two parameters would be constant.

METHODS

Sampling densities were typically three specimens per core section for HPC cores from the first hole, two specimens per section for HPC and XCB cores from the second hole, and one specimen per section for conventional, rotary-drilled cores. Results demonstrate that this sampling density is barely adequate (see, e.g., Site 588 results) despite the very large collection of specimens produced—more than 5900.

Shipboard measurements of the horizontal NRM component (D and H) of whole-core sections was abandoned after Site 588. It became apparent that there was little prospect of improving on the amount of information available from normal subsampling, because the very low remanence intensities were not sufficiently above instrumental noise and rust contamination levels. The shipboard Digico magnetometer was used for NRM measurements of some of the more strongly magnetized material, generally the surficial zone only. All subsequent remanence measurements were made on the three-axis SCT cryogenic magnetometer at the University of Rhode Island. Software modifications were made to permit user-selected integration times to improve the signal-to-noise ratio. To allow longer integration times a two-position (instead of three) measuring sequence was adopted to give full cancellation of vertical holder and induced moments, but incomplete cancellation of the horizontal component of the holder. Thus inclination (Z, to be precise) is better determined than declination. In interpretation, data were discarded if (1) intensities were less than 0.008 μG; (2) the angle between the magnetic vector for each of the two specimen positions exceeded 45°; or (3) an internal measurement variance threshold was exceeded. Despite these very loose criteria, typically 10–15% of the data were discarded. This process is referred to as "filtering."

VRM Tests

To evaluate the importance of viscous remanence (VRM), selected specimens from Sites 590, 593, and 594 were (1) AF demagnetized at 600 Oe; (2) left in a field of 10 Oe for 1000 hr. and measured periodically; (3) placed in the shielded sense region of the cryogenic magnetometer and measured periodically for an interval of 1000 s; (4) returned to the 10-Oe field to restore the VRM; (5) progressively AF demagnetized. Results are summarized in Table 2. An ambient field of 10 Oe was used to produce a more easily measurable remanence. By assuming a linear field dependence of VRM for the time scale concerned (Shimizu, 1960), then VRMs acquired in 0.5-Oe ambient field (i.e., a realistic site value) can be estimated by dividing by 20. As a measure of the relative importance of VRM, the ratio $R = 0.05\ J_V/J_N$ is used, where J_V is the viscous remanence acquired in 10 Oe after 1000 hr. and J_N is the natural remanence. Values greater than 10% are considered to be high. Since sediments are more susceptible to VRM prior to AF demagnetization (e.g., Lowrie and Kent, 1978), our estimates of R should be treated as lower bounds.

Table 2. Summary of NRM and VRM test data.

Sample (level in cm)	Depth (m)	NRM		VRM		$J_V/20 \times J_N$ × 100
		J_N (μG)	MDF_N (Oe)	J_V* (μG)	MDF_V (Oe)	
590-1-4, 130	5.80	0.196	344	1.10	59	28
590A-8-2, 20	95.10	0.046	244	0.52	51	57
590A-12-1, 125	133.05	0.138	130	0.20	69	7
593-1-1, 10	0.10	2.374	300	11.97	43	25
593-1-1, 45	0.45	1.361	>600	1.07	117	4
593-6-2, 125	46.25	0.198	244	0.37	62	9
593-7-6, 25	60.85	0.100	231	0.18	89	9
593-9-6, 25	80.05	0.154	207	0.15	86	5
593-13-5, 75	117.45	0.160	116	0.06	~80	2
593-16-4, 125	145.25	0.103	98	0.08	~70	4
593-22-1, 25	197.35	0.264	217	0.05	119	1
593-28-5, 25	260.95	0.065	185	0.11	100	8
593-31-5, 25	289.75	0.217	175	0.06	146	1
593-36-2, 125	334.25	0.125	469	0.30	96	12
593-40-4, 75	375.15	1.120	95	10.67	62	48
593-44-3, 75	412.05	2.345	276	19.61	153	42
593-45-6, 75	426.15	3.809	~190	21.57	67	28
593-48-3, 75	450.45	0.297	364	3.73	92	63
593-54-3, 25	507.55	0.059	145	0.07	78	6
593-60-3, 125	566.15	0.050	190	0.08	172	8
594-1-1, 25	0.25	0.535	331	3.82	83	36
594-1-1, 75	0.75	0.509		2.09	69	21
594-1-4, 75	5.25	3.686	127	6.31	91	9
594-3-3, 75	19.25	0.509		1.42	64	14
594-3-5, 75	22.25	0.374	300	1.09	61	15
594-5-1, 75	35.45	0.331	178	1.56	61	24
594-5-4, 25	39.45	0.214		1.22	67	29
594-5-4, 75	39.95	1.194	221	1.09	59	5
594-10-2, 25	84.45	0.159	90	1.24	60	39
594-11-1, 75	93.05	0.284	44	1.17	46	21
594-13-4, 125	117.25	0.267	199	1.49	55	28
594-15-5, 25	136.95	0.302	208	1.49	53	25
594-20-3, 125	182.95	0.179	148	1.23	21	34
594-24-5, 25	223.35	0.307	242	0.29	60	5
594-27-5, 25	252.15	0.047	114	0.37	50	40
594-28-1, 125	256.75	0.175		0.35	19	10
594-34-4, 125	318.85	0.374	219	0.28	75	4
594-40-3, 25	373.95	0.432	306	0.26	49	3
594-50-1, 125	467.95	0.174	>600	4.00	136	115

Susceptibility and Q′ Ratio

Initial, low-field magnetic susceptibility measurements were made on most specimens using a Digico bulk susceptibility bridge system. Susceptibilities were commonly dominated by the diamagnetic contributions from water and calcium carbonate. To compensate, an average diamagnetic contribution of $-1.00\ \mu G\ Oe^{-1}$, based on 50% by volume of water and calcium carbonate, respectively, was subtracted from observed susceptibilities, (i.e., the values discussed herein, denoted by χ', refer to the dry noncarbonate component of the sediment). The modified Koenigsberger ratio used is defined as $Q' =$ NRM intensity/χ'.

Orientation and Declination Scatter

Although the Kuster tool used for absolute orientation of cores was moderately successful in producing legible photographic disks, the orientation information generally was inconsistent with paleomagnetic declinations. In agreement with other authors (e.g., Leg 68, Kent and Spariosu, 1982a, b), we conclude that the orientation system is of little or no value. This is a serious handicap for equatorial sites such as Site 586.

Even allowing for the lower precision in measuring declination discussed previously, declination scatter was much greater than for inclination and must be attributed partly to twisting of the sediment column and partial remagnetization during coring, slicing, and handling. For these reasons polarity determination is based almost entirely on inclination data.

AF DEMAGNETIZATION

Alternating magnetic field (AF) cleaning was performed at a peak field of 150 Oe for Holes 586, 586B, 587, 589, and 594, and at 200 Oe for the remaining holes. A few sequences still remain to be cleaned. Stepwise AF demagnetization of individual specimens is preferable to blanket treatment, but rarely leads to more than minor refinements in polarity data from deep-sea sediments and would have been impractical for the present study.

Typical responses of specimens to progressive demagnetization are illustrated in Figure 2, Parts A–E. Hoffman–Day plots depict directions of the magnetic vector removed during successive demagnetization steps (Hoffman and Day, 1978).

A. Single-component stable remanence with a soft overprint of the same polarity. Virtually all specimens showed some evidence of a small soft viscous remanence;

B. As (A), but with soft overprinting of opposite polarity;

C. Two-component remanence with a harder component of very steep inclination, probably imparted during coring. A number of specimens showed this behavior;

D. As (C), but with the softer component imparted during coring—less common.

E. Poor stability, but of constant polarity. Many specimens fell into this class and were considered sufficiently stable to give usable polarity information;

F. Unstable behavior—usually confined to very weakly magnetized sediments and quite common (not illustrated).

The examples chosen illustrate the classes of behavior more clearly than most specimens. Virtually all specimens showed evidence of varying degrees of VRM overprinting, which was easily removed in fields of less than 150 Oe. Surface high-intensity zones and indurated sediments (chalk) toward the bottom of long sequences gave the highest MDFs and greatest directional stability (Fig. 3). However, the large scatter in directions characteristic of much of the latter suggests either that the remanence is not of primary origin or that material was disturbed during drilling.

SCATTER CAUSED BY COMPACTION

Physical compaction of sediments involves juxtaposition of grains to form a more closely packed structure. Magnetic particles in the sediment with a preferential initial alignment will become dispersed in direction during this process. Generally there are enough magnetic particles contributing to the remanence that, provided the directional dispersion is unbiased during compaction, the resultant magnetic vector will be smaller in magnitude but unchanged in direction. However, in sufficiently weakly magnetized sediments such statistical averaging will no longer apply, and compaction may cause significant changes in direction of the magnetic remanence.

To estimate the scale of the effect in Leg 90 sediments, suppose the intensity of magnetization of a 6.5 cm^3 specimen is 0.01 μG. If we neglect grain interaction, the diameter of one saturated magnetite sphere that would account for this is 6.4 μm, which is within the size range of pseudosingle domain behavior. Thus, it is possible that the remanence of many specimens is carried by a very small number of particles and that compaction accounts for much of the scatter observed in the weakly magnetized sediments despite their carrying a hard stable remanence.

MAGNETOSTRATIGRAPHY

Magnetostratigraphy and sedimentation rate summaries are presented in Figures 4 and 5. Results pertaining to particular sites are discussed later. Prior to the first few most recent magnetic reversals at each site, which were self-evident, biostratigraphies were used as a first-order guide for establishing approximate position on the polarity time scale. This became increasingly necessary at greater depths. With few exceptions, final interpretations are generally in good agreement with the biostratigraphies and can be used to refine the assigned time scales. Speculative interpretations are omitted and single-point polarity intervals are ignored except in special circumstances (e.g., supporting evidence from a duplicate hole).

Site 586

Duplicate sequences were recovered: Hole 586 plus Hole 586A (0.0–44.4–305.3 m) and Hole 586B from 0 to 240.3 m. It was suspected that the top of Hole 586B was started 1.4 m below the mudline. The surficial oxidized layer is confined to the upper 0.15 m of Hole 586. Pyrite is common throughout the sequence. Biosiliceous material, mostly radiolarians, is only a minor component but is much more common than at most Leg 90 sites.

NRM measurements were completed for both sequences, and Hole 586 and the upper eight cores of Hole 586B were AF cleaned at 150 Oe (Fig. 6). Inclinations are widely scattered about the axial dipole value of +1.0° (Table 1, Fig. 7). There is no bias to suggest a systematic overprint, and the distribution of inclinations in Hole 586 was affected little by AF cleaning.

Intensities of magnetization are high (~4 μG) in the upper 16 m of Hole 586B, followed by a rapid decrease to about 0.3 μG over the next meter, then a gradual falloff with depth to extremely low values and a corresponding increase in directional scatter. Intensities increase again below 250 m in Hole 586, but directional scatter remains high. In the absence of inclination information and because of high scatter in declinations, only the Brunhes/Matuyama boundary is identified—between 15.0 and 15.75 m (586B-2-3, 100 cm to 586B-2-4, 25 cm). This lies within the upper three cores of Hole 586 that were disturbed and not sampled. Assuming the top of Hole 586B is 1.4 m below the seafloor, a mean sedimentation rate of 22.5 to 23.5 m/m.y. is given, which is in agreement with the biostratigraphically determined rate.

Below the high-intensity surface zone, stability on progressive AF demagnetization was generally poor and lower than at many other sites, despite an average MDF of 173 Oe (for 13 specimens distributed throughout the sequence).

Carbonate contents are relatively low in the upper part of the sequence and show an inverse relationship with intensity of magnetization (J): less than 85% in the upper 10 m where J is high; 85–93% from 10 to 120 m with intermediate–low J; 93–100% below 120 m where extremely low values of J occur. The simple carbonate dilution model discussed earlier can explain most of the variation, but not the transition from high values at the top of the sequence, which must be a diagenetic effect.

Site 587

A single hole was cored at Site 587. Paleomagnetic data were obtained from Cores 587-3 to 587-11 (Fig. 8). Cores 587-1 and 587-2 were completely disturbed and some of the other cores were partially disturbed. Because of this and the high scatter in the data below 40 m, the magnetostratigraphy is poorly defined prior to the Olduvai Subchron. The sequence is devoid of siliceous fossils, and disseminated inclusions of fine-grained authigenic iron sulfide (presumably pyrite) occur occasionally throughout.

The usual surface high-intensity zone presumably was missed in the first two cores. Cores 587-4 and 587-5 contain a high-intensity zone that coincides with high carbonate content (96%). Inclination distributions barely show the expected bipolarity even after AF cleaning (Fig. 9), which is a measure of the poor quality of the data from this site. The normal bias is partly an artifact of the short record length, but probably also indicates incomplete removal of a normal overprint. Median destructive fields are fairly high (217 ±81 Oe (±s.d.) for four specimens) with moderate stability, so the high-directional scatter observed appears to be an intrinsic property of the characteristic remanence. Magnetic susceptibilities of the dry noncarbonate component followed the general trend of NRM intensity variations. Values of Q′ were noticeably higher (typically 0.1–0.9) in the more strongly magnetized sediments above 40 m, which give the best paleomagnetic record. Below this level, Q′ was generally less than 0.1. Such values are higher than at most sites. Six specimens remained diamagnetic even after the susceptibility correction for water and carbonate content.

Because of the incidence of coring disturbance and generally poor magnetic properties, the polarity interpretation is not made with a high degree of confidence. AF cleaning significantly improved the stratigraphy. Preferred polarity assignments are summarized in Figure 10, Scheme A. To conform with NN21/NN19 nannofossil interval (587-3-3, 20 cm to 587-3-4, 20 cm), normal polarities in Core 587-3 must be assigned to the lower part of the Brunhes Chron. Both the Jaramillo and the Olduvai subchrons are therefore lost in Core 587-4, which was badly disturbed, and only three specimens were recovered. Hence, we cannot pinpoint the Pliocene/Pleistocene boundary. Biostratigraphically, the boundary is determined to be either at Samples 587-4,CC to 587-5-1, 44 cm (planktonic foraminifers), or at 587-4-4, 4 cm to 587-4-5, 4 cm (nannofossils). Occurrence of the Matuyama-Gauss reversal at the top of Core 587-5 favors the latter. The base of the Gauss at the bottom of Core 587-5 agrees well with the NN15/NN16 nannofossil zone boundary at Samples 587-5-5, 4 cm to 587-5-6, 4 cm.

Below this the magnetostratigraphy is less clear. The four normal subchrons in the Gilbert are either missing or inadequately resolved (single data points). Optimum consistency with the biostratigraphy is obtained if the lower half of Core 587-7 is assigned to Chron 5 (Magnetic Anomaly 3A), and reversed polarities in the upper half of Core 587-7 represent the upper half of Chron 6. No interpretation is yet made below Core 8. Paleomagnetic placement of the Miocene/Pliocene boundary, which occurs just above Magnetic Anomaly 3A (Chron 5), again favors the nannofossil scheme that puts the boundary at 587-7-4, 4 cm to 587-7-5, 4 cm. This preferred polarity interpretation produces fairly uniform, low sedimentation rates except within the Brunhes and Matuyama chrons. An alternative interpretation (Fig. 10, Scheme B) is to assign the normal interval in Core 587-3 to the Olduvai Subchron. This produces more uniform sedimentation rates during the major intervals, but is a poorer match with the biostratigraphy.

Site 588

Record HPC penetration was achieved: Hole 588 from 0.0 to 236.0 m (9.6-m length cores) followed by Hole 588A from 236.0 to 315.0 m (5 m-length cores from Cores 588A-2 to 588A-15). The remaining three cores of Hole 588A were rotary drilled with the XCB to 344.4 m sub-bottom depth. Duplicate HPC cores obtained to 277.4 m in Hole 588B provided an invaluable cross check on the paleomagnetic results. Rotary drilling was continued in Hole 588C to 488.1 m, but no paleomagnetic data are available yet.

The sequence at Site 588 is characterized by the usual surface layer of brown oxidized material (Unit IA). Siliceous microfossils are almost completely absent down to 469 m (Units IB and IC), but relatively abundant thereafter. Iron sulfides are persistent throughout the section and disseminated volcanic ash and glass occur in Units IB and IC. Light green-gray altered ash layers tend to occur above gray sulfide streaks, suggesting that ash concentrations provide a source of iron during diagenesis. The level of bioturbation is relatively low.

Calcium carbonate content exerts a strong influence on the remanent magnetic properties of the sediments: higher contents correspond to lower NRM intensity (and susceptibility) and high directional scatter. Highest intensities are from 0 to 35 m and 205 to 315 m sub-bottom depth, where carbonate contents are relatively low—approximately 92%. Where the paleomagnetic signal is most scattered (about 70–130 m), intensities are the lowest and carbonate contents are 96–97%. As discussed previously, a simple carbonate dilution model predicts such high sensitivity to small compositional changes in carbonate-rich sediments.

The downcore pattern of intensity variation is: high values (~1 μG) for the first four cores, 0 to 35 m; a fairly rapid decay with depth down to very low values from 75 to 170 m; rise to high values (1 μG) in Core 22 around 207 m; and a gradual increase with depth to about 25 μG at 336 m, which is the limit of current paleomagnetic measurements. Dry noncarbonate susceptibilities (measured for Hole 588 only) were all positive and followed the same pattern of variation as intensities. Modified Q′ ratios were higher than in most sequences, typically 0.3 to 1.0 from 0 to 37 m; 0.01 to 0.2 from 37 to 190 m; and 0.1 to 0.8, increasing with depth below 190 m. These

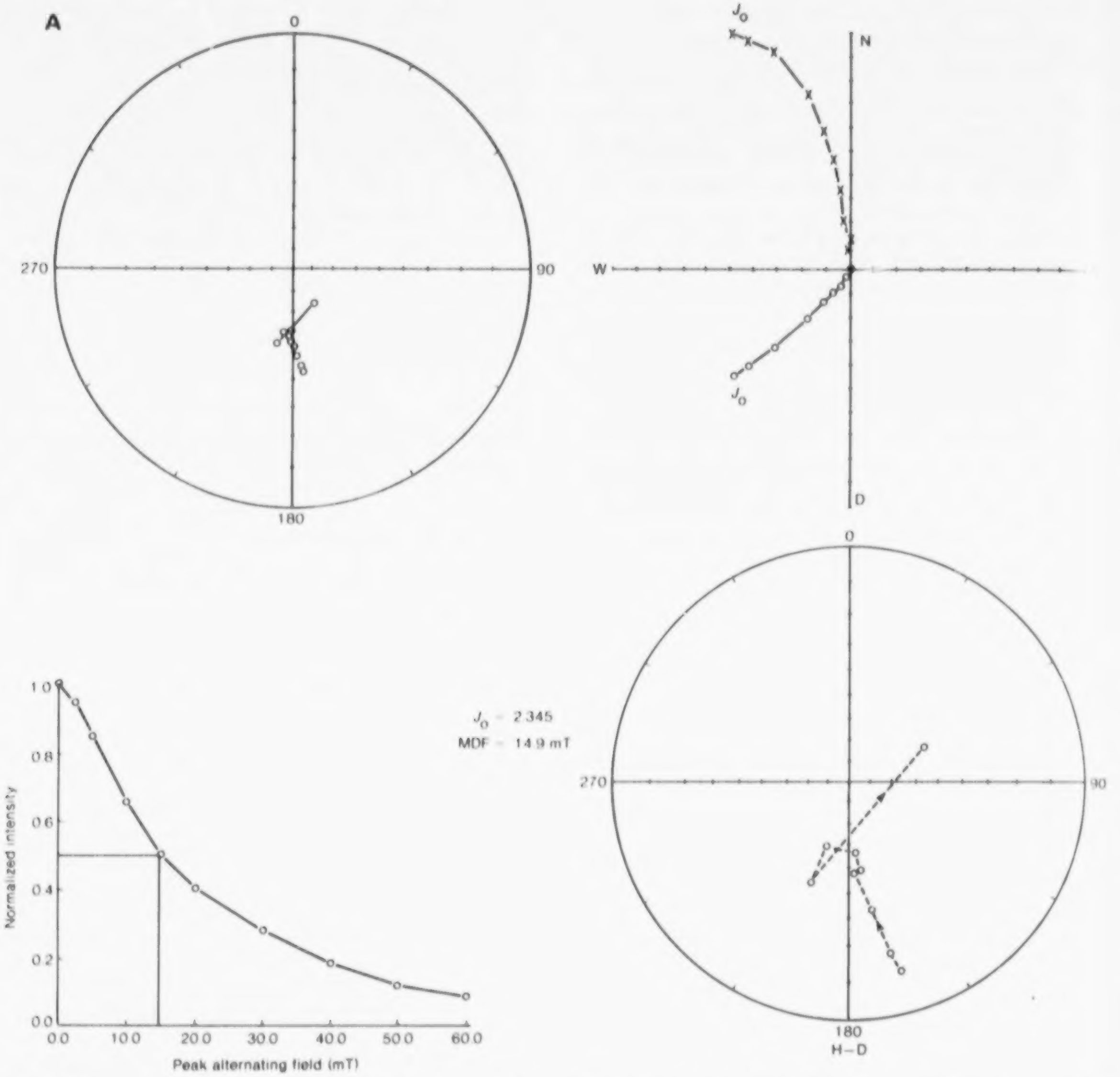

Figure 2. Progressive demagnetization plots for various classes of behavior. On the stereo (top left) and Hoffman–Day (H–D) (bottom right) plots, crosses denote positive inclination. On the Zijderveld plots crosses denote projections on the vertical east–west plane, and circles denote projections on the horizontal plane. The classes of behavior are discussed in the text. A. Sample 588-25-3, 125 cm; depth = 230.65 m. B. Sample 593-1-1, 10 cm; depth = 0.10 m. C. Sample 593-40-4, 75 cm; depth = 375.15 m. D. Sample 594-24-5, 25 cm; depth = 223.35 m. E. Sample 594-6-3, 75 cm; depth = 48.05 m.

relatively high values are reflected in the better quality of the paleomagnetic record and probably result partly from higher concentrations of volcanic material in the sequence.

Inclination distributions (Fig. 11) fail to show the bimodality of a stable primary remanence and reflect the large number of intermediate directions. It is interesting that AF cleaning produces an overall reduction in reverse directions—again indicating a reverse overprint acquired during drilling. The bias toward inclinations steeper than the axial dipole seen in NRM data for Hole 588A further supports the idea of a drilling-induced remanence, but suggests that it may have either polarity.

Progressive AF demagnetization of eight specimens from Hole 588 gave an average MDF of 175 ± 9 Oe (± s.d.) Harder magnetic remanence and greatest stability are associated with the more strongly magnetized sediments at the top and bottom of the sequence. Small, soft components removed at fields of 50 to 100 Oe were common.

AF cleaning (Hole 588 data only) was performed in a peak field of 200 Oe, but produced no substantial

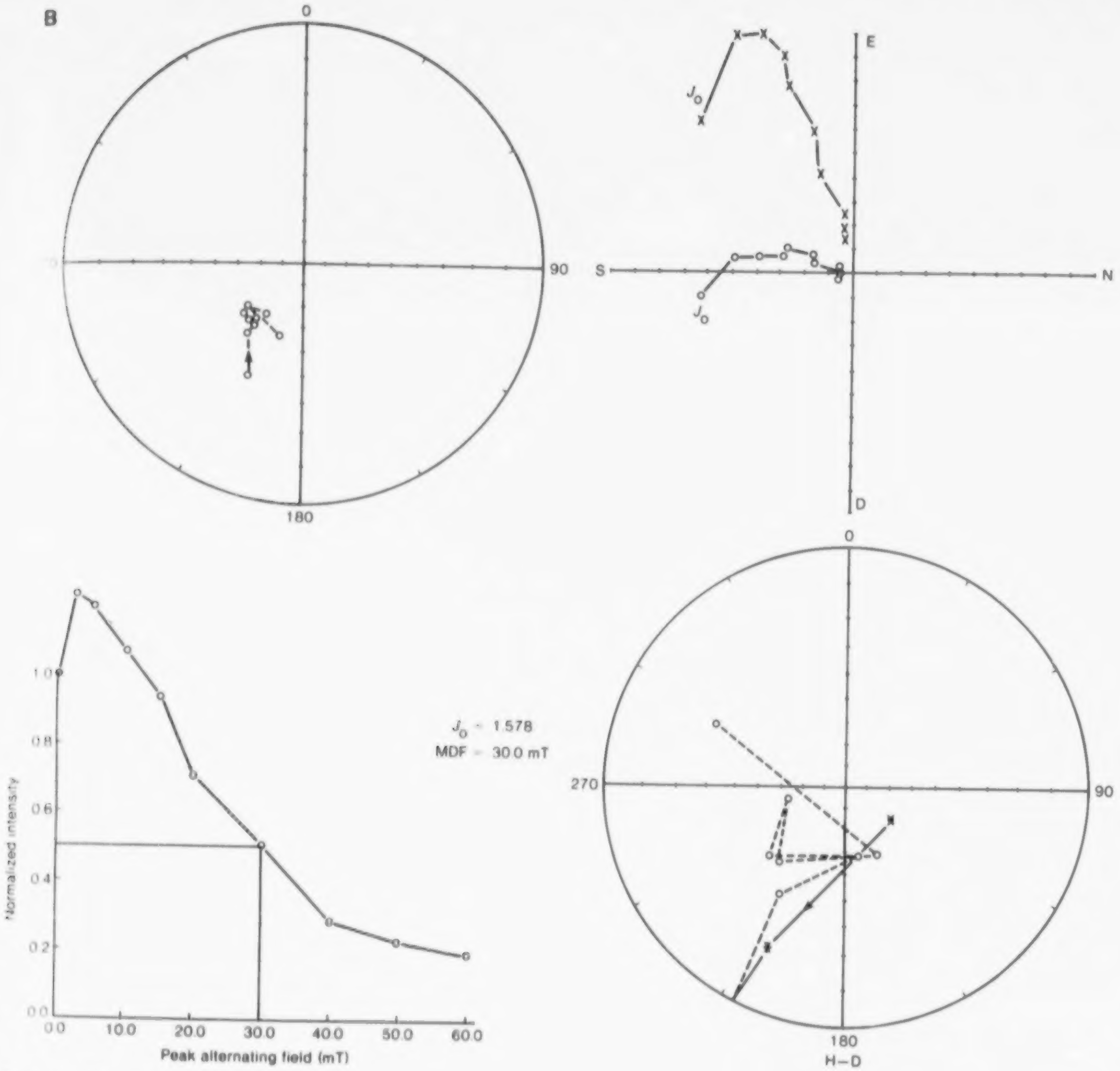

Figure 2. (Continued).

change in the polarity record. In the more weakly magnetized zones, directional scatter was noticeably reduced. A small reverse overprint was evident in the upper 30 m and probably was acquired during coring.

A complete polarity sequence has been identified for Hole 588. This is tentatively extended to the upper five cores ([illegible]0 m) of Hole 588A for which we only have NRM data (Figs. 12, 13). The polarity sequence is consistent with, and further refines, the planktonic nannofossil stratigraphy with the exception of the placement on the polarity time scale of the long normal interval in Cores 588-24 and 588-25. There is a corresponding long normal zone in Cores 588B-24 through 588B-27 and perhaps 588B-28. The length of the zone in Hole 588B indicates that Hole 588A started closer to 242 m sub-bottom rather than 236 m as recorded during drilling operations. Unless the zone coincides precisely with an interval of unusually high deposition, it must correspond to Chron 9 (8.92 to 10.42 Ma) in the early late Miocene, which is the only very long normal polarity interval anywhere near the expected age. (The next best candidate is Chron 19 in the early Miocene.) Our interpretation requires that the middle to late Miocene boundary be placed in the region of Core 588A-5 (265 m) rather than at about 214 m in Core 588-23 as determined from the NN9/NN10 nannofossil zone boundary. Further support for our interpretation lies in the fact that below Chron 9 there is a one-to-one correspondence with the polarity time scale without invoking hiatuses or large departures from uniform sedimentation.

It is not clear why Site 588 produces the longest paleomagnetic record. Biogenic siliceous content is not above

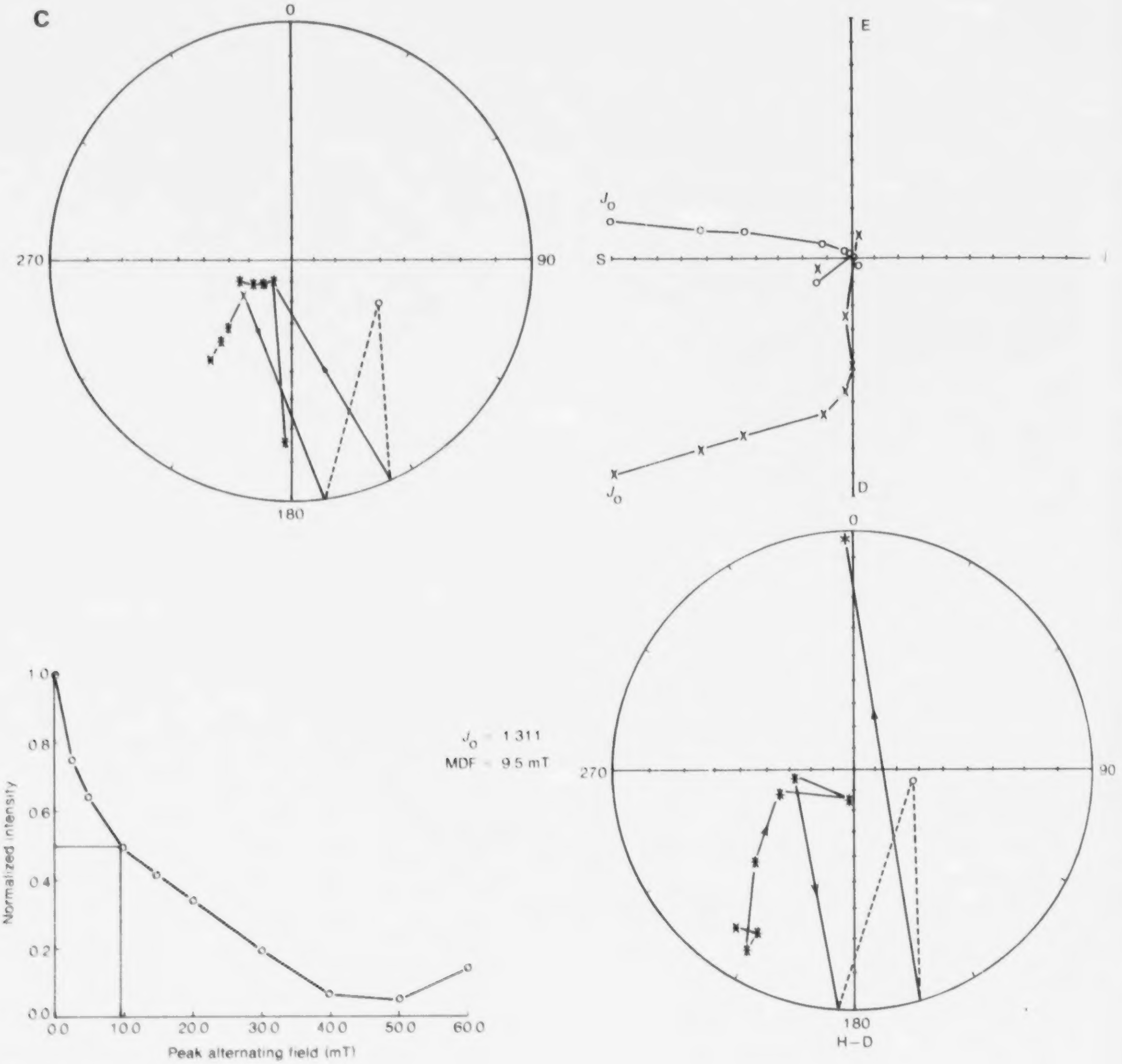

Figure 2. (Continued).

average for the relevant part of the sequence (though it is lower down in Unit II); above the lower high-intensity zone (~200 m) intensities are not noticeably stronger; and behavior during progressive demagnetization did not show any unusual characteristics (although the sample size of eight is not adequate). The only key factor appears to be the above-normal incidence of volcanic ash layers.

Site 589

Four HPC cores were recovered, reaching a sub-bottom depth of 36.1 m. Sediments are similar to those at Site 588 with a surface oxidized layer from 0 to 0.4 m. Median destructive fields at 4.75 and 23.15 m were 431 and 133 Oe, respectively. Q′ ratios were lower than at Site 588: typically 0.07 to 1.75 above 4.8 m and 0.03 to 0.12 below this depth.

The inclination distribution becomes more bimodal after AF cleaning at 150 Oe (Fig. 14), but the vector results (Fig. 15) are not changed significantly. Two polarity interpretations are possible (Fig. 16), depending on whether the normal zone from 31.5 to 34.0 m is assigned to the Olduvai Subchron (Scheme A) or to the normal interval of the upper Gauss (Scheme B), with the Olduvai not recorded. Scheme A gives the better fit to the biostratigraphy, although Scheme B is consistent with more uniform sedimentation. The former is used in Figures 4 and 5.

Site 590

Holes 590 (from 0 to 26.2 m) and 590A gave continuous HPC recovery to a depth of 280.8 m; we have a complete set of AF-cleaned data at 200 Oe. NRM data are available to 335 m in duplicate Hole 590B (HPC to

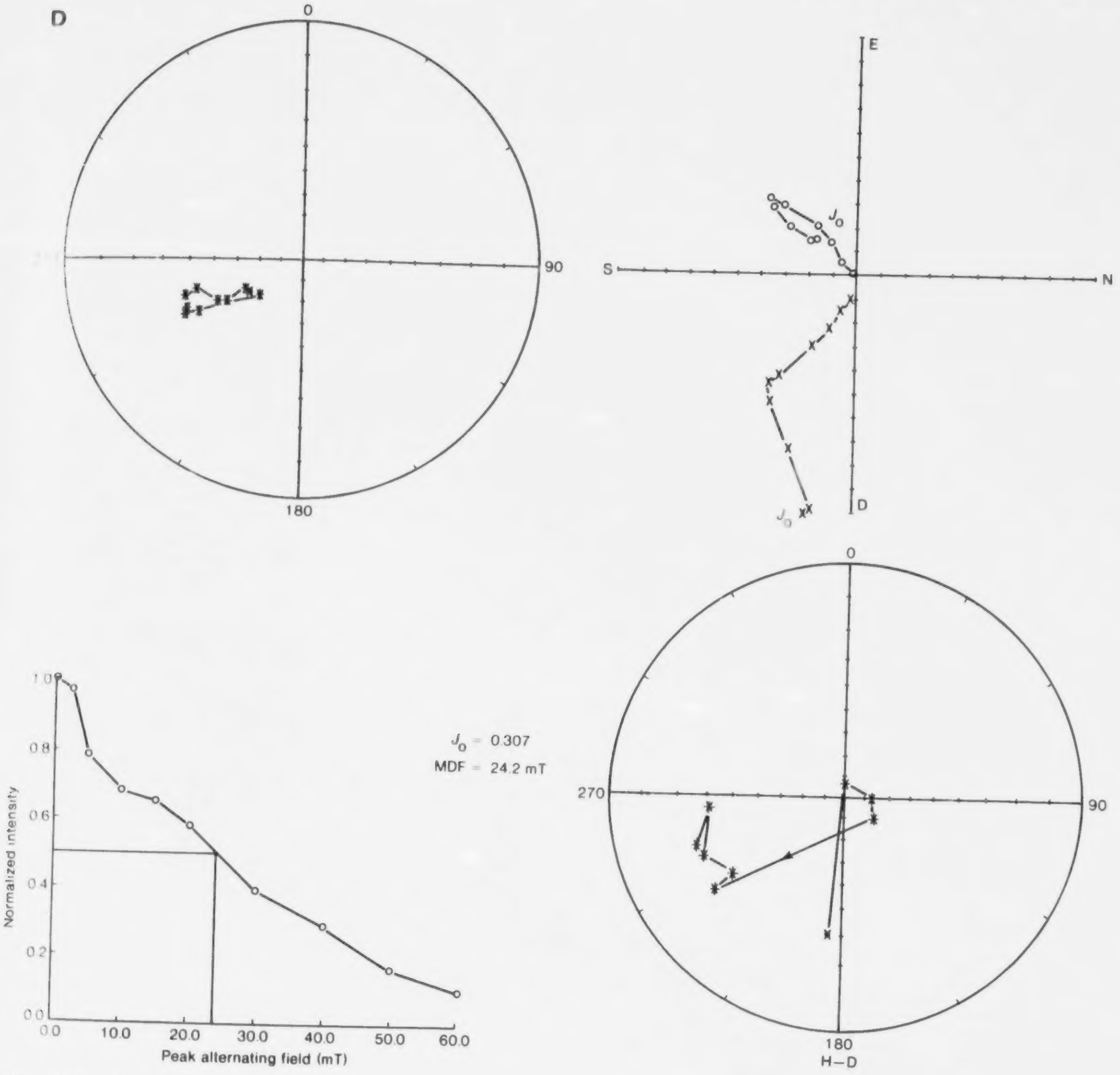

Figure 2. (Continued).

250.7 m then XCB rotary drilling to 499.1 m). This is the shallowest site cored and is not far from Site 589.

The lithology is fairly typical of Leg 90 sites. The surface oxidized layer (Unit IA) occupies the upper 0.4 m of the sequence, whereas the high-intensity zone (~1 μG) extends throughout Core 590-1. A rapid step down to values around 0.1 μG in Core 590-2 suggests that diagenetic alteration of primary iron oxides was unusually rapid at this site. Biosiliceous material is generally absent and authigenic iron sulfides occur throughout in burrows, foraminifer tests, and finely dispersed medium gray streaks and halos. Neither the altered volcanic ash concentrations nor the concretions containing pyrite that are distributed throughout the sequence carry a NRM that is noticeably stronger than that of the surrounding sediments. Bioturbation is slight down to about 200 m, moderate to about 300 m, and intense thereafter.

Progressive demagnetization data for six specimens show MDFs tending to decrease with depth from 421 Oe in the surface oxidized layer to about 116 Oe at 215 m. A very soft VRM is present in most specimens, and there is evidence for a somewhat harder quasivertical overprint, probably acquired during coring. To illustrate more systematically the presence of a fairly soft overprint (e.g., present-day or drilling remanence), a downcore plot was generated of the vector removed by AF cleaning. This difference vector was highly scattered, but showed a normal bias in certain zones: 0–13 m, 30–35 m, 45–62 m, 155–190 m, and 213–240 m. There were only a few short intervals in which the difference vector was systemati-

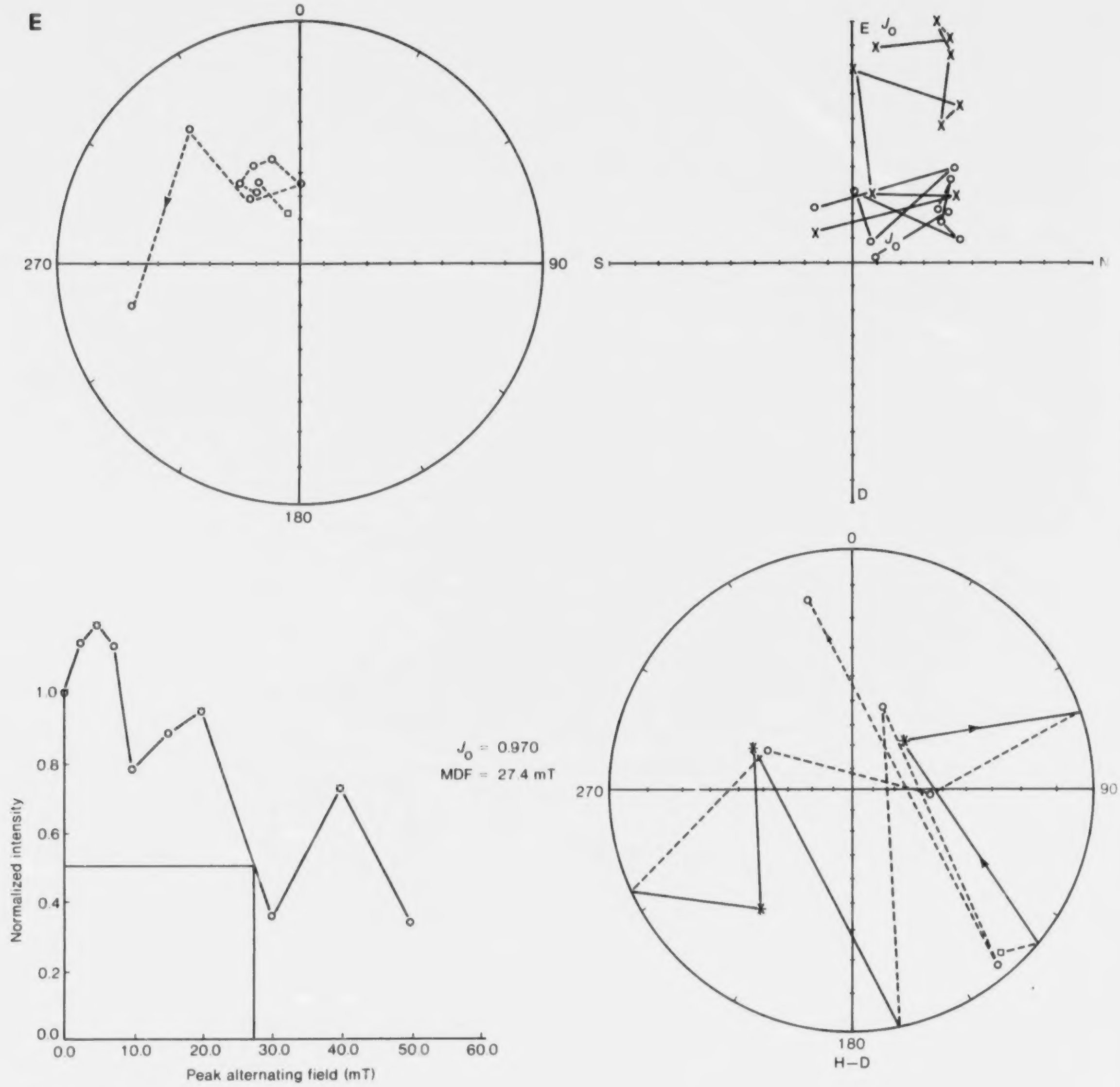

Figure 2. (Continued).

cally reversed. The ratio of the magnitude of the difference vector to the NRM vector (J_D/J_N) varied between about 0.3 to 1.0 within the upper 100 m. This suggests that although a substantial part of the natural remanence is soft, and probably of viscous origin, it is not sufficient to entirely mask the hard (primary?) component. Lower in the sequence, J_D/J_N was slightly higher on the average and more variable. VRM acquisition test results (Table 2) indicate that viscous effects are unlikely to dominate the natural remanence except in the most weakly magnetized sediments.

Above the beginning of the late Pliocene at about 90 m there is a subtle change in lithology, from uniform light gray to white nannofossil ooze to alternating layers of a very pale gray foraminifer-bearing nannofossil ooze and light gray foraminifer–nannofossil ooze (increased current winnowing). The interpretable part of the paleomagnetic record (Fig. 17) is confined to this upper section, where intensities are moderate: typically 0.03 to 0.1 μG, mean MDF is 263 Oe (three specimens) and Q′ is typically 0.02 to 0.15. The polarity sequence down to the base of the Gauss is duplicated in the NRM data from Hole 590B. Evidence for the Cochiti Subchron near the bottom of Core 590A-8 is not confirmed yet in the duplicate core. Prior to this, directions are highly scattered. A more lithified zone of moderate intensity (0.05–0.2 μG) occurs between 270 and 335 m in Hole 590B, which contains a well-defined long interval of nor-

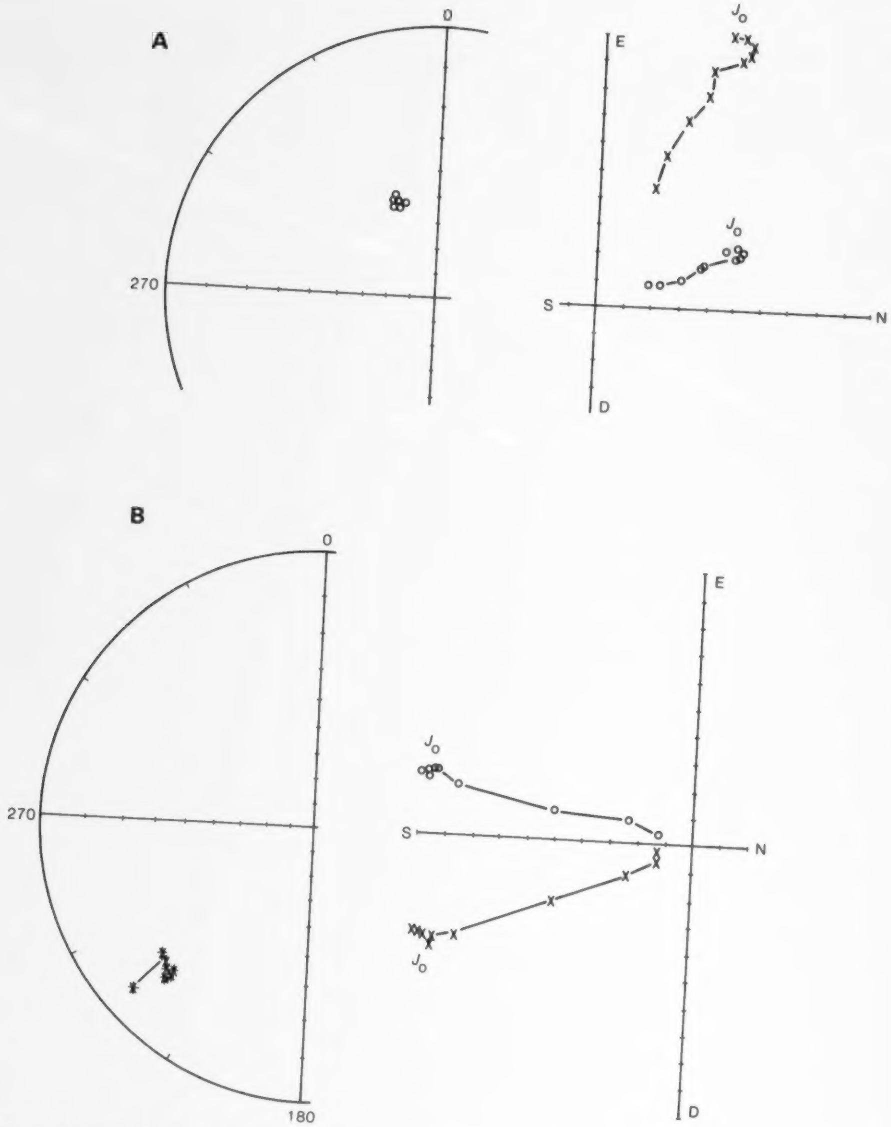

Figure 3. Progressive demagnetization plots. A. Surface high-intensity zone, Sample 593-1-1, 25 cm; depth = 0.25 m. B. Indurated lowermost sediments (chalks), Sample 594-40-3, 25 cm; depth = 373.95 m.

mal polarity that we assign to Chron 9. There is good agreement with the planktonic nannofossil stratigraphy for the site.

Tables 3 and 4 contain the AF-cleaned data for those parts of Holes 590 and 590A that have an interpretable polarity stratigraphy. NRM data for the interval in Hole 590B spanning Chron 9 are listed in Table 5.

Site 591

Although on an eastern spur of the central Lord Howe Rise, Site 591 is in the same general area as Sites 589 and 590. We have AF-cleaned data (at 150 Oe) for the first HPC—Hole 591, 0.0 to 283.1 m; NRM data for the duplicate HPC—Hole 591, 0.0 to 246.5 m; and some NRM data from the rotary drilled cores. Rotary drilling recovered an early Miocene to late Miocene section (17–11 m.y.), but as a result of the low sampling density and high scatter in the data, no polarity interpretation is possible.

Sedimentation rates are somewhat higher than at Site 590 and the surface high-intensity zone is narrower. Otherwise, the magnetic properties of the sequence are similar to Site 590. The zone of enhanced intensity in the middle Miocene at site 588 does not appear at this site. Median destructive fields were fairly high in the surface high-intensity layer (260 Oe) and moderate to low (120–155 Oe) in the very weakly magnetized midhole region. Inclination distribution for Hole 591 became more bi-

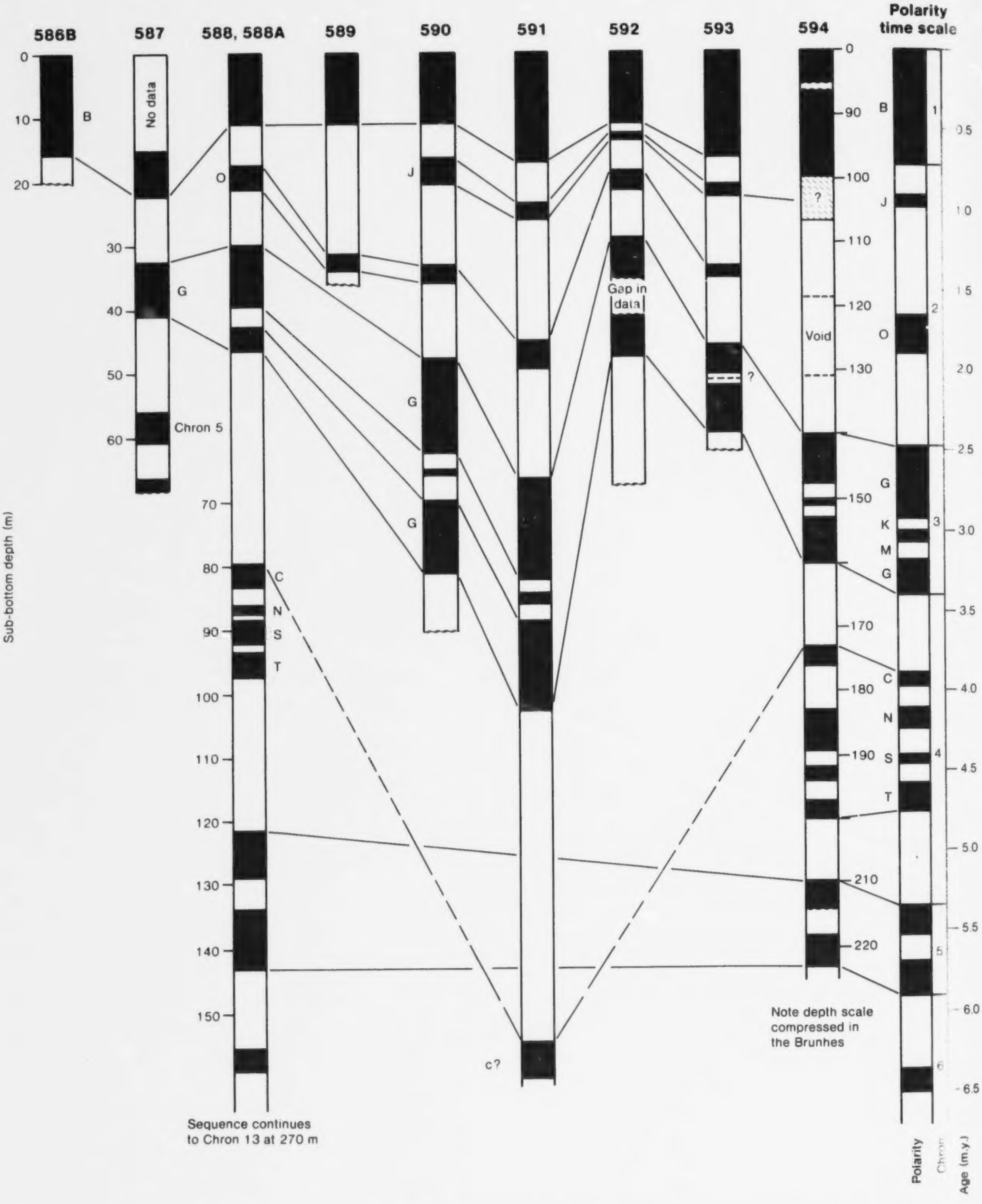

Figure 4. Magnetostratigraphy summary. B = Brunhes, J = Jaramillo, O = Olduvai, G = Gauss, N = Nunivak, S = Sidufjall, T = Thvera. Columns are terminated at levels beyond which no interpretation has yet been possible. The polarity time scale on the right is that of Berggren et al. (1983).

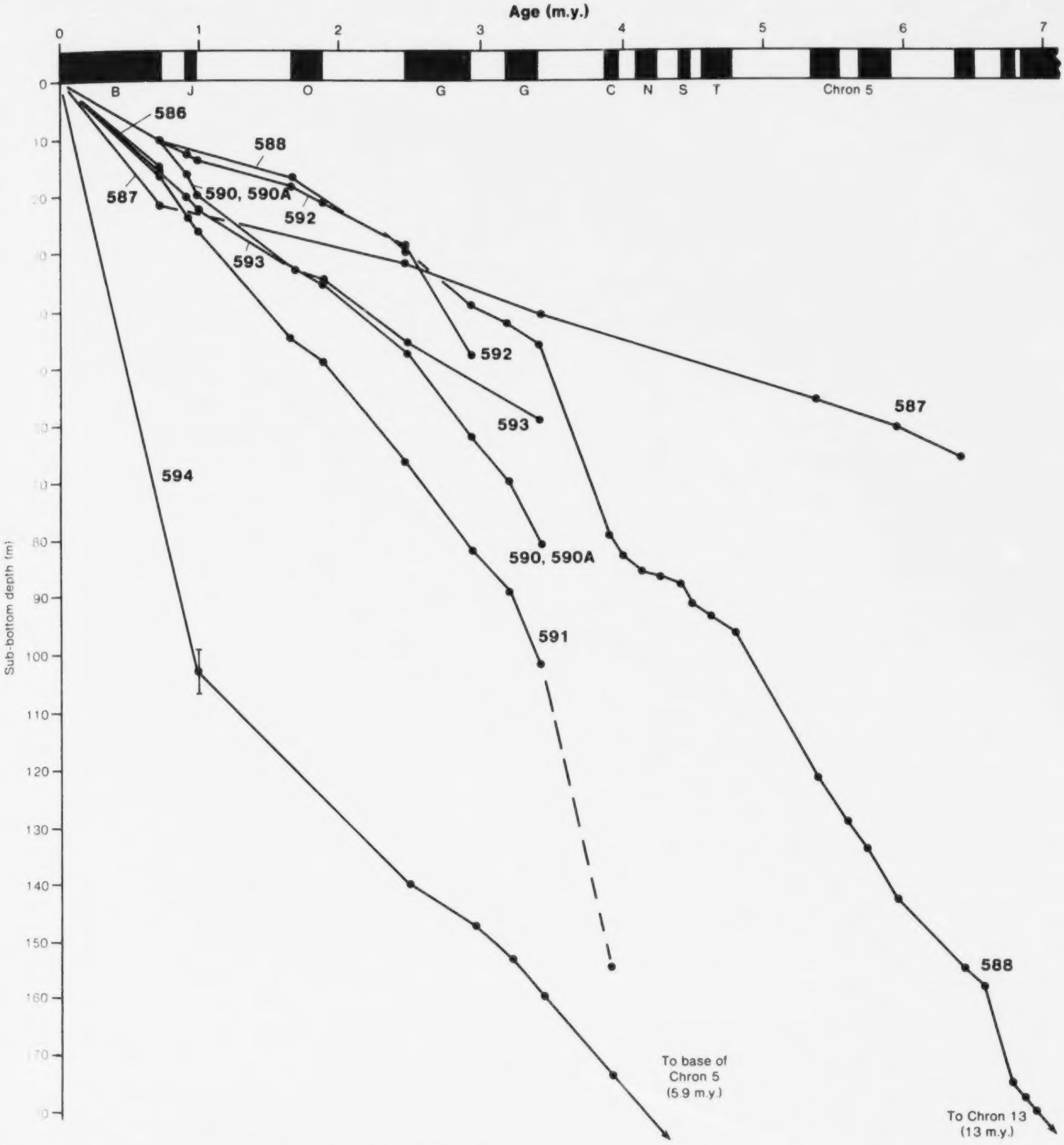

F 5. Sedimentation rate summary based on paleomagnetic data.

m al after AF cleaning (Fig. 18), but there remains a ve high proportion of intermediate directions. In the up r 150 m the distribution is better grouped about the no al and reversed axial dipole directions. Within this re n the inclination of the difference vector, NRM–A racked variations in the AF-cleaned vector (indicatin ingle-component remanence), except in the upper M uyama where it had normal polarity. Throughout the Brunhes Chron, J_D/J_N varies between 10 and 30%, increasing with depth to typically 50 to 80%, although values of 100% are not uncommon. This illustrates the softer and more viscous nature of the weaker sediments.

A polarity sequence in Hole 591 is recognized as far as the upper Gilbert (Fig. 19, the AF-cleaned are given in Table 6), which is reproduced in the NRM data for Hole 591A. Below this, high scatter obscures any corre-

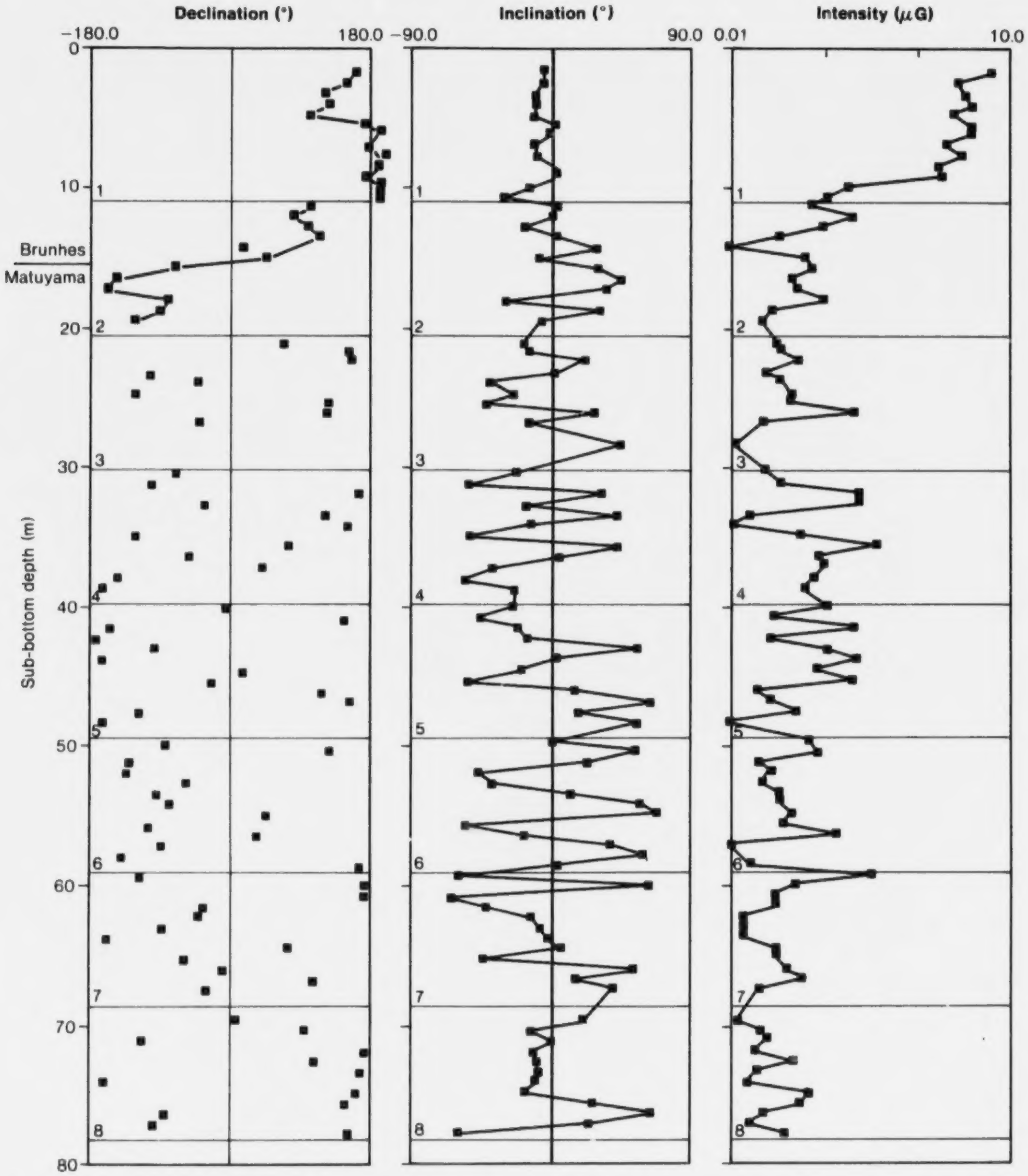

Figure 6. Paleomagnetic data for Hole 586B after AF cleaning at 150 Oe and filtering. Horizontal lines mark core boundaries, numbered in the bottom left; depths are in units of 10 m. Intensities in μG are plotted on a log 10 scale. Declination origins within each core section are arbitrary (i.e., no azimuthal corrections are attempted).

spondence between the two holes. From about 105 m down to 235 m (Cores 591-12 to 591-26), the polarity is predominantly reversed, which is consistent with an extremely high sedimentation rate during the mid- to late-early Pliocene (upper Gilbert) inferred from the nannofossil data. A few normal data points occur during this interval, but these are generally single-point reversals that may not be real. The most probable candidate for the Cochiti Subchron is a 4-point normal interval at 154.7 to 159.5 m.

Site 592

At the single hole cored at this site the HPC was sed down to 234.9 m (Core 25) and the XCB thereaft r to 388.5 m. Three specimens per core section were co ected throughout. Results after AF cleaning at 200 O are available for the first 20 cores (to 186.9 m), with RM data only thereafter.

Magnetic properties are generally similar to tho e at the previous three sites, but with a somewhat stro ger

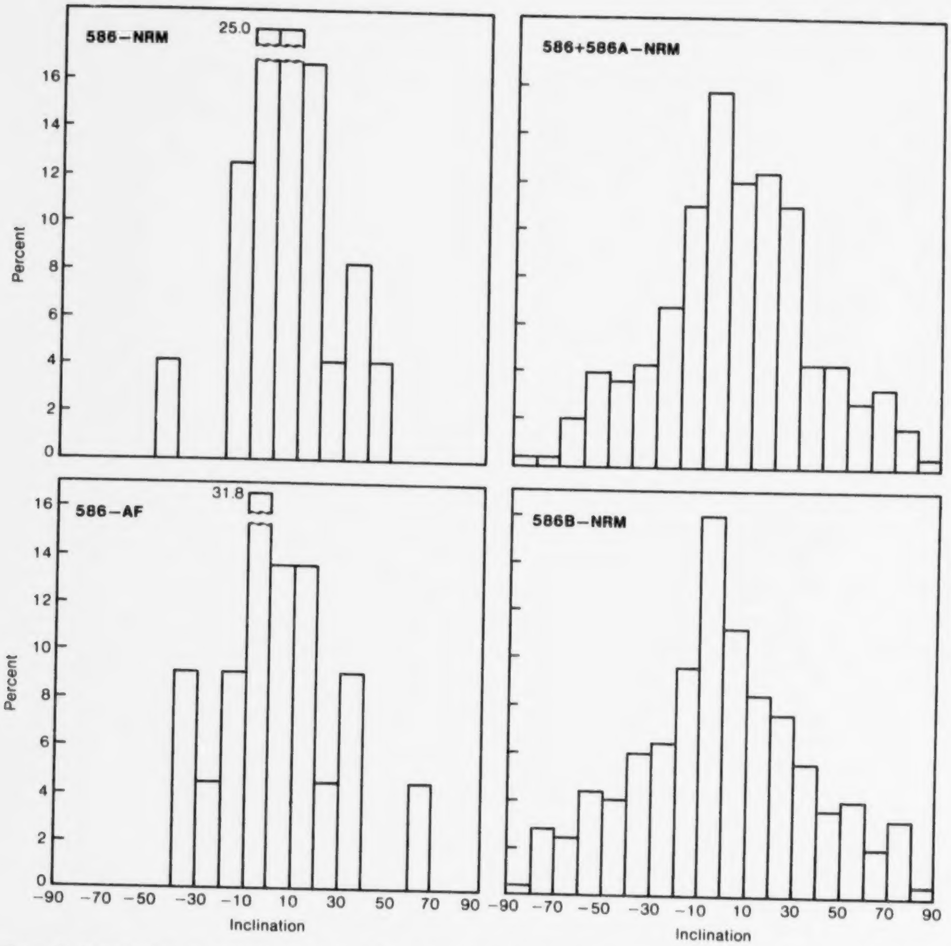

Figure 7. Distribution of inclinations at Site 586. Axial dipole inclination = −1.0°. Histograms for the pre- and postcleaned data are denoted by NRM and AF, respectively.

bias toward intermediate inclinations than in Hole 591 (Fig. 18). Vector difference (NRM–AF) inclinations did not correlate with the NRM vector as at Site 591 and were randomly scattered except between Cores 592-8 and 592-11 (from about 65 to 100 m; Core 8 is largely disturbed), reflecting a VRM component acquired during storage. The ratio J_D/J_N was very scattered and high, with many values greater than 1.0 and poor magnetic stability.

Variations in the dry noncarbonate susceptibility (and Q′) followed the general pattern of intensity changes. Values are typically in the range 0.2–1.0 (Q′ ~0.01–[illegible]), and 11 out of the 595 measurements were still negative (diamagnetic) despite the correction applied.

We identify a polarity sequence down to the upper Gilbert Chron (Fig. 20), which is in good agreement with the nannofossil data. The AF-cleaned data covering this interval are given in Table 7. A notable feature is the very slow sedimentation during the upper Matuyama. Below the Gauss, down to about 65 m, sediments are generally reversely magnetized, but it is not possible to identify subsequent reversal boundaries unambiguously. From 65 to 100 m magnetic stability is poor, as indicated by high values (often 100%) of the ratio J_D/J_N.

A zone of predominantly normal polarity exists within Cores 592-14 and 592-15 (120–140 m) spanning the boundary between nannofossil zones NN11b and NN12 (Miocene/Pliocene boundary), but this is again a region of poor magnetic stability, and without a duplicate HPC for confirmation the interpretation remains tentative. Records in Cores 592-16 to 592-19 are essentially noise, and Cores 592-20 to 592-24 (180–220 m) are predominantly normal but with poor stability so they are probably overprinted. Below 260 m (Core 592-28) intensities are higher (0.05–2 μG) and magnetic stability properties are better, although the data are still very scattered. There is a strong, stably magnetized zone (0.3–2.4 μG) from 263 to 305.8 m containing the early to mid-Miocene chalk Unit IC, which appears to retain a polarity record. However, the NRM data are rather sparse, many of the polarity intervals being supported by one or two data points only, and the interpretation is ambiguous.

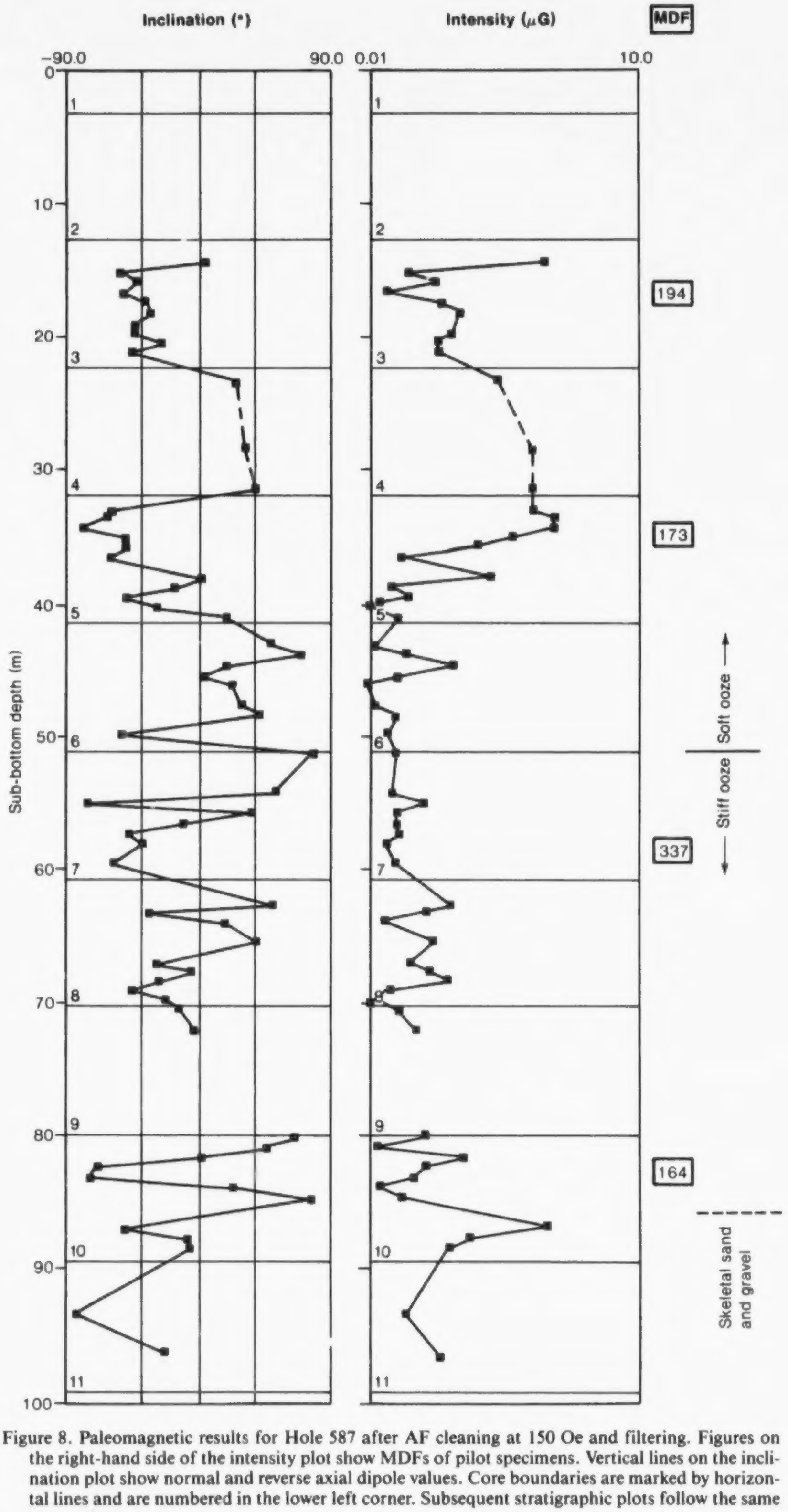

Figure 8. Paleomagnetic results for Hole 587 after AF cleaning at 150 Oe and filtering. Figures on the right-hand side of the intensity plot show MDFs of pilot specimens. Vertical lines on the inclination plot show normal and reverse axial dipole values. Core boundaries are marked by horizontal lines and are numbered in the lower left corner. Subsequent stratigraphic plots follow the same convention.

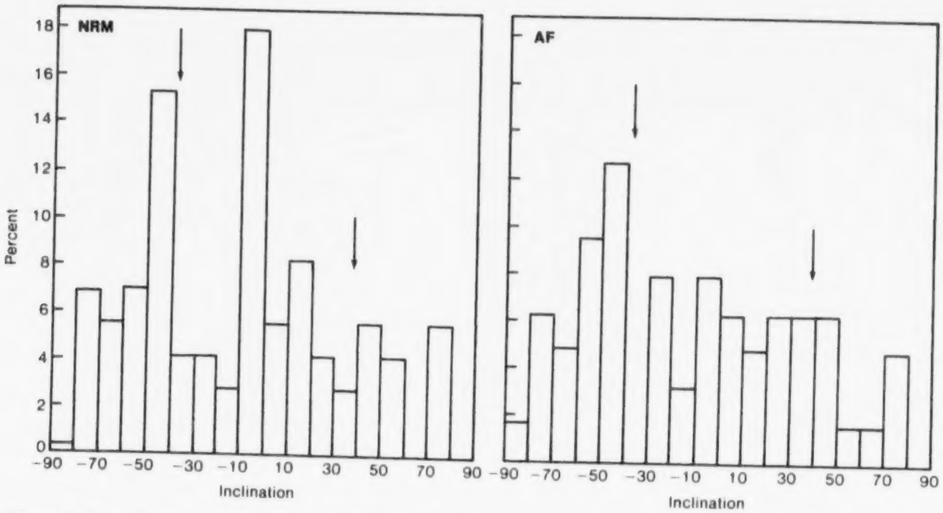

Figure 9. Distribution of inclinations in Hole 587. The axial dipole inclination = −37.8° (arrows).

Site 593

A large data set, AF cleaned at 200 Oe, was obtained from Hole 593: three specimens per section from the 24 HPC cores (0.0–225.9 m) and from the remaining cores recovered by XCB rotary drilling (225.9–571.5 m). Duplicate Hole 593A provided HPC recovery from 0.0 to 103.7 m (Cores 593A-1 to 593A-11, with Cores 593A-8 and 593A-9 being fluid) for which we have AF-cleaned data, and XCB recovery from 448.8 to 257.3 m.

Sediments are similar in character to those at earlier sites. Traces of biosiliceous material occur in a few intervals and foraminifer abundances are lower. Oxidized yellowish gray Subunit IA goes down to 1.5 and 6.0 m in Holes 593 and 593A, respectively. Paleomagnetic inclination and intensity profiles indicate that the vertical offset between the holes is probably no greater than 2 m, hence there must be considerable local variation in thickness of the unit. A unique feature of this sequence is Subunit IC, a pale orange to yellow oxidized nannofossil ooze characterized by unusually high remanent intensities (1.5–3.5 μG). The colored interval (393.8–418 m) is considerably narrower than the interval of elevated intensity (about 360–465 m). The second unique feature is Unit II, Section 593-58-3 to Core 593-60 (545.5–571.5 m), which consists of a black volcanogenic turbidite.

Inclination distributions (Fig. 21) show the highest concentration of intermediate values of any site (except Site 586!), which is a measure of the disappointing quality of this record. The distinct positive bias after AF cleaning arises from a reverse overprint that affects most of the lower half of the sequence (~315–520 m) and was probably acquired during drilling. Evidence for this comes from a consideration of the NRM, AF-cleaned, and vector difference plots, and from AF stability and VRM acquisition tests (see Table 2). This reversely overprinted section encompasses the strongly magnetic Zone D (Table 8) and Subunit IC. Within Zone D magnetic susceptibility, and also Q′, were high, indicating that an increase in the magnetic mineral content is largely responsible for the high magnetization, rather than growth of viscous remanence.

Twenty-four specimens distributed throughout the sequence were subjected to progressive AF demagnetization. Average MDF values are given in Table 8. Specimens with MDF values less than about 150 Oe generally display poor directional stability. In the upper half of the sequence AF cleaning improves the resolution of the polarity sequence, but does not change the overall pattern of reversals. In magnetic Zones A and B the inclination of the NRM–AF difference vector tracked variations in NRM inclination, with a superimposed noise component. Thus, overprinting in the present-day field is not a serious problem. The ratio J_D/J_N increases from about 0.25 at the surface to about 0.75 at about 100 m, with considerable scatter and occasional values greater than 1.0. Below about 100 m values oscillate between about 0.4 and 1.0 with a tendency toward higher values with increasing depth (i.e., the sediments tend to become magnetically softer and/or more viscous with depth). Particularly high values of J_D/J_N occur in certain intervals within the reversely overprinted zone: 357–360 m, 364–369 m, 385–401 m, and 449–454 m. VRM acquisition test results (Table 2) indicate that throughout most of the sequence VRM is unlikely to contribute substantially to the NRM, except at the surface (28% of the NRM acquired in 1000 hr.) and in magnetic Zone D where the VRM contribution can be very large and also magnetically quite hard (MDFs up to 153 Oe). An interesting feature of the VRM acquisition curves (VRM versus log t) was the nature of the departures from linearity. Specimens with low susceptibilities to VRM were quasilinear or slightly convex upward, whereas the highly viscous specimens were clearly concave upward (U-shaped). This demonstrates that the highly magnetic Zone D is associated with a change in magnetic mineralogy and/or grain size and shape.

The magnetic record is generally poorer than at Site 592, but, nevertheless, polarities can be traced back to the base of the Gauss, which are reproducible in both

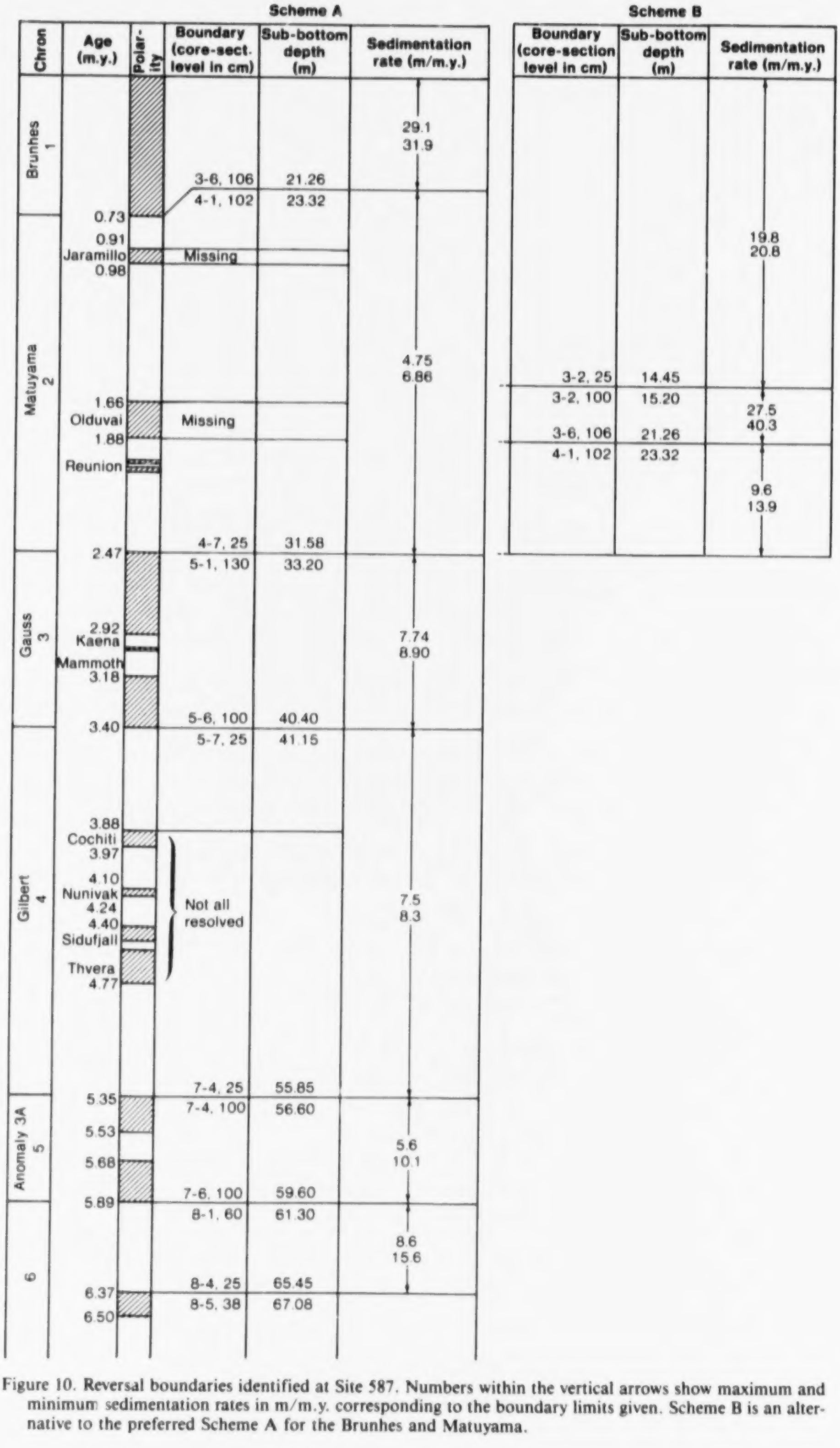

Figure 10. Reversal boundaries identified at Site 587. Numbers within the vertical arrows show maximum and minimum sedimentation rates in m/m.y. corresponding to the boundary limits given. Scheme B is an alternative to the preferred Scheme A for the Brunhes and Matuyama.

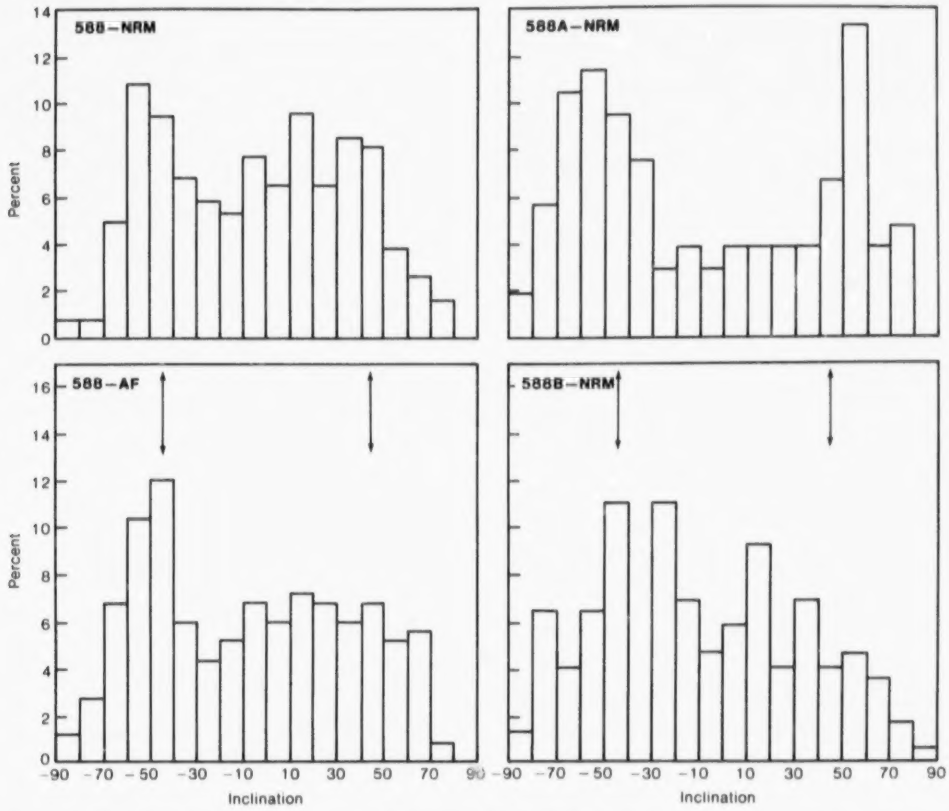

Figure 11. Distribution of inclinations at Site 588. The axial dipole inclination = −44.4° (arrows).

Holes 593 and 593A (Fig. 22). Where the sampled sections overlap below this there is lack of agreement. There is weak evidence for the occurrence of the Kaena and Mammoth subchrons within the Gauss, but it is based only on single-data points of low inclination in each sequence. Table 9 contains the raw data for the upper part of Hole 593.

Volcanogenic Turbidite—Unit II, Hole 593

Special attention was paid to this unit at 545.5–561.9 m in Hole 593, as it is closely associated with the Eocene/Oligocene boundary. Although NRM intensities are igh (up to 10 μG), median destructive fields are very w, ranging from 68 to 95 Oe with one specimen at 166 e (593-59-4, 128 cm—black, very fine grained materi). Shipboard and laboratory remeasurements of NRM owed a substantial decrease over a period of 18 months, ggesting that much of the NRM is a VRM. The isoted band of volcanogenic material below the main unit d the sediments below this level have a harder, more able remanence—MDF = 158 Oe at 564.15 m, and 0 Oe at 566.15 m.

Results after AF cleaning (Fig. 23) indicate that the nit is predominantly of reversed polarity, which is constent with the placement of the Eocene/Oligocene oundary within Chron C13R (following the nomenclaure of LaBrecque et al., 1983). Sediments below Unit II have a spongy consistency that is usually an indicator of coring disturbance. It is, therefore, not clear whether the normal polarity zones in Core 593-60 correspond to Chron C15N. If so, then either there is a short hiatus below the turbidites or the turbidites were deposited prior to the Eocene/Oligocene boundary. Given the poor magnetic stability characteristics of the volcanogenic sediments, the suggested interpretations can only be regarded as speculative. Table 9 contains the raw data for this interval.

Site 594

The site differs from previous sites in that its proximity to New Zealand produced a larger input of terrigenous material. Good HPC recovery extended to 130.7 m in Hole 594 followed by XCB rotary drilling with poor recovery to 207.5 m. Nine HPC cores were recovered from the duplicate Hole 594A from 41.3 to 127.7 m, followed by XCB recovery of the missing intervals in Hole 594 and continuous recovery from 495.5 to 639.5 m.

The lower unit of the sequence (Unit II) is a pelagic foraminifer-nannofossil ooze grading to chalk around 470 m in the middle Miocene, with olive gray turbidite layers below 534 m. This unit is generally similar to the pelagic oozes and chalks at other sites except for a higher biosiliceous component. After the Kaikoura Orogeny, about 6 m.y. (about 169 m in the sequence), the sedi-

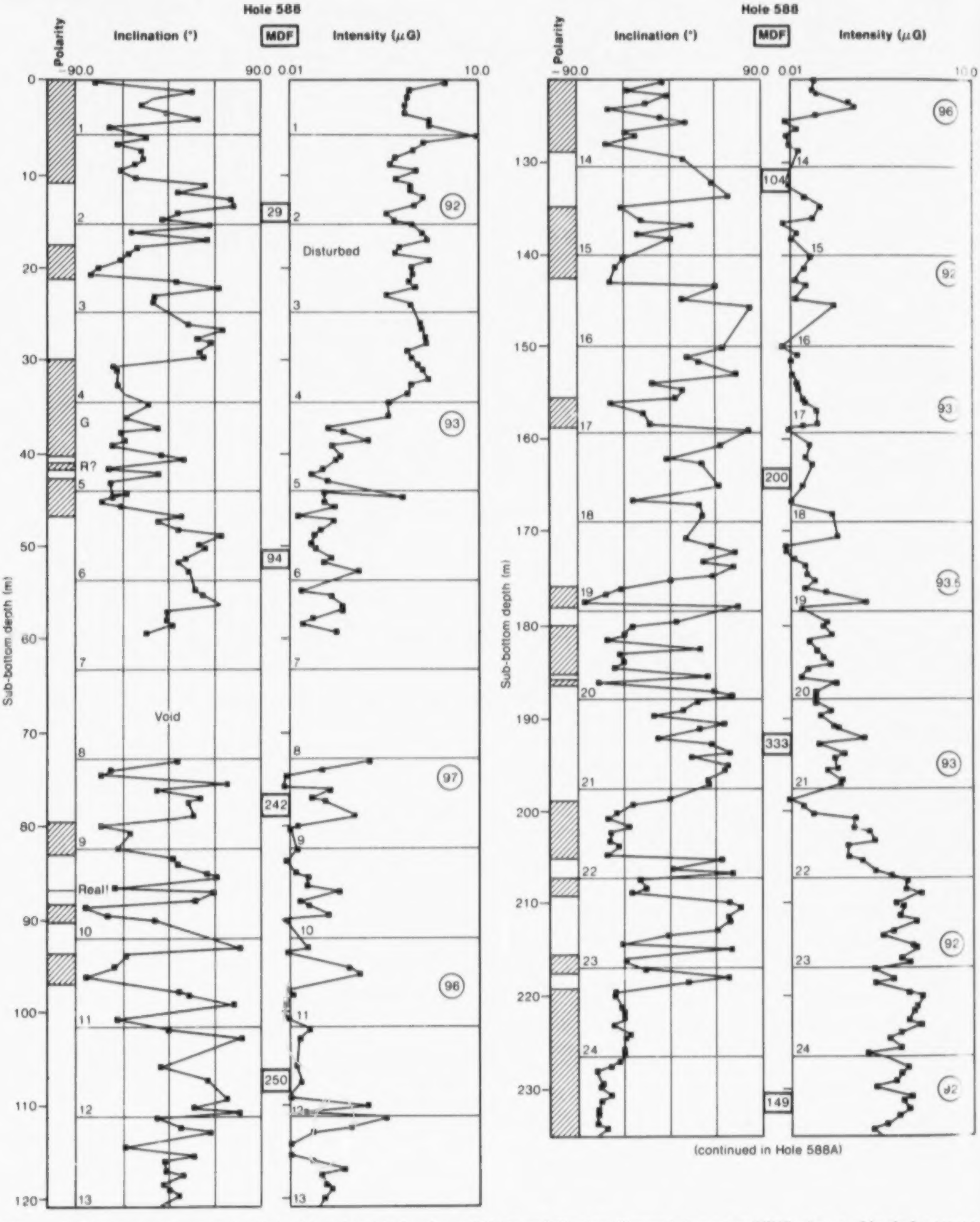

Figure 12. Paleomagnetic results for Hole 588A after AF cleaning at 200 Oe and filtering. Figures in boxes are MDF values and in circles are e carbonate percentages.

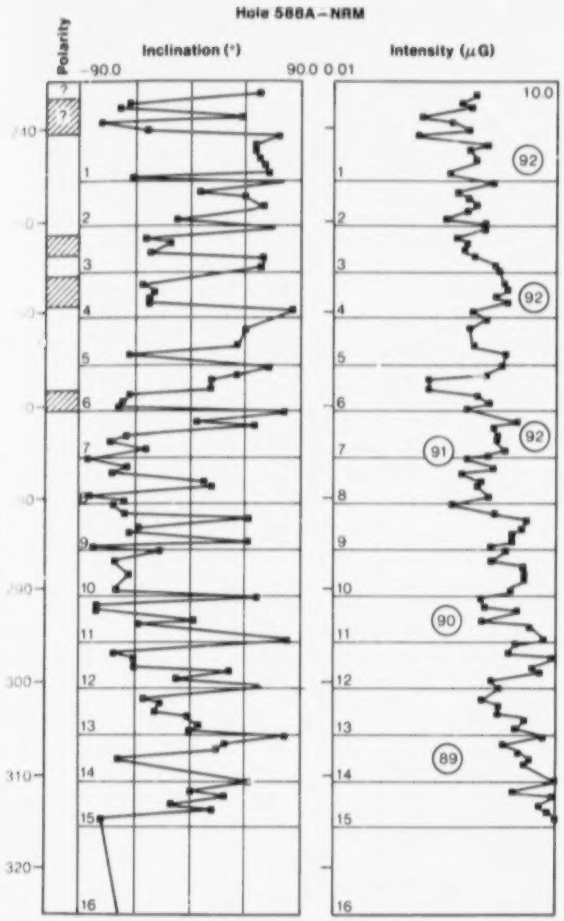

Figure 12. (Continued).

mentation pattern changed with time to alternating pelagic and hemipelagic facies, corresponding to interglacial and glacial conditions, respectively. Enhanced input of terrigenous material is reflected in higher NRM intensities; biosiliceous contents are higher, especially in the hemipelagics; and pyritized streaks and blebs occur throughout the unit.

The distribution of inclinations (Fig. 24) is skewed strongly toward negative (normal polarity) values, with a very large proportion of intermediate inclinations. The rmer is partly due to the occurrence of a very long rmal Brunhes interval (11 cores) and partly to a noral overprint. This is supported by the soft, normal overint observed in reversely magnetized specimens and by inclination distribution in the AF-cleaned data that kewed to a lesser degree than for the NRM data. AF aning reduces the proportion of intermediate inclinans, but it still remains high, reflecting the generally or quality of the paleomagnetic record. Arithmetic an inclinations for NRM and AF-cleaned data are 16.9 and − 15.9°, respectively.

Within Unit I (0–169.1 m), intensities are considera y higher than at similar depths at other sites and show a trend toward lower values with depth (from about 2 to 0.1 μG at the bottom of the unit). The usual surficial layer of a few tens of cm of highly magnetized, oxidized material is not present in Hole 594 and may well be missing since it was suspected that coring started below the mudline. (Duplicate HPCs from Hole 594B have not been opened.) Within the pelagic sediments of Unit II, intensities fall to the usual low values, about 0.01 μG at 260 to 290 m, and thereafter increase somewhat with depth as the sediments become compacted, reaching about 0.05 μG at 490 m.

The long-period variations in susceptibility were of low amplitude and followed a similar pattern to those of NRM intensity, with notably higher values in Unit I (2-15 μG Oe^{-1}), with a small bulge at 400 to 470 m (2-4 μG Oe^{-1}). There is correspondingly little variation in the Q′ ratio: typically 0.01 to 0.04 in Unit I and about 0.01 to 0.20 in Unit II. Generally higher values of Q′ in Unit II are indicative of a larger fraction of fine-grained, single-domain magnetic particles of terrigenous origin.

Downcore variations in inclination of the NRM–AF difference vector and the NRM vector were similar for the upper 250 m of the section. The correspondence is much poorer between the difference vector and the AF-cleaned vector. This indicates that the NRM suffers from a substantial soft overprint at this site. Forty-six pilot specimens were subjected to progressive AF demagnetization. Despite moderate MDF values (mean = 179 ± 99 Oe [± s.d.]), stability was generally poor to bad with widespread evidence for a vertical secondary remanence (up and down) probably imparted during core recovery. AF stability is poorer than at most previous sites, although it improves below 300 m where MDF values are higher. VRM test results (Table 2) indicate that a substantial fraction of the natural remanence could be of viscous origin.

Poor magnetic stability properties combined with unconformities within the section render our interpretation of the paleomagnetic record somewhat tentative, particularly prior to the Pleistocene. Despite this there is sufficient correspondence with the polarity time scale to justify an interpretation.

AF-cleaned data for Hole 594 and our preferred identification of reversed boundaries are illustrated in Figures 25 and 26; (the raw data are given in Table 10). Below Core 594-38 (about 360 m) the record is as yet uninterpretable and is omitted. It is clear from the paleomagnetic data alone that the sequence must contain hiatuses. Except for one short interval (41.95–43.95 m), all cores down to Core 594-11 are normally magnetized. Gaps in the record in Cores 594-7, 594-8, and 594-10 correspond to normal polarity in Hole 594A. According to the radiolarian and diatom stratigraphy there is a hiatus from about 1.6 to 0.74 Ma. If so, the bottom of the long normal interval (101.9 m) corresponds to the base of the Olduvai. An alternative interpretation, which is more consistent with the calcareous nannofossil scheme, is to invoke a very much shorter hiatus and to equate the bottom of the long normal interval with the base of the Jaramillo. This latter alternative is illustrated in Figure 26. It can be argued that the bottom of the normal in-

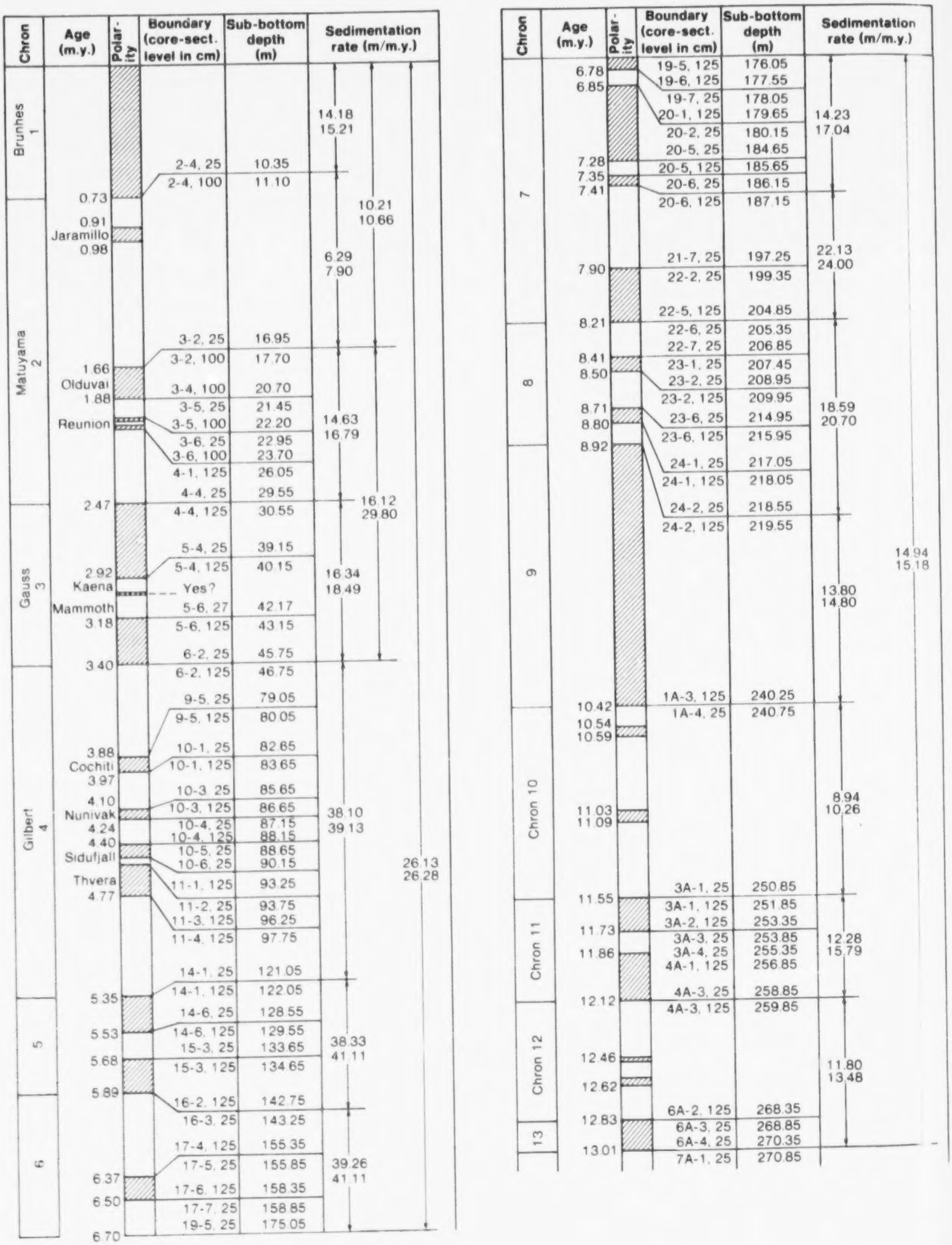

Figure 13. Reversal boundaries for Holes 588 plus 588A.

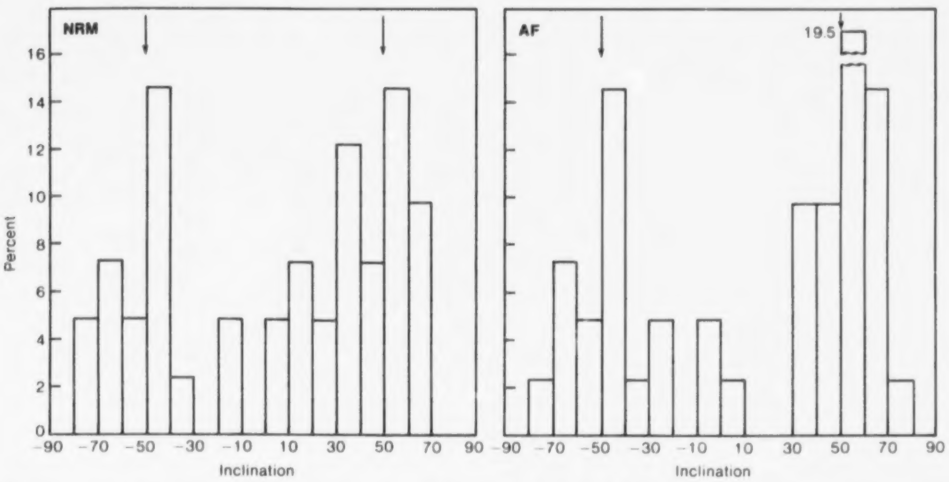

Figure 14. Distribution of inclinations for Hole 589. The axial dipole inclination = −49.9° (arrows).

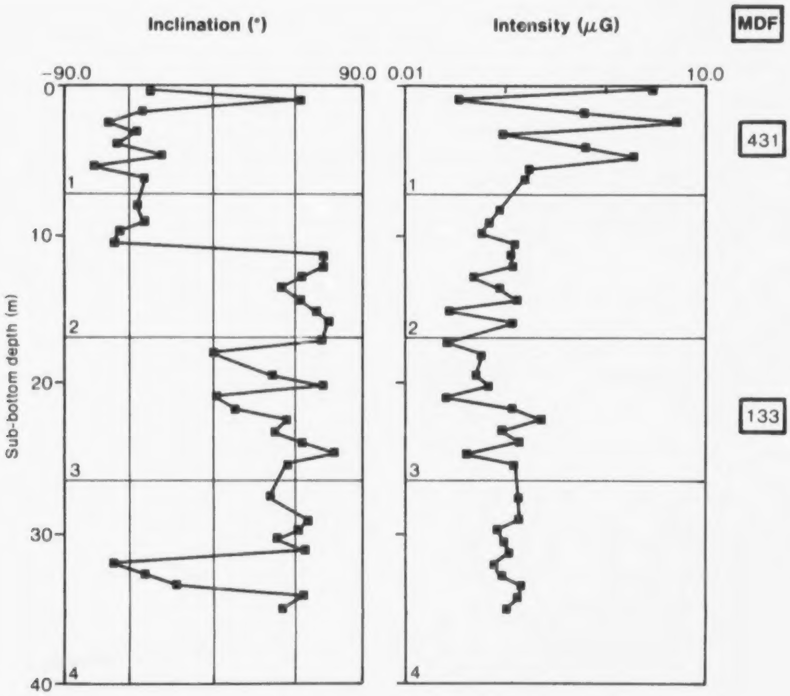

Figure 15. Paleomagnetic results for Hole 589, data AF cleaned at 150 Oe and filtered.

ter[illegible] corresponds to the base of the Brunhes and the Jaramillo is missing.

The scales for the biostratigraphic schemes based on calcareous nannofossils (Site 594 chapter; Martini et al., this volume) and on diatoms and radiolarians (Site 594 chapter; Ciesielski, this volume) disagree. The latter indicates four hiatuses: about 8.3–6.5 Ma, about 5.4–4.5 Ma, about 3.85–2.70 Ma, and about 1.6–0.74 Ma. Despite the mediocre quality of the paleomagnetic data, an intercomparison between the two schemes and the magnetic data is possible (Fig. 27).

In the case of the diatom–radiolarian scheme, the optimum match with the paleomagnetics is plausible except for depth intervals 190–230 m and 245–265 m. In the case of the nannofossil scheme, the match down to the mid-late Miocene boundary is consistent with more uniform sedimentation. The Miocene/Pliocene boundary comes at about 210 m on the magnetic interpreta-

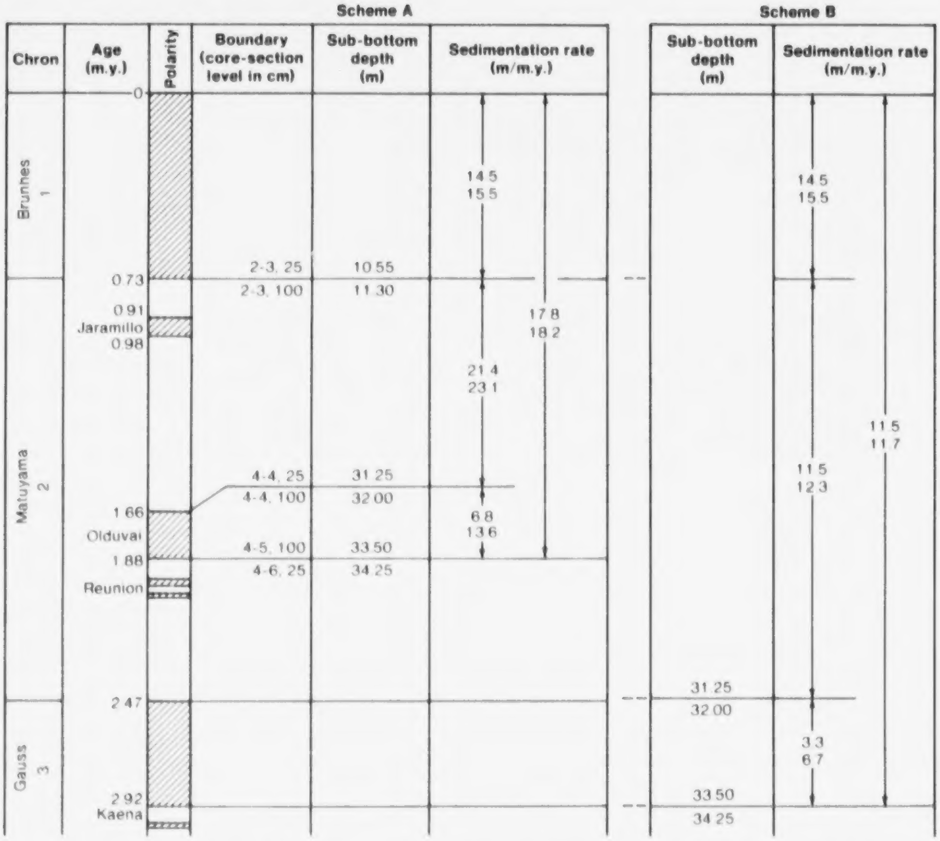

Figure 16. Reversal boundaries for Hole 589—AF. Two interpretations are possible. Scheme A best fits the biostratigraphy.

tion instead of 215 m as on the nannofossil scheme, and the middle Miocene interval on the polarity time scale must be largely missing. Because of its greater simplicity we prefer the combined magneto-nannofossil time scale.

CONCLUSION

The primary objective of this paleomagnetic study is to provide a magnetostratigraphic framework for the transect of sites cored during Leg 90. Excellent recovery, much of it using the HPC, was obtained in the shallow-water carbonate oozes and chalks encountered, extending back to the lower Miocene at most sites and to the upper Eocene at Sites 592 and 593. Despite this, magnetic reversal sequences are recognizable only as far back as the Gilbert (3.4–5.35 m.y.) at most sites. Exceptions to this are Site 588, where we obtained a complete reversal sequence back to the middle Miocene (13 m.y.), and also Site 594, on the southern margin of the Chatham Rise, where the reversal sequence extends to the base of Chron 5 (about 6 m.y., in the late Miocene). There is a very long sequence of 11 cores of Brunhes-age sediments at Site 594. Site 586 on the Ontong-Java Plateau is too close to the equator to use inclination to determine magnetic polarity; the lack of core orientation information was a severe handicap at this site, and only the Brunhes/Matuyama boundary could be identified.

With a few exceptions (e.g., the middle to late Miocene boundary at Site 588) the proposed magnetic chronologies and biostratigraphically determined chronologies are compatible. Volcanogenic turbidite Unit II in Hole 593, associated with the Eocene/Oligocene boundary, is predominantly of reverse polarity, which is consistent with placement of the boundary in Chron C13R (new nomenclature). However, the unit displays poor magnetic stability properties so the evidence is not strong. At Site 594, where there is a conflict between the chronological schemes based on siliceous microfossils (diatoms and radiolarians) and calcareous nannofossils, the magnetic record is in better agreement with the latter.

It is not clear why the paleomagnetic record at Site 588 is so much longer than at other Leg 90 sites on the Lord Howe Rise, all of which are similar sedimentologically. We note that carbonate oozes with a siliceous component studied during previous DSDP Legs give better paleomagnetic records than the almost pure carbonate oozes recovered during Leg 90. This could be related to the stabilizing influence of skeletal siliceous material in the sediment matrix. Such a matrix would be more conducive to the development of a stable postdepositional detrital remanence during compaction. However, sediments from Site 588 were not noticeably more siliceous than from other sites on the Lord Howe Rise.

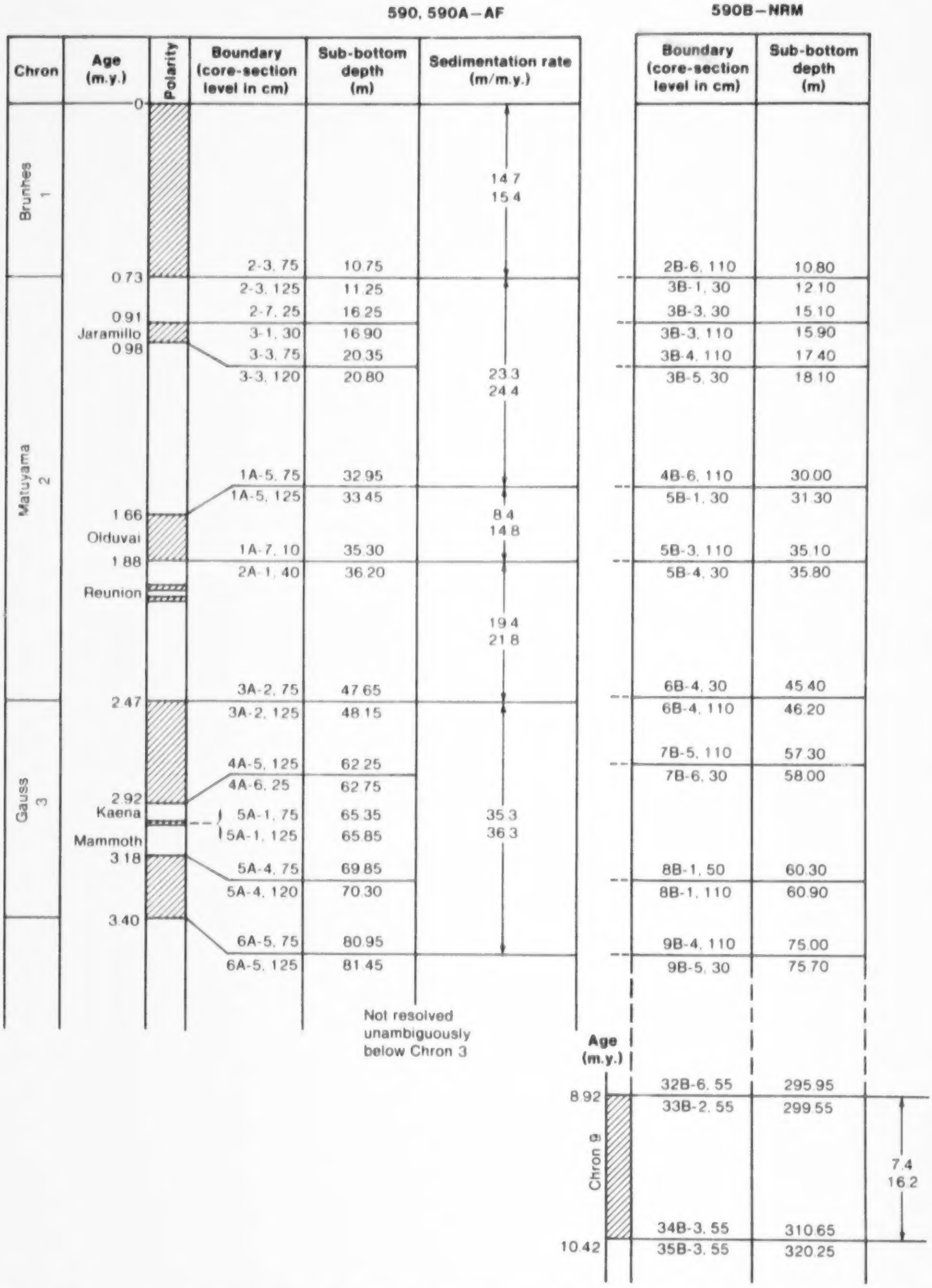

Figure 17. Reversal boundaries identified for Holes 590, 590A, and 590B. Results for Holes 590 and 590A are based on AF-cleaned (200 Oe) and filtered data.

Sequences recovered during Leg 90 were character- ed by very high carbonate contents and correspond- ngly low magnetic remanence, except for a relatively rongly magnetic surficial layer of oxidized material. here is a systematic degradation of the paleomagnetic ignal with depth and an associated decrease of mag- etic remanence which is pronounced in the surface sediments. This is attributed to the combined effects of removal of primary magnetic oxides during sulfate reduction processes (streaks and blebs of pyrite are common), and nonrandom disorientation of magnetic particles in very dilute dispersions during compaction (giving scattered directions with fairly high MDFs). When carbonate contents are very high (close to 100%), a simple car-

Table 3. AF-cleaned data, Hole 590.

Core-Section (interval in cm)	Sub-bottom depth (m)	Declination (°)	Inclination (°)	Intensity (μG)
1-1, 75	0.75	339.4	−17.1	0.231
1-1, 125	1.25	3.2	−74.0	0.596
1-2, 25	1.75	42.8	−76.8	0.402
1-2, 75	2.25	280.2	−52.3	0.161
1-2, 125	2.75	341.1	−66.8	0.806
1-3, 25	3.25	328.7	−50.2	3.503
1-3, 75	3.75	266.7	−59.5	0.191
1-3, 125	4.25	276.6	−51.5	0.046
1-4, 25	4.75	263.4	−53.9	1.458
1-4, 75	5.25	268.8	−29.5	0.400
1-4, 125	5.75	246.6	−71.9	2.493
1-5, 25	6.25	317.3	−54.5	2.287
1-5, 75	6.75	332.7	−65.9	0.107
2-1, 130	8.30	23.2	−55.0	0.076
2-2, 25	8.75	194.8	−57.1	0.090
2-2, 75	9.25	198.5	−56.8	0.095
2-2, 125	9.75	319.5	−57.2	0.090
2-3, 25	10.25	260.6	−52.8	0.124
2-3, 75	10.75	273.9	−63.0	0.195
2-3, 125	11.25	58.6	52.1	0.045
2-4, 25	11.75	94.2	51.8	0.062
2-4, 75	12.25	48.1	−19.8	0.025
2-4, 125	12.75	71.8	−4.8	0.072
2-5, 25	13.25	345.0	45.7	0.090
2-5, 75	13.75	263.4	21.6	0.092
2-5, 125	14.25	289.3	−2.0	0.106
2-6, 25	14.75	197.3	72.1	0.064
2-6, 75	15.25	132.0	43.0	0.069
2-6, 125	15.75	140.4	4.3	0.061
2-7, 25	16.25	193.2	0.3	1.306
3-1, 30	16.90	338.6	−63.8	0.110
3-1, 75	17.35	268.8	−48.0	0.055
3-1, 125	17.85	320.0	−21.0	0.123
3-2, 25	18.35	258.4	−83.9	0.083
3-2, 75	18.85	325.3	−24.5	0.099
3-2, 125	19.35	348.2	−29.0	0.050
3-3, 25	19.85	298.2	−42.0	0.108
3-3, 75	20.35	243.7	−72.6	0.055
3-3, 120	20.80	303.6	29.0	0.061
3-4, 25	21.35	326.7	−33.4	0.072
3-4, 75	21.85	339.2	10.7	0.029
3-4, 125	22.35	126.3	0.2	0.231
3-5, 25	22.85	28.6	61.2	0.032
3-5, 75	23.35	6.8	−62.3	0.057
3-5, 115	23.75	343.1	−36.2	0.067
3-7, 25	25.85	62.4	17.6	0.086

bonate dilution model is sufficient to account for large variations in NRM intensity without invoking any change in the rate of input of magnetic material.

Stratigraphic plots of the vector removed during AF cleaning, inclination histograms, and progressive AF demagnetization and direct VRM tests on selected specimens demonstrate that VRM is common and quite variable within and between sequences, and in some zones is comparable in magnitude to the NRM. A number of specimens contained a vertical component of magnetization, presumably imparted during core recovery, and in some of these this was magnetically the hardest component present. Much of the lower half of the sequence from Hole 593 was affected by a reverse (drilling) overprint. Despite these effects, preliminary polarity results based on NRM data were generally very similar to final ones based on AF-cleaned data. Thus raw NRM data alone may be used for initial shipboard determination of reversal boundaries. Secondly, it was clear that the application of progressive AF demagnetization to all specimens individually, rather than bulk (blanket) AF treat-

Table 4. AF-cleaned data, upper part of Hole 590A.

Core-Section (interval in cm)	Sub-bottom depth (m)	Declination (°)	Inclination (°)	Intensity (μG)
1-1, 100	27.20	287.5	30.6	0.077
1-2, 25	27.95	348.3	16.2	0.052
1-2, 75	28.45	349.7	17.5	0.169
1-2, 125	28.95	40.7	38.0	0.028
1-3, 25	29.45	74.8	66.5	0.065
1-3, 75	29.95	102.4	43.5	0.085
1-3, 125	30.45	100.3	11.8	0.128
1-4, 25	30.95	162.6	65.6	0.116
1-4, 75	31.45	104.7	27.9	0.041
1-5, 25	32.45	113.5	28.6	0.042
1-5, 75	32.95	75.6	45.9	0.043
1-5, 125	33.45	214.2	−28.7	0.105
1-6, 25	33.95	306.1	−42.0	0.203
1-6, 85	34.55	248.9	−30.1	0.100
1-6, 125	34.95	297.8	−56.2	0.093
1-7, 10	35.30	318.1	−27.7	0.089
2-1, 40	36.20	297.5	31.9	0.030
2-1, 120	37.00	291.2	−23.2	0.041
2-2, 25	37.55	281.2	45.0	0.128
2-2, 75	38.05	324.3	18.0	0.037
2-2, 75	38.05	334.4	24.4	0.022
2-2, 125	38.55	263.4	49.2	0.110
2-2, 125	38.55	268.0	43.8	0.119
2-3, 25	39.05	257.7	46.1	0.052
2-3, 25	39.05	248.7	49.2	0.050
2-3, 75	39.55	221.8	−4.8	0.082
2-3, 125	40.05	105.3	35.0	0.030
2-4, 25	40.55	138.2	64.8	0.072
2-4, 75	41.05	4.7	22.1	0.104
2-4, 125	41.55	145.3	42.1	0.086
2-5, 25	42.05	157.6	66.5	0.044
2-5, 75	42.55	165.8	57.9	0.099
2-5, 125	43.05	151.8	20.4	0.048
2-6, 25	43.55	292.2	72.4	0.070
2-6, 75	44.05	122.8	49.0	0.026
2-6, 125	44.55	121.1	65.8	0.059
2-7, 10	44.90	223.6	47.7	0.023
3-1, 25	45.65	313.7	52.8	0.029
3-1, 75	46.15	330.4	−27.5	0.062
3-1, 125	46.65	79.0	55.9	0.053
3-2, 25	47.15	8.6	49.3	0.105
3-2, 75	47.65	317.6	11.6	0.034
3-2, 125	48.15	115.4	−48.8	0.091
3-3, 25	48.65	274.0	−37.4	0.071
3-3, 75	49.15	313.7	−23.5	0.029
3-3, 125	49.65	281.8	−34.2	0.075
3-4, 25	50.15	243.1	−59.0	0.103
3-4, 75	50.65	329.1	−48.2	0.040
3-4, 125	51.15	78.0	4.9	0.027
3-5, 25	51.65	88.7	−80.9	0.103
3-5, 75	52.15	319.4	−76.5	0.067
3-5, 125	52.65	57.2	−77.5	0.091
3-6, 25	53.15	351.5	−41.8	0.077
3-6, 70	53.60	113.5	−57.4	0.121
4-1, 30	55.30	38.3	−27.6	0.11
4-1, 75	55.75	252.4	−74.8	0.08
4-1, 125	56.25	243.7	−83.2	0.07
4-2, 25	56.75	202.7	−19.2	0.07
4-2, 75	57.25	280.1	−47.5	0.07
4-2, 125	57.75	16.7	−40.6	0.06
4-3, 25	58.25	280.7	−33.6	0.07
4-3, 90	58.90	294.7	−28.3	0.08
4-3, 130	59.30	272.3	−49.3	0.10
4-4, 25	59.75	345.3	−37.4	0.18
4-4, 80	60.30	248.6	−34.7	0.04
4-4, 125	60.75	265.7	−16.3	0.05
4-5, 25	61.25	237.5	−39.1	0.05
4-5, 75	61.75	334.5	−40.8	0.02
4-5, 125	62.25	53.6	−10.7	0.05
4-6, 25	62.75	267.2	24.2	0.07
4-6, 85	63.35	282.3	−7.4	0.05
5-1, 75	65.35	264.3	−77.5	0.04
5-1, 125	65.85	259.2	−47.9	0.06
5-2, 25	66.35	286.8	28.1	0.034
5-2, 75	66.85	232.3	53.1	0.029
5-2, 125	67.35	295.0	21.2	0.062
5-3, 25	67.85	215.9	−74.9	0.029

Table 4. (Continued).

Core-Section (interval in cm)	Sub-bottom depth (m)	Declination (°)	Inclination (°)	Intensity (μG)
5-3, 75	68.35	351.7	56.6	0.022
5-3, 125	68.86	252.5	53.1	0.254
5-4, 25	69.35	248.9	46.7	0.043
5-4, 75	69.85	269.3	58.0	0.083
5-4, 120	70.30	184.0	−63.9	0.035
5-5, 25	70.85	86.7	−60.0	0.040
5-5, 75	71.35	137.8	−76.9	0.035
5-5, 125	71.85	45.6	25.3	0.038
5-6, 25	72.35	109.5	−39.5	0.117
5-6, 75	72.85	58.0	−42.4	0.036
5-6, 125	73.35	37.5	−57.4	0.024
6-1, 75	74.95	57.6	−1.0	0.022
6-1, 125	75.45	175.0	−39.8	0.032
6-2, 25	75.95	75.9	−62.5	0.067
6-2, 75	76.45	39.0	−55.5	0.017
6-2, 125	76.95	74.9	−54.2	0.025
6-3, 25	77.45	130.7	32.5	0.141
6-3, 75	77.95	140.4	−78.6	0.012
6-3, 125	78.45	131.7	−49.3	0.027
6-4, 25	78.95	183.8	−67.1	0.012
6-4, 75	79.45	53.6	−80.0	0.031
6-4, 125	79.95	33.1	−41.6	0.023
6-5, 25	80.45	194.9	−39.9	0.045
6-5, 25	80.45	117.1	−73.1	0.037
6-5, 75	80.95	60.6	−36.5	0.025
6-5, 125	81.45	85.4	26.9	0.011
6-6, 25	81.95	298.4	52.7	0.021
6-6, 75	82.45	193.5	43.6	0.038
6-6, 125	82.95	0.5	46.6	0.039
7-1, 25	84.05	12.9	30.0	0.011
7-1, 75	84.55	59.0	43.3	0.009
7-1, 125	85.05	347.7	−69.2	0.063
7-2, 25	85.55	5.1	25.7	0.018
7-2, 75	86.05	0.9	−48.5	0.007
7-2, 125	86.55	191.6	−56.4	0.006
7-3, 25	87.05	316.4	41.7	0.018
7-3, 75	87.55	231.4	81.6	0.050
7-3, 125	88.05	153.9	−2.4	0.060
7-4, 25	88.55	186.9	−8.8	0.018
7-4, 75	89.05	149.1	−18.8	0.018
7-4, 125	89.55	245.4	33.0	0.004
7-5, 25	90.05	29.0	39.7	0.014
7-5, 75	90.55	306.3	20.3	0.012
7-5, 125	91.05	238.8	−10.5	0.010
7-6, 25	91.55	134.5	1.0	0.210
7-6, 75	92.05	28.6	−47.7	0.009
7-6, 125	92.55	215.7	13.5	0.019
8-1, 75	94.15	266.7	−17.8	0.013
8-1, 125	94.65	225.1	15.7	0.023
8-2, 75	95.65	237.1	11.6	0.008
8-2, 125	96.15	277.6	−57.5	0.004
8-3, 25	96.65	309.8	−78.9	0.009
8-3, 75	97.15	307.3	58.2	0.008
8-3, 120	97.60	185.3	−39.4	0.010
8-4, 25	98.15	153.9	54.9	0.007
8-4, 75	98.65	332.6	39.1	0.023
8-4, 125	99.15	227.1	78.9	0.008
8-5, 25	99.65	315.8	49.9	0.112
8-5, 75	100.15	189.3	44.0	0.010
8-5, 125	100.65	232.2	−6.0	0.009
8-6, 25	101.15	103.7	−28.0	0.014
8-6, 75	101.65	104.8	−15.5	0.019
8-6, 125	102.15	114.9	−69.5	0.007
10-1, 25	112.85	182.5	−32.3	0.013
10-1, 75	113.35	188.3	−29.1	0.012
10-1, 125	113.85	275.5	−42.3	0.005
10-2, 25	114.35	148.2	−48.9	0.007
10-2, 75	114.85	300.3	10.5	0.027
10-2, 125	115.35	201.3	57.8	0.011
10-3, 25	115.85	184.2	77.4	0.024
10-3, 75	116.35	50.2	32.8	0.018
10-3, 125	116.85	35.6	−25.4	0.013
10-4, 25	117.35	29.9	47.6	0.185
10-4, 75	117.85	184.7	−0.8	0.013
10-4, 125	118.35	337.9	3.6	0.006
10-5, 25	118.85	339.9	32.7	0.015

Table 4. (Continued).

Core-Section (interval in cm)	Sub-bottom depth (m)	Declination (°)	Inclination (°)	Intensity (μG)
10-5, 75	119.35	71.6	13.6	0.009
10-5, 125	119.85	332.5	21.1	0.004
10-6, 25	120.35	223.7	−13.1	0.010
10-6, 75	120.85	263.4	13.5	0.026

Table 5. NRM data, Hole 590B spanning Chron 9.

Core-Section (interval in cm)	Sub-bottom depth (m)	Declination (°)	Inclination (°)	Intensity (μG)
31-1, 55	278.85	250.1	8.1	0.071
31-2, 55	280.35	261.7	−9.6	0.060
31-3, 55	281.85	263.1	−6.3	0.060
31-4, 55	283.35	262.9	−12.9	0.055
31-5, 55	284.85	257.6	0.7	0.064
32-1, 55	288.45	196.2	3.9	0.088
32-2, 55	289.95	257.8	−2.7	0.061
32-3, 55	291.45	218.7	−9.1	0.049
32-4, 55	292.95	309.9	−14.7	0.024
32-5, 55	294.45	228.0	24.2	0.021
32-6, 55	295.95	246.6	−34.7	0.024
33-1, 55	298.05	247.9	18.4	0.046
33-2, 55	299.55	288.4	−32.8	0.061
33-3, 55	301.05	231.0	−23.9	0.028
33-4, 55	302.55	247.0	−23.7	0.037
33-5, 55	304.05	255.6	−27.5	0.047
33-6, 55	305.55	134.3	−36.4	0.145
34-1, 55	307.65	178.0	−82.5	0.042
34-2, 55	309.15	227.9	−47.5	0.019
34-3, 55	310.65	269.5	−36.4	0.034
34-4, 55	312.15	320.2	25.4	0.045
34-5, 55	313.65	247.8	−29.6	0.028
34-6, 55	315.15	175.1	−13.8	0.048
35-1, 55	317.25	176.6	−14.8	0.018
35-3, 55	320.25	209.0	−8.4	0.025
36-1, 55	326.85	274.0	−14.1	0.855
36-2, 55	328.35	174.9	19.1	0.048
36-3, 55	329.85	275.4	−11.8	0.016
36-4, 55	331.35	212.5	−30.5	0.069
36-5, 55	332.85	246.7	−25.6	0.044
36-6, 55	334.35	356.0	−56.2	0.014

ment such as we used, would lead to only minor refinements in the final polarity interpretation. For studies such as this, involving large collections of specimens, time is better devoted to processing a duplicate core to verify results from the first hole.

The hydraulic piston corer and extended core barrel rotary drilling were very successfully during Leg 90. Although the majority of HPC cores were oriented using the Kuster tool, we found that corrected declination results were no improvement on the raw data for identifying reversal boundaries. We conclude that it is not worthwhile bothering with the Kuster tool in its present form. In comparison with the inclination results, the declination data were more scattered than expected, even allowing for greater experimental uncertainty in the latter. This shows that even with the HPC, large-scale twisting of cores during recovery and/or sampling is common.

ACKNOWLEDGMENTS

We acknowledge with thanks the invaluable role played by the captain and crew of the *Glomar Challenger* during this Christmas voyage, DSDP staff, Peter Aldrich and others for voluntary assistance with

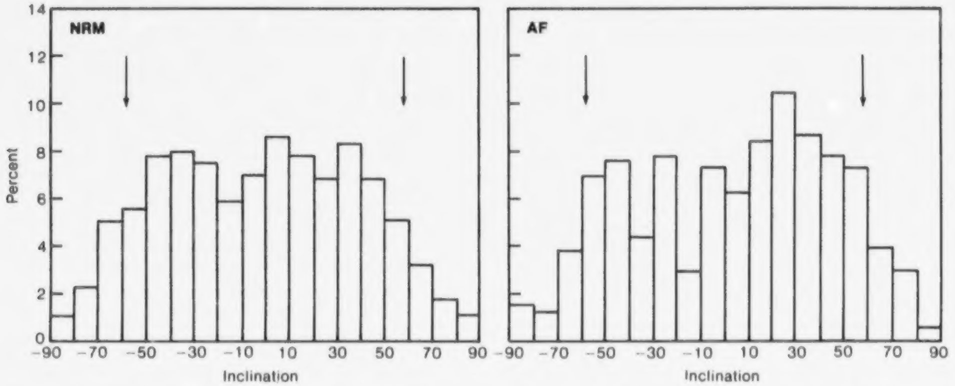

Figure 18. Distribution of inclinations for Hole 591 before and after AF cleaning. The axial dipole inclination = −50.9° (arrows).

laboratory work, and Pat Aldrich for secretarial help. Support came from NSF Grant OCE 8302233.

REFERENCES

Berggren, W. A., Kent, D. V., Flynn, J. F., and Van Couvering, J. A., 1983. Cenozoic geochronology. Woods Hole Oceanogr. Inst., Spec. Publ., Sept. 1983.

________, in press. Cenozoic geochronology. *Geol. Soc. Am. Bull.*

Berggren, W. A., Kent, D. V., and Van Couvering, J. A., in press. Neogene chronology and chronostratigraphy. *In* Snelling, N. J. (Ed.), *Geochronology and the Geological Record*. Geol. Soc. Lond., Spec. Pap.

Berner, R. A., 1964. Stability fields of iron minerals in anaerobic marine sediments. *J. Geol.*, 72:826–834.

Bleil, U., in press. The magnetostratigraphy of NW Pacific sediments, Deep Sea Drilling Project Leg 86. *In* von Huene, R., Aubouin, J., et al., *Init. Repts. DSDP*, 86: Washington (U.S. Govt. Printing Office).

Clement, R. M., and Kent, D. V., 1984. A detailed record of the Lower Jaramillo polarity transition from a southern hemisphere, deep-sea sediment core. *J. Geophys. Res.*, 89:1049–1058.

Hoffman, K. A., and Day, R., 1978. Separation of multicomponent NRM: a general method. *Earth Planet. Sci. Lett.*, 40:433–438.

Karlin, R., and Levi, S., 1983. Diagenesis of magnetic minerals in recent haemipelagic sediments. *Nature*, 303:327–330.

Kent, D. V., and Lowrie, W., 1977. VRM studies in Leg 37 igneous rocks. *In* Aumento, F., Melson, W. G., et al., *Init. Repts. DSDP*, 37: Washington (U.S. Govt. Printing Office), 525–529.

Kent, D. V., and Spariosu, D. J., 1982a. Magnetostratigraphy of Caribbean Site 502 hydraulic piston cores. *In* Prell, W. L., Gardner, J. V., et al., *Init. Repts. DSDP*, 68: Washington (U.S. Govt. Printing Office), 419–433.

________, 1982b. Magnetostratigraphy of equatorial Pacific Site 503 hydraulic piston cores. *In* Prell, W. L., Gardner, J. V., et al., *Init. Repts. DSDP*, 68: Washington (U.S. Govt. Printing Office), 435–440.

LaBrecque, J. L., Hsü, K. J., Carman, M. F., Jr., Karpoff, A., McKenzie, J. A., Percival, S. F., Jr., Petersen, N. P., Pisciotto, K. A., Schreiber, E., Tauxe, L., Tucker, P., Weissert, H. J., and Wright, R., 1983. DSDP Leg 73: Contributions to Paleogene stratigraphy in nomenclature, chronology and sedimentation rates. *Palaeogeogr., Palaeoclimatol., Palaeoecol.*, 42:91–125.

Lowrie, W., and Kent, D. V., 1978. Characteristics of VRM in oceanic basalts. *J. Geophys.*, 44:297–315.

Mayer, L. A., 1982. Physical properties of sediment recovered on Deep Sea Drilling Project Leg 68 with the hydraulic piston corer. *In* Prell, W. L., Gardner, J. V., et al., *Init. Repts. DSDP*, 68: Washington (U.S. Govt. Printing Office), 365–382.

Shimizu, Y., 1960. Magnetic viscosity of magnetite. *J. Geomag. Geoelectr.*, 11:125–138.

Silva, A. J., and Hollister, C. D., 1979. Geotechnical properties of ocean sediments recovered with the giant piston corer: Blake-Bahama Outer Ridge. *Mar. Geol.*, 29:1–22.

Tauxe, L., Tucker, P., and Petersen, N., 1984. Magnetostratigraphy of Leg 73 sediments. *In* Hsü, K. J., LaBrecque, J. L., et al., *Init. Repts. DSDP*, 73: Washington (U.S. Govt. Printing Office), 609–621.

Tauxe, L., Tucker, P., Petersen, N. P., and LaBrecque, J. L., 1983. The magnetostratigraphy of Leg 73 sediments. *Palaeogeogr., Palaeoclimatol., Palaeoecol.*, 42:65–90.

Tucker, P., and Tauxe, L., 1984. The downhole variation of the rock magnetic properties of IPOD Leg 73. *In* Hsü, K. J., LaBrecque, J. L., et al., *Init. Repts. DSDP*, 73: Washington (U.S. Govt. Printing Office), 673–685.

Weinreich, N., and Theyer, F., in press. Paleomagnetism of the Leg 85 sediments: Neogene magnetostratigraphy and tectonic history of the Central Equatorial Pacific. *In* Mayer, L., Theyer, F., et al., *Init. Repts. DSDP*, 85: Washington (U.S. Govt. Printing Office).

Date of Initial Receipt: 25 October 1984
Date of Acceptance: 1 April 1985

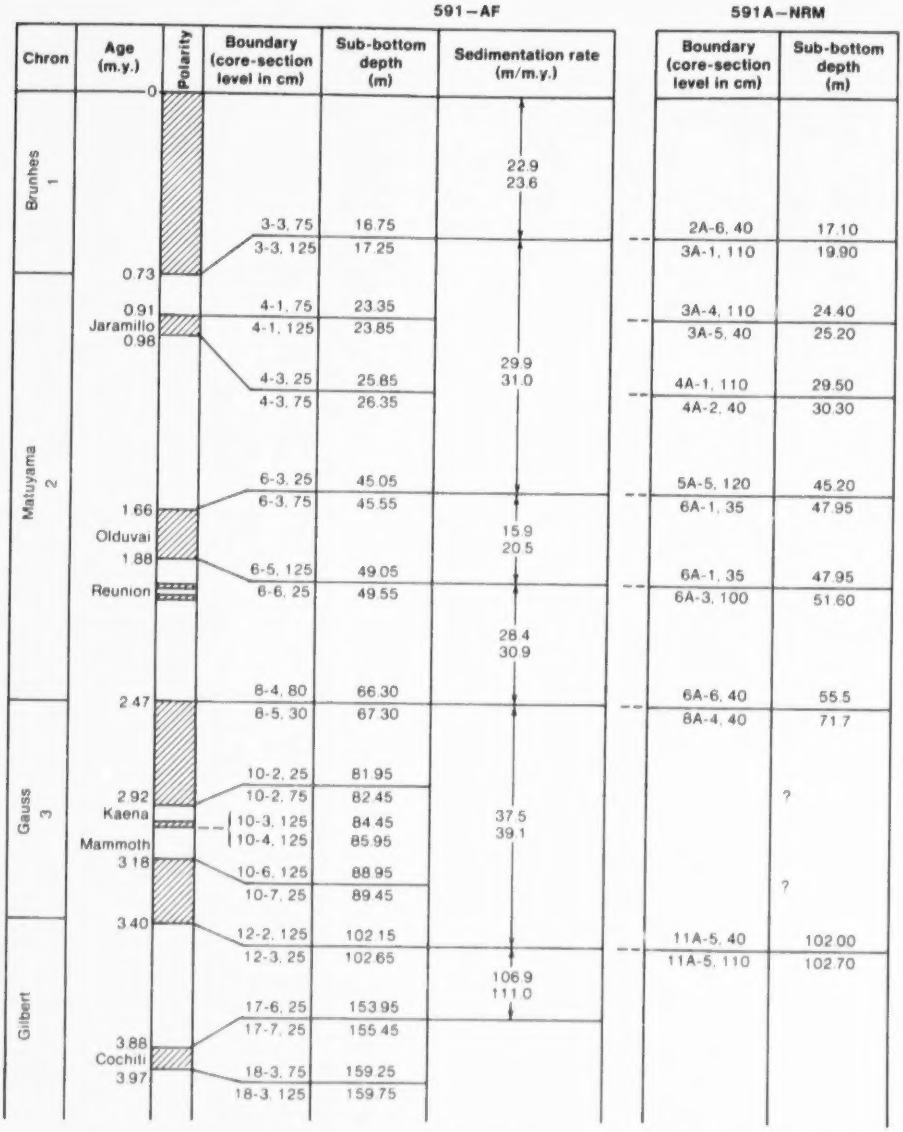

Figure 19. Reversal boundaries for the upper parts of Holes 591 and 591A. Results for Hole 591 are based on AF-cleaned (150 Oe) and filtered data. The polarity sequence is not defined below 167.5 m.

Table 6. AF-cleaned data, upper part of Hole 591.

Core-Section (interval in cm)	Sub-bottom depth (m)	Declination (°)	Inclination (°)	Intensity (μG)
1-1, 80	0.80	58.0	−55.7	3.295
1-1, 125	1.25	253.3	−83.0	0.807
1-2, 25	1.75	56.0	−53.8	4.473
1-2, 80	2.30	41.2	−48.8	7.225
1-2, 125	2.75	64.9	−56.0	0.600
2-1, 25	3.65	36.5	−49.0	2.220
2-1, 25	3.65	36.1	−49.6	2.242
2-1, 75	4.15	43.1	−55.7	0.356
2-1, 125	4.65	93.7	−50.0	0.103
2-2, 25	5.15	105.0	−64.2	0.131
2-2, 75	5.65	96.3	−52.4	0.185
2-3, 25	6.65	58.3	−16.7	0.204
2-3, 75	7.15	91.0	−70.0	0.072
2-3, 125	7.65	83.8	−54.1	0.063
2-4, 25	8.15	62.0	−56.0	0.097
2-4, 75	8.65	55.0	−58.0	0.103
2-4, 125	9.15	62.3	−66.0	0.078
2-5, 25	9.65	40.1	−66.0	0.145
2-5, 75	10.15	27.5	−49.7	0.063
2-5, 125	10.65	341.6	−70.6	0.112
2-6, 25	11.15	45.2	−12.8	0.075
2-6, 75	11.65	337.7	−72.1	0.146
2-7, 25	12.65	61.3	−67.0	0.154
3-1, 25	13.25	165.8	−45.1	0.127
3-1, 75	13.75	189.1	−52.3	0.155
3-1, 125	14.20	198.5	−48.3	0.088
3-2, 25	14.75	188.0	−40.6	0.094
3-2, 75	15.25	196.0	−37.7	0.188
3-2, 125	15.75	140.4	−27.3	0.176
3-3, 25	16.25	205.9	−39.5	0.145
3-3, 75	16.75	250.4	−17.5	0.029
3-3, 125	17.25	324.8	42.7	0.038
3-4, 25	17.75	343.2	47.7	0.096
3-4, 75	18.25	29.9	43.8	0.040
3-4, 125	18.75	359.8	13.6	0.029
3-5, 25	19.25	23.3	57.5	0.057
3-5, 75	19.75	349.3	32.1	0.076
3-5, 125	20.25	282.2	45.9	0.023
3-6, 25	20.75	351.1	26.4	0.035
3-6, 75	21.25	328.6	28.8	0.107
3-6, 125	21.75	131.1	50.8	0.027
4-1, 75	23.35	237.4	−6.9	0.006
4-1, 125	23.85	28.4	−69.7	0.075
4-2, 25	24.35	295.7	−24.2	0.017
4-2, 75	24.85	119.1	−27.2	0.029
4-2, 125	25.35	108.1	−46.7	0.021
4-3, 25	25.85	52.2	−25.5	0.021
4-3, 75	26.35	229.4	41.7	0.032
4-3, 125	26.85	250.1	61.3	0.022
4-4, 25	27.35	191.5	38.4	0.008
4-4, 75	27.85	246.3	35.4	0.006
4-4, 125	28.35	293.7	−23.4	6.906
4-5, 25	28.85	154.2	6.6	0.047
4-5, 75	29.35	212.3	52.6	0.018
4-5, 125	29.85	291.4	7.9	0.010
4-6, 25	30.35	27.2	38.3	0.017
4-6, 75	30.85	23.6	78.5	0.082
4-6, 125	31.35	354.1	30.6	0.020
5-1, 47	32.67	263.7	39.9	0.033
5-1, 75	32.95	144.2	86.6	0.029
5-1, 125	33.45	88.6	63.7	0.032
5-2, 25	33.95	231.3	48.4	0.016
5-2, 75	34.45	253.8	23.3	0.022
5-2, 125	34.95	198.0	−2.3	0.048
5-3, 25	35.45	198.1	51.0	0.027
5-3, 75	35.95	227.7	46.1	0.023
5-3, 125	36.45	221.6	−18.2	0.031
5-4, 25	36.95	167.9	0.0	0.009
5-4, 75	37.45	119.7	83.5	0.027
5-4, 125	37.95	191.4	41.0	0.024
5-5, 25	38.45	115.8	78.2	0.026
5-5, 75	38.95	114.1	63.6	0.036
5-5, 125	39.45	237.4	24.9	0.053
5-6, 25	39.95	243.8	11.3	0.017
5-6, 75	40.45	187.3	32.0	0.038
6-1, 125	43.05	325.7	57.4	0.021

Table 6. (Continued).

Core-Section (interval in cm)	Sub-bottom depth (m)	Declination (°)	Inclination (°)	Intensity (μG)
6-2, 25	43.55	133.5	59.4	0.04
6-2, 75	44.05	113.4	53.9	0.04
6-2, 125	44.55	176.6	14.3	0.03
6-3, 25	45.05	169.3	28.8	0.03
6-3, 75	45.55	154.0	−11.6	0.01
6-3, 125	46.05	229.6	−33.4	0.07
6-4, 25	46.55	266.9	−26.3	0.0
6-4, 75	47.05	253.1	−55.8	0.0
6-4, 125	47.55	290.8	−45.5	0.0
6-5, 25	48.05	280.8	−37.2	0.0
6-5, 75	48.55	277.0	−44.0	0.0
6-5, 125	49.05	261.0	−47.8	0.0
6-6, 25	49.55	283.7	38.0	0.0
6-6, 75	50.05	49.8	58.5	0.0
6-6, 125	50.55	110.9	35.5	0.0
7-1, 75	52.15	13.4	5.6	0.0
7-1, 125	52.65	324.3	37.6	0.0
7-2, 25	53.15	236.5	4.6	0.0
7-2, 75	53.65	172.9	−9.0	0.0
7-2, 125	54.15	305.8	18.0	0.01
7-3, 25	54.65	349.5	39.8	0.013
7-3, 75	55.15	190.6	63.4	0.025
7-3, 125	55.65	210.8	−12.5	0.039
7-4, 25	56.15	348.6	43.6	0.031
7-4, 75	56.65	14.2	55.3	0.011
7-4, 125	57.15	325.7	58.0	0.043
7-5, 25	57.65	256.0	57.2	0.029
7-5, 75	58.15	299.9	44.1	0.017
7-5, 125	58.65	262.8	30.2	0.016
7-6, 25	59.15	293.4	22.5	0.023
7-6, 75	59.65	284.5	37.5	0.039
7-6, 125	60.15	40.8	−31.5	0.008
8-1, 30	61.30	228.1	28.2	0.031
8-1, 80	61.80	78.8	−52.6	0.650
8-1, 130	62.30	263.9	44.8	0.028
8-2, 30	62.80	243.4	38.1	0.034
8-2, 80	63.30	244.0	15.2	0.017
8-2, 130	63.80	109.3	52.6	0.070
8-3, 30	64.30	265.2	4.7	0.069
8-3, 80	64.80	230.9	33.9	0.036
8-3, 130	65.30	210.0	11.5	0.008
8-4, 30	65.80	211.2	30.4	0.022
8-4, 80	66.30	237.7	8.7	0.029
8-5, 30	67.30	278.7	−58.0	0.012
8-5, 80	67.80	6.2	−49.7	0.025
8-5, 130	68.30	105.0	−45.1	0.064
8-6, 30	68.80	304.4	−34.5	0.027
8-6, 80	69.30	158.3	−48.9	0.080
8-6, 130	69.80	298.9	16.0	0.013
9-1, 75	71.35	247.3	−21.5	0.028
9-1, 125	71.85	255.8	25.4	0.009
9-2, 25	72.35	273.1	−37.9	0.031
9-2, 75	72.85	269.3	−34.8	0.015
9-2, 125	73.35	273.4	−31.8	0.042
9-3, 25	73.85	251.1	−36.4	0.029
9-3, 75	74.35	207.6	−6.5	0.017
9-3, 125	74.85	223.3	−7.8	0.017
9-4, 25	75.35	265.6	−64.3	0.0
9-4, 75	75.85	229.6	−41.9	0.0
9-4, 125	76.35	272.8	8.1	0.0
9-5, 25	76.85	199.3	−25.8	0.0
9-5, 75	77.35	238.4	−19.8	0.0
9-5, 125	77.85	265.1	5.2	0.0
9-6, 25	78.35	84.8	−2.0	0.0
9-6, 75	78.85	205.9	−48.7	0.0
9-6, 125	79.35	200.0	−38.3	0.0
10-1, 85	81.05	207.9	0.0	0.0
10-1, 125	81.45	62.9	56.7	0.0
10-2, 25	81.95	220.8	−24.9	0.0
10-2, 75	82.45	336.1	13.3	0.0
10-2, 125	82.95	147.7	61.1	0.0
10-3, 25	83.45	160.3	48.9	0.0
10-3, 75	83.95	317.8	30.2	0.0
10-3, 125	84.45	292.9	−28.6	0.009
10-3, 125	84.45	307.0	−27.7	0.012
10-4, 25	84.95	116.2	−49.2	0.016

Table 6. (Continued).

Core-Section (interval in cm)	Sub-bottom depth (m)	Declination (°)	Inclination (°)	Intensity (μG)
10-4, 75	85.45	93.4	-59.7	0.018
10-4, 125	85.95	187.6	-56.7	0.011
10-5, 25	86.45	248.8	22.8	0.031
10-5, 75	86.95	327.7	12.2	0.009
10-5, 125	87.45	220.6	11.1	0.010
10-6, 25	87.95	266.3	27.4	0.019
10-6, 75	88.45	323.5	14.6	0.023
10-6, 125	88.95	308.1	26.0	0.014
0-7, 25	89.45	298.6	-48.3	0.012
1-1, 75	90.55	325.4	-11.1	0.004
1-1, 125	91.05	215.0	-35.6	0.010
1-2, 25	91.55	350.1	29.4	0.080
1-2, 75	92.05	43.4	-52.7	0.013
1-2, 125	92.55	75.3	-33.6	0.008
1-2, 125	92.55	49.8	-40.9	0.009
1-3, 25	93.05	117.3	-36.4	0.020
1-3, 75	93.55	42.6	-65.0	0.018
1-3, 125	94.05	236.8	16.0	0.062
1-4, 25	94.55	261.3	-35.0	0.022
1-4, 75	95.05	255.5	-59.1	0.048
1-4, 125	95.55	258.2	-57.4	0.013
11-5, 25	96.05	130.2	-5.7	0.016
11-5, 75	96.55	244.7	42.9	0.053
11-5, 125	97.05	167.3	43.3	0.018
11-6, 25	97.55	295.8	-35.3	0.013
11-6, 25	97.55	295.2	-25.3	0.016
11-6, 75	98.05	243.2	2.4	0.009
11-6, 75	98.05	239.0	14.7	0.008
11-6, 125	98.55	295.2	-57.2	0.008
11-6, 125	98.55	333.1	-61.1	0.011
12-1, 125	100.65	319.5	-79.2	0.070
12-2, 25	101.15	142.3	-54.4	0.020
12-2, 75	101.65	157.8	-28.4	0.015
12-2, 75	101.65	166.3	-44.1	0.014
12-2, 75	101.65	157.8	-28.4	0.015
12-2, 125	102.15	1.5	-41.7	0.036
12-3, 25	102.65	118.8	14.5	0.009
12-3, 25	102.65	88.4	27.2	0.006
12-3, 75	103.15	276.6	14.5	0.032
12-3, 125	103.65	268.6	25.2	0.010
12-4, 25	104.15	172.8	48.8	0.007
12-4, 75	104.65	36.6	-11.0	0.006
12-4, 75	104.65	60.3	-5.9	0.006
12-4, 75	104.65	44.1	0.0	0.007
12-4, 125	105.15	115.2	-20.3	0.009
12-4, 125	105.15	107.8	-11.4	0.009
12-5, 25	105.65	172.4	-23.3	0.015
12-6, 25	107.15	202.5	67.5	0.159
12-6, 125	108.15	193.8	53.1	0.105
13-1, 25	109.25	167.0	72.0	0.017
13-1, 75	109.75	347.3	14.3	0.030
13-1, 125	110.25	225.9	37.8	0.018
13-2, 25	110.75	138.0	-19.3	0.011
13-2, 75	111.25	194.0	53.9	0.020
13-2, 125	111.75	263.7	37.6	0.027
13-3, 25	112.25	213.0	10.6	0.019
3, 75	112.75	233.1	-12.9	0.026
3, 125	113.25	284.7	18.6	0.019
4, 25	113.75	230.9	-21.1	0.065
4, 75	114.25	283.7	8.0	0.024
4, 125	114.75	272.9	2.7	0.024
, 25	115.25	280.4	-47.4	0.068
75	115.75	83.4	-4.0	0.016
125	116.25	287.9	18.7	0.025
, 25	116.75	300.8	22.9	0.020
125	117.75	222.1	20.7	0.110
75	119.05	97.7	18.8	0.087
125	119.55	271.9	53.3	0.012
25	120.05	273.7	62.4	0.041
75	120.55	303.4	-9.5	0.024
125	121.05	259.4	-27.7	0.024
25	121.55	349.8	23.4	0.045
75	122.05	322.5	2.5	0.018
125	122.55	242.1	6.8	0.020
25	123.05	279.0	1.8	0.018
75	123.55	269.5	10.1	0.021

Table 6. (Continued).

Core-Section (interval in cm)	Sub-bottom depth (m)	Declination (°)	Inclination (°)	Intensity (μG)
14-4, 125	124.05	263.1	33.2	0.019
14-5, 25	124.55	135.6	8.5	0.022
14-5, 75	125.05	265.0	11.1	0.020
14-5, 125	125.55	249.1	-69.3	0.491
14-6, 25	126.05	316.1	45.6	0.017
14-6, 75	126.55	247.3	26.4	0.019
14-6, 125	127.05	259.2	69.5	0.008
14-7, 25	127.55	90.1	-45.2	0.030
15-1, 75	128.35	323.5	41.9	0.007
15-1, 125	128.85	280.7	10.4	0.096
15-2, 25	129.35	334.7	4.2	0.026
15-2, 75	129.85	298.7	-41.8	0.025
15-2, 125	130.35	84.4	-50.9	0.016
15-3, 25	130.85	301.2	65.7	0.020
15-3, 75	131.35	176.7	-41.3	0.029
15-3, 125	131.85	201.9	44.5	0.017
15-4, 25	132.35	167.1	1.5	0.037
15-4, 75	132.85	212.5	26.6	0.012
15-4, 125	133.35	116.6	21.2	0.012
15-5, 25	133.85	347.1	33.4	0.009
15-5, 75	134.35	223.2	-86.2	0.038
15-5, 125	134.85	32.7	-30.4	0.610
15-6, 25	135.35	277.2	53.4	0.013
15-6, 75	135.85	241.5	-33.4	0.008
15-6, 125	136.35	210.0	52.2	0.012
15-7, 25	136.85	257.3	47.8	0.010
16-1, 30	137.20	312.1	66.5	0.019
16-1, 75	137.65	196.2	61.6	0.011
16-1, 125	138.15	6.8	5.1	0.015
16-2, 25	138.65	178.8	-73.8	0.007
16-2, 75	139.15	88.4	42.8	0.017
16-2, 125	139.65	270.5	72.2	0.061
16-3, 25	140.15	270.0	41.2	0.081
16-3, 75	140.65	110.1	-37.1	0.026
16-3, 125	141.15	182.0	10.8	0.009
16-4, 25	141.65	229.0	-35.5	0.003
16-4, 75	142.15	114.7	-23.5	0.119
16-4, 125	142.65	211.3	-40.0	0.007
16-5, 25	143.15	9.9	30.5	0.039
16-5, 75	143.65	350.5	-62.5	0.246
16-5, 125	144.15	313.3	-23.8	0.009
16-6, 25	144.65	56.0	-8.7	0.033
16-6, 75	145.15	246.5	-3.5	0.028
16-6, 125	145.65	195.4	17.2	0.016
16-7, 25	146.15	140.3	46.1	0.128
17-2, 125	148.95	150.7	43.7	0.025
17-3, 25	149.45	57.7	17.1	0.077
17-3, 75	149.95	193.7	-23.0	0.009
17-3, 75	149.95	181.0	-2.1	0.011
17-3, 125	150.45	9.9	23.0	0.028
17-4, 25	150.95	247.9	-31.1	0.091
17-4, 75	151.45	169.4	54.6	0.010
17-4, 125	151.95	121.3	80.5	0.006
17-5, 25	152.45	336.6	8.8	0.030
17-5, 75	152.95	87.6	17.1	0.052
17-5, 125	153.45	197.9	47.1	0.002
17-6, 25	153.95	205.9	21.5	0.017
17-6, 25	153.95	108.4	72.1	0.018
17-6, 125	154.95	241.9	-67.9	0.005
17-7, 25	155.45	219.1	-64.4	0.009
18-1, 125	156.75	277.8	28.4	0.008
18-2, 75	157.75	28.5	-57.2	0.015
18-3, 25	158.75	258.6	-2.9	0.023
18-3, 75	159.25	257.8	-17.5	0.013
18-3, 75	159.25	254.7	-26.7	0.014
18-3, 125	159.75	195.8	-4.6	0.012
18-4, 25	160.25	355.4	39.5	0.032
18-4, 75	160.75	146.2	2.5	0.009
18-4, 125	161.25	188.2	3.6	0.006
18-4, 125	161.25	177.7	17.1	0.006
18-5, 25	161.75	197.1	34.8	0.006
18-5, 75	162.25	315.9	-6.7	0.055
18-5, 125	162.75	222.7	15.9	0.011
18-6, 25	163.25	228.5	-34.8	0.004
18-6, 75	163.75	329.6	37.4	0.011
18-6, 125	164.25	218.2	-35.3	0.007

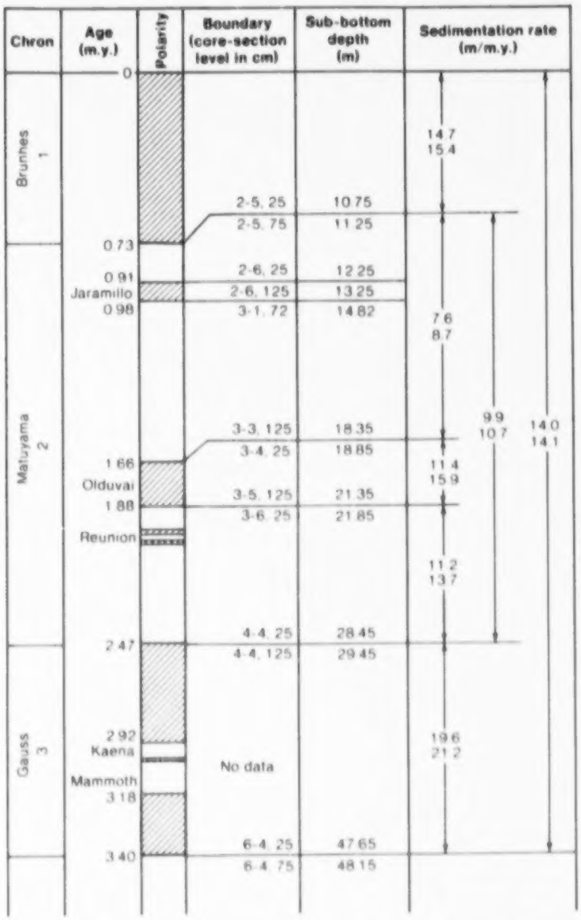

Figure 20. Reversal boundaries for the upper part of Hole 592 based on AF-cleaned (200 Oe) and filtered data. The polarity sequence is not defined below 60.4 m.

Table 7. AF-cleaned data, upper part of Hole 592.

Core-Section (interval in cm)	Sub-bottom depth (m)	Declination (°)	Inclination (°)	Intensity (μG)
1-1, 75	0.75	273.4	−39.4	0.092
1-1, 125	1.25	293.3	−45.1	0.035
1-2, 25	1.75	183.5	−54.2	0.095
1-2, 75	2.25	172.0	−64.6	0.065
1-2, 125	2.75	193.7	−63.6	0.090
1-3, 25	3.25	201.5	−32.4	0.013
1-3, 75	3.75	213.2	−44.3	0.025
1-3, 125	4.25	261.6	−74.8	0.030
2-1, 25	4.75	239.2	−4.1	0.029
2-1, 75	5.25	222.0	−61.2	0.041
2-1, 125	5.75	183.4	−18.4	0.031
2-2, 75	6.75	213.0	−55.4	0.043
2-2, 125	7.25	212.5	−34.7	0.035
2-3, 21	7.71	105.1	−32.8	0.027
2-3, 75	8.25	146.5	−57.8	0.118
2-3, 75	8.25	149.4	−54.0	0.131
2-3, 125	8.75	126.5	23.1	0.044
2-3, 125	8.75	131.4	17.7	0.048
2-4, 25	9.25	175.7	−49.6	0.060
2-4, 125	10.25	341.3	−16.3	0.014
2-5, 75	11.25	0.0	77.0	0.026
2-5, 125	11.75	300.1	44.4	0.0
2-6, 25	12.25	305.5	5.6	0.0
2-6, 125	13.25	159.8	−78.2	0.0
3-1, 72	14.82	189.7	63.9	0.0
3-1, 125	15.35	191.8	54.4	0.0
3-2, 25	15.85	341.9	47.8	0.0
3-2, 75	16.35	349.6	48.3	0.0
3-2, 125	16.85	186.2	49.5	0.1
3-3, 25	17.35	3.0	48.3	0.0
3-3, 75	17.85	36.1	46.2	0.0
3-3, 125	18.35	105.5	54.3	0.0
3-4, 25	18.85	30.5	−20.1	0.0
3-4, 75	19.35	78.5	−35.6	0.0
3-4, 125	19.85	6.9	−6.8	0.0
3-5, 25	20.35	354.7	3.3	0.0
3-5, 75	20.85	113.7	−36.6	0.0
3-5, 125	21.35	234.8	−13.6	0.0
3-6, 25	21.85	6.5	10.2	0.0
3-6, 75	22.35	73.4	36.5	0.0
3-6, 125	22.85	272.6	66.3	0.1
4-1, 75	24.45	319.7	61.9	0.0
4-1, 125	24.95	5.7	53.3	0.01
4-2, 75	25.95	16.1	58.5	0.02
4-2, 125	26.45	74.5	66.5	0.04
4-3, 125	27.95	41.1	12.6	0.02
4-4, 25	28.45	74.9	16.1	0.019
4-4, 125	29.45	243.4	−23.1	0.01
4-5, 75	30.45	169.3	−60.8	0.021
4-5, 125	30.95	283.4	−70.0	0.015
4-5, 125	30.95	281.8	−49.4	0.013
4-6, 25	31.45	254.9	−16.4	0.025
4-6, 75	31.95	195.3	−62.8	0.031
4-6, 125	32.45	274.7	−81.6	0.032
6-1, 75	43.65	188.0	−27.6	0.031
6-1, 125	44.15	143.4	−69.0	0.033
6-2, 25	44.65	258.1	−12.4	0.015
6-2, 75	45.15	248.2	38.2	0.023
6-2, 125	45.65	56.3	−76.5	0.005
6-3, 75	46.65	57.5	−76.7	0.013
6-3, 125	47.15	108.8	−55.8	0.008
6-4, 25	47.65	34.5	−19.7	0.011
6-4, 75	48.15	19.8	12.9	0.009
6-4, 125	48.65	179.2	−39.2	0.015
6-5, 25	49.15	265.2	9.7	0.015
6-5, 75	49.65	59.5	25.9	0.019
6-5, 125	50.15	160.5	37.2	0.010
6-6, 25	50.65	258.3	11.8	0.020
6-6, 75	51.15	158.1	7.7	0.022
6-6, 125	51.65	7.0	23.1	0.015
7-1, 25	52.75	146.9	58.6	0.012
7-1, 75	53.25	302.4	−18.3	0.122
7-1, 125	53.75	85.2	−40.0	0.011
7-2, 25	54.25	252.5	11.6	0.0
7-2, 75	54.75	104.0	−4.5	0.01
7-2, 125	55.25	344.6	−18.1	0.0
7-3, 25	55.75	93.0	17.5	0.0
7-3, 75	56.25	227.1	−0.7	0.0
7-3, 125	56.75	238.4	−46.5	0.0
7-4, 25	57.25	217.8	25.2	0.0
7-4, 75	57.75	162.8	−1.9	0.0
7-4, 125	58.25	144.7	13.2	0.0
7-5, 25	58.75	129.4	58.1	0.0
7-5, 75	59.25	158.8	15.2	0.
8-1, 25	62.35	236.3	5.1	0.
8-1, 30	62.40	287.0	−32.4	0.
8-1, 75	62.85	269.3	−70.4	0.
8-1, 125	63.35	193.2	26.1	0.
8-3, 75	65.85	108.4	−86.8	0.
8-4, 25	66.85	276.8	22.8	0.
8-4, 125	67.85	107.8	26.0	0.
8-5, 25	68.35	172.7	7.0	0.
8-5, 125	69.35	198.6	−55.6	0.
8-6, 25	69.85	300.2	−59.7	0.
8-6, 75	70.35	140.6	−80.4	0.
8-6, 125	70.85	149.4	32.5	0.

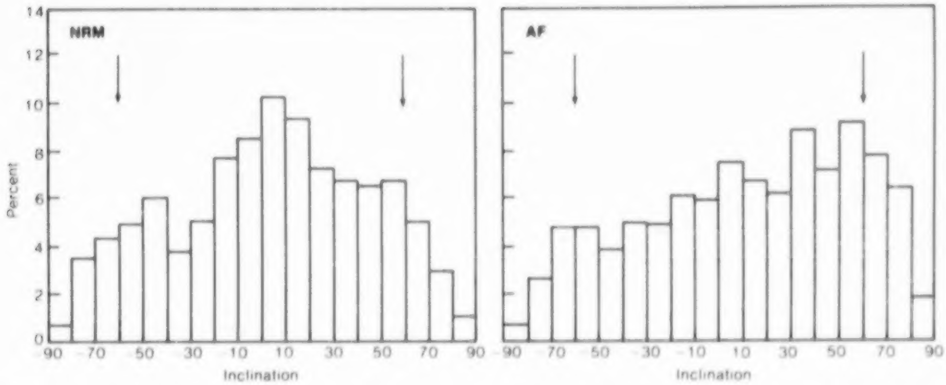

Figure 21. Distribution of inclinations for Hole 593 before and after AF cleaning at 200 Oe. The axial dipole inclination at the site is −59.7° (arrows). The positive bias after AF cleaning is caused by a long interval of reversed overprinting.

Table 8. Magnetic properties, Hole 593.

Magnetic zone	Depth (m)	Ranges J_N (μG)	 χ' (μG Oe^{-1})	 Q' (Oe)	Mean MDF (Oe)	Comment
A	0.0-0.45	1.4-2.3	2.2-3.2	0.63-0.89	~450	Strongly magnetized oxidized surface layer, Subunit IA
B	0.45-75	0.01-0.1	falls to 1	0.01-0.1	265 ± 168	J_N and χ' decrease gradually with depth, Q' initially drops to 0.035 at 0.75 m
C	75-360	0.005-0.02	0.5-1.5	.015-0.2	194 ± 111	Extremely weak magnetization
D	360-470	2-4	1-6	0.2-0.8	231 ± 115	Strongly magnetic, includes colored Subunit IC, very poor magnetic stability, high VRM coefficient
E	>470	0.01-0.1	0.5-1.5	0.02-0.5	221 ± 108	J_N, χ', and Q' increase with depth

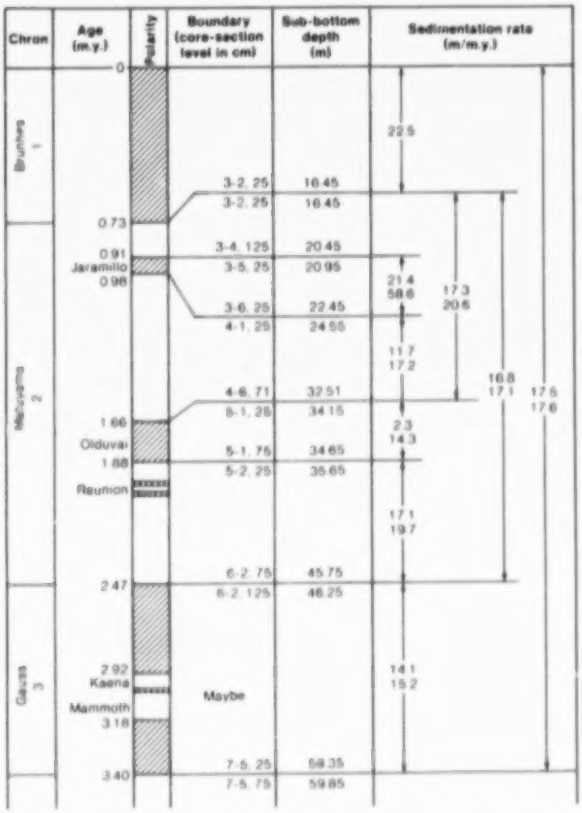
Chron
Age (m.y.)
Polarity
Boundary (core-section level in cm)
Sub-bottom depth (m)
Sedimentation rate (m/m.y.)
Brunhes 1
Matuyama 2
Gauss 3
0
0.73
0.91
Jaramillo
0.98
1.66
Olduvai
1.88
Reunion
2.47
2.92
Kaena
Mammoth
3.18
3.40
3-2, 25
3-2, 25
3-4, 125
3-5, 25
3-6, 25
4-1, 25
4-6, 71
5-1, 25
5-1, 75
5-2, 25
6-2, 75
6-2, 125
Maybe
7-5, 25
7-5, 75
16.45
16.45
20.45
20.95
22.45
24.55
32.51
34.15
34.65
35.65
45.75
46.25
58.35
59.85
22.5
21.4
58.6
17.3
20.6
11.7
17.2
16.8
17.1
17.5
17.6
2.3
14.3
17.1
19.7
14.1
15.2

Figure 22. Reversal boundaries for the upper part of the sequence in Hole 593, based on AF-cleaned (200 Oe) and filtered data. The pattern is duplicated in Hole 593A down to 63 m sub-bottom depth.

Table 9. AF-cleaned data, upper part of Hole 593 and Unit II.

Core-Section (interval in cm)	Sub-bottom depth (m)	Declination (°)	Inclination (°)	Intensity (μG)
1-1, 10	0.10	230.6	−57.6	1.107
1-1, 25	0.25	277.4	−49.2	1.530
1-1, 45	0.45	340.5	−51.4	1.088
1-1, 75	0.75	80.5	−76.8	0.050
1-1, 95	0.95	66.5	−39.8	0.023
1-1, 110	1.10	213.0	−9.4	0.080
1-2, 10	1.60	327.3	−57.8	0.018
1-2, 25	1.75	143.0	−57.6	0.046
1-2, 45	1.95	118.6	−79.5	0.041
1-2, 95	2.45	122.6	2.2	0.138
1-2, 110	2.60	146.4	−61.0	0.113
1-2, 125	2.75	111.6	−55.4	0.077
1-3, 25	3.25	314.8	−21.9	0.051
1-3, 25	3.25	310.6	−23.6	0.048
1-3, 50	3.50	170.3	−57.9	0.038
1-3, 75	3.75	171.2	−40.9	0.043
1-3, 95	3.95	194.9	−40.3	0.166
1-3, 125	4.25	189.6	−48.6	0.067
1-4, 25	4.75	178.0	−62.0	0.051
1-4, 25	4.75	248.4	−76.7	0.033
1-4, 50	5.00	190.5	−39.4	0.048
2-1, 75	5.85	353.9	−50.8	0.038
2-1, 125	6.35	94.4	−32.2	0.020
2-2, 25	6.85	184.8	−80.4	0.019
2-2, 75	7.35	150.7	−2.9	0.023
2-3, 25	8.35	304.8	−54.3	0.032
2-3, 75	8.85	274.1	−33.4	0.074
2-3, 125	9.35	332.0	−64.1	0.046
2-4, 25	9.85	318.9	−37.0	0.032
2-4, 75	10.35	37.7	−51.7	0.015
2-4, 125	10.85	312.4	−15.6	0.038
2-5, 25	11.35	302.6	−31.3	0.019
2-5, 75	11.85	269.1	−41.0	0.040
2-5, 125	12.35	318.2	−21.3	0.044
2-6, 25	12.85	323.5	−6.2	0.034
2-6, 75	13.35	323.6	6.3	0.005
2-6, 125	13.85	339.6	−23.1	0.02
3-1, 75	15.45	135.5	−55.0	0.034
3-2, 25	16.45	200.7	−30.4	0.028
3-2, 75	16.95	308.4	−7.6	0.01
3-2, 125	17.45	310.4	37.5	0.017
3-3, 25	17.95	288.6	37.5	0.03
3-3, 75	18.45	268.9	12.6	0.02
3-3, 125	18.95	280.7	43.0	0.08
3-4, 25	19.45	193.7	54.5	0.016
3-4, 75	19.95	1.7	47.8	0.018
3-4, 125	20.45	339.2	68.2	0.01
3-5, 25	20.95	72.2	−64.6	0.039
3-5, 68	21.38	182.8	−57.7	0.096
3-5, 125	21.95	164.7	−67.1	0.024
3-6, 25	22.45	78.6	−63.4	0.027
3-6, 75	22.95	183.0	−57.2	0.016
3-6, 125	23.45	146.6	−35.4	0.014
4-1, 25	24.55	269.4	61.4	0.163
4-1, 75	25.05	112.6	−8.1	0.179
4-1, 125	25.55	225.6	63.7	0.022
4-2, 25	26.05	249.0	73.0	0.030
4-2, 75	26.55	223.2	32.9	0.042
4-2, 125	27.05	315.2	74.7	0.029
4-3, 25	27.55	282.9	35.0	0.025
4-3, 75	28.05	129.7	66.3	0.020
4-3, 125	28.55	81.4	10.5	0.170
4-4, 25	29.05	103.7	55.8	0.038
4-4, 75	29.55	136.2	33.5	0.031
4-4, 125	30.05	77.3	47.7	0.049
4-5, 25	30.55	305.3	39.4	0.047
4-5, 25	30.55	320.5	34.8	0.057
4-5, 75	31.05	330.6	48.9	0.024
4-5, 75	31.05	341.6	52.7	0.025
4-5, 125	31.55	319.8	62.2	0.015
4-5, 125	31.55	319.7	65.2	0.016
4-6, 25	32.05	356.2	23.1	0.034
4-6, 71	32.51	330.1	39.6	0.043
5-1, 25	34.15	322.1	−18.9	0.042
5-1, 75	34.65	254.4	−53.9	0.036
5-2, 25	35.65	71.2	76.8	0.009
5-2, 75	36.15	115.3	49.9	0.031
5-2, 125	36.65	233.8	28.8	0.019
5-3, 25	37.15	310.2	−13.7	0.01
5-3, 75	37.65	103.9	68.1	0.03
5-3, 125	38.15	159.5	68.8	0.02
5-4, 25	38.65	114.7	−57.9	0.029
5-4, 75	39.15	106.2	68.0	0.02
5-4, 125	39.65	166.2	62.4	0.02
5-5, 25	40.15	284.7	68.7	0.02
5-5, 75	40.65	148.3	63.7	0.03
5-5, 125	41.15	277.9	21.4	0.03
5-6, 25	41.65	41.8	−39.5	0.00
5-6, 75	42.15	155.8	74.9	0.01
5-6, 125	42.65	138.6	6.2	0.1
6-1, 75	44.25	293.3	39.7	0.01
6-1, 125	44.75	26.7	70.5	0.0
6-2, 25	45.25	293.4	2.0	0.0
6-2, 75	45.75	359.1	23.2	0.0
6-2, 125	46.25	336.8	−2.3	0.1
6-3, 25	46.75	275.4	−37.3	0.0
6-3, 75	47.25	261.7	−16.3	0.0
6-3, 121	47.71	224.3	−63.7	0.0
6-3, 125	47.75	164.6	36.1	0.0
6-4, 25	48.25	328.9	−69.9	0.0
6-4, 75	48.75	153.9	−67.6	0.0
6-4, 125	49.25	110.7	−62.3	0.0
6-4, 125	49.25	110.9	−61.6	0.0
6-5, 25	49.75	304.4	−60.5	0.0

Table 9. (Continued).

Core-Section (interval in cm)	Sub-bottom depth (m)	Declination (°)	Inclination (°)	Intensity (μG)
6-5, 75	50.25	135.8	−45.7	0.030
6-5, 125	50.75	231.5	−4.5	0.022
6-6, 25	51.25	242.2	−37.7	0.025
6-6, 75	51.75	205.7	2.2	0.010
6-6, 125	52.25	236.2	−53.3	0.039
7-1, 75	53.85	1.0	−26.1	0.038
7-2, 75	55.35	250.1	−74.5	0.021
7-3, 75	56.85	294.1	−25.9	0.014
7-4, 75	58.35	318.4	−61.2	0.015
7-4, 124	58.84	27.8	−26.0	0.018
7-5, 25	59.35	262.5	−12.7	0.022
7-5, 75	59.85	279.8	40.7	0.026
7-5, 125	60.35	279.7	54.7	0.013
7-6, 25	60.85	85.7	−23.9	0.051
7-6, 75	61.35	283.6	34.0	0.020
7-6, 125	61.85	215.1	18.8	0.013
8-2, 25	64.45	180.0	−66.1	0.009
8-2, 75	64.95	245.0	−50.3	0.012
9-1, 75	73.05	207.7	−23.4	0.011
9-1, 125	73.55	271.7	−4.3	0.013
9-2, 25	74.05	162.6	67.8	0.074
9-2, 75	74.55	140.6	40.1	0.008
9-2, 125	75.05	215.0	23.1	0.008
9-3, 75	76.05	246.0	45.4	0.006
8-3, 125	76.55	229.3	47.7	0.016
9-3, 125	76.55	200.5	29.4	0.012
9-4, 25	77.05	102.3	−55.6	0.174
9-4, 75	77.55	231.8	3.1	0.011
9-4, 125	78.05	18.2	−75.0	0.806
9-5, 25	78.55	164.8	29.8	0.003
9-5, 25	78.55	169.1	37.1	0.004
9-5, 75	79.05	212.2	−13.8	0.009
9-5, 125	79.55	29.4	19.4	0.029
9-6, 25	80.05	141.5	6.5	0.065
58-1, 25	542.95	158.5	−60.2	0.618
58-1, 75	543.45	40.0	17.3	0.008
58-1, 125	543.95	93.1	−5.7	0.029
58-2, 25	544.45	293.1	13.6	0.024
58-2, 85	545.05	224.7	−12.9	0.025
58-2, 125	545.45	212.1	−28.0	0.044
58-3, 72	546.42	66.0	51.0	2.039
59-1, 94	553.24	353.0	67.0	9.320
59-2, 132	555.12	315.0	79.0	8.102
59-3, 50	555.80	340.0	81.0	5.545
59-3, 132	556.62	132.0	61.0	4.734
59-5, 65	558.95	33.0	−62.0	0.179
59-5, 100	559.30	343.0	30.0	0.303
59,CC 10	560.20	126.0	18.0	0.030
60-1, 25	562.15	253.4	6.9	0.016
60-1, 78	562.68	99.3	−20.9	0.034
60-1, 125	563.15	99.4	−55.0	0.071
60-2, 25	563.65	281.4	−59.5	0.265
60-2, 75	564.15	232.0	−39.0	0.078
60-2, 84	564.24	258.8	−17.7	0.024
60-2, 125	564.65	272.0	75.5	0.009
60-3, 25	565.15	102.9	10.4	0.019
60-3, 75	565.65	175.5	−28.1	0.006
60-3, 125	566.15	258.0	33.7	0.022
60-4, 25	566.65	209.5	59.7	0.015
60-4, 70	567.10	69.9	11.9	0.014
60-4, 125	567.65	190.7	−13.3	0.012
60-5, 75	568.65	111.8	−67.5	0.008
60-5, 125	569.15	195.2	−47.0	0.011
60-6, 25	569.65	84.7	1.4	0.077

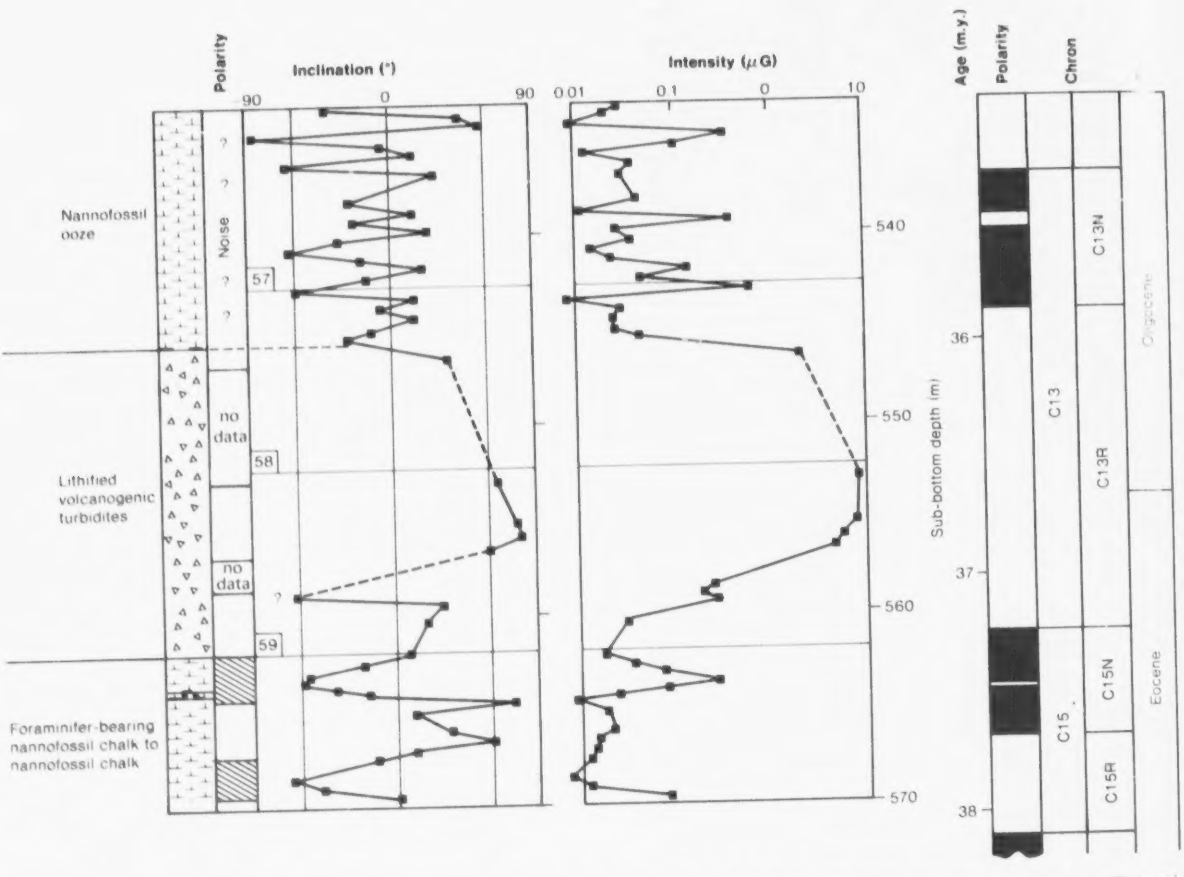

Figure 23. Inclination and intensity data in the vicinity of the volcanogenic turbidite beds in Hole 593, which are thought to mark the Eocene/Oligocene boundary. Core numbers are shown in boxes. Shaded regions are normal polarity. The magnetic polarity time scale is that of Berggren et al. (in press).

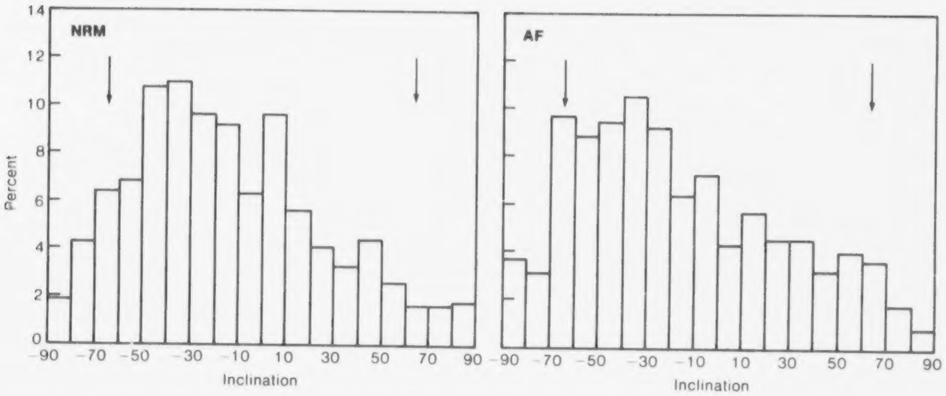

Figure 24. Distribution of inclinations for Hole 594 before and after AF cleaning at 150 Oe. The axial dipole inclination for the site is −63.8° (arrows).

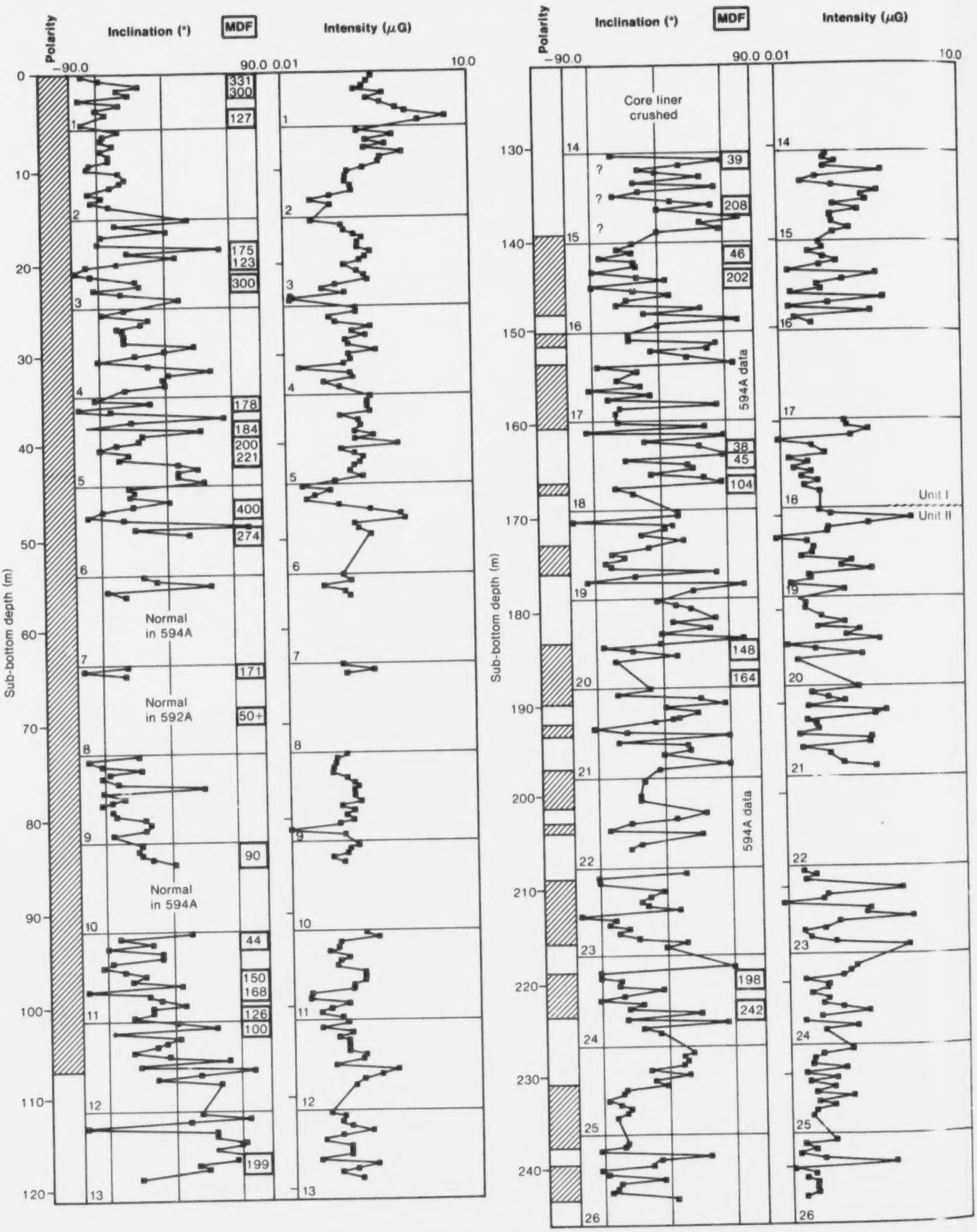

Figure 25. Inclination and intensity data for Hole 594, after AF cleaning at 150 Oe. The polarity record below 360 m is unresolved. Data from Hole 594A have been used to fill in some of the gaps in the record from Hole 594.

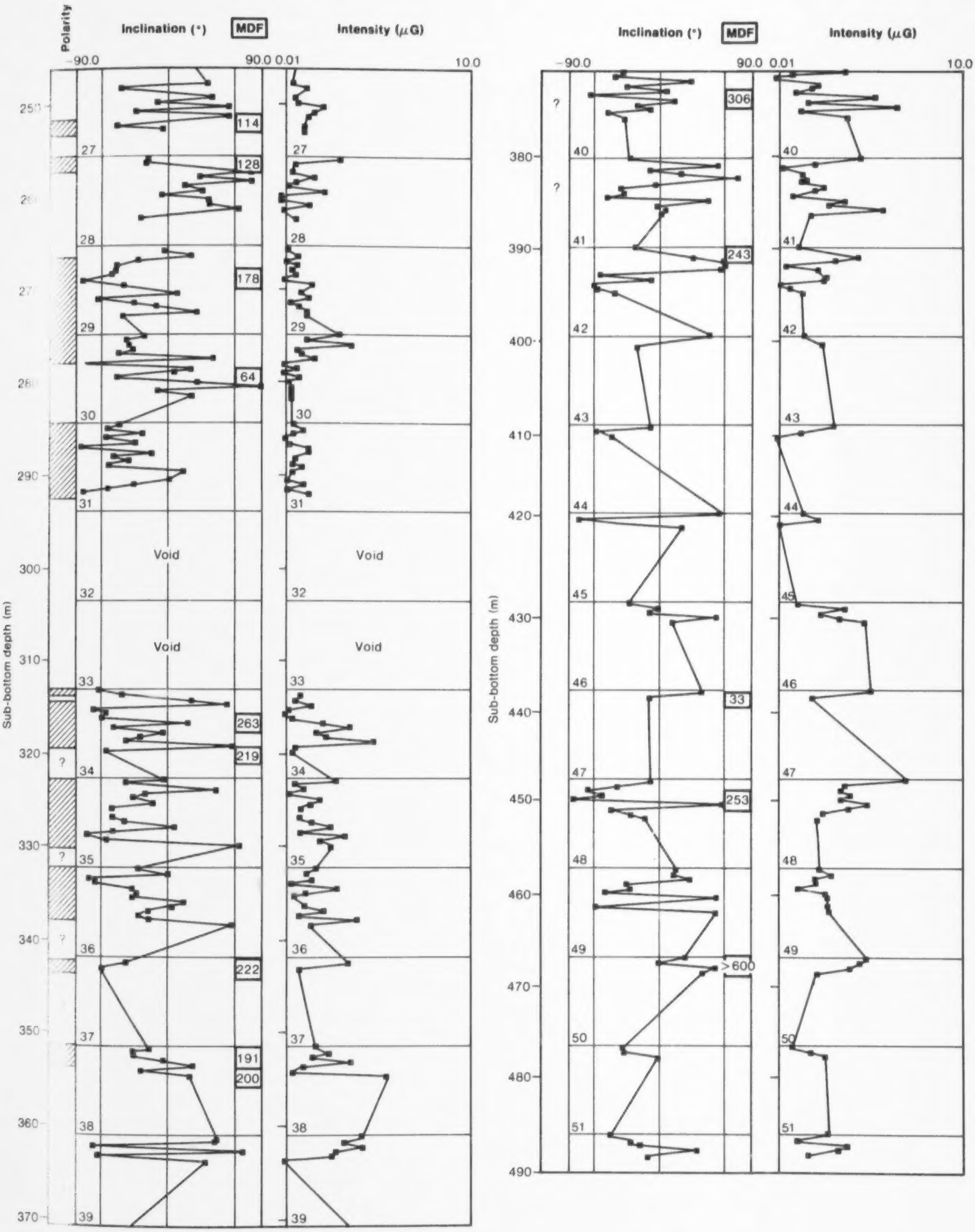

Figure 25 (Continued).

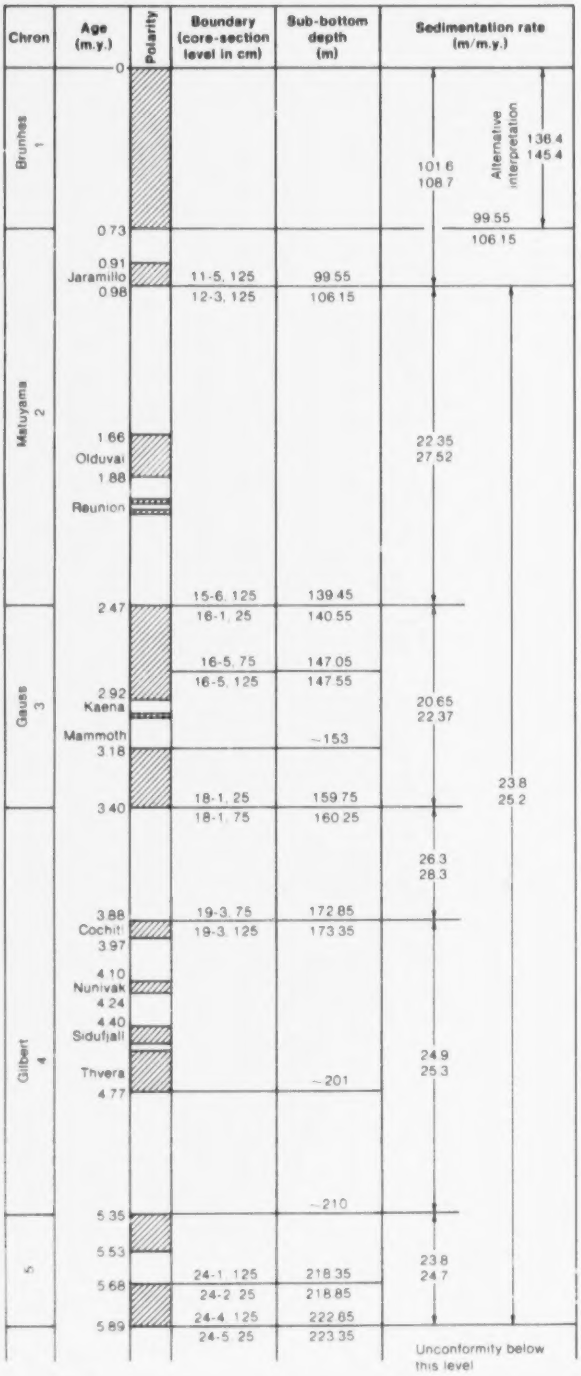
Chron
Age (m.y.)
Polarity
Boundary (core-section level in cm)
Sub-bottom depth (m)
Sedimentation rate (m/m.y.)
Brunhes 1
Matuyama 2
Gauss 3
Gilbert 4
5
0
0.73
0.91
Jaramillo
0.98
1.66
Olduvai
1.88
Reunion
2.47
2.92
Kaena
Mammoth
3.18
3.40
3.88
Cochiti
3.97
4.10
Nunivak
4.24
4.40
Sidufjall
Thvera
4.77
5.35
5.53
5.68
5.89
11-5, 125
12-3, 125
15-6, 125
16-1, 25
16-5, 75
16-5, 125
18-1, 25
18-1, 75
19-3, 75
19-3, 125
24-1, 125
24-2, 25
24-4, 125
24-5, 25
99.55
106.15
139.45
140.55
147.05
147.55
~153
159.75
160.25
172.85
173.35
~201
~210
218.35
218.85
222.85
223.35
101.6
108.7
Alternative interpretation
136.4
145.4
99.55
106.15
22.35
27.52
20.65
22.37
23.8
25.2
26.3
28.3
24.9
25.3
23.8
24.7
Unconformity below this level

Figure 26. Reversal boundaries and sedimentation rates for Hole 594.

Table 10. AF-cleaned data, upper 38 cores of Hole 594.

Core-Section (interval in cm)	Sub-bottom depth (m)	Declination (°)	Inclination (°)	Intens (μG
1-1, 25	0.25	126.0	−75.4	0.28
1-1, 75	0.75	212.0	−61.0	0.2
1-1, 125	1.25	218.1	−20.6	0.20
1-2, 25	1.75	206.1	−46.6	0.14
1-2, 75	2.25	246.8	−33.6	0.4
1-2, 125	2.75	127.4	−84.4	0.2
1-3, 25	3.25	202.2	−41.7	0.3
1-3, 75	3.75	187.5	−67.3	0.6
1-3, 125	4.25	245.0	−56.1	0.8
1-4, 25	4.75	202.3	−67.3	4.4
1-4, 75	5.25	215.4	−83.1	1.4
1-4, 75	5.25	215.0	−83.0	1.4
2-1, 25	6.15	291.8	−43.5	0.1
2-1, 75	6.65	288.2	−58.8	0.62
2-1, 125	7.15	348.4	−63.6	0.20
2-2, 25	7.65	353.4	−49.5	0.44
2-2, 75	8.15	294.2	−61.5	0.17
2-2, 125	8.65	245.1	−53.2	0.85
2-3, 25	9.15	147.1	−52.8	0.31
2-3, 75	9.65	358.6	−74.1	0.34
2-3, 125	10.15	279.0	−76.1	0.19
2-4, 25	10.65	270.9	−44.0	0.10
2-4, 75	11.15	321.5	−38.3	0.090
2-4, 125	11.65	333.5	−42.0	0.092
2-5, 25	12.15	239.4	−51.3	0.111
2-5, 75	12.65	334.1	−74.6	0.129
2-5, 125	13.15	195.9	−60.9	0.051
2-6, 25	13.65	102.6	−73.7	0.026
2-6, 75	14.15	196.9	−53.8	0.053
3-1, 25	15.75	168.7	22.5	0.027
3-1, 75	16.25	189.2	−48.5	0.078
3-1, 125	16.75	158.1	0.9	0.083
3-2, 25	17.25	289.8	−61.2	0.131
3-2, 75	17.75	121.8	−62.4	0.176
3-2, 125	18.25	100.6	−66.7	0.144
3-3, 25	18.75	160.6	55.1	0.138
3-3, 75	19.25	105.0	−35.0	0.216
3-3, 125	19.75	231.9	15.1	0.192
3-4, 25	20.25	108.6	−43.7	0.150
3-4, 75	20.75	128.9	−79.9	0.090
3-4, 125	21.25	12.1	−89.1	0.147
3-5, 25	21.75	151.2	−72.8	0.182
3-5, 75	22.25	187.4	−26.4	0.213
3-5, 125	22.75	142.6	−22.7	0.065
3-6, 25	23.25	245.3	−69.9	0.040
3-6, 75	23.75	336.9	−41.9	0.094
3-6, 125	24.25	286.9	18.6	0.011
4-1, 25	25.35	145.2	−40.1	0.145
4-1, 75	25.85	168.2	−63.2	0.139
4-1, 125	26.35	225.4	−16.6	0.048
4-2, 25	26.85	169.7	−24.3	0.064
4-2, 75	27.35	158.1	−47.6	0.241
4-2, 125	27.85	178.3	−42.2	0.115
4-3, 25	28.35	186.0	−40.8	0.184
4-3, 75	28.85	273.8	−41.3	0.08
4-3, 125	29.35	355.2	30.5	0.09
4-4, 25	29.85	303.3	−3.5	0.30
4-4, 75	30.35	209.7	−29.6	0.0
4-4, 125	30.85	261.9	−65.3	0.10
4-5, 25	31.35	251.9	−17.6	0.07
4-5, 75	31.85	88.2	42.5	0.0
4-5, 125	32.35	211.6	2.0	0.1
4-6, 25	32.85	247.7	−5.1	0.1
4-6, 75	33.35	45.5	−1.0	0.0
4-6, 122	33.82	40.6	−39.6	0.0
5-1, 25	34.95	55.7	−70.1	0.2
5-1, 75	35.45	124.6	−15.8	0.1
5-1, 125	35.95	328.3	−88.7	0.1
5-2, 22	36.42	262.7	−57.2	0.2
5-2, 75	36.95	202.5	55.8	0.0
5-2, 125	37.45	137.1	−35.8	0.1
5-3, 25	37.95	284.7	−80.6	0.1
5-3, 75	38.45	199.8	35.6	0.12
5-3, 125	38.95	282.5	−23.1	0.2
5-4, 25	39.45	121.0	−26.0	0.1
5-4, 75	39.95	64.0	−51.0	0.63
5-4, 125	40.45	180.5	−65.9	0.069

Table 10. (Continued).

Core-Section (interval in cm)	Sub-bottom depth (m)	Declination (°)	Inclination (°)	Intensity (μG)
5-[illegible], 25	40.95	95.9	−36.9	0.121
5-[illegible], 75	41.45	57.3	−46.4	0.171
5-[illegible], 125	41.95	85.4	13.0	0.146
5-[illegible], 25	42.45	114.9	31.1	0.112
5-[illegible], 75	42.95	219.4	9.6	0.101
5-[illegible], 125	43.45	308.1	9.2	0.162
5-[illegible], 25	43.95	295.7	36.8	0.057
6-[illegible], 28	44.58	18.0	−37.9	0.016
6-[illegible], 75	45.05	184.2	−32.4	0.049
6-[illegible], 125	45.55	98.5	−38.2	0.027
6-[illegible], 25	46.05	213.3	3.8	0.020
6-[illegible], 75	46.55	295.9	−34.5	0.065
6-[illegible], 125	47.05	281.6	−64.7	0.199
6-[illegible], 25	47.55	308.0	−81.0	0.720
6-[illegible], 75	48.05	345.0	−43.0	0.854
6-[illegible], 125	48.55	137.5	82.4	0.109
6-[illegible], 25	49.05	222.3	−33.4	0.129
6-[illegible], 74	49.54	249.2	21.2	0.210
[illegible], 25	54.15	201.3	−23.9	0.069
[illegible], 75	54.65	210.4	−10.5	0.105
7-1, 125	55.15	210.1	42.9	0.032
7-[illegible], 25	55.65	9.7	−61.9	0.084
7-2, 75	56.15	101.8	−42.5	0.102
8-1, 25	63.75	358.5	−39.9	0.065
8-1, 75	64.25	58.7	−84.2	0.253
8-1, 125	64.75	274.0	−42.0	0.078
9-1, 25	73.35	7.0	−29.8	0.072
9-1, 75	73.85	348.6	−80.0	0.055
9-1, 125	74.35	349.5	−68.3	0.053
9-2, 25	74.85	47.9	−27.9	0.046
9-2, 75	75.35	312.9	−61.9	0.045
9-2, 125	75.85	40.6	−67.1	0.077
9-3, 25	76.35	220.7	−52.7	0.106
9-3, 75	76.85	121.5	32.0	0.119
9-3, 125	77.35	354.3	−66.7	0.100
9-4, 25	77.85	286.4	−43.2	0.099
9-4, 75	78.35	240.9	−59.1	0.140
9-4, 125	78.85	92.0	−66.0	0.062
9-5, 25	79.35	293.1	−55.8	0.106
9-5, 75	79.85	280.6	−53.7	0.074
9-5, 125	80.35	235.1	−23.9	0.105
9-6, 25	80.85	232.2	−18.9	0.058
9-6, 75	81.35	163.7	−24.6	0.008
9-6, 125	81.85	159.5	−58.7	0.067
10-1, 25	82.95	157.7	−27.3	0.117
10-1, 75	83.45	217.6	−31.8	0.086
10-1, 125	83.95	310.7	−31.1	0.081
10-2, 25	84.45	239.1	−19.5	0.044
10-2, 75	84.95	67.7	3.5	0.063
11-1, 25	92.55	161.6	18.0	0.155
11-1, 75	93.05	234.4	−51.3	0.247
11-1, 125	93.55	292.6	−17.3	0.053
11-2, 25	94.05	313.2	−63.4	0.052
11-2, 75	94.55	250.1	−10.4	0.037
11-2, 125	95.05	145.7	−8.7	0.073
11-3, 25	95.55	116.0	−57.8	0.054
11-3, 75	96.05	326.1	−68.6	0.049
11-[illegible], 125	96.55	312.7	−46.4	0.132
11-[illegible], 25	97.05	198.7	−26.4	0.137
11-[illegible], 75	97.55	232.3	−40.0	0.144
11-[illegible], 125	98.05	143.0	9.0	0.089
11-[illegible], 25	98.55	109.0	−84.5	0.093
11-[illegible], 75	99.05	120.9	−23.3	0.018
11-[illegible], 125	99.55	29.4	−12.5	0.017
11-[illegible], 25	100.05	219.6	11.8	0.081
11-[illegible], 75	100.55	222.7	−20.7	0.038
11-[illegible], 125	101.05	172.6	−20.3	0.026
11-[illegible], 25	101.55	272.8	−38.5	0.056
12-[illegible], 25	102.15	199.0	2.8	0.079
12-[illegible], 75	102.65	160.0	43.0	0.027
12-[illegible], 125	103.15	349.1	−60.5	0.079
12-[illegible], 25	103.65	238.5	5.6	0.053
12-[illegible], 75	104.15	20.3	−7.9	0.075
12-[illegible], 125	104.65	236.8	−16.4	0.072
12-[illegible], 25	105.15	244.2	−40.7	0.082
12-[illegible], 75	105.65	179.3	−3.8	0.134
12-[illegible], 125	106.15	213.2	51.9	0.123

Table 10. (Continued).

Core-Section (interval in cm)	Sub-bottom depth (m)	Declination (°)	Inclination (°)	Intensity (μG)
12-4, 25	106.65	247.4	−34.8	0.044
12-4, 75	107.15	226.4	77.9	0.421
12-4, 125	107.65	226.4	24.1	0.242
12-5, 25	108.15	213.6	−21.8	0.121
12-5, 75	108.65	189.3	44.9	0.092
13-1, 25	111.75	251.0	25.3	0.035
13-1, 75	112.25	275.9	74.5	0.061
13-1, 125	112.75	270.2	14.6	0.050
13-2, 25	113.25	107.0	−86.6	0.072
13-2, 75	113.75	237.7	39.4	0.185
13-2, 125	114.25	235.0	39.3	0.053
13-3, 25	114.75	130.9	65.4	0.028
13-3, 75	115.23	130.6	62.5	0.074
13-3, 125	115.75	55.3	37.0	0.076
13-4, 25	116.25	20.7	69.5	0.074
13-4, 75	116.75	123.4	61.5	0.023
13-4, 125	117.25	331.8	22.5	0.220
13-5, 25	117.75	221.3	32.4	0.095
13-5, 75	118.25	267.0	0.9	0.047
13-5, 125	118.75	318.3	−34.3	0.115
15-1, 25	130.95	122.5	−48.4	0.060
15-1, 75	131.45	117.7	72.8	0.056
15-1, 125	131.95	157.8	23.4	0.087
15-2, 25	132.45	344.8	−17.5	0.052
15-2, 75	132.95	148.5	−0.4	0.510
15-2, 125	133.45	207.6	44.9	0.039
15-3, 25	133.95	205.6	−23.4	0.022
15-3, 75	134.45	280.9	57.7	0.073
15-3, 125	134.95	322.1	−16.5	0.470
15-4, 25	135.45	357.3	−42.5	0.226
15-4, 75	135.95	1.7	15.0	0.287
15-4, 125	136.45	102.9	54.5	0.076
15-5, 25	136.95	339.1	−1.5	0.214
15-5, 75	137.45	267.2	61.4	0.068
15-5, 125	137.95	130.7	78.8	0.069
15-6, 25	138.45	198.7	40.3	0.075
15-6, 75	138.95	310.5	63.1	0.140
15-6, 125	139.45	226.1	−0.9	0.074
16-1, 25	140.55	262.1	−23.6	0.044
16-1, 75	141.05	279.0	−38.1	0.049
16-1, 125	141.55	176.8	−24.1	0.032
16-2, 25	142.05	222.2	−59.0	0.056
16-2, 75	142.55	300.1	−22.2	0.082
16-2, 125	143.05	72.0	−20.0	0.048
16-3, 25	143.55	39.7	−62.2	0.015
16-3, 75	144.05	167.5	−19.3	0.402
16-3, 125	144.55	285.4	8.0	0.105
16-4, 25	145.05	0.1	−64.8	0.042
16-4, 75	145.55	301.0	−23.5	0.048
16-4, 125	146.05	111.4	11.9	0.015
16-5, 25	146.55	277.6	−31.3	0.518
16-5, 75	147.05	85.2	−42.4	0.064
16-5, 125	147.55	149.2	38.7	0.014
16-6, 25	148.05	96.8	−12.8	0.329
16-6, 75	148.55	70.1	79.1	0.017
16-6, 125	149.05	272.3	−3.4	0.032
18-1, 25	159.75	194.5	−41.0	0.104
18-1, 75	160.25	353.0	42.6	0.118
18-1, 125	160.75	95.4	−70.9	0.264
18-2, 25	161.25	116.3	62.4	0.134
18-2, 75	161.75	256.5	−15.3	0.009
18-2, 125	162.25	272.3	35.8	0.031
18-3, 25	162.75	241.5	−40.7	0.005
18-3, 75	163.25	155.7	66.9	0.053
18-3, 125	163.75	179.5	−34.3	0.012
18-4, 25	164.25	236.7	27.4	0.026
18-4, 75	164.75	284.4	34.6	0.014
18-4, 125	165.25	100.3	−10.2	0.027
18-5, 25	165.75	154.3	40.3	0.021
18-5, 75	166.25	169.2	59.4	0.041
18-5, 125	166.75	132.4	−44.8	0.023
18-6, 25	167.25	161.6	−28.8	0.041
19-1, 25	169.35	210.9	14.3	0.040
19-1, 75	169.85	105.7	14.7	0.061
19-1, 125	170.35	315.7	−86.4	1.215
19-2, 25	170.85	265.6	13.6	0.233
19-2, 75	171.35	97.8	3.3	0.057

Table 10. (Continued).

Core-Section (interval in cm)	Sub-bottom depth (m)	Declination (°)	Inclination (°)	Intensity (μG)
19-2, 125	171.85	326.5	−24.7	0.050
19-3, 25	172.35	309.8	21.6	0.008
19-3, 75	172.85	257.7	−2.2	0.026
19-3, 125	173.35	332.2	−13.6	0.030
19-4, 25	173.85	161.0	−51.7	0.028
19-4, 75	174.35	334.6	−35.5	0.021
19-4, 125	174.85	73.9	−58.1	0.129
19-5, 25	175.35	125.9	−51.7	0.086
19-5, 75	175.85	170.7	52.4	0.297
19-5, 125	176.35	80.3	−29.9	0.023
19-6, 25	176.85	114.0	−74.8	0.028
19-6, 75	177.35	289.9	78.8	0.012
19-6, 125	177.85	236.2	31.8	0.101
20-1, 25	178.95	0.3	−5.6	0.016
20-1, 75	179.45	231.7	10.8	0.022
20-1, 125	179.95	241.8	29.4	0.020
20-2, 25	180.45	351.6	−34.8	0.006
20-2, 75	180.95	148.8	48.4	0.043
20-2, 125	181.45	44.2	11.2	0.095
20-3, 25	181.95	102.2	46.8	0.031
20-3, 75	182.45	168.2	−4.3	0.163
20-3, 125	182.95	131.0	77.6	0.088
20-4, 25	183.45	233.9	−2.9	0.416
20-4, 75	183.95	256.5	−62.9	0.010
20-4, 125	184.45	98.7	−31.1	0.028
20-5, 25	184.95	146.5	14.8	0.189
20-5, 75	185.45	209.7	−47.6	0.015
21-1, 25	188.55	338.8	−12.4	0.153
21-1, 75	189.05	251.8	−52.1	0.025
21-1, 125	189.55	63.8	35.0	0.045
21-2, 25	190.05	139.0	57.7	0.094
21-2, 75	190.55	187.9	−3.2	0.020
21-2, 125	191.05	274.3	31.5	0.487
21-3, 25	191.55	179.2	13.3	0.266
21-3, 75	192.05	257.6	−11.5	0.021
21-3, 125	192.55	191.8	−71.8	0.032
21-4, 25	193.05	352.1	−35.9	0.033
21-4, 75	193.55	179.7	61.1	0.016
21-4, 125	194.05	207.0	−47.5	0.250
21-5, 25	194.55	226.9	21.0	0.210
21-5, 75	195.05	216.5	23.7	0.018
21-5, 125	195.55	17.0	−2.9	0.052
21-6, 75	196.55	174.2	63.1	0.078
21-6, 125	197.05	36.5	−6.9	0.289
23-1, 75	208.25	239.9	17.6	0.017
23-1, 125	208.75	340.9	−68.5	0.026
23-2, 25	209.25	243.6	−67.2	0.019
23-2, 75	209.75	300.7	−37.4	0.007
23-2, 125	210.25	314.6	−2.7	0.760
23-3, 25	210.75	347.1	−18.8	0.042
23-3, 75	211.25	87.7	−25.9	0.036
23-3, 125	211.75	180.3	−20.4	0.008
23-4, 25	212.25	230.9	14.6	0.210
23-4, 75	212.75	113.4	−85.8	0.170
23-4, 125	213.25	311.4	−50.7	1.098
23-5, 25	213.75	158.6	−57.7	0.064
23-5, 75	214.25	131.0	−38.4	0.040
23-5, 125	214.75	267.7	−47.0	0.015
23-6, 25	215.25	1.4	−28.0	0.021
23-6, 75	215.75	126.6	18.2	0.049
23-6, 125	216.25	195.8	−4.2	0.940
24-1, 125	218.35	283.6	67.2	0.118
24-2, 25	218.85	200.1	−66.5	0.095
24-2, 75	219.35	272.5	−67.7	0.076
24-2, 125	219.85	157.3	−46.7	0.015
24-3, 25	220.35	173.6	−51.8	0.041
24-3, 75	220.85	123.7	−5.2	0.038
24-3, 125	221.35	287.6	−42.6	0.022
24-4, 25	221.85	132.6	−66.9	0.043
24-4, 75	222.35	234.6	−23.6	0.035
24-4, 125	222.85	170.9	−40.8	0.076
24-5, 25	223.35	244.3	34.1	0.199
24-5, 75	223.85	206.2	−39.3	0.030
24-5, 125	224.35	251.6	57.2	0.016
24-6, 25	224.85	155.4	−29.5	0.119
24-6, 75	225.35	151.7	−10.2	0.033
25-1, 75	227.45	91.8	23.4	0.111

Table 10. (Continued).

Core-Section (interval in cm)	Sub-bottom depth (m)	Declination (°)	Inclination (°)	Intensity (μG)
25-1, 125	227.95	264.9	10.5	0.0[illegible]0
25-2, 25	228.45	253.6	16.2	0.0[illegible]1
25-2, 75	228.95	73.8	13.2	0.0[illegible]0
25-2, 125	229.45	240.9	−18.9	0.0[illegible]8
25-3, 25	229.95	182.3	17.0	0.0[illegible]7
25-3, 75	230.45	272.0	−16.4	0.0[illegible]6
25-3, 125	230.95	98.2	−4.9	0.0[illegible]0
25-4, 25	231.45	343.6	−44.4	0.0[illegible]6
25-4, 75	231.95	168.6	−45.5	0.0[illegible]5
25-4, 125	232.45	201.4	−61.8	0.0[illegible]5
25-5, 25	232.95	207.5	−50.7	0.0[illegible]7
25-5, 75	233.45	178.0	−42.2	0.0[illegible]2
25-5, 125	233.95	178.8	−42.8	0.0[illegible]5
25-6, 25	234.45	153.4	−53.7	0.0[illegible]1
26-1, 75	237.05	177.9	−41.4	0.0[illegible]8
26-1, 125	237.55	227.1	−42.0	0.0[illegible]4
26-2, 25	238.05	238.4	−71.5	0.0[illegible]3
26-2, 75	238.55	263.8	41.0	0.0[illegible]2
26-2, 125	239.05	216.0	−10.8	0.0[illegible]2
26-3, 25	239.55	252.4	−18.7	0.0[illegible]1
26-3, 75	240.05	217.3	−69.1	0.0[illegible]2
26-3, 125	240.55	82.1	−61.2	0.0[illegible]2
26-4, 25	241.05	174.9	−6.1	0.016
26-4, 75	241.55	321.6	−52.1	0.025
26-4, 125	242.05	107.0	−52.7	0.022
26-5, 25	242.55	178.1	−60.5	0.024
26-5, 75	243.05	190.3	5.5	0.016
27-2, 25	247.65	25.4	38.7	0.011
27-2, 75	248.15	239.4	−49.0	0.020
27-2, 125	248.65	199.5	−33.7	0.006
27-3, 25	249.15	169.9	44.1	0.012
27-3, 75	249.65	244.2	−11.3	0.014
27-3, 125	250.15	232.4	60.7	0.040
27-4, 25	250.65	155.5	−32.3	0.025
27-4, 75	251.15	66.1	66.2	0.020
27-4, 125	251.65	211.2	34.6	0.007
27-5, 25	252.15	270.4	−50.3	0.017
27-5, 75	252.65	219.8	−6.3	0.018
27-5, 125	253.15	236.9	−53.8	0.004
28-1, 25	255.75	244.3	−20.3	0.072
28-1, 75	256.25	191.9	−23.7	0.012
28-2, 25	257.25	198.8	80.9	0.011
28-2, 75	257.75	251.8	29.4	0.025
28-2, 125	258.25	308.1	81.5	0.012
28-3, 25	258.75	216.7	16.7	0.010
28-3, 75	259.25	335.3	31.6	0.041
28-3, 125	259.75	172.3	−8.1	0.008
28-4, 25	260.25	124.4	39.5	0.008
28-4, 75	260.75	0.4	38.8	0.025
28-4, 125	261.25	13.5	67.4	0.008
28-5, 25	261.75	271.1	−5.6	0.004
28-5, 75	262.25	266.5	−29.2	0.012
29-1, 75	265.85	187.0	−2.1	0.010
29-1, 125	266.35	220.9	22.4	0.015
29-2, 25	266.85	123.2	−31.0	0.009
29-2, 75	267.35	182.1	−50.5	0.013
29-2, 125	267.85	236.7	−51.2	0.012
29-3, 25	268.35	104.9	−54.1	0.014
29-3, 75	268.85	260.5	−83.2	0.008
29-3, 125	269.35	87.8	−43.0	0.0[illegible]7
29-4, 25	269.85	215.4	27.0	0.006
29-4, 75	270.35	115.4	14.3	0.016
29-4, 125	270.85	274.6	−69.1	0.0[illegible]2
29-5, 25	271.35	148.2	−32.1	0.0[illegible]1
29-5, 75	271.85	185.5	−11.2	0.0[illegible]5
29-5, 125	272.35	87.8	31.1	0.0[illegible]9
29-6, 25	272.85	167.5	−44.3	0.0[illegible]0
29-6, 75	273.35	264.6	−24.1	0.0[illegible]1
29-6, 125	273.85	263.4	−41.4	0.0[illegible]2
30-1, 25	274.95	86.1	−22.5	0.0[illegible]2
30-1, 75	275.45	99.8	−39.1	0.0[illegible]0
30-1, 125	275.95	279.3	−39.6	0.1[illegible]9
30-2, 25	276.45	218.3	−34.7	0.0[illegible]3
30-2, 75	276.95	196.3	−47.4	0.0[illegible]5
30-2, 125	277.45	137.5	43.4	0.0[illegible]6
30-3, 25	277.95	251.6	−81.6	0.0[illegible]8
30-3, 75	278.45	257.8	21.3	0.0[illegible]3

Table 10. (Continued).

Core-Section (interval in cm)	Sub-bottom depth (m)	Declination (°)	Inclination (°)	Intensity (μG)
30-3, 125	278.95	337.7	5.9	0.008
30-4, 25	279.45	195.2	− 50.6	0.016
30-4, 75	279.95	240.9	28.1	0.010
30-4, 125	280.45	93.0	82.4	0.011
30-5, 25	280.95	207.3	− 9.9	0.011
30-5, 75	281.45	161.8	25.4	0.011
30-5, 125	281.95	118.6	72.6	0.003
30-6, 25	282.45	281.6	− 9.5	0.004
31-1, 25	284.55	280.7	− 47.4	0.011
31-1, 75	285.05	110.0	− 59.0	0.017
31-1, 125	285.55	245.3	− 24.3	0.012
31-2, 25	286.05	297.6	− 62.4	0.008
31-2, 75	286.55	61.4	− 30.0	0.010
31-2, 125	287.05	48.6	− 85.4	0.022
31-3, 25	287.55	65.0	− 13.8	0.021
31-3, 75	288.05	120.5	− 53.8	0.013
31-3, 125	288.55	189.1	− 37.6	0.012
31-4, 25	289.05	172.7	− 57.1	0.016
31-4, 75	289.55	114.6	18.0	0.012
31-4, 125	290.05	265.3	− 50.7	0.006
31-5, 25	290.55	289.1	1.1	0.010
31-5, 75	291.05	198.5	− 37.0	0.018
31-5, 125	291.55	127.0	− 56.4	0.009
31-6, 25	292.05	346.0	− 84.5	0.023
34-1, 25	313.35	26.9	− 64.6	0.015
34-1, 75	313.85	294.0	− 41.5	0.017
34-1, 125	314.35	227.4	24.5	0.013
34-2, 25	314.85	303.3	59.9	0.025
34-2, 75	315.35	293.2	− 72.4	0.010
34-2, 125	315.85	106.0	− 59.1	0.009
34-3, 25	316.35	187.4	− 61.8	0.013
34-3, 75	316.85	183.8	20.3	0.038
34-3, 125	317.35	357.0	− 52.8	0.115
34-4, 25	317.85	89.1	1.1	0.029
34-4, 75	318.35	93.6	− 26.4	0.042
34-4, 125	318.85	301.6	− 40.2	0.293
34-5, 25	319.35	307.4	73.1	0.013
34-5, 75	319.85	237.8	− 61.5	0.012
35-1, 25	322.95	101.0	− 2.4	0.060
35-1, 75	323.45	289.5	− 39.2	0.013
35-1, 125	323.95	341.6	51.7	0.018
35-2, 25	324.45	167.9	− 21.0	0.010
35-2, 75	324.95	244.1	− 30.5	0.039
35-2, 125	325.45	54.0	− 11.9	0.024
35-3, 25	325.95	142.7	− 52.6	0.017
35-3, 75	326.45	271.2	− 22.0	0.008
35-3, 125	326.95	328.8	− 52.3	0.015
35-4, 25	327.45	280.2	− 40.7	0.024
35-4, 75	327.95	59.3	7.1	0.060
35-4, 125	328.45	200.2	− 52.1	0.014
35-5, 25	328.95	224.4	− 80.6	0.093
35-5, 75	329.45	250.3	− 56.3	0.033
35-5, 125	329.95	242.0	67.0	0.055
36-1, 25	332.55	264.0	− 31.2	0.027
36-1, 75	333.05	304.6	3.7	0.021
36-1, 125	333.55	310.8	− 74.8	0.026
36-2, 25	334.05	225.8	− 68.7	0.011
36-2, 75	334.55	309.3	− 32.1	0.078
36-2, 125	335.05	203.5	− 27.6	0.021
36-3, 25	335.55	250.5	− 33.1	0.013
36-3, 75	336.05	278.5	21.4	0.017
36-3, 125	336.55	8.3	4.9	0.020
36-4, 25	337.05	296.3	− 18.5	0.041
36-4, 75	337.55	339.5	− 27.0	0.014
36-4, 125	338.05	120.2	− 15.6	0.160
36-5, 25	338.55	237.9	66.8	0.023
37-1, 75	342.65	25.0	− 39.2	0.096
37-1, 125	343.15	240.6	− 65.3	0.015
38-1, 27	351.77	37.2	− 15.8	0.030
38-1, 75	352.25	243.1	− 31.6	0.050
38-1, 125	352.75	72.3	− 33.1	0.024
38-2, 25	353.25	340.0	− 1.6	0.136
38-2, 75	353.75	134.6	29.2	0.019
38-2, 125	354.25	350.6	− 24.0	0.011
38-3, 25	354.75	84.9	23.5	0.448

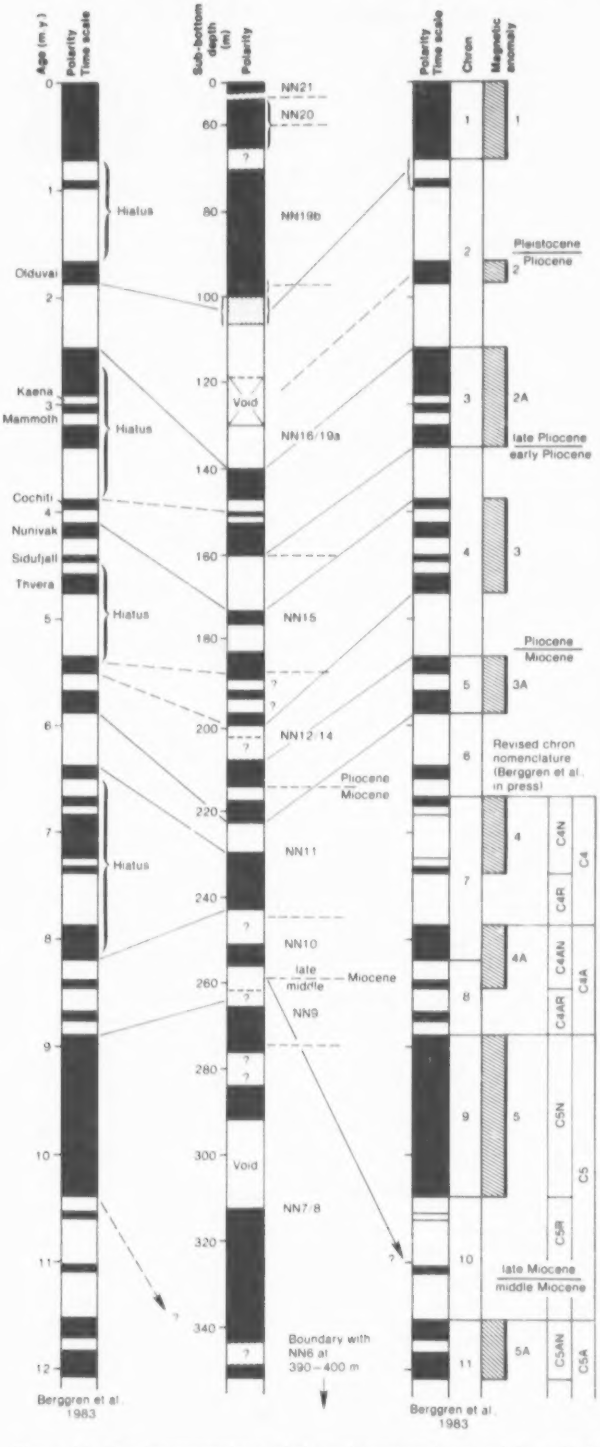

Figure 27. Two interpretations of the paleomagnetic record from Hole 594 (center column). To the left/right is shown the simplest match with the magnetic polarity time scale which is consistent with the diatom-radiolarian/calcareous nannofossil dating schemes, respectively (see text). The diatom-radiolarian scheme incorporates four major hiatuses. The marine magnetic anomaly sequence and the related new magnetic chron nomenclature (Berggren et al., in press) are illustrated on the far right.

37. GEOTHERMAL MEASUREMENTS AT DEEP SEA DRILLING PROJECT SITE 587[1]

Roger H. Morin, Massachusetts Institute of Technology
and
Richard P. Von Herzen, Woods Hole Oceanographic Institution[2]

ABSTRACT

A new WHOI heat flow instrument was successfully used in conjunction with the hydraulic piston corer to obtain temperature–time records for three depths at DSDP Site 587. In order to arrive at an estimate for *in situ*, steady-state temperature, these data are applied to a two-dimensional theoretical formulation that describes the cooling behavior of an annular cylinder surrounded by sediment. An average heat flow of 56.9 mW/m^2 is computed from the resulting temperature profile. This value is in close agreement with the theoretical heat flux of 53.0 mW/m^2 determined from the general heat flow–age relationship. The temperature profile at Site 587 is nonlinear. Examination of the effects of sudden changes in bottom water temperature and upward movement of pore fluid fails to provide convincing solutions to the cause of this nonlinearity. Knowing sediment permeability and extending the theoretical data analysis to three dimensions would improve our ability to understand the geothermal environment at this location.

INTRODUCTION

The Leg 90 scientific program focused primarily on paleoenvironmental studies, requiring extensive use of the hydraulic piston corer (HPC) at several sites traversing tropical to subantarctic regions of the southwest Pacific. A new heat flow instrument, developed at the Woods Hole Oceanographic Institution (WHOI), had originally been designed to be deployed with the HPC and provide information regarding the *in situ* temperature of the sediment column. This tool was initially tested on Leg 86, and its use was incorporated into the Leg 90 schedule because of the possibility of obtaining detailed temperature profiles in conjunction with the planned HPC operations.

The previous method of determining the geothermal gradient involved the separate lowering of temperature-measuring instrumentation (Yokota et al., 1980), with the entire process taking between 1 and 2 hours, depending upon the water depth and operating conditions. The new instrumentation employs a thermistor/microprocessor package that is inserted directly into the wall of the HPC cutting shoe, as shown in Figure 1, recording temperature values at preselected time intervals during the coring operation. With this innovative device, the measurement technique is incorporated directly into the coring procedure and determines the *in situ* temperature, requiring minimum additional operating time (≤10 min.).

Thus, a comprehensive heat flow program was planned for this cruise in conjunction with the ambitious HPC work scheduled along the Lord Howe Rise. Regrettably, one such instrument package had been lost during Leg 89, which left only one remaining aboard ship. This tool was subsequently lost during a coring malfunction at Site 590. Hence, the entire heat flow program was limited to the geothermal measurements determined at Site 587. These data are presented and analyzed in this chapter.

THEORETICAL FORMULATION

The heat flow device measures the temperature inside the coring shoe wall as a function of time. Figure 2A–C depicts the temperature–time records obtained at DSDP Site 587, where temperature values have been recorded every 10 s. These include the temperature of the seawater inside the drill string as the HPC was lowered into the hole. A temperature spike in these plots is caused by frictional heating during HPC sediment penetration. The initial rapid increase to a maximum temperature is followed by a relatively undisturbed decay and, finally, by a sudden deviation from this cooling curve as the piston corer is extracted and returned to the ship. The heat flow instrument package was typically placed in the cutting shoe at every fourth HPC deployment, roughly every 36 m. It was allowed to remain imbedded in the sediment for approximately 10 min. before retrieval to obtain a record of the conductive dissipation of heat to the surrounding sediments.

Horai (personal communication) has investigated, both analytically and numerically, the problem of radial conduction through an annular coring shoe surrounded by sediment. This two-dimensional formulation provides a method of processing the transient record of heat dissipation by fitting to a theoretical temperature decay. The theoretical cooling curve is uniquely determined by the thermal properties and dimensions of the coring shoe material and the adjacent marine sediment. Since the piston corer is retrieved from the ocean bottom before an equilibrium temperature can be reached, this procedure allows extrapolation of the decaying temperature record to yield an estimate for the steady-state *in situ* sediment temperature.

Thermal conductivity values obtained from various depths at Sites 587 and 588 are reported by Morin (this volume). These data are graphically presented here as

---

[1] Kennett, J. P., von der Borch, C. C., et al., *Init. Repts. DSDP*, 90: Washington (U.S. Govt. Printing Office).

[2] Addresses: (Morin, Von Herzen, present address) U.S. Geological Survey, Denver, CO 80225

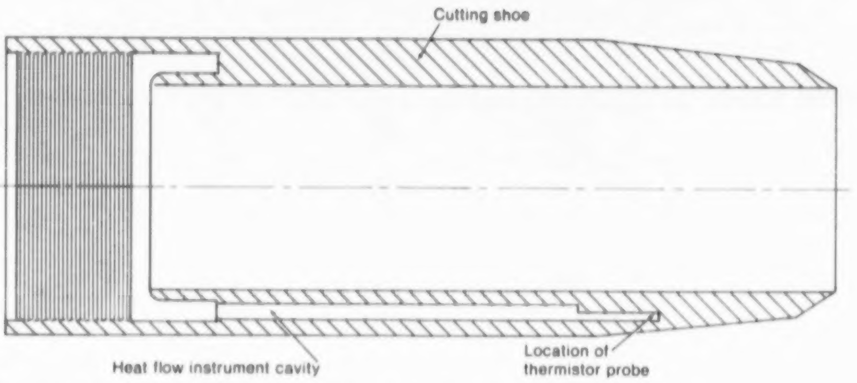

Figure 1. Cross-sectional view of HPC cutting shoe with cavity for heat flow instrument.

well (Fig. 3) and are listed in Table 1. Chaney et al. (1983) describe the experimental technique. Relevant shipboard conductivity measurements were corrected for *in situ* pressure as suggested by Morin and Silva (1984). The magnitude of the correction is a function of porosity and can differ appreciably from that suggested by Ratcliffe (1960) when low-porosity sediments are exposed to substantial hydrostatic pressures. Because of the relatively shallow water depth of 1100 m at Site 587, however, the pressure correction determined by either method proved to be quite small (see Appendix). A temperature coefficient, appropriate within a range of 0 to 30°C, was also applied to the conductivity values determined aboard ship (Macdonald and Simmons, 1972). This adjustment (reduction) to the shipboard thermal conductivity necessitated by the colder *in situ* temperature was slightly offset by the small adjustment (increase) to the shipboard measurement caused by the larger *in situ* pressure (see Appendix). The resulting total correction, a net reduction in thermal conductivity of 2.63%, was employed in computing the proper thermal property values necessary to the theoretical heat transfer formulation.

The corresponding values of sediment thermal diffusivity were estimated by the following linear relationship (Von Herzen and Maxwell, 1959):

$$k = (3.66K - 0.70)(10^{-7})$$

where K is the thermal conductivity and k is the thermal diffusivity in units of W/m°C and m²/s, respectively. Horai's (personal communication) analysis incorporates the following parameters.

$$K_{\text{HPC iron alloy}} = 25.3 \text{ W/m°C}$$

$$k_{\text{HPC iron alloy}} = 10.9 \times 10^{-6} \text{ m}^2\text{/s}$$

$$K_{\text{sediment}} = 1.06 - 1.39 \text{ W/m°C}$$

$$k_{\text{sediment}} = 3.18 - 4.39 \times 10^{-7} \text{ m}^2\text{/s}$$

HPC inside diameter = 6.198 cm

HPC outside diameter = 9.068 cm

In this analytical study of the heat transfer across a composite circular cylinder, the initial temperature of the coring shoe is assumed to be both constant and uniform. In actuality, however, the HPC commonly has an uneven temperature distribution at the instant of sediment penetration. Because of this nonuniform condition, the first few data points, or time steps, recorded by the temperature sensor after penetration are expected to deviate from the predicted values (1 time step = 10 s). In his analysis, Horai has adjusted for the effect of an ambiguous time origin by including a zero-time offset. The theoretical temperatures with shifted time origin are fitted to the recorded data by minimizing the misfit (error), calculated as the rms value:

$$\text{error} = \left[\sum^{n} \frac{(T_i - T_{ti})^2}{n}\right]^{1/2}$$

where T_i is the observed temperature, and T_{ti} is the theoretical temperature.

TEMPERATURE RESULTS

Figure 4A–C displays the results of the three downhole temperature measurements obtained at Site 587. These plots focus upon the decay-curve portions of the data presented in Figure 2. The points represent the temperatures measured by the WHOI instrumentation at 10-s intervals during the coring operation, and the solid lines represent best-fit cooling curves derived from Horai's theoretical analysis in conjunction with the relevant sediment thermal conductivity measurements. The fitting is excellent at a depth of 31.9 m (Fig. 4A), as evidenced by the relatively small residual error, computed from the least-squares analysis to be 0.008. Horai's solution demonstrates that, after 600 s of undisturbed cooling, approximately 78% of the total expected thermal decay has occurred, and an *in situ* temperature of 6.42°C is calculated.

The second temperature-time record (Figs. 2B and 4B) at a sub-bottom depth of 70.3 m shows a disturbance in the thermal decay curve occurring approximately 100 s after HPC penetration. This slight temperature increase is probably caused by movement that has gen-

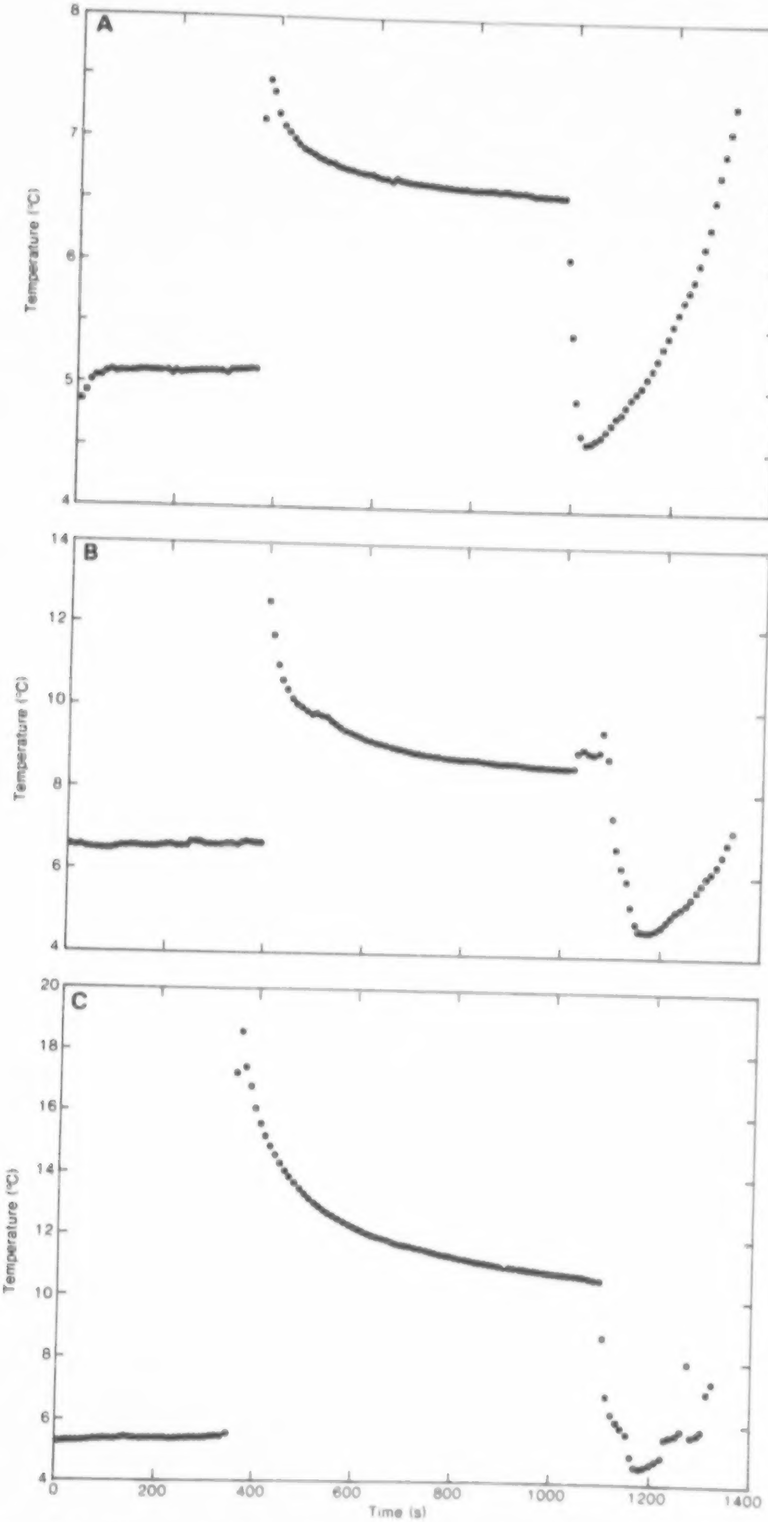

Figure 2. Temperature-time record from WHOI instrument at A. 31.9 m depth, B. 70.3 m depth, C. 108.7 m depth.

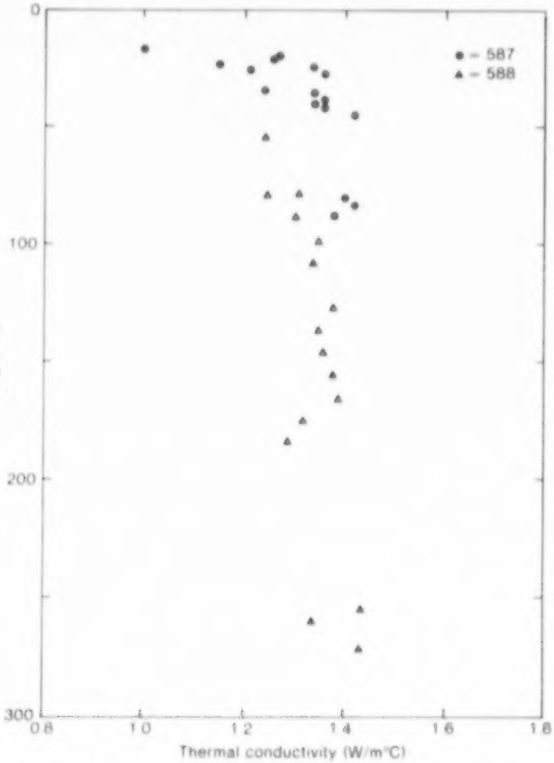

Figure 3. Plot of sediment thermal conductivity (Sites 587 and 588) versus depth.

Table 1. List of sediment thermal conductivity values versus depth for Sites 587 and 588.

Site 587		Site 588	
Depth (m)	Thermal conductivity (W/m°C)	Depth (m)	Thermal conductivity (W/m°C)
16.4	1.00	53.9	1.24
19.4	1.27	78.8	1.31
20.9	1.26	87.8	1.30
23.0	1.15	98.0	1.35
24.5	1.34	107.5	1.34
26.0	1.21	126.8	1.39
27.5	1.36	136.3	1.35
34.1	1.24	146.0	1.36
35.6	1.34	155.5	1.38
38.6	1.36	165.2	1.40
40.1	1.34	174.8	1.32
42.2	1.37	184.3	1.29
45.2	1.42	254.9	1.44
80.6	1.40	260.4	1.34
83.6	1.42	271.6	1.44
88.1	1.39		

erated additional frictional heating. Movement could have been produced by ship motion transmitted through the drill string or simply from settling of the coring gear in the sediment. Horai's analysis is applied to the actual data at the onset of this disturbance in order to achieve a representative fit to the decay curve and, again, a small residual error of 0.008 is calculated. The steady-state temperature at this depth is estimated to be 8.00°C.

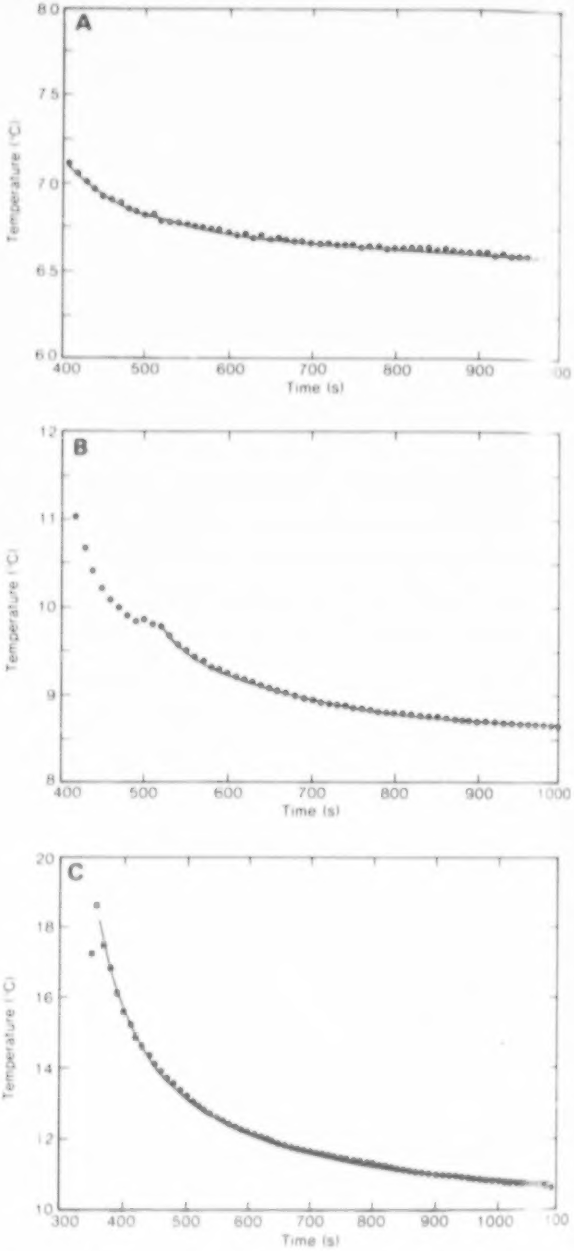

Figure 4. Temperature decay data (points) and corresponding best-fit theoretical solution (solid line) for Site 587. A. 31.9 m depth. B. 70.3 m depth, C. 108.7 m depth.

The WHOI instrument package was deployed for a third time at a depth of 108.7 m. The actual data and the theoretical fit are illustrated in Figure 4C. The associated residual error in this case is 0.068 and an *in situ* temperature of 8.65°C is predicted.

The uncertainties in estimating the *in situ* temperatures can best be considered by applying reasonable constraints to the theoretically derived results. In the three cases discussed previously, the actual temperatures are slightly less than the theoretical ones near the end of the recorded decay curve. Horai employs a two-dimensional model in his analysis, thus assuming that all conductive heat transfer takes place in the radial direction. In reality, however, some degree of axial cooling probably occurs at the base of the cutting shoe, thereby causing temperatures to fall more rapidly than theory has predicted. Hence, the theoretically derived *in situ* temperatures are likely to be slightly less than the actual ones. These former values are considered to be the lower bounds of the *in situ* temperature estimates. An upper bound can be conservatively estimated as being the last value observed during the recorded temperature decay. Thus, appropriate ranges of uncertainty can be attached to the estimated *in situ* temperatures.

Table 2 summarizes the successful geothermal measurements, with the sub-bottom depths obtained from the drillers' logs. The heat flow instrument was immediately lowered into the existing hole during the coring operation and was never permitted to reach thermal equilibrium at the sediment–seawater interface. Therefore, the bottom water temperature was not directly measured at this site. Nevertheless, nearby historical hydrographic data obtained from National Oceanographic Data Center listings give a value of about 4.1 ± 0.1°C at a depth of 1115 m. These data show no observable ($\leq 0.1°C$) long-term variability over the period ranging from approximately 1960 to 1980.

A weighted harmonic mean sediment thermal conductivity was calculated for each depth interval over which the geothermal gradient was determined. A particular sediment porosity has a thermal conductivity value associated with it, and the harmonic means were weighted corresponding to the porosity profile of Hole 587 presented by Morin (this volume). The degrees of uncertainty in estimating these quantities are stated in the footnotes to Table 2.

For purposes of computing thermal gradients through the sediment column across the pertinent depth intervals, assumptions are made regarding the designated temperature constraints. Since the theoretical fits shown in Figure 4 are in close agreement with the actual data, it is anticipated that the true *in situ* temperature will be much closer to $T_{min.}$ than to $T_{max.}$. The following equation is arbitrarily chosen as a subjective approximation to the actual temperature.

$$T_{estimated} = T_{min.} + C(T_{max.} - T_{min.})$$

where C = constant = 0.20. The exact value of C does not significantly affect the final temperature results except at the deepest depth, where the difference between $T_{max.}$ and $T_{min.}$ is greatest. Values of estimated temperatures are included in Table 2 and a plot of the temperature profile for Site 587 is presented in Figure 5.

DISCUSSION

Site 587 is located at 21°11.9′S, 161°20.0′E on the Lansdowne Bank. This geologic feature represents the northernmost part of the Lord Howe Rise and is bordered by the Lord Howe Basin to the west and the New Caledonia Basin to the east. This particular section of the southwest Pacific has a complex tectonic setting, with numerous crustal extensions and discontinuities. Lapouille (1976) has categorized the Lord Howe Rise based upon magnetic variations and crustal thickness (Officer, 1955). Seismic surveys of the New Caledonian margins reveal transitional seismic structures that lie between the proper oceanic domain of the central Pacific and the continental domain forming Australia (Dubois et al., 1974); it is believed that the region that encompasses the Lord Howe Rise and Site 587 probably has a thinned continental structure. Geophysical studies indicate that this zone was detached from Australia by the opening of the Tasman Sea during the Late Cretaceous between 60 and 80 m.y. ago (Hayes and Ringis, 1973). Maestrichtian sediments and rocks recovered from DSDP Sites 207 and 208, also located on the Lord Howe Rise, seem to confirm this age (Burns et al., 1973; Webb, 1973).

It is thus assumed that the crustal age at Site 587 is no younger than Late Cretaceous (65 m.y.) and probably around 80 m.y. Parsons and Sclater (1977) demonstrate that heat flow of normal seafloor can be estimated from crustal age by utilizing the following equation.

$$q(t) = 473/t^{1/2}$$

Table 2. Summary of geothermal data for Site 587.

Core	Depth (m)	$T_{max.}$ (°C)	$T_{min.}$ (°C)	T_{est}[a] (°C)	Thermal gradient (°C/m)	Thermal[b] cond. (W/m°C)	Heat[c] flow (mW/m^2)	Heat[d] flow-avg. (mW/m^2)
Seafloor	0	—	—	4.1 ± 0.1				
					0.074 ± 0.003	1.06 ± 0.08	78.4 ± 7.1	
4	31.9	6.57	6.42	6.45 ± 0.01				
					0.044 ± 0.001	1.39 ± 0.11	61.2 ± 5.1	56.9 ± 5.2
8	70.3	8.64	8.00	8.13 ± 0.02				
					0.025 ± 0.001	1.39 ± 0.11	34.8 ± 3.1	
12	108.7	10.74	8.65	9.08 ± 0.04				

Note: Dashes indicate that no measurement was made.

[a] Uncertainties are subjective estimates based upon accuracy of theoretical fit.

[b] Uncertainty includes standard experimental error of ±4 and ±4% possible systematic error (weighted harmonic mean).

[c] Uncertainty computed as RMS sum of errors in thermal gradient and conductivity.

[d] Uncertainty computed as weighted RMS sum of interval heat flow errors.

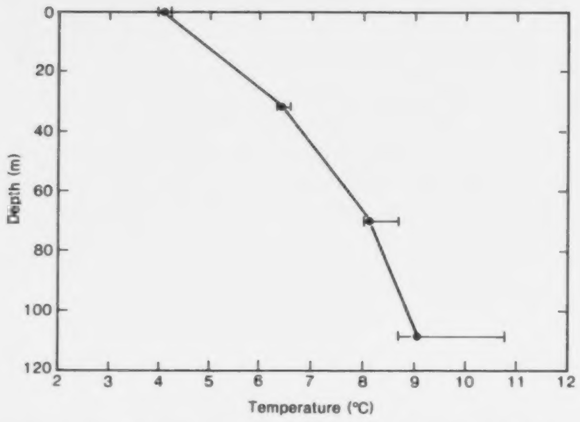

Figure 5. Plot of temperature versus sub-bottom depth for Site 587.

where $q(t)$ = heat flow as a function of time (mW/m^2) and t = age (m.y.)

The associated heat flow predicted for 80-m.y. basement is 53.0 mW/m^2. This theoretical value is in very good agreement with the average heat flow presented in Table 2, computed over the entire 108.7-m depth interval as being 56.9 mW/m^2. There are relatively few heat flow data reported in the literature for this area from which to compare results. Sclater et al. (1972) have reported a heat flux of 42.8 mW/m^2 at a site 230 km to the east, nearer New Caledonia; Von Herzen (1973) has measured a value of 82.2 mW/m^2 at DSDP Site 209, approximately 900 km to the northwest near the Coral Sea Basin.

The temperature profile depicted in Figure 5 is nonlinear. This curvature, although compensated somewhat by changes in thermal conductivity, translates into a nonuniform heat flow distribution with depth. The phenomenon of nonlinear temperature profiles has been vigorously investigated over the past few years (Langseth and Herman, 1981; Anderson et al., 1979; Abbott et al., 1981), although no adequate explanation has been presented yet for this behavior. Factors such as upward percolation of pore fluid through the sedimentary column, changes in bottom water temperature, and variations in thermal conductivity have been suggested as possible causes for the curved temperature profiles. In many cases concerned with marine studies, however, consideration of these factors has yielded inadequate or contradictory explanations.

If it is assumed that the temperatures determined at the two deepest points approach a linear, steady-state distribution, an associated geothermal gradient of 0.020°C/m can be approximated, with a corresponding steady-state bottom water temperature of 6.91°C. In order to justify the temperature profile depicted in Figure 5 to be caused by variations in bottom water temperature, a sudden temperature decrease of about 2.9°C would have to have occurred and have been maintained over the past 100 years. These calculations are computed from the conduction equations for a semi-infinite solid presented by Carslaw and Jaeger (1978, p. 63) and are based on a step change of water temperature superimposed on a medium with uniform thermal diffusivity. Whereas small fluctuations in bottom water temperature may be expected at this site because of the relatively shallow water depth, the magnitude of the deviation required to properly explain the temperature distribution seems unlikely.

Vertical water advection through the sediment column also may produce nonlinear temperature profiles. When the one-dimensional energy balance described by Bredehoeft and Papadopulos (1965) for a medium with uniform thermal properties is applied to the three sediment temperatures listed in Table 2, the upward fluid velocity necessary to generate the resulting profile is computed to the 5.93×10^{-7} cm/s. Unfortunately, permeability has not been determined for the sediments at this site. The material was relatively coarse grained, making retrieval with the HPC difficult. The sediments consisted mostly of skeletal silty sands, composed of corals, calcareous algae, and foraminifers. Because of the coarse grain size and absence of clays, it is anticipated that permeabilities are high. Average porosity through the sediment column is estimated at 60% from the porosity profile of Site 587 presented by Morin (this volume).

Bryant et al. (1975) have classified marine sediment permeabilities in terms of clay content and grain size. For silts and clays that have a significant sand-size fraction, permeability is roughly estimated to be on the order of 10^{-7} cm/s at a porosity of 60%. Robertson (1967) has measured the permeability of an aragonitic sediment during compaction. His results show a permeability on the order of 10^{-5} cm/s at a porosity of 60%. It is difficult to assign a reliable permeability to these Site 587 sediments in light of the wide range of values presented in the literature. For our purposes in this general analysis, however, it is assumed that sediment permeability is on the order of 10^{-6} cm/s. The corresponding hydraulic gradient necessary to generate an upward velocity of 5.93×10^{-7} cm/s is, thus, on the order of 0.1.

$$v = Bi$$

where v = fluid velocity (cm/s), B = sediment permeability (cm/s), and i = hydraulic gradient (dimensionless).

The simple diagram of Figure 6 shows water percolating up through a sediment sample as it travels from points A to C. One-dimensional flow conditions and a uniform permeability are assumed throughout the specimen. We wish to determine the hydraulic gradient necessary to achieve a "quick condition" (no effective stress) at the bottom of the specimen (point B). Conceptually, the height h_2 is gradually increased until the force pushing water up through the sample becomes so great that there is no longer an effective stress in the sediment at point B (i.e., no grain-to grain contacts, with particles suspended in fluid). The threshold value of this height h_2 is determined as follows:

$$\sigma = \sigma' + \mathrm{u} \tag{1}$$

at point B, $\sigma' = 0$, $\sigma = \mathrm{u}$—from (1)

READEX best copy available pages tightly bound

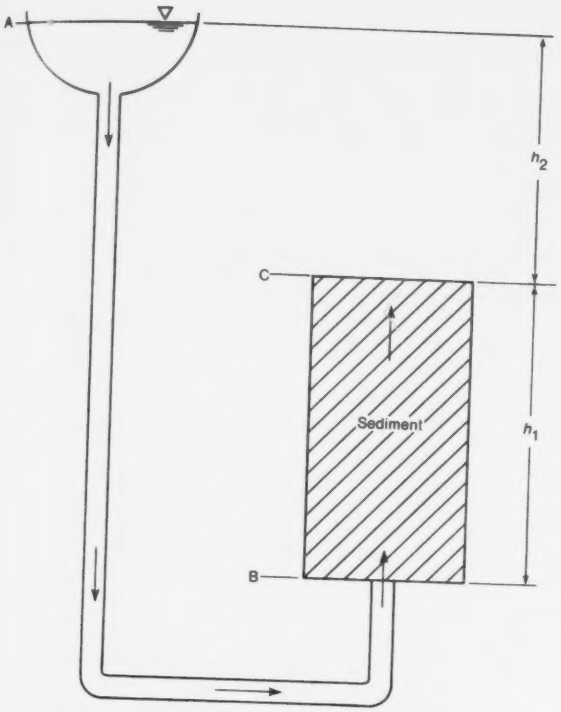

Figure 6. Schematic diagram illustrating water moving up through a sediment sample under a hydraulic pressure gradient. Sketch is used to determine the hydraulic gradient necessary to produce a "quick condition" (see text).

$$u = \gamma_W (h_1 + h_2) \tag{2}$$

$$\sigma = (\gamma_W + \gamma_b)h_1 \tag{3}$$

where σ = total stress, σ' = effective stress, u = pore water pressure, γ_W = unit weight of water, and γ_b = unit weight of sediment in water.

Equating (2) and (3),

$$\gamma_W (h_1 + h_2) = (\gamma_W + \gamma_b)\, h_1$$

$$\gamma_W h_2 = \gamma_b\, h_1$$

$$h_2/h_1 = \gamma_b/\gamma_W$$
$$= \text{threshold hydraulic gradient } i_{\text{quick}}.$$

But

$$\gamma_b = \gamma_W(G - 1)(1 - \Phi)$$
(from Lambe and Whitman, 1969)

where G = specific gravity of solids, Φ = porosity.

$$\therefore\ i_{\text{quick}} = (G - 1)(1 - \Phi) = 0.66$$

assuming $G = 2.65$ and $\Phi = 0.60$.

Thus, a hydraulic gradient larger than 0.66 will cause a "quick condition" on the seafloor. This value is on the same order as that determined necessary to produce the calculated nonlinear temperature profile. Without knowing the permeability more accurately, firm conclusions cannot be reached. If the required gradient is larger than 0.66, this solution is not valid physically. If the gradient needed to generate the appropriate fluid flow is smaller than the threshold gradient, upward percolation through the sediment column may provide a viable explanation for the temperature distribution. This latter condition seems unlikely, however, since an upward flow of 5.93×10^{-7} cm/s implies a local surface heat transfer of about 155 mW/m^2 (Anderson et al., 1979). This value is much higher than all surface heat flow measurements reported for this region and is also much larger than the value calculated from the heat flow versus age relationship presented earlier.

An examination of the effects of variable bottom water temperature and pore fluid movement fails to provide a convincing solution as to the cause of the nonlinear temperature profile at Site 587. Von Herzen (1973) presented a similar profile at Site 206 in the New Caledonia Basin. The large error bar in the predicted temperature at the 108.7-m depth, however, makes it difficult to be certain about the significance of curvature in the profile. Better resolution of this deepest temperature is required before a distinct nonlinear temperature distribution can be confidently assumed. It is to be hoped that a revised, three-dimensional version of Horai's theoretical formulation will permit a re-evaluation of the WHOI instrument data at a future time.

ACKNOWLEDGMENTS

We are grateful to the co-chief scientists of Leg 90, J. Kennett and C. von der Borch, for the opportunity to pursue a heat flow program and make these measurements.

REFERENCES

Abbott, D., Menke, W., Hobart, M., and Anderson, R., 1981. Evidence for excess pore pressures in southwest Indian Ocean sediments. *J. Geophys. Res.*, 86:1813–1827.

Anderson, R. N., Hobart, M. A., and Langseth, M. G., 1979. Geothermal convection through oceanic crust and sediments in the Indian Ocean. *Science*, 204:828–832.

Bredehoeft, J. D., and Papadopulos, J. S., 1965. Rates of vertical groundwater movement estimated from the Earth's thermal profile. *Water Res. Res.*, 2:325–328.

Bryant, W. R., Hottman, W., and Trabant, P., 1975. Permeability of unconsolidated and consolidated marine sediments, Gulf of Mexico. *Mar. Geotech.*, 1:1–13.

Burns, R. E., Andrews, J. E., et al., 1973. *Init. Repts. DSDP*, 21: Washington (U.S. Govt. Printing Office).

Carlsaw, H. S., and Jaeger, J. C., 1978. *Conduction of Heat in Solids* (2nd Ed.): Oxford (Clarendon Press).

Chaney, R. C., Ramanjaneya, G., Hencey, G., Kanchanastit, P., and Fang, H. Y., 1983. Suggested test method for determination of thermal conductivity of soil by thermal-needle procedure. *Geotech. Testing J.*, 6:220–225.

Dubois, J., Ravenne, C., Aubertin, A., Louis, J., Guillaume, R., Launay, J., and Montadert, L., 1974. Continental margins near New Caledonia. *In* Burk, C. A., and Drake, C. L. (Eds.), *The Geology of Continental Margins:* New York (Springer-Verlag), pp. 521–535.

Hayes, D. E., and Ringis, J., 1973. Seafloor spreading in the Tasman Sea. *Nature*, 243:454–458.

Lambe, T. W., and Whitman, R. V., 1969. *Soil Mechanics:* New York (J. Wiley and Sons).

Langseth, M. G., and Herman, B. M., 1981. Heat transfer in the oceanic crust of the Brazil Basin. *J. Geophys. Res.*, 86:10805–10819.

Lapouille, A., 1976. Magnetic surveys over the rises and basins in the South-West Pacific. *Int. Symp. Geodynamics in South-West Pacific*, Noumea (New Caledonia), 15–28.

Macdonald, K., and Simmons, G., 1972. Temperature coefficient of the thermal conductivities of ocean sediments. *Deep-Sea Res.*, 19: 669–671.

Morin, R. H., and Silva, A. J., 1984. The effects of high pressure and high temperature on some physical properties of ocean sediments. *J. Geophys. Res.*, 89;511–526.

Officer, C. B., 1955. Southwest Pacific crustal structure. *Trans. Am. Geophys. Union*, 36:449–459.

Parsons, B., and Sclater, J. G., 1977. An analysis of the variation of ocean floor bathymetry and heat flow with age. *J. Geophys. Res.*, 82:803–827.

Ratcliffe, E. H., 1960. The thermal conductivities of ocean sediments. *J. Geophys. Res.*, 65:1535–1541.

Robertson, E. C., 1967. Laboratory consolidation of carbonate sediment. *In* Richards, A. F. (Ed.), *Marine Geotechnique:* Urbana (Univ. of Ill. Press), pp. 118–127.

Sclater, J. G., Ritter, U. G., and Dixon, F. S., 1972. Heat flow in the southwestern Pacific. *J. Geophys. Res.*, 77:5697–5704.

Von Herzen, R. P., 1973. Geothermal measurements, Leg 21. *In* Burns, R. E., Andrews, J. E., et al., *Init. Repts. DSDP*, 21: Washington (U.S. Govt. Printing Office), 443–457.

Von Herzen, R. P., and Maxwell, A. E., 1959. The measurement of thermal conductivity of deep-sea sediments by a needle-probe method. *J. Geophys. Res.*, 64:1557–1563.

Webb, P. N., 1977. Upper Cretaceous-Paleocene foraminifers from Site 208 (Lord Howe Rise, Tasman Sea). *In* Burns, R. E., Andrews, J. E., et al., *Init. Repts. DSDP*, 21: Washington (U.S. Govt. Printing Office), 541–574.

Yokota, T., Kinoshita, H., and Uyeda, S., 1980. New DSDP downhole temperature probe utilizing ICRAM (Memory) elements. *Bull. Earthquake Res. Inst.*, 55:75–88.

Date of Initial Receipt: 14 May 1984
Date of Acceptance: 20 November 1984

APPENDIX

Sediment Thermal Conductivity Corrections for *In Situ* Pressure and Temperature

Pressure:

assume shipboard thermal conductivity = 1.00 W/m°C
water depth = 1100 m

(from Morin and Silva, 1984)
assume sediment porosity = 0.70

$$\text{pressure corrected therm. cond.} = \text{therm. cond. at 1 atm} + \left(\frac{0.0042\text{W}}{\text{m}^\circ\text{C}}\right)\left(\frac{\text{water depth}}{1000\text{ m}}\right)$$

$$\text{pressure correction} = \left(\frac{0.0042\text{ W}}{\text{m}^\circ\text{C}}\right)\left(\frac{1100\text{ m}}{1000\text{ m}}\right) = \frac{0.0046\text{ W}}{\text{m}^\circ\text{C}}$$

$$\%\text{ correction} = \frac{+0.0046}{1.00} = +0.46\%$$

(from Ratcliffe, 1960)
1% increase in thermal conductivity per 1000 fathoms (1830 m) water depth

$$\%\text{ correction} = (0.01)\left(\frac{1100\text{ m}}{1830\text{ m}}\right) = +0.60\%$$

Temperature:

assume shipboard temperature = 22°C
assume *in situ* temperature = 6°C

(from Macdonald and Simmons, 1972)

$$\text{therm. cond. correction} = \left(\frac{0.193\%}{^\circ\text{C}}\right)(6^\circ\text{C} - 22^\circ\text{C})$$

$$\%\text{ correction} = -3.09\%$$

$$\begin{aligned}\text{Total correction} &= +0.46\%\text{ (pressure)} - 3.09\%\text{ (temperature)}\\ &= -2.63\%\end{aligned}$$

38. SEISMIC STRATIGRAPHY AND STRUCTURE ADJACENT TO AN EVOLVING PLATE BOUNDARY, WESTERN CHATHAM RISE, NEW ZEALAND[1]

K. B. Lewis, New Zealand Oceanographic Institute
D. J. Bennett, Geophysics Division of the Department of Scientific and Industrial Research, New Zealand
R. H. Herzer, New Zealand Geological Survey
and
C. C. von der Borch, Flinders University[2]

ABSTRACT

Seismic profiles obtained from the eastern side of New Zealand, in transit to and from Site 594, illustrate the evolution of the western end of the Chatham Rise and the southern extremity of the Hikurangi Trough. They show several unconformities and several major changes in tectonic and depositional regime. The unconformities represent major changes in oceanic circulation, possibly triggered by large lowerings of sea level in the late Oligocene and late Miocene. Tectonism is exemplified by a Late Cretaceous phase of block faulting, heralding the rift from Gondwanaland, and by Plio–Pleistocene normal faulting on the northern flank of the rise antithetic to the oblique-collision plate boundary in the southern Hikurangi Trough. This active normal faulting may indicate that the northwestern corner of Chatham Rise continental crust is being dragged down with the subducting slab to the north. The depositional regime has changed from Late Cretaceous infilling of fault-angle depressions, through an early Tertiary transgression and mid-Tertiary carbonate drape, to a late Miocene–Recent sequence recording repeated glacial–interglacial events. This upper stratified unit onlaps a late Miocene erosion/phosphatization unconformity toward the crest of the rise. It is locally truncated by a slope-parallel erosion surface, with downslope buildup, which may indicate either current scour and deposition or mass movement.

INTRODUCTION

Background

In transit between Cook Strait and Site 594, the *Glomar Challenger* obtained seismic profiles along approximately 900 km of ship's track. Because they are tied to borehole data and because they cross areas where tracks are sparse, the *Glomar Challenger* profiles provide a significant increase in our understanding of the stratigraphy of eastern New Zealand and of tectonism in continental crust adjacent to an oblique-collision plate boundary.

In this paper we integrate the *Glomar Challenger* profiles with published syntheses, with seismic data obtained by D.S.I.R. divisions, and with compilations of oil company data on open file at the New Zealand Geological Survey. Oil company data used in this study include profiles collected by Mobil Oil Corporation, Magellan Petroleum (New Zealand) Ltd., Australian Gulf Oil company, and B.P. Shell Todd (Chatham Rise) Ltd.

Geomorphological Setting

The *Glomar Challenger* profiles traverse the Mernoo Saddle, a depression between the continental shelf of eastern New Zealand and the east–west-trending Chatham Rise (Fig. 1; Fig. 3, later). The saddle's sill depth is over 500 m deep, contrasting with shelf depths to east and west. It separates the gently sloping head of the Bounty Trough to the south from the steeper-sided head of the Hikurangi Trough to the north. To the east is the flat-topped Mernoo Bank at the western end of the Chatham Rise. To the west is the weathered volcanic mass of Banks Peninsula and beyond lie the Canterbury Plains and the high ramparts of the Southern Alps.

Physical Oceanography

The Chatham Rise is a significant barrier to ocean circulation. Its crest corresponds with a Subtropical Convergence Zone between Subtropic Water, which has flowed around northern New Zealand as the East Cape Current, and mixed Subantarctic Water, which has flowed around southern New Zealand as the Southland Current (Fig. 1; Burling, 1961; Heath, 1972, 1976). Although subtropical species such as flying fish live in the waters off eastern North Island, icebergs large enough to ground on the shallower parts of the Chatham Rise have often been reported off eastern South Island (Brodie and Dawson, 1971) and Antarctic erratics have been dredged from the Chatham Rise (Cullen, 1962).

The Mernoo Saddle is the only significant gap in the barrier. As the main currents turn east along the rise, a branch of the cool Southland Current flows through the gap to mix in complex eddies with water that has flowed from the north and through Cook Strait. In addition, low-salinity water rises from a depth of about 700 m to maintain a slow (0.08 m/s) northward net drift across the deeper parts of the saddle (Heath, 1976). Maximum tidal speeds through the gap reach 0.44 m/s (Heath, 1976), which is more than enough to move sediment (Carter and Herzer, 1979).

---

[1] Kennett, J. P., von der Borch, C. C., et al., *Init. Repts. DSDP*, 90: Washington (U.S. Govt. Printing Office).

[2] Addresses: (Lewis) New Zealand Oceanographic Institute, D.S.I.R., P.O. Box 12-346, Wellington, N.Z.; (Bennett, present address) New Zealand Oil and Gas Ltd., P.O. Box 3149, Wellington, N.Z., (Herzer) New Zealand Geological Survey, D.S.I.R., P.O. Box 30-368, Lower Hutt, N.Z; (von der Borch) Flinders University, Bedford Park, S.A. 5042 , Australia.

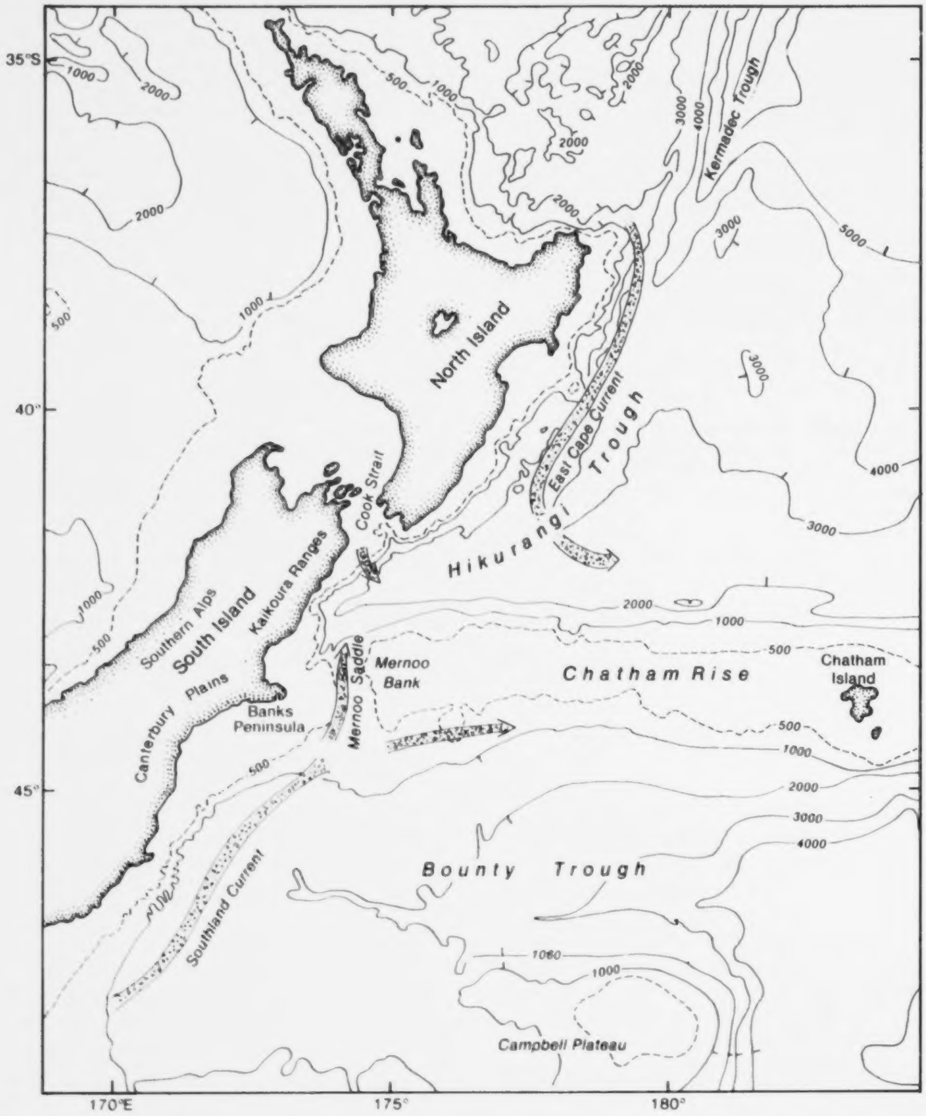
35°S
40°
45°
170°E
175°
180°
North Island
South Island
Cook Strait
Southern Alps
Kaikoura Ranges
Canterbury Plains
Banks Peninsula
Mernoo Saddle
Mernoo Bank
Chatham Rise
Chatham Island
Hikurangi Trough
East Cape Current
Kermadec Trough
Bounty Trough
Southland Current
Campbell Plateau
500
1000
2000
3000
4000
5000

Figure 1. Main topographic features and oceanic circulation off eastern New Zealand. Contours at 1000 m intervals plus broken contour at 500 m depth. (Bathymetry from Carter, 1980, currents from Heath, 1976.)

Along the east coast of South Island, storms are mainly from the south, again producing a net overall northward drift of water and entrained sediment.

During periods of lowered sea level, when the Canterbury Shelf and Mernoo Bank were exposed, flow through the Mernoo Saddle between contrasting water masses could have been even more constricted and more intense than at present. Even if the Subtropical Convergence shifted to the north of New Zealand, the Chatham Rise would still have been a barrier between water masses that had flowed around the northern and southern ends of New Zealand.

Tectonic Setting

The apex of the Hikurangi Trough, just north of the Mernoo Saddle, represents the southern limit of the Tonga–Kermadec–Hikurangi Subduction System (Fig. 2). This system is characterized by subduction of the Pacific Plate beneath the Indo-Australian Plate. Along the sediment-flooded Hikurangi Trough, the Pacific Plate dives beneath the continental crust of northeastern New Zealand, which is being plated with an imbricate-thrust, accretionary prism (Lewis, 1980). The Pacific Plate is probably oceanic crust southward to the latitude of southernmost North Island. The apex of the trough appears to be underlain by downwarped epicontinental crust of the Chatham Rise, which is underthrusting the rapidly rising Kaikoura Ranges.

Along the Hikurangi Margin there is wide zone of deformation where the edge of the Indo-Australian Plate interacts with the obliquely underthrusting Pacific Plate. The outer feather edge is characterized by the accretion-

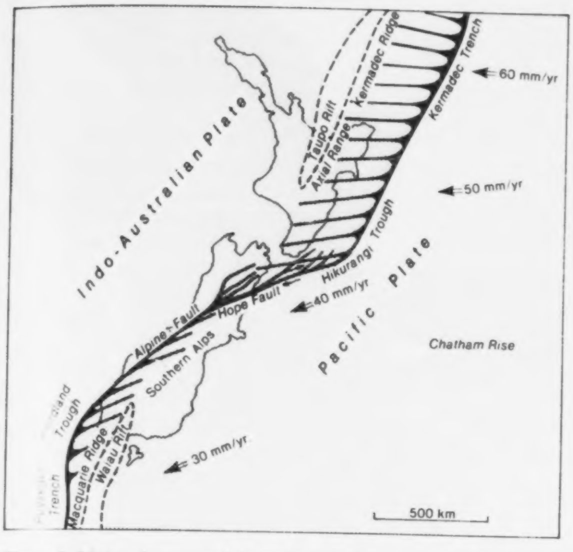

Figure 2. Major elements of the Indo-Australian/Pacific plate boundary in the New Zealand Region. Stippling represents continental crust. Arrows show relative motion of Pacific Plate with respect to the Indo-Australian Plate. Lines represent direction of motion of underthrusting plate (adapted from Walcott, 1978, and Lewis, 1980).

ary prism, which merges landward into a subparallel series of dextral transcurrent faults that link southward into the Alpine Fault (Lewis, 1980). In northeastern South Island the dextral faults form the Marlborough Shear Zone, which is thought to be propagating southward (Ryan and Scholz, 1978) as mirror-image subduction zones north and south of New Zealand move further apart (McKenzie and Morgan, 1969). The underthrust Pacific Plate can be detected beneath the more northerly faults of the Marlborough Shear Zone (Arabasz and Robinson, 1969; Adams and Ware, 1977) but not beneath the southern limit of the zone at the Hope Fault nor at an evolving lineament to the south (Carter and Carter, 1982; Herzer and Bradshaw, in press).

The Alpine Fault is an intracontinental trench–trench transform. In western South Island there is a component of compression across the fault, with the Indo-Australian Plate being thrust under the Pacific Plate (Allis, 1981) and pushing up the edge of the Pacific Plate to form the Southern Alps.

Thus, the western end of the Chatham Rise is on the Pacific Plate close to the northern end of the oblique-collision, trench-trench plate boundary through continental New Zealand. It is to be expected that it will exhibit some structural and stratigraphic evidence of its proximity to this boundary.

Tectonic History

Up to the end of Early Cretaceous Rangitata Orogeny, the history of New Zealand was that of a Pacific margin of Gondwanaland (Spörli, 1980). In the Late Cretaceous, widespread block faulting and graben formation heralded the break-up of this margin (Austin, 1973a, b). The Rangitata Foldbelt, part of which now forms the Chatham Rise, split away from its foreland along a rifted basin, part of which now forms the Bounty Trough (Davey, 1977). The Bounty Trough rift failed and the successful Tasman Sea rift opened up in the foreland to the west. As the Tasman Sea opened in the latest Cretaceous and Paleocene, the foldbelt, the rifted basin, and a segment of foreland rotated together out into the Pacific Ocean (Cullen, 1970; Spörli, 1980) to form the basic elements of the New Zealand Continental Plateau. The southeastern segment of foldbelt has formed the Chatham Rise, the southeastern part of the rifted basin has formed the Bounty Trough, and the Campbell Plateau to the south survives as a remnant of Gondwana foreland.

The Palaeogene was a period of quiescence—of slow subsidence of the New Zealand Plateau as it drifted away from the spreading plate boundary. There was widespread marine transgression and peneplanation of the few remaining low-lying landmasses (Fleming, 1962; Carter and Norris, 1976; Suggate, 1978). With cessation of spreading in the Tasman and opening of the seaway between Australia and Antarctica, the initiation of the Circum-Antarctic Current (Kennett et al., 1975) bought widespread marine erosion, not only in the Southern Ocean but perhaps also on the margins around New Zealand (Carter and Norris, 1976).

At some stage in the Oligocene the present dextrally slipping, trench–trench transform plate boundary bisected the New Zealand continental plateau. In the late Oligocene and early Miocene, there was a component of extension along the boundary that changed to gradually increasing compression after late Miocene times (Carter and Norris, 1976), as the Indo-Pacific pole of rotation moved southward (Walcott, 1978). This increasing compression is expressed as the Plio-Pleistocene Kaikoura Orogeny, which has elevated the mountain chains of New Zealand. The rising mountains have changed patterns of sedimentation on adjacent margins from dominantly calcareous to increasingly coarse clastic debris (Prebble, 1980).

WESTERN CHATHAM RISE

Existing Knowledge

The Chatham Rise is a broad, east–west geanticline with Tertiary formations draped over a core of upper Paleozoic or lower Mesozoic greywacke and chlorite schist of the old Rangitata Foldbelt (Houtz et al., 1967; Cullen, 1980). Samples of schist, of Eocene and lower Miocene limestone, and of phosphatized nodules of Oligocene, lower Miocene, and lower middle Miocene limestone have been dredged from near the ridge crest (Cullen, 1965, 1980; Pasho, 1976). The nature and distribution of limestone on the central rise, on the Chatham Islands, and in central Canterbury suggests that the Chatham Rise was a marginal plateau, remote from large-scale detrital input, for most of the early Tertiary (Suggate, 1978). At some time in middle to late Miocene time there was a phase of erosion with phosphatization of exposed limestone and eroded clasts (Cullen, 1967).

Since the end of the Miocene Epoch, sediments have blanketed the flanks of the rise while the crest has remained largely sediment-free. The northwest corner of the Chatham Rise has been downwarped and buried by up to 4 km of flat-lying Plio-Pleistocene turbidites (Katz, 1974) derived from rapidly rising mountains to the south. This northern margin is heavily faulted but the nature and age of faulting is inconclusive from existing data (Ewing et al., 1969; Davey, 1977).

The westward continuation of the Chatham Rise now lies buried beneath the gravel fans of the Canterbury Plains and the prograding clastic wedge of the Canterbury continental shelf (Herzer, 1981). These deposits have built around the upper Miocene shield volcano (Stipp and McDougall, 1968) of Banks Peninsula. Groups of young, probably upper Cenozoic volcanic knolls occur along the southern flank of the western Chatham Rise, an area heavily scoured by channels and scarred by slope failure (Herzer, 1975).

Importance of *Glomar Challenger* Data

Site 594 (Fig. 3) is the first drill site in the Chatham Rise–Bounty Trough area and it therefore presents an unrivalled opportunity for the stratigraphic interpretation of existing seismic data. Two exploration wells have been drilled on the continental shelf to the west of Site 594 (Anon., 1971, 1975). Both are sited in the thick Neogene clastic wedge and their Neogene stratigraphy is difficult to trace, in seismic sections, to the thin distal facies of the rise and trough. However, the Paleogene stratigraphy can be traced with more success, providing the basis for our interpretation of the deeper seismic stratigraphy. The position of Site 594 was selected on the basis of *Eltanin* profile *E*43 (Fig. 3, 4) (Davey, 1977). Profiles obtained by *Glomar Challenger* in transit to and from Site 594 (Fig. 3; Fig. 5, back pocket) and reported on here show more stratigraphic and structural detail in the upper 1 km or so of sediment than most of the deep-penetration commercial data. The course of *Glomar Challenger* on return from Site 594 was designed to provide increased coverage of the northern flank of the rise, where earlier data indicated structural and erosional complexities in the near-surface layers.

METHODS

Data were collected using a watergun with an 80 cu. in. chamber, firing at 10 s intervals. Firing pressure was 1000 psi, and a 40–160 Hz bandpass filter was employed.

SEISMIC STRATIGRAPHY RESULTS

Seismic Stratigraphy near Site 594

An appraisal of the *Eltanin* site selection profile *E*43 (Fig. 4) and of the southward transit profile (Fig. 5,B–B′) suggest that there are three regional unconformities in the top 1 s or so (two-way traveltime) of seismic section. The unconformities are recognized by local angular discordances in reflectors, such as truncation and baselap, which imply hiatuses in deposition (Vail et al., 1977). In the Bounty Trough they pass into strong reflectors that separate seismic sequences with markedly different characteristics. The unconformities recognized here appear to correlate with the reflectors labeled from the top, Y, X, and A by Davey (1977), A being widely recognized on the eastern Chatham Rise (Austin, 1973a, b). They separate three seismic sequences and an acoustic basement that has markedly different characteristics in different places.

Site 594 lies immediately south and off-structure from a basement high with anticlinal drape of overlying sediments (Fig. 6). Because of the proximity of the high, acoustic reflectors are confused immediately below the drill site. However, the major reflectors and sequences can be extrapolated to the drill site.

The top seismic sequence consists of closely spaced, high-amplitude, near-parallel reflectors with some minor internal convergences or unconformities. It correlates with the "stratified layer" of Davey (1977) and is labeled here acoustic Unit A. At the drill site its acoustic thickness is 320 ms (Fig. 6). The interval velocity in this near-surface layer was measured in core sections and found to be 1500–1600 m/s. Thus, its thickness is about 250 m. Unit A onlaps older sequences toward the north and thins gradually toward the south with development of incised channels in the Bounty Trough (Fig. 4).

Between unconformities Y and X is the Transparent Layer of Davey (1977), characterized by intermittent, widely spaced, low-amplitude reflectors, which are more coherent in the lower half of the sequence. It is labeled here acoustic Unit B. Estimates based on the profile *E*43 and an extrapolation of Reflector X on *Glomar Challenger's* transit profiles (Fig. 6) suggest that Unit B is represented by about 430 ms of seismic penetration at Site 594. Its interval velocity measured in core sections averaged 1600 m/s but refraction data indicate velocities in the range of 1900–2200 m/s (B. W. Davy, Geophysics Division, D.S.I.R., pers. comm., 1984). If an interval velocity of 2000 m/s is used then Unit B must be about 430 m thick, and its base must be about 680 m below the seafloor. Unit B thins rapidly toward the north with apparent onlap onto Reflector X and erosional truncation at Reflector Y, although the diffuse internal reflectors make identification of lapout difficult. It thickens gradually toward the axis of the Bounty Trough (Fig. 4).

Beneath Reflector X is a sequence that for the purposes of the present study can be labeled acoustic Unit C. At most places there is a strong reflector, Reflector A, at its base. At some places the basal reflector has the appearance of volcanic or intrusive knolls, at others of block-faulted Mesozoic basement, and at others of a strong intrasedimentary reflector. Unit C contains only a few low-amplitude reflectors. At the drill site the thickness of Unit C, which was not penetrated by drilling, appears to be represented by a seismic interval of about 190 ms. If a seismic velocity of 3000 m/s is used (B. W. Davy, Geophysics Division, D.S.I.R., pers. comm.) then its thickness is about 280 m.

Correlation with Logs of Site 594

Site 594 was drilled to a total depth of 639.5 m below the seafloor, penetrating acoustic Unit A and most of acoustic Unit B. The boundaries of the seismic sequences described here do not correspond with the bound-

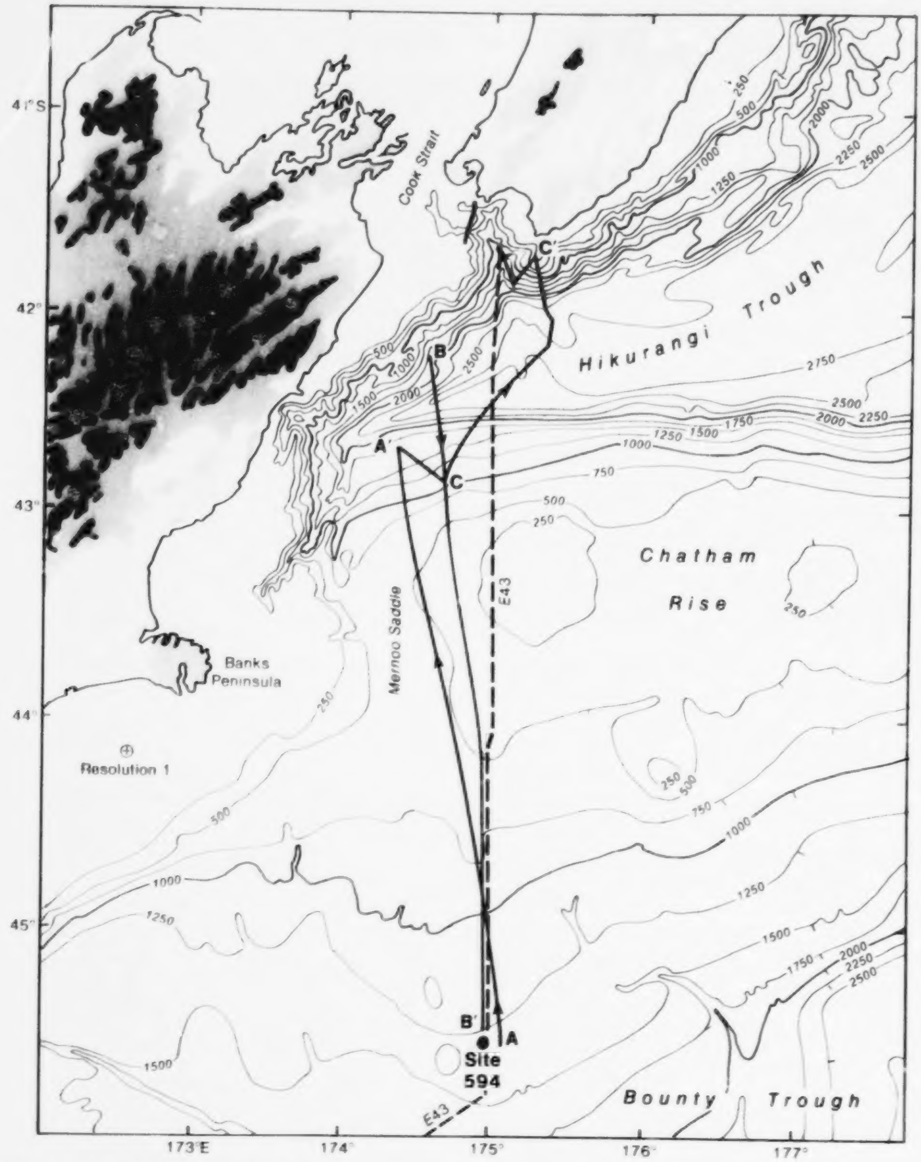
41°S
42°
43°
44°
45°
173°E
174°
175°
176°
177°
Cook Strait
Hikurangi Trough
Chatham Rise
Bounty Trough
Mernoo Saddle
Banks Peninsula
Resolution 1
Site 594
E43
A
A'
B
B'
C
C'
250
500
750
1000
1250
1500
1750
2000
2250
2500
2750

Figure 3. Detailed topography and bathymetry adjacent to the western end of the Chatham Rise with position of *Glomar Challenger* transit profiles A–A′, B–B′, and C–C′ (see Fig. 5), to and from Site 594, and of site selection profile *Eltanin E*43. On land, solid at >1000 m, stippled at 250–1000 m. Isobaths at 250 m intervals from van der Linden (1968) and Krause and Cullen (1970).

aries of designated lithostratigraphic units at the drill site but do correspond with changes in sedimentary regime (Fig. 6).

The stratified acoustic Unit A is represented in the drill samples by stratified upper Miocene to Recent pelagic and hemipelagic oozes (Nelson, Jarrett, et al.; Nelson, Hendy, Cuthbertson et al.; both this volume). The upper half of the acoustic unit correlates with lithostratigraphic Unit I, at 0–160 m sub-bottom depth, consisting of alternating pelagic nannofossil ooze and hemipelagic nannofossil-bearing clayey silt of early Pliocene to Recent age. Individual pelagic–hemipelagic cycles range from 0.5 to 10 m thick and contacts are gradational. They are interpreted as interglacial/glacial cycles, the hemipelagic silty layers representing glacial periods of increased sediment supply from the rising mountain ranges of New Zealand and increased dissolution of pelagic carbonate (Griggs et al., 1983). At least 25 major influxes of silt have occurred during the last 5 Ma.

The lower half of acoustic Unit A, at 160–250 m sub-bottom, may underly a local minor unconformity. It corresponds with the top of lithostratigraphic Unit IIA and consists of uppermost Miocene to basal Pliocene, alternating pure and impure pelagic nannofossil oozes.

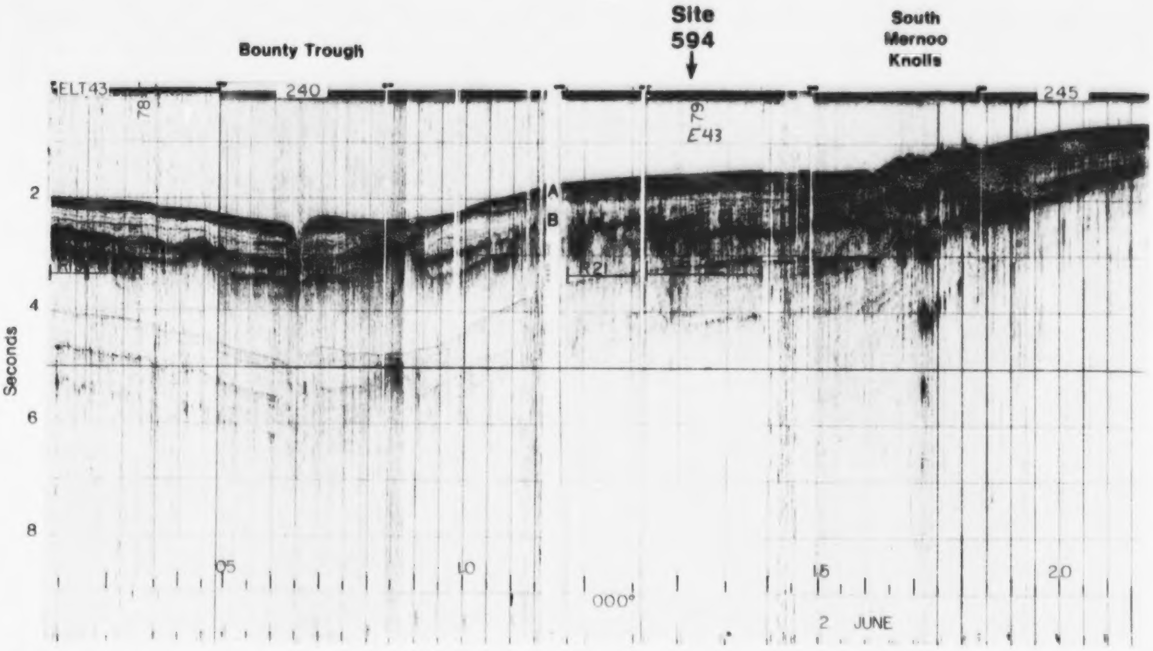

Figure 4. Site selection profile from *Eltanin E*43 showing surface stratified layer (acoustic Unit A) and underlying transparent layer (acoustic Unit B) thinning toward the crest of the Chatham Rise. Lines at 1 s intervals (two-way traveltime) equivalent to 750 m in seawater.

The thin impure intervals are enriched in diatoms, sponge spicules, mica, foraminifers, and/or thin lenses of silt and clay. They are again interpreted as a response to increased glacial-age carbonate dissolution (Griggs et al., 1983). Thus, the closely spaced, high-amplitude signals from acoustic Unit A appear to be a seismic response to the stratification associated with latest Miocene to Recent glacial/interglacial changes. The unconformity Y at its base has a negligible angular difference in dip at the drill site and was not detected in lithostratigraphic or biostratigraphic analysis of core samples.

The "transparent" acoustic Unit B is represented in the core by Miocene nannofossil ooze or, below 470 m, where it is more consolidated, by Miocene nannofossil chalk. The upper part of Unit B, which has only a very few low-amplitude reflectors, corresponds with the almost featureless mid and upper Miocene nannofossil ooze of the lower part of lithostratigraphic Unit IIA. The lower part of acoustic Unit B, which has more coherent low-amplitude reflectors, corresponds with the lower Miocene to basal middle Miocene lithostratigraphic Unit IIB, which is composed of nannofossil chalk with interbeds of silt-bearing clayey nannofossil chalk. The interbeds have sharp erosional bases and are interpreted as turbidite deposits.

The base of acoustic Unit B was not sampled at Site 594, and acoustic Unit C lies well below the total depth of drilling.

South Mernoo Knolls

South of the Mernoo Saddle, there are scattered knolls with positive magnetic anomalies which are considered to be the products of Neogene volcanism (Herzer, 1975). The two *Glomar Challenger* transit profiles (Fig. 5) cross one group of these knolls, and the stratigraphy devised at Site 594 can be traced northward across them only with difficulty. However, correlation is possible on the basis of broad similarities in seismic character and with the help of oil industry profiles in the area.

The uppermost Miocene to Recent acoustic Unit A onlaps unconformity Y at its base toward the knolls (Figs. 5, 6). It can be distinguished to the north of the knolls as a unit of similar seismic character and thickness. Within the group of knolls, channels some 200 m deep appear to have been scoured into the upper sedimentary layers and partly or completely infilled. The channels commonly appear to have been moatlike depressions around individual volcanic pinnacles. Immediately to the north of the group of knolls (Fig. 5A), the presence of a channel with onlap or prograded fill at the uppermost Miocene unconformity Y suggests that the volcanic pinnacles are at least partly older than late Miocene in age. Acoustic Unit B is correlated, with some uncertainty, with a much thinner, more stratified sequence in a similar stratigraphic position north of the knolls. It may be supposed that the different seismic character is the product of a different, perhaps slightly higher energy environment near the rise crest. Convergence of reflectors toward the knolls may indicate some disturbance of the seafloor at this position during the deposition of at least the younger part of acoustic Unit B. Doming of reflectors above the basement high near the drill site could indicate either sheet drape over a pre-existing high in a low-current environment or doming by a magma diapir or velocity pull-up of thermally metamorphosed sediments.

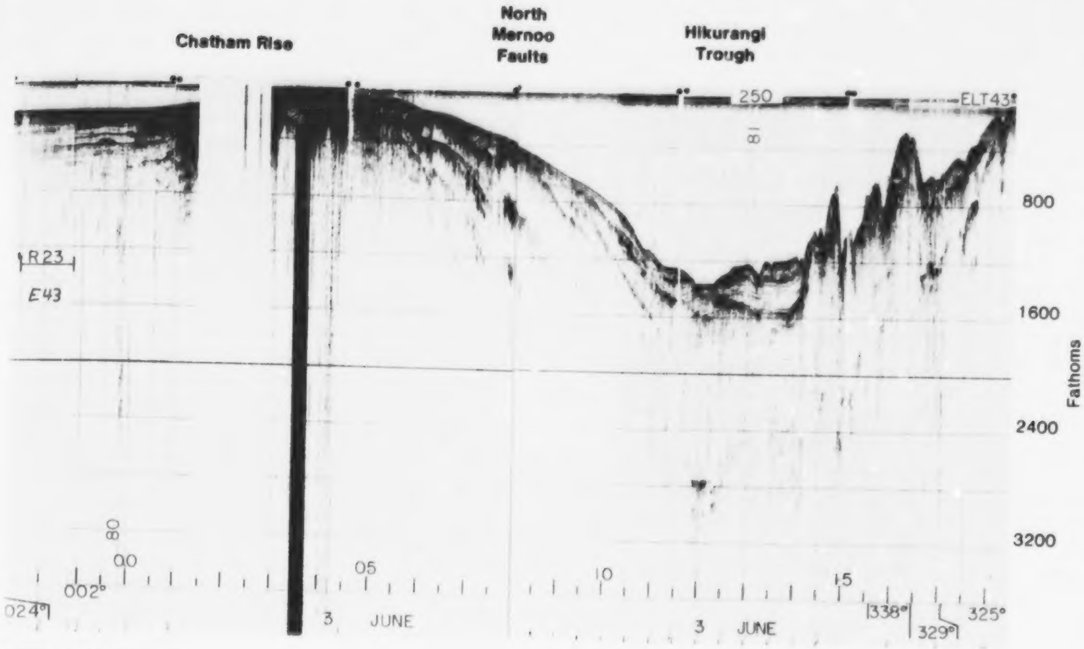

Figure 4. (Continued).

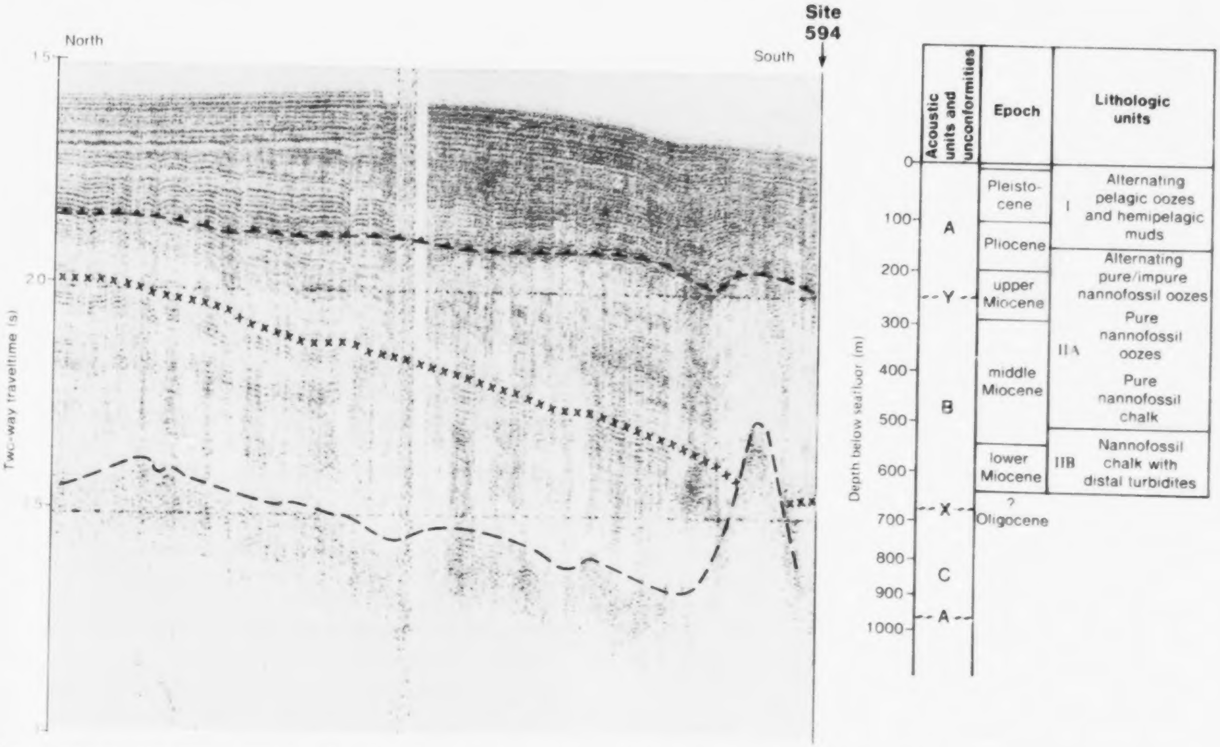
Site 594
North
South
Two-way traveltime (s)
2.0
Acoustic units and unconformities
Epoch
Lithologic units
Depth below seafloor (m)
0
100
200
300
400
500
600
700
800
900
1000
A
Y
B
X
C
A
Pleisto-cene
Pliocene
upper Miocene
middle Miocene
lower Miocene
?
Oligocene
I
Alternating pelagic oozes and hemipelagic muds
Alternating pure/impure nannofossil oozes
IIA
Pure nannofossil oozes
Pure nannofossil chalk
IIB
Nannofossil chalk with distal turbidites

Figure 6. Correlation between seismic stratigraphy in transit profile and borehole stratigraphy at Site 594. Indicated are unconformities Y, X, and A separating acoustic Units A, B, C, and acoustic basement.

Unconformity X, which defines the base of Unit B, can be correlated north of the knolls, although it becomes less seismically reflective toward the crest of the rise and away from the Bounty Trough.

Crest of the Rise

The profiles across the Mernoo Saddle (Fig. 5) show the planed geanticlinal structure typical of the ridge crest further east.

The only rock samples from the vicinity are supposed Permian–Jurassic greywackes dredged from Mernoo Bank (Norris, 1964; McDougall, 1982). These almost certainly correlate with acoustic basement that outcrops at the crest of the saddle. The basement is faulted to form several half-grabens or fault-angle depressions, which are fault-bounded on their northern side; that is, faults are downthrown to the south. Similar tensional faulting in basement occurs at the eastern end of the Chatham Rise, where both fault-angle depression formation and infilling are inferred to be Late Cretaceous in age (Austin et al., 1973a, b). Late Cretaceous fault-angle depressions occur on the southern slopes of the Chatham Rise and into the Bounty Trough (B. W. Davy, Geophysics Division, D.S.I.R., pers. comm.) and on land in South Island (Carter and Norris, 1976), where in each case they are correlated with rifting that preceded opening of the Tasman Sea. Thus, it is assumed that formation of fault-angle depressions and their subsequent infilling is also largely of Late Cretaceous age in the Mernoo Saddle.

The mainly lower and middle Miocene acoustic Unit B and lower Tertiary Unit C onlap and thin toward the crest of the rise but apparently cover much of it. This supports a suggestion (Kennett and Casey, 1969) that the rise has been a submarine bathymetric feature since the early Tertiary.

The uppermost Miocene to Recent acoustic Unit A onlaps the upper Miocene unconformity toward the crest of the rise. The upper Miocene period of planation probably represents the time when lower Oligocene to middle Miocene limestones were exposed at the seabed and phosphatized (Cullen, 1980). Along much of the rise the phosphatized limestones have apparently remained at or near the seabed ever since, but in the Mernoo Saddle they are buried by surficial sediments (McDougall, 1982) too thin to be detected on the present profiles.

North Mernoo Slope

The slope between Mernoo Saddle and the southwestern end of the Hikurangi Trough bears evidence of major Neogene tectonic activity and of post-depositional changes to Neogene sediments. In this it differs significantly from any other areas of the passive Chatham Rise.

The seismic sequences recognized south of the Chatham Rise are tentatively correlated here with a similar sequence north of the rise (Fig. 5). There is an onlapping upper sequence correlated with acoustic Unit A and underlying transparent units between strong reflectors correlated with acoustic Units B and C.

The seismic sequences of the whole slope are fractured by faults that are, with one or two possible exceptions, all downthrown to the south (Figs. 5, 7). The band of faulting extends approximately east–west, and tentative correlations of individual faults suggest a similar trend. The majority of the faults are of late Neogene origin, as they cut acoustic Unit A, some showing evidence of continued growth during deposition of the unit and some producing a scarp at the seabed. The majority do not show evidence of increased throw in units older than late Neogene in age. Some older units thin toward the rise crest, giving a false impression of growth fill in a fault-angle depression. However, there are faults, including several near the rise crest, that show either dislocation of older units only or increased throw in older units, indicating movement on older faults before late Neogene faulting and movement. The age of faulting before the late Neogene is uncertain because of uncertainties in the correlation of seismic sequences below Unit A. However, similar faulting elsewhere on the Chatham Rise is Late Cretaceous in age (Austin et al., 1973a, b).

Plots of earthquake epicenters show that there is significant seismic activity under the area of Neogene faulting (Arabasz and Robinson, 1976). This activity, which is clearly in the Pacific Plate, occurs on the eastern fringe of a diffuse zone of intense activity marking the plate boundary zone to the west. Thus, the seismology indicates active faulting related to the boundary zone. Fault plane solutions, which would show the faulting regime, are not available for this area.

The vertical exaggeration of the transit profiles is such that the dip direction of fault planes is difficult to ascertain, but available oil industry profiles, with low vertical exaggeration (Fig. 7), clearly show the faults to be normal, indicating a tensional regime adjacent to an oblique collision boundary. Industry and D.S.I.R. data show that this band of normal faulting, here termed the North Mernoo Fault Zone, dies out about 100 km east of the *Glomar Challenger* tracks and disappears westward beneath the clastic wedge of the Canterbury shelf.

Besides being offset by faulting, acoustic Unit A is erosionally truncated on the northern slope of the Mernoo Saddle between depths of about 700 m and 1700 m, with increased erosion between 1500 m and 1700 m (Figs. 5, 8). Davey (1977), who described the erosion as a product of slumping, showed that it closely paralleled the contours. Downslope from the scour, Unit A is much thickened, with local discontinuities but still with closely spaced, high-amplitude, sub-parallel reflectors. There are only small patches of contorted bedding both at the seabed and buried within Unit A.

Southern Hikurangi Trough and Accretionary Margin

In the southern extremity of the Hikurangi Trough, the correlative of acoustic Unit A changes character to a thick sequence of near-horizontal reflectors which are deformed along the toe of the eastern margin of New Zealand (Fig. 5). The uppermost Miocene unconformity Y, at the base of Unit A, is too deep to be detected on

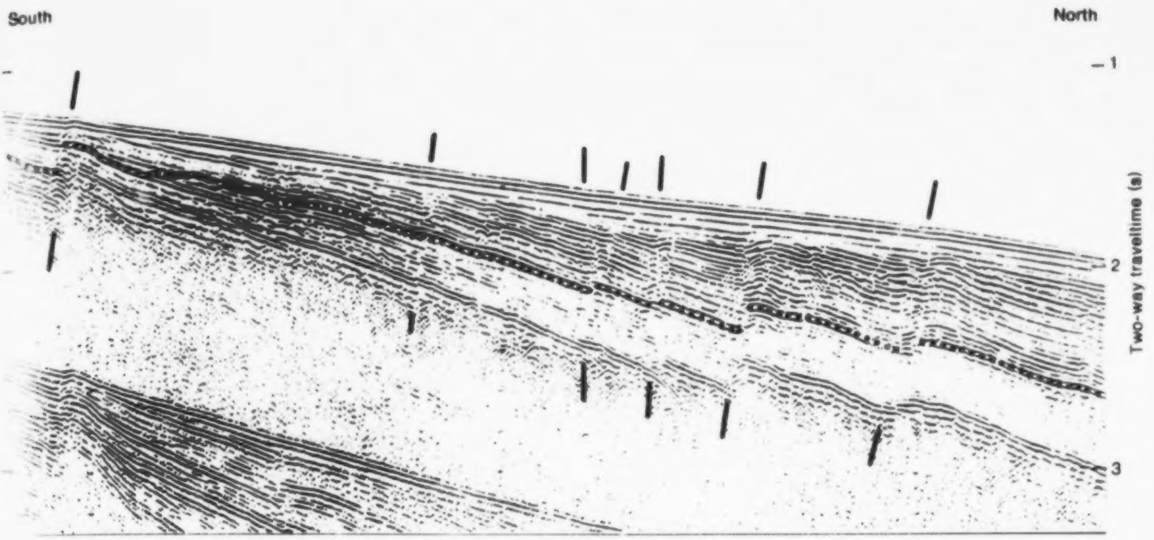

Figure 7. Seismic profile Magellan G-9 across North Mernoo Fault Zone (water depth 800–1450 m) showing dip of most normal faults toward the crest of the Chatham Rise. Unconformity Y, at base of acoustic Unit A, is stippled. Lines at 1 s intervals (two-way traveltime), equivalent to 750 m in seawater.

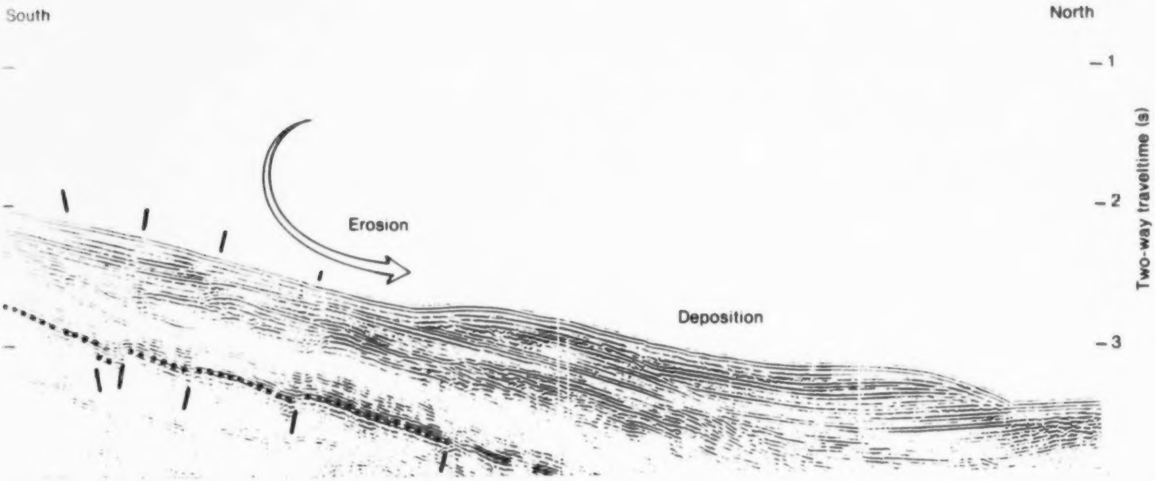

Figure 8. Seismic profile Magellan G-9 across lower North Chatham Slope and adjacent Hikurangi Trough (water depth 1500–2400 m) showing zone of erosion and downslope redeposition. Unconformity Y, at base of acoustic Unit A, is stippled.

the transit profiles. However, on industry profiles an unconformity of about this age can be traced beneath 4 km of Plio–Pleistocene sediments (Katz, 1974).

In the axis of the Hikurangi Trough the thick sequence of near-horizontal reflectors, which is typical of turbidite basin fill, is cut by a channel several hundred meters deep, which has been partly infilled. This channel meanders along the length of the Hikurangi Trough (Houtz et al., 1961; Lewis, 1980).

The deformation along the steep northwestern margin of the trough (Fig. 5B, 5C) is the southern extremity of a zone of imbricate thrusting associated with subduction of the Pacific Plate and accretion of thick slope-toe sediments to the feather edge of the Indo-Australian Plate (Lewis, 1980; Cole and Lewis, 1981).

DISCUSSION

Cycles of Erosion and Deposition

The oldest unconformity on the western Chatham Rise is the surface of the Permian–Jurassic greywackes, planed at the edge of Gondwanaland in the mid-Cretaceous. Initial rifting of New Zealand away from the Australian–Antarctic continent produced tensional half-grabens in the greywacke crust, which filled as the basins developed during the Late Cretaceous (Austin et al., 1973a).

As acoustic Unit C was being deposited in early Cenozoic times, the Chatham Rise was already a submarine ridge with sedimentary layers thinning toward its crest. It lay adjacent to low-lying islands being progressively submerged by the sea and supplying only meager amounts of fine detrital material to the adjacent ocean (Fleming, 1962; Stevens, 1980). Deposition throughout the New Zealand Region was slow and overwhelmingly calcareous, with maximum transgression occurring in middle Oligocene times.

Acoustic unconformity X, the strong reflector that locally corresponds with baselap at the base of acoustic Unit B, was not penetrated at Site 594. However, its stratigraphic position and correlations with exploration wells on the adjacent continental margin indicate a mid to late Oligocene age. The obvious correlation is with the regional "Marshall Paraconformity" (Carter and Landis, 1972), which has been alternatively attributed to either erosion by an initially powerful Circum-Antarctic Current which developed as Australia and Antarctica separated (Carter and Norris, 1976), or erosion arising from increased bottom water activity related to climatic cooling in the Oligocene (Kennett, 1977).

Acoustic Unit B represents another cycle of predominantly fine, calcareous deposition lasting from late Oligocene to late Miocene time. Away from the ridge crest, the monotonous succession exhibits only a few low-amplitude reflectors. Coherent reflectors in the lower part of the unit at the edge of the Bounty Trough can be related to lower Miocene distal turbidites in Site 594. Stronger reflectors on the shallower parts of the rise, where Unit B is much thinner, may indicate marginally more current and/or wave activity along the ridge crest.

Unconformity Y, of late Miocene age, indicates an event that caused either erosion or an hiatus in deposition down to considerable water depths. The dating of this event in the drill log appears to correlate closely with the major eustatic fall in sea level recorded at 6.2 Ma (Loutit and Kennett, 1981a, b). This event marked a major glacioeustatic lowering of sea level in the latest Miocene associated with increased Antarctic glaciation (Kennett, 1967).

The crest of the Chatham Rise was planed at this time and exposed Oligocene to mid-Miocene limestones were phosphatized (Cullen, 1980). Much of the phosphatized limestone has remained exposed at the seafloor since then, but the Mernoo Saddle has a thin covering of surficial sediments on the planed Miocene surface.

The highly "stratified" acoustic Unit A represents a totally new regime of sedimentation dominated by large glacio-eustatic oscillations of sea level and increasing input of hemipelagic detrital debris from the rising Southern Alps. Internal convergence within the sequence indicates some low stands of sea level but the sequence as a whole has gradually onlapped the crest of the rise.

Bottom Current Scour or Mass Movement

There are two alternative explanations for the evident removal of sediment on the northern flank of the rise. The truncated bedding of Unit A could indicate low-angled slope failure, possibly triggered by movement of one of the faults (Davey, 1977). The slope in the area of removal is only just over 1°, but slope failure does occur on slopes of 1° to the north (Lewis, 1973) and to the south (Herzer, 1979) where high rates of sedimentation are considered to have contributed to sediment instability. However, on the northern flank of the Mernoo Saddle, there are no zones of contorted bedding immediately downslope from the truncated bedding; this weighs against, but does not eliminate, the slump hypothesis. An alternative explanation for the truncated bedding is current scour. In favor of this hypothesis is the contour-parallel nature of the feature (Fig. 9; also Davey, 1977, fig. 22), which extends at an approximate depth of 700 to 1700 m deep for at least 50 km northeast of the Mernoo Saddle. Also, downslope from the sediment removal, acoustic Unit A is relatively thick, with sub-parallel and baselapping reflectors. Together, these observations suggest that contour-following currents, analogous to those in the North Atlantic (Davies and Laughton, 1972) are the principal agents of erosion and deposition. If this is correct, then the current responsible may be some variation of the mid-bathyal flow through the saddle described by Heath (1976), possibly a flow constricted during a period of glacially lowered sea level.

The cause of sediment removal on the southern flank of the rise is equally equivocal. Moatlike features around the South Mernoo Knolls are similar to features produced by bottom current scour in the North Atlantic (Davies and Laughton, 1972). There is also evidence that depressions are part of a large sea-valley system, probably related to mass movement of Unit A (Herzer, 1975).

South Mernoo Volcanics

Groups of knolls, interpreted as being volcanic in origin, are common on the slope south of the Mernoo Saddle (Herzer, 1975). The evidence of a scour moat at the base of Unit A indicates that there had been enough volcanic activity to have produced some elevation of the seafloor, and resultant turbulent scour, by the late Miocene. No upper age for the features can be demonstrated. No active volcanism occurs in the region today, but volcanism has occurred in southern New Zealand throughout the Cenozoic (Suggate, 1978); the nearest dated volcanism, 200 km away on Banks Peninsula, is of mainly Miocene age. There is some evidence of a mid-Cenozoic band of alkaline shield volcanoes down the eastern side of New Zealand, and there may be a complementary late Cenozoic band along the edges of the continental crust to the east, perhaps reflecting movement of the Pacific Plate with respect to a linear mantle source (Adams, 1981). Thus, the knolls are most probably mid to late Tertiary in age.

North Mernoo Fault Zone

The North Mernoo Fault Zone was at first puzzling. Its evident seismic activity and its position, which is limited to the northwest corner of the Chatham Rise (Fig. 9), implies that it is active and related to the very oblique collisional plate boundary at the southern end of the

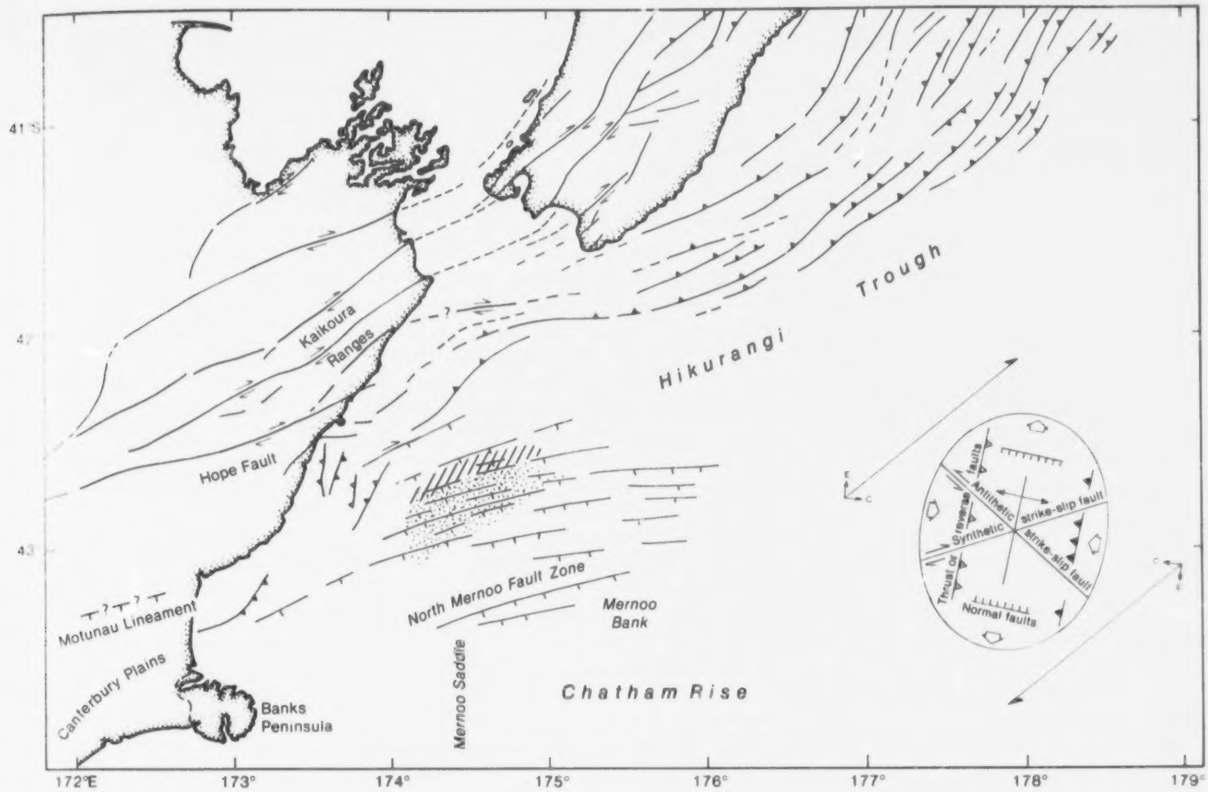

Figure 9. Major faults in vicinity of southern Hikurangi Trough transform plate boundary (from Lewis and Bennett, in press). Tags on faults are down the dip of the fault plane. Triangles are thrust faults and short straight tags are normal faults. Stippling indicates area of erosion and hatching indicates redeposition of top sequence. Inset: structural pattern resulting from a northeast–southwest dextral shear couple (adapted from Reading, 1980).

Hikurangi Trough. But if it is related to a collisional margin, however oblique, why is the faulting apparently tensional?

At many convergent margins, subducting oceanic crust is broken by tensional faults as it is bent and pulled down beneath the overriding plate (Honza, 1980; Schweller et al., 1981; Carey and Dubois, 1981). The faulting pattern is typically one of horsts and grabens, or of normal faults downthrown toward the trench. The northwest corner of the Chatham Rise is not, of course, subducting oceanic crust. However, oceanic crust is being subducted beneath the margin immediately to the north, and the subducted slab has been traced beneath Cook Strait and the northern edge of South Island (Arabasz and Robinson, 1976; Walcott, 1978). It is inferred here that the edge of the continental crust of the Chatham Rise is being pulled down with the contiguous subducting slab of oceanic crust to the north. Certainly the downwarped northwest margin of the Chatham Rise can be traced under thick turbidites in the southern end of the Hikurangi Trough, and the buoyancy of the overridden Chatham Rise may account for the rapid rise of the Kaikoura Ranges.

If this corner of the Chatham Rise is being dragged under the Kaikoura Ranges, why do the normal faults trend east–west? The reason appears to be associated with the fact that the southern Hikurangi segment of the plate boundary is not primarily tensional or compressional but strike–slip (Lewis, 1980). In clay model experiments, strike-slip movement has been shown to produce characteristic structural patterns (Cloos, 1955; Wilcox et al., 1973). A northeast–southwest-trending dextral shear couple (Fig. 9, inset) will produce not only synthetic and antithetic strike–slip faults, but also thrust faults and folds aligned north-northeast–south-southwest, perpendicular to the short, contracting axis of the strain ellipse, and normal faults aligned east-southeast–west-northwest, perpendicular to the expanding axis of the strain ellipse (Reading, 1980). Despite a component of collision at this boundary, a pattern of faults with almost these trends does occur at the southern limit of the Hikurangi Trough (Fig. 9). The north-northeast–south-southwest thrust faults (and anticlines) are most conspicuous at the western end of the trough and on the adjacent land, where they include west-directed, as well as the more common east-directed, thrusted anticlines (Gregg, 1964; Wilson, 1963). The normal faults are most conspicuous on the flank of the Chatham Rise. Their east–west (rather than east-southeast–west-northwest) trend is probably inherited from the strong east–west trend of the Late Cretaceous half-graben system in the underlying basement of the rise.

If the northwest corner of the Chatham Rise is being pulled down while the ridge crest remains buoyant, then why are the faults downthrown toward the crest instead of toward the trough? In fact, in a tensional regime the sense of fault throw matters little. A strain ellipse similar to that for the horizontal components operates in the vertical field, with ordinary synthetic faults downthrown to basin and antithetic faults downthrown updip. Although tensional downbuckling might normally encourage synthetic faulting in an isotropic medium, in this particular case the antithetic system completely dominates. The reason for this is unclear, but the most probable explanation is again that these faults reactivated the Cretaceous structural grain, which is dominated by fault planes with a southerly dip.

CONCLUSIONS

1. The evolution of the western Chatham Rise is clearly illustrated in seismic profiles obtained in transit to and from Site 594. Basement fault-angle depressions and their infill are the products of a Late Cretaceous period of rifting that immediately preceded the rifting of New Zealand away from Gondwanaland. Overlying sequences, draping both the rise and its flanks, are inferred to be predominantly carbonate sediments that accumulated throughout an early and mid-Tertiary period of wide marine transgression, relative tectonic stability, and sporadic volcanism. Nevertheless, conspicuous hiatuses indicate that deposition was interrupted by major falls in sea level and/or major changes in oceanic circulation. The hiatuses are correlated with major events in the late Oligocene (29 Ma) and late Miocene (6.2 Ma). The top sedimentary sequence, present on the flanks of the rise but absent on the crest, is a stratified layer reflecting increased detrital input from the rapidly rising mountain ranges of New Zealand during late Miocene to late Quaternary periods of glacially lowered sea level.

2. The causes of erosion and redeposition of the top sequence are equivocal. The most probable explanation appears to be related to the effects of bottom currents, perhaps during glacial periods of lowered sea level, that move parallel to the contours north of the Mernoo Saddle and are disturbed by volcanic knolls south of the saddle.

3. A group of knolls, the South Mernoo Knolls, on the south flank of the rise are volcanic and were at least partly erupted before late Miocene times. They may be related to alkaline volcanics of similar age down the eastern side of New Zealand.

4. An east–west zone of faults, the Mernoo Fault Zone on the northwest edge of the Chatham Rise, consists of antithetic normal faults downthrown toward the rise crest. It is inferred that tensional faults dominate in this area because the edge of the continental crust of the Chatham Rise is being dragged down under the Kaikoura Ranges by the subducting slab to the north. The antithetic system may dominate because it has reactivated the Cretaceous structural grain of the Chatham Rise basement, which is dominated by east–west normal faults with south-dipping fault planes. The east–west trend, developed along a pre-existing line of weakness, is compatible with the northeast–southwest dextral shear couple at the adjacent transform boundary.

ACKNOWLEDGMENTS

We are indebted to our colleagues Dr. L. Carter, Dr. D. J. Cullen, Dr. F. J. Davey and Dr. B. W. Davy for their willingness to discuss the data, for their many helpful comments and suggestions, and for their constructive criticism of the manuscript.

REFERENCES

Adams, C. J., 1981. Migration of late Cenozoic volcanism in the South Island of New Zealand and the Campbell Plateau. *Nature*, 294: 153–155.

Adams, R. D., and Ware, D. E., 1977. Subcrustal earthquakes beneath New Zealand: locations determined with a laterally inhomogeneous velocity model. *N. Z. J. Geol. Geophys.*, 20:59–8

Allis, R. G., 1981. Continental underthrusting beneath the Southern Alps of New Zealand. *Geology*, 9:303–307.

Anon, 1971. Well Résumé Endeavour-1 B.P. Shell Todd (Canterbury) Ltd. *N. Z. Geol. Surv. Open File Petrol. Rep.* 303.

________, 1975. Well Completion Report. Resolution 1. B.P. Shell Todd (Canterbury) Ltd. *N. Z. Geol. Surv. Open File Petrol. Rep.* 648.

Arabasz, W. J., and Robinson, R., 1976. Microseismicity and geologic structure of northern South Island, New Zealand. *N. Z. J. Geol. Geophys.*, 19:569–609.

Austin, P. M., Sprigg, R. G., and Braithwaite, J. C., 1973a. Structural development of the eastern Chatham Rise and of the New Zealand region. *In* Fraser, R. (Comp.), *Oceanography of the South Pacific, 1972:* Wellington (N. Z. Nat. Comm. for UNESCO), pp. 201–215.

________, 1973b. Structure and petroleum potential of eastern Chatham Rise, New Zealand. *Bull. Am. Assoc. Pet. Geol.*, 57:477–97.

Brodie, W. J., and Dawson, E. W., 1971. Antarctic icebergs near New Zealand. *N. Z. J. Mar. Freshwat. Res.*, 5:80–85.

Carey, E., and Dubois, J., 1981. Behaviour of the oceanic lithosphere at subduction zones: plastic yield strength from finite-element method. *Tectonophysics*, 74:99–110.

Carter, L., 1980. New Zealand Region bathymetry 1:6,000,000 (2nd ed.). *N. Z. Oceanogr. Inst. Chart, Misc. Ser.*, 15.

Carter, L., and Herzer, R. H., 1979. *The Hydraulic Regime and its Potential to Transport Sediment on the Canterbury Continental Shelf.* N. Z. Oceanogr. Inst. Mem., 83.

Carter, R. M., and Carter, L., 1982. The Motunau Fault and other structures at the southern edge of the Australian/Pacific Plate Boundary, offshore Marlborough, New Zealand. *Tectonophysics*, 88:133–159.

Carter, R. M., and Landis, C. A., 1972. Correlative Oligocene unconformities in southern Australasia. *Nature*, 237:12–13.

Carter, R. M., and Norris, R. M., 1976. Cainozoic history of southern New Zealand: an accord between geological observations and plate-tectonic predictions. *Earth Planet. Sci. Lett.*, 31:85–94.

Cloos, E., 1955. Experimental analysis of fracture patterns. *Geol. Soc. Am. Bull.*, 66:241–256.

Cole, J. W., and Lewis, K. B., 1981. Evolution of the Taupo–Hikurangi subduction system. *Tectonophysics*, 72:1–21.

Cullen, D. J., 1962. The significance of a glacial erratic from the Chatham Rise, east of New Zealand. *N. Z. J. Geol. Geophys.* 5:309–313.

________, 1965. Autochthonous rocks from the Chatham Rise east of New Zealand. *N. Z. J. Geol. Geophys.*, 8:465–474.

________, 1967. The age of glauconite from the Chatham Rise east of New Zealand. *N. Z. J. Mar. Freshwat. Res.*, 1:399–406.

________, 1970. A tectonic analysis of the Southwest Pacific. *N. Z. J. Geol. Geophys.*, 13:7–20.

________, 1980. Distribution, composition and age of submarine phosphorites on Chatham Rise. East of New Zealand. *Soc. Econ. Paleont. Mineral., Spec. Publ.*, 29:139–148.

Davey, F. J., 1977. Marine seismic measurements in the New Zealand region. *N. Z. J. Geol. Geophys.*, 20:719–777.

Davies, T. A., and Laughton, A. S., 1972. Sedimentary processes in the North Atlantic. *In* Laughton, A. S., Berggren, W. A., et al., *Init. Repts. DSDP*, 12: Washington (U.S. Govt. Printing Office), 905–934.

Ewing, M., Houtz, R., and Ewing, J., 1969. South Pacific sediment distribution. *J. Geophys. Res.*, 74:2477–2493.

Fleming C. A., 1962. New Zealand biogeography: a paleontologists' approach. *Tuatara*, 10:53–108.

Gregg, D. R., 1964. Hurunui. *N. Z. Geol. Surv. Geological Map 1: 250,000*. Sheet 18.

Griggs, G. B., Carter, L., Kennett, J. P., and Carter, R. M., 1983. Late Quaternary marine stratigraphy southeast of New Zealand. *Geol. Soc. Am. Bull.*, 94:791–797.

Heath, R. A., 1972. The Southland current. *N. Z. J. Mar. Freshwat. Res.*, 6:497–533.

_______, 1976. Oceanic circulation in the head of the Hikurangi Trench, East Coast, New Zealand. *N. Z. J. Mar. Freshwat. Res.*, 10:651–674.

Herzer, R. H., 1975. Uneven submarine topography south of Mernoo Gap—the result of volcanism and submarine sliding (Note). *N. Z. J. Geol. Geophys.*, 18:183–188.

_______, 1979. Submarine slides and submarine canyons on the continental slope off Canterbury, New Zealand. *N. Z. J. Geol. Geophys.*, 22:391–406.

_______, 1981. *Late Quaternary Stratigraphy and Sedimentation of the Canterbury Continental Shelf, New Zealand*. N. Z. Oceanogr. Inst. Mem., 89.

Herzer, R. H., and Bradshaw, J. D., in press. The Motunau Fault and other structures at the southern edge of the Australian/Pacific Plate Boundary, offshore Marlborough, New Zealand-Discussion. *Tectonophysics*.

Honza, E., 1980. Pre-site survey of the Japan Trench transect, Deep Sea Drilling Project. *In* Scientific Party, et al., *Init. Repts. DSDP*, 56, 57 (Pt. 1): Washington (U.S. Govt. Printing Office), 449–458.

Houtz, R., Ewing, J., Ewing, M., and Lonardi, A. G., 1967. Seismic reflection profiles of the New Zealand Plateau. *J. Geophysics.*, 72: 4713–4729.

Katz, R., 1974. Margins of the Southwest Pacific.*In* Burk, C. A., and Drake, C. L. (Eds.), *The Geology of Continental Margins*: New York (Springer-Verlag), pp. 549–565.

Kennett, J. P., 1967. Recognition and correlation of the Kapitean Stage (Upper Miocene, New Zealand). *N. Z. J. Geol. Geophys.*, 10: 1051–1063.

_______, 1977. Cenozoic evolution of Antarctic glaciation and the Circum-Antarctic Ocean and their impact on global paleoceanography. *J. Geophys. Res.*, 82:3843–3859.

Kennett, J. P., and Casey, R. E., 1969. Foraminiferal evidence for a pre-Middle Eocene age of the Chatham Rise, New Zealand. *N. Z. J. Mar. Freshwat. Res.*, 3:20–28.

Kennett, J. P., Houtz, R. E., Andrews, P. B., Edwards, A. R., Gostin, V. A., Hajós, M., Hampton, M., Jenkins, D. G., Margolis, S. V., Ovenshine, A. T., and Perch-Nielsen, K., 1975. Cenozoic paleoceanography in the Southwest Pacific Ocean, Antarctic glaciation, and the development of the Circum-Antarctic Current. *In* Kennett, J. P., Houtz, R. E., et al., *Init. Repts. DSDP*, 29: Washington (U.S. Govt. Printing Office), 1155–1170.

Krause, D. C., and Cullen, D. J., 1970. Bounty bathymetry (2nd ed). *N. Z. Oceanogr. Inst. Chart. Oceanic Series, 1:1,000,000.*

Lewis, K. B., 1973. Slumping on a continental slope inclined at 1°–4°. *Sedimentology*, 16:97–110.

_______, 1980. Quaternary sedimentation on the Hikurangi oblique-subduction and transform margin, New Zealand. *Int. Assoc. Sedimentol., Spec. Publ.*, 4:171–189.

Lewis, K. B., and Bennett, D. J., in press. Structural patterns on the Hikurangi Margin: an interpretation of seismic data. *In* Lewis, K. B., (Ed.), *New Seismic Profiles, Cores and Detailed Rocks from the Hikurangi Margin*. N. Z. Oceanogr. Inst. Field Report.

Loutit, T. S., and Kennett, J. P., 1981a. Australian Cenozoic sedimentary cycles, global sea level changes and the deep sea sedimentary record. *Oceanol. Acta.*, Suppl., pp. 45–63.

_______, 1981b. New Zealand and Australian Cenozoic sedimentary cycles and global sea-level changes. *Am. Assoc. Pet. Geol. Bull.*, 65:1586–1601.

McDougall, J. C., 1982. Bounty sediments. *N. Z. Oceanogr. Inst. Chart. Oceanic Series, 1:1,000,000.*

McKenzie, D. P., and Morgan, W. J., 1969. Evolution of triple junctions. *Nature*, 224:125–133.

Norris, R. M., 1964. *Sediments of Chatham Rise*. N. Z. Dept. Sci. Industr. Res. Bull. 159 (N. Z. Oceanogr. Instr. Mem. 26).

Pasho, D. W., 1976. *Distribution and Morphology of Chatham Rise Phosphorites*. N. Z. Oceanogr. Instr. Mem. 77.

Prebble, W. M., 1980. Late Cainozoic sedimentation and tectonics of the East Coast Deformed Belt, in Marlborough, New Zealand. *Int. Assoc. Sedimentol., Spec. Publ.*, 4:217–228.

Reading, H. R., 1980. Characteristics and recognition of strike-ship fault systems. *Int. Assoc. Sedimentol., Spec. Publ.*, 4:7–26.

Ryan, J. M. W., and Scholz, C. H., 1978. Seismotectonics of Arthur's Pass region, South Island, New Zealand. *Geol. Soc. Am. Bull.*, 89:1373–1388.

Schweller, W. J., Kulm, L. D., and Prince, R. A., 1981. Tectonics, structure and sedimentary framework of the Peru-Chile Trench. *Geol. Soc. Am. Mem.*, 154:327–349.

Spörli, K. B., 1980. New Zealand and oblique-slip margins: tectonic development up to and during the Cainozoic. *Int. Assoc. Sedimentol., Spec. Publ.*, 4:147–170.

Stevens, G. R., 1980. *New Zealand Adrift*: Wellington (Reed).

Stipp, J. J., and McDougall, I., 1968. Geochronology of the Banks Peninsula volcanoes, New Zealand. *N. Z. J. Geol. Geophys.*, 5: 1239–1259.

Suggate, R. P., 1978. *The Geology of New Zealand*: Wellington (Govt. Printer).

Vail, P. R., and Hardenbol, J., 1979. Sea-level changes during the Tertiary. *Oceanus*, 22:71–79.

Vail, P. R., Mitchum, R. M., Todd, R. G., Widmier, J. M., Thompson III, S., Sangree, J. B., Bubb, J. N., and Hatelid, W. G., 1977. Seismic stratigraphy and global changes of sea level. *In* Payton, C. E. (Ed.), *Seismic Stratigraphy-Applications* to *Hydrocarbon Exploration*. Am. Assoc. Pet. Geol. Mem. 26:49–212.

Van der Linden, W. J. M., 1968. Cook bathymetry. *N. Z. Oceanogr. Inst. Chart. Oceanic Series, 1:1,000,000.*

Walcott, R. I., 1978. Present tectonics and late Cenozoic evolution of New Zealand. *Geophys. J. R. Astron. Soc.*, 52:137–164.

_______, 1984. Reconstructions of the New Zealand Region for the Neogene. *Palaeogeogr., Palaeoclimatol., Palaeoecol.*, 46:217–231.

Wilcox, R. E., Harding, T. P., and Seely, D. R., 1973. Basic wrench tectonics. *Am. Assoc. Pet. Geol. Bull.*, 57:74–96.

Wilson, D. D., 1963. *Geology of Waipara*. N. Z. Geol. Surv. Bull., n.s., 64.

Date of Initial Receipt: 25 June 1984
Date of Acceptance: 4 December 1984

39. SEISMIC STRATIGRAPHY OF THE NEOGENE SEQUENCE AT SITE 587[1]

Alain Mignot and Alain Mauffret, Département de Géologie Dynamique, Université Pierre et Marie Curie[2]

INTRODUCTION

The Lord Howe Rise terminates northward against the southeast-trending Fairway Ridge. The Fairway Basin lies to the south of this juncture between the Fairway Ridge and the Lord Howe Rise. Eastward off the Fairway Ridge lies the New Caledonia Basin. Lansdowne Bank, a 137-km-long, 50-km-wide fossil atoll, lies on the northern termination of the Lord Howe Rise at the juncture with the Fairway Ridge (Fig. 1).

These local submarine ridges are isolated from terrigenous input from Australia to the west and New Caledonia to the east. Consequently, they are mantled by undiluted Neogene pelagic sedimentation that records Neogene paleooceanography.

The Comité d'Etudes Pétrolières Marines undertook a seismic investigation in 1981 using two Institut Français du Pétrole Flexichoc sound sources and a 48-trace seismic streamer. Data were processed 24-fold. This survey led to the siting of DSDP Site 587 of Leg 90 (21°11′S, 161°21′E; see Site 587 site chapter, this vol.). This 3000-km survey is not a dense grid; there are about 50-km between each profile. Nevertheless, prior seismic information in this area is scarce (Dubois et al., 1974; Ravenne et al., 1977).

SEISMIC FACIES ANALYSIS AND INTERPRETATION OF THE TRANSPARENT SEISMIC FACIES

The Neogene sequence is thin (about 300 m thick) on top of the ridges, and the low amplitude of reflections from within the sediment sequence suggests a degree of homogeneity in the deposits (Fig. 2, location A). The topographic isolation of the region and shallow-water depth suggest that the most important constituent of the sediment section is calcareous pelagic sediments. These pelagic sediments are reworked by bottom currents that follow small channels (Fig. 2, location B). In the basin along the base of the ridge, the Neogene sequence infills a tilted-block topography. Some high-amplitude reflections indicate that detrital sediments are ponded in these topographic basins (Fig. 3, location A).

SEISMIC FACIES AROUND THE LANSDOWNE BANK

Along the western flank of Lansdowne Bank, chaotic seismic facies suggest that some combination of slumping and canyon erosion are the main sedimentary processes acting at present (Fig. 4, location A). Interbedded strong reflections (Fig. 4, location B), however, make the section appear similar to the basal sequence of the Rhône deep-sea fan (Droz, 1982) and indicate intermittent deposition. In this area the deposits are rare and unstable. Downslope, a fan is formed by the coalescing of sedimentary wedges deposited at the mouths of several canyons. The main channel of the fan is bounded by asymmetrical levees (Fig. 5, locations A and B). Discontinuous reflections within the channel levees indicate an environment of deposition in which presumed fine-grained sediments settle out of turbidity currents while the main channel continues to be the locus of transport and erosion (Mullins et al., 1984).

In the distal parts of the fan, the levee and channel system becomes attenuated (Fig. 6). There possible medium-sized particles and fine-grained sands are deposited among a system of laterally migrating channels (Fig. 6, features labeled B). The seismic facies is typically linked to buried channels and levees. The detrital fraction that passes through the canyons and channels is probably bioclastic material: coral and other neritic remains from Lansdowne Bank.

At the far distal portions of the fan the seafloor becomes flat and shows little evidence of channels (Fig. 7). The pelagic material (the transparent seismic facies) is interbedded with turbidites, and the composite produces a seismic facies characterized by low-frequency reflections of variable amplitude.

EVOLUTION OF THE NEOGENE SEQUENCE

The Neogene section overlies an Oligocene discontinuity (Fig. 8, horizon A) (Mignot, 1984). The basal Neogene is a seismically transparent layer that onlaps horizon A to the northwest (Fig. 8, location E) and is overlain in turn by a series of strong, discontinuous reflections (Fig. 8, location D). The contrasting seismic character probably reflects basal Neogene deposition of homogeneous, fine-grained sediments that become interbedded upward with sandy layers originating from erosion of the Lansdowne Bank. Some channels can be observed (Fig. 8, locations B and C). Assuming a relatively constant sedimentation rate and knowing the sequence thickness and the depth of drilling at Site 587, we estimate the lowest layer of sandy deposits to be late Oligocene to early Miocene in age.

SEISMIC CHARACTER OF SEDIMENTS AT SITE 587

Site 587 was chosen to obtain an uncomplicated, high-resolution record in calcareous sediments of Neogene age

---

[1] Kennett, J. P., von der Borch, C. C., et al., *Init. Repts. DSDP*, 90: Washington (U.S. Govt. Printing Office).

[2] Address: Groupe d'Etude de la Marge Continentale (ERA 605 du CNRS), Département de Géologic Dynamique, Université Pierre et Marie Curie, 4, place Jussieu, 75230, Paris, Cedex 05, France.

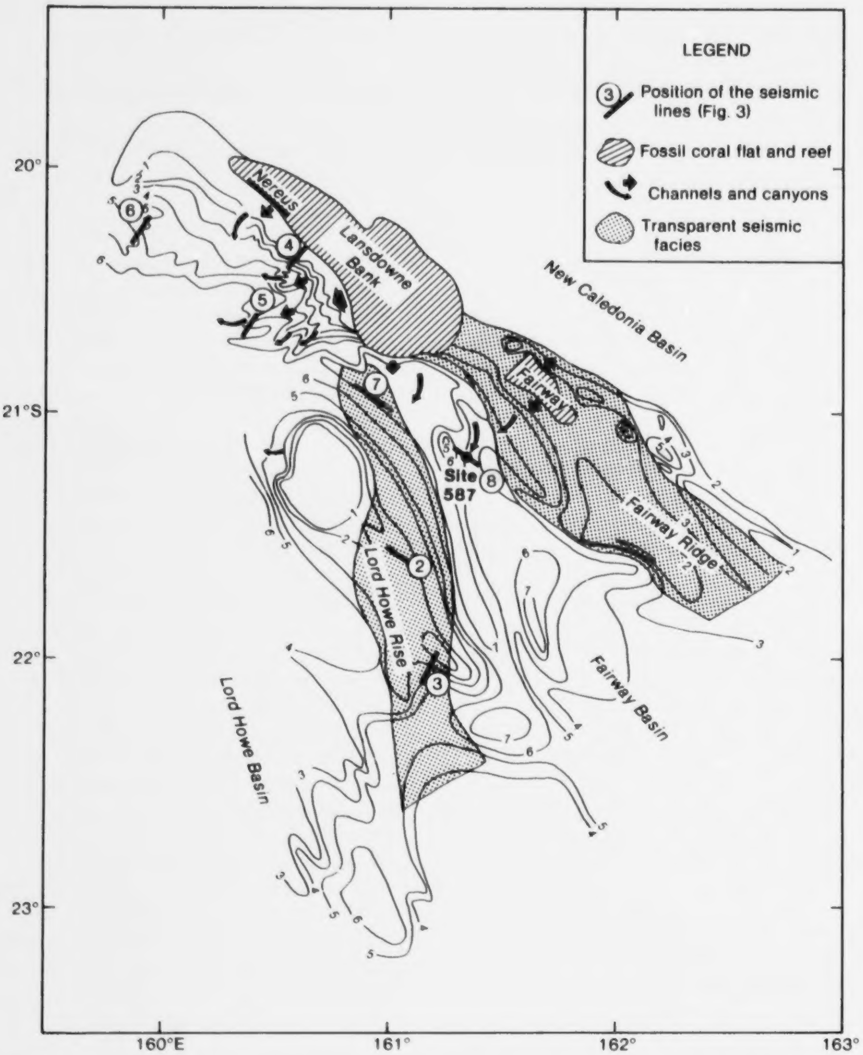
LEGEND
Position of the seismic lines (Fig. 3)
Fossil coral flat and reef
Channels and canyons
Transparent seismic facies
20°
21°S
22°
23°
160°E
161°
162°
163°
Nereus
Lansdowne Bank
New Caledonia Basin
Fairway
Site 587
Fairway Ridge
Lord Howe Rise
Fairway Basin
Lord Howe Basin
①
②
③
④
⑤
⑥
⑦
⑧

Figure 1. Isochron map (0.1 s two-way traveltime) of the Neogene sequence in the area of the northern termination of Lord Howe Rise. Circled numbers refer to figure numbers in this article, which are seismic lines taken at these locations.

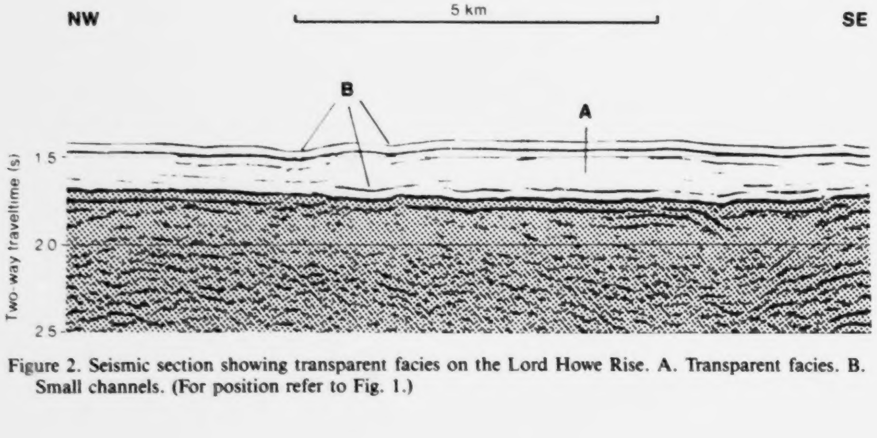

Figure 2. Seismic section showing transparent facies on the Lord Howe Rise. A. Transparent facies. B. Small channels. (For position refer to Fig. 1.)

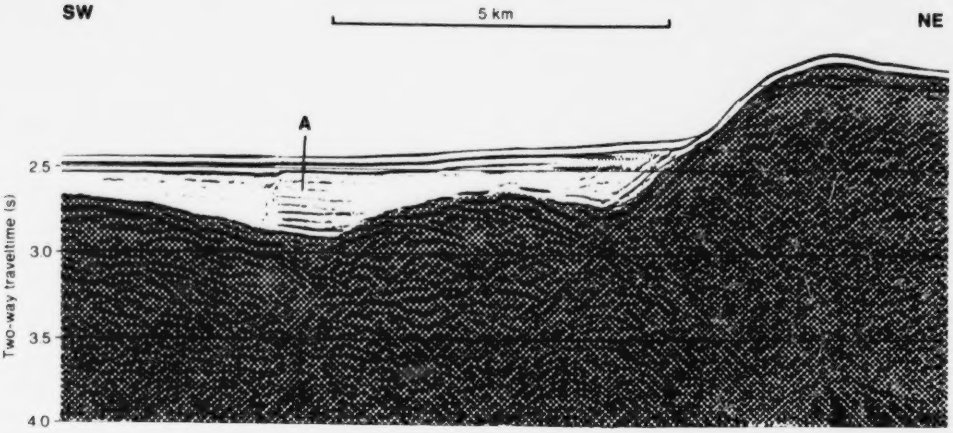

Figure 3. Seismic section showing a transparent layer on the Lord Howe Rise infilling a tilted-block topography. A. Depression infilled with sediments that are coarser than in the surrounding area. (For position refer to Figure 1.)

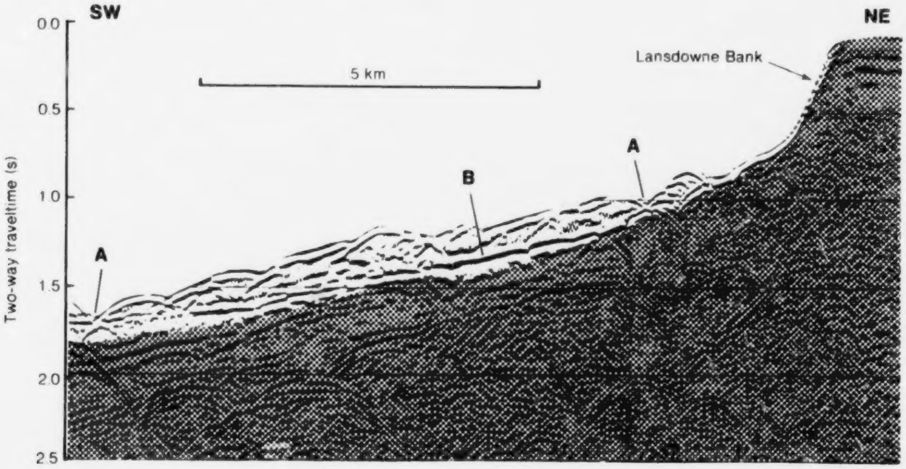

Figure 4. Seismic section showing the western slope of Lansdowne Bank, where slumping and erosion has occurred. (For position refer to Figure 1.) A. Slumps and erosion; B. Interbedded strong reflection.

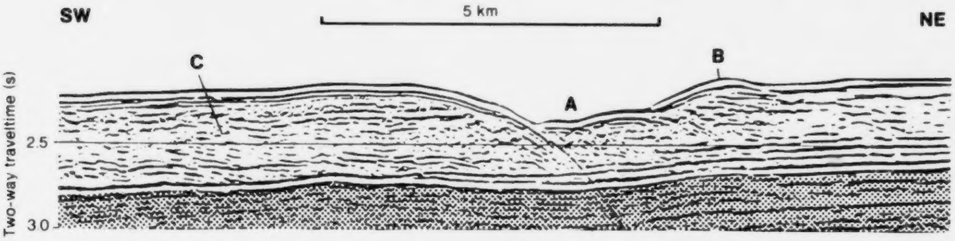

Figure 5. Seismic section showing channels in the fan off Lansdowne Bank. A. Channel. B. Levee. C. Discontinuous reflector indicating high-energy environment. (For position refer to Figure 1.)

between the warm subtropics and the equatorial zone. Unfortunately, Site 587 was located in a channel where detrital sediments from Lansdowne Bank (located upslope) accumulated. This channel could have been avoided if different displays of the seismic data had been consulted. Figure 9 shows the data before and after deconvolution. Deconvolution in this case has obliterated the obvious channel that appears in the seismic section prior to deconvolution.

CONCLUSION

The flank of Lansdowne Bank is a typical bypass carbonate slope that is located upslope from a carbonate fan (Ravenne et al., 1985); Schlager and Ginsburg, 1981).

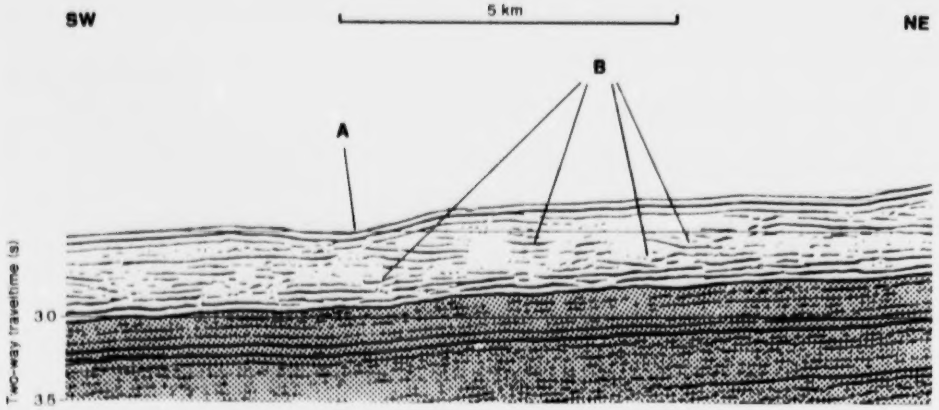

Figure 6. Seismic section showing a small channel in the distal part of the fan. A. Channel. B. Buried channels. (For position refer to Figure 1.)

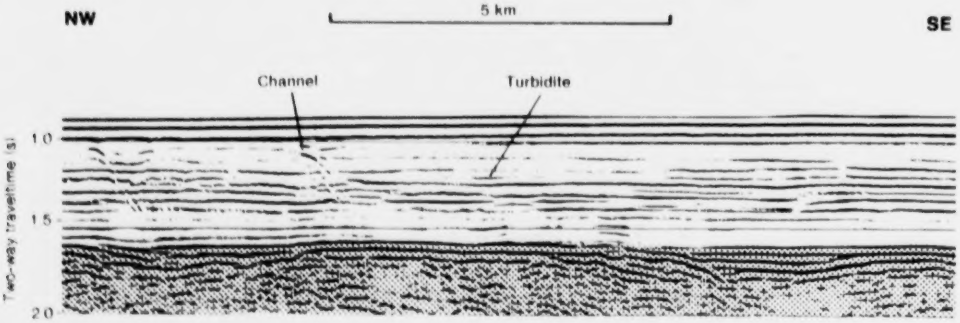

Figure 7. Seismic section showing turbidites interbedded in pelagic sediments south of Lansdowne Bank. (For position refer to Figure 1.)

Site 587 was drilled in a channel where the probability of encountering gravel and sand was high. This explains why only 60% of the cores were recovered and why the hole was abandoned.

ACKNOWLEDGMENTS

We thank the C.E.P.M., which provided and processed the seismic data. We appreciate the many constructive comments on early drafts of the manuscripts by J. Ladd. We also thank J. Ladd and A. Beck for translation and corrections.

REFERENCES

Droz, L., 1983. L'éventail sous-marin profond du Rhône (Golfe du Lion): grands traits morphologiques et structure semi-profonde. *Thèse 3e cycle*, Université Pierre et Marie Curie, Paris.

Dubois, J. Ravenne, C., Aubertin, A., Louis, J., Guillaume, R., Launay, J., and Montadert, L., 1974. Continental Margins near New Caledonia. *In* Burk, C. A., and Drake C. L. (Eds.), *The Geology of Continental Margins*: New York/Berlin (Springer Verlag), pp. 521-535.

Mignot, A., 1984. Sismo-stratigraphie de la terminaison nord de la ride de Lord Howe. Evolution géodynamique du Sud-Ouest Pacifique entre l'Australie et la Nouvelle-Calédonie. *Thèse 3e Cycle*, University, Pierre et Marie Curie, Paris.

Mullins, H. T., Heath, W. C., Van Buren, M., and Newton, C. R., 1984. Anatomy of a modern open ocean carbonate slope: northern Little Bahama Bank. *Sedimentology*, 31:141-168.

Ravenne, C., de Broin, C. E., Dupont, J., Lapouille, A., and Launay, J., 1977. New Caledonia basin-Fairway Ridge: structural and sedimentary study. *International Symposium on Geodynamics in South-West Pacific, Nouméa 1976*: Paris (Technip), pp. 145-154.

Ravenne, C., Le Quellec, P., and Valery, P., 1985. Dépôts carbonatés profonds des Bahamas. *Géodynamique des Caraïbes; Symposium, Paris 5, 8 février 1985*: Paris (Technip), pp. 255-270.

Schlager, W., and Ginsburg, R. N., 1981. Bahama Carbonate Platforms: the deep and the past. *Mar. Geol.* 44:1-24.

Date of Initial Receipt: 1 November 1984
Date of Acceptance: 22 April 1985

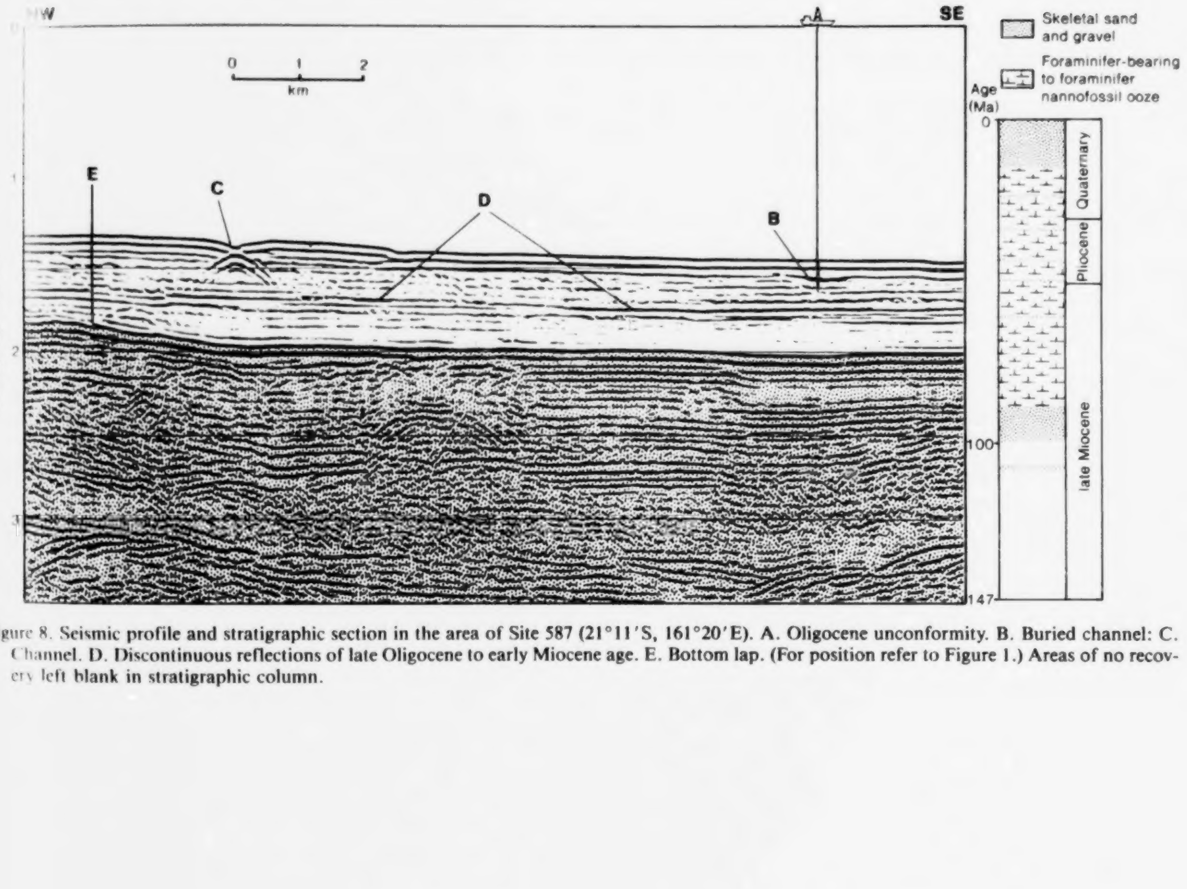
NW
A
SE
0
1
2
km
E
C
D
B
Two-way traveltime (s)
0
1
2
3
Skeletal sand and gravel
Foraminifer-bearing to foraminifer nannofossil ooze
Age (Ma)
0
100
147
Quaternary
Pliocene
late Miocene

Figure 8. Seismic profile and stratigraphic section in the area of Site 587 (21°11'S, 161°20'E). A. Oligocene unconformity. B. Buried channel: C. Channel. D. Discontinuous reflections of late Oligocene to early Miocene age. E. Bottom lap. (For position refer to Figure 1.) Areas of no recovery left blank in stratigraphic column.

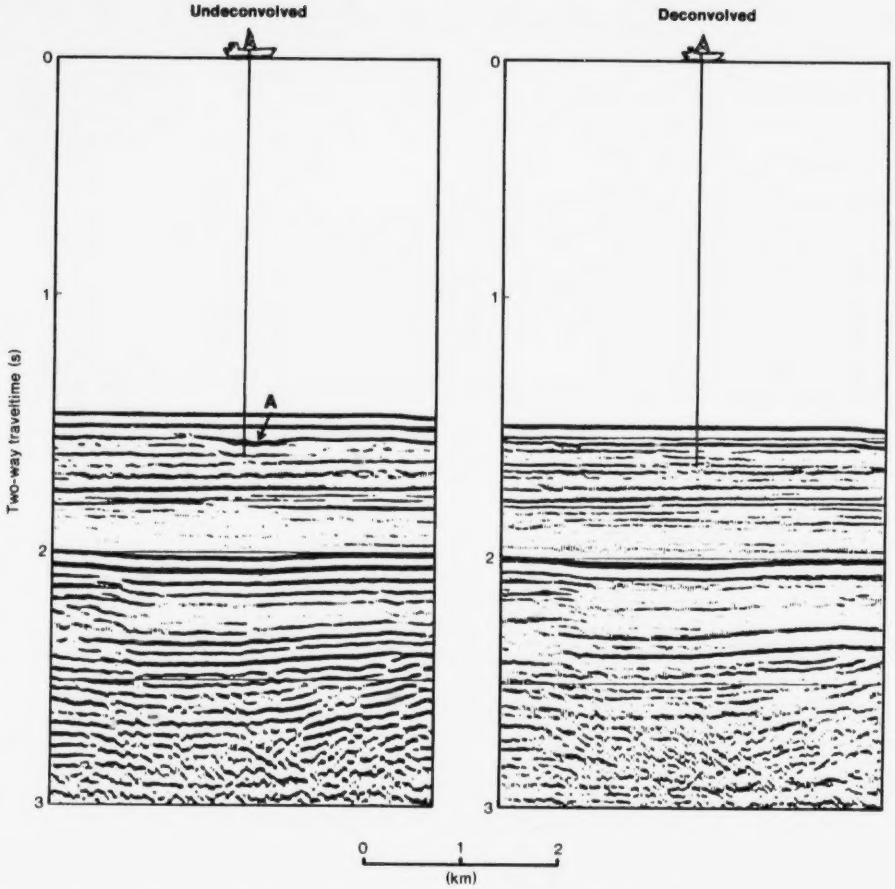
Undeconvolved
Deconvolved
Two-way traveltime (s)
0
1
2
3
A
0
1
2
(km)

Figure 9. Comparison between the undeconvolved seismic section (left) and the deconvolved seismic section (right). Note the channel (A) in the left section that disappears in the right section. (For position refer to Figure 1.)

PART VII: PALEOCEANOGRAPHIC STUDIES

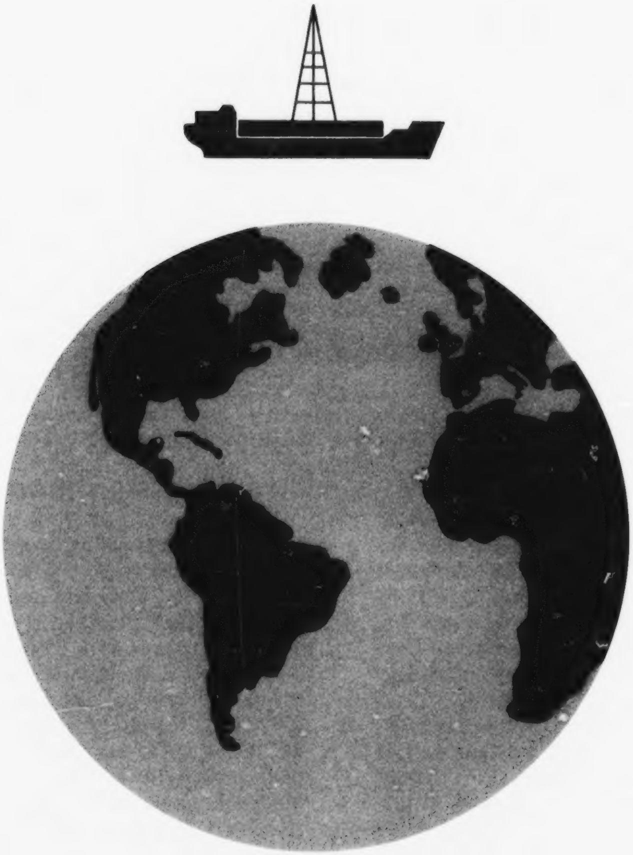

40. DEVELOPMENT OF LATITUDINAL THERMAL GRADIENTS DURING THE OLIGOCENE: OXYGEN-ISOTOPE EVIDENCE FROM THE SOUTHWEST PACIFIC[1]

Margaret G. Murphy and James P. Kennett, University of Rhode Island[2]

ABSTRACT

The late Eocene through earliest Miocene stable-isotope composition of southwest Pacific microfossils has been examined in a traverse of high-quality sedimentary sequences ranging from subantarctic (DSDP Site 277) through temperate regions (DSDP Sites 592 and 593). Changes in oxygen-isotope values, measured in benthic and planktonic foraminifers, document the Oligocene development and strengthening of latitudinal thermal zonation from water masses with broad temperature gradients during the Eocene to the steeper gradients and more distinct latitudinally distributed surface water-mass belts of the Neogene.

The oxygen-isotope records can be divided into three intervals: late Eocene, early Oligocene, and middle to late Oligocene. Each interval represents a successive stage in the evolution of latitudinal thermal gradients between subantarctic and temperate regions in the Southern Hemisphere.

During the late Eocene, oxygen-isotope values at subantarctic Site 277 were similar to those at temperate Sites 592 and 593. The isotope values suggest that, although the inferred paleotemperatures at Site 277 are slightly cooler on average than those at the temperate sites, there is no evidence for a major thermal boundary between the regions at this time. All three sites record the well-known oxygen-isotope enrichment of ~ 1‰ in both planktonic and benthic foraminifers in close association with the Eocene/Oligocene boundary. In contrast to the earliest Oligocene enrichments in the planktonic and benthic oxygen-isotope composition at Site 277, more northern Sites 592 and 593 exhibit a depletion through the early–middle Oligocene. This documents the beginning of thermal segregation as subantarctic waters cooled relative to those at temperate latitudes. During the Oligocene, this surface-water differentiation continued, as measured by planktonic $\delta^{18}O$ values. The oxygen-isotope records of the benthic foraminifers also began to diverge in the earliest Oligocene. The most enriched oxygen-isotope values in all records cluster in the middle Oligocene, marked by oscillating episodes of enrichments >0.5‰ occurring most prominently in the subantarctic record of Site 277. These values can be interpreted as recording either the coldest oceanic temperatures of the Paleogene and/or accumulations of Antarctic ice. After this interval, latitudinal thermal differentiation developed rapidly during the middle Oligocene, especially in the surface waters which actually warmed in temperate areas. If the enriched Oligocene oxygen-isotope values indicate that ice had accumulated, this ice must have disappeared by the early Miocene, when depleted oxygen-isotope values suggest very warm conditions.

The data presented in this chapter document the progressive increase of latitudinal temperature gradients from the late Eocene through the late Oligocene. This pattern of increasing isotopic offset between latitudinally distributed southwest Pacific sites is linked to the establishment and strengthening of the Circum-Antarctic Current, previously considered to have developed during the middle to late Oligocene. The intensification of this current system progressively decoupled the warm subtropical gyres from cool polar circulation, in turn leading to increased Antarctic glaciation.

INTRODUCTION

The record of global Cenozoic climate generally shows the progressive cooling and glaciation of the polar regions. High-latitude cooling, and perhaps some warming in the tropics, led to an increased latitudinal thermal gradient during the Cenozoic. This scenario has been developed from several lines of evidence, including comparisons of changing isotopic values between high and low latitudes during the Cenozoic (Savin et al., 1975; Shackleton and Kennett, 1975; Loutit et al., 1984). Biogeographic patterns of planktonic fossil groups changed from a few broadly distributed provinces in the Paleogene to more numerous, distinct, narrow belts in the Neogene. The changing faunal and floral patterns also indicate cooling of the high-latitude regions as the Antarctic water mass developed (Kaneps, 1975; Kennett, 1978; Sancetta, 1979; Wise et al., 1982).

The cooling of high southern latitudes was a direct result of the developing Circum-Antarctic Current and the related thermal isolation of the Antarctic continent (Kennett, 1977; Kvasov and Verbitsky, 1981). Thus, the development and steepening of the latitudinal thermal gradient was closely linked to development of this Circum-Antarctic Current system. Previous work in the Australasian sector of the Southern Ocean indicated major development of this system during the middle to late Oligocene (Kennett, 1977; 1978), when deep circumantarctic circulation started south of Tasmania and the South Tasman Rise (Kennett et al., 1975). The system continued to expand and intensify as Australia continued its northward drift and the Scotia Sea and Drake Passage became less constricted. The last major Antarctic gateway probably opened through the Drake Passage during the late Oligocene (Barker and Burrell, 1977; Sclater et al., in press). The resulting thermal isolation of Antarctica led to increased glaciation, continental ice accumulation, and sea-ice formation. This, in turn, increased albedo, leading to further cooling, to increased wind strength, and to augmented psychrospheric bottom-water production.

---

[1] Kennett, J. P., von der Borch, C. C., et al., *Init. Repts. DSDP*, 90: Washington (U.S. Govt. Printing Office).

[2] Address: Graduate School of Oceanography, University of Rhode Island, Narragansett, RI 02882-1197.

The purpose of this chapter is to present oxygen- and carbon-isotope data for three sites that form a latitudinal traverse spanning about 12° in the Oligocene. This transect incorporates the modern subantarctic through northern temperate regions. We compared $\delta^{18}O$ data between these sites to decipher changes in latitudinal thermal gradients through the Oligocene in the southwest Pacific and to examine the interrelationships between this thermal history and the developing Circum-Antarctic Current.

Two undisturbed late Eocene to Oligocene sediment sections were collected during Deep Sea Drilling Project (DSDP) Leg 90 (Fig. 1) using the extended core barrel apparatus (XCB). One section (Site 592) was from warm temperate latitudes (36°28.40′S) and the other section (Site 593) was from cooler, southern temperate latitudes (40°30.47′S). The sections were relatively continuous (recovery >70%) and mechanically undisturbed by the XCB technique. The sites were at shallow paleodepths (~1000 m) and are rich in calcareous microfossils. By collecting these temperate sections, we could study the development of late Paleogene latitudinal temperature gradients in conjunction with another site (Site 277) presently located in subantarctic latitudes (52°13.43′S). Site 277 has been used as the standard of reference for high-latitude stable-isotope development (Shackleton and Kennett, 1975). This isotope record was based on analyses of mixed benthic genera and mixed planktonic species of foraminifers. The analysis of mixed planktonic taxa resulted in a generalized isotopic signal because of the averaging effect of combining taxa living at different levels of the water column. The mixture of different benthic genera adds the species-specific disequilibrium value of each taxa to the resulting signal, again producing an averaged record. The late Eocene–early Oligocene portion of Site 277 was reanalyzed by Keigwin (1980) using monospecific samples of *Globigerina angiporoides* and *Oridorsalis umbonatus*. In order to compare this high-latitude section with the two temperate Leg 90 sites, we analyzed the remainder of Site 277 using monospecific samples.

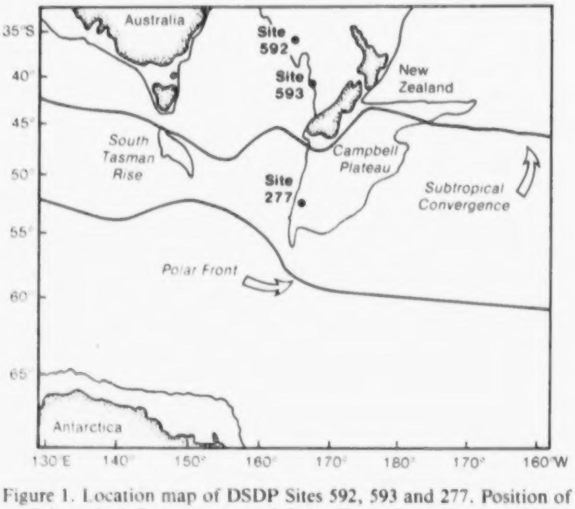

Figure 1. Location map of DSDP Sites 592, 593 and 277. Position of Subtropical Convergence and Polar Front from Gordon (1972); 2000-m isobath is shown.

METHODS

Samples (5 cm^3) were dried in a 50°C oven and weighed after saving a small subsample for calcareous nannofossil analysis. The bulk sample was disaggregated in hog Calgon solution and washed over a 63-μm sieve. The <63-μm residue was retained and centrifuged for future analysis. The >63-μm residue was trapped on filter paper, dried at 50°C, and weighed. The samples were then dry sieved (>250 μm) and the foraminifer species *Globigerina angiporoides* and *Oridorsalis umbonatus* were picked for analysis. These species were chosen for their common occurrence throughout the sections. *G. angiporoides* is believed to have inhabited near-surface waters (Keigwin, 1980), whereas *O. umbonatus* is a distinctive, long-ranging benthic form found to deviate consistently from both $\delta^{18}O$ and $\delta^{13}C$ equilibria (Graham et al., 1981). These monospecific subsamples were sonicated in methanol to remove adhering particles, dried at 50°C, and loaded into stainless steel "boats." The loaded boats were roasted *in vacuo* at 350°C for 60 min., allowed to cool, and placed into the sampling arm for stable isotope analysis.

Each analytical session on the mass spectrometer was preceded and followed by an analysis of the powdered laboratory standard B-1, which has an analytical precision of less than ±0.10‰ for both $\delta^{18}O$ and $\delta^{13}C$. The procedure followed that of Keigwin (1980) with dissolution in phosphoric acid at 50°C, followed by three serial distillations to obtain pure carbon dioxide gas. Analyses were performed on the University of Rhode Island (URI) VG 602D mass spectrometer. Recent recalibration of the URI B-1 standard has resulted in an adjustment of our oxygen-isotope values by +0.29‰ when corrected to Pee Dee belemnite (PDB); the carbon values do not require adjustment. This will affect all analyses of carbonate material published by the URI laboratory between 1980 and September, 1984. The URI reference gas is lighter by 0.59‰ with respect to PDB for $\delta^{18}O$, and heavier by 1.22‰ than PDB for $\delta^{13}C$ (see Appendix).

Sample reproducibility based upon one sigma of the means of 30 sets of *G. angiporoides* and 17 sets of *O. umbonatus* duplicates was ± 0.09‰ for planktonic $\delta^{18}O$ and $\delta^{13}C$; 0.08‰ for benthic $\delta^{18}O$, and 0.13‰ for benthic $\delta^{13}C$. Isotopic results were corrected mathematically for tailing effects as detailed in Craig (1957; Table 1). Samples were checked for possible recrystallization by examination under the scanning electron microscope. Strontium to calcium ratios and strontium-isotope analyses of planktonic foraminifers from Site 593 has also demonstrated the pristine nature of these samples (Hess and Schilling, this volume).

Biostratigraphic zonal nomenclature is after Martini (this volume) and Jenkins and Srinivasan (this volume). Ages are assigned to faunal datum planes after Berggren et al. (in press). For purposes of discussion in this chapter, the Oligocene is divided into three time intervals: early (37.5–33 Ma); middle (33–28 Ma) and late (28–23.5 Ma).

RESULTS OF ISOTOPIC ANALYSES

Site 277

The oxygen-isotope record from Site 277, at subantarctic latitudes (present position 52°13.43′S; 166°11.48′E, 1214 m water depth), was used as the basis for the Eocene–Oligocene portion of the standard Cenozoic high-latitude temperature curve (Shackleton and Kennett, 1975) and has subsequently been included in several global syntheses (e.g., Savin, 1977; Savin and Yeh, 1981; Shackleton et al., 1984). The first step in this study was to reanalyze this important section using monospecific samples and use the resultant curve as a basis of comparison with the record at Sites 592 and 593.

In their analysis of Site 277, Shackleton and Kennett (1975) found relatively constant late Eocene oxygen-iso-

Table 1. Isotopic data from Holes 277, 592, 593, and 593A corrected to PDB.

Sample	Depth	*Globigerina angiporoides*		*Oridorsalis umbonatus*	
		$\delta^{18}O$	$\delta^{13}C$	$\delta^{18}O$	$\delta^{13}C$
Hole 277					
2-2, 140–142	9.9	1.37	1.06	1.72	0.58
2-5, 140–142	14.4	1.29	1.10	1.77	0.41
3-2, 139–140	19.4	1.35	0.74	1.91	−0.41
3-5, 140–142	23.9	1.65	0.94	1.72	−0.52
4-5, 140–142	33.4	1.17	0.86	1.66	0.36
4-5, 140–142	33.4	1.25	0.96	—	—
5-2, 140–142	38.4	1.41	0.86	1.64	0.61
5-5, 140–142	42.9	1.08	0.39	2.05	0.03
6-2, 140–142	46.9	1.19	1.16	1.92	−0.21
6-5, 140–142	52.4	1.04	0.49	1.36	−0.36
7-2, 140–142	57.4	1.20	1.29	1.64	−0.15
7-2, 140–142	57.4	0.81	0.76	—	—
7-5, 140–142	61.9	0.96	1.14	1.46	0.39
8-2, 140–142	66.9	0.87	0.93	1.00	0.11
8-2, 140–142	66.9	1.03	1.09	1.30	0.14
8-5, 140–142	71.4	1.07	1.15	1.77	0.08
8-5, 140–142	71.4	1.20	1.20	2.01	0.74
8-5, 140–142	71.4	1.17	0.98	—	—
9-2, 140–142	76.4	1.62	0.83	1.97	−0.17
9-5, 140–142	80.9	1.04	1.05	1.48	−0.71
10-2, 139–140	85.9	1.04	1.07	1.72	−0.42
10-5, 140–142	90.4	1.08	1.20	1.84	−0.23
10-5, 140–142	90.4	1.17	1.04	—	—
11-2, 140–142	95.4	0.96	1.05	1.51	0.01
11-2, 140–142	95.4	1.16	0.89	1.59	−0.04
11-2, 140–142	95.4	0.98	0.78	—	—
11-5, 140–142	99.9	0.86	1.04	1.03	0.34
11-5, 140–142	99.9	0.95	0.77	1.38	−0.13
12-2, 140–142	104.9	—	—	1.75	−0.13
12-5, 140–142	109.4	1.07	1.18	1.37	0.30
12-5, 140–142	109.4	1.06	1.08	—	—
13-2, 140–142	114.4	0.78	1.04	1.12	0.24
13-5, 140–142	119.4	0.68	1.23	1.35	0.19
14-2, 140–142	123.9	1.13	1.56	1.32	0.54
14-2, 140–142	123.9	1.01	0.31	—	—
14-5, 140–142	128.3	1.18	1.02	1.69	−0.26
15-2, 140–142	133.4	0.80	1.52	1.33	−0.21
15-2, 140–142	133.4	—	—	1.48	0.39
15-5, 141–142	137.9	0.68	0.99	1.62	0.18
16-2, 140–142	142.9	0.79	1.37	1.44	0.19
17-2, 140–142	152.4	0.85	0.94	1.44	0.61
18-2, 140–142	161.9	—	—	1.52	−0.04
19-2, 136–137	171.4	1.14	1.54	1.81	0.13
19-2, 136–137	171.4	1.11	1.43	—	—
20-5, 140–142	185.4	0.65	1.25	0.80	−0.17
20-6, 142–143	186.9	−0.05	0.95	0.95	−0.33
20-6, 142–143	186.9	0.23	1.03	—	—
21-1, 140–141	188.9	0.76	1.21	0.90	−0.22
21-1, 140–141	188.9	0.03	1.04	—	—
21-2, 140–142	190.4	0.26	1.14	0.90	—0.18
22-1, 135–136	198.3	0.24	1.40	0.88	0.20
22-2, 139–140	199.9	0.39	1.40	0.95	0.14
22-3, 140–142	201.4	0.01	1.70	0.76	0.37
Hole 592					
33-3, 35–36	305.46	0.28	1.12	—	—
33-4, 35–36	306.96	0.73	1.15	1.24	0.54
33-5, 35–36	308.46	0.70	1.23	1.20	0.46
34-1, 35–36	312.06	0.77	1.29	1.29	0.47
34-1, 35–36	312.06	—	—	1.24	0.31
34-2, 35–36	313.56	0.74	1.25	1.28	0.37
34-3, 35–36	315.06	0.76	1.27	1.29	0.57
34-4, 35–36	316.56	0.77	1.42	1.31	0.75
34-5, 35–36	318.06	0.79	1.58	1.40	0.84
34-5, 35–36	318.06	—	—	1.26	0.51
34-6, 35–36	319.56	0.86	1.61	1.46	0.69
35-1, 35–36	321.66	0.88	1.77	1.44	0.70
35-1, 35–36	321.66	0.90	1.71	—	—
35-2, 35–36	323.16	0.87	1.51	1.46	0.45
35-3, 35–36	324.66	0.58	1.63	1.03	0.38
35-4, 35–36	326.16	0.54	1.38	1.09	0.67

Table 1. (Continued).

Sample	Depth	*Globigerina angiporoides*		*Oridorsalis umbonatus*	
		$\delta^{18}O$	$\delta^{13}C$	$\delta^{18}O$	$\delta^{13}C$
Hole 592 (cont.)					
35-4, 35–36	326.16	—	—	1.08	0.17
35-5, 35–36	327.66	0.30	1.44	0.95	0.07
35-6, 35–36	329.16	0.35	1.26	1.09	0.10
36-1, 35–36	331.26	0.59	1.43	1.09	0.18
36-1, 35–36	331.26	0.14	1.32	—	—
36-1, 62–63	331.53	0.32	1.31	0.91	0.16
36-1, 92–93	331.83	0.33	1.29	1.05	0.25
36-1, 120–121	332.15	0.47	1.37	1.04	0.12
36-1, 144–145	332.35	0.31	1.16	1.03	0.12
36-1, 144–145	332.35	0.19	1.02	—	—
36-2, 35–36	332.76	0.28	1.12	0.98	0.03
36-2, 63–64	333.04	0.58	1.09	1.09	−0.09
36-2, 86–87	333.27	0.49	1.13	1.14	0.21
36-2, 119–120	333.60	0.33	1.18	1.19	−0.19
36-2, 146–148	333.87	0.37	0.95	1.04	0.01
36-3, 28–29	334.19	0.35	0.91	0.87	−0.27
36-3, 35–36	334.26	0.43	1.05	0.98	−0.17
36-3, 47–48	334.38	0.10	0.85	0.72	−0.39
36-3, 47–48	334.38	0.15	0.94	—	—
36-3, 96–97	334.87	0.11	1.20	0.77	0.20
36-3, 146–147	335.47	0.43	1.28	0.87	0.35
36-3, 146–147	335.47	0.07	1.12	—	—
37-1, 60–61	341.11	−0.16	1.09	0.57	0.15
37-1, 60–61	341.11	0.11	1.13	—	—
37-1, 120–121	341.71	0.02	1.00	0.30	−0.08
37-1, 141–142	341.92	0.25	1.21	0.66	0.09
37-2, 32–33	342.33	0.22	1.11	0.48	−0.04
37-2, 62–63	342.63	0.11	1.14	0.57	0.17
37-2, 62–63	342.63	0.11	0.99	—	—
37-2, 92–93	342.93	0.34	1.16	0.66	−0.10
37-2, 122–123	343.23	0.18	1.22	0.58	0.09
37-2, 142–143	343.43	0.00	1.29	0.61	0.09
37-3, 20–21	343.71	0.18	1.30	1.03	0.58
37-3, 20–21	343.71	—	—	0.78	0.34
37-3, 50–51	344.01	−0.28	1.24	0.72	0.18
37-3, 70–71	344.21	−0.22	1.31	0.71	0.20
37-3, 93–94	344.44	0.16	1.30	0.68	0.03
37-3, 116–117	344.67	−0.05	1.30	0.70	0.11
37-4, 32–33	345.33	0.00	1.21	1.33	0.15
37-4, 32–33	345.33	—	—	0.90	0.09
37-4, 64–65	345.65	0.23	1.28	0.68	0.20
37-4, 64–65	345.65	—	—	0.69	0.29
38-1, 35–36	350.46	0.27	1.43	0.60	0.33
38-2, 35–36	351.96	0.18	1.50	0.70	0.33
38-3, 35–36	353.46	0.19	1.68	0.68	0.43
38-5, 35–36	356.46	−0.01	1.63	0.60	0.45
38-6, 35–36	357.96	−0.02	1.71	0.59	0.56
39-1, 35–36	360.06	−0.08	1.81	0.37	0.85
39-2, 35–36	361.56	−0.17	1.44	0.50	0.44
39-3, 35–36	363.06	0.01	1.68	0.59	0.71
40-1, 35–36	369.66	0.00	1.50	0.27	0.31
40-3, 35–36	372.66	0.08	1.40	0.62	0.22
40-4, 36–38	374.17	0.06	1.31	0.59	0.10
40-5, 36–37	375.67	0.00	1.15	0.65	−0.12
41-1, 35–37	379.26	−0.05	1.31	0.58	0.18
41-3, 35–37	382.26	0.24	1.27	0.63	−0.14
41-4, 35–37	383.26	0.21	1.34	0.73	0.12
41-5, 35–37	385.26	0.30	1.22	0.78	−0.11
41-6, 35–37	386.76	0.15	1.26	0.65	−0.11
Hole 593					
50-3, 35–37	469.26	0.16	1.13	1.12	0.59
50-4, 35–37	470.76	0.04	1.06	1.10	0.09
50-5, 35–37	472.26	0.63	1.67	1.35	0.82
50-6, 35–37	473.76	0.57	0.90	1.33	0.00
52-1, 35–37	485.26	0.56	0.99	1.01	0.29
52-2, 35–37	486.96	0.23	0.74	0.69	−0.45
52-3, 35–37	488.26	0.63	1.06	1.16	−0.15
52-4, 35–37	489.96	0.38	0.75	1.07	−0.34
53-2, 35–37	496.56	0.73	1.12	1.47	−0.07
53-3, 35–37	498.06	0.67	1.40	1.32	−0.08

Table 1. (Continued).

Sample	Depth	*Globigerina angiporoides* $\delta^{18}O$	*Globigerina angiporoides* $\delta^{13}C$	*Oridorsalis umbonatus* $\delta^{18}O$	*Oridorsalis umbonatus* $\delta^{13}C$
Hole 593 (cont.)					
53-3, 35–37	498.06	0.46	1.18	1.33	−0.32
53-4, 35–37	499.56	0.84	1.07	1.49	−0.09
54-1, 35–37	504.66	0.87	0.96	1.46	−0.05
54-1, 35–37	504.66	0.82	1.08	—	—
54-2, 35–37	506.16	0.74	1.08	1.46	−0.02
54-3, 35–37	507.60	0.92	1.23	1.46	0.21
54-3, 35–37	507.60	0.95	1.43	—	—
54-4, 35–37	509.16	0.76	1.13	1.49	0.00
54-5, 35–37	510.66	0.39	0.89	1.05	−0.16
55-1, 35–37	514.26	0.62	1.13	1.32	0.02
55-2, 35–37	515.76	0.36	1.19	1.15	0.15
55-2, 35–37	515.76	0.49	1.52	1.03	0.28
55-4, 35–37	518.76	0.51	1.57	1.39	0.41
55-4, 35–37	518.76	0.59	1.58	1.15	0.77
55-5, 35–37	520.26	0.49	1.21	1.06	0.24
55-5, 35–37	520.26	—	—	1.15	0.14
55-6, 35–37	521.76	0.38	1.18	0.89	−0.04
56-1, 35–37	523.86	0.33	1.03	1.03	0.23
56-2, 35–37	525.36	0.44	0.90	1.13	0.17
56-2, 35–37	525.36	0.39	1.11	—	—
56-3, 35–37	526.86	0.59	0.97	1.08	−0.02
56-4, 35–37	528.36	0.50	1.06	1.08	0.28
56-4, 35–37	528.36	—	—	1.15	0.46
56-5, 35–37	529.86	0.92	1.20	1.00	0.29
56-5, 35–37	529.86	0.60	1.14	—	—
56-6, 35–37	531.36	0.45	0.98	1.38	0.15
57-1, 35–37	533.46	0.63	1.14	0.93	0.13
57-2, 35–37	534.96	0.71	1.34	1.12	0.49
57-3, 35–37	536.46	0.64	1.26	1.36	0.60
57-4, 35–37	537.96	0.71	1.38	1.37	0.28
57-4, 35–37	537.96	0.45	1.59	—	—
57-5, 35–37	539.46	0.98	1.38	1.16	0.22
57-5, 35–37	539.46	0.69	1.44	—	—
57-6, 35–37	540.96	0.51	1.64	1.33	0.76
58-1, 35–37	543.06	0.16	1.14	0.86	0.01
58-2, 35–37	544.56	0.37	0.79	0.67	−0.14
60-1, 35–37	562.26	0.04	0.81	0.68	−0.37
60-2, 35–37	563.76	−0.02	0.78	0.54	−0.26
60-3, 35–37	565.26	0.19	0.74	0.75	−0.66
60-4, 35–37	566.76	0.10	0.46	0.85	−0.66
60-5, 35–37	568.26	0.08	0.98	0.65	−0.35
60-6, 35–37	569.76	0.17	0.95	0.68	−0.13
Hole 593A					
23-2, 35–37	450.60	0.45	1.54	1.53	−0.05
23-3, 35–37	452.26	0.43	1.66	1.37	0.23
23-4, 35–37	453.66	0.13	1.45	1.62	−0.06
24-1, 35–37	458.76	0.32	1.23	1.21	0.02
24-2, 35–37	460.26	0.47	0.98	1.25	0.23
25-1, 35–37	468.36	0.41	0.98	1.33	−0.28
25-2, 35–37	469.86	0.31	0.58	0.90	−0.03
25-3, 35–37	471.36	0.56	0.94	1.67	0.42
25-4, 35–37	472.86	0.46	0.73	1.34	0.25
25-5, 35–37	474.36	0.64	0.90	0.81	0.09
25-6, 35–37	475.86	0.26	0.60	1.15	0.13
26-1, 35–37	477.96	0.19	0.73	0.98	−0.01
26-2, 35–37	479.26	0.11	0.94	0.93	−0.06
26-3, 35–37	480.96	0.52	0.70	1.23	−0.24
26-4, 35–37	482.26	0.52	0.86	1.37	−0.09
26-5, 35–37	483.96	0.65	0.66	1.33	0.03
27-1, 35–37	487.56	0.71	0.98	1.31	0.28
27-2, 35–37	489.06	0.76	0.65	1.36	−0.46
27-2, 35–37	489.06	—	—	1.25	−0.14
27-3, 35–37	490.56	0.64	0.86	1.65	0.01
27-4, 35–37	492.06	0.82	1.17	1.38	−0.27
27-5, 35–37	493.56	0.99	0.76	1.46	−0.19
27-6, 35–37	495.06	0.85	1.34	1.45	−0.23

Note: — means not present.

tope values followed by a rapid 1‰ enrichment in planktonic and benthic $\delta^{18}O$ signals in close association with the Eocene/Oligocene boundary (Fig. 2). The Oligocene values were relatively constant, varying ±0.2‰ and exhibiting no significant trends (Shackleton and Kennett, 1975).

Figure 3 shows our data together with that of Keigwin (1980), based on analyses of monospecific samples at Site 277. These data show relatively constant late Eocene oxygen-isotope values followed by a sudden enrichment of ~1.0‰ at the Eocene/Oligocene boundary. This isotopic shift is characterized by a slight "overshoot" followed by depletion to mean early Oligocene values, which were enriched about 0.6‰ relative to mean late Eocene values. Planktonic and benthic variations of ±0.5‰ are generally parallel through the early and middle Oligocene, exhibiting a slight enrichment trend in $\delta^{18}O$ for a total change of 0.5‰ from the early through the middle Oligocene.

The $\delta^{13}C$ data presented by Shackleton and Kennett (1975) were not discussed and can not be interpreted here because of the mixed taxa analyzed. The major features of our monospecific $\delta^{13}C$ record (Fig. 3) are (1) a 0.8‰ depletion in both planktonic and benthic values immediately prior to the Eocene/Oligocene boundary and (2) a 0.8‰ enrichment in the planktonic carbon record and a 1.0‰ enrichment in the benthic carbon record at the Eocene/Oligocene boundary in synchrony with the oxygen-isotope shift. The remaining planktonic carbon values are relatively constant, whereas the benthic record is characterized by at least three depletion-enrichment cycles during the early to middle Oligocene. The record at this site lacks any parallelism between the planktonic and benthic carbon-isotope variations.

There are several differences between the results of our study and those of Shackleton and Kennett (1975). For the oxygen-isotope data these include larger amplitude variations, a distinct enrichment trend in the middle Oligocene, and the consistently depleted values seen in our monospecific data compared to the mixed species data. Our carbon-isotope records show much greater variability than those of Shackleton and Kennett (1975). These differences are almost certainly a result of the varying composition of the mixed samples analyzed by Shackleton and Kennett (1975).

Site 593

Hole 593, in southern temperate latitudes, was drilled at 40°30.47′S; 167°47′E in 1068 m water depth. Core recovery was good (averaging 72%) except for Core 51 spanning the *Globigerina euapertura* Zone, so a second hole (Hole 593A) was drilled to recover this section. The holes were correlated using faunal datums (Fig. 4). Holes 593 and 593A form a continuous section from the late Eocene through the earliest Miocene. The sediments are foraminifer-rich nannofossil oozes, except for a 16 m sequence of volcaniclastic turbidites, debris flows, and pyroclastic flows emplaced near the Eocene/Oligocene boundary. These flows can be traced on seismic profiles

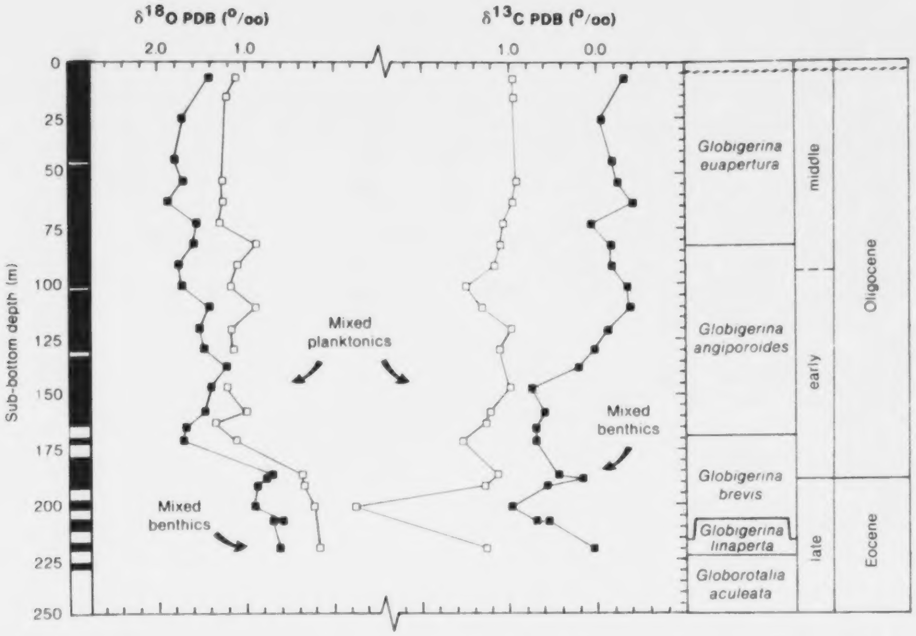

Figure 2. Oxygen- and carbon-isotope data from Shackleton and Kennett (1975) for DSDP Site 277. Foraminiferal stratigraphy after Jenkins (1975). Core recovery shown along left margin.

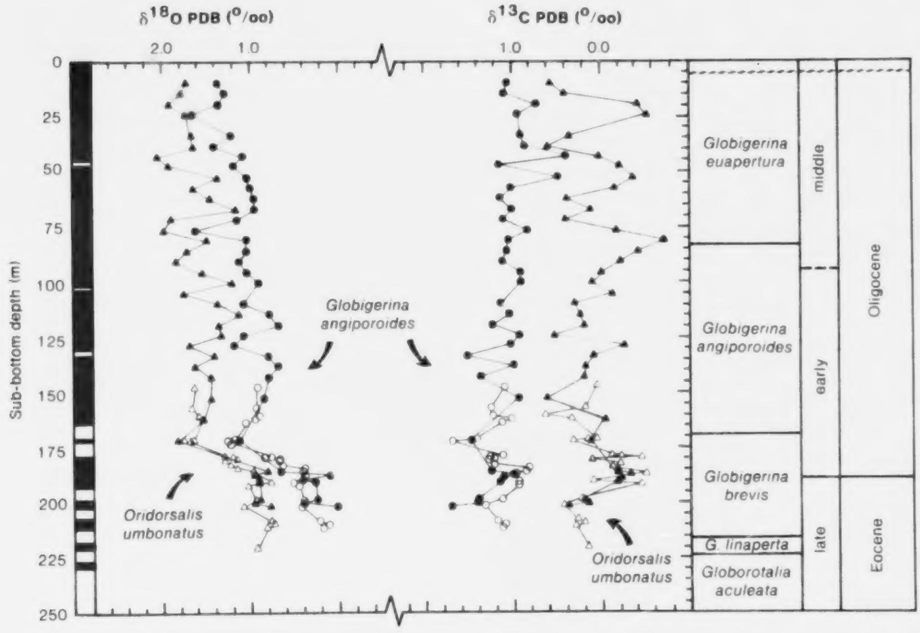

Figure 3. Oxygen- and carbon-isotope data from monospecific analyses of Site 277. Data from Keigwin (1980) indicated by open symbols. Stratigraphy after Jenkins (1975). Core recovery along left margin.

to the buried Lalitha Volcanic Pinnacle approximately 2 km from Site 593.

The δ^{18}O isotope records for both planktonic and benthic foraminifers are remarkably parallel throughout the section, with a clear shift of 1.0‰ beginning in the late Eocene, just below the volcanics, and reaching a maximum in early Oligocene Zones NP22/21. A gradual 0.5‰ depletion in early Oligocene δ^{18}O values was followed by a stepped enrichment of 0.5‰ in the late–early Oligocene; the records gradually deplete 0.6‰ in the middle

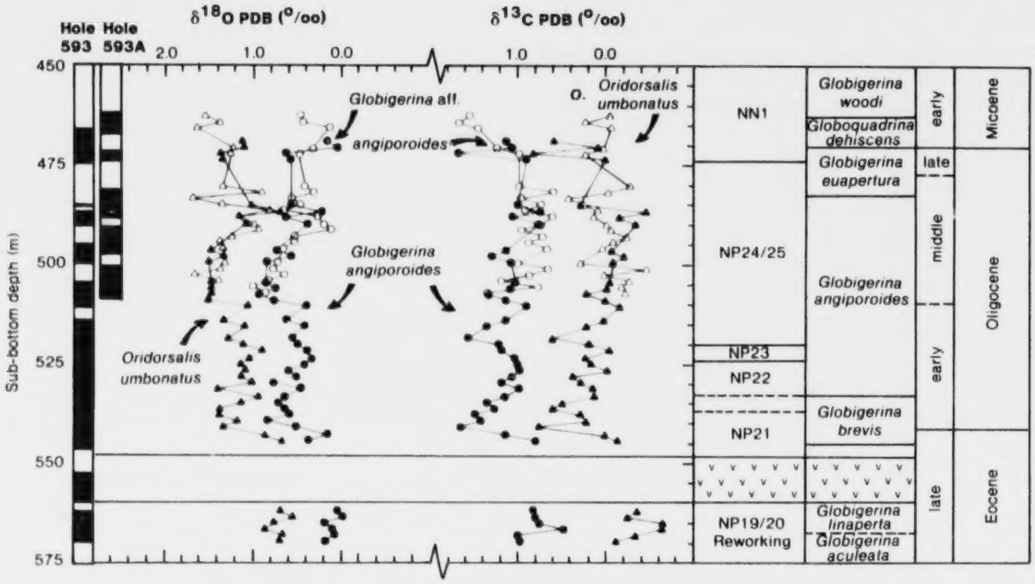

Figure 4. Oxygen- and carbon-isotope data from Holes 593 and 593A. Data from Hole 593A are indicated by open symbols. Calcareous nannoplankton stratigraphy after Martini (this volume). Planktonic foraminiferal stratigraphy after Jenkins and Srinivasan (this volume). Core recovery along left axis.

Oligocene. The late Oligocene benthic values exhibit a slight enrichment in contrast to continued depletion of the planktonic values.

The planktonic and benthic carbon-isotope records were very similar from the Eocene through the middle Oligocene, but diverged in the late Oligocene–early Miocene. A distinct 1.0‰ enrichment was synchronous with the Eocene/Oligocene boundary oxygen-isotope shift, after which the carbon-isotope curves exhibit a general trend toward depleted values. The records diverged in the late Oligocene (*G. euapertura* Zone) when the planktonics showed enrichment, in contrast to a slight depletion in benthic $\delta^{13}C$.

Site 592

Hole 592 was drilled at 36°28.40′S; 165°26.53′E in 1098 m water depth, in the present northern temperate zone. A 90-m section of upper Eocene through lower Oligocene sediments was recovered. This highly expanded section, with an average core recovery of 75%, provided a detailed stable-isotope record.

Figure 5 exhibits the remarkable parallelism of planktonic and benthic oxygen- and carbon-isotope variation at this site (the offset between planktonic and benthic curves varies by only about ±0.17‰). The oxygen-isotope record had relatively constant late Eocene values followed by a rapid depletion (~0.4‰) and a distinct enrichment (~1.0‰) beginning at the base of Zone NP21, which is considered, on the basis of nannofossil biostratigraphy, to represent the Eocene/Oligocene boundary. This oxygen-isotope shift continued until the latest part of Zone NP21. The Eocene/Oligocene boundary, on the basis of planktonic foraminiferal biostratigraphy (last occurrence datum of *Globigerinatheka index*), occurred midway through this oxygen-isotope shift. Martini (this volume) estimates the time period between these two boundary definitions is ~0.4 m.y. The values then deplete slightly (~0.2‰) from the peak associated with the NP21/NP22 boundary and have a depleting trend with little variation in the remaining early Oligocene.

The carbon-isotope record exhibits parallel trends between planktonic and benthic values similar to those seen in the oxygen-isotope data, both planktonic and benthic isotope records exhibit significant enrichments of 0.6–0.8‰ during the early part of the late Eocene *Globigerina linaperta* Zone. This was followed by 0.5‰ depletions in both records to the Eocene/Oligocene boundary (as recognized by the planktonic foraminiferal assemblages). The $\delta^{13}C$ records were enriched by ~1.0‰ in synchrony with the $\delta^{18}O$ shift. These enrichments were followed by an apparent convergence of planktonic and benthic values in the middle Oligocene *G. angiporoides* Zone.

CORRELATION OF ISOTOPIC CURVES

The isotopic curves from the three sites were correlated using a combination of biostratigraphic datums as compiled in the *Initial Reports* of Legs 29 and 90 and isotopic events as detailed in Table 2 using the chronology of Berggren et al. (in press). The main problems encountered in this process were (1) the age of the hiatus at Site 277 and (2) the age of the material below the volcanic sequence at Site 593. Site 277 is marked by a hiatus at 4.5 m. Samples just below the hiatus contain *Chiloguembelina cubensis* (last occurrence datum of 30 Ma: early/late Oligocene boundary; Berggren et al., in press), as well as *Jenkinsina samwelli* which exhibits a very short range in southwest Pacific Hole 282 and on

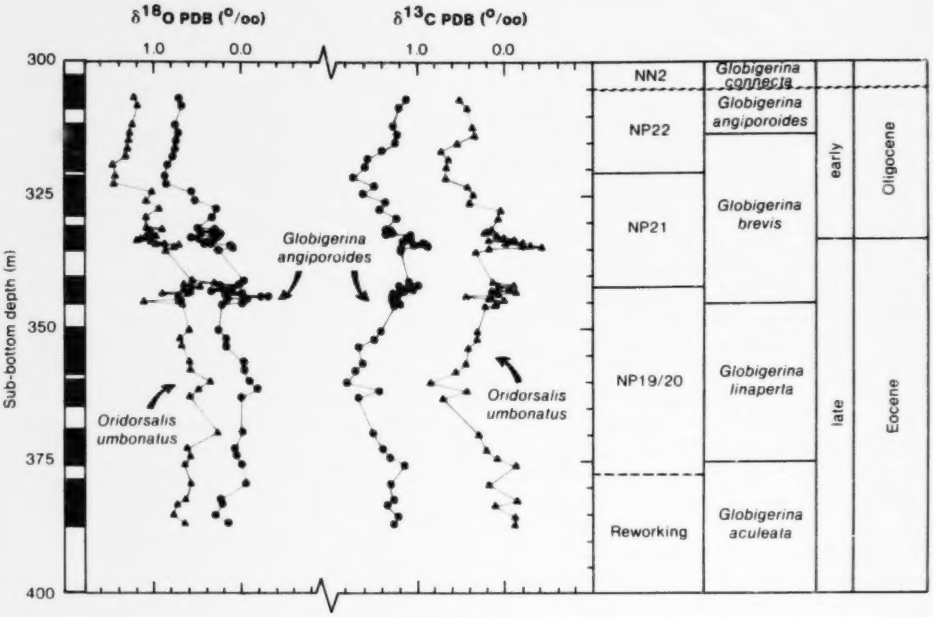

Figure 5. Oxygen- and carbon-isotope data from Site 592. Stratigraphy and recovery as in Figure 4.

Table 2. Chronostratigraphic datums used for correlation between the three sites.

Age (m.y.)	Marker[a]	Hole	Sub-bottom depth (m)	Epoch boundary
23.7	NN1/ /NP23/25	277	Hiatus	
		593	471.7	Oligocene/Miocene boundary
		593A	460.0	
		592	Hiatus	
30.0	LAD *Chiloguembelina cubensis*	277	4.5	
		593	475.0	
		593A	463.2	
		592	Hiatus	
32.0	LAD *Globigerina angiporoides* ss	277	82.05	
		593	489.90	
		592	Hiatus	
—	End of oxygen isotope shift in benthic foraminiferal records following the Eocene/Oligocene Boundary	277	171.0	
		593	539.9	
		592	321.6	
37.0	LAD *Globigerinatheka index*	277	189.6	37 Ma Eocene/Oligocene boundary
		593	542.01	
		592	333.05	
[illegible]	B. *Chiasmolithus oamaruensis*	277	264.0	
		592	347.6	

Note: Ages after Berggren et al. (in press).

[a] LAD = last appearance datum. B. = bottom.

the South Island, New Zealand, disappearing just below *C. cubensis*. The overlapping ranges of these two species at Site 277 suggest that the base of the hiatus is ~31–32 Ma (Jenkins, 1974).

At Site 593, changes in planktonic foraminifer assemblages used to recognize the Eocene/Oligocene boundary occur 3 m above the 16-m volcanogenic sequence (Jenkins and Srinivasan, this volume). In contrast, the calcareous nannofossil forms that mark the upper Eocene occur immediately below and lower Oligocene forms occur immediately above the volcanogenics (Martini, this volume). Comparison of the isotopic curves of Site 277 with those of Sites 592 and 593 suggest that part of the sediment record laid down during the Eocene/Oligocene boundary oxygen-isotope shift at Site 593 has been removed, leaving the beginning and end of the shift in place. Based on this interpretation, Figure 6 shows the oxygen- and carbon-isotope data plotted against age.

DISCUSSION

The correlation of Holes 277, 593/593A, and 592 from the late Eocene through the middle Oligocene is shown is Figures 6A and 6B. The oxygen-isotope records were divided into three stages for discussion: late Eocene to the Eocene/Oligocene boundary (41–37.5 Ma), the early Oligocene (37.5–33 Ma), and the middle Oligocene (33–28 Ma). The carbon-isotope records can be divided at 33 Ma on the basis of the variation in the benthic isotope record.

The surface signals for all three sites overlap as do the intermediate records from the late Eocene through earliest Oligocene (Fig. 6A). This similarity between Site 277 on the Campbell Plateau to the south of New Zealand and Sites 592 and 593 in the Tasman Sea to the north of New Zealand suggests that the sites were influenced by the same surface and intermediate water masses and that no oceanographic front existed between the sites at that time. This conclusion is in agreement with the warm equable climates predicted for the Eocene with low pole-to-equator temperature gradients (Wolfe, 1971; Kennett, 1977; Frakes, 1979; Brass et al., 1982).

A change in thermal structure occurred in the earliest Oligocene (~36.5–36 Ma) when Site 277 began to register consistently enriched ("cooler") isotopic values com-

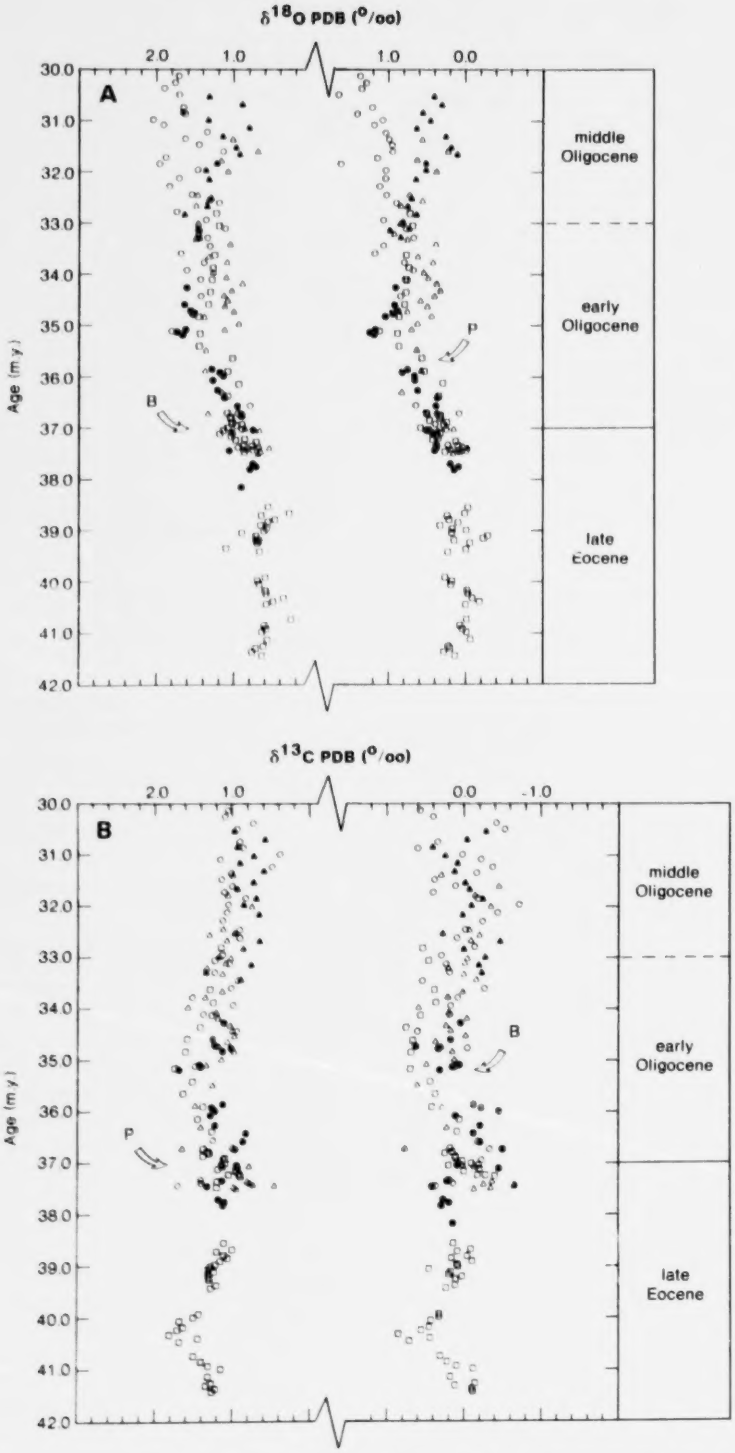

Figure 6. A. Plot of planktonic (P) and benthic (B) foraminiferal δ^{18}O data in late Eocene to middle Oligocene sediments of Sites 277, 593, and 592. Age model given in Table 1. For purposes of discussion, the Oligocene is divided into: early (37–33 Ma), middle (33–28 Ma), and late (28–23.5 Ma) intervals. Note increasing variability of data beginning at ~35 Ma, reaching maximum offset in middle Oligocene. (○) Site 277, this study; (●) Site 277, Keigwin (1980); (□) Site 592, this study; (△) Site 593, this study; (▲) Hole 593A, this study. B. Plot of δ^{13}C data in late Eocene to middle Oligocene sediments of Sites 277, 593, and 592. Age model as described in Figure 6A. Note less scatter in planktonic data (P) in contrast to greater variability of benthic data (B), most of which is due to fluctuations at Site 277 (line). Symbols as explained in Figure 6A.

pared to Sites 592 and 593 to the north. This divergence gradually increased in the planktonic record during the early Oligocene (37.5–33 Ma), while the benthic records fluctuated, with Site 277 maintaining the more enriched values.

At ~33 Ma, oxygen-isotope records at all three sites began to exhibit large variations (±0.4‰), at least until 30.5 Ma. These oscillations overlay a divergence developing between the trend toward enrichment shown by Site 277 and the trend toward depletion exhibited by Site 593 (Fig. 7).

The carbon-isotope data are plotted in Figure 6B. The planktonic values form a narrow band with low-amplitude fluctuations (<0.2‰) about a value of 1.2‰ in the early Oligocene and 0.8% in the middle Oligocene. The benthic $\delta^{13}C$ values were more variable, with the difference between sites increasing in the middle Oligocene (~33 Ma), when Site 277 was characterized by large fluctuations, in contrast to the more constant values from Sites 592 and 593.

TEMPERATURE ANALYSIS

The oxygen-isotope data have been converted to paleotemperature values and plotted in Figure 8. Temperatures have been calculated assuming a lack of any significant ice accumulations in the polar regions during this time interval, as originally modeled by Shackleton and Kennett (1975) and by Savin et al. (1975) using the equation:

$$T(^\circ C) = 16.9 - 4.38(\delta C - \delta W) + 0.1[\delta C - \delta W)^2]$$

where δC = isotopic signal of carbonate deposited in equilibrium with seawater. *Globigerina angiporoides* is assumed to deposit in equilibrium with seawater. The *Oridorsalis umbonatus* data have been corrected to equilibrium calcite by a factor of −0.42‰ in the temperature calculations (Graham et al., 1981). δW = isotopic composition of global ocean. Shackleton and Kennett (1975) have assumed a constant oceanic composition of −1.2‰ in an ice-free world.

This calculation results in minimum estimates of paleotemperatures, since the assumption of a constant δW value throughout the late Paleogene is not correct. It is generally accepted that a major and permanent ice sheet accumulated on East Antarctica during the middle Miocene (15–13 Ma) (Shackleton and Kennett, 1975; Savin et al., 1981; Woodruff and Douglas, 1981; Kennett, 1982). However several workers have argued that there was an Antarctic ice sheet during certain intervals in the Oligocene (Miller and Fairbanks, 1983; Miller and Thomas, in press; Keigwin and Keller, 1984; Shackleton et al., 1984), or even during the entire Paleogene (Matthews and Poore, 1980; Poore and Matthews, 1984). These conclusions were based on isotopically derived bottom-water paleotemperatures cooler than those of the present oceans. These abnormal temperatures were explained by assuming a nonconstant δW resulting from the accumulation of polar ice. Currently, little sedimentary evidence supports the existence of large accumulations of ice on Antarctica during the Paleogene. The marine record is poor in the circum-Antarctic region during the Oligocene. A glacial erosion surface on Antarctica has erased

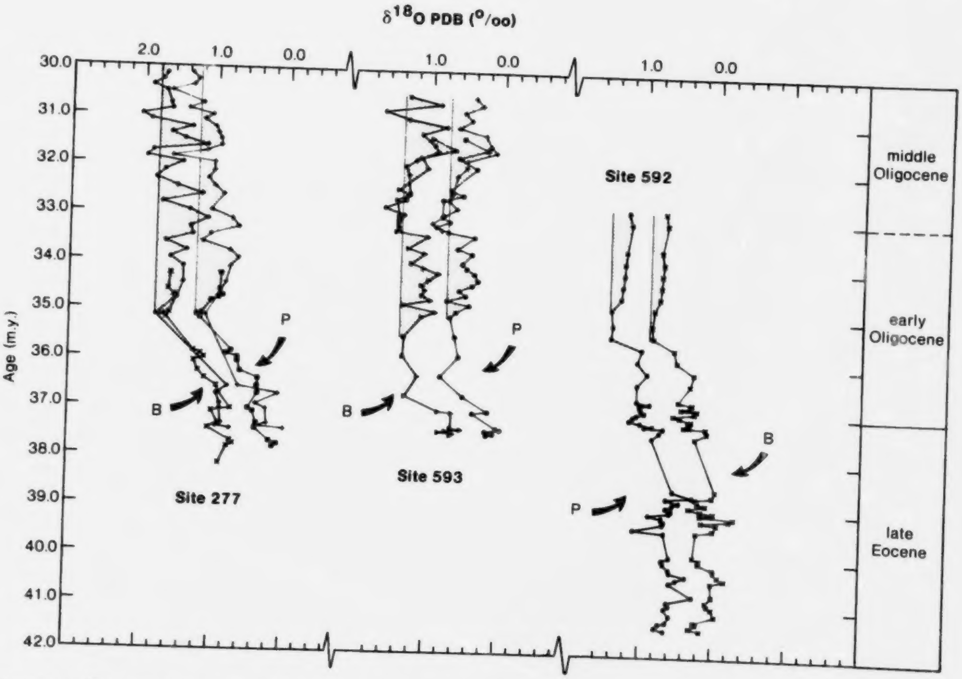

Figure 7. $\delta^{18}O$ records from Sites 277, 593, and 592 plotted against age model described in Figure 6A. Stippled portions denote curves lighter than maximum enrichment attained at Eocene/Oligocene oxygen-isotope shift. Note $\delta^{18}O$ decrease of Site 593 record in middle Oligocene in contrast to increase in Site 277 record.

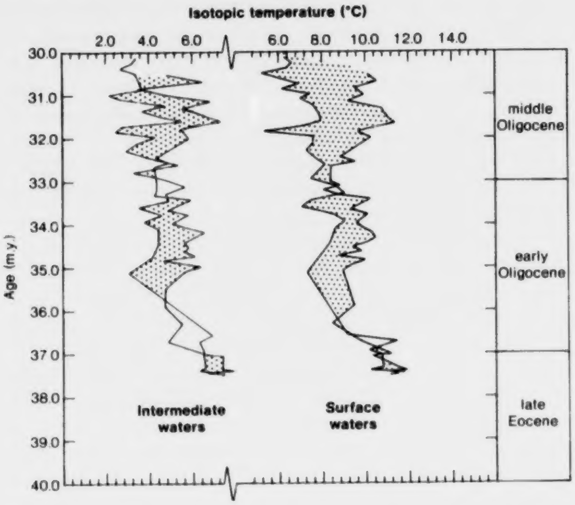

Figure 8. Plot of isotopic temperature gradient between Sites 277 and 593. Note reversal of gradient at ~37–35.5 Ma and at ~33 Ma. Stippled areas, Site 277 cooler than Site 593; white areas, Site 277 warmer than Site 593.

all of the sedimentary record between ~25 and 80 Ma on Marie Byrd Land (LeMasurier and Rex, 1982). Hyaloclastites thought to have been emplaced beneath ice sheets have been radiometrically dated as early Miocene and Oligocene in age, suggesting some ice accumulation during the Paleogene (LeMasurier, 1972). The first dated ice-rafted material in deep-sea sequences drilled around Antarctica is of late Oligocene age and is found in areas close to the continent within the Ross Sea embayment (Hayes and Frakes, 1975). Significant deposits of ice-rafted material have not been found at great distances from Antarctica in sediments older than middle Miocene. Site 278 on the Antarctic Convergence showed the first ice-rafted material at ~15 Ma; the abundance increased rapidly in younger sediments (Margolis, 1975; Kennett, 1978). These data suggest that although the $\delta^{18}O$ of water was probably not constant during the Paleogene, it did not fluctuate greatly in response to large ice-sheet fluctuations.

Table 3 shows the temperature maxima and minima for the southwest Pacific sites calculated using a constant δW of −1.2‰. Benthic values range from a maximum of 9.0°C at Site 592 in the late Eocene (~40.7 Ma) to a low of 2.2°C in the middle Oligocene of Site 277 (~31.0 Ma). Planktonic temperature estimates range from 13.0°C in the late Eocene (~39.1 Ma) at Site 592 to 5.2°C in the middle Oligocene of Site 277 (~30.5 Ma). A comparison of these isotopic paleotemperature estimates with present-day values from the same regions reveals that modern waters at 50 m are warmer than the warmest values from the late Eocene through Oligocene. However, modern intermediate waters have temperatures similar to, but slightly warmer than, the coolest intermediate-water isotopic paleotemperatures estimated during the Oligocene from these sites (Garner, 1962, 1967; Craig et al., 1981).

Table 3. Maximal and minimal oxygen-isotope temperatures for each site assuming $\delta W = -1.2‰$ in an ice-free world and present day temperatures at same locations.

	Eocene-Oligocene isotopic temperatures (°C)			
	Warmest		Coolest	
Site	Planktonic	Benthic	Planktonic	Benthic
592	12.96 (39.1 Ma)	8.98 (40.4 Ma)	8.18 (35.2 Ma)	4.36 (34.8 Ma)
593	11.87 (37.4 Ma)	7.91 (37.4 Ma)	8.02 (33.2 Ma)	3.57 (30.8 Ma)
277	11.75 (37.4 Ma)	7.20 (37.8 Ma)	5.23 (30.5 Ma)	2.17 (30.[illegible] Ma)

Present day			
Site	Position	Surface	Intermedi
NZOI #Di 2730 (Oct., 1950)	35°58′S, 163°39′E	(50 m) 16.90°	(1170 m) 4.[illegible]°
NZOI #A 957 (Feb., 1964)	41°00′S, 165°55′E	(51 m) 14.88°	(1090 m) 4.[illegible]°
GEOSECS 279 (Feb., 1974)	55°60′S, 170°60′E	(50 m) 7.40°	(1103 m) 2.[illegible]°

If there had been accumulation of ice on Antarctica during the time represented by these sediments, there would have been enrichment of ^{18}O in the global ocean, making the paleotemperatures even warmer than those calculated using a constant δW of −1.2‰. An enrichment of global δW values resulting from ice formation would appear as a synchronous enrichment in the surface and intermediate (and deep) oxygen-isotope values at every site (Shackleton and Opdyke, 1973). Each site in the southwest Pacific exhibits strong parallelism of planktonic and benthic oxygen-isotope records until ~33 Ma, at which time they record the coolest isotopic paleotemperatures. After this, however, the records from different sites diverged. We interpret this pattern to be the result of the combined effects of ice accumulation and the progressive decoupling of surface-water temperatures resulting from paleocirculation changes within the region. Clear evidence for the permanent presence of ice sheets is seen only from the middle Miocene (~15 Ma) to the present day. Future drilling in the Antarctic region should help define the nature of large ice accumulations, if any, on Antarctica during the Paleogene and hence assist in the interpretation of absolute paleotemperatures using stable-isotope data.

TEMPERATURE GRADIENTS

The present-day temperature gradient between 35°S (~Site 593) and 55°S (~Site 277) is 9.5°C at 50 m and 1.8°C at ~1000 m (Garner, 1962, 1967; Craig et al., 1981). Throughout the Oligocene, the isotopic paleotemperature at Site 277 was usually cooler than that at Sites 592 or 593, which exhibited similar paleotemperatures (see Table 3). Figure 8 shows the changing surface and intermediate gradients for the latest Eocene through middle Oligocene between Sites 277 and 593. In the late Eocene, northern Sites 592 and 593 recorded temperatures very similar to those at Site 277. By 35 Ma, in the early Oligocene, a gradient of ~1.5°C had developed in both intermediate and surface waters. The surface-water gradients remained at ~1.5°C until 33 Ma while the intermediate-water gradient fluctuated around 1.0°C. The remaining record is characterized by an increasing offset between these sites. A maximum gradient of 4.0°C for surface and 2.4°C for intermediate waters was reached at 31–30 Ma, at which time the planktonic foraminifers at southern Site 277 recorded temperatures nearly as cool as the benthic foraminifers at northern Site 593 (Fig. 8). The greatest amount of latitudinal difference documented in this study occurred at the end of our comparable data at the base of the Site 277 hiatus (~30 Ma, middle Oligocene). The late Oligocene record at Site 593 suggested no major warming or cooling (Fig. 4).

The major steps in the Oligocene development of Southern Ocean latitudinal thermal gradients began at times of "inversion" in the gradient record at 36.0 and 33.0 Ma. These changes in the thermal gradient generally support the paleoceanographic history of the southwest Pacific sector of the Southern Ocean developed by Kennett et al. (1975) and by Kennett (1977, 1978). The proposed paleoceanographic history of the region is summarized in the series of maps shown in Figure 9A–D.

In the late Eocene (Fig. 9A) no Circum-Antarctic Current existed to interfere with the influence of the southward-flowing warm-subtropical arm of the South Pacific gyre (East Australian Current). These warm-subtropical waters were transported close to Antarctica, warming this region and preventing the development of extensive seasonal sea ice (Kennett, 1977). The influence of this gyre resulted in similar temperatures at all three sites during the late Eocene, as recorded by the overlapping values of the oxygen-isotope records.

Kennett et al. (1975) showed that the first high-latitude surface-water communication between the South Indian and South Pacific Oceans occurred in the latest Eocene across the shallow, subsiding South Tasman Rise (Fig. 9B). The opening of the Tasmanian Seaway at shallow depths was a major step in the development of the Circum-Antarctic Current. This allowed passage of relatively cool Indian Ocean waters into the South Pacific, which led to cooling of waters in the South Pacific sector of the Southern Ocean and an initial decoupling of the warm-subtropical gyre from the Southern Ocean (Kennett, 1977, 1978). As a result, the first extensive sea ice and the initial production of cold, dense psychrospheric bottom waters are inferred to have begun in close association with the Eocene/Oligocene boundary in areas adjacent to the Antarctic continent (Shackleton and Kennett, 1975; Kennett, 1978). Thus, the Eocene/Oligocene boundary event, as delineated by the $\delta^{18}O$ shift, is not an isolated event but rather marks the crossing of a threshold in the sequential climatic deterioration seen in the Paleogene paleoclimatic record (Kennett, 1978; Corliss et al., 1984). It has also been proposed that the initial development of the two-layered, thermohaline-driven (psychrospheric) ocean preceded the Eocene/Oligocene boundary, occurring in the latest Eocene (~40 Ma) and that the $\delta^{18}O$ shift at the Eocene/Oligocene boundary marks the shallow water manifestation of this essentially deep-water event (Benson et al., in press). The intermediate records available from the Southwest Pacific cannot resolve this issue.

The continuing separation of Antarctica from Australia led to the further development of the Circum-Antarctic Current. Deep-water circulation developed in the middle to late Oligocene (Fig. 9C), as a deep passage formed south of the South Tasman Rise (Kennett et al., 1975) and the Drake Passage opened (Barker and Burrell, 1977).

Our oxygen-isotope data clearly record the evolution of this system. The paleotemperature difference between Site 277 and the more northern sites continued to increase, in surface waters, through the early to middle Oligocene, except for a reversal of the gradient at ~33 Ma. This divergence resulted from further cooling of high-latitude surface waters as the Southern Ocean continued to expand northward.

A major development in the thermal differentiation occurred ~33 Ma between Site 277 and the northern sites in both surface and intermediate waters as the thermal gradient between these two regions significantly and rapidly increased (Figs. 7 and 8). This is interpreted to reflect a major reorganization of Southern Ocean circulation as proposed earlier by Kennett et al. (1975) and by Kennett (1975) when deep Circum-Antarctic Circulation developed through the Tasmanian Seaway. This led to the formation of widespread hiatuses in the high southern latitudes, northward displacement of the siliceous/calcareous sediment boundary, and the beginning of essentially uninterrupted Neogene biogenic sediment deposition in the Coral and Tasman seas. Resulting intensification of the Circum-Antarctic Current led to further decoupling between the warm-subtropical South Pacific gyre and the cold circumpolar circulation. This decoupling proceeded in both surface and intermediate waters. High-latitude surface waters continued to cool, while those at middle latitudes warmed. At the same time, high-latitude intermediate waters rapidly cooled while those at temperate latitudes gradually warmed. The decoupling of these systems at both surface and intermediate depths led to the parallel development of increasingly cool subpolar regions and increasingly warm subtropics.

During the Miocene, continued decoupling resulted in intensified latitudinal thermal gradients, which doubled from 6 to 12°C between the tropics and the sub-Antarctic (Loutit et al., 1984).

BIOGEOGRAPHY

In the modern ocean there exist a number of surface-water masses bounded by oceanographic fronts that are marked by distinct planktonic fauna and flora. These bioprovinces are arranged with a distinct latitudinal zonality and provide an alternate line of evidence for the water-mass evolution we have proposed. As the pole-to-equator thermal gradient developed during the Cenozoic, there should have been an associated evolution of latitudinal biogeographic zonality. In the present ocean, Site 277 is well within the subantarctic biogeographic province; in contrast, Sites 592 and 593 lie within the temperate (cool subtropical) biogeographic province. Fauna and flora associated with these present-day water masses are quite distinct, the boundary coincides with

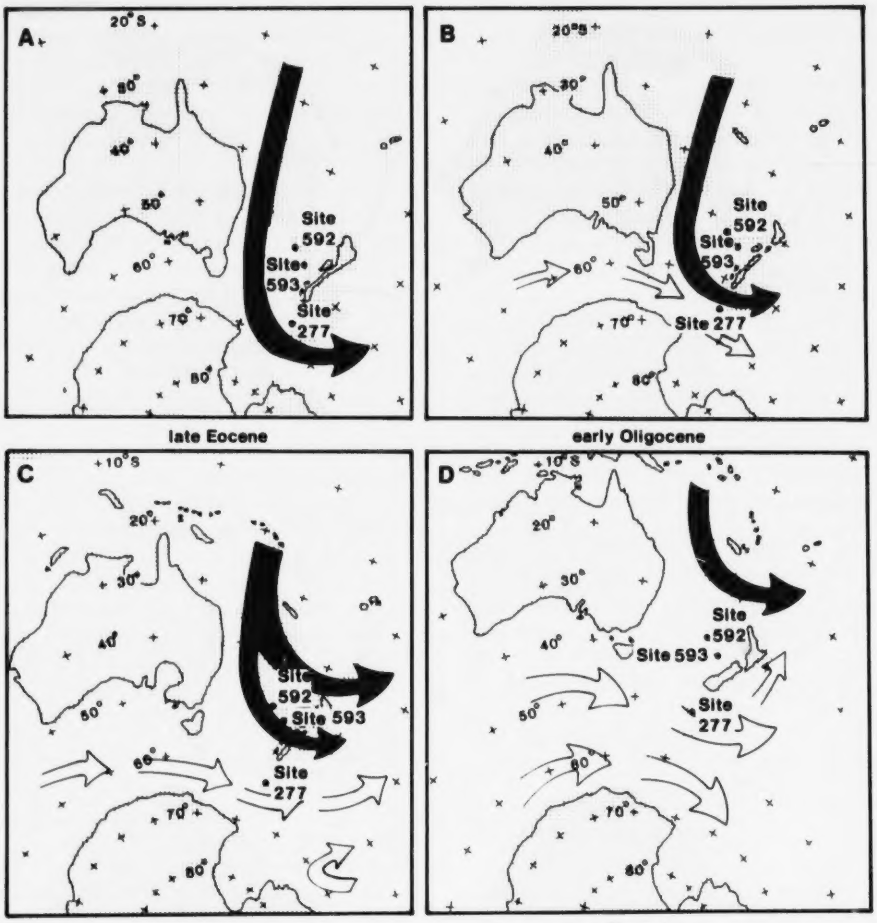

late Eocene

early Oligocene

middle Oligocene

Recent

Figure 9. Proposed model for decoupling of ocean currents affecting temperatures at Sites 592 and 593 versus Site 277. Dark arrows denote warm currents, open arrows denote cool/cold currents, width of arrow indicative of current strength. Land areas and shallow ridges and rises as marked.

the Subtropical Convergence. During the Eocene and Oligocene, these separate biogeographic provinces had not yet developed. Planktonic foraminiferal assemblages at Sites 277 and 593/592 are generally similar during this time and contain most of the same taxa, but in differing proportions (Jenkins, 1975; Jenkins and Srinivasan, this volume). Warm-water elements are more abundant in the northern sites relative to the south, but the assemblages do not suggest the presence of an oceanographic front between the regions as in the modern ocean. The study of the planktonic microfossil sequence at Site 594, drilled in the present-day northern subantarctic waters just south of the Subtropical Convergence, has suggested that this oceanic front developed during the middle Miocene. The Antarctic Convergence (Polar Front) had developed south of Site 277 by the earliest Oligocene, as seen by the faunal assemblages in Hole 267B at 59°S latitude. This front was marked by major faunal differences between relatively high-diversity subantarctic planktonic foraminiferal assemblages to the north and very low-diversity polar assemblages to the south (Kaneps, 1975).

CONCLUSIONS

Oxygen-isotope data document the development of thermal gradients during the Oligocene in the southwest Pacific between subantarctic and temperate latitudes. Isotopic temperature records from these sites diverged in three major steps beginning in the early Oligocene. Late Eocene values overlap; early to middle Oligocene values exhibit a slight divergence as the result of continued temperature decreases at high latitudes but not at temperate latitudes; the middle Oligocene values exhibit major and rapid divergence of both planktonic and benthic signals as the subantarctic region continued to cool and the temperate regions warmed.

This oxygen-isotope history was closely tied to the development of the Circum-Antarctic Current. In the late Eocene, the entire area was bathed by southerly-flowing warm-subtropical gyre waters, uninterrupted by the Circum-Antarctic Current, which had not yet developed. The beginning of latitudinal thermal differentiation occurred after the oxygen-isotope shift associated with the Eocene/Oligocene boundary and is believed to have been related to the development, in the latest Eocene, of surface-water communication between the South Indian and South Pacific sectors. This began to decouple the warm subtropical gyres from the high southern latitudes leading to a cooling of surface- and bottom-water masses. A further major temperature divergence occurred at 33 Ma, when the Circum-Antarctic Current was able to flow south of the South Tasman Rise and affect both deep and shallow waters. This study suggests that there were accumulations of ice during the middle Oligocene, but the diverging oxygen-isotope records after ~33 Ma argue against the establishment of a permanent ice sheet at that time. Further intensification of the cold polar current continued to decouple temperate from subantarctic surface regimes and led to a warming of temperate surface-water masses.

Despite the increase in temperature gradients between Antarctic and temperate regions during the Oligocene, biogeographic similarities in calcareous microfossils suggest that the Subtropical Convergence had not yet formed by the end of the Paleogene. Biostratigraphic evidence suggests formation of this convergence in the middle Miocene. Biogeographic changes, however, do support the existence and development of temperature differences between these latitudes in the Paleogene.

ACKNOWLEDGMENTS

We thank Nancy Meader, Karin Nelson, Robin Rice, Jenny Martin, and Joe Orchardo for their assistance in drafting and editing. Discussion of these ideas with Paul Abell, Allan Cain, and Margaret Leinen was very helpful as was a review by Dave Johnson. Special appreciation is rendered to Ken Miller and Margaret Leinen for their thorough reviews of the manuscript. This research was supported by the National Science Foundation grant #DPP81-12615 from the Division of Polar Programs.

REFERENCES

Barker, P. T., and Burrell, J., 1977. The opening of Drake Passage. *Mar. Geol.*, 25:15–34.

Benson, R. H., Chapman, R. E., and Deck, L. T., 1984. Paleoceanographic events and deep-sea ostracods. *Science*, 224:1334–1336.

Berggren, W. A., Kent, D. V., and Flynn, J. J., in press. Paleogene geochronology and chronostratigraphy. *In* Snelling, N. J. (Ed.), *Geochronology and the Geologic Time Scale.* Geol. Soc. Lond. Spec. Pap.

Blattner, P., and Hulston, J. R., 1978. Proportional variations of geochemical $\delta^{18}O$ scales—An interlaboratory comparison. *Geochim. Cosmochim. Acta*, 42:59–62.

Brass, G. W., Southam, J. R., and Peterson, W. H., 1982. Warm, saline bottom water in the ancient ocean. *Nature (London)*, 296:620–623.

Corliss, B. H., Aubry, M.-P., Berggren, W. A., Fenner, J. M., Keigwin, L. D., Jr., and Keller, G., 1984. The Eocene/Oligocene Boundary event in the deep sea. *Science*, 226:806–810.

Craig, H., 1957. Isotopic standards for carbon and oxygen and correction factors for mass-spectrometric analysis of carbon dioxide. *Geochim. Cosmochim. Acta*, 12:133–140.

Craig, H., Broecker, W. S., and Spencer, D., 1981. Geosecs Pacific Expedition: Hydrographic Data: Washington (Natl. Sci. Found.).

Frakes, L. A., 1979. *Climates throughout Geologic Time.* New York (Elsevier).

Garner, D. M., 1962. Analysis of hydrological observations in the New Zealand Region, 1874–1955. *N. Z. Oceanogr. Inst. Mem.*, 9: 1–45.

________, 1967. Hydrology of the south-east Tasman Sea. *N. Z. Oceanogr. Inst. Mem.*, 48:9–49.

Gordon, A. L., 1972. On the interaction of the Antarctic Circumpolar Current and the Macquarie Ridge. *In* Hayes, D. E. (Ed.), *Antarctic Oceanology II, The Australian-New Zealand Sector.* Am. Geophys. Union Antarct. Res. Ser., 19:71–78.

Graham, D. W., Corliss, B. H., Bender, M. L., and Keigwin, L. D., Jr., 1981. Carbon and oxygen isotopic disequilibria of Recent deep-sea benthic foraminifera. *Mar. Micropaleontol.*, 6:483–497.

Hayes, D. E., and Frakes, L. A., 1975. General synthesis, Deep Sea Drilling Project Leg 28. *In* Hayes, D. E., Frakes, L. A., et al., *Init. Repts. DSDP*, 28: Washington (U.S. Govt. Printing Office), 919–942.

________, 1975. Cenozoic planktonic foraminiferal biostratigraphy of the southwestern Pacific and Tasman Sea—DSDP Leg 29. *In* Kennett, J. P., Houtz, R. E., et al., *Init. Repts. DSDP*, 29: Washington (U.S. Govt. Printing Office), 449–468.

Jenkins, D. G., 1975. Initiation of the proto circum-antarctic current. *Nature (London)*, 252:371–373.

Kaneps, A. G., 1975. Cenozoic planktonic foraminifera from Antarctic deep-sea sediments, Leg 28. *In* Hays, D. E., Frakes, L. A., et al., *Init. Repts. DSDP*, 28: Washington (U.S. Govt. Printing Office), 573–584.

Keigwin, L. D., Jr., 1980. Paleoceanographic change in the Pacific at the Eocene-Oligocene Boundary. *Nature (London)*, 287:722–725.

Keigwin, L. D., Jr., and Keller, G., 1984. Middle Oligocene cooling from Equatorial Pacific DSDP Site 77B. *Geology*, 12:16–19.

Kennett, J. P., 1977. Cenozoic evolution of Antarctic glaciation, the circum-antarctic ocean, and their impact on global paleoceanography. *J. Geophys. Res.*, 82:3843–3860.

________, 1978. The development of planktonic biogeography in the Southern Ocean during the Cenozoic. *Mar. Micropaleontol.*, 3: 301–345.

________, 1982. *Marine Geology*. New Jersey (Prentice-Hall, Inc.).

Kennett, J. P., Houtz, R. E., Andrews, P. B., Edwards, A. R., Gostin, V. A., Hajos, M., Hampton, M., Jenkins, D. G., Margolis, S. V., Ovenshine, A. T., and Perch-Nielsen, K., 1975. Cenozoic paleoceanography in the southwest Pacific Ocean, Antarctic glaciation and the development of the circum-antarctic current. *In* Kennett, J. P., Houtz, R. E., et al., *Init. Repts. DSDP*, 29: Washington (U.S. Govt. Printing Office), 1155–1169.

Kvasov, D. D., and Verbitsky, M. Y., 1981. Causes of Antarctic Glaciation in the Cenozoic. *Quat. Res.*, 15:1–17.

LeMasurier, W. E., 1972. Volcanic record of Cenozoic Glacial History of Marie Byrd Land. *In* Adie, R. J. (Ed.), *Antarctic Geology and Geophysics:* Oslo (Scand. University Books), pp. 251–259.

LeMasurier, W. E., and Rex, D. C., 1982. Rates of uplift and the scale of ice level instabilities recorded by volcanic rocks in Marie Byrd Land, West Antarctica. *In* Craddock, C. (Ed.), *Antarctic Geoscience.* Madison (Univ. Wisconsin Press), 725–734.

Loutit, T. S., Kennett, J. P., and Savin, S. M., 1984. Miocene equatorial and southwest Pacific paleoceanography from stable isotope-evidence. *Mar. Micropaleontol.*, 8:215–223.

Margolis, S. V., 1975. Paleoglacial history of Antarctica inferred from analyses of Leg 29 sediments by scanning-electron microscopy. *In* Kennett, J. P., Houtz, R. E., et al., *Init. Repts. DSDP*, 29: Washington (U.S. Govt. Printing Office), 1039–1048.

Matthews, R. K., and Poore, R. Z., 1980. Tertiary delta O-18 record and glacio-eustatic sea-level fluctuations. *Geology*, 8:501–504.

Miller, K. G., and Fairbanks, R. G., 1983. Evidence for Oligocene-Middle Miocene abyssal circulation changes in the western North Atlantic. *Nature (London)*, 306:250–253.

Miller, K. G., and Thomas, E., in press. Late Eocene to Oligocene benthic foraminiferal isotope record, Site 574, equatorial Pacific. *In* Mayer, L., Theyer, F., et al., *Init. Repts. DSDP*, 85: Washington (U.S. Govt. Printing Office).

Poore, R. Z., and Matthews, R. K., 1984. Late Eocene-Oligocene oxygen and carbon isotopic record from South Atlantic ocean, Deep Sea Drilling Project Site 522. *In* Hsü, K. J., LaBrecque, J. L., et al., *Init. Repts. DSDP*, 73: Washington (U.S. Govt. Printing Office), 725–736.

Sancetta, C., 1979. Paleogene Pacific microfossils and paleoceanography. *Mar. Micropaleontol.*, 4:363–398.

Savin, S. M., 1977. The history of the Earth's surface temperature during the past 100 m.y. *Annu. Rev. Earth Planet. Sci.*, 5:319–355.

Savin, S. M., Douglas, R. G., Keller, G., Killingley, J. S., Shaughnessy, L., Sommer, M. A., Vincent, E., and Woodruff, F., 1981. Miocene benthic foraminiferal isotope records: A synthesis. *Mar. Micropaleontol.*, 6:423–450.

Savin, S. M., Douglas, R. G., and Stehli, F. G., 1975. Tertiary marine paleotemperatures. *Geol. Soc. Am. Bull.*, 86:1499–1510.

Savin, S. M., and Yeh, H. W., 1981. Stable isotopes in ocean sediments. *In* Emiliani, C. (Ed.), *The Sea* (Vol. 7): *The Oceanic Lithosphere:* New York (Wiley-Interscience), 1521–1554.

Sclater, J. G., Meinke, L., Bennett, A., and Murphy, C., in press. The depth of the ocean through the Neogene. *In* Kennett, J. P. (Ed.), *The Miocene Ocean: Paleoceanography and Biogeography (CENOP).* Mem. Geol. Soc. Am., 163

Shackleton, N. J., Hall, M. A., and Boersma, A., 1984. Oxygen and carbon isotope data from Leg 74 foraminifers. *In* Moore, T. C., Jr., Rabinowitz, P. D., et al., *Init. Repts. DSDP*, 74: Washington (U.S. Govt. Printing Office), 599–612.

Shackleton, N. J., and Kennett, J. P., 1975. Paleotemperature history of the Cenozoic and the initiation of Antarctic glaciation: oxygen and carbon isotope analyses in DSDP Sites 277, 279, and 281. *In* Kennett, J. P., Houtz, R. E., et al., *Init. Repts. DSDP*, 29: Washington (U.S. Govt. Printing Office), 743–756.

Shackleton, N. J., and Opdyke, N. D., 1973. Oxygen isotope and palaeomagnetic stratigraphy of equatorial Pacific core V28-238: Oxygen isotope temperatures and ice volumes on a 10^5 year and 10^6 year scale. *Quat. Res.*, 3:39–55.

Wise, S. W., Ciesielski, P. F., MacKenzie, D. T., Wind, F. H., Busen, K. E., Gombos, A. M., Haq, B. U., Lohmann, G. P., Tjalsma, R. C., Harris, W. K., Hedlund, R. W., Beju, D. N., Jones, D. W., Plafker, G., and Sliter, W. V., 1982. Paleontologic and paleoenvironmental synthesis for the southwest Atlantic ocean basin based on Jurassic to Recent faunas and floras from the Falkland Plateau. *In* Craddock, K. (Ed.), *Antarctic Geoscience*. Madison (Univ. of Wisconsin Press), 155–163.

Wolfe, J. A., 1971. Tertiary climatic fluctuations and methods of analysis of Tertiary floras. *Paleogeogr., Paleoclimatol., Paleoecol.*, 9: 27–57.

Woodruff, F., and Douglas, R. G., 1981. Response of deep sea benthic foraminifera to Miocene paleoclimatic events, DSDP Site 289. *Mar. Micropaleontol.*, 6:617–632.

Date of Initial Receipt: 10 August 1984
Date of Acceptance: 7 December 1984

APPENDIX

Calibration of the URI Stable Isotope Standards

J. R. Orchardo

Calibration of the University of Rhode Island's mass spectrometry laboratory reference gas to PDB was accomplished by analysis of national and international standards. These were NBS-20, NBS-19, TKL-1, B-1, Fletton Clay, Brown Yule Marble, and Carrara Marble. Each standard was reacted in fresh 100% orthophosphoric acid at 50 ± 0.5°C. purified, and analysed on a VG Micromass 602D mass spectrometer. The data were corrected following Craig (1957). Conversion to per mil values with respect to PDB was done in two different ways. First, the intercept of a regression of the measured versus literature data was used to correct to PDB. This minimized the uncertainty of the value of NBS-20 to PDB presently in the literature. The second method corrected each standard using only its measured value and the literature value of NBS-20 found in Blattner and Hulston (1978).

It must be noted that the B-1 standard that URI analyzes is a coarse size fraction of that standard. It has recently come to our attention that the delta values of this size fraction differ from the values obtained from the fine size fraction which is more widely analyzed (D. Price, personal communication, 1983). Therefore, we present the B-1 data with respect to our own laboratory calibration of PDB and not with respect to any literature value to PDB.

With the exception of the $\delta^{13}C$ values of TKL-1 and Fletton Clay, the URI results compare well with values reported in the literature (see Table 1).

Table 1. Results of analyses of national and international standards.

Standard	URI measured	Correction by regression to PDB	Correction by NBS-20 to PDB	Literature value to PDB
$\delta^{18}O$				
NBS-20	−3.55 ± 0.02	−4.14	—	−4.18
NBS-19	−1.52 ± 0.02 (4)	−2.11	−2.15	−2.19
TKL-1	−3.56 ± 0.06 (5)	−4.15	−4.19	−4.26
B-1 (coarse fraction)	0.88 ± 0.04 (4)	0.31	0.23	—
Fletton Clay	0.32 ± 0.02 (6)	−0.27	−0.31	−0.24
Brown Yule Marble	−6.00 ± 0.06 (5)	−6.59	−6.63	−6.54
Carrara Marble	−1.29 ± 0.05 (5)	−1.88	−1.92	−1.81
$\delta^{13}C$				
NBS-20	−2.28 ± 0.04	−1.05	—	−1.07
NBS-19	0.71 ± 0.02 (4)	1.93	1.88	1.92
TKL-1	−3.17 ± 0.09 (5)	−1.95	−2.00	−1.69
B-1 (coarse fraction)	−0.58 ± 0.04 (4)	0.64	0.59	—
Fletton Clay	1.02 ± 0.03 (6)	2.24	2.29	1.91
Brown Yule Marble	−3.54 ± 0.05 (5)	−2.32	−2.37	−2.29
Carrara Marble	0.94 ± 0.02 (5)	2.16	2.11	2.16

Note: Standard deviations are listed, with number of replicates in parentheses. Because of continuing questions regarding the value of NBS-20 to PDB, the measured URI values were corrected to PDB using the intercept of a regression of all the measured (URI) values and the measured value of NBS-20 only.

41. LATE NEOGENE PALEOCEANOGRAPHIC EVOLUTION OF SITE 590: SOUTHWEST PACIFIC[1]

Kristin M. Elmstrom and James P. Kennett, Graduate School of Oceanography, University of Rhode Island[2]

ABSTRACT

High biogenic sedimentation rates in the late Neogene at DSDP Site 590 (1293 m) provide an exceptional opportunity to evaluate late Neogene (late Miocene to latest Pliocene) paleoceanography in waters transitional between temperate and warm-subtropical water masses. Oxygen and carbon isotope analyses and quantitative planktonic foraminiferal data have been used to interpret the late Neogene paleoceanographic evolution of this site.

Faunal and isotopic data from Site 590 show a progression of paleoceanographic events between 6.7 and 4.3 Ma, during the latest Miocene and early Pliocene. First, a permanent depletion in both planktonic and benthic foraminiferal $\delta^{13}C$, between 6.7 and 6.2 Ma, can be correlated to the globally recognized late Miocene carbon isotope shift. Second, a 0.5‰ enrichment in benthic foraminiferal $\delta^{18}O$ between 5.6 and 4.7 Ma in the latest Miocene to early Pliocene corresponds to the latest Miocene oxygen isotopic enrichment at Site 284, located in temperate waters south of Site 590. This enrichment in $\delta^{18}O$ coincides with a time of cool surface waters, as is suggested by high frequencies of *Neogloboquadrina pachyderma* and low frequencies of the warmer-water planktonic foraminifers, as well as by an enrichment in planktonic foraminiferal $\delta^{18}O$ relative to the earlier Miocene. By 4.6 Ma, benthic foraminiferal $\delta^{18}O$ values become depleted and remain fairly stable until about 3.8 Ma.

The early Pliocene (~4.3 to 3.2 Ma) is marked by a significant increase in biogenic sedimentation rates (37.7 to 83.3 m/m.y.). During this time, heaviest values in planktonic foraminiferal $\delta^{18}O$ are associated with a decrease in the gradient between surface and intermediate-water $\delta^{13}C$ and $\delta^{18}O$, a 1.0‰ depletion in the $\delta^{13}C$ of two species of planktonic foraminifers, and a mixture of warm and cool planktonic foraminiferal elements. These data suggest that localized upwelling at the Subtropical Divergence produced an increase in surface-water productivity during the early Pliocene.

A two-step enrichment in benthic foraminiferal $\delta^{18}O$ occurs in the late Pliocene sequence at Site 590. A 0.3‰ average enrichment at about 3.6 Ma is followed by a 0.5‰ enrichment at 2.7 Ma. These two events can be correlated with the two-step isotopic enrichment associated with late Pliocene climatic instability and the initiation of Northern Hemisphere glaciation.

INTRODUCTION

Development of the hydraulic piston core (HPC) and the extended core barrel (XCB) have enabled high-quality sedimentary sections to be obtained from the deep sea. Such a high-quality site is DSDP Site 590, located in the southwest Pacific at 1293 m on the eastern flank of the Lord Howe Rise (Fig. 1). The site is located under the present-day position of the Subtropical Divergence (Tasman Front; Denham and Crook, 1976; Stanton, 1979, 1981), which separates temperate surface-water masses to the south from warm-subtropical water masses to the north. The front represents the southern extent of the South Pacific subtropical gyre as the East Australian Current turns to the east, passing to the north of New Zealand. Divergence and associated upwelling at the Subtropical Divergence is caused by the interaction of the eastward-flowing gyral circulation with the Lord Howe Rise (Stanton, 1981) and has created high rates of biogenic productivity during the late Neogene (Kennett et al., 1983). The sedimentary sequence cored at Site 590 ranges in age from early Miocene to Recent and is composed of a nannofossil ooze to foraminifer-bearing nannofossil ooze. Three holes were drilled; Hole 590 terminated after only three cores were taken; Hole 590A, which extends from the earliest Pleistocene to the late Miocene; and Hole 590B, which extends from the late Pleistocene to the early Miocene.

In this chapter we study the paleoceanographic evolution of Hole 590A from the late Miocene (~7.0 Ma) to the latest Pliocene (~1.8 Ma), using quantitative changes in planktonic foraminifers and planktonic and benthic foraminiferal stable isotopes. The position of the site on the Subtropical Divergence separating temperate from warm-subtropical faunal assemblages, the shallow depth of deposition, and the excellent core recovery and microfossil preservation make this site ideal for studying late Neogene paleoceanographic evolution.

Although this is an analysis of nearly the entire late Neogene we are particularly interested in those intervals of major paleoclimatic change. These include the latest Miocene, a time of widespread cooling of surface waters and global glacial increase (Kennett, 1967; Ciesielski et al., 1982; Vincent et al., 1980; Loutit, 1981; Kennett et al., 1979; Adams et al., 1977; and Vail et al., 1977), and the late Pliocene, which was associated with further cooling and oceanic oxygen isotope change resulting from the onset of Northern Hemisphere glaciation (Shackleton and Opdyke, 1977; Kennett et al., 1979; Backman, 1979; Hodell et al., 1983; Shackleton et al., 1984). Much of the early Pliocene was characterized by relative climatic warmth and stability (Shackleton and Kennett, 1975; Kennett, 1978).

---

[1] Kennett, J. P., von der Borch, C. C., et al., *Init. Repts. DSDP*, 90: Washington (U.S. Govt. Printing Office).

[2] Address: Graduate School of Oceanography, University of Rhode Island, Narragansett, RI 02882.

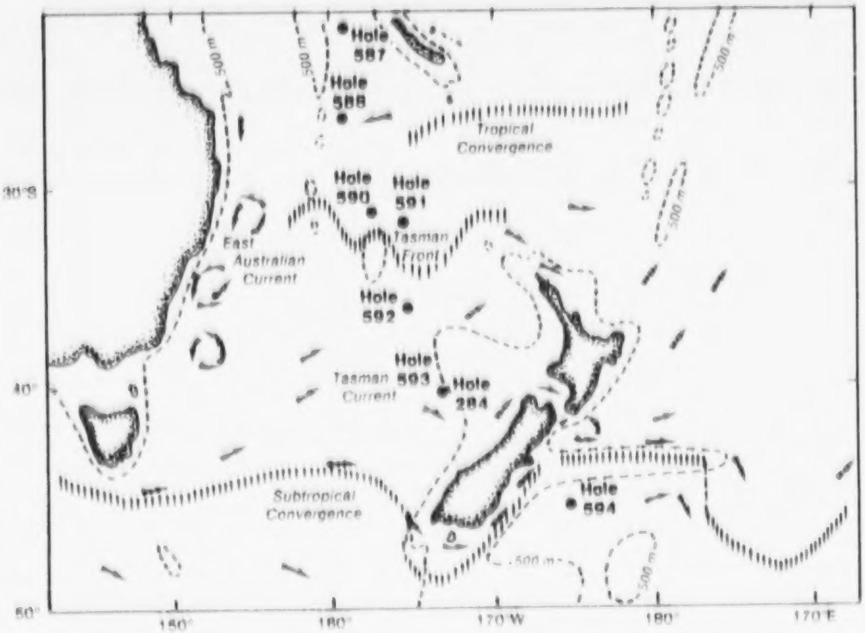

Figure 1. Map showing the location of Site 590 (1293 m) and other DSDP sites in the southwest Pacific. Site 590 is located on the eastern flank of the Lord Howe Rise. Shown also are the present-day positions of the Subtropical Divergence (Tasman Front) and the Subtropical Convergence. Isobath (dotted line) is the 1000 m contour.

BIOSTRATIGRAPHY

We have used, with some minor variations, the planktonic foraminiferal zones established for Site 590 by the shipboard scientific party (Site 590 site chapter, this volume), which are in turn based upon the zonal scheme of Kennett (1973) (Fig. 2).

The *Globorotalia conomiozea* Zone is marked by the first abundant appearance of *G. conomiozea* at 225 m, rather than the 240 m determined in the Site 590 site chapter (this volume). The base of the *G. puncticulata* Zone, marking the Miocene/Pliocene boundary, is based upon the first evolutionary appearance of *G. puncticulata puncticulata* from *G. puncticulata sphericomiozea* at 190 m, as compared to the 194 m determined in the site chapter (this volume). The first appearance of *G. pliozea* also coincides with the first appearance of *G. puncticulata* and the Miocene/Pliocene boundary, whereas the first appearance of *G. margaritae* occurs 4 m below the boundary. The base of the *G. crassaformis* Zone is marked by the first appearance of *G. crassaformis* at 165 m. A gap in core recovery occurs between 113 and 101 m, with the base of the *G. inflata* Zone marked by the first appearance of *G. inflata* at 101 m. The base of the *G. tosaensis* Zone is based upon the first appearance of *G. tosaensis* at 80 m. The first appearance of *G. truncatulinoides* in association with *G. tosaensis* marks the base of the *G. tosaensis–G. truncatulinoides* Overlap Zone. The first appearance of *G. truncatulinoides* has often been taken to represent the Pliocene/Pleistocene boundary, although Rio et al. (1984) demonstrate its first appearance in the late Pliocene. However, at Site 590 the first appearance of this species is within nannofossil Zone NN17 of late Pliocene age, and within the early Matuyama Paleomagnetic Chron. The base of the *G. truncatulinoides–G. tosaensis* Overlap Zone is therefore of late Pliocene age.

CHRONOLOGY

The late Neogene sequence at Site 590 is dated in its upper 81 m using magnetostratigraphy (Barton and Bloemendal, this volume). A magnetostratigraphy could not be determined for the sequence deeper than 81 m at Site 590 because of very low intensities of magnetization. Therefore, the chronology for the earlier part of the late Neogene sequence is based upon ages assigned to specific datum levels. In all, a total of 12 datum levels have been used to provide the chronological framework, and to determine sedimentation rates (Fig. 3, 4). Many of these are summarized in the site chapter, (this volume) and are based upon the compilation of Berggren et al. (in press).

The datum levels used to establish our chronology from oldest to youngest are as follows:

1. The globally recognized late Miocene carbon isotope shift (Haq et al., 1980), dated by Loutit and Kennett (1979) using magnetostratigraphy on an uplifted marine sequence in New Zealand, at 6.3 Ma.

2. The first abundant appearance of *Globorotalia conomiozea* at 225 m, which has been dated at 6.1 Ma by Loutit and Kennett (1979).

3. The base of NN12 at 196 m, which has been assigned an age of 5.2 Ma in the site chapter (this volume).

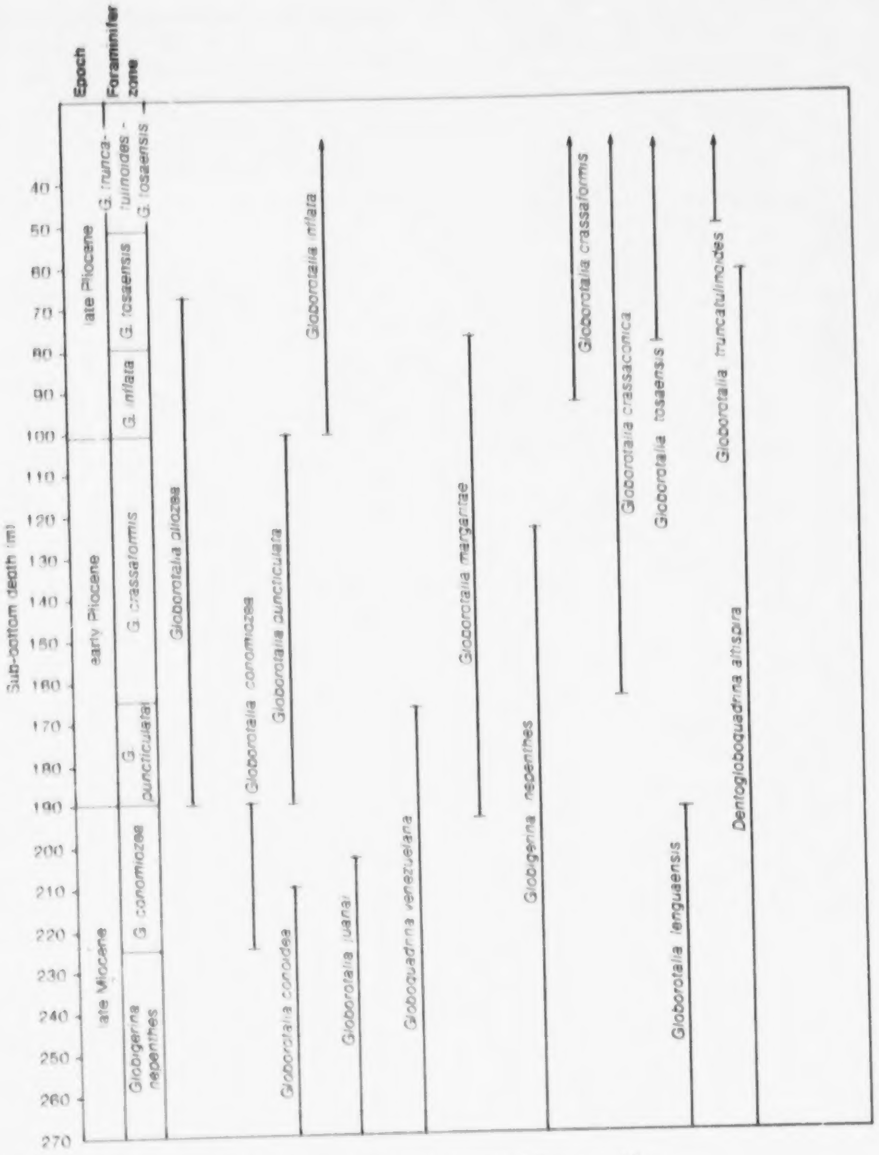

Figure 2. Ranges of certain late Neogene planktonic foraminifers at Site 590.

4. The base of NN13 at 172 m, which has been assigned an age of 4.6 Ma in the site chapter (this volume).

5. The base of NN14 at 151 m, which has been assigned an age of 4.1 Ma in the site chapter (this volume).

6. The base of NN15 at 131 m, which has been assigned an age of 3.65 Ma in the site chapter (this volume).

7. The Gauss/Gilbert Paleomagnetic Chron boundary at 81.2 m, which has been assigned an age of 3.4 Ma by Barton and Bloemendal (this volume).

8. The base of the Mammoth Paleomagnetic Subchron at 70 m, which has been assigned an age of 3.18 Ma by Barton and Bloemendal (this volume).

9. The top of the Kaena Paleomagnetic Subchron at 62.5 m, which has been assigned an age of 2.92 Ma by Barton and Bloemendal (this volume).

10. The Gauss/Matuyama Paleomagnetic Chron boundary at 47.9 m, which has been assigned an age of 2.47 Ma by Barton and Bloemendal (this volume).

11. The base of the Olduvai Paleomagnetic Subchron at 35.75 m, which has been assigned as age of 1.88 Ma by Barton and Bloemendal (this volume).

12. The top of Olduvai Paleomagnetic Subchron at 33 m, which has been assigned an age of 1.66 Ma by Barton and Bloemendal (this volume).

The use of this chronology shows that sedimentation rates at Site 590 range from 22.5 to 83.3 m/m.y. (Fig. 4). The high rates (72.4 m/m.y.) in early late Miocene may

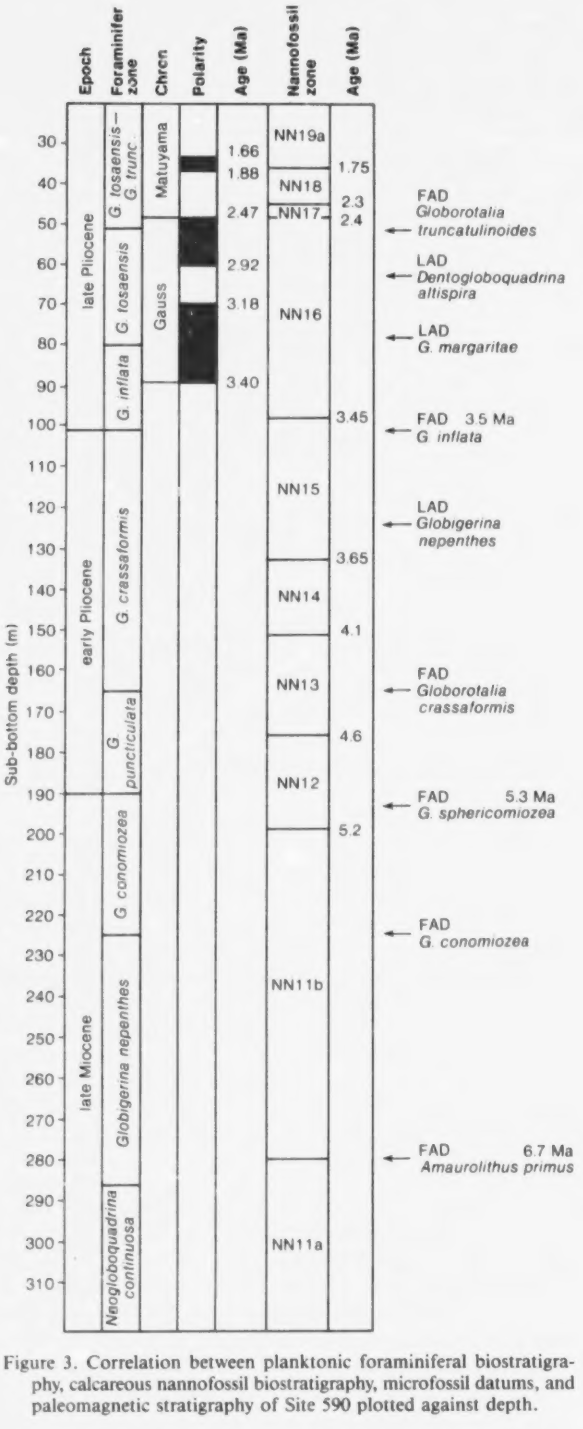
Epoch
Foraminifer zone
Chron
Polarity
Age (Ma)
Nannofossil zone
Age (Ma)
Sub-bottom depth (m)
30
40
50
60
70
80
90
100
110
120
130
140
150
160
170
180
190
200
210
220
230
240
250
260
270
280
290
300
310
late Pliocene
early Pliocene
late Miocene
G. tosaensis — G. trunc.
G. tosaensis
G. inflata
G. crassaformis
G. puncticulata
G. conomiozea
Globigerina nepenthes
Neogloboquadrina continuosa
Matuyama
Gauss
1.66
1.88
2.47
2.92
3.18
3.40
NN19a
NN18
NN17
NN16
NN15
NN14
NN13
NN12
NN11b
NN11a
1.75
2.3
2.4
3.45
3.65
4.1
4.6
5.2
FAD Globorotalia truncatulinoides
LAD Dentoglobоquadrina altispira
LAD G. margaritae
FAD 3.5 Ma G. inflata
LAD Globigerina nepenthes
FAD Globorotalia crassaformis
FAD 5.3 Ma G. sphericomiozea
FAD G. conomiozea
FAD 6.7 Ma Amaurolithus primus

Figure 3. Correlation between planktonic foraminiferal biostratigraphy, calcareous nannofossil biostratigraphy, microfossil datums, and paleomagnetic stratigraphy of Site 590 plotted against depth.

be unreliable because chronological control was poor. The sedimentation rates are based upon the slope of a best-fit regression line (>93% confidence level) through the given datum levels. The curve indicates relatively low sedimentation rates of 37.7 m/m.y. from the latest Miocene (~5.6 Ma) to the early Pliocene (~4.2 Ma). This is followed by unusually high middle to late Pliocene sedimentation rates of 83.3 m/m.y. between 4.2 and 3.2 Ma, which the shipboard party (site chapter, this volume) considered to have resulted from very high rates of calcareous nannofossil productivity caused by intensified upwelling at the Subtropical Divergence. At ~3.2 Ma, sedimentation rates again decrease to lower rates of 22.5 m/m.y.

METHODS

Planktonic foraminiferal counts were made on 112 samples from the latest Miocene to the latest Pliocene. Samples were oven-dried at 60°C, weighed, disaggregated in a hot Calgon solution, washed over a 63-μm Tyler sieve, dried, then reweighed. The >150-μm size fraction was separated and repeatedly placed through a microsplitter to obtain an aliquot of ~300 specimens that were counted. Thirty-eight species of planktonic foraminifers were identified using the taxonomy of Kennett and Srinivasan (1983). Species frequencies were calculated within the total population.

Oxygen and carbon isotope analyses were performed on both planktonic and benthic foraminifers throughout Hole 590A. Planktonic analyses were performed on *Globigerinoides sacculifer* in the fraction from 295 to 417-μm. Material was analyzed from a relatively small size range to decrease potential variability in isotopic composition between different sizes of planktonic foraminifers (Killingley et al., 1981). Analyses were also performed on 15 samples of *Globorotalia puncticulata* from 154 to 180 m to provide a comparison between an inferred deeper-dwelling form *G. puncticulata*, and a known shallow-water species, *Globigerinoides sacculifer*.

Benthic foraminiferal isotopic analyses were performed on *Cibicidoides kullenbergi* from the >250-μm size fraction. When an adequate number of specimens were available for analyses, very large specimens (>400-μm) were not included in the isotopic analyses.

Specimens for isotopic analyses were ultrasonically cleaned in reagent-grade methanol and roasted *in vacuo* at 400° C for 1 hr. The samples were then reacted in 100% orthophosphoric acid at 50°C. The gas was then subject to three distillations in order to purify the remaining CO_2 gas, which was then analyzed for ^{18}O and ^{13}C using an on-line VG Micromass 602D mass spectrometer with an analytical precision of ± 0.1‰ for both $\delta^{18}O$ and $\delta^{13}C$, based upon the analyses of laboratory standard of powdered B-1, which is run at the beginning and end of each day. All isotopic results are expressed as per mil differences from PDB.

FAUNAL RESULTS

Neogloboquadrina pachyderma is an important component in the planktonic foraminiferal assemblage at Site 590, with frequencies ranging up to 50% (Fig. 5, 6; Table 1). Highest frequencies of this species occur during the latest Miocene through early Pliocene (6.1 to 4.5 Ma), moderately high frequencies occur in the early Pliocene between 4.0 and 3.3 Ma, and lowest frequencies (<20%) are generally exhibited during the earlier late Miocene (6.3–6.1 Ma) and again in the latest Pliocene (3.3 to 2.1 Ma). During most of the late Miocene and early Pliocene, the coiling direction of *N. pachyderma* is dominantly sinistral. One brief interval of dominantly dextral coiling occurs during the late Miocene, centered at about 6.0 Ma. There is a rapid switch from dominantly sinistral to dominantly dextral coiling in the early Pliocene (~4.3 Ma), after which populations of *N. pachyderma* are always dominantly dextrally coiled.

Frequency oscillations are also shown in Figure 6 for a group of species that are considered to have a warmer-water tolerance: *Globigerinoides obliquus, G. sacculifer, G. ruber, Globorotalia menardii, Neogloboquadrina acostaensis, N. humerosa, Dentoglobоquadrina altispira,* and

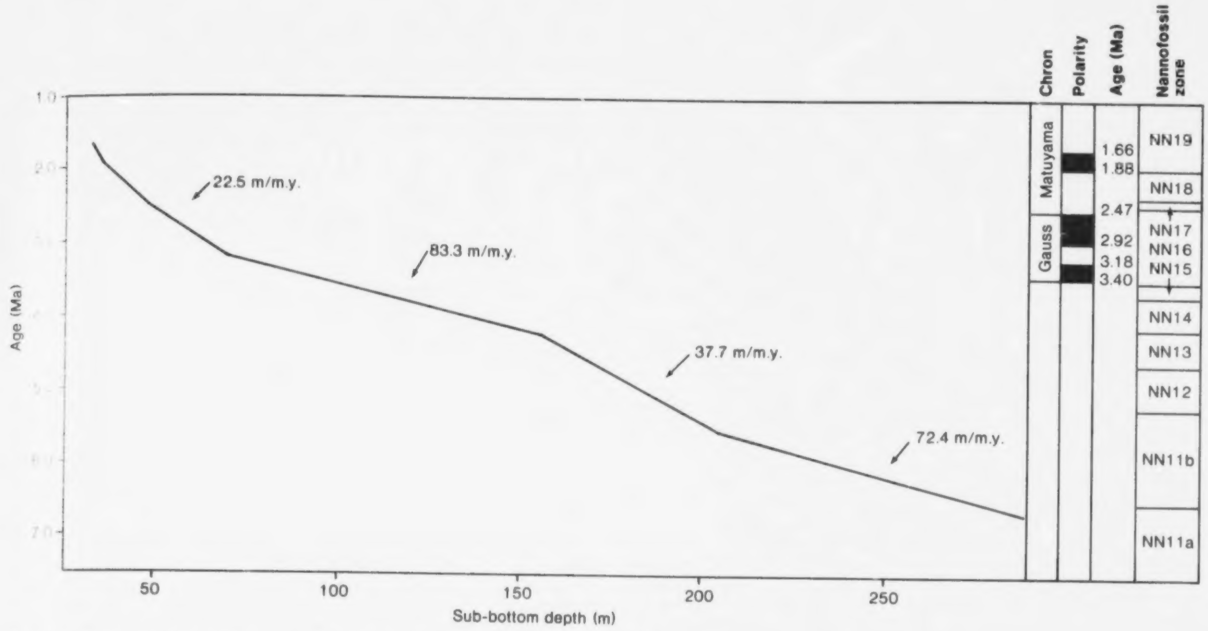

Figure 4. Sedimentation rate diagram for Site 590 based upon 12 datum levels.

Globorotalia margaritae (Kennett and Srinivasan, 1983). Warm-subtropical faunal elements exhibit particularly low frequencies in the latest Miocene through the early Pliocene (5.6 to 4.3 Ma), and in the latest Pliocene (3.3 to 2.1 Ma). Particularly high frequencies of the warm-subtropical fauna occur through the remaining parts of the early Pliocene (4.3 to 3.3 Ma) and the earlier part of the late Miocene (6.3 to 5.6 Ma). The switch in the coiling direction of *N. pachyderma* from dominantly sinistral to dominantly dextral occurs in the early Pliocene coincident with the increase in frequencies of the warm-subtropical fauna and decrease in frequencies of the cold-water form, *N. pachyderma*.

Three important components of the assemblage (*Globigerina woodi, G. bulloides*, and *G. falconensis*) exhibit no clear faunal changes throughout the sequence. Paleoceanographic changes at this latitude were not large enough to cause important frequency oscillations in these forms (Fig. 7) and hence they are of no value as paleoceanographic monitors in this site.

The *Globorotalia* (*Globoconella*) lineage (Kennett and Srinivasan, 1983) is another important element within the assemblage at certain times in the late Neogene (Fig. 7). The lineage consists of an evolutionary transition from *G. conoidea* to *G. conomiozea* to *G. puncticulata sphericomiozea* to *G. puncticulata puncticulata* to *G. inflata*. The evolution is centered in temperate waters, and each species is assumed to have had similar environmental preferences during the late Neogene. Very high frequencies in the early Miocene (6.3 to 6.1 Ma) are followed by relatively low values during the latest Miocene and early Pliocene (6.1 to 3.9 Ma). Two step-like increases occur in the *Globoconella* lineage, one in the late early Pliocene (~3.9 Ma) and the other in the late Pliocene (~3.4 Ma) when the lineage reaches maximum frequencies in the form of *G. inflata*.

Globigerinita glutinata exhibits an increase in frequency across the Miocene/Pliocene boundary and again in the late Pliocene. *Globorotalia margaritae* and *Orbulina universa* both rapidly disappear for a brief interval during the early Pliocene (4.0 to 4.5 Ma), whereas *Globorotalia scitula*, a species known to live deeper in the water column (Williams et al., 1977), increases in frequencies during the same interval.

OXYGEN AND CARBON ISOTOPE RESULTS

Benthic Oxygen Isotopes

Oxygen isotope data for *Cibicidoides kullenbergi* are plotted against depth in Figure 8, and against time in Figure 9 (Table 2). The data are discussed here within a chronological framework. During the last 6.6 Ma, the benthic oxygen isotope record exhibits a number of steps that represent changing average values over specific intervals. These steps are separated by relatively brief intervals of rapid change. Light oxygen isotope values (1.80‰ avg.) are exhibited in the late Miocene between 6.4 and 5.6 Ma. A rapid enrichment in $\delta^{18}O$ occurs at 5.6 Ma, within the latest Miocene, with relatively enriched values exhibited until 4.8 Ma in the early Pliocene. This, in turn, is followed by a depletion in $\delta^{18}O$ at ~4.7 Ma, with lighter and more stable values marking the remaining early Pliocene. A gradual enrichment in $\delta^{18}O$ (0.3‰ avg.) occurs between 3.7 and 3.4 Ma, at the end of the early Pliocene (centered at 3.6 Ma). A second permanent enrichment in $\delta^{18}O$ (0.5‰ avg.) occurs between 2.9 and 2.5 Ma, with heavy values marking the remainder of the Pliocene.

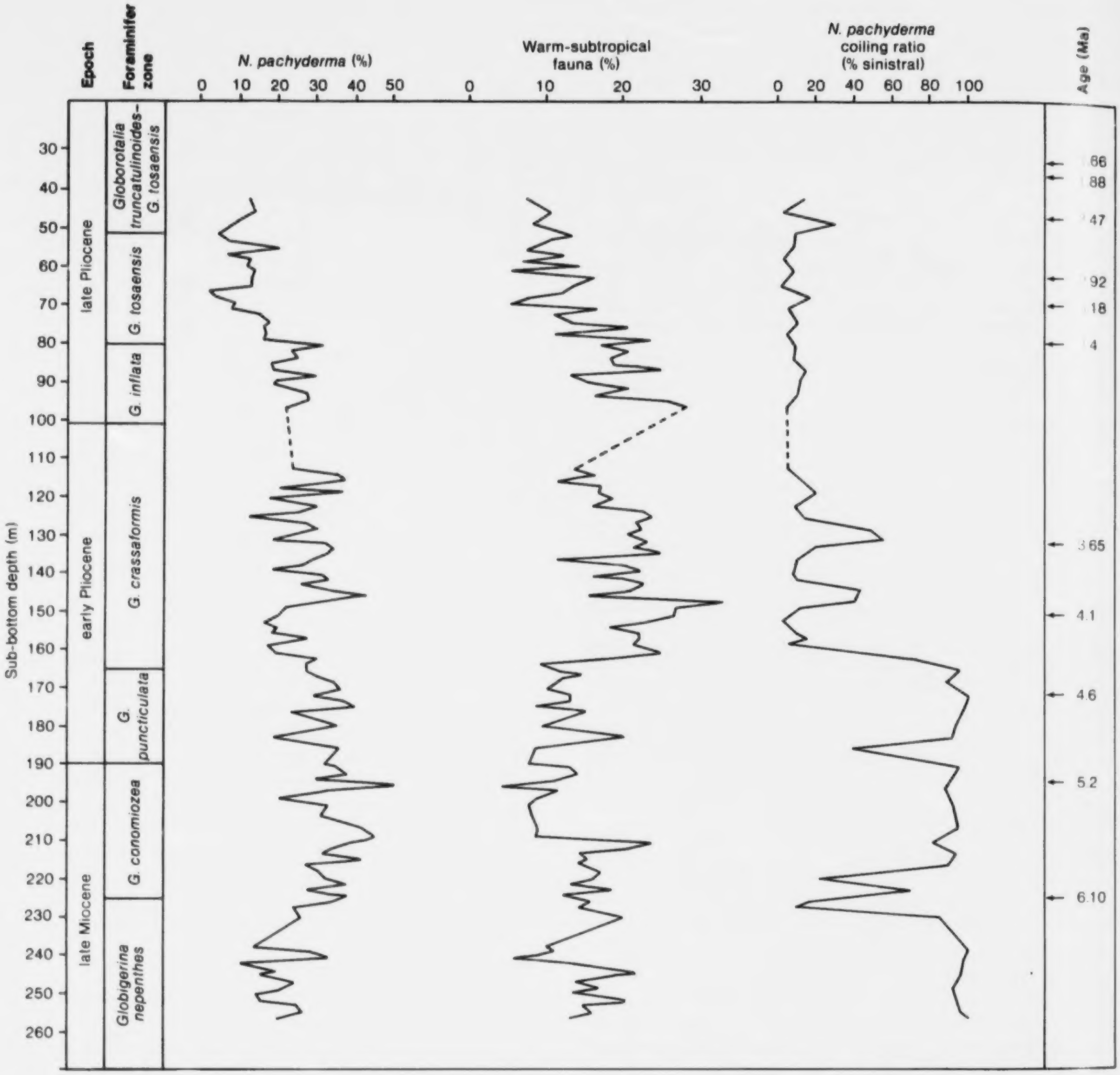

Figure 5. Frequency data for *Neogloboquadrina pachyderma* and warm-subtropical forms and the coiling ratio of *N. pachyderma* plotted against depth at Site 590.

Planktonic Oxygen Isotopes

The planktonic foraminiferal oxygen isotope data for *Globigerinoides sacculifer* are plotted against depth in Figure 8 and against time in Figure 9. The data indicate that the planktonic oxygen isotope record through the entire late Neogene is much more variable than the benthic oxygen isotope record. Such high variability would be expected in a site which is located close to a divergence zone that separates temperate from warm-subtropical waters and is associated with upwelling. The planktonic foraminiferal oxygen isotope record is quite different from the benthic record: it shows no obvious trends through time, and the average values in the latest Pliocene are no heavier than the average values exhibited in the latest Miocene, with average values not changing by more than 0.3‰ between 6.4 and 1.7 Ma. There are, however, slight average differences during various times. The late Miocene, between 6.3 and 5.5 Ma, is represented by average $\delta^{18}O$ values of ≃0.54‰, followed by a slight enrichment at 5.4 Ma to average values of ≃0.40‰ until 3.7 Ma (a distinct brief lightening occurs between 4.9 and 4.6 Ma). Average values lighten to ≃0.66‰ at 3.7 Ma, continuing until 3.1 Ma, when the oxygen isotope values again shift to slightly heavier values of ≃0.57‰ for the remainder of the late Pliocene.

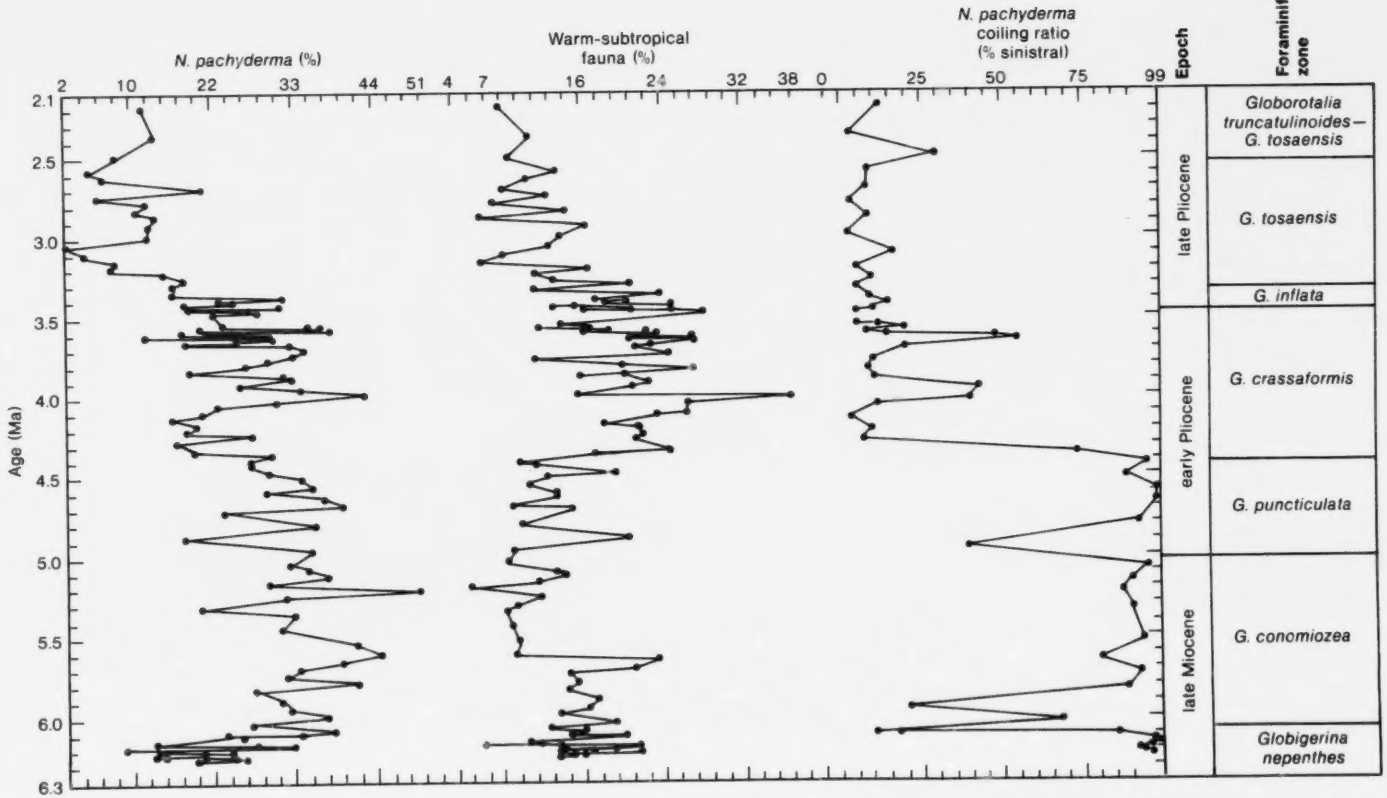

Figure 6. Frequency data for *Neogloboquadrina pachyderma* and warm-subtropical forms (%) and the coiling ratio of *N. pachyderma* (% sinistral) plotted against age at Site 590.

Table 1. Distribution of planktonic foraminifers (frequency in %) in Hole 590A.

Epoch	Foraminifer zone	Sub-bottom depth (m)	Core-Section (level in cm)	*Globigerinoides obliquus*	*G. immaturus*	*G. sacculifer*	*Globigerina woodi*	*G. apertura*	*G. bulloides*	*G. nepenthes*	*G. falconensis*	*G. decoraperta*	*Globorotalia puncticulata*	*G. scitula*	*G. menardii*	*G. margaritae*	*Neogloboquadrina acostaensis*	*Globigerinita glutinata*	*Orbulina universa*	*Dentogloboquadrina altispira*	*Globigerinella aequilateralis*	*Sphaeroidinella seminulina*	*Globoquadrina venezuelana*	*Globorotalia lenguaensis*	*G. cibaoensis*	*G. juanai*	*Beella praedigitata*	*Globigerinoides conglobatus*	*Pulleniatina primalis*	*Globorotalia pliozea*	*G. crassaformis*	*G. tosaensis*	*G. truncatulinoides*	*Globigerinoides ruber*	*Globorotalia crassaconica*	*G. conoidea*	*G. conomiozea*	*G. inflata*	*Neogloboquadrina pachyderma* (sinistral)	*N. pachyderma* (dextral)	*N. humerosa*
late Pliocene	*G. tosaensis*-*G. truncatulinoides*	42.2	2-5, 35	2	1	x	7	0	10	0	16	0	0	x	x	0	0	22	x	0	6	0	0	0	0	0	0	x	0	0	4	0	0	3	1	0	0	12	[illegible]	11	0
		45.8	3-1, 35	2	x	0	9	0	8	0	11	0	0	x	1	0	0	20	2	0	3	0	0	0	0	0	0	x	0	0	0	0	2	7	3	0	0	15	[illegible]	14	0
		48.8	3-3, 35	4	1	1	7	0	7	0	16	0	0	0	0	0	0	11	2	0	5	0	0	0	0	0	0	x	0	0	x	2	6	2	3	0	0	24	[illegible]	6	x
		51.8	3-5, 35	7	0	3	19	0	11	0	8	0	18	1	2	0	0	10	x	0	4	0	0	0	0	0	0	0	0	0	2	2	0	2	5	0	0	18	[illegible]	4	0
	G. tosaensis	53.3	3-6, 35	4	0	2	21	0	7	0	4	0	17	x	x	0	0	17	x	0	5	0	0	0	0	0	0	0	0	0	x	4	0	3	4	0	0	17	[illegible]	4	0
		55.4	4-1, 35	6	0	1	14	0	9	0	4	0	17	x	x	0	0	13	x	0	4	x	0	0	0	0	0	0	0	0	4	x	0	0	2	0	0	17	[illegible]	9	0
		56.9	4-2, 35	7	3	2	10	0	9	0	5	0	28	2	1	0	x	18	x	0	7	0	0	0	0	0	0	0	0	0	1	2	0	1	2	0	0	28	[illegible]	6	x
		58.4	4-3, 35	3	0	2	11	0	7	0	3	0	29	x	x	0	x	15	x	0	7	0	0	0	0	0	0	0	0	0	3	x	0	x	2	0	0	29	[illegible]	12	x
		59.9	4-4, 35	8	0	2	11	0	12	0	9	0	16	x	4	0	0	10	1	0	6	0	0	0	0	0	x	x	0	0	1	1	0	0	2	0	0	16	[illegible]	10	0
		61.4	4-5, 35	3	x	x	10	0	8	0	5	0	24	2	x	2	0	17	2	0	6	0	0	0	0	0	x	0	0	0	3	x	0	x	x	0	0	24	[illegible]	13	0
		62.9	4-6, 35	6	1	4	11	0	5	0	6	0	14	1	5	0	0	12	3	x	8	0	0	0	0	0	0	0	0	0	2	7	0	0	x	0	0	14	[illegible]	12	0
		65.0	5-1, 110	5	x	3	10	0	6	0	9	0	22	1	3	1	0	12	1	x	9	0	0	0	0	0	0	0	x	0	2	x	0	0	0	0	0	22	[illegible]	13	0
		66.5	5-2, 110	5	x	3	6	0	10	0	7	0	33	1	2	x	0	10	x	1	10	x	0	0	0	0	0	0	0	0	6	0	0	0	x	0	0	33	[illegible]	2	0
		68.0	5-3, 110	3	0	2	6	0	6	0	8	0	36	x	1	0	0	14	x	1	12	x	0	0	0	0	x	0	0	1	2	x	0	0	2	0	0	36	[illegible]	3	0
		69.5	5-4, 110	3	0	x	8	0	9	0	11	x	30	2	x	0	0	8	x	1	7	2	0	0	0	0	x	0	x	0	2	0	0	0	3	0	0	30	[illegible]	8	0
		71.0	5-5, 110	7	0	1	9	0	3	0	9	0	21	1	4	0	x	11	x	4	10	2	0	0	0	0	1	0	0	0	6	0	0	0	x	0	0	21	x	7	x
		72.5	5-6, 110	6	0	1	8	0	5	0	12	0	26	x	2	0	0	8	1	1	8	0	0	0	0	0	0	0	0	0	2	0	0	x	1	0	0	26	x	15	0
		74.6	6-1, 55	8	0	1	10	0	7	0	7	0	23	1	x	0	0	10	0	1	7	2	0	0	0	0	0	0	0	0	x	0	0	2	1	0	0	23	2	16	0
		76.1	6-2, 55	7	0	1	16	0	4	0	6	0	10	x	4	0	0	9	x	9	7	1	0	0	0	0	0	0	0	0	3	x	0	x	3	0	0	10	[illegible]	14	0
		77.6	6-3, 55	5	0	1	10	0	6	0	11	0	18	0	2	x	0	10	x	1	6	3	0	0	0	0	0	0	x	0	3	0	0	x	3	0	0	18	x	16	0
		79.1	6-4, 55	6	0	1	6	0	5	0	8	0	17	2	2	x	2	11	0	13	4	0	0	0	0	0	0	x	0	0	4	0	0	0	2	0	0	17	2	14	2
	G. inflata	80.6	6-5, 55	4	x	x	6	0	5	0	6	0	8	2	2	2	x	11	x	7	5	2	0	0	0	0	0	x	x	0	6	0	0	x	x	0	0	8	3	29	x
		82.1	6-6, 55	9	0	2	8	0	6	0	9	0	7	x	3	x	0	11	0	4	6	1	0	0	0	0	0	0	2	x	x	0	0	1	1	0	0	7	3	20	0
		84.2	7-1, 35	9	0	3	8	0	5	0	9	x	18	1	2	x	1	5	x	2	5	x	0	0	0	0	0	x	0	0	2	0	0	1	1	0	0	18	2	23	1
		85.7	7-2, 35	7	0	5	14	0	11	0	11	0	9	1	4	x	0	9	x	1	6	x	0	0	0	0	0	0	x	0	0	0	0	x	0	0	0	9	1	17	0
		87.2	7-3, 35	8	0	8	8	0	8	0	8	0	9	1	2	9	8	9	x	6	6	x	0	0	0	0	0	x	1	x	1	0	0	x	1	0	0	9	3	16	0
		88.7	7-4, 35	7	0	3	8	0	7	0	8	x	8	x	1	x	0	9	x	1	4	0	0	0	0	0	0	0	0	0	4	0	0	x	4	0	0	8	2	30	0
		90.2	7-5, 36	8	0	1	6	0	14	0	14	x	9	x	2	x	0	7	x	4	7	0	0	0	0	0	0	0	1	0	x	0	0	0	5	0	0	9	2	17	0
		91.7	7-6, 35	5	0	11	5	0	5	0	14	0	13	0	4	x	0	9	1	1	8	x	0	0	0	0	0	x	3	0	0	0	0	0	1	0	0	13	3	16	0
		93.8	8-1, 103	7	1	5	10	0	9	0	8	0	9	1	2	x	0	9	x	1	5	x	0	0	0	0	0	0	0	0	3	0	0	0	x	0	0	0	3	24	0
		95.3	8-2, 35	6	4	11	7	0	10	0	7	x	4	1	1	2	x	0	x	x	4	x	0	0	0	0	0	x	x	0	1	0	0	0	1	0	0	0	4	24	x
		96.8	8-3, 35	8	x	4	8	0	9	0	7	0	8	x	4	6	1	9	0	3	4	0	0	0	0	0	0	x	x	0	1	0	0	0	0	0	0	0	x	21	1
early Pliocene	*G. crassaformis*	113.0	10-1, 35	7	0	2	8	0	11	0	7	0	13	2	x	3	x	11	1	x	4	3	0	0	0	0	0	x	x	0	4	0	0	0	0	0	0	0	1	22	x
		114.5	10-2, 35	6	0	2	9	x	7	0	10	x	5	2	4	1	2	4	x	2	2	2	0	0	0	0	0	0	0	0	5	0	0	0	0	0	0	0	2	33	2
		116.0	10-3, 35	4	0	1	7	0	11	0	8	0	2	2	2	2	2	7	x	1	4	x	0	0	0	0	0	0	x	x	8	0	0	0	0	0	0	0	4	33	2
		118.0	10-4, 35	5	0	0	12	0	8	0	11	0	19	x	x	8	x	8	x	x	1	0	0	0	0	0	0	0	0	x	2	0	0	0	0	0	0	0	12	8	x
		119.0	10-5, 35	7	0	x	7	0	4	0	7	x	11	x	6	x	x	7	2	1	3	x	0	0	0	0	0	0	0	0	x	0	0	0	0	0	0	0	8	31	x
		120.5	10-6, 35	6	0	6	9	0	7	0	18	x	14	0	0	6	x	8	x	x	2	x	0	0	0	0	0	0	0	0	4	0	0	0	0	0	0	0	1	16	x
		122.6	11-1, 35	2	0	3	7	0	3	0	14	0	11	x	8	x	2	8	2	0	1	1	0	0	0	0	0	0	0	0	5	0	0	0	0	0	0	0	3	27	2
		124.1	11-2, 35	9	0	5	15	x	9	x	7	x	0	x	3	1	4	7	1	x	3	0	0	0	0	0	0	0	x	0	8	0	0	0	0	0	0	0	3	22	4
		125.6	11-3, 35	9	0	2	9	0	9	0	3	x	23	1	8	4	0	4	1	x	x	0	0	0	0	0	x	0	0	x	10	0	0	0	0	0	0	0	2	11	0
		127.1	11-4, 35	10	0	5	4	0	13	x	4	2	6	1	4	2	0	8	x	1	8	0	0	0	0	0	0	0	0	2	7	0	0	0	0	0	0	0	x	27	0
		128.6	11-5, 35	8	0	4	7	0	7	x	10	x	5	x	3	2	4	4	x	2	3	x	0	0	0	0	x	0	x	0	8	0	0	0	0	0	0	0	15	16	4
		130.1	11-6, 35	3	x	2	9	0	14	0	5	2	14	2	2	8	4	3	0	x	x	x	0	0	0	0	0	0	0	3	x	0	0	0	0	0	0	0	6	19	4
		131.6	11-7, 35	9	0	4	11	0	19	x	7	x	11	0	2	6	5	3	2	x	2	1	0	0	0	0	0	0	0	x	x	0	0	0	0	0	0	0	10	8	5
		132.2	12-1, 35	8	0	3	11	0	10	1	8	1	2	0	2	5	5	3	2	x	2	x	0	0	0	0	0	1	0	3	1	0	0	0	0	0	0	0	12	21	5
		133.7	12-2, 35	7	0	4	8	0	6	0	9	x	5	3	2	4	3	3	1	1	2	0	0	0	0	0	0	0	0	5	1	0	0	0	0	0	0	0	7	28	3
		135.2	12-3, 35	5	0	4	13	0	8	0	5	x	5	x	5	9	1	4	1	x	2	0	0	0	0	0	0	0	0	x	x	0	0	0	0	0	0	0	1	32	1
		136.7	12-4, 35	4	0	1	9	0	13	x	9	x	13	x	2	0	2	4	4	x	2	2	0	0	0	0	x	0	1	x	x	0	0	0	0	0	0	0	3	26	2
		138.2	12-5, 35	7	0	1	15	x	12	x	8	2	2	x	x	10	x	2	2	x	1	x	0	0	0	0	0	0	2	5	0	0	0	0	0	0	0	0	2	24	x
		139.7	12-6, 35	8	x	5	10	0	9	0	12	3	13	2	2	0	4	3	0	3	4	0	0	0	0	0	x	x	x	0	0	0	0	0	0	0	0	0	2	17	4
		141.2	12-7, 35	6	0	3	10	0	14	x	7	x	4	x	3	0	3	4	2	x	4	0	0	0	0	0	0	0	x	5	0	0	0	0	0	0	0	0	14	18	3
		141.8	13-1, 35	14	x	x	13	0	13	0	4	2	7	x	2	0	2	2	4	1	1	x	0	0	0	0	0	0	x	0	0	0	0	0	0	0	0	0	3	30	2
		143.3	13-2, 35	14	0	3	11	0	7	0	9	2	8	x	1	2	x	4	2	2	x	0	0	0	0	0	2	x	x	4	x	0	0	0	0	0	0	0	10	16	x
		144.8	13-3, 35	12	0	2	13	0	6	x	9	3	x	x	3	0	2	2	x	3	2	0	0	0	0	0	0	x	x	5	x	0	0	0	0	0	0	0	15	19	2
		146.3	13-4, 35	8	0	2	10	0	5	0	8	1	1	x	x	x	2	6	x	2	2	0	0	0	0	0	0	x	1	4	0	0	0	0	0	0	0	0	21	22	2
		147.8	13-4, 35	10	0	7	10	0	5	x	x	1	2	x	6	0	3	4	1	7	2	0	0	0	0	0	0	x	x	4	0	0	0	0	0	0	0	0	12	18	3
		149.3	13-6, 35	10	0	4	15	0	2	0	5	2	1	3	x	8	0	8	3	4	3	0	0	0	0	0	0	0	0	7	0	0	0	0	0	0	0	0	3	20	0
		151.4	14-1, 35	12	x	5	9	0	12	0	8	3	6	x	x	6	x	6	1	2	x	x	0	0	0	0	0	x	0	3	0	0	0	0	0	0	0	0	x	19	x
		152.9	14-2, 35	11	0	3	13	0	10	2	8	3	4	1	3	x	4	4	1	2	2	x	0	0	0	0	0	x	2	9	0	0	0	0	0	0	0	0	x	16	4
		154.4	14-3, 35	12	0	2	17	0	5	x	14	2	2	2	2	0	2	6	2	x	1	x	0	0	0	0	0	0	x	7	0	0	0	0	0	0	0	0	2	18	2
		155.9	14-4, 35	10	0	7	10	0	7	x	12	6	x	4	3	0	2	7	1	0	2	0	0	0	0	0	0	x	0	10	0	0	0	0	0	0	0	0	2	16	2
		157.4	14-5, 35	7	x	3	13	0	7	x	6	5	x	x	6	x	2	6	x	3	5	0	0	0	0	0	0	x	1	2	x	0	0	x	0	0	0	0	4	23	2
		158.9	14-6, 35	8	1	4	14	0	9	1	10	6	2	5	7	0	x	7	1	0	1	2	0	0	0	0	0	0	1	x	x	0	0	0	0	0	0	0	1	16	x
		161.0	15-1, 35	14	0	5	11	0	9	x	9	3	2	x	2	0	2	2	2	2	3	2	0	0	0	0	0	0	3	8	x	0	0	0	0	0	0	0	2	17	2
		162.5	15-2, 35	10	1	2	9	x	8	2	4	4	4	x	x	0	x	5	1	3	2	4	0	0	0	0	x	x	x	6	x	0	0	0	0	0	0	0	22	8	x
		164.0	15-3, 35	4	x	2	11	0	18	x	9	2	3	0	x	0	x	6	3	x	2	x	0	0	0	0	0	x	x	5	x	0	0	0	0	0	0	0	23	4	x
		165.5	15-4, 35	7	0	x	20	0	11	2	5	2	2	x	2	0	1	3	5	0	3	x	0	0	0	0	0	x	1	4	x	0	0	0	0	0	0	0	26	[illegible]	1
	G. puncticulata	167.0	15-5, 35	8	x	1	14	x	5	x	3	4	2	x	5	0	1	4	4	2	5	1	2	0	0	0	0	0	0	5	0	0	0	0	0	0	0	0	28	[illegible]	1
		168.5	15-6, 35	3	2	2	15	0	7	2	5	4	x	x	1	0	1	3	3	3	3	x	0	0	0	0	0	0	x	8	0	0	0	0	0	0	0	0	30	[illegible]	1
		170.6	16-1, 35	3	x	3	8	0	10	x	9	3	2	x	0	0	3	3	5	x	4	x	0	0	0	0	0	0	1	7	0	0	0	0	0	0	0	0	34	[illegible]	3
		172.1	16-2, 35	6	x	3	8	0	13	2	8	2	x	0	0	3	x	6	4	0	6	x	0	0	x	0	0	x	2	5	0	0	0	0	0	0	0	0	29	[illegible]	x
		173.6	16-3, 35	6	x	2	13	0	12	x	4	5	x	x	0	5	x	2	3	0	2	0	0	0	0	0	0	0	2	4	0	0	0	0	0	0	0	0	36	[illegible]	x
		175.1	16-4, 35	3	x	x	16	0	9	x	7	3	2	1	0	5	0	3	5	0	4	0	0	0	0	0	0	0	2	0	0	0	0	0	0	0	0	0	39	[illegible]	0
		176.6	16-5, 35	8	2	2	11	0	9	1	x	5	1	0	0	x	0	3	7	2	5	0	3	0	0	0	x	x	0	12	0	0	0	0	0	0	0	0	23	[illegible]	0
		180.2	17-1, 35	6	x	2	12	0	6	x	7	3	0	0	x	0	0	10	4	0	0	x	x	0	1	0	0	0	0	5	0	0	0	0	0	0	0	0	33	[illegible]	0
		183.2	17-3, 35	11	x	4	18	0	8	x	5	2	0	x	4	0	0	8	4	1	3	x	x	0	1	0	0	x	0	8	0	0	0	0	0	0	0	0	16	[illegible]	0
		186.2	17-5, 35	5	0	2	11	1	11	x	6	x	x	0	x	1	0	8	2	0	1	0	0	0	x	0	0	1	0	9	0	0	0	0	0	0	0	0	15	[illegible]	0
		189.8	18-1, 35	4	x	2	6	1	11	x	15	x	9	0	x	1	0	12	3	0	x	x	0	0	0	0	0	0	0	x	0	0	0	0	0	0	0	0	25	[illegible]	0
late Miocene	*G. conomiozea*	191.3	18-2, 35	6	x	2	14	x	8	x	4	1	8	x	2	2	0	10	2	0	2	0	0	0	1	0	0	x	0	0	0	0	0	0	0	0	0	0	34	[illegible]	0
		192.8	18-3, 35	5	2	x	16	0	4	x	8	2	3	0	x	5	x	8	0	0	2	x	0	x	3	0	0	0	x	0	0	0	0	0	0	0	0	0	28	[illegible]	x
		194.3	18-4, 35	3	2	2	18	3	8	x	5	5	1	1	2	2	x	4	6	0	3	0	0	0	3	0	0	0	0	0	0	0	0	0	0	0	1	0	27	[illegible]	x

Table 1. (Continued).

Epo	Foraminifer zone	Sub-bottom depth (m)	Core-Section (level in cm)	*Globigerinoides obliquus*	*G. immaturus*	*G. sacculifer*	*Globigerina woodi*	*G. apertura*	*G. bulloides*	*G. nepenthes*	*G. falconensis*	*G. decoraperta*	*Globorotalia puncticulata*	*G. scitula*	*G. menardii*	*G. margaritae*	*Neogloboquadrina acostaensis*	*Globigerinita glutinata*	*Orbulina universa*	*Dentogloboquadrina altispira*	*Globigerinella aequilateralis*	*Sphaeroidinella seminulina*	*Globoquadrina venezuelana*	*Globorotalia lenguaensis*	*G. cibaoensis*	*G. juanai*	*Beella praedigitata*	*Globigerinoides conglobatus*	*Pulleniatina primalis*	*Globorotalia pliozea*	*G. crassaformis*	*G. tosaensis*	*G. truncatulinoides*	*Globigerinoides ruber*	*Globorotalia crassaconica*	*G. conoidea*	*G. conomiozea*	*G. inflata*	*Neogloboquadrina pachyderma* (sinistral)	*N. pachyderma* (dextral)	*N. humerosa*
late Mioce	*G. conomiozea*	195.8	18-5, 35	2	x	x	10	x	7	1	3	3	5	x	0	0	0	3	3	0	5	x	0	0	x	0	0	0	0	0	0	0	0	0	0	0	5	0	48	3	0
		197.3	18-6, 35	5	3	1	9	x	10	3	9	4	6	0	1	0	1	4	5	0	4	0	0	0	3	0	0	0	0	0	0	0	0	0	0	0	6	0	28	4	1
		199.4	19-1, 35	5	2	1	13	0	8	x	9	x	21	0	x	0	0	8	2	0	4	x	0	x	2	0	0	x	0	0	0	0	0	0	0	0	21	0	17	3	0
		200.9	19-2, 35	5	x	x	14	x	10	x	11	x	5	x	x	0	x	7	4	x	3	x	x	0	1	0	0	0	x	0	0	0	0	0	0	0	5	0	30	3	x
		203.9	19-4, 35	4	x	3	13	0	10	x	9	2	8	0	0	0	x	6	2	x	2	0	1	0	6	x	0	x	x	0	0	0	0	0	0	0	8	0	27	4	x
		206.9	19-6, 35	6	x	2	7	0	5	x	2	3	6	0	x	0	3	4	1	x	2	0	1	0	2	x	0	x	x	0	0	0	0	0	0	x	6	0	39	2	x
		209.0	20-1, 35	5	1	x	9	0	12	1	9	4	1	0	x	0	2	4	x	0	x	x	0	0	2	0	0	0	x	0	0	0	0	0	0	0	1	0	39	6	2
		210.5	20-2, 35	13	3	2	7	3	4	2	2	x	5	0	x	0	5	1	2	x	3	x	x	x	3	1	0	0	0	0	0	0	0	0	0	4	1	0	32	8	5
		212.0	20-3, 35	7	x	2	6	x	7	1	4	3	6	x	7	0	4	1	5	0	2	0	2	x	3	x	x	x	2	0	0	0	0	0	0	3	3	0	31	3	3
		213.5	20-4, 35	8	1	x	11	0	7	0	7	5	5	x	x	0	x	2	3	6	x	1	x	x	x	1	x	x	2	0	0	0	0	0	0	2	3	0	30	2	2
		215.0	20-5, 35	11	1	1	8	1	9	2	5	1	4	0	x	0	1	2	x	0	1	x	x	x	3	0	0	0	x	0	0	0	0	0	0	3	2	0	39	2	x
		216.5	20-6, 35	10	x	x	17	1	10	1	4	3	6	x	2	0	x	2	4	x	2	0	2	0	2	x	0	0	0	0	0	0	0	0	0	5	1	0	24	3	x
		218.6	21-1, 35	8	3	3	11	1	9	x	2	5	8	0	2	0	x	x	2	x	5	x	2	0	3	0	0	0	0	0	0	0	0	0	0	7	1	0	24	7	x
		220.1	21-2, 35	10	4	1	10	2	7	2	5	4	8	0	x	0	x	2	2	x	5	1	x	0	3	0	0	0	0	0	0	0	0	0	0	3	5	0	7	26	x
		221.6	21-3, 35	7	2	3	9	1	10	3	6	2	7	0	x	0	x	2	1	x	4	x	x	x	1	0	0	0	0	0	0	0	0	0	0	5	2	0	35	3	x
		223.1	21-4, 35	13	2	2	13	2	8	2	3	4	5	0	0	0	2	4	4	x	4	0	0	0	4	0	0	0	x	0	0	0	0	0	0	5	0	0	19	8	2
		224.6	21-5, 35	5	2	3	9	x	9	3	4	3	5	0	x	0	2	2	5	0	2	x	x	0	4	0	0	0	0	0	0	0	0	0	0	5	0	0	29	9	1
	G. nepenthes	226.1	21-6, 36	6	x	3	9	x	7	x	3	2	7	0	2	0	4	4	x	x	9	x	1	x	2	x	0	x	0	0	0	0	0	0	0	7	0	0	6	28	3
		227.6	21-7, 35	8	2	2	8	2	7	2	6	3	14	0	1	x	1	4	4	0	5	0	x	x	4	x	0	x	0	0	0	0	0	0	0	14	0	0	2	21	1
		229.7	22-2, 35	9	3	5	12	x	6	1	4	2	10	x	2	0	2	4	3	0	3	0	1	x	3	1	0	0	0	0	0	0	0	0	0	10	0	0	22	4	x
		237.8	23-1, 35	7	x	x	16	1	6	2	4	3	26	2	1	0	x	2	5	x	3	x	0	3	3	2	0	0	0	0	0	0	0	0	0	26	0	0	14	x	x
		239.3	23-2, 35	6	2	0	8	3	7	1	1	2	20	x	1	0	1	4	3	x	7	0	1	1	2	x	0	0	0	0	0	0	0	0	0	20	0	0	27	x	1
		240.8	23-3, 35	3	0	0	11	2	12	1	10	2	3	x	x	0	2	1	3	0	5	x	0	x	9	x	0	0	0	0	0	0	0	0	0	3	0	0	31	2	1
		242.3	23-4, 35	8	1	x	16	1	6	3	4	4	24	0	1	0	3	3	2	x	5	x	0	x	4	x	x	0	0	0	0	0	0	0	0	24	0	0	10	x	3
		244.6	23-5, 122	12	4	2	13	2	5	2	3	2	8	1	2	0	2	4	4	x	9	x	1	x	3	x	0	0	0	0	0	0	0	0	0	8	0	0	19	x	2
		245.3	23-6, 35	12	4	x	15	1	6	x	2	3	15	1	3	x	x	6	2	0	8	0	x	2	3	x	0	0	0	0	0	0	0	0	0	15	0	0	14	x	x
		247.4	24-1, 35	10	2	x	16	3	8	x	6	4	2	3	x	0	x	3	x	0	7	x	x	x	4	2	0	0	0	0	0	0	0	0	0	2	0	0	21	3	x
		248.9	24-2, 35	10	3	x	9	0	8	1	5	3	12	x	1	x	2	5	x	x	8	x	x	0	4	2	0	0	0	0	0	0	0	0	0	12	0	0	19	2	1
		250.4	24-3, 35	5	4	x	23	x	11	3	5	2	5	3	2	0	1	5	3	x	9	0	2	2	0	0	0	0	0	0	0	0	0	0	0	5	0	0	13	x	x
		251.9	24-4, 35	8	4	1	16	1	7	2	4	4	7	4	5	x	2	3	3	1	7	1	2	x	0	0	0	0	0	0	0	0	0	0	0	7	0	0	14	1	1
		253.4	24-5, 35	6	2	x	12	2	6	1	4	2	16	6	1	x	4	4	2	x	5	x	x	x	0	0	0	0	0	0	0	0	0	0	0	16	0	0	24	x	2
		254.9	24-6, 35	8	3	1	14	x	10	2	3	2	9	2	2	1	2	4	3	0	6	x	0	0	0	0	0	0	0	0	0	0	0	0	0	9	0	0	25	1	2
		256.4	24-7, 35	6	x	x	21	2	11	x	6	2	8	5	3	2	3	5	1	x	2	0	x	0	0	0	0	0	0	0	0	0	0	0	0	8	0	0	20	0	x

Note: x refers to values of less than 1%.

Benthic Carbon Isotopes

The benthic carbon isotope data for *Cibicidoides kullenbergi* are plotted against depth in Figure 10 and against time in Figure 11. We will continue to discuss the data within a chronological framework. The benthic carbon isotope record, except in the lower part of the sequence, is very similar throughout the late Neogene, averaging between ~0.7 and 0.9‰, and exhibits moderately high variability. The most distinct change in the benthic carbon isotope record occurs in the late Miocene between 6.7 and 6.2 Ma, representing a dramatic shift in carbon isotope values from 1.35 to 0.45‰ (peak). Lighter carbon isotope values mark the remainder of the late Neogene sequence, although there is a temporary return to heavier average values from 5.2 Ma, until about 4.5 Ma.

Planktonic Carbon Isotopes

The general trends in the planktonic and benthic foraminiferal carbon isotope oscillations are quite similar during the late Miocene and the late Pliocene. However, during the early Pliocene there is a noticeable divergence between the planktonic and benthic records (Fig. 11). The individual oscillations tend to covary quite well throughout the entire record, although the magnitude is often different. The magnitude of the isotopic change in the planktonic record is usually greater than that shown in the benthic record. The planktonic carbon isotope record also exhibits a very large shift from 2.7 to 1.23‰, coincident with the benthic shift (6.7 to 6.2 Ma). Average $\delta^{13}C$ values of about 1.73‰ are exhibited between 6.3 and 4.6 Ma, after which there is a shift to slightly lighter average values of about 1.6‰ through the remainder of the Pliocene. Superimposed upon this lightening is a conspicuous lightening in $\delta^{13}C$ of 1.0‰ in the early Pliocene at 4.2 Ma (Fig. 11). Carbon isotope analyses were performed on *Globorotalia puncticulata* over the interval of the planktonic foraminiferal carbon isotope spike at ~4.2 Ma. The carbon isotope values of *G. puncticulata* are lighter than those of *Globigerinoides sacculifer*, although they display a similar depletion (Fig. 12). A second spike in planktonic $\delta^{13}C$ occurs in the late Pliocene at 2.3 Ma.

DISCUSSION

Paleoclimatic Analyses

The location of Site 590 beneath the Subtropical Divergence, which separates warm-subtropical from temperate waters and is associated with divergence and upwelling, undoubtedly amplifies variability within the faunal assemblages recorded in the sediments. The fau-

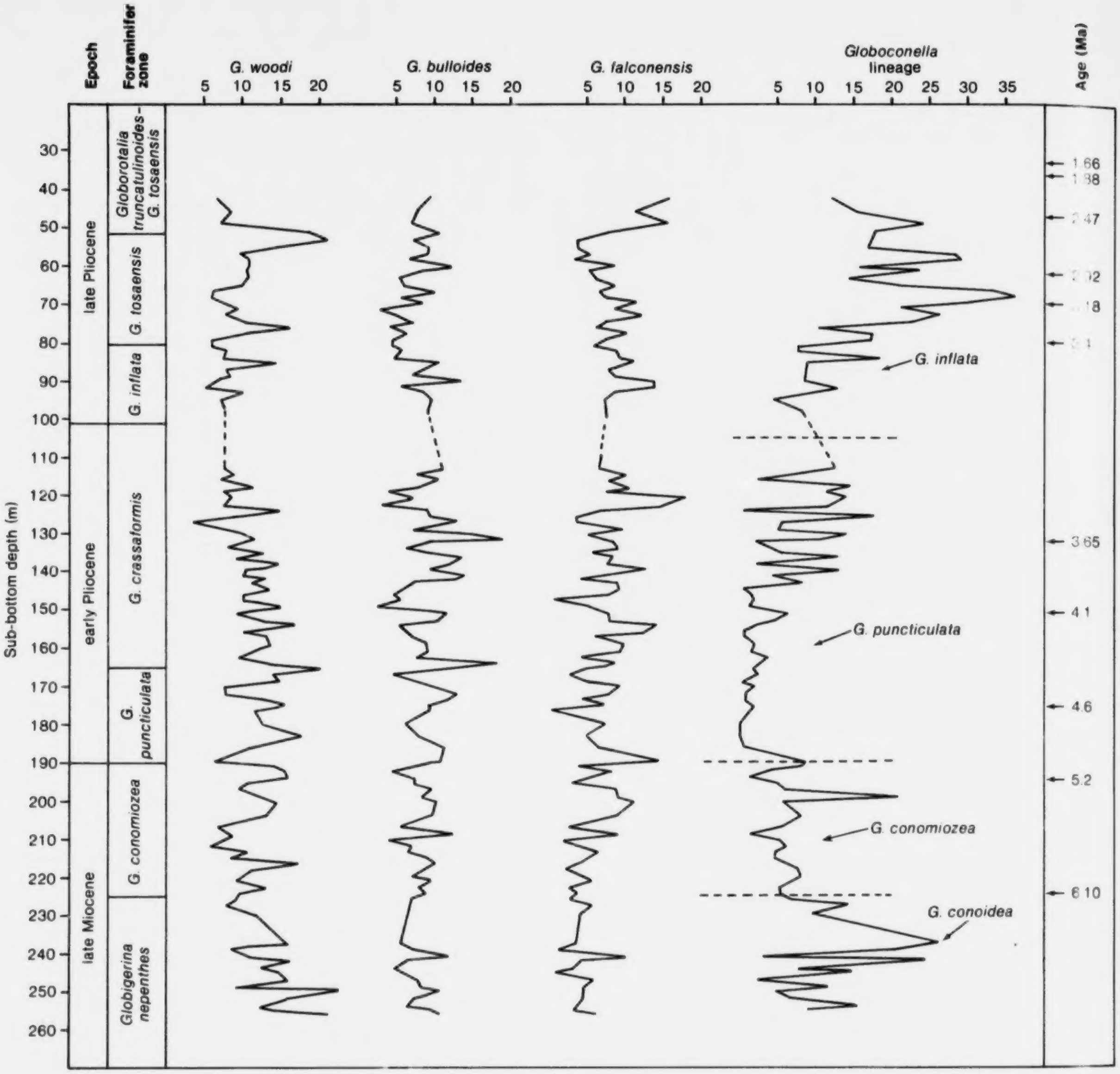

Figure 7. Frequency data for *Globigerina woodi, G. bulloides, G. falconensis*, and the *Globoconella* lineage (all in %) plotted against depth at Site 590 .

nal assemblage at Site 590 is composed of both temperate and warm-subtropical forms; however, the temperate species are most abundant. Frequency oscillations of the cold-water form *Neogloboquadrina pachyderma* and the warm-subtropical fauna serve as sensitive temperature monitors in the late Miocene and early Pliocene and are used to evaluate changes in the temperature of surface waters during this time. The climatic interpretation is much more complex in the middle and late Pliocene at this site, since, as discussed later, the faunal data are reflecting local variability in surface-water temperature arising from changing intensities of upwelling that are not necessarily tied to global temperature changes.

The faunal data indicate that surface waters were relatively warm but cooling during the late Miocene between 6.3 and 5.6 Ma, as indicated by higher frequencies of the warm-subtropical fauna and increasing frequencies of *N. pachyderma*. Surface waters were generally much cooler in the latest Miocene and early Pliocene, between 5.6 and 4.3 Ma, when lowest frequencies of the warm-subtropical fauna coincide with highest frequencies of *N. pachyderma*. From 4.3 to about 3.3 Ma, both the warm subtropical fauna and *N. pachyderma* are equally abundant and exhibit highly variable frequency oscillations (Fig. 6). Higher frequencies of the cool-water form *N. pachyderma* in association with warm-water forms may

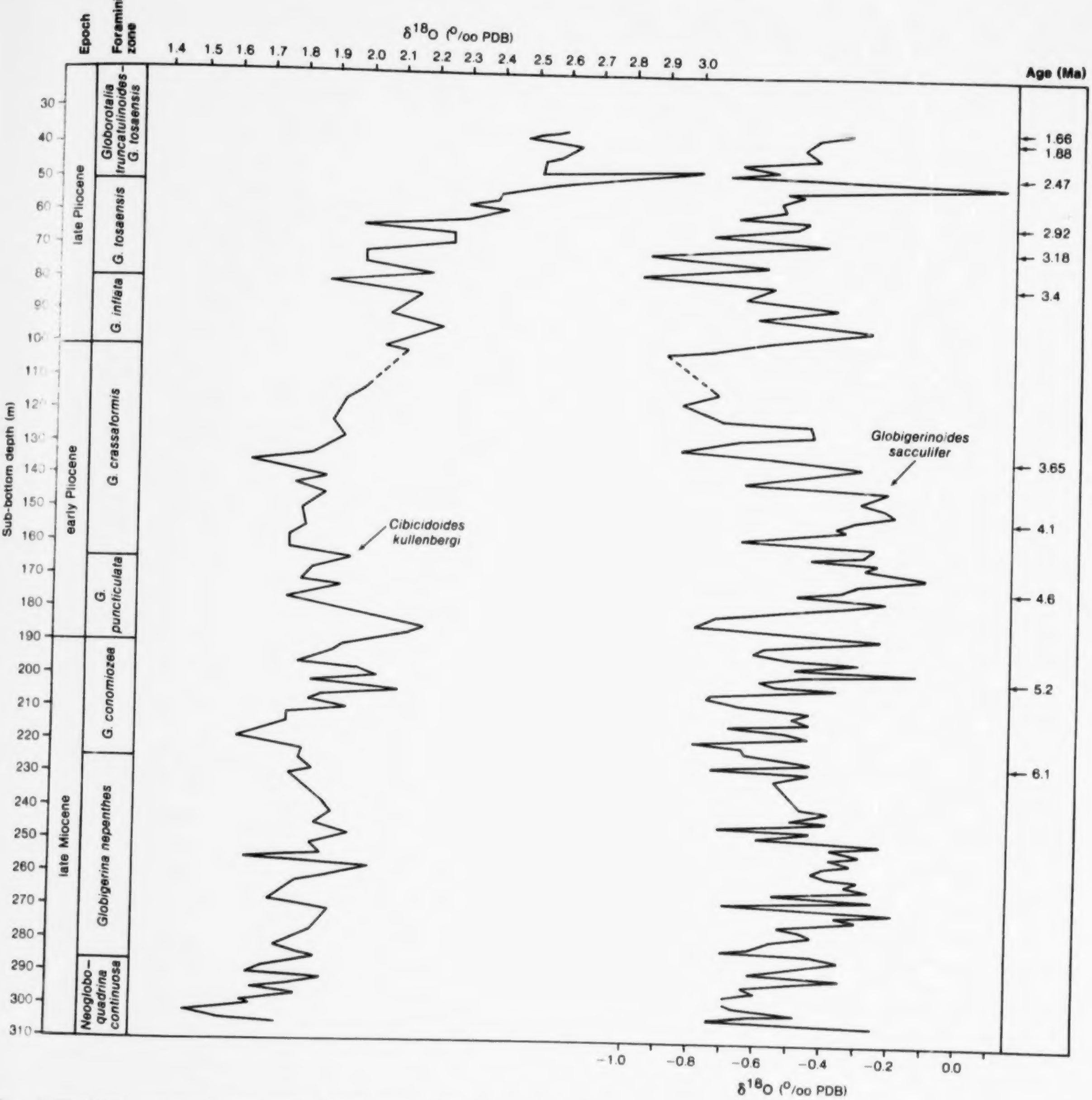

Figure 8. Planktonic and benthic foraminiferal $\delta^{18}O$ plotted against depth at Site 590.

indicate variable temperatures, resulting from changing intensification of the Subtropical Divergence.

N. pachyderma and the warm-subtropical fauna both steadily decrease in frequency between 3.3 and 2.1 Ma, whereas *Globorotalia inflata* significantly increases (Fig. 7). There is no clear climatic interpretation in terms of temperature change represented in the faunal record at this time. The decrease in the frequency of the warm-subtropical forms and *N. pachyderma* may represent a decrease in the intensity of the Subtropical Divergence. Further evidence for this and for the resulting fluctuations within the faunal record will be presented later in a discussion of the increase in biogenic sedimentation rates in the early Pliocene.

Coiling direction changes of *N. pachyderma* at Site 590 exhibit no clear paleotemperature trends. A distinct switch in coiling direction occurs at about 4.3 Ma, in the early Pliocene, when the mode of coiling rapidly changes from dominantly sinistral to dominantly dextral. Kennett and Vella (1975) documented a similar, although more prolonged, switch in the coiling direction of *N. pachyderma* in the later part of the early Pliocene at Site 284 (Fig. 13), which is located in temperate waters south of Site 590. They suggested that this switch

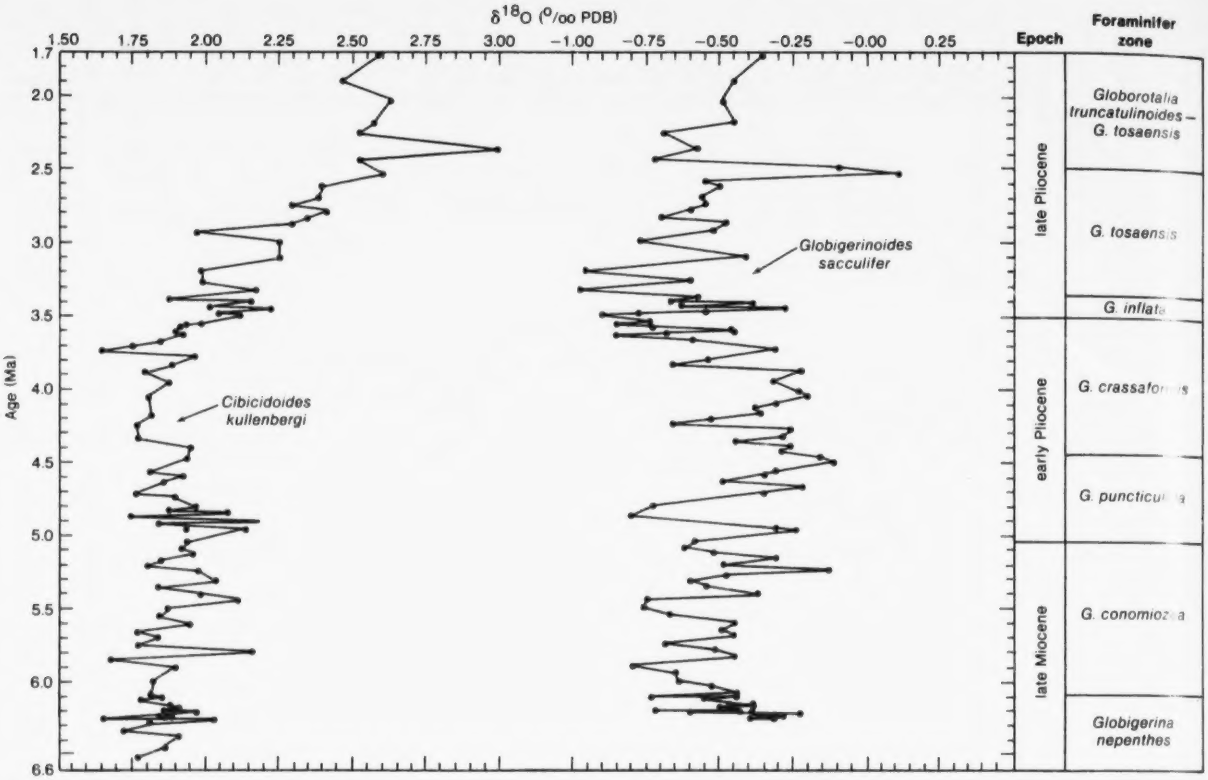

Figure 9. Planktonic and benthic foraminiferal $\delta^{18}O$ plotted against age at Site 590.

reflected the southward migration of the dextral coiling populations as they increased their tolerance for cooler waters and displaced the sinistral populations to the south. Our data from Site 590 supports this interpretation, because the switch to dominantly dextral coiling occurs earlier in the northern site (Site 590) than in the more southern site (Site 284).

Planktonic foraminiferal oxygen isotope analyses were performed on *Globigerinoides sacculifer*, a species which is known to inhabit the upper 50 m of the water column and which contains symbiotic zooxanthellae (Bé et al., 1977). The planktonic foraminiferal oxygen isotope record only generally resembles the faunal climatic record, although both exhibit very high variability in the middle and late Pliocene. The oxygen isotope record exhibits no general trends through the late Neogene, with average values not varying by more than 0.3‰ between the late Miocene and the latest Pliocene (Fig. 9). High variability in the record most likely reflects temperature fluctuations associated with variable rates of upwelling at the Subtropical Divergence.

The climatic record at Site 590 is quite similar to that exhibited at Site 284 (Kennett and Vella, 1975) during the late Miocene through early Pliocene, with both sites indicating cool surface waters at that time. However, the records diverge in the middle Pliocene, when the faunal record at Site 590 seems to exhibit local variation while that of Site 284 indicates warmer conditions through the later part of the early Pliocene and cooler conditions during the late Pliocene in response to climatic cooling in the Northern Hemisphere (Kennett and Vella, 1975).

Benthic Oxygen Isotope Trends

The benthic foraminiferal oxygen isotope record at Site 590 reflects the late Neogene global climatic record, unlike the planktonic foraminiferal oxygen isotope record, which tends to monitor local variability in the temperature of surface waters. The late Neogene benthic foraminiferal oxygen isotope curve monitors oscillations in oceanic isotopic composition caused by continental ice growth and decay, as well as by changes in the temperature of intermediate water masses.

A 0.5‰ increase in benthic foraminiferal $\delta^{18}0$ occurs between 5.6 and 4.8 Ma in the latest Miocene and early Pliocene. A similar isotopic increase was documented at Site 284 (Shackleton and Kennett, 1975) (Fig. 14), and was interpreted to represent a 50% buildup of the West Antarctic ice sheet relative to the present day. This late Miocene isotopic enrichment has not always been found at other sites (Keigwin, 1979; Loutit, 1981), possibly because an unconformity was present at that time, or because sedimentation rates were low. However, further evidence for the late Miocene buildup of the West Antarctic ice sheet is based upon the northward expansion in the distribution of ice-rafted detritus in the Southern Ocean (Ciesielski et al., 1982); a late Miocene age of formation of the Ross Sea disconformity, which is believed to be due to the expansion of a grounded Ross ice shelf

Table 2. Planktonic and benthic foraminiferal oxygen and carbon isotope data, Holes 590A, 590B.

Core-Section (interval in cm)	Depth (m)	*Globigerinoides sacculifer*		*Cibicidoides kullenbergi*	
		$\delta^{18}O$	$\delta^{13}C$	$\delta^{18}O$	$\delta^{13}C$
Hole 590A					
1-6, 35-36	34.0	−0.35	1.90	2.59	0.74
2-1, 35-36	36.2	−0.45	0.95	2.46	0.85
2-3, 35-36	39.2	−0.49	1.42	2.63	0.64
2-5, 35-36	42.2	−0.45	1.50	2.57	0.75
2-6, 35-36	43.7	−0.69	1.58	2.52	0.94
3-1, 35-36	45.8	−0.57	1.57	3.00	0.44
3-2, 35-36	47.3	−0.72	1.66	2.51	0.79
3-3, 35-36	48.8	−0.09	1.39		
3-4, 35-36	50.3	0.11	1.42	2.60	0.61
3-5, 35-36	51.8	−0.55	1.55		
3-6, 35-36	53.3	−0.50	1.67	2.39	0.73
4-1, 35-36	55.4	−0.56	1.52	2.38	0.78
4-2, 35-35	56.9	−0.55	1.74	2.29	0.73
4-3, 35-36	58.4	−0.60	1.24	2.41	0.65
4-4, 35-36	59.9	−0.70	1.57	2.34	0.85
4-5, 35-36	61.4	−0.48	1.44	2.29	0.56
4-6, 35-36	62.9	−0.52	1.36	1.97	0.70
5-1, 110-112	65.7	−0.77	1.39	2.25	0.98
5-3, 110-112	68.7	−0.41	1.56	2.25	0.81
5-5, 110-112	71.7	−0.96	1.49	1.98	0.74
6-1, 55-57	74.8	−0.60	1.59	1.98	0.83
6-3, 55-57	77.8	−0.98	1.50	2.17	0.76
6-5, 55-57	80.8	−0.58	1.75	1.87	0.88
7-1, 35-36	84.2	−0.67	1.58	2.15	0.93
7-3, 35-36	87.2	−0.39	1.45		
7-5, 35-36	90.2	−0.63	1.72	2.01	0.87
8-1, 103-104	94.4	−0.28	1.74	2.22	0.59
8-3, 35-36	96.8	−0.35	1.34		
8-5, 35-36	99.8	−0.78	1.59	2.04	0.99
8-6, 35-36	101.3	−0.90	1.55	2.11	0.80
10-1, 35-36	113.0	−0.74	1.37	1.98	0.73
10-3, 35-36	116.0	−0.85	1.47	1.93	0.69
10-5, 35-36	119.0	−0.73	1.67	1.91	0.76
11-1, 35-36	122.6	−0.46	1.48	1.89	0.91
11-3, 35-36	125.6	−0.45	1.39		
11-4, 35-36	127.0	−0.68	1.73	1.92	0.87
11-6, 35-36	130.0	−0.85	1.37		
12-1, 35-36	132.2	−0.59	1.57	1.84	0.87
12-3, 35-36	135.2	−0.31	1.53	1.64	0.75
12-5, 35-36	138.2	−0.54	1.71		
12-6, 35-36	139.7	−0.66	1.47	1.88	1.06
13-1, 35-36	141.8	−0.22	1.68	1.78	0.94
13-3, 35-36	144.8	−0.32	1.52	1.87	0.86
13-5, 35-36	147.8	−0.23	1.70		
13-6, 35-36	149.3	−0.20	1.32		
14-1, 35-36	151.4	−0.31	1.54	1.80	0.87
14-2, 35-36	152.9	−0.38	1.53		
14-3, 35-36	154.4	−0.36	1.08	1.81	0.77
14-4, 35-36	155.9	−0.53	1.12		
14-5, 35-36	157.4	−0.63	0.83	1.76	0.68
14-6, 35-36	158.9	−0.26	1.45		
15-1, 35-36	161.0	−0.29	1.58	1.76	0.93
15-2, 35-36	162.5	−0.45	1.46		
15-3, 35-36	164.0	−0.26	1.51	1.95	0.63
15-4, 35-36	165.5	−0.29	1.35		
15-5, 35-36	167.0	−0.16	1.59	1.83	1.01
15-6, 35-36	168.5	−0.11	1.58		
16-1, 35-36	170.6	−0.31	1.75	1.80	0.96
16-2, 35-36	172.0	−0.35	1.76	1.92	1.00
16-3, 35-36	173.6	−0.49	1.79	1.85	1.03
16-4, 35-36	175.0	−0.22	1.88		
16-5, 35-36	176.6	−0.35	1.31	1.75	0.82
17-1, 35-36	180.2	−0.73	1.85	1.97	1.15
17-3, 35-36	183.2	−0.81	1.67		
17-3, 121-122	184.1			2.17	0.72
17-5, 35-36	186.2	−0.31	1.43	2.13	0.86
17-5, 121-122	187.0	−0.24	1.98		
18-1, 35-36	189.8	−0.59	2.01	1.93	1.09
18-2, 35-36	191.3	−0.62	2.06	1.91	1.10
18-3, 35-36	192.8	−0.52	1.96		
18-4, 35-36	194.3	−0.31	1.85	1.84	0.78
18-5, 35-36	195.8	−0.49	1.83	1.79	0.88
18-6, 35-36	197.3	−0.13	1.47	1.97	0.47
18-6, 121-122	198.1	−0.48	1.70		
Hole 590A (Cont.)					
19-1, 35-36	199.4	−0.60	1.63	2.03	0.68
19-2, 35-36	200.9	−0.50	1.93	1.83	0.84
19-3, 35-36	202.4	−0.37	1.65	1.97	0.69
19-4, 35-36	203.9	−0.75	1.54	2.10	0.59
19-5, 35-36	205.4	−0.76	1.78	1.86	0.88
19-6, 35-36	206.9	−0.37	2.01	1.83	0.70
20-1, 35-36	209.0	−0.45	1.28	1.94	0.51
20-2, 35-36	210.5	−0.50	1.59	1.76	0.66
20-3, 35-36	212.0	−0.45	1.76		
20-4, 35-36	213.5	−0.69	2.11	1.76	0.88
20-5, 35-36	215.0	−0.52	1.68		
20-6, 35-36	216.5	−0.45	1.59	1.67	0.65
21-1, 35-36	218.6	−0.80	1.84	1.61	0.80
21-2, 35-36	220.1	−0.65	1.57		
21-3, 35-36	221.6	−0.64	1.59	1.81	0.50
21-4, 35-36	223.1	−0.53	1.90		
21-5, 35-36	224.6	−0.44	1.97	1.80	0.93
21-6, 35-36	226.1	−0.74	2.11		
21-7, 35-36	227.6	−0.45	1.76	1.84	0.71
22-2, 35-36	229.7	−0.55	2.01	1.77	0.67
23-1, 35-36	237.8	−0.47	1.73	1.87	0.69
23-2, 35-36	239.3	−0.39	1.78		
23-3, 35-36	240.8	−0.50	1.68	1.90	0.75
23-4, 35-36	242.3	−0.39	1.54		
23-5, 35-36	244.3	−0.72	1.57	1.85	0.70
23-6, 35-36	245.3	−0.17	1.65		
24-1, 35-36	247.4	−0.60	1.26	1.96	0.48
24-2, 35-36	248.9	−0.23	1.56		
24-3, 35-36	250.4	−0.38	1.24	1.84	0.45
24-4, 35-36	251.9	−0.29	1.58		
24-5, 35-36	253.4	−0.38	1.62	1.87	0.46
24-6, 35-36	254.9	−0.32	1.85	1.54	0.60
24-7, 35-36	256.4	−0.40	1.56	1.85	0.54
25-1, 121-122	257.0			2.02	0.69
25-4, 35-36	261.5			1.80	0.77
26-1, 121-122	267.4			1.71	0.79
26-4, 35-36	270.1			1.90	0.70
27-1, 35-36	276.2			1.85	0.82
27-4, 35-36	280.7			1.76	1.02
Hole 590B					
28-5, 35-36	257.03	−0.43	1.92		
28-6, 35-36	258.53	−0.39	2.00		
29-1, 35-36	259.45	−0.29	1.94		
29-2, 35-36	260.95	−0.33	1.59		
29-3, 35-36	262.45	−0.26	1.78		
29-4, 35-36	263.95	−0.55	2.13		
29-5, 35-36	265.45	−0.20	1.87		
29-6, 35-36	266.95	−0.70	2.16		
30-1, 35-36	269.05	−0.19	2.09		
30-2, 35-36	270.55	−0.36	2.30		
30-3, 35-36	272.05	−0.30	2.14		
30-4, 35-36	273.55	−0.53	2.12		
30-5, 35-36	275.05	−0.47	2.20		
30-6, 35-36	276.55	−0.43	2.07		
31-1, 35-36	278.65	−0.56	2.11		
31-2, 35-36	280.15	−0.61	2.24		
31-3, 35-36	281.65	−0.70	2.15	1.73	
31-4, 35-36	283.15	−0.43	2.11	1.78	0.93
31-5, 35-36	284.65	−0.35	2.15	1.86	1.10
32-1, 35-36	288.45	−0.62	2.18	1.69	1.06
32-2, 35-36	289.75	−0.34	2.23	1.65	1.12
32-3, 35-36	291.25	−0.49	2.13	1.88	0.93
32-4, 35-36	292.75	−0.64	2.27	1.77	0.98
32-5, 35-36	294.25	−0.60	2.49	1.66	1.02
32-6, 35-36	295.75	−0.69	2.35	1.81	0.97
33-1, 35-36	297.85	−0.69	2.48	1.63	1.26
33-2, 35-36	299.35	−0.67	2.14	1.66	1.19
33-3, 35-36	300.85	−0.48	2.54	1.49	1.28
33-4, 35-36	301.35	−0.62	2.67	1.46	1.37
33-5, 35-36	302.85	−0.74	2.57	1.55	
33-6, 35-36	304.35	−0.25	2.56	1.71	1.32

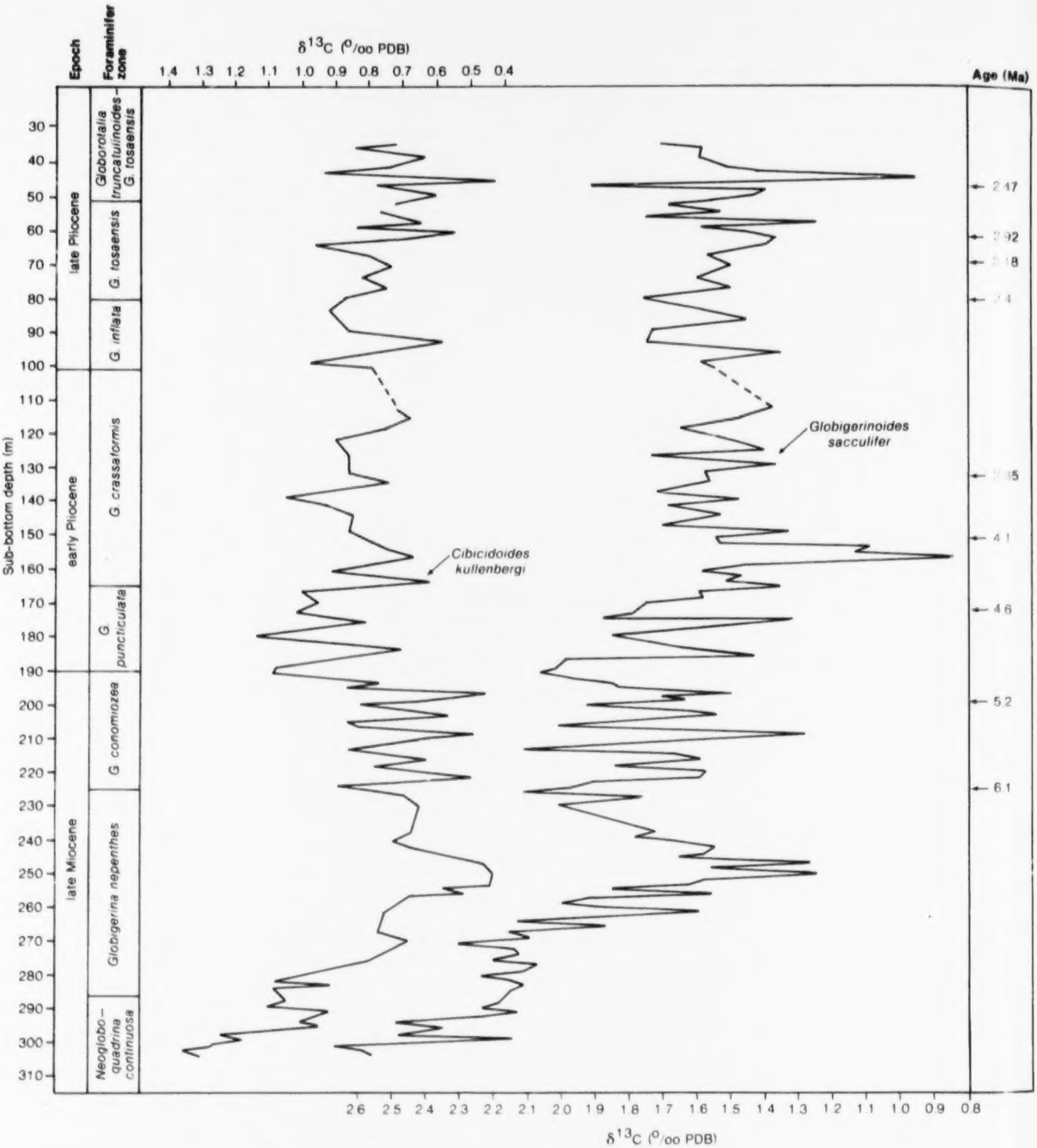

Figure 10. Planktonic and benthic foraminiferal $\delta^{13}C$ plotted against depth at Site 590.

(Hayes and Frakes, 1975); the late Miocene initiation of glaciation in southern Argentina (Mercer and Sutter, 1982); and the northward expansion of the Polar Front and the siliceous biogenic belt (Tucholke et al., 1976; Brewster, 1980). The isotopic enrichment in the latest Miocene and early Pliocene at Site 590 must reflect both the buildup of ice on the West and East Antarctic ice sheets (Shackleton and Kennett, 1975; Ciesielski et al., 1982; Drewry, 1978) and a decrease in the temperature of the intermediate water mass as a result of climatic cooling at this time (Loutit, 1981).

The benthic foraminiferal oxygen isotope record indicates a return to lighter, more stable values by about 4.7 Ma; these continue to about 3.7 Ma. This time of global

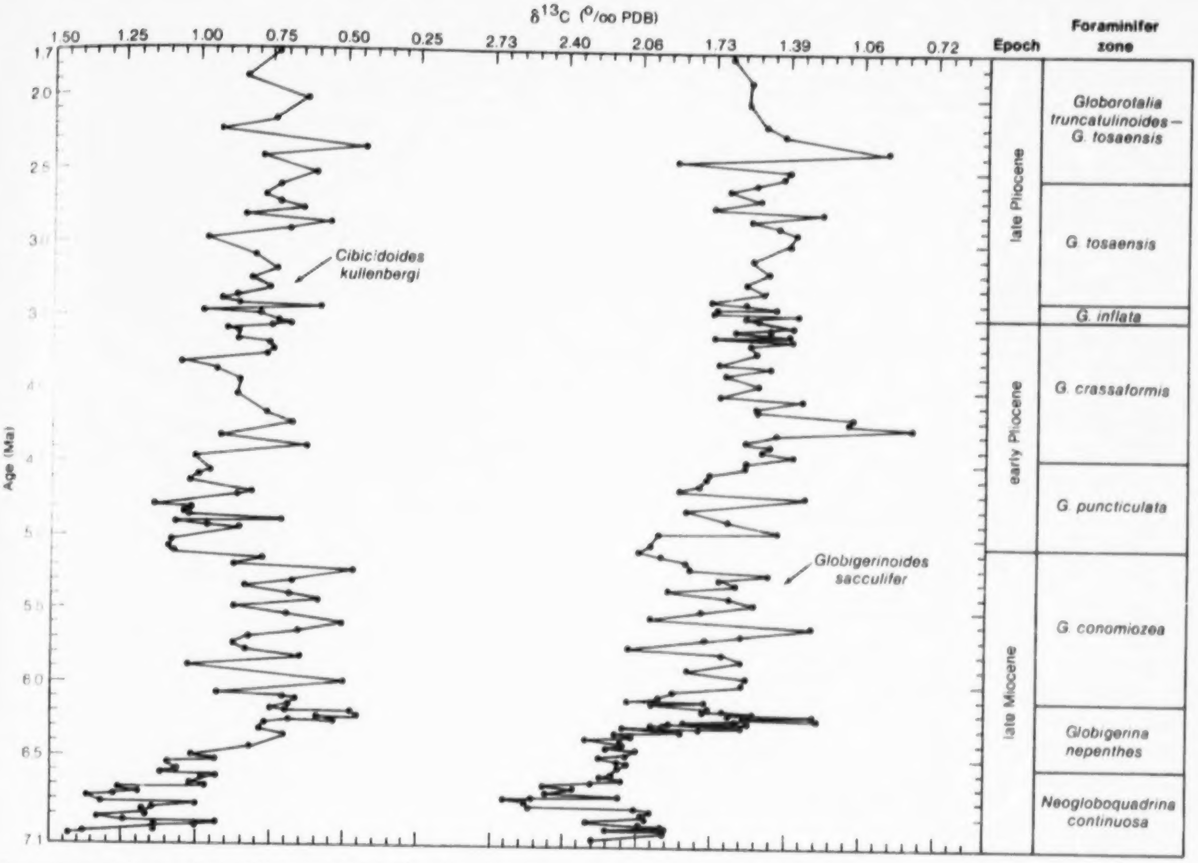

Figure 11. Planktonic and benthic foraminiferal $\delta^{13}C$ plotted against age at Site 590.

climatic warmth and stability was also documented in the benthic foraminiferal oxygen isotope record from Site 284 (Shackleton and Kennett, 1975).

Two distinct changes occur in the benthic foraminiferal oxygen isotope record between 3.7 and 2.4 Ma. The first, between 3.7 and 3.4 represents a 0.3‰ average isotopic enrichment over a 0.3 m.y. period (Fig. 9). The second event, centered at about 2.7 Ma, represented a 0.5‰ average isotopic enrichment. Shackleton and Opdyke (1977) reported two oxygen isotope excursions in the late Pliocene from V28-179, the first at 3.2 Ma, the second at 2.5 Ma. The isotopic enrichment at 3.2 Ma was originally considered to represent the initiation of Northern Hemisphere glaciation, whereas the second isotopic enrichment at 2.5 Ma was believed to reflect an intensification of glaciation on the Northern Hemisphere (Shackleton and Opydke, 1977). Recent evidence suggests that the isotopic enrichment at 3.2 Ma may represent a brief excursion in ice volume rather than a permanent buildup, and/or a change in the character of bottom waters (Prell, 1982; Hodell et al., 1983). The second isotopic shift at 2.5 Ma represents the true initiation of Northern Hemisphere glaciation, because the inception of ice-rafting at high latitudes in the North Atlantic has been redated at 2.5 Ma by Backman (1979), and further isotopic and ice-rafting evidence from the North Atlantic suggest that large ice sheets did not accumulate on the Northern Hemisphere until about 2.5 Ma (Shackleton et al., 1984). The oxygen isotope enrichment centered at 3.6 Ma at Site 590 may be correlated with the isotopic excursion noted by Shackleton and Opdyke (1977) at 3.2 Ma. The second isotopic enrichment at Site 590, centered at 2.7 Ma, reflects the initiation of Northern Hemisphere glaciation.

Late Miocene Carbon Isotope Shift

A permanent depletion in $\delta^{13}C$ in the late Miocene is indicated in the planktonic and benthic foraminiferal carbon isotope records (Fig. 11). The carbon isotope shift in both planktonic and benthic foraminiferal $\delta^{13}C$ is equal in magnitude (0.5 to 0.8‰) and is considered isochronous with the globally recognized carbon isotope shift (Keigwin and Shackleton, 1980; Vincent et al., 1980; Haq et al., 1980) by the following criteria. The first appearance of the calcareous nannofossil *Amaurolithus primus* has been documented to occur prior to the globally recognized carbon shift at many sites (Haq et al., 1980), and at Site 590 this species first appears 15 m below the shift. Keigwin and Shackleton (1980) noted a distinct switch in the coiling direction of *Neogloboquadrina acostaensis* directly above the carbon shift in RC12-66, which is located in the equatorial Pacific. A switch in the coil-

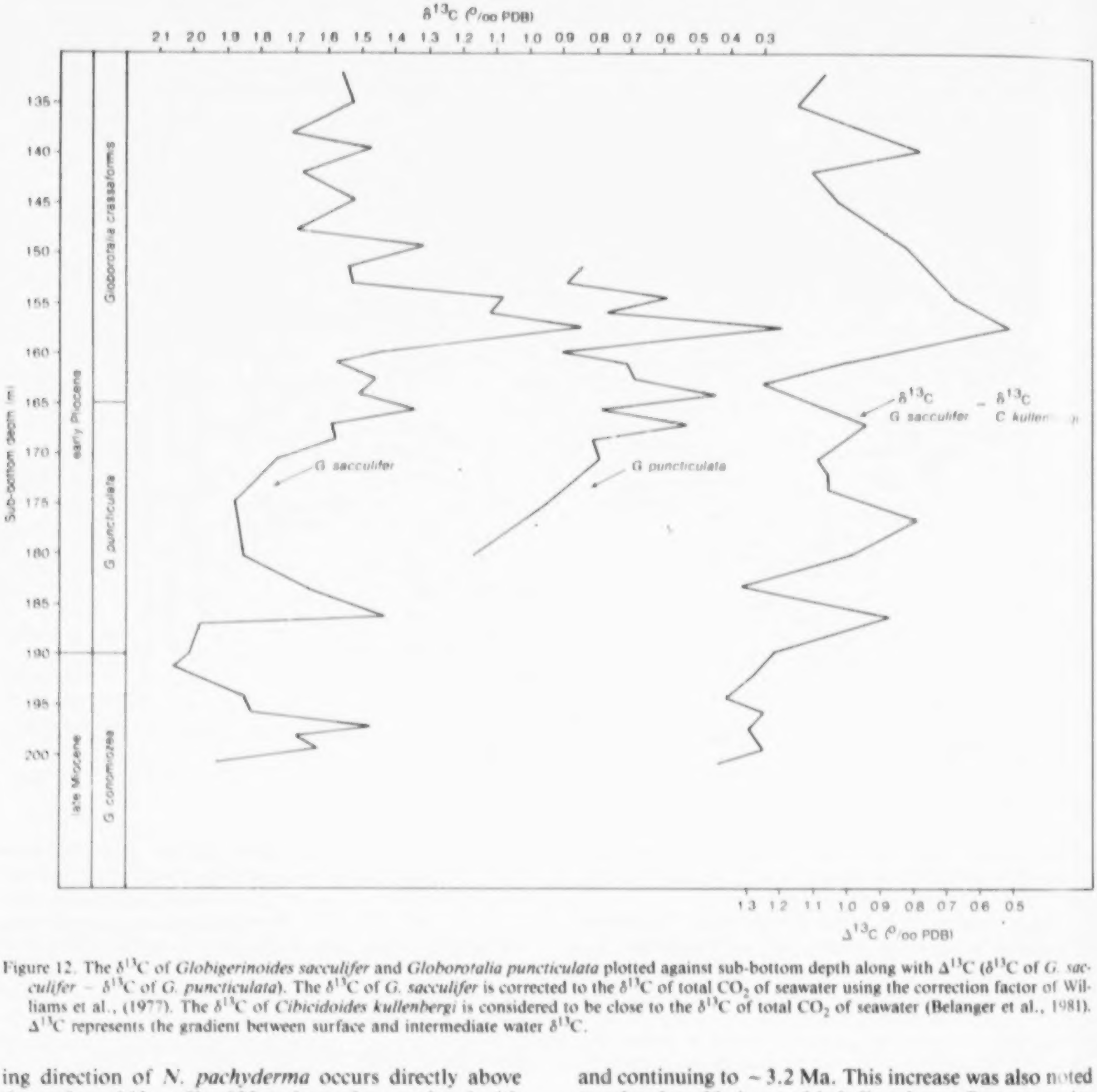

Figure 12. The $\delta^{13}C$ of *Globigerinoides sacculifer* and *Globorotalia puncticulata* plotted against sub-bottom depth along with $\Delta^{13}C$ ($\delta^{13}C$ of *G. sacculifer* − $\delta^{13}C$ of *G. puncticulata*). The $\delta^{13}C$ of *G. sacculifer* is corrected to the $\delta^{13}C$ of total CO_2 of seawater using the correction factor of Williams et al., (1977). The $\delta^{13}C$ of *Cibicidoides kullenbergi* is considered to be close to the $\delta^{13}C$ of total CO_2 of seawater (Belanger et al., 1981). $\Delta^{13}C$ represents the gradient between surface and intermediate water $\delta^{13}C$.

ing direction of *N. pachyderma* occurs directly above the carbon shift at Site 590 and may be correlated with the switch noted at RC12-66. Finally, Loutit and Kennett (1979) and Loutit (1981) noted that the first appearance of *G. conomiozea* occurred directly above the carbon shift at both the Blind River section in New Zealand and at DSDP Site 281. The first appearance of *G. conomiozea* is 40 m above the carbon shift at Site 590. Loutit and Kennett (1979) assigned an age of 6.3 Ma to the late Miocene carbon isotope shift using a paleomagnetically dated marine section in New Zealand, whereas, Haq et al. (1980) assigned an age of 6.1 Ma, also using paleomagnetic stratigraphy.

Early Pliocene Increased Biogenic Sedimentation

A two-fold increase in biogenic sedimentation rates has been documented at Site 590 beginning at ~4.2 Ma and continuing to ~3.2 Ma. This increase was also noted at other Leg 90 sites and is believed to reflect a true increase rather than a chronological problem (site chapter, this volume). The increase was specifically enhanced at the latitude of Site 590 because it is located near the Subtropical Convergence, a zone of upwelling (Kennett et al., 1983). Both the stable isotopic analyses and faunal data from Site 590 indicate that the character of surface waters changed at about the same time as the increase in biogenic sedimentation rates. The faunal data are dominantly composed of both warm- and cool-water taxa and the frequency oscillations are highly variable, a combination normally indicative of seasonal upwelling (Thiede, 1983). The planktonic foraminiferal oxygen isotope values are also highly variable, and heaviest average values are exhibited during this time, which may also indicate upwelling of cooler waters. The gradient be-

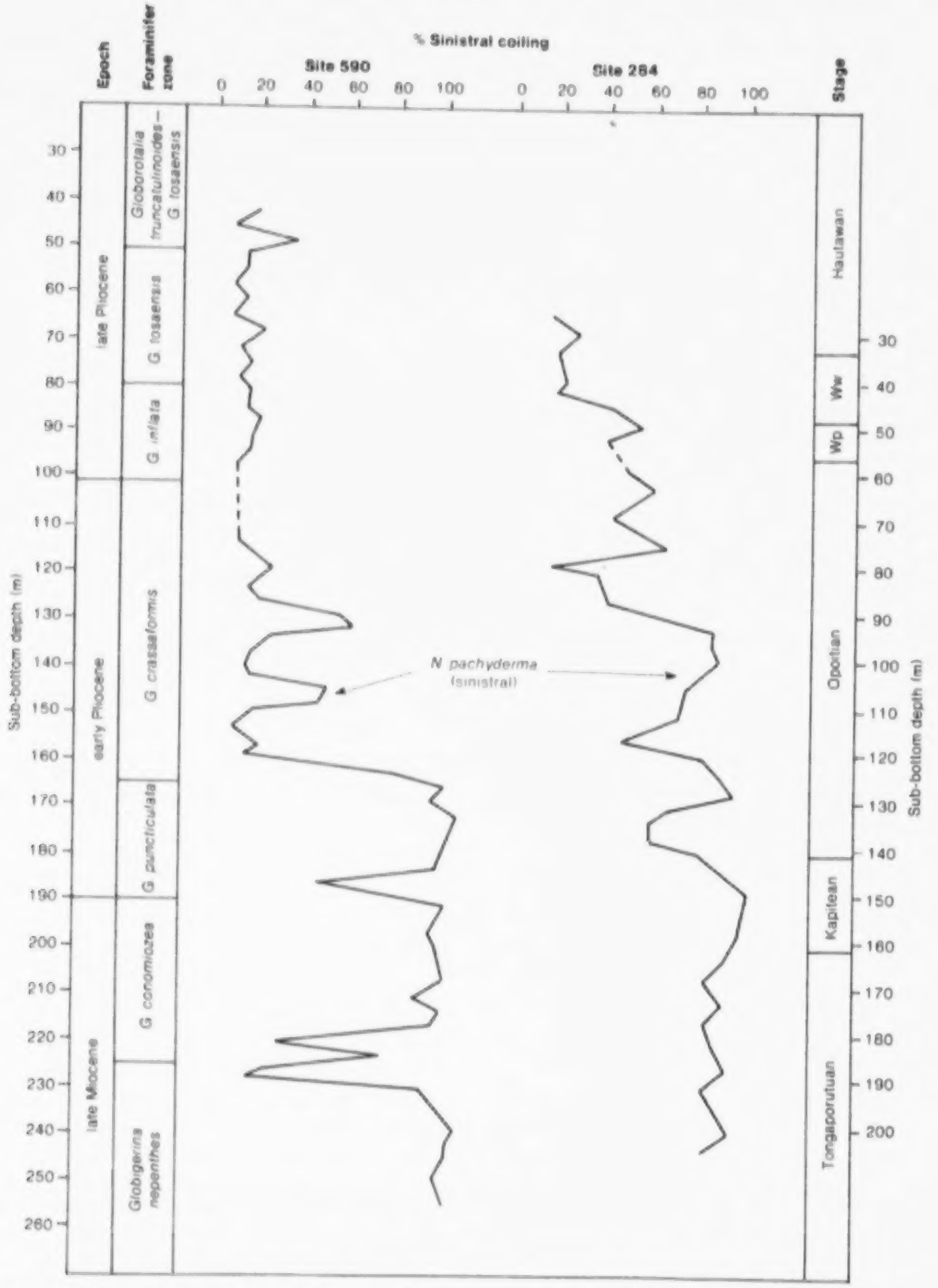

Figure 13. The coiling ratio of *Neogloboquadrina pachyderma* (% sinistral) from Site 590, plotted against depth and the biostratigraphic zonation at Site 590, compared with the coiling ratio of *N. pachyderma* from Site 284, plotted against depth and the New Zealand stages (Kennett and Vella, 1975). The switch in coiling direction from dominantly sinistral to dominantly dextral occurs earlier at Site 590 than it does at Site 284. Ww = Mangapanian; Wp = Waipipian.

tween surface and intermediate-water $\delta^{18}O$ ($\Delta^{18}O$; Fig. 15) decreases during the interval of higher biogenic sedimentation rates. The $\delta^{13}C$ gradient between surface and intermediate waters ($\Delta^{13}C$; Fig. 12) also decreases at the same time as $\Delta^{18}O$, suggesting that there was greater mixing between surface and intermediate waters at that time.

A marked depletion (spike) in planktonic foraminiferal $\delta^{13}C$ ($\sim 1.0‰$) at 4.2 Ma heralds the beginning of lighter carbon isotope values through the Pliocene, and coincides with the onset of the increase in biogenic sedimentation rates. It appears that this spike is only a temporary event: extremely light $\delta^{13}C$ values do not corre-

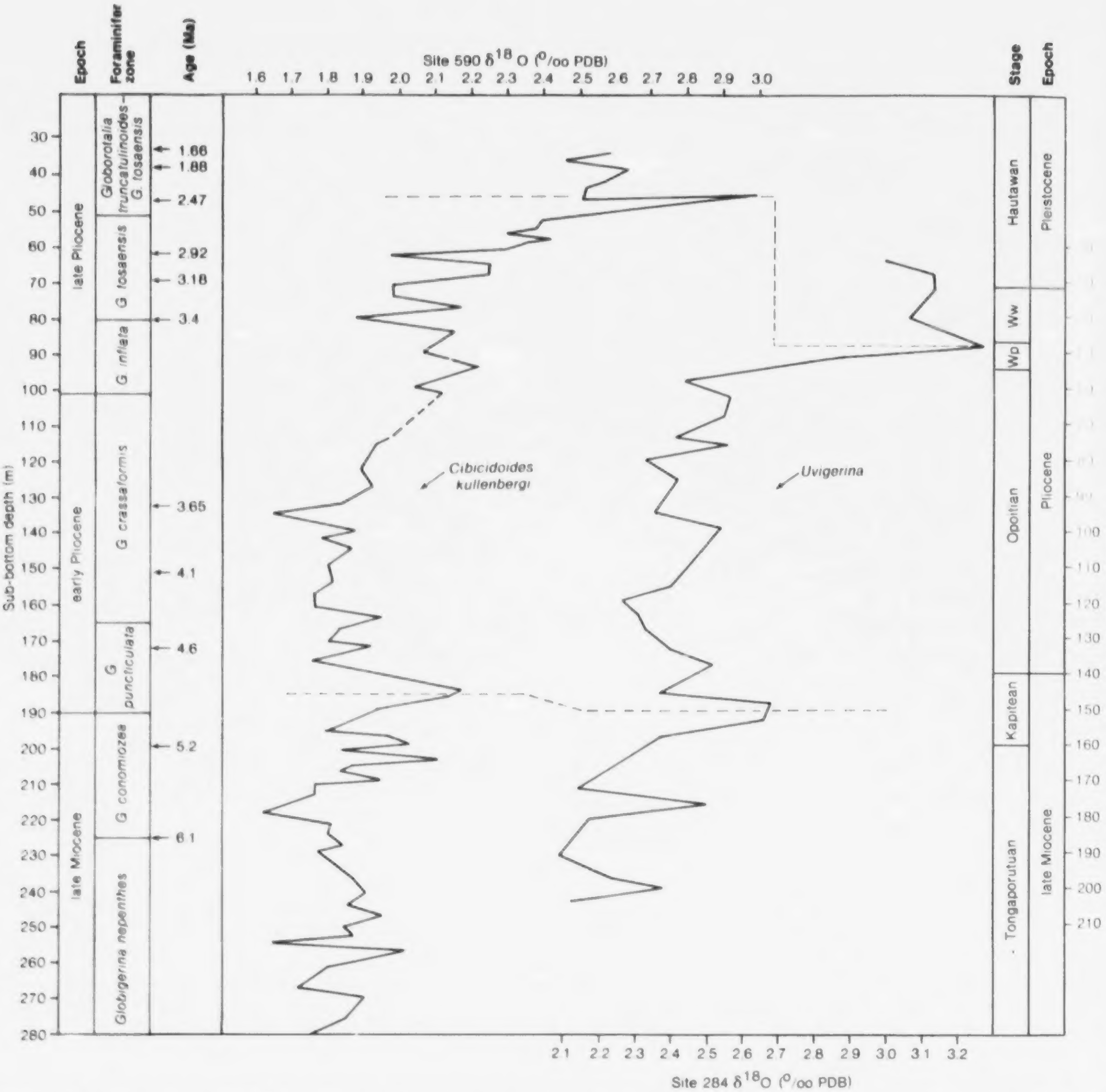

Figure 14. Benthic foraminiferal $\delta^{18}O$ from Site 590 plotted against depth and the biostratigraphic zonation of Site 590, compared with benthic foraminiferal $\delta^{18}O$ for Site 284 plotted against depth and the New Zealand stages (Kennett et al., 1979). Correlation lines refer to periods of maximum oxygen isotope enrichment. Ww = Mangapanian; Wp = Waipipian.

spond to the entire period of higher biogenic sedimentation rates. However, the average $\delta^{13}C$ values are lighter through the remainder of the Pliocene. A major cause for change in the $\delta^{13}C$ of total CO_2 of surface waters is variation in surface-water productivity. The $\delta^{13}C$ of total CO_2 of surface water is a function of the photosynthetic respiration cycle (Kroopnick, 1974). Plants preferentially incorporate the lighter isotope ^{12}C during photosynthesis, leaving the total CO_2 of surface waters enriched in the heavier isotope ^{13}C. The lighter isotope ^{12}C is released to the water column during respiration, thereby producing light $\delta^{13}C$ values in direct association with the O_2 minimum zone (Kroopnick, 1974). During an upwelling event, the lighter isotope ^{12}C is brought back to the surface by the upward advection of water, thus lightening the $\delta^{13}C$ of total CO_2 of surface waters. Ganssen and Sarnthein (1983) investigated $\delta^{13}C$ variations in planktonic foraminifers across the West African upwelling system. They found that *Globorotalia inflata* and *Globigerinoides ruber* both exhibited lighter $\delta^{13}C$ values during periods of upwelling, reflecting the surfacing of waters enriched in ^{12}C. Berger et al. (1978) found similar patterns in $\delta^{13}C$ variations in *G. ruber* in the northwest African upwelling system, interpreting os-

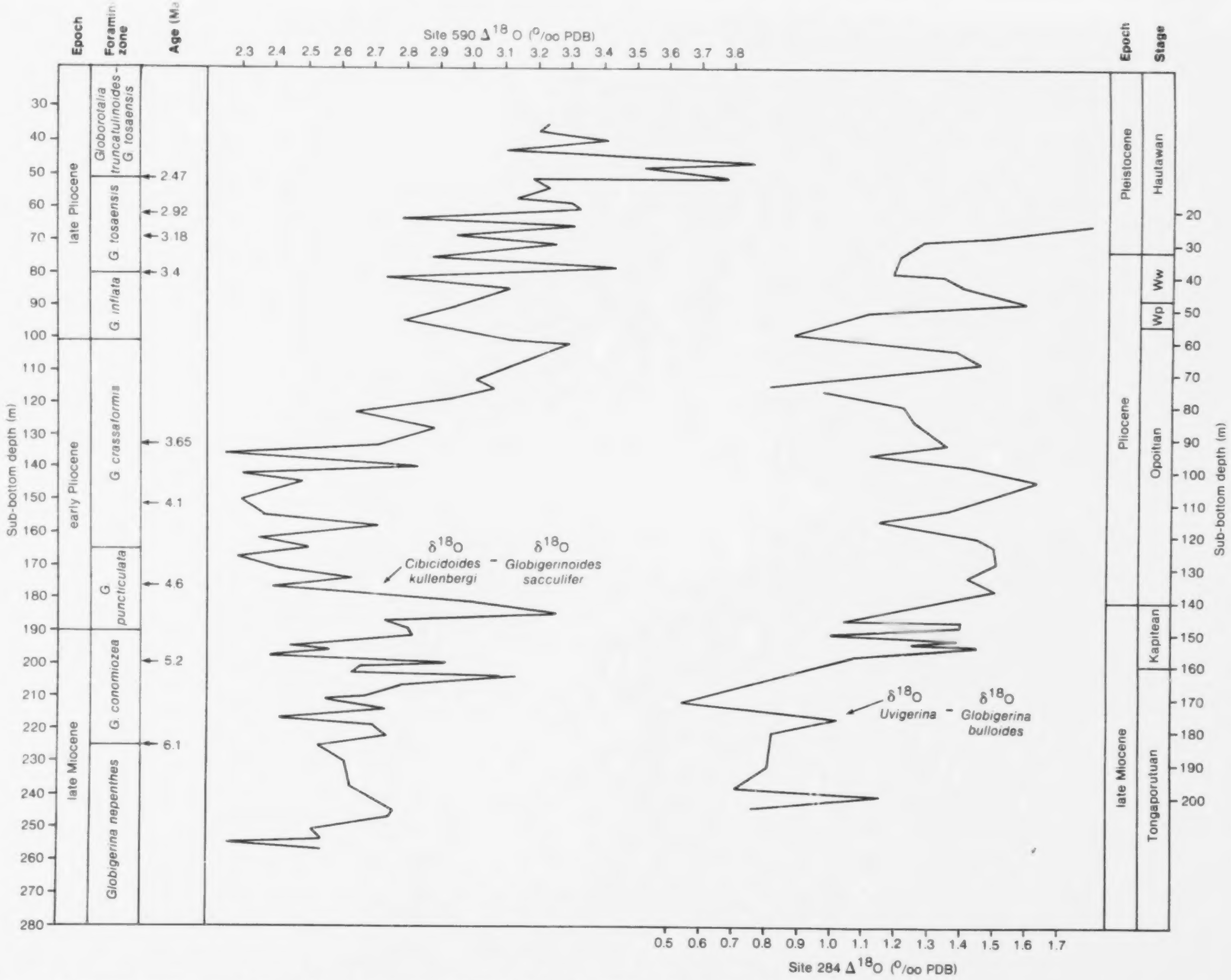

Figure 15. The gradient between surface and intermediate water δ^{18}O (Δ^{18}O) for Site 590 plotted against sub-bottom depth and the biostratigraphic zonation of Site 590, compared with the Δ^{18}O for Site 284 plotted against depth and the New Zealand stages (Kennett et al., 1979).

cillations in the $\delta^{13}C$ of *G. ruber* to represent changes in upwelling intensity during the last glacial–interglacial cycle. On the other hand, Dunbar (1983) and Prell and Curry (1981) found that $\delta^{13}C$ variations in *Globigerina bulloides* did not monitor upwelling events in the Santa Barbara Basin and the Arabian upwelling system, respectively. Prell and Curry (1981) suggested that large stratigraphic variations in planktonic foraminiferal $\delta^{13}C$ may reflect changes in the global carbon cycle and not local surface-water productivity.

To test the validity of the spike in the $\delta^{13}C$ of *Globigerinoides sacculifer*, a second species, *Globorotalia puncticulata*, was analyzed (Fig.12). *G. puncticulata* is a nonspinose species that is inferred to be a deeper dweller than *Globigerinoides sacculifer* (Bé, 1977). The plot shows that *Globorotalia puncticulata* also exhibits a marked decrease in $\delta^{13}C$ of similar magnitude and coincident to the spike in the $\delta^{13}C$ of *Globigerinoides sacculifer*. The marked depletion in $\delta^{13}C$ at ~4.2 Ma, recorded in the $\delta^{13}C$ of two species of planktonic foraminifers, is interpreted as an indicator of upwelling in the early Pliocene at Site 590. This interpretation is also supported by the planktonic foraminiferal oxygen isotope data and the faunal data, as stated earlier. The increase in biogenic sedimentation rates may therefore be associated with upwelling in the early Pliocene, which in turn increased the biogenic productivity of surface waters and produced a highly variable faunal record.

The increase in biogenic productivity is reflected mainly in the calcareous nannofossils, rather than the siliceous taxa, as normally occurs in areas of oceanic upwelling. This may be due to the nature of the upwelling regime. Most areas of siliceous biogenic productivity occur where cold, nutrient-rich, intermediate waters are upwelled. However, at the Subtropical Divergence, the upwelling is occurring over a shallow-water pedestal; thus the source of the upwelling waters is much shallower, and the water is warmer than at most oceanic upwelling regimes, such as the Polar Front, the Equatorial Divergence, and the Eastern Boundary Current systems. It remains to be seen what caused this increase in productivity during a time of known relative global climatic warmth and stability.

CONCLUSIONS

1. Site 590 is located under the present-day position of the Subtropical Divergence, which separates temperate surface water masses to the south from warm-subtropical water masses to the north. We have studied the paleoceanographic evolution of this site from the late Miocene (~7.0 Ma) to the latest Pliocene (~1.8 Ma), using quantitative changes in planktonic foraminifers and planktonic and benthic foraminiferal stable isotopes. Excellent core recovery, a shallow depth of deposition, and excellent microfossil preservation make this site an exceptional location for studying late Neogene paleoceanographic evolution.

2. A permanent depletion in both benthic and planktonic foraminiferal $\delta^{13}C$ occurs between 6.7 and 6.2 Ma, and can be correlated to the globally recognized carbon isotope shift by the criteria which have been associated with the shift in various other localities (Loutit, 1981; Keigwin and Shackleton, 1980; Haq et al., 1980). The shift is located 40 m below the first appearance of *Globorotalia conomiozea* at 6.1 Ma; it is directly below a conspicuous change in the coiling direction of *Neogloboquadrina pachyderma* at 6.0 Ma; it is 15 m above the first appearance of *Amaurolithus primus* at 6.5 Ma, and is of comparable magnitude (0.5 to 0.8‰) to the shift at other sites.

3. The paleoclimatic record from Site 590 indicates that surface waters were cool in the latest Miocene and early Pliocene between 5.6 and 4.3 Ma, as indicated by high frequencies of *N. pachyderma* and low frequency of the warm-subtropical fauna. However, the paleoclimatic interpretation is ambiguous for the remainder of the sequence, since the faunal and planktonic foraminiferal oxygen isotopic data both appear to be reflecting local surface-water temperature variability resulting from interaction with the Subtropical Divergence and not global paleotemperature change.

4. A 0.5‰ enrichment in benthic foraminiferal $\delta^{18}O$ during the latest Miocene and early Pliocene, between 5.6 and 4.8 Ma, reflects the buildup of ice on the Antarctic continent and the cooling of Antarctic Intermediate Waters. The benthic foraminiferal $\delta^{18}O$ record indicates a return to lighter, more stable values by about 4.6 Ma; this continues to about 3.7 Ma.

5. An increase in biogenic sedimentation rates (37.7 to 83.3 m/m.y.) in the early Pliocene at ~4.2 Ma coincides with a decrease in the gradient between surface and intermediate-water $\delta^{13}C$ and $\delta^{18}O$, increased variability within the planktonic foraminiferal frequency data and oxygen isotope data, heaviest values in the planktonic foraminiferal oxygen isotope record, and a 1.0‰ lightening in the $\delta^{13}C$ of two species of planktonic foraminifers. These events reflect localized upwelling at the Subtropical Divergence, which, in turn, produced an increase in the biogenic productivity of surface waters at Site 590.

6. A two-step enrichment occurs in the benthic foraminiferal oxygen isotope record in the late Pliocene at Site 590. The first step represents an average enrichment of 0.3 (0.5 peak)‰, centered at ~3.6 Ma. The second step represents a permanent enrichment of 0.5 (0.8 peak)‰ centered at ~2.7 Ma. These two events may correspond to the well-documented two-step isotopic enrichment associated with late Pliocene climatic cooling and the initiation of Northern Hemisphere glaciation.

ACKNOWLEDGMENTS

The authors would like to thank R. C. Thunell and G. Keller for reviewing the manuscript and Karin Nelson and Robin Rice for general assistance. This research was supported by NSF grant OCE 82-14937 (Marine Geology).

REFERENCES

Adams, C. G., Benson, R. H., Kidd, R. B., Ryan, W. B. F., and Wright, R. C., 1977. The Messinian salinity crisis and evidence of late Miocene eustatic changes in the world oceans. *Nature*, 269: 383–386.

Backman, J., 1979. Pliocene biostratigraphy of DSDP Sites 111 and 116 from the North Atlantic Ocean and the age of Northern Hemisphere glaciation. *Stockholm Contrib. Geol*, 32:115–137.

Bé, A. W. H., 1977. An ecological, zoogeographic, and taxonomic review of Recent planktonic foraminifera. *In* Ramsey A. T. S. (Eds.), *Oceanic Micropaleontology* (Vol. 1): New York (Academic Press), 1-88.

Bé, A. W. H., Hemleben, C. Anderson, O. R., Spindler, M., Hacunda, J., and Tuntivate-Choy, S., 1977. Laboratory an field observations of living planktonic foraminifera. *Micropaleonotology*, 23: 155-179.

Belanger, P. E., Curry, W. B., and Matthews, R. K., 1981. Core-top evaluation of benthic foraminiferal isotope ratios for paleo-oceanographic interpretations. *Palaeogeogr. Palaeoclimatol. Palaeoecol.*, 33:205-220.

Berger, W. H., Diester-Haass, L., and Killingley, J. S., 1978. Upwelling off Northwest Africa: the Holocene decrease as seen in carbon isotopes and sedimentological indicators. *Oceanol. Acta*, 1:1-7.

Berggren, W. A., Kent, D. V., and Van Couvering, J. A., in press. Neogene geochronology and chronostratigraphy. *In* Snelling, N. J., (Ed.), *Geochronology and Geologic Time Scale*. Geol. Soc. London, Spec. Paper.

Brewster, N. A., 1980. Cenozoic biogenic silica sedimentation in the Antarctic Ocean. *Geol. Soc. Am. Bull.*, 91:337-347.

Ciesielski, P. F., Ledbetter, M. T., and Elwood, B. B., 1982. The development of Antarctic glaciation and the Neogene paleoenvironment of the Maurice Ewing Bank. *Mar. Geol.*, 46:1-52.

Denham, R. N., and Crook, F. G., 1976. The Tasman Front. *N. Z. J. Mar. Freshw. Res.*, 10:15-30.

Drewry, D. J., 1978. Aspects of the early evolution of West Antarctic ice. *In* Van Zinderen Balker, E. M., (Ed.), *Antarctic Glacial History and World Paleoenvironments*: Rotterdam (A. A. Balkema), pp. 25-32.

Dunbar, R. B., 1983. Stable isotope record of upwelling and climate from Santa Barbara Basin, California. *In* Suess, E., and Thiede, J. (Eds.), *Costal Upwelling, Its Sediment Record*: New York (Plenum Press), pp. 217-246.

Ganssen, G., and Sarnthein, M., 1983. Stable-isotope composition of foraminifers: The surface and bottom water record of costal upwelling. *In* Suess, E., and Thiede, J. (Eds.), *Costal Upwelling, Its Sediment Record*: New York (Plenum Press), pp. 99-124.

Haq, B. U., Worsley, T. R., Burckle, L. H., Douglas, R., Keigwin, L. D., Jr., Opdyke, N. D., Savin, S. M., Sommer, M. A., II, Vincent, E., and Woodruff, F., 1980. Late Miocene marine carbon isotopic shift and synchroneity of some phytoplanktonic biostratigraphic events. *Geology*, 8:427-431.

Hayes, D. E., and Frakes, L. A., 1975. General synthesis, DSDP Leg 28.*In* Hayes, D. E., Frakes L. A., et al., *Init. Repts. DSDP*, 28: Washington (U.S. Govt. Printing Office), 919-942.

Hodell, D. A., Kennett, J. P., and Leonard, K. A., 1983. Climatically induced changes in vertical water mass structure of the Vema Channel during the Pliocene; Evidence from DSDP Holes 516A, 517, and 518. *In* Barker, P. F., Carlson, R. L., Johnson, D. A., et al., *Init. Repts. DSDP*, 72: Washington (U.S. Govt. Printing Office), 907-919.

Keigwin, L. D., Jr., 1979. Late Cenozoic stable isotopic stratigraphy and paleoceanography of DSDP sites from the east equatorial and central Pacific Ocean. *Earth Planet. Sci. Lett.*, 45:361-382.

Keigwin, L. D., Jr., and Shackleton, N. J., 1980. Uppermost Miocene carbon isotope stratigraphy of a piston core in the equatorial Pacific. *Nature*, 284:613-614.

Kennett, J. P., 1967. Recognition and correlation of the Kapitean Stage (Upper Miocene, New Zealand). *N. Z. J. Geol. Geophys.*, 10: 1051-1063.

_____, 1973. Middle and late Cenozoic planktonic foraminiferal biostratigraphy of the southwest Pacific, DSDP Leg 21. *In* Burns, R. E., Andrews, J. E., et al., *Init. Repts. DSDP*, 21: Washington (U.S. Govt. Printing Office), 575-639.

_____, 1978. The development of planktonic biogeography in the Southern Ocean during the Cenozoic. *Mar. Micropaleontol.*, 3: 301-345.

Kennett, J. P., Shackleton, N. J., Margolis, S. V., Goodney, D. E., Dudley, W. C., and Kroopnick, P. M., 1979. Late Cenozoic oxygen and carbon isotopic history and volcanic ash stratigraphy; DSDP Site 284, South Pacific. *Am. J. Sci.*, 279:52-69.

Kennett, J. P., and Srinivasan, M. S., 1983. *Neogene Planktonic Foraminifera: A Phylogenetic Atlas*: Stroudsburg, Pa. (Hutchinson Ross Pub. Co.).

Kennett, J. P., and Vella, P., 1975. Late Cenozoic planktonic foraminifers and paleoceanography at DSDP Site 284 in the cool subtropical South Pacific. *In* Kennett, J. P., Houtz, R. E., et al., *Init. Repts. DSDP*, 29: Washington (U.S. Govt. Printing Office), 769-799.

Kennett, J. P., von der Borch, C., Baker, P. A., Barton, C. E., Boersma, A., et al., 1983. The South Pacific Cenozoic. *Nature*, 303: 18-19.

Killingley, J. S., Johnson, R. F., and Berger, W. H., 1981. Oxygen and carbon isotopes of individual shells of planktonic foraminifera from Ontong-Java plateau, equatorial Pacific. *Palaeogeogr. Palaeoclimatol. Palaeoecol.*, 33:193-204.

Kroopnick, P., 1974. The dissolved O_2-CO_2 – ^{13}C system in the eastern equatorial Pacific. *Deep-Sea Res.* 21:211-227.

Loutit, T. S., 1981. Late Miocene paleoclimatology: Subantarctic water mass, Southwest Pacific. *Mar. Micropaleontol.*, 6:1-27.

Loutit, T. S., and Kennett, J. P., 1979. Application of carbon isotope stratigraphy to late Miocene shallow marine sediments, New Zealand. *Science*, 204:1196-1199.

Mercer, J. H., and Sutter, J. F., 1982. Late Miocene-earliest Pliocene glaciation in southern Argentina: Implications for global ice-sheet history. *Palaeogeogr. Palaeoclimatol. Palaeoecol.*, 38:185-206.

Prell, W. L., 1982. A reevaluation of the initiation of Northern Hemisphere glaciation at 3.2 m.y. new isotopic evidence. *Geol. Soc. Am. Abstr. Progr.*, 592 (Abstract).

Prell, W. L., and Curry, W. B., 1981. Faunal and isotopic indices of monsoonal upwelling: Western Arabian Sea. *Oceanol. Acta*, 4: 91-98.

Rio, D., Sprovier, R., Di Stefano, E., and Raffi, I., 1964. *Globorotalia truncatulinoides* (d'Orbigny) in the Mediterranean Upper Pliocene geologic record. *Micropaleontology.*, 2:121-137.

Shackleton, N. J., Backman, J., Zimmerman, H., Kent, D. V., Hall, M. A., Roberts, D. G., Schnitger, D., Bauldauf, J. G., Desprairies, A., Homrighausen, R., Huddleston, P., Keene, J. B., Kaltenback, A. J., Krumsiek, K. A. O., Morton, A. C., Murray, J. W., and Westberg-Smith, J., 1984. Oxygen isotopic calibration of the onset of ice rafting and history of glaciation in the North Atlantic region. *Nature*, 307:620-623.

Shackleton, N. J., and Kennett, J. P., 1975. Late Cenozoic oxygen and carbon isotopic changes at DSDP Site 284: Implications for glacial history of the Northern Hemisphere and Antarctica. *In* Kennett, J. P., Houtz, R. E., et al., *Init. Repts. DSDP*, 29: Washington (U.S. Govt. Printing Office), 801-806.

Shackleton, N. J., and Opdyke, N. D., 1977. Oxygen isotopic evidence for early Northern Hemisphere glaciation. *Nature*, 270: 216-219.

Srinivasan, M. S., and Kennett, J. P., 1981. A Review of Neogene planktonic foraminiferal biostratigraphy: Applications in the equatorial and south Pacific. *In* Warme, J. E., Douglas, R. G., and Winterer, E. L. (Eds.), *The Deep Sea Drilling Project: A Decade of Progress*. Soc. Econ. Paleontol. Mineral. Spec. Publ., 32:395-432.

Stanton, B. R., 1979. The Tasman Front. *N. Z. J. Mar. Freshw. Res.*, 138:201-214.

________, 1981. An oceanographic survey of the Tasman Front. *N. Z. J. Mar. Freshw. Res.*, 15:289-297.

Thiede, J., 1983. Skeletal Plankton and Nekton in upwelling water masses of northwestern South America and northwest Africa. *In* Suess, E., and Thiede, J. (Eds.), *Coastal Upwelling, Its Sediment Record*. New York (Plenum Press), pp. 183-207.

Tucholke, B., Hollister, C. D., Weaver, F. M., and Vennum, W. R., 1976. Continental Rise and abyssal plain sedimentation in the southeast Pacific Basin, Leg 35, DSDP. *In* Hollister, C. D., Craddock, C., et al., *Init. Repts. DSDP*, 35: Washington (U.S. Govt. Printing Office), 359-400.

Vail, P. R., Mitchum, R. M., Jr., and Thompson, S., III, 1977. Global cycles of relative changes of sea level. *In* Payton, C. E. (Eds.), *Seismic Stratigraphy-Applications to Hydrocarbon Exploration*, Am. Assoc. Petrol. Geol. Mem., 26:83-97.

Vincent, E., Killingley, J. S., and Berger, W. H., 1980. The magnetic Epoch-6 carbon shift: a change in the oceans $^{13}C/^{12}C$ ratio 6.2 million years ago. *Mar. Micropaleontol.*, 5:185-203.

Williams, D. F., Sommer, M. A., and Bender, M. L., 1977. Carbon isotopic compositions of Recent planktonic foraminifera of the Indian Ocean. *Earth Planet. Sci. Lett.*, 36:391-403.

Date of Initial Receipt: 9 August 1984
Date of Acceptance: 5 December 1984

42. MIOCENE TO EARLY PLIOCENE OXYGEN AND CARBON ISOTOPE STRATIGRAPHY IN THE SOUTHWEST PACIFIC, DEEP SEA DRILLING PROJECT LEG 90[1]

James P. Kennett, Graduate School of Oceanography, University of Rhode Island

ABSTRACT

High-resolution oxygen and carbon isotope stratigraphy is presented for Miocene to early Pliocene sequences at three DSDP sites from the Lord Howe Rise, southwest Pacific, at water depths ranging from 1,300 to 2,000 m. Site 588 is located in the warm subtropics (~26°S), whereas Sites 590 and 591 are positioned in transitional (northern temperate) water masses (~31°S). Benthic foraminiferal oxygen and carbon isotope analyses were conducted on all sites; planktonic foraminiferal isotope data were generated for Site 590 only. Sample resolution in these sequences is on the order of 50,000 yr. or better. The chronological framework employed in this study is based largely upon ages assigned to Neogene calcareous nannoplankton boundaries.

The benthic oxygen isotope record exhibits several major features during the Neogene. During most of the early Miocene, $\delta^{18}O$ values were relatively low, reaching minimum values in the late early Miocene (19.5 to 16.5 Ma), and recording the climax of Neogene warmth. This was followed by a major increase in benthic $\delta^{18}O$ values between ~16.5 and 13.5 Ma, which is interpreted as representing major, permanent accumulation of the East Antarctic ice sheet and cooling of bottom waters. During the 3 m.y. ^{18}O enrichment, surface waters at these middle latitudes warmed between 16 and 14.5 Ma.

During the remainder of the middle and late Miocene, benthic $\delta^{18}O$ values exhibit distinct fluctuations, but the average value remained unchanged. The isotopic data show two distinct episodes of climatic cooling close to the middle/late Miocene boundary. The earliest of these events occurred between 12.5 and 11.5 Ma in the latest middle Miocene. The second cooling event occurred from 11 to 9 Ma, and is marked by some of the highest $\delta^{18}O$ values of the entire Miocene. This was followed by relative warmth during the middle part of the late Miocene. The latest Miocene and earliest Pliocene (6.2 to 4.5 Ma) were marked by relatively high $\delta^{18}O$ values, indicating increased cooling and glaciation.

During the middle Pliocene, at about 3.4 Ma, a 0.4‰ increase in benthic $\delta^{18}O$ documents a net increase in average global ice volume and cooling of bottom waters. During this interval of increased glaciation, surface waters warmed by 2-3°C in southern middle-latitude regions. During the late Pliocene, between 2.6 and 2.4 Ma, a further increase in $\delta^{18}O$ occurred; this has been interpreted by previous workers as heralding the onset of Northern Hemisphere glaciation.

Surface-water warming in the middle latitudes occurred in association with major high-latitude glacial increases in the early middle Miocene (16-14 Ma), middle Pliocene (~3.5 Ma), and late Pliocene (~2.4 Ma). These intervals were also marked by increases in the vertical temperature gradient in the open ocean.

Intersite correlation is enhanced by using carbon isotope stratigraphy. The great similarity of the $\delta^{13}C$ time-series records within and between ocean basins and with water depth clearly indicates that changes in oceanwide average $\delta^{13}C$ of HCO_3 in seawater dominated the records, rather than local effects. Broad changes in the Neogene $\delta^{13}C$ record were caused largely by transfer of organic carbon between continental and oceanic reservoirs. These transfers were caused by marine transgressions and regressions on the continental margins.

The dominant feature of Neogene $\delta^{13}C$ stratigraphy is a broad late early to early middle Miocene increase of about 1‰ between ~19 and 14.5 Ma. This trend occurred contemporaneously with a period of maximum coastal onlap (transgression) and maximum Neogene climatic warmth. The $\delta^{13}C$ trend terminated during the expansion of the Antarctic ice sheet and associated marine regression.

The latest Miocene carbon isotope shift (of up to −0.75‰) at 6.2 Ma is clearly recorded in all sites examined and was followed by relatively low values during the remainder of the Neogene. This shift was caused by a glacioeustatic sea-level lowering that exposed continental margins via regression and ultimately increased the flux of organic carbon to the deep sea. An increase in $\delta^{13}C$ values during the early Pliocene (~5 to 4 Ma) resulted from marine transgression during a time of global warmth.

INTRODUCTION

Cenozoic cooling, which began in the middle Eocene, proceeded gradually, but was punctuated by sudden transitions from one climatic state to another. Global climate underwent major changes during the Miocene Epoch. The most important change occurred during the early middle Miocene, between ~17 and 14 Ma. A marked increase in $\delta^{18}O$ of benthic foraminiferal calcite at this time is commonly interpreted as recording the rapid growth of the East Antarctic ice sheet and associated cooling of high-latitude surface and deep-ocean waters (Savin et al., 1975; Shackleton and Kennett, 1975b; Kennett, 1977; Schnitker, 1980; Keigwin, 1979; Woodruff et al., 1981; Savin et al., 1981). Others have interpreted this increase in $\delta^{18}O$ values as reflecting only a decrease in bottom-water temperatures, unaccompanied by any increase in Antarctic ice (Matthews and Poore, 1980).

Oxygen isotope ratios of benthic and planktonic foraminifers indicate that these events were accompanied by a marked increase in the equator-to-pole thermal gradient and an associated decrease in meridional heat transport (Savin et al., 1975, in press). Tropical Pacific near-surface temperatures increased while high-latitude regions cooled as Antarctic ice volume increased during the middle Miocene (Savin et al., in press). Increased latitudinal temperature gradients are recorded by the progressive divergence of tropical planktonic and benthic foraminiferal $\delta^{18}O$ curves caused by increasing vertical temperature stratification. The early Miocene was marked by limited Antarctic glaciation, gentler equator-to-pole and tropical surface-to-bottom temperature gradients, and warmer high-latitude surface waters. This early Miocene ocean contrasts sharply with that of the late Miocene, which was more similar to the modern ocean (Matthews et al., 1980).

---

[1] Kennett, J. P., von der Borch, C. C., et al., *Init. Repts. DSDP*, 90: Washington (U.S. Govt. Printing Office).

Address: Graduate School of Oceanography, University of Rhode Island, Narragansett, R.I. 92882-1197.

The primary objective of DSDP Leg 90 was to study the Cenozoic paleoceanographic and paleoclimatic evolution of the South Pacific, with emphasis on the Neogene. A latitudinal traverse of carbonate-rich Neogene sequences was cored during Leg 90 on the Lord Howe Rise and New Zealand Platform. Since these sedimentary sequences were obtained using the hydraulic piston corer (HPC) and the extended core barrel (XCB), they are relatively continuous and undisturbed, and are of great value for studies of high-resolution stratigraphy and paleoceanography. HPC sequences in the relatively soft carbonate ooze that blankets this shallow southwest Pacific region were longer than 200 m in each site studied. At Site 588, the HPC sequence is 315 m thick, the longest ever obtained. This sequence contains a continuous, largely uninterrupted record spanning the past 17 m.y. from the late early Miocene to the Quaternary.

This paper presents a detailed study of oxygen and carbon isotope stratigraphy during the Miocene and early Pliocene in three of the Leg 90 sites: 588, 590, and 591 (Fig. 1; Table 1). A number of features of stratigraphic value were identified in the isotopic records of these continuous, high-resolution sequences. The stratigraphic resolution in these sites is much higher than obtained in previous investigations and thus allows a more detailed examination of Miocene paleoceanographic and paleoclimatic history than was previously possible. This paper describes major trends in the isotopic data and discusses causal mechanisms underlying the changes. Future work will consider detailed correlation of the stable isotope records and further examination of cause/effect relationships.

Site Descriptions

The locations of the three sites are shown in Figure 1, with additional relevant information provided in Table 1. The three sequences are composed of relatively uniform, light-colored, foraminifer-bearing to foraminifer-rich nannofossil oozes to chalks throughout the Miocene and Pliocene. Calcium carbonate content is greater than 90% throughout, the terrigenous sedimentary components are virtually nonexistent. Preservation of foraminiferal assemblages is good to excellent in all sections, and deposition always occurred at depths shallower than the foraminiferal lysocline (Kennett and von der Borch, this volume). A noticeable decrease in the quality of preservation of planktonic foraminifers occurs in chalks of early Miocene age at Site 590 and of early middle and early Miocene age at Site 591. Some planktonic foraminiferal specimens from these intervals are slightly recrystallized, but benthic foraminifers show no such change.

Rates of sedimentation show marked changes during the Neogene (Gardner, Dean, et al., this volume). Each of the sites exhibits similar trends. Average early Mio-

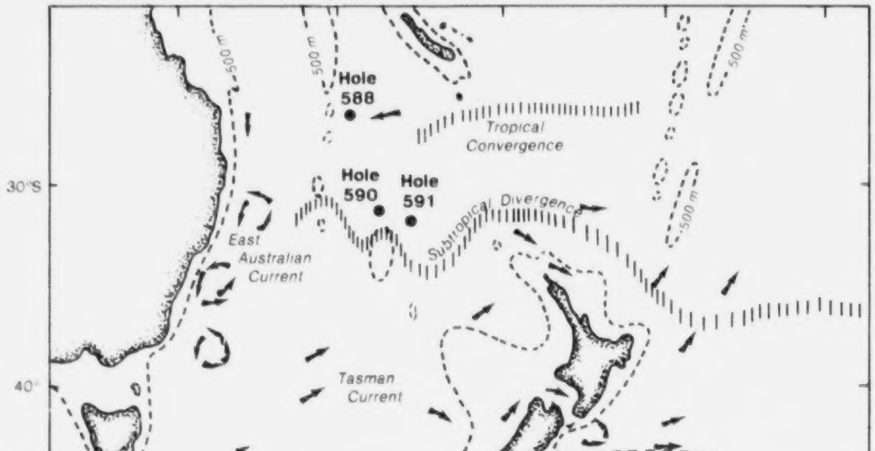

Figure 1. Location of Sites 588, 590, and 591 in relation to modern surface-water boundaries and general circulation in the southwest Pacific (Knox, 1970; Wyrtki, 1974). Dashed line indicates 500 m isobath.

Table 1. Data for sites analyzed in this chapter.

	Site 588	Site 590	Site 591
Latitude (S)	26°06.70′	31°10.02′	31°35.06′
Longitude (E)	161°13.60′	163°21.51′	164°26.92′
Water depth (m)	1533	1299	2131
Modern water mass	Warm-subtropical	Cool-subtropical to transitional	Cool-subtropical to transitional
Thickness of Miocene sequence drilled (m)	288	306	316
Depth at which XCB substituted for HPC (m)	248.6	250.7	283.1
Depth of ooze/chalk transition (m)	260	283.1	290

cene (23 to 16 Ma) carbonate accumulation rates for the open ocean were relatively constant (4.9 g/cm^2 per 10^3 yr.). Accumulation rates were much more variable from about 15 to 10 Ma (middle Miocene) reaching a peak (up to 13 g/cm^2 per 10^3 yr.) at approximately 12 Ma. The late Miocene to earliest Pliocene (10 to 4 Ma) was marked by fairly constant and average rates of accumulation (Gardner, Dean, et al., this volume). At about 5 Ma, near the Miocene/Pliocene boundary, accumulation rates again increased, and widespread, shortlived, remarkably high accumulation rates (up to 27 g/cm^2 per 10^3 yr.) occurred between 4 and 3 Ma (late early Pliocene). This does not simply reflect an artifact of the time scale, because a major modification of the time scale would be required substantially to change the pattern of increased sedimentation rates. Relatively high rates of sedimentation during this interval have also been reported elsewhere for areas such as the Columbia Basin and the Caribbean Sea (Prell, Gardner, et al., 1982). These high rates during the late early Pliocene were particularly pronounced at Sites 590 and 591 and were due to high productivity of calcareous biogenic material (site chapters, this volume), related to the position of the Subtropical Divergence (Tasman Front) that crosses the Tasman Sea in the vicinity of Sites 590 and 591 (Fig. 1). Sedimentation rates are much lower to the north (Site 588) and south (Site 592). Accumulation rates during the late Pliocene were much lower than in the early Pliocene, but remained higher than average Neogene rates.

Oceanographic Setting

The physical oceanography has not been studied in much detail in the region of the three sites used in this study (Fig. 1). Knox (1970) and Wyrtki (1974) showed the position of the major surface-water masses and their boundaries, and directions of surface-water flow in the region (Fig. 1). Site 588 lies within the warm-subtropical water mass, whereas Sites 590 and 591 lie close to the present-day position of the Subtropical Divergence (Tasman Front) that separates warm-subtropical and temperate water masses (Denham and Crook, 1976; Stanton, 1979, 1981). The Subtropical Divergence represents the southern extent of the South Pacific subtropical gyre as the East Australian Current turns to the east, passing to the north of the barrier formed by New Zealand. Upwelling at the Subtropical Divergence is caused by the divergence of the two surface-water masses and the interaction of the eastward-flowing gyral circulation with the Lord Howe Rise (Stanton, 1981). This has created high biogenic sedimentation rates, which in the late Neogene ranged up to 131 m/m.y. at Site 591, the site closest to the Divergence.

Sites 588 and 590 are located in similar water depths, 1500 and 1300 m, respectively, yet bottom-water temperatures at Site 590 are 0.5°C warmer (Site 588 = 3.75°C; Site 590 = 4.25°C), because of the eastward passage across this area of the warm waters contained in the subtropical gyre.

The sites on the Lord Howe Rise have moved about 5° to the north during the Neogene as the result of the movement of the Indo-Australian Plate (Sclater et al., in press). The northward movement of these sites into warmer waters during the Neogene should be reflected by planktonic assemblages indicative of increasingly warm surface water and by lower planktonic $\delta^{18}O$ values, unless the water masses themselves changed latitudinal positions.

Stratigraphy and Chronology

Rich calcareous microfossil assemblages facilitated biostratigraphic subdivision of the sequences. Calcareous nannoplankton and planktonic foraminiferal zonal boundaries are from Lohman (this volume) and Jenkins and Srinivasan (this volume), as summarized in the Introduction (this volume). The nannoplankton zonal boundaries were determined using uneven sample spacing ranging from a few cm to up to 8 m, resulting in varying precision in the placement of individual zonal boundaries. Planktonic foraminiferal zonal boundaries were determined by examining core-catcher samples only (i.e., at 9 m stratigraphic intervals). Minor adjustments were made on zonal boundary positions in the late Miocene and Pliocene of Site 590, as discussed by Elmstrom and Kennett (this volume).

The chronological framework employed here is based upon ages assigned to Neogene calcareous nannoplankton zonal (NN) boundaries (Table 2) by Berggren (1981), and the scheme was uniformly applied by the Leg 90 scientific group (Introduction, this volume). I have also adopted an age of 6.2 Ma for the NN11a/11b boundary. The chronology of the latest Miocene through early Quaternary of Site 590 was that used by Elstrom and Kennett (this volume), with some minor modifications from the scheme used by the Leg 90 group. The chronological

Table 2. Ages assigned to boundaries between nannofossil NN zones to establish chronological framework in this paper.

NN zones	Ma	NN zones	Ma
NN19/20	0.55	NN10/11a	9.50
18/19	1.90	9/10	11.00
17/18	2.30	8/9	12.00
16/17	2.40	7/8	12.20
15/16	3.45	6/7	13.00
14/15	3.65	5/6	15.00
13/14	4.10	4/5	17.00
12/13	4.60	3/4	17.80
11b/12	5.20	2/3	19.00
11a/11b	6.20	1/2	20.50

intercalibration used by Berggren (1981) and most other workers for the past 10 years is based upon a correlation between Chron 9 and Anomaly 5. This scheme places the middle/late Miocene boundary at 11 Ma. After Leg 90 was completed, a major adjustment to the Neogene time scale was made by Berggren, Kent, and Van Couvering (1985), based upon a correlation between Chron 11 and Anomaly 5 (Barron et al., in press). If this correlation is accepted, then an age of 8.92 to 10.42 Ma must be assigned to Chron 11 in accordance with the Berggren, Kent, and Flynn (1985) paleomagnetic time scale. In this scheme, the middle Miocene/late Miocene boundary, which is correlated with upper Chron 11, is assigned an age of 9.5 Ma (Barron et al., in press). This change also requires a shift of about 1.5 to 2 m.y. toward younger ages for much of the late Miocene and late middle Miocene. Nevertheless, to maintain consistency among the Leg 90 contributions, the older time scale is employed here.

All three sites contain continuous sedimentary sequences except for an unconformity at 456 m at Site 590. This unconformity contains the interval from the upper part of the *Globorotalia miozea* Zone (late early Miocene) to the lower part of the *G. fohsi* s.l. Zone (early middle Miocene). The calcareous nannoplankton do not indicate an unconformity at this level, but suggest instead the NN4 and part of NN5 are missing at 470.3 m. In this study I recognize the hiatus at 456 m and place its age between about 18 and 16.5 Ma (latest early Miocene).

Sample intervals for the isotopic analyses in the three sites were, for the most part, evenly spaced at 75 cm (Appendix). The quantity of time represented between samples varies according to changes in sedimentation rates. For much of the Miocene, sedimentation rates ranged from 1.5 to 3 cm/10^3 yr., which provides a sampling interval of about 25 × 10^3 yr. In the Pliocene, sedimentation rates were much higher, ranging from about 5 to 13 cm/10^3 yr. This provides a sampling interval of about 5 to 15 × 10^3 yr. Sampling intervals for isotope analyses are smaller than those used to define the positions of the calcareous nannoplankton boundaries and hence the isotope record is of higher resolution than the chronological framework.

METHODS

Samples were disaggregated by soaking in buffered Calgon solution, washed over a 63 μm sieve, and oven-dried at 50°C.

Isotopic analyses were performed on the planktonic foraminifers of the *Globigerinoides immaturus-G. quadrilobatus-G. sacculifera* lineage in Site 590 in the 295–412 μm fraction. The relatively small size fraction was used to minimize the effect of size on isotopic variability (Berger et al., 1978; Killingley et al., 1981).

Isotopic analyses were performed on four benthic species (> 150 μm size fraction) because no species extends throughout the entire Miocene (Appendix). *Cibicidoides coryelli* or *Oridorsalis umbonatus* were analyzed in the lower portion of the section, incorporating part of the early Miocene; *C. wuellerstorfi* was analyzed in the middle part of the section and *C. kullenbergi* in the upper part of the sequence. The middle part of the sequence of Site 591 was analyzed using either *C. kullenbergi* or *C. wuellerstorfi*. *Cibicidoides wuellerstorfi* and *C. kullenbergi* have been shown to be isotopically indistinguishable within analytical error. The isotopic systematics of *Cibicidoides* spp. and *Oridorsalis* spp. have been discussed by Savin et al. (1981) and Loutit, Kennett, et al., (1983). *C. wuellerstorfi* deposits its test near carbon isotopic equilibrium, but *Oridorsalis* is 1.06‰ lower in $\delta^{13}C$ than *C. wuellerstorfi* (Savin et al., 1981). With respect to $\delta^{18}O$, *C. wuellerstorfi* deposits its test out of oxygen isotopic equilibrium by 0.72‰, whereas *Oridorsalis* is closer to equilibrium (−0.03‰) (Savin et al., 1981).

Almost all analyses in this study were performed on *Cibicidoides* spp. No adjustments were made to the data for disequilibrium effects known for this genus. Because only a few measurements were made on *Oridorsalis* spp., the values of this form were adjusted relative to *Cibicidoides* by adding +1.06‰ for $\delta^{13}C$ and subtracting 0.72 for $\delta^{18}O$ as suggested by Savin et al. (1981).

Specimens selected for isotopic analysis were ultrasonically cleaned in reagent-grade methanol and roasted *in vacuo* at 400°C for 1 h. The samples were then reacted in 100% orthophosphoric acid at [illegible]°C. The evolved CO_2 was purified by distilling four times and was analyzed for $^{18}O/^{16}O$ and $^{13}C/^{12}C$ ratios using an on-line VG Micromass 602D mass spectrometer. The analytical precision of the mass spectrometer is ±0.1‰ for both $\delta^{18}O$ and $\delta^{13}C$, which is based upon the analyses of a laboratory standard of powdered B-1 (Orchardo, in the Appendix to Murphy and Kennett, this volume). This standard was analyzed at the beginning and end of each day. All isotopic results are expressed as per mil difference from PDB.

RESULTS

All isotopic results are presented in the Appendix. For each of the sites, the isotopic data were plotted against both depth and age and a three-point running average of the isotopic data was plotted against age. For Site 588, the data are plotted in Figures 2, 3, and 4; for Site 590 in Figures 5, 6, and 7; and for Site 591 in Figures 8, 9, and 10.

Site 588

Benthic Foraminiferal Oxygen Isotopes

The main features of Miocene benthic oxygen isotope records are exhibited by Figures 3 and 4. During the early Miocene, a slow, progressive decrease in $\delta^{18}O$ values (apparent warming) occurred, reaching several minima (maximum isotopic temperatures) during the late early Miocene between about 19.5 and 17 Ma. Within this interval of optimal Neogene warmth, an episode of slightly higher $\delta^{18}O$ values (apparent cooling) occurred between 19 and 18 Ma.

From 17 Ma (latest early Miocene) to about 13.5 Ma (middle middle Miocene), $\delta^{18}O$ values increased by about 1.5‰. This increase, recognized in most deep-sea sedimentary sections, represents a shift in average values of about 1‰ from the early Miocene to the late Miocene.

From about 13.5 Ma (middle middle Miocene) to about 4 Ma (early Pliocene), the benthic $\delta^{18}O$ values remained permanently offset, but exhibit no apparent long-term trends. There were, however, significant fluctuations during this interval. Within this 13.5 to 4 Ma interval, episodes interpreted as having been warmer and with less polar ice occurred between about 13 and 12 Ma (late middle Miocene), 7.5 and 6.2 (middle late Miocene), and 5.2 and 4 Ma (early Pliocene). Episodes interpreted as having been cooler and with more polar ice occurred from about 11 to 10 Ma (earliest late Miocene) and 6.2 to 5.2 Ma (latest Miocene).

Benthic Foraminiferal Carbon Isotopes

The Miocene benthic carbon isotope record (Figs. 3 and 4) exhibits both short-term and long-term variabili-

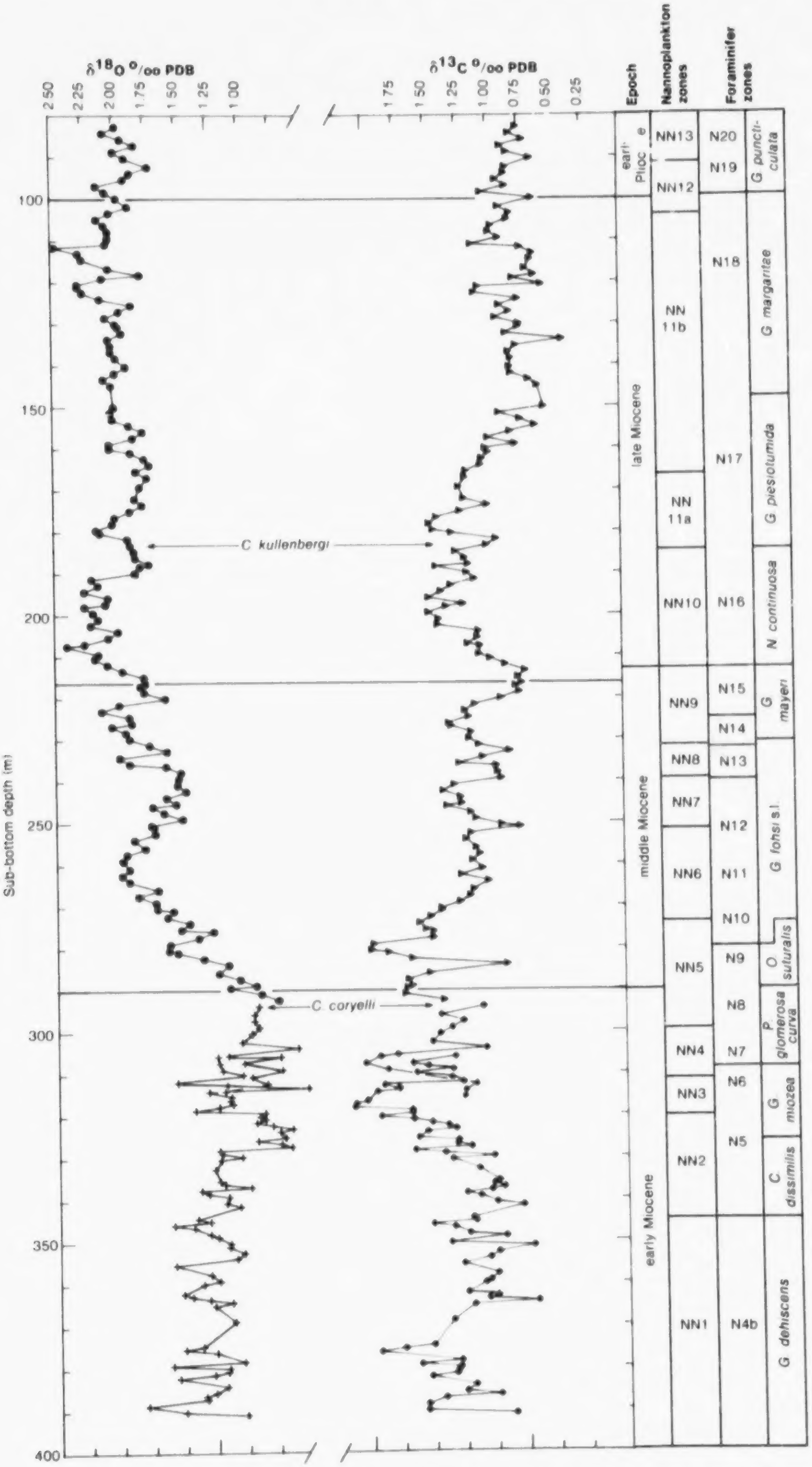

Figure 2. Benthic $\delta^{18}O$ and $\delta^{13}C$ for Holes 588, 588A, and 588C plotted against depth at Site 588 and biostratigraphic zonations for calcareous nannoplankton (Lohman, this volume) and planktonic foraminifers (Jenkins and Srinivasan, this volume).

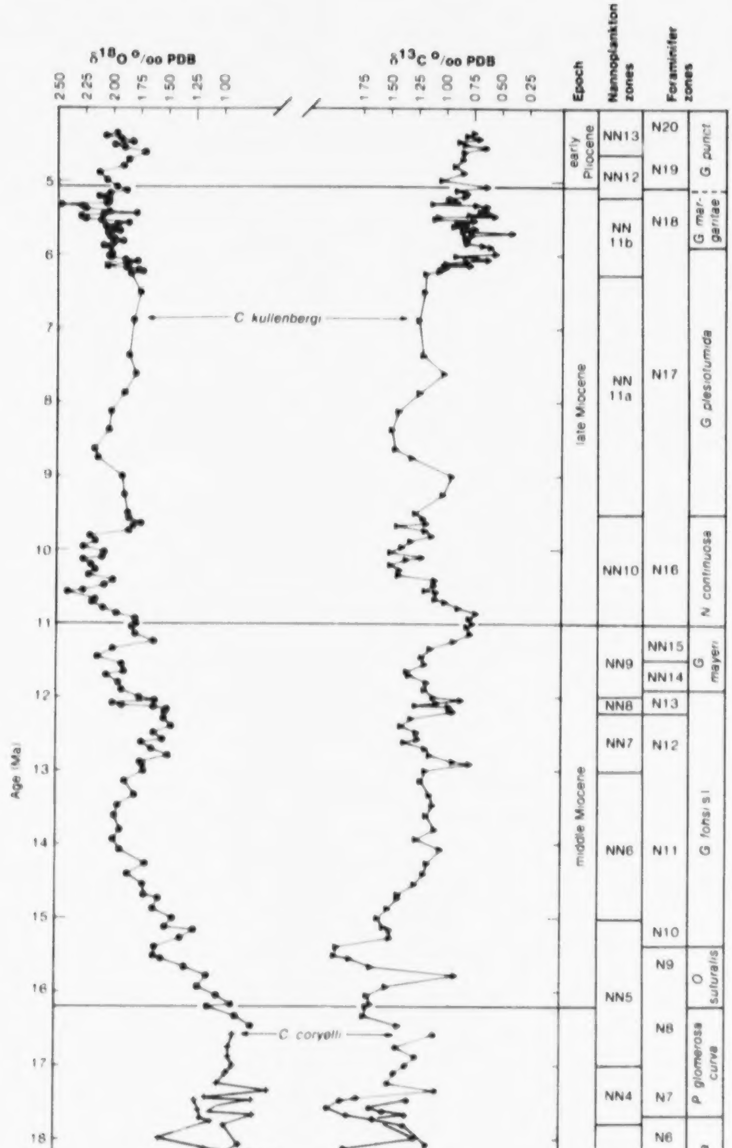

Figure 3. Benthic $\delta^{18}O$ and $\delta^{13}C$ for Holes 588, 588A, and 588C plotted against age at Site 588 and biostratigraphic zonations for calcareous nannoplankton (Lohman, this volume) and planktonic foraminifers (Jenkins and Srinivasan, this volume).

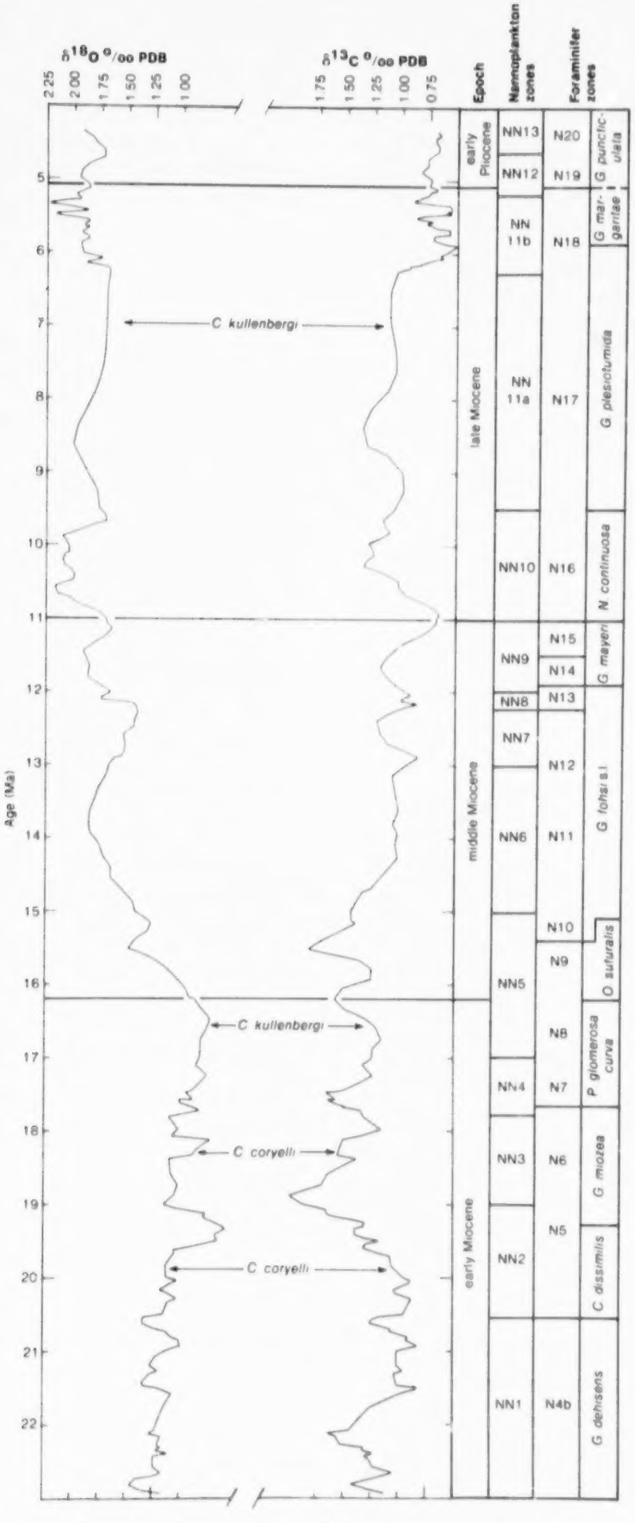

Figure 4. Smoothed benthic $\delta^{18}O$ and $\delta^{13}C$ data (three-point running averages) for Holes 588, 588A, and 588C and biostratigraphic zonations for Site 588, plotted against age.

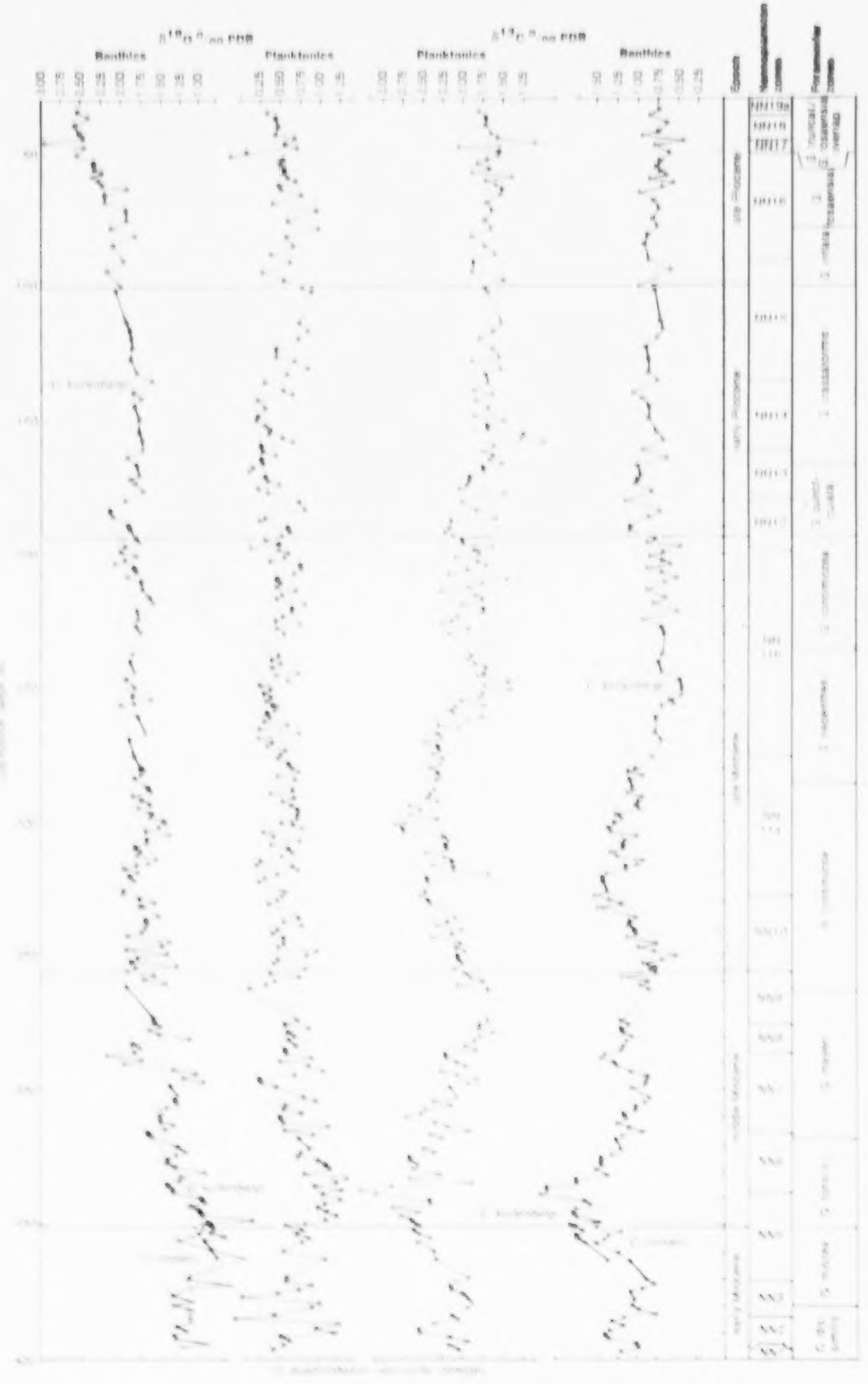

Figure 5. Benthic and planktonic $\delta^{18}O$ and $\delta^{13}C$ for Holes 590A and 590B plotted against depth in Site 590 and biostratigraphic zonations for calcareous nannoplankton (Lohman, this volume) and planktonic foraminifers (Jenkins and Srinivasan, this volume).

ty. Relatively high $\delta^{13}C$ values mark the earliest Miocene between about 23 and 22 Ma, followed by lower values between 22 and 19.5 Ma. This, in turn, was followed by the most conspicuous feature of the Neogene benthic carbon isotope record: a period of increased $\delta^{13}C$ values from the late early Miocene to the early middle Miocene, between 19.5 and 15 Ma. The increase leading to these high $\delta^{13}C$ values consisted of a shift of about 1‰ that occurred between ~19.8 and 18.8 Ma. Although overall values were high during this interval, distinct fluctuations occurred, including minima centered at 18.0, [illegible], and 15.8 Ma. The return to lower values is also distinctive, consisting of a ~1‰ shift between 15.4 and 14.2 in the early middle Miocene. Following this major Neogene episode, there were no such major fluctuations in $\delta^{13}C$ during the remainder of the middle and late Miocene except for a negative peak centered at about [illegible] Ma near the middle/late Miocene boundary. Following this, the most distinctive change in the Neogene benthic carbon isotope record occurred during the late Miocene at about 6.2 Ma, representing a marked shift in $\delta^{13}C$ values of about ~0.7‰. This represents the well-known latest Miocene carbon isotope shift (see Vincent et al., 1980, for review). Generally lower values mark the remainder of the latest Miocene and the early Pliocene, although there was a trend toward slightly higher values during the early Pliocene (5.2 to 4 Ma). The record from Site 588 suggests that the most important events in $\delta^{13}C$ occurred at ~22 to 21.6 Ma; 19.8 to 19 Ma; 15.4 to 14.2 Ma; and 6.2 Ma.

Site 590

Benthic Foraminiferal Oxygen Isotopes

Sedimentation at Site 590 was continuous except for an unconformity centered in the latest early Miocene between about 18 and 16.5 Ma. The early Miocene exhibits relatively low $\delta^{18}O$ values, with the lowest values for the entire Neogene probably dated between about 19 and 18 Ma. From the latest early Miocene (about 16.5 Ma) until about 13 Ma, $\delta^{18}O$ values increased irregularly by about 1‰.

During the remainder of the Miocene and early Pliocene, average values remained unchanged, although important oscillations occurred. These include an episode of lower values (warmer temperatures) centered at about 12.5 Ma followed rapidly by a brief interval of higher values centered at 12.2 Ma. An interval of high values is also centered at about 4.8 Ma in the earliest Pliocene.

Important positive shifts (~0.75‰) occurred during the Pliocene between about 3.5 Ma and 2.2 Ma; these changes are discussed in detail by Elmstrom and Kennett (this volume).

Planktonic Foraminiferal Oxygen Isotopes

The planktonic oxygen isotope record (Figs. 6 and 7) generally exhibits higher variability than the benthic record, especially during the early Miocene, latest Miocene, and Pliocene. The high variability in the early Miocene, between 20 and 18 Ma, of up to 1.3‰, is considered to have resulted from recrystallization of planktonic foraminiferal tests.

The early middle Miocene exhibits distinctly lower values (warmer isotopic temperatures) between 16 and 14.5 Ma. This was followed by the well-known $\delta^{18}O$ increase (of about 1‰), which continued in the $\delta^{18}O$ planktonic record at this site until about 12.4 Ma. Following this, no apparent long-term trends occurred during the latest middle and late Miocene in planktonic $\delta^{18}O$ until 6 Ma. At that time, a distinct positive shift occurred of about 0.5‰ (cooler temperatures). Average latest Miocene to Pliocene values are almost 0.5‰ higher than during the earlier part of the late Miocene. After 6 Ma, several distinct planktonic $\delta^{18}O$ oscillations occurred, including an increase between about 4.6 Ma and 3.7 Ma (0.5‰) and another increase beginning at 3 Ma and continuing to the Pleistocene (at least to 1.8 Ma). Intervals marked by lower values occurred between 5.4 and 5.2, between 4.8 and 4.6, and between 3.7 and 3 Ma. Detailed descriptions of these changes have been made by Elmstrom and Kennett (this volume).

Benthic and Planktonic Foraminiferal Carbon Isotopes

Distinct parallelism occurs between benthic and planktonic carbon isotope records (Figs. 6 and 7), including many of the short-term oscillations, although the amplitude of change often differs. Because of their similarity of change, the records are described as one. The earliest Miocene sequence (20.8 to 18 Ma), preceding the unconformity, exhibits relatively low $\delta^{13}C$ values. A major increase in $\delta^{13}C$ (~1.2‰) occurred during the latest early Miocene to early middle Miocene, with highest values centered at about 15 Ma. This is the most distinct carbon isotope episode of the Neogene. Following this broad early middle Miocene peak, there was a somewhat irregular decrease in $\delta^{13}C$ values, which reached particularly low values between about 11.5 and 10.5 Ma, close to the middle/late Miocene boundary. Values again increased toward a maximum in the middle late Miocene between about 9.5 and 8 Ma. In the latest Miocene at 6.2, a distinct, rapid, negative carbon isotope shift occurred that is synchronous with the Chron 6 carbon isotope shift. The carbon isotope change in the planktonic record (~0.9‰) is almost double that exhibited in the benthic record (~0.4‰). Relatively low $\delta^{13}C$ values mark the remainder of the late Neogene sequence. Following the Miocene/Pliocene boundary, at 5.2 Ma, a temporary increase in $\delta^{13}C$ occurred. This, in turn, was followed by a return to generally lower values typical of the middle and late Pliocene. Details of these changes are described in Elmstrom and Kennett (this volume).

Site 591

Benthic Foraminiferal Oxygen Isotopes

The stable isotope record at Site 591 extends from the late early Miocene (17 Ma) to the middle Pliocene (4 Ma) (Figs. 8–10). The benthic $\delta^{18}O$ record exhibits the lowest values (warmest isotopic temperatures) at about 17 Ma. From 17 Ma (latest early Miocene) to about 14.5 Ma, an irregular increase in $\delta^{18}O$ values of about 1.25‰ occurred, synchronous with the early middle Miocene shift observed in other sites. The time of maximum change occurred between ~16 and 15.2 Ma. Although

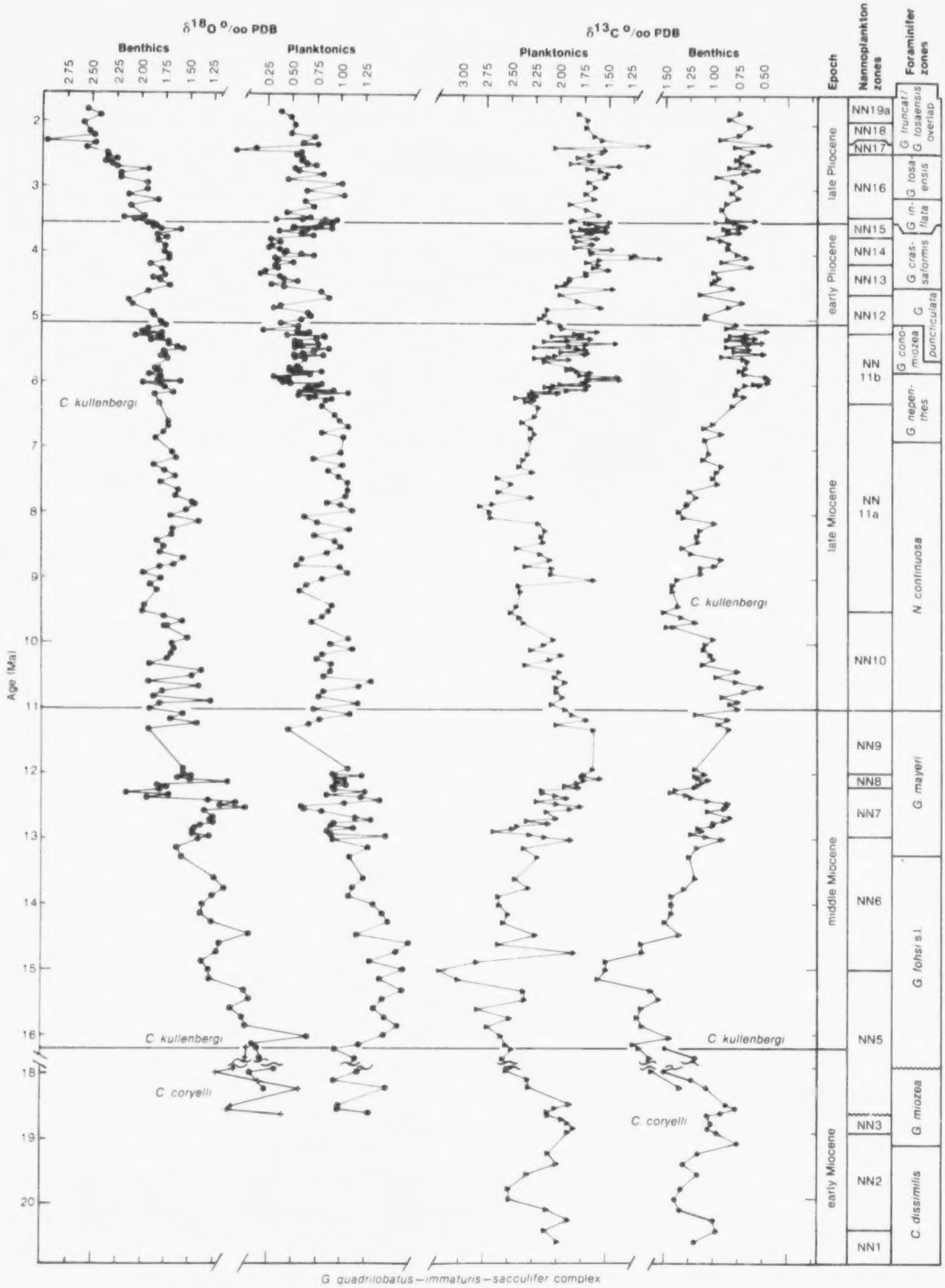

Figure 6. Benthic and planktonic $\delta^{18}O$ and $\delta^{13}C$ for Holes 590A and 590B plotted against age in Site 590 and biostratigraphic zonation for calcareous nannoplankton (Lohman, this volume) and planktonic foraminifers (Jenkins and Srinivasan, this volume). Note unconformity between 16.5 and 18 Ma.

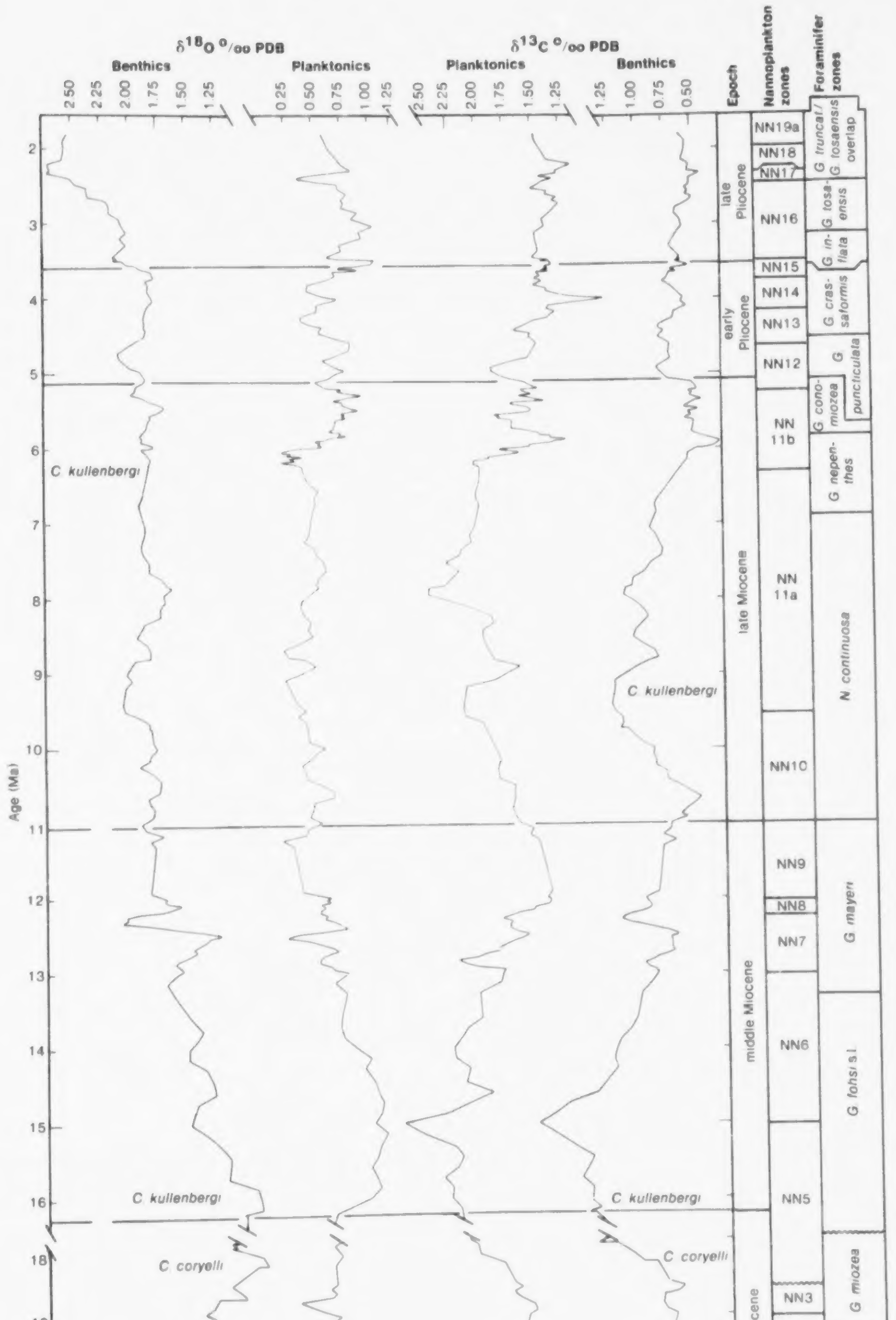

Figure 7. Smoothed benthic and planktonic $\delta^{18}O$ and $\delta^{13}C$ data (three-point running averages) for Holes 590A and 590B and biostratigraphic zonations for Site 590, plotted against age.

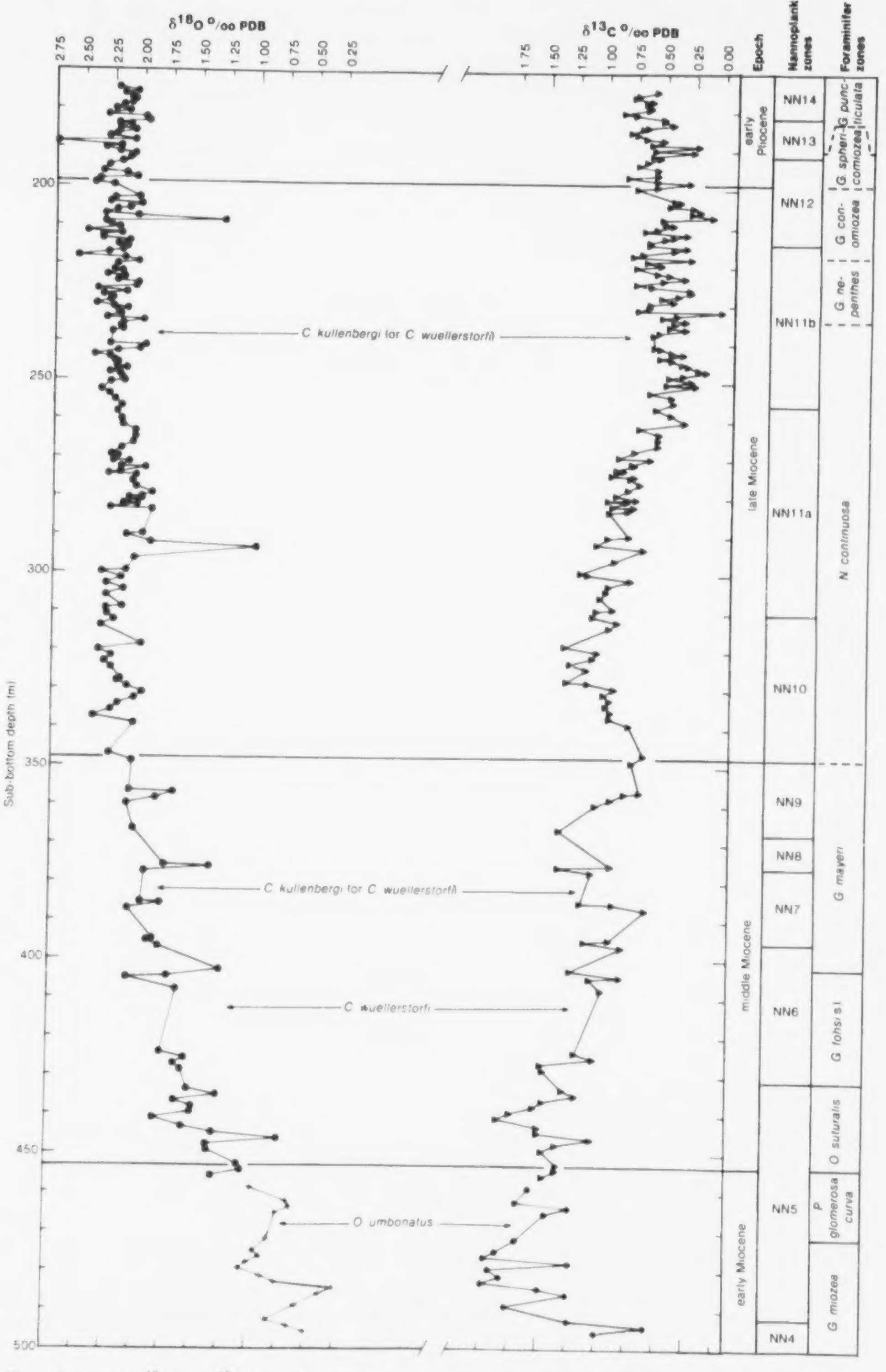

Figure 8. Benthic $\delta^{18}O$ and $\delta^{13}C$ for Holes 591 and 591B plotted against depth in Site 591 and biostratigraphic zonation for calcareous nannoplankton (Lohman, this volume) and planktonic foraminifers (Introduction, this volume). Stable isotope data for *Oridorsalis umbonatus* have been adjusted to that of *Cibicidoides* by adding +1.06‰ for $\delta^{13}C$ and subtracting 0.72 for $\delta^{18}O$ (see text for discussion).

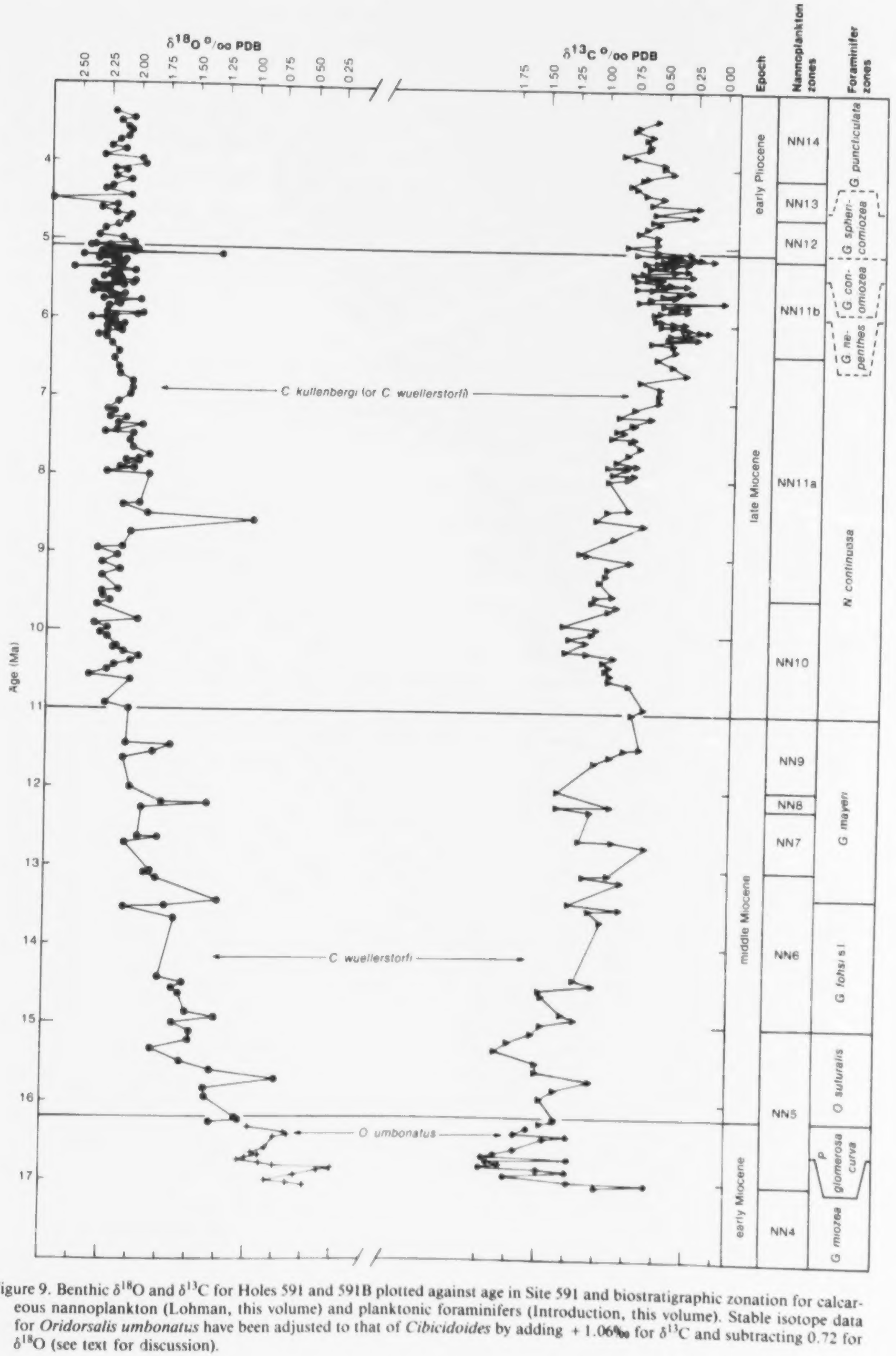

Figure 9. Benthic $\delta^{18}O$ and $\delta^{13}C$ for Holes 591 and 591B plotted against age in Site 591 and biostratigraphic zonation for calcareous nannoplankton (Lohman, this volume) and planktonic foraminifers (Introduction, this volume). Stable isotope data for *Oridorsalis umbonatus* have been adjusted to that of *Cibicidoides* by adding +1.06‰ for $\delta^{13}C$ and subtracting 0.72 for $\delta^{18}O$ (see text for discussion).

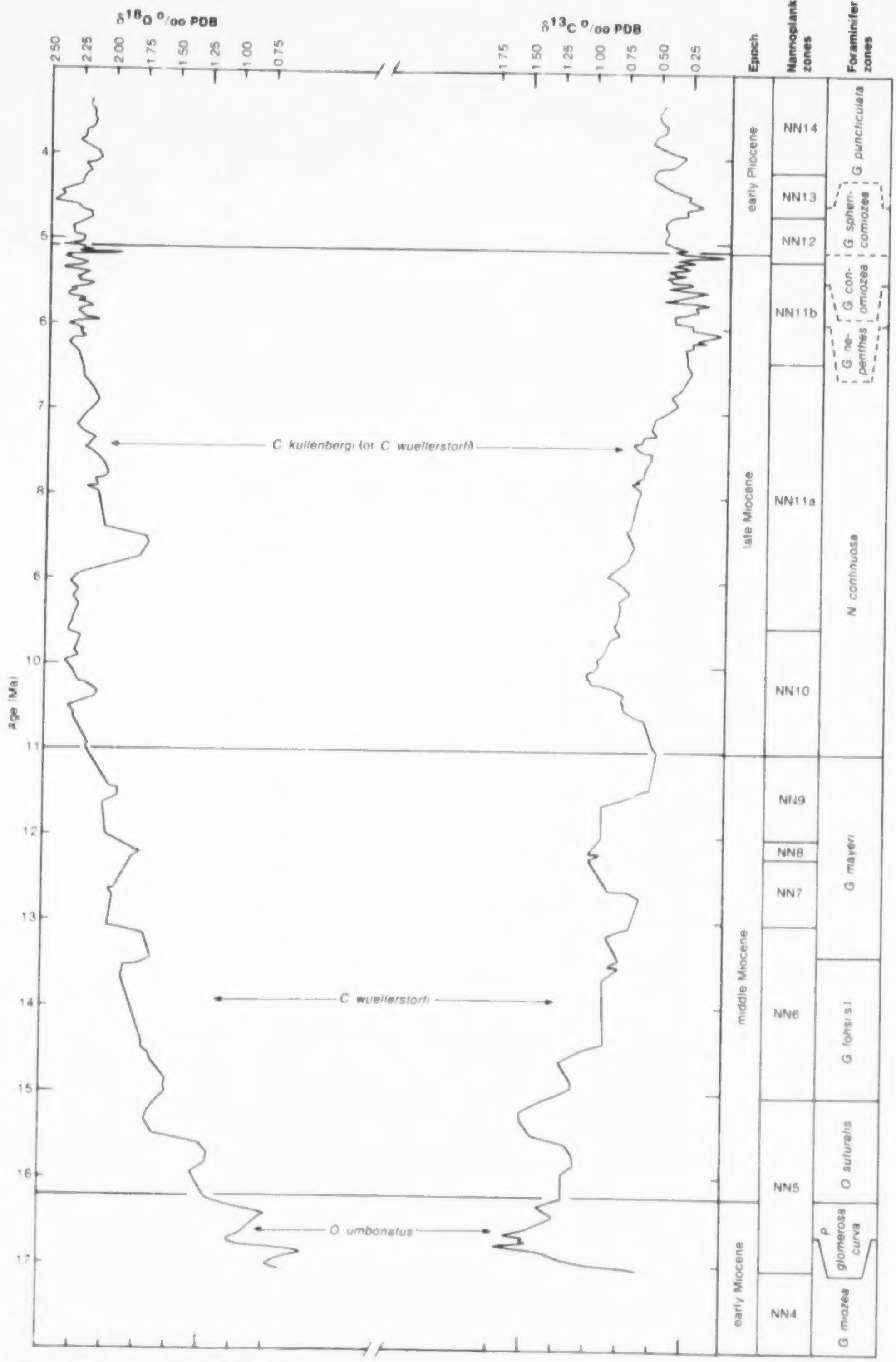

Figure 10. Smoothed benthic $\delta^{18}O$ and $\delta^{13}C$ data (three-point running averages) for Holes 591 and 591B and biostratigraphic zonations for Site 591, plotted against age.

stratigraphic resolution during the middle Miocene at this site is not high, some trends seem to be evident. From 14.5 to 11.5 Ma, the $\delta^{18}O$ values remained much the same or perhaps slightly increased, reaching a maximum close to the middle/late Miocene boundary at ~11.5 Ma. During the late Miocene and the Pliocene, there was relatively little change in $\delta^{18}O$ in this section.

Benthic Foraminiferal Carbon Isotopes

The benthic carbon isotope record at Site 591 (Figs. 8–10) is similar to that of Site 588 and exhibits considerable variability. As at Site 588, the most conspicuous feature of the record is the interval of increased $\delta^{13}C$ values during the late early to early middle Miocene (base of sequence at 17 Ma to 14.5 Ma). During the remainder of the Miocene the $\delta^{13}C$ values generally decreased, reaching a minimum between about 11.6 and 10.6 Ma, associated with the middle/late Miocene boundary. This was followed by a $\delta^{13}C$ maximum at 10.0 Ma and then gradually decreasing values in the late Miocene, culminating in a distinct shift toward low $\delta^{13}C$ values from about 7.5 to 6 Ma. However, unlike the record at the other two sites, this latest Miocene carbon isotope shift was more gradual, rather than sharply defined at 6.2 Ma. A gradual depletion in ^{13}C of 0.4‰ occurred between 7.5 and 6.2, with an additional shift of 0.5‰ centered at 6.2 Ma. During the early Pliocene between 5 and 4 Ma, average $\delta^{13}C$ values were about 0.25‰ higher than latest Miocene values.

DISCUSSION

Oxygen Isotopes

The oxygen isotope composition of calcite is controlled by both the oxygen isotope composition of ambient seawater and its temperature (Epstein et al., 1953). The isotopic composition of the oceans is strongly affected by changes in continental ice volume because ^{16}O is preferentially stored in such ice. An increase in continental ice volume causes an increase in $\delta^{18}O$ values of the ocean. A record of ice volume is provided by benthic foraminiferal oxygen isotope changes during intervals when the temperatures of ocean bottom waters remained constant. Planktonic foraminiferal $\delta^{18}O$ is controlled by local and global changes in the isotopic composition of the oceans and temperature of surface waters. It is difficult to differentiate the effects of temperature from those due to ice volume. The detailed relations provided here between benthic and planktonic $\delta^{18}O$ changes at different latitudes may help differentiate between changes that resulted from ice volume and those that resulted from temperature.

This chapter has no statistically based correlations between the isotope stratigraphies of the individual sites. Nevertheless, visual comparison of the curves shows that many events are easily recognizable in the three sequences. Intersite correlation of these isotopic events also reveals that the assigned ages of individual events, based upon correlations using the nannoplankton biostratigraphy, are not identical in each of the sequences. Individual peaks are often offset by 0.1 to 0.3 m.y. It is clear that intersite correlation could be enhanced by the combined use of $\delta^{13}C$ and $\delta^{18}O$ stratigraphy. More detailed composite isotopic curves will be established in the future by applying quantitative techniques of signal correlation to these and other existing records. In the meantime, visual comparisons of the isotope stratigraphy for the three sites are adequate for interpretation of paleoceanographic history. In the following sections, a synthesis is provided of this history.

Early Miocene

The earliest Miocene (oldest than 19.5 Ma) was marked by relatively high benthic $\delta^{18}O$ values, although the values were lower than those of the late Miocene. This indicates warmer intermediate water and less continental ice during the earliest Miocene than during the late Miocene. A slow, general warming of intermediate water occurred between 23 and 19.5 Ma, leading to the lowest $\delta^{18}O$ values for the entire Neogene between about 19.5 and 16.5 Ma (late early Miocene; late NN2 to middle NN5). This interval represents the optimum of Neogene warmth. Haq (1980) identified a particularly warm interval between 17 and 16 Ma based on mid- to high-latitude Atlantic calcareous nannoplankton biogeography. A minor, cool episode occurred within this warm period between 19 and 18 Ma.

Middle Miocene

The late early Miocene climatic optimum at 16.5 Ma immediately preceded the major middle Miocene episode of increasing $\delta^{18}O$ values, which I interpret to represent major, permanent accumulation of the East Antarctic ice sheet and cooling of bottom waters (Shackleton and Kennett, 1975b; Savin et al., 1975). Thus, sea-surface temperatures at high latitude were relatively warm immediately preceding the buildup of the Antarctic ice sheet, a necessary prerequisite according to Mercer and Suter (1982).

The early middle Miocene $\delta^{18}O$ increase began about 16.5 to 16 Ma, and continued until about 13.5 to 13.2 Ma; the total duration of this event was about 3 m.y. Barron et al. (in press) previously assigned an age of 15.0 to 13.5 Ma to this shift, which encompasses Zones N9 to lower N12. The maximum enrichment in ^{18}O during this event ranged between 1.25 and 1.50‰. This ^{18}O enrichment event has been globally recognized in marine sedimentary sections by Savin et al. (1975); Shackleton and Kennett (1975b), Keigwin (1979), Margolis et al. (1975), Loutit (1981), Loutit, Kennett, et al. (1983); Vincent and Berger (1985); Vincent et al. (in press); Savin et al. (1981), Woodruff et al. (1981), Savin et al. (in press), and many other workers. Haq (1980) identified a cooling trend in mid- to high-latitude Atlantic calcareous nannoplankton assemblages at 15 Ma that he correlated with this isotopic event.

The middle Miocene event has generally been accepted as representing permanent, major buildup of the East Antarctic ice sheet (Savin et al., 1975; Shackleton and Kennett, 1975b) and an associated decrease in bottom-water temperatures related to enhance polar glaciation (Savin et al., 1975). This interpretation was challenged by Matthews and Poore (1980), who suggested that all of the isotopic change was due to the decreasing temperature of intermediate and bottom waters. They attributed none of the isotopic shift to ice accumulation, since they believed that most of the Antarctic ice sheet had formed by at least the earliest Oligocene, and used as supporting evidence the major sea-level fall during the middle Oligocene (Vail and Hardenbol, 1979).

Tropical planktonic $\delta^{18}O$ values decrease, show no change, or exhibit an increase that is smaller in magnitude than the shift observed in high-latitude sequences. Savin et al. (1981, in press), Loutit, Kennett, et al. (1983) and others interpreted these observations as reflecting a warming of tropical sea-surface temperatures. Warming of tropical surface waters during the middle Miocene may have resulted from the progressive thermal isolation of Antarctica and the contraction of the tropical–warm subtropical gyres toward lower latitudes, as the polar and subpolar waters expanded toward the equator. A major question remains, however, as to how much of the $\delta^{18}O$ shift during the early middle Miocene was due to increased ice volume and how much to decreased temperature.

Comparison of planktonic and benthic $\delta^{18}O$ records at Site 590 (Figs. 6 and 7) may assist in separating these effects, although interpretations are not unequivocal. Site 590 is currently located at 31°S, in proximity to the Subtropical Divergence that separates the warm-subtropical and temperate water masses. During the early middle Miocene, this site was located in the present temperate latitudes of about 34°S (Sclater et al., in press). At Site 590, the shift toward higher benthic $\delta^{18}O$ values began at 16 Ma (Figs. 6 and 7) and continued until 13.2 Ma, with a total shift of about 1.25‰. In contrast, the planktonic $\delta^{18}O$ values actually decreased at 16 Ma by about 0.25‰ and remained low until 14.6 Ma. This indicates a distinct warming of surface waters during the early stage of glaciation. The data of Vincent et al. (in press) from the tropical Indian Ocean also exhibit surface-water warming during the first half of the middle Miocene benthic $\delta^{18}O$ increase. At Site 590, planktonic $\delta^{18}O$ values increased irregularly by about 0.65‰ between 14.6 and 13.2 Ma (Figs. 6 and 7). The magnitude of the planktonic $\delta^{18}O$ change was only half that exhibited by benthic $\delta^{18}O$. Based upon these observations, we suggest that the early stage of the middle Miocene $\delta^{18}O$ shift (between 16 and 14.6 Ma) resulted largely from high-latitude cooling, which was followed by a phase in which the benthic isotope record largely reflected ice growth between 14.6 and 13.2 Ma (or 13.6 Ma, as indicated in Site 588). The smaller magnitude of the increase in planktonic $\delta^{18}O$ than benthic $\delta^{18}O$ suggests that surface waters warmed at these sites near the northern edge of the temperate zone during the middle Miocene. Savin et al. (1975), Savin et al. (in press), and Loutit, Kennett, et al. (1983) suggested previously that sea-surface temperatures in the tropical Pacific warmed during the middle Miocene. Assuming an adjustment in ice volume of 0.5‰ and no major changes in the regional variation of the $^{18}O/^{16}O$ ratio of surface waters, then tropical Pacific surface waters typically warmed by 2 to 5°C during the middle Miocene (Savin et al., in press).

The middle Miocene benthic $\delta^{18}O$ shift exhibits numerous oscillations of up to 0.5‰, although these are smaller than the 1‰ changes reported at Site 289 in the western tropical Pacific (Woodruff et al., 1981), where sampling density was higher. A brief but well-defined episode of more positive $\delta^{18}O$ values is centered at 15 (Site 590) or 15.5 Ma (Sites 588 and 591), within the main $\delta^{18}O$ shift, and may be equivalent to the same episode dated at 15 Ma by Savin et al. (1981).

The isotopic data show two more episodes of especially cool surface and deep water close to the middle/late Miocene boundary. The earliest of these, between 12.5 and 11.5 Ma, seems to be equivalent to that dated by Savin et al. (1981) between 13.5 and 12.5 Ma. This event apparently correlates with the early part of paleomagnetic Chron 11 (~11.7 Ma) according to Burckle et al. (1982). Following a period of warming, a second decline of isotopic temperatures (not well defined in Site 590) occurred between 11 and 9 Ma (earliest late Miocene), but this event was dated by Savin et al. (1981) as occurring between 11.8 and 10.5 Ma. This event was correlated with the early part of paleomagnetic Chron 10 (11.4–11 Ma) by Burckle et al. (1982). Some of the highest $\delta^{18}O$ values (coldest isotopic temperatures) for the entire Miocene occur within this interval.

Late Miocene

The late Miocene was marked by large, but variable benthic $\delta^{18}O$ values reflecting a period of prolonged cool climates. Intermediate waters were coldest near the beginning (11 to 9 Ma) and the end of the late Miocene (~6.5 to 4.5 Ma).

During much of the middle late Miocene, between about 9 and 6.5 Ma, average $\delta^{18}O$ values were slightly lower, indicating a general period of relative climatic warmth (this is not observed at Site 590). Haq (1980) also noted warm climate conditions during the middle late Miocene, between 9 and 7 Ma, based upon Atlantic calcareous nannoplankton biogeography.

Further cooling occurred during the latest Miocene, beginning at about 6.2 Ma (shown as 5.5 Ma in Site 590), and continued until about 5 to 4.5 Ma. Similar high $\delta^{18}O$ values were reported by Shackleton and Kennett (1975a) from Site 284, and interpreted to represent a major expansion of the Antarctic ice sheet. This terminal Miocene event was marked by widespread cooling. Moderate to severe cooling of the ocean surface in middle to high latitudes is well documented over wide areas during the latest Miocene (Ingle, 1967, 1973; Keller, 1979; Kennett, 1967; Kennett and Vella, 1975; Loutit and Kennett, 1979; Bandy et al., 1971; Cita and Ryan, 1979; Poore, 1981; Haq, 1980). In Argentina, Patagonian glaciers extended beyond the Andean Mountain front, apparently for the first time, between about 7 and [illegible].2 Ma (Mercer and Sutter, 1982). In Sites 588 (Fig. 3) and 591 (Fig. 9), a number of brief intervals of high $\delta^{18}O$ values between 5.4 and 4.9 Ma are interpreted to represent further increases in Antarctic ice volume (Hodell, Elmstrom, and Kennett, unpublished data). The terminal Miocene event was also marked by marine regression (Kennett, 1967; Adams et al., 1977), growth of the West Antarctic ice sheet (Ciesielski et al., 1982), intensification of oceanic circulation (Brewster, 1980; Savin et al., in press), high sediment accumulation rates (Davies et al., 1977), and the Messinian Salinity Crisis (Hsü et al., 1973; Cita, 1976). The late Miocene was also the time of the distinct latest Miocene carbon isotope shift (Keigwin, 1979).

During the late Miocene until 6.2 Ma, planktonic $\delta^{18}O$ values exhibited large, rapid oscillations about an unchanging average (Figs. 6 and 7). At 6.2 Ma, a marked increase in $\delta^{18}O$ of about 0.5‰ coincided exactly with the late Miocene Chron 6 carbon shift. This represents significant and rapid cooling of surface waters. In Site 588, the carbon shift also coincided with a shift toward higher benthic $\delta^{18}O$ values.

Pliocene

During the early Pliocene, benthic $\delta^{18}O$ values oscillated about an average similar to that of the latest Miocene. At about 3.4 Ma, a 0.4‰ increase (Elmstrom and Kennett, this volume) is documented in the benthic $\delta^{18}O$ record of Site 590 (Figs. 6 and 7). An oxygen isotope shift similar to this has been reported from the equatorial Pacific (Shackleton and Opdyke, 1977; Keigwin, 1979; Prell, 1984), the South Atlantic (Weissert et al., 1984), the North Atlantic (Shackleton and Cita, 1979), and the Mediterranean (Keigwin and Thunell, 1980). This shift almost certainly documents a cooling of intermediate waters (Prell, 1984), but possibly also some additional growth of Antarctic ice (Weissert et al., 1984). Increased glaciation of Antarctica at about 3.5 Ma created a northward shift in the deposition of circum-Antarctic glacial marine sediments (Ciesielski and Weaver, 1974). A glacial increase at about 3.5 Ma is also consistent with the observation by Keany (1978) of cooling of the Southern Ocean at 3.6 Ma, with cooling in temperate areas (Kennett and Vella, 1975; Kennett et al., 1979), and with increased Patagonian glaciation (Mercer, 1976). Significant sediment ice-rafting in the North Atlantic did not seem to occur until 2.5 Ma. Evidence of ice-rafted material prior to 2.4 Ma is negligible and may be due to glaciation unrelated to major Northern Hemisphere ice sheets (Backman, 1979; Shackleton et al., 1984).

The planktonic $\delta^{18}O$ record during the Pliocene is distinctly different from the benthic $\delta^{18}O$ record. First, the planktonic isotopic record is more variable, reflecting rapidly changing surface-water conditions. Secondly, planktonic and benthic records are not parallel. Higher planktonic $\delta^{18}O$ values, reflecting cooler surface waters, occurred between 4.6 and 3.6 Ma. In contrast, benthic $\delta^{18}O$ values show no such trend during this interval. The transition from warm early Pliocene to cooler middle Pliocene intermediate waters is not reflected in the planktonic $\delta^{18}O$ record from Site 590. From 3.4 to 2.2 Ma, the average $\delta^{18}O$ values in the planktonic record were lower (Fig. 6), whereas benthic $\delta^{18}O$ values were increasing. Weissert et al. (1984) also noted this for sequences at similar latitudes (~ 30°S) in the South Atlantic. I concur with their interpretation that surface waters warmed by at least 2°C at these southern latitudes, when high-latitude glaciers were growing and bottom waters were cooling. Between 3.6 and 2.2 Ma at Site 590, a positive shift of 0.4‰ in benthic $\delta^{18}O$ generally coincided with a negative shift of about 0.4‰ in planktonic $\delta^{18}O$. Surface waters could have warmed by as much as 3°C if it is assumed that the oxygen isotope composition of ocean waters increased by 0.4‰ because of ice-volume accumulation. However, since the $\delta^{18}O$ change in benthics was almost certainly caused, in part, by cooling of intermediate waters, the increase in surface waters would have probably been closer to 2°C. Surface waters seem to have warmed over wide latitudinal areas extending from equatorial regions (Vergnaud Grazzini, 1980) to the warm subtropics (Weissert et al., 1984) between 3.4 and 2.2 Ma.

A further increase of about 0.4‰ in benthic $\delta^{18}O$ occurred in the late Pliocene between 2.6 and 2.4 Ma. This isotopic shift heralds the beginning of Northern Hemisphere ice accumulation, as discussed previously (Backman, 1979; Prell, 1984; Shackleton et al., 1984).

The late Pliocene oxygen isotope trends are somewhat comparable to those that occurred during the early middle Miocene between 16 and 14 Ma; that is, they indicate a warming of surface waters at these middle latitudes at times of major ice accumulation at high latitudes.

It is perhaps significant that the transitions between the early and middle Miocene, the middle and late Miocene, the Miocene and Pliocene, and the preglacial and postglacial Pliocene were all marked by episodes of distinct climatic cooling. These stratigraphic boundaries were initially recognized in the classic, shallow-marine sequences exposed on land, on the basis of changes in lithofacies and shallow-water fossils, all susceptible to sea-level change (Loutit and Kennett, 1981) and large-scale climatic change.

Water Column Thermal Gradients

The difference between benthic and planktonic $\delta^{18}O$ values in the same samples ($\Delta^{18}O$ benthics − planktonics) is a measure of the temperature difference between surface and bottom waters, or the vertical temperature gradient. For Site 590 (Figs. 11 and 12), the average vertical $\delta^{18}O$ gradient changed from about 1.75 during the early Miocene to about 2.25 during the middle and late Miocene and for much of the early Pliocene (a shift of 0.5‰). This is equivalent to about a 2°C increase in the vertical temperature gradient between 1300 m and the ocean surface (assuming no salinity change occurred in surface waters). This increase in the southwest Pacific vertical temperature gradient occurred between 16 and 15 Ma, during the early middle Miocene (Fig. 12). During the intervals before and after this shift, the average thermal gradient did not change significantly, although there were large temporary oscillations, such as between 13 and 12 Ma. These results concur with those of Loutit, Kennett, et al. (1983), who suggested that much of the change that occurred in the thermal gradient in the Miocene occurred during the middle Miocene.

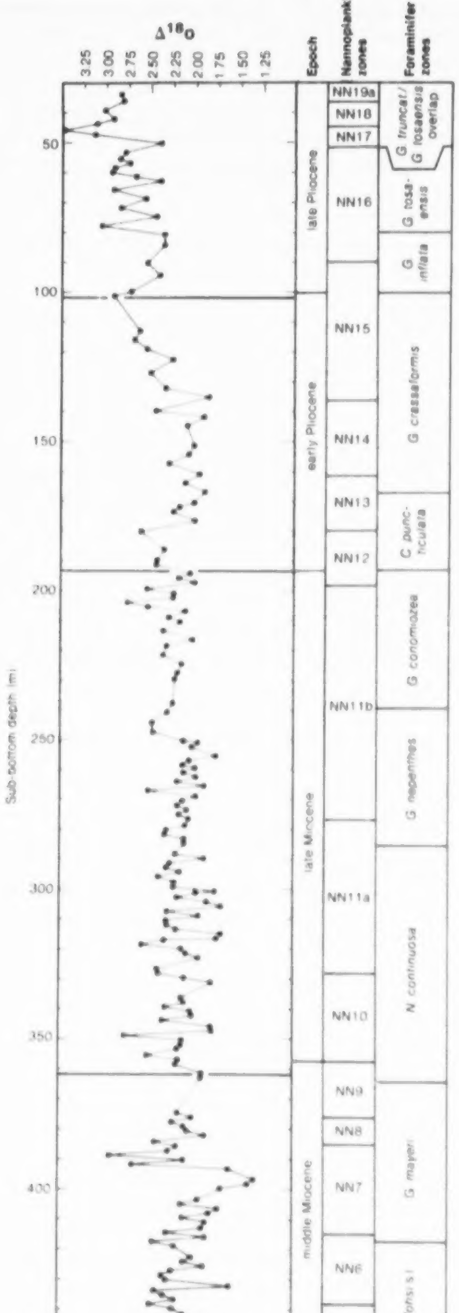

Figure 11. δ18O benthics − planktonics (= Δ18O) for Holes 590A and 590B plotted against depth for Site 590 and biostratigraphic zonations (see caption for Fig. 5). Δ18O represents the δ18O gradient between bottom waters (water depth = 1300 m) and the ocean surface at Site 590.

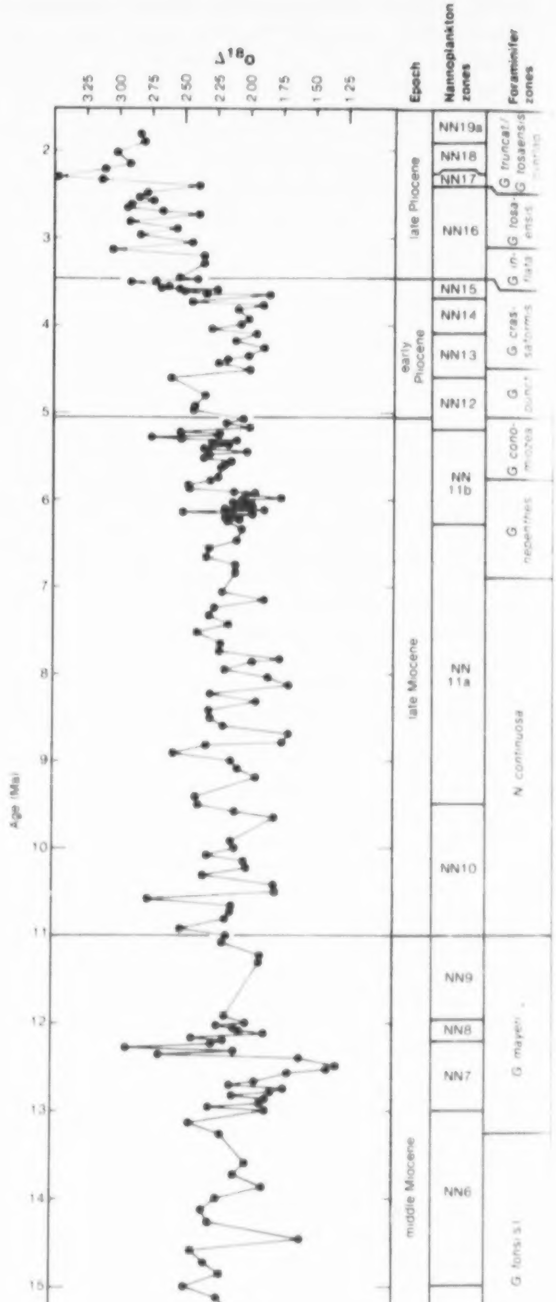

Figure 12. δ18O benthics − planktonics (= Δ18O) for Holes 590A ar 590B plotted against age for Site 590 and biostratigraphic zon tions (see caption for Fig. 5). Δ18O represents the δ18O gradient b tween bottom waters (water depth = 1300 m) and the ocean su face at Site 590. Note unconformity between 16.5 and 18 Ma.

Further distinct changes in the vertical temperature gradient occurred during the middle Pliocene at 3.6 Ma, with the average thermal gradient increasing by another 0.5‰ (~2°C), and during the late Pliocene at 2.4 Ma, with a further shift of 0.25 to 0.5‰ (~1-2°C).

The records therefore document three permanent, rapid shifts in the vertical temperature gradient of the Neogene: (1) between 16 and 15 Ma during the time of major accumulation of the large, permanent East Antarctic ice sheet; (2) at ~3.5 Ma during a time of further increased polar glaciation especially in the Antarctic; and (3) at ~2.4 Ma when Northern Hemisphere ice sheets began to form. There was little change in the average gradient between these three Neogene episodes. The vertical temperature gradient of the open ocean during the Neogene changed permanently only during times of large-scale polar glacial development. As in middle latitudes of the South Atlantic (Hsü et al., 1984), middle-latitude South Pacific locations also record an increase in the vertical temperature gradient during the Neogene.

CARBON ISOTOPES

Work on Leg 90 sites revealed two major characteristics of carbon isotope stratigraphy. First, considerable similarity exists among the $\delta^{13}C$ stratigraphies of all three sites and with those of other regions, especially with respect to the longer-term oscillations (Figs. 3, 6, and 9). Second, the planktonic and benthic $\delta^{13}C$ changes are almost completely parallel, as shown in Site 590 (Fig. 6). This parallelism indicates that both surface and bottom waters are equally affected by changes in $\delta^{13}C$ of oceanic HCO_3^-, although average planktonic $\delta^{13}C$ values are always about 1.25‰ higher than benthic $\delta^{13}C$. The similarity of $\delta^{13}C$ stratigraphies in the Neogene between different sites throughout the ocean basins has been recognized previously (Douglas and Savin, 1973; Loutit, Pisias, et al., 1983; Woodruff and Savin, 1985; Vincent and Berger, 1985). Shackleton and Kennett (1975b) noted a strong parallelism between South Pacific benthic and planktonic $\delta^{13}C$ records during the middle and late Cenozoic, as did Hsü et al. (1984) for the South Atlantic, Barrera et al. (in press) for the northeast Pacific, Vincent et al. (in press) for the tropical Indian Ocean, and Keigwin et al. (in press) for the North Atlantic. The similarity of the $\delta^{13}C$ time-series records within and between ocean basins and between surface and bottom waters clearly indicates that oceanwide changes in average $\delta^{13}C$ of HCO_3^- in seawater, rather than local effects, dominated the records.

A major question concerns the origin of the changes in the benthic and planktonic $\delta^{13}C$ records. Proposed causes of $\delta^{13}C$ change through time include changes in sea level, continental hypsometry, continental biomass, vital effects, and oceanic circulation (Shackleton, 1977; Bender and Keigwin, 1979; Broecker, 1982; Loutit, Pisias, et al., 1983; Vincent et al., in press). Summarizing, Berger (1982) noted that the average oceanic $\delta^{13}C$ composition will change as a result of several processes: the accumulation or release of organic carbon from temporary reservoirs on the continents and in the ocean basins; changes in forest biomass; changes in ocean stratification and fertility; and changes in deep circulation and oxygenation. Oceanic $\delta^{13}C$ values can be changed most rapidly by changing the flux of carbon from major carbon reservoirs: terrigenous carbon having $\delta^{13}C$ values of about −25‰ and marine carbon near −20‰ (Craig, 1953; Sackett, 1964; Wedepohl, 1969). Broecker (1971) suggested that transgressions and regressions across the continental shelf could produce significant changes in open-ocean $\delta^{13}C$ values. During transgressions, the shelves act as sinks for organic carbon. Conversely, during regressions, eroded sediment containing organic material depleted in ^{13}C is supplied to the oceans.

My preferred interpretation of the Neogene $\delta^{13}C$ changes is that they were largely caused by average oceanic compositional changes resulting from fractionation between continental and oceanic organic carbon reservoirs. What caused this fractionation? Loutit, Pisias, et al. (1983) and Woodruff and Savin (1985) have shown that a correlation exists between changes in Neogene carbon isotopic stratigraphy and sea level as inferred from the onlap/offlap curve of Vail and Hardenbol (1979). During marine transgressions, organic carbon accumulated on the continental shelves, and ocean waters became more enriched in ^{13}C by the extraction of organic carbon (enriched in ^{12}C). Conversely, during marine regression, organic carbon was delivered to the ocean basins and thus the oceans became more depleted in ^{13}C. The transgressions and regressions were probably of large magnitude to account for the large changes in oceanic $\delta^{13}C$ values and were controlled by fluctuations in sea level. The magnitude of the $\delta^{13}C$ change depended upon the areas of shallow shelves covered or exposed by a given change in sea level. This, in turn, is directly related to the hypsometry of the continental margins and the magnitude of the sea-level change. A marine transgression that covered wide continental shelves provided a larger area for accumulation of organic carbon, and hence a larger increase in oceanic $\delta^{13}C$ values.

Paleoclimatic change reinforced the $\delta^{13}C$ changes. Global warming probably enhanced the accumulation of organic carbon in the continental reservoir by expansion of the biosphere through greater supply of moisture. Conversely, cooling led to greater aridity and reduction in size of the continental biosphere (Berger, 1982).

Superimposed upon the average $\delta^{13}C$ of the oceans are a number of regional and local effects that have created gradients from region to region and with water depth. For example, Kroopnick (1974, 1980, 1985) documented the fact that different water masses have different $\delta^{13}C$ signatures depending upon source and addition of metabolic CO_2 along the flow path. The mechanisms that controlled this variation in the past are less well understood, but include local and regional differences in biological productivity of surface waters, changes in deep-water circulation patterns, changes in the $\delta^{13}C$ of HCO_3^- in the source regions of bottom-water formation, and the amount of organic carbon that has been oxidized to form ^{12}C-enriched HCO_3^- in deep waters following its formation at high latitudes (Loutit, Pisias, et al., 1983).

Early Neogene Carbon Isotope Excursion

The dominant feature of Neogene carbon isotope stratigraphy is the broad late early to early middle Miocene maximum of about 1‰ which Vincent et al. (in press) and Vincent and Berger (1985) have termed the "Monterey Carbon Isotope Excursion." This excursion is best exhibited at Site 588 (at Site 590, part of the excursion is missing because of the hiatus), where it began as a shift toward increased $\delta^{13}C$ values at about 19.5 Ma (within Zone NN2). The excursion consists of broad peaks centered at 19 Ma, 16.5 Ma, and about 15 to 15.5 Ma. As shown in Sites 588 and 590, the decline from the high values began within the middle Miocene between 15 and 14 Ma and continued with little interruption until 13 Ma. This negative shift began about midway through the distinct, early middle Miocene increase in benthic $\delta^{18}O$ values, and is contemporaneous with the trend toward more positive planktonic $\delta^{18}O$ values (Figs. 3 and 6).

As several previous workers have proposed, I concur that the origin of this carbon isotopic excursion was due to global marine transgression (Loutit, Pisias, et al., 1983; Vincent et al., in press; Woodruff and Savin, 1985). According to Vincent et al. (in press) and Vincent and Berger (1985) widespread transgression during this excursion occurred throughout the circum-Pacific region and created major sinks for organic carbon. Organic and phosphate-rich deposits accumulated within the Monterey Formation of California and other contemporaneous deposits throughout the Pacific margin. Vail and Hardenbol (1979) documented a period of coastal onlap that began at about 19 Ma and terminated about 14 Ma, and was contemporaneous with the interval containing the especially positive $\delta^{13}C$ values (Figs. 3, 6, and 9).

This excursion also corresponded to the maximum ocean temperatures of the Neogene as reflected in benthic and planktonic $\delta^{18}O$ values. Because the late early Miocene was the time of optimum climatic warming during the Neogene, tropical forests were probably widespread and the continental organic biosphere would have been more extensive than at other times. The high continental biomass at this time would have contributed to the positive $\delta^{13}C$ values during this interval. Global cooling during the middle Miocene probably led to greater aridity and reduction of the terrestrial biomass, resulting in a lowering of oceanic $\delta^{13}C$ values during the middle Miocene.

At Site 590, the warming of surface waters during the early stage of the benthic $\delta^{18}O$ shift suggests that the early part of that shift may have resulted largely from decreasing temperatures at high latitudes rather than from increasing ice accumulation. If little ice had accumulated at that point, then glacioeustatic regression would not have occurred. The $\delta^{13}C$ (benthic and planktonic) began to decrease, suggesting regression, at about 14.5 Ma, when the $\delta^{18}O$ shift occurred in both the benthic and planktonic records. It is possible that this synchronous enrichment in both planktonic and benthic $\delta^{18}O$ represents the major ice-growth phase of East Antarctica. If this scenario is correct, then major ice accumulation and resulting regression occurred between 14.5 Ma and 13 Ma.

Following the carbon isotope excursion, during the latest middle Miocene, further changes in $\delta^{13}C$ occurred, including a trend toward lower values that was centered in the earliest late Miocene at 11 Ma. A return to markedly increased benthic $\delta^{13}C$ values occurred during the middle part of the late Miocene, especially between 10 and 7 Ma.

Latest Miocene Carbon Isotope Shift

The latest Miocene at 6.2 Ma is marked by a distinct, rapid $\delta^{13}C$ shift of up to −0.75‰ in all of the southwest Pacific sites, both in the benthic and planktonic records. This depletion in ^{13}C was followed by markedly low values during much of the remainder of the late Neogene, which lead to the suggestion that it was "permanent" (Keigwin, 1979). This well-known late Miocene carbon isotope shift is recorded throughout the Indo-Pacific and South Atlantic (Keigwin, 1979; Bender and Keigwin, 1979; Loutit and Kennett, 1979; Keigwin and Shackleton, 1980; Vincent et al., 1980; Haq et al., 1980; Hodell and Kennett, 1984). This shift, which seems to have occurred within a period of not much more than 100,000 yr. (Vincent et al., 1980), was assigned an age of ~6 Ma by Haq et al. (1980) and of 6.2 Ma by Loutit and Kennett (1979), and was recently estimated at 6.4 Ma (Barron et al., in press). The magnitude of the shift throughout the Indo-Pacific region is generally reported to be about −1‰ (Haq et al., 1980); in the South Atlantic a shift of 0.7‰ has been estimated by Hodell, Elmstrom, and Kennett (unpublished data). Numerous climatic and oceanographic events closely associated with the carbon shift have been summarized by Loutit and Keigwin (1982) (for additional references see therein) and include the following: lowering of sea level; cooling of high- and middle-latitude surface waters; isolation and dessication of the Mediterranean Basin; increase in bottom-water circulation and fertility of the oceans: increase in biogenic siliceous deposits in the Southern Ocean; decrease of biogenic siliceous sedimentation rates in the eastern equatorial Pacific; shoaling of the Isthmus of Panama; a change, in the North Atlantic, from a calcite compensation depth (CCD) shallower than that in the Pacific to one deeper than the Pacific CCD; and an increase in deep-sea sedimentation rates. During the latest Miocene, the CCD experienced a sharp fall of at least several hundred meters (van Andel et al., 1977), or even up to 1 km in the South Atlantic (Hsü et al., 1984).

Numerous hypotheses have been proposed for the cause of the carbon isotope shift, including a change in the rate of organic carbon buried in the oceans and in the rate of upwelling and ocean fertility (Bender and Keigwin, 1979). The carbon shift is believed by some to have been caused by an increase in the flux of organic matter from coastal lowlands and continental shelves exposed by regression (Loutit and Keigwin, 1982; Vincent et al., 1980; Loutit, Pisias, et al., 1983), reinforced by increased oceanic fertility (Vincent et al., 1980). The close temporal association of the carbon shift with global regression (Kennett, 1967; Adams et al., 1977; Vail and Hardenbol, 1979), which is inferred to have resulted from glacioeustatic lowering of sea level (Kennett, 1967; Loutit and Kennett, 1979; Mercer and Sutter, 1982) in the latest Miocene, makes this theory very compelling. Estimates of the magnitude of the marine regression are similar, ranging from 40 to 80 m (Loutit and Kennett, 1979; Berggren and Haq, 1976; Cita and Ryan, 1979).

The drop in the CCD throughout the oceans has an origin similar to that of the carbon isotope shift, having resulted from an increase in the fractionation of carbonate and organic carbon entering the deep basins from the continental shelves during the latest Miocene regression (Berger, 1970; Ciesielski et al., 1982). This sea-level fall was also sufficient to isolate the Mediterranean and initiate the "Messinian Salinity Crisis" (Cita, 1982) between about 5.7 and 5.2 Ma. Previous work has indicated that the sea-level fall was largely glacioeustatic because of the rapidity of the fall and its association with surface-water cooling at middle and high latitudes (Kennett, 1967; Kennett and Watkins, 1974; Loutit and Kennett, 1979; Loutit, 1981) and with a period of relatively high δ^{18}O values (Shackleton and Kennett, 1975a; Kennett et al., 1979; Loutit and Kennett, 1979; Ciesielski et al., 1982; McKenzie et al., 1984).

Early Pliocene Events

During the Pliocene (as shown by Site 590), average benthic δ^{13}C values were lower by about 0.25‰, planktonic δ^{13}C by about 0.75‰, than during the Miocene preceding the carbon shift. An interval of relatively increased values occurred in the early Pliocene, between about 5 and 4 Ma. This interval corresponds with a period of relative global warmth (Kennett, 1967; Loutit and Kennett, 1979; Ingle, 1967; McKenzie et al., 1984); global marine transgression (Kennett, 1967; Kennett and Watkins, 1974; Vail and Hardenbol, 1979); relatively low δ^{18}O values in benthic foraminifers as shown at Site 590 and in records elsewhere (McKenzie et al., 1984; Hodell, Elmstrom, and Kennett, unpublished data), reflecting a decrease in global ice volume; and a marine transgression in the Mediterranean with restoration of pelagic sedimentation. I suggest that the early Pliocene interval of high δ^{13}C values resulted from marine transgression. Details for this interval are provided in Elmstrom and Kennett (this volume).

CONCLUSIONS

1. A high-resolution study of benthic and planktonic oxygen and carbon isotope stratigraphy was conducted for the Miocene to early Pliocene in high-quality DSDP Sites 588, 590, and 591, from the southwest Pacific (warm-subtropical to transitional latitudes). Sample resolution for much of the Miocene is between 25,000 and 50,000 yr. and for the Pliocene between 5,000 and 15,000 yr.

2. The climax of Neogene warmth, marked by the lowest δ^{18}O values of the Neogene, occurred during the late early Miocene, between ~19.5 and 16.5 Ma.

3. This climatic warming was immediately followed by a major increase in δ^{18}O values between ~16.5 and 13.5 Ma. This event is interpreted as representing major, permanent accumulation of the East Antarctic ice sheet and cooling of bottom waters; it lasted 3 m.y. Surface waters at these middle latitudes warmed during the first half of the ice volume increase, but cooled at higher latitudes.

4. The late Miocene began, in the earliest part (11 to 9 Ma), with a distinct climatic cooling that is chronicled by the highest δ^{18}O for the Miocene. This was followed by relative warmth during the middle part of the late Miocene, between ~9 and 6.5 Ma.

5. The latest Miocene and early Pliocene (6.2 to 4.5 Ma) were marked by increased δ^{18}O values, indicating increased cooling and glacial development in the Southern Hemisphere.

6. During the middle Pliocene at about 3.4 Ma, a 0.4‰ increase in benthic δ^{18}O documents a net change in average global ice volume and cooling of bottom waters. During this increase in Southern Hemisphere glaciation, surface waters warmed by 2-3°C in middle-latitude regions of the Southern Hemisphere.

7. During the late Pliocene between 2.6 and 2.4, a further increase in benthic δ^{18}O heralded the development of large ice sheets on the Northern Hemisphere.

8. Surface-water warming in the middle latitudes occurred in association with major high-latitude glacial increases in the early middle Miocene (16-14 Ma), middle Pliocene (~3.5 Ma), and late Pliocene (~2.4 Ma). These intervals were also marked by increases in the vertical temperature gradient in the open ocean. At intervening times, the gradient remained unchanged.

9. Transitions between the early and middle Miocene, the middle and late Miocene, the Miocene and Pliocene, and the "preglacial" and "postglacial" Pliocene were marked by distinct episodes of climatic cooling.

10. A high similarity of the δ^{13}C time-series records within and between ocean basins and between surface and bottom waters clearly indicates that ocean wide changes in the average δ^{13}C of HCO_3^- in seawater dominated the records, rather than local effects. Broad changes in the Neogene δ^{13}C record were caused largely by transfers of organic carbon between continental and oceanic reservoirs. These transfers resulted from marine regressions and transgressions on the continental margins. During transgressions, organic carbon, which has low δ^{13}C values, accumulated on the continental shelves, and ocean waters thus increased in δ^{13}C. Conversely, during marine regressions, organic carbon was delivered to the ocean basins and the oceans became lower in δ^{13}C. Paleoclimatic changes reinforced these δ^{13}C changes by influencing the size of continental biomass.

11. The dominant feature of Neogene δ^{13}C stratigraphy is a broad maximum of about 1‰ between ~19 and 14.5 Ma. This excursion occurred contemporaneously with a period of maximum coastal onlap (transgression) and maximum Neogene climatic warmth. The excursion terminated during the expansion of the Antarctic ice sheet and associated marine regression in the early middle Miocene (15.5-14.5 Ma).

12. The latest Miocene carbon isotope shift (of up to −0.75‰) at 6.2 Ma is clearly recorded in the sites examined, and was followed by generally low δ^{13}C values dur-

ing the remainder of the Neogene. This shift may have been caused by an increase in the flux of organic matter from continental marginal areas exposed by regression, which was, in turn, triggered by glacioeustatic lowering of the sea level.

13. An increase in $\delta^{13}C$ values during the early Pliocene (~5 to 4 Ma) resulted from marine transgression during a time of global warmth.

ACKNOWLEDGMENTS

I wish to thank J. Orchardo for his meticulous care in producing the stable isotope data. Valuable conversations about this work with D. Hodell and N. Shackleton are appreciated. I thank D. Hodell for his most valuable constructive criticism of the manuscript, which was typed by N. Meader. The manuscript also benefited from constructive reviews by L. Keigwin, S. Savin, T. Loutit, and N. Shackleton. Thanks are also due to R. Ross, K. Nelson, and R. Rice for picking foraminifers for the analyses and to K. Nelson for producing the data plots and for general assistance. J. Peck also lent useful general assistance.

This research was supported by the U.S. National Science Foundation Grant No. OCE82-14937 (Submarine Geology and Geophysics).

REFERENCES

Adams, C. G., Benson, R. H., Kidd, R. B., Ryan, W. B. F., and Wright, R. C., 1977. The Messinian salinity crisis and evidence of late Miocene eustatic changes in the world ocean. *Nature*, 269: 383-386.

Backman, J., 1979. Pliocene biostratigraphy of DSDP Sites 111 and 116 from the North Atlantic Ocean and the age of Northern Hemisphere glaciation. *Stockholm Contrib. Geol.*, 32(3):115-135.

Bandy, O. L., Casey, R. E., and Wright, R. C., 1971. *Late Neogene Planktonic Zonation, Magnetic Reversals, and Radiometric Dates, Antarctic to the Tropics*. Am. Geophys. Un. Antarctic Ser., 15.

Barrera, E., Keller, G., and Savin, S. M., in press. Evolution of the Miocene Ocean in the eastern North Pacific as inferred from oxygen and carbon isotopic ratios of foraminifera. *In* Kennett, J. P. (Ed.), *The Miocene Ocean: Paleoceanography and Biogeography*. Geol. Soc. Am. Mem., 163.

Barron, J. A., Keller, G., and Dunn, D. A., in press. A multiple microfossil biochronology for the Miocene. *In* Kennett, J. P. (Ed.), *The Miocene Ocean: Paleoceanography and Biogeography*. Geol. Soc. Am. Mem., 163.

Bender, M. L., and Keigwin, L. D., Jr., 1979. Speculations about the upper Miocene change in abyssal Pacific dissolved bicarbonate $\delta^{13}C$. *Earth Planet. Sci. Lett.*, 45:383-393.

Berger, W. H., 1970. Planktonic Foraminifera in selective solution and the lysocline. *Mar. Geol.*, 8:111-183.

________, 1982. Deep-sea stratigraphy: Cenozoic climate steps and the search for chemo-climatic feedback. *In* Einsele, G., and Seilacher, A. (Eds.), *Cyclic and Event Stratification:* Berlin (Springer-Verlag), pp. 121-157.

Berger, W. H., Killingley, J. S., and Vincent, E., 1978. Stable isotopes in deep-sea carbonates: Box Core ERDC-92, West Equatorial Pacific. *Oceanol. Acta*, 1:203-216.

Berggren, W. A., 1981. Correlation of Atlantic, Mediterranean and Indo-Pacific Neogene stratigraphies: geochronology and chronostratigraphy. *Proc., IGCP-114 Int. Workshop Pacific Neogene Biostratigraphy*, Nov. 25-29, 1981, Osaka, Japan, pp. 29-60.

Berggren, W. A., and Haq, B. U., 1976. The Andalusian Stage (late Miocene): biostratigraphy, biochronology, and paleoecology. *Palaeogeogr., Palaeoclimatol., Palaeoecol.*, 20:67-129.

Berggren, W. A., Kent, D. V., and Flynn, J. J., 1985. Paleogene geochronology and chronostratigraphy. *In* Snelling, N. J. (Ed.), *Geochronology and the Geological Record*. Geol. Soc. London, Spec. Pap.

Berggren, W. A., Kent, D. V., and Van Couvering, J. A., 1985. Neogene geochronology and chronostratigraphy. *In* Snelling, N. J. (Ed.), *Geochronology and the Geologic Time Scale*. Geol. Soc. London, Spec. Pap.

Brewster, N. A., 1980. Cenozoic biogenic silica sedimentation in the Antarctic Ocean, based on two Deep Sea Drilling Project sites. *Geol. Soc. Am. Bull.*, 91:337-347.

Broecker, W. S., 1971. A kinetic model for the chemical composition of seawater. *Quat. Res.*, 1:188-207.

________, 1982. Ocean chemistry during glacial time. *Geochim. Cosmochim. Acta*, 46:1689-1705.

Burckle, L. H., Keigwin, L. D., and Opdyke, N. D., 1982. Middle and late Miocene stable isotope stratigraphy: correlation to the paleomagnetic reversal record. *Micropaleontology*, 28(4):329-33

Ciesielski, P. F., Ledbetter, M. T., and Ellwood, B. B., 1982. The development of Antarctic glaciation and the Neogene paleoenvironment of the Maurice Ewing Bank. *Mar. Geol.*, 46:1-52.

Ciesielski, P. F., and Weaver, F. M., 1974. Early Pliocene temperature changes in the Antarctic seas. *Geology*, 2:511-515.

Cita, M. B., 1976. Biodynamic effects of the Messinian salinity crisis on the evolution of planktonic foraminifers in the Mediterranean. *Palaeogeogr., Palaeoclimatol., Palaeoecol.*, 20:23-42.

________, 1982. The Messinian salinity crisis in the Mediterranean: A review. *Alpine Mediterranean Geodynamics Series* (Vol. 7): Washington (Am. Geophys. Un.), 113-140.

Cita, M. B., and Ryan, W. B. F., 1979. Late Neogene environmental evolution. *In* von Rad, U., Ryan, W. B. F., et al., *Init. Repts. DSDP*, 47 (Pt. 1): Washington (U.S. Govt. Printing Office), 4[illegible]-459.

Craig, H., 1953. The geochemistry of the stable carbon isotopes. *Geochim. Cosmochim. Acta*, 3:53-92.

Davies, T. A., Hay, W. W., Southam, J. R., and Worsley, T. R., 1977. Estimates of Cenozoic oceanic sedimentation rates. *Science*, 197: 53-55.

Denham, R. N., and Crook, F. G., 1976. The Tasman Front. *N.Z.J. Mar. Freshwater Res.*, 10:15-30.

Douglas, R. G., and Savin, S. M., 1973. Oxygen and carbon isotope analyses of Cretaceous and Tertiary Foraminifera from the central north Pacific. *In* Winterer, E. L., Ewing, J. I., et al., *Init. Repts. DSDP*, 17: Washington (U.S. Govt. Printing Office), 591-605.

Epstein, S., Buchsbaum, R., Lowenstam, H. A., and Urey, H. C., 1953. Revised carbonate-water isotopic temperature scale. *Geol. Soc. Am. Bull.*, 64:1315-1326.

Haq, B. U., 1980. Biogeographic history of Miocene calcareous nannoplankton and paleoceanography of the Atlantic Ocean. *Micropaleontology*, 26(4):414-443.

Haq, B. U., Worsley, T. R., Burckle, L. H., Douglas, R. G., Keigwin, L. D., Jr., Opdyke, N. D., Savin, S. M., Sommer, M. A. II, Vincent, E., and Woodruff, F., 1980. Late Miocene marine carbon-isotopic shift and synchroneity of some phytoplanktonic biostratigraphic events. *Geology*, 8:427-431.

Hodell, D., and Kennett, J. P., 1984. Late Miocene carbon shift in DSDP Site 516A, western south Atlantic. *GSA Abstr. Progr.*, 16(6): 540.

Hsü, K. J., Cita, M. B., and Ryan, W. B. F., 1973. The origin of the Mediterranean evaporites. *In* Ryan, W. B. F., Hsü, K. J., et al., *Init. Repts. DSDP*, 13(Pt. 2): Washington (U.S. Govt. Printing Office), 1203-1231.

Hsü, K. J., McKenzie, J. A., Oberhänsli, H., Weissert, H., and Wright, R. C., 1984. South Atlantic Cenozoic paleoceanography. *In* Hsü, K. J., LaBrecque, J. L., et al., *Init. Repts. DSDP*, 73: Washington (U.S. Govt. Printing Office), 771-785.

Ingle, J. C., 1967. Foraminiferal biofacies variation and the Miocene-Pliocene boundary in Southern California. *Bull. Am. Paleontol.*, 52:217-394.

________, 1973. Neogene foraminifera from the northeastern Pacific Ocean, Leg 18, Deep Sea Drilling Project. *In* Kulm, L. D., von Huene, R., et al., *Init. Repts. DSDP*, 18: Washington (U.S. Govt. Printing Office), 517-567.

Keany, J., 1978. Paleoclimatic trends in early and middle Pliocene deep-sea sediments of the Antarctic. *Mar. Micropaleontol.*, 3:35-4

Keigwin, L. D., Jr., 1976. Late Cenozoic planktonic foraminiferal biostratigraphy and paleoceanography of the Panama Basin. *Micropaleontology*, 22:419-440.

________, 1979. Late Cenozoic stable isotope stratigraphy and paleoceanography of DSDP sites from the east equatorial and central north Pacific Ocean. *Earth Planet. Sci. Lett.*, 45:361-382.

Keigwin, L. D., Aubry, M.-P., and Kent, D. V., in press. Upper Miocene stable isotopic stratigraphy, biostratigraphy, and magnetostratigraphy of North Atlantic DSDP Sites. *In* Ruddiman, W. F., Kidd, R. B., et al., *Init. Repts. DSDP*, 94: Washington (U.S. Govt. Printing Office).

Keigwin, L. D., Jr., and Shackleton, N. J., 1980. Uppermost Miocene carbon isotope stratigraphy of a piston core in the equatorial Pacific. *Nature*, 284(5757):613–614.

Keigwin, L. D., Jr., and Thunell, R. C., 1980. Middle Pliocene climatic change from faunal and oxygen isotopic trends: western Mediterranean. *Nature*, 282(5736):294–296.

Keller, G., 1979. Late Neogene planktonic foraminiferal biostratigraphy and paleoceanography of the Northwest Pacific Site 296. *Palaeogeogr., Palaeoclimatol., Palaeoecol.*, 27:129–154.

Kennett, J. P., 1967. Recognition and correlation of the Kapitean Stage (upper Miocene, New Zealand). *N.Z.J. Geol. Geophys.*, 10:1051–1063.

———, 1977. Cenozoic evolution of Antarctic glaciation, the circum-Antarctic ocean and their impact on global paleoceanography. *J. Geophys. Res.*, 82(27):3843–3859.

Kennett, J. P., Keller, G., and Srinivasan, M. S., in press. Miocene planktonic foraminiferal biogeography and paleoceanographic development of the Indo-Pacific region. *In* Kennett, J. P. (Ed.), *The Miocene Ocean: Paleoceanography and Biogeography.* Geol. Soc. Am. Mem., 163.

Kennett, J. P., Shackleton, N. J., Margolis, S. V., Goodney, D. E., Dudley, W. C., and Kroopnick, P. M., 1979. Late Cenozoic oxygen and carbon isotopic history and volcanic ash stratigraphy: DSDP Site 284, South Pacific. *Am. J. Sci.*, 279:52–69.

Kennett, J. P., and Vella, P., 1975. Late Cenozoic planktonic foraminifera and paleoceanography at DSDP Site 284 in the cool subtropical South Pacific. *In* Kennett, J. P., Houtz, R. E., et al., *Init. Repts. DSDP*, 29: Washington (U.S. Govt. Printing Office), 769–799.

Kennett, J. P., and Watkins, N. D., 1974. Late Miocene-early Pliocene paleomagnetic stratigraphy, paleoclimatology, and biostratigraphy in New Zealand. *Geol. Soc. Am. Bull.*, 85:1385–1398.

Killingley, J. S., Johnson, R. F., and Berger, W. H., 1981. Oxygen and carbon isotopes of individual shells of planktonic foraminifera from Ontong-Java plateau, equatorial Pacific. *Palaeogeogr., Palaeoclimatol., Palaeoecol.*, 33:193–204.

Knox, G. A., 1970. Biological oceanography of the South Pacific. *In* Wooster, W. A. (Ed.), *Scientific Exploration of the South Pacific:* Washington (National Academy of Sciences), pp. 155–182.

Kroopnick, P., 1974. The dissolved O_2-CO_2-^{13}C system in the eastern equatorial Pacific. *Deep-Sea Res.*, 21:211–227.

———, 1980. The distribution of δ^{13}C in the Atlantic Ocean. *Earth Planet. Sci. Lett.*, 49:469–484.

———, 1985. The distribution of ^{13}C of ΣCO_2 in the world oceans. *Deep-Sea Res.*, 32:57–84.

Loutit, T. S., 1981. Late Miocene paleoclimatology: subantarctic water mass, southwest Pacific. *Mar. Micropaleontol.*, 6:1–27.

Loutit, T. S., and Keigwin, L. D., Jr., 1982. Stable isotopic evidence for latest Miocene sea-level fall in the Mediterranean region. *Nature*, 300(5888):163–166.

Loutit, T. S., and Kennett, J. P., 1979. Application of carbon isotope stratigraphy to late Miocene shallow marine sediments, New Zealand. *Science*, 204:1196–1199.

———, 1981. New Zealand and Australian Cenozoic sedimentary cycles and global sea-level changes. *Am. Assoc. Pet. Geol. Bull.*, 65:1586–1601.

Loutit, T. S., Kennett, J. P., and Savin, S. M., 1983. Miocene equatorial and southwest Pacific paleoceanography from stable isotope evidence. *Mar. Micropaleontol.*, 8:215–233.

Loutit, T. S., Pisias, N. G., and Kennett, J. P., 1983. Pacific Miocene carbon isotope stratigraphy using benthic foraminifera. *Earth Planet. Sci. Lett.*, 66:48–62.

McKenzie, J. A., Weissert, H., Poore, R. Z., Wright, R. C., Percival, S. F., Jr., Oberhänsli, H., and Casey, M., 1984. Paleoceanographic implications of stable-isotope data from upper Miocene–lower Pliocene sediments from the southeast Atlantic (Deep Sea Drilling Project Site 519). *In* Hsü, K. J., LaBrecque, J. L., et al., *Init. Repts. DSDP*, 73: Washington (U.S. Govt. Printing Office), 717–724.

Margolis, S. V., Kroopnick, P. M., Goodney, D. E., Dudley, W. C., and Mahoney, M. E., 1975. Oxygen and carbon isotopes from calcareous nannofossils as paleoceanographic indicators. *Science*, 189: 555–557.

Matthews, R. K., Curry, W. B., Lohmann, K. C., and Sommer, M. A., 1980. Late Miocene palaeo-oceanography of the Atlantic: oxygen isotope data on planktonic and benthic Foraminifera. *Nature*, 283:555–557.

Matthews, R. K., and Poore, R. Z., 1980. Tertiary δ^{18}O record and glacio-eustatic sea-level fluctuations. *Geology*, 8:501–504.

Mercer, J. H., 1976. Glacial history of southernmost South America. *Quat. Res.*, 6:125–166.

Mercer, J. H., and Sutter, J. F., 1982. Late Miocene–earliest Pliocene glaciation in southern Argentina: implications for global ice-sheet history. *Palaeogeogr., Palaeoclimatol., Palaeoecol.*, 38:185–206.

Poore, R. Z., 1981. Late Miocene biogeography and paleoclimatology of the central North Atlantic. *Mar. Micropaleontol.*, 6:599–616.

Prell, W. L., 1984. Covariance patterns of foraminifera δ^{18}O: an evaluation of Pliocene ice volume changes near 3.2 million years ago. *Science*, 206:692–693.

Prell, W. L., Gardner, J. V., et al., 1982. *Init. Repts. DSDP*, 68: Washington (U.S. Govt. Printing Office).

Sackett, W. M., 1964. The depositional history and isotopic organic carbon composition of marine sediments. *Mar. Geol.*, 2:173–185.

Savin, S. M., Abel, L., Barrera, E., Hodell, D., Keller, G., Kennett, J. P., Killingley, J., Murphy, M., and Vincent, E., in press. The evolution of Miocene surface and near-surface marine temperatures: oxygen isotopic evidence. *In* Kennett, J. P. (Ed.), *The Miocene Ocean: Palaeoceanography and Biogeography*. Geol. Soc. Am. Mem., 163.

Savin, S. M., Douglas, R. G., Keller, G., Killingley, J. S., Shaughnessy, L., Sommer, M. A., Vincent, E., and Woodruff, F., 1981. Miocene benthic foraminiferal isotope records: A synthesis. *Mar. Micropaleontol.*, 6:423–450.

Savin, S. M., Douglas, R. G., and Stehli, F. G., 1975. Tertiary marine paleotemperatures. *Geol. Soc. Am. Bull.*, 86:1499–1510.

Schnitker, D., 1980. North Atlantic oceanography as possible cause of Antarctic glaciation and eutrophication. *Nature*, 287:615–616.

Sclater, J., Meinke, L., Bennett, A., and Murphy, C., in press. The depth of the ocean through the Neogene. *In* Kennett, J. P. (Ed.), *The Miocene Ocean: Paleoceanography and Biogeography.* Geol. Soc. Am. Mem., 163.

Shackleton, N. J., 1977. Carbon-13 in *Uvigerina:* tropical rain forest history and the equatorial Pacific carbonate dissolution cycles. *In* Anderson, N. R., and Malahoff, A. (Eds.), *The Fate of Fossil Fuel CO_2 in the Oceans:* New York (Plenum), pp. 401–427.

Shackleton, N. J., Backman, J., Zimmerman, H., et al., 1984. Oxygen isotope calibration of the onset of ice rafting and history of glaciation in the North Atlantic region. *Nature*, 307(5952):620–623.

Shackleton, N. J., and Cita, M. B., 1979. oxygen and carbon isotope stratigraphy of benthic foraminifers at Site 597: detailed history of climatic change during the late Neogene. *In* von Rad, U., Ryan, W. B. F., et al., *Init. Repts. DSDP*, 47(Pt.1): Washington (U.S. Govt. Printing Office), 433–445.

Shackleton, N. J., and Kennett, J. P., 1975a. Late Cenozoic oxygen and carbon isotopic changes at DSDP Site 284: Implications for glacial history of the Northern Hemisphere and Antarctica. *In* Kennett, J. P., Houtz, R. E., et al., *Init. Repts. DSDP*, 29: Washington (U.S. Govt. Printing Office), 801–806.

———, 1975b. Paleotemperature history of the Cenozoic and the initiation of Antarctic glaciation: Oxygen and carbon isotope analyses in DSDP Sites 277, 279, and 281. *In* Kennett, J. P., Houtz, R. E., et al., *Init. Repts. DSDP*, 29: Washington (U.S. Govt. Printing Office), 743–755.

Shackleton, N. J., and Opdyke, N. D., 1977. Oxygen isotopic and paleomagnetic evidence for early Northern Hemisphere glaciation. *Nature*, 270:216–219.

Stanton, B. R., 1979. The Tasman Front. *N.Z.J. Mar. Freshwater Res.*, 138:201–214.

———, 1981. An oceanographic survey of the Tasman Front. *N.Z.J. Mar. Freshwater Res.*, 15:289–297.

Vail, P. R., and Hardenbol, J., 1979. Sea-level changes during the Tertiary. *Oceanus*, 22:71–79.

van Andel, T. H., Thiede, J., Sclater, J. G., and Hay, W. W., 1977. Depositional history of the South Atlantic ocean during the last 125 million years. *J. Geol.*, 85:651–698.

Vergnaud Grazzini, C., and Rabussier-Lointier, D., 1980. Essai de corrélation stratigraphique par le moyen des iotopes de l'oxygène et du carbone. *Soc. Geol. France*, 22(7):719–730.

Vincent, E., and Berger, W. H., 1985. Carbon dioxide and polar cooling in the Miocene: The Monterey hypothesis. *In* Sundquist, E. T., and Broecker, W. S. (Ed.), *The Carbon Cycle and Atmospheric CO_2: natural Variations Archean to Present:* Am. Geophys. Union Monogr. Ser., 32.

Vincent, E., Killingley, J. S., and Berger, W. H., 1980. The magnetic Epoch-6 carbon shift: a change in the ocean's $^{13}C/^{12}C$ ratio 6.2 million years ago. *Mar. Micropaleontol.*, 5:185–203.

_______, in press. Miocene oxygen and carbon isotope stratigraphy of the tropical Indian Ocean. *In* Kennett, J. P. (Ed.), *The Miocene Ocean: Paleoceanography and Biogeography.* Geol. Soc. Am. Mem., 163.

Wedepohl, K. H. (Ed.), 1969. *Handbook of Geochemistry:* New York (Springer-Verlag), p. II-1(6).

Weissert, H. J., McKenzie, J. A., Wright, R. C., Clark, M., Oberhänsli, H., and Casey, M., 1984. Paleoclimatic record of the Pliocene at Deep Sea Drilling Project Sites 519, 521, 522, and 523 (Central South Atlantic). *In* Hsü, K. J., LaBrecque, J. L., et al., *Init. Repts. DSDP*, 73: Washington (U.S. Govt. Printing Office), 701–715.

Woodruff, F., and Douglas, R. G., 1981. Response of deep-sea benthic foraminifera to Miocene paleoclimatic events, DSDP Site 289. *Mar. Micropaleontol.*, 6:617–632.

Woodruff, F., and Savin, S. M., 1985. $\delta^{13}C$ values of Miocene Pacific benthic foraminifera: correlations with sea level and biological productivity. *Geology*, 13(2):119–122.

Woodruff, F., Savin, S. M., and Douglas, R. G., 1981. Miocene stable isotope record: a detailed deep Pacific Ocean study and its paleoclimatic implications. *Science*, 212:665–668.

Wyrtki, K., 1974. *The Dynamic Topography of the Pacific Ocean and Its Fluctuations.* Hawaii Inst. Geophys. Rep. HIG 74-5.

Date of Initial Receipt: 10 May 1985
Date of Acceptance: 17 May 1985

APPENDIX

Oxygen and Carbon Isotope Composition (‰ PDB) of Benthic and Planktonic Foraminifers, DSDP Sites 588, 590 and 591[1]

SITE 588

Core-Section (interval in cm)	Sub-bottom depth (m)	Age (Ma)	$\delta^{18}O$ (‰ PDB)	$\delta^{13}C$ (‰ PDB)
Hole 588[a]				
10-1, 35–37	82.8	4.34	1.97	0.75
10-2, 35–37	84.3	4.38	2.07	0.81
10-3, 35–37	85.8	4.42	1.93	0.70
10-4, 35–37	87.3	4.46	1.82	0.88
10-5, 35–37	88.8	4.50	1.99	0.83
10-6, 35–37	90.3	4.54	1.90	0.64
11-1, 35–37	92.4	4.60	1.71	0.84
11-2, 35–37	93.9	4.70	1.86	0.85
11-3, 35–37	95.4	4.79	1.91	0.92
11-4, 35–37	96.9	4.88	2.13	0.84
11-5, 35–37	98.4	4.98	2.06	1.04
11-6, 35–37	99.9	5.07	1.97	0.63
12-1, 35–37	101.9	5.12	1.88	0.90
12-2, 35–37	103.4	5.16	2.03	0.81
12-3, 35–37	104.9	5.20	2.13	0.83
12-4, 35–37	106.4	5.23	2.07	0.96
12-5, 35–37	107.9	5.25	2.04	0.98
12-6, 35–37	109.4	5.28	2.04	0.90
12-7, 35–37	110.9	5.30	2.06	1.12
13-1, 35–37	111.6	5.32	2.47	0.73
13-2, 35–37	113.1	5.34	2.28	0.63
13-3, 35–37	114.6	5.37	2.25	0.65
13-4, 110–111	116.8	5.41	2.04	0.69
13-5, 110–111	118.3	5.43	1.79	0.62
13-6, 35–37	119.1	5.45	2.09	0.79
13-7, 35–37	120.6	5.47	2.29	0.56
Hole 588 (Cont.)				
14-1, 35–37	121.1	5.48	2.29	1.07
14-2, 35–37	122.6	5.51	2.25	1.10
14-3, 35–37	124.1	5.53	2.11	0.75
14-4, 35–37	125.6	5.56	1.86	0.90
14-5, 35–37	127.1	5.58	1.96	0.82
14-6, 35–37	128.6	5.61	2.07	0.93
14-7, 35–37	130.1	5.64	1.99	0.74
15-1, 35–37	130.8	5.65	1.97	0.75
15-2, 35–37	132.3	5.67	1.94	0.85
15-3, 35–37	133.8	5.70	2.05	0.40
15-4, 35–37	135.3	5.73	2.03	0.77
15-5, 35–37	136.8	5.75	2.03	0.83
15-6, 35–37	138.3	5.78	1.99	0.81
16-1, 35–37	140.4	5.81	1.91	0.82
16-2, 35–37	141.9	5.84	2.00	0.81
16-3, 35–37	143.4	5.87	2.09	0.67
16-4, 35–37	144.9	5.89	2.03	0.60
17-1, 35–37	150.0	5.98	2.01	0.55
17-2, 35–37	151.5	6.01	2.04	0.91
17-3, 35–37	153.0	6.03	2.02	0.74
17-4, 35–37	154.5	6.06	1.89	0.62
17-5, 35–37	156.0	6.08	1.78	0.82
17-6, 35–37	157.5	6.11	1.86	1.00
17-7, 35–37	159.0	6.14	2.05	0.78
18-1, 35–37	160.0	6.15	2.05	1.02
18-2, 35–37	161.0	6.17	1.88	1.00
18-3, 35–37	162.5	6.20	1.77	1.05
18-4, 35–37	164.0	6.22	1.73	1.06
18-5, 35–37	165.5	6.25	1.84	1.18
18-6, 35–37	167.0	6.50	1.75	1.19
19-1, 50–51	169.3	6.88	1.81	1.24
19-2, 35–37	172.1	7.36	1.85	1.20
19-3, 35–37	173.6	7.61	1.79	1.01
19-4, 35–37	175.1	7.87	1.89	1.23
19-5, 35–37	176.6	8.12	2.01	1.42
19-6, 35–37	178.1	8.37	2.03	1.48
19-7, 35–37	179.6	8.63	2.16	1.45
20-2, 35–37	180.3	8.75	2.13	1.30
20-3, 35–37	181.8	9.00	1.91	0.94
20-4, 35–37	183.3	9.25	1.89	1.02
20-6, 35–37	186.3	9.57	1.85	1.20
20-7, 35–37	187.8	9.64	1.74	1.17
21-1, 35–37	188.4	9.67	1.81	1.43
21-2, 35–37	189.9	9.74	1.85	1.18
21-3, 35–37	191.4	9.81	2.20	1.12
21-4, 35–37	192.9	9.88	2.15	1.31
21-5, 35–37	194.4	9.96	2.26	1.39
21-6, 35–37	195.9	10.03	2.07	1.49
21-7, 35–37	197.4	10.10	2.09	1.21
22-1, 35–37	198.0	10.13	2.26	1.35
22-2, 35–37	199.5	10.20	2.19	1.49
22-3, 35–37	201.0	10.27	2.15	1.41
22-4, 35–37	202.5	10.34	2.21	1.42
22-5, 35–37	204.0	10.41	1.99	1.09
22-6, 35–37	205.0	10.48	2.07	1.10
22-7, 35–37	207.0	10.55	2.26	1.18
23-1, 35–37	207.5	10.57	2.40	1.08
23-2, 35–37	209.5	10.67	2.15	1.09
23-3, 35–37	210.5	10.71	2.18	1.00
23-4, 35–27	212.0	10.79	2.08	0.88
23-5, 35–37	213.5	10.86	1.96	0.72
23-6, 35–37	215.0	10.93	1.79	0.78
23-7, 35–37	216.5	11.00	1.78	0.75
24-1, 35–37	217.1	11.04	1.82	0.80
24-2, 35–37	218.6	11.14	1.79	0.77
24-3, 35–37	220.1	11.24	1.62	0.92
24-4, 35–27	221.6	11.34	1.99	1.13
24-5, 35–37	223.1	11.45	2.13	1.21
24-6, 35–37	224.6	11.55	1.91	1.18
24-7, 35–37	226.1	11.65	1.89	1.34
25-1, 35–37	226.8	11.70	2.05	1.32
25-2, 35–37	228.3	11.80	1.94	1.16
25-3, 35–37	229.8	11.90	1.91	1.18
25-4, 35–37	231.3	12.00	1.75	1.10
25-5, 35–37	232.8	12.04	1.61	0.85
25-6, 35–37	234.3	12.08	1.99	1.07
25-7, 35–37	235.8	12.11	1.91	1.26

[a] *Cibicidoides kullenbergi* (benthic) used except in Sample 588-13-1, 35–37 cm, where *C. wuellerstorfi* was used.

---

[1] Stable isotopic data for *Oridorsalis umbonatus* (Hole 591B) have been adjusted to that of *Cibicidoides* by adding +1.06‰ for $\delta^{13}C$ and subtracting 0.72 for $\delta^{18}O$ (see text for discussion).

Core-Section (interval in cm)	Sub-bottom depth (m)	Age (Ma)	$\delta^{18}O$	$\delta^{13}C$
			(‰ PDB)	
Hole 588A[b]				
1-1, 35–37	236.4	12.13	1.62	0.96
1-2, 35–37	237.9	12.16	1.50	0.95
1-3, 35–37	239.4	12.20	1.52	0.92
1-4, 35–37	240.9	12.29	1.53	1.30
1-5, 35–37	242.4	12.39	1.46	1.39
1-6, 35–37	243.9	12.48	1.62	1.25
1-7, 35–37	245.4	12.57	1.54	1.24
2-1, 35–37	246.0	12.61	1.73	1.36
2-2, 35–37	247.5	12.70	1.64	1.17
2-3, 35–37	249.0	12.79	1.49	1.13
2-4, 35–37	250.5	12.80	1.74	0.92
3-1, 35–37	251.0	12.91	1.72	0.77
3-2, 35–37	252.5	13.00	1.71	1.17
3-3, 35–37	254.0	13.14	1.88	1.21
4-1, 35–37	256.0	13.33	1.79	1.13
4-2, 35–37	257.5	13.47	1.94	1.10
4-3, 35–37	259.0	13.61	1.97	1.16
5-1, 35–37	261.0	13.80	1.92	1.08
5-2, 35–37	262.5	13.93	1.98	1.25
5-3, 35–37	264.0	14.07	1.92	1.03
6-1, 35–37	266.0	14.26	1.69	1.15
6-2, 35–37	267.5	14.40	1.85	1.18
6-3, 35–37	269.0	14.54	1.71	1.26
6-4, 35–37	270.5	14.68	1.70	1.41
7-1, 35–37	271.0	14.73	1.57	1.41
7-2, 35–37	272.5	14.87	1.62	1.50
7-3, 35–37	274.0	15.00	1.44	1.59
7-4, 35–37	275.5	15.12	1.51	1.54
8-1, 35–37	276.0	15.16	1.25	1.48
8-2, 35–37	277.5	15.27	1.37	1.48
8-3, 35–37	279.0	15.39	1.60	1.96
8-4, 35–37	280.5	15.51	1.61	1.98
9-1, 35–37	281.0	15.55	1.54	1.84
9-2, 35–37	282.5	15.66	1.33	1.65
9-3, 35–37	284.0	15.78	1.13	0.89
10-1, 35–37	286.0	15.93	1.21	1.51
10-2, 35–37	287.5	16.05	1.04	1.68
10-3, 35–37	289.0	16.17	0.91	1.65
10-3, 35–37	289.0	16.17	0.91	1.65
10-4, 35–37	289.5	16.20	1.12	1.69
11-1, 35–37	291.0	16.33	0.87	1.71
11-2, 35–37	292.5	16.46	0.73	1.40
11-3, 35–37	294.0	16.58	0.89	1.09
12-1, 35–37	296.0	16.75	0.93	1.43
12-2, 35–37	297.5	16.88	0.93	1.25
12-3, 35–37	299.0	17.00	0.89	1.34
12-4, 35–37	300.5	17.10	0.95	1.44
13-2, 35–37	302.5	17.24	1.03	1.50
13-3, 35–37	304.0	17.34	0.58	1.07
13-4, 35–37	305.5	17.44	1.14	1.78
14-1, 35–37	306.0	17.47	1.23	1.92
14-2, 35–37	307.5	17.57	1.20	2.04
14-3, 35–37	309.0	17.67	1.18	1.86
15-1, 35–37	311.0	17.81	0.97	1.35
15-2, 35–37	312.5	18.07	0.83	1.15
15-3, 35–37	314.0	18.33	1.17	1.24
15-4, 35–37	315.5	18.59	1.12	1.25
Hole 588C[c]				
1-1, 35–37	306.0	17.47	0.72	1.32
1-2, 35–37	307.5	17.57	1.03	1.66
1-2, 110–111	308.3	17.62	1.09	1.54
1-3, 35–37	309.0	17.67	0.71	1.34
1-3, 110–111	309.8	17.72	1.08	1.63
1-5, 35–37	312.0	17.98	1.55	1.26
1-5, 110–111	312.8	18.12	1.14	1.89
1-6, 35–37	313.5	18.24	0.50	1.77
1-6, 110–111	314.3	18.38	1.30	1.95
2-1, 110–111	316.4	18.74	1.13	2.03
2-2, 35–37	317.2	18.88	1.11	2.12
2-2, 110–111	317.9	19.00	1.22	2.13
2-3, 35–37	318.7	19.05	1.41	1.67
Hole 588C (Cont.)				
2-3, 110–111	319.4	19.08	0.85	1.67
2-4, 35–37	320.2	19.13	0.89	1.92
2-4, 110–111	320.9	19.17	0.85	1.66
2-5, 35–37	321.7	19.21	0.92	1.51
2-5, 110–111	322.4	19.25	0.79	1.38
2-6, 35–37	323.2	19.30	0.63	1.32
2-6, 110–111	323.9	19.34	0.73	1.55
3-1, 35–37	325.3	19.42	0.69	1.62
3-1, 110–111	326.0	19.46	0.91	1.30
3-2, 35–37	326.8	19.50	0.72	1.31
3-2, 110–111	327.5	19.54	0.64	1.20
3-3, 35–37	328.3	19.59	1.22	1.65
3-3, 110–111	329.0	19.63	1.20	1.41
3-4, 35–37	329.8	19.67	1.04	1.02
3-4, 110–111	330.5	19.71	1.21	1.35
3-5, 110–111	332.8	19.84	1.26	1.14
3-6, 35–37	335.6	20.00	1.22	0.98
3-6, 110–111	336.3	20.04	1.18	1.02
4-2, 110–111	337.1	20.08	0.97	0.94
4-3, 35–37	337.8	20.12	1.37	1.04
4-3, 110–111	338.6	20.17	1.31	1.24
4-4, 35–37	339.3	20.21	1.15	1.13
4-5, 35–37	340.8	20.29	1.17	1.00
4-5, 110–111	341.6	20.34	1.06	0.79
5-1, 35–37	344.5	20.50	1.40	1.19
5-1, 110–111	345.2	20.54	1.30	1.17
5-2, 35–37	346.0	20.58	1.59	1.51
5-2, 110–111	346.7	20.62	1.43	1.34
5-3, 110–111	348.2	20.70	1.30	1.22
5-4, 35–37	348.9	20.73	1.24	0.93
5-5, 35–37	350.4	20.81	1.14	1.37
5-5, 110–111	351.2	20.85	1.15	0.71
5-6, 110–111	352.7	20.93	1.03	0.99
6-1, 35–37	354.0	21.00	1.09	1.06
6-2, 35–37	355.5	21.08	1.58	1.27
6-3, 110–111	357.8	21.19	1.30	1.00
6-4, 110–111	359.3	21.27	1.23	1.06
6-5, 35–37	360.0	21.31	1.36	1.10
6-6, 110–111	362.3	21.43	1.52	1.24
6-7, 35–37	363.0	21.47	1.45	1.00
7-1, 35–37	363.7	21.50	1.31	1.07
7-1, 110–111	364.4	21.54	1.13	0.68
7-2, 35–37	365.2	21.58	1.27	1.19
7-4, 110–111	368.9	21.77	1.11	1.36
8-2, 35–37	374.8	22.08	1.37	1.52
8-2, 110–111	375.5	22.12	1.51	1.75
8-3, 35–37	376.3	22.16	1.26	1.94
8-4, 110–111	378.5	22.27	1.04	1.30
8-5, 35–37	379.3	22.31	1.61	1.62
8-5, 110–111	380.0	22.35	1.16	1.31
8-6, 35–37	380.8	22.39	1.17	1.33
8-6, 110–111	381.5	22.43	1.28	1.34
8-7, 35–37	382.3	22.47	1.56	1.54
9-2, 35–37	384.3	22.57	1.18	1.19
9-3, 35–37	385.8	22.65	1.27	1.26
9-3, 110–111	386.6	22.69	1.35	0.99
9-4, 35–37	387.3	22.73	1.34	1.43
9-5, 35–37	388.8	22.81	1.81	1.57
9-6, 35–37	390.3	22.89	1.51	1.57
9-6, 110–111	391.1	22.93	1.02	0.87

[b] Samples 588A-1-1, 35–37 cm to 588A-10-4, 35–37 cm, *C. kullenbergi*; Samples 588A-11-3, 35–37 cm and 588A-11-2, 35–37 cm, *C. wuellerstorfi; Samples 588A-1-3, 35-37 cm to 588A-15-4, 35-37 cm, C. coryelli.*

[c] All samples, *C. coryelli.*

SITE 590

Core-Section (interval in cm)	Sub-bottom depth (m)	Age (Ma)	Benthic (‰ PDB)		Planktonic (‰ PDB)	
			$\delta^{18}O$	$\delta^{13}C$	$\delta^{18}O$	$\delta^{13}C$
Hole 590A[a]						
1-6, 35-37	34.1	1.81	2.59	0.74	-0.35	1.90
2-1, 35-37	36.2	1.90	2.46	0.85	-0.45	0.95
2-3, 35-37	39.2	2.02	2.63	0.64	-0.49	1.42

[a] All benthic results measured using *C. kullenbergi*; all planktonic results, *Globigerinoides sacculifer*.

Core-Section (interval in cm)	Sub-bottom depth (m)	Age (Ma)	Benthic (‰ PDB)		Planktonic (‰ PDB)	
			$\delta^{18}O$	$\delta^{13}C$	$\delta^{18}O$	$\delta^{13}C$
Hole 590A (Cont.)						
2-5, 35-37	42.2	2.15	2.57	0.75	-0.45	1.50
2-6, 35-37	43.7	2.21	2.52	0.94	-0.69	1.58
3-1, 35-37	45.8	2.30	3.00	0.44	-0.57	1.57
3-2, 35-37	47.3	2.33	2.51	0.79	-0.72	1.66
3-3, 35-37	48.8	2.37	--	--	-0.09	1.39
3-4, 35-37	50.3	2.40	2.60	0.61	0.11	1.42
3-5, 35-37	51.8	2.44	--	--	-0.55	1.55
3-6, 35-37	53.3	2.48	2.39	0.73	-0.50	1.67
4-1, 35-37	55.3	2.53	2.38	0.78	-0.56	1.52
4-2, 35-37	56.8	2.57	2.29	0.73	-0.55	1.74
4-3, 35-37	58.3	2.61	2.41	0.65	-0.60	1.24
4-4, 35-37	59.8	2.65	2.34	0.85	-0.70	1.57
4-5, 35-37	61.3	2.69	2.29	0.56	-0.48	1.44
4-6, 35-37	62.8	2.73	1.97	0.70	-0.52	1.36
5-1, 110-112	64.9	2.79	2.25	0.98	-0.77	1.39
5-3, 110-112	67.9	2.86	2.25	0.81	-0.31	1.56
5-5, 110-112	70.9	2.94	1.98	0.74	-0.96	1.49
6-1, 55-57	74.6	3.04	1.98	0.83	-0.60	1.59
6-3, 55-57	77.6	3.12	2.17	0.76	-0.98	1.50
6-5, 55-57	80.6	3.20	1.87	0.88	-0.58	1.75
7-1, 35-37	84.1	3.29	2.15	0.93	-0.67	1.58
7-3, 35-37	87.1	3.37	--	--	-0.39	1.45
7-5, 35-37	90.1	3.45	2.01	0.87	-0.63	1.72
8-1, 103-104	93.8	3.47	2.22	0.59	-0.28	1.74
8-3, 35-37	96.8	3.48	--	--	-0.35	1.34
8-5, 35-37	99.8	3.49	2.04	0.99	-0.78	1.59
8-6, 35-37	101.3	3.50	2.11	0.80	-0.90	1.55
10-1, 35-37	112.9	3.55	1.98	0.73	-0.74	1.37
10-3, 35-37	115.9	3.56	1.93	0.69	-0.85	1.47
10-5, 35-37	118.9	3.58	1.91	0.76	-0.73	1.64
11-1, 35-37	122.6	3.59	1.89	0.91	-0.46	1.48
11-3, 35-37	125.6	3.61	--	--	-0.45	1.39
11-4, 35-37	127.1	3.61	1.92	0.87	-0.68	1.73
11-6, 35-37	130.0	3.63	--	--	-0.85	1.37
12-1, 35-37	132.1	3.64	1.84	0.87	-0.59	1.57
12-3, 35-37	135.1	3.65	1.64	0.75	-0.31	1.53
12-5, 35-37	138.1	3.70	--	--	-0.54	1.71
12-6, 35-37	139.6	3.73	1.88	1.06	-0.66	1.47
13-1, 35-37	141.8	3.77	1.78	0.94	-0.22	1.68
13-3, 35-37	144.8	3.82	1.87	0.86	-0.32	1.52
13-5, 35-37	147.8	3.87	--	--	-0.23	1.70
13-6, 35-37	149.3	3.90	1.80	0.87	-0.20	1.32
14-1, 35-37	151.4	3.93	--	--	-0.31	1.54
14-2, 35-37	152.9	3.96	--	--	-0.38	1.53
14-3, 35-37	154.4	3.99	1.81	0.77	-0.36	1.08
14-4, 35-37	155.9	4.01	--	--	-0.53	1.12
14-5, 35-37	157.4	4.04	1.76	0.68	-0.66	0.83
14-6, 35-37	158.9	4.06	--	--	-0.26	1.45
15-1, 35-37	161.0	4.10	1.76	0.93	-0.29	1.58
15-2, 35-37	162.5	4.14	--	--	-0.45	1.46
15-3, 35-37	164.0	4.18	1.95	0.63	-0.26	1.51
15-4, 35-37	165.5	4.22	--	--	-0.29	1.35
15-5, 35-37	167.0	4.26	1.73	1.01	-0.16	1.59
15-6, 35-37	168.5	4.30	--	--	-0.11	1.58
16-1, 35-37	170.6	4.35	1.80	0.96	-0.31	1.75
16-2, 35-37	172.1	4.39	1.92	1.00	-0.35	1.76
16-3, 35-37	173.6	4.43	1.85	1.03	-0.49	1.79
16-4, 35-37	175.1	4.47	--	--	-0.22	1.88
16-5, 35-37	176.6	4.51	1.75	0.82	-0.35	1.31
17-1, 35-37	180.1	4.60	1.97	1.15	-0.73	1.85
17-2, 35-37	183.1	4.70	--	--	-0.80	1.67
17-3, 121-122	184.0	4.73	--	--	2.17	0.72
17-5, 35-37	186.1	4.80	2.13	0.86	-0.31	1.43
18-1, 35-37	189.9	4.92	1.93	1.09	-0.59	2.01
18-2, 35-37	191.3	4.97	1.91	1.10	-0.62	2.06
18-4, 35-37	194.3	5.07	1.84	0.78	-0.31	1.85
18-5, 35-37	195.8	5.12	1.79	0.88	-0.49	1.83
18-6, 35-37	197.3	5.17	1.97	0.47	-0.13	1.47
19-1, 35-36	199.4	5.22	2.03	0.68	-0.60	1.63
19-2, 35-37	200.9	5.24	1.83	0.84	-0.55	1.93
19-3, 35-37	202.4	5.26	1.97	0.69	-0.37	1.65
19-4, 35-37	203.9	5.28	2.10	0.59	-0.75	1.54
19-5, 35-37	205.4	5.30	1.86	0.88	-0.76	1.78
19-6, 35-37	206.9	5.32	1.83	0.70	-0.67	2.01
20-1, 35-37	209.0	5.35	1.94	0.51	-0.45	1.28
20-2, 35-37	210.5	5.37	1.76	0.66	-0.50	1.59
20-4, 35-37	213.5	5.41	1.76	0.88	-0.69	2.11
Hole 590A (Cont.)						
20-6, 35-37	216.5	5.45	1.67	0.65	-0.45	1
21-1, 35-37	218.6	5.48	1.61	0.80	-0.80	1
21-3, 35-37	221.6	5.52	1.81	0.50	-0.64	1
21-5, 35-37	224.6	5.56	1.80	0.93	-0.44	1
21-7, 35-37	227.6	5.60	1.84	0.71	-0.45	1
22-2, 35-37	229.7	5.63	1.77	0.67	-0.55	2
23-1, 35-37	237.8	5.74	1.87	0.69	-0.47	1
23-3, 35-37	240.8	5.78	1.90	0.75	-0.50	1
23-5, 35-37	244.6	5.83	1.85	0.70	-0.72	1
24-1, 35-37	247.4	5.87	1.96	0.48	-0.60	1
24-3, 35-37	250.4	5.91	1.84	0.45	-0.38	1
24-5, 35-37	253.4	5.96	1.87	0.46	-0.38	1
24-6, 35-37	254.9	5.98	1.64	0.60	-0.32	1
24-7, 35-37	256.4	6.00	1.80	0.54	-0.40	1
25-1, 121-122	257.0	6.00	2.02	0.69	-0.13	1
Hole 590B[b]						
28-6, 35-37	258.5	6.02	--	--	-0.39	2
29-1, 35-37	259.5	6.04	--	--	-0.29	1
29-2, 35-37	261.5	6.07	1.80	0.77	-0.33	1
29-3, 35-37	262.5	6.08	--	--	-0.26	1
29-4, 35-37	264.0	6.10	--	--	-0.55	2
29-5, 35-37	265.5	6.12	--	--	-0.20	1.9
29-6, 35-37	267.4	6.15	1.71	0.79	-0.70	2.1
30-1, 35-37	269.0	6.17	--	--	-0.19	2.0
30-2, 35-37	270.0	6.18	1.90	0.70	-0.36	2.30
30-3, 35-37	272.0	6.21	-	--	-0.30	2.14
30-4, 35-37	273.5	6.23	--	--	-0.53	2.12
30-5, 35-37	275.0	6.25	--	--	-0.47	2.20
30-6, 35-37	276.2	6.32	1.85	0.82	-0.43	2.07
31-1, 35-38	278.7	6.48	--	--	-0.56	2.11
31-2, 35-37	280.7	6.60	1.76	1.02	-0.61	2.24
31-3, 35-37	281.7	6.66	1.73	1.11	-0.71	2.15
31-4, 35-37	283.2	6.75	1.78	0.93	-0.43	2.11
31-5, 35-37	284.7	6.84	1.86	1.10	-0.65	2.15
32-1, 35-37	288.3	7.06	1.69	1.06	-0.62	2.18
32-2, 35-37	289.8	7.15	1.65	1.12	-0.34	2.23
32-3, 35-37	291.3	7.25	1.88	0.93	-0.64	2.27
32-4, 35-37	292.8	7.34	1.77	0.98	-0.49	2.13
32-5, 35-37	294.3	7.43	1.66	1.02	-0.60	2.49
32-6, 35-37	295.8	7.52	1.81	0.97	-0.69	2.35
33-1, 35-37	297.8	7.64	1.63	1.26	-0.69	2.48
33-2, 35-37	299.3	7.73	1.66	1.19	-0.67	2.14
33-3, 35-37	300.8	7.83	1.49	1.28	-0.48	2.54
33-4, 35-37	301.3	7.86	1.46	1.29	-0.62	2.67
33-5, 35-37	302.8	7.95	1.55	1.37	-0.74	2.57
33-6, 35-37	304.3	8.04	1.71	1.32	-0.25	2.56
33-7, 35-37	305.8	8.13	1.42	1.00	-0.38	2.07
34-1, 35-37	307.5	8.24	1.69	1.15	-0.71	2.00
34-2, 35-37	309.0	8.33	1.70	1.18	-0.35	2.04
34-3, 35-37	310.5	8.42	1.85	1.17	-0.56	2.0
34-4, 35-37	312.0	8.51	1.78	1.33	-0.62	2.29
34-5, 35-37	313.5	8.60	1.82	1.24	-0.48	2.0
34-6, 35-37	315.0	8.69	1.58	0.93	-0.22	1.9
34,CC	316.6	8.79	1.68	1.00	-0.17	2.20
35-1, 35-37	317.0	8.82	1.82	1.14	-0.61	1.9
35-2, 35-37	318.5	8.91	1.99	1.14	-0.69	1.9
35-3, 35-37	320.0	9.00	1.81	1.38	-0.43	1.5
35-4, 35-37	321.5	9.09	1.92	1.43	-0.27	2.2
35-5, 35-37	323.0	9.18	1.85	1.43	-0.20	2.2
36-1, 35-37	326.7	9.41	1.98	1.37	-0.53	2.2
36-2, 35-37	328.2	9.50	2.00	1.52	-0.49	2.3
36-3, 35-37	329.7	9.58	1.78	1.34	-0.43	2.2
36-4, 35-37	331.2	9.66	1.59	1.19	-0.32	2.2
36-5, 35-37	332.7	9.73	1.75	1.49	--	--
37-1, 35-37	336.3	9.92	1.54	1.01	-0.70	1.9
37-2, 35-37	337.8	10.00	1.70	1.09	-0.51	2.0
37-3, 35-37	339.3	10.08	1.68	1.11	-0.74	2.1
37-4, 35-37	340.8	10.16	1.71	1.04	-0.43	1.8
37-5, 35-37	342.3	10.23	1.75	1.01	-0.37	1.9
37-6, 35-37	343.8	10.31	1.93	1.12	-0.52	2.2
38-1, 35-37	345.9	10.42	1.40	0.76	-0.51	1.8
38-2, 35-37	347.4	10.50	1.50	0.98	-0.44	1.9

[b] All benthic results measured using *C. kullenbergi* except for sample marked with asterisk, where *C. coryelli* was measured. All plankton results, *Globigerinoides quadrilobatus*.

Core-Section (interval in cm)	Sub-bottom depth (m)	Age (Ma)	Benthic (°/oo PDB)		Planktonic (°/oo PDB)	
			$\delta^{18}O$	$\delta^{13}C$	$\delta^{18}O$	$\delta^{13}C$
Hole 590B (Cont.)						
38-3, 35-37	348.9	10.58	1.94	0.78	-0.93	1.79
38-4, 35-37	350.4	10.66	1.43	0.52	-0.80	1.88
38-5, 35-37	351.9	10.73	1.80	0.69	-0.44	1.88
38-6, 35-37	353.4	10.81	1.89	0.92	-0.39	1.82
38-7, 35-37	354.9	10.89	1.31	0.76	--	--
39-1, 35-37	355.5	10.92	1.83	0.84	-0.79	1.93
39-2, 35-37	357.0	11.00	1.93	0.76	-0.34	1.79
39-3, 35-37	358.5	11.08	1.59	1.19	-0.71	1.72
39-4, 35-37	360.0	11.16	1.72	0.86	-0.40	1.57
39-5, 35-37	361.5	11.23	1.45	0.96	-0.29	1.88
39-6, 35-37	363.0	11.31	1.94	0.85	-0.80	1.50
41-1, 35-37	374.7	11.92	1.59	1.20	-0.69	1.51
41-2, 35-37	376.2	12.00	1.59	1.10	-0.53	1.60
41-3, 35-37	377.7	12.03	1.51	1.20	-0.83	1.62
41-4, 35-37	379.2	12.06	1.65	1.17	-0.56	1.43
41-5, 35-37	380.7	12.09	1.52	1.06	-0.65	1.60
41-6, 35-37	382.2	12.13	1.14	1.13	-0.57	1.67
42-1, 35-37	384.3	12.17	1.86	1.17	-0.67	1.79
42-2, 35-37	385.8	12.20	1.76	1.20	-0.53	1.65
42-3, 35-37	387.3	12.24	1.83	1.40	-0.55	2.03
42-4, 35-37	388.8	12.28	2.17	1.45	-0.86	2.02
42-5, 35-37	390.3	12.32	1.74	1.29	-0.47	1.89
42-6, 35-37	391.8	12.36	1.96	1.24	-0.82	1.77
43-1, 35-37	393.8	12.41	1.34	1.07	-1.01	2.08
43-2, 35-37	395.3	12.45	1.06	0.86	-0.65	1.88
43-3, 35-37	396.8	12.49	1.22	0.88	-0.21	1.63
43-4, 35-37	398.3	12.53	0.96	0.90	-0.24	1.74
43-5, 35-37	399.8	12.57	1.38	1.07	-0.42	1.98
44-1, 35-37	403.5	12.67	1.29	0.84	-0.76	1.88
44-2, 35-37	405.0	12.71	1.32	0.90	-0.92	2.18
44-3, 35-37	406.5	12.75	1.29	1.01	-0.54	1.96
44-4, 35-37	408.0	12.79	1.42	1.02	-0.51	2.28
44-5, 35-37	409.5	12.83	1.48	1.17	-0.74	2.33
44-6, 35-37	411.0	12.87	1.50	1.13	-0.47	2.52
45-1, 35-37	413.0	12.92	1.50	1.24	-0.51	2.15
45-2, 35-37	414.5	12.96	1.33	1.09	-1.07	2.00
45-4, 35-37	417.5	13.13	1.66	1.18	-0.89	2.21
45-5, 35-37	419.0	13.27	1.61	1.26	-0.70	2.07
46-1, 35-37	422.7	13.60	1.28	1.20	-0.84	2.30
46-2, 35-37	424.5	13.74	1.18	1.31	-0.73	2.16
46-3, 35-37	425.7	13.87	1.30	1.44	-0.69	2.47
46-4, 35-37	427.2	14.00	1.40	1.44	-0.94	2.46
46-5, 35-37	428.7	14.14	1.42	1.44	-1.03	2.37
46-6, 35-37	430.2	14.27	1.31	1.51	-1.09	2.42
47-1, 35-37	423.3	14.46	0.93	1.36	-0.77	2.09
47-2, 35-37	433.8	14.60	1.23	1.75	-1.30	2.47
47-3, 35-37	435.3	14.73	1.26	1.74	-1.17	1.70
47-4, 35-37	436.8	14.87	1.41	2.11	-0.90	2.69
47-5, 35-37	438.3	15.00	1.34	2.11	-1.24	3.08
47-6, 35-37	439.8	15.14	1.33	2.19	-1.00	2.88
48-1, 35-37	441.8	15.32	0.98	1.65	-1.23	2.21
48-2, 35-37	443.3	15.45	0.93	1.57	-1.03	2.20
48-3, 35-37	444.8	15.59	1.12	1.75	-0.94	2.68
48-4, 35-37	446.3	15.73	1.00	1.79	-1.05	2.35
48-5, 35-37	447.8	15.86	0.97	1.74	-1.18	2.58
48-6, 35-37	449.7	16.00	0.34	1.46	-1.04	2.44
48-7, 35-37	450.8	16.14	0.90	1.83	-0.79	2.39
*49-1, 35-37	451.5	16.20	0.95	1.51	-0.54	2.33
49-1, 35-37	451.5	16.20	--	--	0.85	1.77
49-2, 35-37	453.0	16.34	0.82	1.66	-0.75	2.42
*49-2, 35-37	453.0	16.34	0.96	1.20	--	--
49-3, 35-37	454.5	16.50	0.86	1.75	-0.68	2.35
*49-3, 35-37	454.5	16.50	1.00	1.36	--	--
49-4, 35-37	456.0	18.00	1.09	1.41	-0.83	2.20
49-4, 35-37	456.0	18.00	--	--	-0.68	1.72
*49-5, 35-37	457.5	18.06	1.27	1.52	-0.75	2.37
49-5, 35-37	457.5	18.06	--	--	0.93	1.64
*50-1, 35-37	461.0	18.19	0.84	1.24	-0.51	2.15
*50-3, 35-37	464.0	18.31	0.43	1.09	-1.04	2.14
50-3, 35-37	464.0	18.31	--	--	0.78	1.35
*51-1, 35-37	470.7	18.57	1.11	0.89	-0.56	1.72
*51-2, 35-37	472.2	18.63	1.15	0.79	-0.55	1.87
*51-3, 35-37	474.0	18.69	0.90	0.94	-0.87	1.95
*51-4, 35-37	475.2	18.74	--	--	-0.71	1.94
*51-4, 35-37	475.2	18.74	--	--	1.10	1.08
*51-5, 35-37	476.7	18.80	1.21	1.19	-0.45	1.80
*51-6, 35-37	478.2	18.86	1.34	1.04	-0.00	1.74
*52-1, 35-37	480.3	18.94	1.07	1.07	-0.97	1.68
*52-2, 35-37	481.8	19.00	1.33	0.98	-0.87	1.74
*52-3, 35-37	483.3	19.16	1.07	0.77	--	--
*52-4, 35-37	484.8	19.32	1.10	1.17	-0.41	1.94
*52-5, 35-37	486.3	19.48	1.10	1.32	-0.08	1.85
*52-6, 35-37	487.8	19.64	1.09	1.17	-1.21	2.15
*53-1, 35-37	489.8	19.86	1.28	1.34	-0.92	2.34
*53-2, 35-37	491.3	20.02	1.13	1.40	-1.16	2.33
*53-3, 35-37	492.8	20.18	1.30	1.35	-0.48	1.95
*53-4, 35-37	494.3	20.34	1.28	1.01	-0.60	1.73
*53-5, 35-37	495.8	20.50	0.88	0.98	-0.52	1.97
*53-6, 35-37	497.4	20.67	1.20	1.20	-0.39	1.84

SITE 591

Core-Section (interval in cm)	Sub-bottom depth (m)	Age (Ma)	$\delta^{18}O$ (°/oo PDB)	$\delta^{13}C$ (°/oo PDB)
			$\delta^{18}O$	$\delta^{13}C$
Hole 591[a]				
20-1, 35–37	174.6	3.37	2.27	0.64
20-1, 128–130	175.6	3.45	2.11	0.80
20-2, 35–37	176.1	3.49	2.22	0.83
20-2, 128–130	177.1	3.57	2.16	0.68
20-3, 35–37	177.6	3.61	2.13	0.73
20-3, 128–130	178.6	3.69	2.16	0.70
20-4, 35–37	179.1	3.73	2.23	0.71
20-4, 128–130	180.1	3.81	2.30	0.92
20-5, 35–37	180.6	3.85	2.18	0.82
20-5, 128–130	181.6	3.93	2.36	0.58
20-6, 35–37	182.1	3.97	2.04	0.58
20-6, 128–130	183.1	4.04	2.01	0.50
20,CC	183.8	4.10	2.27	0.72
21-1, 35–37	184.1	4.12	2.17	0.76
21-1, 128–130	185.1	4.20	2.26	0.86
21-2, 35–37	185.6	4.24	2.13	0.81
21-2, 128–130	186.6	4.32	2.29	0.73
21-3, 35–37	187.1	4.36	2.35	0.58
21-3, 128–130	188.1	4.44	2.13	0.68
21-4, 35–37	188.6	4.48	2.79	0.28
21-4, 128–130	189.6	4.56	2.25	0.65
21-5, 35–37	190.1	4.60	2.38	0.32
21-5, 128–130	191.1	4.66	2.26	0.67
21-6, 35–37	191.6	4.69	2.13	0.61
21-6, 128–130	192.6	4.75	2.17	0.72
22-1, 35–37	193.6	4.81	2.24	0.79
22-1, 128–130	194.6	4.86	2.35	0.63
22-2, 128–130	196.1	4.95	2.40	0.63
22-3, 35–37	196.6	4.98	2.20	0.88
22-3, 128–130	197.6	5.04	2.11	0.63
22-4, 35–37	198.1	5.07	2.43	0.35
22-4, 128–130	199.1	5.08	2.47	0.63
22-5, 35–37	199.6	5.08	2.31	0.80
22,CC	202.7	5.11	2.09	0.48
23-1, 35–37	203.0	5.12	2.30	0.43
23-1, 128–130	204.0	5.13	2.34	0.52
23-2, 35–37	204.5	5.13	2.07	0.32
23-2, 128–130	205.5	5.14	2.17	0.26
23-3, 35–37	206.0	5.15	2.28	0.33
23-3, 128–130	207.0	5.16	2.38	0.15
23-4, 35–37	207.5	5.16	2.10	0.58
23-4, 128–130	208.5	5.17	1.35	0.56
23-5, 35–37	209.0	5.18	2.38	0.49
23-5, 128–130	210.0	5.19	2.33	0.63
23-6, 35–37	210.5	5.19	2.26	0.73
23-6, 128–130	211.5	5.20	2.53	0.37
23,CC	212.1	5.22	2.24	0.49
24-1, 35–37	212.5	5.23	2.40	0.56
24-1, 128–130	213.4	5.25	2.40	0.69
24-2, 35–37	214.0	5.26	2.17	0.69
24-2, 128–130	214.9	5.29	2.27	0.37

[a] *Cibicidoides kullenbergi* used except in Samples 591-23-1, 35-37 cm, and 591-25-1, 128-130 cm, where *C. wuellerstorfi* was used.

Core-Section (interval in cm)	Sub-bottom depth (m)	Age (Ma)	$\delta^{18}O$ (‰ PDB) $\delta^{18}O$	$\delta^{13}C$ (‰ PDB) $\delta^{13}C$
Hole 591 (Cont.)				
24-3, 35–37	215.5	5.30	2.19	0.48
24-3, 128–130	216.4	5.32	2.23	0.75
24-4, 35–37	217.0	5.33	2.35	0.83
24-4, 128–130	217.9	5.36	2.61	0.33
24-5, 25–27	218.5	5.37	2.21	0.71
24-5, 128–130	219.4	5.40	2.09	0.59
24-6, 35–37	220.0	5.41	2.27	0.80
24,CC	221.5	5.45	2.30	0.62
25-1, 35–37	221.9	5.46	2.23	0.52
25-1, 128–130	222.8	5.48	2.36	0.38
25-2, 35–37	223.4	5.50	2.21	0.57
25-2, 128–130	224.3	5.52	2.27	0.80
25-3, 35–37	224.9	5.53	2.09	0.67
25-3, 128–130	225.8	5.56	2.11	0.34
25-4, 35–37	226.4	5.57	2.44	0.33
25-4, 128–130	227.3	5.59	2.19	0.44
25-5, 35–37	227.9	5.61	2.39	0.58
25-5, 128–130	228.8	5.63	2.31	0.48
25-6, 35–37	229.4	5.65	2.33	0.68
25-6, 128–130	230.3	5.67	2.45	0.69
25,CC	231.1	5.69	2.30	0.78
26-1, 35-37	231.5	5.70	2.18	0.60
26-1, 128–130	232.4	5.72	2.26	0.45
26-2, 35–37	233.0	5.74	2.24	0.57
26-2, 128–130	233.9	5.76	2.36	0.37
26-3, 35–37	234.5	5.77	2.04	0.47
26-3, 128–130	235.4	5.80	2.22	0.51
26-4, 35–37	236.0	5.81	2.24	0.37
26-4, 128–130	236.9	5.83	2.22	0.60
26-5, 35–37	237.5	5.85	2.31	0.65
26,CC	240.7	5.93	2.33	0.64
27-1, 35–37	241.0	5.94	2.02	0.59
27-1, 128–130	242.0	5.96	2.07	0.49
27-2, 35–37	242.5	5.97	2.26	0.39
27-2, 128–130	243.5	6.00	2.46	0.59
27-3, 35–37	244.0	6.01	2.33	0.49
27-3, 128–130	245.0	6.03	2.29	0.40
27-4, 35–37	245.5	6.05	2.26	0.35
27-4, 128–130	246.5	6.07	2.27	0.26
27-5, 35–37	247.0	6.08	2.18	0.19
27-5, 128–130	248.0	6.11	2.33	0.39
27-6, 35–37	248.5	6.12	2.24	0.51
27-6, 128–130	249.5	6.15	2.22	0.32
27,CC	250.3	6.17	2.20	0.53
28-1, 35–37	250.6	6.17	2.32	0.28
28-2, 35–37	252.5	6.22	2.40	0.67
28-3, 35–37	253.6	6.25	2.33	0.49
28-4, 35–37	255.1	6.33	2.28	0.47
28-5, 35–37	256.7	6.43	2.22	0.62
28-6, 35–37	258.7	6.52	2.26	0.49
29-1, 35–37	260.2	6.63	2.22	0.37
29-2, 35–37	261.7	6.72	2.21	0.76
29-3, 35–37	263.2	6.81	2.10	0.59
29-4, 35–37	264.7	6.90	2.10	0.60
29-5, 35–37	266.2	6.98	2.12	0.60
29-6, 35–37	267.7	7.07	2.22	0.80
29,CC	269.3	7.17	2.31	0.93
30-1, 35–37	269.7	7.19	2.25	0.66
30-2, 35–37	271.2	7.28	2.15	0.80
30-3, 35–37	272.7	7.37	2.01	0.89
30,CC	274.3	7.46	2.33	0.80
31-1, 35–37	274.7	7.48	2.09	0.83
31-2, 35–37	276.2	7.57	2.12	0.75
31-3, 35–37	277.7	7.66	2.09	0.85
31-4, 35–37	279.2	7.75	1.95	0.95
31-5, 35–37	280.7	7.83	2.04	0.86
31-6, 35–37	282.2	7.92	2.08	0.80
31,CC	283.1	7.97	2.31	0.85

Core-Section (interval in cm)	Sub-bottom depth (m)	Age (Ma)	$\delta^{18}O$	$\delta^{13}C$	Species (benthic)
			(‰ PDB)		
Hole 591B					
1-1, 35–37	271.0	7.27	2.29	0.82	*C. kullenbergi*
1-2, 35–37	272.5	7.35	2.22	0.95	*C. kullenbergi*
1-3, 35–37	274.0	7.44	2.23	0.99	*C. kullenbergi*
1,CC	280.2	7.80	2.04	0.78	*C. kullenbergi*
2-1, 35–37	280.5	7.82	2.15	1.02	*C. kullenbergi*
2-2, 35–37	282.0	7.91	2.20	0.98	*C. kullenbergi*
2-3, 35–37	283.5	8.00	1.95	1.01	*C. kullenbergi*
2,CC	289.8	8.37	2.03	0.84	*C. kullenbergi*
3-1, 35–37	290.2	8.39	2.17	1.02	*C. kullenbergi*
3-2, 35–37	292.0	8.50	1.96	1.11	*C. kullenbergi*
3-3, 35–37	293.2	8.57	1.05	0.71	*C. wuellerstorfi*
3-5, 35–37	296.2	8.74	2.10	0.96	*C. wuellerstorfi*
3,CC	299.4	8.93	2.17	1.25	*C. kullenbergi*
4-1, 35–37	299.8	8.95	2.38	1.19	*C. kullenbergi*
4-2, 35–37	301.3	9.04	2.21	0.82	*C. kullenbergi*
4-3, 35–37	302.8	9.13	2.34	1.01	*C. kullenbergi*
4-4, 35–37	304.3	9.22	2.19	1.03	*C. kullenbergi*
4-5, 35–37	305.8	9.30	2.34	1.08	*C. kullenbergi*
4,CC	308.8	9.48	2.20	0.97	*C. wuellerstorfi*
5-1, 35–37	309.2	9.50	2.34	1.11	*C. kullenbergi*
5-2, 35–37	310.7	9.56	2.33	1.14	*C. kullenbergi*
5-3, 35–37	312.2	9.62	2.27	0.93	*C. kullenbergi*
5-4, 35–37	313.7	9.67	2.38	1.00	*C. kullenbergi*
6-1, 35–37	318.5	9.86	2.03	1.38	*C. kullenbergi*
6-2, 35–37	320.0	9.91	2.40	1.10	*C. kullenbergi*
6-3, 35–37	321.5	9.97	2.29	1.14	*C. kullenbergi*
6-4, 35–37	323.0	10.03	2.35	1.33	*C. kullenbergi*
6-5, 35–37	324.5	10.08	2.29	1.19	*C. kullenbergi*
6,CC	327.6	10.20	2.21	1.36	*C. kullenbergi*
7-1, 35–37	328.0	10.22	2.24	1.18	*C. kullenbergi*
7-1, 35–37	328.0	10.22	2.24	1.18	*C. kullenbergi*
7-2, 35–37	329.5	10.27	2.15	0.95	*C. kullenbergi*
7-3, 35–37	331.0	10.33	2.02	1.04	*C. kullenbergi*
7-4, 35–37	332.5	10.39	2.09	0.99	*C. kullenbergi*
7-5, 35–37	334.0	10.44	2.23	1.02	*C. kullenbergi*
7-6, 35–37	335.5	10.50	2.29	0.98	*C. kullenbergi*
7,CC	337.2	10.57	2.44	0.99	*C. kullenbergi*
8-2, 35–37	339.0	10.63	2.09	0.82	*C. kullenbergi*
8,CC	346.8	10.93	2.30	0.69	*C. kullenbergi*
9-2, 35–37	348.7	11.00	2.10	0.79	*C. wuellerstorfi*
9,CC	356.4	11.44	2.12	0.72	*C. wuellerstorfi*
10-1, 35–37	356.8	11.46	1.74	0.85	*C. wuellerstorfi*
10-2, 35–37	358.3	11.55	1.89	0.97	*C. wuellerstorfi*
10-3, 35–37	359.8	11.63	2.14	1.10	*C. wuellerstorfi*
11-1, 35–37	366.3	12.00	2.08	1.41	*C. wuellerstorfi*
11,CC	375.6	12.19	1.81	0.96	*C. kullenbergi*
12-1, 35–37	376.0	12.20	1.42	1.41	*C. kuljenbergi*
12-2, 35–37	377.3	12.26	1.98	1.13	*C. kullenbergi*
12,CC	385.2	12.63	2.01	1.22	*C. kullenbergi*
13-1, 35–37	385.5	12.64	1.84	0.94	*C. kullenbergi*
13-2, 35–37	387.0	12.61	2.12	0.66	*C. kullenbergi*
13,CC	394.8	13.07	1.90	0.97	*C. kullenbergi*
14-1, 35–37	395.2	13.09	1.95	1.18	*C. kullenbergi*
14-2, 35–37	396.7	13.16	1.85	0.86	*C. kullenbergi*
14-6, 35–37	402.7	13.44	1.32	1.30	*C. kullenbergi*
14,CC	404.4	13.51	1.77	0.87	*C. kullenbergi*
15-1, 35–37	404.8	13.53	2.12	1.13	*C. kullenbergi*
15-3, 35–37	407.8	13.67	1.69	1.03	*C. kullenbergi*
17-1, 35–37	424.0	14.42	1.82	1.25	*C. kullenbergi*
17-2, 35–37	425.5	14.49	1.61	1.09	*C. kullenbergi*
17-3, 35–37	427.0	14.56	1.70	1.54	*C. kullenbergi*
17-4, 35–37	428.5	14.63	1.64	1.52	*C. kullenbergi*
18-1, 35–37	433.5	14.86	1.58	1.35	*C.wuellerstorfi*
18-2, 35–37	435.0	14.93	1.33	1.24	*C.wuellerstorfi*
18-3, 35–37	436.5	15.00	1.69	1.52	*C.wuellerstorfi*
18-4, 35–37	438.0	15.11	1.54	1.60	*C.wuellerstorfi*
18-5, 35–37	439.5	15.22	1.55	1.80	*C.wuellerstorfi*
18-6, 35–37	441.0	15.33	1.87	1.91	*C.wuellerstorfi*
19-1, 35–37	443.2	15.49	1.62	1.56	*C.wuellerstorfi*
19-2, 35–37	444.7	15.60	1.36	1.56	*C.wuellerstorfi*
19-4, 35–37	447.7	15.83	1.41	1.40	*C.wuellerstorfi*
19-5, 35–37	449.2	15.94	1.40	1.52	*C.wuellerstorfi*
20-1, 35–37	452.8	16.20	1.14	1.39	*C.wuellerstorfi*
20-2, 35–37	454.3	16.23	1.11	1.40	*C.wuellerstorfi*
20-3, 35–37	455.8	16.26	1.36	1.51	*C.wuellerstorfi*
20-5, 35–37	458.8	16.32	1.02	1.63	*O. umbonatus*
21-1, 35–37	462.3	16.39	0.71	1.74	*O. umbonatus*

Core-Section (interval in cm)	Sub-bottom depth (m)	Age (Ma)	$\delta^{18}O$	$\delta^{13}C$	Species (benthic)
			(‰ PDB)		
Hole 591B (Cont.)					
21-2, 35–37	463.8	16.42	0.68	1.29	*O. umbonatus*
21-3, 35–37	465.3	16.45	0.80	1.49	*O. umbonatus*
22-1, 35–37	472.0	16.59	0.87	1.74	*O. umbonatus*
22-3, 35–37	475.0	16.65	0.99	1.91	*O. umbonatus*
22-4, 35–37	476.5	16.68	0.93	2.01	*O. umbonatus*
22-5, 35–37	478.0	16.71	1.04	2.28	*O. umbonatus*
22-6, 35–37	479.5	16.74	1.11	1.97	*O. umbonatus*
23-1, 35–37	481.5	16.78	0.92	1.87	*O. umbonatus*
23-2, 35–37	483.0	16.81	0.80	2.03	*O. umbonatus*
23-3, 35–37	484.5	16.84	0.30	1.54	*O. umbonatus*
23-4, 35–37	486.0	16.87	0.42	1.30	*O. umbonatus*
23-6, 35–37	489.0	16.93	0.62	1.82	*O. umbonatus*
24-2, 35–37	492.7	17.00	0.87	1.28	*O. umbonatus*
24-3, 35–37	494.2	17.03	0.69	1.63	*O. umbonatus*
24-4, 35–37	495.7	17.06	0.54	1.05	*O. umbonatus*

43. QUATERNARY ISOTOPE STRATIGRAPHY OF HOLE 593, CHALLENGER PLATEAU, SOUTH TASMAN SEA: PRELIMINARY OBSERVATIONS BASED ON FORAMINIFERS AND CALCAREOUS NANNOFOSSILS[1]

Campbell S. Nelson and Chris H. Hendy, University of Waikato
and
Walter C. Dudley, University of Hawaii at Hilo[2]

ABSTRACT

A moderate-resolution isotope stratigraphy (with an average of one sample per 17,500 yr.) derived from the benthic foraminifer *Uvigerina* (or *Cibicides*), the planktonic foraminifer *Globigerina bulloides*, and calcareous nannofossil concentrates is presented for the entire Quaternary (and latest Pliocene) section of mid-upper bathyal calcareous oozes from DSDP Site 593, western Challenger Plateau, south Tasman Sea. Superimposed on a trend of gradually increasing average $\delta^{18}O$ values through the Pleistocene, reflecting the progressive buildup of polar ice sheets, is a record of high-frequency but generally low amplitude (0.5–1‰) isotope fluctuations in the early Quaternary (1.9–1.0 m.y.), followed by a greatly increased intensity (1.5–2.0‰) of glacial-interglacial fluctuations during the late Quaternary (< 1.0 m.y.). The standard late Quaternary isotope stages 1 to 24 are mainly resolvable. Significant excursions in both $\delta^{18}O$ and $\delta^{13}C$ values at various times during the Quaternary are suggested to be due to periodic, fundamental changes in ocean circulation properties over the plateau. For example, intensified upwelling of Antarctic Intermediate Waters during several glacial periods is indicated by the convergence of benthic and planktonic foraminiferal $\delta^{18}O$ data, and productivity variations may account for certain $\delta^{13}C$ spikes in the record. With increasingly higher resolution analysis this core will provide a useful Quaternary isotope reference section for southern temperate waters in the southwest Pacific, centered on New Zealand.

INTRODUCTION

Studies of the stable isotope composition of planktonic and benthic foraminifers, and more recently calcareous nannofossils, have become essential tools for paleoceanographic and paleoclimatic studies and in marine stratigraphic correlation (Kennett, 1982, 1983). The oxygen isotope record contains information on changes in ocean temperature and salinity, and especially on the isotope composition of ocean water as it relates to the extent of continental glaciations, thereby providing a stratigraphic link between on-land sequences and events in the oceans. Carbon isotope data can indicate changes in circulation patterns, productivity, and global carbon budget. Data from different organisms inhabiting specific depth ranges (i.e., coccolithophores, planktonic foraminifers, and benthic foraminifers) should ultimately permit reconstruction of stratification and circulation patterns of ancient oceans and elucidate the evolution of modern circulation patterns.

Detailed stable isotope stratigraphies of the Quaternary are available for much of the Atlantic and parts of the Indian and Pacific oceans (Emiliani and Flint, 1963; Emiliani, 1971; Shackleton and Opdyke, 1976; Prell, 1982; Shackleton et al., 1983; Imbrie et al., in press; Shackleton et al., 1984), but no high-resolution Quaternary isotope data are currently available for the southwest Pacific region. The area is ideal for isotope studies since every major surface water mass between equatorial and subantarctic latitudes is present over a relatively short traverse, and these water masses are underlain by shallow-water (< 2000 m) pedestals with rich calcareous sequences, mainly uncomplicated by dissolution and turbidite input. DSDP Leg 90 drilled these sequences at nine sites (Fig. 1) using the recently developed hydraulic piston corer, which provided both excellent quality cores and high sediment recovery rates of ~90%, prerequisites for high-resolution stratigraphic work.

This chapter reports preliminary isotope results for the Quaternary oozes at cool subtropical (temperate) Site 593. It is proposed ultimately to investigate the Quaternary isotope record at several of the other sites on Leg 90 to obtain an "isotope traverse" for subantarctic to equatorial latitudes. Work is in progress on the subantarctic (Site 594) cores (Nelson, Hendy, Cuthbertson, et al., this volume). These two southern sites (593 and 594) should be particularly useful as stable isotope reference sections against which on-land Quaternary sequences in Australasia, and especially those in New Zealand (Suggate et al., 1978), can be compared and more reliably correlated.

PREVIOUS WORK

Isotope analyses of earlier DSDP core samples from the southwest Pacific area have provided important information on general paleoclimate trends and the history of development of the Antarctic ice sheet through the Cenozoic (Shackleton and Kennett, 1975a, 1975b; Kennett and Shackleton, 1976; Kennett et al., 1979). Two of these studies (Shackleton and Kennett, 1975a; Kennett et al., 1979) dealt specifically with the late Cenozoic isotope history at DSDP Site 284, located close to present Site 593. Their principal result demonstrated three conspicuous episodes of cooling: in the latest Miocene (5.2–6.2 m.y. ago, Loutit and Kennett, 1979) associated with major expansion of Antarctic ice sheet; briefly in the middle Pliocene (~3.5 m.y. ago); and again in the late Pliocene (~2.6 m.y. ago), associated with the initiation of Northern Hemisphere glaciation. Emphasis in these papers was clearly directed at the late Tertiary core interval, and only eight sample points from the Quaternary section provided evidence of glacial oscillations (Kennett et al., 1979).

---

[1] Kennett, J. P., von der Borch, C. C., et al., *Init. Repts. DSDP*, 90: Washington (U.S. Govt. Printing Office).

[2] Addresses: (Nelson) Department of Earth Sciences, University of Waikato, Hamilton, New Zealand; (Hendy) Department of Chemistry, University of Waikato, Hamilton, New Zealand; (Dudley) Natural Sciences Division, University of Hawaii at Hilo, Hilo, Hawaii 96720.

SETTING AND QUATERNARY CORE CHARACTERISTICS AT SITE 593

Modern Oceanographic Setting

Site 593 (40°30.47′S; 167°40.47′E) is located in 1068 m of water near the western margin of Challenger Plateau, 270 km from the nearest land mass of northern South Island, New Zealand (Fig. 1). The site is a reoccupation of Site 284 cored during DSDP Leg 29 (Kennett, Houtz, et al., 1975). It is located some 400 km north of the present-day position of the subtropical convergence in the cool subtropical (temperate) water mass lying midway between true subtropical water masses north of New Zealand and subantarctic waters to the south (Knox, 1970).

Some properties of the water mass structure in the southern Tasman Sea are schematically illustrated in Figure 2. Surface circulation in the vicinity of Site 593 is dominated by the generally northeast-moving Tasman Current. The Current results from interaction of the Subantarctic Surface Water of the West Wind Drift with a complex system of anticyclonic eddies forming off southeastern Australia and fed by the subtropically derived East Australian Current (Stanton, 1973). Biological measurements of near-surface waters over Challenger Plateau show that present-day productivity in the vicinity of Site 593 is generally over twice that of the surrounding waters (Bradford and Roberts, 1978), possibly associated with topographic upwelling along the western edge of the Plateau and in Bellona Gap. The seafloor at Site 593 is presently under the influence of Antarctic Intermediate Water, with low salinity (~34.5‰) and a temperature of 4–5°C.

Lithology and Age

The uppermost six cores from Hole 593 (0–53.1 m sub-bottom depth) recovered Quaternary (Zones NN21–NN19a) through latest Pliocene (top Zone NN16) foraminifer-bearing (5–25%) to foraminifer (25–50%) nannofossil ooze.

Age control for the section (Fig. 3) is provided by both biostratigraphy and paleomagnetic stratigraphy (Site 593 report, this volume). Figure 3 includes a preferred (Curve A) and an alternative but less likely (Curve B), age interpretation for the sequence. At nearby Site 284, drilled on DSDP Leg 29, a middle Pleistocene disconformity was inferred to occur at ~9 m sub-bottom depth (Kennett, Houtz, et al., 1975; Kennett and Vella, 1975; Kennett et al., 1979). Hornibrook (1982) and A. R. Edwards (pers. comm. 1984) have subsequently discounted the evidence for such a hiatus. At Site 593 the shipboard micropaleontologic and lithologic data suggest that no major unconformities occur in the Quaternary sequence, although the Olduvai Subchron (1.66–1.88 m.y.) paleomagnetic event was at first not resolved (Site 593 site chapter, this volume); however, Barton and Bloemendal (this volume) have subsequently recognized an Olduvai interval from about 32–36 m sub-bottom depth. Based on the last occurrence of the nannofossil *Discoaster brouweri* the Plio/Pleistocene boundary is placed near the top of Core 593-6, at 43.9 m sub-bottom depth, giving an average sedimentation rate for the Quaternary of 23 m/m.y. (Fig. 3, Curve A).

A problem concerns the age of 1.45 m.y. for the last occurrence of the nannofossil *Calcidiscus macintyrei* at 17.74 m sub-bottom depth (Lohman, this volume). The date is inconsistent with the paleomagnetic age of about 0.75 m.y. at this level. If, in fact, the Jaramillo Subchron was replaced by the initially unresolved Olduvai Subchron, then the *C. macintyrei* age remains tenable, but necessitates a major (0.7 m.y.) disconformity at about 17 m sub-bottom depth (Fig. 3). This is unlikely for several reasons. In particular, it would demand impossibly high sedimentation rates (1035 m/m.y.) from 43.90 to 23.20 m sub-bottom, followed by unusually low ones through 17.74 m (Fig. 3, Curve B). Moreover, since rare occurrences of *C. macintyrei* are also recorded in topmost Zone NN21 sediments at 0.40 m sub-bottom depth (Lohman, this volume), and the Olduvai event (1.66–1.88 m.y.) has now been tentatively identified from 32–36 m sub-bottom (Barton and Bloemendal, this volume), the stratigraphic significance of the species at Site 593 requires further investigation.

METHODS

During routine shipboard sampling of Hole 593, 131 × 10 cm^3 samples were collected at 30–40-cm intervals from Cores 593-1 through 593-6, averaging four samples per core section or, for the Quaternary period, one sample per 17,500 yr. The very large numbers of samples requested by other scientists from Hole 593 precluded a more detailed sampling program at that time. Additional samples were subsequently obtained to increase the time-stratigraphic resolution in Cores 1 through 3 to about 5000 yr. but results of these will be presented elsewhere.

From 5 to 10 cm^3 of each sample was placed overnight in a 50-ml widemouth flask containing pH 9.4 buffer solution prepared by adding 4 g $NaHCO_3$ and 1 g Na_2CO_3 to 20 l of distilled water (Hay, 1977). Samples were gently agitated on an auto-shaker for 10–15 min. and then washed with buffer solution through a 63-μm mesh sieve. The <63-μm mud fraction (silt plus clay) settled overnight and the supernatant liquid was poured off to give a 50-ml volume suspension. This was shaken, 5-ml aliquot extracted by pipette, and the suspended mud concentrated onto preweighed Millipore filters to determine (× 10) the total weight of mud in the original sample. The remaining mud suspension was split and one portion was washed further over a 25-μm mesh sieve and the <4-μm-sized material siphoned off following settling of the 4-25-μm fraction. A suspension of the latter was examined using a scanning electron microscope (SEM) to note nannofossil abundance, and the remainder was dried and stored at 4°C for isotope analysis.

The sand fraction (>63μm) was washed with distilled water, sonic-probed for 10 s, and rinsed again over a 63-μm-mesh sieve to remove any released fines. The sand was washed on to filter paper, rinsed three times, dried, weighed, and the percentage of sand was deter-

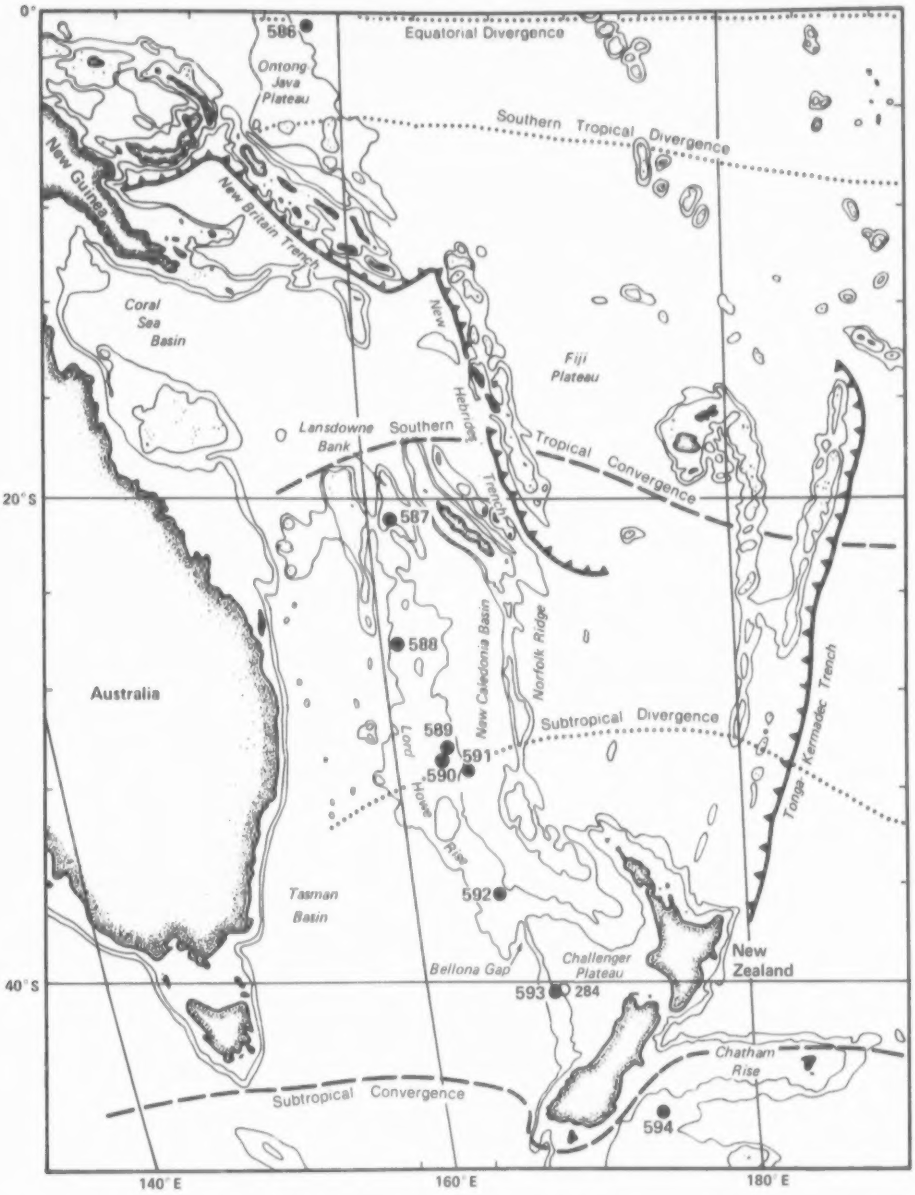
0°
586
Equatorial Divergence
Ontong Java Plateau
Southern Tropical Divergence
New Guinea
New Britain Trench
Coral Sea Basin
New Hebrides Trench
Fiji Plateau
Lansdowne Bank
Southern Tropical Convergence
20°S
587
588
Australia
New Caledonia Basin
Norfolk Ridge
Subtropical Divergence
Tonga-Kermadec Trench
589
591
590
Lord Howe Rise
Tasman Basin
592
Bellona Gap
Challenger Plateau
New Zealand
40°S
593
284
Chatham Rise
Subtropical Convergence
594
140°E
160°E
180°E

Figure 1. Location of Site 593 and Site 284 (Leg 29) with respect to other Leg 90 sites in the southwest Pacific and approximate position of boundaries between present-day surface water masses (after Knox, 1970). Contour lines show depths of 1 and 2 km.

nined. The dry sand was sieved over a 125-μm mesh screen, the >125-m fraction weighed to determine "coarse" sand content, and from it vere picked up to 40 specimens of each of the benthic foraminifer *Uvi- erina* sp. or, where rare or absent, *Cibicides* sp., and a uniform size raction of the planktonic foraminifer *Globigerina bulloides* d'Or- igny. Methanol was added to the vials containing the foraminiferal oncentrates, samples were sonic probed for 2 min., and the methanol vas allowed to evaporate. The cleaned foraminifers were then checked nd recounted, discarding any unsuitable specimens.

Purified foraminiferal samples and ~1 mg of the nannofossil samples were vacuum roasted at 400°C to remove any residual organic contaminants, crushed, and reacted with 100% orthophosphoric acid at 50°C until visible effervescence ceased, typically after 10–30 min. The evolved carbon dioxide and water were immediately removed by freezing at liquid nitrogen temperatures, and noncondensible gases were pumped away. The carbon dioxide was distilled from any other condensible gases at −110°C and passed directly into the cold finger inlet of a VG Micromass 602E mass spectrometer. The sample was compared to a working standard consisting of subsamples of a large volume of carbon dioxide prepared as previously described by reaction of Te Kuiti Limestone (TKL; Blattner and Hulston, 1978). This in turn was checked daily against carbon dioxide from the USGS Toilet Seat Marble standard, equivalent to NBS-19 (Coplen et al., 1983), and/or NBS-20 (Craig, 1957). Results are reported in standard notation as per

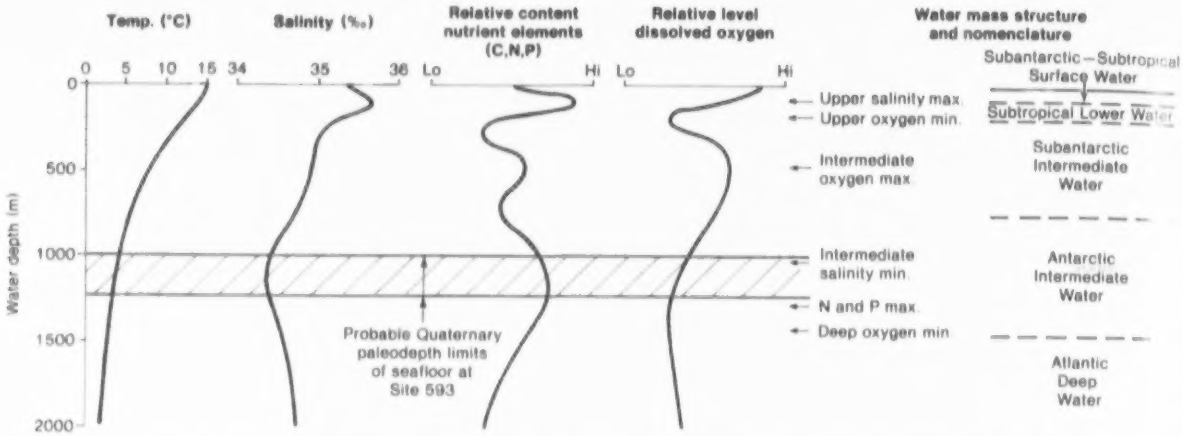

Figure 2. Vertical structure in water mass properties for the southern Tasman Sea in the vicinity of Site 593 (adapted from Rochford, 1960a, 196 Dal Pont and Newell, 1963; Knox, 1970).

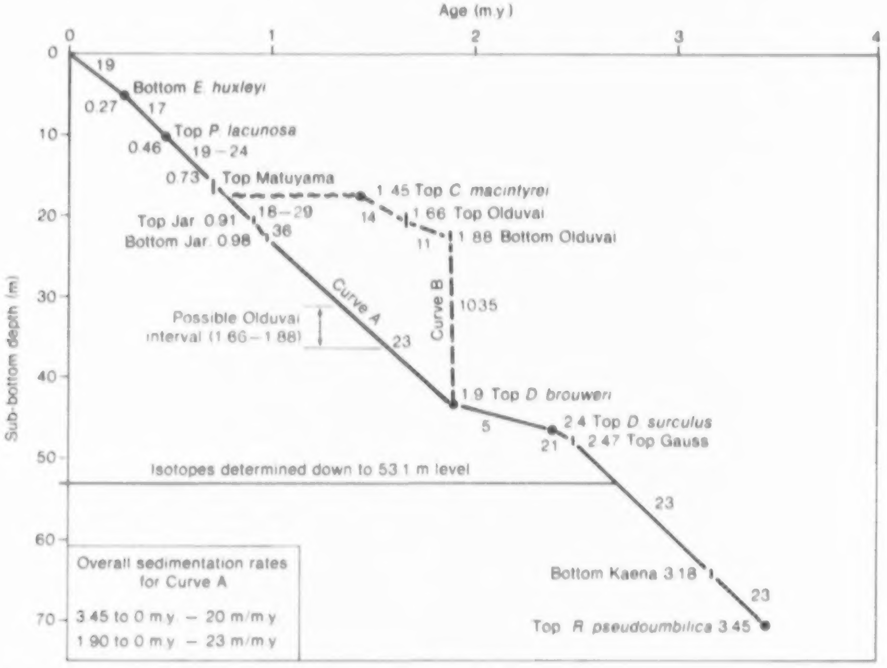

Figure 3. Age versus sub-bottom depth plot for late Pliocene to Recent interval of Hole 593. Whole numbers refer to sedimentation rates (m/m.y.) between the dated (m.y.) calcareous nannofossil and magnetostratigraphic levels. Curve A (solid line) is the preferred relationship; alternative Curve B (dashed line and unconformity) is discounted (see text). After this chapter was completed, Barton and Bloemendal (this volume) tentatively recognized the Olduvai Subchron from about 32-36 m sub-bottom depth, shown against Curve A.

mil (‰) deviations from the international PDB standard. The standard deviation from the mean value for replicate analyses of $\delta^{18}O$ of Toilet Seat Marble was 0.04‰ (n = 42), but for NBS-20 the standard deviation was 0.21‰ (n = 72) which may question the value of NBS-20 as an international isotope standard. This problem is currently being investigated. Replicate analyses of 8 microfossil concentrates gave reproducibility in the range 0.10 ± 0.05‰; however, insufficient replicates have been run to enable a meaningful standard deviation to be calculated.

RESULTS AND INTERPRETATION

Analytical results are listed in Table 1 and graphical displayed in Figure 4.

The benthic foraminifer *Uvigerina* precipitates its te close to oxygen isotope equilibrium with the surroun ing water (Shackleton, 1974) and so is regarded as a rel able indicator of bottom-water composition and/or ten

Table 1. Grain-size ratios (s:m, sand-to-mud; cs:fs, coarse sand-to-fine sand) and oxygen and carbon isotope values (‰) for samples from the latest Pliocene through Quaternary interval of Hole 593.

Sample (core-section, interval in cm)	Sub-bottom depth (m)	Grain-size ratios		Planktonic foraminifers		Benthic foraminifers		Bulk nannofossils	
		s:m	cs:fs	$\delta^{18}O$	$\delta^{13}C$	$\delta^{18}O$	$\delta^{13}C$	$\delta^{18}O$	$\delta^{13}C$
1-1, 30	0.31	0.29	1.81	3.75	1.27	4.18	1.04	3.19	2.18
1-1, 56	0.57	0.97	3.08	3.70	1.13	4.78	0.90	2.75	1.80
1-1, 80	0.81	0.68	1.85	2.97	1.56	4.03	1.10	2.20	1.28
1-1, 128	1.29	0.36	1.89	3.06	1.70	4.21	1.03	2.27	1.38
1-2, 30	1.81	0.43	1.66	2.90	1.54	3.79	1.33	1.70	1.86
1-2, 56	2.07	0.81	2.07	2.22	1.07	3.28	1.42	1.82	1.51
1-2, 80	2.31	0.28	1.83	3.24	1.09	4.56	0.79	2.51	1.88
1-2, 128	2.79	0.26	1.30	2.88	1.22	4.17	0.88	2.68	1.64
1-3, 30	3.31	0.18	1.36	3.17	1.25	4.12	0.29	2.98	2.59
1-3, 56	3.57	0.49	1.80	3.03	1.10	4.02	0.83	2.46	1.58
1-3, 80	3.81	0.69	2.26	2.76	1.17	4.14	0.91	2.04	1.99
1-3, 128	4.29	0.67	1.60	2.62	1.26	4.08	1.12	1.88	1.25
1-4, 30	4.81	0.34	1.93	2.39	0.60	4.11	0.63	3.04	2.08
1-4, 56	5.07	0.58	1.60	2.58	1.00	4.33	−0.49	3.20	2.25
2-1, 30	5.41	0.09	0.05	1.31	1.45	—	—	2.76	2.99
2-1, 80	5.91	0.36	2.08	3.51	1.43	4.35	0.29	3.63	3.38
2-1, 128	6.39	0.16	1.45	2.93	1.13	4.30	−0.07	2.91	2.97
2-1, 143	6.54	1.36	1.39	2.51	1.26	4.07	0.26	2.37	3.08
2-2, 30	6.91	0.42	4.65	2.14	1.15	3.90	0.35	2.75	3.07
2-2, 80	7.41	0.18	1.25	2.24	0.81	—	—	2.18	3.20
2-2, 128	7.89	0.19	1.39	1.55	0.90	—	—	2.76	2.83
2-2, 143	8.04	0.43	1.35	2.74	0.70	—	—	2.88	2.77
2-3, 30	8.41	0.18	1.93	3.46	1.08	4.54*	0.46*	4.33	3.77
2-3, 80	8.91	0.19	2.28	3.27	1.02	4.90*	0.78*	4.76	3.82
2-3, 128	9.39	0.15	1.41	2.59	0.20	3.87*	0.32*	4.25	3.83
2-3, 143	9.54	0.36	1.21	2.25	0.50	3.95*	−0.74*	3.90	3.47
2-4, 30	9.91	0.22	1.57	2.55	1.31	—	0.71	3.30	3.23
2-4, 80	10.41	0.15	1.28	3.03	1.40	3.55	1.06	2.93	3.02
2-4, 128	10.89	0.13	1.28	2.36	1.76	2.99	1.27	2.75	3.63
2-4, 143	11.04	0.43	1.23	2.54	1.01	3.41	0.38	2.31	3.57
2-5, 30	11.41	0.14	1.49	1.17	1.39	2.85	0.98	2.35	3.57
2-5, 80	11.91	0.21	1.04	2.30	0.34	3.55	0.43	3.34	3.54
2-5, 128	12.39	0.19	1.16	1.35	—	3.31	0.87	2.45	3.01
2-5, 143	12.54	0.68	1.43	1.16	1.71	3.35	0.44	3.60	3.06
2-6, 30	12.91	0.25	1.41	1.73	1.31	4.24	0.94	3.40	3.39
2-6, 80	13.41	0.76	1.54	0.66	0.41	3.47	0.74	2.44	2.28
2-6, 128	13.89	0.52	1.73	0.89	0.54	3.59	1.33	2.35	2.55
3-1, 30	15.00	0.81	2.33	1.81	0.37	3.64	0.68	2.77	1.29
3-1, 56	15.26	1.24	1.38	1.23	−0.16	3.46	0.55	1.90	0.75
3-1, 80	15.50	0.64	1.77	1.24	0.57	3.50	0.64	2.39	1.37
3-1, 128	15.98	0.24	1.94	1.96	1.28	2.88	0.95	2.24	1.84
3-2, 30	16.50	1.20	1.32	3.01	1.17	4.18	0.63	3.57	2.66
3-2, 56	16.76	0.42	1.34	3.01	1.21	3.89	0.33	3.81	3.05
3-2, 80	17.00	0.20	1.32	2.31	0.50	—	—	2.28	2.28
3-2, 128	17.48	0.53	1.33	2.33	0.88	2.47*	1.23*	1.59	1.49
3-3, 30	18.00	0.62	1.91	3.59	1.14	3.40*	1.15*	2.42	1.55
3-3, 56	18.26	0.81	1.54	3.32	1.08	3.73	0.42	2.53	1.52
3-3, 80	18.50	0.48	1.57	2.68	1.13	3.72	0.26	2.54	1.84
3-3, 128	18.98	0.46	1.93	2.42	1.08	4.14	0.37	2.71	1.98
3-4, 30	19.50	0.25	1.34	2.12	1.30	3.75	—	2.52	1.92
3-4, 56	19.76	0.47	1.51	2.57	1.69	2.74	1.10	2.44	2.02
3-4, 80	20.00	0.30	1.73	3.02	1.94	3.19	1.32	2.04	2.07
3-4, 128	20.48	0.16	4.34	2.04	1.06	2.82	1.20	1.58	1.84
3-5, 30	21.00	0.31	1.33	2.09	1.51	2.95	0.92	1.92	2.45
3-5, 56	21.26	0.33	0.67	1.26	0.97	3.21	0.84	2.17	2.24
3-5, 80	21.50	1.74	0.05	1.96	0.12	—	—	3.45	2.01
3-5, 128	21.98	0.21	1.53	2.92	1.68	2.35*	1.74*	2.43	2.25
3-6, 30	22.50	0.29	1.45	2.20	1.06	3.43	0.52	1.85	2.18
3-6, 56	22.76	1.05	1.82	2.19	1.15	3.77	0.53	2.65	2.19
3-6, 80	23.00	0.48	2.61	1.42	1.04	3.50	0.80	3.06	2.24
3-6, 128	23.48	0.25	1.52	0.52	0.65	2.33	1.13	2.53	3.07
4-1, 30	24.61	0.32	1.82	1.83	1.47	2.77	1.29	2.56	2.11
4-1, 56	24.87	1.01	0.88	2.13	1.45	3.69	0.91	2.46	2.46
4-1, 80	25.11	0.25	1.28	2.02	0.89	3.86	0.73	2.16	2.03
4-1, 128	25.59	0.40	1.57	1.59	1.14	2.99	1.14	2.22	1.95
4-2, 30	26.11	0.44	2.88	2.13	1.03	4.05	0.79	3.30	2.13
4-2, 56	26.37	0.68	3.94	2.13	1.50	3.38	0.83	2.92	2.26
4-2, 80	26.61	0.32	1.86	1.55	1.22	3.02	0.96	1.86	2.25
4-2, 128	27.09	0.37	1.69	1.87	1.47	3.02	0.53	1.73	2.21
4-3, 30	27.61	0.33	4.06	1.85	1.41	3.31	0.53	1.49	1.08
4-3, 56	27.87	0.53	1.73	1.44	1.54	—	—	1.65	1.70
4-3, 80	28.11	0.19	1.20	2.06	1.30	3.35	0.52	3.01	1.87
4-3, 128	28.59	0.36	1.46	1.85	1.47	2.69	0.55	1.50	1.77
4-4, 30	29.11	0.41	1.80	1.54	1.59	3.02	0.79	1.15	1.62
4-4, 56	29.37	0.61	1.81	2.01	1.53	3.30	0.79	1.47	1.60
4-4, 80	29.61	1.37	0.90	1.44	2.12	2.55	1.31	1.24	1.57
4-4, 128	30.09	0.45	1.66	2.13	1.96	3.57	1.19	1.68	1.89
4-5, 30	30.61	0.56	1.84	2.21	1.52	3.68	0.80	2.00	1.76
4-5, 56	30.86	0.65	1.34	1.96	1.81	3.10	1.26	1.20	1.83
4-5, 80	31.11	0.76	2.07	1.91	1.69	3.16	1.32	1.51	1.91
4-5, 128	31.59	0.41	1.95	1.78	1.80	3.08	1.39	1.35	1.39
4-6, 30	32.11	0.98	1.43	1.76	0.90	3.19	1.01	1.28	0.76
4-6, 56	32.37	0.85	1.29	1.75	0.97	3.14	0.97	1.26	0.08
4-6, 80	32.61	0.62	1.44	2.22	1.27	3.43	0.98	2.26	1.67
5-1, 30	34.21	0.44	1.91	2.06	1.51	2.93	1.09	2.50	1.69
5-1, 56	34.47	0.37	1.43	1.53	1.52	2.95	0.96	2.13	1.32
5-2, 80	34.71	0.45	1.77	2.48	1.36	2.86	0.13	2.06	1.50
5-2, 128	35.19	0.19	1.40	1.91	1.50	2.27	0.67	2.05	1.93
5-2, 30	35.71	0.11	1.11	1.62	1.64	2.48*	2.20*	2.39	2.65
5-2, 56	35.97	0.28	1.32	1.48	1.48	2.19*	2.06*	1.80	2.54
5-2, 80	36.21	0.26	1.27	1.92	1.55	2.15*	2.08*	3.09	2.70

Table 1. (Continued).

Sample (core-section, interval in cm)	Sub-bottom depth (m)	Grain-size ratios		Planktonic foraminifers		Benthic foraminifers		Bulk nannofossils	
		s:m	cs:fs	$\delta^{18}O$	$\delta^{13}C$	$\delta^{18}O$	$\delta^{13}C$	$\delta^{18}O$	$\delta^{13}C$
5-2, 128	36.69	0.34	1.37	1.27	1.73	2.67	0.91	2.03	2.28
5-3, 30	37.21	0.83	0.69	2.01	1.35	2.47*	1.16*	1.71	1.58
5-3, 56	37.47	0.94	1.42	2.03	1.54	2.22*	1.78*	2.04	1.65
5-3, 80	37.71	0.60	2.74	1.47	1.30	2.08*	1.77*	1.53	1.17
5-3, 128	38.19	0.31	1.22	1.77	1.43	2.41*	1.91*	2.23	2.18
5-4, 30	38.71	0.30	1.15	1.98	1.72	2.41*	1.49*	1.53	1.75
5-4, 56	38.97	0.20	1.65	1.51	1.39	2.37*	1.50*	1.93	1.71
5-4, 80	39.21	0.25	1.50	1.21	1.35	2.17*	1.63*	1.94	1.89
5-4, 128	39.69	0.19	1.60	1.74	1.06	2.07*	1.51*	2.04	1.79
5-5, 30	40.21	0.14	1.29	0.93	1.32	2.10*	1.75*	1.77	1.93
5-5, 56	40.47	0.36	1.69	1.22	1.22	2.07*	1.54*	1.57	1.70
5-5, 80	40.71	0.34	2.06	1.77	0.90	2.98	0.52	1.81	1.19
5-5, 128	41.19	0.24	1.54	1.32	0.37	2.56*	1.56*	1.56	1.48
5-6, 30	41.71	0.25	1.55	1.40	0.37	2.89*	1.43*	2.62	1.92
5-6, 56	41.97	0.33	1.81	1.28	0.67	2.55*	1.52*	1.72	1.64
5-6, 80	42.21	0.28	1.73	1.11	0.65	2.24*	1.66*	1.59	1.61
5-6, 128	42.69	0.28	1.48	1.39	1.13	2.46*	1.75*	1.87	1.90
6-1, 56	44.07	0.23	1.66	1.81	0.83	3.32	0.12	2.12	0.82
6-1, 80	44.31	0.30	1.49	1.39	1.27	2.83	0.93	1.79	1.63
6-1, 128	44.79	0.26	2.91	1.56	0.78	3.22	0.19	2.63	1.81
6-2, 30	45.31	0.26	1.97	1.37	1.16	2.60	0.13	1.69	1.31
6-2, 56	45.57	0.36	2.12	1.25	1.14	2.83	0.71	1.61	1.72
6-2, 80	45.81	0.36	1.75	1.22	1.30	2.70	0.76	2.27	1.79
6-2, 128	46.29	0.27	2.12	1.44	1.13	2.32	0.56	1.67	1.84
6-3, 30	46.81	0.27	2.18	1.02	0.91	1.97	0.50	1.56	1.55
6-3, 56	47.07	0.51	2.87	1.38	0.90	2.67	0.54	1.91	1.35
6-3, 80	47.31	0.25	2.16	1.06	1.23	2.44	0.79	1.70	1.76
6-3, 128	47.79	0.36	2.13	1.32	1.19	3.07	0.99	1.58	2.15
6-4, 30	48.31	0.23	1.98	1.51	1.12	3.57	0.45	1.73	1.95
6-4, 56	48.57	0.30	—	1.33	1.28	2.01	0.97	1.36	1.51
6-4, 80	48.81	0.20	1.21	0.75	0.91	—	—	1.71	1.67
6-4, 128	49.29	0.14	1.39	0.99	1.09	—	—	1.51	1.89
6-5, 30	49.81	0.22	1.72	0.68	1.19	—	—	1.37	1.53
6-5, 56	50.07	0.40	2.12	1.54	1.18	2.15	0.83	1.24	1.79
6-5, 80	50.31	0.15	1.54	0.96	1.39	2.99	0.61	1.51	1.92
6-5, 128	50.29	0.13	1.59	1.74	1.16	1.97*	0.73*	1.28	1.77
6-6, 30	51.31	0.12	0.99	1.14	1.33	1.16*	0.34*	1.60	1.92
6-6, 56	51.57	0.08	1.71	0.88	1.14	1.45*	1.18*	1.50	1.81
6-6, 80	51.81	0.11	1.32	1.34	1.01	2.26*	1.22*	1.59	1.76
6-6, 128	52.29	0.22	1.48	0.69	0.93	2.58	0.46	1.64	1.77

Note: Measurements for planktonic foraminifers are on *Globigerina bulloides*, for benthic foraminifers on *Uvigerina* sp. and, where asterisked, *Cibicides* sp., and for bulk calcareous nannofossil concentrates from the 4-25 μm sediment-size fraction. —, not determined.

perature (Vincent et al., 1981; Duplessy et al., 1984). Where *Cibicides* specimens had to be analyzed because of low abundance of *Uvigerina* in samples, their isotope values have been converted to nominal *Uvigerina* values for display purposes by the addition of 0.64‰ to the *Cibicides* $\delta^{18}O$ values and by subtracting 0.90‰ from the *Cibicides* $\delta^{13}C$ results (Shackleton and Opdyke, 1973; Shackleton and Cita, 1979; Duplessy et al., 1984).

Globigerina bulloides is a common species of the modern subantarctic assemblages of planktonic foraminifers (Kennett, 1969; Kennett and Vella, 1975; Vella et al., 1975). It has been widely used previously in isotope studies of cores from the Southern Ocean as an indicator of near-surface water mass characteristics (e.g., Hays et al., 1976a, 1976b; Kennett et al., 1979), although Kennett et al. (1979) suggested that the species may have undergone some vertical migration in the water column relative to other planktonic foraminifers.

The isotope results for the nannofossils are bulk values derived from relatively pure (>90%) polyspecific calcareous nannofossil concentrates. Since Dudley et al. (1980, 1982) have shown differing biological fractionations for different nannofossil species, the isotope composition of the bulk nannofossil samples cannot be interpreted as a function of ocean composition and temperature until species abundances are known.

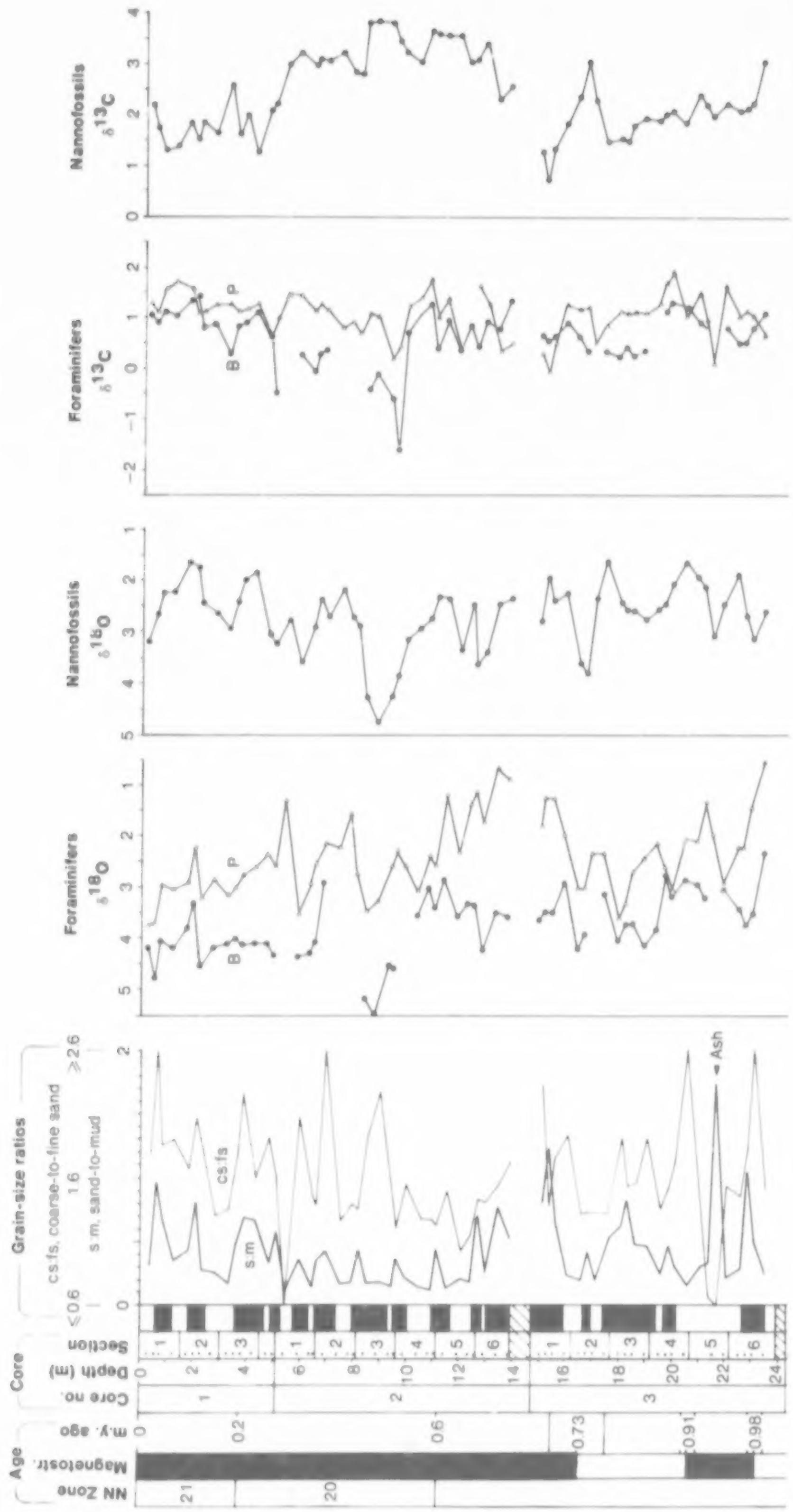
Nannofossils
$\delta^{13}C$
0
1
2
3
4
Foraminifers
$\delta^{13}C$
-2
-1
0
1
2
P
B
Nannofossils
$\delta^{18}O$
1
2
3
4
5
Foraminifers
$\delta^{18}O$
1
2
3
4
5
P
B
Grain-size ratios
cs:fs, coarse-to-fine sand
s:m, sand-to-mud
≤0.6
1.6
≥2.6
0
2
cs:fs
s:m
Ash
Core
Section
Depth (m)
Core no.
1 2 3 1 2 3 4 5 6 1 2 3 4 5 6
0 2 4 6 8 10 12 14 16 18 20 22 24
1
2
3
Age
m.y. ago
Magnetostr.
NN Zone
0
0.2
0.6
0.73
0.91
0.98
21
20

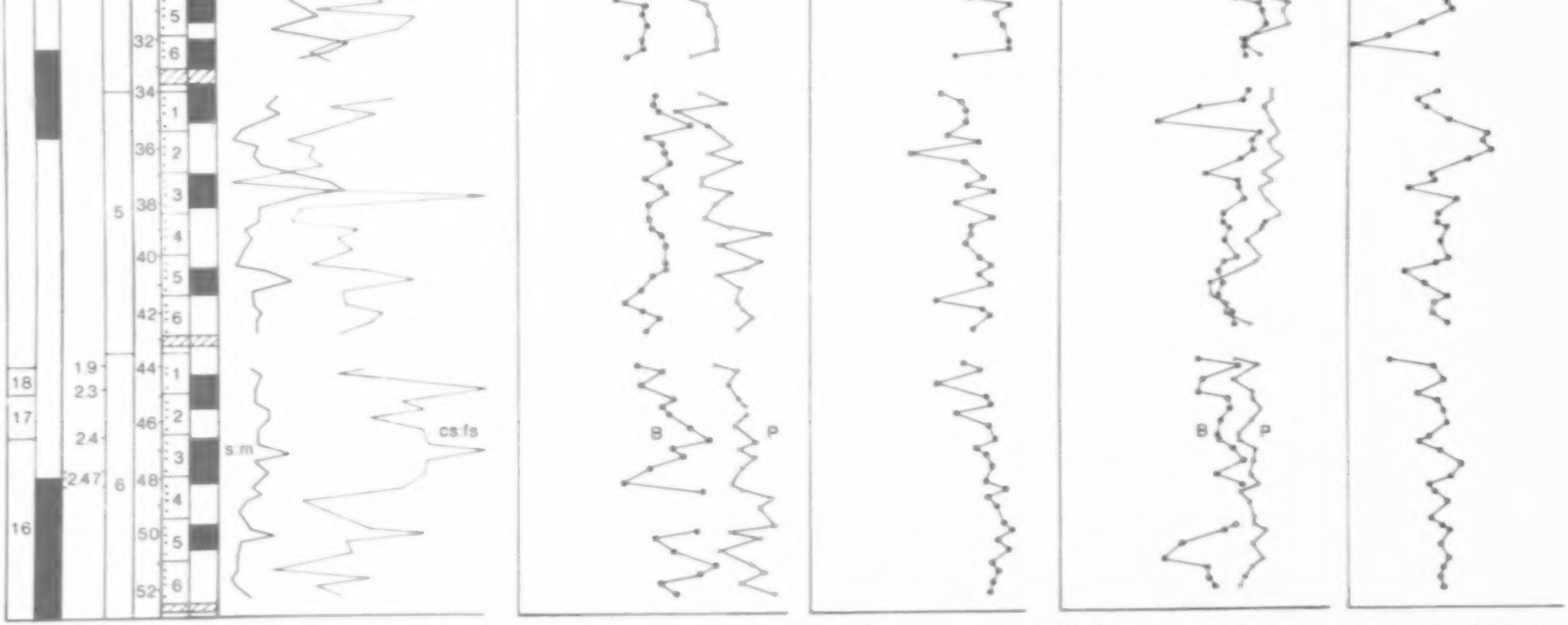

Figure 4. Sediment texture and oxygen and carbon stratigraphic logs for the latest Pliocene through Quaternary interval of Hole 593. Magnetic record shows in black from top to bottom the Brunhes Normal Chron, the Jaramillo Normal Subchron, possible Olduvai Normal Subchron (1.66–1.88 m.y.; Barton and Bloemendal, this volume), and the upper part of the Gauss Normal Chron. Alternating black-and-white intervals down the grain-size log correspond to relatively coarser and finer sediment zones, respectively. Isotope values are in per mil deviations (‰) from the international PDB standard. B, benthic foraminiferal curve based on *Uvigerina* sp. and sometimes *Cibicides* sp. (see Table 1), the latter having been converted to nominal *Uvigerina* values for display purposes (see text for explanation); P, planktonic foraminiferal curve based upon *Globigerina bulloides*.

Sediment Texture

Detailed textural analysis of the samples is in progress and only the ratios of sand (>63 μm) to mud (<63 μm) and of coarse (>125 μm) to fine (63–125 μm) sand are mentioned briefly here. Variations in both ratios reflect mainly the changing abundances of foraminifers in samples. An increase in the sand-to-mud (s:m) ratio corresponds with an increase in the content of both whole and broken foraminifers in samples, whereas the higher ratios of coarse-to-fine sand (cs:fs) reflect mainly larger numbers of mature, whole foraminifers in samples. In the vicinity of two ash layers (Fig. 4) the sand fraction includes, or is dominated by, glass shards (Nelson, Froggatt, et al., this volume).

Cyclical changes in the s:m and cs:fs ratios occur in the core (Fig. 4). The sand content of samples varies from about 10 to rarely as much as 50% and is dominated mainly by coarse sand, forming 50–70% of the sand fraction. With some exceptions the two ratio curves are broadly in phase, although the intensity of ratio fluctuations is more marked for the cs:fs curve. A very tentative scheme of alternating grain-size zones, each characterized by an overall relative increase or decrease in sediment coarseness compared to its neighboring zone, is suggested in Figure 4. The coarser textured intervals are generally more conspicuously burrowed and darker colored (light gray to greenish gray) than the finer oozes (very light gray) and, from the broad relationship between sediment color and isotope stages (Table 2), the coarser oozes apparently are associated mainly with glacial periods.

In other Pacific Ocean cores, glacial stage sediments are generally characterized by less dissolution of foraminifers than are interglacial ones (e.g., Thompson and Saito, 1974; Shackleton and Opdyke, 1976; Volat et al., 1980) and they are therefore relatively coarser grained. The shallowness (1068 m) of Site 593, well above the lysocline depth of about 2500 m at 40°S in the Pacific (Berger, 1976), as well as the excellent preservation of both foraminifers and nannofossils in Challenger Plateau cores (see the Site 593 report, this volume; Jenkins, 1975; Kennett and Vella, 1975; Hornibrook, 1982), argue against dissolution as a major factor controlling the grain-size variations. Instead, the topographic elevation of the site (Fig. 1) and its coincidence in depth with the north-flowing core of Antarctic Intermediate Water (Fig. 2) suggest that changes in the rates of lateral transport or intensity of winnowing by bottom currents may have been the principal factors determining sediment texture. The general correspondence between darker colored oozes, relatively coarser sediment intervals, and glacial isotope stages at Site 593 is then compatible with the more intensified patterns of ocean circulation commonly ascribed to glacial conditions (Valencia, 1977; Volat et al., 1980).

Table 2. Relationship between isotope stages and sediment color in the top 19 m of core in Hole 593.

Interglacial isotope stage	Sediment color[a]			Glacial isotope stage	Sediment color		
	N8	N7	5GY		N8	N7	5GY
1	X			2		X	
3			X	4			X
5	X	X		6		X	X
7	X	X		8			X
9	X			10		X	X
11	X		X	12	X		
13	X			14	X		
15	X			16			X
17			X	18		X	
19	X			20	X		X
21	X			22	X		
23		X	X				

[a] N8 = very light gray; N7 = light gray; 5GY = greenish gray.

Oxygen Isotope Stratigraphy

The foraminiferal oxygen isotope record for the last 1 m.y. has been compared (Fig. 5) to the records from other long-duration cores, in particular those from the western Caribbean DSDP Hole 502 (Prell, 1982) and the equatorial Pacific Core V28-239 (Shackleton and Opdyke, 1976). It is evident that despite our rather large sampling interval of about 17,500 yr., sufficient detail is present to allow tentative identification of most of the standard isotope stages (Emiliani, 1955; Shackleton and Opdyke, 1976). In particular, the major glacial–interglacial transitions are recognizable with the exception of boundary 17/18, which appears to fall within the gap between Cores 593-2 and 593-3, and of transition 11/12, which is subdued. The coarse sampling interval dictated by DSDP shipboard sampling restrictions has provided only about 3 to 6 points per glacial–interglacial cycle. This has made detailed correlation between this record and those of other cores difficult as the highs, lows, and fine structure of each glacial–interglacial cycle are not necessarily located. Furthermore, it is not possible to distinguish between the loss of parts of isotope stages through winnowing as opposed to absence occasioned by their lying between sample points.

Correlation is aided by the magnetostratigraphy (Fig. 5), which enables placement of the 19/20 boundary at the conclusion of the Matuyama Chron, and of the 23/24 boundary at the close of the Jaramillo Subchron, and is further strengthened by the last appearance of *Pseudoemiliania lacunosa* at 9.91 m at the isotope stage 11/12 boundary, and the first appearance of *Emiliania huxleyi* at 5.07 m within isotope stage 7. These are consistent with the results of Thierstein et al. (1977) who found *P. lacunosa* extinction during isotope stage 12 and the first appearance of *E. huxleyi* during isotope stage 8. It has proved difficult to resolve positively the isotope stages between the base of the Brunhes and the base of the Jaramillo, because at Site 593 only one glacial stage was identified within the Jaramillo, and three were identified between the top of the Jaramillo and the base of the Brunhes. It is our opinion that isotope stage 23 occurs at about 20 m sub-bottom, and that the apparent discrepancy between this and the level of the top of the Jaramillo may be resolved by sampling at closer intervals. Below the Jaramillo our oxygen isotope record is of little assistance in establishing a chronology for the core since the magnitude of glacial–interglacial changes in $\delta^{18}O$ is smaller and their frequency greater, a situation seen also in the other cores (Fig. 5) and elsewhere (e.g.,

READEX best copy available pages tightly bound

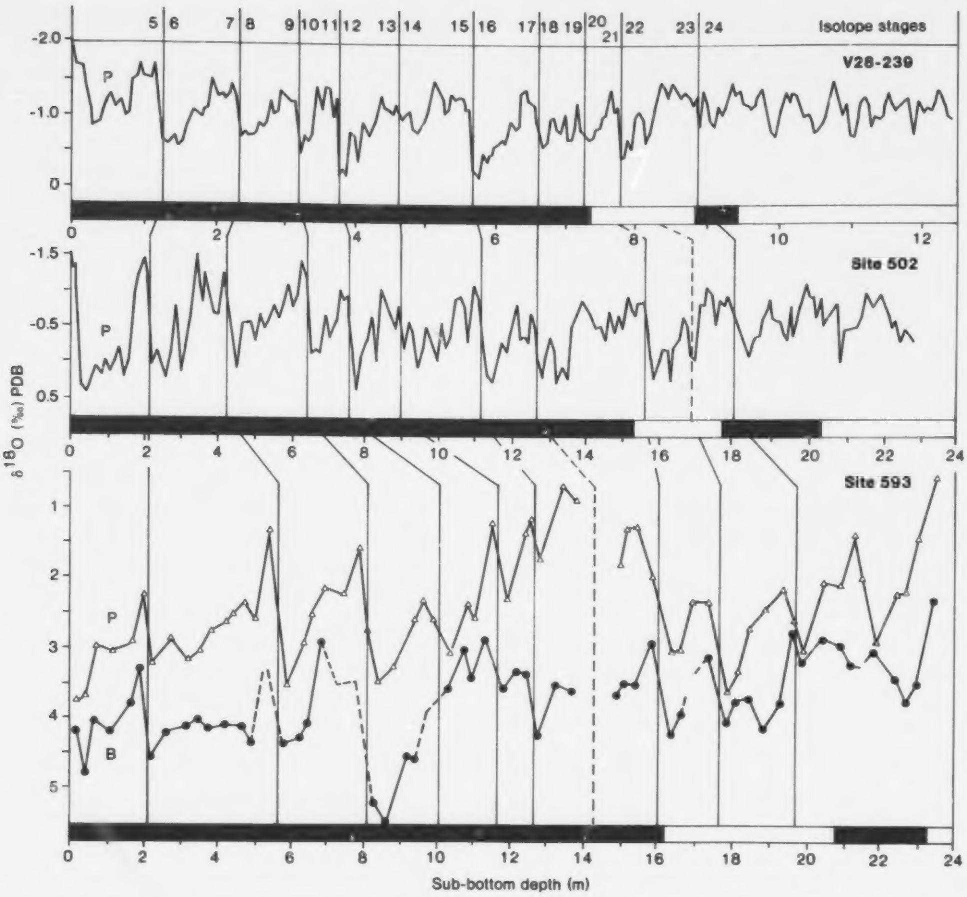

Figure 5. Occurrence of numbered standard isotope stages in late Pleistocene interval of Hole 593 based on correlation with cores at DSDP Site 502 (Prell, 1982) and Core V28-239 (Shackleton and Opdyke, 1976). Note the increasing scale of thickness from Core V28-239 to DSDP Sites 502 and 593. Black bars correspond to Brunhes Normal Chron (0–0.73 m.y.) and Jaramillo Normal Subchron (0.91–0.98 m.y.) intervals. B, benthic foraminiferal curve; P, planktonic foraminiferal curve.

Van Donk, 1976). The importance of this shift in average and amplitude of the $\delta^{18}O$ signal at about 900 × 10^3 yr. ago has been emphasized by Pisias and Moore (1981) and Prell (1982). It reflects a fundamental change in the global ice budget between the early and late Quaternary and has been related to major expansion of Arctic ice sheets and development of large floating Arctic Ocean ice masses at about the time of the Jaramillo Subchron (Williams et al., 1981).

Despite the limitations in identification of isotope stage boundaries, we have used those indicated in Figure 5, in conjunction with the established ages of the isotope stage boundaries (Imbrie et al., in press) and the magnetic datum points, to estimate average sedimentation rates in the core (Table 3). These vary between 1.66 and 3.13 cm/10^3 yr. and are sufficiently high to minimize the smoothing of the isotope record as a result of sediment mixing by organisms (Shackleton and Opdyke, 1976), especially since bioturbation is apparently not intensive in the cores (Nelson, this volume). Consequently, the coarse sampling intervals have tended to yield a more er-

Table 3. Average sedimentation rates at various times in the Quaternary of Hole 593 based mainly on the position of late Pleistocene isotope stages and their probable ages (Imbrie et al., in press).

Stratigraphic interval	Sub-bottom depth (cm)	Age range (× 10^3 yr.)	Sedimentation rate (cm/10^3 yr.)
Present-5/6	0–215	0–128	1.68
5/6–7/8	215–565	128–245	2.99
7/8–9/10	565–795	245–338	2.47
9/10–11/12	795–1010*	338–427	2.42
11/12–13/14	1010*–1185	427–508	2.16
13/14–15/16	1185–1380	508–620	1.74
15/16–19/20	1380–1620	620–737	2.05
19/20–21/22	1620–1770	737–785	3.13
21/22–Base Jar	1770–2325	785–980	2.85
Base Jar–M/G	2325–4800	980–2470	1.66

Note: Jar, M, and G refer to Jaramillo, Matuyama, and Gauss magnetic periods; 5/6 = boundary between stages 5 and 6, etc.
* position inferred.

ratic curve with a larger spread of $\delta^{18}O$ values than either Core V28-239 or DSDP Hole 502 (Fig. 5). Furthermore, it appears that no unconformities of more than a few tens of centimeters are possible above the base of the Jaramillo Subchron.

The fluctuations in the $\delta^{18}O$ record of the planktonic and benthic foraminifers and of the calcareous nannofossils are mainly concordant and match those found in the many deep-sea cores that have been analyzed over the last 30 yr. The isotope fluctuations are a response to the combined effects of changing $^{18}O/^{16}O$ ratio of ocean water due to the growth and waning of the major ice sheets, and of changing temperature due to climate and ocean circulation changes. The dominant effect during the late Pleistocene has been the growth and recession of ice sheets (Shackleton, 1967), which has resulted in fluctuations in the $\delta^{18}O$ of benthic and planktonic foraminifers of about 1.6‰ on a time scale of approximately 100 × 10^3 yr. per cycle.

Several features of the $\delta^{18}O$ record of Hole 593 deserve comment. Throughout the Pleistocene there is a gradual increase in the average $\delta^{18}O$ value in all three of the isotope records. Comparing the mean values from below the Jaramillo (23.4–52.3 m) to those within the Brunhes (0–16.3 m), the planktonic foraminifers increase from 1.56 to 2.41‰, the benthic foraminifers increase from 2.93 to 3.95‰, and the calcareous nannofossils increase from 1.86 to 2.82‰. This long-term increase in $\delta^{18}O$ is also evident in many other long cores (e.g., Van Donk, 1976; Prell, 1982; Shackleton et al., 1984) and presumably reflects mainly an overall gradual increase in polar ice volume through the Quaternary. For our planktonic foraminiferal record the increase is brought about by a progressively greater difference between the interglacial and glacial values, with the interglacial values remaining within the range of +1.0 to +1.5‰ throughout, whereas the glacial values increase from a range of +2.0 to +2.5‰ in the early Pleistocene to a range of +3.0 to +3.5‰ in the late Pleistocene. Again, a generally similar situation is evident in records from the Indian (Imbrie et al., in press), eastern Pacific (Shackleton and Hall, 1982), and Atlantic (Prell, 1982) oceans.

Compared to the *Globigerina bulloides* values, the *Uvigerina* $\delta^{18}O$ values generally remain approximately 1.5‰ more positive during the late Pleistocene interglacial periods and 1.3‰ more positive during glacial periods. The difference is less than might be predicted from the modern observed temperature gradient of about 10°C between surface and bottom waters at Site 593 (Fig. 2). Both records fall within the range of isotope values reported by Kennett et al. (1979) on the basis of their few Quaternary analyses at nearby Site 284. Since *Uvigerina* has been shown to deposit its test in isotopic equilibrium with seawater (Shackleton, 1974) and is restricted to living at the seafloor, the discrepancy between the planktonic and benthic curves may result from *G. bulloides* depositing at least some of its carbonate at a depth within the water column or within a restricted temperature season. If, however, *G. bulloides* maintained much the same depth habitat and seasonal growth patterns throughout, the change in the difference between the planktonic and benthic curves suggests a glacial–interglacial change in temperature gradient between surface waters and bottom waters of only about 1°C in the vicinity of Site 593 throughout the late Pleistocene. This value is less than the 2–4° cooling of sea-surface temperatures estimated by CLIMAP Project Members (1981) to have occurred in the south Tasman Sea about 18 × 10^3 yr. ago compared to the present day, but may be achieved by a modest cooling of bottom waters (currently 4–5°C) by 1–3°C.

Whereas the benthic foraminiferal $\delta^{18}O$ record is generally 1.3 to 1.5‰ more positive than the planktonic record, there are several intervals in the core where the two records converge. This is particularly apparent at 35 m, at 22 m (isotope stage ?26), at 20 m (isotope stage 24), at 18 m (isotope stage 22), and at 10.4 m (isotope stage 12). In each of these instances the isotope convergence has occurred during a glacial period and in three cases it has resulted in a simultaneous decrease in the benthic and increase in the planktonic $\delta^{18}O$ record. We interpret this as evidence for the development of periods of intensified upwelling over the shallow Challenger Plateau and thus for possible significant changes in the pattern or intensity of circulation of the intermediate waters in the southwest Pacific (Fig. 2) during several of the Pleistocene glaciations. More vigorous current activity at these times can explain the frequent association of coarser oozes with glacial periods as a result of fine sediment winnowing, as mentioned earlier.

An extremely positive excursion of $\delta^{18}O$ values is recorded in the benthic curve during isotope stage 10 (Fig. 5), with $\delta^{18}O$ values approximately 1‰ greater than for other glacial periods. This positive $\delta^{18}O$ anomaly is matched also by the bulk calcareous nannofossil $\delta^{18}O$ data (Fig. 4), by the sudden absence of *Uvigerina* specimens from the benthic foraminiferal population (Table 1), and partly by the occurrence of rather low foraminiferal $\delta^{13}C$ values over this interval (Fig. 4). We interpret the anomaly as representing the appearance of a major pulse of much colder (by as much as 4°C) bottom waters on the Challenger Plateau at this time (about 350 × 10^3 yr. ago), although we do not understand the greatly increased nannofossil $\delta^{18}O$ at this time.

The significant positive $\delta^{18}O$ excursion of about 1.5‰ at 48.5 m depth occurs close to the Matuyama/Gauss boundary (2.47 m.y.) and is probably an expression of the rapid expansion of Northern Hemisphere ice sheets from about 2.6 to 2.4 m.y. ago (Shackleton and Kennett, 1975a), which involved also the first extensive calving of icebergs into the North Atlantic (Shackleton et al., 1984). Since no corresponding excursion appears in either the planktonic or nannofossil record, we assume that the benthic excursion was the result of a decrease in bottom-water temperatures, with perhaps the appearance of Atlantic Deep Water at Site 593.

The $\delta^{18}O$ record of the calcareous nannofossils roughly parallels the foraminiferal isotope curves, showing the same long-term increase in $\delta^{18}O$ through the Pleistocene, and the increasing amplitude of glacial–interglacial cycles over the last 1 m.y. Phase correspondence of the $\delta^{18}O$ signal with the planktonic foraminiferal record is good in Cores 593-1, -2, and -4, and fair in Cores 593-3, -5, and -6. The overall amplitude of the nannofossil cycles is about 50% greater than that of the planktonic foraminifers. This probably reflects the consistently shallower (< 150 m) depth habitat of the coccolithophores, which should therefore record the largest glacial–interglacial paleotemperature change, as well as perhaps a damping of the paleotemperature signal provided by the planktonic foraminifers because of migration to different depths during interglacial and glacial periods (Emiliani, 1966). More precise interpretations of the nannofossil curve will have to take into account the effect of species-specific "vital effects" (Dudley et al., 1982) on the overall isotope composition of the nannofossil assemblages sampled.

Carbon Isotope Stratigraphy

Although the determination of $\delta^{18}O$ on carbonates usually requires the simultaneous determination of $\delta^{13}C$, very much less is known about the significance of carbon isotope stratigraphy of oceanic cores, and much of the data produced as a consequence of the oxygen isotope studies remains unpublished. No attempt is made here to interpret the $\delta^{13}C$ stratigraphy, but the analyses are presented in Table 1 and Figure 4 for completeness.

SUMMARY

1. The Quaternary section of Hole 593 comprises 43.9 m of foraminifer-bearing nannofossil oozes, deposited in about 1000 m water depth at an average rate of 2.3 cm/10^3 yr., from which has been obtained a moderate-resolution (sample/17,500 yr.) isotope stratigraphy for the entire Quaternary (and latest Pliocene) based on analyses of the benthic foraminifer *Uvigerina* (or *Cibicides*), the planktonic foraminifer *Globigerina bulloides*, and bulk calcareous nannofossil samples (4–25μm).

2. All the records show a gradual increase in the average $\delta^{18}O$ value through the Pleistocene in response to a progressive increase in the volume of ice locked in polar ice sheets. However, despite this long-term increase, maximum interglacial $\delta^{18}O$ values remain similarly low throughout the record. Two modes of Quaternary $\delta^{18}O$ variation (Prell, 1982) are evident: low values with generally low variability in the early Quaternary (1.9–1.0 m.y.), and higher values with high variability during the late Quaternary (< 1.0 m.y.). The greatly increased intensity of glacial–interglacial fluctuations since about the start of the Jaramillo Subchron has been related to significant growth of sea ice in the Arctic Ocean (Williams et al., 1981).

3. The standard late Quaternary isotope stages 1–24 are generally resolvable, but uncertainties remain since the coarse sampling intervals have resulted in much of the fine structure being missed.

4. With some exceptions, the benthic and planktonic foraminiferal $\delta^{18}O$ trends roughly parallel each other, indicating generally little change in the temperature difference between surface and bottom (intermediate) water masses at the site. However, during at least five periods, the $\delta^{18}O$ values for the benthic and planktonic foraminifers converge closely. These all occur during planktonic $\delta^{18}O$ maxima, a fact suggestive of intensified upwelling of Antarctic Intermediate Waters over the Challenger Plateau during some glacials. Highly positive $\delta^{18}O$ values of benthic foraminifers during isotope stage 10 indicate a major, but temporary, intrusion of bottom waters near 0°C on to the Plateau around 350 × 10^3 yr. ago.

5. The calcareous nannofossil $\delta^{18}O$ record is in good to fair agreement with the foraminiferal curves. The isotope cycles are of greater amplitude, possibly because of an increased temperature effect on the record.

6. Compared to the interglacial oozes (very light gray), the oozes of glacial stages are often darker colored (light gray to greenish gray), more conspicuously burrowed, and coarser grained (foraminifer-enriched). The coarse sediment intervals are ascribed to periods of increased intensity of winnowing by Antarctic Intermediate Bottom Waters.

ACKNOWLEDGMENTS

We gratefully thank Mark Lawrence, Scott Nodder, Alison Cuthbertson, and Steve Bergin for considerable assistance with sample preparation and operation of the mass spectrometer; Dr. Graham Gibson (Geology Department, University of Auckland) for verification of foraminiferal identifications; Tony Edwards (N.Z. Geological Survey, Lower Hutt) and Dr. Bill Lohman (Marathon Oil Co., Denver) for information relevant to refining microfossil age datums in the core; and Professor Warren Prell (Department of Geological Sciences, Brown University) and an anonymous reviewer for comments of this manuscript. The work was partly financed by University Grants Committee research number 88/125 to C. S. Nelson and by the U.S.–New Zealand Cooperative Science Program (No. 80-N2-05), Division of International Programs, U.S. National Science Foundation.

REFERENCES

Berger, A. H., 1976. Biogenous deep-sea sediments: production, preservation, interpretation. *In* Riley, J. P., and Chester, R. (Eds.), *Chemical Oceanography* (2nd Ed.) London (Academic Press), 5: 265–387.

Blattner, P., and Hulston, J. R., 1978. Proportional variations of geochemical $\delta^{18}O$ scales—an interlaboratory comparison. *Geochim. Cosmochim. Acta*, 42:59–62.

Bradford, J. M., and Roberts, P. E., 1978. Distribution of reactive phosphorus and plankton in relation to upwelling and surface circulation around New Zealand. *N.Z. J. Mar. Freshw. Res.*, 12:1–15.

CLIMAP Project Members, 1981. Seasonal reconstructions of the earth's surface at the last glacial maximum. *Geol. Soc. Am. Map Chart Ser*, MC-36.

Coplen, T. B., Kendall, C., and Hopple, J., 1983. Comparison of stable isotope reference samples. *Nature*, 302:236–238.

Craig, H., 1957. Isotopic standards for carbon and oxygen and correction factors for mass-spectrometric analysis of carbon dioxide. *Geochim. Cosmochim. Acta*, 12:133–140.

Dal Pont, G., and Newell, B., 1963. Suspended organic matter in the Tasman Sea. *Aust. J. Mar. Freshw. Res.*, 14:155–165.

Dudley, W. C., Brand, L. E., Blackwelder, P. L., Duplessy, J.-C., and Guillard, R. R. L., 1982. Re-evaluation of calcareous nannofossil oxygen isotope data. *Geol. Soc. Am. Abstr. Progr.* (Abstract)

Dudley, W. C., Duplessy, J.-C., Blackwelder, P. L., Brand L. E., and Guillard, R. R. L., 1980. Coccoliths in Pleistocene–Holocene nannofossil assemblages. *Nature*, 285:222–223.

Duplessy, J.-C., Shackleton, N. J., Mathews, R. K., Prell, W., Ruddiman, W. F., Caralp, M., and Hendy, C. H., 1984. ^{13}C Record of benthic foraminifera in the last interglacial ocean: implications for the carbon cycle and the global deep water circulation. *Quat. Res.*, 21:225–243.

Emiliani, C., 1955. Pleistocene temperatures. *J. Geol.*, 63:538–578.

________, 1966. Paleotemperature analysis of Caribbean Cores P6304-8 and P6304-9 and a generalized temperature curve for the past 425,000 years. *J. Geol.*, 74:109–124.

________, 1971. The amplitude of Pleistocene climatic cycles at low latitudes and the isotopic composition of glacial ice. *In* Turekian,

K. K. (Ed.), *Late Cenozoic Glacial Ages*: Hartford (Yale University Press), pp. 183–197.

Emiliani, C., and Flint, R. F., 1963. The Pleistocene record. *In* Hill, M. N. (Ed.), *The Sea* (Vol. 3): New York (Wiley), pp. 888–919.

Hay, W. W., 1977. Calcareous nannofossils. *In* Ramsay, A. T. S. (Ed.), *Oceanic Micropalentology*, (Vol. 2): London (Academic Press), 1055–1200.

Hays, J. D., Imbrie, J., Shackleton, N. J., 1976a. Variations in the earth's orbit: pacemaker of the ice ages. *Science*, 194:1121–1132.

Hays, J. D., Lozano, J., Shackleton, N. J., and Irving, G., 1976b. Reconstruction of the Atlantic Ocean and western Indian Ocean sectors of the 18000 B.P. Antarctic Ocean. *In* Cline, R. M., and Hays, J. D. (Eds.), *Investigation of Late Quaternary Paleoceanography and Paleoclimatology.* Geol. Soc. Am. Mem., 145:337–372.

Hornibrook, N. de B., 1982. Late Miocene to Pleistocene *Globorotalia* (Foraminiferida) from DSDP Leg 29, Site 284, Southwest Pacific. *N.Z. J. Geol. Geophys.*, 25:83–99.

Imbrie, J., Shackleton, N. J., Pisias, N. G., Morley, J. J., Prell, W. L., et al., in press. The orbital theory of Pleistocene climate: support from a revised chronology of the marine $\delta^{18}O$ record. *In* Imbrie, J., and Berger, A. (Eds.), *Milankovitch and Climate Change*: Amsterdam (Elsevier).

Jenkins, D. G., 1975. Cenozoic planktonic foraminiferal biostratigraphy of the South Western Pacific and Tasman Sea—DSDP Leg 29. *In* Kennett, J. P., Houtz, R. E., et al., *Init. Repts. DSDP*, 29: Washington (U.S. Govt. Printing Office), 449–467.

Kennett, J. P., 1969. Distribution of planktonic foraminifera in surface sediments to the southeast of New Zealand. *In* Brönniman, P., and Renz, H. H. (Eds.), *Proc. First Int. Conf. Plankt. Microfossils, Geneva 1967*, 2:307–322.

________, 1983. Paleo-oceanography: global ocean evolution. *Rev. Geophys. Space Phys.*, 21:1258–1274.

________, 1982. *Marine Geology*: Englewood Cliffs, N.J. (Prentice Hall).

Kennett, J. P., Shackleton, N. J., Margolis, S. V., Goodney, D. E., Dudley, W. C., and Kroopnick, P. M., 1979. Late Cenozoic oxygen and carbon isotopic history and volcanic ash stratigraphy: DSDP Site 284, South Pacific. *Am. J. Sci.*, 179:52–69.

Kennett, J. P., and Shackleton, N. J., 1976. Oxygen isotopic evidence for the development of the psychrosphere 38 M yr ago. *Nature*, 260:513–515.

Kennett, J. P., Houtz, R. E., et al., 1975. *Init. Repts. DSDP*, 29: Washington (U.S. Govt. Printing Office).

Kennett, J. P., and Vella, P., 1975. Late Cenozoic planktonic foraminifera and paleoceanography at DSDP Site 284 in the cool subtropical South Pacific. *In* Kennett, J. P., Houtz, R. E., et al., *Init. Repts. DSDP*, 29: Washington (U.S. Govt. Printing Office), 769–799.

Knox, G. A., 1970. Biological oceanography of the South Pacific. *In* Wooster, W. S., (Ed.), *Scientific Exploration of the South Pacific*: Washington (National Academy of Sciences), pp. 155–182.

Loutit, T. S., and Kennett, J. P., 1979. Application of carbon isotope stratigraphy to late Miocene shallow marine sediments, New Zealand. *Science*, 204:1196–1199.

Pisias, N. G., and Moore, T. C., Jr., 1981. The evolution of Pleistocene climate: a time series approach. *Earth Planet. Sci. Lett.*, 52: 450–458.

Prell, W. L., 1982. Oxygen and carbon isotope stratigraphy for the Quaternary of Hole 502B: evidence for two modes of isotopic variability. *In* Prell, W. L., Gardner, J. V., et al., *Init. Repts. DSDP*, 68: Washington (U.S. Govt. Printing Office), 455–464.

Rochford, D. J., 1960a. The intermediate depth water of the Tasman and Coral Seas. I. The 27.20 σT surface. *Aust. J. Mar. Freshw. Res.*, 11:127–147.

________, 1960b. The intermediate depth waters of the Tasman and Coral Seas II. The 26.80 σ_T surface. *Aust. J. Freshw. Res.*, 11: 148–165.

Shackleton, N. J., 1967. Oxygen isotope analyses and Pleistocene temperatures reassessed. *Nature*, 215:15–17.

________, 1974. Attainment of isotopic equilibrium between ocean water and the benthonic foraminifera genus *Uvigerina*: isotopic changes in the ocean during the last glacial. *Coll. Internat. Centre Nat. Rech. Sci.*, 219:203–210.

Shackleton, N. J., Backman, J., Zimmerman, H., Kent, D. V., Hall, M. A., Roberts, D. G., Schnitker, D., Baldauf, J. G., Desprairies, A., Homrighausen, R., Huddlestun, P., Keene, J. B., Kaltenback, A. J., Krumsiek, K. A. O., Morton, A. C., Murray, J. W., and Westberg-Smith, J., 1984. Oxygen isotope calibration of the onset of ice-rafting history of glaciation in the North Atlantic region. *Nature*, 307:620–623.

Shackleton, N. J., and Cita, M. B., 1979. Oxygen and carbon isotope stratigraphy of benthic foraminifers at Site 397: detailed history of climatic change during the late Neogene. *In* von Rad, U., Ryan, W. B. F., et al., *Init. Repts. DSDP*, 47, Pt. 1: Washington (U.S. Govt. Printing Office), 433–445.

Shackleton, N. J., and Hall, M. A., 1982. Stable isotope record of Hole 504 sediments: high resolution record of the Pleistocene. *In* Cann, J. R., Langseth, M. G., Honnorez, J., Von Herzen, R. ., White, S. M., et al., *Init. Repts. DSDP*, 69: Washington (U.S. Govt. Printing Office), 431–441.

Shackleton, N. J., Imbrie, J., and Hall, M. A., 1983. Oxygen and carbon isotope record of East Pacific core V19-30: implications for the formation of deep water in the late Pleistocene North Atlantic. *Earth Planet. Sci. Lett.*, 65:233–244.

Shackleton, N. J., and Kennett, J. P., 1975a. Late Cenozoic oxygen and carbon isotope changes at DSDP Site 284: implications for glacial history of the Northern Hemisphere and Antarctica. *In* Kennett, J. P., Houtz, R. E., et al., *Init. Repts. DSDP*, 29: Washington (U.S. Govt. Printing Office), 801–807.

________, 1975b. Paleotemperature history of the Cenozoic and the initiation of Antarctic glaciation: oxygen and carbon isotope analyses in DSDP Sites 277, 279, and 281. *In* Kennett, J. P., Houtz, R. E., et al., *Init. Repts. DSDP*, 29: Washington (U.S. Govt. Printing Office), 743–755.

Shackleton, N. J., and Opdyke, N. D., 1973. Oxygen isotope and palaeomagnetic stratigraphy of Equatorial Pacific core V28-238: oxygen isotope temperatures and ice volumes on a 10^5 year and 10^6 year scale. *Quat. Res.*, 39–55.

________, 1976. Oxygen isotope and paleomagnetic stratigraphy of Pacific core V28-239, late Pliocene to latest Pleistocene. *In* Cline, R. M., and Hays, J. D. (Eds.), *Investigation of Late Quaternary Paleoceanography and Paleoclimatology:* Geol. Soc. Am. Mem., 145:449–464.

Stanton, B. R., 1973. Circulation along the eastern boundary of the Tasman Sea. *In* Fraser, R. (Ed.), *Oceanography of the South Pacific 1972*: Wellington (N.Z. Commission for UNESCO), pp. 141–147.

Suggate, R. P., Stevens, G. R., and Te Punga, M. T. (Eds.), 1978. *The Geology of New Zealand* (Vol. 2): Wellington (Govt. Printer), pp. 541–626.

Thierstein, H. R., Geitsenauer, K. R., Molfino, B., and Shackleton, N. J., 1977. Global synchroneity of late Quaternary coccolith datum levels: Validation by oxygen isotopes. *Geology*, 5:400–404.

Thompson, P. R., and Saito, T., 1974. Pacific Pleistocene sediments: planktonic foraminifera dissolution cycles and geochronology. *Geology*, 2:333–335.

Valencia, M. J., 1977. Pacific Pleistocene paleoclimatic stratigraphies: a comparative analysis of results. *Quat. Res.*, 8:339–354.

Van Donk, J., 1976. O^{18} record of the Atlantic Ocean for the entire Pleistocene epoch. *In* Cline, R. M., and Hays, J. D. (Eds.), *Investigation of Late Quaternary Paleoceanography and Paleoclimatology.* Geol. Soc. Am. Mem., 145:147–163.

Vella, P., Ellwood, B. B., and Watkins, N. D., 1975. Surface-water temperature changes in the Southern Ocean southwest of Australia during the last one million years. *In* Suggate, R. P., and Cresw , M. M. (Eds.), *Quaternary Studies*: Wellington (The Roy. Soc. N.Z), pp. 297–309.

Vincent, E., Killingley, J. S., and Berger, W. H., 1981. Stable isotope composition of benthic foraminifera from the equatorial Pacific. *Nature*, 289:639–643.

Volat, J.-L., Pastouret, L., and Vergnaud-Grassini, C., 1980. Dissolution and carbonate fluctuations in Pleistocene deep-sea cores: a review. *Mar. Geol.*, 34:1–28.

Williams, D. F., Moore, W. S., and Fillon, R. H., 1981. Role of glacial Arctic Ocean ice sheets in Pleistocene oxygen isotope and sea level records. *Earth Planet. Sci. Lett.*, 56:157–166.

Date of Initial Receipt: 11 June 1984
Date of Acceptance: 29 October 1984

44. LATE QUATERNARY CARBONATE AND ISOTOPE STRATIGRAPHY, SUBANTARCTIC SITE 594, SOUTHWEST PACIFIC[1]

Campbell S. Nelson, Chris H. Hendy, Alison M. Cuthbertson, and Grant R. Jarrett, University of Waikato, Hamilton, New Zealand[2]

ABSTRACT

The late Quaternary sequence off eastern South Island, New Zealand, consists of ~100 m of alternating bluish gray pelagic oozes and greenish gray hemipelagic oozes that extend uninterruptedly back to the Brunhes/Matuyama boundary (0.73 m.y.). A very high resolution (~2400 yr.) record of sediment texture, calcium carbonate content, and planktonic and benthic foraminiferal oxygen and carbon isotope composition demonstrates an in-phase cyclical fluctuation between the sedimentary parameters that closely correspond to the pelagic–hemipelagic sedimentation cycles and the isotope composition. Pelagic oozes, formed during interglacial periods of high eustatic sea level, are characterized by calcareous microfossils, relative enrichment in sand and clay sizes, high carbonate contents, reduced δ^{18}O values, and increased δ^{13}C values. Hemipelagic oozes, associated with glacial episodes and lowered eustatic sea level, include common terrigenous material and siliceous microfossils, are enriched in silt sizes, have low carbonate contents, high δ^{18}O values, and low δ^{13} values. The history of alpine glaciations and associated erosion of the South Island of New Zealand, as expressed by the appearance of hemipelagic oozes, can be correlated directly with the major fluctuations of Northern Hemisphere ice sheets as expressed by the influence of eustatic sea-level changes on the oxygen isotope composition of both planktonic and benthic foraminifers. This high-accumulation-rate record contains conspicuous intervals of high-frequency, high-amplitude isotope variability including the presence of multiple glacial/interglacial intervals within single isotope stages, and offers one of the best sections cored to date for detailed study of the evolution and history of climate change over the last 0.75 m.y.

INTRODUCTION

Site 594 (45°31.41′S, 174°56.88′E) is located 300 km east of South Island, New Zealand, on the southern margin of Chatham Rise in a water depth of 1204 m (Fig. 1). The site lies in the subantarctic water mass immediately south of the Subtropical Convergence and is the southernmost site of a north–south transect (Sites 586–594) drilled on Leg 90 in the southwest Pacific. Because of its proximity to the New Zealand landmass, sedimentation at the site has been influenced by both oceanic and terrigenous processes. In particular, the 170-m-thick Pliocene–Quaternary interval, drilled with almost 100% recovery using the hydraulic piston corer, comprises an alternating sequence of pelagic and hemipelagic sediments (Fig. 2) whose major characteristics are listed and contrasted in Table 1. The sedimentary cycles are probably sensitive indicators of glacial–interglacial climate fluctuations (Griggs et al., 1983) with the pelagic lithofacies forming during interglacial periods and the hemipelagic lithofacies during glacial episodes. If this is true, then Site 594 offers an extremely detailed oceanic record of climate change through the latest Cenozoic with excellent potential for correlation with the continental and marine Plio–Pleistocene and Holocene sequences of New Zealand.

The climate signature contained in the alternating pelagic–hemipelagic sedimentary sequence is currently being investigated using three approaches: sediment particle-size characteristics; calcium carbonate content; and oxygen and carbon stable isotope analysis of planktonic (*Globigerina bulloides* d'Orbigny) and benthic (*Uvigerina* or *Cibicides* spp.) foraminifers. Details of analytical procedures are described fully by Nelson, Hendy, and Dudley (this volume), although here the content of silt- (4–63 μm) and clay- (<4 μm) sized particles in samples has been determined automatically using a Shimadzu Centrifugal Particle Size Analyzer SA-CP2 (Healy et al., 1983), and the calcium carbonate values were determined by back titration following sample acidification using a Mettler DL40RC automatic titrator.

RESULTS

This chapter is only a preview of some of the sedimentary and isotope results obtained to date on the late Quaternary samples from Site 594. The data are given in Table 2 and are summarized on a stratigraphic log (Fig. 3) which extends back to straddle the Brunhes/Matuyama boundary (0.73 m.y.) at a sub-bottom depth of 99.3 m.

Some biostratigraphic data pertinent to age control within the sequence are summarized in Table 3. The anomalous occurrence of the calcareous nannofossil *Calcidiscus macintyrei* at the bottom of the sequence is explanable in terms of sediment reworking associated with formation of the major Matuyama disconformity (~1.6 to ~0.74 m.y.) immediately below the Brunhes/Matuyama boundary (Site 594 report, this volume). The last occurrence of both the radiolarian *Stylatractus universus* and the calcareous nannofossil *Pseudoemiliania lacunosa* is at about 54 m sub-bottom in an interval corresponding to one of the most glacial periods in the isotope record (Fig. 3). Elsewhere, these bioevents have been

---

[1] Kennett, J. P., von der Borch, C. C., et al., *Init. Repts. DSDP*, 90: Washington (U.S. Govt. Printing Office).

[2] Addresses: (Nelson, Jarrett) Department of Earth Sciences, University of Waikato, Hamilton, New Zealand; (Hendy, Cuthbertson) Department of Chemistry, University of Waikato, Hamilton, New Zealand.

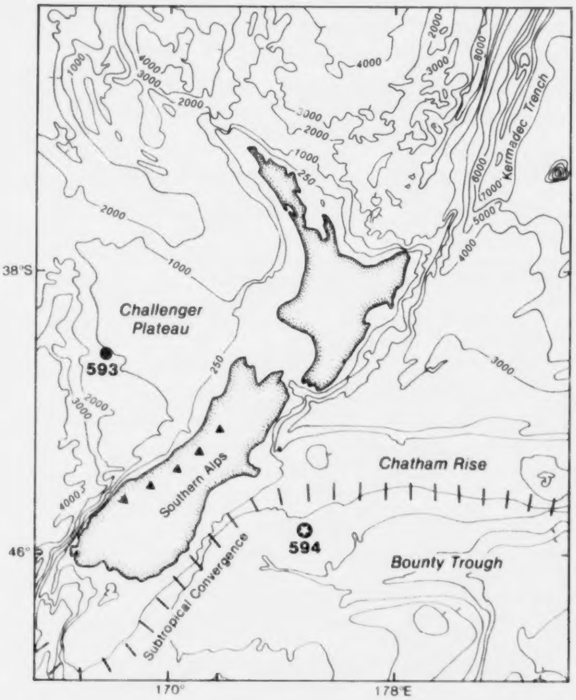

Figure 1. Location of Site 594 off southeastern New Zealand showing also some relevant physiographic features and the approximate position of the Subtropical Convergence.

Table 1. General sediment properties of the late Quaternary pelagic and hemipelagic oozes at Site 594.

Property	Pelagic lithofacies	Hemipelagic lithofacies
Color	Bluish gray (5B 7/1 to 5B 5/1)	Greenish gray (5G 6/1 to 5G 4/1)
Grain size		
Sand	Rare to common	Rare
Silt	Abundant	Abundant
Clay	Common to abundant	Rare to common
$CaCO_3$ content	Moderate to very high	Very low to moderate
Nannofossils	Abundant	Rare to abundant
Foraminifers	Common	Rare
Siliceous microfossils	Absent to rare	Rare to common
Terrigenous sediment	Rare to common	Common to abundant
Dominant sediment types	Foraminiferal-bearing nannofossil ooze; foraminifer- and clay-bearing nannofossil ooze; foraminifer-bearing clayey nannofossil ooze	Clay-, silt-, and/or diat bearing nannofossil ooze; nannofossil-, diatom-, and/or sponge-spicule-bear clayey silt

shown to have occurred between ~0.41 and 0.46 m.y. ago, typically within isotope stage 12 (Hays and Shackleton, 1976; Gartner, 1977; Shackleton, 1977b; Thierstein et al., 1977) which is characterized by extreme ^{18}O enrichment (e.g., Prell, 1982; Imbrie et al., in press). About 10 m above this level a few specimens of the calcareous nannofossil *Emiliania huxleyi* are recorded by Lohman (this volume), although the taxon does not become common until 37 m sub-bottom and abundant un-

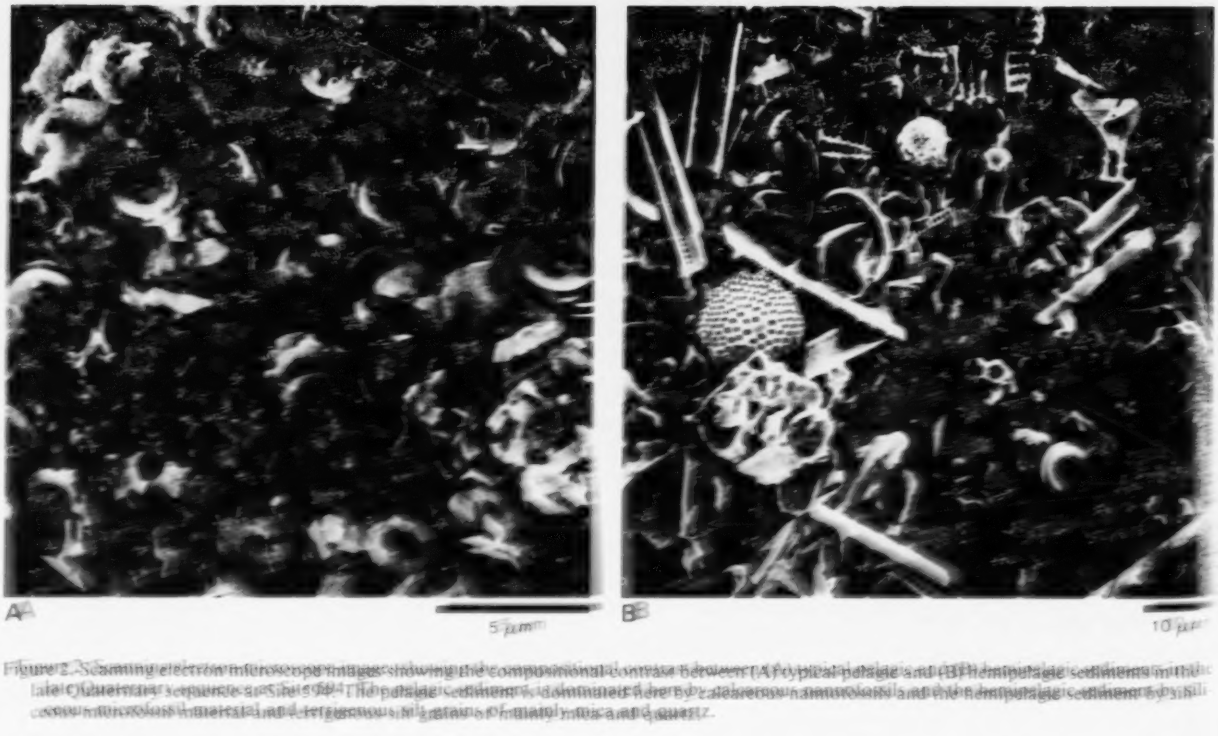

Figure 2. Scanning electron microscope images showing the compositional contrast between (A) typical pelagic and (B) hemipelagic sediments in the late Quaternary sequence at Site 594. The pelagic sediment is dominated here by calcareous nannofossils and the hemipelagic sediment by siliceous microfossil material and terrigenous silt grains of mainly mica and quartz.

Table 2. Carbon and oxygen data (per mil deviations from the PDB standard) for foraminifers, and calcium carbonate and textural (sand, >63 μm; silt, 4–63 μm; clay, <4 μm) data for bulk samples from the late Quaternary interval of Holes 594 and 594A.

Core-Section (level in cm)	Corrected sub-bottom depth (m)	Planktonic foraminifers		Benthic foraminifers		$CaCO_3$ (%)	Texture (%)		
		$\delta^{18}O$	$\delta^{13}C$	$\delta^{18}O$	$\delta^{13}C$		Silt	Clay	Sand
Hole 594									
1-1, 30	0.31	1.61	1.44	3.04	0.50	—	63.7	22.7	13.6
1-1, 52	0.53	1.48	1.21	2.77	0.44	40.2	67.0	19.6	13.4
1-1, 80	0.81	1.72	0.77	3.22	0.16	41.8	71.3	22.0	6.7
1-1, 105	1.06	2.06	0.91	3.30	0.22	42.6	69.4	23.7	6.9
1-1, 130	1.31	2.92	1.04	3.86	0.31	37.9	67.8	23.7	8.5
1-2, 30	1.81	3.02	0.63	4.65	0.12	6.6	80.2	16.1	3.7
1-2, 52	2.03	3.02	0.02	4.75	0.09	6.8	83.3	15.2	1.5
1-2, 80	2.31	3.12	−0.34	4.80	0.01	7.8	74.3	23.9	1.8
1-2, 105	2.56	3.32	0.10	4.68	0.05	11.3	78.1	17.8	4.1
1-2, 130	2.81	2.73	0.16	4.71	0.24	7.1	81.8	15.5	2.7
1-3, 30	3.31	3.27	0.99	5.10	0.26	7.1	80.3	17.7	2.0
1-3, 52	3.53	3.12	0.01	4.50	0.45	3.2	78.3	20.2	1.5
1-3, 80	3.81	3.65	1.15	4.28	0.23	9.5	83.6	13.0	3.4
1-3, 105	4.06	3.37	1.40	4.44	0.65	14.3	81.6	15.5	2.9
1-3, 130	4.31	2.93	0.70	4.25	1.41	6.2	80.2	18.3	1.5
1-4, 30	4.81	3.31	1.32	4.12	0.33	9.9	78.3	19.2	2.5
1-4, 52	5.03	2.89	0.46	4.25	0.51	10.3	80.3	15.6	4.1
1-4, 80	5.31	3.45	1.48	4.47	0.69	8.6	80.0	17.0	3.0
1-4, 105	5.56	2.42	1.07	4.04	0.55	22.3	78.0	17.9	4.1
2-1, 30	6.21	2.61	0.82	3.92	0.37	—	65.8	25.4	8.8
2-1, 52	6.43	2.54	1.45	3.97	0.67	21.8	75.0	19.9	5.1
2-1, 80	6.71	2.52	0.31	4.11	0.48	14.5	76.9	20.2	2.9
2-1, 105	6.96	2.62	0.85	3.77*	0.59*	26.0	71.1	21.1	7.8
2-1, 130	7.21	2.70	1.38	3.75	0.40	29.4	70.8	22.5	6.7
2-2, 30	7.71	2.50	1.17	3.84	0.34	31.6	66.4	26.5	7.1
2-2, 52	7.93	2.93	1.18	3.90	0.30	35.9	65.7	27.9	6.4
2-2, 80	8.21	2.88, 2.97	1.05, 1.06	4.05	0.15	12.8	74.2	22.5	3.3
2-2, 105	8.46	2.63, 2.79	0.98, 0.76	4.04	0.30	7.2	75.1	23.0	1.9
2-2, 130	8.71	2.95, 2.94	0.80, 0.65	3.91	−0.11	10.3	74.4	24.2	1.4
2-3, 30	9.21	3.28	0.85	4.01	0.13	7.0	74.2	25.0	0.8
2-3, 52	9.43	3.23	1.00	4.44	0.20	7.9	78.1	20.8	1.1
2-3, 80	9.71	3.29	0.52	4.30	0.16	10.0	78.3	20.5	1.2
2-3, 105	9.96	3.25, 3.08	0.11, 0.97	4.49	0.14	11.2	78.4	19.9	1.7
2-3, 130	10.21	2.97, 3.01	0.13, 0.88	4.27	0.31	15.4	75.0	23.4	1.6
2-4, 30	10.71	2.97, 2.99	1.38, 1.70	4.03	0.29	35.6	67.6	26.2	6.2
2-4, 52	10.93	2.63, 2.74	1.20, 1.79	3.33	0.40	48.0	52.5	39.9	7.6
2-4, 80	11.21	2.77	1.79	3.76	0.44	42.2	52.9	35.4	11.7
2-4, 105	11.46	2.78	1.75	3.50	0.27	45.1	59.2	36.6	4.2
2-4, 130	11.71	2.40	1.26	3.69	0.20	47.6	58.3	33.2	8.5
2-5, 30	12.21	2.52	1.51	3.53	0.39	55.3	60.8	34.2	5.0
2-5, 52	12.43	2.69	1.85	3.96	0.65	53.6	60.5	33.2	6.3
2-5, 80	12.71	2.58	1.75	3.77	0.61	28.0	61.7	24.4	13.9
2-5, 105	12.96	2.68	1.68	3.87	0.39	38.3	53.9	34.7	11.4
2-5, 130	13.21	2.26	1.69	3.81	0.47	21.5	61.7	32.5	5.8
2-6, 30	13.71	2.24	1.67	3.38	0.57	51.5	49.8	38.7	11.5
2-6, 52	13.93	2.55	1.62	3.39	0.29	54.4	49.8	35.3	14.9
2-6, 80	14.21	2.39	1.26	2.92	−0.13	45.0	46.1	30.1	23.8
2-6, 105	14.46	2.58	1.41	3.08	0.25	44.6	63.4	27.2	9.4
3-1, 30	15.81	2.54	1.44	3.21	−0.43	22.1	62.3	11.4	26.3
3-1, 52	16.03	1.35	0.71	2.83*	−0.08*	55.4	58.9	24.6	16.5
3-1, 80	16.30	1.59	0.49	2.94	0.12	60.7	63.7	30.6	5.7
3-1, 105	16.56	2.97	0.85	4.00	0.10	45.2	69.7	23.0	7.3
3-1, 130	16.81	3.20	0.88	4.27	0.25	28.1	78.8	17.5	3.7
3-2, 30	17.31	3.17, 3.16	1.01, 0.93	3.96	0.21	4.5	73.5	22.2	4.3
3-2, 52	17.53	2.35, 2.39	0.85, 1.08	3.80*	0.50*	6.1	80.3	16.8	2.9
3-2, 80	17.80	2.71, 2.47	1.02, 0.91	3.97	0.07	8.9	75.7	21.1	3.2
3-2, 105	18.06	3.22, 3.03	0.70, 1.17	3.63	−0.16	20.5	76.0	17.7	6.3
3-2, 130	18.31	2.97	0.68	4.35	−0.07	19.8	75.5	18.6	5.9
3-3, 30	18.81	3.26, 3.31	0.69, 0.55	4.43	−0.15	4.7	81.8	16.0	2.2
3-3, 52	19.03	3.20, 2.89	0.72, 0.80	4.28	0.33	20.5	75.1	19.4	5.5
3-3, 80	19.31	3.04, 3.03	0.80, 0.93	4.40	0.15	12.2	74.9	21.7	3.4
3-3, 105	19.80	2.79, 2.92	0.78, 0.95	—	—	5.9	79.3	19.0	1.7
3-3, 130	19.81	3.51, 3.01	0.24, 0.11	—	—	4.0	80.4	17.6	2.0
3-4, 30	20.31	3.24, 3.45	1.10, 0.86	4.00	−0.09	30.7	73.2	18.2	8.6
3-4, 52	20.53	2.68, 3.23	0.51, 1.09	3.83	0.18	15.7	79.5	14.3	6.2
3-4, 80	20.80	3.02, 2.94	0.90, 1.01	4.08	0.11	8.2	77.4	18.8	3.8
3-4, 105	21.06	3.47, 3.13	0.97, 1.11	3.91	0.01	9.8	77.2	14.9	7.9
3-4, 140	21.40	2.68, 3.09	1.20, 0.85	3.68	0.13	22.7	73.1	15.5	11.4
3-5, 30	21.81	2.35, 2.27	1.20, 1.09	4.63	−0.95	4.8	76.0	22.7	1.3
3-5, 52	22.03	3.28, 3.10	1.08, 1.10	—	—	8.2	78.0	13.2	8.8
3-5, 80	22.30	3.09, 3.21	0.83, 0.99	—	—	6.0	80.0	17.3	2.7
3-5, 105	22.56	3.47, 2.88	0.85, 0.84	3.62	0.10	19.6	77.5	14.8	7.7

Table 2. (Continued).

Core-Section (level in cm)	Corrected sub-bottom depth (m)	Planktonic foraminifers		Benthic foraminifers		$CaCO_3$ (%)	Texture (%)		
		$\delta^{18}O$	$\delta^{13}C$	$\delta^{18}O$	$\delta^{13}C$		Silt	Clay	Sand
Hole 594 (Cont).									
3-5, 130	22.81	2.99, 3.22	0.83, 1.02	4.25	−0.39	5.2	77.0	18.0	5.0
3-6, 30	23.31	1.23	0.68	2.96*	−0.60*	56.8	68.3	16.8	14.9
3-6, 52	23.53	2.03	0.83	3.30*	0.49*	40.5	44.4	11.3	44.3
3-6, 80	23.80	1.48	0.46	3.13*	0.28*	44.9	60.4	15.0	24.6
3-6, 105	24.06	2.44	1.07	3.21*	0.75*	48.7	58.6	24.4	17.0
3-6, 130	24.31	2.19	0.95	3.29*	0.09*	—	60.3	15.4	24.3
4-1, 30	25.41	2.27	1.08	—	—	34.1	66.2	23.8	10.0
4-1, 52	25.63	2.11	0.97	—	—	47.1	56.2	17.8	26.0
4-1, 80	25.91	2.27	0.90	2.82*	0.21*	50.0	61.7	23.0	15.3
4-1, 105	26.16	1.98	0.75	2.83*	−0.21*	53.7	68.2	23.6	8.2
4-1, 130	26.41	1.61	0.66	2.70	0.25	56.8	68.0	27.6	4.4
4-2, 30	26.91	2.53	0.74	3.75	0.13	21.9	78.2	15.8	6.0
4-2, 52	27.13	2.71	0.76	3.76	0.23	31.1	72.7	19.3	8.0
4-2, 80	27.41	2.38	0.69	—	—	8.7	81.6	16.3	2.1
4-2, 105	27.66	2.61, 2.72	0.94, 0.71	3.55	−0.01	12.1	79.6	17.1	3.3
4-2, 130	27.91	3.27, 2.86	0.45, 0.30	3.77	−0.25	12.9	78.3	15.7	6.0
4-3, 30	28.41	2.67, 2.45	0.70, 0.58	4.04	0.24	9.9	79.6	16.6	3.8
4-3, 52	28.63	3.17, 3.09	1.02, 0.84	4.08	0.14	24.6	71.3	20.0	8.7
4-3, 80	28.91	3.38, 3.49	0.99, 0.82	3.85	0.05	20.3	74.3	19.1	6.6
4-3, 130	29.41	3.02, 2.71	0.89, 0.41	3.98	−0.01	8.5	79.3	18.2	2.5
4-4, 30	29.91	2.65, 2.38	0.70, 0.31	3.72	−0.05	4.2	79.0	19.0	2.0
4-4, 52	30.13	2.71, 2.42	0.57, 0.60	—	—	2.9	77.2	20.5	2.3
4-4, 80	30.41	2.84, 2.87	0.46, 0.93	4.43	0.14	2.6	82.5	15.3	2.2
4-4, 105	30.66	2.95	1.05	—	—	5.1	80.2	17.0	2.8
4-4, 130	30.91	3.19	0.58	4.44	0.18	4.4	80.9	17.4	1.7
4-5, 30	31.41	2.49, 3.07	1.63, 1.52	4.03	0.52	30.6	64.9	19.4	15.7
4-5, 52	31.63	2.60, 2.72	1.58, 1.44	—	—	48.6	58.0	25.9	16.1
4-5, 80	31.91	2.68, 2.79	1.46, 1.75	—	—	46.0	64.4	28.4	7.2
4-5, 105	32.16	2.56, 2.56	1.51, 1.49	3.52*	−0.47*	31.4	64.7	22.2	13.1
4-5, 130	32.41	2.68	1.34	3.18	−0.07	29.0	67.9	23.5	8.6
4-6, 30	32.91	2.27	1.77	—	—	49.0	61.2	29.7	9.1
4-6, 52	33.13	2.32, 2.82	1.67, 1.61	—	—	42.5	56.8	27.1	16.1
4-6, 80	33.41	2.26, 2.54	1.63, 1.34	—	—	43.8	54.9	24.2	20.9
4-6, 105	33.66	1.95, 2.10	1.63, 1.12	—	—	45.8	57.1	24.4	18.5
5-1, 52	35.23	2.30, 2.77	1.06, 1.26	—	—	8.1	83.7	13.4	2.9
5-1, 80	35.51	2.61, 2.52	1.03, 1.08	—	—	12.8	81.1	15.9	3.0
5-1, 105	35.76	2.23, 2.63	1.48, 1.27	4.30	0.20	15.5	76.4	21.9	1.7
5-1, 132	36.03	3.48	1.06	—	—	9.3	82.2	15.8	2.0
5-2, 30	36.51	2.31	1.28	—	—	2.7	54.3	7.6	38.1
5-2, 52	36.73	3.44	0.66	—	—	19.6	79.4	18.7	1.9
5-2, 80	37.01	3.04	1.29	4.25	−0.14	22.6	73.3	25.4	1.3
5-2, 105	37.26	3.17	1.96	4.42	0.12	38.3	—	—	3.2
5-2, 132	37.53	3.24	1.38	4.10	0.09	39.7	61.4	35.2	3.4
5-3, 30	38.01	3.31	1.48	3.57*	−0.05*	32.3	70.4	26.3	3.3
5-3, 52	38.23	2.94	1.44	4.08*	0.35*	22.8	62.1	34.7	3.2
5-3, 80	38.51	2.42	1.14	—	—	16.0	71.6	27.4	1.0
5-3, 105	38.76	2.93	1.30	4.26	0.14	18.4	76.4	21.4	2.2
5-3, 132	39.03	3.41	1.23	—	—	16.0	79.0	19.6	1.4
5-4, 30	39.51	2.91	1.62	4.18	0.27	17.6	74.7	23.2	2.1
5-4, 52	39.73	2.92	1.79	—	—	20.5	78.0	20.5	1.5
5-4, 80	40.01	3.02	1.63	—	—	23.4	72.1	26.1	1.8
5-4, 132	40.53	2.73	1.63	—	—	45.5	57.8	39.7	2.5
5-5, 30	41.01	2.93	1.71	4.07	0.23	24.3	70.7	27.5	1.8
5-5, 52	41.23	2.72	1.94	—	—	26.4	70.8	25.2	4.0
5-5, 80	41.51	2.70	1.56	4.20	−0.12	35.0	69.7	22.6	7.7
5-5, 105	41.76	2.45	1.58	3.92	−0.08	41.3	69.9	21.4	8.7
5-5, 132	42.03	2.49	1.81	3.68	0.08	52.3	70.0	27.6	2.4
5-6, 30	42.51	2.94	1.71	3.93	0.07	—	62.0	31.2	6.8
5-6, 52	42.73	2.89	1.67	3.62	0.18	57.9	59.9	34.1	6.0
5-6, 80	43.01	2.87	1.68	—	—	60.4	43.2	46.5	10.3
5-6, 105	43.26	2.61	1.65	3.95*	0.26*	68.0	55.5	38.5	6.0
5-6, 132	43.53	2.52	1.79	3.65	0.30	60.2	47.3	45.0	7.7
5-7, 30	44.01	2.68	1.81	3.65	0.27	63.3	—	—	3.9
9-1, 52	73.63	2.03	0.40	4.35	0.13	41.1	66.8	28.8	4.4
9-1, 80	73.91	2.23	0.43	3.84	0.15	54.9	56.5	39.2	4.3
9-1, 105	74.16	1.83	0.42	3.62	0.37	60.4	52.7	36.9	10.4
9-1, 130	74.41	1.50	0.24	3.39	0.30	56.9	53.3	39.5	7.2
9-2, 30	74.91	1.78	0.54	3.39	0.44	61.7	49.0	40.7	10.3
9-2, 52	75.13	1.42	0.38	3.08	0.72	68.4	58.9	39.2	1.9
9-2, 80	75.41	1.76	0.24	3.61	0.42	70.1	49.1	39.7	11.2
9-2, 105	75.66	2.08	0.01	3.49	0.03	47.2	71.6	19.8	8.6
9-2, 130	75.91	2.45	0.16	3.77	−0.14	41.8	69.9	23.6	6.5
9-3, 30	76.41	2.14	—	—	—	4.8	84.0	15.0	1.0
9-3, 52	76.63	3.57	—	—	—	4.0	72.6	26.2	1.2

Table 2. (Continued).

Core-Section (level in cm)	Corrected sub-bottom depth (m)	Planktonic foraminifers		Benthic foraminifers		$CaCO_3$ (%)	Texture (%)		
		$\delta^{18}O$	$\delta^{13}C$	$\delta^{18}O$	$\delta^{13}C$		Silt	Clay	Sand
Hole 594 (Cont).									
9-3, 80	76.91	3.18	—	—	—	10.6	84.7	13.8	1.5
9-3, 105	77.16	3.37	0.71	3.61	0.02	53.3	73.4	17.6	9.0
9-3, 130	77.41	2.68	0.28	3.22	−0.16	49.0	73.6	23.4	3.0
9-4, 30	77.91	2.71	0.16	3.85	−0.04	26.6	77.9	13.3	8.8
9-4, 80	78.41	3.01	0.13	4.63	0.17	9.5	83.7	12.4	3.9
9-4, 105	78.66	3.47	0.67	—	—	7.7	83.3	15.2	1.5
9-4, 130	78.91	3.89	0.34	4.39	−0.41	8.9	83.9	14.5	1.6
9-5, 30	79.41	3.03	0.56	—	—	9.1	81.7	14.7	3.6
9-5, 52	79.63	3.65	0.72	4.30	−0.28	13.1	84.7	12.3	3.0
9-5, 80	79.91	3.22	0.86	—	—	15.2	83.0	13.9	3.1
9-5, 105	80.16	2.86	0.74	4.23	−0.29	15.9	83.2	14.5	2.3
9-5, 130	80.41	2.50	0.31	3.53	0.26	42.8	75.6	15.9	8.5
9-6, 30	80.91	2.11	0.38	3.29	0.26	56.6	61.8	24.0	14.2
9-6, 52	81.13	2.25	0.27	3.82	−0.10	62.3	51.7	29.3	19.0
9-6, 80	81.41	2.14	0.53	3.00	−0.26	68.7	45.2	41.0	13.8
9-6, 105	81.66	1.63	0.74	2.94	0.06	70.0	50.4	33.0	16.6
9-6, 130	81.91	1.59	0.47	3.54	0.30	74.9	52.3	43.0	4.7
11-1, 52	92.83	2.63	0.54	—	—	2.0	84.0	14.6	1.4
11-1, 80	93.11	—	—	—	—	3.3	82.5	15.7	1.8
11-1, 105	93.36	2.23	0.97	3.81	−0.23	16.1	78.4	14.7	6.9
11-1, 130	93.61	2.63	1.23	3.67	−0.18	46.7	68.9	19.7	11.4
11-2, 30	94.11	1.91	0.62	3.67	0.25	50.6	58.6	18.7	22.7
11-2, 52	94.33	2.64	0.82	3.72	0.07	16.6	79.5	17.3	3.2
11-2, 80	94.61	2.50	1.34	3.09	0.60	45.5	73.2	14.6	12.2
11-2, 105	94.86	2.59	1.21	2.86	0.25	36.2	72.0	12.3	15.7
11-2, 130	95.11	2.62	1.26	3.23	0.39	40.1	67.5	12.9	19.6
11-3, 30	95.61	2.48	1.23	3.34	0.60	42.4	72.6	14.8	12.6
11-3, 52	95.83	2.42	0.71	3.29*	−0.12*	43.9	76.1	13.7	10.2
11-3, 80	96.11	2.59	1.04	3.39	−0.43	21.8	80.8	13.8	5.4
11-3, 105	96.36	2.62	0.46	3.62	−0.52	19.4	79.6	16.2	4.2
11-3, 130	96.61	2.19	−0.47	3.84	−0.32	12.3	83.6	14.8	1.6
11-4, 30	97.11	2.61	0.59	3.94	−0.02	13.4	84.9	12.4	2.7
11-4, 52	97.33	2.70	0.47	3.82	−0.36	38.2	83.7	13.6	2.7
11-4, 80	97.61	2.45	0.73	3.94	−0.09	36.0	75.9	18.8	5.3
11-4, 105	97.86	1.98	1.19	3.40	0.23	64.0	64.9	26.2	8.9
11-4, 130	98.11	2.03	0.99	3.15	0.10	76.9	62.1	30.3	7.6
11-5, 30	98.61	1.43	0.40	—	—	69.2	53.0	38.2	8.8
11-5, 52	98.83	2.18	1.16	3.51	−0.02	59.8	69.7	22.2	8.1
11-5, 80	99.11	2.63	1.08	3.52	0.19	38.3	69.5	24.1	6.4
11-5, 105	99.36	2.37	0.72	3.46	−0.18	27.0	69.8	23.8	6.4
11-5, 130	99.61	3.27	1.18	3.69	0.52	39.5	66.6	18.4	15.0
11-6, 30	100.11	2.72	0.89	3.79	−0.11	22.4	78.3	11.2	10.5
11-6, 52	100.33	2.06	1.01	3.99	−0.24	17.2	76.6	14.2	9.2
11-6, 80	100.61	2.46	1.04	3.95	−0.37	12.6	83.8	13.3	2.9
11-6, 105	100.86	2.26	1.22	3.65	0.25	29.9	73.5	11.8	14.7
11-6, 130	101.11	1.98	1.31	—	—	54.0	63.4	19.6	17.0
11-7, 30	101.61	1.42	0.83	—	—	54.5	56.6	17.4	26.0
Hole 594A									
1-3, 30	44.61	2.11	1.88	3.22	0.43	77.4	53.8	40.8	5.4
1-3, 52	44.83	2.11	1.37	2.77	0.38	81.9	47.1	48.1	4.8
1-3, 80	45.11	0.96	0.54	2.77	0.79	76.1	49.0	44.1	6.9
1-3, 105	45.36	1.72	1.38	2.86	0.84	75.3	56.7	37.6	5.7
1-3, 130	45.61	1.94	1.67	3.02	1.03	76.6	55.5	39.7	4.8
1-4, 30	46.11	1.73	0.98	—	—	77.6	51.6	44.3	4.1
1-4, 52	46.33	2.27	1.01	—	—	69.1	55.7	37.5	6.8
1-4, 80	46.61	2.68	1.19	—	—	60.1	64.3	28.5	7.2
1-4, 105	46.86	2.26	0.57	—	—	58.3	61.2	32.9	5.9
1-4, 130	47.11	3.32	1.09	4.28*	0.13*	45.9	62.8	34.6	2.6
1-5, 30	47.61	3.30	0.86	—	—	19.5	79.3	17.8	2.9
1-5, 52	47.83	3.06	−0.01	—	—	16.1	82.3	16.2	1.5
1-5, 80	48.11	3.48	0.85	—	—	7.7	—	—	—
1-5, 105	48.36	3.45	0.66	—	—	6.5	85.1	13.2	1.7
1-5, 130	48.61	2.90	0.70	—	—	5.9	82.0	16.9	1.1
1-6, 30	49.11	3.23	0.50	—	—	2.5	80.8	18.2	1.0
1-6, 52	49.33	3.07	0.39	—	—	11.3	82.3	16.3	1.4
1-6, 80	49.61	3.60	0.69	4.91	−0.14	5.8	81.3	17.9	0.8
1-6, 105	49.86	3.13	0.61	4.93	−0.05	10.5	77.9	20.0	2.1
1-7, 30	50.30	2.93	0.67	—	—	—	84.3	13.1	2.6
1-7, 52	50.61	2.96	0.54	—	—	4.8	83.5	15.3	1.2
2-1, 30	51.21	2.83	0.99	—	—	14.3	77.9	20.3	1.8
2-1, 52	51.43	3.37	0.91	5.10	−0.04	22.6	79.9	17.4	2.7
2-1, 80	51.71	3.03	0.34	4.46	0.01	11.5	82.3	16.5	1.2

Table 2. (Continued).

Core-Section (level in cm)	Corrected sub-bottom depth (m)	Planktonic foraminifers		Benthic foraminifers		$CaCO_3$ (%)	Texture (%)		
		$\delta^{18}O$	$\delta^{13}C$	$\delta^{18}O$	$\delta^{13}C$		Silt	Clay	Sand
Hole 594A (Cont).									
2-1, 105	51.96	3.22	0.54	4.54	−0.02	15.9	78.3	19.8	1.9
2-1, 130	52.21	3.38	1.44	4.42	0.01	24.8	72.3	24.4	3.3
2-2, 30	52.71	2.94	0.37	4.72	0.16	19.4	—	—	3.6
2-2, 52	52.93	2.78	0.82	4.30	−0.02	15.0	74.9	22.4	2.7
2-2, 80	53.11	—	—	4.44	0.16	8.8	70.8	16.4	12.8
2-2, 105	53.46	2.64	0.30	4.34	0.10	7.0	82.0	16.6	1.4
2-2, 130	53.71	2.58	1.44	4.35	0.07	8.7	82.6	15.9	1.5
2-3, 30	54.21	2.67	1.37	4.13	0.10	17.3	70.4	25.7	3.9
2-3, 52	54.43	2.56	1.02	4.33	0.16	12.2	77.4	20.0	2.6
2-3, 80	54.71	2.26	0.49	4.54	0.21	7.5	79.2	16.5	4.3
2-3, 105	54.96	2.74	1.47	4.16	0.26	12.8	79.3	18.7	2.0
2-3, 130	55.21	—	—	4.31	0.21	14.0	78.7	19.0	2.3
2-4, 30	55.71	2.10	1.42	3.46	0.23	54.1	62.3	32.1	5.6
2-4, 52	55.93	2.58	1.88	3.38	0.61	76.2	53.4	41.8	4.8
2-4, 80	56.21	2.40	1.73	3.08	0.94	60.3	55.8	36.1	8.1
2-4, 105	56.46	2.32	1.85	3.13	0.76	70.3	55.1	37.1	7.8
2-4, 130	56.71	1.97	1.32	3.32	0.67	66.7	62.0	30.6	7.4
2-5, 30	57.21	2.31	1.46	3.46	0.50	52.8	61.5	28.0	10.5
2-5, 52	57.43	2.85	1.20	3.59	0.41	46.8	66.6	27.4	6.0
2-5, 80	57.71	2.39	1.60	3.86	0.55	50.0	64.6	29.2	6.2
2-5, 105	57.96	2.12	1.52	4.21	0.52	44.0	69.6	26.0	4.4
2-5, 130	58.21	2.70	2.02	3.82	0.56	52.3	46.0	34.6	19.4
2-6, 30	58.71	2.57	1.20	3.74	0.62	51.4	66.3	22.2	11.5
2-6, 80	59.21	2.41	0.74	3.62	0.35	41.5	62.1	28.9	9.0
2-6, 105	59.46	2.54	0.12	4.47	−0.05	23.8	77.9	18.4	3.7
2-6, 130	59.71	2.35	1.20	4.11	0.11	10.6	81.0	17.0	2.0
3-1, 30	60.81	2.28	0.51	—	—	13.3	82.4	15.1	2.5
3-1, 52	61.03	2.42	0.75	4.06	0.47	4.6	81.3	16.5	2.2
3-1, 80	61.31	3.28	1.21	—	—	8.6	84.0	13.7	2.3
3-1, 132	61.83	2.29	−0.13	4.03	−0.05	12.9	79.6	15.7	4.7
3-2, 30	62.31	1.94	0.88	3.41	0.32	37.6	63.5	18.9	17.6
3-2, 52	62.53	2.27	0.55	3.31	0.34	30.1	80.6	13.3	6.1
3-2, 80	62.81	1.81	0.84	2.79	0.38	51.2	63.1	20.2	16.7
3-2, 105	63.06	1.76	0.57	2.72	0.16	50.5	68.9	20.2	10.9
3-2, 132	63.33	1.90	0.55	3.67	0.25	29.5	74.4	15.2	10.4
3-3, 30	63.81	2.44	0.66	3.60	−0.07	38.1	73.1	12.9	14.0
3-3, 52	64.03	2.31	0.37	—	—	37.7	67.5	14.7	17.8
3-3, 80	64.31	2.83	0.64	4.02	0.02	22.0	72.8	11.0	16.2
3-3, 105	64.56	3.44	−0.31	3.57	−0.01	37.2	65.2	10.7	24.1
3-3, 132	64.83	2.42	0.65	3.40	0.17	46.8	68.7	11.4	19.9
3-4, 30	65.31	2.69	0.25	3.29	0.37	42.3	73.0	16.0	11.0
3-4, 52	65.53	2.74	−0.18	3.47	0.10	56.2	76.1	16.1	7.8
3-4, 80	65.81	2.40	−0.18	4.08	−0.06	38.8	74.9	16.6	8.5
3-4, 105	66.06	2.72	−0.01	4.46	−0.02	14.6	81.7	15.8	2.5
3-4, 132	66.33	2.31	0.00	—	—	10.7	79.6	17.1	3.3
3-5, 30	66.81	3.02	0.21	—	—	19.3	—	—	—
3-5, 52	67.03	3.47	1.18	—	—	10.0	79.0	18.2	2.8
3-5, 80	67.31	2.61	0.15	—	—	7.1	82.8	15.5	1.7
3-5, 105	67.56	2.99	0.40	4.59	−0.23	5.5	76.1	20.8	3.1
3-5, 132	67.83	2.84	0.52	4.37	−0.17	21.1	80.7	14.7	4.6
3-6, 30	68.31	3.55	0.29	4.32	−0.01	6.0	77.4	20.8	1.8
4-1, 30	70.41	2.73	−0.09	4.35*	−1.45*	15.8	79.4	15.1	5.5
4-1, 52	70.63	3.14	−0.19	4.13*	−0.39*	17.7	79.7	15.4	4.9
4-1, 80	70.91	2.74	−0.45	—	—	12.5	82.8	14.9	2.3
4-1, 105	71.16	2.48	0.20	—	—	4.9	82.8	15.8	1.4
4-1, 132	71.43	3.01	0.00	4.33	−0.34	10.3	82.7	13.9	3.4
4-2, 30	71.91	2.95	−0.03	4.66	0.03	14.7	77.8	16.5	5.7
4-2, 52	72.13	2.31	0.04	—	—	17.0	78.3	16.6	5.1
4-2, 80	72.41	2.79	0.15	—	—	9.7	82.0	14.9	3.1
4-2, 105	72.66	2.61	−0.62	3.92	−0.21	12.2	80.4	16.1	3.5
4-2, 132	72.93	3.24	0.33	—	—	6.9	—	—	—
5-3, 30	83.01	1.79	0.20	3.19	0.09	65.5	50.7	32.8	16.5
5-3, 52	83.23	1.78	−0.15	3.33	0.33	72.0	45.2	41.1	13.7
5-3, 80	83.51	1.57	0.34	2.65	0.92	68.7	49.6	34.2	16.2
5-3, 105	83.76	1.28	0.16	3.44	0.36	75.6	52.3	39.1	8.6
5-3, 132	84.03	2.16	0.37	3.83	0.18	52.7	63.0	29.4	7.6
5-4, 30	84.51	2.94	0.48	—	—	11.8	78.8	18.2	3.0
5-4, 52	84.73	2.93	0.19	—	—	11.4	77.6	19.7	2.7
5-4, 80	85.01	—	—	5.21	−0.12	11.5	78.9	18.4	2.7
5-4, 105	85.26	3.16	0.47	—	—	7.1	82.4	15.4	2.2
5-4, 132	85.53	3.27	0.46	—	—	5.6	74.9	20.0	5.1
5-5, 30	86.01	2.75	0.43	—	—	7.1	81.3	16.9	1.8
5-5, 52	86.23	2.78	0.03	4.25	−0.25	7.1	80.4	17.3	2.3
5-5, 80	86.51	2.31	0.96	4.00	−0.35	10.5	84.4	14.0	1.6

Table 2. (Continued).

Core-Section	Corrected sub-bottom	Planktonic foraminifers		Benthic foraminifers		CaCO$_3$	Texture (%)		
(level in cm)	depth (m)	$\delta^{18}O$	$\delta^{13}C$	$\delta^{18}O$	$\delta^{13}C$	(%)	Silt	Clay	Sand
Hole 594A (Cont).									
5-5, 105	86.76	2.53	0.35	4.16	−0.29	10.9	83.0	15.3	1.7
5-5, 132	87.03	1.94	0.16	3.56	−0.30	20.2	73.5	22.6	3.9
5-6, 30	87.51	2.13	0.40	3.34	0.23	43.5	62.9	25.9	11.2
5-6, 52	87.73	1.70	0.05	3.44	0.19	45.0	63.2	27.5	9.3
5-6, 80	88.01	1.43	0.22	3.53	−0.10	33.4	67.5	21.8	10.7
5-6, 105	88.26	1.72	0.37	3.64	0.01	48.5	61.4	28.0	10.6
5-6, 132	88.53	1.57	0.50	3.58	−0.02	53.7	59.9	28.7	11.4
6-1, 30	89.61	1.97	1.17	3.20	−0.13	63.4	54.5	28.9	16.6
6-1, 52	89.83	1.97	1.21	3.30	−0.09	69.2	42.7	44.3	13.0
6-1, 80	90.11	2.19	1.07	3.29	0.06	6.5	56.4	32.1	11.5
6-1, 105	90.36	1.94	0.64	3.68	0.03	—	55.9	22.8	21.3
6-1, 132	90.63	2.40	0.08	3.95	−0.50	—	82.3	14.8	2.9
6-2, 30	91.11	3.15	0.30	4.48	−0.36	—	77.8	19.7	2.5
6-2, 52	91.33	2.82	0.37	4.34	−0.11	9.3	79.8	14.5	5.7
6-2, 80	91.61	2.55	0.23	4.64	−0.43	6.9	79.1	11.8	9.1
6-2, 105	91.86	2.85	0.71	4.02	−0.06	14.9	76.8	12.2	11.0
6-2, 132	92.13	2.54	0.25	4.09	−0.09	16.4	78.7	12.6	8.7

Note: Planktonic foraminiferal measurements are on *Globigerina bulloides* (125–250 μm); benthic measurements are on *Uvigerina* sp. (125–250 μm), and, for asterisked values only, on *Cibicides* sp. (125–250 μm). Where duplicate isotope results are shown for samples the average value has been plotted on Figs. 3 and 4. Where benthic foraminiferal isotope values are not given, the samples contained too few suitable specimens for analysis. Details of isotope analytical procedures are recorded in Nelson, Hendy, and Dudley, (this volume). —, not determined.

til 25 m sub-bottom. According to Thierstein et al. (1977), *E. huxleyi* evolved about 0.27 m.y. ago, during isotope stage 8. At Site 594 such an evolutionary age appears to be inconsistent with the interpretation of the isotope curve presented here, which in its central portion has been positioned on the basis of the *P. lacunosa/S. universus* bioevents defining isotope stage 12 (cf. Figs. 3 and 4). The distribution and age significance of *E. huxleyi* in the core require more detailed study, particularly as the subantarctic location of the site is known to have complicated the chronostratigraphic interpretation of several other microfossil zonal species in the core (Site 594 report, this volume).

The paleomagnetic and biostratigraphic data give average rates of sedimentation for the Brunhes normal Chron of 13.4 cm/10^3 yr. so an extremely high resolution stratigraphy is available compared with those of most deep-sea cores spanning the same time interval. Analytical results for 315 samples are included on Figure 3, with a sample interval of one sample every 30 cm of core, or a mean age resolution of one sample per 2400 yr.

DISCUSSION OF RESULTS

The summary stratigraphic log (Fig. 3) shows a remarkably consistent downcore correlation between the changes in sediment color represented by the alternating zones of pelagic and hemipelagic oozes, and each of the textural, carbonate, and isotope parameters analyzed. Despite rather wide variations in the absolute values of these properties, the pelagic sediments are always relatively enriched in sand- (dominantly foraminifers) and clay- (dominantly calcareous nannofossils and clay minerals) sized material, in calcium carbonate, in ^{16}O (lower $\delta^{18}O$ values), and in ^{13}C (higher $\delta^{13}C$ values) compared to the adjacent hemipelagic intervals. Typical ranges in values are given in Table 4. The oxygen isotope data clearly indicate that the major pelagic intervals are associated with interglacial periods. By implication, therefore, the sediment properties of high carbonate content and increased sand fraction also equate with interglacial episodes. This association is opposite to that generally reported from Pacific cores (e.g., Hays, et al., 1969; Thompson and Saito, 1974; Shackleton and Opdyke, 1976; Valencia, 1977; Volat et al., 1980).

Griggs et al. (1983) have discussed the stratigraphy of short piston cores spanning the last 30 × 10^3 yr. or so from the same general area as Site 594. They developed a "sedimentary model" to explain the occurrence of contrasting sediment facies in their cores. We believe that this model can be extended back over at least the past 0.75 m.y. to account for the interrelationships between texture, carbonate content, and oxygen isotope values documented here. During glacial periods of lowered sea level (^{18}O enrichment), glaciation in the Southern Alps of South Island greatly increased the volume of terrigenous sediments delivered by rivers and wind to the east coast shelf and beyond, particularly the content of silt-sized mica and quartz derived from a schist-dominated provenance. Micaceous hemipelagic sediments accumulated offshore with a proportionately reduced biogenic component dominated by diatoms, sponge spicules, and/or radiolarians rather than planktonic foraminifers and coccolithophorids (Fig. 2). The preponderance of siliceous microfossils may be attributed to a greatly enhanced concentration of silicic acid (compared to nitrate) in Subantarctic Surface Waters (e.g., Zentara and Kamykowski, 1981) as a result of accelerated erosion of the adjacent landmass (Suggate et al., 1978), as well as generally lowered water temperatures and possibly increased dissolution of the carbonate microfossils (Griggs et al., 1983).

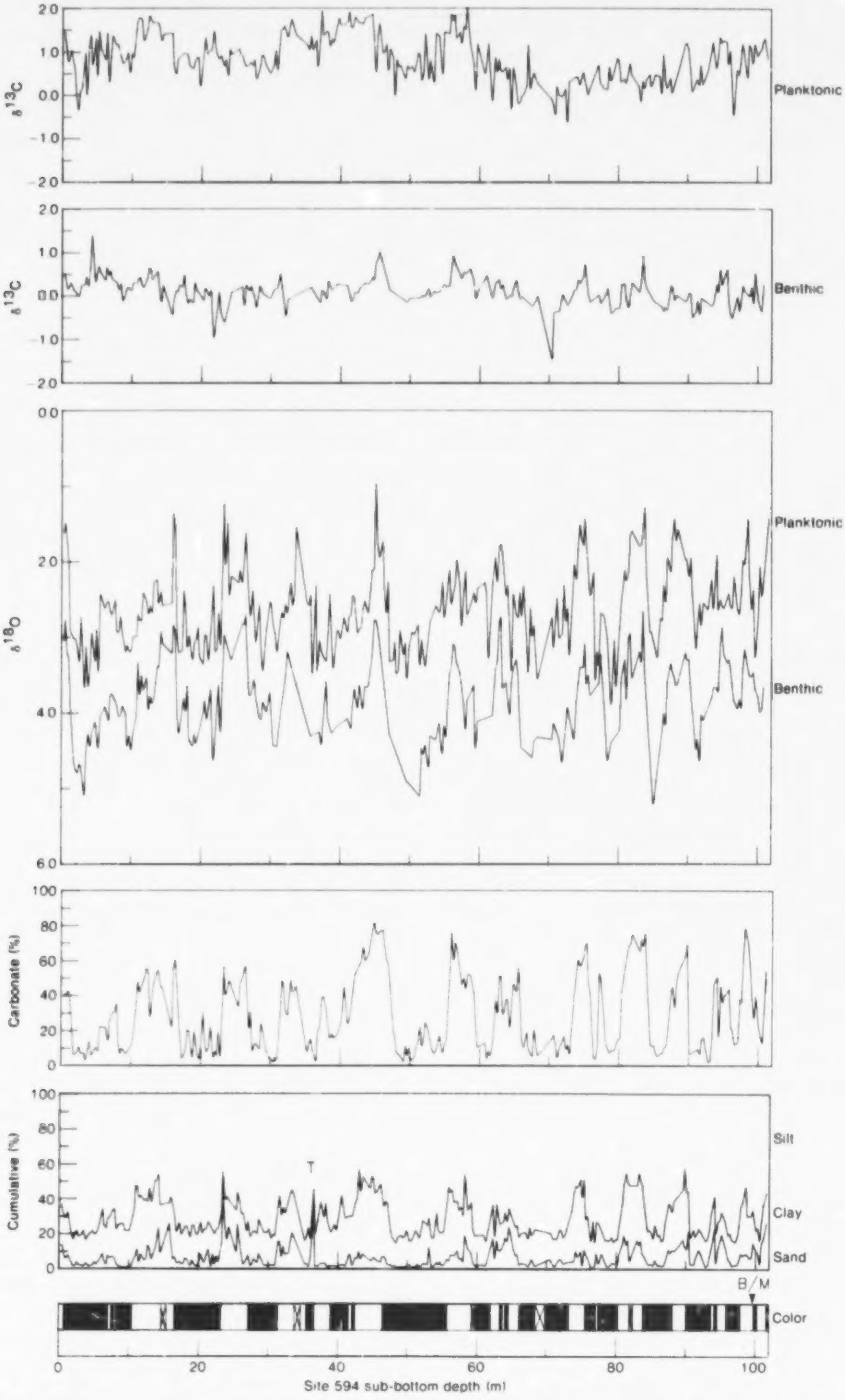

Figure 3. Summary stratigraphic logs of the color, texture, and calcium carbonate content of bulk core samples and of the oxygen and carbon isotope variations of planktonic (*Globigerina bulloides*) and benthic (*Uvigerina* sp.) foraminifers in the late Quaternary oozes at Site 594 (data from Table 2). B/M, Brunhes/Matuyama boundary (730 × 10^3 yr.) at 99.3 m sub-bottom depth. T, sand-rich tephra bed. The color variation is simplified: white intervals are dominantly bluish gray pelagic oozes; black intervals are mainly greenish gray hemipelagic oozes. Crosses indicate gaps in the cored sequence. Isotope values are in per mil deviations (‰) from the international PDB standard. In this plot, the *Cibicides* isotope results (Table 2) have been converted to nominal *Uvigerina* values (Nelson, Hendy, and Dudley, this volume).

Table 3. Distribution of some Quaternary zonal microfossil species at Site 594 and their possible age significance as adopted elsewhere.

Index species	Appearance datum	Suggested age (m.y.)	Isotope stage	Core sample	Sub-bottom depth (m)	Abundance
Emiliania huxleyi	First	0.27	8	6-1, 25 cm	44.56	Rare
				6-3, 3 cm	47.34	Absent
Stylatractus universus	Last	0.41	11/12	7-1	~54.6	Absent
				7-2	~55.9	Rare
Pseudoemiliania lacunosa	Last	0.46	12	7-1, 3 cm	53.94	Absent
				7-1, CC	63.50	Rare
				6-1, 33 cm[a]	44.63	Absent
				7-1, 31 cm[a]	54.21	Present
Calcidiscus macintyrei	Last	1.45	—	11-3, 3 cm	95.34	Absent
				11-5, 3 cm	98.34	Rare

Note: Distributions from Site 594 site report, this volume; Lohman, this volume, and A. R. Edwards, pers. comm., 1983. Age significance after Hays and Shackleton, 1976; Gartner, 1977; Shackleton, 1977b; and Thierstein et al., 1977.

[a] From A. R. Edwards (pers. comm., 1983).

Table 4. Typical range of values of textural, carbonate, and isotope parameters for the late Quaternary pelagic and hemipelagic oozes at Site 594.

Property	Pelagic lithofacies	Hemipelagic lithofacies
Sand sizes (%)	10–30	0–10
Silt sizes (%)	50–70	70–90
Clay sizes (%)	25–50	10–25
$CaCO_3$ (%)	40–80	0–25
$\delta^{18}O$ (‰)		
Planktonic foraminifers	1.5–2.5	2.5–3.5
Benthic foraminifers	3.0–4.0	4.0–5.0
$\delta^{13}C$ (‰)		
Planktonic foraminifers	1.0–2.0	0–1.0
Benthic foraminifers	0–1.0	−0.5–0.5

During interglacial episodes and higher sea levels, erosion along the alpine chain was much less severe and the terrigenous sediment was mainly trapped on extensive piedmont plains or in glacial lakes. Apart from fine clays, the supply of terrigenous material to offshore basins was reduced. Coincidentally, there was a decrease in siliceous biogenic productivity and, according to Griggs et al. (1983), carbonate dissolution, with deposition of predominantly foraminifer-bearing nannofossil pelagic oozes (Fig. 2). Thus, the entire late Quaternary sedimentary record at Site 594 is dominated by paleoclimate influences that have controlled sea level and isotope composition, terrigenous input, calcium carbonate content, and biogenic productivity and composition. The three factors of dilution by noncarbonate material, calcareous plankton productivity, and intensity of carbonate dissolution together have determined the calcium carbonate stratigraphy at the site, but dilution by terrigenous and, to a lesser extent, siliceous microfossil materials is regarded as the dominant factor. Evidence for this can be gauged from Table 5, which shows that glacial isotope stages have overall sedimentation rates that were two to three times greater than interglacial isotope stages, but had calcium carbonate accumulation rates only about half those of the interglacial stages. Moreover, it is particularly relevant that the pulses of terrigenous sediment derived ultimately from glacial and periglacial erosion in the South Island have accompanied every period of relatively increased $\delta^{18}O$ values corresponding to lowered sea levels. This demonstrates a direct link throughout the last 0.75 m.y. between the fluctuations of the major Northern Hemisphere ice sheets and the advance and retreat of small alpine glaciers on a remote, temperate-latitude island in the South Pacific.

Tentative correlation between the planktonic and benthic $\delta^{18}O$ fluctuations and the standard isotope stages is presented in Figure 4. For comparison, our $\delta^{18}O$ isotope records are plotted alongside the planktonic foraminiferal record from DSDP Site 502 in the western Caribbean (Prell, 1982) as well as "SPECMAP"—a synthesis of the $\delta^{18}O$ records from five cores (including DSDP Site 502) plotted as a function of time (Imbrie et al., in press). The isotope stage boundaries for DSDP Site 502 cores are from Prell (1982). It should be noted however, that Prell's positions for several of the stage boundaries at Site 502 in Figure 4 are at considerable variance with those given by Imbrie et al. (in press, table 6, column 7), which may be in error.

The proximity of Site 594 to the Subtropical Convergence and the very high sedimentation rate (average 13.4 cm/10^3 yr.), which has enabled a 30-cm sampling interval, thus eliminating intersample mixing and reducing smoothing of the isotope signature by bioturbation (Shackleton and Opdyke, 1976), has resulted in some important differences between the Site 594 $\delta^{18}O$ record and those of most other cores penetrating the Brunhes/Matuyama boundary:

1. Some additional full glacial/interglacial cycles are recognizable in the late Quaternary. This is particularly apparent during isotope stage 15 (tentative correlation only), where the $\delta^{18}O$ record twice reaches full glacial values during an interglacial stage, and in glacial stages 14 and 18 (tentative correlations only), where prominent interglacial $\delta^{18}O$ peaks are recorded.
2. The magnitude of the glacial to interglacial $\delta^{18}O$ fluctuations remains more or less constant at 2.0 to 2.2‰ throughout the entire Brunhes Chron and contrasts with the "SPECMAP" synthesis, which shows a decreasing $\delta^{18}O$ amplitude with age. This latter is probably mainly a consequence of the diminishing resolution with age of the data base used by Imbrie et al. (in press).
3. The $\delta^{18}O$ isotope record includes the common occurrence of short-term fluctuations (within a few to sev-

Table 5. Tentative scheme of isotope stage positions and sedimentation rates for the late Quaternary oozes at Site 594.

Isotope stage boundary			Isotope stage					
Position	Depth (cm)	Age[a] (10^3 yr.)	Number	Thickness (cm)	Duration (10^3 yr.)	Bulk sed. rate (cm/10^3 yr.)	$CaCO_3$ (mean %)	$CaCO_3$ sed. rate (cm/10^3 yr.)
			1	144	12	12.0	34.5	4.1
1/2	144	12						
			2	404	12	33.7	8.4	2.8
2/3	548	24						
			3	315	35	9.0	22.3	2.0
3/4	863	59						
			4	227	12	18.9	10.3	1.9
4/5	1090	71						
			5	570	57	10.0	45.6	4.6
5/6	1660	128						
			6	640	58	11.0	12.7	1.4
6/7	2300	186						
			7	396	59	6.7	45.5	3.0
7/8	2696	245						
			8	491	58	8.5	10.6	0.9
8/9	3187	303						
			9	428	36	11.9	33.6	4.0
9/10	3615	339						
			10	525	23	22.8	24.6	5.6
10/11	4140	362						
			11	522	61	8.6	64.6	5.6
11/12	4662	423						
			12	856	55	15.6	11.8	1.8
12/13	5518	478						
			13	398	46	8.7	55.5	4.8
13/14	5916	524						
			14	1418	41	34.6	21.4	7.4
14/15	7334	565						
			15	1071	55	19.5	42.4	8.3
15/16	8405	620						
			16	244	39	6.3	8.6	0.5
16/17	8649	659						
			17	425	30	14.2	39.4	5.6
17/18	9074	689						
			18	679	37	18.4	24.0	4.4
18/19	9753	726						
			19	187	10	18.7	52.8	9.9
19/20	9940	736						

[a] Based on Imbrie et al. (in press).

eral thousand years) with an amplitude of about 0.7‰. Some of these fluctuations occur concurrently in the planktonic and benthic records, which would suggest that high-frequency fluctuations in ice volumes and eustatic sea levels may be an intrinsic feature of the late Quaternary. In addition, a number of the planktonic short-term fluctuations are not evident in the benthic record and may result from changes in surface water temperatures, perhaps associated with shifts in the location of the Subtropical Convergence over Site 594 (Fig. 1).

The foraminiferal $\delta^{13}C$ record shows some significant variations and, as plotted, is broadly in phase with the $\delta^{18}O$ curve (Fig. 3). Intervals of reduced $\delta^{13}C$ values correspond to glacial episodes, while relatively higher $\delta^{13}C$ values accompany interglacials. Near-surface waters in this region probably have $\delta^{13}C$ values in the range 1.0–2.0‰ for dissolved bicarbonate (Kroopnick, 1971; Kennett et al., 1979). This overlaps with the majority of interglacial values for the *Globigerina bulloides* calcite at the site and may indicate that the species deposited its carbonate close to carbon isotope equilibrium with dissolved bicarbonate. The *Uvigerina* calcite has $\delta^{13}C$ values that are generally about 1‰ lower than those of *G. bulloides* and display a more subdued response to glacial/interglacial changes than do *G. bulloides*. Similar depletions of ^{13}C in planktonic and benthic foraminifers during glacial stages have been observed in other cores and have been interpreted by Shackleton (1977a) to result from a decrease in the organic carbon stored on land. Changes in the productivity of surface waters can also result in changes in the $\delta^{13}C$ values of both planktonic and benthic foraminifers (Fontugne and Duplessy, 1981), although the effect of this is difficult to assess at Site 594 since decreased carbonate productivity during glacial stages is matched by increased siliceous microorganism productivity. The higher frequency fluctuations in $\delta^{13}C$ probably do relate to short-term changes in primary productivity, which presently shows considerable spatial and temporal variability in response to nutrient availability, depth of vertical mixing, circulation patterns, and water transparency (Bradford, 1983).

CONCLUSIONS

1. The Brunhes normal Chron (last 730 × 10^3 yr.) at Site 594 off southeast New Zealand consists of a 99.3-m-thick sequence of oozes that alternate between pelagic

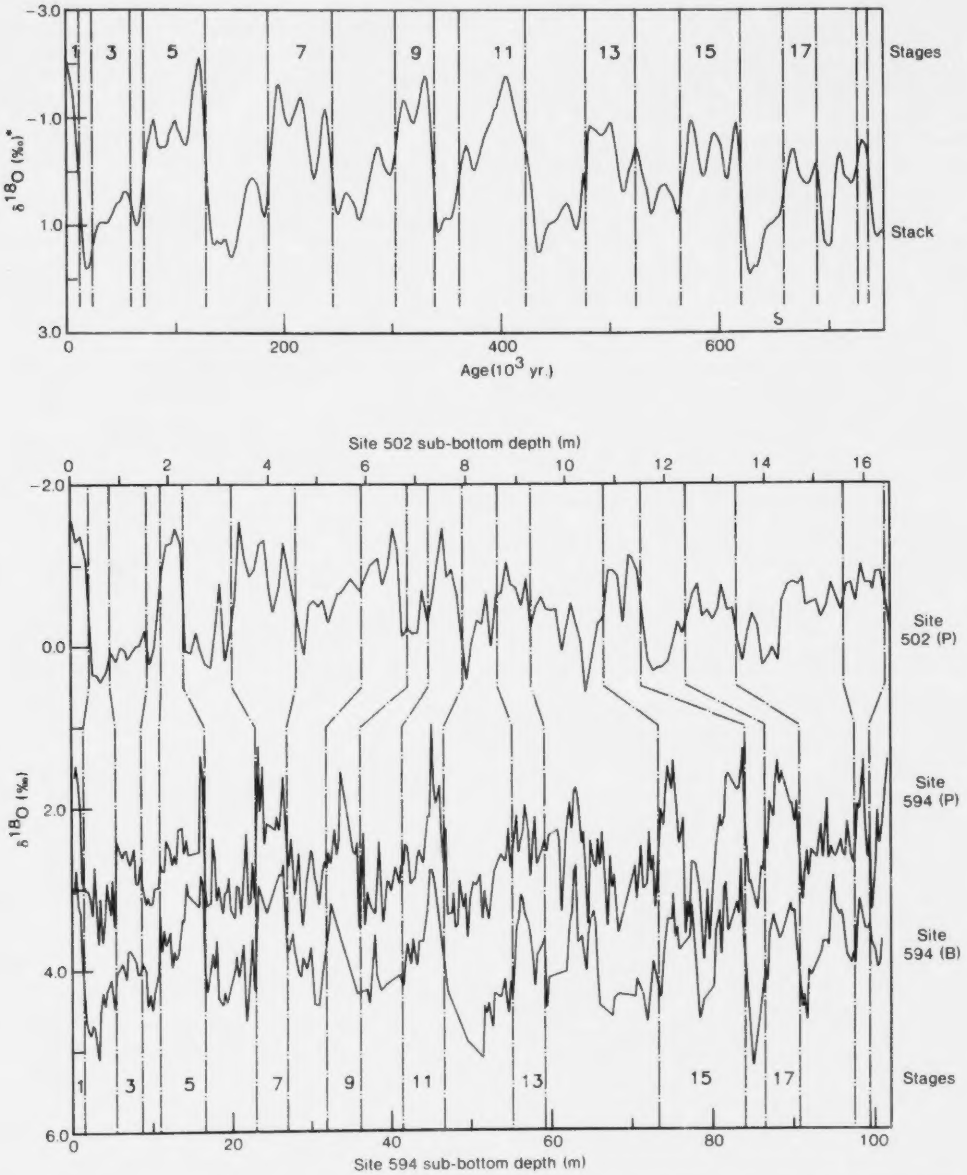

Figure 4. Tentative correlation scheme of late Quaternary isotope stages 1 to 19 defined for the age-based "SPECMAC" $\delta^{18}O$ isotope stack (Imbrie et al., in press) and for the planktonic (P) foraminiferal $\delta^{18}O$ record from DSDP Site 502 in the western Caribbean (Prell, 1982) with the planktonic (P) and benthic (B) foraminiferal $\delta^{18}O$ records at DSDP Site 594, southeastern New Zealand. Note the significant difference in the sub-bottom depth scales for the same time period between DSDP Sites 502 and 594. *Note that the "SPECMAC" $\delta^{18}O$ stack curve is expressed as standard deviation units (after Imbrie et al., in press).

and hemipelagic type as a result of paleoclimate fluctuations.

2. Hemipelagic sediments were deposited during glacial episodes and lowered eustatic sea level and are characterized by siliceous microfossils, low (0–25%) $CaCO_3$ contents, and common terrigenous silt derived principally from accelerated physical erosion in South Island, New Zealand. Sedimentation rates at these times were typically 10–35 cm/10^3 yr.

3. Pelagic sediments formed during interglacial periods of high eustatic sea level and are characterized by calcareous microfossils, high (50–80%) $CaCO_3$ contents, and a reduced terrigenous fraction that was predominantly clay-sized material. Sedimentation rates were typically 5–10 cm/10^3 yr.

4. The history of alpine glaciations and associated erosion in South Island, recorded by the hemipelagic ooze intervals, appears to be closely in phase with major fluc-

tuations of the Pleistocene ice sheets as expressed by the influence of eustatic sea-level changes on the oxygen isotope composition of foraminifers in the core.

5. The Site 594 benthic and planktonic foraminiferal $\delta^{18}O$ records include at least three additional full glacial–interglacial cycles compared to the standard isotope stage scheme for the late Quaternary. The intensity of glacial to interglacial fluctuations has remained similar throughout this entire period. Moreover, superimposed high-frequency $\delta^{18}O$ fluctuations of $\sim 0.7‰$ amplitude suggest that rapid eustatic sea-level oscillations of up to 50 m may be an important feature of the late Quaternary.

ACKNOWLEDGMENTS

We thank Scott Nodder and Steve Bergin (University of Waikato) for assistance with sample processing; Lionel Carter and Janet Bradford (N. Z. Oceanographic Institute, Wellington) for helpful discussions on the oceanography and bottom sediments off eastern South Island; Tony Edwards (N.Z. Geological Survey, Lower Hutt) for providing some preliminary information on calcareous nannoplankton in core-top samples; and Carolyn Beltz (University of Waikato) for SEM assistance. The review comments on this manuscript by Nick Pisias (Oregon State University, Corvallis) were much appreciated. Research was supported partly by Grant 83/125 to C.S. Nelson from the N.Z. University Grants Committee.

REFERENCES

Bradford, J. M., 1983. Plankton and primary productivity in the vicinity of the Chatham Rise. *N.Z. Oceanogr. Inst. Oceanogr. Summary*, 21:1–14.

Fontugne, M. F., and Duplessy, J. C., 1981. Organic carbon isotopic fractionation by marine plankton in the temperature range −1 to 31°C. *Oceanologica Acta*, 4:85–90.

Gartner, S., 1977. Calcareous nannofossil biostratigraphy and revised zonation of the Pleistocene. *Mar. Micropaleontol.*, 2:1–25.

Griggs, G. B., Carter, L., Kennett, J. P., and Carter, R. V., 1983. Late Quaternary marine stratigraphy southeast of New Zealand. *Geol. Soc. Am. Bull.*, 94:791–797.

Hays, J. D., Saito, T., Opdyke, N. D., and Burckle, L. H., 1969. Pliocene-Pleistocene sediments of the equatorial Pacific: their paleomagnetic, biostratigraphic and climatic record. *Geol. Soc. Am. Bull.*, 80:1481–1514.

Hays, J. D., and Shackleton, N. J., 1976. The globally synchronous extinction of *Stylatractus universus*. *Geology*, 4:649–652.

Healy, T. R., Nelson, C. S., de Lange, W., and McArthur, W., 1983. The University of Waikato rapid sediment analysis system for particle size analysis. *Geol. Soc. N.Z. Misc. Publ.*, 30A:57.

Imbrie, J., Shackleton, N. J., Pisias, N. G., Morley, J. J., Prell, W. L., Martinson, D. G., Hays, J. D., McIntyre, A., and Mix, A. C., in press. The orbital theory of Pleistocene climate: support from a revised chronology of the marine $\delta^{18}O$ record. *In* Imbrie, J., and Berger, A. (Eds.), *Milankovitch and Climate Change*: Amsterdam (Elsevier).

Kennett, J. P., Shackleton, N. J., Margolis, S. V., Goodney, D. E., Dudley, W. C., and Kroopnick, P. M., 1979. Late Cenozoic oxygen and carbon isotopic history and volcanic ash stratigraphy: DSDP Site 284, South Pacific. *Am. J. Sci.*, 179:52–69.

Kroopnick, P. M., 1971. Oxygen and carbon in the oceans and atmosphere: stable isotopes as tracers for consumption, production and circulation models [Ph.D. dissert.]. University of California, San Diego.

Prell, W. L., 1982. Oxygen and carbon isotope stratigraphy for the Quaternary of Hole 502B: evidence for two modes of isotopic variability. *In* Prell, W. L., Gardner, J. V., et al., *Init. Repts. DSDP*, 68: Washington (U.S. Govt. Printing Office), 455–464.

Shackleton, N. J., 1977a. Carbon-13 in *Uvigerina*: tropical rainforest history and equatorial Pacific carbonate dissolution cycles. *In* Anderson, N. R., and Malahoff, A. (Eds.), *The Fate of Fossil Fuel CO_2 in the Oceans*: New York (Plenum Press), pp. 401–427.

———, 1977b. Oxygen isotope stratigraphy of the middle Pleistocene. *In* Shotton, F. W. (Ed.), *British Quaternary Studies—Recent Advances*: Oxford (Clarendon Press), pp. 1–16.

Shackleton, N. J., and Opdyke, N. D., 1976. Oxygen isotope and paleomagnetic stratigraphy of Pacific core V28-239, late Pliocene to latest Pleistocene. *In* Cline, R. M., and Hays, J. D. (Eds.), *Investigation of Late Quaternary Paleoceanography and Paleoclimatology*. Geol. Soc. Am. Mem., 145:449–464.

Suggate, R. P., Stevens, G. R., and Te Punga, M. T. (Eds.), 1978. *The Geology of New Zealand*, 2. New Zealand Geological Survey, Department of Scientific and Industrial Research, Wellington.

Theirstein, H. R., Geitzenauer, K. R., Molfino, B., and Shackleton, N. J., 1977. Global synchroneity of late Quaternary coccolith datum levels: validation by oxygen isotopes. *Geology*, 5:400–404.

Thompson, P. R., and Saito, T., 1974. Pacific Pleistocene sediments: planktonic foraminifera dissolution cycles and geochronology. *Geology*, 2:333–335.

Valencia, M. J., 1977. Pacific Pleistocene paleoclimatic stratigraphies: a comparative analysis of results. *Quat. Res.*, 8:339–354.

Volat, J.-L., Pastouret, L., and Vergnaud-Grassini, C., 1980. Dissolution and carbonate fluctuations in Pleistocene deep-sea cores: a review. *Mar. Geol.*, 34:1–28.

Zentara, S. J., and Kamykowski, D., 1981. Geographic variations in the relationship between silicic acid and nitrate in the South Pacific Ocean. *Deep-Sea Res.*, 28A:455–465.

Date of Initial Receipt: 8 June 1984
Date of Acceptance: 5 December 1984

45. SILICICLASTIC SEDIMENTS AT SITES 588, 590, AND 591: NEOGENE AND PALEOGENE EVOLUTION IN THE SOUTHWEST PACIFIC AND AUSTRALIAN CLIMATE[1]

R. Stein, Geologisch-Palaeontologisches Institut Kiel
and
C. Robert, Géologie Marine, Faculté des Sciences de Luminy, Marseille[2]

ABSTRACT

Clay minerals, grain sizes, and flux rates of terrigenous sediments in the Lord Howe Rise area provide important information about the Neogene evolution of climate and physical processes in the southwest Pacific region. Temporal variations in these data suggest that the Neogene history of desertification in Australia was controlled by both the northward drift of the Indo-Australian Plate and the buildup of Antarctic ice sheets. Increased aridity, as defined by a distinct decrease in smectite/illite ratios and increased accumulation rates of terrigenous matter, occurred in northern Australia about 13 m.y. ago, expanding to the south during the late Miocene. Periods of maximum aridity coincided with major cooling events near 12, 9, 5, and 3 m.y. ago. Increased eolian sediment supply and intensified atmospheric circulation are inferred from the grain size and flux rates of the terrigenous sediments at Site 591 during the last 4 m.y., that is, about 0.8 m.y. earlier than similar observations recorded in the Northern Hemisphere. An enhanced oceanic intermediate-water circulation is inferred from decreased accumulation rates and a coarsening of both the bulk-sediment and the terrigenous-sediment fraction at Sites 588 and 590 during the last 3 m.y.

Volcanic activity increased in the southwest Pacific region during the Miocene (21 to 9 m.y. ago) and in the Quaternary (0.4 m.y. ago).

INTRODUCTION

During Leg 90 of the Deep Sea Drilling Project, Sites 588, 590, 591, and 592 were drilled along a latitudinal transect on the Lord Howe Rise between 26 and 36°S at water depths between about 1000 and 2100 m (Fig. 1, Table 1). The sediments range in age from the middle Eocene (Site 588) or early Miocene (Sites 590, 591) to the Pleistocene and consist of foraminifer-bearing nannofossil oozes and chalks to nannofossil oozes and chalks (site chapters, this vol.). The use of the hydraulic piston corer (HPC) and—in greater sub-bottom depths—the extended core barrel (XCB) facilitated a very good recovery and high quality for all sediment sections and provided excellent material for studying the paleoclimatology and paleoceanography of the southwest Pacific region.

The purpose of this study is to reconstruct paleoenvironments from the investigation of the mineralogy, grain size, and flux rate of the terrigenous (i.e., carbonate-free, nonauthigenic, inorganic) sediment fraction (Fig. 2). The main objectives were to understand (1) the evolution of the Australian climate, (2) changes in atmospheric and oceanic circulation in the southwest Pacific region, (3) phases of volcanic activities, and (4) the northward drift of the Indo-Australian Plate as reflected in the marine terrigenous sediments at the Lord Howe Rise.

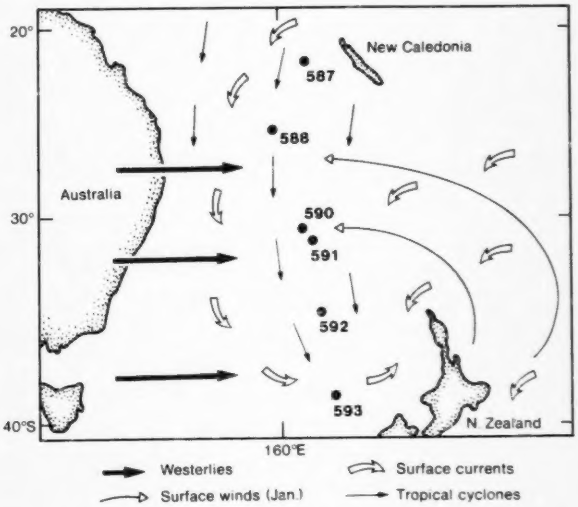

Figure 1. Positions of the Leg 90 sites drilled on the Lord Howe Rise, and the dominant atmospheric and oceanic surface circulation patterns in the southwest Pacific (according to Knox, 1970; Ramage, 1970).

As shown by previous studies from other ocean regions, investigations of the terrigenous sediment fraction can provide a useful record of paleoclimate and paleoceanography. Clay mineral analyses can provide information about the origin of detrital minerals and the climate of the source area as well as volcanic and tectonic activity (Biscaye, 1965; Griffin et al., 1968; Chamley, 1979; Chamley and Robert, 1979; Leinen and Heath, 1981; Lange, 1982; Robert, 1982; Sarnthein et al., 1982; Maillot and Robert, 1984; Stein, 1984; Stein and Sarnthein, 1984a). If the terrigenous sediment supply is mainly eolian in origin, wind intensity of past times can be

---

[1] Kennett, J. P., von der Borch, C. C., et al., *Init. Repts. DSDP*, 90: Washington (U.S. Govt. Printing Office).

[2] Addresses: (Stein, present address) Institute for Petroleum and Organic Geochemistry (CH 5), Kernforschungsanlage Jülich GmbH, P.O. Box 1913, 5170 Jülich, Federal Republic of Germany; (Robert) Géologie Marine, URA CNRS 41, Faculté des Sciences de Luminy, Case 901, 13288 Marseille Cedex 9, France.

Table 1. Site locations and water depths.

Site	Latitude (S)	Longitude (E)	Water depth (m)
588	26°06.70′	161°13.60′	1533
590	31°10.02′	163°21.51′	1299
591	31°35.06′	164°26.92′	2131
592	36′28.40′	165°26.53′	1098

deduced from the grain-size distribution of the terrigenous matter (Parkin, 1974; Leinen and Heath, 1981; Sarnthein et al., 1981; Rea and Janecek, 1982; Janecek and Rea, 1983; Lever and McCave, 1983; Stein 1984, 1985a). The flux rates of dust may yield additional information on the aridity of the source area because erosion initially increases as vegetation cover decreases (Parkin and Padgham, 1975; Leinen and Heath, 1981; Rea and Janecek, 1982; Stein and Sarnthein, 1984a). In contrast, the dust flux from a mature sand and stone desert is minor, although still significantly more than from a humid vegetation area. Therefore, maximum dust-flux rates are recorded in areas of semiarid climate such as in the southern Sahara and the Sahelian zone (Carlson and Prospero, 1977; Sarnthein et al., 1982).

THE MODERN REGIME OF SEDIMENT DISTRIBUTION PATTERNS IN THE SOUTHWEST PACIFIC

Origin and Significance of Clay Minerals

Smectite can be formed by the weathering of volcanic products and by pedogenic processes in a humid to semiarid climatic regime characterized by areas with low relief and poorly drained environments (Millot, 1964; Chamley et al., 1984). Climatic conditions favorable for the formation of smectite are found in the north and northeast regions of Australia and in the semiarid belts enclosing the central Australian deserts (Pedro, 1968) as well as in southern Australia (Moriarty, 1977).

Regions with high relief and active tectonism as well as areas with temperate to cold or hot, dry climatic conditions, that is, areas with dominant physical weathering, favor the formation of illite, chlorite, and irregular mixed-layer clays (Chamley, 1979; Robert, 1982).

Kaolinite is preferentially formed under tropical conditions where chemical weathering dominates, such as in the lateritic zones in equatorial Africa (Millot, 1964; Biscaye, 1965; Chester et al., 1971). Thus, kaolinite-rich soils found today in arid to semiarid areas of central Australia (Griffin et al., 1968; Moriarty, 1977) may have been formed during earlier, more humid climatic periods.

Sources of Detrital Materials at the Lord Howe Rise

Several source areas of terrigenous matter and different transport systems must be distinguished if the variations in the terrigenous sediments at the Lord Howe Rise are to be used as a record of paleoclimate and paleoceanography (Fig. 1).

1. Eolian Sediment Supply

The importance of wind-borne material for the sediment budget of siliciclastic matter in the southwest Pacific region has been recorded in several previous studies (Marshall and Kidson, 1929; Kidson, 1930; Loewe, 1943;

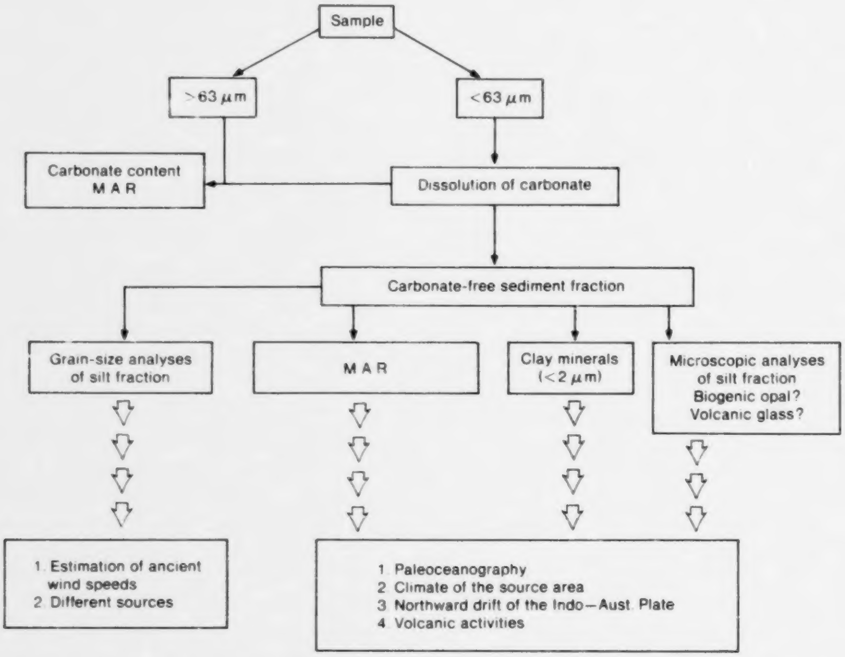
Sample
>63 μm
<63 μm
Carbonate content
MAR
Dissolution of carbonate
Carbonate-free sediment fraction
Grain-size analyses of silt fraction
MAR
Clay minerals (<2 μm)
Microscopic analyses of silt fraction
Biogenic opal?
Volcanic glass?
1. Estimation of ancient wind speeds
2. Different sources
1. Paleoceanography
2. Climate of the source area
3. Northward drift of the Indo-Aust. Plate
4. Volcanic activities

Figure 2. Flow chart of the methods used to determine grain size and composition of the carbonate-free silt fraction, mass accumulation rates (MAR), and clay mineralogy.

Healy, 1970; Glasby, 1971; Walker and Costin, 1971; Thiede, 1979).

The terrigenous sediment supply in the area investigated is restricted mainly to eolian dust, because the Lord Howe Rise lies more than 1000 km offshore and is separated from the Australian continental margin by the Tasman Abyssal Plain. This prevents a supply of fluvial terrigenous matter by turbidity currents. At present, the eolian sediment flux is dominated by westerly winds bringing dust from the Australian deserts and semideserts (Fig. 1; Healy, 1970; Glasby, 1971; Sprigg, 1982). The eolian origin of the sediments is also indicated by the (eolian) quartz content in recent deep-sea sediments from the Tasman Sea, which show a distinct decrease from the Australian continent toward the east (Thiede, 1979). Kaolinite and illite in the dust are probably derived from the western and central deserts and semidesert regions and the eastern highlands of Australia, where they are dominant components of the fine-sediment fraction (Griffin et al., 1968; Moriarty, 1977; Mienert, 1981). The clay mineralogy of dust samples collected from snowfields in southeastern Australia is also dominated by illite and kaolinite (Walker and Costin, 1971).

In addition to the eolian sediment supplied by the westerlies, dust may be supplied by two other wind systems. Surface winds may carry dust from New Zealand during the southern summer, and tropical cyclones may supply dust from the northern tropical regions (e.g., the Melanesian islands) (Fig. 1; Ramage, 1970). Today, the eolian sediment flux of these two transport systems is negligible because the vegetation cover is thick in these areas and volcanicity is absent. However, during phases of volcanic activity in the tropical southwest Pacific regions and in New Zealand and during phases of both tectonic events and more arid climatic conditions in New Zealand, the two wind systems may have become important agents of eolian transport toward the Lord Howe Rise (see Nelson et al., this vol.).

2. Advective Transport of Detritus by Currents

In addition to the eolian sediment supply by winds, oceanic currents may also influence the terrigenous sediment balance at the Lord Howe Rise (Fig. 1). The East Australian Current flows southward off the eastern coast of Australia; it reaches maximum velocities of about 175 cm/s in the upper 100 m and decreases to 10-20 cm/s in 1200-m water depth (Fig. 1; Hamon, 1970). This current may supply clay-sized material from tropical regions north of the Lord Howe Rise and from Australia. Antarctic Intermediate Water enters the region from the east between 10 and 30°S (Wyrtki, 1962) and may also influence the flux of siliciclastic matter. Or if the currents reach a critical velocity, they may also winnow the fine fraction; this may be indicated by reduced bulk accumulation rates and a parallel coarsening of the grain sizes of both the bulk sediment and the terrigenous sediment fraction (Stein, 1984; Stein and Sarnthein, 1984b). At present, the advective transport of detritus toward the Lord Howe Rise seems to be of minor importance, as can be inferred from the similarity of dust-flux rates and terrigenous accumulation rates in the southwest Pacific region (Windom, 1969; Glasby, 1971). Thus, the carbonate- and biogenic-opal-free, nonauthigenic sediment fraction on the Lord Howe Rise is probably mainly eolian in origin.

METHODS

The methodology used for this study is outlined in Figure 2. Because the carbonate-free sediment fraction was very small, it was not possible to determine all sediment parameters from the same sample. Thus, one set of samples was used for carbonate measurements, grain-size analyses, and component analyses of the carbonate-free silt fraction, and another set of samples was used for clay mineral analyses.

Clay Mineral Analyses

The fraction less than 63 μm was decalcified in 0.2 hydrochloric acid and the excess acid removed by repeated washing and centrifugation followed by homogenization. The fraction less than 2 μm was separated by decantation and was fixed as oriented aggregates on glass slides. Three X-ray diffractograms were made using (1) an untreated sample, (2) a glycolated sample, and (3) a sample heated for 2 hr. at 490°C. A C.G.R. Theta 60 diffractometer (copper Kα radiation focused by a quartz curved monochromator) was used at scanning speeds of 1° 2θ/min. A receiving slit of 1.25 mm allowed a more precise resolution of poorly crystallized minerals. Semiquantitative evaluations were based on the peak heights and areas. The data presented in Figures 4 through 6 are given in percentages, with the relative error being ±5% per total clay. The relative abundances of smectite versus illite (S/I index) and of kaolinite versus illite (K/I index) were obtained from the ratios of the 001 smectite (18 Å), illite (10 Å), and kaolinite (7 Å) peaks on the glycolated sample.

The morphology of the smectites was studied by transmission electron microscope (Chamley, 1980; Chamley et al., 1984; Holtzapffel et al., 1984). The fraction less than 8 μm was separated by decantation and the particles were scattered in a solution of tert-Butylamin. A drop of the suspension was then deposited on a copper grid which had been previously recovered by a membrane of Collodion. The analyses were performed using a Philips EM 300 electron microscope.

Carbonate Content

Total carbonate-CO_2 and carbonate-CO_2 of the fraction less than 63 μm were determined from a subsample by infrared absorption of CO_2 after carbonates were dissolved in hot phosphoric acid. A factor of 2.274 was used to convert CO_2 values into $CaCO_3$ values, taking calcite as the predominant carbonate mineral. The analytical precision of this method is about ±2% (Stein, 1984).

Composition and Grain Size of the Carbonate-Free Sediment Fraction

The samples were washed through a 63-μm sieve. The fraction less than 63 μm was treated successively with hydrogen peroxide and acetic acid to remove organic matter and calcium carbonate. The carbonate-free sediment fraction was separated into >6 μm and <6 μm subfractions by the Atterberg method (Mueller, 1967). The >6 μm fraction was analyzed for the percentage of biogenic opal and volcanic glass by smear-slide counts under a microscope. The terrigenous sediment fraction >6 μm presented in Figure 9 was calculated by subtracting biogenic opal >6 μm from the carbonate-free sediment fraction >6 μm. The grain-size distribution of the 6 to 63 μm size-fraction was determined using a Coulter Counter, Model T (McCave and Jarvis, 1973; Stein, 1985b).

Mass Accumulation Rates

Linear sedimentation rates (LSR) and mass accumulation rates (MAR) can be used to describe the rate of deposition of sediment in the ocean. The LSR, that is, the thickness of a sediment section per time interval, does not take into account the compaction of the accumulated sediment with increasing overburden and age. Thus, it is not meaningful to compare LSR from different sub-bottom depths (van

Andel et al., 1975). Using MAR, the compaction problem can be eliminated, and a comparison of sediment accumulation on both a temporal and areal basis is possible.

The MAR were calculated according to van Andel et al. (1975) and Thiede et al. (1982) using mean porosity (*Po*) and wet-bulk density (ρ_{wet}) data of Morin (site chapters, this vol.) and the LSR (Fig. 3):

$$\begin{aligned} \text{MAR } (\text{g} \cdot \text{cm}^{-2}\ 10^{-3}\ \text{y}^{-1}) &= \text{LSR} \cdot \rho_{dry} \\ &= \text{LSR} \cdot \left(\rho_{wet} - 1.026 \cdot \frac{Po}{100}\right), \end{aligned}$$

whereby LSR = sedimentation rate (cm $\cdot$ 10^{-3} y^{-1}), ρ_{dry} = dry-bulk density (g $\cdot$ cm^{-3}), and 1.026 = density of interstitial water (g $\cdot$ cm^{-3}). The LSR (Fig. 3) were based on the nannofossil biostratigraphy of Lohman (this vol.) and Martini (this vol.). The MAR of the carbonate-free sediment fraction can then be calculated by multiplying the MAR by the wt.% total carbonate-free (i.e., mainly terrigenous) sediment fraction:

$$\text{MART} = \text{MAR} \cdot \frac{\%\ \text{terrigenous sediment}}{100}.$$

That is, we interpret the MAR of the carbonate-free sediment as the MAR of the terrigenous matter (MART), an assumption which seems to be permissible because (1) the carbonate-free sediment fraction contains almost no authigenic clay minerals (zeolites are absent or occur only in trace amounts; Figs. 4 to 6) and (2) biogenic opal is generally absent or occurs only in minor quantities (Figs. 4 to 6). An exception may be the late Miocene time interval at Site 591 (i.e., 350 to 200 m sub-bottom; Fig. 6) where higher abundances of biogenic opal were recorded. This would imply that the already low MART of this time interval (see Fig. 11, later) would become even lower.

RESULTS[3]

Coarse Fraction Abundance

The contents of the fraction greater than 63 μm, mainly planktonic foraminifers, vary between 5 and 50% at all three sites (Figs. 4, 5, 6, and 7). Values of less than 10% are observed in the late Oligocene (Site 588) and in the late Miocene to Pliocene, between 8 and 3.5 m.y. ago (Sites 588, 590, and 591). Moderate percentages of coarse fraction (10 to 20%) occur between 20 and 8 m.y. ago (Site 588). It was not meaningful to determine the >63-μm percentages by wet sieving for samples from Sites 590 and 591 from core depths greater than 280 m (8 m.y.) and 340 m (10 m.y.), respectively, because of diagenetic formation of aggregates (Fig. 7). These levels coincide with the transition from ooze to chalk (site chapters, this vol.). A more or less distinct increase in the coarse fraction has occurred in all Leg 90 sites at the Lord Howe Rise during the last 3 m.y. This increase is more distinct at the shallower Sites 588, 590, and 592 than at the deeper Site 591 (Fig. 7).

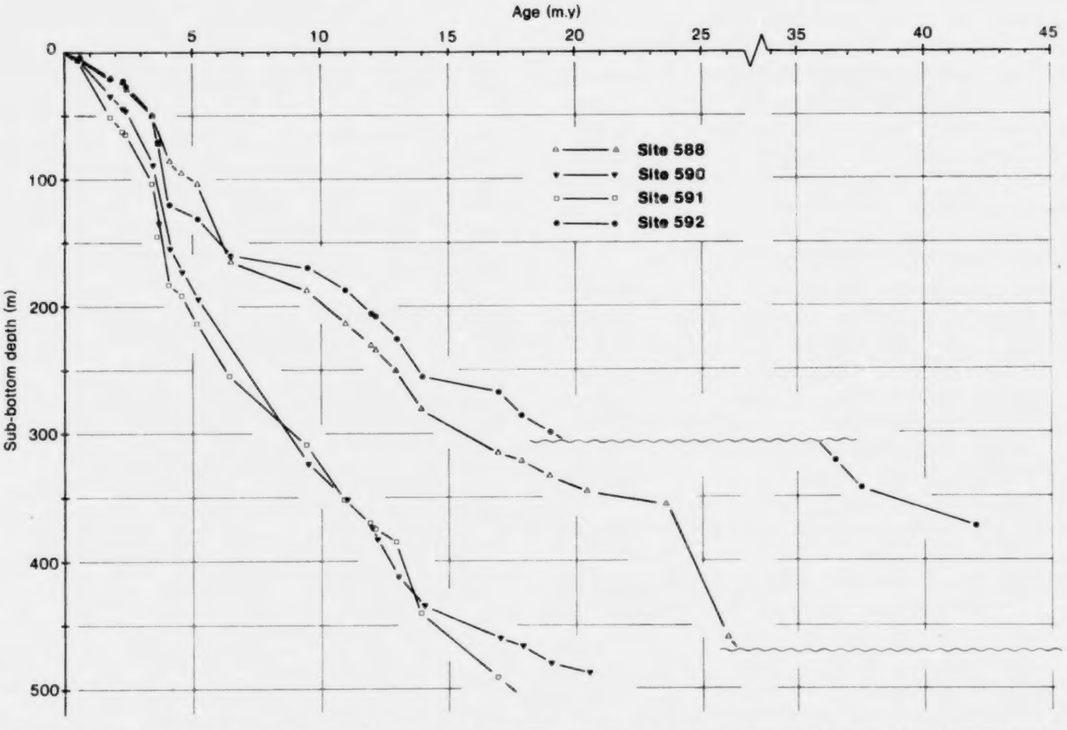

Figure 3. Linear sedimentation rates of bulk sediments at Sites 588, 590, 591, and 592 according to the nannofossil biostratigraphy (Lohman, this vol., and Martini, this vol.).

---

[3] The data for Site 592 are presented and discussed in detail in the context of the results for Sites 593 and 594, because the sediment records of these three sites are controlled mainly by the tectonic evolution of the New Zealand islands (Robert et al., this vol.). However, the paleoenvironmental history of the area near Site 592 was influenced by eolian and oceanographic processes characteristic of the evolution at the central Lord Howe Rise region that is discussed in this paper. Thus, some overlapping in the discussion of results from Site 592 is inevitable.

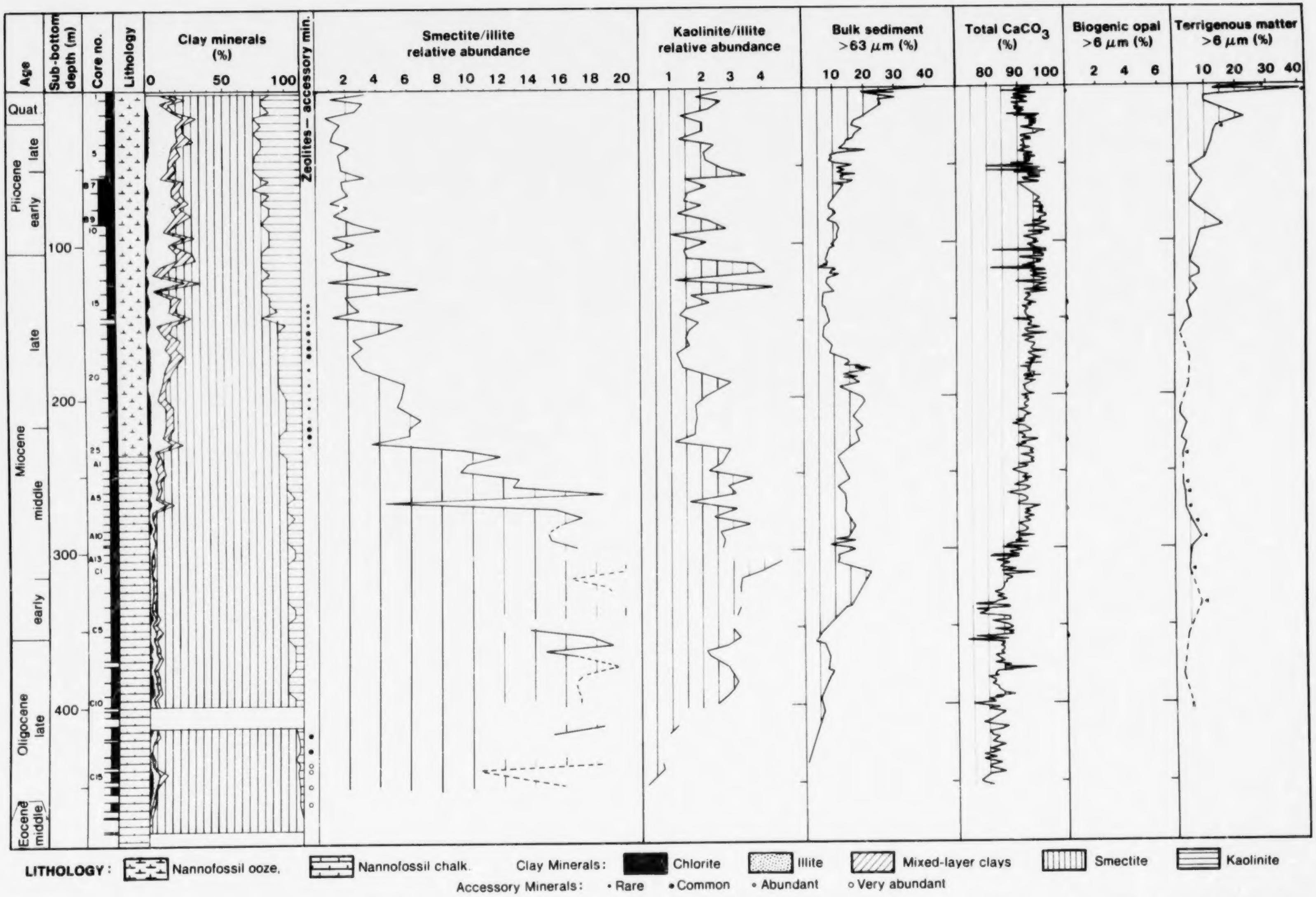

Figure 4. Site 588 results. Carbonate concentration values of bulk sediment samples are shipboard data (determined by carbonate bomb; see site chapter, this vol.), supplemented by the author's data of 138 $CaCO_3$ measurements. Contents of biogenic opal and terrigenous matter are percentages of the carbonate-free sediment fraction <63 µm. Solid triangles indicate samples with amounts of volcanic glass. Letters A, B, C before core number indicate Holes 588A, B, C, respectively.

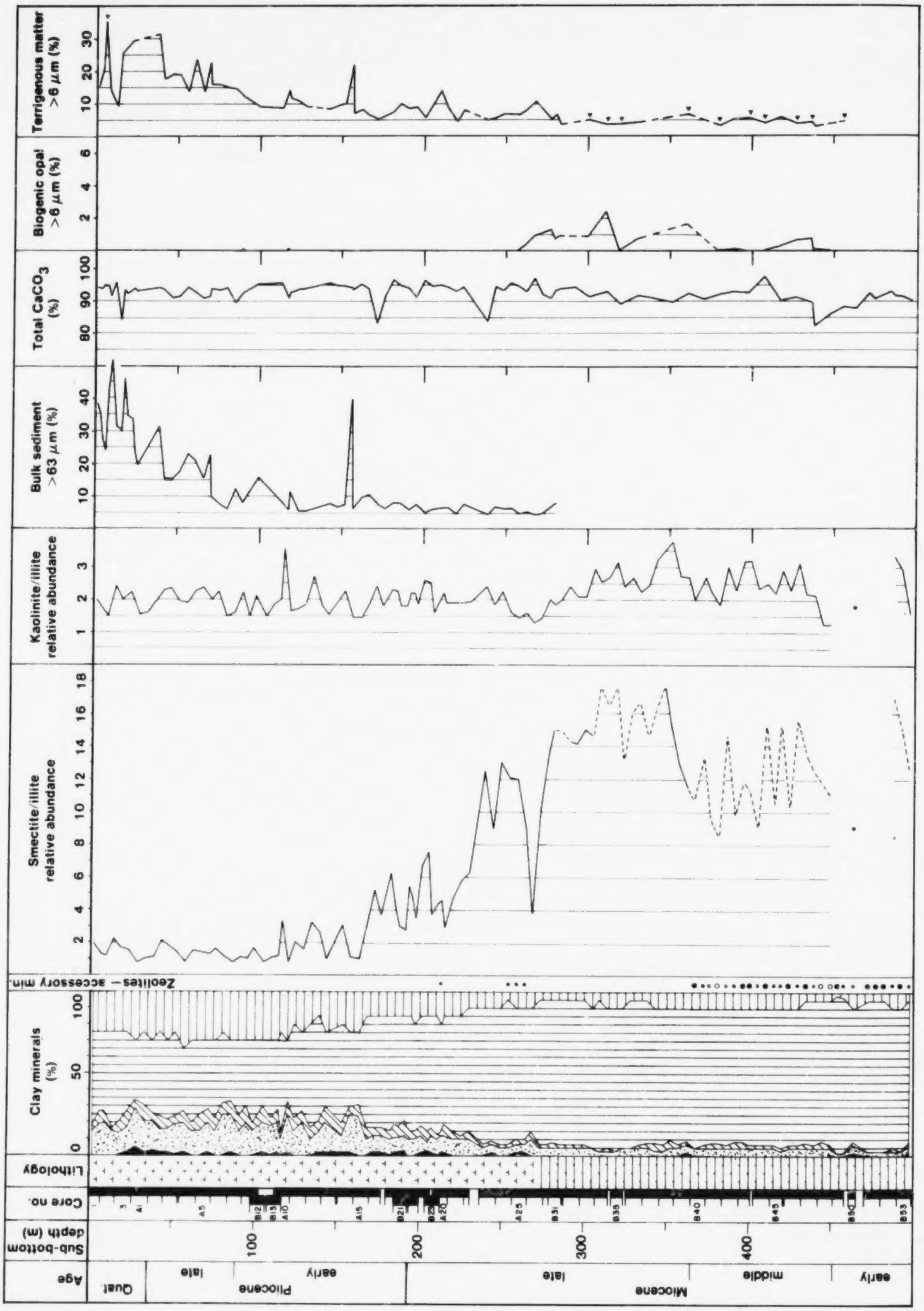

Figure 5. Site 590 results. For explanation of symbols see Figure 4. Contents of biogenic opal >6 μm and terrigenous matter >6 μm in percentages of the carbonate-free sediment fraction <63 μm.

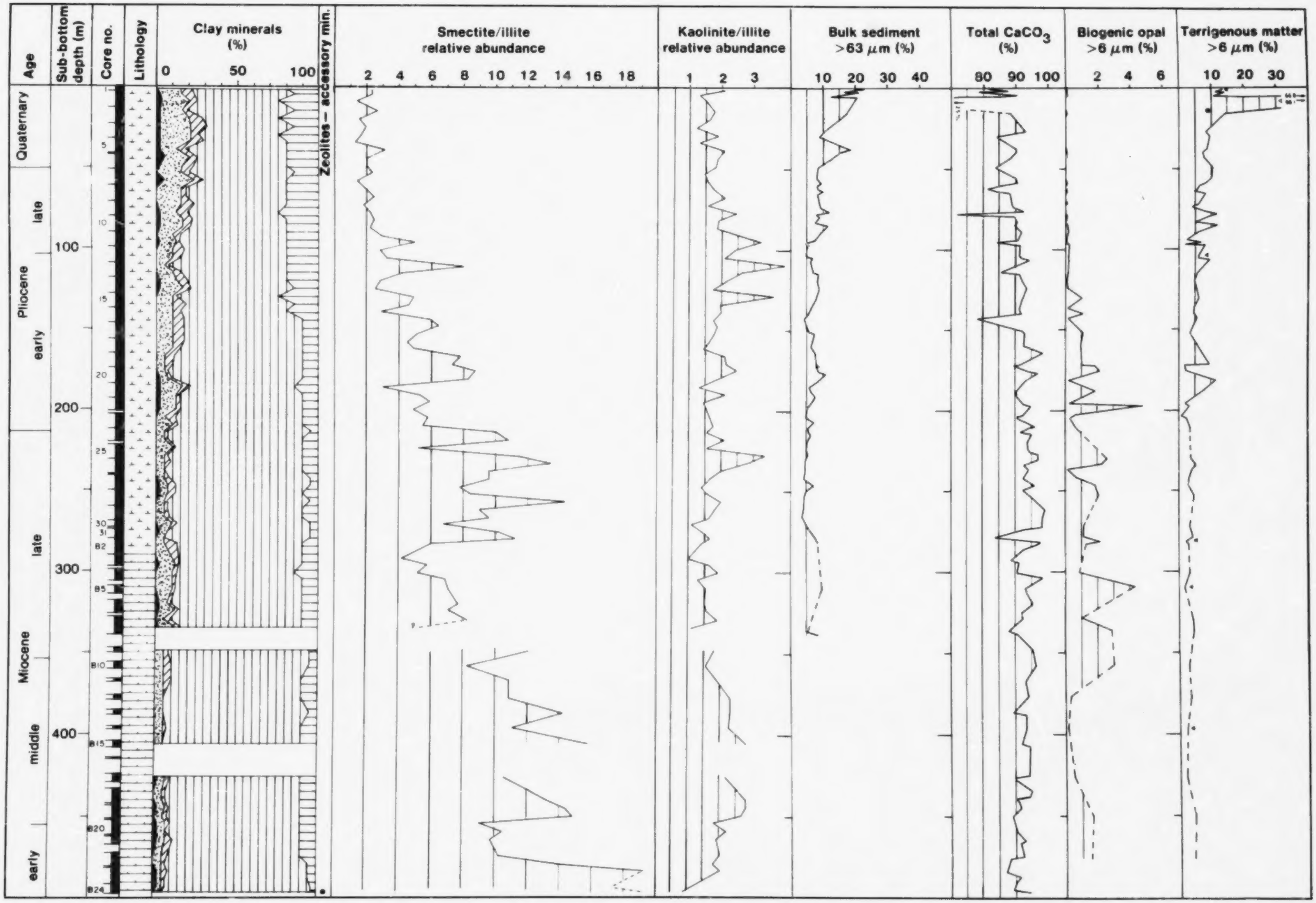

Figure 6. Site 591 results. For explanation of symbols see Figure 4. Content of biogenic opal >6 μm and terrigenous matter >6 μm in percentages of the carbonate-free sediment fraction <63 μm.

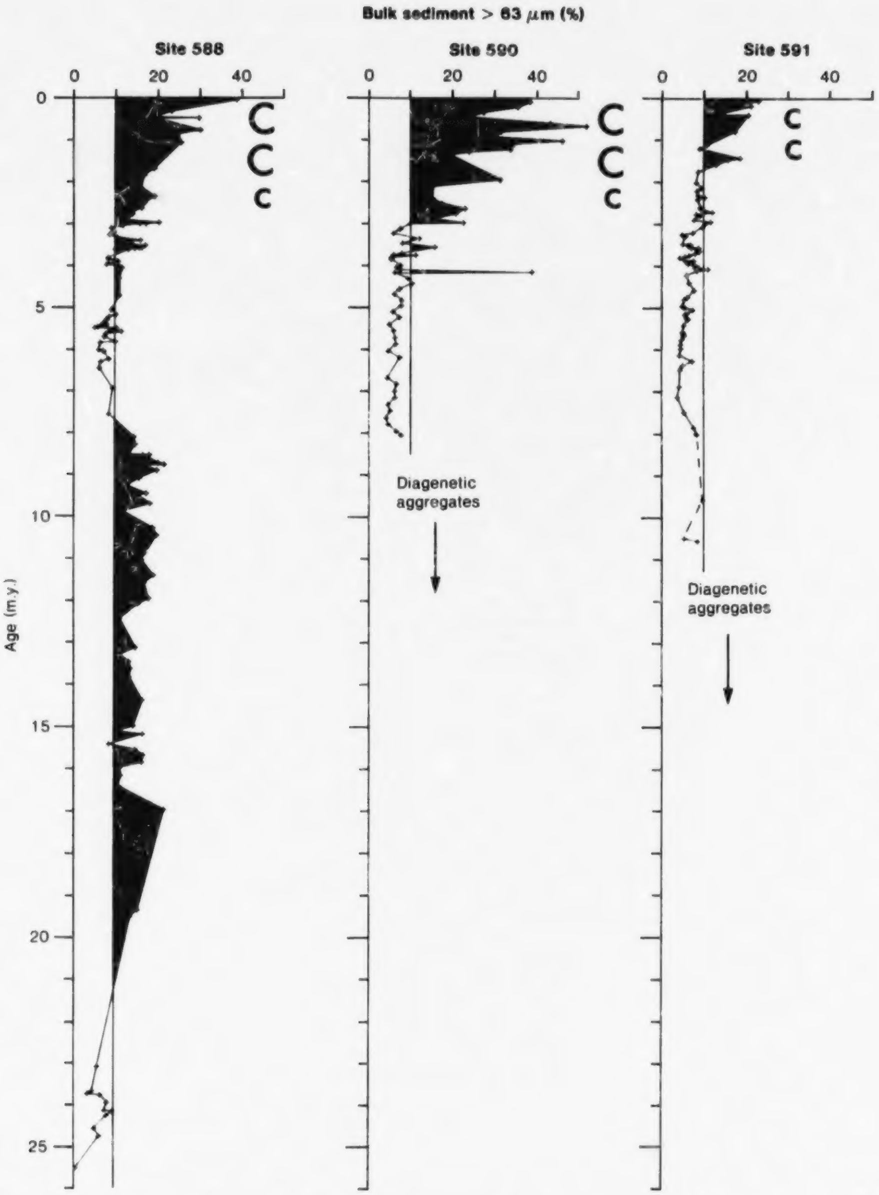

Figure 7. Percentages of sediment coarse fraction >63 μm. "C" indicates intervals with a distinct coarsening of the bulk sediment fractions, interpreted as winnowing of the fine fraction by increased ("c") or strongly increased ("C") currents (cf. Fig. 9).

Calcium Carbonate Content

In general, all Leg 90 Sites at the Lord Howe Rise are characterized by high carbonate contents. The Neogene sediment sequences usually consist of more than about 90% calcium carbonate (Figs. 4, 5, and 6). Only in the late Oligocene to early Miocene of Site 588 are lower values of 75 to 90% $CaCO_3$ observed (Fig. 4; for detailed investigations of short-term and long-term cyclic variations of $CaCO_3$, see Gardner, this vol.).

Clay Minerals

Smectites (40 to 100%) are the dominant clay minerals at Sites 588, 590, and 591 (Figs. 4, 5, and 6). Fleecy particles, generally pedogenic, are often abundant in recent sediments and become sparse in older sediments. Fine laths, transparent and brittle, sometimes associated in geometrical figures, are rarely present in Quaternary sediments but are very abundant in Miocene and Paleogene sediments (Plate 1). As in the New Zealand section of the Tasman Sea, fleecy particles and very fine laths correspond to different morphological types of smectites. These laths were formed during *in situ* recrystallization of smectites within the interstitial sedimentary environment, without significant chemical or mineralogical change (Holtzapffel et al., in press). On the Lord Howe Rise, as around New Zealand, recrystallization processes occur in sediments which are characterized by high sedimentation rates and where the terrigenous components are highly diluted by the biogenic elements (Robert et al., this vol.). There is no apparent modification in the recrystallization of the smectites at Sites 590 and 591 during the early Miocene, when recrystallization of the carbonates began. Nor is there any change in the S/I index that can be related to the beginning and the development of the recrystallization of the smectites. This phenomenon does not influence the paleoenvironmental significance of the clay minerals. Thick-lathed particles, as well as globular packs of fine laths (Plate 1) are also present. These morphological types of particles become more abundant in levels where volcanic glass is present and in the vicinity of greenish gray laminae of devitrified volcanic ash (site chapters, this vol.) and probably correspond to smectites formed during alteration processes of volcanic products. The scarcity of these particles means that this mechanism is not a major contributor to smectite genesis in the sediments from the Lord Howe Rise.

Smectites are accompanied by kaolinite (0–35%), illite (0–25%), irregular mixed-layer clays (0–10%), and chlorite (0–5%). During the Neogene, illite, irregular mixed-layer clays, and kaolinite increase gradually, whereas the abundance of smectite decreases (Fig. 4, 5, and 6). Electron micrographs show the presence of very long and flexuous elements. Rarely present, these fibers are sometimes associated in clusters (Plate 1). They are very similar to palygorskite or sepiolite particles but are not abundant enough to be determined by X-ray diffraction.

The clay mineral assemblages suggest that the sediments of Sites 588, 590, and 591 can be separated into the following major intervals:

1. Middle Eocene and late Oligocene

During the middle Eocene, smectite is the only clay mineral found in the sediments of Site 588. Illite (5%) and kaolinite (10%) are first recorded in the late Oligocene (Fig. 4).

2. Early Miocene to early Pliocene

Illite and kaolinite both show a further increase from % in the early Miocene to 30% in the early Pliocene (Figs. 4, 5, and 6). Mixed-layer minerals occur in trace amounts up to about 10%. This time interval is characterized by distinct changes in the relative abundances of clay minerals (S/I, K/I ratios; Figs. 4, 5, 6, and 8). These changes are not synchronous at all sites. A decrease in the S/I ratio near the early/middle Miocene boundary (15 m.y.) is paralleled by K/I minima at Sites 588 and 590. A drastic change in the S/I ratios from values between 19 and 16 to values of about 4 occurs in sediments deposited during the middle Miocene at Site 588 and during the late Miocene at Sites 590 and 591 (Figs. 4–6). These major changes coincide with lesser decreases in the K/I ratios (Figs. 4, 5, 6, and 8). At site 591, the early Miocene decrease in S/I is followed by an increase of the S/I ratio to about 14 in the latest Miocene, followed by a decrease to 2 during the early Pliocene (Figs. 6 and 8). More or less distinct maxima in the K/I ratios are observed in all three sites near 5.5 and 3.5 m.y. (Figs. 4–6).

3. Pliocene to Quaternary

The youngest sediment sections at all three sites are characterized by clay mineral assemblages of smectite (40–50%), kaolinite (20–35%), and illite (about 20%) (Figs. 4–6). The S/I ratios show relatively constant, low mean values of 1.5 to 2 (Fig. 8). The change to these low S/I ratios is asynchronous, like the middle Miocene change, and occurs at Site 588 near 5.5, at Site 590 near 4, and at Site 591 near 3 m.y ago (Fig. 8).

Composition, Grain Sizes, and Flux Rates of the Carbonate-free Sediment Fraction

The main proportion of the carbonate-free silt fraction is siliciclastic. Biogenic opal is also abundant in several core intervals (Figs. 5 and 6).

The content of biogenic opal in the 6- to 63-μm fraction is negligible in the carbonate-free sediment fractions of Site 588 (Fig. 4). Significant concentrations of biogenic opal are observed at Sites 590 and 591 during the time interval between 14 and 3.6 m.y. These concentrations are clearly greater in the sediments deposited at 2130 m water depth than in those deposited at 1300 m (Figs. 5 and 6).

Yellowish volcanic glass shards are observed in the Neogene sections prior to 9 m.y. and are more common in the northern than in the southern Lord Howe Rise region (Fig. 9; Robert et al., this vol.). A further distinct volcanic event is indicated by a high content of light volcanic glass near 0.4 m.y. ago (Fig. 9). However, both the amount and the grain size of the Quaternary volcanic glass particles decrease toward the north, unlike the early and middle Miocene glass shards.

The grain size of the terrigenous silt fraction has remained almost unchanged in all sites of the Lord Howe Rise during the last 15 m.y. (compare histograms in Fig. 10). In general, the grain-size modes lie near 18 μm. The similarity of the modes may suggest the same provenance region for the terrigenous silt-sized matter (see Dauphin, 1980; Sarnthein et al., 1982), that is probably the Australian continent by analogy to the recent and subrecent supply regime (Healy, 1970; Glasby, 1971; Thiede, 1979). The grain size of volcanic glass shards observed in middle Miocene and Quaternary time intervals is significantly coarser than the grain size of the terrigenous matter supplied from the Australian continent: the modes lie near 40 μm (Fig. 10). The amount of terrigenous medium- and coarse-sized silt (i.e., >6 μm) varies between 2 and 10% at all three sites prior to 4 m.y. Between 3 and 4 m.y, the >6 μm fraction at Sites 588 and 590 increases to more than 10%, reaching maximum values of 30% at Site 590 near 2 m.y. (Fig. 9; Robert et al.,

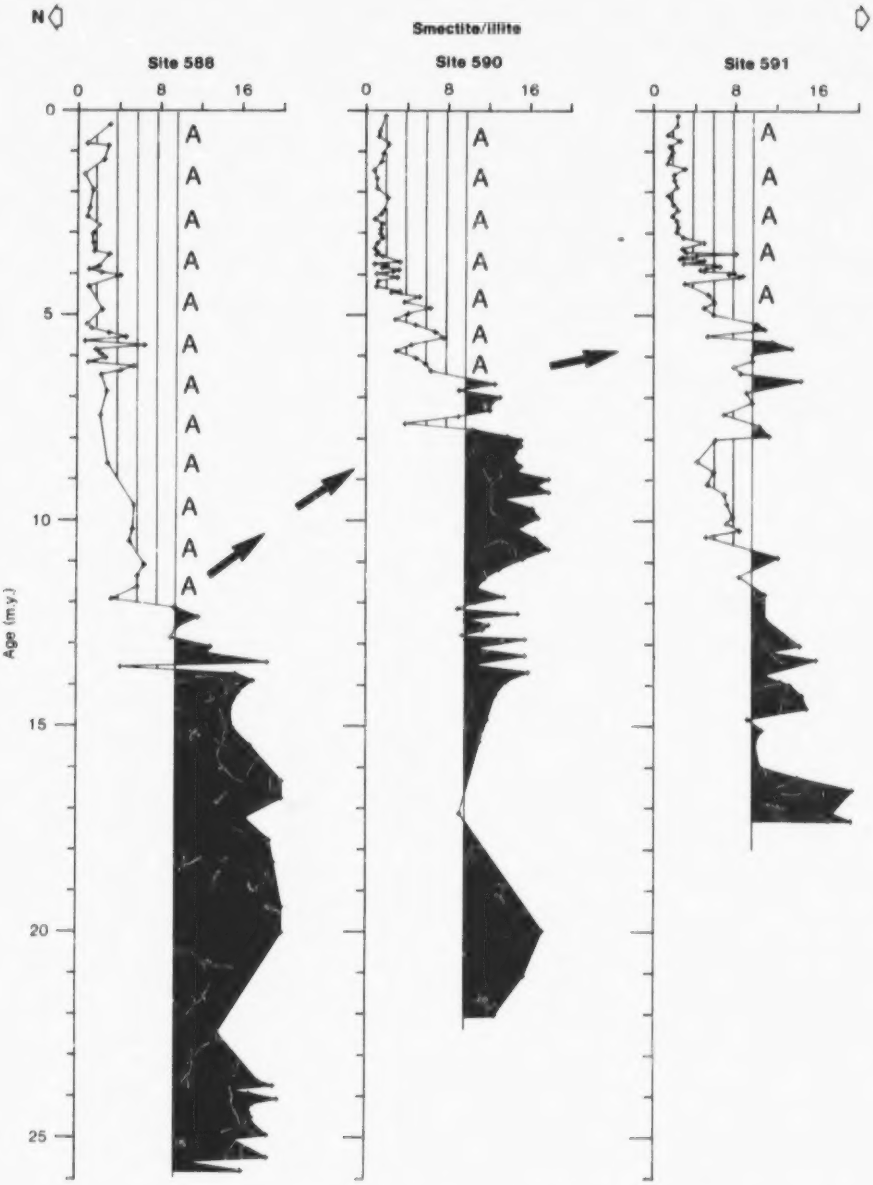

Figure 8. Smectite/illite (S/I) ratios of clay mineral assemblages at the Lord Howe Rise. Black arrows mark the boundary between dominantly high and extremely low S/I ratios. The latter are interpreted as representative of dominantly arid climate ("A"). Furthermore, those arrows should indicate the southward expansion of Australian deserts during middle and late Miocene time (cf. Fig. 12).

this vol.). At Site 591, the >6 μm values are significantly lower. The maximum values near 0.4 m.y. ago at all three sites mark a coarse-sized ash layer (Fig. 9).

Changes in the mass accumulation rates of the carbonate-free sediment fraction mainly reflect variations in the terrigenous sediment supply. Maximum MART are recorded in the latest Oligocene (up to 1.5 g · cm^{-2} 10^{-3} y^{-1}). A drastic decrease of the MART occurs at Site 588 near the Oligocene/Miocene boundary (Fig. 11). This decrease resulted from a change in the LSR (Fig. 3) so abrupt that it is possibly an artefact of the time scale applied. The earliest Miocene is characterized by very low MART (0.05–0.08 g · cm^{-2} 10^{-3} y^{-1}), followed by a slight increase to about 0.2 g · cm^{-2} 10^{-3} y^{-1} near 20 m.y. ago (Site 588, Fig. 11). A distinct maximum of MART of up to 0.5 g · cm^{-2} 10^{-3} y^{-1} at Site 588, 0.25 g · cm^{-2} 10^{-3} y^{-1} at Site 590, and 0.7 g · cm^{-2} 10^{-3} y^{-1} at Site 591 occurs at 14–13 m.y. (Fig. 11). Values between 0.2 and 0.4 g · cm^{-2} 10^{-3} y^{-1} dominate at Sites 590 and 591 between 11 and 4 m.y. ago (Fig. 11). At Site

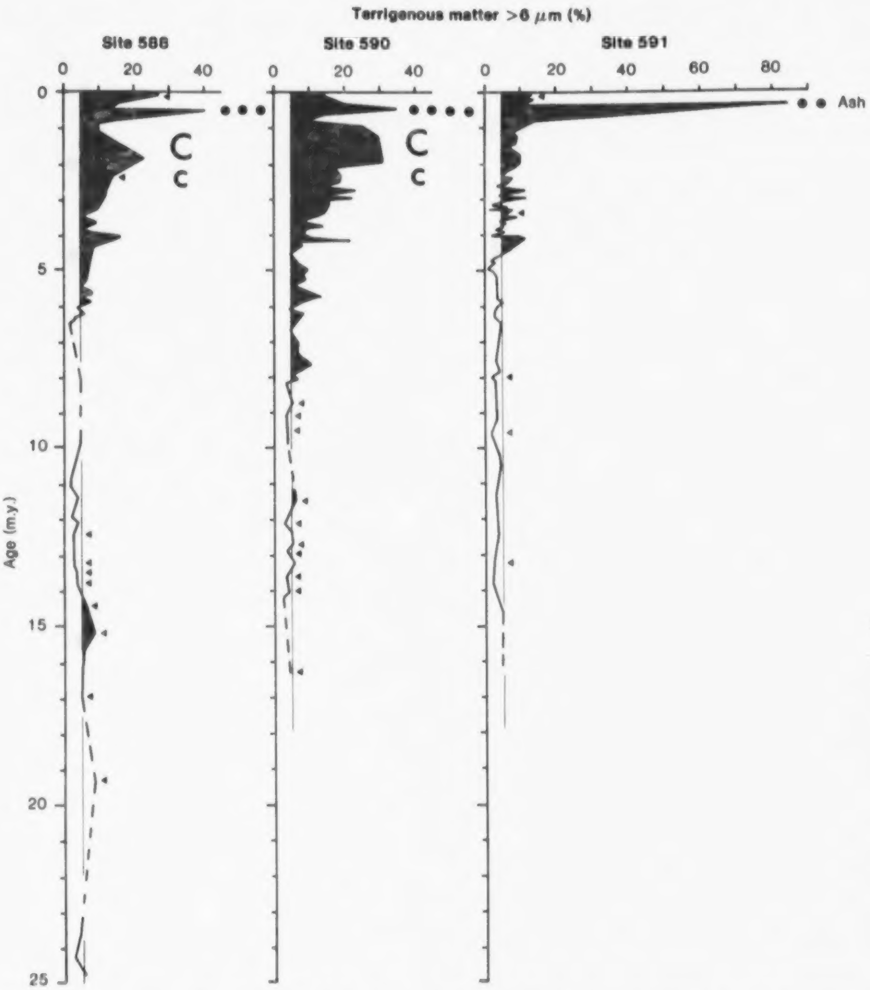

Figure 9. Terrigenous sediment fraction >6 μm (i.e., carbonate-free sediment fraction >6 μm minus biogenic opal >6 μm) in percentages of the carbonate-free sediment fraction <63 μm. Triangles indicate samples with amounts of volcanic glass. Black dots mark a distinct Quaternary ash layer observed in all three sites. The increased >6 μm values during the last 3 m.y. are probably caused by intensified oceanic currents ("C"), resulting in winnowing of the fine fraction (cf. Fig. 7).

588 the MART gradually decreases between 13 and 9.5 m.y., and values of less than 0.1 g · cm^{-2} 10^{-3} y^{-1} occur between 9.5 and 6.5 m.y. ago. Further distinct maxima of MART are observed at Site 588 near 6 and 4 m.y. ago. The latter maximum is also recorded at Sites 590 and 591 (Fig. 11, more than 1 g · cm^{-2} 10^{-3} y^{-1}). The last 3 m.y. are characterized by reduced MART at the shallower Sites 588, 590, and 592, whereas the MART at the deeper Site 591 continue to be relatively high (but lower than those at 4 m.y.) (Fig. 11). In the uppermost sediment sequences of all four sites (last 500,000 yr.) the MART values are low, varying from 0.04 to 0.2 g · cm^{-2} 10^{-3} y^{-1}, which is similar to the modern rates of eolian-dust accumulation in the southwest Pacific (0.08 g · cm^{-2} 10^{-3} y^{-1}; according to Windom [1969], using the porosity and wet-bulk density data of the near-surface samples of the Lord Howe Rise sites). This suggests that most of the terrigenous sediments at the Lord Howe Rise have been supplied by winds.

NEOGENE EVOLUTION OF PALEOENVIRONMENTS AT THE CENTRAL LORD HOWE RISE

Table 2 summarizes the Neogene evolution of climate and oceanic circulation in the southwest Pacific region that can be deduced from the terrigenous-sediment fraction at the Lord Howe Rise.

Oligocene

During the latest Oligocene, the dominance of pedogenic smectite in the northern Lord Howe Rise area suggests predominantly warm climatic conditions with al-

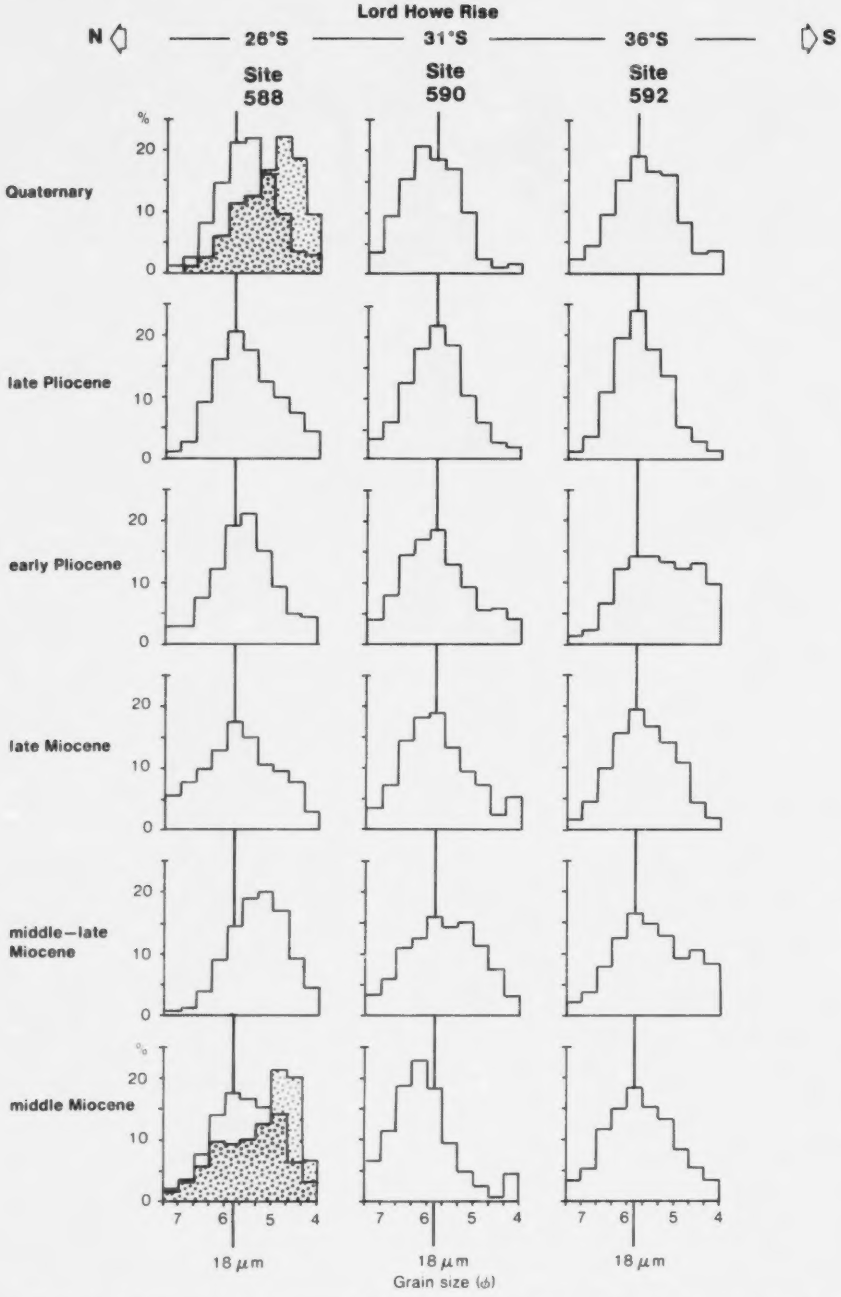

Figure 10. Typical grain-size distributions of the carbonate-free silt fractions from the Lord Howe Rise Sites for different time intervals, figured as histograms. Site 588 histograms defined by open circles (middle Miocene and Quaternary) show grain-size distributions of samples rich in volcanic glass.

ternating periods of humidity and aridity in a source area characterized by low relief (i.e., Australia). This climatic pattern is similar to that found at present in southern Morocco (Paquet, 1969) and the Chad Basin (Gac, 1979). The gradual increase of the K/I ratio during the Oligocene at Site 588 (Fig. 4) may have been caused by the gradual northward drift of the Indo-Australian Plate toward lower latitudes, resulting in an increased admixture of kaolinite from tropical areas by southward-flowing oceanic currents or by tropical cyclones. High mass accumulation rates of terrigenous, mainly clay-sized matter at Site 588 (Fig. 11), if not an artefact of the time scale applied (see above), are possibly also related to stronger southward-flowing surface currents in the Tasman Sea during the Oligocene (Kennett, 1978b). The lower percentages of $CaCO_3$ during the late Oligocene (Fig. 4)

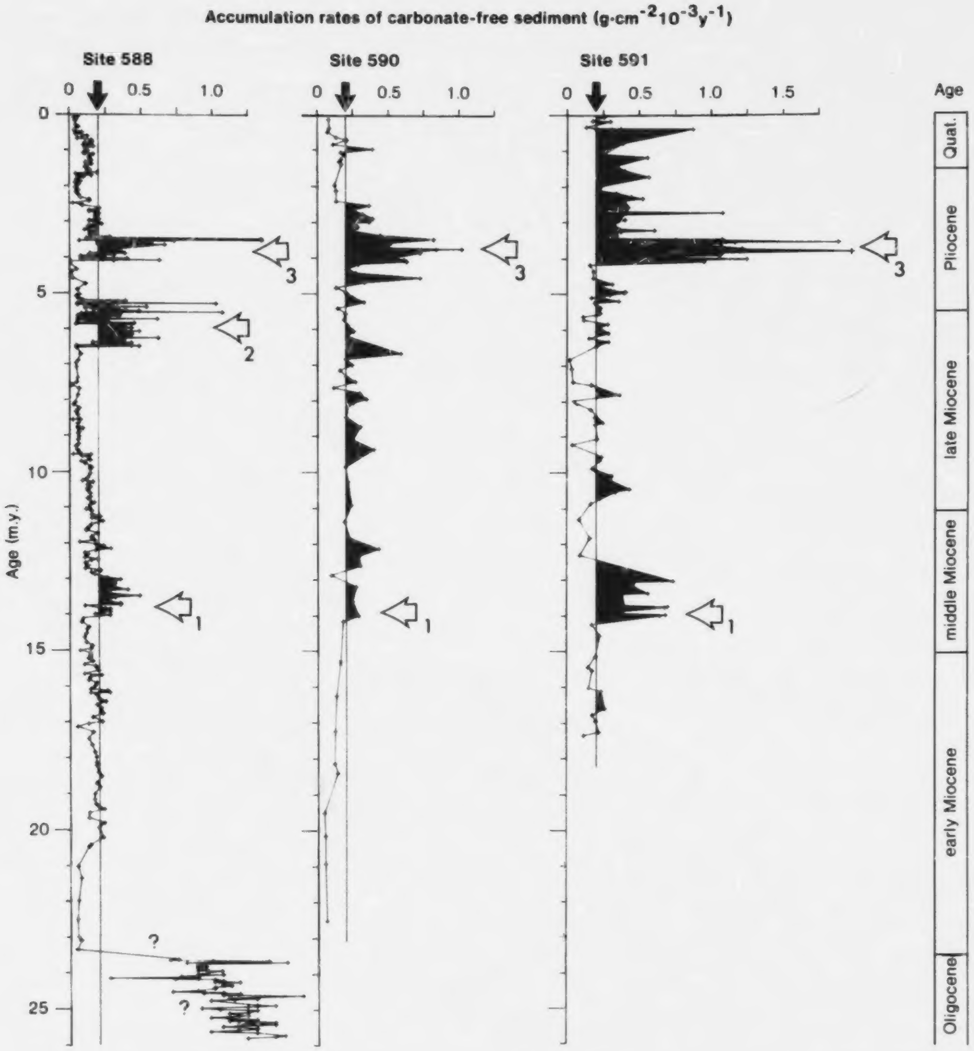

Figure 11. Mass accumulation rates of the carbonate-free (mainly terrigenous) sediment fraction (MART) at the Lord Howe Rise during Neogene times. Black arrows mark the maximum value of recent accumulation rates of terrigenous matter recorded in the Pacific (0.01 to 0.2 g·cm^{-2} 10^{-3} y^{-1}; Folger, 1978). Open arrows indicate (1) the first occurrence of distinct maximum values of MART in the middle Miocene, (2) distinct late Miocene maximum of MART at Site 588, and (3) extreme maxima of MART in the early Pliocene. The change of the MART at Site 588 near the Oligocene/Miocene boundary is so abrupt that it is possibly an artefact of the time scale applied(?).

nay be the result of dilution by this increased terrigeous supply. The reduction in mass accumulation rates t the Oligocene/Miocene boundary (Fig. 11) coincided ith a change of circulation regime in the Tasman Sea. he southward-flowing currents dominating during the ligocene decreased in intensity. The intensity of the orthward-flowing bottom waters through the Tasman ea also decreased as the western boundary current beame strongly established east of New Zealand (Kennett, 977, 1978b; cf. Robert et al., this vol.).

arly and Middle Miocene

An increase in explosive volcanism in the early and niddle Miocene is suggested by the abundance of volcanic glass in sediments on the Lord Howe Rise (Fig. 9). At the same time, higher abundances of greenish gray laminae, defined as volcanic ash or diagenetically altered volcanic ash (Gardner et al., this vol.), as well as of volcanogenic smectite are observed. Volcanic glass occurs more frequently in samples at the northern sites than at the southern sites. This fact, along with the coarseness of the volcanic glass shards, suggest a high-energy transport system from north to south like, for example, the tropical cyclones which today reach wind speeds exceeding Beaufort force 9, that is, 20 to 24 m/s (Ramage, 1970). The suggestion that volcanic ash may have been supplied by tropical cyclones from the north is further supported by the fact that the volcanic glass in the Lord

Table 2. Major changes in paleoenvironment and climatic events and their signals in the sediments at the Lord Howe Rise.

Age (m.y.)	Signals in the sediment	Interpretations	Major events	Plate tectonic drift and related events
0	Abundant light volcanic glass (decrease of both thickness of ash layer and grain size from Site 591 to Site 588)	Intensive volcanism in southern regions	Quaternary volcanism on North Island of New Zealand (Nelson and Hume, 1977)	
	Decrease of S/I ratios to Quaternary values; coarsening of grain sizes of terrigenous and carbonate sediment fractions	Dominantly arid climate in much of Australia; increased oceanic intermediate-water circulation	Development of major Arctic ice sheets (Shackleton and Kennett, 1975; Shackleton and Opdyke, 1977)	
5	Minimum values of S/I ratios and K/I ratios; increased MART	Expansion of deserts and semideserts in Australia	Expansion of Antarctic ice sheets (Shackleton and Kennett, 1977; Mercer and Sutter, 1982); increased aridity in South Australia (Kemp, 1978)	
10	Distinct S/I minimum at Site 591	Increased supply of illite (probably from New Zealand)	Major cooling in high northern latitudes (Denton and Armstrong, 1969; Mudie and Helgason, 1983). Buildup of AA ice sheets essentially complete (Shackleton and Kennett, 1975)	Northward drift of the Indo-Australian Plate into drier climatic belts Southward expansion of Australian deserts and semideserts through time
15	Distinct increase of MART; decrease of S/I and K/I ratios at Site 588	Expansion of deserts and semideserts in northern Australia	Development of major Antarctic ice sheets (Shackleton and Kennett, 1975; Woodruff et al., 1981); desertification in northern parts of Australia (Kemp, 1978)	
20	Coarse yellowish volcanic glass (more frequent at Sites 588 and 590 than at Sites 591 and 592)	Volcanic activity in tropical regions of the southwest Pacific (and New Zealand)	Tectonism and volcanism in the Melanesian and New Hebrides regions (Crook and Belbin, 1978); volcanism in North Island of New Zealand (Crook and Feary, 1982)	
	Distinct increase of K/I ratios at Site 588	Increased supply of kaolinite from tropical regions		

Note: MART = mass accumulation rates of terrigenous matter; x = interval characterized by the occurrence of yellowish volcanic glass.

Howe Rise sediments occurred contemporaneously with tectonic and volcanic activities in the Melanesian and New Hebrides islands (Crook and Belbin, 1978; cf. Nelson et al., this vol.). New Zealand may also have been a source area of volcanic ash, because volcanic activity was prevalent on the North Island of New Zealand during those times (Crook and Feary, 1982). However, this explanation is less probable for the northern Sites on the Lord Howe Rise, because the transport energy of the surface winds needed to carry dust from New Zealand (Fig. 1) would be unrealistically high for the long-distance transport of coarse-silt-sized grains to Site 588 (the downwind distance from New Zealand to Site 588 exceeds 2500 km).

The distinct increase of illite at Site 588 during the middle Miocene near 12.5 m.y. (Fig. 8) suggests increased desertification in the source area, the northern to central parts of Australia (Figs. 8 and 12). Southern Australia may still have been dominated by alternating humid and semiarid climatic conditions, however, as is indicated by the continuously high amounts of pedogenic smectite at the more southern Site 590 (Figs. 8, 12). Increased desertification in northern and northwestern areas of Australia at this time was also inferred from palynological data (Kemp, 1978) and from investigations of ancient drainage systems (van de Graaff et al., 1977). The expansion of aridity in northern Australia may have been caused by both the northward drift of the Indo-

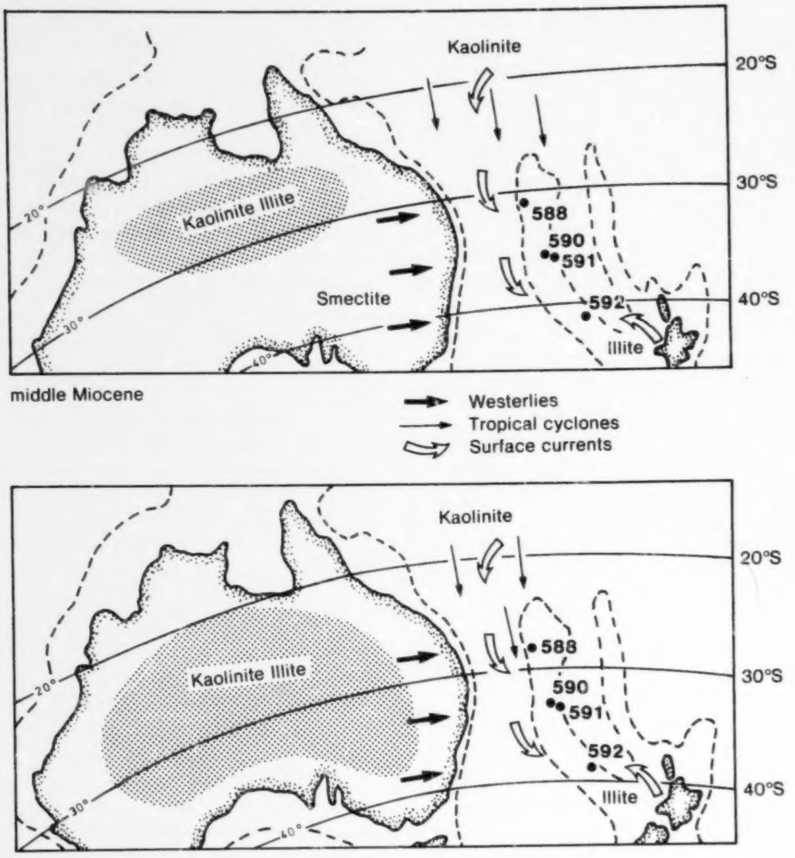

Figure 12. Interpretation of clay mineral data of Miocene sediments from the Lord Howe Rise. Paleogeography from Kemp (1978), according to Hayes and Ringis (1973) and Weissel and Hayes (1972). For atmospheric and oceanic circulation see Figure 1. Dashed line approximates the 3000 m isobath (Kemp, 1978).

Australian Plate into a drier climatic belt and the development of major Antarctic ice sheets during that time (Shackleton and Kennett, 1975; Kennett, 1977; Savin et al., 1981; Woodruff et al., 1981). The *transition* from a dominantly humid climate to a more semiarid and arid climate resulted in a reduced vegetation cover and increased availability of eolian sediments in the source area. This transition is indicated by increased flux rates of terrigenous matter at the Lord Howe Rise near 14 to 13 m.y., that is about 1 m.y. before maximum aridity developed in northern and central Australia (Fig. 11). Concomitant with the buildup of the Antarctic ice sheets, upwelling at the Subtropical Divergence Zone (Burkov, 1966; Knox, 1970) may have intensified, increasing the fertility of surface waters and generating greater productivity, which is reflected in increased deposition of biogenic opal at Sites 590 and 591 between 14 and 3.6 m.y. ago (Figs. 5 and 6).

The distinct S/I minimum at Site 591 near 9 m.y. was not recorded at nearby Site 590 (Fig. 8). The change in the clay mineral assemblage at Site 591 may have been caused by an increased admixture of illite from eastern or southeastern regions by oceanic currents in water depths below 1300 m. Because Site 591 is not located in the same water mass as the shallower Sites 588 and 590, it may be influenced more by Antarctic or New Zealand sources than the other two sites. This paleoenvironmental change coincided with a phase of major cooling in northern high latitudes (Denton and Armstrong, 1969; Mudie and Helgason, 1983). The buildup of the middle to late Miocene Antarctic ice cap was essentially complete near 9 m.y. (Shackleton and Kennett, 1975; Kennett, 1978a).

Late Miocene to Early Pliocene

The sharp decrease of the S/I index at Site 590 during the late Miocene can be interpreted as an increased input of illite, eroded from central Australia as the desert areas expanded southward (Figs. 8, 12). Extremely low S/I ratios, similar to those of Pleistocene time, occurred at all three sites during the latest Miocene (Site 588) to early Pliocene (Sites 590 and 591) (Fig. 8). They suggest a major expansion of the Australian deserts and semideserts, a view which is also supported by land data.

From palynological data, Kemp (1978) has deduced a general increase of aridity in central Australia as well as in the Murray and Gippsland basins. In addition, Locker and Martini (this vol.) recorded an increase in the supply of opal phytoliths to the Lord Howe Rise, interpreted as indicating expanded aridity in Australia. This change in paleoenvironment was probably related to the maximum buildup of Antarctic ice masses during latest Miocene-earliest Pliocene times (Kennett et al., 1975, Shackleton and Kennett, 1975; Mercer and Sutter, 1982). Maximum accumulation rates of terrigenous matter are observed at all sites at the Lord Howe Rise near 4 m.y. ago (Fig. 11), just after the phase of maximum Antarctic glaciation and aridity in Australia, but contemporaneously with a major cooling trend in the southwest Atlantic sector of the Southern Ocean (Ciesielski and Wise, 1977). This increase of eolian sediment supply from Australian deserts toward the Lord Howe Rise (i.e., Southern Hemisphere) occurs about 0.8 m.y. earlier than a similar increase of eolian sediment supply from the Saharan desert toward the northeast Atlantic (i.e., Northern Hemisphere; Stein, 1985a).

Pliocene to Quaternary

A major change in paleoceanography in the southwest Pacific near 3 m.y. coincided with the development of major ice sheets in the Northern Hemisphere (Shackleton and Kennett, 1975; Shackleton and Opdyke, 1977; Keigwin, 1979, 1982; Shackleton et al., 1984) and continental evidence of glaciation in southern South America (Mercer, 1976). The extremely low accumulation rates (Fig. 11) and the concomitant coarsening of both bulk sediment (Fig. 7) and the terrigenous sediment fractions in water depths between 1100 m and 1530 m (Fig. 9) suggest winnowing by intensified currents at these water depths during the last 3 m.y. This may indicate an intensified advection of water masses in intermediate water depths (probably the East Australian Current and/or Antarctic Intermediate Water). Thus, the grain size of the terrigenous sediments at Sites 588 and 590 allows no interpretation in terms of intensity of atmospheric circulation during that time. At Site 591, however, in water depths below the influence of the East Australian Current, the intermediate-water circulation was less enhanced (Figs. 7 and 9). At this site, the accumulation rates of terrigenous matter remained high through the Pliocene and Pleistocene (Fig. 11) and could be interpreted as continuously high eolian dust input to the central Lord Howe Rise and/or a supply of clay-sized material by deeper-water currents.

The low S/I ratios at all Leg 90 sites from the Lord Howe Rise during the last 3 m.y. may imply dominantly arid climatic conditions in large parts of Australia during late Pliocene and Quaternary times. The relatively high amounts of the terrigenous coarser-silt fraction at Site 591 (Fig. 9) may suggest enhanced atmospheric circulation during the last 4 m.y. It is interesting that increased atmospheric circulation and mass flux of dust were recorded in Northern Hemisphere eolian sediments from the North Pacific and northeast Atlantic about 0.8 m.y. later (Leinen and Heath, 1981; Rea and Harrsch, 1981; Rea and Janecek, 1982; Janecek and Rea, 1983; Stein, 1984, 1985a; Stein and Sarnthein, 1984a).

A conspicuous volcanic event was recorded at the Lord Howe Rise during Quaternary times. Distinct amounts of light volcanic glass occurred in the sediments of Sites 588, 590, and 591 near 0.4 m.y.; thickness of ash layers (site chapters, this vol.) and grain size of volcanic glass particles both decrease from south to north (Fig. 9). This pattern suggests that the volcanism was centered in southern regions. One possible source area is the North Island of New Zealand, where Nelson and Hume (1977) have reported Quaternary volcanism connected with the formation of the Taupo Graben and the Havre Trough.

CONCLUSIONS

1. Two processes were of major importance for the Neogene evolution of climate and oceanic circulation in the southwest Pacific: (1) the continued northward drift of the Indo-Australian Plate and (2) the development of the Antarctic ice sheets.

2. Desertification in Australia started in the northern parts of the continent near 14 m.y. and expanded southward during the late Miocene. Maximum phases of aridity coincided with major cooling events near 12, 9, 5, and 3 m.y., as indicated by distinct minima of the S/I ratios. Accumulation rates of terrigenous sediments at the Lord Howe Rise increase during the transition from a dominantly humid to a more arid climate during the last 4 m.y., and during the last 3 m.y. the climate of most of Australia has been dominated by aridity.

3. Upwelling at the Subtropical Convergence Zone may have been intensified between 14 and 3.6 m.y., resulting in increased productivity, as indicated by significant amounts of biogenic opal at Sites 590 and 591.

4. Enhanced oceanic intermediate-water circulation during the last 3 m.y. is inferred from decreased accumulation rates and a coarsening of both bulk and terrigenous sediment fractions at Sites 588 and 590.

5. Periods of explosive volcanicity in the Southwest Pacific occurred between 21 and 9 m.y. and near 0.4 m.y., as is suggested by increased input of volcanic glass to the Lord Howe Rise sediments.

ACKNOWLEDGMENTS

We would like to thank Drs. H. Chamley and M. Sarnthein for critical discussions. For technical assistance, we gratefully acknowledge M. Acquaviva, T. Allert, J. P. Ripert, F. Sirocko, R. Spielhagen, and M. Stransky. We thank our reviewers T. Janecek and M. Leinen for their numerous constructive suggestions for improving the manuscript. Financial support for this study was provided by the Deutsche Forschungsgemeinschaft and the Centre National de la Recherche Scientifique (A.T.P. Géologie et Géophysique des Océans).

REFERENCES

Albertsson, K. J., 1981. Hambrey, M. J., and Harland, W. B. (Eds.), *Earth's Pre-Pleistocene Glacial Record:* Cambridge (Cambridge University Press), pp. 53-56.

Biscaye, P. E., 1965. Mineralogy and sedimentation of the recent deep-sea clay in the Atlantic Ocean and adjacent seas and oceans. *Geol. Soc. Am. Bull.*, 76:803-832.

Burkov, V. A., 1966. Structure and nomenclature of Pacific Ocean currents. *Oceanology*, 6:1-10.

Carlson, T., and Prospero, J. M., 1977. Saharan air outbreaks: meteorology, aerosols, and radiation. *Rept. US GATE Central Progr. Workshop (NCAR), Boulder, Colorado*, pp. 57-78.

Chamley, H., 1979. North Atlantic clay sedimentation and paleoenvironment since the Late Jurassic. *In* Talwani, M., Hay, W., Ryan, W. B. F. (Eds.), *Deep Drilling Results in the Atlantic Ocean: Continental Margins and Paleoenvironment*. Am. Geophys. Un., Maurice Ewing Ser., 3:342–361.

________, 1980. Clay sedimentation and paleoenvironment in the area of Daito Ridge (northwestern Philippine Sea) since the early Eocene. *In* Klein, G. deV., Kobayashi, K., et al., *Init. Repts. DSDP*, 58: Washington (U.S. Govt. Printing Office), 683–693.

Chamley, H., Maillot, H., Duée, G., and Robert, C., 1984. Paleoenvironmental history of the Walvis Ridge at the Cretaceous/Tertiary transition, from mineralogical and geochemical investigations. *In* Moore, T. C., Jr., Rabinowitz, P. D., et al., *Init. Repts. DSDP*, 74: Washington (U.S. Govt. Printing Office), 685–695.

Chamley, H., and Robert, C., 1979. Late Cretaceous to early Paleogene environmental evolution expressed by the Atlantic clay sedimentation. *In* Christensen, W. K., and Birkelund, T. (Eds.), *Cretaceous/Tertiary Boundary Events Symposium, University of Copenhagen* (Vol. 2), 71–77.

Chester, R., Elderfield, H., Griffin, J. J., Johnson, L. R., and Padgham, R. C., 1972. Eolian dust along Atlantic eastern margins. *Mar. Geol.*, 13:91–106.

Ciesielski, P. F., and Wise, S. W., Jr., 1977. Geologic history of the Maurice Ewing Bank of the Falkland Plateau (southwest Atlantic sector of the Southern Ocean) based on piston and drill cores. *Mar. Geol.*, 25:175–207.

Crook, K. A. W., and Belbin, L., 1978. The southwest Pacific area during the last 90 mill. years. *J. Geol. Soc. Aust.*, 25:23–40.

Crook, K. A. W., and Feary, D. A., 1982. Development of New Zealand according to the fore-arc model of crustal evolution. *Tectonophysics*, 37:65–107.

Dauphin, J. P., 1980. Size Distribution of chemically extracted quartz used to characterize fine-grained sediments. *J. Sed. Petrol.*, 50: 205–214.

Denton, G. H., and Armstrong, R. L., 1969. Miocene–Pliocene glaciations in southern Alaska. *Am. J. Sci.*, 267:1121–1142.

Folger, D. W., 1978. Eolian dust in Marine sediments. *In* Fairbridge, R. W., and Bourgeois, J. (Eds.) *The Encyclopedia of Sedimentology.* Encyclopedia of Earth Sciences Series (Vol. 6): Stroudsburg, Pa (Dowden, Hutchinson, and Ross).

Gac, J. Y., 1979. Geochimie du bassin du lac Tchad: Bilan de l'altération, de l'érosion, et de la sédimentation [D.Sc. thesis]. Université de Strasbourg.

Glasby, G. P., 1971. The influence of aeolian transport of dust particles on marine sedimentation in the southwest Pacific. *J. R. Soc. N. Z.*, 1:285–300.

Griffin, J. J., Windom, H., and Goldberg, E. D., 1968. The distribution of clay minerals in the World Ocean. *Deep-Sea Res.*, 15: 433–459.

Hamon, B. V., 1970. Western boundary currents in the South Pacific. *In* Wooster, W. S. (Ed.), *Scientific Exploration of the South Pacific:* Washington (National Academy of Sciences), pp. 50–59.

Hayes, D. E., and Ringis, J., 1973. Sea-floor spreading in the Tasman Sea. *Nature*, 243:454–458.

Healy, T. R., 1970. Dust from Australia. *Earth Sci. J.*, 4:106–116.

Holtzapffel, T., Bonnot-Courtois, C., Chamley, H., and Clauer, N., in press. Heritage et diagénèse dans la constitution des smectites nord-atlantiques (Crétacé–Paléogène). *Bull. Soc. Geol. Fr.*

Janecek, T. R., and Rea, D. K., 1983. Eolian deposition in the northeast Pacific Ocean: Cenozoic history of atmospheric circulation. *Geol. Soc. Am. Bull.*, 94:730–738.

Keigwin, L. D., Jr., 1979. Late Cenozoic stable isotope stratigraphy and paleooceanography of DSDP sites from the east equatorial and north central Pacific Ocean. *Earth Planet. Sci. Lett.*, 45:361–382.

________, 1982. Stable isotope Stratigraphy and paleoceanography of Sites 502 and 503. *In* Prell, W. L., Gardner, J. V., et al., *Init. Repts. DSDP*, 68: Washington (U.S. Govt. Printing Office), 445–453.

Kemp, E. M., 1978. Tertiary climatic evolution and vegetation history in the Southeast Indian Ocean region. *Palaeogeogr., Palaeoclimatol., Palaeoecol.*, 24:169–208.

Kennett, J. P., 1977. Cenozoic evolution of Antarctic glaciation, the Circum-Antarctic Ocean, and their impact on global paleoceanography. *J. Geophys. Res.*, 82:3843–3860.

________, 1978a. Cenozoic evolution of circumantarctic paleoceanography. *In* van Zinderen Bakker, E. M. (Ed.), *Antarctic Glacial History and Paleoenvironments:* Rotterdam (Balkema), pp. 41–56.

________, 1978b. The development of planktonic biogeography in the Southern Ocean during the Cenozoic. *Mar. Micropaleontol.*, 3: 301–345.

Kennett, J. P., Houtz, R. E., Andrews, P. B., Edwards, A. R., Gostin, V. A., Hajós, M., Hampton, M., Jenkins, D. G., Margolis, S. V., Ovenshine, A. T., and Perch-Nielsen, K., 1975. Cenozoic paleoceanography in the southwest Pacific Ocean, Antarctic glaciation, and the development of the Circum-Antarctic Current. *In* Kennett, J. P., Houtz, R. E., et al., *Init. Repts. DSDP*, 29: Washington (U.S. Govt. Printing Office), 1155–1170.

Kidson, E., 1930. Dust from Australia. *N.Z. Sci. Tech.*, 11:417–418.

Knox, G. A., 1970. Biological oceanography of the South Pacific. *In* Wooster, W. S. (Ed.), *Scientific Exploration of the South Pacific:* Washington (National Academy of Sciences), pp. 155–182.

Lange, H., 1982. Distribution of chlorite and kaolinite in eastern Atlantic sediments off North Africa. *Sedimentology*, 29:427–432.

Leinen, M., and Heath, G. P., 1981. Sedimentary indicators of atmospheric activity in the Northern Hemisphere during the Cenozoic. *Palaeogeogr., Palaeoclimatol., Palaeoecol.*, 36:1–21.

Lever, A., and McCave, I. N., 1983. Eolian components in Cretaceous and Tertiary North Atlantic sediments. *J. Sed. Petrol.*, 53:811–832.

Loewe, F., 1943. *Duststorms in Australia*. Commonwealth Met. Bur., Bull. 28.

McCave, J. N., and Jarvis, J., 1973. Use of the Model T Coulter Counter in size analysis of the fine to coarse sand. *Sedimentology*, 20: 305–315.

Maillot, H., and Robert, C., 1984. Paleoenvironmental evolution of the Walvis Ridge deduced from inorganic geochemical and clay mineralogical data, Deep Sea Drilling Project Leg 74, Southwest Atlantic. *In* Moore, T. C., Jr., Rabinowitz, P. D., et al., *Init. Repts. DSDP*, 74: Washington (U.S. Govt. Printing Office), 663–683.

Marshall, P., and Kidson, E., 1929. The duststorm of October, 1929. *N.Z. J. Sci. Tech.*, 10:291–299.

Mercer, J. H., 1976. Glacial history of southernmost South America. *Quat. Res.*, 6:125–166.

Mercer, J. H., and Sutter, J. F., 1982. Late Miocene–earliest Pliocene glaciation in southern Argentina: implications for global ice-sheet history. *Palaeogeogr., Palaeoclimatol., Palaeoecol.*, 38:185–206.

Mienert, J., 1981. Wind- und Flussfracht in rezenten und jungquartaeren Sedimenten im Kuestenbereich NW-Australiens [Diplomarbeit]. University of Kiel.

Millot, G., 1964. *Geologie des argiles:* Paris (Masson).

Moriarty, K. C., 1977. Clay minerals in southeast Indian Ocean sediments, transport mechanisms and depositional environments. *Mar. Geol.*, 25:149–174.

Mudie, P. J., and Helgason, J., 1983. Palynological evidence for Miocene climatic cooling in eastern Iceland about 9.8 Myr ago. *Nature*, 303:689–692.

Mueller, G., 1967. Methods in sedimentary petrology. *In* Engelhardt, W. V., Fuechtbauer, H., and Mueller, G. (Eds.), *Sedimentary Petrology* (Part I): Stuttgart (Schweizerbart'sche Verlagsbuchhandlung).

Nelson, C. S., and Hume, T. M., 1977. Relative intensity of tectonic events revealed by the Tertiary sedimentary record in the Wanganui Basin and adjacent areas, New Zealand. *N. Z. J. Geol. Geophys.*, 20:369–392.

Paquet, H., 1969. *Evolution Géochimique des Minéraux Argilaux dans les Altérations et les Sols des Climats Mediterranéens et Tropicaux à Saisons Contrastées.* Sci. Geol. Strasbourg, Mem. 30.

Parkin, D. W., 1974. Trade winds during the glacial cycles. *Proc. R. Soc. London, Ser. A*, 337:73–100.

Parkin, D. W., and Padgham, R. C., 1975. Further studies on trade winds during glacial cycles. *Proc. R. Soc. London, Ser. A*, 346: 245–260.

Pedro, G., 1968. Distribution des principaux types d'altération chimique à la surface du globe. Présentation d'une esquisse géographique. *Rev. Geogr. Phys. Geol. Dyn.*, 10:457–470.

Ramage, C. S., 1970. Meteorology of the South Pacific tropical and middle latitudes. *In* Wooster, W. S. (Ed.), *Scientific Exploration of the South Pacific:* Washington (National Academy of Sciences), 16–29.

Rea, D. K., and Harrsch, E. C., 1981. Mass-accumulation rates of the non-authigenic inorganic crystalline (eolian) components of deep-sea sediments from Hess Rise, Deep Sea Drilling Project Sites 464, 465, and 466. *In* Thiede, J., Vallier, T. L., et al., *Init. Repts. DSDP*, 62: Washington (U.S. Govt. Printing Office), 661–668.

Rea, D. K., and Janecek, T. R., 1982. Late Cenozoic changes in atmospheric circulation deduced from North Pacific eolian sediments. *Mar. Geol.*, 49:149–167.

Robert, C., 1982. Modalité de la sédimentation argileuse en relation avec l'histoire géologique de l'Atlantique sud [thesis]. Université d'Aix-Marseille.

Sarnthein, M., Tetzlaff, G., Koopmann, B., Wolter, K., and Pflaumann, U., 1981. Glacial and interglacial wind regimes over the eastern subtropical Atlantic and Northwest Africa. *Nature*, 293: 193–196.

Sarnthein, M., Thiede, J., Pflaumann, U., Erlenkeuser, H., Fuetterer, D., Koopmann, B., Lange, H., and Seibold, E., 1982. Atmospheric and oceanic circulation patterns off Northwest Africa during the past 25 million years. *In* von Rad, U., Hinz, K., Sarnthein, M., and Seibold, E. (Eds.), *Geology of the Northwest African Continental Margin:* Berlin (Springer Verlag), pp. 545–604.

Savin, S. M., Douglas, R. G., Keller, G., Killingley, J. S., Shaughnessy, L., Sommer, M. A., Vincent, E., and Woodruff, F., 1981. Miocene benthic foraminiferal isotope records: a synthesis. *Mar. Micropaleontol.*, 6:423–450.

Shackleton, N. J., Backman, J., Zimmerman, H., Kent, D. V., Hall, M. A., Roberts, D. G., Schnitker, D., Baldauff, J. G., Desprairies, A., Homrighausen, R., Huddlestun, P., Keene, J. B., Kaltenback, A. J., Krumsiek, K. A. O., Morton, A. C., Murray, J. W., and Westberg-Smith, J., 1984. Oxygen isotope calibration of the onset of ice-rafting and history of glaciation in the North Atlantic region. *Nature*, 307:620–623.

Shackleton, N. J., and Kennett, J. P., 1975. Paleotemperature history of the Cenozoic and the initiation of Antarctic glaciation: oxygen and carbon isotope analyses in DSDP Sites 277, 279, and 281. *In* Kennett, J. P., Houtz, R. E., et al., *Init. Repts. DSDP*, 29: Washington (U.S. Govt. Printing Office), 743–755.

Shackleton, N. J., and Opdyke, N. D., 1977. Oxygen isotope and paleomagnetic evidence for early northern hemisphere glaciation. *Nature*, 270:216–219.

Sprigg, R. C., 1982. Alternating wind cycles of the Quaternary era and their influences on aeolian sedimentation in and around the dune deserts of southeastern Australia. *In* Wasson, R. J. (Ed.), *Quaternary Dust Mantles of China, New Zealand and Australia:* Canberra, pp. 211–240.

Stein, R., 1984. *Zur neogenen Klimaentwicklung in Nordwest-Afrika und Palaeo-Ozeanographie im Nordost-Atlantik: Ergebnisse von DSDP-Sites 141, 366, 397 und 544B.* Berichte-Reports, Geol. Pal. Inst. Univ. Kiel, 4.

________, 1985a. Late Neogene changes of paleoclimate and paleoproductivity off Northwest Africa (DSDP Site 397). *Palaeogeogr., Palaeoclimatol., Palaeoecol.*, 49:47–59.

________, 1985b. Rapid grain-size analyses of silt and clay fractions by SediGraph 5000D: Comparison with Coulter Counter and Atterberg methods. *J. Sed. Petrol.*

Stein, R., and Sarnthein, M., 1984a. Late Neogene events of atmospheric and oceanic circulation offshore Northwest Africa: high-resolution record from deep-sea sediments. *In* Coetzee, J. A., an van Zinderen Bakker, E. M. (Eds.), *Palaeoecology of Africa* (Vo 16): Rotterdam (A. A. Balkema), 16:9–36.

________, 1984b. Late Neogene oxygen isotope stratigraphy and te rigenous flux rates at Site 544B off Morocco. *In* Hinz, K., Winte er, E. L., et al., *Init. Repts. DSDP*, 79: Washington (U.S. Gov Printing Office), 385–394.

Thiede, J., 1979. Wind regimes over the late Quaternary southwest Pa cific Ocean. *Geology*, 7:259–262.

Thiede, J., Suess, E., and Mueller, P., 1982. Late Quaternary fluxes o major sediment components to the sea floor at the Northwest A rican continental slope. *In* von Rad, U., Hinz, K., Sarnthein, M. and Seibold, E. (Eds.), *Geology of the Northwest African Cont nental Margin:* Berlin (Springer Verlag), pp. 605–631.

van Andel, T. H., Heath, G. R., and Moore, T. C., 1975. *Cenozoi History and Paleoceanography of the Central Equatorial Pacifi Ocean*. Geol. Soc. Am. Mem., 143.

van de Graaff, W. J. E., Crowe, R. W. A., Bunting, J. A., and Jack son, M. J., 1977. Relict Early Cainozoic drainages in arid Western Australia. *Z. Geomorphol. N.F.*, 21:379–400.

Walker, P. H., and Costin, A. B., 1971. Atmospheric dust accession in south-eastern Australia. *Aust. J. Soil Res.*, 9:1–5.

Weissel, J. K., and Hayes, D. E., 1972. Magnetic anomalies in the Southeast Indian Ocean. *In* Hayes, D. E. (Ed.), *Antarctic Oceanology, II: The Australian-New Zealand Sector.* Antarct. Res. Ser., 19: Washington (Am. Geophys. Un.), 165–196.

Windom, H. L., 1969. Atmospheric dust records in permanent snow fields: implications to marine sedimentation. *Geol. Soc. Am. Bull.*, 80:761–782.

Woodruff, F., Savin, S. M., and Douglas, R. G., 1981. Miocene stable isotope record: a detailed deep Pacific Ocean study and its paleoclimate implications. *Science*, 212:665–667.

Wyrtki, K., 1962. The subsurface water masses in the Western South Pacific. *Aust. J. Mar. Freshwater Res.*, 13:18–48.

Date of Initial Receipt: 2 August 1984
Date of Acceptance: 15 February 1985

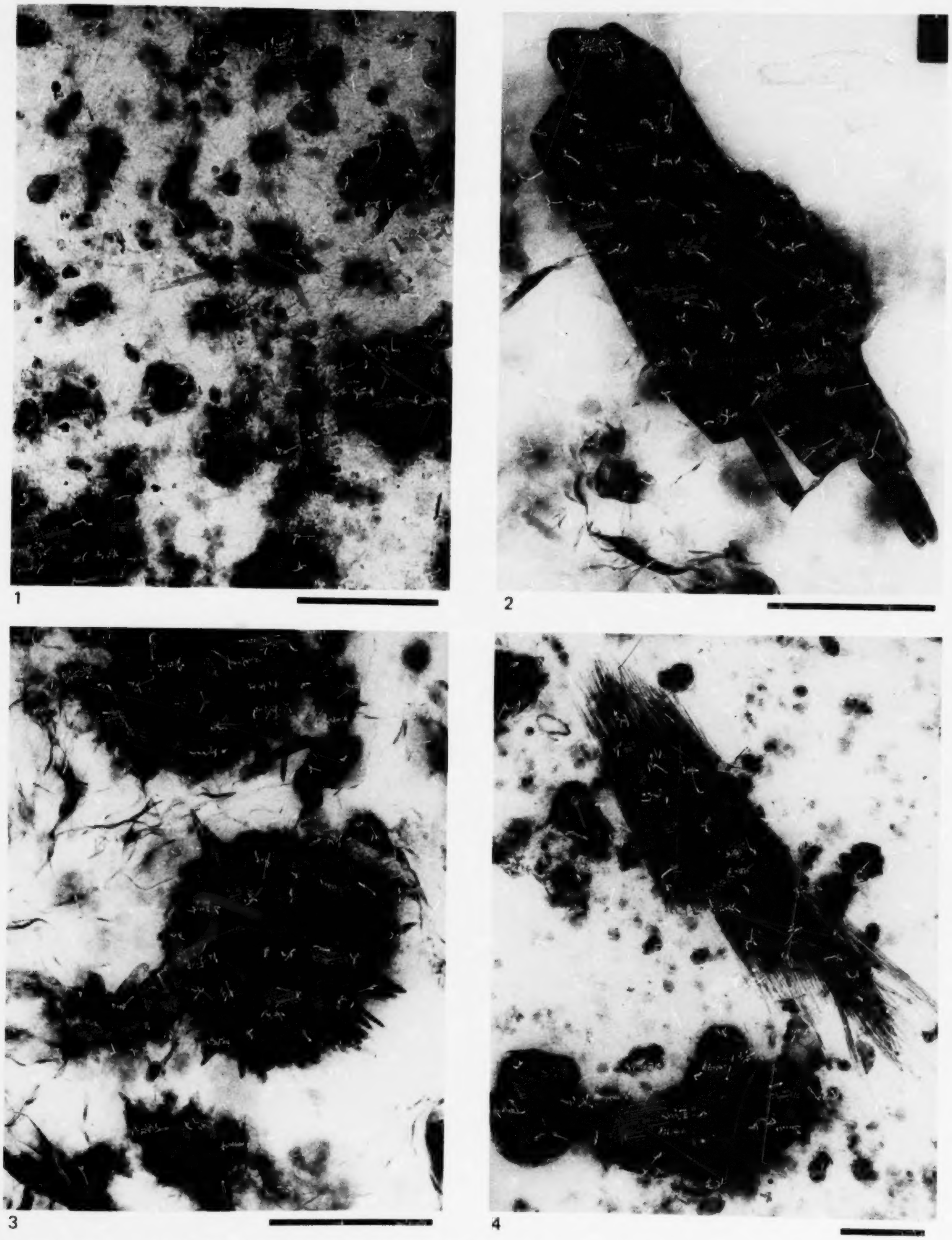

Plate 1. (Scale bar = 1 μm.) **1.** Sample 588-16-5, 80 cm (×25000); late Miocene; very fine laths, dispersed in the background or associated in geometrical figures in this clay fraction, containing 50% smectites associated with 25% illite and 25% kaolinite. **2.** Sample 588-16-5, 80 cm (×32000); late Miocene; thick-lathed particle. **3.** Sample 590A-14-2, 50 cm (×32000); early Pliocene; globular packs of fine laths in this sample, containing 65% smectites, 10% illite, 5% irregular mixed-layer clays and 20% kaolinite. **4.** Sample 591-16-5, 50 cm (×12500); early Pliocene; cluster of fibers resembling palygorskite/sepiolite.

PART VIII: SYNTHESES

46. BIOSTRATIGRAPHIC SYNTHESIS, DEEP SEA DRILLING PROJECT LEG 90 IN THE SOUTHWEST PACIFIC OCEAN[1]

Erlend Martini, Geologisch-Paläontologisches Institut der Universität, Frankfurt am Main
and
D. Graham Jenkins, Department of Earth Sciences, Open University[2]

ABSTRACT

During Leg 90 the sequences cored at Sites 587 to 594, drilled in subtropical to subantarctic waters, were dated by analyses of calcareous nannoplankton and planktonic foraminifers. We summarize the general stratigraphic distribution of these and other fossil groups, including fish otoliths, mollusks, pteropods, ostracodes, echinoids, benthic foraminifers, radiolarians, diatoms, silicoflagellates, ebridians, actiniscidians, sponge spicules, and phytoliths.

Placement of the four major epoch boundaries from late Eocene to Pleistocene at the different sites was based mainly on calcareous nannoplankton and planktonic foraminifers. We discuss the various taxa used to define these boundaries and the biostratigraphic problems involved in correlating sequences in a latitudinal traverse that ranges from 21° to 45°S.

Hiatuses at Sites 588 (late Eocene/late Oligocene) and 592 (late Oligocene/early Miocene) are recorded, and the factors that may have formed these unconformities are briefly described.

INTRODUCTION

During Leg 90 of the Deep Sea Drilling Project, eight sites were occupied and 18 holes drilled in the New Caledonia and New Zealand regions (Fig. 1, Table 1). All sites have yielded abundant calcareous nannoplankton and foraminifers, whereas radiolarians, diatoms, silicoflagellates, and some other groups are restricted to certain sites and stratigraphic levels. The occurrences and general trends of each group are discussed below.

In a traverse between equatorial and northern subantarctic water masses in the southwest Pacific, high-quality middle to late Cenozoic sections were obtained at all Leg 90 sites and at Site 586, drilled during Leg 89 but incorporated in the *Initial Reports* for Legs 89 and 90. At all sites, sediments are presently deposited well above the CCD; this is also true for the middle Eocene and younger sediments cored. Time intervals covered by the cores are shown for each site in Figure 2. However, one of the main objectives of Leg 90 was not achieved. It proved impossible to correlate the biostratigraphic events with the paleomagnetic record; generally, the original paleomagnetic signatures in the sediments were too weak to measure (Barton and Bloemendal, this volume). Thus it was not possible to demonstrate accurately the degree to which some taxa were diachronous.

OCCURRENCE AND GENERAL TRENDS OF VARIOUS GROUPS

Calcareous plankton are abundant and benthic foraminifers widespread at all sites and all levels cored. However, siliceous plankton are restricted to certain areas and levels. Diatoms, silicoflagellates, radiolarians, ebridians, actiniscidians, and sponge spicules are present only in sediments from the middle Eocene at Site 588, the middle Miocene to early Pliocene at Site 591, and the middle Miocene to early Quaternary at the southernmost Site 594. Radiolarians also occur in lower frequencies in Miocene sediments at Site 590 and in the upper Eocene at Site 592.

Site 594 is just south of the present-day Subtropical Convergence. This site exhibits typical cold-water flora and fauna, in which siliceous groups are normally well represented, dating back to the middle Miocene. The occurrence of siliceous plankton in the middle Miocene to lower Pliocene of Site 591 and in the lower Miocene to lower Pleistocene of adjacent Site 206 (Leg 21) is important, because neither nearby Site 590 to the west nor Site 588 to the north and Site 592 to the south show similar occurrences during these intervals. At the moment, no obvious explanation can be offered for local occurrences, although upwelling may have enhanced biogenic productivity.

Fish Otoliths

Fish otoliths, predominantly belonging to the Lanternfishes (Myctophidae), were found in the Quaternary of Sites 587 and 594. Most of the otoliths are badly worn, but some are fairly well preserved and could be identified generically and in some cases specifically (Martini and Gaemers, this volume).

Mollusks

Mollusk fragments were noted in Core 592-34, of early Oligocene age. The better-preserved specimens were tentatively identified as *Ostrea* sp. A few juvenile *Chlamys* were found in the late Quaternary at Site 594.

---

[1] Kennett, J. P., von der Borch, C. C., et al., *Init. Repts. DSDP*, 90: Washington (U.S. Govt. Printing Office).

[2] Addresses: (Martini) Geologisch-Paläontologisches Institut der Universität, Senckenberg-Anlage 32-34, D6000 Frankfurt am Main, Federal Republic of Germany; (Jenkins) Department of Earth Sciences, Open University, Walton Hall, Milton Keynes MK7 6AA, Buckinghamshire, England.

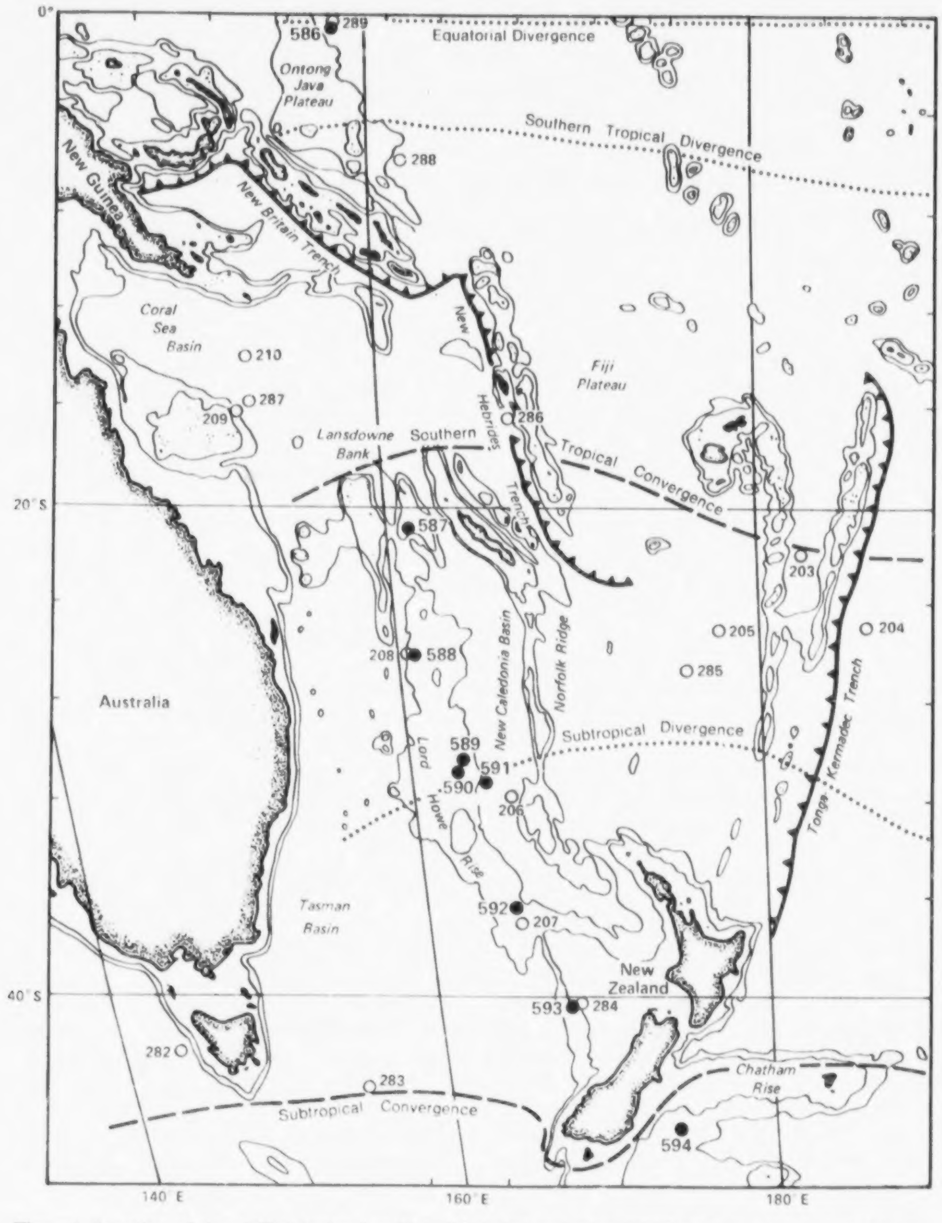
0°
586
289
Equatorial Divergence
Ontong Java Plateau
Southern Tropical Divergence
288
New Guinea
New Britain Trench
Coral Sea Basin
210
287
209
Lansdowne Bank
Southern
New Hebrides Trench
286
Tropical Convergence
Fiji Plateau
20°S
587
203
205
204
208
588
285
Australia
New Caledonia Basin
Norfolk Ridge
Subtropical Divergence
Tonga-Kermadec Trench
589
591
590
206
Lord Howe Rise
Tasman Basin
592
207
New Zealand
40°S
593
284
282
283
Chatham Rise
Subtropical Convergence
594
140°E
160°E
180°E

Figure 1. Location of sites drilled during Leg 90 (solid circles) and other DSDP drill sites (open circles) in the southwest Pacific.

Pteropods, Ostracodes, and Echinoids

Representatives of these groups were noted in Quaternary samples from several holes but were not investigated in detail. Pteropods are especially common in the uppermost samples of Site 587. They include the circumtropical species *Diacria quadridentata*, and *Creseis* cf. *virgula* as well as the Indo-Pacific species *Atlanta turriculata*. Pteropods were not found at the southernmost Site 594, where ostracodes and echinoid spines form a varying but constant constituent in the Quaternary samples.

Planktonic Foraminifers

In general, samples from Site 586 in the tropical province to Site 594 in subantarctic waters yielded excellen planktonic foraminiferal faunas. Because of the change in the faunas from the equatorial region to Site 594 a latitude 45°S, five zonal schemes were used, and intersite correlation was established by using selected datum species. Most of the extinctions and initial appearance of datum species appear to be relatively isochronous, except at the paleogeographic limits of some species, where a few were demonstrably diachronous, including the ap-

Table 1. Locations and water depths of Leg 90 sites.

Site	Latitude (S)	Longitude (E)	Water depth (m)
586	00°29.84′	158°29.89′	2207
587	21°11.87′	161°19.99′	1101
588	26°06.7′	161°13.6′	1533
589	30°42.72′	163°38.39′	1391
590	31°10.02′	163°21.51′	1299
591	31°35.06′	164°26.92′	2131
592	36°28.40′	165°26.53′	1098
593	40°30.47′	167°40.47′	1068
594	45°31.41′	174°56.88′	1204

earances of *Globorotalia truncatulinoides* at Site 594 nd *G. inflata* at Site 587 (Jenkins and Srinivasan, this olume).

Stratigraphic range charts of Sites 586 to 594 are pro-ided, selected taxonomic problems are discussed, and 39 species are illustrated in Jenkins and Srinivasan (this volume). Some details of the last or first occurrences of important species around the major boundaries from the Eocene onward are also discussed below and are illustrated in Figures 3 to 8.

Benthic Foraminifers

Benthic foraminifers are present at all sites and cored intervals. Redeposited shallow-water foraminifers were noted at Site 587. Assemblages and regional differences along the traverse from Site 586 to the southernmost Site 594 are described in detail by Boersma (this volume).

Calcareous Nannoplankton

Calcareous nannoplankton are present in all holes and are described in detail for the Neogene and Quaternary by Lohman (this volume) and for the Paleogene by Martini (this volume). The standard nannoplankton zonation (Martini, 1971) is used at all sites to identify nanno-

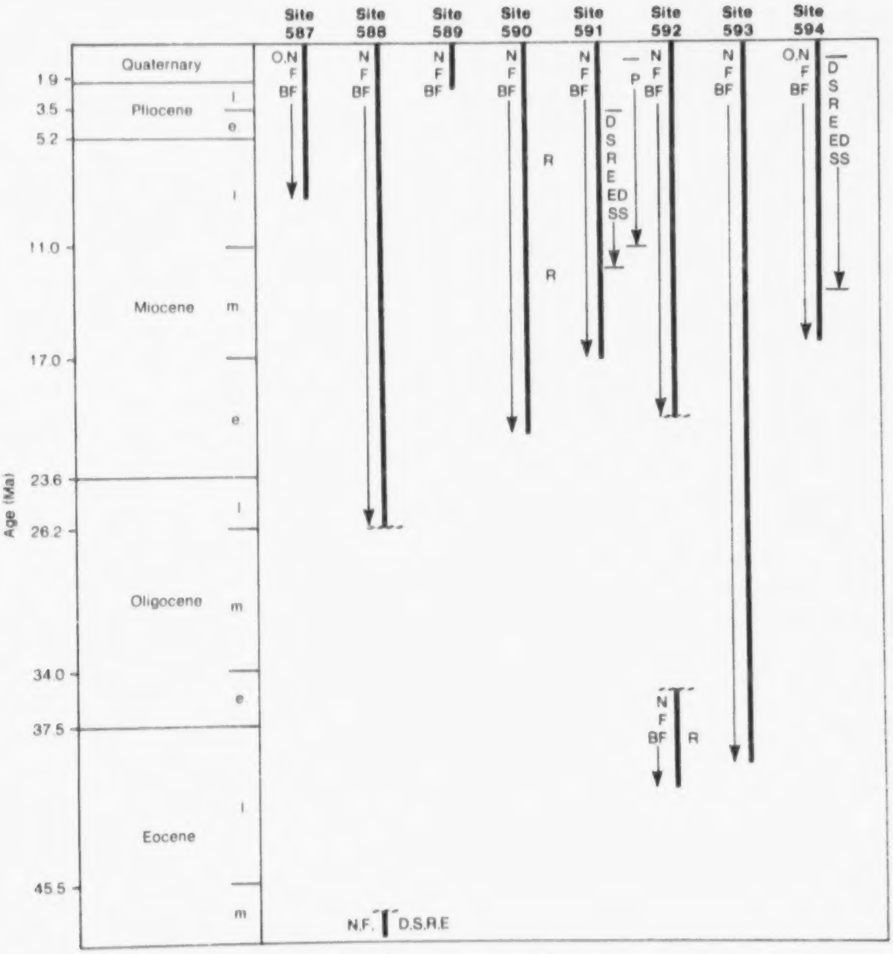

Figure 2. Intervals recovered during Leg 90 in the southwest Pacific, and occurrence of various fossil groups. O = fish otoliths, N = calcareous nannoplankton, F = planktonic foraminifers, BF = benthic foraminifers, D = diatoms, S = silicoflagellates, R = radiolarians, E = ebridians, ED = endoskeletal dinoflagellates, SS = sponge spicules, P = phytoliths. Mollusks, pteropods, ostracodes, and echinoids omitted.

plankton zones. However, from Site 592 (36°28.40′S) southward, zones based on *Discoaster, Ceratolithus, Catinaster*, and *Sphenolithus* species had in some cases to be combined, because most of these species do not occur in subantarctic waters. In the middle and late Oligocene of Site 593, sphenoliths and *Helicosphaera recta* are either rare or missing, and substitute species such as *Blackites tenuis* and *Zygrhablithus bijugatus* were used. In the Miocene and especially in the Pliocene at Site 594 (45°31.41′S) and, to a lesser extent, at Site 593 (40°30.47′S), discoasters are missing or occur only as rare specimens, not reliable for zonation. Thus large intervals had to be combined, as in the nannoplankton zonation used in the northern high latitudes of the Atlantic and the Norwegian-Greenland Sea (Leg 38, Müller, 1976; Leg 49, Martini, 1979). This poses a particular problem for the identification of the Pliocene/Pleistocene boundary, which elsewhere is commonly placed at the last occurrence of discoasters (see later discussion).

In the Quaternary, calcareous nannoplankton are generally well preserved at all sites. However, as depth increases preservation changes from good to moderate in the Pliocene and deteriorates to poor in some of the early Miocene assemblages. Preservation in the Paleogene at Sites 588, 592, and 593 varies between poor and moderate. In Hole 588C, discoasters, especially in the Oligocene, are overgrown, as are some of the Oligocene *Discolithina* specimens.

Radiolarians

Radiolarians were noted during routine shipboard work in the middle Eocene section of Hole 588C and below Sample 590B-25,CC (middle upper Miocene) at Site 590, but do not occur in sufficient numbers for detailed investigations. Fragments of radiolarians were found in smear slides from various levels at Site 591, indicating that this group was present throughout most of the section cored; in Sample 591B-5,CC (upper Miocene), for example, radiolarians are rather common but were not investigated in detail. At Site 592, radiolarians are present only in part of the upper Eocene and are not very different from the tropical faunas. Hence the classic biostratigraphy of Riedel and Sanfilippo (1971) has been used. At Site 594, radiolarians are rare throughout the cores because of the great dilution by terrigenous material. Equatorial and high-latitude assemblages were mixed and, accordingly, zonations proposed for both regions have been employed (Caulet, this volume). Subantarctic or antarctic species are recognized only in Plio/Pleistocene samples, whereas radiolarian faunas below Section 594-23-1 are composed of temperate species. This change occurs near the Miocene/Pliocene boundary.

Diatoms

Diatoms are present in the middle Eocene of Hole 588C and are especially common in Core 588C-19, where representatives of *Triceratium, Actinoptychus, Trochosira*, and *Thalassiosira* are included in the well-diversified assemblage. At Site 591, diatoms occur in fair numbers throughout most of the section, but the occurrences are heavily masked by vast numbers of foraminifers and calcareous nannoplankton. Diatoms are present also in most Site 594 samples from the middle Miocene up to the Quaternary (Ciesielski, this volume). Reworked Eocene and Oligocene diatoms are common throughout the sequence.

Silicoflagellates

Silicoflagellates are rather frequent in the middle Eocene from Site 588, in the middle Miocene to lower Pliocene from Site 591, and in the middle Miocene to Quaternary at Site 594. At Sites 591 and 594 a detailed silicoflagellate zonation is possible, although because of the latitudinal change some differences are obvious in the silicoflagellate assemblages at the sites. Comparison between the sequences recovered at Sites 591 and 206 (Leg 21) revealed two hiatuses in the latter, but helped to establish a zonation for this area from the early Miocene to the Pleistocene and a correlation to standard nannoplankton zones. Two new genera, two new subspecies, and three new forms are described from this material (Locker and Martini, this volume). Reworked Eocene and Oligocene silicoflagellates were noted in most of the Neogene and Quaternary samples of Site 594.

Ebridians and Actiniscidians

Ebridians and actiniscidians (so-called endoskeletal dinoflagellates) were found at three sites. Hole 588C yielded middle Eocene ebridians. At Site 591, ebridians and actiniscidians are rather common in the middle Miocene and lower Pliocene and are investigated in detail (Locker and Martini, this volume). In Holes 594 and 594A both groups were noted sporadically in the middle Miocene to Pleistocene, including reworked forms from the Paleogene. The middle Miocene to lower Pliocene at Site 591 can be subdivided into five ebridian–actiniscidian zones. Five new species are described from this material.

Sponge Spicules

Sponge spicules were noted in the middle Eocene of Hole 588C and at Sites 591 and 594, where they are associated with diatoms, silicoflagellates, and ebridians. A few specimens are figured by Locker and Martini (this volume).

Phytoliths

Phytoliths were found in fair numbers in Holes 591, 591A, and 591B, and very sporadically also in Hole 594A, but were investigated only in the first three holes (Locker and Martini, this volume). They are derived from the semiarid regions of Australia, whence they were blown by westerly winds into the Tasman Sea area. The stratigraphic record ranges from the middle Miocene (~14 Ma) to the early Pleistocene.

MAJOR BOUNDARIES

All major boundaries from the Eocene onward were encountered at Leg 90 and are discussed with respect to planktonic foraminifers and calcareous nannoplankton.

Eocene/Oligocene Boundary

The Eocene/Oligocene boundary as identified by calcareous nannoplankton is commonly placed at the last occurrence of the rosette-shaped discoasters which dominate in the Eocene, especially the last occurrence of *Discoaster saipanensis* (top of Zone NP20; Martini, 1971) in deep-sea sediments and land-based sections of low and middle latitudes. Several authors that have discussed the dating of the Eocene/Oligocene boundary by calcareous nannoplankton and foraminifers (e.g., Bombita and Rusu, 1981; Snyder et al., 1984) have shown that the boundary determined using planktonic foraminifers (commonly the last occurrence of *Globorotalia cerroazulensis*) is slightly younger than that determined using calcareous nannoplankton and occurs in the lower part of nannoplankton Zone NP21. The time-span between the two boundary "events" is about 0.4 m.y. as determined from the sedimentation rate at Site 592 (Martini, this volume). In high latitudes, discoasters are generally rare or are missing and thus not so reliable for indicating the position of the Eocene/Oligocene boundary. However, *Cribrocentrum reticulatum* last occurs just below the Eocene/Oligocene boundary (top of Zone NP20, last occurrence of *D. saipanensis*) in low and middle latitudes and can also be used as a reliable substitute species at high latitudes (Müller, 1978).

At Sites 592 and 593 the extinction of *Globigerinatheka index* was used to mark the boundary, following the work of Finlay (1939), Hornibrook (1958), and Jenkins (1963, 1966) in New Zealand. Other taxa such as *Hantkenina* and *Globorotalia cerroazulensis* s.l. became extinct below the boundary in the late Eocene in the mid to high latitudes of the southwest Pacific. At Site 592 the last occurrences of *D. saipanensis* and *D. barbadiensis* were used to define the nannoplankton-based Eocene/Oligocene boundary at Sample 592-37-2, 33–34 cm (Fig. 3). In contrast, at Site 593, the last rare occurrences of these species are in Core 60, *below* the last occurrence of *C. reticulatum* in Sample 593-59,CC (see Fig. 4). Thus the disappearances of these two *Discoaster* species are slightly diachronous at these latitudes with respect to the extinction of *C. reticulatum* and not reliable at this site.

It has been fairly well established that there was a significant lowering of oceanic temperature in the earliest Oligocene, coinciding with paleomagnetic Anomaly 13 at Site 522 in the South Atlantic (Poore and Matthews, 1983), after the extinctions of *Globigerinatheka index, Hantkenina*, and *Globorotalia cerroazulensis*. This drop in temperature is detected at Site 592 in Core 35, after the extinction of *G. index* is noted in Sample 592-36-3, 90–91 cm (Murphy and Kennett, this volume). At Site 593, the same set of extinctions occurs, that is, *D. barbadiensis* and *D. saipanensis* followed by *G. index*.

Oligocene/Miocene Boundary

At Sites 586, 588, and 593 the Oligocene/Miocene boundary was encountered. Details on last and first occurrences of calcareous nannoplankton and planktonic foraminifers near the boundary are presented in Figures 5 and 6.

At Sites 586, 588, and 593 the initial appearance of *Globoquadrina dehiscens* was used to mark the boundary; this follows the work of Jenkins (1966, 1971) and Srinivasan and Kennett (1983). Jenkins (1971, 1981) has suggested that *G. dehiscens* evolved and appeared earlier in the middle latitudes, compared with its cryptogenic appearance at low latitudes.

The Oligocene/Miocene boundary as defined by calcareous nannoplankton is generally placed at the top of nannoplankton Zone NP25 (Steininger, 1982), where several nannoplankton species, such as *Sphenolithus ciperoensis, Helicosphaera recta*, and *Zygrhablithus bijugatus*, have their last occurrences. *Dictyococcites dictyodus*, which may be used in certain areas as an additional boundary indicator, is not very reliable because of its varying last occurrence. For example, in the central Pacific it last occurs at the top of Zone NP23 (DSDP Site 317), whereas in the southwest Pacific the last occurrence is well within Zone NN1 (DSDP Site 593). Some workers, such as Okada (1980), identify the *Cyclicargolithus abisectus* Acme Zone of Bukry (1973) as the last zone within the Oligocene. Although *C. abisectus* ranges up to the lower part of Zone NN6 (*Discoaster exilis* Zone), it has several acmes up to this level and cannot be used to define a useful zone near the Oligocene/Miocene boundary.

At Site 593, the boundary was identified by the last occurrence of *H. recta* and *Z. bijugatus* and is very close to the boundary as defined by the first appearance of *Globoquadrina dehiscens*. However, in Hole 588C, the boundary identified by calcareous nannoplankton has a considerable offset compared with that identified by planktonic foraminifers (Fig. 5). Detailed nannoplankton studies from Cores 4 to 9 reveal a consistent presence of *H. recta* up to Sample 588C-6-2, 0–1 cm, but rather scattered occurrences of *Z. bijugatus* and *Discolithina enormis* in Cores 6 to 9. The last common occurrence of *Z. bijugatus* (Sample 588C-10-2, 24 cm and the first occurrence of *Sphenolithus capricornutus* (Sample 588C-9,CC) were noted close to the first appearance of *G. dehiscens* in Sample 588C-9-3, 40–41 cm, in a similar position to that found in Hole 593 (Fig. 6).

Miocene/Pliocene Boundary

The placement of this boundary using planktonic foraminifers presented some problems on Leg 90. At the tropical/subtropical Sites 586 and 587 the first appearance of *Globorotalia tumida* was used, but it became progressively rarer in the southward traverse and at the other Sites 588 and 590 and 594 the boundary was placed by the extinction of *G. conomiozea*, a species which commonly occurs also in New Zealand sections of late Miocene age (Hornibrook, 1984).

Without reliable paleomagnetic data it is difficult to prove, but Jenkins and Srinivasan (this volume) believe that this extinction was probably diachronous. Data for some important calcareous nannoplankton species around the Miocene/Pliocene boundary seem to support this assumption (Fig. 7). The first appearance of *G. tumida* seems to be an unreliable marker, since its datum line crosses the datum lines of *Ceratholithus rugosus* (FAD) and *Discoaster quinqueramus* (LAD) between Sites 587 and 588. Both are crossed back again by the *G. conomiozea* datum (LAD) between Sites 588 and 591. At Site 594 the extinction level of *G. conomiozea* was noted even

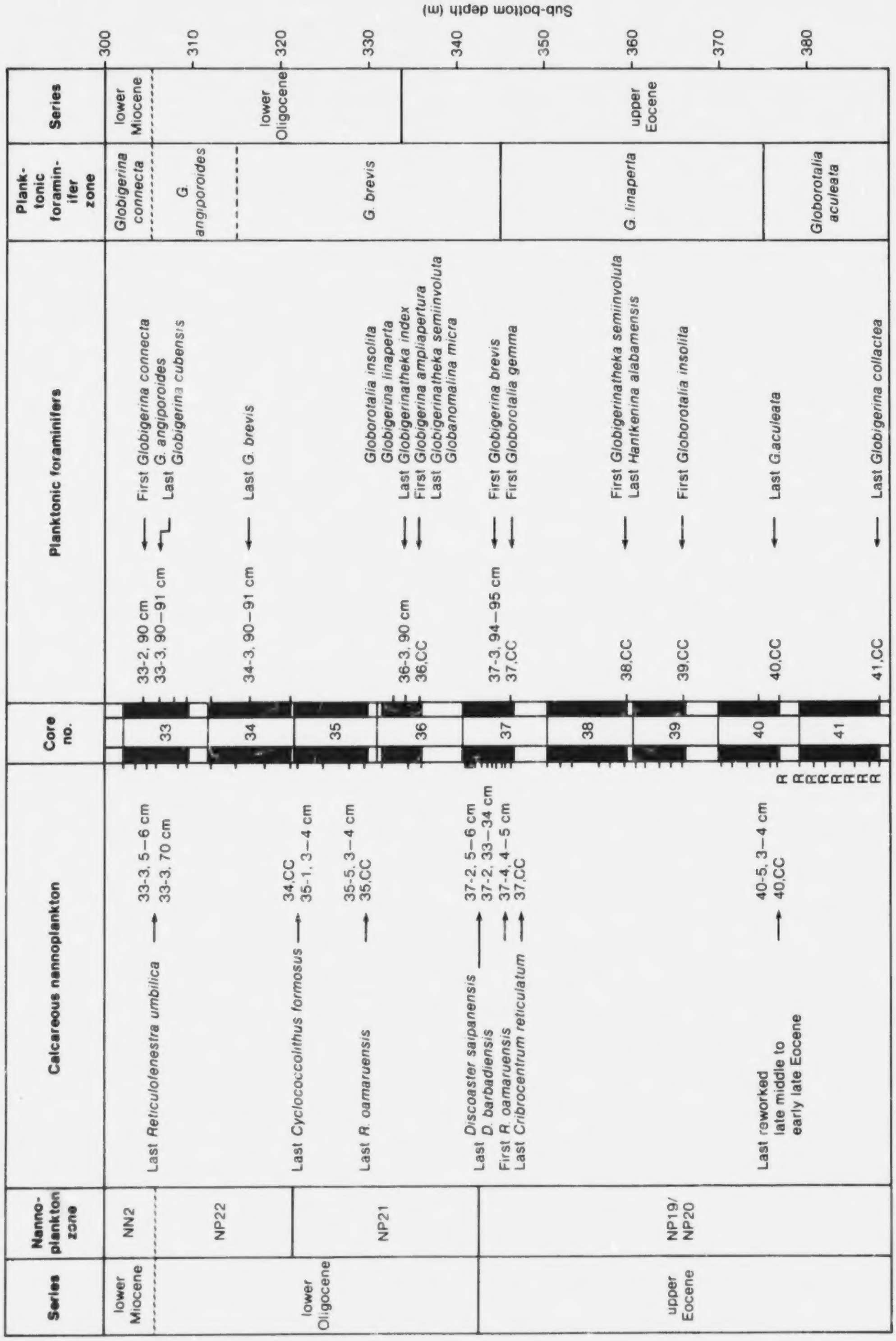

Figure 3. Last or first occurrences of important calcareous nannoplankton and planktonic foraminiferal species about the Eocene/Oligocene boundary in Hole 592, at 36°28.40′S. Black = recovered material, R = reworked middle to early late Eocene calcareous nannoplankton.

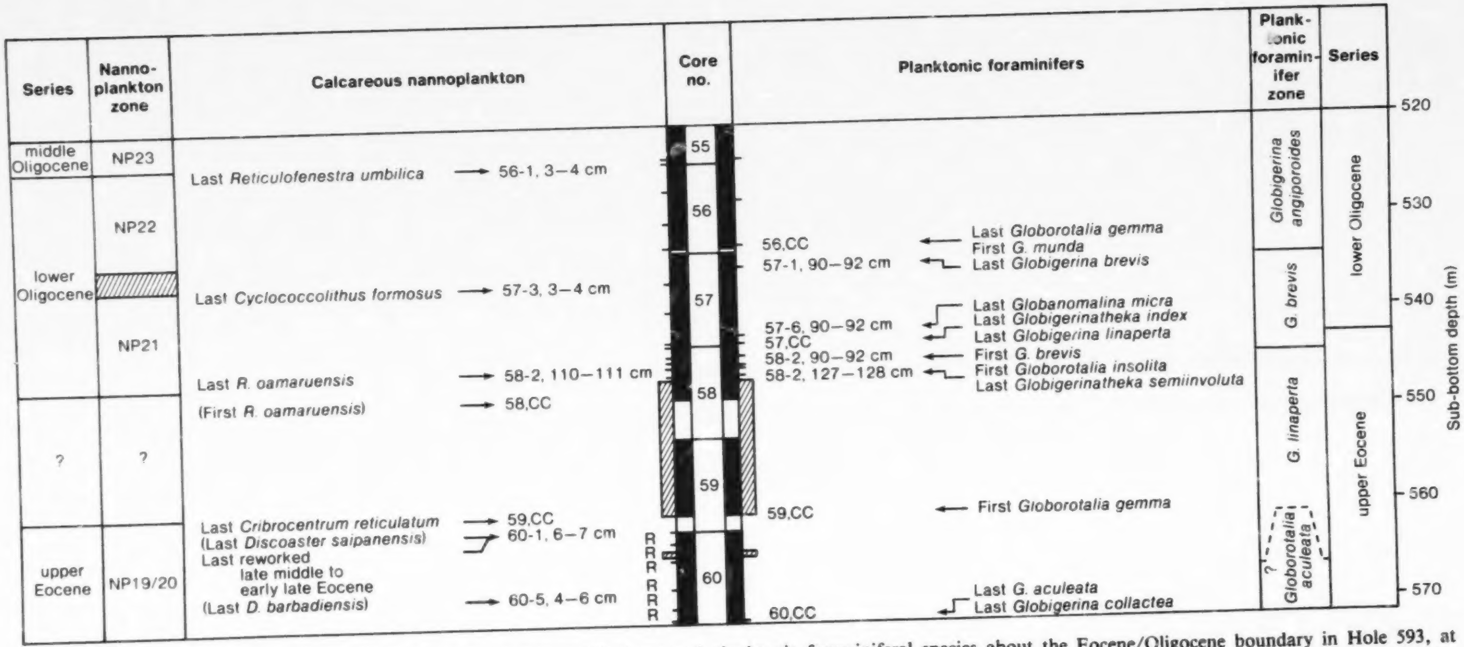

Figure 4. Last or first occurrences of important calcareous nannoplankton and planktonic foraminiferal species about the Eocene/Oligocene boundary in Hole 593, at 40°30.47′S. Black = recovered material, hachures = volcanogenic material, R = reworked middle to early late Eocene calcareous nannoplankton, parentheses indicate that species are too rare and too poorly preserved to be sure of last occurrence.

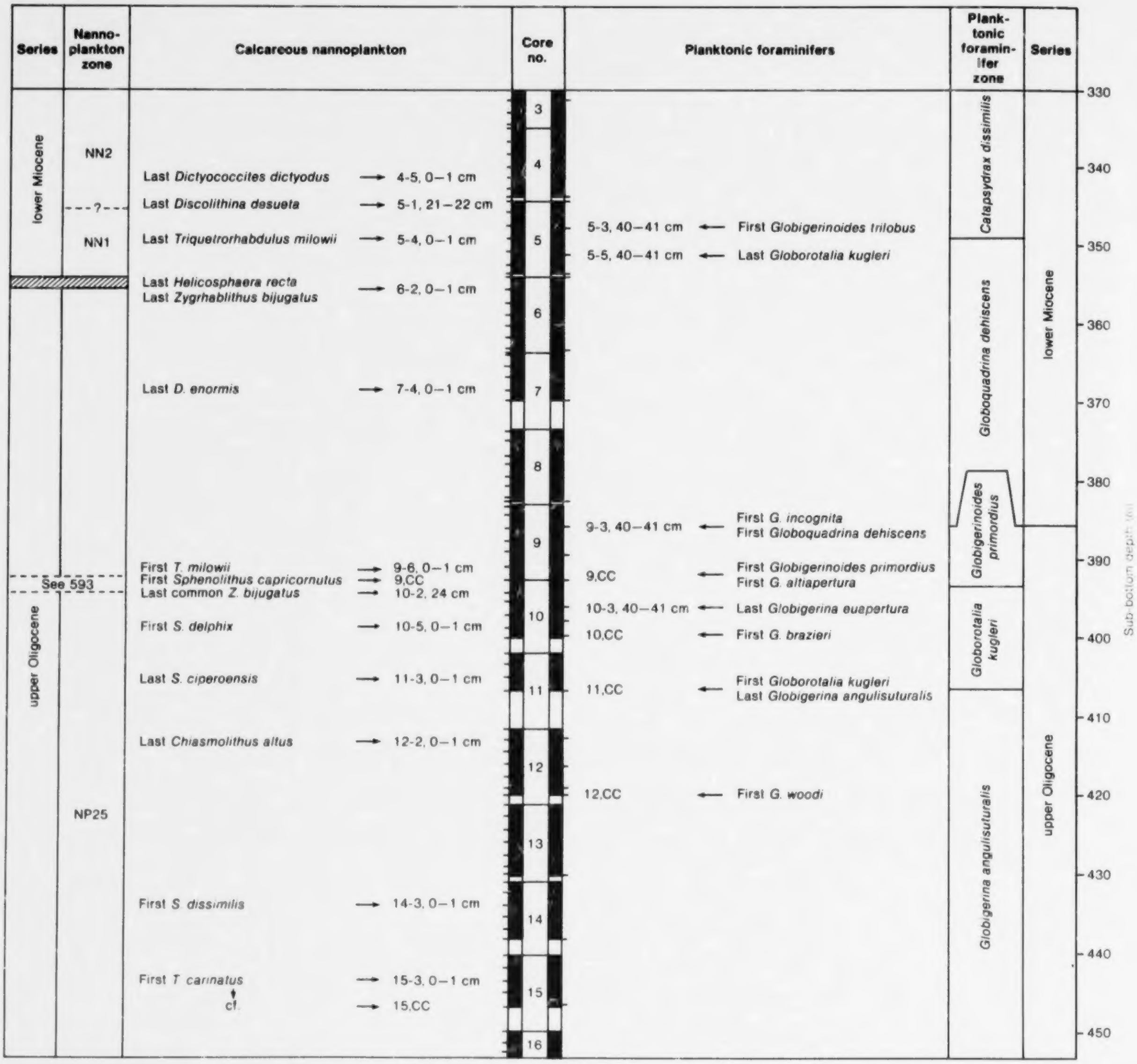

Figure 5. Last or first occurrences of important calcareous nannoplankton and planktonic foraminiferal species about the Oligocene/Miocene boundary in Hole 588C at 26°06.7′S. Black = recovered material.

above the last occurrence of *C. tricorniculatus*, although the latter is not a reliable marker in this high-latitude position.

Pliocene/Pleistocene Boundary

Until recently the first evolutionary appearance of *Globorotalia truncatulinoides* has been used to position the Pliocene/Pleistocene boundary at approximately 1.8 Ma, and this method was used during Leg 90. At Sites 586 to 592 the boundary can be located with confidence, because *G. tosaensis*, the ancestor of the marker, is present; at Site 593 the ancestor is present in low numbers and at Site 594 it is absent, making placement of the boundary unreliable.

The Pliocene/Pleistocene boundary as identified by calcareous nannoplankton is commonly marked by the last occurrence of *Discoaster brouweri* in low and middle latitudes. This datum level is close to the first evolutionary appearance of *Globorotalia truncatulinoides* and near the base of the Olduvai Paleomagnetic Chron. In high latitudes, discoasters are rare or even missing and are not very reliable for identification of the Pliocene/Pleistocene boundary. However, *Cyclococcolithus macintyrei* (which seems to have its last occurrence consistently above the last occurrence of *D. brouweri* near the top of the Olduvai Chron) was recently dated as 1.45 Ma by Backman and Shackleton (1983). This species may serve in high latitudes to approximate the Pliocene/

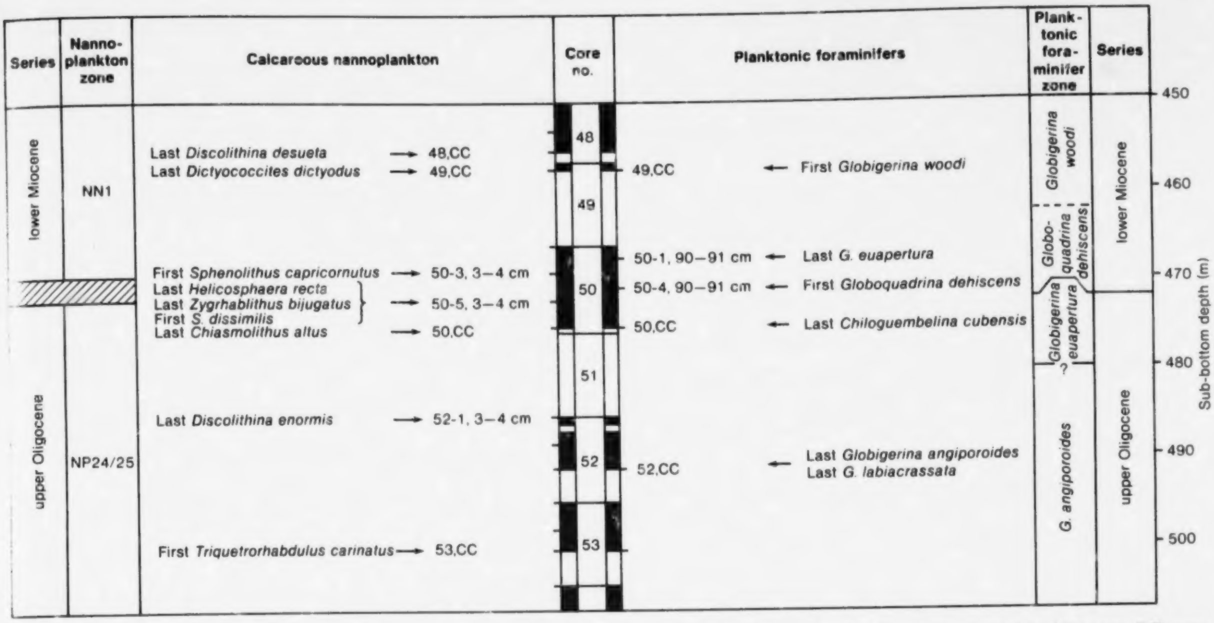

Figure 6. Last or first occurrences of important calcareous nannoplankton and planktonic foraminiferal species around the Oligocene/Miocene boundary in Hole 593, at 40°30.47′S. Black = recovered material.

Pleistocene boundary, as it serves also to subdivide nannoplankton Zone NN19 into a short lower (NN19a) and longer-lasting upper (NN19b) interval. Figure 8 clearly demonstrates these difficulties in higher latitudes, where, between Sites 592 and 593, the *D. brouweri* datum crosses the *G. truncatulinoides* datum, which in turn crosses that of *C. macintyrei* between Sites 593 and 594.

Hiatuses

The mechanisms that cause hiatuses are under scrutiny, but the subject is still under the influence of the idea of large changes in sea level proposed by Vail et al. (1977). On Leg 90 two unconformities were detected.

The first hiatus was noted at Site 588 in Core 588C-18, about 470 m sub-bottom, separating sediments of the late Oligocene *Chiloguembelina cubensis* Zone (and Zone NP24) from the middle Eocene calcareous nannoplankton Zone NP15/NP16. The unconformity represents a time-gap of about 19 m.y. A similar unconformity was found at nearby Site 208 on Leg 21 (Fig. 1).

The second hiatus detected at Site 592 in Core 33 separates the Oligocene *Globigerina angiporoides* Zone (and NP22) sediments below from the lower Miocene *Globigerina connecta* Zone (and Zone NN2) above; this unconformity represents an interval of about 15 m.y.

The areal extent and the various interpretations regarding the cause or causes of the unconformity at about 30 Ma in the southwest Pacific have been discussed by a number of workers (Carter and Landis, 1972; Kennett et al., 1974; Kennett, Houtz, et al. 1975; Edwards, 1975; Jenkins, 1975; Findlay, 1980; Loutit and Kennett, 1981; Carter and Landis, 1982; Lewis and Bellis, 1984). An unconformity in deep-sea deposits such as the one at Site 592 was probably caused by erosion and nondeposition arising from active bottom waters, whereas in the shallower continental shelf deposits nondeposition was caused by a lowering of sea level.

The factors which caused the late Oligocene unconformity are probably related to events which were taking place on and around Antarctica at this time. The active bottom water and the lowering of the sea level were probably related to a combination of the development of the Circum-Antarctic Current at about 30 Ma (Jenkins, 1974, 1978a, b) and the development of initial continental ice sheets on Antarctica at about 29–30 Ma (Keigwin and Keller, 1984; Miller and Thomas, in press).

ACKNOWLEDGMENTS

Data summarized here include that obtained by our colleagues J. P. Caulet, Paul Ciesielski, William Lohman, and M. S. Srinivasan during shipboard studies or during and after the postcruise meeting at Scripps Institution of Oceanography. Martina Bundschuh helped to assemble the data for the drafts of Figures 3 to 8. Thanks are also due to the Deutsche Forschungsgemeinschaft for supporting this study.

REFERENCES

Backman, J., and Shackleton, N. J., 1983. Quantitative biochronology of Pliocene and early Pleistocene calcareous nannoplankton from the Atlantic, Indian and Pacific Oceans. *Mar. Micropaleontol.*, 8: 141–170.

Bombita, G., and Rusu, A., 1981. New data on the Eocene/Oligocene boundary in the Romanian Carpathians. *Palaeogeogr., Palaeoclimatol. Palaeoecol.*, 36:213–222.

Bukry, D., 1973. Low-latitude coccolith biostratigraphic zonation. *In* Edgar, N. T., Saunders, J. B., et al., *Init. Repts. DSDP*, 15: Washington (U.S. Govt. Printing Office), 685–703.

Carter, R. M., and Landis, C. A., 1971. Correlative Oligocene unconformities in southern Australasia. *Nature (Physical Sci.)*, 237:12–13.

________, 1982. Appendix: Oligocene unconformities in the South Island. *J. R. Soc. N. Z.*, 12:42–46.

Findlay, R. H., 1980. The Marshall Paraconformity (Note). *N.Z. J. Geol. Geophys.*, 23:125–133.

Finlay, H. J., 1939. New Zealand Foraminifera: key species in stratigraphy, No. 3. *Trans. R. Soc. N. Z.*, 69(3):309-329.

Hornibrook, N. de B., 1958. New Zealand Upper Cretaceous and Tertiary foraminiferal zones and some overseas correlations. *Micropaleontology*, 4(1):25-38.

________, 1984. *Globorotalia* (planktic foraminifera) at the Miocene/Pliocene boundary in New Zealand. *Palaeogeogr., Palaeoclimatol., Palaeoecol.*, 46:107-117.

Jenkins, D. G., 1963. The Eocene-Oligocene boundary in New Zealand. *N. Z. J. Geol. Geophys.*, 6:107.

________, 1966. Planktonic foraminiferal zones and new taxa from the Danian to lower Miocene of New Zealand. *N. Z. J. Geol. Geophys.*, 8:1088-1125.

________, 1971. *Cenozoic Planktonic Foraminifera of New Zealand.* N. Z. Geol. Surv. Paleontol. Bull., 42.

________, 1974. Initiation of the proto-Circum-Antarctic Current. *Nature*, 252(5482):371-373.

________, 1975. Age and correlation of some unconformities in the New Zealand region. *Geol. Soc. N. Z. Newsl.*, 39:45-47.

________, 1978a. *Guembelitria* aff. *stavensis* Bandy, a paleoceanographic marker of the initiation of the Circum-Antarctic Current and the opening of Drake Passage. *In* Bolli, H. M., Ryan, W. B. F., *Init. Repts. DSDP*, Supply to Vols. 38, 39, 40, and 41: Washington (U.S. Govt. Printing Office), 687-693.

________, 1978b. *Guembelitria samwelli* Jenkins, a new species from the Oligocene of the southern Hemisphere. *J. Foraminiferal Res.*, 8(2):132-137.

________, 1981. Planktonic foraminifera and the Palaeogene/Neogene boundary in the southwest Pacific. *In Search of the Palaeogene/Neogene Boundary Stratotype. Giorn. Geol., Ser. 2a*, 44:205-210.

Keigwin, L. D., and Keller, G., 1984. Middle Oligocene climatic change from equatorial Pacific DSDP Site 77. *Geology*, 12:16-19.

Kennett, J. P., Houtz, R. E., Andrews, P. B., Edwards, A. R., Gostin, V. A., et al., 1974. Development of the Circum-Antarctic Current. *Science*, 186:144-147.

Kennett, J. P., Houtz, R. E., Andrews, P. B., Edwards, A. R., Gostin, V. A., et al., 1975. Cenozoic paleoceanography in the southwest Pacific Ocean, Antarctic glaciation, and the development of the Circum-Antarctic current. *In* Kennett, J. P., Houtz, R. E., et al., *Init. Repts. DSDP*, 29: Washington (U.S. Govt. Printing Office), 1155-1169.

Lewis, D. W., and Bellis, S. E., 1984. Mid-Tertiary unconformities in the Waitaki Subdivision, North Otago. *J. R. Soc. N. Z.*, 14(3): 251-276.

Loutit, T. S., and Kennett, J. P., 1981. New Zealand and Australian Cenozoic sedimentary cycles and global sea-level changes. *Am. Assoc. Pet. Geol. Bull.*, 65:1586-1601.

Martini, E., 1971. Standard Tertiary and Quaternary calcareous nannoplankton zonation. *In* Farinacci, A. (Ed.), *Proc. II Planktonic Conf., Roma 1970* (Vol. 2): Rome (Edizioni Tecnoscienza), pp. 739-785.

________, 1979. Calcareous nannoplankton and silicoflagellate biostratigraphy at Reykjanes Ridge, northeastern North Atlantic (DSDP Leg 49, Sites 407 and 409). *In* Luyendyk, B. P., Cann, J. R., et al., *Init. Repts. DSDP*, 49: Washington (U.S. Govt. Printing Office), 533-549.

Miller, K. G., and Thomas, E., in press. Late Eocene to Oligocene benthic foraminiferal isotopic record, Site 574 equatorial Pacific. *In* Mayer, L., Theyer, F., et al., *Init. Repts. DSDP*, 85: Washington (U.S. Govt. Printing Office).

Müller, C., 1976. Tertiary and Quaternary calcareous nannoplankton in the Norweigian-Greenland Sea, DSDP, Leg 38. *In* Talwani, M., Udintsev, G., et al., *Init. Repts. DSDP*, 38: Washington (U.S. Govt. Printing Office), 823-841.

________, 1978. Remarks on biostratigraphically useful nannofossils in the Paleogene of the northern hemisphere. *Newsl. Stratigr.*, 7: 45-52.

Okada, H., 1980. Calcareous nannofossils from Deep Sea Drilling Project Sites 442 through 446, Philippine Sea. *In* Klein, G. deV., Kobayashi, K., et al., *Init. Repts. DSDP*, 58: Washington (U.S. Govt. Printing Office), 549-565.

Poore, R. A., and Matthews, R. K., 1983. Late Eocene–Oligocene oxygen- and carbon-isotope record from South Atlantic Ocean, Deep Sea Drilling Project Site 522. *In* Hsü, K. J., LaBrecque, J. L., et al., *Init. Repts. DSDP*, 73: Washington (U.S. Govt. Printing Office), 725-735.

Riedel, W. R., and Sanfilippo, A., 1971. Cenozoic radiolaria from the western tropical Pacific, Leg 7. *In* Winterer, E. L., Riedel, W. R., et al., *Init. Repts. DSDP*, 7, Pt 2: Washington (U.S. Govt. Printing Office), 1529-1672.

Snyder, S. W., Müller, C., and Miller, K. G., 1984. Eocene-Oligocene boundary: biostratigraphic recognition and gradual paleoceanographic change at DSDP Site 459. *Geology*, 12:112-115.

Srinivasan, M. S., and Kennett, J. P., 1983. The Oligocene-Miocene boundary in the South Pacific. *Geol. Soc. Am. Bull.*, 94:798-812.

Steininger, F. F., 1982. The Palaeogene-Neogene (Oligocene-Miocene) boundary. *In* Odin, G. S. (Ed.), *Numerical Dating in Stratigraphy*: New York (John Wiley), pp. 652-658.

Vail, R. P., Mitchum, R. M., and Thompson, S., 1977. Seismic stratigraphy and global changes in sea level, Part 4: global cycles of relative changes in sea level. *In* Plyton, C. E. (Ed.), *Seismic Stratigraphy*. Am. Assoc. Pet. Geol. Mem., 26:83-97.

Date of Initial Receipt: 6 March 1985
Date of Acceptance: 21 May 1985

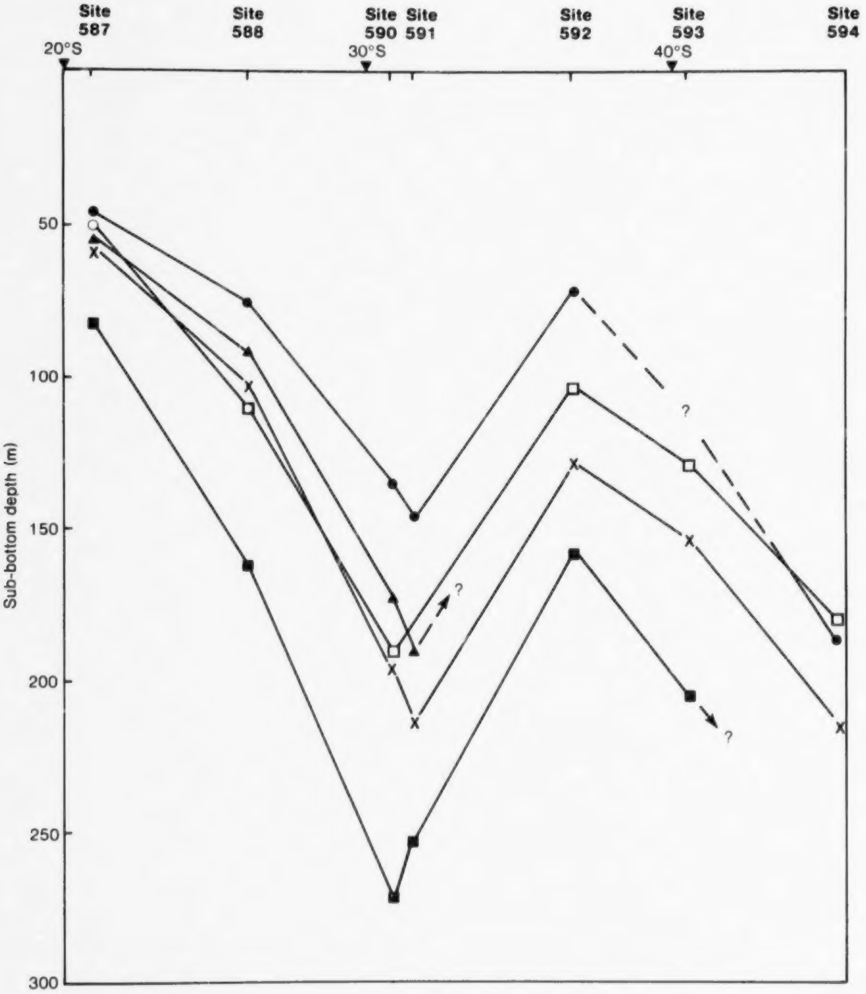

Figure 7. Occurrence of important calcareous nannoplankton and planktonic foraminiferal species about the Miocene/Pliocene boundary at Sites 587 through 594. ● = last occurrence of *Ceratolithus tricorniculatus*, ▲ = first occurrence of *C. rugosus*, X = last occurrence of *Discoaster quinqueramus*, ■ = first occurrence of *C. primus*, O = first occurrence of *Globorotalia tumida*, □ = last occurrence of *G. conomiozea*. Diagram not corrected to sedimentation rates.

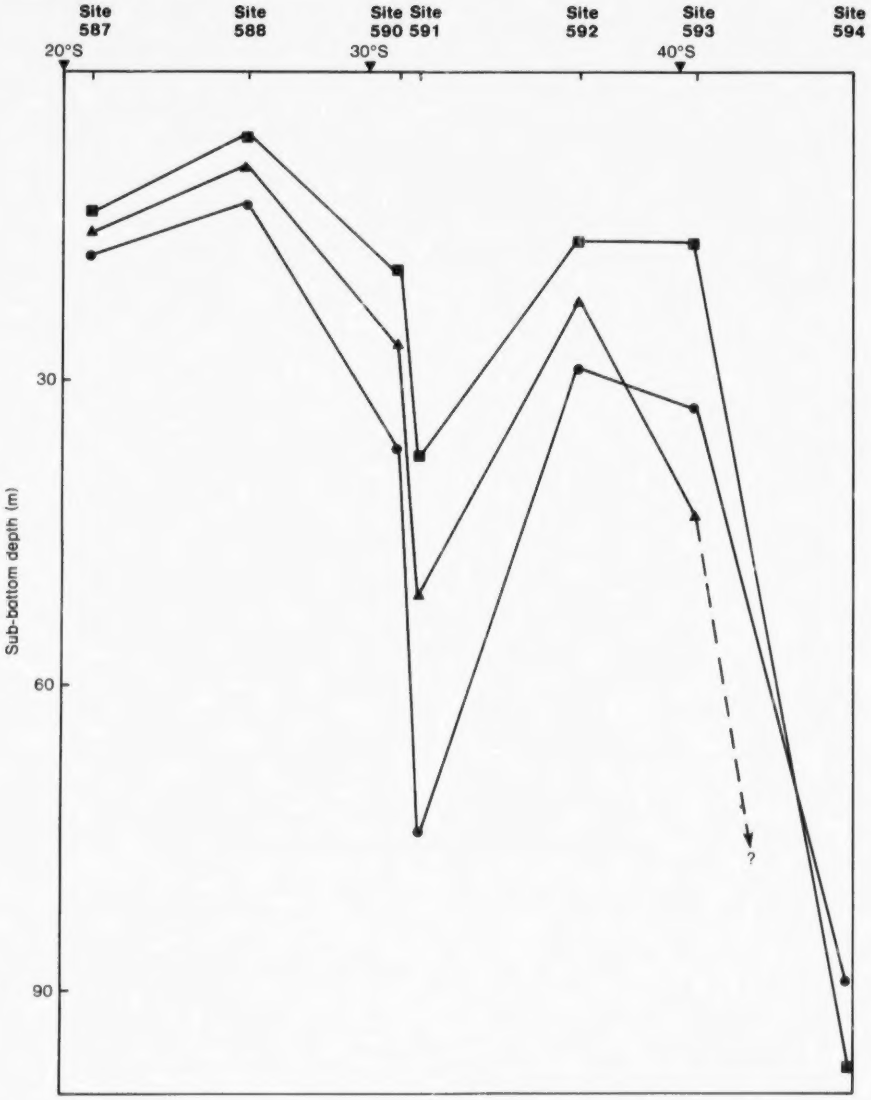

Figure 8. Occurrence of important calcareous nannoplankton and planktonic foraminiferal species about the Pliocene/Pleistocene boundary at Sites 587 through 594. ■ = last occurrence of *Cyclococcolithus macintyrei*, ▲ = last occurrence of *Discoaster brouweri*, ● = first evolutionary appearance of *Globorotalia truncatulinoides*. Diagram not corrected to sedimentation rates.

47. LITHOSTRATIGRAPHY OF DEEP SEA DRILLING PROJECT LEG 90 DRILL SITES IN THE SOUTHWEST PACIFIC: AN OVERVIEW[1]

Campbell S. Nelson, Department of Earth Sciences, University of Waikato[2]

ABSTRACT

Leg 90 recovered approximately 3705 m of core at eight sites lying at middle bathyal depths (1000–2200 m) (Sites 587 to 594) in a traverse from subtropical to subantarctic latitudes in the southwest Pacific region, chiefly on Lord Howe Rise in the Tasman Sea. This chapter summarizes some preliminary lithostratigraphic results of the leg and includes data from Site 586, drilled during DSDP Leg 89 on the Ontong-Java Plateau that forms the northern equatorial point of the latitudinal traverse.

The lithofacies consist almost exclusively of continuous sections of very pure (>95% $CaCO_3$) pelagic calcareous sediment, typically foraminifer-bearing nannofossil ooze (or chalk) and nannofossil ooze (or chalk), which is mainly of Neogene age but extends back into the Eocene at Sites 588, 592, and 593. Only at Site 594 off southeastern New Zealand is there local development of hemipelagic sediments and several late Neogene unconformities. Increased contents of foraminifers in Leg 90 sediments, notably in the Quaternary interval, correspond to periods of enhanced winnowing by bottom currents. Significant changes in the rates of sediment accumulation and in the character and intensity of sediment bioturbation within and between sites probably reflect changes in calcareous biogenic productivity as a result of fundamental paleoceanographic events in the region during the Neogene.

Burial lithification is expressed by a decrease in sediment porosity from about 70 to 45% with depth. Concomitantly, microfossil preservation slowly deteriorates as a result of selective dissolution or recrystallization of some skeletons and the progressive appearance of secondary calcite overgrowths, first about discoasters and sphenoliths, and ultimately on portions of coccoliths. The ooze/chalk transition occurs at about 270 m sub-bottom depth at each of the northern sites (Sites 586 to 592) but is delayed until about twice this depth at the two southern sites (Sites 593 and 594). A possible explanation for this difference between geographic areas is the paucity of discoasters and sphenoliths at the southern sites; these nannofossil elements provide ideal nucleation sites for calcite overgrowths. Toward the bottom of some holes, dissolution seams and flasers appear in recrystallized chalks.

The very minor terrigenous fraction of the sediment consists of silt- through clay-sized quartz, feldspar, mica, and clay minerals (smectite, illite, kaolinite, and chlorite), supplied as eolian dust from the Australian continent and by wind and ocean currents from erosion on South Island, New Zealand. Changes in the mass accumulation rates of terrigenous sediment and in clay mineral assemblages through time are related to various external controls, such as the continued northward drift of the Indo-Australian Plate, the development of Antarctic ice sheets, the increased desertification of the Australian continent after 14 m.y. ago, and the progressive increase in tectonic relief of New Zealand through the late Cenozoic.

Disseminated glass shards and (altered) tephra layers occur in Leg 90 cores. They were derived from major silicic eruptions in North Island, New Zealand, and from basic to intermediate explosive volcanism along the Melanesian island chains. The tephrostratigraphic record suggests episodes of increased volcanicity in the southwest Pacific centered near 17, 13, 10, 5 and 1 m.y. ago, especially in the middle and early late Miocene. In addition, submarine basaltic volcanism was widespread in the southeast Tasman Sea around the Eocene/Oligocene boundary, possibly related to the propagation of the Southeast Indian Ridge through western New Zealand as a continental rift system.

INTRODUCTION

This chapter highlights the general lithologic nature of Leg 90 deposits and also briefly comments on some other more specific items of lithologic interest in the cores. The intention has been to collate and summarize much of the lithostratigraphic information contained in several of the site chapters and specialist reports in this volume. A detailed discussion of specific topics has been avoided but I hope that there is sufficient information to direct the interested reader to relevant chapters and core materials.

Leg 90 is one of several complementary DSDP legs organized to study global paleoceanographic changes during the Cenozoic. Previous rotary drilling during DSDP Legs 21 and 29 (Burns, Andrews, et al., 1973; Kennett, Houtz, et al., 1975) demonstrated that the southwest Pacific region is optimal for the study of thick, relatively uncomplicated, and continuously deposited pelagic carbonate sequences of Neogene age between the equator and the subantarctic. Unlike in most other oceanic regions, shallow-water platforms extend latitudinally over vast distances, providing an opportunity for drilling into oceanic pelagic sediments at relatively shallow depths.

With this background as basis, DSDP Leg 90 successfully obtained a traverse of middle to late Cenozoic sections between subequatorial and subantarctic water masses at eight sites (Sites 587 to 594) in the southwest Pacific region (Fig. 1). An additional site (Site 586) was for logistical reasons drilled on Leg 89; it is included in the Leg 90 *Initial Report* because it forms the northern equatorial point of the latitudinal traverse. Together these sites collected sediments beneath every major surface water mass between the tropics and the subantarctic, permitting paleoceanographic records to be analyzed for each

---

[1] Kennett, J. P., von der Borch, C. C., et al., *Init. Repts. DSDP*, 90: Washington (U.S. Govt. Printing Office).

[2] Address: Dept. of Earth Sciences, University of Waikato, Private Bag, Hamilton, New Zealand.

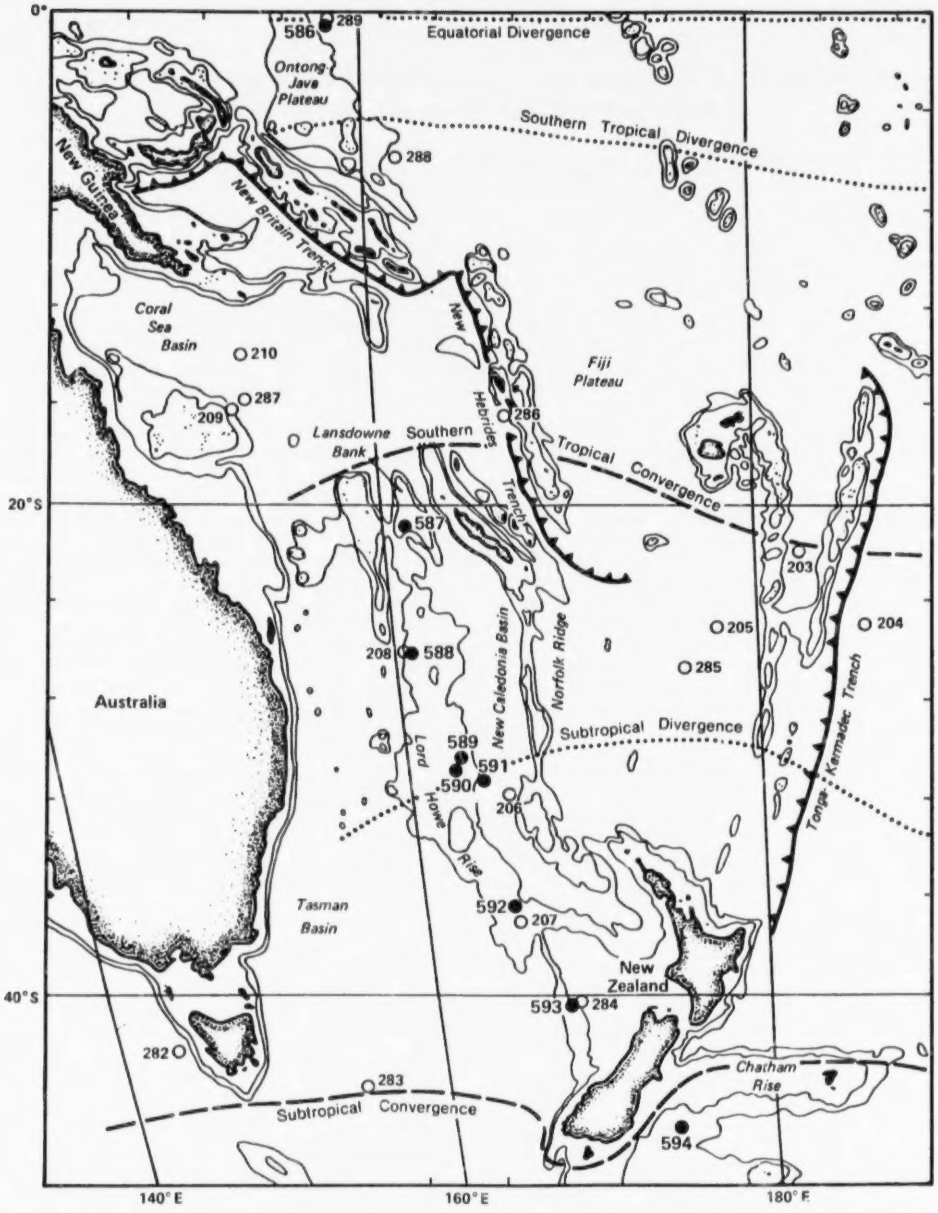
0°
586
289
Equatorial Divergence
Ontong-Java Plateau
Southern Tropical Divergence
288
New Guinea
New Britain Trench
Coral Sea Basin
210
287
209
Lansdowne Bank
Southern Tropical Convergence
New Hebrides Trench
286
Fiji Plateau
20°S
587
203
New Caledonia Basin
Norfolk Ridge
205
204
208
588
285
Australia
Subtropical Divergence
Tonga-Kermadec Trench
589
591
590
206
Lord Howe Rise
Tasman Basin
592
207
New Zealand
40°S
593
284
282
283
Chatham Rise
Subtropical Convergence
594
140° E
160° E
180° E

Figure 1. Location of Leg 90 drill sites (solid circles) and other DSDP sites (open circles) in the southwest Pacific region in relation to approximate positions of major surface water mass boundaries. Depth contours are for 1 and 2 km.

water mass. In addition, this distribution of sites allows correlation of sections across a wide range of latitudes. A vertical traverse of sediment from water depths of 1299 m (Site 590), 2131 m (Site 591), and 3196 m (Site 206 of Leg 21) was also recovered at the mid latitudes.

Leg 90 recovered 3705 m of core, the longest for any drilling leg. Average core recovery for the entire leg was about 90% of the drilled section except for the Chatham Rise site (Site 594), where only about 65% core recovery was achieved. Some drill site statistics are summarized in Table 1. Cores were obtained mainly with the hydraulic piston corer and extended core barrel systems (see introductory chapter, this volume), which provide sections of generally excellent quality with minimal core disturbance. The Leg 90 cores represent the most complete and coherent latitudinal traverse of Neogene sections from equator to subpole yet collected from the oceans.

All sites were drilled in middle bathyal water depths, from 1000 to 2200 m on submarine plateaus, which include Ontong-Java Plateau (Site 586) at the equator, Lord Howe Rise (Sites 587 to 592) and Challenger Plateau (Site 593) in the Tasman Sea, and southwestern

Table 1. Summary of Leg 90 drilling.

Hole	Latitude (S)	Longitude (E)	Water depth (m)	Penetration (m)	No. of cores	Meters cored	Meters recovered	Percentage recovered
586[a]	00°29.84′	158°29.89′	2207	44.4	5	39.3	38.98	99.2
586A[a]	00°29.84′	158°29.89′	2207	305.3	31	260.9	257.03	98.5
586B[a]	00°29.84′	158°29.89′	2207	240.3	25	240.3	234.93	97.8
586C[a]	00°29.84′	158°29.89′	2207	623.1	1	9.6	2.18	22.7
587	21°11.87′	161°19.99′	1101	147.0	17	147.0	88.81	60.4
588	26°06.70′	161°13.6′	1533	236.0	26	236.0	220.76	93.5
588A	26°06.70′	161°13.6′	1533	344.4	18	108.4	84.27	77.7
588B	26°06.70′	161°13.6′	1533	277.4	31	277.4	255.87	92.2
588C	26°06.70′	161°13.6′	1533	488.1	19	182.4	134.61	73.8
589	30°42.72′	163°38.39′	1391	36.1	4	36.1	35.08	97.2
590	31°10.02′	163°21.51′	1299	26.2	3	26.2	26.36	100.0
590A	31°10.02′	163°21.51′	1299	280.8	27	254.6	224.17	88.0
590B	31°10.02′	163°21.51′	1299	499.1	53	499.1	465.26	93.2
591	31°35.06′	164°26.92′	2131	283.1	31	283.1	278.21	98.3
591A	31°35.06′	164°26.92′	2131	284.6	30	284.6	233.15	81.9
591B	31°35.06′	164°26.92′	2131	500.4	24	229.8	130.86	56.9
592	36°28.40′	165°26.53′	1098	388.5	41	388.5	340.12	87.5
593	40°30.47′	167°40.47′	1068	571.5	60	571.5	468.21	81.9
593A	40°30.47′	167°40.47′	1068	496.8	27	257.3	227.71	88.5
594	45°31.41′	174°56.88′	1204	505.1	53	505.1	299.72	59.3
594A	45°31.41′	174°56.88′	1204	639.5	26	249.6	161.55	64.7
594B	45°31.41′	174°56.88′	1204	42.9	5	42.9	34.18	79.6

[a] For logistical reasons, Site 586 was cored on Leg 89.

Chatham Rise (Site 594) east of New Zealand. The sites lie well above the modern southwest Pacific lysocline depth of 2500 to 3500 m (Berger, 1976). Apart from Site 594 off southeastern New Zealand, the sediments are mainly free of turbidites and have received negligible inputs of terrigenous sediment.

SITE LITHOSTRATIGRAPHIES

Stratigraphic Logs

A variety of lithologic information for the nine drill sites in the southwest Pacific has been summarized on stratigraphic sections (Fig. 2). In addition to standard lithologic data, the figures include degree of sediment induration (soft, firm or stiff ooze, chalk, and recrystallized chalk); average sedimentation rates (m/m.y.) uncorrected for sediment porosity and calculated mainly from calcareous nannofossil zonal boundaries; the degree of sediment bioturbation; the state of preservation of planktonic foraminifers, benthic foraminifers, and calcareous nannoplankton and the relative abundance of pale green laminae representing altered tephra layers.

Lithostratigraphic Subdivisions

The lithostratigraphic succession at most sites is simple and they are broadly similar to one another (Figs. 2 and 3). The sections represent one correlatable lithostratigraphic unit that consists mainly of foraminifer-bearing nannofossil oozes (or chalks) and nannofossil oozes (or chalks) (Plates 1 and 2). This lithostratigraphic unit can be subdivided into as many as three subunits on the basis of color and degree of induration. The upper subunit is a thin (0.2 to 7.0 m thick) surficial zone of soft foraminifer-bearing or foraminifer–nannofossil ooze with a distinctive pale brown to orange color. The middle subunit is a thick (250 to 550 m), soft to firm, light gray to white, foraminifer-bearing nannofossil ooze or nannofossil ooze. The lower subunit consists of light gray to white chalk, compositionally similar to the middle ooze subunit. Diagenesis controls the downcore distinction among these subunits, from the upper oxidized to the middle and lower reduced subunits, and from the weakly lithified ooze of the middle subunit to the more indurated chalk of the lower subunit. Repetition of these zones at Sites 592 and 593 makes it necessary to define additional subunits.

Other lithostratigraphic units were defined for Leg 90 sections but they are of only local significance. These minor lithostratigraphic units include siliceous chalks at the bottom of Site 592, a sequence of volcanogenic turbidites at the bottom of Site 593, and a thick (169 m) succession of alternations of hemipelagic and pelagic oozes at the top of Site 594.

Unconformities

Calcareous nannofossil and planktonic foraminiferal biostratigraphy at Sites 586 through 593, supported by diatom and radiolarian biostratigraphy at Site 594, shows that all but two of the Neogene sections appear to be continuous (Fig. 3). Site 590 contains a 3 m.y. hiatus at the early/middle Miocene boundary. The section at Site 594 is interrupted by at least four unconformities, including a 2 m.y. gap in the middle late Miocene, and a 1 m.y. hiatus at the Miocene/Pliocene boundary, another between the early and late Pliocene, and another within the early Quaternary. None of these unconformities shows a lithologic expression.

Only three Leg 90 sites were drilled deep enough to potentially encounter the well-documented Paleogene–Neogene regional unconformity (Kennett et al., 1975). The unconformity was recovered at Sites 588 and 592, where it represents an hiatus of about 19 m.y. (from middle Eocene to late Oligocene) and 15 m.y. (from early Oligocene to late early Miocene), respectively. However, the unconformity is absent from Site 593 on Challenger Plateau, suggesting that the bottom currents that eroded

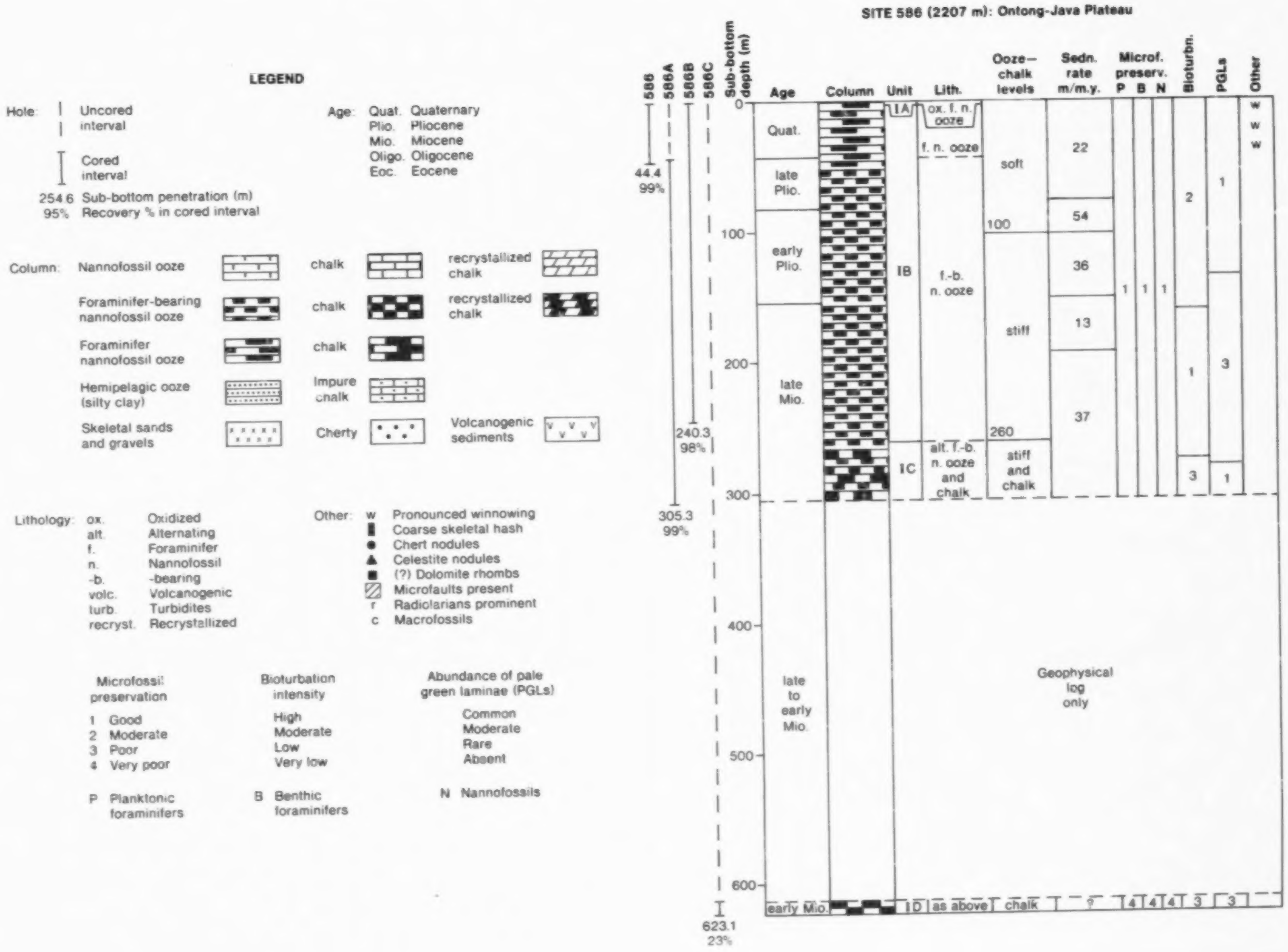

SITE 586 (2207 m): Ontong-Java Plateau
586
586A
586B
586C
Sub-bottom depth (m)
Age
Column
Unit
Lith.
Ooze–chalk levels
Sedn. rate m/m.y.
Microf. preserv. P B N
Bioturbn.
PGLs
Other
0
100
200
300
400
500
600
44.4
99%
240.3
98%
305.3
99%
623.1
23%
Quat.
late Plio.
early Plio.
late Mio.
late to early Mio.
early Mio.
IA
IB
IC
ID
ox. f. n. ooze
f. n. ooze
f.-b. n. ooze
alt. f.-b. n. ooze and chalk
as above
soft
100
stiff
260
stiff and chalk
chalk
22
54
36
13
37
?
1 1 1
4 4 4
2
1
3
3
1
3
1
3
w w w
Geophysical log only
LEGEND
Hole:
Uncored interval
Cored interval
254.6 Sub-bottom penetration (m)
95% Recovery % in cored interval
Age:
Quat. Quaternary
Plio. Pliocene
Mio. Miocene
Oligo. Oligocene
Eoc. Eocene
Column:
Nannofossil ooze
Foraminifer-bearing nannofossil ooze
Foraminifer nannofossil ooze
Hemipelagic ooze (silty clay)
Skeletal sands and gravels
chalk
chalk
chalk
Impure chalk
Cherty
recrystallized chalk
recrystallized chalk
Volcanogenic sediments
Lithology:
ox. Oxidized
alt. Alternating
f. Foraminifer
n. Nannofossil
-b. -bearing
volc. Volcanogenic
turb. Turbidites
recryst. Recrystallized
Other:
w Pronounced winnowing
Coarse skeletal hash
Chert nodules
Celestite nodules
(?) Dolomite rhombs
Microfaults present
r Radiolarians prominent
c Macrofossils
Microfossil preservation
1 Good
2 Moderate
3 Poor
4 Very poor
Bioturbation intensity
High
Moderate
Low
Very low
Abundance of pale green laminae (PGLs)
Common
Moderate
Rare
Absent
P Planktonic foraminifers
B Benthic foraminifers
N Nannofossils

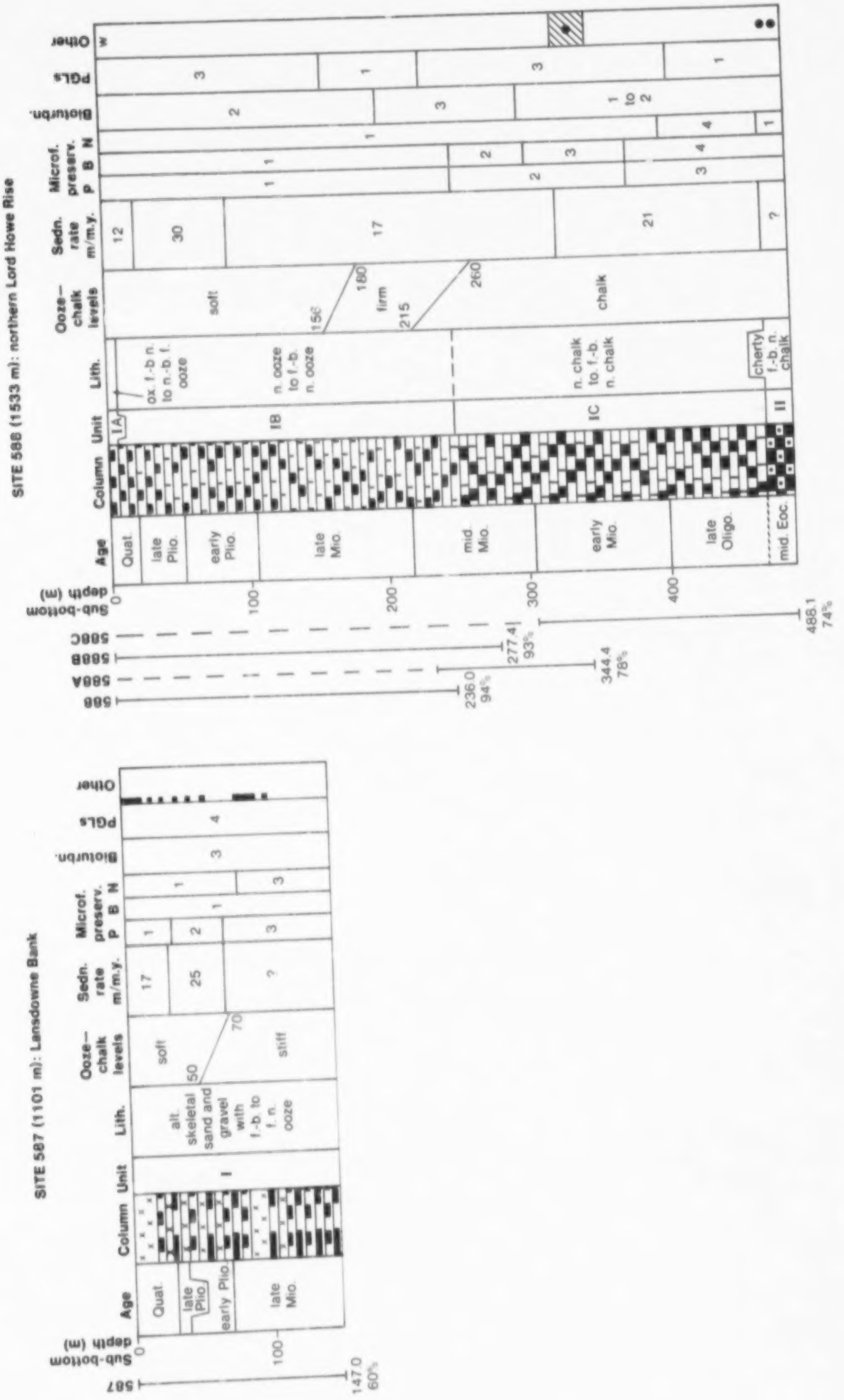

Figure 2. Summary stratigraphic logs for Leg 90 drill sites.

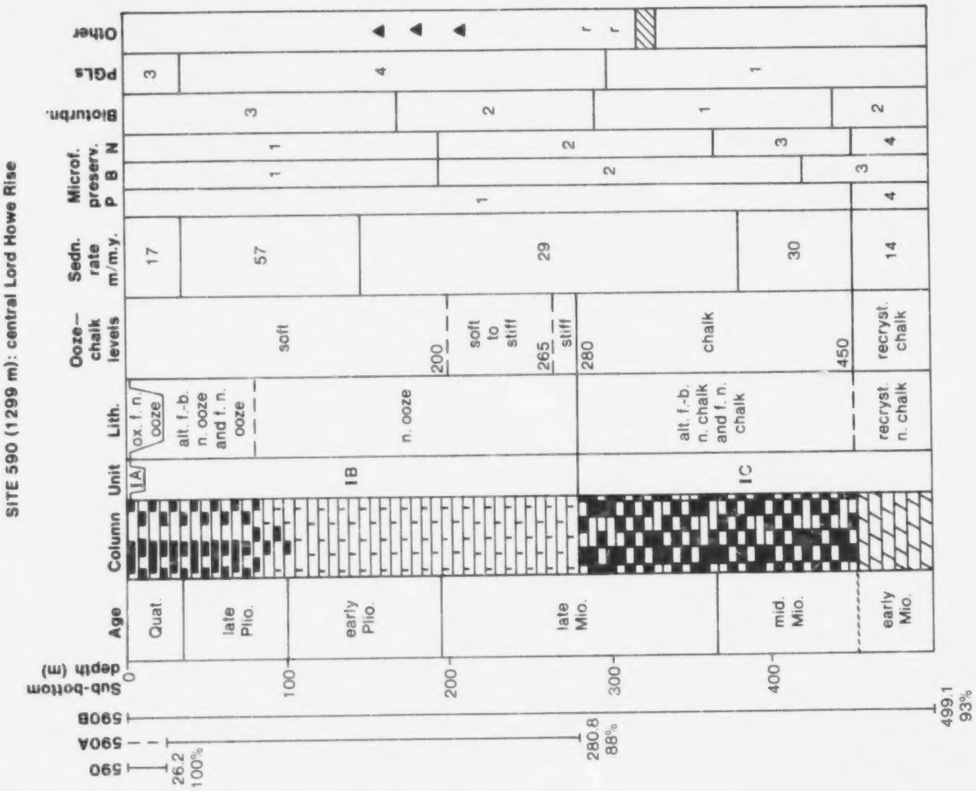
SITE 590 (1299 m): central Lord Howe Rise
590
590A
590B
26.2
100%
280.8
88%
499.1
93%
Sub-bottom depth (m)
0
100
200
300
400
Age
Quat.
late Plio.
early Plio.
late Mio.
mid. Mio.
early Mio.
Column
Unit
IA
IB
IC
Lith.
ox. f. n. ooze
alt. f.-b. n. ooze and f. n. ooze
n. ooze
alt. f.-b. n. chalk and f. n. chalk
recryst. n. chalk
Ooze–chalk levels
soft
200
soft to stiff
265
stiff
280
chalk
450
recryst. chalk
Sedn. rate m/m.y.
17
57
29
30
14
Microf. preserv. P B N
1
4
1
2
3
2
3
4
Bioturbn.
3
2
1
2
PGLs
3
4
1
Other
r
r

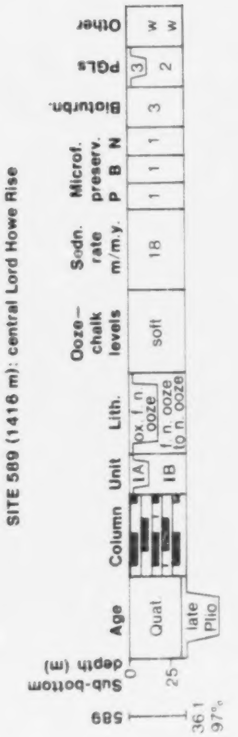
SITE 589 (1416 m): central Lord Howe Rise
589
36.1
97%
Sub-bottom depth (m)
0
25
Age
Quat.
late Plio.
Column
Unit
IA
IB
Lith.
ox. f. n. ooze
f. n. ooze to n. ooze
Ooze–chalk levels
soft
Sedn. rate m/m.y.
18
Microf. preserv. P B N
1
1
1
Bioturbn.
3
PGLs
3
2
Other
w
w

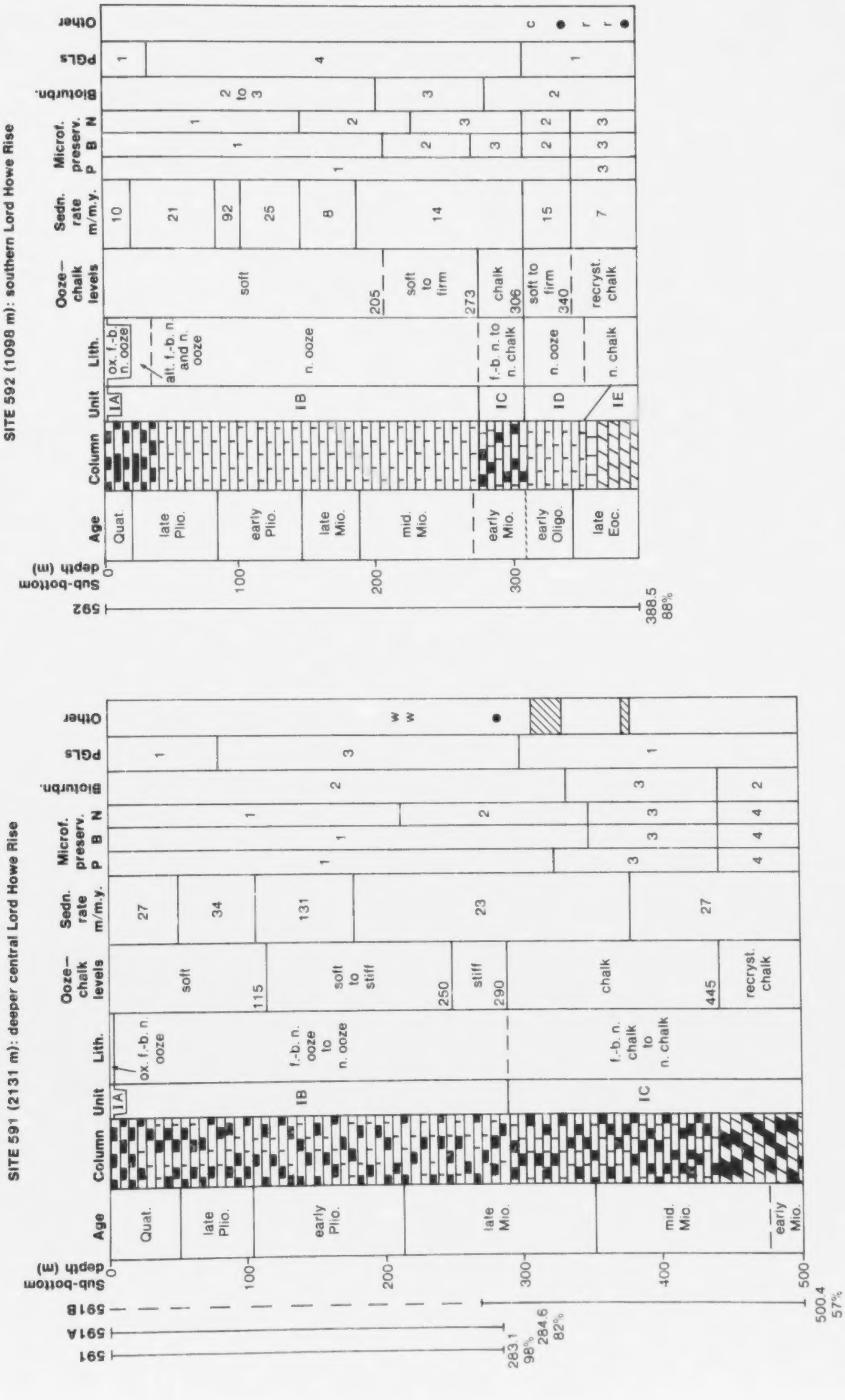
SITE 592 (1098 m): southern Lord Howe Rise
592
388.5
88%
Sub-bottom depth (m)
0
100
200
300
Age
Column
Unit
Lith.
Ooze–chalk levels
Sedn. rate m/m.y.
Microf. preserv. P B N
Bioturbn.
PGLs
Other
Quat.
late Plio.
early Plio.
late Mio.
mid. Mio.
early Mio.
early Oligo.
late Eoc.
IA
IB
IC
ID
IE
ox. f.-b. n. ooze
alt. f.-b. n. and n. ooze
n. ooze
f.-b. n. to n. chalk
n. ooze
n. chalk
soft
205
soft to firm
273
chalk
306
soft to firm
340
recryst. chalk
10
21
92
25
8
14
15
7
1
2
3
2 to 3
4
c
r
SITE 591 (2131 m): deeper central Lord Howe Rise
591
591A
591B
283.1
98%
284.6
82%
500.4
57%
0
100
200
300
400
500
Quat.
late Plio.
early Plio.
late Mio.
mid. Mio.
early Mio.
IA
IB
IC
ox. f.-b. n. ooze
f.-b. n. ooze to n. ooze
f.-b. n. chalk to n. chalk
soft
115
soft to stiff
250
stiff
290
chalk
445
recryst. chalk
27
34
131
23
27
4
w
w

Figure 2. (Continued).

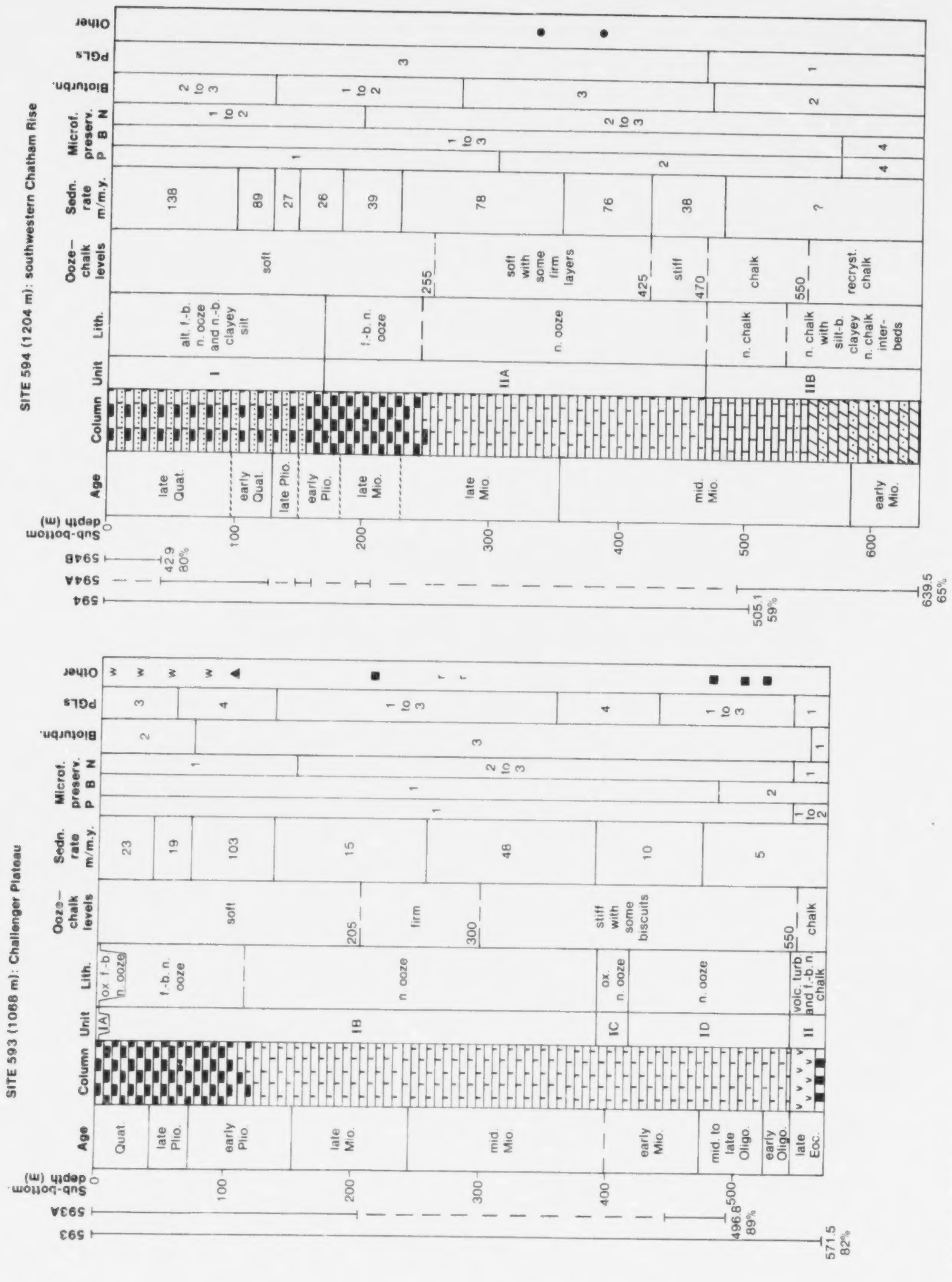

Figure 2. (Continued).

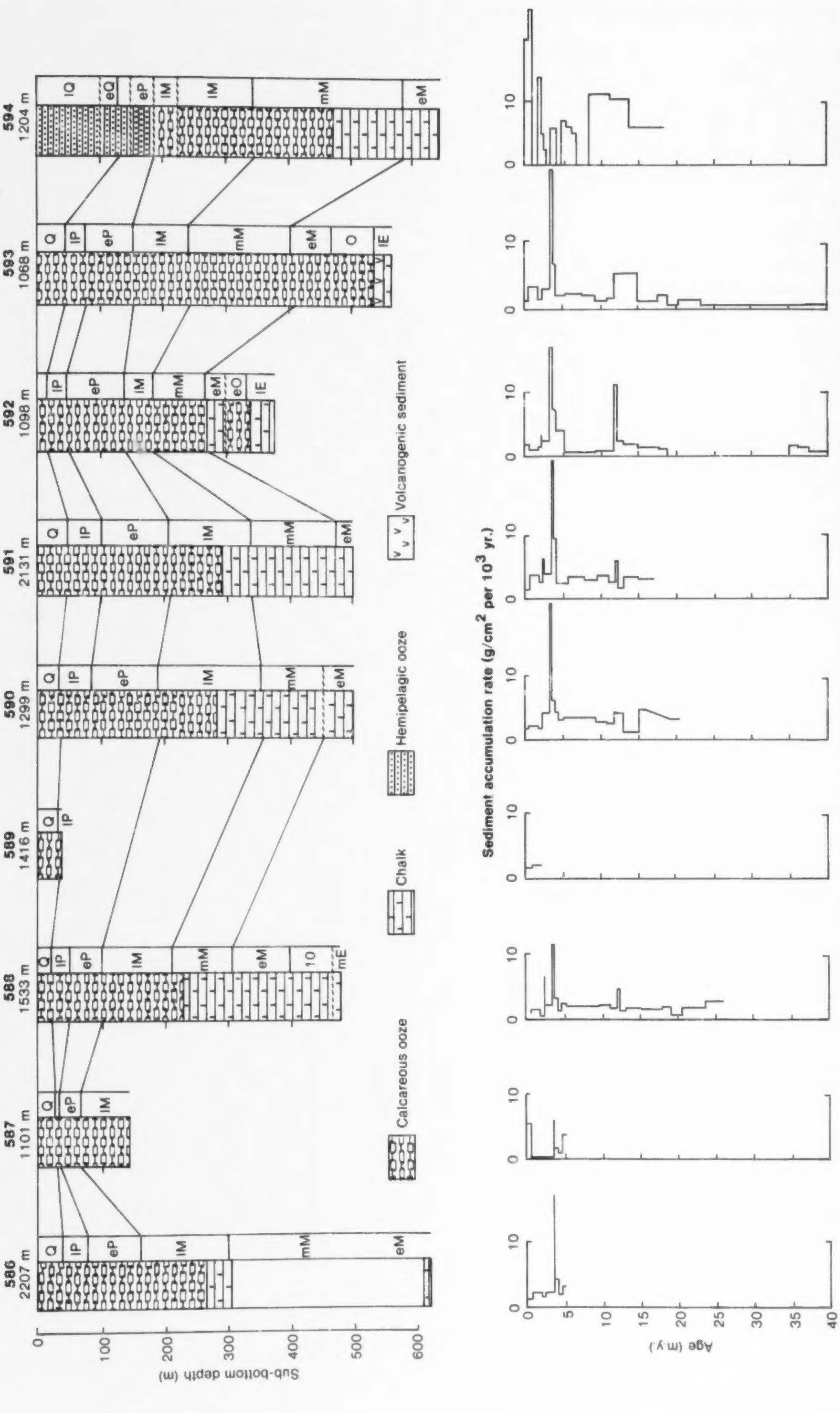

Figure 3. Schematic sections showing the relationships between bulk lithology, ages, and mass accumulation rates of sediments at Leg 90 drill sites. Q = Quaternary, P = Pliocene, M = Miocene, O = Oligocene, E = Eocene. l = late, m = middle, e = early.

the regional hiatus in Tasman Sea did not extend that far to the east.

MAJOR LITHOLOGIES

Calcareous Oozes and Chalks

Almost all sediment cored on Leg 90 is light-colored calcareous ooze or its more lithified equivalent, chalk (Table 2; Plates 1 and 2). Munsell sediment colors are typically white (N9), very light gray (N8), or light gray (N7), sometimes with subtle bluish (5B 7/1 to 5B 9/1) or greenish (5GY 7/1) tones. Skeletal material is completely dominated by calcareous nannofossils, with variable but small (<5%) to moderate (5–25%) quantities of foraminifers, so that the sediment is mainly nannofossil ooze (chalk) or foraminifer-bearing nannofossil ooze (chalk). Foraminifer-bearing nannofossil oozes (chalks) are more prevalent at the northern sites (Sites 586 to 591), and nannofossil oozes (chalks) prevail at the southern sites (Sites 592 to 594). Higher contents (25–50%) of foraminifers occasionally occur and are associated with periods of intensified winnowing by bottom currents (Gardner, Dean, et al.; Stein and Robert; both this volume). Winnowing is especially evident in the Quaternary interval at several sites where alternating sequences of foraminifer and foraminifer-bearing nannofossil oozes are developed. Minor amounts of other calcareous microfossils, including dinoflagellates (calcispheres), ostracodes, and pteropods locally occur in the calcareous pelagic sediment.

The calcium carbonate contents of Leg 90 oozes and chalks range from about 90 to 98% (Gardner, Dean, et al.; Stein and Robert; both this volume). The small quantities of acid-insoluble material in the sediments are composed of terrigenous grains, some siliceous biogenic skeletons, and minor authigenic minerals. The terrigenous material includes quartz, feldspar, clay minerals, volcanic glass, mica, and very rare ferromagnesian minerals.

With the exception of some of the glass shards, which can range in size up to fine sand (Nelson, Froggatt, et al., this volume), the siliciclastic components are silt- and clay-sized. The grain-size distribution of the siliciclastic silt remained very similar (modal size about 18 μm or medium silt) at all Lord Howe Rise silts throughout the Neogene. This silt, dominated by quartz and feldspar, was supplied mainly as eolian dust from the Australian continent (Stein and Robert, this volume). Distinct peaks in the mass accumulation rates of the terrigenous sediment occur in the middle Miocene (14 m.y.), latest Miocene (7–5 m.y.), and early Pliocene (4–3 m.y.) from Lord Howe Rise. These increases in mass accumulation rate are interpreted by Stein and Robert (this volume) to be the result of enhanced atmospheric circulation during maximum phases of aridity on the Australian continent, more or less coincident with major global cooling events. The terrigenous silt mode at Site 594 is commonly coarser (30–50 μm) than on Lord Howe Rise because the site is close to New Zealand. The silt at Site 594 is dominated by chlorite, muscovite, and quartz, with lesser amounts of feldspar, reflecting the wide distribution of low-rank metamorphic rocks in South Island (Jarrett, 1985).

Table 2. Percentage occurrence of different lithologies in sections drilled at Leg 90 sites.

Site	Sub-bottom depth (m)	Pelagic calcareous oozes	Pelagic chalks	Hemipelagic oozes	Skeletal sands and gravels
586	305.3	92	8	—	—
587	147.0	80	—	—	20
588[a]	488.1	51	45	—	—
589	36.1	100	—	—	—
590	499.1	56	44	—	—
591	500.4	58	42	—	—
592	388.5	82	18	—	—
593[b]	571.5	95	2	—	—
594[c]	639.5	47	26	26	—

[a] Sediments also include 4% siliceous chalks.
[b] Sediments also include 3% volcanogenic turbidites.
[c] Sediments also include 1% chalk turbidites.

Trace quantities of volcanic shards are the most ubiquitous of all terrigenous components in Leg 90 sediments and may dominate the minor siliciclastic silt (to fine sand) fraction over thick sections of core (Gardner, Nelson, et al., this volume). Colorless shards dominate, but yellowish shards occur in several of the early Neogene sections, especially on northern Lord Howe Rise. It is likely that the shards were dispersed through the sediment by bioturbation. The tephras originated from explosive volcanic activity in North Island, New Zealand, and along the Melanesian island chains in the southwest Pacific (see section on tephras, later).

The siliciclastic clay fraction (<2 μm) of Leg 90 sediments is dominated by clay minerals with some quartz, feldspar, and zeolites (Stein and Robert; Robert et al.; both this volume; Jarrett, 1985). Smectites are the most abundant clay minerals (typically 30–100%), with illite (0–45%), kaolinite (0–35%), chlorite (0–35%), and irregular mixed-layer clays (0–20%) making up a smaller component. Despite some chemical modification during burial diagenesis, especially of smectite, the clays are primarily of detrital origin, transported by winds and ocean currents from Australia (Sites 587 to 593) and New Zealand (Sites 592 to 594) (Stein and Robert; Robert et al., this volume). The strong influence of a detrital supply of clays from New Zealand at southern sites is suggested by the occurrence of small amounts of stilpnomelane, a diagnostic accessory mineral in South Island schists. Stilpnomelane is found in sediment from the middle Miocene to Quaternary at Sites 593 and 594, and in Quaternary sediment at Site 592 (Robert et al., this volume).

At least three morphologic varieties of smectite occur in the sediments, suggesting it has different origins (Stein and Robert; Robert et al.; both this volume). Fleecy particles, of probable pedogenic detrital origin, are rare and restricted to the youngest cores. The dominant smectite variety occurs as very fine, delicate laths, sometimes grouped in distinctive geometric figures. The laths are only occasionally present in Quaternary and Pliocene ooze, but become especially abundant in Miocene and

Paleogene sediment. The fine laths are interpreted by Stein and Robert (this volume) as having formed from the *in situ* recrystallization of (fleecy) detrital smectites in the sediment. It is also possible that a proportion of this smectite was neoformed in association with the selective dissolution of calcareous microfossil components during burial diagenesis, in the manner described by Marchig and Rösch (1983). The third smectite variety is thick laths or globular packs of fine laths that formed from the alteration of volcanic components. This volcanogenic smectite is most evident in sediment that is relatively enriched in glass shards or that contains greenish gray laminae of devitrified volcanic ash (see section on tephras, later).

Variations in the relative proportions of the different clay mineral species through time are related by Stein and Robert and Robert et al. (both this volume) to important changes in the locations and relief of landmasses, as well as to climatic conditions and patterns of ocean circulation. For example, at Sites 588 to 591 on northern Lord Howe Rise, the gradual increases in the content of illite and kaolinite at the expense of smectite in sediment younger than middle Miocene (~14 m.y.) resulted from the onset and southward expansion of desertification in Australia, together with the continued northward drift of that continent into more tropical latitudes. At Sites 592 to 594, nearer to New Zealand, the sudden and progressive increase of illite and chlorite at the expense of smectite after the end of the Oligocene occurred at the same time that the boundary between the Indo-Australian and Pacific plates in its present form (the Alpine Fault Zone) propagated through New Zealand and generated significant topographic relief. Moreover, the evolution from a predominantly oblique strike-slip boundary to an increasingly compressive one from the late Miocene onwards (the Kaikoura Orogeny) coincided with the period when smectite rapidly disappeared from the clay mineral record. The clay mineral evolution with time is very similar to that recorded by Nelson and Hume (1977) from New Zealand Cenozoic sequences on land.

Biosiliceous material is typically rare or absent in Leg 90 sediments. Biogenic components consist of radiolarians, sponge spicules, diatoms, silicoflagellates, and ebridians. Small amounts of siliceous microfossils persist throughout the sections at subantarctic Site 594 and the two deeper-water sites (Sites 586 and 591). The scarcity of biosiliceous material in Neogene sediments at all other Lord Howe Rise sites is surprising considering the relatively fast sediment accumulation rates, which suggest high productivity. The lack of siliceous biogenic components may be the result of postdepositional dissolution of opaline silica at the sea bed, possibly associated with the impingement of silica-undersaturated Antarctic Intermediate Waters onto the Rise (Gardner, Nelson, et al., this volume). The more consistent occurrence of siliceous microfossils in the Paleogene chalks on Lord Howe Rise (see also Burns, Andrews et al., 1973) suggests that an equivalent intermediate water mass was not developed at that time.

Hemipelagic Oozes

Because Site 594 is close to the South Island of New Zealand, sedimentation at the site has been influenced by both oceanic and terrigenous processes (Table 2). In particular, the topmost 169 m of Pliocene and Quaternary ooze includes a significant amount of silt- and clay-sized terrigenous material, dominantly chlorite, quartz, muscovite, feldspar, and illite, delivered to the site by prevailing westerly winds and ocean currents from the uplifted schist-dominated mountain chains of South Island (Griggs et al., 1983; Jarrett, 1985; Nelson, Hendy, Cuthbertson, et al., this volume). In detail, this section contains many fluctuations of hemipelagic and impure pelagic lithofacies that are evident from color changes in the core and calcium carbonate stratigraphy (Fig. 4; Nelson, Hendy, Cuthbertson, et al., this volume). The hemipelagic sediments are typically greenish gray (5G 6/1) nannofossil-bearing clayey silts, rich in mica and quartz, often having diatoms and sponge spicules (Plate 1, Fig. 2). The $CaCO_3$ contents in the hemipelagic sediments range from 0 to 25%. In contrast, the pelagic interbeds are mainly bluish gray (5B 7/1) foraminifer-bearing nannofossil oozes with reduced but variable amounts of terrigenous material and only trace quantities of biosiliceous components. The $CaCO_3$ contents of these sediments range between 50 and 80%. Oxygen isotope analyses (Fig. 4; Nelson, Hendy, Cuthbertson, et al., this volume) confirm that the hemipelagic sediment accumulated during lowered eustatic sea level of glacial periods and that the impure pelagic sediment was deposited during times of high eustatic sea level of interglacial periods. The history of alpine glaciations and associated erosion in South Island, represented by the hemipelagic oozes, can be correlated via isotope stages with the major fluctuations of Northern Hemisphere ice sheets (e.g., Imbrie et al., 1985). The existence of strong 100, 41, and 23 × 10^3 yr. (Milankovitch) cycles in the carbonate and isotope records of this high-accumulation section (Nelson et al., 1984) makes it valuable for very detailed study of late Quaternary climate changes.

MINOR LITHOLOGIES

Skeletal Sands and Gravels

At least 20% of the recovered section at Site 587 on Lansdowne Bank, northernmost Lord Howe Rise, consists of yellowish to pinkish gray coarse-grained skeletal carbonate debris with silty sand, sand, sandy gravel, or gravel textures. These sediments occur in massive or normally graded beds, less than 1 to 2 m thick, that alternate with a dominant lithofacies of foraminifer (-bearing) nannofossil ooze. Many of the sediment components in the coarse interbeds are of shallow-marine origin and include broken and/or abraded tests of large benthic foraminifers, fragments of calcareous red and green algae (including *Halimeda*), corals, bryozoans, and echinoderm material, and carbonate lithoclasts of chalk and skeletal packstone and wackestone. They represent re-

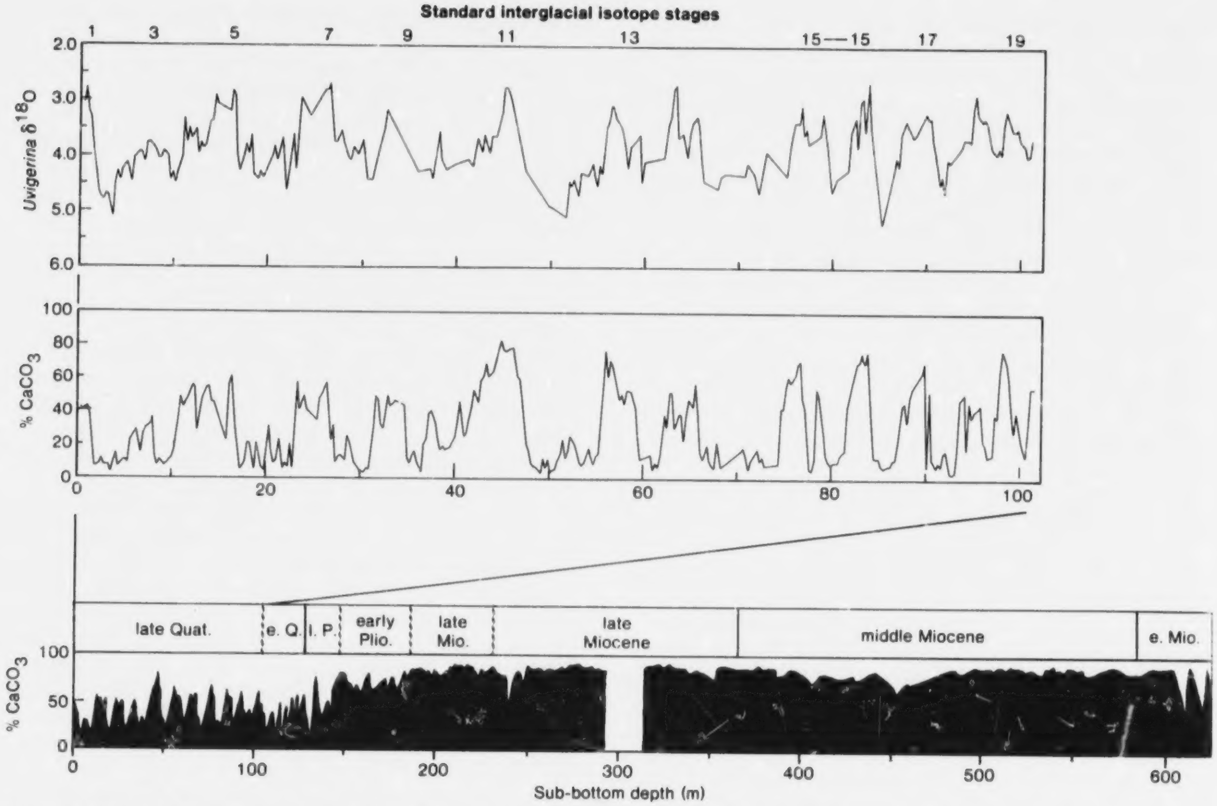

Figure 4. Calcium carbonate stratigraphy at Site 594, southeastern New Zealand (from Jarrett, 1985), including high-resolution carbonate and benthic foraminiferal (*Uvigerina* sp.) oxygen isotope stratigraphies for the top 100 m of section (from Nelson, Hendy, et al., this volume). Note that (1) the calcareous oozes and chalks are generally less pure (80–90%) than most other Leg 90 calcareous sediments because the site is close to New Zealand (increased terrigenous content) and in subantarctic waters (increased biosiliceous material); (2) fluctuating $CaCO_3$ values in the late early Miocene are due to interbeds of impure chalk turbidites; (3) the overall decrease in $CaCO_3$ content after the latest Miocene (~6 m.y.) corresponds to the Kaikoura Orogeny, with progressive elevation of the New Zealand Southern Alps along the Alpine Fault zone; (4) the drop in $CaCO_3$ content in the late Pliocene (~3 m.y.) may correlate with the oldest known late Cenozoic glacial sediments (the Ross glacial deposits) on South Island and the onset of the Northern Hemisphere Ice Age; and (5) the cyclic alternations of high-carbonate impure pelagic oozes and low-carbonate hemipelagic oozes in the late Quaternary correspond to fluctuating interglacial and glacial episodes, respectively, indicated by the isotope record. Standard interglacial isotope stages tentatively identified on the isotope record are discussed by Nelson, Hendy, et al. (this volume).

worked and redeposited sediment derived from the photic zone of nearby banks and transported downslope, possibly during low stands of sea level. Surficial and buried channels are seen on the seismic profile near Site 587.

Siliceous Chalks

Siliceous sediment is extremely rare in Leg 90 cores, but isolated chert nodules were recovered from a few stratigraphic levels at Sites 588, 591, 592, and 594 (Fig. 2). The chalk from the bottom 19 m of Site 588 includes common siliceous material, mainly sponge spicules, diatoms, and diagenetic chert (Plate 2, Fig. 3), and the chalk at the base of Site 592 contains rare radiolarians and chert nodules. The cherty beds at Sites 588 and 592 are both Eocene and lie below the regional unconformity that represents a significant portion of the Paleogene succession. The siliceous lithologies and chronostratigraphies are identical to those recorded at Sites 206 to 210, drilled in the Tasman and Coral seas on DSDP Leg 21 (Burns, Andrews, et al., 1973; van der Lingen et al., 1973).

Chalk Turbidites

Below about 534 m sub-bottom and continuing to the bottom (640 m) of the section at Site 594, the otherwise relatively pure nannofossil chalks of late early to early middle Miocene age include occasional conspicuous "chocolate-colored" (olive gray 5Y 4/1) interbeds of silt-bearing clayey nannofossil chalk that are sometimes sponge-spicule-bearing (Figs. 2 and 4). The terrigenous components of the interbeds are common mica and clay minerals (illite and smectite), some quartz, and feldspar. This mineralogy is broadly similar to the siliciclastic mineralogy of the Pliocene–Quaternary hemipelagic oozes at the top of the section. Individual interbeds have sharp erosional bases, range in thickness from a few to 90 cm, and are normally graded from medium to very fine silty and eventually clay-dominated and bioturbated sediment which passes imperceptibly into overlying chalk containing reworked microfaunas. The sedimentary structures suggest that these impure chalk interbeds are turbidites. A pronounced habitat stratification of infaunal burrow types occurs in the upper portion of the thicker beds, with Planolites between 0 and about 5 cm down, Chondrites below to depths of 10 cm, and Zoophycos to depths of 15 to 20 cm in the bed (Nelson, this volume, Plate 1, Figs. 11, 12), similar to that reported elsewhere for the burrowed tops of turbidite deposits (Seilacher, 1978).

The impure chalk turbidites may record an early Neogene phase of active fan progradation into the head of the Bounty Trough (Carter and Carter, 1984). Tectonic movements and erosion occurred on nearby South Island of New Zealand, so that periodically large volumes of fine terrigenous sediment were supplied to the area of Site 594.

Volcanogenic Turbidites

The only noncarbonate lithostratigraphic unit drilled on Leg 90 was a 16.4 m section of thinly bedded, grayish black (N2) to grayish green (10G 4/2), lithified volcanogenic sandstone, mudstone, and occasional breccia at the bottom of Site 593, Challenger Plateau, southern Tasman Sea (Nelson, Briggs, et al., this volume). The sequence was rapidly emplaced at bathyal depths at about the time of the Eocene/Oligocene boundary, 37 to 36 m.y. ago. Late Eocene nannofossil chalk occurs below, and early Oligocene nannofossil ooze is found above the volcanogenic unit. It comprises at least 35 sharp-based and normally graded volcanogenic sandstone–mudstone couplets or turbidites, each typically 20–50 cm thick and with common Bouma A, B, and E divisions. Rarer thick beds of massive or inversely graded, unsorted breccia were probably deposited from highly concentrated laminar suspensions resembling debris flows. The turbidites and debris flows almost certainly originated on the slopes of "Lalitha pinnacle," a now-buried volcanic shield 500 m high (av. 6–8° slopes), situated only a few kilometers from Site 593. A variety of evidence supports a basaltic origin for the sequence, but the basic glassy components that form the bulk of the deposits have been pervasively palagonitized and replaced by phillipsite, smectite, and calcite as a result of low-temperature oxidative alteration by pore fluids, presumably during early diagenesis. Seismic evidence indicates that buried volcanoes of similar character and age to "Lalitha pinnacle" are widespread on southern Lord Howe Rise and Challenger Plateau, suggesting a significant period of submarine basaltic volcanism in the southeast Tasman Sea region about 37 m.y. ago. Nelson, Briggs, et al. (this volume) view the volcanic activity as off-rift volcanism related to regional extension and formation of a major continental rift system through western New Zealand in the late Eocene–early Oligocene. These tectonic adjustments were the result of the eastward propagation of the Southeast Indian Ridge into the south Tasman Sea and through the New Zealand subcontinent. Analogous occurrences of submarine Eocene–Oligocene basalts east of the rift system now crop out on land in eastern South Island, New Zealand.

Tephras

Megascopic Vitric Tephras

Explosive volcanism has characterized large areas of the southwest Pacific region throughout the late Cenozoic (Churkin and Packham, 1973; Coleman and Packham, 1976) and so it is not surprising that glass shards are ubiquitous in the sediment at most sites drilled on Leg 90. The stratigraphic occurrence of glass shards in smear slides of sediments for five sites on Lord Howe Rise has been summarized by Gardner, Nelson, et al. (this volume). The shards typically occur in trace amounts ($<1\%$) only and are mainly dispersed through the sediment, probably by bioturbation of thin ash layers. Careful processing of channel samples from cores may ultimately provide a useful tephrostratigraphy based on the frequency distribution of this dispersed volcanic glass fraction.

Occasional discrete, 1–10 cm thick layers of glass-dominated tephra occur in the cores. Eighteen of these megascopic tephras have been studied in detail by Nelson, Froggatt, et al. (this volume). The majority are silicic (75 to 78% SiO_2), with abundant clear glass shards and a biotite ± hypersthene ± green hornblende ferromagnesian mineralogy. The megascopic tephras were derived from Miocene through Quaternary eruptions in North Island, New Zealand. Several of the Quaternary silicic tephras can be correlated to one another, and at least two can be matched to the widespread on-land Mt. Curl tephra (~ 0.25 m.y. ago), with a probable source in Lake Taupo. The occurrence of North-Island-derived tephras in central and northern Lord Howe Rise sites suggests that ash normally transported eastward into the Pacific by the prevailing westerly airflow across New Zealand may also be diverted northwest and west on entering the Southeast Trade wind belt to be deposited ultimately in the Tasman Sea region. Moreover, the occurrence of correlative silicic tephras up to 3500 km apart at sites on northern Lord Howe Rise (Sites 588 to 591) and off eastern South Island (Site 594) is evidence of occasional exceptionally large eruptions. Nelson, Foggatt, et al. (this volume) have suggested that some ash in the eruptive column ascended above 20 km altitude and may have been directly carried toward the Tasman Sea by stratospheric winds, while coeval lower-level ash drifted east of New Zealand into the southern Pacific Ocean.

Only three of the megascopic tephras analyzed were nonsilicic. They occur in Neogene sediments at northern sites (Sites 586 to 588) and are composed of altered (partially devitrified and pyritized) basic shards and common labradorite crystals derived from explosive basaltic to andesitic volcanism at nearby ocean island or ridge sources, probably in the Ontong-Java Plateau and Vanuatu regions. Considering that basic to intermediate volcanic activity overwhelmingly preponderates in the southwest Pacific, notably along the volcanic island chains of the Melanesian Borderland at the boundary between the Indo-Australian and Pacific plates (Coleman and Packham, 1976), the apparent paucity of more basic tephras in Leg 90 sediments appears at first to be anomalous. The situation may be explainable by the occurrence of pale green layers in the sediments.

Pale Green Laminae

During the shipboard descriptions of the calcareous oozes and chalks on Leg 90, numerous pale green laminations (PGLs) were noted to recur persistently throughout long intervals of many cores (Fig. 2). The laminae are isolated or occur in composite sets, are typically 0.5 to 2 mm thick, are horizontal or nearly so, and commonly are associated with underlying concentrations of iron sulfides. The stratigraphic distribution and origin of PGLs at Lord Howe Rise sites are discussed in detail by Gardner, Nelson, et al. (this volume) and their composite PGL stratigraphy is summarized here in Figure 5.

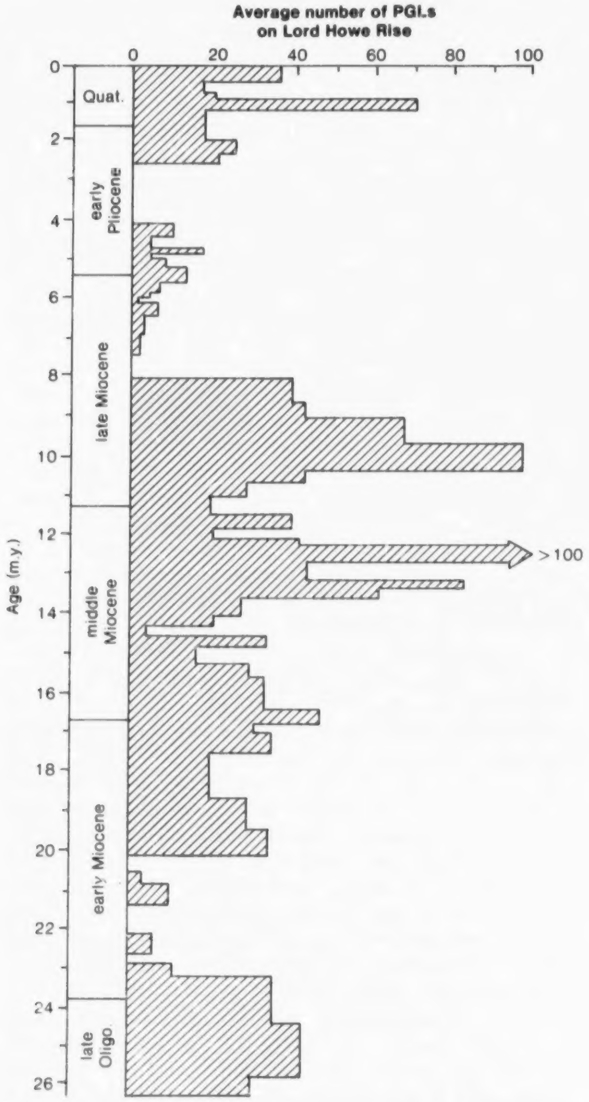

Figure 5. The overall distribution of pale green laminae (PGLs) interpreted as altered ash layers in Leg 90 drill sites on Lord Howe Rise (from Gardner, Nelson, et al., this volume). Note major episodes of explosive volcanism centered near 10 and 13 m.y. ago.

They argue that the PGLs represent diagenetically altered volcanic ash layers from regional volcanic events, principally on the basis that (1) the laminae are completely dominated by authigenic smectite and are therefore equivalent to bentonite layers; (2) because terrigenous components are absent in the sediment, the iron necessary for the formation of the associated iron sulfides could only be supplied by alteration of the overlying volcanic ash, the sulfur being supplied by sulfate reduction of pore water; and (3) the times at which the laminae occur closely match periods of reported volcanism from the southwest Pacific and circum-Pacific (Kennett et al., 1977). Volcanicity peaked in the latest early Miocene to early middle Miocene (18–15 m.y.), the late middle Miocene (14–12 m.y.), the early late Miocene (11–9 m.y.), and the latest Pliocene to Quaternary (3–0 m.y.). However, the PGL tephrostratigraphy of the region is considerably more complex and detailed than was previously known; in particular, it suggests that middle and early late Miocene volcanism was much more active in this sector of the southwest Pacific than it was during the Quaternary (cf. Kennett et al., 1977). A broad correlation is evident between maxima in the PGL record and periods of increased intensity of convergence at the boundary between the Indo-Australian and Pacific plates in the southwest Pacific (Gardner, Nelson, et al., this volume).

Because fresh silicic glass shards are widely disseminated although rare in Leg 90 sediments (Nelson, Froggatt, et al., this volume), it may be inferred that the PGLs are principally a record of basic to intermediate explosive volcanicity and that these more basic shards had very low preservation potential in the calcareous sediments during burial diagenesis.

SEDIMENTATION RATES

Figure 2 includes values for the average rates of sedimentation (m/m.y.), uncorrected for sediment porosity, based on ages of nannoplankton zones (radiolarian/diatom zones at Site 594). Rates of sedimentation for pelagic carbonates range from as low as about 5 m/m.y. in the Paleogene of Site 593, to as high as 131 m/m.y. in the late early Pliocene of Site 591. Overall, sedimentation rates range between 15 and 30 m/m.y., although consistently higher rates of biogenic carbonate sedimentation are characteristic of certain times, especially in the late early Pliocene.

The physical property data for porosity and wet-bulk density of sediments enable calculations of mass accumulation rates (MAR) (g/cm^2 per 10^3 yr.). Because the CaCO$_3$ content of most cores exceeds 95%, changes in MAR largely represent changes in carbonate flux. Good intercore comparisons of accumulation rates for the Neogene at Leg 90 sites have been made (Fig. 3). The early Miocene (23–16 m.y.) has fairly constant MAR of about 2 to 3 g/cm^2 per 10^3 yr., which began to fluctuate about 15 to 10 m.y. ago (middle Miocene). A major peak of up to 12 g/cm^2 per 10^3 yr. is centered at 12 m.y. The late Miocene (10 to 7 m.y.) section has fairly constant MAR of about 3 g/cm^2 per 10^3 yr. In the latest Miocene, at about 6 m.y., accumulation rates again increase to between about 5 and 10 g/cm^2 per 10^3 yr. and by the late early Pliocene (4 to 3 m.y.) there is a remarkably widespread and brief peak of mass accumulation of up to 27 g/cm^2 per 10^3 yr. Accumulation rates during the late Pliocene fall to much lower values, but are still consistently higher than average Neogene MAR. Except for Site 594, Quaternary MAR are generally much lower and are variable.

Apart from Site 594, the MAR probably reflect actual changes in calcareous biogenic productivity associated with fundamental paleoceanographic events that occurred during the Neogene in the southwest Pacific region (Kennett and von der Borch, this volume). The large MAR are not due to dilution from noncarbonate sources, because the noncarbonate materials occur in only minor amounts, and they do not reflect redeposition from winnowed areas, because there is little evidence of reworking of microfossils. The fast MAR are unlikely to be artefacts of an imprecise chronostratigraphy because the age boundaries have to be substantially changed to affect the pattern of increased MAR. The paleoceanographic reason for such high productivity in the late early Pliocene remains unclear. Relatively high MAR have also been reported elsewhere at this time, in the Colombia Basin, for example (Prell, Gardner, et al., 1982).

Sedimentation rates (both m/m.y. and MAR) in the north-south transect are generally highest throughout the Neogene at Site 586 on the equator and at Sites 590 and 591 at about 31°S. The increased biogenic productivity probably relates to the location of these sites in nutrient-enriched waters near major divergences, the Equatorial Divergence in the western Pacific and the Subtropical Divergence (or Tasman Front) crossing the central Tasman Sea (Fig. 1).

The relatively reduced rates of sedimentation (both m/m.y. and MAR) in the Quaternary (and latest Pliocene) compared to the remainder of the Neogene at most sites in the Tasman Sea are due to increased winnowing by bottom currents at this time, related to stimulated circulation of Antarctic Intermediate Water, as evidenced by the overall coarsening of both bulk carbonate sediment and terrigenous sediment fractions at this time (Stein and Robert, this volume; Gardner, Dean, et al., this volume). Intervals of winnowed sediment are noticeably enriched in whole and fragmented foraminiferal tests, and interbedding of foraminifer and foraminifer-bearing nannofossil oozes or of foraminifer-bearing and nannofossil oozes is common, correlated to the alternation of glacial and interglacial episodes, respectively (e.g., Nelson, Hendy, and Dudley, this volume). The unusually high MAR in the Quaternary at Site 587 (Fig. 3) are a result of downslope transport of coarse-grained, shallow-marine bioclastic carbonate from the Lansdowne Bank.

Sedimentation rates (both m/m.y. and MAR) at subantarctic Site 594 are considerably higher (40 to 150 m/m.y. or 6 to 24 g/cm^2 per 10^3 yr.) than at other Leg 90 sites. Lowest rates (30 to 40 m/m.y. or 2 to 6 g/cm^2 per 10^3 yr.) occur in the latest Neogene, an interval interrupted by at least three disconformities. The high rates of sediment accumulation reflect (1) the proximity of Site 594 to South Island, New Zealand; (2) the generally high nutrient level of subantarctic waters near the Subtropical Convergence (Bradford, 1983), which probably developed during the middle Miocene (Kennett and von der Borch, this volume); and (3) the evidence (Site 594 chapter, this volume) for considerable amounts of local reworking and redeposition of older microfossils, certainly in the basal 150 m of section and to a lesser extent in the Quaternary interval of the core.

BIOTURBATION

Bioturbation is ubiquitous in Leg 90 sediments and has been reviewed by Nelson (this volume). Cores are dominated by a range of taxonomically nondiagnostic traces identified by subtle diagenetic color contrasts with the host sediment. These structures include abundant mottles, blebs, and spots, common streaks and wisps, and rare threads, tubes, rinds, halos, rings, and pockets. Some represent sections through Planolites and Trichichnus burrows. The trace fossils Planolites, Chondrites, and Zoophycos typically occur in association below a definite but variable sub-bottom depth at most sites.

The degree of bioturbation varies widely, both within and among sites. The principal controlling factors may be variations in bulk sediment flux and the flux of organic matter. Overall increases in these parameters during the Neogene can also explain the upward disappearance of the Planolites-Chondrites-Zoophycos association and its replacement by predominantly Planolites (-like) and nondiagnostic traces of indiscriminate burrowers. The timing of the changeover between the two burrowing assemblages varies from site to site (Nelson, this volume) and may be tied to the initiation and evolution of the various surface and intermediate water masses in the southwest Pacific region during the middle and late Cenozoic (Kennett and von der Borch, this volume).

ASPECTS OF DIAGENESIS

Oxidized Versus Reduced Sediment

Almost all the sites drilled on Leg 90 have a surficial oxidized zone of oozes directly resting on a thick reduced section of sediment. The oxidized zone is typically 30 to 60 cm thick, but reaches as much as 6 or 7 m at Sites 588 and 593, and is distinguished by its distinctive pale brown (5Y 8/1, 10Y 6/2), pale orange (10Y 8/2, 10YR 8/2, 10Y 7/4), or yellow gray (5Y 7/2) color. Pyrite is absent in the oxidized zone, but the underlying reduced sediment contains disseminated fine-grained pyrite and is typically light gray (N7) to white (N9). The surface oxidized zone probably corresponds to a redox front that represents the level below which aerobic combustion of organic matter by microorganisms has depleted the available oxygen in the interstitial waters. Intensities of magnetization are relatively high (1 to 10 μG) within the oxidized zone, but they quickly drop to very low values (<0.05 μG) in the anoxic sediments (Barton and Bloemendal, this volume), presumably as a consequence of the two-stage reduction of sulfates and iron oxides to pyrite (Karlin and Levi, 1983).

Site 593 is of particular interest because it also contains a distinctive, pale orange nannofossil ooze (Subunit IC) from about 394 to 418 m sub-bottom depth, interbedded with normal light gray to white nannofossil oozes of otherwise identical lithology (Fig. 2). The pale orange nannofossil ooze has relatively high intensities of magnetization. It formed between 15.5 and 15 m.y. ago and was not postdepositionally reduced, presumably because a change occurred in the balance between available dissolved oxygen supplied to the seafloor and available organic carbon supplied to the infauna, epifauna, and bacteria within the sediment. The subunit was deposited during a time of major ice buildup in Antarctica and it may be that the oxidizing event was associated with the brief development or intensification of an oceanographic front close to Site 593 that produced intermediate waters sufficiently oxygenated to prevent postdepositional reduction within the sediments. The thicker than normal (up to 6 m) surficial oxidized zone at Site 593 may likewise reflect the present-day impingement of the northward flow of oxygen-charged Antarctic Intermediate Water on Challenger Plateau at about 1000 m water depth.

Microfossil Preservation

The qualitative assessment of downcore variations in the preservation of foraminiferal and calcareous nannoplankton microfossils included in Figure 2 is based on brief comments contained in the Biostratigraphy sections of the site reports (this volume). Preservation of the microfossils is generally very good in the thick sections of calcareous oozes; below them, it slowly deteriorates. Preservation in chalk ranges from moderately good to very poor. The relationship between degree of sediment lithification and microfossil quality is emphasized by the better preservation of shell material in oozes that persist below the ooze/chalk transition depth (e.g., Site 592). In addition, microfossil preservation significantly deteriorates in hard, recrystallized chalk sections at the bottom of several holes (e.g., Holes 590B, 591A, 592, and 594A). The recrystallized chalks include a large proportion of micritic carbonate particles, or micarb (Matter, 1974), which presumably represent disaggregated crystals freed by dissolution along element or segment sutures of small coccolith plates and foraminiferal fragments (Plates 1 and 2).

Preservation of the dominant calcareous nannofossil fraction varies systematically with depth. In general, discoasters, sphenoliths, and the rod-shaped genus *Triquetrorhabdulus* are the first to show secondary calcite overgrowths. In most Leg 90 sites, overgrowths begin in sections as young as the early Pliocene, probably because of the high mass accumulation rates of pelagic carbonate at this time (Fig. 3). Heavy overcalcification occurs from the middle Miocene downward, with discoasters showing fused rays and crystal faces, especially in the firmer nannofossil oozes and chalks (Plate 2). At this level the coccoliths also exhibit varying degress of secondary calcite overgrowths. In the Oligocene section of Sites 588 and 593, calcite overgrowths are prominent on all nannofossil species. In the middle Eocene section of Site 588, the early Oligocene section of Site 592, and the late Eocene section of Site 593, the preservation is good regardless of burial depth. In the first two cases the sediments include significant biosiliceous material and underlie the regional unconformity, and in the last a sequence of volcanogenic turbidites occurs immediately above the chalk containing the better-preserved calcareous nannoplankton, so that perhaps these local factors have somehow enhanced preservation.

Authigenic Nodules

Occasional nodules of chert and celestite ($SrSO_4$), up to 5 cm in size, were recovered at a few sites (Fig. 2). Biogenic silica has been dissolved in many Leg 90 sediments (Baker, this volume; Gardner, Nelson, et al., this volume) and forms the most obvious source of silica for local precipitation of opal-CT in chert nodules. The strontium for celestite formation is derived from the dissolution or recrystallization of biogenic calcite. Baker (this volume) shows that the concentration of dissolved Sr^{2+} in pore waters increases with depth at all sites and that as long as microbial sulfate reduction is relatively unimportant, celestite precipitation is possible.

Minor amounts of pyrite form ubiquitous, noncarbonate, authigenic mineral phases in Leg 90 sediments. Pyrite occurs as scattered framboids and micronodules, up to 1 to 2 mm across, commonly as small solid tubes 1 to 2 mm in diameter and several centimeters long, and rarely as larger nodules, sometimes in association with celestite. In many cases the pyrite is intimately associated with bioturbation structures (Nelson, this volume), suggesting precipitation of iron sulfide minerals within and about the preferred sites of sulfate reduction provided by the organic-matter-rich burrows.

The Ooze/Chalk Transition

The recovery of several continuous and largely undisturbed sections of pure carbonate sediments uncontaminated by significant quantities of biosiliceous and fine terrigenous material provides an excellent opportunity for the detailed study of the diagenetic processes that occur during the transformation of ooze into chalk (Plates 1 and 2). Some physical and chemical information relevant to the diagenesis of Leg 90 sediments is contained in the chapters by Baker (this volume) and Morin (this volume).

The general trend that pelagic carbonate sediments become increasingly lithified with greater depth of burial (e.g., Garrison, 1981) is well substantiated. Some relevant statistics are summarized in Table 3. The transition from soft to firm or stiff oozes ranges between 100 and 255 m sub-bottom depth. Generally, the further south the site is located, the deeper this transition occurs (Fig. 6). Also, at sites south of Site 590, the firmness of the oozes commonly varies below the first transition level, with variable-scale interbedding of soft and firm oozes.

At five sites (Sites 586, 588, and 590–592), the depth of the ooze/chalk transformation averages about 270 m, with a total range of variation of only about 20 m (Fig. 6). The age of this transformation varies from about 8 m.y. at Sites 586 and 590 to almost 17 m.y. at Site 592, averaging 11 m.y. over the same five sites. Sites 593 and 594, the two southernmost sections, have oozes that persist to depths of 562 and 476 m respectively. Moreover,

Table 3. Approximate sub-bottom depths and ages of the transition of soft to firm ooze and of firm ooze to chalk at Leg 90 sites.

Site	Water depth (m)	Latitude (°S)	Total core penetration (m)	Soft-firm ooze transition		Ooze-chalk transition		Avg. sedn. rate for site (m/m.y.)
				Depth (m)	~ Age (m.y.)	Depth (m)	~ Age (m.y.)	
586	2207	0.0	305.3	100	3.6	260	8.0	25
587	1101	21.0	147.0	?50	3.5	—	—	21
588	1533	26.0	488.1	165	8.0	245	13.0	17
590	1299	31.0	499.1	200	6.0	269	8.0	25
591	2131	31.5	500.4	175	4.0	290	9.0	29
592	1098	36.5	388.5	205	12.0	273	17.0	16
593	1068	40.5	571.5	205	9.0	562	40.0	14
594	1204	45.5	639.5	255	10.0	476	13.0	46

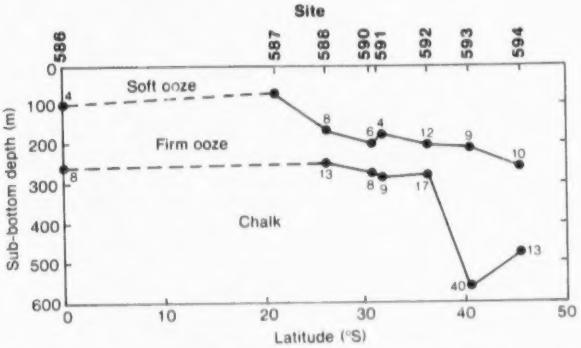

Figure 6. Changing sub-bottom depths with latitude of the transition level of soft to firm calcareous ooze and of firm ooze into chalk at Leg 90 sites. The numbers within the diagram are the approximate ages (in m.y.) of the transition depths at each site. Note the tendency for depths of transformation to increase with increasing southern latitude.

at Site 593 the age of the transition is as old as 40 m.y., but at Site 594 it is only 13 m.y.

Possibly delayed lithification may be related to the decreased content of discoasters and sphenoliths in the calcareous sediments at the southern sites. Both of these nannofossil groups, and especially the discoasters, provide ideal nucleation sites for calcite overgrowth and cementation during diagenesis (Schlanger and Douglas, 1974; Matter et al., 1975; Garrison, 1981). In Leg 90 sediments discoasters and sphenoliths are common only at warm-water sites; their low abundance and diversity at temperate Site 593 and subantarctic Site 594 (Fig. 7; Lohman, this volume) may be responsible for forestalling calcite crystallization in these sediments. In general it is anticipated that high-latitude pelagic carbonates will remain oozes to deeper burial depths than those in lower latitudes.

The same situation may also explain the reversal in the trend of increased lithification with burial depth that occurred at Site 592. Between about 305 and 360 m sub-bottom, early Oligocene soft to firm nannofossil ooze unconformably underlies early Miocene nannofossil chalk. The Oligocene ooze at the site is dominated by cold-water taxa with few discoasters and sphenoliths, so that calcite crystallization has been relatively inhibited. It is unlikely that this reversal in lithification is in any way associated with the regional unconformity (Packham and van der Lingen, 1973).

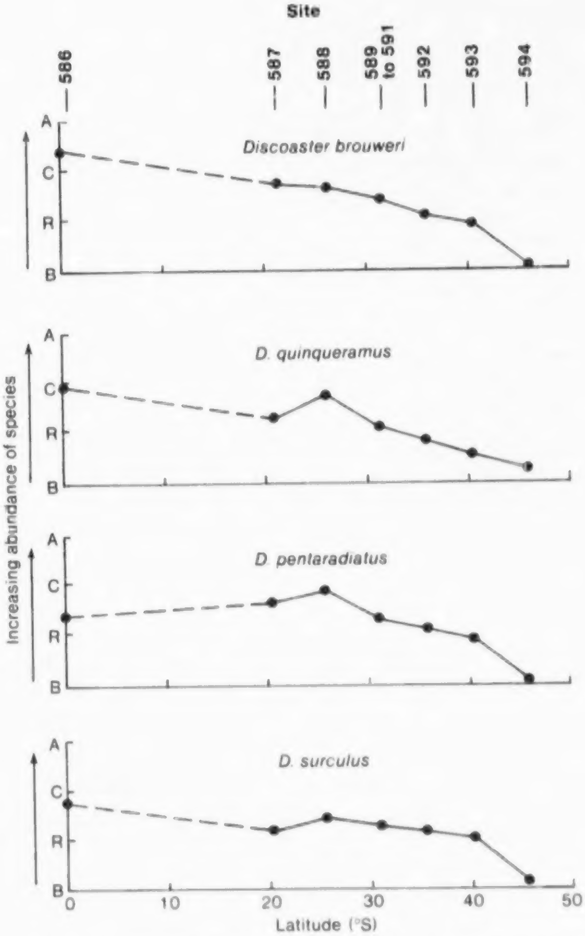

Figure 7. Examples of latitudinal abundance trends (A, abundant; C, common; R, rare; B, barren) for four important zone-defining species of discoasters in Leg 90 sediments (adapted from Lohman, this volume). Note the generally steady decline with higher latitude: the discoasters become extremely rare by 45°S.

Burial lithification is reflected by the very gradual decline in sediment porosity with depth and the reciprocating rise in bulk density (Morin, this volume). Porosities range from about 70 to 45% and are in the range of 50 to 53% at the depth where ooze becomes chalk. The transition is sudden and, across a very narrow porosity range of only 1 to 2%, properties that relate to sediment rigidity, such as shear strength and compressional acoustic velocity, sharply increase.

Instances occur where porosity remains essentially constant over hundreds of meters of section, and there is no evidence of systematic compaction of the sediments although overburden stress substantially increases (e.g., Sites 590 and 593 from 200 to 450 m and 50 to 350 m sub-bottom depths, respectively). Among other reasons, Morin (this volume) suggests that this may be a consequence of locally very high sedimentation rates that, on the one hand, probably caused excess pore pressures that retarded initial compaction and promoted the formation of a competent sediment matrix and, on the other hand, increased the diagenetic potential of the carbonates (Schlanger and Douglas, 1974, p. 133), which accelerated point-to-point cementation between grains and increased sediment rigidity.

Apart from diagenetic color contrasts, associated commonly with organic traces, and the laminae of pale green altered tephras, the oozes and chalks are structurally almost homogeneous. However, below about 350, 440, and 550 m in the chalks at Sites 588, 591, and 594, respectively, flaserlike bedding occurs locally in the form of small elliptical nodules or "eyes" of purer chalk surrounded by wispy dissolution seams, relatively enriched in insoluble clay materials (Fig. 8). The flasers are associated with the progressive alteration of biogenic material in the recrystallized chalks and attest to more wholesale pressure-dissolution of carbonate sediment along horizons relatively enriched in terrigenous clays. Flasers are widely reported from many chalk sequences on land (e.g., Garrison and Kennedy, 1977). By about 600 m sub-bottom depth at Site 594, the flaser bedding is more pronounced and begins to resemble stylolite seams (Fig. 8).

In the early Miocene of Site 588 and the early late Miocene of Sites 590 and 591, short intervals of chalk are cut by suites of microfaults, some with slickensided surfaces. The faults are high-angle (>60°) and normal, with apparent dip-slip offsets of a few millimeters to centimeters. Sometimes the microfractures are healed by secondary minerals, including iron sulfides and possibly rhodochrosite. A tectonic origin is favored for these features, although some of the fractures may have been artificially produced by drilling.

ACKNOWLEDGMENTS

This review chapter could only be prepared by having access to much of the shipboard and shore-based lithologic data collected by my scientific colleagues on DSDP Leg 90. Their major contribution in this regard is gratefully acknowledged. I particularly thank Jim Kennett and Jim Gardner for their helpful comments on a draft copy of the review.

REFERENCES

Berger, W. H., 1976. Biogenous deep-sea sediments: production, preservation, interpretation. *In* Riley, J. P., and Chester, R. (Eds.), *Chemical Oceanography* (Vol. 5): London (Academic Press), 265-387.

Bradford, J. M., 1983. Plankton and primary productivity in the vicinity of the Chatham Rise. *N.Z. Oceanogr. Inst. Oceanogr. Summary*, 21:1-14.

Burns, R. E., Andrews, J. E., et al., 1973. *Init. Repts. DSDP*, 21: Washington (U.S. Govt. Printing Office).

Carter, R. M., and Carter, L., 1984. Tectonic and sedimentary controls on the evolution of the Bounty Channel, southwestern Pacific Basin. *Geol. Soc. N.Z. Misc. Publ.*, 31A:34. (Abstract.)

Churkin, M., Jr., and Packham, G. H., 1973. Volcanic rocks and volcanic constituents in sediments, Leg 21, Deep Sea Drilling Project. *In* Burns, R. E., Andrews, J. E., et al., *Init. Repts. DSDP*, 21 Washington (U.S. Govt. Printing Office), 481-493.

Coleman, P. J., and Packham, G. H., 1976. The Melanesian border lands and India-Pacific plates' boundary. *Earth Sci. Rev.*, 12:19 233.

Garrison, R. E., 1981. Diagenesis of ocean carbonate sediments: a r view of the DSDP perspective. *In* Warme, J. E., Douglas, R. G and Winterer, E. L. (Eds.), *The Deep Sea Drilling Project: A De ade of Progress*. Soc. Econ. Paleont. Mineral. Spec. Publ., 3 181-207.

Garrison, R. E., and Kennedy, W. J., 1977. Origin of solution sean and flaser structure in Upper Cretaceous chalks of southern En gland. *Sediment. Geol.*, 19:107-137.

Griggs, G. B., Carter, L., Kennett, J. P., and Carter, R. V., 1983. La Quaternary marine stratigraphy southeast of New Zealand. *Geo Soc. Am. Bull.*, 94:791-797.

Imbrie, J., Shackleton, N. J., Pisias, N. G., Morley, J. J., Prell, W. L Martinson, D. G., Hays, J. D., McIntyre, A., and Mix, A. C 1985. The orbital theory of Pleistocene climate: support from a revised chronology of the marine $\delta^{18}O$ record. *In* Imbrie, J., and Berger, A. (Eds.), *Milankovitch and Climate Change:* Amsterdam (Elsevier).

Jarrett, G. R., 1985. Late Cenozoic lithostratigraphy of DSDP Site 594, southwestern Chatham Rise, New Zealand, with emphasis on the paleoenvironmental significance of the late Quaternary sequence [M.Sc. thesis]. University of Waikato, Hamilton, New Zealand.

Karlin, R., and Levi, S., 1983. Diagenesis of magnetic minerals in Recent hemipelagic sediments. *Nature*, 303:327-330.

Kennett, J. P., Houtz, R. E., et al., 1975. *Init. Repts. DSDP*, 29: Washington (U.S. Govt. Printing Office).

Kennett, J. P., Houtz, R. E., Andrews, P. B., Edwards, A. R., Gostin, V. A., Hajós, M., Hampton, M., Jenkins, D. G., Margolis, S. V., Ovenshine, A. T., and Perch-Nielsen, K., 1975. Cenozoic paleoceanography in the southwest Pacific Ocean, Antarctic glaciation, and the development of the Circum-Antarctic Current. *In* Kennett, J. P., Houtz, R. E., et al., *Init. Repts. DSDP*, 29: Washington (U.S. Govt. Printing Office), 1155-1169.

Kennett, J. P., McBirney, A. R., and Thunell, R. C., 1977. Episodes of Cenozoic volcanism in the circum-Pacific region. *J. Volc. Geothermal Res.*, 2:145-163.

Marchig, V., and Rösch, H., 1983. Formation of clay minerals during early diagenesis of a calcareous ooze. *Sediment. Geol.*, 34:283-299.

Matter, A., 1974. Burial diagenesis of pelitic and carbonate deep-sea sediments from the Arabian Sea. *In* Whitmarsh, R. B., Weser, O. E., Ross, D. A., et al., *Init. Repts. DSDP*, 23: Washington (U.S. Govt. Printing Office), 421-470.

Matter, A., Douglas, R. G., and Perch-Nielsen, K., 1975. Fossil preservation, geochemistry, and diagenesis of pelagic carbonates from Shatsky Rise, northwest Pacific. *In* Larson, R. L., Moberly, R., et al., *Init. Repts. DSDP*, 32: Washington (U.S. Govt. Printing Office), 891-922.

Nelson, C. S., Hendy, C. H., Cuthbertson, A. M., Jarrett, G. R., and Black, K. P., 1984. A mid-late Quaternary isotope reference section for New Zealand: DSDP Site 594, eastern South Island. *Geol. Soc. N.Z. Misc. Publ.*, 31A:88. (Abstract)

Nelson, C. S., and Hume, T. M., 1977. Relative intensity of tectonic events revealed by the Tertiary sedimentary record in the North Wanganui Basin and adjacent areas, New Zealand. *N.Z. J. Geol. Geophys.*, 20:369-392.

Packham, G. H., and van der Lingen, G. J., 1973. Progressive carbonate diagenesis at Deep Sea Drilling Sites 206, 207, 208, and 210 in the southwest Pacific and its relationship to sediment physical properties and seismic reflectors. *In* Burns, R. E., Andrews, J. E., et al., *Init. Repts. DSDP*, 21: Washington (U.S. Govt. Printing Office), 495-521.

Prell, W. L., Gardner, J. V., et al., 1982. *Init. Repts. DSDP*, 68: Washington (U.S. Govt. Printing Office).

Schlanger, S. O., and Douglas, R. G., 1974. The pelagic ooze-chalk-limestone transition and its implications for marine stratigraphy. *In* Hsü, K. J., and Jenkyns, H. C. (Eds.), *Pelagic Sediments: on Land and under the Sea*. Int. Assoc. Sed. Spec. Publ., 1:117-148.

Seilacher, A., 1978. Use of trace fossil assemblages for recognizing depositional environments. *In* Basan, P. (Ed.), *Trace Fossil Concepts*. Soc. Econ. Paleontol. Mineral. Short Course, 5:167-181.

van der Lingen, G. J., Andrews, J. E., Burns, R. E., Churkin, M., Jr., Davies, T. A., Dumitrică, P., Edwards, A. R., Galehouse, J. S., Kennett, J. P., and Packham, G. H., 1973. Lithostratigraphy of eight drill sites in the South-west Pacific—preliminary results of Leg 21 of the Deep Sea Drilling Project. *In* Fraser, R. (Ed.), *Oceanography of the South Pacific 1972:* Wellington (N.Z. National Commission for UNESCO), pp. 299-313.

Date of Initial Receipt: 28 February 1985
Date of Acceptance: 6 June 1985

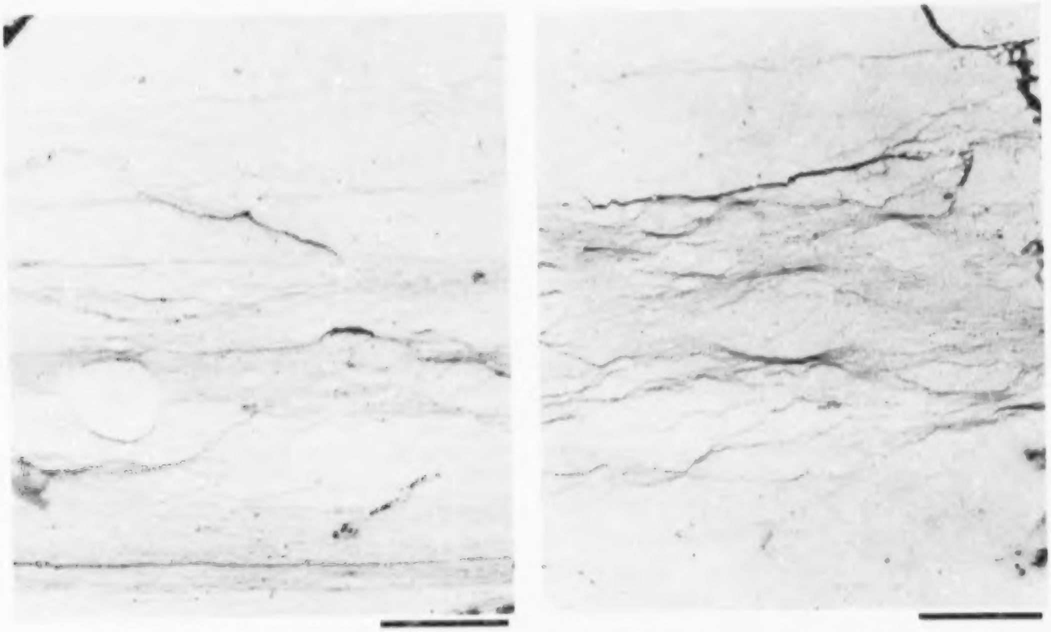

Figure 8. Examples of flaser structure and composite clay-rich dissolution seams in nannofossil chalks of late early Miocene age at about 630 m sub-bottom depth in Hole 594A off southeastern New Zealand. Bar scale 1 cm.

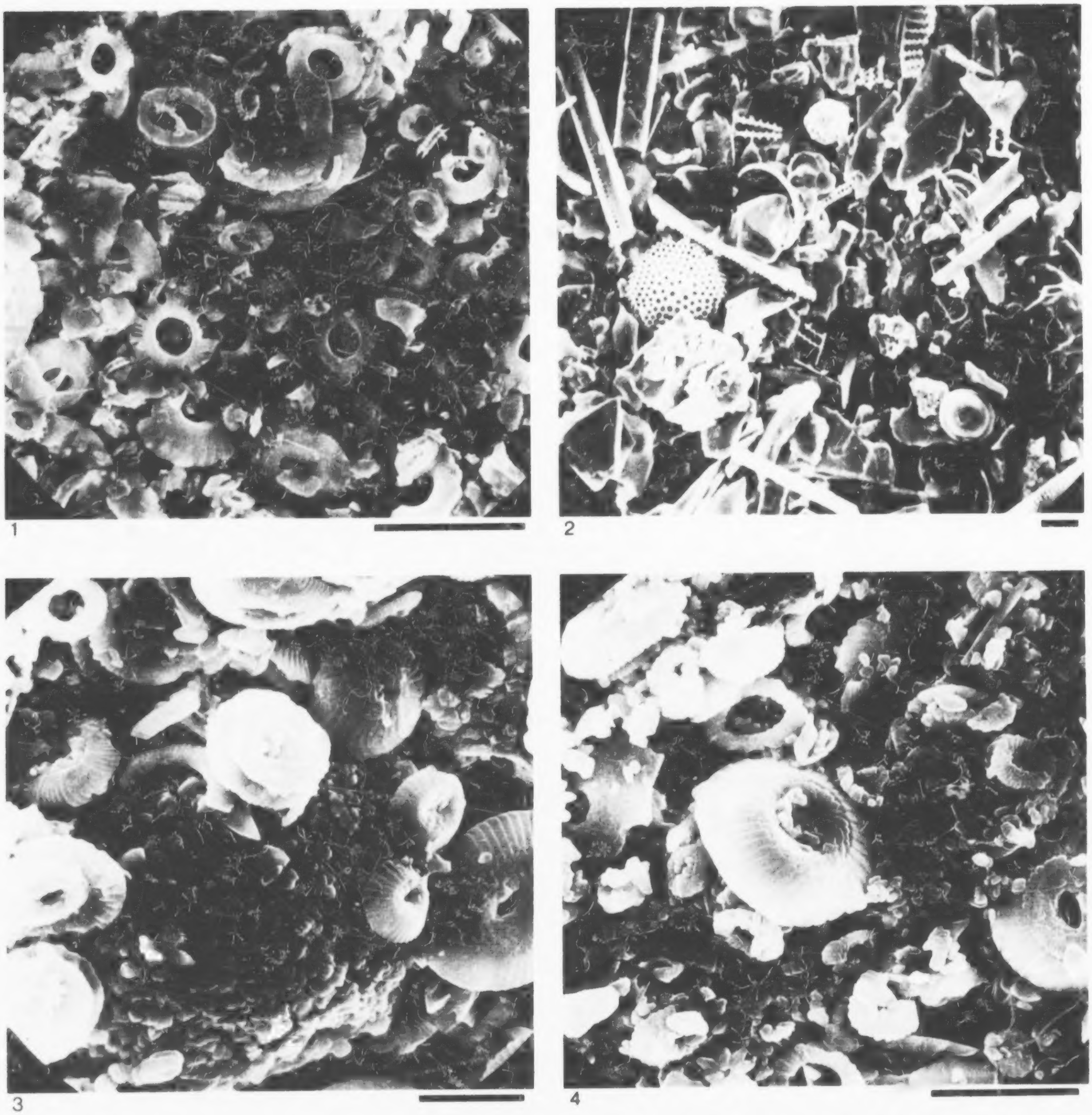

Plate 1. Scanning electron micrographs of fracture surfaces of Leg 90 oozes, in order of increasing burial depth. Bar scale 5 μm. **1.** Soft nannofossil ooze dominated by whole and broken coccolith shields, some exhibiting peripheral dissolution; Sample 588-2-4, 70 cm, early Quaternary; burial depth 10.80 m. **2.** Soft hemipelagic ooze of biosiliceous-material-bearing clayey silt; terrigenous matter is dominated by quartz and mica, and siliceous microfossils include diatoms, sponge spicules, and radiolarians; Sample 594-9-4, 80 cm, late Quaternary; burial depth 78.41 m. **3.** Soft foraminifer-bearing nannofossil ooze showing well-preserved whole and some broken coccolith shields and a portion of a foraminifer wall with evidence of strong dissolution; calcite crystals freed in this manner are probably an important source of micarb particles; Sample 592-11-3, 141 cm, early Pliocene; burial depth 95.32 m. **4.** Stiff nannofossil ooze comprising coccolith shields, some showing marginal corrosion and dissolution of central structures, a slightly calcite-overgrown sphenolith (bottom left), and abundant micarb particles; Sample 591-30-2, 140 cm, late Miocene; burial depth 272.21 m.

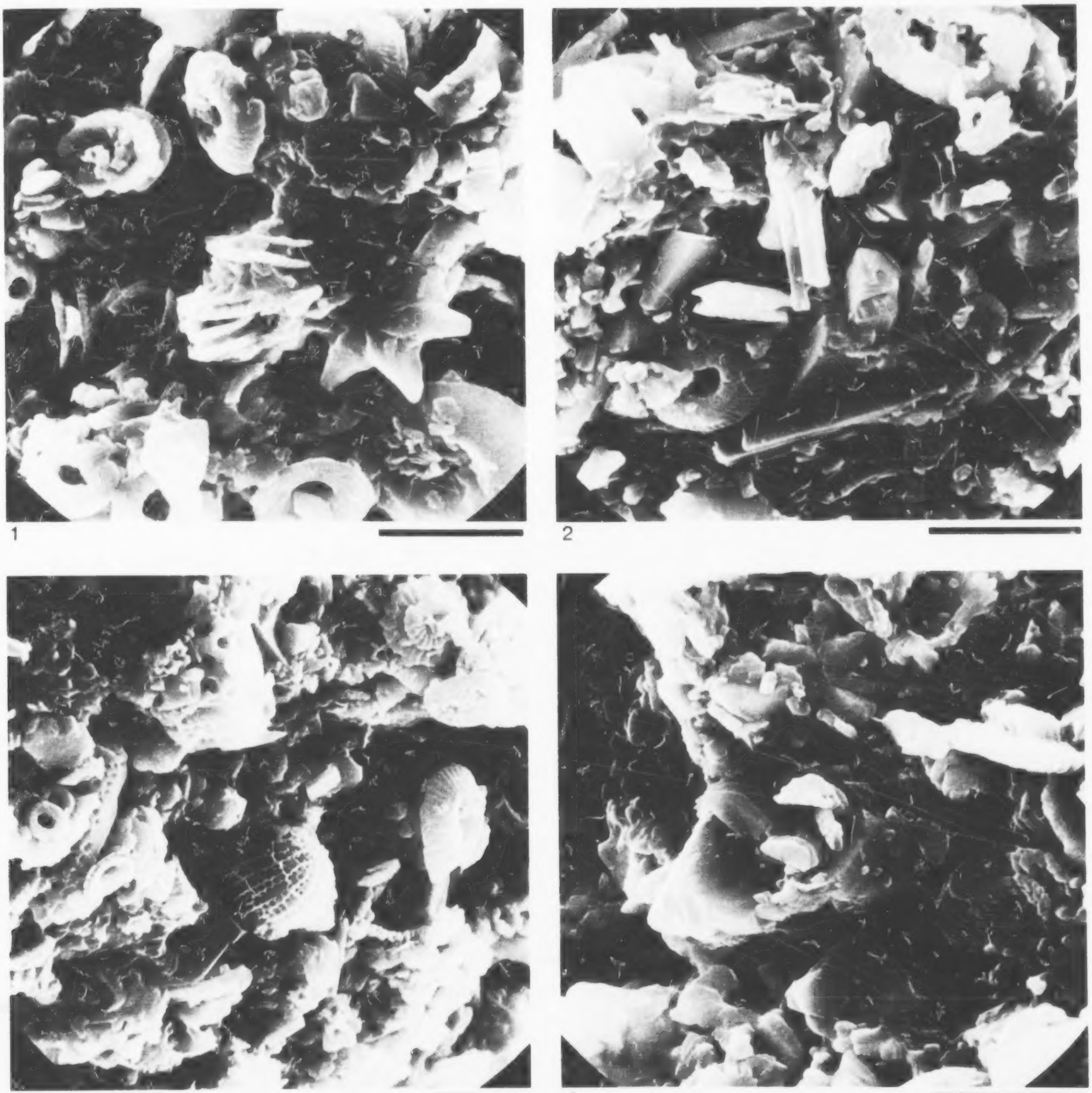

Plate 2. Scanning electron micrographs of fracture surfaces of Leg 90 chalks, in order of increasing burial depth. Bar scale 5 μm. **1.** Nannofossil chalk showing selective fusion of portions of the nannoplankton elements as a result of calcite overgrowth about the discoaster and between several coccolith shields; Sample 588A-9-3, 30 cm, middle Miocene; burial depth 283.90 m. **2.** Nannofossil chalk showing fusion and overgrowth of several nannoplankton elements and a moderately advanced stage of pore plugging by large crystals of rhombic calcite cement; Sample 588C-14-4, 77 cm, late Oligocene; burial depth 435.79 m. **3.** Biosiliceous-material-bearing nannofossil chalk showing both corroded and overgrown coccoliths and some radiolarian and diatom material differentially cemented by microgranular calcite; Sample 588C-19-1, 49 cm, middle Eocene; burial depth 479.00 m. **4.** Very hard nannofossil chalk in which extensive calcite cement overgrowths about discoasters in particular have poikilitically enclosed surrounding nannofossil and micarb material; Sample 591B-24-4, 136 cm, early Miocene; burial depth 496.67 m.

48. SOUTHWEST PACIFIC CENOZOIC PALEOCEANOGRAPHY[1]

James P. Kennett, Graduate School of Oceanography, University of Rhode Island
and
Christopher C. von der Borch, School of Earth Sciences, Flinders University[2]

ABSTRACT

This is a synthesis of major middle and late Cenozoic oceanographic and climatic events revealed in a diverse suite of studies by Leg 90 investigators and involving analyses of oxygen and carbon isotopes, sediment character, and accumulation rates and microfossils.

The benthic $\delta^{18}O$ record in Leg 90 sites exhibits a number of large changes that reflect the sequential development of polar glaciation and cooling of bottom waters beginning in the latest Eocene-earliest Oligocene. Major climatic cooling events in the Leg 90 sequences include the Terminal Eocene Event (37 Ma); middle Oligocene cooling events clustered close to 31 Ma; the Middle Miocene Event (16.5-13.5 Ma); further temporary cooling events during the late middle Miocene (12.5 to 11.5 Ma) and the earliest late Miocene (11-9 Ma); the Terminal Miocene Event (~6.2-5.0 Ma), the Middle Pliocene Cooling Event at 3.4 Ma; the Late Pliocene Event at 2.6-2.4 Ma; and amplification of glacial-interglacial oscillations during the Quaternary at 0.9 Ma (Jaramillo Paleomagnetic Subchron). The climax of Neogene warmth occurred during the early Miocene, especially between 19.5 and 16.5 Ma.

The sequences record the development during the Cenozoic of latitudinal and vertical thermal gradients in the southwest Pacific region. Major, permanent increases in the vertical temperature gradients occurred in association with the Middle Miocene Event (16.5-13.5 Ma), the Middle Pliocene Cooling Event (3.4 Ma) and the Late Pliocene Event (2.6-2.4 Ma).

Deep-sea benthic foraminiferal assemblages underwent important changes near the Eocene/Oligocene boundary and during the earliest Middle Miocene, the latest Miocene, and the late Pliocene and Quaternary. Late Neogene benthic foraminiferal changes are, in part, related to changes in the organic flux rates that accompanied changes in biogenic sedimentation rates and inferred surface-water productivity.

Changes in clay mineralogy, wind-blown terrigenous sediments, and opal phytoliths in the Lord Howe Rise Sites record a general expansion of Australian deserts. Important steps in aridification occurred during the Middle Miocene Event; the Terminal Miocene Event (~5 Ma), and the Middle Pliocene Cooling Event (~3.4 Ma).

INTRODUCTION

Cenozoic oceanographic and climatic evolution is largely a record of progressive cooling and glaciation of the polar regions and perhaps some warming in the tropics, resulting in an increase in the planet's latitudinal thermal gradient (Savin et al., 1975; Shackleton and Kennett, 1975b; Loutit, Kennett, et al., 1983). This global climatic evolution did not proceed uniformly but was marked, in part, by discrete and sudden coolings that appear to have resulted from changes in the geometry of the ocean basins and associated changes in ocean circulation. Although the tectonic changes served as triggering mechanisms, strong, positive climatic feedback mechanisms such as changes in albedo must have been actuated. Previous work by many investigators has led to the development of general scenarios of Cenozoic climatic evolution (for example, Kennett, 1982; Haq, 1984) that must be tested by this and future drilling expeditions. Such scenarios can be expected to change, especially as a result of future high-latitude drilling. One of the most prominent changes took place near the Eocene/Oligocene boundary (38 Ma), when cold, deep water began to form in the ice-covered sea surrounding Antarctica. Subsequent coolings occurred during the middle Miocene (~15 Ma), when it is likely that much of the East Antarctic ice sheet accumulated; the latest Miocene (~6-5 Ma), when a substantial West Antarctic ice sheet may have accumulated; and during the late Pliocene to Quaternary (2.4 Ma to the present), when large ice sheets formed on the Northern Hemisphere and further ice accumulated over Antarctica.

The cooling of high southern latitudes resulted from the development of the Circum-Antarctic Current and related thermal isolation of Antarctica (Kennett, 1977; Kvasov and Verbitsky, 1981). The steepening of the oceanic latitudinal thermal gradient was thus closely linked to development of the Circum-Antarctic Current system.

The primary objective of DSDP Leg 90 was to study Cenozoic oceanographic and climatic evolution of the southwest Pacific (Table 1). This contribution synthesizes the main paleoceanographic results from many of the Leg 90 investigations, outlining the major events in the order in which they occurred through geologic time (Table 2); thus it provides a paleoceanographic history of the southwest Pacific based upon Leg 90 discoveries.

Leg 90 of the Deep Sea Drilling Project obtained a traverse of eight high-quality sections of middle to late Cenozoic age (from Sites 587-594) between equatorial and northern subantarctic water masses (Fig. 1; Table 1). For logistical reasons, Leg 89 cored an additional Site 586 at the equator (Ontong-Java Plateau), forming

---

[1] Kennett, J. P., von der Borch, C. C., et al., *Init. Repts. DSDP*, 90: Washington (U.S. Govt. Printing Office).

[2] Addresses: (Kennett) Graduate School of Oceanography, University of Rhode Island, Narragansett, RI 02882-1197; (von der Borch) School of Earth Sciences, Flinders University, Bedford Park, South Australia 5042.

Table 1. Summary of Leg 90 drilling.

Hole	Latitude (S)	Longitude (E)	Water depth (m)	Penetration (m)	No. of cores	Meters cored	Meters recovered	Percentage recovered
586[a]	00°29.84′	158°29.89′	2207	44.4	5	44.4	38.98	87.8
586A[a]	00°29.84′	158°29.89′	2207	305.2	31	260.9	257.03	98.5
586B[a]	00°29.84′	158°29.89′	2207	240.3	25	240.3	234.93	97.8
586C[a]	00°29.84′	158°29.89′	2207	623.1	1	9.6	2.18	22.7
587	21°11.87′	161°19.99′	1101	147.0	17	147.0	88.81	60.4
588	26°06.70′	161°13.6′	1533	245.7	26	236.0	220.76	93.5
588A	26°06.70′	161°13.6′	1533	344.4	18	108.4	84.27	77.7
588B	26°06.70′	161°13.6′	1533	277.4	31	277.4	255.87	92.2
588C	26°06.70′	161°13.6′	1533	488.1	19	182.4	134.61	73.8
589	30°42.72′	163°38.39′	1391	36.1	4	36.1	35.08	97.2
590	31°10.02′	163°21.51′	1299	26.2	3	26.2	26.36	100.0
590A	31°10.02′	163°21.51′	1299	280.8	27	254.6	224.17	88.0
590B	31°10.02′	163°21.51′	1299	499.1	53	499.1	465.26	93.2
591	31°35.06′	164°26.92′	2131	283.1	31	283.1	278.21	98.3
591A	31°35.06′	164°26.92′	2131	284.6	30	284.6	233.15	81.9
591B	31°35.06′	164°26.92′	2131	500.4	24	229.8	130.86	56.9
592	36°28.40′	165°26.53′	1098	388.5	41	388.5	340.12	87.5
593	40°30.47′	167°40.47′	1068	571.5	60	571.5	468.21	81.9
593A	40°30.47′	167°40.47′	1068	496.8	27	257.3	227.71	88.5
594	45°31.41′	174°56.88′	1204	505.1	53	505.1	299.72	59.3
594A	45°31.41′	174°56.88′	1204	639.5	26	249.6	161.5	64.7
594B	45°31.41′	174°56.88′	1204	42.9	5	42.9	34.18	79.6

[a] For logistical reasons, Site 586 was cored on Leg 89.

the northern limit of the latitudinal traverse. Previous rotary drilling during DSDP Legs 21 and 29 (Burns, Andrews, et al., 1973; Kennett, Houtz et al., 1975) demonstrated that the southwest Pacific region is optimal for the study of thick, relatively uncomplicated and continuously deposited pelagic carbonate sequences of Neogene and Quaternary age between the equator and subantarctic. The sections are all located on shallow-water pedestals (between 1000 and 2000 m) that include Ontong-Java Plateau (Site 586) at the equator; Lord Howe Rise (Sites 587 through 592); the Challenger Plateau west of New Zealand (Site 593); and Chatham Rise east of New Zealand (Site 594). Sediment was collected from beneath every major surface water mass between the equator and subantarctic, permitting paleoceanographic records to be analyzed for each water mass. Recovered sections also form a vertical traverse at mid-latitudes from water depths of 1299 m (Site 590), 2131 m (Site 591), and 3196 m (Site 206, which was drilled during Leg 21).

Because these sedimentary sequences were obtained using the Hydraulic Piston Corer (HPC) and the Extended Core Barrel (XCB), they are relatively continuous and undisturbed and are of great value for studies of high-resolution stratigraphy and paleoceanography. HPC sequences in the soft carbonate ooze that blankets this shallow southwest Pacific region were longer than 200 m in each site. At Site 588, the HPC sequence is 315 m thick, the longest ever obtained. This sequence contains a continuous, largely uninterrupted record spanning the past 17 m.y. from the late early Miocene to the Quaternary.

Leg 90 recovered 3705 m of core, the longest for any drilling leg. Average core recovery for the entire leg was about 90% of the drilled section except for the Chatham Rise site (Site 594), where only 68% core recovery was achieved. Core quality is generally excellent with minimal core disturbance. The sites lie well above the modern southwest Pacific lysocline depth of 2500 to 3500 m (Berger, 1976).

Almost all sediment cored during Leg 90 is light-colored calcareous ooze or its more lithified equivalent, chalk. Foraminifers generally range from 5 to 15% with higher percentages during winnowed sedimentary intervals. Calcium carbonate content is greater than 90% in most sediments, which are mainly free of turbidites and received negligible amounts of terrigenous sediments. Siliceous biogenic material is usually absent and where present is found only in trace quantities. It usually consists only of radiolarians and sponge spicules. Diatoms are rare in these sediments. Bioturbation is ubiquitous in Leg 90 sediments and varies widely, both within and between sites (Nelson, this volume). Laminae are almost always volcanic ash or altered volcanic ash and provide a valuable measure for the amount of mechanical or biological disturbance. Most are relatively sharp, suggesting bioturbation or core disturbance had minimal influence.

Oceanographic Setting

The physical oceanography is not well known in the southwest Pacific region north of New Zealand but has been extensively studied in the area adjacent to New Zealand. Knox (1970) and Wyrki (1974) showed the position of the major surface water masses, their boundaries, and the directions of surface water flow in the region (Fig. 1). Site 588 lies within the warm-subtropical water mass, whereas Sites 590 and 591 lie close to the present-day position of the Subtropical Divergence (Tasman Front) that separates warm-subtropical temperate water masses (Denham and Crook, 1976; Stanton, 1979; 1981). The Subtropical Divergence represents the southern extent of the South Pacific subtropical gyre as the East Australian Current turns to the east, at about 30°S (Hamon, 1970), passing to the north of the barrier formed by New Zealand. The east Australian Current reaches maximum velocities of about 175 cm/s in the upper 100 m, and decreases to 10–20 cm/s at 1200 m water depth (Hamon, 1970). Upwelling at the Subtropical Divergence is caused by the divergence of the two surface-water masses and the interaction of the eastward-flowing gyral circulation with the Lord Howe Rise (Stanton, 1981). Upwelling in this region has created high biogenic sedimentation rates, which in the late Neogene ranged up to 131 m/m.y. in Site 591, the site closest to the Divergence.

Sites 588 and 590 are located in similar water depths, 1500 m and 1300 m, respectively, yet bottom-water temperatures at Site 590 are 0.5°C warmer (Site 588 = 3.75°C; Site 590 = 4.25°C; Rochford, 1960). The warmer bottom-water temperatures at Site 590 are due to the eastward passage of warm waters contained in the subtropical gyre and derived from the East Australian Current. Sites 592 and 593 are located well within the temperate (cool-subtropical) surface water mass and are under the influence of the eastward-flowing Tasman Current (Fig. 1). Site 593 is positioned within Antarctic Intermediate Water derived from cooling and sinking of surface waters at the Antarctic Convergence to the south. Temperatures at this depth range from 3 to 5°C (Ridgway, 1969). Site 594 is located in subantarctic waters to the south of the Subtropical Convergence which trends eastward across the Chatham Rise.

The sites on the Lord Howe Rise have moved about 5° to the north during the Neogene as a result of the movement of the Indo-Australian Plate (Sclater et al., in press). The northward movement of these sites into warmer waters during the Neogene should be reflected by planktonic assemblages indicative of increasingly warm surface water and by lower planktonic $\delta^{18}O$ values, unless the water masses themselves changed latitudinal positions.

Stratigraphic Continuity

Calcareous nannofossil biostratigraphy at all sites, planktonic foraminiferal biostratigraphy at Sites 586 through 593, and diatom and radiolarian biostratigraphy at Site 594 suggest that all but three of the Neogene to late Oligocene sections are completely continuous (Fig. 2). Site 590 contains a 1.5 m.y. hiatus in the latest early Miocene (18 to 16.5 Ma). Site 592 encountered the well-documented late Paleogene Tasman Sea regional unconformity (Kennett et al., 1975; Fig. 2). In this site, a 14.5 m.y. hiatus extends from the early Oligocene to the late early Miocene. We also penetrated the regional unconformity at Site 588 (= Site 208), which exhibits a hiatus of 19 m.y. from the middle Eocene to the late Oligocene. The regional unconformity is absent from Site 593 on Challenger Plateau, suggesting that bottom currents responsible for the erosional hiatus in the Tasman Sea did not extend far to the east. The section at Site 594 is interrupted by at least four unconformities, which include a 2 m.y. gap in the middle late Miocene, a 1 m.y. hiatus at the Miocene/Pliocene boundary, another between the early and late Pliocene, and another within the early Quaternary.

SUMMARY OF SOUTHWEST PACIFIC PALEOCEANOGRAPHIC HISTORY

Late Eocene Warm Climates

During the last Eocene, oxygen isotope values of planktonic and benthic foraminifers of Site 277 in the subantarctic south of New Zealand (Fig. 1) were similar to those of Sites 592 and 593 in the Tasman Sea to the northwest of New Zealand. This similarity of inferred surface and intermediate-water temperatures suggests that the sites were influenced by the same surface and intermediate-water masses, and that no surface water front existed between the sites at this time (Murphy and Kennett, this volume). Temperate radiolarian assemblages of late Eocene age, which are similar to those of the tropics (Caulet, this volume), also indicate low surface water temperature gradients between the tropics and temperate areas. This conclusion is in agreement with the warm, equable climates predicted for the Eocene, with low pole-to-equator temperature gradients (Wolfe, 1971; Kennett, 1977; Frakes, 1979; Brass et al., 1982).

During the late Eocene, no Circum-Antarctic Current existed to interfere with the influence of the southward-flowing warm-subtropical arm of the South Pacific gyre (East Australian Current; Fig. 1). These warm-subtropical waters were transported close to Antarctica, warming this region and preventing the development of extensive seasonal sea ice (Kennett, 1977). The influence of this gyre resulted in similar temperatures through the southwest Pacific during the late Eocene, as recorded by the similar oxygen isotope values (Murphy and Kennett, this volume).

Terminal Eocene Event

The terminal Eocene event is well represented in Sites 592 and 593 (and subantarctic Site 277) and is marked by a rapid, distinct $\delta^{18}O$ enrichment of about 1‰ in both planktonic and benthic foraminifers. Sequential changes in various biotic elements in these sites mark the transition from the relatively warm conditions of the late Eocene to the distinctly cooler conditions of the Oligocene (Murphy and Kennett; Martini; both this volume). The oxygen isotope shift, isochronous throughout the oceans according to planktonic foraminiferal biostratigraphy, gave rise to maximum earliest Oligocene $\delta^{18}O$ values, which were followed by lower (lighter) values later in the Oligocene (Corliss and Keigwin, 1983). Oxygen isotope and faunal evidence indicates that the cold waters of the oceans (psychrosphere) were generated during the late Eocene to earliest Oligocene, when a glacial threshold was crossed in the Antarctic (Kennett and Shackleton, 1976; Benson et al., 1984).

No clear paleomagnetic age for the Eocene/Oligocene boundary was determined for the southwest Pacific sites, but the age of 36.5 to 37 Ma that has been suggested for the Eocene/Oligocene boundary (Berggren et al., in press) is close to that determined by the DSDP Leg 73 staff based upon Subchron C-13R (37.1–37.2 Ma), (LaBrecque, Hsü, et al., 1983). The extinction of *Globigerinatheka index*, marking the Eocene/Oligocene boundary occurs

Table 2. Major oceanographic and climatic events of the Cenozoic revealed in Leg 90 investigations.

Ma	Age	Oxygen isotope changes	Carbon isotope changes	Glacial and climatic interpretations	Surface water changes: Southwest Pacific	Bottom and intermediate water mass changes	Biotic changes	Australasian continental climatic changes	Other changes: Southwest Pacific	Other changes
1	Quaternary	Late Quaternary higher values and higher variability Early Quaternary lower values and lower variability		Major glacial/interglacial episodes ← Increase in polar ice volume. Expansion of Northern Hemisphere ice sheets				Warm/cold cycles in New Zealand vegetation and glaciation Dominantly arid climate over much of Australia	Increased winnowing of sediments Distinct cycles in sediments More distinct cycles in sediment	
2	late Pliocene	← Increase of 0.4 $^{0}/oo$ (Late Pliocene Event)		← Major Northern Hemisphere ice accumulation		← Increase in vertical temperature gradient	Further changes in benthic foraminifer assemblages			
3	middle Pliocene	← Increase of 0.4$^{0}/oo$ (middle Pliocene event)		← Cooling at high latitudes, warming at low latitudes. Some Antarctic ice-volume increase	← Warming of surface waters Increased upwelling	← Cooling of intermediate waters; increase in vertical temperature gradient	← Major turnover of benthic foraminifer assemblages		Major increase in biogenic sedimentation and mass accumulation rates; high biogenic productivity	← Antarctic glacial increase; cooling of AABW
4 5	early Pliocene	Minimum Pliocene values		Global warmth Decreased ice volume			High diversity, highest Neogene nannoplankton diversity	Major increase in opal phytoliths (Lord Howe Rise)		Marine transgression
6	late Miocene	Highly variable, enriched values 0.4 $^{0}/oo$ more enriched than modern equilibrium $\delta^{18}O$ values at each site	← Distinct, rapid $\delta^{13}C$ decrease, up to -0.75 $^{0}/oo$ (late Miocene Carbon Isotope Shift)	Increase in Antarctic ice volume in West Antarctica Global temperature decrease	Cooling ← Cooling, increased upwelling. Intensification of upwelling at Subtropical Convergence		← Major turnover of benthic foraminifer assemblages	Increased Australian aridity/expansion of deserts. Increase in opal phytoliths. Cooler, drier New Zealand climates Low smectite/illite ratios in Australia, such as in Quaternary	← Increased biogenic sedimentation Greater organic flux to deep-sea sediments	Isolation and dessication of Mediterranean Basin Glacioeustatic marine regression; increased Antarctic glaciation
7 8		Lower values		Relative warmth				Increased aridity of Australia	Biogenic sedimentation rates typical of carbonate platforms outside regions of high productivity	
9 10 11		Very high values (average 2.25 $^{0}/oo$)		Greater ice volumes and/or cooler temperatures than modern ocean						

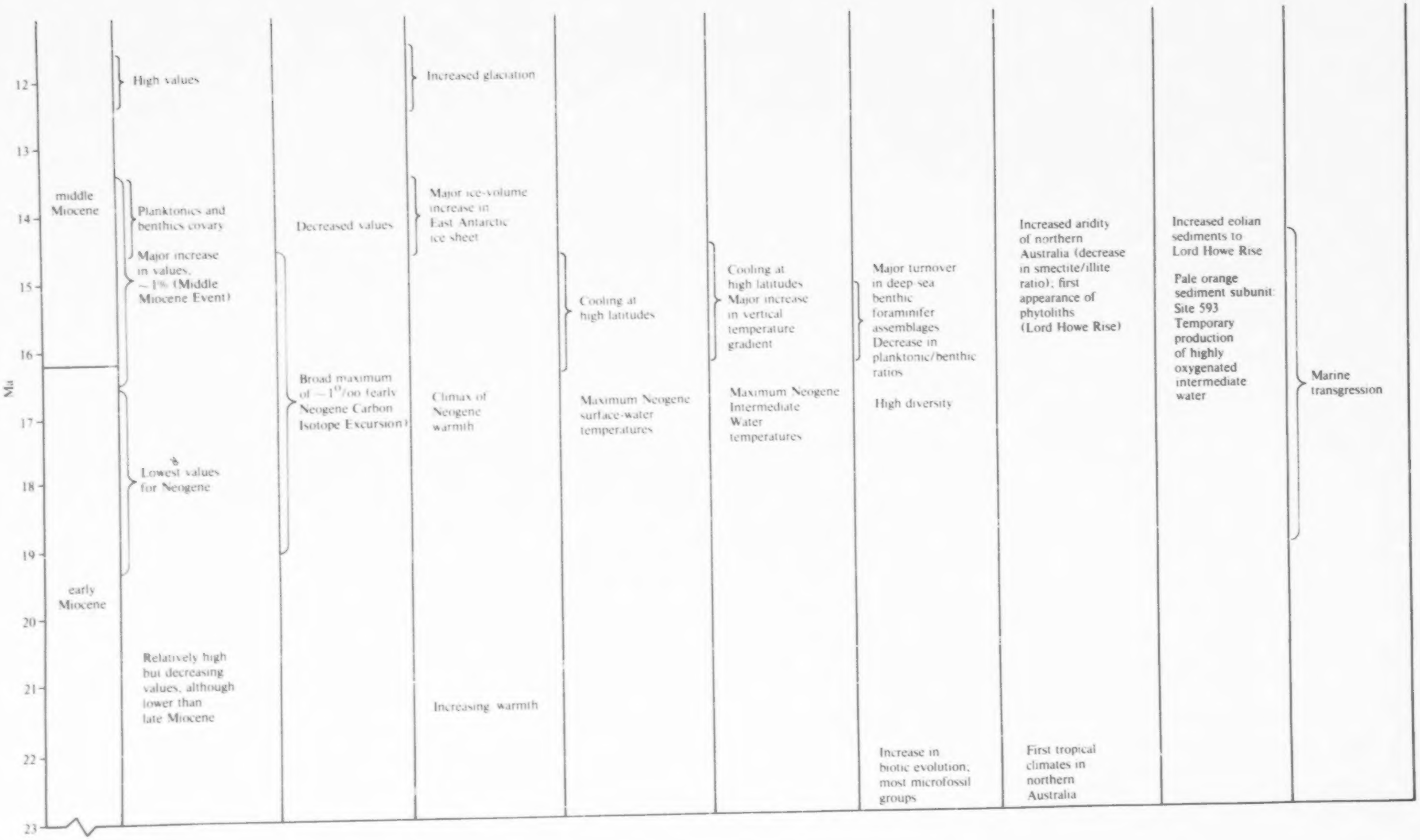

High values

Planktonics and benthics covary

Major increase in values, ~1‰ (Middle Miocene Event)

Lowest values for Neogene

Relatively high but decreasing values, although lower than late Miocene

Decreased values

Broad maximum of ~1‰ (early Neogene Carbon Isotope Excursion)

Increased glaciation

Major ice-volume increase in East Antarctic ice sheet

Climax of Neogene warmth

Increasing warmth

Cooling at high latitudes

Maximum Neogene surface-water temperatures

Cooling at high latitudes
Major increase in vertical temperature gradient

Maximum Neogene Intermediate Water temperatures

Major turnover in deep-sea benthic foraminifer assemblages
Decrease in planktonic/benthic ratios

High diversity

Increase in biotic evolution; most microfossil groups

Increased aridity of northern Australia (decrease in smectite/illite ratio); first appearance of phytoliths (Lord Howe Rise)

First tropical climates in northern Australia

Increased eolian sediments to Lord Howe Rise

Pale orange sediment subunit: Site 593
Temporary production of highly oxygenated intermediate water

Marine transgression

Table 2. (Continued).

Ma	Age	Oxygen isotope changes	Carbon isotope changes	Glacial and climatic interpretations	Surface water changes: Southwest Pacific	Bottom and intermediate water mass changes	Biotic changes	Australasian continental climatic changes	Other changes: Southwest Pacific	Other changes
					Little information for this age					
30 31 32	middle Oligocene	Highest values of Paleogene record Oscillating episodes (>0.5‰)		Coldest oceanic temperatures of Paleogene Perhaps some accumulation of Antarctic ice	Strengthening of Circum-Antarctic Current					
33 34	early Oligocene	← Increase in isotopic divergence of surface and intermediate waters between temperate and subantarctic areas		Subantarctic region cooled, temperate region warmed	Development and strengthening of latitudinal thermal zonation in southwest Pacific subantarctic and temperate water masses. Warming at temperate latitudes, cooling at high latitudes	Vertical thermal gradients increased			↑ Northward drift of Australia toward tropics ↑	Deep opening of Tasmanian Seaway
35 36		← Increase in isotopic divergence of surface and intermediate waters between temperate and subantarctic areas					Low-diversity planktonic assemblages			
37		← Rapid increase of ~1‰ in planktonics and benthics at Sites 277, 592, and 593	← Temporary shift toward higher values	← Rapid cooling Major glacial increase of Antarctica First extensive sea ice	← Cooling. Initial decoupling of warm subtropical gyre from the Southern Ocean	← Major generation of cold bottom waters of oceans 2000 m drop in CCD	← Disappearance of numerous planktonics in middle- to high-latitude regions, reduction in diversity Distinct changes in benthic foraminifer faunas		← Reduction in siliceous biogenic sediment component	Shallow opening of Tasmanian Seaway
38 39 40	late Eocene	Very low values		Warm, equable climates Low pole-to-equator temperature gradient	No oceanographic front between temperate and subantarctic areas Warm subtropical gyre extended to high latitudes		Warm faunas and floras, high biotic diversity at high latitudes			

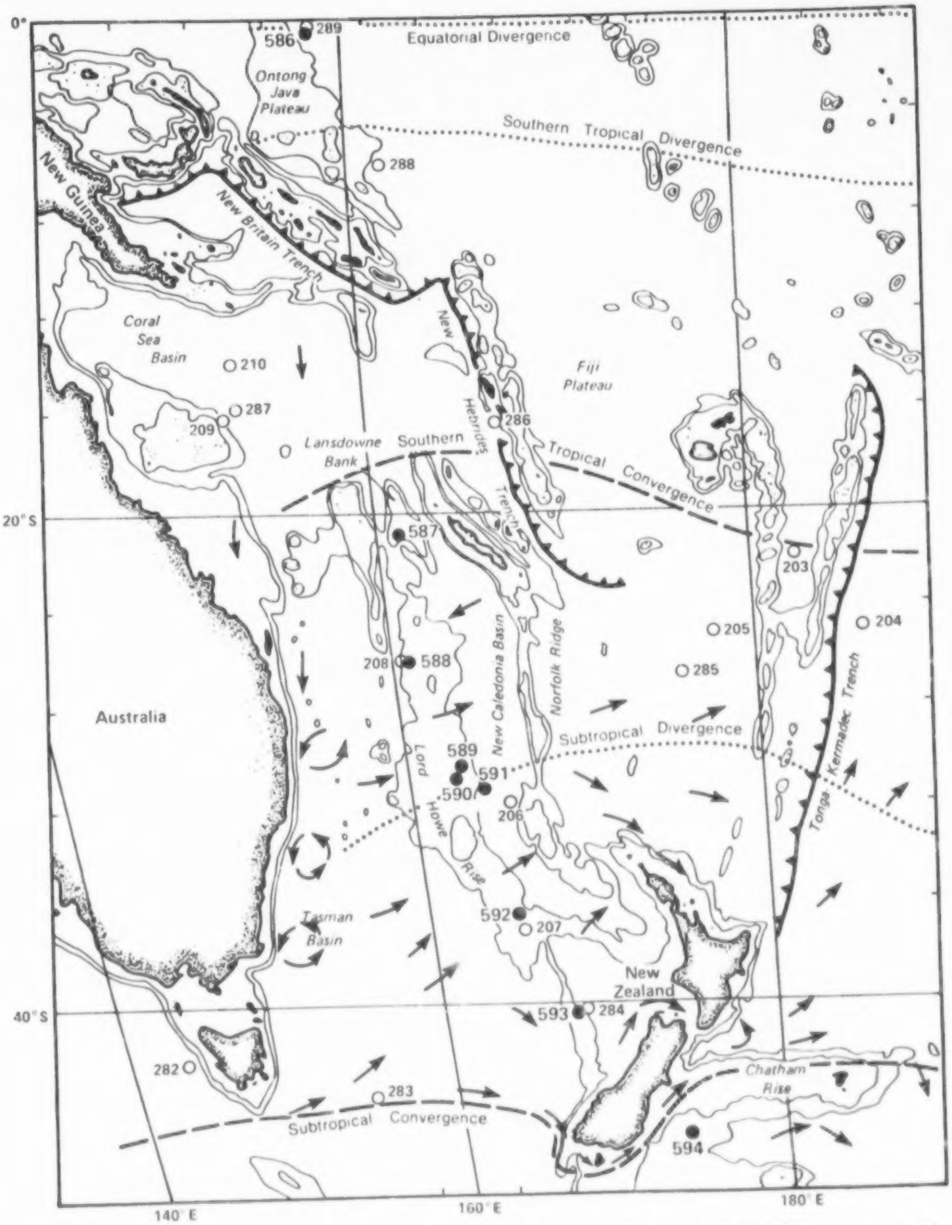
0°
20°S
40°S
140°E
160°E
180°E
586
289
Equatorial Divergence
Ontong Java Plateau
Southern Tropical Divergence
288
New Guinea
New Britain Trench
Coral Sea Basin
210
287
209
Lansdowne Bank
Southern Tropical Convergence
New Hebrides Trench
286
Fiji Plateau
587
203
204
205
285
208
588
Australia
Lord Howe Rise
New Caledonia Basin
Norfolk Ridge
Subtropical Divergence
Tonga-Kermadec Trench
589
591
590
206
Tasman Basin
592
207
New Zealand
593
284
282
283
Chatham Rise
Subtropical Convergence
594

Figure 1. Location of DSDP Leg 90 drill sites (solid circles) and sites drilled on other DSDP legs (open circles) in the southwest Pacific in relation to approximate positions of major surface water mass boundaries and circulation. Shown also are 1000 m and 500 m isobaths.

about 0.4 m.y. after the extinction of *Discoaster saipanensis* and *D. barbadiensis* (Martini, this volume), although the disappearance of these discoasters may be slightly diachronous across latitudes in relation to the stratigraphic position of the Eocene/Oligocene boundary (Martini and Jenkins, this volume).

The benthic foraminiferal assemblages also exhibit significant changes at the Eocene/Oligocene boundary (Boersma, this volume). At Site 593, the globocassidulinids were replaced by a fauna consisting of hispidocostate uvigerinids, a relatively large number of anomalinids, and a large percentage of long-lived Tertiary cosmopolitan forms.

Site 592 contains a highly expanded 90 m section of late Eocene through early Oligocene sediment. The $\delta^{18}O$ record at Site 592 (Murphy and Kennett, this volume) exhibits relatively constant late Eocene values followed by a rapid decrease ($-0.4‰$) in the latest Eocene, and then a distinct increase ($\sim 1.0‰$) beginning at the base of Zone NP21, which is considered to represent the Eocene/Oligocene boundary according to calcareous nannoplankton biostratigraphy. This oxygen isotope shift con-

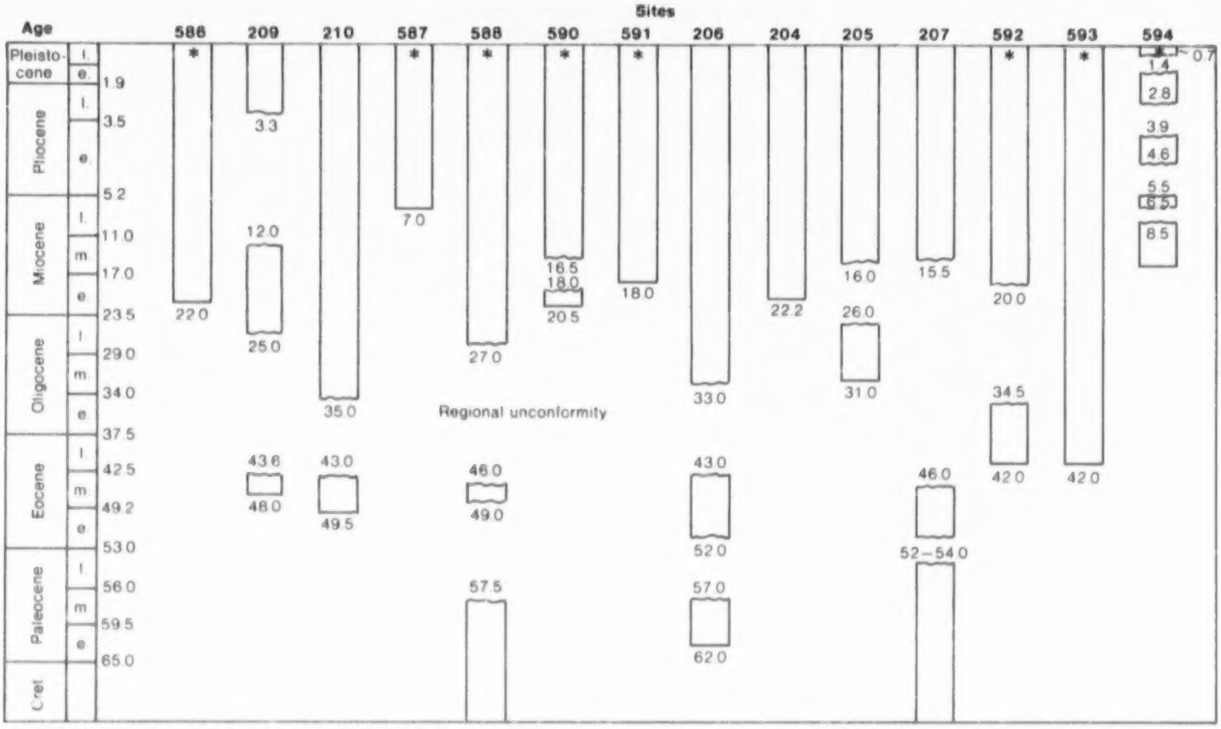

Figure 2. Age ranges represented in each of the Leg 90 drill sites (asterisk) and other sites in the southwest Pacific. Ages of contained unconformities shown in each case. Paleogene regional unconformity is clearly evident. Ages of stratigraphic boundaries were those used during Leg 90.

tinued until the latest part of Zone NP21. The Eocene/Oligocene boundary based upon planktonic foraminifers (last appearance of *G. index*) was placed near the beginning of this oxygen isotope shift. Oxygen isotope values decreased slightly ($\sim 0.2‰$) from the peak associated with the NP21/NP22 boundary and then steadily decreased with little variation during the remaining early Oligocene. Planktonic and benthic oxygen isotope variations are remarkably parallel.

Faunal and floral assemblages underwent distinct but not drastic changes at the Eocene/Oligocene boundary. Various planktonic faunal and floral assemblages exhibit reduced diversity across the boundary (Jenkins and Srinivasan, this volume; Martini, this volume) and cool-water forms increased in abundance to replace warmer-water late Eocene elements. The Eocene/Oligocene boundary is biostratigraphically linked with the last appearances (LAD) of *Globorotalia cerroazulensis-G. cocoaensis* group, *Hantkenina*, *Globigerinatheka*, and the rosette-shaped discoasters including *D. barbadiensis* and *D. saipanensis* (Berggren et al., in press).

A significant drop of up to 2000 m in the calcium carbonate compensation depth and related oceanwide lithofacies changes were associated with the Eocene/Oligocene boundary (Berger and Winterer, 1974). The late Eocene sedimentary sequences are largely represented by nannofossil chalk containing siliceous microfossils such as Radiolaria and sponge spicules, whereas the Oligocene is represented by surprisingly soft nannofossil ooze lacking biosiliceous material.

The terminal Eocene event may have had its origin in paleoceanographic changes that occurred in the high-latitude southwest Pacific sector of the Southern Ocean (Murphy and Kennett, this volume). Kennett et al. (1975) showed that the first high-latitude surface-water communication between the South Indian and South Pacific oceans occurred in the latest Eocene across the shallow, subsiding South Tasman Rise (Fig. 3). The opening of the Tasmanian Seaway at shallow depths was a major step in the development of the Circum-Antarctic Current, allowing relatively cool Indian Ocean waters to pass into the South Pacific. This led to cooling of waters in the South Pacific sector of the Southern Ocean and initial decoupling of the warm-subtropical gyre from the Southern Ocean (Kennett, 1977, 1978). It is inferred that, as a result, the first extensive sea ice appeared and cold, dense, oceanic psychrospheric bottom waters began to be produced in close association with the Eocene/Oligocene boundary in areas adjacent to the Antarctic continent (Shackleton and Kennett, 1975b; Kennett, 1978). The Eocene/Oligocene boundary event, as delineated by the $\delta^{18}O$ shift, is not isolated but rather marks the crossing of a threshold in the sequential deterioration seen in the Paleogene climatic record (Kennett, 1978; Corliss et al., 1984; Murphy and Kennett, this volume).

Oligocene Increase in the Thermal Gradient of Southwest Pacific Surface Waters

As discussed by Murphy and Kennett (this volume), changes in oxygen isotope values, measured in benthic

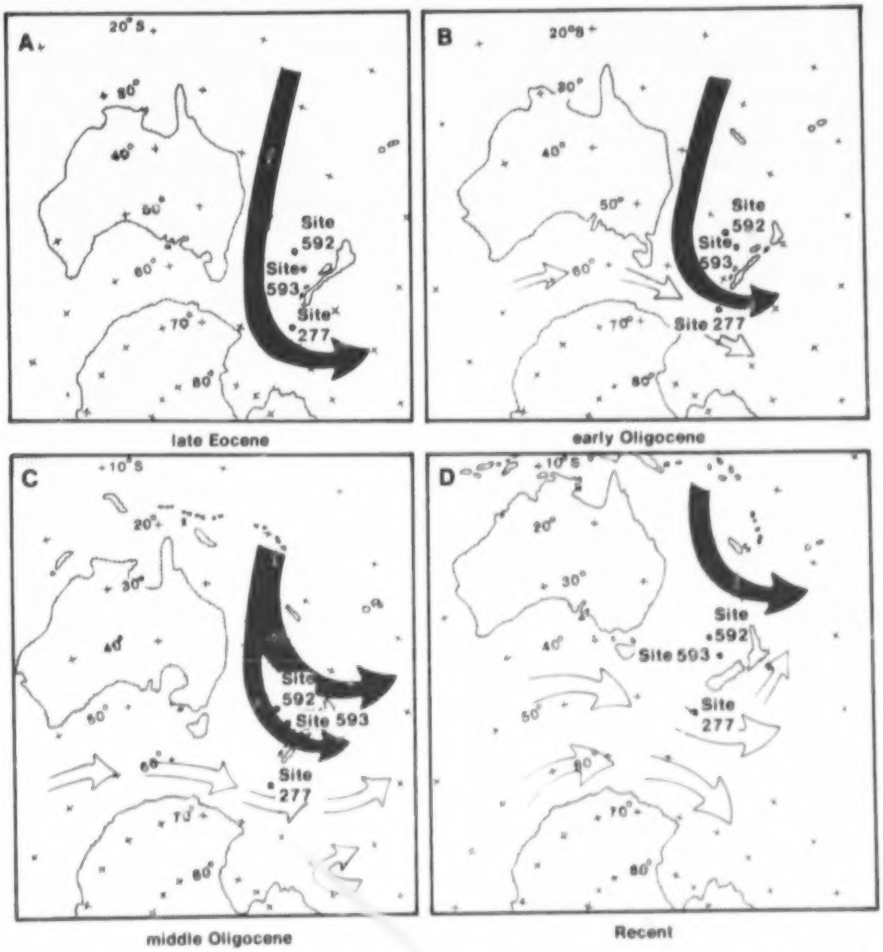

late Eocene

early Oligocene

middle Oligocene

Recent

Figure 3. Changes in surface-water circulation during the Cenozoic proposed by Murphy and Kennett (this volume) to account for the decoupling of warm gyral surface currents from the Antarctic-subantarctic region. Dark arrows indicate warm currents; open arrows cold currents. Locations of Sites 592, 593 and 277 are indicated.

and planktonic foraminifers, document the Oligocene development and strengthening of latitudinal thermal zonation in southwest Pacific subantarctic and temperate water masses. The oxygen isotope trends are not considered to have been affected by diagenesis, for reasons discussed in Murphy and Kennett (this volume) and Nelson (this volume). Weak temperature gradients of the Eocene are transformed, during the Oligocene, to the steeper gradients of the Neogene, with more distinct, latitudinally distributed surface water mass belts. The thermal structure changed in the earliest Oligocene (~36.5–36 Ma) immediately after the oxygen isotope shift associated with the Eocene/Oligocene boundary, when Site 277 began to record consistently higher ("cooler") oxygen isotope values compared to Sites 592 and 593 to the north. Sites 592 and 593 exhibit a decrease in $\delta^{18}O$ values during the early to middle Oligocene (Fig. 4). The temperature difference between Site 277 and the more northern sites continued to increase, in surface waters, during the early to middle Oligocene (37.5–33 Ma), except for a temporary reversal of the gradient at ~33 Ma. The oxygen isotope records of the benthic foraminifers also began to diverge in the earliest Oligocene. These trends also document the beginning of vertical thermal segregation as subantarctic waters cooled relative to those at temperate latitudes.

Isotopic temperature records from these sites diverged in two major steps at 36 Ma and 33 Ma, representing successive stages in the evolution of latitudinal thermal gradients between subantarctic and temperate regions in the Southern Hemisphere. Early to middle Oligocene values diverge slightly because temperatures continued to decrease at high latitudes but not at temperate latitudes. For the middle Oligocene, Oxygen isotope values between sites exhibit major, rapid divergence of both planktonic and benthic signals because the subantarctic region continued to cool and the temperate regions warmed.

This pattern of increasing isotopic offset between latitudinally distributed southwest Pacific sites is linked to the establishment and strengthening of the Circum-Antarctic Current, previously considered to have developed during the middle to late Oligocene (Kennett, 1977). As Australia and Antarctica continued to separate and the Southern Ocean expanded northward, the intensification of this current system progressively decoupled the warm subtropical gyres from the polar region and eventually led to increased Antarctic glaciation.

At ~33 Ma, in both surface and intermediate waters, the thermal gradient between Site 277 and the northern sites significantly and rapidly increased (Fig. 4). This is interpreted as reflecting a major reorganization of Southern Ocean circulation, as proposed earlier by Kennett et al. (1975) and by Kennett (1977, 1978), when deep circum-Antarctic circulation developed through the Tasmanian Seaway.

Despite the increase in temperature gradients between subantarctic and temperate regions during the Oligocene, biogeographic similarities in calcareous microfossils (Jenkins, 1975; Jenkins and Srinivasan, this volume) suggest that the Subtropical Convergence had not yet formed by the end of the Paleogene and that separate biogeographic provinces had not yet developed.

Oligocene Climate and Glacial Episodes

Murphy and Kennett (this volume) have shown that the highest $\delta^{18}O$ values in all of the Paleogene records for the southwest Pacific cluster in the middle Oligocene, marked by oscillating episodes of enrichments >0.5‰, occurring most prominently in the subantarctic record of Site 277. These values can be interpreted as recording either the coldest oceanic temperatures of the Paleogene, accumulations of Antarctic ice, or both. Several workers have argued that an Antarctic ice sheet existed at certain times during the Oligocene (Miller and Fairbanks, 1983; Keigwin and Keller, 1984; Miller and Thomas, in press; Shackleton et al., 1984). These conclusions were based upon isotopically derived bottom-water paleotemperatures cooler than those of the present oceans, although there is little sedimentary evidence to support the existence of large accumulations of Antarctic ice during the Paleogene (Kennett, Houtz et al., 1975; Hayes and Frakes, 1975).

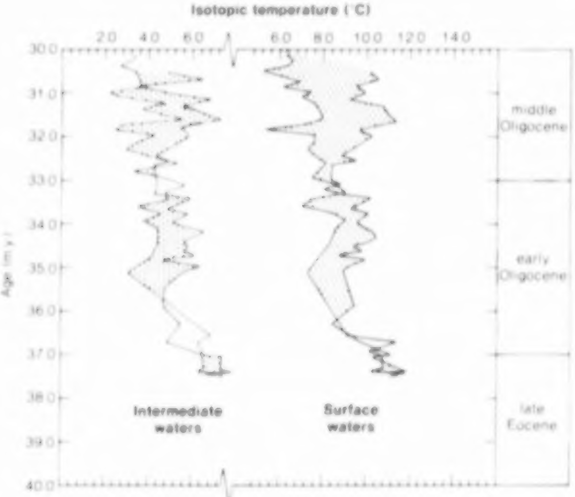

Figure 4. Isotopic temperature gradient from late Eocene to middle Oligocene between Sites 277 (more southern site) and 593 (from Murphy and Kennett, this volume). Reversals in gradient occur at ~37 to 35.5 Ma and ~33 Ma.

The data of Murphy and Kennett suggest that there may have been accumulations of Antarctic ice during the middle Oligocene, although Sites 277 and 593 do not seem to include the interval from 30 to 29 Ma in which other workers (Miller and Thomas, in press) have reported even higher $\delta^{18}O$ values. An enrichment of global δW values as a result of ice formation would appear as a synchronous enrichment in the surface and intermediate (and deep) oxygen isotope values at every site (Shackleton and Opdyke, 1973). Each site in the southwest Pacific exhibits strongly parallel planktonic and benthic oxygen isotope records until ~33 Ma, at which time they record the coolest isotopic temperatures (Murphy and Kennett, this volume). After this, the records from different sites diverge, and the cause is interpreted to be the combined effects of ice accumulation and the progressive decoupling of surface water temperatures resulting from circulation changes within the region. Furthermore, if the enriched Oligocene oxygen isotope values do indicate that ice had accumulated, this ice must have disappeared by the early Miocene, when depleted oxygen isotope values suggest very warm conditions (Kennett, this volume).

The climatic conditions of Australia also changed during the Oligocene in response to the combined effects of global climatic change and the northward movement of the Australian continent into lower latitudes. Stein and Robert (this volume) show that changes in clay mineralogy at Site 588 on the northern Lord Howe Rise monitor climatic changes occurring on Australia, the source region for the clays. During the latest Oligocene, dominant pedogenic smectite suggests dominantly warm climatic conditions with alternating periods of humidity and aridity in a low-relief area. Toward the end of the Oligocene, a gradual increase of the kaolinite/illite ratio is interpreted by Stein and Robert (this volume) to represent more tropical climates in northern Australia, leading to increased weathering and the formation of lateritic soils. The northward drift of Australia into the tropics created these changes.

Late Paleogene Regional Hiatus

It is quite well documented that the ocean basins of the southwest Pacific are marked by numerous unconformities that cut the Paleogene sequence, whereas the Neogene sequence is largely complete. The best-documented unconformity of the Paleogene removed much of the Oligocene and is commonly referred to as the Tasman Sea regional unconformity (Fig. 2; Burns, Andrews, et al., 1973; Kennett et al., 1972) or the Marshall paraconformity (Carter and Landis, 1972). Only three Leg 90 sites were drilled deep enough to potentially encounter the unconformity. At two of these (Sites 588 and 592) the unconformity was encountered whereas it is absent in the other (Site 593).

In Hole 588C, the hiatus separates sediments of middle Eocene age (Zone NP15/NP16) from those of late Oligocene age (Zone NP24, or *Chiloguembelina cuben-*

sis Zone) representing a time gap of 19 m.y. (Martini, this volume; Jenkins and Srinivasan, this volume).

The hiatus at Site 592 is of interest because it ranges in age from the early or middle Oligocene (NP22, or *Globigerina angiporoides* Zone) to the early Miocene (NN2, or *Globigerinoides trilobus* Zone), representing a time gap of about 15 m.y. Erosion at this site did not remove the Eocene/Oligocene boundary, unlike all of the other sites. At this location, erosion commenced after the time of the Eocene/Oligocene boundary.

The regional unconformity may have been formed by bottom-water masses that flowed northward through the Tasman Sea at times during the Paleogene. These water masses were activated by cooling that began at the beginning of the Oligocene (Kennett et al., 1972). The sequence at Site 592 is significant because it shows that at least in that area, bottom-water velocities were insufficient to erode sediment until the Oligocene, rather than at the Eocene/Oligocene boundary.

The absence of the unconformity in Site 593 on the Challenger Plateau indicates, as previously suggested by Kennett et al. (1975), that the bottom currents that cut the hiatus did not extend so far to the east.

Early Miocene Climatic Maximum

The earliest Miocene (older than 19.5 Ma) was marked by relatively high benthic $\delta^{18}O$ values, although the values were much lower than those of the late Miocene (Kennett, this volume; Fig. 5). This indicates warmer intermediate water and less continental ice during the earliest Miocene than during the late Miocene. A slow, general warming of intermediate water occurred between 23 and 19.5 Ma (Fig. 5), leading to the lowest $\delta^{18}O$ values for the entire Neogene between about 19.5 and 16.5 Ma (late early Miocene; late NN2 to middle NN5; Kennett, this volume). This interval represents the climax of Neogene warmth.

Warm early Miocene climates are also reflected in the pollen assemblages recovered at Site 594, to the east of South Island, New Zealand (Heusser, this volume). The pollen assemblages represent a mixture of subtropical (frost-intolerant) vegetation (trees similar to those now growing in New Guinea and New Caledonia) and temperate vegetation (trees now growing in lowland and montane parts of New Zealand). The early Miocene floras of New Zealand were thus transitional between warm-temperate to subtropical early Cenozoic vegetation and temperate vegetation of the late Cenozoic (Heusser, this volume).

Many benthic foraminiferal species first occur close to the Oligocene/Miocene boundary at Sites 588 and 593 (Boersma, this volume). This evolutionary radiation parallels that of other groups at the beginning of the Neogene, such as the planktonic foraminifers (Kennett and Srinivasan, 1983; Wei and Kennett, in press).

Early Neogene Carbon Isotope Excursion

One of the dominant features of the Neogene isotopic record (Fig. 6) is a broad $\delta^{13}C$ maximum of about 1‰ between about 19 and 14.5 Ma, from the late early to early middle Miocene, and best exhibited at Site 588, where it consists of broad peaks centered at 19 Ma, 16.5 Ma, and about 15 to 15.5 Ma (Kennett, this volume). The carbon isotope excursion corresponded to the maximum Neogene ocean temperatures as reflected in benthic and planktonic $\delta^{18}O$ values. This excursion has been recognized in other ocean basins and has been termed the "Monterey Carbon Isotopic Excursion" by Vincent et al. (in press) and Vincent and Berger (in press). The great similarity of the broad-scale Neogene $\delta^{13}C$ time-series records within and between ocean basins and with water depth clearly indicates that changes in ocean-wide average $\delta^{13}C$ of HCO_3^- in seawater dominated the records, rather than local effects.

In concurrence with other workers, Kennett (this volume) considers that this carbon isotope excursion resulted from an increase in the ratio of carbon leaving the oceans in the form of organic carbon as opposed to carbonate carbon. This increase was probably modulated by a marine transgression (Loutit, Pisias, et al., 1983; Vincent et al., in press; Woodruff and Savin, 1985). According to Vincent et al. (in press) and Vincent and Berger (in press), widespread transgression during this excursion occurred throughout the circum-Pacific region, creating major sinks for organic carbon. Organic and phosphate-rich deposits accumulated within the Monterey Formation of California and contemporaneous deposits throughout the Pacific margin. Vail and Hardenbol (1979) documented a period of coastal onlap that began at about 19 Ma, terminated about 14 Ma, and was contemporaneous with the interval containing the especially positive $\delta^{13}C$ values. The excursion thus occurred contemporaneously with a period of maximum coastal onlap (transgression) and maximum Neogene climatic warmth. Because the late early Miocene was the time of optimum climatic warming during the Neogene, tropical forests were probably widespread, and the continental organic biosphere would have been more extensive than at other times. The high continental biomass at this time would also have contributed to the positive $\delta^{13}C$ values.

The carbon isotope excursion terminated during the expansion of the Antarctic ice sheet and associated marine regression in the early middle Miocene (15.5–14.5 Ma); the decline from high values continued with little interruption until about 13 Ma. Associated global cooling probably led to greater aridity and reduced the terrestrial biomass, so that oceanic $\delta^{13}C$ values dropped during the middle Miocene.

Middle Miocene Event

The Middle Miocene Event, between about 16.5 and 13.5 Ma, represents a critical threshold in Cenozoic climatic evolution. At this time, the Leg 90 sites (588, 590, and 591) saw a major increase in $\delta^{18}O$ values (Fig. 5) interpreted by Kennett (this volume) and by numerous other workers (e.g., Savin et al., 1975; Shackleton and Kennett, 1975b) as representing a major, permanent accumulation of the East Antarctic ice sheet and cooling of bottom waters. This event lasted 3 m.y., and the average enrichment in ^{18}O was about 1.0‰. This ^{18}O enrichment event has been globally recognized in marine sedimentary sections by Savin et al. (1975); Shackleton and Ken-

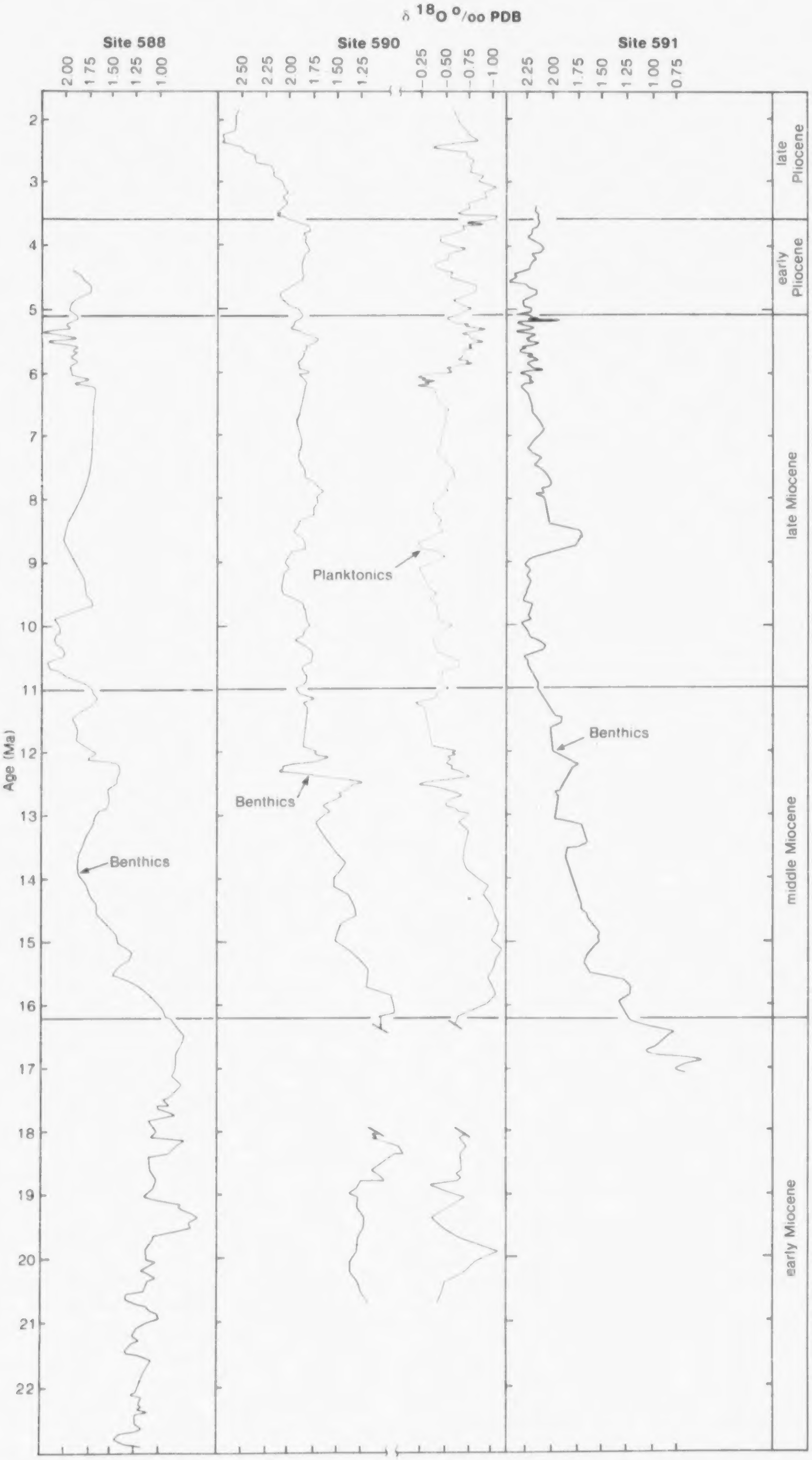

Figure 5. Smoothed $\delta^{18}O$ data (three-point running averages) for Sites 588, 590, and 591 plotted against age (from Kennett, this volume). For further details, see Kennett (this volume).

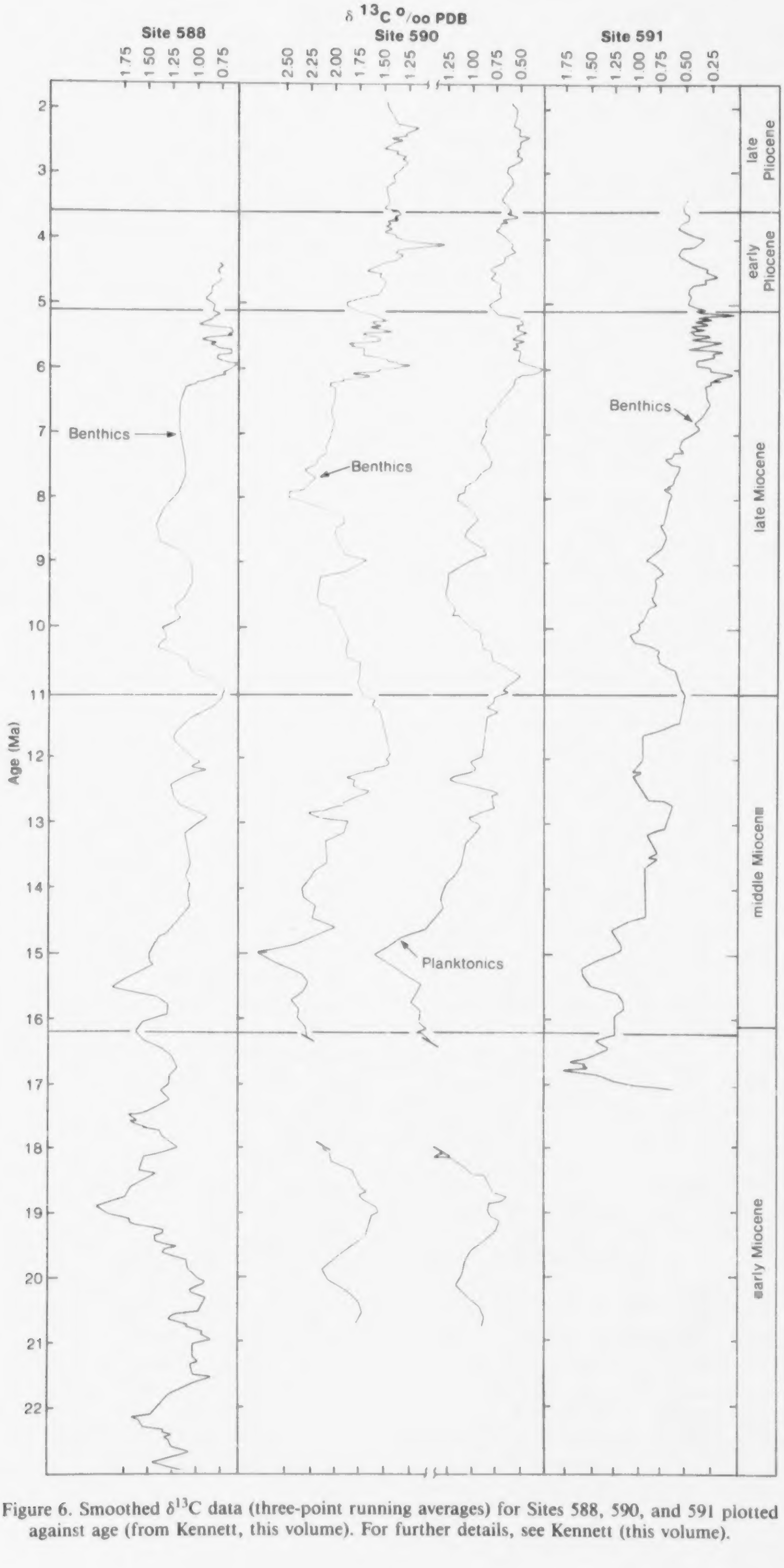

Figure 6. Smoothed $\delta^{13}C$ data (three-point running averages) for Sites 588, 590, and 591 plotted against age (from Kennett, this volume). For further details, see Kennett (this volume).

nett (1975b), Keigwin (1979), Margolis et al. (1975), Loutit (1981), Loutit, Kennett, et al. (1983), Vincent and Berger (in press), Vincent et al. (in press), Savin et al. (1981), Woodruff et al. (1981), Savin et al. (in press), and many other workers. The oxygen isotope shift was immediately preceded by the late early Miocene climatic optimum, from 19.5 to 16.5 Ma. Thus, sea-surface temperatures at high latitudes were relatively warm immediately preceding the buildup of the Antarctic ice sheet. Mercer and Sutter (1982) suggest that warm temperatures may be a necessary prerequisite for such ice accumulation.

Savin et al. (1975), Savin et al. (in press), and Loutit, Kennett, et al. (1983) have suggested that sea-surface temperatures in the tropical Pacific warmed during the middle Miocene. Tropical planktonic $\delta^{18}O$ values either decrease, show no change, or exhibit an increase that is smaller in magnitude than the shift observed in high-latitude sequences (Kennett, this volume). Warming of tropical surface waters during the middle Miocene may have resulted from the progressive thermal isolation of Antarctica and the contraction of the tropical-to-warm-subtropical gyres toward lower latitudes, as the polar and subpolar waters expanded toward the equator. Ocean circulation became less efficient at removing heat from the tropical regions. A major question remains, however: how much of the $\delta^{18}O$ shift during the early middle Miocene was due to an ice volume increase and how much was due to temperature decrease? Comparison of planktonic and benthic $\delta^{18}O$ records in Site 590 (Kennett, this volume) may assist in separating these effects, although interpretations are not unequivocal. At Site 590, the warming of surface waters during the early stage of the benthic $\delta^{18}O$ shift suggests that that part of the shift may have resulted largely from a decrease in temperature at high latitudes rather than an increase in ice accumulation. If little ice had then accumulated, glacioeustatic regression would not have occurred. $\delta^{13}C$ (benthic and planktonic) began to decrease, suggesting regression (assuming that $\delta^{13}C$ changes are related to sea level), at about 14.5 Ma, when the $\delta^{18}O$ shift occurred in both the benthic and planktonic records (Kennett, this volume). It is possible that this synchronous enrichment in both planktonic and benthic $\delta^{18}O$ represents the major ice-growth phase of East Antarctica. If this scenario is correct, then major ice accumulation and resulting regression occurred between 14.5 Ma ands 13 Ma.

In Site 593, 24 m of distinctive, pale orange nannofossil ooze is interbedded with normal, light gray to white nannofossil oozes of otherwise identical lithology. This pale orange sedimentary subunit was deposited between 15.5 and 15 Ma, contemporaneously with the early part of the middle Miocene oxygen isotope shift. It is interpreted as representing an increase in pore-water oxygen concentrations that were not subsequently reduced by postdepositional diagenesis. In the modern ocean, an orange oxidized layer is found in core-tops throughout the southwest Pacific (Nelson, this volume). We suggest that the relationship between the oxidizing event and the middle Miocene oxygen isotope shift is not coincidental. Since O_2 concentrations are controlled largely by temperature in the source area of bottom-water formation, the temperature drop between 15.5 and 15.0 Ma may have produced intermediate waters sufficiently oxygenated to prevent postdepositional reduction within the sediment. The origin of the oxidized sediment layer may, therefore, be related to temporary water mass changes connected with this major early middle Miocene development of Antarctic glaciation.

The middle Miocene development of the East Antarctic ice sheet was intimately associated with a number of other changes, including surface-water cooling—an inference based upon middle- to high-latitude Atlantic calcareous nannoplankton assemblages (Haq, 1980)—a marked steepening of the planetary temperature gradient (Savin et al., 1975), a major change in deep-sea benthic foraminiferal assemblages (Woodruff et al., 1981), an increase in hiatus abundance (van Andel et al., 1975), a shoaling of the CCD in the equatorial Pacific (Berger and Winterer, 1974), and an intensification in atmospheric circulation (Brewster, 1980). Several of these changes were also recognized in Leg 90 studies.

In Site 590, between 16 and 15 Ma, the average vertical $\delta^{18}O$ gradient ($\Delta\delta^{18}O$ benthics—planktonics) changed from about 1.75 during the early Miocene to about 2.25 during the middle and late Miocene (Kennett, this volume). This is equivalent to about a 2°C increase in the vertical temperature gradient between 1300 m and the ocean surface (assuming no salinity change occurred in surface waters). The average thermal gradient did not change significantly during the intervals before and after this event. Our results concur with those of Loutit, Kennett, et al. (1983), who suggested that much of the increase in thermal gradient during the Miocene (doubling of gradient from 6 to 12°C between the tropics and the subantarctic) took place in the middle Miocene.

An increase in upwelling, beginning in the middle Miocene ($\sim$14 Ma), in Sites 590 and 591 is indicated by a significant increase in biogenic opal (Stein and Robert, this volume), reflecting increased fertility of surface waters at the Subtropical Divergence.

A major change in deep-sea benthic foraminiferal assemblages also coincided with the Middle Miocene Event, according to the studies of Kurihara and Kennett (this volume) and Boersma (this volume). Boersma (this volume) found that the largest number of first appearances of the entire Tertiary were in Zone NN6 and, to a lesser extent, NN7 during the middle Miocene oxygen isotope shift. This interval, furthermore, heralded an increasing subdivision of bathyal benthic assemblages into bioprovinces with both depth and latitude. Differences became more pronounced between the assemblages of the lower and middle bathyal zones during this event. Kurihara and Kennett (this volume) found that *Globocassidulina subglobosa*, a dominant early Miocene element on the Lord Howe Rise sequences, became less dominant in the shallower sites (Sites 590 and 591), whereas *Epistominella exigua*, which was associated with the bottom waters of the New Caledonia Basin, migrated upslope and became dominant at these shallower depths. This suggests that the deeper water masses within the New Caledonia Basin became shallower, reaching water depths of about

1300 m during the early middle Miocene. These faunal changes occurred during the beginning of the $\delta^{18}O$ shift (NN5) at Sites 590 and 591, close to the early/middle Miocene boundary. The inferred change in vertical water mass structure that created the faunal changes was probably related to high-latitude surface-water cooling caused by increased Antarctic glaciation.

These changes in intermediate waters also markedly decreased planktonic/benthic ratios during the Middle Miocene Event (Kurihara and Kennett, this volume). Relatively higher numbers of benthic foraminifers after the early middle Miocene may have resulted from higher nutrient levels in deep-sea sediments caused by increased surface-water productivity which in turn resulted from increased upwelling at that time.

Middle Miocene paleoclimatic changes also had a marked impact upon the terrestrial climates of Australia (Stein and Robert, this volume). During the early middle Miocene, a distinct increase of illite at Site 588 is considered by Stein and Robert (this volume) to represent an increase in aridity in northern and central Australia. In contrast, high content of pedogenic smectite at Site 590, to the south, indicates that southern Australian continental climates were dominated by alternating humid and semiarid conditions. The expansion of aridity in northern Australia was almost certainly related to the expansion of the East Antarctic ice sheet in the middle Miocene. Increased availability of eolian sediments in Australia also increased the flux rates of terrigenous sediments to the Lord Howe Rise region (Stein and Robert, this volume). Increased aridity of Australia during the middle Miocene is also suggested by the first appearance of opal phytoliths in Lord Howe Rise sequences during Zone NN6 at 14.5 Ma (Locker and Martini, this volume). According to Locker and Martini (this volume) this record indicates the initial development of open grasslands in Australia. Westerly winds transported phytolith-bearing dust from the arid and semiarid regions of Australia more than 1000 km to the Lord Howe Rise region.

Late Miocene Paleoclimates

Following the Middle Miocene Event, during the remainder of the middle and late Miocene benthic $\delta^{18}O$ values underwent distinct fluctuations (Fig. 5), but the average value remained unchanged and the relatively enriched values reflect a period of prolonged, cool climates. The isotopic data show two distinct episodes of climatic cooling close to the middle/late Miocene boundary. The earliest of these events occurred between 12.5 and 11.5 Ma in the latest middle Miocene (Kennett, this volume).

The second cooling event, at the beginning of the late Miocene between 11 and 9 Ma, is marked by some of the highest $\delta^{18}O$ values of the entire Miocene. This was followed by relative warmth during the middle part of the late Miocene between about 9 and 6.5 Ma, as revealed by slightly lower $\delta^{18}O$ values. Relative warmth in the middle late Miocene (9–7 Ma) was also inferred by Haq (1980) from Atlantic calcareous nannoplankton biogeography.

During the early and middle late Miocene (10.5 to 6.5 Ma), sedimentation rates at Sites 586 (Ontong-Java Plateau) and 591 (Lord Howe Rise) were typical of carbonate platforms outside regions of high productivity (Gardner et al., this volume). The sedimentation rate on Lord Howe Rise was about 20 m/m.y., on the Ontong-Java Plateau about 25 m/m.y. The bulk-sediment mass accumulation rates of the two areas were about 2500 g/cm^2 per m.y. for Lord Howe Rise and about 3000 g/cm^2 per m.y. for Ontong-Java Plateau. These mass accumulation rates are typical for the southwestern Pacific at that time (Worsley and Davies, 1979). Changes in clay mineralogy and rates of accumulation of terrigenous sediments in Lord Howe Rise sequences (Stein and Robert, this volume) indicate that desertification of Australia continued to increase during the late Miocene. A sharp decrease in the smectite/illite (S/I) ratio during the middle to late Neogene in Lord Howe Rise sediments was interpreted by Stein and Robert (this volume) to represent increased transport of illite from Australia. The trends also indicate that the desert areas expanded southward (Fig. 7). By the middle late Miocene ($\sim$7.5 Ma), very low S/I ratios like those of the Quaternary occurred in all of the Lord Howe Rise sites (Sites 588, 590, 591) examined by Stein and Robert (this volume). During the late Miocene, the abundance of opal phytoliths on the Lord Howe Rise displayed a slight but noticeable increase compared with the middle Miocene (Locker and Martini, this volume), also reflecting increased aridity in Australia. Kemp (1978) made a similar finding for the Neogene, based upon palynological data. Distinct minima of the S/I ratios and increased accumulation rates of terrigenous sediments on the Lord Howe Rise suggest a maximum in aridity occurred between about 10 and 9 Ma in the early late Miocene, coinciding with the major cooling episode evidenced in the oxygen isotope record.

Terminal Miocene Event

During the latest Miocene, numerous oceanographic changes occurred within a relatively narrow time interval of only 1.3 m.y. Between about 6.3 and 5.0 Ma, evidence exists for conspicuous global cooling, worldwide regression, permanent depletion in carbon isotope values, intensification of oceanic circulation, possible development of the West Antarctic ice sheet, isolation/dessication of the Mediterranean Basin ("Messinian Salinity Crisis"), and several other oceanographic and climatic changes.

Studies of Leg 90 sequences also revealed an association of numerous oceanographic, climatic, and biotic changes during the latest Miocene. They are summarized in the following sections.

Carbon Isotope Shift

The latest Miocene at 6.2 Ma is marked by a distinct, rapid $\delta^{13}C$ shift of up to $-0.75‰$ in all of the southwest Pacific sites (Fig. 6), both in the benthic and planktonic records (Kennett, this volume; Elmstrom and Kennett, this volume). This depletion in ^{13}C was followed by markedly low values during much of the remainder of the late Neogene, which has led to the suggestion that the carbon isotope change was "permanent" (Keigwin, 1979). This well-known late Miocene carbon isotope shift is re-

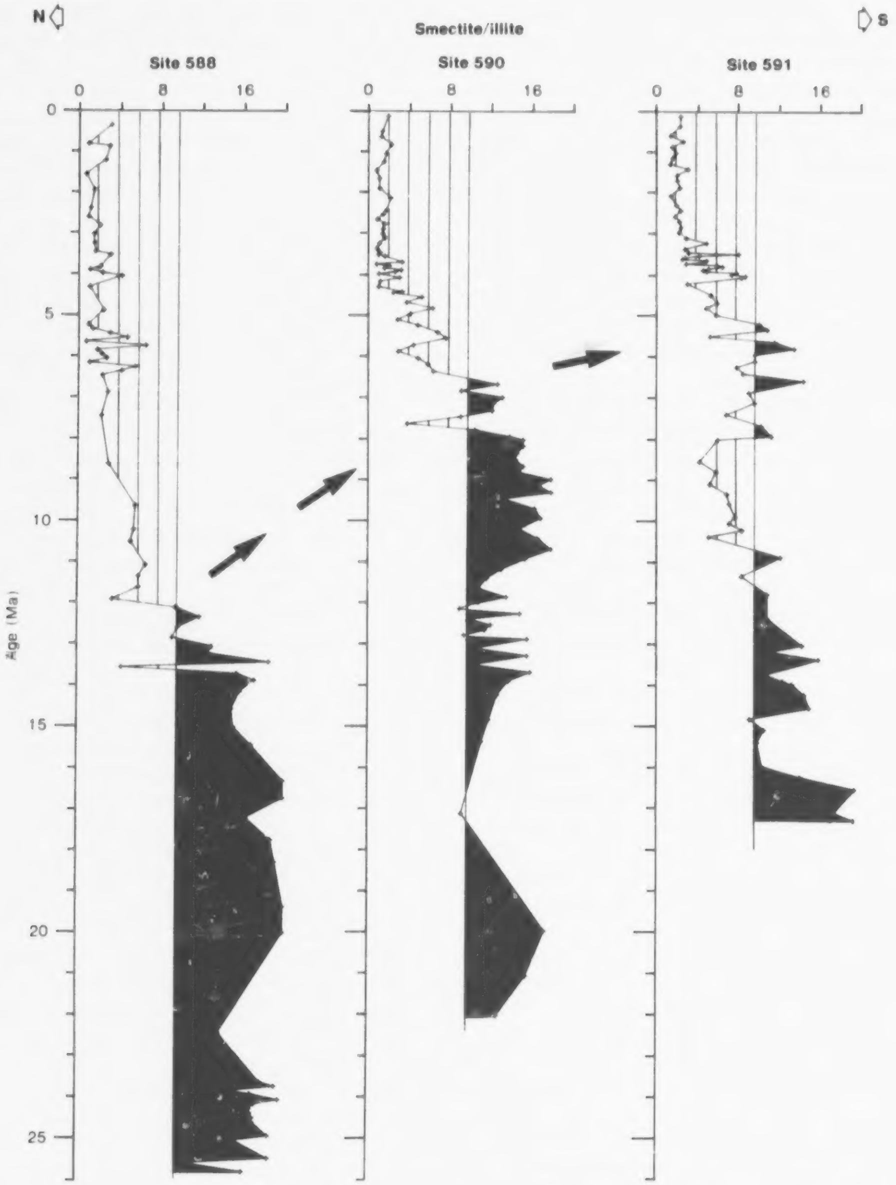

Figure 7. Smectite/illite ratios (S/I) of clay mineral assemblages in Sites 588, 590, and 591 from the Lord Howe Rise. Low S/I ratios reflect dominantly arid Australian continental climates. Note inferred expansion of continental aridity toward the south during the late Neogene (from Stein and Robert, this volume).

corded throughout the Indo-Pacific and South Atlantic and is considered to have been isochronous (Keigwin, 1979; Bender and Keigwin, 1979; Loutit and Kennett, 1979; Keigwin and Shackleton, 1980; Vincent et al., 1980; Haq et al., 1980; Hodell and Kennett, 1984). This shift, which seems to have occurred within a period of not much more than 100,000 yr. (Vincent et al., 1980), was assigned an age of ~6 Ma by Haq et al. (1980) and 6.2 Ma by Loutit and Kennett (1979), and is estimated at 6.4 Ma by Barron et al., (in press). The magnitude of the shift throughout the Indo-Pacific region is generally reported to be about −1‰ (Haq et al., 1980); in the South Atlantic a shift of 0.7‰ has been reported by Hodell and Kennett, 1984; in the North Atlantic a shift of 1.0‰ has now been identified by Keigwin et al., in press.

At Site 590, the shift occurs in close association with a number of biostratigraphic events that have been previously recognized to occur near the time of the carbon shift (Elmstrom and Kennett, this volume). These events include the first evolutionary appearance of *Globorotalia conomiozea* (Loutit and Kennett, 1979; Loutit, 1981); the first appearance of *Amaurolithus primus* (Haq et al., 1980); and a distinct switch in the coiling direction of *Neogloboquadrina pachyderma*.

Numerous hypotheses have been proposed to explain the cause of the carbon isotope shift, including a change in the rate of organic carbon burial and a change in the rate of upwelling and ocean fertility (Bender and Keigwin, 1979). The carbon shift is believed by some to have been caused by an increase in the flux of organic matter from coastal lowlands and continental shelves exposed by regression (Loutit and Keigwin, 1982; Vincent et al., 1980; Loutit, Pisias, et al., 1983), reinforced by increased oceanic fertility (Vincent et al., 1980). Kennett (this volume) found this theory very compelling because of the close temporal association of the carbon shift with global regression (Kennett, 1967; Adams et al., 1977; Vail and Hardenbol, 1979), inferred to have resulted from glacioeustatic lowering of sea level (Kennett, 1967; Loutit and Kennett, 1979; Mercer and Sutter, 1982) in the latest Miocene. Estimates of the magnitude of the marine regression are similar, ranging from 40 to 80 m (Loutit and Kennett, 1979; Berggren and Haq, 1976; Cita and Ryan, 1979).

The drop in the CCD throughout the oceans has an origin similar to that of the carbon isotope shift, having resulted from an increase in the fractionation of carbonate and organic carbon entering the deep basins from the continental shelves during the latest Miocene regression (Berger, 1970; Ciesielski et al., 1982).

Increased Sedimentation Rates and Benthic Foraminiferal Faunal Turnover

Also associated with the carbon isotope shift was an increase in sedimentation rates in both the fine and coarse biogenic sediment fraction (Gardner et al., this volume). This increase, general throughout the southwest Pacific (Fig. 8), was caused by higher biogenic productivity that resulted, at least in part, from an increase in upwelling at the Subtropical Divergence and the Equatorial Divergence.

Coincident with the carbon isotope shift and increase in biogenic sedimentation rates was a major turnover of the benthic foraminiferal assemblages (Kurihara and Kennett; Boersma; both this volume) near the NN11a/NN11b boundary (6.3 Ma). At this time, new uvigerinid and/or miliolid faunal elements evolved at all sites, but less so at Site 593 where, instead, the less ornamented brizalinids replaced the reticulate species in importance (Boersma, this volume). The uvigerinids particularly included the more hispid, spinose, or costate forms, rather than the hispido-costate forms that appeared slightly later in the latest Miocene. The uvigerinids are present only during the latest Miocene and permanently reappear again in late Pliocene to Quaternary assemblages. They are known to have appeared in increased abundances in many areas of the world's oceans during the latest Miocene in association with the $\delta^{13}C$ shift (Keigwin, 1979), reflecting increases in organic carbon flux rates that accompanied increases in global accumulation rates. Boersma (this volume) suggests that a direct relation exists among benthic faunal composition, increased biogenic sediment supply, and inferred surface-water productivity. This conclusion is largely based upon the increased abundance of uvigerinids (including *Rectuvigerina*), which have been shown to be related to episodes of high productivity and increased sedimentation during the Paleogene and Quaternary in other regions.

Epistominella exigua was also replaced during the late Miocene *Globigerina nepenthes* Zone at Site 590 by *E. rotunda* (Kurihara and Kennett, this volume). Synchronous with this faunal change, assemblages at Site 206 became temporarily dominated by *E. umbonifera*. This species is abundant in Cenozoic sections of deeper DSDP sites of the Pacific (Resig, 1976), and is associated with Antarctic Bottom Water in the Atlantic Ocean (Streeter, 1973; Schnitker, 1974) and in the Indian Ocean (Corliss, 1978). The temporary dominance of *E. umbonifera* at Site 206 may indicate the influence of deep water masses, probably Antarctic Bottom Water, during the latest Miocene. Bottom-water temperatures seemed to have cooled at the three sites during this time.

Climatic Cooling

At 6.2 Ma, a marked increase of planktonic $\delta^{18}O$ of about 0.5‰ occurred in the Lord Howe Rise sites, which coincides exactly with the late Miocene Epoch 6 carbon shift. This represents a significant and rapid cooling of surface waters from the latest Miocene to earliest Pliocene (6.2 to 4.5 Ma). In Site 588, the carbon shift also coincided with a shift toward higher benthic $\delta^{18}O$ values (Fig. 5; Kennett; Elmstrom and Kennett; both this volume). Similar high $\delta^{18}O$ values are reported by Shackleton and Kennett (1975a) from Site 284 and are interpreted to represent a major expansion of the Antarctic ice sheet. In Site 590, this enrichment in $\delta^{18}O$ coincided with a time of cool surface waters, suggested by high frequencies of *Neogloboquadrina pachyderma* and low frequencies of the warmer-water planktonic foraminifers (Elmstrom and Kennett, this volume).

The Terminal Miocene Event was marked by widespread cooling at high and middle latitudes (Ingle, 1967, 1973; Barron, 1973; Keller, 1979; Kennett, 1967; Kennett and Vella, 1975; Loutit and Kennett, 1979; Bandy et al., 1971; Cita and Ryan, 1979; Poore, 1981; Haq, 1980). In Argentina, Patagonian glaciers extended beyond the Andean Mountain front, apparently for the first time, between about 7 and 5.2 Ma (Mercer and Sutter, 1982). In Sites 588 and 590, a number of brief intervals of high $\delta^{18}O$ values between 5.4 and 4.9 Ma are interpreted to represent further increases in Antarctic ice volume, although the variability of the $\delta^{18}O$ record reflects instability in this ice (Hodell et al., in press). Much of this ice buildup may have been related to the expansion of the West Antarctic ice sheet (Ciesielski et al., 1982). This conclusion is based upon a variety of observations, including the northward expansion of ice-rafted debris in the Southern Ocean (Ciesielski et al., 1982); a northward migration of the Antarctic Convergence, inferred from a rapid equatorward displacement of the Antarctic siliceous biogenic belt (Tucholke et al., 1976; Kemp et al., 1975); a conspicuous increase in biogenic opal production (Kennett et al., 1975; Brewster, 1980); and a late Miocene age for the formation of the Ross

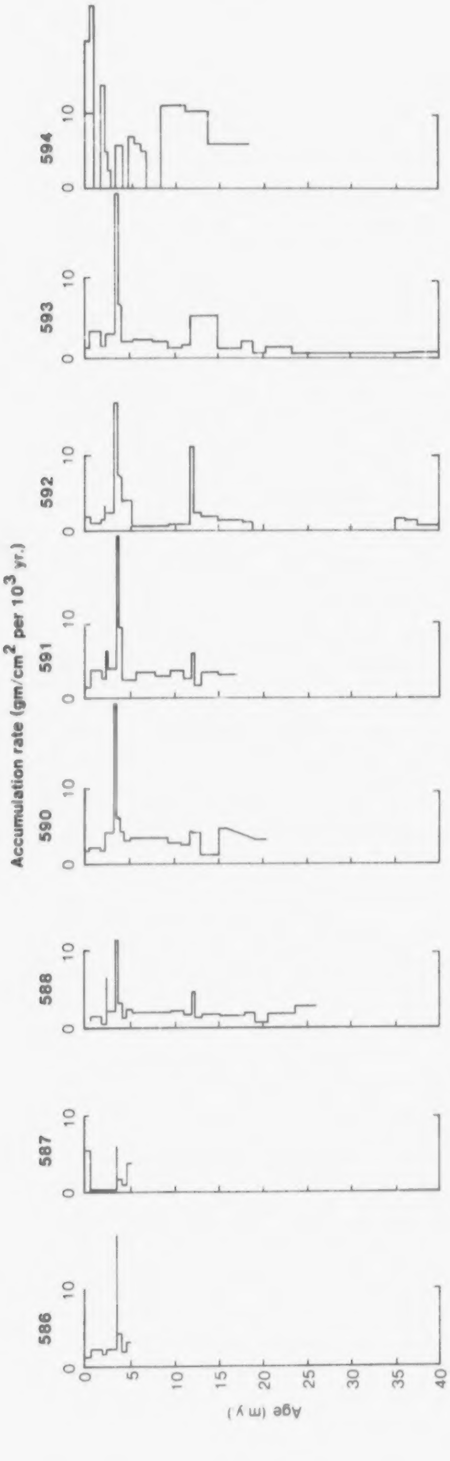

Figure 8. Mass accumulation rates of sediments at Leg 90 drill sites.

Sea disconformity, which is believed to be due to the expansion of a grounded Ross ice shelf (Hayes and Frakes, 1975).

Other climatic and oceanographic events closely associated with the Terminal Miocene Event include intensified oceanic circulation (Brewster, 1980; Savin et al., in press), high sediment accumulation rates (Davies et al., 1977), and marine regression (Kennett, 1967; Adams et al., 1977; Berggren and Haq, 1976). The latest sea-level fall was sufficient to isolate the Mediterranean and initiate the "Messinian Salinity Crisis" (Cita, 1982) between about 5.7 and 5.2 Ma. Previous work has indicated that this sea-level fall was largely glacioeustatic because of its rapidity and its association with surface-water cooling at middle and high latitudes (Kennett, 1967; Kennett and Watkins, 1974; Loutit and Kennett, 1979; Loutit, 1981) and with a period of relatively high $\delta^{18}O$ values (Shackleton and Kennett, 1975a; Kennett et al., 1979; Loutit and Kennett, 1979; Loutit and Keigwin, 1982; Ciesielski et al., 1982; McKenzie et al., 1984; Hodell et al., in press).

Continental Aridity

The latest Miocene to early Pliocene was also a time of increased cooling and aridity of the New Zealand and Australian land masses. Changes in pollens at Site 594 (Heusser, this volume) document a warm, moist climate in the earlier late Miocene, followed by cooler, drier conditions in the latest Miocene, when herbs and shrubs developed and temperate forests expanded. In Australia, the latest Miocene (close to 5 Ma) was marked by an episode of increased aridity, judging by increased accumulation rates of wind-blown, terrigenous sediments in the Lord Howe Rise region (Stein and Robert, this volume). At 5.1 Ma (close to the Miocene/Pliocene boundary), a sudden increase in opal phytolith abundance in Lord Howe Rise sequences reflected further aridification of Australia (Locker and Martini, this volume).

Early Pliocene Increased Biogenic Sedimentation

During the Pliocene (as shown by Site 590), average benthic $\delta^{13}C$ values were lower by about 0.25‰ and planktonic $\delta^{13}C$ by about 0.75‰ than during the Miocene preceding the carbon shift (Elmstrom and Kennett, this volume). An interval of relatively low values occurred during the early Pliocene between about 5 and 4 Ma. This interval corresponds with a period of relative global warmth (Kennett, 1967; Loutit and Kennett, 1979; Ingle, 1967; McKenzie et al., 1984), in which occurred the highest calcareous nannofossil diversity for the Neogene (Lohman, this volume), global marine transgressions (Kennett, 1967; Kennett and Watkins, 1974; Vail and Hardenbol, 1979), and relatively low $\delta^{18}O$ values in benthic foraminifers, as is shown at Site 590 and elsewhere (McKenzie et al., 1984; Hodell et al., in press). This depletion in ^{18}O values probably reflects a decrease in global ice volume and a marine transgression into the Mediterranean that restored pelagic sedimentation. This early Pliocene interval is also marked by relatively high $\delta^{13}C$ values, which Kennett (this volume) suggests may have resulted from marine transgression.

During the early Pliocene between 4 and 3 Ma, there was a remarkable, widespread increase in sedimentation rates (up to 131 m/m.y. at Site 591) and mass accumulation rates (MAR) in the Lord Howe Rise sequences (Fig. 8). At Site 591, the <63 um MAR increased from about 2100 to >8000 g/cm^2 per m.y. (Gardner et al., this volume). During this same interval, the >63 um MAR rose from less than 200 to about 800 g/cm^2 per m.y. Less dramatic, but significant increases in size-fraction MARs also occurred on Ontong-Java Plateau (Site 586) where the <63 um MAR increased from 2000 to 3000 g/cm^2 per m.y., and the >63 um MAR increased from 700 to 1100 g/cm^2 per m.y. (Gardner et al., this volume). The ratio of the coarse- to fine-fraction components underwent little change during this increase.

The large MARs are not due to dilution from noncarbonate components because noncarbonate material comprises only a minor amount of the sediment. Nor do they reflect variations in calcium carbonate dissolution, because the sites are located well above the lysocline and show little evidence of dissolution other than that caused by burial diagenesis. Redeposition from winnowed areas seems not to be a factor, because there is little evidence of reworking of microfossils. We do not believe that the high sedimentation rates are an artifact of an imprecise chronology, because the age boundaries would have to be substantially changed to offset the pattern of increased MAR rates. This early Pliocene episode of increased biogenic sedimentation on the Lord Howe Rise and Ontong-Java Plateau corresponds to a period of maximum sedimentation rates in the Columbia Basin (Prell, Gardner, et al., 1982), the Falkland Plateau (Ciesielski et al., 1982), the Walvis Ridge area (Moore et al., 1983; Shackleton et al., 1984), and maximum carbonate MAR averaged for the Pacific Ocean (Davies and Worsley, 1981).

The increases in sedimentation rates and bulk-sediment MARs on the Lord Howe Rise and Ontong Java Plateau were due to increased biogenic productivity of both calcareous nannoplankton and foraminifers (Gardner et al.; Elmstrom and Kennett; Nelson; all this volume). The increased productivity on the Lord Howe Rise probably was caused by increased upwelling at the Subtropical Divergence and that on the Ontong-Java Plateau by increased upwelling at the Equatorial Divergence. If planktonic foraminifers increased their productivity, then the planktonic/benthic foraminiferal ratio (P/B) should also have increased. However, the average P/B ratio of Site 591 in the early Pliocene, the time of highest calculated sedimentation rates, is only slightly higher than ratios in the Quaternary and the late Pliocene, and is comparable to late Miocene estimates (Kurihara and Kennett, this volume). To maintain constant ratios, the productivity of benthic foraminifers must have increased proportionally with planktonic productivity.

The early Pliocene between 4 and 3 Ma was also marked by maximum accumulation rates of wind-blown, non-carbonate terrigenous sediment in all sites of the Lord Howe Rise (Stein and Robert, this volume). This suggests an increase in wind strength and/or aridity at the time biogenic productivity increased in the southwest Pacific.

Both the stable isotope data and faunal analyses from Site 590 indicate that the character of surface waters changed during the time when biogenic sedimentation rates increased (Elmstrom and Kennett, this volume). Changes included a distinct increase in $\delta^{18}O$ of planktonic foraminifers; a decrease in the gradient between surface and intermediate water $\delta^{13}C$ and $\delta^{18}O$; a 1.0‰ depletion of the $\delta^{13}C$ of two species of planktonic foraminifers; mixing of warm and cool planktonic foraminiferal elements, which normally indicates seasonal upwelling (Thiede, 1983); and high variability in planktonic foraminiferal species frequencies and in planktonic oxygen isotope values, reflecting temperature fluctuations associated with variable rates of upwelling. These data suggest that surface-water productivity, induced by localized upwelling at the Subtropical and Tropical divergences, significantly increased during the early Pliocene.

The increase in biogenic productivity is reflected mainly in the calcareous fossils, rather than in the siliceous forms more typical of areas of oceanic upwelling. Elmstrom and Kennett (this volume) suggest that this may be due to the nature of the upwelling regime. Most areas of siliceous biogenic productivity occur where cold, nutrient-rich intermediate waters are upwelled. In the southwest Pacific, the upwelling occurs over a shallow-water pedestal; thus, the upwelled waters are both shallow and warm, being associated with the East Australian Current. The upwelled water is thus warmer than in most oceanic upwelling regimes such as the Antarctic Convergence, the Equatorial Divergence, and the Eastern Boundary Current systems. It remains unclear why upwelling (and biogenic productivity) increased during the early Pliocene between about 4 and 3 Ma, a time of relative global climatic warmth and stability.

Middle to Late Pliocene Climatic Coolings

During the middle Pliocene at about 3.4 Ma, a 0.4‰ increase is recorded in the benthic $\delta^{18}O$ record of Site 590 (Fig. 5), documenting a net increase in average global ice volume and cooling of bottom waters (Elmstrom and Kennett; Kennett; both this volume). A similar oxygen isotope shift has been reported from the equatorial Pacific (Shackleton and Opdyke, 1977; Keigwin, 1979; Prell, 1984), the South Atlantic (Weissert et al., 1984), the North Atlantic (Shackleton and Cita, 1979), and the Mediterranean (Keigwin and Thunell, 1980). This shift almost certainly documents a cooling of intermediate waters (Prell, 1984), but possibly also some additional growth of Antarctic ice (Weissert et al., 1984). Increased glaciation ofAntarctica at about 3.5 Ma created a northward shift in the deposition of circum-Antarctic glacial marine sediments (Ciesielski and Weaver, 1974). A glacial increase at about 3.5 Ma is also consistent with the observation of cooling of the Southern Ocean at 3.6 Ma (Keany, 1978) and in temperate areas (Kennett and Vella, 1975; Kennett et al., 1979), and increased Patagonian glaciation (Mercer, 1976).

The planktonic $\delta^{18}O$ record during the Pliocene (as recorded in Site 590) is more variable than the benthic $\delta^{18}O$ record, and exhibits different trends. Between 3.6 and 2.2 Ma at Site 590, a positive shift of 0.4‰ in benthic $\delta^{18}O$ generally coincided with a negative shift of about 0.4‰ in planktonic $\delta^{18}O$ (Elmstrom and Kennett, this volume). This is interpreted by Kennett (this volume) to represent a surface-water warming of at least 2°C at these latitudes, in concurrence with the observation of Weissert et al. (1984) at similar latitudes (~30°S) in the South Atlantic. This warming occurred when high-latitude glaciers were growing.

During the late Pliocene between 2.6 and 2.4 Ma, $\delta^{18}O$ again increased ~0.4‰ (Elmstrom and Kennett, this volume). This isotopic shift heralded the beginning of major Northern Hemisphere ice accumulation (Backman, 1979; Prell, 1984; Shackleton et al., 1984). A decrease in the frequencies of warm-subtropical planktonic foraminifers and *Neogloboquadrina pachyderma* at this time may represent a decrease in the intensity of upwelling at the Subtropical Divergence (Elmstrom and Kennett, this volume).

Further distinct changes in the vertical temperature gradient occurred both during the middle Pliocene at 3.6 Ma, whereby the average thermal gradient increased by another 0.5‰ (~2°C), and during the late Pliocene at 2.4 Ma, with a further shift of 0.25 to 0.5‰ (~1-2°C) (Fig. 5; Kennett, this volume). Thus, the late Pliocene oxygen isotope trends are somewhat comparable to that which occurred during the early middle Miocene (16 to 14 Ma); that is, they indicate that surface waters warmed at these middle latitudes at times when large amounts of ice accumulated at high latitudes and that the vertical temperature gradient of the open ocean showed a major, permanent increase.

Mass accumulation rates during the late Pliocene are much reduced from early Pliocene values but are still higher than average Neogene rates. After about 3.5 to 3 Ma, the fine-sediment fraction decreased and values of the coarse fraction were persistently high, suggesting a significant episode of winnowing by bottom currents (Gardner et al.; Stein and Robert; both this volume). This persisted for the remainder of the Neogene and almost certainly reflects enhanced oceanic circulation associated with the further development of polar glaciation. Further major changes in benthic foraminiferal assemblages are associated with this change on the Lord Howe Rise, especially marked by an increase in uvigerinid abundance.

Australian continental climate from 3 Ma to the present was dominantly arid, based upon consistently low S/I ratios and high amounts of eolian terrigenous sediments on the Lord Howe Rise (Stein and Robert, this volume). Opal phytoliths increase drastically in late Pliocene sediments, peaking at 2.5 Ma (Locker and Martini, this volume) and indicating further expansion of Australian grassland areas and intensified transport of dust to the Lord Howe Rise area.

Quaternary Glacial-Interglacial Oscillations

Oxygen isotope studies of the Quaternary at Site 593 (Nelson et al., this volume) clearly exhibit two modes of Quaternary $\delta^{18}O$ variation (Prell, 1982): depleted values with generally low variability in the early Quaternary

(1.9–0.9 Ma), and enriched values with high variability during the late Quaternary (0.9–0 Ma). At Site 593, the major glacial–interglacial episodes are clearly recognizable. Correlation with magnetostratigraphy (Barton and Bloemendale, this volume) makes it possible to place the Stage 19/20 boundary at the Brunhes/Matuyama Chron boundary and the Stage 23/24 boundary at the end of the Jaramillo Subchron. The shift toward much more intense glacial–interglacial fluctuations near the beginning of the Jaramillo Subchron reflects a fundamental change in global ice budget and must be linked to an expansion of the Northern Hemisphere ice sheets, including perhaps the development of an Arctic Ocean ice sheet during glacial episodes (Williams et al., 1981). In Site 593, the Quaternary carbonate oozes display a cyclical variation in texture consisting of alternating zones of relatively enriched and impoverished sand-sized material, mainly foraminifers (Nelson et al., this volume). Carbonate dissolution is unimportant at these shallow water depths on the Challenger Plateau, and the coarser intervals are considered by Nelson et al. (this volume) to result from episodes of intensified winnowing by bottom currents, particularly during glaciation.

Sedimentary cycles during the Quaternary (and the remainder of the late Neogene) are also very conspicuous at Site 594. The section contains many fluctuations of hemipelagic and impure pelagic lithofacies that are evident from color changes in the core and calcium carbonate stratigraphy (Nelson et al., this volume). The hemipelagic sediments are typically greenish gray nannofossil-bearing clayey silts, rich in mica and quartz, and often diatom- or sponge-spicule-bearing. The $CaCO_3$ content in the hemipelagic sediments ranges from 0 to 25%. In content, the pelagic interbeds are mainly bluish gray foraminifer-bearing nannofossil oozes with reduced, but variable, amounts of terrigeneous material and only trace quantities of biosiliceous components. The $CaCO_3$ of these sediments ranges between 50 and 80%. Individual pelagic to hemipelagic cycles (at least 25 major hemipelagic sediment episodes during the last 6 m.y.) range from 0.5 to 10 m in thickness.

Oxygen isotope analyses of the last 0.7 m.y. (Nelson et al., this volume) confirm that the hemipelagic sediment intervals, marked by high $\delta^{18}O$ values, accumulated during glacial episodes when sea level was low, whereas the pelagic interbeds, marked by lower $\delta^{18}O$ values, were deposited during interglacial episodes when sea level was high. As with other Quaternary isotopic records (e.g., Shackleton, 1977), the $\delta^{13}C$ of Site 594 exhibits oscillations that are related to glacial-interglacial episodes; lower $\delta^{13}C$ values are associated with glacial intervals.

Fluctuating climatic modes were inferred by Heusser (this volume) from high-frequency changes in arboreal pollen in the upper 200 m of Site 594. High values in the podocarp/*Nothofagus* ratio are interpreted to represent warm climatic intervals (Heusser, this volume), and low values to represent cold climatic intervals (Mildenhall, 1976). Heusser (this volume) demonstrates that a close correlation exists between cool-temperate (glacial) pollen assemblages and hemipelagic oozes, low carbonate content, high $\delta^{18}O$, and low $\delta^{13}C$. Warm-temperate (interstadial and interglacial) pollen assemblages are associated with pelagic oozes, high carbonate content, low $\delta^{18}O$), and high $\delta^{13}C$ (Nelson et al., this volume). The history of alpine glaciations, cool vegetation, and associated erosion in South Island are contained within the hemipelagic oozes, which can be correlated with major fluctuations of Northern Hemisphere ice sheets, as evidenced by the marine oxygen isotope record.

The late Quaternary (0.7 Ma to present) of the Lord Howe Rise sites are marked by intensified winnowing, as is shown by substantial decreases in the mass accumulation rates of both the fine and coarse fractions (Gardner et al., this volume). This is due to intensified circulation of intermediate waters in the Lord Howe Rise region, but not on the Ontong-Java Plateau, where evidence for increased winnowing is lacking (Gardner et al., this volume).

SUMMARY

Leg 90 of the Deep Sea Drilling Project obtained a traverse of eight middle to late Cenozoic sections from relatively shallow water pedestals (1000 to 2000 m) in the southwest Pacific between tropical and northern subantarctic water masses. The sequences are largely calcareous ooze or chalk, relatively continuous and undisturbed, having been collected using the Hydraulic Piston Corer and the Extended Core Barrel. Sediment was collected during Leg 90 from beneath every major surface water mass between the equator and the subantarctic, permitting paleoceanographic records to be analyzed for each water mass. Paleoceanographic and paleoclimatic investigations of Leg 90 material have involved analyses of oxygen and carbon isotopes, sediment character and accumulation rates, and microfossils.

The benthic $\delta^{18}O$ record in Leg 90 sites exhibits a number of large changes that reflect the sequential development of polar glaciation and cooling of bottom waters beginning in the latest Eocene–earliest Oligocene. The late Eocene was marked by warm, equable climates with low surface-water temperature gradients between tropical and subantarctic regions. Major climatic cooling events in the Leg 90 sequences include the Terminal Eocene Event (37 Ma) which marks the transition from warm Eocene to cooler Oligocene conditions; middle Oligocene cooling events, clustered close to 31 Ma, and which may, in part, represent temporary accumulations of Antarctic ice; the Middle Miocene Event (16.5–13.5 Ma) representing a major, permanent accumulation of the East Antarctic ice sheet and cooling of bottom waters; further temporary cooling events during the late middle Miocene (12.5 to 11.5 Ma) and the earliest late Miocene (11–9 Ma); the Terminal Miocene Event (~6.2–5.0 Ma) marked by cooling, permanent depletion in carbon isotope values, intensification of oceanic circulation, increased biogenic sedimentation rates, and important biotic changes in the surface and deep oceans; the Middle Pliocene Cooling Event at 3.4 Ma, documenting an increase in average global ice volume and cooling of bottom waters; the Late Pliocene Event at 2.6–2.4 Ma, heralding the beginning of major Northern Hemisphere ice accumulation; and amplification of glacial–interglacial oscillations during the Quaternary at 0.9 Ma (Jaramillo Paleomagnetic Subchron).

The sequences record the development during the Cenozoic of latitudinal and vertical thermal gradients in the southwest Pacific region. During the Oligocene, latitudinal thermal gradients developed and strengthened between subantarctic and temperate water masses. A pattern of increasing offset between latitudinally distributed southwest Pacific sites is linked to the establishment and strengthening of the Circum-Antarctic Current during the Oligocene. Major, permanent increases in the vertical temperature gradients of the open ocean occurred in association with the Middle Miocene Event (16.5–13.5), the Middle Pliocene Cooling Event (3.4 Ma) and the Late Pliocene Event (2.6–2.4 Ma). The oxygen isotope records indicate that surface waters in middle latitudes warmed at these times of major ice accumulation or cooling at high latitudes.

The climax of Neogene warmth occurred during the early Miocene, especially between 19.5 and 16.5 Ma, as reflected in the oxygen isotope record and pollen assemblages from southern New Zealand. The middle late Miocene (9 to 6.5 Ma) and the early Pliocene (~5–4 Ma) were also times of relatively warm climatic conditions.

Deep-sea benthic foraminiferal assemblages underwent important changes near the Eocene/Oligocene boundary and during the earliest Middle Miocene, the latest Miocene, and the late Pliocene and Quaternary. The faunal changes associated with the Middle Miocene Event occurred during the early part of the $\delta^{18}O$ shift, which is interpreted to be largely a result of bottom-water cooling. The later part of the $\delta^{18}O$ shift probably largely reflects ice accumulation on East Antarctica. Late Neogene benthic foraminiferal changes are, in part, related to changes in the organic flux rates that accompanied changes in biogenic sedimentation rates and inferred surface-water productivity.

Changes in clay mineralogy, wind-blown terrigenous sediments, and opal phytoliths in the Lord Howe Rise sites record a general evolution of Australian continental climates during the middle and late Cenozoic. Tropical conditions developed during the late Oligocene in northern Australia as the continent migrated northward into the tropical region. During the Neogene, a series of changes led to continental aridity and expansion of grasslands. Important steps occurred during the Middle Miocene Event; the Terminal Miocene Event (~5 Ma), and the Middle Pliocene Event (~3 Ma). Increased continental aridity was linked to global climatic changes related to the sequential glacial development of the polar regions, especially Antarctica.

ACKNOWLEDGMENTS

We appreciate the scientific professionalism and camaraderie of our Leg 90 scientific colleagues. This paleoceanographic synthesis results from all of their contributions. We also thank Captain J. Clark, the crew of the *Glomar Challenger*, and the shipboard technicians for their most professional assistance during DSDP Leg 90, and D. Huey, engineer and Cruise Operations Manager, who successfully completed the development of the extended core barrel (XCB) during Leg 90.

We thank D. Hodell for his valuable constructive criticism of the manuscript, K. Nelson for general assistance, and N. Meader for typing the manuscript.

This research was partly supported by the U.S. National Science Foundation Grants OCE82-14937 (Submarine Geology and Geophysics) and DPP84-16687 (Division of Polar Programs).

REFERENCES

Adams, C. G., Benson, R. H., Kidd, R. B., Ryan, W. B. F., and Wright, R. C., 1977. The Messinian salinity crisis and evidence of late Miocene eustatic changes in the world ocean. *Nature*, 269: 383–386.

Backman, J., 1979. Pliocene biostratigraphy of DSDP Sites 111 and 116 from the North Atlantic Ocean and the age of Northern Hemisphere glaciation. *Stockholm Contrib. Geol.*, 32(3):115–137.

Bandy, O. L., Casey, R. E., and Wright, R. C., 1971. Late Neogene planktonic zonation, magnetic reversals, and radiometric dates, Antarctic to the tropics. *In* Reid, J. L. (Ed.), *Antarctic Oceanology.* Am. Geophys. Un. Antarctic Res. Ser., 15:1–26.

Barron, J. A., 1973. Late Miocene–early Pliocene paleotemperatures for California from marine diatom evidence. *Palaeogeogr., Palaeoclimatol., Palaeoecol.*, 14:277–291.

Barron, J. A., Keller, G., and Dunn, D. A., in press. A multiple microfossil biochronology for the Miocene. *In* Kennett, J. P. (Ed.), *The Miocene Ocean: Paleoceanography and Biogeography.* Geol. Soc. Am. Mem., 163.

Bender, M. L., and Keigwin, L. D., Jr., 1979. Speculations about the upper Miocene change in abyssal Pacific dissolved bicarbonate $\delta^{13}C$. *Earth Planet. Sci. Lett.*, 45:383–393.

Benson, R. H., Chapman, R. E., and Deck, L. T., 1984. Paleoceanographic events and deep-sea ostracodes. *Science*, 224(4655):1334–1336.

Berger, W. H., 1970. Planktonic Foraminifera in selective solution and the lysocline. *Mar. Geol.*, 8:111–183.

________, 1976. Biogenous deep-sea sediments: production, preservation, interpretation. *In* Riley, J. P., and Chester, R. (Eds.), *Chemical Oceanography* (2nd Ed., Vol. 5): London (Academic Press), 265–387.

Berger, W. H., and Winterer, E. L., 1974. Plate stratigraphy and the fluctuating carbonate line. *In* Hsü, K. L., and Jenkyns, H. C. (Eds.), *Pelagic Sediments: On Land and Under the Sea:* Oxford (Blackwell), pp. 11–98.

Berggren, W. A., and Haq, B. U., 1976. The Andalusian Stage (late Miocene): biostratigraphy, biochronology, and paleoecology. *Palaeogeogr. Palaeoclimatol. Palaeoecol.*, 20:67–129.

Berggren, W. A., Kent, D. V., and Flynn, J. J., in press. Paleogene geochronology and chronostratigraphy. *In* Snelling, N. J. (Ed.), *Geochronology and the Geologic Time Scale.* Geol. Soc. London, Spec. Pap.

Brass, G. W., Southam, J. R., and Peterson, W. H., 1982. Warm, saline bottom water in the ancient ocean. *Nature*, 296:620–623.

Brewster, N. A., 1980. Cenozoic biogenic silica sedimentation in the Antarctic Ocean, based on two Deep Sea Drilling Project sites. *Geol. Soc. Am. Bull.*, 91:337–347.

Burns, R. E., Andrews, J. E., et al., 1973. *Init. Repts. DSDP*, 21: Washington (U.S. Govt. Printing Office).

Carter, R. M., and Landis, C. A., 1972. Correlative Oligocene unconformities in southern Australia. *Nature (Phys. Sci.)*, 237(70):12–13.

Ciesielski, P. F., Ledbetter, M. T., and Ellwood, B. B., 1982. The development of Antarctic glaciation and the Neogene paleoenvironment of the Maurice Ewing Bank. *Mar. Geol.*, 46:1–52.

Ciesielski, P. F., and Weaver, F. M., 1974. Early Pliocene temperature changes in the Antarctic Seas. *Geology*, 2:511–515.

Cita, M. B., 1982. The Messinian salinity crisis in the Mediterranean: A review. *Alpine Mediterranean Geodynamics Series* (Vol. 7): Washington (Am. Geophys. Un.), 113–140.

Cita, M. B., and Ryan, W. B. F., 1979. Late Neogene environmental evolution. *In* von Rad, U., Ryan, W. B. F., et al., *Init. Repts. DSDP*, 47, Pt. 1: Washington (U.S. Govt. Printing Office), 447–459.

Corliss, B. H., 1978. Studies of deep-sea benthonic foraminifera in the southeast Indian Ocean. *Antarctic J. U.S.*, 13:116–118.

Corliss, B. H., Aubry, M.-P., Berggren, W. A., Fenner, J. M., Keigwin, L. D., Jr., and Keller, G., 1984. The Eocene/Oligocene Boundary event in the deep sea. *Science*, 226:806–810.

Corliss, B. H., and Keigwin, L. D., Jr., 1983. Eocene-Oligocene benthonic foraminifera: implications for deep-water circulation history. *Am. Assoc. Pet. Geol. Bull.*, 67(3):443-444. (Abstr.)

Davies, T. A., Hay, W. W., Southam, J. R., and Worsley, T. R., 1977. Estimates of Cenozoic oceanic sedimentation rates. *Science*, 197: 53-55.

Davies, T. A., and Worsley, T. R., 1981. Paleoenvironmental implications of oceanic carbonate sedimentation rates. *In* Warme, J. E., Douglas, R. G., and Winterer, E. L. (Eds.), *The Deep Sea Drilling Project: A Decade of Progress.* Soc. Econ. Paleontol. Mineral. Spec. Publ., 32:169-179.

Denham, R. N., and Crook, F. G., 1976. The Tasman Front. *N.Z.J. Mar. Freshwater Res.*, 10:15-30.

Frakes, L. A., 1979. *Climates Throughout Geologic Time:* New York (Elsevier).

Hamon, B. V., 1970. Western boundary currents in the South Pacific. *In* Wooster, W. S. (Ed.), *Scientific Exploration of the South Pacific:* Washington (National Academy of Sciences), pp. 50-59.

Haq, B. U., 1980. Biogeographic history of Miocene calcareous nannoplankton and paleoceanography of the Atlantic Ocean. *Micropaleontology*, 26(4):414-443.

———, 1984. Paleoceanography: a synoptic overview of 200 million years of ocean history. *In* Haq, B. U., and Milliman, J. (Eds.), *Marine Geology and Oceanography of Arabian Sea and Coastal Pakistan:* New York (van Nostrand Reinhold), pp. 201-231.

Haq, B. U., Worsley, T. R., Burckle, L. H., Douglas, R. G., Keigwin, L. D., Jr., Opdyke, N. D., Savin, S. M., Sommer, M. A. II, Vincent, E., and Woodruff, F., 1980. Late Miocene marine carbon-isotopic shift and synchroneity of some phytoplanktonic biostratigraphic events. *Geology*, 8:427-431.

Hayes, D. E., and Frakes, L. A., 1975. General synthesis, Deep Sea Drilling Project Leg 28. *In* Hayes, D. E., Frakes, L. A., et al., *Init., Repts. DSDP*, 28: Washington (U.S. Govt. Printing Office), 919-942.

Hodell, D., Elmstrom, K. M., and Kennett, J. P., in press. Latest Miocene $\delta^{18}O$ variability, global ice volume, sea level, and the "Messinian Salinity Crisis." *Nature.*

Hodell, D., and Kennett, J. P., 1984. Late Miocene carbon shift in DSDP Site 516A, western south Atlantic. *Geol. Soc. Am. Abstr. Prog.*, 16(6):540.

Hodell, D. A., Williams, D. F., and Kennett, J. P., 1985. Late Pliocene reorganization of deep vertical water-mass structure in the western South Atlantic: faunal and isotopic evidence. *Geol. Soc. Am. Bull.*, 96:495-503.

Ingle, J. C., 1967. Foraminiferal biofacies variation and the Miocene-Pliocene boundary in Southern California. *Bull. Am. Paleontol.*, 52:217-394.

———, 1973. Neogene foraminifera from the northeastern Pacific Ocean, Leg 18, Deep Sea Drilling Project. *In* Kulm, L. D., von Huene, R., et al., *Init. Repts. DSDP*, 18: Washington (U.S. Govt. Printing Office), 517-567.

Jenkins, D. G., 1975. Cenozoic planktonic foraminiferal biostratigraphy of the southwestern Pacific and Tasman Sea—DSDP Leg 29. *In* Kennett, J. P., Houtz, R. E., et al., *Init. Repts. DSDP*, 29: Washington (U.S. Govt. Printing Office), 449-467.

Keany, J., 1978. Paleoclimatic trends in early and middle Pliocene deep-sea sediments of the Antarctic. *Mar. Micropaleontol.*, 3:35-49.

Keigwin, L. D., Jr., 1979. Late Cenozoic stable isotope stratigraphy and paleoceanography of DSDP sites from the east equatorial and central north Pacific Ocean. *Earth Planet. Sci. Lett.*, 45:361-382.

Keigwin, L. D., Aubry, M.-P., and Kent, D. V., in press. Upper Miocene stable isotopic stratigraphy, biostratigraphy, and magnetostratigraphy of North Atlantic DSDP Sites. *In* Ruddiman, W. F., Kidd, R. B., et al., *Init. Repts. DSDP*, 94: Washington (U.S. Govt. Printing Office).

Keigwin, L. D., Jr., and Keller, G., 1984. Middle Oligocene cooling from Equatorial Pacific DSDP Site 77B. *Geology*, 12:16-19.

Keigwin, L. D., Jr., and Shackleton, N. J., 1980. Uppermost Miocene carbon isotope stratigraphy of a piston core in the equatorial Pacific. *Nature*, 284(5757):613-614.

Keigwin, L. D., Jr., and Thunell, R. C., 1980. Middle Pliocene climatic change from faunal and oxygen isotopic trends: western Mediterranean. *Nature*, 282(5736):294-296.

Keller, G., 1979. Late Neogene planktonic foraminiferal biostratigraphy and paleoceanography of the northwest Pacific Site 296. *Palaeogeogr., Palaeoclimatol., Palaeoecol.*, 27:129-154.

Kemp, E. M., 1978. Tertiary climatic evolution and vegetation history in the Southeast Indian Ocean region. *Palaeogeogr. Palaeoclimatol. Palaeoecol.*, 24:169-208.

Kemp, E. M., Frakes, L. A., and Hayes, D. E., 1975. Paleoclimatic significance of diachronous biogenic facies, Leg 28, Deep Sea Drilling Project. *In* Hayes, D. E., Frakes, L. A., et al., *Init. Repts. DSDP*, 28: Washington (U.S. Govt. Printing Office), 909-917.

Kennett, J. P., 1967. Recognition and correlation of the Kapitean Stage (upper Miocene, New Zealand). *N.Z.J. Geol. Geophys.*, 10:1051-1063.

———, 1977. Cenozoic evolution of Antarctic glaciation, the circum-Antarctic Ocean, and their impact on global paleoceanography. *J. Geophys. Res.*, 82:3843-3860.

———, 1978. The development of planktonic biogeography in the Southern Ocean during the Cenozoic. *Mar. Micropaleontol.*, 3: 301-345.

———, 1982. *Marine Geology:* Englewood Cliffs, N. J. (Prentice-Hall).

Kennett, J. P., Burns, R. E., Andrews, J. E., Churkin, M., Jr., Davies, T. A., Dumitrică, P., Edwards, A. R., Galehouse, J. S., Packham, G. M., and van der Lingen, G. J., 1972. Australian-Antarctic continental drift, palaeocirculation changes and Oligocene deep-sea erosion. *Nat. (Phys. Sci.)*, 239(91):51-55.

Kennett, J. P., Houtz, R. E., et al., 1975. *Init. Repts. DSDP*, 29: Washington (U.S. Govt. Printing Office).

Kennett, J. P., Houtz, R. E., Andrews, P. B., Edwards, A. R., Gostin, V. A., Hajós, M., Hampton, M., Jenkins, D. G., Margolis, S. V., Ovenshine, A. T., and Perch-Nielsen, K., 1975. Cenozoic paleoceanography in the southwest Pacific Ocean, Antarctic glaciation, and the development of the circum-Antarctic current. *In* Kennett, J. P., Houtz, R. E., et al., *Init. Repts. DSDP*, 29: Washington (U.S. Govt. Printing Office), 1155-1169.

Kennett, J. P., and Shackleton, N. J., 1976. Oxygen isotopic evidence of the development of the psychrosphere 38 m.y. ago. *Nature*, 260: 513-515.

Kennett, J. P., Shackleton, N. J., Margolis, S. V., Goodney, D. E., Dudley, W. C., and Kroopnick, P. M., 1979. Late Cenozoic oxygen and carbon isotopic history and volcanic ash stratigraphy: DSDP Site 284, South Pacific. *Am. J. Sci.*, 279:52-69.

Kennett, J. P., and Srinivasan, M. S., 1983. *Neogene Planktonic Foraminifera: A Phylogenetic Atlas:* Stroudsburg, PA (Hutchinson Ross).

Kennett, J. P., and Vella, P., 1975. Late Cenozoic planktonic foraminifera and paleoceanography at DSDP Site 284 in the cool subtropical South Pacific. *In* Kennett, J. P., Houtz, R. E., et al., *Init. Repts. DSDP*, 29: Washington (U.S. Govt. Printing Office), 769-799.

Kennett, J. P., and Watkins, N. D., 1974. Late Miocene-early Pliocene paleomagnetic stratigraphy, paleoclimatology, and biostratigraphy in New Zealand. *Geol. Soc. Am. Bull.*, 85:1385-1398.

Knox, G. A., 1970. Biological oceanography of the South Pacific. *In* Wooster, W. A. (Ed.), *Scientific Exploration of the South Pacific:* Washington (National Academy of Sciences), pp. 155-182.

Kvasov, D. D., and Verbitsky, M. Y., 1981. Causes of Antarctic glaciation in the Cenozoic. *Quat. Res.*, 15:1-17.

LaBrecque, J., Hsü, K. J., Carman, M. F., Karpoff, A. M., McKenzie, J. A., et al., 1983. DSDP Leg 73: Contributions to Paleogene stratigraphy and nomenclature, chronology and sedimentation rates. *Palaeogeogr., Palaeoclimatol., Palaeoecol.*, 42(1/2):91-125.

Loutit, T. S., 1981. Late Miocene paleoclimatology: subantarctic water mass, southwest Pacific. *Mar. Micropaleontol.*, 6:1-27.

Loutit, T. S., and Keigwin, L. D., Jr., 1982. Stable isotopic evidence for latest Miocene sea-level fall in the Mediterranean region. *Nature*, 300(5888):163-166.

Loutit, T. S., and Kennett, J. P., 1979. Application of carbon isotope stratigraphy to late Miocene shallow marine sediments, New Zealand. *Science*, 204:1196-1199.

Loutit, T. S., Kennett, J. P., and Savin, S. M., 1983. Miocene equatorial and southwest Pacific paleoceanography from stable isotope evidence. *Mar. Micropaleontol.*, 8:215-233.

Loutit, T. S., Pisias, N. G., and Kennett, J. P., 1983. Pacific Miocene carbon isotope stratigraphy using benthic foraminifera. *Earth Planet. Sci. Lett.*, 66:48–62.

McKenzie, J. A., Weissert, H., Poore, R. Z., Wright, R. C., Percival, S. F., Jr., Oberhänsli, H., and Casey, M., 1984. Paleoceanographic implications of stable-isotope data from upper Miocene–lower Pliocene sediments from the southeast Atlantic (Deep Sea Drilling Project Site 519). *In* Hsü, K. J., LaBrecque, J. L., et al., *Init. Repts. DSDP*, 73: Washington (U.S. Govt. Printing Office), 717–724.

Margolis, S. V., Kroopnick, P. M., Goodney, D. E., Dudley, W. C., and Mahoney, M. E., 1975. Oxygen and carbon isotopes from calcareous nannofossils as paleoceanographic indicators. *Science*, 189:555–557.

Mercer, J. H., 1976. Glacial history of southernmost South America. *Quat. Res.*, 6:125–166.

Mercer, J. H., and Sutter, J. F., 1982. Late Miocene–earliest Pliocene glaciation in southern Argentina: implications for global ice-sheet history. *Palaeogeogr., Palaeoclimatol., Palaeoecol.*, 38:185–206.

Mildenhall, D. C., 1976. Exotic pollen rain on the Chatham Islands during the Late Pleistocene. *N.Z.J. Geol. Geophys.*, 19:327–333.

Miller, K. G., and Fairbanks, R. G., 1983. Evidence for Oligocene-middle Miocene abyssal circulation changes in the western North Atlantic. *Nature*, 306:250–253.

Miller, K. G., and Thomas, E., in press. Late Eocene to Oligocene benthic foraminiferal isotope record, Site 574, equatorial Pacific. *In* Mayer, L., Theyer, G., et al., *Init. Repts. DSDP*, 85: Washington (U.S. Govt. Printing Office), 771–778.

Moore, T. C., Jr., Rabinowitz, P. D., and Shipboard Scientific Party, 1983. The Walvis transect, Deep Sea Drilling Project Leg 74: the geologic evolution of an oceanic plateau in the south Atlantic Ocean. *Geol. Soc. Am. Bull.*, 94:907–925.

Poore, R. Z., 1981. Late Miocene biogeography and paleoclimatology of the central North Atlantic. *Mar. Micropaleontol.*, 6:599–616.

Prell, W. L., 1982. Oxygen and carbon isotope stratigraphy for the Quaternary of Hole 502B: evidence for two modes of isotopic variability. *In* Prell, W. L., Gardner, J. V., et al., *Init. Repts. DSDP*, 68: Washington (U.S. Govt. Printing Office), 455–464.

________, 1984. Covariance patterns of foraminifera $\delta^{18}O$: an evaluation of Pliocene ice volume changes near 3.2 million years ago. *Science*, 206:692–693.

Prell, W. L., Gardner, J. V., et al., 1982. *Init. Repts. DSDP*, 68: Washington (U.S. Govt. Printing Office).

Resig, J. M., 1976. Benthic foraminiferal stratigraphy, eastern margin, Nazca Plate. *In* Yeats, R. S., Hart, S. R., et al., *Init. Repts. DSDP*, 34: Washington (U.S. Govt. Printing Office), 743–759.

Ridgway, N. M., 1969. Temperature and salinity of sea water at the ocean floor in the New Zealand region. *N.Z.J. Mar. Freshwater Res.*, 3:57–72.

Rochford, D. J., 1960. Some aspects of the deep circulation of the Tasman and Coral Seas. *Aust. J. Mar. Freshwater Res.*, 11:166–181.

Savin, S. M., Abel, L., Barrera, E., Hodell, D., Keller, G., Kennett, J. P., Killingley, J., Murphy, M., and Vincent, E., in press. The evolution of Miocene surface and near-surface marine temperatures: oxygen isotopic evidence. *In* Kennett, J. P. (Ed.), *The Miocene Ocean: Paleoceanography and Biogeography.* Geol. Soc. Am. Mem., 163.

Savin, S. M., Douglas, R. G., Keller, G., Killingley, J. S., Shaughnessy, L., Sommer, M. A., Vincent, E., and Woodruff, F., 1981. Miocene benthic foraminiferal isotope records: a synthesis. *Mar. Micropaleontol.*, 6:423–450.

Savin, S. M., Douglas, R. G., and Stehli, F. G., 1975. Tertiary marine paleotemperatures. *Geol. Soc. Am. Bull.*, 86:1499–1510.

Schnitker, D., 1974. West Atlantic abyssal circulation during the past 120,000 years. *Nature*, 248:385–387.

Sclater, J., Meinke, L., Bennett, A., and Murphy, C., in press. The depth of the ocean through the Neogene. *In* Kennett, J. P. (Ed.), *The Miocene Ocean: Paleoceanography and Biogeography.* Geol. Soc. Am. Mem., 163.

Shackleton, N. J., 1977. Carbon-13 in *Uvigerina:* Tropical rain forest history and the equatorial Pacific carbonate dissolution cycles. *In* Anderson, N. R., and Malahoff, A. (Eds.), *The Fate of Fossil Fuel CO_2 in the Oceans:* New York (Plenum), pp. 401–427.

Shackleton, N. J., Backman, J., Zimmerman, H., Kent, D. V., Hall, M. A., et al., 1984. Oxygen isotope calibration of the onset of ice-rafting and history of glaciation in the North Atlantic region. *Nature*, 307(5952):620–623.

Shackleton, N. J., and Cita, M. B., 1979. Oxygen and carbon isotopic stratigraphy of benthic foraminifers at Site 397: detailed history of climatic change during the late Neogene. *In* von Rad, U., Ryan, W. B. F., et al., *Init. Repts. DSDP*, 47, Pt. 1: Washington (U.S. Govt. Printing Office), 433–445.

Shackleton, N. J., Hall, M. A., and Boersma, A., 1984. Oxygen and carbon isotope data from Leg 74 foraminifers. *In* Moore, T. C., Jr., Rabinowitz, P. D., et al., *Init. Repts. DSDP*, 74: Washington (U.S. Govt. Printing Office), 599–612.

Shackleton, N. J., and Kennett, J. P., 1975a. Late Cenozoic oxygen and carbon isotopic changes at DSDP Site 284: implications for glacial history of the Northern Hemisphere and Antarctica. *In* Kennett, J. P., Houtz, R. E., et al., *Init. Repts. DSDP*, 29: Washington (U.S. Govt. Printing Office), 801–806.

________, 1975b. Paleotemperature history of the Cenozoic and the initiation of Antarctic glaciation: oxygen and carbon isotope analyses in DSDP Sites 277, 279, and 281. *In* Kennett, J. P., Houtz, R. E., et al., *Init. Repts. DSDP*, 29: Washington (U.S. Govt. Printing Office), 743–755.

Shackleton, N. J., and Members of the Shipboard Scientific Party, 1984. Accumulation rates in Leg 74 sediments. *In* Moore, T. C., Jr., Rabinowitz, P. D., et al., *Init. Repts. DSDP*, 74: Washington (U.S. Govt. Printing Office), 621–644.

Shackleton, N. J., and Opdyke, N. D., 1973. Oxygen isotope and palaeomagnetic stratigraphy of equatorial Pacific core V28-238: oxygen isotope temperatures and ice volumes on a 10^5 year and 10^6 year scale. *Quat. Res.*, 3:39–55.

________, 1977. Oxygen isotopic and paleomagnetic evidence for early Northern Hemisphere glaciation. *Nature*, 270:216–219.

Stanton, B. R., 1979. The Tasman Front. *N.Z.J. Mar. Freshwater Res.*, 138:201–214.

________, 1981. An oceanographic survey of the Tasman Front. *N.Z.J. Mar. Freshwater Res.*, 15:289–297.

Streeter, S. S., 1973. Bottom water and benthonic foraminifera in the North Atlantic—glacial-interglacial contrasts. *Quat. Res.*, 3:131–141.

Thiede, J., 1983. Skeletal plankton and nekton in upwelling water masses of northwestern South America and northwest Africa. *In* Suess, E., and Thiede, J. (Eds.), *Coastal Upwelling, Its Sediment Record:* New York (Plenum Press), pp. 183–207.

Tucholke, B. E., Hollister, C. D., Weaver, F. M., and Vennum, W. R., 1976. Continental rise and abyssal plain sedimentation in the southeast Pacific basin, Leg 35, Deep Sea Drilling Project. *In* Hollister, C. D., Craddock, C., et al., *Init. Repts. DSDP*, 35: Washington (U.S. Govt. Printing Office), 359–400.

Vail, P. R., and Hardenbol, J., 1979. Sea-level changes during the Tertiary. *Oceanus*, 22:71–79.

van Andel, T. H., Heath, G. R., and Moore, T. C., Jr., 1975. *Cenozoic History and Paleoceanography of the Central Equatorial Pacific Ocean.* Geol. Soc. Am. Mem., 143.

Vincent, E., and Berger, W. H., in press. Carbon dioxide and polar cooling in the Miocene: the Monterey hypothesis. *In* Sundquist, E. T., and Broecker, W. S. (Eds.), *The Carbon Cycle and Atmospheric Co_2: Natural Variations Archean to Present.* Am. Geophys. Un. Monogr., 32.

Vincent, E., Killingley, J. S., and Berger, W. H., 1980. The magnetic Epoch-6 carbon shift: a change in the ocean's $^{13}C/^{12}C$ ratio 6.2 million years ago. *Mar. Micropaleontol.*, 5:185–203.

________, in press. Miocene oxygen and carbon isotope stratigraphy of the tropical Indian Ocean. *In* Kennett, J. P. (Ed.), *The Miocene Ocean: Paleoceanography and Biogeography.* Geol. Soc. Am. Mem., 163.

Wei, K.-Y., and Kennett, J. P., in press. Taxonomic evolution of Neogene planktonic foraminifera and paleoceanographic relations. *Paleobiology.*

Weissert, H. J., McKenzie, J. A., Wright, R. C., Clark, M., Oberhänsli, H., and Casey, M., 1984. Paleoclimatic record of the Pliocene at Deep Sea Drilling Project Sites 519, 521, 522, and 523 (Central

South Atlantic). *In* Hsü, K. J., LaBrecque, J. L., et al., *Init. Repts. DSDP*, 73: Washington (U.S. Govt. Printing Office), 701–715.

Williams, D. F., Moore, W. S., and Fillon, R. H., 1981. Role of glacial Arctic Ocean ice sheets in Pleistocene oxygen isotope and sea level records. *Earth Planet. Sci. Lett.*, 56:157–166.

Wolfe, J. A., 1971. Tertiary climatic fluctuations and methods of analysis of Tertiary floras. *Palaeogeogr., Palaeoclimatol., Palaeoecol.* 9:27–57.

Woodruff, F., and Savin, S. M., 1985. $\delta^{13}C$ values of Miocene Pacific benthic foraminifera: correlations with sea level and biological productivity. *Geology*, 13(2):119–122.

Woodruff, F., Savin, S. M., and Douglas, R. G., 1981. Miocene stable isotope record: a detailed deep Pacific Ocean study and its paleoclimatic implications. *Science*, 212:665–668.

Worsley, T. R., and Davies, T. A., 1979. Cenozoic sedimentation in the Pacific Ocean: steps toward a quantitative evaluation. *J. Sed. Petrol.*, 49:1131–1146.

Wyrtki, K., 1974. *The Dynamic Topography of the Pacific Ocean and Its Fluctuations.* Hawaii Inst. Geophys. Rep. HIG 74-5.

Date of Acceptance: 14 June 1985

Drilling locations

Leg	Location	Sites
Phase 1 1968–1970		
1	North Atlantic	1–7
2	North Atlantic	8–12
3	South Atlantic	13–22
4	Central Atlantic	23–31
5	North Pacific	32–43
6	North Pacific	44–60
7	Central Pacific	61–67
8	Central Pacific	68–75
9	Central Pacific	76–84
Phase 2 1970–1972		
10	Gulf of Mexico	85–97
11	North Atlantic	98–108
Re-entry trials		109–110
12	North Atlantic	111–119
13	Mediterranean	120–134
14	Central Atlantic	135–144
15	Caribbean	146–154
16	Central Pacific	155–163
17	Central Pacific	164–171
18	North Pacific	172–182
19	North Pacific	183–193
20	North Pacific	194–202
21	Coral Sea	203–210
22	Indian Ocean	211–218
23	Arabian Sea	219–230
24	Indian Ocean	231–238
25	Indian Ocean	239–249
Phase 3 1972–1975		
26	Indian Ocean	250–258
27	Indian Ocean	259–263
28	Antarctic	264–274
29	Tasman Sea	275–284
30	South Pacific	285–289
31	North Pacific	290–302
32	North Pacific	303–313
33	North Pacific	314–318
34	South Pacific	319–321
35	South Pacific	322–325
36	South Atlantic	326–331
37	North Atlantic	332–335
38	Arctic	336–352
39	Atlantic	353–359
40	South Atlantic	360–365
41	South Atlantic	366–370
42A	Mediterranean	371–378
42B	Black Sea	379–381
43	North Atlantic	382–387
44	North Atlantic	388–392
44A	North Atlantic	393–394
IPOD I 1975–present		
45	North Atlantic	395–396
46	North Atlantic	396A–396B
47	North Atlantic	397–398
48	North Atlantic	399–406
49	North Atlantic	407–414
50	North Atlantic	415–416
51A	North Atlantic	417–417A
51B	North Atlantic	417B–417D
52	North Atlantic	417D–418A
53	North Atlantic	418A–418B
54	Central Pacific	419–429
55	North Pacific	430–433
56	North Pacific	434–437
57	North Pacific	438–441
58	North Pacific	442–446
59	North Pacific	447–451
60	North Pacific	452–461
61	Central Pacific	462
62	North Pacific	463–466
63	North Pacific	467–473
64	Gulf of California	474–481
65	Gulf of California	482–485
66	Central Pacific	486–493
67	Central Pacific	494–500
68	Central Pacific	502–503
69	Central Pacific	504–505, 501
70	Central Pacific	506–510, 504B
71	South Atlantic	511–514
72	South Atlantic	515–518
73	South Atlantic	519–524
74	South Atlantic	525–529
75	South Atlantic	530–532
76	North Atlantic	533–534
77	Caribbean	535–540
78	North Atlantic	541–543, 395A, B
79	North Atlantic	544–547
80	North Atlantic	548–551
81	North Atlantic	552–555
82	North Atlantic	556–564
83	Central Pacific	504B
84	Central Pacific	565–570
85	Central Pacific	571–575
86	North Pacific	576–581
87	North Pacific	582–584
88	North Pacific	581
89	Central Pacific	585–586, 462A
90	South Pacific	587–594

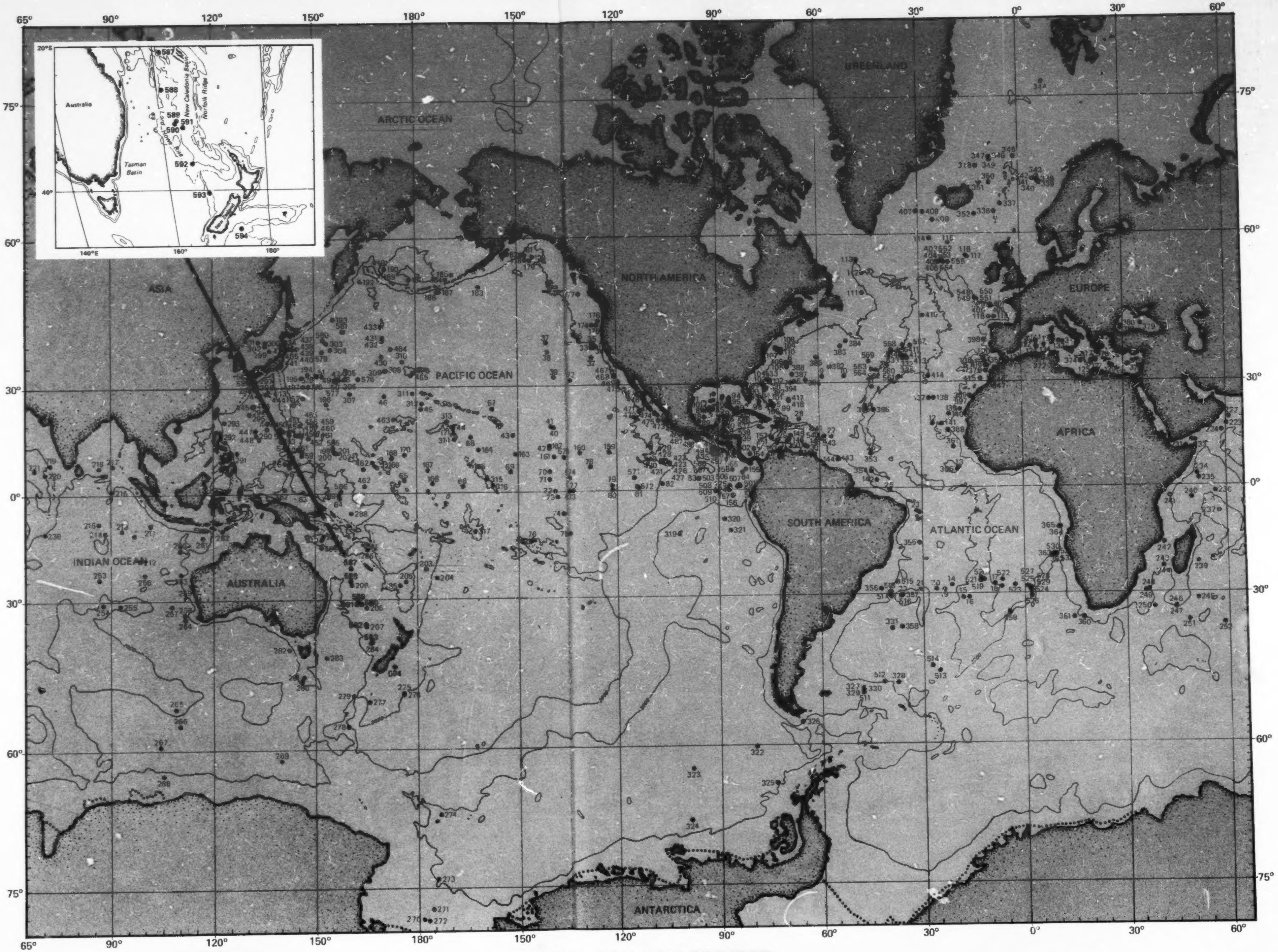
ARCTIC OCEAN
GREENLAND
NORTH AMERICA
ASIA
EUROPE
PACIFIC OCEAN
AFRICA
INDIAN OCEAN
AUSTRALIA
SOUTH AMERICA
ATLANTIC OCEAN
ANTARCTICA
Australia
Tasman Basin
Lord Howe Rise
New Caledonia Basin
Norfolk Ridge
20°S
40°
140°E
160°
180°
587
588
589
590
591
592
593
594
65°
90°
120°
150°
180°
150°
120°
90°
60°
30°
0°
30°
60°
75°
60°
30°
0°
30°
60°
75°

DEEP SEA DRILLING PROJECT

READEX best copy available

Volume 90: Chapter 15: Figure 3. Positions of selected diatom, radiolarian, silicoflagellate, and foraminiferal datums in the late Miocene and Pliocene to Quaternary of Holes 594 and 594A and their correlation to paleomagnetic stratigraphy. Radiolarian datums from Caulet (this volume) and foraminiferal datum from Jenkins and Srinivasan (this volume). Reference key: (1) Tauxe et al., 1983; (2) LaBrecque et al., 1977, and Theyer and Hammond, 1974; (3) Berggren et al., in press; (4) Ciesielski, 1983.

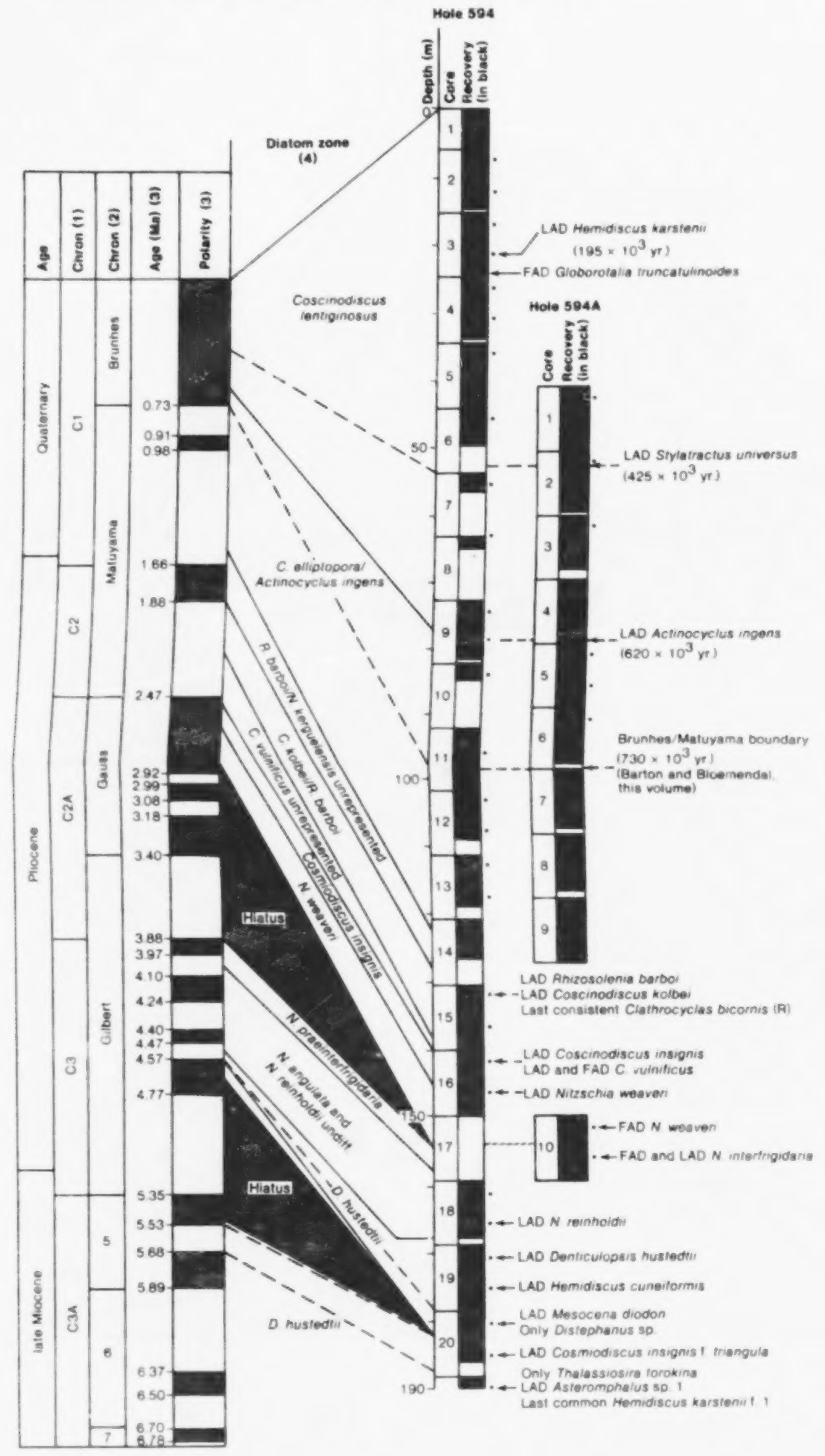

Volume 90: Chapter 15: Figure 4. Positions of selected diatom, radiolarian, silicoflagellate, and calcareous nannofossil datums in the middle to late Miocene of Holes 594 and 594A and their correlation to paleomagnetic stratigraphy. Diatom and silicoflagellate datums (this chapter), radiolarians (Caulet, this volume), calcareous nannofossils (Martini, this volume). Ages and correlations of important datums to paleomagnetic stratigraphy are cited in Table 3. Reference key: (1) Tauxe et al., 1983; (2) LaBrecque et al., 1977, and Theyer and Hammond, 1974; (3) Berggren et al., 1984. Numbers on correlation lines from cores to the paleomagnetic stratigraphy refer to corresponding datums numbered in Table 3.

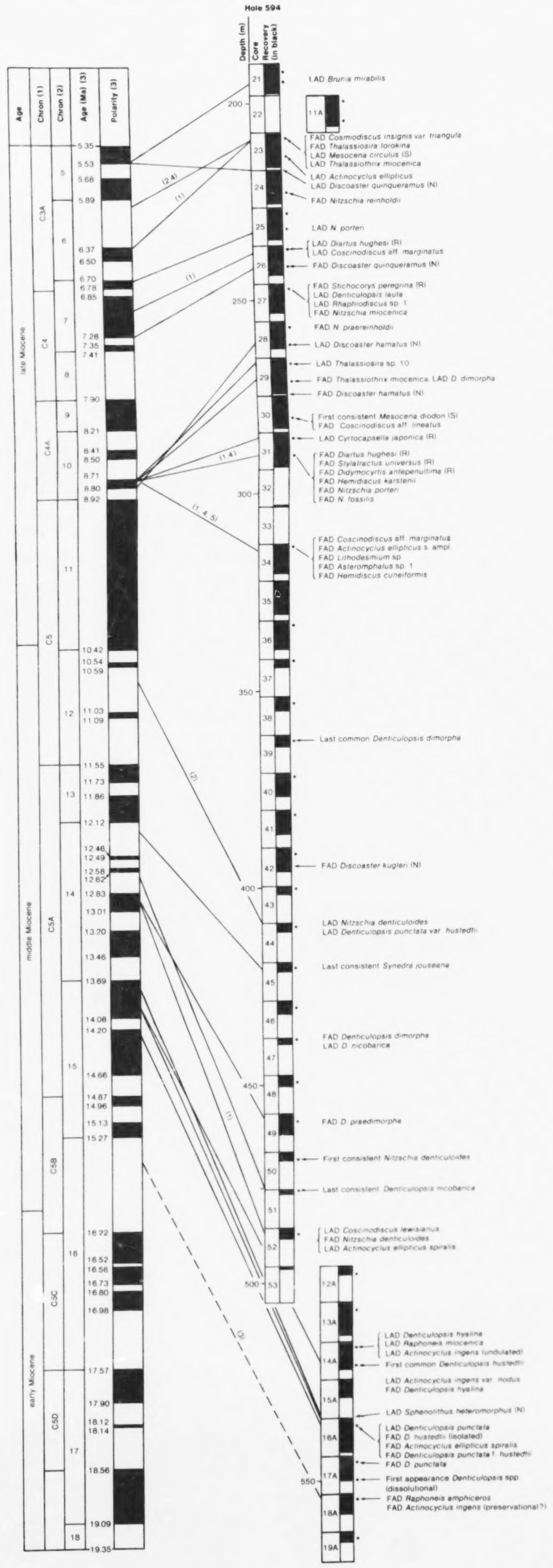

Volume 90: Chapter 38: Figure 5. Tracings of *Glomar Challenger* transit profiles between Cook Strait and Site 594 east of New Zealand, showing main seismic sequences, faults, and unconformities patterned for clarity. Lines at 1 s intervals (two-way traveltime) equivalent to 750 m in seawater.

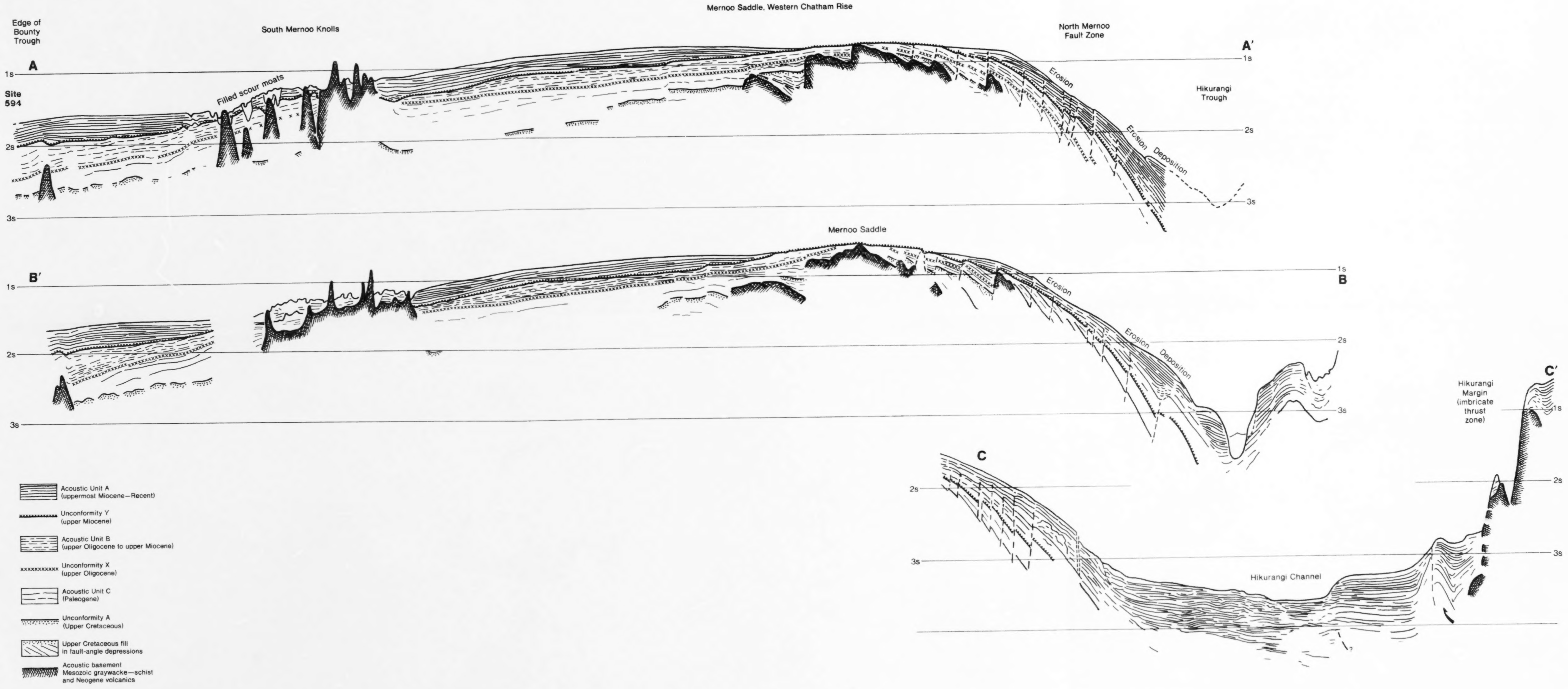
Mernoo Saddle, Western Chatham Rise
Edge of Bounty Trough
South Mernoo Knolls
North Mernoo Fault Zone
A
A′
1s
Site 594
Filled scour moats
Erosion
Erosion
Deposition
Hikurangi Trough
2s
3s
Mernoo Saddle
B′
B
1s
2s
3s
Erosion
Erosion
Deposition
C
C′
Hikurangi Margin (imbricate thrust zone)
Hikurangi Channel
1s
2s
3s
Acoustic Unit A (uppermost Miocene—Recent)
Unconformity Y (upper Miocene)
Acoustic Unit B (upper Oligocene to upper Miocene)
Unconformity X (upper Oligocene)
Acoustic Unit C (Paleogene)
Unconformity A (Upper Cretaceous)
Upper Cretaceous fill in fault-angle depressions
Acoustic basement Mesozoic graywacke—schist and Neogene volcanics